MH370 COLLECTION

OFFICIAL REPORTS
ANALYSIS
DATA
HISTORICAL

COMPILED BY GRIDER BROWNING
X : HIGHEARTHORBIT_
r/garygundark

Table of Contents

SAFETY REPORT2018 MH370 26
1 I - Contents 27
1.1 i. Table of Contents 27
1.2 ii. List of Appendices 38
2 II. Synopsis 40
3 III. Dedication 44
4 IV. Acknowledegment 45
5 V. Objective 46
6 VI. Disclaimer 47
7 VII. Glossary of Terms 48
8 VIII. Abbreviations & Codes 54
9 IX. The Malaysian ICAO Annex 13 Safety Investigation Team for MH370 (9M-MRO) 70
10 Section 1.1 - History of Flight 72
10.1 1.1.1 Introduction 72
10.2 1.1.2 Actions by HCM ACC and KL ACC 74
10.3 1.1.3 Diversion from Filed Flight Plan Route 74
10.3.1 1) Malaysian Military Radar 74
10.3.2 2) DCA Civilian Radar from Kota Bharu-Sultan Ismail Petra Airport Runway 77
10.3.3 3) Ho Chi Minh Air Traffic Services 86
10.3.4 4) Kuala Lumpur ACC Radar 88
10.3.5 5) Medan Air Traffic Control Radar 89
10.3.6 6) Bangkok Air Traffic Control Radar 89
10.3.7 7) Singapore Air Traffic Services 90
10.4 1.1.4 Role of Malaysian Military 90
10.5 1.1.5 Detection of Hand Phone Signal 91
10.6 1.1.6 Search for Aircraft 91
11 Section 1.2 - Injuries to Persons 93

12 Section 1.3 - Damage to Aircraft 94
13 Section 1.4 - Other Damages 95
14 Section 1.5 - Personnel Information 96
14.1 1.5.1 Introduction 96
14.2 1.5.2 Malaysia Airlines Training and Check Records 96
14.3 1.5.3 Pilot-in-Command 97
14.3.1 1) Personal Profile of Pilot-in-Command 97
14.3.2 2) Royal Malaysia Police's Report on Flight Simulator of PIC 98
14.4 1.5.4 First Officer 100
14.4.1 1) Personal Profile of First Officer 101
14.5 1.5.5 Summary of Work Schedule for Flight Crew of MH370 101
14.6 1.5.6 Cabin Crew and Personal Profiles 101
14.6.1 1) In-flight Supervisor (IFS) 102
14.6.2 2) Chief Steward (CS) 102
14.6.3 3) Chief Stewardess (CSS) 103
14.6.4 4) Leading Steward (LS) 103
14.6.5 5) Leading Stewardess (LSS) 104
14.6.6 6) Flight Stewardess (FSS) 1 104
14.6.7 7) Flight Stewardess (FSS) 2 105
14.6.8 8) Flight Steward (FS) 1 105
14.6.9 9) Flight Steward (FS) 2 106
14.6.10 10) Flight Steward (FS) 3 106
14.7 1.5.7 Disciplinary/Administrative Actions 107
14.8 1.5.8 Financial Background and Insurance Cover 107
14.9 1.5.9 Significant Past Medical and Medication History 107
14.10 1.5.10 Psychological and Social Events 108
14.11 1.5.11 Behavioural Events 108
14.12 1.5.12 Voice Recognition of the Radio Transmissions between MH370 and Air Traffic Control 109
15 Section 1.6 - Aircraft Information 110

15.1 1.6.1 Airframe 110
15.2 1.6.2 Engine 110
15.3 1.6.3 Auxiliary Power Unit 110
15.4 1.6.4 Airworthiness and Maintenance 111
15.4.1 1) Aircraft Maintenance Schedule 111
15.4.2 2) Major Repair 115
15.4.3 3) Cabin Configuration Change 116
15.4.4 4) Mandatory Occurrence Reports 116
15.4.5 5) Airworthiness Directives 117
15.4.6 6) Technical Log 118
15.4.7 7) Deferred Defects (Maintenance Report 2) 119
15.4.8 8) Engine Health Monitoring 120
15.4.9 9) Central Maintenance Computing System 120
15.5 1.6.5 Weight and Balance 121
15.6 1.6.6 Fuel 122
15.7 1.6.7 Emergency Locator Transmitter 123
15.7.1 1) Review of Effectiveness of Emergency Locator Transmitters 125
15.8 1.6.8 Aircraft Systems Description 127
15.8.1 1) Air Conditioning and Pressurisation 128
15.8.2 2) Autopilot Flight Director System 129
15.8.3 3) Electrical Power 138
15.8.4 4) Cabin and Cargo Compartments 146
15.8.5 5) Flight Controls 147
15.8.6 6) Fuel System 149
15.8.7 7) Hydraulics 151
15.8.8 8) Instrumentation 152
15.8.9 9) Airplane Information Management System 156
15.8.10 10) Navigation Systems 157
15.8.11 11) Oxygen Systems 159

15.8.12 12) Central Maintenance Computing System 161
15.8.13 13) Engines 161
15.8.14 14) Auxiliary Power Unit 163
15.9 1.6.9 Aircraft Performance 164
15.10 1.6.10 Boeing Patent on Remote Control Take-over of Aircraft 165
16 Section 1.7 - Meteorological Information 167
16.1 1.7.1 Meteorological Situation 167
16.2 1.7.2 Comments on the Information Available 170
16.2.1 1) Forecast Charts 170
16.2.2 2) Significant Meteorological Information 171
16.2.3 3) Volcanic Ash Advisory 172
16.3 1.7.3 Availability of Meteorological Information 172
17 Section 1.8 - Aids to Navigation 173
18 Section 1.9 - Communications 174
18.1 1.9.1 High Frequency System 174
18.2 1.9.2 Very High Frequency System 174
18.3 1.9.3 Air Traffic Control/Mode S Transponder System 175
18.4 1.9.4 Aircraft Communications Addressing and Reporting System 176
18.4.1 1) ACARS Traffic Log 179
18.5 1.9.5 Satellite Communications 186
18.5.1 1) Satellite Communications System Description 186
18.5.2 2) SATCOM Ground Station Logs of Event - Introduction 190
18.5.3 3) SATCOM Ground Station Logs of the Event - Summary 192
18.5.4 4) SATCOM Ground Station Logs - Key Observations 195
18.5.5 5) Frequencies of Log-On Bursts 201
19 Section 1.10 - Aerodrome Information 203
20 Section 1.11 Flight Recorders 204
20.1 1.11.1 Solid State Flight Data Recorder 204

20.2 1.11.2 Solid State Cockpit Voice Recorder 205
20.3 1.11.3 Underwater Locator Beacons 207
20.3.1 1) Solid State Flight Data Recorder Underwater Locator Beacon Battery Expiry 208
21 Section 1.12 - Wreckage and Impact Information 209
21.1 1.12.1 Introduction 209
21.2 1.12.2 Location of Where the Debris were Found 210
21.3 1.12.3 Details of the Debris 225
21.4 1.12.4 Process for Recovery of Debris 238
22 Section 1.13 - Medical and Pathological Information 239
23 Section 1.14 - Fire 241
24 Section 1.15 - Survivability 242
25 Section 1.16 - Test and Research 243
26 Section 1.17 - Organisational and Management Information 244
26.1 1.17.1 Department of Civil Avaition Malaysia 244
26.1.1 1) Introduction 244
26.1.2 2) Functions and Responsibilities of Department of Civil Aviation 245
26.1.3 3) Sectors and Division of Department of Civil Aviation 246
26.1.4 4) Areas of Focus 246
26.1.5 5) Air Traffic Management Sector 246
26.1.6 6) Airworthiness Sector 261
26.1.7 7) Flight Operations Sector 265
26.2 1.17.2 Malaysia Airlines 267
26.2.1 1) Introduction 267
26.2.2 2) Engineering & Maintenance 268
26.2.3 3) Operations 273
27 Section 1.18 - Additional Information 299
27.1 1.18.1 Provision of Air Traffic Services and Areas of Responsibilities 299
27.1.1 1) Introduction 299

27.1.2 2) Sector 3 Area of Responsibility 300
27.1.3 3) Sector 5 Area of Responsibility 303
27.1.4 4) Air Traffic Services Operations 306
27.1.5 5) KL ATSC Duty Shift System for Air Traffic Controllers 307
27.1.6 6) Chronology of Activities after notification by HCM ACC 313
27.1.7 7) Activation of KL Aeronautical Rescue Coordination Centre 318
27.1.8 8) Recorded Telephone Conversations 320
27.1.9 9) Watch Supervisor Air Traffic Services and Sector (3 & 5) Logbook 321
27.1.10 10) Flight Progress Strip 321
27.2 1.18.2 Aircraft Cargo Consignment 323
27.2.1 1) Introduction 323
27.2.2 2) Lithium Ion Batteries 325
27.2.3 3) Mangosteen Fruits 330
27.3 1.18.3 Crew and Passengers on board MH370 334
28 Section 1.19 - New Investigation Techniques 345
29 Section 2 - Analysis Introduction 346
30 Section 2.1 - Diversion from Filed Flight Plan 347
30.1 2.1.1 Seven Simulator Sessions 347
30.1.1 1) Recreating the Left turn past Waypoint IGARI - Session 1 347
30.1.2 2) Session 2 348
30.1.3 3) Session 3 349
30.1.4 4) Session 4 349
30.1.5 5) Session 5 (Manual Flying) 350
30.1.6 6) Session 6 (Manual Flying) 351
30.1.7 7) Analysis on Re-enactment Sessions (Sessions 1-6) 351
30.1.8 8) Session 7 - Recreating the Right Turn South of Penang Island 354

30.2 2.1.2 Ho Chi Minh Air Traffic Services Operations 355
31 Section 2.2 Air Traffic Services Operations 356
31.1 2.2.1 Review of Flight MH370 before its Disapperance 356
31.2 2.2.2 Chronology of ATC Events before the Disappearance of Flight MH370 357
31.3 2.2.3 Filed Flight Plan of MH370 360
31.4 2.2.4 Departure Message of MH370 365
31.5 2.2.5 Waypoints - Geographical Coordinates of MH370 Filed Flight Plan 366
31.6 2.2.6 Analysis on FPL Message of MH370 366
31.7 2.2.7 Chronology of Events following the Disappearance of MH370 369
31.8 2.2.8 ATS Operational Issues after Last Radio Communication with MH370 and subsequent ATS Activities/Actions 372
31.8.1 1) Analysis of ATS Operational Issues after Last Radio Communication with MH370 and subsequent Activities/Actions taken 373
31.8.1.1 a) Transfer of Control Point at Waypoint IGARI 373
31.8.1.2 b) Responsibilities of Accepting Air Traffic Control Service Unit on Establishment of Communications 382
31.8.1.3 c) Marking on MH370 Flight Progress Strip 383
31.8.1.4 d) Responsibilities of Air Traffic Controllers 386
31.8.1.5 e) Recognising Emergency Situations and Air Traffic Control Actions 387
31.8.1.6 f) Information to be passed to other Radar Units - Civil and Military 393
31.8.1.7 g) Provision of Alerting Service for Flight operating through more than one FIRs and ATC Actions 394
31.8.1.8 h) Actions taken by Air Traffic Service Centre Duty Watch Supervisor 395
31.8.1.9 i) Flight Following System of Malaysia Airlines 396
31.8.1.10 j) Communication Exchanges between KL ACC and HCM ACC, and KL ACC and MAS Operations Despatch Centre on MH370 398

31.8.1.11 k) Delegation of Airspace by Singapore Area Control Centre to KL ACC 406
31.8.1.12 l) ATC Actions on Strayed/Unidentified Aircraft (Primary Radar Target) within the Area of Responsibility 408
31.8.1.13 m) KL ATSC Duty Shift System for Air Traffic Controllers 410
31.8.1.14 n) Roles played by the Duty ATSC Watch Supervisor 415
31.8.1.15 o) Activation of Aeronautical Rescue Coordination Centre 416
31.8.1.16 p) Play-back of Radar and Radiotelephony Recordings by ATSC Duty Watch Supervisor 418
31.8.1.17 q) Entries in ATS Logbooks of ATSC Watch Supervisor and Sector 3 Controller Working Position 418
31.8.1.18 r) Distress Message 422
31.8.1.19 s) Issues with Manual of Air Traffic Services (MATS) 428
32 Section 2.3 - Medical/Human Factors Issues 429
32.1 2.3.1 Introduction 429
32.2 2.3.2 General Human Performance Issues 429
32.3 2.3.3 Specific Human Factors Issues 431
32.4 2.3.4 Human Factor Aspects of Air Traffic Control Recordings 433
33 Section 2.4 - Airworthiness & Maintenance and Aircraft Systems 434
33.1 2.4.1 Airworthiness & Maintenance 434
33.2 2.4.2 Emergency Locator Transmitters 436
33.3 2.4.3 Aircraft Health Monitoring 437
33.4 2.4.4 Aircraft Systems Analysis 438
33.4.1 1) Air-conditioning, Pressurisation and Oxygen 438
33.4.2 2) Autoflight 440
33.4.3 3) Electrical Power 440
33.4.4 4) Flight Controls and Hydraulics 441
33.4.5 5) Instrumentation 442
33.4.6 6) Navigation 442

33.4.7 7) Engines 443
33.4.8 8) Fuel Systems 443
33.4.9 9) Auxiliary Power Unit 443
33.4.10 10) Communications 444
33.4.11 11) Airplane Information Management System 448
33.5 2.4.5 Summary 450
34 Section 2.5 - Satellite Communications Analysis 451
34.1 2.5.1 Summary of Key Observations of the SATCOM Ground Station Logs 451
34.2 2.5.2 Possible Reasons for the 1825 and 0019 Log-On Events and Preceding Link Losses 454
34.3 2.5.3 Summary Assessment of Doppler for 1825 and 0019 Log-On Events 456
35 Section 2.6 - Wreckage and Impact Information 463
35.1 2.6.1 Debris Considered for Detailed Examination 463
35.2 2.6.2 Location of Debris with respect to Aircraft 464
35.3 2.6.3 Damage Analysis of Significant Debris 466
35.4 2.6.4 Marine Life Examination 467
36 Section 2.7 - Organisation and Management of Department of Civil Aviation and Malaysia Airlines 468
36.1 2.7.1 Department of Civil Aviation Malaysia 468
36.1.1 1) Introduction 468
36.1.2 2) Department of Civil Aviation Organisation Structure 468
36.1.3 3) Air Traffic Management Sector 469
36.1.4 4) Air Traffic Inspectorate Division 470
36.1.5 5) Search and Rescue 471
36.1.6 6) Kuala Lumpur Air Traffic Control Centre 475
36.1.7 7) Airworthiness Sector 477
36.1.8 8) Flight Operations Sector 484
36.2 2.7.2 Malaysia Airlines 486
36.2.1 1) Engineering & Maintenance 486

36.2.2 2) Flight Operations Management 486
36.2.3 3) In-flight Services 491
37 Section 2.8 Aircraft Cargo Consignment 494
37.1 2.8.1 Cargo on Board MH370 494
37.2 2.8.2 Li-ion Batteries on Board MH370 495
37.3 2.8.3 Mangosteen Fruits on Board MH370 496
37.4 2.8.4 Dangerous Goods 496
37.5 2.8.5 Laboratory Tests Conducted 496
37.6 2.8.6 Effects of Close Proximity of Li-ion Batteries and Mangosteens in Cargo Consignment 499
38 Section 3 - Findings and Conclusion 500
38.1 3.1 Findings 500
38.1.1 3.1.1 Diversion from Filed Flight Plan Route 500
38.1.2 3.1.2 Air Traffic Services Operations 501
38.1.2.1 1) Kuala Lumpur Air Traffic Services 501
38.1.2.2 2) Ho Chi Minh Air Traffic Services 501
38.1.3 3.1.3 Flight Crew Profile 502
38.1.3.1 1) General and Specific Human Factors Issues 502
38.1.3.2 2) Human Factor Aspects of Air Traffic Control Recordings 502
38.1.4 3.1.4 Airworthiness & Maintenance and Aircraft Systems 503
38.1.5 3.1.5 Satellite Communications 505
38.1.6 3.1.6 Wreckage and Impact Information 506
38.1.7 3.1.7 Organisational and Management Information 507
38.1.7.1 1) Department of Civil Aviation 507
38.1.7.2 2) Malaysia Airlines 508
38.1.8 3.1.8 Aircraft Cargo Consignment (Lithium Ion Batteries and Mangosteen Fruits) 510
38.2 3.2 Conclusion 511
39 Section 4 - Safety Recommendations 515
39.1 4.1 Safety Recommendation of Preliminary Report 515

39.2 4.2 Safety Recommendations of this Report 517
39.2.1 4.2.1 Department of Civil Aviation - SR #01-07 517
39.2.2 4.2.2 Civil Aviation Authority of Viet Nam - SR #08-09 518
39.2.3 4.2.3 Malaysia Airlines Berhad - SR #10-17 518
39.2.4 4.2.4 Malaysia Airports Holdings Berhad - SR #18 519
39.2.5 4.2.5 International Civil Aviation Oganization - SR #19 519
39.2.6 Section 5 - Comments to the Report as required by ICAO Annex 13, para 6.3 520
MH370 Flight Path Analaysis - 30th August 2023 521
MH370 TRAJECTORIES 753
1 1 Introduction 760
2 2 Overview of the flight 761
3 3 The known trajectory 769
3.1 3.1 Introduction 769
3.2 3.2 From Kuala Lumpur to IGARI 769
3.2.1 3.2.1 Flight plan and clearances until the transfer 769
3.2.2 3.2.2 From the ATC transfer to Waypoint IGARI 770
3.3 3.3 Diversion from the flight plan at IGARI: The U-Turn 770
3.3.1 3.3.1 Introduction 770
3.3.2 3.3.2 Available data 771
3.3.2.1 3.3.2.1 Military primary radar plots 771
3.3.2.2 3.3.2.2 The official Entry and Exit points 772
3.3.2.3 3.3.2.3 Boeing simulations 773
3.3.2.4 3.3.2.4 FIRs boundaries 774
3.3.2.5 3.3.2.5 The Thailand ADIZ 774
3.3.2.6 3.3.2.6 ADS-B data unavailable due to transponder switched to stand-by. 775
3.3.2.7 3.3.2.7 GDAS Meteo data 775
3.3.2.8 3.3.2.8 Civilian approach radar data 776
3.3.3 3.3.3 Subsequent Hypotheses 776
3.3.3.1 3.3.3.1 Analytical review of the data 776

3.3.3.1.1 What happened at IGARI? 776
3.3.3.1.2 Why a sharp U-turn? 777
3.3.3.1.3 Manual U-turn 778
3.3.3.2 3.3.3.2 Hypotheses on the U-turn 779
3.3.4 3.3.4 Simulations 779
3.3.4.1 3.3.4.1 Parameters settings in our simulations 779
3.3.4.2 3.3.4.2 Simulations using Prepar3D 780
3.3.4.3 3.3.4.3 Fixed based simulator 781
3.3.4.4 3.3.4.4 Results of all simulations 781
3.3.4.5 3.3.4.5 Fuel consumption estimation 783
3.3.5 3.3.5 Conclusions on the U-turn after waypoint IGARI 785
3.4 3.4 From the Exit Waypoint to the last radar contact 785
3.4.1 3.4.1 Available data 785
3.4.1.1 3.4.1.1 Military primary radar plots 785
3.4.1.2 3.4.1.2 Civil Primary Radar Data Plots (RDP) 786
3.4.1.3 3.4.1.3 Military radar “blips” 788
3.4.1.4 3.4.1.4 Detection of the co-pilot’s mobile phone 788
3.4.1.5 3.4.1.5 Undisputable Facts on Distance and timing 790
3.4.2 3.4.2 From the U-turn Exit waypoint to Penang 791
3.4.2.1 3.4.2.1 Hypotheses 791
3.4.2.2 3.4.2.2 No electromagnetic emissions 791
3.4.2.3 3.4.2.3 Depressurised aircraft and descent until Kota Bharu 792
3.4.2.4 3.4.2.4 From Kota Bharu to South of Penang 793
3.4.2.5 3.4.2.5 Fuel consumption 794
3.4.2.6 3.4.2.6 Simulations 794
3.4.3 3.4.3 From Penang to the Last Radar Plot 795
3.4.3.1 3.4.3.1 Hypotheses 795
3.4.3.2 3.4.3.2 From South of Penang to VAMPI 795
3.4.3.3 3.4.3.3 From VAMPI to the last radar plot (LSTRP) 796

3.4.3.4 3.4.3.4 Geometric considerations 797
3.4.3.5 3.4.3.5 Time and velocity considerations 798
3.4.3.6 3.4.3.6 Simulations 798
3.4.4 3.4.4 Conclusions on the leg from the Exit Waypoint to the last radar contact 800
3.5 3.5 Conclusions on the known trajectory 800
4 4 The unknown and recalculated trajectory 801
4.1 4.1 Introduction 801
4.2 4.2 Available data 801
4.2.1 4.2.1 Inmarsat data 801
4.2.2 4.2.2 FIRs 802
4.2.3 4.2.3 Southeast India ADIZ11F 803
4.2.4 4.2.4 Routes and Waypoints 804
4.3 4.3 The « Final Major Turn12F » (FMT) 805
4.3.1 4.3.1 Hypotheses at the Last Radar Plot 806
4.3.2 4.3.2 From Last Radar Plot to the electrical power restoration 806
4.3.2.1 4.3.2.1 The flown path 807
4.3.3 4.3.3 From the electrical power restoration to the Arc1-Crossing 807
4.3.3.1 4.3.3.1 The flown path 808
4.3.3.2 4.3.3.2 Person in command’s workload in the cockpit 808
4.3.4 4.3.4 From Arc1-Crossing to Arc1.2-Crossing… a manual turn 811
4.3.5 4.3.5 From Arc1.2-Crossing to POVUS 812
4.3.6 4.3.6 From POVUS to the Phone call-1 location 813
4.3.7 4.3.7 Compliance with Inmarsat data 815
4.3.8 4.3.8 Simulations 815
4.3.9 4.3.9 Conclusions 816
4.4 4.4 En-route at 188 from Phone Call 1 to Arc6 817
4.4.1 4.4.1 Speed and Altitude Computation 817

4.4.2 4.4.2 Reconstructing the “Southern Leg” 821
4.4.3 4.4.3 Validation of the “southern leg” with Inmarsat data 823
4.5 4.5 The Final Descent to the End of the Flight 826
4.5.1 4.5.1 Hypotheses and basic parameters: 826
4.5.2 4.5.2 Profile of the descent 827
4.5.3 4.5.3 Estimated point of ditching 829
4.5.4 4.5.4 Simulations 830
5 5 The proposed new search zone 830
6 6 Conclusions 832
7 7 Additional elements of interest 833
7.1 7.1 Visual detection of satellite images 833
7.2 7.2 How does our trajectory compare with Boeing Performance Analysis? 833
8 8 Annex 1: Variant 2 of the End of the Flight 837
9 9 References 839
10 10 Abbreviations and Index 841
RECONSTRUCTING FLIGHT TRAJECTORY BY OPTIMAL SEARCH 844
1 Reconstructing the Malaysian 370 Flight Trajectory by Optimal Search 844
1.1 INTRODUCTION 844
1.2 MH370 FLIGHT FACTS 845
1.3 CALCULATION OF QUASI-CIRCLES 848
1.4 SOLVING TRAJECTORY EQUATIONS 849
1.4.1 The Time to Turn Unknown (TTT) 849
1.4.2 The Track Unknown (TK) 851
1.4.3 The Flight Level Unknown (FL) 851
1.4.4 The Mach Number Unknown (M) 852
1.4.5 Assumptions for the Last Segment of the Flight 852
1.4.6 Trajectory Equations 852
1.5 THE DYNAMIC MODEL FLIGHT SIMULATOR 854

1.6 ANALYSIS OF RESULTS 856
1.7 CONCLUSIONS 865
1.8 ACKNOWLEDGEMENTS 865
1.9 REFERENCES 866
CONTROLLED EASTWARD VEERING DESCENT AFTER 6TH ARC 867
WATER ENTRY OF AN AIRLINER 879
THE OPERATIONAL SEARCH FOR MH370 894
1 Appendix A - Search vessel.pdf
1.1 Search vessels 1064
1.1.1 Fugro Equator 1064
1.1.1.1 Ship details 1064
1.1.2 GO Phoenix 1065
1.1.2.1 Ship details 1065
1.1.3 Fugro Discovery 1066
1.1.3.1 Ship details 1066
1.1.4 Fugro Supporter 1067
1.1.4.1 Ship details 1067
1.1.5 Havila Harmony 1068
1.1.5.1 Ship details 1068
1.1.6 Dong Hai Jiu 101 1069
1.1.6.1 Ship details 1069
2 Appendix C - BFO Doppler model development.pdf
2.1 Burst Frequency Offset (BFO) doppler model development0F 1091
2.1.1 BFO doppler model summary 1091
2.1.2 BFO doppler model chronology 1092
2.1.2.1 21 Mar 2014 Differential Doppler Analysis 1092
2.1.2.2 22 Mar 2014 Differential Doppler Analysis Release 2 (OAMS) 1092
2.1.2.3 25 Mar 2014 Differential Doppler Analysis EXT 1093
2.1.2.4 3 Apr 2014 Differential Doppler Analysis ADJ_EXT 1093

2.1.2.5 8 Apr 2014 ECLIPSE_1 Differential Doppler Analysis 1093
2.1.2.6 8 Apr 2014 ECLIPSE_2 Differential Doppler Analysis 1093
Eclipse 2 Sensitivity 1094
Eclipse 2 Model Reference Data 1094
Verification 1095
2.1.2.7 23 May 2014 ECLIPSE_3 Differential Doppler Analysis 1095
2.1.2.8 19 Jun 2014 BFO Analysis UNIFIED 1095
2.1.2.9 20 Jun 2014 BFO Analysis UNIFIED 2x 1096
2.1.2.10 21 Jul 2014 BFO Analysis UNIFIED 3x 1096
2.1.2.11 30 Jul 2014 BFO Analysis UNIFIED 4x 1096
3 Appendix D - FRPT GP1500_SUM_Vol7_Summary Report (Rev 0) with Appendices.pdf
3.1 FRPT GP1500-SUM_Vol7_Summary Report (Rev 0) 1098
3.1.1 1. INTRODUCTION 1105
3.1.1.1 1.1 Project Description 1105
3.1.1.2 1.2 Project Objectives 1107
3.1.1.3 1.3 Scope of Work 1107
3.1.1.4 1.4 Survey Operations 1108
3.1.1.5 1.5 Report Structure 1109
3.1.2 2. HEALTH, SAFETY AND ENVIRONMENTAL MANAGEMENT 1110
3.1.2.1 2.1 Health, Safety and Environmental Performance (HSE) 1110
3.1.3 3. SURVEY OPERATIONS 1113
3.1.3.1 3.1 Sequence of Events 1113
3.1.3.2 3.2 Vessel Swings 1114
3.1.3.3 3.3 Mobilisations 1115
3.1.3.4 3.4 Production Summary 1116
3.1.3.5 3.5 Project Time Allocation 1121

3.1.3.6 3.6 Survey Coverage 1121
3.6.1 Port Calls 1123
3.1.3.7 3.7 Processing and Reporting 1123
3.1.3.8 3.8 Data Transfer Ashore 1124
3.1.3.9 3.9 Demobilisation 1125
3.1.4 4. STATISTICAL SUMMARIES 1126
3.1.4.1 4.1 Data Holiday Types and Extents 1126
4.1.1 Remaining Holidays 1126
3.1.4.2 4.2 Contact Summary 1128
3.1.4.3 4.3 Findings 1129
4.3.1 Shipwreck #1 1129
4.3.2 Shipwreck #2 1132
4.3.3 Shipwreck #3 1134
4.3.4 Shipwreck #4 1135
4.3.5 Small Target Detection 1136
3.1.4.4 4.4 Sound Velocity Profiles 1137
3.1.4.5 4.5 Seabed Features 1139
3.1.4.6 4.6 Transit Distance 1140
3.1.4.7 4.7 Personnel Hours 1140
3.1.4.8 4.8 Equipment – Deep Tow and AUV 1141
3.1.4.9 4.9 MBES Coverage 1143
3.1.4.10 4.10 Extreme Sea Condition 1145
3.1.4.11 4.11 Time Spent On Line Turns 1146
3.1.4.12 4.12 Fuel Consumption 1147
3.1.5 5. SURVEY PARAMETERS 1148
3.1.5.1 5.1 Geodetic and Projection Parameters 1148
3.1.5.2 5.2 Vertical Control 1149
3.1.6 6. SURVEY EQUIPMENT, VESSEL AND PERSONNEL 1150
3.1.6.1 6.1 Vessels 1150
6.1.1 Fugro Equator 1150

6.1.2 Fugro Discovery 1151
6.1.3 Fugro Supporter 1152
6.1.4 Havila Harmony 1152
3.1.6.2 6.2 Personnel 1153
3.1.7 7. DATA HANDLING 1154
3.1.8 8. DISTRIBUTION 1156
3.2 APPENDIX 1157
3.2.1 A. SOUND VELOCITY PROFILES 1158
4 Appendix G - Summary of Analyses Undertaken on Debris_Final_GA.pdf
4.1 Summary of Analyses Undertaken on Debris Recovered During the Search for Flight MH370 1205
4.1.1 A collation of reports describing quarantine and parts analysis undertaken by Geoscience Australia 1205
4.2 Abbreviations 1207
4.3 Acknowledgements 1208
4.4 Contents 1209
4.5 1 Executive Summary 1211
4.6 2 Review of Sediment on Aircraft Pieces from Mozambique, Mossel Bay and Mauritius (Items 2 to 5) 1213
4.6.1 2.1 Summary 1213
4.6.2 2.2 Methods 1213
4.6.2.1 2.2.1 Establishing Geological Context 1213
4.6.2.2 2.2.2 Sediment Analysis 1214
4.6.3 2.3 Results for Items 2 and 3 1214
4.6.3.1 2.3.1 Geological Context: Mozambique 1214
4.6.3.2 2.3.2 Sediment Analysis Results 1216
4.6.3.3 2.3.3 Discussion 1219
4.6.3.4 2.3.4 Conclusion 1220
4.6.4 2.4 Item 4 1221
4.6.4.1 2.4.1 Geological Context: Mossel Bay, South Africa 1221
4.6.4.2 2.4.2 Sediment Analysis Results 1221

4.6.4.3 2.4.3 Discussion 1221
4.6.4.4 2.4.4 Conclusion 1221
4.6.5 2.5 Item 5 1222
4.6.5.1 2.5.1 Geological Context: Rodrigues Island 1222
4.6.5.2 2.5.2 Sediment Analysis Results 1223
4.6.5.3 2.5.3 Discussion 1223
4.6.5.4 2.5.4 Conclusions 1224
4.6.6 2.6 References 1225
4.7 3 Review of Macrofauna on Pieces from Mozambique (Item 2 and 3) 1228
4.7.1 3.1 Summary 1228
4.7.2 3.2 Method 1229
4.7.3 3.3 Results 1229
4.7.3.1 3.3.1 Item 2: Recovered From Daghatane Beach, Mozambique 1229
Crustacea: 1229
Mollusc: 1230
Bryozoa: 1230
4.7.3.2 3.3.2 Item 3 (Right Horizontal Stabilizer Panel): Recovered From a Beach in the Mozambique Channel 1232
Molluscs and Annelids: 1232
Crustacea: 1234
Bryozoa: 1234
4.7.4 3.4 References 1243
4.8 4 Stable Isotope Analyses of Paints on Aircraft Pieces From Mozambique (Items 2 and 3) and Mauritius (Item 5) 1244
4.8.1 4.1 Summary 1244
4.8.2 4.2 Method 1244
4.8.2.1 4.2.1 Sub-Sampling Items 2 and 3 1244
4.8.2.2 4.2.2 Sub-sampling Item 5 and Control Sample 1245
4.8.2.3 4.2.3 Isotopic Analysis of Items 2, 3 and 5 and the Control Sample 1245

4.8.3 4.3 Results 1246
4.9 5 Analyses of Organic Compounds on Aircraft Pieces From Mozambique (Item 2) 1248
4.9.1 5.1 Summary 1248
4.9.2 5.2 Methodology 1248
4.9.3 5.3 Results 1248
4.9.4 5.4 References: 1252
4.10 6 Review of Macrofauna on Aircraft Pieces Found on Mauritius and South Africa (Item 5) 1253
4.10.1 6.1 Summary 1253
4.10.2 6.2 Method 1254
4.10.3 6.3 Results 1258
4.10.3.1 6.3.1 Item 4 (External Engine Cowling) 1258
4.10.3.2 6.3.2 Item 5 (Door R1 Stowage Closet) 1258
4.10.4 6.4 References 1260
5 Appendix H - CMST 1308 Report 2014-30 MH370 PassiveAcoustics - Final.pdf
5.1 1 Introduction 1266
5.2 2 Signal descriptions and analysis 1267
5.3 3 Automated signal detection algorithm 1272
5.3.1 3.1 General description 1272
5.3.2 3.2 Mathematical derivation 1273
5.3.3 3.3 Results 1274
5.4 4 Independent time calibration check 1275
5.5 5 Estimate of the probability that events at HA01 and RCS are from the same source 1278
5.6 6 Analysis of data from HA08S 1281
5.7 7 Discussion 1286
5.8 8 Conclusions 1292
6 Blank Page 1332
SAR RESPONSE TO MH370 1334
SEARCH FOR MH370 1344

SEARCH AND DEBRIS UPDATE NOV 2016 1366
DRIFT SIMULATION OF DEBRIS USING SUPERENSEMBLE TECHNIQUES 1391
1 Abstract 1391
2 Introduction 1391
3 Modelling 1392
3.1 Drift trajectories 1392
3.2 Superensemble 1393
3.2.1 Model coefficients 1393
3.2.2 Initial conditions and parameters 1393
3.3 Forcing field data 1393
4 Results 1393
4.1 First debris discovery 1393
4.2 Including further discoveries 1395
5 Conclusions 1396
6 Acknowledgements 1396
7 References 1396
SEARCH STRATEGY IN DYNAMIC ENVIRON 1397
1 I Introduction 1397
2 II Related research 1397
2.1 II-A Stationary targets 1398
2.2 II-B Non-stationary targets 1398
3 III Search in dynamic environments 1399
4 IV Spectral Multi-scale Coverage path planning 1400
5 V Search for MH370 (Results) 1401
5.1 V-A Problem Definition of Search for MH370 1401
5.2 V-B Drift model 1402
5.3 V-C The search 1402
6 VI Effect of delayed search on the success rate 1403
7 VII Conclusion 1404
8 References 1408

SPACE SURVEILLANCE DURING SEARCH 1409
1 Slide 1 1409
2 Slide 2 1410
3 Slide 3 1411
4 Slide 4 1412
5 Slide 5 1413
6 Slide 7 1415
7 Slide 8 1416
8 Slide 9 1417
9 Slide 10 1418
10 Slide 11 1419
11 Slide 12 1420
12 Slide 13 1421
13 Slide 14 1422
14 Slide 17 1425
15 Slide 18 1426
16 Slide 19 1427
17 Slide 21 1429
18 Slide 22 1430
19 Slide 23 1431
20 Slide 24 1432
21 Slide 26 1434
22 Slide 27 1435
23 Slide 28 1436
24 Slide 30 1438
25 Slide 31 1439
26 Slide 32 1440
27 Slide 33 1441
28 Slide 38 1446
29 Slide 39 1447

30 Slide 41 1449
31 Slide 42 1450
32 Slide 43 1451
33 Slide 45 1453
34 Slide 46 1454
35 Slide 47 1455
36 Slide 48 1456
37 Slide 49 1457
38 Slide 50 1458
39 Slide 52 1460
40 Slide 53 1461
41 Slide 54 1462
42 Slide 55 1463
43 Slide 56 1464
Article-MH370-Final-Edition-Image-980x998 1465
Blelly-Analysis-of-Flight-MH370 1466
1 1 Introduction 1468
2 2 The « Final Major Turn2F » (FMT) 1469
3 3 The Southern Part of the Trajectory 1472
3.1 3.1 Speed and Altitude Computation 1472
3.2 3.2 Reconstructing the “Southern Leg” 1475
3.3 3.3 Validation of the “southern leg” with Inmarsat data 1477
4 4 The Final Descent to the End of Flight 1480
5 5 The proposed new search zone 1483
6 6 Additional elements of interest 1484
7 Annex 1: Variant 2 of the End of Flight 1485
8 References 1486
BURST FREQUENCY OFFSET ANALYSIS AND IMPLICATIONS ON DESCENT RATE AT END OF FLIGHT 1487
1 I Introduction 1487

2 II Timeline of Events During the Accident Flight 1488
3 III Review of SATCOM Model 1488
3.1 III-A Review of BFO Statistics 1488
4 IV Effects of Aircraft Position and Velocity on the Burst Frequency Offset 1488
4.1 IV-A Mathematical Description of the BFO 1488
4.2 IV-B Effect of uncompensated vertical velocity 1489
4.3 IV-C Effect of track angle on BFO towards end-of-flight 1490
4.4 IV-D BFO Trend During the MH370 Flight 1490
5 V Effect of SDU Startup on the BFO 1491
5.1 V-A Detailed Analysis of SDU Startup Effects on the BFO 1491
5.2 V-B Summary of SDU Startup Effects on the BFO 1493
6 VI Bounding the Descent Rates of MH370 1493
6.1 VI-A Hypothesis 1: SATCOM outage due to insufficient fuel 1494
6.2 VI-B Hypothesis 2: SATCOM outage due to some other reason 1494
6.3 VI-C Summary of Descent Rate Bounds 1494
6.4 VI-D Estimated Downwards Acceleration 1494
7 VII Conclusion 1494
8 References 1495
9 Biographies 1495
9.1 Ian D. Holland 1495
CAPTIO-Analysis 1497
INFRASOUND SEARCH FOR MH370 1498
MH370ResearchV3.4 1503
MH370-SkyVector-Chart-SIO-980x844 1516
SEAFLOOR IN MH370 SEARCH AREA 1517
USING LANDSAT PLUS GOOG EARTH TO LOCATE DOWNED AIRCRAFT 1520
MH370SIAMReviewSep15 1539
Bill-Tracy-ZS-Home-Flight-Simulator-806x675 1566
PUBLIC DATA RELEASE FLIGHT PATH 1567

MH370 PASSENGER LIST 1646
RADIO TRANSCRIPT 1654
MH370 A CONTENT ANALYSIS OF MALAYSIAN CHINESE AND US MEDIA 1656
PSCHOLOGY BEHIND MH370 CONSPIRACIES 1683
MH370 WIKI 1687

SAFETY INVESTIGATION REPORT

Malaysia Airlines Boeing B777-200ER (9M-MRO)
08 March 2014

By

The Malaysian ICAO Annex 13 Safety Investigation Team for MH370

Issued on 02 July 2018
MH370/01/2018

The Malaysian ICAO Annex 13
Safety Investigation Team for MH370
Email: *MH370SafetyInvestigation@mot.gov.my*

I. CONTENTS

i - TABLE OF CONTENTS

NO.	TITLE	PAGE/S
I.	i. Table of Contents	i-xi
	ii. List of Appendices	xii-xiii
II.	Synopsis	xiv-xvii
III.	Dedication	xviii
IV.	Acknowledgement	xix
V.	Objective	xx
VI.	Disclaimer	xxi
VII.	Glossary of Terms	xxii-xxvii
VIII	Abbreviations and Codes	xxviii-xliii
IX	The Malaysian ICAO Annex 13 Safety Investigation Team for MH370	xliv-xlv

SECTION	TITLE	PAGE/S
1	**FACTUAL INFORMATION**	**1-273**
1.1	**HISTORY OF THE FLIGHT**	**1-21**
1.1.1	Introduction	1
1.1.2	Actions by HCM ACC and KL ACC	3
1.1.3	Diversion from Filed Flight Plan Route	3
	1) Malaysian Military Radar	3
	2) DCA Civilian Radar Data from Kota Bharu – Sultan Ismail Petra Airport Runway	6
	3) Ho Chi Minh Air Traffic Services	15
	4) Kuala Lumpur ACC Radar	17
	5) Medan Air Traffic Control Radar	18
	6) Bangkok Air Traffic Control Radar	18
	7) Singapore Air Traffic Services	19
1.1.4	Role of the Malaysian Military	19
1.1.5	Detection of Hand Phone Signal	20
1.1.6	Search for Aircraft	20
1.2	**INJURIES TO PERSONS**	**22**
1.3	**DAMAGE TO AIRCRAFT**	**23**
1.4	**OTHER DAMAGES**	**24**

SECTION	TITLE	PAGE/S
1.5	**PERSONNEL INFORMATION**	**25-38**
1.5.1	Introduction	25
1.5.2	Malaysia Airlines Training and Check Records	25
1.5.3	Pilot-in-Command	26
	1) Personal Profile of Pilot-in-Command	26
	2) Royal Malaysia Police's Report on Flight Simulator of PIC	27
1.5.4	First Officer	29
	1) Personal Profile of First Officer	30
1.5.5	Summary of Work Schedule for Flight Crew of MH370	30
1.5.6	Cabin Crew and Personal Profiles	30
.	1) In-flight Supervisor (IFS)	31
	2) Chief Steward (CS)	31
	3) Chief Stewardess (CSS)	32
	4) Leading Steward (LS)	32
	5) Leading Stewardess (LSS)	33
	6) Flight Stewardess (FSS) 1	33
	7) Flight Stewardess (FSS) 2	34
	8) Flight Steward (FS) 1	34
	9) Flight Steward (FS) 2	35
	10) Flight Steward (FS) 3	35
1.5.7	Disciplinary/Administrative Actions	36
1.5.8	Financial Background and Insurance Cover	36
1.5.9	Significant Past Medical and Medication History	36
1.5.10	Psychological and Social Events	37
1.5.11	Behavioural Events	37
1.5.12	Voice Recognition of the Radio Transmissions between MH370 and Air Traffic Control	38
1.6	**AIRCRAFT INFORMATION**	**39-95**
1.6.1	Airframe	39
1.6.2	Engine	39
1.6.3	Auxiliary Power Unit	39
1.6.4	Airworthiness and Maintenance	40
	1) Aircraft Maintenance Schedule	40
	2) Major Repair	44
	3) Cabin Configuration Change	45
	4) Mandatory Occurrence Reports	45
	5) Airworthiness Directives	46
	6) Technical Log	47
	7) Deferred Defects (Maintenance Report 2)	48

SECTION	TITLE	PAGE/S
1.6.4	8) Engine Health Monitoring	49
cont.	9) Central Maintenance Computing System	49
1.6.5	Weight and Balance	50
1.6.6	Fuel	51
1.6.7	Emergency Locator Transmitter	52
	1) Review of Effectiveness of Emergency Locator Transmitters	54
1.6.8	Aircraft Systems Description	56
.	1) Air Conditioning and Pressurisation	57
	2) Autopilot Flight Director System	58
	a) Take-off Mode	59
	b) Roll Modes	59
	c) Pitch Modes	61
	d) Landing Modes	63
	e) Autothrottle (Thrust Management Computing Function)	64
	f) Autothrottle Modes	65
	3) Electrical Power	67
	a) Electrical Load Management System	69
	b) Alternating Current Electrical System Power Sources	69
	c) Integrated Drive Generators	69
	d) Auxiliary Power Unit Generator	70
	e) Alternating Current Electrical Power Distribution	70
	f) Autoland	71
	g) Backup Alternating Current Electrical System	71
	h) Backup Generators	71
	i) Direct Current Electrical System	72
	j) Batteries	73
	k) Flight Control Direct Current Electrical System	73
	l) Standby Electrical System	73
	4) Cabin and Cargo Compartments	75
	5) Flight Controls	76
	6) Fuel System	78
	7) Hydraulics	80
	8) Instrumentation	81
	9) Airplane Information Management System	85
	10) Navigation Systems	86
	11) Oxygen Systems	88
	12) Central Maintenance Computing System	90

SECTION	TITLE	PAGE/S
1.6.8 *cont.*	13) Engines	90
	14) Auxiliary Power Unit	92
	15) Communications	93
1.6.9	Aircraft Performance	93
1.6.10	Boeing Patent on Remote Control Takeover of Aircraft	94
1.7	**METEOROLOGICAL INFORMATION**	**96-101**
1.7.1	Meteorological Situation	96
1.7.2	Comments on the Information Available	99
	1) Forecast Charts	99
	a) Significant Weather Chart	99
	b) Wind and Temperature Forecast Chart	100
	2) Significant Meteorological Information	100
	3) Volcanic Ash Advisory	101
1.7.3	Availability of Meteorological Information	101
1.8	**AIDS TO NAVIGATION –** Not applicable	**102**
1.9	**COMMUNICATIONS**	**103-131**
1.9.1	High Frequency System	103
1.9.2	Very High Frequency System	103
1.9.3	Air Traffic Control/Mode S Transponder System	104
1.9.4	Aircraft Communications Addressing and Reporting System	105
	1) Aircraft Communications Addressing and Reporting System Traffic Log	108
1.9.5	Satellite Communications	115
	1) Satellite Communications System Description	115
	2) Satellite Communications Ground Station Logs of the Event – Introduction	119
	3) Satellite Communications Ground Station Logs of the Event – Summary	121
	4) Satellite Communications Ground Station Logs – Key Observations in Chronological Order	124
	5) Frequencies of Log-on Bursts	130
1.10	**AERODROME INFORMATION -** Not applicable	**132**
1.11	**FLIGHT RECORDERS**	**133-137**
1.11.1	Solid State Flight Data Recorder	133
1.11.2	Solid State Cockpit Voice Recorder	134
1.11.3	Underwater Locator Beacons	136
	1) Solid State Data Recorder Underwater Locator Beacon Battery Expiry	137
1.12	**WRECKAGE AND IMPACT INFORMATION**	**138-167**
1.12.1	Introduction	138

SECTION	TITLE	PAGE/S
1.12.2	Location of Where the Debris were Found	139
1.12.3	Details of the Debris	154
1.12.4	Process for Recovery of Debris	167
1.13	**MEDICAL AND PATHOLOGICAL INFORMATION**	**168-169**
1.14	**FIRE**	**170**
1.15	**SURVIVABILITY**	**171**
1.16	**TESTS AND RESEARCH -** Not applicable	**172**
1.17	**ORGANISATIONAL AND MANAGEMENT INFORMATION**	**173-227**
1.17.1.	Department of Civil Aviation Malaysia	173
	1) Introduction	173
	2) Functions and Responsibilities of Department of Civil Aviation	174
	3) Sectors and Divisions of Department of Civil Aviation	175
	4) Areas of Focus	175
	5) Air Traffic Management Sector	175
	a) Air Traffic Inspectorate Division	177
	6) Airworthiness Sector	190
	7) Flight Operations Sector	194
1.17.2	Malaysia Airlines	196
	1) Introduction	196
	2) Engineering & Maintenance	197
	a) Organisation Structure	197
	b) Maintenance and Design Approval	197
	c) Training	199
	d) Base Maintenance	200
	e) Line Maintenance	200
	f) Maintenance Authorisation	201
	g) Safety Management System	201
	3) Operations	202
	a) Flight Operations	202
	i) Flight Operations Management	202
	ii) Organisation and Management related to B777 Operations	203
	iii) Technical Crew	204
	iv) Technical Crew of MH370	207
	v) Working Schedule/Roster Schedule and Management	208
	vi) Safety Management System	209

SECTION	TITLE	PAGE/S
1.17.2 *cont.*	vii) Confidential Human Factors Incident Report	210
	viii) Flight Operations Quality Assurance	212
	ix) Line Operations Safety Audit	213
	x) Crew Resources Management	213
	xi) Training and Standards	215
	xii) MAS B777 Training and Standards	216
	xiii) Multi-Crew Operation MH370	218
	xiv) Safety and Emergency Procedures	219
	xv) Technical and Development	220
	xvi) Fuel Policy	220
	xvii) Flight Plan Routing	221
	xviii) Hijack and Sabotage Security Procedures	221
	b) In-flight Services	221
	i) Cabin Crew Training	221
	ii) Crew Performance Appraisal	223
	iii) In-flight Operation	224
	iv) Flight and Duty Time Limitations Scheme for Cabin Crew	226
	v) Safety Report	227
1.18	**ADDITIONAL INFORMATION**	**228-273**
1.18.1	Provision of Air Traffic Services and Areas of Responsibilities	228
	1) Introduction	228
	2) Sector 3 Area of Responsibility	229
	3) Sector 5 Area of Responsibility	232
	4) Air Traffic Services Operations	235
	5) KL ATSC Duty Shift System for Air Traffic Controllers	236
	6) Chronology of Activities after Notification by HCM ACC	242
	7) Activation of KL Aeronautical Rescue Coordination Centre	247
	8) Recorded Telephone Conversations	249
	9) Watch Supervisor Air Traffic Services and Sector (3 & 5) Logbook	250
	10) Flight Progress Strip	250
1.18.2	Air Cargo Consignment	252
	1) Introduction	252

SECTION	TITLE	PAGE/S
1.18.2 *cont.*	2) Lithium Ion Batteries	254
	3) Mangosteen Fruits	259
1.18.3	Crew and Passengers on Board MH370	263
	1) Total Number of Crew and Passengers	263
	2) Nationalities of the Crew and Passengers	263
	a) Crew	264
	b) Passengers	264
	c) Passengers' Seating Positions	264
1.19	**NEW INVESTIGATION TECHNIQUES** – Not applicable	274
2	**ANALYSIS**	**275-428**
	Introduction	275
2.1	**DIVERSION FROM FILED FLIGHT PLAN**	**276-284**
2.1.1	Seven Simulator Sessions	276
	1) Recreating the Left Turn past Waypoint IGARI	276
	a) Session 1	276
	2) Session 2	277
	3) Session 3	278
	4) Session 4	278
	5) Session 5 (Manual Flying)	279
	6) Session 6 (Manual Flying)	280
	7) Analysis on Re-enactment Sessions (Sessions 1-6)	280
	8) Session 7 – Recreating the Right Turn South of Penang Island	283
2.1.2	Ho Chi Minh Air Traffic Services Operation	284
2.2	**AIR TRAFFIC SERVICES OPERATIONS**	**285-357**
2.2.1	Review of Flight MH370 before its Disappearance	286
2.2.2	Chronology of ATC Events before the Disappearance of Flight MH370	288
2.2.3	Filed Flight Plan of MH370	289
	1) Message Code of FPL of MH370 and Meaning	290
2.2.4	Departure message of MH370	294
	1) Message Code of Departure message of MH370 and Meaning	294
2.2.5	Waypoints - Geographical Coordinates (LAT/LONG) of MH370 Filed Flight Plan	295
2.2.6	Analysis on FPL Message of MH370	295

SECTION	TITLE	PAGE/S
2.2.7	Chronology of ATC Events following the Disappearance of MH370	298
2.2.8	ATS Operational Issues after Last Radio Communication with MH370 and subsequent ATS Activities/Actions	301
	1) Analysis of ATS Operational Issues after Last Radio Communication with MH370 and subsequent Activities/ Actions	302
	a) Transfer of Control Point at Waypoint IGARI	302
	b) Responsibilities of Accepting Air Traffic Control Service Unit on Establishment of Communications	311
	c) Marking on MH370 Flight Progress Strip	312
	d) Responsibilities of Air Traffic Controllers	315
	e) Recognising Emergency Situations and Air Traffic Control Actions	316
	f) Information to be passed to other Radar Units – Civil and Military	322
	g) Provision of Alerting Service for Flight operating through more than one FIRs and ATC actions	323
	h) Actions taken by Air Traffic Service Centre Duty Watch Supervisor	324
	i) Flight-Following System of Malaysia Airlines	325
	j) Communication Exchanges between KL ACC and HCM ACC and KL ACC and MAS Operations Despatch Centre on MH370	327
	k) Delegation of Airspace by Singapore Area Control Centre to KL ACC	335
	l) ATC Actions on Strayed/Unidentified Aircraft (Primary Radar Target) within the Area of Responsibility	337
	m) KL ATSC Duty Shift System for Air Traffic Controllers	339
	n) Roles played by the Duty ATSC Watch Supervisor	344
	o) Activation of Aeronautical Rescue Coordination Centre	345
	p) Play-back of Radar and Radiotelephony Recordings by ATSC Duty Watch Supervisor	347
	q) Entries in ATS Logbooks of ATSC Watch Supervisor and Sector 3 Controller Working Position	347
	r) Distress Message	351
	s) Issues with Manual of Air Traffic Services (MATS)	357

SECTION	TITLE	PAGE/S
2.3	**MEDICAL/HUMAN FACTORS ISSUES**	**358-362**
2.3.1	Introduction	358
2.3.2	General Human Performance Issues	358
2.3.3	Specific Human Factors Issues	360
2.3.4	Human Factor Aspects of Air Traffic Control Recordings	362
2.4	**AIRWORTHINESS & MAINTENANCE AND AIRCRAFT SYSTEMS**	**363-379**
2.4.1	Airworthiness & Maintenance	363
2.4.2	Emergency Locator Transmitters	365
2.4.3	Aircraft Health Monitoring	366
2.4.4	Aircraft Systems Analysis	367
	1) Air-conditioning, Pressurisation and Oxygen	367
	2) Autoflight	369
	3) Electrical Power	369
	4) Flight Control and Hydraulics	370
	5) Instrumentation	371
	6) Navigation	371
	7) Engines	372
	8) Fuel Systems	372
	9) Auxiliary Power Unit	372
	10) Communications	373
	11) Airplane Information Management System	377
2.4.5	Summary	379
2.5	**SATELLITE COMMUNICATIONS ANALYSIS**	**380-391**
2.5.1	Summary of Key Observations of the SATCOM Ground Station Logs	380
2.5.2	Possible Reasons for the 1825 and 0019 Log-On Events and Preceding Link Losses	383
2.5.3	Summary Assessment of Doppler for 1825 and 0019 Log-On Events	385
2.6	**WRECKAGE AND IMPACT INFORMATION**	**392-396**
2.6.1	Debris Considered for Detailed Examination	392
2.6.2	Location of Debris with respect to Aircraft	393
2.6.3	Damage Analysis of Significant Debris	395
2.6.4	Marine Life Examination	396
2.7	**ORGANISATION AND MANAGEMENT OF DEPARTMENT OF CIVIL AVIATION AND MALAYSIA AIRLINES**	**397-422**
2.7.1	Department of Civil Aviation Malaysia	397

SECTION	TITLE	PAGE/S
2.7.1 *cont.*	1) Introduction	397
	2) Department of Civil Aviation Organisation Structure	397
	3) Air Traffic Management Sector	398
	4) Air Traffic Inspectorate Division	399
	5) Search and Rescue	400
	6) Kuala Lumpur Air Traffic Service Centre	404
	7) Airworthiness Sector	406
	8) Flight Operations Sector	413
2.7.2	Malaysia Airlines	415
	1) Engineering & Maintenance	415
	2) Flight Operations Management	415
	3) In-flight Services	420
2.8	**AIRCRAFT CARGO CONSIGNMENT**	**423-428**
2.8.1	Cargo on Board MH370	423
2.8.2	Li-ion Batteries on Board MH370	424
2.8.3	Mangosteen Fruits on Board MH370	425
2.8.4	Dangerous Goods	425
2.8.5	Laboratory Tests Conducted	425
	1) Li-ion Batteries	426
	2) Mangosteen Fruits	427
2.8.6	Effects of Close Proximity of Li-ion Batteries and Mangosteens in Cargo Consignment	428
	1) Location of Cargo	428
	2) Results of Tests	428
3	**FINDINGS AND CONCLUSION**	**429-443**
3.1	**Findings**	**429-439**
3.1.1	Diversion from Filed Flight Plan Route	429
3.1.2	Air Traffic Services Operations	430
	1) Kuala Lumpur Air Traffic Services	430
	2) Ho Chi Minh Traffic Services	430
3.1.3	Flight Crew Profile	431
	1) General and Specific Human Factors Issues	431
	2) Human Factor Aspects of Air Traffic Control Recordings	431
3.1.4	Airworthiness & Maintenance and Aircraft Systems	432
3.1.5	Satellite Communications	434
3.1.6	Wreckage and Impact Information	435
3.1.7	Organisational & Management Information	436
	1) Department of Civil Aviation	436

SECTION	TITLE	PAGE/S
3.1.7 *cont.*	2) Malaysia Airlines	437
3.1.8	Aircraft Cargo Consignment (Lithium Ion Batteries and Mangosteen Fruits)	439
3.2	**Conclusion**	**440-443**
4	**SAFETY RECOMMENDATIONS**	**444-448**
4.1	**Safety Recommendation of Preliminary Report**	**444-445**
4.2	**Safety Recommendations of this Report**	**446-448**
4.2.1	Department of Civil Aviation - SR #01-07	446
4.2.2	Civil Aviation Authority of Viet Nam - SR #08-09	447
4.2.3	Malaysia Airlines Berhad - SR #10-17	447
4.2.4	Malaysia Airports Holdings Berhad - SR #18	448
4.2.5	International Civil Aviation Organization - SR #19	448
5	**COMMENTS TO THE REPORT AS REQUIRED BY ICAO ANNEX 13, PARAGRAPH 6.3**	449

ii – LIST OF APPENDICES

APPENDIX	TITLE	TOTAL PAGE/S
1.1A	Letter of Agreement between Department of Civil Aviation Malaysia and View Nam Air Traffic Management	14
1.6A	Recent Technical Log Entries	4
1.6B	Engine Health Monitoring	4
1.6C	9M-MRO Radio Licence	1
1.6D	ELT Activation Summary (Source ICAO)	2
1.6E	Aircraft Performance Analysis - MH370	8
1.9A	ACARS Traffic Log	14
1.12A-1	Debris Examination Item 1 - Flaperon Identification	16
1.12A-2	Debris Examination Item 1 - Flaperon	240
1.12B	Debris Examination Items 2 & 3 – No. 7 Flap Support Fairing & Right Horizontal Stabilizer Panel	5
1.12C	Debris Examination Items 4 & 5 – Engine Nose Cowl & Door R1 Stowage Closet	6
1.12D	Debris Examination Item 6 - Right Hand Engine Fan Cowling	5
1.12E	Debris Examination Item 7 - Wing to Body Fairing	5
1.12F	Debris Examination Item 8 - No. 1 Flap Support Fairing Tail Cone	4
1.12G	Debris Examination Items 9 & 15 - Left & Right Wing Trailing Edge Panels	7
1.12H	Debris Examination Item 10 - Left Outboard Aft Flap	3
1.12I	Debris Examination Item 11 - Seat Back Trim Panel (IFE Monitor)	4
1.12J	Debris Examination Item 12 – Bottom Panel of Wing or Horizontal Stabilizer	4
1.12K	Debris Examination Item 13 - Unidentified Part	4
1.12L	Debris Examination Item 14 - Unidentified Part	3
1.12M	Debris Examination Items 16 & 17 - Cabin Interior Panel & Unidentified Part	4
1.12N	Debris Examination Item 18 - Right Forward Nose Landing Gear Door	5
1.12O	Debris Examination Item 19 - Right Outboard Flap	5
1.12P	Debris Examination Item 20 - Right Aft Wing to Body Fairing	4

cont…

APPENDIX	TITLE	TOTAL PAGE/S
1.12Q	Debris Examination Item 21 - Unidentified Part	3
1.12R	Debris Examination Item 22 - Right Vertical Stabilizer Panel	6
1.12S	Debris Examination Item 23 - Unidentified Part	4
1.12T	Debris Examination Item 24 - Unidentified Part	6
1.12U	Debris Examination Item 25 - Unidentified Part	3
1.12V	Debris Examination Item 26 - Right Aileron	7
1.12W	Debris Examination Item 27 - No. 7 Flap Support Fairing	9
1.18A	Air-Ground Communication - Airways Clearance Delivery	9
1.18B	Air-Ground Communication - Lumpur Ground	23
1.18C	Air-Ground Communication - Lumpur Tower	14
1.18D	Air-Ground Communication - Approach Radar	14
1.18E	Air-Ground Communication - Lumpur Radar	29
1.18F	Air-Ground Communication - Lumpur Radar and Radar Direct Line	125
1.18G	Direct Line Coordination Communication – KL ATCC Sectors 3+5 Planner	164
1.18H	Cargo Manifest and Associated Documents	18
1.18I	Lithium Battery Guidance Document	3
1.18J	Airways Bills (from January to May 2014)	7
2.6A	Marine Biologist Report 1	11
2.6B	Marine Biologist Report 2	50
2.6C	Search and Debris Examination Update (including Right Outboard Flap Failure Analysis)	25
2.8A	Certificate of Compliance	2
2.8B	Director General Directive No. 1A/2013	2
2.8C	Director General Directive No. 2/2013	2
2.8D	Special Load Notification to Captain	1
2.8E	Laboratory Tests on Li-ion Batteries and Mangosteens	20

II. SYNOPSIS

On 08 March 2014, a scheduled passenger flight from Kuala Lumpur to Beijing, operated by Malaysia Airlines (MAS) and designated flight MH370, went missing soon after a routine handover from the Malaysian Air Traffic Control (ATC) to Viet Nam ATC. The aircraft operating the flight was a Boeing 777-200 ER, registered as 9M-MRO. On board the aircraft were 12 crew and 227 passengers (239 persons in total). A review of available radar and satellite communications indicated that the aircraft flew back across the Malaysian Peninsula and subsequently travelled to the southern Indian Ocean. Despite an extensive air and sea search, the location of the aircraft and occupants remains unknown. However, some debris have been recovered consistent with having drifted over nearly two years from the area in which impact is thought to have occurred.

By international convention, the investigation of aircraft accidents and incidents is conducted in accordance with Annex 13 to the Convention on International Civil Aviation, *Aircraft Accident and Incident Investigation.* The Standards and Recommended Practices (SARPs) in Annex 13 are applied in Malaysia through Part XII of the Malaysian Civil Aviation Regulations (MCAR) 1996.

In accordance with the MCAR 1996, an independent international investigation team (The Team) comprising 19 Malaysians and 7 Accredited Representatives (ARs) of 7 safety investigation authorities from 7 countries was established by the Malaysian Minister of Transport to investigate the disappearance of MH370. The ARs appointed are from the:

- Air Accidents Investigation Branch (AAIB) of United Kingdom
- Australian Transport Safety Bureau (ATSB) of Australia;
- Bureau d'Enquêtes et d'Analyses pour la Sécurité de l'Aviation civile (BEA) of France;
- Civil Aviation Administration of the People's Republic of China (CAAC);
- National Transportation Safety Board (NTSB) of United States of America;
- National Transportation Safety Committee (NTSC) of Indonesia; and
- Transport Safety Investigation Bureau (TSIB) of Singapore (formerly Air Accident Investigation Bureau [AAIB]).

Advisors to the ARs were appointed from the States' investigation agencies, as well as the aircraft, engine and satellite communications systems manufacturers.

While this investigation report documents the safety investigation aspects as noted above, the Team is aware of other investigations being undertaken for other purposes, including criminal investigations.

Investigation Organisation

The investigation was organised in accordance with the ICAO Manual of Accident Investigation and Incident Investigation (Doc. 9756-AN965) practices and comprised an Investigator-in-Charge (IIC) and three main Committees, comprising:

- Airworthiness;
- Flight Operations; and
- Medical/Human Factors.

Preliminary Report

On 09 April 2014, the Malaysian Ministry of Transport released the **Preliminary Report** into the investigation activities at that time. The Preliminary Report contained a Safety Recommendation to ICAO in regard to in-flight tracking of large commercial aircraft. A copy of the **Preliminary Report** is available on the Department of Civil Aviation website here:

- *http://www.dca.gov.my/wp-content/uploads/2015/02/Preliminary-Report1.pdf*

1st Interim Statement and Factual Information Report

On 08 March 2015, the Team released the **1st Interim Statement** and a **Factual Information Report** detailing the factual information available at that time. The report contained no analysis, findings/conclusions or safety recommendations. Copies of both the **Interim Statement** and the **Factual Information Report** are available from the Malaysian Ministry of Transport's two websites here:

- *http://mh370.mot.gov.my*
- *http://www.mh370.gov.my*

2nd Interim Statement

On 08 March 2016, the Team released the **2nd Interim Statement**.

3rd Interim Statement

On 08 March 2017, the Team released the ***3rd Interim Statement***.

4th Interim Statement

On 08 March 2018, the Team released the ***4th Interim Statement.***

Safety Investigation Report

This **Safety Investigation Report** (Report) builds on the previous ***Factual Information Report*** and extends the available information publicly released to include analysis, findings/conclusions and safety recommendations. Recognising that at the time of issue of this Report, the main aircraft wreckage, including the aircraft's Flight Data Recorder (FDR) and Cockpit Voice Recorder (CVR) have not yet been located, this Report will necessarily be limited by a significant lack of evidence.

Based on the available evidence, the analysis of factors considered relevant to the disappearance of MH370 include:

- Diversion from Filed Flight Plan Route;
- Air Traffic Services Operations;
- Flight Crew Profile;
- Airworthiness & Maintenance and Aircraft Systems;
- Satellite Communications;
- Wreckage and Impact Information;
- Organisation and Management Information of DCA and MAS; and
- Aircraft Cargo Consignment.

Other factors examined by the investigation and not considered relevant include the aircraft weight and balance, the amount and quality of fuel on-board and meteorological conditions.

Significant Issues and Safety Recommendations

In the analysis of the above factors, several significant issues were identified that could affect the safety of international commercial aviation, including the lack of effectiveness of certified Emergency Locator Transmitters (ELT) if a large commercial aircraft ditches or crashes into the ocean.

While this issue is currently being addressed by ICAO and the international aviation industry, the Team is of the view that work needs to be expedited in this area to implement effective changes to enhance aviation safety into the future.

Additionally, a number of issues were identified that could affect the monitoring and timely initiation of search and rescue of commercial aircraft in Malaysian airspace by the Air Navigation Services provider. Issues were also identified in the Airline Operations. They include the following:

- Malaysian and adjacent air traffic management;
- Cargo screening;
- Flight crew medical and training records;
- Reporting and following-up of crew mental health;
- Flight following system;
- Quick reference for operations control; and
- Emergency locator transmitter effectiveness.

As a result of the issues identified in the investigation and in accordance with para. 6.8 of Annex 13 which states that: "*At any stage of the investigation of an accident or incident, the accident investigation authority of the State conducting the investigation shall recommend in a dated transmittal correspondence to the appropriate authorities, including those in other States, any preventive action that it considers necessary to be taken promptly to enhance aviation safety",* a number of safety recommendations (*Section 4 - Safety Recommendations),* have been made to the Department of Civil Aviation (DCA), Civil Aviation Authority of Viet Nam, Malaysian Airlines Berhad (MAB, formerly MAS), the Malaysia Airports Holdings Berhad (MAHB) and the International Civil Aviation Organization (ICAO) to enhance aviation safety.

III. DEDICATION

This report is dedicated to the memory of the 239 passengers and crew missing on MH370 (9M-MRO) on 08 March 2014. They will be forever missed by their families, friends and colleagues, but never forgotten.

IV. ACKNOWLEDGEMENT

The Malaysian ICAO Annex 13 Safety Investigation Team for MH370 would like to acknowledge the work carried out by the Search Strategy Group in the analysis of the satellite data and the search teams involved in the search for MH370. The search was unprecedented in its scale and their dedication was a remarkable effort.

We trust that MH370 will be located to provide answers to the families of the passengers and crew of MH370 and bring closure to this event.

V. OBJECTIVE

The sole objective of the investigation of an accident or incident shall be the prevention of accidents and incidents. It is not the purpose of this activity to apportion blame or liability.

Annex 13, Section 3.1 page 3-1

VI. DISCLAIMER

This **Safety Investigation Report** contains facts which have been determined up to the time of issue and is published to inform the aviation industry and the public of the safety investigation and the safety issues raised thus far. Therefore, the report may be subject to alteration or correction if additional and credible evidence becomes available.

Extracts can be published without specific permission providing that the source is duly acknowledged.

VII. GLOSSARY OF TERMS

When the following terms are used, they have the following meaning:

Accident

An occurrence associated with the operation of an aircraft which, in the case of a manned aircraft, takes place between the time any person boards the aircraft with the intention of flight until such time as all such persons have disembarked, or in the case of an unmanned aircraft, takes place between the time the aircraft is ready to move with the purpose of flight until such time as it comes to rest at the end of the flight and the primary propulsion system is shut down, in which:

a) a person is fatally or seriously injured as a result of:

- being in the aircraft, or
- direct contact with any part of the aircraft, including parts which have become detached from the aircraft, or
- direct exposure to jet blast,

Except when the injuries are from natural causes, self-inflicted or inflicted by other persons, or when the injuries are to stowaways hiding outside the areas normally available to the passengers and crew; or

b) the aircraft sustains damage or structural failure which:

- adversely affects the structural strength, performance or flight characteristics of the aircraft, and would normally require major repair or replacement of the affected component,

  except for engine failure or damage, when the damage is limited to a single engine (including its cowlings or accessories), to propellers, wing tips, antennas, probes, vanes, tires, brakes, wheels, fairings, panels, landing gear doors, windscreens, the aircraft skin (such as small dents or puncture holes), or for minor damages to main rotor blades, tail rotor blades, landing gear, and those resulting from hail or bird strike (including holes in the radome); or

c) The aircraft is missing or is completely inaccessible.

Note 1 - For statistical uniformity only, an injury resulting in death within thirty days of the date of the accident is classified, by ICAO, as a fatal injury.

Note 2 - An aircraft is considered to be missing when the official search has been terminated and the wreckage has not been located.

cont...

Note 3 - The type of unmanned aircraft system to be investigated is addressed in Annex 13, para 5.1.

Note 4 - Guidance for the determination of aircraft damage can be found in Annex 13, Attachment E.

Accredited Representative

A person designated by a State, on the basis of his or her qualifications, for the purpose of participating in an investigation conducted by another State. Where the State has been established an accident investigation authority, the designated accredited representative would normally be from that authority.

Advisor

A person appointed by a State, on the basis of his or her qualifications, for the purpose of assisting its accredited representative in an investigation.

Aeronautical fixed telecommunication network (AFTN)

A worldwide system of aeronautical fixed circuit provided, as part of the aeronautical fixed service, for the exchange of messages and/or digital data between aeronautical fixed stations having the same or compatible communications characteristics.

Air-ground communication

Two-way communication between aircraft and stations or locations on the surface of the earth.

Aircraft

Any machine that can give derive support in the atmosphere from the reactions of the air other than the reactions of the air against the earth’s surface.

Alert Phase

A situation wherein apprehension exists as to the safety of an aircraft and its occupants.

Alerting Post

Any facility intended to serve as an intermediary between a person reporting an emergency and a rescue co-ordination centre or rescue sub-centre.

cont...

Blind Transmission

A transmission from one station to another station in circumstances where two-way communication cannot be established but where it is believed that the called station is able to receive the transmission.

Cabin Crew Member

A crew member who performs, in the interest of safety passengers, duties assigned by the operator or the pilot-in-command of the aircraft, but who shall not act as a flight crew member.

Cargo

Any property carried on an aircraft other than mail, stores and accompanied or mishandled baggage.

Causes

Actions, omissions, events, conditioning, or a combination of thereof, which led to the accident or incident. The identification of causes does not imply the assignment of fault or the determination of administrative, civil or criminal liability.

Co-ordinated Universal Time (UTC)

International term for time at the prime meridian.

Conversion Training

Training required when a pilot is posted to a different aircraft type or model

DETRESFA

The code word used to designate a distress phase

Distress Phase

A situation wherein there is reasonable certainty than an aircraft and its occupants are threatened by grave and imminent danger or require immediate assistance.

Emergency Phase

A generic term meaning, as the case may be, uncertainty phase, alert phase or distress phase

cont...

Filed Flight Plan

The flight plan as filed with an ATS unit by the pilot or a designated representative, without any subsequent changes.

Flight Plan

Specified information provided to air traffic units, relative to an intended flight or portion of a flight of an aircraft.

Flight Recorder

Any type of recorder installed in the aircraft for the purpose of complementing accident/incident investigation - *Annex 6, Parts I, II and III, for specifications relating to flight recorders.*

Incident

An occurrence, other than an accident, associated with the operation of an aircraft which affects or could affect the safety of operation.

Note: *The types of incidents which are of main interest to the International Civil Aviation Organization for accident prevention studies are listed in Accident/Incident Reporting Manual (Doc. 9156).*

Investigation

A process conducted for the purpose of accident prevention which includes the gathering and analysis of information, the drawing of conclusions, including the determination of causes and/or contributing factors and, when appropriate, the making of safety recommendations.

Investigator-in-Charge

A person charged, on the basis of his or her qualifications, with the responsibility for the organisation, conduct and control of an investigation

Note - *Nothing in the above definition is intended to preclude the functions of an investigator-in-charge being assigned to a commission or other body.*

Knot (kt)

A unit of speed equal to one nautical mile per hour.

cont...

NOTAM

A notice distributed by means of telecommunication containing information concerning the establishment, condition of change in any aeronautical facility, service, procedure or hazard, the timely knowledge of which is essential to personnel concerned with flight operations.

Operator

A person, organization or enterprise engaged in or offering to engage in an aircraft operation.

Pilot-in-Command

The pilot responsible for the operation and the safety of the aircraft during flight time.

Safety Recommendation

A proposal of an accident investigation authority based on information derived from an investigation, made with the intention of preventing accidents or incidents and which in no case has the purpose of creating a presumption of blame or liability for an accident or incident. In addition to safety recommendations arising from accident and incident investigations, safety recommendations may result from diverse sources, including safety studies. *(Annex 13, Chapter 1, page 1-3).*

State of Design

The State having jurisdiction over the organization responsible for the type design.

State of Manufacture

The State having jurisdiction over the organization responsible for the final assembly of the aircraft.

State of Occurrence

The State in the territory of which an accident or incident occurs.

State of the Operator

The State in which the operator’s principal place of business is located or, if there is no such place of business, the operator’s permanent residence.

cont...

State of Registry

The State on whose register the aircraft is entered.

Note: *In the case of the registration of aircraft of an international operating agency on other than a national basis, the States constituting the agency are jointly and severally bound to assume the obligations which, under the Chicago Convention, attach to a State of Registry. See, in this regard, the Council Resolution of 14 December 1967 on Nationality and Registration of Aircraft Operated by International Operating Agencies which can be found in Policy and Guidance Material on the Economic Regulation of International Air Transport (Doc 9587).*

State Safety Programme (SSP)

An integrated set of regulations and activities aimed at improving safety.

Uncertainty Phase

A situation wherein doubt exists as to the safety of an aircraft or marine vessel, and of the persons on board.

VIII. ABBREVIATIONS & CODES

A

A300	Airbus 300
A/P	Autopilot
A-SAR	Aeronautical Search and Rescue
A/T	Autothrottle
AAIB	Air Accidents Investigation Branch (United Kingdom)
AC	Alternating Current
ACARS	Aircraft Communications Addressing and Reporting System
ACC	Area Control Centre
ACD	Airways Clearance Delivery
ACE	Actuator Control Electronic
ACIPS	Airfoil Cowl Ice Protection System
ACMP	Alternating Current Motor Pump
ACMS	Aircraft Condition Monitoring System
ACP	Audio Control Panel
AD	Airworthiness Directive
ADF	Automatic Direction Finder
ADFR	Automatic Deployable Flight Recorder
ADI	Attitude Director Indicator
ADIRS	Air Data Inertial Reference System
ADIRU	Air Data Inertial Reference Unit
ADM	Airworthiness Departmental Manual
ADP	Air Driven Pump
ADS-B	Automatic Dependent Surveillance-Broadcast
ADS-C	Automatic Dependent Surveillance-Contract
AED	Airworthiness Engineering Division
AEG	Airline Engineering Group
AES	Airborne Earth Station
AFD	Assistant Flight Data
AFDC	Autopilot Flight Director Computer
AFDS	Autopilot Flight Director System
AFS	Aeronautical Fixed Service
AFTN	Aeronautical Fixed Telecommunication Network
AIC	Aeronautical Information Circular
AID	Airworthiness Inspection Division
AIMS	Airplane Information Management System
AIP	Aeronautical Information Publication
AIS	Aeronautical Information Service

A *(cont…)*

A (cont...)

ALERFA	Alert Phase
ADF	Automatic Direction Finder
ALR	Alerting
ALT	Altitude
AM	Amplitude Modification
AMC	Acceptable Means of Compliance
AMEL	Aircraft Maintenance Engineer's Licence
AMO	Approved Maintenance Organisation
AMU	Audio Management Unit
AN	Aircraft Number; Airworthiness Notice
ANS	Air Navigation Services
AOA	Angle of Attack
AOC	Air Operator Certificate
AOR	Area of Responsibility
APP	Approach
APU	Auxiliary Power Unit
APUC	Auxiliary Power Unit Controller
AR	Accredited Representative/s
AR	Approach Radar
ARCC	Aeronautical Rescue Coordination Centre
ARSC	Aeronautical Rescue Sub-Centre
ARINC	Aeronautical Incorporated
ASB	Amanah Saham Bumiputra (A People's Trust Council of the Malaysian Government)
ASDI	Aircraft Situation Display Information
ASL	Air Service Licence
ASN	Amanah Saham Nasional (a Government-back National Trust Fund)
ASR	Air Safety Report
ASCPC	Air Supply Cabin Pressure Controller
ATC	Air Traffic Control
ATC	Air Traffic Controller/s
ATC-ATO	Air Traffic Control - Approved Training Organisation
ATCC	Air Traffic Control Centre
ATCO	Air Traffic Control Officer
ATD	Actual Time of Departure
ATI	Air Traffic Inspectorate
ATIS	Automatic Terminal Information Broadcast
ATM	Air Traffic Management
ATSB	Australian Transport Safety Bureau
ATN	Aeronautical Telecommunication Network
ATO	Approved Training Organisation

A *(cont).*

A *(cont...)*

ATPL	Air Transport Pilot Licence
ATS	Air Traffic Services
ATSC	Air Traffic Services Centre
ATSU	Air Traffic Service Unit
ATTN	Attenuator
AUTO	Automatic
AVBL	Available
AWL	Airworthiness Limitation
AWY	Airway

B

BEA	Bureau d'Enquêtes et d'Analyses pour la Sécurité de l'Aviation civile (France)
BER	Bit Error Rate
BEW	Basic Empty Weight
BFO	Burst Frequency Offset
BKK	IATA Airport Designator for Suvarnahbumi International Airport
BITE	Built In Test Equipment
BOI	Board of Inquiry
BSCU	Brake System Control Unit
BSU	Beam Steering Unit
BTO	Burst Timing Offset

C

C	Degree Celsius (Centigrade)
C of A	Certificate of Airworthiness
C of G	Centre of Gravity
C of R	Certificate of Registration
CA	Collective Agreement
CAA	Civil Aviation Act
CAAC	Civil Aviation Authority of the Republic of China
CAAS	Civil Aviation Authority Singapore
CAM	Cockpit Area Microphone
CAR 1996	Civil Aviation Regulations 1996

A *(cont...)*

A *(cont...)*

CAR 2016	Civil Aviation Regulations 2016
CAS	Calibrated Airspeed
CASA	Civil Aviation Safety Authority
CASR	Civil Aviation Safety Requirements
CAT	Clear Air Turbulence
CB	Circuit Breaker
CCD	Cursor Control Device
CCTV	Closed Circuit Television
CDS	Central Deposit System
CDU	Control Display Unit
CEO	Chief Executive Officer
CHIRPS	Confidential Human Factors Accident Incident Reporting System
CLB	Climb
Cm	Centimetre
CMCS	Central Maintenance Computing System
CMR	Certificate Maintenance Requirement
CMS	Central Maintenance System
COSPAS	Space System for Search of Vessels in Distress
CPA	Crew Performance Appraiser
CPDLC	Controller Pilot Data Link Communications
CPL	Commercial Pilot Licence
CPM	Core Processor Module
CPMU	Cabin Passenger Management Unit
CRM	Crew Resource Management
CRZ	Cruise
CSR	Cabin Safety Report
CTR	Control Zone
CTRL	Control
CTU	Cabin Telecommunications Unit
CVR	Cockpit Voice Recorder
CX	C Extended
CWP	Controller Working Position

D

DARD	Direct Access Radar Data
dB	decibel

A *(cont...)*

DC	Direct Current
DCGF	Data Conversion Gateway Function
DCMF	Data Communication Management Function
DCMS	Data Communication Management System
Deg	Degree
DEOR	Daily Engineering Operations Report
DES	Descent
DETRESFA	Distress Phase
DFDAF	Digital Flight Data Acquisition Function
DFDAU	Digital Flight Data Acquisition Unit
DG	Dangerous Goods
DGCA	Director General of Civil Aviation
DGTA	General Delegate of Armament Aeronautical Technique
DIP	Diplexer
DLNA	Diplexer Low Noise Amplifier
DME	Distance Measuring Equipment
DOW	Dry Operating Weight
DTG	Date-Time-Group

E

EASA	European Aviation Safety Agency
ECL	Electronic Checklist
EDIU	Engine Data Interface Unit
EDP	Engine Driven Pump
EEC	Electronic Engine Control
EFIS	Electronic Flight Instrument System
EFS	Electronic Flight Strips
EHM	Engine Health Monitoring
EICAS	Engine Indicating and Crew Alerting System

E (cont...)

ELMS	Electrical Load Management System

E *(cont…)*

ELP	English Language Proficiency
ELT	Emergency Locator Transmitter
EMD	Engineering & Maintenance Department
EMS	Engineering Maintenance System
ENR	En-route
EOL	End-of-Lease
EEZ	Exclusive Economic Zone
EPF	Employees Provident Fund
EPR	Engine Pressure Ratio
EQIS	Fuel Quantity Indicating System
EST	Estimate
ETA	Estimated Time of Arrival
ETOPS	Extended Twin Engine Operations
EXT	External

F

FAA	Federal Aviation Administration
FANS 1/A	Future Air Navigation System 1/A
FAR	Federal Aviation Regulations
FDEVSS	Flight Deck Entry Video Surveillance System
FDP	Flight Data Processing/Flight Duty Period
FDR	Flight Data Recorder
FFS	Flight-Following System
FPL	Filed Flight Plan (*message type designator – used in AFS message)*
FIR	Flight Information Region
FIS	Flight Information Service
FL	Flight Level
FMC	Flight Management Computer
FLCH	Flight Level Change
FMCF	Flight Management Control Function
FMCS	Flight Management Control System
FMS	Flight Management System
FO	Flight Officer

F *(cont…)*

F (cont…)

FOQA	Flight Operations Quality Assurance
FOS	Flight Operations Sector
FOSI	Flight Operations Surveillance Inspector
FPA	Flight Path Angle
FSCU	Flap Slat Control Unit
FSEU	Flap Slat Electronic Unit
FPS	Flight Progress Strip
FS	Flight Steward
FSS	Flight Stewardess
ft	Feet (*dimensional unit*)
FTL	Flight Time Limitation

G

G/S	Glide Slope
GA	Go Around
GADSS	Global Aeronautical Distress and Safety System
GCC	Golden Class Club
GEN	Generator
GES	Ground Earth Station
GHz	Giga Hertz
GM	Guidance Material
GMT	Greenwich Mean Time
GNSS	Global Navigation Satellite System
GPS	Global Positioning System
GPWS	Ground Proximity Warning System
GSP	Ground Service Provider
GSR	Ground Safety Report
GWT	Gross Weight

H

hPa	Hectopascal
HPA	High Power Attenuator
HCM	IATA Airport Designator for Ho Chi Minh International Airport
HDG	Heading
HF	High Frequency
HF/AMSS	High Frequency Aeronautical Mobile Service Station
HGA	High Gain Antenna
HLCS	High Lift Control System
HPA	High Power Amplifier
HR	Hours
HYDIM	Hydraulic Interface Module
Hz	Hertz
HZR	Hazard Report

I

i.u.	Index unit
IAMSAR	International Aeronautical and Maritime Search and Rescue
IMARSAT	International Mobile Satellite Organisation
IAS	Indicated Airspeed
IATA	International Air Transport Association
ICAO	International Civil Aviation Organisation
ID	Identification
IDG	Integrated Drive Generator
IFE	In-flight Entertainment
IFS	In-flight Supervisor
IGV	Inlet Guide Vane
ILS	Instrument Landing System
IMO	International Maritime Organisation
In.	Inches
INCERFA	Uncertainty Phase
IOM	Input/output Module
IOR	Indian Oceanic Region
IRP	Incident Review Panel
IRP	Integrated Refuel Panel
ISLN	Isolation

J

JATCC	Joint Air Traffic Control Centre

K

KHz	Kilo Hertz
KLIA	KL International Airport
kg	Kilogram
KPI	Key Performance Indicator
kt	Knot
km^2	Kilometer square
KVA	Kilo Volt Ampere

L

LAME	Licenced Aircraft Maintenance Engineer
LAT	Latitude
lb	Pound
LDW	Landing Weight
LFA	Langkawi Flying Academy
LGA	Low Gain Antenna
LH	Left Hand
LLAR	Lower Lobe Attendant Rest
LNA	Low Noise Amplifier
LNAV	Lateral Navigation
LOA	Letters of Agreement
LOC	Localiser
LONG	Longitude

L *(cont...)*

L (cont...)

LOPA	Lay Out of Passenger Accommodation
LOSA	Line Operations Safety Audit
LRM	Line Replaceable Module
LRU	Line Replaceable Unit
LS	Leading Steward
LSS	Leading Stewardess
LR	Lumpur Radar
LT	Lumpur Tower

M

M	Metre
MAB	Malaysia Airlines Berhad (formerly MAS)
MAC	Mean Aerodynamic Chord
MAHB	Malaysia Airports Holdings Berhad
MAL	Malaysia Airways Limited
MARA	Majlis Amanah Rakyat (An agency of the Malaysian Government)
MAS	Malaysia Airlines (now Malaysia Airlines Berhad [MAB])
MASEU	Malaysia Airlines Employees Union
MATS	Manual of Air Traffic Services
MCC	Maintenance Control Centre
MCDU	Multi-purpose/function Control Display Unit
MCE	Malaysian Certificate of Education
MCP	Mode Control Panel
MEC	Main Equipment Centre
MEL	Minimum Equipment List
MET	Meteorological or meteorology
METAR	Aerodrome routine meteorological report
MFA	Malaysian Flying Academy
MFD	Multi-Function Display
MGSCU	Main Gear Steering Control Unit
MHz	Megahertz
Min	Minute

M *(cont.)*

M (cont.)

MMEA	Malaysian Maritime Enforcement Agency
MMOE	Maintenance Management Organisation Exposition
MNPS	Minimum Navigation Performance Specification
MOC	MAS Operations Centre
MOR	Mandatory Occurrence Report
MOU	Memorandum of Understanding
MPD	Maintenance Planning Document
MR1	Maintenance Report 1
MR2	Maintenance Report 2
MRB	Maintenance Review Board
MRO	Maintenance Repair and Overhaul
MRCC	Maritime Rescue Coordination Centre
MRSC	Maritime Rescue Sub-Centre
ms	meter per second
MSA	Malaysia-Singapore Airlines
MSRR	Maritime Search and Rescue Region
MTSAT	Multifunctional Transport Satellites of Japan Meteorological Agency (JMA)
MU	Management Unit
MYT	Malaysia Time

N

NCR	Non Compliance Record
ND	Navigation Display
NDB	Non-directional Beacon
NDT	Non Destructive Testing
nm	Nautical Mile
NOTAM	Notice to Airmen
NOTOC	Notice to Crew
NSC	National Security Council
NTC	Notes to Crew
NTSB	National Transportation Safety Board (United States of America)
NTSC	National Transportation Safety Committee (Indonesia)

O

OCC	Operations Control Centre
OCXO	Oven Controlled Crystal Oscillator
ODA	Organization Designation Authorisation
OPR	Operator
OPS	Operations
OOOI	Out, Off, On, In

P

P/N	Part Number
PAN-ATM	Procedures for Air Navigation Services - Air Traffic Management
PASS	Passenger(s)
PBN	Performance-based Navigation
PCU	Power Control Units
PDS	Primary Display System
PDU	Power Drive Unit
PFC	Primary Flight Computer
PFCS	Primary Flight Control System
PFD	Primary Flight Display
PIC	Pilot in Command
PLN	Flight Plan
PMG	Permanent Magnet Generator
POA	Production Organisation Approval
POB	Person on Board
POR	Pacific Oceanic Region
ppm	parts per million
PSA	Power Supply Assembly
PSEU	Proximity Switch Electronic Unit
psi	Pounds per square inch
PSR	Primary Surveillance Radar
PSU	Passenger Service Unit
PTT	Push to Talk
PWR	Power
PWS	Predictive Windshear

Q

QA	Quality Assurance
Q & A	Questions and Answers
QAE	Quality Assurance Engineer

R

RAT	Ram Air Turbine
RCC	Rescue Coordination Centre
RDP	Radar Data Plot
REF	Reference
RF	Radio Frequency
RF ATTN	Radio Frequency Attenuator
RFS	Radio Frequency Splitter
RFU	Radio Frequency U nit
RH	Right Hand
RHP	Radar Data Head Processor
rms	Root Mean Square
R n R	Rest and Recreation
RTP	Radio Tuning Panel
RVSM	Reduced Vertical Separation Minima
RQS	Request Supplementary Flight Plan
RADAR	Radio Detection and Ranging
RSC	Rescue Sub-Centre
RMAF	Royal Malaysia Air Force
RNAV	Area Navigation
RTP	Radio Tuning Panel
RVSM	Reduced Vertical Separation Minima
RWY	Runway

S

SAP	Safety Awareness Programme
SAR	Search and Rescue
SAREX	Search and Rescue Exercise
SARPs	Standard and Recommended Practices
SARSAT	Search and Rescue Satellite-Added Tracking
SAT	Static Air Temperature
SATCOM	Satellite Communications
SC	SAR Coordinator
SCP	Safety Change Process
SCSC	South China Sea Corridor
SDU	Satellite Data Unit
SEA 1	South East Asia 1
SEA 2	South East Asia 2
SEL	Select
SELCAL	Selective Calling System
SEP	Safety Engineering Procedures
SIGMET	Significant meteorological information
SIGWX	Significant weather chart
SMC	Search and Rescue Mission Coordinator
SME	Site Maintenance Engineer
SOC	Statement of Compliance
SOI	Supplementary Operations Instructions
SOP	Standard Operating Procedures
SPD	Speed
SR	Safety Recommendations
SRB	Safety Review Boards
SRR	Search and Rescue Region
SSM	Sign Status Matrix
SSP	State Safety Programme
SSR	Secondary Surveillance Radar
STC	Supplemental Type Certificate
STRIDE	Science & Technology Research Institute for Defence
SZB	Subang Airport

T

T	Tonne
TAC	Thrust Augmentation Computer
TAT	Total Air Temperature
TCAS	Traffic Collision Avoidance System
TCP	Transfer of Control Point
THDG	True Heading
TMA	Terminal Control Area
TMCF	Thrust Management Computing Function
THR	Thrust
THR REF	Thrust Reference
TMCF	Thrust Management Control Function
TO	Take-off
TOTFW	Total Remaining Fuel Weight
TRE	Type Rating Examiner
TRI	Type Rating Instructor
TRK	Track
TRTO	Type Rating Training Organization
TRU	Transformer Rectifier Unit
TSIB	Transport Safety Investigation Bureau of Singapore (formerly Air Accident Investigation Bureau [AAIB])
TSO	Technical Standard Order

U

UA	Unstabilized Approach
UAI	Unit Administrative Instruction
UHF	Ultra High Frequency
ULB	Underwater Locator Beacon
ULD	Unit Load Device
USB	Upper Side Band
UTC	Coordinated Universal Time

V

V	Volt
V/S	Vertical Speed
VAAC	Volcanic Ash Advisory Centre
VDL	VHF Digital Link
VHF	Very High Frequency
VNAV	Vertical Navigation
VOR	VHF Omni Directional Radio Range

W

W	Watt
WAFC	World Area Forecast Centre
WHCU	Window Heat Control Unit
WINDIR	Wind Direction
WINDSP	Wind Speed
WMKC	ICAO 4-letter location indicator for Kota Bharu Airport
WMKK	ICAO 4-letter location indicator for KL International Airport WMKN
WMKN	ICAO 4-letter location indicator for Kuala Terengganu Airport
WMKP	ICAO 4-letter location indicator for Penang International Airport
WS	Watch Supervisor
WSSS	ICAO 4-letter location indicator for Changi International Airport Singapore
WWW	Worldwide web
WXR	Weather (Meteorological messages)
WX	Weather

X

-

Y

-

Z

ZBAA	ICAO 4-letter location indicator of Peking-Capital International Airport
ZFW	Zero Fuel Weight
Z	Coordinated Universal Time (*in meteorological messages)*

IX. THE MALAYSIAN ICAO ANNEX 13 SAFETY INVESTIGATION TEAM FOR MH370 (9M-MRO)

- **The Malaysian Members**

Dato' Ir. Kok Soo Chon	Investigator-in-Charge
Capt. Abdul Wahab Ibrahim	Senior Investigator/ Chairman of Operations Committee
Mr. Mohan Suppiah	Senior Investigator/ Chairman of Airworthiness Committee
Datuk Dr. Mohd Shah Mahmood	Senior Investigator/ Chairman of Medical/Human Factors Committee
Assoc. Prof. Ir. Abu Hanifah Hj Abdullah	Investigator, Airworthiness
Mr. Amirudin Ab Ghani	Investigator, Airworthiness
Mr. Aslam Basha Khan	Investigator, Airworthiness
Dato' Capt. Jalil Mat Dom	Investigator, Operations
Mr. Khaw Sim Min	Investigator, Operations
Ms. Khoo Lay See	Investigator, Medical/Human Factors
Mr. Lim Kim Seang	Investigator, Operations
Dato' SAC Mohd Rafique Ramli Ariffin	Investigator, Operations
Mr. Muhammad Imran Ismail	Investigator, Operations
Ms. Norwalena Abdul Wahab	Investigator, Operations
Prof. Dr. Pathmanathan Rajadurai	Investigator, Medical/Human Factors
Dato' Dr. Suarn Singh A/L Jasmit Singh	Investigator, Medical/Human Factors
Ms. Swandra Kim Chu Ramachandran	Investigator, Operations (from January 2018)
Mr. Tan Huvi Vein	Investigator, Operations
Dr. Toh Chin Lee	Investigator, Medical/Human Factors
Capt. Abdul Razak Hashim	Investigator, Operations (April 2014 - April 2015)

- **The Accredited Representatives**

Air Accidents Investigation Branch (AAIB)	United Kingdom
Australian Transport Safety Bureau (ATSB)	Australia
Bureau d'Enquêtes et d'Analyses pour la sécurité d l'aviation civile (BEA)	France
Civil Aviation Administration of the People's Republic of China	China
National Transportation Safety Board (NTSB)	United States of America
National Transportation Safety Committee (NTSC)	Indonesia
Transport Safety Investigation Bureau (TSIB) (*formerly Air Accident Investigation Bureau [AAIB])*	Singapore

SECTION 1 – FACTUAL INFORMATION

1.1 HISTORY OF THE FLIGHT

1.1.1 Introduction

On 07 March 2014 at 1642 UTC[1] [0042 MYT, 08 March 2014], Malaysia Airlines (MAS) Flight MH370 Beijing-bound international scheduled passenger flight departed from Runway 32 Right, KL International Airport (KLIA) with a total of 239 persons on board (227 passengers and 12 crew). The aircraft was a Boeing 777-200ER, registered as 9M-MRO.

The Pilot-in-Command (PIC) signed in for duty at 1450 UTC [2250 MYT], 07 March 2014 followed by the First Officer (FO) who signed in 25 minutes later. The MAS Operations Despatch Centre (ODC) released the flight at around 1515 UTC [2315 MYT].

The PIC, an authorised examiner for the Department of Civil Aviation (DCA), Malaysia, was conducting the last phase of line training for the FO, who was transitioning to the Boeing 777 (B777) aircraft type from the Airbus A330. As the FO was certified functional during his last line training flight, no additional pilot was required as safety pilot on MH370. It has been established that the PIC had assigned the FO to be the Pilot Flying for this flight.

The PIC ordered 49,100 kilograms (kg) of fuel for the flight that gave an endurance of 07 hours and 31 minutes including reserves (as per computerised flight plan). The planned flight duration was 05 hours and 34 minutes.

The recorded radio transmissions between the Air Traffic Controllers at Kuala Lumpur Area Control Centre (KL ACC) and the FO showed that an airways clearance request to Lumpur Airways Clearance Delivery was made at 1625:52 UTC [0025:52 MYT] and a pushback and start clearance request to Lumpur Ground was made at 1627:37 UTC [0027:37 MYT].

Note:

In accordance with the Standard Operating Procedures (SOP) of MAS, radio

[1] Unless specified, all times in this report are in Coordinated Universal Time (UTC). The Malaysian Time (MYT) is UTC+08 hours.

communication on the ground is the responsibility of the FO. In the air, the role is reversed when the assigned pilot flying is the FO.

Lumpur Tower cleared MH370 for take-off at 1640:37 UTC [0040:37 MYT]. At 1642:53 UTC [0042:53 MYT] Lumpur Departure cleared MH370 to climb to Flight Level (FL) 180 (the aviation term for 18,000 feet [ft.]) and to cancel the Standard Instrument Departure (SID) clearance by tracking direct to waypoint[2] IGARI.

At 1643:31 UTC [0043:31 MYT], KL ACC Sector 3 Planner coordinated with Ho Chi Minh (Viet Nam) Area Control Centre (HCM ACC) on the Direct Speech Circuit (direct telephone line) relaying the estimated time of arrival (ETA) of MH370 for waypoint IGARI as 1722 UTC [0122 MYT] and the assigned Secondary Surveillance Radar (SSR) transponder code A2157.

MH370 was transferred to Lumpur Radar at 1646:39 UTC [0046:39 MYT].

At 1646:58 UTC [0046:58 MYT], MH370 was cleared to climb to FL250 and subsequently to FL350 at 1650:08 UTC [0050:08 MYT]. MH370 reported maintaining FL350 at 1701:17 UTC [0101:17 MYT] and reported maintaining FL350 again at 1707:56 UTC [0107:56 MYT].

At 1719:26 UTC [0119:26 MYT], MH370 was instructed to contact HCM ACC on the radio frequency 120.9 MHz.

At 1719:30 UTC [0119:30 MYT], MH370 acknowledged with "*Good night Malaysian Three Seven Zero*". This was the last recorded radio transmission from MH370.

Radar recording showed that MH370 passed through waypoint IGARI at 1720:31 UTC [0120:31 MYT].

Based on the reconstruction of the flight profile conducted on the B777 simulator, the flight would be at waypoint IGARI one minute earlier than the original ETA of 1722 UTC [0122 MYT].

[2] Waypoint - A specified geographical location used to define an area navigation route or the flight path of an aircraft employing area navigation. Waypoints are identified as either:

- *Fly-by waypoint - A waypoint which requires turn anticipation to allow tangential interception of the next segment of a route or procedure, or*
- *Flyover waypoint - A waypoint at which a turn is initiated in order to join the next segment of a route or procedure.*

The Mode S symbol of MH370 dropped off from radar display at 1720:36 UTC [0120:36 MYT], and the last secondary radar position symbol of MH370 was recorded at 1721:13 UTC [0121:13 MYT].

The disappearance of the radar position symbol of MH370 was captured by the KL ACC radar at 1721:13 UTC [0121:13 MYT]. The Malaysian military radar and radar sources from two other countries, namely Viet Nam and Thailand, also captured the disappearance of the radar position symbol of MH370. The Bangkok radar target drop occurred at 1721:13 UTC [0121:13 MYT] and Viet Nam's at 1720:59 UTC [0120:59 MYT].

The last Aircraft Communication Addressing and Reporting System (ACARS) (refer to *Section 1.9.4 - ACARS*) transmission was made through the aircraft's satellite communication system at 1707:29 UTC [0107:29 MYT].

Figure 1.1A (below) shows the *Chronological Sequence of Events of the Disappearance of MH370 (in pictorial form and not to scale)*

1.1.2 Actions by HCM ACC and KL ACC

At 1739:06 UTC [0139:06 MYT] HCM ACC queried KL ACC on the whereabouts of MH370. KL ACC contacted MAS ODC to check on the whereabouts of MH370.

HCM ACC had also contacted Hong Kong (China) ACC and Phnom Penh (Cambodia) ACC in an attempt to establish the location of MH370. However, no contact had been established by any of the ATC units.

Kuala Lumpur Aeronautical Rescue Coordination Centre (KL ARCC) was activated at 2130 UTC [0530 MYT]. There is no evidence to show HCM ACC activated its Rescue Coordination Centre.

1.1.3 Diversion from Filed Flight Plan Route

1) Malaysian Military Radar

The Military radar data provided more extensive details of what was termed as "Air Turn Back". It became very apparent, however, that the recorded altitude and speed change "blip" to "blip" were well beyond the

capability of the aircraft. It was highlighted to the Team that the altitude and speed extracted from the data are subjected to inherent error. The only useful information obtained from the Military radar was the latitude and longitude position of the aircraft as this data is reasonably accurate.

At 1721:13 UTC [0121:13 MYT] the Military radar showed the radar return of MH370 turning right but shortly after, making a constant left turn to heading of 273°, flying parallel to Airway M765 to VKB (Kota Bharu).

Between 1724:57 UTC [0124; 57 MYT] to 1737:35 UTC [0137:35 MYT] the “blip” (a spot of light on a radar screen indicating the position of a detected aircraft) made heading changes that varied between 8° and 20°, and a ground speed that varied from 451 kt to 529 kt. The Military data also recorded a significant height variation from 31,150 to 39,116 ft.

The Military data further identified the “blip” on a heading of 239° at 1737:59 UTC [0137:59 MYT] parallel to Airway B219 towards VPG (VOR Penang). Heading of this “blip” varied from 239° to 255° at a speed from 532 to 571 kt. The height of this “blip” was recorded between 24,450 ft and 47,500 ft.

At 1752:31 UTC [0152:31 MYT] the “blip” was observed to be at 10 nm south of Penang Island on a heading of 261°, speed of 525 kt and at a height of 44,700 ft.

At 1801:59 UTC [0201:59 MYT] the data showed the “blip” on a heading of 022°, speed of 492 kt and altitude at 4,800 ft. This is supported by the “blip” detected by Military radar in the area of Pulau Perak at altitude 4,800 ft at 1801:59 UTC [0201:59 MYT]. At 1803:09 UTC [0203:09 MYT] the “blip” disappeared, only to reappear at 1815:25 UTC [0215:25 MYT] until 1822:12 UTC [0222:12 MYT], about 195 nm from Butterworth, on a heading of 285°, speed of 516 kt and at an altitude of 29,500 ft.

9	At 1721:13 UTC [0121:13 MYT], 3.2 nm after passing IGARI, the radar position symbol of MH370 dropped off
8	MH370 Mode S symbol dropped off at 1720:36 UTC [0120:36 MYT]
7	MH370 over waypoint IGARI at 1720:31 UTC [0120:31 MYT]
6	At 1719:26 UTC [0119:26 MYT], 8.6 nm to waypoint IGARI, KL ACC instructed MH370 to contact HCM ACC MH370 acknowledged with '*Good night Malaysian Three Seven Zero*' at 1719:30 UTC [0119:30 MYT]
5	MH370 maintaining FL350 at 1701:17 UTC [0101:17 MYT] MH370 reported again maintaining FL350 at 1707:56 UTC [0107:56 MYT]
4	MH370 climbing to FL350 at 1650:11 UTC [0050:11 MYT]
3	MH370 climbing to FL250 at 1647:03 UTC [0047:03 MYT]
2	MH370 climbing to FL180 at 1643:01 UTC [0043:01 MYT]
1	Lumpur Tower cleared for take-off at 1640:37 UTC [0040:37 MYT] and MH370 departed at 1642 UTC [0042 MYT]

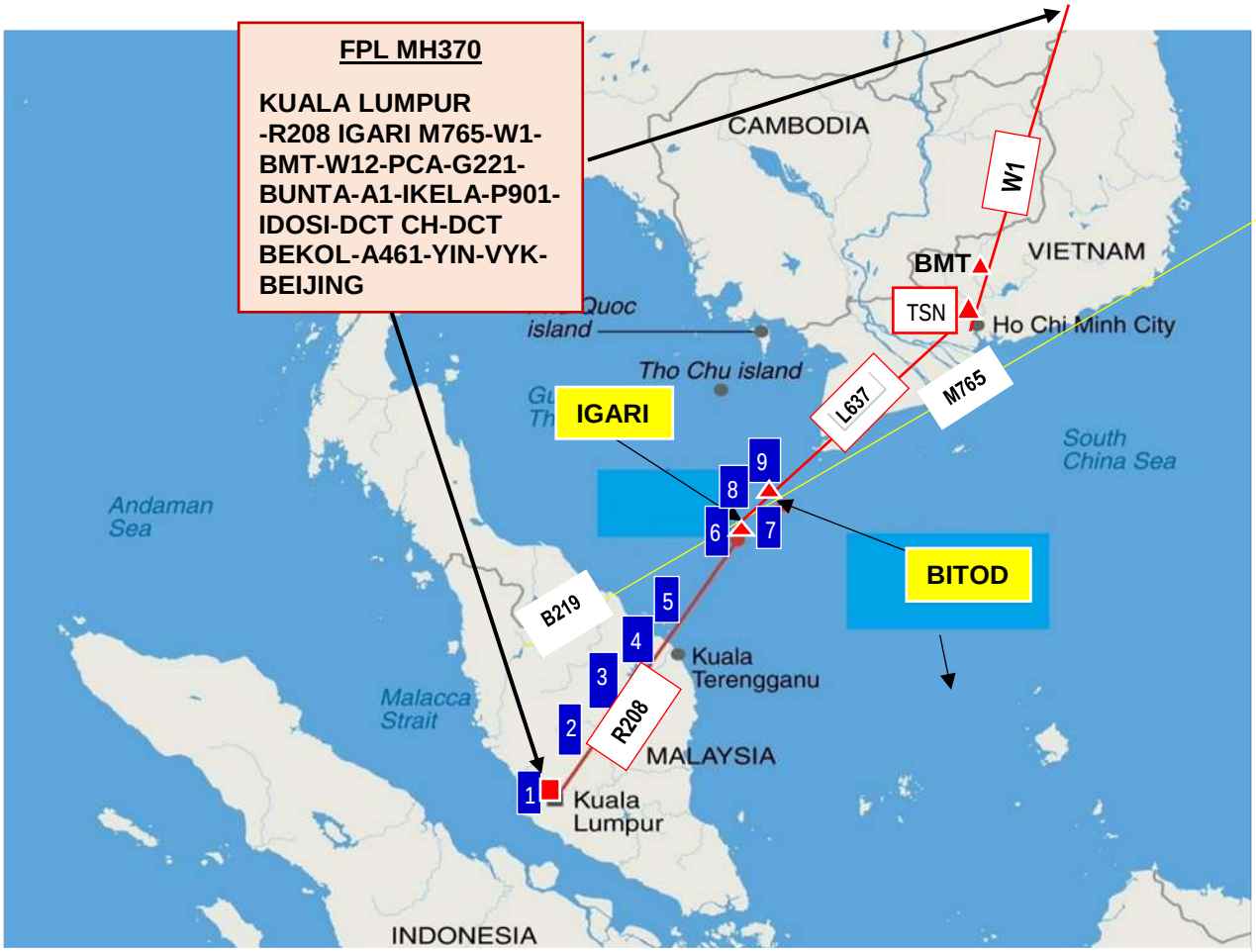

Figure 1.1A - Chronological Sequence of Events of Disappearance of MH370 (in pictorial form and not to scale)

Figure 1.1A – Chronological Sequence of Events of Disappearance of MH370 (in pictorial form and not to scale)

The tracking by the Military continued as the “blip” was observed to be heading towards waypoint MEKAR on Airway N571 when it finally disappeared at 1822:12 UTC [0222:12 MYT], 10 nm after waypoint MEKAR.

On the day of the disappearance of MH370, the Military radar system recognised the ‘blip’ that appeared west after the left turn over IGARI was that of MH370. Even with the loss of SSR data, the Military long range air defence radar with Primary Surveillance Radar (PSR) capabilities affirmed that it was MH370 based on its track behaviour, characteristics and constant/continuous track pattern/trend. Therefore, the Military did not pursue to intercept the aircraft since it was ‘friendly’ and did not pose any threat to national airspace security, integrity and sovereignty.

Based on the Malaysian Military data, a reconstruction of the profile was conducted on a Boeing 777 simulator. *Figure 1.1B* (below) in chart form shows the *Profile Chart of Data from Malaysian Military Radar.* Some of the speed and height variations were not achievable even after repeated simulator sessions.

It was also noted that, in the absence of autopilot or continuous manual control, an aircraft is very unlikely to maintain straight and level flight. Further, it is extremely unlikely for an aircraft to enter and maintain a turn and then return to straight and level flight for any significant period of time.

2) DCA Civilian Radar Data from Kota Bharu - Sultan Ismail Petra Airport Runway

The aircraft diversion from the filed flight plan route was recorded on the DCA radar playback:

a) From 1730:37 UTC [0130:37 MYT] to 1744:52 UTC [0144:52 MYT] a primary aircraft target was captured by the Terminal Primary Approach Radar located to the south of the Kota Bharu – Sultan Ismail Petra Airport runway.

b) The appearance of an aircraft target on the KL ACC radar display, coded as P3362, was recorded at 1730:37 UTC [0130:37 MYT] but the aircraft target disappeared from the radar display at 1737:22 UTC [0137:22 MYT].

c) At 1738:56 UTC [0138:56 MYT] an aircraft target, coded as P3401, appeared on the KL ACC radar display and disappeared at 1744:52 UTC [0144:52 MYT].

d) At 1747:02 UTC [0147:02 MYT] an aircraft target, coded as P3415, appeared on the KL ACC radar display but disappeared at 1748:39 UTC [0148:39 MYT], which appeared to be the continuity of the same target.

e) At 1751:45 UTC [0151:45 MYT] an aircraft target, coded as P3426, appeared on the KL ACC radar display but disappeared at 1752:35 UTC [0152:35 MYT].

Figure 1.1C (below) shows *Diversion from Filed Flight Plan Route (in pictorial form and not to scale).*

It has been confirmed by DCA and its radar maintenance contractor, Advanced Air Traffic Systems (M) Sdn. Bhd. (AAT), that it was the 60 nm Terminal Primary Approach Radar, co-mounted with 200 nm monopulse SSR[3] located to the south of Kota Bharu - Sultan Ismail Petra Airport runway, which captured the above-mentioned primary aircraft targets.

[3] *SSR (Secondary Surveillance Radar) - A surveillance radar system which uses transmitters/receivers system (interrogators) and transponders*.

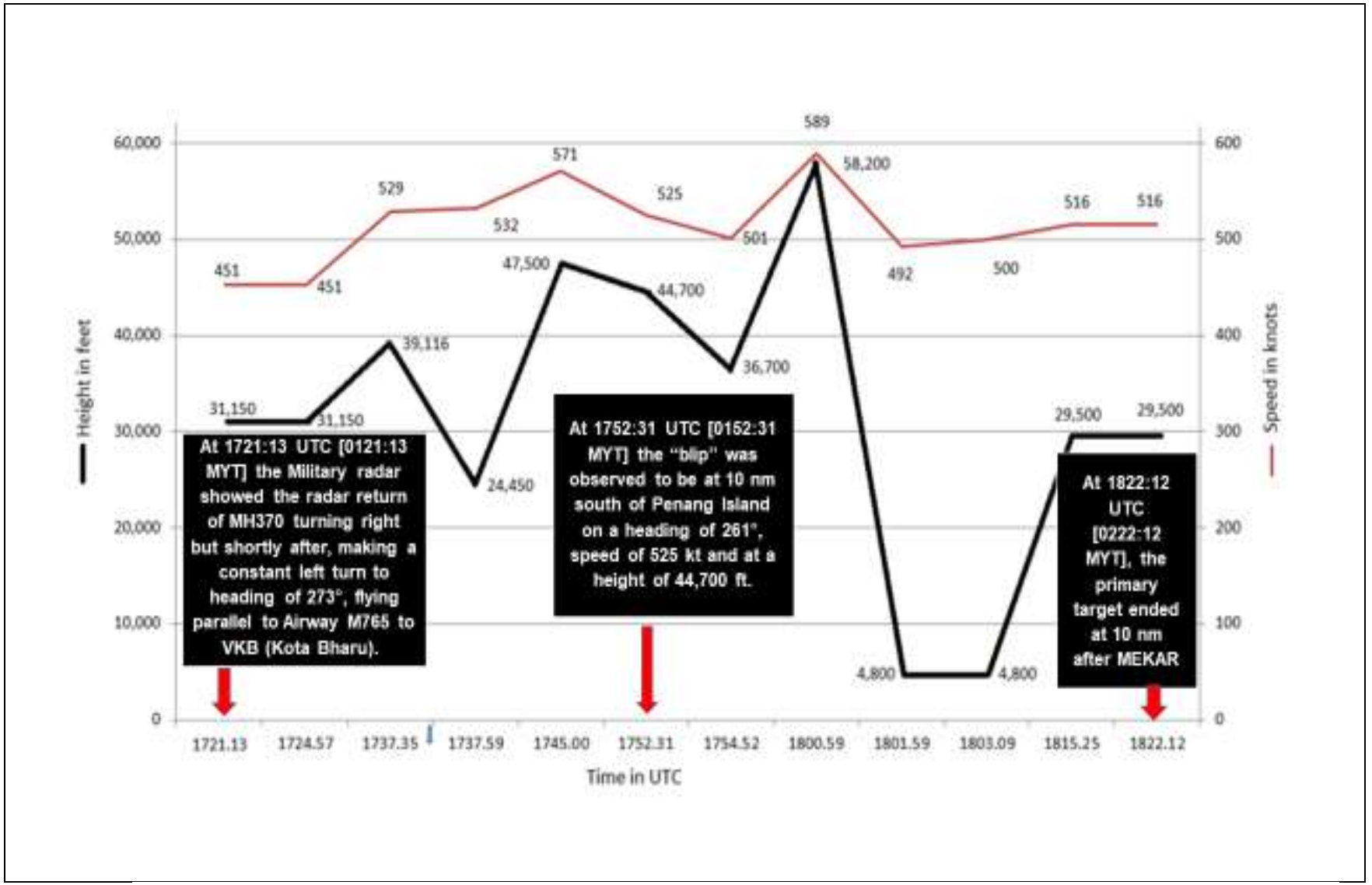

Figure 1.1B - Profile Chart of Data from Malaysian Military Radar (not to scale).

1	P3362: Appeared at 1730:37 UTC [0130:37 MYT]
2	P3362: Coasted at 1737:12 UTC [0137:12 MYT] Dropped at 1737:22 UTC [0137:22 MYT]
3	P3401: Appeared at 1738:56 UTC [0138:56 MYT]
4	P3401: Coasted at 1744:42 UTC [0144:42 MYT] Dropped at 1744:52 UTC [0144:52 MYT]
5	P3415: Appeared at 1747:02 UTC [0147:02 MYT]
6	P3415: Coasted at 1748:29 UTC [0148:29 MYT] Dropped at 1748:39 UTC [0148:39 MYT]
7	P3426: Appeared at 1751:45 UTC [0151:45 MYT]
8	P3426: Coasted at 1752:25 UTC [0152:25 MYT] Dropped at 1752:35 UTC [0152:35 MYT] P3426 last seen on radar display Approximately 6 nm south of Penang
9	The primary target (military radar) appeared to track west-northwest direction joining RNAV Route N571 at waypoint VAMPI thence to 10 nm north MEKAR *Source: RMAF*
10	The primary target ended at 10 nm after MEKAR at 1822:12 UTC [0222:12 MYT] *Source: RMAF*

	Filed Flight Plan Route
	Diversion route
	Radar target appearance
	Radar target coasted/dropped off

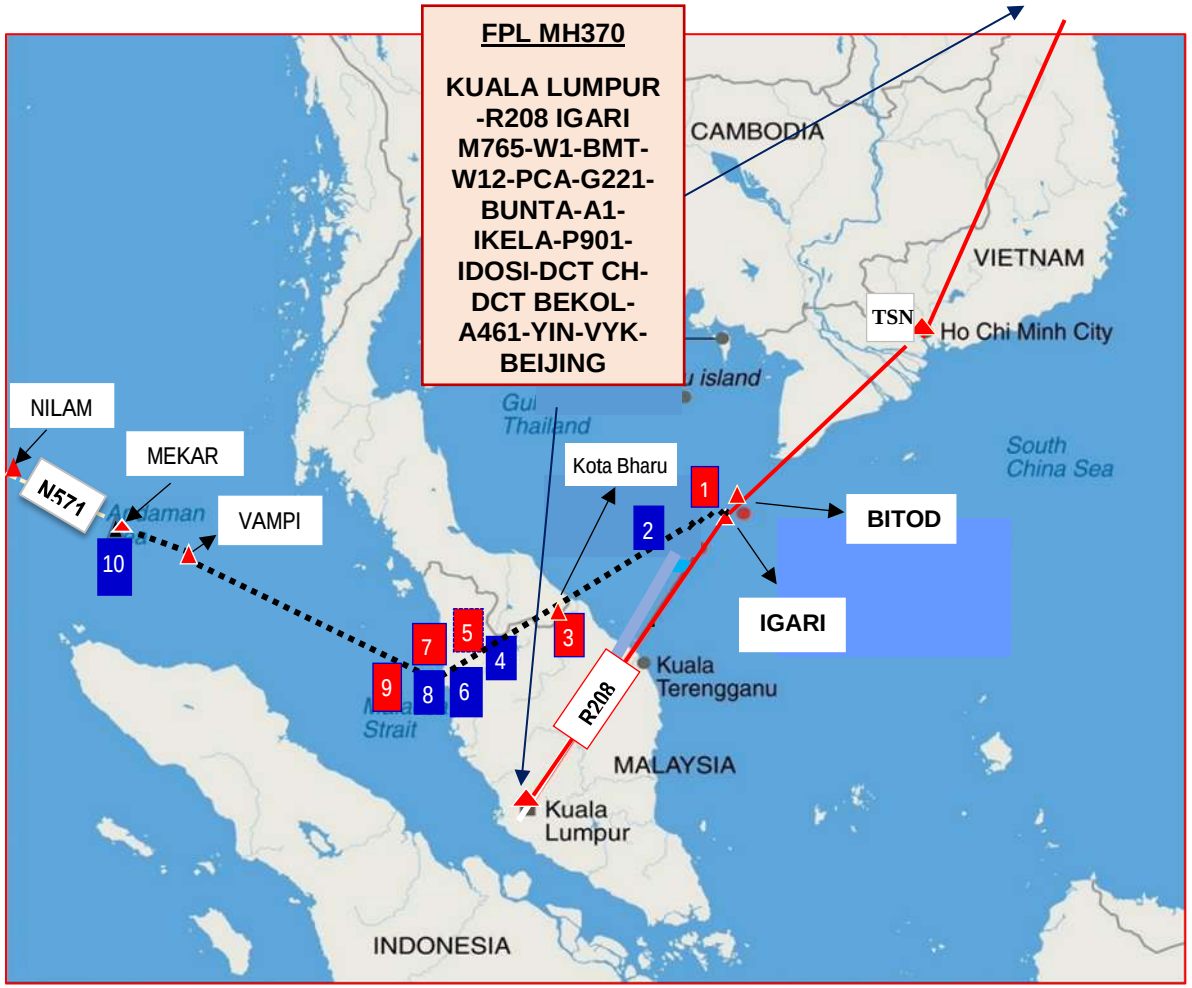

Figure 1.1C - Diversion from Filed Flight Plan Route - Civilian Radar (in pictorial form and not to scale)

Figure 1.1D (below) shows the suitable airports for emergency en-route diversion.

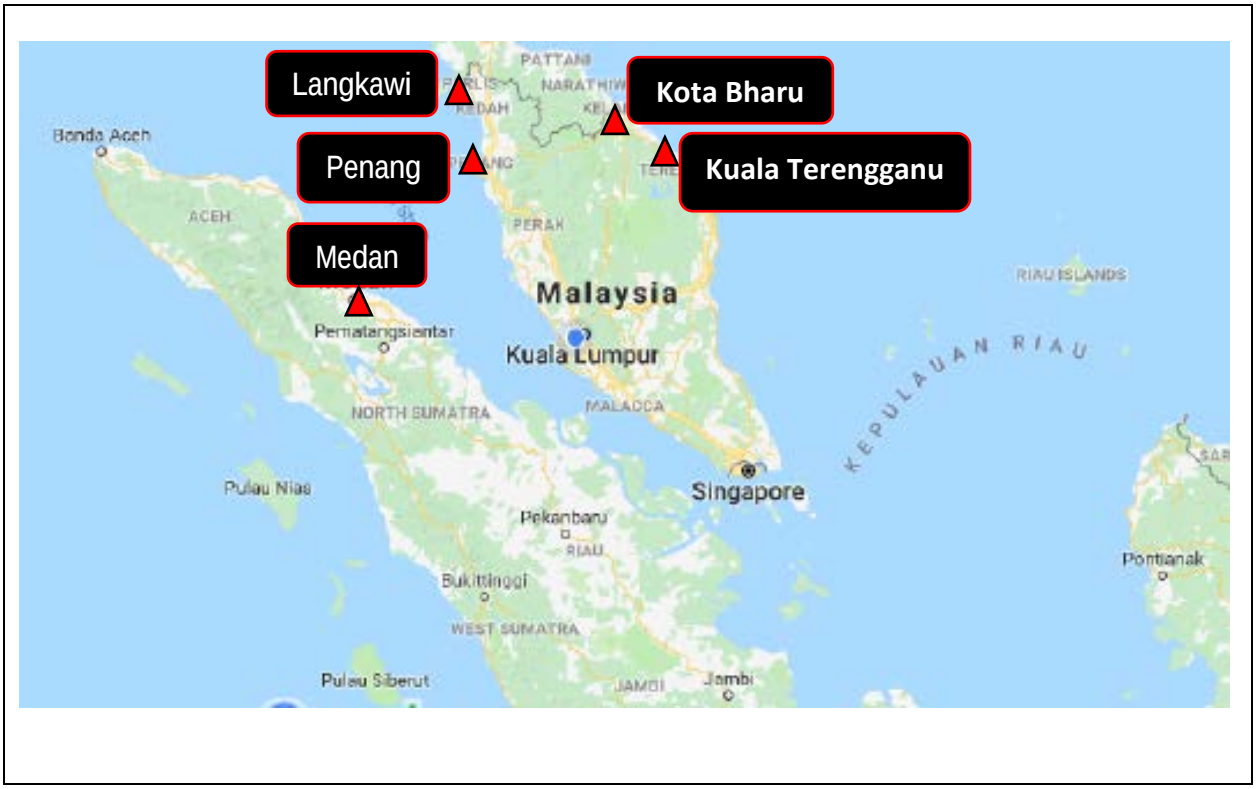

Figure 1.1D - Airports for Emergency Landing along the Flightpath of MH370 (chart not to scale)

Figure 1.1E (below) shows the *Filed Flight Plan message of MH370*.

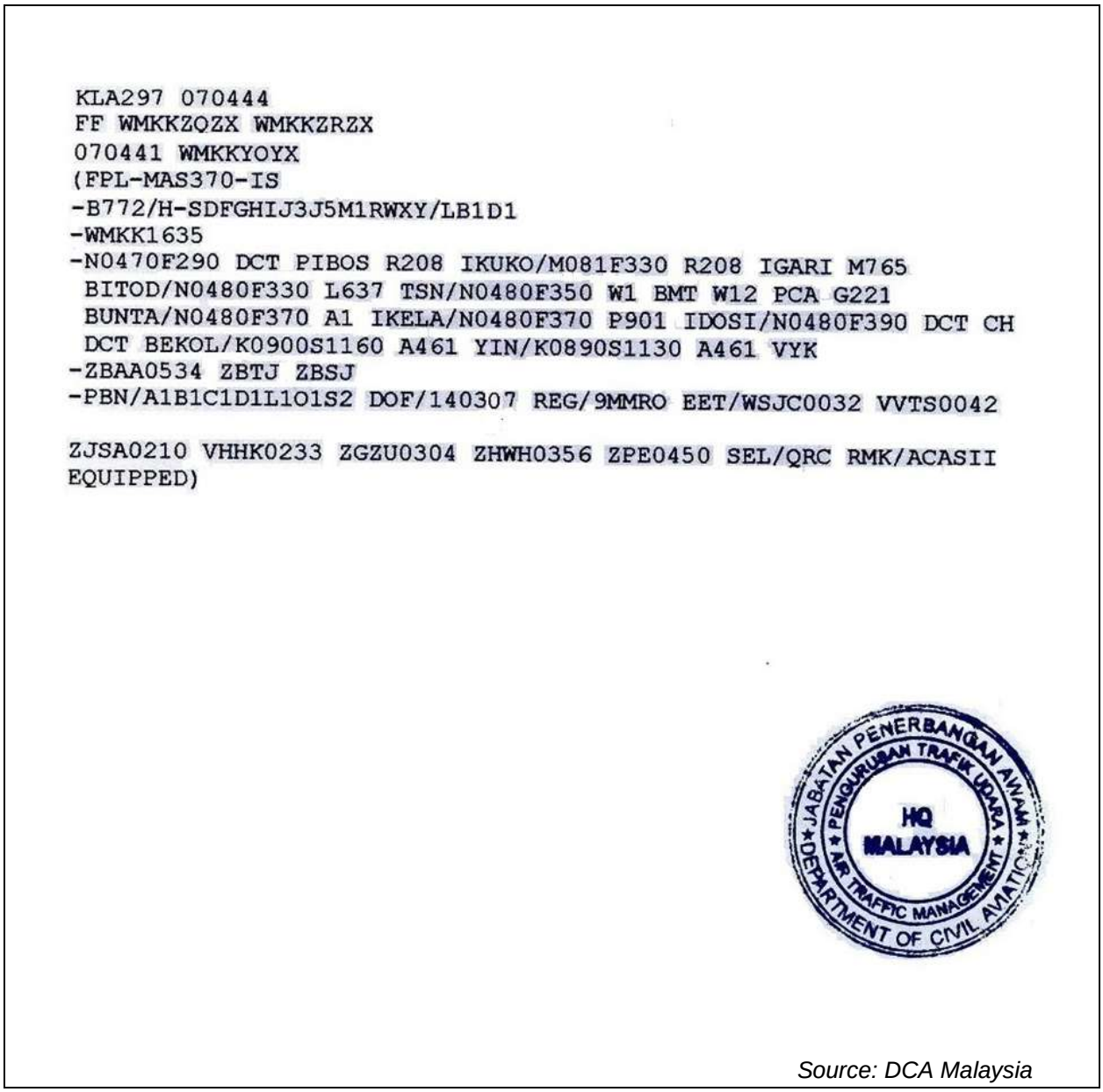

```
KLA297 070444
FF WMKKZQZX WMKKZRZX
070441 WMKKYOYX
(FPL-MAS370-IS
-B772/H-SDFGHIJ3J5M1RWXY/LB1D1
-WMKK1635
-N0470F290 DCT PIBOS R208 IKUKO/M081F330 R208 IGARI M765
 BITOD/N0480F330 L637 TSN/N0480F350 W1 BMT W12 PCA G221
 BUNTA/N0480F370 A1 IKELA/N0480F370 P901 IDOSI/N0480F390 DCT CH
 DCT BEKOL/K0900S1160 A461 YIN/K0890S1130 A461 VYK
-ZBAA0534 ZBTJ ZBSJ
-PBN/A1B1C1D1L1O1S2 DOF/140307 REG/9MMRO EET/WSJC0032 VVTS0042

ZJSA0210 VHHK0233 ZGZU0304 ZHWH0356 ZPE0450 SEL/QRC RMK/ACASII
EQUIPPED)
```


Source: DCA Malaysia

Figure 1.1E - Filed Flight Plan message of MH370.

Figure 1.1F (below) shows Radar Data Plots (RDP) Tracks from the 60 nm Terminal Primary Approach Radar co-mounted with 200 nm monopulse SSR located to the south of Kota Bharu - Sultan Ismail Petra Airport runway after Diversion and *Figure 1.1G* (below) shows RDP Tracks from Kuala Lumpur after take-off.

All the primary aircraft targets that were recorded by the DCA radar are consistent with those of the military data that were made available to the Investigation Team.

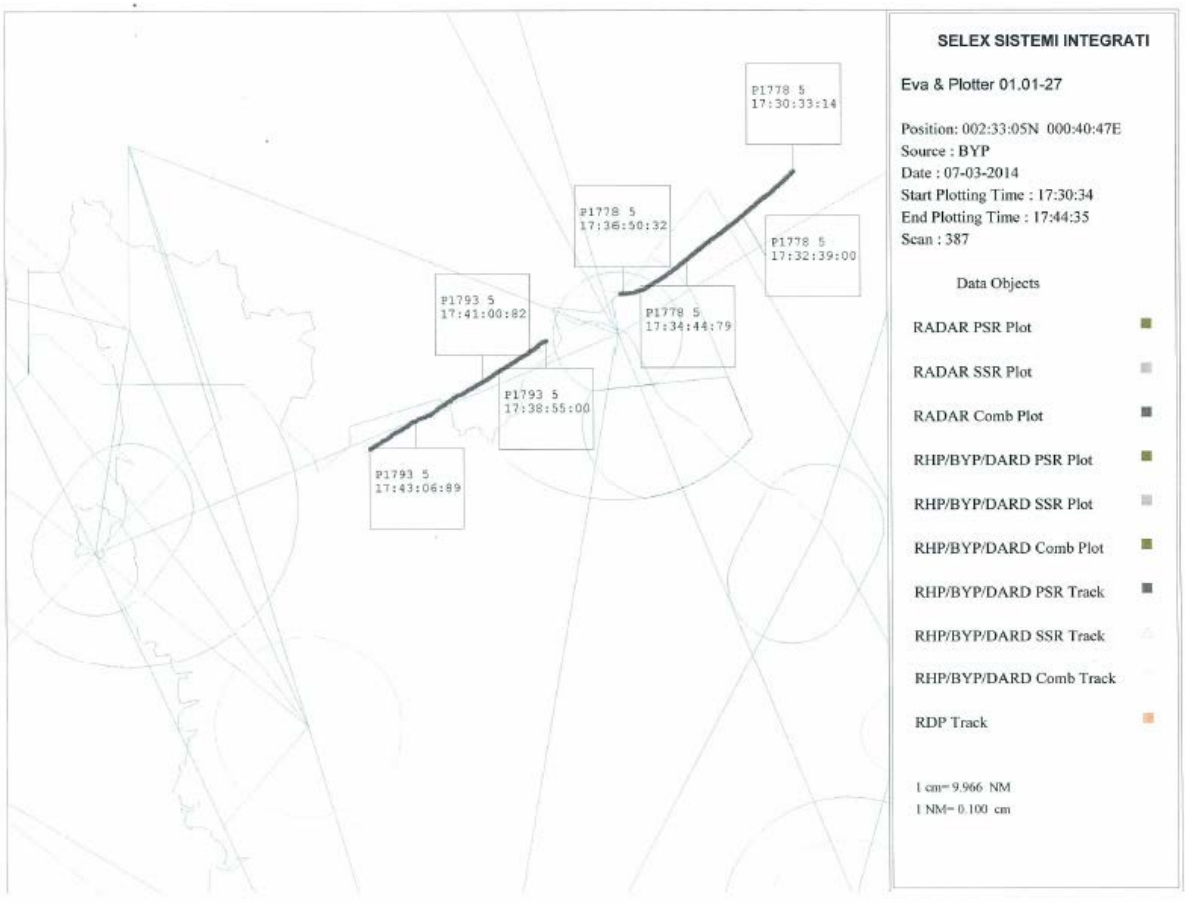

Source: Advanced Air Traffic Systems (M) Sdn. Bhd. (AAT)

Figure 1.1F - Radar Data Plots (RDP) Tracks from the 60 nm Terminal Primary Approach Radar co-mounted with 200 nm monopulse SSR located to the south of Kota Bharu - Sultan Ismail Petra Airport runway after Diversion.

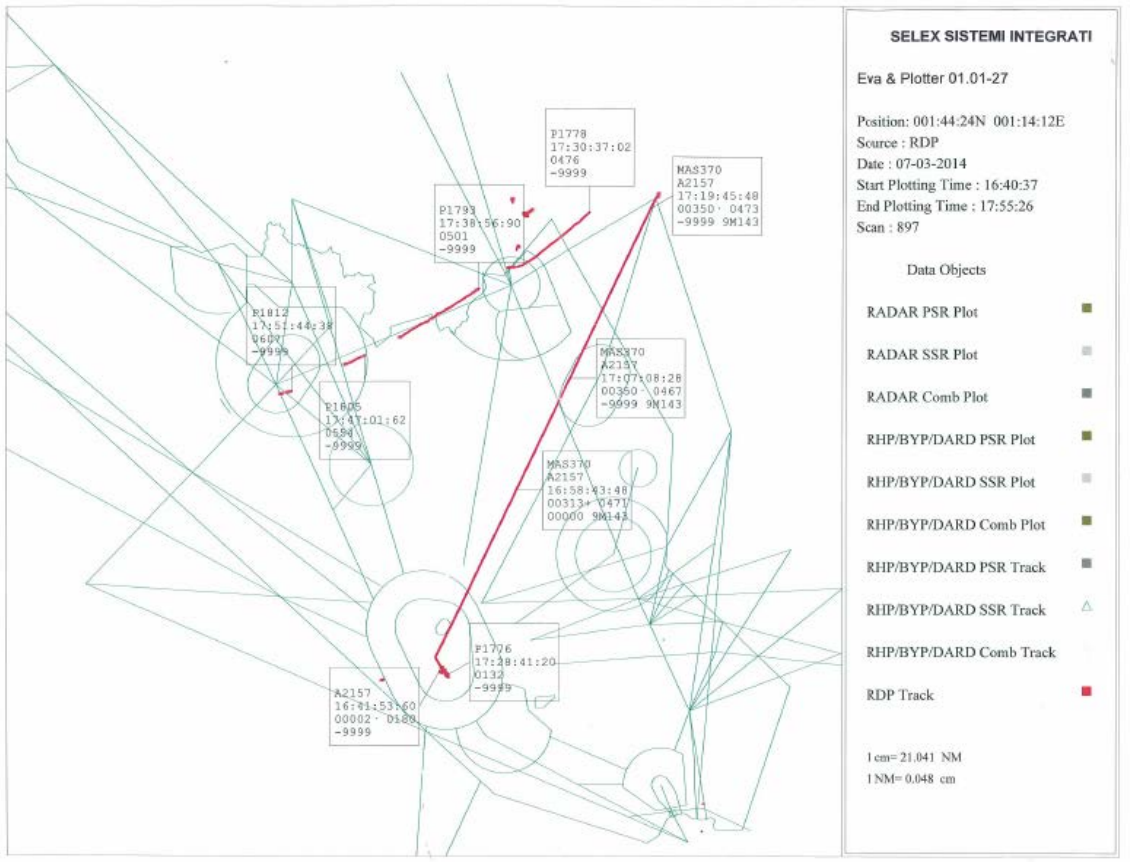

Source: Advanced Air Traffic Systems (M) Sdn. Bhd. (AAT)

Figure 1.1G - Radar Data Plots (RDP) Tracks from Kuala Lumpur after take-off

Reference:

The Malaysia Aeronautical Information Publication [AIP] ENR 1.6 dated 05 June 2008, AIP AMDT 2/2008 on the Provision of Radar Services and Procedures states that, in paragraph 1.1.4:

> "*In the Kuala Lumpur and Kota Kinabalu FIRs, radar services are provided using the following civil/military ATC Radars:*
>
> *g) A 60 nm Terminal Primary Approach Radar co-mounted with 200 nm monopulse SSR located to the south of Kota Bharu - Sultan Ismail Petra Airport runway.".*

Figure 1.1H (below) shows the Radar Coverage Chart of Kuala Lumpur and Kota Kinabalu FIRs.

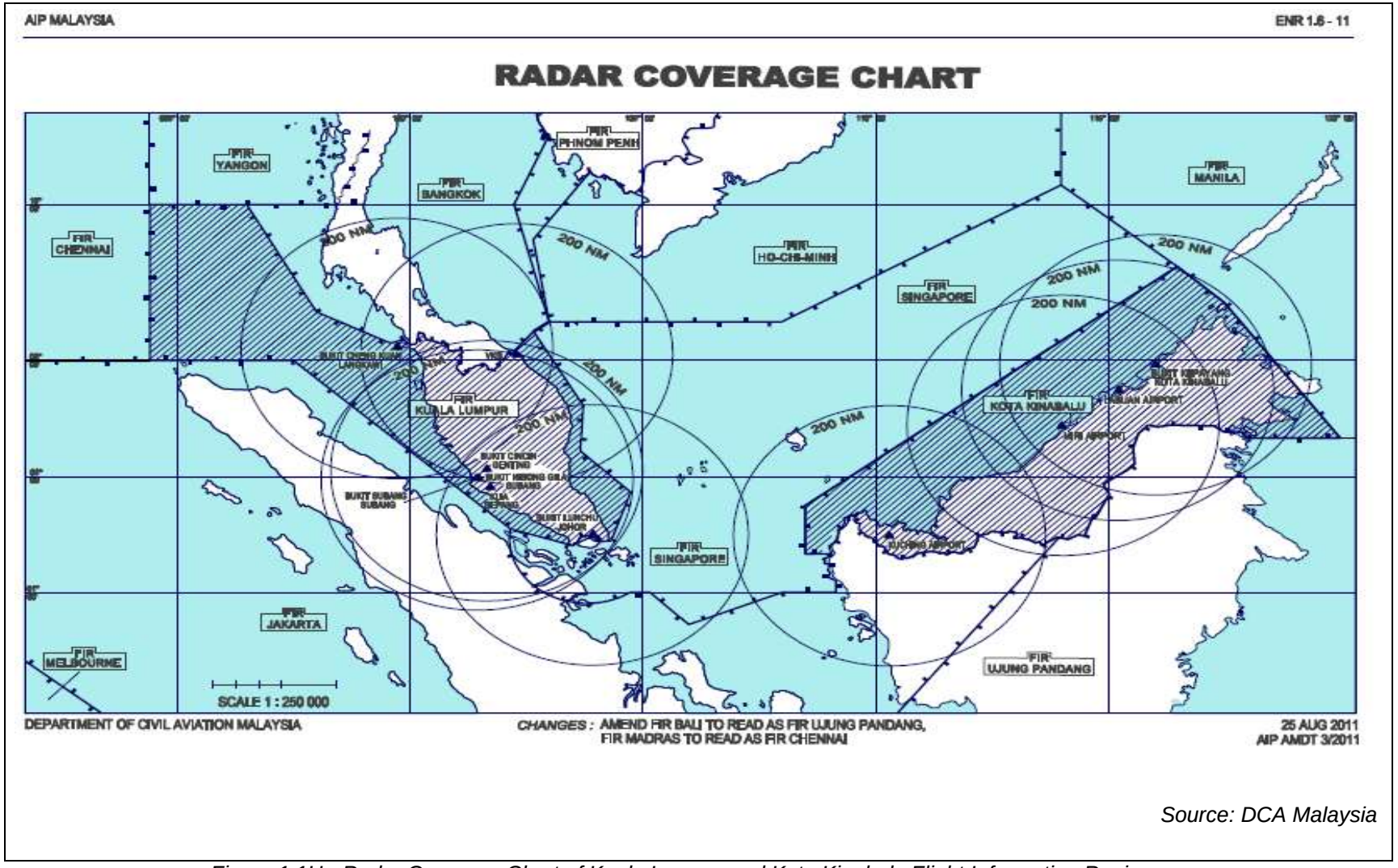

Source: DCA Malaysia

Figure 1.1H - Radar Coverage Chart of Kuala Lumpur and Kota Kinabalu Flight Information Regions

3) Ho Chi Minh Air Traffic Services

The tracking of MH370 was captured by HCM ACC Secondary Radar at Tan Son Nhut and at Camau Province, and Automatic Dependent Surveillance- Broadcast (ADS-B) located at Conson Island/range 270 nm) at 1711:59 UTC [0111:59 MYT] as it was heading for waypoint IGARI.

At 1720:59 UTC [0120:45 MYT] the "blip" from MH370 from both SSR and ADS-B radar position symbols disappeared from the radar display.

A visit was made to the office of the Vietnamese Civil Aviation Authority (CAAV) in Ho Chi Minh City on 10 September 2014. In interviews, the Duty HCM Duty ACC Controller who was handling MH370 on that night could not explain why he did not initiate any call to MH370 within the standard 5 minutes as specified in the Letter of Agreement (LOA) between Department of Civil Aviation Malaysia and Viet Nam Air Traffic Management dated 07 July 2001 and effective on 01 November 2001 (Refer *Appendix 1.1A - Letter of Agreement between DCA Malaysia and Viet Nam*). It was noted that he had only initiated an enquiry on the whereabouts of MH370 at 1739:03 UTC [0139:03 MYT] after a lapse of 12 minutes.

The Duty Controller however had stated that he had initiated calls to other aircraft on the existing frequency and on the emergency frequency of 121.5 MHz. This was neither supported nor collaborated by any documents.

The landline recorded transcripts between KL ACC and HCM ACC suggested that there were confusions on the position of MH370. This was evident when HCM ACC requested KL ACC for information on MH370 at 1739:06 UTC [0139:06 MYT]. This conversation took place:

KL ACC: *"MH370 already transferred to you rite?"*

HCM ACC: *"Yeah…yeah…I know at time two zero but we have no just about in contact up to BITOD…we have radar lost with him…the one we have to track identified via radar*."

When pointed out that neither HCM ACC SSR nor ADS-B showed any presence of a "blip" of MH370, the Duty Controller could not explain why he mentioned BITOD.

MH370 was operating within the Singapore FIR, in that portion of the airspace which has been delegated to Malaysia (Refer to *Figure 2.2K - Singapore Airspace delegated to Malaysia)* for the provision of air traffic

services when the last air-ground radio contact was made at 1719 UTC [0119 MYT]. As such, KL ACC should be responsible for the alerting service which would mean that KL ACC would have to declare the Distress Phase at 1827 UTC [0227 MYT] when HCM ACC informed that there had been no two-way radio communications with MH37O.

The *DETRESFA* was only declared at 2232 UTC [0632 MYT]. Refer to para. 2.2.7 Table 2.2C, No. 26-28 - Chronology of ATC Events following the Disappearance of MH370; and to para. 2.2.8 1) o) - Activation of Aeronautical Rescue Coordination Centre, for details.

Reference:

Manual of Air Traffic Services, Part 9 - Emergencies, para. 9-6-5, Para, 6.7.2 dated 15/3/2009 states:

> *If alerting service is required for an aircraft that is flight planned to operate through more than one FIR including the airspace delegate to the Kuala Lumpur and Kota Kinabalu ATSCs and the position of the aircraft is in doubt, the responsibility for co-ordinating such service shall normally rest with the ATSC of the respective FIRs:*
>
> - *within which the aircraft was flying at the time of last air-ground radio contact;*
> - *that the aircraft was about to enter when last air-ground contact was established at or close to the boundary of two FIRs or control areas;*
> - *within which the aircraft's intermediate stop or final destination point is located:*
>
> *1) if the aircraft was not equipped with suitable two-way radio communication, or*
>
> *2) was not under obligations to transmit position reports.*

and

ICAO Doc 4444 ATM/501 Procedures for Air Navigation - Air Traffic Management (PANS-ATM), page 9-6, para 9.2.2.2, dated 22/11/07 states*:*

> *When alerting services is required in respect of a flight operated through more than one FIR or control area, and when the position of the aircraft is in doubt, responsibility for coordinating such service*

shall rest with the ATS unit of the FIR or control area within which the aircraft was flying at the time of last air-ground radio contact:

a) that the aircraft was about to enter when last air-ground contact was established at or close to the boundary of two FIRs or control areas;

b) within which the aircraft's intermediate stop or final destination point is located:

1) if the aircraft was not equipped with suitable two-way radio communication, or

2) was not under obligations to transmit position reports.

Based on interviews, HCM ACC had stated that it did not initiate any emergency actions as it did not receive any change of the transfer of control time of IGARI, MH370 did not contact the Centre at the stated time, and it was unable to establish radio communication with MH370.

MH370 was also operating in the airspace delegated to KL ACC and the last air-ground radio contact was with KL ACC. Hence the provision of alerting service for MH370 rests with KL ACC.

These uncertainties were further compounded by the Duty Despatcher, based on MAS Flight Following System (FFS), who mentioned that the aircraft was over the Cambodian airspace when in fact the filed flight plan routing did not include flying over the Cambodian airspace.

Added to these confusions, for reasons best known to him, the MAS Captain from the Technical and Development Department, Flight Operations spoke to KL ACC saying that the aircraft did not leave the Malaysian airspace. When interviewed, the Captain insisted that he was asking a question rather than making a statement. This conversation was recorded at 0521.23 MYT:

KL ACC: *"…had never leave Lumpur airspace?"*

MAS Captain: *"…yea he has not left Lumpur airspace because he has failed to call Ho Chi Minh."*

4) Kuala Lumpur ACC Radar

KL ACC Radar captured the disappearance of MH370 at 1721:13 UTC [0121:13 MYT]. In interviews with the Duty KL ACC Radar Controller, he stated that he did not notice the "blip" disappearance as MH370 was out

of radar coverage and would be in contact with HCM ACC after the transfer of responsibility was effected.

From 1730:37 UTC [0130:37 MYT] to 1752:35 UTC [0152:35 MYT], what appeared to be MH370 was captured on KL ACC primary radar, coded as P3362, P3401, P1415, P3415 and P3426 (P signifies Primary Radar). *Figure 1.1C - Diversion from Filed Flight Plan Route.*

The appearance of a “blip” coded as P3362 was recorded at 1730:37 UTC [0130:37 MYT)] but disappeared abruptly at 1737:22 UTC [0137:22 MYT].

At 1738:56 UTC [0138:56 MYT], a “blip” identified as P3401 was tracked by KL ACC but disappeared at 1744:52 UTC [0144:52 MYT].

Shortly after, another “blip” coded as P3451 appeared at 1747.02 UTC [0147:02 MYT] but disappeared at 1748:39 UTC [0148:39 MYT].

At 1751:45 UTC [0151:45 MYT], a “blip” coded as P3426 appeared south of Penang Island but disappeared at 1752:35 UTC [0152:35 MYT].

5) Medan Air Traffic Control Radar

The Medan ATC Radar has a range of 240 nm, but for unknown reasons, did not pick up any radar return bearing the SSR transponder code A2157 of MH370.

The Indonesian Military however stated that they picked up MH370 earlier as it was heading towards waypoint IGARI.

No other information was made available.

6) Bangkok Air Traffic Control Radar

The radar position symbol with SSR transponder code A2157 was detected on the Aeronautical Radio of Thailand Limited (AEROTHAI) radar display at 1711 UTC [0111 MYT] as the aircraft was tracking for waypoint IGARI.

Thailand DCA is a government agency whereas AEROTHAI is a state enterprise under the Ministry of Transport and Communications. AEROTHAI is the air navigation service provider responsible for the provision of Air Traffic Services within the Bangkok Flight Information Region (FIR).

As the flight plan of MH370 did not fall under the purview of Thailand's FIR, Bangkok ACC did not pay attention to this flight. On playback of the radar recording it was noted that the radar position symbol of A2157 disappeared at 1721:13 UTC [0121:13 MYT].

7) Singapore Air Traffic Services

The Team visited Singapore to conduct interviews with officers from Civil Aviation Authority of Singapore (CAAS) and the Air Traffic Controllers on duty on 07 March 2014. The following were noted:

i) Singapore ACC did not have radar coverage over the South China Sea. (*ADS and CPDLC services are available to suitably equipped aircraft operating outside radar cover over the South China Sea …);*

Reference:

AIP Singapore page 94 GEN 3.4-2, 10 MAR 11, para 3.2.2 d.

ii) At 2104:00 UTC [0504:00 MYT], Singapore ACC received a call from Hong Kong ACC enquiring any knowledge of a missing Malaysian aircraft MH370. Hong Kong ACC then requested assistance from Singapore ACC to contact Lumpur ACC for detailed information. It was evident that Singapore ACC was not aware of the problem until this call was received. Hong Kong ACC however had the knowledge of the missing Aircraft earlier after receiving unconfirmed information from HCM ACC;

iii) At 2109:13 UTC [0509:13 MYT], Singapore ACC contacted Lumpur ACC to relay the query from Hong Kong ACC.

Reference

Radiotelephony transcripts between Sin*gapore ACC and KL ACC Sector 3+5 Planner - Appendix 1.18G* on *Direct Line Coordination Communication,* pages 109 to 114.

1.1.4 Role of Malaysian Military

On the day of the disappearance of MH370, the Military radar system recognised the 'blip' that appeared west after the left turn over IGARI was that of MH370. Even with the loss of SSR data, the Military long range air defence radar with Primary Surveillance Radar (PSR) capabilities affirmed that it was MH370 based on its track behaviour, characteristics and constant/

continuous track pattern/trend. Therefore, the Military did not pursue to intercept the aircraft since it was 'friendly' and did not pose any threat to national airspace security, integrity and sovereignty.

1.1.5 Detection of Hand Phone Signal

A Telco service provider in an interview with the RMP confirmed a signal "hit" occurred at 0152:27 MYT on 08 March 2014, coming from the mobile phone tower (LBS Location Base station) at Bandar Baru Farlim Penang. The signal "hit" however did not record any communication except to confirm that it was in the ON mode signal related to the "hit". The phone number *xxxxxxx* was later traced to that registered under the FO. This was supported by the RMP's report.

To ascertain the probability of making calls inside an aircraft from different altitudes, a reconstructed flight using a King Air 350 over the said area and during the same time when the signal "hit" happened was carried out shortly after the disappearance of MH370. The flight was conducted from an altitude of 24,000 ft with step descents every 4,000 ft until 8,000 ft. The next descent was to 5,000 ft but at 1,000 ft interval. An expert from a Telco service provider conducted the test using three different brands of phone and related equipment that were carried on board the King Air 350. Test call will be automatically answered by the server in the event of connectivity.

In summary, during the tests, it was found that it was difficult to maintain successful call connectivity above 8,000 ft. However, one brand of phone was able to make a call at 20,000 ft. Only one cell phone service provider recorded the highest call attempts using their 3G network above 8,000 ft. Two service providers could only provide connection below 8,000 ft.

The Telco service provider expert cautioned the Team that the tests would be difficult to conclude and use as scientific/theoretical assumptions for the case of MH370, as the measurement results were only valid for that specific time, flight path, speed, altitude, devices used, and environment during the tests.

1.1.6 Search for Aircraft

Extensive work done by the MH370 Search Strategy Group, coordinated by the Australian Transport Safety Bureau (ATSB), by analysing signals transmitted by the aircraft's satellite communications terminal to Inmarsat's Indian Ocean Region satellite indicated that the aircraft continued to fly for

several hours after loss of contact. The analysis showed the aircraft changed course shortly after it passed the northern tip of Sumatra (Indonesia) and travelled in a southerly direction until it ran out of fuel in the southern Indian Ocean west of Australia. Details of this work can be found in the ATSB's report: AE-2014-054 dated 26 June 2014, and in subsequent updates, available at ATSB's website:
http://www.atsb.gov.au/publications/investigation_reports/2014/aair/ae-2014-054/

On 03 October 2017, the ATSB published a report detailing the history of the search and made conclusions and recommendations relating to the search activities. This is contained in the report titled "***The Operational Search for MH370".*** The report and relevant attachments are available at ATSB's website:
https://www.atsb.gov.au/newsroom/news-items/2017/chapter-closes-on-mh370/

The search for Malaysia Airlines flight MH370 commenced on 8 March 2014 and continued for 1,046 days until 17 January 2017 when it was suspended in accordance with a decision made by the Governments of Malaysia, Australia and the People's Republic of China. This involved surface searches in the South China Sea, Straits of Malacca and the southern Indian Ocean. The 52 days of the surface search involving aircraft and surface vessels covered an area of several million square kilometres. A sub surface search for the aircraft's underwater locator beacons was also conducted during the surface search. The underwater search started with a bathymetry survey which mapped a total of 710,000 square kilometres of Indian Ocean seafloor and continued with a high-resolution sonar search which covered an area in excess of 120,000 square kilometres. The last search vessel left the underwater search area on 17 January 2017 without locating the missing aircraft. Although combined scientific studies continued to refine areas of probability, there was no new information at that date to determine the specific location of the aircraft.

On 10 January 2018, the Malaysian Government entered into an agreement with the US company, Ocean Infinity, to conduct a 90-day underwater search in an area that was considered the most likely location for the wreckage. This search which commenced in the identified search area on 22 January 2018 was completed on 29 May 2018 without locating the missing aircraft. The search utilising the most advance underwater search technology currently available covered an area in excess of 112,000 square kilometres.

Details on the whole search effort for the aircraft have been documented elsewhere, in particular in the Australian Transport Safety Bureau report, "The Operational Search for MH370", in relation to the search in the southern Indian Ocean and the weekly updates provided by the MH370 Response Team in relation to the re-activated search by Ocean Infinity, and are separate and distinct from this Safety Investigation Report.

SECTION 1 – FACTUAL INFORMATION

1.2 INJURIES TO PERSONS

While injuries to persons on the flight could not be established as no survivors or bodies were found to date, the fact remains that there are 239 persons still missing.

SECTION 1 – FACTUAL INFORMATION

1.3 DAMAGE TO AIRCRAFT

Several pieces of debris were found washed ashore the south eastern coasts of Africa (South Africa, Mozambique and Tanzania), the Islands of Madagascar, Mauritius and Réunion, suggesting that the aircraft had suffered damage.

Refer to *Section 1.12* - *Wreckage and Impact Information* for the list of significant debris possibly/confirmed belonging to MH370, recovered and examined to date.

SECTION 1 – FACTUAL INFORMATION

1.4 OTHER DAMAGES

Other damages could not be established as the main wreckage of the aircraft had not been found. There was no reported ground impact or damage to any ground facilities or properties.

SECTION 1 – FACTUAL INFORMATION

1.5 PERSONNEL INFORMATION

1.5.1 Introduction

This investigation emphasised on the Pilot-in-Command (PIC), First Officer (FO) and the 10 cabin crew but did not include the passengers on board Flight MH370. The factual information of the crew was gathered from the following sources:

1) **Personal records/files of the Pilot-in-Command, First Officer and the Cabin Crew from Malaysia Airlines**

   These documents included the log book, certificates, licences, medical records and any disciplinary/administrative actions;

2) **Investigation details from the Polis Di Raja Malaysia (Royal Malaysia Police)**

   These were statements obtained from the next-of-kin and relatives, doctors/ care givers, co-workers, friends and acquaintances; financial records of the flight crew; Closed Circuit Television (CCTV) recordings at KLIA; and analysis of the radio transmission made between MH370 and ground air traffic control;

3) **Medical records from private health care facilities and from the Malaysia Airlines Medical Centre; and**

4) **Interviews with Malaysia Airlines staff and several of the next-of-kin of the crew**

The facts obtained were in relation to the demographic and employment history, financial background and insurance cover, significant past medical and medication history, psychological, social and behavioural pattern of the crew.

1.5.2 Malaysia Airlines Training and Check Records

As professional pilots, the two Malaysia Airlines (MAS) flight crew were subjected to periodic checks when flying on the type of aircraft at least on a bi-annual basis to revalidate the currency of their licences. These performance checks were conducted in approved flight simulators and in

addition, further checks are conducted on route flying duties on normal commercial flights on a yearly basis.

1.5.3 Pilot-in-Command

The PIC was born in the Island of Penang. He completed his Malaysian Certificate of Education (MCE) - the equivalent of the United Kingdom Ordinary (UK 'O') Level - at the Penang Free School, where he sat for his MCE Examination in 1978. In 1981 he was accepted as a Cadet Pilot with MAS under the sponsorship of Majlis Amanah Rakyat (MARA), a People's Trust Council of the Malaysian Government.

1) Personal Profile of Pilot-in-Command

Sex	Male
Age	53 years
Marital Status	Married with 3 children
Date of joining MAS	15 June 1981
Licence country of issues	Malaysia
Licence type	Air Transport Pilot Licence (ATPL)
Licence number	A751
Validity Period of Licence	14 May 2014
Ratings	Boeing B777
Medical Certificate	First Class (valid until 30 June 2014)
Aeronautical experience	18423:40 hours
Experience on type	8659:40 hours
Last 24 hours	0:00:00 hours
Last 72 hours	07:00:00 hours
Last 07 days	20:39:00 hours
Last 28 days	91:04:00 hours
Last 90 days	303:09:00 hours
Last line check	08 April 2013
Instrument rating check	15 November 2013
Last proficiency	15 November 2013
Last promotion	B777 Captain (22 September 1998)

The PIC was sent to Manila in the Philippines to be provided ab-initio pilot training and graduated 2 years later with a Commercial Pilot Licence & Instrument Rating (CPL & IR). He joined MAS as a Second Officer in 1983 and was posted on the F27 where he obtained his initial airline flying experience. He was then posted to the B737-200 in 1985, thereafter the A300B4, and stayed on as First Officer (FO) until March 1990. In July 1990

he was promoted to captain and took his first command on the F50 aircraft.

By the end of 1991 he was promoted to Captain on the B737-400 until December 1996. His next promotion was to the A330-300 and stayed on the fleet until September 1998 when he was promoted to the B777-200ER fleet until the day of the event. By virtue of his good track record and seniority he was made a Type Rating Instructor (TRI) and Type Rating Examiner (TRE) on this present fleet effective November 2007.

The PIC's flying record for the last 72 hours and preceding 28 days' cycle were well within the Company's specified limits. His last flight as an operating PIC was to Denpasar, Bali, in the Republic of Indonesia on 03 March 2014. This was a daily return flight with a sector time of approximately 3 hours. On the day of the event, he was conducting training for the FO who was functionally checked out.

2) Royal Malaysia Police's Report on Flight Simulator of PIC

The Royal Malaysia Police (RMP) seized the PIC's home flight simulator from the residence of the PIC on 15 March 2014.

The RMP Forensic Report dated 19 May 2014 documented more than 2,700 coordinates retrieved from separate file fragments and most of them are default game coordinates.

It was also discovered that there were seven 'manually programmed' waypoint[4] coordinates (*Figure 1.5A* [below), that when connected together, will create a flight path from KLIA to an area south of the Indian Ocean through the Andaman Sea. These coordinates were stored in the Volume Shadow Information (VSI) file dated 03 February 2014. The function of this file was to save information when a computer is left idle for more than 15 minutes. Hence, the RMP Forensic Report could not determine if the waypoints came from one or more files.

The RMP Forensic Report on the simulator also did not find any data that showed the aircraft was performing climb, attitude or heading manoeuvres, nor did they find any data that showed a similar route flown by MH370.

The RMP Forensic Report concluded that there were no unusual activities other than game-related flight simulations.

[4] **'**Manually programmed waypoints' - Manually programmed waypoints are waypoints that are not published in Airway Charts

Figure 1.5A - Snapshot of Seven Manually Programmed 'Waypoints'

Source: Royal Malaysia Police

1.5.4 First Officer

The FO was born in the State of Kelantan and had his basic primary education in Segamat, Johor. He completed his secondary Education in Maktab Rendah Sains MARA (MRSM) or MARA Junior Science College, in Taiping, Perak, where he left in 2004 with the Sijil Pelajaran Malaysia (SPM) or Malaysia Certificate of Education, which is equivalent to the UK 'O' Level. He was accepted as a MAS Cadet Pilot and completed his flying training at the Langkawi Aerospace Training Centre, Langkawi in 2008.

His first fleet posting was on the B737-400 as a Second Officer until May 2010 He was promoted to FO in May 2010 and was on the fleet until August 2012. Between the end of 2012 to November 2013, he was promoted to the A330-300 and the B777-200.

On the day of the flight, he was operating his last training flight before he was scheduled to be checked out on his next scheduled flight. His flying record for the last 72 hours and preceding 28 days cycle were well within the Company's specified limits. His previous flight as a functional FO under Line Training, was to Frankfurt, Germany, on 01 March 2014 and he returned to Malaysia on 02 March 2014. All his required licences and certificates were valid when he was assigned to operate this flight to Beijing.

1) Personal Profile of First Officer

Sex	Male
Age	27 years
Marital Status	Single
Date of joining MAS	23 July 2007
Licence type	Air Transport Pilot Licence (ATPL)
Licence number	A3550
Validity Period of Licence	26 July 2014
Ratings	Boeing B777
Medical Certificate	First Class (valid until 31 October 2014)
Aeronautical experience	2813:42 hours
Experience on type	39:11 hours
Last 24 hours	0:00:00 hours
Last 72 hours	0:00:00 hours
Last 07 days	28:47:00 hours
Last 28 days	51:17:00 hours
Last 90 days	158:46:00 hours
Last line check*	22 July 2013 (A330)
Instrument rating check*	04 December 2012 (A330)
Last proficiency	26 January 2014
Last promotion	B777 FO (04 November 2013)

* *No record on B777*

1.5.5 Summary of Work Schedule for Flight Crew of MH370

A summary of the work schedule for the PIC and the FO, three months prior to the eventful flight, is available in *Table* 1.5A (below).

Rank	24	72	7	28	90	SEP Validity
	Hours		Days			
Pilot-in-Command	0:00:00	07:00:00	20:39:00	91:04:00	303:09:00	14 May 2014
First Officer	0:00:00	0:00:00	28:47:00	51:17:00	158:46:00	26 July 2014

Table 1.5A - 3 Months Work Schedule of PIC and FO

1.5.6 Cabin Crew and Personal Profiles

The cabin crews' flying experiences spread from 13 years for the most junior member to 35 years for the most senior member. A review of their records in MAS reveals that all certificates, which include Safety Emergency Procedures (SEP) training, Crew Resource Management (CRM), Safety Awareness Programme (SAP), are valid as per the requirement stated in

the Company's document. CRM & SAP incorporate Human Factors as part of the training modules. The flying records which were monitored by the Scheduling Office indicated that all the cabin crew were well-rested before operating the flight.

1) In-flight Supervisor (IFS)

Sex	Male
Age	55 years
Marital status	Married with 4 children
Date of Joining MAS	19 November 1979
Aircraft Ratings	A330/B777/B747
Crew Performance Appraisal	Rating: 4
Validity period of licence	28 April 2014
Aeronautical experience	35 years
Medical History	43 days medical leave including 6 days hospitalisation in 2013
Last 24 hours	0:00:00 hours
Last 72 hours	8:00:00 hours
Last 07 days	19:44:00 hours
Last 28days	82:43:00 hours
Last 90 days	305:06:00 hours
Last promotion	IFS (27 March 2000)

2) Chief Steward (CS)

Sex	Male
Age	49 years
Marital status	Married with 2 children
Date of Joining MAS	13 November 1989
Aircraft Ratings	A330/B777/A380
Crew Performance Appraisal	Rating 4
Validity period of licence	26 June 2014
Aeronautical experience	25 years
Last 24 hours	0:00:00 hours
Last 72 hours	0:00:00 hours
Last 07 days	30:56:00 hours
Last 28 days	124:35:00 hours
Last 90 days	408:32:00 hours
Last promotion	CS (06 March 2000)

3) Chief Stewardess (CSS)

Sex	Female
Age	49 years
Marital status	Married with a child
Date of Joining MAS	02 January 1990
Aircraft Ratings	A330/B777/A380
Crew Performance Appraisal	Rating 5
Validity period of licence	23 October 2014
Aeronautical experience	24 years
Last 24 hours	0:00:00 hours
Last 72 hours	0:00:00 hours
Last 7 days	30:55:00 hours
Last 28 days	118:02:00 hours
Last 90 days	355:23:00 hours
Last promotion	CSS (22 October 2003)

4) Leading Steward (LS)

Sex	Male
Age	42 years
Marital status	Married with 4 children
Date of Joining MAS	05 October 1995
Aircraft Ratings	B737/B777/A380
Crew Performance Appraisal	Rating 4
Validity period of licence	22 August 2014
Aeronautical experience	19 years
Last 24 hours	00:00:00 hours
Last 72 hours	10:47:00 hours
Last 7 days	38:38:00 hours
Last 28 days	106:10:00 hours
Last 90 days	365:51:00 hours
Last promotion	LS (28 May 2005)

5) Leading Stewardess (LSS)

Sex	Female
Age	42 Years
Marital status	Married with 2 children
Date of Joining MAS	18 August 1992
Aircraft Ratings	B737/B777/A380
Crew Performance Appraisal	Rating 5
Validity period of licence	01 November2014
Aeronautical experience	22 years
Last 24 hours	0:00:00 hours
Last 72 hours	11:36:00 hours
Last 7 days	41:27:00 hours
Last 28 days	140:11:00 hours
Last 90 days	443:23:00 hours
Last promotion	LSS (09 May 2004)

6) Flight Stewardess (FSS) 1

Sex	Female
Age	42 years
Marital status	Married with 2 children
Date of Joining MAS	18 January 1992
Aircraft Ratings	A330/B777/A380
Crew Performance Appraisal	Rating 4
Validity period of licence	27 June 2014
Aeronautical experience	22 years
Last 24 hours	0:00:00 hours
Last 72 hours	9:39:00 hours
Last 7 days	34:22:00 hours
Last 28 days	93:50:00 hours
Last 90 days	327:18:00 hours
Last promotion	FSS wide-body aircraft (18 January 1993)

7) Flight Stewardess (FSS) 2

Sex	Female
Age	39 years
Marital status	Married with 2 children
Date of Joining MAS	16 April 1996
Aircraft Ratings	A330/B777/A380
Crew Performance Appraisal	Rating 4
Validity period of licence	11 May 2014
Aeronautical experience	18 years
Last 24 hours	0:00:00 hours
Last 72 hours	0:00:00 hours
Last 7 days	16:12:00 hours
Last 28 days	112:11:00 hours
Last 90 days	323:55:00 hours
Last promotion	FSS Wide-body aircraft (01 October 2001)

8) Flight Steward (FS) 1

Sex	Male
Age	46 years
Marital status	Married with 3 children
Date of Joining MAS	16 April 1996
Aircraft Ratings	B737/B777/A380
Crew Performance Appraisal	Rating 5
Validity period of licence	24 October 2014
Aeronautical experience	18 years
Last 24 hours	0:00:00 hours
Last 72 hours	11:02:00 hours
Last 7 days	30:58:00 hours
Last 28 days	119:27:00 hours
Last 90 days	429:15:00 hours
Last promotion	FS Wide-body aircraft (03 December 2001)

9) Flight Steward (FS) 2

Sex	Male
Age	41 years
Marital status	Married with 2 children
Date of Joining MAS	13 February 1997
Aircraft Ratings	B737/B777/A380
Crew Performance Appraisal	Rating 5
Validity period of licence	03 November 2014
Aeronautical experience	17 years
Last 24 hours	0:00:00 hours
Last 72 hours	0:00:00 hours
Last 7 days	30:36:00 hours
Last 28 days	122:22:00 hours
Last 90 days	391:20:00 hours
Last promotion	FS Wide-body aircraft (15 February 2002)

10) Flight Steward (FS) 3

Sex	Male
Age	34 years
Marital status	Married with 2 children
Date of Joining MAS	27 September 2001
Aircraft Ratings	B737/B777/A380
Crew Performance Appraisal	Rating 5
Validity period of licence	06 February 2015
Aeronautical experience	13 years
Last 24 hours	0:00:00 hours
Last 72 hours	10:47:00 hours
Last 7 days	26:24:00 hours
Last 28 days	125:01:00 hours
Last 90 days	435:43:00 hours

1.5.7 Disciplinary/Administrative Actions

There were no major disciplinary records on any of the flight and cabin crew. However, there were minor disciplinary issues among the cabin crew, where cautionary administrative letters were issued.

1.5.8 Financial Background and Insurance Cover

The PIC held bank accounts, two savings accounts, one current account, two national trust funds (ASB and ASN) and a joint account with his wife. He had a credit card. He was contributing to the Employees Provident Fund (EPF). There is no record of him having secured a life insurance policy. He had 2 houses, one in Shah Alam and the other in Subang Jaya. He had taken a bank loan on one of his houses and had a mortgage insurance policy on this loan. He also had 3 vehicles. His gross monthly income and out-of-pocket expenses indicated nothing unusual.

The PIC also had a trading account with an investment bank. The Central Depository System (CDS) and Trading accounts were opened since 13 February 1998 and 19 March 1998 respectively. The CDS account was inactive whereas the last transaction of the trading account was noted on 03 February 2000.

The FO had two saving accounts and a national trust fund (ASB) account. He contributed to the EPF. He owned two cars and spent money on the upkeep of his cars. He did not have much savings in his bank account. He had a life insurance policy and a mortgage insurance policy for a loan he took for his car.

The cabin crew had bank accounts and loans. However, the gross monthly income and out-of-pocket expenses indicated nothing unusual. There is also no evidence of recent or imminent significant financial transactions carried out.

1.5.9 Significant Past Medical and Medication History

The PIC had received treatment for minor medical ailments and was diagnosed as having osteoarthritis on 05 May 2007. He had a spinal injury on 28 January 2007 in a paragliding event. He sustained a fracture of the 2nd lumbar vertebra and underwent surgery on 30 January 2007 in a private health care facility. He was discharged on 05 February 2007 and went for a follow-up as advised. He was certified fit to fly in mid-2007 and went regularly for his six-monthly medical examinations for his continued

licensure as a pilot. For his pain he was noted to have taken analgesics on an irregular basis. Based on available information, he was not on any regular long-term medication for any chronic medical illness.

There was no significant health-related issue for the FO. He went regularly for his yearly medical examinations for his continued licensure to fly.

Based on the medical records from MAS, there were no unusual health-related issues for the cabin crew, except for the in-flight supervisor who had a history of first onset of seizures on 09 June 2013. He was admitted on the same day in a private health care facility and was treated by a Consultant Neurologist. He was discharged on 14 June 2013 and went for a follow-up as advised. He had not experienced any further seizures since his discharge. He was certified fit to fly on 06 August 2013.

1.5.10 Psychological and Social Events

The PIC's ability to handle stress at work and home was reported to be good. There was no known history of apathy, anxiety, or irritability. There were no significant changes in his lifestyle, interpersonal conflict or family stresses.

Similarly, the FO's ability and professional approach to work was reported to be good. This was evident with the rapid fleet promotion within 3 years as a professional pilot. There were no reports on recent changes in his behaviour or lifestyle.

1.5.11 Behavioural Events

There were no behavioural signs of social isolation, change in habits or interest, self-neglect, drug or alcohol abuse of the PIC, FO and the cabin crew.

The CCTV recordings at KLIA on 07 March 2014 were evaluated to assess the behavioural pattern of the PIC, and the FO from the time of arrival at KLIA until boarding time.

Three previous CCTV recordings of the movements of the PIC in KLIA were also viewed to see the behavioural pattern and were compared with the CCTV recordings on 07 March 2014.

The PIC's movement was captured on CCTV at KLIA on the following days:

- 07 March 2014 - To Beijing

- 03 March 2014 - To Denpasar
- 26 February 2014 - To Melbourne
- 21 February 2014 - To Beijing

On studying the PIC's behavioural pattern on the CCTV recordings on the day of the flight and prior 3 flights there were no significant behavioural changes observed. On all the CCTV recordings the appearance was similar, i.e. well-groomed and attired. The gait, posture, facial expressions and mannerism were his normal characteristics.

The FO's movement captured on CCTV at KLIA on 07 March 2014 was observed. The FO's behavioural pattern on CCTV recordings on the day of the flight showed no significant behavioural changes.

1.5.12 Voice Recognition of the Radio Transmissions between MH370 and Air Traffic Control

The radio transmissions made between MH370 and the air traffic control were studied. The Team used pilot friends, family members, and an expert report of objective analysis of the radio transmissions in the voice recognition of the transmissions made between MH370 and air traffic control.

Five sets of audio recordings were analysed starting from Airway Clearance Delivery at 1625:52 UTC [0025:52 MYT] till the last utterance from Lumpur Radar at 1719:30 UTC [0119:30 MYT]. There was a total of 23 utterances as follows:

No.	Audio Recordings	Frequency (MHz)	Utterances	
1.	Airway Clearance Delivery (ACD)	126.0	→	4
2.	Lumpur Ground (LG)	122.27	→	6
3.	Lumpur Tower (LT)	118.8	→	4
4.	Approach Radar (AR)	121.25	→	3
5.	Lumpur Radar (LR)	132.5	→	6

From the information available, the first 3 sets of audio recordings (ACD, LG, LT), the speech segments are those of the FO before take-off, and the 4th & 5th (AR & LR) sets of the audio recordings originated from the PIC after take-off.

SECTION 1 – FACTUAL INFORMATION

1.6 AIRCRAFT INFORMATION

1.6.1 Airframe

Manufacturer	Boeing Company
Model	777-2H6ER
Serial Number	28420
Manufacturer's Line No.	404
Variable No.	WB175
Registration	9M-MRO
Date of manufacture	29 May 2002
Date of delivery to MAS	Delivered new on 31 May 2002
Certificate of Airworthiness	M.0938 valid to 02 June 2014
Certificate of registration	M.1124 issued 23 August 2006. Replacement of Certificate issued on 17 June 2002
Last Maintenance check	A1 Check on 23 February 2014 at 53,301:17 hours and 7,494 cycles
Total airframe hours/cycles	53,471.6 hours/7,526 cycles (as of 07 March 2014)

1.6.2 Engine

Manufacturer	Rolls-Royce
Model	RB211 Trent 892B-17
Engine 1 (Left)	
Serial Number	51463
Date of Construction	November 2004
Date Installed	08 May 2013
Last Shop Visit	06 September 2010 to 21 November 2010
Time in Service	40,779 hours, 5,574 cycles (as of 07 March 2014)
Engine 2 (Right)	
Serial Number	51462
Date of Construction	October 2004
Date Installed	15 June 2010
Last Shop Visit	05 February 2010 to 14 April 2010
Time in Service	40,046 hours, 5,508 cycles (as of 07 March 2014)

1.6.3 Auxiliary Power Unit

Manufacturer	Allied Signal
Model	GTCP 331-500B
Serial Number	P1196
APU Hours	22,093 (as of 07 March 2014)

1.6.4 Airworthiness and Maintenance

The aircraft, Serial Number 28420, was issued with a Federal Aviation Administration (FAA) Export Certificate of Airworthiness No: E370249 on 29 May 2002 and placed on the Malaysian aircraft register as 9M-MRO on 03 June 2002. Ownership of the aircraft, as stated on the Certification of Registration (C of R), was Malaysian Airline System Berhad. The ownership was subsequently changed to Aircraft Business Malaysia Sdn. Bhd., as the lessor, and leased and operated by MAS. A new C of R to reflect the new owner was issued on 17 June 2002.

A Certificate of Airworthiness (C of A) in the 'PRIVATE' category was initially issued on 03 June 2002. The aircraft was then flown to Kuala Lumpur, Malaysia where a C of A in 'TRANSPORT PASSENGER' category was issued by the DCA Malaysia on 12 June 2002 after the pre-service modifications were accomplished.

The C of A was subjected to annual renewal by DCA Malaysia and its renewal was subjected to compliance to the DCA Malaysia Airworthiness Notice No. 2 - Certificate of Airworthiness Renewal Procedure. The operator was required to declare the aircraft, engine, APU and equipment maintenance status as per the approved Maintenance Schedule, and that they complied with all the mandatory inspections and modifications originating from the State of Manufacture and State of Registry. The Quality Assurance Department of MAS was required to submit an 'Aircraft Physical Inspection for the Purpose of C of A Issue/Renewal' prior to the expiry of the C of A. An 'Aircraft Survey Report for Certificate of Airworthiness' will be issued by the DCA Inspector after a satisfactory physical inspection on the aircraft has been carried out. At times, the physical aircraft inspection has to coincide with the aircraft scheduled check at base or line maintenance.

The last C of A document review by DCA Inspector was carried out on 15 May 2013 for the C of A renewal and the aircraft physical inspection was carried out by MAS Quality Assurance Engineer (QAE) on 12 April 2013. The only inspection defect noted was a torn left hand flaperon inboard seal which was subsequently replaced. The aircraft C of A was renewed with no airworthiness issues identified.

1) Aircraft Maintenance Schedule

Brief description of the sections follows:

a) Section 1

The definition and introduction of the routine check types. Check intervals and limitations at which the maintenance tasks are to be carried out.

b) Section 2

Task Maintenance Requirements relating to on-wing tasks or tasks to be performed on parts after removal from the aircraft, their intervals and control in the routine maintenance check or independently.

c) Section 3

Component Maintenance Requirements on tasks to be performed on components, their intervals and controlled independently.

d) Section 4

Registers all the applicable job cards which are tied up to the maintenance Checks or Phases of inspections or tasks. The job cards/task cards cover the system, power plants, structural and zonal tasks.

The Master document of the approved Maintenance Schedule is stored in the Engineering Maintenance System (EMS) computer system bank and subject to regular revisions.

In addition to the Maintenance Schedule, a Supplementary Maintenance Schedule covered MAS' own generated tasks, non-mandatory manufacturer/vendor recommended tasks and non-airworthiness items.

The Maintenance check cycles are translated into the routine Transit Check, Stayover Check, Equalised 'A' Check, 'C' Check, 'C Extended' Check and 'D' Check. *Table 1.6A* (below) summarises the maintenance check intervals.

Transit	Stay-over	A Check	C Check	CX (Extended) Check	D Check
Whenever aircraft is on transit	6 hours planned or 12 hours unplanned	In 4 parts A1 thru A4 • A1 to A2 = 550 hours • A2 to A3 = 550 hours • A3 to A4 = 550 hours • A4 to A1 = 550 hours	In 2 parts C1 and C2 • C1 to C2 = 13 months • C2 to C1 = 13 months	52 months	8 years

Table 1.6A - Maintenance Check Intervals

No.	Type of Aircraft Checks	Date of aircraft Checks	Airframe Hours	Landing Cycles
1.	A1	23 February 2014	53,301:17	7,494
2.	A4	14 - 16 January 2014	52,785:37	7,422
3.	A3	13 December 2013	52,323:00	7,359
4.	A2	04 November 2013	51,766:29	7,282
5.	C1 and A1	29 August-26 September 2013	51,270:15	7,208
6.	A4	24 - 25 July 2013	50,810:19	7,132
7.	A3	19 June 2013	50,372:07	7,069
8.	A2	14 May 2013	49,840:28	6,994
9.	A1	04 April 2013	49,331:52	6,910
10.	A4	19 - 20 February 2013	48,836:23	6,840
11.	A3	10 January 2013	48,291:37	6,766
12.	A2	03 December 2012	47,749:39	6,693
13.	A1	25 October 2012	47,214:27	6,617
14.	A1, A4 and C2	06 - 22 July 2012	46,727:16	6,552
15.	A4, C2, CX and D	25 May - 26 June 2010	37,014:15	5,304

Table 1.6B - Recent Aircraft Checks

A review of the maintenance records for 9M-MRO revealed the following sequence of recent checks (*Table 1.6B* [above]) carried out by MAS prior to the disappearance of the aircraft on the 08 March 2014. No significant defects were noted during the checks including the turn-around transit checks.

The Maintenance Schedule incorporated the Structural Inspection Programme based on the B777 Maintenance Review Board Report and B777 Maintenance Planning Document, which are categorised as Structural Inspection Items, Corrosion Prevention and Control Items and Fatigue Related Inspection Items. Inspection findings would be evaluated by the MAS Reliability Section of the Technical Services Department and the department would recommend any follow-up actions as necessary and report to Boeing Company of all significant structural discrepancies.

The Maintenance Schedule also included compliance procedures for Airworthiness Directives[5], Airworthiness Limitations (AWL)[6] and Structural Inspections with Provisions for Damage Tolerance Rating. It also included Certification Maintenance Requirement Compliance to the Extended Twin Engine Operations (ETOPS)[7] operational approval, which was obtained from DCA Malaysia. The MAS B777 ETOPS Maintenance Manual specified the maintenance policies, procedures and requirements for ETOPS operations. A policy to prevent the same personnel to perform or certify certain tasks on multiple similar systems at the same downtime is stipulated. ETOPS task intervals cannot be exceeded. If a concession is given for a check that contains ETOPS task or for individual ETOPS task, the aircraft must be downgraded to non-ETOPS status. 9M-MRO was approved and had no limitations for ETOPS operations at the time of departure from Kuala Lumpur to Beijing. It was not on an ETOPS flight plan. MAS and its fleet of B777 were approved for Reduced Vertical Separation Minimum (RVSM) operation.

[5] An AD is a notification to owners and operators of certified aircraft that a known safety deficiency with a particular model of aircraft, engine, avionics or other system exists and must be corrected. It is mandatory in nature.

[6] AWLs are items that the Certificate process has defined as critical from a fatigue or damage tolerance assessment.

[7] ETOPS is an aviation rule that allows twin-engine airliners to fly long distance routes that were previously off-limits to twin-engine aircraft.

2) Major Repair

There was an entry in the Aircraft Log Book on 09 August 2012 that the aircraft right wing tip was damaged during taxiing at Pudong, Shanghai Airport. The aircraft collided with a China Eastern Airlines A340-600, registered B-6050. The right wing tip of 9M-MRO ran into the left horizontal stabilizer of B-6050. Part of the aircraft wing tip was ruptured and stuck at the left elevator of the B-6050. *Figures 1.6A* and *1.6B* (below) show the wing tip damages.

Figure 1.6A - Right Wing Tip Damage

Figure 1.6B - Damaged Wing Tip

Boeing produced an Aircraft Survey Report reference WB175/W8134/LN404 on 15 August 2012 and the repair was carried out by Boeing Aircraft-On-Ground (AOG) Team at Pudong, Boeing Shanghai facility from 22 September to 03 October 2012. The Boeing repair scheme was approved under DCA Malaysia's Statement of Compliance (SOC) Reference Number SC/2012/081 issued on 03 September 2012. At the time of the incident, the recorded airframe hours were at 46,975:43 and landing cycles at 6,585.

There was a requirement for damage tolerance[8] information to be incorporated in the aircraft maintenance programme within 24 months from 02 October 2012 as stated in the FAA Form - Organization Designation Authorization (ODA). This damage tolerance information was not yet included in the maintenance programme for the aircraft at the time of the occurrence.

3) Cabin Configuration Change

The fleet of B777 of MAS went through a cabin interior retrofit programme which converted the configuration from 12 First Class seats/33 Business Class seats/233 Economy Class seats to 35 Business Class and 247 Economy Class seats. On 9M-MRO, this re-configuration started on 17 August 2006 and was completed on 08 September 2006. The modification was approved under FAA Supplemental Type Certificate (STC) No. STO1493SE dated 24 January 2005 and DCA's SOC No. SC2004/98.

4) Mandatory Occurrence Reports

A review of the Mandatory Occurrence Reports (MORs) for the B777 fleet raised by the Engineering & Maintenance Quality Assurance Department of MAS revealed that only one was raised for 9M-MRO, and this was related to the right wing tip damage stated above. A total of 77 MORs were raised for the MAS fleet of 17 B777 aircraft. MORs raised by the Quality Assurance department are primarily related to technical issues with the fleet. The average age of the B777 fleet as of 01 March 2014 was 14.35 years. 9M-MRO was 11.75 years old.

[8] Damage tolerance means that the structure has been evaluated to ensure that should serious fatigue, corrosion or accidental damage occurs within the operational life of the aircraft, the remaining structure can withstand reasonable loads without failure or excessive structural deformation until the damage is detected.

5) Airworthiness Directives

Maintenance and Inspection records provided by MAS indicated that at the time the aircraft 9M-MRO went missing, the aircraft and engines were fully compliant with all applicable Airworthiness Directives (AD).

The most recent AD, which was accomplished on 17 January 2014, was FAA AD 2012-13-05 which made mandatory the accomplishment of Boeing Service Bulletin 777-35A0027 which requires replacement of low pressure oxygen hoses in the cockpit. The changes provided in the service bulletin are to prevent damage to the low pressure oxygen hoses that may be subjected to electrical current. An electrical current condition in the low pressure oxygen hose can cause the low pressure oxygen hose to melt or burn. This could result in smoke and/or fire in the flight compartment. An operator (not MAS) reported that a fire originated near the first officer's area which caused extensive damage to the cockpit. One scenario of the causes being considered is that an electrical fault or short circuit resulted in electrical heating of the low pressure oxygen hoses in the flight crew oxygen system. This service bulletin is to replace low pressure oxygen hoses with non-conductive low pressure oxygen hoses located in the cockpit. The replacement of the low pressure oxygen hoses will prevent electrical current from passing through the low pressure oxygen hose internal anti-collapse spring which can cause the low pressure oxygen hose to melt or burn.

An FAA AD 2014-05-03 was issued and became effective on 09 April 2014. This AD made mandatory the accomplishment of Boeing Service Bulletin 777-53A0068 which addresses a crack in the fuselage skin under the SATCOM antenna adapter. The Service Bulletin was issued on 12 June 2013. The AD was issued to detect and correct cracking and corrosion in the fuselage skin, which could lead to rapid decompression and loss of structural integrity of the aircraft. However, this AD was not applicable to 9M-MRO as the location and configuration of the antenna on the aircraft, as delivered by Boeing ex-production, were different and not affected by the issues highlighted in the Service Bulletin.

6) Technical Log

a) MR1 and MR2

The MAS Technical Log Book was divided into Maintenance Report 1 (MR1) and Maintenance Report 2 (MR2). The MR1 has provision for the flight crew to enter any aircraft defects for each flight phase. It can also be used to enter maintenance required and rectifications by the Licenced Aircraft Maintenance Engineers (LAME) or Approval Holders, or defer defects within the Minimum Equipment List (MEL) procedures to the Maintenance Report 2 (MR2) section.

A review of the Technical Log entries for 9M-MRO since the last D check in June 2010 did not reveal any significant defects or trend.

The most recent entries made in the Technical Log Book for 9M-MRO are listed in *Appendix 1.6A.*

b) Oxygen System Replenishment

A Technical Log entry of interest, made on 07 March 2014, is the replenishment of crew oxygen system. This replenishment was reviewed in detail together with information gathered from the interview of the LAME who performed the task. Replenishment (servicing) of the crew oxygen system is a routine procedure, carried out before the minimum pressure required for departure is reached, usually carried out during a Stayover check. The minimum pressure for despatch as per the MAS Minimum Equipment List (MEL) is 310 psi at 35°C for 2-man crew and with a 2-cylinder configuration (as installed on MAS B777 fleet).

It has been the practice of the airline to service the oxygen system whenever time permits, even if the pressure is above the minimum required for despatch.

During the Stayover check on 07 March 2014, the servicing on 9M-MRO was performed by the LAME with the assistance of a mechanic, as the pressure reading was 1120 psi. The servicing was normal and nothing unusual was noticed. There was no leak in the oxygen system and the decay in pressure from the nominal value of 1850 psi was not unusual. The system was topped up to 1800 psi. Before this servicing, maintenance records showed that

the system was last serviced on 14 January 2014 during an A4 check.

A small amount of oxygen is normally expended during pre-departure checks of the oxygen masks by the flight crew. Oxygen pressure is also dissipated by a bleed valve in the system for a few seconds during engine start following the end of a flight.

7) Deferred Defects (Maintenance Report 2)

A review of the aircraft records from the MAS Maintenance Control Centre (MCC) showed that the following defects were outstanding on 9M-MRO and deferred to the Deferred Defect Log (*Table 1.6C,* [below]). The hole found on the right engine acoustic panel, mentioned below in item 7, was of dimension of approximately 1 inch by 1 inch and is allowed to be deferred by the B777 Maintenance Manual until permanent repair is carried out within 500 flight hours. This minor damage is considered normal wear and tear of the engine nacelles and does not pose any hazard to the engine.

No.	Deferred Date	Defect
1.	25 Sep 2013	To carry out installation test for aft water quantity gauge.
2.	31 Oct 2013	In-Flight Entertainment (IFE) Airshow does not show arrival time/time to destination logged time & problem still persists.
3.	07 Nov 2013	From Daily Engineering Operations Report (DEOR) - Right engine consumes average 1.5T more fuel per/hour compared to left engine
4.	21 Jan 2014	Toilet 3F-1L mirror light lens broken
5.	30 Jan 2014	Pre-departure F/O seat power adjustment (fwd/aft) found inoperative.
6.	05 Mar 2014	Please check alignment for left runway turn/off light.
7.	05 Mar 2014	Hole found at 6 o'clock position of the right engine acoustic panel.

Table 1.6C - Deferred Defects

8) Engine Health Monitoring

Engine Health Monitoring (EHM) was contracted out to Rolls Royce, the engine manufacturer. Engine data 'snapshot' reports were generated by the Aircraft Condition Monitoring System (ACMS) and transmitted via ACARS to MAS, who then submitted them to Rolls Royce for analysis on its behalf. The transmitted engine parameters primarily used to assess engine health are:

- Turbine Gas Temperature
- Shaft Speeds
- Shaft Vibration (Low Pressure, Intermediate Pressure and High Pressure)
- Oil Pressure
- Oil Temperature

The EHM system trend reports over the last 3 months which covered 'snapshot' data points gathered at take-off, climb and cruise received through the ACMS show no evidence of unusual engine behaviour for both engines. On the occurrence flight, 2 EHM reports were transmitted; the first was a Take-off report generated at 1641:58 UTC, 07 March 2014 [0041:58 MYT, 08 March 2014] and the second was a Climb report at 1652:21 UTC, 07 March 2014 [0052:21 MYT, 08 March 2014]. Reports are transmitted by ACARS at convenient times during the flight (not necessarily at the time of generation/data capture). Both reports did not show any unusual engine behaviour. The data transmitted on these reports are shown in *Appendix 1.6B - Engine Health Monitoring Decoded Data for Take-off and Climb Reports*. The ACMS will also generate other pre-defined engine reports including engine parameters' exceedance reports. However, no such EHM reports were received during the flight. Position reports are also transmitted, via ACARS, every 30 minutes. Refer to *Section 1.9.4* for further details.

9) Central Maintenance Computing System

The Central Maintenance Computing System (CMCS) collects and stores information from most of the aircraft systems. It can store fault histories as well as monitor and conduct tests on the various systems. The fault history contains details of warnings, cautions and maintenance messages.

At regular intervals, during flight, the CMCS transmits any recorded fault messages, via the ACARS, to the Maintenance Control Centre (MCC) of MAS. This helps in the planning and preparation for the rectification of any potential aircraft defects at the main base or line stations.

The traffic log of maintenance messages transmitted for the last 10 flights on 9M-MRO were reviewed. There were messages transmitted, indicating that the CMCS was functioning prior to the occurrence flight. However, no maintenance messages were transmitted during the occurrence flight. These messages are transmitted in real time that is, as the faults occur.

Maintenance messages are not displayed on the Engine Indicating and Crew Alerting System (EICAS) in the cockpit and they are not used to determine the airworthiness of the aircraft. They provide diagnostic information useful in troubleshooting or maintenance planning. Only maintenance messages which trigger EICAS Alert messages require maintenance action (including deferment, if allowable) prior to despatch.

1.6.5 Weight and Balance

The aircraft underwent a scheduled reweighing on 28 April 2009 at the MAS maintenance facility at KLIA. The next aircraft re-weighing was due on or before 27 April 2014. The aircraft Weight Schedule dated 12 June 2009 was reviewed with the following pertinent details (also refer to *Table 1.6D* [below]):

- Basic Empty Weight (BEW) of 138,918.7 kg
- Centre of Gravity (C of G) position of 1,248.8 Inches
- Index of 60.07 I.U.
- C of G of 26.7 % Mean Aerodynamic Chord (MAC) Dry Operating Weight (DOW) of 145,150 kg and Index 61.13

The maximum authorised take-off weight was 286,897 kg. On the occurrence flight, the aircraft departed with a calculated take-off weight of 223,469 kg. This take-off weight was broken down as follows:

	Actual (kg)	Maximum (kg)
Take-off Weight (TOW)	223,469	286,897
Zero Fuel Weight (ZFW)	174,369	195,044
Take-off Fuel	49,100	-
Landing Weight (LDW)	186,269	208,652
Trip Fuel	37,200	-
Total Traffic Load	31,086	-
Total Payload (Load in compartment)	14,296	-
Passenger & Luggage	16,790	-
Dry Operating Weight (DOW)	143,283	-

Table 1.6D - Aircraft Weight

The balance corresponding to the aircraft take-off weight and shown on the final loadsheet (after Last Minute Changes) was 33.78% of the Mean Aerodynamic Chord (MAC) which was within limits.

During take-off, the aircraft Basic Empty Weight (BEW) was 138,918.7 kg and the C of G position was 1,248.8 inches (C of G MAC was 26.7%). Total moment was 173,478,288.65 kg in. This indicates the planned weight and balance of the aircraft was within the allowable limits. The planned cargo weight (load in compartment) of 14,296 kg and distribution matched the recorded cargo weight and distribution.

Based on the available data, the aircraft weight and balance for the take-off from Kuala Lumpur was found to be normal and within the allowable limits.

1.6.6 Fuel

The aircraft used Jet A-1 fuel. Following the previous flight, as per records in the Transit Check and Fuel Log, the total remaining fuel before refuelling as per the cockpit indication was 8,200 kg (Left Tank was 3,700 kg and Right Tank was 4,500 kg). Total departure fuel after refuelling was 49,700 kg (Left Tank was 24,900 kg and Right Tank was 24,800 kg) as indicated in the cockpit.

The fuel weight on board corresponded to a planned trip-fuel of 37,200 kg. Based on MH370 ATC flight plan dated 07 March 2014, the take-off fuel recorded was 49,100 kg. This figure differed slightly from the take-off fuel figure of 49,200 kg generated by the Aircraft Condition Monitoring System (ACMS) and transmitted by Aircraft Communications Addressing and Reporting System (ACARS). The difference was due to the actual time the fuel figure was taken from the aircraft fuel quantity indication system, by Operations for the load sheet, and by the ACMS for the ACARS report,

considering fluctuations in the fuel quantity indication. The investigation estimated that the aircraft would have had 41,500 kg fuel remaining after 41 minutes flying from KLIA to IGARI.

The last position report transmitted via ACARS at 1707:29 UTC, 07 March 2014 [0107:29 MYT, 08 March 2014] recorded remaining fuel of 43,800 kg at 35,004 ft altitude.

ATC flight plan forecast recorded remaining fuel of 11,900 kg at landing, including 7,700 kg of diversion fuel. The first alternate airport, Jinan Yaoqiang International Airport (China), was estimated to be 46 minutes from the diversion point with 4,800 kg fuel required and the second alternate airport, Hangzhou Xiaoshan International Airport (China) was estimated to be 1 hour 45 minutes with 10,700 kg fuel required.

The fuel carried on board for the flight met the regulatory requirements on the minimum required, taking into account the use of possible diversion airports. There was also no evidence that more than the reasonable amount required was carried.

1.6.7 Emergency Locator Transmitter

An emergency locator transmitter (ELT) is a radio beacon that when activated will transmit digital distress signals. These signals can be tracked in order to aid the detection and localisation of an aircraft in distress.

The Fixed and Portable ELT radio beacons interface worldwide with the international Cospas-Sarsat satellite system for Search and Rescue (SAR). When activated and under satellite coverage, such beacons send out a distress signal which can be detected by satellites. The satellite receivers send this information to ground stations. This signal is transmitted to Mission Control Centres (MCC) located in six regions worldwide. The MCC covering the Indian Ocean is managed by the Australian Maritime Safety Authority based in Canberra, Australia.

ELTs are mandatory safety items carried on board the aircraft. The cabin and the technical crew attend compulsory safety emergency procedure (SEP) training and have to remain current by attending refresher SEP courses. Operation and functioning of the ELT is part of the SEP training module.

The specifications for the ELT are contained in FAA Technical Standard Orders TSO-C126 and TSO-C91A.

The ELT is a radio beacon; like all other radio equipment installed on-board, its usage is approved by the Malaysian Communications and Multimedia Commission through the Aircraft Radio Licence.

Appendix 1.6C - Copy of the Radio Licence issued for 9M-MRO.

9M-MRO had four ELTs installed. They were located as follows:

- **One FIXED ELT** located above ceiling of the aft passenger cabin at STA 1880.

  The aircraft was delivered without a fixed ELT; this component was added by MAS later (between December 2004 and July 2005). This unit is mounted to aircraft structure at the aft passenger cabin at STA 1880.

  A control switch installed in the cockpit (flight deck) aft overhead panel provides the command signal. This switch is guarded in the ARMED position. If required, the flight crew can select the ELT to ON by moving the guarded switch from ARMED to ON.

  The fixed ELT is manufactured by ELTA FRANCE and is of the 406 series, part number is 01N65900. The unit is connected to an Omni-directional, triple frequency blade antenna located at the rear fuselage forward of the vertical stabilizer at station 1881. The ELT will activate upon a sudden deceleration force per the Technical Standard Order.

  This ELT has the provision to operate on the satellite frequency of 406 MHz when activated. The transmission includes the ELT identifier, aircraft nationality and registration markings. It will also transmit on 121.5 MHz and 243 MHz when activated and these signals may be detected by air, sea or ground receivers. Transmissions on VHF frequency (121.5/243 MHz) are line of sight and effective only in close proximity (about 20 km radius).

  The battery expiry date for the FIXED ELT was November 2014.

  One PORTABLE ELT located in the forward cabin right hand coat closet.

  This closet is used by the cabin crew.

  This unit is bracket-mounted to the inside of the coat closet door. A label fixed on the coat closet door identifies the ELT. The installation allows quick removal. The Portable ELT is manufactured by ELTA FRANCE and is of the 406 series. It is identical to the fixed ELT except

that this unit has its own foldable antenna. The operations and function are the same. The manufacturer part number is 01N65910.

The portable ELT has a control switch on the front face. It is normally in the OFF position. When needed, the switch can be selected to the ON position to activate the ELT transmission.

The battery expiry date for the PORTABLE ELT was November 2014.

- **Two SLIDE RAFT** mounted ELTs located at Door 1 Left and Door 4 Right (packed within the slide raft assembly).

The slide raft mounted ELT will only be available when the slide rafts at doors 1 Left or 4 Right are deployed. The ELT transmission is not satellite enabled. The transmission signal is on 121.5 MHz and 243 MHz which may be monitored with air, sea and ground-based receivers. The slide raft ELT is automatically armed when the slide raft is deployed and inflated. Once armed the ELT is automatically activated by a water sensor coming in contact with water. This ELT is not activated by deceleration. The slide raft ELTs (Part No.: P3-03-0029-10) are manufactured by DME Corporation and the battery expiry dates are as follows:

- Door 1 Left - August 2016
- Door 4 Right - May 2017

No relevant ELT beacon signals from the aircraft were reported from the responsible Search and Rescue agencies or any other aircraft.

1) Review of Effectiveness of Emergency Locator Transmitters

In general, Emergency Locator Transmitters (ELT) are intended for use on land or on the surface of water, and neither portable nor fixed ELT signals are detectable when the ELT is submerged in deep water. Portable ELT is equipped with a floatation device and can be activated by immersion in water. For effective signal transmission, the antenna of the ELT must remain above water. Damage to an ELT or its associated wiring and antenna, or shielding by aircraft wreckage or terrain, may also prevent or degrade transmission. If the portable ELT is activated within a closed aircraft the shielding effect of the aircraft structure may degrade the transmission.

a) A review of ICAO accident records over the last 30 years indicates that of the 114 accidents in which the status of ELTs was known, only 39 cases recorded effective ELT activation. This implies that of the total accidents in which ELTs were carried, only about 34% of the ELTs operated effectively (*Appendix 1.6D*).

b) The Cospas-Sarsat system has been helpful for search and rescue teams in numerous aircraft accidents on a world-wide basis. Despite these successes, the detection of ELT signals after an aircraft crash remains problematic. Several reports have identified malfunctions of the beacon triggering system, disconnection of the beacon from its antenna or destruction of the beacon as a result of accidents where aircraft was destroyed or substantially damaged. Even when the beacon and its antenna are functioning properly, signals may not be adequately transmitted to the Cospas-Sarsat satellites because of physical blockage from aircraft debris obstructing the beacon antenna or when the antenna is under water.

Source: Global Aeronautical Distress and Safety System (GADSS document)

Note:

In the aftermath of the disappearance of MH370, following a multi-disciplinary meeting in May 2014, ICAO formed an Ad-hoc Working Group on Flight Tracking with the mandate to develop a Concept of Operation on the sequence of events before and after the occurrence of an accident which should include all identified phases of such a sequence including detection of an abnormal situation, alert phase, distress phase, and search and rescue activities. This Concept of Operation is GADSS.

c) ELT can be activated automatically by shock typically encountered during aircraft crashes or manually. It is possible for Flight Crew to manually activate the ELT; however existing flight operating procedures do not call for activation of the ELT until the incident has occurred.

d) The Cospas-Sarsat system does not provide a complete coverage of the earth at all times. As a consequence, beacons located outside the areas covered by these satellites at a given moment cannot be immediately detected

and must continue to transmit until a satellite passes overhead.

e) The global distress beacon detection system, Cospas-Sarsat, no longer detects 121.5 MHz distress signals. Only 406 MHz digital distress beacons are now capable of detection by satellite. Analogue beacon signals may be received by other aircraft within VHF range but there may not be such aircraft within range at the time of beacon transmission and monitoring 121.5 MHz.

1.6.8 Aircraft Systems Description

Most of the electronic equipment on the aircraft are mounted on equipment racks in the various equipment centres.

The Main Equipment Centre (MEC) contains most of the electronics equipment on the aircraft. The MEC is below the passenger cabin, rear of the nose wheel well and forward of the forward cargo compartment. Access to the MEC is possible on ground or in flight. The equipment in the MEC includes electronics for these functions:

- Information Management
- Generator Control
- Transformer Rectifier
- Flight control and autopilot
- Environmental control
- Recording
- Navigation
- Communication
- Cabin Management
- Weight and balance
- Air data
- Inertial data
- Warning
- Proximity sensing
- Engine control
- Electrical Load Management.

The Forward Equipment Centre is forward of the nose wheel well and contains the two weather radar receiver/transmitters. Access to the

Forward Equipment Centre is through the access door forward of the nose landing gear or through the MEC.

The passenger compartment above the Door 3 cross-aisle at station 1530 on the left of the aircraft centre line contains the satellite communication equipment.

A rack in the passenger compartment above the rear galley at station 2100 on the right side of the aircraft contains the flight recorders.

There are also equipment racks adjacent to the forward, aft and bulk cargo doors. The forward cargo racks contain the primary flight control, actuator control, radio altitude, fuel quantity and cargo handling electronics. The aft cargo racks contain the HF communication, brake and tire and main gear steering electronics. The bulk cargo racks contain the APU battery and charger.

1) Air Conditioning and Pressurisation

The aircraft has two air conditioning systems divided into left pack and right pack. Engine bleed air provides the pneumatic source for air conditioning and pressurisation.

There are two electronic Controllers, each of which can provide both pack and zone control. Each Controller has two channels that alternate command cycle. Cockpit and cabin temperature selection is monitored, and the Air cycle machine and temperature control valves will be commanded to deliver temperature conditioned air to the various cabin zones.

Conditioned air is also used for electronic equipment cooling. This is supplied through a series of pneumatic valves with supply and exhaust fans. Exhaust air from the equipment cooling flow is routed to the forward cargo and used for forward cargo compartment heating.

Two cabin pressure Controllers regulate the aircraft pressurisation and command the pneumatic system. System operation is automatic and works in conjunction with the forward and aft outflow valves that are used for pressurisation. The outflow valves can also be manually operated from the cockpit by switches on the overhead panel.

Loss of cabin pressure will be indicated to the flight crew by a Cabin Altitude warning message on the Engine Indicating and Crew Alerting System (EICAS) display together with the associated aural warning.

2) Autopilot Flight Director System

The autopilot is engaged by operation of either of two A/P pushbutton switches on the Mode Control Panel (MCP) located on the glareshield panel (*Figure 1.6C* [below]). Once engaged the autopilot can control the aircraft in various modes selected on the MCP. Normal autopilot disengagement is through either control wheel autopilot disengage switch. The autopilot can disengage if the flight crew override an

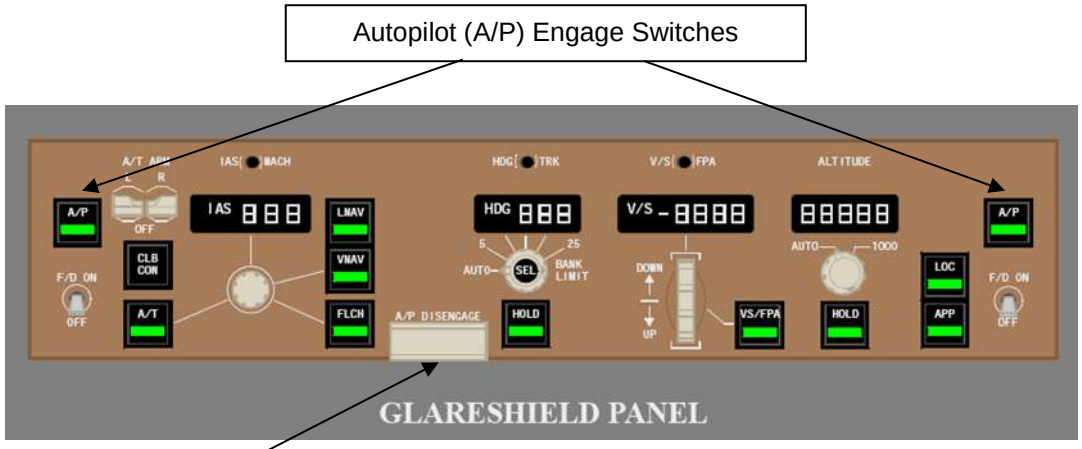

Copyright © Boeing. Reprinted with permission of The Boeing Company

Figure 1.6C - Autopilot Mode Control Panel

autopilot command through the use of the control column, control wheel or rudder pedals (when the yaw axis is engaged for approach).

The autopilot can also be disengaged by pulling down on the A/P Disengage Bar on the MCP. The autopilot will also disengage automatically for failures of systems on which it relies upon for specific operations. The Autopilot Flight Director System (AFDS) consists of three Autopilot Flight Director Computers (AFDCs), one MCP, and six backdrive actuators (one each for the Captain's and First Officer's control column, control wheel, and rudder pedals). The left and right 28V DC buses power the left and right AFDCs, respectively and the MCP while the 28V DC battery bus powers the centre AFDC.

Emergency power from the Ram Air Turbine (RAT) generator does not power these busses and as a result the autopilot will not function with RAT electrical power.

a) Take-off Mode

The Take-off (TO/GA) mode controls roll and pitch during take-off. Also, the Thrust Management Computing Function (TMCF) controls thrust during take-off. Turning a flight director on while the aircraft is on the ground, or activating either TO/GA switch while on the ground, will engage Take-off mode.

b) Roll Modes

The following AFDS roll modes are available during climb, cruise and descent (*Figure 1.6D* [below]*):*

i) Lateral Navigation

Pushing the Lateral Navigation (LNAV) switch arms or disarms the LNAV mode. The commands come from the active Flight Management Computing Function (FMCF) when there is a valid navigation data base and an active flight plan.

ii) Heading Hold/Track Hold

Pushing the Heading Hold (HDG HOLD)/Track hold (TRK HOLD) switch selects Heading or Track hold. In this mode, the aircraft holds either heading (HDG) or track (TRK). If the HDG/TRK display on the MCP shows TRK, the aircraft holds track. If the HDG/TRK display on the MCP shows HDG, the aircraft holds heading.

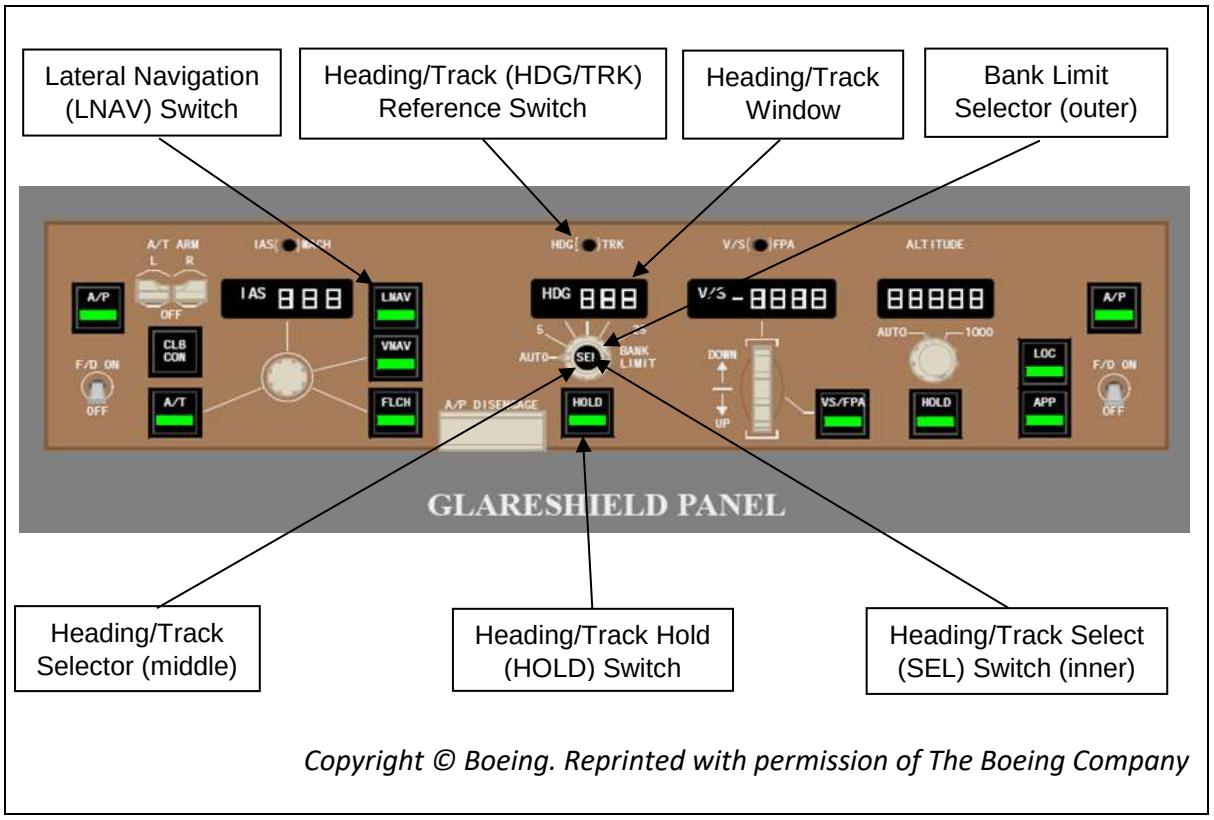

Copyright © Boeing. Reprinted with permission of The Boeing Company

Figure 1.6D - Lateral Mode Switches and Indicators

iii) Heading Select/Track Select

Pushing the Heading Select (HDG SEL)/Track Select (TRK SEL) switch (inner) selects Heading Select or Track Select modes. In this mode, the aircraft turns to the heading or track that shows in the heading/track window. Pushing the Heading/Track (HDG/TRK) Reference switch alternately changes the heading/track reference between heading and track. Rotating the Heading/Track selector (middle) sets the heading or track in the heading/track window. If the HDG/TRK display shows HDG, the aircraft goes to and holds the heading that shows in the heading/track window. If the HDG/TRK display shows TRK, the aircraft goes to and holds the track that shows in the heading/track window. Rotating the Bank Limit selector (outer) sets the bank limit when in the Heading Select or Track Select modes. In the AUTO position, the limit varies between 15 - 25°, depending on True Airspeed. When the other detented positions are selected, the value is the maximum, regardless of airspeed.

iv) Roll Attitude Hold

The Roll Attitude Hold mode is used to hold the roll attitude that exists at the time the flight director is first turned on, or the autopilot is first engaged. The Roll Attitude Hold mode is activated, and ATT annunciated, if the bank angle is greater than 5 degrees when either:

- A flight director is turned on with the autopilot not engaged; or
- The autopilot is initially engaged with no flight director on.

c) Pitch Modes

The following AFDS pitch modes are available during climb, cruise and descent (*Figure 1.6E* [below]):

i) Vertical Navigation

Pushing the vertical navigation (VNAV) switch arms or disarms the VNAV mode. In this mode, the AFDS uses vertical steering commands provided by the Flight Management Computer Function (FMCF). The FMCF vertical steering commands come from the active FMCF based on the navigation data and the active flight plan.

ii) Vertical Speed/Flight Path Angle

Pushing the Vertical Speed/Flight Path Angle (V/S-FPA) switch selects the V/S or FPA mode. Rotating the V/S-FPA selector Up or Down sets the vertical speed or flight path angle in the vertical speed/flight path angle window. Pushing the V/S-FPA Reference switch alternately changes vertical speed/flight path angle window references between vertical speed and flight path angle. The vertical speed or flight path angle command is an elevator command. The pilot uses this mode to change flight levels. The pilot must set the engine thrust necessary to hold the vertical speed or flight path angle command. When the V/S/FPA display shows V/S, the aircraft goes to and holds the vertical speed that shows on the vertical speed/flight path angle window.

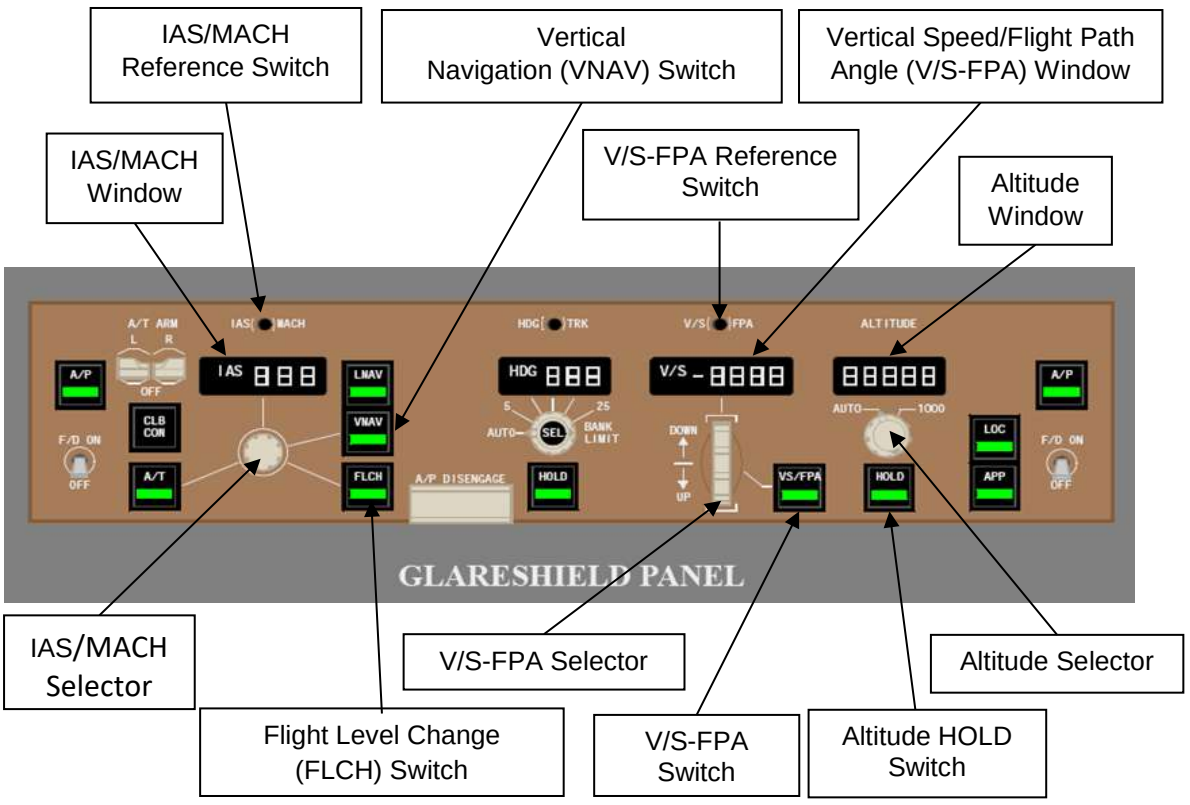

Copyright © Boeing. Reprinted with permission of The Boeing Company

Figure 1.6E - Vertical Mode Switches and Indicators

iii) Flight Level Change

Pushing the Flight Level Change (FLCH) switch selects the FLCH mode. In this mode, the AFDS will control to the speed target in the IAS/MACH window, providing climb and descent guidance and control. FLCH mode may be used with autothrottles, or with manual throttle control. When the IAS/MACH display shows IAS, the elevator command holds the speed that shows on the IAS/MACH window. When the IAS/MACH display shows MACH, the elevator command holds the MACH that shows on the IAS/MACH window. Rotating the IAS/MACH selector sets the speed in the IAS/MACH window. Pushing the IAS/MACH Reference switch alternately changes the IAS/MACH window between IAS and MACH. The Thrust Management Computing Function (TMCF) supplies the engine thrust commands.

iv) Altitude Hold

Pushing the Altitude Hold (ALT) switch selects the Altitude hold mode. In this mode, the aircraft holds the barometric altitude present when the pilot pushes the altitude HOLD switch. Altitude Capture and Hold can also be engaged from a climb or descent as the aircraft approaches the altitude that is selected and displayed in the altitude window.

d) Landing Modes

The following AFDS functions are available for landing:

i) Localizer

The Localizer (LOC) mode captures and holds the aircraft to a localizer flight path.

ii) Glideslope

The Glideslope (G/S) mode captures and holds the aircraft to a vertical descent flight path.

iii) Flare

The flare (FLARE) mode controls the aircraft to a smooth touchdown at a point past the glideslope antenna. This is a computed command and is not part of the glideslope mode.

iv) Runway Alignment

In crosswind conditions, the runway alignment mode supplies roll and yaw control to decrease the aircraft crab angle for touchdown. The runway alignment mode also includes roll and yaw control for an engine failure in approach during autoland.

v) Rollout

After touchdown, the rollout **(**ROLLOUT) mode controls the aircraft to the runway centre line. Aircraft deviation from the localizer centre line supplies rudder and nose wheel steering signals.

vi) Go-Around

The go-around (TO/GA) mode controls roll and pitch after an aborted approach. Also, the TMCF controls thrust during go-around.

Pushing the LOC switch arms or disarms the localizer as roll mode. Pushing the Approach (APP) switch arms or disarms the localizer as roll mode and G/S as pitch mode (*Figure 1.6F* [below]*).*

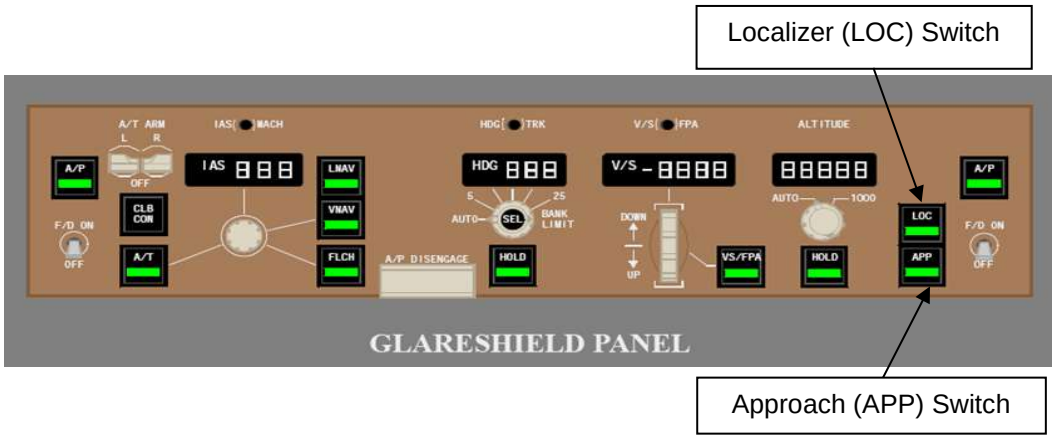

Copyright © Boeing. Reprinted with permission of The Boeing Company

Figure 1.6F - Approach Mode Switches

e) Autothrottle (Thrust Management Computing Function)

The autothrottle (A/T) commands the thrust levers to achieve an engine thrust setting, or a selected airspeed. The A/T is armed by raising one or both A/T Arm switches, and is engaged by a pushbutton switch on the MCP (*Figure 1.6G* [below]).

During normal flight operations, the flight crew uses the Thrust Management Computing Function (TMCF) to perform several routine or normal operations and tasks. These operations or tasks relate to autothrottle modes. The A/T modes operate in these flight phases:

Copyright © Boeing. Reprinted with permission of The Boeing Company

Figure 1.6G - Autothrottle Switches

- Take-off (TO)
- Climb (CLB)
- Cruise (CRZ)
- Descent (DES)
- Approach (APP)
- Go-around (GA)

Autothrottle thrust mode annunciations relate to pitch mode annunciations on the Primary Flight Display (PFD).

f) Autothrottle Modes

i) Take-off

In take-off (TO), the autothrottle controls thrust to the TO thrust limit. The autothrottle mode annunciation on the PFD is thrust reference (THR REF). At a threshold air speed, the autothrottle mode annunciation on the PFD changes to HOLD.

ii) Climb

These are the three autothrottle mode selections in climb (CLB):

- Vertical navigation (VNAV)
- Flight level change (FLCH)

- Autothrottle (MCP) speed mode or thrust mode.

These are the autothrottle mode annunciations for these modes:

- THR REF when VNAV engages
- THR when FLCH engages
- SPD or THR REF when autothrottle mode engages.

The autothrottle speed mode only engages when VNAV, FLCH, and TO/GA are not active, and the aircraft is in the air.

iii) Cruise

In cruise, the pitch mode could be VNAV PTH, VNAV ALT or MCP ALT; the corresponding A/T mode is SPD.

iv) Descent

These are the three autothrottle modes in descent (DES):

- VNAV
- FLCH
- Autothrottle speed mode

These are the autothrottle mode annunciations in descent:

- IDLE, THR, SPD or HOLD shows for VNAV
- THR, or HOLD shows for FLCH
- SPD shows for V/S, FPA or no AFDS mode

v) Approach

SPD is normal mode in approach with glideslope active or in a manual approach (APP).

- **Go-Around**

A go-around (GA) mode request causes the autothrottle mode to change to THR. A second GA request causes the autothrottle mode to change to THR REF. The TO/GA switch must be pushed to request GA.

- **Flare Retard**

  Flare retard occurs when a specified altitude threshold has been achieved when in SPD mode, or during an Autoland approach with a command from the autopilot flight director system (AFDS). The autothrottle mode changes to IDLE during a flare retard.

vi) Autothrottle Disconnect

The autothrottle disconnects when there is a manual autothrottle disconnect or when there is thrust reverser application. This occurs after initial touchdown during rollout. The autothrottle will disconnect automatically for certain system faults.

3) Electrical Power

The electrical system generates and distributes AC and DC power to other aircraft systems, and is comprised of: main AC power, backup power, DC power, standby power, and flight controls power. System operation is automatic. Electrical faults are automatically detected and isolated. The AC electrical system is the main source for aircraft electrical power. *Figure 1.6H* (below) shows the cockpit electrical panel where electrical switching can be made. It also shows the associated lights.

As the various aircraft systems rely on electrical power, failure of the electrical buses will affect the systems operation which will in turn trigger the corresponding fault messages. These messages are collected by the CMCS which will transmit the messages, via the ACARS, to the Maintenance Control Centre (MCC).

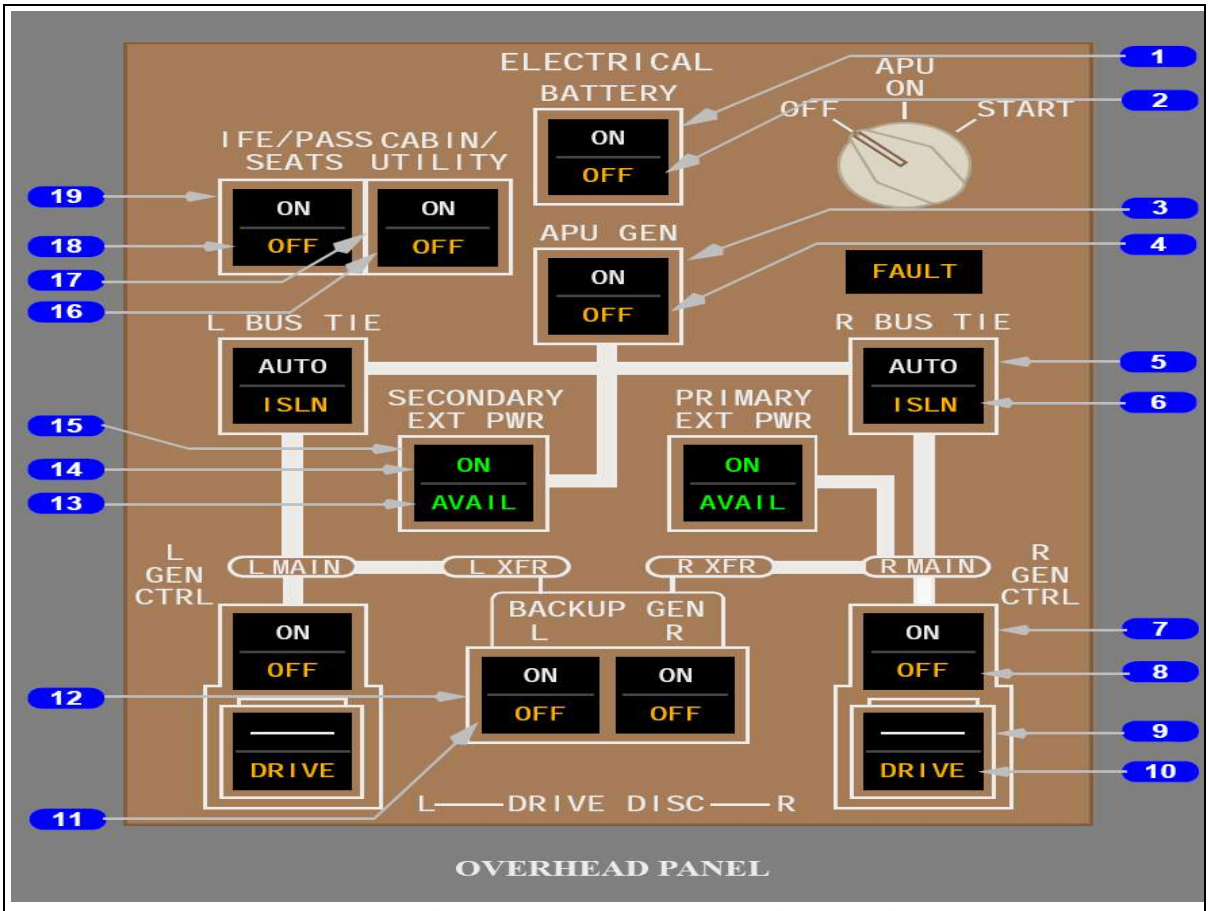

Electrical Power Panel Switches/Lights

1.	Battery Switch	11.	Backup Generator OFF Lights
2.	Battery OFF Light	12.	Backup Generator (BACKUP GEN) Switches
3.	APU Generator (APU GEN) Switch	13.	External Power AVAIL Lights
4.	APU Generator OFF Light	14.	External Power ON Lights
5.	BUS TIE Switches	15.	External Power (EXT PWR) Switches
6.	BUS Isolation (ISLN) Lights	16.	CABIN/UTILITY Power OFF Light
7.	Generator Control (GEN CTRL) Switches	17.	Cabin/Utility (CABIN/UTILITY) Power Switch
8.	Generator OFF Lights	18.	IFE/PASS SEATS OFF Light
9.	Drive Disconnect Switches	19.	In Flight Entertainment System/ Passenger Seats (IFE/PASS SEATS) Power Switch
10.	Generator DRIVE Lights		

Copyright © Boeing. Reprinted with permission of The Boeing Company

Figure 1.6H - Electrical Power Panel Switches/Lights

a) Electrical Load Management System

The Electrical Load Management System (ELMS) provides load management and protection to ensure power is available to critical and essential equipment. If the electrical loads exceed the power available (aircraft or external), ELMS automatically shed AC loads by priority until the loads are within the capacity of the aircraft or ground power generators. The load shedding is non-essential equipment first, then utility busses. Utility busses are followed by individual equipment items powered by the main AC busses. When an additional power source becomes available or the loads decrease, ELMS restores power to shed systems (in the reverse order). The message LOAD SHED displays on the electrical synoptic when load shed conditions exist.

b) Alternating Current Electrical System Power Sources

The entire aircraft alternating current (AC) electrical load can be supplied by any two main AC power sources. The main AC electrical power sources are:

- left and right engine integrated drive generators (IDGs)
- APU generator
- primary and secondary external power

The power sources normally operate isolated from one another. During power source transfers on the ground (such as switching from the APU generator to an engine generator) operating sources are momentarily paralleled to prevent power interruption.

c) Integrated Drive Generators

Each engine has an Integrated Drive Generator (IDG). Each IDG has automatic control and system protection functions. When an engine starts, with the GENERATOR CONTROL switch selected ON, the IDG automatically powers the respective main bus. The previous power source is disconnected from that bus.

The IDG can be electrically disconnected from the busses by pushing the GENERATOR CONTROL switch to OFF. The IDG can also be electrically disconnected from its respective bus by selecting an available external power source prior to engine

shutdown. The DRIVE light illuminates and the EICAS message ELEC GEN DRIVE L or R displays when low oil pressure is detected in an IDG. The IDG drive can be disconnected from the engine by pushing the respective DRIVE DISCONNECT switch. The IDG cannot be reconnected by the flight crew. High drive temperature causes the IDG to disconnect automatically.

d) Auxiliary Power Unit Generator

The Auxiliary Power Unit (APU) generator is electrically identical to the IDG generators. The APU generator can power either or both main busses and may be used in flight as a replacement to an IDG source. If no other power source is available when the APU generator becomes available, the APU generator automatically connects to both main AC busses. If the primary external source is powering both main busses, the APU powers the left main bus, and the primary external source continues to power the right main bus. If the primary external source is powering the right main bus, and the secondary external source is powering the left main bus, the APU then powers the left main bus and the primary external source continues to power the right main bus. If the secondary external source is powering both main busses, the APU then powers both main busses.

The APU generator OFF light illuminates when the APU is operating and the APU generator breaker is open because of a fault or the APU GENERATOR switch is selected OFF. When the APU GENERATOR switch is ON and a fault is detected, the APU generator cannot connect to the busses.

In flight, when both transfer busses are unpowered, the APU starts automatically, regardless of APU selector position.

e) Alternating Current Electrical Power Distribution

The AC power is distributed through the left and right main busses and the ground service bus. The right IDG normally powers the right main bus and the left IDG normally powers the left main bus. The APU normally powers both main busses when they are not powered by any other source.

Bus tie relays, controlled by BUS TIE switches, isolate or parallel the right and left main busses. When both BUS TIE switches are

set to AUTO, the bus tie system operates automatically to maintain power to both main busses.

Power transfers are made without interruption when the aircraft is on the ground, except when switching between primary and secondary external power sources. The source order for powering left and right main busses in flight is the:

- respective IDG
- APU generator
- opposite IDG

f) Autoland

During autoland, the busses isolate to allow three independent sources to power the three autopilots:

- the left IDG powers the left AC transfer bus, the left main DC bus, and the captain's flight instrument bus;
- the right IDG powers the battery bus and AC standby bus through the main battery charger; and
- the back-up system powers the right AC transfer bus, the right DC bus, and the first officer's flight instrument bus.

g) Backup Alternating Current Electrical System

The electrical system is highly reconfigurable to accommodate multiple failures. The electrical system is designed to automatically provide power to selected aircraft systems. The electrical system automatically powers one or both transfer busses when:

- only one main AC generator (includes APU) is available;
- power to one or both of the main AC busses is lost;
- approach (APP) mode is selected for autoland; and
- the system is automatically tested after engine starts

The system automatically transfers power without interruption.

h) Backup Generators

Backup power is provided by one variable speed, variable frequency generator mounted on each engine. A frequency

converter converts the generator frequency to a constant 400 Hz. Only one backup generator can power the converter at a time.

Each backup generator contains two permanent magnet generators (PMGs) that supply power to the flight control DC electrical system (refer to DC Electrical System). If both IDGs and the APU generator are inoperative, a backup generator powers essential aircraft equipment. To reduce electrical loading on the backup generator, the following systems are inoperative:

- TCAS
- SATCOM
- Right HF radio

i) Direct Current Electrical System

The direct current (DC) electrical system includes the main DC electrical system and the flight control DC electrical system. The main DC electrical system uses four transformer-rectifier units (TRUs) to produce DC power. The TRUs are powered by the AC transfer busses.

TRU DC electrical power is distributed to various DC busses as follows:

(1) The left TRU powers the left main DC bus, which provides a second DC power source for:

- left flight control power supply assembly (PSA)
- right main DC bus.

(2) The right TRU powers the right main DC bus, which provides a second DC power source for:

- right flight control PSA
- left main DC bus.

(3) The C1 TRU powers the captain's flight instrument bus and the battery bus. The captain's flight instrument bus provides a second DC power source for:

- centre flight control PSA
- first officer's flight instrument bus

The C2 TRU powers the first officer's flight instrument bus, which provides a second DC power source for the captain's instrument bus.

j) Batteries

The main battery is connected directly to the hot battery bus and provides standby power to other busses. The main battery charger normally powers the hot battery bus and maintains the main battery fully charged.

The APU battery is connected directly to the APU battery bus and provides dedicated power to the APU electric starter, which is used when sufficient bleed air duct pressure is unavailable for the APU air turbine starter. The APU battery charger normally powers the APU battery bus and maintains the APU battery fully charged.

k) Flight Control Direct Current Electrical System

The flight control DC electrical system is a dedicated power source for the primary flight control system. Primary power for the flight control DC electrical system comes from permanent magnet generators (PMGs) housed within each backup generator. Variable frequency PMG AC power is used by individual power supply assemblies (PSAs) to provide DC power to the three flight control DC busses. To ensure a high level of system reliability, each PSA also has multiple DC power sources. If primary PMG AC power is not available, secondary power for the left and right PSAs is provided by the related main DC bus. Secondary power for the centre PSA is provided by the captain's flight instrument bus. The hot battery bus provides additional backup power for the left and centre PSAs only. Each PSA also uses a dedicated battery to prevent power interruptions to the related flight control DC bus. The batteries have limited capacity and are incorporated to supply power for brief periods during PSA power source transfers.

l) Standby Electrical System

The standby electrical system can supply AC and DC power to selected flight instruments, communications and navigation systems, and the flight control system, if there are primary

electrical power system failures. The standby electrical system consists of:

- the main battery
- the standby inverter
- the RAT generator and its associated generator control unit
- the C1 and C2 TRUs

(1) Main Battery

The main battery provides standby power to the:

- hot battery bus
- battery bus
- captain's flight instrument bus
- left and centre flight control PSAs
- standby inverter.

Note:

The main battery can power the standby system for a minimum of 10 minutes.

(2) Standby Inverter

The standby inverter converts DC power to AC power. The inverter powers the AC standby bus if the left transfer bus is not powered.

(3) Ram Air Turbine Generator

The ram air turbine (RAT) generator provides standby power to the C1 and C2 TRUs. The RAT can supply electrical and hydraulic power simultaneously. If the RAT is unable to maintain RPM, the RAT generator electrical load is shed until RPM is satisfactory. Power for standby electrical loads is provided by the main battery during deployment of the RAT and when RAT generator loads are shed. The RAT is deployed automatically if both AC transfer busses lose power in flight. The RAT can be manually deployed by using the RAM AIR TURBINE switch on the overhead panel.

(4) Cabin Systems and Utility Power

Electrical power to some cabin and utility systems are controlled from the cockpit. The IFE/PASS SEATS Power switch controls power to the IFE and passenger seats. The CABIN/UTILITY Power switch controls power to cabin and utility systems.

4) Cabin and Cargo Compartments

The aircraft, 9M-MRO was configured to 35 business class and 247 economy class seats. The business class and economy class seats were procured from BE Aerospace. An approved Lay Out of Passenger Accommodation (LOPA) determines the cabin interior configuration. Safety and emergency equipment are fitted and positioned throughout the cabin.

There is one crew rest area in the forward cabin behind the cockpit. There is a cabin crew rest area in the aft cabin lower lobe. Access is through a compartment door adjacent to Door 3R.

The cockpit door provides selective entry to the cockpit and is resistant to ballistic penetration. When closed, the door locks when electrical power is available and unlocks when electrical power is removed. A viewing lens in the door allows observation of the cabin. The door can be manually opened from the cockpit by turning the door handle.

An emergency access code is used to gain access to the cockpit in case of pilot incapacitation. Access is provided by the use of a Keypad Access System which consists of a numeric keypad outside the cockpit area and a chime module and electric strike that is not accessible from outside the cockpit. The chime module provides an audible alert to the pilots that the correct code has been entered into the keypad. There is also an indicator light in the cockpit and a Light Emitting Diode (LED) on the keypad that indicates that the correct code has been entered.

The pilots have a 3-position switch by which they can open the door lock, close the door lock, or permanently lock the door for a specified amount of time to prevent access by anyone regardless if the correct code is entered into the keypad.

The door has blowout panels that will open in the event of a rapid decompression of the passenger compartment. A pressure sensor controls an electric strike and allows the door to open inward in the event of a rapid decompression in the cockpit. These features serve to equalise the pressure between the passenger compartment and the cockpit in case of decompression either side of the door.

The aircraft is also fitted with a Flight Deck Entry Video Surveillance System (FDEVSS) which provides the pilots surveillance capability of the cockpit doorway and the forward galley areas. This allows the pilots to see the person who wants to access the cockpit before they allow entry.

There are four Type A passenger and service doors on each side of the aircraft. Each door has a window. The passenger compartment has windows along both sides of the passenger compartment. Each exit is fitted with a slide raft system for emergency use.

The overhead passenger cabin is fitted with Passenger Service Units (PSU) above each seat row. They are hinged and secured by a magnetic latch that is electrically controlled. In the event of cabin depressurisation, the PSU magnetic latch will be electrically released and allow the oxygen masks to drop for passenger use.

The aircraft cabin lighting system comprises of ceiling lights, sidewall lights, entry lights and emergency lights. The cabin management system (CMS) controls the passenger cabin lighting.

The lower section of the fuselage houses forward, aft and bulk cargo compartments. A cargo handling system is fitted for the forward and aft cargo to command power drive units (PDU) to move cargo containers laterally and longitudinally.

Cargo compartment sidewalls, ceilings and walkways are constructed of fire resistant materials. There is a smoke detection warning system and fire extinguishing system installed to contain any smoke or fire eventualities.

5) Flight Controls

The flight control system is an electronic fly by wire system. It is divided into two separate systems to control the aircraft in flight.

Primary Flight control system (PFCS) is a modern three axis, fly by wire system. It controls the roll, yaw and pitch commands using the ailerons, flaperons, spoilers, elevators, rudder and horizontal stabilizer. The high lift control system (HLCS) comprises of inboard and outboard trailing edge flaps, leading edge flaps and Kruger flaps. It supplies increased lift at lower speeds for take-off and landing.

The PFCS and HLCS use 3 dedicated ARINC 629[9] Flight Control digital busses to transmit data signals to command the flight controls. Mechanical control is available to two spoilers and horizontal stabilizers.

The PFCS has three operational modes of command - Normal mode, Secondary mode and Direct mode. The PFCS command signals are computed by three redundant Primary Flight Computers (PFCs) in Normal and Secondary modes and directed through four Actuator Control Electronic (ACE) units. In Direct mode, the control surface command signals are computed by the ACEs without reliance on the PFCs.

The PFC also receives airspeed, altitude and inertial reference data from Airplane Information Management System (AIMS), Air Data Inertial Reference Unit (ADIRU) and Secondary Attitude and Air Data Reference unit (SAARU). The PFCs calculate the flight control commands based on control laws, augmentation and envelop protections. The digital command signals from the PFCs go to the ACEs that will change the digital signal to analogue format and send to the power control units (PCU) that will command the control surface movement.

The HLCS operates in three modes, primary, secondary and alternate. Command signals are transmitted from the flap lever to two Flap Slat Electronic Units (FSEU).

The FSEU process the flap command and control the sequence of flaps and slats operation. It also commands auto slat, load relief and asymmetry protection.

Two spoilers and the horizontal stabilizer receive mechanical control signals from pilots input.

[9] *Aeronautical Radio, Incorporated (ARINC) 629 is an aeronautical standard which specifies multi-transmitter data bus protocol where up to 128 units can share the same bus.*

6) Fuel System

The fuel system has three fuel tanks, two integral wing tanks and one centre tank. The tanks are part of the wing structure and have many fuel system components located inside the tanks and on the rear spar. The fuel tanks are vented through channels in the wing to allow near ambient pressure during all phases of flight.

An integrated refuel panel (IRP) on the lower left wing and two refuel receptacles on each wing allows rapid pressure refueling of the aircraft. The refueling operation is automatic with fuel load selection on the IRP. Fuel quantity indicating system (FQIS) processor unit controls all fueling operations and measuring of fuel quantity.

Several enhanced features were incorporated in the design to include the following:

- Ultrasonic Fuel Quantity Indicating system
- Automatic centre tank scavenge system
- Ultrasonic water detection system
- Densitometers
- Jettison system

Fuel quantity is displayed on the fuel synoptic page and the upper EICAS fuel block.

a) Engine Fuel Feed System

There are two boost pumps for each main tank and two override/ jettison pumps in the center tank to supply fuel to the engines. The fuel flows through the crossfeed manifold to the engines. Redundant crossfeed valves isolate the left and right sides of the manifold.

At the start of a flight, when all the tanks are full, the normal procedure is to turn on all the fuel pumps. The override/jettison pumps supply center tank fuel to both engines. This occurs because the override/jettison pumps have a higher output pressure than the main tank boost pumps. When the override/jettison pump output pressure decreases because of low fuel quantity in the center tank, the boost pumps automatically supply fuel to both engines from the main tanks.

b) Auxiliary Power Unit Fuel Feed System

The Auxiliary Power Unit (APU) can receive fuel from any tank. A DC pump supplies fuel from the left main tank if no AC power is available. APU fuel is supplied from the left fuel manifold. APU fuel can be provided by any AC fuel pump supplying fuel to the left fuel manifold or by the left main tank DC fuel pump. On the ground, with the APU switch ON and no AC power available, the DC pump runs automatically. With AC power available, the left forward AC fuel pump operates automatically, regardless of fuel pump switch position, and the DC fuel pump turns off. In flight, the DC fuel pump operates automatically for quick left engine relight with the loss of both engines and all AC power. *Figure 1.6I* (below) shows the Engine and APU Fuel Feed System.

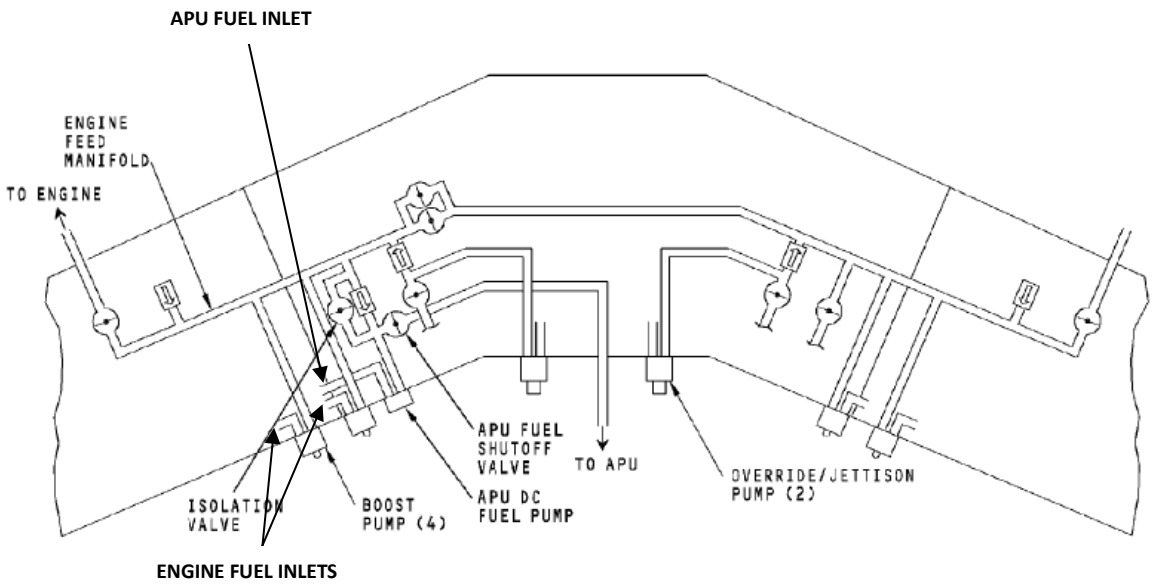

Copyright © Boeing. Reprinted with permission of The Boeing Company

Figure 1.6I - Engine and APU Fuel Feed

c) Fuel Inlets

The fuel intake inlet for the APU (in the left main tank) is located lower than that for the engine. As the fuel level drops below the engine fuel intake level the engine will be starved of fuel, however fuel will still be available for the APU as its fuel intake is lower. This difference in level between the engine and APU

fuel intakes, accounts for approximately 30 pounds of fuel in a standard flight attitude (1° pitch). The APU is estimated to consume (when electrically loaded) approximately 2 pounds of fuel in 55 seconds which will amount to a maximum APU run time of 13 minutes and 45 seconds. The pitch attitude and in-flight accelerations can affect the actual amount available for the APU.

7) Hydraulics

There are three independent hydraulic systems using electrical, pneumatics or engine driven power source. They are identified as Left, Centre and Right. Each hydraulic system can independently operate the flight controls for safe flight and landing.

Each hydraulic system uses a Hydraulic Interface Module Electronics Card (HYDIM) for automatic control and indications. The three systems operate independently at 3000 psi nominal pressure.

The left system is powered by an engine driven pump (EDP) and an electric motor pump (ACMP). The right system is also powered by an EDP and ACMP. The centre system has two ACMP and two air driven pumps (ADP) and a ram air turbine (RAT) pump.

Hydraulic pumps control and indication are on the P5 overhead panel. During normal operation the flight crew will select the switches to the auto position before flight. The pressure and quantity indication is provided on the hydraulic synoptic page and the status page.

The primary pumps are the EDPs in the left and right system and the ACMPs for the centre system. These pumps operate continuously. The demand pumps are the ACMPs for the left and right systems and the ADPs for the centre system. These pumps normally operate only during heavy system demands. The operation logic is controlled and monitored by the HYDIM cards.

The RAT deploys automatically during flight when both engines are shutdown or for loss of all three hydraulic power. The RAT hydraulic pump supplies hydraulic power to some of the center hydraulic system flight controls. When the aircraft is operating on RAT power only, the flap drive hydraulic motor is isolated from the center hydraulic system and as a result the flaps will not respond to the cockpit flap handle inputs.

8) Instrumentation

The flight instruments and displays supply information to the flight crew on six flat panel liquid crystal display units:

- Captain and First Officer Primary Flight Display (PFD)
- Captain and First Officer Navigation Display (ND)
- Engine Indication and Crew Alerting System (EICAS)
- the Multifunction Display (MFD)

Standby Flight Instruments provide information on separate indicators. Clocks display Airplane Information Management System (AIMS) generated UTC time and date, or manually set time and date.

a) Primary Flight Display

The Primary Flight Display (PFD) presents a dynamic color display of all the parameters necessary for flight path control. The PFDs provide the following information:

- flight mode annunciation
- airspeed
- altitude
- vertical speed
- attitude
- steering information
- radio altitude
- instrument landing system display
- approach minimums
- heading/track indications, engine fail, Ground Proximity Warning System (GPWS), and Predictive Windshear (PWS) alerts.

Failure flags are displayed for aircraft system failures. Displayed information is removed or replaced by dashes if no valid information is available to the display system (because of out-of-range or malfunctioning navigation aids). Displays are removed when a source fails or when no system source information is available.

b) Navigation Display

The navigation displays (ND) provide a mode-selectable color flight progress display. The modes are:

- MAP
- VOR
- APP (approach)
- PLN (plan)

The MAP, VOR, and APP modes can be switched between an expanded mode with a partial compass rose and a centered mode with a full compass rose.

c) Engine Indication and Crew Alerting System

The Engine Indication and Crew Alerting System (EICAS) consolidates engine and aircraft system indications and is the primary means of displaying system indications and alerts to the flight crew. The most important indications are displayed on EICAS which is normally displayed on the upper centre display.

i) System Alert Level Definitions

(1) Time Critical Warnings

Time critical warnings alert the crew of a non-normal operational condition requiring immediate crew awareness and corrective action to maintain safe flight. Master warning lights, voice alerts, and ADI indications or stick shakers announce time critical conditions.

(2) Warnings

Warnings alert the crew to a non-normal operational or system condition requiring immediate crew awareness and corrective action.

(3) Cautions

Cautions alert the crew to a non-normal operational or system condition requiring immediate crew awareness. Corrective action may be required.

(4) Advisories

Advisories alert the crew to a non-normal operational or system condition requiring routine crew awareness. Corrective action may be required.

(5) Engine Indication and Crew Alerting System Messages

Systems conditions and configuration information are provided to the crew by four types of EICAS messages:

- EICAS alert messages are the primary method to alert the crew to non-normal conditions.
- EICAS communication messages direct the crew to normal communication conditions and messages.
- EICAS memo messages are crew reminders of certain flight crew selected normal conditions.
- EICAS status messages indicate equipment faults which may affect aircraft capability.

An EICAS alert, communications, or memo message is no longer displayed when the respective condition no longer exists.

d) Multifunction Display

The electronic checklist (ECL) system shows normal and non-normal checklists on a multifunction display (MFD). The electronic checklist system is not required for, and a paper checklist or other approved backup checklist must be available in the cockpit.

The checklist display switch on the display select panel opens the electronic checklist. The flight crew operates the checklist with the cursor control devices (CCDs).

The MFD has also communications functions which are used to control data link features. Data link messages not processed by the Flight Management Computer (FMC) are received, accepted, rejected, reviewed, composed, sent, and printed using communications functions on the MFD. ACARS and data link radio management functions are provided through communications management menus. The COMM display switch, located on the display select panel, displays the communications main menu on the selected MFD.

Communications functions are selected using the cursor control device. Message text entry is accomplished by entering data into the Control Display Unit (CDU) scratchpad and transferring it to the appropriate area. Messages can be printed on the cockpit printer. Incoming message traffic is annunciated by EICAS communications messages.

e) Standby Flight Instruments

The standby flight instruments include:

- standby attitude indicator
- standby airspeed indicator
- standby altimeter
- standby magnetic compass

An external Power Supply Assembly supplies power to the standby attitude and airspeed indicators and the standby altimeter. The standby magnetic compass does not require any electrical power except for its lighting.

(1) Standby Attitude Indicator

The Standby Attitude Indicator displays Secondary Attitude Air Data Reference Unit (SAARU) attitude. A bank indicator and pitch scale are provided.

(2) Standby Airspeed Indicator

The Standby Airspeed Indicator displays airspeed calculated from two standby air data modules (one pitot and one static). It provides current airspeed in knots as a digital readout box with an airspeed pointer.

(3) Standby Altimeter

The standby altimeter displays altitude from the standby (static) air data module. Current altitude is displayed digitally. A pointer indicates altitude in hundreds of feet. The pointer makes one complete revolution at appropriate intervals.

(4) Standby Magnetic Compass

A standard liquid–damped magnetic standby compass is provided. A card located near the compass provides heading correction factors.

f) Clock

A clock is located on each forward panel. Each clock displays Airplane Information Management System (AIMS) generated UTC time and date, or manually set time and date. The AIMS UTC time comes from the global positioning system (GPS). In addition to time, the clocks also provide alternating day-month and year, elapsed time, and chronograph functions.

9) Airplane Information Management System

The Airplane Information Management System (AIMS) collects and calculates large quantities of data. The AIMS manages this data for several integrated avionics systems. These systems are the:

- Primary display system (PDS)
- Central maintenance computing system (CMCS)
- Airplane condition monitoring system (ACMS)
- Flight data recorder system (FDRS)
- Data communication management system (DCMS) - including ACARS datalink
- Flight management computing system (FMCS)
- Thrust management computing system (TMCS)

The AIMS has software functions that do the calculation for each of these avionics systems. The AIMS supplies one other software function that many aircraft systems use. It is the data conversion gateway function (DCGF).

The AIMS has two cabinets, for redundancy, which do the calculations for other avionic systems. The Left cabinet is located in the forward rack of the Main Equipment Centre (MEC) while the Right cabinet is located in rear rack of the MEC. To do these calculations, each AIMS cabinet has the following:

- A cabinet chassis
- Four Input/output modules (IOM)

- Four Core processor modules (CPM)

The IOMs and CPMs are considered Line Replaceable Modules (LRM). The IOM transfers data between the software functions in the AIMS CPMs and external signal sources. The CPMs supply the software and hardware to do the calculations for several avionic systems. The software is called functions. To keep a necessary separation between the functions, each function is partitioned. The partitions permit multiple functions to use the same hardware and be in the same CPM.

The Left AIMS cabinet gets electrical power from the 28V DC Capt Flight Instrument bus and the 28V DC F/O Flight Instrument bus. The Right AIMS cabinet gets electrical power from the 28V DC Left bus and the 28V DC Right bus. Each cabinet receives the power from four 28V DC circuit breakers in the overhead circuit breaker panel. The four 28V DC bus inputs are known as power 1 through power 4. Power 1 and power 2 enter the cabinet through a connector on the left side of the cabinet and therefore they are considered as left power. Power 3 and power 4 enter the cabinet through a connector on the right side of the cabinet and are considered as right power.

Each LRM receives power from four sources, two for main power and two for monitor power. The main circuitry uses the main power. Special circuits that monitor the condition of the power supply in the LRM use the monitor power. The two main and two monitor sources of power for each LRM come from different power sources.

Each AIMS cabinet also receives power through one hot battery bus circuit breaker in the standby power management panel. The connection to the hot battery bus keeps the LRMs internal memories active. The hot battery bus also makes the AIMS cabinet less likely to have faults due to power transients.

10) Navigation Systems

The Navigation systems of interest include Global Positioning System (GPS), Air Data Inertial Reference System (ADIRS) and the Flight Management System (FMS).

a) Global Positioning System

The Left and right GPS receivers are independent and use navigation satellites to supply very accurate position data to the

FMC. One is powered by the 115V AC Standby bus and the other by the 115V AC Transfer bus. They pass data to aircraft systems including the ADIRS via the AIMS. GPS tuning is automatic. If the Air Data Inertial Reference Unit (ADIRU) becomes inoperative during flight, the EICAS displays the message NAV ADIRU INERTIAL and the FMC uses only GPS data to navigate.

b) Inertial System

The ADIRS calculates aircraft altitude, airspeed, attitude, heading, and position data for the displays, flight management system, flight controls, engine controls, and other systems. The major components of ADIRS are the ADIRU, Secondary Attitude and Air Data Reference Unit (SAARU), and air data modules. The ADIRU supplies primary flight data, inertial reference, and air data. The ADIRU is fault-tolerant and fully redundant. The SAARU is a secondary source of critical flight data for displays, flight control systems, and other systems. If the ADIRU fails, the SAARU automatically supplies attitude, heading, and air data. SAARU heading must be manually set to the standby compass magnetic heading periodically. The ADIRU and SAARU receive air data from the same three sources. The ADIRU and SAARU validate the air data before it may be used for navigation. The three air data sources are the left, centre, and right pitot and static systems.

c) Flight Management System

The FMS aids the flight crew with navigation, in-flight performance optimisation, automatic fuel monitoring, and cockpit displays. Automatic flight functions manage the aircraft lateral flight path (LNAV) and vertical flight path (VNAV). The displays include a map for aircraft orientation and command markers on the airspeed, altitude, and thrust indicators to help in flying efficient profiles. The flight crew enters the applicable route and flight data into the CDUs. The FMS then uses the navigation database, aircraft position, and supporting system data to calculate commands for manual and automatic flight path control. The FMS tunes the navigation radios and sets courses. The FMS navigation database supplies the necessary data to fly routes, SIDs, STARs, holding patterns, and procedure turns. Cruise altitudes and crossing altitude restrictions are used to

calculate VNAV commands. Lateral offsets from the programmed route can be calculated and commanded.

The basis of the flight management system is the flight management computer function. Under normal conditions, one Flight Management Computer (FMC) accomplishes the flight management tasks while the other FMC monitors. The second FMC is ready to replace the first FMC if system faults occur. The FMC uses flight crew-entered flight plan data, aircraft systems data, and data from the FMC navigation database to calculate aircraft present position and pitch, roll, and thrust commands necessary to fly an optimum flight profile. The FMC sends these commands to the autothrottle, autopilot, and flight director. Map and route data are sent to the NDs. The EFIS control panels select the necessary data for the ND. The mode control panel selects the autothrottle, autopilot, and flight director operating modes.

Crew Procedure on the operations and programming of the Flight Management System safeguards and protects against incorrect execution of erroneous Information for the Navigation and Performance Data Input. Different levels of verification and cross checking between the Captain and Co-Pilot ensure that any error would be captured and corrected during the crew preparation.

In addition, system logics will also prevent the crew against selection of the wrong co-ordinates from the stored Navigation Database if a particular waypoint code happens to be used by many different places worldwide.

11) Oxygen Systems

a) Flight Crew Oxygen System

The flight crew oxygen system provides oxygen to the flight crew for emergencies and other procedures which make its use necessary. The oxygen is supplied by two cylinders located in the left side of the main equipment centre. Each cylinder is made of composite material and holds 115 cubic feet (3,256 litres) of oxygen at 1,850 psi. The oxygen is supplied, through regulators, to four oxygen masks in the cockpit, one each for the Captain, the First Officer, the First Observer and the Second Observer. The mask has a dilution control which is normally set at ‘Normal’ position. In this position the oxygen is diluted with

ambient air according to the pressure altitude in the cockpit. It can also be selected to '100%', in which case 100% oxygen will be supplied. *Table 1.6E* (below) shows the expected duration of oxygen supply from the two cylinders with the dilution control in 'Normal' position.

AIRCRAFT ALTITUDE: 36,000 ft			
Cabin Altitude: 8,000 ft.		**Cabin Altitude: 36,000 ft.**	
No. of Crew Members	**Expected Duration (hour)**	**No. of Crew Members**	**Expected Duration (hour)**
1	42	1	27
2	21	2	13
3	14	3	9
4	10.5	4	6.5

Table 1.6E - Expected Duration of Crew Oxygen

Aircraft altitude is assumed to be 36,000 ft. A cabin altitude of 8,000 ft. would indicate a normally pressurised cabin and a cabin altitude of 36,000 ft. would indicate an unpressurised cabin. At this cabin altitude of 36,000 ft, 100% oxygen will be supplied even with the dilution control in the 'Normal' position.

b) Passenger Oxygen System

The passenger oxygen system is supplied by separate and individual chemical oxygen generators. The oxygen system provides oxygen to:

- passenger seats
- attendant stations
- lower crew rest compartment
- lavatory service units

The passenger oxygen masks and chemical oxygen generators are located in passenger service units (PSUs). A door with an electrically operated latch keeps the masks in a box until the oxygen deployment circuit operates. The deployment circuit operates, and the masks automatically drop from the PSUs if cabin altitude exceeds approximately 13,500 feet. The passenger masks can be manually deployed from the cockpit by pushing the overhead panel PASSENGER OXYGEN switch to the ON position. Oxygen flows from a PSU generator

when any mask hanging from that PSU is pulled. Oxygen is available for approximately 22 minutes. The electrical power to the latch is supplied through a circuit breaker located in the Main Equipment Centre. It is not possible to deactivate automatic deployment of the masks from the cockpit.

c) Portable Oxygen

Portable oxygen cylinder lets the flight attendants move in the aircraft when oxygen is in use. It is also a gaseous oxygen supply for medical emergencies. The bottle is fitted with disposable mask. 15 cylinders are located throughout the passenger cabin. Each cylinder is of 11 cubic ft (310 litres) capacity. The flow of oxygen can be controlled by an 'Off-On' knob which can be rotated to control the flow from 0 to 20 litres per minute. Therefore, the minimum time for the portable oxygen supply from full is 15.5 minutes.

12) Central Maintenance Computing System

The Central Maintenance Computing System (CMCS) collects and stores information from most of the aircraft systems. It can store fault histories as well as monitor and conduct tests on the various systems. The fault history contains details of warnings, cautions and maintenance messages.

At regular intervals, during flight, the CMCS transmits any recorded fault messages, via the Aircraft Communications Addressing and Reporting System (ACARS), to the Maintenance Control Centre (MCC) of Malaysia Airlines. This helps in the planning and preparation for the rectification of any potential aircraft defects at the main base or line stations. Refer also to *Section 1.6.4 para. 9)*.

13) Engines

The aircraft is fitted with two engines (Model: RB211 TRENT 892B-17) manufactured by Rolls-Royce. The RB211 TRENT 892B-17 engine is a high bypass turbofan (bypass ratio of 6.4:1 at a typical cruise thrust) axial flow, three-rotor with a single low pressure fan driven by a five-stage, low-pressure turbine.

The engine has an eight-stage intermediate pressure compressor driven by a single-stage turbine and a six-stage high pressure compressor driven by a single-stage turbine.

The engine take-off thrust is 92,800 lb and weighing approximately 15,700 lb (7,136 kg). The engines are certified in accordance with the US FAA Type Certificate E00050EN.

The FAA Type Certificate Data Sheet certifies that the engines meet the smoke and gaseous emission requirements of the US FAR 34. The engine is certified under FAR Part 36 Stage 3 Noise regulation.

The engine is fitted with a digital Electronic Engine Fuel Control System and it interfaces with many systems and components in the form of primary analogue or ARINC 629 buses.

The following analogue engine fuel and control system interfaces and correlates with the other systems for supply and feedback:

- Engine ignition - ignition unit power
- Engine air - actuator and valves
- Engine controls - resolver excitation and position
- Engine indicating - engine parameter data
- Engine exhaust - thrust reverser operations
- Engine oil - oil cooling and indications
- Engine starting - auto-start and manual start
- Electrical power - aircraft power from the Electrical Load Management System (ELMS)

The following ARINC 629 engine fuel and control system interfaces and correlates with other systems for supply, control and indication data:

- AIMS - indication, air data and flight management control
- Cockpit controls - switch position and indication
- Flap Slat Electronic Unit (FSEU) - Flap indication
- Proximity Switch Electronic Unit (PSEU) - Landing gear lever position
- Air Supply Cabin Pressure Controller (ASCPC) - Pneumatic system demand

The RB211 TRENT 892B-17 engine Electronic Engine Control (EEC) serves as the primary component of the engine fuel control system and uses data from the engine sensors and aircraft systems

to control the engine operations. The EEC controls most of the engine components and receives feedback from them. These digital data go to the Engine Data Interface Unit (EDIU) and send the signal to the AIMS. The AIMS transmits and receives a large amount of data to and from the EEC. These include:

- Engine bleed status - EEC thrust limit calculations
- Air data - EEC thrust limit calculations
- Engine data – system requirements
- Autothrottle Engine Pressure Ratio (EPR) trim - thrust balancing
- Condition monitoring - performance tracking
- Maintenance data - trouble shooting
- Primary display system data - indication.

14) Auxiliary Power Unit

The aircraft is fitted with an Auxiliary Power Unit (APU) - Model: GTCP 331-500 - manufactured by Allied Signal. The Allied Signal GTCP 331-500 gas turbine APU is a two-stage centrifugal flow compressor, a reverse flow annular combustion chamber and a three-stage axial flow turbine. It supplies the auxiliary power system for the aircraft pneumatic and electrical power. This permits independent operations from the ground external power sources or the main engines.

The APU generator supplies 120 KVA electrical power at any altitude. The APU can start at all altitudes up to the service ceiling of the aircraft (43,100 ft/13,100 m). Electrical power is available up to the service ceiling and pneumatic power is available up to 22,000 ft (6,700 m).

The ELMS contains the APU autostart logic and sends signal to the APU Controller (APUC).

The APU Controller serves to control the APU functions for:

- Starting and ignition
- Fuel metering
- Surge control
- Inlet guide vane (IGV) control
- Data storage
- Protective shutdown
- BITE/Fault reporting

- APU indication

The APU is designed to automatically start when certain logic conditions are met when the aircraft is in the air or electrical power removed from left and right transfer buses from respective No. 1 and No. 2 engine generators.

15) Communications

For Communications Systems description, refer to *Section 1.9*.

1.6.9 Aircraft Performance

The detailed Boeing Performance analysis of the aircraft is provided in *Appendix 1.6E.* This section summarises the aircraft performance and range capability of MH370.

The following data were available to help analyse the possible flight paths of the aircraft: ACARS data, radar data, and satellite data. Wind data were incorporated along the paths to determine the true airspeed which was incorporated into the performance fuel burn and range analysis.

The ACARS data provided the quantity of fuel on board after approximately 25 minutes of flight following take-off from KUL.

The radar data provided information about the flight path and ground speed after the last ACARS transmission and captured the left turn off of the scheduled route until the data ended over the Straits of Malacca. The analysis of the radar data allowed for an estimation of the fuel burn during that portion of the flight. However, that estimation was built on many assumptions, including flying at constant altitude and constant airspeed during each flight segment.

The satellite data provided evidence that the satellite was in communication with the aircraft until the last transmission at time 0019:29.42 UTC, approximately 7 hours and 37 minutes after take-off from KUL. Refer to *Section 1.9.5*.

The performance range capability of the aircraft, along with the satellite data, allowed for the creation of multiple flight path profiles that demonstrate that the aircraft had the range capability to reach the 7th Arc[10].

[10] Arcs - Lines created along the earth representing a set of possible aircraft positions at the time of satellite communication based on Burst Timing Offset (BTO). Refer to *Appendix 1.6E* for further details.

Many assumptions were also made during the flight path profile creation, including but not limited to, constant altitude and constant speed from Arc 1 to Arc 7, with the restriction that there were no course changes between the arcs. Additional analyses were conducted in Boeing and MAS simulators that continued the analysis after fuel exhaustion and assumed no intervention in the cockpit.

The results of the simulator session showed that the aircraft would roll gently to the left due to residual rudder deflection commanded by the Thrust Asymmetry Compensation (TAC) with the end of flight occurring within a 100 nm^2 box that extended 10 nm beyond fuel exhaustion and 10 nm to the left of the flight path. The maximum range after dual engine flame-out would have been achieved through driftdown, with manual control keeping the aircraft in wings level flight, and would extend the range of the aircraft by approximately 120 nm beyond the location of the dual engine flame-out.

1.6.10 Boeing Patent on Remote Control Take-over of Aircraft

There have been speculations that MH370 could have been taken over control remotely in order to foil a hijack attempt. Some of these speculations have mentioned a US patent that Boeing filed for in February 2003 and received (US 7,142,971 B2) in November 2006 for a system that, once activated, would remove all controls from pilots and automatically fly and land the aircraft at a predetermined location.

According to the patent, existing preventative measures such as bullet-proof doors and the carriage of air marshals on board may have vulnerabilities. The flight crew could decide to open a lockable bullet-proof cockpit door [refer to *Section 1.6.8, para. 4*)] and air marshals, if used, might be over-powered. In light of the potential that unauthorised persons might be able to access the flight controls of an aircraft, the inventors conceived of a technique to avoid this risk by removing any form of human decision process that may be influenced by the circumstances of the situation, including threats or violence on-board.

The ‘uninterruptible’ autopilot envisioned by the patent could be activated, either by pilots, on-board sensors or remotely via radio or satellite links by the airline or government agencies if there were attempts to forcibly gain control of the cockpit. This system once activated would disallow pilot inputs and prevent anyone on-board from interrupting the automatic take-over. Thus, the personnel on-board could not be forced into carrying out the demands of any unauthorised person(s). To make it fully independent,

the system described in the patent would have its own power supply, inaccessible in-flight, so that it could not be disengaged by tripping circuit breakers accessible on-board the aircraft. The aircraft would remain in automatic mode until after landing when ground crew working in conjunction with authorised personnel would be called to disengage the system.

Boeing has confirmed that it has not implemented the patented system or any other technology to remotely pilot a commercial aircraft and is not aware of any Boeing commercial aircraft that has incorporated such technology. The technology was never installed on an aircraft.

It should also be noted that the aircraft 9M-MRO was delivered in May 2002 to MAS before the patent was issued in 2006. The aircraft was under the control of MAS for the entire time after delivery except for a short duration at Pudong, Shanghai Airport, China in August 2012, when it underwent wing tip repair by Boeing [refer to *Section 1.6.4, para. 2*)]. Even then the repair was under the oversight of MAS engineers. Aircraft modification installation data do not indicate that any systems like that described in the patent were installed on the aircraft post delivery and during in-service. Airworthiness protocols require that all modifications are approved for installation and a record kept of each modification incorporated. There is no reason to believe any systems like that described in the patent either were or could have been incorporated without the knowledge of MAS.

From the foregoing, there is no evidence to support the belief that control of the aircraft 9M-MRO (operating as MH370) could have been or was taken over remotely as the technology was not implemented on commercial aircraft.

SECTION 1 – FACTUAL INFORMATION

1.7 METEOROLOGICAL INFORMATION

1.7.1 Meteorological Situation

Climatologically for the month of March, the position of the sub-tropical high is located over the Gulf of Thailand. The weather is generally dry with very little clouds. The winds are generally light from the surface to the height of 40,000 ft above sea level.

The infra-red image taken by the geostationary satellite Multifunctional Transport Satellites (MTSAT) 1R of Japan Meteorological Agency (JMA) at 1732 UTC 07 March 2014 [0132 MYT 08 March 2014] *(Figure 1.7A* [below]*)* showed that there were no significant clouds at the last civil radar point at 1722 UTC, 07 March 2014 [0122 MYT, 08 March 2014].

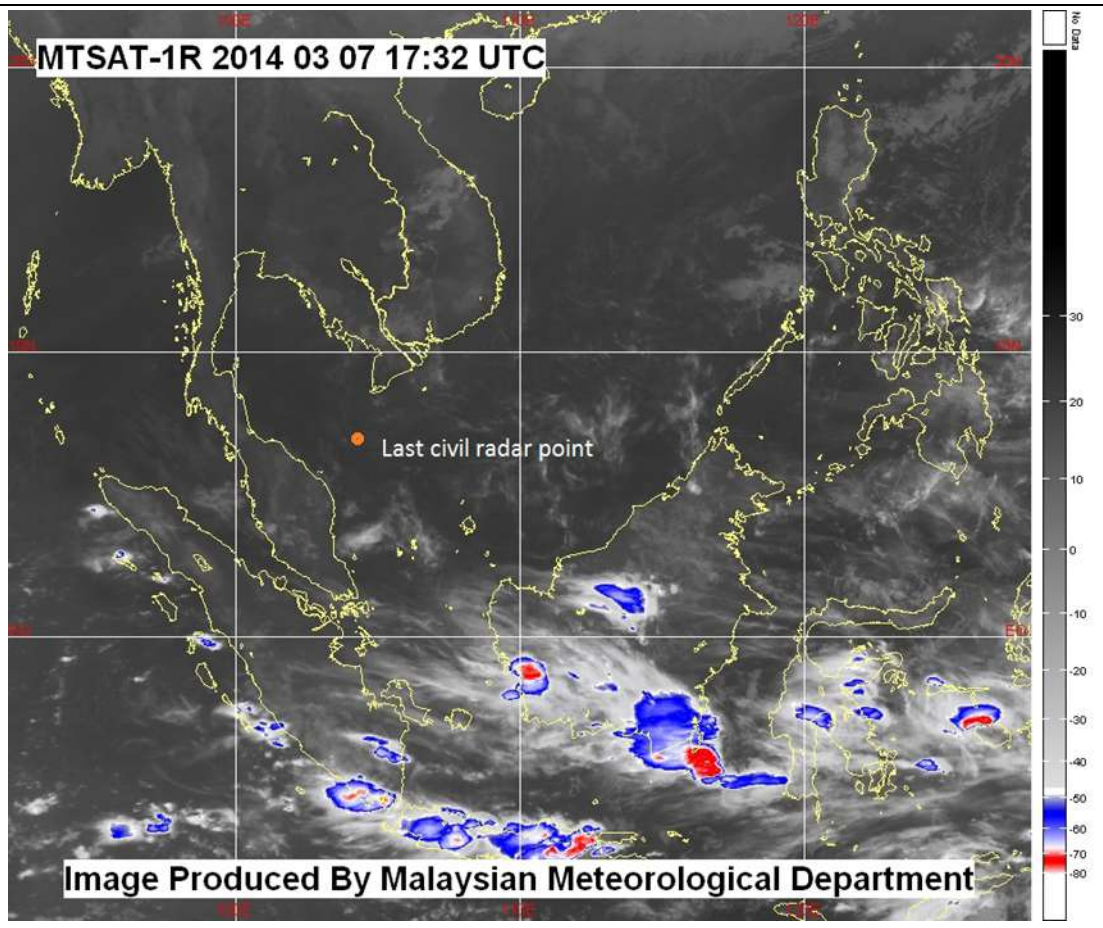

Source: Malaysian Meteorological Department

Figure 1.7A - Infrared Satellite image taken by MTSAT at 1732 UTC 07 March 2014 [0132 MYT, 08 March2014]

The meteorological radar image taken at 1722 UTC, 07 March 2014 [0122 MYT, 08 March 2014] (*Figure 1.7B* [below]) showed that no rain occurred at the last civil radar point.

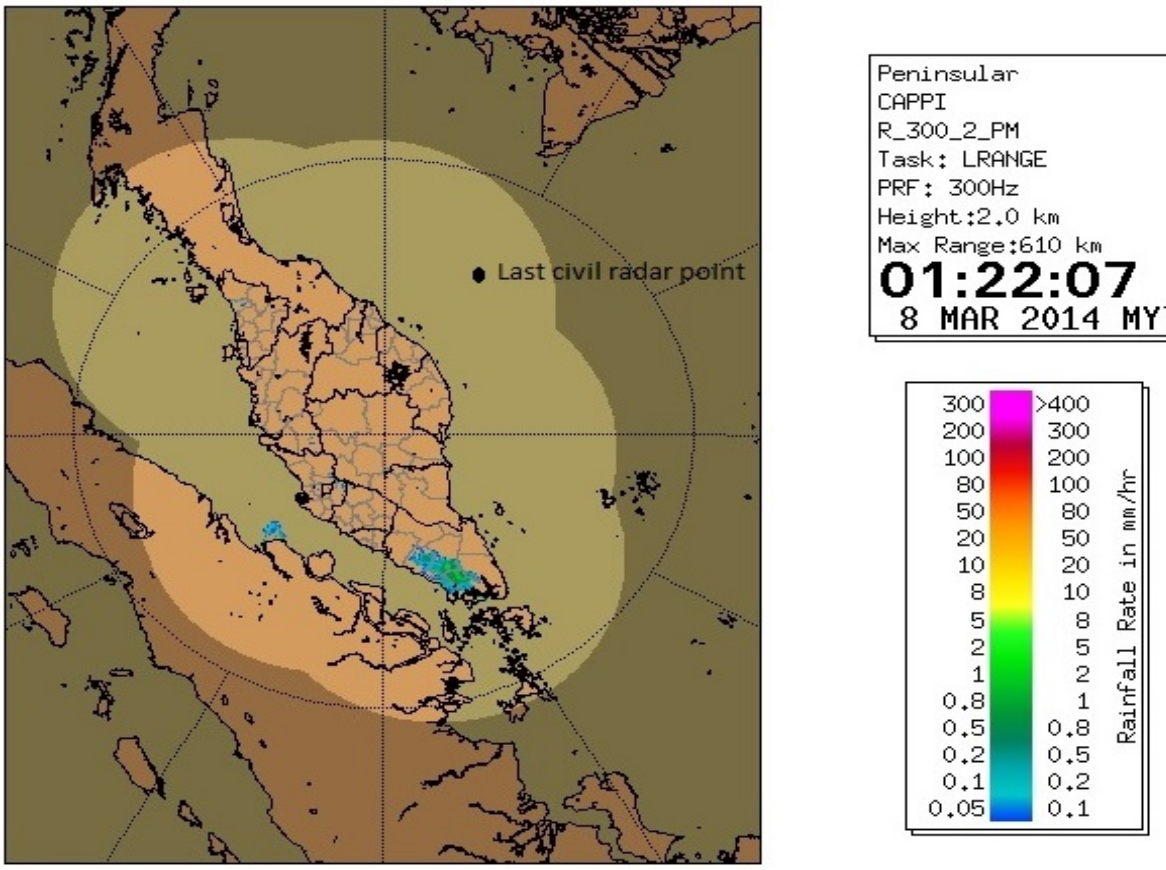

Source: Malaysian Meteorological Department

Figure 1.7B - Meteorological Radar Image at 1722 UTC 07 March 2014 [0122 MYT, 08 March 2014]

No lightning discharges were detected by the Lightning Detection System of the Malaysia Meteorological Department at the vicinity of last civil radar point from 1600 to 2159 UTC, 07 March 2014 [0000 to 0559 MYT, 08 March 2014]. *Figure 1.7C* (below) *Blue symbol* shows the lightning detected 1700 UTC to 1800 UTC, 07 March 2014 [0100 to 0200 MYT, 08 March 2014].

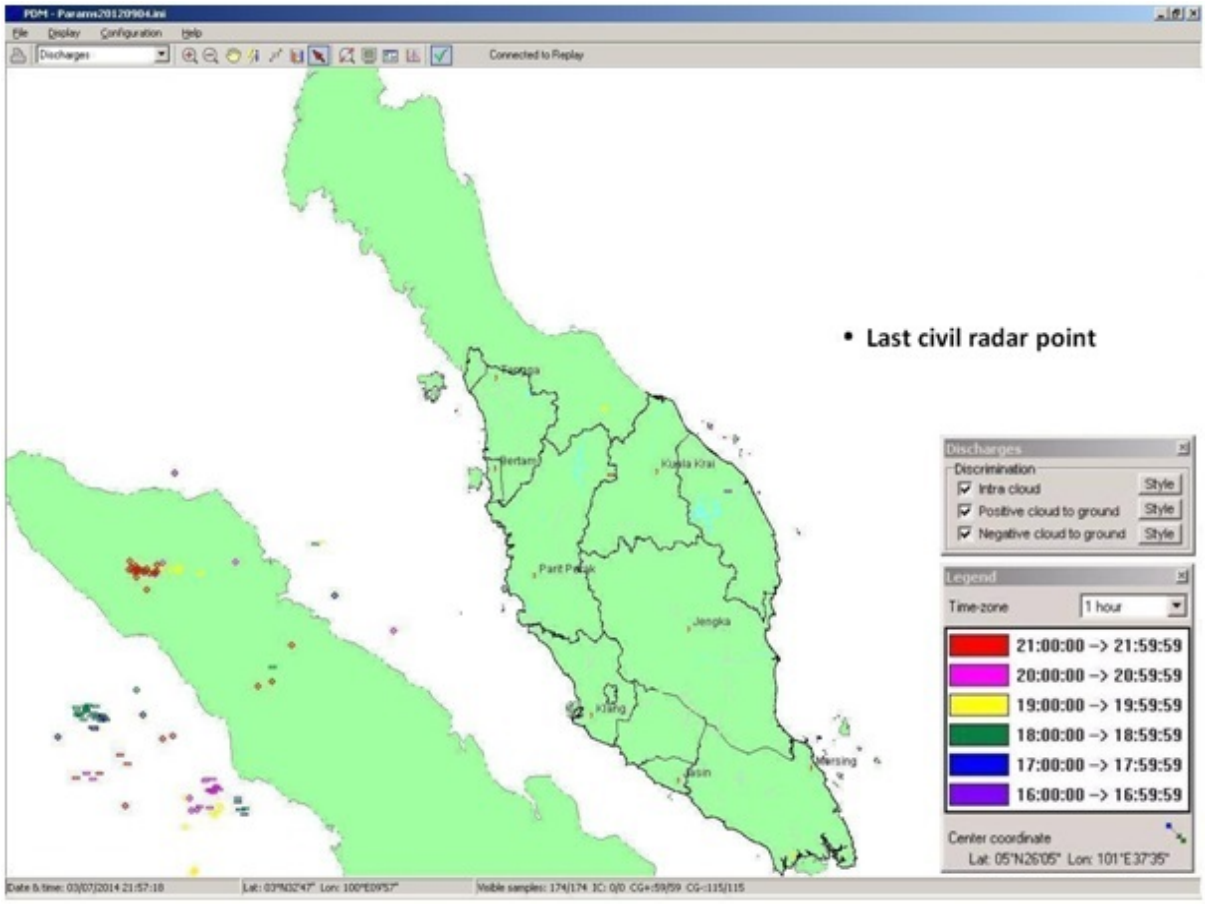

Source: Malaysian Meteorological Department

Figure 1.7C - Lightning Detection Map from 1600 to 2159 UTC 07 March 2014 [0000 to 0559, 08 March 2014]

The Meteorological Aerodrome Report (METAR) issued at 1600, 1700 and 1800 UTC [0000, 0100 and 0200 MYT, 08 March 2014] from Kota Bharu Sultan Ismail Petra Airport (WMKC), Kuala Terengganu Airport (WMKN), Penang International Airport (WMKP) and KLIA (WMKK) (*Figure 1.7D* [below]) did not report any significant weather phenomena.

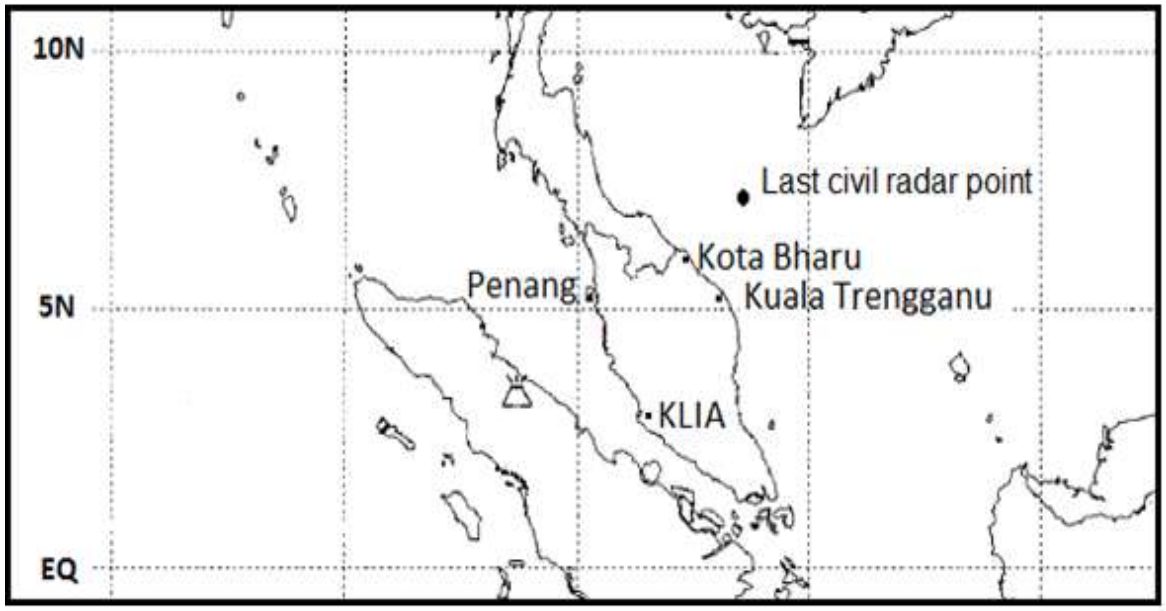

Source: Malaysian Meteorological Department

Figure 1.7D - Locations of METAR Reports

There was no direct observation of the wind conditions at the last civil radar point, the closest upper air observation was at the Kota Bharu Meteorological Station, taken at 1200 UTC, 07 March 2014 and at 0000 UTC, 08 March 2014 [2000 MYT, 07 March 2014 and 0800 MYT, 08 March 2014] respectively, both reported a temperature of -40ºC and wind from the north-east at 15 kt or less at 36,000 ft above sea level.

1.7.2 Comments on the Information Available

1) Forecast Charts

a) Significant Weather Chart

The Significant Weather Chart (SIGWX) *PGCE05 EGRR 061800* issued by World Area Forecast Centre (WAFC) London Fixed Time Prognostic Chart ICAO Area G SIGWX for FL250-630 (25,000 ft to 63,000 ft above standard sea-level pressure) valid 1800 UTC, 07 March 2014 [0200 MYT, 08 March 2014] showed that the filed flight plan route (red dotted line - *Figure. 1.7E* [below]) passed through a westerly jet stream with wind speed of up to 150 kt at latitude 30°N at FL390. Another westerly jet stream with wind speed of up to 100 kt at FL310 at the destination. Light clear air turbulence (CAT) might be expected from 25°N onwards

to the destination. However, no significant adverse weather phenomenon was expected for the whole planned flight route.

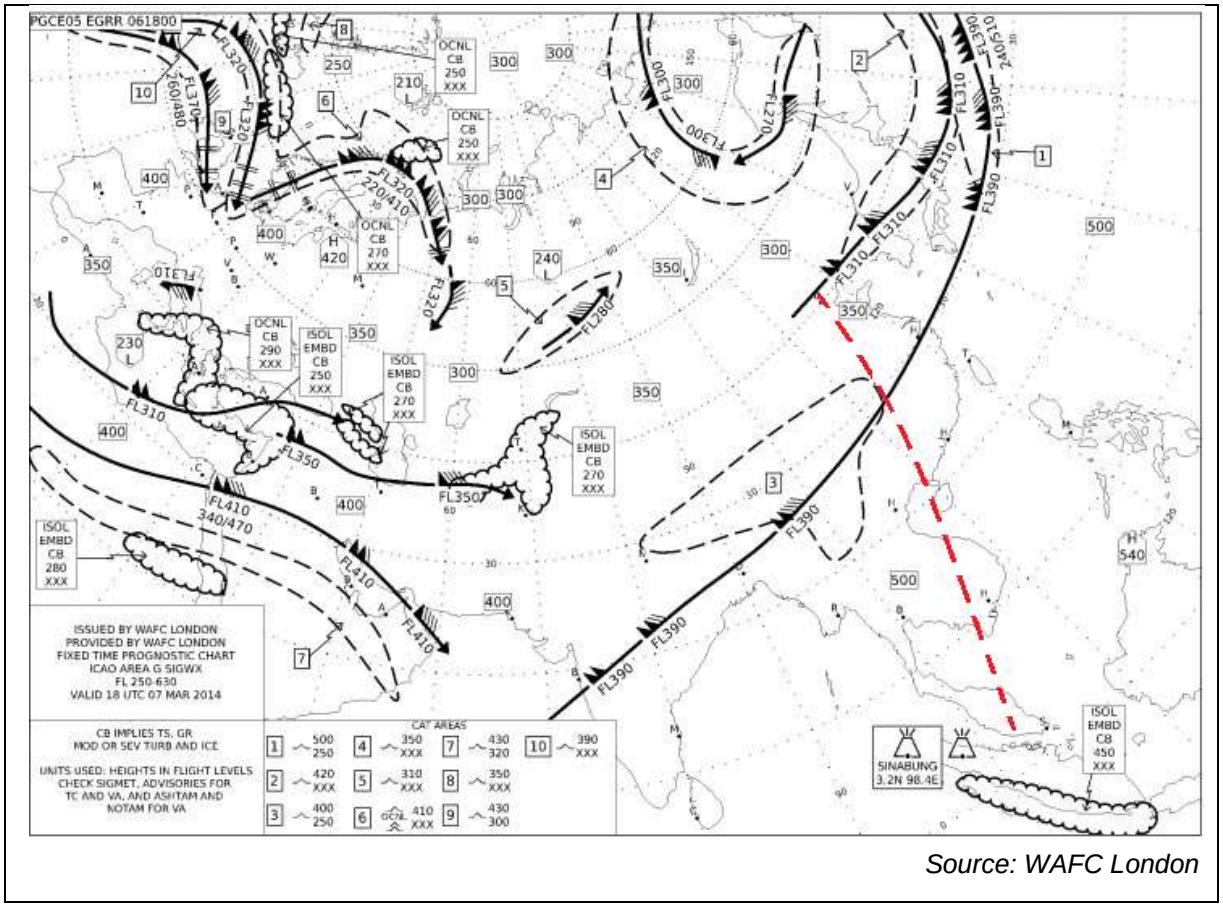

Source: WAFC London

Figure 1.7E - Significant Weather Chart PGCE05 Issued by WAFC London Fixed Time ICAO Area G Prognostic Chart SIGWX FL250-630 valid 1800 UTC, 07 March 2014 [0200 MYT, 08 March 2014

b) Wind and Temperature Forecast Chart

The wind and temperature forecast chart PWGE25 for FL340 valid 1800 UTC, 07 March 2014 issued by WAFC Washington showed the jet stream as in the significant weather chart above. The forecast winds at the last civil radar point and last air defence radar point were below 20 kt *(Figure 1.7F* [below]).

2) Significant Meteorological Information

Significant Meteorological Information (SIGMET) 3 was issued for the GUANGZHOU FIR valid from 12:45 to 16:45 UTC, 07 March 2014 [0200 MYT, 08 March 2014] indicated a thunderstorm forecast north of latitude 27°N and moving eastwards at 50 km/h in the layer with cloud tops at FL260.

3) Volcanic Ash Advisory

Volcanic ash advisories issued by Darwin Volcanic Ash Advisory Centre (VAAC) on 07 March 2014 at 06:27 and 18:37 UTC [2045 MYT, 07 March 2014 and 0045 MYT, 08 March 2014] for Sinabung (Sumatra, Indonesia) highlighted volcanic eruption located at 3.10°N 98.23°E (*Figure 1.7E* [above]*)* and volcanic ash plume observed up to FL120 and the plume was extending toward the west.

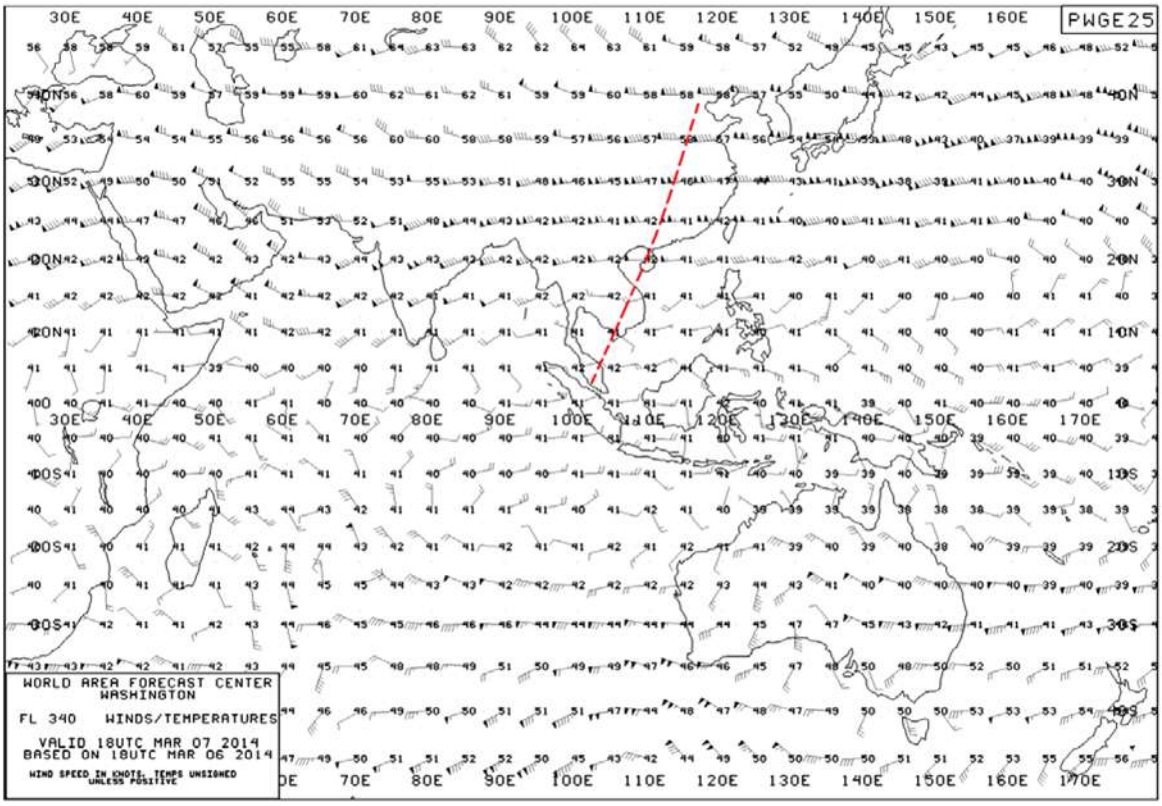

Source: WAFC Washington

Figure 1.7F - The wind and temperature forecast chart PWGE25 issued by WAFC Washington for FL340 valid 1800 UTC 07 March 2014 [0200 MYT, 08 March 2014]

1.7.3 Availability of Meteorological Information

The necessary meteorological information was made available to the crew.

SECTION 1 – FACTUAL INFORMATION

1.8 AIDS TO NAVIGATION

Not applicable.

SECTION 1 – FACTUAL INFORMATION

1.9 COMMUNICATIONS

1.9.1 High Frequency System

This aircraft was installed with Collins HFS-900 High Frequency (HF) System. The HF communication system on this aircraft uses two HF systems with a common HF antenna to transmit and receive radio frequency (RF) signals in the HF range.

The HF transceiver operates within the frequency range of 2,000 MHz to 29,999 MHz and one KHz channel spacing.

The Left Transfer bus sends 115V AC three-phase power to the Left HF communication system. The Left HF communication transceiver supplies 115V AC single phase to the Left HF antenna coupler for operational power. It also supplies 28V DC for the key interlock function. The Right HF communication system is the same as the Left, except that it uses power from the Right AC Sec 2 bus.

1.9.2 Very High Frequency System

This aircraft was installed with Collins VHF-900B VHF System. The very high frequency (VHF) communication system permits voice and data communication over line-of-sight distances. It permits communication between aircraft or between ground stations and aircraft. The VHF system operates in the VHF aeronautical frequency range of 118.000 MHz to 136.992 MHz.

The VHF communication system on this aircraft uses three VHF systems. Each VHF system has a VHF antenna and a VHF communication transceiver.

The VHF communication system connects with Selective Calling Equipment (SELCAL) decoder that starts an alert when a call comes in for that aircraft.

The captain’s flight instrument bus sends 28V DC to the Left VHF communication transceiver and the Left Radio Tuning Panel (RTP). The Left Main DC bus sends 28V DC to the centre VHF communication transceiver and the centre RTP.

The Right Main DC bus sends 28V DC to the right VHF communication transceiver and the right RTP.

1.9.3 Air Traffic Control/Mode S Transponder System

This aircraft was installed with a Bendix/King TRA-67A Mode S transponder. The Air Traffic Control (ATC) ground stations interrogate the airborne ATC/Mode S transponder system as shown in *Figure 1.9A* (below).

The ATC/Mode S transponder replies to the interrogations in the form of coded information that the ground station uses. The ground station uses a Primary Surveillance Radar (PSR) to get radar returns from aircraft within the radar range. To make a communication link with the aircraft in the radar range, the ground station uses a Secondary Surveillance Radar (SSR) to interrogate the ATC/Mode S transponder. The ground station transmits a side lobe suppression signal to inhibit close ATC replies that come from a SSR side lobe transmission.

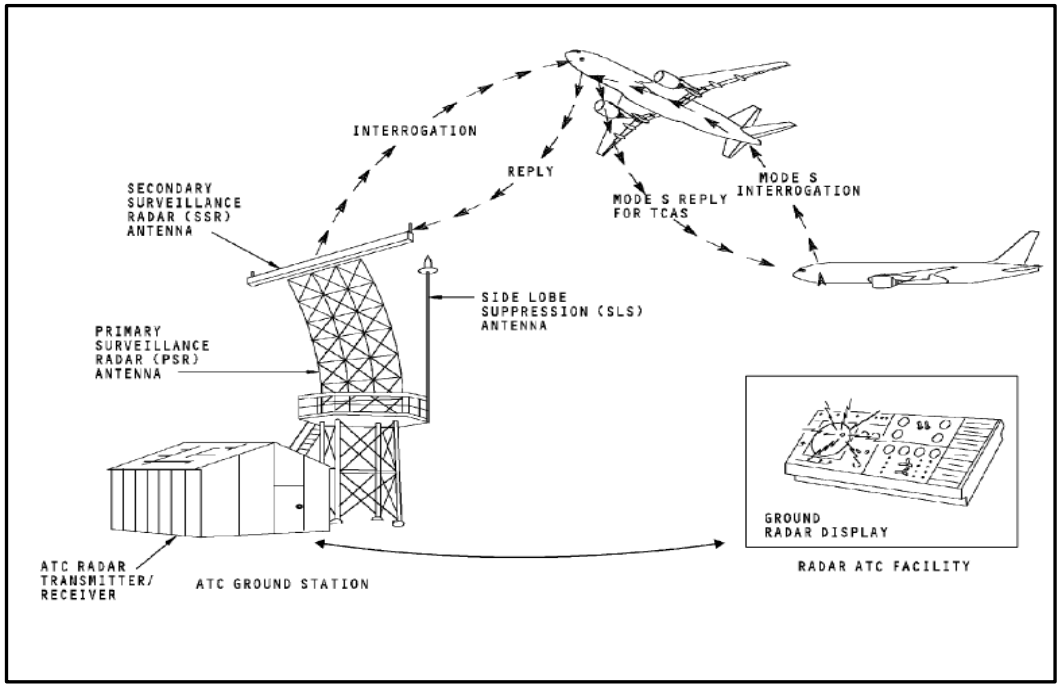

Copyright © Boeing. Reprinted with permission of The Boeing Company

Figure 1.9A - Air Traffic Control/Mode S Transponder System

On the ground radar display, the Air Traffic Controller (ATC) sees the radar returns, altitude, and a four digit aircraft identifier. The ATC also sees aircraft derived Enhanced Surveillance downlink data on the ground station radar display, such as Magnetic Heading, Air Speed (Indicated Air Speed and Mach number), Ground Speed, Roll Angle, Selected Altitude, True Track Angle, and Vertical Rate.

The ATC/Mode S transponder also replies to mode S interrogations from the Traffic Alert and Collision Avoidance Systems (TCAS) of other aircraft. ATC/Mode S transponders with Extended Squitter function provide broadcast of Global Position System (GPS) position and velocity data.

Two transponders are installed on the aircraft. A Transponder selector switch on the Transponder panel in the cockpit allows selection of either the left or the right transponder. During normal operations the crew procedure is to leave the left transponder selected on the panel. There is no automatic switching between the transponders if one fails. It must be done manually by the pilots. Failure of either of the transponders will be annunciated in the cockpit. The Left ATC/Mode S transponder gets 115V AC power from the AC Standby bus. The Right ATC/Mode S transponder gets 115V AC power from the Right AC Transfer bus. The dual transponder panel gets 115V AC power from the AC Standby bus. The two transponders are powered by highly reconfigurable AC buses; the left one can be powered by the battery if the left AC bus is unavailable (the AC Standby bus can be powered by the left Transfer bus or the battery), and the AC Transfer busses also have their alternate sources.

This system can be deactivated (turned OFF) by pulling the circuit breakers located at the P11 overhead circuit breaker panel or by selecting the Transponder Mode Selector (Transponder Panel) to “STBY” position. The transponder on the occurrence flight was operating satisfactorily up to the time it was lost on the ATC radar screen at 1721.13 UTC, 07 March 2014 [0121:13 MYT, 08 March 2014]. There was no message received from the aircraft to report a system failure.

1.9.4 Aircraft Communications Addressing and Reporting System

The Aircraft Communications Addressing and Reporting System (ACARS) is a digital data-link system that manages flight plan and maintenance data between the aircraft and the Ground Service Provider (GSP) by using radio i.e. VHF or satellite communications (SATCOM) as shown in *Figure 1.9B* (below).

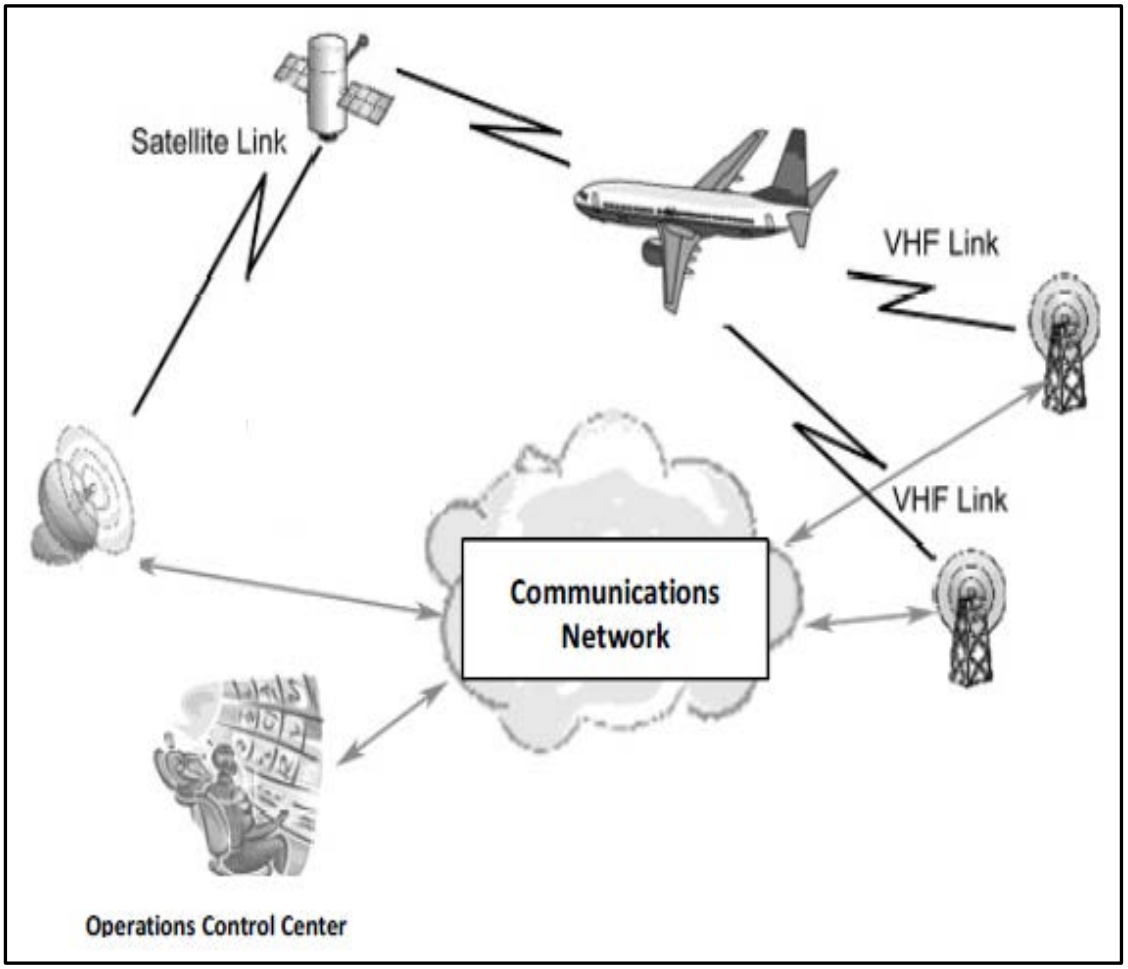

Figure 1.9B - ACARS System

ACARS provides message communication between aircraft and its base (ground). The following messages are transmitted:

- **O**ut of the gate, **O**ff the ground, **O**n the ground, and **I**nto the gate (OOOI) events:
  - **O**ut of the gate event: Departure from the gate with all doors closed and parking brake released;
  - **O**ff the ground event: Take-off with the nose gear squat switch extended;
  - **O**n the ground event: Touch down with the nose gear squat switch compressed; and
  - **I**nto the gate event**:** Parked at the gate with the parking brake set and the door open.

- Flight plans: ACARS interfaces with Flight Management Systems (FMS) acting as the communication system for flight plans to be sent from the ground to the FMS. This enables the aircraft to update the FMS while in flight and allows the flight crew to evaluate the alternative flight plans including the status of connecting flights.

- Weather information: ACARS interfaces with FMS, acting as the communication system for weather information to be sent from the ground to the FMS. This enables the aircraft to update the FMS while in flight and allows the flight crew to evaluate new weather conditions.

- Equipment health: ACARS is used to send information from the aircraft to ground stations about the conditions of various aircraft systems and sensors in real-time. Maintenance faults and abnormal events are also transmitted to ground stations along with detailed messages, which are used by MAS for monitoring equipment health, and to better plan the repair and maintenance activities.

- Aircraft positions which provide latitude and longitude, altitude, speed, total air temperature, total remaining fuel, wind direction and speed and heading.

- Engine performance data which provide engine data during take-off, climb, cruise and approach.

ACARS interfaces with the Multifunction Display (MFD) in the cockpit, which flight crew can use to send and receive technical messages and reports to or from ground stations, such as a request for weather information or clearances or the status of connecting flights. The response from the ground station is received on the aircraft via ACARS as well. The ACARS Manager page in the Communications main menu on the selected Multifunction Display (MFD) is used for this purpose. The COMM display switch, located on the display select panel, displays the communications main menu on the selected MFD. The ACARS Manager page allows the flight crew to independently select/deselect VHF or SATCOM transmission of data.

The ACARS communicates through either the VHF or the SATCOM systems. The ACARS datalink connects to the Satellite Data Unit (SDU) of the SATCOM system and the Center and Right VHF Communication Transceivers of the VHF systems. The Center VHF exchanges data with the ACARS modem in the Communications Core Processor Module (CPM/Comm) of the Left AIMS cabinet. The right VHF exchanges data with

the ACARS modem in the CPM/Comm of the Right AIMS cabinet. The ACARS does not interface with the Left VHF Transceiver.

For the ACARS operation the Data Communication Management Function (DCMF) of the AIMS uses the voice/data select to set the VHF Communication Transceiver to the data signal mode. At power-up, the DCMF sets the Center VHF Communication Transceiver to the data signal mode. If the Center VHF Communication Transceiver fails, or voice is selected manually by the flight crew, the DCMF selects SATCOM for data transmissions. If SATCOM fails, the DCMF selects the Right VHF Communication Transceiver for data transmissions. The Left VHF Communication Transceiver is voice only. On the event flight, as instructed by Ground Operations via text message shown on the MFD (shown as 'Switch VHF3 to Voice'), the flight crew would have selected voice on the Center VHF resulting in SATCOM being used for the data transmissions. Refer to page 1 of *Appendix 1.9A – ACARS Traffic Log*. The use of SATCOM for the ACARS transmissions is evident in the SATCOM Ground Station Logs [refer to *Section 1.9.5*, *para. 4*)]. This switching from VHF to SATCOM for the data transmissions is normal practice in MAS for commercial reasons.

In the event that the aircraft ACARS unit has been silent for longer than a pre-set time interval, the ground station can ping the aircraft (directly or via satellite). A ping response indicates a healthy ACARS communication. This ping is different from the Satellite ping or handshake.

Pre-set time interval for MAS B777 is 30 minutes. When the aircraft ACARS is silent for more than 30 minutes, MAS Operation Control Centre (OCC) is required to send a text message via ACARS to the cockpit or to call the cockpit via SATCOM.

1) Aircraft Communications Addressing & Reporting System Traffic Log

ACARS traffic log messages sent/received to/from 9M-MRO between 1554:41 UTC, 07 March 2014 [2354:41 MYT, 07 March 2014] until 1815:25 UTC, 07 March 2014 [0215:25 MYT, 08 March 2014] is shown in *Appendix 1.9A*. Some key events are extracted and explained below.

At 1554:41 UTC, 07 March 2014, ACARS data link was fully established on SATCOM transmission and at 1556:08 UTC the flight information (FI) MH0370 and Aircraft Number (AN) 9M-MRO were keyed in by the crew as per *Figure 1.9C* (below).

Figure 1.9C - ACARS data link established SATCOM transmission

Notice to Crew (NOTOC) was sent at 1606:15 UTC on 07 March 2014 [0006:15 MYT, 08 March 2014] direct to the aircraft printer and to be printed out by the crew.

NOTOC from the ground station to the cockpit stated the special loads of total 4,566 kg of mangosteens were carried on board. Details of the mangosteens were:

- 1,128 kg at station 41L,
- 1,152 kg at station 41R,
- 1,148 kg at station 43L, and
- 1,138 kg at 44L respectively.

(Refer to *Section 1.18.2* for details of cargo carried).

Declaration of *"there is no evidence that any damaged or leaking packages containing dangerous goods have been loaded on the aircraft at this station"* was also written in the NOTOC message. *Figure 1.9D* (below) shows the snapshot of the ACARS NOTOC message.

Aircraft final loadsheet was sent via ACARS at 1606:32 UTC, 07 March 2014 [0006:32 MYT, 08 March 2014] direct to the aircraft printer and to be printed out by the crew. Details of aircraft weight as stated in the final loadsheet are discussed in *Section 1.6.5*.

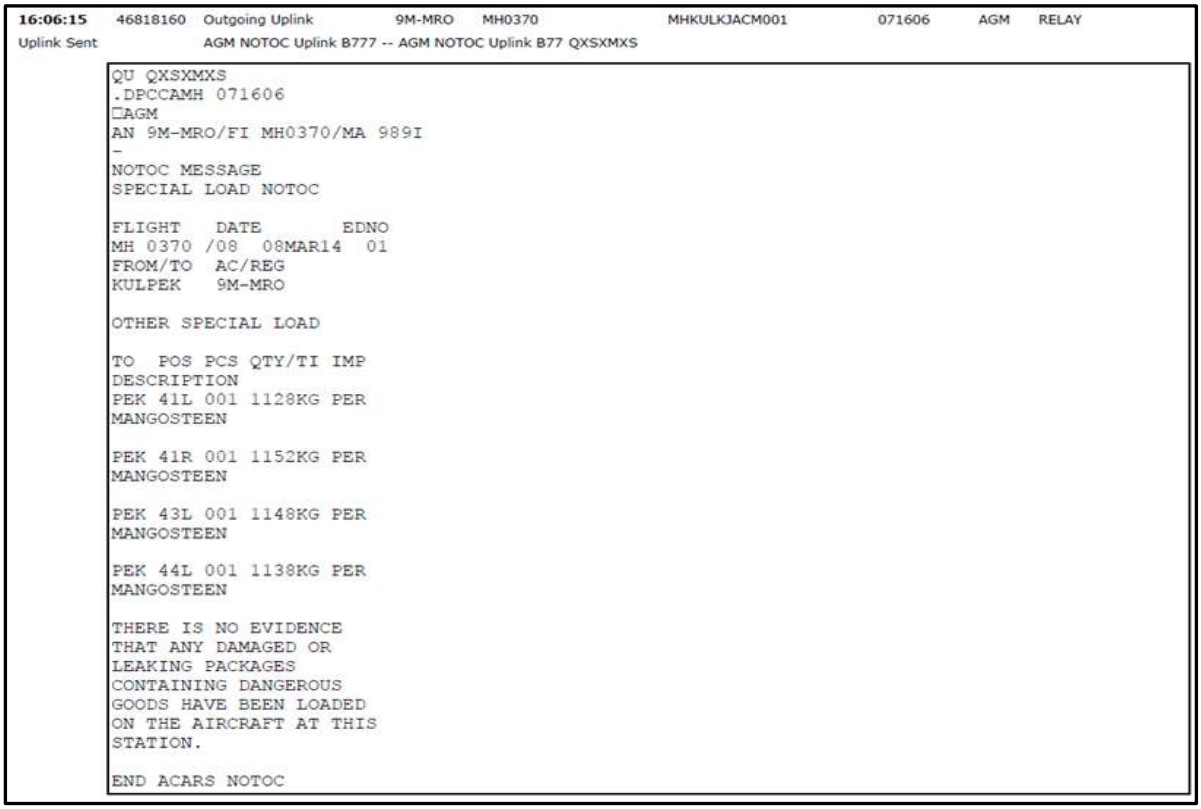

16:06:15 46818160 Outgoing Uplink 9M-MRO MH0370 MHKULKJACM001 071606 AGM RELAY
Uplink Sent AGM NOTOC Uplink B777 -- AGM NOTOC Uplink B77 QXSXMXS

```
QU QXSXMXS
.DPCCAMH 071606
□AGM
AN 9M-MRO/FI MH0370/MA 989I
-
NOTOC MESSAGE
SPECIAL LOAD NOTOC

FLIGHT   DATE       EDNO
MH 0370 /08  08MAR14  01
FROM/TO  AC/REG
KULPEK   9M-MRO

OTHER SPECIAL LOAD

TO  POS PCS QTY/TI IMP
DESCRIPTION
PEK 41L 001 1128KG PER
MANGOSTEEN

PEK 41R 001 1152KG PER
MANGOSTEEN

PEK 43L 001 1148KG PER
MANGOSTEEN

PEK 44L 001 1138KG PER
MANGOSTEEN

THERE IS NO EVIDENCE
THAT ANY DAMAGED OR
LEAKING PACKAGES
CONTAINING DANGEROUS
GOODS HAVE BEEN LOADED
ON THE AIRCRAFT AT THIS
STATION.

END ACARS NOTOC
```

Figure 1.9D - Snapshot of ACARS NOTOC message

Figure 1.9E (below) shows the snapshot of the final loadsheet of this aircraft.

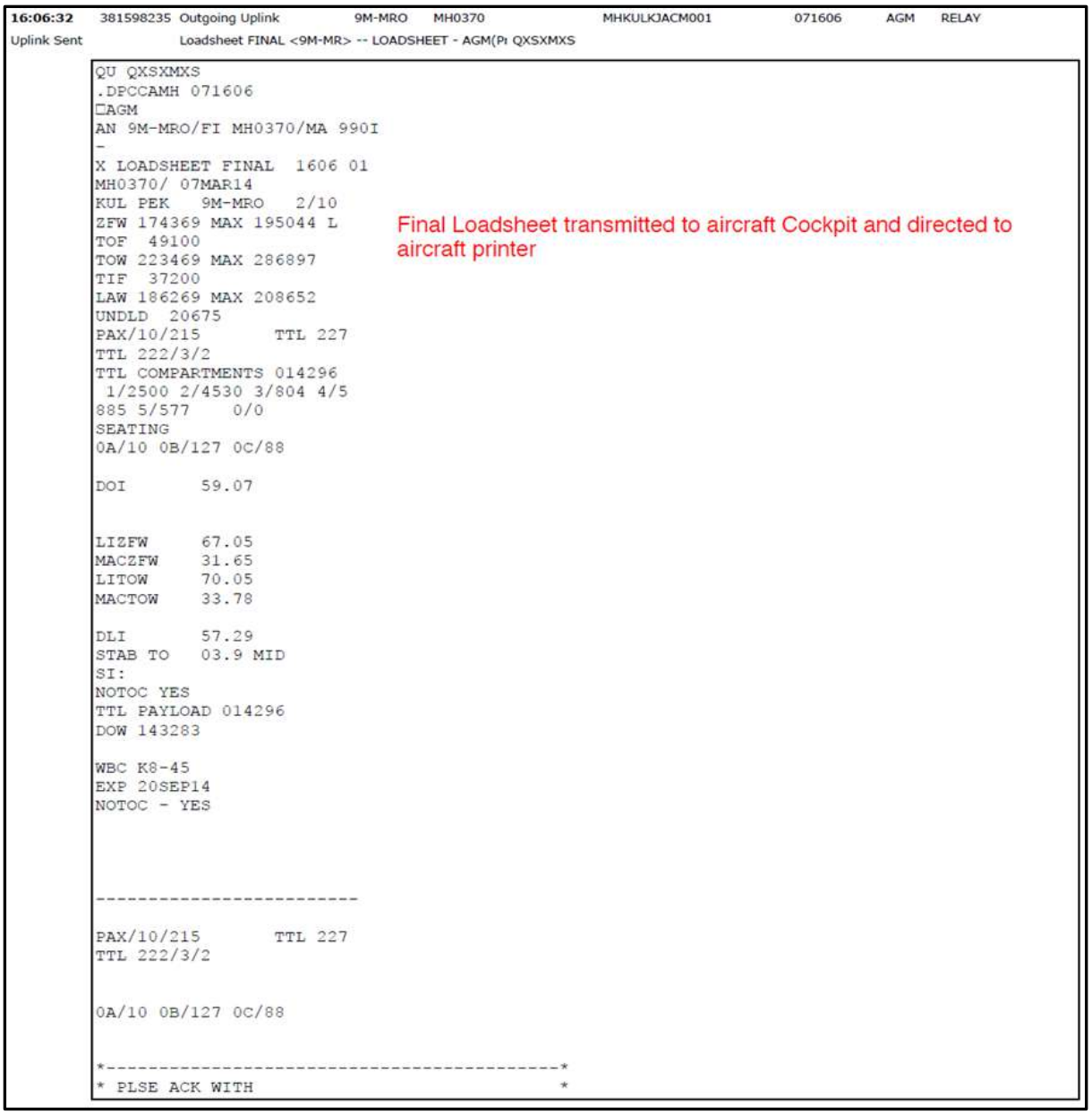

16:06:32 381598235 Outgoing Uplink 9M-MRO MH0370 MHKULKJACM001 071606 AGM RELAY
Uplink Sent Loadsheet FINAL <9M-MR> -- LOADSHEET - AGM(P1 QXSXMXS

```
QU QXSXMXS
.DPCCAMH 071606
□AGM
AN 9M-MRO/FI MH0370/MA 990I
-
X LOADSHEET FINAL  1606 01
MH0370/ 07MAR14
KUL PEK   9M-MRO   2/10
ZFW 174369 MAX 195044 L
TOF  49100
TOW 223469 MAX 286897
TIF  37200
LAW 186269 MAX 208652
UNDLD  20675
PAX/10/215       TTL 227
TTL 222/3/2
TTL COMPARTMENTS 014296
 1/2500 2/4530 3/804 4/5
885 5/577    0/0
SEATING
0A/10 0B/127 0C/88

DOI       59.07


LIZFW     67.05
MACZFW    31.65
LITOW     70.05
MACTOW    33.78

DLI       57.29
STAB TO   03.9 MID
SI:
NOTOC YES
TTL PAYLOAD 014296
DOW 143283

WBC K8-45
EXP 20SEP14
NOTOC - YES



-------------------------

PAX/10/215       TTL 227
TTL 222/3/2


0A/10 0B/127 0C/88


*--------------------------------------------*
* PLSE ACK WITH                              *
```

Final Loadsheet transmitted to aircraft Cockpit and directed to aircraft printer

Figure 1.9E - Final Loadsheet

Pilot acknowledgement and confirmation of the final loadsheet is shown in the ACARS snapshot in *Figure 1.9F* (below).

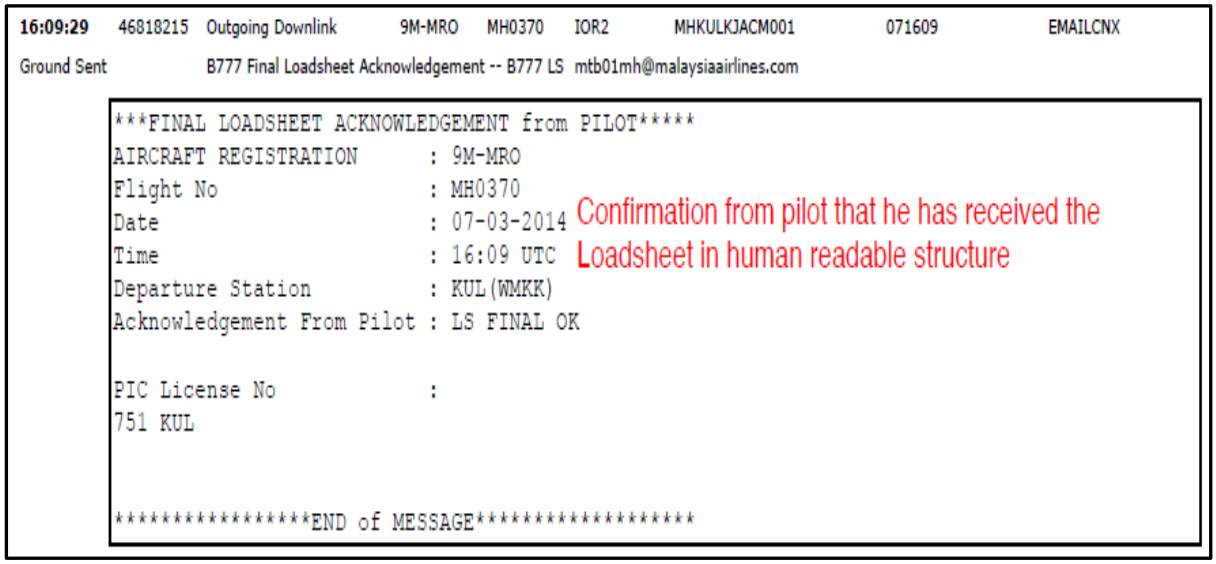

16:09:29 46818215 Outgoing Downlink 9M-MRO MH0370 IOR2 MHKULKJACM001 071609 EMAILCNX

Ground Sent B777 Final Loadsheet Acknowledgement -- B777 LS mtb01mh@malaysiaairlines.com

```
***FINAL LOADSHEET ACKNOWLEDGEMENT from PILOT*****
AIRCRAFT REGISTRATION      : 9M-MRO
Flight No                  : MH0370
Date                       : 07-03-2014
Time                       : 16:09 UTC
Departure Station          : KUL(WMKK)
Acknowledgement From Pilot : LS FINAL OK

PIC License No             :
751 KUL


*****************END of MESSAGE*******************
```

Confirmation from pilot that he has received the Loadsheet in human readable structure

Figure 1.9F - Final Loadsheet Acknowledgement

Data on aircraft APU is shown in *Figure 1.9G* (below). APU report generated by ACMS sent via ACARS at 1629:33 UTC stated the total APU cycles and hours were 15,699 cycles and 22,093 hours. APU hours for the previous flight was 4 hours.

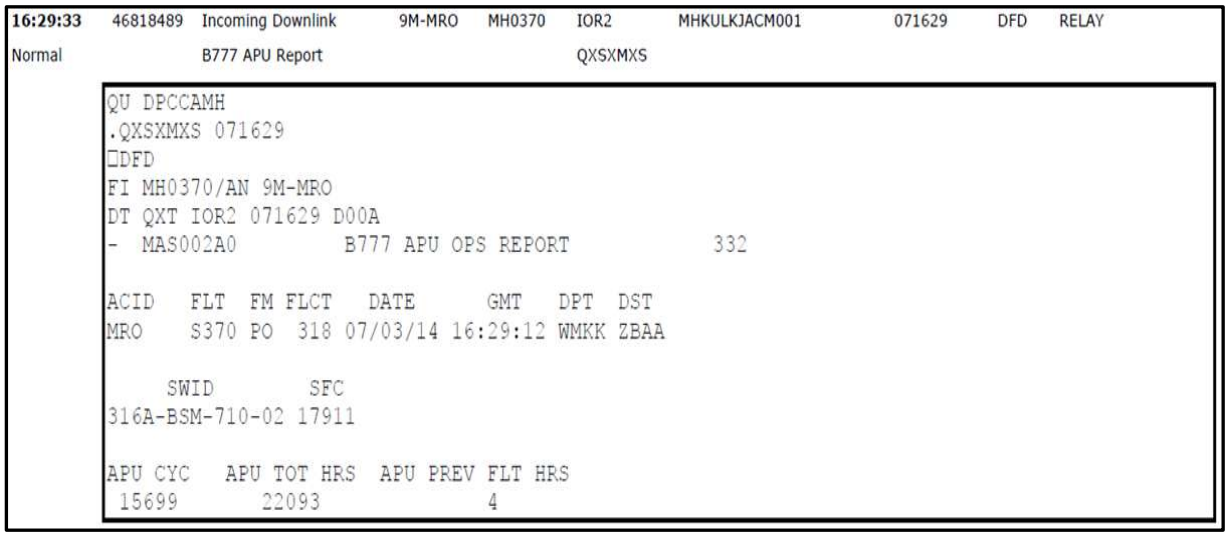

16:29:33 46818489 Incoming Downlink 9M-MRO MH0370 IOR2 MHKULKJACM001 071629 DFD RELAY

Normal B777 APU Report QXSXMXS

```
QU DPCCAMH
.QXSXMXS 071629
□DFD
FI MH0370/AN 9M-MRO
DT QXT IOR2 071629 D00A
-  MAS002A0          B777 APU OPS REPORT            332

ACID    FLT  FM FLCT   DATE       GMT    DPT  DST
MRO     S370 PO  318 07/03/14 16:29:12 WMKK ZBAA

     SWID         SFC
316A-BSM-710-02 17911

APU CYC    APU TOT HRS   APU PREV FLT HRS
 15699        22093              4
```

Figure 1.9G - APU Report

Engine take-off and climb reports transmitted via ACARS are explained in *Section 1.6.4 para. 8*). Engine parameter reports were transmitted to MAS and then to Rolls Royce for Engine Health Monitoring (EHM). *Appendix 1.9A* shows these data in coded form. The decoded data are shown in *Appendix 1.6B*.

The first (which was also the last) position report was transmitted via ACARS at 1707:29 UTC, 07 March 2014 [0107:29 MYT, 08 March 2014]. This was a collation of 6 reports generated at 5-minute intervals by the system at 1641:43 UTC, 1646:43 UTC, 1651:43 UTC, 1656:43 UTC, 1701:43 UTC and 1706:43 UTC, 07 March 2014. Parameters transmitted are as per *Table 1.9A* (below). The actual traffic log on the position report is reproduced in *Figure 1.9H* (below). Position reports were programmed to be transmitted every 30 minutes.

Note:

Aircraft position information is also included in the EHM take-off and climb reports.

Greenwich Mean Time (GMT) - UTC	**1641:43**	**1646:43**	**1651:43**	**1656:43**	**1701:43**	**1706:43**
Altitude (ALT) – Feet	103	10,582	21,193	28,938	34,998	35,004
Calibrated Airspeed (CAS) - Knots.	168.4	261.8	301.1	303.1	278.0	278.4
MACH	0.255	0.478	0.669	0.783	0.819	0.821
Total Air Temperature (TAT) - °C	31.1	23.4	11.6	2.5	-13.4	-13.1
Static Air Temperature (SAT) - °C	27.3	10.4	-11.8	-27.4	-43.9	-43.8
Latitude (LAT)	2.667	3.074	3.553	4.109	4.708	5.299
Longitude (LONG)	101.715	101.760	01.988	102.251	102.434	102.713
Gross Weight (GWT) – lb	492,520	489,200	486,240	483,840	481,880	480,600
Total Remaining Fuel Weight (TOTFW) - kg	49,200	47,800	46,500	45,400	44,500	43,800
Wind Direction (WINDIR)	140.3	107.6	1.8	58.4	69.6	70.0
Wind Speed (WINDSP)	1.25	9.38	19.50	10.63	17.38	17.13
True Heading (THDG)	-33.5	27.7	27.8	26.0	26.8	26.7

Table 1.9A - ACARS Position Report

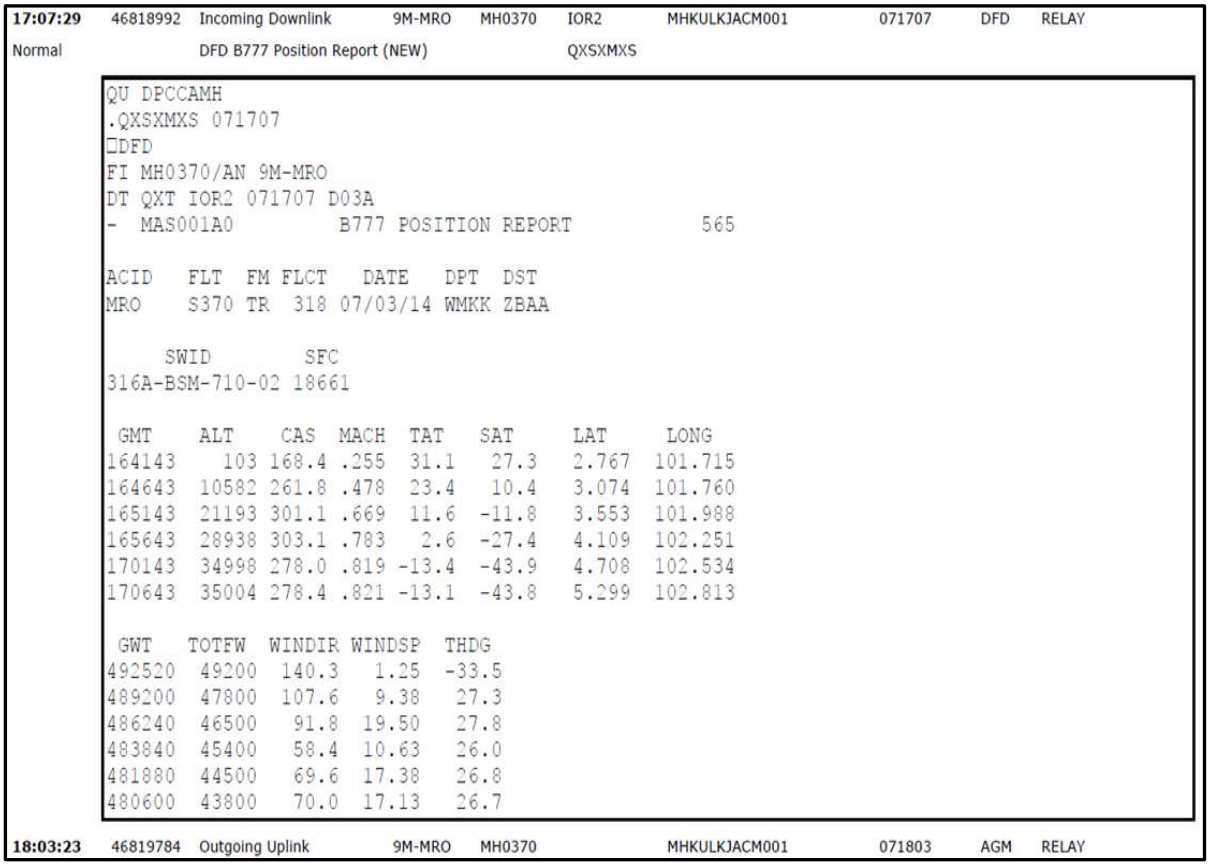

17:07:29 46818992 Incoming Downlink 9M-MRO MH0370 IOR2 MHKULKJACM001 071707 DFD RELAY
Normal DFD B777 Position Report (NEW) QXSXMXS

```
QU DPCCAMH
.QXSXMXS 071707
□DFD
FI MH0370/AN 9M-MRO
DT QXT IOR2 071707 D03A
-  MAS001A0          B777 POSITION REPORT           565

ACID   FLT  FM FLCT   DATE   DPT  DST
MRO    S370 TR  318 07/03/14 WMKK ZBAA

     SWID         SFC
316A-BSM-710-02 18661

 GMT    ALT    CAS  MACH  TAT   SAT     LAT     LONG
164143    103 168.4 .255  31.1   27.3   2.767  101.715
164643  10582 261.8 .478  23.4   10.4   3.074  101.760
165143  21193 301.1 .669  11.6  -11.8   3.553  101.988
165643  28938 303.1 .783   2.6  -27.4   4.109  102.251
170143  34998 278.0 .819 -13.4  -43.9   4.708  102.534
170643  35004 278.4 .821 -13.1  -43.8   5.299  102.813

 GWT   TOTFW  WINDIR WINDSP  THDG
492520  49200  140.3   1.25  -33.5
489200  47800  107.6   9.38   27.3
486240  46500   91.8  19.50   27.8
483840  45400   58.4  10.63   26.0
481880  44500   69.6  17.38   26.8
480600  43800   70.0  17.13   26.7
```

18:03:23 46819784 Outgoing Uplink 9M-MRO MH0370 MHKULKJACM001 071803 AGM RELAY

Figure 1.9H - Position Report

The first message sent to the aircraft cockpit printer from the MAS ODC was at 1803:23 UTC. The ACARS message requested the crew to contact the HCM ACC immediately. The incoming downlink message at 1803:24 UTC showed the message failed to reach the aircraft. Messages are auto transmitted every 2 minutes and the message was retransmitted until 1843:33 UTC but all messages failed to get a response. Automated downlink message by ACARS showed ‘failed’. Message sent to the aircraft cockpit printer and the Automated Downlink messages are shown in *Figures 1.9I* and *1.9J* (below), respectively.

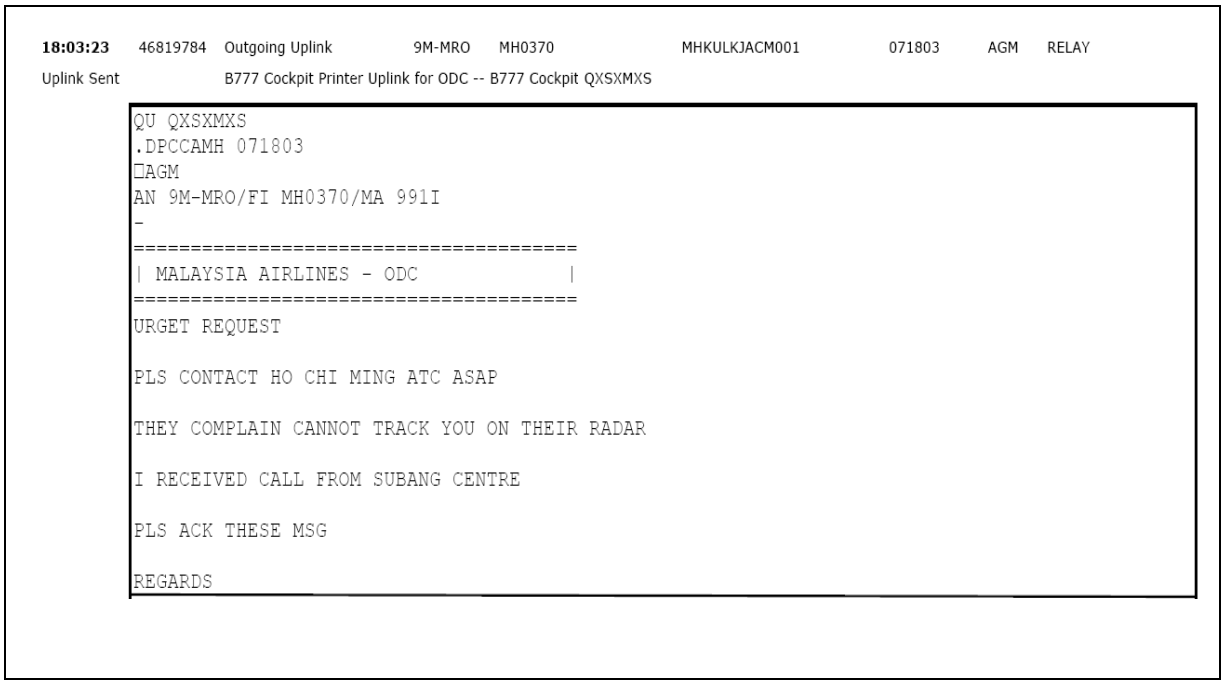

18:03:23 46819784 Outgoing Uplink 9M-MRO MH0370 MHKULKJACM001 071803 AGM RELAY
Uplink Sent B777 Cockpit Printer Uplink for ODC -- B777 Cockpit QXSXMXS

```
QU QXSXMXS
.DPCCAMH 071803
□AGM
AN 9M-MRO/FI MH0370/MA 991I
-
======================================
| MALAYSIA AIRLINES - ODC             |
======================================
URGET REQUEST

PLS CONTACT HO CHI MING ATC ASAP

THEY COMPLAIN CANNOT TRACK YOU ON THEIR RADAR

I RECEIVED CALL FROM SUBANG CENTRE

PLS ACK THESE MSG

REGARDS
```

Figure 1.9I - Message from MH ODC

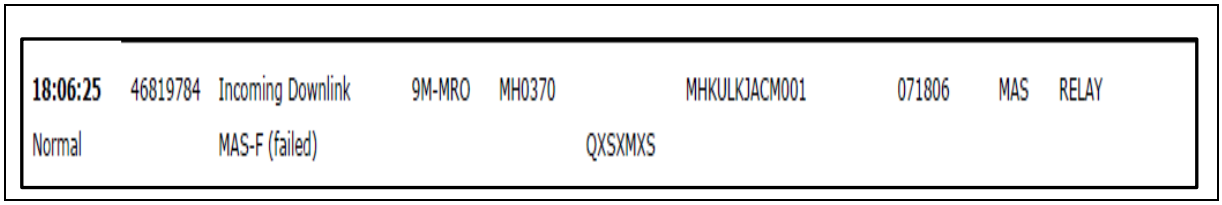

18:06:25 46819784 Incoming Downlink 9M-MRO MH0370 MHKULKJACM001 071806 MAS RELAY
Normal MAS-F (failed) QXSXMXS

Figure 1.9J - Automated Downlink Message

1.9.5 Satellite Communications

1) Satellite Communications System Description

Satellite Communications (SATCOM) is an acronym of, and generic term for, satellite communications. SATCOM operates by using satellites to relay radio signals between the sender and receiver. It can cover far more distance and wider areas than other radios. SATCOM can be used to transmit words, pictures and other forms of information.

The aircraft, 9M-MRO, was equipped with a SATCOM terminal that used the Inmarsat Classic Aero system. The Inmarsat system utilises a constellation of satellites to provide nearly global coverage, the exception being polar areas. The aircraft SATCOM system, also referred to as an Airborne Earth Station (AES) operates on L Band, transmits at 1.6 GHz and receives at 1.5 GHz. For this aircraft, the

SATCOM system provided a total of five voice channels and one data channel. The satellite link provides the following functions:

- Audio and text communication;
- ACARS data; and
- In-flight Entertainment (IFE) Equipment connectivity.

The Earth or Ground Station uses C Band, transmits at 6 GHz and receives at 4 GHz. Inmarsat uses a network of Ground Earth Stations (GES) to communicate with the satellites and connect the SATCOM signal to other terrestrial data networks such as telephone systems, internet, etc.

When the SATCOM AES is first powered on, it sends a log-on request to the GES to initiate service.

There are a number of channels available for messages to be sent between the Satellite and Earth Station. One of the channels is called the ‘common access channel’, which aircraft will constantly listen to when able to do so.

If the GES has not heard from an aircraft for an hour after the last communication, it automatically transmits a ‘log on interrogation’ (“ping”) message on the common access frequency using the aircraft’s unique identifier. If the aircraft receives its ‘unique identifier’, it returns a short message that it is still logged onto the network. Both the initial log-on request and the hourly ping have been termed as a ‘handshake'.

The SATCOM AES consists of the following equipment: Radio frequency unit (RFU), Radio frequency attenuator (RF ATTN), Radio frequency splitter (RFS), Class C high power amplifier (HPA), Class A high power amplifier (HPA), High power relay (HPR), three low noise amplifier/diplexers (LNA/DIPs), Low gain antenna (LGA), two beam steering units (BSUs), two high gain antennas (HGAs), Radio frequency combiner (RFC) and Satellite data unit (SDU).

The SATCOM avionics are located on the E11 rack, which is in the crown area aft of doors 3 left/right. The High Gain antennas are mounted above door 3 left and door 3 right. The Low Gain antenna is mounted on the fuselage centreline. The SATCOM Circuit Breakers (CB) are located in the Main Equipment Center (MEC).

The Satellite Data Unit (SDU) receives 115V AC from the Left Main bus. In flight, this bus can be powered by engine mounted generators or the APU generator. Neither the aircraft battery nor the ram air turbine will power the SATCOM system.

The diagram in *Figure 1.9K* (below) shows the complete set of SATCOM units, including avionics, High Gain Antenna Subsystem and Low Gain Antenna Subsystem. It also shows interfaces to the aircraft cockpit and cabin systems and functions. The following notes are intended to be read in conjunction with *Figure 1.9K* (below)*:*

a) CDU (3) are the three Control Display Units, otherwise known as Multi-function Control Display Units (MCDUs).

b) CPMU is Cabin Passenger Management Unit, which provides an interface between the Panasonic IFE and the SDU, for any Data-3 SMS/e-mail messages.

c) AMU is the Audio Management Unit, which feeds cockpit audio to and from the SDU.

d) CTU is the Cabin Telecommunications Unit, which provides an interface between the in-seat handsets and the SDU, for cabin telephony calls, were that functions available. In the case of 9M-MRO, the in-seat phones can only be used for seat-to-seat calling.

e) AIMS Cabinet is one of two Airplane Information Management System cabinets, which route numerous information to and from the SDU, including ACARS data, Navigational data, AES ID and Flight ID.

f) SATCOM Maintenance Switch is not relevant to this document, as no maintenance activity is possible in flight.

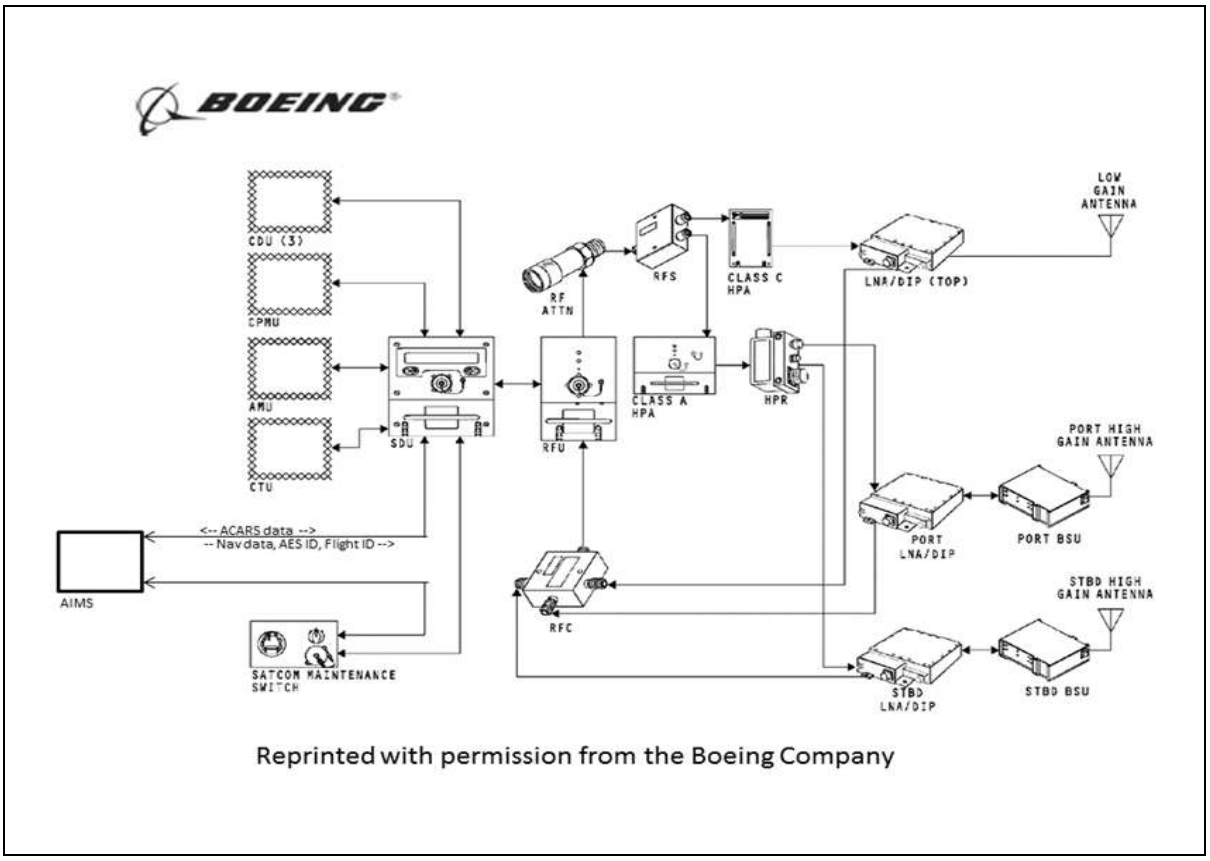

Figure 1.9K - SATCOM System

The photo in *Figure 1.9L* (below) shows the Honeywell/Racal (Honeywell/Thales) MCS-6000 SATCOM Units - RFU (left), SDU (centre) and HPA (right).

Figure 1.9L - RFU (left), SDU (centre) and HPA (right)

2) Satellite Communications Ground Station Logs of the Event - Introduction

Throughout the flight of MH370, the aircraft communicated through the Inmarsat Indian Ocean Region (IOR) I-3 Satellite and the GES in Perth, Australia.

Figure 1.9M (below) shows the Inmarsat I-3 IOR Satellite Coverage Map. The blue lines represent the elevation angle to the IOR satellite for a SATCOM unit on the ground or in the air. Due to the satellite inclination, the elevation angles are approximate.

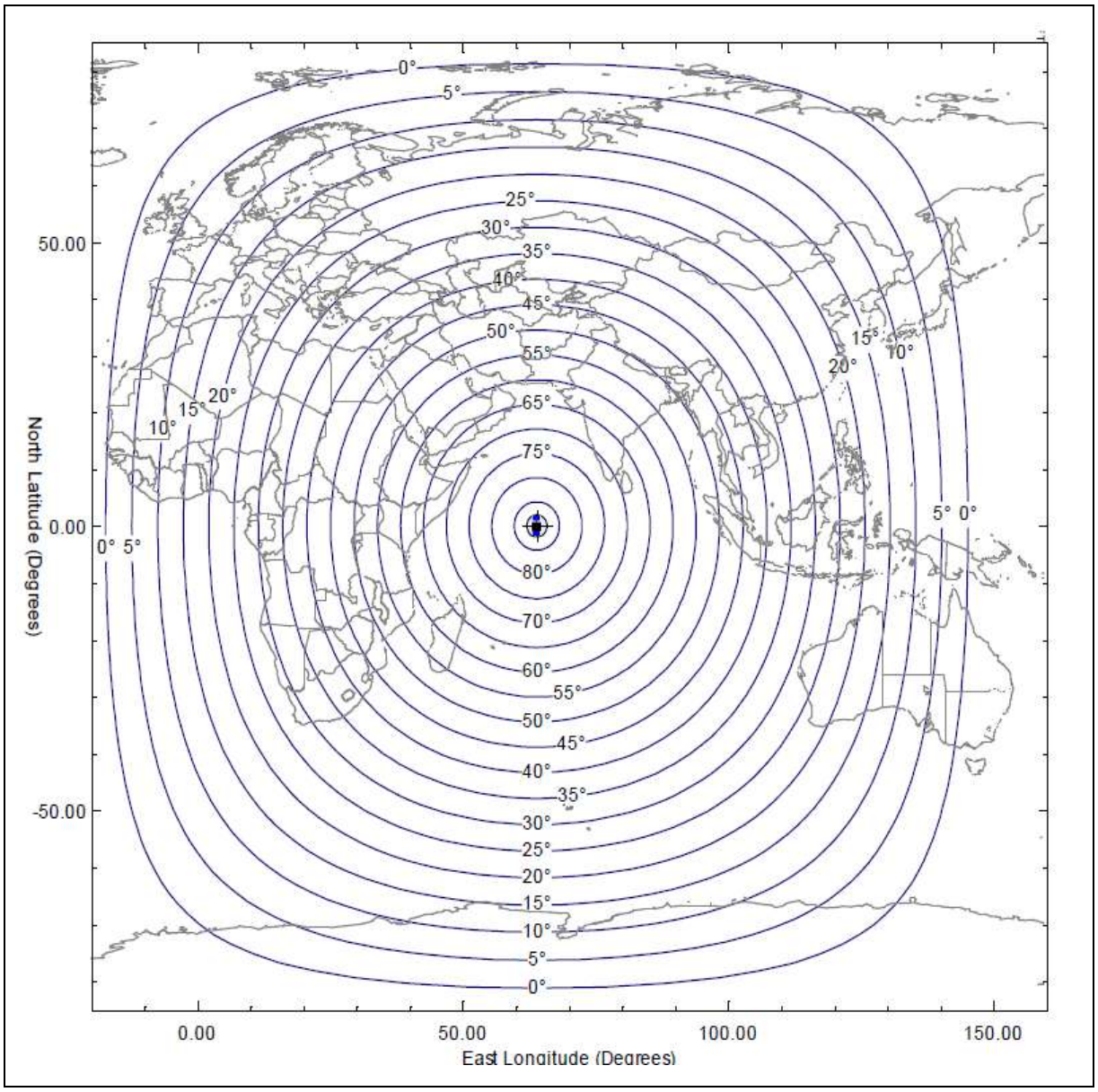

Figure 1.9M - Inmarsat I-3 IOR Satellite Coverage Map

MH370 departed KLIA at 1642 UTC [0042 MYT, 08 March 2014]. At 1707 UTC, the SATCOM system was used to send a standard ACARS report, normally sent every 30 minutes. The message also indicated the remaining fuel on-board.

The ACARS reports expected at 1737 UTC and 1807 UTC were not received. The next SATCOM communication was a log-on request from the aircraft at 1825 UTC. From that point until 0011 UTC, SATCOM transmissions indicate that the link was available, although not used for any voice, ACARS or other data services apart from two unanswered ground-to-air telephone calls. At 0019 UTC, the AES initiated another log-on request. The log-on acknowledge was the last transmission from the SATCOM.

The SATCOM link was available for most of the flight, excluding a period of between 22 and 78 minutes leading up to 1825 UTC, 07 March and a period of less than 8 minutes leading up to 0019 UTC, 08 March 2014. The absence of any aircraft-initiated handshakes, and on-going success of ground-initiated handshakes, indicates that power to the SATCOM was maintained other than the two periods stated above.

Data from the last seven ‘handshakes’ were used to help establish the most probable location of the aircraft. Initially only the first six of these ‘handshakes’ were considered to be complete. The seventh and last ‘handshake’ that was automatically initiated by the aircraft, was originally assessed as a partial ‘handshake’. Subsequent analysis confirmed the 7th handshake could be used to help determine the most probable flight path. Two unanswered ground-to-air telephone calls had the effect of resetting the activity log and hence increased the period between the ground initiated ‘handshakes’. The significant times used to identify the most probable final location of the aircraft are tabulated in *Table 1.9B* below. Details of the event’s SATCOM ground station logs are provided in *Section 1.9.5 para. 3) and 4)* (below).

SATCOM TRANSMISSIONS		TIME	
		UTC	MYT*
1.	Aircraft departed KLIA	1642	0042
2.	Last ACARS transmission	1707	0107
3.	1st handshake - log-on initiated by the aircraft	1825	0225
4.	Unanswered ground-to-air telephone call	1839	0239
5.	2nd handshake initiated by ground station	1941	0341
6.	3rd handshake initiated by ground station	2041	0441
7.	4th handshake initiated by ground station	2141	0541
8.	5th handshake initiated by ground station	2241	0641
9.	Unanswered ground-to-air telephone call	2313	0713
10.	6th handshake initiated by ground station	0011*	0811
11.	7th handshake - log-on initiated by the aircraft	0019*	0819
12.	Aircraft did not respond to 'handshake' from Satellite Earth Ground Station	0115*	0915
* 08 March 2014			

Table 1.9B - SATCOM 'Handshakes'

3) Satellite Communications Ground Station Logs of the Event - Summary

The SATCOM utilised the Inmarsat Indian Ocean Region (IOR) I-3 satellite and the associated Perth Ground Earth Station (GES) throughout the flight. Inmarsat has confirmed that during the flight, no SATCOM signalling or traffic was routed via any other satellites (including MTSAT) to any other GESs (including MTSAT[11] GESs).

The SATCOM provides the Satellite link for the following functions:

- Cockpit Voice - Call control via the Multi-function Control and Display Units (MCDUs) and audio via the cockpit Audio Management Unit (AMU) and associated headsets;
- Cockpit Packet Data (Data-2) - Interface via the ACARS Management Unit (MU); and

[11] MTSAT - A series of Japanese weather and aviation satellites and GESs. MTSAT-1R and MTSAT-2 satellites are interoperable with Inmarsat satellites.

- Cabin Packet Data (Data-3) - Interface via the Panasonic System 3000i IFE equipment:
  - SMS/e-Mail
  - BITE-offload

The GES logs contain the following key information for each transmission to and from the aircraft:

- Time tag, Satellite and GES (Note: the timestamp accuracy does vary between the different logs, but should always be <1 second, and usually to a few milliseconds);
- Channel Type, Channel Number (frequency), Received Carrier/Noise Density Ratio (C/No), channel Bit-Error-Rate (BER), Burst Frequency Offset (BFO) and Burst Timing Offset (BTO, or round trip delay); and
- All payload data (excluding voice frames) contained within the transmission - these are known as the Signal Unit contents.

The events are summarised below. All times are in UTC. In the summary below, times are truncated to the nearest minute (the format is Hours Minutes) and in *Section 1.9.5 para. 4)*, times are truncated to the nearest second (the format is Hours Minutes:Seconds).

No.	Summary of SATCOM Ground Station Logs
1.	Prior to take-off, the SATCOM Logged On (normally) a number of times, the last time being at 1600, when it sent a valid Flight ID to the GES. The SATCOM link was available for both voice and data (known as Log-On Class 3).
2.	After take-off, the IFE SMS email application sent a normal beginning-of-flight message at 1642 (containing the correct Airborne Earth Station [AES ID], Flight ID "MAS370", origin airport "WMKK", and destination airport "ZBAA"), indicating that the IFE was receiving the valid Flight ID, origin airport and destination airport from AIMS and the ICAO (AES) ID from the Satellite Data Unit (SDU) at this time.
3.	The SATCOM link was available for most of the flight, excluding periods leading up to 1825 UTC, 07 March and 0019 UTC, 08 March 2014.

cont…

No.	Summary of SATCOM Ground Station Logs
4.	When the SATCOM link was re-established at the above times, no Flight ID was present
5.	During each of the two in-flight Log Ons at 1825 UTC and 0019 UTC, the GES recorded abnormal frequency offsets for the burst transmission from the SATCOM.
6.	There is no indication of the SATCOM link being manually Logged Off from the cockpit (via an MCDU). Such activity would have been captured in the GES logs, but it was not.
7.	No Data - 2 ACARS traffic was observed after 1707 UTC 07 March 2014.
8.	The IFE equipment set up two ground connections over SATCOM [for the SMS e-mail application and Built-In Test Equipment (BITE) application] after the SATCOM re-established the link at 1825 UTC, 07 March 2014 (normal), but not after the SATCOM re-established the link at 0019 UTC, 08 March (abnormal). At no time during the flight was any user data sent over the link by means of the SMS/e-Mail application.
9.	Two Ground-to-Air Telephone Calls were placed to the cockpit from MAS Operations Centre (MOC) at Airline Operational Communications (AOC) Q10 priority level at 1839 UTC and at 2313 UTC, 07 March 2014. Neither of the calls was answered.
10.	The SATCOM responded normally to a series of roughly hourly Log-On Interrogations from the Perth GES, up to and including a Log-On Interrogation at 0011 UTC, 08 March 2014. The two unanswered ground to air calls at 1839 UTC and 2313 UTC reset the Perth GES inactivity timer and hence the Log-On Interrogations were not always hourly.
11.	The last transmission received from the SATCOM occurred at 0019 UTC, 08 March 2014 and the SATCOM failed to respond to a series of three Log-On interrogations starting at 0115 UTC, 08 March 2014.

4) Satellite Communications Ground Station Logs – Key Observations (in chronological order) *(Table 1.9C* [below]*)*

No.	Time (UTC)	Key Observations - Satellite Ground Station Logs
1.	1250:19	Prior to take-off, the SATCOM initiates a normal Log-On as Class 1 (data only capable) via the Pacific Ocean Region (POR) I-3 satellite, using the Low Gain Antenna (LGA) subsystem, suggesting that ADIRU (Air Data Inertial Reference Unit) navigation data was not available to the SDU at this time. No flight ID is sent to the GES at this time. This is the first SATCOM activity recorded at the GES since 0802:27, suggesting that the SATCOM was not powered for a period of several hours, whilst the aircraft was on ground. This is quite normal.
2.	1555:57	The SATCOM initiates a normal Log On Renewal as Class 1 (data only capable) via the POR I-3 satellite, using the LGA subsystem, this time with a valid Flight ID.
3.	1557:49	The SATCOM initiates a normal Log-On as Class 3 (voice and data capable) via the POR I-3 satellite, using the High Gain Antenna (HGA) subsystem, with a valid Flight ID. This suggests that the ADIRU derived navigation data has become available at this time.
4.	1559:57	The SATCOM initiates a Log-On handover as Class 3 (voice and data capable) to the IOR I-3 satellite, using the HGA subsystem, with a valid Flight ID. This suggests that the IOR is now considered to be the best available satellite. This is probably because either the line of sight to the IOR satellite is now clearer than that to the POR satellite, or the antenna gain in the direction of the IOR satellite has become higher than the antenna gain in the direction of the POR satellite.
5.	1642:04	After take-off, the IFE SMS e-mail application sends a normal beginning-of-flight message. a. The message contained the correct AES ID, Flight ID "MAS370", origin airport "WMKK", and destination airport "ZBAA". b. This indicates that the IFE was receiving the Flight ID, origin airport and destination airport from AIMS and the ICAO (AES) ID from the SDU at this time.

Table 1.9C - Chronology of Satellite Communications Ground Station Logs

cont…

No.	Time (UTC)	Key Observations - Satellite Ground Station Logs
6.	1707:48	Last DATA-2 ACARS Message received at the GES. No further SATCOM Data-2 ACARS messages or acknowledgements were received at the GES for the remainder of the flight. This is abnormal and suggests that the on-board ACARS equipment either failed, or was disabled or powered down at some time between 1707:48 and around 1825:00.
7.	1803:41	GES initiates a DATA-2 ACARS transmission (uplink), but receives no acknowledgement from the SATCOM. a. Therefore, the SATCOM Link was lost at sometime between 1707:48 and 1803:41. b. There is no evidence of a cockpit-initiated manual Log-Off of the SATCOM. c. Note that even if the on-board ACARs equipment was failed, disabled or powered down at this time, it would not prevent the SATCOM from acknowledging the ACARS-related P-Channel transmissions from the GES.
8.	1805:11	GES initiates a DATA-2 ACARS transmission, but receives no acknowledgement from the SATCOM, indicating that there is still no SATCOM link at this time.
9.	1825:27	SATCOM Log-On, initiated from the aircraft terminal. a. This is the first 'handshake'. b. This marks the end of the link lost period that began at sometime between 1707:48 and 1803:41. c. This log-on request suggests that whatever caused the SATCOM link loss to occur between 1707:48 and 1803:41 had been reversed.
10.	1825:34	SATCOM Log-On, successfully completed. a. The SATCOM link becomes available (for both voice and data - Class 3) once more and normal SATCOM operation resumes (except that there is no Data-2 ACARS traffic). b. No Flight ID was sent to the GES during the Log-On. This implies that the SDU stopped receiving a valid Flight ID from the AIMS at sometime between 1642:04 and 1825:00. *cont…*

Table 1.9C - Chronology of Satellite Communications Ground Station Logs

cont…

No.	Time (UTC)	Key Observations - Satellite Ground Station Logs
10. *cont…*	1825:34	c. The possible reasons for the link loss and the subsequent Log-On that took place at 1825:00 have been investigated and are detailed in *Table 2.5A*. There are many quite complicated scenarios that could have caused the 1825:00 Log-On. However, the most likely reason is a power interrupt to the SATCOM avionics, of a duration greater than 22 minutes (the time between events 7 and 9) and less than 78 minutes (the time between events 6 and 9). d. The GES recorded an abnormal BFO for the SATCOM Log-On Acknowledge transmissions (*Sections 1.9.5 para.* 5) and *2.5.3*). • 1825:00 Log-On Acknowledge - Most likely due to the power-on drift of the Oven Controlled Crystal Oscillator (OCXO), thus endorsing the belief that the 1825:00 Log-On was preceded by a lengthy power interrupt. An OCXO provides a stable reference frequency for the SDU Radio Frequency (RF) transmit and receive circuits and also for SDU modem timing. Within the OCXO, a regulated oven keeps the crystal at an almost constant temperature if the ambient temperature in the crown area is between the ranges -55°C up to above +70°C. The oven also contains extra electrical regulation and isolation to ensure frequency accuracy and stability. The OCXO includes an oven ready flag, which triggers the Log-On initiation when the OCXO reaches its operating temperature. Extensive laboratory testing has revealed that during warm up, the OCXO frequency may vary non-linearly with time, but then settles with almost negligible variation. At power-on, the OCXO can exhibit either a rising or falling frequency gradient, before decaying over time to its normal steady state value. The testing has indicated that reasonable stability (within 2Hz/minute) is typically reached by around five minutes after an initial peak or overshoot. The testing has also shown that there can still be a significant frequency offset at the time that the oven ready flag initiates the Log-On process, so the Log-On request, Log-On Acknowledge and subsequent data bursts can all exhibit significant frequency offsets.

Table 1.9C - Chronology of Satellite Communications Ground Station Logs

cont…

No.	Time (UTC)	Key Observations - Satellite Ground Station Logs
11.	1827:03	The IFE sets up a Data-3 ground connection (X.25 circuit) over SATCOM for an SMS/e-mail application after the SATCOM link is re-established.
12.	1828:05	The IFE sets up a Data-3 ground connection (X.25 circuit) over SATCOM for a BITE application after the SATCOM link is re-established.
13.	1839:52	Ground-to-air telephony call placed from a number with country code 60 (Malaysia) a. Q10 Airline Operational Communications (AOC) Priority Level b. The Perth GES logs indicate that a good link is likely to have existed at this time. c. This call would have been routed to the cockpit and should have resulted in a chime and an incoming visual annunciation on the Audio Control Panels (ACPs), and, if the appropriate SATCOM page was selected, then also on one or more MCDU. d. The GES logs show zero duration, indicating that the call went unanswered. Note that there are two methods for the answering of an incoming call: Either by pressing the relevant Line Select Key on an MCDU, or by keying a microphone.
14.	1840:56	The GES logs show that the unanswered Ground-to-Air telephony call was cleared by the calling party.
15.	1941:00	Log-On Interrogation by the Perth GES, with a response from the SATCOM a. This is the second ‘handshake’, whereby the GES inactivity timer has expired and the GES has sent a message to interrogate the status of the SATCOM. b. The SATCOM responded normally and the SATCOM link was therefore available at this time.
16.	2041:02	Log-On Interrogation by the Perth GES, with a response from the SATCOM a. This is the third ‘handshake’. b. The SATCOM responded normally and the SATCOM link was therefore available at this time.

Table 1.9C - Chronology of Satellite Communications Ground Station Logs

cont…

No.	Time (UTC)	Key Observations - Satellite Ground Station Logs
17.	2141:24	Log-On Interrogation by the Perth GES, with a response from the SATCOM a. This is the fourth 'handshake'. b. The SATCOM responded normally and the SATCOM link was therefore available at this time.
18.	2241:19	Log-On Interrogation by the Perth GES, with a response from the SATCOM a. This is the fifth 'handshake'. b. The SATCOM responded normally and the SATCOM link was therefore available at this time.
19.	2313:58	Ground-to-air telephony call placed from a number with country code 60 (Malaysia) a. Q10 AOC Priority Level. b. The Perth GES logs indicate that a good link is likely to have existed at this time. c. This call would have been routed to the cockpit and should have resulted in a chime and an incoming visual annunciation on the Audio Control Panels, and, if the appropriate SATCOM page was selected, then also on one or more MCDU. d. The GES logs show zero duration, indicating that the call went unanswered. Note that there are two methods for the answering of an incoming call: Either by pressing the relevant Line Select Key on an MCDU, or by keying a microphone.
20.	2315:02	The GES logs show that the unanswered Ground to Air telephony call was cleared by the calling party.
21.	0010:58	Log-On Interrogation by the Perth GES, with a response from the SATCOM a. This is the sixth 'handshake'. b. The SATCOM responded normally and the SATCOM link was therefore available at this time.

Table 1.9C - Chronology of Satellite Communications Ground Station Log

cont…

No.	Time (UTC)	Key Observations - Satellite Ground Station Logs
22.	0019:29	SATCOM Log-On, initiated from the aircraft terminal. This is the seventh 'handshake'. a. For there to have been a Log-On at this time, there must have been a prior loss of the SATCOM link. This link loss must have occurred at some time after 0010:58, when the SATCOM responded to a Log-On interrogation. b. This Log-On request suggests that whatever caused the SATCOM link loss to occur had been reversed.
23.	0019:37	SATCOM Log-On, successfully completed a. The SATCOM link becomes available (for voice and data – Class 3) once more and normal SATCOM operation resumes. b. No Flight ID was sent to the GES during the Log-On. This infers that the SDU was still not receiving the Flight ID from AIMS. c. The possible reasons for the link loss and the subsequent Log-On that took place at 0019:00 have been investigated and are detailed in Section 2.5.2. There are many quite complicated scenarios that could have caused the 0019:00 Log-On with no Flight ID. However, the most likely reason is a power interrupt to the SATCOM avionics, of a duration less than 8 minutes. d. The GES recorded an abnormal frequency offset for the SATCOM Log-On Request and Acknowledge transmissions (see *Sections 1.9.5 para. 5) and 2.5.3*). The abnormal BFOs for the 0019 Log-On Request and Log-On Acknowledge are more likely due to a combination of uncompensated vertical velocity (descent) and OCXO warm up drift. e) The IFE did not subsequently establish the two Data-3 X.25 connections over the SATCOM, which it normally does if it is functional. It can be inferred that the IFE was either not operating at this time (powered off, not being powered whilst the SATCOM was being powered by the APU, failed, or still resetting after a power cycle), or the SATCOM and/or the IFE became inoperative before the IFE was able to establish the Data-3 connection <u>Note:</u> This is the last transmission received from the aircraft terminal.

Table 1.9C - Chronology of Satellite Communications Ground Station Logs

cont…

No.	Time (UTC)	Key Observations - Satellite Ground Station Logs
24.	0115:56	Log-On Interrogation by the Perth GES, with no response from the SATCOM a. The SATCOM Link was lost at sometime between 0019:37 and 0115:56. b. There is no evidence of a cockpit-initiated manual Log-Off of the SATCOM. c. The loss of SATCOM link was due to one of the following: i. The SATCOM stopped receiving the P-Channel transmission from the satellite ii. SATCOM input power (115VAC 400Hz) was removed iii. The SATCOM experienced a BITE failure.
25.	0116:06	Log-On Interrogation by the Perth GES, with no response from the SATCOM.
26.	0116:15	Log-On Interrogation by the Perth GES, with no response from the SATCOM.

Table 1.9C - Chronology of Satellite Communications Ground Station Logs

5) Frequencies of Log-On Bursts

During each of the two in-flight Log-Ons that occurred at 1825 and 0019, the GES recorded abnormal frequency offsets for the SATCOM transmissions. This is in contrast with the 'normal' Log-On behaviour.

Table 1.9D (below) shows the frequencies of these Log-On bursts, as measured at the GES, plus differences from assumed reference frequencies (closest stable values in time, where the aircraft is assumed to be in level flight). The table also shows the very high delta frequencies between the respective Log-On Request and Log-On Acknowledge bursts.

Log-On Time	1825	0019
BFO used as a reference (closest stable value, assume level flight)	144Hz @ 1828:05	252Hz @ 0010:59
Log-On Request BFO	142Hz @ 1825:27	182Hz @ 0019:29
Log-On Request C/No recorded at GES	30.28	40.59
Log-On Request Channel BER recorded at GES	5	0
Log-On Request Difference Frequency (from BFO reference)	-2Hz @ 1825:27	-70Hz @ 0019:29
Log-On Acknowledge BFO	273Hz @ 1825:34	-2Hz @ 0019:37
Log-On Acknowledge C/No recorded at GES	42.55	43.38
Log-On Acknowledge Channel BER recorded at GES	0	0
Log-On Acknowledge Difference Frequency (from BFO reference)	+129Hz @ 1825:34	-254Hz @ 0019:37
Delta frequency between the Log-On Request and the Log-On Acknowledge bursts, plus time period	+131Hz over 7 seconds	-184Hz over 8 seconds

Table 1.9D - Log-On Bursts

SECTION 1 – FACTUAL INFORMATION

1.10 AERODROME INFORMATION

Not applicable.

SECTION 1 – FACTUAL INFORMATION

1.11 FLIGHT RECORDERS

The aircraft was equipped with two crash-protected recorders:

- Solid State Flight Data Recorder (SSFDR)
- Solid State Cockpit Voice Recorder (SSCVR)

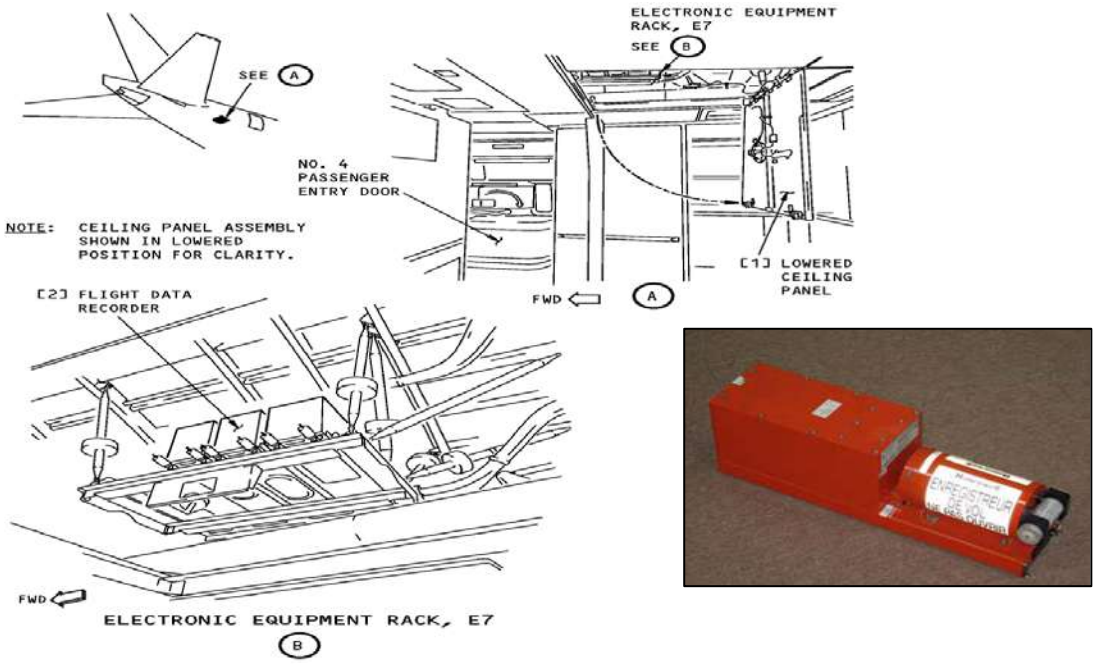

Copyright © Boeing. Reprinted with permission of The Boeing Company

Figure 1.11A - Location of Solid State Flight Data Recorder

1.11.1 Solid State Flight Data Recorder

The solid state flight data recorder (SSFDR) is located in the Electronic Equipment rack, E7, which is in the aft cabin above the ceiling (*Figure. 1.11A* [above]).

The SSFDR receives and stores selected aircraft parameters from various aircraft systems and sensors in a crash-protected solid state memory.

The flight data recorder system (FDRS) operates during any engine start, while any engine is running, during test or when the aircraft is in the air. The SSFDR is powered from the right AC transfer bus which is powered

by the engine generators or the APU generator. If none of these generators are functioning due to non-operation of the engines and APU then the bus will not be powered and the SSFDR will not operate in the air.

This is a solid state flight data recorder (SSFDR) with a recording capacity of at least twenty-five hours.

The SSFDR records the most recent 25 hours of flight and records more than 1300 parameters. The SSFDR is a 256 word per second (wps) data rate recorder. The most recent flight data recorder download for this aircraft was in September 2013 and this was carried out for the annual readout. The annual readout extracts 151 parameters for evaluation. Details of the SSFDR installed and specifications are as follows:

- Manufacturer: Honeywell
- Model: SSFDR Model 4700
- Part Number (P/N): 980-4700-042
- Serial Number (S/N): SSFDR-08636
- Date last installed on aircraft: 26 August 2012
- Weight: 6.8 kg
- Electricity Consumption: 15 W, 115 VAC 400 Hz
- Impact Shock: 3400 G for 6.5 ms
- Fire Temperature: Max 1100°C (30 min)
- Deep Sea Pressure and Sea Water Immersion: 20,000 ft.

1.11.2 Solid State Cockpit Voice Recorder

The solid state cockpit voice recorder (SSCVR) is in the Electronic Equipment Rack, E7, in the aft cabin above the ceiling and located adjacent to the SSFDR (*Figure 1-11B* [below]).

The SSCVR has a recording capacity of at least two hours in standard quality and thirty minutes in high quality.

The voice recorder system receives cockpit sounds and flight crew communications. It keeps this audio in a solid state memory.

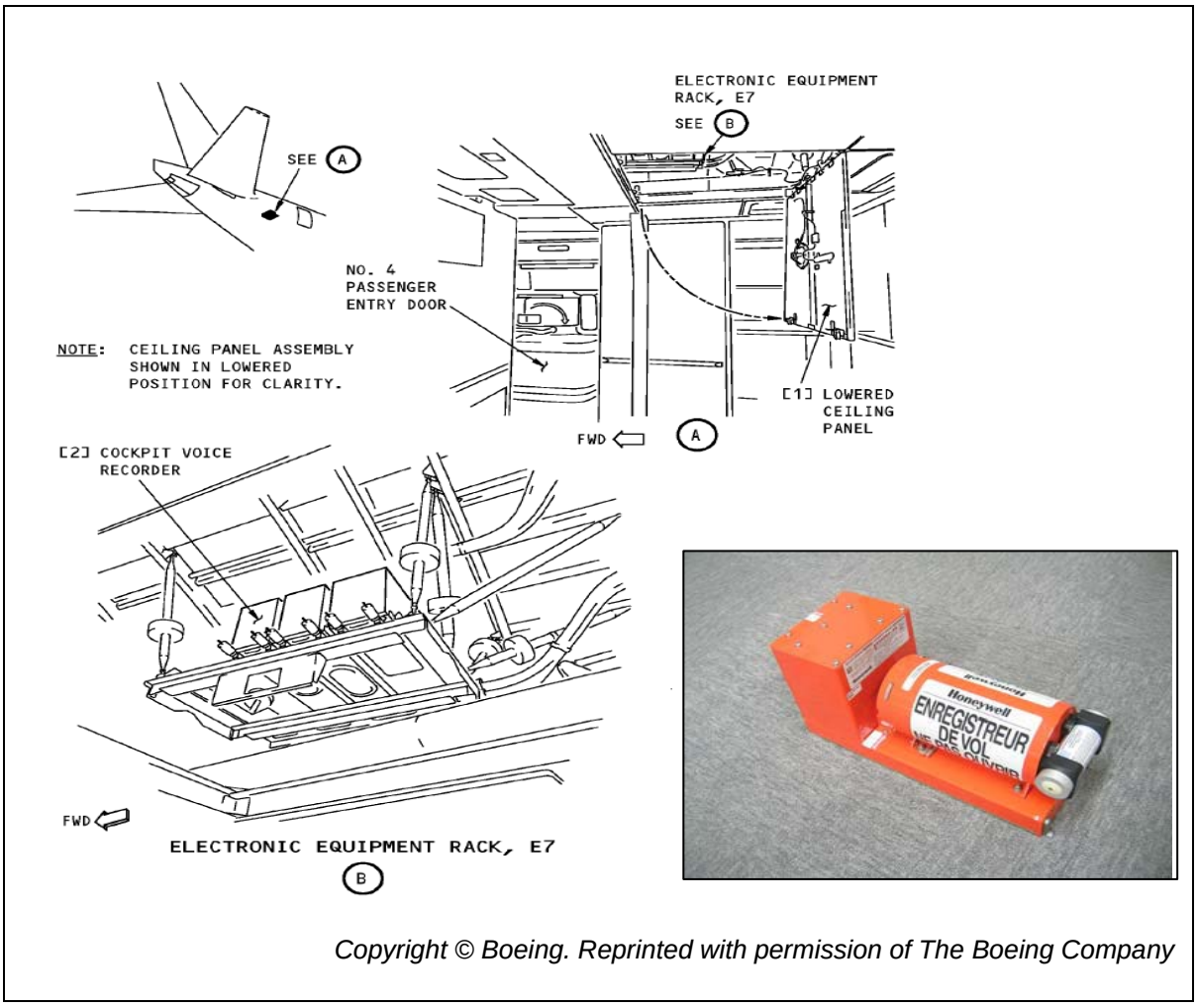

Copyright © Boeing. Reprinted with permission of The Boeing Company

Figure 1.11B - Location of Solid State Cockpit Voice Recorder

Four audio channels go to the SSCVR. Channel 1, 2, and 3 audio is from the audio management unit (AMU). Each channel carries audio from one crew member's flight interphone audio. The audio on each channel is the sum of these signals:

- Hot mic audio (microphone audio when there is no press-to-talk [PTT])
- Received audio as selected on the crew member's audio control panel (ACP)
- Side tone audio to the crew member

Channel 4 audio is from the Cockpit Area Microphone (CAM). The CAM sends cockpit area audio to the SSCVR. The SSCVR operates any time power is available on the Left AC transfer bus. This bus is not powered from batteries or the Ram Air Turbine (RAT).

Details of the SSCVR installed and the specifications are as follows:

- Manufacturer: Honeywell
- Model: SSCVR Model 6022
- Part Number (P/N): 980-6022-001
- Serial Number (S/N): 2677
- Date last installed on aircraft: 26 August 2012
- Weight: 5.9 kg Electricity Consumption: 8 W, 115 VAC 400 Hz
- Impact Shock: 3400 G for 6.5 ms
- Fire Temperature: Max 1100°C (30 min)
- Deep Sea Pressure and Sea Water Immersion: 20,000 ft.

1.11.3 Underwater Locator Beacons

Both crash-protected recorders were equipped as provided by the regulations with underwater locator beacons (ULB) whose transmission time is at least 30 days, on the 37.5 kHz frequency, operating depth up to 20,000 ft (6096 m) and activated with fresh or salt water immersion. Detail specifications are as per below:

- Manufacturer: Dukane
- Model: DK-100 / DK-120
- Operating Frequency: 37.5 kHz ± 1 kHz
- Operating Depth: Surface to 20,000 ft. (6,096 meters)
- Pulse Length: 10 milliseconds + 10%
- Pulse Repetition Rate: Not less than 0.9 Pulse/Sec
- Operating Life: 30 days (minimum)
- Battery Life In Beacon: 6 Years
- Acoustic Output, Initial: 1060 dynes/cm² rms pressure at 1 meter (160.5 dB)
- Acoustic Output After 30 Days: 700 dynes/cm² rms pressure at 1 meter (157.0 dB)
- Operating Temperature Range: +28°F (-2.2°C) to +100°F (+37.8°C)
- Actuation: Fresh or salt water
- Radiation Pattern: Rated output over 80 percent of sphere
- Size: 1.30 inches (3.30 cm) diameter x 3.92 inches (9.95 cm) long (less mount)
- Weight, Beacon: 6.7 ounces (190 grams)
- Storage Temperature Range: -65°F (-54°C) to 160°F (71°C)

The SSFDR was attached with a ULB as below:

- S/N: SC26210
- ULB Expiry Date: December 2012

The SSCVR was attached with ULB as below:

- S/N: Not Recorded
- ULB Expiry Date: June 2014

1) Solid State Flight Data Recorder Underwater Locator Beacon Battery Expiry

According to maintenance records, the solid state flight data recorder (SSFDR) Underwater Locator Beacon's (ULB) battery expired in December 2012. There is no evidence to suggest that the SSFDR ULB battery had been replaced before the expiry date. The SSCVR ULB battery however was replaced, as scheduled, with the next expiry in June 2014.

Technical Log records showed that the SSFDR (together with the ULB) was replaced on the aircraft on 29 February 2008. Component installation records for the ULB showed that at the time the SSFDR was replaced on aircraft the expiry date for the battery was December 2012.

SECTION 1 – FACTUAL INFORMATION

1.12 WRECKAGE AND IMPACT INFORMATION

1.12.1 Introduction

Extensive work by the the MH370 Search Strategy Group, coordinated by the ATSB, by analysing signals transmitted by the aircraft's satellite communications terminal to Inmarsat's Indian Ocean Region satellite indicated that the aircraft ended its flight in the Southern Indian Ocean.

The ATSB led the underwater search for MH370 in the southern Indian Ocean. The search area, as shown (below) in *Figure 1.12A*, covered in excess of 120,000 sq. km at the 7th Arc.

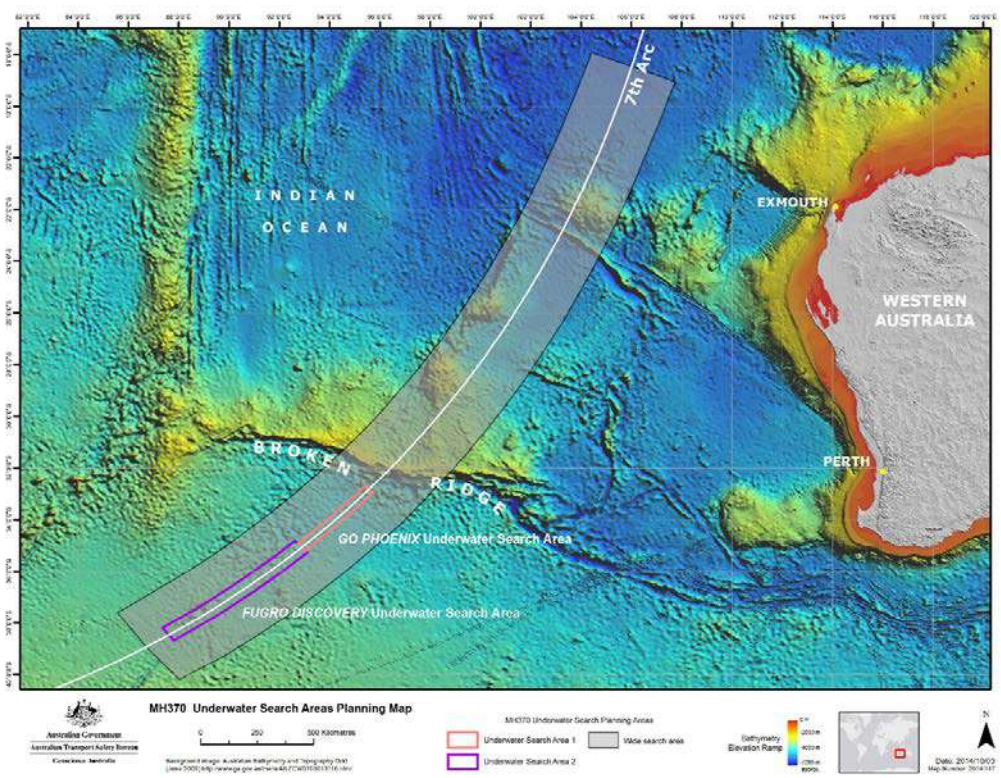

Source: ATSB

Figure 1.12A - MH370 Search Area

Further search was carried out by the US company, Ocean Infinity, which covered an area of more than 112,000 sq. km towards the north of the area covered by ATSB on the 7th arc.

No wreckage of the aircraft has been found after the completion of the search. However, several floating components and debris

confirmed/possibly from MH370 have been found as far as the south eastern coast of Africa. Refer to *Figure 1.12B* (below).

1.12.2 Location of Where the Debris were Found

After a number of assessments, more than 20 items were considered for further examination. These items were found in the north west corner of the Indian Ocean, namely in Réunion Island, Mozambique, Tanzania,

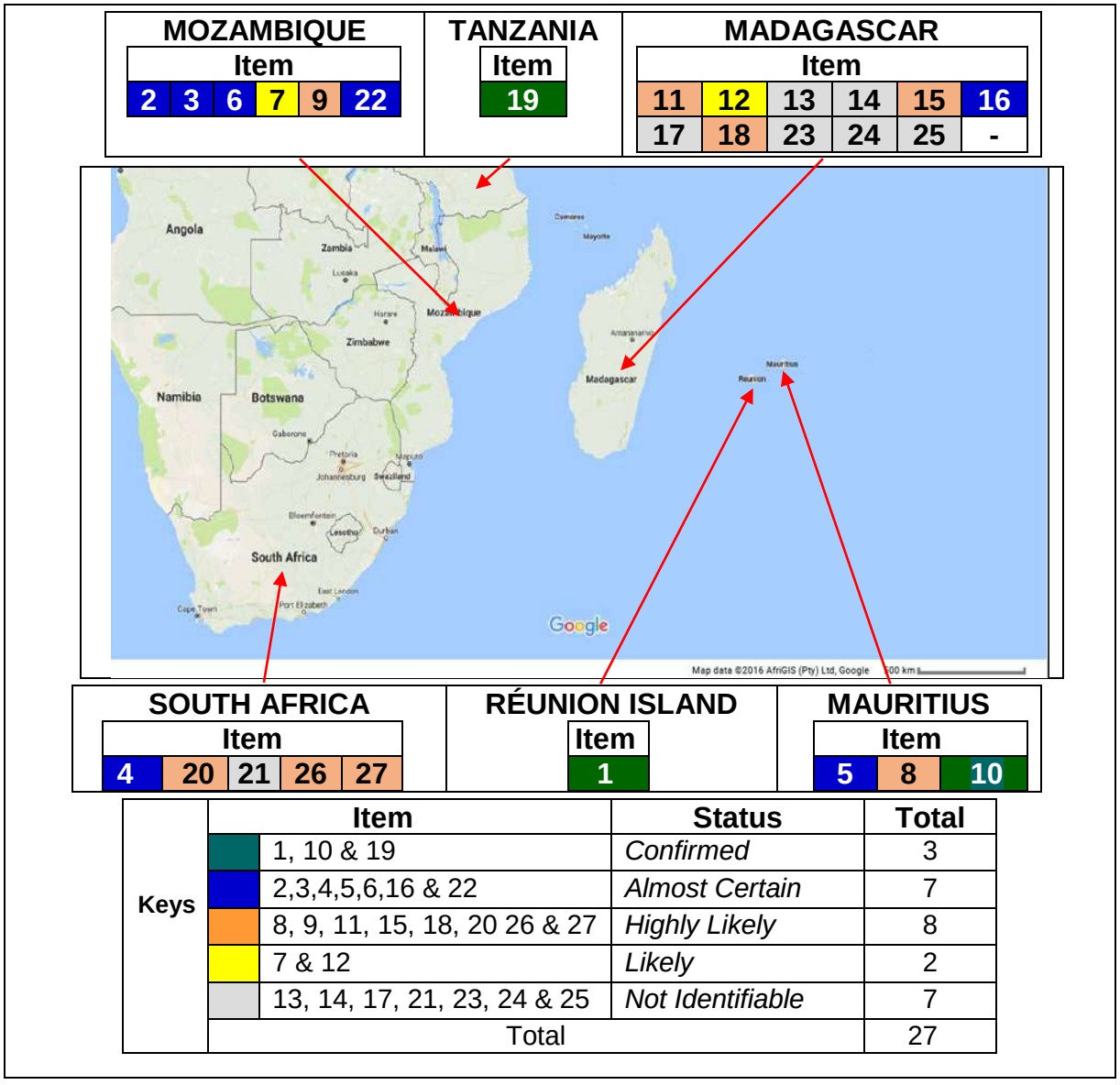

Keys	Item	Status	Total
	1, 10 & 19	*Confirmed*	3
	2,3,4,5,6,16 & 22	*Almost Certain*	7
	8, 9, 11, 15, 18, 20 26 & 27	*Highly Likely*	8
	7 & 12	*Likely*	2
	13, 14, 17, 21, 23, 24 & 25	*Not Identifiable*	7
	Total		27

Figure 1.12B - Locations and Status of Identification of the Debris

South Africa, Madagascar and Mauritius. *Figure 1.12B* (above) shows the distribution of the debris found in the above respective areas. *Table 1.12A* (below) provides a summary of the items of debris examined.

Ref.	Date Found	Debris	Location	Remarks
Item 1	29 July 2015	Right Flaperon	Saint-Denis, Réunion Island	• *Confirmed* by French Judicial Authority belonging to MH370 on 03 September 2015 • Refer to *Appendix 1.12A-1* and *Appendix 1.12A-2*
Item 2	27 December 2015	Right Wing No. 7 Flap Support Fairing	Daghatane Beach, Mozambique	• Examination showed that part is *almost certain* from MH370 • Refer to *Appendix 1.12B*

Table 1.12A - Items of Debris

cont…

Ref.	Date Found	Debris	Location	Remarks
Item 3	27 February 2016	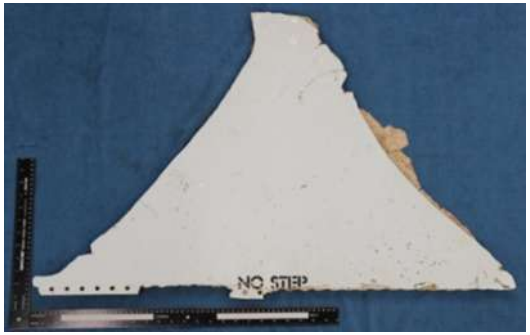 Right Horizontal Stabiliser Panel	Valankulo, Paluma Sandbank, Mozambique	• Examination showed that part is *almost certain* from MH370 • Refer to *Appendix 1.12B*
Item 4	22 March 2016	Engine Nose Cowl	Mossel Bay, South Africa	• Examination showed that part is *almost certain* from MH370 • Refer to *Appendix 1.12C*

Table 1.12A - Items of Debris

cont...

Ref.	Date Found	Debris	Location	Remarks
Item 5	30 March 2016	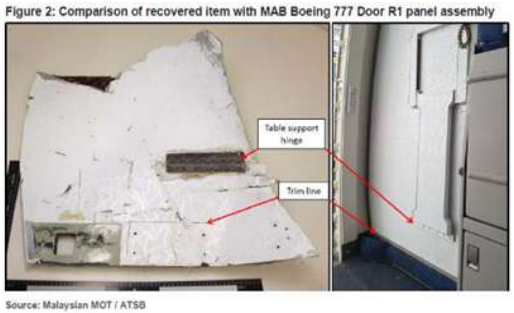 Door R1 Stowage Closet	Rodrigues, Mauritius	• Examination showed that part is *almost certain* from MH370 • Refer to *Appendix 1.12C*
Item 6	24 April 2016	Right Hand Engine Fan Cowling	South of Chidenguele, Mozambique	• Examination showed that part is *almost certain* from MH370 • Refer to *Appendix 1.12D*

Table 1.12A - Items of Debris

cont…

Ref.	Date Found	Debris	Location	Remarks
Item 7	30 April 2016	Wing to Body Fairing	Anvil Bay, Chemucane, Mozambique	• Examination showed that part is *likely* from MH370 • Refer to *Appendix 1.12E*
Item 8	24 May 2016	No. 1 Flap Support Fairing Tail Cone	Gris Gris Beach, Mauritius	• Examination showed that part is *highly likely* from MH370 • Refer to *Appendix 1.12F*

Table 1.12A - Items of Debris

cont...

Ref.	Date Found	Debris	Location	Remarks
Item 9	22 May 2016	Left Wing Trailing Edge Panel	Macenta Peninsular, Mozambique	• Examination showed that part is *highly likely* from MH370 • Refer to *Appendix 1.12G*
Item 10	10 May 2016	Left Outboard Flap	Ilot Bernache, Mauritius	• This part is *confirmed* from MH370 • Refer to *Appendix 1.12H*

Table 1.12A - Items of Debris

cont…

Ref.	Date Found	Debris	Location	Remarks
Item 11	06 June 2016	Seat Back Trim Panel encasing IFE Monitor	Riake beach, Nosy Boraha Island, Madagascar	• Examination showed that part is *highly likely* from MH370 • Refer to *Appendix 1.12I*
Item 12	06 June 2016	Bottom panel on the Wing or Horizontal Stabilizer	Riake beach, Nosy Boraha Island, Madagascar	• Examination showed that part is *likely* from MH370 • Refer to *Appendix 1.12J*

Table 1.12A - Items of Debris

cont…

Ref.	Date Found	Debris	Location	Remarks
Item 13	12 June 2016	Unidentified part	Riake beach, Nosy Boraha Island, Madagascar	• Not identifiable • Refer to *Appendix 1.12K*
Item 14	12 June 2016	Unidentified part	Riake beach, Nosy Boraha Island, Madagascar	• Not identifiable • Refer to *Appendix 1.12L*

Table 1.12A - Items of Debris

cont...

Ref.	Date Found	Debris	Location	Remarks
Item 15	06 June 2016	Right Wing Trailing Edge Panel	Riake beach, Nosy Boraha Island, Madagascar	• Examination showed that part is *highly likely* from MH370 • Refer to *Appendix 1.12G*
Item 16	12 June 2016	Cabin Interior Panel	Antsiraka beach, Madagascar	• Examination showed that part is *almost certain* from MH370 • Refer to *Appendix 1.12M*

Table 1.12A - Items of Debris

cont…

Ref.	Date Found	Debris	Location	Remarks
Item 17	12 June 2016	 Unidentified part	 Antsiraka beach, Madagascar	• Not identifiable • Refer to *Appendix 1.12M*
Item 18	12 June 2016	 Right Forward Nose Landing Gear Door	 Antsiraka beach, Madagascar	• Examination showed that part is *highly likely* from MH370 • Refer to *Appendix 1.12N*

Table 1.12A - Items of Debris

cont…

Ref.	Date Found	Debris	Location	Remarks
Item 19	20 June 2016	 Right Outboard Flap	 Pemba Island, East of Tanzania	• The part is *confirmed* from MH370 • Refer to *Appendix 1.12O*
Item 20	21 June 2016	 Right Aft Wing to Body Fairing	 Kosi Bay Mouth, Kwa Zulu Natal, South Africa	• Examination showed that part is *highly likely* from MH370 • Refer to *Appendix 1.12P*

Table 1.12A - Items of Debris

cont…

Ref.	Date Found	Debris	Location	Remarks
Item 21	18 July 2016	 Unidentified Part	 Northern Kwa Zulu Natal, South Africa	• Not identifiable • Refer to *Appendix 1.12Q*
Item 22	26 August 2016	 Right Vertical Stabilizer Panel	 Linga Linga beach Mozambique	• Examination showed that part is *almost certain* from MH370 • Refer to *Appendix 1.12R*

Table 1.12A - Items of Debris

cont…

Ref.	Date Found	Debris	Location	Remarks
Item 23	October 2016	Unidentified Part	Riake beach, Nosy Boraha Island, Madagascar	• Not identifiable • Refer to *Appendix 1.12S*
Item 24	February 2016	Unidentified Part	Saint Luce, Madagascar	• Not Identifiable • Refer to *Appendix 1.12T*

Table 1.12A - Items of Debris

cont...

Ref.	Date Found	Debris	Location	Remarks
Item 25	July 2016	Unidentified Part	Riake beach, Nosy Boraha Island, Madagascar	• Not identifiable • Refer to *Appendix 1.12U*
Item 26	23 December 2016	Right Aileron	Nautilus Bay, South Africa	• Examination showed that part is *highly likely* from MH370 • Refer to *Appendix 1.12V*

Table 1.12A - Items of Debris

cont…

Ref.	Date Found	Debris	Location	Remarks
Item 27	27 January 2017	Right Wing No. 7 Flap Support Fairing	Mpame Beach, South Africa	• Examination showed that part is *highly likely* from MH370 • Refer to *Appendix 1.12W*

Table 1.12A - Items of Debris

1.12.3 Details of the Debris

The debris are briefly described in the following paragraphs. The details of the parts will be found in the *Appendix 1.12A* to *Appendix 1.12W* of this report.

1) Item 1 - Right Flaperon

Item No. 1 was found on 29 July 2015 in Saint-Denis, Réunion Island. Réunion Island is a French territory in the Indian Ocean.

This item was one of the biggest and complete part of an aircraft found washed ashore. The item was retrieved by the local French authorities and shipped to General Delegate of Armament Aeronautical Technique (DGA/TA) facility in Toulouse for detailed examination. Because of a court case pending in Paris, the part was taken custody by the French Investigative Judge, as evidence for a criminal investigation.

The part identification, detailed examination and analysis were carried out at DGA/TA in Toulouse under the directive and jurisdiction of the French Investigative judge. Although the name plate was missing, which could have provided immediate traceability to the aircraft (9M-MRO), the part was *confirmed* to be a right flaperon of the aircraft 9M-MRO, by tracing the identification numbers of the internal parts of the flaperon to their manufacturing records at EADS CASA, Spain. Refer to *Appendix 1.12A-1.*

The examination of the flaperon at DGA/TA revealed the following damages:

a) the inboard and outboard hinge fittings were fractured in two places; at the level of the leading edge and on the lower surface of the flaperon;

b) the fracture surfaces on the hinge fittings were highly corroded;

c) the ribs at the edge of the flaperon showed, in their metallic area, holes due to corrosion;

d) the leading edge showed dents and cracks;

e) the trailing edge was generally broken;

f) the lower and upper surface panels showed localised dents and the upper surface had a large crack; and

g) the mounting attachment zones on each side of the flaperon were damaged or broken off.

In addition, the flaperon was covered with a colony of barnacles. Most of them were on the upper surface (extrados).

Refer to *Appendix 1.12A-2* for details.

2) Item 2 - Right Wing No. 7 Flap Support Fairing

Item No. 2 was found on 27 December 2015 in Daghatane Beach, Mozambique.

The item was brought to ATSB Laboratory in Canberra for detailed examination and analysis. The part was identified from a number stencilled on the part (676EB), as a segment from a Boeing 777 flap track (support) fairing (Fairing No. 7) from the right wing. All measurable dimensions, materials, construction and other identifiable features conformed to the applicable Boeing drawings for the identified fairing. It was concluded that the item is *almost certain* from MAS B777 aircraft, registered 9M-MRO.

Refer to *Appendix 1.12B* for details.

3) Item 3 - Right Horizontal Stabilizer Panel Piece

Item No. 3 was found on 27 February 2016 in Valankulo, Paluma Sandbank, Mozambique.

The item was brought to ATSB Laboratory in Canberra for detailed examination and analysis. The part was primarily identified from images showing the materials, construction and “NO STEP” stencil, as a segment of a Boeing 777 right horizontal stabilizer panel. All measurable dimensions, materials, construction and other identifiable features conformed to the Boeing drawings for the stabiliser panel. It was concluded that the item is *almost certain* from MAS B777 aircraft, registered 9M-MRO.

Refer to *Appendix 1.12B* for details.

4) Item 4 - Engine Nose Cowl

Item No. 4 was found on 22 March 2016 in Mossel Bay, South Africa.

The item was brought to ATSB Laboratory in Canberra for detailed examination and analysis. The part was identified from the partial Rolls-Royce stencil as a segment from an aircraft engine cowling. The panel thickness, materials and construction conformed to the applicable drawings for Boeing 777 engine cowlings. There were no identifiers on the engine cowling segment that were unique to 9M-MRO, however the Rolls-Royce stencil font and detail did not match the original from manufacture. The stencil was consistent with that developed and used by MAS and closely matched exemplar stencils on other MAS B777 aircraft. There were no significant differentiators on the cowling segment to assist in determining whether the item of debris was from the left or right side of the aircraft, or the inboard or outboard side of the cowling. It was concluded that the item is *almost certain* from MAS B777 aircraft, registered 9M-MRO.

Refer to *Appendix 1.12C* for details.

5) Item 5 - Door R1 Stowage Closet

Item No. 5 was found on 30 March 2016 in Rodrigues Island of Mauritius.

The item was brought to ATSB Laboratory in Canberra for detailed examination and analysis. The part was identified by the decorative laminate as an interior panel from the main cabin. The location of a piano hinge on the part surface was consistent with a work-table support leg, utilised on the exterior of the MAS Door R1 (forward, right hand) closet panel. The part materials, dimensions, construction and fasteners were all consistent with the drawing for the panel assembly and matched that installed on other MAS Boeing 777 aircraft at the Door R1 location.

There were no identifiers on the panel segment that were unique to 9M-MRO, however the pattern, colour and texture of the laminate was only specified by MAS for use on Boeing 747 and 777 aircraft. There is no record of the laminate being used by any other Boeing 777 customers.

It was concluded that the item is *almost certain* from MAS B777 aircraft, registered 9M-MRO.

Refer to *Appendix 1.12C* for details.

6) Item 6 - Right Hand Engine Fan Cowling

Item No. 6 was found on 24 April 2016, south of Chidenguele, Mozambique. The item was brought back to Malaysia for identification and further examination by the Team. The possible location of the debris on a MAS B777 aircraft was determined. The hinge bracket, number of fasteners and fasteners' pitch on the part were consistent with those on the right engine fan cowl on the aircraft. The mount found on the part was also consistent with the mount of the fan cowl "Hold-Open Stay Rod" in regards to its location, shape and size of the mounting bracket. The words "HOIST POINT" were still visible and in the correct location. The fonts used for the words on the part matched those on the fan cowl of the aircraft. The part was brought near to the right fan cowl and was found to physically resemble it in terms of shape, size, colour and features.

It has been concluded that the debris is part of the Right Fan Cowl of a B777. As the right fan cowls on both the engines are similar, there is no conclusive evidence to determine whether it belongs to the left (No. 1) or right (No. 2) engine. Based on the other features on the recovered part it has also been determined that the part is *almost certain* from MH370 (aircraft registered as 9M-MRO).

Refer to *Appendix 1.12D* for details.

7) Item 7 - Unidentified Part

Item No. 7 was found on 30 April 2016 on Anvil Bay, Chemucane, Mozambique. The item was brought back to Malaysia for identification and further examination by the Team.

The exact location of the debris on a MAS B777 aircraft could not be identified since it did not have any markings or numbers and there were no peculiar features which could match it on the aircraft except for one edge of the part which had a distinct radius, which suggested that the joining part would be at an angle.

While the construction was similar to a B777 part, there was no conclusive evidence to determine the origin of this part with respect to the aircraft. After review of the B777 Illustrated Parts Catalogue (IPC), the most possible location of the part was determined to be the wing to fuselage body fairing.

There is no conclusive evidence to determine the origin of this part with respect to the aircraft however it is likely to be a part of a panel of the wing to body fairing on a B777 and it is *likely* to be from MH370 (aircraft registered as 9M-MRO).

Refer to *Appendix 1.12E* for details.

8) Item 8 - Flap Support Fairing Tail Cone

Item No. 8 was found on 24 May 2016 on Gris Gris Beach, Mauritius. The item was brought back to Malaysia for identification and further examination by the Team.

Initial assessment indicated that this could be a flap support fairing tail cone of a B777. The part was identified from the legible numbers that were observed on the inner surface. The following part number 113W9154-401 and serial number 407 were visible on one side. The profile of the part resembled the wing flap support fairing tail cone.

The part number was cross referenced to the Boeing component maintenance manual and drawings. This identified it as a component of the wing flap fairing assembly and the fit closely matched that of the No. 1 flap support fairing. As the records of where these fairing tail cones are fitted are not normally kept by airlines, the serial number 407 could not be tracked to any particular aircraft.

Based on the legible numbers and the fit, it is confirmed that it is the tail cone of the No. 1 flap support fairing of B777 and *highly likely* to be from MH370 (aircraft registered as 9M-MRO).

Refer to *Appendix 1.12F* for details.

9) Item 9 - Left Wing Trailing Edge Panel

The item was found on 22 May 2016 in Macenta Peninsular, Mozambique. The item was brought back to Malaysia for identification and further examination by the Team.

The item matched the left part (outboard section) of the Upper Fixed Panel forward of the flaperon on the left wing. It was observed that the outboard side was fractured and on the inboard side the fastener holes were still visible with a pitch of 1 in. This fastener pitch matched that on the inboard side of the panel of the aircraft. The fasteners' pitch on the outboard side is 2 in. The raised portion of the core of the section of the panel of length 18 in. also matched with that on the aircraft panel.

The item is confirmed to be the outboard section of the "Upper Fixed Panel forward of the flaperon" on the left wing. The debris is *highly likely* to be from MH370 (aircraft registered as 9M-MRO).

Refer to *Appendix 1.12G* for details.

10) Item 10 - Left Outboard Flap

Item No. 10 was found on 08 May 2016 at Ilot Bernache, Mauritius. A part number was identified on a section of the debris, identifying it as a trailing edge splice strap, incorporated into the rear spar assembly of a Boeing 777 left outboard flap. This was consistent with the appearance and construction of the debris.

Adjacent to the part number was a second part identifier. The flap manufacturer supplied records indicating that this identifier was a unique work order number and that the referred part was incorporated into the outboard flap shipset line number 404 which corresponded to the Boeing 777 aircraft line number 404, registered 9M-MRO and operating as MH370.

Refer to *Appendix 1.12H* for details.

11) Item 11 - Seat Back Trim Panel Encasing IFE Monitor

Item No. 11 was found on 06 June 2016 on Riake beach, Nosy Boraha Island, Madagascar.

The item was brought back to Malaysia for the identification and further examination by the Team.

The part was identified as the seat back trim panel which encases the In-Flight Entertainment (IFE) monitor. There was a small fragment of fabric around the coat hanger on the debris, which was greenish in colour. This colour matched the seat fabric used on the MAS B777 on the centre seats. The location of the coat hanger on the left conforms to the Right Hand, Triple Seat Assembly column in the Economy (EY) class.

This part is confirmed to be the seat back trim panel for encasing the IFE monitor and is *highly likely* to be from MH370 (aircraft registered as 9M-MRO).

Refer to *Appendix 1.12I* for details.

12) Item 12 - Bottom Panel on Wing or Horizontal Stabilizer

Item No. 12 was found on 06 June 2016 on Riake beach, Nosy Boraha Island, Madagascar.

The item was brought back to Malaysia for identification and further examination by the Team. The letters “FB” were clearly visible on the part which indicates that it is a bottom panel on the wing or horizontal stabilizer. An attempt was made to match the part to all the wing and horizontal stabilizer panels with the identification marks ending with “FB”. The thickness and profile of the part did not match any of those panels on the aircraft. However, it could be confirmed that it is very likely to be a part from a Boeing aircraft and *likely* to be from MH370 (aircraft registered as 9M-MRO).

Refer to *Appendix 1.12J* for details.

13) Item 13 - Unidentified Part

Item No. 13 was found on 06 June 2016 on Riake beach, Nosy Boraha Island, Madagascar.

The item was brought back to Malaysia for the further examination and identification by the Team. The part could not be matched exactly to any part on a MAS B777 aircraft. There were also no identification numbers on the part.

Refer to *Appendix 1.12K* for details.

14) Item 14 - Unidentified Part

Item No. 14 was found on 06 June 2016 in Riake beach, Nosy Boraha Island, Madagascar.

The item was brought back to Malaysia for identification and further examination by the Team. The part did not have any distinguishing features to match any on a MAS B777 aircraft. It did not have any identification numbers. The part resembled a cabin interior piece based on the decorative finish, however there was insufficient evidence to positively identify the part to be from an aircraft.

Refer to *Appendix 1.12L* for details.

15) Item 15 - Right Wing Trailing Edge Panel

Item No. 15 was found on 06 June 2016 in Riake beach, Nosy Boraha Island, Madagascar.

The item was brought back to Malaysia for identification and further examination by the Team.

It was identified to be the outboard section of the “Upper Fixed Panel forward of the flaperon” on the right wing of a MAS B777 aircraft. The pitch of the fasteners’ holes on the right side (outboard) of the panel was measured to be 2 in. and that matched that on the debris. The debris is *highly likely* to be from MH370 (aircraft registered as 9M-MRO).

Refer to *Appendix 1.12G* for details.

16) Item 16 - Cabin Interior Panel

Item No. 16 was found on 12 June 2016 on Antsiraka beach, Madagascar.

The piece was small and did not have any evidence of part number printed on it. The vinyl cover showed a unique pattern of interior decorative panel on one side and white vinyl on the other side of the piece. The pattern was similar to the one used on MAS 777 cabin interior panels. There were also 'insert' holes visible on one of the sides. The part has been determined to be *almost certain* from MH370.

The detailed examination was conducted by the Team in collaboration with Science & Technology Research Institute for Defence (STRIDE).

Refer to *Appendix 1.12M* for details.

17) Item 17 - Unidentified Part

Item No. 17 was found on 12 June 2016 on Antsiraka beach, Madagascar.

This item is a sandwich structure panel with Nomex Honeycomb core of typical aircraft composite structure. No markings were found on this item. Further analysis on this item is difficult due to lack of features to indicate that it could be a B777 part.

Refer to *Appendix 1.12M* for details.

18) Item 18 - Right Forward Nose Landing Gear Door

Item No. 18 was found on 12 June 2016 in Antsiraka beach, Madagascar.

The item was brought back to Malaysia for the identification and further examination by the Team.

The part did not have any identification numbers on it. However, the features on the part resembled the Right Nose Gear Forward Door of a MAS B777 aircraft. The oval depressions on the inner skin and the

orientation of a diagonal, raised bar matched that on the Right Nose Gear Forward Door on the aircraft.

The part is positively identified as the Right Hand Nose Gear Forward Door of a B777. It is *highly likely* to be from MH370 (aircraft registered as 9M-MRO).

Refer to *Appendix 1.12N* for details.

19) Item 19 - Right Outboard Flap

Item No. 19 was found on 21 June 2016 in Pemba Island, East of Tanzania. This is the largest piece found after the flaperon and has been determined to be part of the inboard section of the right outboard flap of a B777. The Italian part manufacturer build records for the numbers located on the part *confirm* that all of the numbers relate to the same serial number outboard flap that was shipped to Boeing as line number 404. Aircraft line number 404 was delivered to MAS and registered as 9M-MRO.

Refer to *Appendix 1.12O* for details

A fibreglass and aluminium seal pan located at the inboard end of this outboard flap was found damaged. Two adjacent aluminium stiffeners within this inboard seal pan area also exhibited damage which was due to impact.

Refer to *Appendix 2.5C* for details.

20) Item 20 - Right Aft Wing to Body Fairing

Item No. 20 was found on 21 June 2016 on Kosi Bay Mouth, Kwa Zulu Natal, South Africa.

The item was brought back to Malaysia for identification and further examination by the Team. Part of the identification number was visible on the debris indicating that it is part of the right aft wing to body fairing panel, 196 MR. Part of the part number, 149W5232-1, was visible with the letter ‘R’ below it, indicating it is a panel on the right side of the aircraft.

This item is confirmed to be part of the right aft wing to body fairing panel from a B777 aircraft. It is *highly likely* to be from MH370 (aircraft registered as 9M-MRO).

Refer to *Appendix 1.12P* for details.

21) Item 21 - Unidentified Part

Item No. 21 was found on 18 July 2016 in Northern Kwa Zulu Natal, South Africa.

The item was brought back to Malaysia for identification and further examination by the Team. Based on the structure construction, this part could be a small section of a panel from an aircraft. There were no identification numbers on the part and it could not be positively determined from which aircraft and which section it could have come from. It could not be positively determined whether the debris could be from a B777 aircraft.

Refer to *Appendix 1.12Q* for details.

22) Item 22 - Vertical Stabilizer Panel

Item No. 22 was found on 26 August 2016 on Linga Linga beach Mozambique.

The item was brought back to Malaysia for the identification and further examination by the Team.

On the interior side of the part, there was still a decal with part identification numbers. The Assembly (Assy) Number 177W3103-8 was visible. When referred to the Boeing 777 Illustrated Parts Catalog (IPC) this part was confirmed to be the right vertical stabilizer panel between the auxiliary and front spar. The red/white paint on the panel and the paint configuration appeared to match that of the MAS ‘kite’ logo on the right side of the vertical stabilizer.

The debris is confirmed to be part of the right vertical stabilizer panel of a B777. Based on the red/white livery on the panel it is determined to be *almost certain* from MH370 (aircraft registered as 9M-MRO).

Refer to *Appendix 1.12R* for details.

23) Item 23 - Unidentified Part

This item was recovered from Riake Beach, Nosy Bohara Island, Madagascar in October 2016.

The item was brought back to Malaysia for the identification and further examination by the Team.

The part structure construction characteristics showed that it was not part of the aircraft structure. It appeared more likely to be from the aircraft interior based on the vinyl and edge sealant which was on the part. The vinyl and sealant colour on the part matched that of the parts generally used in aircraft galleys. Although it appeared to be part of an aircraft interior there is no conclusive evidence to indicate whether the part could have actually originated from an aircraft.

Refer to *Appendix 1.12S* for details.

24) Item 24 - Unidentified Part

Two items of fibreglass-honeycomb composite debris were recovered near Sainte Luce on the south-east coast of Madagascar, having reportedly washed ashore in February 2016.

They were hand-delivered to the ATSB on 12 September 2016. The items were initially reported in the media as being burnt.

No manufacturing identifiers, such as a part numbers or serial numbers were present on either item that may have provided direct clues as to their origin. Despite no evidence of overall gross heat damage, two small (<10mm) marks on one side of the larger item and one on the reverse side were identified as damage resulting from localised heating. A burnt odour emanating from the large item was isolated to these discrete areas. The origin and age of these marks was not apparent. However, it was considered that burning odours would generally dissipate after an extended period of environmental exposure, including salt water immersion, as expected for items originating from 9M-MRO.

Refer to *Appendix 1.12T* for details.

25) Item 25 - Unidentified Part

This item was recovered from Riake beach, Nosy Boraha Island, Madagascar in July 2016.

The item was brought back to Malaysia for examination and identification by the Team. There were no identification numbers on the part and with the available features it could not be matched to any part on a MAS B777 aircraft.

Refer to *Appendix 1.12U* for details.

26) Item 26 - Right Aileron

This item was recovered from Nautilus bay, South Africa on 23 December 2016.

The item was brought back to Malaysia for identification and further examination by the Team. The debris closely matched the inboard section of the Right Aileron on a MAS B777 aircraft.

The numbers on the head of the fasteners on the debris were compared with those on the inboard section of the right aileron on the aircraft. These numbers matched. Additionally, the spacing of the fasteners on the aileron also matched those on the debris. The core and its dimensions also matched those on the inboard section of the right aileron. These confirmed that the debris is part of the inboard section of the right aileron of a B777 aircraft.

Based on the dimensions and fit on the aircraft and the visible fasteners it could be confirmed that the debris is part of the inboard section of the right aileron of a B777 aircraft. It was also determined to be *highly likely* from MH370 (aircraft registered as 9M-MRO).

Refer to *Appendix 1.12V* for details.

27) Item 27 - Right Wing No. 7 Flap Support Fairing

This item was recovered from Mpame beach, South Africa on 27 January 2017.

The item was brought back to Malaysia for identification and further examination by the Team. The possible location of the part on a MAS B777 aircraft was determined.

It was easily matched to the fixed, forward portion of the No. 7 flap support fairing. Item No. 2, found on 27 December 2015 at Daghatane Beach, Mozambique, is also part of the same fairing; however, it is part of the rear, moveable section.

The debris was thoroughly cleaned to reveal any identification numbers. After cleaning, the numbers 113W9211-402, S/N: 406 were found on the inside surface of the debris. The part number 113W9211-402 indicated that the debris was indeed a part of the No. 7 flap support fairing of a B777 aircraft. The serial number, 406 could not be used to link it to any particular aircraft as there were no records available to confirm this.

Based on the legible part number and the match of the part on the aircraft it is confirmed that the debris is part of the fixed, forward No. 7 flap support fairing of a B777 aircraft, and also determined to be *highly likely* to be from MH370 (aircraft registered as 9M-MRO).

Refer to *Appendix 1.12W* for details.

1.12.4 Process for Recovery of Debris

At the time of writing of this report, the possibility exists that more debris might be found washed ashore, especially at the coasts of south east Africa. Arrangements have been made with the Civil Aviation Authorities there to retrieve and secure the debris and to be delivered to the Team for examination.

SECTION 1 – FACTUAL INFORMATION

1.13 MEDICAL AND PATHOLOGICAL INFORMATION

Medical information relating to the crew is under *Section 1.5.*

Loss of aircraft cabin pressure, or depressurisation, is a potentially serious emergency in an aircraft flying at normal cruising altitude. Depressurisation, also known as decompression, is the reduction of atmospheric pressure inside a contained space such as the cabin of a pressurised aircraft. The cabins of modern passenger aircraft are pressurised in order to create an environment which is physiologically suitable for humans. The higher the aircraft flies, the higher the pressure differential that needs to be maintained and the higher the stress on the aircraft structure. Without a fully functional pressurised cabin, passengers and crew need to use oxygen systems during cruise. The composition of atmospheric air remains constant as air pressure reduces with increasing altitude. Since the partial pressure of oxygen also reduces, the absolute amount of oxygen also reduces. The reduction in air pressure reduces the flow of oxygen across lung tissue and into the human bloodstream. A significant reduction in the normal concentration of oxygen in the bloodstream is called hypoxia.

Hypoxia is a condition in which the body or a region of the body is deprived of adequate oxygen supply at the tissue level. The major symptoms and signs of hypoxia include light headedness or dizziness, blurred or tunnel vision, headache or nausea, diminished hearing and tingling or numbness of finger tips. The effects of hypoxia become more significant when exposed to an altitude above 10,000 ft.

Time of useful consciousness or also known as effective performance time is the amount of time crew and passengers can continue to conduct duties and activities in an environment with inadequate oxygen. It is measured from the time when the occupants of the aircraft are exposed to a low-pressure environment to the time when the occupants have lost the capability to take corrective and protective actions, such as self-administration of oxygen. The time of useful consciousness is dependent on the pressure altitude inside the cabin following depressurisation (Refer to *Table 1.13A* below). Hypoxia symptoms can be worse and time of useful consciousness shorter for people with respiratory or heart conditions, who are smokers and unfit, or have been drinking alcohol.

There was no evidence that physiological factors or incapacitation affected the performance of flight crew members on MH370.

Cabin Pressure Altitude (ft)	*Time of Useful Consciousness (TUC)*
15,000	More than 30 min
18,000	20 – 30 min
22,000	10 min
25,000	3 – 5 min
28,000	2.5 – 3 min
30,000	1 – 2 min
35,000	30 sec – 1 min
40,000	15 – 20 sec
Source: Reinhart, R.O. 1996. Basic Flight Pathology. 2nd Edition. McGraw-Hill: New York.	

Table 1.13A: Time of Useful Consciousness

SECTION 1 – FACTUAL INFORMATION

1.14 FIRE

Aircraft fire could not be established as there was no reported air or ground fire.

SECTION 1 – FACTUAL INFORMATION

1.15 SURVIVABILITY

Survivability of persons on board could not be established as the aircraft has not been found.

SECTION 1 – FACTUAL INFORMATION

1.16 TESTS AND RESEARCH

Not applicable.

SECTION 1 – FACTUAL INFORMATION

1.17 ORGANISATIONAL AND MANAGEMENT INFORMATION

1.17.1 Department of Civil Aviation Malaysia

1) Introduction

The Department of Civil Aviation **(**DCA) is an agency under the purview of the Ministry of Transport (MOT) with the authority to regulate and oversee all technical-operational aspects of the civil aviation industry in Malaysia.

As a Contracting State of the International Civil Aviation Organization (ICAO) since 1958 Malaysia through DCA is responsible to ensure that the safety and security of flights are consistently maintained at the highest level possible, and at the same time, to ensure the safety of the Malaysian airspace for aircraft operations in conformity to the requirements of ICAO in all aspect of polices, regulations and Standards and Recommended Practices (SARPs).

Malaysia's civil aviation system is based on the Federal Constitution as the supreme law. The legal framework in place consists of the following legislations enacted by Parliament:

- Civil Aviation Act 1969 (Act 3), last amended 01 June 2003
- Aviation Offences Act 1984 (Act 307);
- Airport and Aviation Services (Operating Company) Act 1991 (Act 467); and
- Carriage by Air Act 1974 (Act 148).

Specifically, Section 3 of the *Civil Aviation Act 1969* empowers the Minister of Transport *"to give effect to the Chicago Convention and regulate civil aviation."* Under the authority conferred by the same provision, the Minister of Transport also enacted the *Civil Aviation Regulations 1996 (CAR) [P.U. (A) 139/96].*

CAR 201 stipulates the use of '*ipso facto*' to address ICAO Annexes 1 to 19, including the application of not only ICAO Standards, but also the recommended practices, provided that a regulation has not already been established in CAR and that a difference has not been notified to ICAO. In

particular, DCA relies completely on CAR 201 for the implementation of Annexes 3, 4, 5 and 12.

The *Civil Aviation Act 1969* or Act 3 also empowers the Minister of Transport to make rules providing for *"the investigation in such manner as may be prescribed, including by means of a tribunal established for the purpose, of any accident either occurring in Malaysia or occurring to Malaysian aircraft."* In addition, this Act provides the Minister of Transport, the Chief Inspector of Air Accidents Investigation Bureau (AAIB) with the proper authority and legal tools to conduct investigations effectively, and in compliance with Annex 13.

CAR defines which accidents and incidents shall be reported and empowers the Minister of Transport to appoint a Chief Inspector of Air Accidents and Incidents. CAR provides for the Chief Inspector to *"determine whether or not an investigation shall be carried out in respect of any accident to which these regulations apply and the form of the investigation"*. The Chief Inspector may carry out, or may cause another Inspector to carry out, an investigation of any such accident. CAR also makes provision for the mandatory submission of a report to the Director-General of Civil Aviation (DGCA) in respect of any reportable occurrence. No provision is however made for a voluntary non-punitive reporting system.

2) Functions and Responsibilities of Department of Civil Aviation

The functions and responsibilities of DCA are, as follows:

- To exercise regulatory functions in respect of civil aviation and airport and aviation services including the establishment of standards and their enforcement;

- To represent the Government in respect of civil aviation matters and to do all things necessary for this purpose;

- To ensure the safe and orderly growth of civil aviation throughout Malaysia;

- To encourage the development of airways, airport and air navigation facilities for civil aviation;

- To promote the provision of efficient airport and aviation services by the licensed Company; and

- To promote the interests of users of airport and aviation services in Malaysia in respect of the prices charged for, and the quality and variety of, services provided by the licensed Company.

3) Sectors and Divisions of Department of Civil Aviation

<table>
<tr><th colspan="2">Sectors and Divisions of DCA</th></tr>
<tr><td>1. Flight Operations Sector</td><td rowspan="3">Grouped under a broader unit called Engineering and Flight Operations</td></tr>
<tr><td>2. Airworthiness Sector</td></tr>
<tr><td>3. Flight Calibration Division</td></tr>
<tr><td colspan="2">4. Air Traffic Management Sector</td></tr>
<tr><td colspan="2">5. Air Traffic Management Inspectorate Division</td></tr>
<tr><td colspan="2">6. Aviation Security Division</td></tr>
<tr><td colspan="2">7. Airport Standards Division</td></tr>
<tr><td colspan="2">8. Malaysian Aviation Academy Division</td></tr>
</table>

4) Areas of Focus

Section 1.17.1 will focus on three Sectors of DCA, as below:

a) Air Traffic Management Sector,

b) Airworthiness Sector, and

c) Flight Operations Sector.

5) Air Traffic Management Sector

The Director of the Air Traffic Management (ATM) Sector is responsible to the DGCA for the planning, implementation and operation of the air traffic services systems in the two Malaysian Flight Information Regions (FIRs), i.e. Kuala Lumpur and Kota Kinabalu FIRs respectively, in accordance with the ICAO Standards and Recommended Practices (SARPs).

The function of the ATM Sector is responsible for the provision of air traffic service for the safe and efficient conduct of flight within Malaysian airspace pursuant to the Chicago Convention 1944.

The Malaysian airspace is divided into the Kuala Lumpur and Kota Kinabalu FIRs, where operations are associated with air traffic control units. There are two Air Traffic Control Centres; in Kuala Lumpur and Kota Kinabalu, a sub-centre in Kuching as well as 12 Control Towers in Peninsular Malaysia, 4 in Sabah and 8 in Sarawak.

The Director of ATM Sector is supported by Regional Director I (Peninsular Malaysia), Regional Director II (Sabah), Regional Director III (Sarawak), Director KLIA and Director of KL ATSC in the functionality of the Sector.

Supporting the Regional Directors/Directors are ATSC Chiefs, Supervisors, DCA Managers, Unit Chiefs, Operational Controllers and support staff. Other entities, including Aeronautical Information Service (AIS), Procedures for Air Navigation Services and Operations (PANS-OPS), Cartography and SAR are under the direct responsibility of the Director of ATM Sector. The ICAO SARPs associated with the responsibility of ATM Sector are those contained in:

- Annex 1 - Personnel licensing;
- Annex 2 - Rules of the Air;
- Annex 3 - Meteorological Service for International Air Navigation;
- Annex 4 - Aeronautical Charts;
- Annex 5 - Units of Measurement to be used in Air and Ground Operations
- Annex 10 - Aeronautical Telecommunications Volume I & II;
- Annex 11 - Air Traffic Services;
- Annex 12 - Search and Rescue;
- Annex 14 - Aerodromes; and
- Annex 15 - Aeronautical Information Services.

Other relevant documents are:

- DOC 4444 - Procedures for Air Navigation Services - Air Traffic Management (PANS-ATM);
- DOC 9859 - Safety Management System Manual;
- CIR 314 - Threat and Error Management (TEM);
- DOC 9910 - Normal Operations Survey (NOSS);
- DOC 9426 - Air Traffic Services Planning Manual; and
- DOC 9683 - Human Factors Training Manual.

a) Air Traffic Inspectorate Division

The Air Traffic Inspectorate (ATI) Division is the regulatory body that oversees the provision of Air Navigation Services (ANS) by the ANS providers to ensure compliance with the national legislations, namely the Civil Aviation Act 1969 and the Civil Aviation Regulations 1996, and ANS-related ICAO Annexes to the Chicago Convention.

The ATI Division develops and establishes the ANS safety standards and performs safety oversight and surveillance activities with the sole aim of regulating the ANS providers. The regulatory Manual of ANS Inspectorate contains the requirements and procedures pertaining to the provision of the ANS, based on the SARPs of ICAO Annexes to the Chicago Convention, other ICAO documents and best practices, as may be determined by the ATI Division which develops and establishes the ANS safety standards and performs safety oversight to be applicable in Malaysia. From time to time the ATI Division develops and establishes the ANS safety standards and performs safety oversight and may supplement these ANS safety standards in the form of safety publications such as Air Traffic Inspectorate Directives (ATIDS) or Aeronautical Information Circulars (AIC). Where appropriate, these safety publications will be incorporated into the Manual by amendments.

i) Audits/Inspections

The audits/inspections utilise protocols questions and compliance checklists to evaluate the level of adherence to stipulated national legislations, and ANS-related ICAO Annexes to the Chicago Convention and ICAO documents, including best practices. The ATI Division also conducts oversight of the ANS provider's safety management system (SMS) to ensure its formal and systematic implementation by all ATSUs, including compliance with stipulated requirements. Currently, the ANS providers that are regulated by the ATI Division include Air Traffic Management Sector of DCA, Malaysian Meteorology Department, Royal Malaysian Air Force (RMAF) and the Malaysian Army.

ii) Personnel Licensing

Personnel Licensing for ATCOs provisions was promulgated in the Malaysia Civil Aviation Regulations (MCAR) 1996. The ATI Division is the authority for issuance, renewal, endorsement and validation of an ATC Licence and an ATC Trainee Licence (implemented since 01 April 2011), in accordance with ICAO Annex 1 to the Chicago Convention.

(1) Air Traffic Control Examination activities include all ATC courses at ATC organisations that are approved by the DGCA and operational ATC examinations at ATS units that control civil air traffic. However, some functions are delegated to designated ATC Check Officers who are appointed on a two-year basis by the DGCA.

(2) Air Traffic Control Licensing provisions were promulgated in the MCAR 1996. The ATI Division is the authority for issuance, renewal, endorsement and validation of an ATC Licence and an ATC Trainee Licence in accordance with ICAO Annex 1 to the Chicago Convention, as follows:

(3) Class 3 Medical Assessment for ATCOs, as part of the pre-requisite for an ATC Licence and an ATC Trainee Licence,

shall only be issued by a Designated Aviation Medical Examiner (DAME). The ATI Division develops and establishes the ANS safety standards and performs safety oversight and maintains a comprehensive database of licensing information for all licensed holders, and

(4) English Language Proficiency (ELP) Assessment is required for ATCOs and aeronautical station operators, and they must meet the minimum required proficiency level for radiotelephony communications i.e. Level 4 in accordance with ICAO Annex 1 to the Chicago Convention.

iii) Certification and Audit of ATC Approved Training Organisation

The Certification and Audit of ATC Approved Training Organisation (ATC-ATO) is responsible for the training of ATCOs. It provides ATC training by holding ATC-ATO approval certificate that is issued by the DGCA. The ATI Division conducts a regular oversight programme on the approved ATC-ATO to ensure continuing compliance with the approval requirements.

iv) Air Traffic Control Incident Investigations

Air Traffic Control Incident Investigations are carried out for ATC safety-related occurrences to evaluate the effectiveness of the ATC system and its components, as well as recommending mitigation actions towards enhancements. The investigative process includes the Incident Review Panel (IRP), The Board of Inquiry (BOI) and the Safety Review Boards (SRB).

In addition to the licensing and validation of ATCOs, the ATI Division develops and establishes the ANS safety standards and performs safety oversight and is responsible for regulating the checks and standards units at various ATS facilities. It also conducts safety oversight of military ATCOs who are charged with the responsibility of providing air traffic services to civil flights in selected portions of the airspace.

The ATI Division develops and establishes the ANS safety standards and performs safety oversight and has also developed appropriate processes and procedures to enable the division to carry out its safety oversight functions in accordance with established requirements and in a standardised manner. The Division has the necessary facilities and equipment to enable the personnel to carry out their safety oversight functions in an effective manner. All necessary procedures, including guidance material, have been developed.

v) Search and Rescue

With respect to Search and Rescue (SAR), no legislation specifically addresses the provision of assistance to aircraft in distress. However, in Malaysia, aeronautical SAR (A-SAR) is provided in accordance with Annex 12 to the Convention of ICAO and International Aeronautical and Maritime Search and Rescue (IAMSAR) Manual Vol. I to IV.

As a signatory to the Chicago Convention, Malaysia is obligated to provide A-SAR services on a 24-hour basis, within the Malaysian Aeronautical Search and Rescue Regions (SRR), (defined within the Kuala Lumpur and Kota Kinabalu FIRs).

With the implementation of National Security Council (NSC) Directive No. 20 effective 11 May 1977, A-SAR Operational procedures have been amended to harmonise with inter-agency actions during an aeronautical incident.

vi) Primary Aeronautical and Maritime Search and Rescue Agencies

(1) National Security Council

The National Security Council (NSC) is the body responsible for establishing, developing and maintaining Aeronautical and Maritime SAR Organisation in Malaysia. The Cabinet, through the Secretary of the National Security Council, directs the NSC on policy, international agreements, conventions and operational matter. The

NSC is responsible to the Cabinet on all matters pertaining to Aeronautical and Maritime SAR.

Note:

The National Security Council Act 2016 was enacted by the Parliament of Malaysia and published in the *Gazette* on 07 June 2016.

(2) Department of Civil Aviation

DCA is the SAR Authority for aeronautical incidents and shall be responsible for the provision of Aeronautical SAR service within Malaysia's Aeronautical Search and Rescue Regions (SRRs). As such DCA shall co-ordinate, liaise, train, equip, staff, maintain, develop procedures and operations and conduct exercises for A-SAR. DCA shall also assist the Maritime SAR Authority, when requested.

(3) Malaysian Maritime Enforcement Agency

The Malaysia Maritime Enforcement Agency (MMEA) is the SAR Authority for maritime incidents and shall be responsible for the provision of Maritime SAR service within Malaysia's Maritime SRRs. As such MMEA shall co-ordinate, liaise, train, equip, staff, maintain, develop procedures and operations and conduct exercises for maritime SAR. MMEA shall also assist the Aeronautical SAR Authority, when required.

vii) Aeronautical Search and Rescue Plan of Operation

The purpose of this plan is to provide a set of specific Aeronautical SAR Operation Procedures in all SAR missions within the Malaysian SRRs, for which DCA is the SAR Authority for aeronautical incidents and, acts as Chairman to the Aeronautical SAR Working Group. However, this plan is, by no means, exhaustive in nature, and is to be used in conjunction with IAMSAR MANUAL VOLUMES I, II, and III and as well as other departmental documents issued from time to time. Operational Letters of Agreements have also been signed with

neighbouring States/SAR Regions. The preparedness and training of all entities is ensured through regular exercise and training.

viii) International Search and Rescue Treaties, Conventions and Agreements

DCA Malaysia had participated in a number of international organisations such as ICAO, and in accordance with the Convention on international Civil Aviation has adopted search and rescue (SAR) standards and practices. Additionally, there are SAR bilateral agreements between Malaysia and the ASEAN countries (Indonesia, Singapore, Thailand, Brunei and the Philippines) SAR agencies to enhance coordination, cooperation and mutual support for operations along commons borders.

(1) Search and Rescue Agreements:

(a) Multilateral

As a member state of the Association of South East Asia Nations (ASEAN), and in line with the Declaration of ASEAN Concord for Cooperation between the member states of Indonesia, Philippines, Singapore and Thailand, Malaysia has formalised the following on aeronautical and maritime SAR:

ASEAN Agreements for the facilitations of search for aircraft in distress and rescue of survivors of aircraft accidents, signed in Singapore on 14 April 1972; and

ASEAN Agreements for the facilitations of search for ships in distress and rescue of survivors of accidents, signed in Kuala Lumpur on May 1975.

(b) Bilateral

Malaysia has also signed Bilateral Aeronautical SAR Agreements with the following countries:

1.	Singapore	11 August 1984
2.	Thailand	09 August 1985
3.	Indonesia	29 August 1985
4.	Philippines	09 December 1985
5.	Brunei Darussalam	16 December 1998

(c) Other Arrangements

Special operational procedures for border SAR Malaysia/Indonesia by the General Border Committee, resulting from the special arrangements between the Malaysia/Indonesia SAR Working Group of both countries.

Under the Operational Letter of Agreements between Singapore and Malaysia pertaining to aeronautical SAR service in the South China Sea Corridor Area[12], Kuala Lumpur ACC shall take alerting actions while Singapore RCC shall conduct the aeronautical SAR mission (AIP Malaysia Volume I ENR 2.2-3).

It is noted that the SAR responsibilities over the high seas/Malaysia Exclusive Economic Zone (EEZ) within the KL FIR/ASRR over Malaysia Maritime SAR Region (MSRR) shall be under the jurisdiction of Malaysia SAR authorities.

[12] South China Sea Corridor Area is defined as the area West of 105E at flight level 150 to Ground/Sea Level and East of 105E at flight level 200 to Ground/Sea Level, within the dimensions of 023600N 1044500E to 020000N 107000E and along 020000N till the Singapore/Kota Kinabalu FIR boundary - thence along 060000N till the Singapore/ Kuala Lumpur FIR Boundary - thence along this boundary to 023600N1044500E)

(d) Area of Responsibility

In accordance with ICAO agreements, the international boundaries for the provision of the search and rescue (SAR) services in Malaysia and adjacent ocean areas are divided into two search and rescue regions (SRRs) for aeronautical coordination.

(e) Search and Rescue Regions of Malaysia

As promulgated in the ICAO's Regional Air Navigation Plan, the Search and Rescue Regions of Malaysia are defined as the areas coincide with the boundaries of the Kuala Lumpur and Kota Kinabalu Flight Information Regions; airspace as delegated by Aeronautical SAR Region (ASRR) Appendix ICAO under Malaysia's jurisdiction. The Malaysia ASRR area of responsibility is, as *Figure 1.17A* (below).

(f) Maritime Search and Rescue Regions

The Malaysia Maritime Search and Rescue Regions (MSSR) - *Figure 1.17B* (below), include the waters of Malaysia and the areas declared as the Continental Shelf Boundary and also the waters under the FIRs delegated to Malaysia. This information is published in IMO SAR Plan.

(g) Responsibilities of Department of Civil Aviation on Search and Rescue

The responsibilities of DCA on Search and Rescue are as follows:

- Developing SAR policies;
- Developing A-SAR bilateral agreements with adjacent states;

- Establishing, staffing, equipment and managing the A-SAR system;
- Conduct training courses in search and rescue at the Civil Aviation Academy and refresher courses at the ARCC;
- Coordinate for SAR training and refresher courses;
- Establishing of ARCCs and ARSC;
- Arranging for SAR facilities; Conduct and coordinate all SAR missions involving civil aircraft within its areas of responsibility.
- Assist in the conduct of all SAR missions involving military aircraft, when requested by RMAF;
- Assist in the conduct of SAR missions involving vessel when requested by MRCC/MRSC;
- Provision and maintenance of the KL ARCC, KK ARCC and Kuching ARSC; and
- Tasking of SAR participating aircraft or vessel for search and rescue operations:
    - Provision of survival equipment; and
    - Periodically conduct national and international search and rescue exercises (SAREX).

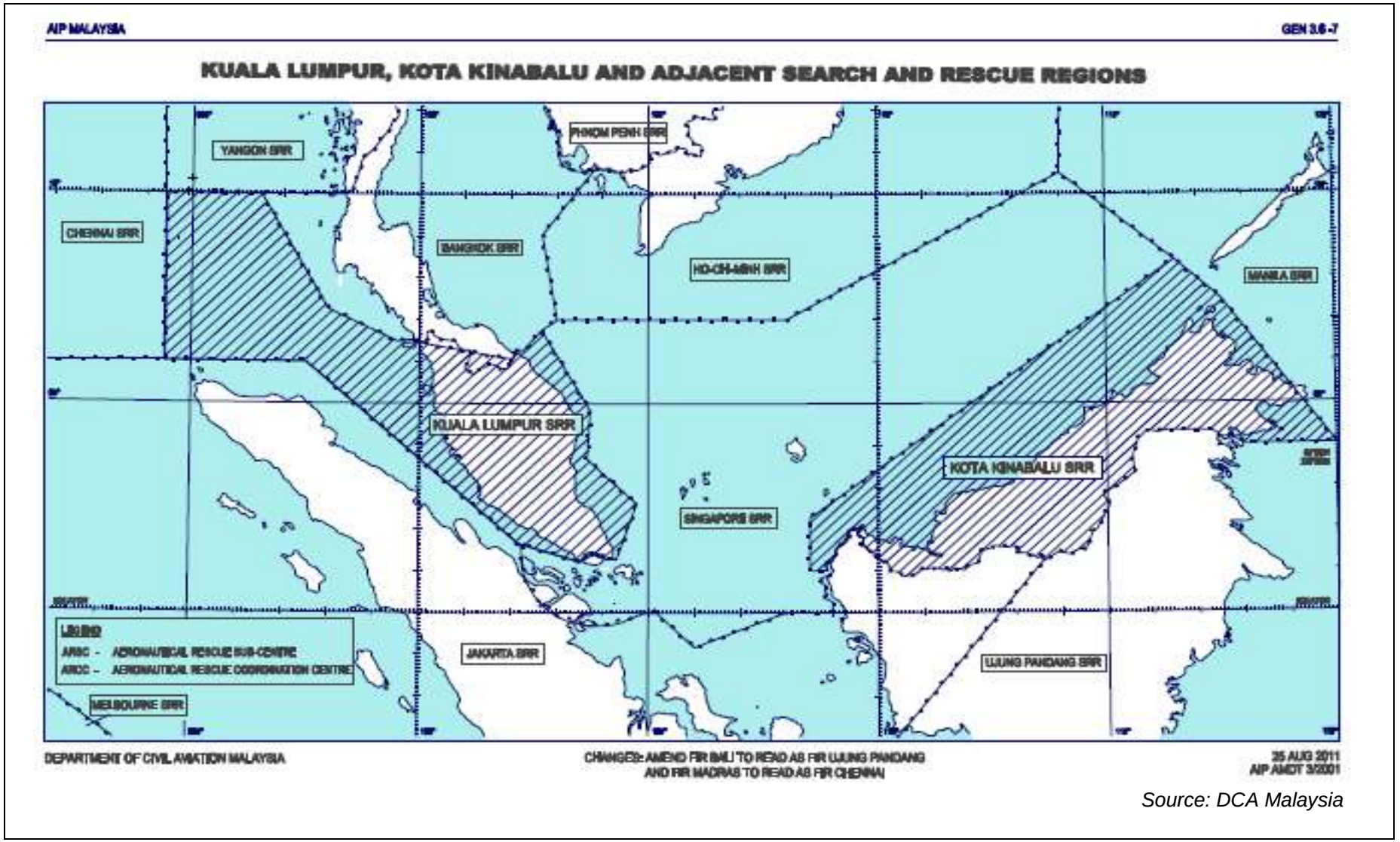

Source: DCA Malaysia

Figure 1.17A - Malaysia Aeronautical Search and Rescue Region

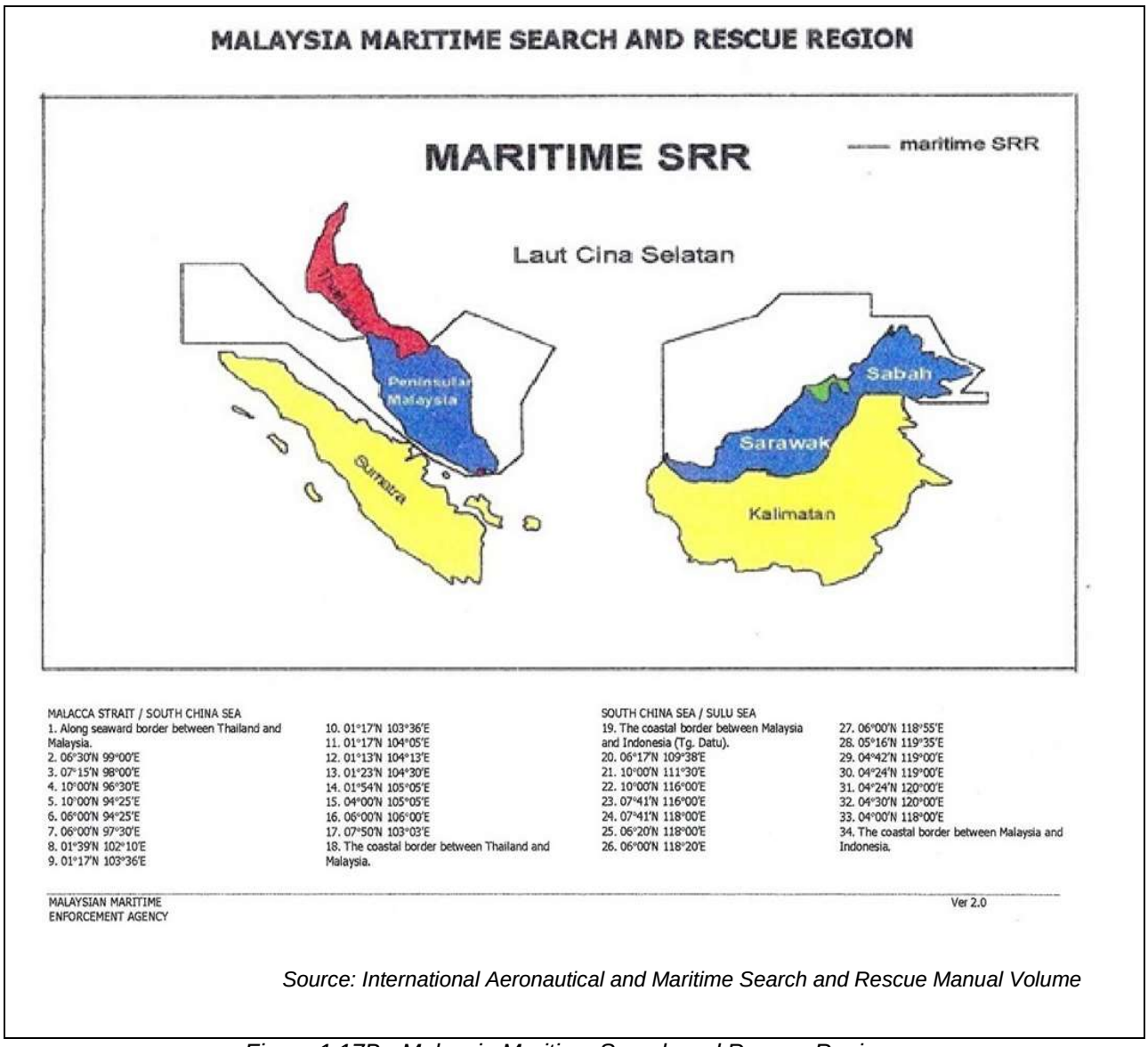

Source: International Aeronautical and Maritime Search and Rescue Manual Volume

Figure 1.17B - Malaysia Maritime Search and Rescue Regions

h) Kuala Lumpur Air Traffic Service Centre

The Kuala Lumpur Air Traffic Service Centre (KL ATSC) is headed by a Director and supported by two deputies - Deputy Director for ATSC and Deputy Director for KL TMA - and 243 ATCOs of various grades. The total number of the ATCO posts approved by the Government was 353. As of March 2014, there were 110 vacant posts.

The KL ATSC's Controller Working Positions (CWPs):

(i) Approach Control Surveillance

- TMA Supervisor
- Aproach North
- Approach South
- Approach Low
- Approach Radar (Flow Control)

(ii) Area Control Surveilliance

- Sector 1 Area Control Surveilliance
- Sector 2 Area Control Surveilliance
- Sector 3 Area Control Surveillance
- Sector 4 Area Control Surveillance
- Sector 5 Area Control Surveillance
- Sector 6 Area Control Surveillance (Sector 1 Upper)
- Sector 7 Area Control Surveilliance

(iii) Area Control Procedural

- Sector 1 Area Control Procedural
- Sector 2 Area Control Procedural
- Sector 3 Area Control Procedural
- Sector 4 Area Control Procedural
- Sector 5 Area Control Procedural

(iv) Sector Flight Data Assistant/Clearance Delivery

- Sector 1 Flight Data Assistant
- Sector 2 Flight Data Assistant
- Sector 3 Flight Data Assistant
- Sector 4 Flight Data Assistant
- Sector 5 Flight Data Assistant
- Sector 6 Flight Data Assistant
- Flight Data Processing
- Clearance Delivery
- Assistant Clearance Delivery
- Assistant Flight Information Services

(v) Working Positions (No Rating required)

- Watch Manager
- Controller-Pilot Data Link Communications
- Flight Information Services
- High Frequency/Aeronautical Mobile Services Station (HF/AMSS) South East Asia (SEA)1 and HF/AMSS SEA 2 Aeronautical Fixed Telecommunications Networks (AFTN) 1 and AFTN 2

(vi) Butterworth Terminal Area

To enable the Military to meet its national operational requirements, a number of control zones, training areas and danger areas have been established. Operational

control of these airspaces and responsibility for the provision of air traffic services within these airspaces have been delegated to the military. Coordination procedures between the civil and military authorities have also been established as follows:

Provision of approach control service within lateral limits of Butterworth Control Zone:

- Ground/Sea - 5,500 ft. altitude - FL245,
- Elsewhere 2,500 ft altitude - FL245 with Butterworth Terminal Area.

Air traffic to/from the civilian Penang International Airport (PIA), Alor Setar Airport and Langkawi International Airport is provided by military ATCOs who have been licensed by the ATI Division, which develops and establishes the ANS safety standards and performs safety oversight and to ensure the provision of services to civil traffic. The rationale for such an arrangement is based on the military activities at Butterworth Military Airport (BMA) which is in close proximity to PIA, and other military activities carried out over the high seas in danger areas WMD 412A and WMD 413A (permanently established). Furthermore, the final approach segments of both the PIA and the BMA intersect. No major incident has been recorded with the present arrangement/delegation of authority.

6) Airworthiness Sector

The Civil Aviation Act of 1969 empowered the DGCA to exercise its statutory powers to regulate the civil aviation and airport services including the establishment of standards and its enforcement.

The Civil Aviation Regulation (CAR) of 1996 was derived from the United Kingdom Air Navigation Order (ANO) of the mid-nineties and adopted with certain provisions for the Malaysian requirements. The CAR Fifth Schedule - Aircraft Equipment and Sixth Schedule - Radio and Radio Navigation Equipment to be carried in aircraft, and the DGCA issued Airworthiness Notices (ANs) specifically AN. No. 1 - Aircraft Certification, forms the basis for aircraft airworthiness and design standard for acceptance into Malaysian registry.

A comprehensive review of the MCAR 1996 by consultants was carried out in March 2013 and the submission of the final report was completed in January 2014. It was anticipated that the introduction of the CAR 2016 would streamline the DCA regulatory functions on similar approach to the European Aviation Safety Agency (EASA) requirements. This would include the introduction of CASR (Civil Aircraft Safety Requirements, AMC (Acceptable Means of Compliance) and GM (Guidance Materials) as part of the Malaysian regulatory framework, requirements and procedures.

The Director of Airworthiness Sector reports directly to the DGCA and is responsible for the operations of five divisions, namely: Continuing Airworthiness, Engineering, Maintenance Repair and Overhaul (MRO), Licensing and Standards.

The primary functions of the Airworthiness Sector include surveillance oversight of the aircraft maintenance activities on scheduled and non-scheduled air carriers, MROs, and the licensing of Aircraft Maintenance Engineers (AMEs). The sector is also responsible for the management of the aircraft register and joint technical audits with the Flight Operations Sector and Air Transport Sector for the issue or renewal of Air Operating Certificate.

With respect to aircraft accidents or incidents investigation, officers with specific trade and specialisation may be called upon, to assist the Air Accident Investigation Bureau, which is under the Ministry of Transport.

The Airworthiness Sector has established a minimum qualification of a university engineering degree or an Aircraft Maintenance Engineer's Licence (AMEL) for the posts of Airworthiness Engineers or

Airworthiness Inspectors respectively, and in addition, a minimum of five to seven years hands-on aviation industry experience. 37 of the 40 posts had been filled to support an 8% annual rate of growth of aircraft increment for the local air transport industry.

The Airworthiness Sector has developed a good working relationship with the local aviation organisations whereby, the newly recruited technical staff have been given the exposure to work closely with industry players. The DCA has made provisions in the AN. No. 1 Aircraft Certification, for the operator to bear the cost of training for DCA officers, specifically for the airworthiness engineers, inspectors and pilots for new aircraft type to be placed on the Malaysian register. This serves to keep them abreast with the latest development on the local airlines or operators fleet expansion programme.

The DCA Airworthiness Division Manual (ADM) provides guidance and procedures to airworthiness inspectors and airworthiness engineers to carry out their duties and function responsibilities.

The Sector emplaces a fairly comprehensive audit plan for the local and international organisations requiring DCA approvals. These approved organisations are subject to an annual audit. The audit includes local and international base maintenance and line stations. These audits may be scheduled on mutual arrangement with the organisation or be carried out on an opportunity basis when the DCA officers are in the vicinity of that organisation during the auditing period.

Any audit findings or deficiencies will be recorded in the NCRs (Non-Conformance Reports) and categorised into the respective levels of Level 1, Level 2 or Level 3. The Level 1 NCR requires urgent and mandatory compliance to a major deficiency in the audit findings. The Sector would review the corrective actions and reschedule an audit of the organisation before closing the finding as acceptable.

The ANs are published on a regular basis in the DCA website and would serve to notify any current changes on airworthiness policies or requirements for the Aircraft Maintenance Engineers and the aviation organisations to comply with as applicable. Some of the Airworthiness Notices issued by the Airworthiness Sector may originate from Original

Equipment Manufacturers' (OEMs) service bulletins or in-service difficulties arising from incident or accident reports which may affect aviation safety. The Airworthiness Notices form part of the Malaysian regulatory framework and the expedient means for the aviation industry to comply with at short notice.

The AN. No. 11 - Mandatory Occurrence Reporting, requires Air Operators and Maintenance Organisations to transmit information on faults, malfunctions, defects and other occurrences which cause or might cause adverse effects on the continuing airworthiness of the aircraft to the DCA.

With respect to ICAO Annex 19 - Safety Management, the Airworthiness Sector has implemented the requirement under AN No. 101 - Safety Management Systems (SMS) For Approved Maintenance Organisation (AMO) including Approved Training Organisations (ATOs) in March 2008. The SMS was made effective on 01 January 2009.

The Sector has been actively involved in the audits of 176 local and international Approved Maintenance Organisations (AMOs) that hold the DCA approvals; continuing airworthiness surveillance of 892 aircraft (of which 839 aircraft are active in operations), 12 Approved Training Organisations (ATOs) for Aircraft Maintenance Engineers and Technicians ab-initio training and also aircraft type training programme. There were 4,212 Licensed Aircraft Maintenance Engineers issued with DCA licence, but 2,374 licensed holders remain current. CAR 30 requires that inspection, overhaul, repair, replacement and modification works on a Malaysian-registered aircraft, including the engines, propellers and aircraft components, are carried out by an approved person or organisation, specifically, under the AMO maintenance organisation exposition procedures. The DCA requires the release of an aircraft 'Certificate of Release to Service' to be issued by an approved or authorised personnel, type-rated on the aircraft type under a DCA approved AMO procedures. The introduction of the new CARs would also address the training requirements and certification responsibilities of both Aircraft Maintenance Engineers in Category B and Aircraft Maintenance Technicians in Category A in their respective trades. The DCA Malaysia Part 66 engineers and

technicians licensing system is based on the EASA Part 66 syllabus and training requirements.

7) Flight Operations Sector

The Director of Flight Operations reports directly to the DGCA and is responsible for the operations of five divisions, namely:

- Flight Crew Licensing,
- Air Operator Regulatory,
- Flight Simulator,
- General Aviation, and
- Flight Calibration.

The primary functions of the Flight Operations Sector include surveillance oversight on scheduled and non-scheduled air carriers, flight test and simulator training of pilots, flight crew licensing on examinations standards, General Aviation activities, airfields and airways calibration and the conduct of a joint technical audit with the Airworthiness Sector and Air Transport Sector for the issue or renewal of Air Operating Certificate (AOC) for scheduled and non-scheduled air carriers. With respect to aircraft accidents or incidents investigation, pilots from this sector may be called upon, to assist the Air Accident Investigation Bureau, under the Ministry of Transport.

The Sector has established the procedures for Mandatory Occurrence Reporting (MOR) Scheme Guidelines in the Flight Operations Notice for the air operators to comply with in DCA Malaysia website.

With respect to ICAO Annex 19 - Safety Management, the Flight Operations Sector had implemented the requirement under the Aeronautical Information Circular (AIC) No: 06/2008. In conjunction with ICAO Annex 6 Part 1 Chapter 3 paragraphs 3.2.3 and 3.2.4 and Part III Chapter 1 paragraphs 1.2.3 and 1.2.4 with effect from 1 January 2009, it requires all Malaysian AOC Holders to implement an integrated Safety Management Systems (SMS).

To date, 8 of the AOC Scheduled Operators have complied with the SMS requirements and approved by the Sector. The implementation of the SMS for the 16 Non-Scheduled Operators is being incorporated in stages.

The following documents form part of the sector procedure manual in carrying out their surveillance responsibilities:

- Flight Operations Surveillance Inspector Handbook,
- Flight Crew Licensing Handbook,
- Flight Operations Policy, and
- Procedure Manual and Ramp Inspection Handbook.

As stated in the authorised Flight Examiner Handbook, each flight examiner is required to conduct at least six instrument flight checks and two type rating checks over the three-year period of their authorisation. In addition, they have to submit a quarterly activity report. In accordance with the Handbook, the authorised examiner has to pass an initial test upon appointment and a renewal test, to be conducted six months prior to the expiration of the authorisation. In between the tests, the examiner will also be the subject of one observation session to be conducted by the inspector.

The present activities of the Flight Operations Sector for surveillance oversight includes 8 Scheduled Operators, 21 Non-Scheduled Operators 8 Approved Flying Training Organisations, 16 new AOC applicants, 12 Flying Clubs, international flight en-route Inspections, domestic and international Station Facility Inspections and Ramp Inspections.

The frequency for Station Facility is once in every 2 years, the RAMP Inspection is 4 inspections at every originating en-route or destination stops, 4 inspections annually at every location but may depend on the safety performance of the operator while Base Inspection for Scheduled Operations and Non-Schedule Operations to be carried out on annual basis.

The Sector has a total establishment of 28 pilot posts to manage the various divisions, and of which only 16 posts had been filled. The need for experienced pilots to fill up the various posts had been an issue for most authority bodies worldwide, unless better incentives are offered.

1.17.2 Malaysia Airlines

1) Introduction

Malaysia Airlines (MAS) began in 1937, when the Straits Steamship Company and Imperial Airways formed Malayan Airways Limited (MAL) in Malaya. MAL evolved through many changes to Malaysia-Singapore Airlines (MSA) until Singapore gained its independence in 1965, where its Malaysian part became Malaysian Airline System (MAS) Berhad. In 1987 the Company took the commercial name of 'Malaysia Airlines' in line with the international promotion of the country.

MAS held an Air Service Licence (ASL) and Air Operators Certificate (AOC) for scheduled and non-scheduled operations. It was public-listed in 1985 with the Government holding a golden share. At its peak, MAS had an extensive network of operations with more than 100 destinations spanning over 5 continents around the world. The recession in 1994 affected the airline's business significantly when its operations were drastically scaled down.

The airline's performance for the past years had been a subject of great interest as it had suffered financial losses. Competition from emerging low-cost operators significantly contributed to the negative performance of the Company. MAS had in its fleet the A380, A330, B747-400, B777-200ER, B737-400 and B737-800. Its subsidiaries Firefly & MASWings operated the ATR-72 plying most of the domestic network in Peninsular and East Malaysia.

In spite of its scaled-down operations it was still a fairly large organisation (*Figure 1.17C* [below] shows the *Organisation Structure of MAS*), with a staff strength of more than 20,000 employees. It was headed by a Group Chief Executive Officer (CEO) who reported to the Board. Eight Directors reported to him, each heading a Division. The Divisions were, as follows:

- Group CEO Office
- Commercial
- Operations
- Corporate Services
- Customer Services

- Finance
- Human Resources
- MAS Aerospace Engineering (Engineering & Maintenance Division)

2) Engineering & Maintenance

a) Organisation Structure

The Engineering & Maintenance Department (EMD), also known as MAS Aerospace Engineering, was headed by a Chief Executive Officer (CEO), assisted by a Deputy CEO (Airlines Operations) and Senior Vice President (SVP) MRO Operations. The Finance, Engineering Materials, Business Support, Business Development, Legal and Warranty departments of the EMD reported direct to the CEO of the EMD. Heavy Maintenance, Engineering, Commercial, Training, Special Project, Engineering Facility and Workshop departments reported to the SVP (MRO Operations). The Technical Services, Maintenance Operations, Aircraft & Engine Maintenance Planning, Quality Assurance, Aircraft Project, Lease Planning, End-of-Lease (EOL)/Airline Engineering Group (AEG) Special Project and EOL Project Departments reported to the Deputy CEO (Airlines Operations). The organisation's management structure encompassed all the relevant areas befitting a maintenance management and maintenance organisation and was manned by suitable and experienced personnel. Key positions (post holders) as required for the Air Operators Certificate (AOC) holder and maintenance organisation were nominated by MAS and approved by DCA Malaysia. These key positions were further supported downstream by departmental managers and their executives.

b) Maintenance and Design Approval

The EMD was responsible to manage and carry out the maintenance of the MAS fleet of aircraft, which consisted of B747-400, B777-200ER, B737-400, B737-800, A330 and A380. The Maintenance and Management approval was issued by the DCA Malaysia in 1971. The approval was based on the approved quality

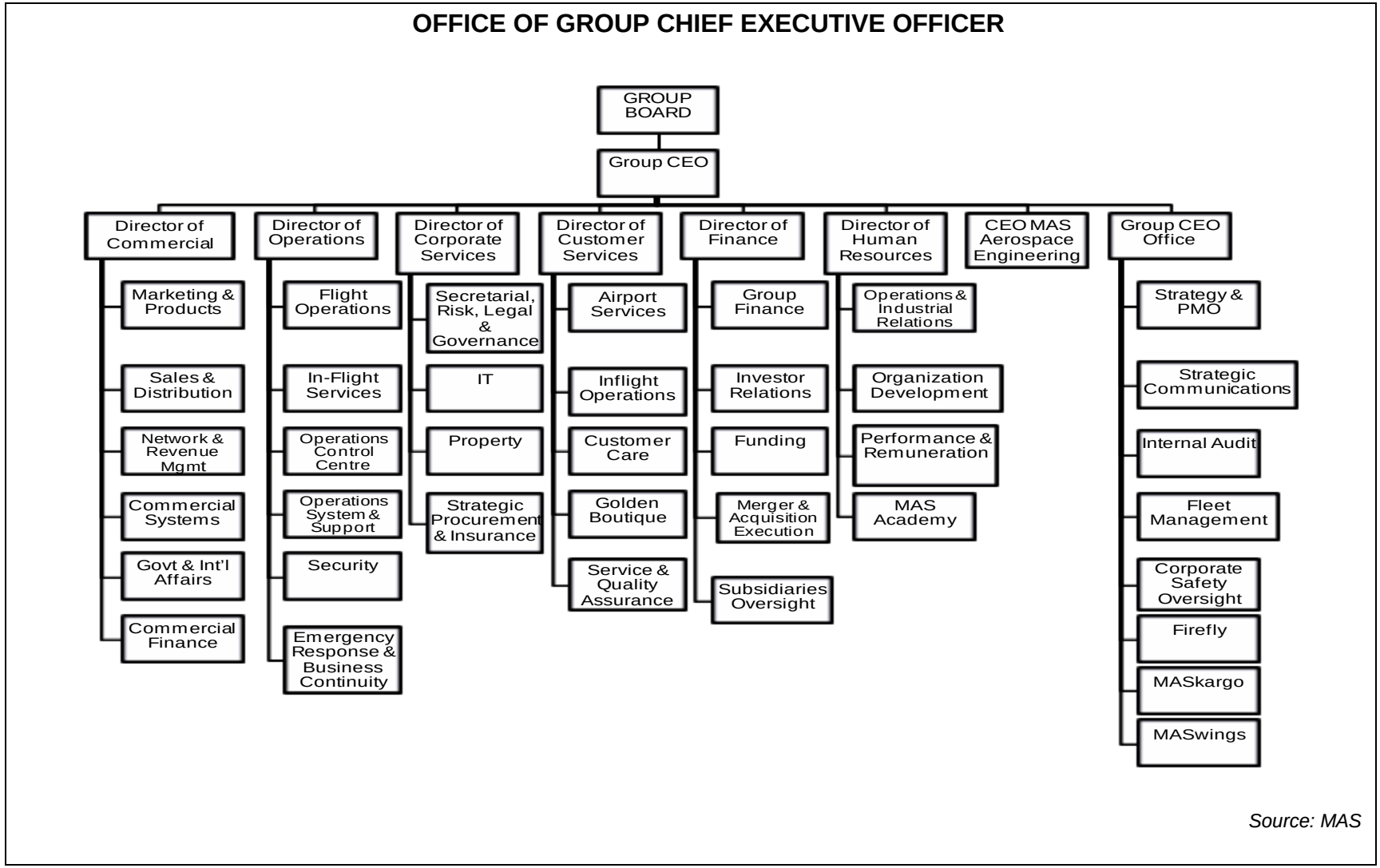

Figure 1.17C - Organisation structure of MAS

system laid out in the Maintenance Management Organisation Exposition (MMOE). The quality management system as detailed in the MMOE was under the responsibility of the Head of the Quality Assurance, who had direct access to the CEO of the EMD.

In the quest to undertake third party maintenance business the EMD also carried out maintenance of foreign registered aircraft under their respective National Aviation Maintenance Organisation Approvals. These approvals are from the European Aviation Safety Agency (EASA), the Federal Aviation Administration (FAA) of the United States of America (USA), the Civil Aviation and Safety Authority (CASA) of Australia and others. All these approvals had their independent approval process of initial approval, revalidation and surveillance.

The oversight of these maintenance activities was by regular audits and surveillance by the internal auditors of the Quality Assurance department and by DCA Malaysia, as well as the National Aviation Authorities of the various countries whose aircraft were maintained by MAS. In some cases, the audits were also carried out by the respective customers. There have not been any findings significant enough for any regulatory actions to be taken against the EMD for issues arising out of aircraft maintenance.

The EMD was also issued with Design Organisation Approval by DCA Malaysia. This allows the EMD to make minor design changes on the MAS fleet. To administer this, a team of engineers in the Technical Services Department of the EMD were qualified and approved in the various aviation disciplines such as Structures, Systems and Avionics.

c) Training

The EMD had its own Training school which provided ab-initio training to qualify selected candidates to obtain the DCA Malaysia Maintenance Engineers' licenses in the Mechanical or Avionics category. There were also training programmes for

aircraft and workshop technicians as well as approval holders. The Training School also provided continuation training which was required for all staff working on aircraft and in workshops, and in addition, aircraft type training and training for external parties. The training requirements were laid down in the DCA Part 66, which is similar to the EASA Part 66 requirements.

d) Base Maintenance

The EMD had two main bases for base maintenance: KLIA in Sepang and Subang Airport (SZB) in Subang.

The Kota Kinabalu (BKI) base in Sabah was an extension of the KLIA base. These bases were equipped with the hangars and facilities as required in the scope of the approval. The SZB base had 4 hangars to accommodate all aircraft in the MAS fleet. The SZB facility also accommodated all the support workshops for the required maintenance. The KLIA base had 2 hangars, one of which could accommodate the A380-800. The KLIA base had some limited support workshops for maintenance activity under the scope of approval. The BKI, extension of KLIA, had one smaller hangar only capable to accommodate B737 series aircraft or its equivalent.

e) Line Maintenance

Other than the main bases, there were also line stations according to the regions around the world. These were, as follows:

- Peninsular Malaysia,
- Sabah and Sarawak,
- South East Asian,
- Far Eastern,
- America and Pacific,
- Australian and New Zealand,
- Indo-Pakistan/Mideast and African, and
- European.

Line maintenance of aircraft at international line stations was contracted out to the local maintenance organisations. These line maintenance organisations were approved by DCA Malaysia before they took over the task. The organisations were also subjected to regular audits by MAS and DCA Malaysia.

f) Maintenance Authorisation

The EMD had approximately 4000 staff; distributed among the SZB base, KLIA base and the BKI extension base. There were approximately 1240 certifying staff at both SZB and KLIA bases and 41 certifying staff in BKI. The certifying staff consisted of the following:

- Licenced Aircraft Maintenance Engineers,
- Workshop approval holders,
- Certifying mechanics,
- Stores Inspectors,
- Non Destructive Testing (NDT) approval holders,
- Welders.

Authorisation of certifying staff for aircraft and component maintenance was carried out by the EMD's Quality Assurance department. This was strictly in accordance with the requirements laid down in the MMOE. These requirements, which were in line with the EASA requirements, were approved by DCA Malaysia. This process of authorisation was subjected to internal audit by independent quality auditors within the organisation, as well as by the DCA and other National Aviation authorities.

The Head of Quality Assurance (QA) was responsible for the administration and control of the Certifying staff.

g) Safety Management System

The EMD had implemented the Safety Management System as documented in the Safety Management Manual and as required by DCA Malaysia Airworthiness Notice No. 101. This safety

management was a part of the Company-wide Corporate Safety Management led by the Corporate Safety Oversight department which reports to the Group CEO's office. There was an internal reporting system in place for occurrences and hazards which encompassed provisions for confidential reporting. Regular safety meetings were conducted within the organisation as well as representing the division within the overall corporate system. Safety Management was supported by Occupational Safety, as required by the Occupational Safety and Health Act 1994. Safety actions were deliberated during these meetings and mitigating actions were discussed and followed up.

3) Operations

This division was headed by the Director of Operations and supported by Flight Operations, In-flight Services, Operations Control Centre, Operations System & Support, Security, and Director of Operations Office.

a) Flight Operations

The structure consisted of 6 Senior Managerial positions namely Quality Assurance & Regulatory Affairs, Training & Standards, Flight Safety & Human Factors, Technical & Development, Crew Planning & Deployment and Line Operations.

i) Flight Operations Management

The Flight Operations Management Structure *(Figure 1.17D* below*)* met the Air Operators Certificate (AOC) requirement as stipulated in the MCAR 1996. The key post holder positions in MAS were manned by captains who possessed outstanding credentials, senior in rank and had held several aircraft type rating in the airline's fleet. Their extensive exposure was therefore an asset to the airline's operations.

MAS Operations Manual A, Part 1.4.11 defined the guidelines for management pilots' office coverage and flying duties. As an example, the guideline stipulated that a Flight Operation

Manager (FOM) would be rostered 9 days flying duties (excluding weekend) and 13 days on office duties.

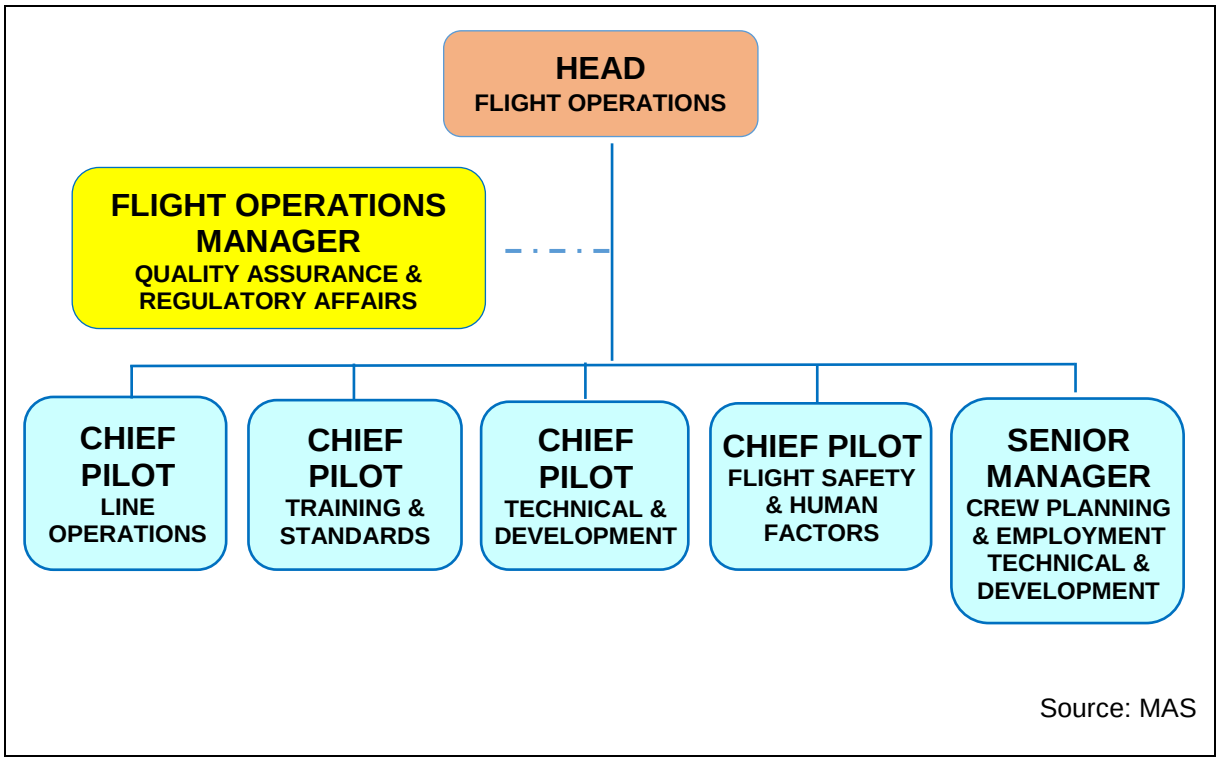

Figure 1.17D - Organisation of Flight Operations Management

ii) Organisation and Management related to B777 Operations

All the fleets in the Company were under the purview of Chief Pilot Line Operations. The fleet was headed by a Fleet Manager B777 who would report to the Chief Pilot Line Operations. The Fleet Manager B777 had been with the Company for the past 17 years and until March 2014 the fleet comprised of 17 aircraft. The Fleet Manager (with more than 10 years Command experience on the B777) was supported by non-flying staff in the day-to-day management of the fleet co-ordinated by Flight Operations Controllers (*Figure 1.17E* [below]).

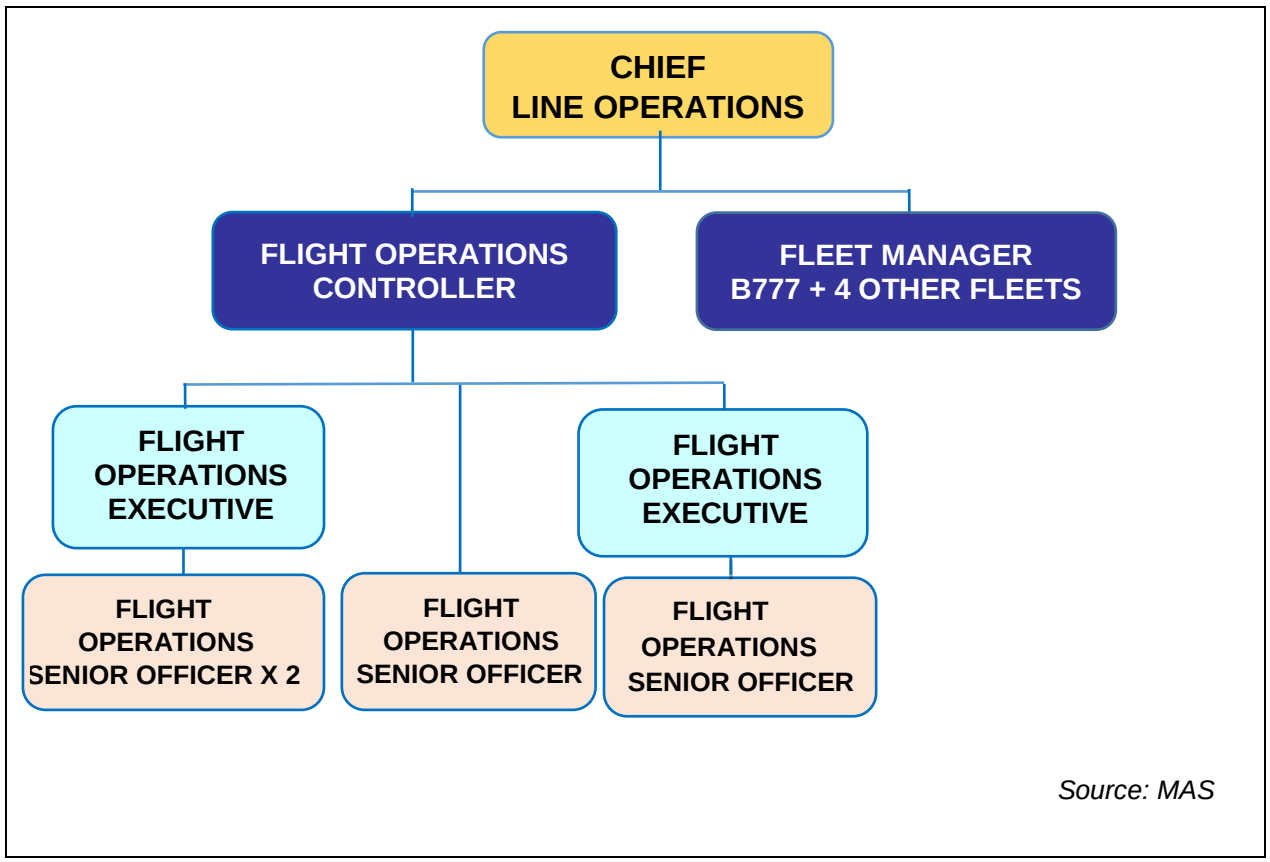

Figure 1.17E - Line Operations, Administration & Support (as of January 2014)

iii) Technical Crew

The airline technical crew were pioneered by pilots who crossed over to MAS when the then Malaysia-Singapore Airlines (MSA) split in 1972 to become MAS and SIA respectively. In the early days of MAS up to the mid-1980s a majority of MAS pilots came from MAS-sponsored cadets. These trainee pilots were normally sent to reputed Flying Colleges/Academies, mainly in Australia, Philippines, Scotland and Indonesia. These candidates were put through stringent pre-hire recruitment processes which included aptitude tests, psychomotor skills, as well as interviews by a panel comprising of Management Pilots and Human Resource Managers and/or Executives. In later years, the process became even more stringent with the inclusion of simulator evaluation and psychological tests.

After the mid-1980s, the emergence of local flying schools had resulted in most of the sponsored cadets undergoing their basic training in Malacca at the Malaysian Flying Academy (MFA). The MFA had also provided training for foreign students from Singapore, Indonesia, Bangladesh and India. This had benefited MAS in terms of costs and the ability to graduate ab initio qualified pilots in a shorter time compared to overseas flying schools.

In the last ten years, more flying colleges or academies were set up, such as in Kota Bahru and Langkawi. MAS-sponsored cadets were eventually trained at these places in tandem and then absorbed as trainee pilots into MAS, including a small number of self-sponsored students who made the grade. These cadets would pass out with a Frozen ATPL (Air Transport Pilot Licence) and by the time they had accumulated a total of 1,500 hours or more, the full authorisation of the licence would take effect giving the holder the privilege of its full coverage.

From the early days of operations, MAS started with domestic and regional services. Thus, the fleet of aircraft had always included small propeller aircraft to service remote towns that were equipped with short field aerodromes and short-haul twin engine jets. Generally, a career of a pilot in MAS began as a co-pilot on the smallest Turbo Props, or sometimes when the demand and the promotion was rapid, suitable candidates would be posted direct to the B737 upon entry into the airline. A co-pilot would need to serve for at least 5 to 7 years in the Company on the lower fleet before one could be considered for promotion to the B777. Before the arrival of the new generation aircraft, the career progression would start with the F27/50, then the 737 classics as their first jet aircraft experience, then to either A300B4 or the DC10/B747-200. After the introduction of the new generation aircraft, they were normally promoted from the B737/200/400/800 to the A330 or B777 fleet then the B747-400/A380 depending on the Company's individual

fleet requirement.

The pilot promotion policy had since changed to include individual pilot's bidding for promotion to larger aircraft, which was not the case in the past.

The pre-hire test also applied to those joining the airline with previous flying experience from other flying organisations. A significant percentage of MAS pilots came from the Royal Malaysian Air Force (RMAF), mainly those who had served the Air Force as short-commissioned officers. After about seven to ten years of service in the RMAF, they were able to join MAS with recognised flying hours and experience to be accepted as First Officers in the lowest fleet. After accumulating sufficient airline flying hours, they would be ready for promotion to Captain on the lowest fleet, e.g. F27/50, or direct to the B737 jet. A small percentage of pilots came from a general aviation background and needed to go through the similar stringent pre-hire process before commencing their training to the appropriate fleet.

On the average it would take at least 15 years of flying in the Company before a pilot could be promoted to command the B777. Among the factors for career progression is eligibility in terms of total command hours, base check and line check competencies, seniority in the pilot ranking and the airlines expansion plan. In Malaysia Airlines, no young fresh ab-initio pilot would be posted direct to the big wide-body jet (i.e. B777) without the smaller twin jets experience. By the time a captain was ready for the B777, he would have at least flown F50, B737 or A330 or combination of all the 3 aircraft with at least a total of 5,500 hours, part of which had to be a minimum of 1,500 command hours and 2 years operational on the MAS B737.

By normal career progression, the Captain that was flying on this aircraft would have met the full pre-requisites to be on the elite fleet of the B747-400 or the A380. However, it was his choice that he preferred to remain on the B777 fleet

as he did not bid for position on the two higher fleets.

iv) Technical Crew of MH370

The PIC of MH370 graduated in May 1981 from the Philippines Flying School under the MAS sponsorship programme during that era. He started his career with MAS upon graduation and served MAS until the day of the eventful flight.

The FO of MH370 graduated from the Langkawi Aerospace Training Centre (LATC) on the Island of Langkawi, Kedah, Malaysia in June 2007. LATC has been in existence for the last 12 years. MAS had sponsored at least ten batches of pilots at an average of 12 trainees per batch. These graduates had been flying with MAS upon graduation. Graduates from LATC generally met the standards set by MAS, proven by the numbers joining the airline as trainees and eventually becoming qualified First Officers. Since the last 5 or 6 years there were also pilots being sponsored and trained in the Asia Pacific Flight Training (APFT) Kota Bahru, one of the latest additions to the number of flying schools available locally.

The fleet carried sufficient numbers of Type Rating Examiners (TRE) and Type Rating Instructors (TRI) to fulfil the licensing requirements. TRE and TRI were Captains from within the airline, appointed with approval from the Licensing Section of the DCA. They were also tasked with monitoring the overall standards to be maintained by the fleet. This responsibility is under the jurisdiction of the Training and Standards Department, which is headed by a Chief Pilot. On the day of this eventful flight, the Captain was conducting the last phase of the Co-pilot's training as a B777 First Officer, in the capacity of a TRE.

v) Working Schedule/Roster Schedule and Management

The working schedule and rest requirement to manage crew fatigue was highly regulated and normally bounded by guidelines stipulated by the CAA UK CAP 371 and the Malaysian Civil Aviation Regulations (MCAR) 1996. The MCAR 1996 adapted the CAA CAP 371. With the formation of the Joint Aviation Requirements (JAR), DCA Malaysia had gradually migrated towards regulations stipulated in the JAR. Duty and Flight Time Limitation (FTL) was strictly guided by these published regulatory documents. In general, MAS has since its inception, adopted a more stringent and restrictive FTL based on the Memorandum of Understanding (MoU) between the Pilots Association and the adequately rested before they were scheduled to any assigned flight duties. The Pilots Association played an important role to ensure compliance to the limits were met.

In the case of MH370, the expected flight and duty time was less than 8 hours, with a single leg of one take-off and one landing. The Regulatory requirement and MAS Operations Manual A, Part 7.1.20 and MoU would only require one set of crew to man the flight. Standard Company's practice, in compliance with FTL, would call for the whole set of crew to be allocated a stop-over duration of 24 hours (more than the minimum rest period required) in Beijing before returning to Kuala Lumpur. Beijing was a destination that MAS operated with the same aircraft type on a daily basis.

The guidelines for Technical Crew complement requirements based on Maximum Schedule Block Time were as follows:

- Less than 8 hours: 2 crew (1 Captain and 1 Co-pilot);
- Between 8 to 12 hours: 3 crew (2 Captains and 1 Co-pilot); and
- More than 12 hours (3 Captains and 2 Co-pilots).

The Technical Crew were required to undergo medical check-up by approved aviation doctors for their license renewal. The medical certificate issued forms part of the validity of a pilot flying license.

A summary of the work schedule for the PIC and the FO, three months prior to the eventful flight, is available in *Table 1.17A* (below).

Rank	24	72	7	28	90	SEP Validity
	Hours		Days			
Pilot-in-Command	0:00:00	7:00:00	20:39:00	91:04:00	303:09:00	14 May 2014
First Officer	0:00:00	0:00:00	28:47:00	51:17:00	158:46:00	26 July 2014

Table 1.17A - 3 Months FTL Data

vi) Safety Management System

MAS Safety Management System (SMS) had been designed to comply with the framework as per ICAO in Annex 6, Appendix 7 (Currently Annex 19), Framework for Safety Management Systems and the expanded guidance found in the ICAO Doc.9859 Safety Management Manual (SMM) and IATA SMS Implementation Guide. In addition, this system was consistent with the requirements of the DCA Malaysia's Aeronautical Information Circular (AIC) document number 06-2008: SMS. MAS had established these requirements to ensure positive control and continuous improvement for safe and secure operations, including the operations of its subsidiaries, MASWings, Firefly, MAS Aerospace Engineering and MASkargo. This document had formed an integral part of the Corporate Safety Policy Manual.

The SMS encouraged an open reporting policy or commonly referred by industry as non-punitive reporting system. This assured employees that reports of unpremeditated or inadvertent errors would not result in disciplinary or punitive

action being taken against the reporter or other individuals involved. Employees were–assured that the identity, or information leading to the identity, of any employee who reported an error under this policy was never disclosed unless agreed to by the employee or required by law. The Open Reporting Policy encouraged individuals to report hazards and operational deficiencies to management. It also assured personnel that their candid input was highly desired and vital towards safe and secure operations.

The organisation had a proactive reporting system in place. Refer to *Figure 1.17F* (below):

- The SMS' guidelines resided in the Corporate Safety Manual. There were various reporting channels for the staff to transmit safety-related reports to account holders or their designates;

- The reporting channels were well-structured and covered all areas of operations:
  - Air Safety Report (ASR)
  - Cabin Safety Report (CSR)
  - Ground Safety Report (GSR)
  - Hazard report (Hazard/HZR)
  - Confidential Human Factors Incident Report Programme (CHIRPs); and
  - Flight Operations Quality Assurance (FOQA).

vii) Confidential Human Factors Incident Report

The flight crew and cabin crew were constantly being encouraged and reminded to utilise this reporting channel during their CRM and Safety classes (refer *SEP Manual; Part 7.15.2*). The Confidential Human Factors Incident Report (CHIRP), (refer to *Table 1.17B* [below]*)*, being a highly confidential report, had become the most appropriate

tool for identifying potential human factor issues, especially on the behavioural patterns of flight and cabin crew.

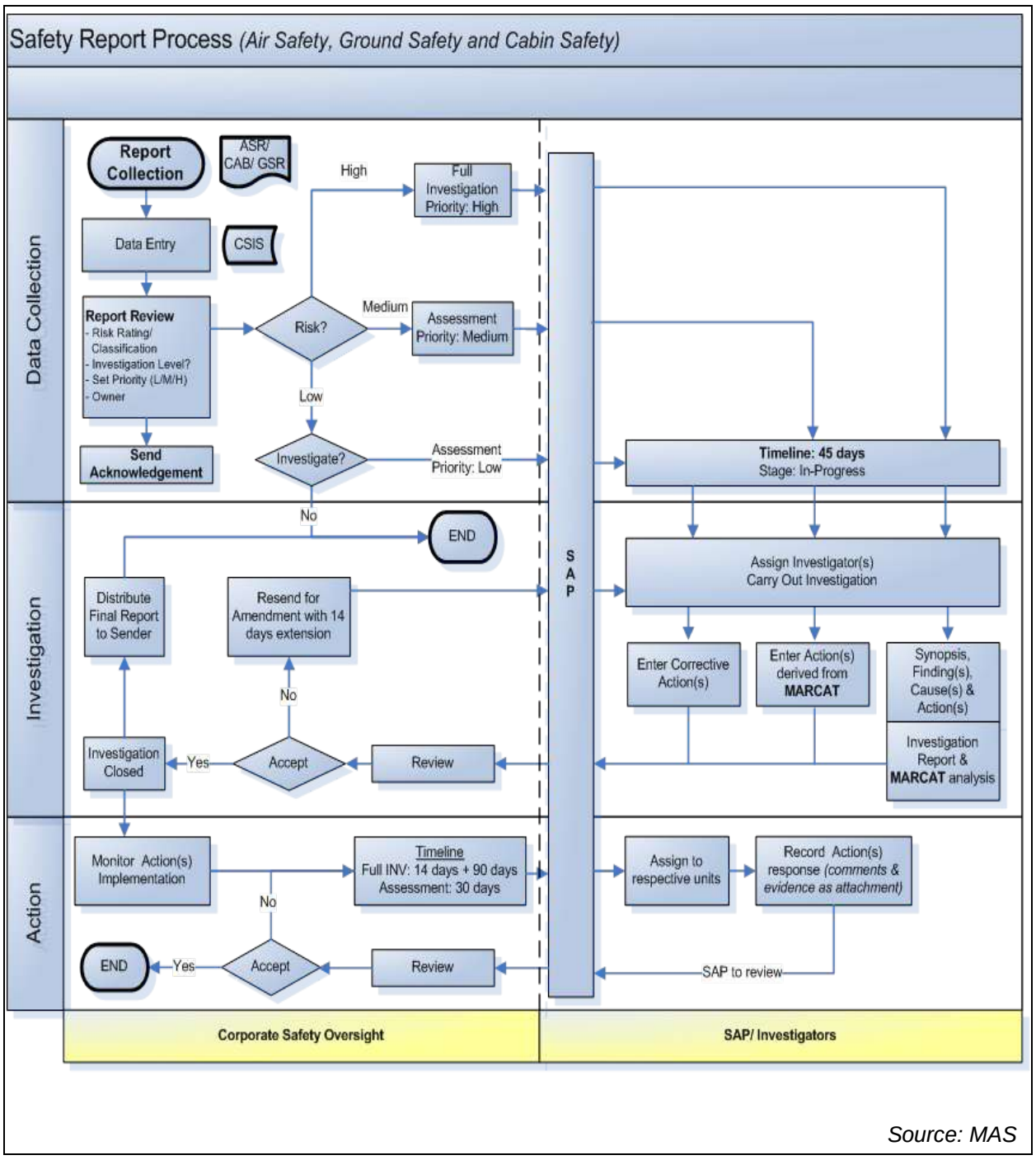

Figure 1.17F - Safety Report Process

	Year 2013				Year 2014		
	Sep	Oct	Nov	Dec	Jan	Feb	Mar
CHIRPS	**4**	**-**	**2**	**-**	**-**	**-**	**-**
10 September 2013	Communication issues between Tech Crew and Cabin Crew (1 report received)						
23 September 2013	Cabin Crew to be offloaded by Tech Crew (3 reports received)						
15 November 2013	Mis-communication between Technician and Cabin Crew during ground servicing (2 reports received)						

Table 1.17B - List of CHIRPs 2013 & 2014

viii) Flight Operations Quality Assurance

The airline had acknowledged the importance of safety as its utmost priority. Like most other airlines, with statistics showing Human Factor as the main contributor to air accidents, the Flight Operations Quality Assurance (FOQA) programme was introduced. This system had contributed tremendously even in non-eventful cases where impending trend towards an unsafe situation could be recorded. With this system in place investigations of events that could lead to an incident would be undertaken and remedial actions and recommendations put into place.

The FOQA programme was introduced in 2010. The objective of FOQA was to promote safety and accident prevention by identifying operational safety trends during normal line operations.

MAS considered FOQA as an important safety reporting culture where safety is enhanced in a non-punitive manner (reference: *MAS Operations Manual A, Part 2.2.4.2*). FOQA protocol, a written document under the custody of the Flight Safety and Human Factor Department (dated 07 July 2010) stipulated manners at which corrective and timely strategies

were implemented following a risk or potential hazardous trend.

The statistics of FOQA events in the last 2-year period (April 2012-March 2014) is as in *Table 1.17C* (below).

ix) Line Operations Safety Audit

The Line Operations Safety Audit (LOSA) was first introduced in 2004 in collaboration with the University of Texas, USA. The results were fruitful, and recommendations were implemented via Safety Change Process (SCP). MAS conducted LOSA every 2 years but not later than 5 years. LOSA was conducted by taking random samplings of all aspects of operations including random audit of normal scheduled commercial flights.

The last LOSA (2nd LOSA) was carried out between March and August 2011. The objective of LOSA was for MAS to diagnose its level of resilience to systemic threats, operational risks, and front-line personnel errors, thus providing a data driven approach to prioritise and implement actions to primarily enhance safety. This was carried out system-wide with no emphasis on any specific fleet.

x) Crew Resources Management

MAS considered Crew Resources Management (CRM) as a critical component of flight safety during operations and introduced it more than 20 years ago. The training programme for the pilots included the Cabin crew & Dispatchers. For new recruits there was a 3-day programme for CRM. Recurrent training was conducted on a yearly basis. The Safety Awareness Programme (SAP) conducted on a yearly basis would include the recurrent for the CRM training/ refresher. This programme had been in the system ever since the release of ICAO Annex 6 Part 1.

It started off with the pilots only to improve the cockpit culture. It was considered essential then as the airline had

Flight Operation Quality Assurance (FOQA) data statistic 2 years before the incident date.

i. Number of Triggers
ii. Total numbers of flight.
iii. percentage of trigger

Rate per 10,000 flight cycles			2012									Year 2013												Year 2014		
			Apr	May	Jun	Jul	Aug	Sep	Oct	Nov	Dec	Jan	Feb	Mar	Apr	May	Jun	Jul	Aug	Sep	Oct	Nov	Dec	Jan	Feb	Mar
1	Flight Cycles		798	780	789	811	813	785	817	852	799	836	672	809	779	842	837	826	812	659	684	792	811	837	772	831
2	UA	#	1	-	3	1	1	1	1	-	3	1	-	1	1	-	-	1	4	2	2	1	3	-	1	3
		Rate	12.53	-	38.02	12.33	12.3	12.74	12.24	-	37.55	11.96	-	12.36	12.84	-	-	12.11	49.26	30.35	29.24	12.63	36.99	-	12.95	36.1
3	Hard Landing	#	2	-	1	-	-	-	1	-	-	1	-	1	1	1	2	1	-	1	-	1	-	2	2	-
		Rate	25.06	-	12.67	-	-	-	12.24	-	-	11.96	-	12.36	12.84	11.88	23.89	12.11	-	15.17	-	12.63	-	23.89	25.91	-
4	Long Flare	#	9	19	11	8	10	7	13	9	10	7	10	9	11	17	15	17	10	9	10	11	8	10	7	7
		Rate	112.8	243.6	139.4	98.64	123	89.17	159.1	105.6	125.2	83.73	148.8	111.2	141.2	201.9	179.2	205.8	123.2	136.6	146.2	138.9	98.64	119.5	90.67	84.24
5	Late Land Flap	#	1	-	2	-	2	-	1	-	2	1	-	-	1	-	-	1	1	-	-	1	-	-	-	-
		Rate	12.53	-	25.35	-	24.6	-	12.24	-	25.03	11.96	-	-	12.84	-	-	12.11	12.32	-	-	12.63	-	-	-	-
6	Winshear	#	-	-	-	-	-	-	-	-	-	-	1	-	-	-	-	-	-	-	-	-	-	-	-	-
		Rate	-	-	-	-	-	-	-	-	-	-	14.88	-	-	-	-	-	-	-	-	-	-	-	-	-
7	TCAS	#	1	-	-	-	-	-	1	1	-	-	-	-	-	-	-	-	1	1	2	2	-	-	1	2
		Rate	12.53	-	-	-	-	-	12.24	11.74	-	-	-	-	-	-	-	-	12.32	15.17	29.24	25.25	-	-	12.95	24.07

Source: MAS

Table 1.17C - Statistics of FOQA Events in the Last 2-Year Period (April 2012-March 2014)

significant numbers of expatriate community serving MAS from a diverse culture. Later, the training programme also included Cabin crew & Despatchers. For new recruits there was a 3-day programme for the Initial CRM. Recurrent CRM training (1 day) also known as Safety Awareness Programme (SAP) was conducted regularly to cater for flight crew, cabin crew and flight despatchers. JAR-OPS Subpart N, JAR-OPS 1/3.965 stated that all major CRM topics should be covered every 3 years for technical crew, every 2 years for cabin crew and annually for flight despatchers.

xi) Training and Standards

MAS managed its entire training requirement in-house including the mandatory requirement for the flight crew. MAS had its own Training Centre for pilots as well as engineers. It was equipped with various Full Flight Simulators for all the fleet in the Company with most of the Flight training devices certified to FAA Level D, capable of zero flight time training. This Training Centre had been established for more than 40 years and had been certified by many countries as an approved Type Rating Training Organization (TRTO.)

Type Rating Instructors (TRI) & Type Rating Examiners (TRE) normally came from within the airline and they require stringent training and check before being approved by the DCA Licensing Division. Besides the availability as a TRTO, the Simulators were utilised by neighbouring airlines and smaller organisations within the region to fulfill their training and checking requirements.

Competency of pilots, as per regulatory requirements worldwide, is normally monitored every 6 months. MAS training policy required 2 Simulator sessions every 6 months. The two training sorties every 6 months consisted of 1 review and training followed by proficiency check session.

xii) MAS B777 Training and Standards

The training package for the B777 conversion training followed the Boeing Training Recommendations. During the introduction period, representatives from the Boeing Flight Training Department oversaw the operations. The first crew trained by Boeing comprised a project team of four pilots from the Company and one representative from DCA, the regulatory authority. The team members were then responsible for managing the introduction of the new aircraft into operation. Part of their responsibility was to ensure that the subsequent training and recurrent requirements were addressed according to the recommendations of the aircraft manufacturer, consistent with the mandatory requirements of the DCA Licensing Authority. When the B777 was introduced, the simulator was also procured, and it arrived at the MAS training premises before the first aircraft entered into commercial service. At the introduction phase of the B777 into MAS, the airline had sought assistance from the Boeing Flight Training Department to kick-start the training of new pilots locally.

In MAS, all aircraft purchased came with a package that included the respective simulator, except the B747-200/300 and Fokker F27. Like most other established airlines, MAS considered training as vital tool to maintain good pilot skills and standards.

The pilot's upgrade policy of having to serve on the smaller fleets at point of entry helped in preparing captains and co-pilots to handle larger machines, such as the B777. During the day of the event, the co-pilot was on his last training flight before he was due for a check flight on his next flight duty assignment. The Team had recorded that the FO was assigned to be the flying pilot for Kuala Lumpur/Beijing sector on the ill-fated flight.

Throughout a pilot's career, should the pilot's performance during Simulator and Line operational checks fell below the minimum standards, the Company would provide adequate retraining to ensure the required regulatory

competency was maintained.

It is important to note that there were 3 phases of training when a pilot was undergoing conversion training to a new fleet in MAS. The FO's last fleet was the A330 and he was undergoing the final phase of training to be qualified as a co-pilot on the B777. The three training phases were:

- Ground School & Computer Base Training (CBT);
- Simulator Training; and
- Initial Operation Experience (IOE) Phase 1 and Phase 2.

The IOE was for the trainee to be trained during line operations on a passenger scheduled flight commanded by a TRE or TRI-qualified Captain.

During the initial part of the IOE, it was the Company's policy that the flight had to be accompanied by an additional experienced co-pilot or captain to support the flight in case the trainee needed any supervision and, most importantly, if the TRE or TRI was incapacitated. This policy guaranteed that in such an untoward incident, there would always be a qualified Pilot to take over command of the aircraft and proceed with the next safe course of action.

As the training progressed, and if the trainee's performance was above average, and deemed safe, the carriage of the third pilot would not be necessary beyond this stage of training, based on the recommendation of the earlier trainer (TRI/TRE) in accordance with the training policy.

In such a case, a trainee pilot under IOE would not need a third pilot to accompany the flight, even though he was effectively still in the training phase. This was the case on the day of the eventful flight.

On the B777 a pilot under training normally would require to operate a certain number of minimum sectors before he could be certified to be fully functional as a line operational pilot (end-of-training). Depending on the

previous aircraft flown, the minimum and maximum number of required training sectors were, as follows:

- Last aircraft flown B737: Minimum 10 sectors, Maximum 14 sectors; and
- Last aircraft flown A330: Minimum 8 sectors, Maximum 14 sectors.

xiii) Multi-crew Operation MH370

During the day of the eventful flight, the FO was on his last training flight before he was due for a check flight on his next flight duty assignment. Record shows that he was assigned to be the flying pilot during that first leg from Kuala Lumpur to Beijing. The airline encouraged Captain to allow First Officer a fair share of flying and handling of the aircraft. Under normal practice, if the duty pattern involves more than 1 sectors, it is quite common that the additional sector will be flown by the First Officer. The decision of who to carry out the take-off and landing was solely at the discretion of the Captain. The assignment of duty regarding who was going to be the flying pilot for the first flight out normally decided during the pre-flight briefing at the despatch office.

If the decision was made that the First Officer was going to be the Pilot Flying, the MAS Flight Operations policy required that the Captain would start and taxi the aircraft up to the take-off point on the runway, after which control of the aircraft would be handed over to the co-pilot to perform the take-off and eventually the landing at the destination. Up to the take-off position at the beginning of the runway, radio communications with the ATC would be the responsibility of the co-pilot. It was a MAS' written procedure during this phase of the flight that the throttle would be handled by the Captain as PIC, a policy to ease and expedite the rejected take-off manoeuvre if so required. The First Officer would control the rudder and control column as the pilot flying.

As soon as control was handed over to the co-pilot at the take-off point, the ATC communication became the

responsibility of the Captain. Evidence from the KL ATSC's voice recording indicated clearly (in interviews with the Captain's colleagues, friends and son), that the voice recorded was that of the Captain after the aircraft took off.

xiv) Safety and Emergency Procedures

Proficiency in Safety and Emergency Procedures (SEP) was also a part of the mandatory training requirement which was conducted every 12 months. It was based on the Aircraft Type that the pilot was rated on. This recurrent training required a minimum of 3 days which covered all aspects of emergencies including medical and first aid knowledge. This section of Training fell under the purview of Flight Safety and Human Factor.

(1) Operation Control Centre

The Operation Control Centre (OCC) was where the briefing of flight crew and cabin crew took place. A team of Licensed Aircraft Despatchers were stationed in this Department.

Besides the crew formalities required prior to departure, the flight crew would be working in tandem with the assigned despatcher to review all documentations related to the assigned flight which influenced the decision on the finalised routing and fuel ordered by the Captain of the flight.

(2) Flight-Following System

In MAS, the FFS was an integrated approach which enabled flight operations Controllers to easily monitor the status of flights and gain a better view of impending operational problems, and making the process of resolving them much more efficient. A 24-hour OCC maintained operational control of all fleets in MAS by providing support for the pilots before and during flights. The FFS played the foundational role in OCC. The system is a product from Sabre and utilises position input to update the aircraft's geographical position. Position updates come from two sources namely:

- ASDI (Aircraft Situation Display Information) sourced from the FAA for aircraft flying in the United States, and
- ACARS update from individual Company aircraft flying anywhere in the world.

The information was available on a monitor mounted in the ODC and was also available on all Despatchers' positions via selections to be displayed on individual monitors.

- Projected flight plan against hazardous weather and published prohibited or restricted areas en-route;
- Actual flight data; and
- Pertinent data related to the flight, and allows direct communications with aircraft via satellite phone or ACARS communications.

xv) Technical and Development

Technical data and aircraft performance were under the control of the Operations Engineering Department. This Department worked closely with the Technical Services Department of the Engineering Division and Aircraft Manufacturers on Performance Engineering matters. The Technical and Development Department participated in the evaluation of new Aircraft Type and Aircraft Equipment.

xvi) Fuel Policy

The fuel policy defined in the *MAS Operations Manual A (Part 8.1.7)* met the minimum required for aircraft despatch. A Captain has the privilege of carrying extra fuel if he feels that there is justification to do so, based on expected weather forecast enroute and at the destination. Extra Fuel carriage can also be due to aircraft performance penalty as required by MEL or specific ATC requirement at some destination airports.

xvii) Flight Plan Routing

The Company's policy required the despatcher to evaluate the flight routing for the best economy routes to Beijing based on the OCC Flight Management System. As there was no known enroute weather forecast that could pose a threat for MH370, the usual standard routing was chosen. This was normally done by the computer system to give the despatcher the recommended routing unless otherwise modified.

xviii) Hijack and Sabotage Security Procedures

The Hijack and Sabotage Security Procedures and Guidelines in MAS's SEP Manual (Part 4.3) were recommended by the world's aviation security authorities based on in-depth studies of actual hijack and sabotage incidents. These authorities included ICAO Annex 17, IATA, TSA, FAA, Malaysia Airlines Security Programme and the Aviation Offences Act 1984 (Act 307).

The procedures stipulated that security precautions against both hijack and sabotage cannot be maintained at maximum level at all times without disrupting operational functions and public goodwill.

b) In-flight Services

i) Cabin Crew Training

Cabin crew were required to be present on public transport flights to perform duties in the interest of passengers' safety. They must be well-informed about safety and Policies of the Company. Each cabin crew member shall:

- Be well-prepared and fit for the flight;
- Ensure adherence of "Fasten Seat Belt" and "No Smoking" signs;
- Ensure the comfort and safety of all passengers; and

- Ensure passengers safely escape in an emergency evacuation.

A cabin crew member is a person employed to facilitate the safety of passengers whose duties are detailed by the Company or the aircraft Commander. Cabin crew will not act as a member of the flight crew.

At the point of recruitment, the candidate would have to undergo through a thorough interview and medical check-up. Once selected, a comprehensive training of safety and service procedures would be provided by the airline for the duration of 3 months and he/she would graduate and leave the academy as a qualified cabin crew assigned to the selected fleet that he/she was trained for.

MAS had the policy of fleet grouping for cabin crew in the following order:

- Narrow Body - B737
- Wide Body - A330, B777 & B747/A380

Upon graduation, the cabin crew would be given a flight duty roster on a monthly basis. The roster was managed by the Crew Planning & Deployment Section.

Initially, a cabin crew was required to operate the domestic and the regional flights known as the Narrow Body Fleet for a minimum of 2 years. With sufficient experience gained on the narrow body fleet he/she might be eligible for promotion to the wide-body fleets. These new wide-body may include long-haul flights to international destinations. The selection of cabin crew for promotion normally depends on merit, track record and seniority.

A cabin crew would be provided with proper training on Safety and First Aid. He/she would be trained to handle:

- Safety and emergency evacuation
- Disruptive/Difficult passengers
- Medical emergency (Provide First Aid)

On a yearly basis, the cabin crew was required to go through a safety recurrent training on their Safety Emergency Procedures (SEP) at the academy in order to keep his/her licence and training validated by certified instructors. It was mandatory for the crew to achieve the required minimum safety and emergency procedures and knowledge which were assessed through examinations. This recurrent training included first aid training and examination, to get the certificate renewed. There were also "Safety Awareness Programme" and "Crew Resources Management" classes that were compulsory for the cabin crew to attend every 2 years. These two programmes were basically similar, and they were incorporated within the 3 days of training.

The cabin crew would be issued with a Safety Card endorsed by the Safety and Human Factors Department of MAS as well as a Crew Performance Card issued by the Cabin Crew Line Operation and Performance Department. The crew would be expected to carry these two documents at all times for flight duty.

Excellent service awards won by the Company's cabin staff for several years stood as a testimony for the quality of the training and the service standards acquired. MAS' reputation had attracted foreign established top-rated airlines for secondment of cabin crew.

ii) Crew Performance Appraisal

The Crew Performance Appraisal (CPA) was an established process in the organisation, monitoring crew performance and standards including safety knowledge. To maintain and achieve a high standard of service and safety, each and every cabin crew was required to have a CPA which was done twice a year. The assessment was carried out by the crew in charge on board during the flight.

Refer *Table 1.17D* (below) on Rating Score.

The cabin crew would be checked on aspects such as safety and service procedure, product knowledge,

Customs, Immigration and Quarantine, station documents, grooming and leadership skills. The crew in charge would conduct the checking on the crew by Questions & Answers (Q & A) and how the individual performed as part of the operational crew member in his/her assigned capacity.

Ratings	Category	Range of Score
5	Amongst the Best	98% and above
4	Highly Effective	93%-97.90%
3	Fully Productive	87%-92.90%
2	Needs Improvement	80%-86.90%
1	Unacceptable	<80%

Table 1.17D - Crew Rating Score

iii) In-flight Operation

On board a Boeing 777-200ER aircraft the standard operating cabin crew of 11 was required. The normal cabin crew complement for the Boeing 777-200ER aircraft was as follows:

- 1 In-flight Supervisor
- 2 Chief Steward/Chief Stewardess
- 2 Leading Steward/Leading Stewardess
- 6 Flight Steward/Flight Stewardess

The 777-200ER fleet had a two-class cabin configuration, namely Golden Class Club (GCC) and Economy Class (EY). Four cabin crew would be designated to work in GCC and six in EY.

The In-flight Supervisor would be in charge of the whole cabin. Two Chief Stewards/Chief Stewardesses looked after the GCC assisted by two cabin crew. Six cabin crew were designated to work in EY class. The EY class was divided into two sections and each section was looked after by one Leading Steward/Leading Stewardess and assisted by two cabin crew.

The In-flight Supervisor was the person responsible to manage the cabin safety and report to the Commander of the aircraft.

He or she shall:

- have the overall responsibility to the aircraft commander for the conduct, coordination and performance of the cabin operations and the safety duties;
- verify that all the cabin crew members are fit for flight and with all relevant documents valid for flight duty; and
- coordinate and organise the functions and tasks of all cabin crew members:
  - Execute cabin crew briefing;
  - Nominate positions and working areas;
  - Nominate in-flight service duties;
  - Checking of emergency equipment, pre-flight safety briefing and reporting matters concerning safety (irregularities and malfunctions) to the Commander;
  - Debriefing the cabin crew members when required;
  - Ensuring efficient communication with crew members and ground personnel; and
  - Ensuring contact with the cockpit on a regular basis.

As per Civil Aviation Regulations 1996 the minimum requirement of the operating cabin crew for B777-200ER fleet is 8 based on the number of exit doors available on the aircraft.

Notwithstanding the above, many other airlines carry additional cabin crew above the minimum required in the interest of customer services.

iv) Flight and Duty Time Limitations Scheme for Cabin Crew

The prime objective of a flight time limitations scheme is to ensure that crew members are adequately rested at the beginning of each flying duty period, and whilst flying, be sufficiently free from fatigue so that they could operate to a satisfactory level of efficiency and safety in all normal and abnormal situations.

The maximum duty hours for cabin crew should not exceed:

- 60 hours in 7 consecutive days;
- 105 hours in any 14 consecutive days; and
- 210 hours in any 28 consecutive days.

Cabin crew would be notified in advance of a flying duty period so that sufficient and uninterrupted pre-flight rest can be assured in preparation for the flight. When away from base, opportunities and facilities for adequate pre-flight rest would be provided by the Company with suitable accommodation.

The minimum rest period which must be taken before undertaking a flying duty period shall be:

- At least as long as the preceding duty period, or
- 12 hours, whichever is the greater.

The minimum rest period would be the highest of pre-flight or post-flight rest. It was not cumulative of both rests.

The minimum rest period which must be provided before undertaking a flight, at home base would be:

Flight	Rest Period
Pre-flight	40 hours (inclusive 2-local nights)
Post-flight	72 hours (inclusive 3-local nights)

The minimum rest period which must be provided after performing a flight, out of base would be:

Flight	Rest Period
Post-flight	24 hours

MAS Employee Union (MASEU) was the recognised union certified by MAS to represent the cabin crew. Flight Time Limitation and working conditions were governed by the Collective Agreement (CA) signed between the union and MAS, in compliance with CAR or whichever was more limiting.

v) Safety Report

(1) Accident/Incident/Hazard Reports Form

MAS managed an in-house reporting system to identify many of these accidents/incidents/hazards by collecting and then analysing hazard and incident reports to audit incidents encountered during flight. The Incident reporting system was one of the most effective tools for pro-active hazard identification. Cabin crew were required to fill up this form and to submit it at the end of the flight within 24 hours.

(2) Confidential Human Factors Incident Reporting Programme

Confidential Human Factors Incident Reporting Programme (CHIRPs) applicable for the flight crew, cabin crew and engineering personnel only. It was a non-disclosure type of document where one could use and submit to the Company to report any complaints and issues. CHIRPs could only be used for human factor and safety issues, errors and unsafe practices and where some actions might potentially infringe regulatory practises. It was not to be used for mandatory incidents reporting, personality conflicts, industrial issues and employment problems. It would be reviewed by the members of the CHIRPs staff and action would be taken accordingly.

All these reports were managed by the Corporate Safety Oversight and Human Factors Department.

SECTION 1 – FACTUAL INFORMATION

1.18 ADDITIONAL INFORMATION

1.18.1 Provision of Air Traffic Services and Areas of Responsibilities

1) Introduction

For the provision of Air Traffic Services (ATS), the Kuala Lumpur FIR is divided into seven Sectors, namely Sector 1, Sector 2, Sector 3, Sector 4, Sector 5, Sector 6 and Sector 7.

Each Sector has a specified area of responsibility. Sectors 1 to 5 are manned by Sector Planning and Radar Controller jointly responsible for the safe, efficient and orderly provision of air traffic control service, flight information service and alerting service in their Sectors. Each Sector has an Assistant Flight Data (AFD) Controller.

Sector 6 is manned by a Radar Controller and supported by the Sector 1 Planning Controller and Sector 1 AFD Controller. Sector 7 is manned by a Radar Controller and supported by the Sector 2 Planning Controller and Sector 2 AFD Controller.

a) Responsibilities of Sector Radar Controller:

- Handle all radiotelephony functions;
- When necessary, coordinate to effect transfer of radar identity and control;
- Monitor the Sector Inbound List (SIL) to ensure appropriate action for orderly acceptance, control and transfer of aircraft; and
- Comply with instructions issued by FLOW control.

b) Responsibilities of Sector Planning Controller:

- Plan and coordinate as necessary for the management of all flights that will operate in their sectors; and
- Ensure that the information on the electronic flight strips (EFS) is updated.

The Radar and Planning Controllers will make available to each other information that is essential to enable them to carry out their responsibilities, e.g. change in cruising level/altitude or revision to transfer of control point estimates.

c) Responsibilities of Controllers at AFD Position:

- Assist the Planning Controller by ensuring that information displayed on the EFS is kept updated in a timely manner;
- Ensure that essential information found on the EFS is also available on the paper strips;
- Display the paper strips on the display board in the correct manner;
- Make paper strips available to the EXE Controller if requested;
- Wrap up all used strips, and place them at a common place for collection; and
- Clear wrong ADP Message Queues as follows:
  - AFD Sector 2 - wrong AFTN Message Queue
  - AFD Sector 5 - wrong METEO and AIS Message Queue
  - AFD Sectors 1 & 4 - wrong FDP Message Queue

2) Sector 3 Area of Responsibility

a) Sector 3 is responsible for the provision of air traffic services in controlled airspace and outside controlled airspace above FL145 within:

That airspace from VKL to PIBOS then to 033658N 1022253E then to 040051N 1034109E at the border of Peninsular Malaysia/Singapore International Boundary, thence southwards along the FIR boundary to 012652N 1034540E thence northwards to 021958N 1034235E (10 nm west of VMR) thence westwards to DAMAL thence northwards along the airway R325 to SAROX (but

excluding ATS Route R325) thence along the airway G334 to VKL but excluding the Kuantan TMA.

b) Sector 3 is also responsible for the provision of FIS and Alerting Service in the South China Sea Corridor (SCSC). The lateral and vertical limits of the SCSC (Refer *Table 1.18A* [below]) are as follows:

Laterals Limits	Vertical Limits
From 023600N 1044500E to 020000N1070000E and along 020000N till the Singapore/Kota Kinabalu FIR Boundary, thence along this Boundary to 060000N 1132000E, thence along 060000N till the Singapore/Kuala Lumpur FIR Boundary, thence along this Boundary to 023600N 1044500E	West of 105E FL150 GND/SL East of 105E FL200 GND/SL

Table 1.18A - Lateral and Vertical Limits of South China Sea Corridor

c) Sector 3 encompasses the following ATS routes or route segments *(Table 1.18B* [below]*):*

Routes	Segments	Routes	Segments
A224	VMR - VJR	N884	VMR – LENDA
B338	VTK - VMR	N891	PU – MANIM
B469	VPK - PU	N892	KIBOL - VMR
G334	VKL - UKASA - VPT - KIBOL	R221	VMR - VPT
G582	Sector 1 boundary - VPK	R325	MATSU - SAROX (FL280 & below)
G584	VKL – VPK	W533	VKL - VKN - VKE
L629	VPK - BUVAL	W540	VPK - A/VKE (FL235 & below)
L635	VPK - DOVOL	Y331	PIBOS - TAXUL
L642	VMR - EGOLO	Y332	TAXUL - PADLI
M751	VPK - A/VKE (FL240 & above)	Y333	PADLI - BUVAL
M758	VPK - ISDEL	Y334	PADLI - DOVOL
M761	VPK - KETOD	Y335	PADLI - IDSEL
M763	VPK - TAXUL	Y336	ISTAN - PADLI - KETOD
M771	VMR - RAXIM	-	-

Table 1.18B - ATS routes or route segments of Sector 3

Note:

SAROX is not a waypoint on R325. It is a waypoint on G334 that intersects R325. It is used here for ease of reference.

d) Delegation of Airspace and Communication Watch

i) Delegation of Airspace from Kuala Lumpur ACC (Sector 3) to Singapore ACC

The contiguous airspace Areas A, C, E and H along eastern Johor/South China Sea and responsibility for provision of air traffic services in these areas remains delegated to Singapore.

ii) Communication Watch

To ease air traffic management, communications watch shall be maintained by Singapore HF, Lumpur Sector 3 and Lumpur HF within South China Sea Corridor (AIP Malaysia ENR 2.1-13 [below]*).*

AREAS WITHIN THE SINGAPORE FIR FOR WHICH LUMPUR ACC IS RESPONSIBLE FOR PROVIDING ATS.					
SOUTH CHINA SEA CORRIDOR Fm 023600N 1044500E to 020000N 1070000E and along 020000N till the Singapore / Kota Kinabalu FIR BDRY - thence along this BDRY to 060000N 1130000E, thence along 060000N till the Singapore/Kuala Lumpur FIR BDRY - thence along this BDRY to 023600N 1044500E.	W of 105E FL 150 GND / SEA E of 105E FL 200 GND / SEA	Lumpur ACC	Lumpur Control Lumpur Radio English H24	132.6 MHz HF 5655 KHz 8942 KHZ 11396 KHz	Lumpur ACC shall be responsible for the provision of air traffic services to flights operating within the South China Sea Corridor.

Extract from Malaysia AIP ENR 2.1-13

iii) Singapore will pass to Sector 3 Estimate for flights bound for the Natuna and Matak Islands. Sector 3 in turn, shall notify Aeronautical Mobile Service (AMS) High Frequency (HF) who shall provide additional communications watch in order to discharge its Flight Information Service (FIS)/Alerting Service functions.

3) Sector 5 Area of Responsibility

a) Sector 5 is responsible for the provision of air traffic services in controlled airspace and outside controlled airspace above FL145 within:

That airspace from VKL to PIBOS then to 033658N 1022253E then to 040051N 1034109E at the border of Peninsular Malaysia/Singapore International Boundary, thence northwards along the FIR boundary, thence westwards along the Peninsular Malaysia/Thailand International Boundary to 054342N 1010038E thence southwards to 044021N 1012704E, then to VKL but excluding the Kota Bharu TMA/Terengganu and Kerteh CTRs. Sectors 5 encompasses the following ATS routes or route segments *(Table 1.18C* [below]*)*:

Routes	Segments
A334	PASVA – VKB
B219	Butterwort TMA Boundary East – VKB
B463	KADAX – VKB
G466	VKL – VKB
M644	VKB – ABTOK
M751	A/VKE – VKB – GOLUD (FL240 and above)
M765	VKB – VENLI – IGARI
R208	VKL – GUNBO – VKR – IKUKO – IGARI
R325	ANSOM – MATSU (FL 280 and below)
W540	A/VKE – VKB (FL235 and below)

Table 1.18C - ATS routes or route segments

b) Delegation of Airspace

i) Delegation of Airspace from Singapore ACC to Kuala Lumpur ACC (Sector 5)

RNAV route M765 between VENLI and IGARI has been delegated by Singapore ACC. Lumpur Sector 5 shall provide air traffic services and carry out coordination with Ho Chi Minh ACC.

ii) Route segment between IKUKO and IGARI on ATS R208 is released by Singapore ACC subject to daily coordination between Singapore ACC and Kuala Lumpur ACC.

iii) Communication Watch

To ease air traffic management, communication watch is maintained by Lumpur Sector 5 and Lumpur HF between IKUMI and IGARI along N89. Refer *Figure 1.18A - Sector 3 and 5 Area of Responsibilities* (below).

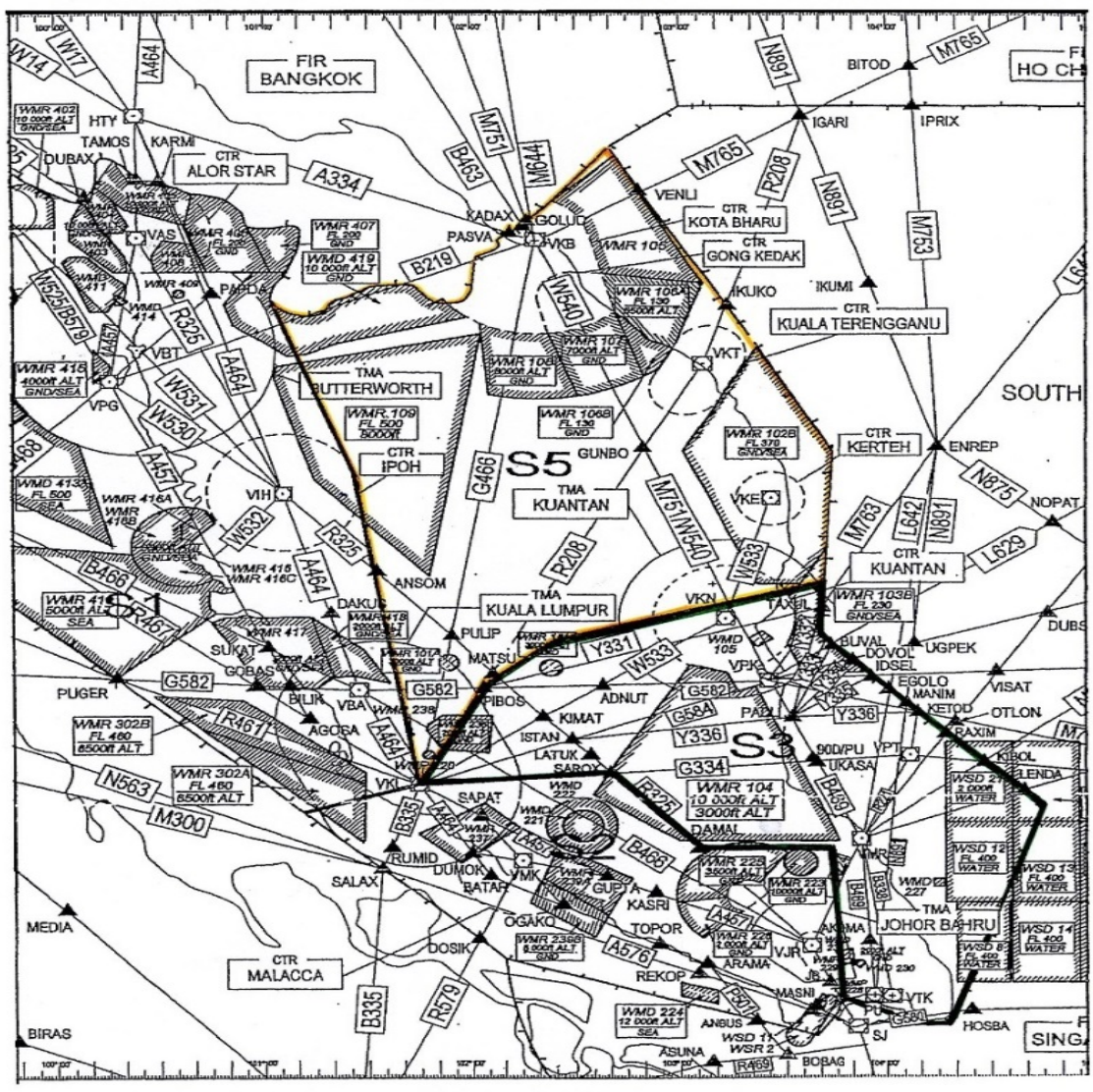

Source: DCA Malaysia

Figure 1.18A - Sector 3 and 5 Area of Responsibilities

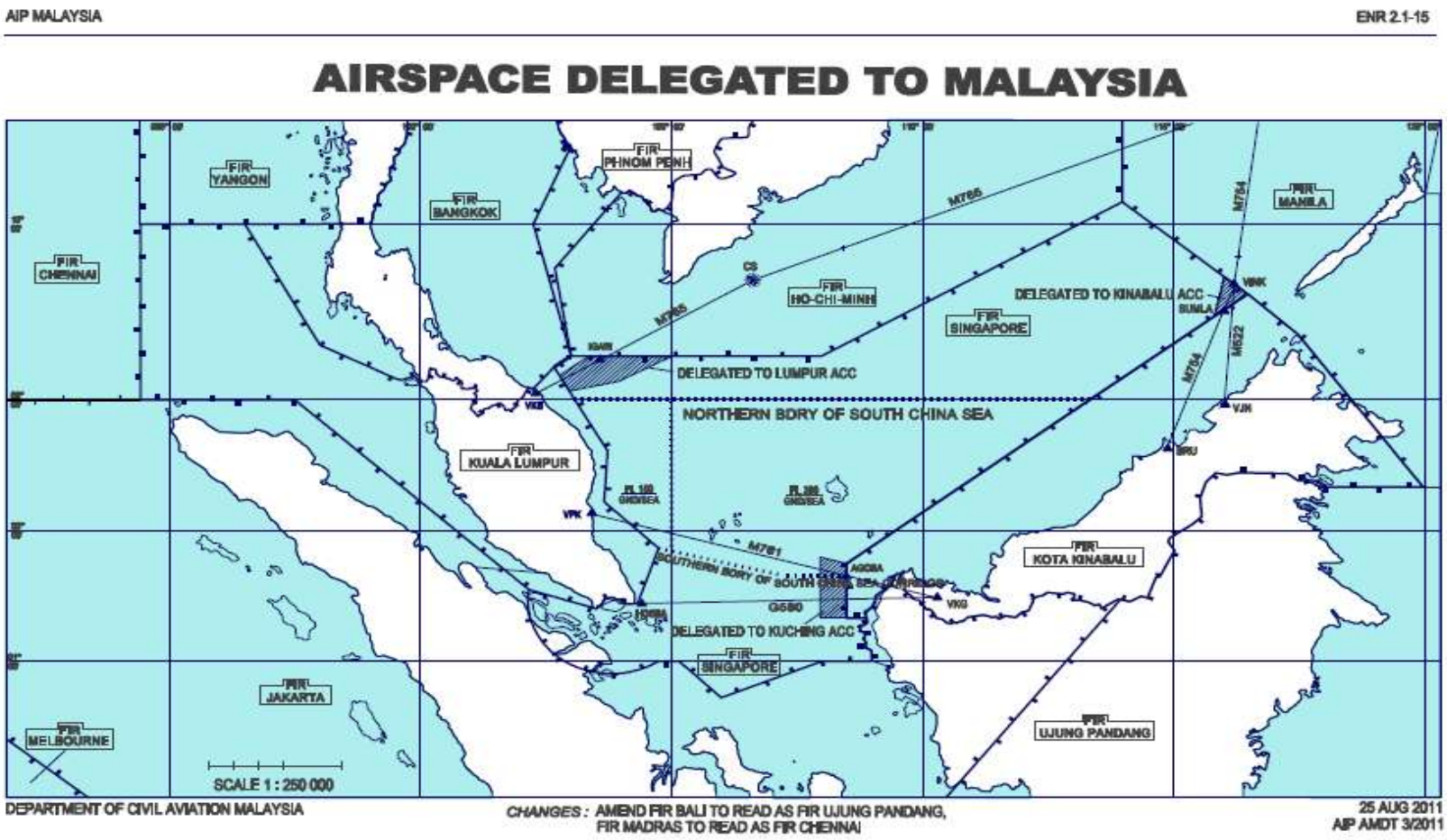

Source: DCA Malaysia

Figure 1.18B - Airspace Delegated to Malaysia by Singapore

4) Air Traffic Services Operations

a) The disappearance of MH370 occurred in the Singapore FIR where the airspace is delegated to KL ACC. The portion of airspace delegated is RNAV route M765 between VENLI[13] and IGARI[14], and the portion released is ATS route R208 between IKUKO[15] and IGARI. (References: Malaysia Aeronautical Information Publication (AIP) ENR 2.1-15 (*Figure 1.18B* [below]), ENR 3.1-10 and ENR 3.3-5 and Manual of Air Traffic Services [MATS] Vol. 2 page 2-2-10 paragraphs 2.4.3.1 & 2.4.3.2).

b) KL ACC is responsible for the provision of Air Traffic Control Service, Flight Information Service and Alerting Service to all aircraft within Kuala Lumpur FIR and the "released airspace" on ATS route R208 and the "delegated airspace" on RNAV route M765 (*Figure 1.18B* [above]).

c) MATS part 9, page 9-6-5 para 6.7.2 states that:

> "*If alerting service is required for an aircraft that is flight planned to operate through more than one FIR including the airspace delegated to the Kuala Lumpur and Kota Kinabalu ATSCs and, the position of the aircraft is in doubt, the responsibility for coordinating such service shall normally rest with the ATSC of the respective FIRs:*
>
> *a) Within which the aircraft was flying at the time of last radio contact;*
>
> *b) That the aircraft was about to enter when last radio contact was established at or close to the boundary of the two FIRs.*

d) Operational Letter of Agreement for the Provision of Search and Rescue Services between the Department of Civil Aviation Malaysia and the Department of Civil Aviation Singapore dated August 1984 page 6 para. 7.1 states that:

[13] Coordinates VENLI: 062846N 1024900E
[14] Coordinates IGARI: 065612N 1033506E
[15] Coordinates IKUKO: 054512N 1031324E

"In the event of an aircraft emergency occurring within

the South China Sea Corridor (SCSC), the KL ATSC shall be responsible to take initial alerting action whilst the Singapore RCC shall be responsible for subsequent coordination of all SAR efforts. While the responsibility for the provision of SAR service within the SCSC rests with Singapore RCC, the Singapore RCC may as provided for in paragraph 3.2.2 delegate responsibility for the overall control of the SAR mission to Kuala Lumpur RCC or Kota Kinabalu RCC, whichever is deemed appropriate"

Para. 3.2.2, page 3 of the same agreement, para. (d) above states that:

"*When a transfer of responsibility for the overall SAR co-ordination is to take place, either from subsequent establishment of an aircraft's position or movement, or because an RCC other than the one initiating the action is more favourably placed to assume control of the mission by reason of better communication, proximity to the search area, more readily available facilities or any other reasons, the following procedures shall be adopted:*

i. direct discussions, wherever possible, shall take place between the Search and Rescue Mission Co-ordinators (SMCs) concerned to determine the course of action.

ii. if it decided that a transfer of responsibility is appropriate for the whole mission or part thereof, full details of the SAR mission shall be exchanged.

iii. the initiating RCC shall continue to retain responsibility until the accepting RCC formally assumes control for the mission.

5) KL ATSC Duty Shift System for Air Traffic Controllers

a) The duty shift system *(Table 1.18D* [below]*)* on 07 March 2014 for Air Traffic Controllers was as follows:

Sectors 1, 2, 3, 4 and 5 were manned by a Radar Controller, a Planning Controller and an Assistant Flight Data Controller in each Sector from 1100-1600 UTC [1900-2400 MYT]. Sector

6 was manned by a Radar Controller and Sector 7 was not manned.

Day	Shift	Period
1	Afternoon	• 0500 UTC [1300 MYT] - 1100 UTC [1900 MYT]
2	Morning & Night	• 2300 UTC [0700 MYT] - 0500 UTC [1300 MYT] and • 1100 UTC [1900 MYT] - 1600 UTC [2400 MYT]
3	Midnight shift	• 1600 UTC [0000 MYT] - 2300 UTC [0700 MYT]
4	Off duty	

Table 1.18D - Duty Shift System for Air Traffic Controllers

b) From 1600 UTC [0000 MYT] until 2200 UTC [0600 MYT], the number of Controllers in the KL ATSC were scaled down by or to half to enable the Controllers to take a rostered break - the first half from 1600 UTC [0000 MYT] to 1900 UTC [0300 MYT] and the second half from 1900 UTC [0300 MYT] to 2200 UTC [0600 MYT], as follows:

- Sector 1, Sector 2 and Sector 4 each were manned by a Radar Controller with an AFD Controller.
- Sector 3 and Sector 5 were combined and operating from a Controller working position with a Radar Controller and an AFD Controller.
- The area of responsibility would be that of Sector 3 and Sector 5. Between 1600 UTC [0000 MYT] and 2200 UTC [0200 MYT], Sectors 3 and 5 Assistant Flight Data Controller carried out the duty of Planning Controller.

c) The last radio transmission between KL ACC and MH370 took place at 1719:30 UTC [0119:30 MYT]. A contact should have occurred at around 1722 UTC [0122 MYT] at waypoint IGARI.

Reference is made to Malaysia AIP ENR 6, En-route Charts - IGARI has been designated as a compulsory reporting point, and MATS page 8-2-6, Part 8 Surveillance para 2.4.1 - Controllers may instruct a radar identified aircraft to omit making compulsory position reports unless:

- *the position report is required for control purposes.*

There was no instruction by the KL ACC Controller to MH370 to omit making compulsory position report as stated in MATS.

KL ACC should have declared the Distress Phase[16] at 1827 UTC [0227 MYT] and the transmission of the *DETRESFA*[17] message, as KL ACC was the ATS unit last in contact with MH370 at 1719:30 UTC [0119:30 MYT] when MH370 acknowledged the transfer of control by KL ACC at 1719:26 UTC [0119:26 MYT].

MH370 did not contact Ho Chi Minh ACC on radio frequency 120.9 MHz. and Ho Chi Minh ACC was not able to establish two-way communication with MH370.

Reference

Manual of Air Traffic Services, Part 9 - Emergencies, page 9-6-5, para. 6.7.2 dated 15/3/2009 No.1 states:

> *If alerting service is required for an aircraft that is flight planned to operate through more than one FIR including the airspace delegate to the Kuala Lumpur and Kota Kinabalu ATSCs and the position of the aircraft is in doubt, the responsibility for co-ordinating such service shall normally rest with the ATSC of the respective FIRs:*
>
> - *within which the aircraft was flying at the time of last air-ground radio contact;*
> - *that the aircraft was about to enter when last air-ground contact was established at or close to the boundary of two FIRs or control areas;*
> - *within which the aircraft's intermediate stop or final destination point is located:*
>
> *1) if the aircraft was not equipped with suitable two-way radio communication, or*

[16] *Distress Phase - A situation wherein there is a reasonable certainty that an aircraft and its occupants are threatened by grave and imminent danger and require immediate assistance.*

[17] *DETRESFA - The code for a Distress Phase*

2) was not under obligations to transmit position reports.

and

ICAO Doc 4444 ATM/501 Procedures for Air Navigation - Air Traffic Management (PANS-ATM), page 9-6, para 9.2.2.2, dated 22/11/07 states:

When alerting services is required in respect of a flight operated through more than one FIR or control area, and when the position of the aircraft is in doubt, responsibility for coordinating such service shall rest with the ATS unit of the FIR or control area:

a) within which the aircraft was flying at the time of last air-ground radio contact;

b) that the aircraft was about to enter when last air-ground contact was established at or close to the boundary of two FIRs or control areas;

c) within which the aircraft's intermediate stop or final destination point is located:

1) if the aircraft was not equipped with suitable two-way radio communication, or

2) was not under obligations to transmit position reports.

The Team noted that MH370 was operating in the airspace delegated to KL ACC and the last air-ground radio contact was with KL ACC. MH370 did not contact Ho Chi Minh ACC and Ho Chi Minh ACC was unable to establish radio communication with MH370.

Hence KL ACC shall be responsible for the provision of alerting service for MH370.

At 2232 UTC [0632 MYT] KL ARCC transmitted the first *DETRESFA* message. A total of 4 hours and 05 minutes had passed from the time the Distress Phase should have been declared.

d) As the 'custodian' of the airspace, the KL ACC transferred MH370 to HCM ACC 3 minutes before the estimated time of arrival over the Transfer of Control Point[18] (TCP).

The estimate[19] of the aircraft for IGARI which was 1722 UTC [0122 MYT] had been passed to, by KL ACC, and duly acknowledged by HCM ACC, as stipulated in the Operational Letter of Agreement between DCA Malaysia and Viet Nam Air Traffic Management.

e) Page 11 of *Appendix 1.1A - Establishment of Communication* in the Operational Letter of Agreement between DCA Malaysia and Viet Nam Air Traffic Management stipulates that:

> *"The accepting unit shall notify the transferring unit if two-way communication is not established within five (5) minutes of the estimated time over the TCP".*

At 1739:03 UTC [0139:03 MYT] HCM ACC queried KL ACC for news on MH370.

After MH370 was transferred to HCM ACC, the time of transfer was not recorded manually on the paper Flight Progress Strip as stipulated in MATS Part 2-Gen Section 11 FLIGHT PROGRESS STRIPS.

Manual of Air Traffic Services Part 9, Table 9-2.2 Overdue Action - Radio Equipped Aircraft preliminary action stipulates that:

> "*When an aircraft fails to make a position report when it is expected, commence actions not later than the ETA*[20] *for the reporting point plus 3 minutes"* and
>
> *a) The following actions shall be taken:*

---

[18] *Transfer of Control Point - A defined point located along the flight path of an aircraft, at which the responsibility for providing air traffic control service to the aircraft is transferred from one control unit or control position to the next.*

[19] *Estimate - The time at which it is estimated that an aircraft will be over a position or over the destination.*

[20] *ETA* - Estimated time of Arrival.

(1) request information from other ATS units and likely aerodromes;

(2) notify the RCC that the Uncertainty Phase[21] exists;

(3) ensure that RQS[22] message is sent.

b) Full Overdue Action: not later than 30 minutes after the declaration of the Uncertainty Phase:

i. notify the RCC that the Alert Phase[23] exists.

ii. notify the RCC that Distress Phase exists if:

-1 hour has elapsed beyond the last ETA for the destination; or

- the fuel is considered exhausted; or

- 1 hour has elapsed since the declaration of the Uncertainty Phase.

MATS Part 9 para 6.2.3 stipulates that:

"*If Controllers have reason to believe that an aircraft is lost, overdue or experiencing communication failure, they shall:*

a) inform appropriate radar units (civil and military) of the circumstances,

b) request the units to watch out for emergency SSR code display or the triangular radio failure pattern, and

c) notify these units when their services are no longer required."

[21] *Uncertainty phase - A situation wherein doubt exists as to the safety of an aircraft or a marine vessel, and the Persons on board.*

[22] *RQS - Request Supplementary Flight Plan.*

[23] *Alert phase - A situation wherein apprehension exists as to the safety of an aircraft or marine vessel and of the persons on board.*

At 1741:23 UTC [0141:23 MYT] KL ACC Sector (3 & 5) Controller made a call on the radio frequency 132.5 MHz to MH370 but there was no response from the aircraft.

Event that followed was at the time of 1804:39 UTC [0204:39 MYT] when KL ACC Radar Controller informed HCM ACC:

> *"…reference to the Company Malaysian Airlines the aircraft is still flying, is over somewhere over Cambodia*".

Thirty-one minutes later, at 1835:52 UTC [0235:52 MYT] MAS Operations Centre (MOC) informed the position of the aircraft was at latitude N14.9 0000 and longitude E109 15500 which was somewhere east of Vietnam. This information was relayed to HCM ACC. At 1930 UTC [0330 MYT] MOC called in and spoke to the Radar Controller, "…*admitting that the 'flight tracker'*[24] *is based on projection and could not be relied for actual positioning or search."* (*Watch Supervisor Logbook's entry*).

6) Chronology of Activities after Notification by HCM ACC

The paragraphs (*Table 1.18E* [below]) describe the chronology of activities after notification by HCM ACC leading to the initiation of the Search and Rescue operations (SAR) and deployment of resources for the MH370 search.

Refer Radiotelephony Transcripts - *Appendices 1.18A to 1.18G - Air-Ground Communications.*

[24] *MAS Operations Centre used the name 'Flight Explore*r'.

a) Chronology of ATC Activities after Notification by HCM ACC

No.	Time	Activities
1.	1739:03 UTC [0139:03 MYT]	Ho Chi Minh ACC first enquired about MH370 and informed KL ACC that verbal contact was not established with MH370 and the radar target was last seen at BITOD.
2.	1741:22 UTC [0141:22 MYT]	Ho Chi Minh enquired for information on MH370 and KL ACC informed HCM ACC that after waypoint IGARI, MH370 did not return to Lumpur Radar frequency.
3.	1741:23 UTC [0141:23 MYT]	KL ACC Radar Controller made a “blind transmission” to MH370.
4.	1746:47 UTC [0146:47 MYT]	HCM ACC queried about MH370 again, stating that radar contact was established over IGARI but there was no verbal contact. HCM ACC advised that the observed radar blip disappeared at waypoint BITOD. HCM ACC stated that efforts to establish communication were made by calling MH370 many times for more than twenty (20) minutes.
5.	1750:28 UTC [0150:28 MYT]	KL ACC queried HCM ACC if there had been any contact with MH370, HCM ACC’s reply was “negative”**.**
6.	1757:49 UTC [0157:49 MYT]	HCM ACC informed KL ACC that there was officially no contact with MH370 until this time. Attempts on many frequencies and through other aircraft in the vicinity received no response from MH370.
7.	1803:48 UTC [0203:48 MYT]	KL ACC queried HCM ACC on the status of MH370, HCM ACC confirmed there was no radar contact at this time and no verbal communication was established. KL ACC relayed the information received from Malaysia Airlines Operations that the aircraft was in the Cambodian airspace.
8.	1807:47 UTC [0207:47 MYT]	HCM ACC queried for confirmation that MH370 was in Phnom Penh FIR as Phnom Penh did not have any information on MH370. KL ACC indicated it would check further with the supervisor.

Table 1.18E – ATC Activities after Notification by HCM ACC

cont…

a) Chronology of ATC Activities after Notification by HCM ACC *(cont…)*

No.	Time	Activities
9.	1812:15 UTC [0212:15 MYT]	KL ACC informed HCM ACC that there was no update on the status of MH370.
10.	1815 UTC [0215 MYT]	(*No voice recording*). Extracted from the Watch Supervisor Log Book: KL ATSC Watch Supervisor queried Malaysia Airlines Operations who informed that MH370 was able to exchange signals with the Flight Explorer.
11.	1818:50 UTC [0218:50 MYT]	KL ACC queried if the flight plan routing of MH370 was supposed to enter Cambodian airspace. HCM ACC confirmed that the planned route was only through the Vietnamese airspace. HCM ACC had checked and Cambodia had advised that it had no information or contact with MH370. HCM ACC confirmed earlier information that radar contact was lost after BITOD and radio contact was never established. KL ACC queried if HCM ACC was taking Radio Failure action, but the query didn't seem to be understood by the personnel. HCM ACC suggested KL ACC to call Malaysia Airlines Operations and was advised that it had already been done.
12.	1833:59 UTC [0233:59 MYT]	KL ACC Radar Controller enquired with Malaysia Airlines Operations Centre about the communication status with MH370 but the personnel was unsure if the message went through successfully or not. Malaysia Airlines Operations Centre informed that the aircraft was still sending the movement message indicating it was somewhere in Vietnam and giving the last position as coordinates N14.90000 E109 15500 at time of 1833 UTC [0233 MYT].
13.	1834:56 UTC [0234:56 MYT]	HCM ACC queried about the status of MH370 and was informed that the Watch Supervisor was talking to the Company at this time.

Table 1.18E – ATC Activities after Notification by HCM ACC

cont…

a) Chronology of ATC Activities after Notification by HCM ACC (*cont*…)

No.	Time	Activities
14.	1837:34 UTC [0237:34 MYT]	KL ACC informed HCM ACC that MH370 was still flying and that the aircraft was continuing to send position reports to the airline, and relayed to HCM ACC the latitude and longitude as advised by Malaysian Airlines Operations.
15.	1853:48 UTC [0253:48 MYT]	MH386 which was enroute from KLIA to Shanghai and within HCM FIR was requested by HCM ACC to try to establish contact with MH370 on Lumpur Radar radio frequency. KL ACC then requested MH386 to try on emergency frequencies as well.
16.	1930 UTC [0330 MYT]	(*No voice recording*) Extract from Watch Supervisor's Log Book: MAS Operations Centre informed KL ACC that the flight tracker information was based on flight projection and was not reliable for aircraft positioning.
17.	1930:03 UTC [0330:03 MYT]	KL ACC queried if HCM ACC had checked with next FIR Hainan.
18.	1948:52 UTC [0348:52 MYT]	When KL ACC queried whether HCM ACC had checked with the Sanya FIR, HCM ACC informed KL ACC that there was no response until now. At 1956:13 UTC [0356:13 MYT] KL ACC queried Malaysia Airlines Operations for any latest information or contact with MH370.
19.	2025:22 UTC [0425:22 MYT]	HCM ACC Supervisor queried KL ACC on the last position that MH370 was in contact with KL ACC.
20.	2118:32 UTC [0518:32 MYT]	When HCM ACC queried for information on MH370, KL ACC also queried if any information had been received from Hong Kong or Beijing.
21.	2109:13 UTC [0509:13 MYT]	Singapore, on behalf of Hong Kong, enquired for information on MH370.

Table 1.18E – ATC Activities after Notification by HCM ACC

cont…

a) Chronology of ATC Activities after Notification by HCM ACC (*cont*…)

No.	Time	Activities
22.	2120:16 UTC [0520:16 MYT]	Capt. *xxxx [name redacted]* of MAS requested for information on MH370. He opined that based on known information, *"MH370 never left Malaysian airspace".*
23.	2130 UTC [0530 MYT]	Watch Supervisor activated the Kuala Lumpur Aeronautical Rescue Coordination Centre (ARCC).
24.	2141:20 UTC [0541:20 MYT]	HCM ACC queried for any updates.
25.	2214:13 UTC [0614:13 MYT]	KL ACC queried HCM ACC if SAR was activated.
26.	2232 UTC [0632 MYT]	KL ARCC issued a *DETRESFA* message (*Figure 1.18C* [below]).

Table 1.18E – ATC Activities after Notification by HCM ACC

b) *DETRESFA* Message of MH370

```
KLA637 072232
SS WMKKZQZX WMKKZRZX
072232 WMFCZQZX
(ALR-DESTRESFA/WMFCZQZX/MISSING
-FPL-MAS370-IS
-B772/H-SDFGHIJ3J5M1RWXY/LB1D1
-WMKK1635
-N0470F290 DCT PIBOS R208 IKUKO/M081F330 R208 IGARI M765
 BITOD/N0480F330 L637 TSN/N0480F350 W1 BMT W12 PCA G221
 BUNTA/N0480F370 A1 IKELA/N0480F370 P901 IDOSI/N0480F390 DCT CH
 DCT BEKOL/K0900S1160 A461 YIN/K0890S1130 A461 VYK
-ZBAA0534 ZBTJ ZBSJ
-PBN/A1B1C1D1L1O1S2 DOF/140307 REG/9MMRO EET/WSJC0032 VVTS0042
 ZJSA0210 VHHK0233 ZGZU0304 ZHWH0356 ZPE0450 SEL/QRCS
 RMK/ACASII EQUIPPED
-E/0710 P/TBN R/UVE S/M J/LF D/8 290 GREY A/WHITE WITH RED AND
 BLUE STRIPE C/TBN)
```

Source: DCA Malaysia

Figure 1.18C - DETRESFA Message

7) Activation of KL Aeronautical Rescue Coordination Centre

KL ARCC was activated at 2130 UTC [0530 MYT]. The *DETRES*FA message was disseminated via the AFTN at 2232 UTC [0632 MYT], 01 hour and 02 minutes later. No activity was recorded in the RCC Logbook between 2130 UTC [0530 MYT] and 2232 UTC [0632 MYT].

The Kuala Lumpur Aeronautical Rescue Co-ordination Centre, Standard Operating Procedure for Search and Rescue, page 11, para 3.1 stipulated:

"The search and Rescue Mission Co-ordinator (SMC) is the officer assigned to co-ordinate response to an actual or apparent distress situation.

In aeronautical search and rescue operations, the SMC is usually in the best position to assess the circumstances of a particular case, and to take whatever steps necessary to promote the safety of life and prevent further loss of property.

The SMC must use his/her best judgment in initiating and coordination operations to ensure use of the most suitable method of planning with least possible delay.

Initial Actions

On receipt of information regarding aircraft in difficulties normally from the Watch Supervisor in the ATCC, or from request of assistance from RSCs, MRCC (vessel or person - maritime distress) or from any adjacent RCCs and is aware that assistance is required the SMC shall act as follows:

- *Activate the SAR operation room;*
- *Appraise the situation.*

Continue to take the following actions if emergency situation involves civil aviation accident:

- *Declare the Distress phase if not done yet by the Duty Watch Supervisor;*
- *Notify the SAR Chief and the SAR Co-ordinator (SC);*
- *Request Supervisor to recall SAR trained staff if deemed necessary;*
- *Initiate ARCC activation message;*
- *Assign specific position accordingly (SMC, ASMC… etc.);*
- *Initiate NOTAM[25] actions;*

[25] *NOTAM (Notice to Airmen) - A notice issued by, or with the authority of the State and containing information or instruction concerning the establishment, condition change in any aeronautical facility, service, procedure or hazard, the timely knowledge of which is essential to persons concerned with flight operations. NOTAM is distributed by AFTN. (Aeronautical Fixed Telecommunication Network).*

- *Initiate RQS[26] request from AIS[27] and weather report from Meteorological Office if not done yet by the Supervisor;*
- *Obtain information of aircraft position if necessary by:*
  - *Information contained in the flight plan or notification;*
  - *Check all airports or possible alighting areas along the route of flight and within the possible flight range of the aircraft concerned;*
  - *Notify other aircraft or agencies to attempt establishment of the aircraft's position, informing them of all known frequencies, request for aircraft lookout made through the ATCC Watch Supervisor);*
  - *Notify the Police, along the route of flight, and request them to verify alighting areas, or obtain information on the aircraft and its occupants;*
  - *Request MRCC[28] to alert the vessels in the area if the flight is over or near water;*
  - *Ascertain the type of emergency equipment carried by the missing or distressed craft;*
  - *When required, request Radar assistance for search from appropriate radar station or Radar Plot.*

8) Recorded Telephone Conversations

From the recorded telephone conversations between the KL ACC Radar Controller and MAS Operations Centre, the Radar Controller at 2123:18 UTC [0523:18 MYT] indicated that he would inform the Watch Supervisor to check on when was the last contact with MH370.

[26] RQS - Request Supplementary Flight Plan.

[27] AIS - Aeronautical Information Service.

[28] MRCC - Maritime Rescue Coordination Centre.

9) Watch Supervisor Air Traffic Services and Sector (3 & 5) Logbook

MATS Part 1 - Admin, page 1-1-7 para 1.7 for recording of entries in the logbook as follows:

a) The time of entries shall be based on UTC and events recorded in a chronological order;

b) Entries shall give sufficient details to give readers a full understanding of all actions taken;

c) The time an incident occurred and the time at which each action was initiated shall be stated.

10) Flight Progress Strip

The FPS (*Figure 1.18D* below) of MH370 on 07 March 2014.contains essential flight and control data and is the basic tool to enable Air Traffic Controllers to visualise the disposition of traffic within their area of responsibility including traffic arriving and departing an aerodrome, assess conflicts and control aircraft in a safe manner.

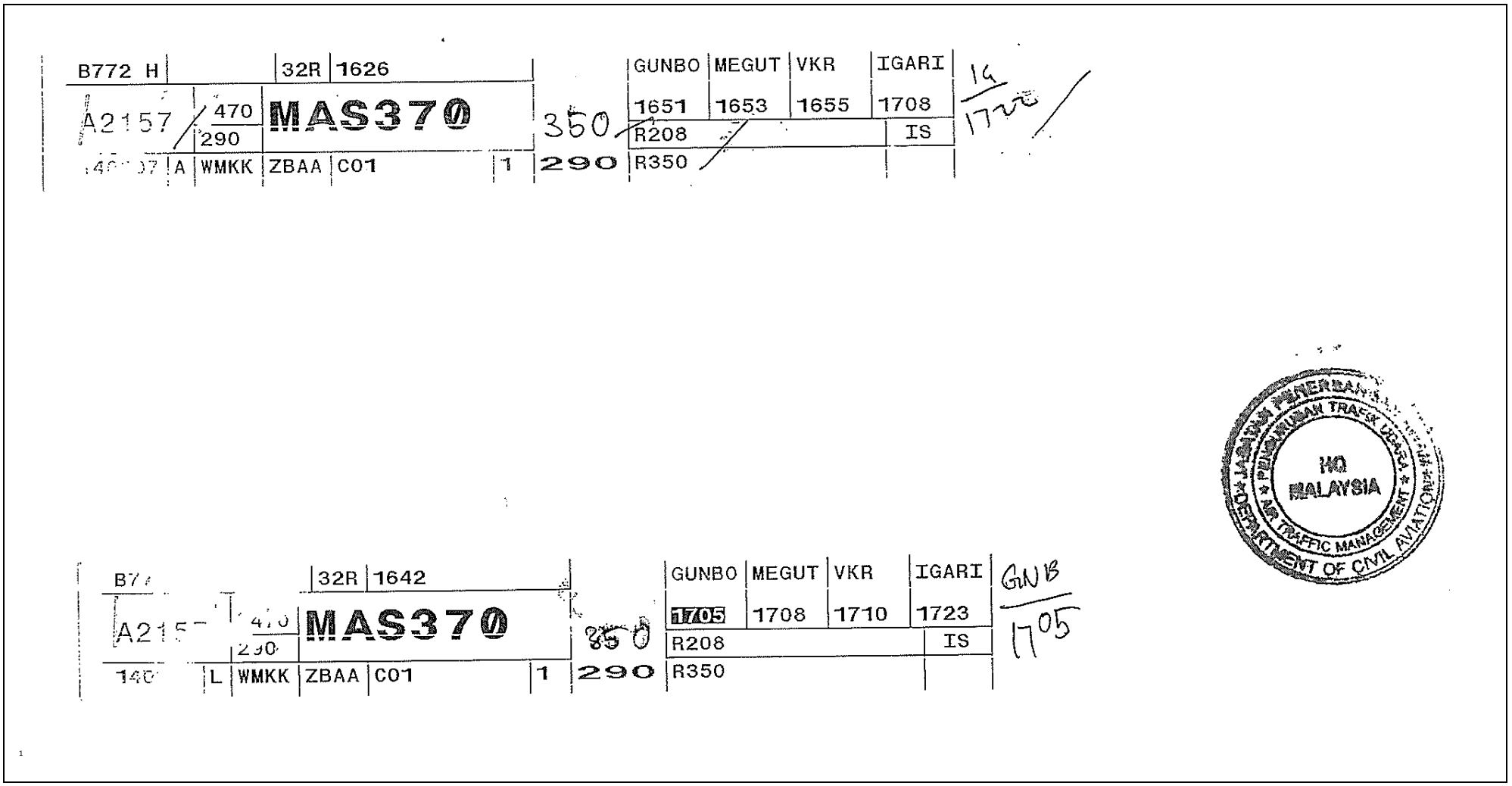

Figure 1.18D - Flight Progress Strip of MH370 on 07 March 2014

1.18.2 Aircraft Cargo Consignment

1) Introduction

During the course of the investigation the Team visited and interviewed the relevant people in MAS at KLIA Sepang, Motorola Solutions Penang, MASkargo Sdn. Bhd. (MASkargo) Penang, NNR Global Logistic (M) Sdn. Bhd. Penang, Poh Seng Kian, Muar, Johore (supplier of mangosteen fruit), Freescale Semiconductor, Petaling Jaya, JHJ International Transportation Co. Ltd. Beijing, China (forwarding agent of Motorola Solutions China), Motorola Solutions China, TianJin, China and Beijing GuangChangMing Trading Co. Ltd. Beijing, China.

On 08 March 2014, MAS B777-200ER MH370 was on a scheduled flight from KLIA to Beijing, China. The aircraft was carrying 227 passengers with a tabulated passenger weight of 17,015 kg, baggage 3,324 kg, cargo 10,806 kg (gross weight) and Max Take-off Weight of 223,469 kg. All these are stipulated in the cargo manifest attached as *Appendix 1.18H*.

The lists of cargo, Airway Bill, Local Agent and Final Destination, are tabulated in *Table 1.18F (*below).

The cargo that had generated interest were:

- Lithium ion Batteries (Li-Ion) and Accessories - 2,453 kg; and
- Mangosteens - 4,566 kg.

No.	COMPANY (MALAYSIA)	AIRWAY BILL	AGENT TRANSPORTER (MALAYSIA)	ITEMS	WEIGHT (nett)
1.	Grolier (M) SB Balakong Selangor	232-2009141	Kerry Logistics (M) Subang Jaya, Selangor	Scholastic assorted books	2,250 kg
2.	Motorola Solutions (M) Bayan Lepas Penang	232-0677085	NNR Global Logistic Batu Maung Penang	Lithium Ion batteries-walkie-talkie accessories & chargers	2,453 kg
3.	Panasonic Industrial Devices Sales, Shah Alam, Selangor	232-12022382	Panalpina Transport (M) MAS Cargo, KLIA,	Electrical parts capacitors	26 kg
4.	Freescale Semiconductor Petaling Jaya, Selangor	232-12022404	Panalpina Transport (M) MAS Cargo, KLIA	Vehicle electronic chips	6 kg
5.	Agilents Technologies Bayan Baru, Penang	232-10664905	Kintetsu World Express MAS Cargo Penang	Electronic measurements	646 kg
6.	Poh Seng Kian Muar, Johore	232-12007306	Poh Seng Kian Muar, Johore	Fresh mangosteens	4,566 kg
7.	Malaysian Express Worldwide, Subang Jaya Selangor	232-11873632	Malaysian Express Worldwide, Subang Jaya, Selangor	Courier materials - documents	6 kg

Table 1.18F - List of Cargo on Board MH370

2) Lithium Ion Batteries

Li-Ion Batteries carried on MH370 were from Motorola Solution Penang. Of the total consignment of 2,453 kg, only 221 kg were Li-ion batteries, the rest were chargers and radio accessories.

The batteries were fabricated in the factory before being packed for export. *Figure 1.18E* (below) shows a raw single cell battery.

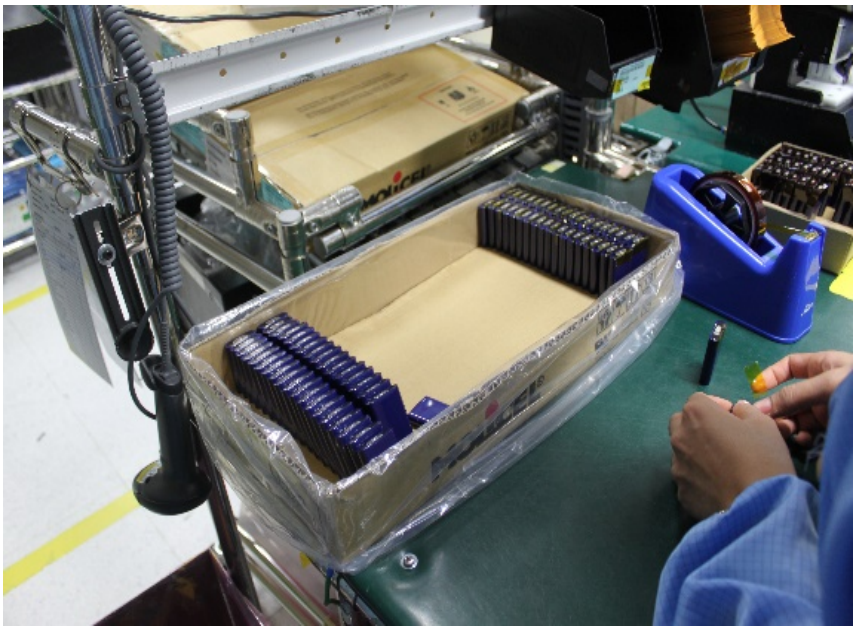

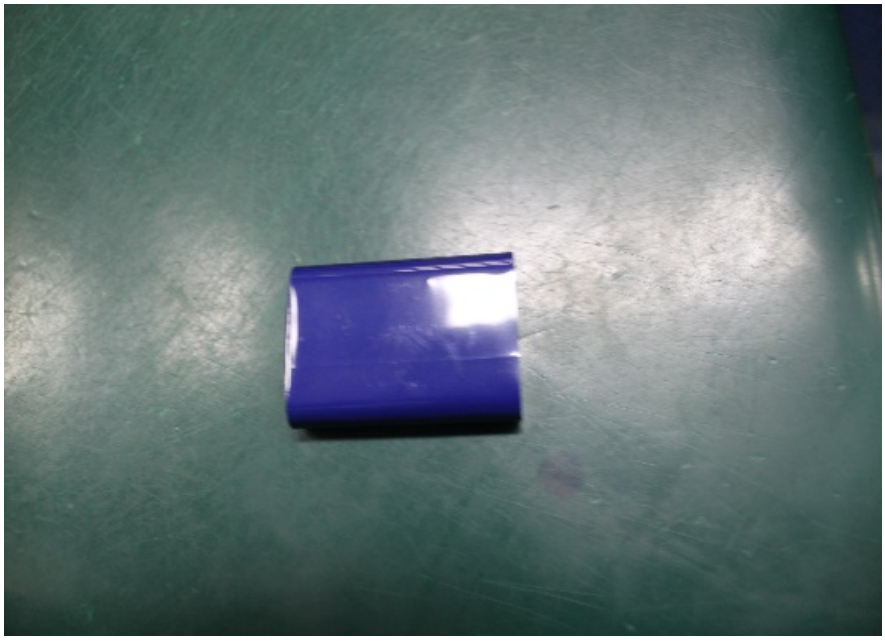

Figure 1.18E - Raw Single Cell Battery

The step-by-step process of fabricating 2 single cell batteries together to form a battery pack for shipment is shown in *Figure 1.18F* (below).

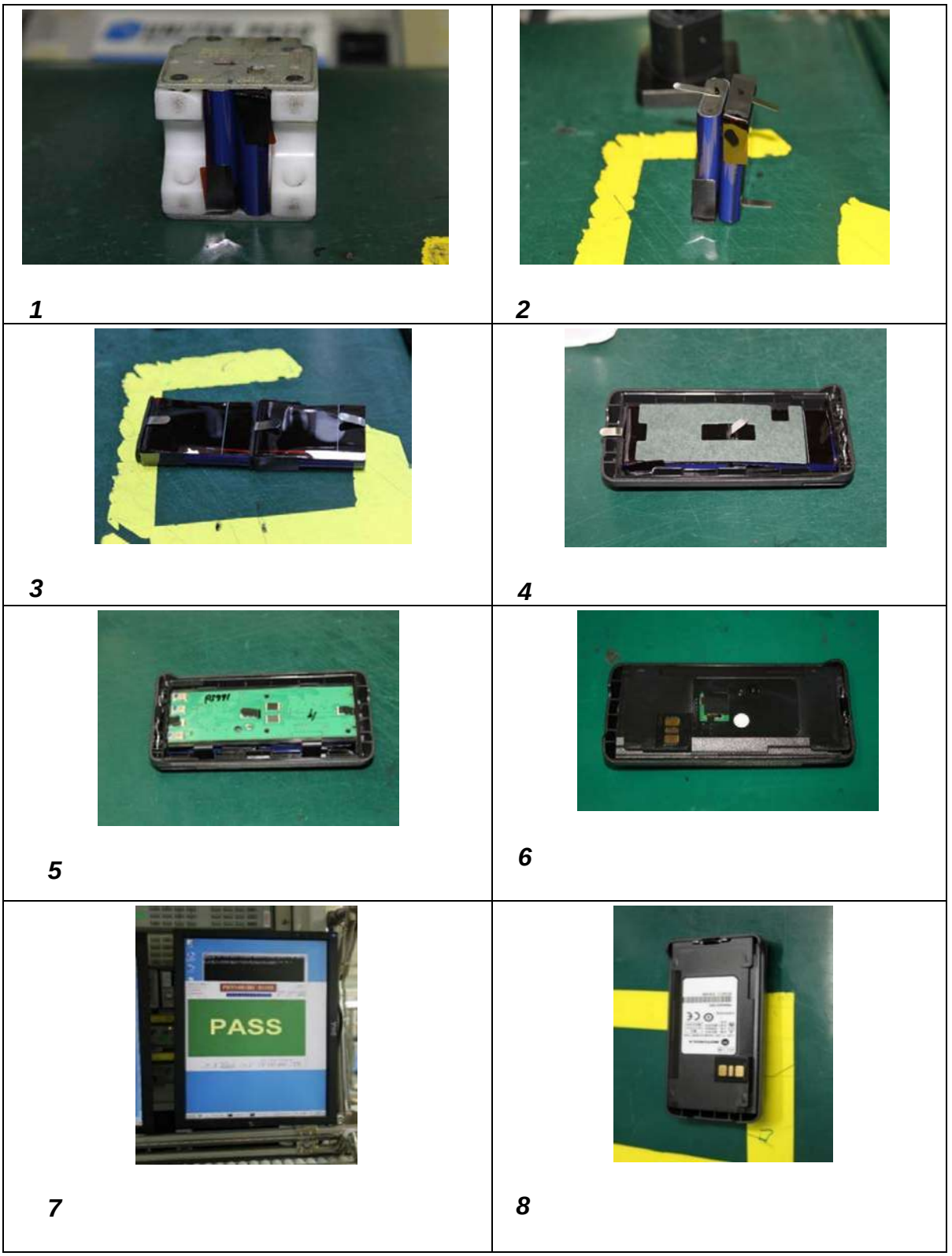

Figure 1.18F - Step-by-step Process of Fabricating 2 Single Cell Batteries to form a Battery Pack for Shipment

The Li-Ion batteries from Motorola Solutions Penang were assembled on 07 March 2014 before being packed, the built-up consigments placed on wooden pallets and delivered by the forwarding agent (NNR Global Logistic (M) Sdn. Bhd.) to MASkargo Penang and subsequently transported by MASkargo truck '*MH6803*' to MAS Cargo Complex, KLIA, Sepang. The shipment did not go through security screening in Penang but was inspected physically by MASkargo personnel and went through Customs' inspection and clearance before the truck was sealed and allowed to leave the Penang Cargo Complex.

The shipment arrived at KLIA Cargo Complex on the evening of 07 March 2014 before being loaded onto MH370 without going through additional security screening.

The Motorola Solutions consignments were loaded in the Aircraft at 90348C (47R) and PMC5871 (23L, 23R) as per Loading Instruction/Report. Illustration as shown in *Figure 1.18G* (below).

There were two (2) different models of Li-Ion battery consignment on MH370 on 08 March 2014:

- PMNN4073AR Li-ion batteries rated at 7.4V, 11.8Wh; and
- PMNN4081BRC Li-ion batteries rated at 7.4V, 11.1Wh.

Both of the batteries were not regulated as Dangerous Goods because the packing had adhered to the guidelines as per Lithium Battery Guidance Document (3. Section II - Packing Instructions 965-970). This document is based on the provisions set out in the 2013-2014 Edition of the ICAO Technical Instructions for Safe Transport of Dangerous Goods by Air and the 55th Edition of the IATA Dangerous Goods Regulations (DGR). The ICAO and IATA documents are as per *Appendix 1.18I.*

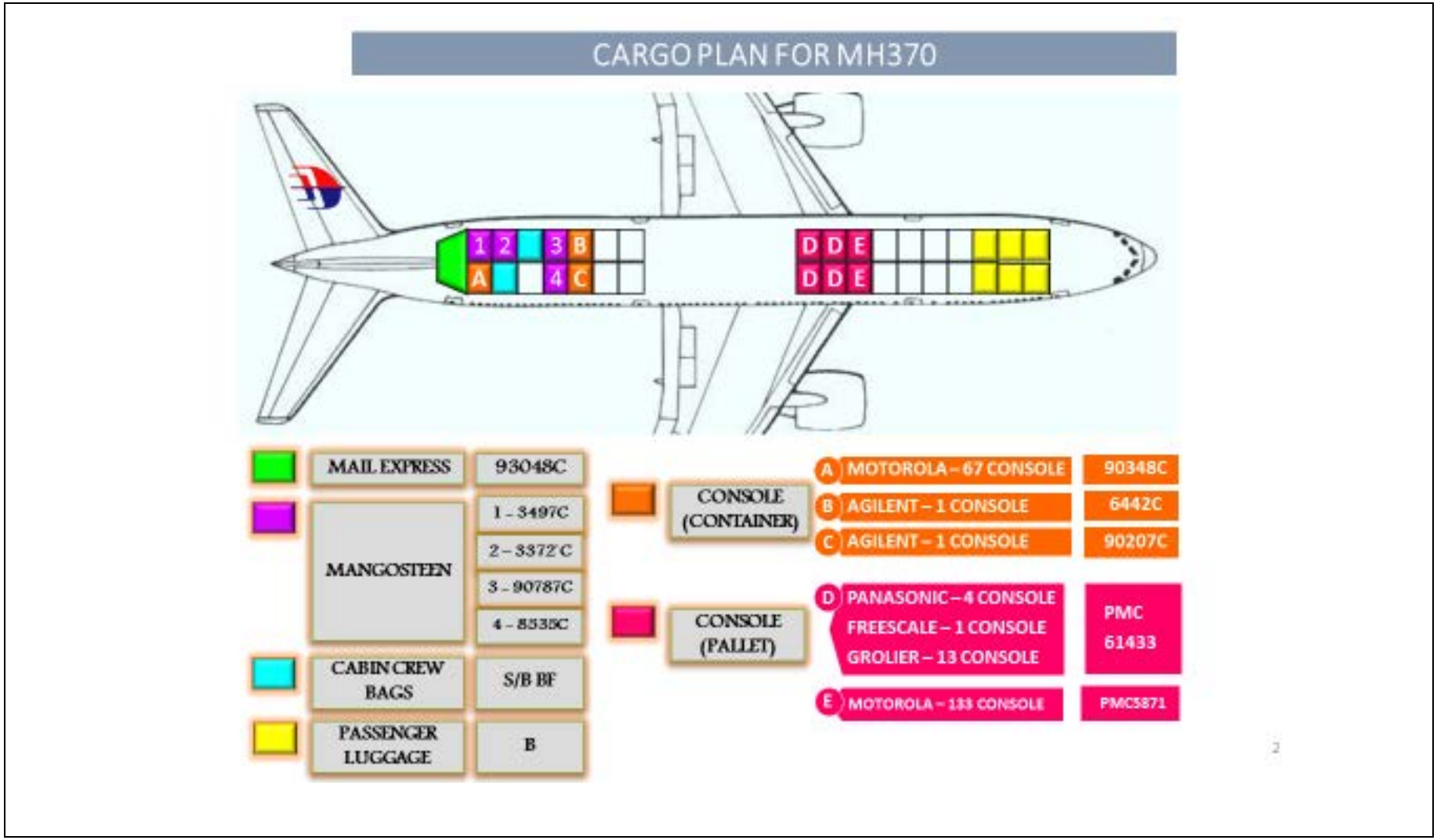

Figure 1.18G - Motorola Solutions Consignment Loading

The packing of the batteries by Motorola Solutions is shown in *Figure 1.18H* (below).

Picture 1	*Picture 2*	*Picture 3*
Picture 4	*Picture 5*	*Picture 6*

Figure 1.18H - Packing of Batteries by Motorola Solutions

Each Li-Ion battery was placed in a white window box (*Picture 1* [above]) and two of these filled boxes were then placed in a brown box (*Picture 2* [above]) printed with Li-Ion battery warning shipping information (*Picture 3* [above]). The brown box filled with two Li-Ion batteries each was then packed into a larger box. Each box contained twenty-four Li-ion batteries (12 boxes x 2 = 24, *Picture 4, Figure 1.18H* [above]), sealed and weighed (*Picture 5, Figure 1.18H* [above]). All the sealed boxes were placed on a wooden pallet and the built-up consignment was wrapped with plastic and polystyrene sheets for protection (*Picture 6, Figure 1.18H* [above]). They were then scanned, with the number of batteries determined by means of weighing the boxes.

From January 2014 to May 2014 there were ninety-nine shipments of Li-ion Batteries on MAS flights to Beijing.

Refer *Appendix 1.18J - List of Airways Bills.*

3) Mangosteen Fruits

The mangosteens on board MH370 on 08 March 2014 originated from Poh Seng Kian of No.79, 6¼ mile Kesang, 84000 Muar, Johore, Malaysia. About 2,500 kg of the fruit were harvested from Muar and the rest from Sumatra, Indonesia. Photographs of the mangosteen orchard and a typical mangosteen plant are shown as *Figures 1.18I* and *1.18J* (below) respectively.

Figure 1.18I - Mangosteen Orchard in Muar, Johor, Malaysia

Figure 1.18J - Mangosteen Plant/Fruit

The mangosteens were packed in plastic baskets of between 8 to 9 kg per basket with a piece of sponge soaked with water placed on top of the mangosteens to maintain their freshness (*Figures 1.18K and 1.18L* [below]*)*. The packed mangosteens were then loaded on the trucks which proceeded to MASkargo Complex at KLIA, Sepang. At the complex, four ULD containers were provided by MASKargo staff to the forwarding agent. The forwarding agent then loaded the packed fruit into the ULD containers (*Figure 1.18M* [below]). The consignment was then inspected by the Federal Agriculture Marketing Authority (FAMA) of Malaysia. After obtaining the clearance, the forwarding agent handed over the consignments to the MAS loaders for loading into the aircraft.

Figure 1.18K - Plastic Baskets of Mangosteens

Figure 1.18L - Piece of Soaked Sponge placed on Top of Mangosteens

1. MASkargo Perishable Warehouse	**2.** Unloading crates of mangosteens from plantation	**3**. Crates of mangosteens ready for loading into ULD
4. Placing large plastic sheet in ULD before loading	**5**. Loading crates of mangosteens into ULD	**6**. Filling up crates into ULD .
7. Secured crates of mangosteens with plastic sheets before latching ULD cover.	**8**. Another piece of plastic sheet to cover ULD	**9.** ULD secured with labels for uploading into aircraft

Figure 1.18M - Processing of Packed Crates of Mangosteens into ULD before Uploaded to Aircraft

Flight MH370 on 08 March 2014 carried four ULD containers of mangosteens - ULD AKE3497MH weighing 1,128 kg was placed at cargo bay 41L, ULD AKE90787MH weighing 1,152 kg at cargo bay 41F, ULD AKE3372MH weighing 1,148 kg at cargo bay 43L and ULD AKE8535MH weighing 1,138 kg at cargo bay 44L. The loading arrangement is shown in *Figure 1.18N* (below). Loading Instruction/Report is shown in the MH370 cargo manifest (*Appendix 1.18H*).

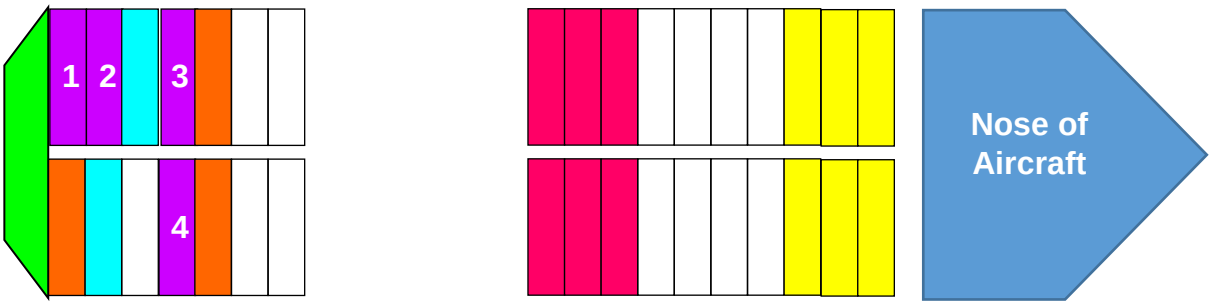

No.	ULD	WEIGHT (KG)	POSITION
1	AKE3497MH	1,128	41F
2	AKE90787MH	1,152	41L
3	AKE3372MH	1,148	43L
4	AKE8535MH	1,138	44L

Figure 1.18N - Loading Arrangement of ULDs of Mangosteens

From January 2014 till May 2014 there were a total of eighty-five shipments of mangosteens to Beijing, China. The list of Airway Bills is shown in *Appendix 1.18J*. The combination of the two cargo shipments (Li-ion Batteries and mangosteens) carried together from January to May 2014 were thirty-six times (*highlighted in red in Appendix 1.18J).*

1.18.3 Crew and Passengers on Board MH370

1) Total Number of Crew and Passengers

Total number crew and passengers on board MH370 are shown in *Table 1.18G* (below).

Crew		Passengers	Total
Flight	Cabin		
2	10	227	239

Table 1.18G - Total Number of Crew and Passengers

2) Nationalities of the Crew and Passengers

The nationalities of the flight crew and passengers on board MH370 are shown in *Table 1.18H* (below).

Countries		Crew		Passengers	Total
		Flight	Cabin		
1.	China	-	-	153	153
2.	Malaysia	2	10	38	50
3.	Indonesia	-	-	7	7
4.	Australia	-	-	6	6
5.	India	-	-	5	5
6.	France	-	-	4	4
7.	United States of America	-	-	3	3
8.	Ukraine	-	-	2	2
9.	Canada	-	-	2	2
10.	New Zealand	-	-	2	2
11.	Netherland	-	-	1	1
12.	Russia	-	-	1	1
13.	Chinese Taipei	-	-	1	1
14.	Italy* (Iran)	-	-	1	1
15.	Austria* (Iran)	-	-	1	1
Total		2	10	227	**239**

Table 1.18H - Breakdown of Nationalities of Passengers

* Travelling on stolen passports and discovered to be Iranian citizen *(Figures 1.18V & W* [below] *on Passengers' Seating Positions).*

a) Crew

All the 12 crew (including the two pilots) were Malaysians.

b) Passengers

A total of 227 passengers (including 3 children and 2 infants) were on board with the majority of them from China, followed by Malaysia and other citizens from different countries.

c) Passengers' Seating Positions

The aircraft was compartmentalised into 2 categories of seating, namely the business class with a total of 35 seats and the economy class with a total of 249 seats. Passengers from the 14 countries were seated throughout the aircraft from Row 1 to Row 41. (*Figure 1.18O* [below]).

A total of 10 passengers were seated in the Business Class in the front portion of the aircraft, from Row 1 to Row 4. (*Figure 1.18P* [below]).

In the middle portion of the aircraft, the Economy seating started from Row 11 to Row 27. A total of 127 passengers were seated in this middle portion of the aircraft. There were 2 children on seats 17F and 18F respectively (*Figures 1.18Q, 1.18R, 1.18S and 1.18T* [below]).

The rear portion of the aircraft accommodated 90 passengers from Row 29 to Row 41. 2 infants were on board accompanied by adults seated on seats 30E and 37D respectively. There was a child on seat 30H in the rear portion of the aircraft. (*Figures 1.18U, 1.18V and 1.18W* [below]).

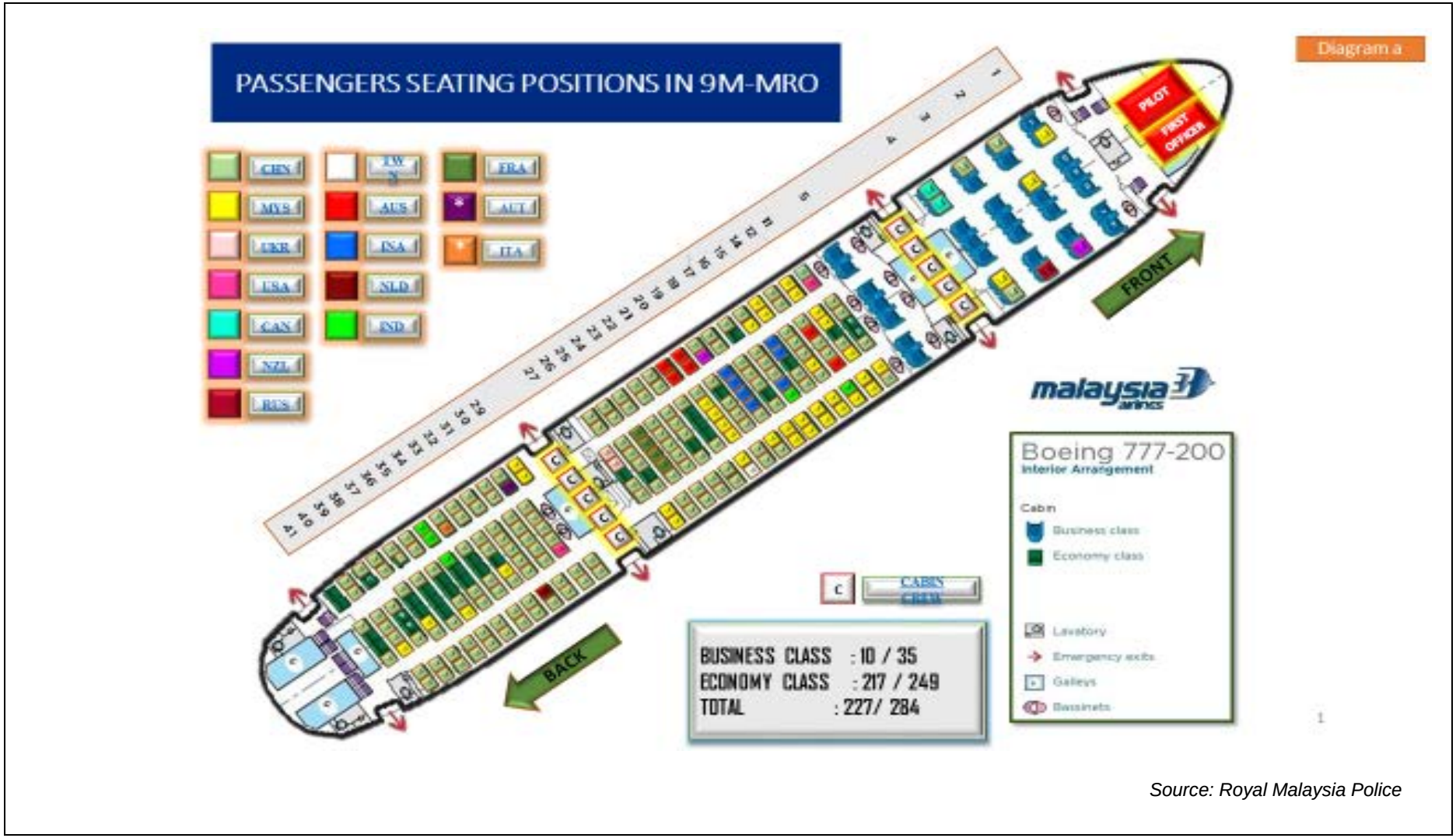

Figure 1.18O - Passengers' Seating Positions

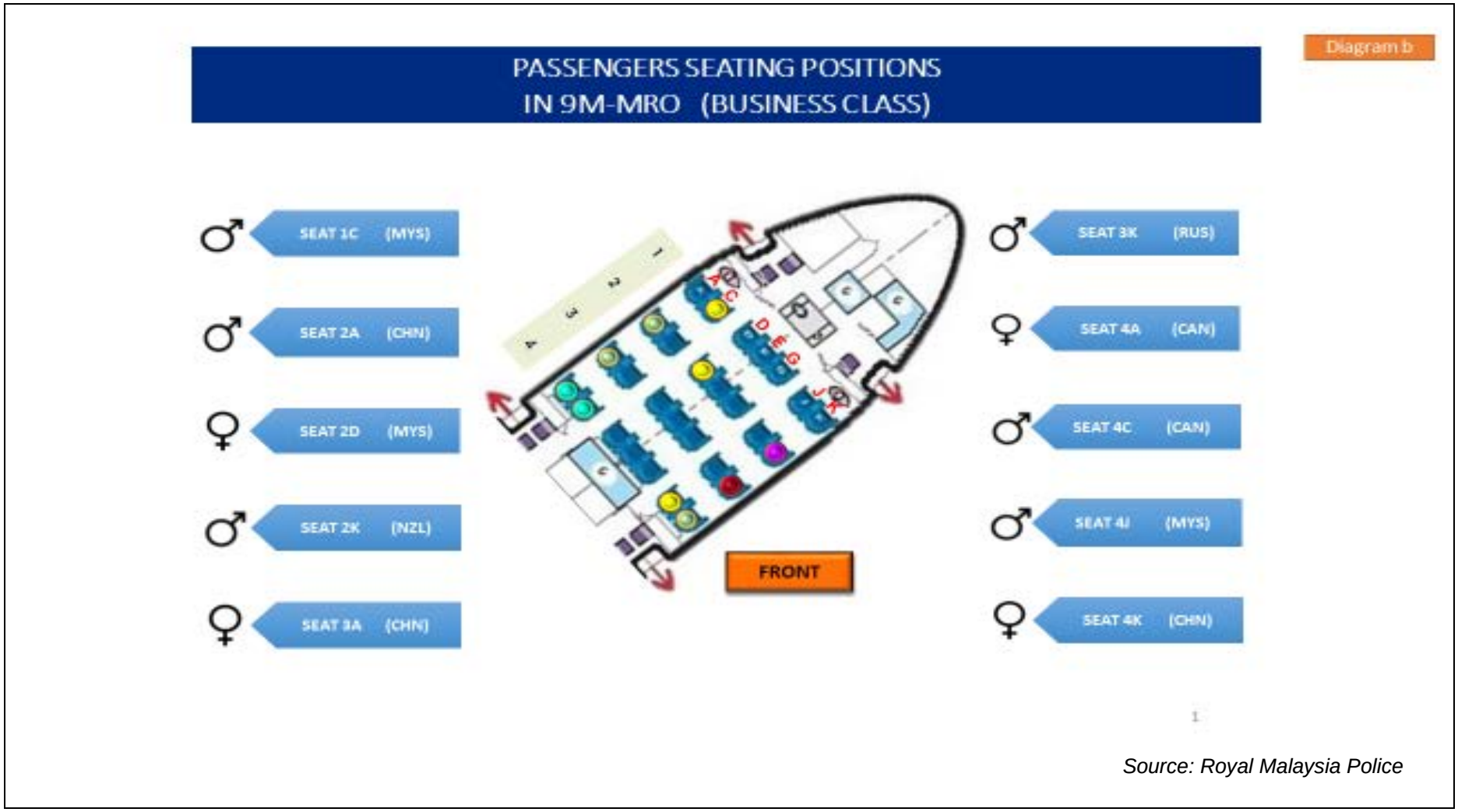

Figure 1.18P - Passengers' Seating Positions (Business Class)

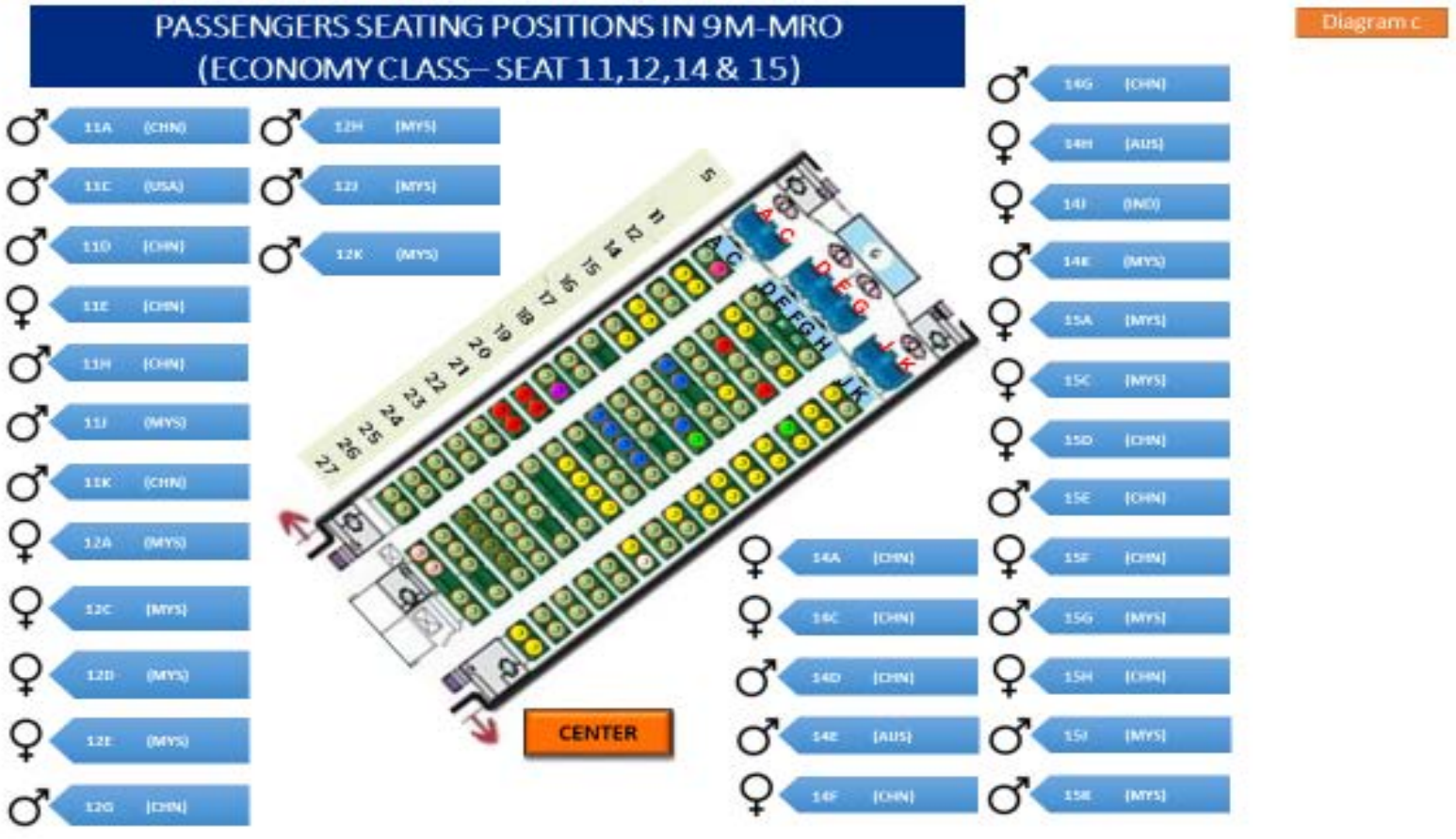

Figure 1.18Q - Passengers' Seating Positions (Economy Class - Seats 11, 12, 14 & 15)

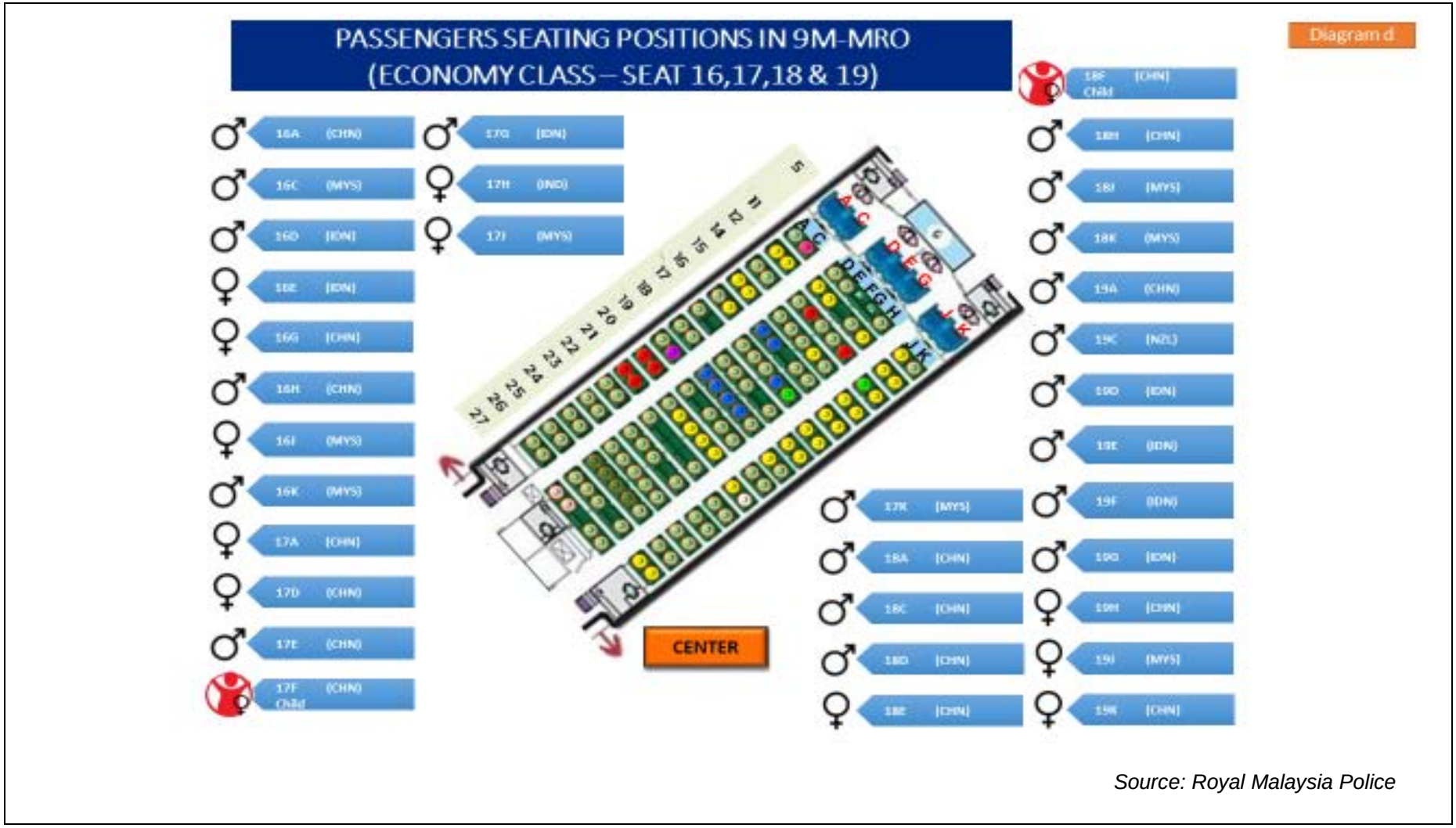

Figure 1.18R - Passengers' Seating Positions (Economy Class - Seats 16, 17, 18 & 19)

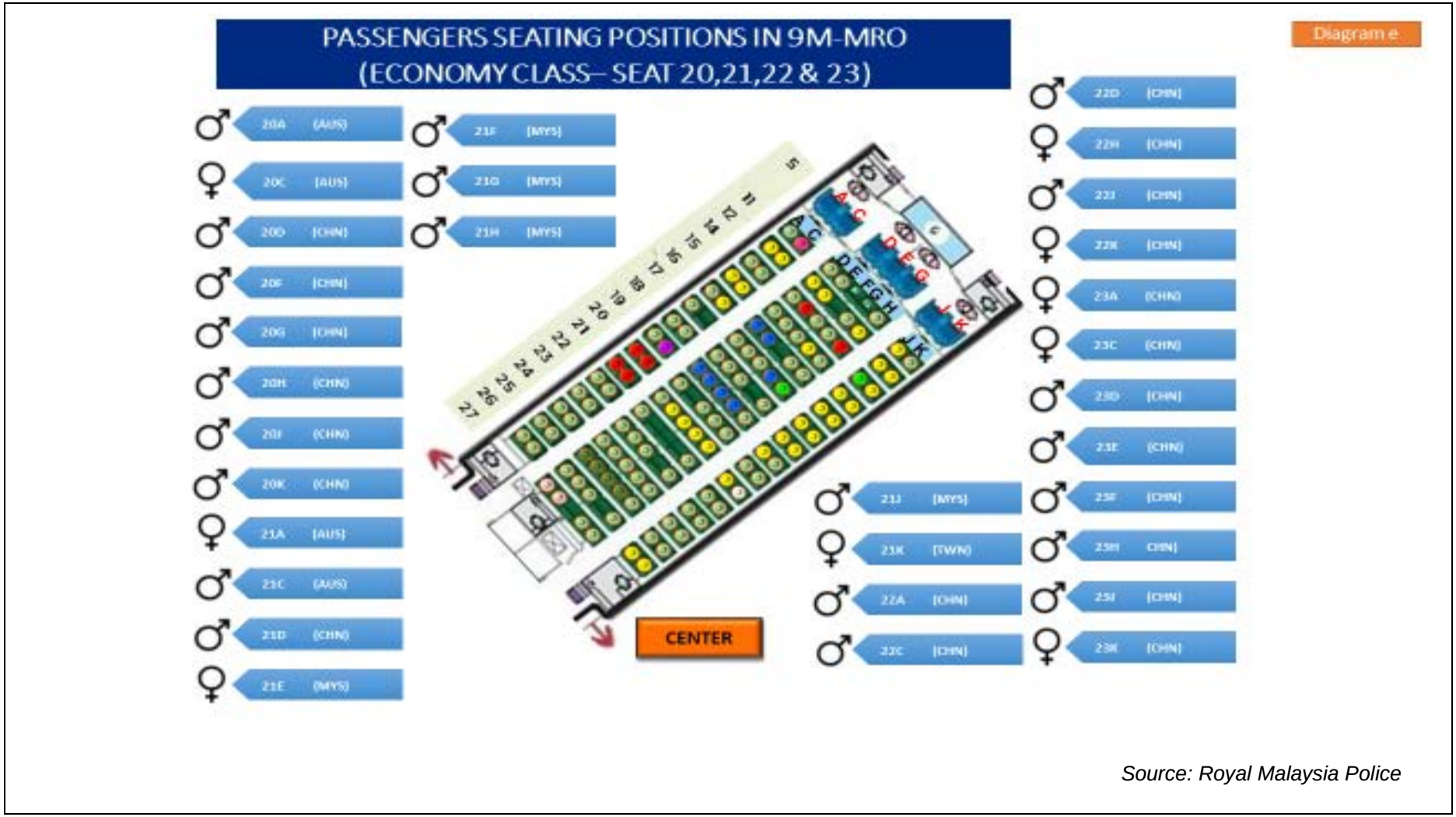

Figure 1.18S - Passengers' Seating Positions (Economy Class - Seats 20, 21, 22 & 23)

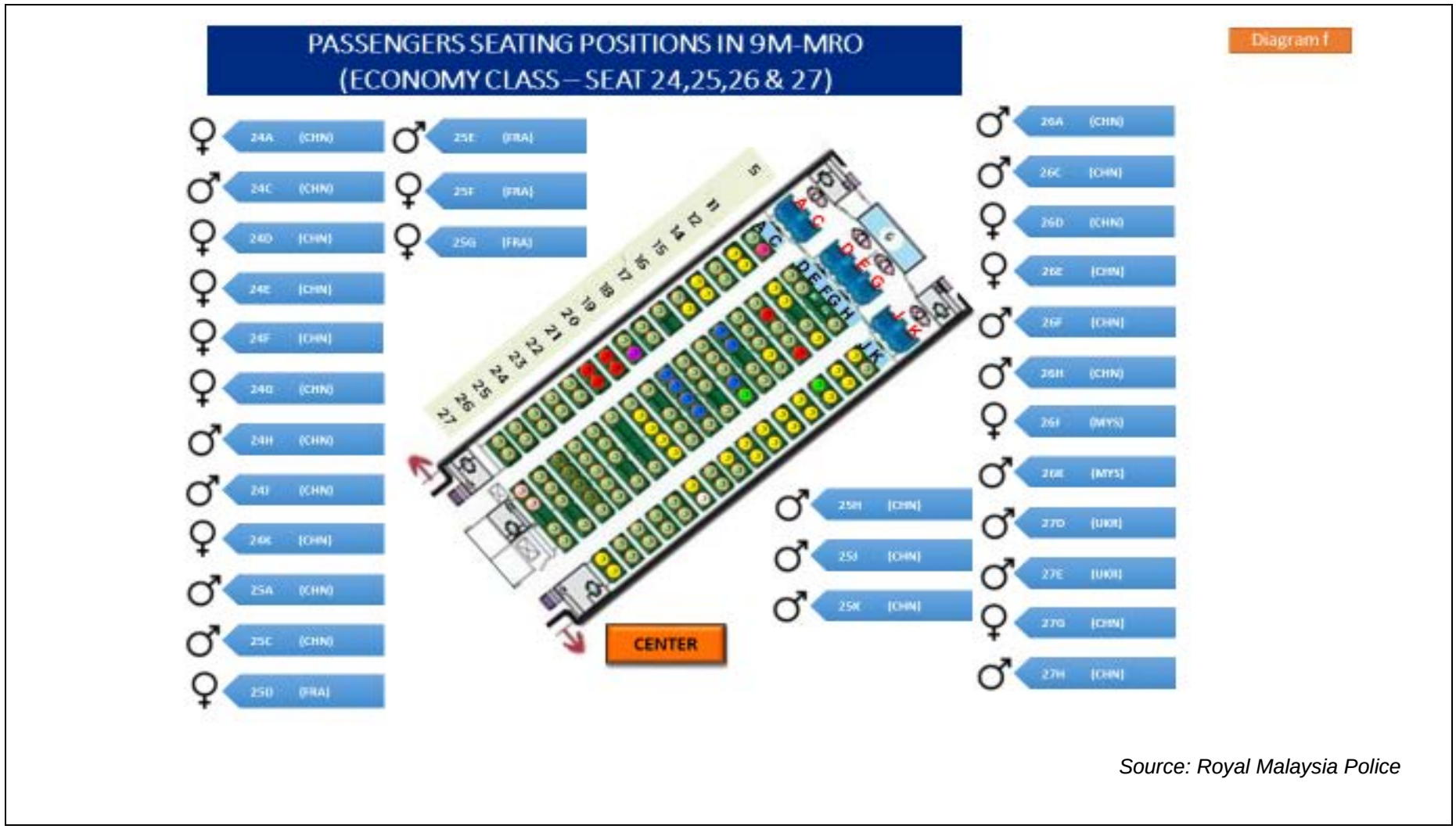

Figure 1.18T - Passengers' Seating Positions (Economy Class - Seats 24, 25, 26 & 27)

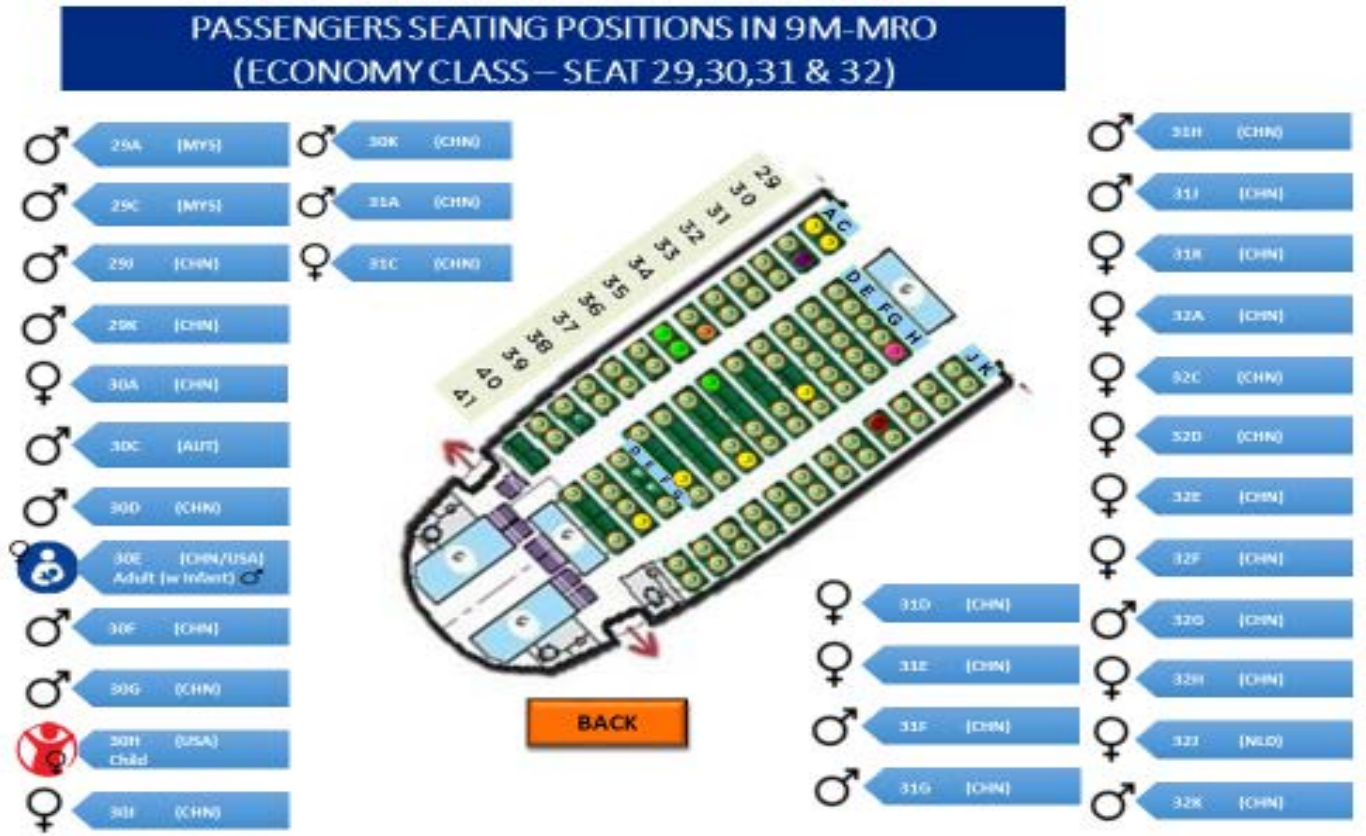

Source: Royal Malaysia Police

Figure 1.18U - Passengers' Seating Positions (Economy Class - Seats 29, 30, 31 & 32)

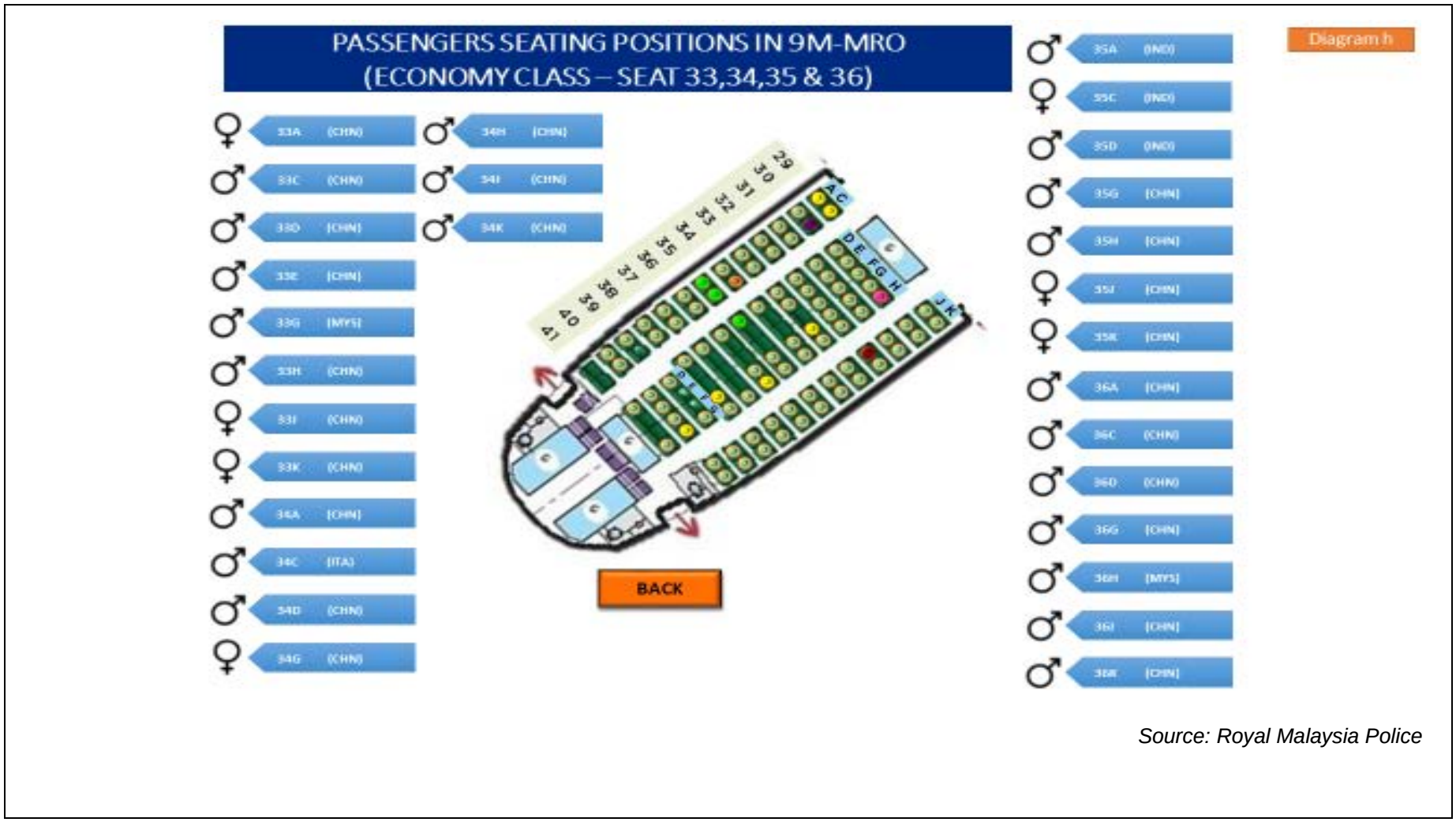

Source: Royal Malaysia Police

Figure 1.18V - Passengers' Seating Positions (Economy Class - Seats 33, 34, 35 & 36)

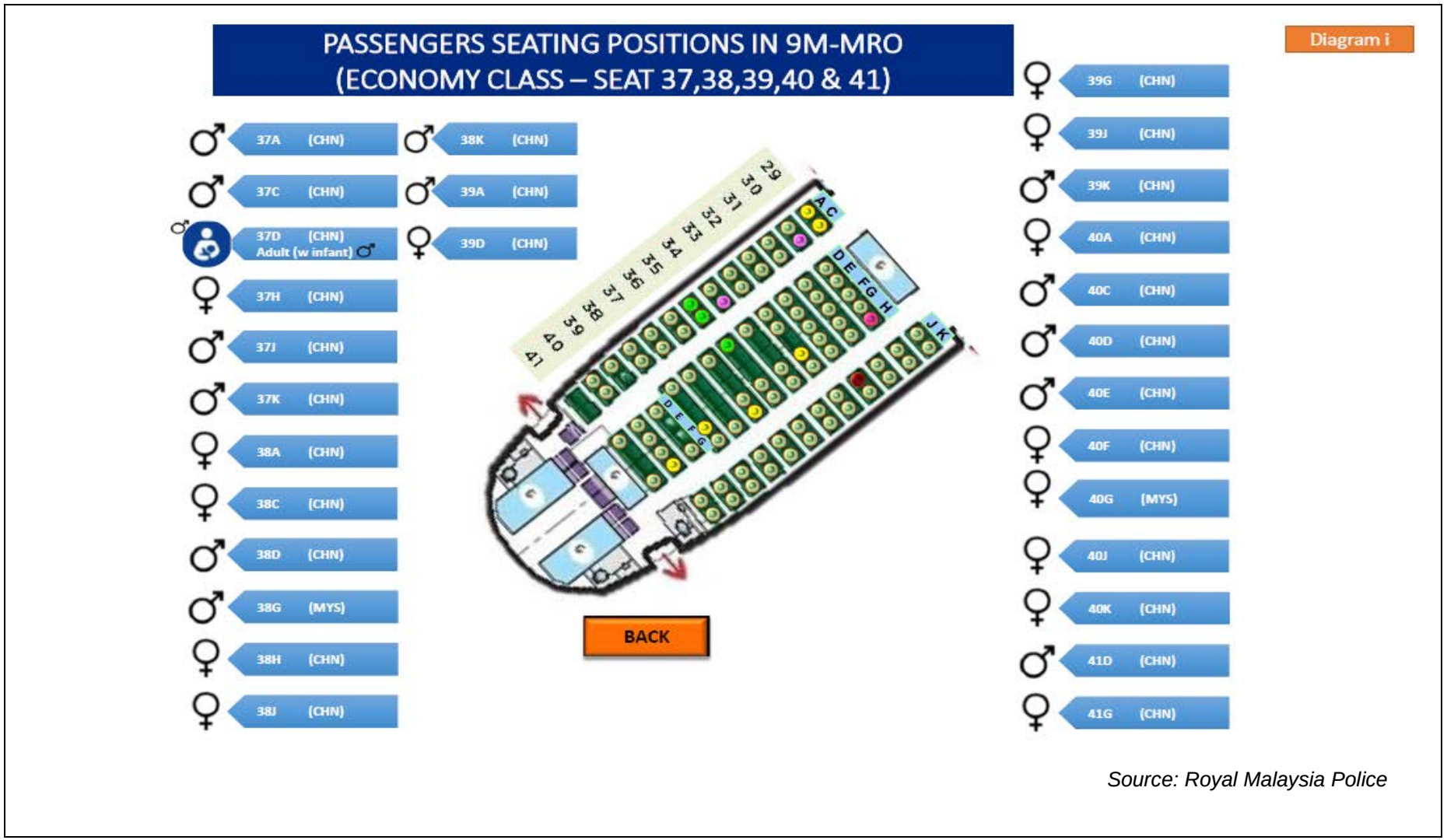

Figure 1.18W - Passengers' Seating Positions (Economy Class - Seats 37, 38, 39, 40 & 41)

SECTION 1 – FACTUAL INFORMATION

1.19 NEW INVESTIGATION TECHNIQUES

Not applicable.

SECTION 2 – ANALYSIS

INTRODUCTION

Section 2 analyses the relevant issues associated with the disappearance of B777-200ER aircraft, registered as 9M-MRO, and operating as Flight MH370 on 08 March 2014. Recognising that at the time of issue of this Report, the main aircraft wreckage, including the Flight Data Recorder (FDR) and Cockpit Voice Recorder (CVR) have not been located, this analysis will necessarily be limited by a significant lack of evidence.

The issues that will be covered in this Section include the following:

1. Diversion from Filed Flight Plan Route;
2. Air Traffic Services Operations;
3. Flight Crew Profile;
4. Airworthiness & Maintenance and Aircraft Systems;
5. Satellite Communications;
6. Wreckage and Impact Information;
7. Organisation and Management of Department of Civil Aviation and Malaysia Airlines; and
8. Aircraft Cargo Consignment.

SECTION 2 – ANALYSIS

2.1 DIVERSION FROM FILED FLIGHT PLAN

2.1.1 Seven Simulator Sessions

To analyse further on how MH370 had diverted from the Filed Flight Plan (FPL) route, the Team conducted a total of seven flight simulator sessions to recreate the two turns of MH370, i.e. six sessions on the left turn past waypoint IGARI and one session on the right turn on reaching the south of Penang Island. Three of the seven sessions were conducted at high speed and the remainders at low speed. The turns were based on the recorded primary radar data that recorded a primary target conducting a left turn from where the SSR code ceased, shortly after the aircraft passed waypoint IGARI. The following data (*Tables 2.1A to 2.1F* [below] on data input for the first six sessions respectively) were introduced to simulate an actual environment:

- Actual weight and meteorological condition prevailing at the time of the turn (extracted from the computerised flight plan); and
- Different speed and rate of turns to determine scenarios closest were made available to the Team.

1) Recreating the Left turn past Waypoint IGARI – Session 1

Initial conditions

Fuel	41,200 kg
Gross weight	215,410 kg
Height	35,000 ft
Speed	IAS 271 (475 knots ground speed)
Simulator setup	Speed/Lateral Navigation/Vertical Navigation (SPD/LNAV/VNAV), autopilot engaged, autothrottle engaged
Entry waypoint	N07.05.7 E103.47.1
Exit waypoint	N07.12.7 E103.38.7

Table 2.1A - Data Input for Session 1

To get the 'aircraft' to track correctly, a flight path from waypoint IGARI to waypoint BITOD was generated with the entry and exit waypoints entered.

The simulation commenced before IGARI and the 'aircraft' turned right on LNAV and tracked to the entry waypoint. Once over the waypoint, the flight management computer (FMC) was directed to fly "direct to" to the exit waypoint. The 'aircraft' entered a left turn, with a maximum bank-angle of 26° (maximum bank-angle in LNAV is 25°).

About half-way through the turn, it was obvious that the 'aircraft' was not going to make it through the exit waypoint as it was overshooting as there was no tracking information in the FMC. The simulator session was then terminated.

2) Session 2

Initial conditions (identical to Session 1)

Fuel	41,200 kg
Gross weight	215,410 kg
Height	35,000 ft
Speed	IAS 271 (475 knots ground speed)
Simulator setup	SPD/LNAV/VNAV, autopilot engaged, autothrottle engaged
Entry waypoint	N07.05.7 E103.47.1
Exit waypoint	N07.12.7 E103.38.7
Additional waypoint	N05.15.6 E100.27.5

Table 2.1B - Data Input for Session 2

To get the 'aircraft' to track correctly, a flight path from waypoint IGARI to waypoint BITOD was generated with the entry and exit waypoint entered. A further waypoint was entered along a track of 244° at the commencement of the right turn south of Penang.

The simulation commenced before IGARI and the 'aircraft' turned right on LNAV and tracked to the entry waypoint. Once over the waypoint, the FMC was directed to fly "direct to", to the exit waypoint. The 'aircraft' entered a left turn, with a maximum bank-angle of 26° (maximum bank-angle in LNAV is 25°).

The 'aircraft' made the exit waypoint; however, it took 3 minutes and 45 seconds to achieve it (the recorded radar time was 2 minutes 10 seconds).

3) Session 3

Initial conditions

Fuel	41,200 kg
Gross weight	215,410 kg
Height	35,000 ft
Speed	IAS 250 (425 knots groundspeed)
Simulator setup	SPD/LNAV/VNAV, autopilot engaged, autothrottle engaged
Entry waypoint	N07.05.7 E103.47.1
Exit waypoint	N07.12.7 E103.38.7
Additional waypoint	N05.15.6 E100.27.5

Table 2.1C - Data Input for Session 3

Following discussions, it was decided to reduce the speed in the turn to see if the rate of turn would increase. In this session, the speed was reduced to 250 knots IAS (ground speed of 425 knots). Similar set up as Session 2.

The simulation commenced before IGARI and the 'aircraft' turned right on LNAV and tracked to the entry waypoint. Once over the waypoint, the FMC was directed to fly "direct to" to the exit waypoint. The 'aircraft' entered a left turn, with a maximum bank-angle of 28° (maximum bank-angle in LNAV is 25°). The 'aircraft' made the exit waypoint. However, it took 3 minutes and 3 seconds to achieve it.

4) Session 4

Following further discussions, it was decided to further reduce the speed in the turn.

The simulation commenced before IGARI and the 'aircraft' turned right on and tracked to the entry waypoint. Once over the waypoint, the FMC was directed to fly "direct to", to the exit waypoint. The 'aircraft' entered a left turn, with a maximum bank-angle of 23° (maximum bank-angle in LNAV is 25°).

Initial conditions

Fuel	41,200 kg
Gross weight	215,410 kg
Height	35,000 ft
Speed	IAS 220 (400 knots groundspeed)
Simulator setup	SPD/LNAV/VNAV, autopilot engaged, autothrottle engaged
Entry waypoint	N07.05.7 E103.47.1
Exit waypoint	N07.12.7 E103.38.7
Additional waypoint	N05.15.6 E100.27.5

Table 2.1D - Data Input for Session 4

The 'aircraft' made the exit waypoint. However, it took 3 minutes and 30 seconds to achieve it.

5) Session 5 (Manual Flying)

Following discussions, it was agreed that the turn could be executed in LNAV, but not in 2 minutes. It was decided that the bank-angle needed to be increased to reduce the time and that could only be achieved with the autopilot disengaged and the 'aircraft' manually flown, with the auto-thrust managing the speed. Similar set-up as Session 2.

Initial conditions

Fuel	41,200 kg
Gross weight	215,410 kg
Height	35,000 ft
Speed	IAS 271 (475 knots ground speed)
Simulator setup	SPD/LNAV/VNAV, autopilot engaged, then autothrottle engaged
Entry waypoint	N07.05.7 E103.47.1
Exit waypoint	N07.12.7 E103.38.7
Additional waypoint	N05.15.6 E100.27.5

Table 2.1E - Data Input for Session 5

The simulation commenced before IGARI with autopilot and autothrottle engaged and the 'aircraft' turned right on LNAV and tracked to the entry waypoint. Once over the waypoint, the autopilot was disconnected and the 'aircraft' manually turned to the left. Bank-angles around 30°-32° were used. As the entry and exit waypoints were displaced slightly laterally (i.e. not exactly aligned 180° apart), the 'aircraft's wings were rolled level

when aligned to intercept the exit waypoint. This was at 2 minutes and 10 seconds. The 'aircraft' then intercepted the exit waypoint at 2 minutes and 40 seconds.

6) Session 6 (Manual Flying)

Finally, it was agreed that the same turn should be executed manually but at a lower speed of 250 knots with the autopilot disengaged and the 'aircraft' manually flown, with the autothrottle managing the speed. Same set-up as Session 2.

Initial conditions

Fuel	41,200 kg
Gross weight	215,410 kg
Height	35,000 ft
Speed	IAS 250 (425 knots ground speed)
Simulator setup	SPD/LNAV/VNAV, then autopilot disengaged, autothrottle engaged
Entry waypoint	N07.05.7 E103.47.1
Exit waypoint	N07.12.7 E103.38.7
Additional waypoint	N05.15.6 E100.27.5

Table 2.1F - Data Input for Session 6

The simulation commenced before IGARI with autopilot and autothrottle engaged and the 'aircraft' turned right on LNAV and tracked to the entry waypoint. Once over the waypoint, the autopilot was disengaged and the 'aircraft' manually turned to the left. Bank-angle around 35° was used (bank-angle warnings sounded several times).

At about half way through the turn (1 minute mark), the stick-shaker activated. The 'aircraft' intercepted the exit waypoint at 2 minutes and 28 seconds.

7) Analysis on Re-enactment Sessions (Sessions 1 - 6)

a) From the various re-enactment sessions tested, it is apparent that the 'aircraft' could make the turn in LNAV, but took a longer time due to bank-angle limitations (25°) and also required the need to reduce speed (Session 3 was the closest at 3 minutes and 3 seconds) in the turn.

b) However, there were issues with the entry waypoint being off the direct track IGARI to BITOD (to the south-east) and this resulted in the 'aircraft' being in a slight right bank when overflying the waypoint and then starting the left turn. This would have increased the time to make the left turn as the 'aircraft' had to roll through level, before rolling west.

c) The 'aircraft' could also make the turn and achieve a closer time to the recorded radar data with the autopilot disengaged and manually flown (Session 5 was closest with 2 minutes 10 seconds to wings-level and 2 minutes and 40 seconds to the exit waypoint).

d) Again, there were issues with the positioning of the entry and exit waypoints as they were not aligned (i.e. not 180° apart) leaving a short straight segment before the 'aircraft' intersected the exit waypoint.

e) Summary of 6 Simulator Re-enactment Sessions and Common Factors

Based on the six simulator re-enactment sessions conducted as summarised in *Table 2.1G* (below) and on the common factors in *Table 2.1H* (below), the Team concluded the following:

i) The turn would have been carried out with the autopilot disengaged, as it was not possible to achieve a turn time of 2 minutes and 10 seconds (as suggested by recorded data) using autopilot. The manoeuvre can be performed by a single pilot. The Team also noted that the aircraft's flight path from after the turn was consistent with the navigation being set to LNAV and/or heading mode, following published and/or manual waypoints that are not normally used with normal route (published airways between Kota Bharu and Penang).

Re-enactment	**Session**					
	1	**2**	**3**	**4**	**5**	**6**
Ground Speed (in knots)	475	475	425	400	475	425
Autopilot Engaged	✓	✓	✓	✓	x	X
Additional Waypoint	x	x	X	N05.15.6 E100.27.5	✓	✓
Bank angle (in degrees)	26º	26º	28º	23º	30-32º	35º
Exit Waypoint Time	Over-Shooting	2 min 45 sec	3 min 3 sec	3 min 30 sec	2 min 40 sec	2 min 28 sec

Table 2.1G - Re-enactment Sessions

Common Factors		
1.	Fuel	41,200 kg
2.	Gross Weight	215,410 kg
3.	Height	35,000 ft
4.	Entry Point	N07.05.7º E103.47.1º
	Exit Point	N07.12.7º E103.38.7º
5.	Autothrottle Engaged	

Table 2.1H - Common Factors

ii) From the data it was determined that the 'aircraft' was on heading mode that varied from 239º to 255º as it flew to the south of Penang where it continued westerly to Waypoint MEKAR where it finally disappeared completely at 1822:12 UTC [0222:12 MYT], about 10 nautical miles north of MEKAR.

iii) Based on the Team's review of the Military recorded radar display and printout, the aircraft's flight path could not be determined, and there is no evidence of rapid altitude and/or speed changes to indicate that MH370 was evading radar.

iv) Without further evidence, the reason for the transponder information from the aircraft ceasing could not be determined;

v) It is determined that only the transponder signal of MH370 ceased from the ATC Controller display whilst displays from other aircraft were still available; and

vi) There is also no evidence to suggest that the aircraft was flown by anyone other than the designated MAS pilots. However, the Team does not exclude the possibility of intervention by a third party.

8) Session 7 – Recreating the Right Turn South of Penang Island

Initial conditions

Fuel	36,000 kg
Gross weight	210,200 kg
Height	35,000 ft
Speed	IAS294 (525 knots groundspeed) M0.86 Note: A tailwind of 30 knots was needed to achieve this
Simulator setup	SPD/LNAV/VNAV, autopilot engaged, autothrottle engaged.
Entry waypoint	N05.15.6 E100.27.5
Exit waypoint	N05.12.0 E100.01.5

Table 2.1I - Data Input for Session 7

To get the 'aircraft' to track correctly (*Table 2.1I* [above]), both the entry and exit waypoints were entered, without a track between them in the FMC. The 'aircraft' was flown on heading mode to turn gently to intercept the exit waypoint.

The simulation commenced before the entry waypoint. Once crossing the waypoint, a heading change to the right was initiated to achieve a bank-angle of 5°. During the turn, the bank-angle was increased to a maximum of 10°. The exit waypoint was easily intercepted at 3 minutes and 5 seconds (the recorded radar time was 3 minutes). No further simulations were done on this turn.

2.1.2 Ho Chi Minh Air Traffic Services Operations

Based on the on-site interviews and briefing from the Team's visit to the Office of the Vietnamese Civil Aviation Authority in Ho Chi Minh City, it was noted that the radar position symbol for MH370 dropped from the radar display at 1720:59 UTC (0120:59 MYT). MH370 had not reached waypoint BITOD which is 37 nm from waypoint IGARI and based on the aircraft speed of 480 kt, it would take approximately five minutes for MH370 to travel from IGARI to BITOD.

The Direct Line Coordination Communication transcripts between KL ACC and Ho Chi Minh ACC suggested that there were uncertainties on the position of the aircraft. This could come about from the level of understanding of the English language. The HCM Duty Controller also could not communicate effectively during the interviews and an interpreter was there to assist him.

Reference:

Ho Chi Minh radar data recording, page 33 to 41 and page 51 to 61 of the Direct Line Coordination Communication KL ACC Sector 3+5 Planner (*Appendix 1.18G*) transcripts between Kuala Lumpur ACC and Ho Chi Minh ACC)

SECTION 2 – ANALYSIS

2.2 AIR TRAFFIC SERVICES OPERATIONS

2.2.1 Review of Flight MH370 before its Disappearance

1) The MH370 from Kuala Lumpur to Beijing was a normal daily scheduled flight. It took off at 1642 UTC [0042 MYT].

2) There was no indication of any unusual operations prior to departure and during the flight until the last secondary radar position symbol was recorded by ATC at 1721 UTC [0121 MYT] as detailed in *Table 2.2A - Chronological of events before disappearance of MH370* below.

3) Preparation of the flight was in order from the time the Filed Flight Plan[29] (FPL) message was filed and transmitted 12 hours before the flight.

4) The flight crew reported on time for duty and there was no delay in the departure of the flight (*Figure 2.2C* [below] - *Departure message*).

5) There was also no report of any significant or unusual health-related issues for the flight and cabin crew.

6) The radiotelephony speech segments from the cockpit with KL ACC were determined from the voice analysis of the ATC radiotelephony communications recording to be that of the FO before take-off and the PIC after take-off.

7) The transfer of control was effected three minutes before the estimate for IGARI. There was no recording of transmission (voice or in written form) of KL ACC informing HCM ACC (via direct land line) when MH370 was transferred 3 minutes earlier than the estimate for the Transfer of Control Point (TCP).

Note:

Based on reconstruction *(Section 2.1)* of the flight profile conducted on the B777 simulator, the flight would be at waypoint IGARI one minute earlier than the original estimate of 1722 UTC [0122 MYT].

[29] Filed Flight Plan – The flight plan as filed with an ATS unit by the pilot or his designated representative, without any subsequent changes.

2.2.2 Chronology of ATC Events before the Disappearance of Flight MH370

No.	Time	Event	Remarks
1.	0444 UTC [1244 MYT]	Filed Flight Plan (FPL) of scheduled flight of MH370 transmitted at 070444 UTC [071244 MYT], about 12 hours earlier over the Aeronautical Fixed Telecommunications Network (AFTN).	As required under Annex 10, Volume II.
		Flight planned on ATS/RNAV Routes R208 IGARI M765 BITOD L637 TSN… ZBAA.	Filed Flight Plan (*Figure 2.2A*)
2.	1450 UTC [2250 MYT]	PIC of MH370 signed in for duty.	As per operational requirements.
3.	1515 UTC [2315 MYT]	FO of MH370 signed in for duty.	
		MAS Operations Despatch Centre (ODC) released flight.	
4.	1625:52 UTC [0025:52 MYT]	Airway clearance request to Lumpur Airways Clearance Delivery.	
5.	1625:52 UTC [0025:52 MYT]	Airway clearance request to Lumpur Airways Clearance Delivery.	.
6.	1627:31 UTC [0027:31 MYT]	Pushback and start-up clearance request to Lumpur Ground.	As per operational requirements.
7.	1640:31 UTC [0040:31 MYT]	Lumpur Tower cleared MH370 for take-off.	
8.	1642 UTC [0042 MYT]	MH370 departed from Runway Three Two Right KLIA.	Departure message (*Figure 2.2C*)
9.	1642:53 UTC [0042:53 MYT]	Lumpur Departure cleared MH370 to climb to FL180 and to cancel the Standard Instrument Departure (SID) clearance by tracking direct to waypoint (*Figure 2.2A*) IGARI.	Normal ATC practice for track shortening.

Table 2.2A - Chronology of ATC Events before the Disappearance of Flight MH370

cont…

2.2.2 Chronology of ATC Events before the Disappearance of Flight MH370 *(cont.)*

No.	Time	Event	Remarks
10.	1643:31 UTC [0043:31 MYT]	KL ACC Sector 3+5 coordinated with HCM ACC via direct land line the estimate of MH370 for waypoint IGARI at 1722 UTC on [0122 MYT], request flight level 350 and the assigned SSR Code 2157.	As per Letter of Agreement between Malaysia and Viet Nam. (*Appendix 1.1A*)
11.	1646:39 UTC [0046:39 MYT]	MH370 transferred to Lumpur Radar (Sector 3+5).	As per operational requirement.
12.	1646:58 UTC [0046:58 MYT]	Lumpur Radar (Sector 3+5) cleared MH370 to climb to FL250.	As per operational requirement.
13.	1650:08 UTC [0050:08 MYT]	Lumpur Radar (Sector 3+5) cleared MH370 to climb to FL350.	
14.	1701:17 UTC [0101:17 MYT]	MH370 reported maintaining FL350.	It was noticed that the PIC made the same statement of "*maintaining flight level three five zero'* twice at 1701:17 UTC [0101.17 MYT] and at 1707:56 UTC [0107:56 MYT].
15.	1707:56 UTC- [0107:56 MYT]	MH370 reported maintaining FL350.	• However, the Team did not find any significance of that statement spoken twice by PIC in a short interval of 6.39 minutes.

Table 2.2A - Chronology of ATC Events before the Disappearance of Flight MH370

cont…

2.2.2 Chronology of ATC Events before the Disappearance of Flight MH370 *(cont.)*

No.	Time	Event	Remarks
15. *cont.*	1707:56 UTC- [0107:56 MYT]	MH370 reported maintaining FL350.	• Also refer *para. 2.2.9 para 1) a) (1-6)* on Radiotelephony Readback on frequency changes for more details.
16.	1719:26 UTC [0119:26 MYT]	The KL ACC radar Controller transferred MH370 to HCM ACC by instructing MH370 to contact Ho Chi Minh on the VHF radio frequency 120.9 MHz.	• Transfer of control was effected 3 minutes before the estimate for IGARI. • KL ACC passed to HCM ACC estimate for IGARI as 1722 UTC. • Transfer of control to HCM ACC was effected at 1719 UTC before MH370 was over IGARI. • There was no arrangement between KL ACC and HCM ACC for an “electronic handoff” or other methods to hand over the radar picture.
17.	1719:30 UTC [0119:30 MYT]	MH370 responded with: “*Good night Malaysian Three Seven Zero”.*	Thereafter there was no further voice communication.

Table 2.2A - Chronology of ATC Events before the Disappearance of Flight MH370

2.2.3 Filed Flight Plan of MH370

```
KLA297 070444
FF WMKKZQZX WMKKZRZX
070441 WMKKYOYX
(FPL-MAS370-IS
-B772/H-SDFGHIJ3J5M1RWXY/LB1D1
-WMKK1635
-N0470F290 DCT PIBOS R208 IKUKO/M081F330 R208 IGARI M765
 BITOD/N0480F330 L637 TSN/N0480F350 W1 BMT W12 PCA G221
 BUNTA/N0480F370 A1 IKELA/N0480F370 P901 IDOSI/N0480F390 DCT CH
 DCT BEKOL/K0900S1160 A461 YIN/K0890S1130 A461 VYK
-ZBAA0534 ZBTJ ZBSJ
-PBN/A1B1C1D1L1O1S2 DOF/140307 REG/9MMRO EET/WSJC0032 VVTS0042

ZJSA0210 VHHK0233 ZGZU0304 ZHWH0356 ZPE0450 SEL/QRC RMK/ACASII
EQUIPPED)
```

Source: DCA Malaysia

Figure 2.2A - Filed Flight Plan of MH370

1) Message Code of FPL of MH370 and Meaning

Message Code	Meaning
KLA297 070444	
KL	*KLIA message*
A	*Series*
297	*Sequence Number*
070444	*Date-time-group or the transmission time of the filed flight plan message at 070444UTC*

FF WMKKZQZX WMKKZRZX	
FF	*Priority Indicator for the message category*
WMKKZQZX	*8-letter addressee for Lumpur "Area Control Centre".*
WMKKZRZ*X*	*8-letter addressee for Lumpur "Approach Radar Office".*

070441 WMKKYOYX	
070441	*Message Filling Time (in UTC)*
WMKKYOYX	*8-letter Message Originator for KLIA Aeronautical Information Office*

Field Type 3 - Message type, number and reference data	
(FPL	*Filed Flight Plan Message*
WMKKYOYX	*Message Originator Indicator i.e. KLIA Aeronautical Information Service Office.*

- Field Type 7- Aircraft Identification and SSR mode and code	
-MAS370	*Aircraft identification Malaysian 370*

-Field Type 8 - Flight rules and type of flight	
-I	*Instrument Flight Rules*
-S	*Status: - Scheduled Air Transport*

Field Type 9 - Number and type of aircraft and wake turbulence category	
-B772/H	*Boeing 777-200/wake turbulence category/Heavy*

Figure 2.2B - Message Code of Filed Flight Plan of MH370 and Meaning

cont…

1) Message Code of FPL of MH370 and Meaning (*cont...*)

Message Code	Meaning
Field Type 10 - Equipment and capabilities	
(a) **Radio communication, navigation and approach aid equipment and capabilities**	
-SDFGHIJ3J5M1RWXY/LB1D1	
-S	Equipped with: *Standard COM/NAV/approach aid equipment for the route is carried and serviceable. Standard equipment is considered to be VHF RTF, VOR and ILS.*
D	*DME*
F	*ADF*
G	*GNSS*
H	*HF RTF*
I	*Inertial Navigation*
J3	*CPDLC FANS 1/A VDL Mode 4*
J5	*CPDLC FANS 1/A SATCOM (INMARSAT)*
M1	*ATC RTF SATCOM (INMARSAT)*
R	*PBN approved.*
W	*RVSM approved*
X	*MNPS approved*
Y	*VHF with 8.33 kHz. channel spacing capability/*
(b) Surveillance equipment and capabilities	
L	*Transponder Mode S, including aircraft identification, pressure-altitude, extended squitter (ADS-B) and enhanced surveillance capability*
B1	*ADS-B with dedicated 1090 MHz ADS-B "out" capability*
D1	*ADS-C with FANS 1/A capabilities*
Field Type 13 - Departure aerodrome and time	
-WMKK1635	*-Departure aerodrome KLIA estimated off-block time 1635 UTC*

Figure 2.2B - Message Code of Filed Flight Plan of MH370 and Meaning

cont…

1) Message Code of FPL of MH370 and Meaning (*cont...*)

Message Code	Meaning
Field Type 15 – Route	
-N0470F290 DCT PIBOS R208 IKUKO/M081F330 R208 IGARI M765 BITOD/N0480F330 L637 TSN/N0480F350 W1 BMT W12 PCA G221 BUNTA/N0480F370 A1 IKELA/N0480F370 P901 IDOSI/N0480F390 DCT CH DCT BEKOL/K0900S1160 A461 YIN/K0890S1130 A461 VYK	
-airspeed 470 knots requested flight level 290 - the flight will proceed direct to waypoint PIBOS joining Airway R208 and to waypoint IKUKO, thence the airspeed will be Mach 0.81 flight level 330 on Airway R208 to waypoint IGARI joining Airway M765 thence to waypoint BITOD. Thence the airspeed will be 480 knots and flight level 330 on Airways L637 and proceed to TSN (Tansonnhat), thence the airspeed will be 480 knots and flight level 350. Thence on Airway W1 to BMT (Buon Ma Thout), thence Airway W12 to PCA (Phu Cat), thence on Airway G221 to waypoint BUNTA, thence airspeed will be 480 knots and flight level 370, thence proceed via Airway A1 to waypoint IKELA, thence airspeed will be 480 knots and flight level 370, thence via Airway P901 to waypoint ISODI, airspeed 480 knots and flight level 390. Thence track direct to CH (Cheung Chau), and direct to waypoint BEKOL. Thence the airspeed will be 900 kilometres per hour and level 11600 meters on Airway A461, thence to YIN (Yingde). Thence, the airspeed will be 890 kilometres per hour and level 11300 metres on Airway A461 to VYK (Dawangzhuang).	
Field Type 16 - Destination aerodrome and total estimated elapsed time, destination alternate aerodrome(s)	
-ZBAA0534 ZBTJ ZBSJ	
-Destination aerodrome ZBAA - Beijing Capital International Airport and total estimated elapsed time 5 hours and 34 minutes *Destination alternate aerodrome(s)* *ZBTJ* - Tianjin Binhai International Airport, and *ZBSJ* - Shijiazhuang Zhengding International Airport	

Figure 2.2B - Message Code of Filed Flight Plan of MH370 and Meaning

cont...

1) Message Code of FPL of MH370 and Meaning (*cont...*)

Message Code	Meaning
Field Type 18 – Other information	
PBN/A1B1C1D1L1O1S2 DOF/140307 REG/9MMRO EET/WSJC0032 VVTS0042 ZJSA0210 VHHK0233 ZGZU0304 ZHWH0356 ZBPE0450 SEL/QRC RMK/ACASII EQUIPPED)	
PBN	*Performance Based Navigation/Indication of RNAV and or RNP capabilities.*
	RNAV Specifications
A1	*RNAV 10 (RNP 10)*
B1	*RNAV 5 all permitted sensors*
C1	*RNAV 2 all permitted sensors*
D1	*RNAV 1 all permitted sensors*
	RNP Specifications
L1	*RNP 4*
O1	*Basic RNP 1 all permitted sensors*
S2	*RNP APCH with BARCO-VNAV*
DOF/140307	*Date of flight/2014 March 7th*
REG/9MMRO	*Aircraft registration 9MMRO*
EET	FIR boundary designators and accumulated *estimated elapsed times from take-off to such FIR boundaries.* *Singapore FIR 32 minutes* *Ho Chi Minh FIR 42 minutes* *Sanya FIR 2 hours 10 minutes* *Hong Kong FIR 2 hours 33 minutes* *Guangzhou FIR 3 hours 4 minutes* *Wuhan FIR 3 hours 56 minutes* *Beijing FIR 4 hours 50 minutes*
SEL/QRC	*Selective Calling code/QRC*
RMK/ACAS II EQUIPPED	*Equipped with ACAS II)*

Figure 2.2B - Message Code of Filed Flight Plan of MH370 and Meaning

2.2.4 Departure Message of MH370

Legal Recording ATS-Message

Type: DEP Priority: FF
Originator: WMFDYFYX Operator: 1A
Filing Time: 071642 Last Stordate: 14-03-07 16:42
Legal Recording Informations:
Date: 14-03-07 16:42:44 Action: Creation

ATS Message

(DEP-MAS370/A2157-WMKK1642-ZBAA-DOF/140307)

End of Report

Source : Dca Malaysia

Figure 2.2C - Departure Message of MH370

1) Message Code of Departure Message of MH370 and Meaning

Message Code	Meaning
(DEP	(Departure
-MAS370/A2157	-Aircraft identification MH370/Secondary Surveillance Radar Code A2157
-WMKK1642	-KLIA1642 (UTC)
-ZBAA	-destination aerodrome: Beijing/Capital
-DOF140307)	-Date of flight 2014March07)

Figure 2.2D - Message Code of Departure Message of MH370 and Meaning

2.2.5 Waypoints - Geographical Coordinates (LAT/LONG) of MH370 Filed Flight Plan

No.	WAYPOINT	LAT	LONG	AIRWAY
1.	PIBOS	N0320.5	E10203.1	R208
2.	IKUKO	N0545.2	E10313.4	R208
3.	IGARI	N0656.2	E10335.1	R208
4.	BITOD	N0715.4	E10407.1	M765
5.	TSN	N1049.0	E10638.7	L637
6.	BMT	N1240.0	E10807.4	W1
7.	PCA	N1357.4	E10902.5	W12
8.	BUNTA	N1650.0	E10923.7	G221
9.	IKELA	N1839.7	E11214.7	A1
10.	IDOSI	N1900.0	E11230.0	P901
11.	CH	N2213.2	E11401.8	DCT
12.	BEKOL	N2232.5	E11408.0	DCT
13.	YIN	N2411.4	E11324.9	A461
14.	VYK	N3911.7	E11634.3	A461

Table 2.2B - Waypoints of MH370 FPL

2.2.6 Analysis on FPL Message of MH370

1) The MH370 FPL had been filed in accordance with the Doc 4444 ATM/501, Procedures for Air Navigation Services - Air Traffic Management (PANS-ATM).

2) However, there are two airways designated as A1/P901 within Hong Kong Flight Information Region (FIR) which required examination. Both airways (A1 and P901) are within the Hong Kong FIR, and have the same alignment and share the same waypoints. The waypoints are IKELA, IDOSI and CH (CHEUNG CHAU). The differences between the two airways are the lower limits and upper limits. The lower limit of A1 is 8,000 ft, and the upper limit is FL285 whereas the lower limit of P901 is FL285 and upper limit unlimited.

Note:

Refer to the following for details:

- *Figure 2.2E* (below) - *Route Segment of ATS Route A1 and Performance Based Navigation (PBN) Route P901;* and

- *Figure 2.2F* (below) - *Longitudinal Cross Section of ATS Route A1 and PBN Route P901*

3) It is observed that the fifth group of alphabet/number, written as ZPE0450, in line 13th of the FPL message of MH370 should read ZBPE0450. However, the missing alphabet B from the original text message does not invalidate the FPL.

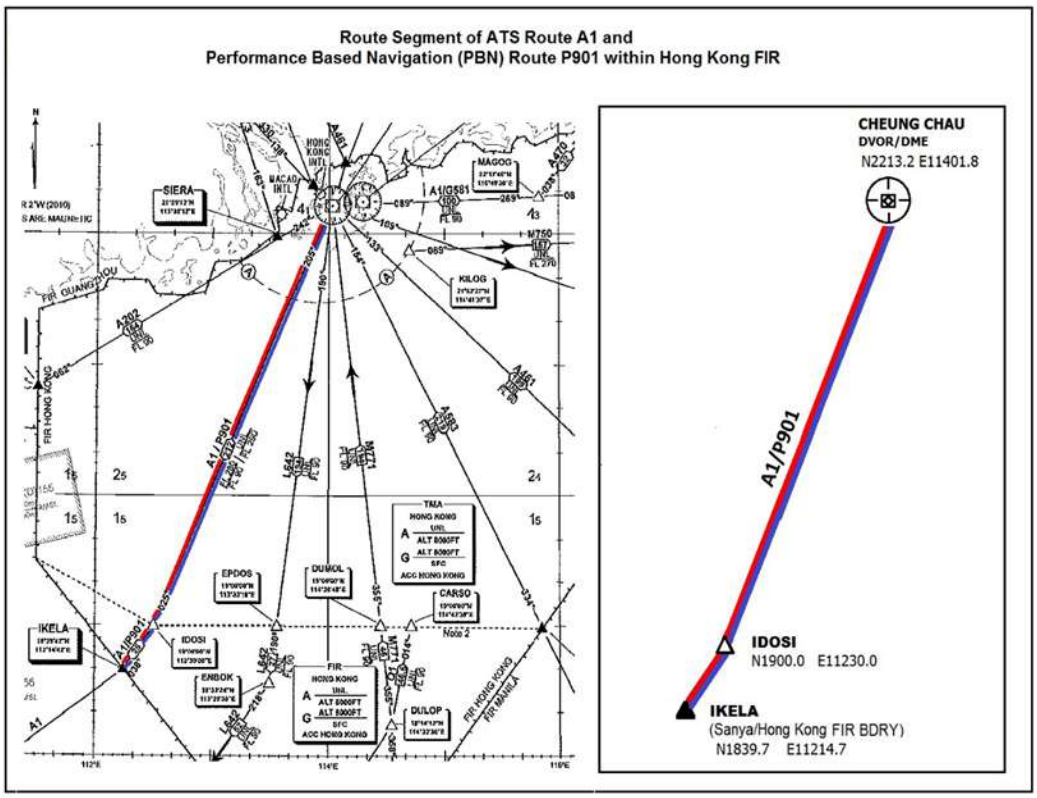

Figure 2.2E - Route Segment of ATS Route A1 and PBN Route P901

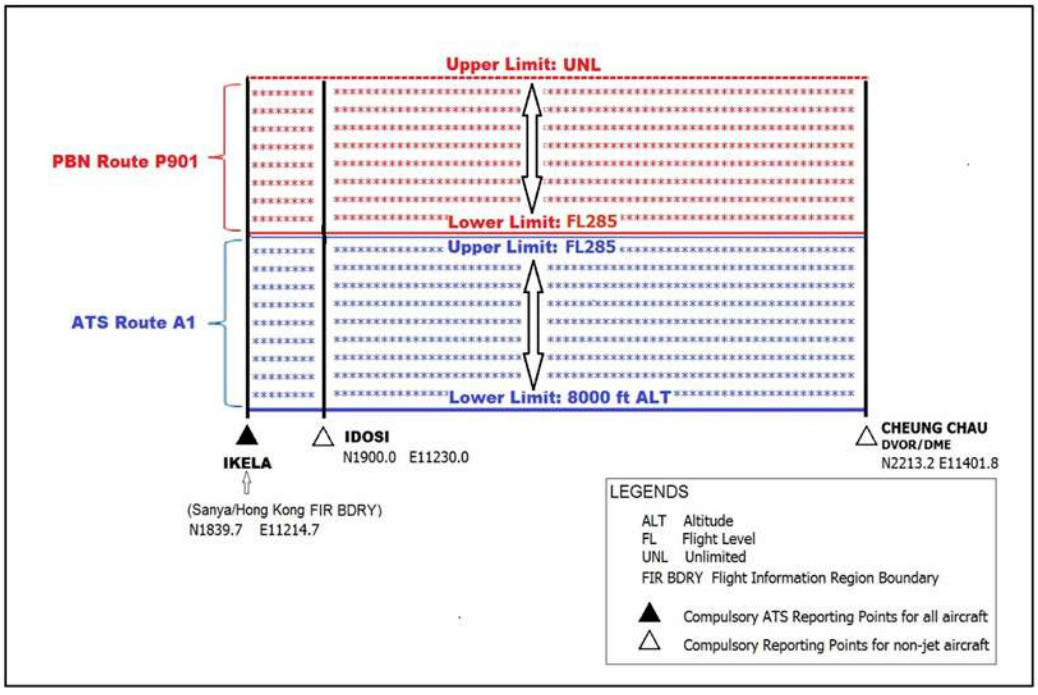

Figure 2.2F - Longitudinal Cross Section of ATS Route A1 and PBN Route P901

2.2.7 Chronology of ATC Events following the Disappearance of MH370 (*Table 2.2C*, below)

No.	Time	Event
1.	1720:31 UTC [0120:31 MYT]	Radar recording showed MH370 passed over waypoint IGARI.
2.	1720:36 UTC [0120:36 MYT]	Mode S radar symbol of MH370 dropped off from radar display.
3.	1721:13 UTC [0121:13 MYT]	3.2 nm after passing IGARI, SSR radar position symbol of MH370 dropped off from radar display. Two radar sources, from Viet Nam and Thailand respectively, captured the disappearance of the radar position symbol of MH370 vis-à-vis Bangkok radar target drop at 1721:13 UTC [0121:13 MYT] and Viet Nam's at 1720:59 UTC [0120:59 MYT].
4.	1739:03 UTC [0139:03 MYT]	HCM ACC queried KL ACC on whereabouts of MH370 and informed KL ACC that verbal contact with MH370 was not established and the radar target was last seen at waypoint BITOD. Note: MH370 did not arrive over waypoint BITOD (Refer to *Item 3* above).
5.	1741:22 UTC [0141:22 MYT]	HCM ACC enquired for information on MH370. KL ACC informed HCM ACC that after waypoint IGARI, MH370 did not return to Lumpur radar frequency.
6.	1741:23 UTC [0141:23 MYT]	KL ACC Radar Controller made a 'blind transmission'[30] to MH370.
7.	1746:47 UTC [0146:47 MYT]	HCM ACC queried on MH370 again, stating that radar contact was established at IGARI but there was no verbal contact. HCM ACC advised that the observed radar blip disappeared at waypoint BITOD. HCM ACC also stated that efforts had been made to establish communications by calling MH370 several times for more than twenty minutes.

Table 2.2C Chronology of ATC Events following the Disappearance of MH370

cont…

[30] Blind transmission - A transmission from one station to another station in circumstances where two-way communications cannot be established but where it is believed that the called station is able to receive the transmission.

2.2.7 Chronology of ATC Events following the Disappearance of MH370 (*Table 2.2C*, below)

No.	Time	Event
8.	1750:28 UTC [0150:28 MYT]	KL ACC queried HCM ACC if there was any contact with MH370. HCM ACC's reply was: "*Negative*".
9.	1757:49 UTC [0157:49 MYT]	HCM ACC informed that there was officially no contact with MH370 until this time. Attempts on many frequencies and aircraft in the vicinity received no response from MH370.
10.	1803:48 UTC [0203:48 MYT]	KL ACC queried HCM ACC on status of MH370. HCM ACC confirmed there was no radar contact at this time and no verbal communications was established. KL ACC relayed the information received from Malaysia Airlines Operations that aircraft was in Cambodian airspace.
11.	1807:47 UTC [0207:47 MYT]	HCM ACC queried for confirmation that MH370 was in Phnom Penh FIR as Phnom Penh did not have any information on MH370. KL ACC indicated it would check further with the supervisor.
12.	1812:15 UTC [0212:15 MYT]	KL ACC informed HCM ACC that there was no update on status of MH370.
13.	1815 UTC [0215 MYT]	Extract from Watch Supervisor Log Book (in written form only, no voice recording): *KL ATSC WS queried Malaysia Airlines Operations who informed that MH370 was able to exchange signals with the Flight Explorer.*
14.	1818:50 UTC [0218:50 MYT]	KL ACC queried if flight planned routing of MH370 was supposed to enter the Cambodian airspace. HCM ACC confirmed that planned route was only through the Vietnamese airspace. HCM ACC had checked and Cambodian had advised that it had no information on or contact with MH370. HCM ACC confirmed earlier information that radar contact was lost after BITOD and radio contact was never established.
15.	1833:59 UTC [0233:59 MYT]	KL ACC Radar Controller enquired with MAS Operations Despatch Centre (ODC) on communications status on MH370. Personnel was not sure if the message went through successfully. ODC informed that aircraft was still sending movement message indicating it was somewhere

Table 2.2C - Chronology of ATC Events following the Disappearance of MH370

cont...

2.2.7 Chronology of ATC Events following the Disappearance of MH370 (*Table 2.2C*, below)

No.	Time	Event
15. *cont..*	1833:59 UTC [0233:59 MYT]	in Viet Nam, and that its last position was at coordinates N14.90000 E109 15500 at 071833 UTC [080233 MYT].
16.	1834:56 UTC [0234:56 MYT]	HCM ACC queried on the status of MH370 and was advised that the Watch Supervisor was talking to the Company at this time.
17.	1854:28 UTC [0254:28 MYT]	Requested MH386, which was then in the HCM FIR, to try to establish contact with MH370 on emergency frequencies.
18.	1930 UTC [0330 MYT]	Extract from KL ACC Watch Supervisor ATS logbook: *MAS Operations Centre informed KL ACC that the flight tracker was based on flight projection and not reliable for aircraft positioning.*
19.	1930:03 UTC [0330:03 MYT]	KL ACC queried if HCM ACC had checked with next FIR HAINAN.
20.	1948:52 UTC [0348:52 MYT]	KL ACC queried if HCM ACC had checked with the SANYA FIR. HCM ACC informed KL ACC that there was no response until then.
21.	1956:13 UTC [0356:13 MYT]	KL ACC queried MAS Operations Centre for any latest information or contact with MH370.
22.	2025:22 UTC [0425:22 MYT]	HCM ACC Supervisor queried KL ACC on the last position that MH370 was in contact with KL ACC.
23.	2109:13 UTC [0509:13 MYT]	Singapore, on behalf of Hong Kong ACC enquired for information on MH370.
24.	2118:32 UTC [0518:32 MYT]	HCM ACC queried for information on MH370, KL ACC queried if any information had been received from Hong Kong or Beijing.
25.	2120:16 UTC [0520:16 MYT]	Capt. *xxxx* [*name redacted*] of MAS requested for information on MH370. He opined that based on known information,"*MH370 never left Malaysian airspace*."
26.	2130 UTC [0530 MYT]	Duty ATSC Watch Supervisor activated the Kuala Lumpur Aeronautical Rescue Coordination Centre (ARCC).

Table 2.2C - Chronology of ATC events following the disappearance of MH370

cont...

2.2.7 Chronology of ATC Events following the Disappearance of MH370 (*Table 2.2C*, below)

No.	Time	Event
27.	2214:13 UTC [0614:13 MYT]	KL ACC queried HCM ACC if SAR was activated.
28.	2232 UTC [0632 MYT]	KL ARCC issued a *DETRESFA* message.

Table 2.2C - Chronology of ATC Events following the Disappearance of MH370

2.2.8 ATS Operational Issues after Last Radio Communication with MH370 and subsequent ATS Activities/Actions

The following analysis are based on the ICAO Doc 4444 ATM/501, Procedures for Air Navigation Services - Air Traffic Management (PANS-ATM), Annex 11 - Air Traffic Services, Aeronautical Information Publication, MATS and MATS Vol 2 Malaysia. Operation Letter of Agreement between DCA Malaysia and Viet Nam Air Traffic Management (effective 1 November 2011/, Letters of Operational Agreement Malaysia - Singapore dated August 1984 DCA/SAR01-84/Doc 04 (a).

They also include the Chronology of events following the disappearance of MH370, as tabulated above (*Table 2.2A)*, the Team had gathered these operational issues regarding activities/actions taken by KL ACC, HCM ACC and others as follows:

No.	Operational Issues
1.	Transfer of Control Point[31] at Waypoint IGARI
2.	Responsibilities of Accepting Air Traffic Control Service Unit on 'Establishment of Communications'
3.	Marking of MH370 Flight Progress Strips[32]
4.	Responsibilities of Air Traffic Controller
5.	Recognising Emergency Situations and ATC Actions

[31] Transfer of Control Point - A defined point located along the flight path of an aircraft at which the responsibility for providing air traffic control service to the aircraft is transferred from one control unit or control position to the next.

[32] Flight Progress Strip - It contains essential flight and control data and is the basic tool which enables Controllers to visualize the disposition of traffic within their area of responsibility including traffic arriving and departing an aerodrome, assess conflicts and control aircraft in a safe manner.

cont..

No.	Operational Issues
6.	Information to be passed to other Radar Stations - Civil and Military
7.	Provision of Alerting Service by an ATSU for flights operated through more than one FIR and ATC actions
8.	Actions taken by Duty ATSC Watch Supervisor
9.	Flight-following System of Malaysia Airlines
10.	Communications Exchanges between KL ACC and HCM ACC, and KL ACC and Malaysia Airlines Operations Centre on MH370
11.	Delegation of Airspace from Singapore ACC to KL ACC
12.	ATC Actions on Strayed/Unidentified Aircraft (Primary Radar Target) within Area of Responsibility
13.	KL ATSC Duty Shift System for Air Traffic Controllers
14.	Roles played by the ATSC Duty Watch Supervisor
15.	Activation of Aeronautical Rescue Coordination Centre
16.	Playback of Radar and Radio Telephony Recordings by Duty ATSC Watch Supervisor
17.	Entries in Air Traffic Services Logbooks of ATSC Duty Watch Supervisor and Sector 3 Controller Working Position
18.	Distress Message
19.	Issues with the Manual of Air Traffic Services

1) Analysis of ATS Operational Issues ~~a~~fter Last Radio Communication with MH370 and subsequent Activities/Actions taken

a) Transfer of Control Point at Waypoint IGARI

i) The MH370 flight from Kuala Lumpur to Beijing was planned on ATS/RNAV Routes R208 IGARI M765 BITOD L637 TSN…ZBAA. About one and a half minutes after MH370 took off at 1642 [0042 MYT], KL ACC conveyed to HCM ACC via the direct land line the estimate for waypoint IGARI as 1722 UTC [0122MYT], and requested Flight Level three five zero and Squawk two one five seven. HCM ACC acknowledged: "*two one five seven, three five zero is approved, one seven two two*".

ii) The Transfer of Control Point (TCP) for flights on route R208 IGARI M765 BITOD L637 TSN…ZBAA is IGARI. Aircraft operating on this route shall be transferred by KL ACC to HCM ACC when the Radar Controller observes on the radar display that the aircraft is over IGARI or when the aircraft reports over IGARI.

iii) The transfer of control by KL ACC to HCM ACC is by way of instructing the aircraft concerned on the control VHF (very high frequency) radio frequency 132.5 MHz to contact HCM ACC on VHF radio frequency 120.9 MHz. The ATS infrastructure in KL ACC was not equipped to perform an "electronic handoff" of aircraft or other method to hand over the radar picture to HCM ACC.

References:

MATS Vol. 2, Part 2 KL ATSC - Coordination, para. 3.5.8, page 2-3-53 Coordination between Sector 5 Position and HCM ACC dated 15 March 2013 (*Table 2.2E)* as shown below.

The LOA (*Appendix 1.1A*) between DCA Malaysia and Vietnam Air Traffic Management dated 18 July 2001 and effective on 01 November 2001, para Transfer of Control Point *(Table 2.2D* [below]*),* page 7, as below:

Co-ordination Procedures

Transfer of Control Point

Route	TCP
M765	IGARI (065612N 1033512E)
N891	
R208 / M765	

Table 2.2D - Coordination Procedures

3.5.8 Coordination Between Sector 5 and Ho Chi Minh ACC

Sector 5's Actions				
Destination	Route	Pass EST for	Transfer To	Transfer At
Entering Ho Chi Minh FIR	R208 (E)	IGARI	Ho Chi Minh Sector 3	IGARI
	M765 (E)			
	N891 (N)			

Ho Chi Minh ACC's Actions				
Destination	Route	Pass EST for	Transfer To	Transfer At
Entering Kuala Lumpur FIR/AOR	M765 (W)	IGARI	Lumpur Sector 5	IGARI
	N891 (S)			

3.5.9 Coordination Between Sector 5 and Singapore ACC

Sector 5's Actions				
Destination	Route	Pass EST for	Transfer To	Transfer At
Entering Singapore FIR	N891 (S)	IGARI	Singapore Sector 3	IKUMI
	M904 (S)	TIDAR		A/Beam IKUMI

Singapore ACC's Actions				
Destination	Route	Pass EST for	Transfer To	Transfer At
Entering Kuala Lumpur FIR	N891 (N) N891 (S)	IGARI	Lumpur Sector 5	IKUMI
	M904 (N)	A/Beam IKUMI		A/Beam IKUMI

Table 2.2E - Coordination between Sector 5 and Ho Chi Minh ACC

(1) The Transfer of Control Point as stated in the Doc 4444 Chapter 10 - Coordination, paragraph, 10.1.2.2, page 10-3 dated 10/11/16 is as follows:

10.1.2.2.1 The responsibility for the control of an aircraft shall be transferred from the ATC unit to the next unit at the time of crossing the common control area boundary as determined by the unit having control of the aircraft or at such other point or time as has been agreed between the two units.

10.1.2.2.2 Where specified in letters of agreement between the ATC units concerned, and when transferring an aircraft, the transferring unit shall notify the accepting unit that the aircraft is in position to be transferred, and specify that the responsibility for control should be assumed by the accepting unit forthwith at the time of crossing the control boundary or other transfer control point specified in letters of agreement between the ATC units or at such other point or time coordinated between the two units.

10.1.2.2.3 If the transfer of control time or point is other than forthwith, the accepting ATC unit shall not alter the clearance of the aircraft prior to the agreed transfer of control time or point without the approval of the transferring unit.

10.1.2.2.4 If transfer of communication is used to transfer an aircraft to a receiving ATC unit, responsibility for control shall not be assumed until the time of crossing the control area boundary or other transfer of control point specified in letters of agreement between the ATC units.

(2) KL ACC transferred MH370 to HCM ACC by instructing MH370 to contact Ho Chi Minh on the VHF radio frequency 120.9 MHz at 1719:26 UTC [0119:26 MYT].

(3) MATS Vol. 2, Part 2 KL ATSC and Operational Letter of Agreement between DCA Malaysia and Viet Nam Air

Traffic Management do not have provision for KL ACC to effect transfer of communication of an aircraft to HCM ACC. It is noted that MH370 was transferred to HCM ACC three minutes before the Transfer of Control Point.

(4) The recorded landline communications between KL ACC and HCM ACC suggested that there were confusions on the position of MH370. This was evident when HCM ACC requested KL ACC for information on MH370 at 1739:06 UTC [0139:06].

(5) The following timings were based on recordings vis-à-vis landline/radiotelephony communications and radar recording:

(a) 1643 UTC - KL ACC passed MH370's estimated time over IGARI at 1722 UTC to Ho Chi Minh ACC.

(b) 1719:26 UTC - MH370 was instructed by KL ACC to contact Ho Chi Minh ACC.

(c) 1719:30 UTC - MH370 acknowledged.

(d) 1720:31 UTC - MH370 passed over IGARI.

From the above timings, it is evident that there was a 3-minute lapse from the time MH370 was instructed to HCM ACC and the original estimate.[33]

(6) Radiotelephony Readback

(a) Readback Messages

MATS Part 10 - COM, page 10-3-3 para 3.4.4 states that:

Pilots are required to read back in full messages containing any of the following:

a) Level instructions;

b) Heading instructions;

c) Speed instructions;

d) Airways or route clearances;

[33] See *Table 2.2A* – Chronology of ATC Events before the Disappearance of Flight MH370 for detailed timeline plot.

e) Runway in use;

f) Clearance to enter, land on, take-off, backtrack, cross or hold short of an active runway;

g) SSR operating instructions;

h) Altimeter settings;

i) Frequency Changes

(b) Readback on Frequency Changes

Annex 11 - Air Traffic Services, page 3-7 para 3.7.3 states:

Readback of clearances and safety-related information.

3.7.3.1 The flight crew shall read back to the Air Traffic Controller safety-related parts of ATC clearances and instructions which are transmitted by voice. The following items shall always be read back:

a) ATC route clearances;

b) clearances and instructions to enter, land on, take-off from, hold short of, cross and backtrack on any runway; and

c) runway-in use, altimeter settings, SSR codes, level instructions, heading and speed instructions and, whether issued by the Controller or contained in ATIS broadcasts, transition levels.

3.7.3.1.1 Other clearances or instructions, including conditional clearances, shall be read back or acknowledged in a manner to clearly indicate that they have been understood and will be complied with.

(c) Doc 4444 Air Traffic Management (PANS-ATM) Pages 4-8 para 4.5.7.5 states that:

4.5.7.5.1 The flight crew shall read back to the Air Traffic Controller safety-related parts of ATC clearances and instructions which are

transmitted by voice. The following items shall always be read back:

a) ATC route clearances;

b) clearances and instructions to enter, land on, take-off from, hold short of, cross and backtrack on any runway; and

c) runway-in-use, altimeter settings, SSR codes, level instructions, heading and speed instructions and, whether issued by the Controller or contained in automatic terminal information service (ATIS) broadcasts, transition levels.

4.5.7.5.1.1 Other clearances or instructions, including conditional clearances, shall be read back or acknowledged in a manner to clearly indicate that they have been understood and will be complied with.

(d) Pilot's Readback on Frequency Changes

MATS clearly stipulates that pilots are required to read back radio frequency changes. Similarly, ICAO Annex 11 and ICAO Doc 4444 also stipulate that:

"other clearances or instructions shall be read back or acknowledged in a manner to clearly indicate that they have been understood and will be complied with".

At 1719:26 UTC KL ACC had instructed MH370 to contact Ho Chi Minh on radio frequency one two zero decimal nine (120.9). MH370 was therefore required to read back the frequency change as an acknowledgment and thereby had complied with the instruction. There was no readback from MH370.

There were altogether five instances where MH370 had to change radio frequencies when transferred from an ATC unit to another. They are as follows:

- From Airways Clearance Delivery to Lumpur Ground (*Note 1*, below);

- From Lumpur Ground to Lumpur Tower (*Note 2* below);
- From Lumpur Tower to Lumpur Approach (*Note 3* below);
- From Lumpur Approach to Lumpur Radar (Sector 3+5) [*Note 4* below]; and
- From Lumpur Radar (Sector 3+5) to Ho Chi Minh (*Note 5*, below).

Note 1

When Airways Clearance Delivery transferred MH370 to Lumpur Ground, the radio frequency of Lumpur Ground was not mentioned by the ATC. MH370 responded by transmitting *"Good day sir."*

Note 2

When Lumpur Ground transferred MH370 to Lumpur Tower, the Lumpur Tower radio frequency was transmitted by the Controller even though it was unintelligible in the RT recording, MH370 read back the radio frequency, *"One one eight eight Malaysian Three Seven Zero thank you."*

Note 3

When Lumpur Tower transferred MH370 to Lumpur Approach Control, ATC transmitted the take-off clearance, no radio frequency was included in the take-off clearance and the pilot read back the take-off clearance, *"Three Two Right clear for take-off Malaysian Three Seven Zero thank you bye."*

Note 4

When Lumpur Approach Control transferred MH370 to Lumpur Radar (Sector 3+5), the Sector 3+5 radio frequency was transmitted by Lumpur Approach Control and MH370 read back the radio frequency, *"Night one three two six Malaysian err… Three Seven Zero".*

Note 5

When Lumpur Radar (Sector 3+5) transferred MH370 to Ho Chi Minh, the radio frequency of Ho Chi Minh was transmitted by Lumpur Radar (Sector 3+5), MH370 responded with *"Good night Malaysian Three Seven Zero",* the radio frequency of Ho Chi Minh was not read back by MH370.

There were two instances when radio frequency was not included in the ATC instructions and three instances when radio frequency was included in the ATC instructions, MH370 had read back the radio frequency on two of the instances but did not on the last radio transmission. The Team could not conclude any reason for the absence of the read-back at this stage of the flight but noted that it was not consistent with the previous frequency changes.

(e) Maintaining FL350 Transmitted Twice

At 1701:17 UTC [0101:17 MYT] MH370 made a radio transmission: "*Maintaining flight level three five zero three seven zero"* and again at 1707:56 UTC [0107:56 MYT].

The MAS Standard Operating Procedures (SOPs) for flight crew dictated that the PIC and the FO would have to be on-seat during the following phrases of flight:

- Take-off;
- Climbing and descending; and
- Approach and landing.

However, one of the flight crew could leave the cockpit for a break once the aircraft had maintained the assigned cruising level.

The voice recognition process (*para 1.5.11*) has established that the PIC made the radio transmission of *maintaining flight level three five zero* at 1701:17 UTC [0101:17 MYT] and again at 1707:56 UTC [0107:56 MYT].

The interval between the first and second radio transmission was 6 minutes and 39 seconds.

Repetition of radiotelephony communications happens occasionally. While the Team could not determine the reason for the additional transmission at this stage of the flight, it was noted that it was anomalous at this time.

b) Responsibilities of Accepting Air Traffic Control Service Unit on Establishment of Communications

i) The 3rd paragraph of page 11 of the LOA between DCA Malaysia and Viet Nam Air Traffic Management (*Appendix 1.1A*), titled Establishment of Communication states that:

a. "*The accepting unit shall notify the transferring unit if two-way communication is not established within five (5) minutes of the estimated time for the TCP".*

ii) Since HCM ACC had earlier received from KL ACC MH370's estimate (as 1722 UTC [0122 MYT] for IGARI and also had not been able to establish two-way communication with the aircraft, HC ACC should have notified KL ACC by 1727 UTC [0127 MYT], i.e. 1722 UTC [0127 MYT] plus 5 minutes. Instead HCM only notified KL ACC at 1739 UTC [0139].

iii) The direct line coordination between KL ATCC Sector 3+5 Planner states that, at 1747:09 UTC [0147 MYT]. HCM ATCC informed KL ATCC that: "*we call him many times until na…more than 20 minutes."* This shows that HCM ATCC had commenced communication search for MH370 FROM 1727 UTC [0127 MYT].

iv) At 1757:51 [0157:51 MYT], HCM ATCC again informed KL ATCC: "*Yes sir, we officially no contact from Malaysian Three Seven Zero until now and we try on many frequencies and all the aircraft calling, no response from Malaysian Three Seven Zero."*

v) The 12 minutes lapse on the part of HCM ACC to notify KL ATCC could have come about by their actions to carry out

communication search and thereby had resulted in their failure to notify KL ATCC by 1727 UTC [0127 MYT.

Note

The 12 minutes interval is derived from the timings of the two-way radio communication recording between HCM ACC and KL ACC *(para 2.2.9 para. b) i)* above for details.

c) Marking on MH370 Flight Progress Strip

i) Two markings have been left out on the flight progress strip (FPS), *Figure 2.2G,* (below) of MH370:

(1) The actual time (1721) when MH370 passed over IGARI - FPS' Estimate IG (abbreviation for IGARI) 1722, and

(2) The transfer of control time (1719) on the FPS.

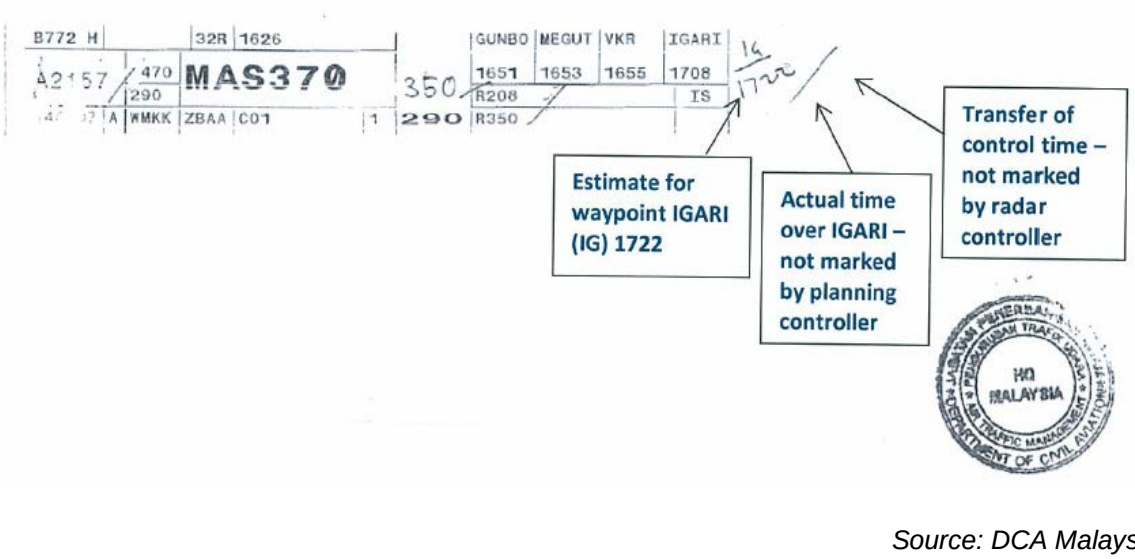

Source: DCA Malaysia

Figure 2.2G - Flight Progress Strip on MH370 from KL ACC

(3) Strip Marking on Flight Progress Strips

MATS Vol 2, Part 2 KL ATSC - General, page 2-1-8 para 1.4 dated 15 March 2009 and page 2-1-9 dated 15 March 2009 shows example of how the flight progress strip of a flight is marked.

Refer (below): *Figure 2.2H - Strip Marking on Flight Progress Strips generated by FDPS,* and *Figure 2.2I - Example on how the PLN strip will appear and Example on how the EXE strip will appear.*

Manual of Air Traffic Services — Part 2 KL ATSC – General

1.4 STRIP MARKING ON FLIGHT PROGRESS STRIPS (FPS) GENERATED BY FDPS

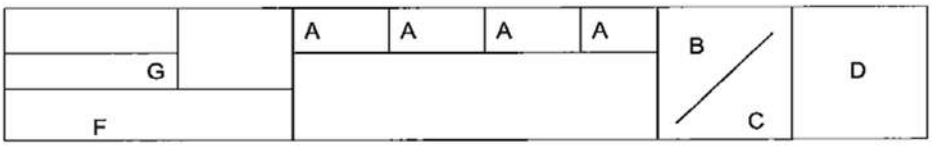

BOX	PLAN	EXE
A		Estimated time over fix
B	Estimated time over fix	Miscellaneous
C	Actual time over fix	
D	Flight level	
E	ATC restriction / requested level / lowest	
F	Level approved	
G	SSR code	

Note : The estimates in Box A are not necessarily accurate. PLN shall use Box B to write down the estimated time over a single fix whereas. EXE will write down the estimated time over the multiple fixes in Boxes A. The actual time over a fix will be reflected in PLN's Box C.

Example of a FPS generated by the FDPS

MAS 72	PE 000	PULIP	VKB	BASIR	IGARI		
	140	0056	0116	0121	0124		
1 / B747 / H		WMKK	G466/M765		VHHH		
IS N503 0045	330			PULIP 32R			

Department of Civil Aviation Malaysia — 2 - 1 - 8 — 15 March 2009

Figure 2.2H - Strip Marking on Flight Progress Strips generated by FDPS

MATS Vol 2, Part 2 KL ATSC - General, page 2-10-9 para contd. 1.4 dated 15 March 2009:

Example of how the PLN strip will appear

MAS 72	AR	**GUNBO**	**VKR**	**IKUKO**	**IGARI**	IGARI	
	140	**0107**	**0111**	**0115**	**0124**	0126 27	330
1/B747/H A2134		WMKK		R208	VHHH	27	~~270~~
IS N503 0045	270	RL330MAS84P10					

Box	Meaning
B	MAS 72 estimates IGARI 0126 and revised to 0127
C	MAS 72 passed IGARI 0127
D	MAS 72 was assigned FL270 initially and recleared FL330
E	Restriction for MAS 72 to depart 10 minutes after MAS 84
F	FL 270 has been approved by ACD
G	Transponder Code A 2134 was assigned by the FDP

Example of how the EXE strip will appear

MAS 73	AR	**IGARI**	**IKUKO**	**GUNBO**	**PIBOS**	IGARI	380
	150	**1010**	**1018**	**1026**	**1037**	1010	
1/B747/H A3003		VHHH	R208		WMKK		
IS N503 0045	380				PIBOS 32R	10	150

Box	Meaning
A	MAS 73 estimates IGARI 1010 IKUKO 1018 GUNBO 1026 PIBOS1037
B	MAS 73 passed over IGARI 1010
D	MAS 73 is at FL 380 and has been cleared down to FL 150

Figure 2.2I - Example on how the PLN strip will appear and Example on how the EXE strip will appear

Since the two recordings on the Flight Progress Strip for MH370 were not marked by the Air Traffic Controllers (Planner and Radar) KL ACC did not have the record of the time of the last radio contact and the actual time of MH370 passing over waypoint IGARI.

d) Responsibilities of Air Traffic Controllers

i) MATS Vol. 1, Part 1 - ADMIN, para 1.2.2, page 1-1-4, which states as below:

Air Traffic Controller is responsible:

- *for maintaining a continuous watch on their assigned communications channels or radar displays.* [Refer para. v) below].

ii) In interviews conducted with the Air Traffic Control Officer (ATCO) who was on duty on the night of the disappearance of MH370, the Sector 3+5 Radar Controller stated that he did not continuously monitor the progress of MH370 because he had to shift his focus to another area, viz. VPK[34] (approximately 214 nm south-southwest of IGARI), as there were four other flights over that area that required his attention.

iii) The radiotelephony transcripts of this sector confirmed that there were other four other flights - one at 1723 UTC [0123 MYT] proceeding to VPK and contacting Lumpur Radar and three others at 1726 UTC [0126 MYT], 1742 UTC [0142 MYT] and 1746 UTC [0146 MYT] respectively.

iv) MH370 was operating in the Sector 3+5 Area of Responsibility (AOR) when the Radar Controller transferred the aircraft to HCM ACC. As he had not been monitoring the progress of the flight of MH370, the Sector 3+5 Radar Controller was not aware when MH370 passed the TCP IGARI, and when the MH370 radar display symbol started to “coast” and dropped from the radar display.

[34] VPK - Pekan DVOR/DME coordinates 032259N 1032524E.

v) Notwithstanding the fact that he had to shift his focus to another area within his AOR, the Radar Controller was still required to monitor the progress of MH370. The responsibility of the Sector 3+5 Radar Controller for MH370 did not end with the transfer of control to HCM ACC. The process of transfer of control is only with regard to Air Traffic Control Service. Therefore, the Sector 3+5 Radar Controller was still responsible for the provision of alerting service to MH370 as it was still operating within his AOR. The responsibility of the provision of alerting service would end when MH370 had a two-way radio communication with HCM ACC.

vi) The Radar Controller was not aware when MH370 radar position symbol dropped off from the radar display.

e) Recognising Emergency Situations and Air Traffic Control Actions

i) Upon receipt of the query from HCM ACC at 1739 UTC [0139 MYT] that HCM ACC had not been able to establish two-way radio communications with MH370, the Lumpur Sector 3+5 Radar Controller should have realised that MH370 could be experiencing an emergency situation. This was especially so after he had tried to establish radio communication with MH370 by making a 'blind transmission' on the VHF radio frequency 132.5 MHz at 1741:23 UTC [0141:23 MYT], without success.

ii) Under such circumstances and upon notification from HCM ACC that there were no two-way radio communications with the aircraft and/or subsequent inquiries to other sources had failed to reveal any news of the aircraft, the Sector 3+5 Radar Controller should have immediately notified the ATSC Duty Watch Supervisor and ARCC that an *Uncertainty Phase* had existed. By then, the Radar Controller should have commenced full overdue action (not later than 30 minutes after the declaration of an *Uncertainty Phase*), i.e. notify the KL ARCC that an *Alert Phase* existed.

iii) Manual of Air Traffic Services, Part 9 - Emergencies, page 9-6-5, para. 6.7.2 dated 15/3/2009 states:

If alerting service is required for an aircraft that is flight planned to operate through more than one FIR including the airspace delegate to the Kuala Lumpur and Kota Kinabalu ATSCs and the position of the aircraft is in doubt, the responsibility for co-ordinating such service shall normally rest with the ATSC of the respective FIRs:

within which the aircraft was flying at the time of last air-ground radio contact.

Reference

Manual of Air Traffic Services, Part 9 - Emergencies, page 9-6-5, para. 6.7.2 dated 15/3/2009 No. 1 states:

If alerting service is required for an aircraft that is flight planned to operate through more than one FIR including the airspace delegate to the Kuala Lumpur and Kota Kinabalu ATSCs and the position of the aircraft is in doubt, the responsibility for co-ordinating such service shall normally rest with the ATSC of the respective FIRs:

- *within which the aircraft was flying at the time of last air-ground radio contact;*
- *that the aircraft was about to enter when last air-ground contact was established at or close to the boundary of two FIRs or control areas;*
- *within which the aircraft's intermediate stop or final destination point is located:*

  1) if the aircraft was not equipped with suitable two-way radio communication, or

  2) was not under obligations to transmit position reports.

and

ICAO Doc 4444 ATM/501 Procedures for Air Navigation - Air Traffic Management (PANS-ATM), page 9-6, para 9.2.2.2, dated 22/11/07 states:

When alerting services is required in respect of a flight operated through more than one FIR or control area, and when the position of the aircraft is in doubt, responsibility for coordinating such service shall rest with the ATS unit of the FIR or control area within which the aircraft was flying at the time of last air-ground radio contact:

a) that the aircraft was about to enter when last air-ground contact was established at or close to the boundary of two FIRs or control areas;

b) within which the aircraft's intermediate stop or final destination point is located:

1) if the aircraft was not equipped with suitable two-way radio communication, or

2) was not under obligations to transmit position reports.

The responsibility for the provision of alerting service for MH370 therefore rested on KL ACC.

iv) Following the *Alert Phase*, the *Distress Phase* should be declared by the Radar Controller after further unsuccessful attempts to establish communication with the aircraft and more widespread unsuccessful inquiries pointed to the probability that the aircraft was in distress.

References

(1) MATS, PART 9 - EMERGENCIES, para 1.3.1 a) and b) page 9-1-2 Ver.01 stipulates that:

Controller may suspect that an aircraft is experiencing an emergency situation or that an emergency situation exists if one of the following situations becomes apparent:

a) *when radio contact is not established at the time it is expected to be established;*

b) *radio or radar contact is lost;*

c) *pilot reports a malfunction or unusual behaviour of person(s) on board;*

d) *pilot reports of unlawful interference;*

e) *aircraft is observed or reported to be behaving erratically;*

f) *aircraft is overdue at an aerodrome; and*

g) *an ELT signal is heard or is reported.*

(2) MATS PART 9 - EMERGENCIES, SECTION 2 OVERDUE AIRCRAFT, para. 2.1.1, page 9-2-1, No.1, dated 15/03/2009 stipulates that:

ATC action with respect to an aircraft that is overdue should not be considered in isolation, and the emergency actions described in other sections, in particular radio failure procedures, should be applied if they are appropriate. For example, if a radio-equipped aircraft fails to make an expected report, continuous attempts should be made to re-establish communications while at the same time initiating overdue action.

(3) MATS PART 9 - EMERGENCIES, SECTION 2 OVERDUE AIRCRAFT, para. 2.1.3, page 9-2-1, also stipulates that:

Overdue action must be commenced not later than the times stipulated in the procedure herein. Controllers may at their own discretion consider initiating actions before the times stated. The following consideration will assist Controllers in making a decision:

Route - The need for prompt action if the route is over sparsely populated area, mountainous country, and long stretches of water.

(4) MATS PART 9 - EMERGENCIES, Table 9-2-2, page 9-2-3 OVERDUE ACTION - RADIO EQUIPPED AIRCRAFT

ATSC Procedures

Preliminary action

When an aircraft fails to make a position report when it is expected, commence action not later than the ETA for the reporting point plus 3 minutes:

- *Confirm ATD and time of last contact with preceding ATS unit if appropriate;*
- *Request information from other ATS units and likely aerodromes;*
- *Notify the RCC that the Uncertainty Phase exists; and*
- *Ensure that RQS message is sent.*

Full overdue Action

Commence full overdue action not later than 30 minutes after the declaration of the Uncertainty Phase or when advised by the Aerodrome that the aircraft is fully overdue:

- *Notify the RCC that the Alert Phase exists;*
- *Notify the RCC that the Distress Phase exists if:*

i) 1 hour has elapsed beyond the last ETA for the destination; or

ii) the fuel is considered exhausted; or

iii) 1 hour has elapsed since the declaration of the Uncertainty Phase.

(5) ATC actions on the declaration of emergency phases should be taken as shown below:

MATS PART 9 - EMERGENCIES, page 9-6-2 – para

9-6-4, para 6.4 and Annex 11, page 5-1, para 5.2.1 states:

a) Uncertainty Phase when:

1) no communication has been received from an aircraft within a period of thirty minutes after the time a communication should have been received, or from the time an unsuccessful attempt to establish communication with such aircraft was first made, whichever is the earlier, or when an aircraft fails to arrive within thirty minutes of the estimated time of arrival last notified to or estimated by air traffic units, whichever is the earlier, except when no doubt exits as to the safety of the aircraft and its occupants.

b) Alert Phase when:

1) following the uncertainty phase, subsequent attempts to establish communication with the aircraft or inquiries to other relevant sources have failed to reveal any news of the aircraft, or when

2) an aircraft has been cleared to land and fails to land within five minutes of the estimated time of landing and communication has not been re-established with the aircraft, or when

3) information has been received which indicates that the operating efficiency of the aircraft has been impaired, but not to the extent that a forced landing is likely, except when evidence exists that would allay apprehension as to the safety of the aircraft and its occupants, or when

4) an aircraft is known or believed to be the subject of unlawful interference.

c) Distress Phase when:

1) following the alert phase, further unsuccessful attempts to establish communication with the aircraft and more widespread unsuccessful inquiries point to the probability that the aircraft is in distress, or when

2) the fuel on board is considered to be exhausted, or to be insufficient to enable the aircraft to reach safety, or when

3) information is received which indicate that the operating efficiency of the aircraft has been impaired to the extent that a forced landing is likely, or when

4) information is received or it is reasonably certain that the aircraft is about to make or has made a forced landing except when there is reasonable certainty that the aircraft and its occupants are not threatened by grave and imminent danger and do not require immediate assistance.

f) Information to be passed to other Radar Units - Civil and Military

The Sector 3+5 Radar Controller did not inform other radar units, civil and military, of the circumstances surrounding MH370. MATS PART 9 - EMERGENCIES, para 6.2.3, page 9-6-2, stipulates that:

If Controllers have reason to believe that an aircraft is lost, overdue or experiencing a communication failure, they shall:

a) inform appropriate radar units (civil and military) of the circumstances.

b) request the units to watch out for emergency SSR code display or the triangular radio failure pattern.

c) notify these units when their services is no longer required.

g) Provision of Alerting Service for Flight operating through more than one FIRs and ATC Actions

MH370 was operating within the Singapore FIR, in that portion of the airspace which has been delegated to Malaysia (refer to *Figure 2.2K - Singapore Airspace delegated to Malaysia*) for the provision of air traffic services when the last air-ground radio contact was made at 1719 UTC [0119 MYT]. As such, KL ACC should be responsible for the alerting service which would mean that KL ACC would have to declare the Distress Phase at 1827 UTC [0227 MYT] when HCM ACC informed that there had been no two-way radio communications with MH370.

Reference

Manual of Air Traffic Services, Part 9 - Emergencies, page 9-6-5, para. 6.7.2 dated 15/3/2009 No. 1 states:

> *If alerting service is required for an aircraft that is flight planned to operate through more than one FIR including the airspace delegate to the Kuala Lumpur and Kota Kinabalu ATSCs and the position of the aircraft is in doubt, the responsibility for co-ordinating such service shall normally rest with the ATSC of the respective FIRs:*
>
> - *within which the aircraft was flying at the time of last air-ground radio contact;*
> - *that the aircraft was about to enter when last air-ground contact was established at or close to the boundary of two FIRs or control areas;*
> - *within which the aircraft's intermediate stop or final destination point is located:*
>
> *3) if the aircraft was not equipped with suitable two-way radio communication, or*
>
> *4) was not under obligations to transmit position reports.*

and

ICAO Doc 4444 ATM/501 Procedures for Air Navigation - Air Traffic Management (PANS-ATM), page 9-6, para 9.2.2.2, dated 22/11/07 states:

When alerting services is required in respect of a flight operated through more than one FIR or control area, and when the position of the aircraft is in doubt, responsibility for coordinating such service shall rest with the ATS unit of the FIR or control area within which the aircraft was flying at the time of last air-ground radio contact:

c) that the aircraft was about to enter when last air-ground contact was established at or close to the boundary of two FIRs or control areas;

d) within which the aircraft's intermediate stop or final destination point is located:

3) if the aircraft was not equipped with suitable two-way radio communication, or

4) was not under obligations to transmit position reports.

The responsibility for the provision of alerting service for MH370 therefore rested on KL ACC.

h) Actions taken by Air Traffic Service Centre Duty Watch Supervisor

In interviews conducted with the Duty Air Traffic Controllers on that night, the Team recorded the following:

i) At about 1800 UTC [0200 MYT], the Sector 3+5 Radar Controller had instructed a junior Controller to inform the ATSC Duty Watch Supervisor - who was then in the rest area[35] - on HCM ACC's query on the status of MH370;

ii) The ATSC Duty Watch Supervisor stated that he subsequently left the rest area and returned to the ATSC. He contacted MAS Operations Despatch Centre (ODC) by telephone (albeit not tape-recorded) to inform that HCM ACC had not been able to establish radio and radar contact with MH370. In response ODC informed that the Flight-following System (FFS) or *Flight Explorer* of MAS showed that: "*aircraft in Cambodian airspace*" and added that he

[35] Rest area - It is located in the same building adjacent to ATSC and is furnished with 3 x double-decker beds for the night shift Controllers to rest/sleep during break in between shift.

(ODC) would try to use the ACARS to contact MH370 and also to request the aircraft to contact HCM ACC. The ATSC Duty Watch Supervisor stated that he was satisfied with the information that MH370 was still flying and therefore did not take any further actions.

iii) The junior Controller (who had earlier informed the ATSC Duty Watch Supervisor in the rest area) stated that the ATSC Duty Watch Supervisor then returned to the rest area at around 1830 UTC [0230 MYT] until about 2130 UTC [0530 MYT].

iv) At 2130 UTC [0530 MYT], the ATSC Duty Watch Supervisor initiated the alerting action by instructing the SAR-trained Controller to activate the KL ARCC.

v) At 2232 UTC [0632 MYT], the *DETRESFA* message was disseminated

i) Flight-Following System of Malaysia Airlines

(1) In interviews conducted with the MAS duty personnel in charge of the FFS on the night of 07 March 2014, he was not able to explain clearly on the operations of the system due to "*lack of training*". The Team was also informed that all the personnel in this unit were not adequately trained to operate this system. The MAS personnel also informed the Team that the FFS could not track aircraft on a real-time basis and that the position information was computer-projected, based on the flight plan of aircraft. He added that the status of an aircraft position would only be updated every thirty (30) minutes. He admitted that he had informed KL ACC that MH370 was in Cambodian airspace as during: *"…that point in time, I did not notice that the position was actually projected movement and not actual"*.

Even with this admission, MAS ODC continued to provide information to KL ACC that the aircraft was "*still sending movement messages*", and stated that:

> "*It was somewhere in Vietnam and coordinates of its position as N14.90000 E109 15500 at time 1833 UTC [0233 MYT]".*

(2) KL ACC then relayed the position information to HCM ACC at 1837:41 UTC [0237:41 MYT] informing HCM ACC that MH370 was still flying.

(3) To understand how the *Flight Explorer* works, the Team requested for a copy of the *Flight Explorer User Manual* and was informed that there was none in the office. Later, a copy of the *Flight Explorer User Manual* was provided to the Team.

Note:

Flight Explorer is a computer-based system which is also known as "Flight-Following System" to track aircraft based on input of the aircraft's Flight Plan data into the computer. The Flight Plan data generates the flight profile and position of the aircraft and updates every 30 minutes. However, the system does not provide real-time tracking.

(4) Whilst air traffic Controllers' communication with airline operators to obtain flight information is a normal occurrence, however information provided ought to be evaluated and assessed with due diligence as to its accuracy and relevancy. The information of the FFS on MH370 was derived from the *Flight Explorer* which did not provide real-time tracking. The *Flight Explorer* was neither a part of the ATS system nor documented in the Manual of ATS (MATS), International Aeronautical and Maritime Search and Rescue (IAMSAR) Manual Volume IV, Standard Operating Procedure for SAR, Supplementary Operations Instructions (SOIs) or other documents. Therefore, the information derived from the FFS from ODC did not help at all but, instead, further complicated the situation**.**

The Team noted that MAS FFS was not part of the KL ACC Air Traffic Services system and it did not provide real-time tracking of flight. The position information of MH370 provided to KL ACC were computer-generated and not actual.

j) Communication Exchanges between KL ACC and HCM ACC and KL ACC and MAS Operations Despatch Centre on MH370

(1) The period between 1739 UTC [0139 MYT] and 2120 UTC [0520 MYT] revolved with ATC communications activities between HCM ACC and KL ACC, and. between KL ACC and ODC, for information on MH370. It also included KL ACC requesting HCM ACC to check with the adjacent FIRs namely SANYA, HONG KONG and BEIJING.

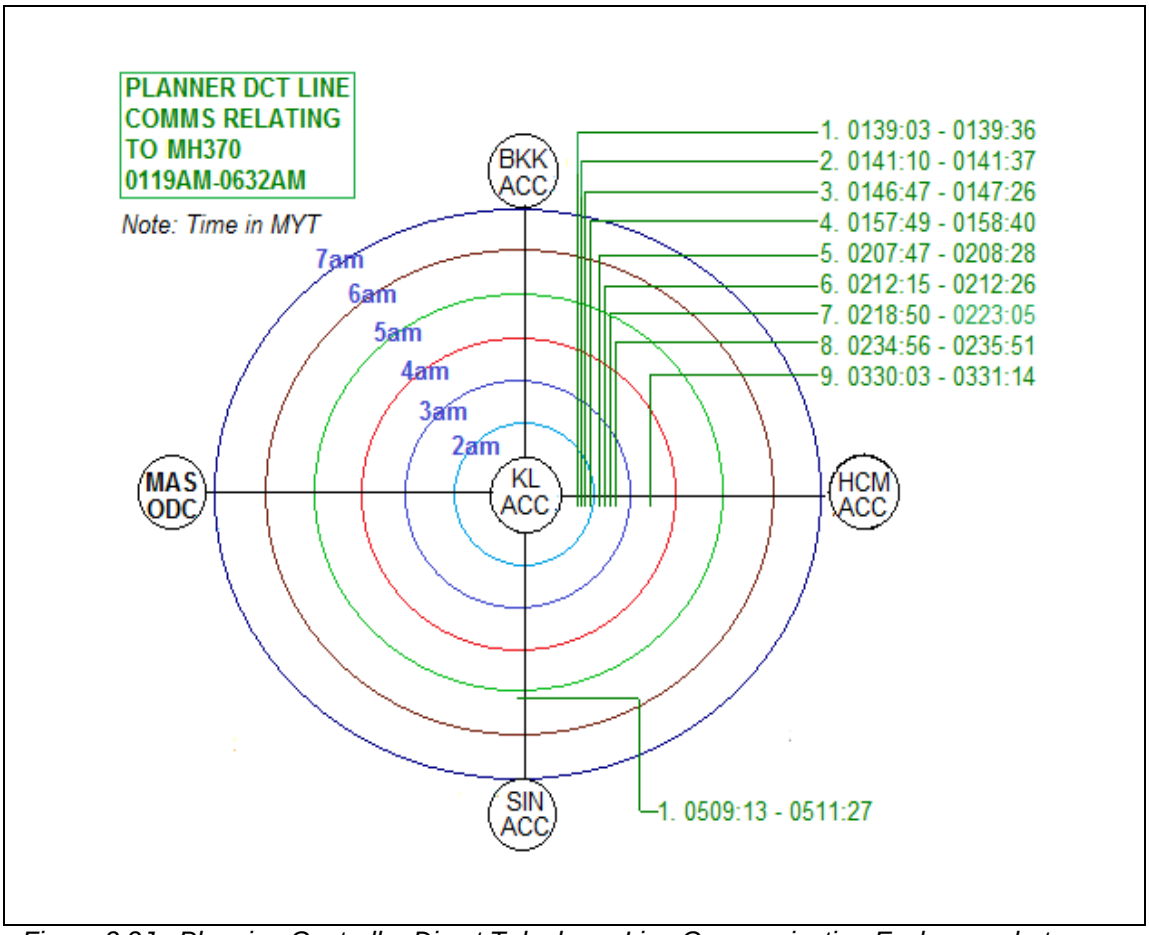

Figure 2.2J - Planning Controller Direct Telephone Line Communication Exchanges between KL ACC and HCM ACC, KL ACC and Singapore ACC from 0119 to 0632 [MYT]

(2) The time and the Planning Controller's direct line communications exchanges with HCM ACC, and Singapore ACC, from 1719 to 2232 UTC [0119 to 0632 MYT], is illustrated in concentric circles *(Figure 2.2J above)* when MH370 went missing. The illustrations at 0100 (MYT) begins with the innermost concentric circle followed by 0200 [MYT] on the next concentric circle with 0700 [MYT] on the outermost concentric circle (it depicts the timeline for 08 March 2014 on the KL ACC Planning Controller's direct line

communication exchanges with HCM ACC and with Singapore ACC from 0119 to 0632 [MYT] when MH370 was missing).

(3) Direct line communication exchanges (time in MYT) between KL ACC Planning Controller and HCM ACC.

No.	Time [MYT]	Direct-Line Communication Exchanges
1.	0139:03 - 0139:36	HCM ACC initiated the call to enquire about MH370 and notified KL ACC verbal contact was not established with MH370 and the radar target was last seen at BITOD.
2.	0141:10 - 0141:37	KL ACC initiated the call to inform HCM ACC that MH370 did not contact KL ACC after IGARI. HCM ACC informed KL ACC that "*we have radar contact but not verbal contact until BITOD, we are no ADS-B identity and no radar contact."*
3.	0146:47 - 0147:26	HCM ACC initiated the call /query about MH370 and stated that *"we have radar contact over IGARI not verbal contact and after BITOD we have no radar ident also ADS-B identity. And we call him many times until more than 20 minutes".* KL ACC responded: *"Okay, I will try...give a call and then."*
4.	0157:49 - 0158:40	HCM ACC initiated the call/query and stated: "*we officially no contact from MH370 until now, and we tried on many frequencies and all the aircraft - calling no response from MH370."* HCM ACC added and requested by saying: *"Could you check back for your side?"* KL ACC responded: "*Okay we will do that and the first at IGARI did you ever in contact with the aircraft or not first place."* HCM ACC replied: "*Negative sir, we have radar contact only but not verbal contact."* KL ACC responded: "*But no when passed IGARI, did the aircraft call you?"* HCM ACC replied: *"Negative sir."* KL ACC responded: *"Negative. Why you didn't tell me first within five minutes you should be called me?"* KL ACC, before ending the conversation, indicated that he would try to call the Company.

Table 2.2F - Direct Line Communication Exchanges between KL ACC and HCM ACC

cont…

(3) Direct line communication exchanges (time in MYT) between KL ACC Planning Controller and HCM ACC *(cont…)*

No.	Time [MYT]	Direct-Line Communication Exchanges
5.	0207:47 - 0208:28	HCM ACC initiated the call query to KL ACC for confirmation that MH370 was in Phnom Penh FIR as Phnom Penh did not have any information on MH370.KL ACC responded that he would check with his supervisor again.
6.	0212:15 - 0212:26	KL ACC while coordinating with HCM ACC on another traffic informed that there was no update on the status of MH370.
7.	0218:50 - 0223:05	KL ACC initiated the call and queried if the flight plan routing of MH370 was supposed to enter Cambodian airspace. HCM ACC confirmed that the planned route was only through the Vietnamese airspace. HCM ACC also informed that it had checked and also been advised by Cambodia that it had no information or contact with MH370. HCM ACC confirmed that earlier information on loss of radar contact after BITOD, and radio contact, was never established. KL ACC queried if HCM ACC was taking Radio Failure action but the query did not seem to be understood by the personnel. HCM ACC suggested KL ACC to call MAS Operations and was advised that it had already been done.
8.	0234:56 - 0235:51	HCM ACC initiated the call and queried about the status of MH370 and was informed by KL ACC that the Watch Supervisor was talking to the Company at that time.
9.	0330:03 - 0331:14	KL ACC initiated the call and enquired on news of MH370 and HCM ACC responded: "*not yet.*" KL ACC queried whether HCM ACC had checked with the next FIR Hainan.

Table 2.2F - Direct Line Communication Exchanges between KL ACC and HCM ACC

(4) Direct line communication exchange (time in MYT) relating to MH370 between KL ACC and Singapore ACC *(Table 2.2G* below)

No	Time [MYT]	Direct-Line Communications Exchanges
1.	0509:13 - 0511:27	Singapore ACC initiated the call and informed that it was first alerted by Hong Kong ACC who had made enquiries to ascertain the status of MH370. KL ACC confirmed that it was in contact with MH370 until transferred at IGARI and that MAS on the ground had also no contact with MH370.

Table 2.2G - Direct Line Communication Exchanges between KL ACC and Singapore ACC

(5) *Figure 2.2K* below illustrates the time and the Radar Controller's direct line communications exchanges relating to the missing MH370 between KL ACC and HCM ACC, and between KL ACC and ODC.

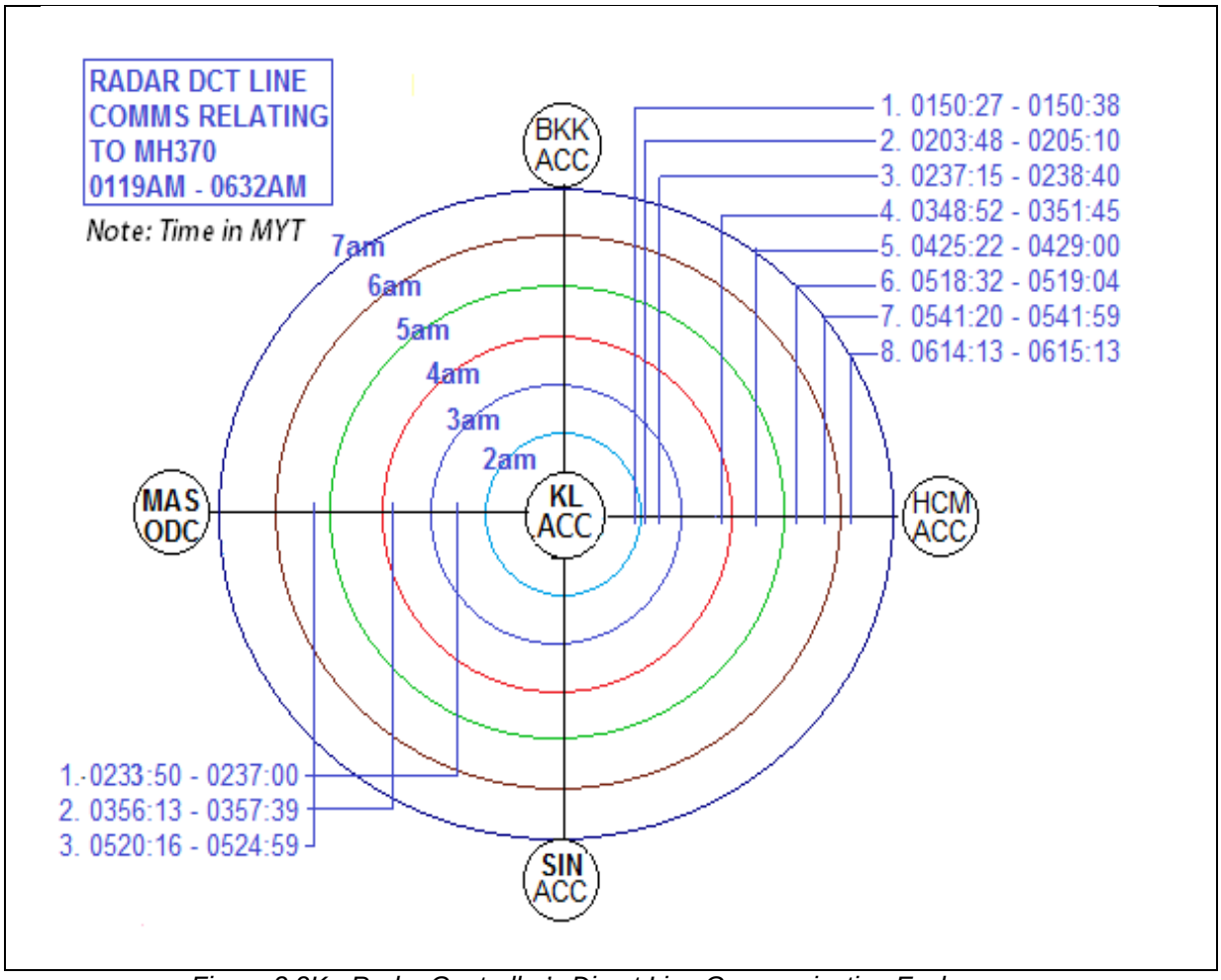

Figure 2.2K - Radar Controller's Direct Line Communication Exchanges

It begins with 0100 [MYT] at the innermost concentric circle followed by 0200 [MYT] on the next concentric circle with 0700 [MYT] on the outermost concentric circle (it depicts the timeline for 08 March 2014 on the KL ACC Radar Controller direct line communication exchanges with HCM ACC and ODC 0119 to 0632 [MYT] when MH370 went missing).

(6) Direct line communication exchanges between KL ACC Radar Controller and HCM ACC (*Table 2.2H*, below)

No.	Time [MYT]	Direct-Line Communications Exchanges
1.	0150:27 - 0150:38	KL ACC initiated the call to enquire about MH370 and HCM ACC replied: "*negative contact.*"
2.	0203:48 - 0205:10	KL ACC initiated the call query to HCM ACC on the status of MH370. HCM ACC confirmed there was no radar contact at that time and no verbal communication was established. KL ACC relayed the information received from MAS Operations that MH370 was in Cambodian airspace.
3.	0237:15 - 0238:40	KL ACC initiated the call and informed HCM ACC that MH370 was still flying, and that the aircraft was sending position reports to the airline. KL ACC then relayed to HCM ACC the position of MH370 in latitude and longitude as advised by MAS Operations Centre.
4.	0348:52 - 0351:45	KL ACC initiated the call and queried HCM ACC for news of MH370. HCM ACC replied: "*Until now nothing.*" KL ACC suggested checking with the next FIR and HCM ACC advised: "*It was SANYA FIR and he had checked with SANYA FIR but no response until now*."
5.	0425:22 - 0429:00	HCM ACC initiated the call and queried to confirm the last position that MH370 was in contact with KL ACC. KL ACC replied: *"The last position we contact that was about IGARI."*

Table 2.2H - Direct Line Communication Exchanges between KL ACC Radar Controller and HCM ACC

cont…

(6) Direct line communication exchanges between KL ACC Radar Controller and HCM ACC (*Table 2.2H*, below)..*cont.*

No.	Time [MYT]	Direct-Line Communications Exchanges
6.	0518:32 - 0519:04	HCM ACC initiated the call and queried for information on MH370. KL ACC queried if any information had been received from Hong Kong or Beijing.
7.	0541:20 - 0541:59	HCM ACC initiated the call and queried for any updates.
8.	0614:13 - 0615:13	KL ACC initiated the call and queried HCM ACC if SAR was activated.

Table 2.2H - Direct Line Communication Exchanges between KL ACC Radar Controller and HCM ACC

(7) Direct line communication exchanges between KL ACC and ODC (*Table 2.2I* below)

No.	Time [MYT]	Direct-Line Communications Exchanges
1.	0233:50 - 0237:00	KL ACC informed MAS that HCM ACC still had no contact with MH370. MAS informed that the aircraft was still sending movement messages and providing latitude 14.90000 longitude 109.15500 at 1833 UTC [0233 MYT].
2.	0356:13 - 0357:39	KL ACC initiated the call and enquired about MH370. MAS replied: *"Not yet".*
3.	0520:16 - 0524:59	KL ACC initiated the call and queried MAS for news on MH370. The Technical Captain said: *"Whatever we have here suggest that the aircraft had never leave Lumpur airspace because he has failed to call Ho Chi Minh"* and suggested to KL ATSC to trace back the record, voice recording and time of the positive handover to Ho Chi Minh. KL ACC replied: *"I wake up my supervisor and ask him to check again to go to the room and check what, what the last contact all this thing."*

Table 2.2I - Direct Line Communications Exchanges between KL ACC and ODC

Investigation revealed that between 0119 and 0632 MYT, the following ATC communications activities on MH370, between HCM ACC and KL ACC, and between KL ACC and ODC, took place:

- There were nine instances KL ACC Sector 3+5 planner Controller communicated with HCM ACC and one with Singapore ACC relating to MH370, and

- There were eight instances KL ACC Sector 3+5 Radar Controller communicated with HCM ACC and three with ODC relating to MH370,

Figure 2.2L (below) illustrates the time and the Radar Controller's direct line communications exchanges, though not relating to the missing MH370, with HCM ACC and Singapore ACC, from 0119 to 0632 [MYT].

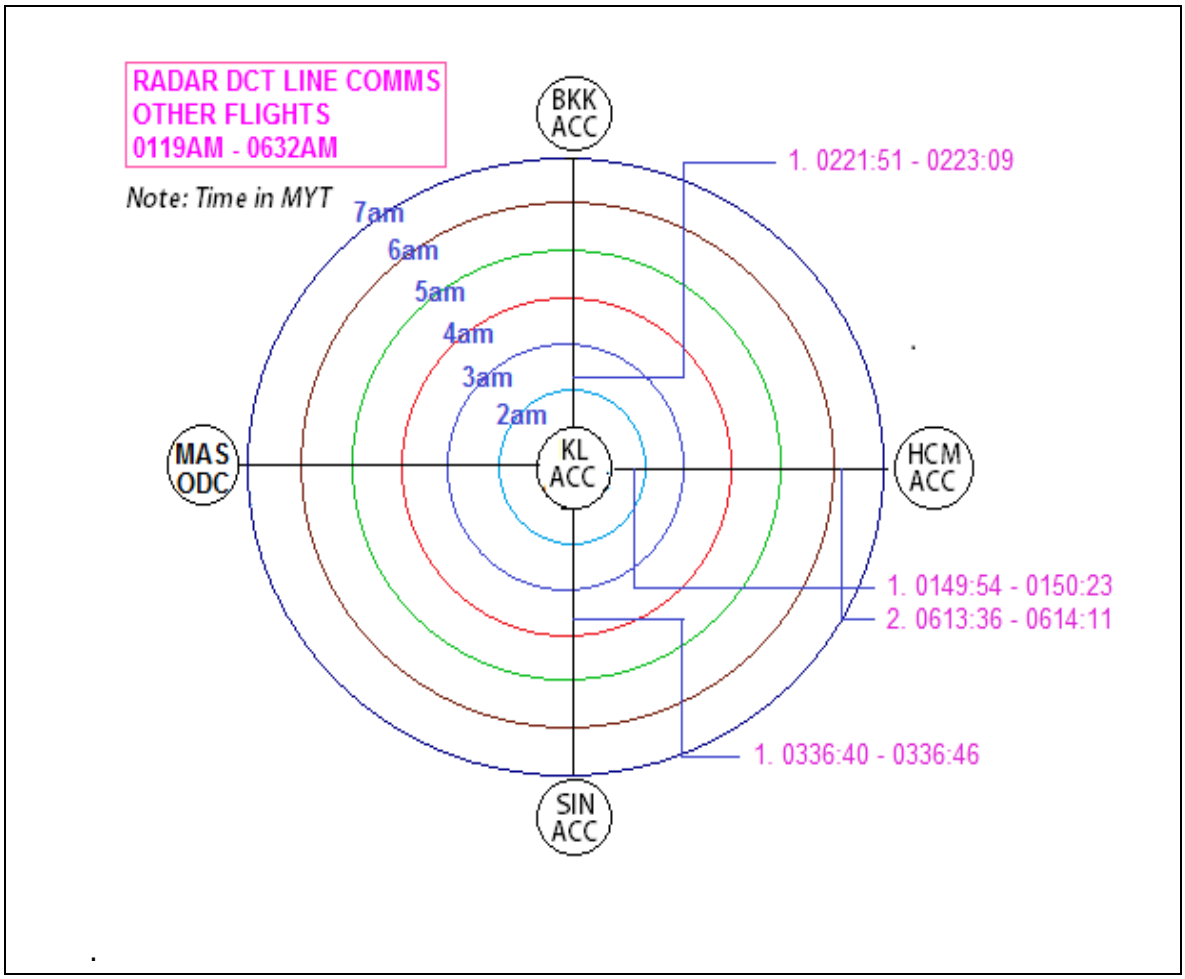

Figure 2.2L - Radar Controller direct telephone line communications exchanges between KL ACC and HCM ACC, KL ACC and Bangkok ACC, KL ACC and Singapore ACC from 0119 to 0632 [MYT] not related to MH370

Figure 2.2M (below) illustrates the time and the Planning Controller's direct line communications exchanges not relating to the missing MH370 with HCM ACC, Singapore ACC and Bangkok ACC, from 0119 to 0632 [MYT]. It begins at 0100am at the innermost concentric circle followed by 0200 [MYT] on the next concentric circle with 0700 [MYT] on the outermost concentric circle (it depicts the timeline for 08 March 2014 on KL ACC Planning Controller direct line communications exchanges with between KL ACC and HCM ACC, KL ACC and Bangkok ACC, KL ACC and Singapore ACC from 0119 to 0632 [MYT] when MH370 went missing).

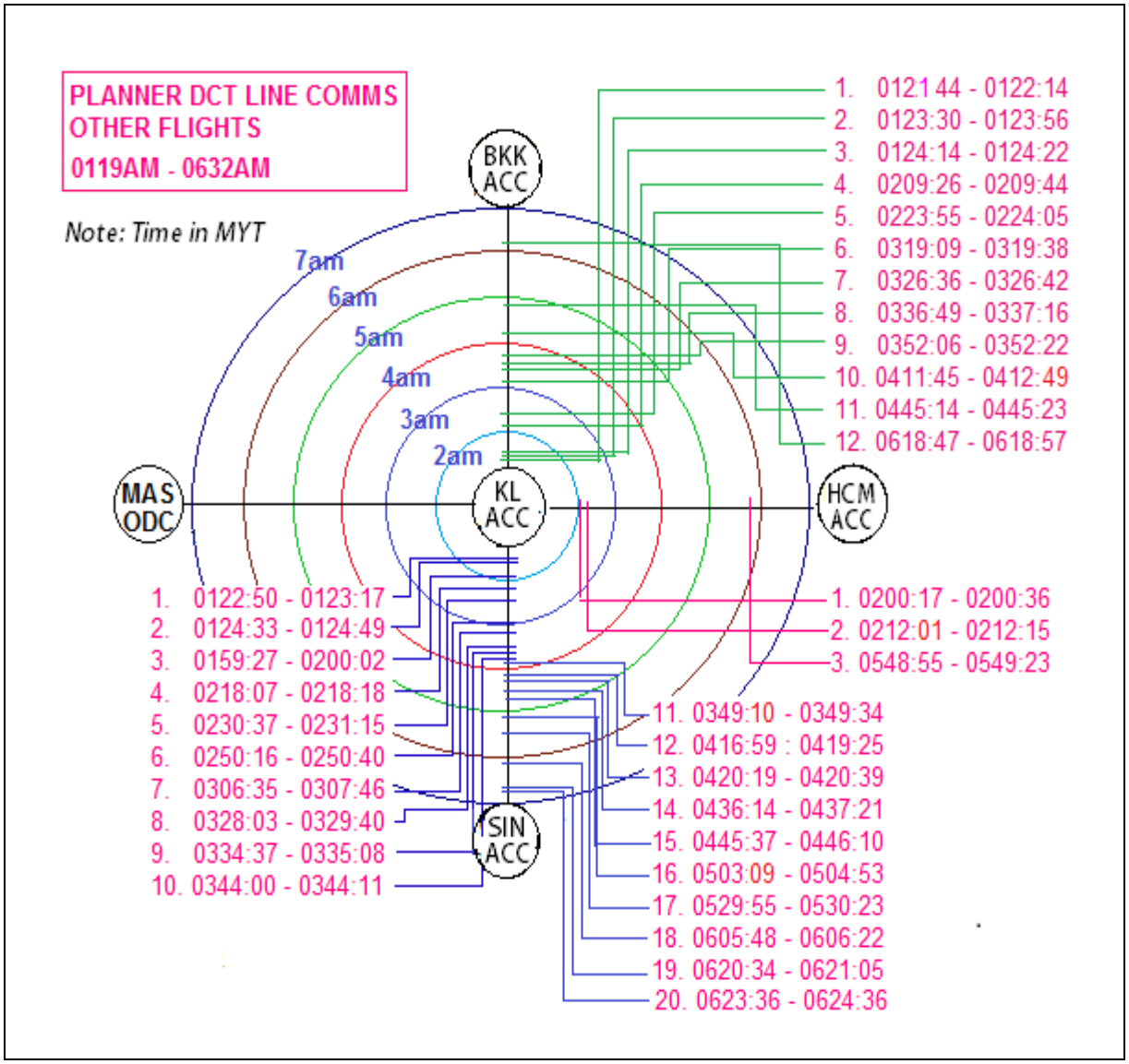

Figure 2.2M - Planning Controller's direct telephone line communications exchanges between KL ACC and HCM ACC, KL ACC and Bangkok ACC, KL ACC and Singapore ACC from 0119 to 0632 [MYT] not related to MH370

It begins at 0100 [MYT] at the innermost concentric followed by 0200 [MYT] on the next circle with 0700 [MYT] on the outermost concentric circle (it depicts the timeline for 08 March 2014 on KL ACC Radar Controller direct line communications exchanges between KL ACC and HCM ACC, KL ACC and Bangkok ACC, KL ACC and Singapore ACC, from 0119 to 0632 [MYT] when MH370 went missing).

The Team noted that between 0119 and 0632 MYT:

- there were two instances KL ACC Sector 3+5 Radar Controller communicated with HCM ACC, one with Bangkok ACC and another with Singapore ACC relating to other flights; and
- there were three instances Sector 3+5 planner Controller communicated with HCM ACC, twelve instances with Bangkok ACC and twenty with Singapore ACC relating to other flights.

k) Delegation of Airspace by Singapore Area Control Centre to KL ACC

i) The delegated airspace *(Figure 2.2N* below) is a portion of airspace within the Singapore FIR over the South China Sea. IGARI is a waypoint along airway M765 which is within the delegated airspace. KL ACC is responsible for the provision of air traffic services to flights operating within the delegated airspace and Singapore ACC is responsible for the provision of SAR service.

ii) At 2109:13 UTC [0509:13 MYT] Singapore ACC contacted KL ACC for information on MH370 following an enquiry on the status of the aircraft by Hong Kong ACC four minutes earlier. By then, over three and a half hours had lapsed.

iii) At 0230 UTC 08 March 2014, KL ARCC advised Singapore RCC on the situation relating to MH370. Singapore RCC informed that a Hercules aircraft (C-130) would be launched to the search area with clearance from Ho Chi Minh. The Hercules aircraft (C-130) was assigned the radiotelephony callsign as *Rescue 71* by Lumpur ARCC.

iv) Although Singapore ACC is responsible for the provision of SAR service within the delegated airspace, KL ACC did not inform Singapore ACC when MH370 was overdue. Nevertheless, Singapore RCC launched a search and rescue

aircraft to the search area after KL ARCC advised on the situation relating to MH370.

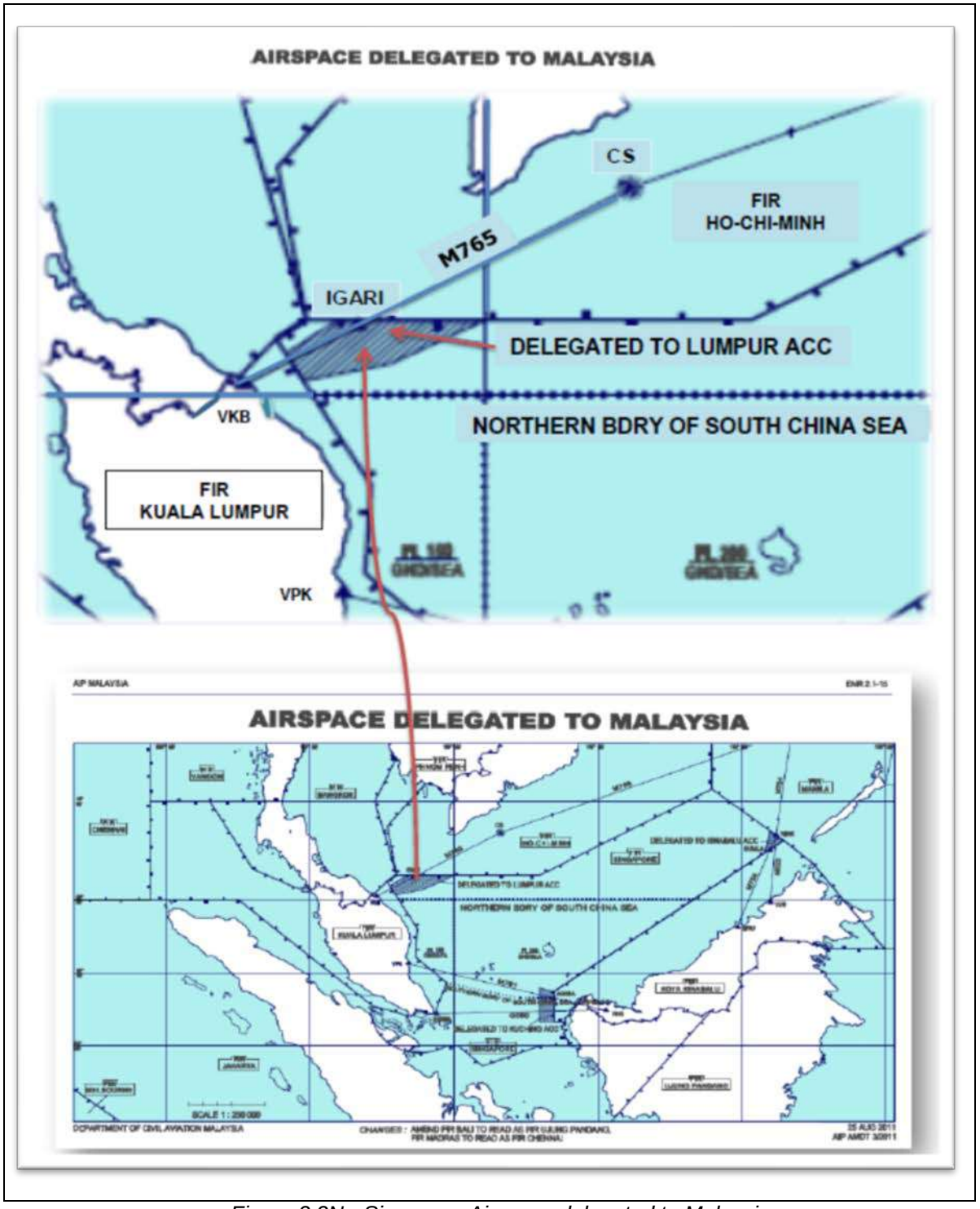

Figure 2.2N - Singapore Airspace delegated to Malaysia

Source: DCA Malaysia

l) ATC Actions on Strayed/Unidentified Aircraft (Primary Radar Target) within the Area of Responsibility

i) At 1730:37 UTC [0130:37 MYT] a strayed/unidentified aircraft (primary radar target) appeared on the Sector 3+5 radar display at approximately 57 nm north east of Kota Bahru and heading to Kota Bahru. This aircraft target dropped off from the radar display at 1737:22 UTC [0137:22 MYT]. It reappeared at 1738:56 UTC [0138:56 MYT], on airway B219 heading towards VPG[36] and dropped off at 1744:52 UTC [0144:52 MYT]. The appearances and reappearances of these strayed/unidentified primary targets on Lumpur Sector 3+5 radar display were for a duration of 6 minutes 45 seconds and 5 minutes 56 seconds respectively. The duration of the strayed/unidentified aircraft appearing on the Lumpur Sector 3+5 radar display was 12 minutes and 41 seconds. When the strayed/unidentified aircraft continued its journey towards VPG, it entered into the Lumpur Sector 1 Area of Responsibility.

ii) On the Lumpur Sector 1 radar display, the strayed/ unidentified aircraft (primary radar target) appeared at 1747:02 UTC [0147 MYT] and dropped off at 1748:39 UTC [0148:39 MYT]; and reappeared at 1751:45 UTC [0151:45 MYT] and dropped off at 1752:35 UTC [0152:35 MYT]. The duration of the strayed/ unidentified aircraft appearing on Lumpur Sector 1 radar display was 2 minutes 27 seconds.

Note

Information on strayed/unidentified aircraft (primary radar target) was obtained from radar recording playback.

iii) In interviews with the ATCOs on duty, the Sector 3+5 and Sector 1 Radar Controllers informed that they were unaware of the strayed/unidentified aircraft (primary radar target) transiting their AORs.

The Sector 3+5 Radar Controller acknowledged that he had to shift his attention to four other aircraft in another area, viz. VPK approximately 214 nm south of IGARI). As such, he did

[36] VPG – Penang DVOR/DME coordinates 051646.7N 1001537.4E.

not observe the strayed/unidentified aircraft (primary radar target).

The Sector 1 Radar Controller stated that he did not observe the strayed/unidentified aircraft (primary radar target) even though he remained at the Controller working position.

MATS Vol 1, Part 1 - ADMIN page 1-1-4 para 1.2.2 which stipulates that:

> *Air Traffic Controller is responsible*:
>
> - *for maintaining a continuous watch on their assigned communications channels or radar displays.* (Point No. 5)

MATS PART 9 - EMERGENCIES, SECTION 15, page 9-15-1 (and ICAO Annex 11 - Air Traffic Services Chapter 2, para. 2.24.1, page 2-14) on *Strayed or unidentified aircraft* states:

> *1.5.2 The terms "strayed aircraft" and "unidentified aircraft" have the following meanings:*
>
> *a) Strayed aircraft - An aircraft that has deviated significantly from its intended track or which reports that it is lost.*
>
> b) *Unidentified aircraft - An aircraft that has been observed or reported to be operating in a given area but whose identity has not been established.*

ATS PART 9 – EMERGENCIES, SECTION 15, para 15.4, page 9–15–2 (also ICAO Annex 11 - Air Traffic Services Chapter 2, para. 2.24.1.2, page 2-15) stipulates*:*

> *15.4 As soon as Controllers become aware of an unidentified aircraft operating in their area of responsibility, they shall endeavour to establish the identity of the aircraft for the provision of air traffic services or as required by the appropriate military authorities in accordance with local instructions. Towards this end, Controllers shall take such action as appropriate to establish two-way communication with the aircraft:*

a) inquire of other ATS units within the FIR about the flight and request their assistance to establish two-way communication with the aircraft;

b) inquire of ATS units in adjacent FIRs about the flight and request their assistance to establish two-way communication with the aircraft;

c) attempt to obtain information from other aircraft in the area; and

d) notify the appropriate military unit as soon as the identity of the aircraft has been established.

m) KL ATSC Duty Shift System for Air Traffic Controllers

i) 4-cycle Shift System

The 4-cycle shift system (*Table 2.2J* below) for the KL ATSC was, as follows:

Day	Shift	Start	End
1	Afternoon	0500 UTC [1300 MYT]	1100 UTC [1900 MYT]
2	Morning	2300 UTC [0700 MYT]	0500 UTC [1300 MYT]
	Night	1100 UTC [1900 MYT]	1600 UTC [2400 MYT]
3	Morning	1600 UTC [0000 MYT]	2400 UTC [0700 MYT]
4	Off Duty		

Table 2.2J - 4-cycle Shift System of KL ATSC

ii) Operations in Restricted/Collapsed Mode

(1) From 1600 UTC [0000 MYT] until 2200 UTC [0600 MYT] the number of Controllers in the KL ATSC was scaled down by half to enable the Controllers to take a scheduled break from duty:

- the first group from 1600 UTC [0000 MYT] to 1900 UTC [0300 MYT] and
- the second group from 1900 UTC [0300 MYT] to 2200 UTC [0600 MYT].

This practice had been approved by DCA. According to DCA, the scale-down of personnel during lean hours is a norm in air traffic control centres all around

the world where air traffic services can continue safely.

(2) MATS 1 Part 2 Section 2 para. 2.3.6, page 2-2-3 stipulates that:

The Supervisor may give periods of relief during a shift to personnel:

- *by arranging for relief personnel if possible; or by combining operating positions provided current and anticipated workload permits and the personnel on relief can be recalled quickly; or*
- *by rotating personnel to less active positions.*

(3) DCA Unit Administrative Instruction UAI 7/2010 details on how shift duty Air Traffic Controllers have their breaks during night shift work where the number of traffic movements is substantially reduced during the early morning period between 0000-0600 hours. Between the hours of 1600-1900 UTC [0000-0300 MYT] and 1900-2200 UTC [0300-0600 MYT], the shift is undertaken by two teams by combining the six working positions into four. However, though combined, they still would cover all the working positions.

(4) The 'Shift Break Time' in *Table 2.2K* below illustrated the manner the Controller working positions was managed. Based on this table, the Controller working positions on the 07 March 2014 is tabulated as shown in the two tables below:

- *Table 2.2L - Controller Working Positions between 1600-1900 UTC [0000-0300 MYT],* and
- *Table 2.2M - Controller Working Position between 1900-2200 UTC [0300-0600 MYT].*

From 1600 to 1900 UTC [0000-0600 MYT] Sectors 3 and 5 were combined while Sectors 1, 2 and 4 remained status quo.

FORM ATCC/OPS(IV)plnd.1/10

SHIFT BREAK TIME

TPP BERTUGAS

NO	NAME	POSITION	POSITION TO BE COVERED	TIME
1		BC	BA	0000 - 0300
2		CA	CA	
3		BD	BB & CB	
4		CD	CD & EB	
5		BE	BC	
6		BF	CC	
7		ED	ED	
8		EE	EC	
9		EA	EA	
10		EF1	EI & EF	
11		EH1	EH	
12		FA3	EB (0000-0200)	
1		BB	BA	0300 -0600
2		CB	CD	
3		BA	BB	
4		CE	BC &CC	
5		CC	CA	
6		EB	ED	
7		EF2	EC & EE	
8		EI	EI & EF	
9		EH2	EH	
10		EC	EB	
1		AF	APP	0000 - 0115
2		AN	APP	0115 - 0230
3		AL	APP	0230 - 0345
4		AS	APP	0345-0500
5		AA	APP	0500-0615
1		EG	CB	0000-0200
2		FB	CPDLC	
1		EG	ANY POSN	0530-0630
2		FB	ANY POSN	
TRAINING / FAMILIARIZATION				
1			ANY POSN	0000 - 0130 & 0530-0630
2				
3				
4				
5				

NOTE 1: Fs SHALL BREAK INTO 2 DURING RESTRICTED WATCH.HOWEVER IF B3 IS NOT AVAILABLE; F SHALL COVER CD POSITION UNTIL 0200 AND BE BACK BY 0530.THE OTHER F SHALL COVER 'C' FROM 0000-0200.

NOTE 2 THE 2ND RESTRICTED WATCH SHIFT SHALL REMAIN AT THEIR RESPECTIVE P(UNTIL RELEIVED BY 1ST RESTRICTED WATCH SHIFT

NOTE 3: WHEN W/S IS RESTING THE SHIFT LEADER SHALL TAKE CHARGE. IF URGENT W/S SHALL BE INFORMED IMMEDIATELY.

NOTE 4: WHEN TFC PERMIT X SHALL PERFORM CPDLC TRIAL FROM 0200-0300

NOTE 5: C3 SHALL REMAIN AT 'U' PSN 1100-0000

APPROVED BY :

.....

WATCH MANAGER
ATCC KL FIR

Legends

FS	ATSC Supervisor	**BA**	Sector 1 Radar	**CA**	Sector 1 Area Proc	**FB**	CPDLC
AA	TMA Supervisor	**BB**	Sector 2 Radar	**CB**	Sector 2 Area Proc	**EG**	Clearance Delivery
AN	Approach North	**BC**	Sector 3 Radar	**CC**	Sector 3 Area Proc	**RC**	Relief
AS	Approach South	**BD**	Sector 4 Radar	**CD**	Sector 4 Area Proc	**P**	Check Officer/ Candidate
AL	Approach Low	**BE**	Sector 5 Radar	**CE**	Sector 5 Area Proc	**T**	Training
AF	Flow Control	**BF**	Sector 6 Radar (Sec 1 Upper)	**CR**	Area Proc Relief	**FAM**	Familiarisation
AR	APC ADAR Relief	**BG**	Sector 7 Radar			**F**	Extra Controller
		BH	Area Radar Relief				

Table 2.2K - Shift Break Time

No.	Position	Position To Be Covered	Time (MYT)
1.	Sector 1 Planner	Sector 1 Planner	0000 - 0300
2.	Sector 4 Planner	Sector 4 Planner and Sector 2 AFD	
3.	Sector 3 Radar	Sector 1 Radar	
4.	Sector 4 Radar	Sector 2 Planner and Radar	
5.	Sector 5 Radar	Sector 3 + 5 Radar	
6.	Sector 6 Radar	Sector 3 + 5 Planner (working position not covered by Sector 6 Radar)	
7.	Sector 4 AFD	Sector 4 AFD	
8.	Sector 5 AFD	Sector 3 + 5 AFD and also cover as Sector 3 + 5 Planner	
9.	Sector 1 AFD	Sector 1 AFD	
10.	AFD/FDP 1	Assist FIS & AFD/FDP	
11.	Assist Clearance Delivery 1	Assist Clearance Delivery	
12.	FIS 3	AFD (0000-0200 UTC)	

Table 2.2L - Controller Working Positions between 0000-0300 MYT

No.	Position	Position To Be Covered	Time (MYT)
1.	Sector 2 Radar	Sector 1 Radar	0300 - 0600
2.	Sector 2 Planner	Sector 4 Planner	
3.	Sector 1 Radar	Sector 2 Radar	
4.	Sector 5 Planner	Sector 3+5 Planner and Sector 3+5 Radar.	
5.	Sector 3 Planner	Sector 1 Planner	
6.	Sector 2 AFD	Sector 4 AFD	
7.	AFD/FDP	Sector 3+5 AFD and also cover as 3+5 Planner	
8.	Assist FIS	Assist FIS & AFD/FDP	
9.	Assist Clearance Delivery	Assist Clearance Delivery	
10.	Sector 3 AFD	Sector 2 AFD	

Table 2.2M - Controller Working Positions between 0300-0600 MYT

(5) This analysis is based on the Air Traffic Controller Duty Roster for the month of March 2014, DCA Unit Administrative Instruction UAI 7/2010 and the entry recorded by the WS in the WS ATS logbook on 07 March 2014. From 1500 UTC [2300 MYT] until 1900 UTC [0300 MYT] and 1900 UTC [0300 MYT] until 2200 UTC [0600 MYT] the Sector 3+5 radar working position was manned by a radar-rated Controller. The Controller working positions (CWPs) between 0000 - 0300 MYT on the night of 07 March 2014, as shown in item 6 of *Table 2.2K* above revealed that the Sector 6 Radar Controller who was supposed to cover the Sector 3+5 planner position was not rostered by the ATSC Duty Watch Supervisor (the Radar Controller was rostered to work between 0300 - 0600 MYT). Consequently, the CWP for Sector 3 which was combined with Sector 5 at 1500 UTC [2300 MYT] was manned by a Radar Controller and an assistant flight data (AFD) Controller. Since the CWP planner was not covered (item 8 of *Table 2.2G* above), the AFD Controller stepped in as Sector 3+5 planner (albeit untrained for the planner position). From 1900-2200 UTC [0300 - 0600 MYT], a Radar Controller had to cover the Sector 3+5 radar and planner position (refer item 4 of *Table 2.2H*, above with an AFD Controller (refer to item 7 of *Table 2.2M*) who also stepped in as Sector 3+5 planner.

(6) In interviews with the ATCOs, the Team noted that when the planner positions were not covered, the AFD Controllers would step in as planners to assist the Radar Controllers as this had been the practice.

Shift personnel during scheduled break are allowed to rest in the rest area adjacent to the ATSC. The ATSC Duty Watch Supervisor maintains his/her watch at the Operational Centre until 1730 UTC [0130 MYT]. He/she takes his/her break until 2130 UTC [0530 MYT]. During his/her absence, a shift leader (usually the most senior Controller) is appointed to take charge but the ATSC Duty Watch Supervisor can be recalled at a moment's notice should the need arises.

(7) On the night of 07 March 2014, at 1500 UTC [2300 MYT] the Subang ATSC radar maintenance contractor at KL ATSC received a request from the Sector 5 Air Traffic Controller to absorb functions of control for Sector 5 into Sector 3. The request was successfully executed by the Site Maintenance Engineer (SME).

(8) In interviews with the ATCOs and on listening from the play-back of the direct telephone line recording on the Planning Controller working position, it is confirmed that, from 1600 UTC [0000 MYT] till 2200 UTC [0600 MYT], the Planning Controller working position (*Table 2.2N,* [below]) was manned by unrated Air Traffic Controllers as follows:

No.	Time	Sector 3 + 5 Planner Position
1	1600 UTC [0000 MYT] until 1730 UTC [0130 MYT]	Manned by an unrated ATCO
2.	1730 UTC [0130 MYT] until 1900 UTC [0300 MYT]	Manned by AFD Controller - untrained and unrated.
3.	1900 UTC [0300 MYT] until 2200 UTC [0600 MYT]	

Table 2.2N - Planning Controller Position between 1600-2200 UTC

The Team noted that during the operations in restricted/collapsed mode between 1600 UTC [0000 MYT] and 2200 UTC [0600 MYT], untrained and unrated Air Traffic Controller were manning the Planning Controller working position

n) Roles played by the Duty ATSC Watch Supervisor

i) Refer to *para. 2.2.2 para. l) (5).* b) MATS PART 1 - ADMIN, para 1.2.2, page 1-1-3 stipulates that:

Watch Supervisor - responsible for:

- *ensuring that the operating positions are manned adequately by personnel qualified and current in practice.* (Point No. 3).
- *ensuring that staff are operationally proficient (Point No. 4).*

ii) In interviews with the ATCOs on shift duty on the day of the disappearance of MH370, the AFD Controllers confirmed that they were performing the functions as Planning Controller for Sector 3+5 from 1600 UTC [0000 MYT] to 2200 UTC [0600 MYT].

iii) Based on transcripts of the planner's direct telephone line (refer *Factual Information, Appendix 1.18G, pages 1-164*), from 1620 UTC [0020 MYT] to 2200 UTC [0600 MYT], a total of forty-one (*Table 2.2O* below) Planning Controller's direct telephone line exchanges took place - thirty-eight by three ATCOs (one trainee and two AFD Controllers performing the functions of Planning Controller) and the remaining three by a Radar Controller.

No.	**ATCO**			**REMARKS**
	Radar	**Planning (3+5)**	**Trainee & AFD**	
1.	2	8	-	Relating to MH370
2.	1	25	5	Not relating to MH370 (mainly coordination with BKK, HCM and SIN
Sub-Total	**3**	**33**	**5**	
Total	**41**			

Table 2.2O - Planner Direct Line Telephone Exchanges

o) Activation of Aeronautical Rescue Coordination Centre

In interviews conducted with the SAR-trained Controller, the Team noted that the Aeronautical Rescue Coordination Centre (ARCC) was activated (*Figure 2.2O - ARCC Activation Form,* below) at 2130 UTC [0530 MYT]. After the activation, the Search and Rescue Mission Coordinator (SARMC) did not have sufficient details to act upon before the distress message was disseminated at 2232 UTC [0632 MYT]. The SARMC also informed the Team that the ARCC did not receive any alerting message from Ho Chi Minh via the Aeronautical Fixed Telecommunication Network (AFTN).

DCA/ASAR/FORM/01

JABATAN PENERBANGAN AWAM MALAYSIA
Department of Civil Aviation Malaysia (DCA)
AERONAUTICAL RESCUE COORDINATION CENTRE
BLOK B, KOMPLEKS KAWALAN TRAFIK UDARA
LAPANGAN TERBANG SULTAN ABDUL AZIZ SHAH
47200 SUBANG, SELANGOR DARUL EHSAN

Telephone No:
xx-xxxx xxxx (number redacted)
Fax No:
xx-xxxx xxxx (number redacted)

AIRCRAFT INCIDENT NOTIFICATION AND AERONAUTICAL RESCUE COORDINATION CENTRE ACTIVATION

TO :

	AGENCY	FAX	TEL
1	POTU	xx-xxxx xxxx (number redacted)	xx-xxxx xxxx (number redacted)
2	MRCC	xx-xxxx xxxx (number redacted)	xx-xxxx xxxx (number redacted)
3	MCC	xx-xxxx xxxx (number redacted)	xx-xxxx xxxx (number redacted)
4	UNIT UDARA BOMBA	xx-xxxx xxxx (number redacted)	xx-xxxx xxxx (number redacted)
5			

REF NO
1
DATE
8/3/2014
PAGE
1

1 DISTRESS STAGE

	ALERTFA
	INCERFA
X	DISTRESFA

INFORMATION OF THE INCIDENT			
Date	:	7/3/2014	
Time	:	17:19	UTC
		01:19AM	Local
Last Known Position	:	07 01' 36"	N
		103 31' 23"	E

2 NATURE OF DISTRESS

AIRCRAFT MISSING AFTER PASSED WAY POINT IGARI. NO DISTRESS CALL FROM THE PILOT REPORTED. KL ARCC ACTIVATED AT 0530 UTC.

3 AIRCRAFT DETAILS

Craft Callsign:	:	MAS 370
Type:	:	B777-200
Point of Dep:	:	WMKK, KUALA LUMPUR
Destination:	:	ZBAA, BEIJING
Route:	:	R208 - IGARI - BITOD

Crew	:	12
Passenger	:	227
Operator	:	MALAYSIA AIRLINE
Colour/Marking	:	WHITE/RED/BLUE
Survival Equipment	:	

SUBMITTED BY : *xxxxxx (Name redacted)*
DUTY SAR MISSION CO-ORDINATOR
KUALA LUMPUR ARCC

TIME SUBMITTED	
21:30	UTC
5:30 AM	LOCAL

COMPLETE THE SECTION BELOW AND RETURN BY FAX TO RCC, IF APPLICABLE

4 Request details on SRUs that are available for deployment for SAR:

	Search Unit Craft/Personnel	DEPARTURE & ARRIVAL LOCATION		ETD	POB	Fuel	Cruise Speed	Search Speed
		Departure	Arrival					
1								
2								
3								
4								

5	*Please mark 'YES' if , NIL SRUs AT ALL, WILL ADVISE WHEN AVAILABLE*	YES

Note: PILOT TO BE PRESENT FOR PREFLIGHT BRIEFING AT THE KL AERONAUTICAL RESCUE COORDINATION CENTRE (KLARCC), SUBANG (TIME: BEFORE FLIGHT)

Figure 2.2O - Aircraft Incident and ARCC Activation Form

The Team noted that the distress message was disseminated an hour and two minutes after KL ARCC was activated. There was no alerting message from Ho Chi Minh RCC.

p) Play-back of Radar and Radiotelephony Recordings by ATSC Duty Watch Supervisor

At 2145 UTC [0545 MYT], the ATSC Duty Watch Supervisor requested from the radar maintenance personnel to carry out radar data play-back (with permission granted by KL ATSC's Chief Assistant Director). The SME successfully restored the desired file from the recording play-back back-up hard disc. At 2200 UTC [0600 MYT] the ATSC Duty Watch Supervisor performed radar data and voice recording play-back at the D40 Controller Working Position (D40 CWP).

q) Entries in ATS Logbooks of ATSC Watch Supervisor and Sector 3 Controller Working Position

MATS Part 1 - Admin, page 1-1-7 para 1.7 on recording of entries in the logbook states, as follows:

i. The time of entries shall be based on UTC and events recorded in a chronological order;

ii. Entries shall give sufficient details to give readers a full understanding of all actions taken;

iii. The time an incident occurred and the time at which each action was initiated shall be stated.

MATS PART 1 - ADMIN, para 1.7, page 1-1-7 further states that:

The ATS logbook serves to record all significant occurrences and actions relating to operations, facilities, equipment and staff at an ATS unit. It is an official document and, unless otherwise authorised, its content shall be restricted to those personnel requiring access to the information. All personnel should read those log entries of concern to them, which were made during the period since their last tour of duty before accepting responsibility for an operating position.

1.7.2 Where there is more than one unit within a facility, a logbook shall be maintained for each unit.

1.7.3 The Supervisor or the senior Controller on duty shall be responsible for opening, closing and maintaining the log as applicable. Any Controller may make an entry but all entries shall be made in an indelible manner and no erasure is permitted. Incorrect information shall be struck out and the correct information inserted and initiated.

1.7.4 Information to be recorded in the ATS log should, as appropriate to the facility, include such matters as:

a) Incidents, accidents, non-compliance with regulations or air traffic control clearance, regardless of whether an additional separate report is required;

b) Aerodrome inspection reports, details of work in progress, aerodrome closures, and other essential aerodrome information;

c) Changes in the status of facilities, service or procedure including communications difficulties and tests;

d) Time of receipt of significant meteorological reports, e.g. SIGMET;

e) Any occurrence of a significant nature;

f) Configuration and reconfiguration of operation positions;

g) Any dispensation against the regulations, or special authorisation given by the Director General;

h) Details of approval for Special VFR operations; and

i) Opening and closing of shift or watch.

1.7.5 Controllers should follow the following procedures for recording of entries in the log:

a) Each entry should be accompanied by the signature or the authorised initials of the Controller making the entry.

b) The time of entries shall be based on UTC and events recorded in a chronological order;

c) Entries shall give sufficient details to give readers a full understanding of all actions taken;

d) The time and incident occurred and the times at which each action was initiate shall be stated; and

e) An entry needs to be brought to the attention of the unit chief shall be so annotated to enable him to take follow up action.

1.7.6 If during an emergency or busy period, it is not possible to make detailed entries in the log at the time of occurrence, Controllers are permitted to keep rough notes with exact times. As soon as possible thereafter, a detailed entry shall be made in the log.

a) Extract from the Watch Supervisor Logbook

i. Entry 11 at 1600 - Restricted watch

1st: named
12 names for the "2nd" half)

ii. Entry redacted (12 names for the "1st" half) and 2nd named redacted (12 at 1800:

*At 1800UTC, I was informed by S3 radar (name redacted) Controller then Ho Chi Minh is enquiring the position of MAS370 B777 reg. 9MMRO estimate for IGARI 1720, with a cleared level 35,000 ft. MAS370 is from KLIA to Beijing (ZBBB) with 239 POB. The fact is at time 1719 UTC, Mr. xxxx (name redacted) made a transfer of comm. instruction to MAS370 (MAS370 contact HO Chi Minh 120.9) and the pilot acknowledged by reading its callsign (MAS370). (*The radar label as it rosses Igari eastbound was good, but about 4 to 5 miles east of Igari the radar label starts 'coasting'. *base on radar video recording).*

*Prior to opening up the *replay, Ho Chi Minh indicated the Mr. xxxx (name redacted) that they saw the target until Bitod. At 1815, I check with MAS OPS Centre in KLIA Mr. xxxx, (name redacted) and he mentioned that MAS370 is on their flight tracker and he was able to exchange signals with the flight.*

At 1930 UTC Mr. xxxx (name redacted) MAS OPS Centre call in and spoke to Mr. xxxx (name redacted), admitting that the 'flight tracker' is based on projection and could not be relied for actual positioning or search.

At 2130 I activated RCC by instructing Pn. xxxx (name redacted) to handle this case.

Until 2245 still no cospas sarsat signal receive at ATCC Subang and ATCC Singapore. I spoke to Mr xxxx (name redacted) - watch supervisor Singapore (night shift), he confirmed that the was no cospas sarsat signal pickup on aviation target, only maritime hits was observed.

At 2250 I spoke to Ho Chi Minh W/sup, and advise him that based of video recording, the target starts to coast out about 4 to 5 miles east of Igari.

L/E at 2200, PTU Mr. xxxx (name redacted) who is in xxxx (name of place redacted) was informed, PP En. xxxx (name redacted) was informed by xxxx (name redacted).

Late entry - note - at 1840 Mr. xxxx (name redacted) (MAS OPS) confirmed that MAS370 download from acft giving a coordinate of N14.9000 1091500E timed 1833.

Conclusion - Our response to this incident is based on input by Ho Chi Minh and MAS Operations Centre using their 'flight tracker'. MAS370 was well transferred comms to Ho Chi Minh and acknowledged the instruction by pilot. And lastly the

radar label started to coast about 5 NM. east of IGARI. Lumpur RCC responsibility is to assist Ho Chi Minh to locating the acft posn.

r) Distress Message

i) The distress message (*DETRESFA*) is intended to convey pertinent information to the recipients that there is a situation wherein there is a reasonable certainty that an aircraft and its occupants are threatened by grave and imminent danger and require immediate assistance.

ii) The *DETRESFA* message with a date-time-group (DTG) 072232 UTC was transmitted at 2232 UTC [0632 MYT].

iii) The contents of the *DETRESFA* message, as shown in *Figure 2.2P* below was not composed in accordance with the standard specified in ICAO DOC 4444, Air Traffic Management (PANS-ATM) Chapter 11, Air Traffic Services Messages, Appendix 3 (*Figure 2.2Q* below). The errors are, as below:

(1) Appendix 3, page A3-9 (*Figure 2.2P* below)

Field type 7 - Aircraft identification and SSR mode and code FPL–MAS370–IS should be “MAS370/A2157”

(2) Appendix 3, page A3-14 (*Figure 2.2P* below)

Field type 13 - Departure aerodrome and time WMKK1635 should be “WMKK1642”

(3) Appendix 3, page A3-29 & A3-30 (*Figure 2.2P* below)

Omission of Field Type 20 - Alerting search and rescue information. This field consists of the following sequence of elements separated by spaces. Any information not available should be shown as “NIL” or “NOT KNOWN” and not simply omitted.

(4) Spelling of ***DESTRESFA*** should read ***DETRESFA*** (*Figure 2.2P* below)

```
KLA637 072232
SS WMKKZQZX WMKKZRZX
072232 WMFCZQZX
(ALR-DESTRESFA/WMFCZQZX/MISSING
-FPL-MAS370-IS
-B772/H-SDFGHIJ3J5M1RWXY/LB1D1
-WMKK1635
-N0470F290 DCT PIBOS R208 IKUKO/M081F330 R208 IGARI M765
 BITOD/N0480F330 L637 TSN/N0480F350 W1 BMT W12 PCA G221
 BUNTA/N0480F370 A1 IKELA/N0480F370 P901 IDOSI/N0480F390 DCT CH
 DCT BEKOL/K0900S1160 A461 YIN/K0890S1130 A461 VYK
-ZBAA0534 ZBTJ ZBSJ
-PBN/A1B1C1D1L1O1S2 DOF/140307 REG/9MMRO EET/WSJC0032 VVTS0042
 ZJSA0210 VHHK0233 ZGZU0304 ZHWH0356 ZPE0450 SEL/QRCS
 RMK/ACASII EQUIPPED
-E/0710 P/TBN R/UVE S/M J/LF D/8 290 GREY A/WHITE WITH RED AND
 BLUE STRIPE C/TBN)
```

JABATAN PENERBANGAN AWAM MALAYSIA
PENGURUSAN TRAFIK UDARA
HQ
AIR TRAFFIC MANAGEMENT
DEPARTMENT OF CIVIL AVIATION

Source: DCA Malaysia

Figure 2.2P - DETRESFA Message sent over AFTN

Excerpt from ICAO DOC 4444, Air Traffic Management (PANS-ATM) Chapter 10, Air Traffic Services Messages, Appendix 3, Field Type 7

Appendix 3 *A3-9*

Field Type 7 — Aircraft identification and SSR mode and code

Format: – (a) Max. 7 characters* / b c

SINGLE HYPHEN

(a) *Aircraft identification*

NOT MORE THAN 7 CHARACTERS, being the aircraft identification shown in the filed flight plan and composed as specified in Appendix 2, Section 2.

* This field may be terminated here in messages relating to flights operating within areas where SSR is not used, or when the SSR code information is not known or would not be meaningful to the accepting unit.

OBLIQUE STROKE

(b) *SSR mode*

LETTER A giving the SSR mode related to (c).

(c) *SSR code*

4 NUMERICS giving the SSR code assigned to the aircraft by ATS and transmitted in the mode given in (b).

Examples: –BAW902
–SAS912/A5100

FIELD TYPE 7

Previous type of field or symbol	*This type of field is used in*	*Next type of field or symbol*
5	ALR	8
3	RCF	21
3	FPL	8
3	CHG	13
3	CNL	13
3	DLA	13
3	DEP	13
3	ARR	13
3	CPL	8
3	EST	13
3	CDN	13
3	ACP	13
3	RQP	13
3	RQS	13
3	SPL	13

Figure 2.2Q - ATS Messages

Excerpt from ICAO DOC 4444, Air Traffic Management (PANS-ATM) Chapter 10, Air Traffic Services Messages, Appendix 3, Field Type 13 below

Field Type 13 — Departure aerodrome and time

FIELD TYPE 13

Format: – a b *

SINGLE HYPHEN

(a) *Departure aerodrome*

4 LETTERS, being

the ICAO four-letter location indicator allocated to the departure aerodrome, as specified in Doc 7910, *Location Indicators*, or

ZZZZ if no ICAO location indicator has been allocated (*see Note 1*) or if the departure aerodrome is not known, or

AFIL if the flight plan has been filed in the air (*see Note 2*).

Note 1.— If ZZZZ is used, the name and location of the departure aerodrome is to be shown in the Other Information Field (see Field Type 18) if this Field Type is contained in the message.

Note 2.— If AFIL is used, the ATS unit from which supplementary flight data can be obtained is to be shown in the Other Information Field (Field Type 18).

* This field shall be terminated here in message types CPL, EST, CDN and ACP. It shall be terminated here in message type RQP if the estimated off-block time is not known.

(b) *Time*

4 NUMERICS giving

the estimated off-block time (EOBT) at the aerodrome in (a) in FPL, ARR, CHG, CNL, DLA and RQS messages and in RQP message, if known, or

the actual time of departure from the aerodrome in (a) in ALR, DEP and SPL messages, or

the actual or estimated time of departure from the first point shown in the Route Field (see Field Type 15) in FPL messages derived from flight plans filed in the air, as shown by the letters AFIL in (a).

Examples: –EHAM0730
–AFIL1625

Previous type of field or symbol	*This type of field is used in*	*Next type of field or symbol*
10	ALR	15
10	FPL	15
7	CHG	16
7	CNL	16
7	DLA	16
7	DEP	16
7	ARR	(16)**
		17
10	CPL	14
7	EST	14
7	CDN	16
7	ACP	16
7	RQP	16
7	RQS	16
7	SPL	16

** Only in case of a diversionary landing

Figure 2.2R - ATS Messages

Excerpt from ICAO DOC 4444, Air Traffic Management (PANS-ATM) Chapter 10, Air Traffic Services Messages, Appendix 3, Field Type 20

Appendix 3 *A3-29*

Field Type 20 — Alerting search and rescue information

FIELD TYPE 20

Previous type of field or symbol	*This type of field is used in*	*Next type of field or symbol*
19	ALR	)

Format: – [ ] (sp) [ ] (sp) * (sp) [ ]

(*EIGHT elements in all)

This field consists of the following specified sequence of elements separated by spaces. Any information not available should be shown as "NIL" or "NOT KNOWN" and not simply omitted.

SINGLE HYPHEN

(a) *Identity of operator*

The ICAO two-letter designator of the aircraft operating agency or, if this has not been assigned, the name of the operator.

(b) *Unit which made last contact*

6 LETTERS consisting of the 4-letter ICAO location indicator followed by the 2-letter designator which together identify the ATS unit which made the last two-way contact or, if these are not available, some other description of the unit.

(c) *Time of last two-way contact*

4 NUMERICS giving the time of the last two-way contact.

(d) *Frequency of last contact*

NUMERICS as necessary giving the transmitting/receiving frequency of the last contact.

(e) *Last reported position*

The last reported position expressed in one of the data conventions of 1.6 of this Appendix followed by the time over that position.

Figure 2.2S - ATS Messages

cont…

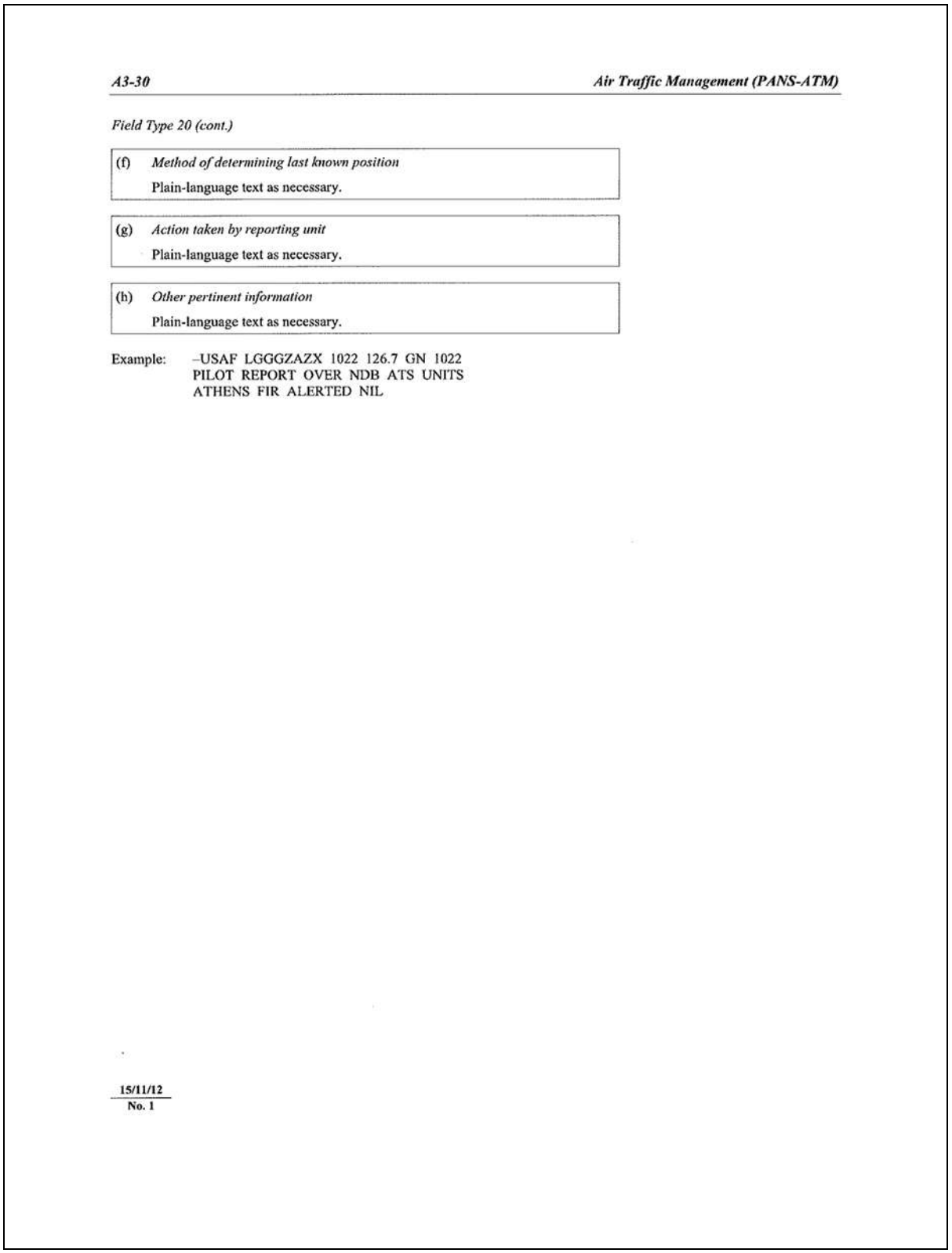

A3-30 *Air Traffic Management (PANS-ATM)*

Field Type 20 (cont.)

(f) *Method of determining last known position*
Plain-language text as necessary.

(g) *Action taken by reporting unit*
Plain-language text as necessary.

(h) *Other pertinent information*
Plain-language text as necessary.

Example: –USAF LGGGZAZX 1022 126.7 GN 1022
PILOT REPORT OVER NDB ATS UNITS
ATHENS FIR ALERTED NIL

15/11/12
No. 1

Figure 2.2T - ATS Messages

s) Issues with Manual of Air Traffic Services (MATS)

i) MATS 1 PART 2 - GEN, page 2-2-1 stipulates that:

2.1.2 Controllers and other operational staff shall:

a. apply as appropriate the rules, procedures, separation minima and guidance material contained in this manual in the control of air traffic and in the provision of other air traffic service; and

b. additionally comply with directive detailed in SOIs, ROIs, and UOIs and in Operational Letters of Agreement.

2.1.3 Controllers shall not deviate from a rule or separation minima, but may however deviate from a procedure if in the opinion of the Controller the situation warrants.

2.1.4 if a situation that is not covered in this Manual arises, Controllers shall use their best judgement as to the procedure to be applied to handle the situation.

In any uneventful situations, there are specific actions that require ATC personnel to maintain a continuous watch in their respective working positions and not to rely on information from MAS ODC.

SECTION 2 – ANALYSIS

2.3 MEDICAL/HUMAN FACTORS ISSUES

2.3.1 Introduction

This section analyses general human performance issues such as the medical history, professional qualifications, training, factors related to mental and physical fatigue, crew-to-ground communications, psycho-social events, and other relevant factors.

The analysis was done based on the following sources gathered from:

1) Personal records/files of the PIC, FO and the cabin crew from MAS. These documents included the log book, certificates, licenses, medical records and any disciplinary/administrative actions;

2) Investigation details from the Polis Di Raja Malaysia (PDRM) - Royal Malaysia Police. These were statements obtained from the next of kin and relatives, doctors/care givers, co-workers, friends and acquaintances; financial records of the flight crew, CCTV recordings at KLIA and analysis of the radio transmission made between MH370 and ground Air Traffic Control;

3) Medical records from private health care facility and from MAS Medical Centre; and

4) Interviews with MAS staff and several of the next of kin of the crew.

The analysis attained from documentations, CCTV recordings and interviews were conducted ethically, based on professional assessments code of practice of the Team.

2.3.2 General Human Performance Issues

1) The flight-crew's medical background and recent activities were examined. All medical files reviewed showed no significant health-related issues. Information derived from interviews with the medical health care professionals in the MAS organisation, members of the family and some friends of the flight crew, and study of the available medical records indicate that the PIC and FO were in good health and certified fit to fly at the time of the flight.

2) The Team noted that the medical records or reports of the flight crew obtained from the MAS Medical Centre facility did not include medical records or reports from other medical facilities. In fact, the Team has found a medical record of the PIC from another private medical centre which was not recorded in the MAS Medical Centre. The records from the MAS Medical Centre as well as the records from private clinics regularly visited by both the flight crew also seemed to be mainly records related to minor ailments such as coughs and colds and may not be reflective of the complete medical record of the individuals in question.

3) Based on the available medical records, only one cabin crew member, the In-Flight Supervisor, was known to have a history of previous seizures in 2013 but was subsequently certified fit to fly. However, all the cabin crew were fit to fly at the time of the flight.

    a) All cabin crew were adequately rested before the flight based on the flying records.

    b) There is no evidence that members of the cabin crew had received any flight training, based on the '*Basic Flying Training*' and '*Aircraft Type Conversion Training'* (B777) records of the Company and records of DCA.

4) Both the PIC and FO held valid airman licenses and medical certification. They had received all the required training. It was concluded that both the PIC and FO were properly trained, licensed and qualified to conduct the flight.

5) Based on the flying records from the Scheduling Office, both the PIC and FO were within duty-time limits and therefore were adequately rested before the flight.

6) The interpersonal relationship between the PIC and FO was examined. There were no reports of any conflicts or problems between the PIC and FO prior to the flight or before the day of the flight. This is the first time the PIC and FO have flown together after the latter completed his upgraded training to the B777. The Team did not find any evidence of a strain in the relationship between the two. It was the FO's last Line Training flight before he was scheduled to be checked out. The FO's training progress was within the performance of new FOs promoted to the B777 from the smaller fleet.

2.3.3 Specific Human Factors Issues

In this section, the specific personal relationships, financial background, personal insurance coverage and benefits, past medical and medication history, as well as the recent behaviour of the PIC, FO and all the cabin crew were examined.

1) Personal Relationships

Information obtained from family and friends of both the PIC and FO suggested no recent changes or difficulties in personal relationships. There was nothing significant observed by the family and friends of the crew. The PIC and FO as well as the crew were not experiencing difficulties in any personal relationships.

2) Pilot-in-Command

The investigation into the personal and professional career revealed that the PIC had flawless safety records with a smooth career pathway to his existing position as a Type Rating Examiner on the B777 and has been well respected throughout his flying career. He was considered a leading pilot who was given privileges to be an instructor and examiner.

3) First Officer

The investigation into the personal and professional career revealed that the FO had a good safety record with a smooth career pathway to his existing position as a Co-pilot under training on the B777-200ER. The investigation into the FO's personal and professional history revealed no disciplinary records.

4) Cabin Crew

There is no evidence to suggest that any members of the cabin crew had experienced career-related incidents or mishaps resulting in major disciplinary records.

5) Financial Background and Insurance Coverage

Information obtained on the financial background for the PIC, FO and all the cabin crew showed no evidence of financial

stresses or impending insolvency. Analysis of the bank financial statements did not reveal any incidents of unusual financial transactions.

Based on the available data, investment or trading accounts owned by the PIC were mainly inactive or dormant. The FO and cabin crew have no investment or trading accounts. Insurance coverage records were unremarkable which include generally life insurance policy, motor vehicle insurance policy, medical insurance policy and personal accident policy. There is no evidence of recent or additional insurance cover purchased by the PIC, FO or any members of the cabin crew.

6) Past medical and medication history

In the course of the investigation, it was confirmed that the PIC sustained a spinal injury as a result of a paragliding accident in January 2007. He was medically certified to have recovered from the injury, and there is no record of him being on long term medication for this, or other medical ailments. Scrutiny of his credit card transactions failed to reveal a pattern of regular purchase of over-the-counter medication of any significance, either in local or overseas pharmacies. The possibility that such medication may have been purchased by cash cannot be excluded.

The Team has further investigated the overseas over-the-counter prescriptions as there was no recorded transaction on the PIC's credit card on any medications purchased. The Team specifically investigated the possibility of mental/stress-related ailments in the PIC and concluded that there is no medical record or other documentation of the PIC having received psychiatric treatment.

Similarly, there was no documented unusual health-related issues involving the FO. Other than the Inflight Supervisor, the other members of the cabin crew have no significant health-related issues.

7) Recent Behaviour

According to family members and work associates who interacted with the PIC, FO and the cabin crew on the day of the flight and on their most recent flights, there were no behavioural signs of social isolation, change in habits or interest, self-neglect,

involvement in drug or alcohol abuse. There were no significant behavioural changes observed on all the CCTV recordings for the PIC, FO and cabin crew related to the flight.

8) Overall Comments

Evidence from the medical/human factors issues showed no unusual issues on the PIC, FO and cabin crew.

2.3.4 Human Factor Aspects of Air Traffic Control Recordings

1) Voice analysis

No Cockpit Voice Recorder (CVR) and Flight Data Recorder (FDR) analysis could be done as the wreckage is yet to be found. From the available information, the speech segments for the first 3 sets of audio recordings (Airway Clearance Delivery, Lumpur Ground and Lumpur Tower) were those of the FO before take-off and the 4th and 5th sets of the audio recordings (Approach Radar and Lumpur Radar) originated from the PIC after take-off.

The Team has noted nothing unusual in the conversations by the PIC and the FO with the assigned traffic Controllers. The last sentence of "*Good Night Malaysian Three Seven Zero"* was spoken by the PIC at 1719:30 UTC [0119:30 MYT].

2) Air Traffic Control Recordings

Radiotelephony recordings between the flight crew and the Air Traffic Controllers were analysed for voice recognition and it was verified that the words spoken before take-off and after take-off were that of the FO and PIC respectively. The Team has made comparison of the voice sample analysis recorded previously and found no evidence that there was any stress or anxiety detected in the conversations. It was noticed that the PIC made the same statement of "maintaining flight level three five zero' twice at 1701.17 UTC [0107.57 UTC [0107.56 MYT]. However, the Team did not find any significance of that statement spoken twice by PIC in a short interval of 6.39 minutes.

SECTION 2 – ANALYSIS

2.4 AIRWORTHINESS & MAINTENANCE AND AIRCRAFT SYSTEMS

2.4.1 Airworthiness & Maintenance

The review of the aircraft Airworthiness and Maintenance records revealed the following:

1) No current airworthiness issues were noted. There was no evidence of any pre-existing aircraft defects that would affect the safety of the flight.

2) An assessment of the Aircraft Log Book since the original issue of the Certificate of Airworthiness by the Department of Civil Aviation, Malaysia on 03 June 2002 indicated that the aircraft maintenance was carried out in accordance with the approved manufacturer's Maintenance Planning Document and in compliance with the Department of Civil Aviation Malaysia Approved Maintenance Schedule requirements. The Certificate of Airworthiness was valid at the time of the occurrence and the next Certificate of Airworthiness was due on 02 June 2014.

3) The last A1 Check was carried out on 23 February 2014 at 53,301:17 hours and 7,494 cycles. It was also noted that the last A4 Check was carried out at Malaysia Airlines Base Maintenance at KLIA, Sepang from 14 to 16 January 2014 at 52,785:37 airframe hours and 7,422 cycles respectively.

4) The right wing tip which was damaged during taxi at Pudong, Shanghai Airport on 09 August 2012 was assessed and repaired by Boeing AOG Team at Pudong, Boeing Shanghai facility from 22 September to 03 October 2012 as per MAS-RE-1209619 instructions. The Boeing repair scheme was approved under DCAM Statement of Compliance Reference Number SC/2012/081. There was no evidence of structural anomaly in the repair scheme. The repair had no bearing on the observed events on the event flight, i.e. it would not have affected any of the on-board equipment. There was a requirement, however, for damage tolerance information to be incorporated in the aircraft maintenance programme within 24 months from 02 October 2012, as stated in the FAA Form 8100-9 for the approval of the repair by the FAA Organisation Designation Authorization (ODA). This damage

tolerance information was not yet included in the maintenance programme for the aircraft at the time of the occurrence. The due date for the incorporation would be by 02 October 2014. Incorporation of the information in the maintenance programme would address any maintenance that becomes necessary as a result of the damage tolerance assessment. However, the investigation assessed that this had no effect on the occurrence flight.

5) The cabin re-configuration was approved under the FAA STC and DCAM SOC and there is no evidence of any documented deviation from stipulated design changes.

6) A review of aircraft concessions during the last year of operation revealed that Malaysia Airlines Quality Assurance Department had requested from the Department of Civil Aviation, Malaysia for a 10-day or 100-hour extension for a C1 check from 22 August to 01 September 2013. This request was approved. There were no other concessions recorded in the Aircraft Log Book.

7) A review of Malaysia Airlines Airworthiness Directives indicated that all the applicable Airworthiness Directives for mandatory compliance were complied with.

8) A review of the recent Technical Log Book entries by the flight and ground crew did not reveal any significant defects or trends.

9) A review of Malaysia Airlines list of Hard Time Components installed on the aircraft showed that the SSFDR ULB battery life was overdue at the time of the occurrence. There was no evidence of other overdue maintenance.

10) According to maintenance records, the SSFDR ULB battery expired in December 2012. There is no evidence to suggest that the SSFDR ULB battery had been replaced before the expiry date. The SSCVR ULB battery however was replaced, as scheduled, with the next expiry in June 2014. There is some extra margin in the design to account for battery life variability and ensure that the unit will meet the minimum requirement. However, once beyond the expiry date, the ULB effectiveness decreases so it may operate, for a reduced time period until it finally discharges. While there is a definite possibility that a ULB will operate past the expiry date on the device, it is not guaranteed that it will work or that it would meet the 30-day minimum requirement.

There is also limited assurance that the nature of the signal (characteristics such as frequency and power) will remain within specification when battery voltage drops below the nominal 30-day level.

Technical Log records showed that the SSFDR (together with the ULB) was replaced on the aircraft on 29 February 2008. Component installation records for the ULB showed that at the time the SSFDR was replaced on the aircraft the expiry date for the battery was December 2012.

Interviews were held with the MAS Engineering Technical records staff to determine why the ULB battery was not replaced before the expiry. It was revealed that the Engineering Maintenance System (EMS, a computer system used to track and call out maintenance) was not updated correctly when the SSFDR was replaced on 29 February 2008. The update involves 'removal' of the old unit in the system followed by 'installation' of the new unit. In this particular instance, although the old unit was 'removed', the new unit was inadvertently not recorded as 'installed' in the system. If the system was updated correctly on the installation, the next due date for removal would have been for the replacement of the ULB battery. Since the system was not updated it did not trigger the removal of the SSFDR for replacement of the ULB battery when it was due. ULB battery replacement is normally done in the workshop by routing the removed SSFDR, together with the ULB, to the workshop. This oversight was not noted until after the disappearance of MH370 when details of the ULBs were requested.

Subsequently, MAS Engineering Technical records staff carried out a fleet-wide record inspection for the ULBs to ensure all records for other aircraft were updated accordingly.

2.4.2 Emergency Locator Transmitters

The aircraft was fitted with four Emergency Locator Transmitters (ELTs) meeting the current ICAO and regulatory requirements at the time. All four ELT battery lives were within the required expiry dates. No ELT signal from 9M-MRO was reported by the responsible Search and Rescue agencies or any other aircraft. There have been reported difficulties with

the transmission of ELT signals if an aircraft enters the water, such as in the case of Air France flight AF447. In these instances, the ELT does not activate, or the transmission is ineffective as a result of being submerged under water. Furthermore, the ELT itself could be damaged or, very commonly in the case of fixed ELTs, the antenna or antenna cables become disconnected or broken. This significantly hampers any search and rescue effort and may mean the aircraft location remains undetected for a considerable time. A review of ICAO accident records (refer to *Appendix 1.6D*) over the last 30 years indicates that of 173 accidents involving aircraft fitted with ELTs, only 39 cases recorded effective ELT activation.

Following the disappearance of MH370 and in line with Global Aeronautical Distress and Safety System (GADSS) recommendation an amendment to ICAO Annex 6, Part 1 has been proposed for an Automatic Deployable Flight Recorder (ADFR). The ADFR is a combination recorder fitted into a crash-protected container that would deploy from an aircraft during significant deformation of the aircraft in an accident scenario. Considering the design and deployment features of a deployable recorder, the recorder is usually fitted externally, flush with the outer skin towards the tail of the aircraft. To find a deployed ADFR, an Emergency Locator Transmitter (ELT) is integrated in the ADFR. This ELT has the added advantage to assist in locating the accident site and facilitate search and rescue efforts. In the case of a new generation ELT being fitted, the ELT will provide emergency tracking data before the impact. Furthermore, if the wreckage becomes submerged in water, the traditional ELT signal will be undetectable, but with the deployable recorder being floatable, the ELT signal would still be detectable, and the deployable recorder would be recovered quicker. As the ADFR is floatable, there is no requirement for an underwater locating device.

2.4.3 Aircraft Health Monitoring

The Maintenance Control Centre (MCC) of Malaysia Airlines did not receive any fault messages through ACARS during the event flight even up to the time the last ACARS report was transmitted. Depending on the type of failure, failure of the ACARS itself can be reported by the system. However, no such reports were received for the flight. The traffic log of maintenance messages transmitted for the last 10 flights for the aircraft indicated that the CMCS was functioning appropriately before the event flight. On an average, 11 maintenance messages, of various systems, were transmitted on each flight. A review of the maintenance history showed no evidence of a defect trend on the CMCS.

2.4.4 Aircraft Systems Analysis

The aircraft systems analysis is severely limited by the lack of available evidence. The information in this section is primarily inferred from SATCOM transmissions, aircraft system characteristics, radar data, and the absence of other communications from the aircraft for the majority of the flight.

1) Air-conditioning, Pressurisation and Oxygen

The SATCOM handshake data indicated that the aircraft was airborne for approximately 7 hours, 37 minutes (Take-off: 0042 MYT to Last SATCOM Handshake: 0819 MYT). That the aircraft flew quite some distance over a long period suggests that it flew at high altitude. Refer to the aircraft performance section in *Section 1.6.9*.

There is no evidence from the limited data available on the status of the aircraft air-conditioning and pressurisation systems during the flight. There was no Mandatory Occurrence report raised for this aircraft on pressurisation issues. A review of the Technical Log entries since the last D check in June 2010 did not reveal any defect trends in the air conditioning or the pressurisation systems. There were also no such defects reported prior to the event flight. There was an FAA Airworthiness Directive (AD) issued which made mandatory the accomplishment of Boeing Service Bulletin 777-53A0068 which addresses a crack in the fuselage skin under the SATCOM antenna adapter. This Service Bulletin was issued on 12 June 2013. A crack in the fuselage skin could lead to rapid decompression and loss of structural integrity of the aircraft. However, this AD or the Service Bulletin was not applicable to 9M-MRO due to a different configuration and location of the SATCOM antennas.

In the event of a complete pressurisation failure, however, oxygen would be available for the flight crew through the flight crew oxygen system and masks. Two cylinders located in the left side of the main equipment centre, each of 115 cubic feet (3256 litres), would be able to supply oxygen to a single person for a duration of 27 hours, or for 2 persons for a duration of 13 hours.

For the passengers, oxygen could be supplied by chemical oxygen generators located in passenger service units (PSUs). A door with an electrically operated latch keeps the masks in a box until the oxygen

deployment circuit operates. The deployment circuit would operate, and the masks automatically drop from the PSUs if cabin altitude were to exceed approximately 13,500 ft. Oxygen would flow when any mask hanging from that PSU was pulled. Oxygen would be available for approximately 22 minutes. The passenger masks can be manually deployed from the cockpit by pushing the overhead panel PASSENGER OXYGEN switch to the ON position. The electrical power to the latch is supplied through a circuit breaker located in the Main Equipment Centre. It is not possible to deactivate automatic deployment of the masks from the cockpit.

There are also portable oxygen cylinders located throughout the cabin which let the flight attendants move in the aircraft when oxygen is in use. It is also a gaseous oxygen supply for medical emergencies. The cylinders are fitted with a disposable mask. 15 cylinders are located throughout the passenger cabin. Each cylinder is of 11 cubic feet (310 litres) capacity. The flow of oxygen can be controlled by an 'Off-On' knob which can be rotated to control the flow from 0 to 20 liters per minute.

A review was carried out of whether there could have been an oxygen leak in the crew oxygen system. A leak of oxygen is a potential source for fire to break-out. A review of the Technical Log entries since the last D check in June 2010 did not reveal any oxygen leak in the system. There had been the usual servicing of the oxygen system when the pressure had dropped from the nominal level. The Stayover check, which is carried out whenever the aircraft planned ground time exceeds 6 hours, calls for the crew oxygen pressure to be checked. It has been the practice of the airline to service the oxygen system whenever time permits, even if the pressure is above the minimum required for dispatch (310 psi at 35°C). Tech Log entries showed that the system was serviced when the pressure dropped to, on an average, 1100 psi. On 07 March 2014, prior to the last flight, the pressure was noted to be 1120 psi and serviced to 1800 psi. However, it was not possible to eliminate the possibility of an oxygen leak on the event flight.

Another potential source of fire fed by oxygen is the issue highlighted in FAA AD 2012-13-05 which made mandatory the accomplishment of Boeing Service Bulletin 777-35A0027, as highlighted in *Section 1.6.4 para. 5)*. An electrical fault or short circuit can result in electrical heating of the low pressure oxygen hoses in the flight crew oxygen system and can cause the low pressure oxygen hose to melt or burn.

This can result in smoke and/or fire in the flight compartment. This service bulletin was already accomplished on 9M-MRO on 17 January 2014 by replacing the low pressure oxygen hoses with non-conductive low pressure oxygen hoses, reducing the likelihood of this potential source of fire.

2) Autoflight

The turn after IGARI was made from a heading of about 060° to a final heading of about 240° (a change of 180°) based on recorded radar data. Simulator sessions indicated that a bank angle of at least 30° is required to accomplish a half rate turn, of 180° in 2 minutes with a Ground speed of about 470 knots. Such a turn is not possible using autopilot as the bank angle is limited up to a maximum of 25° in any of the autopilot modes, such as LNAV or HDG SEL. Using LNAV mode, the time taken to make the turn is greater than 3 minutes. At an Indicated airspeed (IAS) of 250 knots (groundspeed – GS, of 425 knots) it took 3 minutes 3 seconds while at an IAS of 220 knots (GS of 400 knots) it took 3 minutes 30 seconds. Both manoeuvres were at 35,000 ft. Refer to *Section 2.1* on a discussion on this. From the simulator sessions it is evident that the turn itself was most likely made with the autopilot disengaged.

It is unclear how the aircraft was flown for the remainder of the flight, however the aircraft made several other turns and rolled out to level flight after the turn after IGARI. The SATCOM data indicated that the aircraft was airborne for more than 7 hours suggesting that the autopilot was probably functioning, at least in the basic modes.

3) Electrical Power

As the aircraft SATCOM system was providing log-on information to the INMARSAT satellites it can be deduced that at least part of the SATCOM system had electrical power. The SATCOM system components including the Satellite Data Unit (SDU), Radio Frequency Unit (RFU), High Power Amplifier (HPA), Low Noise Amplifier/Diplexer (LNA/DIP) and the Beam Steering Unit (BSO) are powered by the 115V AC, Left Main AC bus. This bus is normally powered by the Left Engine Generator, however a failure of the generator or the power feed to it will cause the Bus Tie Breakers to close and automatically let the Right Engine Generator power the bus.

This bus can also be powered by the Auxiliary Power Unit (APU) Generator, if the APU is started manually or automatically (such as a loss of power to both engines).

The above suggests that at least one generator was operating and providing the power to the SATCOM system after power was restored at 1825 UTC following the interrupt of between 22 to 78 minutes.

SATCOM operation, especially the electronic steering of the Radio Frequency signals through the antenna to the satellite, requires the Air Data Inertial Reference Unit (ADIRU) to be functioning. The ADIRU, which is a single unit on this aircraft, is an integrated unit having internal redundancy and provides the air data and inertial reference functions. It is powered either by the Right 28 Volt DC bus, the Left 28 Volt DC bus or the hot battery bus (a direct connection to the aircraft battery). The DC busses can be powered by the respective Main AC busses (after being rectified to DC) or by automatic switching (in case of failure of the respective AC bus) by the opposite Main AC bus. The battery itself can only supply power for a short duration, so it is highly likely that the source of power for the ADIRU was one of the generators as the SATCOM system was powered for many hours.

The operation of the SATCOM not only depends on the supply of power to its own system, it also depends on the supply of power to other systems feeding it, such as the ADIRUs. This inter-dependency of operation suggests that significant parts of the aircraft electrical power system were probably functioning throughout the flight.

4) Flight Controls and Hydraulics

The primary flight control system is highly redundant, with three operating modes: normal mode, secondary mode, and direct mode. The primary flight controls are powered by redundant hydraulic sources. The hydraulic systems are pressurised from the engines and the electrical actuation systems are similarly highly redundant. The secondary flight controls, high lift devices consisting of flaps and slats, are hydraulically powered with an electrically powered backup system. It is highly likely that the primary flight controls were functional as the aircraft altered the flight path several times and maintained flight for a long duration.

5) Instrumentation

Flight instruments are required only to fly the aircraft manually. The aircraft was equipped with Standby flight instruments which operate independently of the Primary flight instruments. Operation of the autopilot is not dependent on operation of the flight instrument displays.

Due to the lack of available evidence, it was not possible to determine the extent to which the instrumentation was operable throughout the flight. However, the instrumentation system, and the system that feed information to it, are highly redundant and driven from multiple automatically-reconfigurable electrical power sources. Based on the findings that several systems (particularly ADIRS, AIMS and SATCOM) were operable for some or all of the flight, it is very likely that some or all instrumentation was available.

6) Navigation

The main systems that are relevant for consideration are the Air Data Inertial Reference System (ADIRS), the Flight Management System (FMS) and the Global Positioning System (GPS).

If the autopilot (at least the basic modes) was functional, the ADIRS must have been operating satisfactorily because an essential input to the autopilot is the aircraft attitude which is provided by the ADIRU, the main unit of the ADIRS. In addition, the SATCOM continued to transmit during the flight as evidenced by the handshakes (*Section 1.9.5*). The SATCOM was using the High Gain Antenna for tuning. This shows that the ADIRU was operable, otherwise the Low Gain Antenna (LGA) would have been used.

As for the Flight Management System, it is unclear whether the system was functioning properly throughout the flight. This system is not essential for the operation of the autopilot.

The GPS is required for position updates of the FMS. Accurate navigation is dependent on GPS inputs. However, the ADIRU can provide the navigation reference without GPS inputs, although with lesser accuracy.

7) Engines

The aircraft satellite transmission associated with the 7th arc is most likely associated with power interruptions on board the aircraft caused by fuel exhaustion (*Section 2.4.4 para. 9)*. The time of this transmission is consistent with the maximum flight times expected for the MH370 flight, based on the total weight of fuel remaining during the last ACARS transmission at 1707 UTC. It is highly likely that both the engines were operating for the aircraft to have flown for more than 7 hours with that amount of fuel on board.

The Engine Health Monitoring (EHM) system trend reports over the last 3 months which cover 'snapshot' data points gathered at take-off, climb and cruise also showed no evidence of unusual engine behaviour for both engines. Similarly, the last report (Climb report) received at 1652 UTC on 07 March 2014 (0052 MYT on 08 March 2014) and the earlier Take-off report, do not show any unusual engine behaviour. Furthermore, there were no fault messages transmitted by the CMCS to indicate any engine abnormalities, before the ACARS last transmission.

8) Fuel Systems

The fuel systems were most probably functioning satisfactorily as the performance of the engines was dependent on this. It is unlikely that there were any problems in these based on the premise that the aircraft most likely flew to fuel exhaustion, as explained in *Section 2.4.4 para. 9)*.

9) Auxiliary Power Unit

The operation of the Auxiliary Power Unit (APU) during the majority of the flight is uncertain although it is possible that it started up automatically (as it should) after both engines shutdown due to fuel exhaustion at the end of the flight. This start-up and power-up of the electrical buses most likely caused the 7th and last, aircraft initiated SATCOM handshake.

Performance calculations indicate the possibility that the aircraft would have reached fuel exhaustion at, or before the time of the 7th handshake. After a single engine shutdown, automatic switching of the electrical tie breakers would ensure the Left and the Right Main busses and the Left and Right Transfer busses were still powered by the remaining generator driven by the running engine. After the

shutdown of the second engine following fuel exhaustion, the Main busses and the Transfer busses would have de-energised as there would be no generators powering these busses. An electronic logic in the APU starting system would automatically start the APU, if the aircraft was in the air, and both the Left and Right Transfer busses were not powered. As the fuel inlet for the APU is below that of the engines (left engine main fuel inlet in the left tank) the APU can start up and run for about 14 minutes even though the aircraft engines themselves are exhausted of fuel from the fuel tanks as the difference in the fuel intake levels would provide about 30 pounds of fuel. It would take about 1 minute for the APU to start up and power the busses and once powered, the Satellite Data Unit (SDU) of the SATCOM would take approximately another 1 minute to initiate the 'handshake', which would have been the 7th and last SATCOM handshake. Both the APU start up and the initialisation of the handshake by the SDU would have happened within the 14 minutes of running time available from the 30 pounds of fuel, after which the APU would have shut down due to its own fuel exhaustion.

10) Communications

The aircraft was fitted with many communication systems, available to the flight crew. Among them were the High Frequency (HF) system, the Very High Frequency (VHF) system, the Air Traffic Control system including the Mode S Transponder, the ACARs and the SATCOM. The SATCOM phone in the cabin was available for the cabin crew. Despite the availability of all these systems no communications were received from the aircraft after the last communication at 1719:30 UTC, 07 March 2014 (0119:30 MYT on 08 March 2014) except for the 'handshakes' received from the SATCOM system.

a) High Frequency System

Communication with ATC after take-off is normally through the VHF. The HF system is for communication with ground stations or other aircraft during long overwater flights. There was no evidence to indicate that the HF systems (Left or Right) were used prior to the aircraft's last communication at 1719:30 UTC on 07 March 2014. This communication was through VHF. There was no message received from the aircraft to report on a HF system failure or system technical error prior to the last voice or ACARS communication. There was also no recent defect trend on the HF systems.

b) Very High Frequency System

The aircraft VHF system was operating satisfactorily as evidenced by the communication by the flight crew to ATC up to the last communication at 1719:30 UTC, 07 March 2014 (0119:30 MYT, 08 March 2014). There were three independent VHF communication systems on the aircraft. The crew normal procedure is to use the Left VHF for communications. There was no message received from the aircraft to report on the VHF system failure or system technical error prior to the last voice or ACARS communication. There was also no recent defect trend on the VHF systems.

c) Air Traffic Control/Mode S Transponder System

The aircraft transponder was operating satisfactorily up to the time it was lost on the ATC radar screen at 1720.36 UTC, 07 March 2014 (0120:36 MYT, 08 March 2014). There was no message received from the aircraft to report a system failure prior to the last voice or ACARS communication. The crew procedure for normal operations is to select the left system on the control panel so the left system was likely in use. Failure of the system will be annunciated in the cockpit so that the crew can select the operating system.

The Left ATC/Mode S transponder gets 115V AC power from the AC Standby bus. The Right ATC/Mode S transponder gets 115V AC power from the Right AC Transfer bus. The dual transponder panel gets 115V AC power from the AC Standby bus. The two transponders are powered by highly reconfigurable AC buses; the left one can be powered by the battery if the left AC bus is unavailable (the AC Standby bus can be powered by the left Transfer bus or the battery), and the AC Transfer busses also have their alternate sources (the Main AC busses). It is likely that the Right Main AC bus was available because otherwise the ADIRU would have lost alignment (which it did not). It is likely that the power sources for one or both transponders were available.

This system can be deactivated (turned OFF) by pulling the circuit breakers located at the P11 overhead circuit breaker panel in the cockpit or by selecting the Transponder Mode

Selector (Transponder Panel) to “STBY” position. Selecting the Mode Selector to “STBY” will deactivate both the transponders.

d) Aircraft Communications Addressing and Reporting System

The ACARS communicates through either the VHF or the SATCOM systems. The ACARS datalink connects to the Satellite Data Unit (SDU) of the SATCOM system and the Center and Right VHF Communication Transceivers of the VHF systems. The Center VHF exchanges data with the ACARS modem in the Communications Core Processor Module (CPM/Comm) of the Left AIMS cabinet. The right VHF exchanges data with the ACARS modem in the CPM/Comm of the Right AIMS cabinet. The ACARS does not interface with the Left VHF Transceiver.

For the ACARS operation the Data Communication Management Function (DCMF) of the AIMS uses the voice/data select to set the VHF Communication Transceiver to the data signal mode. At power-up, the DCMF sets the Center VHF Communication Transceiver to the data signal mode. If the Center VHF Communication Transceiver fails, or voice is selected manually by the flight crew, the DCMF selects SATCOM for data transmissions. If SATCOM fails, the DCMF selects the Right VHF Communication Transceiver for data transmissions. The Left VHF Communication Transceiver is voice only. On the event flight, voice was selected for the Center VHF on the ground which resulted in the ACARS using SATCOM for the data transmissions, as shown in the SATCOM Ground Station Logs (refer to *Section 1.9.4*).

As the ACARS function is part of the AIMS there is no direct way of removing electrical power from the ACARS. This would require removing power to the AIMS which would disable many other systems as the AIMS manages data for several integrated avionics systems. However, it is possible to deactivate the ACARS downlink function from the ACARS Manager page in the Communications main menu on the selected Multifunction Display (MFD) in the cockpit. However, this will not affect the SATCOM handshakes. The COMM display switch, located on the display select panel, displays the communications main menu on the selected MFD. The

ACARS Manager page allows the flight crew to select/deselect VHF or SATCOM transmission of data (*Figure 2.4A* below). ACARS is set to auto mode (both boxes selected) at power-up or during a manual data communication system reset. Normally, this permits ACARS to automatically use VHF or SATCOM (if VHF is unavailable). If both boxes are deselected, ACARS loses the capability to send downlink messages, but can receive and display uplink messages.

Once deselected, a power interruption, will not cause the ACARS to be set to auto mode (both the VHF and SATCOM boxes selected) again. For the ACARS to be set to auto mode, either a data communication system reset or a power-up is done. The system does an automatic data link system reset 10 minutes after last engine shutdown and first passenger door open. This would explain why the power resumption at 1825 UTC following the interruption (*Section 1.9.5 para. 4*) did not activate the ACARS downlink again (with the assumption that both the VHF and SATCOM boxes were deselected).

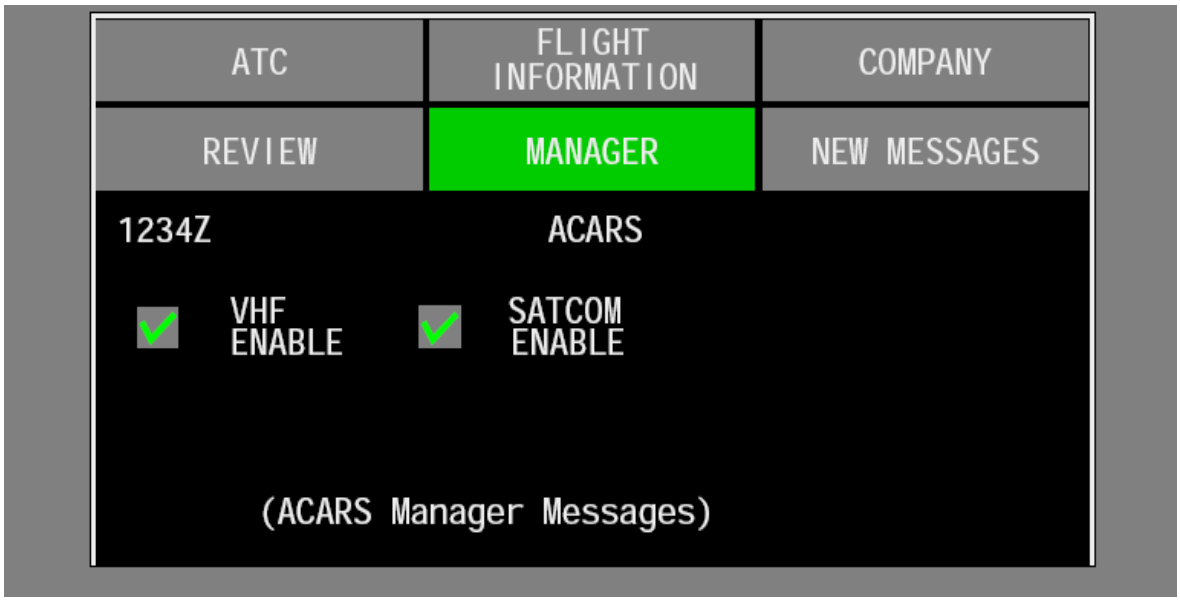

Copyright © Boeing. Reprinted with permission of The Boeing Company

Figure 2.4A - ACARS Manager Page on MFD

The last position report transmitted via ACARS was at 1707:29 UTC, 07 March 2014 (0107:29 MYT, 08 March 2014). Parameters recorded (*Table 2.3A*) were as follows:

Greenwich Mean Time (GMT)	1706:43 UTC
Altitude (ALT)	35004 feet
Calibrated Airspeed (CAS)	278.4 knots
MACH	0.821 Mach
Total Air Temperature (TAT)	-13.1° C
Static Air Temperature (SAT)	-43.8° C
Latitude (LAT)	5.299
Longitude (LONG)	102.713
Gross Weight (GWT)	480,600 lb
Total Remaining Fuel Weight (TOTFW)	43,800 kg
Wind Direction (WINDIR)	70.0
Wind Speed (WINDSP)	17.13
True Heading (THDG)	26.7

Table 2.4A - Last Position Report from ACARS

All programmed communications via ACARS prior to 1707:29 UTC were working satisfactorily.

After this last automatic ACARS transmission over the SATCOM, either the ACARS was turned off or the AIMS had a fault that prevented ACARS transmissions while certain other functions such as inertial data forwarding did not appear to be significantly affected.

e) Satellite Communication System

Refer to *Section 2.5* for the detailed analysis of SATCOM.

11) Airplane Information Management System

The Airplane Information Management System (AIMS) is designed with several redundancies to be failure tolerant. The system consists of two cabinets performing almost identical operations. The signal outputs of these cabinets are fed onto common busses which are shared by the various systems. These two cabinets are also isolated in location, the Left AIMs is located in the forward rack of the Main Equipment Centre (MEC) while the Right AIMS is located in the rear rack of the MEC.

The AIMS cabinets also receive electrical power from different busses. The Left AIMS cabinet gets electrical power from the 28V

DC Capt Flight Instrument bus and the 28V DC F/O Flight Instrument bus. The Right AIMS cabinet gets electrical power from the 28V DC Left bus and the 28V DC Right bus. Each cabinet receives the power from four 28V DC circuit breakers in the overhead circuit breaker panel. The four 28V DC bus inputs, known as power 1 through power 4 enter the cabinets through different routings. Power 1 and power 2, known as left power, enter the cabinet through a connector on the left side of the cabinet. Power 3 and power 4, known as right power, enter the cabinet through a connector on the right side of the cabinet.

Each AIMS cabinet has four Input/Output modules (IOM) and four Core Processor Modules (CPM). These are Line Replaceable Modules (LRM). The IOM transfers data between the software functions in the AIMS CPMs and external signal sources. The CPMs supply the software and hardware to do the calculations for several avionic systems. The software is called functions. To keep a necessary separation between the functions, each function is partitioned. The partitions permit multiple functions to use the same hardware and be in the same CPM. Each LRM receives power from four sources, two for main power and two for monitor power. The main circuitry uses the main power. Special circuits that monitor the condition of the power supply in the LRM use the monitor power. The two main and two monitor sources of power for each LRM come from different power sources. Each LRM must have at least one main and one monitor power input to operate. The loss of any one of the four power buses to the backplane power bus or to any one LRM has no effect on the function of the LRMs. The loss of two power inputs from the same side of the cabinet, left or right, has no effect on the function of the LRMs. The loss of one power input from the left side and one power input from the right side results in the loss of function in four LRMs. The loss of three or four of the power buses to the cabinet chassis power backplane results in the loss of function of all the LRMs.

Each AIMS cabinet also receives power through one hot battery bus circuit breaker in the standby power management panel. The connection to the hot battery bus keeps the LRMs internal memories active. The hot battery bus also makes the AIMS cabinet less likely to have faults due to power transients.

Given the preceding arrangement of dual and distant location of the AIMS cabinets, independent and multiple power sources and

separation of the computing functions the likelihood of failure of the AIMS operation is remote. Furthermore, operation of the SATCOM is reliant on satisfactory operation of the AIMS. Regular SATCOM 'handshakes' were present, till the 7th and last handshake at 0019 UTC. This indicates that the AIMS, or at least part of it, was operational.

2.4.5 Summary

From the foregoing discussion it can be generally deduced that there is no evidence to suggest that a malfunction had caused the aircraft to divert from its filed flight plan route. The aircraft's maintenance history and events prior to the last flight do not show any issues that could have contributed and resulted in the deviation and subsequent changes in the flight path. Although it cannot be conclusively ruled out that an aircraft or system malfunction was a cause, based on the limited evidence available, it is more likely that the loss of communication (VHF and HF communications, ACARS, SATCOM and Transponder) prior to the diversion is due to the systems being manually turned off or power interrupted to them or additionally in the case of VHF and HF, not used, whether with intent or otherwise.

Similarly, the recorded changes in the aircraft flight path following waypoint IGARI, heading back across peninsular Malaysia, turning south of Penang to the north-west and a subsequent turn towards the Southern Indian Ocean are difficult to attribute to any specific aircraft system failures. It is more likely that such manoeuvres are due to the systems being manipulated.

The analysis of the relevant aircraft systems taking into account the route followed by the aircraft and the height at which it flew, constrained by its performance and range capability, does not suggest a mechanical problem with the aircraft.

SECTION 2 – ANALYSIS

2.5 SATELLITE COMMUNICATIONS ANALYSIS

2.5.1 Summary of Key Observations of the SATCOM Ground Station Logs

The key observations of the SATCOM Ground Station Logs, with an assessment, are summarised below:

1) Prior to take-off, the SATCOM Logged On (normally) a number of times, the last time being at 1600, when it sent a valid Flight ID to the Ground Earth Station (GES). The SATCOM link was available for both voice and data (known as Log-On Class 3).

2) After take-off, the In-Flight Entertainment System (IFE) Short Messaging System (SMS) e-mail application sent a normal beginning of flight message at 1642 (containing the correct Airborne Earth Station (AES ID), Flight ID “MAS370”, origin airport “WMKK”, and destination airport “ZBAA”), indicating that the IFE was receiving the valid Flight ID, origin airport and destination airport from Airplane Integrated Management System (AIMS) and the ICAO (AES) ID from the Satellite Data Unit (SDU) at this time.

3) The SATCOM link was available for most of the flight, excluding periods leading up to 1825 on 07 March 2014 and 0019 on 08 March 2014.

4) When the SATCOM link was re-established at the above times, no Flight ID was present. This implies that a valid Flight ID probably stopped being sent to SATCOM at some time between 1642 (when the IFE reported the correct Flight ID) and 1825 (when the SATCOM Logged On with no Flight ID) on 07 March 2014. The possible reasons for the link losses and the subsequent Log-Ons that took place at 1825 and 0019 have been investigated and are detailed in tables in *Section 2.5.2.* There are many quite complicated scenarios that could have caused the 1825 Log-On. However, the most likely reason is a lengthy power interrupt to the SATCOM. The most likely reason for the 0019 Log-On was also a power interrupt to the SATCOM.

5) During the two in-flight Log-Ons at 1825 and 0019, the GES recorded abnormal frequency offsets for four burst transmissions from the SATCOM. After extensive analysis, the following explanations have emerged.

The 1825 Log-On Request had a non-zero BER and could therefore have been logged at the Ground station with a BFO measurement error suggesting that the BFO figure may not be reliable.

a) 1825 Log-On Acknowledge - Most likely due to the power-on drift of the SDU Oven Controlled Crystal Oscillator (OCXO), thus endorsing the belief that the 1825 Log-On was preceded by a lengthy power interrupt.

b) 0019 Log-On Request - Could have been due to uncompensated vertical velocity, indicating that the aircraft was likely to be descending at this time. Alternatively, it could have been due to the OCXO warm up drift, or it could have been due to a combination of uncompensated vertical velocity and OCXO warm up drift.

c) 0019 Log-On Acknowledge - Could have been due to uncompensated vertical velocity, indicating that the aircraft was likely to be descending at this time. Alternatively, it could have been due to the OCXO warm up drift, or it could have been due to a combination of uncompensated vertical velocity and OCXO warm up drift.

d) It has not been possible to attribute specific correction values to the 1825 Log-On Acknowledge and 0019 Log-on Request and Log-On Acknowledge BFOs, so it was excluded from the Doppler calculations undertaken by the Aircraft Flight Path/Performance Subgroup. In the case of the 1825 Log-On Acknowledge, the following subsequent bursts were used instead, as the frequency is more stable at these times:

i) 1828:05.904 Data-3 R-Channel burst.

ii) 1828:14.905 Data-3 R-Channel burst.

6) There is no indication of the SATCOM link being manually Logged Off from the cockpit (via a Multi-function Control Display Unit [MCDU]). Such activity would have been captured in the GES logs, but it was not.

7) No Data-2 Aircraft Communications Addressing and Reporting System (ACARS) traffic was observed after 1707 on 07 March 2014.

8) The IFE equipment set up two ground connections over SATCOM (for the SMS e-mail application and Built-In Test Equipment (BITE) application) after the SATCOM re-established the link at 1825 on 07 March 2014 (normal), but not after the SATCOM re-established the link at 0019 on 08 March 2014 (abnormal). In the 0019 case, it is possible that the IFE was no longer powered, or failed, or that the IFE and/or the SATCOM became inoperative before the connections could be set up. At no time during the flight was any user data sent over the link by means of the SMS/e-mail application.

9) Two Ground-to-Air Telephony Calls were placed to the cockpit from the MAS Airline Operations Centre at Airline Operational Communications (AOC) Q10 priority level at 1839 and at 2313 on 07 March 2014. Neither of the calls was answered.

10) The SATCOM responded normally to a series of roughly hourly Log-On Interrogations from the Perth GES, up to and including a Log-On Interrogation at 0011 on 08 March 2014. The two unanswered ground to air calls at 1839 and 2313 reset the Perth GES inactivity timer and hence the Log-On Interrogations were not always hourly.

11) The SATCOM transmissions during the two in-flight Log-Ons and five Log-On Interrogations form the seven ‘handshakes’ that have been used by the Flight Path/Performance Subgroup to calculate the seven geographical ‘arcs’.

12) The last transmission received from the SATCOM occurred at 0019 on 08 March 2014 and the SATCOM failed to respond to a series of three Log-On interrogations starting at 0115 on 08 March 2014. This implies that the SATCOM probably became inoperative at sometime between 0019 and 0115 on 08 March 2014.

2.5.2 Possible Reasons for the 1825 and 0019 Log-On Events and Preceding Link Losses

1) First In-Flight Log-On at 1825 on 07 March 2014

Flight ID Status Change Description	Log-On Reason	Likelihood	Comments
Flight ID stopped being received from AIMS, or being received, but with the Sign Status Matrix (SSM) field not set to Normal Operation.	Power Interrupt	Medium	CBs are not readily accessible, but could have been due to power interrupt.
	Sysfail (software fail)	Very low	Sysfail is a very rare event and usually results in only a few minutes loss of link.
	Loss of Minop[37] or Loss of Link	Not possible	Loss of Minop or link would have resulted in the original Flight ID being sent to the GES at Log-On.
Flight ID received from AIMS, but with null value (zeros) and Sign Status Matrix (SSM) field set to Normal Operation	Power Interrupt	Low	Flight ID would have to have transitioned to null value whilst the SDU was not powered.
	Sysfail (software fail)	Very low	Flight ID would have to have transitioned to null value whilst the SDU was in Sysfail (which is a rare event in itself).
	Loss of Minop or Loss of Link	Low	Flight ID would have to have been cleared whilst the SDU was in loss of Minop or experiencing loss of link (duration at least 22 minutes). Otherwise a Log-On Renewal would have occurred and the GES log shows that a Log-On renewal did not occur.
Flight ID manually cleared via the MCDU	Power Interrupt or Sysfail (software fail)	Not possible	SDU needs to be operational to accept null Flight ID via an MCDU.
	Loss of Minop or Loss of Link	Low	Flight ID would have to have been manually cleared whilst the SDU was in loss of Minop or experiencing loss of link (duration between 22 and 78 minutes). Otherwise a Log-On Renewal would have occurred and the GES log shows that a Log-On Renewal did not occur.

Table 2.5A - Possible Reasons for the 1825 Log-On Events and Preceding Link Losses

From the above table, the most likely reason for the 1825 Log-On is a power interrupt.

[37] Loss of Minop - Is the inability of the AES to Log-On, because of one or more missing or failed resources, (e.g. equipment BITE failure).

2) Second In-Flight Log-On at 0019 on 08 March 2014

Log-On Reason	Likelihood	Comments
Power Interrupt	Medium	The SATCOM CBs are not readily accessible and are therefore unlikely to have been cycled. However, given that MH370 could have been low on fuel at this time, some form of generator transfer may have occurred, resulting in a SATCOM power interrupt.
Sysfail (software fail)	Very low	Sysfail is a very rare event.
Loss of Minop	Low	Loss of Minop - Normally a very low likelihood, but given that MH370 could have been low on fuel at this time, some form of generator-related abnormal operation of a peripheral system (e.g. AIMS) may have occurred.
Loss of Link	Low	Loss of Link would have prompted a new Log-On attempt via the Low Gain Antenna (LGA) subsystem. From the GES records, the subsequent Log-On is known to have been via the High Gain Antenna (HGA) subsystem, so for loss of link to be the Log-On reason, both the HGA and LGA subsystems would have had to have failed to close the link for a while. This is only likely in the case of an abnormal aircraft attitude, but given that MH370 could have been low on fuel at this time, this is a plausible reason.

Table 2.5B - Possible Reasons for the 0019 Log-On Events and Preceding Link Losses

From the above table, the most likely reason for the 0019 Log-On is a power interrupt.

Note:

The above table does not include the 'Flight ID Status Change Description' column that appears in the previous table, as there is no change of Flight ID Status for this second in-flight Log-On.

3) Preceding Link Losses

Although the link loss that is believed to have preceded the 1825 Log-On is most likely to have been due to a power interrupt, for completeness, other possible reasons for the link loss are considered in the following table (*Table 2.5C*).

Link Loss Reason	Likelihood	Comments
Automatic Satellite/GES Handover	Very low	Had the SDU initiated a handover, a Log-Off Request should have been recorded in the GES log. No such request was recorded.
Manual Log-Off, via the MCDU	Very low	Had a manual Log-Off been initiated via the MCDU, a Log-Off Request should have been recorded in the GES log. No such request was recorded.

Table 2.5C – Other Reasons for the Link Loss

The above table confirms that the link loss that is believed to have preceded the 1825 Log-On was not due to Satellite/GES handover or manual intervention via the MCDU.

2.5.3 Summary Assessment of Doppler for 1825 and 0019 Log-On Events

1) During each of the two in-flight Log-Ons that occurred during flight MH370, the GES recorded abnormal frequency offsets for the SATCOM transmissions. This is in contrast with the 'normal' Log-On behaviour.

2) *Table 1.9D* in *Section 1.9.5* shows the frequencies of these Log-On bursts, as measured at the GES, plus differences from assumed reference frequencies. The table also shows the very high delta frequencies between the respective Log-On Request and Log-On Acknowledge bursts.

3) The following graph *(Figure 2.5A)* shows the delta frequencies between pairs of Log-On Request and Log-On Acknowledge bursts for over one hundred Log-Ons of the SATCOM on-board 9M-MRO, up to and including the two during flight MH370. In every case prior to MH370 the delta frequencies were fairly small. Only the last two pairs of transmissions (the 1825 and 0019 Log-Ons) show significant deltas. Note that for ease of display, only the magnitude is shown for the two MH370 Log-On frequency deltas.

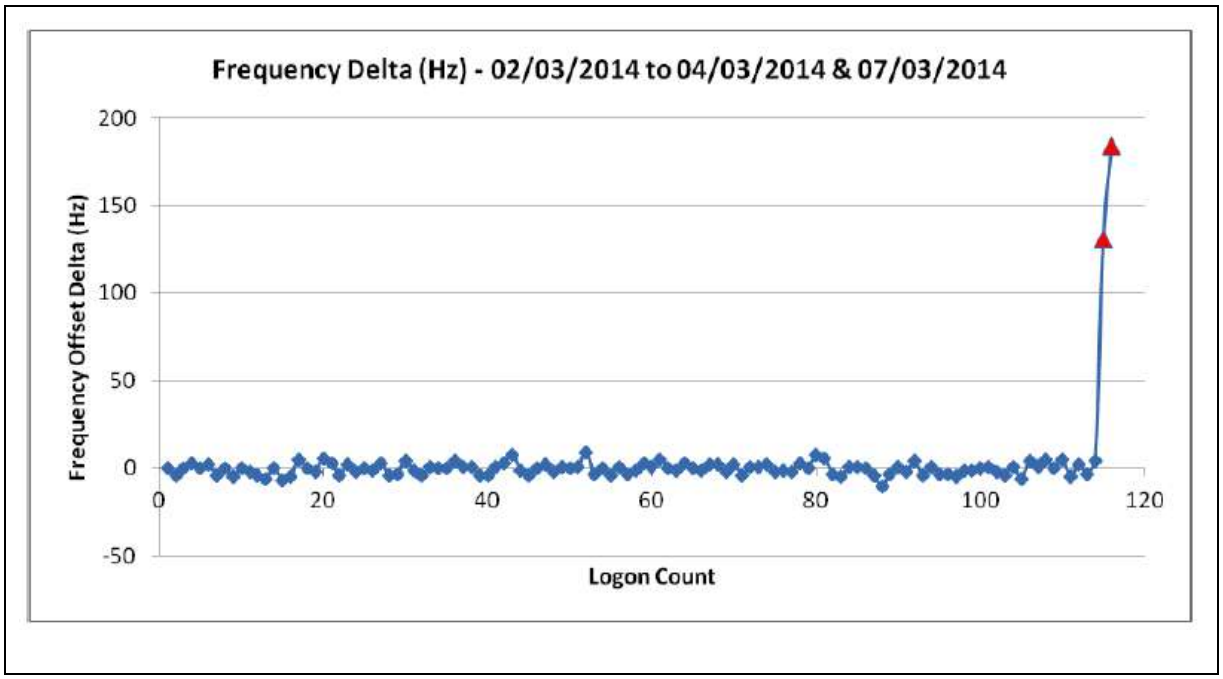

Figure 2.5A – Delta Frequencies between Pairs of Log-On Request and Log-On Acknowledge

4) From the Perth GES logs, the AES is known to have Logged-On as Class 3 (Voice & Packet Data). In order to have done so, the SDU must have been receiving valid Air Data Inertial Reference Unit (ADIRU) data from AIMS. In this case, the AES would apply open loop Doppler compensation, whereby it uses the ADIRU data in order to calculate the transmit frequency Doppler offset.

5) An OCXO provides a stable reference frequency for the SDU Radio Frequency (RF) transmit and receive circuits and also for

SDU modem timing. Within the OCXO, a regulated oven keeps the crystal at an almost constant temperature if the ambient temperature in the crown area is between the ranges -55^{0}C up to above +70^{0}C. The oven also contains extra electrical regulation and isolation to ensure frequency accuracy and stability. The OCXO includes an oven ready flag, which triggers the Log-On initiation when the OCXO reaches its operating temperature. Extensive laboratory testing has revealed that during warm up, the OCXO frequency may vary non-linearly with time, but then settles with almost negligible variation. At power-on, the OCXO can exhibit either a rising or falling frequency gradient, before decaying over time to its normal steady state value. The testing has indicated that reasonable stability (within 2Hz/minute) is typically reached by around five minutes after an initial peak or overshoot. The testing has also shown that there can still be a significant frequency offset at the time that the oven ready flag initiates the Log-On process, so the Log-On request, Log-On Acknowledge and subsequent data bursts can all exhibit significant frequency offsets.

6) These frequency offsets can be seen in the plot (*Figure 2.5B)* below, for a 9M-MRO SATCOM Log-On (believed to have taken place after a lengthy power down), at 1250 on 07 March, whilst the aircraft was on the ground at Kuala Lumpur, prior to the departure of MH370. The frequency has stabilised to a value of around 350Hz, within three minutes of the Log-On Request.

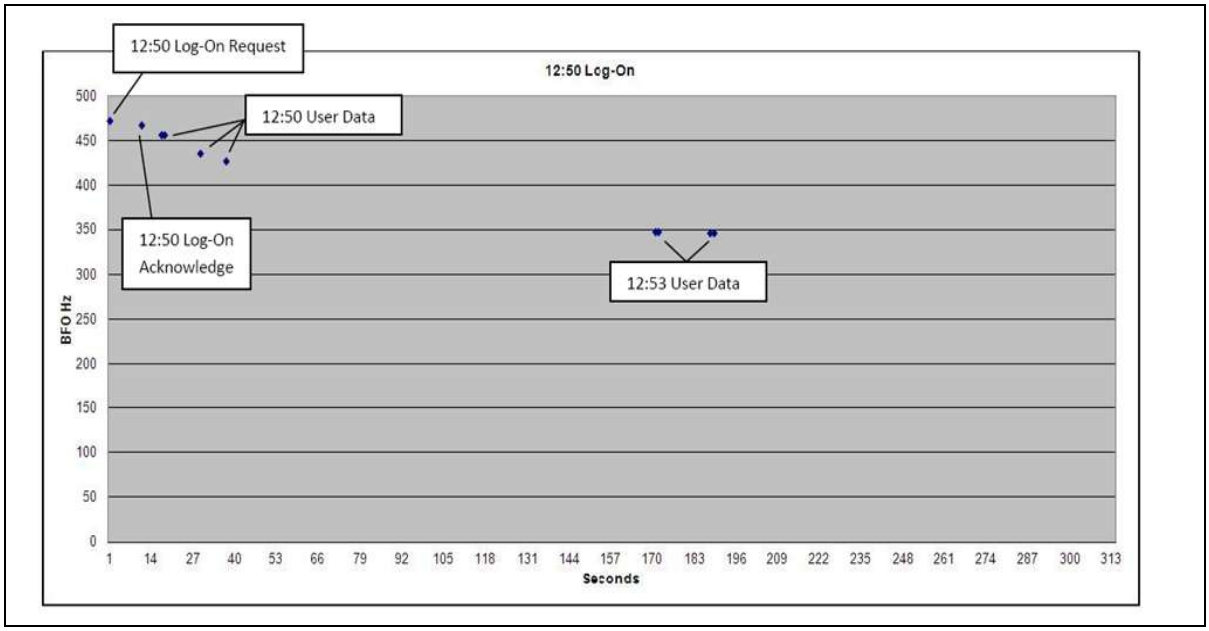

Figure 2.5B - SATCOM Log-On Frequency Offsets at 1250, 07 March 2014

7) These frequency offsets can also be seen in the plot (*Figure 2.5C)* below for the MH370 1825 Log-On. As with the 1250 Log-On, the frequency has stabilised within three minutes of the Log-On Request, this time at around 150Hz.

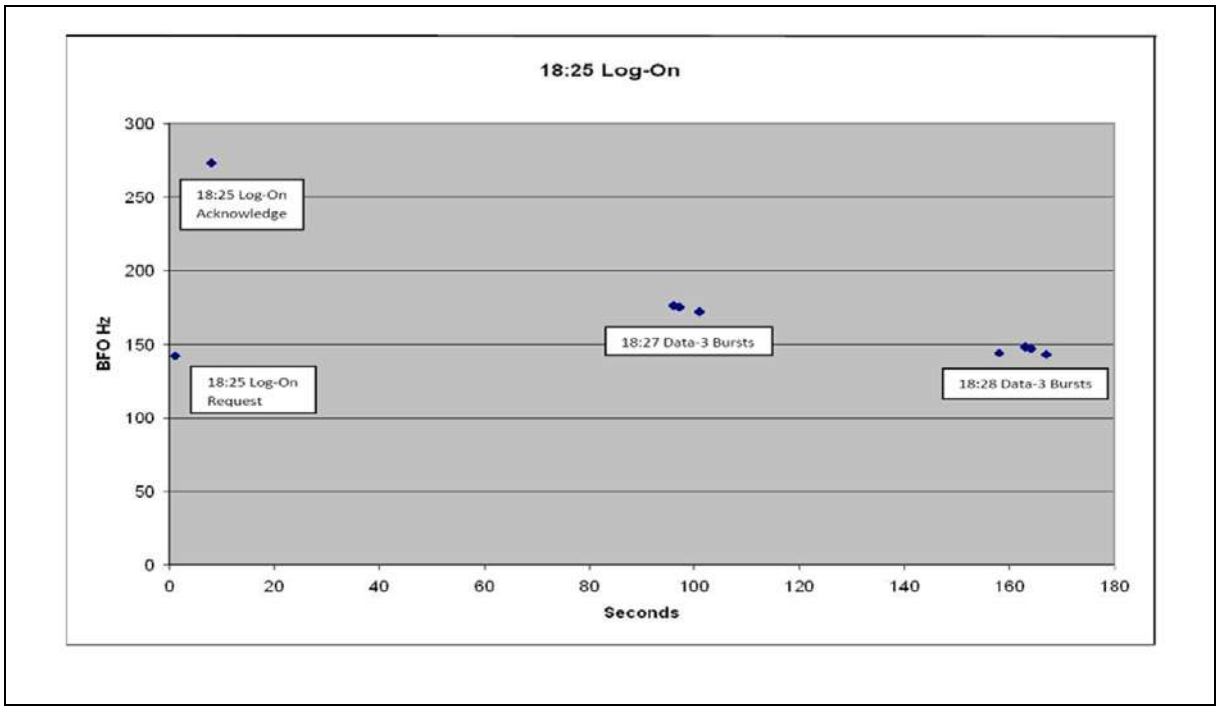

Figure 2.5C - SATCOM Log-On Frequency Offsets at 1825, 07 March 2014

8) The 1825 Log-On Acknowledge and the subsequent Data-3 transmissions exhibit a frequency offset, which decays to the steady state value. This frequency decay endorses the belief that the SATCOM had been powered down prior to the 1825 Log-On.

9) The 1825 Log-On Request does not exhibit the frequency offset decay though. However, it is possible that the OCXO frequency was rising at this time, prior to decaying to its steady state value. It is noted that the 1825 Log-On Request was received at the GES with a low Received Carrier/Noise Density Ratio (C/No) and a channel Bit-Error-Rate (BER) of 5 and could therefore have been logged at the Ground station with a BFO measurement error suggesting that the BFO figure may not be reliable. Non-zero channel BER transmissions are not uncommon for a satellite link. The C/No (and hence channel BER) can be impacted by the gain of the SATCOM antenna and also atmospheric effects, as well as interference due to collisions with a (lower power) burst from another aircraft.

10) In the seven days leading up to flight MH370, 235 out of 6803 (3%) of 9M-MRO SATCOM Class 3 transmissions (via HGA) were received at a GES with a non-zero channel BER and during flight MH370, 5 out of 112 (4%) of transmissions were received at a GES with a non-zero channel BER. So, the MH370 SATCOM performance from a channel BER perspective appears to have been normal.

11) The plot *(Figure 2.5D)* below shows a series of MH370 Log-On Interrogation transmissions, which steadily rise in frequency (due to the satellite ephemeris). However, the 0019 Log-On Request and Log-On Acknowledge transmissions diverge from the steady state slope.

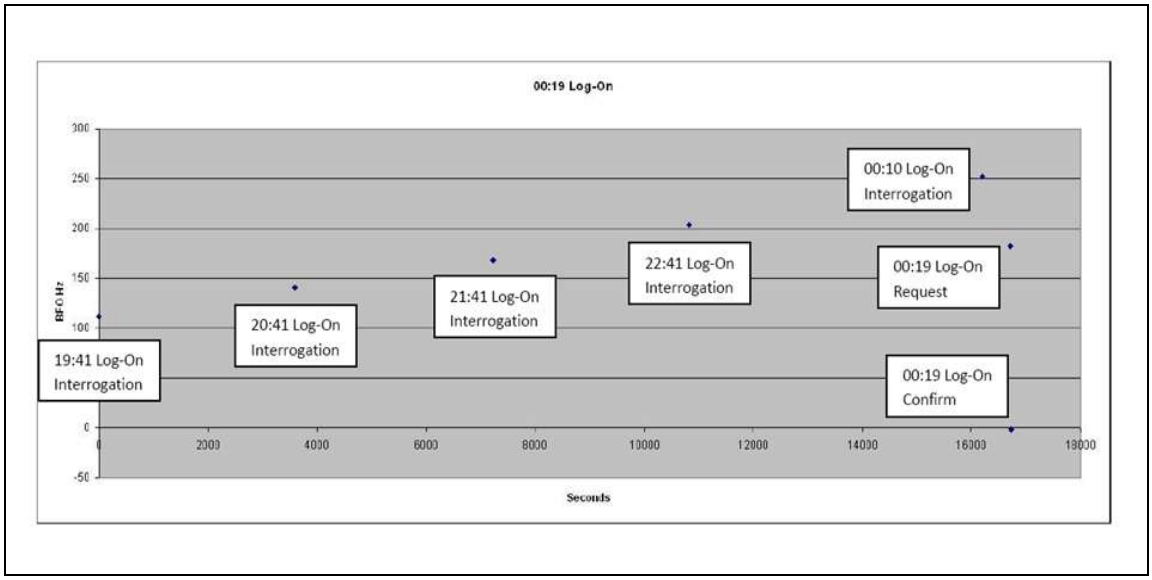

Figure 2.5D - Log-On Interrogation Transmissions

12) For the 0019 BFOs, the following possible error contributions are considered:

a) GES Measurement Errors - There is only evidence to suggest a significant GES measurement error in the case of a burst that is received at the GES with a non-zero channel BER, as in the case of the 1825 Log-On Request. This was not the case with the 0019 BFOs, so it can be discounted.

b) SDU OCXO Reference Error – OCXO stability has been measured over both temperature (circa -0.65Hz/deg. C) and time (as described above). The OCXO double

inflection warm up drift could explain at least part of the 0019 Log-On Request and Log-On Acknowledge frequency offsets.

c) Satellite Doppler Towards SDU and GES - Doppler frequency offset due to the relative movement of the satellite could not account for the >100Hz frequency shift in the <10 seconds between the 0019 Log-On Request and the Log-On Acknowledge bursts.

d) Doppler Error due to ADIRU Drift - If the aircraft ADIRU is assumed to have a maximum drift of 2kts (1m/s), then the worst case Doppler offset is 16Hz, significantly smaller magnitude than the >100Hz frequency shift in the <10 seconds between the 0019 Log-On Request and the Log-On Acknowledge bursts.

e) Doppler due to erroneous ADIRU Data - From a SATCOM perspective, the SDU will not use navigation data unless the Sign Status Matrix (SSM) for every one of the required ARINC 429 words (Latitude, Longitude, Groundspeed, Track, Pitch, Roll and Heading) is set to Normal Operation. It is “extremely improbable” that an ADIRU will send erroneous data with the SSM set to normal. In this case, we can conclude that the abnormal frequency offsets are extremely unlikely to be as a result of the SDU receiving or acting upon erroneous navigation data from an ADIRU.

f) Uncompensated Vertical Velocity - The SATCOM SDU does not consider vertical velocity in its Doppler calculation. It has been calculated that a vertical velocity of +100ft/min causes about a +2Hz change in the Doppler shift. Therefore, under normal circumstances, only a small frequency error results from the uncompensated vertical velocity. For example, an ascent or descent rate of 2000ft/minute would cause a 40Hz offset. In the case of MH370, a significant vertical velocity could explain at least part of the 0019 Log-On Request and Log-On Acknowledge frequency offsets.

13) In summary, the abnormal BFOs for the 1825 and 0019 Log-Ons can be explained as follows:

    a) The 1825 Log-On Acknowledge - Most likely due to the power-on drift of the OCXO.

    b) 0019 Log-On Request and Log-On Acknowledge - Could have been due to uncompensated vertical velocity, indicating that the aircraft was likely to be descending at this time. Alternatively, it could have been due to the OCXO warm up drift, or it could have been due to a combination of uncompensated vertical velocity and OCXO warm up drift.

14) It has not been possible to attribute specific correction values to the 1825 Log-On Acknowledge and 0019 Log-on Request and Log-On Acknowledge BFOs, so it was excluded from the Doppler calculations undertaken by the Aircraft Flight Path/Performance Subgroup. In the case of the 1825 Log-On Acknowledge, the following subsequent bursts were used instead, as the frequency is more stable at these times:

    - 1828:05.904 Data-3 R-Channel burst.
    - 1828:14.905 Data-3 R-Channel burst.

SECTION 2 – ANALYSIS

2.6 WRECKAGE AND IMPACT INFORMATION

2.6.1 Debris Considered for Detailed Examination

After the completion of the underwater search no wreckage belonging to MH370 was found. However, a number of debris were washed ashore near and onto the coast of south east Africa. Only the right flaperon, part of the right outboard flap and a section of the left outboard flap were confirmed to be from MH370. So far, 7 other pieces were also determined to be *almost certain* from MH370. To date, 27 items were considered significant for evaluation and the table below lists them and the status.

Ref.	Debris	Status
Item 1	Right Flaperon	*Confirmed*
Item 2	Right Wing No. 7 Flap Support Fairing	*Almost certain*
Item 3	Right Horizontal Stabiliser panel piece	*Almost certain*
Item 4	Engine Nose Cowl	*Almost certain*
Item 5	Door R1 Stowage Closet	*Almost certain*
Item 6	Right Hand Engine Fan Cowling	*Almost certain*
Item 7	Wing Body Fairing	*Likely*
Item 8	No. 1 Flap Support Fairing Tail Cone	*Highly Likely*
Item 9	Left Wing Trailing Edge Panel	*Highly Likely*
Item 10	Left Outboard Aft Flap Section	*Confirmed*
Item 11	Seat Back Trim Panel Encasing IFE Monitor	*Highly Likely*
Item 12	Bottom Panel of Wing or Horizontal Stabilizer	*Likely*
Item 13	Unidentified Part	*Not Identifiable*
Item 14	Unidentified Part	*Not Identifiable*
Item 15	Right Wing Trailing Edge Panel	*Highly Likely*
Item 16	Cabin Interior Panel	*Almost certain*
Item 17	Unidentified Part	*Not Identifiable*
Item 18	Right Forward Nose Landing Gear Door	*Highly Likely*
Item 19	Right Outboard Flap	*Confirmed*
Item 20	Right Aft Wing to Body Fairing	*Highly Likely*
Item 21	Unidentified Part	*Not Identifiable*
Item 22	Right Vertical Stabilizer Panel	*Almost Certain*
Item 23	Unidentified Part	*Not Identifiable*
Item 24	Unidentified Part	*Not Identifiable*
Item 25	Unidentified Part	*Not Identifiable*
Item 26	Right Aileron	*Highly Likely*
Item 27	Right Wing No. 7 Flap Support Fairing	*Highly Likely*

Table 2.6A - List of Debris Found and Considered for Detailed Examination

Examination, analysis and test were conducted by ATSB in Canberra, Australia and MH370 Safety Investigation Team in collaboration with STRIDE of Malaysia.

2.6.2 Location of Debris with respect to Aircraft

Figure 2.6A (below) shows the locations of the debris with respect to the aircraft.

Item 4 (part of the Engine Nose Cowl) is depicted to be from the right engine. There were no significant differentiators on the cowling segment to assist in determining whether the item of debris was from the left or right side of the aircraft, or the inboard or outboard side the cowling. Similarly, although Item 6 (part of the RH fan cowl) is depicted to be from the right engine in *Figure 2.6A,* there is a possibility that it could also be from the left engine. As for Item 7 - Wing body fairing - this too could be from either side of the aircraft.

Based on the identification of the parts and debris found, it shows that most of those parts and debris were from the right hand side of the aircraft.

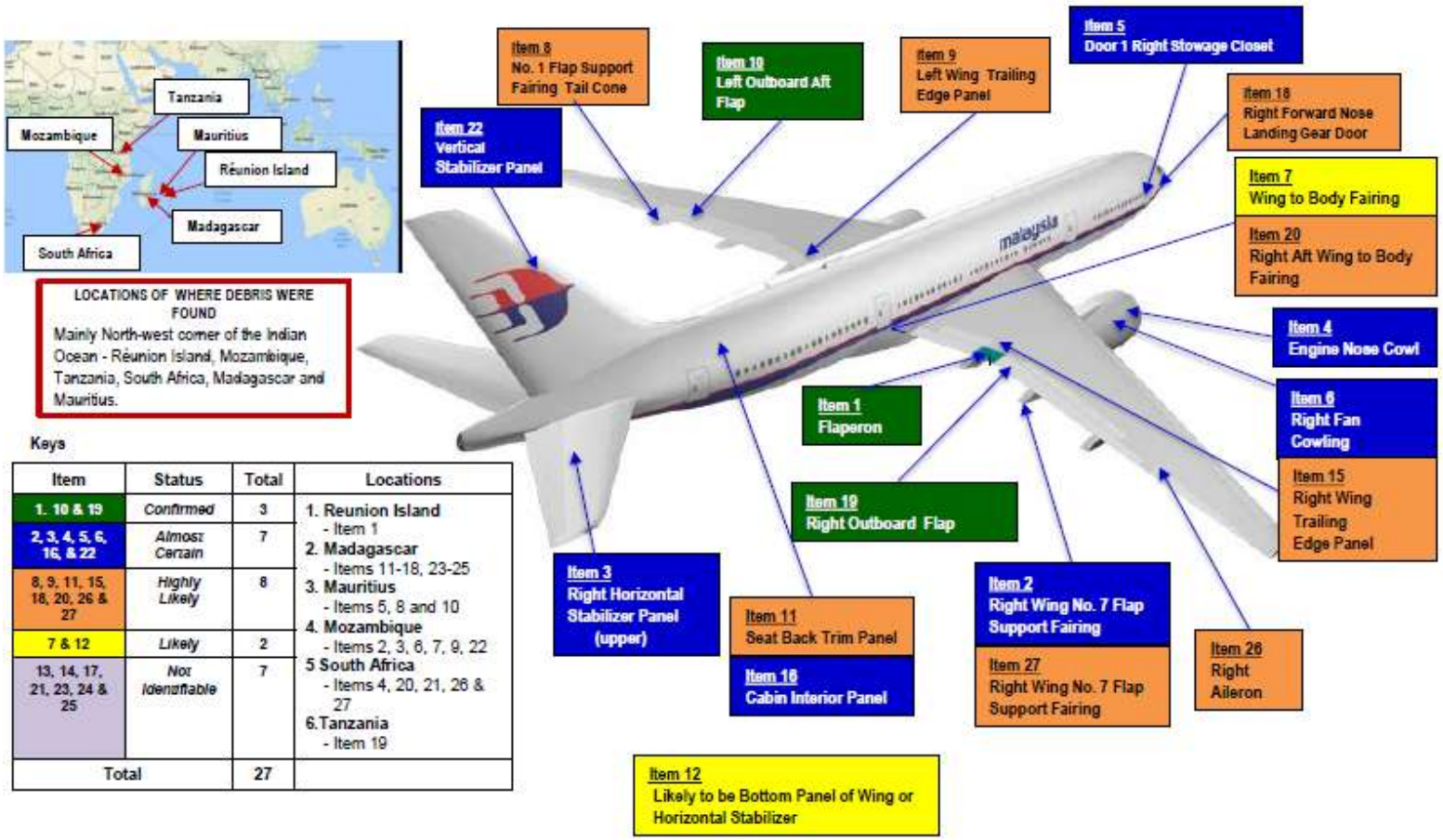

Figure 2.6A - Location of Parts and Debris Found with respect to Aircraft

2.6.3 Damage Analysis of Significant Debris

Damage examination on the recovered part of the right outboard flap (Item 19), together with the damage found on the right flaperon (Item 1) indicates that the right outboard flap was most likely in the retracted position and the right flaperon was probably at, or close to, the neutral position, at the time they separated from the wing. This conclusion is based on the following findings and analysis.

There were damages to the internal seal pan components at the inboard end of the outboard flap which were possible with the auxiliary support track fully inserted into the flap. The damages were consistent with contact between the support track and flap, with the flap in the retracted position. The possibility of the damages originating from a more complex failure sequence, commencing with the flaps extended, were considered much less likely.

With the flap in the retracted position, alignment of the flap and flaperon rear spar lines, along with the close proximity of the two parts, indicated a probable relationship between two areas of damage around the rear spars of the parts. This was consistent with contact between the two parts during the aircraft breakup sequence, indicating that the flaperon was probably aligned with the flap, at or close to the neutral (faired) position. Refer to ATSB's report on the Outboard Flap Failure Analysis (*Appendix 2.6C)* for further details.

It should be noted that the DGA/TA, after examining the flaperon soon after it was found in July 2015, had concluded that the flaperon was likely to be deflected at the time of impact. This was primarily based on the damage observed on the trailing edge of the flaperon. However, this scenario was considered a hypothesis only due to lack of corroborating information, and more importantly, it was done without the benefit of the damage information available from the right outboard flap which was found much later. Additionally, the flaperon being rear of the engine, left some doubt as to its loading during the aircraft impact with the water and the phenomena at issue being highly dynamic and thus difficult to exploit. Refer to *Appendix 1.12A-2* for further details.

Two pieces of debris are *almost certain* from the cabin interior suggesting that the aircraft might have broken up. However, there is insufficient information to determine if the aircraft broke up in the air or during impact with the ocean.

Of the pieces tested so far, no traces of explosion were found.

2.6.4 Marine Life Examination

The marine organisms (barnacles) found on the flaperon were examined in detail by marine biologists, under the directive of the French Investigative judge. Below is a summary of the analysis.

The barnacles present on the flaperon belonged to the species *Lepas (Anatifa) anatifera striata*. This sub-species is strictly pelagic, always living on floating objects. It is a cosmopolitan species, widespread in worldwide oceans at tropical and temperate latitudes, in water temperatures above 18-20°C. The size of the biggest specimen indicated that the initial settlement could have occurred 15-16 months prior *to* the discovery of the flaperon at Reunion Island. The locations of the *Lepas* colony on the flaperon indicated that the flaperon was floating with its "belly face" up (the lower surface [intrados] was up, the upper surface [extrados] was immersed). Refer to *Appendix 2.6A* for details.

Temperatures during the growth of the youngest valves and the terminal fringe of the biggest adult valves (25.4 +/- 1°C) were consistent with temperatures observed off the Reunion Island. These results suggest that the barnacles ended up their developments in waters whose thermal characteristics were similar to waters close to Reunion Island, before the discovery of the flaperon.

At the beginning of their growth, the barnacles were immersed in waters with a temperature close to 28.5 +/- 1°C. Temperature distribution maps in the months preceding the discovery of the flaperon suggest that it has drifted in waters located East-North East of Reunion Island.

There are however no elements to determine precisely the duration of the growth of the valves examined, and therefore the period covered by the most developed valves. However, based on two experimental studies dealing with growth speeds of pelagic anatifas (Evans, 1958, Inatsuchi et al., 2010), the biggest valves (scutum) could have grown over a few months period. Refer to *Appendix 2.6B* for details.

SECTION 2 – ANALYSIS

2.7 ORGANISATION AND MANAGEMENT OF DEPARTMENT OF CIVIL AVIATION AND MALAYSIA AIRLINES

2.7.1 Department of Civil Aviation Malaysia

1) Introduction

In light of the disappearance of MH370 on 08 March 2014 [MYT], Malaysia as the State of Registry, State of Operator and State of Occurrence was obliged to conduct an investigation into the incident. Accordingly, the Minister of Transport had on 25 April 2014, instituted an independent international Investigation Team known as *The Malaysian ICAO Annex 13 Safety Investigation Team for MH370* with the sole objective of "prevention of future accidents or incidents and not for the purpose to apportion blame or liability." The Team, headed by an Investigator-in-Charge, comprised of nineteen Malaysians and seven international Accredited Representatives (AR) of seven safety investigation authorities from seven countries (Australia, China, France, Indonesia, Singapore, the United Kingdom, and the United States of America).

2) Department of Civil Aviation Organisation Structure

a) The Department of Civil Aviation (DCA) organisation structure at headquarters and operations resembles a flat or horizontal organisation structure which enables the officers to know what their respective responsibilities are since individual officers are assigned specific roles and functions. It enables the coordination of all activities within the DCA so that there is minimal duplication of effort or conflict and avoids overlapping of functions. As this structure creates fewer management levels, quick decisions and prompt actions can be taken without delay. Fast and clear communication is possible among these few levels of management and subordinates who are free from close and strict supervision and control.

b) This organisation structure is suitable for DCA at headquarters as the activities are rather routine and standardised. The officers at headquarters are assigned specific roles and functions enabling them to carry out their duty efficiently.

c) The DCA does not have sufficient technical personnel to effectively carry out all of its safety oversight tasks and functions due to resignations, delays in the filling of existing vacant posts, and difficulty in increasing the number of established posts in response to the growth of the industry. Uncompetitive employment conditions and the current practice of accepting technical personnel on rotational secondment from other government departments and short-term contracts from industry create difficulties in recruiting and retaining qualified and experienced technical personnel.

d) DCA is looking into the State Safety Programme (SSP) in accordance with Chapter 3, Annex 19 to the Convention on International Civil Aviation which will be applicable on 07 November 2019.

3) Air Traffic Management Sector

a) Organisation Structure

The organisation structure of the Air Traffic Manager (ATM) Sector at headquarters and operations resembles a flat or horizontal organisation structure which enables the officers to know what their responsibilities are since individual officers are assigned specific roles and functions. It enables the coordination of all activities within the ATM headquarters so that there is minimal duplication of effort or conflict and avoids overlapping of functions. As this structure creates fewer management levels, quick decisions and prompt actions can be taken without delay. Fast and clear communication is possible among these few levels of management and subordinates are free from close and strict supervision and control.

b) The ATM Sector at headquarters has a total establishment of 19 posts to manage the ATSUs in Kuala Lumpur and Kota Kinabalu FIRs and all the posts are filled and are sufficiently staffed.

c) This organisation structure is suitable for ATM headquarters as the activities are rather routine and standardised. The officers in this Sector are assigned specific roles and functions enabling them to carry out their duty efficiently. However, the personnel in ATM headquarters should closely monitor the Air Traffic Services Units (ATSUs) in the Kuala Lumpur and Kota Kinabalu

FIRs to ensure that the rules and established procedures are strictly adhered to. Periodical reminders and surprise visits to the respective ATSUs should be carried out so that the operational personnel would not lose touch with current procedures.

d) The ATM headquarters' responsibility with regard to MH370 is through the KL ATSC Director in adherence to and compliance with the rules and established procedures in the MATS Vol. 1 and Vol. 2, ICAO Annexes and Documents, Operational Letter of Agreements and Departmental Directives and Instructions, Supplementary Operations Instructions and Administration Instructions.

4) Air Traffic Inspectorate Division

a) The Air Traffic Inspectorate (ATI) Division organisation resembles a flat or horizontal organisation structure which enables the officers to know what their responsibilities are since individual officers are assigned specific roles and functions. It enables the coordination of all activities within the Division so that there is minimal duplication of effort or conflict and avoids overlapping of functions. As this structure has fewer management levels, quick decisions and prompt actions can be taken without delay. Fast and clear communication is possible among these few levels of management and subordinates are free from close and strict supervision and control. This organisation structure is suitable for the ATI Division as the activities are rather routine and standardised.

b) The ATI Division is headed by a Director and assisted by a Deputy Director. There are three units viz. Safety Oversight of ANS Providers, ATC Examination, ATC Licensing and Safety. There are three Principal Assistant Directors and three Senior Assistant Directors.

c) The ATI Division has conducted six Safety Oversight Audits on the Kuala Lumpur ATSC (KL ATSC). The last audit was conducted from 22 - 25 April 2013. The objective of the audit is to ensure conformity with ATMS prescribed standards and requirements in the provisions of ATMS by the ATM service provider.

d) The relevant ICAO Annexes, Documents and Manuals were used to identify differences between KL ATSC practices and those established by the ATM Sector, and ICAO Standard and Recommended Practices (SARPs).

e) During the on-site audit, the audit team made 6 observations, with only one having a bearing on the ongoing investigation by the Team. The observation was that the "*Direct line at Watch Supervisor console was not connected to recording facility*". During the course of the audit, there were 8 Manual of Air Traffic Services' (MATS) non-compliance reports (NCRs), 21 Annex 4's NCRs (16 Annex Chapter and 5 Annex Chapter 21), 6 Doc 9426 - ATSC Facilities NCRs and 2 ANS Regulatory NCRs. There was a total of 37 new NCRs' findings for the audit conducted in 2013. However, for the audit that was conducted in 2010, 9 out of 11 MATS' NCRs and the entire 8 Doc 9426's NCRs still remain open. There were a total of 17 NCRs still remaining open. There were 6 NCRs brought forward from 2005/2006. KL ATSC has accumulated altogether a total of 60 NCRs after the audit conducted in April A2013.

Notwithstanding the above, the Team does not find any direct link between the NCRs and the disappearance of MH370.

f) There has not been any direct link as to the functions of the ATI Division with regard to the disappearance of MH370. The ATI Division has issued ATC licenses to the ATC personnel in accordance with Personnel Licensing under Regulation 92(1) of the Malaysian Civil Aviation Regulations 1996.

5) Search and Rescue

a) Although there is no legislation specifically to address the provision of assistance to aircraft in distress, Aeronautical SAR (A-SAR) in Malaysia is provided in accordance with ICAO Annex 12 and the International Aeronautical and Maritime Search and Rescue (IAMSAR) Manual Vol. I – III (ICAO Doc 9731-AN958). It should be noted that CAR 201 stipulates the use of *'ipso facto'* to address ICAO Annexes 1 to 18, including the application of ICAO Standards and Recommended Practices (SARPs), provided that a regulation has not already been established in CAR and that a difference has not been

notified to ICAO. In particular, DCA relies completely on CAR 201 for the implementation of Annexes 3, 4, 5 and 12.

b) IAMSAR Vol. IV - The National Aeronautical and Maritime Search and Rescue Manual (Malaysia), prepared under the direction of the National Search and Rescue Committee, National Security Council (NSC) and the Prime Minister's Department in March 2008, provides guidance to federal agencies concerning the implementation of the National Search and Rescue Plan. This Plan provides specific additional national standards and guidance that build upon the base line established by the International Aeronautical and Maritime Search and Rescue (IAMSAR) Manual. The IAMSAR Manual is a three-volume set published jointly by both the International Civil Aviation Organisation (ICAO) and the International Maritime Organisation (IMO) for use by all countries. This Plan provides guidance to all federal forces, military and civilian, that support civil search and rescue (SAR) operations. It should be noted that the land (populated areas) and military SAR elements, under the portfolio of its respective ministries, are intentionally excluded from this document.

c) The IAMSAR Vol. IV is a very comprehensive national SAR manual covering areas viz.:

Part One	Aeronautical and Maritime SAR Authority and Administration;
Part Two	Aeronautical and Maritime SAR Policy
Part Three	Aeronautical and Maritime SAR Resources
Part Four	Aeronautical and Maritime SAR Communications
Part Five	Special Procedures
Part Six	Memoranda of Understanding
Plan of Operation	Part 1 - Aeronautical Part 2 - Maritime

Over the South China Sea, within the Singapore FIR, there are two distinct areas namely the South China Sea Corridor (SCSC) and the airspace delegated to KL ACC by Singapore ACC known as the "Delegated Airspace". There are special arrangements whereby the roles and responsibilities of KL

ARCC and Singapore RCC have been defined in terms of alerting service and SAR operations as follows:

i) South China Sea Corridor

The arrangement for aeronautical search and rescue service by way of the Operational Letter of Agreement between Malaysia and Singapore for the part of the South China Sea (which is within the Singapore FIR) was in force since 1984. The agreement specified the designated area, known as the South China Sea Corridor (SCSC) and stipulates that in the event of an aircraft emergency occurring within the SCSC, the KL ACC shall be responsible to take initial alerting action whilst Singapore RCC shall be responsible for subsequent coordination of all SAR efforts. Whist the responsibility for the provision of search and rescue service within the SCSC rests with the Singapore RCC, the Singapore RCC may delegate responsibility for the overall control of the SAR mission to Kuala Lumpur RCC or Kota Kinabalu RCC, whichever is deemed appropriate.

Letter of Agreement Para 3.2.2 states that*:*

When a transfer of responsibility for the overall SAR coordination is to take place, either from subsequent establishment of an aircraft's position or movement, or because an RCC other than the one initiating the action is more favourably placed to assume control of the mission by reason of better communication, proximity to the search area, more readily available facilities or any other reasons, the following procedures shall be adopted:

i) direct discussions, wherever possible, shall take place between the Search and Rescue Mission Coordinators (SMCs) concerned to determine the course of action,

ii) if it is decided that a transfer of responsibility is appropriate for the whole mission or part thereof, full details of the SAR mission shall be exchanged, the initiating RCC shall continue to retain responsibility until the accepting RCC formally assumes control for the mission.

ii) "Delegated Airspace" in Singapore FIR

The **"**Delegated Airspace" is a defined airspace over the South China Sea within the Singapore FIR that has been delegated by Singapore to Malaysia for the purpose of Air Traffic Services. SAR service is provided by Singapore.

Figure 2.7A - Kuala Lumpur - Aeronautical Rescue Coordination Centre (ARCC)

On 08 March 2014 [MYT], MH370 operated within the "Delegated Airspace". The radar position symbol dropped from the radar display at 1721:13 UTC [0121:13 MYT]. Though the KL ACC was responsible for the provision of Air Traffic Services, no alerting action was taken. At 2130 UTC [0530 MYT] the KL ATSC Duty Watch Supervisor directed the Search and Rescue Mission Coordinator (SARMC) to activate the ARCC (*Figure 2.7A* above and *Figure 2.7B* below). After the ARCC was activated, and due to a lack of details from the KL ATSC Duty Watch Supervisor, the SARMC only managed to disseminate the distress message at 2232 UTC [0632 MYT], an hour and two minutes later.

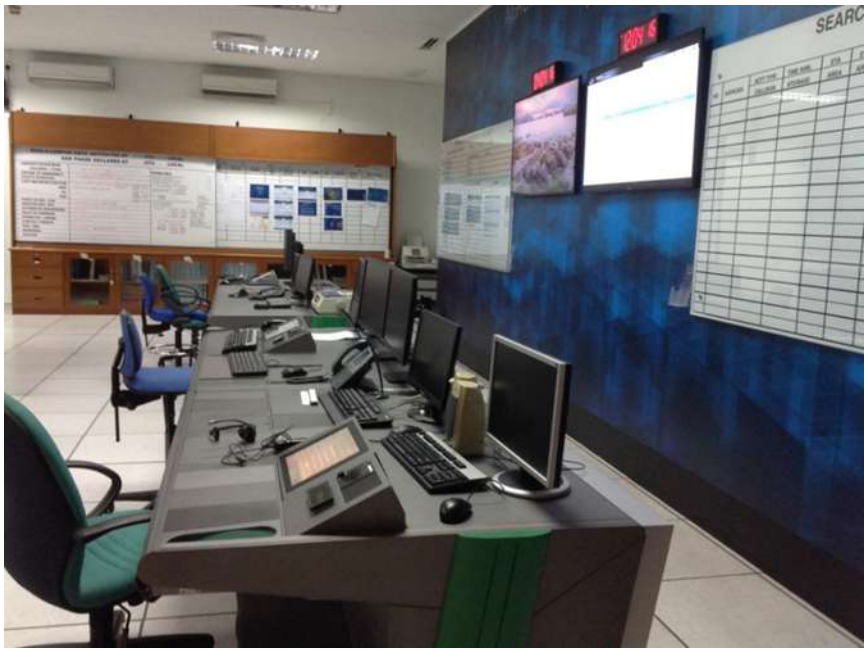

Figure 2.7B - Kuala Lumpur ARCC Work Stations

6) Kuala Lumpur Air Traffic Service Centre

a) Staffing

This analysis on the Organisation Structure of the Kuala Lumpur Air Traffic Service Centre - *Figure 2.7C* below - is based on information obtained from the Department of Civil Aviation. There are altogether 353 approved ATS posts of various grades in the KL ATSC. As of March 2015, there were 110 vacancies and 64 as of December 2014. The reason cited for the posts not being filled was *"considering the opening of klia2, DCA has managed to obtain new posts for KL ACC (Area and Approach) and KLIA on 08 May 2013. But due to the delay of klia2 opening the promotion exercise was also delayed".*

b) Findings of Safety Oversight Audit

The findings of the Final Report of the Safety Oversight Audit (Follow-up) of KL ATSC in April 2013 state that:

- *the organisational charts do not reflect the task currently assigned to and being performed by the ATS staff who are also assigned secondary posts with specific duties.*

- *KL ATCC had not conducted any Refresher Course for its Controllers. There is no training programme developed for ATC staff. All training is conducted on operational and opportunity basis. In addition, training records for ATC staff were not systematically maintained.*

- *No internal audit conducted however it is noted that an audit team will be established consisting of personnel who had previously attended audit course.*

The reasons cited in the audit report were inadequate staffing and inadequate resources to run the programme.

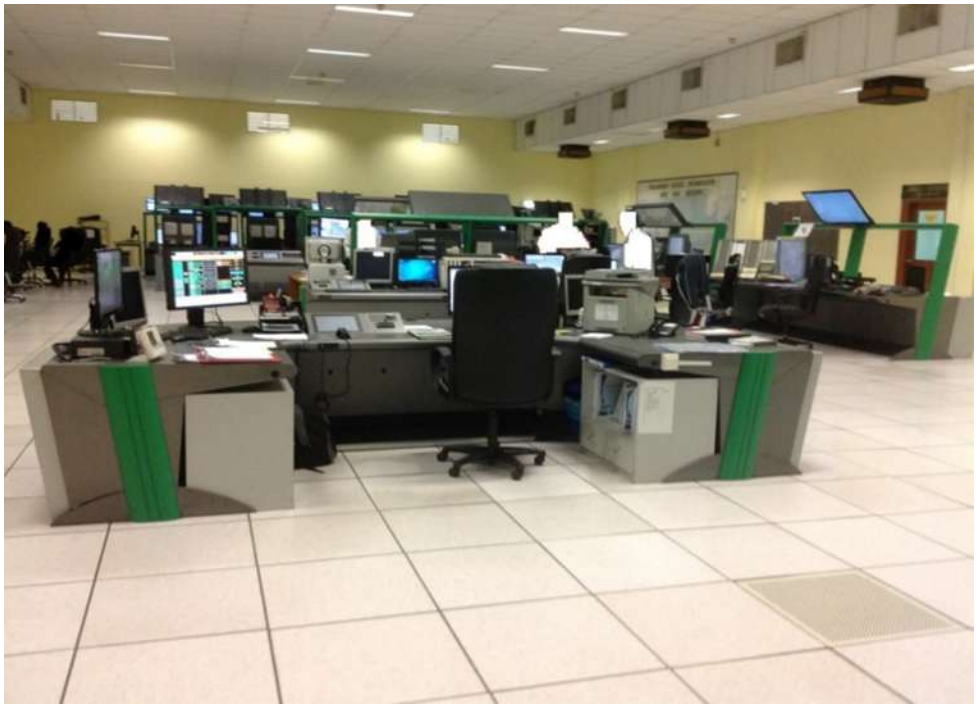

Figure 2.7C - Overview of Kuala Lumpur Air Traffic Control Centre

c) Duty Roster for March 2014

i) This analysis is based on the KL ATSC duty roster for Air Traffic Controllers for the month of March 2014. The Team acknowledges that the duty roster was prepared with the number of Controller working positions (CWPs) in the KL ATSC being filled by qualified Controllers at all CWPs.

ii) On the night of 07 March 2014, at 1500 UTC [2300 MYT] the functions of control for Sector 5 was absorbed into

Sector 3. There was no issue from this time other than that the combination of these two CWPs was carried out an hour earlier than scheduled. From 1600 UTC [0000 MYT] until 1900 UTC [0300 MYT] and 1900 UTC [0300 MYT] to 2200 UTC [0600 MYT] the Sector 3+5 radar working position was manned by radar-rated Controllers. However, it is confirmed that, from 1600 UTC [0000 MYT] till 2200 UTC [0600 MYT], the Sector 3+5 Planning Position was manned by an *OJT Controller* and an *AFD Officer* as the qualified Controllers were having their respective breaks.

Figure 2.7D - Kuala Lumpur Air Traffic Control Centre – Area Control CWPs

7) Airworthiness Sector

a) The Airworthiness Sector is not involved in the frontline operations of the aircraft. Organisational weaknesses or shortcomings of the Airworthiness Sector however may contribute to accidents due to weaknesses in the management systems and culture.

b) Areas Analysed

The following areas were analysed for latent conditions:

- Corporate goals
- Organisational Structure
- Communication
- Planning

- Control and monitoring
- Procedures
- Resources, which include:
  - Regulations
  - Safety Management

i) Corporate Goals

The Airworthiness Sector does not have specific corporate goals. It shares the Vision, Mission and values of the parent DCA. The DCA's Vision is "*to be the world's leading aviation aut*hority". Its Mission is "*to continuously enhance safety, security and efficiency for sustainable aviation industry*". These Vision and Mission do not specifically relate to the roles and functions of the Airworthiness Sector, which is to carry out "*the regulatory function in respect of airworthiness through the establishment of standards recommended practices and guidelines, and their enforcement as required by the Civil Aviation Act [CAA] 1969".* The organisational Vision and Mission are normally related to corporate goals. It is very important to instil values in each staff to achieve the corporate objectives. However, there is no direct evidence that any missing corporate goals in terms of Vision and Mission may contribute to any latent conditions which can lead to the potential failure of the system.

ii) Organisational Structure

The organisational structure of an Airworthiness Organisation is detailed in the ICAO Document 9760. The Airworthiness organisation is divided into the Airworthiness Engineering Division (AED) and Airworthiness Inspection Division (AID), as shown in *Figure 2.7E - Setup of the Airworthiness Organisation (ICAO Document 9760)*.

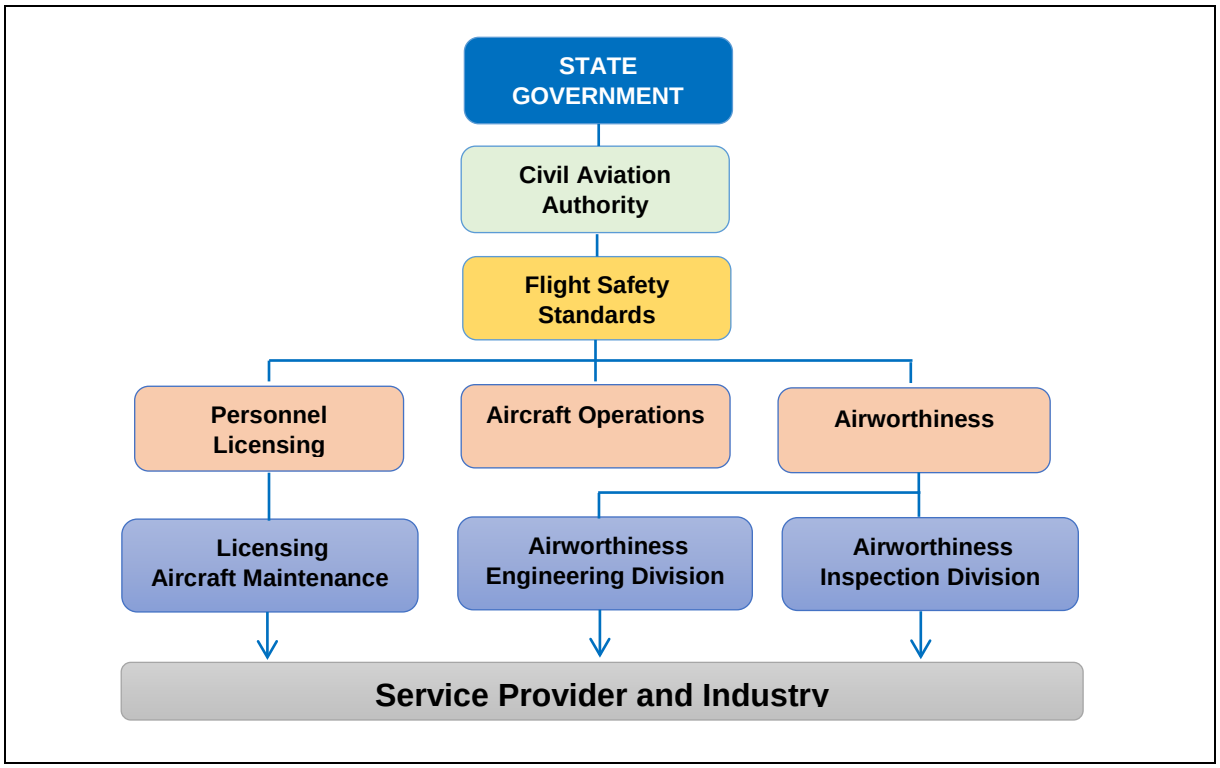

Figure 2.7E - Setup of the Airworthiness Organisation (ICAO Document 9760)

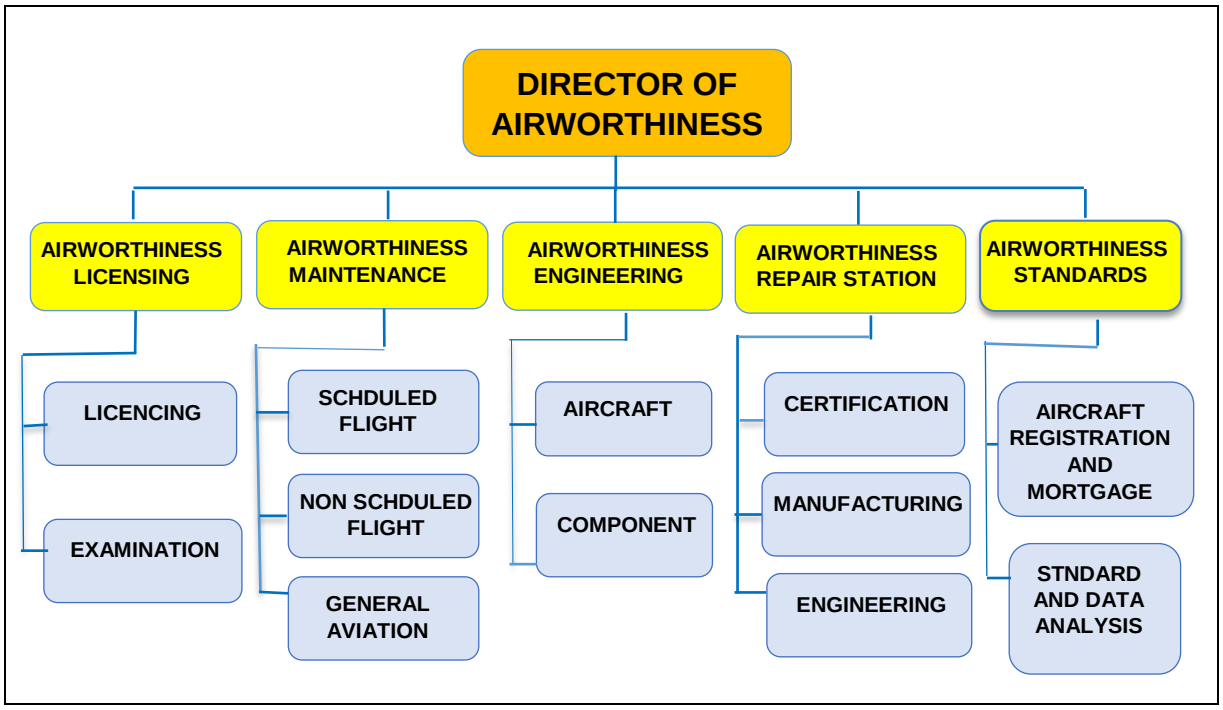

Figure 2.7F - DCA Airworthiness Sector

The DCA Airworthiness Sector is divided into 5 divisions: Airworthiness Licensing, Airworthiness Maintenance, Airworthiness Engineering, Airworthiness Repair Station, and Airworthiness Standards as in *Figure 2.7F* above.

The roles and responsibilities of each division are as follows:

- **Airworthiness Licensing** is responsible for examination of engineers, approval of training organisations, and issuance of licensing of aircraft maintenance engineers.

- **Airworthiness Maintenance** is responsible in initial issuance and renewal of Airworthiness Certificates and approval of aircraft maintenance and facilities, continuing airworthiness maintenance and investigation of incidents and defects.

- **Airworthiness Engineering** is responsible for certification of aeronautical products, issue of Airworthiness Directives (AD), approval of modification and repair, and approval of Design Organisations (DOA) and Production Organisations (POA).

- **Airworthiness Repair Station** is responsible for investigation of incidents and defects and approval of maintenance organizations/repair stations (MRO).

- **Airworthiness Standards** is responsible for registration of all civil aircraft and aircraft mortgage, to develop and update standards, requirement and procedures, analyse airworthiness data, including all occurrence reporting, service difficulties reporting, malfunction and defects.

The organisational structure of the DCA Airworthiness Sector does not clearly show the divisions of AED and AID. The licensing of aircraft maintenance is in the Airworthiness Sector. However, the analysis of the current Airworthiness Sector organisation structure indicates there are elements of AED and AID in the organisation. The AID elements are available in

Airworthiness Maintenance, and Airworthiness Repair Stations. The Airworthiness Standards cover both the AED and AID. The Airworthiness Licensing should be in the Airworthiness Sector because the DCA has a dedicated division to handle all licensing matters. Based on the organisation structure and the roles and responsibilities of each of the divisions within the Airworthiness Sector, there is no evidence of any aspects or characteristics which may lead to a latent condition.

iii) Communication

The effective external and internal communication is essential because ineffective communication and miscommunication have shown to result in unsafe condition. The Airworthiness Sector external and internal communication have been shown to be effective formally by letter and email. The internal communication is by means of meetings and discussions between the staff. The work process and activities are consistent since the Airworthiness Division Manual (ADM) is used by the airworthiness engineers and inspectors as their procedure manual when carrying out their respective tasks. Therefore, there is no evidence of any unsafe condition with respect to communication.

iv) Planning

The Airworthiness Sector carries out continuing airworthiness and surveillance oversight of aircraft maintenance activities of 8 Scheduled Operators and 21 Non-Scheduled Operators, 176 (local and international) Approved Maintenance Organisations (AMO) and 12 Approved Training Organisations (ATO). MAS was one of the major airline operators. The Airworthiness Sector also provides technical audit support in conjunction with the Flight Operations Sector and Air Transport Division to issue an Air Operating Certificate (AOC). The above activities are adequately planned and conducted, based on the schedule established for each organisation.

For the initial airworthiness certification, airworthiness inspectors and airworthiness engineers carry out new aircraft type design certification or the validation of Aircraft

Type Certificate before the aircraft is registered. The Airworthiness Sector also reviews new applications for minor or major modifications and monitoring the applicability of mandatory Airworthiness Directives issued by the State of Design.

The audit and surveillance of the organisation (i.e. MRO, ATO and AOC) and aircraft inspection for Certificate of Airworthiness (C of A) renewal are conducted on a regular basis of at least once a year. The Airworthiness Sector establishes a detailed annual audit and surveillance programme.

In the case of 9M-MRO, it was noted that the last C of A renewal for aircraft physical inspection was not carried out by the Airworthiness Inspector but was renewed based on document submission and a physical inspection report by MAS. The last aircraft physical inspection on 9M-MRO was carried out more than one year prior to the aircraft's disappearance. This is an acceptable practice by the Airworthiness Sector because the annual renewal of the Certificate of Airworthiness is normally supported by an aircraft document/physical inspection report. The mutual arrangement with the operators would indicate that the Sector has a close working relationship with the aviation industry and this arrangement serves to expedite the Certificate of Airworthiness' renewal process. Based on the above analysis, the system of planning and accomplishment are in order and there is no evidence of any latent condition which may contribute any failures.

v) Control and Monitoring

The control and monitoring mechanism requires the organisation to have key performance indicators (KPI) of its performance, hazards identification and risk management policies and programme. The aspects of hazards identification and risk management are essential for the organisation in decision making of its functions and responsibilities. The aspect of organisation key performance indicators is clearly discernible.

vi) Procedures

The Airworthiness Sector uses Airworthiness Department Manuals (ADM) as internal documented policies and procedures for the Airworthiness Engineers and Inspectors. The ADM has detailed most of the Airworthiness Sector's working procedures. However, it has not been reviewed regularly and updated in line with technological advancement. There is no specific unsafe condition, but it could be a latent condition.

vii) Resources

ICAO through Doc 9760 has recommended that inspectors and engineers possess relevant knowledge, experience and competency. The Airworthiness Sector has recruited a number of fresh engineers and inspectors to fill up the relevant posts. These new engineers/inspectors need to undergo training required under ICAO requirements.

Regulation is one aspect of the important resources required by the Airworthiness Sector. All the activities of the Sector were based on the Civil Aviation Act 1969. The Act requires compliance with the ICAO Annexes. The Act also requires the Minister of Transport to make regulations based on ICAO SARPS (Standards and Recommended Practices. The Minister of Transport formulated the Civil Aviation Regulations 1996 under the provisions of the Civil Aviation Act 1969. The analysis on the Malaysian civil aviation laws and regulations indicate that the Civil Aviation Act 1969 and CARs of 1996 may be outdated by present international regulatory standards and practices.

It is anticipated that the future introduction of the Civil Aviation Safety Requirements (CASR), Acceptable Means of Compliance (AMC) and Guidance Materials (GM) would serve to streamline the Malaysian regulatory framework, requirements and procedures, similar to the approach of the European Aviation Safety Agency (EASA) requirements. In the absence of new regulations in CAR 1996, the Airworthiness Sector has adopted and

adapted other countries' laws and regulations (i.e. United States of America, European Union) and published these regulations either in notices, circulars, directives or information and issued them under section 240 (Publication of Notices) of the Civil Aviation Act 1969.

8) Flight Operations Sector

a) Corporate goals

The Flight Operations Sector (FOS) is one of the sectors of DCA Malaysia. It does not have specific corporate goals, vision or mission. It rides on the DCA Vision and Mission, which are not specific to the functions and responsibilities of the FOS. A specific vision and mission would focus the FOS inspectors on common values and practices. There is no evidence of any significant safety issue with the absence of a specific Vision and Mission for the FOS. It has no direct bearing on the disappearance of MH370.

b) Organisational structure

The FOS is divided into 5 divisions namely: Flight Crew Licensing, Air Operator Regulations, Flight Simulator, General Aviation and Flight Calibrations.

The FOS is responsible primarily for ICAO Annex 6 (Aircraft Operation) and ICAO Annex 1 (Personnel Licensing) for the flight crew. There is an operational division in the FOS - Flight Calibration Division - which operates a number of aircraft for calibration of airfields and airways. FOS is considered a mixed mode of authority-cum-operator.

c) Resources

The FOS lacks the required number of experienced inspectors (pilots). The shortage of personnel may affect the flight safety standard of the Air Operating Certificate (AOC) holders, especially with respect to the frequency of audit involving station facility inspection, RAMP Inspection for en-route and destination stop, annual inspection at every location, and base inspection for Scheduled Operations and Non-Scheduled Operations. Similarly, the shortage of flight examiners may also affect the standard of the training establishments.

The Flight Operations' Aeronautical Information Circular (AIC) No. 30/2005 November 2015 - Inspections and Investigation of Air Accidents, reiterates the statutory powers of the Minister of Transport to investigate aircraft accidents and serious incidents that occur in Malaysia regardless of nationality of aircraft registration. With respect to aircraft accidents or incidents investigation, the inspectors from the FOS may be called upon to assist the Air Accident Investigation Bureau (AAIB) under the Ministry of Transport. This function would create some constraint to the FOS in view of the shortage of experienced pilots in the Sector. This shortage is potentially a latent condition, which if not addressed, may lead to potential unsafe conditions.

Regulations is another important resource issue with the FOS working within the Civil Aviation Act 1969 and MCAR 1996. The MCAR 1996 is unable to cope with the rapid development in international aviation regulations and practices. Under the provision of section 240 of the Civil Aviation Act 1969, the AICs are published by the DCA. This practice of supplementing the CAR 1996 has been successful. However, it is still unable to cope with the up-to-date rules and regulations in Europe and North America. This condition could not have contributed to the disappearance of MH370. However, this is a latent condition which needs to be appropriately addressed.

Safety management is another important aspect in the organisation. The ICAO Annex 19 (Safety Management) has mandated the aircraft operators to develop their organisations' SMS by January 2009. To comply with the ICAO requirements, the FOS has developed the AIC No. 06/2008 which was issued under section 240 of the Civil Aviation Act 1969 for all Malaysian Air Operating Certificate (AOC) holders to establish their organisational Safety Management System (SMS). Notably, MAS had implemented the SMS into their procedures manual. The requirement for the operators to establish SMS by the FOS is adequate. However, the FOS has to establish its own safety management programme.

2.7.2 Malaysia Airlines

1) Engineering & Maintenance

Based on the factual information provided in *Section 1.17.2 para. 2)* the Engineering & Maintenance Division was well-structured appropriate to a maintenance management and maintenance organisation with key positions manned by persons approved by the Department of Civil Aviation (DCA), Malaysia. The required oversight of the maintenance activities was provided both by internal Quality auditors, as well as by the DCA Malaysia. This was further supported by audits by foreign auditors, such as from the EASA and FAA. There were no significant audit findings suggesting that the organisation was well managed. It is not unusual to have findings during audits; the purpose is to continuously improve by instituting corrective and preventive actions.

Maintenance personnel were appropriately trained and qualified in accordance with approved procedures, as documented in the Maintenance Management and Organisation Exposition (MMOE).

Although recently introduced in the year 2009, Safety Management had been embraced in the organisation and in line with the corporate system.

2) Flight Operations Management

The Flight Operations Management (FOM) office positions were sufficiently manned by qualified individuals and the working guidelines ensure their effectiveness in carrying out duties in their respective management positions. The fleet manager, being on the B777 for more than 10 years and having held the post of Type Rating Examiner (TRE), attests to his level of competency and seniority.

a) Technical Crew of Malaysia Airlines

There was no evidence of irregularities in the standards, performance and capability of pilots in Malaysia Airlines **(**MAS).

b) Medical Check-up

There was no evidence of irregularities in terms of medical and licensing validity of pilots in MAS.

c) Roster Schedule & Management

Data collected indicate that the pilots' roster and rest period are in compliance with MCAR FTL requirements.

There is no evidence to suggest that any of the two pilots infringed any of the required MCAR FTL limits.

d) Confidential Human Factors Incident Report System

In September 2013 to March 2014 over a period of six months, there were a total of six reports submitted, mainly on communications issues between staff.

This suggests that the CHIRPS was capturing adequate data to meet its objective.

There was no evidence to suggest that any of the two pilots were subjected to CHIRP's surveillance.

e) Flight Operations Quality Assurance

Sampling of FOQA data over a 2-year period prior to the event was studied. Capture rates were close to 100% and it is evident that the system works and justifies its role in identifying non-normal operations either deliberate or due to environment factors.

The overall rate for B777 has its average figure comparative to the industry standards.

As an example, the highest event of UA (Unstablised Approach) occurred in the month of August 2013 at a rate of 49.26 per 10,000 flight cycles. This is equivalent to 0.49% for the month.

The highest FOQA trigger was the long flare event which occurred in the month of May 2012 at 243.6 per 10,000 flight cycles. This is equivalent to 2.3% for the month.

Based on these findings, enhanced training on the proper corrective measures was introduced during recurrent simulator checks.

f) Line Operations Safety Audit

The findings were very relevant, and recommendations were implemented via Safety Change Process (SCP). MAS on the average had less findings compared with the other 5 airlines in the Line Operations Safety Audit (LOSA) archive. Safety Change Process was carried out to mitigate the findings. LOSA findings also revealed low prevalence in terms of overall mismanagement rate (unsafe operations) in the B777 fleet as reported in MAS LOSA Report 2011. LOSA was conducted by taking a random sampling

on all fleets including the B777. MAS had met the average safety standards of most international airlines.

g) Crew Resources Management

The Team's analysis reveals that the CRM programme had been implemented and had produced positive results over the years. These awareness and regular recurrent training programmes had inculcated good interpersonal relationships between flight crew members and had contributed significantly to the overall safety of the flight operations.

Both the technical and cabin crew were in compliance with CRM requirements.

h) Safety and Emergency Procedures

Findings have indicated that both the technical and cabin crew were in compliance with SEP validity. The training syllabus had met all the regulatory requirements.

i) Flight Deck Security Procedures

At the time of flight MH370, there were no requirements for an additional crew member in the cockpit in the event when one of two pilots were to leave the cockpit. However, in response to flight MH370, MAS has, since introduced this requirement into its safety procedures effective 27 March 2014, a procedure subsequently introduced by other airlines following the GermanWings Flight 9525 accident on 24 March 2015.

j) MAS B777 Training and Standards

The fleet carried sufficient numbers of Type Rating Examiners (TRE) and Type Rating Instructors (TRI) to fulfil the licensing requirements. TRE and TRI were Captains from within the airline, appointed with approval from the Licensing Section of the DCA. They were also tasked with monitoring the overall standards to be maintained by the fleet. This responsibility was under the jurisdiction of the Training and Standards Department, which was headed by a Chief Pilot.

k) Multi-crew Operation MH370

Flight MH370 was operated on a normal 2-man crew operation with one PIC and one FO. A third pilot was not required as a safety pilot as the trainee's performance was reported to be above average and deemed safe by the previous Training Captain.

The duration of the scheduled flight with FDP (Flight Duty Period) of less than 8 hours also justified the 2-man crew operations.

l) Operation Control Centre

During the day of the disappearance of MH370, it was established that the FFS was programmed to receive a download from the aircraft at 30 minute intervals. The last download was transmitted at 1707:29 UTC [0107:29 MYT]. As a result, the track and position shown on the monitor after this time was only the predicted track and position.

Facts gathered during interviews with despatchers on duty during the incident suggested that with the exception of hijack and bomb hoax, there were no quick references to guide the frontline operations staff to react to emergency situations such as a lost aircraft and a crash.

The FFS was observed to be in accordance ICAO Annex 6 Part 1 Chapter 4, AIC 10/2002 dated 25 July 2002 and FOSI[38] Handbook, Vol 3, Chapter 4, para 6. Personal interviews with individual despatchers suggested increased workload which could

[38] This order is referred to as a handbook and directs the activities of Flight Operations Surveillance Inspectors (FOSI) who are responsible for the certification, technical administration, and surveillance of scheduled air carriers and certain other air operators who conduct their operations in accordance with the Malaysian Civil Aviation Regulations 1996, made under the Civil Aviation Act 1969.

have affected the quality of work. There is evidence that the Supervisor/Despatcher-in-charge oversaw an average of 30 flights on that particular night shift, including monitoring seven to eight different flights at one time on the Orient Sector. This suggests the existence of an element of overworked condition.

The Team's investigation into the basic capability of the FFS suggested that there are bound to be discrepancies between the actual aircraft position compared to the projected flight path in the FFS once an automatic update stops. This could explain the state of confusion and uncertainties among all parties involved during the incident. These discrepancies suggest two hypotheses:

- Data downlink failure from the ACARS communication.
- Intentional or unintentional deactivation of ACARS Communications.

The position update on the FFS was programmed at 30 minute intervals on the B777. This interval is the same as the B747-400 but comparatively longer than other aircraft (A380: 10 mins; A330: 10 mins; B737-800: 10 mins).

The displayed aircraft position was erroneous right from the point where the ACARS communication was lost.

m) Fuel Policy

There is no evidence to suggest that the PIC had ordered or carried any extra amount of fuel beyond the minimum amount recommended by the Computerized Flight Plan. This was in compliance with the Company's fuel policy.

No irregularities were found in the fuel computation and fuel flight plan.

n) Flight Plan Routing

There is no evidence in terms of out-of-normal flight planning on the KUL/PEK sector nor any deliberate rerouting to suggest that the PIC might have the intention to carry extra fuel. Nonetheless, it is a captain's authority to carry additional fuel if he thinks it is justified and to override the despatcher's decision.

No irregularities were found in the aircraft flight plan.

3) In-flight Services

a) Cabin Crew Training

The cabin crew of MH370 were provided with proper training on Safety and First Aid. They were also trained to handle:

i) Safety and emergency evacuation.
ii) Disruptive/difficult passengers.
iii) Medical emergency (provision of First Aid).

Crew Resource Management (CRM) is part of the mandatory programme in cabin crew training. It is on record that the IFS did his CRM a day before the departure of the MH370 flight (the most current in the CRM recorded was from the IFS where it was noted that he did his CRM a day before the departure of the MH370 flight).

All the cabin crew of MH370 were trained with Safety procedures and in compliance with regulatory and Company's requirements.

b) Crew Performance Appraiser

The Crew Performance Appraiser (CPA) system was an established process in the organisation to monitor crew performance and standards including safety knowledge.

The organisation had a clear system on the CPA monitoring process that, if a crew member had failed to carry out the required CPA, the crew member was reminded by the system or the Ward Leader[39] to follow up on the crew member apart from alerting the Crew-in-charge to ensure that the crew member would have to fulfil the requirement within the stipulated cycle in a year.

There is no evidence to indicate that the disappearance of MH370 was attributed to poor crew performance.

c) Medical Record

The cabin crew of MH370 had undergone a medical check-up as a requirement during the initial crew training. However, medical check-up was never made compulsory as a yearly pre-requisite. There is no evidence to suggest that the disappearance of MH370 was attributed to medical conditions of the cabin crew.

[39] Ward Leader – An executive assigned to monitor the performance, discipline and welfare of cabin crew.

d) In-flight Operation

To efficiently carry out the duties that include in-flight customer services including serving passenger meals, MAS had established the need to carry 11 cabin crew members. MH370 however departed with only 10 cabin crew members, 1 less than the normal compliment. It is an established fact that, based on regulation, the minimum crew required are 8, consistent with the number of doors/Emergency Exits available on the B777. It is unlikely that any of the crew were subjected to exhaustion before or while on duty on the ill-fated flight.

MAS was then facing acute shortage of cabin crew resulting in flights departing with under-strength crew complements from the numbers normally required on many of their aircraft operations in the past year.

The flight departed within the legal minimum crew requirement as per the local Civil Aviation Requirement. Shortage of manpower can lead to personnel fatigue even though it is within the legal requirement and acceptable operations.

Nevertheless, there is no evidence to indicate that exposure to stress and overwork had contributed to the disappearance of MH370.

e) Flight Time Limitation

The Malaysia Airlines Employee Union (MASEU) was the recognised Union Organisation endorsed by MAS to represent the cabin crew. The Flight Time Limitation (FTL) and the working conditions were governed by the Collective Agreement (CA) signed between the Union and MAS in accordance with the Civil Aviation Regulations 1996, whichever was the more limiting.

Another Union - the National Union Flight Attendants Malaysia (NUFAM) - was later formed and sought recognition to represent the crew's Collective Agreement (CA). A secret ballot was held in July 2013 and NUFAM won the election with a majority of 60% indicating the cabin crew's preference. However, MAS Management did not recognise the Union. This stalemate had delayed the renewal of the Collective Agreement which expired in August 2013.

There was no infringement of the FTL. The cabin crew were in

compliance with the requirements of the Civil Aviation Regulations 1996.

There is no evidence to indicate that the disappearance of MH370 was attributed to insufficient rest or exceeding permitted working hours.

FTL is not a contributing factor to the disappearance of MH370. However, the crew's working conditions and FTL were subject to each organisation's MOU with the approval of the DCA as a regulator. The crew were in compliance with the requirements of the Civil Aviation Regulations 1996.

SECTION 2 – ANALYSIS

2.8 AIRCRAFT CARGO CONSIGNMENT

2.8.1 Cargo on Board MH370

1) The gross weight of the cargo carried on board MH370 was 10806 kg (cargo plus packing materials, pallets and ULDs).

2) The nett and gross weight of the cargo are as depicted in *Table 2.8A* (below).

CARGO ITEMS	WEIGHT (in kg)	
	NETT	GROSS
Scholastic Assorted Books	2,250	2,320
Lithium Ion Batteries	221	2,650
Walkie Talkie and Radio Accessories and Chargers	2,232	
Electrical Parts (Capacitors)	26*	(410 + 394) 804
Vehicle Electronic Chips	6*	
Electronic Measurements	646*	
Fresh Mangosteens	4,566	4,926
Courier Materials - Documents	6	6
Total	**9,953**	**10,806**

Table 2.8A - Cargo List

* *shared cargo position*

3) There were 2 items of concern viz. Lithium Ion (Li-ion) batteries and mangosteen fruit. The batteries were speculated to be a fire hazard and the mangosteens were also speculated to be out of season at that time of the year.

4) A total of 36 shipments of Li-ion batteries and accessories and mangosteens were flown together to China on previous flights (*Appendix 1.18J - Airways Bills from January to May 2014)***.** There were no reports of any incidents concerning these cargo shipments.

5) During the Team's visit to NNR Logistics, Tianjin, China the forwarding agent for Motorola confirmed that they had reserved cargo space on all MH370 departures out of Kuala Lumpur to Peking for the carriage of Motorola products. NNR Logistics had also highlighted that, in compliance with Motorola's stringent Standard Operating Procedures

(SOP), any damaged boxes would be rejected during physical inspection and loading.

2.8.2 Li-ion Batteries on Board MH370

1) Of the total consignment of 2,453 kg from Motorola Solutions Penang, only 221 kg were Li-ion batteries in compliance with Section II of Packing Instruction 965; the rest comprised Radio Accessories and Chargers.

2) Testing of the Li-ion batteries was carried out by the Company's Research & Development Department in the United States of America as per Certificate of Compliance, Certificate No. 12GEM0185 with Issue Date: 12-09-2012 for PMNN4081BRC; and Certificate No. 13GEM0300 with Issue Date: 2013.10.25 for PMNN4073AR. *Appendix 2.8A - Certificates of Compliance (Rev 14 and 15).*

3) The shipments from Motorola Solutions, transported to the Penang MASkargo Complex by NNR were physically (external visual inspection but did not involve the breaking down of the cargo) inspected by the MASkargo handlers in Penang but not screened by MAS security personnel by means of an x-ray screening machine. At that time there were no available x-ray machines on the landside large enough to screen the consignments. In June 2014, Penang MASkargo had acquired three machines capable of screening large consignments which were fully operational in July 2014.

4) The security procedures are in accordance with Amendment 13 of ICAO Annex 17 which came into force on 15 July 2013 where all cargo are required to undergo physical security screening as per DCA Director General Directive No. 1A/2013 (AVSEC) Physical Security Screening-Enhanced. There is also a Director General Directive No. 2/2013 (AVSEC) on Air Cargo Transhipment in Malaysia effective 15 July 2013 which allows this procedure (*Appendix 2.8B - Director General Directive No. 1A/2013 and Appendix 2.8C - Director General Directives No. 2/2013*).

   After the physical inspection by MASkargo personnel, the loaded consignments went through Customs inspection and clearance. The truck was then sealed by Customs and MAS Security before being allowed to leave the Penang cargo complex enroute to KLIA under escort. The truck made a routine resting stop at Rest and Recreation

(R n R) Centre, Tapah, Perak on the North-South Highway. The two drivers interviewed revealed that the truck was never left unguarded by them or the security escort. The shipment arrived at KLIA Cargo Complex on the evening of 07 March 2014, before the seals were broken and the cargo loaded onto MH370 without further screening.

The security procedures for the cargo from Motorola Solutions to KLIA, Sepang were reviewed and found in accordance to the standard operating procedures.

2.8.3 Mangosteen Fruits on Board MH370

The Team confirmed that MH370 was carrying mangosteens to China. Contrary to speculations that the fruits were out of season, it was found to be in season in Muar, Johore and neighbouring countries. At the time of writing of this report the fruits are still being exported by the same company to Beijing, China.

2.8.4 Dangerous Goods

1) The Li-ion batteries carried on board MH370 were not listed as dangerous goods (DG) and as such they were in compliance with Section II of Packing Instruction 965. Hence, there was no requirement for the pilots to be informed. However, the mangosteens were declared in the Special Load Notification to Captain (Doc. DVC-17957 1529 07Mar14 (*Appendix 2.8D*) and the Letter and Directive by the Director General (*Appendices 2.8B and 2.8C*) as it is classified as a perishable item.

2) Both pilots were trained on DG procedures and were periodically updated (once every two years) in their Safety and Emergency Procedures (SEP) training programme. *Table 2.8B (*below) shows the training programme.

Crew	SEP Expiry Date	CRM Date Attended	DG Cat 10
Pilot	17 August 2014	07 September 2011	24 February 2014

Table 2.8B - Table for Technical Crew SEP/CRM/DG CAT

2.8.5 Laboratory Tests Conducted

After the disappearance of MH370, laboratory tests on Li-ion batteries and mangosteens were conducted by STRIDE, Malaysia to determine their

individual and/or combined reactions under certain conditions. Refer to *Appendix 2.8E Laboratory test on Li-ion batteries and mangosteens.* The test results are as follows:

1) Li-ion Batteries

a) High Temperature Tests

i) Point of bulging was at 175º C;

ii) Point of fuming was at 187º C;

iii) Point of eruption was at 207º C;

iv) At peak, release of carbon monoxide (CO) was at 176.5 ppm;

v) At peak, release of carbon dioxide (CO2) was at 471 ppm.

b) Functional and Voltage Capacity Tests

i) All the batteries tested were functioning normally.

ii) Average capacity of 60% or about 7.3V from full capacity of 11V.

c) Drop Tests

The tests were carried out with batteries (window white box in brown box *(Figure 2.8A*, [below]) dropped at a height of 120.92 cm (48 inches) on to a wooden platform. It was found that the batteries had no observable physical damage and functioned normally.

i) Short Circuit Tests

- The batteries produced sparks when electrodes (Positive and Negative) touched directly.
- The batteries did not produce sparks when the electrodes were touched with cardboard soaked in water from sponge or mangosteen extract.

ii) Built-in Voltage and Current Protection Circuit Tests

- The batteries also have a built-in voltage and current protection circuit. "…*Cell protection features consist of internally trimmed charge and discharge voltage limits,*

discharge limit with a delayed shutdown and an ultra-low current sleep mode state when the cell is discharged."

Figure 2.8A - 2 Batteries in window white box and placed in a brown box

2) Mangosteen Fruits

a) pH Value Tests

Water from the sponge used to keep the fruit fresh was tested and found to have a pH value of 6 and the mangosteen juice had a pH value of 3.

b) Conductivity Tests

- When current was passed through distilled water, the current flow indicator did not light up (distilled water was not conductive);
- When current was passed through mangosteen extracts, the current flow indicator lit up (mangosteen extract was conductive);
- When current was passed through water from the sponge, the current flow indicator lit up (water from the sponge was conductive).

2.8.6 Effects of Close Proximity of Li-ion Batteries and Mangosteens in Cargo Consignment

1) Location of Cargo

In one of the cargo compartments on MH370 the Motorola Solutions batteries and mangosteens were placed next to each other (No. 1 and 'A'). Even though they were placed next to each other in the aircraft (*Figure 2.8B* [below]), the mangosteens were packed in plastic crates and placed in Unit Load Device (ULD) containers. The consignment was also wrapped in a plastic sheet to make it water-proof to a certain extent.

Figure 2.8B - Sample ULD and Batteries placed next to each other

2) Results of Tests

There were concerns that the mangosteen extracts could have got into contact with the batteries and produced hazardous fumes or in a worst case scenario caused a short circuit and/or fire. These tests were carried out and the results are as follows:

i) This was highly improbable on board MH370 with a comparatively short flight duration and under controlled conditions.

ii) After carrying out the tests, STRIDE was convinced that the two items tested could not be the cause in the disappearance of MH370. The Team concurs with STRIDE's findings.

SECTION 3 – FINDINGS AND CONCLUSION

3.1 Findings

3.1.1 Diversion from Filed Flight Plan Route

1) Flight MH370 had diverted from the Filed Flight Plan route.

2) There is no evidence to indicate that MH370 was evading radar.

3) Only the transponder signal of MH370 disappeared from the ATC Controller radar display whilst the (radar) position symbols from other aircraft were still available.

4) The reason for the transponder information disappearing from the aircraft could not be established.

5) It could not be established whether the aircraft was flown by anyone other than the pilots.

6) The reconstruction flight conducted on the B777 flight simulator had established that the turn back was likely made while the aircraft was under manual control and not the autopilot. However, it could not be established that the other two turns over the south of Penang and the north of MEKAR were made under manual control or autopilot.

7) The aircraft primary radar target was designated as ‘friendly’ by the Royal Malaysian Air Force as it did not pose any threat to national airspace security, integrity and sovereignty.

8) There were uncertainties on the position of MH370 by both Kuala Lumpur ACC and Ho Chi Minh ACC.

3.1.2 Air Traffic Services Operations

1) Kuala Lumpur Air Traffic Services

a) KL ATSC operation was normal with no significant observation until 1720 UTC [0120 MYT].

b) KL ACC controllers transferred MH370 to Ho Chi Minh ACC at 1719:26 UTC, 3 minutes before the original estimate time of the transfer of the control point.

c) HCM ACC did not notify KL ACC when two-way communication was not established with MH370 within five minutes of the estimated time for the transfer of control point.

d) KL ACC controllers relied solely on position information of the aircraft provided by MAS Flight Operations Despatch Centre rather than checking up with other ATC authorities.

e) The Air Traffic controllers did not initiate, in a timely manner, the three standard emergency phases in accordance with the standard operating procedures.

f) There is no record to suggest that the KL ACC controllers took any action to alert the RMAF Joint Air Traffic Control Centre (JATCC).

g) There is no evidence to suggest that the Air Traffic controllers at KL ACC had kept continuous watch on the radar display.

h) KL ACC controllers did not comply fully with established ATC procedures.

2) Ho Chi Minh Air Traffic Services

a) There were uncertainties on the position of MH370 by both KL ACC and HCM ACC.

b) The command of the English language in the coordination process between KL ACC and HCM ACC needs improvement.

c) HCM ACC did not notify KL ACC when two-way communication was not established with MH370 within five (5) minutes of the estimated time for the transfer of control point.

3.1.3 Flight Crew Profile

1) General and Specific Human Factors Issues

a) There is no evidence to suggest any recent behavioural changes for the PIC, FO and cabin crew.

b) There is no evidence to suggest a pattern of regular over-the-counter medication purchase by the PIC. However, the possibility that such medication may have been purchased by cash cannot be excluded.

2) Human Factor Aspects of Air Traffic Control Recordings

a) The voice transmission for the first 3 sets of recordings were those of the FO before take-off and the 4th and 5th sets were from the PIC after take-off.

b) The last radio transmission "*Good Night Malaysian Three Seven Zero"* was spoken by the PIC. However, he did not readback the assigned frequency, which was inconsistent with radio-telephony procedures.

c) The radio-telephony communications conducted by the PIC and the FO with the Air Traffic Controllers revealed no evidence of anxiety or stress detected in the conversations.

3.1.4 Airworthiness & Maintenance and Aircraft Systems

1) The maintenance records indicated that the aircraft was equipped and maintained in accordance with existing regulations and approved procedures, except for the instance of the Solid-state Flight Data Recorder Underwater Locating Beacon (SSFDR ULB) battery which had expired in December 2012.

2) The aircraft had a valid Certificate of Airworthiness.

3) The aircraft was airworthy when dispatched for the flight.

4) The mass and the centre of gravity of the aircraft were within the prescribed limits.

5) Although it cannot be conclusively ruled out that an aircraft or system malfunction was a cause, based on the limited evidence available, it is more likely that the loss of communication (VHF and HF communications, ACARS, SATCOM and Transponder) prior to the diversion is due to the systems being manually turned off or power interrupted to them or additionally in the case of VHF and HF, not used, whether with intent or otherwise.

6) The recorded changes in the aircraft flight path following waypoint IGARI, heading back across Peninsular Malaysia, turning south of Penang to the north-west and a subsequent turn towards the Southern Indian Ocean are difficult to attribute to any specific aircraft system failures. It is more likely that such manoeuvres are due to the systems being manipulated.

7) The SATCOM data indicated that the aircraft was airborne for more than 7 hours suggesting that the autopilot was probably functioning, at least in the basic modes, for the aircraft to be flown for such a long duration. This in turn suggests that the air and inertial data were probably available to the autopilot system and/or the crew.

8) The inter-dependency of operation of the various aircraft systems suggests that significant parts of the aircraft electrical power system were likely to be functioning throughout the flight.

9) Without the benefit of the examination of the aircraft wreckage and recorded flight data information, the investigation is unable to determine any plausible aircraft or systems failure mode that would lead to the observed systems deactivation, diversion from the filed flight plan route and the subsequent flight path taken by the aircraft.

10) No Emergency Locator Transmitter (ELT) signal from the aircraft was reported by the responsible Search and Rescue agencies or any other aircraft.

3.1.5 Satellite Communications

1) Throughout the flight of MH370 the aircraft communicated through the Inmarsat Indian Ocean Region (IOR) I-3 Satellite and the Ground Earth Station (GES) in Perth, Australia.

2) At 1707 UTC (07 March 2014), the SATCOM system was used to send a standard ACARS report, normally sent at every 30 minutes. The ACARS reports expected at 1737 UTC and subsequently were not received. The next SATCOM communication was a log-on request from the aircraft at 1825 UTC, followed by two IFE Data-3 channel setups. From that point until 0011 UTC (08 March 2014), SATCOM transmissions indicate that the link was available, although not used for any voice, ACARS or other data services apart from two unanswered ground-to-air telephone calls. At 0019 UTC, the Airborne Earth Station (AES) initiated another log-on request. This was the last SATCOM transmission received from the AES.

3) Data from the last seven ‘handshakes’ were used to help establish the most probable location of the aircraft. Both the initial log-on request and the hourly ping have been termed as a ‘handshake'. Two unanswered ground-to-air telephone calls at 1839 and 2313 UTC (07 March 2014) had the effect of resetting the activity log and hence increased the period between the ground initiated ‘handshakes’.

4) The two Log-Ons, at 1825 UTC (07 March 2014) and 0019 UTC (08 March 2014), were initiated by the aircraft most likely due to power interruptions to the SATCOM avionics.

5) The power interruption leading up to 1825 UTC was probably due to power bus cycling, the reason for it being unknown. The power interruption leading up to 0019 UTC was probably due to low fuel at this time resulting in the loss of both engines and their respective generators. There was probably enough fuel for the APU to start up and run long enough for its generator to power the SATCOM avionics (SATCOM AES) to initiate a log-on request.

3.1.6 Wreckage and Impact Information

1) The main wreckage belonging to MH370 has so far not been found. However, a number of debris were found washed ashore near and onto the south eastern coast of Africa.

2) Only the parts washed ashore on La Reunion Island (the right flaperon), Tanzania (part of the right outboard flap) and Mauritius (a section of the left outboard flap) were confirmed to be from MH370. Although the name plate was missing, which could have provided immediate traceability to the accident aircraft, the flaperon was confirmed to be from the aircraft 9M-MRO, by tracing the identification numbers of the internal parts of the flaperon to their manufacturing records at EADS, CASA, Spain. Similarly, the Italian part manufacturer build records for the numbers located on the right outboard flap part confirmed that all of the numbers related to the same serial number outboard flap shipped to Boeing for aircraft 9M-MRO. As for the section of the left outboard flap, a part identifier on it matched the flap manufacturer supplied records which indicated a unique work order number and that the referred part was incorporated into the outboard flap shipset line 404 which corresponded to the Boeing 777 aircraft line number 404, registered 9M-MRO and operating as MH370.

3) To date, 27 items of debris were considered significant for examination. Of these, other than the flaperon, a part of the right outboard flap and a section of the left outboard flap, 7 items were also considered *almost certain* to be from MH370.

4) Damage examination on the recovered part of the right outboard flap, together with the damage found on the right flaperon indicates that the right outboard flap was most likely in the retracted position and the right flaperon was probably at, or close to, the neutral position, at the time they separated from the wing.

5) Recovery of the cabin interior debris suggests that the aircraft was likely to have broken up. However, there is insufficient information to determine if the aircraft broke up in the air or during impact with the ocean.

3.1.7 Organisational and Management Information

1) Department of Civil Aviation

a) The regulatory system in Malaysia includes Regulation 201 of MCAR 1996 that applies ICAO Annex 1 to 18 "*ipso facto*". However, the resulting regulatory framework under this *"ipso facto"* regulation in Malaysia does not enable an effective implementation of all ICAO Annex provisions. With the introduction of Annex 19 dedicated to a Safety Management System, applicability date 14 November 2013, the *"ipso facto"* provision does not include Annex 19.

b) DCA is looking into the establishment of a State Safety Programme (SSP) for the management of safety in the State that will be applicable on 07 November 2019.

c) The organisation structure is suitable for DCA at headquarters as the activities are routine and standardised.

d) On Search and Rescue, there is a comprehensive arrangement in dealing with an aircraft emergency between Malaysia and neighbouring States which requires the provision of A-SAR services on a 24-hours daily basis fulfilling the international obligations.

e) Kuala Lumpur Air Traffic Control Centre

i) DCA has a policy of retaining retiring ATCOs on a contract basis to ensure that the number of qualified and rated Controllers remains status quo and that there is a transfer of technology, experience and expertise.

ii) Although no internal audit had been conducted, it is noted that an audit team will be established consisting of personnel who had previously attended audit courses.

iii) All ATC training courses were conducted on operational and opportunity basis.

2) Malaysia Airlines

a) Engineering & Maintenance

i) The Engineering & Maintenance Division was a well-structured maintenance management and maintenance organisation with key positions manned by persons approved by the Department of Civil Aviation (DCA), Malaysia.

ii) Proper oversight was provided both by internal and external audits. There were no significant audit findings.

iii) Maintenance personnel were appropriately trained and qualified in accordance with approved procedures.

b) Flight Operations

i) There is no evidence of irregularities of both the pilots in terms of their capability, performance and standard to assume command of a B777 and as First Officer respectively prior to the disappearance of MH370.

ii) There is no evidence of irregularities in terms of Medical & Licencing Validity of both the pilots prior to the disappearance of MH370.

iii) There is no evidence of irregularities in Roster Schedule and Management.

iv) The findings of LOSA were very relevant and recommendations were implemented via a Safety Change Process (SCP). MAS had met the average safety standards of most international airlines.

v) Both the Technical Crew & Cabin Crew were in compliance with CRM requirements.

vi) During the period of the incident there was no enhanced special security alert status declared by MAS.

vii) there were no training records available for the FO from the beginning of his simulator training and initial operating experience (IOE) to his present fleet where he was still under training. All the training reports were with him in his personal training file on board the flight.

viii) Based on past training records, there is no evidence that both the pilots' performance was below the Company's standard since their employment with MAS.

ix) The duration of the scheduled flight with Flight Duty Period (FDP) of less than 8 hours and the training policy justify the 2-man crew operations.

x) An element of overworked condition in the MAS Operation Control Centre existed.

xi) The displayed aircraft position on the Flight-Following System was erroneous right from the point where ACARS communication was lost.

xii) No irregularities were found in the fuel computation and fuel flight plan.

xiii) No irregularities were found in the aircraft flight plan.

xiv) The cabin crew were subjected to thorough medical check-ups as a requirement during the initial recruitment before employment and neither the Company nor the Regulatory body made it a requirement after being employed. However, there was no strict monitoring on the crew's health and mental health in the Standard Operating Procedures (SOP).

xv) The flight departed within the legal minimum cabin crew requirement.

3.1.8 Aircraft Cargo Consignment (Lithium Ion Batteries and Mangosteen Fruits)

1) The two cargo items in question which were carried on MH370 had also been transported via scheduled flights on MAS before and after the event.

2) The Lithium ion batteries (listed as non-dangerous goods), were packed and land-transported out from the production factory to KLIA Sepang in accordance with existing and approved regulations and procedures.

3) Extensive tests conducted on the mangosteens packed with water-soaked foam and juice extracts of mangosteens in contact with Lithium ion batteries revealed that this could only be hazardous if exposed to a certain extreme condition and over a long period of time. This was highly improbable on board MH370 which had a comparatively shorter duration of flight time and was under controlled conditions.

4) There was no cargo classified as dangerous goods on board MH370. The batteries on board were not classified as Dangerous Goods because the packing adhered to the guidelines as stipulated in the Lithium Battery Guidance Document.

SECTION 3.2 – Conclusion

On 08 March 2014, MH370, a scheduled passenger flight from Kuala Lumpur to Beijing, operated by MAS went missing soon after a routine handover from the Malaysian ATC to Viet Nam ATC. Communications with the aircraft were lost after it passed waypoint IGARI, less than 40 minutes after take-off. The aircraft operating the flight was a Boeing 777-200ER, registered 9M-MRO. On board the aircraft were 12 crew and 227 passengers (239 persons in total).

Evidence shows that Flight MH370 diverted from the Filed Flight Plan route. The aircraft's transponder signal ceased for reasons that could not be established and was then no longer visible on the ATC radar display. The changes in the aircraft flight path after the aircraft passed waypoint IGARI were captured by both civilian and military radars. These changes, evidently seen as turning slightly to the right first and then to the left and flying across the Peninsular Malaysia, followed by a right turn south of Penang Island to the north-west and a subsequent (unrecorded) turn towards the Southern Indian Ocean, are difficult to attribute to anomalous system issues alone. It could not be established whether the aircraft was flown by anyone other than the pilots. Later flight simulator trials established that the turn back was likely made while the aircraft was under manual control and not the autopilot.

KL ATSC operation was normal with no significant observation until the handover to Viet Nam ATC. Being *the accepting unit*, HCM ACC did not notify *the transferring unit* (KL ATSC) when two-way communication was not established with MH370 within five minutes of the estimated time of the transfer of control point (Establishment of Communications, page 11 of Operational LOA between DCA Malaysia and Vietnam Air Traffic Management effective 1 November 2001). Likewise, KL ATSC should have taken action to contact HCM ACC, instead, relied on position information of the aircraft provided by MAS Flight Operations. By this time, the aircraft had left the range of radars visible to the KL ATSC. It is noted that about one minute elapsed from the last transmission from MH370 and the SSR being lost from the radar display. The Air Traffic Controllers of both Centres did not initiate the various emergency phases as required then, thereby delaying the activation of the alerting and Search and Rescue operations.

The PIC and FO held valid airman licences and medical certification. There is no evidence to suggest that the PIC and FO experienced recent changes or difficulties in personal relationships or that there were any conflicts or problems between them. All the flight and cabin crew were certified fit to fly and were within duty-time limits at the time of the flight and were adequately rested. There had been no financial stress or impending insolvency, recent or additional insurance coverage purchased or recent behavioural changes for the crew. The radio-telephony communications conducted by

the PIC and the FO with the Air Traffic Controllers conformed to the routine procedure and no evidence of anxiety or stress was detected in the communications.

The aircraft maintenance records indicated that the aircraft was equipped and maintained in accordance with existing regulations and approved procedures, except for the instance of the SSFDR ULB battery which had expired. The aircraft had a valid Certificate of Airworthiness and was airworthy when released for the flight and there was no record or report of any defect or malfunction in the aircraft that could have contributed to the event. Although it cannot be conclusively ruled out that an aircraft or system malfunction was a cause, based on the limited evidence available, it is more likely that the loss of communications (VHF and HF communications, ACARS, SATCOM and Transponder) prior to the diversion is due to the systems being manually turned off or power interrupted to them or additionally in the case of VHF and HF, not used, whether with intent or otherwise. No ELT signal from the aircraft was reported by the Search and Rescue agencies or any other aircraft. The SATCOM data indicated that the aircraft was airborne for more than 7 hours suggesting that the autopilot was probably functioning, at least in the basic modes, for the aircraft to be flown for such a long duration. This in turn suggests that the air and inertial data were probably available to the autopilot system and/or the crew. The inter-dependency of operation of the various aircraft systems suggests that significant parts of the aircraft electrical power system were likely to be functioning throughout the flight. The analysis of the relevant aircraft systems taking into account the route followed by the aircraft and the height at which it flew, constrained by its performance and range capability, does not suggest a mechanical problem with the aircraft’s airframe, control systems, fuel or engines.

Except for the first report, the ACARS reports normally sent every 30 minutes by the SATCOM system were not received. Data from the last seven SATCOM ‘handshakes’ were used to help establish the approximate path of the aircraft over the Indian Ocean. The initial log-on request and the hourly pings have been termed as ‘handshakes'. SATCOM transmissions indicated that a link was available from 1825 UTC on 07 March 2014 to 0011 UTC on 08 March 2014 although not used for any voice, ACARS or other data services apart from two unanswered ground-to-air telephone calls. Two log-ons, at 1825 UTC (07 March 2014) and 0019 UTC (08 March 2014), were initiated by the aircraft most likely due to power interruptions to the SATCOM avionics. The power interruption leading up to 1825 UTC was probably due to power bus cycling, the reason for it being unknown. The power interruption leading up to 0019 UTC was probably due to low fuel at this time resulting in the loss of both engines and their respective generators. There was probably enough fuel for the APU to start up and run long enough for its generator to power the SATCOM avionics to initiate a log-on request.

To date, the main wreckage of MH370 has still not been found despite a 4-year search in the South Indian Ocean. However, items of debris possibly from MH370, have been found as far north as the eastern coast of Tanzania and far south as the eastern coast of South Africa. This is in addition to several islands and island nations off the east coast of the African continent. Of these, the flaperon, a part of the right outboard flap and a section of the left outboard flap were confirmed to be from MH370. A few other pieces of debris were determined to be almost certain from MH370 which included some cabin interior items. Damage examination on the recovered part of the right outboard flap, together with the damage found on the right flaperon has led to the conclusion that the right outboard flap was most likely in the retracted position and the right flaperon was probably at, or close to, the neutral position at the time they separated from the wing. Recovery of the cabin interior debris suggests that the aircraft was likely to have broken up. However, there is insufficient information to determine if the aircraft broke up in the air or during impact with the ocean. Apart from the above, no other information about in-flight emergencies, aircraft configuration or impact could be inferred from the nature and damage of the debris.

MH370 did not carry any cargo classified as dangerous goods. Two cargo items of interest (the Lithium ion Batteries and Mangosteens) which were carried on MH370 had also been transported via scheduled flights on MAS before and after the event. These items were packed and loaded according to standard operating procedures.

As a result of the identified issues, the investigation has issued safety recommendations to enhance the safety of the aviation system. The recommendations made address the Malaysian and foreign air traffic surveillance systems, cargo scanning, flight crew medical and training records, reporting and following-up of crew mental health, flight-following system, development of a Quick Reference for Operations Control and ELT effectiveness.

It should be recognised that there is a significant lack of evidence available to the Team to determine with any certainty the reasons that the aircraft diverted from its filed flight plan route. However, the change in flight path likely resulted from manual inputs. The lack of evidence includes the exact location and disposition of the main aircraft wreckage and the evidence that it could provide, the information recorded on the Flight Data Recorder, Cockpit Voice Recorder and other recording devices on the aircraft and the absence of any aircraft voice or data transmissions that could indicate why the aircraft flew to the Southern Indian Ocean.

Without the benefit of the examination of the aircraft wreckage and recorded flight data information, the investigation was unable to identify any plausible aircraft or systems failure mode that would lead to the observed systems deactivation, diversion from the filed flight plan route and the subsequent flight path taken by the aircraft. However,

the same lack of evidence precluded the investigation from definitely eliminating that possibility. The possibility of intervention by a third party cannot be excluded either.

The disappearance of MH370 and the search effort are unprecedented in commercial aviation history. Improvements must be undertaken to ensure that this type of event is identified as soon as possible, and mechanisms are in place to track an aircraft that is not following its filed flight plan for any reason.

In recent years, several States have expended significant amounts of funds and resources searching for missing commercial aircraft in remote oceanic locations, including AF447 and MH370. In this technological epoch, the international aviation community needs to provide assurance to the travelling public that the location of current-generation commercial aircraft is always known. It is unacceptable to do otherwise.

In conclusion, the Team is unable to determine the real cause for the disappearance of MH370.

SECTION 4 - SAFETY RECOMMENDATIONS

4.1 Safety Recommendation of Preliminary Report

On 09 April 2014, the Ministry of Transport, Malaysia, issued a Preliminary Report that contained the following Safety Recommendation to the International Civil Aviation Organization (ICAO):

> *"It is recommended that the International Civil Aviation Organization examine the safety benefits of introducing a standard for real-time tracking of commercial air transport aircraft".*

Based on the above recommendation, the ICAO Council has adopted Amendments 40 and 42 on 02 March 2016 and 27 February 2017, respectively, to the International Standards and Recommended Practices, Operation of Aircraft - International Commercial Air Transport - Aeroplanes (Annex 6, Part I to the Convention on International Civil Aviation). Excerpts of the amendments are listed below.

Amendment 40

"**6.18 Location of an aeroplane in distress**
(Applicable on 10 November 2016)

6.18.1 All aeroplanes of a maximum certificated take-off mass of over 27 000 kg for which the individual certificate of airworthiness is first issued on or after 1 January 2021, shall autonomously transmit information from which a position can be determined by the operator at least once every minute, when in distress, in accordance with Appendix 9.

6.18.2 **Recommendation.** - *All aeroplanes of a maximum certificated take-off mass of over 5 700 kg for which the individual certificate of airworthiness is first issued on or after 1 January 2021, should autonomously transmit information from which a position can be determined at least once every minute, when in distress, in accordance with Appendix 9.*

6.18.3 The operator shall make position information of a flight in distress available to the appropriate organizations, as established by the State of the Operator."

Amendment 42

"3.5 AIRCRAFT TRACKING
(Applicable on 8 November 2018)

3.5.1 The operator shall establish an aircraft tracking capability to track aeroplanes throughout its area of operations.

3.5.2 **Recommendation.** — *The operator should track the position of an aeroplane through automated reporting at least every 15 minutes for the portion(s) of the in-flight operation(s) under the following conditions:*

a) the aeroplane has a maximum certificated take-off mass of over 27 000 kg and a seating capacity greater than 19; and

b) where an ATS unit obtains aeroplane position information at greater than 15 minute intervals.

3.5.3 The operator shall track the position of an aeroplane through automated reporting at least every 15 minutes for the portion(s) of the in-flight operation(s) that is planned in an oceanic area(s) under the following conditions:

a) the aeroplane has a maximum certificated take-off mass of over 45 500 kg and a seating capacity greater than 19; and

b) where an ATS unit obtains aeroplane position information at greater than 15 minute intervals.”

4.2 Safety Recommendations of this Report

As a result of the issues identified in the investigation and in order to enhance greater aviation safety and benefits, the investigation has made the following Safety Recommendations (SR) to the following organisations:

4.2.1 Department of Civil Aviation - SR #01-07

SR	Safety Recommendation
#01	To review the existing coordination procedures/establish new procedures between KL ATSC and Joint Air Traffic Control Centre (JATCC) with regard to unidentified primary target observed by the Radar Controller.
#02	To review the present Duty Roster System for KL ATSC with the objective of improving the working conditions.
#03	To develop a comprehensive *Quick Reference* on ATC actions relating to aircraft emergency to be available at all Controller working positions.
#04	Air Traffic Controllers are to be provided refresher training to ensure established procedures are always complied with.
#05	To review and enhance the training syllabi of the courses for Lead-in and On-the-job training to include ATC actions during aircraft emergencies for ATS personnel at KL ATSC.
#06	To review and introduce more stringent security measures for cargo scanning at Penang International Airport/all airports and the point of entry into airside at KLIA/all airports.
#07	To review the privileging process of the appointment of the designated aviation medical examiners on a regular basis.

4.2.2 Civil Aviation Authority of Viet Nam - SR #08 - 09

SR	Safety Recommendation
#08	To observe the provisions of the Operational Letter of Agreement between Civil Aviation Authorities of adjacent Flight Information Regions.
#09	To observe the requirement of Language Proficiency as outlined from the following document: d) ICAO Annex 1 Personnel Licencing Chapter 1 paragraph 1.2.9.2 Language Proficiency; ii) ICAO Doc 9835 AN/53 Manual on the Implementation of ICAO Language Proficiency Requirements Chapter 6 - Language Testing Criteria for Global Harmonization.

4.2.3 Malaysia Airlines Berhad - SR #10-17

SR	Safety Recommendation
#10	To ensure that the flight crew report to MAB Flight Operations of any serious ailment that can cause medical incapacitation and therapy prescribed at MAB medical facilities as well as MAB-appointed panel clinics.
#11	To ensure that the medical records of the flight crew maintained by the MAB Medical Centre to include records maintained by different panel clinics. The complete medical record of the individual flight crew shall show all visits to any panel clinics, the details of ailments and therapy prescribed.
#12	To review the process of reporting system and the action flow when flight crew and cabin crew's health may become a risk factor for the safety of the aircraft operations.
#13	The personnel manning the Flight-Following System/*Flight Explorer* should be adequately trained and qualified to enable them to provide information relating to flights to the relevant authorities and/or organisations.
#14	The current Flight-Following System/ *Flight Explorer* should be upgraded to the Global real-time Tracking System.

4.2.3 Malaysia Airlines Berhad - SR #10-17 (*cont*…)

SR	Safety Recommendation
#15	To review and introduce new security measures for cargo scanning at Penang International Airport/all airports and the point of entry into airside at KLIA/all airports.
#16	A document back-up system should be implemented on every training sorties, simulator trainings, and flight trainings completed by a trainee should have their original form submitted to the Training Department and a copy retained by the trainee in his personal training file.
#17	To develop a comprehensive *Quick Reference* for the Operations Control Centre that covers every aspect of abnormal operations/situations.

4.2.4 Malaysia Airports Holdings Berhad - SR #18

SR	Safety Recommendation
#18	To review and introduce new security procedures for the scanning of cargo at the point of entry at all airports and the point of entry into the airside at KLIA/all airports in Malaysia.

4.2.5 International Civil Aviation Organization - SR #19

SR	Safety Recommendation
#19	To review the effectiveness of current ELTs fitted to passenger aircraft and consider ways to more effectively determine the location of an aircraft that enters water. Note: The Investigation Team is cognizant of the fact that this effort is already underway.

SECTION 5 – COMMENTS TO THE REPORT AS REQUIRED BY ICAO ANNEX 13, PARAGRAPH 6.3

As required by ICAO Annex 13, paragraph 6.3, the draft Report was sent to the Accredited Representatives of the States participating in the investigation inviting their significant and substantiated comments on the Report. The following is the status of the comments received.

Organisations participating in the Investigation	**Status of Significant and Substantiated Comments**
Air Accidents Investigation Branch (AAIB) of United Kingdom	Accepted and Incorporated
Australian Transport Safety Bureau (ATSB) of Australia	Accepted and Incorporated
Bureau d'Enquêtes et d'Analyses pour la Sécurité de l'Aviation civile (BEA) of France	Accepted and Incorporated
Civil Aviation Administration of the People's Republic of China (CAAC)	Accepted and Incorporated
National Transportation Safety Board (NTSB) of United States of America	Accepted and Incorporated
National Transportation Safety Committee (NTSC) of Indonesia	No comments received
Transport Safety Investigation Bureau (TSIB) of Singapore (formerly Air Accident Investigation Bureau [AAIB])	Accepted and Incorporated

MH370 Flight Path Analysis
Case Study

by Richard Godfrey, Dr. Hannes Coetzee (ZS6BZP) and Prof. Simon Maskell

30th August 2023

1. Introduction.

MH370 is one of the greatest aviation mysteries of all time. Malaysian Airlines flight MH370 was operated by a Boeing 777-200ER aircraft with the registration 9M-MRO. The aircraft departed Kuala Lumpur International Airport, Malaysia on 7th March 2014 at 16:41:43 UTC (8th March 2014 00:41:43 local time) and was scheduled to arrive in Beijing Capital International Airport, China at 06.30 local time after 5 hours 34 minutes flying time. There were 227 passengers and 12 crew on board from 14 different nations including 153 passengers from China and 38 passengers and 12 crew from Malaysia.

This work is dedicated to the families and friends of those lost in this tragic incident.

At 17:19:26 UTC Malaysian Air Traffic Control (ATC) at the Lumpur Radar station contacted MH370 with a routine message: “Malaysian Three Seven Zero contact Ho Chi Minh one two zero decimal niner good night.” Captain Zaharie Shah responded at 17:19:30 UTC: “Good night Malaysian Three Seven Zero.” At 17:20:36 UTC, just 66 seconds later, the Mode S transponder symbol of MH370 dropped off the Malaysian ATC radar display. MH370 had gone ‘dark’ and disappeared into the night sky diverting back over Malaysia to the Malacca Strait according to primary civilian and military radar data.

In previous case studies we have successfully detected and tracked both large and small aircraft, such as Emirates flight EK421, which was a Boeing 777-300ER [1], a small aircraft such as a Diamond DA40 [2], a private jet, which was a Cessna 551 Citation II/SP [3], an Alouette II helicopter SE313B [4] and Qatar Airways flight QTR901, a Boeing 777-300ER [5].

This case study examines the use of radio waves from the Weak Signal Propagation Reporter (WSPR) and the historic database called WSPRnet. WSPR data can be used as a multi-static passive radar system to detect and track aircraft, where WSPR links between radio transmitters and receivers align with the aircraft position along a great circle path. Signal level and signal frequency modulations can result, when an aircraft flight path intersects with the propagation path of a WSPR link. Together with the Boeing aircraft performance data, the MAS Operations fuel and engineering data, the weather data enroute, the Inmarsat satellite data and the drift analysis of the 41 items of possible MH370 floating debris that have been recovered from around the Indian Ocean, a comprehensive picture of the final hours of flight MH370 can be collated.

The purpose of detecting and tracking MH370 across the Indian Ocean is to ensure the reliability of the flight path analysis during the 7 hours 46 minutes the aircraft was in the air and therefore the accuracy of the end point position, where MH370 ran out of fuel after 7 hours 35 minutes and then subsequently crashed around 11 minutes later. The alignment of the WSPR analysis with the analyses from Boeing, Inmarsat and the drift analysis from the University of Western Australia is a significant multi-disciplinary outcome, which all point to the same crash area. There have been 41 items of confirmed or possible MH370 floating debris recovered from round the Indian Ocean.

Flight MH370 was diverted to the Indian Ocean, where it crashed after fuel exhaustion on 8th March 2014 at some point after the last satellite signal was received at 00:19:37 UTC. At the time of writing of this case study, MH370 still has not been found despite extensive surface and underwater searches. Around 10 million commercial passengers fly every day and the safety of the airline industry relies on finding the cause of every aircraft accident.

2. Summary of Results.

The last known position of MH370, based on the Butterworth primary civilian radar, was 5.589118°N 99.165228°E at 18:01 UTC. The regional radar data contains 1,394 regular estimates of latitude and longitude at approximately 3 second intervals from 16:41:43 UTC to 18:00:51 UTC from four radar stations with two small gaps. A single additional latitude and longitude position was reported at 18:22:12 UTC but discounted due to the large gap to the penultimate radar position and possible inaccuracy due to the long range.

From this point at 18:01 UTC onwards there are 67 positions, comprising a total of 125 anomalous WSPR links, which intersect with the MH370 flight path at the estimated position of MH370.

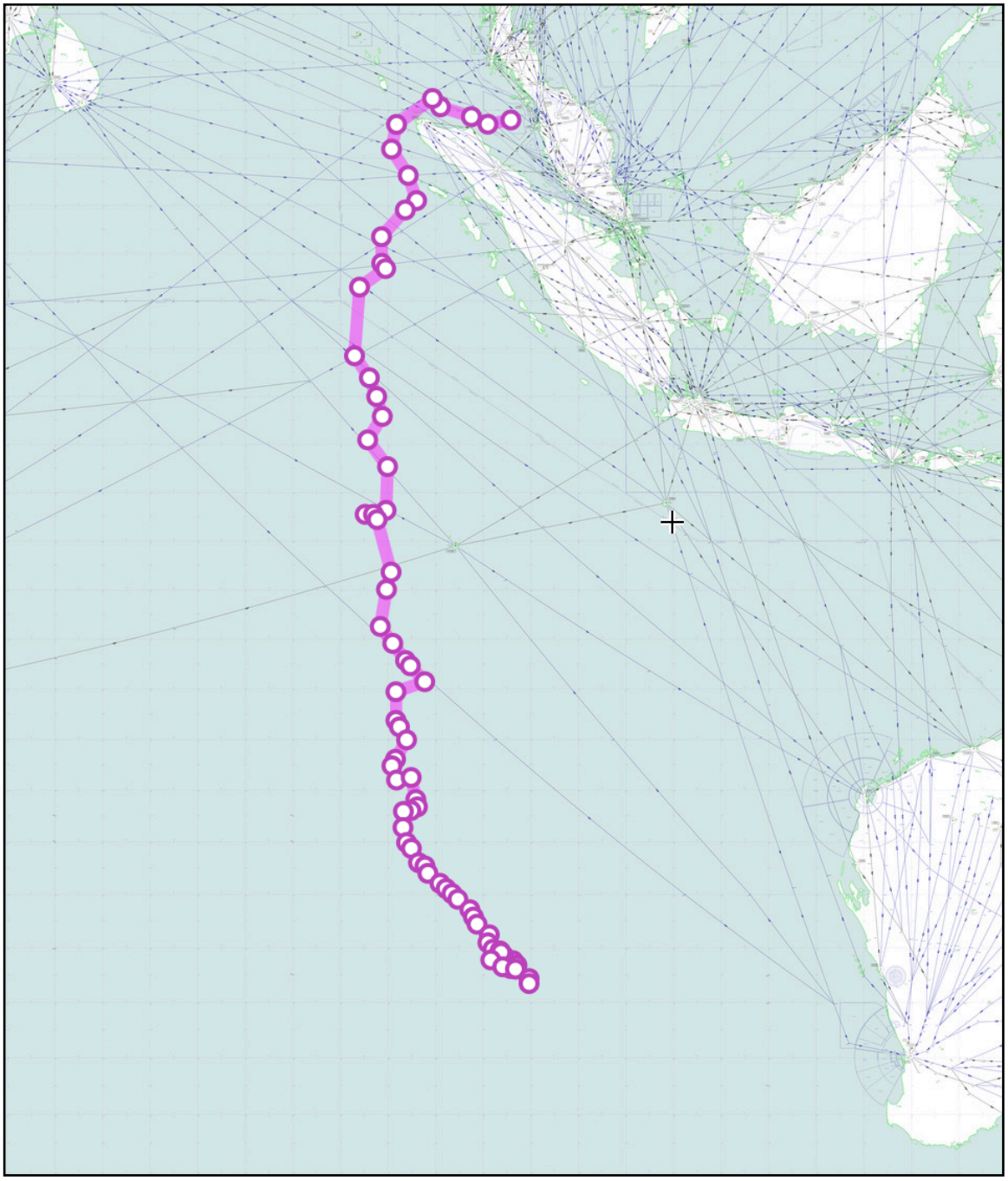

Figure 1: Sky Vector MH370 estimated Flight Path Overview Map.

The location of anomalous WSPR links aligned with all 7 positions, where the MH370 flight path crossed the arcs defined by the distance from the Inmarsat satellite calculated from the Burst Timing Offset (BTO) data. The anomalous WSPR links also aligned with 2 further positions, where the MH370 estimated track aligned with the calculation from the Inmarsat satellite Burst Frequency Offset (BFO) data. MH370 was thought to have most likely crashed close to the 7th Arc as defined by the last Inmarsat satellite BTO data. This position aligns with the point of fuel exhaustion. We know from the Inmarsat BFO data at 00:19:29 UTC and 00:19:37 UTC as well as the WSPR data at 00:20 UTC, that MH370 was in an accelerating descent of -14,517 fpm on a track of 99.6°T at a ground speed of 435.1 knots. Ian Holland of the DSTG, Australia in his paper titled "MH370 Burst Frequency Offset Analysis and Implications on Descent Rate at End-of-Flight" dated 15th January 2018 showed the rate of descent was at least -13,800 fpm, but could be up to -25,300 fpm depending on the final track and was accelerating at around 0.68 g [6].

This WSPR results at 00:26 UTC indicate a possible recovery from this descent, with a position indicator at the intersection of 3 anomalous WSPR links from 3 different transmitters and 3 different receivers at a position of 29.128°S 99.934°E, which is 44.27 nmi from the 7th Arc on a track of 124.4°T. At 00:28 UTC there was a potential progress indicator with 4 WSPR anomalous links but all from the same transmitter W4MO and all on a similar bearing.

A single anomalous WSPR signal is termed a progress indicator, as it only indicates possible progress. Multiple WSPR signals that are all aligned on the same bearing do not give a position, and are also referred to as a progress indicator. There is always the chance that WSPR signals may have been disturbed by other air traffic between the transmitter, aircraft and the receiver. This chance is significantly reduced when multiple anomalous WSPR links intersect at a significant angle at the same point and at the same time, which is termed a position indicator.

A SNR anomaly is defined as a deviation by ≥ 0.75 standard deviation from the mean taken over a 6 hour time period based on the test datum ± 3 hours. If there are less than 5 results in the result set, then the time period is extended to ± 3 days but at the same ± 3 hours each day. A drift anomaly is defined as a temporary non-zero drift. A permanent or almost permanent non-zero drift is discarded as a possible transmitter problem.

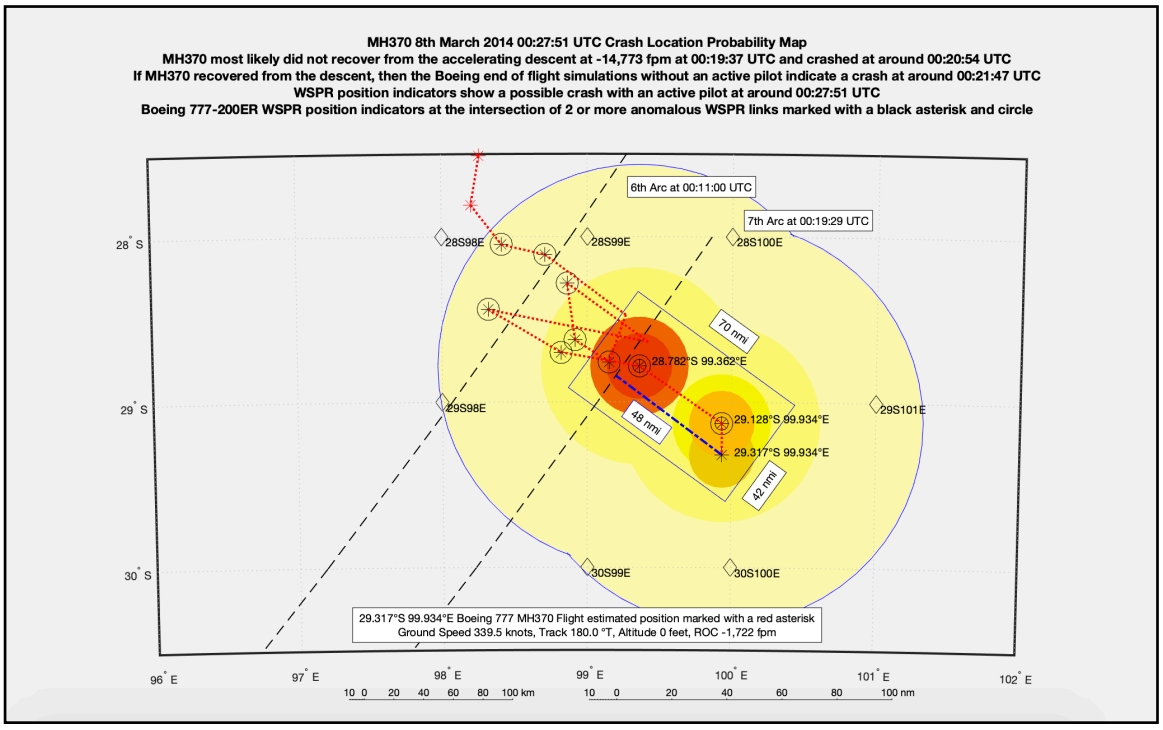

Figure 2: MH370 Crash Location Probability Map.

Boeing performed 10 end of flight simulations with various criteria of starting altitude, ground speed, autopilot disengagement timing at 1st engine flameout or 2nd engine flameout, alternate electrical configuration and turbulence setting. In 5 cases (Case 3, 4, 5 ,6 and 10) the aircraft recovered from a rate of descent of over -15,000 fpm. In Case 5 the aircraft only recovered after the 11th swoop right at the end.

The average for Case 3, 4, 6 and 10 was a glide range of 58.5 nmi and glide duration of 471.8 seconds [7]. The average flight duration from the point of first reaching a rate of descent of -15,000 fpm was a further 129.5 seconds. This would imply a crash at around 00:21:46 UTC. With an active pilot, this time could be extended to 00:27:51 UTC and the ground speed reduced to a more reasonable ground speed of 163 knots on impact with a descent rate of - 1,722 fpm, without lowering the flaps, assuming a 19° glide slope and average altitude recovery of 19,636 feet after the first descent from 40,000 feet (or for Case 6 from a start altitude of 35,000 feet).

Significantly, if an active pilot recovered from the high descent rate of -14,773 fpm and then controlled the aircraft on a glide slope with flaps partially lowered to attempt a ditching across the waves at a more normal landing speed of 135 knots, then the aircraft could have remained relatively intact.

The surface wind at 29.128°S 99.934°E on 8th March 2014 at 00:00 UTC was 17.8 knots from 150°T. The wind was a fresh breeze and the wave height would be just over 1.1 m, with small waves becoming longer and with numerous white caps.

The 41 floating debris items recovered show however a complete break up of the aircraft with parts from both the exterior and interior of the aircraft. There were items externally from the nose, wings, engines and tail, as well as items internally from cabin dividers, flooring, seat back video trim, clothing, shoes and hand luggage.

A crash location around 29.0°S 99.5°E is within the area defined by Prof. Pattiaratchi and Prof. Wijeratne of the University of Western Australia in their drift analysis, which was between 28°S and 33°S along the 7th Arc [8]. When Captain Sullenberger performed a controlled ditching on the Hudson River at 124.2 knots, there was a complete absence of floating debris from any part of the aircraft. Of course, the Hudson River does not experience the same wave height as the Indian Ocean and a Boeing 777-200ER is a larger aircraft than an Airbus A320-214.

The average weight of the 41 items of floating debris recovered is 4.9 kg. The zero fuel weight of the Boeing 777-200ER was 174,369 kg. This implies up to around 36,000 items of debris, which in turn implies a severe impact. If an attempt to ditch the aircraft was made in order to reduce the amount of floating debris, then it appears the bid is likely to have failed.

3. Background.

3.1 Weak Signal Propagation Reporter (WSPR).

The WSPR protocol was invented by Prof. Joe Taylor and is used to confirm a radio wave propagation between appropriately equipped transmitters and receivers. Propagation distances over 19,000 km are common place in the WSPRnet database. WSPR signals are sent every two minutes and are synchronised with GPS to start one second after every even UTC minute. The transmission of the WSPR protocol takes 110.484 seconds. The WSPRnet historic database is publicly available and goes back to 2008.

Each WSPR transmission contains the call sign of the transmitter, the location of the transmitter using a Maidenhead Grid code and the power level of the transmission. The receiver station augments this data with the call sign of the receiver, the location of the receiver using a Maidenhead Grid code, the received frequency, the frequency drift and the Signal to Noise Ratio (SNR) of the received signal. The Maidenhead Grid code is a 4 character code in the first transmission and a 6 character code in the second transmission. A 4 character code has a precision better than ± 120 km and a 6 character code is better than ± 5.2 km. Neither has the precision required to determine the great circle path between transmitter and receiver for the purpose of detecting and tracking aircraft. We therefore decided to build a database with transmitter and receiver antenna locations, where the precision of the latitude and longitude is given to 6 decimal places (better than ± 1 m).

3.2 WSPR based Aircraft Detection and Tracking.

Signal level and signal frequency modulations can result, when an aircraft flight path intersects with the propagation path of a WSPR link. This is evident from anomalies in either the reported SNR or the frequency drift over a short time period. Commercial aircraft typically cruise at altitudes up to 43,000 feet (13.1 km), whereas typical multi-hop ionospheric propagation extends to an altitude of at least around 100 km and usually much higher. Generally the E-layer starts at around 85 km and the F-layer ends at around 600 km above the Earth's surface. Only a small proportion of the ionospheric propagation path will be disturbed by an aircraft. The signal level and frequency level disturbances can result from forward or back scatter at the target aircraft.

Typical multi-hop ionospheric propagation ranges vary between 1,500 km and 3,000 km per hop. Depending on the ray take off angle, less than 10% of the propagation path will be within aircraft altitudes. A 3D intersection calculation is required to see if the aircraft track actually intersects with the WSPR propagation path. The great circle path of an aircraft is usually calculated using the WGS84 geodetic model of the Earth as an oblate spheroid and WSPR links are calculated with a spherical model of the Earth. We use Proplab Pro V3.2 software for High Frequency (HF) radio propagation ray tracing produced by Solar Terrestrial Dispatch, which is a useful tool for tracing multi-hop ionospheric WSPR propagations. We use Matlab software for mapping the aircraft track and the anomalous WSPR links relevant to the aircraft detection and tracking. We use an online Vincenty calculator to determine the initial and final bearings of propagation paths between transmitter, aircraft and receiver. The software system has several components and is collectively known as the Global Tracking and Detection of Aircraft Anywhere Anytime (GDTAAA).

3.3 Antenna Location Source Data.

The best source data for antenna location is the radio amateur who implemented the antenna. Some radio amateurs have more than one antenna and use more than one location. Some antennas are static and other antennas are mobile, having been implemented as portable devices or on vehicles, ships or balloons. Some antennas are connected by repeater or relay to a remote location. Care was taken to check the antenna location in 2014 matched the grid locator in the historic WSPRnet database from 7th/8th March 2014, as some of the amateur radio operated have since moved to a new location.

4. Method.

In the timeframe of interest for the MH370 flight path analysis, between 7th March 2014 17:52 UTC and 8th March 2014 00:34 UTC, there were 202 WSPR data sets every 2 minutes. In total there were 75,822 WSPR links globally, between 10,799 distinct transmitter receiver pairs. There were 2,401 WSPR links crossing the target area around the MH370 estimated position each 2 minutes defined by a moving grid with a latitude of ± 1.0° and a longitude of ± 2.0°.

The ground speed and track of MH370 are calculated every two minutes and updated from the distance covered in two minutes as indicated by the WSPR position and progress data. The true air speed and heading are calculated, given the wind speed and direction for that position, altitude and time. The Mach setting was calculated from the True Air Speed (TAS) and the static outside air temperature for that position, altitude and time.

The wind and air temperature data are derived from the NOAA GDAS historic database and interpolated over a 1° latitude x 1° longitude position grid, 5 pressure altitude levels between 350 hPa (nominally 26,631 feet), 300 hPa (nominally 30,065 feet), 250 hPa (nominally 33,999 feet), 200 hPa (nominally 38,661 feet), 150 hPa (nominally 44,645 feet), for each latitude from 15°N to 40°S, each longitude from 80°E to 105°E and for each 3 hour time period from 7th March 2014 18:00 UTC to 8th March 2014 03:00 UTC. This resulted in 5,824 x 4 measurements of wind speed, wind direction, air temperature and ∂SAT at each position (latitude, longitude, altitude) and time.

The fuel consumption in each engine is calculated each minute from the actual aircraft weight, delta static outside air temperature, Mach setting and MAS Engineering data for the two engines installed on 9M-MRO. The two engines had slightly different fuel consumptions, where the right engine was estimated to flame out at 00:07:17 UTC and the left engine at 00:16:38 UTC, assuming no fuel rebalancing between the right and left fuel tanks.

The MH370 estimated position was updated ever two minutes to align with the WSPR data. A total of 987 WSPR links are analysed that crossed within a radius of the MH370 estimated position defined by the distance covered from the last known position at the maximum possible ground speed.

We use the http://wspr.rocks/livequeries/ front end, which exposes the WSPRnet database for SQL based queries. The WSPRnet data for any particular two minute timeframe is downloaded and exported to a spreadsheet. A sample SQL WSPR Download script is shown in Appendix A.

We then augment the spreadsheet by adding the transmitter and receiver antenna latitudes and longitudes. These positions are derived from the master antenna locations database. A sample Matlab Call Sign script is shown in Appendix B. We then process all the WSPR links in the target area and this script generates a set of function calls. A sample Matlab Target Area script is shown in Appendix C. These function calls, which each define a WSPR link are imported into the Matlab Mapping script. This script can display either a local view in the target area or a global view of the WSPR links. In the local view, the MH370 track and the relevant waypoints and Inmarsat satellite arcs are also depicted. A sample Matlab Mapping script is shown in Appendix D.

Finally we analyse each WSPR link over a time frame of ± 3 hours to see if there is either a SNR anomaly or a drift anomaly or both. A sample SQL WSPR Anomaly Checking script is shown in Appendix E.

A plausibility check is performed on the anomalous WSPR links using the Proplab Pro V3.2 software. The propagation path between transmitter and aircraft as well as aircraft and receiver is analysed using the International Reference Ionosphere (IRI) 2007 model as well as a topographic model of the Earth. The transmission frequency is checked to be within the Maximum Usable Frequency (MUF) and a multi-hop ionospheric path is confirmed at an Elevation Angle (EA) to be within the specified range. The EA is sometimes called the take off angle.

5. Worked Example.

At 22:42 UTC MH370 is estimated to be at a position of 20.788°S 94.319°E at the intersection of the 5th Arc and the anomalous WSPR link between the transmitter OX3XR and N2NOM with a SNR showing a deviation from the mean by a factor of 2.31standard deviations (SD) over a ± 3 hour timeframe. At 22:44 UTC there is a further progress indicator with a SNR anomaly of 0.86 SD and again at 22:48 UTC a SNR anomaly of 2.65 SD. By 22:50 UTC the estimated position of MH370 is 21.882°S 94.456°E.

The worked example at 22:52 UTC starts from this previous position at 22:50 UTC. The first step is using the SQL WSPR Download script for 22:52 UTC, which produces 286 rows of data. The Matlab Call Sign script is run to augment this data with the latitude and longitude of each transmitter and receiver. This also shows that there are no call signs missing in the call sign database. The Matlab Target Area script is run for the target area defined by a bottom left hand corner at 22°S 93°E to a top right corner at 20°S 97°E. This produces 28 rows of data as shown in Table 1 below.

WSPR_Link_GCV9_Function('0','1','51.27083335','6.79166664','52.33746900','-2.27851600','DF2JP','G1ZRN');
WSPR_Link_GCV9_Function('1','1','50.78080100','0.10020200','49.52370266','8.24777591','G3JKF','DK6UG');
WSPR_Link_GCV9_Function('1','0','51.35188900','-0.15826000','44.39583336','26.20833333','G4FKK','YO3ITD');
WSPR_Link_GCV9_Function('1','0','52.40423508','0.27702300','51.43750003','6.95833330','G4KPX','DC0DX/A');
WSPR_Link_GCV9_Function('1','0','52.40423508','0.27702300','51.35416669','8.12500000','G4KPX','DL1DBC');
WSPR_Link_GCV9_Function('1','1','52.40423508','0.27702300','51.80847356','4.70791832','G4KPX','PA3ABK/2');
WSPR_Link_GCV9_Function('1','1','50.86820200','-0.13595600','26.96563955','-82.32011327','G4WCP','W4AC');
WSPR_Link_GCV9_Function('0','1','50.93750007','-1.29166669','49.52370266','8.24777591','G6RRL','DK6UG');
WSPR_Link_GCV9_Function('1','1','51.50048800','-0.31508400','26.96563955','-82.32011327','G8VDQ','W4AC');
WSPR_Link_GCV9_Function('1','0','36.33690300','139.01551900','32.72916672','-95.04166670','JH1GYE','KD6RF');
WSPR_Link_GCV9_Function('1','1','36.33690300','139.01551900','29.72522500','-95.39439000','JH1GYE','KE5HPY');
WSPR_Link_GCV9_Function('1','0','-38.11628400','145.16138100','-31.85416666','115.79166660','VK3DXE','VK6ZRY');
WSPR_Link_GCV9_Function('1','1','27.10306700','-82.39671500','52.47916670','-2.04166674','W4MO','2E0DSS');
WSPR_Link_GCV9_Function('1','0','27.10306700','-82.39671500','53.47916670','-2.54166672','W4MO','2E1CJF');
WSPR_Link_GCV9_Function('1','1','27.10306700','-82.39671500','57.52083330','-4.37500000','W4MO','GM4SFW');
WSPR_Link_GCV9_Function('1','1','27.10306700','-82.39671500','38.35372470','-78.45945496','W4MO','K4RCG');
WSPR_Link_GCV9_Function('1','0','27.10306700','-82.39671500','53.47916670','-1.12500003','W4MO','M5ADA');
WSPR_Link_GCV9_Function('1','1','27.10306700','-82.39671500','51.20351600','-0.33178500','W4MO','M6NNB');
WSPR_Link_GCV9_Function('1','0','27.10306700','-82.39671500','48.68750005','15.62499994','W4MO','OE3VMS');
WSPR_Link_GCV9_Function('1','1','27.10306700','-82.39671500','55.24975200','12.30082000','W4MO','OZ7IT');
WSPR_Link_GCV9_Function('1','1','27.10306700','-82.39671500','52.23807201','6.85770275','W4MO','PI4THT');
WSPR_Link_GCV9_Function('1','0','27.10306700','-82.39671500','59.47916670','17.70833327','W4MO','SM3ULC');
WSPR_Link_GCV9_Function('1','0','27.10306700','-82.39671500','44.77083339','-63.70833334','W4MO','VE1AIM');
WSPR_Link_GCV9_Function('1','1','27.10306700','-82.39671500','39.46108700','-76.80855118','W4MO','W3GXT');
WSPR_Link_GCV9_Function('0','0','39.56250004','-104.87500004','32.97916674','-97.12500003','W5OLF','AD4PT');
WSPR_Link_GCV9_Function('1','1','34.77307873','-86.69914586','40.11087200','-88.19699300','WD0UG','K9AN');
WSPR_Link_GCV9_Function('1','1','34.77307873','-86.69914586','44.37883000','-88.18698700','WD0UG','KB9VLR');
WSPR_Link_GCV9_Function('1','1','36.19872900','-79.83413800','38.35372470','-78.45945496','WD4ELG','K4RCG');

Table 1: Worked Example at 22:52 UTC showing all WSPR Links in the vicinity of MH370.

The Matlab Mapping script is run with the 28 rows shown in Table 1, which are function calls imported into the Matlab Mapping script and use the Matlab WSPR_Link_GCV9_Function shown in Appendix F.

There is one function call for each WSPR link. The function call depicts each WSPR link on either a local or global Mercator projection of the world. The WSPR links are shown as great circle paths using a spherical model of the earth.

The function call defines the colour of the WSPR links which are initially set to red where the location of both the transmitter and receiver antenna are known precisely, orange where only one is known precisely and the other is calculated from the 6 character Maidenhead grid locator and grey if both are calculated from the 6 character Maidenhead grid locator. This process allows for the correction of the antenna location, if there was a less precise location on a particular anomalous WSPR link of interest.

The 28 links are depicted in Figure 3 below.

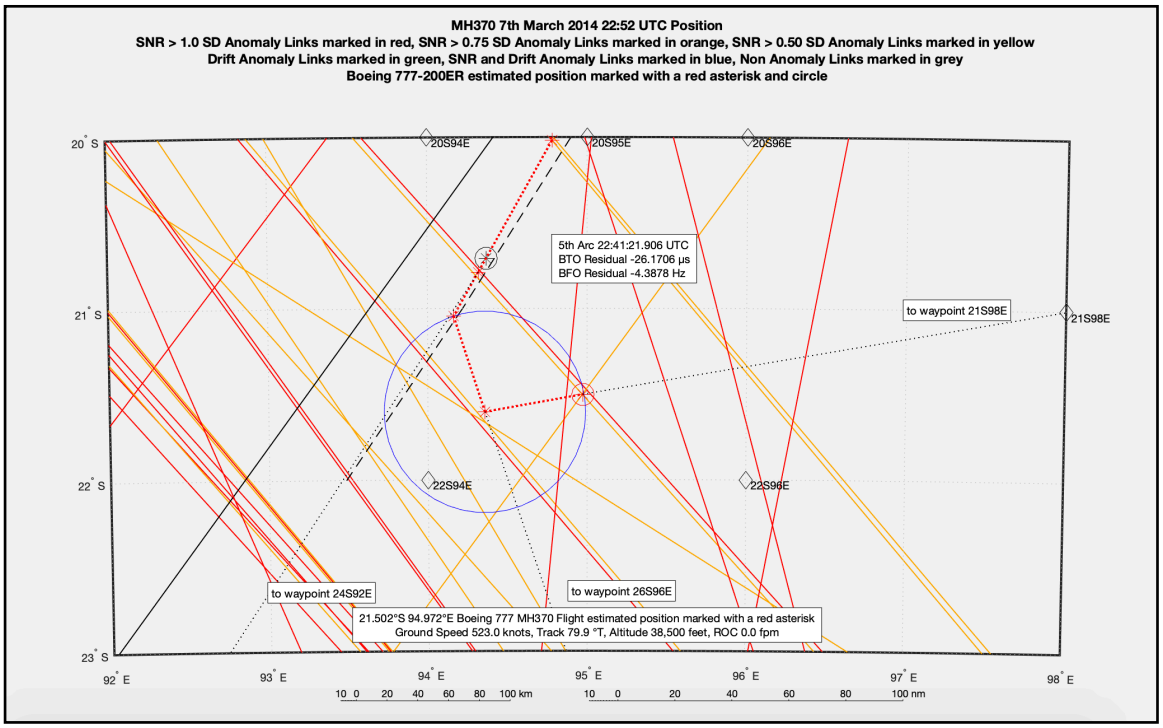

Figure 3: Worked Example at 22:52 UTC showing all WSPR Links in the vicinity of MH370.

Page 528 of 1738

The next step is to analyse the links within possible range marked with a blue circle and defined by the maximum distance MH370 could fly since the previous known position.

WSPR_Link_GCV9_Function('1','1','50.78080100','0.10020200','49.52370266','8.24777591','G3JKF','DK6UG');
WSPR_Link_GCV9_Function('1','0','51.35188900','-0.15826000','44.39583336','26.20833333','G4FKK','YO3ITD');
WSPR_Link_GCV9_Function('1','0','52.40423508','0.27702300','51.43750003','6.95833330','G4KPX','DC0DX/A');
WSPR_Link_GCV9_Function('1','1','52.40423508','0.27702300','51.80847356','4.70791832','G4KPX','PA3ABK/2');
WSPR_Link_GCV9_Function('0','1','50.93750007','-1.29166669','49.52370266','8.24777591','G6RRL','DK6UG');
WSPR_Link_GCV9_Function('1','0','36.33690300','139.01551900','32.72916672','-95.04166670','JH1GYE','KD6RF');
WSPR_Link_GCV9_Function('1','0','-38.11628400','145.16138100','-31.85416666','115.79166660','VK3DXE','VK6ZRY');
WSPR_Link_GCV9_Function('1','0','27.10306700','-82.39671500','59.47916670','17.70833327','W4MO','SM3ULC');
WSPR_Link_GCV9_Function('1','1','34.77307873','-86.69914586','44.37883000','-88.18698700','WD0UG','KB9VLR');

Table 2: Worked Example at 22:52 UTC showing WSPR Links within the possible range.

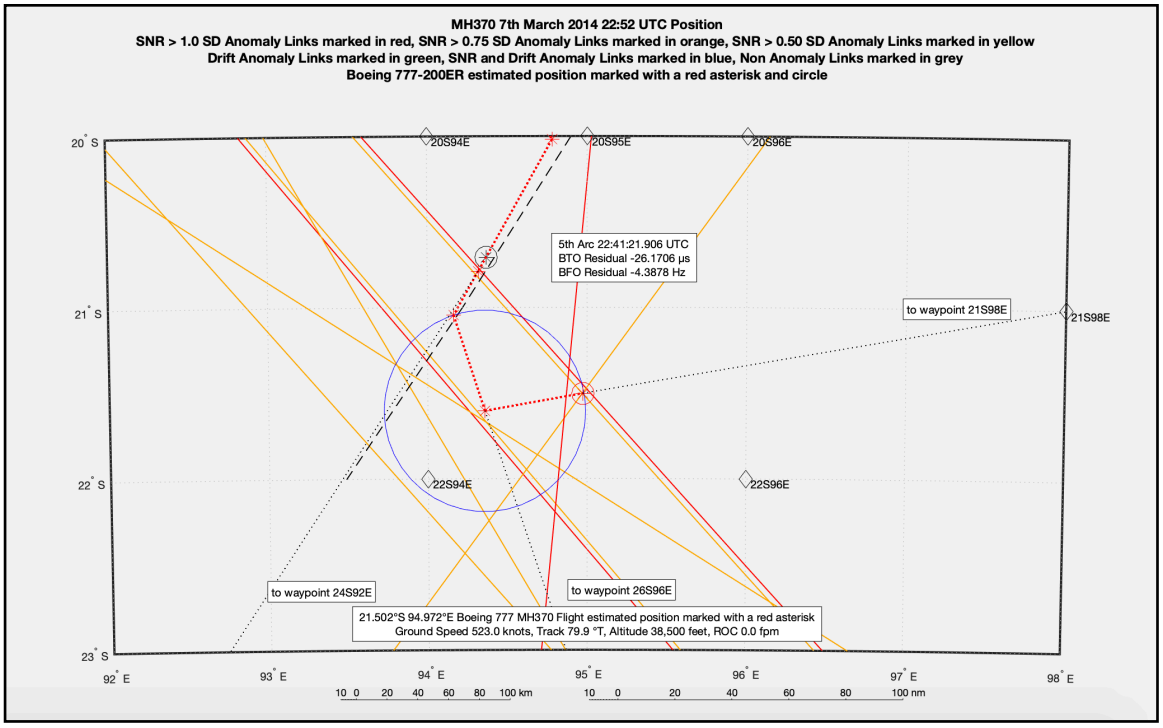

Figure 4: Worked Example at 22:52 UTC showing all WSPR Links within the possible range.

Each WSPR link is then analysed to see if there was a SNR or drift anomaly over a ± 3 hour time period. There are 3 SNR anomalies with deviations of 2.68 SD, 1.23 SD and 0.85 SD that intersect close to the edge of the blue circle.

A summary of the 9 WSPR links in the timeframe analysis is shown in Table 3 below. The details of each of the 9 WSPR links in the timeframe analysis are shown in Appendix G.

WSPR Link	Results	Timeframe	Action	SND % SD	Drift	Drift Type	Anomaly Type	Colour
WSPR_Link_GCV9_Function('1','1','50.78080100','0.10020200','49.52370266','8.24777591','G3JKF','DK6UG');	15	± 3 hours	Accepted	-54	0		None	Yellow
WSPR_Link_GCV9_Function('1','0','51.35188900','-0.15826000','44.39583336','26.20833333','G4FKK','YO3ITD');	14	± 3 hours	Accepted	37	-1	Temporary	Drift	Green
WSPR_Link_GCV9_Function('1','0','52.40423508','0.27702300','51.43750003','6.95833330','G4KPX','DC0DX/A');	3	± 3 days ± 3 hours	Discarded				None	Grey
WSPR_Link_GCV9_Function('1','1','52.40423508','0.27702300','51.80847356','4.70791832','G4KPX','PA3ABK/2');	37	± 3 hours	Accepted	-21	0		None	Grey
WSPR_Link_GCV9_Function('0','1','50.93750007','-1.29166669','49.52370266','8.24777591','G6RRL','DK6UG');	11	± 3 hours	Accepted	268	0		SNR	Red
WSPR_Link_GCV9_Function('1','0','36.33690300','139.01551900','32.72916672','-95.04166670','JH1GYE','KD6RF');	22	± 3 hours	Accepted	-123	0		SNR	Red
WSPR_Link_GCV9_Function('1','0','-38.11628400','145.16138100','-31.85416666','115.79166660','VK3DXE','VK6ZRY');	10	± 3 hours	Accepted	-51	-2	Permanent	None	Yellow
WSPR_Link_GCV9_Function('1','0','27.10306700','-82.39671500','59.47916670','17.70833327','W4MO','SM3ULC');	3	± 3 days ± 3 hours	Discarded				None	Grey
WSPR_Link_GCV9_Function('1','1','34.77307873','-86.69914586','44.37883000','-88.18698700','WD0UG','KB9VLR');	12	± 3 hours	Accepted	-85	-2	Permanent	SNR	Orange

Table 3: Worked Example at 22:52 UTC showing WSPR Links analysis results.

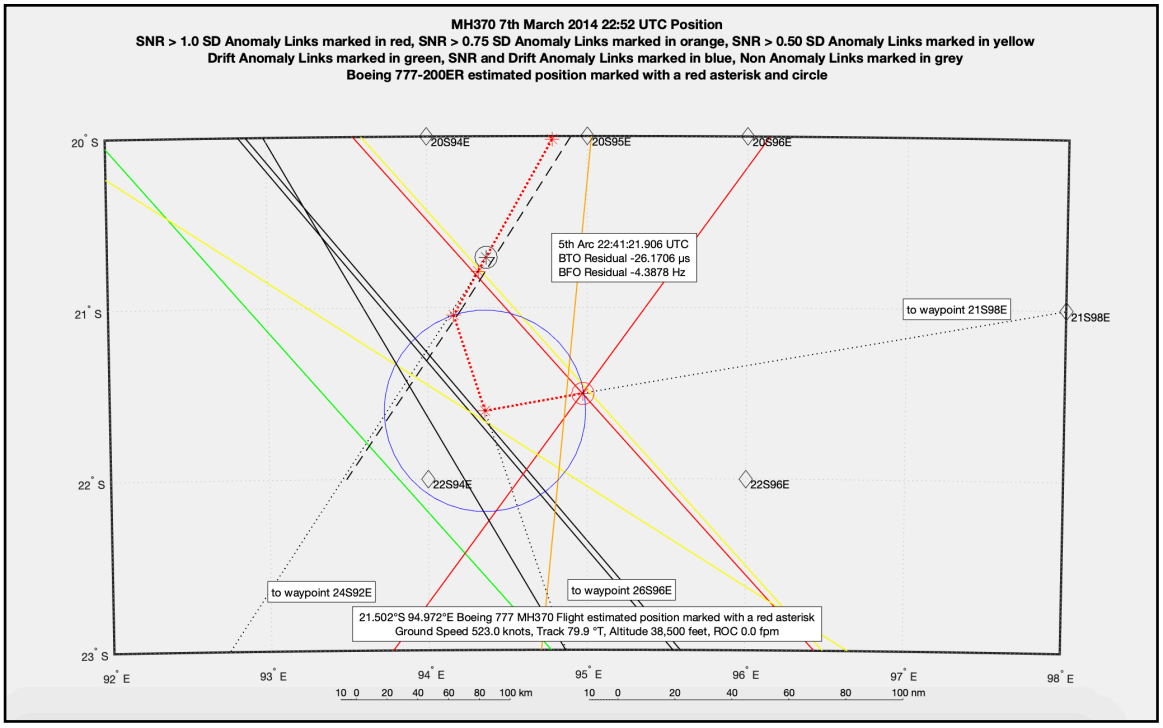

Figure 5: Worked Example at 22:52 UTC showing WSPR Links analysis results.

There are 3 anomalous WSPR links intersecting within the possible range and this point defines the new MH370 position at 22:52 UTC at 21.502°S 94.972°E. The ground speed of 523.0 knots and track of 79.9°T are calculated from the previous known position and the alignment to the geographical waypoint 21S98E is noted.

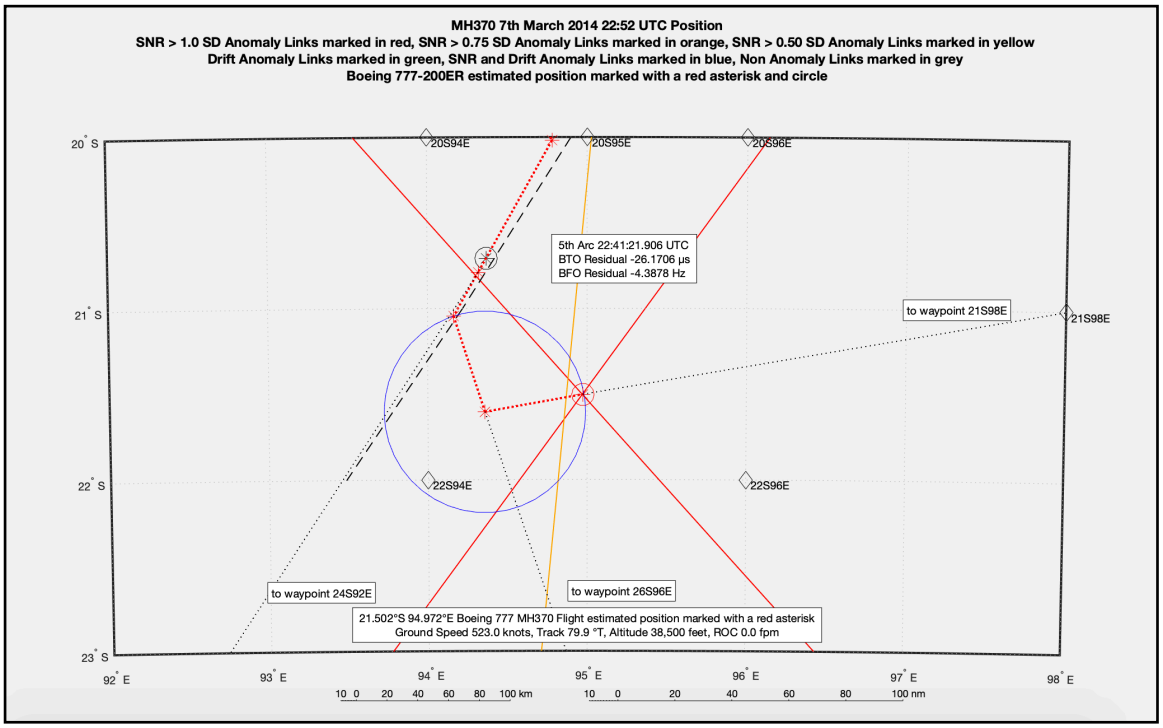

Figure 6: Worked Example at 22:52 UTC showing 3 WSPR Links anomalies.

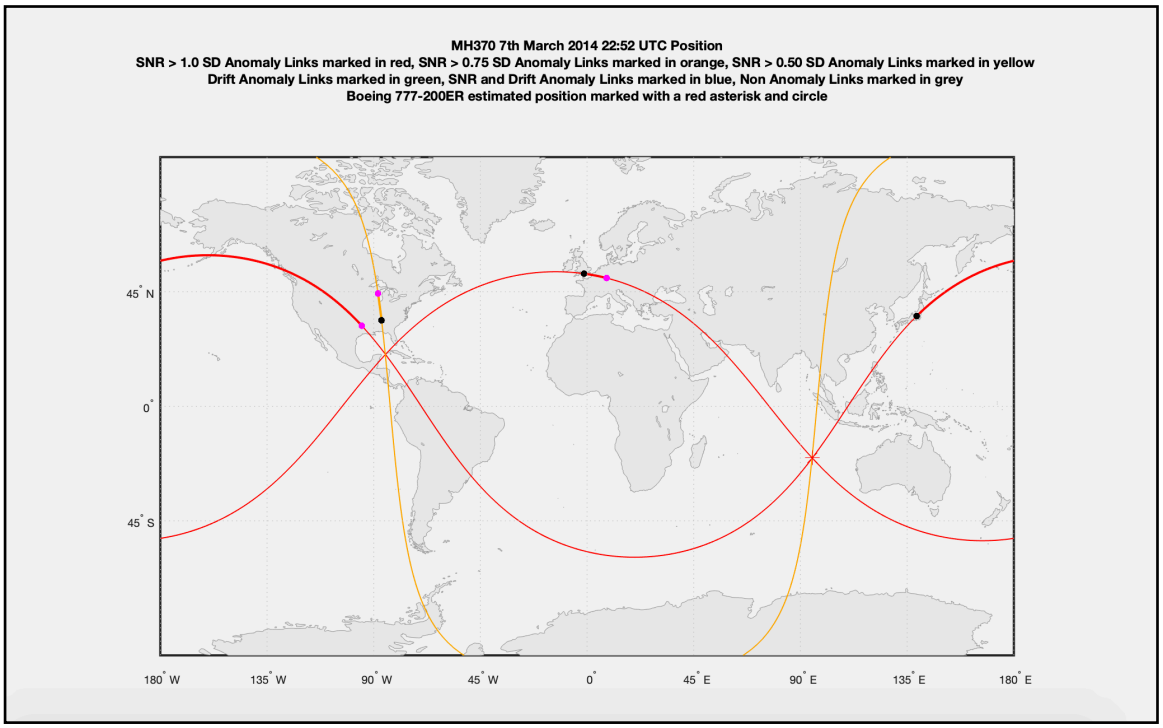

Figure 7: Worked Example at 22:52 UTC showing 3 WSPR Links anomalies in a global view.

Page 531 of 1738

The WSPR link with the identifier 186192616 between the transmitter G6RRL, the receiver DK6UG and the MH370 position at 21.502°S 94.972°E is analysed using Proplab Pro V3.2. This link showed a SNR anomaly of 2.68 SD. The aircraft is located within the grey zone. The grey zone or twilight zone at dawn and dusk is known to enhance propagation.

The Proplab Pro V3.2 analysis is used as a plausibility check to ensure the maximum usable frequency is not exceeded and the elevation angle is within expectations.

row	id	time	tx_sign	tx_loc	rx_sign	rx_loc	frequency	power	snr	drift	distance	azimuth	band	version	code
107	186192616	2014-03-07 22:52:00	G6RRL	IO90iw	DK6UG	JN49cm	3594078	33	-22	0	693	99	3	2.21_r2286	0

Table 4: Worked Example at 22:52 UTC showing WSPR Link ID 186192616.

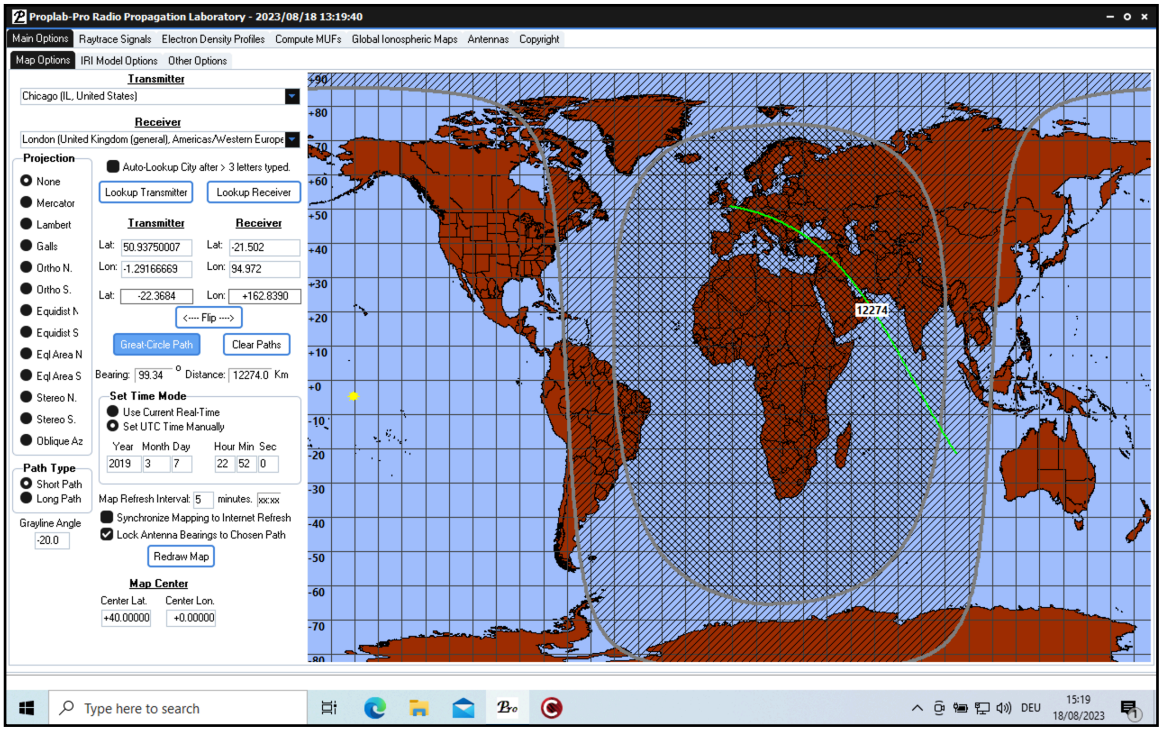

Figure 8: Worked Example at 22:52 UTC showing WSPR Link ID 186192616.

The WSPR link ID 186192616 was transmitted at 3.594078 MHz and was within the maximum usable frequency at 7th March 2014 22:52 UTC of around 6.75 MHz. The elevation angle is 1.981° and within the specified elevation angle of around 3.5°. The ionospheric propagation from transmitter to MH370 required 5 hops reaching a maximum height of around 235 km above the Earth's surface.

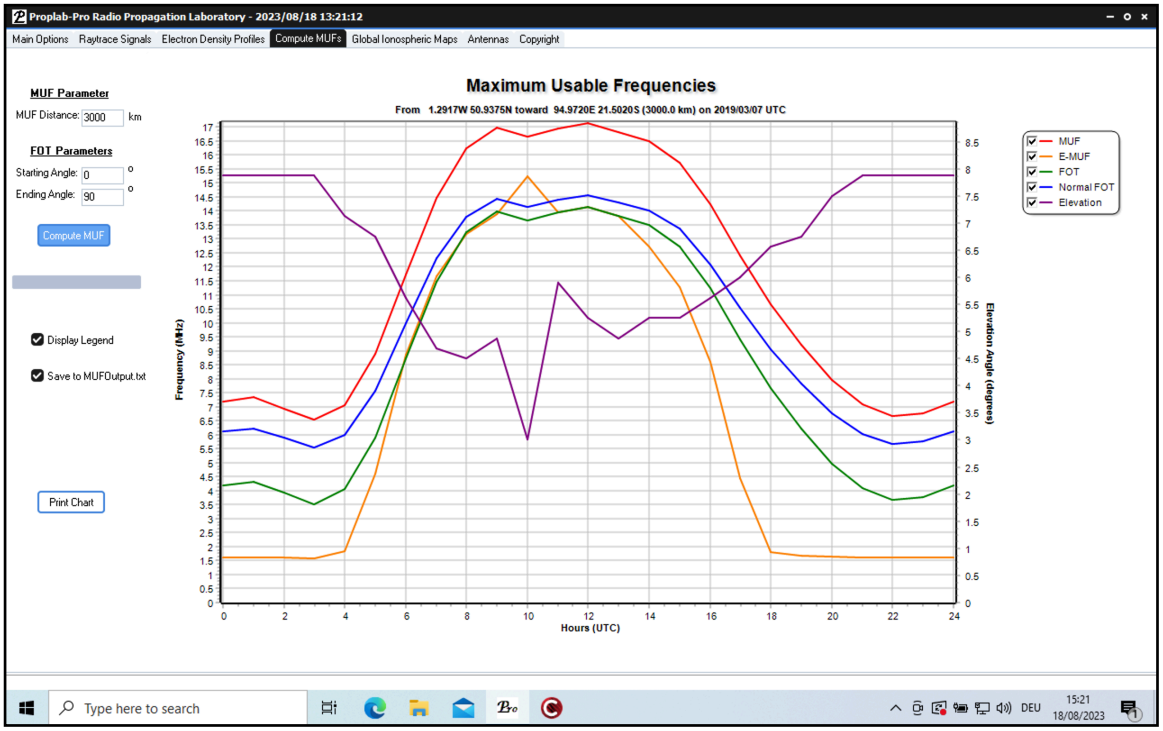

Figure 9: Worked Example at 22:52 UTC showing WSPR Link ID 186192616 MUF and EA.

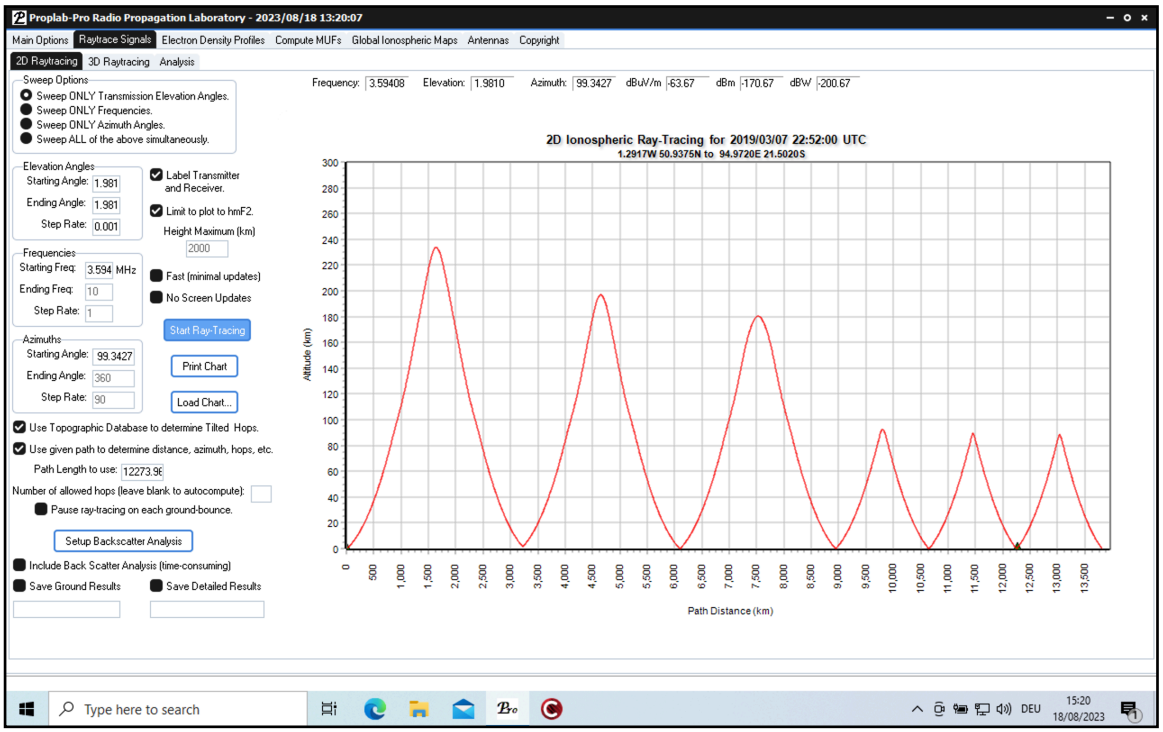

Figure 10: Worked Example at 22:52 UTC showing WSPR Link ID 186192616 Ray Tracing Results.

6. Results.

MH370 passed Penang Airport at around 17:52 UTC where the WSPR based tracking starts. MH370 was still being tracked by military and civilian primary radar, although it had gone 'dark'. The Copilot's mobile phone was detected by the BBFARLIM2 base station at Bandar Baru Air Itam on Penang Island at 17:52:27 UTC. Just after 18:01 UTC as MH370 approached Pulau Perak the aircraft turned toward waypoint DUAMO in Indonesia. At 18:14 UTC on approaching the Indonesian coast MH370 turned North West and tracked the coastline towards waypoint MEKAR.

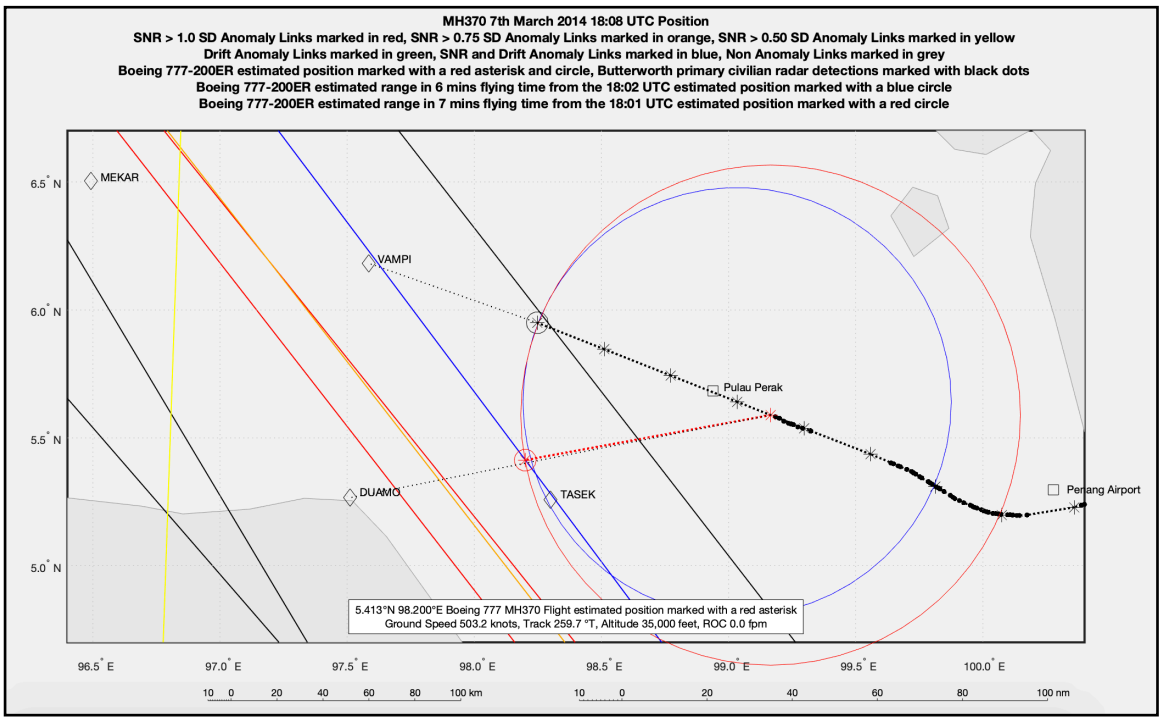

Figure 11: MH370 estimated position at 18:08 UTC.

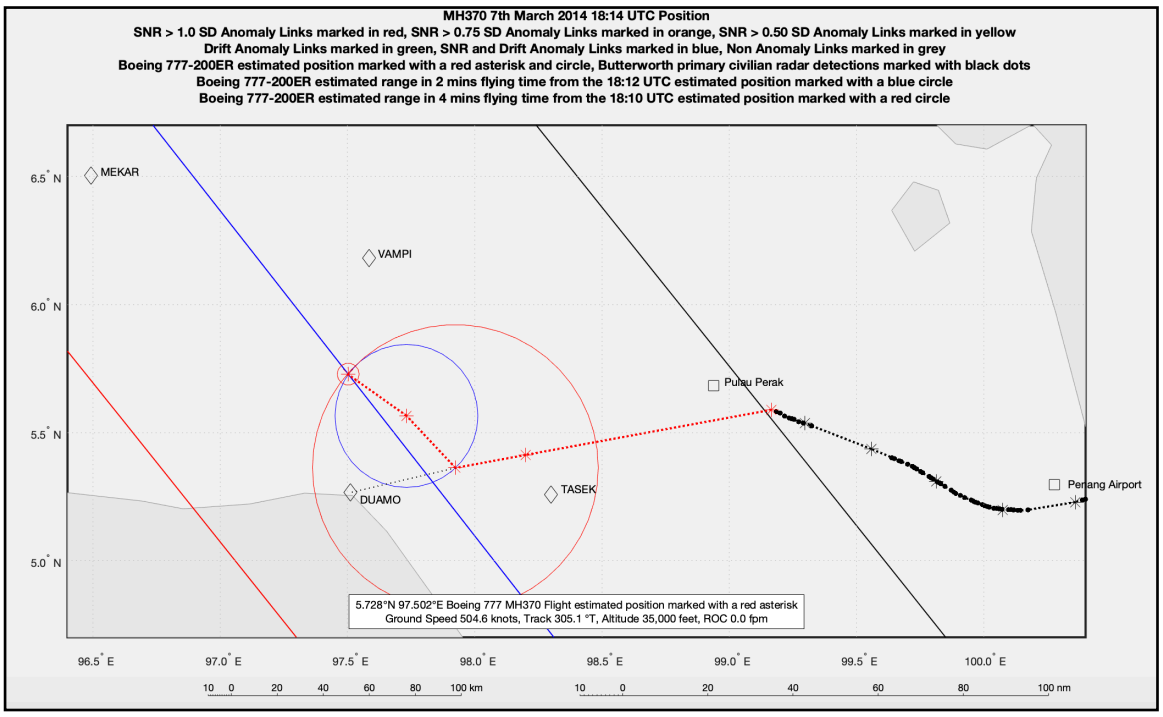

Figure 12: MH370 estimated position at 18:14 UTC.

At 18:24 UTC MH370 was tracking towards waypoint SANOB. At 18:28:15 UTC MH370 crosses the 1st Arc as defined by the Inmarsat satellite BTO data. MH370 appears to slow down from the previous ground speed of 502.0 knots to 432.2 knots. The altitude at this point is assumed to be around 35,000 feet, which is the last known altitude prior to diversion. The actual altitude may well have changed and it is conceivable that an interim altitude of 34,500 feet or 35,500 feet was adopted to avoid other air traffic in the vicinity.

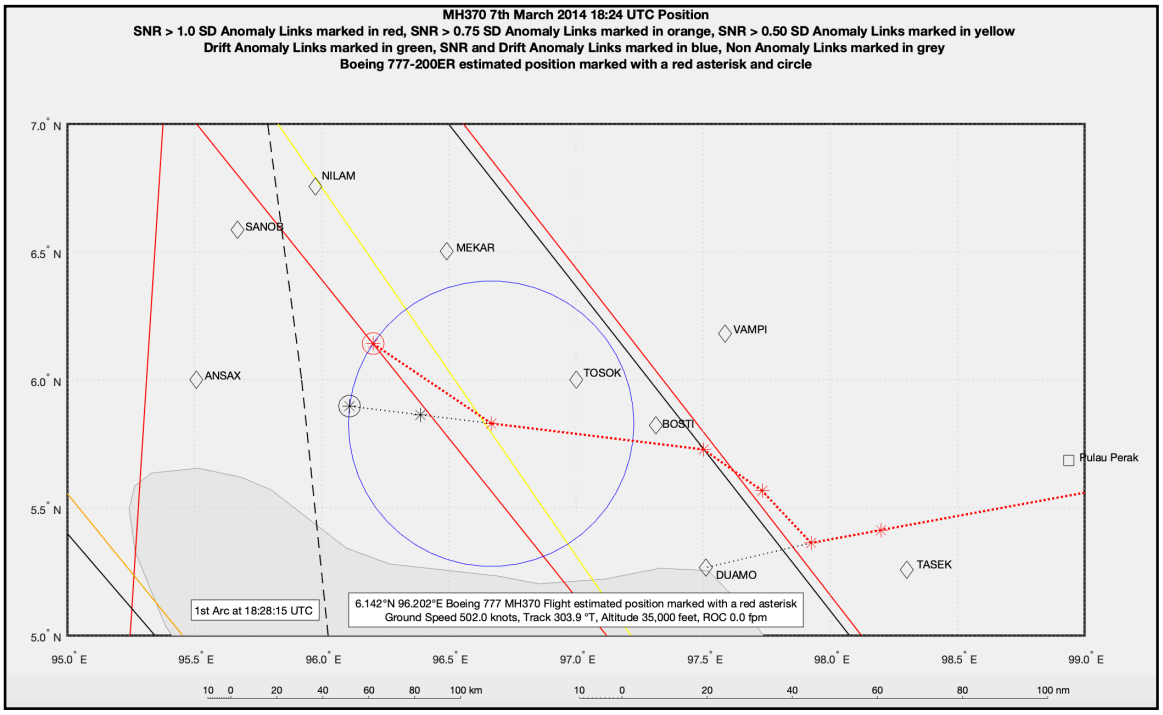

Figure 13: MH370 estimated position at 18:24 UTC.

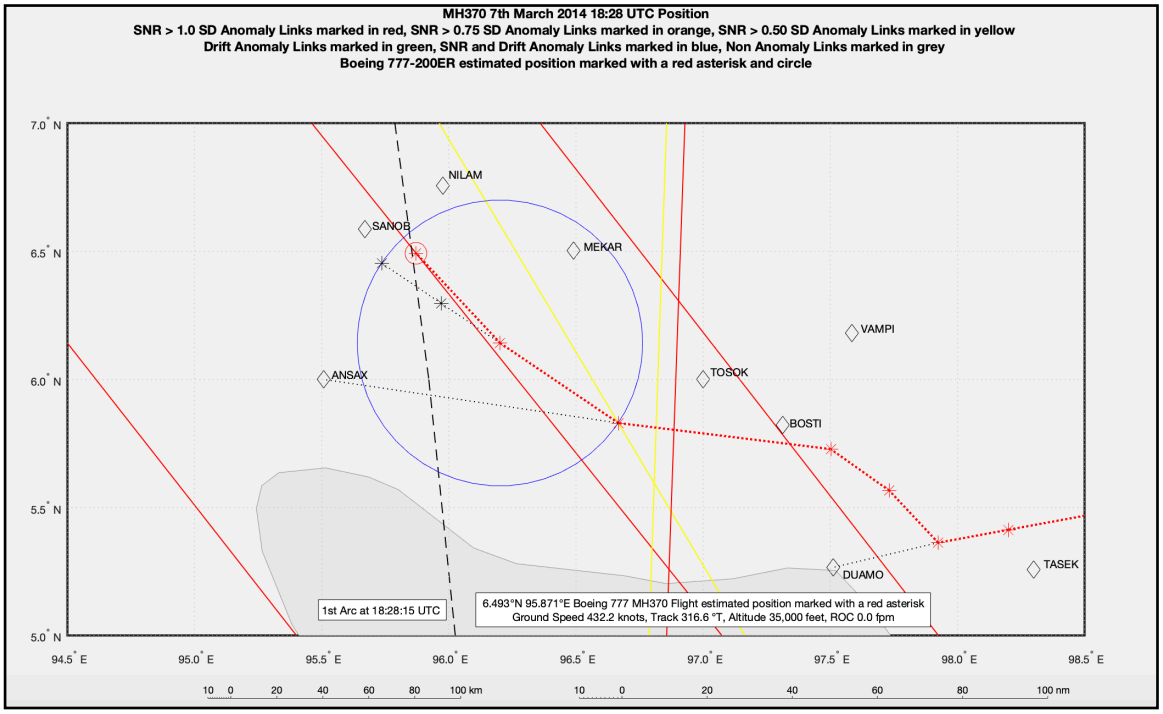

Figure 14: MH370 estimated position at 18:28 UTC.

At 16:42 UTC just after MH370 took off, there were 18 other flights in the vicinity. All the 6 flights heading out over the Malacca Strait were at flight levels between FL229 and FL 350. By the time MH370 reached the area close to Penang Airport (VPG) at 17:52 UTC there were only 3 other flights heading out over the Malacca Strait at flight levels between FL300 and FL350. An interim flight level of FL345 or FL355 would suffice in order to avoid other air traffic. The data is sourced from the ADS-B data for the region between 7th March 2014 15:39 UTC and 21:38 UTC.

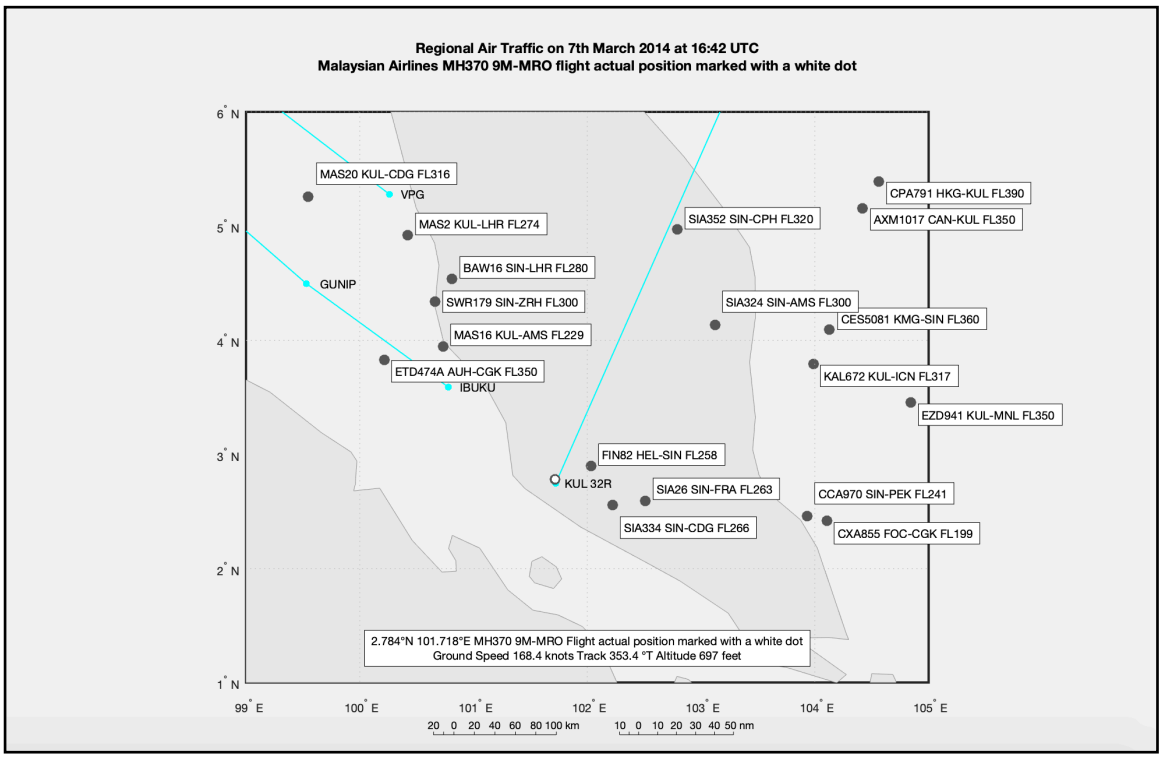

Figure 15: Regional Air Traffic when MH370 had just taken off at 16:42 UTC.

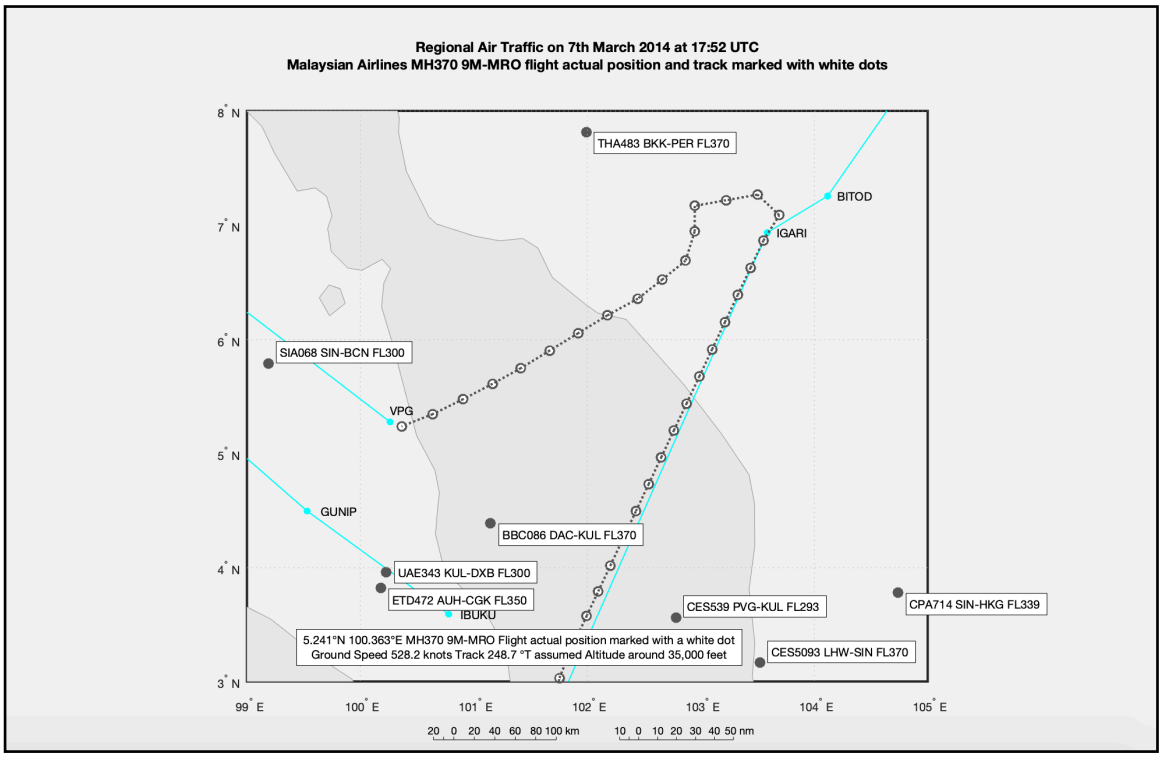

Figure 16: Regional Air Traffic when MH370 reached the Penang Airport (VPG) area at 17:52 UTC.

As MH370 passes the 1st Arc the BTO residual was -1.0368 μs (a horizontal error of approximately 207 m) and the BFO residual was -0.0030 Hz based on a turn onto a track of 300.2°T. The BTO tolerance is around ± 50 μs (99% confidence level), which translates into a horizontal error of ± 10 km. The BFO tolerance is around ± 7 Hz, which translates into a track error of ± 13.2 ° or a rate of climb/descent error of ± 313 fpm. At 18:40 UTC during the first SATCOM call the BFO residual was 1.5182 Hz. The BFO data shows a constant flight path (51 data points, mean BFO 87.8235 Hz, standard deviation 1.2603 Hz).

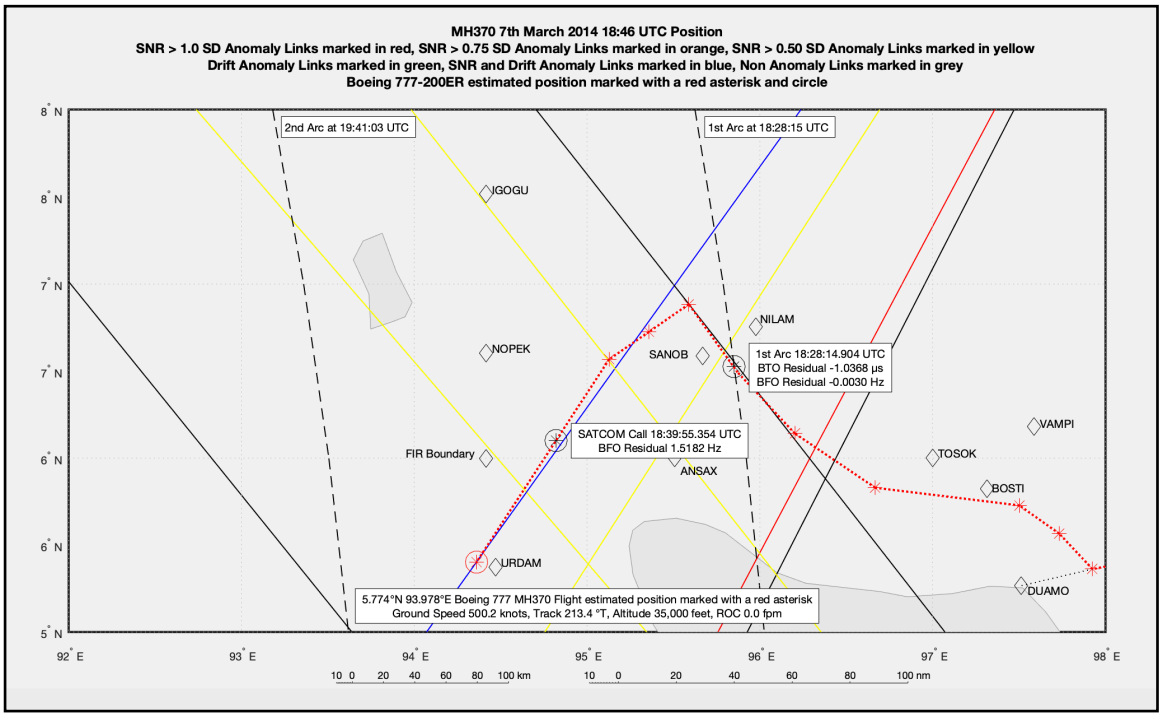

Figure 17: MH370 estimated position at 18:46 UTC.

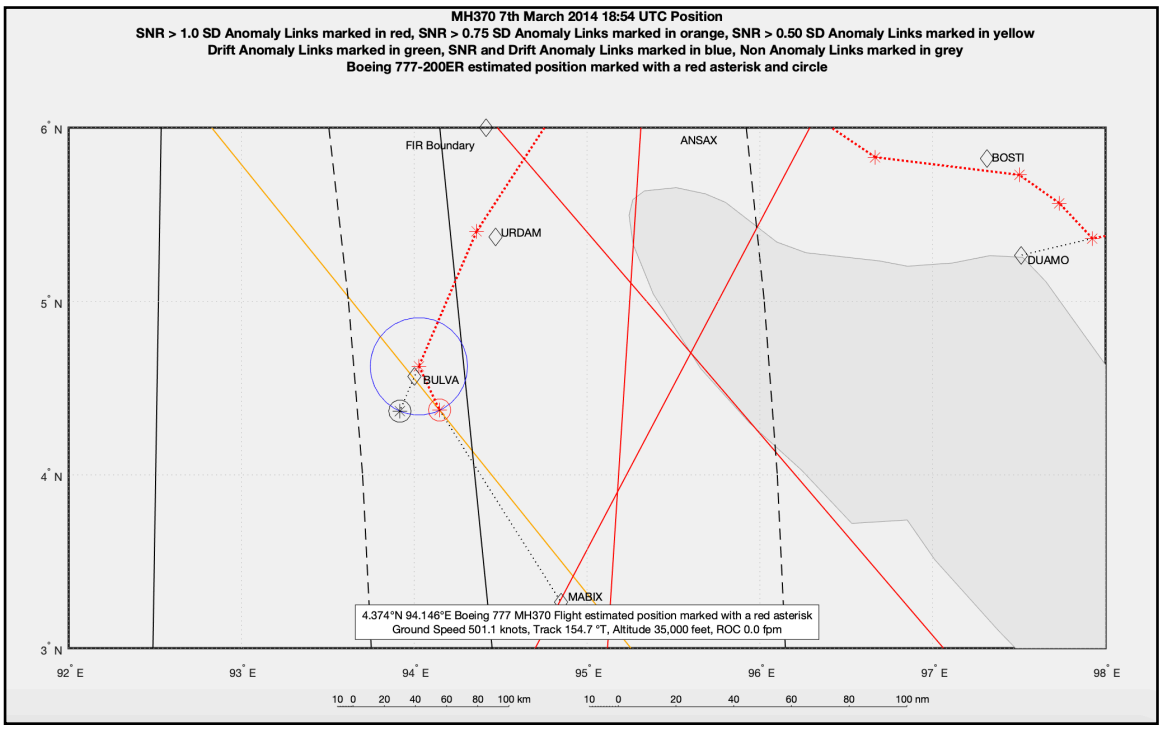

Figure 18: MH370 estimated position at 18:54 UTC.

By 19:16 UTC MH370 had tracked around Indonesia using waypoints DUAMO, ANSAX, SANOB, URDAM, BULVA and MABIX. At 19:16 UTC MH370 turned towards the FIR boundary at 2°S 92°E where the Melbourne FIR meets the Colombo FIR and the Jakarta FIR. At 19:28 UTC MH370 turns towards waypoint BASEV. Every turn is toward a waypoint and it appears that every waypoint was carefully selected not to follow a flight route, but only to cross over a flight route. The pilot was knowledgable of all the regional waypoints and carefully planned a flight path avoiding other traffic and busy flight routes.

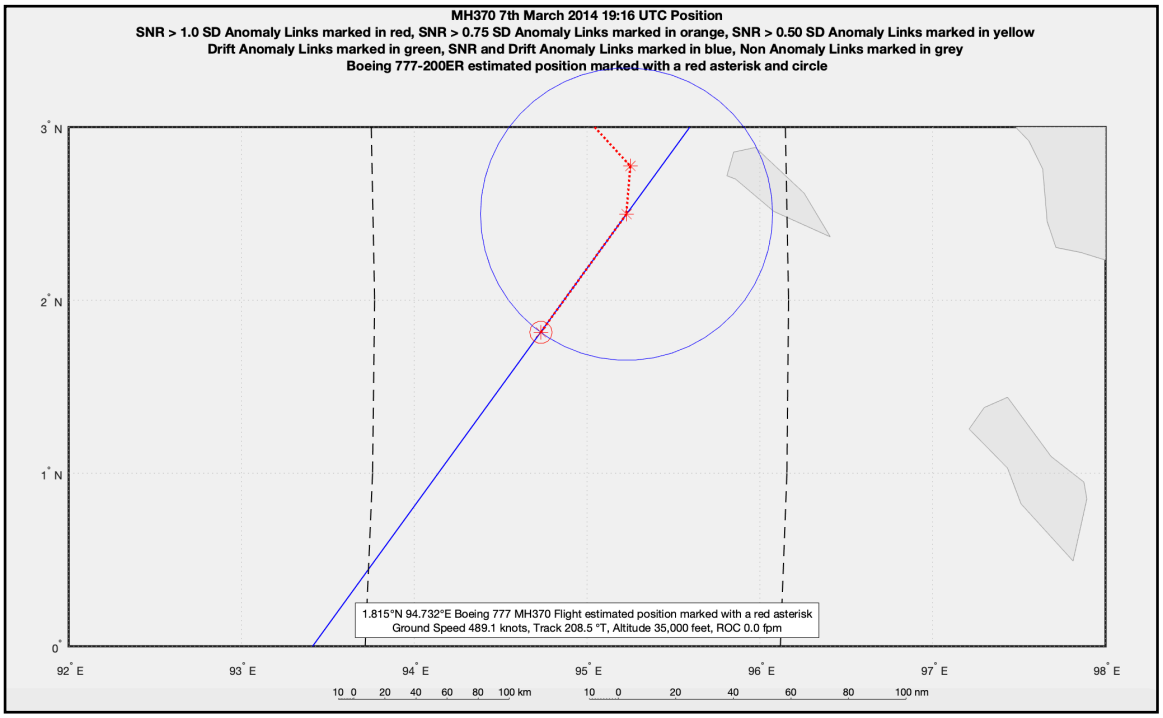

Figure 19: MH370 estimated position at 19:16 UTC.

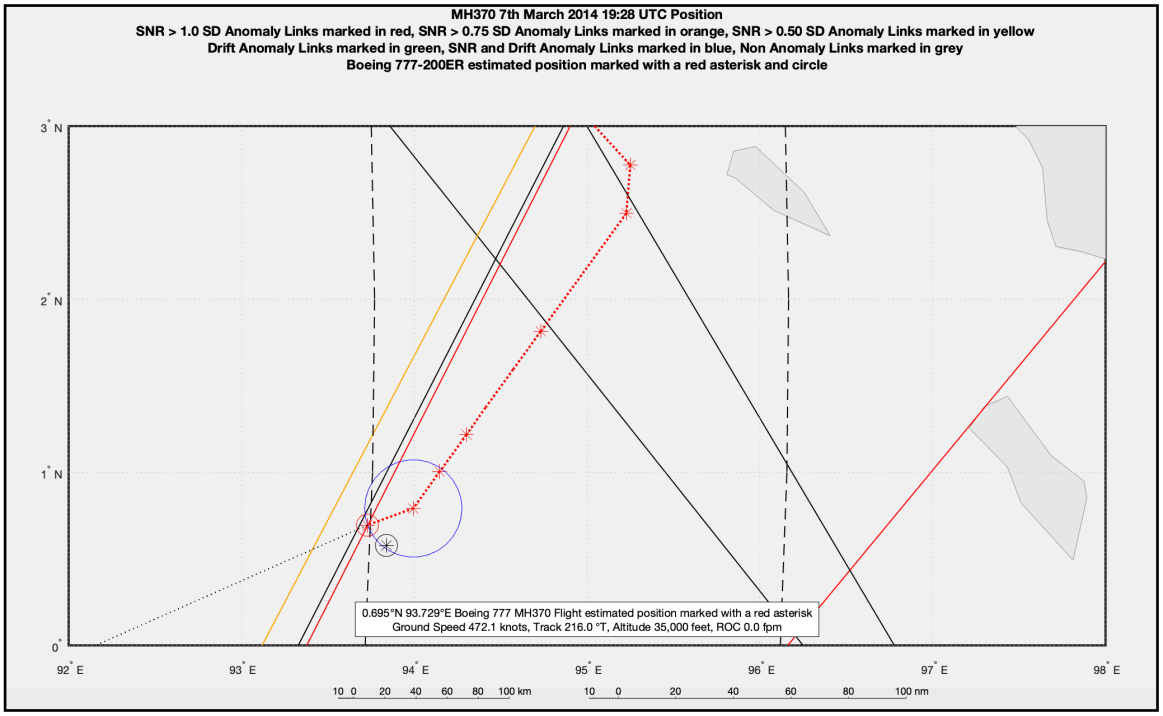

Figure 20: MH370 estimated position at 19:28 UTC.

At 19:38 UTC MH370 turns towards waypoint TATOD, between Cocos Island and Christmas Island. At 19:40 UTC MH370 is heading again towards the FIR boundary waypoint at 2°S 92°E. The pilot appears to have been extremely cautious not to be detected and if by chance there was a detection, then to at least mislead everyone as to the intended destination.

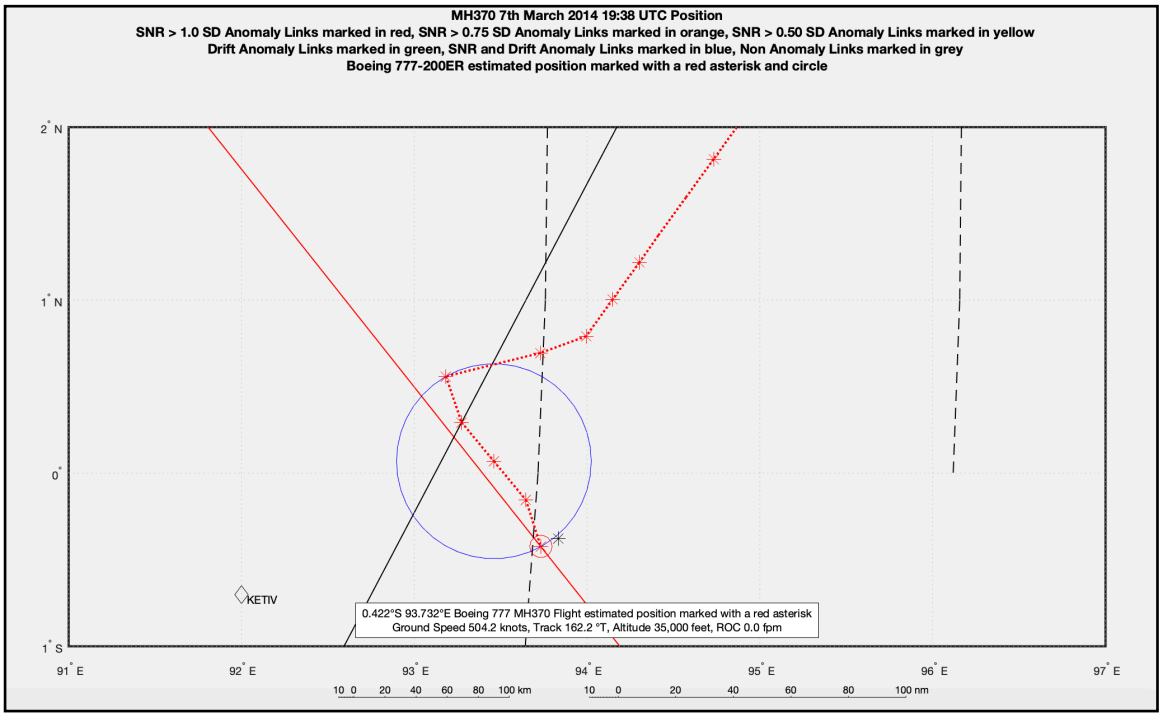

Figure 21: MH370 estimated position at 19:38 UTC.

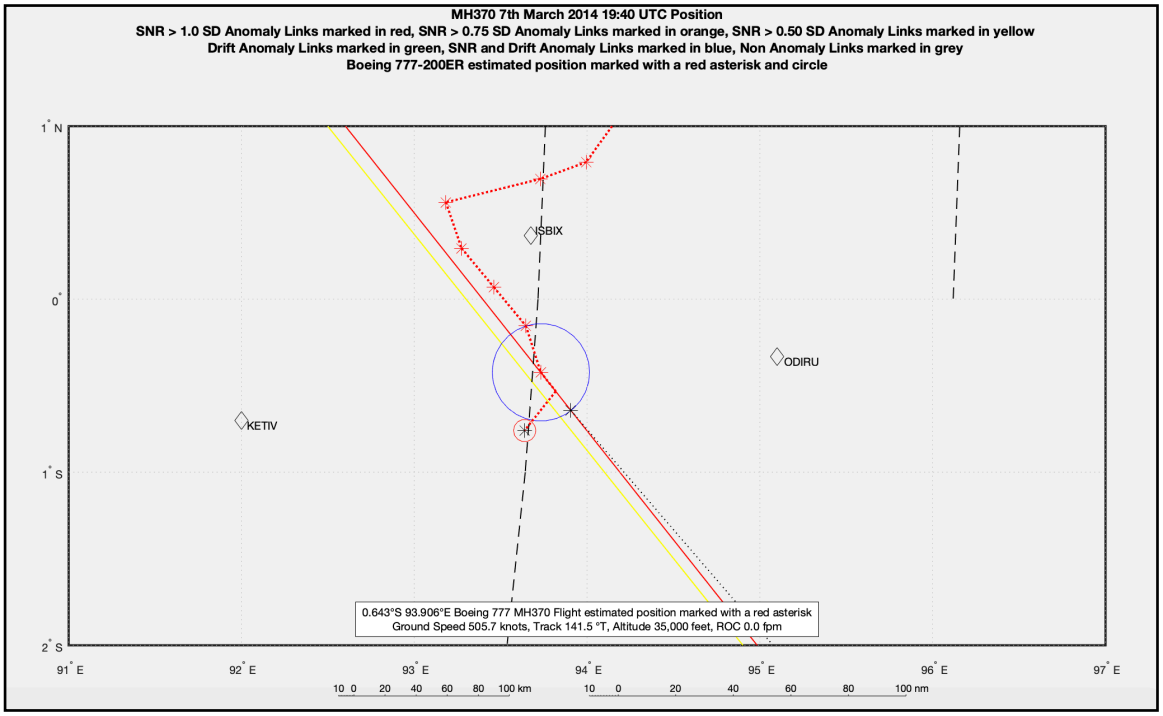

Figure 22: MH370 estimated position at 19:40 UTC.

At 19:48 UTC MH370 is heading again towards the FIR boundary waypoint at 2°S 92°E. The Inmarsat satellite data is matched at the 2nd Arc at 19:41:03 UTC. At 20:16 UTC MH370 is close to waypoint PIPOV and crossing the flight route N663 which runs via waypoints MUTMI and PIPOV. There are two anomalous WSPR links intersecting at this location.

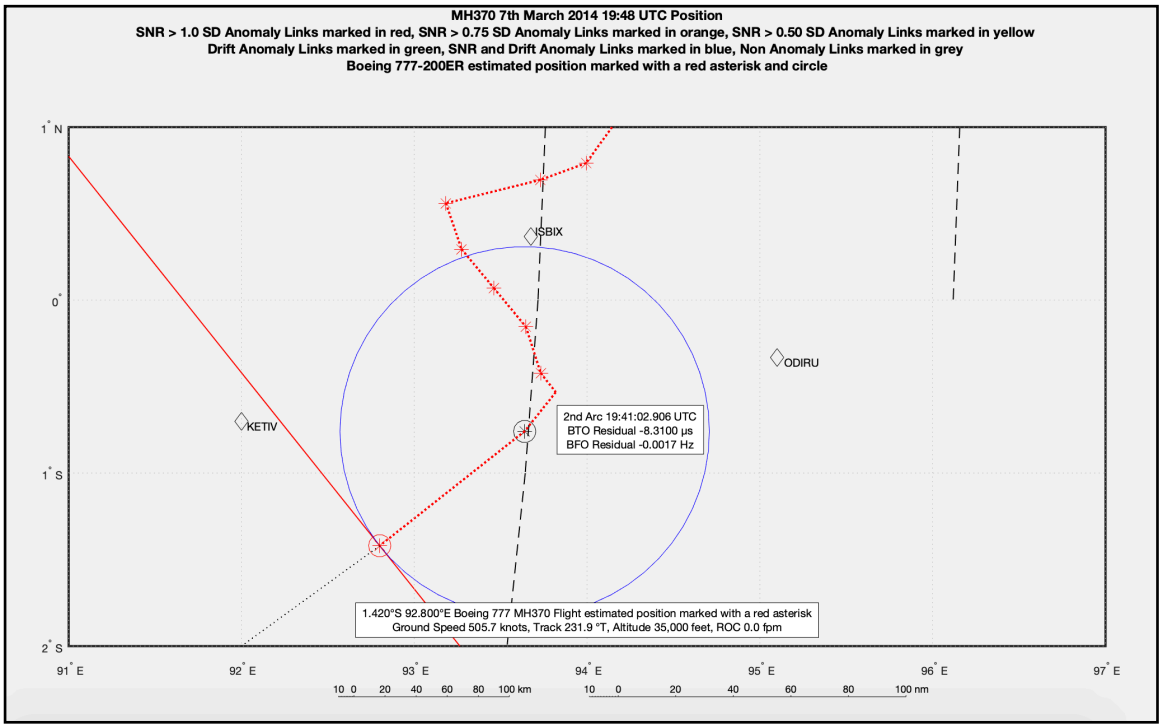

Figure 23: MH370 estimated position at 19:48 UTC.

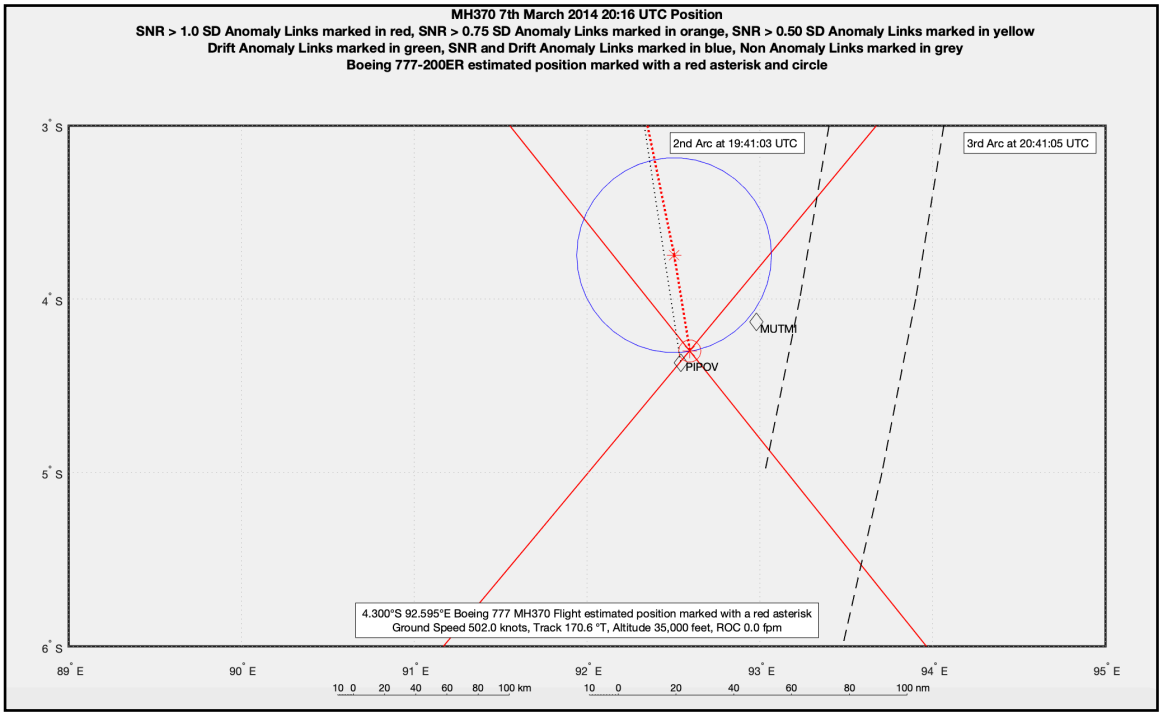

Figure 24: MH370 estimated position at 20:16 UTC.

At 20:24 UTC MH370 had just passed waypoint PIPOV and tracking towards waypoint POROR. At this juncture MH370 is within 4 minutes flying time from another aircraft SQ478 flying from Singapore to Johannesburg. SQ478 was at 36,000 feet and MH370 was possibly at an interim altitude such as 34,500 feet. SQ478 did not report any near miss and there was obviously sufficient horizontal and vertical separation between the aircraft.

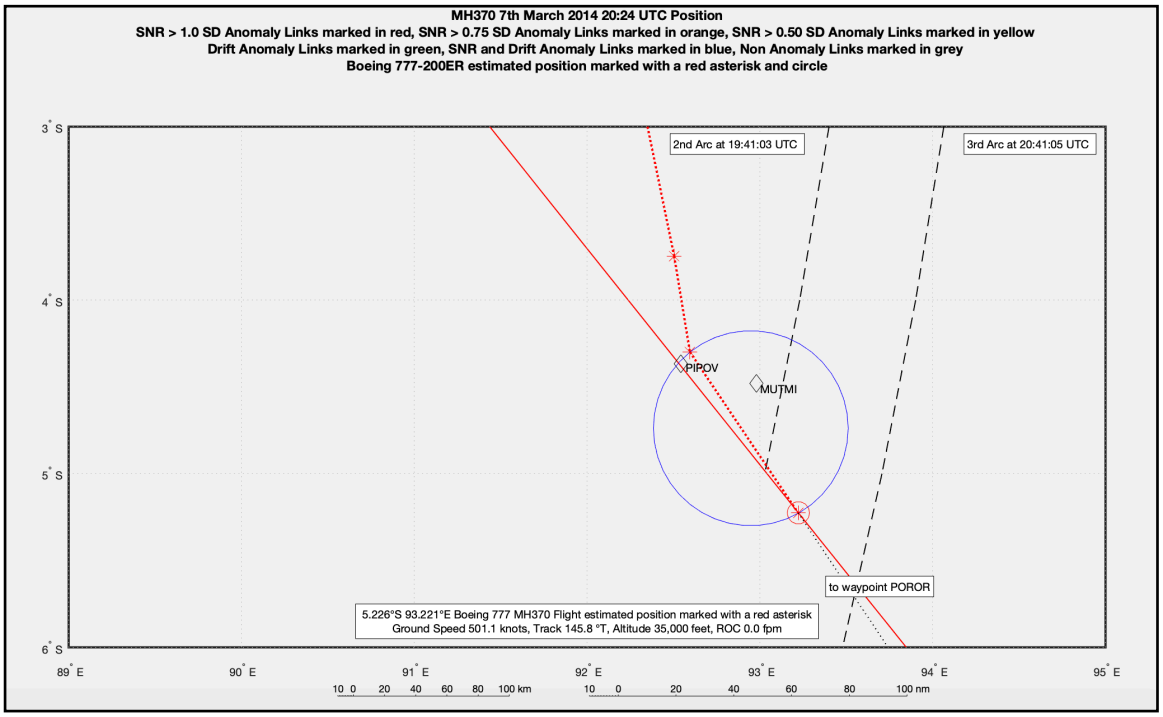

Figure 25: MH370 estimated position at 20:24 UTC.

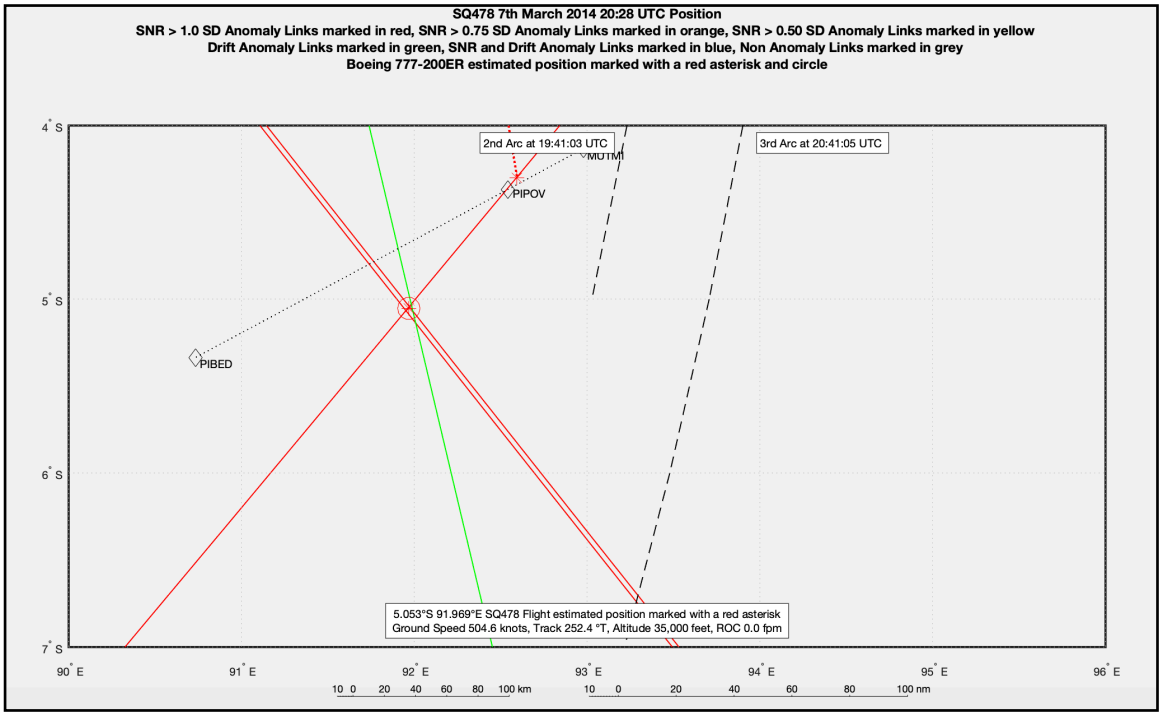

Figure 26: SQ478 estimated position at 20:28 UTC.

At 20:30 UTC MH370 is heading toward waypoint POLUM. At 20:36 UTC MH370 is heading toward waypoint RUNUT. The anomalous SNR WSPR link is marked with a red line and the track to the next waypoint is marked with a black dotted line.

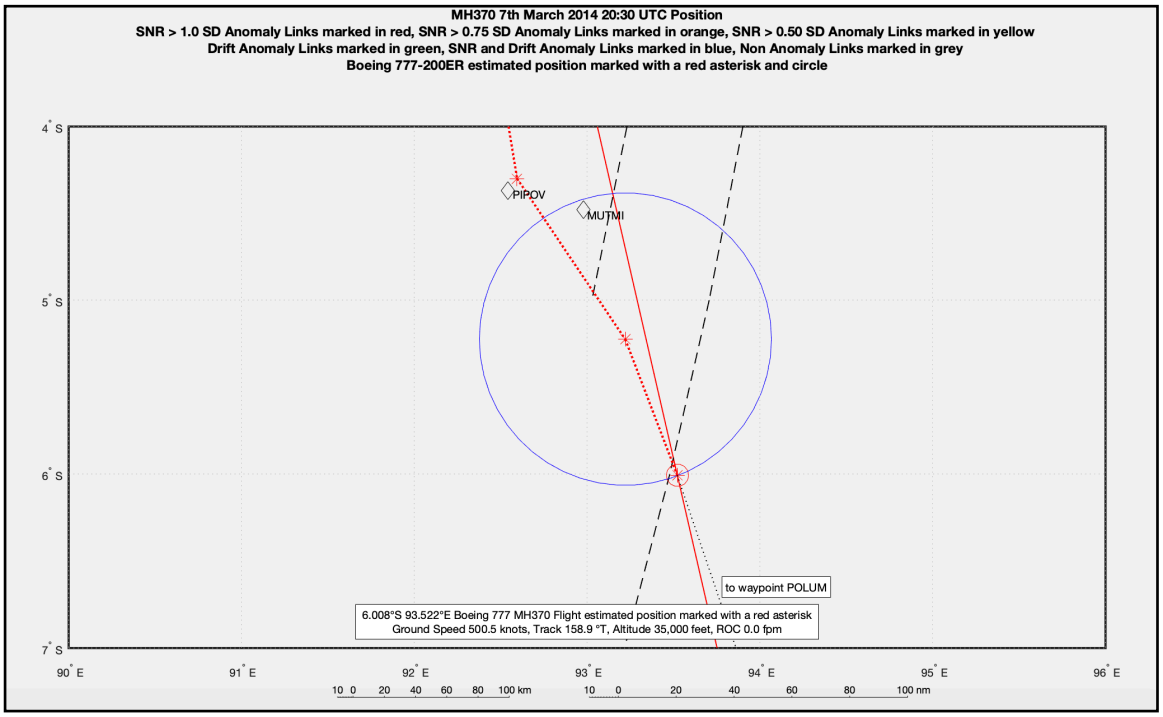

Figure 27: MH370 estimated position at 20:30 UTC.

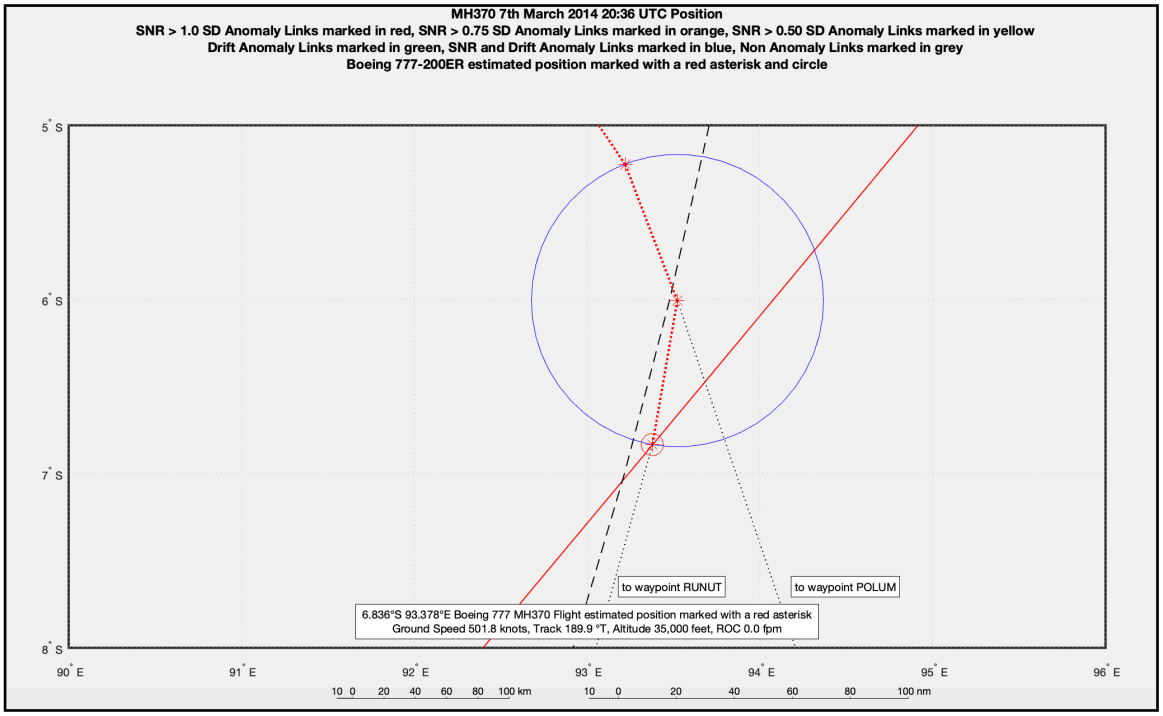

Figure 28: MH370 estimated position at 20:36 UTC.

At 20:44 UTC MH370 is heading toward waypoint SOLIT and then waypoint BEBIM. The Inmarsat satellite data is matched at the 3rd Arc. At 20:54 UTC MH370 is close to flight route M641 which runs towards the Cocos Islands. The pilot appears to be continually changing direction but always towards waypoints and always to cross flight routes, but not to precisely follow flight routes.

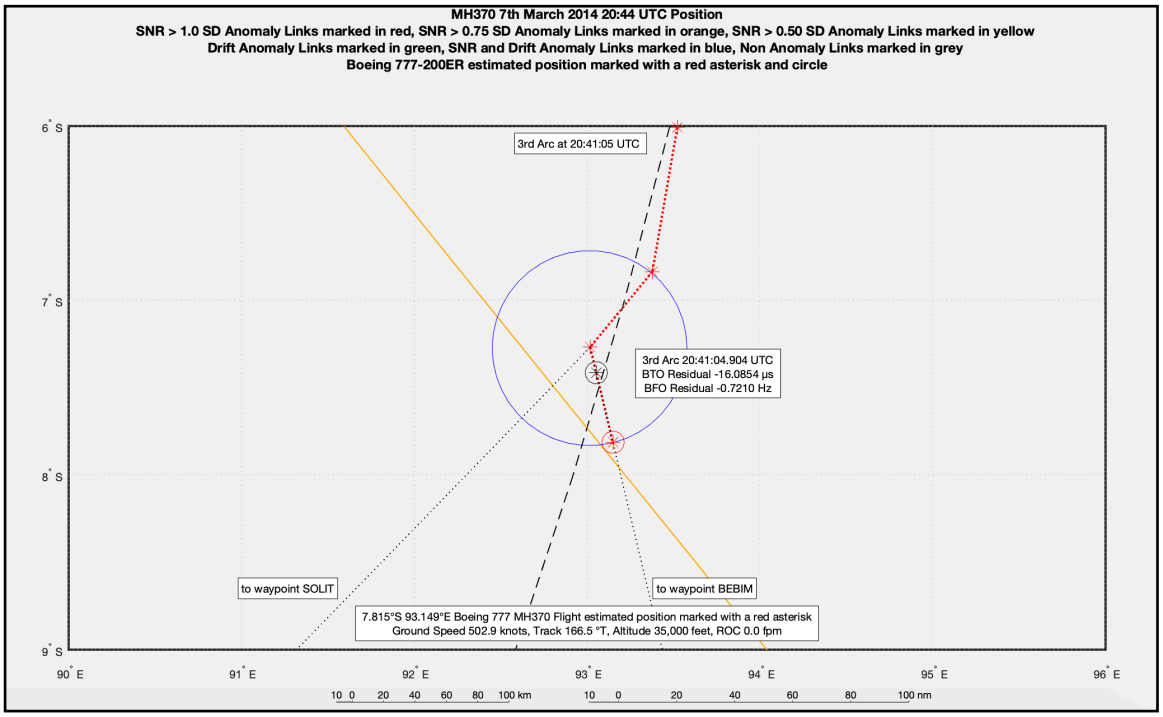

Figure 29: MH370 estimated position at 20:44 UTC.

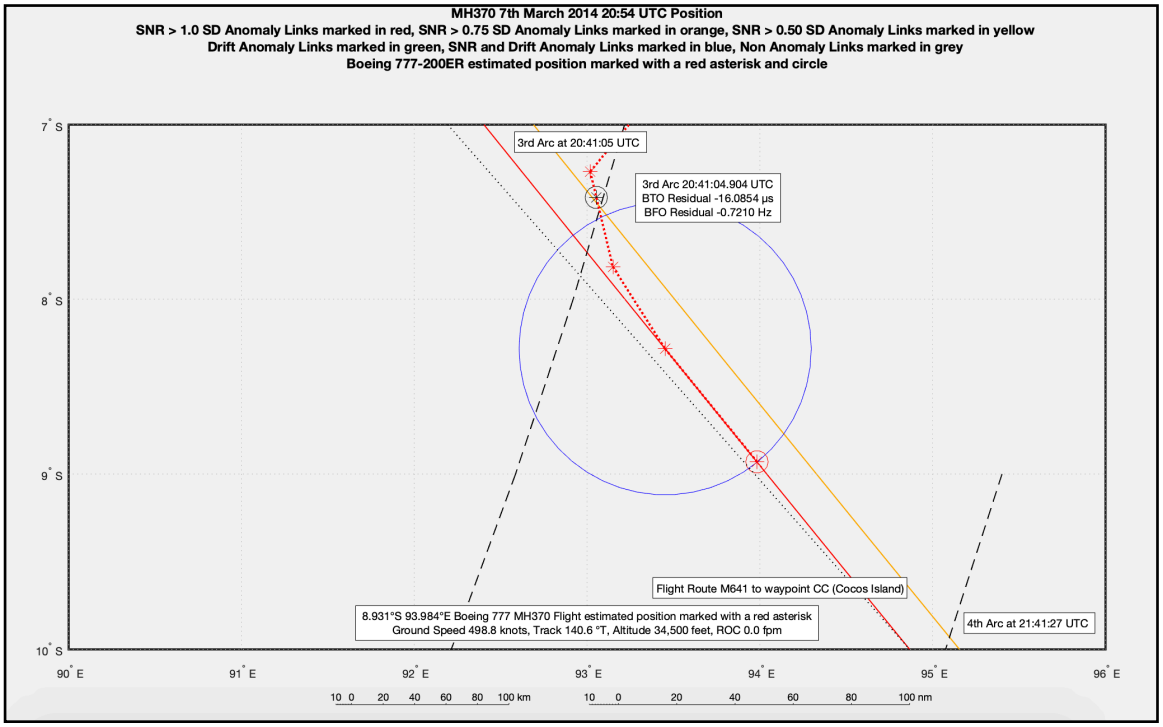

Figure 30: MH370 estimated position at 20:54 UTC.

At 21:10 UTC MH370 is close to waypoint BEBIM and again heading towards waypoint RUNUT. Another aircraft is detected (marked in blue) on a direct flight route from Colombo to Sydney via waypoint 07S88E to 14S101E and would typically be at either FL350 or FL370. This would support the hypothesis that the pilot of MH370 selected an interim flight level such as 34,500 feet in order to avoid other traffic. At 21:14 UTC MH370 turns towards waypoint UVUBI. There is an intersection of two anomalous WSPR signals at this point. MH370 slows from 500.2 knots to 482.6 knots and it appears there may be a step climb taking place.

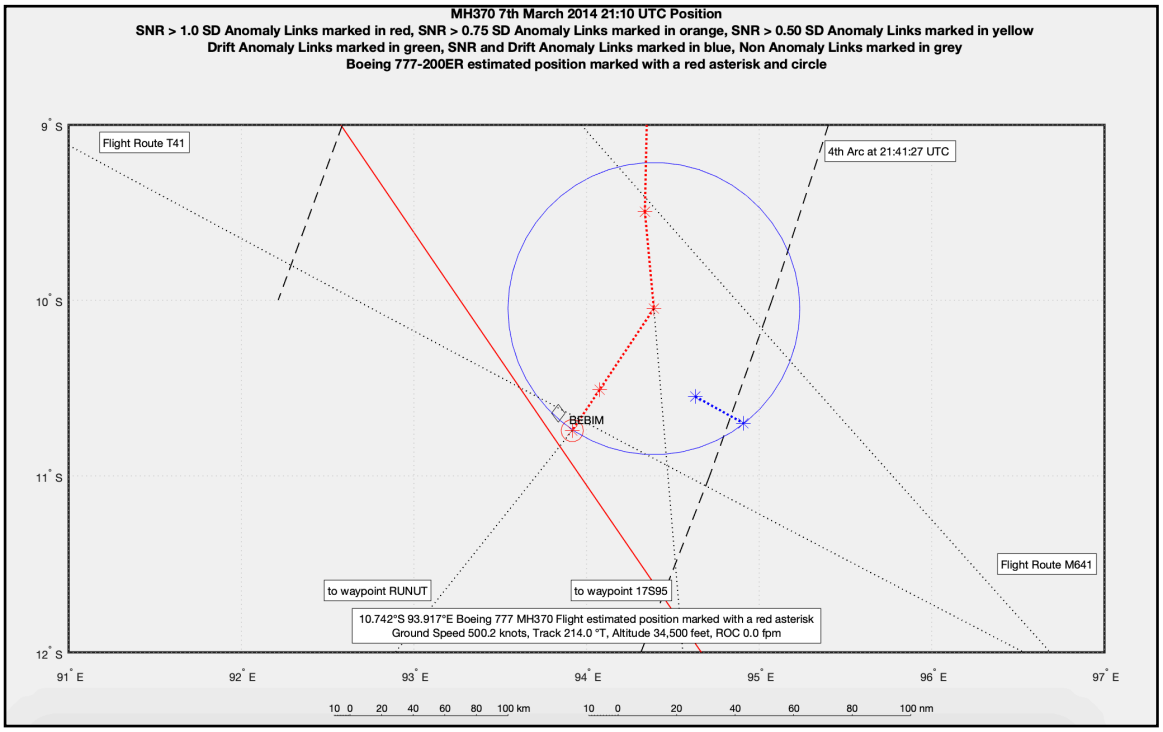

Figure 31: MH370 estimated position at 21:10 UTC.

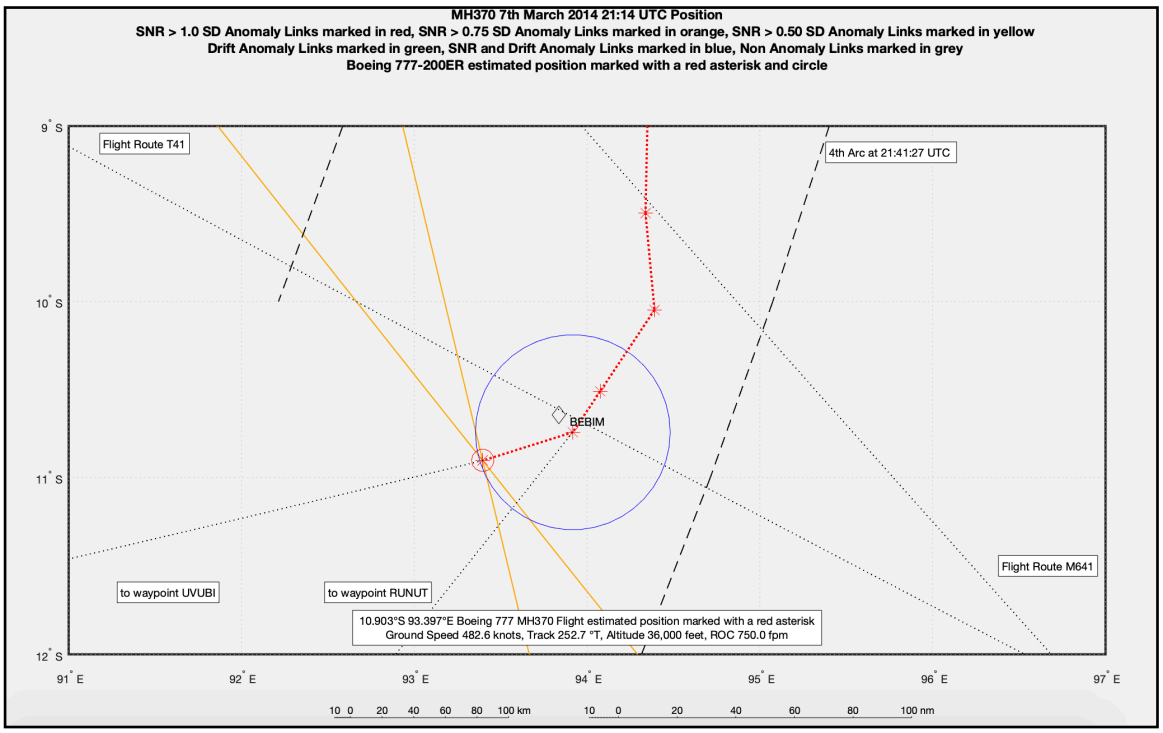

Figure 32: MH370 estimated position at 21:14 UTC.

Waypoint RUNUT is the most southerly aeronautical waypoint in this part of the Indian Ocean region. At 21:16 UTC MH370 turns towards the geographical waypoint 16S097E. There is again an intersection of two anomalous WSPR signals at this point. MH370 slows to 461.9 knots confirming a step climb is being executed. The duration and temporary speed reduction indicate a step climb of around 4,000 feet, for example from FL345 to FL385 (38,500 feet). At 21:38 UTC MH370 turns again towards the geographical waypoint 14S093E. There is again an intersection of two anomalous WSPR signals at this point.

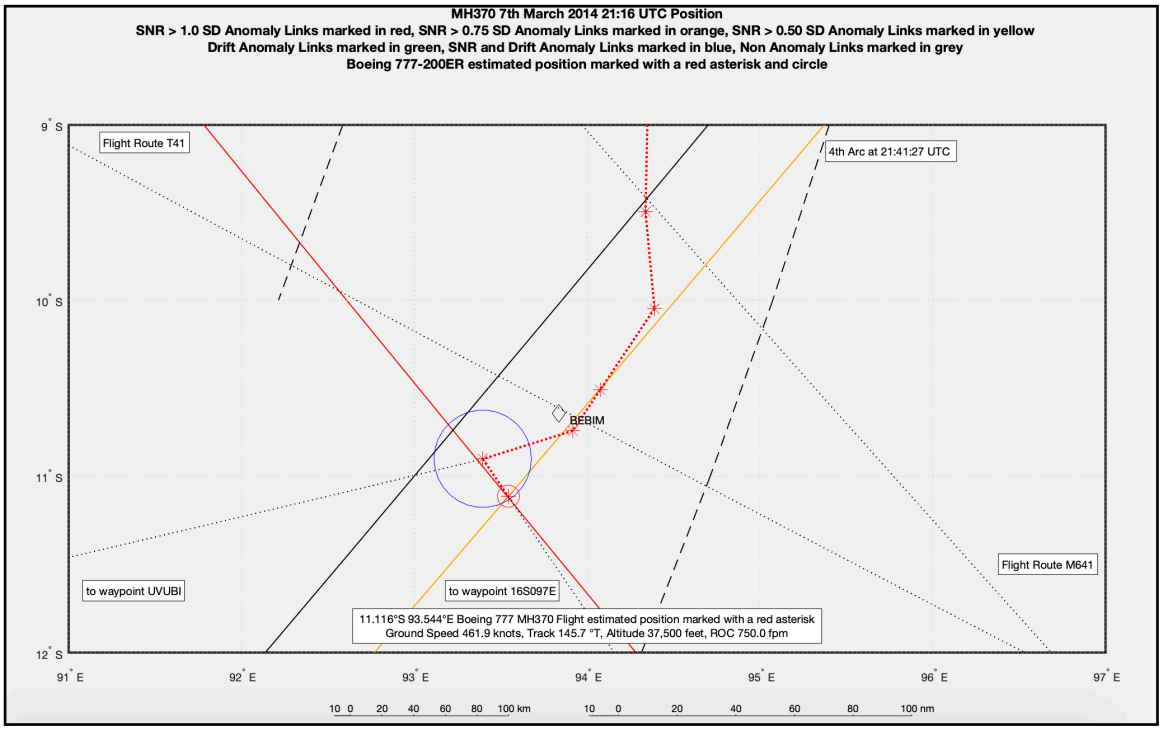

Figure 33: MH370 estimated position at 21:16 UTC.

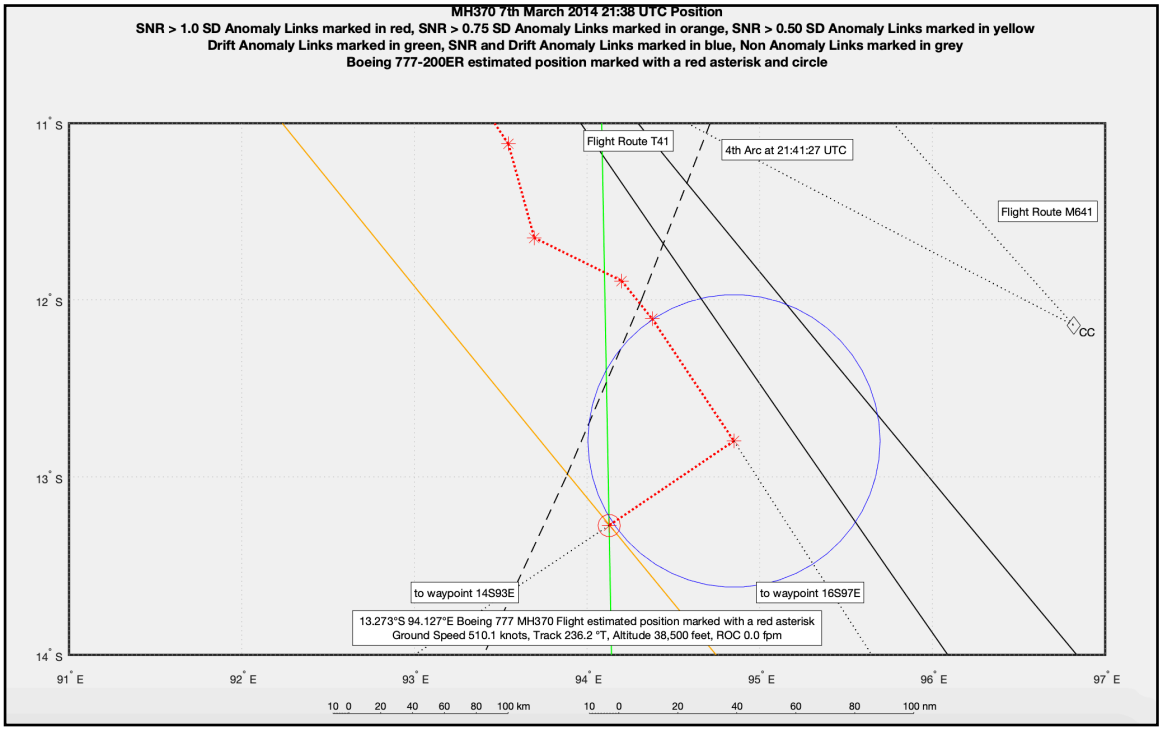

Figure 34: MH370 estimated position at 21:38 UTC.

At 21:44 UTC MH370 turns towards the geographical waypoint 16S095E. The Inmarsat satellite data is matched at the 4th Arc. At 21:50 UTC MH370 is detected by a WSPR SNR anomaly with a 2.16 standard deviation (SD) from the mean over ± 3 hours and is tracking towards waypoint 18S91E. It appears that the goal of the pilot is not to go as far as possible, but to lose the aircraft in a location that is not easily predictable. If you fly in a straight line as far as you can into the southern Indian Ocean, your final location is predictable. We have looked in these predictable straight line flight path locations and not found MH370.

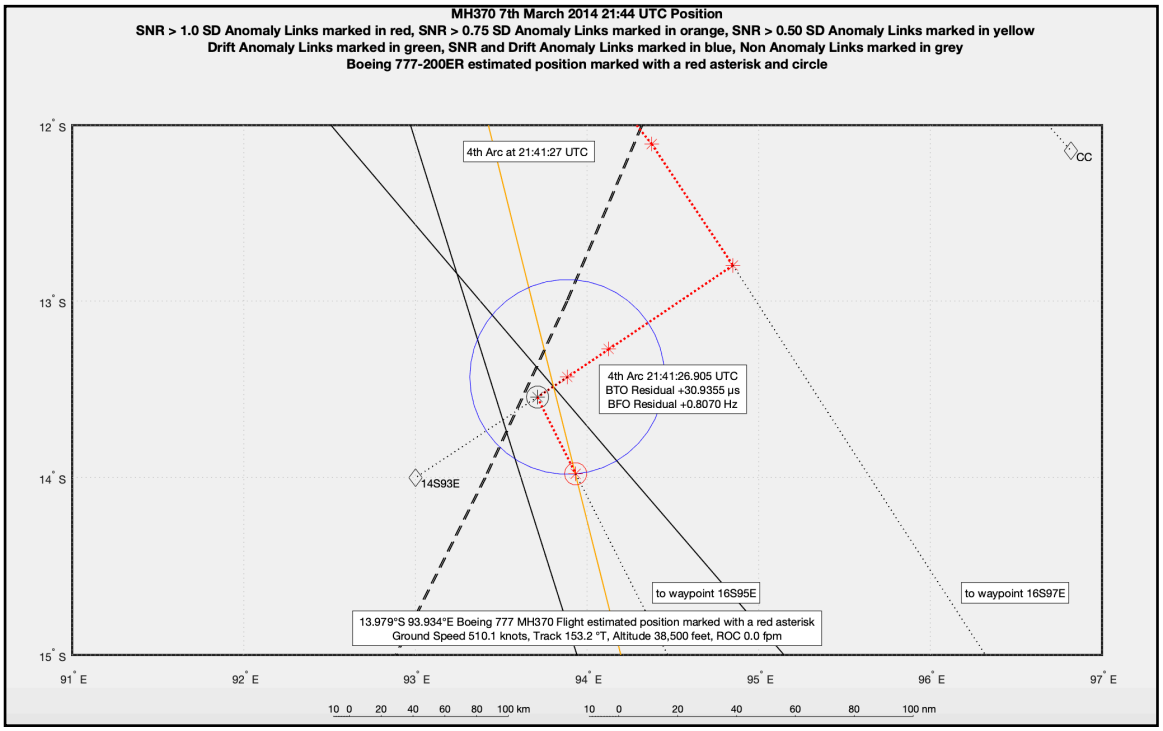

Figure 35: MH370 estimated position at 21:44 UTC.

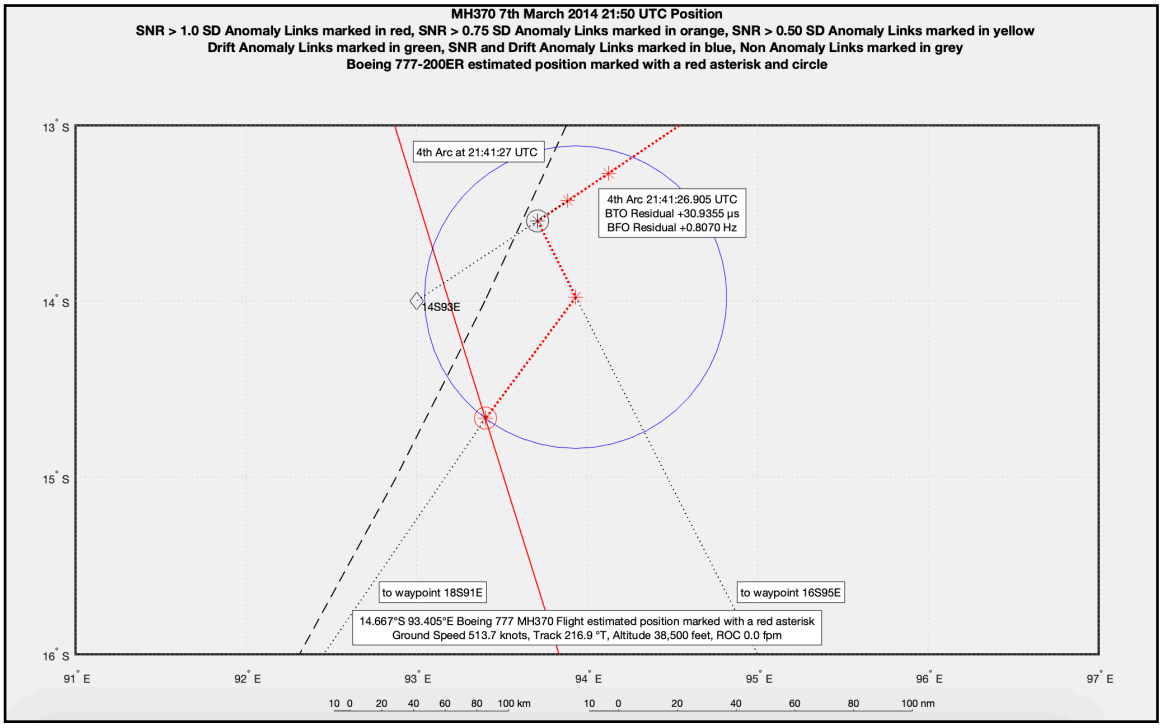

Figure 36: MH370 estimated position at 21:50 UTC.

At 21:56 UTC MH370 is detected by a WSPR SNR anomaly with a 0.86 SD from the mean over ± 3 hours and is tracking towards waypoint 20S95E. At 22:02 UTC MH370 is detected by a WSPR SNR anomaly with a 1.06 SD and another with 0.92 SD and is tracking towards waypoint 20S97E.

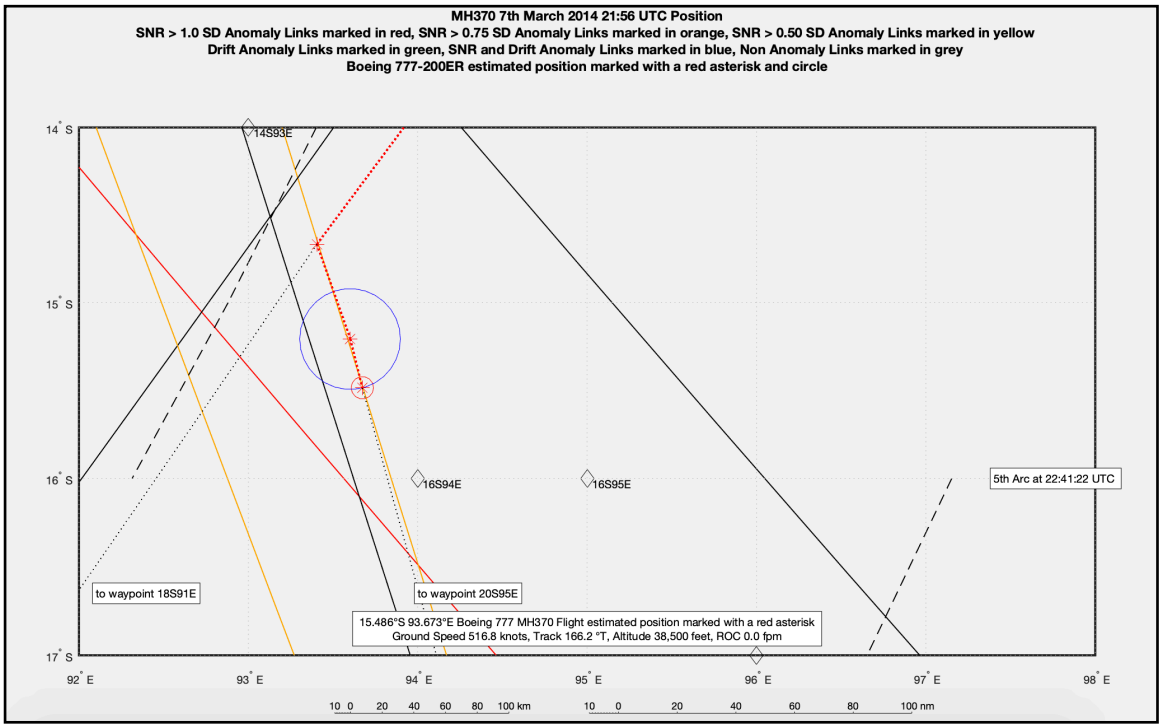

Figure 37: MH370 estimated position at 21:56 UTC.

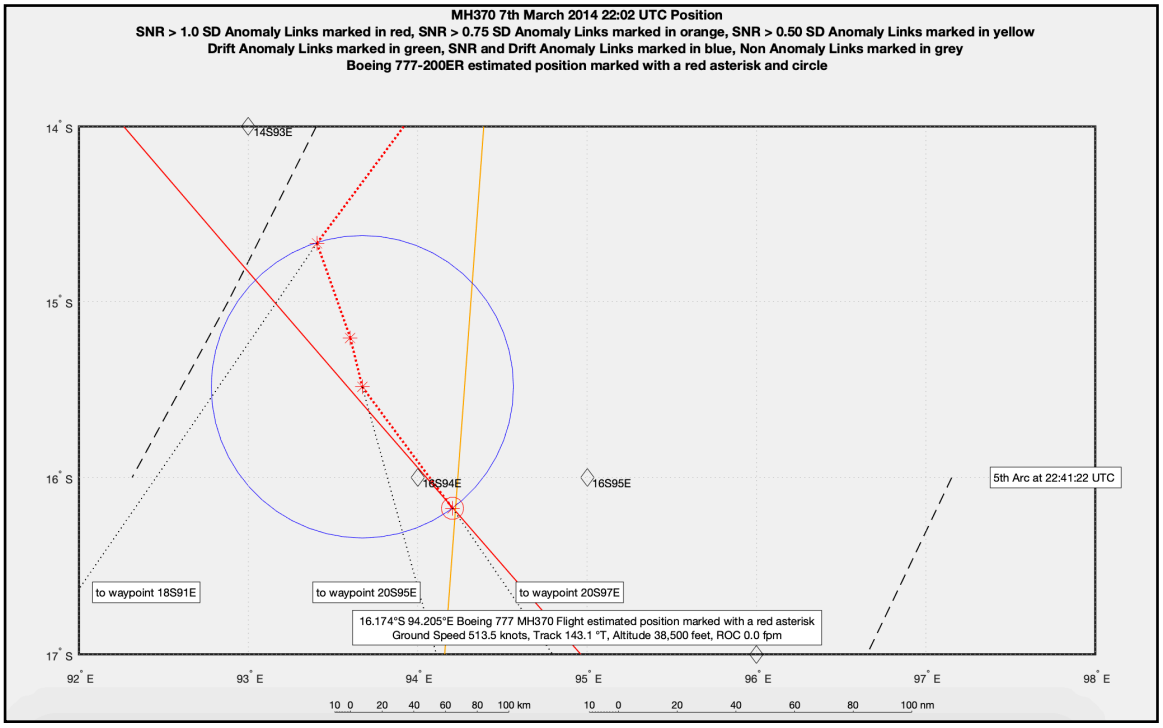

Figure 38: MH370 estimated position at 22:02 UTC.

At 22:08 UTC MH370 is detected by a WSPR SNR anomaly with a 1.14 SD and is tracking towards waypoint 20S97E. At 22:10 UTC MH370 is detected by a WSPR SNR anomaly with a 1.41 SD and is tracking towards waypoint 22S99E.

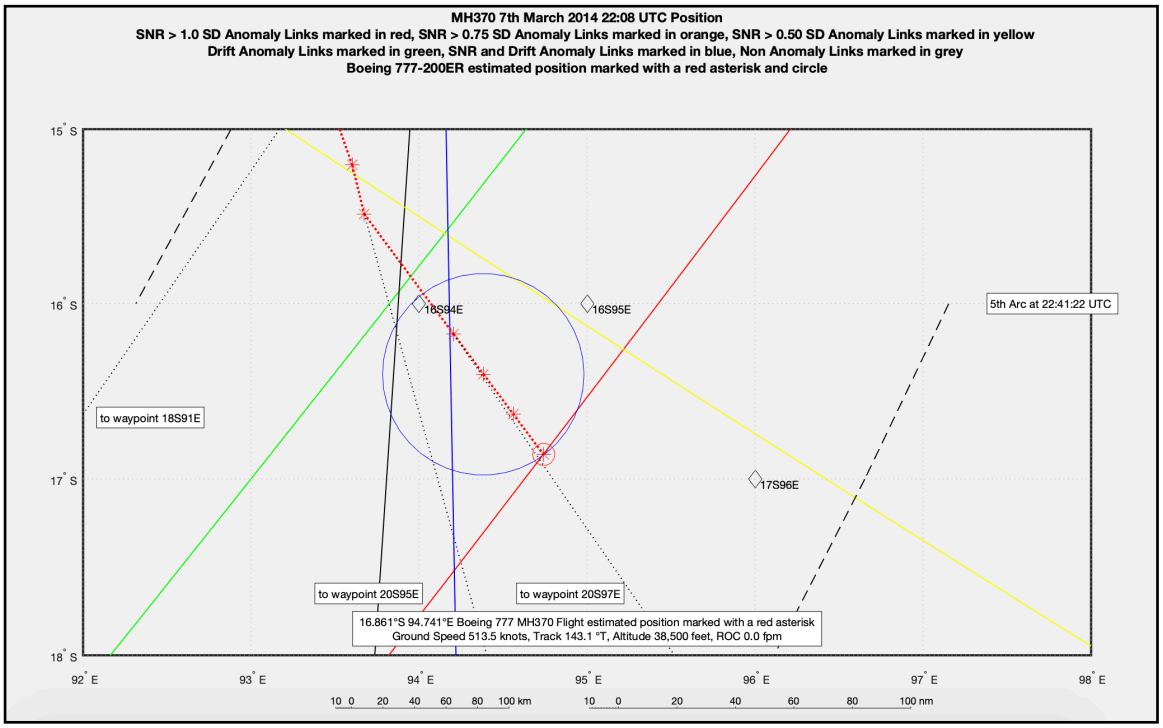

Figure 39: MH370 estimated position at 22:08 UTC.

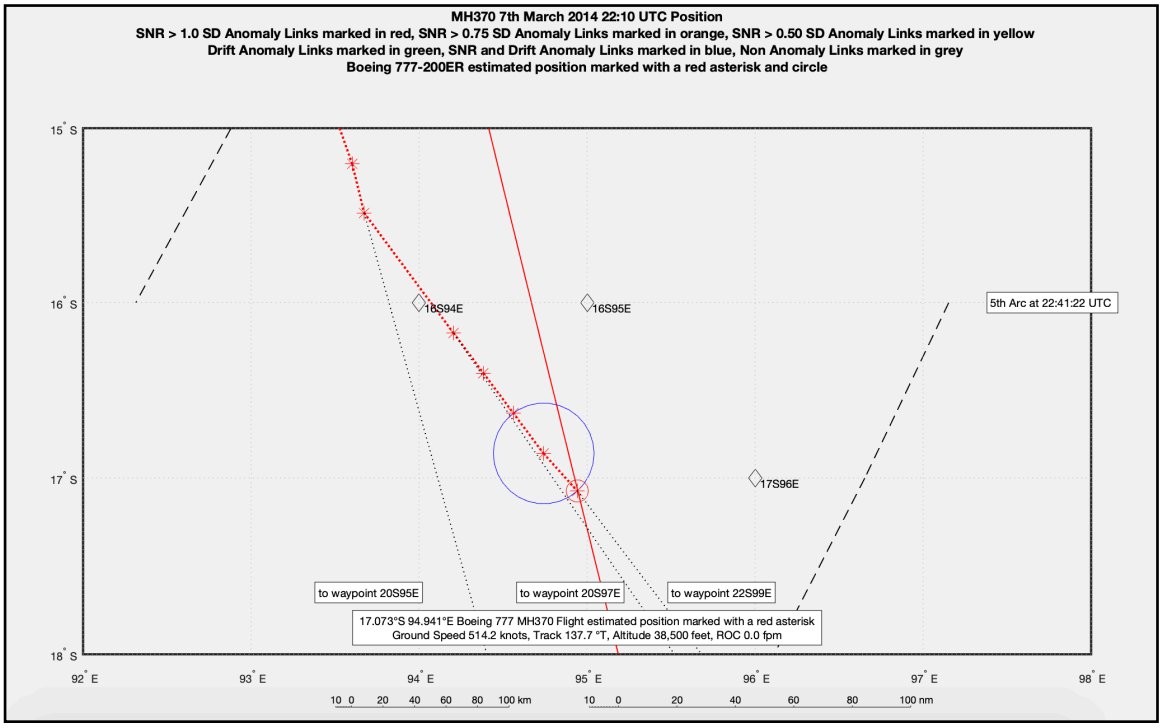

Figure 40: MH370 estimated position at 22:10 UTC.

At 22:16 UTC MH370 is detected by a WSPR SNR anomaly with a 0.94 SD and is tracking towards waypoint 20S96E. MH370 passes over the Flight Route L894 which runs from waypoint RUNUT to waypoint POLUM and is used for flights to/from Perth. There are no more flight routes to cross south of this point. The flight routes between South Africa and Australia are much further south and out of range. At 22:22 UTC MH370 is detected by a WSPR SNR anomaly with a 1.76 SD and two others with 0.73 SD and 0.66 SD and is tracking towards waypoint 19S90E.

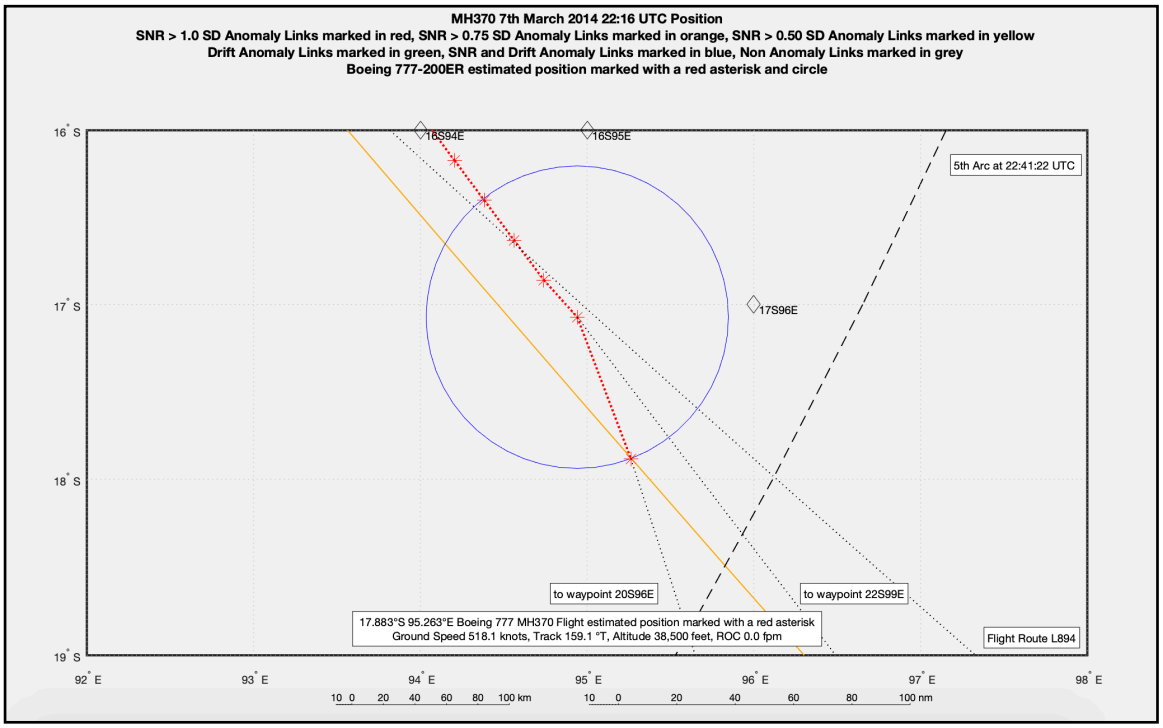

Figure 41: MH370 estimated position at 22:16 UTC.

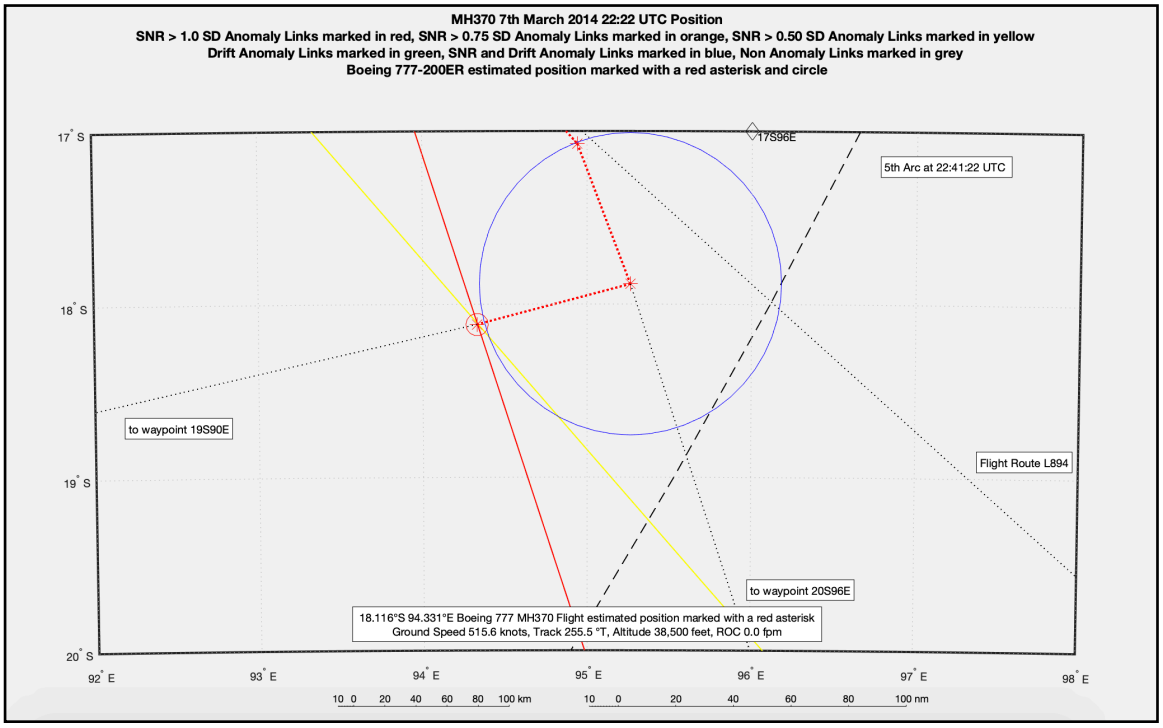

Figure 42: MH370 estimated position at 22:22 UTC.

At 22:30 UTC MH370 is detected by a WSPR SNR anomaly with a 1.13 SD and is tracking towards waypoint 22S94E. At 22:32 UTC MH370 is detected by a WSPR SNR anomaly with a 1.15 SD and is tracking towards waypoint 22S96E.

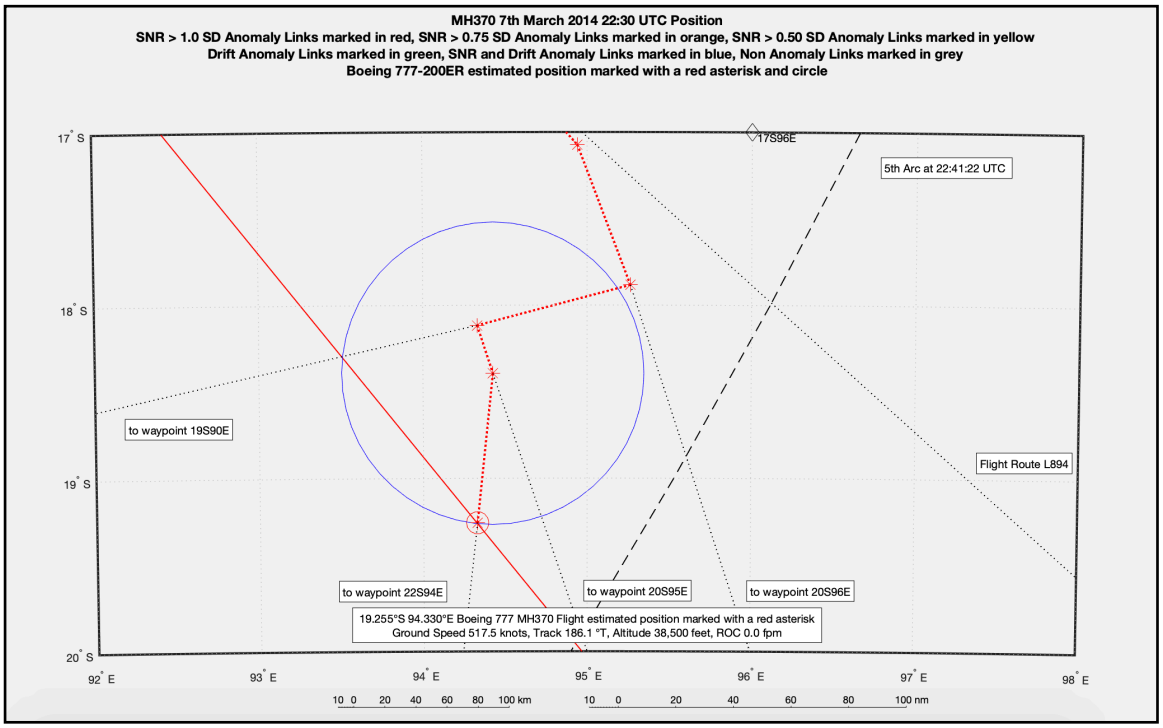

Figure 43: MH370 estimated position at 22:30 UTC.

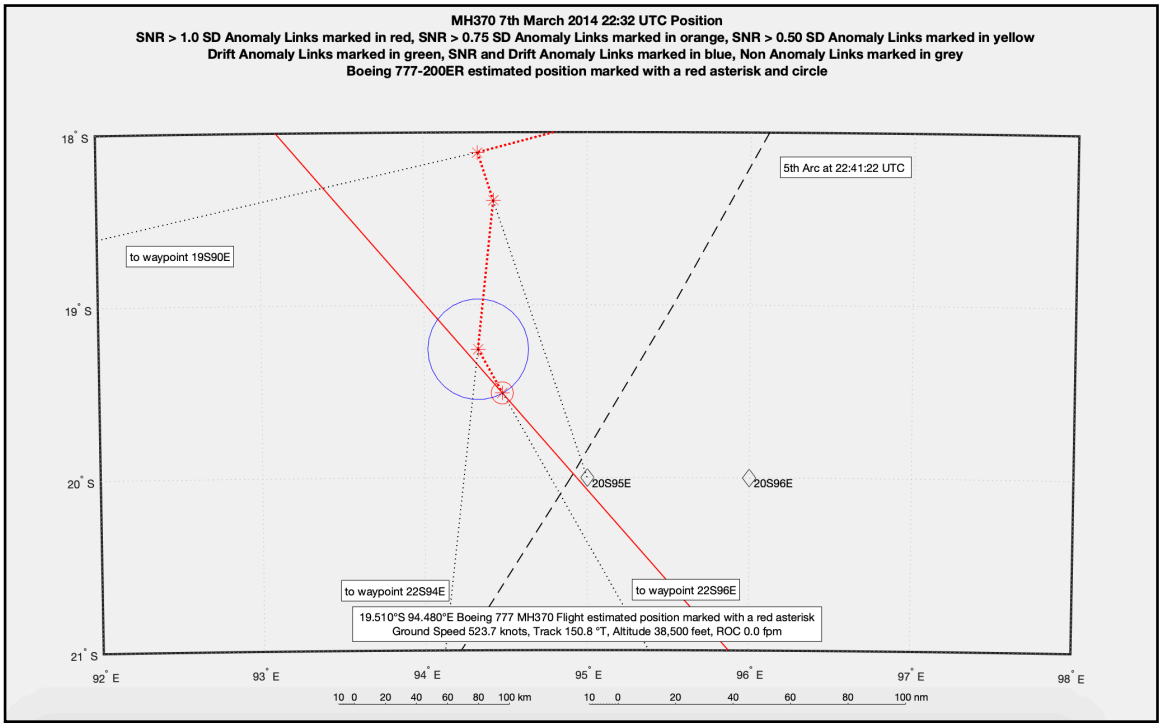

Figure 44: MH370 estimated position at 22:32 UTC.

At 22:36 UTC MH370 is detected by a WSPR SNR anomaly with a 2.80 SD and is tracking towards waypoint 22S96E. At 22:42 UTC MH370 is detected by a WSPR SNR anomaly with a 2.31 SD and is tracking towards waypoint 24S92E. The Inmarsat data is matched at the 5th Arc. At this stage the pilot no longer had sufficient fuel to reach Australia, but could still have turned back and reached Cocos Island. The pilot continues to change course every few minutes. The pilot possibly thinks that the Australian Over-the-Horizon Radar (OTHR) system JORN might have been tracking MH370. JORN was not operational at the time of the aircraft's disappearance.

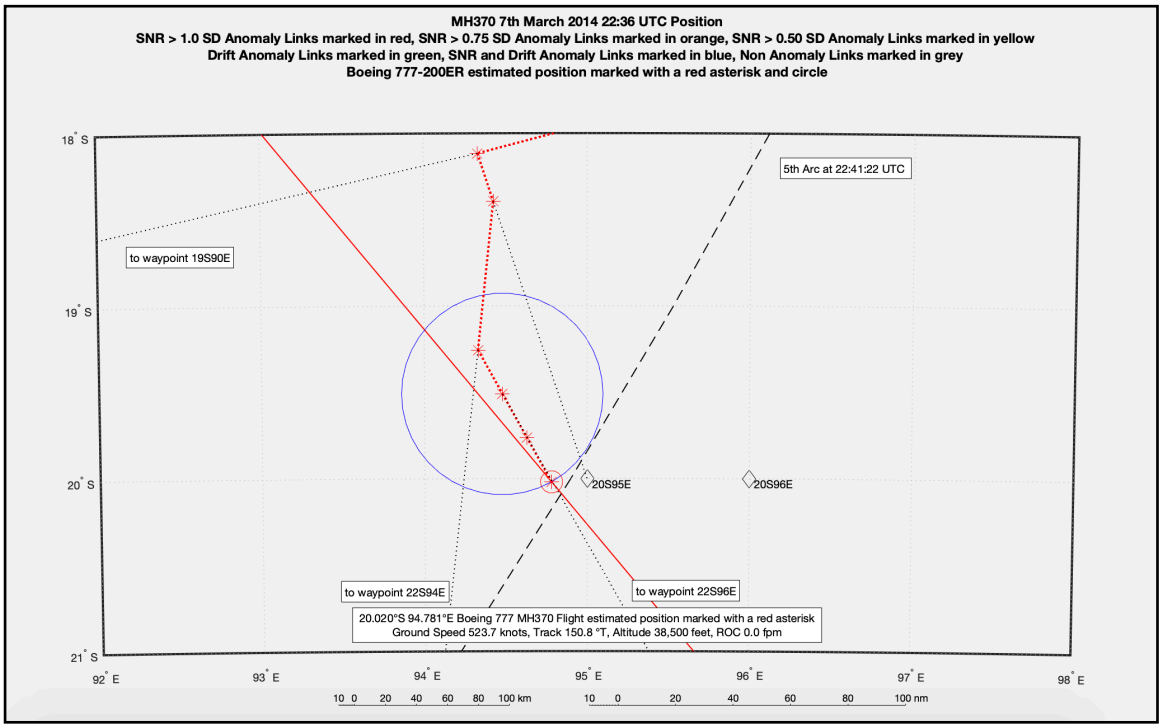

Figure 45: MH370 estimated position at 22:36 UTC.

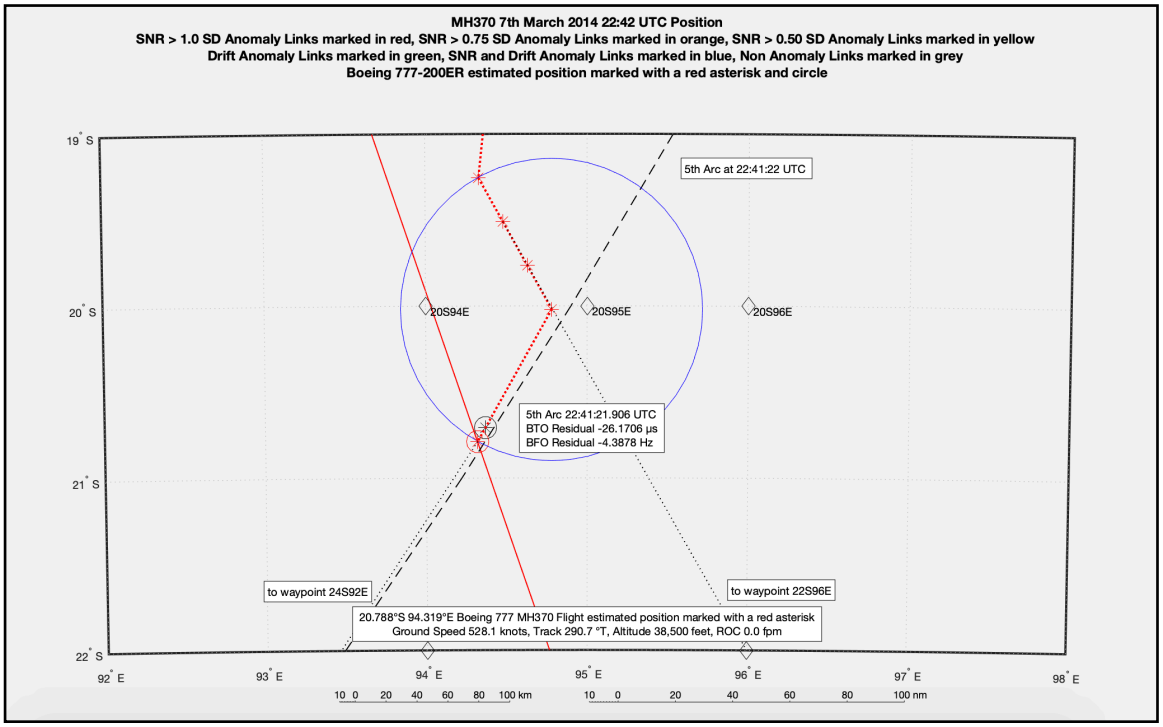

Figure 46: MH370 estimated position at 22:42 UTC.

At 22:44 UTC MH370 is detected by a WSPR SNR anomaly with a 0.86 standard deviation (SD) and is tracking towards waypoint 24S92E. At 22:48 UTC MH370 is detected by a WSPR SNR anomaly with a 2.65 SD and is tracking towards waypoint 26S96E.

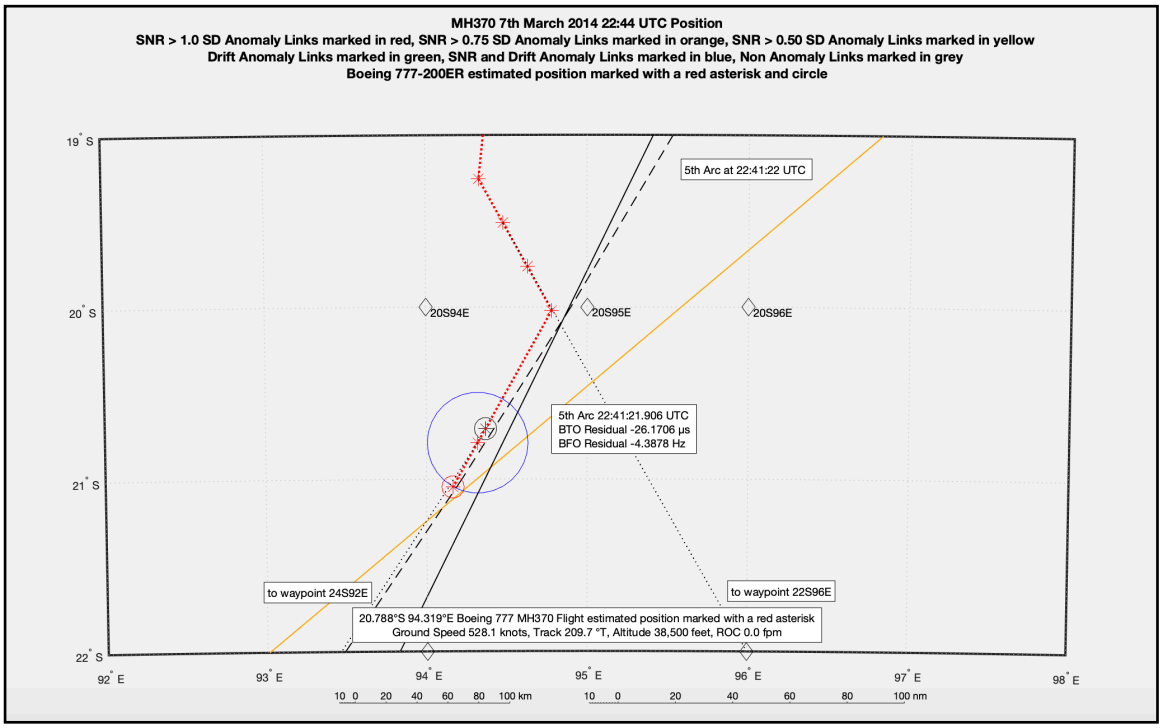

Figure 47: MH370 estimated position at 22:44 UTC.

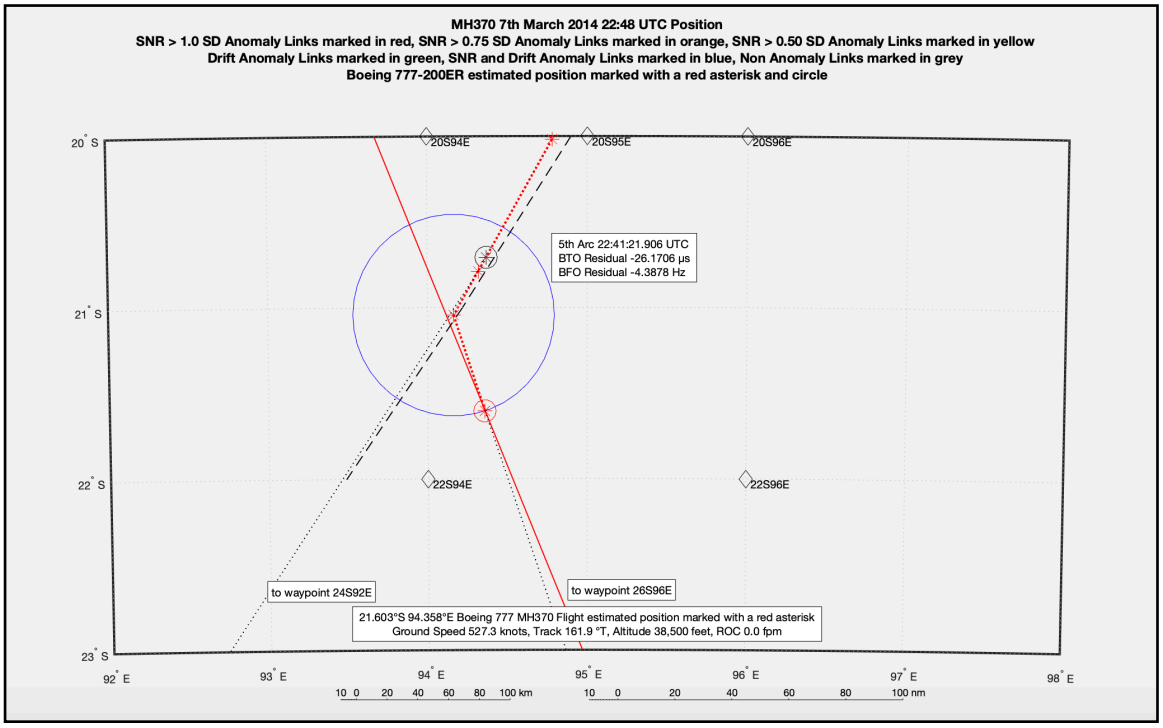

Figure 48: MH370 estimated position at 22:48 UTC.

At 22:52 UTC MH370 is detected by 3 WSPR SNR anomalies with 2.68, 1.23 and 0.85 SD and is tracking towards waypoint 21S98E. This point was subject of the worked example in section 5 above. At 22:58 UTC MH370 is detected by 2 WSPR SNR anomalies with 1.47 and 1.12 SD and is tracking towards waypoint 26S96E again.

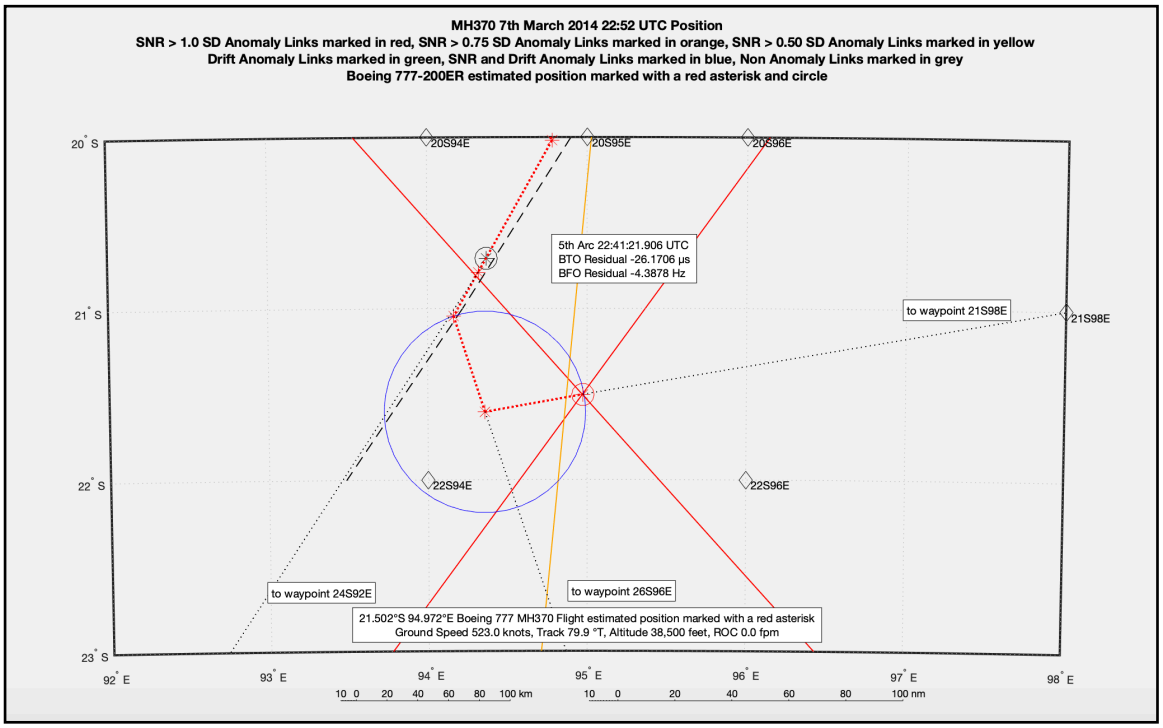

Figure 49: MH370 estimated position at 22:52 UTC.

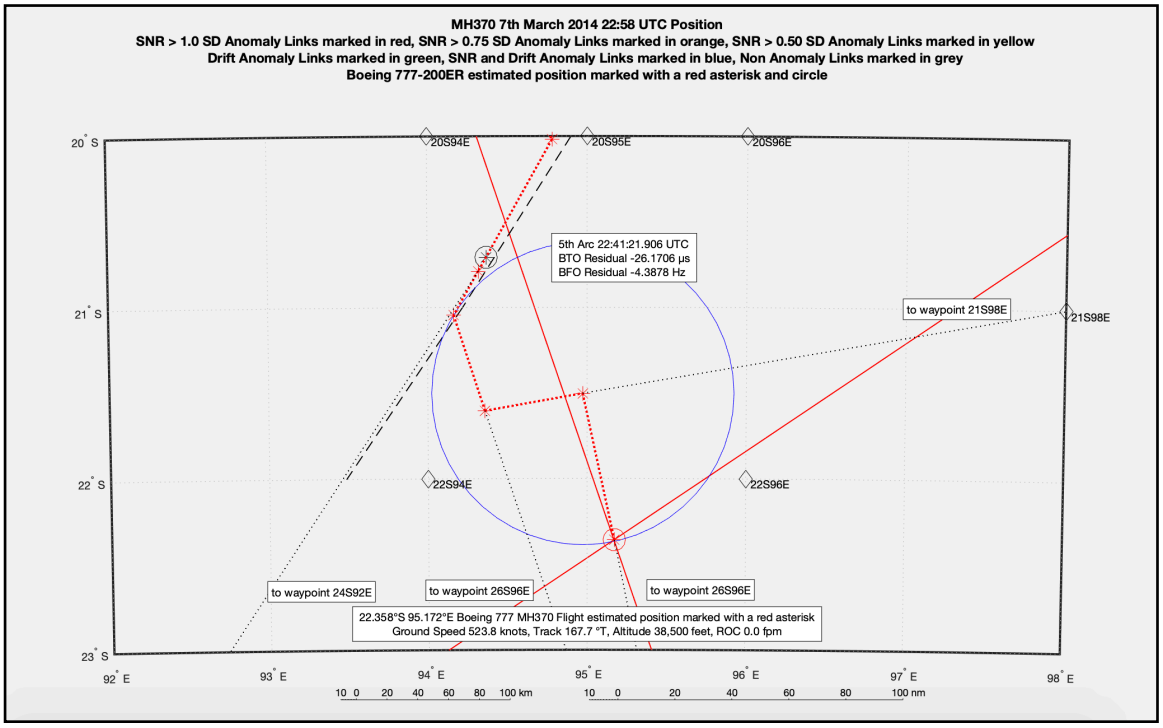

Figure 50: MH370 estimated position at 22:58 UTC.

Page 553 of 1738

At 23:00 UTC MH370 is detected by a WSPR SNR anomaly with 1.45 SD and is tracking towards waypoint 26S96E. At 23:02 UTC MH370 is detected by a WSPR SNR anomaly with 1.34 SD and is tracking towards waypoint 24S92E.

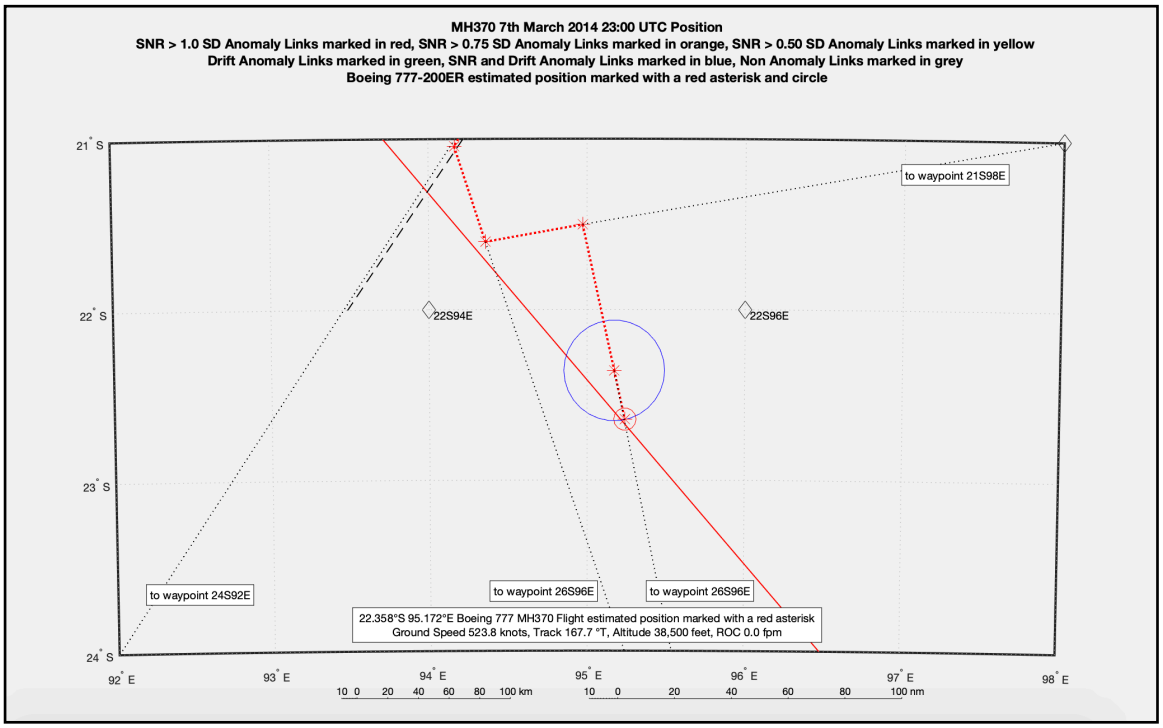

Figure 51: MH370 estimated position at 23:00 UTC.

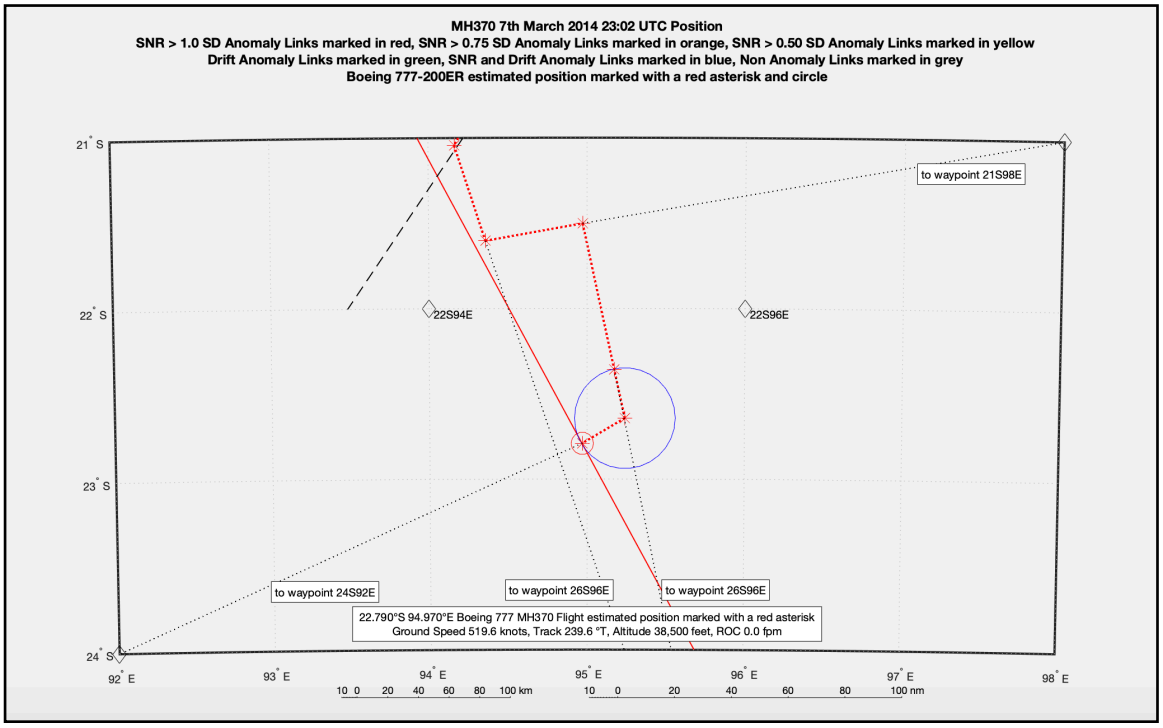

Figure 52: MH370 estimated position at 23:02 UTC.

At 23:04 UTC MH370 is detected by 3 WSPR SNR anomalies with 2.39, a drift of -1 Hz/min and another SNR anomaly of 0.94 SD and is tracking towards waypoint 23S92E. At 23:08 UTC MH370 is detected by 3 WSPR SNR anomalies with 2.27 and another SNR anomaly of 1.04 SD with a drift of -1 Hz/min and is tracking towards waypoint 38S94E.

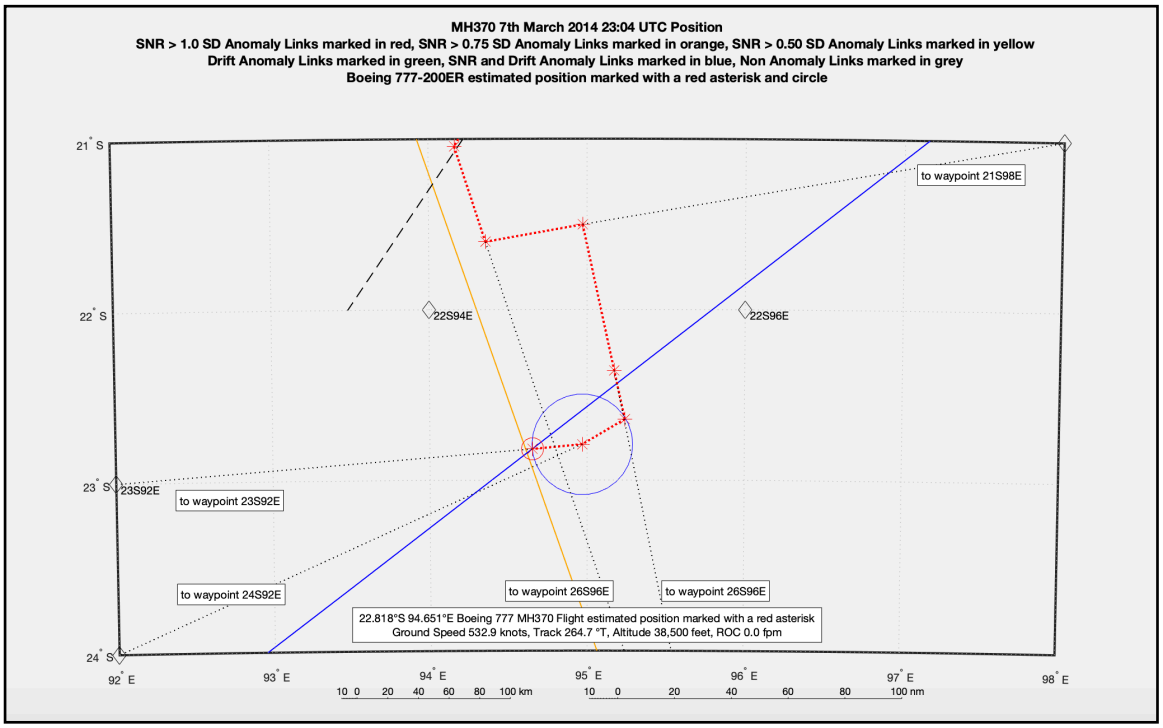

Figure 53: MH370 estimated position at 23:04 UTC.

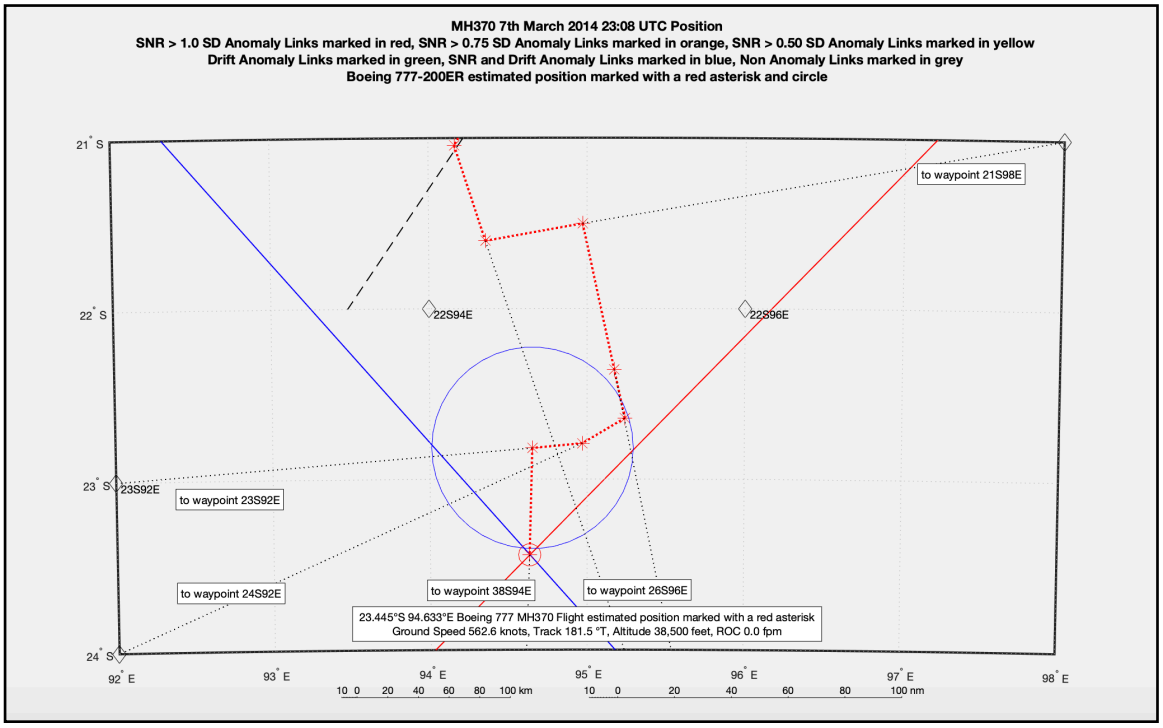

Figure 54: MH370 estimated position at 23:08 UTC.

At 23:12 UTC MH370 is detected by 3 WSPR SNR anomalies with 1.09, 1.04 and 0.95 SD as well as a drift of +1 Hz/min close to the turning point and is tracking towards waypoint 28S96E. At 23:14 UTC MH370 is detected by a WSPR SNR anomaly with a 2.41 SD and is tracking towards waypoint 30S101E. The Inmarsat data is matched during the SATCOM call at 23:14:01 UTC. At this point the estimated remaining fuel is 5,329 kg, with a range of around 922 km and is insufficient to reach either the Cocos Islands (1,348 km) or Learmonth Airport, Western Australia (1,967 km).

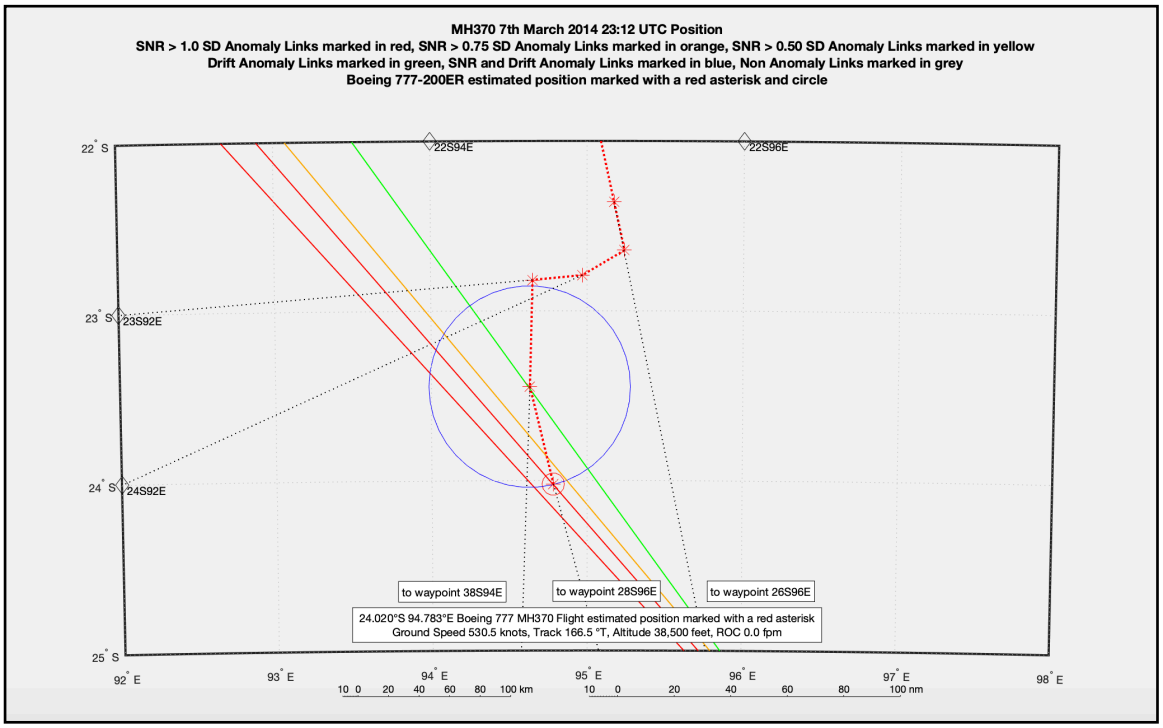

Figure 55: MH370 estimated position at 23:12 UTC.

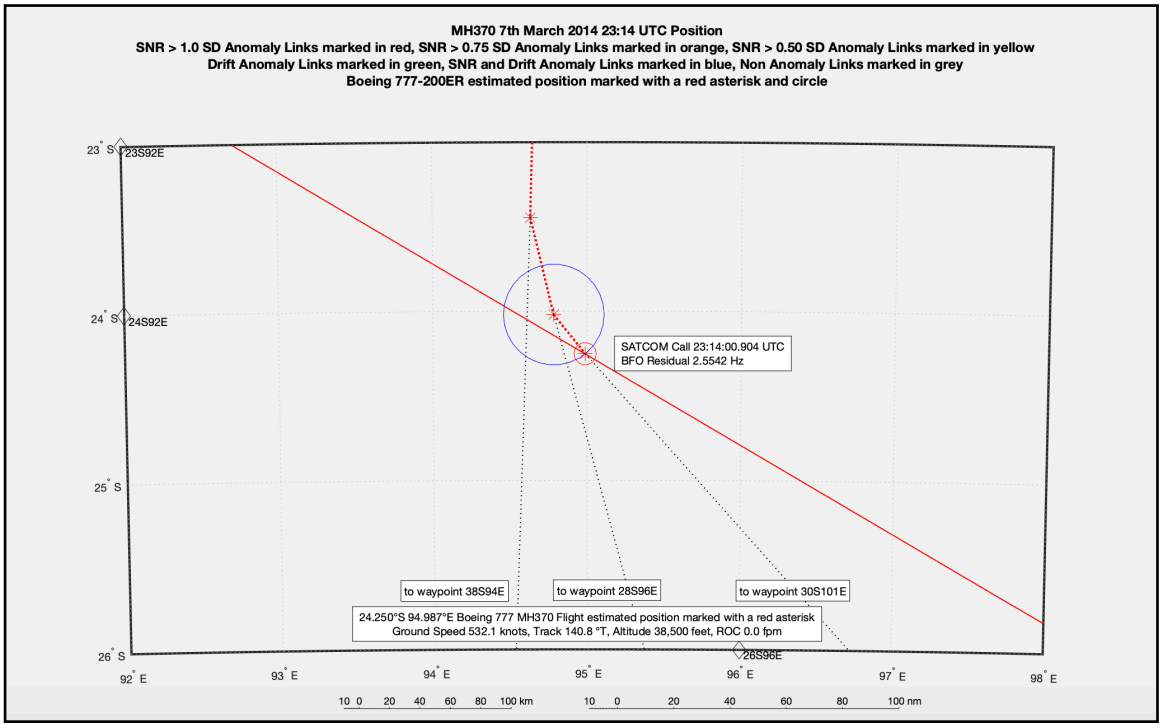

Figure 56: MH370 estimated position at 23:14 UTC.

At 23:18 UTC MH370 is detected by 3 WSPR anomalies with 2 SNR anomalies of 1.01 and 0.89 standard deviation (SD) from the mean over ± 3 hours as well as a drift anomaly at -1 Hz/minute and is tracking towards waypoint 26S96E again. At 23:20 UTC MH370 is detected by 5 WSPR SNR anomalies with a 1.33, 1.32, 1.11, 1.07 and 1.03 SD and is tracking towards waypoint 26S98E. The aircraft's ground speed slows by 33.7 knots over a 4 minute period indicative of a step climb of 2,000 feet to FL405 (40,500 feet). The change in ground speed cannot be explained by a change in the wind speed or wind direction.

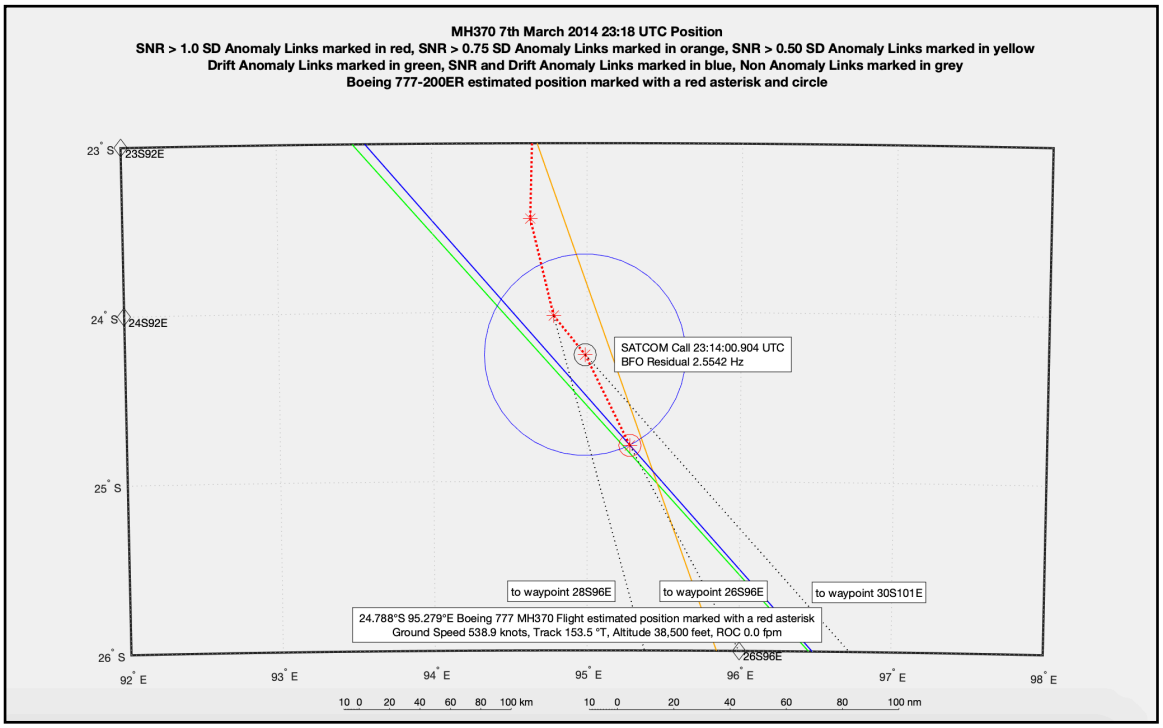

Figure 57: MH370 estimated position at 23:18 UTC.

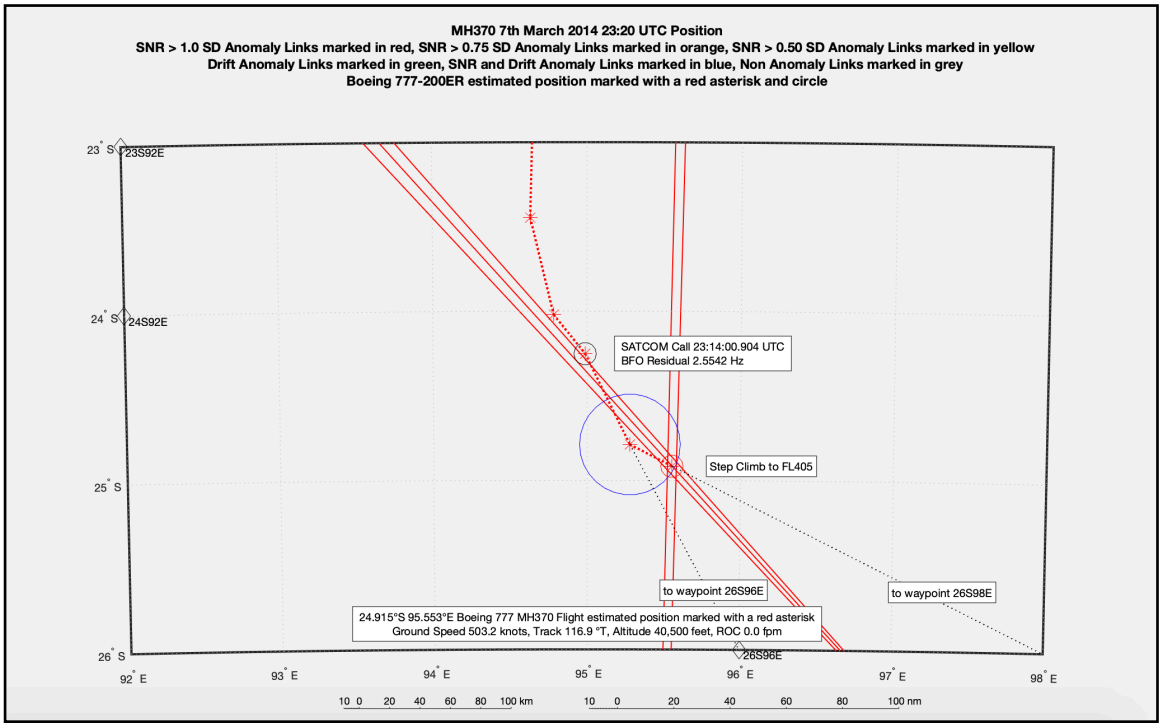

Figure 58: MH370 estimated position at 23:20 UTC.

At 23:22 UTC MH370 is detected by 5 WSPR SNR anomalies with a 1.38, 1.35, 1.07, 0.83 and 0.83 SD and is tracking towards waypoint 26S96E again. At 23:26 UTC MH370 is detected by 2 WSPR SNR anomalies with a 1.64 and 1.61 SD and is tracking towards waypoint 27S98E.

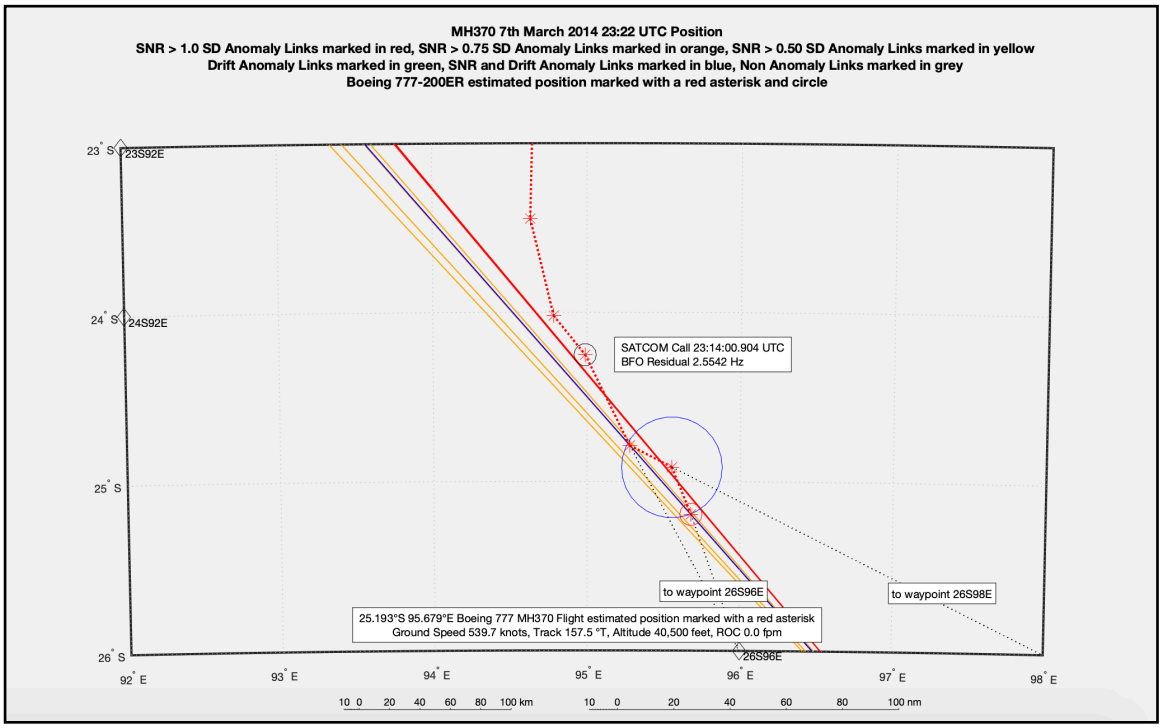

Figure 59: MH370 estimated position at 23:22 UTC.

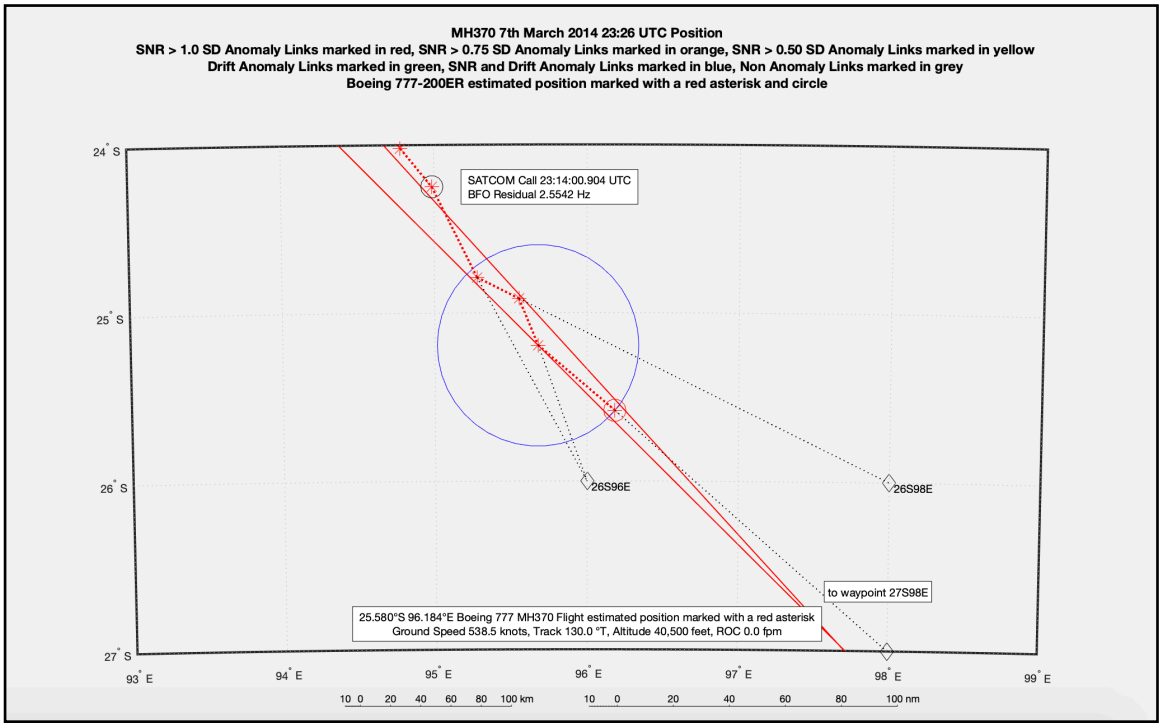

Figure 60: MH370 estimated position at 23:26 UTC.

At 23:28 UTC MH370 is detected by 3 WSPR SNR anomalies with a 2.00, 1.50 and 1.43 SD and is tracking towards waypoint 27S98E. At 23:30 UTC MH370 is detected by 2 WSPR SNR anomalies with a 1.48 and 1.24 SD and is tracking towards waypoint 27S98E.

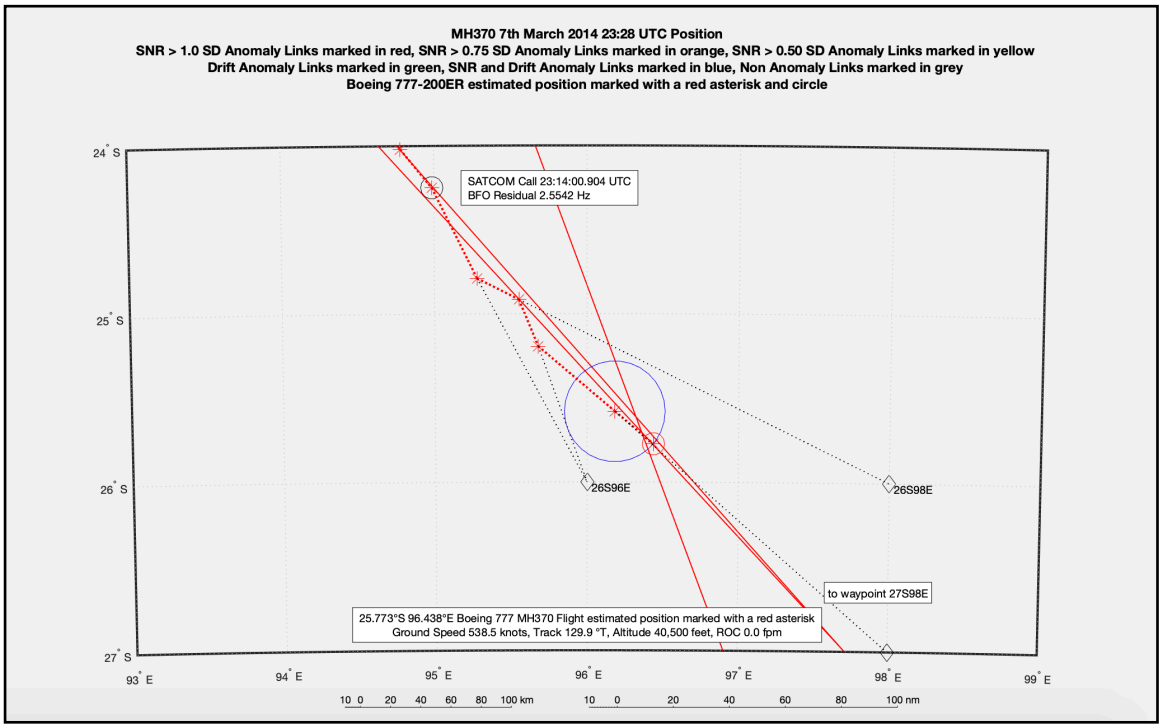

Figure 61: MH370 estimated position at 23:28 UTC.

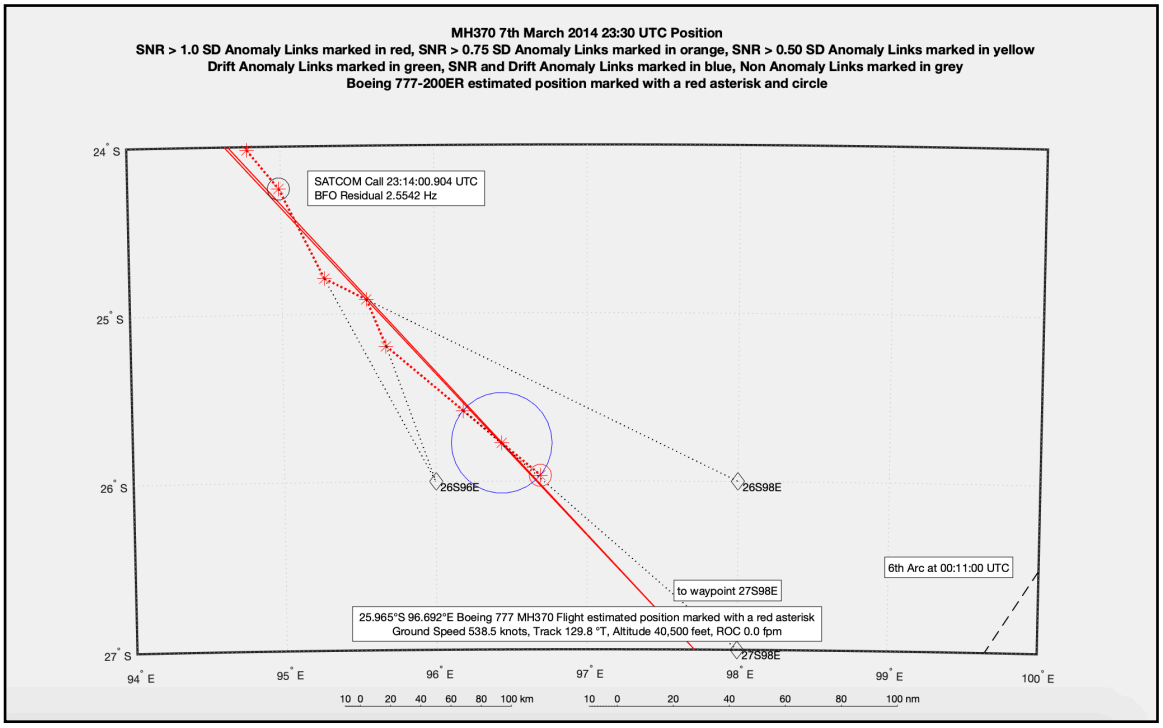

Figure 62: MH370 estimated position at 23:30 UTC.

At 23:32 UTC MH370 is detected by 2 WSPR SNR anomalies with a 2.08 and 1.89 SD and is tracking towards waypoint 27S98E. At 23:36 UTC MH370 is detected by a WSPR SNR anomaly with a 1.51 SD and is tracking towards waypoint 27S98E.

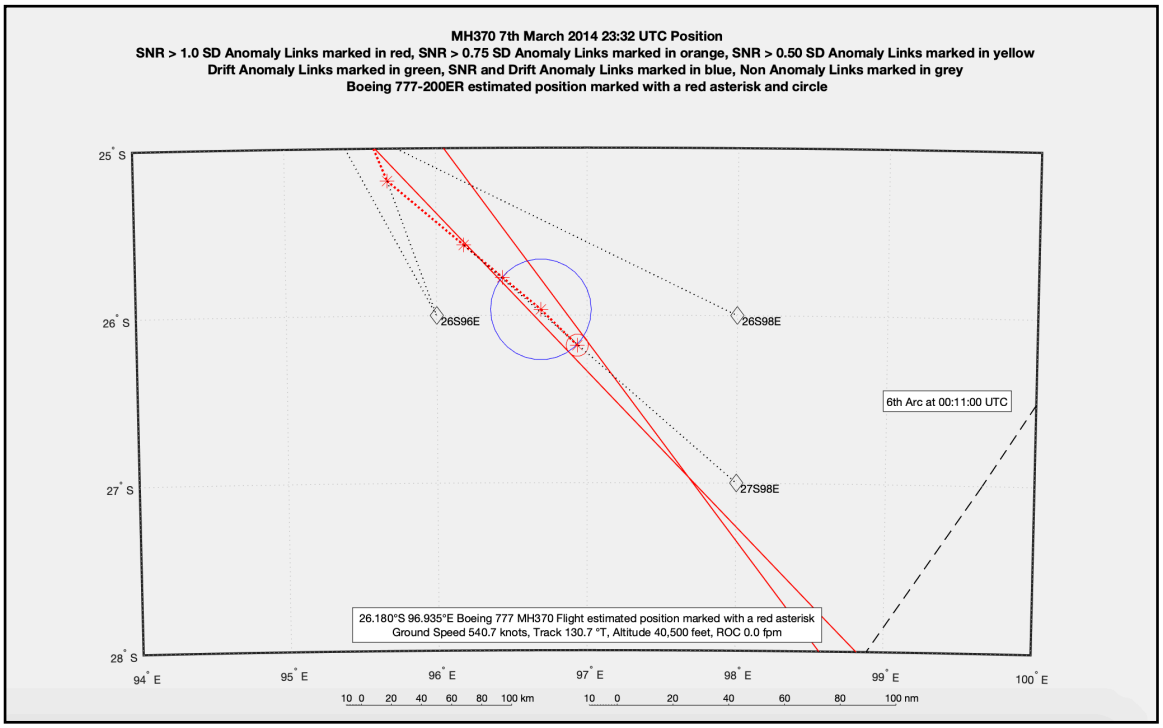

Figure 63: MH370 estimated position at 23:32 UTC.

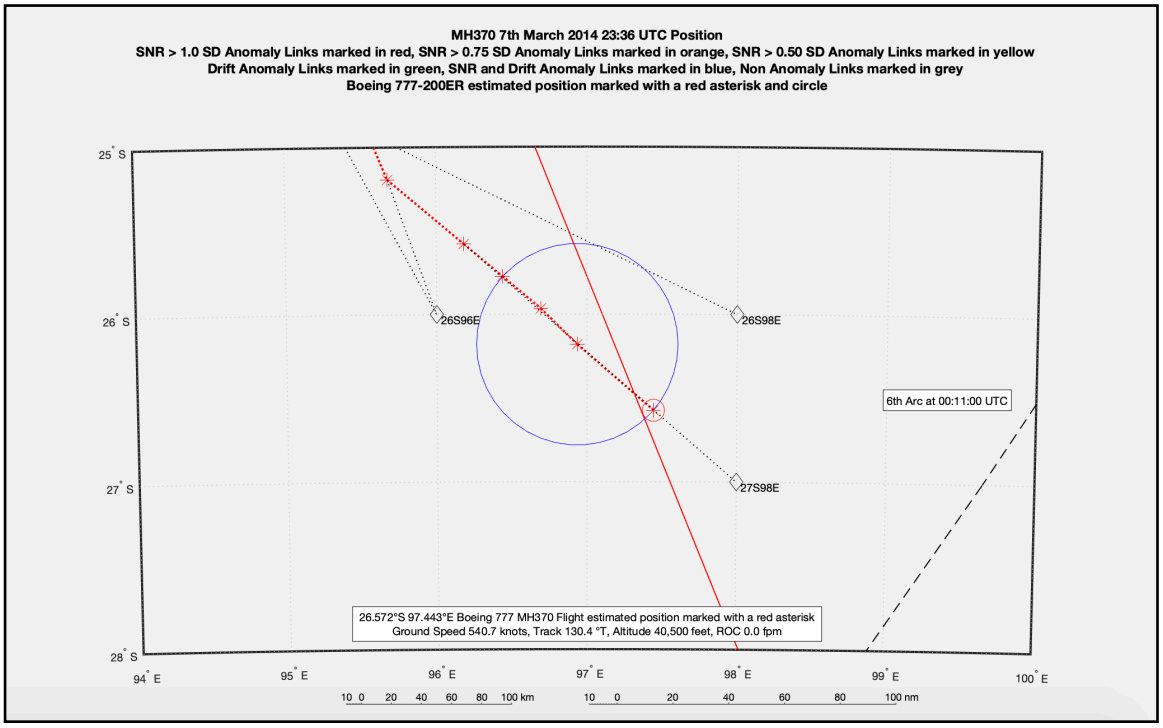

Figure 64: MH370 estimated position at 23:36 UTC.

At 23:38 UTC there was a position indicator at the intersection of 4 WSPR SNR anomalous links with standard deviations (SD) of 1.97, 1.76, 1.69 and 1.66 from the mean over ± 3 hours and MH370 is tracking towards waypoint 30S99E. At 23:40 UTC there was a position indicator at the intersection of 3 WSPR SNR anomalous links with 1.54, 1.08 and 0.81 SD as well as 1 WSPR drift anomaly of -1 Hz/minute and MH370 is still tracking towards waypoint 30S99E.

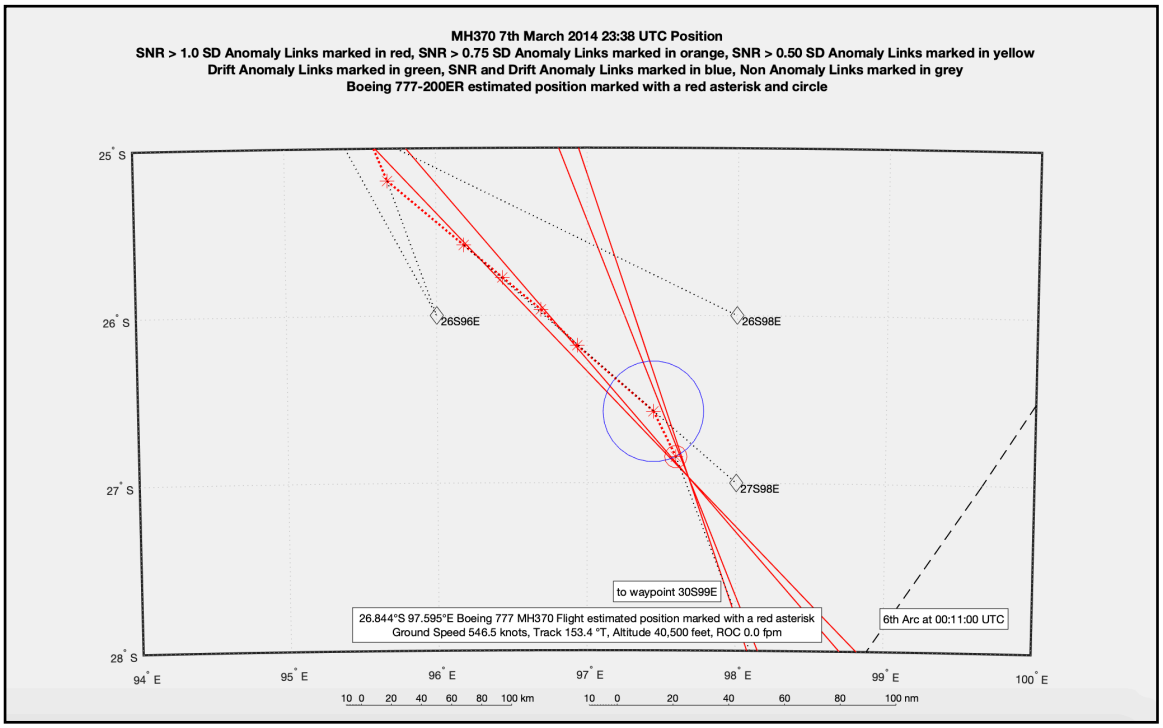

Figure 65: MH370 estimated position at 23:38 UTC.

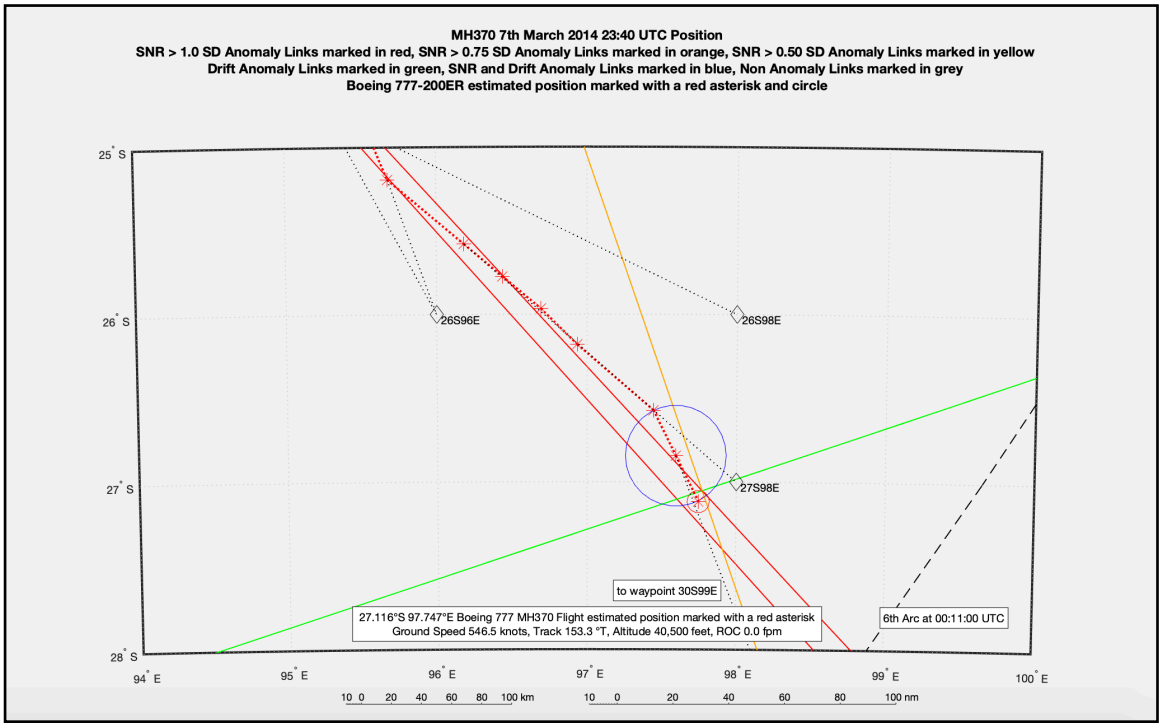

Figure 66: MH370 estimated position at 23:40 UTC.

At 23:44 UTC there was a progress indicator with 1 WSPR dual SNR and drift anomalous link with 0.82 and -1 Hz/minute. At the same time there were 3 WSPR SNR anomalous links with 1.43, 0.76 and a third again with a 0.76 SD. MH370 is tracking towards waypoint 28S99E. At 23:46 UTC there was a progress indicator with 2 WSPR SNR anomalous links with 1.80 and 0.93 SD and MH370 is tracking towards waypoint 29S98E.

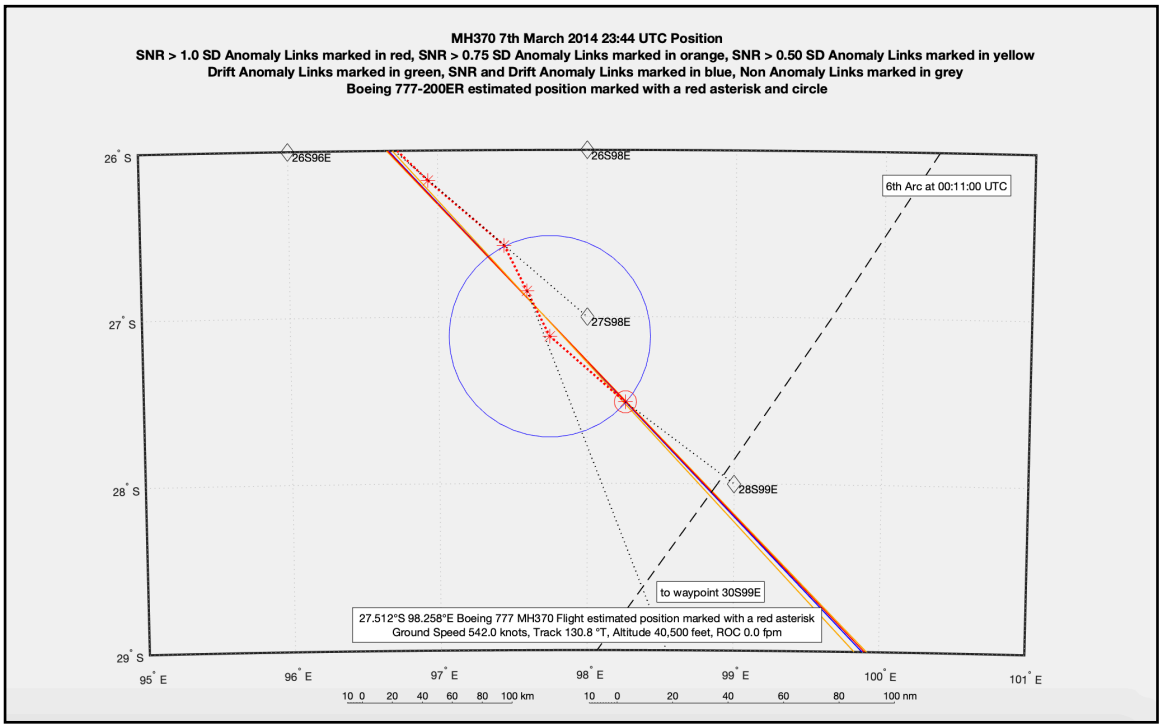

Figure 67: MH370 estimated position at 23:44 UTC.

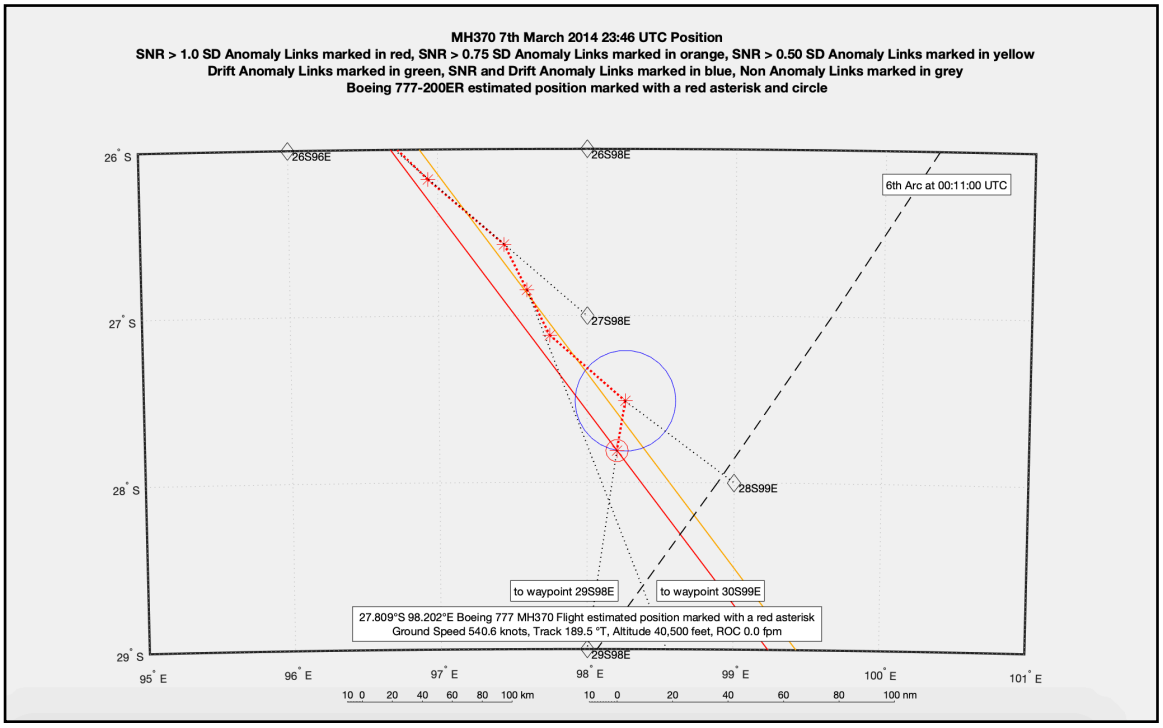

Figure 68: MH370 estimated position at 23:46 UTC.

At 23:48 UTC there was a position indicator at the intersection of 3 WSPR SNR anomalous links with 1.89, 1.56 and 0.98 SD and MH370 is tracking towards waypoint 30S100E. At 23:50 UTC there was a position indicator at the intersection of 5 WSPR SNR anomalous links with 2.02, 1.51, 1.05, 1.04 and 0.90 SD and MH370 is tracking towards waypoint MERIB, which is close to Perth, Australia.

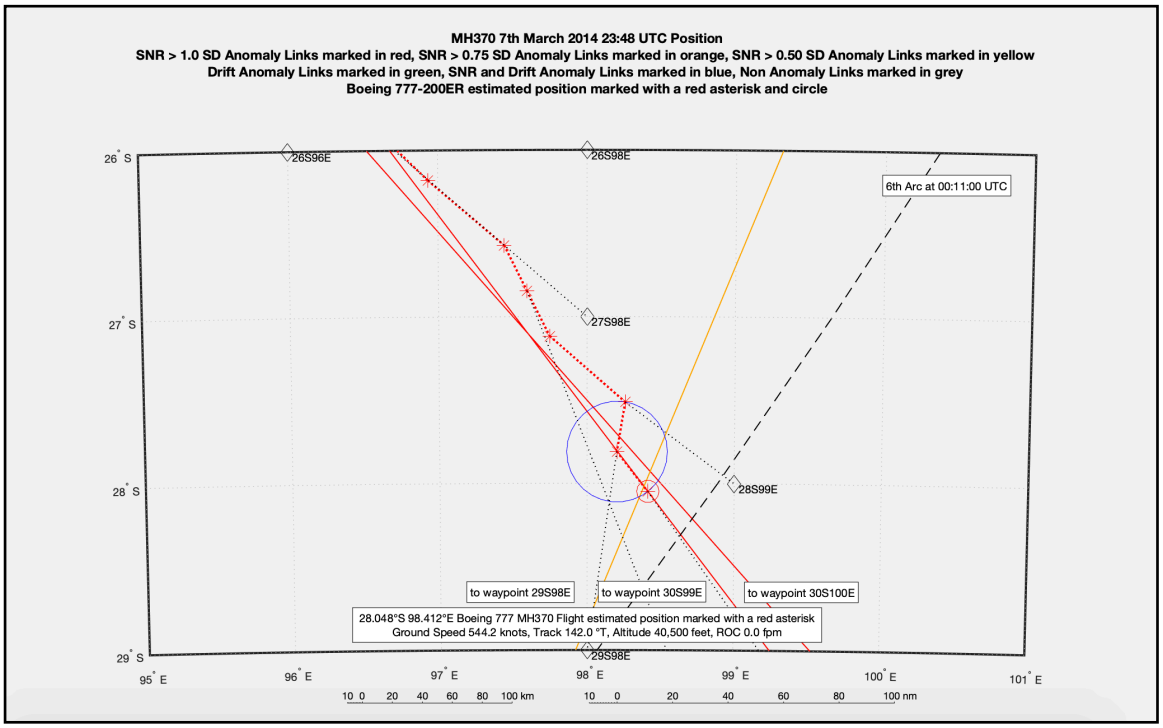

Figure 69: MH370 estimated position at 23:48 UTC.

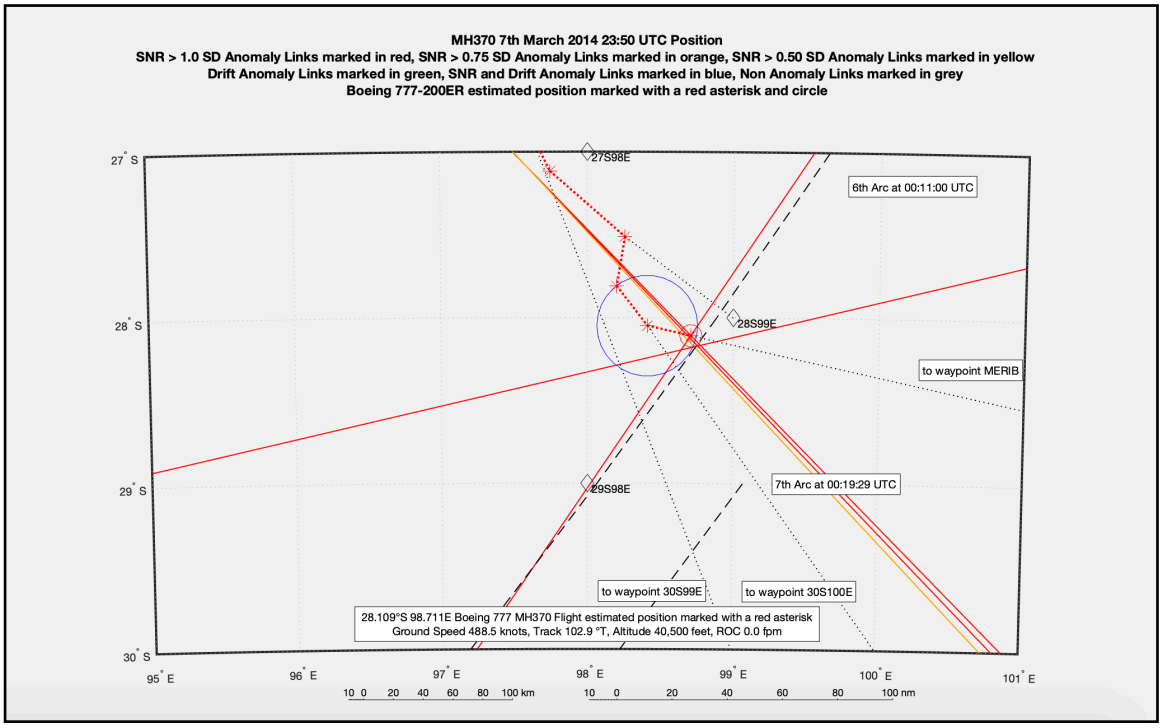

Figure 70: MH370 estimated position at 23:50 UTC.

At 23:54 UTC there was a progress indicator with 1 WSPR SNR anomalous link with 0.94 SD and MH370 is tracking towards waypoint 29S100E. At 23:56 UTC there was a position indicator at the intersection of 2 WSPR SNR anomalous links with 1.93 and 1.58 SD and MH370 is tracking towards waypoint 32S98E. One possible explanation of the number of turns is that the pilot was intermittently using the TCAS System to see what other traffic was in the vicinity. The pilot would be detected by any other aircraft within range as soon as the TCAS system was switched on and therefore wanted to always be on a different track in case the position and track were reported.

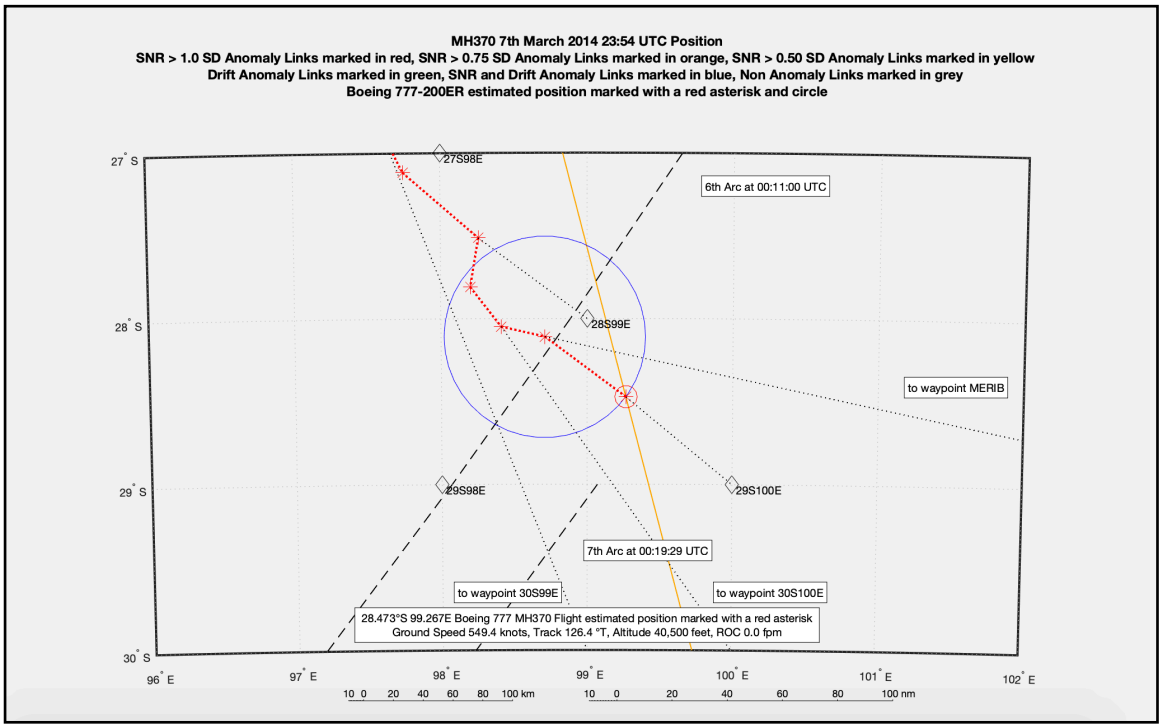

Figure 71: MH370 estimated position at 23:54 UTC.

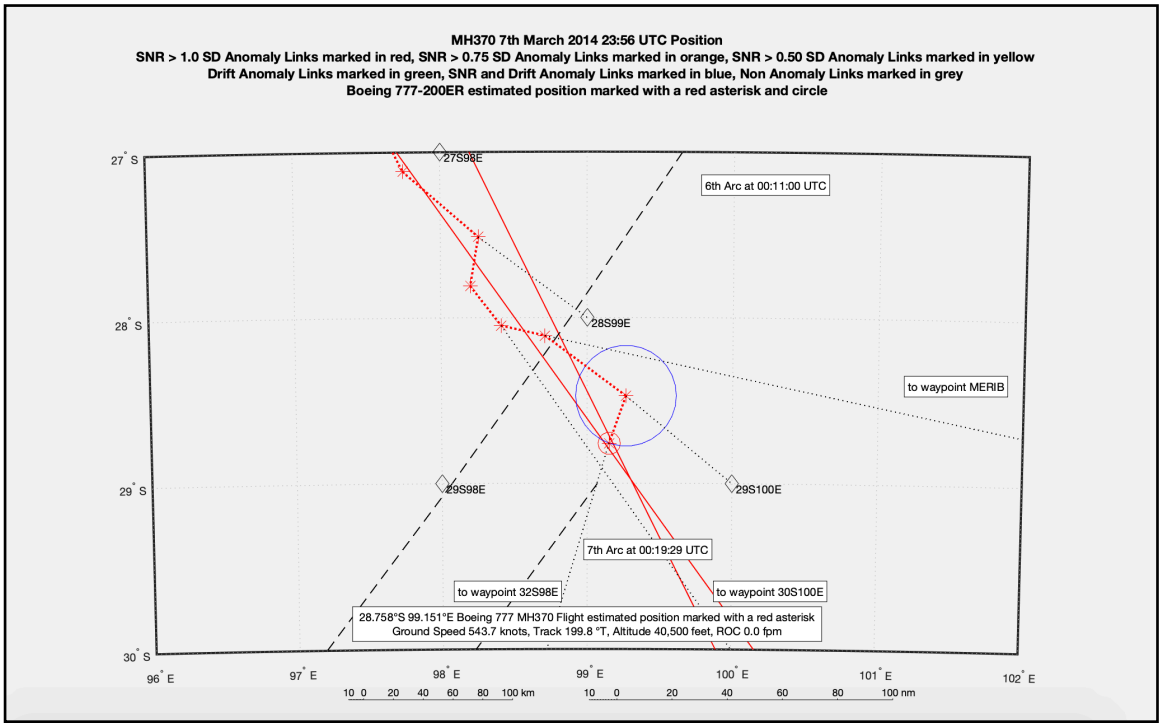

Figure 72: MH370 estimated position at 23:56 UTC.

At 23:58 UTC there was a position indicator at the intersection of 2 WSPR SNR anomalous links with 2.00 and 1.22 SD and indications are that MH370 is starting to circle. At this stage there was an estimated 432.1 kg of fuel remaining with a fuel range of 70.4 nmi until the right engine flame out and 132.6 nmi until the left engine flame out. At 00:00 UTC there was a position indicator at the intersection of 2 WSPR SNR anomalous links with 1.94 and 1.59 SD.

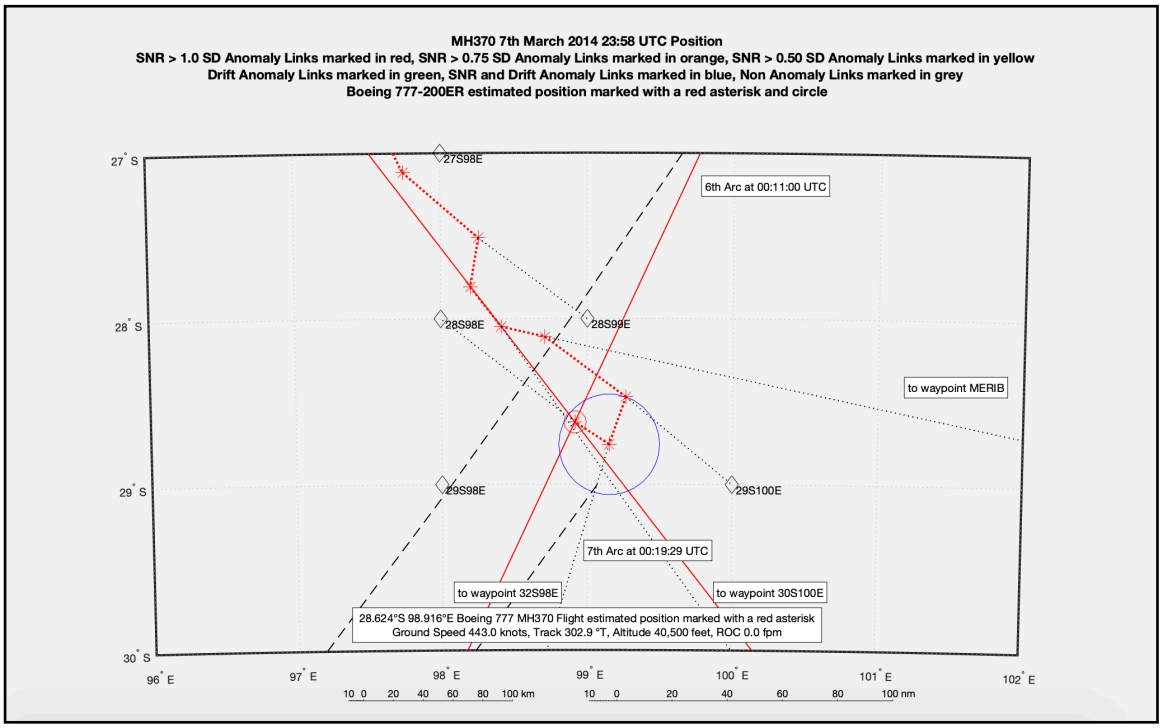

Figure 73: MH370 estimated position at 23:58 UTC.

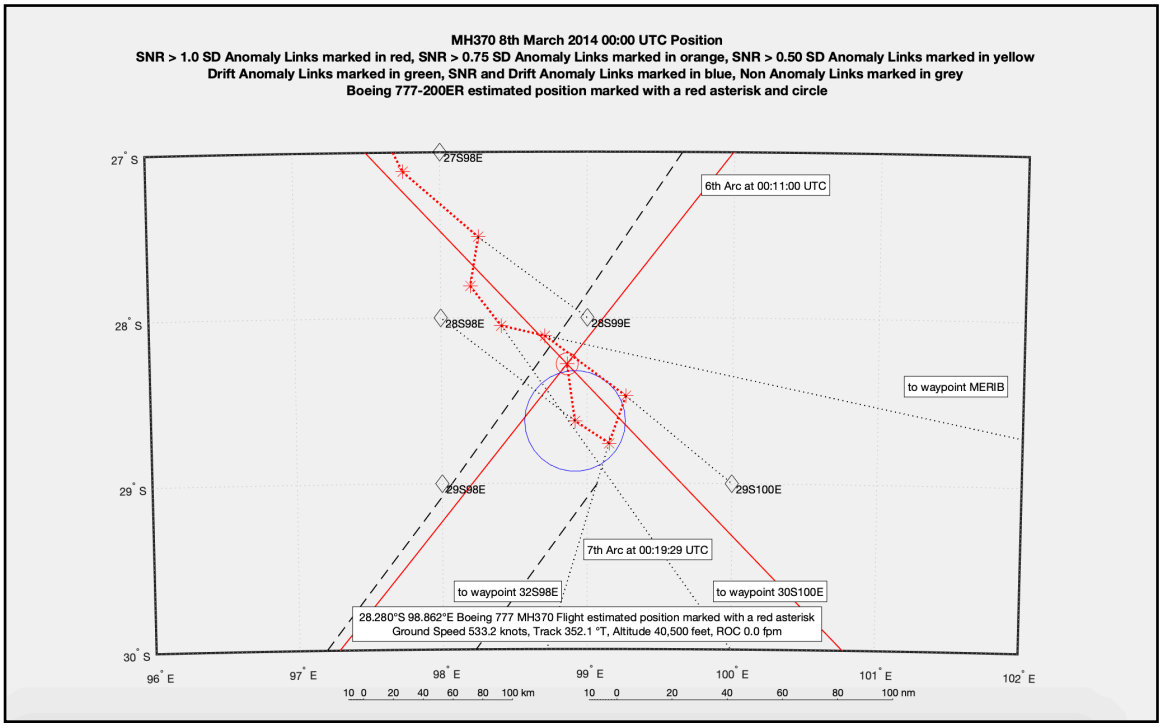

Figure 74: MH370 estimated position at 8th March 2014 00:00 UTC.

At 00:04 UTC there was a progress indicator with 6 WSPR SNR and drift anomalous links with 2.04, 1.43, 1.43, 1.03 SD as well as -2 Hz/minute, 0.96 and 0.95 SD. At 00:12 UTC there was a progress indicator with 2 WSPR SNR anomalous links with 2.31 and 1.44 SD. The Inmarsat data is matched at the 6th Arc. The right engine flameout is estimated at 00:07:27 UTC and the left engine flame out at 00:16:38 UTC.

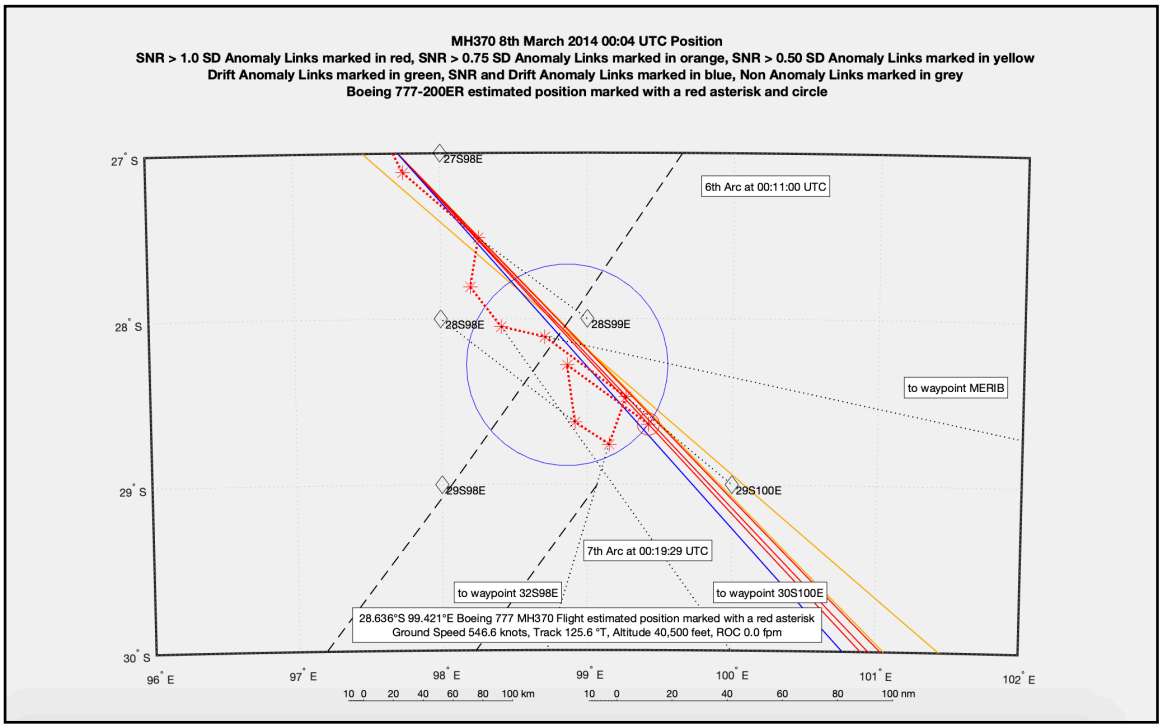

Figure 75: MH370 estimated position at 8th March 2014 00:04 UTC.

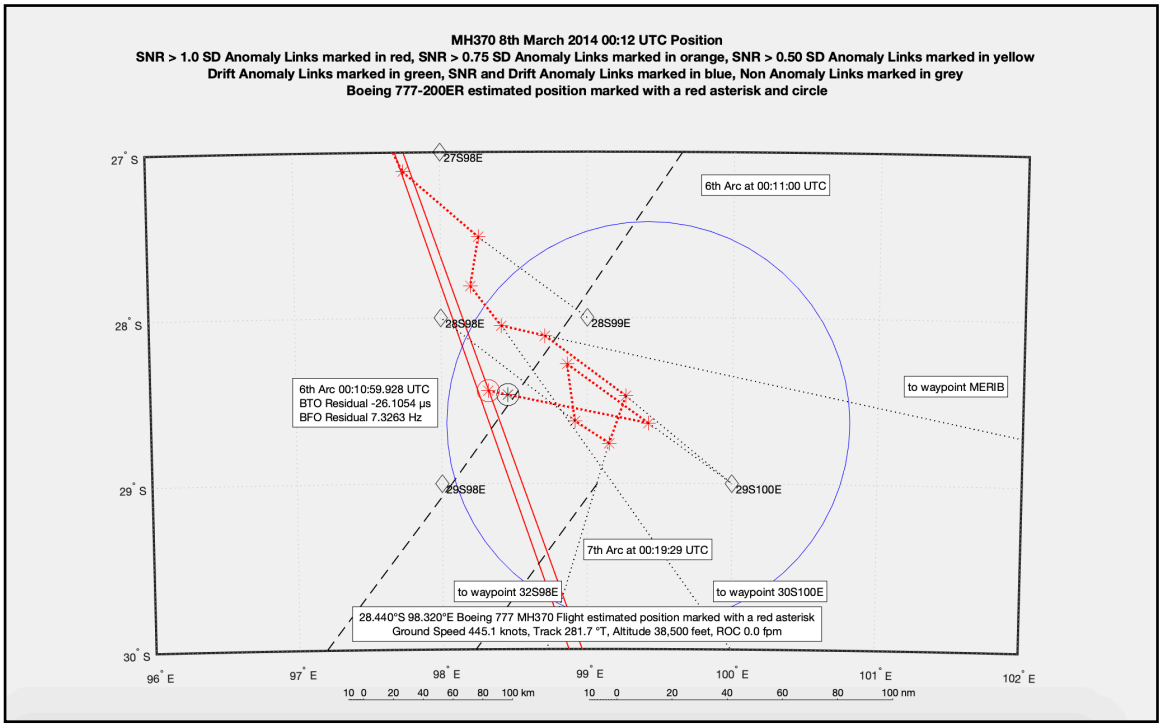

Figure 76: MH370 estimated position at 00:12 UTC.

At 00:16 UTC there was a position indicator at the intersection of 2 WSPR SNR anomalous links with 1.41 and 1.13 SD. At 00:20 UTC there was a position indicator at the intersection of 2 WSPR SNR anomalous links with 1.64 and 1.19 SD. The Inmarsat data is matched at the 7th Arc at both 00:19:29 UTC and 00:19:37 UTC (Note: The BFO residual at the 7th Arc has been zeroised to obtain the rate of descent).

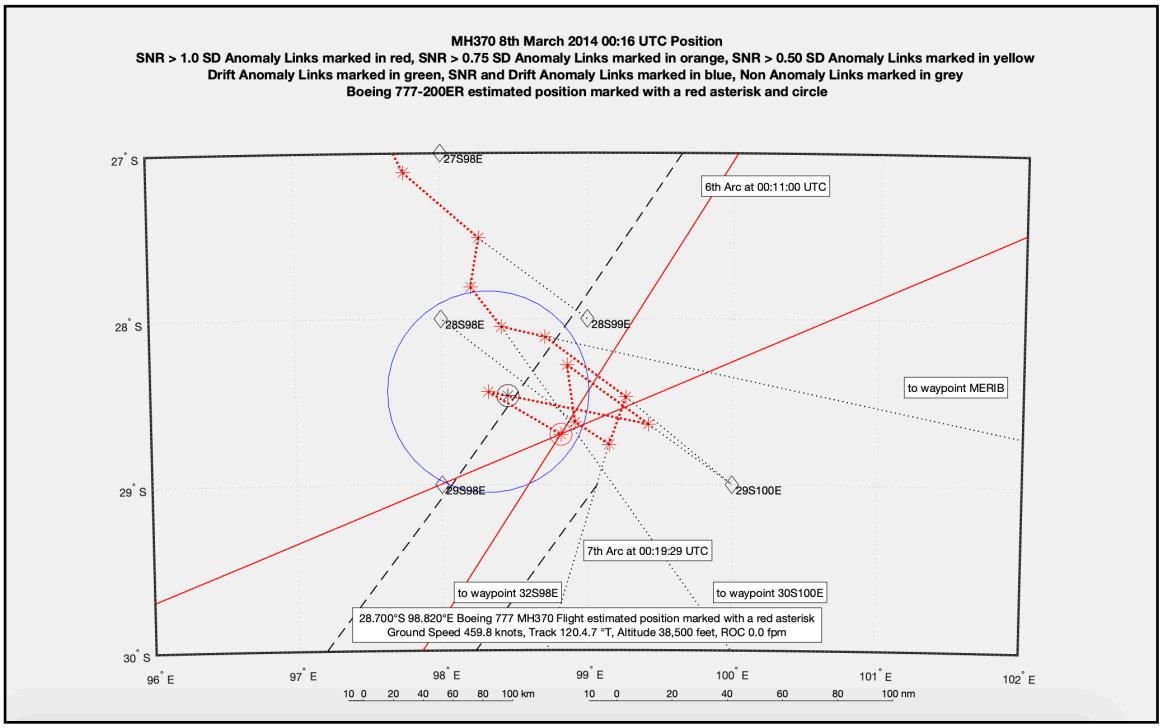

Figure 77: MH370 estimated position at 00:16 UTC.

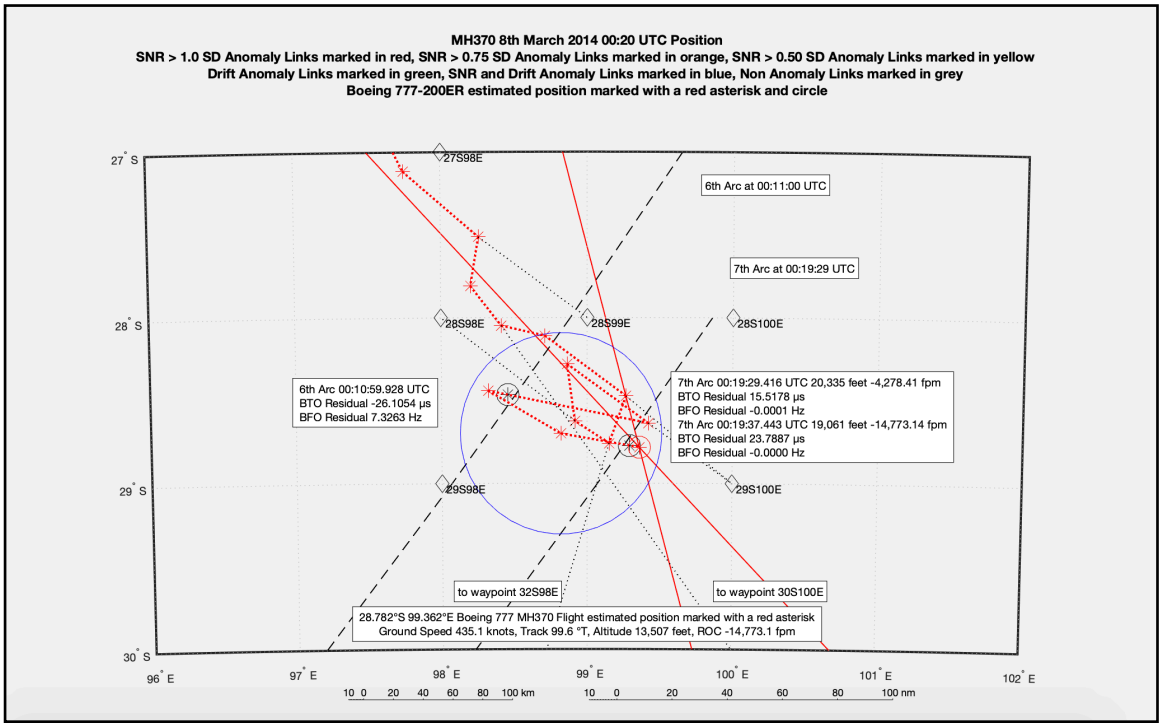

Figure 78: MH370 estimated position at 00:20 UTC.

The IFE signal was not received at 00:21:06 UTC because either the IFE was switched off or the IFE and SDU were no longer powered by the APU or both. At 00:26 UTC there was a position indicator at the intersection of 3 independent WSPR SNR anomalous links with 1.67, 1.46 and 1.15 SD from 3 separate transmitters to 3 separate receivers (NH7SR - KE7KRF, KK4U - YV4GJN, HB9CZF - W4MO). This result indicates a possible recovery from the accelerating rate of descent of -14,773 fpm at 00:19:37 UTC. At 00:28 UTC there was a progress indicator with 4 WSPR SNR anomalous links but all from the same transmitter W4MO.

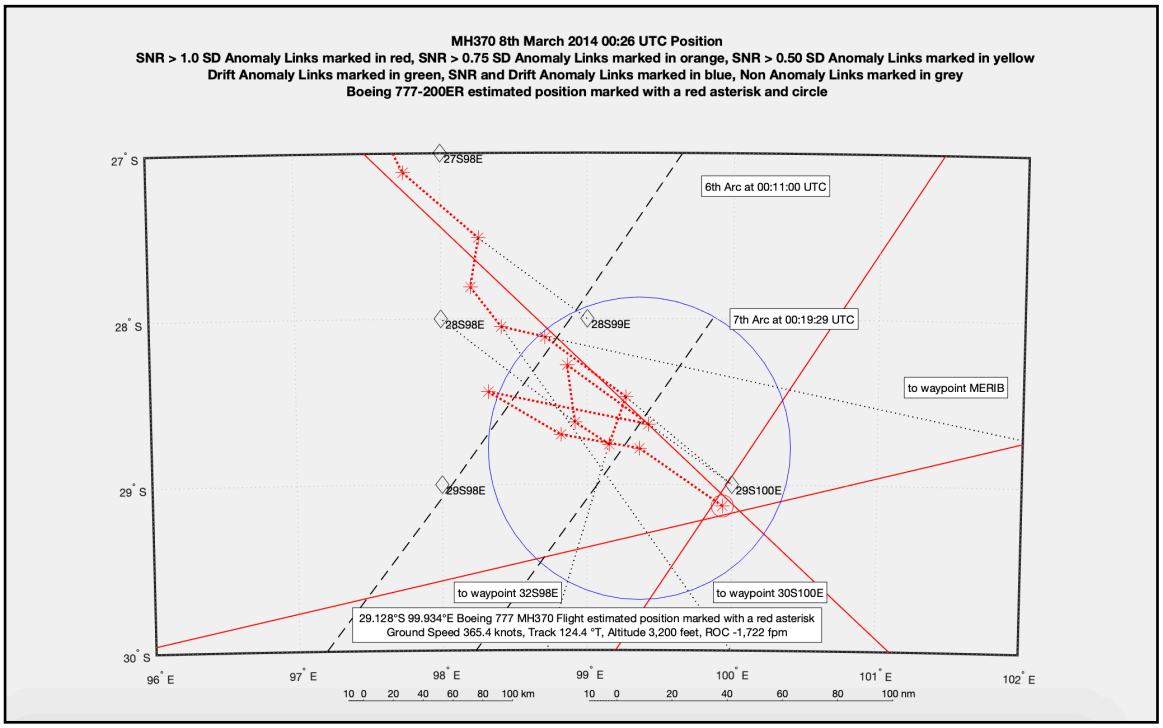

Figure 79: MH370 estimated position at 00:26 UTC.

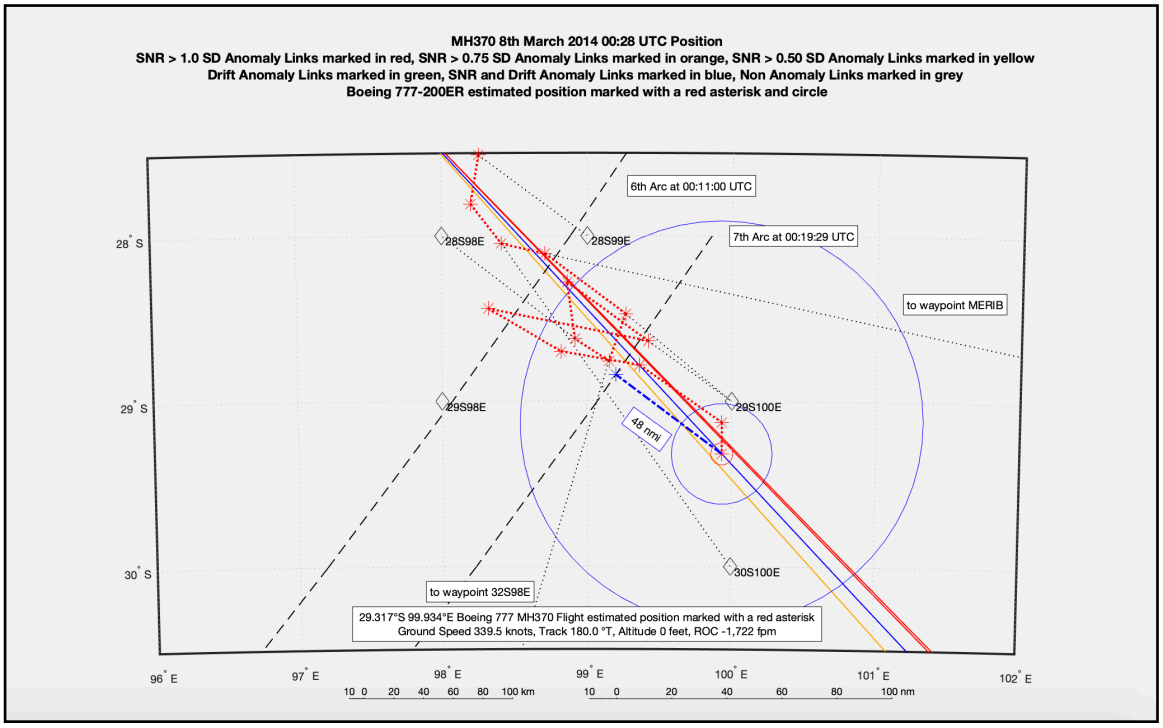

Figure 80: MH370 estimated position at 00:28 UTC.

Boeing performed 10 end of flight simulations with various criteria of starting altitude, ground speed, autopilot disengagement timing at 1st engine flameout or 2nd engine flameout and turbulence setting. In 5 cases (Case 3, 4, 5 ,6 and 10) the aircraft recovered from a rate of descent of over -15,000 fpm. In Case 5 the aircraft only recovered after the 11th swoop right at the end.

The average for Case 3, 4, 6 and 10 was a glide range of 58.5 nmi and glide duration of 471.8 seconds. The average flight duration from the point of first reaching a rate of descent of -15,000 fpm was a further 129.5 seconds. This would imply a crash at around 00:21:46 UTC. With an active pilot this time could be extended to 00:27:51 UTC, depending on the horizontal ground speed and assuming a 19° glide slope and average altitude recovery of 19,636 feet after the first descent from 40,000 feet (for Case 6 the start altitude was 35,000 feet).

There were no further WSPR anomalies that align to a possible flight path of MH370 at 00:30 UTC, 00:32 UTC and 00:34 UTC. A wide scale search at 00:34 UTC revealed only one WSPR anomaly at 30.300°S 99.650°E just inside the outer edge of the least likely search area marked in a pale yellow colour. This anomaly was discarded because it was 60.7 nmi further south than the last anomaly at 00:28 UTC on a bearing of 194.1°T, requiring an average ground speed of 607 knots to reach this position and another recovery from a high descent rate.

The crash location probability map is centred on the estimated position of MH370 at 00:20 UTC, with a possible position at 00:26 UTC and a less likely position at 00:28 UTC. There are 9 anomalous WSPR position indicators within the coloured area marked on the crash location probability map. The key areas are bounded by a rectangle 70 nmi x 42 nmi (10,084 km2).

The approximate depths at each point are:

1. 2,939 m at 28.672°S 99.362°E.
2. 3,768 m at 29.128°S 99.934°E.
3. 3,879 m at 29.317°S 99.934 °E.

Table 5 on the next 4 pages lists all 67 positions and 125 anomalous WSPR links used to define the MH370 flight path and crash location. The details of each of the 125 anomalous links over a ± 3 hour timeframe can be found in Appendix H.

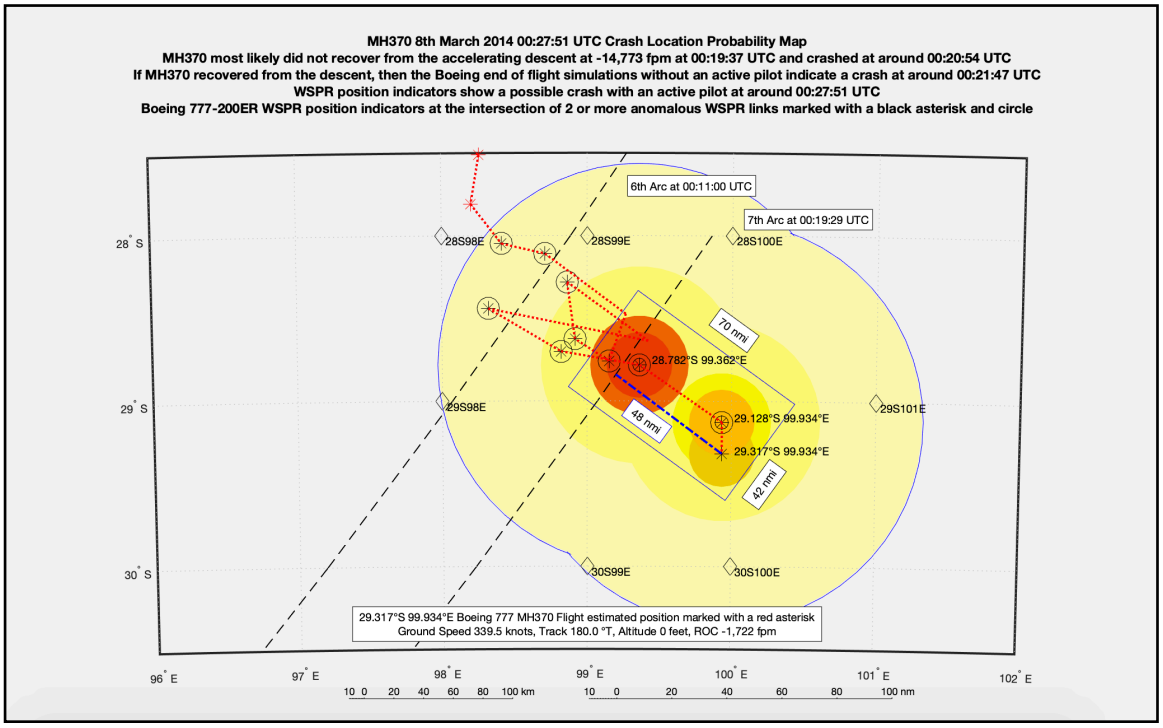

Figure 81: MH370 estimated crash location at 00:27:51 UTC.

ID	Tx	Rx	Date	UTC	File Links	Type	Latitude	Longitude	Sky Vector
1			07/03/2014	1801		00	5.589117920	99.165228400	053521S0990955E
2	DC5BN	2E0DSS	07/03/2014	1808	DC5BN2E0DSS1808	21	5.413	98.200	052447S0981200E
3	G8VDQ	DO6RPS	07/03/2014	1814	G8VDQDO6RPS1814	21	5.728	97.502	054341N0973007E
4	G8YTR	DL8YCA	07/03/2014	1824	G8YTRDL8YCA1824	11	6.142	96.202	060831N0961207E
5	DL8SEL	G8YTR	07/03/2014	1828	DL8SELG8YTR1828	11	6.493	95.871	062935N0955216E
6	HS0ZKM	KC6KGE	07/03/2014	1846	HS0ZKMKC6KGE1846	21	5.402	94.360	052407N0942136E
7	DF2JP	G3SXH	07/03/2014	1854	DF2JPG3SXH1854	01	4.374	94.146	042226N0940846E
8	N7SCQ	CX2ABP	07/03/2014	1916	N7SCQCX2ABP1916	21	1.815	94.732	014854N0944355E
9	HS0ZKM	K7UEB/20	07/03/2014	1928	HS0ZKMK7UEB/201928	11	0.695	93.729	004142N0934344E
10	G8VDQ	G0MQW	07/03/2014	1938	G8VDQG0MQW1938	11	-0.422	93.732	002519S0934353E
11	G8VDQ	G0MQW	07/03/2014	1940	G8VDQG0MQW1940	11	-0.643	93.906	003835S0935422E
12	G4FKK	ON7KB	07/03/2014	1948	G4FKKON7KB1948	11	-1.420	92.800	012512S0924800E
13	G4ZXE	ON7KB	07/03/2014	2016	G4ZXEON7KB2016	11	-4.300	92.595	041800S0923504E
14	KC6KGE	AG6IF	07/03/2014	2016	KC6KGEAG6IF2016	11			
15	OK2SAM	ON7KB	07/03/2014	2024	OK2SAMON7KB2024	11	-5.226	93.221	051334S0931316E
16	W3CSW	N2NOM	07/03/2014	2030	W3CSWN2NOM2030	11	-6.008	93.522	060029S0933119E
17	N7SCQ	ZP5BAB	07/03/2014	2036	N7SCQZP5BAB2036	11	-6.836	93.758	065010S0934529E
18	ON7KO	G4ZXE	07/03/2014	2044	ON7KOG4ZXE2044	10	-7.815	93.149	074854S0930856E
19	ON7KO	G4ZXE	07/03/2014	2054	ON7KOG4ZXE2054	11	-8.931	93.984	085552S0935902E
20	US3IRX	OZ7IT	07/03/2014	2110	US3IRXOZ7IT2110	11	-10.742	93.917	104431S0935501E
21	K4RCG	W4AC	07/03/2014	2114	K4RCGW4AC2114	10	-10.903	93.397	105411S0932349E
22	OK2SAM	M0BLP	07/03/2014	2114	OK2SAMM0BLP2114	10			
23	G4ZXE	G4FKK	07/03/2014	2116	G4ZXEG4FKK2116	11	-11.116	93.544	110658S0933238E
24	KI7CI	JG1TWP/1	07/03/2014	2116	KI7CIJG1TWP/12116	10			
25	ON7KB	DK4TJ	07/03/2014	2138	ON7KBDK4TJ2138	10	-13.273	94.127	131623S0940737E
26	WA8RC	AI4RY	07/03/2014	2138	WA8RCAI4RY2138	31			
27	W4MO	K4RCG	07/03/2014	2144	W4MOK4RCG2144	10	-13.979	93.934	135844S0935602E
28	W3GXT	W4AC	07/03/2014	2150	W3GXTW4AC2150	11	-14.667	93.405	144001S0932418E
29	KC3AVT	W4AC	07/03/2014	2156	KC3AVTW4AC2156	01	-15.486	93.673	152910S0934023E
30	G3SXH	DK6UG	07/03/2014	2202	G3SXHDK6UG2202	11	-16.174	94.205	161026S0941218E
31	VA3ROM	KB9AMG	07/03/2014	2202	VA3ROMKB9AMG2202	10			
32	JH1GYE	WA5NGP	07/03/2014	2208	JH1GYEWA5NGP2208	11	-16.861	94.741	165140S0944428E

Table 5: WSPR Anomalous Links and MH370 Positions.

ID	Tx	Rx	Date	UTC	File Links	Type	Latitude	Longitude	Sky Vector
33	K4RCG	W4AC	07/03/2014	2210	K4RCGW4AC2210	11	-17.073	94.941	170423S0945628E
34	DH5RAE	OE1MSB	07/03/2014	2216	DH5RAEOE1MSB2216	10	-17.709	95.545	174232S0953242E
35	W4MO	KC3AVT	07/03/2014	2222	W4MOKC3AVT2222	11	-18.116	94.331	180658S0941952E
36	OK2SAM	PI4THT	07/03/2014	2230	OK2SAMPI4THT2230	11	-19.255	94.330	191518S0941948E
37	G3NZP	DH5RAE	07/03/2014	2232	G3NZPDH5RAE2232	11	-19.510	94.480	193036S0942848E
38	G4KPX	DL1DBC	07/03/2014	2236	G4KPXDL1DBC2236	11	-20.020	94.781	200112S0944652E
39	OX3XR	N2NOM	07/03/2014	2242	OX3XRN2NOM2242	11	-20.788	94.319	204717S0941908E
40	KI7CI	KB4RG	07/03/2014	2244	KI7CIKB4RG2244	10	-21.044	94.164	210238S0940950E
41	W3HH	W3BI	07/03/2014	2248	W3HHW3BI2248	11	-21.603	94.358	213611S0942129E
42	G6RRL	DK6UG	07/03/2014	2252	G6RRLDK6UG2252	11	-21.502	94.972	213007S0945819E
43	JH1GYE	KD6RF	07/03/2014	2252	JH1GYEKD6RF2252	11			
44	WD0UG	KB9VLR	07/03/2014	2252	WD0UGKB9VLR2252	10			
45	KI6STW	KB4RG	07/03/2014	2258	KI6STWKB4RG2258	11	-22.358	95.172	222129S0951019E
46	W3HH	OX3XR	07/03/2014	2258	W3HHOX3XR2258	11			
47	G4KPX	PA3ABK/2	07/03/2014	2300	G4KPXPA3ABK/22300	11	-22.643	95.239	223835S0951420E
48	KB1CHU	W4MO	07/03/2014	2302	KB1CHUW4MO2302	11	-22.790	94.970	224724S0945812E
49	K4RCG	OX3XR	07/03/2014	2304	K4RCGOX3XR2304	10	-22.818	94.651	224905S0943904E
50	KI7CI	WA5NGP	07/03/2014	2304	KI7CIWA5NGP2304	21			
51	AD4PT	W7ZWW	07/03/2014	2308	AD4PTW7ZWW2308	11	-23.445	94.633	232642S0943759E
52	G8VDQ	YO3ITD	07/03/2014	2308	G8VDQYO3ITD2308	20			
53	W4AC	2E0DSS	07/03/2014	2312	W4AC2E0DSS2312	11	-24.020	94.783	240112S0944659E
54	VK3DXE	ZL1AML	07/03/2014	2314	VK3DXEZL1AML2314	11	-24.250	94.987	241500S0945913E
55	G8VDQ	W4MO	07/03/2014	2318	G8VDQW4MO2318	31	-24.788	95.279	244717S0951644E
56	K4RCG	OX3XR	07/03/2014	2318	K4RCGOX3XR2318	01			
57	ON7KB	W4MO	07/03/2014	2318	ON7KBW4MO2318	21			
58	W4AC	M6NNB	07/03/2014	2320	W4ACM6NNB2320	11	-24.915	95.553	245454S0953311E
59	W4AC	OE6PWD	07/03/2014	2320	W4ACOE6PWD2320	11			
60	W4AC	ON4SAR	07/03/2014	2320	W4ACON4SAR2320	11			
61	W9HLY	K4EH	07/03/2014	2320	W9HLYK4EH2320	11			
62	W9HLY	KB1MVX	07/03/2014	2320	W9HLYKB1MVX2320	11			
63	W4MO	2E0DSS	07/03/2014	2322	W4MO2E0DSS2322	10	-25.193	95.679	251135S0954044E
64	W4MO	DK6UG	07/03/2014	2322	W4MODK6UG2322	10			

Table 5: WSPR Anomalous Links and MH370 Positions (continued).

ID	Tx	Rx	Date	UTC	File Links	Type	Latitude	Longitude	Sky Vector
65	W4MO	M5ADA	07/03/2014	2322	W4MOM5ADA2322	11			
66	W4MO	OE3VMS	07/03/2014	2322	W4MOOE3VMS2322	10			
67	W4MO	OE6PWD	07/03/2014	2322	W4MOOE6PWD2322	10			
68	W4MO	ON7KB	07/03/2014	2322	W4MOON7KB2322	21			
69	W4MO	PI4THT	07/03/2014	2322	W4MOPI4THT2322	11			
70	G8VDQ	W4AC	07/03/2014	2326	G8VDQW4AC2326	11	-25.580	96.184	253448S0961102E
71	HB9CZF	W4AC	07/03/2014	2326	HB9CZFW4AC2326	11			
72	W3HH	W3CSW	07/03/2014	2328	W3HHW3CSW2328	11	-25.773	96.438	254623S0962617E
73	W4AC	2E0DSS	07/03/2014	2328	W4AC2E0DSS2328	11			
74	W4AC	M6NNB	07/03/2014	2328	W4ACM6NNB2328	11			
75	DK0SC	W4AC	07/03/2014	2330	DK0SCW4AC2330	11	-25.965	96.692	255754S0964131E
76	G4ANN	W4AC	07/03/2014	2330	G4ANNW4AC2330	11			
77	DG7RJ	W4AC	07/03/2014	2332	DG7RJW4AC2332	11	-26.180	96.935	261048S0965606E
78	OZ7IT	W4AC	07/03/2014	2332	OZ7ITW4AC2332	11			
79	WA3DNM	W4MO	07/03/2014	2336	WA3DNMW4MO2336	11	-26.572	97.443	263419S0972635E
80	W4AC	DG7RJ	07/03/2014	2338	W4ACDG7RJ2338	11	-26.844	97.595	265038S0973542E
81	W4AC	M5ADA	07/03/2014	2338	W4ACM5ADA2338	11			
82	W4AC	W3GXT	07/03/2014	2338	W4ACW3GXT2338	11			
83	W4AC	WA3DNM	07/03/2014	2338	W4ACWA3DNM2338	11			
84	2E0DSS	W4MO	07/03/2014	2340	2E0DSSW4MO2340	11	-27.116	97.747	270658S0974449E
85	AA7FV	W4MO	07/03/2014	2340	AA7FVW4MO2340	31			
86	G8VDQ	W4AC	07/03/2014	2340	G8VDQW4AC2340	11			
87	KZ3X	OX3XR	07/03/2014	2340	KZ3XOX3XR2340	01			
88	W4AC	DK0SC	07/03/2014	2344	W4ACDK0SC2344	21	-27.512	98.258	273043S0981529E
89	W4AC	DK6UG	07/03/2014	2344	W4ACDK6UG2344	01			
90	W4AC	M6NNB	07/03/2014	2344	W4ACM6NNB2344	11			
91	W4AC	ON7KB	07/03/2014	2344	W4ACON7KB2344	01			
92	GM4SFW	W4MO	07/03/2014	2346	GM4SFWW4MO2346	11	-27.809	98.202	274832S0981207E
93	G4JVF	W4MO	07/03/2014	2348	G4JVFW4MO2348	11	-28.048	98.412	280253S0982443E
94	OZ7IT	W4MO	07/03/2014	2348	OZ7ITW4MO2348	11			
95	WD4LHT	K9AN	07/03/2014	2348	WD4LHTK9AN2348	10			

Table 5: WSPR Anomalous Links and MH370 Positions (continued).

ID	Tx	Rx	Date	UTC	File Links	Type	Latitude	Longitude	Sky Vector
96	NH7SR	WA5NGP	07/03/2014	2350	NH7SRWA5NGP2350	11	-28.109	98.711	280632S0984240E
97	W4MO	DG7RJ	07/03/2014	2350	W4MODG7RJ2350	11			
98	W4MO	M6NNB	07/03/2014	2350	W4MOM6NNB2350	11			
99	W4MO	ON4SAR	07/03/2014	2350	W4MOON4SAR2350	10			
100	WB8ELK	VE6PDQ/1	07/03/2014	2350	WB8ELKVE6PDQ/12350	11			
101	W3CSW	N2NOM	07/03/2014	2354	W3CSWN2NOM2354	10	-28.473	99.267	282823S0991601E
102	N1NCO	OH7AZL	07/03/2014	2356	N1NCOOH7AZL2356	11	-28.758	99.151	284529S0990904E
103	W4AC	VE1AIM	07/03/2014	2356	W4ACVE1AIM2356	11			
104	K9AN	VE4KE	07/03/2014	2358	K9ANVE4KE2358	11	-28.624	98.916	283726S0985458E
105	W4MO	OZ7IT	07/03/2014	2358	W4MOOZ7IT2358	11			
106	G8VDQ	W4MO	08/03/2014	0000	G8VDQW4MO0000	11	-28.280	98.862	281648S0985143E
107	WD4LHT	KV0S	08/03/2014	0000	WD4LHTKV0S0000	11			
108	IK1NET	W4MO	08/03/2014	0004	IK1NETW4MO0004	01	-28.636	99.421	283810S0992516E
109	W4AC	2E0DSS	08/03/2014	0004	W4AC2E0DSS0004	11			
110	W4AC	DK6UG	08/03/2014	0004	W4ACDK6UG0004	01			
111	W4AC	M6NNB	08/03/2014	0004	W4ACM6NNB0004	11			
112	W4AC	ON4SAR	08/03/2014	0004	W4ACON4SAR0004	11			
113	W4AC	PI4THT	08/03/2014	0004	W4ACPI4THT0004	21			
114	KZ3X	OX3XR	08/03/2014	0012	KZ3XOX3XR0012	11	-28.440	98.320	282624S0981912E
115	W3GXT	W4AC	08/03/2014	0012	W3GXTW4AC0012	11			
116	JH1GYE	VE6PDQ	08/03/2014	0016	JH1GYEVE6PDQ0016	11	-28.700	98.820	284200S0984912E
117	W3HH	KK5MR	08/03/2014	0016	W3HHKK5MR0016	11			
118	W3CSW	N2NOM	08/03/2014	0020	W3CSWN2NOM0020	11	-28.782	99.362	284655S0992143E
119	W4MO	2E0DSS	08/03/2014	0020	W4MO2E0DSS0020	11			
120	HB9CZF	W4MO	08/03/2014	0026	HB9CZFW4MO0026	11	-29.128	99.934	290741S0995602E
121	KK4U	YV4GJN	08/03/2014	0026	KK4UYV4GJN0026	11			
122	NH7SR	KE7KRF	08/03/2014	0026	NH7SRKE7KRF0026	11			
123	W4MO	2E0DSS	08/03/2014	0028	W4MO2E0DSS0028	21	-29.317	99.934	291901S0995602E
124	W4MO	DK6UG	08/03/2014	0028	W4MODK6UG0028	11			
125	W4MO	M6NNB	08/03/2014	0028	W4MOM6NNB0028	11			
126	W4MO	Pi4THT	08/03/2014	0028	W4MOPI4THT0028	01			

Table 5: WSPR Anomalous Links and MH370 Positions (continued).

7. Reproducibility.

The code, data and associated files can be made available free of charge to bona fide academic researchers, who wish to reproduce the results in their own environments. The code package of Matlab scripts and data is 687 files (22.6 MB). The case study comprises 2,434 files (710.8 MB).

Applications are invited via either the website invitation page at https://www.mh370search.com/invitation/ or email richard@mh370search.com.

Applicants will be required to give their full name, street address, academic affiliation and a valid email that aligns with their proper name. Data is available in both Microsoft Windows Excel and Apple Mac Numbers data format. Code is only available in Matlab format. Delivery is via Dropbox.

8. Discussion of Results.

Part of the crash area shown in Figure 81 has been searched before by Ocean Infinity on 10th May 2018. The search width either side of the 7th Arc was around 22 nmi at this latitude. As no points of interest were found during the previous search, it is therefore reasonable to start with that part of the new search area further out than 22 nmi from the 7th Arc and not previously scoured by the Autonomous Underwater Vehicles (AUVs) from Ocean Infinity.

In Figure 82 the track of the Ocean Infinity vessel Seabed Constructor is marked in red and the points where the ship stopped to launch or collect AUVs are marked with black and white dots. The bathymetric data is only partially available for this location and there is an underwater sea mount in the vicinity of the 7th Arc marked with a dotted yellow line. The depths in the areas coloured orange are down to 3,000 m depth, coloured yellow are down to 3,500 m depth and coloured blue are down to 4,000 m depth.

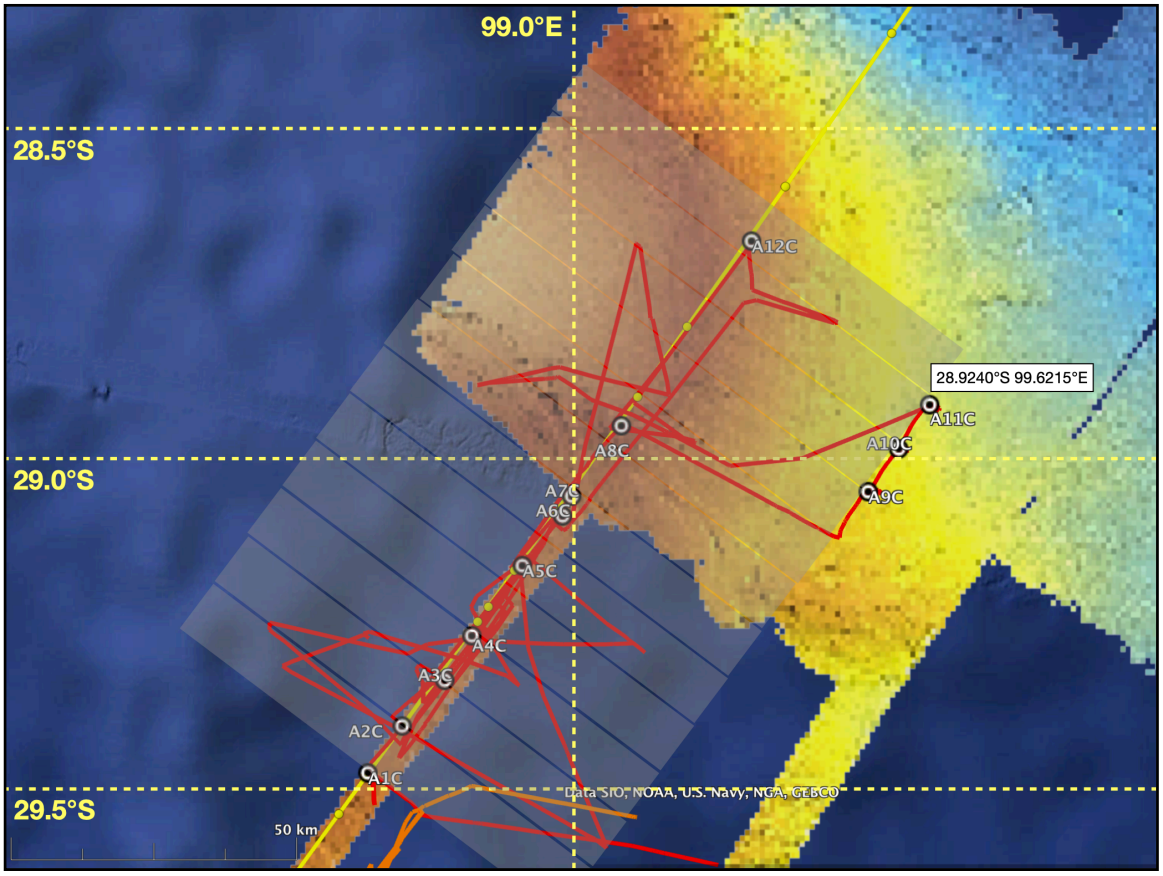

Figure 82: Previous Search Area covered by Ocean Infinity on 10th May 2018.

A .kml file of the search area is available for download at the following link:

https://www.dropbox.com/scl/fi/9in2j4oealrbqc8wg8huk/MH370_Search_Area.kml?rlkey=65doypmdfym2m9z0ewqy25hew&dl=0

The .kml file can be viewed with Google Earth as shown in Figure 83. The Altitude Mode is specified as relative to sea level. The World Geodetic System 1984 (WGS84) is specified for the .kml output. This results in a small area of sea being displayed in Google Earth around an underwater sea mount, which is shown more clearly in Figure 84.

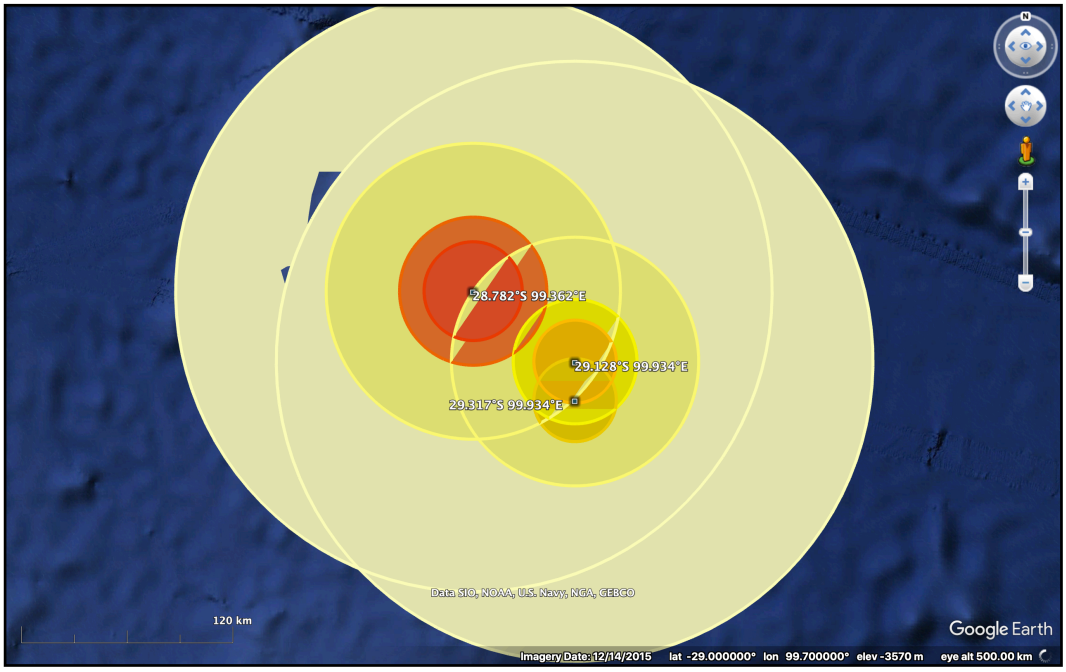

Figure 83: Google Earth View of proposed MH370 Search Area .

Figure 84: Google Earth View of Sea Mount in the MH370 Search Area .

There are 16 WSPR anomalies with a SNR of more than two standard deviations from the mean over a ± 3 hour timeframe. These are mostly when MH370 was turning or circling. In nearly all cases either the transmitter or MH370 or both were on the grey line. HF ionospheric transmissions experience better propagation at either dawn or dusk in the twilight or grey zone. The propagation distances from transmitter to aircraft and back to the receiver are shown in Table 6 below and range from 12,157 km to 38,026 km. An example propagation path is shown in Figure 85. The transmitter W3HH, receiver W3CSW and MH370 are all on the grey line.

ID	UTC	Tx	Rx	AC Lat	AC Lon	AC Alt	AC Trk	AC	Scatter	SNR SD %	Signal	Action	Route	Great Circle Distance (km)	Tx to AC Take Off IB	Tx to AC Landing FB	Tx to C Landing FB Rev	AC to Rx Take Off IB	Comment
1	19:48	G4FKK	ON7KB	-1.420	92.800	34,500	231.9	Straight	Back	-221	Enhanced	Reflection	Europe-Asia-Indian Ocean-Asia-Europe	20357	88.426	141.261	321.261	321.254	Tx Grey Line
2	21:10	US3IRX	OZ7IT	-10.742	93.917	34,500	214.0	Turning	Back	-217	Enhanced	Reflection	Asia-Indian Ocean-Asia-Europe	18992	123.135	145.399	325.399	325.464	Night
3	21:50	W3GXT	W4AC	-14.667	93.405	38,500	216.9	Turning		-216	Enhanced	Reflection	USA-Artic-Europe-Asia-Indian Ocean-Asia-Europe-Artic-USA	17097	21.567	162.921	342.921	343.266	TX and AC Grey Line
4	22:36	G4KPX	DL1DBC	-20.020	94.781	38,500	150.8	Turning	Back	-280	Enhanced	Reflection	Europe-Asia-Indian Ocean-Asia-Europe	23543	98.944	140.019	320.019	320.006	Tx Grey Line
5	22:42	OX3XR	N2NOM	-20.788	94.319	38,500	290.7	Turning	Back	231	Diminished	Deflection	Artic-Europe-Asia-Indian Ocean-Asia-Europe-Artic-USA	32024	43.732	161.169	341.169	341.387	TX and AC Grey Line
6	22:48	W3HH	W3BI	-21.603	94.358	38,500	161.9	Turning	Back	265	Diminished	Deflection	USA-Artic-Europe-Asia-Indian Ocean-Asia-Europe-Artic-USA	36812	22.285	159.107	339.107	338.360	TX and AC Grey Line
7	22:52	G6RRL	DK6UG	-21.502	94.972	38,500	79.9	Turning	Back	268	Diminished	Deflection	Europe-Asia-Indian Ocean-Asia-Europe	23835	99.160	137.955	317.955	317.938	AC Grey Line
8	23:04	KI7CI	WA5NGP	-22.818	94.651	38,500	264.7	Turning	Back	239	Diminished	Deflection	USA-Pacific Ocean-Asia-Indian Ocean-Asia-Pacific Ocean-USA	34813	289.525	232.364	52.364	51.566	AC Grey Line
9	23:08	AD4PT	W7ZWW	-23.445	94.633	38,500	181.5	Turning	Back	-227	Enhanced	Reflection	USA-Pacific Ocean-Asia-Indian Ocean-Asia-Pacific Ocean-USA	34339	310.590	224.001	44.001	44.655	AC Grey Line
10	23:14	VK3DXE	ZL1AML	-24.250	94.987	38,500	140.8	Turning	Back	241	Diminished	Deflection	Australia-Indian Ocean-Australia-New Zealand	12517	272.966	300.418	120.418	120.463	AC Grey Line
11	23:28	W3HH	W3CSW	-25.773	96.438	40,500	129.9	Straight	Back	200	Diminished	Deflection	USA-Artic-Europe-Asia-Indian Ocean-Asia-Europe-Artic-USA	38026	18.303	162.250	342.250	340.018	TX and AC Grey Line
12	23:32	DG7RJ	W4AC	-26.180	96.935	40,500	130.7	Straight	Back	-208	Enhanced	Reflection	Europe-Asia-Indian Ocean-Asia-Europe-Atlantic Ocean-USA	31704	111.099	136.180	316.180	331.147	AC Grey Line
13	23:50	W4MO	DG7RJ	-28.109	98.711	40,500	102.9	Turning	Forward	-202	Enhanced	Reflection	USA-Pacific Ocean-Indian Ocean-Asia-Europe	31940	35.093	324.537	144.537	135.303	TX and AC Grey Line
14	23:58	W4MO	OZ7IT	-28.624	98.916	40,500	320.9	Circling	Forward	200	Diminished	Deflection	USA-Pacific Ocean-Indian Ocean-Asia-Europe	32165	30.957	328.559	148.559	142.230	TX and AC Grey Line
15	00:04	W4AC	2E0DSS	-28.636	99.421	40,500	125.6	Circling	Forward	204	Diminished	Deflection	USA-Pacific Ocean-Indian Ocean-Asia-Europe	32994	36.745	322.593	142.593	136.808	TX and AC Grey Line
16	00:12	KZ3X	OX3XR	-28.440	98.320	40,500	281.7	Circling	Back	-231	Enhanced	Reflection	USA-Artic-Europe-Asia-Indian Ocean-Asia-Europe-Artic	34097	22.171	160.885	340.885	340.448	TX and AC Grey Line

Table 6: WSPR Anomalous Links with greater than 2.0 SD SNR anomalies.

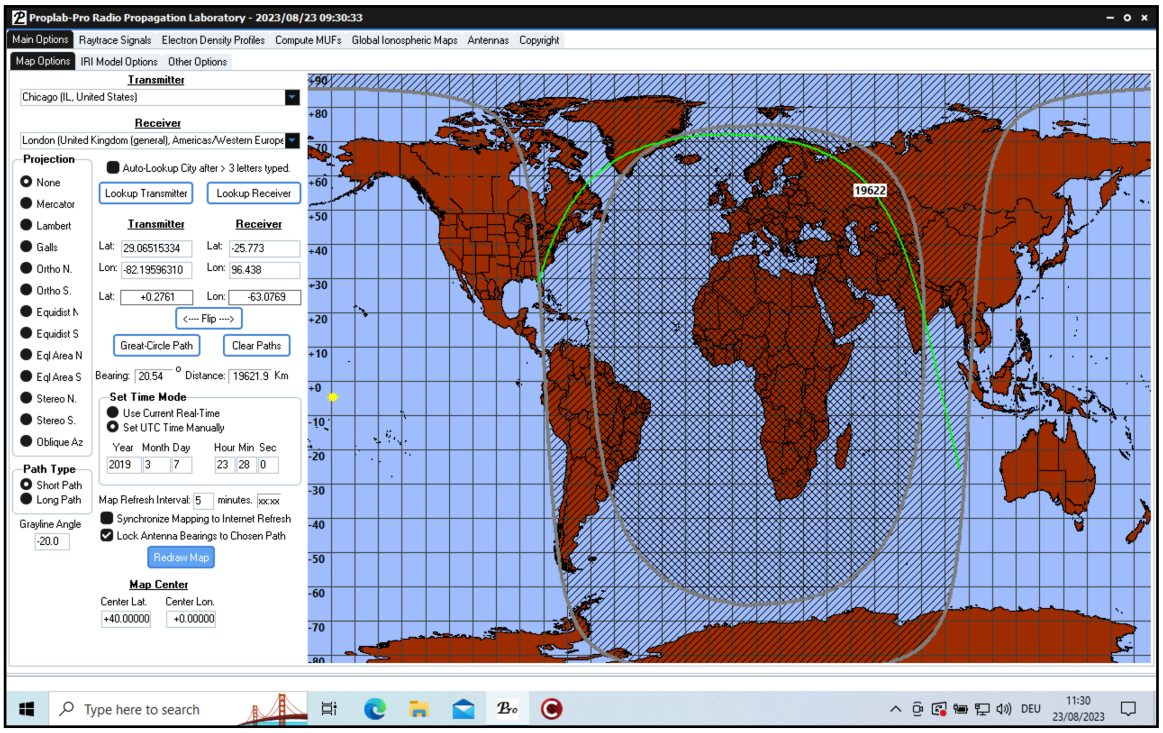

Figure 85: Propagation Path between W3HH to W3CSW to MH370 at 23:28 UTC.

Page 577 of 1738

The MH370 positions where the 16 WSPR anomalies with a SNR of more than two standard deviations from the mean over a ± 3 hour timeframe are shown in Figure 86 below. The starting point is the last known point from the Butterworth primary civilian radar. The MH370 estimated positions crossing each of the seven Arcs defined by the Inmarsat satellite BTO data are also included.

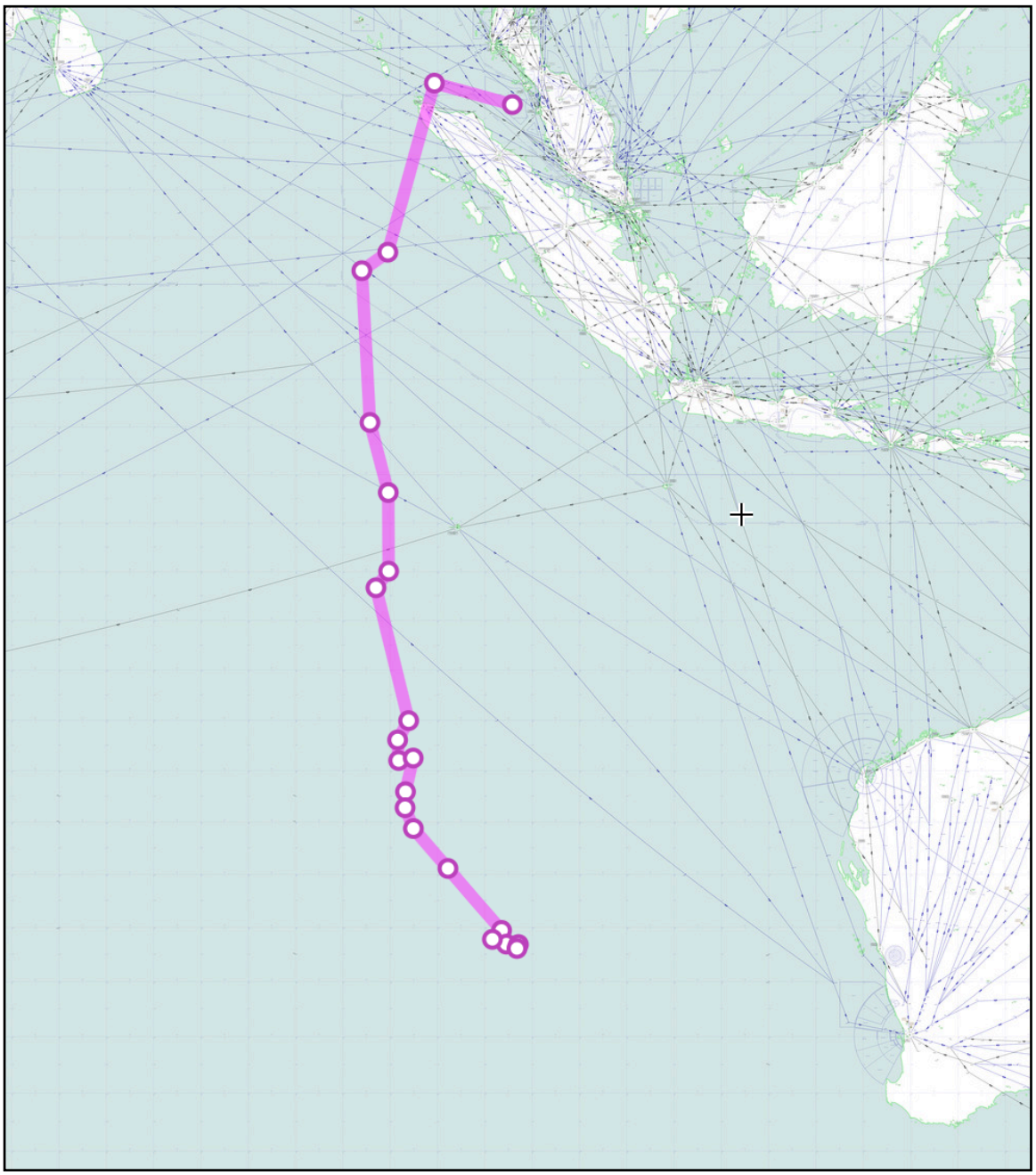

Figure 86: Sky Vector of MH370 positions with WSPR SNR anomalies greater than 2.0 SD.

From the Inmarsat satellite data we know that the Satellite Data Unit (SDU) experienced a power up reboot starting at 18:25:27.421 UTC and which was completed at 18:28:14.904 UTC. When the BTO data settled at 18:28:05.904 UTC, Boeing calculated the remaining fuel at this point in time was 73,908 lbs or 33,524 kg assuming a flight level of FL300, Mach 0.838 and TAS 494 knots.

The estimated fuel range at 18:28 UTC assuming a constant flight at Mach 0.838, flight level FL350 and based on the winds encountered on a 180°T track was 5,117 km centred on a position at 6.493°N 95.871°E. However the WSPR analysis indicates that there was neither a constant straight line flight path, nor a constant flight level. On the contrary, there were a large number of turns and two step climbs at around 21:14 UTC and 23:18 UTC, which will have significantly changed the fuel range. By 21:14 UTC at a position of 14.0°S 93.945°E close to waypoint 14S93E the estimated fuel range was 2,149 km. By 23:30 UTC at a position of 26.0°S 96.731558°E close to waypoint 26S96E the estimated fuel range was 619 km.

Towards the end of flight the pilot circled twice over the end location, which will have again required further fuel. One possible explanation of the circling is that the pilot was checking for any shipping in the vicinity. There was no cloud cover at this location and time according to the GDAS cloud cover map. There was substantial cloud cover further south and west, which may also be a reason for selecting this end location around 29.0°S 99.5°E. The pilot may have been checking for any shipping that might observe the crash of MH370.

A map showing the MH370 flight paths from the preliminary WSPR findings dated 30th November 2021, as compared with the report dated 8th September 2022 and the results presented in this case study is shown in Figure 87 below. The technique was continually refined and improved after feedback from various persons and entities and as a result of a large number of trials and case studies conducted. Major improvements resulted from a tighter definition of a WSPR link anomaly and the more precise antenna database. Both the presence and absence of anomalous WSPR links in the target area are included in the analysis. The aircraft performance, WSPR detection, waypoint navigation and Inmarsat data all align.

The fuel range at 18:28 UTC of 5,117 km from a position estimated at 6.493°N 95.871°E, reducing to a fuel range of 2,149 km at 21:44 UTC and further reducing to a fuel range of 619 km at 23:30 UTC is also depicted in Figure 87 marked with a red line.

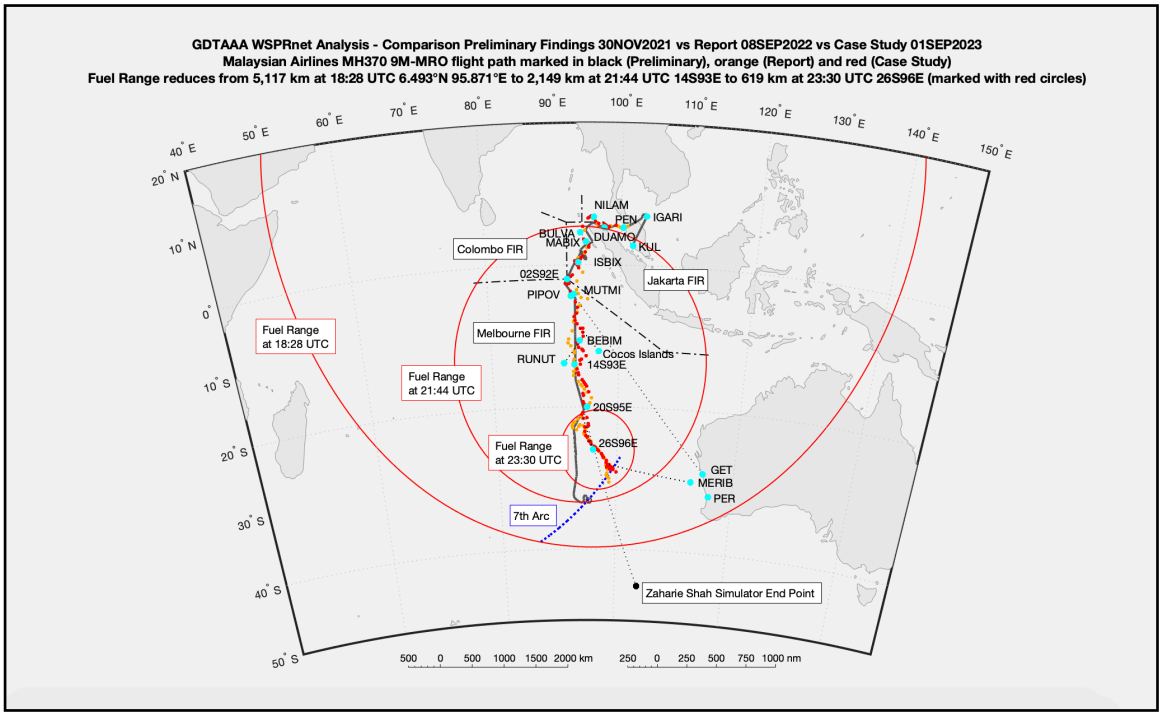

Figure 87: Comparison of WSPR Preliminary Findings, Report and Case Study.

There were 36 SDU Logons in the last 24 hours of 9M-MRO operations, covering both the MH371 and MH370 flights. Out of these 36, there were 22 normal SDU Logons with processing lasting an average of 75 seconds.

There were 3 time periods in this 24 hours where the SDU was powered down completely:

(a) For an outage of up to 3h 48m 30s ending at 07/03/2014 12:50:19 UTC.

(b) For an outage of up to 1h 17m 39s ending at 07/03/2014 18:25:27 UTC.

(c) For an outage of up to 8m 29s ending at 08/03/2014 00:19:29 UTC.

The Logon process time following a power outage is quite different from the normal time of 75 seconds. The SDU Logon took 235.495 seconds at 12:50:19 UTC, 167.483 seconds at 18:25:27 UTC and was incomplete after only 8.991 seconds at 00:19:29 UTC.

There are four information steps in the Logon process:

(a) Confirmation of the 9M-MRO identification.

(b) Confirmation of the Flight Number e.g. MH370.

(c) Confirmation of the Aircraft Time e.g. 16:00 UTC.

(d) Confirmation of the In Flight Entertainment (IFE) Logon.

The final Logon at 15:59:55 UTC to the IOR satellite prior to the departure of MH370 from Kuala Lumpur completed all the information steps taking a little longer than the average process time at 84 seconds.

The Logon process at 12:50:19 UTC missed out steps (b) and (c). The Logon process at 18:25:27 UTC missed out steps (a), (b) and (c). The Logon process at 00:19:29 UTC missed out all the information steps.

The Electrical Load Management System (ELMS) provides load management and protection to ensure power is available to critical and essential equipment. If the electrical loads exceed the power available, ELMS automatically sheds AC loads by priority until the loads are within the capacity of the airplane or ground power generators.

Each engine has an Integrated Drive Generator (IDG). Each IDG has automatic control and system protection functions. The Auxiliary Power Unit (APU) generator is electrically identical to the IDG generators. The APU generator can power either or both main busses, and may be used in flight as a replacement to an IDG source.

If both IDGs and the APU generator are inoperative, a backup generator powers essential airplane equipment. To reduce electrical loading on the backup generator, the following systems are inoperative: TCAS, SATCOM and Right HF radio.

It is possible that the backup generator configuration was selected at diversion and the TCAS and SDU were switched off until the backup generator configuration was deselected at 18:25:27 UTC. This selection can be made on the overhead control panel in the cockpit. The TCAS can also separately be switched off from the overhead circuit breaker panel in the cockpit. The circuit breaker for the SDU is in the Main Equipment Center (MEC) and not in the cockpit.

https://www.dropbox.com/scl/fi/0flhdblfqiml2z2x4rho9/Electrical-Systems-Power-Distribution.png?rlkey=k4jyaxpgbdl38hjdwhpfh3qsi&dl=0

9. Conclusion.

This case study uses ground breaking WSPR technology to detect and track flight MH370. This WSPR technology has been developed over the last 3 years and therefore the results presented in this paper represent credible new evidence in the search for MH370.

From a known radar position at 18:01 UTC, the case study presents 67 positions for MH370 over the next 6 hours 27 minutes of flight, as detected by a total of 125 anomalous WSPR links.

The results of this case study align with the analyses by Boeing, Inmarsat and the drift analysis by the University of Western Australia of the MH370 floating debris that has been recovered from around the Indian Ocean.

Dr. Robert Westphal, an expert in passive radar systems, first proposed the idea of using WSPR transmissions to detect and track MH370 in July 2020. Dr. Westphal presented his ideas in a paper titled "Geocaching in the Ionosphere" to the HamSCI conference in 2021. Dr. Westphal had previously written a paper in 2015 proposing using GPS satellite signals as a passive radar system and holds several related patents. The idea of using amateur radio signals as a passive radar system to detect and track aircraft was first proposed in a NATO paper written by the Finnish Air Defence Academy in 2016.

Prof. Simon Maskell is developing a variant of the algorithm developed by DSTG and presented in their paper titled “Bayesian Methods in the Search for MH370” and dated 30th November 2015, but modified to incorporate the WSPR data. The plan is that the paper will be independently reviewed and that the results will be presented in a separate paper in due course.

10. Acknowledgements.

This study would not have been possible without the data supplied to the WSPRnet database by the following radio amateur call signs from all over the world.

Call Sign	Detections	Type
W4AC	32	Tx and Rx
W4MO	30	Tx and Rx
2E0DSS	8	Tx and Rx
G8VDQ	8	Tx
ON7KB	7	Tx and Rx
DK6UG	6	Rx
M6NNB	6	Rx
OX3XR	6	Tx and Rx
K4RCG	5	Tx and Rx
G4ZXE	4	Tx and Rx
N2NOM	4	Rx
OZ7IT	4	Tx and Rx
PI4THT	4	Rx
W3CSW	4	Tx and Rx
W3HH	4	Tx
DG7RJ	3	Tx and Rx
JH1GYE	3	Tx
KI7CI	3	Tx
OK2SAM	3	Tx
ON4SAR	3	Rx
W3GXT	3	Tx and Rx
WA5NGP	3	Rx
DH5RAE	2	Tx and Rx
DK0SC	2	Tx and Rx
G0MQW	2	Rx
G3SXH	2	Tx and Rx
G4FKK	2	Tx and Rx
G4KPX	2	Tx
G8YTR	2	Tx and Rx
HB9CZF	2	Tx
HS0ZKM	2	Tx
K9AN	2	Tx and Rx
KB4RG	2	Rx
KC3AVT	2	Tx and Rx
KC6KGE	2	Tx and Rx
KZ3X	2	Tx
M5ADA	2	Rx
N7SCQ	2	Tx
NH7SR	2	Tx
OE6PWD	2	Rx
ON7KO	2	Tx
W9HLY	2	Tx
WA3DNM	2	Tx and Rx
WD4LHT	2	Tx
AA7FV	1	Tx
AD4PT	1	Tx
AG6IF	1	Rx
AI4RY	1	Rx

Call Sign	Detections	Type
CX2ABP	1	Rx
DC5BN	1	Tx
DF2JP	1	Tx
DK4TJ	1	Rx
DL1DBC	1	Rx
DL8SEL	1	Tx
DL8YCA	1	Rx
DO6RPS	1	Rx
G3NZP	1	Tx
G4ANN	1	Tx
G4JVF	1	Tx
G6RRL	1	Tx
GM4SFW	1	Tx
IK1NET	1	Tx
JG1TWP/1	1	Rx
K4EH	1	Rx
K7UEB/20	1	Rx
KB1CHU	1	Tx
KB1MVX	1	Rx
KB9AMG	1	Rx
KB9VLR	1	Rx
KD6RF	1	Rx
KE7KRF	1	Rx
KI6STW	1	Tx
KK4U	1	Tx
KK5MR	1	Rx
KV0S	1	Rx
M0BLP	1	Rx
N1NCO	1	Tx
OE1MSB	1	Rx
OE3VMS	1	Rx
OH7AZL	1	Rx
PA3ABK/2	1	Rx
US3IRX	1	Tx
VA3ROM	1	Tx
VE1AIM	1	Rx
VE4KE	1	Rx
VE6PDQ	1	Rx
VE6PDQ/1	1	Rx
VK3DXE	1	Tx
W3BI	1	Rx
W7ZWW	1	Rx
WA8RC	1	Tx
WB8ELK	1	Tx
WD0UG	1	Tx
YO3ITD	1	Rx
YV4GJN	1	Rx
ZL1AML	1	Rx
ZP5BAB	1	Rx

Particular thanks for the help and advice from Rob DJ4FF, Karl DL2NGT, Dominik HB9CZF, Christian DL3MBG and Phil VK7JJ.

Thanks to all the people at WSPRnet.org, WSPR.live, WSPR.rocks, QRZ.com, QRZCQ.com, HamCall.net, DXMAPS.com, kiwisdr.com, RepeaterBook.com and VOACAP.com and the radio amateur registration authorities in a number of countries.

11. References.

[1] Richard Godfrey, Dr. Hannes Coetzee (2022) Emirates Flight EK421 GDTAAA WSPRnet Analysis - Case Study.

https://www.dropbox.com/s/z3cfnj7qee30ke0/Emirates%20Flight%20EK421%20GDTAAA%20WSPRnet%20Analysis%20-%20Case%20Study%20-%2023rd%20June%202022.pdf?dl=0

[2] Richard Godfrey, Dr. Hannes Coetzee (2022) Roanoke Flight N395JP GDTAAA WSPRnet Analysis - Case Study.

https://www.dropbox.com/s/h0raiqmhcamma06/Roanoke%20Flight%20N395JP%20GDTAAA%20WSPRnet%20Analysis%20-%20Case%20Study%20-%2013th%20July%202022.pdf?dl=0

[3] Richard Godfrey, Dr. Hannes Coetzee (2022) Flight OE-FGR GDTAAA WSPRnet Analysis - Case Study.

https://www.dropbox.com/s/hlfi1amubynkjvo/Flight%20OE-FGR%20GDTAAA%20WSPRnet%20Analysis%20-%20Case%20Study%20-%2030th%20October%202022.pdf?dl=0

[4] Richard Godfrey, Dr. Hannes Coetzee, Prof. Simon Maskell (2023) Flight N45VX GDTAAA WSPRnet Analysis - Case Study.

https://www.dropbox.com/s/m53aiwvmhv0842k/Flight%20N45VX%20GDTAAA%20WSPRnet%20Analysis%20-%20Case%20Study%20-%2018th%20April%202023.pdf?dl=0

[5] Richard Godfrey, Dr. Hannes Coetzee, Prof. Simon Maskell (2023) Flight QTR901 GDTAAA WSPRnet Analysis - Case Study

https://www.dropbox.com/s/224qont4xrgv54u/Boeing%20777-300ER%20QTR901%20PER%20DOH%2001NOV2022%20Detection%20and%20Tracking%20-%208th%20June%202023.pdf?dl=0

[6] Ian Holland (2018) MH370 Burst Frequency Offset Analysis and Implications on Descent Rate at End-of-Flight.
https://www.dropbox.com/scl/fi/x1ekixakr24yd2763gw94/Ian-Holland-DSTG-Revised-Version-V3-15JAN2018.pdf?rlkey=m6t5y8yl4ga1ll9ypx64hbkzw&dl=0

[7] Boeing End of Flight Simulations (2016)

Case 3
https://www.dropbox.com/scl/fi/ics1h3m256z5c2ioz7h91/Case-03.csv?rlkey=v5afih5g5qpcipv74op2rfx4v&dl=0

Case 4
https://www.dropbox.com/scl/fi/a65k59pd4bmnk8ua9aqsp/Case-04.csv?rlkey=dp2sncut8epjdtqupb4vmk4i2&dl=0

Case 6
https://www.dropbox.com/scl/fi/tve2u4gfbkmibpyyrl8ny/Case-06.csv?rlkey=pjs9wwbqy9kblwmupwn08dqow&dl=0

Case 10
https://www.dropbox.com/scl/fi/eupezyxasd5ruw20ogt3i/Case-10.csv?rlkey=mzhhxpxjx36f6gx7hoffo9xey&dl=0

[8] Prof. Charitha Pattiaratchi, Prof. Ems Wijeratne (2016) Ocean currents suggest where we should be looking for missing flight MH370.
https://theconversation.com/ocean-currents-suggest-where-we-should-be-looking-for-missing-flight-mh370-63100

12. List of Appendices.

A. Sample SQL Script for WSPR Download.

B. Sample Matlab Script for Call Sign processing.

C. Sample Matlab Script for Target Area processing.

D. Sample Matlab Script for Local or Global Mapping.

E. Sample SQL Script for WSPR Anomaly Checking.

F. Matlab Function Call WSPR_Link_GCV9_Function for Mapping.

G. Worked Example WSPR Link Timeframe Analysis.

H. Anomalous WSPR Link Timeframe Analysis.

A. Sample SQL Script for WSPR Download.

```
select
        id, time, tx_sign, tx_loc, rx_sign, rx_loc, frequency, power, snr, drift, distance,
azimuth, band, version, code
from wspr.rx where
        time = '2014-03-08 00:34:00'
order by tx_sign, rx_sign
limit 2000
```

B. Sample Matlab Script for Call Sign processing.

```
load("WSPR_0034_UTC.mat");
load("call_sign.mat");

call_sign_sz = size(call_sign);
s = call_sign_sz(1);

WSPR_sz = size(WSPR);
t = WSPR_sz(1);

%Missing Call Signs
sz = [200 3];
varT = {'string','string','string'};
call_signs_missing = table('Size',sz,'VariableTypes',varT);


cs_i = 1;

for m=1:t

   tx_sign = string(WSPR{m,4});

   n = 1;

   while n < s
      token = string(call_sign{n,"CallSign"});
      if token == tx_sign
         break
      end
      n=n+1;
   end

   if n >= s
      tx_loc = string(WSPR{m,5});
      call_signs_missing(cs_i,1) = {"Tx Call Sign"};
      call_signs_missing(cs_i,2) = {tx_sign};
      call_signs_missing(cs_i,3) = {tx_loc};
      cs_i = cs_i + 1;
   end

   tx_lat=double(call_sign{n,3});
   tx_lon=double(call_sign{n,4});
   tx_status=single(call_sign{n,5});

   WSPR{m,"tx_lat"}=tx_lat;
   WSPR{m,"tx_lon"}=tx_lon;
   WSPR{m,"tx_status"}=tx_status;

end

for m=1:t

   rx_sign = string(WSPR{m,6});

   n = 1;

   while n < s
      token = string(call_sign{n,"CallSign"});
```

```
        if token == rx_sign
            break
        end
        n=n+1;
    end

    if n >= s
        rx_loc = string(WSPR{m,7});
        call_signs_missing(cs_i,1) = {"Rx Call Sign"};
        call_signs_missing(cs_i,2) = {rx_sign};
        call_signs_missing(cs_i,3) = {rx_loc};
        cs_i = cs_i + 1;
    end


    rx_lat=double(call_sign{n,3});
    rx_lon=double(call_sign{n,4});
    rx_status=single(call_sign{n,5});

    WSPR{m,"rx_lat"}=rx_lat;
    WSPR{m,"rx_lon"}=rx_lon;
    WSPR{m,"rx_status"}=rx_status;

end

writetable(call_signs_missing,"Call Signs Missing.xlsx");
```

C. Sample Matlab Script for Target Area processing.

```
% Target Area (2° latitude x 4° longitude)
start_lat = -30.0;
start_lon = 98.0;

% Earth Reference Sphere
s = referenceSphere('Earth');
R=6378137;
s.LengthUnit = 'meter';
s.Radius=R;

%Targets
sz = [100 1];
varT = {'string'};
targets = table('Size',sz,'VariableTypes',varT);

target_i = 1;

for wspr_i = 1:m

   slat = WSPR{wspr_i,"tx_lat"};
   slon = WSPR{wspr_i,"tx_lon"};
   elat = WSPR{wspr_i,"rx_lat"};
   elon = WSPR{wspr_i,"rx_lon"};

   %Great Circle Tracks Short Path
   [arclen,az] = distance(slat,slon,elat,elon,s);

   %Great Circle Tracks Long Path
   arclenlp=40075016-arclen;
   azlp = azimuth(elat,elon,slat,slon,s)-180;

   %Great Circle Tracks Short Path Track Points
   [lttrk,lntrk] = track1(slat,slon,az,arclen,s,'degrees',300);

   for p_i = 1:300
      if round(lttrk(p_i),0) == start_lat
         if round(lntrk(p_i),0) == start_lon
            break
         end
      end
   end

   if p_i < 300
      s1 = "WSPR_Link_GCV9_Function('";
      s2 = WSPR{wspr_i,"tx_status"};
      s3 = "','";
      s4 = WSPR{wspr_i,"rx_status"};
      s5 = "','";
      s6 = num2str(WSPR{wspr_i,"tx_lat"},'%.8f');
      s7 = "','";
      s8 = num2str(WSPR{wspr_i,"tx_lon"},'%.8f');
      s9 = "','";
      s10 = num2str(WSPR{wspr_i,"rx_lat"},'%.8f');
      s11 = "','";
      s12 = num2str(WSPR{wspr_i,"rx_lon"},'%.8f');
      s13 = "','";
      s14 = WSPR{wspr_i,"tx_sign"};
```

```
    s15 = "','";
    s16 = WSPR{wspr_i,"rx_sign"};
    s17 = "');";
    sp_s = {s1 + s2 + s3 + s4 + s5 + s6 + s7 + s8 + s9 + s10 + s11 + s12 + s13 + s14 + s15 + s16 + s17};
    targets(target_i,1) = sp_s;
    target_i = target_i + 1;
end

for p_i = 1:300
    if round(lttrk(p_i),0) == start_lat
        if round(lntrk(p_i),0) == start_lon + 1
            break
        end
    end
end

if p_i < 300
    s1 = "WSPR_Link_GCV9_Function('";
    s2 = WSPR{wspr_i,"tx_status"};
    s3 = "','";
    s4 = WSPR{wspr_i,"rx_status"};
    s5 = "','";
    s6 = num2str(WSPR{wspr_i,"tx_lat"},'%.8f');
    s7 = "','";
    s8 = num2str(WSPR{wspr_i,"tx_lon"},'%.8f');
    s9 = "','";
    s10 = num2str(WSPR{wspr_i,"rx_lat"},'%.8f');
    s11 = "','";
    s12 = num2str(WSPR{wspr_i,"rx_lon"},'%.8f');
    s13 = "','";
    s14 = WSPR{wspr_i,"tx_sign"};
    s15 = "','";
    s16 = WSPR{wspr_i,"rx_sign"};
    s17 = "');";
    sp_s = {s1 + s2 + s3 + s4 + s5 + s6 + s7 + s8 + s9 + s10 + s11 + s12 + s13 + s14 + s15 + s16 + s17};
    targets(target_i,1) = sp_s;
    target_i = target_i + 1;
end

for p_i = 1:300
    if round(lttrk(p_i),0) == start_lat
        if round(lntrk(p_i),0) == start_lon + 2
            break
        end
    end
end

if p_i < 300
    s1 = "WSPR_Link_GCV9_Function('";
    s2 = WSPR{wspr_i,"tx_status"};
    s3 = "','";
    s4 = WSPR{wspr_i,"rx_status"};
    s5 = "','";
    s6 = num2str(WSPR{wspr_i,"tx_lat"},'%.8f');
    s7 = "','";
    s8 = num2str(WSPR{wspr_i,"tx_lon"},'%.8f');
    s9 = "','";
    s10 = num2str(WSPR{wspr_i,"rx_lat"},'%.8f');
    s11 = "','";
    s12 = num2str(WSPR{wspr_i,"rx_lon"},'%.8f');
```

```
    s13 = "','";
    s14 = WSPR{wspr_i,"tx_sign"};
    s15 = "','";
    s16 = WSPR{wspr_i,"rx_sign"};
    s17 = "');";
    sp_s = {s1 + s2 + s3 + s4 + s5 + s6 + s7 + s8 + s9 + s10 + s11 + s12 + s13 + s14 + s15 + s16 + s17};
    targets(target_i,1) = sp_s;
    target_i = target_i + 1;
end

for p_i = 1:300
    if round(lttrk(p_i),0) == start_lat
        if round(lntrk(p_i),0) == start_lon + 3
            break
        end
    end
end

if p_i < 300
    s1 = "WSPR_Link_GCV9_Function('";
    s2 = WSPR{wspr_i,"tx_status"};
    s3 = "','";
    s4 = WSPR{wspr_i,"rx_status"};
    s5 = "','";
    s6 = num2str(WSPR{wspr_i,"tx_lat"},'%.8f');
    s7 = "','";
    s8 = num2str(WSPR{wspr_i,"tx_lon"},'%.8f');
    s9 = "','";
    s10 = num2str(WSPR{wspr_i,"rx_lat"},'%.8f');
    s11 = "','";
    s12 = num2str(WSPR{wspr_i,"rx_lon"},'%.8f');
    s13 = "','";
    s14 = WSPR{wspr_i,"tx_sign"};
    s15 = "','";
    s16 = WSPR{wspr_i,"rx_sign"};
    s17 = "');";
    sp_s = {s1 + s2 + s3 + s4 + s5 + s6 + s7 + s8 + s9 + s10 + s11 + s12 + s13 + s14 + s15 + s16 + s17};
    targets(target_i,1) = sp_s;
    target_i = target_i + 1;
end

for p_i = 1:300
    if round(lttrk(p_i),0) == start_lat + 1
        if round(lntrk(p_i),0) == start_lon
            break
        end
    end
end

 if p_i < 300
    s1 = "WSPR_Link_GCV9_Function('";
    s2 = WSPR{wspr_i,"tx_status"};
    s3 = "','";
    s4 = WSPR{wspr_i,"rx_status"};
    s5 = "','";
    s6 = num2str(WSPR{wspr_i,"tx_lat"},'%.8f');
    s7 = "','";
    s8 = num2str(WSPR{wspr_i,"tx_lon"},'%.8f');
    s9 = "','";
    s10 = num2str(WSPR{wspr_i,"rx_lat"},'%.8f');
```

```
   s11 = "',';
   s12 = num2str(WSPR{wspr_i,"rx_lon"},'%.8f');
   s13 = "',';
   s14 = WSPR{wspr_i,"tx_sign"};
   s15 = "',';
   s16 = WSPR{wspr_i,"rx_sign"};
   s17 = "');";
   sp_s = {s1 + s2 + s3 + s4 + s5 + s6 + s7 + s8 + s9 + s10 + s11 + s12 + s13 + s14 + s15 + s16 + s17};
   targets(target_i,1) = sp_s;
   target_i = target_i + 1;
end

for p_i = 1:300
   if round(lttrk(p_i),0) == start_lat + 1
      if round(lntrk(p_i),0) == start_lon + 1
         break
      end
   end
end

if p_i < 300
   s1 = "WSPR_Link_GCV9_Function('";
   s2 = WSPR{wspr_i,"tx_status"};
   s3 = "',';
   s4 = WSPR{wspr_i,"rx_status"};
   s5 = "',';
   s6 = num2str(WSPR{wspr_i,"tx_lat"},'%.8f');
   s7 = "',';
   s8 = num2str(WSPR{wspr_i,"tx_lon"},'%.8f');
   s9 = "',';
   s10 = num2str(WSPR{wspr_i,"rx_lat"},'%.8f');
   s11 = "',';
   s12 = num2str(WSPR{wspr_i,"rx_lon"},'%.8f');
   s13 = "',';
   s14 = WSPR{wspr_i,"tx_sign"};
   s15 = "',';
   s16 = WSPR{wspr_i,"rx_sign"};
   s17 = "');";
   sp_s = {s1 + s2 + s3 + s4 + s5 + s6 + s7 + s8 + s9 + s10 + s11 + s12 + s13 + s14 + s15 + s16 + s17};
   targets(target_i,1) = sp_s;
   target_i = target_i + 1;
end

for p_i = 1:300
   if round(lttrk(p_i),0) == start_lat + 1
      if round(lntrk(p_i),0) == start_lon + 2
         break
      end
   end
end

if p_i < 300
   s1 = "WSPR_Link_GCV9_Function('";
   s2 = WSPR{wspr_i,"tx_status"};
   s3 = "',';
   s4 = WSPR{wspr_i,"rx_status"};
   s5 = "',';
   s6 = num2str(WSPR{wspr_i,"tx_lat"},'%.8f');
   s7 = "',';
   s8 = num2str(WSPR{wspr_i,"tx_lon"},'%.8f');
```

```
    s9 = "','";
    s10 = num2str(WSPR{wspr_i,"rx_lat"},'%.8f');
    s11 = "','";
    s12 = num2str(WSPR{wspr_i,"rx_lon"},'%.8f');
    s13 = "','";
    s14 = WSPR{wspr_i,"tx_sign"};
    s15 = "','";
    s16 = WSPR{wspr_i,"rx_sign"};
    s17 = "');";
    sp_s = {s1 + s2 + s3 + s4 + s5 + s6 + s7 + s8 + s9 + s10 + s11 + s12 + s13 + s14 + s15 + s16 + s17};
    targets(target_i,1) = sp_s;
    target_i = target_i + 1;
end


for p_i = 1:300
    if round(lttrk(p_i),0) == start_lat + 1
        if round(lntrk(p_i),0) == start_lon + 3
            break
        end
    end
end

if p_i < 300
    s1 = "WSPR_Link_GCV9_Function('";
    s2 = WSPR{wspr_i,"tx_status"};
    s3 = "','";
    s4 = WSPR{wspr_i,"rx_status"};
    s5 = "','";
    s6 = num2str(WSPR{wspr_i,"tx_lat"},'%.8f');
    s7 = "','";
    s8 = num2str(WSPR{wspr_i,"tx_lon"},'%.8f');
    s9 = "','";
    s10 = num2str(WSPR{wspr_i,"rx_lat"},'%.8f');
    s11 = "','";
    s12 = num2str(WSPR{wspr_i,"rx_lon"},'%.8f');
    s13 = "','";
    s14 = WSPR{wspr_i,"tx_sign"};
    s15 = "','";
    s16 = WSPR{wspr_i,"rx_sign"};
    s17 = "');";
    sp_s = {s1 + s2 + s3 + s4 + s5 + s6 + s7 + s8 + s9 + s10 + s11 + s12 + s13 + s14 + s15 + s16 + s17};
    targets(target_i,1) = sp_s;
    target_i = target_i + 1;
end

%Great Circle Tracks Long Path Track Points
[lttrk,lntrk] = track1(elat,elon,azlp,arclenlp,s,'degrees',300);

for p_i = 1:300
    if round(lttrk(p_i),0) == start_lat
        if round(lntrk(p_i),0) == start_lon
            break
        end
    end
end

if p_i < 300
    s1 = "WSPR_Link_GCV9_Function('";
    s2 = WSPR{wspr_i,"tx_status"};
```

```
    s3 = "','";
    s4 = WSPR{wspr_i,"rx_status"};
    s5 = "','";
    s6 = num2str(WSPR{wspr_i,"tx_lat"},'%.8f');
    s7 = "','";
    s8 = num2str(WSPR{wspr_i,"tx_lon"},'%.8f');
    s9 = "','";
    s10 = num2str(WSPR{wspr_i,"rx_lat"},'%.8f');
    s11 = "','";
    s12 = num2str(WSPR{wspr_i,"rx_lon"},'%.8f');
    s13 = "','";
    s14 = WSPR{wspr_i,"tx_sign"};
    s15 = "','";
    s16 = WSPR{wspr_i,"rx_sign"};
    s17 = "');";
    lp_s = {s1 + s2 + s3 + s4 + s5 + s6 + s7 + s8 + s9 + s10 + s11 + s12 + s13 + s14 + s15 + s16 + s17};
    targets(target_i,1) = lp_s;
    target_i = target_i + 1;
end

for p_i = 1:300
    if round(lttrk(p_i),0) == start_lat
        if round(lntrk(p_i),0) == start_lon + 1
            break
        end
    end
end

if p_i < 300
    s1 = "WSPR_Link_GCV9_Function('";
    s2 = WSPR{wspr_i,"tx_status"};
    s3 = "','";
    s4 = WSPR{wspr_i,"rx_status"};
    s5 = "','";
    s6 = num2str(WSPR{wspr_i,"tx_lat"},'%.8f');
    s7 = "','";
    s8 = num2str(WSPR{wspr_i,"tx_lon"},'%.8f');
    s9 = "','";
    s10 = num2str(WSPR{wspr_i,"rx_lat"},'%.8f');
    s11 = "','";
    s12 = num2str(WSPR{wspr_i,"rx_lon"},'%.8f');
    s13 = "','";
    s14 = WSPR{wspr_i,"tx_sign"};
    s15 = "','";
    s16 = WSPR{wspr_i,"rx_sign"};
    s17 = "');";
    lp_s = {s1 + s2 + s3 + s4 + s5 + s6 + s7 + s8 + s9 + s10 + s11 + s12 + s13 + s14 + s15 + s16 + s17};
    targets(target_i,1) = lp_s;
    target_i = target_i + 1;
end

for p_i = 1:300
    if round(lttrk(p_i),0) == start_lat
        if round(lntrk(p_i),0) == start_lon + 2
            break
        end
    end
end

if p_i < 300
```

```
    s1 = "WSPR_Link_GCV9_Function('";
    s2 = WSPR{wspr_i,"tx_status"};
    s3 = "','";
    s4 = WSPR{wspr_i,"rx_status"};
    s5 = "','";
    s6 = num2str(WSPR{wspr_i,"tx_lat"},'%.8f');
    s7 = "','";
    s8 = num2str(WSPR{wspr_i,"tx_lon"},'%.8f');
    s9 = "','";
    s10 = num2str(WSPR{wspr_i,"rx_lat"},'%.8f');
    s11 = "','";
    s12 = num2str(WSPR{wspr_i,"rx_lon"},'%.8f');
    s13 = "','";
    s14 = WSPR{wspr_i,"tx_sign"};
    s15 = "','";
    s16 = WSPR{wspr_i,"rx_sign"};
    s17 = "');";
    lp_s = {s1 + s2 + s3 + s4 + s5 + s6 + s7 + s8 + s9 + s10 + s11 + s12 + s13 + s14 + s15 + s16 + s17};
    targets(target_i,1) = lp_s;
    target_i = target_i + 1;
end

for p_i = 1:300
    if round(lttrk(p_i),0) == start_lat
        if round(lntrk(p_i),0) == start_lon + 3
            break
        end
    end
end

if p_i < 300
    s1 = "WSPR_Link_GCV9_Function('";
    s2 = WSPR{wspr_i,"tx_status"};
    s3 = "','";
    s4 = WSPR{wspr_i,"rx_status"};
    s5 = "','";
    s6 = num2str(WSPR{wspr_i,"tx_lat"},'%.8f');
    s7 = "','";
    s8 = num2str(WSPR{wspr_i,"tx_lon"},'%.8f');
    s9 = "','";
    s10 = num2str(WSPR{wspr_i,"rx_lat"},'%.8f');
    s11 = "','";
    s12 = num2str(WSPR{wspr_i,"rx_lon"},'%.8f');
    s13 = "','";
    s14 = WSPR{wspr_i,"tx_sign"};
    s15 = "','";
    s16 = WSPR{wspr_i,"rx_sign"};
    s17 = "');";
    lp_s = {s1 + s2 + s3 + s4 + s5 + s6 + s7 + s8 + s9 + s10 + s11 + s12 + s13 + s14 + s15 + s16 + s17};
    targets(target_i,1) = lp_s;
    target_i = target_i + 1;
end

for p_i = 1:300
    if round(lttrk(p_i),0) == start_lat + 1
        if round(lntrk(p_i),0) == start_lon
            break
        end
    end
end
```

```
if p_i < 300
   s1 = "WSPR_Link_GCV9_Function('";
   s2 = WSPR{wspr_i,"tx_status"};
   s3 = "','";
   s4 = WSPR{wspr_i,"rx_status"};
   s5 = "','";
   s6 = num2str(WSPR{wspr_i,"tx_lat"},'%.8f');
   s7 = "','";
   s8 = num2str(WSPR{wspr_i,"tx_lon"},'%.8f');
   s9 = "','";
   s10 = num2str(WSPR{wspr_i,"rx_lat"},'%.8f');
   s11 = "','";
   s12 = num2str(WSPR{wspr_i,"rx_lon"},'%.8f');
   s13 = "','";
   s14 = WSPR{wspr_i,"tx_sign"};
   s15 = "','";
   s16 = WSPR{wspr_i,"rx_sign"};
   s17 = "');";
   lp_s = {s1 + s2 + s3 + s4 + s5 + s6 + s7 + s8 + s9 + s10 + s11 + s12 + s13 + s14 + s15 + s16 + s17};
   targets(target_i,1) = lp_s;
   target_i = target_i + 1;
end

for p_i = 1:300
   if round(lttrk(p_i),0) == start_lat + 1
      if round(lntrk(p_i),0) == start_lon + 1
         break
      end
   end
end

if p_i < 300
   s1 = "WSPR_Link_GCV9_Function('";
   s2 = WSPR{wspr_i,"tx_status"};
   s3 = "','";
   s4 = WSPR{wspr_i,"rx_status"};
   s5 = "','";
   s6 = num2str(WSPR{wspr_i,"tx_lat"},'%.8f');
   s7 = "','";
   s8 = num2str(WSPR{wspr_i,"tx_lon"},'%.8f');
   s9 = "','";
   s10 = num2str(WSPR{wspr_i,"rx_lat"},'%.8f');
   s11 = "','";
   s12 = num2str(WSPR{wspr_i,"rx_lon"},'%.8f');
   s13 = "','";
   s14 = WSPR{wspr_i,"tx_sign"};
   s15 = "','";
   s16 = WSPR{wspr_i,"rx_sign"};
   s17 = "');";
   lp_s = {s1 + s2 + s3 + s4 + s5 + s6 + s7 + s8 + s9 + s10 + s11 + s12 + s13 + s14 + s15 + s16 + s17};
   targets(target_i,1) = lp_s;
   target_i = target_i + 1;
end

for p_i = 1:300
   if round(lttrk(p_i),0) == start_lat + 1
      if round(lntrk(p_i),0) == start_lon + 2
         break
      end
```

```
        end
    end

    if p_i < 300
        s1 = "WSPR_Link_GCV9_Function('";
        s2 = WSPR{wspr_i,"tx_status"};
        s3 = "','";
        s4 = WSPR{wspr_i,"rx_status"};
        s5 = "','";
        s6 = num2str(WSPR{wspr_i,"tx_lat"},'%.8f');
        s7 = "','";
        s8 = num2str(WSPR{wspr_i,"tx_lon"},'%.8f');
        s9 = "','";
        s10 = num2str(WSPR{wspr_i,"rx_lat"},'%.8f');
        s11 = "','";
        s12 = num2str(WSPR{wspr_i,"rx_lon"},'%.8f');
        s13 = "','";
        s14 = WSPR{wspr_i,"tx_sign"};
        s15 = "','";
        s16 = WSPR{wspr_i,"rx_sign"};
        s17 = "')";";
        lp_s = {s1 + s2 + s3 + s4 + s5 + s6 + s7 + s8 + s9 + s10 + s11 + s12 + s13 + s14 + s15 + s16 + s17};
        targets(target_i,1) = lp_s;
        target_i = target_i + 1;
    end

    for p_i = 1:300
        if round(lttrk(p_i),0) == start_lat + 1
            if round(lntrk(p_i),0) == start_lon + 3
                break
            end
        end
    end

    if p_i < 300
        s1 = "WSPR_Link_GCV9_Function('";
        s2 = WSPR{wspr_i,"tx_status"};
        s3 = "','";
        s4 = WSPR{wspr_i,"rx_status"};
        s5 = "','";
        s6 = num2str(WSPR{wspr_i,"tx_lat"},'%.8f');
        s7 = "','";
        s8 = num2str(WSPR{wspr_i,"tx_lon"},'%.8f');
        s9 = "','";
        s10 = num2str(WSPR{wspr_i,"rx_lat"},'%.8f');
        s11 = "','";
        s12 = num2str(WSPR{wspr_i,"rx_lon"},'%.8f');
        s13 = "','";
        s14 = WSPR{wspr_i,"tx_sign"};
        s15 = "','";
        s16 = WSPR{wspr_i,"rx_sign"};
        s17 = "')";";
        lp_s = {s1 + s2 + s3 + s4 + s5 + s6 + s7 + s8 + s9 + s10 + s11 + s12 + s13 + s14 + s15 + s16 + s17};
        targets(target_i,1) = lp_s;
        target_i = target_i + 1;
    end
end

writetable(targets,"WSPR Targets.xlsx");
```

D. Sample Matlab Script for Local or Global Mapping.

```
figure('Name','GDTAAA Flight Path Analysis','Position',[50,50,1200,800]);

glob = '0';

if glob == '1'
   LatLimit=[-80 80];
   LonLimit=[-180 180];
   h=worldmap(LatLimit,LonLimit);
   setm(h,'MLabelParallel',-80.0);
else
   LatLimit=[-23.0 -20.0];
   LonLimit=[92.0 98.0];
   h=worldmap(LatLimit,LonLimit);
   setm(h,'MLabelParallel',-23.0);
   setm(h,'PLabelLocation',[-23.0, -22.0, -21.0, -20.0]);
   setm(h,'MLabelLocation',[92.0, 93.0, 94.0, 95.0, 96.0, 97.0, 98.0]);
end

landareas = shaperead('landareas.shp','UseGeoCoords',true);
geoshow(landareas,'FaceColor',[.9 .9 .9],'EdgeColor',[.6 .6 .6]);

if glob == '0'
   scaleruler on
   h=handlem('scaleruler1');
   setm(h,'XLoc',-0.150e+06);
   setm(h,'YLoc',-25.900e+05);
   setm(h,'MajorTick',0:20:100);
   setm(h,'MinorTick',0:1:10);
   setm(h,'MajorTickLength',1);
   setm(h,'MinorTickLength',0.5);
   setm(h,'TickDir','up');
   scaleruler('units','nm');
   h=handlem('scaleruler2');
   setm(h,'XLoc',0.020e+06);
   setm(h,'YLoc',-25.900e+05);
   setm(h,'MajorTick',0:20:100);
   setm(h,'MinorTick',0:1:10);
   setm(h,'MajorTickLength',km2nm(1));
   setm(h,'MinorTickLength',km2nm(0.5));
   setm(h,'TickDir','up');
end


% WSPR Links

% WSPR_Link_GCV9_Function('0','1','51.27083335','6.79166664','52.33746900','-2.27851600','DF2JP','G1ZRN');
% WSPR_Link_GCV9_Function('4','1','50.78080100','0.10020200','49.52370266','8.24777591','G3JKF','DK6UG');
% WSPR_Link_GCV9_Function('1','0','50.78080100','0.10020200','50.97916674','-1.37500002','G3JKF','G8JNJ/A');
% WSPR_Link_GCV9_Function('3','0','51.35188900','-0.15826000','44.39583336','26.20833333','G4FKK','YO3ITD');
% WSPR_Link_GCV9_Function('0','0','52.40423508','0.27702300','51.43750003','6.95833330','G4KPX','DC0DX/A');
% WSPR_Link_GCV9_Function('1','0','52.40423508','0.27702300','51.35416669','8.12500000','G4KPX','DL1DBC');
% WSPR_Link_GCV9_Function('0','0','52.40423508','0.27702300','51.80847356','4.70791832','G4KPX','PA3ABK/2');
% WSPR_Link_GCV9_Function('1','1','50.86820200','-0.13595600','26.96563955','-82.32011327','G4WCP','W4AC');
WSPR_Link_GCV9_Function('1','1','50.93750007','-1.29166669','49.52370266','8.24777591','G6RRL','DK6UG');
% WSPR_Link_GCV9_Function('1','1','51.50048800','-0.31508400','26.96563955','-82.32011327','G8VDQ','W4AC');
WSPR_Link_GCV9_Function('1','1','36.33690300','139.01551900','32.72916672','-95.04166670','JH1GYE','KD6RF');
% WSPR_Link_GCV9_Function('1','1','51.39158150','-2.95518072','49.52370266','8.24777591','M0NDE','DK6UG');
% WSPR_Link_GCV9_Function('4','0','-38.11628400','145.16138100','-31.85416666','115.79166660','VK3DXE','VK6ZRY');
% WSPR_Link_GCV9_Function('1','1','27.10306700','-82.39671500','52.47916670','-2.04166674','W4MO','2E0DSS');
% WSPR_Link_GCV9_Function('1','0','27.10306700','-82.39671500','53.47916670','-2.54166672','W4MO','2E1CJF');
% WSPR_Link_GCV9_Function('1','1','27.10306700','-82.39671500','32.78086100','34.99031300','W4MO','4X1RF');
% WSPR_Link_GCV9_Function('1','1','27.10306700','-82.39671500','49.52370266','8.24777591','W4MO','DK6UG');
% WSPR_Link_GCV9_Function('1','0','27.10306700','-82.39671500','50.60416670','-3.87500000','W4MO','G4DND');
% WSPR_Link_GCV9_Function('1','1','27.10306700','-82.39671500','57.52083330','-4.37500000','W4MO','GM4SFW');
% WSPR_Link_GCV9_Function('1','0','27.10306700','-82.39671500','44.85416673','7.54166661','W4MO','IK1NET');
% WSPR_Link_GCV9_Function('1','1','27.10306700','-82.39671500','38.35372470','-78.45945496','W4MO','K4RCG');
% WSPR_Link_GCV9_Function('1','0','27.10306700','-82.39671500','53.47916670','-1.12500003','W4MO','M5ADA');
% WSPR_Link_GCV9_Function('1','1','27.10306700','-82.39671500','51.20351600','-0.33178500','W4MO','M6NNB');
% WSPR_Link_GCV9_Function('1','0','27.10306700','-82.39671500','48.68750005','15.62499994','W4MO','OE3VMS');
```

```
% WSPR_Link_GCV9_Function('1','1','27.10306700','-82.39671500','51.18750001','4.20833333','W4MO','ON4SAR');
% WSPR_Link_GCV9_Function('1','1','27.10306700','-82.39671500','55.24975200','12.30082000','W4MO','OZ7IT');
% WSPR_Link_GCV9_Function('1','1','27.10306700','-82.39671500','52.23807201','6.85770275','W4MO','PI4THT');
% WSPR_Link_GCV9_Function('0','0','27.10306700','-82.39671500','59.47916670','17.70833327','W4MO','SM3ULC');
% WSPR_Link_GCV9_Function('1','0','27.10306700','-82.39671500','44.77083339','-63.70833334','W4MO','VE1AIM');
% WSPR_Link_GCV9_Function('1','1','27.10306700','-82.39671500','39.46108700','-76.80855118','W4MO','W3GXT');
% WSPR_Link_GCV9_Function('0','0','39.56250004','-104.87500004','32.97916674','-97.12500003','W5OLF','AD4PT');
% WSPR_Link_GCV9_Function('1','1','34.77307873','-86.69914586','40.11087200','-88.19699300','WD0UG','K9AN');
WSPR_Link_GCV9_Function('1','0','34.77307873','-86.69914586','44.37883000','-88.18698700','WD0UG','KB9VLR');
% WSPR_Link_GCV9_Function('1','1','36.19872900','-79.83413800','38.35372470','-78.45945496','WD4ELG','K4RCG');


if glob == '0'


% Waypoints


   geoshow(5.29674258,100.27632618,'Marker','square','color','k','MarkerSize',12);
   textm(5.30,100.33,'Penang Airport');

   geoshow(5.68424584,98.93855228,'Marker','square','color','k','MarkerSize',12);
   textm(5.70,98.98,'Pulau Perak');

   geoshow(6.18200000,97.58550000,'Marker','diamond','color','k','MarkerSize',12);
   textm(6.20,97.62,'VAMPI');

   geoshow(6.50366667,96.49133333,'Marker','diamond','color','k','MarkerSize',12);
   textm(6.52,96.53,'MEKAR');

   geoshow(5.25833333,98.30016667,'Marker','diamond','color','k','MarkerSize',12);
   textm(5.28,98.34,'TASEK');

   geoshow(5.26600000,97.51133333,'Marker','diamond','color','k','MarkerSize',12);
   textm(5.24,97.55,'DUAMO');

   geoshow(6.75633333,95.97650000,'Marker','diamond','color','k','MarkerSize',12);
   textm(6.80,96.00,'NILAM');

   geoshow(5.82366667,97.31366667,'Marker','diamond','color','k','MarkerSize',12);
   textm(5.83,97.34,'BOSTI');

   geoshow(6.00016667,95.50800000,'Marker','diamond','color','k','MarkerSize',12);
   textm(5.93,95.54,'ANSAX');

   geoshow(6.58600000,95.66900000,'Marker','diamond','color','k','MarkerSize',12);
   textm(6.60,95.36,'SANOB');

   geoshow(6.00016667,97.00000000,'Marker','diamond','color','k','MarkerSize',12);
   textm(6.03,97.03,'TOSOK');

   geoshow(7.51716667,94.41650000,'Marker','diamond','color','k','MarkerSize',12);
   textm(7.54,94.45,'IGOGU');

   geoshow(6.60400000,94.41650000,'Marker','diamond','color','k','MarkerSize',12);
   textm(6.63,94.45,'NOPEK');

   geoshow(6.00000000,94.41650000,'Marker','diamond','color','k','MarkerSize',12);
   textm(5.90,93.95,'FIR Boundary');

   geoshow(5.37266667,94.47200000,'Marker','diamond','color','k','MarkerSize',12);
   textm(5.40,94.50,'URDAM');

   geoshow(4.56650000,94.00016667,'Marker','diamond','color','k','MarkerSize',12);
   textm(4.55,94.05,'BULVA');

   geoshow(3.26616667,94.84883333,'Marker','diamond','color','k','MarkerSize',12);
   textm(3.30,94.89,'MABIX');

   geoshow(-0.70000000,92.00000000,'Marker','diamond','color','k','MarkerSize',12);
   textm(-0.73,92.03,'KETIV');
```

```
geoshow(0.36700000,93.67500000,'Marker','diamond','color','k','MarkerSize',12);
textm(0.40,93.70,'ISBIX');

geoshow(-0.33016667,95.10100000,'Marker','diamond','color','k','MarkerSize',12);
textm(-0.36,95.14,'ODIRU');

geoshow(-2.00000000,92.00000000,'Marker','diamond','color','k','MarkerSize',12);
textm(-2.03,92.03,'FIR Boundary 02S92E');

geoshow(-1.99983333,89.96150000,'Marker','diamond','color','k','MarkerSize',12);
textm(-1.96,89.99,'ELATI');

geoshow(-4.36833333,92.54166667,'Marker','diamond','color','k','MarkerSize',12);
textm(-4.39,92.57,'PIPOV');

geoshow(-4.48000000,92.97833333,'Marker','diamond','color','k','MarkerSize',12);
textm(-4.51,93.00,'MUTMI');

geoshow(-5.33666667,90.73316667,'Marker','diamond','color','k','MarkerSize',12);
textm(-5.37,91.00,'PIBED');

geoshow(-12.14533333,96.81950000,'Marker','diamond','color','k','MarkerSize',12);
textm(-12.18,96.85,'CC');

geoshow(-10.64433333,93.83533333,'Marker','diamond','color','k','MarkerSize',12);
textm(-10.68,93.90,'BEBIM');

geoshow(-14.0,93.0,'Marker','diamond','color','k','MarkerSize',12);
textm(-14.03,93.03,'14S93E');

geoshow(-16.0,95.0,'Marker','diamond','color','k','MarkerSize',12);
textm(-16.03,95.03,'16S95E');

geoshow(-16.0,94.0,'Marker','diamond','color','k','MarkerSize',12);
textm(-16.03,94.03,'16S94E');

geoshow(-17.0,96.0,'Marker','diamond','color','k','MarkerSize',12);
textm(-17.03,96.03,'17S96E');

geoshow(-20.0,95.0,'Marker','diamond','color','k','MarkerSize',12);
textm(-20.03,95.03,'20S95E');

geoshow(-20.0,96.0,'Marker','diamond','color','k','MarkerSize',12);
textm(-20.03,96.03,'20S96E');

geoshow(-20.0,94.0,'Marker','diamond','color','k','MarkerSize',12);
textm(-20.03,94.03,'20S94E');

geoshow(-22.0,94.0,'Marker','diamond','color','k','MarkerSize',12);
textm(-22.03,94.03,'22S94E');

geoshow(-22.0,96.0,'Marker','diamond','color','k','MarkerSize',12);
textm(-22.03,96.03,'22S96E');

geoshow(-21.0,98.0,'Marker','diamond','color','k','MarkerSize',12);
textm(-21.03,98.03,'21S98E');


%Arcs


waypoints = [10.0,95.204601; 9.0,95.430192];
[lttrk,lntrk] = track('gc',waypoints,'degrees');
geoshow(lttrk,lntrk,'DisplayType','line','LineStyle','--','color','k','LineWidth',1);
waypoints = [9.0,95.430192; 8.0,95.624242];
[lttrk,lntrk] = track('gc',waypoints,'degrees');
geoshow(lttrk,lntrk,'DisplayType','line','LineStyle','--','color','k','LineWidth',1);
waypoints = [8.0,95.624242; 7.0,95.787636];
[lttrk,lntrk] = track('gc',waypoints,'degrees');
geoshow(lttrk,lntrk,'DisplayType','line','LineStyle','--','color','k','LineWidth',1);
waypoints = [7.0,95.787636; 6.0,95.921108];
```

```
[lttrk,lntrk] = track('gc',waypoints,'degrees');
geoshow(lttrk,lntrk,'DisplayType','line','LineStyle','--','color','k','LineWidth',1);
waypoints = [6.0,95.921108; 5.0,96.025255];
[lttrk,lntrk] = track('gc',waypoints,'degrees');
geoshow(lttrk,lntrk,'DisplayType','line','LineStyle','--','color','k','LineWidth',1);
waypoints = [5.0,96.025255; 4.0,96.100549];
[lttrk,lntrk] = track('gc',waypoints,'degrees');
geoshow(lttrk,lntrk,'DisplayType','line','LineStyle','--','color','k','LineWidth',1);
waypoints = [4.0,96.100549; 3.0,96.147336];
[lttrk,lntrk] = track('gc',waypoints,'degrees');
geoshow(lttrk,lntrk,'DisplayType','line','LineStyle','--','color','k','LineWidth',1);
waypoints = [3.0,96.147336; 2.0,96.165852];
[lttrk,lntrk] = track('gc',waypoints,'degrees');
geoshow(lttrk,lntrk,'DisplayType','line','LineStyle','--','color','k','LineWidth',1);
waypoints = [2.0,96.165852; 1.0,96.156217];
[lttrk,lntrk] = track('gc',waypoints,'degrees');
geoshow(lttrk,lntrk,'DisplayType','line','LineStyle','--','color','k','LineWidth',1);
waypoints = [1.0,96.156217; 0.0,96.118440];
[lttrk,lntrk] = track('gc',waypoints,'degrees');
geoshow(lttrk,lntrk,'DisplayType','line','LineStyle','--','color','k','LineWidth',1);

textm(6.9,95.9,'1st Arc at 18:28:15 UTC ','EdgeColor','k','BackgroundColor','w','HorizontalAlignment','left');


waypoints = [10.0,92.719602; 9.0,92.967769];
[lttrk,lntrk] = track('gc',waypoints,'degrees');
geoshow(lttrk,lntrk,'DisplayType','line','LineStyle','--','color','k','LineWidth',1);
waypoints = [9.0,92.967769; 8.0,93.180803];
[lttrk,lntrk] = track('gc',waypoints,'degrees');
geoshow(lttrk,lntrk,'DisplayType','line','LineStyle','--','color','k','LineWidth',1);
waypoints = [8.0,93.180803; 7.0,93.359809];
[lttrk,lntrk] = track('gc',waypoints,'degrees');
geoshow(lttrk,lntrk,'DisplayType','line','LineStyle','--','color','k','LineWidth',1);
waypoints = [7.0,93.359809; 6.0,93.505697];
[lttrk,lntrk] = track('gc',waypoints,'degrees');
geoshow(lttrk,lntrk,'DisplayType','line','LineStyle','--','color','k','LineWidth',1);
waypoints = [6.0,93.505697; 5.0,93.619204];
[lttrk,lntrk] = track('gc',waypoints,'degrees');
geoshow(lttrk,lntrk,'DisplayType','line','LineStyle','--','color','k','LineWidth',1);
waypoints = [5.0,93.619204; 4.0,93.700905];
[lttrk,lntrk] = track('gc',waypoints,'degrees');
geoshow(lttrk,lntrk,'DisplayType','line','LineStyle','--','color','k','LineWidth',1);
waypoints = [4.0,93.700905; 3.0,93.751222];
[lttrk,lntrk] = track('gc',waypoints,'degrees');
geoshow(lttrk,lntrk,'DisplayType','line','LineStyle','--','color','k','LineWidth',1);
waypoints = [3.0,93.751222; 2.0,93.770435];
[lttrk,lntrk] = track('gc',waypoints,'degrees');
geoshow(lttrk,lntrk,'DisplayType','line','LineStyle','--','color','k','LineWidth',1);
waypoints = [2.0,93.770435; 1.0,93.758682];
[lttrk,lntrk] = track('gc',waypoints,'degrees');
geoshow(lttrk,lntrk,'DisplayType','line','LineStyle','--','color','k','LineWidth',1);
waypoints = [1.0,93.758682; 0.0,93.715965];
[lttrk,lntrk] = track('gc',waypoints,'degrees');
geoshow(lttrk,lntrk,'DisplayType','line','LineStyle','--','color','k','LineWidth',1);
waypoints = [0.0,93.715965; -1.0,93.642149];
[lttrk,lntrk] = track('gc',waypoints,'degrees');
geoshow(lttrk,lntrk,'DisplayType','line','LineStyle','--','color','k','LineWidth',1);
waypoints = [-1.0,93.642149; -2.0,93.536956];
[lttrk,lntrk] = track('gc',waypoints,'degrees');
geoshow(lttrk,lntrk,'DisplayType','line','LineStyle','--','color','k','LineWidth',1);
waypoints = [-2.0,93.536956; -3.0,93.399966];
[lttrk,lntrk] = track('gc',waypoints,'degrees');
geoshow(lttrk,lntrk,'DisplayType','line','LineStyle','--','color','k','LineWidth',1);
waypoints = [-3.0,93.399966; -4.0,93.230606];
[lttrk,lntrk] = track('gc',waypoints,'degrees');
geoshow(lttrk,lntrk,'DisplayType','line','LineStyle','--','color','k','LineWidth',1);
waypoints = [-4.0,93.230606; -5.0,93.028139];
[lttrk,lntrk] = track('gc',waypoints,'degrees');
geoshow(lttrk,lntrk,'DisplayType','line','LineStyle','--','color','k','LineWidth',1);

textm(-3.1,92.50,'2nd Arc at 19:41:03 UTC ','EdgeColor','k','BackgroundColor','w','HorizontalAlignment','left');
```

```
waypoints = [-1.0,94.295993;-2.0,94.195528];
[lttrk,lntrk] = track('gc',waypoints,'degrees');
geoshow(lttrk,lntrk,'DisplayType','line','LineStyle','--','color','k','LineWidth',1);
waypoints = [-2.0,94.195528;-3.0,94.064163];
[lttrk,lntrk] = track('gc',waypoints,'degrees');
geoshow(lttrk,lntrk,'DisplayType','line','LineStyle','--','color','k','LineWidth',1);
waypoints = [-3.0,94.064163; -4.0,93.901368];
[lttrk,lntrk] = track('gc',waypoints,'degrees');
geoshow(lttrk,lntrk,'DisplayType','line','LineStyle','--','color','k','LineWidth',1);
waypoints = [-4.0,93.901368; -5.0,93.706464];
[lttrk,lntrk] = track('gc',waypoints,'degrees');
geoshow(lttrk,lntrk,'DisplayType','line','LineStyle','--','color','k','LineWidth',1);
waypoints = [-5.0,93.706464; -6.0,93.478606];
[lttrk,lntrk] = track('gc',waypoints,'degrees');
geoshow(lttrk,lntrk,'DisplayType','line','LineStyle','--','color','k','LineWidth',1);
waypoints = [-6.0,93.478606; -7.0,93.216772];
[lttrk,lntrk] = track('gc',waypoints,'degrees');
geoshow(lttrk,lntrk,'DisplayType','line','LineStyle','--','color','k','LineWidth',1);
waypoints = [-7.0,93.216772; -8.0,92.919740];
[lttrk,lntrk] = track('gc',waypoints,'degrees');
geoshow(lttrk,lntrk,'DisplayType','line','LineStyle','--','color','k','LineWidth',1);
waypoints = [-8.0,92.919740; -9.0,92.586062];
[lttrk,lntrk] = track('gc',waypoints,'degrees');
geoshow(lttrk,lntrk,'DisplayType','line','LineStyle','--','color','k','LineWidth',1);
waypoints = [-9.0,92.586062; -10.0,92.214036];
[lttrk,lntrk] = track('gc',waypoints,'degrees');
geoshow(lttrk,lntrk,'DisplayType','line','LineStyle','--','color','k','LineWidth',1);

textm(-7.1,92.60,'3rd Arc at 20:41:05 UTC ','EdgeColor','k','BackgroundColor','w','HorizontalAlignment','left');

waypoints = [-9.0,95.400910; -10.0,95.074252];
[lttrk,lntrk] = track('gc',waypoints,'degrees');
geoshow(lttrk,lntrk,'DisplayType','line','LineStyle','--','color','k','LineWidth',1);
waypoints = [-10.0,95.074252; -11.0,94.712797];
[lttrk,lntrk] = track('gc',waypoints,'degrees');
geoshow(lttrk,lntrk,'DisplayType','line','LineStyle','--','color','k','LineWidth',1);
waypoints = [-11.0,94.712797; -12.0,94.314850];
[lttrk,lntrk] = track('gc',waypoints,'degrees');
geoshow(lttrk,lntrk,'DisplayType','line','LineStyle','--','color','k','LineWidth',1);
waypoints = [-12.0,94.314850; -13.0,93.878443];
[lttrk,lntrk] = track('gc',waypoints,'degrees');
geoshow(lttrk,lntrk,'DisplayType','line','LineStyle','--','color','k','LineWidth',1);
waypoints = [-13.0,93.878443; -14.0,93.401296];
[lttrk,lntrk] = track('gc',waypoints,'degrees');
geoshow(lttrk,lntrk,'DisplayType','line','LineStyle','--','color','k','LineWidth',1);
waypoints = [-14.0,93.401296; -15.0,92.880756];
[lttrk,lntrk] = track('gc',waypoints,'degrees');
geoshow(lttrk,lntrk,'DisplayType','line','LineStyle','--','color','k','LineWidth',1);
waypoints = [-15.0,92.880756; -16.0,92.313720];
[lttrk,lntrk] = track('gc',waypoints,'degrees');
geoshow(lttrk,lntrk,'DisplayType','line','LineStyle','--','color','k','LineWidth',1);

textm(-13.15,93.0,'4th Arc at 21:41:27 UTC ','EdgeColor','k','BackgroundColor','w','HorizontalAlignment','left');


waypoints = [-16.0,97.152797; -17.0,96.653230];
[lttrk,lntrk] = track('gc',waypoints,'degrees');
geoshow(lttrk,lntrk,'DisplayType','line','LineStyle','--','color','k','LineWidth',1);
waypoints = [-17.0,96.653230; -18.0,96.113237];
[lttrk,lntrk] = track('gc',waypoints,'degrees');
geoshow(lttrk,lntrk,'DisplayType','line','LineStyle','--','color','k','LineWidth',1);
waypoints = [-18.0,96.113237; -19.0,95.529978];
[lttrk,lntrk] = track('gc',waypoints,'degrees');
geoshow(lttrk,lntrk,'DisplayType','line','LineStyle','--','color','k','LineWidth',1);
waypoints = [-19.0,95.529978; -20.0,94.900162];
[lttrk,lntrk] = track('gc',waypoints,'degrees');
geoshow(lttrk,lntrk,'DisplayType','line','LineStyle','--','color','k','LineWidth',1);
waypoints = [-20.0,94.900162; -21.0,94.219947];
[lttrk,lntrk] = track('gc',waypoints,'degrees');
geoshow(lttrk,lntrk,'DisplayType','line','LineStyle','--','color','k','LineWidth',1);
waypoints = [-21.0,94.219947; -22.0,93.484818];
```

```
[lttrk,lntrk] = track('gc',waypoints,'degrees');
geoshow(lttrk,lntrk,'DisplayType','line','LineStyle','--','color','k','LineWidth',1);

textm(-19.2,95.6,'5th Arc at 22:41:22 UTC ' ,'EdgeColor','k','BackgroundColor','w','HorizontalAlignment','left');

waypoints = [-23.0,102.224997; -24.0,101.644677];
[lttrk,lntrk] = track('gc',waypoints,'degrees');
geoshow(lttrk,lntrk,'DisplayType','line','LineStyle',':','color','b','LineWidth',2);
waypoints = [-24.0,101.644677; -25.0,101.023959];
[lttrk,lntrk] = track('gc',waypoints,'degrees');
geoshow(lttrk,lntrk,'DisplayType','line','LineStyle',':','color','b','LineWidth',2);
waypoints = [-25.0,101.023959; -26.0,100.359782];
[lttrk,lntrk] = track('gc',waypoints,'degrees');
geoshow(lttrk,lntrk,'DisplayType','line','LineStyle',':','color','b','LineWidth',2);
waypoints = [-26.0,100.359782; -27.0,99.648631];
[lttrk,lntrk] = track('gc',waypoints,'degrees');
geoshow(lttrk,lntrk,'DisplayType','line','LineStyle',':','color','b','LineWidth',2);
waypoints = [-27.0,99.648631; -28.0,98.886445];
[lttrk,lntrk] = track('gc',waypoints,'degrees');
geoshow(lttrk,lntrk,'DisplayType','line','LineStyle',':','color','b','LineWidth',2);
waypoints = [-28.0,98.886445; -29.0,98.068491];
[lttrk,lntrk] = track('gc',waypoints,'degrees');
geoshow(lttrk,lntrk,'DisplayType','line','LineStyle',':','color','b','LineWidth',2);
waypoints = [-29.0,98.068491; -30.0,97.189202];
[lttrk,lntrk] = track('gc',waypoints,'degrees');
geoshow(lttrk,lntrk,'DisplayType','line','LineStyle',':','color','b','LineWidth',2);
waypoints = [-30.0,97.189202; -31.0,96.241966];
[lttrk,lntrk] = track('gc',waypoints,'degrees');
geoshow(lttrk,lntrk,'DisplayType','line','LineStyle',':','color','b','LineWidth',2);
waypoints = [-31.0,96.241966; -32.0,95.218821];
[lttrk,lntrk] = track('gc',waypoints,'degrees');
geoshow(lttrk,lntrk,'DisplayType','line','LineStyle',':','color','b','LineWidth',2);
waypoints = [-32.0,95.218821; -33.0,94.110040];
[lttrk,lntrk] = track('gc',waypoints,'degrees');
geoshow(lttrk,lntrk,'DisplayType','line','LineStyle',':','color','b','LineWidth',2);
waypoints = [-33.0,94.110040; -34.0,92.903528];
[lttrk,lntrk] = track('gc',waypoints,'degrees');
geoshow(lttrk,lntrk,'DisplayType','line','LineStyle',':','color','b','LineWidth',2);

textm(-23.0,103.0,'6th Arc ' ,'EdgeColor','k','BackgroundColor','w','HorizontalAlignment','left');

% Flight Track Points


geoshow(5.58911792,99.16522840,'Marker','*','color','r','MarkerSize',12);
geoshow(5.413,98.200,'Marker','*','color','r','MarkerSize',12);
geoshow(5.36239182,97.92430148,'Marker','*','color','r','MarkerSize',12);
geoshow(5.566,97.732,'Marker','*','color','r','MarkerSize',12);
geoshow(5.728,97.502,'Marker','*','color','r','MarkerSize',12);
geoshow(5.830,96.667,'Marker','*','color','r','MarkerSize',12);
geoshow(6.142,96.202,'Marker','*','color','r','MarkerSize',12);

geoshow(6.525,95.850,'Marker','*','color','k','MarkerSize',12);
geoshow(6.525,95.850,'Marker','o','color','k','MarkerSize',20);
str={' 1st Arc 18:28:14.904 UTC ', ...
    ' BTO Residual -1.0368 µs ', ...
    ' BFO Residual -0.0030 Hz '};
textm(6.52,96.35,str,'EdgeColor','k','BackgroundColor','w','HorizontalAlignment','center');

geoshow(6.88431518,95.58854742,'Marker','*','color','r','MarkerSize',12);
geoshow(6.726,95.358,'Marker','*','color','r','MarkerSize',12);
geoshow(6.56757525,95.12760184,'Marker','*','color','r','MarkerSize',12);

geoshow(6.10148080,94.82016820,'Marker','*','color','k','MarkerSize',12);
geoshow(6.10148080,94.82016820,'Marker','o','color','k','MarkerSize',20);
str={' SATCOM Call 18:39:55.354 UTC ', ...
    ' BFO Residual 1.5182 Hz '};
textm(6.10,95.42,str,'EdgeColor','k','BackgroundColor','w','HorizontalAlignment','center');

geoshow(5.402,94.360,'Marker','*','color','r','MarkerSize',12);
geoshow(4.627,94.027,'Marker','*','color','r','MarkerSize',12);
geoshow(4.374,94.146,'Marker','*','color','r','MarkerSize',12);
```

```
geoshow(3.603,94.489,'Marker','*','color','r','MarkerSize',12);
geoshow(2.775,95.250,'Marker','*','color','r','MarkerSize',12);
geoshow(2.4965,95.227,'Marker','*','color','r','MarkerSize',12);
geoshow(1.815,94.732,'Marker','*','color','r','MarkerSize',12);
geoshow(1.218,94.302,'Marker','*','color','r','MarkerSize',12);
geoshow(1.00487505,94.14794281,'Marker','*','color','r','MarkerSize',12);
geoshow(0.79174251,93.99390559,'Marker','*','color','r','MarkerSize',12);
geoshow(0.695,93.729,'Marker','*','color','r','MarkerSize',12);
geoshow(0.560,93.183,'Marker','*','color','r','MarkerSize',12);
geoshow(0.294,93.274,'Marker','*','color','r','MarkerSize',12);
geoshow(0.070,93.460,'Marker','*','color','r','MarkerSize',12);
geoshow(-0.15400077,93.64599824,'Marker','*','color','r','MarkerSize',12);
geoshow(-0.422,93.7315,'Marker','*','color','r','MarkerSize',12);

geoshow(-0.758,93.639,'Marker','*','color','k','MarkerSize',12);
geoshow(-0.758,93.639,'Marker','o','color','k','MarkerSize',20);
str={' 2nd Arc 19:41:02.906 UTC ', ...
    ' BTO Residual -8.3100 μs ', ...
    ' BFO Residual -0.0017 Hz '};
textm(-0.75,94.25,str,'EdgeColor','k','BackgroundColor','w','HorizontalAlignment','center');

geoshow(-1.420,92.800,'Marker','*','color','r','MarkerSize',12);
geoshow(-1.626,92.516,'Marker','*','color','r','MarkerSize',12);
geoshow(-1.676,92.241,'Marker','*','color','r','MarkerSize',12);
geoshow(-2.105,91.880,'Marker','*','color','r','MarkerSize',12);
geoshow(-2.645,91.725,'Marker','*','color','r','MarkerSize',12);
geoshow(-2.70,92.00,'Marker','*','color','r','MarkerSize',12);
geoshow(-2.648,92.277,'Marker','*','color','r','MarkerSize',12);
geoshow(-3.747,92.504,'Marker','*','color','r','MarkerSize',12);
geoshow(-4.300,92.595,'Marker','*','color','r','MarkerSize',12);
geoshow(-5.226,93.221,'Marker','*','color','r','MarkerSize',12);
geoshow(-6.008,93.522,'Marker','*','color','r','MarkerSize',12);
geoshow(-6.836,93.378,'Marker','*','color','r','MarkerSize',12);
geoshow(-7.269,93.018,'Marker','*','color','r','MarkerSize',12);

geoshow(-7.41664131,93.05347689,'Marker','*','color','k','MarkerSize',12);
geoshow(-7.41664131,93.05347689,'Marker','o','color','k','MarkerSize',20);
str={' 3rd Arc 20:41:04.904 UTC ', ...
    ' BTO Residual -16.0854 μs ', ...
    ' BFO Residual -0.7210 Hz '};
textm(-7.42,93.70,str,'EdgeColor','k','BackgroundColor','w','HorizontalAlignment','center');

geoshow(-7.81494345,93.14918533,'Marker','*','color','r','MarkerSize',12);
geoshow(-8.285,93.452,'Marker','*','color','r','MarkerSize',12);
geoshow(-8.931,93.984,'Marker','*','color','r','MarkerSize',12);
geoshow(-8.939,94.350,'Marker','*','color','r','MarkerSize',12);
geoshow(-9.495,94.338,'Marker','*','color','r','MarkerSize',12);
geoshow(-10.048,94.390,'Marker','*','color','r','MarkerSize',12);
geoshow(-10.511,94.075,'Marker','*','color','r','MarkerSize',12);
geoshow(-10.74237833,93.91715046,'Marker','*','color','r','MarkerSize',12);
geoshow(-10.903,93.397,'Marker','*','color','r','MarkerSize',12);
geoshow(-11.116,93.544,'Marker','*','color','r','MarkerSize',12);
geoshow(-11.649,93.694,'Marker','*','color','r','MarkerSize',12);
geoshow(-11.893,94.2005,'Marker','*','color','r','MarkerSize',12);
geoshow(-12.107,94.376,'Marker','*','color','r','MarkerSize',12);
geoshow(-12.797,94.850,'Marker','*','color','r','MarkerSize',12);
geoshow(-13.273,94.127,'Marker','*','color','r','MarkerSize',12);
geoshow(-13.43120922,93.88537951,'Marker','*','color','r','MarkerSize',12);

geoshow(-13.54561623,93.71016665,'Marker','*','color','k','MarkerSize',12);
geoshow(-13.54561623,93.71016665,'Marker','o','color','k','MarkerSize',20);
str={' 4th Arc 21:41:26.905 UTC ', ...
    ' BTO Residual +30.9355 μs ', ...
    ' BFO Residual +0.8070 Hz '};
textm(-13.50,94.50,str,'EdgeColor','k','BackgroundColor','w','HorizontalAlignment','center');

geoshow(-13.979,93.934,'Marker','*','color','r','MarkerSize',12);
geoshow(-14.667,93.405,'Marker','*','color','r','MarkerSize',12);
geoshow(-15.206,93.602,'Marker','*','color','r','MarkerSize',12);
geoshow(-15.486,93.673,'Marker','*','color','r','MarkerSize',12);
geoshow(-16.174,94.205,'Marker','*','color','r','MarkerSize',12);
geoshow(-16.40302944,94.38314466,'Marker','*','color','r','MarkerSize',12);
```

```
   geoshow(-16.63190256,94.56170633,'Marker','*','color','r','MarkerSize',12);
   geoshow(-16.86061673,94.74069188,'Marker','*','color','r','MarkerSize',12);
   geoshow(-17.073,94.941,'Marker','*','color','r','MarkerSize',12);
   geoshow(-17.883,95.263,'Marker','*','color','r','MarkerSize',12);
   geoshow(-18.116,94.331,'Marker','*','color','r','MarkerSize',12);
   geoshow(-18.394,94.426,'Marker','*','color','r','MarkerSize',12);
   geoshow(-19.255,94.330,'Marker','*','color','r','MarkerSize',12);
   geoshow(-19.510,94.480,'Marker','*','color','r','MarkerSize',12);
   geoshow(-19.76486807,94.63047087,'Marker','*','color','r','MarkerSize',12);
   geoshow(-20.01960198,94.78142055,'Marker','*','color','r','MarkerSize',12);

   geoshow(-20.706691,94.367932,'Marker','*','color','k','MarkerSize',12);
   geoshow(-20.706691,94.367932,'Marker','o','color','k','MarkerSize',20);
   str={' 5th Arc 22:41:21.906 UTC ', ...
       ' BTO Residual -26.1706 µs ', ...
       ' BFO Residual -4.3878 Hz '};
   textm(-20.71,94.80,str,'EdgeColor','k','BackgroundColor','w','HorizontalAlignment','left');

   geoshow(-20.788,94.319,'Marker','*','color','r','MarkerSize',12);
   geoshow(-21.04384104,94.16382653,'Marker','*','color','r','MarkerSize',12);
   geoshow(-21.603,94.358,'Marker','*','color','r','MarkerSize',12);



% Current Position Limit Markers

   geoshow(-21.502,94.972,'Marker','o','color','r','MarkerSize',20);
   geoshow(-21.603,94.358,'Marker','o','color','b','MarkerSize',180);

end


% Current Position Marker


geoshow(-21.502,94.972,'Marker','*','color','r','MarkerSize',12);


if glob == '0'


% Flight Track Lines

   waypoints = [5.47472811,100.89183367;5.25434271,100.45004693];
   [lttrk,lntrk] = track('gc',waypoints,'degrees');
   geoshow(lttrk,lntrk,'DisplayType','line','color','k','LineWidth',2,'LineStyle',':');

   waypoints = [5.25434271,100.45004693;5.25196956,100.43974800];
   [lttrk,lntrk] = track('gc',waypoints,'degrees');
   geoshow(lttrk,lntrk,'DisplayType','line','color','k','LineWidth',2,'LineStyle',':');

   waypoints = [5.25196956,100.43974800;5.24822535,100.42924017];
   [lttrk,lntrk] = track('gc',waypoints,'degrees');
   geoshow(lttrk,lntrk,'DisplayType','line','color','k','LineWidth',2,'LineStyle',':');

   waypoints = [5.24822535,100.42924017;5.24507545,100.41926510];
   [lttrk,lntrk] = track('gc',waypoints,'degrees');
   geoshow(lttrk,lntrk,'DisplayType','line','color','k','LineWidth',2,'LineStyle',':');

   waypoints = [5.24507545,100.41926510;5.24237736,100.40907553];
   [lttrk,lntrk] = track('gc',waypoints,'degrees');
   geoshow(lttrk,lntrk,'DisplayType','line','color','k','LineWidth',2,'LineStyle',':');

   waypoints = [5.24237736,100.40907553;5.24015961,100.39950012];
   [lttrk,lntrk] = track('gc',waypoints,'degrees');
   geoshow(lttrk,lntrk,'DisplayType','line','color','k','LineWidth',2,'LineStyle',':');

   waypoints = [5.24015961,100.39950012;5.23658986,100.38767545];
   [lttrk,lntrk] = track('gc',waypoints,'degrees');
   geoshow(lttrk,lntrk,'DisplayType','line','color','k','LineWidth',2,'LineStyle',':');

   waypoints = [5.23658986,100.38767545;5.22853875,100.35940772];
```

```
[lttrk,lntrk] = track('gc',waypoints,'degrees');
geoshow(lttrk,lntrk,'DisplayType','line','color','k','LineWidth',2,'LineStyle',':');

waypoints = [5.22853875,100.35940772;5.19844115,100.17349006];
[lttrk,lntrk] = track('gc',waypoints,'degrees');
geoshow(lttrk,lntrk,'DisplayType','line','color','k','LineWidth',2,'LineStyle',':');

waypoints = [5.19844115,100.17349006;5.19671047,100.14368928];
[lttrk,lntrk] = track('gc',waypoints,'degrees');
geoshow(lttrk,lntrk,'DisplayType','line','color','k','LineWidth',2,'LineStyle',':');

waypoints = [5.19671047,100.14368928;5.19657320,100.13370932];
[lttrk,lntrk] = track('gc',waypoints,'degrees');
geoshow(lttrk,lntrk,'DisplayType','line','color','k','LineWidth',2,'LineStyle',':');

waypoints = [5.19657320,100.13370932;5.19812122,100.11737592];
[lttrk,lntrk] = track('gc',waypoints,'degrees');
geoshow(lttrk,lntrk,'DisplayType','line','color','k','LineWidth',2,'LineStyle',':');

waypoints = [5.19812122,100.11737592;5.19926161,100.10670992];
[lttrk,lntrk] = track('gc',waypoints,'degrees');
geoshow(lttrk,lntrk,'DisplayType','line','color','k','LineWidth',2,'LineStyle',':');

waypoints = [5.19926161,100.10670992;5.19917267,100.09739918];
[lttrk,lntrk] = track('gc',waypoints,'degrees');
geoshow(lttrk,lntrk,'DisplayType','line','color','k','LineWidth',2,'LineStyle',':');

waypoints = [5.19917267,100.09739918;5.19896331,100.07529101];
[lttrk,lntrk] = track('gc',waypoints,'degrees');
geoshow(lttrk,lntrk,'DisplayType','line','color','k','LineWidth',2,'LineStyle',':');

waypoints = [5.19896331,100.07529101;5.21452286,100.00331029];
[lttrk,lntrk] = track('gc',waypoints,'degrees');
geoshow(lttrk,lntrk,'DisplayType','line','color','k','LineWidth',2,'LineStyle',':');

waypoints = [5.21452286,100.00331029;5.24653523,99.92479600];
[lttrk,lntrk] = track('gc',waypoints,'degrees');
geoshow(lttrk,lntrk,'DisplayType','line','color','k','LineWidth',2,'LineStyle',':');

waypoints = [5.24653523,99.92479600;5.27526160,99.87200435];
[lttrk,lntrk] = track('gc',waypoints,'degrees');
geoshow(lttrk,lntrk,'DisplayType','line','color','k','LineWidth',2,'LineStyle',':');

waypoints = [5.27526160,99.87200435;5.30975116,99.81418601];
[lttrk,lntrk] = track('gc',waypoints,'degrees');
geoshow(lttrk,lntrk,'DisplayType','line','color','k','LineWidth',2,'LineStyle',':');

waypoints = [5.30975116,99.81418601;5.34376189,99.75938739];
[lttrk,lntrk] = track('gc',waypoints,'degrees');
geoshow(lttrk,lntrk,'DisplayType','line','color','k','LineWidth',2,'LineStyle',':');

waypoints = [5.34376189,99.75938739;5.36851655,99.71900578];
[lttrk,lntrk] = track('gc',waypoints,'degrees');
geoshow(lttrk,lntrk,'DisplayType','line','color','k','LineWidth',2,'LineStyle',':');

waypoints = [5.36851655,99.71900578;5.39885124,99.64895222];
[lttrk,lntrk] = track('gc',waypoints,'degrees');
geoshow(lttrk,lntrk,'DisplayType','line','color','k','LineWidth',2,'LineStyle',':');

waypoints = [5.39885124,99.64895222;5.43673126,99.55760530];
[lttrk,lntrk] = track('gc',waypoints,'degrees');
geoshow(lttrk,lntrk,'DisplayType','line','color','k','LineWidth',2,'LineStyle',':');

waypoints = [5.43673126,99.55760530;5.53749203,99.29607774];
[lttrk,lntrk] = track('gc',waypoints,'degrees');
geoshow(lttrk,lntrk,'DisplayType','line','color','k','LineWidth',2,'LineStyle',':');

waypoints = [5.58911792,99.16522840;5.413,98.200];
[lttrk,lntrk] = track('gc',waypoints,'degrees');
geoshow(lttrk,lntrk,'DisplayType','line','color','r','LineWidth',2,'LineStyle',':');

waypoints = [5.413,98.200;5.36239182,97.92430148];
```

```
[lttrk,lntrk] = track('gc',waypoints,'degrees');
geoshow(lttrk,lntrk,'DisplayType','line','color','r','LineWidth',2,'LineStyle',':');

waypoints = [5.36239182,97.92430148;5.26600000,97.51133333];
[lttrk,lntrk] = track('gc',waypoints,'degrees');
geoshow(lttrk,lntrk,'DisplayType','line','color','k','LineWidth',1,'LineStyle',':');

waypoints = [5.36239182,97.92430148;5.566,97.732];
[lttrk,lntrk] = track('gc',waypoints,'degrees');
geoshow(lttrk,lntrk,'DisplayType','line','color','r','LineWidth',2,'LineStyle',':');

waypoints = [5.566,97.732;5.728,97.502];
[lttrk,lntrk] = track('gc',waypoints,'degrees');
geoshow(lttrk,lntrk,'DisplayType','line','color','r','LineWidth',2,'LineStyle',':');

waypoints = [5.728,97.502;5.830,96.667];
[lttrk,lntrk] = track('gc',waypoints,'degrees');
geoshow(lttrk,lntrk,'DisplayType','line','color','r','LineWidth',2,'LineStyle',':');

waypoints = [5.830,96.667;6.142,96.202];
[lttrk,lntrk] = track('gc',waypoints,'degrees');
geoshow(lttrk,lntrk,'DisplayType','line','color','r','LineWidth',2,'LineStyle',':');

waypoints = [6.142,96.202;6.493,95.871];
[lttrk,lntrk] = track('gc',waypoints,'degrees');
geoshow(lttrk,lntrk,'DisplayType','line','color','r','LineWidth',2,'LineStyle',':');

waypoints = [6.493,95.871;6.88431518,95.58854742];
[lttrk,lntrk] = track('gc',waypoints,'degrees');
geoshow(lttrk,lntrk,'DisplayType','line','color','r','LineWidth',2,'LineStyle',':');

waypoints = [6.88431518,95.58854742;6.726,95.358];
[lttrk,lntrk] = track('gc',waypoints,'degrees');
geoshow(lttrk,lntrk,'DisplayType','line','color','r','LineWidth',2,'LineStyle',':');

waypoints = [6.726,95.358;6.56757525,95.12760184];
[lttrk,lntrk] = track('gc',waypoints,'degrees');
geoshow(lttrk,lntrk,'DisplayType','line','color','r','LineWidth',2,'LineStyle',':');

waypoints = [6.56757525,95.12760184;5.402,94.360];
[lttrk,lntrk] = track('gc',waypoints,'degrees');
geoshow(lttrk,lntrk,'DisplayType','line','color','r','LineWidth',2,'LineStyle',':');

waypoints = [5.402,94.360;4.627,94.027];
[lttrk,lntrk] = track('gc',waypoints,'degrees');
geoshow(lttrk,lntrk,'DisplayType','line','color','r','LineWidth',2,'LineStyle',':');

waypoints = [4.627,94.027;4.374,94.146];
[lttrk,lntrk] = track('gc',waypoints,'degrees');
geoshow(lttrk,lntrk,'DisplayType','line','color','r','LineWidth',2,'LineStyle',':');

waypoints = [4.374,94.146;4.12097938,94.26492017];
[lttrk,lntrk] = track('gc',waypoints,'degrees');
geoshow(lttrk,lntrk,'DisplayType','line','color','r','LineWidth',2,'LineStyle',':');

waypoints = [4.374,94.146;3.603,94.489];
[lttrk,lntrk] = track('gc',waypoints,'degrees');
geoshow(lttrk,lntrk,'DisplayType','line','color','r','LineWidth',2,'LineStyle',':');

waypoints = [3.603,94.489;2.775,95.250];
[lttrk,lntrk] = track('gc',waypoints,'degrees');
geoshow(lttrk,lntrk,'DisplayType','line','color','r','LineWidth',2,'LineStyle',':');

waypoints = [2.775,95.250;2.4965,95.227];
[lttrk,lntrk] = track('gc',waypoints,'degrees');
geoshow(lttrk,lntrk,'DisplayType','line','color','r','LineWidth',2,'LineStyle',':');

waypoints = [2.4965,95.227;1.815,94.732];
[lttrk,lntrk] = track('gc',waypoints,'degrees');
geoshow(lttrk,lntrk,'DisplayType','line','color','r','LineWidth',2,'LineStyle',':');

waypoints = [1.815,94.732;1.59448304,94.57193986];
```

```
[lttrk,lntrk] = track('gc',waypoints,'degrees');
geoshow(lttrk,lntrk,'DisplayType','line','color','r','LineWidth',2,'LineStyle',':');

waypoints = [1.59448304,94.57193986;1.37395309,94.41191378];
[lttrk,lntrk] = track('gc',waypoints,'degrees');
geoshow(lttrk,lntrk,'DisplayType','line','color','r','LineWidth',2,'LineStyle',':');

waypoints = [1.37395309,94.41191378;1.218,94.302];
[lttrk,lntrk] = track('gc',waypoints,'degrees');
geoshow(lttrk,lntrk,'DisplayType','line','color','r','LineWidth',2,'LineStyle',':');

waypoints = [1.218,94.302;1.00487505,94.14794281];
[lttrk,lntrk] = track('gc',waypoints,'degrees');
geoshow(lttrk,lntrk,'DisplayType','line','color','r','LineWidth',2,'LineStyle',':');

waypoints = [1.00487505,94.14794281;0.79174251,93.99390559];
[lttrk,lntrk] = track('gc',waypoints,'degrees');
geoshow(lttrk,lntrk,'DisplayType','line','color','r','LineWidth',2,'LineStyle',':');

waypoints = [0.79174251,93.99390559;0.695,93.729];
[lttrk,lntrk] = track('gc',waypoints,'degrees');
geoshow(lttrk,lntrk,'DisplayType','line','color','r','LineWidth',2,'LineStyle',':');

waypoints = [0.695,93.729;0.560,93.183];
[lttrk,lntrk] = track('gc',waypoints,'degrees');
geoshow(lttrk,lntrk,'DisplayType','line','color','r','LineWidth',2,'LineStyle',':');

waypoints = [0.560,93.183;0.294,93.274];
[lttrk,lntrk] = track('gc',waypoints,'degrees');
geoshow(lttrk,lntrk,'DisplayType','line','color','r','LineWidth',2,'LineStyle',':');

waypoints = [0.294,93.274;0.070,93.460];
[lttrk,lntrk] = track('gc',waypoints,'degrees');
geoshow(lttrk,lntrk,'DisplayType','line','color','r','LineWidth',2,'LineStyle',':');

waypoints = [0.070,93.460;-0.15400077,93.64599824];
[lttrk,lntrk] = track('gc',waypoints,'degrees');
geoshow(lttrk,lntrk,'DisplayType','line','color','r','LineWidth',2,'LineStyle',':');

waypoints = [-0.15400077,93.64599824;-0.422,93.7315];
[lttrk,lntrk] = track('gc',waypoints,'degrees');
geoshow(lttrk,lntrk,'DisplayType','line','color','r','LineWidth',2,'LineStyle',':');

waypoints = [-0.422,93.7315;-0.5325,93.81875];
[lttrk,lntrk] = track('gc',waypoints,'degrees');
geoshow(lttrk,lntrk,'DisplayType','line','color','r','LineWidth',2,'LineStyle',':');

waypoints = [-0.5325,93.81875;-0.75778425,93.63885080];
[lttrk,lntrk] = track('gc',waypoints,'degrees');
geoshow(lttrk,lntrk,'DisplayType','line','color','r','LineWidth',2,'LineStyle',':');

waypoints = [-0.75778425,93.63885080;-1.420,92.800];
[lttrk,lntrk] = track('gc',waypoints,'degrees');
geoshow(lttrk,lntrk,'DisplayType','line','color','r','LineWidth',2,'LineStyle',':');

waypoints = [-1.420,92.800;-1.626,92.516];
[lttrk,lntrk] = track('gc',waypoints,'degrees');
geoshow(lttrk,lntrk,'DisplayType','line','color','r','LineWidth',2,'LineStyle',':');

waypoints = [-1.626,92.516;-1.676,92.241];
[lttrk,lntrk] = track('gc',waypoints,'degrees');
geoshow(lttrk,lntrk,'DisplayType','line','color','r','LineWidth',2,'LineStyle',':');

waypoints = [-1.676,92.241;-2.105,91.880];
[lttrk,lntrk] = track('gc',waypoints,'degrees');
geoshow(lttrk,lntrk,'DisplayType','line','color','r','LineWidth',2,'LineStyle',':');

waypoints = [-2.105,91.880;-2.645,91.725];
[lttrk,lntrk] = track('gc',waypoints,'degrees');
geoshow(lttrk,lntrk,'DisplayType','line','color','r','LineWidth',2,'LineStyle',':');

waypoints = [-2.645,91.725;-2.70,92.00];
```

```
[lttrk,lntrk] = track('gc',waypoints,'degrees');
geoshow(lttrk,lntrk,'DisplayType','line','color','r','LineWidth',2,'LineStyle',':');

waypoints = [-2.70,92.00;-2.648,92.277];
[lttrk,lntrk] = track('gc',waypoints,'degrees');
geoshow(lttrk,lntrk,'DisplayType','line','color','r','LineWidth',2,'LineStyle',':');

waypoints = [-2.648,92.277;-3.747,92.504];
[lttrk,lntrk] = track('gc',waypoints,'degrees');
geoshow(lttrk,lntrk,'DisplayType','line','color','r','LineWidth',2,'LineStyle',':');

waypoints = [-3.747,92.504;-4.300,92.595];
[lttrk,lntrk] = track('gc',waypoints,'degrees');
geoshow(lttrk,lntrk,'DisplayType','line','color','r','LineWidth',2,'LineStyle',':');

waypoints = [-4.300,92.595;-5.226,93.221];
[lttrk,lntrk] = track('gc',waypoints,'degrees');
geoshow(lttrk,lntrk,'DisplayType','line','color','r','LineWidth',2,'LineStyle',':');

waypoints = [-5.226,93.221;-6.008,93.522];
[lttrk,lntrk] = track('gc',waypoints,'degrees');
geoshow(lttrk,lntrk,'DisplayType','line','color','r','LineWidth',2,'LineStyle',':');

waypoints = [-6.008,93.522;-6.836,93.378];
[lttrk,lntrk] = track('gc',waypoints,'degrees');
geoshow(lttrk,lntrk,'DisplayType','line','color','r','LineWidth',2,'LineStyle',':');

waypoints = [-6.836,93.378;-7.269,93.018];
[lttrk,lntrk] = track('gc',waypoints,'degrees');
geoshow(lttrk,lntrk,'DisplayType','line','color','r','LineWidth',2,'LineStyle',':');

waypoints = [-7.269,93.018;-7.81494345,93.14918533];
[lttrk,lntrk] = track('gc',waypoints,'degrees');
geoshow(lttrk,lntrk,'DisplayType','line','color','r','LineWidth',2,'LineStyle',':');

waypoints = [-7.81494345,93.14918533;-8.285,93.452];
[lttrk,lntrk] = track('gc',waypoints,'degrees');
geoshow(lttrk,lntrk,'DisplayType','line','color','r','LineWidth',2,'LineStyle',':');

waypoints = [-8.285,93.452;-8.931,93.984];
[lttrk,lntrk] = track('gc',waypoints,'degrees');
geoshow(lttrk,lntrk,'DisplayType','line','color','r','LineWidth',2,'LineStyle',':');

waypoints = [-8.931,93.984;-8.939,94.350];
[lttrk,lntrk] = track('gc',waypoints,'degrees');
geoshow(lttrk,lntrk,'DisplayType','line','color','r','LineWidth',2,'LineStyle',':');

waypoints = [-8.939,94.350;-9.495,94.338];
[lttrk,lntrk] = track('gc',waypoints,'degrees');
geoshow(lttrk,lntrk,'DisplayType','line','color','r','LineWidth',2,'LineStyle',':');

waypoints = [-9.495,94.338;-10.048,94.390];
[lttrk,lntrk] = track('gc',waypoints,'degrees');
geoshow(lttrk,lntrk,'DisplayType','line','color','r','LineWidth',2,'LineStyle',':');

waypoints = [-10.048,94.390;-10.511,94.075];
[lttrk,lntrk] = track('gc',waypoints,'degrees');
geoshow(lttrk,lntrk,'DisplayType','line','color','r','LineWidth',2,'LineStyle',':');

waypoints = [-10.511,94.075;-10.74237833,93.91715046];
[lttrk,lntrk] = track('gc',waypoints,'degrees');
geoshow(lttrk,lntrk,'DisplayType','line','color','r','LineWidth',2,'LineStyle',':');

waypoints = [-10.74237833,93.91715046;-10.903,93.397];
[lttrk,lntrk] = track('gc',waypoints,'degrees');
geoshow(lttrk,lntrk,'DisplayType','line','color','r','LineWidth',2,'LineStyle',':');

waypoints = [-10.903,93.397;-11.116,93.544];
[lttrk,lntrk] = track('gc',waypoints,'degrees');
geoshow(lttrk,lntrk,'DisplayType','line','color','r','LineWidth',2,'LineStyle',':');

waypoints = [-11.116,93.544;-11.649,93.694];
```

```
[lttrk,lntrk] = track('gc',waypoints,'degrees');
geoshow(lttrk,lntrk,'DisplayType','line','color','r','LineWidth',2,'LineStyle',':');

waypoints = [-11.649,93.694;-11.893,94.2005];
[lttrk,lntrk] = track('gc',waypoints,'degrees');
geoshow(lttrk,lntrk,'DisplayType','line','color','r','LineWidth',2,'LineStyle',':');

waypoints = [-11.893,94.2005;-12.107,94.376];
[lttrk,lntrk] = track('gc',waypoints,'degrees');
geoshow(lttrk,lntrk,'DisplayType','line','color','r','LineWidth',2,'LineStyle',':');

waypoints = [-12.107,94.376;-12.797,94.850];
[lttrk,lntrk] = track('gc',waypoints,'degrees');
geoshow(lttrk,lntrk,'DisplayType','line','color','r','LineWidth',2,'LineStyle',':');

waypoints = [-12.797,94.850;-13.273,94.127];
[lttrk,lntrk] = track('gc',waypoints,'degrees');
geoshow(lttrk,lntrk,'DisplayType','line','color','r','LineWidth',2,'LineStyle',':');

waypoints = [-13.273,94.127;-13.54561623,93.71016665];
[lttrk,lntrk] = track('gc',waypoints,'degrees');
geoshow(lttrk,lntrk,'DisplayType','line','color','r','LineWidth',2,'LineStyle',':');

waypoints = [-13.54561623,93.71016665;-13.979,93.934];
[lttrk,lntrk] = track('gc',waypoints,'degrees');
geoshow(lttrk,lntrk,'DisplayType','line','color','r','LineWidth',2,'LineStyle',':');

waypoints = [-13.979,93.934;-14.667,93.405];
[lttrk,lntrk] = track('gc',waypoints,'degrees');
geoshow(lttrk,lntrk,'DisplayType','line','color','r','LineWidth',2,'LineStyle',':');

waypoints = [-14.667,93.405;-15.206,93.602];
[lttrk,lntrk] = track('gc',waypoints,'degrees');
geoshow(lttrk,lntrk,'DisplayType','line','color','r','LineWidth',2,'LineStyle',':');

waypoints = [-15.206,93.602;-15.486,93.673];
[lttrk,lntrk] = track('gc',waypoints,'degrees');
geoshow(lttrk,lntrk,'DisplayType','line','color','r','LineWidth',2,'LineStyle',':');

waypoints = [-15.486,93.673;-16.174,94.205];
[lttrk,lntrk] = track('gc',waypoints,'degrees');
geoshow(lttrk,lntrk,'DisplayType','line','color','r','LineWidth',2,'LineStyle',':');

waypoints = [-16.174,94.205;-16.40302944,94.38314466];
[lttrk,lntrk] = track('gc',waypoints,'degrees');
geoshow(lttrk,lntrk,'DisplayType','line','color','r','LineWidth',2,'LineStyle',':');

waypoints = [-16.40302944,94.38314466;-16.86061673,94.74069188];
[lttrk,lntrk] = track('gc',waypoints,'degrees');
geoshow(lttrk,lntrk,'DisplayType','line','color','r','LineWidth',2,'LineStyle',':');

waypoints = [-16.86061673,94.74069188;-17.073,94.941];
[lttrk,lntrk] = track('gc',waypoints,'degrees');
geoshow(lttrk,lntrk,'DisplayType','line','color','r','LineWidth',2,'LineStyle',':');

waypoints = [-17.073,94.941;-17.883,95.263];
[lttrk,lntrk] = track('gc',waypoints,'degrees');
geoshow(lttrk,lntrk,'DisplayType','line','color','r','LineWidth',2,'LineStyle',':');

waypoints = [-17.883,95.263;-18.116,94.331];
[lttrk,lntrk] = track('gc',waypoints,'degrees');
geoshow(lttrk,lntrk,'DisplayType','line','color','r','LineWidth',2,'LineStyle',':');

waypoints = [-18.116,94.331;-18.394,94.426];
[lttrk,lntrk] = track('gc',waypoints,'degrees');
geoshow(lttrk,lntrk,'DisplayType','line','color','r','LineWidth',2,'LineStyle',':');

waypoints = [-18.394,94.426;-19.255,94.330];
[lttrk,lntrk] = track('gc',waypoints,'degrees');
geoshow(lttrk,lntrk,'DisplayType','line','color','r','LineWidth',2,'LineStyle',':');

waypoints = [-19.255,94.330;-19.510,94.480];
```

```
   [lttrk,lntrk] = track('gc',waypoints,'degrees');
   geoshow(lttrk,lntrk,'DisplayType','line','color','r','LineWidth',2,'LineStyle',':');

   waypoints = [-19.510,94.480;-20.01960198,94.78142055];
   [lttrk,lntrk] = track('gc',waypoints,'degrees');
   geoshow(lttrk,lntrk,'DisplayType','line','color','r','LineWidth',2,'LineStyle',':');

   waypoints = [-20.01960198,94.78142055;-20.788,94.319];
   [lttrk,lntrk] = track('gc',waypoints,'degrees');
   geoshow(lttrk,lntrk,'DisplayType','line','color','r','LineWidth',2,'LineStyle',':');

   waypoints = [-20.788,94.319;-21.04384104,94.16382653];
   [lttrk,lntrk] = track('gc',waypoints,'degrees');
   geoshow(lttrk,lntrk,'DisplayType','line','color','r','LineWidth',2,'LineStyle',':');

   waypoints = [-21.04384104,94.16382653;-21.603,94.358];
   [lttrk,lntrk] = track('gc',waypoints,'degrees');
   geoshow(lttrk,lntrk,'DisplayType','line','color','r','LineWidth',2,'LineStyle',':');

   waypoints = [-21.603,94.358;-21.502,94.972];
   [lttrk,lntrk] = track('gc',waypoints,'degrees');
   geoshow(lttrk,lntrk,'DisplayType','line','color','r','LineWidth',2,'LineStyle',':');


% Waypoint Tracks

   waypoints = [-21.502,94.972;-21.0,98.0];
   [lttrk,lntrk] = track('gc',waypoints,'degrees');
   geoshow(lttrk,lntrk,'DisplayType','line','color','k','LineWidth',1,'LineStyle',':');

   textm(-21.00,97.00,'to waypoint 21S98E','EdgeColor','k','BackgroundColor','w','HorizontalAlignment','left');


   waypoints = [-21.603,94.358;-26.0,96.0];
   [lttrk,lntrk] = track('gc',waypoints,'degrees');
   geoshow(lttrk,lntrk,'DisplayType','line','color','k','LineWidth',1,'LineStyle',':');

   textm(-22.65,94.90,'to waypoint 26S96E','EdgeColor','k','BackgroundColor','w','HorizontalAlignment','left');

   waypoints = [-20.788,94.319;-24.0,92.0];
   [lttrk,lntrk] = track('gc',waypoints,'degrees');
   geoshow(lttrk,lntrk,'DisplayType','line','color','k','LineWidth',1,'LineStyle',':');

   textm(-22.65,93.00,'to waypoint 24S92E','EdgeColor','k','BackgroundColor','w','HorizontalAlignment','left');


% Footer Label

   str={' 21.502°S 94.972°E Boeing 777 MH370 Flight estimated position marked with a red asterisk ', ...
       [' Ground Speed 523.0 knots, Track 79.9 °T, Altitude 38,500 feet, ROC 0.0 fpm ']};
   textm(-22.85,95.0,str,'EdgeColor','k','BackgroundColor','w','HorizontalAlignment','center');

end


% Title

titstring1=' ';
titstring2=' ';
titstring3=' MH370 7th March 2014 22:52 UTC Position ';
titstring4=' SNR > 1.0 SD Anomaly Links marked in red, SNR > 0.75 SD Anomaly Links marked in orange, SNR > 0.50 SD
Anomaly Links marked in yellow  ';
titstring5=' Drift Anomaly Links marked in green, SNR and Drift Anomaly Links marked in blue, Non Anomaly Links marked in
grey  ';
titstring6=' Boeing 777-200ER estimated position marked with a red asterisk and circle ';
titstring7=' ';
titstring8=' ';
titstring9=' ';

title({titstring1;titstring2;titstring3;titstring4;titstring5;titstring6;titstring7;titstring8;titstring9},'fontsize',12,'fontweight','bold');
```

E. Sample SQL Script for WSPR Anomaly Checking.

```
select
        id, time, tx_sign, tx_loc, rx_sign, rx_loc, frequency, power, snr, drift, distance,
azimuth, band, version, code
from wspr.rx where
        time between '2014-03-07 21:34:00' and '2014-03-08 03:34:00'
        and tx_sign = 'AD4PT'
        and rx_sign = 'N6RY'
        and band = '21'
order by time
limit 2000
```

F. Matlab Function Call WSPR_Link_GCV9_Function for Mapping.

```
function [slat,slon,arclen,az] = WSPR_Link_GCV9_Function(tc,rc,sslat, sslon, selat,
selon,tx_sign,rx_sign)

warning('off');

start = -85.0;
finish = 85.0;

rev='0';

% Earth Reference Sphere
s = referenceSphere('Earth');
R=6378137;
s.LengthUnit = 'meter';
s.Radius=R;

az=0;

slat=str2double(sslat);
slon=str2double(sslon);
elat=str2double(selat);
elon=str2double(selon);

if and(slat>start, slat<=finish)

% LineColour

if tc == '0'
   if rc == '1'
      LineColour = [1,0.65,0];
   else
      LineColour = [0,0,0];
   end
elseif tc == '1'
   if rc == '1'
      LineColour = [1,0,0];
   else
      LineColour = [1,0.65,0];
   end
elseif tc == '2'
   LineColour = [0,0,1];
elseif tc == '3'
   LineColour = [0,1,0];
elseif tc == '4'
   LineColour = [1,1,0];
else
   error(LineColour);
   return;
end
```

```
%Great Circle Tracks
[arclen,az] = distance(slat,slon,elat,elon,s);

% az

arclenlp=40075016-arclen;
azlp = azimuth(elat,elon,slat,slon,s)-180;


[lttrk,lntrk] = track1(slat,slon,az,arclen,s,'degrees',100);
geoshow(lttrk,lntrk,'DisplayType','line','color',LineColour,'LineWidth',2,'LineStyle','-');

[lttrk,lntrk] = track1(elat,elon,azlp,arclenlp,s,'degrees',300);
geoshow(lttrk,lntrk,'DisplayType','line','color',LineColour,'LineWidth',1,'LineStyle','-');

geoshow(slat,slon,'Marker','.','color','k','MarkerSize',16);
geoshow(elat,elon,'Marker','.','color','m','MarkerSize',16);

end
```

G. Worked Example WSPR Link Timeframe Analysis.

(in alphanumeric order of the Transmitter and Receiver call signs and hour of detection)

row	id	time	tx_sign	tx_loc	rx_sign	rx_loc	frequency	power	snr	drift	distance	azimuth	band	version	code
1	186190476	2014-03-07 22:38:00	G3JKF	JO00bs	DK6UG	JN49cm	3594150	37	-5	0	592	100	3	2.21_r2286	0
2	186191134	2014-03-07 22:42:00	G3JKF	JO00bs	DK6UG	JN49cm	3594150	37	-6	0	592	100	3	2.21_r2286	0
3	186191992	2014-03-07 22:48:00	G3JKF	JO00bs	DK6UG	JN49cm	3594150	37	-13	0	592	100	3	2.21_r2286	0
4	186192650	2014-03-07 22:52:00	G3JKF	JO00bs	DK6UG	JN49cm	3594150	37	-3	0	592	100	3	2.21_r2286	0
5	186193474	2014-03-07 22:58:00	G3JKF	JO00bs	DK6UG	JN49cm	3594150	37	-4	0	592	100	3	2.21_r2286	0
6	186194501	2014-03-07 23:04:00	G3JKF	JO00bs	DK6UG	JN49cm	3594150	37	-3	0	592	100	3	2.21_r2286	0
7	186195432	2014-03-07 23:10:00	G3JKF	JO00bs	DK6UG	JN49cm	3594173	37	-3	0	592	100	3	2.21_r2286	0
8	186196701	2014-03-07 23:18:00	G3JKF	JO00bs	DK6UG	JN49cm	3594173	37	0	0	592	100	3	2.21_r2286	0
9	186197498	2014-03-07 23:24:00	G3JKF	JO00bs	DK6UG	JN49cm	3594173	37	-3	0	592	100	3	2.21_r2286	0
10	186198079	2014-03-07 23:28:00	G3JKF	JO00bs	DK6UG	JN49cm	3594173	37	-3	0	592	100	3	2.21_r2286	0
11	186199099	2014-03-07 23:34:00	G3JKF	JO00bs	DK6UG	JN49cm	3594173	37	-7	0	592	100	3	2.21_r2286	0
12	186200012	2014-03-07 23:38:00	G3JKF	JO00bs	DK6UG	JN49cm	3594173	37	-9	0	592	100	3	2.21_r2286	0
13	186200877	2014-03-07 23:44:00	G3JKF	JO00bs	DK6UG	JN49cm	3594173	37	-3	0	592	100	3	2.21_r2286	0
14	186201978	2014-03-07 23:50:00	G3JKF	JO00bs	DK6UG	JN49cm	3594173	37	-4	0	592	100	3	2.21_r2286	0
15	186203248	2014-03-07 23:58:00	G3JKF	JO00bs	DK6UG	JN49cm	3594173	37	-4	0	592	100	3	2.21_r2286	0
								Mean	-4.6667						
								SD	3.1091						
								AD	-1.6667						
								AD%	-54						

row	id	time	tx_sign	tx_loc	rx_sign	rx_loc	frequency	power	snr	drift	distance	azimuth	band	version	code
1	186191093	2014-03-07 22:42:00	G4FKK	IO91wi	YO3ITD	KN34cj	7040052	33	-6	0	2097	101	7	2.11_r2263	0
2	186192608	2014-03-07 22:52:00	G4FKK	IO91wi	YO3ITD	KN34cj	7040048	33	-9	-1	2097	101	7	2.11_r2263	0
3	186194499	2014-03-07 23:04:00	G4FKK	IO91wi	YO3ITD	KN34cj	7040052	33	-9	0	2097	101	7	2.11_r2263	0
4	186196013	2014-03-07 23:14:00	G4FKK	IO91wi	YO3ITD	KN34cj	7040050	33	-8	0	2097	101	7	2.11_r2263	0
5	186197890	2014-03-07 23:26:00	G4FKK	IO91wi	YO3ITD	KN34cj	7040052	33	-9	0	2097	101	7	2.11_r2263	0
6	186199815	2014-03-07 23:38:00	G4FKK	IO91wi	YO3ITD	KN34cj	7040052	33	-12	0	2097	101	7	2.11_r2263	0
7	186201107	2014-03-07 23:46:00	G4FKK	IO91wi	YO3ITD	KN34cj	7040052	33	-6	0	2097	101	7	2.11_r2263	0
8	186203222	2014-03-07 23:58:00	G4FKK	IO91wi	YO3ITD	KN34cj	7040052	33	-10	0	2097	101	7	2.11_r2263	0
9	186207550	2014-03-08 00:26:00	G4FKK	IO91wi	YO3ITD	KN34cj	7040052	33	-7	0	2097	101	7	2.11_r2263	0
10	186208814	2014-03-08 00:34:00	G4FKK	IO91wi	YO3ITD	KN34cj	7040049	33	-9	0	2097	101	7	2.11_r2263	0
11	186210532	2014-03-08 00:46:00	G4FKK	IO91wi	YO3ITD	KN34cj	7040053	33	-10	0	2097	101	7	2.11_r2263	0
12	186211717	2014-03-08 00:54:00	G4FKK	IO91wi	YO3ITD	KN34cj	7040051	33	-6	-1	2097	101	7	2.11_r2263	0
13	186214388	2014-03-08 01:14:00	G4FKK	IO91wi	YO3ITD	KN34cj	7040050	33	-1	-1	2097	101	7	2.11_r2263	0
14	186216773	2014-03-08 01:32:00	G4FKK	IO91wi	YO3ITD	KN34cj	7040051	33	-10	-1	2097	101	7	2.11_r2263	0
								Mean	-8.0000						
								SD	2.6890						
								AD	1.0000						
								AD%	37						

row	id	time	tx_sign	tx_loc	rx_sign	rx_loc	frequency	power	snr	drift	distance	azimuth	band	version	code
1	186177821	2014-03-07 21:40:00	G4KPX	JO02dj	DC0DX/A	JO31lk	475618	0	-26	0	469	100	0	4.0 r3015	0
2	186180717	2014-03-07 21:48:00	G4KPX	JO02dj	DC0DX/A	JO31lk	475618	0	-29	0	469	100	0	4.0 r3015	0
3	186192571	2014-03-07 22:52:00	G4KPX	JO02dj	DC0DX/A	JO31lk	475619	0	-23	0	469	100	0	4.0 r3015	0
								Mean	-26.0000						
								SD	3.0000						
								AD	-3.0000						
								AD%	-100						

row	id	time	tx_sign	tx_loc	rx_sign	rx_loc	frequency	power	snr	drift	distance	azimuth	band	version	code
1	186158662	2014-03-07 19:56:00	G4KPX	JO02dj	PA3ABK/2	JO21it	475617	0	-21	0	308	100	0	2.11_r2263	0
2	186160136	2014-03-07 20:04:00	G4KPX	JO02dj	PA3ABK/2	JO21it	475617	0	-23	0	308	100	0	2.11_r2263	0
3	186161677	2014-03-07 20:12:00	G4KPX	JO02dj	PA3ABK/2	JO21it	475617	0	-19	0	308	100	0	2.11_r2263	0
4	186162966	2014-03-07 20:20:00	G4KPX	JO02dj	PA3ABK/2	JO21it	475617	0	-19	0	308	100	0	2.11_r2263	0
5	186164557	2014-03-07 20:28:00	G4KPX	JO02dj	PA3ABK/2	JO21it	475617	0	-19	0	308	100	0	2.11_r2263	0
6	186166177	2014-03-07 20:36:00	G4KPX	JO02dj	PA3ABK/2	JO21it	475617	0	-19	0	308	100	0	2.11_r2263	0
7	186169159	2014-03-07 20:52:00	G4KPX	JO02dj	PA3ABK/2	JO21it	475617	0	-25	0	308	100	0	2.11_r2263	0
8	186173554	2014-03-07 21:16:00	G4KPX	JO02dj	PA3ABK/2	JO21it	475617	0	-17	0	308	100	0	2.11_r2263	0
9	186175120	2014-03-07 21:24:00	G4KPX	JO02dj	PA3ABK/2	JO21it	475617	0	-13	0	308	100	0	2.11_r2263	0
10	186176647	2014-03-07 21:32:00	G4KPX	JO02dj	PA3ABK/2	JO21it	475617	0	-14	0	308	100	0	2.11_r2263	0
11	186177917	2014-03-07 21:40:00	G4KPX	JO02dj	PA3ABK/2	JO21it	475617	0	-18	0	308	100	0	2.11_r2263	0
12	186180738	2014-03-07 21:48:00	G4KPX	JO02dj	PA3ABK/2	JO21it	475617	0	-21	0	308	100	0	2.11_r2263	0
13	186185112	2014-03-07 22:04:00	G4KPX	JO02dj	PA3ABK/2	JO21it	475617	0	-19	0	308	100	0	2.11_r2263	0
14	186186534	2014-03-07 22:12:00	G4KPX	JO02dj	PA3ABK/2	JO21it	475617	0	-16	0	308	100	0	2.11_r2263	0
15	186187834	2014-03-07 22:20:00	G4KPX	JO02dj	PA3ABK/2	JO21it	475617	0	-20	0	308	100	0	2.11_r2263	0
16	186188938	2014-03-07 22:28:00	G4KPX	JO02dj	PA3ABK/2	JO21it	475617	0	-23	0	308	100	0	2.11_r2263	0
17	186190276	2014-03-07 22:36:00	G4KPX	JO02dj	PA3ABK/2	JO21it	475617	0	-16	0	308	100	0	2.11_r2263	0
18	186192721	2014-03-07 22:52:00	G4KPX	JO02dj	PA3ABK/2	JO21it	475617	0	-15	0	308	100	0	2.11_r2263	0
19	186193990	2014-03-07 23:00:00	G4KPX	JO02dj	PA3ABK/2	JO21it	475617	0	-23	0	308	100	0	2.11_r2263	0
20	186195146	2014-03-07 23:08:00	G4KPX	JO02dj	PA3ABK/2	JO21it	475617	0	-17	0	308	100	0	2.11_r2263	0
21	186196266	2014-03-07 23:16:00	G4KPX	JO02dj	PA3ABK/2	JO21it	475617	0	-14	0	308	100	0	2.11_r2263	0
22	186197462	2014-03-07 23:24:00	G4KPX	JO02dj	PA3ABK/2	JO21it	475617	0	-10	0	308	100	0	2.11_r2263	0
23	186198961	2014-03-07 23:32:00	G4KPX	JO02dj	PA3ABK/2	JO21it	475617	0	-11	0	308	100	0	2.11_r2263	0
24	186200398	2014-03-07 23:40:00	G4KPX	JO02dj	PA3ABK/2	JO21it	475617	0	-10	0	308	100	0	2.11_r2263	0
25	186201668	2014-03-07 23:48:00	G4KPX	JO02dj	PA3ABK/2	JO21it	475617	0	-13	0	308	100	0	2.11_r2263	0
26	186203036	2014-03-07 23:56:00	G4KPX	JO02dj	PA3ABK/2	JO21it	475617	0	-10	0	308	100	0	2.11_r2263	0
27	186204246	2014-03-08 00:04:00	G4KPX	JO02dj	PA3ABK/2	JO21it	475617	0	-18	0	308	100	0	2.11_r2263	0
28	186205306	2014-03-08 00:12:00	G4KPX	JO02dj	PA3ABK/2	JO21it	475617	0	-16	0	308	100	0	2.11_r2263	0
29	186206699	2014-03-08 00:20:00	G4KPX	JO02dj	PA3ABK/2	JO21it	475617	0	-16	0	308	100	0	2.11_r2263	0
30	186207951	2014-03-08 00:28:00	G4KPX	JO02dj	PA3ABK/2	JO21it	475617	0	-17	0	308	100	0	2.11_r2263	0
31	186209211	2014-03-08 00:36:00	G4KPX	JO02dj	PA3ABK/2	JO21it	475617	0	-16	0	308	100	0	2.11_r2263	0
32	186213745	2014-03-08 01:08:00	G4KPX	JO02dj	PA3ABK/2	JO21it	475617	0	-12	0	308	100	0	2.11_r2263	0
33	186214711	2014-03-08 01:16:00	G4KPX	JO02dj	PA3ABK/2	JO21it	475617	0	-11	0	308	100	0	2.11_r2263	0
34	186215719	2014-03-08 01:24:00	G4KPX	JO02dj	PA3ABK/2	JO21it	475617	0	-19	0	308	100	0	2.11_r2263	0
35	186216800	2014-03-08 01:32:00	G4KPX	JO02dj	PA3ABK/2	JO21it	475617	0	-20	0	308	100	0	2.11_r2263	0
36	186217845	2014-03-08 01:40:00	G4KPX	JO02dj	PA3ABK/2	JO21it	475617	0	-15	0	308	100	0	2.11_r2263	0
37	186218942	2014-03-08 01:48:00	G4KPX	JO02dj	PA3ABK/2	JO21it	475617	0	-18	0	308	100	0	2.11_r2263	0
								Mean	-16.8378						
								SD	3.9265						
								AD	-0.8378						
								AD%	-21						

row	id	time	tx_sign	tx_loc	rx_sign	rx_loc	frequency	power	snr	drift	distance	azimuth	band	version
1	186188233	2014-03-07 22:22:00	G6RRL	IO90iw	DK6UG	JN49cm	3594082	33	-4	0	693	99	3	2.21_r2286
2	186189710	2014-03-07 22:32:00	G6RRL	IO90iw	DK6UG	JN49cm	3594081	33	-12	0	693	99	3	2.21_r2286
3	186192616	2014-03-07 22:52:00	G6RRL	IO90iw	DK6UG	JN49cm	3594078	33	-22	0	693	99	3	2.21_r2286
4	186194484	2014-03-07 23:04:00	G6RRL	IO90iw	DK6UG	JN49cm	3594077	33	-8	0	693	99	3	2.21_r2286
5	186195696	2014-03-07 23:12:00	G6RRL	IO90iw	DK6UG	JN49cm	3594076	33	-6	0	693	99	3	2.21_r2286
6	186197307	2014-03-07 23:22:00	G6RRL	IO90iw	DK6UG	JN49cm	3594075	33	-9	0	693	99	3	2.21_r2286
7	186198808	2014-03-07 23:32:00	G6RRL	IO90iw	DK6UG	JN49cm	3594075	33	-4	0	693	99	3	2.21_r2286
8	186200229	2014-03-07 23:40:00	G6RRL	IO90iw	DK6UG	JN49cm	3594074	33	-8	0	693	99	3	2.21_r2286
9	186202149	2014-03-07 23:52:00	G6RRL	IO90iw	DK6UG	JN49cm	3594074	33	-7	0	693	99	3	2.21_r2286
10	186203661	2014-03-08 00:00:00	G6RRL	IO90iw	DK6UG	JN49cm	3594074	33	-7	0	693	99	3	2.21_r2286
11	186204473	2014-03-08 00:06:00	G6RRL	IO90iw	DK6UG	JN49cm	3594073	33	-5	0	693	99	3	2.21_r2286
								Mean	-8.3636					
								SD	5.0847					
								AD	13.6364					
								AD%	268					

row	id	time	tx_sign	tx_loc	rx_sign	rx_loc	frequency	power	snr	drift	distance	azimuth	band	version	code
1	186185841	2014-03-07 22:08:00	JH1GYE	PM96mi	KD6RF	CM97cq	28126134	37	11	0	8326	54	28	2.11_r2263	0
2	186187617	2014-03-07 22:18:00	JH1GYE	PM96mi	KD6RF	CM97cq	28126134	37	9	0	8326	54	28	2.11_r2263	0
3	186189183	2014-03-07 22:28:00	JH1GYE	PM96mi	KD6RF	CM97cq	28126134	37	10	0	8326	54	28	2.11_r2263	0
4	186190346	2014-03-07 22:36:00	JH1GYE	PM96mi	KD6RF	CM97cq	28126134	37	4	0	8326	54	28	2.11_r2263	0
5	186191486	2014-03-07 22:44:00	JH1GYE	PM96mi	KD6RF	CM97cq	28126134	37	1	0	8326	54	28	2.11_r2263	0
6	186192574	2014-03-07 22:52:00	JH1GYE	PM96mi	KD6RF	CM97cq	28126133	37	10	0	8326	54	28	2.11_r2263	0
7	186195680	2014-03-07 23:12:00	JH1GYE	PM96mi	KD6RF	CM97cq	28126134	37	1	0	8326	54	28	2.11_r2263	0
8	186197623	2014-03-07 23:24:00	JH1GYE	PM96mi	KD6RF	CM97cq	28126134	37	2	0	8326	54	28	2.11_r2263	0
9	186199237	2014-03-07 23:34:00	JH1GYE	PM96mi	KD6RF	CM97cq	28126134	37	2	0	8326	54	28	2.11_r2263	0
10	186200921	2014-03-07 23:44:00	JH1GYE	PM96mi	KD6RF	CM97cq	28126134	37	5	0	8326	54	28	2.11_r2263	0
11	186202933	2014-03-07 23:56:00	JH1GYE	PM96mi	KD6RF	CM97cq	28126134	37	10	0	8326	54	28	2.11_r2263	0
12	186205921	2014-03-08 00:16:00	JH1GYE	PM96mi	KD6RF	CM97cq	28126134	37	5	0	8326	54	28	2.11_r2263	0
13	186207367	2014-03-08 00:24:00	JH1GYE	PM96mi	KD6RF	CM97cq	28126134	37	11	0	8326	54	28	2.11_r2263	0
14	186208984	2014-03-08 00:34:00	JH1GYE	PM96mi	KD6RF	CM97cq	28126133	37	8	0	8326	54	28	2.11_r2263	0
15	186210181	2014-03-08 00:42:00	JH1GYE	PM96mi	KD6RF	CM97cq	28126134	37	-2	0	8326	54	28	2.11_r2263	0
16	186211262	2014-03-08 00:50:00	JH1GYE	PM96mi	KD6RF	CM97cq	28126134	37	-1	0	8326	54	28	2.11_r2263	0
17	186212984	2014-03-08 01:02:00	JH1GYE	PM96mi	KD6RF	CM97cq	28126134	37	4	0	8326	54	28	2.11_r2263	0
18	186215300	2014-03-08 01:20:00	JH1GYE	PM96mi	KD6RF	CM97cq	28126134	37	-4	0	8326	54	28	2.11_r2263	0
19	186216228	2014-03-08 01:28:00	JH1GYE	PM96mi	KD6RF	CM97cq	28126134	37	-2	0	8326	54	28	2.11_r2263	0
20	186217288	2014-03-08 01:36:00	JH1GYE	PM96mi	KD6RF	CM97cq	28126134	37	-1	0	8326	54	28	2.11_r2263	0
21	186218521	2014-03-08 01:44:00	JH1GYE	PM96mi	KD6RF	CM97cq	28126133	37	5	0	8326	54	28	2.11_r2263	0
22	186219503	2014-03-08 01:52:00	JH1GYE	PM96mi	KD6RF	CM97cq	28126134	37	5	0	8326	54	28	2.11_r2263	0
								Mean	4.2273						
								SD	4.6897						
								AD	-5.7727						
								AD%	-123						

row	id	time	tx_sign	tx_loc	rx_sign	rx_loc	frequency	power	snr	drift	distance	azimuth	band	version	code
1	186160575	2014-03-07 20:08:00	VK3DXE	QF21nv	VK6ZRY	OF78vd	14097175	37	-23	-1	2749	276	14	0.8_r3058	0
2	186164555	2014-03-07 20:28:00	VK3DXE	QF21nv	VK6ZRY	OF78vd	14097176	37	-22	-1	2749	276	14	0.8_r3058	0
3	186174325	2014-03-07 21:20:00	VK3DXE	QF21nv	VK6ZRY	OF78vd	14097024	37	-12	-1	2749	276	14	0.8_r3058	0
4	186176522	2014-03-07 21:32:00	VK3DXE	QF21nv	VK6ZRY	OF78vd	14097025	37	-11	-2	2749	276	14	0.8_r3058	0
5	186180260	2014-03-07 21:46:00	VK3DXE	QF21nv	VK6ZRY	OF78vd	14097025	37	-15	-2	2749	276	14	0.8_r3058	0
6	186184221	2014-03-07 22:00:00	VK3DXE	QF21nv	VK6ZRY	OF78vd	14097024	37	-20	-2	2749	276	14	0.8_r3058	0
7	186186441	2014-03-07 22:12:00	VK3DXE	QF21nv	VK6ZRY	OF78vd	14097024	37	-18	-2	2749	276	14	0.8_r3058	0
8	186188796	2014-03-07 22:26:00	VK3DXE	QF21nv	VK6ZRY	OF78vd	14097025	37	-12	-1	2749	276	14	0.8_r3058	0
9	186190576	2014-03-07 22:38:00	VK3DXE	QF21nv	VK6ZRY	OF78vd	14097024	37	-9	-1	2749	276	14	0.8_r3058	0
10	186192696	2014-03-07 22:52:00	VK3DXE	QF21nv	VK6ZRY	OF78vd	14097024	37	-13	-2	2749	276	14	0.8_r3058	0
								Mean	-15.5000						
								SD	4.9272						
								AD	-2.5000						
								AD%	-51						

row	id	time	tx_sign	tx_loc	rx_sign	rx_loc	frequency	power	snr	drift	distance	azimuth	band	version	code
1	186190800	2014-03-07 22:40:00	W4MO	EL87tc	SM3ULC	JO89ul	14097123	33	-14	1	7977	32	14	2.11_r2263	0
2	186192673	2014-03-07 22:52:00	W4MO	EL87tc	SM3ULC	JO89ul	14097123	33	-24	0	7977	32	14	2.11_r2263	0
3	186193839	2014-03-07 23:00:00	W4MO	EL87tc	SM3ULC	JO89ul	14097122	33	-15	0	7977	32	14	2.11_r2263	0
								Mean	-17.6667						
								SD	5.5076						
								AD	6.3333						
								AD%	115						

row	id	time	tx_sign	tx_loc	rx_sign	rx_loc	frequency	power	snr	drift	distance	azimuth	band	version	code
1	186157819	2014-03-07 19:52:00	WD0UG	EM64	KB9VLR	EN54vj	10140163	30	-11	-3	1107	355	10	2.0_r1714	0
2	186159654	2014-03-07 20:02:00	WD0UG	EM64	KB9VLR	EN54vj	10140163	30	-6	-1	1107	355	10	2.0_r1714	0
3	186163580	2014-03-07 20:22:00	WD0UG	EM64	KB9VLR	EN54vj	10140162	30	-11	-1	1107	355	10	2.0_r1714	0
4	186172767	2014-03-07 21:12:00	WD0UG	EM64	KB9VLR	EN54vj	10140160	30	-6	-2	1107	355	10	2.0_r1714	0
5	186184744	2014-03-07 22:02:00	WD0UG	EM64	KB9VLR	EN54vj	10140160	30	-7	-1	1107	355	10	2.0_r1714	0
6	186188196	2014-03-07 22:22:00	WD0UG	EM64	KB9VLR	EN54vj	10140161	30	-7	-4	1107	355	10	2.0_r1714	0
7	186189900	2014-03-07 22:32:00	WD0UG	EM64	KB9VLR	EN54vj	10140161	30	-10	-1	1107	355	10	2.0_r1714	0
8	186192732	2014-03-07 22:52:00	WD0UG	EM64	KB9VLR	EN54vj	10140161	30	-5	-2	1107	355	10	2.0_r1714	0
9	186194065	2014-03-07 23:02:00	WD0UG	EM64	KB9VLR	EN54vj	10140161	30	-5	-2	1107	355	10	2.0_r1714	0
10	186197349	2014-03-07 23:22:00	WD0UG	EM64	KB9VLR	EN54vj	10140162	30	-11	-4	1107	355	10	2.0_r1714	0
11	186200624	2014-03-07 23:42:00	WD0UG	EM64	KB9VLR	EN54vj	10140161	30	-3	-2	1107	355	10	2.0_r1714	0
12	186203905	2014-03-08 00:02:00	WD0UG	EM64	KB9VLR	EN54vj	10140162	30	-6	-3	1107	355	10	2.0_r1714	0
								Mean	-7.3333						
								SD	2.7414						
								AD	-2.3333						
								AD%	-85						

H. Anomalous WSPR Link Timeframe Analysis.

(in alphanumeric order of the Transmitter and Receiver call signs and hour of detection)

row	id	time	tx_sign	tx_loc	rx_sign	rx_loc	frequency	power	snr	drift	distance	azimuth	band	version	code
1	186194966	2014-03-07 23:08:00	2E0DSS	IO82xl	W4MO	EL87	14097065	33	-21	0	7030	281	14	2.21_r2286	0
2	186200146	2014-03-07 23:40:00	2E0DSS	IO82xl	W4MO	EL87	14097065	33	-11	0	7030	281	14	2.21_r2286	0
3	186208633	2014-03-08 00:32:00	2E0DSS	IO82xl	W4MO	EL87	14097065	33	-13	0	7030	281	14	2.21_r2286	0
4	186212543	2014-03-08 01:00:00	2E0DSS	IO82xl	W4MO	EL87	14097065	33	-14	0	7030	281	14	2.21_r2286	0
5	186220003	2014-03-08 01:56:00	2E0DSS	IO82xl	W4MO	EL87	14097066	33	-20	0	7030	281	14	2.21_r2286	0
								Mean	-15.8000						
								SD	4.4385						
								AD	-4.8000						
								AD%	-108						

row	id	time	tx_sign	tx_loc	rx_sign	rx_loc	frequency	power	snr	drift	distance	azimuth	band	version	code
1	186196090	2014-03-07 23:14:00	AA7FV	DM42pg	W4MO	EL87	14097189	33	-13	0	2712	94	14	2.21_r2286	0
2	186200184	2014-03-07 23:40:00	AA7FV	DM42pg	W4MO	EL87	14097189	33	-9	-1	2712	94	14	2.21_r2286	0
3	186205705	2014-03-08 00:14:00	AA7FV	DM42pg	W4MO	EL87	14097188	33	-12	0	2712	94	14	2.21_r2286	0
4	186213832	2014-03-08 01:10:00	AA7FV	DM42pg	W4MO	EL87	14097189	33	-10	0	2712	94	14	2.21_r2286	0
5	186217776	2014-03-08 01:40:00	AA7FV	DM42pg	W4MO	EL87	14097189	33	-9	0	2712	94	14	2.21_r2286	0
6	186222554	2014-03-08 02:14:00	AA7FV	DM42pg	W4MO	EL87	14097189	33	-7	1	2712	94	14	2.21_r2286	0
								Mean	-10.0000						
								SD	2.1909						
								AD	-1.0000						
								AD%	-46						

row	id	time	tx_sign	tx_loc	rx_sign	rx_loc	frequency	power	snr	drift	distance	azimuth	band	version	code
1	186177065	2014-03-07 21:34:00	AD4PT	EM12kx	W7ZWW	CN85rh	14097125	37	-18	0	2569	310	14	2.0_r1714	0
2	186178465	2014-03-07 21:42:00	AD4PT	EM12kx	W7ZWW	CN85rh	14097126	37	-18	0	2569	310	14	2.0_r1714	0
3	186182802	2014-03-07 21:52:00	AD4PT	EM12kx	W7ZWW	CN85rh	14097127	37	-15	0	2569	310	14	2.0_r1714	0
4	186184348	2014-03-07 22:00:00	AD4PT	EM12kx	W7ZWW	CN85rh	14097128	37	-16	0	2569	310	14	2.0_r1714	0
5	186186176	2014-03-07 22:10:00	AD4PT	EM12kx	W7ZWW	CN85rh	14097129	37	-16	0	2569	310	14	2.0_r1714	0
6	186187980	2014-03-07 22:20:00	AD4PT	EM12kx	W7ZWW	CN85rh	14097129	37	-15	0	2569	310	14	2.0_r1714	0
7	186189607	2014-03-07 22:30:00	AD4PT	EM12kx	W7ZWW	CN85rh	14097129	37	-15	0	2569	310	14	2.0_r1714	0
8	186190592	2014-03-07 22:38:00	AD4PT	EM12kx	W7ZWW	CN85rh	14097130	37	-15	0	2569	310	14	2.0_r1714	0
9	186191885	2014-03-07 22:46:00	AD4PT	EM12kx	W7ZWW	CN85rh	14097131	37	-12	0	2569	310	14	2.0_r1714	0
10	186193638	2014-03-07 22:58:00	AD4PT	EM12kx	W7ZWW	CN85rh	14097130	37	-15	0	2569	310	14	2.0_r1714	0
11	186195213	2014-03-07 23:08:00	AD4PT	EM12kx	W7ZWW	CN85rh	14097131	37	-10	0	2569	310	14	2.0_r1714	0
12	186196442	2014-03-07 23:16:00	AD4PT	EM12kx	W7ZWW	CN85rh	14097131	37	-18	0	2569	310	14	2.0_r1714	0
13	186197571	2014-03-07 23:24:00	AD4PT	EM12kx	W7ZWW	CN85rh	14097131	37	-18	0	2569	310	14	2.0_r1714	0
								Mean	-15.4615						
								SD	2.4019						
								AD	-5.4615						
								AD%	-227						

Page 626 of 1738

row	id	time	tx_sign	tx_loc	rx_sign	rx_loc	frequency	power	snr	drift	distance	azimuth	band	version	code
1	186088393	2014-03-07 15:10:00	DC5BN	JO43rh	2E0DSS	IO82xl	14097180	37	3	1	776	268	14	2.0_r1714	0
2	186095682	2014-03-07 15:38:00	DC5BN	JO43rh	2E0DSS	IO82xl	14097183	37	4	0	776	268	14	2.0_r1714	0
3	186102877	2014-03-07 16:02:00	DC5BN	JO43rh	2E0DSS	IO82xl	14097181	37	3	0	776	268	14	2.0_r1714	0
4	186108444	2014-03-07 16:22:00	DC5BN	JO43rh	2E0DSS	IO82xl	14097180	37	7	1	776	268	14	2.0_r1714	0
5	186114499	2014-03-07 16:44:00	DC5BN	JO43rh	2E0DSS	IO82xl	14097180	37	9	1	776	268	14	2.0_r1714	0
6	186120045	2014-03-07 17:04:00	DC5BN	JO43rh	2E0DSS	IO82xl	14097180	37	5	1	776	268	14	2.0_r1714	0
7	186125686	2014-03-07 17:26:00	DC5BN	JO43rh	2E0DSS	IO82xl	14097179	37	10	1	776	268	14	2.0_r1714	0
8	186131313	2014-03-07 17:48:00	DC5BN	JO43rh	2E0DSS	IO82xl	14097179	37	-16	0	776	268	14	2.0_r1714	0
9	186136587	2014-03-07 18:08:00	DC5BN	JO43rh	2E0DSS	IO82xl	14097179	37	-20	1	776	268	14	2.0_r1714	0
10	186141406	2014-03-07 18:30:00	DC5BN	JO43rh	2E0DSS	IO82xl	14097178	37	-23	1	776	268	14	2.0_r1714	0
								Mean	-1.8000						
								SD	12.6561						
								AD	18.2000						
								AD%	144						

row	id	time	tx_sign	tx_loc	rx_sign	rx_loc	frequency	power	snr	drift	distance	azimuth	band	version	code
1	186136229	2014-03-07 18:08:00	DF2JP	JO31jg	G3SXH	IO80	1838021	33	-17	0	695	267	1	2.0_r1714	0
2	186137937	2014-03-07 18:16:00	DF2JP	JO31jg	G3SXH	IO80	1838021	33	-19	0	695	267	1	2.0_r1714	0
3	186140378	2014-03-07 18:26:00	DF2JP	JO31jg	G3SXH	IO80	1838021	33	-20	0	695	267	1	2.0_r1714	0
4	186141844	2014-03-07 18:32:00	DF2JP	JO31jg	G3SXH	IO80	1838020	33	-18	1	695	267	1	2.0_r1714	0
5	186142956	2014-03-07 18:38:00	DF2JP	JO31jg	G3SXH	IO80	1838020	33	-17	0	695	267	1	2.0_r1714	0
6	186144839	2014-03-07 18:46:00	DF2JP	JO31jg	G3SXH	IO80	1838021	33	-15	0	695	267	1	2.0_r1714	0
7	186146270	2014-03-07 18:54:00	DF2JP	JO31jg	G3SXH	IO80	1838020	33	-11	0	695	267	1	2.0_r1714	0
8	186147756	2014-03-07 19:00:00	DF2JP	JO31jg	G3SXH	IO80	1838020	33	-15	0	695	267	1	2.0_r1714	0
9	186148776	2014-03-07 19:06:00	DF2JP	JO31jg	G3SXH	IO80	1838021	33	-12	0	695	267	1	2.0_r1714	0
10	186151045	2014-03-07 19:16:00	DF2JP	JO31jg	G3SXH	IO80	1838020	33	-9	0	695	267	1	2.0_r1714	0
11	186152940	2014-03-07 19:26:00	DF2JP	JO31jg	G3SXH	IO80	1838021	33	-9	0	695	267	1	2.0_r1714	0
12	186154243	2014-03-07 19:34:00	DF2JP	JO31jg	G3SXH	IO80	1838020	33	-16	0	695	267	1	2.0_r1714	0
13	186156273	2014-03-07 19:44:00	DF2JP	JO31jg	G3SXH	IO80	1838020	33	-12	0	695	267	1	2.0_r1714	0
14	186157168	2014-03-07 19:50:00	DF2JP	JO31jg	G3SXH	IO80	1838021	33	-14	0	695	267	1	2.0_r1714	0
15	186158891	2014-03-07 19:58:00	DF2JP	JO31jg	G3SXH	IO80	1838020	33	-12	0	695	267	1	2.0_r1714	0
16	186160694	2014-03-07 20:08:00	DF2JP	JO31jg	G3SXH	IO80	1838021	33	-12	0	695	267	1	2.0_r1714	0
17	186162164	2014-03-07 20:16:00	DF2JP	JO31jg	G3SXH	IO80	1838020	33	-14	0	695	267	1	2.0_r1714	0
18	186163435	2014-03-07 20:22:00	DF2JP	JO31jg	G3SXH	IO80	1838020	33	-16	0	695	267	1	2.0_r1714	0
19	186165012	2014-03-07 20:30:00	DF2JP	JO31jg	G3SXH	IO80	1838021	33	-14	0	695	267	1	2.0_r1714	0
20	186165953	2014-03-07 20:36:00	DF2JP	JO31jg	G3SXH	IO80	1838020	33	-17	0	695	267	1	2.0_r1714	0
21	186169144	2014-03-07 20:52:00	DF2JP	JO31jg	G3SXH	IO80	1838020	33	-10	0	695	267	1	2.0_r1714	0
22	186172856	2014-03-07 21:12:00	DF2JP	JO31jg	G3SXH	IO80	1838020	33	-9	0	695	267	1	2.0_r1714	0
23	186174262	2014-03-07 21:20:00	DF2JP	JO31jg	G3SXH	IO80	1838020	33	-9	0	695	267	1	2.0_r1714	0
24	186176297	2014-03-07 21:30:00	DF2JP	JO31jg	G3SXH	IO80	1838021	33	-12	0	695	267	1	2.0_r1714	0
25	186177508	2014-03-07 21:38:00	DF2JP	JO31jg	G3SXH	IO80	1838020	33	-14	0	695	267	1	2.0_r1714	0
26	186178583	2014-03-07 21:44:00	DF2JP	JO31jg	G3SXH	IO80	1838021	33	-15	0	695	267	1	2.0_r1714	0
27	186183165	2014-03-07 21:54:00	DF2JP	JO31jg	G3SXH	IO80	1838020	33	-13	0	695	267	1	2.0_r1714	0
								Mean	-13.7407						
								SD	3.1573						
								AD	-2.7407						
								AD%	-87						

row	id	time	tx_sign	tx_loc	rx_sign	rx_loc	frequency	power	snr	drift	distance	azimuth	band	version	code
1	186165656	2014-03-07 20:34:00	DG7RJ	JN58th	W4AC	EL86	14097186	33	-22	0	8169	291	14	2.21_r2286	0
2	186171487	2014-03-07 21:04:00	DG7RJ	JN58th	W4AC	EL86	14097186	33	-22	0	8169	291	14	2.21_r2286	0
3	186173309	2014-03-07 21:14:00	DG7RJ	JN58th	W4AC	EL86	14097186	33	-18	0	8169	291	14	2.21_r2286	0
4	186186540	2014-03-07 22:12:00	DG7RJ	JN58th	W4AC	EL86	14097186	33	-20	0	8169	291	14	2.21_r2286	0
5	186188616	2014-03-07 22:24:00	DG7RJ	JN58th	W4AC	EL86	14097186	33	-25	0	8169	291	14	2.21_r2286	0
6	186194259	2014-03-07 23:02:00	DG7RJ	JN58th	W4AC	EL86	14097186	33	-27	0	8169	291	14	2.21_r2286	0
7	186195956	2014-03-07 23:14:00	DG7RJ	JN58th	W4AC	EL86	14097186	33	-27	0	8169	291	14	2.21_r2286	0
8	186198720	2014-03-07 23:32:00	DG7RJ	JN58th	W4AC	EL86	14097186	33	-14	0	8169	291	14	2.21_r2286	0
9	186200213	2014-03-07 23:40:00	DG7RJ	JN58th	W4AC	EL86	14097186	33	-24	0	8169	291	14	2.21_r2286	0
10	186203910	2014-03-08 00:02:00	DG7RJ	JN58th	W4AC	EL86	14097186	33	-22	0	8169	291	14	2.21_r2286	0
11	186205417	2014-03-08 00:12:00	DG7RJ	JN58th	W4AC	EL86	14097186	33	-21	0	8169	291	14	2.21_r2286	0
								Mean	-22.0000						
								SD	3.8471						
								AD	-8.0000						
								AD%	-208						

row	id	time	tx_sign	tx_loc	rx_sign	rx_loc	frequency	power	snr	drift	distance	azimuth	band	version	code
1	186162803	2014-03-07 20:18:00	DH5RAE	JN68qv	OE1MSB	JN88df	1838151	37	-6	0	227	108	1	0.8_r3058	0
2	186165050	2014-03-07 20:30:00	DH5RAE	JN68qv	OE1MSB	JN88df	1838151	37	-8	0	227	108	1	0.8_r3058	0
3	186167383	2014-03-07 20:42:00	DH5RAE	JN68qv	OE1MSB	JN88df	1838151	37	-11	0	227	108	1	0.8_r3058	0
4	186169998	2014-03-07 20:56:00	DH5RAE	JN68qv	OE1MSB	JN88df	1838151	37	-3	0	227	108	1	0.8_r3058	0
5	186172192	2014-03-07 21:08:00	DH5RAE	JN68qv	OE1MSB	JN88df	1838151	37	-7	0	227	108	1	0.8_r3058	0
6	186172765	2014-03-07 21:12:00	DH5RAE	JN68qv	OE1MSB	JN88df	1838151	37	-2	0	227	108	1	0.8_r3058	0
7	186174269	2014-03-07 21:20:00	DH5RAE	JN68qv	OE1MSB	JN88df	1838151	37	-1	0	227	108	1	0.8_r3058	0
8	186176765	2014-03-07 21:34:00	DH5RAE	JN68qv	OE1MSB	JN88df	1838151	37	-1	0	227	108	1	0.8_r3058	0
9	186178729	2014-03-07 21:44:00	DH5RAE	JN68qv	OE1MSB	JN88df	1838151	37	-3	0	227	108	1	0.8_r3058	0
10	186183579	2014-03-07 21:56:00	DH5RAE	JN68qv	OE1MSB	JN88df	1838151	37	5	0	227	108	1	0.8_r3058	0
11	186185446	2014-03-07 22:06:00	DH5RAE	JN68qv	OE1MSB	JN88df	1838151	37	-1	0	227	108	1	0.8_r3058	0
12	186187128	2014-03-07 22:16:00	DH5RAE	JN68qv	OE1MSB	JN88df	1838151	37	1	0	227	108	1	0.8_r3058	0
13	186189525	2014-03-07 22:30:00	DH5RAE	JN68qv	OE1MSB	JN88df	1838151	37	-1	0	227	108	1	0.8_r3058	0
								Mean	-2.9231						
								SD	4.1925						
								AD	-3.9231						
								AD%	-94						

row	id	time	tx_sign	tx_loc	rx_sign	rx_loc	frequency	power	snr	drift	distance	azimuth	band	version	code
1	185897451	2014-03-06 21:32:00	DK0SC	JN59mf	W4AC	EL86	14097108	37	-16	0	8093	291	14	2.21_r2286	0
2	186172496	2014-03-07 21:10:00	DK0SC	JN59mf	W4AC	EL86	14097108	37	-18	0	8093	291	14	2.21_r2286	0
3	186176045	2014-03-07 21:30:00	DK0SC	JN59mf	W4AC	EL86	14097107	37	-16	0	8093	291	14	2.21_r2286	0
4	186189409	2014-03-07 22:30:00	DK0SC	JN59mf	W4AC	EL86	14097109	37	-15	0	8093	291	14	2.21_r2286	0
5	186198561	2014-03-07 23:30:00	DK0SC	JN59mf	W4AC	EL86	14097109	37	-21	0	8093	291	14	2.21_r2286	0
6	186725024	2014-03-09 20:56:00	DK0SC	JN59mf	W4AC	EL86	14097109	37	-13	0	8093	291	14	2.21_r2286	0
7	186730783	2014-03-09 21:26:00	DK0SC	JN59mf	W4AC	EL86	14097108	37	-14	-1	8093	291	14	2.21_r2286	0
8	186735126	2014-03-09 21:50:00	DK0SC	JN59mf	W4AC	EL86	14097107	37	-17	0	8093	291	14	2.21_r2286	0
9	186751827	2014-03-09 23:12:00	DK0SC	JN59mf	W4AC	EL86	14097108	37	-20	0	8093	291	14	2.21_r2286	0
10	186754940	2014-03-09 23:30:00	DK0SC	JN59mf	W4AC	EL86	14097108	37	-11	0	8093	291	14	2.21_r2286	0
11	186769440	2014-03-10 00:42:00	DK0SC	JN59mf	W4AC	EL86	14097110	37	-3	0	8093	291	14	2.21_r2286	0
								Mean	-14.9091						
								SD	4.9082						
								AD	6.0909						
								AD%	124						

row	id	time	tx_sign	tx_loc	rx_sign	rx_loc	frequency	power	snr	drift	distance	azimuth	band	version	code
1	188318569	2014-03-07 15:36:00	DL8SEL	JO31vl	G8YTR	IO90lv	10140175	23	-25	-1	619	267	10	0.8_r3058	0
2	188318602	2014-03-07 15:52:00	DL8SEL	JO31vl	G8YTR	IO90lv	10140175	23	-26	-1	619	267	10	0.8_r3058	0
3	188318653	2014-03-07 16:20:00	DL8SEL	JO31vl	G8YTR	IO90lv	10140176	23	-21	-1	619	267	10	0.8_r3058	0
4	188319086	2014-03-07 18:12:00	DL8SEL	JO31vl	G8YTR	IO90lv	10140174	23	-24	-1	619	267	10	0.8_r3058	0
5	188319124	2014-03-07 18:20:00	DL8SEL	JO31vl	G8YTR	IO90lv	10140175	23	-21	-2	619	267	10	0.8_r3058	0
6	188319142	2014-03-07 18:28:00	DL8SEL	JO31vl	G8YTR	IO90lv	10140174	23	-18	-1	619	267	10	0.8_r3058	0
7	188319165	2014-03-07 18:36:00	DL8SEL	JO31vl	G8YTR	IO90lv	10140175	23	-22	-1	619	267	10	0.8_r3058	0
8	188319208	2014-03-07 18:52:00	DL8SEL	JO31vl	G8YTR	IO90lv	10140176	23	-22	-2	619	267	10	0.8_r3058	0
9	188319223	2014-03-07 19:04:00	DL8SEL	JO31vl	G8YTR	IO90lv	10140177	23	-19	-2	619	267	10	0.8_r3058	0
								Mean	-22.0000						
								SD	2.6458						
								AD	-4.0000						
								AD%	-151						

Page 632 of 1738

row	id	time	tx_sign	tx_loc	rx_sign	rx_loc	frequency	power	snr	drift	distance	azimuth	band	version	code
1	186163588	2014-03-07 20:22:00	G3NZP	IO91wc	DH5RAE	JN68qv	1838129	27	-19	0	994	99	1	0.8_r3058	0
2	186165275	2014-03-07 20:32:00	G3NZP	IO91wc	DH5RAE	JN68qv	1838129	27	-13	0	994	99	1	0.8_r3058	0
3	186173436	2014-03-07 20:52:00	G3NZP	IO91wc	DH5RAE	JN68qv	1838129	27	-17	0	994	99	1	0.8_r3058	0
4	186173447	2014-03-07 21:02:00	G3NZP	IO91wc	DH5RAE	JN68qv	1838129	27	-18	0	994	99	1	0.8_r3058	0
5	186174844	2014-03-07 21:22:00	G3NZP	IO91wc	DH5RAE	JN68qv	1838129	27	-12	0	994	99	1	0.8_r3058	0
6	186176630	2014-03-07 21:32:00	G3NZP	IO91wc	DH5RAE	JN68qv	1838129	27	-19	0	994	99	1	0.8_r3058	0
7	186178181	2014-03-07 21:42:00	G3NZP	IO91wc	DH5RAE	JN68qv	1838129	27	-12	0	994	99	1	0.8_r3058	0
8	186182660	2014-03-07 21:52:00	G3NZP	IO91wc	DH5RAE	JN68qv	1838129	27	-14	0	994	99	1	0.8_r3058	0
9	186184689	2014-03-07 22:02:00	G3NZP	IO91wc	DH5RAE	JN68qv	1838129	27	-15	0	994	99	1	0.8_r3058	0
10	186186587	2014-03-07 22:12:00	G3NZP	IO91wc	DH5RAE	JN68qv	1838129	27	-17	0	994	99	1	0.8_r3058	0
11	186188250	2014-03-07 22:22:00	G3NZP	IO91wc	DH5RAE	JN68qv	1838129	27	-17	0	994	99	1	0.8_r3058	0
12	186189895	2014-03-07 22:32:00	G3NZP	IO91wc	DH5RAE	JN68qv	1838129	27	-20	0	994	99	1	0.8_r3058	0
13	186215423	2014-03-08 01:22:00	G3NZP	IO91wc	DH5RAE	JN68qv	1838129	27	-6	0	994	99	1	0.8_r3058	0
14	186216829	2014-03-08 01:32:00	G3NZP	IO91wc	DH5RAE	JN68qv	1838129	27	-4	0	994	99	1	0.8_r3058	0
								Mean	-14.5000						
								SD	4.7998						
								AD	5.5000						
								AD%	115						

row	id	time	tx_sign	tx_loc	rx_sign	rx_loc	frequency	power	snr	drift	distance	azimuth	band	version	code
1	186171176	2014-03-07 21:02:00	G3SXH	IO80fr	DK6UG	JN49cm	1838043	30	-23	0	847	95	1	2.21_r2286	0
2	186174760	2014-03-07 21:22:00	G3SXH	IO80fr	DK6UG	JN49cm	1838043	30	-23	0	847	95	1	2.21_r2286	0
3	186178298	2014-03-07 21:42:00	G3SXH	IO80fr	DK6UG	JN49cm	1838043	30	-26	0	847	95	1	2.21_r2286	0
4	186184636	2014-03-07 22:02:00	G3SXH	IO80fr	DK6UG	JN49cm	1838043	30	-22	0	847	95	1	2.21_r2286	0
5	186197694	2014-03-07 23:26:00	G3SXH	IO80fr	DK6UG	JN49cm	1838043	30	-26	0	847	95	1	2.21_r2286	0
6	186203734	2014-03-08 00:02:00	G3SXH	IO80fr	DK6UG	JN49cm	1838042	30	-28	0	847	95	1	2.21_r2286	0
7	186207240	2014-03-08 00:24:00	G3SXH	IO80fr	DK6UG	JN49cm	1838043	30	-27	0	847	95	1	2.21_r2286	0
8	186210341	2014-03-08 00:44:00	G3SXH	IO80fr	DK6UG	JN49cm	1838043	30	-21	0	847	95	1	2.21_r2286	0
9	186212836	2014-03-08 01:02:00	G3SXH	IO80fr	DK6UG	JN49cm	1838042	30	-25	0	847	95	1	2.21_r2286	0
								Mean	-24.5556						
								SD	2.4037						
								AD	-2.5556						
								AD%	-106						

row	id	time	tx_sign	tx_loc	rx_sign	rx_loc	frequency	power	snr	drift	distance	azimuth	band	version	code
1	186170820	2014-03-07 21:00:00	G4ANN	IO91wd	W4AC	EL86	14097117	23	-25	1	7271	282	14	2.21_r2286	0
2	186184216	2014-03-07 22:00:00	G4ANN	IO91wd	W4AC	EL86	14097118	23	-23	1	7271	282	14	2.21_r2286	0
3	186198564	2014-03-07 23:30:00	G4ANN	IO91wd	W4AC	EL86	14097118	23	-27	1	7271	282	14	2.21_r2286	0
4	186201809	2014-03-07 23:50:00	G4ANN	IO91wd	W4AC	EL86	14097118	23	-20	1	7271	282	14	2.21_r2286	0
5	186738736	2014-03-09 22:10:00	G4ANN	IO91wd	W4AC	EL86	14097118	23	-15	1	7271	282	14	2.21_r2286	0
6	186746501	2014-03-09 22:40:00	G4ANN	IO91wd	W4AC	EL86	14097118	23	-17	1	7271	282	14	2.21_r2286	0
7	186772113	2014-03-10 01:00:00	G4ANN	IO91wd	W4AC	EL86	14097118	23	-14	1	7271	282	14	2.21_r2286	0
8	186777886	2014-03-10 01:40:00	G4ANN	IO91wd	W4AC	EL86	14097117	23	-16	0	7271	282	14	2.21_r2286	0
9	186780435	2014-03-10 02:00:00	G4ANN	IO91wd	W4AC	EL86	14097118	23	-20	0	7271	282	14	2.21_r2286	0
								Mean	-19.6667						
								SD	4.5826						
								AD	7.3333						
								AD%	160						

row	id	time	tx_sign	tx_loc	rx_sign	rx_loc	frequency	power	snr	drift	distance	azimuth	band	version	code
1	186116561	2014-03-07 16:52:00	G4FKK	IO91wi	ON7KB	JO21ei	7040048	33	-6	0	312	88	7	0.8_r3058	0
2	186120023	2014-03-07 17:04:00	G4FKK	IO91wi	ON7KB	JO21ei	7040047	33	-5	0	312	88	7	0.8_r3058	0
3	186121736	2014-03-07 17:12:00	G4FKK	IO91wi	ON7KB	JO21ei	7040048	33	-8	0	312	88	7	0.8_r3058	0
4	186128020	2014-03-07 17:34:00	G4FKK	IO91wi	ON7KB	JO21ei	7040048	33	-6	0	312	88	7	0.8_r3058	0
5	186130940	2014-03-07 17:46:00	G4FKK	IO91wi	ON7KB	JO21ei	7040047	33	-3	0	312	88	7	0.8_r3058	0
6	186132788	2014-03-07 17:54:00	G4FKK	IO91wi	ON7KB	JO21ei	7040048	33	-4	0	312	88	7	0.8_r3058	0
7	186146297	2014-03-07 18:54:00	G4FKK	IO91wi	ON7KB	JO21ei	7040046	33	-2	0	312	88	7	0.8_r3058	0
8	186149186	2014-03-07 19:06:00	G4FKK	IO91wi	ON7KB	JO21ei	7040047	33	-7	0	312	88	7	0.8_r3058	0
9	186153443	2014-03-07 19:30:00	G4FKK	IO91wi	ON7KB	JO21ei	7040047	33	-3	0	312	88	7	0.8_r3058	0
10	186155519	2014-03-07 19:40:00	G4FKK	IO91wi	ON7KB	JO21ei	7040047	33	-7	0	312	88	7	0.8_r3058	0
11	186157125	2014-03-07 19:48:00	G4FKK	IO91wi	ON7KB	JO21ei	7040048	33	0	0	312	88	7	0.8_r3058	0
12	186160581	2014-03-07 20:08:00	G4FKK	IO91wi	ON7KB	JO21ei	7040048	33	-6	0	312	88	7	0.8_r3058	0
13	186162341	2014-03-07 20:16:00	G4FKK	IO91wi	ON7KB	JO21ei	7040049	33	-9	0	312	88	7	0.8_r3058	0
14	186164073	2014-03-07 20:26:00	G4FKK	IO91wi	ON7KB	JO21ei	7040049	33	-6	0	312	88	7	0.8_r3058	0
15	186165628	2014-03-07 20:34:00	G4FKK	IO91wi	ON7KB	JO21ei	7040049	33	-8	0	312	88	7	0.8_r3058	0
16	186168823	2014-03-07 20:50:00	G4FKK	IO91wi	ON7KB	JO21ei	7040051	33	-10	0	312	88	7	0.8_r3058	0
17	186172137	2014-03-07 21:08:00	G4FKK	IO91wi	ON7KB	JO21ei	7040050	33	-6	0	312	88	7	0.8_r3058	0
18	186174113	2014-03-07 21:18:00	G4FKK	IO91wi	ON7KB	JO21ei	7040049	33	-9	0	312	88	7	0.8_r3058	0
								Mean	-5.8333						
								SD	2.6402						
								AD	-5.8333						
								AD%	-221						

row	id	time	tx_sign	tx_loc	rx_sign	rx_loc	frequency	power	snr	drift	distance	azimuth	band	version	code
1	186186508	2014-03-07 22:12:00	G4JVF	IO93if	W4MO	EL87	14097106	23	-25	0	7064	281	14	2.21_r2286	0
2	186187789	2014-03-07 22:20:00	G4JVF	IO93if	W4MO	EL87	14097107	23	-23	0	7064	281	14	2.21_r2286	0
3	186189823	2014-03-07 22:32:00	G4JVF	IO93if	W4MO	EL87	14097110	23	-24	0	7064	281	14	2.21_r2286	0
4	186201432	2014-03-07 23:48:00	G4JVF	IO93if	W4MO	EL87	14097110	23	-28	0	7064	281	14	2.21_r2286	0
5	186219429	2014-03-08 01:52:00	G4JVF	IO93if	W4MO	EL87	14097112	23	-22	0	7064	281	14	2.21_r2286	0
								Mean	-24.4000						
								SD	2.3022						
								AD	3.6000						
								AD%	156						

row	id	time	tx_sign	tx_loc	rx_sign	rx_loc	frequency	power	snr	drift	distance	azimuth	band	version	code
1	186156997	2014-03-07 19:48:00	G4KPX	JO02dj	DL1DBC	JO41bi	475617	0	-27	0	550	99	0	2.0_r1714	0
2	186160063	2014-03-07 20:04:00	G4KPX	JO02dj	DL1DBC	JO41bi	475617	0	-32	0	550	99	0	2.0_r1714	0
3	186161660	2014-03-07 20:12:00	G4KPX	JO02dj	DL1DBC	JO41bi	475617	0	-27	0	550	99	0	2.0_r1714	0
4	186163199	2014-03-07 20:20:00	G4KPX	JO02dj	DL1DBC	JO41bi	475617	0	-26	0	550	99	0	2.0_r1714	0
5	186164686	2014-03-07 20:28:00	G4KPX	JO02dj	DL1DBC	JO41bi	475617	0	-23	0	550	99	0	2.0_r1714	0
6	186166245	2014-03-07 20:36:00	G4KPX	JO02dj	DL1DBC	JO41bi	475617	0	-21	0	550	99	0	2.0_r1714	0
7	186170568	2014-03-07 21:00:00	G4KPX	JO02dj	DL1DBC	JO41bi	475617	0	-27	0	550	99	0	2.0_r1714	0
8	186173518	2014-03-07 21:16:00	G4KPX	JO02dj	DL1DBC	JO41bi	475617	0	-22	0	550	99	0	2.0_r1714	0
9	186176601	2014-03-07 21:32:00	G4KPX	JO02dj	DL1DBC	JO41bi	475617	0	-21	0	550	99	0	2.0_r1714	0
10	186178121	2014-03-07 21:40:00	G4KPX	JO02dj	DL1DBC	JO41bi	475617	0	-23	0	550	99	0	2.0_r1714	0
11	186180543	2014-03-07 21:48:00	G4KPX	JO02dj	DL1DBC	JO41bi	475617	0	-26	0	550	99	0	2.0_r1714	0
12	186186710	2014-03-07 22:12:00	G4KPX	JO02dj	DL1DBC	JO41bi	475617	0	-26	0	550	99	0	2.0_r1714	0
13	186187896	2014-03-07 22:20:00	G4KPX	JO02dj	DL1DBC	JO41bi	475617	0	-27	0	550	99	0	2.0_r1714	0
14	186189220	2014-03-07 22:28:00	G4KPX	JO02dj	DL1DBC	JO41bi	475617	0	-21	0	550	99	0	2.0_r1714	0
15	186190392	2014-03-07 22:36:00	G4KPX	JO02dj	DL1DBC	JO41bi	475617	0	-16	0	550	99	0	2.0_r1714	0
16	186192739	2014-03-07 22:52:00	G4KPX	JO02dj	DL1DBC	JO41bi	475617	0	-26	0	550	99	0	2.0_r1714	0
17	186193752	2014-03-07 23:00:00	G4KPX	JO02dj	DL1DBC	JO41bi	475617	0	-21	0	550	99	0	2.0_r1714	0
18	186195126	2014-03-07 23:08:00	G4KPX	JO02dj	DL1DBC	JO41bi	475617	0	-28	0	550	99	0	2.0_r1714	0
19	186196447	2014-03-07 23:16:00	G4KPX	JO02dj	DL1DBC	JO41bi	475617	0	-24	0	550	99	0	2.0_r1714	0
20	186197439	2014-03-07 23:24:00	G4KPX	JO02dj	DL1DBC	JO41bi	475617	0	-23	0	550	99	0	2.0_r1714	0
21	186198986	2014-03-07 23:32:00	G4KPX	JO02dj	DL1DBC	JO41bi	475617	0	-23	0	550	99	0	2.0_r1714	0
22	186200344	2014-03-07 23:40:00	G4KPX	JO02dj	DL1DBC	JO41bi	475617	0	-25	0	550	99	0	2.0_r1714	0
23	186201687	2014-03-07 23:48:00	G4KPX	JO02dj	DL1DBC	JO41bi	475617	0	-27	0	550	99	0	2.0_r1714	0
24	186203048	2014-03-07 23:56:00	G4KPX	JO02dj	DL1DBC	JO41bi	475617	0	-28	0	550	99	0	2.0_r1714	0
25	186204227	2014-03-08 00:04:00	G4KPX	JO02dj	DL1DBC	JO41bi	475617	0	-28	0	550	99	0	2.0_r1714	0
26	186205524	2014-03-08 00:12:00	G4KPX	JO02dj	DL1DBC	JO41bi	475617	0	-28	0	550	99	0	2.0_r1714	0
27	186206848	2014-03-08 00:20:00	G4KPX	JO02dj	DL1DBC	JO41bi	475617	0	-22	0	550	99	0	2.0_r1714	0
28	186208027	2014-03-08 00:28:00	G4KPX	JO02dj	DL1DBC	JO41bi	475617	0	-26	0	550	99	0	2.0_r1714	0
29	186209243	2014-03-08 00:36:00	G4KPX	JO02dj	DL1DBC	JO41bi	475617	0	-25	0	550	99	0	2.0_r1714	0
30	186211536	2014-03-08 00:52:00	G4KPX	JO02dj	DL1DBC	JO41bi	475617	0	-22	0	550	99	0	2.0_r1714	0
31	186212671	2014-03-08 01:00:00	G4KPX	JO02dj	DL1DBC	JO41bi	475617	0	-25	0	550	99	0	2.0_r1714	0
32	186213508	2014-03-08 01:08:00	G4KPX	JO02dj	DL1DBC	JO41bi	475617	0	-22	0	550	99	0	2.0_r1714	0
33	186214751	2014-03-08 01:16:00	G4KPX	JO02dj	DL1DBC	JO41bi	475617	0	-23	0	550	99	0	2.0_r1714	0
34	186216910	2014-03-08 01:32:00	G4KPX	JO02dj	DL1DBC	JO41bi	475617	0	-28	0	550	99	0	2.0_r1714	0
								Mean	-24.6765						
								SD	3.1015						
								AD	-8.6765						
								AD%	-280						

row	id	time	tx_sign	tx_loc	rx_sign	rx_loc	frequency	power	snr	drift	distance	azimuth	band	version	code
1	186160136	2014-03-07 20:04:00	G4KPX	JO02dj	PA3ABK/2	JO21it	475617	0	-23	0	308	100	0	2.11_r2263	0
2	186161677	2014-03-07 20:12:00	G4KPX	JO02dj	PA3ABK/2	JO21it	475617	0	-19	0	308	100	0	2.11_r2263	0
3	186162966	2014-03-07 20:20:00	G4KPX	JO02dj	PA3ABK/2	JO21it	475617	0	-19	0	308	100	0	2.11_r2263	0
4	186164557	2014-03-07 20:28:00	G4KPX	JO02dj	PA3ABK/2	JO21it	475617	0	-19	0	308	100	0	2.11_r2263	0
5	186166177	2014-03-07 20:36:00	G4KPX	JO02dj	PA3ABK/2	JO21it	475617	0	-19	0	308	100	0	2.11_r2263	0
6	186169159	2014-03-07 20:52:00	G4KPX	JO02dj	PA3ABK/2	JO21it	475617	0	-25	0	308	100	0	2.11_r2263	0
7	186173554	2014-03-07 21:16:00	G4KPX	JO02dj	PA3ABK/2	JO21it	475617	0	-17	0	308	100	0	2.11_r2263	0
8	186175120	2014-03-07 21:24:00	G4KPX	JO02dj	PA3ABK/2	JO21it	475617	0	-13	0	308	100	0	2.11_r2263	0
9	186176647	2014-03-07 21:32:00	G4KPX	JO02dj	PA3ABK/2	JO21it	475617	0	-14	0	308	100	0	2.11_r2263	0
10	186177917	2014-03-07 21:40:00	G4KPX	JO02dj	PA3ABK/2	JO21it	475617	0	-18	0	308	100	0	2.11_r2263	0
11	186180738	2014-03-07 21:48:00	G4KPX	JO02dj	PA3ABK/2	JO21it	475617	0	-21	0	308	100	0	2.11_r2263	0
12	186185112	2014-03-07 22:04:00	G4KPX	JO02dj	PA3ABK/2	JO21it	475617	0	-19	0	308	100	0	2.11_r2263	0
13	186186534	2014-03-07 22:12:00	G4KPX	JO02dj	PA3ABK/2	JO21it	475617	0	-16	0	308	100	0	2.11_r2263	0
14	186187834	2014-03-07 22:20:00	G4KPX	JO02dj	PA3ABK/2	JO21it	475617	0	-20	0	308	100	0	2.11_r2263	0
15	186188938	2014-03-07 22:28:00	G4KPX	JO02dj	PA3ABK/2	JO21it	475617	0	-23	0	308	100	0	2.11_r2263	0
16	186190276	2014-03-07 22:36:00	G4KPX	JO02dj	PA3ABK/2	JO21it	475617	0	-16	0	308	100	0	2.11_r2263	0
17	186192721	2014-03-07 22:52:00	G4KPX	JO02dj	PA3ABK/2	JO21it	475617	0	-15	0	308	100	0	2.11_r2263	0
18	186193990	2014-03-07 23:00:00	G4KPX	JO02dj	PA3ABK/2	JO21it	475617	0	-23	0	308	100	0	2.11_r2263	0
19	186195146	2014-03-07 23:08:00	G4KPX	JO02dj	PA3ABK/2	JO21it	475617	0	-17	0	308	100	0	2.11_r2263	0
20	186196266	2014-03-07 23:16:00	G4KPX	JO02dj	PA3ABK/2	JO21it	475617	0	-14	0	308	100	0	2.11_r2263	0
21	186197462	2014-03-07 23:24:00	G4KPX	JO02dj	PA3ABK/2	JO21it	475617	0	-10	0	308	100	0	2.11_r2263	0
22	186198961	2014-03-07 23:32:00	G4KPX	JO02dj	PA3ABK/2	JO21it	475617	0	-11	0	308	100	0	2.11_r2263	0
23	186200398	2014-03-07 23:40:00	G4KPX	JO02dj	PA3ABK/2	JO21it	475617	0	-10	0	308	100	0	2.11_r2263	0
24	186201668	2014-03-07 23:48:00	G4KPX	JO02dj	PA3ABK/2	JO21it	475617	0	-13	0	308	100	0	2.11_r2263	0
25	186203036	2014-03-07 23:56:00	G4KPX	JO02dj	PA3ABK/2	JO21it	475617	0	-10	0	308	100	0	2.11_r2263	0
26	186204246	2014-03-08 00:04:00	G4KPX	JO02dj	PA3ABK/2	JO21it	475617	0	-18	0	308	100	0	2.11_r2263	0
27	186205306	2014-03-08 00:12:00	G4KPX	JO02dj	PA3ABK/2	JO21it	475617	0	-16	0	308	100	0	2.11_r2263	0
28	186206699	2014-03-08 00:20:00	G4KPX	JO02dj	PA3ABK/2	JO21it	475617	0	-16	0	308	100	0	2.11_r2263	0
29	186207951	2014-03-08 00:28:00	G4KPX	JO02dj	PA3ABK/2	JO21it	475617	0	-17	0	308	100	0	2.11_r2263	0
30	186209211	2014-03-08 00:36:00	G4KPX	JO02dj	PA3ABK/2	JO21it	475617	0	-16	0	308	100	0	2.11_r2263	0
31	186213745	2014-03-08 01:08:00	G4KPX	JO02dj	PA3ABK/2	JO21it	475617	0	-12	0	308	100	0	2.11_r2263	0
32	186214711	2014-03-08 01:16:00	G4KPX	JO02dj	PA3ABK/2	JO21it	475617	0	-11	0	308	100	0	2.11_r2263	0
33	186215719	2014-03-08 01:24:00	G4KPX	JO02dj	PA3ABK/2	JO21it	475617	0	-19	0	308	100	0	2.11_r2263	0
34	186216800	2014-03-08 01:32:00	G4KPX	JO02dj	PA3ABK/2	JO21it	475617	0	-20	0	308	100	0	2.11_r2263	0
35	186217845	2014-03-08 01:40:00	G4KPX	JO02dj	PA3ABK/2	JO21it	475617	0	-15	0	308	100	0	2.11_r2263	0
36	186218942	2014-03-08 01:48:00	G4KPX	JO02dj	PA3ABK/2	JO21it	475617	0	-18	0	308	100	0	2.11_r2263	0
37	186220186	2014-03-08 01:56:00	G4KPX	JO02dj	PA3ABK/2	JO21it	475617	0	-26	0	308	100	0	2.11_r2263	0
								Mean	-16.9730						
								SD	4.1532						
								AD	6.0270						
								AD%	145						

row	id	time	tx_sign	tx_loc	rx_sign	rx_loc	frequency	power	snr	drift	distance	azimuth	band	version	code
1	186148140	2014-03-07 19:02:00	G4ZXE	IO81qk	G4FKK	IO91wi	7040058	37	3	0	174	92	7	2.0_r1714	0
2	186150504	2014-03-07 19:14:00	G4ZXE	IO81qk	G4FKK	IO91wi	7040058	37	1	0	174	92	7	2.0_r1714	0
3	186152543	2014-03-07 19:24:00	G4ZXE	IO81qk	G4FKK	IO91wi	7040057	37	5	0	174	92	7	2.0_r1714	0
4	186154163	2014-03-07 19:32:00	G4ZXE	IO81qk	G4FKK	IO91wi	7040057	37	2	0	174	92	7	2.0_r1714	0
5	186156086	2014-03-07 19:44:00	G4ZXE	IO81qk	G4FKK	IO91wi	7040056	37	3	0	174	92	7	2.0_r1714	0
6	186157921	2014-03-07 19:52:00	G4ZXE	IO81qk	G4FKK	IO91wi	7040055	37	1	0	174	92	7	2.0_r1714	0
7	186160055	2014-03-07 20:04:00	G4ZXE	IO81qk	G4FKK	IO91wi	7040055	37	4	0	174	92	7	2.0_r1714	0
8	186163774	2014-03-07 20:24:00	G4ZXE	IO81qk	G4FKK	IO91wi	7040055	37	-4	0	174	92	7	2.0_r1714	0
9	186165272	2014-03-07 20:32:00	G4ZXE	IO81qk	G4FKK	IO91wi	7040055	37	1	0	174	92	7	2.0_r1714	0
10	186167003	2014-03-07 20:40:00	G4ZXE	IO81qk	G4FKK	IO91wi	7040055	37	-2	0	174	92	7	2.0_r1714	0
11	186170338	2014-03-07 20:58:00	G4ZXE	IO81qk	G4FKK	IO91wi	7040055	37	-3	0	174	92	7	2.0_r1714	0
12	186171883	2014-03-07 21:06:00	G4ZXE	IO81qk	G4FKK	IO91wi	7040055	37	-2	0	174	92	7	2.0_r1714	0
13	186173688	2014-03-07 21:16:00	G4ZXE	IO81qk	G4FKK	IO91wi	7040044	37	-5	0	174	92	7	2.0_r1714	0
14	186175519	2014-03-07 21:26:00	G4ZXE	IO81qk	G4FKK	IO91wi	7040044	37	-4	0	174	92	7	2.0_r1714	0
								Mean	0.0000						
								SD	3.2817						
								AD	5.0000						
								AD%	152						

row	id	time	tx_sign	tx_loc	rx_sign	rx_loc	frequency	power	snr	drift	distance	azimuth	band	version	code
1	186132792	2014-03-07 17:54:00	G4ZXE	IO81qk	ON7KB	JO21ei	7040163	37	-1	0	486	88	7	0.8_r3058	0
2	186141190	2014-03-07 18:30:00	G4ZXE	IO81qk	ON7KB	JO21ei	7040079	37	-4	0	486	88	7	0.8_r3058	0
3	186148363	2014-03-07 19:02:00	G4ZXE	IO81qk	ON7KB	JO21ei	7040081	37	-5	0	486	88	7	0.8_r3058	0
4	186150892	2014-03-07 19:14:00	G4ZXE	IO81qk	ON7KB	JO21ei	7040080	37	-3	0	486	88	7	0.8_r3058	0
5	186152724	2014-03-07 19:24:00	G4ZXE	IO81qk	ON7KB	JO21ei	7040080	37	-1	0	486	88	7	0.8_r3058	0
6	186156082	2014-03-07 19:44:00	G4ZXE	IO81qk	ON7KB	JO21ei	7040079	37	-4	0	486	88	7	0.8_r3058	0
7	186157968	2014-03-07 19:52:00	G4ZXE	IO81qk	ON7KB	JO21ei	7040080	37	-5	0	486	88	7	0.8_r3058	0
8	186160132	2014-03-07 20:04:00	G4ZXE	IO81qk	ON7KB	JO21ei	7040079	37	-1	0	486	88	7	0.8_r3058	0
9	186162347	2014-03-07 20:16:00	G4ZXE	IO81qk	ON7KB	JO21ei	7040080	37	-8	0	486	88	7	0.8_r3058	0
10	186163887	2014-03-07 20:24:00	G4ZXE	IO81qk	ON7KB	JO21ei	7040080	37	-3	0	486	88	7	0.8_r3058	0
11	186165423	2014-03-07 20:32:00	G4ZXE	IO81qk	ON7KB	JO21ei	7040080	37	-3	0	486	88	7	0.8_r3058	0
12	186167029	2014-03-07 20:40:00	G4ZXE	IO81qk	ON7KB	JO21ei	7040080	37	-6	0	486	88	7	0.8_r3058	0
13	186168830	2014-03-07 20:50:00	G4ZXE	IO81qk	ON7KB	JO21ei	7040080	37	-4	0	486	88	7	0.8_r3058	0
14	186170392	2014-03-07 20:58:00	G4ZXE	IO81qk	ON7KB	JO21ei	7040080	37	-7	0	486	88	7	0.8_r3058	0
15	186171771	2014-03-07 21:06:00	G4ZXE	IO81qk	ON7KB	JO21ei	7040080	37	-7	0	486	88	7	0.8_r3058	0
16	186173730	2014-03-07 21:16:00	G4ZXE	IO81qk	ON7KB	JO21ei	7040069	37	-4	0	486	88	7	0.8_r3058	0
17	186175309	2014-03-07 21:26:00	G4ZXE	IO81qk	ON7KB	JO21ei	7040069	37	-7	0	486	88	7	0.8_r3058	0
								Mean	-4.2941						
								SD	2.2013						
								AD	3.7059						
								AD%	168						

Page 641 of 1738

row	id	time	tx_sign	tx_loc	rx_sign	rx_loc	frequency	power	snr	drift	distance	azimuth	band	version	code
1	186188233	2014-03-07 22:22:00	G6RRL	IO90iw	DK6UG	JN49cm	3594082	33	-4	0	693	99	3	2.21_r2286	0
2	186189710	2014-03-07 22:32:00	G6RRL	IO90iw	DK6UG	JN49cm	3594081	33	-12	0	693	99	3	2.21_r2286	0
3	186192616	2014-03-07 22:52:00	G6RRL	IO90iw	DK6UG	JN49cm	3594078	33	-22	0	693	99	3	2.21_r2286	0
4	186194484	2014-03-07 23:04:00	G6RRL	IO90iw	DK6UG	JN49cm	3594077	33	-8	0	693	99	3	2.21_r2286	0
5	186195696	2014-03-07 23:12:00	G6RRL	IO90iw	DK6UG	JN49cm	3594076	33	-6	0	693	99	3	2.21_r2286	0
6	186197307	2014-03-07 23:22:00	G6RRL	IO90iw	DK6UG	JN49cm	3594075	33	-9	0	693	99	3	2.21_r2286	0
7	186198808	2014-03-07 23:32:00	G6RRL	IO90iw	DK6UG	JN49cm	3594075	33	-4	0	693	99	3	2.21_r2286	0
8	186200229	2014-03-07 23:40:00	G6RRL	IO90iw	DK6UG	JN49cm	3594074	33	-8	0	693	99	3	2.21_r2286	0
9	186202149	2014-03-07 23:52:00	G6RRL	IO90iw	DK6UG	JN49cm	3594074	33	-7	0	693	99	3	2.21_r2286	0
10	186203661	2014-03-08 00:00:00	G6RRL	IO90iw	DK6UG	JN49cm	3594074	33	-7	0	693	99	3	2.21_r2286	0
11	186204473	2014-03-08 00:06:00	G6RRL	IO90iw	DK6UG	JN49cm	3594073	33	-5	0	693	99	3	2.21_r2286	0
								Mean	-8.3636						
								SD	5.0847						
								AD	13.6364						
								AD%	268						

Page 642 of 1738

row	id	time	tx_sign	tx_loc	rx_sign	rx_loc	frequency	power	snr	drift	distance	azimuth	band	version	code
1	186127704	2014-03-07 17:34:00	G8VDQ	IO91um	DO6RPS	JO42ic	3594041	37	-23	0	622	80	3	0.8_r3058	0
2	186130169	2014-03-07 17:44:00	G8VDQ	IO91um	DO6RPS	JO42ic	3594047	37	-21	1	622	80	3	0.8_r3058	0
3	186132600	2014-03-07 17:54:00	G8VDQ	IO91um	DO6RPS	JO42ic	3594050	37	-20	0	622	80	3	0.8_r3058	0
4	186137651	2014-03-07 18:14:00	G8VDQ	IO91um	DO6RPS	JO42ic	3594054	37	-17	1	622	80	3	0.8_r3058	0
5	186139964	2014-03-07 18:24:00	G8VDQ	IO91um	DO6RPS	JO42ic	3594054	37	-20	0	622	80	3	0.8_r3058	0
6	186142372	2014-03-07 18:34:00	G8VDQ	IO91um	DO6RPS	JO42ic	3594054	37	-21	0	622	80	3	0.8_r3058	0
7	186144238	2014-03-07 18:44:00	G8VDQ	IO91um	DO6RPS	JO42ic	3594054	37	-17	0	622	80	3	0.8_r3058	0
8	186146251	2014-03-07 18:54:00	G8VDQ	IO91um	DO6RPS	JO42ic	3594055	37	-22	0	622	80	3	0.8_r3058	0
9	186148494	2014-03-07 19:04:00	G8VDQ	IO91um	DO6RPS	JO42ic	3594055	37	-21	0	622	80	3	0.8_r3058	0
10	186150501	2014-03-07 19:14:00	G8VDQ	IO91um	DO6RPS	JO42ic	3594054	37	-19	1	622	80	3	0.8_r3058	0
11	186152402	2014-03-07 19:24:00	G8VDQ	IO91um	DO6RPS	JO42ic	3594054	37	-20	0	622	80	3	0.8_r3058	0
12	186154346	2014-03-07 19:34:00	G8VDQ	IO91um	DO6RPS	JO42ic	3594055	37	-20	0	622	80	3	0.8_r3058	0
13	186156192	2014-03-07 19:44:00	G8VDQ	IO91um	DO6RPS	JO42ic	3594054	37	-19	0	622	80	3	0.8_r3058	0
14	186160147	2014-03-07 20:04:00	G8VDQ	IO91um	DO6RPS	JO42ic	3594054	37	-18	0	622	80	3	0.8_r3058	0
15	186161851	2014-03-07 20:14:00	G8VDQ	IO91um	DO6RPS	JO42ic	3594054	37	-17	0	622	80	3	0.8_r3058	0
16	186165889	2014-03-07 20:34:00	G8VDQ	IO91um	DO6RPS	JO42ic	3594055	37	-19	0	622	80	3	0.8_r3058	0
								Mean	-19.6250						
								SD	1.7842						
								AD	-2.6250						
								AD%	-147						

row	id	time	tx_sign	tx_loc	rx_sign	rx_loc	frequency	power	snr	drift	distance	azimuth	band	version	code
1	186116492	2014-03-07 16:52:00	G8VDQ	IO91um	G0MQW	IO91ml	10140149	37	-21	0	46	265	10	2.0_r1714	0
2	186118471	2014-03-07 16:58:00	G8VDQ	IO91um	G0MQW	IO91ml	10140149	37	-17	0	46	265	10	2.0_r1714	0
3	186120323	2014-03-07 17:06:00	G8VDQ	IO91um	G0MQW	IO91ml	10140149	37	-16	0	46	265	10	2.0_r1714	0
4	186122186	2014-03-07 17:12:00	G8VDQ	IO91um	G0MQW	IO91ml	10140149	37	-22	0	46	265	10	2.0_r1714	0
5	186125761	2014-03-07 17:26:00	G8VDQ	IO91um	G0MQW	IO91ml	10140149	37	-18	0	46	265	10	2.0_r1714	0
6	186127557	2014-03-07 17:32:00	G8VDQ	IO91um	G0MQW	IO91ml	10140149	37	-16	0	46	265	10	2.0_r1714	0
7	186129153	2014-03-07 17:40:00	G8VDQ	IO91um	G0MQW	IO91ml	10140149	37	-17	0	46	265	10	2.0_r1714	0
8	186132561	2014-03-07 17:52:00	G8VDQ	IO91um	G0MQW	IO91ml	10140149	37	-23	0	46	265	10	2.0_r1714	0
9	186134492	2014-03-07 18:00:00	G8VDQ	IO91um	G0MQW	IO91ml	10140149	37	-18	0	46	265	10	2.0_r1714	0
10	186139357	2014-03-07 18:20:00	G8VDQ	IO91um	G0MQW	IO91ml	10140149	37	-25	0	46	265	10	2.0_r1714	0
11	186147467	2014-03-07 18:58:00	G8VDQ	IO91um	G0MQW	IO91ml	10140149	37	-26	0	46	265	10	2.0_r1714	0
12	186155238	2014-03-07 19:38:00	G8VDQ	IO91um	G0MQW	IO91ml	10140149	37	-25	0	46	265	10	2.0_r1714	0
13	186155548	2014-03-07 19:40:00	G8VDQ	IO91um	G0MQW	IO91ml	10140149	37	-26	0	46	265	10	2.0_r1714	0
								Mean	-20.7692						
								SD	3.9403						
								AD	4.2308						
								AD%	107						

row	id	time	tx_sign	tx_loc	rx_sign	rx_loc	frequency	power	snr	drift	distance	azimuth	band	version	code
1	186116492	2014-03-07 16:52:00	G8VDQ	IO91um	G0MQW	IO91ml	10140149	37	-21	0	46	265	10	2.0_r1714	0
2	186118471	2014-03-07 16:58:00	G8VDQ	IO91um	G0MQW	IO91ml	10140149	37	-17	0	46	265	10	2.0_r1714	0
3	186120323	2014-03-07 17:06:00	G8VDQ	IO91um	G0MQW	IO91ml	10140149	37	-16	0	46	265	10	2.0_r1714	0
4	186122186	2014-03-07 17:12:00	G8VDQ	IO91um	G0MQW	IO91ml	10140149	37	-22	0	46	265	10	2.0_r1714	0
5	186125761	2014-03-07 17:26:00	G8VDQ	IO91um	G0MQW	IO91ml	10140149	37	-18	0	46	265	10	2.0_r1714	0
6	186127557	2014-03-07 17:32:00	G8VDQ	IO91um	G0MQW	IO91ml	10140149	37	-16	0	46	265	10	2.0_r1714	0
7	186129153	2014-03-07 17:40:00	G8VDQ	IO91um	G0MQW	IO91ml	10140149	37	-17	0	46	265	10	2.0_r1714	0
8	186132561	2014-03-07 17:52:00	G8VDQ	IO91um	G0MQW	IO91ml	10140149	37	-23	0	46	265	10	2.0_r1714	0
9	186134492	2014-03-07 18:00:00	G8VDQ	IO91um	G0MQW	IO91ml	10140149	37	-18	0	46	265	10	2.0_r1714	0
10	186139357	2014-03-07 18:20:00	G8VDQ	IO91um	G0MQW	IO91ml	10140149	37	-25	0	46	265	10	2.0_r1714	0
11	186147467	2014-03-07 18:58:00	G8VDQ	IO91um	G0MQW	IO91ml	10140149	37	-26	0	46	265	10	2.0_r1714	0
12	186155238	2014-03-07 19:38:00	G8VDQ	IO91um	G0MQW	IO91ml	10140149	37	-25	0	46	265	10	2.0_r1714	0
13	186155548	2014-03-07 19:40:00	G8VDQ	IO91um	G0MQW	IO91ml	10140149	37	-26	0	46	265	10	2.0_r1714	0
								Mean	-20.7692						
								SD	3.9403						
								AD	5.2308						
								AD%	133						

row	id	time	tx_sign	tx_loc	rx_sign	rx_loc	frequency	power	snr	drift	distance	azimuth	band	version	code
1	186164120	2014-03-07 20:26:00	G8VDQ	IO91um	W4AC	EL86	14097053	37	-18	0	7251	282	14	2.21_r2286	0
2	186165451	2014-03-07 20:32:00	G8VDQ	IO91um	W4AC	EL86	14097054	37	-13	0	7251	282	14	2.21_r2286	0
3	186166896	2014-03-07 20:40:00	G8VDQ	IO91um	W4AC	EL86	14097054	37	-11	0	7251	282	14	2.21_r2286	0
4	186169105	2014-03-07 20:52:00	G8VDQ	IO91um	W4AC	EL86	14097054	37	-13	0	7251	282	14	2.21_r2286	0
5	186170775	2014-03-07 21:00:00	G8VDQ	IO91um	W4AC	EL86	14097054	37	-14	0	7251	282	14	2.21_r2286	0
6	186171816	2014-03-07 21:06:00	G8VDQ	IO91um	W4AC	EL86	14097053	37	-12	0	7251	282	14	2.21_r2286	0
7	186172974	2014-03-07 21:12:00	G8VDQ	IO91um	W4AC	EL86	14097052	37	-11	0	7251	282	14	2.21_r2286	0
8	186173913	2014-03-07 21:18:00	G8VDQ	IO91um	W4AC	EL86	14097053	37	-14	0	7251	282	14	2.21_r2286	0
9	186177492	2014-03-07 21:38:00	G8VDQ	IO91um	W4AC	EL86	14097054	37	-12	0	7251	282	14	2.21_r2286	0
10	186177998	2014-03-07 21:40:00	G8VDQ	IO91um	W4AC	EL86	14097053	37	-12	0	7251	282	14	2.21_r2286	0
11	186183927	2014-03-07 21:58:00	G8VDQ	IO91um	W4AC	EL86	14097054	37	-16	0	7251	282	14	2.21_r2286	0
12	186184211	2014-03-07 22:00:00	G8VDQ	IO91um	W4AC	EL86	14097053	37	-10	0	7251	282	14	2.21_r2286	0
13	186185520	2014-03-07 22:06:00	G8VDQ	IO91um	W4AC	EL86	14097054	37	-11	0	7251	282	14	2.21_r2286	0
14	186186509	2014-03-07 22:12:00	G8VDQ	IO91um	W4AC	EL86	14097054	37	-8	0	7251	282	14	2.21_r2286	0
15	186187397	2014-03-07 22:18:00	G8VDQ	IO91um	W4AC	EL86	14097054	37	-13	0	7251	282	14	2.21_r2286	0
16	186187849	2014-03-07 22:20:00	G8VDQ	IO91um	W4AC	EL86	14097054	37	-11	0	7251	282	14	2.21_r2286	0
17	186188831	2014-03-07 22:26:00	G8VDQ	IO91um	W4AC	EL86	14097055	37	-8	0	7251	282	14	2.21_r2286	0
18	186189715	2014-03-07 22:32:00	G8VDQ	IO91um	W4AC	EL86	14097054	37	-7	-1	7251	282	14	2.21_r2286	0
19	186190623	2014-03-07 22:38:00	G8VDQ	IO91um	W4AC	EL86	14097054	37	-15	0	7251	282	14	2.21_r2286	0
20	186191808	2014-03-07 22:46:00	G8VDQ	IO91um	W4AC	EL86	14097055	37	-12	0	7251	282	14	2.21_r2286	0
21	186192712	2014-03-07 22:52:00	G8VDQ	IO91um	W4AC	EL86	14097054	37	-14	0	7251	282	14	2.21_r2286	0
22	186193893	2014-03-07 23:00:00	G8VDQ	IO91um	W4AC	EL86	14097055	37	-20	0	7251	282	14	2.21_r2286	0
23	186194857	2014-03-07 23:06:00	G8VDQ	IO91um	W4AC	EL86	14097055	37	-16	0	7251	282	14	2.21_r2286	0
24	186196670	2014-03-07 23:18:00	G8VDQ	IO91um	W4AC	EL86	14097054	37	-15	-1	7251	282	14	2.21_r2286	0
25	186197805	2014-03-07 23:26:00	G8VDQ	IO91um	W4AC	EL86	14097054	37	-19	0	7251	282	14	2.21_r2286	0
26	186198711	2014-03-07 23:32:00	G8VDQ	IO91um	W4AC	EL86	14097055	37	-14	0	7251	282	14	2.21_r2286	0
27	186200173	2014-03-07 23:40:00	G8VDQ	IO91um	W4AC	EL86	14097055	37	-7	0	7251	282	14	2.21_r2286	0
28	186201125	2014-03-07 23:46:00	G8VDQ	IO91um	W4AC	EL86	14097055	37	-11	0	7251	282	14	2.21_r2286	0
29	186202337	2014-03-07 23:52:00	G8VDQ	IO91um	W4AC	EL86	14097055	37	-14	0	7251	282	14	2.21_r2286	0
30	186203513	2014-03-08 00:00:00	G8VDQ	IO91um	W4AC	EL86	14097054	37	-23	0	7251	282	14	2.21_r2286	0
31	186205403	2014-03-08 00:12:00	G8VDQ	IO91um	W4AC	EL86	14097055	37	-8	0	7251	282	14	2.21_r2286	0
								Mean	-12.9677						
								SD	3.7460						
								AD	6.0323						
								AD%	161						

row	id	time	tx_sign	tx_loc	rx_sign	rx_loc	frequency	power	snr	drift	distance	azimuth	band	version	code
1	186166896	2014-03-07 20:40:00	G8VDQ	IO91um	W4AC	EL86	14097054	37	-11	0	7251	282	14	2.21_r2286	0
2	186169105	2014-03-07 20:52:00	G8VDQ	IO91um	W4AC	EL86	14097054	37	-13	0	7251	282	14	2.21_r2286	0
3	186170775	2014-03-07 21:00:00	G8VDQ	IO91um	W4AC	EL86	14097054	37	-14	0	7251	282	14	2.21_r2286	0
4	186171816	2014-03-07 21:06:00	G8VDQ	IO91um	W4AC	EL86	14097053	37	-12	0	7251	282	14	2.21_r2286	0
5	186172974	2014-03-07 21:12:00	G8VDQ	IO91um	W4AC	EL86	14097052	37	-11	0	7251	282	14	2.21_r2286	0
6	186173913	2014-03-07 21:18:00	G8VDQ	IO91um	W4AC	EL86	14097053	37	-14	0	7251	282	14	2.21_r2286	0
7	186177492	2014-03-07 21:38:00	G8VDQ	IO91um	W4AC	EL86	14097054	37	-12	0	7251	282	14	2.21_r2286	0
8	186177998	2014-03-07 21:40:00	G8VDQ	IO91um	W4AC	EL86	14097053	37	-12	0	7251	282	14	2.21_r2286	0
9	186183927	2014-03-07 21:58:00	G8VDQ	IO91um	W4AC	EL86	14097054	37	-16	0	7251	282	14	2.21_r2286	0
10	186184211	2014-03-07 22:00:00	G8VDQ	IO91um	W4AC	EL86	14097053	37	-10	0	7251	282	14	2.21_r2286	0
11	186185520	2014-03-07 22:06:00	G8VDQ	IO91um	W4AC	EL86	14097054	37	-11	0	7251	282	14	2.21_r2286	0
12	186186509	2014-03-07 22:12:00	G8VDQ	IO91um	W4AC	EL86	14097054	37	-8	0	7251	282	14	2.21_r2286	0
13	186187397	2014-03-07 22:18:00	G8VDQ	IO91um	W4AC	EL86	14097054	37	-13	0	7251	282	14	2.21_r2286	0
14	186187849	2014-03-07 22:20:00	G8VDQ	IO91um	W4AC	EL86	14097054	37	-11	0	7251	282	14	2.21_r2286	0
15	186188831	2014-03-07 22:26:00	G8VDQ	IO91um	W4AC	EL86	14097055	37	-8	0	7251	282	14	2.21_r2286	0
16	186189715	2014-03-07 22:32:00	G8VDQ	IO91um	W4AC	EL86	14097054	37	-7	-1	7251	282	14	2.21_r2286	0
17	186190623	2014-03-07 22:38:00	G8VDQ	IO91um	W4AC	EL86	14097054	37	-15	0	7251	282	14	2.21_r2286	0
18	186191808	2014-03-07 22:46:00	G8VDQ	IO91um	W4AC	EL86	14097055	37	-12	0	7251	282	14	2.21_r2286	0
19	186192712	2014-03-07 22:52:00	G8VDQ	IO91um	W4AC	EL86	14097054	37	-14	0	7251	282	14	2.21_r2286	0
20	186193893	2014-03-07 23:00:00	G8VDQ	IO91um	W4AC	EL86	14097055	37	-20	0	7251	282	14	2.21_r2286	0
21	186194857	2014-03-07 23:06:00	G8VDQ	IO91um	W4AC	EL86	14097055	37	-16	0	7251	282	14	2.21_r2286	0
22	186196670	2014-03-07 23:18:00	G8VDQ	IO91um	W4AC	EL86	14097054	37	-15	-1	7251	282	14	2.21_r2286	0
23	186197805	2014-03-07 23:26:00	G8VDQ	IO91um	W4AC	EL86	14097054	37	-19	0	7251	282	14	2.21_r2286	0
24	186198711	2014-03-07 23:32:00	G8VDQ	IO91um	W4AC	EL86	14097055	37	-14	0	7251	282	14	2.21_r2286	0
25	186200173	2014-03-07 23:40:00	G8VDQ	IO91um	W4AC	EL86	14097055	37	-7	0	7251	282	14	2.21_r2286	0
26	186201125	2014-03-07 23:46:00	G8VDQ	IO91um	W4AC	EL86	14097055	37	-11	0	7251	282	14	2.21_r2286	0
27	186202337	2014-03-07 23:52:00	G8VDQ	IO91um	W4AC	EL86	14097055	37	-14	0	7251	282	14	2.21_r2286	0
28	186203513	2014-03-08 00:00:00	G8VDQ	IO91um	W4AC	EL86	14097054	37	-23	0	7251	282	14	2.21_r2286	0
29	186205403	2014-03-08 00:12:00	G8VDQ	IO91um	W4AC	EL86	14097055	37	-8	0	7251	282	14	2.21_r2286	0
								Mean	-12.7931						
								SD	3.7548						
								AD	-5.7931						
								AD%	-154						

row	id	time	tx_sign	tx_loc	rx_sign	rx_loc	frequency	power	snr	drift	distance	azimuth	band	version	code
1	186184285	2014-03-07 22:00:00	G8VDQ	IO91um	W4MO	EL87	14097062	37	-9	0	7169	283	14	2.21_r2286	0
2	186185395	2014-03-07 22:06:00	G8VDQ	IO91um	W4MO	EL87	14097065	37	-9	0	7169	283	14	2.21_r2286	0
3	186186506	2014-03-07 22:12:00	G8VDQ	IO91um	W4MO	EL87	14097067	37	-4	0	7169	283	14	2.21_r2286	0
4	186187516	2014-03-07 22:18:00	G8VDQ	IO91um	W4MO	EL87	14097068	37	-11	0	7169	283	14	2.21_r2286	0
5	186187786	2014-03-07 22:20:00	G8VDQ	IO91um	W4MO	EL87	14097068	37	-6	0	7169	283	14	2.21_r2286	0
6	186188687	2014-03-07 22:26:00	G8VDQ	IO91um	W4MO	EL87	14097070	37	-13	0	7169	283	14	2.21_r2286	0
7	186189819	2014-03-07 22:32:00	G8VDQ	IO91um	W4MO	EL87	14097071	37	-7	0	7169	283	14	2.21_r2286	0
8	186190439	2014-03-07 22:38:00	G8VDQ	IO91um	W4MO	EL87	14097071	37	-20	0	7169	283	14	2.21_r2286	0
9	186191630	2014-03-07 22:46:00	G8VDQ	IO91um	W4MO	EL87	14097072	37	-14	0	7169	283	14	2.21_r2286	0
10	186195594	2014-03-07 23:12:00	G8VDQ	IO91um	W4MO	EL87	14097072	37	-16	0	7169	283	14	2.21_r2286	0
11	186196684	2014-03-07 23:18:00	G8VDQ	IO91um	W4MO	EL87	14097071	37	-14	-1	7169	283	14	2.21_r2286	0
12	186197842	2014-03-07 23:26:00	G8VDQ	IO91um	W4MO	EL87	14097071	37	-11	0	7169	283	14	2.21_r2286	0
13	186200157	2014-03-07 23:40:00	G8VDQ	IO91um	W4MO	EL87	14097072	37	-10	0	7169	283	14	2.21_r2286	0
14	186201134	2014-03-07 23:46:00	G8VDQ	IO91um	W4MO	EL87	14097072	37	-17	0	7169	283	14	2.21_r2286	0
15	186202106	2014-03-07 23:52:00	G8VDQ	IO91um	W4MO	EL87	14097071	37	-12	0	7169	283	14	2.21_r2286	0
16	186203505	2014-03-08 00:00:00	G8VDQ	IO91um	W4MO	EL87	14097071	37	-24	0	7169	283	14	2.21_r2286	0
17	186205277	2014-03-08 00:12:00	G8VDQ	IO91um	W4MO	EL87	14097071	37	-6	0	7169	283	14	2.21_r2286	0
18	186206308	2014-03-08 00:18:00	G8VDQ	IO91um	W4MO	EL87	14097073	37	-9	0	7169	283	14	2.21_r2286	0
19	186207553	2014-03-08 00:26:00	G8VDQ	IO91um	W4MO	EL87	14097073	37	-16	0	7169	283	14	2.21_r2286	0
20	186208634	2014-03-08 00:32:00	G8VDQ	IO91um	W4MO	EL87	14097073	37	-14	0	7169	283	14	2.21_r2286	0
21	186209728	2014-03-08 00:40:00	G8VDQ	IO91um	W4MO	EL87	14097073	37	-10	0	7169	283	14	2.21_r2286	0
22	186211364	2014-03-08 00:52:00	G8VDQ	IO91um	W4MO	EL87	14097071	37	-14	0	7169	283	14	2.21_r2286	0
23	186212126	2014-03-08 00:58:00	G8VDQ	IO91um	W4MO	EL87	14097071	37	-16	0	7169	283	14	2.21_r2286	0
24	186216060	2014-03-08 01:26:00	G8VDQ	IO91um	W4MO	EL87	14097072	37	-22	0	7169	283	14	2.21_r2286	0
25	186216828	2014-03-08 01:32:00	G8VDQ	IO91um	W4MO	EL87	14097073	37	-24	0	7169	283	14	2.21_r2286	0
26	186217771	2014-03-08 01:40:00	G8VDQ	IO91um	W4MO	EL87	14097073	37	-15	0	7169	283	14	2.21_r2286	0
27	186219428	2014-03-08 01:52:00	G8VDQ	IO91um	W4MO	EL87	14097072	37	-17	0	7169	283	14	2.21_r2286	0
28	186220215	2014-03-08 01:58:00	G8VDQ	IO91um	W4MO	EL87	14097072	37	-11	0	7169	283	14	2.21_r2286	0
29	186221605	2014-03-08 02:06:00	G8VDQ	IO91um	W4MO	EL87	14097073	37	-18	0	7169	283	14	2.21_r2286	0
30	186223140	2014-03-08 02:18:00	G8VDQ	IO91um	W4MO	EL87	14097073	37	-18	0	7169	283	14	2.21_r2286	0
31	186223485	2014-03-08 02:20:00	G8VDQ	IO91um	W4MO	EL87	14097072	37	-21	0	7169	283	14	2.21_r2286	0
								Mean	-13.8065						
								SD	5.2499						
								AD	10.1935						
								AD%	194						

row	id	time	tx_sign	tx_loc	rx_sign	rx_loc	frequency	power	snr	drift	distance	azimuth	band	version	code
1	186184285	2014-03-07 22:00:00	G8VDQ	IO91um	W4MO	EL87	14097062	37	-9	0	7169	283	14	2.21_r2286	0
2	186185395	2014-03-07 22:06:00	G8VDQ	IO91um	W4MO	EL87	14097065	37	-9	0	7169	283	14	2.21_r2286	0
3	186186506	2014-03-07 22:12:00	G8VDQ	IO91um	W4MO	EL87	14097067	37	-4	0	7169	283	14	2.21_r2286	0
4	186187516	2014-03-07 22:18:00	G8VDQ	IO91um	W4MO	EL87	14097068	37	-11	0	7169	283	14	2.21_r2286	0
5	186187786	2014-03-07 22:20:00	G8VDQ	IO91um	W4MO	EL87	14097068	37	-6	0	7169	283	14	2.21_r2286	0
6	186188687	2014-03-07 22:26:00	G8VDQ	IO91um	W4MO	EL87	14097070	37	-13	0	7169	283	14	2.21_r2286	0
7	186189819	2014-03-07 22:32:00	G8VDQ	IO91um	W4MO	EL87	14097071	37	-7	0	7169	283	14	2.21_r2286	0
8	186190439	2014-03-07 22:38:00	G8VDQ	IO91um	W4MO	EL87	14097071	37	-20	0	7169	283	14	2.21_r2286	0
9	186191630	2014-03-07 22:46:00	G8VDQ	IO91um	W4MO	EL87	14097072	37	-14	0	7169	283	14	2.21_r2286	0
10	186195594	2014-03-07 23:12:00	G8VDQ	IO91um	W4MO	EL87	14097072	37	-16	0	7169	283	14	2.21_r2286	0
11	186196684	2014-03-07 23:18:00	G8VDQ	IO91um	W4MO	EL87	14097071	37	-14	-1	7169	283	14	2.21_r2286	0
12	186197842	2014-03-07 23:26:00	G8VDQ	IO91um	W4MO	EL87	14097071	37	-11	0	7169	283	14	2.21_r2286	0
13	186200157	2014-03-07 23:40:00	G8VDQ	IO91um	W4MO	EL87	14097072	37	-10	0	7169	283	14	2.21_r2286	0
14	186201134	2014-03-07 23:46:00	G8VDQ	IO91um	W4MO	EL87	14097072	37	-17	0	7169	283	14	2.21_r2286	0
15	186202106	2014-03-07 23:52:00	G8VDQ	IO91um	W4MO	EL87	14097071	37	-12	0	7169	283	14	2.21_r2286	0
16	186203505	2014-03-08 00:00:00	G8VDQ	IO91um	W4MO	EL87	14097071	37	-24	0	7169	283	14	2.21_r2286	0
17	186205277	2014-03-08 00:12:00	G8VDQ	IO91um	W4MO	EL87	14097071	37	-6	0	7169	283	14	2.21_r2286	0
18	186206308	2014-03-08 00:18:00	G8VDQ	IO91um	W4MO	EL87	14097073	37	-9	0	7169	283	14	2.21_r2286	0
19	186207553	2014-03-08 00:26:00	G8VDQ	IO91um	W4MO	EL87	14097073	37	-16	0	7169	283	14	2.21_r2286	0
20	186208634	2014-03-08 00:32:00	G8VDQ	IO91um	W4MO	EL87	14097073	37	-14	0	7169	283	14	2.21_r2286	0
21	186209728	2014-03-08 00:40:00	G8VDQ	IO91um	W4MO	EL87	14097073	37	-10	0	7169	283	14	2.21_r2286	0
22	186211364	2014-03-08 00:52:00	G8VDQ	IO91um	W4MO	EL87	14097071	37	-14	0	7169	283	14	2.21_r2286	0
23	186212126	2014-03-08 00:58:00	G8VDQ	IO91um	W4MO	EL87	14097071	37	-16	0	7169	283	14	2.21_r2286	0
24	186216060	2014-03-08 01:26:00	G8VDQ	IO91um	W4MO	EL87	14097072	37	-22	0	7169	283	14	2.21_r2286	0
25	186216828	2014-03-08 01:32:00	G8VDQ	IO91um	W4MO	EL87	14097073	37	-24	0	7169	283	14	2.21_r2286	0
26	186217771	2014-03-08 01:40:00	G8VDQ	IO91um	W4MO	EL87	14097073	37	-15	0	7169	283	14	2.21_r2286	0
27	186219428	2014-03-08 01:52:00	G8VDQ	IO91um	W4MO	EL87	14097072	37	-17	0	7169	283	14	2.21_r2286	0
28	186220215	2014-03-08 01:58:00	G8VDQ	IO91um	W4MO	EL87	14097072	37	-11	0	7169	283	14	2.21_r2286	0
29	186221605	2014-03-08 02:06:00	G8VDQ	IO91um	W4MO	EL87	14097073	37	-18	0	7169	283	14	2.21_r2286	0
30	186223140	2014-03-08 02:18:00	G8VDQ	IO91um	W4MO	EL87	14097073	37	-18	0	7169	283	14	2.21_r2286	0
								Mean	-13.5667						
								SD	5.1641						
								AD	0.4333						
								AD%	8						

Page 649 of 1738

row	id	time	tx_sign	tx_loc	rx_sign	rx_loc	frequency	power	snr	drift	distance	azimuth	band	version	code
1	186189147	2014-03-07 22:28:00	G8VDQ	IO91um	YO3ITD	KN34cj	7040057	37	-11	-1	2112	102	7	2.11_r2263	0
2	186195161	2014-03-07 23:08:00	G8VDQ	IO91um	YO3ITD	KN34cj	7040059	37	-11	-1	2112	102	7	2.11_r2263	0
3	186199819	2014-03-07 23:38:00	G8VDQ	IO91um	YO3ITD	KN34cj	7040060	37	-19	0	2112	102	7	2.11_r2263	0
4	186203229	2014-03-07 23:58:00	G8VDQ	IO91um	YO3ITD	KN34cj	7040060	37	-14	0	2112	102	7	2.11_r2263	0
5	186204849	2014-03-08 00:08:00	G8VDQ	IO91um	YO3ITD	KN34cj	7040059	37	-13	-1	2112	102	7	2.11_r2263	0
6	186210909	2014-03-08 00:48:00	G8VDQ	IO91um	YO3ITD	KN34cj	7040060	37	-16	0	2112	102	7	2.11_r2263	0
7	186212178	2014-03-08 00:58:00	G8VDQ	IO91um	YO3ITD	KN34cj	7040058	37	-14	0	2112	102	7	2.11_r2263	0
8	186213733	2014-03-08 01:08:00	G8VDQ	IO91um	YO3ITD	KN34cj	7040060	37	-13	0	2112	102	7	2.11_r2263	0
9	186216198	2014-03-08 01:28:00	G8VDQ	IO91um	YO3ITD	KN34cj	7040060	37	-19	0	2112	102	7	2.11_r2263	0
10	186217522	2014-03-08 01:38:00	G8VDQ	IO91um	YO3ITD	KN34cj	7040058	37	-13	1	2112	102	7	2.11_r2263	0
11	186221696	2014-03-08 02:08:00	G8VDQ	IO91um	YO3ITD	KN34cj	7040060	37	-12	0	2112	102	7	2.11_r2263	0
								Mean	-14.0909						
								SD	2.8091						
								AD	-3.0909						
								AD%	-110						

row	id	time	tx_sign	tx_loc	rx_sign	rx_loc	frequency	power	snr	drift	distance	azimuth	band	version	code
1	186100401	2014-03-07 15:54:00	G8YTR	IO90lv	DL8YCA	JO43aq	10140106	33	-26	0	691	60	10	2.12_r3617	0
2	186103227	2014-03-07 16:04:00	G8YTR	IO90lv	DL8YCA	JO43aq	10140105	33	-23	0	691	60	10	2.12_r3617	0
3	186105194	2014-03-07 16:10:00	G8YTR	IO90lv	DL8YCA	JO43aq	10140105	33	-24	0	691	60	10	2.12_r3617	0
4	186106528	2014-03-07 16:16:00	G8YTR	IO90lv	DL8YCA	JO43aq	10140105	33	-24	0	691	60	10	2.12_r3617	0
5	186110909	2014-03-07 16:32:00	G8YTR	IO90lv	DL8YCA	JO43aq	10140105	33	-23	0	691	60	10	2.12_r3617	0
6	186116177	2014-03-07 16:50:00	G8YTR	IO90lv	DL8YCA	JO43aq	10140106	33	-24	0	691	60	10	2.12_r3617	0
7	186139948	2014-03-07 18:24:00	G8YTR	IO90lv	DL8YCA	JO43aq	10140105	33	-25	0	691	60	10	2.12_r3617	0
8	186141382	2014-03-07 18:30:00	G8YTR	IO90lv	DL8YCA	JO43aq	10140105	33	-22	0	691	60	10	2.12_r3617	0
9	186144289	2014-03-07 18:44:00	G8YTR	IO90lv	DL8YCA	JO43aq	10140105	33	-21	0	691	60	10	2.12_r3617	0
10	186145637	2014-03-07 18:50:00	G8YTR	IO90lv	DL8YCA	JO43aq	10140105	33	-22	0	691	60	10	2.12_r3617	0
11	186147266	2014-03-07 18:58:00	G8YTR	IO90lv	DL8YCA	JO43aq	10140105	33	-21	0	691	60	10	2.12_r3617	0
12	186148890	2014-03-07 19:06:00	G8YTR	IO90lv	DL8YCA	JO43aq	10140105	33	-20	0	691	60	10	2.12_r3617	0
								Mean	-22.9167						
								SD	1.7816						
								AD	2.0833						
								AD%	117						

row	id	time	tx_sign	tx_loc	rx_sign	rx_loc	frequency	power	snr	drift	distance	azimuth	band	version	code
1	186169995	2014-03-07 20:56:00	GM4SFW	IO77tm	W4MO	EL87	14097046	30	-15	0	6797	277	14	2.21_r2286	0
2	186175712	2014-03-07 21:28:00	GM4SFW	IO77tm	W4MO	EL87	14097045	30	-12	0	6797	277	14	2.21_r2286	0
3	186187267	2014-03-07 22:16:00	GM4SFW	IO77sn	W4MO	EL87	14097175	30	-14	-1	6792	277	14	2.21_r2286	0
4	186188333	2014-03-07 22:24:00	GM4SFW	IO77sn	W4MO	EL87	14097176	30	-16	0	6792	277	14	2.21_r2286	0
5	186189989	2014-03-07 22:34:00	GM4SFW	IO77sn	W4MO	EL87	14097179	30	-11	0	6792	277	14	2.21_r2286	0
6	186192812	2014-03-07 22:54:00	GM4SFW	IO77sn	W4MO	EL87	14097181	30	-17	-1	6792	277	14	2.21_r2286	0
7	186201147	2014-03-07 23:46:00	GM4SFW	IO77sn	W4MO	EL87	14097182	30	-24	0	6792	277	14	2.21_r2286	0
8	186204108	2014-03-08 00:04:00	GM4SFW	IO77tm	W4MO	EL87	14097184	30	-13	0	6797	277	14	2.21_r2286	0
9	186211165	2014-03-08 00:50:00	GM4SFW	IO77sn	W4MO	EL87	14097186	30	-20	0	6792	277	14	2.21_r2286	0
10	186212547	2014-03-08 01:00:00	GM4SFW	IO77tm	W4MO	EL87	14097186	30	-25	-1	6797	277	14	2.21_r2286	0
11	186219431	2014-03-08 01:52:00	GM4SFW	IO77sn	W4MO	EL87	14097187	30	-13	0	6792	277	14	2.21_r2286	0
12	186220751	2014-03-08 02:00:00	GM4SFW	IO77sn	W4MO	EL87	14097187	30	-12	0	6792	277	14	2.21_r2286	0
13	186223488	2014-03-08 02:20:00	GM4SFW	IO77sn	W4MO	EL87	14097188	30	-15	-1	6792	277	14	2.21_r2286	0
								Mean	-15.9231						
								SD	4.4993						
								AD	8.0769						
								AD%	180						

row	id	time	tx_sign	tx_loc	rx_sign	rx_loc	frequency	power	snr	drift	distance	azimuth	band	version	code
1	186166164	2014-03-07 20:36:00	HB9CZF	JN47ch	W4AC	EL86	14097096	30	-17	-1	7969	289	14	2.21_r2286	0
2	186169912	2014-03-07 20:56:00	HB9CZF	JN47ch	W4AC	EL86	14097096	30	-14	-1	7969	289	14	2.21_r2286	0
3	186173705	2014-03-07 21:16:00	HB9CZF	JN47ch	W4AC	EL86	14097096	30	-18	-1	7969	289	14	2.21_r2286	0
4	186175269	2014-03-07 21:26:00	HB9CZF	JN47ch	W4AC	EL86	14097096	30	-15	-2	7969	289	14	2.21_r2286	0
5	186177203	2014-03-07 21:36:00	HB9CZF	JN47ch	W4AC	EL86	14097093	30	-7	-1	7969	289	14	2.21_r2286	0
6	186183567	2014-03-07 21:56:00	HB9CZF	JN47ch	W4AC	EL86	14097093	30	-11	-1	7969	289	14	2.21_r2286	0
7	186185525	2014-03-07 22:06:00	HB9CZF	JN47ch	W4AC	EL86	14097096	30	-14	-1	7969	289	14	2.21_r2286	0
8	186187223	2014-03-07 22:16:00	HB9CZF	JN47ch	W4AC	EL86	14097096	30	-13	-1	7969	289	14	2.21_r2286	0
9	186191811	2014-03-07 22:46:00	HB9CZF	JN47ch	W4AC	EL86	14097099	30	-19	-1	7969	289	14	2.21_r2286	0
10	186197812	2014-03-07 23:26:00	HB9CZF	JN47ch	W4AC	EL86	14097094	30	-22	-1	7969	289	14	2.21_r2286	0
								Mean	-15.0000						
								SD	4.2687						
								AD	7.0000						
								AD%	164						

row	id	time	tx_sign	tx_loc	rx_sign	rx_loc	frequency	power	snr	drift	distance	azimuth	band	version	code
1	186183432	2014-03-07 21:56:00	HB9CZF	JN47ch	W4MO	EL87	14097099	30	-13	-1	7892	290	14	2.21_r2286	0
2	186185421	2014-03-07 22:06:00	HB9CZF	JN47ch	W4MO	EL87	14097107	30	-13	-1	7892	290	14	2.21_r2286	0
3	186187262	2014-03-07 22:16:00	HB9CZF	JN47ch	W4MO	EL87	14097110	30	-14	-1	7892	290	14	2.21_r2286	0
4	186191634	2014-03-07 22:46:00	HB9CZF	JN47ch	W4MO	EL87	14097116	30	-20	-1	7892	290	14	2.21_r2286	0
5	186197847	2014-03-07 23:26:00	HB9CZF	JN47ch	W4MO	EL87	14097111	30	-21	-1	7892	290	14	2.21_r2286	0
6	186207557	2014-03-08 00:26:00	HB9CZF	JN47ch	W4MO	EL87	14097115	30	-21	-1	7892	290	14	2.21_r2286	0
7	186210433	2014-03-08 00:46:00	HB9CZF	JN47ch	W4MO	EL87	14097117	30	-22	-1	7892	290	14	2.21_r2286	0
8	186214591	2014-03-08 01:16:00	HB9CZF	JN47ch	W4MO	EL87	14097111	30	-16	-1	7892	290	14	2.21_r2286	0
9	186216063	2014-03-08 01:26:00	HB9CZF	JN47ch	W4MO	EL87	14097115	30	-17	-1	7892	290	14	2.21_r2286	0
10	186220009	2014-03-08 01:56:00	HB9CZF	JN47ch	W4MO	EL87	14097109	30	-15	-1	7892	290	14	2.21_r2286	0
11	186221608	2014-03-08 02:06:00	HB9CZF	JN47ch	W4MO	EL87	14097115	30	-13	-1	7892	290	14	2.21_r2286	0
12	186222830	2014-03-08 02:16:00	HB9CZF	JN47ch	W4MO	EL87	14097115	30	-19	-1	7892	290	14	2.21_r2286	0
								Mean	-17.0000						
								SD	3.4641						
								AD	4.0000						
								AD%	115						

row	id	time	tx_sign	tx_loc	rx_sign	rx_loc	frequency	power	snr	drift	distance	azimuth	band	version	code
1	186116899	2014-03-07 16:54:00	HS0ZKM	OK03gr	K7UEB/20	DN06tb	14097160	37	-25	1	12310	28	14	3.00_r2326	0
2	186124629	2014-03-07 17:22:00	HS0ZKM	OK03gr	K7UEB/20	DN06tb	14097153	37	-27	0	12310	28	14	3.00_r2326	0
3	186142754	2014-03-07 18:36:00	HS0ZKM	OK03gr	K7UEB/20	DN06tb	14097156	37	-27	0	12310	28	14	3.00_r2326	0
4	186144899	2014-03-07 18:46:00	HS0ZKM	OK03gr	K7UEB/20	DN06tb	14097153	37	-25	0	12310	28	14	3.00_r2326	0
5	186148043	2014-03-07 19:02:00	HS0ZKM	OK03gr	K7UEB/20	DN06tb	14097153	37	-25	0	12310	28	14	3.00_r2326	0
6	186153337	2014-03-07 19:28:00	HS0ZKM	OK03gr	K7UEB/20	DN06tb	14097153	37	-22	0	12310	28	14	3.00_r2326	0
7	186154374	2014-03-07 19:34:00	HS0ZKM	OK03gr	K7UEB/20	DN06tb	14097153	37	-20	0	12310	28	14	3.00_r2326	0
8	186157823	2014-03-07 19:52:00	HS0ZKM	OK03gr	K7UEB/20	DN06tb	14097154	37	-26	1	12310	28	14	3.00_r2326	0
9	186166073	2014-03-07 20:36:00	HS0ZKM	OK03gr	K7UEB/20	DN06tb	14097153	37	-26	0	12310	28	14	3.00_r2326	0
								Mean	-24.7778						
								SD	2.3333						
								AD	-2.7778						
								AD%	-119						

row	id	time	tx_sign	tx_loc	rx_sign	rx_loc	frequency	power	snr	drift	distance	azimuth	band	version	code
1	186115302	2014-03-07 16:48:00	HS0ZKM	OK03gr	KC6KGE	DM05gd	14097110	37	-19	0	13138	37	14	0.8_r3058	0
2	186119146	2014-03-07 17:02:00	HS0ZKM	OK03gr	KC6KGE	DM05gd	14097114	37	-26	1	13138	37	14	0.8_r3058	0
3	186144772	2014-03-07 18:46:00	HS0ZKM	OK03gr	KC6KGE	DM05gd	14097111	37	-25	-1	13138	37	14	0.8_r3058	0
4	186391388	2014-03-08 16:08:00	HS0ZKM	OK03gr	KC6KGE	DM05gd	14097113	37	-22	1	13138	37	14	0.8_r3058	0
5	186393380	2014-03-08 16:16:00	HS0ZKM	OK03gr	KC6KGE	DM05gd	14097113	37	-19	1	13138	37	14	0.8_r3058	0
6	186395509	2014-03-08 16:26:00	HS0ZKM	OK03gr	KC6KGE	DM05gd	14097114	37	-18	1	13138	37	14	0.8_r3058	0
7	186397452	2014-03-08 16:36:00	HS0ZKM	OK03gr	KC6KGE	DM05gd	14097114	37	-18	-1	13138	37	14	0.8_r3058	0
8	186399302	2014-03-08 16:44:00	HS0ZKM	OK03gr	KC6KGE	DM05gd	14097113	37	-19	-1	13138	37	14	0.8_r3058	0
9	186400963	2014-03-08 16:52:00	HS0ZKM	OK03gr	KC6KGE	DM05gd	14097114	37	-21	1	13138	37	14	0.8_r3058	0
10	186403129	2014-03-08 17:02:00	HS0ZKM	OK03gr	KC6KGE	DM05gd	14097113	37	-20	-1	13138	37	14	0.8_r3058	0
11	186430823	2014-03-08 19:04:00	HS0ZKM	OK03gr	KC6KGE	DM05gd	14097115	37	-24	1	13138	37	14	0.8_r3058	0
								Mean	-21.0000						
								SD	2.8636						
								AD	4.0000						
								AD%	140						

row	id	time	tx_sign	tx_loc	rx_sign	rx_loc	frequency	power	snr	drift	distance	azimuth	band	version	code
1	186189980	2014-03-07 22:34:00	IK1NET	JN34su	W4MO	EL87	14097129	30	-10	0	7939	291	14	2.21_r2286	0
2	186191636	2014-03-07 22:46:00	IK1NET	JN34su	W4MO	EL87	14097131	30	-17	0	7939	291	14	2.21_r2286	0
3	186199215	2014-03-07 23:34:00	IK1NET	JN34su	W4MO	EL87	14097130	30	-13	0	7939	291	14	2.21_r2286	0
4	186201140	2014-03-07 23:46:00	IK1NET	JN34su	W4MO	EL87	14097131	30	-18	0	7939	291	14	2.21_r2286	0
5	186204067	2014-03-08 00:04:00	IK1NET	JN34su	W4MO	EL87	14097131	30	-19	0	7939	291	14	2.21_r2286	0
								Mean	-15.4000						
								SD	3.7815						
								AD	3.6000						
								AD%	95						

row	id	time	tx_sign	tx_loc	rx_sign	rx_loc	frequency	power	snr	drift	distance	azimuth	band	version	code
1	186185841	2014-03-07 22:08:00	JH1GYE	PM96mi	KD6RF	CM97cq	28126134	37	11	0	8326	54	28	2.11_r2263	0
2	186187617	2014-03-07 22:18:00	JH1GYE	PM96mi	KD6RF	CM97cq	28126134	37	9	0	8326	54	28	2.11_r2263	0
3	186189183	2014-03-07 22:28:00	JH1GYE	PM96mi	KD6RF	CM97cq	28126134	37	10	0	8326	54	28	2.11_r2263	0
4	186190346	2014-03-07 22:36:00	JH1GYE	PM96mi	KD6RF	CM97cq	28126134	37	4	0	8326	54	28	2.11_r2263	0
5	186191486	2014-03-07 22:44:00	JH1GYE	PM96mi	KD6RF	CM97cq	28126134	37	1	0	8326	54	28	2.11_r2263	0
6	186192574	2014-03-07 22:52:00	JH1GYE	PM96mi	KD6RF	CM97cq	28126133	37	10	0	8326	54	28	2.11_r2263	0
7	186195680	2014-03-07 23:12:00	JH1GYE	PM96mi	KD6RF	CM97cq	28126134	37	1	0	8326	54	28	2.11_r2263	0
8	186197623	2014-03-07 23:24:00	JH1GYE	PM96mi	KD6RF	CM97cq	28126134	37	2	0	8326	54	28	2.11_r2263	0
9	186199237	2014-03-07 23:34:00	JH1GYE	PM96mi	KD6RF	CM97cq	28126134	37	2	0	8326	54	28	2.11_r2263	0
10	186200921	2014-03-07 23:44:00	JH1GYE	PM96mi	KD6RF	CM97cq	28126134	37	5	0	8326	54	28	2.11_r2263	0
11	186202933	2014-03-07 23:56:00	JH1GYE	PM96mi	KD6RF	CM97cq	28126134	37	10	0	8326	54	28	2.11_r2263	0
12	186205921	2014-03-08 00:16:00	JH1GYE	PM96mi	KD6RF	CM97cq	28126134	37	5	0	8326	54	28	2.11_r2263	0
13	186207367	2014-03-08 00:24:00	JH1GYE	PM96mi	KD6RF	CM97cq	28126134	37	11	0	8326	54	28	2.11_r2263	0
14	186208984	2014-03-08 00:34:00	JH1GYE	PM96mi	KD6RF	CM97cq	28126133	37	8	0	8326	54	28	2.11_r2263	0
15	186210181	2014-03-08 00:42:00	JH1GYE	PM96mi	KD6RF	CM97cq	28126134	37	-2	0	8326	54	28	2.11_r2263	0
16	186211262	2014-03-08 00:50:00	JH1GYE	PM96mi	KD6RF	CM97cq	28126134	37	-1	0	8326	54	28	2.11_r2263	0
17	186212984	2014-03-08 01:02:00	JH1GYE	PM96mi	KD6RF	CM97cq	28126134	37	4	0	8326	54	28	2.11_r2263	0
18	186215300	2014-03-08 01:20:00	JH1GYE	PM96mi	KD6RF	CM97cq	28126134	37	-4	0	8326	54	28	2.11_r2263	0
19	186216228	2014-03-08 01:28:00	JH1GYE	PM96mi	KD6RF	CM97cq	28126134	37	-2	0	8326	54	28	2.11_r2263	0
20	186217288	2014-03-08 01:36:00	JH1GYE	PM96mi	KD6RF	CM97cq	28126134	37	-1	0	8326	54	28	2.11_r2263	0
21	186218521	2014-03-08 01:44:00	JH1GYE	PM96mi	KD6RF	CM97cq	28126133	37	5	0	8326	54	28	2.11_r2263	0
22	186219503	2014-03-08 01:52:00	JH1GYE	PM96mi	KD6RF	CM97cq	28126134	37	5	0	8326	54	28	2.11_r2263	0
								Mean	4.2273						
								SD	4.6897						
								AD	-5.7727						
								AD%	-123						

row	id	time	tx_sign	tx_loc	rx_sign	rx_loc	frequency	power	snr	drift	distance	azimuth	band	version	code
1	186187590	2014-03-07 22:18:00	JH1GYE	PM96mi	VE6PDQ	DO34ir	28126131	37	-14	0	7778	36	28	3.00_r2485	0
2	186206131	2014-03-08 00:16:00	JH1GYE	PM96mi	VE6PDQ	DO34ir	28126129	37	-9	0	7778	36	28	3.00_r2485	0
3	186209988	2014-03-08 00:42:00	JH1GYE	PM96mi	VE6PDQ	DO34ir	28126130	37	-11	0	7778	36	28	3.00_r2485	0
4	186211058	2014-03-08 00:50:00	JH1GYE	PM96mi	VE6PDQ	DO34ir	28126129	37	-12	0	7778	36	28	3.00_r2485	0
5	186212908	2014-03-08 01:02:00	JH1GYE	PM96mi	VE6PDQ	DO34ir	28126129	37	-14	0	7778	36	28	3.00_r2485	0
								Mean	-12.0000						
								SD	2.1213						
								AD	-3.0000						
								AD%	-141						

Page 659 of 1738

row	id	time	tx_sign	tx_loc	rx_sign	rx_loc	frequency	power	snr	drift	distance	azimuth	band	version	code
1	186185742	2014-03-07 22:08:00	JH1GYE	PM96mi	WA5NGP	EM10cn	28126129	37	-12	0	10505	46	28	2.0_r1714	0
2	186187569	2014-03-07 22:18:00	JH1GYE	PM96mi	WA5NGP	EM10cn	28126131	37	-7	0	10505	46	28	2.0_r1714	0
3	186199055	2014-03-07 23:34:00	JH1GYE	PM96mi	WA5NGP	EM10cn	28126129	37	-12	1	10505	46	28	2.0_r1714	0
4	186200954	2014-03-07 23:44:00	JH1GYE	PM96mi	WA5NGP	EM10cn	28126131	37	-12	0	10505	46	28	2.0_r1714	0
5	186202843	2014-03-07 23:56:00	JH1GYE	PM96mi	WA5NGP	EM10cn	28126132	37	-10	1	10505	46	28	2.0_r1714	0
6	186205976	2014-03-08 00:16:00	JH1GYE	PM96mi	WA5NGP	EM10cn	28126130	37	-3	1	10505	46	28	2.0_r1714	0
7	186207380	2014-03-08 00:24:00	JH1GYE	PM96mi	WA5NGP	EM10cn	28126129	37	0	0	10505	46	28	2.0_r1714	0
8	186208790	2014-03-08 00:34:00	JH1GYE	PM96mi	WA5NGP	EM10cn	28126129	37	-5	1	10505	46	28	2.0_r1714	0
9	186209974	2014-03-08 00:42:00	JH1GYE	PM96mi	WA5NGP	EM10cn	28126128	37	-8	0	10505	46	28	2.0_r1714	0
10	186211174	2014-03-08 00:50:00	JH1GYE	PM96mi	WA5NGP	EM10cn	28126126	37	-8	0	10505	46	28	2.0_r1714	0
11	186212939	2014-03-08 01:02:00	JH1GYE	PM96mi	WA5NGP	EM10cn	28126129	37	-6	0	10505	46	28	2.0_r1714	0
								Mean	-7.5455						
								SD	3.9080						
								AD	4.4545						
								AD%	114						

row	id	time	tx_sign	tx_loc	rx_sign	rx_loc	frequency	power	snr	drift	distance	azimuth	band	version	code
1	186331932	2014-03-07 20:04:00	K4RCG	FM08xl	OX3XR	GP44de	10140229	37	-30	0	3341	23	10		0
2	186331863	2014-03-07 20:44:00	K4RCG	FM08xl	OX3XR	GP44de	10140229	37	-19	0	3341	23	10		0
3	186331806	2014-03-07 21:10:00	K4RCG	FM08xl	OX3XR	GP44de	10140229	37	-19	0	3341	23	10		0
4	186331785	2014-03-07 21:20:00	K4RCG	FM08xl	OX3XR	GP44de	10140228	37	-15	0	3341	23	10		0
5	186331758	2014-03-07 21:32:00	K4RCG	FM08xl	OX3XR	GP44de	10140228	37	-15	0	3341	23	10		0
6	186331722	2014-03-07 21:48:00	K4RCG	FM08xl	OX3XR	GP44de	10140228	37	-13	0	3341	23	10		0
7	186331677	2014-03-07 22:04:00	K4RCG	FM08xl	OX3XR	GP44de	10140228	37	-9	0	3341	23	10		0
8	186331562	2014-03-07 23:04:00	K4RCG	FM08xl	OX3XR	GP44de	10140229	37	-7	0	3341	23	10		0
9	186331543	2014-03-07 23:18:00	K4RCG	FM08xl	OX3XR	GP44de	10140229	37	-15	0	3341	23	10		0
10	186331523	2014-03-07 23:34:00	K4RCG	FM08xl	OX3XR	GP44de	10140229	37	-11	0	3341	23	10		0
11	186331493	2014-03-07 23:46:00	K4RCG	FM08xl	OX3XR	GP44de	10140229	37	-13	0	3341	23	10		0
12	186331458	2014-03-08 00:02:00	K4RCG	FM08xl	OX3XR	GP44de	10140229	37	-9	0	3341	23	10		0
13	186331431	2014-03-08 00:16:00	K4RCG	FM08xl	OX3XR	GP44de	10140229	37	-8	0	3341	23	10		0
14	186331397	2014-03-08 00:46:00	K4RCG	FM08xl	OX3XR	GP44de	10140229	37	-8	0	3341	23	10		0
15	186331376	2014-03-08 01:00:00	K4RCG	FM08xl	OX3XR	GP44de	10140229	37	-7	0	3341	23	10		0
16	186331364	2014-03-08 01:12:00	K4RCG	FM08xl	OX3XR	GP44de	10140229	37	-8	0	3341	23	10		0
17	186331323	2014-03-08 01:52:00	K4RCG	FM08xl	OX3XR	GP44de	10140229	37	-10	0	3341	23	10		0
18	186331306	2014-03-08 02:04:00	K4RCG	FM08xl	OX3XR	GP44de	10140229	37	-9	0	3341	23	10		0
								Mean	-12.5000						
								SD	5.8234						
								AD	-5.5000						
								AD%	-94						

row	id	time	tx_sign	tx_loc	rx_sign	rx_loc	frequency	power	snr	drift	distance	azimuth	band	version	code
1	186331863	2014-03-07 20:44:00	K4RCG	FM08xl	OX3XR	GP44de	10140229	37	-19	0	3341	23	10		0
2	186331806	2014-03-07 21:10:00	K4RCG	FM08xl	OX3XR	GP44de	10140229	37	-19	0	3341	23	10		0
3	186331785	2014-03-07 21:20:00	K4RCG	FM08xl	OX3XR	GP44de	10140228	37	-15	0	3341	23	10		0
4	186331758	2014-03-07 21:32:00	K4RCG	FM08xl	OX3XR	GP44de	10140228	37	-15	0	3341	23	10		0
5	186331722	2014-03-07 21:48:00	K4RCG	FM08xl	OX3XR	GP44de	10140228	37	-13	0	3341	23	10		0
6	186331677	2014-03-07 22:04:00	K4RCG	FM08xl	OX3XR	GP44de	10140228	37	-9	0	3341	23	10		0
7	186331562	2014-03-07 23:04:00	K4RCG	FM08xl	OX3XR	GP44de	10140229	37	-7	0	3341	23	10		0
8	186331543	2014-03-07 23:18:00	K4RCG	FM08xl	OX3XR	GP44de	10140229	37	-15	0	3341	23	10		0
9	186331523	2014-03-07 23:34:00	K4RCG	FM08xl	OX3XR	GP44de	10140229	37	-11	0	3341	23	10		0
10	186331493	2014-03-07 23:46:00	K4RCG	FM08xl	OX3XR	GP44de	10140229	37	-13	0	3341	23	10		0
11	186331458	2014-03-08 00:02:00	K4RCG	FM08xl	OX3XR	GP44de	10140229	37	-9	0	3341	23	10		0
12	186331431	2014-03-08 00:16:00	K4RCG	FM08xl	OX3XR	GP44de	10140229	37	-8	0	3341	23	10		0
13	186331397	2014-03-08 00:46:00	K4RCG	FM08xl	OX3XR	GP44de	10140229	37	-8	0	3341	23	10		0
14	186331376	2014-03-08 01:00:00	K4RCG	FM08xl	OX3XR	GP44de	10140229	37	-7	0	3341	23	10		0
15	186331364	2014-03-08 01:12:00	K4RCG	FM08xl	OX3XR	GP44de	10140229	37	-8	0	3341	23	10		0
16	186331323	2014-03-08 01:52:00	K4RCG	FM08xl	OX3XR	GP44de	10140229	37	-10	0	3341	23	10		0
17	186331306	2014-03-08 02:04:00	K4RCG	FM08xl	OX3XR	GP44de	10140229	37	-9	0	3341	23	10		0
								Mean	-11.4706						
								SD	3.9705						
								AD	3.5294						
								AD%	89						

Page 662 of 1738

row	id	time	tx_sign	tx_loc	rx_sign	rx_loc	frequency	power	snr	drift	distance	azimuth	band	version	code
1	186138595	2014-03-07 18:18:00	K4RCG	FM08xl	W4AC	EL86	14097136	37	1	0	1414	201	14	2.21_r2286	0
2	186141290	2014-03-07 18:30:00	K4RCG	FM08xl	W4AC	EL86	14097135	37	3	0	1414	201	14	2.21_r2286	0
3	186144268	2014-03-07 18:44:00	K4RCG	FM08xl	W4AC	EL86	14097135	37	6	0	1414	201	14	2.21_r2286	0
4	186147696	2014-03-07 19:00:00	K4RCG	FM08xl	W4AC	EL86	14097135	37	5	0	1414	201	14	2.21_r2286	0
5	186150579	2014-03-07 19:14:00	K4RCG	FM08xl	W4AC	EL86	14097135	37	3	0	1414	201	14	2.21_r2286	0
6	186152938	2014-03-07 19:26:00	K4RCG	FM08xl	W4AC	EL86	14097135	37	2	0	1414	201	14	2.21_r2286	0
7	186157207	2014-03-07 19:50:00	K4RCG	FM08xl	W4AC	EL86	14097126	37	4	1	1414	201	14	2.21_r2286	0
8	186159639	2014-03-07 20:02:00	K4RCG	FM08xl	W4AC	EL86	14097126	37	1	1	1414	201	14	2.21_r2286	0
9	186163454	2014-03-07 20:22:00	K4RCG	FM08xl	W4AC	EL86	14097126	37	8	1	1414	201	14	2.21_r2286	0
10	186164782	2014-03-07 20:30:00	K4RCG	FM08xl	W4AC	EL86	14097126	37	1	1	1414	201	14	2.21_r2286	0
11	186167222	2014-03-07 20:42:00	K4RCG	FM08xl	W4AC	EL86	14097126	37	2	1	1414	201	14	2.21_r2286	0
12	186168753	2014-03-07 20:50:00	K4RCG	FM08xl	W4AC	EL86	14097127	37	6	0	1414	201	14	2.21_r2286	0
13	186171122	2014-03-07 21:02:00	K4RCG	FM08xl	W4AC	EL86	14097126	37	1	1	1414	201	14	2.21_r2286	0
14	186173284	2014-03-07 21:14:00	K4RCG	FM08xl	W4AC	EL86	14097126	37	5	1	1414	201	14	2.21_r2286	0
15	186174747	2014-03-07 21:22:00	K4RCG	FM08xl	W4AC	EL86	14097127	37	3	1	1414	201	14	2.21_r2286	0
16	186178318	2014-03-07 21:42:00	K4RCG	FM08xl	W4AC	EL86	14097126	37	8	1	1414	201	14	2.21_r2286	0
17	186183253	2014-03-07 21:54:00	K4RCG	FM08xl	W4AC	EL86	14097126	37	2	1	1414	201	14	2.21_r2286	0
18	186184755	2014-03-07 22:02:00	K4RCG	FM08xl	W4AC	EL86	14097126	37	-1	1	1414	201	14	2.21_r2286	0
19	186186190	2014-03-07 22:10:00	K4RCG	FM08xl	W4AC	EL86	14097126	37	-2	1	1414	201	14	2.21_r2286	0
20	186189416	2014-03-07 22:30:00	K4RCG	FM08xl	W4AC	EL86	14097126	37	2	1	1414	201	14	2.21_r2286	0
21	186195120	2014-03-07 23:08:00	K4RCG	FM08xl	W4AC	EL86	14097126	37	2	0	1414	201	14	2.21_r2286	0
22	186197821	2014-03-07 23:26:00	K4RCG	FM08xl	W4AC	EL86	14097126	37	-4	0	1414	201	14	2.21_r2286	0
								Mean	2.6364						
								SD	2.9688						
								AD	-2.3636						
								AD%	-80						

row	id	time	tx_sign	tx_loc	rx_sign	rx_loc	frequency	power	snr	drift	distance	azimuth	band	version	code
1	186150579	2014-03-07 19:14:00	K4RCG	FM08xl	W4AC	EL86	14097135	37	3	0	1414	201	14	2.21_r2286	0
2	186152938	2014-03-07 19:26:00	K4RCG	FM08xl	W4AC	EL86	14097135	37	2	0	1414	201	14	2.21_r2286	0
3	186157207	2014-03-07 19:50:00	K4RCG	FM08xl	W4AC	EL86	14097126	37	4	1	1414	201	14	2.21_r2286	0
4	186159639	2014-03-07 20:02:00	K4RCG	FM08xl	W4AC	EL86	14097126	37	1	1	1414	201	14	2.21_r2286	0
5	186163454	2014-03-07 20:22:00	K4RCG	FM08xl	W4AC	EL86	14097126	37	8	1	1414	201	14	2.21_r2286	0
6	186164782	2014-03-07 20:30:00	K4RCG	FM08xl	W4AC	EL86	14097126	37	1	1	1414	201	14	2.21_r2286	0
7	186167222	2014-03-07 20:42:00	K4RCG	FM08xl	W4AC	EL86	14097126	37	2	1	1414	201	14	2.21_r2286	0
8	186168753	2014-03-07 20:50:00	K4RCG	FM08xl	W4AC	EL86	14097127	37	6	0	1414	201	14	2.21_r2286	0
9	186171122	2014-03-07 21:02:00	K4RCG	FM08xl	W4AC	EL86	14097126	37	1	1	1414	201	14	2.21_r2286	0
10	186173284	2014-03-07 21:14:00	K4RCG	FM08xl	W4AC	EL86	14097126	37	5	1	1414	201	14	2.21_r2286	0
11	186174747	2014-03-07 21:22:00	K4RCG	FM08xl	W4AC	EL86	14097127	37	3	1	1414	201	14	2.21_r2286	0
12	186178318	2014-03-07 21:42:00	K4RCG	FM08xl	W4AC	EL86	14097126	37	8	1	1414	201	14	2.21_r2286	0
13	186183253	2014-03-07 21:54:00	K4RCG	FM08xl	W4AC	EL86	14097126	37	2	1	1414	201	14	2.21_r2286	0
14	186184755	2014-03-07 22:02:00	K4RCG	FM08xl	W4AC	EL86	14097126	37	-1	1	1414	201	14	2.21_r2286	0
15	186186190	2014-03-07 22:10:00	K4RCG	FM08xl	W4AC	EL86	14097126	37	-2	1	1414	201	14	2.21_r2286	0
16	186189416	2014-03-07 22:30:00	K4RCG	FM08xl	W4AC	EL86	14097126	37	2	1	1414	201	14	2.21_r2286	0
17	186195120	2014-03-07 23:08:00	K4RCG	FM08xl	W4AC	EL86	14097126	37	2	0	1414	201	14	2.21_r2286	0
18	186197821	2014-03-07 23:26:00	K4RCG	FM08xl	W4AC	EL86	14097126	37	-4	0	1414	201	14	2.21_r2286	0
								Mean	2.3889						
								SD	3.1086						
								AD	4.3889						
								AD%	141						

Page 664 of 1738

row	id	time	tx_sign	tx_loc	rx_sign	rx_loc	frequency	power	snr	drift	distance	azimuth	band	version	code
1	185682697	2014-03-06 01:58:00	K9AN	EN50wc	VE4KE	EO01te	28126099	30	-19	-2	1464	331	28	2.11_r2263	0
2	185894962	2014-03-06 21:18:00	K9AN	EN50wc	VE4KE	EO01te	28126088	30	-20	0	1464	331	28	2.11_r2263	0
3	185915111	2014-03-06 23:06:00	K9AN	EN50wc	VE4KE	EO01te	28126088	30	-16	0	1464	331	28	2.11_r2263	0
4	185920324	2014-03-06 23:38:00	K9AN	EN50wc	VE4KE	EO01te	28126087	30	-19	0	1464	331	28	2.11_r2263	0
5	185929388	2014-03-07 00:38:00	K9AN	EN50wc	VE4KE	EO01te	28126087	30	-19	0	1464	331	28	2.11_r2263	0
6	186170235	2014-03-07 20:58:00	K9AN	EN50wc	VE4KE	EO01te	28126091	30	-17	0	1464	331	28	2.11_r2263	0
7	186180309	2014-03-07 21:46:00	K9AN	EN50wc	VE4KE	EO01te	28126090	30	-17	0	1464	331	28	2.11_r2263	0
8	186190670	2014-03-07 22:38:00	K9AN	EN50wc	VE4KE	EO01te	28126091	30	-16	0	1464	331	28	2.11_r2263	0
9	186203244	2014-03-07 23:58:00	K9AN	EN50wc	VE4KE	EO01te	28126092	30	-13	0	1464	331	28	2.11_r2263	0
10	186458122	2014-03-08 21:22:00	K9AN	EN50wc	VE4KE	EO01te	28126087	30	-10	0	1464	331	28	2.11_r2263	0
11	186464096	2014-03-08 21:58:00	K9AN	EN50wc	VE4KE	EO01te	28126088	30	-13	0	1464	331	28	2.11_r2263	0
12	186464839	2014-03-08 22:04:00	K9AN	EN50wc	VE4KE	EO01te	28126086	30	-13	0	1464	331	28	2.11_r2263	0
13	186479292	2014-03-08 23:18:00	K9AN	EN50wc	VE4KE	EO01te	28126088	30	-21	0	1464	331	28	2.11_r2263	0
14	186479585	2014-03-08 23:20:00	K9AN	EN50wc	VE4KE	EO01te	28126087	30	-20	0	1464	331	28	2.11_r2263	0
15	186485476	2014-03-08 23:58:00	K9AN	EN50wc	VE4KE	EO01te	28126090	30	-19	-1	1464	331	28	2.11_r2263	0
16	186492352	2014-03-09 00:38:00	K9AN	EN50wc	VE4KE	EO01te	28126088	30	-27	-1	1464	331	28	2.11_r2263	0
17	186729371	2014-03-09 21:18:00	K9AN	EN50wc	VE4KE	EO01te	28126088	30	-17	-1	1464	331	28	2.11_r2263	0
18	186737105	2014-03-09 22:00:00	K9AN	EN50wc	VE4KE	EO01te	28126085	30	-18	0	1464	331	28	2.11_r2263	0
19	186747984	2014-03-09 22:48:00	K9AN	EN50wc	VE4KE	EO01te	28126085	30	-19	0	1464	331	28	2.11_r2263	0
								Mean	-17.5263						
								SD	3.7174						
								AD	-4.5263						
								AD%	-122						

row	id	time	tx_sign	tx_loc	rx_sign	rx_loc	frequency	power	snr	drift	distance	azimuth	band	version	code
1	186184562	2014-03-07 22:02:00	KB1CHU	FN42pb	W4MO	EL87	14097075	30	-9	-1	1970	219	14	2.21_r2286	0
2	186189168	2014-03-07 22:28:00	KB1CHU	FN42pb	W4MO	EL87	14097088	30	-5	-2	1970	219	14	2.21_r2286	0
3	186194276	2014-03-07 23:02:00	KB1CHU	FN42pb	W4MO	EL87	14097083	30	-3	-1	1970	219	14	2.21_r2286	0
4	186208635	2014-03-08 00:32:00	KB1CHU	FN42pb	W4MO	EL87	14097084	30	-14	-1	1970	219	14	2.21_r2286	0
5	186212809	2014-03-08 01:02:00	KB1CHU	FN42pb	W4MO	EL87	14097085	30	-11	-2	1970	219	14	2.21_r2286	0
6	186216151	2014-03-08 01:28:00	KB1CHU	FN42pb	W4MO	EL87	14097093	30	-14	-4	1970	219	14	2.21_r2286	0
7	186220216	2014-03-08 01:58:00	KB1CHU	FN42pb	W4MO	EL87	14097093	30	-6	-4	1970	219	14	2.21_r2286	0
								Mean	-8.8571						
								SD	4.3753						
								AD	-5.8571						
								AD%	-134						

row	id	time	tx_sign	tx_loc	rx_sign	rx_loc	frequency	power	snr	drift	distance	azimuth	band	version	code
1	186148079	2014-03-07 19:02:00	KC3AVT	FM19la	W4AC	EL86	14097138	37	-2	0	1502	204	14	2.21_r2286	0
2	186150097	2014-03-07 19:12:00	KC3AVT	FM19la	W4AC	EL86	14097138	37	-2	0	1502	204	14	2.21_r2286	0
3	186151839	2014-03-07 19:20:00	KC3AVT	FM19la	W4AC	EL86	14097138	37	-1	0	1502	204	14	2.21_r2286	0
4	186153481	2014-03-07 19:30:00	KC3AVT	FM19la	W4AC	EL86	14097138	37	-1	0	1502	204	14	2.21_r2286	0
5	186155997	2014-03-07 19:44:00	KC3AVT	FM19la	W4AC	EL86	14097137	37	0	1	1502	204	14	2.21_r2286	0
6	186157664	2014-03-07 19:52:00	KC3AVT	FM19la	W4AC	EL86	14097138	37	-4	0	1502	204	14	2.21_r2286	0
7	186159375	2014-03-07 20:00:00	KC3AVT	FM19la	W4AC	EL86	14097138	37	-5	0	1502	204	14	2.21_r2286	0
8	186162150	2014-03-07 20:16:00	KC3AVT	FM19la	W4AC	EL86	14097138	37	-2	0	1502	204	14	2.21_r2286	0
9	186164784	2014-03-07 20:30:00	KC3AVT	FM19la	W4AC	EL86	14097138	37	-7	1	1502	204	14	2.21_r2286	0
10	186167691	2014-03-07 20:44:00	KC3AVT	FM19la	W4AC	EL86	14097139	37	1	0	1502	204	14	2.21_r2286	0
11	186169915	2014-03-07 20:56:00	KC3AVT	FM19la	W4AC	EL86	14097138	37	-2	1	1502	204	14	2.21_r2286	0
12	186174751	2014-03-07 21:22:00	KC3AVT	FM19la	W4AC	EL86	14097139	37	-10	0	1502	204	14	2.21_r2286	0
13	186178321	2014-03-07 21:42:00	KC3AVT	FM19la	W4AC	EL86	14097140	37	-5	0	1502	204	14	2.21_r2286	0
14	186183586	2014-03-07 21:56:00	KC3AVT	FM19la	W4AC	EL86	14097140	37	0	0	1502	204	14	2.21_r2286	0
15	186186532	2014-03-07 22:12:00	KC3AVT	FM19la	W4AC	EL86	14097140	37	1	0	1502	204	14	2.21_r2286	0
16	186188453	2014-03-07 22:24:00	KC3AVT	FM19la	W4AC	EL86	14097140	37	-2	0	1502	204	14	2.21_r2286	0
								Mean	-2.5625						
								SD	2.9882						
								AD	-2.5625						
								AD%	-86						

Page 667 of 1738

row	id	time	tx_sign	tx_loc	rx_sign	rx_loc	frequency	power	snr	drift	distance	azimuth	band	version	code
1	186123062	2014-03-07 17:16:00	KC6KGE	DM05gd	AG6IF	DM13II	10140256	30	-11	0	289	129	10	2.12_r3617	0
2	186125713	2014-03-07 17:26:00	KC6KGE	DM05gd	AG6IF	DM13II	10140256	30	-12	0	289	129	10	2.12_r3617	0
3	186127362	2014-03-07 17:32:00	KC6KGE	DM05gd	AG6IF	DM13II	10140256	30	-11	0	289	129	10	2.12_r3617	0
4	186129202	2014-03-07 17:40:00	KC6KGE	DM05gd	AG6IF	DM13II	10140255	30	-14	0	289	129	10	2.12_r3617	0
5	186131221	2014-03-07 17:48:00	KC6KGE	DM05gd	AG6IF	DM13II	10140255	30	-11	0	289	129	10	2.12_r3617	0
6	186133483	2014-03-07 17:56:00	KC6KGE	DM05gd	AG6IF	DM13II	10140255	30	-16	0	289	129	10	2.12_r3617	0
7	186134856	2014-03-07 18:02:00	KC6KGE	DM05gd	AG6IF	DM13II	10140255	30	-11	0	289	129	10	2.12_r3617	0
8	186137201	2014-03-07 18:12:00	KC6KGE	DM05gd	AG6IF	DM13II	10140255	30	-13	0	289	129	10	2.12_r3617	0
9	186139006	2014-03-07 18:20:00	KC6KGE	DM05gd	AG6IF	DM13II	10140256	30	-11	0	289	129	10	2.12_r3617	0
10	186140699	2014-03-07 18:28:00	KC6KGE	DM05gd	AG6IF	DM13II	10140255	30	-16	0	289	129	10	2.12_r3617	0
11	186142383	2014-03-07 18:34:00	KC6KGE	DM05gd	AG6IF	DM13II	10140255	30	-14	0	289	129	10	2.12_r3617	0
12	186143951	2014-03-07 18:42:00	KC6KGE	DM05gd	AG6IF	DM13II	10140255	30	-15	0	289	129	10	2.12_r3617	0
13	186146003	2014-03-07 18:52:00	KC6KGE	DM05gd	AG6IF	DM13II	10140255	30	-17	0	289	129	10	2.12_r3617	0
14	186147819	2014-03-07 19:00:00	KC6KGE	DM05gd	AG6IF	DM13II	10140256	30	-13	0	289	129	10	2.12_r3617	0
15	186149615	2014-03-07 19:10:00	KC6KGE	DM05gd	AG6IF	DM13II	10140256	30	-13	0	289	129	10	2.12_r3617	0
16	186151953	2014-03-07 19:20:00	KC6KGE	DM05gd	AG6IF	DM13II	10140256	30	-15	0	289	129	10	2.12_r3617	0
17	186153256	2014-03-07 19:28:00	KC6KGE	DM05gd	AG6IF	DM13II	10140256	30	-17	0	289	129	10	2.12_r3617	0
18	186154852	2014-03-07 19:36:00	KC6KGE	DM05gd	AG6IF	DM13II	10140255	30	-20	0	289	129	10	2.12_r3617	0
19	186156735	2014-03-07 19:46:00	KC6KGE	DM05gd	AG6IF	DM13II	10140255	30	-12	0	289	129	10	2.12_r3617	0
20	186157962	2014-03-07 19:52:00	KC6KGE	DM05gd	AG6IF	DM13II	10140256	30	-13	0	289	129	10	2.12_r3617	0
21	186158966	2014-03-07 19:58:00	KC6KGE	DM05gd	AG6IF	DM13II	10140256	30	-14	0	289	129	10	2.12_r3617	0
22	186160402	2014-03-07 20:06:00	KC6KGE	DM05gd	AG6IF	DM13II	10140256	30	-18	0	289	129	10	2.12_r3617	0
23	186162381	2014-03-07 20:16:00	KC6KGE	DM05gd	AG6IF	DM13II	10140255	30	-18	0	289	129	10	2.12_r3617	0
24	186163538	2014-03-07 20:22:00	KC6KGE	DM05gd	AG6IF	DM13II	10140255	30	-13	0	289	129	10	2.12_r3617	0
25	186164638	2014-03-07 20:28:00	KC6KGE	DM05gd	AG6IF	DM13II	10140256	30	-11	0	289	129	10	2.12_r3617	0
26	186166141	2014-03-07 20:36:00	KC6KGE	DM05gd	AG6IF	DM13II	10140256	30	-16	0	289	129	10	2.12_r3617	0
27	186167747	2014-03-07 20:44:00	KC6KGE	DM05gd	AG6IF	DM13II	10140256	30	-14	0	289	129	10	2.12_r3617	0
28	186173990	2014-03-07 21:18:00	KC6KGE	DM05gd	AG6IF	DM13II	10140259	30	-12	0	289	129	10	2.12_r3617	0
29	186175060	2014-03-07 21:24:00	KC6KGE	DM05gd	AG6IF	DM13II	10140257	30	-15	0	289	129	10	2.12_r3617	0
30	186177061	2014-03-07 21:34:00	KC6KGE	DM05gd	AG6IF	DM13II	10140257	30	-12	0	289	129	10	2.12_r3617	0
31	186178881	2014-03-07 21:44:00	KC6KGE	DM05gd	AG6IF	DM13II	10140257	30	-15	0	289	129	10	2.12_r3617	0
32	186182522	2014-03-07 21:50:00	KC6KGE	DM05gd	AG6IF	DM13II	10140257	30	-12	0	289	129	10	2.12_r3617	0
33	186183961	2014-03-07 21:58:00	KC6KGE	DM05gd	AG6IF	DM13II	10140257	30	-15	0	289	129	10	2.12_r3617	0
								Mean	-13.9394						
								SD	2.3841						
								AD	4.0606						
								AD%	170						

row	id	time	tx_sign	tx_loc	rx_sign	rx_loc	frequency	power	snr	drift	distance	azimuth	band	version	code
1	186158894	2014-03-07 19:58:00	KI6STW	CM97bk	KB4RG	EL09wn	28126109	30	-17	-1	2362	105	28	2.12_r3617	0
2	186162579	2014-03-07 20:18:00	KI6STW	CM97bk	KB4RG	EL09wn	28126110	30	-12	-1	2362	105	28	2.12_r3617	0
3	186170151	2014-03-07 20:58:00	KI6STW	CM97bk	KB4RG	EL09wn	28126109	30	-12	0	2362	105	28	2.12_r3617	0
4	186187512	2014-03-07 22:18:00	KI6STW	CM97bk	KB4RG	EL09wn	28126109	33	-10	0	2362	105	28	2.12_r3617	0
5	186190493	2014-03-07 22:38:00	KI6STW	CM97bk	KB4RG	EL09wn	28126109	33	-10	0	2362	105	28	2.12_r3617	0
6	186193406	2014-03-07 22:58:00	KI6STW	CM97bk	KB4RG	EL09wn	28126109	33	-6	0	2362	105	28	2.12_r3617	0
7	186196624	2014-03-07 23:18:00	KI6STW	CM97bk	KB4RG	EL09wn	28126109	33	-10	0	2362	105	28	2.12_r3617	0
8	186203292	2014-03-07 23:58:00	KI6STW	CM97bk	KB4RG	EL09wn	28126108	33	-11	0	2362	105	28	2.12_r3617	0
9	186209518	2014-03-08 00:38:00	KI6STW	CM97bk	KB4RG	EL09wn	28126109	33	-6	0	2362	105	28	2.12_r3617	0
10	186212197	2014-03-08 00:58:00	KI6STW	CM97bk	KB4RG	EL09wn	28126109	33	-10	-1	2362	105	28	2.12_r3617	0
11	186217597	2014-03-08 01:38:00	KI6STW	CM97bk	KB4RG	EL09wn	28126109	33	-10	0	2362	105	28	2.12_r3617	0
								Mean	-10.3636						
								SD	2.9757						
								AD	-4.3636						
								AD%	-147						

row	id	time	tx_sign	tx_loc	rx_sign	rx_loc	frequency	power	snr	drift	distance	azimuth	band	version	code
1	186138508	2014-03-07 18:18:00	KI7CI	DM09ch	JG1TWP/1	PM95rq	14097146	40	-28	0	8382	304	14	2.11_r2263	0
2	186142988	2014-03-07 18:38:00	KI7CI	DM09ch	JG1TWP/1	PM95rq	14097145	40	-17	0	8382	304	14	2.11_r2263	0
3	186145506	2014-03-07 18:50:00	KI7CI	DM09ch	JG1TWP/1	PM95rq	14097145	40	-25	0	8382	304	14	2.11_r2263	0
4	186147710	2014-03-07 19:00:00	KI7CI	DM09ch	JG1TWP/1	PM95rq	14097144	40	-26	0	8382	304	14	2.11_r2263	0
5	186149208	2014-03-07 19:08:00	KI7CI	DM09ch	JG1TWP/1	PM95rq	14097144	40	-26	0	8382	304	14	2.11_r2263	0
6	186151366	2014-03-07 19:18:00	KI7CI	DM09ch	JG1TWP/1	PM95rq	14097144	40	-26	0	8382	304	14	2.11_r2263	0
7	186153551	2014-03-07 19:30:00	KI7CI	DM09ch	JG1TWP/1	PM95rq	14097144	40	-28	0	8382	304	14	2.11_r2263	0
8	186155857	2014-03-07 19:42:00	KI7CI	DM09ch	JG1TWP/1	PM95rq	14097144	40	-21	0	8382	304	14	2.11_r2263	0
9	186158178	2014-03-07 19:54:00	KI7CI	DM09ch	JG1TWP/1	PM95rq	14097145	40	-26	0	8382	304	14	2.11_r2263	0
10	186168116	2014-03-07 20:46:00	KI7CI	DM09ch	JG1TWP/1	PM95rq	14097142	40	-24	0	8382	304	14	2.11_r2263	0
11	186171404	2014-03-07 21:04:00	KI7CI	DM09ch	JG1TWP/1	PM95rq	14097141	40	-25	0	8382	304	14	2.11_r2263	0
12	186173672	2014-03-07 21:16:00	KI7CI	DM09ch	JG1TWP/1	PM95rq	14097140	40	-27	0	8382	304	14	2.11_r2263	0
13	186175662	2014-03-07 21:28:00	KI7CI	DM09ch	JG1TWP/1	PM95rq	14097140	40	-24	0	8382	304	14	2.11_r2263	0
14	186177216	2014-03-07 21:36:00	KI7CI	DM09ch	JG1TWP/1	PM95rq	14097140	40	-23	0	8382	304	14	2.11_r2263	0
								Mean	-24.7143						
								SD	2.9202						
								AD	2.2857						
								AD%	78						

row	id	time	tx_sign	tx_loc	rx_sign	rx_loc	frequency	power	snr	drift	distance	azimuth	band	version	code
1	186178727	2014-03-07 21:44:00	KI7CI	DM09ch	KB4RG	EL09wn	28126137	40	8	0	2255	112	28	2.12_r3617	0
2	186182897	2014-03-07 21:52:00	KI7CI	DM09ch	KB4RG	EL09wn	28126137	40	5	0	2255	112	28	2.12_r3617	0
3	186184943	2014-03-07 22:04:00	KI7CI	DM09ch	KB4RG	EL09wn	28126137	40	11	1	2255	112	28	2.12_r3617	0
4	186186458	2014-03-07 22:12:00	KI7CI	DM09ch	KB4RG	EL09wn	28126136	40	5	0	2255	112	28	2.12_r3617	0
5	186189709	2014-03-07 22:32:00	KI7CI	DM09ch	KB4RG	EL09wn	28126136	40	9	0	2255	112	28	2.12_r3617	0
6	186191328	2014-03-07 22:44:00	KI7CI	DM09ch	KB4RG	EL09wn	28126136	40	5	0	2255	112	28	2.12_r3617	0
7	186192897	2014-03-07 22:54:00	KI7CI	DM09ch	KB4RG	EL09wn	28126136	40	3	0	2255	112	28	2.12_r3617	0
8	186194388	2014-03-07 23:04:00	KI7CI	DM09ch	KB4RG	EL09wn	28126137	40	10	0	2255	112	28	2.12_r3617	0
9	186198336	2014-03-07 23:30:00	KI7CI	DM09ch	KB4RG	EL09wn	28126136	40	8	0	2255	112	28	2.12_r3617	0
10	186200161	2014-03-07 23:40:00	KI7CI	DM09ch	KB4RG	EL09wn	28126137	40	5	0	2255	112	28	2.12_r3617	0
11	186202242	2014-03-07 23:52:00	KI7CI	DM09ch	KB4RG	EL09wn	28126137	40	1	0	2255	112	28	2.12_r3617	0
12	186205689	2014-03-08 00:14:00	KI7CI	DM09ch	KB4RG	EL09wn	28126137	40	11	0	2255	112	28	2.12_r3617	0
13	186206969	2014-03-08 00:22:00	KI7CI	DM09ch	KB4RG	EL09wn	28126137	40	7	0	2255	112	28	2.12_r3617	0
14	186208531	2014-03-08 00:32:00	KI7CI	DM09ch	KB4RG	EL09wn	28126136	40	9	0	2255	112	28	2.12_r3617	0
15	186209578	2014-03-08 00:40:00	KI7CI	DM09ch	KB4RG	EL09wn	28126136	40	9	0	2255	112	28	2.12_r3617	0
16	186211358	2014-03-08 00:52:00	KI7CI	DM09ch	KB4RG	EL09wn	28126137	40	8	0	2255	112	28	2.12_r3617	0
17	186213159	2014-03-08 01:04:00	KI7CI	DM09ch	KB4RG	EL09wn	28126137	40	10	0	2255	112	28	2.12_r3617	0
18	186214611	2014-03-08 01:16:00	KI7CI	DM09ch	KB4RG	EL09wn	28126137	40	11	0	2255	112	28	2.12_r3617	0
								Mean	7.5000						
								SD	2.9155						
								AD	2.5000						
								AD%	86						

row	id	time	tx_sign	tx_loc	rx_sign	rx_loc	frequency	power	snr	drift	distance	azimuth	band	version	code
1	186182892	2014-03-07 21:52:00	KI7CI	DM09ch	WA5NGP	EM10cn	28126100	40	-2	0	2221	109	28	2.0_r1714	0
2	186184926	2014-03-07 22:04:00	KI7CI	DM09ch	WA5NGP	EM10cn	28126099	40	-10	-1	2221	109	28	2.0_r1714	0
3	186186419	2014-03-07 22:12:00	KI7CI	DM09ch	WA5NGP	EM10cn	28126099	40	-3	1	2221	109	28	2.0_r1714	0
4	186187833	2014-03-07 22:20:00	KI7CI	DM09ch	WA5NGP	EM10cn	28126099	40	-2	-1	2221	109	28	2.0_r1714	0
5	186189837	2014-03-07 22:32:00	KI7CI	DM09ch	WA5NGP	EM10cn	28126097	40	0	0	2221	109	28	2.0_r1714	0
6	186191334	2014-03-07 22:44:00	KI7CI	DM09ch	WA5NGP	EM10cn	28126100	40	-3	-1	2221	109	28	2.0_r1714	0
7	186192987	2014-03-07 22:54:00	KI7CI	DM09ch	WA5NGP	EM10cn	28126099	40	-1	0	2221	109	28	2.0_r1714	0
8	186194379	2014-03-07 23:04:00	KI7CI	DM09ch	WA5NGP	EM10cn	28126100	40	-2	0	2221	109	28	2.0_r1714	0
9	186195580	2014-03-07 23:12:00	KI7CI	DM09ch	WA5NGP	EM10cn	28126102	40	-3	0	2221	109	28	2.0_r1714	0
10	186197260	2014-03-07 23:22:00	KI7CI	DM09ch	WA5NGP	EM10cn	28126101	40	-1	0	2221	109	28	2.0_r1714	0
11	186198589	2014-03-07 23:30:00	KI7CI	DM09ch	WA5NGP	EM10cn	28126098	40	0	0	2221	109	28	2.0_r1714	0
12	186200139	2014-03-07 23:40:00	KI7CI	DM09ch	WA5NGP	EM10cn	28126098	40	-2	0	2221	109	28	2.0_r1714	0
13	186202171	2014-03-07 23:52:00	KI7CI	DM09ch	WA5NGP	EM10cn	28126099	40	-8	0	2221	109	28	2.0_r1714	0
14	186203857	2014-03-08 00:02:00	KI7CI	DM09ch	WA5NGP	EM10cn	28126099	40	-5	0	2221	109	28	2.0_r1714	0
15	186205712	2014-03-08 00:14:00	KI7CI	DM09ch	WA5NGP	EM10cn	28126099	40	-3	-1	2221	109	28	2.0_r1714	0
16	186206971	2014-03-08 00:22:00	KI7CI	DM09ch	WA5NGP	EM10cn	28126099	40	2	-1	2221	109	28	2.0_r1714	0
17	186208600	2014-03-08 00:32:00	KI7CI	DM09ch	WA5NGP	EM10cn	28126096	40	2	0	2221	109	28	2.0_r1714	0
18	186209599	2014-03-08 00:40:00	KI7CI	DM09ch	WA5NGP	EM10cn	28126096	40	3	0	2221	109	28	2.0_r1714	0
19	186211477	2014-03-08 00:52:00	KI7CI	DM09ch	WA5NGP	EM10cn	28126095	40	1	0	2221	109	28	2.0_r1714	0
20	186213233	2014-03-08 01:04:00	KI7CI	DM09ch	WA5NGP	EM10cn	28126097	40	4	0	2221	109	28	2.0_r1714	0
21	186214687	2014-03-08 01:16:00	KI7CI	DM09ch	WA5NGP	EM10cn	28126096	40	4	0	2221	109	28	2.0_r1714	0
22	186216079	2014-03-08 01:26:00	KI7CI	DM09ch	WA5NGP	EM10cn	28126096	40	5	1	2221	109	28	2.0_r1714	0
								Mean	-1.0909						
								SD	3.7277						
								AD	8.9091						
								AD%	239						

Page 672 of 1738

row	id	time	tx_sign	tx_loc	rx_sign	rx_loc	frequency	power	snr	drift	distance	azimuth	band	version	code
1	186206840	2014-03-08 00:20:00	KK4U	EM83av	YV4GJN	FK50	10140191	37	-12	0	3014	146	10	2.0_r1714	0
2	186207647	2014-03-08 00:26:00	KK4U	EM83av	YV4GJN	FK50	10140192	37	-10	0	3014	146	10	2.0_r1714	0
3	186210370	2014-03-08 00:44:00	KK4U	EM83av	YV4GJN	FK50	10140152	37	-16	0	3014	146	10	2.0_r1714	0
4	186212633	2014-03-08 01:00:00	KK4U	EM83av	YV4GJN	FK50	10140153	37	-14	0	3014	146	10	2.0_r1714	0
5	186215167	2014-03-08 01:20:00	KK4U	EM83av	YV4GJN	FK50	10140153	37	-15	0	3014	146	10	2.0_r1714	0
6	186216711	2014-03-08 01:32:00	KK4U	EM83av	YV4GJN	FK50	10140153	37	-18	0	3014	146	10	2.0_r1714	0
								Mean	-14.1667						
								SD	2.8577						
								AD	-4.1667						
								AD%	-146						

row	id	time	tx_sign	tx_loc	rx_sign	rx_loc	frequency	power	snr	drift	distance	azimuth	band	version	code
1	186333729	2014-03-06 23:10:00	KZ3X	FN10wh	OX3XR	GP44de	10140283	30	-14	0	3089	23	10		0
2	186333718	2014-03-06 23:22:00	KZ3X	FN10wh	OX3XR	GP44de	10140283	30	-12	0	3089	23	10		0
3	186333699	2014-03-06 23:34:00	KZ3X	FN10wh	OX3XR	GP44de	10140283	30	-11	-1	3089	23	10		0
4	186333666	2014-03-06 23:50:00	KZ3X	FN10wh	OX3XR	GP44de	10140283	30	-9	0	3089	23	10		0
5	186333654	2014-03-07 00:00:00	KZ3X	FN10wh	OX3XR	GP44de	10140283	30	-11	0	3089	23	10		0
6	186333620	2014-03-07 00:22:00	KZ3X	FN10wh	OX3XR	GP44de	10140283	30	-10	0	3089	23	10		0
7	186331503	2014-03-07 23:40:00	KZ3X	FN10wh	OX3XR	GP44de	10140285	30	-13	0	3089	23	10		0
8	186331475	2014-03-07 23:52:00	KZ3X	FN10wh	OX3XR	GP44de	10140284	30	-13	0	3089	23	10		0
9	186331463	2014-03-08 00:00:00	KZ3X	FN10wh	OX3XR	GP44de	10140283	30	-8	0	3089	23	10		0
10	186331437	2014-03-08 00:12:00	KZ3X	FN10wh	OX3XR	GP44de	10140283	30	-3	0	3089	23	10		0
								Mean	-10.4000						
								SD	3.2042						
								AD	-7.4000						
								AD%	-231						

row	id	time	tx_sign	tx_loc	rx_sign	rx_loc	frequency	power	snr	drift	distance	azimuth	band	version	code
1	186333729	2014-03-06 23:10:00	KZ3X	FN10wh	OX3XR	GP44de	10140283	30	-14	0	3089	23	10		0
2	186333718	2014-03-06 23:22:00	KZ3X	FN10wh	OX3XR	GP44de	10140283	30	-12	0	3089	23	10		0
3	186333699	2014-03-06 23:34:00	KZ3X	FN10wh	OX3XR	GP44de	10140283	30	-11	-1	3089	23	10		0
4	186333666	2014-03-06 23:50:00	KZ3X	FN10wh	OX3XR	GP44de	10140283	30	-9	0	3089	23	10		0
5	186333654	2014-03-07 00:00:00	KZ3X	FN10wh	OX3XR	GP44de	10140283	30	-11	0	3089	23	10		0
6	186333620	2014-03-07 00:22:00	KZ3X	FN10wh	OX3XR	GP44de	10140283	30	-10	0	3089	23	10		0
7	186331503	2014-03-07 23:40:00	KZ3X	FN10wh	OX3XR	GP44de	10140285	30	-13	0	3089	23	10		0
8	186331475	2014-03-07 23:52:00	KZ3X	FN10wh	OX3XR	GP44de	10140284	30	-13	0	3089	23	10		0
9	186331463	2014-03-08 00:00:00	KZ3X	FN10wh	OX3XR	GP44de	10140283	30	-8	0	3089	23	10		0
10	186331437	2014-03-08 00:12:00	KZ3X	FN10wh	OX3XR	GP44de	10140283	30	-3	0	3089	23	10		0
								Mean	-10.4000						
								SD	3.2042						
								AD	2.6000						
								AD%	81						

row	id	time	tx_sign	tx_loc	rx_sign	rx_loc	frequency	power	snr	drift	distance	azimuth	band	version	code
1	186202838	2014-03-07 23:56:00	N1NCO	FN42gl	OH7AZL	KP33on	10140201	37	-17	0	6257	32	10	2.0_r1714	0
2	186204761	2014-03-08 00:08:00	N1NCO	FN42gl	OH7AZL	KP33on	10140201	37	-22	0	6257	32	10	2.0_r1714	0
3	186206149	2014-03-08 00:16:00	N1NCO	FN42gl	OH7AZL	KP33on	10140201	37	-23	0	6257	32	10	2.0_r1714	0
4	186212257	2014-03-08 00:58:00	N1NCO	FN42gl	OH7AZL	KP33on	10140201	37	-23	0	6257	32	10	2.0_r1714	0
5	186216682	2014-03-08 01:32:00	N1NCO	FN42gl	OH7AZL	KP33on	10140201	37	-21	0	6257	32	10	2.0_r1714	0
6	186221366	2014-03-08 02:06:00	N1NCO	FN42gl	OH7AZL	KP33on	10140201	37	-22	0	6257	32	10	2.0_r1714	0
								Mean	-21.3333						
								SD	2.2509						
								AD	-4.3333						
								AD%	-193						

row	id	time	tx_sign	tx_loc	rx_sign	rx_loc	frequency	power	snr	drift	distance	azimuth	band	version	code
1	186125639	2014-03-07 17:26:00	N7SCQ	CM98ck	CX2ABP	GF15wc	28126094	30	-21	1	10588	131	28	2.21_r2286	0
2	186126891	2014-03-07 17:30:00	N7SCQ	CM98ck	CX2ABP	GF15wc	28126096	30	-25	1	10588	131	28	2.21_r2286	0
3	186133442	2014-03-07 17:56:00	N7SCQ	CM98ck	CX2ABP	GF15wc	28126092	30	-26	-1	10588	131	28	2.21_r2286	0
4	186138347	2014-03-07 18:16:00	N7SCQ	CM98ck	CX2ABP	GF15wc	28126094	30	-24	-2	10588	131	28	2.21_r2286	0
5	186138995	2014-03-07 18:20:00	N7SCQ	CM98ck	CX2ABP	GF15wc	28126090	30	-25	0	10588	131	28	2.21_r2286	0
6	186140551	2014-03-07 18:26:00	N7SCQ	CM98ck	CX2ABP	GF15wc	28126094	30	-24	1	10588	131	28	2.21_r2286	0
7	186143659	2014-03-07 18:40:00	N7SCQ	CM98ck	CX2ABP	GF15wc	28126093	30	-22	-1	10588	131	28	2.21_r2286	0
8	186145804	2014-03-07 18:50:00	N7SCQ	CM98ck	CX2ABP	GF15wc	28126096	30	-23	0	10588	131	28	2.21_r2286	0
9	186146976	2014-03-07 18:56:00	N7SCQ	CM98ck	CX2ABP	GF15wc	28126095	30	-25	-1	10588	131	28	2.21_r2286	0
10	186149031	2014-03-07 19:06:00	N7SCQ	CM98ck	CX2ABP	GF15wc	28126095	30	-24	0	10588	131	28	2.21_r2286	0
11	186149756	2014-03-07 19:10:00	N7SCQ	CM98ck	CX2ABP	GF15wc	28126096	30	-25	1	10588	131	28	2.21_r2286	0
12	186151215	2014-03-07 19:16:00	N7SCQ	CM98ck	CX2ABP	GF15wc	28126095	30	-24	-1	10588	131	28	2.21_r2286	0
13	186151702	2014-03-07 19:20:00	N7SCQ	CM98ck	CX2ABP	GF15wc	28126091	30	-23	1	10588	131	28	2.21_r2286	0
14	186152895	2014-03-07 19:26:00	N7SCQ	CM98ck	CX2ABP	GF15wc	28126094	30	-22	1	10588	131	28	2.21_r2286	0
15	186153769	2014-03-07 19:30:00	N7SCQ	CM98ck	CX2ABP	GF15wc	28126096	30	-22	0	10588	131	28	2.21_r2286	0
16	186154746	2014-03-07 19:36:00	N7SCQ	CM98ck	CX2ABP	GF15wc	28126095	30	-19	-1	10588	131	28	2.21_r2286	0
17	186155321	2014-03-07 19:40:00	N7SCQ	CM98ck	CX2ABP	GF15wc	28126092	30	-20	0	10588	131	28	2.21_r2286	0
18	186156452	2014-03-07 19:46:00	N7SCQ	CM98ck	CX2ABP	GF15wc	28126095	30	-18	1	10588	131	28	2.21_r2286	0
19	186157295	2014-03-07 19:50:00	N7SCQ	CM98ck	CX2ABP	GF15wc	28126097	30	-20	0	10588	131	28	2.21_r2286	0
20	186158645	2014-03-07 19:56:00	N7SCQ	CM98ck	CX2ABP	GF15wc	28126093	30	-19	-1	10588	131	28	2.21_r2286	0
21	186159304	2014-03-07 20:00:00	N7SCQ	CM98ck	CX2ABP	GF15wc	28126093	30	-18	1	10588	131	28	2.21_r2286	0
22	186160469	2014-03-07 20:06:00	N7SCQ	CM98ck	CX2ABP	GF15wc	28126096	30	-19	1	10588	131	28	2.21_r2286	0
23	186162137	2014-03-07 20:16:00	N7SCQ	CM98ck	CX2ABP	GF15wc	28126093	30	-21	-1	10588	131	28	2.21_r2286	0
24	186162989	2014-03-07 20:20:00	N7SCQ	CM98ck	CX2ABP	GF15wc	28126093	30	-21	1	10588	131	28	2.21_r2286	0
25	186164084	2014-03-07 20:26:00	N7SCQ	CM98ck	CX2ABP	GF15wc	28126097	30	-22	0	10588	131	28	2.21_r2286	0
26	186165025	2014-03-07 20:30:00	N7SCQ	CM98ck	CX2ABP	GF15wc	28126099	30	-19	0	10588	131	28	2.21_r2286	0
27	186166183	2014-03-07 20:36:00	N7SCQ	CM98ck	CX2ABP	GF15wc	28126094	30	-18	-1	10588	131	28	2.21_r2286	0
28	186166969	2014-03-07 20:40:00	N7SCQ	CM98ck	CX2ABP	GF15wc	28126094	30	-18	1	10588	131	28	2.21_r2286	0
29	186167881	2014-03-07 20:46:00	N7SCQ	CM98ck	CX2ABP	GF15wc	28126098	30	-23	1	10588	131	28	2.21_r2286	0
30	186168979	2014-03-07 20:50:00	N7SCQ	CM98ck	CX2ABP	GF15wc	28126099	30	-24	0	10588	131	28	2.21_r2286	0
31	186169813	2014-03-07 20:56:00	N7SCQ	CM98ck	CX2ABP	GF15wc	28126098	30	-19	-1	10588	131	28	2.21_r2286	0
32	186170560	2014-03-07 21:00:00	N7SCQ	CM98ck	CX2ABP	GF15wc	28126094	30	-18	0	10588	131	28	2.21_r2286	0
33	186171657	2014-03-07 21:06:00	N7SCQ	CM98ck	CX2ABP	GF15wc	28126097	30	-18	0	10588	131	28	2.21_r2286	0
34	186172570	2014-03-07 21:10:00	N7SCQ	CM98ck	CX2ABP	GF15wc	28126099	30	-18	0	10588	131	28	2.21_r2286	0
35	186173616	2014-03-07 21:16:00	N7SCQ	CM98ck	CX2ABP	GF15wc	28126098	30	-19	-1	10588	131	28	2.21_r2286	0
36	186174512	2014-03-07 21:20:00	N7SCQ	CM98ck	CX2ABP	GF15wc	28126094	30	-18	0	10588	131	28	2.21_r2286	0
37	186175458	2014-03-07 21:26:00	N7SCQ	CM98ck	CX2ABP	GF15wc	28126097	30	-18	0	10588	131	28	2.21_r2286	0
38	186176113	2014-03-07 21:30:00	N7SCQ	CM98ck	CX2ABP	GF15wc	28126099	30	-18	0	10588	131	28	2.21_r2286	0
39	186177134	2014-03-07 21:36:00	N7SCQ	CM98ck	CX2ABP	GF15wc	28126098	30	-16	-1	10588	131	28	2.21_r2286	0
40	186177905	2014-03-07 21:40:00	N7SCQ	CM98ck	CX2ABP	GF15wc	28126094	30	-16	0	10588	131	28	2.21_r2286	0
41	186180280	2014-03-07 21:46:00	N7SCQ	CM98ck	CX2ABP	GF15wc	28126098	30	-23	1	10588	131	28	2.21_r2286	0
42	186182565	2014-03-07 21:50:00	N7SCQ	CM98ck	CX2ABP	GF15wc	28126100	30	-22	1	10588	131	28	2.21_r2286	0
43	186184369	2014-03-07 22:00:00	N7SCQ	CM98ck	CX2ABP	GF15wc	28126096	30	-23	1	10588	131	28	2.21_r2286	0
44	186185314	2014-03-07 22:06:00	N7SCQ	CM98ck	CX2ABP	GF15wc	28126099	30	-21	0	10588	131	28	2.21_r2286	0
45	186187093	2014-03-07 22:16:00	N7SCQ	CM98ck	CX2ABP	GF15wc	28126096	30	-22	-1	10588	131	28	2.21_r2286	0

Mean	-20.9556
SD	2.7216
AD	3.0444
AD%	112

row	id	time	tx_sign	tx_loc	rx_sign	rx_loc	frequency	power	snr	drift	distance	azimuth	band	version	code
1	186131899	2014-03-07 17:50:00	N7SCQ	CM98ck	ZP5BAB	GG14hc	28126117	30	-26	0	9799	126	28	0.8_r3058	0
2	186135804	2014-03-07 18:06:00	N7SCQ	CM98ck	ZP5BAB	GG14hc	28126117	30	-21	0	9799	126	28	0.8_r3058	0
3	186138215	2014-03-07 18:16:00	N7SCQ	CM98ck	ZP5BAB	GG14hc	28126117	30	-23	0	9799	126	28	0.8_r3058	0
4	186139185	2014-03-07 18:20:00	N7SCQ	CM98ck	ZP5BAB	GG14hc	28126117	30	-21	0	9799	126	28	0.8_r3058	0
5	186140434	2014-03-07 18:26:00	N7SCQ	CM98ck	ZP5BAB	GG14hc	28126117	30	-22	0	9799	126	28	0.8_r3058	0
6	186142596	2014-03-07 18:36:00	N7SCQ	CM98ck	ZP5BAB	GG14hc	28126117	30	-16	0	9799	126	28	0.8_r3058	0
7	186143419	2014-03-07 18:40:00	N7SCQ	CM98ck	ZP5BAB	GG14hc	28126118	30	-21	0	9799	126	28	0.8_r3058	0
8	186144720	2014-03-07 18:46:00	N7SCQ	CM98ck	ZP5BAB	GG14hc	28126118	30	-22	0	9799	126	28	0.8_r3058	0
9	186146894	2014-03-07 18:56:00	N7SCQ	CM98ck	ZP5BAB	GG14hc	28126117	30	-22	0	9799	126	28	0.8_r3058	0
10	186147718	2014-03-07 19:00:00	N7SCQ	CM98ck	ZP5BAB	GG14hc	28126117	30	-20	0	9799	126	28	0.8_r3058	0
11	186148769	2014-03-07 19:06:00	N7SCQ	CM98ck	ZP5BAB	GG14hc	28126117	30	-23	0	9799	126	28	0.8_r3058	0
12	186150910	2014-03-07 19:16:00	N7SCQ	CM98ck	ZP5BAB	GG14hc	28126117	30	-19	0	9799	126	28	0.8_r3058	0
13	186151797	2014-03-07 19:20:00	N7SCQ	CM98ck	ZP5BAB	GG14hc	28126118	30	-20	0	9799	126	28	0.8_r3058	0
14	186152792	2014-03-07 19:26:00	N7SCQ	CM98ck	ZP5BAB	GG14hc	28126118	30	-16	0	9799	126	28	0.8_r3058	0
15	186153700	2014-03-07 19:30:00	N7SCQ	CM98ck	ZP5BAB	GG14hc	28126118	30	-16	0	9799	126	28	0.8_r3058	0
16	186154747	2014-03-07 19:36:00	N7SCQ	CM98ck	ZP5BAB	GG14hc	28126118	30	-19	0	9799	126	28	0.8_r3058	0
17	186155254	2014-03-07 19:40:00	N7SCQ	CM98ck	ZP5BAB	GG14hc	28126118	30	-18	0	9799	126	28	0.8_r3058	0
18	186156630	2014-03-07 19:46:00	N7SCQ	CM98ck	ZP5BAB	GG14hc	28126118	30	-18	0	9799	126	28	0.8_r3058	0
19	186157195	2014-03-07 19:50:00	N7SCQ	CM98ck	ZP5BAB	GG14hc	28126118	30	-19	0	9799	126	28	0.8_r3058	0
20	186158387	2014-03-07 19:56:00	N7SCQ	CM98ck	ZP5BAB	GG14hc	28126118	30	-20	0	9799	126	28	0.8_r3058	0
21	186159267	2014-03-07 20:00:00	N7SCQ	CM98ck	ZP5BAB	GG14hc	28126118	30	-18	0	9799	126	28	0.8_r3058	0
22	186160352	2014-03-07 20:06:00	N7SCQ	CM98ck	ZP5BAB	GG14hc	28126118	30	-21	0	9799	126	28	0.8_r3058	0
23	186161255	2014-03-07 20:10:00	N7SCQ	CM98ck	ZP5BAB	GG14hc	28126118	30	-22	0	9799	126	28	0.8_r3058	0
24	186162141	2014-03-07 20:16:00	N7SCQ	CM98ck	ZP5BAB	GG14hc	28126118	30	-20	0	9799	126	28	0.8_r3058	0
25	186162897	2014-03-07 20:20:00	N7SCQ	CM98ck	ZP5BAB	GG14hc	28126118	30	-18	0	9799	126	28	0.8_r3058	0
26	186164140	2014-03-07 20:26:00	N7SCQ	CM98ck	ZP5BAB	GG14hc	28126118	30	-19	0	9799	126	28	0.8_r3058	0
27	186164936	2014-03-07 20:30:00	N7SCQ	CM98ck	ZP5BAB	GG14hc	28126118	30	-16	0	9799	126	28	0.8_r3058	0
28	186166102	2014-03-07 20:36:00	N7SCQ	CM98ck	ZP5BAB	GG14hc	28126119	30	-14	0	9799	126	28	0.8_r3058	0
29	186166841	2014-03-07 20:40:00	N7SCQ	CM98ck	ZP5BAB	GG14hc	28126119	30	-15	0	9799	126	28	0.8_r3058	0
30	186167949	2014-03-07 20:46:00	N7SCQ	CM98ck	ZP5BAB	GG14hc	28126119	30	-18	0	9799	126	28	0.8_r3058	0
31	186168658	2014-03-07 20:50:00	N7SCQ	CM98ck	ZP5BAB	GG14hc	28126119	30	-20	0	9799	126	28	0.8_r3058	0
32	186169822	2014-03-07 20:56:00	N7SCQ	CM98ck	ZP5BAB	GG14hc	28126120	30	-21	0	9799	126	28	0.8_r3058	0
33	186170586	2014-03-07 21:00:00	N7SCQ	CM98ck	ZP5BAB	GG14hc	28126119	30	-21	0	9799	126	28	0.8_r3058	0
34	186171710	2014-03-07 21:06:00	N7SCQ	CM98ck	ZP5BAB	GG14hc	28126120	30	-18	0	9799	126	28	0.8_r3058	0
35	186172469	2014-03-07 21:10:00	N7SCQ	CM98ck	ZP5BAB	GG14hc	28126119	30	-24	0	9799	126	28	0.8_r3058	0
36	186173643	2014-03-07 21:16:00	N7SCQ	CM98ck	ZP5BAB	GG14hc	28126120	30	-20	0	9799	126	28	0.8_r3058	0
37	186174350	2014-03-07 21:20:00	N7SCQ	CM98ck	ZP5BAB	GG14hc	28126120	30	-20	0	9799	126	28	0.8_r3058	0
38	186175381	2014-03-07 21:26:00	N7SCQ	CM98ck	ZP5BAB	GG14hc	28126120	30	-17	0	9799	126	28	0.8_r3058	0
39	186175999	2014-03-07 21:30:00	N7SCQ	CM98ck	ZP5BAB	GG14hc	28126120	30	-18	0	9799	126	28	0.8_r3058	0
40	186177258	2014-03-07 21:36:00	N7SCQ	CM98ck	ZP5BAB	GG14hc	28126120	30	-17	0	9799	126	28	0.8_r3058	0
41	186177822	2014-03-07 21:40:00	N7SCQ	CM98ck	ZP5BAB	GG14hc	28126120	30	-16	0	9799	126	28	0.8_r3058	0
42	186180101	2014-03-07 21:46:00	N7SCQ	CM98ck	ZP5BAB	GG14hc	28126120	30	-17	0	9799	126	28	0.8_r3058	0
43	186182410	2014-03-07 21:50:00	N7SCQ	CM98ck	ZP5BAB	GG14hc	28126120	30	-17	0	9799	126	28	0.8_r3058	0
44	186183372	2014-03-07 21:56:00	N7SCQ	CM98ck	ZP5BAB	GG14hc	28126120	30	-16	0	9799	126	28	0.8_r3058	0
45	186184193	2014-03-07 22:00:00	N7SCQ	CM98ck	ZP5BAB	GG14hc	28126120	30	-17	0	9799	126	28	0.8_r3058	0
46	186185222	2014-03-07 22:06:00	N7SCQ	CM98ck	ZP5BAB	GG14hc	28126120	30	-18	0	9799	126	28	0.8_r3058	0
47	186186074	2014-03-07 22:10:00	N7SCQ	CM98ck	ZP5BAB	GG14hc	28126120	30	-22	0	9799	126	28	0.8_r3058	0
48	186187066	2014-03-07 22:16:00	N7SCQ	CM98ck	ZP5BAB	GG14hc	28126120	30	-24	0	9799	126	28	0.8_r3058	0
49	186187673	2014-03-07 22:20:00	N7SCQ	CM98ck	ZP5BAB	GG14hc	28126120	30	-25	0	9799	126	28	0.8_r3058	0
								Mean	-19.4082						
								SD	2.7304						
								AD	-5.4082						
								AD%	-198						

row	id	time	tx_sign	tx_loc	rx_sign	rx_loc	frequency	power	snr	drift	distance	azimuth	band	version	code
1	186183640	2014-03-07 21:58:00	NH7SR	BL11ch	KE7KRF	DM51kw	28126110	37	-26	0	4938	66	28	2.0_r1714	0
2	186185969	2014-03-07 22:10:00	NH7SR	BL11ch	KE7KRF	DM51kw	28126110	37	-23	0	4938	66	28	2.0_r1714	0
3	186189262	2014-03-07 22:30:00	NH7SR	BL11ch	KE7KRF	DM51kw	28126110	37	-15	0	4938	66	28	2.0_r1714	0
4	186190587	2014-03-07 22:38:00	NH7SR	BL11ch	KE7KRF	DM51kw	28126110	37	-21	0	4938	66	28	2.0_r1714	0
5	186193625	2014-03-07 22:58:00	NH7SR	BL11ch	KE7KRF	DM51kw	28126110	37	-23	0	4938	66	28	2.0_r1714	0
6	186195254	2014-03-07 23:10:00	NH7SR	BL11ch	KE7KRF	DM51kw	28126110	37	-24	0	4938	66	28	2.0_r1714	0
7	186199715	2014-03-07 23:38:00	NH7SR	BL11ch	KE7KRF	DM51kw	28126110	37	-20	0	4938	66	28	2.0_r1714	0
8	186201760	2014-03-07 23:50:00	NH7SR	BL11ch	KE7KRF	DM51kw	28126109	37	-25	0	4938	66	28	2.0_r1714	0
9	186202928	2014-03-07 23:56:00	NH7SR	BL11ch	KE7KRF	DM51kw	28126109	37	-12	0	4938	66	28	2.0_r1714	0
10	186203152	2014-03-07 23:58:00	NH7SR	BL11ch	KE7KRF	DM51kw	28126109	37	-13	0	4938	66	28	2.0_r1714	0
11	186204540	2014-03-08 00:06:00	NH7SR	BL11ch	KE7KRF	DM51kw	28126110	37	-17	0	4938	66	28	2.0_r1714	0
12	186207572	2014-03-08 00:26:00	NH7SR	BL11ch	KE7KRF	DM51kw	28126110	37	-11	0	4938	66	28	2.0_r1714	0
13	186208745	2014-03-08 00:34:00	NH7SR	BL11ch	KE7KRF	DM51kw	28126110	37	-20	0	4938	66	28	2.0_r1714	0
14	186209395	2014-03-08 00:38:00	NH7SR	BL11ch	KE7KRF	DM51kw	28126110	37	-19	0	4938	66	28	2.0_r1714	0
								Mean	-19.2143						
								SD	4.9331						
								AD	-8.2143						
								AD%	-167						

Page 679 of 1738

row	id	time	tx_sign	tx_loc	rx_sign	rx_loc	frequency	power	snr	drift	distance	azimuth	band	version	code
1	186168965	2014-03-07 20:50:00	NH7SR	BL11ch	WA5NGP	EM10cn	28126121	37	-17	1	6019	67	28	2.0_r1714	0
2	186170173	2014-03-07 20:58:00	NH7SR	BL11ch	WA5NGP	EM10cn	28126121	37	-18	0	6019	67	28	2.0_r1714	0
3	186173626	2014-03-07 21:16:00	NH7SR	BL11ch	WA5NGP	EM10cn	28126121	37	-16	0	6019	67	28	2.0_r1714	0
4	186182540	2014-03-07 21:50:00	NH7SR	BL11ch	WA5NGP	EM10cn	28126115	37	-20	-1	6019	67	28	2.0_r1714	0
5	186183897	2014-03-07 21:58:00	NH7SR	BL11ch	WA5NGP	EM10cn	28126115	37	-16	1	6019	67	28	2.0_r1714	0
6	186191615	2014-03-07 22:46:00	NH7SR	BL11ch	WA5NGP	EM10cn	28126116	37	-17	0	6019	67	28	2.0_r1714	0
7	186193454	2014-03-07 22:58:00	NH7SR	BL11ch	WA5NGP	EM10cn	28126116	37	-15	0	6019	67	28	2.0_r1714	0
8	186195438	2014-03-07 23:10:00	NH7SR	BL11ch	WA5NGP	EM10cn	28126119	37	-16	0	6019	67	28	2.0_r1714	0
9	186196511	2014-03-07 23:18:00	NH7SR	BL11ch	WA5NGP	EM10cn	28126116	37	-19	0	6019	67	28	2.0_r1714	0
10	186198593	2014-03-07 23:30:00	NH7SR	BL11ch	WA5NGP	EM10cn	28126115	37	-14	-1	6019	67	28	2.0_r1714	0
11	186200034	2014-03-07 23:38:00	NH7SR	BL11ch	WA5NGP	EM10cn	28126114	37	-20	0	6019	67	28	2.0_r1714	0
12	186201813	2014-03-07 23:50:00	NH7SR	BL11ch	WA5NGP	EM10cn	28126115	37	-21	0	6019	67	28	2.0_r1714	0
13	186202840	2014-03-07 23:56:00	NH7SR	BL11ch	WA5NGP	EM10cn	28126117	37	-10	1	6019	67	28	2.0_r1714	0
14	186203178	2014-03-07 23:58:00	NH7SR	BL11ch	WA5NGP	EM10cn	28126117	37	-14	0	6019	67	28	2.0_r1714	0
15	186207543	2014-03-08 00:26:00	NH7SR	BL11ch	WA5NGP	EM10cn	28126115	37	-19	0	6019	67	28	2.0_r1714	0
16	186208783	2014-03-08 00:34:00	NH7SR	BL11ch	WA5NGP	EM10cn	28126114	37	-13	0	6019	67	28	2.0_r1714	0
17	186209414	2014-03-08 00:38:00	NH7SR	BL11ch	WA5NGP	EM10cn	28126113	37	-12	0	6019	67	28	2.0_r1714	0
18	186210596	2014-03-08 00:46:00	NH7SR	BL11ch	WA5NGP	EM10cn	28126112	37	-9	0	6019	67	28	2.0_r1714	0
19	186211736	2014-03-08 00:54:00	NH7SR	BL11ch	WA5NGP	EM10cn	28126112	37	-13	0	6019	67	28	2.0_r1714	0
20	186212324	2014-03-08 00:58:00	NH7SR	BL11ch	WA5NGP	EM10cn	28126115	37	-11	0	6019	67	28	2.0_r1714	0
21	186213697	2014-03-08 01:08:00	NH7SR	BL11ch	WA5NGP	EM10cn	28126114	37	-24	0	6019	67	28	2.0_r1714	0
22	186222819	2014-03-08 02:16:00	NH7SR	BL11ch	WA5NGP	EM10cn	28126119	37	-20	-1	6019	67	28	2.0_r1714	0
23	186222989	2014-03-08 02:18:00	NH7SR	BL11ch	WA5NGP	EM10cn	28126118	37	-26	-1	6019	67	28	2.0_r1714	0
								Mean	-16.5217						
								SD	4.3051						
								AD	4.4783						
								AD%	104						

row	id	time	tx_sign	tx_loc	rx_sign	rx_loc	frequency	power	snr	drift	distance	azimuth	band	version	code
1	186137823	2014-03-07 18:14:00	OK2SAM	JN99du	M0BLP	JO02ad	10140228	27	-24	0	1299	288	10	2.11_r2263	0
2	186140072	2014-03-07 18:24:00	OK2SAM	JN99du	M0BLP	JO02ad	10140227	27	-22	0	1299	288	10	2.11_r2263	0
3	186156289	2014-03-07 19:44:00	OK2SAM	JN99du	M0BLP	JO02ad	10140229	27	-27	0	1299	288	10	2.11_r2263	0
4	186158181	2014-03-07 19:54:00	OK2SAM	JN99du	M0BLP	JO02ad	10140229	27	-28	0	1299	288	10	2.11_r2263	0
5	186163780	2014-03-07 20:24:00	OK2SAM	JN99du	M0BLP	JO02ad	10140229	27	-27	0	1299	288	10	2.11_r2263	0
6	186165712	2014-03-07 20:34:00	OK2SAM	JN99du	M0BLP	JO02ad	10140229	27	-25	0	1299	288	10	2.11_r2263	0
7	186167752	2014-03-07 20:44:00	OK2SAM	JN99du	M0BLP	JO02ad	10140229	27	-25	0	1299	288	10	2.11_r2263	0
8	186169645	2014-03-07 20:54:00	OK2SAM	JN99du	M0BLP	JO02ad	10140229	27	-26	0	1299	288	10	2.11_r2263	0
9	186171483	2014-03-07 21:04:00	OK2SAM	JN99du	M0BLP	JO02ad	10140229	27	-26	0	1299	288	10	2.11_r2263	0
10	186173211	2014-03-07 21:14:00	OK2SAM	JN99du	M0BLP	JO02ad	10140229	27	-23	0	1299	288	10	2.11_r2263	0
11	186175040	2014-03-07 21:24:00	OK2SAM	JN99du	M0BLP	JO02ad	10140229	27	-21	0	1299	288	10	2.11_r2263	0
								Mean	-24.9091						
								SD	2.2115						
								AD	-1.9091						
								AD%	-86						

row	id	time	tx_sign	tx_loc	rx_sign	rx_loc	frequency	power	snr	drift	distance	azimuth	band	version	code
1	186125200	2014-03-07 17:24:00	OK2SAM	JN99du	ON7KB	JO21ei	10140198	27	-20	0	995	285	10	0.8_r3058	0
2	186132654	2014-03-07 17:54:00	OK2SAM	JN99du	ON7KB	JO21ei	10140197	27	-21	0	995	285	10	0.8_r3058	0
3	186146356	2014-03-07 18:54:00	OK2SAM	JN99du	ON7KB	JO21ei	10140198	27	-18	0	995	285	10	0.8_r3058	0
4	186148648	2014-03-07 19:04:00	OK2SAM	JN99du	ON7KB	JO21ei	10140198	27	-14	0	995	285	10	0.8_r3058	0
5	186150665	2014-03-07 19:14:00	OK2SAM	JN99du	ON7KB	JO21ei	10140198	27	-20	0	995	285	10	0.8_r3058	0
6	186152541	2014-03-07 19:24:00	OK2SAM	JN99du	ON7KB	JO21ei	10140198	27	-10	0	995	285	10	0.8_r3058	0
7	186154264	2014-03-07 19:34:00	OK2SAM	JN99du	ON7KB	JO21ei	10140198	27	-17	0	995	285	10	0.8_r3058	0
8	186155972	2014-03-07 19:44:00	OK2SAM	JN99du	ON7KB	JO21ei	10140198	27	-16	0	995	285	10	0.8_r3058	0
9	186158097	2014-03-07 19:54:00	OK2SAM	JN99du	ON7KB	JO21ei	10140198	27	-11	0	995	285	10	0.8_r3058	0
10	186159996	2014-03-07 20:04:00	OK2SAM	JN99du	ON7KB	JO21ei	10140197	27	-20	0	995	285	10	0.8_r3058	0
11	186161785	2014-03-07 20:14:00	OK2SAM	JN99du	ON7KB	JO21ei	10140198	27	-9	0	995	285	10	0.8_r3058	0
12	186163676	2014-03-07 20:24:00	OK2SAM	JN99du	ON7KB	JO21ei	10140198	27	-7	0	995	285	10	0.8_r3058	0
								Mean	-15.2500						
								SD	4.9198						
								AD	-8.2500						
								AD%	-168						

row	id	time	tx_sign	tx_loc	rx_sign	rx_loc	frequency	power	snr	drift	distance	azimuth	band	version	code
1	186172745	2014-03-07 21:10:00	OK2SAM	JN99du	PI4THT	JO32kf	3594150	27	-20	0	840	293	3	0.6	0
2	186178156	2014-03-07 21:40:00	OK2SAM	JN99du	PI4THT	JO32kf	3594150	27	-23	0	840	293	3	0.6	0
3	186182641	2014-03-07 21:50:00	OK2SAM	JN99du	PI4THT	JO32kf	3594150	27	-24	0	840	293	3	0.6	0
4	186186357	2014-03-07 22:10:00	OK2SAM	JN99du	PI4THT	JO32kf	3594150	27	-20	0	840	293	3	0.6	0
5	186189631	2014-03-07 22:30:00	OK2SAM	JN99du	PI4THT	JO32kf	3594150	27	-25	0	840	293	3	0.6	0
6	186191059	2014-03-07 22:40:00	OK2SAM	JN99du	PI4THT	JO32kf	3594150	27	-28	0	840	293	3	0.6	0
7	186192489	2014-03-07 22:50:00	OK2SAM	JN99du	PI4THT	JO32kf	3594150	27	-21	0	840	293	3	0.6	0
8	186194004	2014-03-07 23:00:00	OK2SAM	JN99du	PI4THT	JO32kf	3594150	27	-20	0	840	293	3	0.6	0
9	186195522	2014-03-07 23:10:00	OK2SAM	JN99du	PI4THT	JO32kf	3594150	27	-23	0	840	293	3	0.6	0
10	186197065	2014-03-07 23:20:00	OK2SAM	JN99du	PI4THT	JO32kf	3594150	27	-23	0	840	293	3	0.6	0
11	186198664	2014-03-07 23:30:00	OK2SAM	JN99du	PI4THT	JO32kf	3594150	27	-25	0	840	293	3	0.6	0
12	186202024	2014-03-07 23:50:00	OK2SAM	JN99du	PI4THT	JO32kf	3594150	27	-22	0	840	293	3	0.6	0
13	186205250	2014-03-08 00:10:00	OK2SAM	JN99du	PI4THT	JO32kf	3594150	27	-24	0	840	293	3	0.6	0
14	186208398	2014-03-08 00:30:00	OK2SAM	JN99du	PI4THT	JO32kf	3594150	27	-23	0	840	293	3	0.6	0
15	186209910	2014-03-08 00:40:00	OK2SAM	JN99du	PI4THT	JO32kf	3594150	27	-20	0	840	293	3	0.6	0
16	186211280	2014-03-08 00:50:00	OK2SAM	JN99du	PI4THT	JO32kf	3594150	27	-21	0	840	293	3	0.6	0
17	186212734	2014-03-08 01:00:00	OK2SAM	JN99du	PI4THT	JO32kf	3594150	27	-21	0	840	293	3	0.6	0
18	186214045	2014-03-08 01:10:00	OK2SAM	JN99du	PI4THT	JO32kf	3594150	27	-25	0	840	293	3	0.6	0
19	186215395	2014-03-08 01:20:00	OK2SAM	JN99du	PI4THT	JO32kf	3594150	27	-20	0	840	293	3	0.6	0
20	186216668	2014-03-08 01:30:00	OK2SAM	JN99du	PI4THT	JO32kf	3594150	27	-22	0	840	293	3	0.6	0
								Mean	-22.5000						
								SD	2.2124						
								AD	2.5000						
								AD%	113						

row	id	time	tx_sign	tx_loc	rx_sign	rx_loc	frequency	power	snr	drift	distance	azimuth	band	version	code
1	186154062	2014-03-07 19:32:00	ON7KB	JO21ei	DK4TJ	JO31fc	10140209	33	-20	0	148	100	10	2.0_r1714	0
2	186157842	2014-03-07 19:52:00	ON7KB	JO21ei	DK4TJ	JO31fc	10140211	33	-17	0	148	100	10	2.0_r1714	0
3	186168905	2014-03-07 20:50:00	ON7KB	JO21ei	DK4TJ	JO31fc	10140211	33	-21	0	148	100	10	2.0_r1714	0
4	186175498	2014-03-07 21:26:00	ON7KB	JO21ei	DK4TJ	JO31fc	10140210	33	-21	0	148	100	10	2.0_r1714	0
5	186177665	2014-03-07 21:38:00	ON7KB	JO21ei	DK4TJ	JO31fc	10140209	33	-22	0	148	100	10	2.0_r1714	0
								Mean	-20.2000						
								SD	1.9235						
								AD	1.8000						
								AD%	94						

row	id	time	tx_sign	tx_loc	rx_sign	rx_loc	frequency	power	snr	drift	distance	azimuth	band	version	code
1	186164185	2014-03-07 20:26:00	ON7KB	JO21ei	W4MO	EL87	14097029	33	-5	1	7487	286	14	2.21_r2286	0
2	186170170	2014-03-07 20:58:00	ON7KB	JO21ei	W4MO	EL87	14097030	33	-11	1	7487	286	14	2.21_r2286	0
3	186171726	2014-03-07 21:06:00	ON7KB	JO21ei	W4MO	EL87	14097027	33	-7	1	7487	286	14	2.21_r2286	0
4	186185439	2014-03-07 22:06:00	ON7KB	JO21ei	W4MO	EL87	14097160	33	-3	0	7487	286	14	2.21_r2286	0
5	186186867	2014-03-07 22:14:00	ON7KB	JO21ei	W4MO	EL87	14097163	33	-10	0	7487	286	14	2.21_r2286	0
6	186194285	2014-03-07 23:02:00	ON7KB	JO21ei	W4MO	EL87	14097167	33	-19	0	7487	286	14	2.21_r2286	0
7	186196685	2014-03-07 23:18:00	ON7KB	JO21ei	W4MO	EL87	14097168	33	-4	-1	7487	286	14	2.21_r2286	0
8	186198110	2014-03-07 23:28:00	ON7KB	JO21ei	W4MO	EL87	14097167	33	-13	0	7487	286	14	2.21_r2286	0
9	186199688	2014-03-07 23:38:00	ON7KB	JO21ei	W4MO	EL87	14097167	33	-10	0	7487	286	14	2.21_r2286	0
								Mean	-9.1111						
								SD	5.0360						
								AD	-5.1111						
								AD%	-101						

row	id	time	tx_sign	tx_loc	rx_sign	rx_loc	frequency	power	snr	drift	distance	azimuth	band	version	code
1	186133918	2014-03-07 17:58:00	ON7KO	JO21ce	G4ZXE	IO81qk	7040109	37	-8	1	476	276	7	2.0_r1714	0
2	186141803	2014-03-07 18:32:00	ON7KO	JO21ce	G4ZXE	IO81qk	7040110	37	-3	0	476	276	7	2.0_r1714	0
3	186145906	2014-03-07 18:52:00	ON7KO	JO21ce	G4ZXE	IO81qk	7040110	37	-5	0	476	276	7	2.0_r1714	0
4	186147668	2014-03-07 19:00:00	ON7KO	JO21ce	G4ZXE	IO81qk	7040110	37	-3	1	476	276	7	2.0_r1714	0
5	186150462	2014-03-07 19:12:00	ON7KO	JO21ce	G4ZXE	IO81qk	7040110	37	-5	0	476	276	7	2.0_r1714	0
6	186152304	2014-03-07 19:22:00	ON7KO	JO21ce	G4ZXE	IO81qk	7040110	37	-5	0	476	276	7	2.0_r1714	0
7	186158596	2014-03-07 19:56:00	ON7KO	JO21ce	G4ZXE	IO81qk	7040110	37	-6	0	476	276	7	2.0_r1714	0
8	186160753	2014-03-07 20:08:00	ON7KO	JO21ce	G4ZXE	IO81qk	7040110	37	-5	0	476	276	7	2.0_r1714	0
9	186162625	2014-03-07 20:18:00	ON7KO	JO21ce	G4ZXE	IO81qk	7040110	37	-6	0	476	276	7	2.0_r1714	0
10	186167811	2014-03-07 20:44:00	ON7KO	JO21ce	G4ZXE	IO81qk	7040110	37	-7	0	476	276	7	2.0_r1714	0
11	186169567	2014-03-07 20:54:00	ON7KO	JO21ce	G4ZXE	IO81qk	7040110	37	-8	0	476	276	7	2.0_r1714	0
12	186173384	2014-03-07 21:14:00	ON7KO	JO21ce	G4ZXE	IO81qk	7040110	37	-6	0	476	276	7	2.0_r1714	0
								Mean	-5.5833						
								SD	1.6214						
								AD	1.4167						
								AD%	87						

row	id	time	tx_sign	tx_loc	rx_sign	rx_loc	frequency	power	snr	drift	distance	azimuth	band	version	code
1	186133918	2014-03-07 17:58:00	ON7KO	JO21ce	G4ZXE	IO81qk	7040109	37	-8	1	476	276	7	2.0_r1714	0
2	186141803	2014-03-07 18:32:00	ON7KO	JO21ce	G4ZXE	IO81qk	7040110	37	-3	0	476	276	7	2.0_r1714	0
3	186145906	2014-03-07 18:52:00	ON7KO	JO21ce	G4ZXE	IO81qk	7040110	37	-5	0	476	276	7	2.0_r1714	0
4	186147668	2014-03-07 19:00:00	ON7KO	JO21ce	G4ZXE	IO81qk	7040110	37	-3	1	476	276	7	2.0_r1714	0
5	186150462	2014-03-07 19:12:00	ON7KO	JO21ce	G4ZXE	IO81qk	7040110	37	-5	0	476	276	7	2.0_r1714	0
6	186152304	2014-03-07 19:22:00	ON7KO	JO21ce	G4ZXE	IO81qk	7040110	37	-5	0	476	276	7	2.0_r1714	0
7	186158596	2014-03-07 19:56:00	ON7KO	JO21ce	G4ZXE	IO81qk	7040110	37	-6	0	476	276	7	2.0_r1714	0
8	186160753	2014-03-07 20:08:00	ON7KO	JO21ce	G4ZXE	IO81qk	7040110	37	-5	0	476	276	7	2.0_r1714	0
9	186162625	2014-03-07 20:18:00	ON7KO	JO21ce	G4ZXE	IO81qk	7040110	37	-6	0	476	276	7	2.0_r1714	0
10	186167811	2014-03-07 20:44:00	ON7KO	JO21ce	G4ZXE	IO81qk	7040110	37	-7	0	476	276	7	2.0_r1714	0
11	186169567	2014-03-07 20:54:00	ON7KO	JO21ce	G4ZXE	IO81qk	7040110	37	-8	0	476	276	7	2.0_r1714	0
12	186173384	2014-03-07 21:14:00	ON7KO	JO21ce	G4ZXE	IO81qk	7040110	37	-6	0	476	276	7	2.0_r1714	0
								Mean	-5.5833						
								SD	1.6214						
								AD	2.4167						
								AD%	149						

row	id	time	tx_sign	tx_loc	rx_sign	rx_loc	frequency	power	snr	drift	distance	azimuth	band	version	code
1	186175423	2014-03-07 21:26:00	OX3XR	GP44de	N2NOM	FN22bg	10140104	33	-23	0	2881	224	10	2.11_r2263	0
2	186177859	2014-03-07 21:40:00	OX3XR	GP44de	N2NOM	FN22bg	10140103	33	-21	0	2881	224	10	2.11_r2263	0
3	186183035	2014-03-07 21:54:00	OX3XR	GP44de	N2NOM	FN22bg	10140105	33	-22	0	2881	224	10	2.11_r2263	0
4	186185284	2014-03-07 22:06:00	OX3XR	GP44de	N2NOM	FN22bg	10140105	33	-21	0	2881	224	10	2.11_r2263	0
5	186189114	2014-03-07 22:28:00	OX3XR	GP44de	N2NOM	FN22bg	10140102	33	-25	0	2881	224	10	2.11_r2263	0
6	186191217	2014-03-07 22:42:00	OX3XR	GP44de	N2NOM	FN22bg	10140103	33	-33	0	2881	224	10	2.11_r2263	0
7	186192784	2014-03-07 22:54:00	OX3XR	GP44de	N2NOM	FN22bg	10140101	33	-20	0	2881	224	10	2.11_r2263	0
8	186194660	2014-03-07 23:06:00	OX3XR	GP44de	N2NOM	FN22bg	10140102	33	-25	0	2881	224	10	2.11_r2263	0
9	186196099	2014-03-07 23:14:00	OX3XR	GP44de	N2NOM	FN22bg	10140103	33	-31	0	2881	224	10	2.11_r2263	0
10	186200888	2014-03-07 23:44:00	OX3XR	GP44de	N2NOM	FN22bg	10140101	33	-28	0	2881	224	10	2.11_r2263	0
11	186204533	2014-03-08 00:06:00	OX3XR	GP44de	N2NOM	FN22bg	10140103	33	-21	0	2881	224	10	2.11_r2263	0
12	186206760	2014-03-08 00:20:00	OX3XR	GP44de	N2NOM	FN22bg	10140105	33	-23	0	2881	224	10	2.11_r2263	0
13	186208148	2014-03-08 00:30:00	OX3XR	GP44de	N2NOM	FN22bg	10140103	33	-25	-1	2881	224	10	2.11_r2263	0
14	186211893	2014-03-08 00:56:00	OX3XR	GP44de	N2NOM	FN22bg	10140105	33	-23	0	2881	224	10	2.11_r2263	0
15	186213526	2014-03-08 01:08:00	OX3XR	GP44de	N2NOM	FN22bg	10140105	33	-24	0	2881	224	10	2.11_r2263	0
								Mean	-24.3333						
								SD	3.7544						
								AD	8.6667						
								AD%	231						

row	id	time	tx_sign	tx_loc	rx_sign	rx_loc	frequency	power	snr	drift	distance	azimuth	band	version	code
1	186168759	2014-03-07 20:50:00	OZ7IT	JO65df	W4AC	EL86	14097167	37	-3	0	7940	290	14	2.21_r2286	0
2	186176052	2014-03-07 21:30:00	OZ7IT	JO65df	W4AC	EL86	14097166	37	-5	-1	7940	290	14	2.21_r2286	0
3	186183271	2014-03-07 21:54:00	OZ7IT	JO65df	W4AC	EL86	14097167	37	-5	-1	7940	290	14	2.21_r2286	0
4	186185529	2014-03-07 22:06:00	OZ7IT	JO65df	W4AC	EL86	14097167	37	-8	-1	7940	290	14	2.21_r2286	0
5	186187410	2014-03-07 22:18:00	OZ7IT	JO65df	W4AC	EL86	14097167	37	-9	-1	7940	290	14	2.21_r2286	0
6	186189721	2014-03-07 22:32:00	OZ7IT	JO65df	W4AC	EL86	14097166	37	-9	0	7940	290	14	2.21_r2286	0
7	186194255	2014-03-07 23:02:00	OZ7IT	JO65df	W4AC	EL86	14097167	37	-11	0	7940	290	14	2.21_r2286	0
8	186198719	2014-03-07 23:32:00	OZ7IT	JO65df	W4AC	EL86	14097167	37	-16	0	7940	290	14	2.21_r2286	0
								Mean	-8.2500						
								SD	4.0970						
								AD	7.7500						
								AD%	189						

row	id	time	tx_sign	tx_loc	rx_sign	rx_loc	frequency	power	snr	drift	distance	azimuth	band	version	code
1	186168856	2014-03-07 20:50:00	OZ7IT	JO65df	W4MO	EL87	14097051	37	-5	-1	7851	291	14	2.21_r2286	0
2	186185451	2014-03-07 22:06:00	OZ7IT	JO65df	W4MO	EL87	14097178	37	-6	-1	7851	291	14	2.21_r2286	0
3	186187599	2014-03-07 22:18:00	OZ7IT	JO65df	W4MO	EL87	14097181	37	-8	-1	7851	291	14	2.21_r2286	0
4	186189835	2014-03-07 22:32:00	OZ7IT	JO65df	W4MO	EL87	14097183	37	-6	0	7851	291	14	2.21_r2286	0
5	186191390	2014-03-07 22:44:00	OZ7IT	JO65df	W4MO	EL87	14097183	37	-8	0	7851	291	14	2.21_r2286	0
6	186194288	2014-03-07 23:02:00	OZ7IT	JO65df	W4MO	EL87	14097184	37	-13	0	7851	291	14	2.21_r2286	0
7	186195600	2014-03-07 23:12:00	OZ7IT	JO65df	W4MO	EL87	14097184	37	-8	1	7851	291	14	2.21_r2286	0
8	186201435	2014-03-07 23:48:00	OZ7IT	JO65df	W4MO	EL87	14097187	37	-28	0	7851	291	14	2.21_r2286	0
9	186206958	2014-03-08 00:22:00	OZ7IT	JO65df	W4MO	EL87	14097187	37	-20	0	7851	291	14	2.21_r2286	0
10	186208638	2014-03-08 00:32:00	OZ7IT	JO65df	W4MO	EL87	14097188	37	-23	0	7851	291	14	2.21_r2286	0
								Mean	-12.5000						
								SD	8.2226						
								AD	15.5000						
								AD%	189						

row	id	time	tx_sign	tx_loc	rx_sign	rx_loc	frequency	power	snr	drift	distance	azimuth	band	version	code
1	186136927	2014-03-07 18:10:00	US3IRX	KN88xh	OZ7IT	JO65df	7040183	37	-13	0	1912	303	7	2.21_r2286	0
2	186145678	2014-03-07 18:50:00	US3IRX	KN88xh	OZ7IT	JO65df	7040183	37	-12	0	1912	303	7	2.21_r2286	0
3	186148247	2014-03-07 19:02:00	US3IRX	KN88xh	OZ7IT	JO65df	7040183	37	-11	0	1912	303	7	2.21_r2286	0
4	186149846	2014-03-07 19:10:00	US3IRX	KN88xh	OZ7IT	JO65df	7040183	37	-13	0	1912	303	7	2.21_r2286	0
5	186152217	2014-03-07 19:22:00	US3IRX	KN88xh	OZ7IT	JO65df	7040183	37	-16	0	1912	303	7	2.21_r2286	0
6	186155831	2014-03-07 19:42:00	US3IRX	KN88xh	OZ7IT	JO65df	7040183	37	-9	0	1912	303	7	2.21_r2286	0
7	186157232	2014-03-07 19:50:00	US3IRX	KN88xh	OZ7IT	JO65df	7040183	37	-11	0	1912	303	7	2.21_r2286	0
8	186158984	2014-03-07 19:58:00	US3IRX	KN88xh	OZ7IT	JO65df	7040183	37	-10	0	1912	303	7	2.21_r2286	0
9	186161194	2014-03-07 20:10:00	US3IRX	KN88xh	OZ7IT	JO65df	7040183	37	-9	0	1912	303	7	2.21_r2286	0
10	186163247	2014-03-07 20:20:00	US3IRX	KN88xh	OZ7IT	JO65df	7040183	37	-6	0	1912	303	7	2.21_r2286	0
11	186164898	2014-03-07 20:30:00	US3IRX	KN88xh	OZ7IT	JO65df	7040182	37	-3	0	1912	303	7	2.21_r2286	0
12	186167289	2014-03-07 20:42:00	US3IRX	KN88xh	OZ7IT	JO65df	7040182	37	-10	0	1912	303	7	2.21_r2286	0
13	186172081	2014-03-07 21:08:00	US3IRX	KN88xh	OZ7IT	JO65df	7040181	37	-1	0	1912	303	7	2.21_r2286	0
14	186172683	2014-03-07 21:10:00	US3IRX	KN88xh	OZ7IT	JO65df	7040181	37	1	0	1912	303	7	2.21_r2286	0
15	186175864	2014-03-07 21:28:00	US3IRX	KN88xh	OZ7IT	JO65df	7040181	37	-9	0	1912	303	7	2.21_r2286	0
16	186177581	2014-03-07 21:38:00	US3IRX	KN88xh	OZ7IT	JO65df	7040181	37	-10	0	1912	303	7	2.21_r2286	0
								Mean	-8.8750						
								SD	4.5442						
								AD	-9.8750						
								AD%	-217						

row	id	time	tx_sign	tx_loc	rx_sign	rx_loc	frequency	power	snr	drift	distance	azimuth	band	version	code
1	186151033	2014-03-07 19:16:00	VA3ROM	EN58jk	KB9AMG	EN52tx	28126135	27	-29	0	610	174	28	2.0_r1714	0
2	186170591	2014-03-07 21:00:00	VA3ROM	EN58jk	KB9AMG	EN52tx	28126134	27	-27	0	610	174	28	2.0_r1714	0
3	186172650	2014-03-07 21:10:00	VA3ROM	EN58jk	KB9AMG	EN52tx	28126135	27	-28	0	610	174	28	2.0_r1714	0
4	186184608	2014-03-07 22:02:00	VA3ROM	EN58jk	KB9AMG	EN52tx	28126135	27	-26	0	610	174	28	2.0_r1714	0
5	186199174	2014-03-07 23:34:00	VA3ROM	EN58jk	KB9AMG	EN52tx	28126136	27	-26	0	610	174	28	2.0_r1714	0
								Mean	-27.2000						
								SD	1.3038						
								AD	-1.2000						
								AD%	-92						

row	id	time	tx_sign	tx_loc	rx_sign	rx_loc	frequency	power	snr	drift	distance	azimuth	band	version	code
1	186160575	2014-03-07 20:08:00	VK3DXE	QF21nv	VK6ZRY	OF78vd	14097175	37	-23	-1	2749	276	14	0.8_r3058	0
2	186164555	2014-03-07 20:28:00	VK3DXE	QF21nv	VK6ZRY	OF78vd	14097176	37	-22	-1	2749	276	14	0.8_r3058	0
3	186174325	2014-03-07 21:20:00	VK3DXE	QF21nv	VK6ZRY	OF78vd	14097024	37	-12	-1	2749	276	14	0.8_r3058	0
4	186176522	2014-03-07 21:32:00	VK3DXE	QF21nv	VK6ZRY	OF78vd	14097025	37	-11	-2	2749	276	14	0.8_r3058	0
5	186180260	2014-03-07 21:46:00	VK3DXE	QF21nv	VK6ZRY	OF78vd	14097025	37	-15	-2	2749	276	14	0.8_r3058	0
6	186184221	2014-03-07 22:00:00	VK3DXE	QF21nv	VK6ZRY	OF78vd	14097024	37	-20	-2	2749	276	14	0.8_r3058	0
7	186186441	2014-03-07 22:12:00	VK3DXE	QF21nv	VK6ZRY	OF78vd	14097024	37	-18	-2	2749	276	14	0.8_r3058	0
8	186188796	2014-03-07 22:26:00	VK3DXE	QF21nv	VK6ZRY	OF78vd	14097025	37	-12	-1	2749	276	14	0.8_r3058	0
9	186190576	2014-03-07 22:38:00	VK3DXE	QF21nv	VK6ZRY	OF78vd	14097024	37	-9	-1	2749	276	14	0.8_r3058	0
10	186192696	2014-03-07 22:52:00	VK3DXE	QF21nv	VK6ZRY	OF78vd	14097024	37	-13	-2	2749	276	14	0.8_r3058	0
								Mean	-15.5000						
								SD	4.9272						
								AD	-2.5000						
								AD%	-51						

row	id	time	tx_sign	tx_loc	rx_sign	rx_loc	frequency	power	snr	drift	distance	azimuth	band	version	code
1	186194907	2014-03-07 23:06:00	VK3DXE	QF21nv	ZL1AML	RF73gb	28126012	37	7	-3	2587	96	28	2.11_r2263	0
2	186196157	2014-03-07 23:14:00	VK3DXE	QF21nv	ZL1AML	RF73gb	28126012	37	-10	-2	2587	96	28	2.11_r2263	0
3	186210198	2014-03-08 00:42:00	VK3DXE	QF21nv	ZL1AML	RF73gb	28126154	37	9	-3	2587	96	28	2.11_r2263	0
4	186211289	2014-03-08 00:50:00	VK3DXE	QF21nv	ZL1AML	RF73gb	28126154	37	8	-3	2587	96	28	2.11_r2263	0
5	186214037	2014-03-08 01:10:00	VK3DXE	QF21nv	ZL1AML	RF73gb	28126156	37	10	-3	2587	96	28	2.11_r2263	0
6	186215616	2014-03-08 01:22:00	VK3DXE	QF21nv	ZL1AML	RF73gb	28126156	37	9	-3	2587	96	28	2.11_r2263	0
7	186216659	2014-03-08 01:30:00	VK3DXE	QF21nv	ZL1AML	RF73gb	28126156	37	8	-2	2587	96	28	2.11_r2263	0
8	186220165	2014-03-08 01:56:00	VK3DXE	QF21nv	ZL1AML	RF73gb	28126156	37	5	-3	2587	96	28	2.11_r2263	0
								Mean	5.7500						
								SD	6.5411						
								AD	15.7500						
								AD%	241						

row	id	time	tx_sign	tx_loc	rx_sign	rx_loc	frequency	power	snr	drift	distance	azimuth	band	version	code
1	186198601	2014-03-07 23:30:00	W3CSW	FM19kd	N2NOM	FN22bg	10140271	33	5	0	363	16	10	2.11_r2263	0
2	186200616	2014-03-07 23:42:00	W3CSW	FM19kd	N2NOM	FN22bg	10140269	33	8	0	363	16	10	2.11_r2263	0
3	186202536	2014-03-07 23:54:00	W3CSW	FM19kd	N2NOM	FN22bg	10140267	33	9	0	363	16	10	2.11_r2263	0
4	186204169	2014-03-08 00:04:00	W3CSW	FM19kd	N2NOM	FN22bg	10140269	33	4	0	363	16	10	2.11_r2263	0
5	186206787	2014-03-08 00:20:00	W3CSW	FM19kd	N2NOM	FN22bg	10140272	33	-8	0	363	16	10	2.11_r2263	0
6	186208927	2014-03-08 00:34:00	W3CSW	FM19kd	N2NOM	FN22bg	10140270	33	-9	0	363	16	10	2.11_r2263	0
								Mean	1.5000						
								SD	7.9687						
								AD	9.5000						
								AD%	119						

row	id	time	tx_sign	tx_loc	rx_sign	rx_loc	frequency	power	snr	drift	distance	azimuth	band	version	code
1	186134595	2014-03-07 18:02:00	W3CSW	FM19kd	N2NOM	FN22bg	28126169	33	-17	0	363	16	28	2.11_r2263	0
2	186141840	2014-03-07 18:32:00	W3CSW	FM19kd	N2NOM	FN22bg	28126169	33	-18	0	363	16	28	2.11_r2263	0
3	186148059	2014-03-07 19:02:00	W3CSW	FM19kd	N2NOM	FN22bg	28126169	33	-15	0	363	16	28	2.11_r2263	0
4	186151423	2014-03-07 19:18:00	W3CSW	FM19kd	N2NOM	FN22bg	28126170	33	-18	0	363	16	28	2.11_r2263	0
5	186154261	2014-03-07 19:34:00	W3CSW	FM19kd	N2NOM	FN22bg	28126172	33	-14	0	363	16	28	2.11_r2263	0
6	186157310	2014-03-07 19:50:00	W3CSW	FM19kd	N2NOM	FN22bg	28126173	33	-20	0	363	16	28	2.11_r2263	0
7	186159711	2014-03-07 20:02:00	W3CSW	FM19kd	N2NOM	FN22bg	28126173	33	-13	0	363	16	28	2.11_r2263	0
8	186161985	2014-03-07 20:14:00	W3CSW	FM19kd	N2NOM	FN22bg	28126173	33	-18	0	363	16	28	2.11_r2263	0
9	186164886	2014-03-07 20:30:00	W3CSW	FM19kd	N2NOM	FN22bg	28126174	33	-20	0	363	16	28	2.11_r2263	0
10	186168315	2014-03-07 20:48:00	W3CSW	FM19kd	N2NOM	FN22bg	28126175	33	-13	0	363	16	28	2.11_r2263	0
11	186170571	2014-03-07 21:00:00	W3CSW	FM19kd	N2NOM	FN22bg	28126175	33	-19	0	363	16	28	2.11_r2263	0
12	186173317	2014-03-07 21:14:00	W3CSW	FM19kd	N2NOM	FN22bg	28126175	33	-16	0	363	16	28	2.11_r2263	0
								Mean	-16.7500						
								SD	2.5271						
								AD	3.2500						
								AD%	129						

row	id	time	tx_sign	tx_loc	rx_sign	rx_loc	frequency	power	snr	drift	distance	azimuth	band	version	code
1	186198601	2014-03-07 23:30:00	W3CSW	FM19kd	N2NOM	FN22bg	10140271	33	5	0	363	16	10	2.11_r2263	0
2	186200616	2014-03-07 23:42:00	W3CSW	FM19kd	N2NOM	FN22bg	10140269	33	8	0	363	16	10	2.11_r2263	0
3	186202536	2014-03-07 23:54:00	W3CSW	FM19kd	N2NOM	FN22bg	10140267	33	9	0	363	16	10	2.11_r2263	0
4	186204169	2014-03-08 00:04:00	W3CSW	FM19kd	N2NOM	FN22bg	10140269	33	4	0	363	16	10	2.11_r2263	0
5	186206787	2014-03-08 00:20:00	W3CSW	FM19kd	N2NOM	FN22bg	10140272	33	-8	0	363	16	10	2.11_r2263	0
6	186208927	2014-03-08 00:34:00	W3CSW	FM19kd	N2NOM	FN22bg	10140270	33	-9	0	363	16	10	2.11_r2263	0
								Mean	1.5000						
								SD	7.9687						
								AD	-7.5000						
								AD%	-94						

Page 697 of 1738

row	id	time	tx_sign	tx_loc	rx_sign	rx_loc	frequency	power	snr	drift	distance	azimuth	band	version	code
1	186174016	2014-03-07 21:18:00	W3GXT	FM19ol	W4AC	EL86	14097123	37	-2	0	1558	204	14	2.21_r2286	0
2	186175276	2014-03-07 21:26:00	W3GXT	FM19ol	W4AC	EL86	14097123	37	-3	0	1558	204	14	2.21_r2286	0
3	186176884	2014-03-07 21:34:00	W3GXT	FM19ol	W4AC	EL86	14097123	37	1	0	1558	204	14	2.21_r2286	0
4	186182370	2014-03-07 21:50:00	W3GXT	FM19ol	W4AC	EL86	14097123	37	6	0	1558	204	14	2.21_r2286	0
5	186187867	2014-03-07 22:20:00	W3GXT	FM19ol	W4AC	EL86	14097123	37	2	0	1558	204	14	2.21_r2286	0
6	186191817	2014-03-07 22:46:00	W3GXT	FM19ol	W4AC	EL86	14097124	37	0	0	1558	204	14	2.21_r2286	0
7	186196369	2014-03-07 23:16:00	W3GXT	FM19ol	W4AC	EL86	14097124	37	-4	0	1558	204	14	2.21_r2286	0
8	186197509	2014-03-07 23:24:00	W3GXT	FM19ol	W4AC	EL86	14097123	37	0	0	1558	204	14	2.21_r2286	0
9	186199069	2014-03-07 23:34:00	W3GXT	FM19ol	W4AC	EL86	14097124	37	2	0	1558	204	14	2.21_r2286	0
10	186202354	2014-03-07 23:52:00	W3GXT	FM19ol	W4AC	EL86	14097123	37	0	0	1558	204	14	2.21_r2286	0
11	186203542	2014-03-08 00:00:00	W3GXT	FM19ol	W4AC	EL86	14097123	37	2	0	1558	204	14	2.21_r2286	0
12	186205408	2014-03-08 00:12:00	W3GXT	FM19ol	W4AC	EL86	14097124	37	5	0	1558	204	14	2.21_r2286	0
								Mean	0.7500						
								SD	2.9580						
								AD	-4.2500						
								AD%	-144						

row	id	time	tx_sign	tx_loc	rx_sign	rx_loc	frequency	power	snr	drift	distance	azimuth	band	version	code
1	186145623	2014-03-07 18:50:00	W3GXT	FM19ol	W4AC	EL86	14097123	37	-3	0	1558	204	14	2.21_r2286	0
2	186149056	2014-03-07 19:06:00	W3GXT	FM19ol	W4AC	EL86	14097123	37	-2	0	1558	204	14	2.21_r2286	0
3	186150565	2014-03-07 19:14:00	W3GXT	FM19ol	W4AC	EL86	14097123	37	0	0	1558	204	14	2.21_r2286	0
4	186152058	2014-03-07 19:22:00	W3GXT	FM19ol	W4AC	EL86	14097124	37	0	0	1558	204	14	2.21_r2286	0
5	186154099	2014-03-07 19:32:00	W3GXT	FM19ol	W4AC	EL86	14097123	37	-2	0	1558	204	14	2.21_r2286	0
6	186155418	2014-03-07 19:40:00	W3GXT	FM19ol	W4AC	EL86	14097123	37	2	0	1558	204	14	2.21_r2286	0
7	186158753	2014-03-07 19:58:00	W3GXT	FM19ol	W4AC	EL86	14097123	37	3	0	1558	204	14	2.21_r2286	0
8	186160804	2014-03-07 20:08:00	W3GXT	FM19ol	W4AC	EL86	14097123	37	2	0	1558	204	14	2.21_r2286	0
9	186162146	2014-03-07 20:16:00	W3GXT	FM19ol	W4AC	EL86	14097123	37	-2	0	1558	204	14	2.21_r2286	0
10	186164124	2014-03-07 20:26:00	W3GXT	FM19ol	W4AC	EL86	14097123	37	3	0	1558	204	14	2.21_r2286	0
11	186169657	2014-03-07 20:54:00	W3GXT	FM19ol	W4AC	EL86	14097123	37	-4	0	1558	204	14	2.21_r2286	0
12	186172497	2014-03-07 21:10:00	W3GXT	FM19ol	W4AC	EL86	14097123	37	-1	0	1558	204	14	2.21_r2286	0
13	186174016	2014-03-07 21:18:00	W3GXT	FM19ol	W4AC	EL86	14097123	37	-2	0	1558	204	14	2.21_r2286	0
14	186175276	2014-03-07 21:26:00	W3GXT	FM19ol	W4AC	EL86	14097123	37	-3	0	1558	204	14	2.21_r2286	0
15	186176884	2014-03-07 21:34:00	W3GXT	FM19ol	W4AC	EL86	14097123	37	1	0	1558	204	14	2.21_r2286	0
16	186182370	2014-03-07 21:50:00	W3GXT	FM19ol	W4AC	EL86	14097123	37	6	0	1558	204	14	2.21_r2286	0
17	186187867	2014-03-07 22:20:00	W3GXT	FM19ol	W4AC	EL86	14097123	37	2	0	1558	204	14	2.21_r2286	0
18	186191817	2014-03-07 22:46:00	W3GXT	FM19ol	W4AC	EL86	14097124	37	0	0	1558	204	14	2.21_r2286	0
19	186196369	2014-03-07 23:16:00	W3GXT	FM19ol	W4AC	EL86	14097124	37	-4	0	1558	204	14	2.21_r2286	0
20	186197509	2014-03-07 23:24:00	W3GXT	FM19ol	W4AC	EL86	14097123	37	0	0	1558	204	14	2.21_r2286	0
21	186199069	2014-03-07 23:34:00	W3GXT	FM19ol	W4AC	EL86	14097124	37	2	0	1558	204	14	2.21_r2286	0
22	186202354	2014-03-07 23:52:00	W3GXT	FM19ol	W4AC	EL86	14097123	37	0	0	1558	204	14	2.21_r2286	0
23	186203542	2014-03-08 00:00:00	W3GXT	FM19ol	W4AC	EL86	14097123	37	2	0	1558	204	14	2.21_r2286	0
24	186205408	2014-03-08 00:12:00	W3GXT	FM19ol	W4AC	EL86	14097124	37	5	0	1558	204	14	2.21_r2286	0
								Mean	0.2083						
								SD	2.6862						
								AD	-5.7917						
								AD%	-216						

row	id	time	tx_sign	tx_loc	rx_sign	rx_loc	frequency	power	snr	drift	distance	azimuth	band	version	code
1	186188803	2014-03-07 22:26:00	W3HH	EL89vb	KK5MR	EM13wc	10140297	30	-17	0	1398	292	10	2.10_r2179	0
2	186191963	2014-03-07 22:48:00	W3HH	EL89vb	KK5MR	EM13wc	10140297	30	-15	0	1398	292	10	2.10_r2179	0
3	186193678	2014-03-07 22:58:00	W3HH	EL89vb	KK5MR	EM13wc	10140297	30	-12	0	1398	292	10	2.10_r2179	0
4	186205972	2014-03-08 00:16:00	W3HH	EL89vb	KK5MR	EM13wc	10140298	30	-12	0	1398	292	10	2.10_r2179	0
5	186207855	2014-03-08 00:28:00	W3HH	EL89vb	KK5MR	EM13wc	10140298	30	-14	0	1398	292	10	2.10_r2179	0
6	186209485	2014-03-08 00:38:00	W3HH	EL89vb	KK5MR	EM13wc	10140297	30	-17	0	1398	292	10	2.10_r2179	0
7	186212338	2014-03-08 00:58:00	W3HH	EL89vb	KK5MR	EM13wc	10140297	30	-17	0	1398	292	10	2.10_r2179	0
8	186214927	2014-03-08 01:18:00	W3HH	EL89vb	KK5MR	EM13wc	10140297	30	-13	0	1398	292	10	2.10_r2179	0
9	186217298	2014-03-08 01:36:00	W3HH	EL89vb	KK5MR	EM13wc	10140298	30	-12	0	1398	292	10	2.10_r2179	0
10	186218531	2014-03-08 01:44:00	W3HH	EL89vb	KK5MR	EM13wc	10140298	30	-13	0	1398	292	10	2.10_r2179	0
11	186219480	2014-03-08 01:52:00	W3HH	EL89vb	KK5MR	EM13wc	10140298	30	-17	0	1398	292	10	2.10_r2179	0
12	186221025	2014-03-08 02:02:00	W3HH	EL89vb	KK5MR	EM13wc	10140297	30	-18	0	1398	292	10	2.10_r2179	0
13	186222201	2014-03-08 02:12:00	W3HH	EL89vb	KK5MR	EM13wc	10140297	30	-18	0	1398	292	10	2.10_r2179	0
14	186223292	2014-03-08 02:20:00	W3HH	EL89vb	KK5MR	EM13wc	10140297	30	-16	0	1398	292	10	2.10_r2179	0
15	186224463	2014-03-08 02:28:00	W3HH	EL89vb	KK5MR	EM13wc	10140298	30	-11	0	1398	292	10	2.10_r2179	0
16	186225696	2014-03-08 02:36:00	W3HH	EL89vb	KK5MR	EM13wc	10140298	30	-12	0	1398	292	10	2.10_r2179	0
17	186227041	2014-03-08 02:46:00	W3HH	EL89vb	KK5MR	EM13wc	10140298	30	-15	0	1398	292	10	2.10_r2179	0
18	186228025	2014-03-08 02:54:00	W3HH	EL89vb	KK5MR	EM13wc	10140298	30	-13	0	1398	292	10	2.10_r2179	0
19	186229490	2014-03-08 03:06:00	W3HH	EL89vb	KK5MR	EM13wc	10140298	30	-16	0	1398	292	10	2.10_r2179	0
								Mean	-14.6316						
								SD	2.3383						
								AD	-2.6316						
								AD%	-113						

row	id	time	tx_sign	tx_loc	rx_sign	rx_loc	frequency	power	snr	drift	distance	azimuth	band	version	code
1	186331580	2014-03-07 22:58:00	W3HH	EL89vb	OX3XR	GP44de	10140298	30	-25	0	4456	20	10		0
2	186331510	2014-03-07 23:38:00	W3HH	EL89vb	OX3XR	GP44de	10140298	30	-24	0	4456	20	10		0
3	186331492	2014-03-07 23:46:00	W3HH	EL89vb	OX3XR	GP44de	10140298	30	-26	0	4456	20	10		0
4	186331448	2014-03-08 00:08:00	W3HH	EL89vb	OX3XR	GP44de	10140298	30	-22	0	4456	20	10		0
5	186331389	2014-03-08 00:50:00	W3HH	EL89vb	OX3XR	GP44de	10140298	30	-21	0	4456	20	10		0
6	186331380	2014-03-08 00:58:00	W3HH	EL89vb	OX3XR	GP44de	10140298	30	-16	0	4456	20	10		0
7	186331342	2014-03-08 01:36:00	W3HH	EL89vb	OX3XR	GP44de	10140299	30	-20	0	4456	20	10		0
8	186331333	2014-03-08 01:44:00	W3HH	EL89vb	OX3XR	GP44de	10140299	30	-18	0	4456	20	10		0
9	186331320	2014-03-08 01:52:00	W3HH	EL89vb	OX3XR	GP44de	10140299	30	-20	0	4456	20	10		0
								Mean	-21.3333						
								SD	3.2787						
								AD	3.6667						
								AD%	112						

Page 701 of 1738

row	id	time	tx_sign	tx_loc	rx_sign	rx_loc	frequency	power	snr	drift	distance	azimuth	band	version	code
1	186161543	2014-03-07 20:12:00	W3HH	EL89vb	W3BI	FN20en	10140282	30	-18	0	1412	23	10	2.0_r1714	0
2	186163052	2014-03-07 20:20:00	W3HH	EL89vb	W3BI	FN20en	10140283	30	-14	0	1412	23	10	2.0_r1714	0
3	186165529	2014-03-07 20:32:00	W3HH	EL89vb	W3BI	FN20en	10140282	30	-13	0	1412	23	10	2.0_r1714	0
4	186169312	2014-03-07 20:52:00	W3HH	EL89vb	W3BI	FN20en	10140282	30	-14	0	1412	23	10	2.0_r1714	0
5	186177014	2014-03-07 21:34:00	W3HH	EL89vb	W3BI	FN20en	10140282	30	-6	0	1412	23	10	2.0_r1714	0
6	186178248	2014-03-07 21:42:00	W3HH	EL89vb	W3BI	FN20en	10140282	30	-13	0	1412	23	10	2.0_r1714	0
7	186185350	2014-03-07 22:06:00	W3HH	EL89vb	W3BI	FN20en	10140282	30	-11	0	1412	23	10	2.0_r1714	0
8	186187612	2014-03-07 22:18:00	W3HH	EL89vb	W3BI	FN20en	10140283	30	-11	0	1412	23	10	2.0_r1714	0
9	186188677	2014-03-07 22:26:00	W3HH	EL89vb	W3BI	FN20en	10140282	30	-7	0	1412	23	10	2.0_r1714	0
10	186192167	2014-03-07 22:48:00	W3HH	EL89vb	W3BI	FN20en	10140282	30	-22	0	1412	23	10	2.0_r1714	0
11	186194738	2014-03-07 23:06:00	W3HH	EL89vb	W3BI	FN20en	10140282	30	-13	0	1412	23	10	2.0_r1714	0
12	186196451	2014-03-07 23:16:00	W3HH	EL89vb	W3BI	FN20en	10140282	30	-9	0	1412	23	10	2.0_r1714	0
13	186198227	2014-03-07 23:28:00	W3HH	EL89vb	W3BI	FN20en	10140283	30	-12	0	1412	23	10	2.0_r1714	0
14	186200018	2014-03-07 23:38:00	W3HH	EL89vb	W3BI	FN20en	10140283	30	-5	0	1412	23	10	2.0_r1714	0
15	186201331	2014-03-07 23:46:00	W3HH	EL89vb	W3BI	FN20en	10140283	30	-4	0	1412	23	10	2.0_r1714	0
16	186203024	2014-03-07 23:56:00	W3HH	EL89vb	W3BI	FN20en	10140283	30	-10	0	1412	23	10	2.0_r1714	0
17	186204684	2014-03-08 00:08:00	W3HH	EL89vb	W3BI	FN20en	10140282	30	-8	-1	1412	23	10	2.0_r1714	0
18	186207890	2014-03-08 00:28:00	W3HH	EL89vb	W3BI	FN20en	10140283	30	-12	0	1412	23	10	2.0_r1714	0
19	186209507	2014-03-08 00:38:00	W3HH	EL89vb	W3BI	FN20en	10140282	30	-4	0	1412	23	10	2.0_r1714	0
20	186211197	2014-03-08 00:50:00	W3HH	EL89vb	W3BI	FN20en	10140283	30	-6	0	1412	23	10	2.0_r1714	0
21	186212278	2014-03-08 00:58:00	W3HH	EL89vb	W3BI	FN20en	10140283	30	-3	0	1412	23	10	2.0_r1714	0
22	186213607	2014-03-08 01:08:00	W3HH	EL89vb	W3BI	FN20en	10140283	30	-8	0	1412	23	10	2.0_r1714	0
23	186214856	2014-03-08 01:18:00	W3HH	EL89vb	W3BI	FN20en	10140282	30	-7	0	1412	23	10	2.0_r1714	0
24	186216312	2014-03-08 01:28:00	W3HH	EL89vb	W3BI	FN20en	10140283	30	-6	0	1412	23	10	2.0_r1714	0
25	186217447	2014-03-08 01:36:00	W3HH	EL89vb	W3BI	FN20en	10140283	30	-14	0	1412	23	10	2.0_r1714	0
26	186218412	2014-03-08 01:44:00	W3HH	EL89vb	W3BI	FN20en	10140283	30	-10	0	1412	23	10	2.0_r1714	0
								Mean	-10.0000						
								SD	4.5343						
								AD	12.0000						
								AD%	265						

row	id	time	tx_sign	tx_loc	rx_sign	rx_loc	frequency	power	snr	drift	distance	azimuth	band	version	code
1	186198233	2014-03-07 23:28:00	W3HH	EL89vb	W3CSW	FM19kd	10140288	30	-15	0	1214	21	10	2.12_r3617	0
2	186199920	2014-03-07 23:38:00	W3HH	EL89vb	W3CSW	FM19kd	10140287	30	-4	0	1214	21	10	2.12_r3617	0
3	186201321	2014-03-07 23:46:00	W3HH	EL89vb	W3CSW	FM19kd	10140288	30	-4	0	1214	21	10	2.12_r3617	0
4	186202964	2014-03-07 23:56:00	W3HH	EL89vb	W3CSW	FM19kd	10140288	30	-6	0	1214	21	10	2.12_r3617	0
5	186204724	2014-03-08 00:08:00	W3HH	EL89vb	W3CSW	FM19kd	10140288	30	-3	0	1214	21	10	2.12_r3617	0
6	186206079	2014-03-08 00:16:00	W3HH	EL89vb	W3CSW	FM19kd	10140288	30	-7	0	1214	21	10	2.12_r3617	0
7	186207919	2014-03-08 00:28:00	W3HH	EL89vb	W3CSW	FM19kd	10140288	30	0	0	1214	21	10	2.12_r3617	0
								Mean	-5.5714						
								SD	4.7208						
								AD	9.4286						
								AD%	200						

row	id	time	tx_sign	tx_loc	rx_sign	rx_loc	frequency	power	snr	drift	distance	azimuth	band	version	code
1	186172367	2014-03-07 21:08:00	W4AC	EL86ux	2E0DSS	IO82xl	14097077	30	-12	0	7021	42	14	2.0_r1714	0
2	186174261	2014-03-07 21:20:00	W4AC	EL86ux	2E0DSS	IO82xl	14097077	30	-23	0	7021	42	14	2.0_r1714	0
3	186176552	2014-03-07 21:32:00	W4AC	EL86ux	2E0DSS	IO82xl	14097077	30	-15	0	7021	42	14	2.0_r1714	0
4	186185191	2014-03-07 22:04:00	W4AC	EL86ux	2E0DSS	IO82xl	14097077	30	-18	0	7021	42	14	2.0_r1714	0
5	186186787	2014-03-07 22:14:00	W4AC	EL86ux	2E0DSS	IO82xl	14097077	30	-17	0	7021	42	14	2.0_r1714	0
6	186188014	2014-03-07 22:22:00	W4AC	EL86ux	2E0DSS	IO82xl	14097077	30	-16	0	7021	42	14	2.0_r1714	0
7	186191613	2014-03-07 22:44:00	W4AC	EL86ux	2E0DSS	IO82xl	14097077	30	-17	0	7021	42	14	2.0_r1714	0
8	186192974	2014-03-07 22:54:00	W4AC	EL86ux	2E0DSS	IO82xl	14097078	30	-13	0	7021	42	14	2.0_r1714	0
9	186194463	2014-03-07 23:04:00	W4AC	EL86ux	2E0DSS	IO82xl	14097077	30	-24	0	7021	42	14	2.0_r1714	0
10	186195719	2014-03-07 23:12:00	W4AC	EL86ux	2E0DSS	IO82xl	14097077	30	-24	0	7021	42	14	2.0_r1714	0
11	186196863	2014-03-07 23:20:00	W4AC	EL86ux	2E0DSS	IO82xl	14097077	30	-20	0	7021	42	14	2.0_r1714	0
12	186198026	2014-03-07 23:28:00	W4AC	EL86ux	2E0DSS	IO82xl	14097077	30	-12	0	7021	42	14	2.0_r1714	0
13	186199846	2014-03-07 23:38:00	W4AC	EL86ux	2E0DSS	IO82xl	14097077	30	-15	0	7021	42	14	2.0_r1714	0
14	186200801	2014-03-07 23:44:00	W4AC	EL86ux	2E0DSS	IO82xl	14097077	30	-19	0	7021	42	14	2.0_r1714	0
15	186204383	2014-03-08 00:04:00	W4AC	EL86ux	2E0DSS	IO82xl	14097077	30	-28	0	7021	42	14	2.0_r1714	0
								Mean	-18.2000						
								SD	4.7988						
								AD	9.8000						
								AD%	204						

row	id	time	tx_sign	tx_loc	rx_sign	rx_loc	frequency	power	snr	drift	distance	azimuth	band	version	code
1	186164707	2014-03-07 20:28:00	W4AC	EL86ux	2E0DSS	IO82xl	14097077	30	-23	0	7021	42	14	2.0_r1714	0
2	186166448	2014-03-07 20:38:00	W4AC	EL86ux	2E0DSS	IO82xl	14097077	30	-20	0	7021	42	14	2.0_r1714	0
3	186168228	2014-03-07 20:46:00	W4AC	EL86ux	2E0DSS	IO82xl	14097077	30	-19	0	7021	42	14	2.0_r1714	0
4	186170479	2014-03-07 20:58:00	W4AC	EL86ux	2E0DSS	IO82xl	14097077	30	-25	0	7021	42	14	2.0_r1714	0
5	186172367	2014-03-07 21:08:00	W4AC	EL86ux	2E0DSS	IO82xl	14097077	30	-12	0	7021	42	14	2.0_r1714	0
6	186174261	2014-03-07 21:20:00	W4AC	EL86ux	2E0DSS	IO82xl	14097077	30	-23	0	7021	42	14	2.0_r1714	0
7	186176552	2014-03-07 21:32:00	W4AC	EL86ux	2E0DSS	IO82xl	14097077	30	-15	0	7021	42	14	2.0_r1714	0
8	186185191	2014-03-07 22:04:00	W4AC	EL86ux	2E0DSS	IO82xl	14097077	30	-18	0	7021	42	14	2.0_r1714	0
9	186186787	2014-03-07 22:14:00	W4AC	EL86ux	2E0DSS	IO82xl	14097077	30	-17	0	7021	42	14	2.0_r1714	0
10	186188014	2014-03-07 22:22:00	W4AC	EL86ux	2E0DSS	IO82xl	14097077	30	-16	0	7021	42	14	2.0_r1714	0
11	186191613	2014-03-07 22:44:00	W4AC	EL86ux	2E0DSS	IO82xl	14097077	30	-17	0	7021	42	14	2.0_r1714	0
12	186192974	2014-03-07 22:54:00	W4AC	EL86ux	2E0DSS	IO82xl	14097078	30	-13	0	7021	42	14	2.0_r1714	0
13	186194463	2014-03-07 23:04:00	W4AC	EL86ux	2E0DSS	IO82xl	14097077	30	-24	0	7021	42	14	2.0_r1714	0
14	186195719	2014-03-07 23:12:00	W4AC	EL86ux	2E0DSS	IO82xl	14097077	30	-24	0	7021	42	14	2.0_r1714	0
15	186196863	2014-03-07 23:20:00	W4AC	EL86ux	2E0DSS	IO82xl	14097077	30	-20	0	7021	42	14	2.0_r1714	0
16	186198026	2014-03-07 23:28:00	W4AC	EL86ux	2E0DSS	IO82xl	14097077	30	-12	0	7021	42	14	2.0_r1714	0
17	186199846	2014-03-07 23:38:00	W4AC	EL86ux	2E0DSS	IO82xl	14097077	30	-15	0	7021	42	14	2.0_r1714	0
18	186200801	2014-03-07 23:44:00	W4AC	EL86ux	2E0DSS	IO82xl	14097077	30	-19	0	7021	42	14	2.0_r1714	0
19	186204383	2014-03-08 00:04:00	W4AC	EL86ux	2E0DSS	IO82xl	14097077	30	-28	0	7021	42	14	2.0_r1714	0
								Mean	-18.9474						
								SD	4.6245						
								AD	5.0526						
								AD%	109						

row	id	time	tx_sign	tx_loc	rx_sign	rx_loc	frequency	power	snr	drift	distance	azimuth	band	version	code
1	186164707	2014-03-07 20:28:00	W4AC	EL86ux	2E0DSS	IO82xl	14097077	30	-23	0	7021	42	14	2.0_r1714	0
2	186166448	2014-03-07 20:38:00	W4AC	EL86ux	2E0DSS	IO82xl	14097077	30	-20	0	7021	42	14	2.0_r1714	0
3	186168228	2014-03-07 20:46:00	W4AC	EL86ux	2E0DSS	IO82xl	14097077	30	-19	0	7021	42	14	2.0_r1714	0
4	186170479	2014-03-07 20:58:00	W4AC	EL86ux	2E0DSS	IO82xl	14097077	30	-25	0	7021	42	14	2.0_r1714	0
5	186172367	2014-03-07 21:08:00	W4AC	EL86ux	2E0DSS	IO82xl	14097077	30	-12	0	7021	42	14	2.0_r1714	0
6	186174261	2014-03-07 21:20:00	W4AC	EL86ux	2E0DSS	IO82xl	14097077	30	-23	0	7021	42	14	2.0_r1714	0
7	186176552	2014-03-07 21:32:00	W4AC	EL86ux	2E0DSS	IO82xl	14097077	30	-15	0	7021	42	14	2.0_r1714	0
8	186185191	2014-03-07 22:04:00	W4AC	EL86ux	2E0DSS	IO82xl	14097077	30	-18	0	7021	42	14	2.0_r1714	0
9	186186787	2014-03-07 22:14:00	W4AC	EL86ux	2E0DSS	IO82xl	14097077	30	-17	0	7021	42	14	2.0_r1714	0
10	186188014	2014-03-07 22:22:00	W4AC	EL86ux	2E0DSS	IO82xl	14097077	30	-16	0	7021	42	14	2.0_r1714	0
11	186191613	2014-03-07 22:44:00	W4AC	EL86ux	2E0DSS	IO82xl	14097077	30	-17	0	7021	42	14	2.0_r1714	0
12	186192974	2014-03-07 22:54:00	W4AC	EL86ux	2E0DSS	IO82xl	14097078	30	-13	0	7021	42	14	2.0_r1714	0
13	186194463	2014-03-07 23:04:00	W4AC	EL86ux	2E0DSS	IO82xl	14097077	30	-24	0	7021	42	14	2.0_r1714	0
14	186195719	2014-03-07 23:12:00	W4AC	EL86ux	2E0DSS	IO82xl	14097077	30	-24	0	7021	42	14	2.0_r1714	0
15	186196863	2014-03-07 23:20:00	W4AC	EL86ux	2E0DSS	IO82xl	14097077	30	-20	0	7021	42	14	2.0_r1714	0
16	186198026	2014-03-07 23:28:00	W4AC	EL86ux	2E0DSS	IO82xl	14097077	30	-12	0	7021	42	14	2.0_r1714	0
17	186199846	2014-03-07 23:38:00	W4AC	EL86ux	2E0DSS	IO82xl	14097077	30	-15	0	7021	42	14	2.0_r1714	0
18	186200801	2014-03-07 23:44:00	W4AC	EL86ux	2E0DSS	IO82xl	14097077	30	-19	0	7021	42	14	2.0_r1714	0
19	186204383	2014-03-08 00:04:00	W4AC	EL86ux	2E0DSS	IO82xl	14097077	30	-28	0	7021	42	14	2.0_r1714	0
								Mean	-18.9474						
								SD	4.6245						
								AD	-6.9474						
								AD%	-150						

row	id	time	tx_sign	tx_loc	rx_sign	rx_loc	frequency	power	snr	drift	distance	azimuth	band	version	code
1	186170458	2014-03-07 20:58:00	W4AC	EL86ux	DG7RJ	JN58th	14097079	30	-26	0	8078	44	14	2.11_r2263	0
2	186174406	2014-03-07 21:20:00	W4AC	EL86ux	DG7RJ	JN58th	14097078	30	-27	0	8078	44	14	2.11_r2263	0
3	186185137	2014-03-07 22:04:00	W4AC	EL86ux	DG7RJ	JN58th	14097077	30	-23	0	8078	44	14	2.11_r2263	0
4	186187006	2014-03-07 22:14:00	W4AC	EL86ux	DG7RJ	JN58th	14097078	30	-25	0	8078	44	14	2.11_r2263	0
5	186193062	2014-03-07 22:54:00	W4AC	EL86ux	DG7RJ	JN58th	14097078	30	-26	0	8078	44	14	2.11_r2263	0
6	186199816	2014-03-07 23:38:00	W4AC	EL86ux	DG7RJ	JN58th	14097077	30	-29	0	8078	44	14	2.11_r2263	0
7	186200752	2014-03-07 23:44:00	W4AC	EL86ux	DG7RJ	JN58th	14097077	30	-25	0	8078	44	14	2.11_r2263	0
								Mean	-25.8571						
								SD	1.8645						
								AD	3.1429						
								AD%	169						

Page 707 of 1738

row	id	time	tx_sign	tx_loc	rx_sign	rx_loc	frequency	power	snr	drift	distance	azimuth	band	version	code
1	186172345	2014-03-07 21:08:00	W4AC	EL86ux	DK0SC	JN59mf	14097090	30	-19	0	8001	43	14	2.21_r2286	0
2	186174602	2014-03-07 21:20:00	W4AC	EL86ux	DK0SC	JN59mf	14097090	30	-17	0	8001	43	14	2.21_r2286	0
3	186191530	2014-03-07 22:44:00	W4AC	EL86ux	DK0SC	JN59mf	14097090	30	-17	0	8001	43	14	2.21_r2286	0
4	186200748	2014-03-07 23:44:00	W4AC	EL86ux	DK0SC	JN59mf	14097089	30	-14	-1	8001	43	14	2.21_r2286	0
5	186203023	2014-03-07 23:56:00	W4AC	EL86ux	DK0SC	JN59mf	14097090	30	-13	0	8001	43	14	2.21_r2286	0
								Mean	-16.0000						
								SD	2.4495						
								AD	-2.0000						
								AD%	-82						

Page 708 of 1738

row	id	time	tx_sign	tx_loc	rx_sign	rx_loc	frequency	power	snr	drift	distance	azimuth	band	version	code
1	186174441	2014-03-07 21:20:00	W4AC	EL86ux	DK6UG	JN49cm	14097077	30	-6	0	7797	44	14	2.21_r2286	0
2	186176590	2014-03-07 21:32:00	W4AC	EL86ux	DK6UG	JN49cm	14097077	30	-8	0	7797	44	14	2.21_r2286	0
3	186182766	2014-03-07 21:52:00	W4AC	EL86ux	DK6UG	JN49cm	14097077	30	-2	0	7797	44	14	2.21_r2286	0
4	186184965	2014-03-07 22:04:00	W4AC	EL86ux	DK6UG	JN49cm	14097076	30	-3	0	7797	44	14	2.21_r2286	0
5	186186762	2014-03-07 22:14:00	W4AC	EL86ux	DK6UG	JN49cm	14097077	30	-9	0	7797	44	14	2.21_r2286	0
6	186188186	2014-03-07 22:22:00	W4AC	EL86ux	DK6UG	JN49cm	14097077	30	-8	0	7797	44	14	2.21_r2286	0
7	186190017	2014-03-07 22:34:00	W4AC	EL86ux	DK6UG	JN49cm	14097077	30	-5	0	7797	44	14	2.21_r2286	0
8	186191346	2014-03-07 22:44:00	W4AC	EL86ux	DK6UG	JN49cm	14097077	30	-7	0	7797	44	14	2.21_r2286	0
9	186192860	2014-03-07 22:54:00	W4AC	EL86ux	DK6UG	JN49cm	14097077	30	-11	0	7797	44	14	2.21_r2286	0
10	186194412	2014-03-07 23:04:00	W4AC	EL86ux	DK6UG	JN49cm	14097077	30	-12	0	7797	44	14	2.21_r2286	0
11	186195612	2014-03-07 23:12:00	W4AC	EL86ux	DK6UG	JN49cm	14097076	30	-12	0	7797	44	14	2.21_r2286	0
12	186196951	2014-03-07 23:20:00	W4AC	EL86ux	DK6UG	JN49cm	14097076	30	-8	0	7797	44	14	2.21_r2286	0
13	186199830	2014-03-07 23:38:00	W4AC	EL86ux	DK6UG	JN49cm	14097076	30	-11	0	7797	44	14	2.21_r2286	0
14	186200874	2014-03-07 23:44:00	W4AC	EL86ux	DK6UG	JN49cm	14097075	30	-11	0	7797	44	14	2.21_r2286	0
15	186202858	2014-03-07 23:56:00	W4AC	EL86ux	DK6UG	JN49cm	14097076	30	-11	0	7797	44	14	2.21_r2286	0
16	186204044	2014-03-08 00:04:00	W4AC	EL86ux	DK6UG	JN49cm	14097075	30	-5	0	7797	44	14	2.21_r2286	0
								Mean	-8.0625						
								SD	3.1931						
								AD	-3.0625						
								AD%	-96						

Page 709 of 1738

row	id	time	tx_sign	tx_loc	rx_sign	rx_loc	frequency	power	snr	drift	distance	azimuth	band	version	code
1	186170207	2014-03-07 20:58:00	W4AC	EL86ux	DK6UG	JN49cm	14097077	30	-14	0	7797	44	14	2.21_r2286	0
2	186174441	2014-03-07 21:20:00	W4AC	EL86ux	DK6UG	JN49cm	14097077	30	-6	0	7797	44	14	2.21_r2286	0
3	186176590	2014-03-07 21:32:00	W4AC	EL86ux	DK6UG	JN49cm	14097077	30	-8	0	7797	44	14	2.21_r2286	0
4	186182766	2014-03-07 21:52:00	W4AC	EL86ux	DK6UG	JN49cm	14097077	30	-2	0	7797	44	14	2.21_r2286	0
5	186184965	2014-03-07 22:04:00	W4AC	EL86ux	DK6UG	JN49cm	14097076	30	-3	0	7797	44	14	2.21_r2286	0
6	186186762	2014-03-07 22:14:00	W4AC	EL86ux	DK6UG	JN49cm	14097077	30	-9	0	7797	44	14	2.21_r2286	0
7	186188186	2014-03-07 22:22:00	W4AC	EL86ux	DK6UG	JN49cm	14097077	30	-8	0	7797	44	14	2.21_r2286	0
8	186190017	2014-03-07 22:34:00	W4AC	EL86ux	DK6UG	JN49cm	14097077	30	-5	0	7797	44	14	2.21_r2286	0
9	186191346	2014-03-07 22:44:00	W4AC	EL86ux	DK6UG	JN49cm	14097077	30	-7	0	7797	44	14	2.21_r2286	0
10	186192860	2014-03-07 22:54:00	W4AC	EL86ux	DK6UG	JN49cm	14097077	30	-11	0	7797	44	14	2.21_r2286	0
11	186194412	2014-03-07 23:04:00	W4AC	EL86ux	DK6UG	JN49cm	14097077	30	-12	0	7797	44	14	2.21_r2286	0
12	186195612	2014-03-07 23:12:00	W4AC	EL86ux	DK6UG	JN49cm	14097076	30	-12	0	7797	44	14	2.21_r2286	0
13	186196951	2014-03-07 23:20:00	W4AC	EL86ux	DK6UG	JN49cm	14097076	30	-8	0	7797	44	14	2.21_r2286	0
14	186199830	2014-03-07 23:38:00	W4AC	EL86ux	DK6UG	JN49cm	14097076	30	-11	0	7797	44	14	2.21_r2286	0
15	186200874	2014-03-07 23:44:00	W4AC	EL86ux	DK6UG	JN49cm	14097075	30	-11	0	7797	44	14	2.21_r2286	0
16	186202858	2014-03-07 23:56:00	W4AC	EL86ux	DK6UG	JN49cm	14097076	30	-11	0	7797	44	14	2.21_r2286	0
17	186204044	2014-03-08 00:04:00	W4AC	EL86ux	DK6UG	JN49cm	14097075	30	-5	0	7797	44	14	2.21_r2286	0
								Mean	-8.4118						
								SD	3.4106						
								AD	2.5882						
								AD%	76						

row	id	time	tx_sign	tx_loc	rx_sign	rx_loc	frequency	power	snr	drift	distance	azimuth	band	version	code
1	186166613	2014-03-07 20:38:00	W4AC	EL86ux	M5ADA	IO93kl	14097090	30	-22	0	7062	41	14	3.0.1_r255	0
2	186168066	2014-03-07 20:46:00	W4AC	EL86ux	M5ADA	IO93kl	14097090	30	-24	0	7062	41	14	3.0.1_r255	0
3	186170443	2014-03-07 20:58:00	W4AC	EL86ux	M5ADA	IO93kl	14097090	30	-28	0	7062	41	14	3.0.1_r255	0
4	186174403	2014-03-07 21:20:00	W4AC	EL86ux	M5ADA	IO93kl	14097089	30	-21	0	7062	41	14	3.0.1_r255	0
5	186176594	2014-03-07 21:32:00	W4AC	EL86ux	M5ADA	IO93kl	14097090	30	-24	0	7062	41	14	3.0.1_r255	0
6	186182649	2014-03-07 21:52:00	W4AC	EL86ux	M5ADA	IO93kl	14097090	30	-17	0	7062	41	14	3.0.1_r255	0
7	186184949	2014-03-07 22:04:00	W4AC	EL86ux	M5ADA	IO93kl	14097089	30	-23	0	7062	41	14	3.0.1_r255	0
8	186189954	2014-03-07 22:34:00	W4AC	EL86ux	M5ADA	IO93kl	14097090	30	-25	0	7062	41	14	3.0.1_r255	0
9	186191322	2014-03-07 22:44:00	W4AC	EL86ux	M5ADA	IO93kl	14097090	30	-28	0	7062	41	14	3.0.1_r255	0
10	186196953	2014-03-07 23:20:00	W4AC	EL86ux	M5ADA	IO93kl	14097089	30	-25	0	7062	41	14	3.0.1_r255	0
11	186198129	2014-03-07 23:28:00	W4AC	EL86ux	M5ADA	IO93kl	14097090	30	-24	0	7062	41	14	3.0.1_r255	0
12	186199940	2014-03-07 23:38:00	W4AC	EL86ux	M5ADA	IO93kl	14097089	30	-31	0	7062	41	14	3.0.1_r255	0
13	186202800	2014-03-07 23:56:00	W4AC	EL86ux	M5ADA	IO93kl	14097090	30	-28	0	7062	41	14	3.0.1_r255	0
								Mean	-24.6154						
								SD	3.6180						
								AD	6.3846						
								AD%	176						

Page 711 of 1738

row	id	time	tx_sign	tx_loc	rx_sign	rx_loc	frequency	power	snr	drift	distance	azimuth	band	version	code
1	186172262	2014-03-07 21:08:00	W4AC	EL86ux	M6NNB	IO91ue	14097096	30	-23	0	7167	43	14	2.11_r2263	0
2	186174535	2014-03-07 21:20:00	W4AC	EL86ux	M6NNB	IO91ue	14097097	30	-20	0	7167	43	14	2.11_r2263	0
3	186182691	2014-03-07 21:52:00	W4AC	EL86ux	M6NNB	IO91ue	14097097	30	-21	0	7167	43	14	2.11_r2263	0
4	186185088	2014-03-07 22:04:00	W4AC	EL86ux	M6NNB	IO91ue	14097097	30	-23	0	7167	43	14	2.11_r2263	0
5	186188041	2014-03-07 22:22:00	W4AC	EL86ux	M6NNB	IO91ue	14097097	30	-23	0	7167	43	14	2.11_r2263	0
6	186189982	2014-03-07 22:34:00	W4AC	EL86ux	M6NNB	IO91ue	14097098	30	-24	0	7167	43	14	2.11_r2263	0
7	186191348	2014-03-07 22:44:00	W4AC	EL86ux	M6NNB	IO91ue	14097097	30	-23	0	7167	43	14	2.11_r2263	0
8	186194445	2014-03-07 23:04:00	W4AC	EL86ux	M6NNB	IO91ue	14097098	30	-25	0	7167	43	14	2.11_r2263	0
9	186196906	2014-03-07 23:20:00	W4AC	EL86ux	M6NNB	IO91ue	14097097	30	-20	0	7167	43	14	2.11_r2263	0
10	186198184	2014-03-07 23:28:00	W4AC	EL86ux	M6NNB	IO91ue	14097097	30	-29	0	7167	43	14	2.11_r2263	0
11	186199981	2014-03-07 23:38:00	W4AC	EL86ux	M6NNB	IO91ue	14097097	30	-27	0	7167	43	14	2.11_r2263	0
12	186200850	2014-03-07 23:44:00	W4AC	EL86ux	M6NNB	IO91ue	14097096	30	-29	0	7167	43	14	2.11_r2263	0
13	186204017	2014-03-08 00:04:00	W4AC	EL86ux	M6NNB	IO91ue	14097096	30	-29	0	7167	43	14	2.11_r2263	0
								Mean	-24.3077						
								SD	3.2758						
								AD	4.6923						
								AD%	143						

Page 712 of 1738

row	id	time	tx_sign	tx_loc	rx_sign	rx_loc	frequency	power	snr	drift	distance	azimuth	band	version	code
1	186172262	2014-03-07 21:08:00	W4AC	EL86ux	M6NNB	IO91ue	14097096	30	-23	0	7167	43	14	2.11_r2263	0
2	186174535	2014-03-07 21:20:00	W4AC	EL86ux	M6NNB	IO91ue	14097097	30	-20	0	7167	43	14	2.11_r2263	0
3	186182691	2014-03-07 21:52:00	W4AC	EL86ux	M6NNB	IO91ue	14097097	30	-21	0	7167	43	14	2.11_r2263	0
4	186185088	2014-03-07 22:04:00	W4AC	EL86ux	M6NNB	IO91ue	14097097	30	-23	0	7167	43	14	2.11_r2263	0
5	186188041	2014-03-07 22:22:00	W4AC	EL86ux	M6NNB	IO91ue	14097097	30	-23	0	7167	43	14	2.11_r2263	0
6	186189982	2014-03-07 22:34:00	W4AC	EL86ux	M6NNB	IO91ue	14097098	30	-24	0	7167	43	14	2.11_r2263	0
7	186191348	2014-03-07 22:44:00	W4AC	EL86ux	M6NNB	IO91ue	14097097	30	-23	0	7167	43	14	2.11_r2263	0
8	186194445	2014-03-07 23:04:00	W4AC	EL86ux	M6NNB	IO91ue	14097098	30	-25	0	7167	43	14	2.11_r2263	0
9	186196906	2014-03-07 23:20:00	W4AC	EL86ux	M6NNB	IO91ue	14097097	30	-20	0	7167	43	14	2.11_r2263	0
10	186198184	2014-03-07 23:28:00	W4AC	EL86ux	M6NNB	IO91ue	14097097	30	-29	0	7167	43	14	2.11_r2263	0
11	186199981	2014-03-07 23:38:00	W4AC	EL86ux	M6NNB	IO91ue	14097097	30	-27	0	7167	43	14	2.11_r2263	0
12	186200850	2014-03-07 23:44:00	W4AC	EL86ux	M6NNB	IO91ue	14097096	30	-29	0	7167	43	14	2.11_r2263	0
13	186204017	2014-03-08 00:04:00	W4AC	EL86ux	M6NNB	IO91ue	14097096	30	-29	0	7167	43	14	2.11_r2263	0
								Mean	-24.3077						
								SD	3.2758						
								AD	-4.3077						
								AD%	-132						

Page 713 of 1738

row	id	time	tx_sign	tx_loc	rx_sign	rx_loc	frequency	power	snr	drift	distance	azimuth	band	version	code
1	186172262	2014-03-07 21:08:00	W4AC	EL86ux	M6NNB	IO91ue	14097096	30	-23	0	7167	43	14	2.11_r2263	0
2	186174535	2014-03-07 21:20:00	W4AC	EL86ux	M6NNB	IO91ue	14097097	30	-20	0	7167	43	14	2.11_r2263	0
3	186182691	2014-03-07 21:52:00	W4AC	EL86ux	M6NNB	IO91ue	14097097	30	-21	0	7167	43	14	2.11_r2263	0
4	186185088	2014-03-07 22:04:00	W4AC	EL86ux	M6NNB	IO91ue	14097097	30	-23	0	7167	43	14	2.11_r2263	0
5	186188041	2014-03-07 22:22:00	W4AC	EL86ux	M6NNB	IO91ue	14097097	30	-23	0	7167	43	14	2.11_r2263	0
6	186189982	2014-03-07 22:34:00	W4AC	EL86ux	M6NNB	IO91ue	14097098	30	-24	0	7167	43	14	2.11_r2263	0
7	186191348	2014-03-07 22:44:00	W4AC	EL86ux	M6NNB	IO91ue	14097097	30	-23	0	7167	43	14	2.11_r2263	0
8	186194445	2014-03-07 23:04:00	W4AC	EL86ux	M6NNB	IO91ue	14097098	30	-25	0	7167	43	14	2.11_r2263	0
9	186196906	2014-03-07 23:20:00	W4AC	EL86ux	M6NNB	IO91ue	14097097	30	-20	0	7167	43	14	2.11_r2263	0
10	186198184	2014-03-07 23:28:00	W4AC	EL86ux	M6NNB	IO91ue	14097097	30	-29	0	7167	43	14	2.11_r2263	0
11	186199981	2014-03-07 23:38:00	W4AC	EL86ux	M6NNB	IO91ue	14097097	30	-27	0	7167	43	14	2.11_r2263	0
12	186200850	2014-03-07 23:44:00	W4AC	EL86ux	M6NNB	IO91ue	14097096	30	-29	0	7167	43	14	2.11_r2263	0
13	186204017	2014-03-08 00:04:00	W4AC	EL86ux	M6NNB	IO91ue	14097096	30	-29	0	7167	43	14	2.11_r2263	0
								Mean	-24.3077						
								SD	3.2758						
								AD	4.6923						
								AD%	143						

row	id	time	tx_sign	tx_loc	rx_sign	rx_loc	frequency	power	snr	drift	distance	azimuth	band	version	code
1	186172262	2014-03-07 21:08:00	W4AC	EL86ux	M6NNB	IO91ue	14097096	30	-23	0	7167	43	14	2.11_r2263	0
2	186174535	2014-03-07 21:20:00	W4AC	EL86ux	M6NNB	IO91ue	14097097	30	-20	0	7167	43	14	2.11_r2263	0
3	186182691	2014-03-07 21:52:00	W4AC	EL86ux	M6NNB	IO91ue	14097097	30	-21	0	7167	43	14	2.11_r2263	0
4	186185088	2014-03-07 22:04:00	W4AC	EL86ux	M6NNB	IO91ue	14097097	30	-23	0	7167	43	14	2.11_r2263	0
5	186188041	2014-03-07 22:22:00	W4AC	EL86ux	M6NNB	IO91ue	14097097	30	-23	0	7167	43	14	2.11_r2263	0
6	186189982	2014-03-07 22:34:00	W4AC	EL86ux	M6NNB	IO91ue	14097098	30	-24	0	7167	43	14	2.11_r2263	0
7	186191348	2014-03-07 22:44:00	W4AC	EL86ux	M6NNB	IO91ue	14097097	30	-23	0	7167	43	14	2.11_r2263	0
8	186194445	2014-03-07 23:04:00	W4AC	EL86ux	M6NNB	IO91ue	14097098	30	-25	0	7167	43	14	2.11_r2263	0
9	186196906	2014-03-07 23:20:00	W4AC	EL86ux	M6NNB	IO91ue	14097097	30	-20	0	7167	43	14	2.11_r2263	0
10	186198184	2014-03-07 23:28:00	W4AC	EL86ux	M6NNB	IO91ue	14097097	30	-29	0	7167	43	14	2.11_r2263	0
11	186199981	2014-03-07 23:38:00	W4AC	EL86ux	M6NNB	IO91ue	14097097	30	-27	0	7167	43	14	2.11_r2263	0
12	186200850	2014-03-07 23:44:00	W4AC	EL86ux	M6NNB	IO91ue	14097096	30	-29	0	7167	43	14	2.11_r2263	0
13	186204017	2014-03-08 00:04:00	W4AC	EL86ux	M6NNB	IO91ue	14097096	30	-29	0	7167	43	14	2.11_r2263	0
								Mean	-24.3077						
								SD	3.2758						
								AD	4.6923						
								AD%	143						

row	id	time	tx_sign	tx_loc	rx_sign	rx_loc	frequency	power	snr	drift	distance	azimuth	band	version	code
1	185675623	2014-03-06 01:06:00	W4AC	EL86ux	OE6PWD	JN77rb	14097085	30	-27	0	8396	44	14	4.0 r3015	0
2	185678357	2014-03-06 01:24:00	W4AC	EL86ux	OE6PWD	JN77rb	14097085	30	-24	0	8396	44	14	4.0 r3015	0
3	185679363	2014-03-06 01:32:00	W4AC	EL86ux	OE6PWD	JN77rb	14097086	30	-25	0	8396	44	14	4.0 r3015	0
4	185684819	2014-03-06 02:14:00	W4AC	EL86ux	OE6PWD	JN77rb	14097085	30	-22	0	8396	44	14	4.0 r3015	0
5	185919625	2014-03-06 23:34:00	W4AC	EL86ux	OE6PWD	JN77rb	14097085	30	-24	0	8396	44	14	4.0 r3015	0
6	185943331	2014-03-07 02:20:00	W4AC	EL86ux	OE6PWD	JN77rb	14097085	30	-23	0	8396	44	14	4.0 r3015	0
7	186196831	2014-03-07 23:20:00	W4AC	EL86ux	OE6PWD	JN77rb	14097085	30	-27	0	8396	44	14	4.0 r3015	0
8	186737973	2014-03-09 22:06:00	W4AC	EL86ux	OE6PWD	JN77rb	14097085	30	-27	0	8396	44	14	4.0 r3015	0
9	186752328	2014-03-09 23:16:00	W4AC	EL86ux	OE6PWD	JN77rb	14097085	30	-26	0	8396	44	14	4.0 r3015	0
								Mean	-25.0000						
								SD	1.8708						
								AD	2.0000						
								AD%	107						

Page 716 of 1738

row	id	time	tx_sign	tx_loc	rx_sign	rx_loc	frequency	power	snr	drift	distance	azimuth	band	version	code
1	186172154	2014-03-07 21:08:00	W4AC	EL86ux	ON4SAR	JO21ce	14097107	30	-19	0	7472	43	14	0.8_r3058	0
2	186174456	2014-03-07 21:20:00	W4AC	EL86ux	ON4SAR	JO21ce	14097107	30	-28	0	7472	43	14	0.8_r3058	0
3	186176534	2014-03-07 21:32:00	W4AC	EL86ux	ON4SAR	JO21ce	14097107	30	-21	0	7472	43	14	0.8_r3058	0
4	186182929	2014-03-07 21:52:00	W4AC	EL86ux	ON4SAR	JO21ce	14097107	30	-23	0	7472	43	14	0.8_r3058	0
5	186185121	2014-03-07 22:04:00	W4AC	EL86ux	ON4SAR	JO21ce	14097107	30	-23	0	7472	43	14	0.8_r3058	0
6	186186892	2014-03-07 22:14:00	W4AC	EL86ux	ON4SAR	JO21ce	14097107	30	-22	0	7472	43	14	0.8_r3058	0
7	186188126	2014-03-07 22:22:00	W4AC	EL86ux	ON4SAR	JO21ce	14097106	30	-20	0	7472	43	14	0.8_r3058	0
8	186191500	2014-03-07 22:44:00	W4AC	EL86ux	ON4SAR	JO21ce	14097107	30	-22	0	7472	43	14	0.8_r3058	0
9	186196985	2014-03-07 23:20:00	W4AC	EL86ux	ON4SAR	JO21ce	14097106	30	-18	0	7472	43	14	0.8_r3058	0
10	186199693	2014-03-07 23:38:00	W4AC	EL86ux	ON4SAR	JO21ce	14097106	30	-22	0	7472	43	14	0.8_r3058	0
11	186200895	2014-03-07 23:44:00	W4AC	EL86ux	ON4SAR	JO21ce	14097106	30	-20	0	7472	43	14	0.8_r3058	0
12	186204100	2014-03-08 00:04:00	W4AC	EL86ux	ON4SAR	JO21ce	14097105	30	-18	0	7472	43	14	0.8_r3058	0
								Mean	-21.3333						
								SD	2.7414						
								AD	-3.3333						
								AD%	-122						

Page 717 of 1738

row	id	time	tx_sign	tx_loc	rx_sign	rx_loc	frequency	power	snr	drift	distance	azimuth	band	version	code
1	186164728	2014-03-07 20:28:00	W4AC	EL86ux	ON4SAR	JO21ce	14097107	30	-27	0	7472	43	14	0.8_r3058	0
2	186166568	2014-03-07 20:38:00	W4AC	EL86ux	ON4SAR	JO21ce	14097107	30	-21	0	7472	43	14	0.8_r3058	0
3	186170428	2014-03-07 20:58:00	W4AC	EL86ux	ON4SAR	JO21ce	14097107	30	-23	0	7472	43	14	0.8_r3058	0
4	186172154	2014-03-07 21:08:00	W4AC	EL86ux	ON4SAR	JO21ce	14097107	30	-19	0	7472	43	14	0.8_r3058	0
5	186174456	2014-03-07 21:20:00	W4AC	EL86ux	ON4SAR	JO21ce	14097107	30	-28	0	7472	43	14	0.8_r3058	0
6	186176534	2014-03-07 21:32:00	W4AC	EL86ux	ON4SAR	JO21ce	14097107	30	-21	0	7472	43	14	0.8_r3058	0
7	186182929	2014-03-07 21:52:00	W4AC	EL86ux	ON4SAR	JO21ce	14097107	30	-23	0	7472	43	14	0.8_r3058	0
8	186185121	2014-03-07 22:04:00	W4AC	EL86ux	ON4SAR	JO21ce	14097107	30	-23	0	7472	43	14	0.8_r3058	0
9	186186892	2014-03-07 22:14:00	W4AC	EL86ux	ON4SAR	JO21ce	14097107	30	-22	0	7472	43	14	0.8_r3058	0
10	186188126	2014-03-07 22:22:00	W4AC	EL86ux	ON4SAR	JO21ce	14097106	30	-20	0	7472	43	14	0.8_r3058	0
11	186191500	2014-03-07 22:44:00	W4AC	EL86ux	ON4SAR	JO21ce	14097107	30	-22	0	7472	43	14	0.8_r3058	0
12	186196985	2014-03-07 23:20:00	W4AC	EL86ux	ON4SAR	JO21ce	14097106	30	-18	0	7472	43	14	0.8_r3058	0
13	186199693	2014-03-07 23:38:00	W4AC	EL86ux	ON4SAR	JO21ce	14097106	30	-22	0	7472	43	14	0.8_r3058	0
14	186200895	2014-03-07 23:44:00	W4AC	EL86ux	ON4SAR	JO21ce	14097106	30	-20	0	7472	43	14	0.8_r3058	0
15	186204100	2014-03-08 00:04:00	W4AC	EL86ux	ON4SAR	JO21ce	14097105	30	-18	0	7472	43	14	0.8_r3058	0
								Mean	-21.8000						
								SD	2.8586						
								AD	-3.8000						
								AD%	-133						

Page 718 of 1738

row	id	time	tx_sign	tx_loc	rx_sign	rx_loc	frequency	power	snr	drift	distance	azimuth	band	version	code
1	185669892	2014-03-06 00:22:00	W4AC	EL86ux	ON7KB	JO21ei	14097054	30	-25	0	7478	43	14	0.8_r3058	0
2	185670648	2014-03-06 00:28:00	W4AC	EL86ux	ON7KB	JO21ei	14097053	30	-26	0	7478	43	14	0.8_r3058	0
3	185671934	2014-03-06 00:38:00	W4AC	EL86ux	ON7KB	JO21ei	14097053	30	-28	-1	7478	43	14	0.8_r3058	0
4	185674624	2014-03-06 00:58:00	W4AC	EL86ux	ON7KB	JO21ei	14097055	30	-28	0	7478	43	14	0.8_r3058	0
5	185893779	2014-03-06 21:12:00	W4AC	EL86ux	ON7KB	JO21ei	14097051	30	-27	0	7478	43	14	0.8_r3058	0
6	185908006	2014-03-06 22:24:00	W4AC	EL86ux	ON7KB	JO21ei	14097051	30	-25	0	7478	43	14	0.8_r3058	0
7	185919640	2014-03-06 23:34:00	W4AC	EL86ux	ON7KB	JO21ei	14097051	30	-22	0	7478	43	14	0.8_r3058	0
8	186176586	2014-03-07 21:32:00	W4AC	EL86ux	ON7KB	JO21ei	14097053	30	-25	-1	7478	43	14	0.8_r3058	0
9	186185013	2014-03-07 22:04:00	W4AC	EL86ux	ON7KB	JO21ei	14097052	30	-21	1	7478	43	14	0.8_r3058	0
10	186200853	2014-03-07 23:44:00	W4AC	EL86ux	ON7KB	JO21ei	14097050	30	-28	0	7478	43	14	0.8_r3058	0
11	186744550	2014-03-09 22:30:00	W4AC	EL86ux	ON7KB	JO21ei	14097052	30	-21	0	7478	43	14	0.8_r3058	0
12	186746804	2014-03-09 22:42:00	W4AC	EL86ux	ON7KB	JO21ei	14097052	30	-28	0	7478	43	14	0.8_r3058	0
13	186748969	2014-03-09 22:54:00	W4AC	EL86ux	ON7KB	JO21ei	14097052	30	-20	0	7478	43	14	0.8_r3058	0
14	186757942	2014-03-09 23:50:00	W4AC	EL86ux	ON7KB	JO21ei	14097051	30	-31	0	7478	43	14	0.8_r3058	0
15	186769011	2014-03-10 00:40:00	W4AC	EL86ux	ON7KB	JO21ei	14097051	30	-28	0	7478	43	14	0.8_r3058	0
								Mean	-25.5333						
								SD	3.2484						
								AD	2.4667						
								AD%	76						

Page 719 of 1738

row	id	time	tx_sign	tx_loc	rx_sign	rx_loc	frequency	power	snr	drift	distance	azimuth	band	version	code
1	186174637	2014-03-07 21:20:00	W4AC	EL86ux	PI4THT	JO32kf	14097084	30	-27	0	7617	41	14	0.6	0
2	186176750	2014-03-07 21:32:00	W4AC	EL86ux	PI4THT	JO32kf	14097084	30	-16	0	7617	41	14	0.6	0
3	186183002	2014-03-07 21:52:00	W4AC	EL86ux	PI4THT	JO32kf	14097083	30	-20	0	7617	41	14	0.6	0
4	186185201	2014-03-07 22:04:00	W4AC	EL86ux	PI4THT	JO32kf	14097084	30	-13	0	7617	41	14	0.6	0
5	186187032	2014-03-07 22:14:00	W4AC	EL86ux	PI4THT	JO32kf	14097083	30	-18	0	7617	41	14	0.6	0
6	186190177	2014-03-07 22:34:00	W4AC	EL86ux	PI4THT	JO32kf	14097084	30	-14	0	7617	41	14	0.6	0
7	186195864	2014-03-07 23:12:00	W4AC	EL86ux	PI4THT	JO32kf	14097082	30	-23	0	7617	41	14	0.6	0
8	186197067	2014-03-07 23:20:00	W4AC	EL86ux	PI4THT	JO32kf	14097082	30	-21	0	7617	41	14	0.6	0
9	186200053	2014-03-07 23:38:00	W4AC	EL86ux	PI4THT	JO32kf	14097082	30	-19	0	7617	41	14	0.6	0
10	186201050	2014-03-07 23:44:00	W4AC	EL86ux	PI4THT	JO32kf	14097082	30	-17	0	7617	41	14	0.6	0
11	186204435	2014-03-08 00:04:00	W4AC	EL86ux	PI4THT	JO32kf	14097083	30	-14	-2	7617	41	14	0.6	0
								Mean	-18.3636						
								SD	4.2491						
								AD	-4.3636						
								AD%	-103						

row	id	time	tx_sign	tx_loc	rx_sign	rx_loc	frequency	power	snr	drift	distance	azimuth	band	version	code
1	186170107	2014-03-07 20:58:00	W4AC	EL86ux	VE1AIM	FN84ds	14097090	30	-20	0	2579	35	14	2.0_r1714	0
2	186172324	2014-03-07 21:08:00	W4AC	EL86ux	VE1AIM	FN84ds	14097089	30	-15	0	2579	35	14	2.0_r1714	0
3	186174467	2014-03-07 21:20:00	W4AC	EL86ux	VE1AIM	FN84ds	14097089	30	-22	0	2579	35	14	2.0_r1714	0
4	186176442	2014-03-07 21:32:00	W4AC	EL86ux	VE1AIM	FN84ds	14097088	30	-23	0	2579	35	14	2.0_r1714	0
5	186191295	2014-03-07 22:44:00	W4AC	EL86ux	VE1AIM	FN84ds	14097085	30	-9	0	2579	35	14	2.0_r1714	0
6	186192905	2014-03-07 22:54:00	W4AC	EL86ux	VE1AIM	FN84ds	14097085	30	-20	0	2579	35	14	2.0_r1714	0
7	186194369	2014-03-07 23:04:00	W4AC	EL86ux	VE1AIM	FN84ds	14097085	30	-19	0	2579	35	14	2.0_r1714	0
8	186195579	2014-03-07 23:12:00	W4AC	EL86ux	VE1AIM	FN84ds	14097084	30	-14	0	2579	35	14	2.0_r1714	0
9	186196847	2014-03-07 23:20:00	W4AC	EL86ux	VE1AIM	FN84ds	14097083	30	-13	0	2579	35	14	2.0_r1714	0
10	186199694	2014-03-07 23:38:00	W4AC	EL86ux	VE1AIM	FN84ds	14097083	30	-19	0	2579	35	14	2.0_r1714	0
11	186200720	2014-03-07 23:44:00	W4AC	EL86ux	VE1AIM	FN84ds	14097082	30	-22	0	2579	35	14	2.0_r1714	0
12	186202867	2014-03-07 23:56:00	W4AC	EL86ux	VE1AIM	FN84ds	14097083	30	-26	0	2579	35	14	2.0_r1714	0
13	186204148	2014-03-08 00:04:00	W4AC	EL86ux	VE1AIM	FN84ds	14097082	30	-20	0	2579	35	14	2.0_r1714	0
								Mean	-18.6154						
								SD	4.6644						
								AD	7.3846						
								AD%	158						

row	id	time	tx_sign	tx_loc	rx_sign	rx_loc	frequency	power	snr	drift	distance	azimuth	band	version	code
1	186170467	2014-03-07 20:58:00	W4AC	EL86ux	W3GXT	FM19ol	14097077	30	-2	0	1480	19	14	2.0_r1714	0
2	186174532	2014-03-07 21:20:00	W4AC	EL86ux	W3GXT	FM19ol	14097077	30	-4	0	1480	19	14	2.0_r1714	0
3	186176538	2014-03-07 21:32:00	W4AC	EL86ux	W3GXT	FM19ol	14097077	30	0	0	1480	19	14	2.0_r1714	0
4	186192932	2014-03-07 22:54:00	W4AC	EL86ux	W3GXT	FM19ol	14097077	30	-1	0	1480	19	14	2.0_r1714	0
5	186194425	2014-03-07 23:04:00	W4AC	EL86ux	W3GXT	FM19ol	14097077	30	0	0	1480	19	14	2.0_r1714	0
6	186195628	2014-03-07 23:12:00	W4AC	EL86ux	W3GXT	FM19ol	14097076	30	2	0	1480	19	14	2.0_r1714	0
7	186197040	2014-03-07 23:20:00	W4AC	EL86ux	W3GXT	FM19ol	14097076	30	1	0	1480	19	14	2.0_r1714	0
8	186199769	2014-03-07 23:38:00	W4AC	EL86ux	W3GXT	FM19ol	14097076	30	-7	0	1480	19	14	2.0_r1714	0
9	186202997	2014-03-07 23:56:00	W4AC	EL86ux	W3GXT	FM19ol	14097076	30	3	0	1480	19	14	2.0_r1714	0
10	186204009	2014-03-08 00:04:00	W4AC	EL86ux	W3GXT	FM19ol	14097076	30	-3	0	1480	19	14	2.0_r1714	0
								Mean	-1.1000						
								SD	2.9981						
								AD	5.9000						
								AD%	197						

row	id	time	tx_sign	tx_loc	rx_sign	rx_loc	frequency	power	snr	drift	distance	azimuth	band	version	code
1	185667967	2014-03-06 00:10:00	W4AC	EL86ux	WA3DNM	FM29	14097078	30	-2	0	1543	24	14	2.11_r2263	0
2	185672087	2014-03-06 00:38:00	W4AC	EL86ux	WA3DNM	FM29	14097077	30	-1	0	1543	24	14	2.11_r2263	0
3	185678428	2014-03-06 01:24:00	W4AC	EL86ux	WA3DNM	FM29	14097077	30	-1	0	1543	24	14	2.11_r2263	0
4	185679405	2014-03-06 01:32:00	W4AC	EL86ux	WA3DNM	FM29	14097077	30	-3	0	1543	24	14	2.11_r2263	0
5	185682221	2014-03-06 01:54:00	W4AC	EL86ux	WA3DNM	FM29	14097077	30	3	0	1543	24	14	2.11_r2263	0
6	185888572	2014-03-06 20:42:00	W4AC	EL86ux	WA3DNM	FM29	14097077	30	-3	0	1543	24	14	2.11_r2263	0
7	185895312	2014-03-06 21:20:00	W4AC	EL86ux	WA3DNM	FM29	14097077	30	-2	0	1543	24	14	2.11_r2263	0
8	185899962	2014-03-06 21:48:00	W4AC	EL86ux	WA3DNM	FM29	14097077	30	-5	0	1543	24	14	2.11_r2263	0
9	185906502	2014-03-06 22:14:00	W4AC	EL86ux	WA3DNM	FM29	14097077	30	2	0	1543	24	14	2.11_r2263	0
10	185907963	2014-03-06 22:24:00	W4AC	EL86ux	WA3DNM	FM29	14097077	30	-9	0	1543	24	14	2.11_r2263	0
11	185909926	2014-03-06 22:36:00	W4AC	EL86ux	WA3DNM	FM29	14097077	30	-2	0	1543	24	14	2.11_r2263	0
12	185911737	2014-03-06 22:46:00	W4AC	EL86ux	WA3DNM	FM29	14097077	30	-8	0	1543	24	14	2.11_r2263	0
13	185913683	2014-03-06 22:58:00	W4AC	EL86ux	WA3DNM	FM29	14097077	30	-2	0	1543	24	14	2.11_r2263	0
14	185915213	2014-03-06 23:08:00	W4AC	EL86ux	WA3DNM	FM29	14097077	30	-4	0	1543	24	14	2.11_r2263	0
15	185919695	2014-03-06 23:34:00	W4AC	EL86ux	WA3DNM	FM29	14097077	30	2	0	1543	24	14	2.11_r2263	0
16	185921458	2014-03-06 23:46:00	W4AC	EL86ux	WA3DNM	FM29	14097077	30	0	0	1543	24	14	2.11_r2263	0
17	185924506	2014-03-07 00:06:00	W4AC	EL86ux	WA3DNM	FM29	14097077	30	-1	0	1543	24	14	2.11_r2263	0
18	185927997	2014-03-07 00:28:00	W4AC	EL86ux	WA3DNM	FM29	14097077	30	0	0	1543	24	14	2.11_r2263	0
19	185930708	2014-03-07 00:46:00	W4AC	EL86ux	WA3DNM	FM29	14097077	30	4	0	1543	24	14	2.11_r2263	0
20	185932249	2014-03-07 00:58:00	W4AC	EL86ux	WA3DNM	FM29	14097077	30	-2	0	1543	24	14	2.11_r2263	0
21	185934933	2014-03-07 01:16:00	W4AC	EL86ux	WA3DNM	FM29	14097077	30	2	0	1543	24	14	2.11_r2263	0
22	185936230	2014-03-07 01:26:00	W4AC	EL86ux	WA3DNM	FM29	14097077	30	-1	0	1543	24	14	2.11_r2263	0
23	185937729	2014-03-07 01:38:00	W4AC	EL86ux	WA3DNM	FM29	14097077	30	1	0	1543	24	14	2.11_r2263	0
24	185938686	2014-03-07 01:46:00	W4AC	EL86ux	WA3DNM	FM29	14097077	30	-2	0	1543	24	14	2.11_r2263	0
25	185940382	2014-03-07 01:58:00	W4AC	EL86ux	WA3DNM	FM29	14097077	30	3	0	1543	24	14	2.11_r2263	0
26	185941611	2014-03-07 02:08:00	W4AC	EL86ux	WA3DNM	FM29	14097077	30	0	0	1543	24	14	2.11_r2263	0
27	185943178	2014-03-07 02:20:00	W4AC	EL86ux	WA3DNM	FM29	14097077	30	2	0	1543	24	14	2.11_r2263	0
28	185944175	2014-03-07 02:28:00	W4AC	EL86ux	WA3DNM	FM29	14097077	30	2	0	1543	24	14	2.11_r2263	0
29	185945320	2014-03-07 02:36:00	W4AC	EL86ux	WA3DNM	FM29	14097077	30	2	0	1543	24	14	2.11_r2263	0
30	186196988	2014-03-07 23:20:00	W4AC	EL86ux	WA3DNM	FM29	14097077	30	-3	0	1543	24	14	2.11_r2263	0
31	186199912	2014-03-07 23:38:00	W4AC	EL86ux	WA3DNM	FM29	14097077	30	-8	0	1543	24	14	2.11_r2263	0
32	186202834	2014-03-07 23:56:00	W4AC	EL86ux	WA3DNM	FM29	14097077	30	-1	0	1543	24	14	2.11_r2263	0
33	186204096	2014-03-08 00:04:00	W4AC	EL86ux	WA3DNM	FM29	14097077	30	-6	0	1543	24	14	2.11_r2263	0
34	186459246	2014-03-08 21:30:00	W4AC	EL86ux	WA3DNM	FM29	14097077	30	-8	0	1543	24	14	2.11_r2263	0
35	186487324	2014-03-09 00:10:00	W4AC	EL86ux	WA3DNM	FM29	14097077	30	-3	0	1543	24	14	2.11_r2263	0
36	186488943	2014-03-09 00:20:00	W4AC	EL86ux	WA3DNM	FM29	14097077	30	-4	0	1543	24	14	2.11_r2263	0
37	186491236	2014-03-09 00:32:00	W4AC	EL86ux	WA3DNM	FM29	14097077	30	-4	0	1543	24	14	2.11_r2263	0
38	186497744	2014-03-09 01:10:00	W4AC	EL86ux	WA3DNM	FM29	14097077	30	-3	0	1543	24	14	2.11_r2263	0
39	186498986	2014-03-09 01:18:00	W4AC	EL86ux	WA3DNM	FM29	14097077	30	0	0	1543	24	14	2.11_r2263	0
40	186721151	2014-03-09 20:38:00	W4AC	EL86ux	WA3DNM	FM29	14097077	30	-15	0	1543	24	14	2.11_r2263	0
41	186723854	2014-03-09 20:50:00	W4AC	EL86ux	WA3DNM	FM29	14097077	30	-7	0	1543	24	14	2.11_r2263	0
42	186725895	2014-03-09 21:00:00	W4AC	EL86ux	WA3DNM	FM29	14097077	30	-5	0	1543	24	14	2.11_r2263	0
43	186727846	2014-03-09 21:10:00	W4AC	EL86ux	WA3DNM	FM29	14097077	30	-6	0	1543	24	14	2.11_r2263	0
44	186731199	2014-03-09 21:28:00	W4AC	EL86ux	WA3DNM	FM29	14097077	30	-6	0	1543	24	14	2.11_r2263	0
45	186738189	2014-03-09 22:06:00	W4AC	EL86ux	WA3DNM	FM29	14097077	30	-4	0	1543	24	14	2.11_r2263	0
46	186740224	2014-03-09 22:18:00	W4AC	EL86ux	WA3DNM	FM29	14097077	30	-6	0	1543	24	14	2.11_r2263	0
47	186750414	2014-03-09 23:04:00	W4AC	EL86ux	WA3DNM	FM29	14097077	30	-1	0	1543	24	14	2.11_r2263	0
48	186752461	2014-03-09 23:16:00	W4AC	EL86ux	WA3DNM	FM29	14097077	30	-3	0	1543	24	14	2.11_r2263	0
49	186754395	2014-03-09 23:28:00	W4AC	EL86ux	WA3DNM	FM29	14097077	30	2	0	1543	24	14	2.11_r2263	0
50	186757967	2014-03-09 23:50:00	W4AC	EL86ux	WA3DNM	FM29	14097077	30	-1	0	1543	24	14	2.11_r2263	0
51	186759173	2014-03-09 23:58:00	W4AC	EL86ux	WA3DNM	FM29	14097077	30	0	0	1543	24	14	2.11_r2263	0
52	186764701	2014-03-10 00:10:00	W4AC	EL86ux	WA3DNM	FM29	14097077	30	-2	0	1543	24	14	2.11_r2263	0
53	186765716	2014-03-10 00:18:00	W4AC	EL86ux	WA3DNM	FM29	14097077	30	3	0	1543	24	14	2.11_r2263	0
54	186768992	2014-03-10 00:40:00	W4AC	EL86ux	WA3DNM	FM29	14097077	30	0	0	1543	24	14	2.11_r2263	0
55	186770578	2014-03-10 00:50:00	W4AC	EL86ux	WA3DNM	FM29	14097077	30	0	0	1543	24	14	2.11_r2263	0
56	186772349	2014-03-10 01:02:00	W4AC	EL86ux	WA3DNM	FM29	14097077	30	-2	0	1543	24	14	2.11_r2263	0
57	186775046	2014-03-10 01:20:00	W4AC	EL86ux	WA3DNM	FM29	14097077	30	-1	0	1543	24	14	2.11_r2263	0
58	186776683	2014-03-10 01:32:00	W4AC	EL86ux	WA3DNM	FM29	14097077	30	2	0	1543	24	14	2.11_r2263	0
								Mean	-2.0172						
								SD	3.6006						
								AD	5.9828						
								AD%	166						

row	id	time	tx_sign	tx_loc	rx_sign	rx_loc	frequency	power	snr	drift	distance	azimuth	band	version	code
1	186174662	2014-03-07 21:22:00	W4MO	EL87tc	2E0DSS	IO82xl	14097194	33	-10	1	7017	42	14	2.0_r1714	0
2	186176244	2014-03-07 21:30:00	W4MO	EL87tc	2E0DSS	IO82xl	14097195	33	-8	1	7017	42	14	2.0_r1714	0
3	186178647	2014-03-07 21:44:00	W4MO	EL87tc	2E0DSS	IO82xl	14097074	33	-11	-1	7017	42	14	2.0_r1714	0
4	186184008	2014-03-07 21:58:00	W4MO	EL87tc	2E0DSS	IO82xl	14097071	33	-11	-1	7017	42	14	2.0_r1714	0
5	186188013	2014-03-07 22:22:00	W4MO	EL87tc	2E0DSS	IO82xl	14097063	33	-14	0	7017	42	14	2.0_r1714	0
6	186192759	2014-03-07 22:52:00	W4MO	EL87tc	2E0DSS	IO82xl	14097060	33	-11	1	7017	42	14	2.0_r1714	0
7	186193992	2014-03-07 23:00:00	W4MO	EL87tc	2E0DSS	IO82xl	14097060	33	-16	0	7017	42	14	2.0_r1714	0
8	186197366	2014-03-07 23:22:00	W4MO	EL87tc	2E0DSS	IO82xl	14097060	33	-10	1	7017	42	14	2.0_r1714	0
9	186198844	2014-03-07 23:32:00	W4MO	EL87tc	2E0DSS	IO82xl	14097060	33	-13	1	7017	42	14	2.0_r1714	0
10	186201926	2014-03-07 23:50:00	W4MO	EL87tc	2E0DSS	IO82xl	14097060	33	-15	1	7017	42	14	2.0_r1714	0
11	186203313	2014-03-07 23:58:00	W4MO	EL87tc	2E0DSS	IO82xl	14097060	33	-23	1	7017	42	14	2.0_r1714	0
12	186206796	2014-03-08 00:20:00	W4MO	EL87tc	2E0DSS	IO82xl	14097060	33	-5	0	7017	42	14	2.0_r1714	0
13	186207814	2014-03-08 00:28:00	W4MO	EL87tc	2E0DSS	IO82xl	14097059	33	-6	1	7017	42	14	2.0_r1714	0
14	186210739	2014-03-08 00:48:00	W4MO	EL87tc	2E0DSS	IO82xl	14097059	33	-17	1	7017	42	14	2.0_r1714	0
15	186211862	2014-03-08 00:56:00	W4MO	EL87tc	2E0DSS	IO82xl	14097058	33	-20	1	7017	42	14	2.0_r1714	0
16	186214490	2014-03-08 01:14:00	W4MO	EL87tc	2E0DSS	IO82xl	14097058	33	-24	1	7017	42	14	2.0_r1714	0
17	186215744	2014-03-08 01:24:00	W4MO	EL87tc	2E0DSS	IO82xl	14097058	33	-22	1	7017	42	14	2.0_r1714	0
18	186218721	2014-03-08 01:46:00	W4MO	EL87tc	2E0DSS	IO82xl	14097058	33	-12	1	7017	42	14	2.0_r1714	0
19	186219849	2014-03-08 01:54:00	W4MO	EL87tc	2E0DSS	IO82xl	14097058	33	-14	1	7017	42	14	2.0_r1714	0
20	186220929	2014-03-08 02:02:00	W4MO	EL87tc	2E0DSS	IO82xl	14097058	33	-21	1	7017	42	14	2.0_r1714	0
								Mean	-14.1500						
								SD	5.5656						
								AD	-9.1500						
								AD%	-164						

row	id	time	tx_sign	tx_loc	rx_sign	rx_loc	frequency	power	snr	drift	distance	azimuth	band	version	code
1	186176244	2014-03-07 21:30:00	W4MO	EL87tc	2E0DSS	IO82xl	14097195	33	-8	1	7017	42	14	2.0_r1714	0
2	186178647	2014-03-07 21:44:00	W4MO	EL87tc	2E0DSS	IO82xl	14097074	33	-11	-1	7017	42	14	2.0_r1714	0
3	186184008	2014-03-07 21:58:00	W4MO	EL87tc	2E0DSS	IO82xl	14097071	33	-11	-1	7017	42	14	2.0_r1714	0
4	186188013	2014-03-07 22:22:00	W4MO	EL87tc	2E0DSS	IO82xl	14097063	33	-14	0	7017	42	14	2.0_r1714	0
5	186192759	2014-03-07 22:52:00	W4MO	EL87tc	2E0DSS	IO82xl	14097060	33	-11	1	7017	42	14	2.0_r1714	0
6	186193992	2014-03-07 23:00:00	W4MO	EL87tc	2E0DSS	IO82xl	14097060	33	-16	0	7017	42	14	2.0_r1714	0
7	186197366	2014-03-07 23:22:00	W4MO	EL87tc	2E0DSS	IO82xl	14097060	33	-10	1	7017	42	14	2.0_r1714	0
8	186198844	2014-03-07 23:32:00	W4MO	EL87tc	2E0DSS	IO82xl	14097060	33	-13	1	7017	42	14	2.0_r1714	0
9	186201926	2014-03-07 23:50:00	W4MO	EL87tc	2E0DSS	IO82xl	14097060	33	-15	1	7017	42	14	2.0_r1714	0
10	186203313	2014-03-07 23:58:00	W4MO	EL87tc	2E0DSS	IO82xl	14097060	33	-23	1	7017	42	14	2.0_r1714	0
11	186206796	2014-03-08 00:20:00	W4MO	EL87tc	2E0DSS	IO82xl	14097060	33	-5	0	7017	42	14	2.0_r1714	0
12	186207814	2014-03-08 00:28:00	W4MO	EL87tc	2E0DSS	IO82xl	14097059	33	-6	1	7017	42	14	2.0_r1714	0
13	186210739	2014-03-08 00:48:00	W4MO	EL87tc	2E0DSS	IO82xl	14097059	33	-17	1	7017	42	14	2.0_r1714	0
14	186211862	2014-03-08 00:56:00	W4MO	EL87tc	2E0DSS	IO82xl	14097058	33	-20	1	7017	42	14	2.0_r1714	0
15	186214490	2014-03-08 01:14:00	W4MO	EL87tc	2E0DSS	IO82xl	14097058	33	-24	1	7017	42	14	2.0_r1714	0
16	186215744	2014-03-08 01:24:00	W4MO	EL87tc	2E0DSS	IO82xl	14097058	33	-22	1	7017	42	14	2.0_r1714	0
17	186218721	2014-03-08 01:46:00	W4MO	EL87tc	2E0DSS	IO82xl	14097058	33	-12	1	7017	42	14	2.0_r1714	0
18	186219849	2014-03-08 01:54:00	W4MO	EL87tc	2E0DSS	IO82xl	14097058	33	-14	1	7017	42	14	2.0_r1714	0
19	186220929	2014-03-08 02:02:00	W4MO	EL87tc	2E0DSS	IO82xl	14097058	33	-21	1	7017	42	14	2.0_r1714	0
								Mean	-14.3684						
								SD	5.6294						
								AD	-8.3684						
								AD%	-149						

row	id	time	tx_sign	tx_loc	rx_sign	rx_loc	frequency	power	snr	drift	distance	azimuth	band	version	code
1	186164708	2014-03-07 20:28:00	W4MO	EL87tc	2E0DSS	IO82xl	14097194	33	-14	1	7017	42	14	2.0_r1714	0
2	186167081	2014-03-07 20:40:00	W4MO	EL87tc	2E0DSS	IO82xl	14097192	33	-15	1	7017	42	14	2.0_r1714	0
3	186169177	2014-03-07 20:52:00	W4MO	EL87tc	2E0DSS	IO82xl	14097192	33	-17	1	7017	42	14	2.0_r1714	0
4	186171251	2014-03-07 21:02:00	W4MO	EL87tc	2E0DSS	IO82xl	14097192	33	-14	1	7017	42	14	2.0_r1714	0
5	186172558	2014-03-07 21:10:00	W4MO	EL87tc	2E0DSS	IO82xl	14097196	33	-11	1	7017	42	14	2.0_r1714	0
6	186174662	2014-03-07 21:22:00	W4MO	EL87tc	2E0DSS	IO82xl	14097194	33	-10	1	7017	42	14	2.0_r1714	0
7	186176244	2014-03-07 21:30:00	W4MO	EL87tc	2E0DSS	IO82xl	14097195	33	-8	1	7017	42	14	2.0_r1714	0
8	186178647	2014-03-07 21:44:00	W4MO	EL87tc	2E0DSS	IO82xl	14097074	33	-11	-1	7017	42	14	2.0_r1714	0
9	186184008	2014-03-07 21:58:00	W4MO	EL87tc	2E0DSS	IO82xl	14097071	33	-11	-1	7017	42	14	2.0_r1714	0
10	186188013	2014-03-07 22:22:00	W4MO	EL87tc	2E0DSS	IO82xl	14097063	33	-14	0	7017	42	14	2.0_r1714	0
11	186192759	2014-03-07 22:52:00	W4MO	EL87tc	2E0DSS	IO82xl	14097060	33	-11	1	7017	42	14	2.0_r1714	0
12	186193992	2014-03-07 23:00:00	W4MO	EL87tc	2E0DSS	IO82xl	14097060	33	-16	0	7017	42	14	2.0_r1714	0
13	186197366	2014-03-07 23:22:00	W4MO	EL87tc	2E0DSS	IO82xl	14097060	33	-10	1	7017	42	14	2.0_r1714	0
14	186198844	2014-03-07 23:32:00	W4MO	EL87tc	2E0DSS	IO82xl	14097060	33	-13	1	7017	42	14	2.0_r1714	0
15	186201926	2014-03-07 23:50:00	W4MO	EL87tc	2E0DSS	IO82xl	14097060	33	-15	1	7017	42	14	2.0_r1714	0
16	186203313	2014-03-07 23:58:00	W4MO	EL87tc	2E0DSS	IO82xl	14097060	33	-23	1	7017	42	14	2.0_r1714	0
17	186206796	2014-03-08 00:20:00	W4MO	EL87tc	2E0DSS	IO82xl	14097060	33	-5	0	7017	42	14	2.0_r1714	0
18	186207814	2014-03-08 00:28:00	W4MO	EL87tc	2E0DSS	IO82xl	14097059	33	-6	1	7017	42	14	2.0_r1714	0
19	186210739	2014-03-08 00:48:00	W4MO	EL87tc	2E0DSS	IO82xl	14097059	33	-17	1	7017	42	14	2.0_r1714	0
20	186211862	2014-03-08 00:56:00	W4MO	EL87tc	2E0DSS	IO82xl	14097058	33	-20	1	7017	42	14	2.0_r1714	0
21	186214490	2014-03-08 01:14:00	W4MO	EL87tc	2E0DSS	IO82xl	14097058	33	-24	1	7017	42	14	2.0_r1714	0
22	186215744	2014-03-08 01:24:00	W4MO	EL87tc	2E0DSS	IO82xl	14097058	33	-22	1	7017	42	14	2.0_r1714	0
23	186218721	2014-03-08 01:46:00	W4MO	EL87tc	2E0DSS	IO82xl	14097058	33	-12	1	7017	42	14	2.0_r1714	0
24	186219849	2014-03-08 01:54:00	W4MO	EL87tc	2E0DSS	IO82xl	14097058	33	-14	1	7017	42	14	2.0_r1714	0
25	186220929	2014-03-08 02:02:00	W4MO	EL87tc	2E0DSS	IO82xl	14097058	33	-21	1	7017	42	14	2.0_r1714	0
								Mean	-14.1600						
								SD	5.0306						
								AD	-4.1600						
								AD%	-83						

row	id	time	tx_sign	tx_loc	rx_sign	rx_loc	frequency	power	snr	drift	distance	azimuth	band	version	code
1	186169280	2014-03-07 20:52:00	W4MO	EL87tc	DG7RJ	JN58th	14097194	33	-24	1	8073	44	14	2.11_r2263	0
2	186171243	2014-03-07 21:02:00	W4MO	EL87tc	DG7RJ	JN58th	14097194	33	-25	1	8073	44	14	2.11_r2263	0
3	186176293	2014-03-07 21:30:00	W4MO	EL87tc	DG7RJ	JN58th	14097196	33	-22	0	8073	44	14	2.11_r2263	0
4	186178837	2014-03-07 21:44:00	W4MO	EL87tc	DG7RJ	JN58th	14097074	33	-21	-1	8073	44	14	2.11_r2263	0
5	186183967	2014-03-07 21:58:00	W4MO	EL87tc	DG7RJ	JN58th	14097071	33	-21	-1	8073	44	14	2.11_r2263	0
6	186186105	2014-03-07 22:10:00	W4MO	EL87tc	DG7RJ	JN58th	14097066	33	-18	-1	8073	44	14	2.11_r2263	0
7	186189517	2014-03-07 22:30:00	W4MO	EL87tc	DG7RJ	JN58th	14097062	33	-25	0	8073	44	14	2.11_r2263	0
8	186190819	2014-03-07 22:40:00	W4MO	EL87tc	DG7RJ	JN58th	14097060	33	-20	1	8073	44	14	2.11_r2263	0
9	186193891	2014-03-07 23:00:00	W4MO	EL87tc	DG7RJ	JN58th	14097060	33	-19	1	8073	44	14	2.11_r2263	0
10	186197134	2014-03-07 23:22:00	W4MO	EL87tc	DG7RJ	JN58th	14097060	33	-21	0	8073	44	14	2.11_r2263	0
11	186201759	2014-03-07 23:50:00	W4MO	EL87tc	DG7RJ	JN58th	14097060	33	-14	1	8073	44	14	2.11_r2263	0
12	186203351	2014-03-07 23:58:00	W4MO	EL87tc	DG7RJ	JN58th	14097059	33	-24	1	8073	44	14	2.11_r2263	0
13	186208047	2014-03-08 00:28:00	W4MO	EL87tc	DG7RJ	JN58th	14097060	33	-20	0	8073	44	14	2.11_r2263	0
14	186212039	2014-03-08 00:56:00	W4MO	EL87tc	DG7RJ	JN58th	14097060	33	-25	1	8073	44	14	2.11_r2263	0
15	186219854	2014-03-08 01:54:00	W4MO	EL87tc	DG7RJ	JN58th	14097060	33	-19	1	8073	44	14	2.11_r2263	0
16	186223741	2014-03-08 02:22:00	W4MO	EL87tc	DG7RJ	JN58th	14097060	33	-15	1	8073	44	14	2.11_r2263	0
								Mean	-20.8125						
								SD	3.3708						
								AD	-6.8125						
								AD%	-202						

row	id	time	tx_sign	tx_loc	rx_sign	rx_loc	frequency	power	snr	drift	distance	azimuth	band	version	code
1	186176278	2014-03-07 21:30:00	W4MO	EL87tc	DK6UG	JN49cm	14097194	33	-3	1	7793	44	14	2.21_r2286	0
2	186178675	2014-03-07 21:44:00	W4MO	EL87tc	DK6UG	JN49cm	14097073	33	-1	-1	7793	44	14	2.21_r2286	0
3	186183668	2014-03-07 21:58:00	W4MO	EL87tc	DK6UG	JN49cm	14097069	33	-4	-1	7793	44	14	2.21_r2286	0
4	186186219	2014-03-07 22:10:00	W4MO	EL87tc	DK6UG	JN49cm	14097064	33	-3	-1	7793	44	14	2.21_r2286	0
5	186188182	2014-03-07 22:22:00	W4MO	EL87tc	DK6UG	JN49cm	14097062	33	-1	0	7793	44	14	2.21_r2286	0
6	186189396	2014-03-07 22:30:00	W4MO	EL87tc	DK6UG	JN49cm	14097060	33	-6	0	7793	44	14	2.21_r2286	0
7	186190949	2014-03-07 22:40:00	W4MO	EL87tc	DK6UG	JN49cm	14097059	33	-5	1	7793	44	14	2.21_r2286	0
8	186192602	2014-03-07 22:52:00	W4MO	EL87tc	DK6UG	JN49cm	14097059	33	-5	0	7793	44	14	2.21_r2286	0
9	186193824	2014-03-07 23:00:00	W4MO	EL87tc	DK6UG	JN49cm	14097058	33	-4	1	7793	44	14	2.21_r2286	0
10	186197105	2014-03-07 23:22:00	W4MO	EL87tc	DK6UG	JN49cm	14097059	33	0	1	7793	44	14	2.21_r2286	0
11	186198889	2014-03-07 23:32:00	W4MO	EL87tc	DK6UG	JN49cm	14097059	33	3	1	7793	44	14	2.21_r2286	0
12	186201850	2014-03-07 23:50:00	W4MO	EL87tc	DK6UG	JN49cm	14097058	33	-6	1	7793	44	14	2.21_r2286	0
13	186203135	2014-03-07 23:58:00	W4MO	EL87tc	DK6UG	JN49cm	14097058	33	-2	0	7793	44	14	2.21_r2286	0
14	186204983	2014-03-08 00:10:00	W4MO	EL87tc	DK6UG	JN49cm	14097058	33	-5	1	7793	44	14	2.21_r2286	0
15	186207924	2014-03-08 00:28:00	W4MO	EL87tc	DK6UG	JN49cm	14097058	33	1	1	7793	44	14	2.21_r2286	0
16	186210829	2014-03-08 00:48:00	W4MO	EL87tc	DK6UG	JN49cm	14097058	33	-9	1	7793	44	14	2.21_r2286	0
17	186211785	2014-03-08 00:56:00	W4MO	EL87tc	DK6UG	JN49cm	14097058	33	-3	1	7793	44	14	2.21_r2286	0
18	186213337	2014-03-08 01:06:00	W4MO	EL87tc	DK6UG	JN49cm	14097057	33	-3	1	7793	44	14	2.21_r2286	0
19	186214441	2014-03-08 01:14:00	W4MO	EL87tc	DK6UG	JN49cm	14097057	33	-3	1	7793	44	14	2.21_r2286	0
20	186215799	2014-03-08 01:24:00	W4MO	EL87tc	DK6UG	JN49cm	14097058	33	-1	1	7793	44	14	2.21_r2286	0
21	186218728	2014-03-08 01:46:00	W4MO	EL87tc	DK6UG	JN49cm	14097059	33	-10	1	7793	44	14	2.21_r2286	0
22	186219898	2014-03-08 01:54:00	W4MO	EL87tc	DK6UG	JN49cm	14097058	33	-14	1	7793	44	14	2.21_r2286	0
23	186220902	2014-03-08 02:02:00	W4MO	EL87tc	DK6UG	JN49cm	14097058	33	-21	1	7793	44	14	2.21_r2286	0
24	186223578	2014-03-08 02:22:00	W4MO	EL87tc	DK6UG	JN49cm	14097059	33	2	1	7793	44	14	2.21_r2286	0
								Mean	-4.2917						
								SD	5.1960						
								AD	-5.2917						
								AD%	-102						

row	id	time	tx_sign	tx_loc	rx_sign	rx_loc	frequency	power	snr	drift	distance	azimuth	band	version	code
1	186164669	2014-03-07 20:28:00	W4MO	EL87tc	DK6UG	JN49cm	14097196	33	-7	1	7793	44	14	2.21_r2286	0
2	186166828	2014-03-07 20:40:00	W4MO	EL87tc	DK6UG	JN49cm	14097193	33	-7	1	7793	44	14	2.21_r2286	0
3	186169324	2014-03-07 20:52:00	W4MO	EL87tc	DK6UG	JN49cm	14097193	33	5	1	7793	44	14	2.21_r2286	0
4	186171030	2014-03-07 21:02:00	W4MO	EL87tc	DK6UG	JN49cm	14097194	33	-5	1	7793	44	14	2.21_r2286	0
5	186172574	2014-03-07 21:10:00	W4MO	EL87tc	DK6UG	JN49cm	14097196	33	-2	1	7793	44	14	2.21_r2286	0
6	186174694	2014-03-07 21:22:00	W4MO	EL87tc	DK6UG	JN49cm	14097194	33	-7	1	7793	44	14	2.21_r2286	0
7	186176278	2014-03-07 21:30:00	W4MO	EL87tc	DK6UG	JN49cm	14097194	33	-3	1	7793	44	14	2.21_r2286	0
8	186178675	2014-03-07 21:44:00	W4MO	EL87tc	DK6UG	JN49cm	14097073	33	-1	-1	7793	44	14	2.21_r2286	0
9	186183668	2014-03-07 21:58:00	W4MO	EL87tc	DK6UG	JN49cm	14097069	33	-4	-1	7793	44	14	2.21_r2286	0
10	186186219	2014-03-07 22:10:00	W4MO	EL87tc	DK6UG	JN49cm	14097064	33	-3	-1	7793	44	14	2.21_r2286	0
11	186188182	2014-03-07 22:22:00	W4MO	EL87tc	DK6UG	JN49cm	14097062	33	-1	0	7793	44	14	2.21_r2286	0
12	186189396	2014-03-07 22:30:00	W4MO	EL87tc	DK6UG	JN49cm	14097060	33	-6	0	7793	44	14	2.21_r2286	0
13	186190949	2014-03-07 22:40:00	W4MO	EL87tc	DK6UG	JN49cm	14097059	33	-5	1	7793	44	14	2.21_r2286	0
14	186192602	2014-03-07 22:52:00	W4MO	EL87tc	DK6UG	JN49cm	14097059	33	-5	0	7793	44	14	2.21_r2286	0
15	186193824	2014-03-07 23:00:00	W4MO	EL87tc	DK6UG	JN49cm	14097058	33	-4	1	7793	44	14	2.21_r2286	0
16	186197105	2014-03-07 23:22:00	W4MO	EL87tc	DK6UG	JN49cm	14097059	33	0	1	7793	44	14	2.21_r2286	0
17	186198889	2014-03-07 23:32:00	W4MO	EL87tc	DK6UG	JN49cm	14097059	33	3	1	7793	44	14	2.21_r2286	0
18	186201850	2014-03-07 23:50:00	W4MO	EL87tc	DK6UG	JN49cm	14097058	33	-6	1	7793	44	14	2.21_r2286	0
19	186203135	2014-03-07 23:58:00	W4MO	EL87tc	DK6UG	JN49cm	14097058	33	-2	0	7793	44	14	2.21_r2286	0
20	186204983	2014-03-08 00:10:00	W4MO	EL87tc	DK6UG	JN49cm	14097058	33	-5	1	7793	44	14	2.21_r2286	0
21	186207924	2014-03-08 00:28:00	W4MO	EL87tc	DK6UG	JN49cm	14097058	33	1	1	7793	44	14	2.21_r2286	0
22	186210829	2014-03-08 00:48:00	W4MO	EL87tc	DK6UG	JN49cm	14097058	33	-9	1	7793	44	14	2.21_r2286	0
23	186211785	2014-03-08 00:56:00	W4MO	EL87tc	DK6UG	JN49cm	14097058	33	-3	1	7793	44	14	2.21_r2286	0
24	186213337	2014-03-08 01:06:00	W4MO	EL87tc	DK6UG	JN49cm	14097057	33	-3	1	7793	44	14	2.21_r2286	0
25	186214441	2014-03-08 01:14:00	W4MO	EL87tc	DK6UG	JN49cm	14097057	33	-3	1	7793	44	14	2.21_r2286	0
26	186215799	2014-03-08 01:24:00	W4MO	EL87tc	DK6UG	JN49cm	14097058	33	-1	1	7793	44	14	2.21_r2286	0
27	186218728	2014-03-08 01:46:00	W4MO	EL87tc	DK6UG	JN49cm	14097059	33	-10	1	7793	44	14	2.21_r2286	0
28	186219898	2014-03-08 01:54:00	W4MO	EL87tc	DK6UG	JN49cm	14097058	33	-14	1	7793	44	14	2.21_r2286	0
29	186220902	2014-03-08 02:02:00	W4MO	EL87tc	DK6UG	JN49cm	14097058	33	-21	1	7793	44	14	2.21_r2286	0
30	186223578	2014-03-08 02:22:00	W4MO	EL87tc	DK6UG	JN49cm	14097059	33	2	1	7793	44	14	2.21_r2286	0
								Mean	-4.2000						
								SD	5.0337						
								AD	-4.2000						
								AD%	-83						

Page 729 of 1738

row	id	time	tx_sign	tx_loc	rx_sign	rx_loc	frequency	power	snr	drift	distance	azimuth	band	version	code
1	186178571	2014-03-07 21:44:00	W4MO	EL87tc	K4RCG	FM08xl	14097084	33	-1	-1	1328	17	14	2.21_r2286	0
2	186190818	2014-03-07 22:40:00	W4MO	EL87tc	K4RCG	FM08xl	14097070	33	-5	1	1328	17	14	2.21_r2286	0
3	186192582	2014-03-07 22:52:00	W4MO	EL87tc	K4RCG	FM08xl	14097071	33	5	1	1328	17	14	2.21_r2286	0
4	186193954	2014-03-07 23:00:00	W4MO	EL87tc	K4RCG	FM08xl	14097070	33	-4	0	1328	17	14	2.21_r2286	0
5	186197228	2014-03-07 23:22:00	W4MO	EL87tc	K4RCG	FM08xl	14097071	33	-23	1	1328	17	14	2.21_r2286	0
6	186198983	2014-03-07 23:32:00	W4MO	EL87tc	K4RCG	FM08xl	14097071	33	-10	1	1328	17	14	2.21_r2286	0
7	186201847	2014-03-07 23:50:00	W4MO	EL87tc	K4RCG	FM08xl	14097071	33	-7	1	1328	17	14	2.21_r2286	0
8	186203107	2014-03-07 23:58:00	W4MO	EL87tc	K4RCG	FM08xl	14097071	33	-21	1	1328	17	14	2.21_r2286	0
9	186205145	2014-03-08 00:10:00	W4MO	EL87tc	K4RCG	FM08xl	14097071	33	-7	1	1328	17	14	2.21_r2286	0
10	186206756	2014-03-08 00:20:00	W4MO	EL87tc	K4RCG	FM08xl	14097071	33	-4	1	1328	17	14	2.21_r2286	0
11	186207801	2014-03-08 00:28:00	W4MO	EL87tc	K4RCG	FM08xl	14097070	33	-6	1	1328	17	14	2.21_r2286	0
								Mean	-7.5455						
								SD	8.1285						
								AD	-6.5455						
								AD%	-81						

row	id	time	tx_sign	tx_loc	rx_sign	rx_loc	frequency	power	snr	drift	distance	azimuth	band	version	code
1	186154174	2014-03-07 19:32:00	W4MO	EL87tc	KC3AVT	FM19la	14097197	33	-15	0	1414	19	14	0.9_r3827	0
2	186159940	2014-03-07 20:02:00	W4MO	EL87tc	KC3AVT	FM19la	14097198	33	-11	1	1414	19	14	0.9_r3827	0
3	186161647	2014-03-07 20:12:00	W4MO	EL87tc	KC3AVT	FM19la	14097199	33	-7	1	1414	19	14	0.9_r3827	0
4	186166984	2014-03-07 20:40:00	W4MO	EL87tc	KC3AVT	FM19la	14097198	33	-5	1	1414	19	14	0.9_r3827	0
5	186169344	2014-03-07 20:52:00	W4MO	EL87tc	KC3AVT	FM19la	14097197	33	-3	1	1414	19	14	0.9_r3827	0
6	186171185	2014-03-07 21:02:00	W4MO	EL87tc	KC3AVT	FM19la	14097198	33	-13	1	1414	19	14	0.9_r3827	0
7	186172714	2014-03-07 21:10:00	W4MO	EL87tc	KC3AVT	FM19la	14097200	33	-10	1	1414	19	14	0.9_r3827	0
8	186176326	2014-03-07 21:30:00	W4MO	EL87tc	KC3AVT	FM19la	14097200	33	-10	1	1414	19	14	0.9_r3827	0
9	186186125	2014-03-07 22:10:00	W4MO	EL87tc	KC3AVT	FM19la	14097069	33	-8	-1	1414	19	14	0.9_r3827	0
10	186188216	2014-03-07 22:22:00	W4MO	EL87tc	KC3AVT	FM19la	14097066	33	-1	0	1414	19	14	0.9_r3827	0
11	186189583	2014-03-07 22:30:00	W4MO	EL87tc	KC3AVT	FM19la	14097064	33	-9	0	1414	19	14	0.9_r3827	0
								Mean	-8.3636						
								SD	4.1779						
								AD	-7.3636						
								AD%	-176						

row	id	time	tx_sign	tx_loc	rx_sign	rx_loc	frequency	power	snr	drift	distance	azimuth	band	version	code
1	186178649	2014-03-07 21:44:00	W4MO	EL87tc	M5ADA	IO93kl	14097085	33	-15	-1	7057	41	14	3.0.1_r255	0
2	186183863	2014-03-07 21:58:00	W4MO	EL87tc	M5ADA	IO93kl	14097082	33	-14	-1	7057	41	14	3.0.1_r255	0
3	186188066	2014-03-07 22:22:00	W4MO	EL87tc	M5ADA	IO93kl	14097075	33	-19	0	7057	41	14	3.0.1_r255	0
4	186190893	2014-03-07 22:40:00	W4MO	EL87tc	M5ADA	IO93kl	14097072	33	-22	0	7057	41	14	3.0.1_r255	0
5	186192671	2014-03-07 22:52:00	W4MO	EL87tc	M5ADA	IO93kl	14097072	33	-23	1	7057	41	14	3.0.1_r255	0
6	186197239	2014-03-07 23:22:00	W4MO	EL87tc	M5ADA	IO93kl	14097072	33	-15	1	7057	41	14	3.0.1_r255	0
7	186198944	2014-03-07 23:32:00	W4MO	EL87tc	M5ADA	IO93kl	14097071	33	-19	1	7057	41	14	3.0.1_r255	0
8	186203079	2014-03-07 23:58:00	W4MO	EL87tc	M5ADA	IO93kl	14097071	33	-23	1	7057	41	14	3.0.1_r255	0
9	186211930	2014-03-08 00:56:00	W4MO	EL87tc	M5ADA	IO93kl	14097071	33	-23	1	7057	41	14	3.0.1_r255	0
10	186218693	2014-03-08 01:46:00	W4MO	EL87tc	M5ADA	IO93kl	14097072	33	-22	0	7057	41	14	3.0.1_r255	0
11	186219815	2014-03-08 01:54:00	W4MO	EL87tc	M5ADA	IO93kl	14097072	33	-22	1	7057	41	14	3.0.1_r255	0
12	186221059	2014-03-08 02:02:00	W4MO	EL87tc	M5ADA	IO93kl	14097072	33	-12	1	7057	41	14	3.0.1_r255	0
13	186223642	2014-03-08 02:22:00	W4MO	EL87tc	M5ADA	IO93kl	14097072	33	-20	1	7057	41	14	3.0.1_r255	0
								Mean	-19.1538						
								SD	3.8911						
								AD	-4.1538						
								AD%	-107						

row	id	time	tx_sign	tx_loc	rx_sign	rx_loc	frequency	power	snr	drift	distance	azimuth	band	version	code
1	186183734	2014-03-07 21:58:00	W4MO	EL87tc	M6NNB	IO91ue	14097090	33	-11	-1	7163	43	14	2.11_r2263	0
2	186186133	2014-03-07 22:10:00	W4MO	EL87tc	M6NNB	IO91ue	14097085	33	-14	-1	7163	43	14	2.11_r2263	0
3	186188039	2014-03-07 22:22:00	W4MO	EL87tc	M6NNB	IO91ue	14097082	33	-18	0	7163	43	14	2.11_r2263	0
4	186189559	2014-03-07 22:30:00	W4MO	EL87tc	M6NNB	IO91ue	14097081	33	-17	0	7163	43	14	2.11_r2263	0
5	186190883	2014-03-07 22:40:00	W4MO	EL87tc	M6NNB	IO91ue	14097080	33	-20	1	7163	43	14	2.11_r2263	0
6	186192566	2014-03-07 22:52:00	W4MO	EL87tc	M6NNB	IO91ue	14097080	33	-22	1	7163	43	14	2.11_r2263	0
7	186197149	2014-03-07 23:22:00	W4MO	EL87tc	M6NNB	IO91ue	14097079	33	-16	0	7163	43	14	2.11_r2263	0
8	186198847	2014-03-07 23:32:00	W4MO	EL87tc	M6NNB	IO91ue	14097079	33	-21	1	7163	43	14	2.11_r2263	0
9	186201792	2014-03-07 23:50:00	W4MO	EL87tc	M6NNB	IO91ue	14097079	33	-24	1	7163	43	14	2.11_r2263	0
10	186205144	2014-03-08 00:10:00	W4MO	EL87tc	M6NNB	IO91ue	14097079	33	-14	1	7163	43	14	2.11_r2263	0
11	186207945	2014-03-08 00:28:00	W4MO	EL87tc	M6NNB	IO91ue	14097079	33	-25	1	7163	43	14	2.11_r2263	0
12	186210779	2014-03-08 00:48:00	W4MO	EL87tc	M6NNB	IO91ue	14097080	33	-14	1	7163	43	14	2.11_r2263	0
13	186211998	2014-03-08 00:56:00	W4MO	EL87tc	M6NNB	IO91ue	14097079	33	-16	1	7163	43	14	2.11_r2263	0
14	186218647	2014-03-08 01:46:00	W4MO	EL87tc	M6NNB	IO91ue	14097080	33	-23	1	7163	43	14	2.11_r2263	0
15	186219891	2014-03-08 01:54:00	W4MO	EL87tc	M6NNB	IO91ue	14097079	33	-17	1	7163	43	14	2.11_r2263	0
16	186220969	2014-03-08 02:02:00	W4MO	EL87tc	M6NNB	IO91ue	14097079	33	-27	1	7163	43	14	2.11_r2263	0
17	186223640	2014-03-08 02:22:00	W4MO	EL87tc	M6NNB	IO91ue	14097080	33	-25	1	7163	43	14	2.11_r2263	0
								Mean	-19.0588						
								SD	4.7232						
								AD	-5.0588						
								AD%	-107						

row	id	time	tx_sign	tx_loc	rx_sign	rx_loc	frequency	power	snr	drift	distance	azimuth	band	version	code
1	186183734	2014-03-07 21:58:00	W4MO	EL87tc	M6NNB	IO91ue	14097090	33	-11	-1	7163	43	14	2.11_r2263	0
2	186186133	2014-03-07 22:10:00	W4MO	EL87tc	M6NNB	IO91ue	14097085	33	-14	-1	7163	43	14	2.11_r2263	0
3	186188039	2014-03-07 22:22:00	W4MO	EL87tc	M6NNB	IO91ue	14097082	33	-18	0	7163	43	14	2.11_r2263	0
4	186189559	2014-03-07 22:30:00	W4MO	EL87tc	M6NNB	IO91ue	14097081	33	-17	0	7163	43	14	2.11_r2263	0
5	186190883	2014-03-07 22:40:00	W4MO	EL87tc	M6NNB	IO91ue	14097080	33	-20	1	7163	43	14	2.11_r2263	0
6	186192566	2014-03-07 22:52:00	W4MO	EL87tc	M6NNB	IO91ue	14097080	33	-22	1	7163	43	14	2.11_r2263	0
7	186197149	2014-03-07 23:22:00	W4MO	EL87tc	M6NNB	IO91ue	14097079	33	-16	0	7163	43	14	2.11_r2263	0
8	186198847	2014-03-07 23:32:00	W4MO	EL87tc	M6NNB	IO91ue	14097079	33	-21	1	7163	43	14	2.11_r2263	0
9	186201792	2014-03-07 23:50:00	W4MO	EL87tc	M6NNB	IO91ue	14097079	33	-24	1	7163	43	14	2.11_r2263	0
10	186205144	2014-03-08 00:10:00	W4MO	EL87tc	M6NNB	IO91ue	14097079	33	-14	1	7163	43	14	2.11_r2263	0
11	186207945	2014-03-08 00:28:00	W4MO	EL87tc	M6NNB	IO91ue	14097079	33	-25	1	7163	43	14	2.11_r2263	0
12	186210779	2014-03-08 00:48:00	W4MO	EL87tc	M6NNB	IO91ue	14097080	33	-14	1	7163	43	14	2.11_r2263	0
13	186211998	2014-03-08 00:56:00	W4MO	EL87tc	M6NNB	IO91ue	14097079	33	-16	1	7163	43	14	2.11_r2263	0
14	186218647	2014-03-08 01:46:00	W4MO	EL87tc	M6NNB	IO91ue	14097080	33	-23	1	7163	43	14	2.11_r2263	0
15	186219891	2014-03-08 01:54:00	W4MO	EL87tc	M6NNB	IO91ue	14097079	33	-17	1	7163	43	14	2.11_r2263	0
16	186220969	2014-03-08 02:02:00	W4MO	EL87tc	M6NNB	IO91ue	14097079	33	-27	1	7163	43	14	2.11_r2263	0
17	186223640	2014-03-08 02:22:00	W4MO	EL87tc	M6NNB	IO91ue	14097080	33	-25	1	7163	43	14	2.11_r2263	0
								Mean	-19.0588						
								SD	4.7232						
								AD	5.9412						
								AD%	126						

row	id	time	tx_sign	tx_loc	rx_sign	rx_loc	frequency	power	snr	drift	distance	azimuth	band	version	code
1	186183734	2014-03-07 21:58:00	W4MO	EL87tc	M6NNB	IO91ue	14097090	33	-11	-1	7163	43	14	2.11_r2263	0
2	186186133	2014-03-07 22:10:00	W4MO	EL87tc	M6NNB	IO91ue	14097085	33	-14	-1	7163	43	14	2.11_r2263	0
3	186188039	2014-03-07 22:22:00	W4MO	EL87tc	M6NNB	IO91ue	14097082	33	-18	0	7163	43	14	2.11_r2263	0
4	186189559	2014-03-07 22:30:00	W4MO	EL87tc	M6NNB	IO91ue	14097081	33	-17	0	7163	43	14	2.11_r2263	0
5	186190883	2014-03-07 22:40:00	W4MO	EL87tc	M6NNB	IO91ue	14097080	33	-20	1	7163	43	14	2.11_r2263	0
6	186192566	2014-03-07 22:52:00	W4MO	EL87tc	M6NNB	IO91ue	14097080	33	-22	1	7163	43	14	2.11_r2263	0
7	186197149	2014-03-07 23:22:00	W4MO	EL87tc	M6NNB	IO91ue	14097079	33	-16	0	7163	43	14	2.11_r2263	0
8	186198847	2014-03-07 23:32:00	W4MO	EL87tc	M6NNB	IO91ue	14097079	33	-21	1	7163	43	14	2.11_r2263	0
9	186201792	2014-03-07 23:50:00	W4MO	EL87tc	M6NNB	IO91ue	14097079	33	-24	1	7163	43	14	2.11_r2263	0
10	186205144	2014-03-08 00:10:00	W4MO	EL87tc	M6NNB	IO91ue	14097079	33	-14	1	7163	43	14	2.11_r2263	0
11	186207945	2014-03-08 00:28:00	W4MO	EL87tc	M6NNB	IO91ue	14097079	33	-25	1	7163	43	14	2.11_r2263	0
12	186210779	2014-03-08 00:48:00	W4MO	EL87tc	M6NNB	IO91ue	14097080	33	-14	1	7163	43	14	2.11_r2263	0
13	186211998	2014-03-08 00:56:00	W4MO	EL87tc	M6NNB	IO91ue	14097079	33	-16	1	7163	43	14	2.11_r2263	0
14	186218647	2014-03-08 01:46:00	W4MO	EL87tc	M6NNB	IO91ue	14097080	33	-23	1	7163	43	14	2.11_r2263	0
15	186219891	2014-03-08 01:54:00	W4MO	EL87tc	M6NNB	IO91ue	14097079	33	-17	1	7163	43	14	2.11_r2263	0
16	186220969	2014-03-08 02:02:00	W4MO	EL87tc	M6NNB	IO91ue	14097079	33	-27	1	7163	43	14	2.11_r2263	0
17	186223640	2014-03-08 02:22:00	W4MO	EL87tc	M6NNB	IO91ue	14097080	33	-25	1	7163	43	14	2.11_r2263	0
								Mean	-19.0588						
								SD	4.7232						
								AD	4.9412						
								AD%	105						

row	id	time	tx_sign	tx_loc	rx_sign	rx_loc	frequency	power	snr	drift	distance	azimuth	band	version	code
1	186172674	2014-03-07 21:10:00	W4MO	EL87tc	OE3VMS	JN78tq	14097197	33	-22	1	8329	43	14	2.11_r2263	0
2	186174773	2014-03-07 21:22:00	W4MO	EL87tc	OE3VMS	JN78tq	14097196	33	-24	1	8329	43	14	2.11_r2263	0
3	186178684	2014-03-07 21:44:00	W4MO	EL87tc	OE3VMS	JN78tq	14097074	33	-20	-1	8329	43	14	2.11_r2263	0
4	186183996	2014-03-07 21:58:00	W4MO	EL87tc	OE3VMS	JN78tq	14097071	33	-21	-1	8329	43	14	2.11_r2263	0
5	186186195	2014-03-07 22:10:00	W4MO	EL87tc	OE3VMS	JN78tq	14097066	33	-23	-1	8329	43	14	2.11_r2263	0
6	186188190	2014-03-07 22:22:00	W4MO	EL87tc	OE3VMS	JN78tq	14097063	33	-20	0	8329	43	14	2.11_r2263	0
7	186192698	2014-03-07 22:52:00	W4MO	EL87tc	OE3VMS	JN78tq	14097060	33	-24	1	8329	43	14	2.11_r2263	0
8	186193892	2014-03-07 23:00:00	W4MO	EL87tc	OE3VMS	JN78tq	14097060	33	-27	0	8329	43	14	2.11_r2263	0
9	186197257	2014-03-07 23:22:00	W4MO	EL87tc	OE3VMS	JN78tq	14097061	33	-24	1	8329	43	14	2.11_r2263	0
10	186198814	2014-03-07 23:32:00	W4MO	EL87tc	OE3VMS	JN78tq	14097060	33	-24	1	8329	43	14	2.11_r2263	0
11	186204992	2014-03-08 00:10:00	W4MO	EL87tc	OE3VMS	JN78tq	14097060	33	-21	1	8329	43	14	2.11_r2263	0
12	186210768	2014-03-08 00:48:00	W4MO	EL87tc	OE3VMS	JN78tq	14097061	33	-21	0	8329	43	14	2.11_r2263	0
13	186212027	2014-03-08 00:56:00	W4MO	EL87tc	OE3VMS	JN78tq	14097060	33	-22	1	8329	43	14	2.11_r2263	0
14	186213420	2014-03-08 01:06:00	W4MO	EL87tc	OE3VMS	JN78tq	14097060	33	-21	1	8329	43	14	2.11_r2263	0
15	186218689	2014-03-08 01:46:00	W4MO	EL87tc	OE3VMS	JN78tq	14097061	33	-22	1	8329	43	14	2.11_r2263	0
16	186219746	2014-03-08 01:54:00	W4MO	EL87tc	OE3VMS	JN78tq	14097060	33	-23	1	8329	43	14	2.11_r2263	0
								Mean	-22.4375						
								SD	1.8608						
								AD	-1.4375						
								AD%	-77						

row	id	time	tx_sign	tx_loc	rx_sign	rx_loc	frequency	power	snr	drift	distance	azimuth	band	version	code
1	186166950	2014-03-07 20:40:00	W4MO	EL87tc	OE3VMS	JN78tq	14097194	33	-24	1	8329	43	14	2.11_r2263	0
2	186169273	2014-03-07 20:52:00	W4MO	EL87tc	OE3VMS	JN78tq	14097194	33	-20	1	8329	43	14	2.11_r2263	0
3	186172674	2014-03-07 21:10:00	W4MO	EL87tc	OE3VMS	JN78tq	14097197	33	-22	1	8329	43	14	2.11_r2263	0
4	186174773	2014-03-07 21:22:00	W4MO	EL87tc	OE3VMS	JN78tq	14097196	33	-24	1	8329	43	14	2.11_r2263	0
5	186178684	2014-03-07 21:44:00	W4MO	EL87tc	OE3VMS	JN78tq	14097074	33	-20	-1	8329	43	14	2.11_r2263	0
6	186183996	2014-03-07 21:58:00	W4MO	EL87tc	OE3VMS	JN78tq	14097071	33	-21	-1	8329	43	14	2.11_r2263	0
7	186186195	2014-03-07 22:10:00	W4MO	EL87tc	OE3VMS	JN78tq	14097066	33	-23	-1	8329	43	14	2.11_r2263	0
8	186188190	2014-03-07 22:22:00	W4MO	EL87tc	OE3VMS	JN78tq	14097063	33	-20	0	8329	43	14	2.11_r2263	0
9	186192698	2014-03-07 22:52:00	W4MO	EL87tc	OE3VMS	JN78tq	14097060	33	-24	1	8329	43	14	2.11_r2263	0
10	186193892	2014-03-07 23:00:00	W4MO	EL87tc	OE3VMS	JN78tq	14097060	33	-27	0	8329	43	14	2.11_r2263	0
11	186197257	2014-03-07 23:22:00	W4MO	EL87tc	OE3VMS	JN78tq	14097061	33	-24	1	8329	43	14	2.11_r2263	0
12	186198814	2014-03-07 23:32:00	W4MO	EL87tc	OE3VMS	JN78tq	14097060	33	-24	1	8329	43	14	2.11_r2263	0
13	186204992	2014-03-08 00:10:00	W4MO	EL87tc	OE3VMS	JN78tq	14097060	33	-21	1	8329	43	14	2.11_r2263	0
14	186210768	2014-03-08 00:48:00	W4MO	EL87tc	OE3VMS	JN78tq	14097061	33	-21	0	8329	43	14	2.11_r2263	0
15	186212027	2014-03-08 00:56:00	W4MO	EL87tc	OE3VMS	JN78tq	14097060	33	-22	1	8329	43	14	2.11_r2263	0
16	186213420	2014-03-08 01:06:00	W4MO	EL87tc	OE3VMS	JN78tq	14097060	33	-21	1	8329	43	14	2.11_r2263	0
17	186218689	2014-03-08 01:46:00	W4MO	EL87tc	OE3VMS	JN78tq	14097061	33	-22	1	8329	43	14	2.11_r2263	0
18	186219746	2014-03-08 01:54:00	W4MO	EL87tc	OE3VMS	JN78tq	14097060	33	-23	1	8329	43	14	2.11_r2263	0
								Mean	-22.3889						
								SD	1.8830						
								AD	1.6111						
								AD%	86						

row	id	time	tx_sign	tx_loc	rx_sign	rx_loc	frequency	power	snr	drift	distance	azimuth	band	version	code
1	185904741	2014-03-06 22:04:00	W4MO	EL87tc	OE6PWD	JN77rb	14097102	33	-26	1	8392	44	14	4.0 r3015	0
2	185908324	2014-03-06 22:26:00	W4MO	EL87tc	OE6PWD	JN77rb	14097103	33	-25	1	8392	44	14	4.0 r3015	0
3	185910326	2014-03-06 22:38:00	W4MO	EL87tc	OE6PWD	JN77rb	14097103	33	-29	1	8392	44	14	4.0 r3015	0
4	185917591	2014-03-06 23:22:00	W4MO	EL87tc	OE6PWD	JN77rb	14097103	33	-27	1	8392	44	14	4.0 r3015	0
5	185925791	2014-03-07 00:14:00	W4MO	EL87tc	OE6PWD	JN77rb	14097104	33	-28	1	8392	44	14	4.0 r3015	0
6	185927724	2014-03-07 00:26:00	W4MO	EL87tc	OE6PWD	JN77rb	14097103	33	-19	1	8392	44	14	4.0 r3015	0
7	185937869	2014-03-07 01:40:00	W4MO	EL87tc	OE6PWD	JN77rb	14097104	33	-24	1	8392	44	14	4.0 r3015	0
8	186188038	2014-03-07 22:22:00	W4MO	EL87tc	OE6PWD	JN77rb	14097071	33	-25	0	8392	44	14	4.0 r3015	0
9	186197184	2014-03-07 23:22:00	W4MO	EL87tc	OE6PWD	JN77rb	14097069	33	-23	0	8392	44	14	4.0 r3015	0
10	186223654	2014-03-08 02:22:00	W4MO	EL87tc	OE6PWD	JN77rb	14097068	33	-27	1	8392	44	14	4.0 r3015	0
								Mean	-25.3000						
								SD	2.8694						
								AD	-2.3000						
								AD%	-80						

row	id	time	tx_sign	tx_loc	rx_sign	rx_loc	frequency	power	snr	drift	distance	azimuth	band	version	code
1	186178877	2014-03-07 21:44:00	W4MO	EL87tc	ON4SAR	JO21ce	14097102	33	-17	-1	7467	43	14	0.8_r3058	0
2	186183844	2014-03-07 21:58:00	W4MO	EL87tc	ON4SAR	JO21ce	14097099	33	-13	-1	7467	43	14	0.8_r3058	0
3	186186119	2014-03-07 22:10:00	W4MO	EL87tc	ON4SAR	JO21ce	14097094	33	-22	-1	7467	43	14	0.8_r3058	0
4	186188123	2014-03-07 22:22:00	W4MO	EL87tc	ON4SAR	JO21ce	14097092	33	-16	0	7467	43	14	0.8_r3058	0
5	186189270	2014-03-07 22:30:00	W4MO	EL87tc	ON4SAR	JO21ce	14097090	33	-20	0	7467	43	14	0.8_r3058	0
6	186190988	2014-03-07 22:40:00	W4MO	EL87tc	ON4SAR	JO21ce	14097089	33	-26	0	7467	43	14	0.8_r3058	0
7	186192513	2014-03-07 22:52:00	W4MO	EL87tc	ON4SAR	JO21ce	14097089	33	-24	1	7467	43	14	0.8_r3058	0
8	186197147	2014-03-07 23:22:00	W4MO	EL87tc	ON4SAR	JO21ce	14097089	33	-14	1	7467	43	14	0.8_r3058	0
9	186198764	2014-03-07 23:32:00	W4MO	EL87tc	ON4SAR	JO21ce	14097088	33	-21	1	7467	43	14	0.8_r3058	0
10	186201785	2014-03-07 23:50:00	W4MO	EL87tc	ON4SAR	JO21ce	14097088	33	-24	1	7467	43	14	0.8_r3058	0
11	186203267	2014-03-07 23:58:00	W4MO	EL87tc	ON4SAR	JO21ce	14097088	33	-20	0	7467	43	14	0.8_r3058	0
12	186207985	2014-03-08 00:28:00	W4MO	EL87tc	ON4SAR	JO21ce	14097088	33	-20	1	7467	43	14	0.8_r3058	0
13	186210762	2014-03-08 00:48:00	W4MO	EL87tc	ON4SAR	JO21ce	14097088	33	-23	1	7467	43	14	0.8_r3058	0
14	186218761	2014-03-08 01:46:00	W4MO	EL87tc	ON4SAR	JO21ce	14097088	33	-25	0	7467	43	14	0.8_r3058	0
								Mean	-20.3571						
								SD	4.0688						
								AD	3.6429						
								AD%	90						

row	id	time	tx_sign	tx_loc	rx_sign	rx_loc	frequency	power	snr	drift	distance	azimuth	band	version	code
1	186170961	2014-03-07 21:02:00	W4MO	EL87tc	ON7KB	JO21ei	14097169	33	-28	1	7473	43	14	0.8_r3058	0
2	186178833	2014-03-07 21:44:00	W4MO	EL87tc	ON7KB	JO21ei	14097047	33	-23	-1	7473	43	14	0.8_r3058	0
3	186185902	2014-03-07 22:10:00	W4MO	EL87tc	ON7KB	JO21ei	14097039	33	-27	-1	7473	43	14	0.8_r3058	0
4	186189410	2014-03-07 22:30:00	W4MO	EL87tc	ON7KB	JO21ei	14097034	33	-27	0	7473	43	14	0.8_r3058	0
5	186197267	2014-03-07 23:22:00	W4MO	EL87tc	ON7KB	JO21ei	14097033	33	-21	1	7473	43	14	0.8_r3058	0
								Mean	-25.2000						
								SD	3.0332						
								AD	-4.2000						
								AD%	-138						

row	id	time	tx_sign	tx_loc	rx_sign	rx_loc	frequency	power	snr	drift	distance	azimuth	band	version	code
1	186172667	2014-03-07 21:10:00	W4MO	EL87tc	OZ7IT	JO65df	14097199	33	-4	1	7845	37	14	2.21_r2286	0
2	186174675	2014-03-07 21:22:00	W4MO	EL87tc	OZ7IT	JO65df	14097197	33	-5	1	7845	37	14	2.21_r2286	0
3	186178670	2014-03-07 21:44:00	W4MO	EL87tc	OZ7IT	JO65df	14097077	33	-1	-1	7845	37	14	2.21_r2286	0
4	186183747	2014-03-07 21:58:00	W4MO	EL87tc	OZ7IT	JO65df	14097073	33	-2	-1	7845	37	14	2.21_r2286	0
5	186186012	2014-03-07 22:10:00	W4MO	EL87tc	OZ7IT	JO65df	14097069	33	-6	0	7845	37	14	2.21_r2286	0
6	186188053	2014-03-07 22:22:00	W4MO	EL87tc	OZ7IT	JO65df	14097066	33	2	0	7845	37	14	2.21_r2286	0
7	186189531	2014-03-07 22:30:00	W4MO	EL87tc	OZ7IT	JO65df	14097064	33	0	0	7845	37	14	2.21_r2286	0
8	186190778	2014-03-07 22:40:00	W4MO	EL87tc	OZ7IT	JO65df	14097063	33	-3	0	7845	37	14	2.21_r2286	0
9	186192620	2014-03-07 22:52:00	W4MO	EL87tc	OZ7IT	JO65df	14097063	33	-1	1	7845	37	14	2.21_r2286	0
10	186193979	2014-03-07 23:00:00	W4MO	EL87tc	OZ7IT	JO65df	14097063	33	-4	1	7845	37	14	2.21_r2286	0
11	186197169	2014-03-07 23:22:00	W4MO	EL87tc	OZ7IT	JO65df	14097062	33	-5	1	7845	37	14	2.21_r2286	0
12	186201758	2014-03-07 23:50:00	W4MO	EL87tc	OZ7IT	JO65df	14097060	33	-22	1	7845	37	14	2.21_r2286	0
13	186203112	2014-03-07 23:58:00	W4MO	EL87tc	OZ7IT	JO65df	14097060	33	-20	1	7845	37	14	2.21_r2286	0
								Mean	-5.4615						
								SD	7.2642						
								AD	14.5385						
								AD%	200						

row	id	time	tx_sign	tx_loc	rx_sign	rx_loc	frequency	power	snr	drift	distance	azimuth	band	version	code
1	186178915	2014-03-07 21:44:00	W4MO	EL87tc	PI4THT	JO32kf	14097079	33	-13	-1	7612	41	14	0.6	0
2	186183991	2014-03-07 21:58:00	W4MO	EL87tc	PI4THT	JO32kf	14097076	33	-10	-1	7612	41	14	0.6	0
3	186186364	2014-03-07 22:10:00	W4MO	EL87tc	PI4THT	JO32kf	14097071	33	-11	0	7612	41	14	0.6	0
4	186188285	2014-03-07 22:22:00	W4MO	EL87tc	PI4THT	JO32kf	14097069	33	-15	0	7612	41	14	0.6	0
5	186189638	2014-03-07 22:30:00	W4MO	EL87tc	PI4THT	JO32kf	14097067	33	-17	0	7612	41	14	0.6	0
6	186191063	2014-03-07 22:40:00	W4MO	EL87tc	PI4THT	JO32kf	14097066	33	-15	1	7612	41	14	0.6	0
7	186192773	2014-03-07 22:52:00	W4MO	EL87tc	PI4THT	JO32kf	14097065	33	-20	0	7612	41	14	0.6	0
8	186194007	2014-03-07 23:00:00	W4MO	EL87tc	PI4THT	JO32kf	14097065	33	-23	1	7612	41	14	0.6	0
9	186197395	2014-03-07 23:22:00	W4MO	EL87tc	PI4THT	JO32kf	14097065	33	-12	1	7612	41	14	0.6	0
10	186199032	2014-03-07 23:32:00	W4MO	EL87tc	PI4THT	JO32kf	14097065	33	-21	1	7612	41	14	0.6	0
11	186202028	2014-03-07 23:50:00	W4MO	EL87tc	PI4THT	JO32kf	14097065	33	-21	1	7612	41	14	0.6	0
12	186203371	2014-03-07 23:58:00	W4MO	EL87tc	PI4THT	JO32kf	14097065	33	-17	1	7612	41	14	0.6	0
13	186208074	2014-03-08 00:28:00	W4MO	EL87tc	PI4THT	JO32kf	14097065	33	-22	1	7612	41	14	0.6	0
14	186210965	2014-03-08 00:48:00	W4MO	EL87tc	PI4THT	JO32kf	14097065	33	-25	1	7612	41	14	0.6	0
15	186215905	2014-03-08 01:24:00	W4MO	EL87tc	PI4THT	JO32kf	14097065	33	-24	1	7612	41	14	0.6	0
16	186218837	2014-03-08 01:46:00	W4MO	EL87tc	PI4THT	JO32kf	14097065	33	-21	1	7612	41	14	0.6	0
17	186219962	2014-03-08 01:54:00	W4MO	EL87tc	PI4THT	JO32kf	14097065	33	-17	1	7612	41	14	0.6	0
18	186221127	2014-03-08 02:02:00	W4MO	EL87tc	PI4THT	JO32kf	14097065	33	-18	1	7612	41	14	0.6	0
19	186223848	2014-03-08 02:22:00	W4MO	EL87tc	PI4THT	JO32kf	14097065	33	-20	1	7612	41	14	0.6	0
								Mean	-18.0000						
								SD	4.4472						
								AD	4.0000						
								AD%	90						

row	id	time	tx_sign	tx_loc	rx_sign	rx_loc	frequency	power	snr	drift	distance	azimuth	band	version	code
1	186178915	2014-03-07 21:44:00	W4MO	EL87tc	PI4THT	JO32kf	14097079	33	-13	-1	7612	41	14	0.6	0
2	186183991	2014-03-07 21:58:00	W4MO	EL87tc	PI4THT	JO32kf	14097076	33	-10	-1	7612	41	14	0.6	0
3	186186364	2014-03-07 22:10:00	W4MO	EL87tc	PI4THT	JO32kf	14097071	33	-11	0	7612	41	14	0.6	0
4	186188285	2014-03-07 22:22:00	W4MO	EL87tc	PI4THT	JO32kf	14097069	33	-15	0	7612	41	14	0.6	0
5	186189638	2014-03-07 22:30:00	W4MO	EL87tc	PI4THT	JO32kf	14097067	33	-17	0	7612	41	14	0.6	0
6	186191063	2014-03-07 22:40:00	W4MO	EL87tc	PI4THT	JO32kf	14097066	33	-15	1	7612	41	14	0.6	0
7	186192773	2014-03-07 22:52:00	W4MO	EL87tc	PI4THT	JO32kf	14097065	33	-20	0	7612	41	14	0.6	0
8	186194007	2014-03-07 23:00:00	W4MO	EL87tc	PI4THT	JO32kf	14097065	33	-23	1	7612	41	14	0.6	0
9	186197395	2014-03-07 23:22:00	W4MO	EL87tc	PI4THT	JO32kf	14097065	33	-12	1	7612	41	14	0.6	0
10	186199032	2014-03-07 23:32:00	W4MO	EL87tc	PI4THT	JO32kf	14097065	33	-21	1	7612	41	14	0.6	0
11	186202028	2014-03-07 23:50:00	W4MO	EL87tc	PI4THT	JO32kf	14097065	33	-21	1	7612	41	14	0.6	0
12	186203371	2014-03-07 23:58:00	W4MO	EL87tc	PI4THT	JO32kf	14097065	33	-17	1	7612	41	14	0.6	0
13	186208074	2014-03-08 00:28:00	W4MO	EL87tc	PI4THT	JO32kf	14097065	33	-22	1	7612	41	14	0.6	0
14	186210965	2014-03-08 00:48:00	W4MO	EL87tc	PI4THT	JO32kf	14097065	33	-25	1	7612	41	14	0.6	0
15	186215905	2014-03-08 01:24:00	W4MO	EL87tc	PI4THT	JO32kf	14097065	33	-24	1	7612	41	14	0.6	0
16	186218837	2014-03-08 01:46:00	W4MO	EL87tc	PI4THT	JO32kf	14097065	33	-21	1	7612	41	14	0.6	0
17	186219962	2014-03-08 01:54:00	W4MO	EL87tc	PI4THT	JO32kf	14097065	33	-17	1	7612	41	14	0.6	0
18	186221127	2014-03-08 02:02:00	W4MO	EL87tc	PI4THT	JO32kf	14097065	33	-18	1	7612	41	14	0.6	0
19	186223848	2014-03-08 02:22:00	W4MO	EL87tc	PI4THT	JO32kf	14097065	33	-20	1	7612	41	14	0.6	0
								Mean	-18.0000						
								SD	4.4472						
								AD	-6.0000						
								AD%	-135						

row	id	time	tx_sign	tx_loc	rx_sign	rx_loc	frequency	power	snr	drift	distance	azimuth	band	version	code
1	186190800	2014-03-07 22:40:00	W4MO	EL87tc	SM3ULC	JO89ul	14097123	33	-14	1	7977	32	14	2.11_r2263	0
2	186192673	2014-03-07 22:52:00	W4MO	EL87tc	SM3ULC	JO89ul	14097123	33	-24	0	7977	32	14	2.11_r2263	0
3	186193839	2014-03-07 23:00:00	W4MO	EL87tc	SM3ULC	JO89ul	14097122	33	-15	0	7977	32	14	2.11_r2263	0
								Mean	-17.6667						
								SD	5.5076						
								AD	6.3333						
								AD%	115						

row	id	time	tx_sign	tx_loc	rx_sign	rx_loc	frequency	power	snr	drift	distance	azimuth	band	version	code
1	186186996	2014-03-07 22:14:00	W9HLY	EN70mt	K4EH	EM73	14097051	30	3	0	815	181	14	2.21_r2286	0
2	186192837	2014-03-07 22:54:00	W9HLY	EN70mt	K4EH	EM73	14097052	30	3	0	815	181	14	2.21_r2286	0
3	186196971	2014-03-07 23:20:00	W9HLY	EN70mt	K4EH	EM73	14097052	30	0	0	815	181	14	2.21_r2286	0
4	186199002	2014-03-07 23:32:00	W9HLY	EN70mt	K4EH	EM73	14097051	30	1	0	815	181	14	2.21_r2286	0
5	186203305	2014-03-07 23:58:00	W9HLY	EN70mt	K4EH	EM73	14097052	30	3	0	815	181	14	2.21_r2286	0
6	186205816	2014-03-08 00:14:00	W9HLY	EN70mt	K4EH	EM73	14097052	30	0	0	815	181	14	2.21_r2286	0
								Mean	1.6667						
								SD	1.5055						
								AD	1.6667						
								AD%	111						

row	id	time	tx_sign	tx_loc	rx_sign	rx_loc	frequency	power	snr	drift	distance	azimuth	band	version	code
1	185634293	2014-03-05 20:28:00	W9HLY	EN70mt	KB1MVX	EM73	14097012	30	-12	0	815	181	14	2.11_r2263	0
2	185642870	2014-03-05 21:30:00	W9HLY	EN70mt	KB1MVX	EM73	14097013	30	-15	0	815	181	14	2.11_r2263	0
3	185645193	2014-03-05 21:46:00	W9HLY	EN70mt	KB1MVX	EM73	14097011	30	-18	0	815	181	14	2.11_r2263	0
4	185652264	2014-03-05 22:36:00	W9HLY	EN70mt	KB1MVX	EM73	14097012	30	-26	0	815	181	14	2.11_r2263	0
5	185653897	2014-03-05 22:48:00	W9HLY	EN70mt	KB1MVX	EM73	14097011	30	-17	0	815	181	14	2.11_r2263	0
6	185660367	2014-03-05 23:14:00	W9HLY	EN70mt	KB1MVX	EM73	14097010	30	-22	0	815	181	14	2.11_r2263	0
7	185666778	2014-03-06 00:00:00	W9HLY	EN70mt	KB1MVX	EM73	14097011	30	-16	0	815	181	14	2.11_r2263	0
8	185668461	2014-03-06 00:12:00	W9HLY	EN70mt	KB1MVX	EM73	14097011	30	-26	-1	815	181	14	2.11_r2263	0
9	186193017	2014-03-07 22:54:00	W9HLY	EN70mt	KB1MVX	EM73	14097013	30	-5	0	815	181	14	2.11_r2263	0
10	186196977	2014-03-07 23:20:00	W9HLY	EN70mt	KB1MVX	EM73	14097014	30	4	0	815	181	14	2.11_r2263	0
11	186199033	2014-03-07 23:32:00	W9HLY	EN70mt	KB1MVX	EM73	14097011	30	5	0	815	181	14	2.11_r2263	0
12	186459211	2014-03-08 21:28:00	W9HLY	EN70mt	KB1MVX	EM73	14097014	30	7	0	815	181	14	2.11_r2263	0
13	186461637	2014-03-08 21:42:00	W9HLY	EN70mt	KB1MVX	EM73	14097013	30	-11	0	815	181	14	2.11_r2263	0
14	186465634	2014-03-08 22:08:00	W9HLY	EN70mt	KB1MVX	EM73	14097014	30	-4	0	815	181	14	2.11_r2263	0
15	186480712	2014-03-08 23:26:00	W9HLY	EN70mt	KB1MVX	EM73	14097014	30	2	0	815	181	14	2.11_r2263	0
16	186482599	2014-03-08 23:38:00	W9HLY	EN70mt	KB1MVX	EM73	14097014	30	5	0	815	181	14	2.11_r2263	0
17	186726372	2014-03-09 21:02:00	W9HLY	EN70mt	KB1MVX	EM73	14097019	30	-6	0	815	181	14	2.11_r2263	0
18	186728525	2014-03-09 21:12:00	W9HLY	EN70mt	KB1MVX	EM73	14097017	30	3	0	815	181	14	2.11_r2263	0
19	186730656	2014-03-09 21:24:00	W9HLY	EN70mt	KB1MVX	EM73	14097017	30	-2	0	815	181	14	2.11_r2263	0
20	186733343	2014-03-09 21:38:00	W9HLY	EN70mt	KB1MVX	EM73	14097017	30	1	0	815	181	14	2.11_r2263	0
21	186735437	2014-03-09 21:50:00	W9HLY	EN70mt	KB1MVX	EM73	14097018	30	-4	0	815	181	14	2.11_r2263	0
22	186738054	2014-03-09 22:06:00	W9HLY	EN70mt	KB1MVX	EM73	14097018	30	-1	0	815	181	14	2.11_r2263	0
23	186747215	2014-03-09 22:44:00	W9HLY	EN70mt	KB1MVX	EM73	14097016	30	0	0	815	181	14	2.11_r2263	0
24	186751045	2014-03-09 23:06:00	W9HLY	EN70mt	KB1MVX	EM73	14097015	30	-1	0	815	181	14	2.11_r2263	0
25	186760159	2014-03-10 00:04:00	W9HLY	EN70mt	KB1MVX	EM73	14097016	30	1	0	815	181	14	2.11_r2263	0
								Mean	-6.3200						
								SD	10.0529						
								AD	-10.3200						
								AD%	-103						

row	id	time	tx_sign	tx_loc	rx_sign	rx_loc	frequency	power	snr	drift	distance	azimuth	band	version	code
1	186196250	2014-03-07 23:16:00	WA3DNM	FM29fw	W4MO	EL87	14097096	37	1	0	1548	209	14	2.21_r2286	0
2	186198108	2014-03-07 23:28:00	WA3DNM	FM29fw	W4MO	EL87	14097096	37	1	0	1548	209	14	2.21_r2286	0
3	186199474	2014-03-07 23:36:00	WA3DNM	FM29fw	W4MO	EL87	14097096	37	-1	0	1548	209	14	2.21_r2286	0
4	186200776	2014-03-07 23:44:00	WA3DNM	FM29fw	W4MO	EL87	14097096	37	1	0	1548	209	14	2.21_r2286	0
5	186202109	2014-03-07 23:52:00	WA3DNM	FM29fw	W4MO	EL87	14097096	37	0	0	1548	209	14	2.21_r2286	0
6	186203904	2014-03-08 00:02:00	WA3DNM	FM29fw	W4MO	EL87	14097096	37	5	0	1548	209	14	2.21_r2286	0
7	186208636	2014-03-08 00:32:00	WA3DNM	FM29fw	W4MO	EL87	14097097	37	4	0	1548	209	14	2.21_r2286	0
8	186210065	2014-03-08 00:42:00	WA3DNM	FM29fw	W4MO	EL87	14097097	37	4	0	1548	209	14	2.21_r2286	0
9	186211153	2014-03-08 00:50:00	WA3DNM	FM29fw	W4MO	EL87	14097096	37	4	0	1548	209	14	2.21_r2286	0
10	186212129	2014-03-08 00:58:00	WA3DNM	FM29fw	W4MO	EL87	14097096	37	5	0	1548	209	14	2.21_r2286	0
11	186218404	2014-03-08 01:44:00	WA3DNM	FM29fw	W4MO	EL87	14097096	37	7	0	1548	209	14	2.21_r2286	0
								Mean	2.8182						
								SD	2.5226						
								AD	3.8182						
								AD%	151						

row	id	time	tx_sign	tx_loc	rx_sign	rx_loc	frequency	power	snr	drift	distance	azimuth	band	version	code
1	186168370	2014-03-07 20:48:00	WA8RC	EN72jh	AI4RY	EM72go	14097104	23	-4	0	1080	181	14	0.8_r3058	0
2	186170214	2014-03-07 20:58:00	WA8RC	EN72jh	AI4RY	EM72go	14097108	23	-7	0	1080	181	14	0.8_r3058	0
3	186172131	2014-03-07 21:08:00	WA8RC	EN72jh	AI4RY	EM72go	14097107	23	-9	-1	1080	181	14	0.8_r3058	0
4	186175719	2014-03-07 21:28:00	WA8RC	EN72jh	AI4RY	EM72go	14097110	23	-4	0	1080	181	14	0.8_r3058	0
5	186177509	2014-03-07 21:38:00	WA8RC	EN72jh	AI4RY	EM72go	14097106	23	-3	-1	1080	181	14	0.8_r3058	0
6	186185811	2014-03-07 22:08:00	WA8RC	EN72jh	AI4RY	EM72go	14097107	23	1	-1	1080	181	14	0.8_r3058	0
7	186187398	2014-03-07 22:18:00	WA8RC	EN72jh	AI4RY	EM72go	14097106	23	-5	0	1080	181	14	0.8_r3058	0
8	186189080	2014-03-07 22:28:00	WA8RC	EN72jh	AI4RY	EM72go	14097104	23	-5	-1	1080	181	14	0.8_r3058	0
								Mean	-4.5000						
								SD	2.9277						
								AD	-1.5000						
								AD%	-51						

row	id	time	tx_sign	tx_loc	rx_sign	rx_loc	frequency	power	snr	drift	distance	azimuth	band	version	code
1	186168642	2014-03-07 20:50:00	WB8ELK	EM64oj	VE6PDQ/1	DO33fl	14097121	23	-23	-1	2981	324	14	3.00_r2485	0
2	186172583	2014-03-07 21:10:00	WB8ELK	EM64oj	VE6PDQ/1	DO33fl	14097122	23	-29	-1	2981	324	14	3.00_r2485	0
3	186180257	2014-03-07 21:46:00	WB8ELK	EM64oj	VE6PDQ/1	DO33fl	14097123	23	-26	0	2981	324	14	3.00_r2485	0
4	186184231	2014-03-07 22:00:00	WB8ELK	EM64oj	VE6PDQ/1	DO33fl	14097121	23	-20	-1	2981	324	14	3.00_r2485	0
5	186185129	2014-03-07 22:04:00	WB8ELK	EM64oj	VE6PDQ/1	DO33fl	14097121	23	-25	-1	2981	324	14	3.00_r2485	0
6	186185925	2014-03-07 22:10:00	WB8ELK	EM64oj	VE6PDQ/1	DO33fl	14097124	23	-24	0	2981	324	14	3.00_r2485	0
7	186195410	2014-03-07 23:10:00	WB8ELK	EM64oj	VE6PDQ/1	DO33fl	14097124	23	-20	-1	2981	324	14	3.00_r2485	0
8	186197569	2014-03-07 23:24:00	WB8ELK	EM64oj	VE6PDQ/1	DO33fl	14097123	23	-17	-1	2981	324	14	3.00_r2485	0
9	186200937	2014-03-07 23:44:00	WB8ELK	EM64oj	VE6PDQ/1	DO33fl	14097121	23	-18	-1	2981	324	14	3.00_r2485	0
10	186201210	2014-03-07 23:46:00	WB8ELK	EM64oj	VE6PDQ/1	DO33fl	14097120	23	-17	0	2981	324	14	3.00_r2485	0
11	186201894	2014-03-07 23:50:00	WB8ELK	EM64oj	VE6PDQ/1	DO33fl	14097122	23	-16	-1	2981	324	14	3.00_r2485	0
12	186211286	2014-03-08 00:50:00	WB8ELK	EM64oj	VE6PDQ/1	DO33fl	14097120	23	-21	0	2981	324	14	3.00_r2485	0
13	186213839	2014-03-08 01:10:00	WB8ELK	EM64oj	VE6PDQ/1	DO33fl	14097122	23	-22	-1	2981	324	14	3.00_r2485	0
14	186221307	2014-03-08 02:04:00	WB8ELK	EM64oj	VE6PDQ/1	DO33fl	14097125	23	-20	-1	2981	324	14	3.00_r2485	0
15	186224870	2014-03-08 02:30:00	WB8ELK	EM64oj	VE6PDQ/1	DO33fl	14097123	23	-25	-1	2981	324	14	3.00_r2485	0
16	186227449	2014-03-08 02:50:00	WB8ELK	EM64oj	VE6PDQ/1	DO33fl	14097123	23	-21	-1	2981	324	14	3.00_r2485	0
								Mean	-21.5000						
								SD	3.6515						
								AD	-5.5000						
								AD%	-151						

row	id	time	tx_sign	tx_loc	rx_sign	rx_loc	frequency	power	snr	drift	distance	azimuth	band	version	code
1	186157819	2014-03-07 19:52:00	WD0UG	EM64	KB9VLR	EN54vj	10140163	30	-11	-3	1107	355	10	2.0_r1714	0
2	186159654	2014-03-07 20:02:00	WD0UG	EM64	KB9VLR	EN54vj	10140163	30	-6	-1	1107	355	10	2.0_r1714	0
3	186163580	2014-03-07 20:22:00	WD0UG	EM64	KB9VLR	EN54vj	10140162	30	-11	-1	1107	355	10	2.0_r1714	0
4	186172767	2014-03-07 21:12:00	WD0UG	EM64	KB9VLR	EN54vj	10140160	30	-6	-2	1107	355	10	2.0_r1714	0
5	186184744	2014-03-07 22:02:00	WD0UG	EM64	KB9VLR	EN54vj	10140160	30	-7	-1	1107	355	10	2.0_r1714	0
6	186188196	2014-03-07 22:22:00	WD0UG	EM64	KB9VLR	EN54vj	10140161	30	-7	-4	1107	355	10	2.0_r1714	0
7	186189900	2014-03-07 22:32:00	WD0UG	EM64	KB9VLR	EN54vj	10140161	30	-10	-1	1107	355	10	2.0_r1714	0
8	186192732	2014-03-07 22:52:00	WD0UG	EM64	KB9VLR	EN54vj	10140161	30	-5	-2	1107	355	10	2.0_r1714	0
9	186194065	2014-03-07 23:02:00	WD0UG	EM64	KB9VLR	EN54vj	10140161	30	-5	-2	1107	355	10	2.0_r1714	0
10	186197349	2014-03-07 23:22:00	WD0UG	EM64	KB9VLR	EN54vj	10140162	30	-11	-4	1107	355	10	2.0_r1714	0
11	186200624	2014-03-07 23:42:00	WD0UG	EM64	KB9VLR	EN54vj	10140161	30	-3	-2	1107	355	10	2.0_r1714	0
12	186203905	2014-03-08 00:02:00	WD0UG	EM64	KB9VLR	EN54vj	10140162	30	-6	-3	1107	355	10	2.0_r1714	0
								Mean	-7.3333						
								SD	2.7414						
								AD	-2.3333						
								AD%	-85						

row	id	time	tx_sign	tx_loc	rx_sign	rx_loc	frequency	power	snr	drift	distance	azimuth	band	version	code
1	186168931	2014-03-07 20:50:00	WD4LHT	EL89tp	K9AN	EN50wc	10140229	30	-14	0	1275	337	10		0
2	186170127	2014-03-07 20:58:00	WD4LHT	EL89tp	K9AN	EN50wc	10140229	30	-16	0	1275	337	10		0
3	186172677	2014-03-07 21:10:00	WD4LHT	EL89tp	K9AN	EN50wc	10140229	30	-14	0	1275	337	10		0
4	186174422	2014-03-07 21:20:00	WD4LHT	EL89tp	K9AN	EN50wc	10140229	30	-12	0	1275	337	10		0
5	186175754	2014-03-07 21:28:00	WD4LHT	EL89tp	K9AN	EN50wc	10140229	30	-14	0	1275	337	10		0
6	186177689	2014-03-07 21:38:00	WD4LHT	EL89tp	K9AN	EN50wc	10140229	30	-13	0	1275	337	10		0
7	186180625	2014-03-07 21:48:00	WD4LHT	EL89tp	K9AN	EN50wc	10140229	30	-16	0	1275	337	10		0
8	186184330	2014-03-07 22:00:00	WD4LHT	EL89tp	K9AN	EN50wc	10140229	30	-11	0	1275	337	10		0
9	186185648	2014-03-07 22:08:00	WD4LHT	EL89tp	K9AN	EN50wc	10140229	30	-9	0	1275	337	10		0
10	186187249	2014-03-07 22:16:00	WD4LHT	EL89tp	K9AN	EN50wc	10140229	30	-14	0	1275	337	10		0
11	186188986	2014-03-07 22:28:00	WD4LHT	EL89tp	K9AN	EN50wc	10140229	30	-11	0	1275	337	10		0
12	186193417	2014-03-07 22:58:00	WD4LHT	EL89tp	K9AN	EN50wc	10140229	30	-12	0	1275	337	10		0
13	186194673	2014-03-07 23:06:00	WD4LHT	EL89tp	K9AN	EN50wc	10140229	30	-11	0	1275	337	10		0
14	186196142	2014-03-07 23:14:00	WD4LHT	EL89tp	K9AN	EN50wc	10140229	30	-18	0	1275	337	10		0
15	186197928	2014-03-07 23:26:00	WD4LHT	EL89tp	K9AN	EN50wc	10140229	30	-19	0	1275	337	10		0
16	186199623	2014-03-07 23:36:00	WD4LHT	EL89tp	K9AN	EN50wc	10140229	30	-9	0	1275	337	10		0
17	186201553	2014-03-07 23:48:00	WD4LHT	EL89tp	K9AN	EN50wc	10140229	30	-17	0	1275	337	10		0
18	186203550	2014-03-08 00:00:00	WD4LHT	EL89tp	K9AN	EN50wc	10140229	30	-10	0	1275	337	10		0
19	186204787	2014-03-08 00:08:00	WD4LHT	EL89tp	K9AN	EN50wc	10140229	30	-11	0	1275	337	10		0
20	186206868	2014-03-08 00:20:00	WD4LHT	EL89tp	K9AN	EN50wc	10140229	30	-13	1	1275	337	10		0
21	186209675	2014-03-08 00:40:00	WD4LHT	EL89tp	K9AN	EN50wc	10140229	30	-6	0	1275	337	10		0
22	186211257	2014-03-08 00:50:00	WD4LHT	EL89tp	K9AN	EN50wc	10140229	30	-15	0	1275	337	10		0
23	186213721	2014-03-08 01:08:00	WD4LHT	EL89tp	K9AN	EN50wc	10140229	30	-13	0	1275	337	10		0
24	186215188	2014-03-08 01:20:00	WD4LHT	EL89tp	K9AN	EN50wc	10140229	30	-14	0	1275	337	10		0
25	186216649	2014-03-08 01:30:00	WD4LHT	EL89tp	K9AN	EN50wc	10140229	30	-12	0	1275	337	10		0
26	186218021	2014-03-08 01:40:00	WD4LHT	EL89tp	K9AN	EN50wc	10140229	30	-19	0	1275	337	10		0
27	186221325	2014-03-08 02:04:00	WD4LHT	EL89tp	K9AN	EN50wc	10140230	30	-11	0	1275	337	10	3.0.1_r246	0
28	186222294	2014-03-08 02:12:00	WD4LHT	EL89tp	K9AN	EN50wc	10140229	30	-21	0	1275	337	10		0
29	186225050	2014-03-08 02:32:00	WD4LHT	EL89tp	K9AN	EN50wc	10140229	30	-19	0	1275	337	10		0
30	186226654	2014-03-08 02:44:00	WD4LHT	EL89tp	K9AN	EN50wc	10140229	30	-15	0	1275	337	10		0
								Mean	-13.6333						
								SD	3.4490						
								AD	3.3667						
								AD%	98						

row	id	time	tx_sign	tx_loc	rx_sign	rx_loc	frequency	power	snr	drift	distance	azimuth	band	version	code
1	186172437	2014-03-07 21:10:00	WD4LHT	EL89tp	KV0S	EM38	10140254	30	-15	1	1387	318	10	4.0 r3015	0
2	186177758	2014-03-07 21:38:00	WD4LHT	EL89tp	KV0S	EM38	10140255	30	-14	0	1387	318	10	4.0 r3015	0
3	186184349	2014-03-07 22:00:00	WD4LHT	EL89tp	KV0S	EM38	10140255	30	-11	0	1387	318	10	4.0 r3015	0
4	186196156	2014-03-07 23:14:00	WD4LHT	EL89tp	KV0S	EM38	10140256	30	-10	0	1387	318	10	4.0 r3015	0
5	186197953	2014-03-07 23:26:00	WD4LHT	EL89tp	KV0S	EM38	10140256	30	-11	0	1387	318	10	4.0 r3015	0
6	186199635	2014-03-07 23:36:00	WD4LHT	EL89tp	KV0S	EM38	10140256	30	-13	0	1387	318	10	4.0 r3015	0
7	186203689	2014-03-08 00:00:00	WD4LHT	EL89tp	KV0S	EM38	10140256	30	-6	0	1387	318	10	4.0 r3015	0
8	186206883	2014-03-08 00:20:00	WD4LHT	EL89tp	KV0S	EM38	10140255	30	-10	0	1387	318	10	4.0 r3015	0
9	186208339	2014-03-08 00:30:00	WD4LHT	EL89tp	KV0S	EM38	10140255	30	-2	1	1387	318	10	4.0 r3015	0
10	186211284	2014-03-08 00:50:00	WD4LHT	EL89tp	KV0S	EM38	10140255	30	-12	1	1387	318	10	4.0 r3015	0
11	186212603	2014-03-08 01:00:00	WD4LHT	EL89tp	KV0S	EM38	10140256	30	-8	0	1387	318	10	4.0 r3015	0
12	186215324	2014-03-08 01:20:00	WD4LHT	EL89tp	KV0S	EM38	10140256	30	-14	1	1387	318	10	4.0 r3015	0
13	186216647	2014-03-08 01:30:00	WD4LHT	EL89tp	KV0S	EM38	10140256	30	-13	1	1387	318	10	4.0 r3015	0
14	186218005	2014-03-08 01:40:00	WD4LHT	EL89tp	KV0S	EM38	10140257	30	-13	1	1387	318	10	4.0 r3015	0
15	186219669	2014-03-08 01:52:00	WD4LHT	EL89tp	KV0S	EM38	10140257	30	-15	0	1387	318	10	4.0 r3015	0
16	186222332	2014-03-08 02:12:00	WD4LHT	EL89tp	KV0S	EM38	10140257	30	-19	1	1387	318	10	4.0 r3015	0
17	186225222	2014-03-08 02:32:00	WD4LHT	EL89tp	KV0S	EM38	10140257	30	-16	1	1387	318	10	4.0 r3015	0
18	186226700	2014-03-08 02:44:00	WD4LHT	EL89tp	KV0S	EM38	10140256	30	-16	0	1387	318	10	4.0 r3015	0
19	186228059	2014-03-08 02:54:00	WD4LHT	EL89tp	KV0S	EM38	10140257	30	-15	0	1387	318	10	4.0 r3015	0
								Mean	-12.2632						
								SD	3.9418						
								AD	-6.2632						
								AD%	-159						

Analysis of the trajectory of Flight MH370

Technical and Aeronautical analysis from take-off to the end of the flight

by

Captain Patrick Blelly (r) and Jean-Luc Marchand, MSc

patrick.blelly@protonmail.com, jean-luc.marchand@mh370-caption.net

Version 2.0 – 16 February 2023 – updated 22 March 2023

To the families of the victims …

Credit cover photo
Wikimedia commons creative license
Auteur :
Paul Rowbotham, CC BY-SA 2.0

Note: Part of this document may be used or copied with no restriction under the condition that its full title, its version number and date and the author's name are included on all such copies and derivative work.[1]

[1] *The authors are grateful to Peter Hotham (BSc(Hons), PgDip, FRAeS) for his review*

Executive Summary:

The known part and the recalculated unknown part of the trajectory

Reconstructing the proposed probable trajectory took four years and was made possible thanks to publicly available material and information. The main findings of this study and some complementary aspects have been recently published in a book [1]. This paper presents the methods used, the computations with their justification as well as the results in more details.

The following elements have been addressed:

1. The known trajectory from waypoint IGARI until the last radar contact in the north of Sumatra has been analysed in detail. It is shown that the U-turn during the rerouting of the aircraft was most likely performed manually. After a short descent, the aircraft flew at FL300 at a constant IAS of 310kt and slightly accelerated after 18h21' UTC. This matches the timing from the official Exit point after the U-Turn to the last radar contact.

2. The reconstructed unknown trajectory using proven aeronautical computations is based on:
    a. Our estimation of the fuel quantity at 18h28 UTC using weather data on that day.
    b. The Inmarsat satellite arcs which are considered trustworthy.
    c. Meteorological information of the day used by pilots and data collected a posteriori by satellites (wind maps, temperature reports, Global Data Assimilation System-GDAS, etc.)
    d. "In Flight Performance" tables for the B777-200ER powered by Rolls-Royce Trent 892 engines.
    e. 9M-MRO Specific technical data like the fuel consumption performance factor

3. BTO and BFO[2] values computed along our recalculated trajectory match the official measured values since they are within Inmarsat defined margins of +/-50 µs and +/- 7 Hz respectively.

The following conclusions were drawn:

1. The reconstructed trajectory is a quasi-straight continuous track, initially a magnetic track at 188° then true at 178°. It is somehow similar to Inmarsat's example published in the report "the Search for MH370" [3]. Figure 1 below allows comparing the reconstructed trajectory in yellow with Inmarsat's example in red.

2. Thus, Inmarsat "loss of contact point" is very close to the reconstructed unknown trajectory path and it coincides well with our estimated location where the second engine was voluntarily shut down (c.f. Figure 3).

3. The northernmost probable point of impact (POI) identified in this study is located at approximately [35°31'S ; 93°02'E]. It is also very close to the POI computed by CSIRO forward drift analysis reported in their report n°III of 26 June 2017. In addition, potential debris have been photographed by the French CNES Pléiades 1A satellite in this area.

[2] *BTO: Burst Time Offset; BFO: Burst Frequency Offset*

4. Concerning the end of the flight, two slightly different possible scenarios have been elaborated. Both include a gliding phase with a final controlled ditching producing little debris. Scenario 1 is illustrated in Figure 2.
5. From these scenarios, a zone for a new search of the wreckage is proposed (Green area in Figure 3) which extends the already searched area in 2018 to the south by about 25Nm. Its width is ~15Nm. The estimated duration to scan this area of ~350Nm^2 is approximately 5 days according to recent information provided by Ocean Infinity which was the last company searching in the field in 2018.

All of this forms a coherent and realistic piloted trajectory.

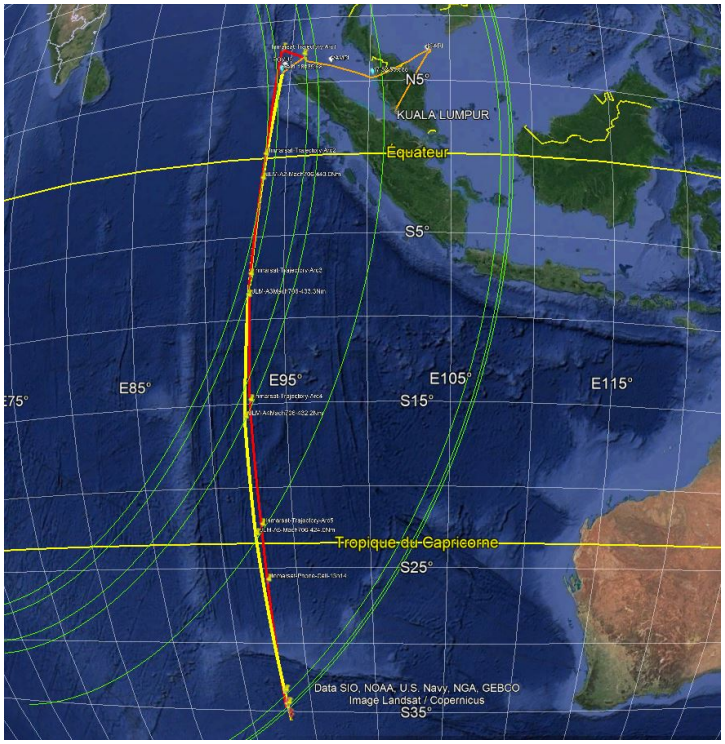

Figure 1: Reconstructed trajectory (Yellow) and Inmarsat example (Red)

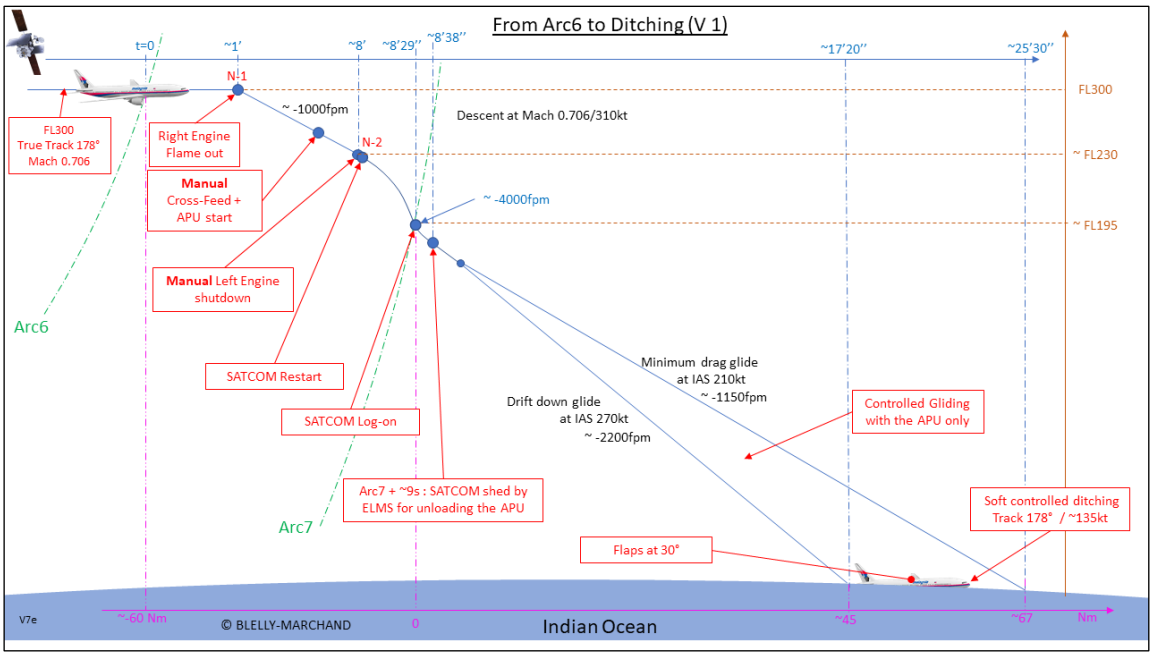

Figure 2: Scenario 1 of the probable final descent of MH370 with a glide

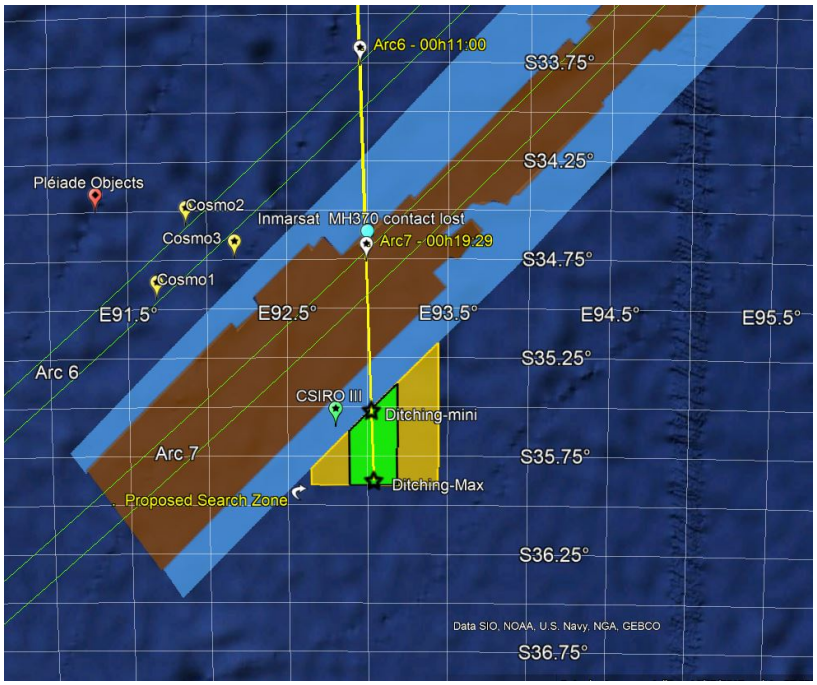

Figure 3: Proposed search zone (Green, ~300Nm2) and CSIRO III estimated Point of Impact Contact

Table of Contents

1 Introduction 8
2 Overview of the flight 9
3 The known trajectory 17
3.1 Introduction 17
3.2 From Kuala Lumpur to IGARI 17
3.2.1 Flight plan and clearances until the transfer 17
3.2.2 From the ATC transfer to Waypoint IGARI 18
3.3 Diversion from the flight plan at IGARI: The U-Turn 18
3.3.1 Introduction 18
3.3.2 Available data 19
3.3.3 Subsequent Hypotheses 24
3.3.4 Simulations 27
3.3.5 Conclusions on the U-turn after waypoint IGARI 33
3.4 From the Exit Waypoint to the last radar contact 33
3.4.1 Available data 33
3.4.2 From the U-turn Exit waypoint to Penang 39
3.4.3 From Penang to the Last Radar Plot 43
3.4.4 Conclusions on the leg from the Exit Waypoint to the last radar contact 48
3.5 Conclusions on the known trajectory 48
4 The unknown and recalculated trajectory 49
4.1 Introduction 49
4.2 Available data 49
4.2.1 Inmarsat data 49
4.2.2 FIRs 50
4.2.3 Southeast India ADIZ 51
4.2.4 Routes and Waypoints 52
4.3 The « Final Major Turn » (FMT) 53
4.3.1 Hypotheses at the Last Radar Plot 54
4.3.2 From Last Radar Plot to the electrical power restoration 54
4.3.3 From the electrical power restoration to the Arc1-Crossing 55
4.3.4 From Arc1-Crossing to Arc1.2-Crossing… a manual turn 59
4.3.5 From Arc1.2-Crossing to POVUS 60
4.3.6 From POVUS to the Phone call-1 location 61
4.3.7 Compliance with Inmarsat data 63

4.3.8 Simulations 63
4.3.9 Conclusions 64
4.4 En-route at 188° from Phone Call 1 to Arc6 65
4.4.1 Speed and Altitude Computation 65
4.4.2 Reconstructing the “Southern Leg” 69
4.4.3 Validation of the “southern leg” with Inmarsat data 71
4.5 The Final Descent to the End of the Flight 74
4.5.1 Hypotheses and basic parameters: 74
4.5.2 Profile of the descent 75
4.5.3 Estimated point of ditching 77
4.5.4 Simulations 78
5 The proposed new search zone 78
6 Conclusions 80
7 Additional elements of interest …. 81
7.1 Visual detection of satellite images 81
7.2 How does our trajectory compare with Boeing Performance Analysis? 81
8 Annex 1: Variant 2 of the End of the Flight 85
9 References 87
10 Abbreviations and Index 89

1 Introduction

This paper presents the results of a study by Captain Patrick Blelly and Jean-Luc Marchand, MSc, performed during several years.

The aim is to demonstrate that a probable cause of flight MH370's disappearance was a well-prepared hijacking by a highly skilled aeronautical person and most probably a professional pilot. The main driving hypothesis is this person in command went for a nefarious one-way journey with the aim to make the plane disappear without any trace in the South of the Indian Ocean.

Our approach is humble and based on realistic hypotheses with an attempt to unify and consolidate aeronautical operational elements. We used all available officially published technical satellite data within a demonstrable scenario with no identified flaw to our knowledge, as explained in Chapter 2.

It was found important to provide our findings not only for the unknown part of the flight but also for the known part as both form a coherent scenario.

Thus, the trajectory includes two major parts:

- The verified known trajectory segment

  This part of the flight begins at Kuala Lumpur and lasts until the last recorded radar plot as known thanks to published official radar data. It is addressed in Chapter 3.

- The recalculated unknown trajectory

  Chapter 4 explains the unknown trajectory reconstruction mainly based on aeronautical data validated by the published Inmarsat satellite data. It begins at the exit of the radar coverage in the northwest of the Malacca Straight and ends by a ditching in the south of the Indian Ocean.

In addition, Chapter 5 details the new zone proposed for future search of the wreck.

Some additional elements of interest are also provided in Chapter 7.

This contribution is to be considered as a working hypothesis to support any future search for the wreck. Our hope is to provide solid elements to help manifesting the truth about this disappearance.

2 Overview of the flight

Our reading of the events is that the person in command followed a well thought, well-prepared diverted flight as analysed in Captain Blelly's book [1].

The main driving hypothesis is made that the person in command went for a nefarious one-way journey with the aim to make the plane disappear without any trace.

This work represents some years of work still it does not pretend to be the truth. We have reconstructed the first part of the MH370 flight by using the published radar tracks, by re-computing the aeronautical parameters of the aircraft as well as by taking into account the airspace structure. For the "unknown" second part of the trajectory, we have computed a path until the end of the flight and ensured that all Inmarsat data were matched. This was done to help potential future search for the wreck and also for the families of the victims. It is our humble contribution.

The key elements of this flight are presented below as numbered bullets points for the sake of simplicity:

1. The leg from take-off at Kuala Lumpur to abeam waypoint IGARI was flown, according to the filed flight plan, as shown in Figure 4. Some additional clearances were given to the pilot like a more direct route to waypoint IGARI or a final flight level at FL350, above the one originally requested.

2. Abeam waypoint IGARI, the transponder was manually switched to stand-by making the aircraft disappear from the screens of the civil air traffic controllers. In addition, the right turn towards waypoint BITOD was interrupted and was shortly followed by a U-turn to the left.

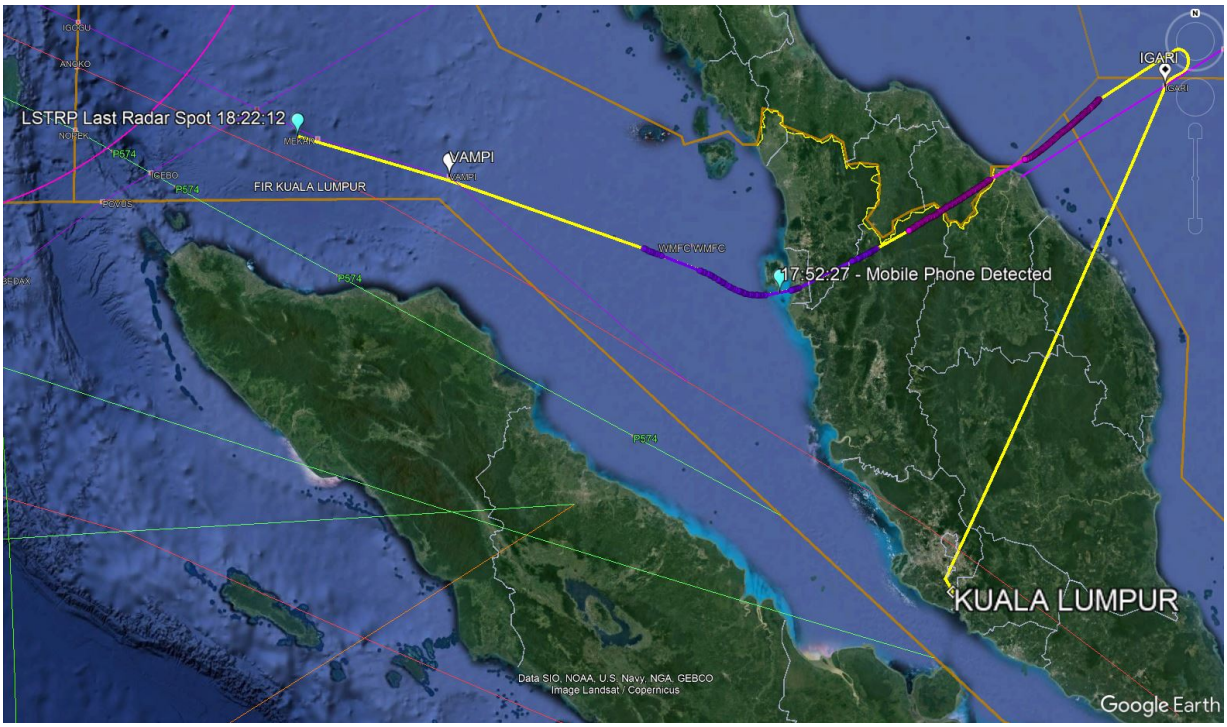

Figure 4: Known trajectory of Flight MH370 from Kuala Lumpur till the last radar plot

3. This U-turn is considered to have started earlier than the “official” entry point defined in the Malaysian official report [2]. Most likely, it started just after the overshoot of waypoint IGARI. The turn was performed manually as the military radar track shows a geometrical shape of a turn with a banking up to its maximum i.e. ~38°. This is incompatible with a standard LNAV (with the auto-pilot) manoeuvre which limits the banking to 25°. In fact, the presence of the Thai Air Defence Identification Zone (Thai ADIZ) in the vicinity is a clear constraint for the turn and explains why the person in command avoided trespassing it and performed a very sharp manual turn. The turn finished at the “official” exit point when the aircraft was on direct track to Kota Bharu. We supposed the flight maintained a constant flight level FL350 (i.e. ~35000ft) during the U-turn.

4. After having overflown the official “exit” point and because of the high banking turn the aircraft speed had probably dropped down to M0.787.

5. Most likely, it was then the time when the person in command carried out a series of technical actions: total power outage by disconnecting the two main generators control push-buttons and the two back-up generators control push-buttons. In addition, he prevented the auto start of the auxiliary power unit (APU) by turning its knob to On and Off successively. The electrical outage would have triggered the Ram Air Turbine (RAT) automatic deployment. The RAT is a small windmill generator used as last resort. Flying with the electricity power provided by the RAT only and with the full hydraulic power from the main engines is manageable for an experienced pilot. Carrying out these actions before the turn is unlikely as performing this high banking U-turn without electricity in a degraded control mode would have been difficult. Additionally, depressurising the aircraft before the turn would have required the person in command to wear his full-face oxygen mask and reducing his flying capabilities. Thus, we believe these actions were performed after the U-turn.

6. The way-out trajectory began at the official exit point and the aircraft approximately overflew waypoint GOLUD and continued towards the south of Penang Island. Because the aircraft was being depressurised after the U-Turn at waypoint IGARI, the person in command probably started descending to FL300 (~30000ft approx.).

7. From the beginning of the descent, the A/P was disconnected due to the electrical power outage and subsequently the throttle was probably in a steady state. Thus, the aircraft accelerated up to about ~M0.85 most likely and reached the IAS (Indicated Air Speed) speed of 310kt which was further manually maintained steadily as the reference speed until waypoint VAMPI.

8. But rate of descent must have been low between 300fpm and 500fpm for two reasons: a sustainable pain in the ears of the person in command due to the change of pressure and also to avoid that passengers’ mobile phones could get connected to a terrestrial telecom network close to Kota Bharu revealing his presence and possibly placing calls to alert third parties. The bottom of the descent is probably in the vicinity of Kota Bharu.

9. The chosen flight level FL300 (30000ft with altimeter reference at 1013.25hpa) is in the low-level part of the airways followed by long haul flights reducing the probability of conflicts.

10. Also, this allowed a better ground speed for a given Mach with the best specific fuel consumption.

11. In addition, as the meteorological conditions were excellent at that time, Kota Bharu city lights might have been a landmark in the first place and allowed the person in command to fly visually just above the Thai boundary. Later, a more precise navigation was required to stay within the boundary area without trespassing the Thailand airspace and the most likely, efficient means is to use Penang radial VOR (VPG) which also explains the small path deviations mentioned in the Malaysian report [2] as the aircraft did not follow specific routes.

12. Still manually piloted, the aircraft circumvented Penang Island to the south. Then it took a heading at 301° intercepting the VPG outbound radial at ~291°/292°. At that moment, it was away from any IFR[3] airway. During the leg Penang to waypoint VAMPI, the latter could have been targeted thanks to its icon visible on the navigational display (ND), consolidating the manual flight path using the VPG 291° radial outbound. The flight level was still maintained at FL300 and the IAS was maintained at ~310kt. Waypoint VAMPI is 170Nm away from Penang and thus is well within VPG range. Thus, overflying waypoint VAMPI was an easy task.

15. Shortly after waypoint VAMPI, the aircraft exited the VPG range making the radio navigation impossible for the intended flight path any more. Thus, the person in command was left with the MEKAR icon on the ND screen with the inertial navigation function due to the RAT. Subsequently, his route was less precise considering also the potential inertial drifting (triple mixing) affecting the actual position of the MEKAR icon in particular. This is why the aircraft flew a little south of MEKAR as shown on the Lido hotel official image shown to the Next of Kin (cf Figure 23).

16. It is our understanding that the person in command's intent was to overfly waypoints VAMPI, MEKAR, NILAM (all on route N571), SANOB, IGEBO, POVUS (all on route P627) and then a constant track to the south of the Indian Ocean after passing Banda Aceh (Sumatra) as illustrated in Figure 4 and in Figure 5. The selected magnetic track was most probably at ~188° to avoid adverse meteorological conditions reported in the southwest of Banda Aceh. Following route P627 from waypoint NILAM would ensure not to enter the South-India ADIZ and also to only cross one FIR boundary i.e. the one between FIR Kuala Lumpur and FIR Jakarta

[3] IFR: Instrument Flight Rules

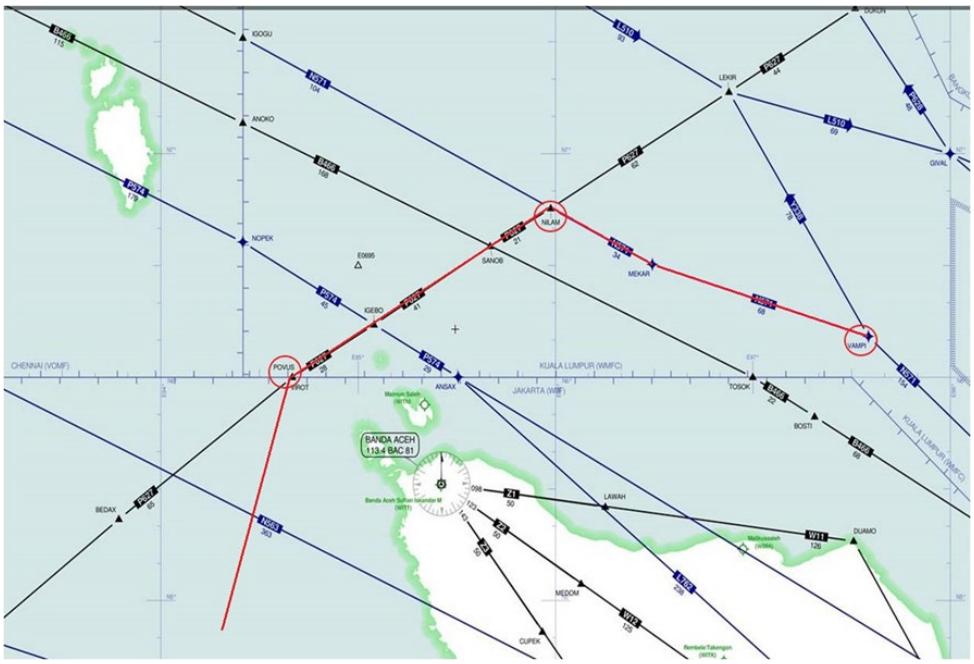

Figure 5: Flight intent after waypoint VAMPI to get around Sumatra without ATC drawing attention

17. To stay on his intended path, the person in command had to reactivate the LNAV function at some point after having restored the full electrical power. The Inmarsat data records show that it was decided to do so at about 18h23 UTC after having passed abeam waypoint MEKAR and being out of range of Butterworth military radar (Penang Island). It is also noticeable that this is basically one hour after exiting the U-turn at IGARI.

18. From waypoint VAMPI, the flown path appears to indicate that the aircraft flew the intended path like any commercial airliner would do in this region respecting the airmen rules to avoid drawing military controller's attention by an abnormal behaviour. The transponder is meant to be on standby still and thus was not responding to any civil SSR (secondary Surveillance Radar) interrogation leading to the absence of tag on the Indonesian civilian ATC controller's screen. Furthermore, staying on airways N571 and then on P627 would ensure that the aircraft would not enter in the range of Car Nicobar military radar or trespass the Indian ADIZ.

19. As soon as the electrical power was restored, a kind of countdown was triggered for the person in command to react in a minimum time and quickly configure and engage the autopilot for safely managing the aircraft trajectory. This was needed to create an opportunity for disabling as soon as possible all communication systems before they could broadcast any message, and therefore stay undetected. The intent was to make the aircraft follow published local airways with the LNAV function. In addition, also restoring the pressure was most probably on its way at this time (automatically or manually). Blocking the communications before the Satellite Data Communication Unit (SDU) became operational was probably done thanks to a data link reset via the Communication Manager page on the MFD (Multi Function Display) which, in flight, has a side effect of erasing the flight and company information and in particular the flight identification (Flight ID). It should be noted that this is the unique way to have the Flight ID erased and missing in the SDU signal units as reported in the Malaysian report [2].

20. In our opinion, the Inmarsat BFO for Arc-1 at 18h25:27 can be used and provides a trustful indication on the potential trajectory. Therefore, we included it in our recalculation of the flight path at that time.

21. Thus, in the rush for completing these tasks, the person in command is likely to have had difficulty to properly control the trajectory during two minutes approximately and probably did not pay attention to the actual position of the aircraft relative to Route N571. We make this hypothesis because we think that the person in command had to look down to complete his tasks on the MFD and FMC and did not pay sufficient attention to the evolution of the aircraft track.

22. When the FMC was fully operational, the most logical first waypoint entered was probably NILAM. Thus, the person in command had sequentially keyed NILAM in, then pressed "Execute" on the MCDU and pressed the "LNAV" button on the MCP commanding the aircraft to pass by waypoint NILAM automatically. Thus, being in the south of the route, the aircraft had to turn right to the north in direction to NILAM as revealed by the Inmarsat BFO value at Arc-1 time. We don't think it is a coincidence that waypoint NILAM was basically overflown, it was a properly executed route. In addition, as the reference IAS is reset to 200kt at power-up on the MCP, the person in command had to manually increase the requested speed to a much more adequate value. Thanks to Inmarsat data, we estimate this value to be close to 325kt and surely below the maximum operating speed of VMO 330kt up to flight level FL300. This is in line with the behaviour of someone keen to escape quickly, but things did not go exactly as planned.

23. A second hitch comes from the fact that, at power-up, the FMC grasps the instantaneous rate of descent (or climb) and keeps it as the reference value on the MCP. At that time, it was around -1000fpm in descent as indicated by Inmarsat data. The descent lasted around 2.5 minutes leading the aircraft to ~FL270 (~27000ft). This could be explained by one of these following reasons:

    - Either the person in command voluntarily triggered a descent when he saw the lights of the Indigo traffic coming ahead. As he thought he was on Route N571, as MH370 was not detectable by the other aircraft due to the TCAS standby state and lights off and as he could not know what was the Indigo's flight level, a potential collision was possible. Descending was safe and would be seen by ATC as a normal behaviour.
    - Or, in the rush and with the oxygen mask on, the person in command did not pay attention or was focused on the MFD and MCDU displays while the aircraft was descending as mentioned above.

Figure 6: Heading to waypoint NILAM after electrical power restoration

24. A few minutes after the electrical power was restored and after having completed the urgent actions with head down, the person in command likely realised the aircraft was heading north while descending and reaching ~FL270. Immediately, the auto-pilot was disengaged and a manual left turn was started with a high banking along with a climb to get back to FL300. The Inmarsat BTOs indicate that the turn had to be sharp especially towards the end, probably to stay as close as possible to route P627 by a direct to waypoint POVUS. Doing so put him close to his intended path at the planned flight level in quasi-normal flight conditions.

25. After this first part of the FMT, the time tags show that the aircraft strongly accelerated probably to cross the straight between Andaman Islands and Sumatra Island and get out as quickly as possible of this area where its recovered awkward manoeuvre took place. Our analysis shows that the reference IAS was ~325kt which is close to Mach 0.850. Let's remember that the LNAV function became operational again. The person in command keyed in "direct to waypoint POVUS" on the MCDU followed by "Execute" and then engaged the LNAV function of the A/P.

26. After the first part of the FMT, the aircraft made a speedy direct to waypoint POVUS.

27. Then, it is most probable that at waypoint POVUS, the aircraft started the second part of the FMT by turning left to a southerly direction. Several studies suggested that its heading was established at 180°. But to avoid encountering dangerous meteorological phenomena developing around [4.25N;95.5E] in the south/southwest of Banda Aceh in the form of a cumulonimbus, the person in command probably selected at different track at ~188°. In addition, this was a safe way to avoid detection by the military radars located on Sumatra west coast in particular Sibolga radar.

28. Shortly after overflying waypoint POVUS, and en-route on track ~188°, the person in command kept this magnetic track constant until crossing about 25° South parallel. At this latitude, the strong increase in magnetic declination forced him to switch to true (track/heading) function. Thus, the aircraft followed an almost-linear southern trajectory from 18h40 UTC onwards.

29. As reported in the Malaysian report [2], the right engine consumed more fuel than the left one leading to the right engine starvation in the first place. We think that according to Captain

Blelly's book [1] the APU was then started manually before voluntarily shutting down the left engine. Thus, the APU had enough fuel to power all systems allowing a fully controlled final ditching i.e. probably about 200kg.

30. Based on the Inmarsat data between Arc6 and Arc7, two possible piloted trajectories of descent could be envisaged including a low speed or a high-speed segment. In fact, the last BFO (-2Hz) at 0h19:37 reported in Inmarsat report [3] raises questions and appears to indicate that aircraft was in a high diving for few seconds followed by a safe aircraft recovery by the person in command.

The major events of the recalculated trajectory are summarised in Table 1.

Table 1: Synopsis of the recalculated trajectory

Time UTC	Location	Event/decision	Comment
17h07:49		Last radio voice communication from the aircraft	Official
17h20:34	IGARI	Transponder manually switched to Standby abeam IGARI	Official
~17h21:53	U-Turn actual start		Estimated
17h22:30	U-Turn Entry point		Official
17h24:40	U-turn Exit Point	End of the U-Turn after IGARI	Official
~17h36:50	~GOLUD (Kota-Bharu)	Bottom of Descent to FL300	Estimated
17h52:27	South of Penang	Co-pilot mobile phone connected to network	Official
~18h02:40	~Pulau Perak Island		Estimated
~18h13:00	VAMPI		Estimated
18h21:00	MEKAR		Estimated
18h22:12	10Nm after MEKAR	Accelerating in descent	LSTRP, Official timing, approximate official location
~18h23:30	6°34'32"N/96°8.00'E	Electrical power restored	Estimated
		Autopilot engaged	In descent
		Data Link Reset	En-route to NILAM - descending
18h25:27	~NILAM (FL270)	Arc-1 Ab-initio Logon	Official timing only - Heading north
~18h25:40	6°46.90'N/95°58.53'E	FMT part1: Manual turn	To correct towards route P627
18h27:05	6°54.77'N/95°51.58'E	Arc1.1	Official timing only - turning and climbing
~18h27:35	6°53.41'N/95°48.06'E	End of FMT part1	Estimated - still climbing (FL280)
		En-route to POVUS	Heading 233° - still climbing
18h28:06	6°50.90'N/95°44.81'E	Arc1-Boeing	Official timing only - still climbing (FL295)
18h28:15	6°50.19'N/95°43.86'E	Arc1.2	Official - still climbing (FL297)
~18h28:25	6°49.26'N/95°42.64'E	Levelled at FL300	Estimated
~18h37:40	POVUS	FMT part2	Estimated
18h39:58	5°45.75'N/94°29.57'E	Phone Call-1	Official timing only – En-route heading 188°
19h41:03	1°34.61'S/93°31.74'E	Arc-2	Official timing only
20h41:05	8°48.60'S/92°42.17'E	Arc-3	Official timing only
21h41:27	16°03.39'S/92°13.74'E	Arc-4	Official timing only
22h41:22	23°09.83'S/92°24.81'E	Arc-5	Official timing only
23h14:30		Phone Call-2	Official timing only
00h11:00	33°45.88'S/92°57.09'E	Arc-6	Official timing only
00h19:29	34°45.40'S/92°59.56'E	Arc-7	Official timing only
		Controlled Ditching/EoF	Estimated

3 The known trajectory

3.1 Introduction

This chapter addresses the part of the trajectory fully known thanks to published ATC information and radar data.

The objective is to reconstruct a realistic trajectory using available official data as well as data from public sources in particular the Boeing trials to simulate the U-turn. We have validated this trajectory by simulation sessions using three different simulators (Prepar3D, FsX and a fixed based simulator in the city of Nantes with an active airliner B777 captain).

3.2 From Kuala Lumpur to IGARI

The segment from take-off to abeam waypoint IGARI is perfectly known due to the radar data, the surveillance ADS-B data and the testimony of the controllers in charge of this flight.

3.2.1 Flight plan and clearances until the transfer

Before the flight, Malaysian airlines filed the ATC flight plan as provided in Figure 7.

```
KLA297 070444
FF WMKKZQZX WMKKZRZX
070441 WMKKYOYX
(FPL-MAS370-IS
-B772/H-SDFGHIJ3J5M1RWXY/LB1D1
-WMKK1635
-N0470F290 DCT PIBOS R208 IKUKO/M081F330 R208 IGARI M765
 BITOD/N0480F330 L637 TSN/N0480F350 W1 BMT W12 PCA G221
 BUNTA/N0480F370 A1 IKELA/N0480F370 P901 IDOSI/N0480F390 DCT CH
 DCT BEKOL/K0900S1160 A461 YIN/K0890S1130 A461 VYK
-ZBAA0534 ZBTJ ZBSJ
-PBN/A1B1C1D1L1O1S2 DOF/140307 REG/9MMRO EET/WSJC0032 VVTS0042

ZJSA0210 VHHK0233 ZGZU0304 ZHWH0356 ZPE0450 SEL/QRC RMK/ACASII
EQUIPPED)
```

Figure 7:MH370 ATC Filed Flight Plan for 7-mar-2014 at 16h35 UTC

Until waypoint IGARI and as stated by the Malaysian report [2], MH370 was a normal flight following its filed ATC flight plan according to the aviation rules until its transfer by Kuala Lumpur ATC to Ho Chi Minh ATC.

In our opinion, this particular moment is the most appropriate time to hijack the aircraft because the flight was not in contact with the Malaysian controller and not yet in contact with the Vietnamese controller.

3.2.2 From the ATC transfer to Waypoint IGARI

Thanks to the transponder on-board the aircraft which responds to the interrogations of the secondary surveillance Radar (SSR) and which also cooperatively broadcasts ADS-B[4] data including the aircraft position in time, the aircraft actual route is precisely known until the last ADS-B message transmitted at 17h20:34 UTC when the transponder knob was manually put on stand-by.

At that time, the aircraft was located exactly abeam waypoint IGARI after having started a turn to the right to follow route M765 to the next planned waypoint i.e. BITOD.

The perfectly known trajectory until that time is illustrated in Yellow in Figure 8.

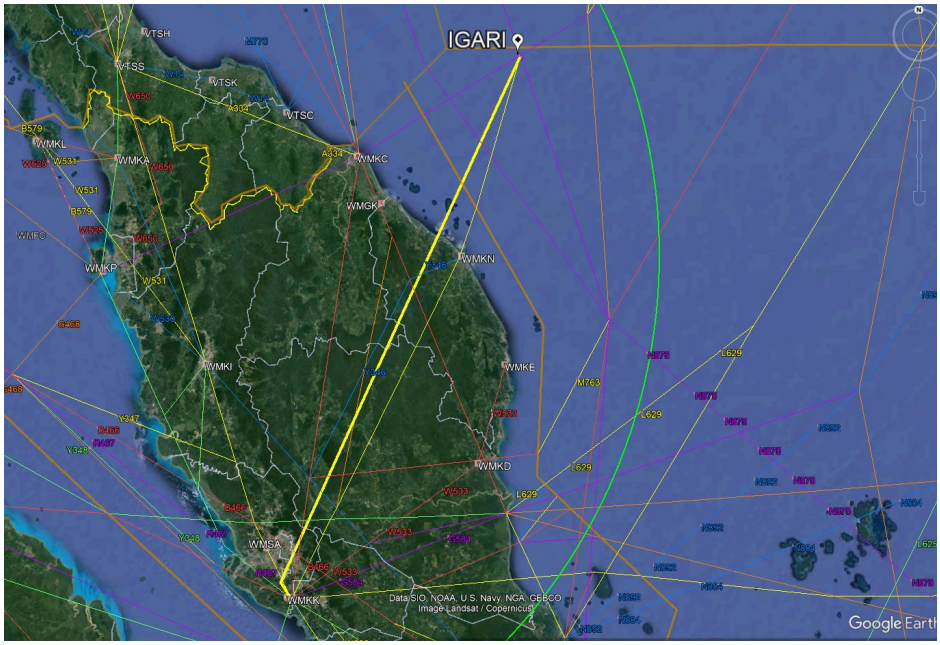

Figure 8: Perfectly known trajectory of MH370 from Kuala Lumpur until abeam waypoint IGARI

3.3 Diversion from the flight plan at IGARI: The U-Turn

3.3.1 Introduction

This section presents the findings of our study focused on reconstructing the portion of the trajectory, which started shortly after 17h20 UTC when the aircraft was abeam waypoint IGARI. A U-turn was performed in less than five minutes. During this time interval the radar data shows that the aircraft performed a sharp U-turn to the left heading abeam northern to Kota Bharu in Malaysia.

The unique available data of this turn is provided on page 3 of the Australian report [4] in a very low-resolution image illustrating the radar track drawn on a GoogleEarth map. Figure 9 presents a zoom of this image, which depicts the aircraft passing abeam waypoint IGARI until the end of its U-turn towards Kota Bharu. A few extra key elements for the analysis have also been added on this image. Unfortunately, the military and the civilian authorities did not officially release any primary radar data.

[4] *ADS-B: "Automatic Dependent Surveillance – Broadcast" is a cooperative system for aircraft information dissemination*

According to the Malaysian final report [2], the six trials performed by Boeing to simulate such a turn have not been conclusive. It is believed here that it comes from the use of only two officially identified waypoints called “Entry waypoint” and “Exit waypoint” separated by 2min 10 sec. But, when considering the shape of the radar track and the geometry of the U-turn, a new, more detailed analysis is required considering an earlier start of the turn i.e. before the “Entry waypoint”.

3.3.2 Available data

This detailed analysis is based on information provided by the ATSB Transport Safety Report published in June 2014 p3 [4], the Malaysian Safety Investigation Report [2] and its Appendix-1.6E including the results of the Boeing Performance-Analysis [5], the navigation chart for airmen, the ADS-B data published by the Independent Group [6], the GDAS meteorological data provided by Nullschool [7] and the civilian approach radar data provided by the Independent Group [8]. They are reviewed one by one in this section.

3.3.2.1 Military primary radar plots

The unique source of information on the actual aircraft trajectory at, and after, waypoint IGARI is provided on page 3 of the Australian report [4] in a low-resolution image reproduced in Figure 9.

In this unique image, the aircraft position - as acquired and forecasted by the radar - is shown by quasi-white fuzzy successive spots. This path exhibits an unrealistic steep angle impossible to be flown by such an aircraft of this weight. This shape is due to the “coasting” algorithm (i.e. predictive) of the radar tracking system which probably received low-quality echoes from the aircraft at this point in time - or even lost them - probably because being - or close to be - out of range of the radar (cf Figure 10). Thus, the radar extrapolated the path based on the last reliable echoes and also on the a-priori knowledge of the next waypoint via the ATC filed flight plan. When the plots acquisition resumed, the prediction did not match anymore. Thus, the algorithm “jumped” to and restarted from the updated real location of the aircraft and filled the gap of the trajectory with straight lines for reconstructing a continuous track which was not actually flown. This explains the strange shape of the trajectory with such a steep angle.

Figure 9 : Military primary radar tracking during the U-Turn between waypoints IGARI and BITOD

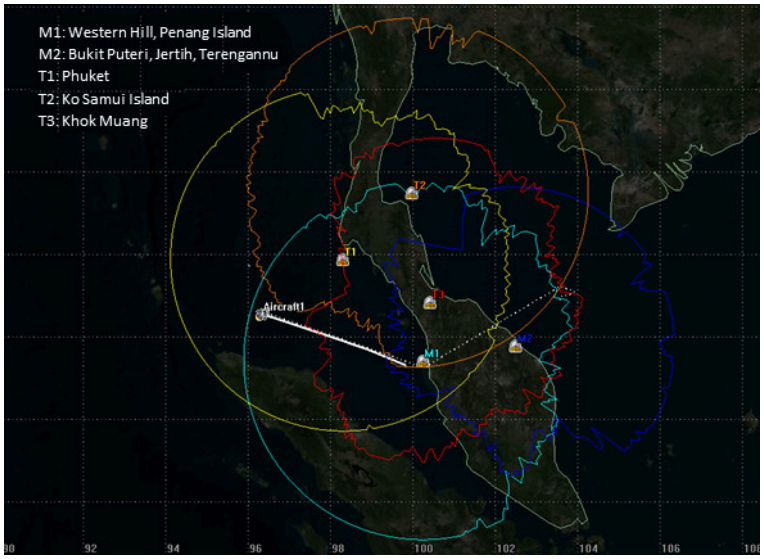

Figure 10: Range of military radar sites for an aircraft at 37,000ft (source B. Hall)

Nevertheless, this low-quality path image is very useful to the overall understanding because it allowed the Malaysian investigators team to define two useful waypoints in the U-Turn. On our side, we have used this image also to "shape" the path to be followed during our simulations according to the best-fit principle especially with the actual acquired plots, ignoring the predicted part.

3.3.2.2 The official Entry and Exit points

The official Malaysian report [2] presents Boeing trials results to simulate the complete U-Turn. They were principally based on those two specific theoretical reference waypoints defined for this occasion and officially called "Entry Point" and "Exit Point". They are located as indicated in Figure 9 and their

coordinates are recalled in Table 2 as determined by Boeing. Their time separating interval is 2:10 minutes.

Table 2: Official reference waypoints defined for analysing the U-Turn at IGARI

	Latitude	Longitude
Entry Point	N07.05.7	E103.47.1
Exit Point	N07.12.7	E103.38.7

We have used these two waypoints in our simulations as mandatory waypoints to be overflown.

3.3.2.3 Boeing simulations

Section 2.1 of the Malaysian report [2] presents the detailed results of the six attempts by Boeing to simulate the diversion from the flight plan. A summary is presented in Figure 11. Four attempts were performed with the autopilot engaged and two with a manual piloting. None of the six simulations could match the 2:10 minutes timing between the Entry and Exit points. It should be noted that, by definition, Boeing considered the U-turn to have started precisely at the Entry point.

In its lower part, Figure 11 recalls also the common factors and flight parameters used for the sessions.

SAFETY INVESTIGATION REPORT
MH370 (9M-MRO)

Re-enactment	Session					
	1	2	3	4	5	6
Ground Speed (in knots)	475	475	425	400	475	425
Autopilot Engaged	✓	✓	✓	✓	x	X
Additional Waypoint	x	x	X	N05.15.6 E100.27.5	✓	✓
Bank angle (in degrees)	26°	26°	28°	23°	30-32°	35°
Exit Waypoint Time	Over-Shooting	2 min 45 sec	3 min 3 sec	3 min 30 sec	2 min 40 sec	2 min 28 sec

Table 2.1G - Re-enactment Sessions

Common Factors		
1.	Fuel	41,200 kg
2.	Gross Weight	215,410 kg
3.	Height	35,000 ft
4.	Entry Point	N07.05.7° E103.47.1°
	Exit Point	N07.12.7° E103.38.7°
5.	Autothrottle Engaged	

Table 2.1H - Common Factors

Figure 11: Summary of Boeing unsuccessful sessions to match the U-turn timing (Source Report [2])

These results compared to the geometry of the radar track led us to a new analysis with a new perspective considering an earlier start of the U-turn. This would make the official "Entry point" a simple point to be overflown in the course of the turn (c.f. Figure 9).

During our simulations, the same aircraft configuration was used at flight level FL350.

3.3.2.4 FIRs boundaries

As already underlined by the authors in several previous studies, the choice of the location to perform the U-Turn is particularly well chosen for whoever wants to escape from the civilian ATC and also from Military ATC at night. The U-turn started just after crossing the Kuala-Lumpur FIR northern boundary (c.f. the thick blue-green line in Figure 12) where the Malaysian controller would not pay attention any more as he had "transferred" the flight to the next control sector according to the rules. The turn started before executing the mandatory self-identification by the aircraft to the Vietnamese ATC and hence before calling for his attention. This timely "in-between" tiny location was thus temporarily without sustained attention from both controllers. This transfer would normally be executed within one minute. Actually, the ATC Vietnamese controller reacted 14 minutes later.

3.3.2.5 The Thailand ADIZ

Furthermore, this tiny geographical location must be considered in a wider perspective taking into account the surrounding airspace structure. In this area, another important constraint is imposed to the airmen by the Thai military authorities. Thailand has defined an air defence identification zone (ADIZ) named TADIZ. It provides an early warning system to detect possible incursion into Thai sovereign airspace. ADIZ are not part of any international treaty or body.

To enter TADIZ any intruder must satisfy specific formalities (ATC filed flight plan, early warning and in particular to have an active transponder in working condition, etc.) and being known in advance to the Thai military controller before entering. Its southern boundary is located at about 18Nm north of waypoint IGARI as illustrated in Figure 12 by the double dotted purple line and the red arrow.

The existence of the Thailand ADIZ is a new element brought by the analysis presented here. To our knowledge, none of the previous studies considered it as a constraint for the turn. But we think it was.

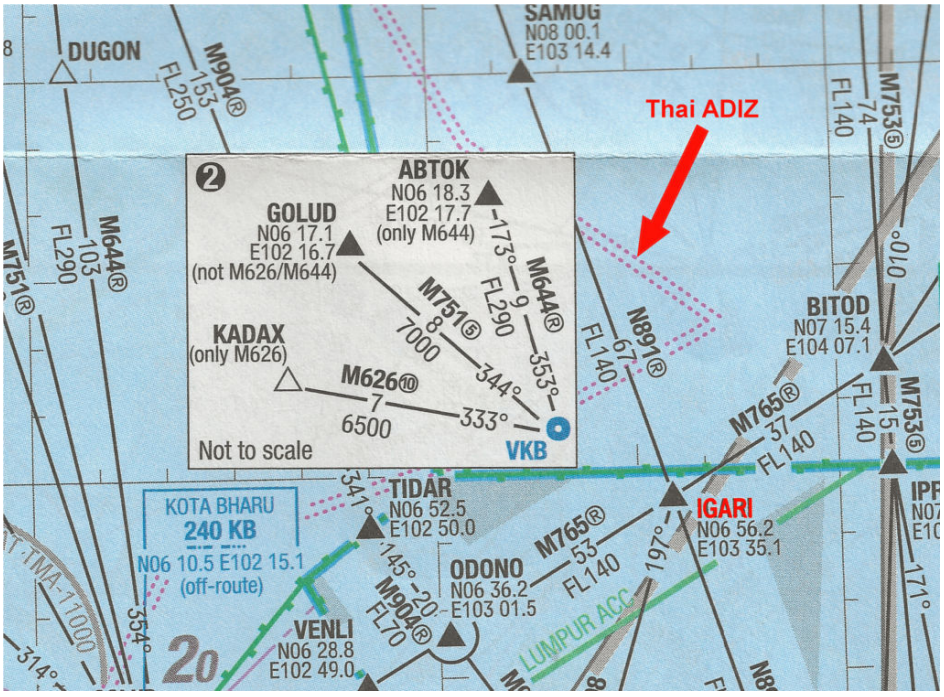

Figure 12: Location of waypoint IGARI at ~18Nm south of the Thailand ADIZ boundary (source: Aeronautical map from Lido/RouteManual AS 14HL 20-04-2017)

The presence of this boundary imposes a high constraint for a person in command planning a U-Turn in this area requiring the turn diameter to be less than 18Nm to avoid drawing Thai military

controller‘s attention. Thai Khok Muang military PSR radar is covering this area with a potential backup from the Ko Samui Island radar PSR.

Due to no compliance to these formalities, the aircraft had to avoid entering the ADIZ absolutely if it wanted to remain discreet.

3.3.2.6 ADS-B data unavailable due to transponder switched to stand-by.

As explained above, until some point in time, the aircraft was transmitting the required information to the air traffic control (ATC) via its transponder as part of the collaborative surveillance system called ADS-B for Automatic Dependent Surveillance – Broadcast. This information (different from ACARS) provides detailed numerical values on the aircraft situation. This includes its call sign, its aircraft type, its precise position, its speed, its flight level and its intent. When this information is actually coming from the aircraft, the controller in charge is informed by a specific icon (usually a “@”) enlightened in the aircraft label on his screen.

Thanks to the Independent Group (IG), records of ADS-B data received at the Malaysian ATC station in Terengganu (c.f. Figure 13) have been made publicly available [6]. In addition, the IG clearly demonstrated that the transponder was manually and gradually switched to standby before the last ADS-B data transmission which took place at 17:20:34:55 UTC via an ADS-B point message with no altitude report.

This constitutes an additional element towards a deliberate human action as opposed to an automatic switch off due to a system or electrical failure which would have prevented such an altitude message to be sent.

Figure 13: ADS-B receiving stations (red spots) when the aircraft stopped broadcasting its position (source IG and RMC Story Channel [14])

3.3.2.7 GDAS Meteo data

In our simulations, we have used meteorological data produced by the Global Data Assimilation System (GDAS) accessible via the website earth.nullschool.net [7]. Due to the sampling of the data, Runge-Kuta interpolations were performed both in time and in space (i.e. 4D) at flight level FL350.

The data shows that during the U-turn the meteorological conditions were stable, but not favourable, pushing the aircraft to the west towards the Thai ADIZ with an easterly wind of 11kt from 95°.

3.3.2.8 Civilian approach radar data

To complete the data set, we have used the civilian approach primary radar data as provided by the Independent Group on their web site [8]. The data helps verifying the correct execution of the simulations in checking that the simulated flight was in accordance with the first points of the radar plots after it had finished the U-turn.

This was of great help also for scaling and positioning the unique low-resolution image of the turn on the Google-Earth globe.

3.3.3 Subsequent Hypotheses

3.3.3.1 Analytical review of the data

3.3.3.1.1 What happened at IGARI?

Referring to Figure 14 resulting from the analysis of the ADS-B data by the IG [22] at IGARI the turn initially started as a normal "fly-by" procedure heading to the next waypoint BITOD on route M765 according to the ATC filed flight plan. When abeam waypoint IGARI, the last ADS-B message was sent at 17h20:34:55 UTC. As recalled in section 3.3.2.6 "ADS-B data", this was the result of a deliberate action to switch the transponder to standby.

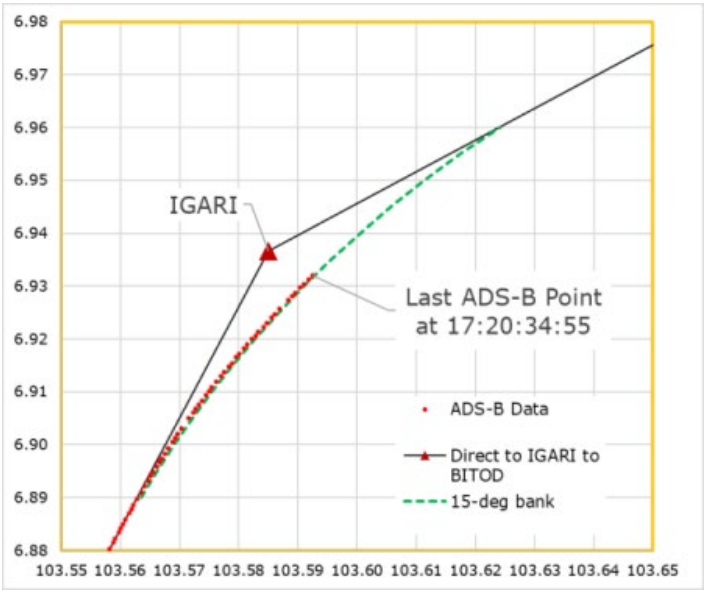

Figure 14: Aircraft Position when transmitting the last ADS-B message (source mh370.radiantphysics.com)

Should the aircraft have continued directly to waypoint BITOD, its trajectory would have been similar to the green dotted trajectory of Figure 14 and the yellow line illustrated in Figure 15. But, comparing this yellow extrapolated path towards waypoint BITOD with the actual path recorded by the radar as illustrated in green in Figure 15, a clear overshoot of waypoint IGARI is visible with a straight-line segment as if the turn was interrupted in its course during few seconds before resuming later. The path appears to follow a broken line heading first at ~36° and then with an evolving heading between ~63° and ~67°.

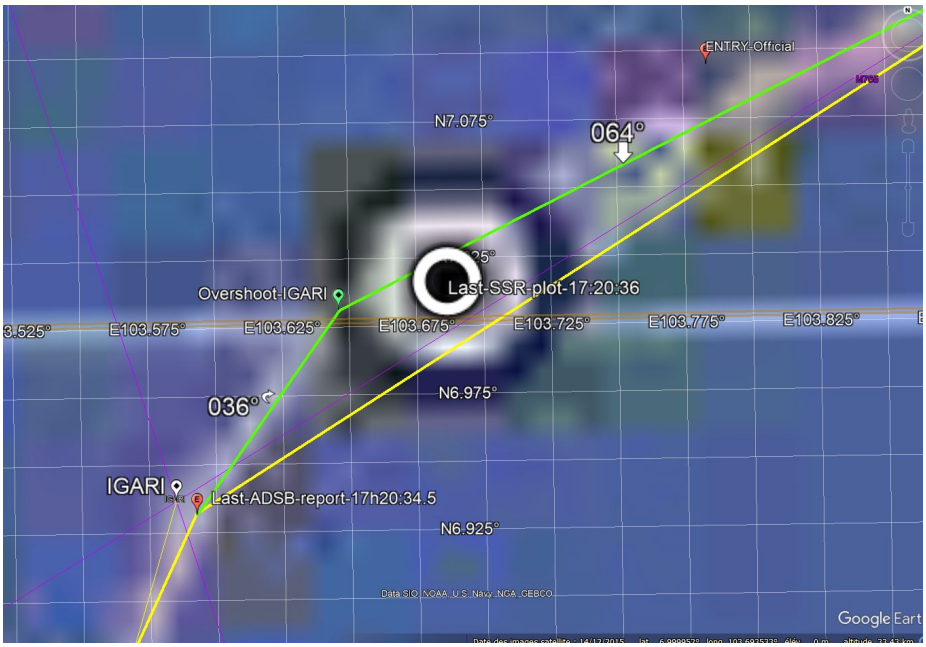

Figure 15: Actual trajectory according to the radar records posting an overshoot at IGARI

In our view, the most probable interpretation of this unusual trajectory cannot be explained by the bad radar data quality only. It is better explained by considering that the turn to waypoint BITOD started initially with the A/P engaged in LNAV and then was interrupted by the person in command by pushing the Heading Hold button which commanded the aircraft to maintain the current heading which was around ~36° at that time.

At this point in time, the person in command was most probably busy preparing the planned U-turn and successive actions to come.

The person in command then corrected the heading manually to the right in direction to route M765 i.e. up to ~67°.

3.3.3.1.2 Why a sharp U-turn?

When scaling and overlaying Figure 9 onto Figure 12, the most probable reason for the sharpness of the U-turn appears clearly in Figure 16. The person in command had to execute a demanding manoeuvre to stay outside of the Thai ADIZ and shows a behaviour as if he was under the Malaysian control. The radar plots indicate a direction remarkably parallel to the Thai ADIZ boundary.

Figure 16: The radar track indicates a sharp turn avoiding the Military Thai ADIZ

3.3.3.1.3 Manual U-turn

Within the constraints identified so far, would the aircraft be able to perform such a U-turn with its autopilot engaged? Simulations have been run to determine the behaviour and the trajectory of the aircraft with the configuration and context described in the official report (weight, speed, met etc.).

All simulations demonstrated that, with the autopilot engaged, the turn is performed at a maximum angle of 25° and that either the trajectory enters the Thai ADIZ or it passes very close to its boundary at a distance of less than 2 Nm depending on the initial conditions. Two extreme examples are provided in Figure 17 illustrating these findings. The red line illustrates the trajectory simulated on our Prepar3D simulator with the "full auto LNAV" function while the white line is with the autopilot and using the track/heading function.

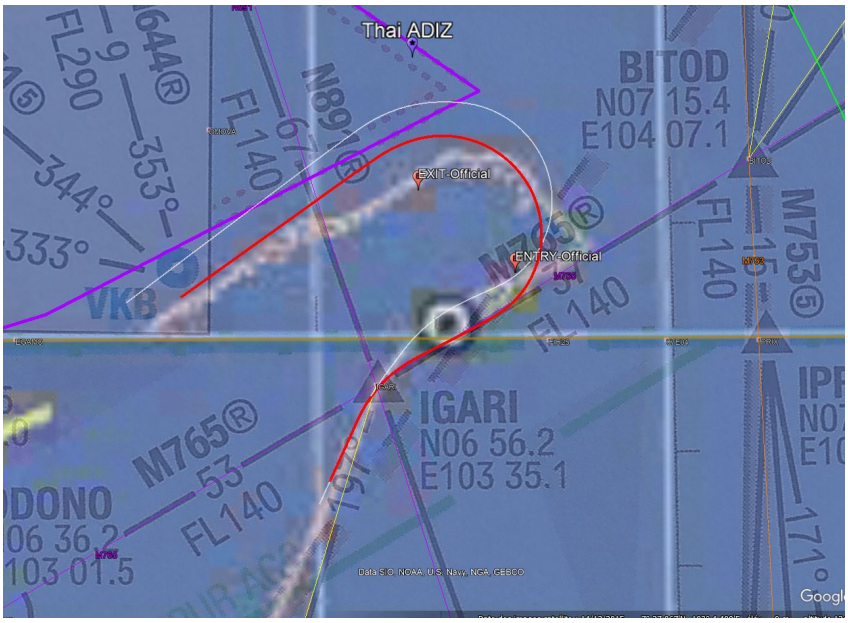

Figure 17: Simulations of U-turn with Autopilot engaged (max banking at 25°)

In addition, Figure 17 illustrates the impossibility to overfly both the official Entry point and Exit point within the measured 2min10s documented in the Malaysian official report [2].

The solution to satisfy the above constraints and match the radar track is to increase the maximum banking angle during the turn.

As the risk to enter the Thai ADIZ is considered too high to keep the autopilot engaged and as the banking angle should be above 25°, the turn was most probably achieved with a manual piloting. Let's recall also that Boeing's conclusion (c) in section 2.1 of report [2] claims that the best time-matching was achieved when manually flown.

3.3.3.2 Hypotheses on the U-turn

Based on this preliminary analysis, the following hypotheses are made:

a. The turn was manually executed to avoid entering the Thai Military ADIZ.
b. The turn started earlier than the official Entry point.
c. There was an overshoot of waypoint IGARI as shown by the radar plots because of the manual intervention.
d. The flying time of 2min10s between the Entry and Exit waypoints is a given data.
e. The aircraft flew back in the small corridor between route M765 and the Thai ADIZ boundary
f. Considering the radar track, the turn was not in circle but was performed with a gradually increasing banking angle leading to a sort of spiral turn making the turn "effective" radius shorter.
g. The initial conditions were identical to those used for the Boeing sessions except two of them which were not sufficiently accurate and had to be corrected thanks to the last ACARS report and extrapolations from GDAS weather data.
h. During the turn, the aircraft did not descend and stayed levelled at about FL350.

3.3.4 Simulations

Several simulations were performed in order to validate the hypothesis of a manual execution of the U-turn. Three different simulators were used.

3.3.4.1 Parameters settings in our simulations

The set of parameters used as initial conditions for the simulations is posted in Table 3:

Table 3: Aircraft and context input parameters for the simulations

Aircraft configuration		***Comment***
Fuel	42,250 kg	Consumption ~6.8 t/h *(cf our detailed computation in Section 3.3.4.5 below)*
Gross Weight	216,650 kg	
Altitude	35,000 ft	
Indicated Air Speed	IAS 280	The IAS 271 given in report [2] was found erroneous as confirmed by our computation and by the simulations *(c.f. Section 3.3.4.5 below)*
Ground Speed	475kt	Initial ground speed from report [2]
Simulator setup		
Autopilot	Engaged then disengaged	Heading hold when abeam IGARI and then disengaged before the U-turn to the left
Auto-throttle	Engaged	
Local conditions		
Wind direction	95°	GDAS data show that the wind was stable during the time of the turn and in its vicinity
Wind Magnitude	11 kt	
Waypoints		
Actual start of the turn	N07.02.13/ E103.42.88	Heuristically defined by tests & trials
Entry point	N07.05.7/ E103. 47.01	As defined p276 in Malaysian report [2]
Exit point	N07.12.7/ E103.38.70	As defined p276 in Malaysian report [2]
Time from Entry to Exit pts	2min 10sec	As defined p278 in Malaysian report [2]

3.3.4.2 Simulations using Prepar3D

The simulations were performed with a personal computer and the Prepar3D software from Lockheed-Martin enhanced with the PMDG add-on including a B777-200ER model equipped with Rolls-Royce TRENT-892 engines. This configuration is similar to the actual 9M-MRO aircraft.

Several runs were performed by airliner Captain Blelly to scan the different possibilities of performing such a sharp U-turn manually. As the result, executing such a turn is feasible and can be repeated identically at will. But this requires professional pilot's skills in order to maintain the aircraft level during the turn while gradually increasing the banking angle reaching the maximum banking limit in the second portion of the turn, especially at night.

Figure 18 illustrates the particular situation where the banking angle has been progressively increased from 25° at the start of the turn until between ~35° and ~38° which is at the limit. The full video is available at www.mh370-Caption.net (*01-Virage-IGARI-2022-12-07-Prepar3D.mp4*). The visible waypoint ahead of the aircraft is the official Exit waypoint. The timer of the aircraft was triggered when overflying the Entry waypoint. Increasing gradually the banking angle offers the best fit with the known radar track as shown in Figure 19.

Figure 18: Snapshot of the Prepar3D simulator in the U-Turn at time stamp 1min30s after overflying the Entry point

3.3.4.3 Fixed based simulator

During a simulator session organised in Autumn 2022, an active B777-rated airliner Captain was asked to execute such a turn. The initial conditions were those given in Table 3. The simulator is a fixed based simulator located at Skyway Simulation, in the city of Nantes, France. The core of the simulator is the Lockheed- Martin Prepar3D software enhanced with the full cockpit equipment suite FDS-B777-FTD from Flightdeck Solutions.

In a unique trial, the Captain did execute properly the turn overflying the two official Entry and Exit waypoints in 2min 10sec after overflying the newly defined starting waypoint of the turn. This provides an additional evidence supporting the hypothesis that this turn was executed manually.

A video clip of this particular turn is available at www.mh370-caption.net (*02-virage-IGARI-2022-09-Nantes.mp4*).

3.3.4.4 Results of all simulations

The flown trajectory resulting from the different sessions is illustrated by an example in Yellow in Figure 19. It encompasses the overshoot after passing abeam waypoint IGARI and the newly defined starting point of the U-turn earlier that the official Entry waypoint. In addition, both official Entry point and Exit points were mandatory waypoints to be overflown.

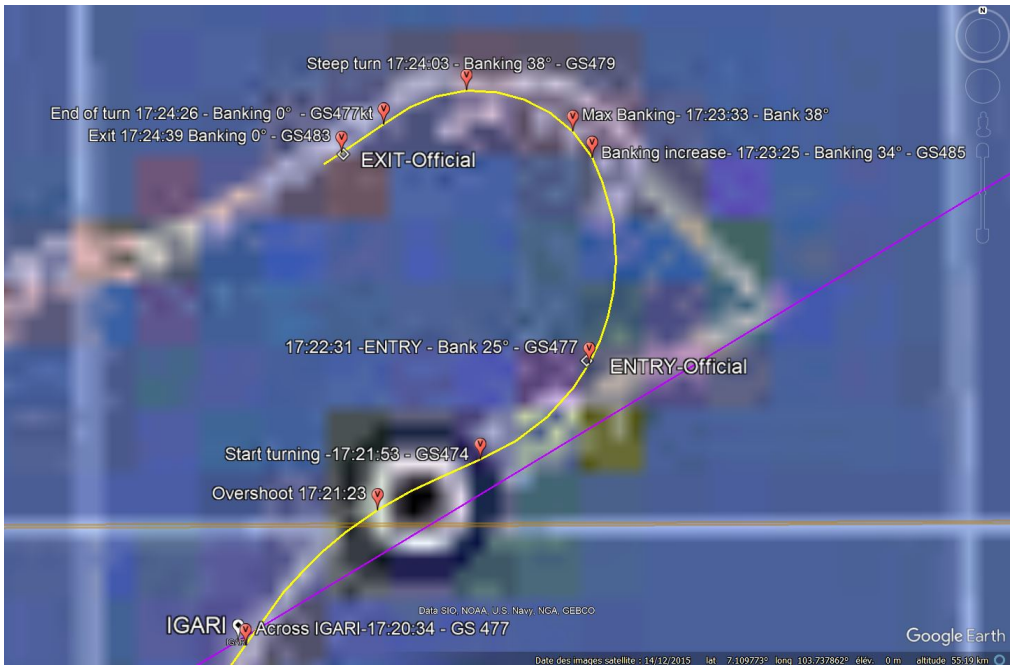

Figure 19: Spiral trajectory flown with Prepar3D simulator (gradual increasing of the banking angle)

The executed trajectory time tags from the video have been converted in UTC time in order to provide better readability for each navigational waypoint.

The first noticeable visual result is the excellent match between the path built from the "acquired" radar plots and the flown trajectory in the simulations. This validates the hypothesis of a high banking turn with an increasing bank angle from 25° up to the acceptable banking limit i.e. ~38°. This is just outside the banking alarm making this situation as a demanding one.

Furthermore, in this example like in a large number of simulation exercises, the timing between the two official Entry and Exit waypoints matched the mandatory interval of 2min10sec within +/- 2sec.

The aircraft parameters at different key points along the trajectory during the U-turn are posted in Table 4. The fuel calculation is justified in Section *3.3.4.5 below*. The flight level was successfully kept constant at ~35000 ft (i.e. ~FL350).

Table 4: Aircraft parameters along the U-turn manually executed

Time (UTC)	***Location***	***Ground Speed (kt)***	***Heading (°)***	***Fuel (t)***	***Banking (°)***
17h20:34	Abeam IGARI	477	025 to ~036	42.3	
17h21:23	Overshoot	476	~057		
17h21:53	Start Turn point	474	~064	42.1	0
17h22:30	Entry point	477	~029	42.0	25
17h23:25	Intermediate	485	~329		34
17h23:33	Intermediate	481	~315		max~38
17h24:03	Intermediate	479	~269		max~38
17h24:26	Intermediate	479	~237		0
17h24:40	Exit point *(+2'10" after Entry)*	483	~236	41.8	0

3.3.4.5 *Fuel consumption estimation*

To be as accurate as possible, the estimation of fuel is worth dedicating some attention for the most realistic reconstruction of the trajectory as possible. To that effect, and like all other existing studies, our computations are based on the last known value of fuel on-aboard which is 43.8t as reported at 17h06:43 UTC in the last aircraft ACARS message which is presented in Table 5 from [15].

Table 5: Last ACARS position report including the fuel on-board (last column) [15]

Greenwich Mean Time (GMT) - UTC	1641:43	1646:43	1651:43	1656:43	1701:43	1706:43
Altitude (ALT) – Feet	103	10,582	21,193	28,938	34,998	35,004
Calibrated Airspeed (CAS) - Knots.	168.4	261.8	301.1	303.1	278.0	278.4
MACH	0.255	0.478	0.669	0.783	0.819	0.821
Total Air Temperature (TAT) - °C	31.1	23.4	11.6	2.5	-13.4	-13.1
Static Air Temperature (SAT) - °C	27.3	10.4	-11.8	-27.4	-43.9	-43.8
Latitude (LAT)	2.667	3.074	3.553	4.109	4.708	5.299
Longitude (LONG)	101.715	101.760	01.988	102.251	102.434	102.713
Gross Weight (GWT) – lb	492,520	489,200	486,240	483,840	481,880	480,600
Total Remaining Fuel Weight (TOTFW) - kg	49,200	47,800	46,500	45,400	44,500	43,800
Wind Direction (WINDIR)	140.3	107.6	1.8	58.4	69.6	70.0
Wind Speed (WINDSP)	1.25	9.38	19.50	10.63	17.38	17.13
True Heading (THDG)	-33.5	27.7	27.8	26.0	26.8	26.7

Table 1.9A - ACARS Position Report

The Exit point was overflown at 17h24:40 UTC i.e. 2min10s after the Entry point. Thus, the time interval between 17h06:43 and the time at the Exit point is basically ~18 min.

In the operational flight plan (OFP) filed by the company less than two hours before departure and signed by Zaharie Shah, the estimation of fuel consumption for this particular flight was made taking into account the meteorological forecast of the day as well as the performance factor due to the overconsumption of the aging engines.

Let's consider the two waypoints "AC" and "PCA" planned to be overflown at about 40min past IGARI when the aircraft was supposed to have reached FL350 and be levelled. Table 6 presents the fuel estimation figures at those two locations (highlighted in green).

Table 6: Fuel estimation made in the filed operational flight plan for the "en-route" after IGARI

MAS 0370 / 1		PAGE 5 / 9 (07MAR14 15:05)							7 MAR 2014	
WPT	AWY	TTRK	SAT	WS	WC	GS	DIST	ZEET	TOTM	FUELRM
LAT/LONG		MTRK	TDV	TP	WIND	FL	ZATA	ZETA	MOCA	RQFUEL
AC	W1	077	M45	0	M002	481	0033	0:04	1:23	
N1056.3	E10711.3	078	P09	52	016/005	350			042	36.5
BMT	W1	028	M45	0	M004	479	0117	0:15	1:38	26 minutes
N1240.0	E10807.4	028	P09	53	016/005	350			104	34.9
PCA	W12	035	M45	0	P008	490	0094	0:11	1:49	
N1357.4	E10902.6	035	P09	58	272/016	350			104	33.6

This table shows that for the planned travel time of 26min between waypoints AC and PCA, the fuel consumption was estimated at 2.9t (i.e. 36.5t – 33.6t). This means ~112kg/minute or 6,8t/h. Somehow, this is confirmed by the model of the simulator which posts a figure of 2 x 3.4t/h = 6.8t/h as shown in Figure 20 and reported in Table 3 as well as by our Constraint Assessment Tool[5] (CAT) as reported in Table 7.

Figure 20: Cross-checking of our computation with the simulator model

If we make the hypothesis that the fuel consumption per time unit abeam waypoint IGARI would have been very close to the one between waypoints AC and PCA as the aircraft configuration is almost identical, then we can induce that to reach the Exit point from the location of the last ACARS message in 18 minutes, the aircraft consumed ~2,016kg of fuel. Thus, at the Exit point the fuel on-board was most probably 43.8 – 2.0 = 41.8t.

Similarly, the journey between the location at the last ACARS message and waypoint IGARI leads to a fuel consumption equal to ~1,570kg. Thus, abeam waypoint IGARI the fuel on-board was ~42,230kg rounded at 42.2t. This figure was used in our simulations replacing the estimated value of 41,200kg posted by Boeing in the Malaysian report [2] which is probably due to a transcription error.

To complement the fuel consumption analysis, we have performed a second computation thanks to an improved version of the CAT tool at the same constant flight level of FL350. The CAT is based on IG member Dr Ulich's fuel consumption model and it computes the consumption every second also taking into account the GDAS meteorological data. The results are provided in Table 7.

Table 7: On-board Fuel estimation by the CAT tool

Name	Longitude °	Latitude °	Time UTC	Wind Speed (kt)	Wind Direction °	Delta-Isa	Fuel (kg)
Abeam IGARI	103.5933	6.9310	17:20:34	11.5	95.4	11	42,229
Overshoot-IGARI	103.6469	7.0071	17:21:16	11.4	95.4	11	42,149
ENTRY-Official	103.7835	7.0950	17:22:30	11.4	95.3	11	42,003
EXIT-Official	103.6450	7.2117	17:24:40	11.4	95.2	11	41,755

[5] CAT tool : specific software developed for trajectory and fuel consumption calculation

Thus, the two sets of figures - computed separately- are in accordance with each other by less than 25kg and have been used in place of Boeing's figures as initial conditions for the performed simulations (c.f. Table 3). These figures have been confirmed by the Prepar3D simulator model also.

3.3.5 Conclusions on the U-turn after waypoint IGARI

The results of the analysis above show that considering a manual execution of the U-turn after crossing IGARI is well justified and probably the most likely action performed by the person in command at this point in time to turn and avoid entering the Thai ADIZ. Different simulations on different simulators performed by airliner Captains have validated such a hypothesis. It required skills from experienced pilots but it is possible within the measured timing.

Consequently, a manual U-turn is the hypothesis retained for the rest of the study.

3.4 From the Exit Waypoint to the last radar contact

In this section, our analysis focuses particularly on the leg starting at the exit of the U-turn estimated at 17h24:40 UTC and finishing at the last known position of the aircraft at about 10 Nm after waypoint MEKAR at 18h22:12 UTC as reported in the Malaysian report [2] which we call LaST Report Point (LSTPR). This is the second part of the MH370 known trajectory.

3.4.1 Available data

From the last transponder message received at 17h20:34 UTC when abeam waypoint IGARI, the aircraft was still tracked by the military. And today, the trajectory can be reconstructed thanks to additional radar data sources and one extra piece of information coming from the Celcom mobile telecommunication company at Penang. This complete set of available data is reviewed below.

3.4.1.1 Military primary radar plots

The first source of information is still the image provided in a low-resolution on page 3 of the Australian report [4]. However, this time the full picture presented in Figure 21 will be considered because it covers the aircraft flight path until the last radar contact after waypoint MEKAR. The two segments of interest are

a) the short visible path after the Exit point (end of the Pink line) and then

b) after the gap, the path followed by the aircraft from 17h30:33 till 18h22:12 UTC (Yellow line).

The location of the aircraft at 18h22:12 UTC is the last known position and it will be referred as the last primary radar plot or LSTRP waypoint in this study.

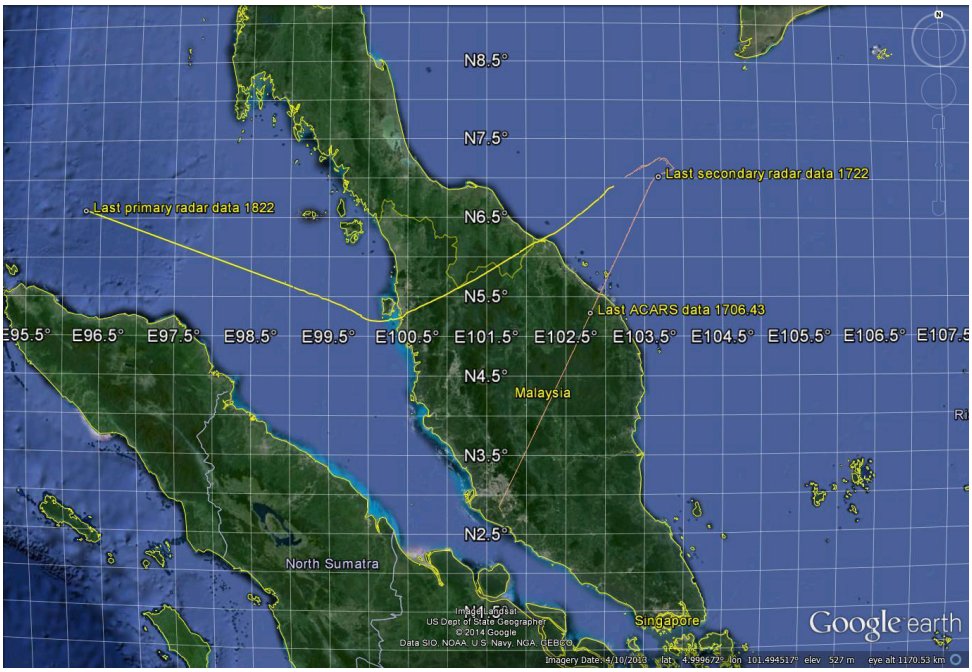

Figure 21: MH370 flight path derived from primary and secondary radar data (source ASTB)

Unfortunately, the military authorities did not release any primary radar data officially except the picture captured at the Lido Hotel conference (c.f. Figure 23).

3.4.1.2 Civil Primary Radar Data Plots (RDP)

Thanks to the Independent Group, civil primary radar data has been made publicly available on their web site [8]. An overlay of this data on top of the military plots shows the very good match of the respective paths. A deeper analysis was made by the Independent Group in [8] providing trust in this information and confirming the same conclusion stated in section 1.1.3 of the Malaysian report [2] on the localisation of the track but also on the high level of "noise" in the measuring of the time stamps.

The data comes from the Terminal Primary Approach Radar at Kota Bharu airport and at Butterworth airbase. The range of these systems is approximately 60 Nm and 80Nm respectively. They are calibrated to track aircraft at a shorter range and lower altitude than MH370 was flying.

Unfortunately, the data includes some gaps, but it comes into six useful data sets providing time and distance in slant range. Furthermore, the time stamps include irregularities and the distance measurements are provided as raw data without any post-processing that usually a radar system does before presenting the data on the controller screen. Nevertheless, the graphical fusion of the military data and the civil data shows a remarkable match as illustrated in Figure 22.

Figure 22: Comparison of military primary radar (yellow) and civil primary radar (magenta and purple)

Like the military data, for which a warning is made in the Malaysian report [2], the civil radar data are subject to inherent measurement uncertainties both in time and slant range. Thus, the computed instantaneous ground speed magnitude based on the raw data with no filtering posts scattered values outside the flight envelope of the aircraft.

Computing altitude and speed from 2D-Radar data without complementary SSR data is not possible without making assumption on one or the other. Furthermore, the provided time data is too erratic leading to computed speed values which are not realistic. In a short study [26], we have shown that in numerous segments these values are above the upper limit of the flight envelope (overspeed) and in one segment the speed is too low and very close to the manoeuvrability speed limit.

Thus, we consider that the speed computations cannot be made on solid ground as the data is not timewise reliable.

It is very important to keep in mind that “no matter what”, a pilot will never go outside the flight envelope and the fact that the MH370 flew during so many hours proves that the person in command respected this rule. Taking into account the local wind at that time, considering a TAS speed above ~535kt should not be an option. In addition, the certified maximum operating altitude for a B777 is 43,100 ft.

Building on the airmen’s way of managing the speed (or the Mach) and also on Captain Blelly’s experience, we only used the time stamps known as key information such as the time of exiting the U-turn at 17h24:40 UTC, the detection of the co-pilot’s mobile phone at Penang at 17h52:27 UTC and the last radar plot at 18h22:12 UTC. This data can be used to establish average ground speeds which we used further to tune the possible TAS or Mach on successive segments. Average speeds are routinely used by a pilot. For example, after the U-turn and during the descent, the person in command increased the IAS up to ~310kt which was further maintained steadily in the cruise at FL300 until waypoint VAMPI. This IAS is the recommended minimum consumption speed for descent by Boeing.

3.4.1.3 Military radar "blips"

The last radar information available is still the pictural element shown to the Next of Kin during a conference in 2014 and replicated in Figure 23. This time the radar blips are represented as yellow dots with fuzzy unreadable labels. The set is incomplete, probably due to a malfunctioning element of the radar elevation beam forming, but the most important information provided is the last radar blip (LSTRP) at 18h22:12 UTC located at about 10Nm after waypoint MEKAR.

At this particular point, we will use the data provided in the Malaysian report [2]:

- Time = 18h22:12 UTC
- Heading = 285°
- Distance = About 10 Nm after MEKAR (i.e. ~251Nm from Butterworth and not 200Nm)
- Ground speed = 516kt
- Altitude = 29,500ft (QNH)

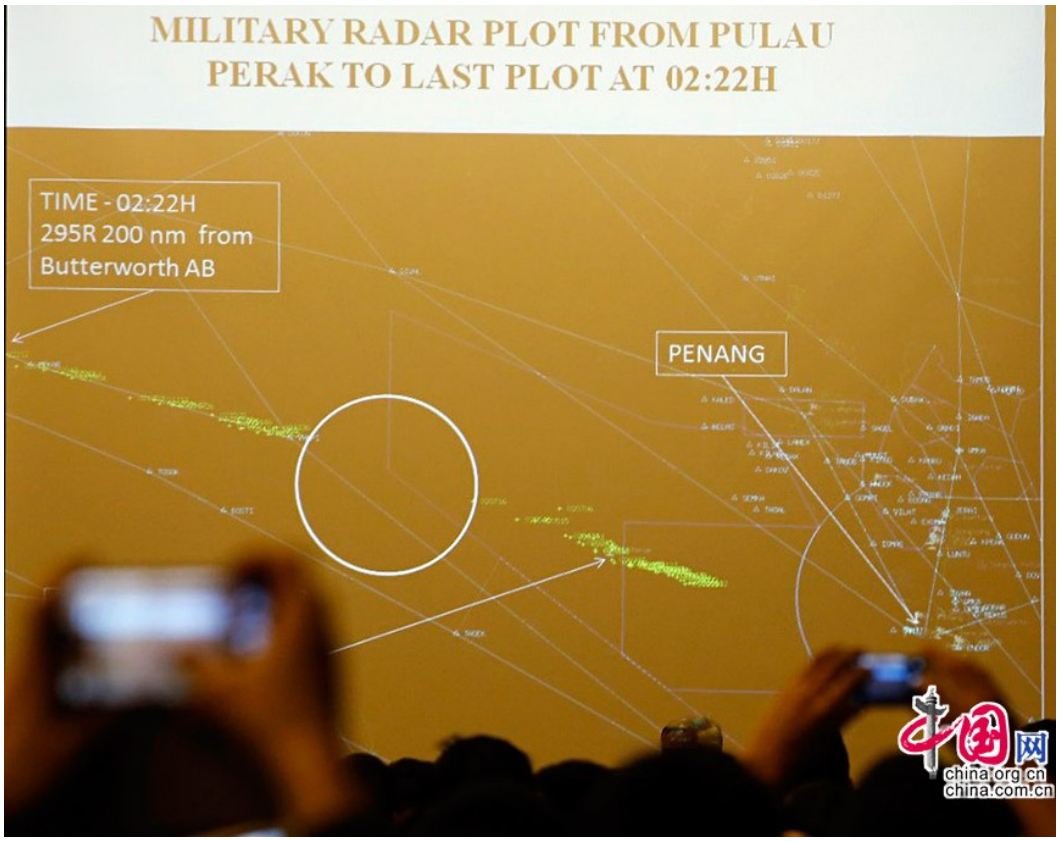

Figure 23: Military Radar records shown to Next of Kin at Lido Hotel, Beijing on 21st March, 2014

3.4.1.4 Detection of the co-pilot's mobile phone

An additional piece of key information is provided by the Malaysian Police report. It is the brief connection of the co-pilot's mobile phone at 17h52:27 UTC to a Celcom Location Base Station in Penang Island. The BBFARLIM2 station sectorial range is indicated to be approximately 32km i.e. ~17.3Nm on the ground (c.f. the boundaries of the primary lobe in Red in Figure 24).

Using the radar plot locations around this time stamp, one can derive an approximate location of the aircraft at 17h52:27 UTC as illustrated in Figure 24. Its coordinates are [5.2187°N; 100.2919°E] approximately 10Nm in the south of the Celcom terrestrial antenna.

Following the airmen's way of flying, this point was used as a mandatory timely waypoint in the trajectory reconstruction.

One could ask why the co-pilot's mobile phone was detected there? According to Captain Blelly's investigation [1], there is a high probability that the co-pilot who had been trained for depressurised cabin situation could have used small portable oxygen tanks. Some of them are available to cabin crew for moving along the aisles in emergency situations. Thus, he could have tried to place a phone call through one of the cabin windows. At this point in time (17h52 UTC) the oxygen supply capacity for the passengers was exhausted, thus the co-pilot had to use a portable oxygen tank.

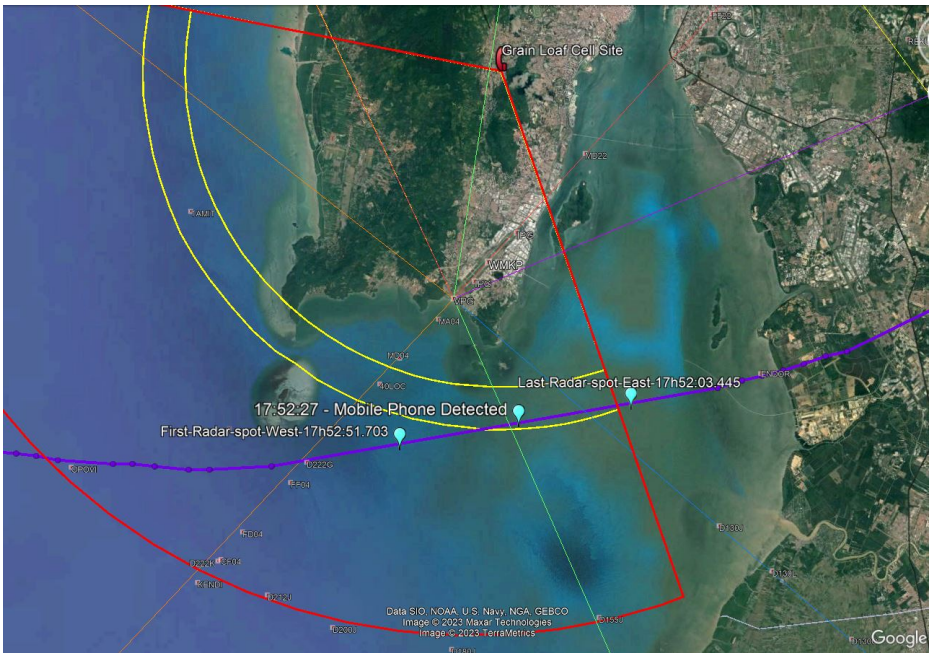

Figure 24: Estimated aircraft position when the mobile phone was detected at 17h52:27UTC

How the mobile phone could succeed to get connected and why the call did not go through? Figure 25 presents an approximate extrapolation of the terrestrial cell antenna secondary lobe power diagram versus the elevation. By design, the power level of this "1 bar" lobe is not strong enough to be received above 32000ft in true height. One can see in Figure 25 that at FL300, which was ~31500ft in true height, the beam could just barely be detected at a location between 9 to 10Nm approximately.

The possible geographical ring where a mobile phone could get connected is illustrated by its two Yellow boundaries in Figure 24 and between the two Orange vertical lines in Figure 25. The aircraft crossed it marginally during ~30 seconds only. This explains why a phone call could not be completed.

In addition, this event is an extra evidence that the aircraft was below the height of 32000 ft as he could not have succeeded to be connected at a higher altitude.

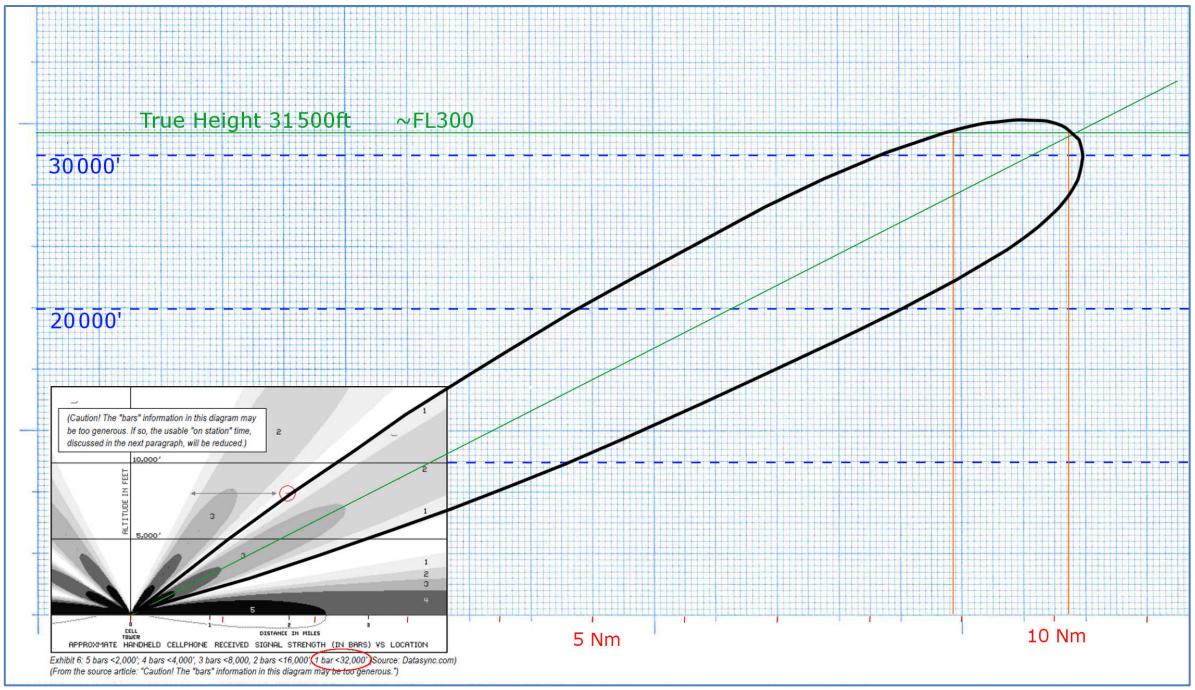

Figure 25: Extrapolation of the Celcom terrestrial antenna secondary lobe power diagram (source Datasync.com)

For information, the correspondence between the flight level and the true height (i.e. above mean sea level) during the path from the U-turn to Pulau Perak is provided in Table 8. At that time, in the south of Penang, the delta ISA was 11°.

Table 8: correspondence between the flight level and the true height above sea level

Flight Level	True height (ft)	Delta ISA °
FL350	36,540	11
FL330	34,450	11
FL300	31,320	11
FL300	30,840	7
FL300	31,560	13

3.4.1.5 Undisputable Facts on Distance and timing

There are absolute distance and timing figures between the Exit point and the last radar contact at 18h22:12 UTC. According to the above data, the aircraft flew 485.4Nm between the Exit point after the U-turn and the last radar contact position at 10Nm northwest of MEKAR. Furthermore, the time interval between these two locations is 57min32sec.

Thus, following the pilots' way of estimating legs, the reference value of the average ground speed for this leg is 485.4Nm flown in 57'32" = 506kt.

3.4.2 From the U-turn Exit waypoint to Penang

In this section, a plausible manually piloted trajectory will be reconstructed from the Exit point of the U-turn estimated at 17h24:40 UTC and the estimated location where the co-pilot's mobile phone was detected at 17h52:27 UTC.

3.4.2.1 Hypotheses

According to Captain Blelly's investigation [1], the person in command triggered several actions as soon as possible in order to make the aircraft invisible and undetectable by the civil ATC. Firstly, he disconnected all electrical generators from the electrical network to create a situation difficult for both the crew and passengers. This also triggered the deployment of the RAM Air Turbine (RAT) to provide the necessary power to manually pilot the aircraft.

Secondly, the person in command voluntarily depressurised the aircraft to simulate a pressure incident to keep the passengers and the crew seated with their oxygen masks on and later suffering hypoxia when the oxygen exhausted approximately 22 minutes later. The aircraft then descended to FL300, probably to be able to better sustain the low pressure inside the cockpit. It is not compulsory to switch off the Air Conditioning systems (packs) to depressurise the aircraft. This can be done manually, thus keeping the temperature drop acceptable inside the cockpit.

When each of these particular actions took place is difficult to evaluate precisely. Below is the list of their results and their consequences provided as the basic hypotheses for our analysis:

- No more electro-magnetic emissions from the aircraft including aircraft position lights because the electrical generators were disconnected
- The electricity was provided by the RAT and led to a manual piloting
- Descent to a lower altitude ~ FL300 in approximately 15min
- Constant FL300 from Kota Bharu to South Penang
- Depressurised aircraft and oxygen mask put on (27h oxygen endurance for a single pilot in the cockpit)
- No need to put the air conditioning packs off for aircraft depressurisation: only manual full opening of the outflow valves.
- Low flow for air conditioning is always available in the aircraft to maintain a bearable temperature
- The radar plots show lateral irregularities which are unusual for an aircraft controlled by the autopilot, this is an additional element supporting the manual piloting hypothesis
- The navigation was made via the Captain's Navigation Display in using some waypoints as visual targets in conjunction with Penang VOR (VOR In, then VOR Out) mainly.
- The flight passed to the South of Penang Island at about ~10Nm when the co-pilot's mobile phone got connected very briefly at 17h52:27 UTC with no call going through.
- The average ground speed between the exit of the U-Turn and South Penang is thus estimated at ~506kt +/-2.5kt.

3.4.2.2 No electromagnetic emissions

As explained above, the U-turn required the full attention and dedication of the person in command. Thus, it is most probable the person in command waited for the U-turn to be completed before making sure that the aircraft ceased emitting any detectable signal and remained "electromagnetically" silent. This encompasses the telecoms (including the ACARS, IFE, etc.), the lights but also the DME (Distance Measuring Equipment).

For a pilot, the simplest and the most effective way to be sure to switch off all systems at once is to disconnect the electrical circuits from the four generators (main and backup). By successively pressing the button of each generator on the overhead panel, the person in command ensured the disabling of all systems capable of communicating outside without any exception. This supposes the APU rotating knob had been turned on and then off just after to avoid its auto-restart. This implies also that subsequently the aircraft was flown with the sole electrical power provided by the RAT (Ram Air Turbine) but also in parallel with the full hydraulic power of the properly working engines. This implies a subsequent manual piloting. The RAT was deployed either automatically or manually.

Regularly pilots are trained to fly in such conditions during flight simulator training sessions. So, it is believed that the PIC was well trained for this. In addition, let's remind the LATAM B777 flight 8084 in December 2018 from Sao Paulo to London which flew about ~50 minutes with the RAT power only without any problem.

3.4.2.3 Depressurised aircraft and descent until Kota Bharu

The scenario including a descent after the U-turn executed at FL350 down to a lower level at about FL300 fits well with the hypothesis of depressurisation. The increase of speed until 17h37 UTC matches well with a descent with the throttle kept in a fixed position due to the disconnection of the auto throttle when the electrical power went off. Also, the autopilot was not available anymore.

Nevertheless, it should be noticed that during our simulations of the U-Turn, the ground speed at the Exit waypoint point was in fact at about ~476kt at Mach 0.787 on average (c.f. Figure 18). This is a higher speed at the exit than the radar computed value of ~458kt. Noticeably, in this manoeuvre the instantaneous speed is very variable.

At such a flight level, the most logical operational speed reference to use is the Mach number. At waypoint IGARI the Mach was set at ~0.821. Our analysis shows that during the descent, the aircraft accelerated with an average Mach of 0.835 until reaching IAS 310kt as illustrated by a screen capture taken during one of our simulations in Figure 26.

Figure 26: Flight parameters in the late part of the descent to FL300

This makes the average ground speed equal to 507kt with a standard deviation σ = ± 2 kt for the descent. This is well below the maximum possible Mach of 0.870. The meteorological data indicates a tail wind evolving from 11kt from 95° to 17kt from 75°. Overall, the average TAS was about ~495kt according to our computation.

To be levelled at FL300 at Kota Bharu, the rate of descent is estimated between 300 to 500 feet per minute (fpm) during 15 minutes approximately.

During this leg, the navigation could have been a mix of visual usage of the navigational display waypoint icons of Kota Bharu as a global direction and of the Penang VOR-In radial as the aircraft was well within its range. The light of the city of Koa Bharu could have been of help too.

An interesting question is why the person in command chose to level at FL300? Our answers could take the form of a chess player preparing several moves in advance. First, as explained above, this level was probably an acceptable level for sustaining the low pressure and a bearable temperature in the cockpit. Second, FL300 is sufficiently high to behave as normal En-route traffic above Kota Bharu and Penang terminal areas. Thirdly, FL300 is a low flight level for the targeted Malacca Straight area and its routes thus staying safe and below the long-haul traffic usually flying above. Fourthly, FL300 offers the highest ground speed for any selected IAS or Mach for the best specific fuel consumption. Finally, FL300 is judiciously chosen with a good ratio consumption/range as no climb would be necessary afterwards as demonstrated in the chapter dedicated on the unknown trajectory later in this report (c.f. Chapter 4).

3.4.2.4 From Kota Bharu to South of Penang

At Kota Bharu, and levelled at FL300, the operational speed reference to consider is now the Indicated AirSpeed (IAS) as the aircraft normally switches automatically from Mach to IAS when arriving at an IAS of 310kt. Our analysis shows that in this leg the average IAS was ~310 ± 1 kt. Thus, it appears that the person in command flew manually at that quasi-constant IAS acquired during the descent at FL300. It is a safe way of flying well below the maximum possible IAS of 330kt.

Overall, the average ground speed of this leg is equal to ~506kt with a standard deviation σ = ± 2.5 kt. Our simulations confirmed that an average IAS of ~310kt is the best fit.

The leg “Exit Waypoint to South of Penang” is illustrated in Figure 27. Some small trajectory lateral adjustments are mentioned in the Malaysian report [2] which we read as the result of manual flying and following a radial-In to VOR Penang (the autopilot was unavailable).

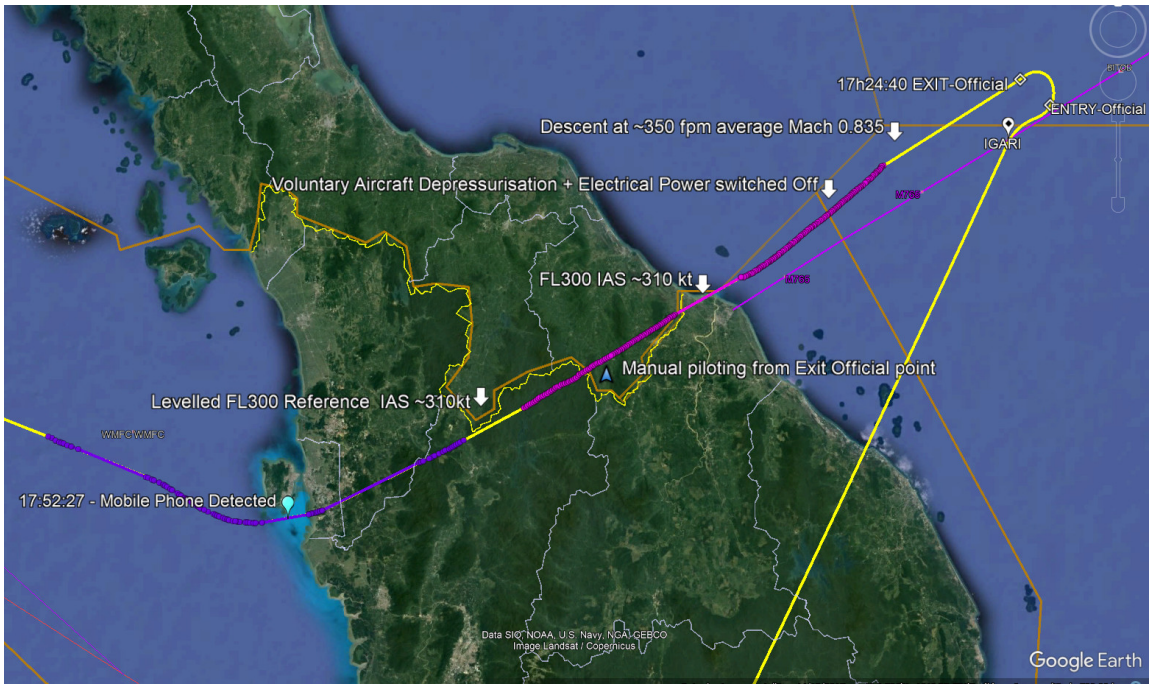

Figure 27: Path and scenario between Exit Waypoint and South of Penang

3.4.2.5 Fuel consumption

To evaluate the fuel consumption the same method was used as above. Three types of computations were performed: the airmen's method, our CAT tool fuel consumption model and the measurement of the fuel indicated by the FMC of our simulator. The results are posted in Table 9.

Table 9: On-board fuel during the leg Exit Waypoint to South Penang

Time	***Location***	***Fuel On-Board (t)***		
		Airmen's	*CAT Tool*	*Simulator*
17h24:40	U-Turn Exit waypoint	41.8	41.8	41.8
17h37:00	Kota Bharu	-	40.5	40.4
17h52:27	South Penang (Phone detected)	38.5	38.6	38.4

The different methods are in accordance about the hourly fuel consumption which is evaluated between 6.9t to 7.3t. Thus, in spite of the descent, the aircraft consumed above average because it was at lower levels than the optimised ones.

3.4.2.6 Simulations

Several simulations were run according to the flight profile and hypotheses described above. A video of one run is available at www.mh370-caption.net (*03-Exit-to-VAMPI-manual-506GS.mp4*). The lessons learned from the simulations are that the person in command must have changed the Mach number along the descent in order to keep the aircraft within the speed envelope without gaining too much speed as the auto-throttle was disengaged. Thus, on this leg the Mach number decreased from 0.850 initially down to 0.815 in cruise.

Mach 0.815 at the bottom of the descent at FL300 led to an IAS of 310kt, which is due to the average wind conditions used for this leg i.e. a constant wind of 14kt from 85° underestimating its positive evolution. Changing the meteorological conditions in the Prepar3D simulator is not straightforward. Nevertheless, under manual piloting, our simulator overflew the point of the mobile phone's connection in just 5 seconds ahead of schedule.

3.4.3 From Penang to the Last Radar Plot

In this section, the analysis focuses on the second leg starting at the estimated location where the co-pilot's mobile phone got connected at 17h52:27 UTC in the south of Penang until the last known position of the aircraft at about 10 Nm after waypoint MEKAR at 18h22:12 UTC which is the last bit of information about the MH370's known trajectory.

3.4.3.1 Hypotheses

For this leg, the only available data includes two "large field of view" images and one set of civil primary radar raw data with low precision time stamps. According to the Malaysian report [2], the aircraft was turning to the northwest direction at 17h52:27 UTC. Then it flew on a quasi-direct route to waypoint VAMPI and disappeared from the radar after waypoint MEKAR.

Even though the numerical radar data provided by the IG [8] is raw with unreliable time tags, its geographical location matches well the military radar track. Both show lateral excursions of the aircraft which cannot come only from the imprecision of these plot measurements. An aircraft controlled via the LNAV function on a direct route to waypoint VAMPI would not present such lateral deviations. It is concluded that in continuity with the previous leg, the person in command was still manually controlling the aircraft following a radial-out from VOR Penang.

Building on the above conclusions and to maintain continuity, the following hypotheses form the basis to our analysis of this leg:

- The aircraft was still manually piloted as the radar plots show lateral irregularities which are unusual for an aircraft controlled with LNAV
- The aircraft was still depressurised and the person in command was still wearing his oxygen mask
- The electrical power was still provided by the RAT only
- No electro-magnetic emission was possible still
- The flight level was maintained constant at FL300 from South Penang to waypoint MEKAR
- The navigation was still made via the pilot Nav Display by visually using waypoint VAMPI icon as a target in conjunction with Penang VOR-Out
- Knowing the time difference from South of Penang to LSTRP, the average ground speed is estimated at ~508kt.

3.4.3.2 From South of Penang to VAMPI

The path flown by the aircraft is clearly identified by the radar plots as presented in Figure 28. The lateral deviation just after the turn is not a typical trajectory flown with the LNAV function activated. This is also visible on the image at the Lido Hotel in Figure 23 above. Under LNAV, the aircraft would have taken a more direct route to waypoint VAMPI as illustrated by the Red line in Figure 28.

Figure 28: Civil Primary radar track overlaid on the military radar track from South of Penang to waypoint VAMPI (source ATSB [4])

As there is still no evidence of electrical power restoration, the person in command was still piloting the aircraft manually, using the navigation tools at their disposal i.e. waypoints icons on the navigation display as visual aids and the radial out from VOR Penang. Just after the turn at Penang, the pilot most probably used the "track select" function for adjusting at best his route to waypoint VAMPI.

Remark: The aircraft path displayed in Figure 28 is represented by a perfect straight line while the display in Figure 23 show irregular locations around the line direction to VAMPI. Thus, we believe that the image provided by ASTB [4] in Figure 28 has been edited and a broken line at VAMPI has been simply drawn from the last radar plot before Pulau Perak until the LSTRP via VAMPI. This will be addressed in more details in section 4.3.4 below.

Based on the available information on the route followed and the time difference between the location of the connection of the mobile phone at Penang and the LSTRP position, the average ground speed has been estimated at ~508kt. This implies that the aircraft flew abeam waypoint VAMPI at about ~18h13:00 UTC. Taking into account the necessary final acceleration between waypoint VAMPI and LSTRP leading to a ground speed at 516kt (Malaysian Report [2]), the simulation sessions showed that the average ground speed between South of Penang and waypoint VAMPI was actually ~506kt.

Taking into account the wind characteristics along the path, this would mean that the aircraft was manually piloted still using the IAS reference of ~310kt.

3.4.3.3 From VAMPI to the last radar plot (LSTRP)

For simplicity and because it does not impact the trajectory too much- and like many other studies -we considered that waypoint VAMPI has been overflown in order to stay well within the FIR Kuala Lumpur. Using the poor-quality data at hand, the IG member B. Holland succeeded to overlay timestamps on the Lido Hotel image as shown in Figure 29.

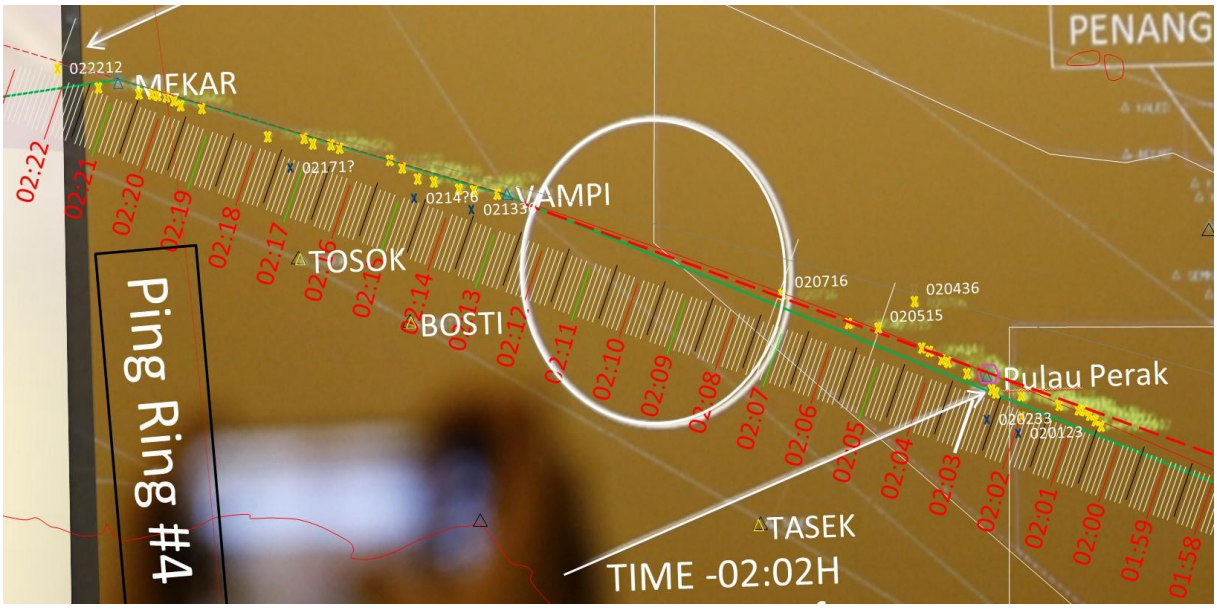

Figure 29: Enlarged Lido Hotel image with timestamps (source Bill Holland)

3.4.3.4 Geometric considerations

Let us consider the yellow crosses in the first place i.e. the location aspects of Figure 29. They represent the aircraft locations as reported by the military radar. The timestamp 18h22:12 as mentioned in the Malaysian report [2] had to be extrapolated in the top left corner and is supposedly positioned at 10Nm from waypoint MEKAR in the continuation of his current route.

Getting closer, it is possible to mix this information with the data provided in the Malaysian report [2] in which it is stated that at the last radar plot (LSTRP) the aircraft's track was 285°, its ground speed was 516kt and its altitude was 29,500ft without more details. The most logical assumption is to consider it as a QNH altitude. Figure 30 provides a data fusion image on GoogleEarth and presents the trajectory that best fits with the available information. The green line is a visual best fit of the yellow crosses from VAMPI to MEKAR and from MEKAR it follows the track at 285°. One can see that the aircraft was initially a little south of route N571 at 286° then further south of it after MEKAR at 285°.

This is coherent with the hypothesis of a manual flying because if LNAV was engaged the trajectory would have been much closer to route N571 and the waypoints VAMPI and MEKAR would have been more closely overflown and the aircraft would have turned to the right towards NILAM.

This slightly offset trajectory will be used in our simulations later in section 3.4.3.6 Simulations

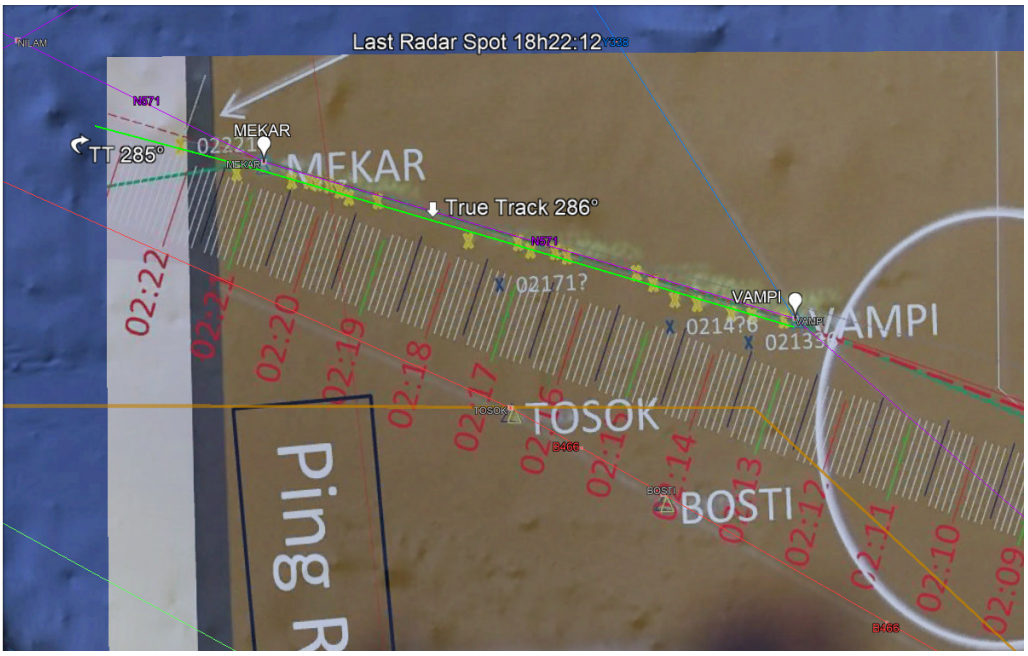

Figure 30: Induced trajectory between VAMPI and LSTRP (Green broken line at MEKAR)

3.4.3.5 Time and velocity considerations

Considering the ground speed of 516kt at the LSTRP (c.f. Malaysian Report [2]), we made the hypothesis that the IAS was kept quasi-constant between South of Penang and waypoint VAMPI and that an acceleration tool place afterwards as indicated above. The computation, as a simulation would do, includes the fuel consumption and the wind changes along the path. Table 10 presents the results of the computations.

Table 10: Estimation of the IAS, ground speed and on-board fuel between 17h52:27 and 18h21:00

Time	***Location***	***IAS (kt)***	***Ground Speed (kt)***	***On-board Fuel (t)***
17h52:27	CPMPh (South of Penang)	310	506	38.6
		310 ± 1	506 ± 1	
18h13:00[6]	VAMPI	310	506	35.9
18h21:00[7]	Abeam MEKAR	316	509	34.8

From waypoint VAMPI to the LSTRP, the aircraft slightly accelerated and after waypoint MEKAR it started a slow descent. The segment from south of Penang to MEKAR was at FL300 and the radar data detected altitude 29,500 ft at LSTRP, thus a 500 ft descent had to take place.

This scenario and figures were selected for our simulations.

3.4.3.6 Simulations

To verify these assumptions, several sessions of simulations were performed with the Prepar3D simulator and its PMDG add-on according to the flight profile described above. A video of one of the runs until VAMPI is available at www.mh370-caption.net (*03-Exit-to-VAMPI-manual-506GS.mp4*). The simulations confirmed that the person in command used a constant reference IAS of about 310kt

[6] *This timestamp is computed by the CAT and confirmed by our simulations*
[7] *Idem as footnote above*

until waypoint VAMPI. Thus, on this leg, the Mach number was stable at ~0.815 (GS=506kt). A screenshot taken during one simulation is provided in Figure 31 illustrating the different parameters values (in Red circles) and the aircraft condition manually piloted.

Figure 31: Screenshot of the simulator between South of Penang (CPMPh) and VAMPI with the RAT deployed

For this segment, the wind was considered constant with the average values of 15kt from 76°, this explains the difference between the IAS estimated by the CAT and the simulator value. Under these conditions, Captain Blelly could achieve reaching waypoint MEKAR at 18h21:00 UTC as expected under a fully manual piloting.

From waypoint MEKAR to the LSTRP, the Malaysian report [2] indicates a distance of 10Nm and a final ground speed of 516kt. The simulation of a descent manually piloted from the vicinity of waypoint MEKAR confirms the estimated figures above (IAS 326kt and ground speed 517kt) as illustrated in Figure 32 taken when approaching LSTRP waypoint.

Figure 32: Screenshot of a simulation manually piloted at the end of the descent to 29,500 QNH at LSTRP (18h22:12)

3.4.4 Conclusions on the leg from the Exit Waypoint to the last radar contact

The results of the analysis above show that considering a manual piloting from the end of the U-turn after crossing waypoint IGARI until the last radar contact is well justified and is probably most likely. Different simulations performed by an airliner Captain have validated such a hypothesis.

In summary, the estimated parameters of the trajectory leading to a successful match of the timing at the reference locations are reported in Table 11.

Table 11: Estimation of the IAS, ground speed and on-board fuel between 17h52:27 and 18h21:00

Time	***Location***	***Velocity (kt)***	***Ground Speed (kt)***	***On-board Fuel (t)***	
				Estimated	***Simulation***
17h24:40	U-Turn Exit waypoint			41.8	41.8
		M0.835	506		
17h37:00[8]	Kota Bharu			40.5	40.4
		IAS 310	506		
17h52:27	South of Penang			38.6	38.4
		IAS 310	506		
18h13:00[9]	VAMPI	IAS 310	508	36.0	35.8
18h21:00[10]	Abeam MEKAR	IAS 317	509	35.0	34.8

3.5 Conclusions on the known trajectory

It has been shown that this known trajectory could been flown manually by an excellent qualified pilot maintaining the flight parameters quasi-constant on these two segments (Altitude, speed and track) in a difficult meteorological environment and with a degraded electrical power system and in depressurised conditions.

[8] *This timestamp is computed by the CAT and confirmed by the simulations*
[9] *Idem as footnote above*
[10] *Idem as footnote above*

4 The unknown and recalculated trajectory

4.1 Introduction

This chapter addresses the part of the trajectory recalculated thanks to the published Inmarsat data measured via their communications satellite and thanks to our aeronautical operational computations.

The main objective of this chapter is to reconstruct an operationally realistic piloted trajectory using the few pieces of data available either from official sources or from other public sources and in particular, the Inmarsat report [3]. The validation of such an inferred trajectory is also addressed thanks to the many simulation sessions based on the Prepar3D[11] model with the PMDG add-on.

The focus of our study is on the part of the trajectory starting shortly before 18h22:12 UTC when the aircraft exited the Malaysian radar coverage. The aircraft radar blip was lost a little bit more than one minute after passing abeam waypoint MEKAR.

But to ease the understanding, the starting point of this chapter was chosen to be waypoint MEKAR at the estimated time around 18h21:00 UTC on March 7th, 2014. The study is organised as follows:

1. Section 4.2 reviews the reduced set of data available and recalls the context when the aircraft passed abeam waypoint MEKAR
2. Section 4.3 addresses the leg from the last radar plot (waypoint LSTRP) until the phone call of the ground at around 18h40 UTC. It includes a series of three turning manoeuvres leading to the south and which is commonly called FMT (Final Major Turn).
3. Section 4.4 details the reconstructed trajectory after the FMT, which is a quasi-straight-line path to the south.
4. Section 4.5 presents the different possibilities for the final descent and the related actions performed by the person in command leading to a probable soft ditching and creating a minimum number of pieces of debris.

One should keep in mind that what is presented in this report is a highly probable inferred, reconstructed trajectory. However, until the moment the wreckage is found, it remains a hypothesis.

4.2 Available data

Once any trace of the aircraft was lost by the Malaysian military surveillance system, the only available undisputable data comes from two sets of measurements made by Inmarsat.

In addition to this data, other sources of information were found valuable for the analysis in particular the controlled airspace structures.

4.2.1 Inmarsat data

This study will often refer to the only public source of information provided by Inmarsat in a cornerstone document [3] in which the numerical values of the BTOs and BFOs measurements are provided among other important information.

[11] *B777-200ER Simulator from Lockheed Martin with Rolls-Royce engines*

In short, the Burst Time Offsets (BTOs) provide an estimation of the distance between the aircraft and the satellite while the Burst Frequency Offsets (BFOs) provide an estimation of the frequency shift of the signal (Doppler effect) due to the relative velocity between the aircraft and the satellite.

During each stage of this analysis, validation sessions were performed for consolidating our recalculated trajectory. The method consists in comparing Inmarsat measurements with an estimation of the values of BTOs and BFOs at key moments well defined by Inmarsat itself in [3] and called the Arc crossings (for ex. Arc1-crossing).

To estimate the numerical values, we have developed specific tools as explained in Section 4.4.3 below.

During the reconstruction of the FMT, the following Inmarsat data have been used with a specific nomenclature as presented in Table 12.

Table 12: Inmarsat BTOs/BFOs considered for the FMT reconstruction

Time (UTC)	Name	BTO (µs)	BFO (Hz)	CBFO (c.f. [9])
18:25:27	Arc1*	12520	142	Not calibrated
18:27:04	Arc1.1	12520	175	156
18:28:06	Arc1-Boeing	12500	144	144
18:28:15	Arc1.2	12480	143	143

*: In spite of some discussion on Arc1 BFO possibly impacted by packet collision as well as by some adjustment due to the OCXO (Oscillator Cristal Oven) behaviour of the aircraft satellite communication system as discussed by Bobby Ulich in [9], this data has been taken into account to shape the turn.

4.2.2 FIRs

Other important data comes from the airspace structure along the reconstructed trajectory. In particular, the FIRs (Flight Information Regions) in which the aircraft flew (or avoided) are worth considering. As explain in the report [2], with the exception of a short 5 minutes excursion in Ho Chi Minh FIR, the person in command ensured to stay within the FIR Kuala Lumpur until waypoint MEKAR and onwards to the west.

In doing so, the person in command did not draw other FIRs controller's attention. But at MEKAR, the aircraft was approaching the boundaries of FIR Chennai in India and of FIR Jakarta in Indonesia. Figure 33 presents the main elements of the airspace structure in the vicinity of the last radar plot LSTRP at 18h22:12 UTC.

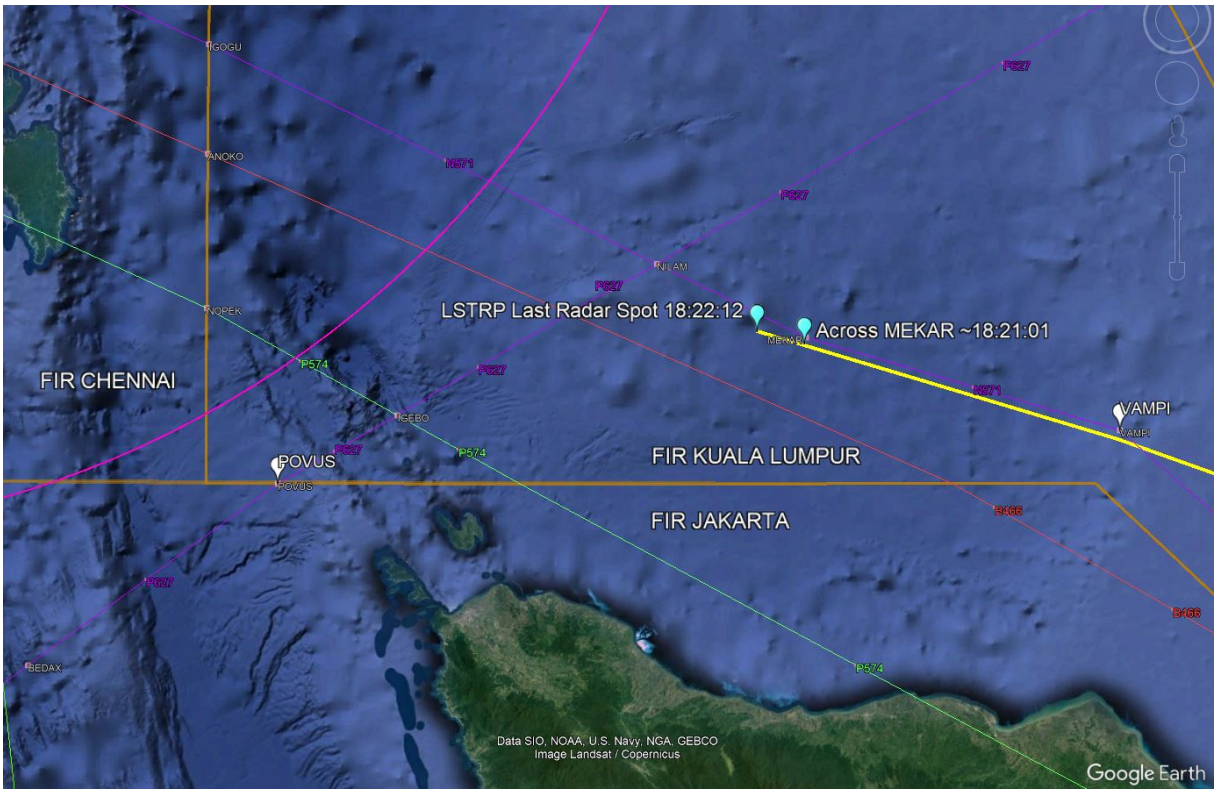

Figure 33: Airspace structure in the vicinity of the last radar plot LSTRP at 18h22:12 UTC

For a pilot who wanted to stay the least visible as possible and drawing the least attention as possible, crossing the minimum number of FIR boundaries is most probably the best choice.

Another noticeable element to be avoided is the Indian military radar based at Car Nicobar whose maximum range at FL300 is represented in purple in Figure 33.

4.2.3 Southeast India ADIZ[12]

In addition, in the vicinity of the FMT, an additional constraint comes from the sovereign limit imposed by the Indian military authorities. In particular, India has defined the Southeast India ADIZ whose boundary coincides exactly with the FIR Chennai boundary. As MH370 transponder (normally broadcasting the flight parameters) was on standby and as no ATC flight plan had been filed, the aircraft had to avoid entering FIR Chennai by any means avoiding drawing Indian military controllers' attention. Figure 34 highlights the location of the ADIZ illustrated by the Purple double dotted line.

Subsequently, one can apply this constraint to all waypoints located on the FIR Chennai boundary and conclude that they could not have been overflown without drawing the attention of the Indian controller. In particular, this encompasses the following waypoints: IGOGU, ANOKO and NOPEK as visible in Figure 34.

[12] Air Defense Identification Zone c.f. [16] for definition and more details

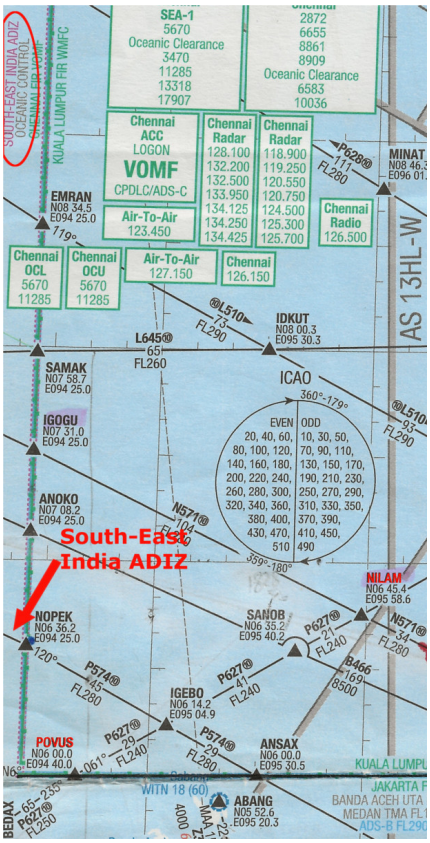

Figure 34: Boundary of South-East India ADIZ (Source Lido/Route Manual AS 14HL Apr. 2017)

4.2.4 Routes and Waypoints

Keeping in view that at waypoint LSTRP the aircraft was on its way to entering a new FIR and the person in command's care to be seen as the least threatening as possible, the best way of crossing a FIR boundary is to follow a registered airway. Two routes are possible: continuing on Route N571 or turning to the southwest on Route P627 in light purple in Figure 33, in Figure 34 and also in Figure 35.

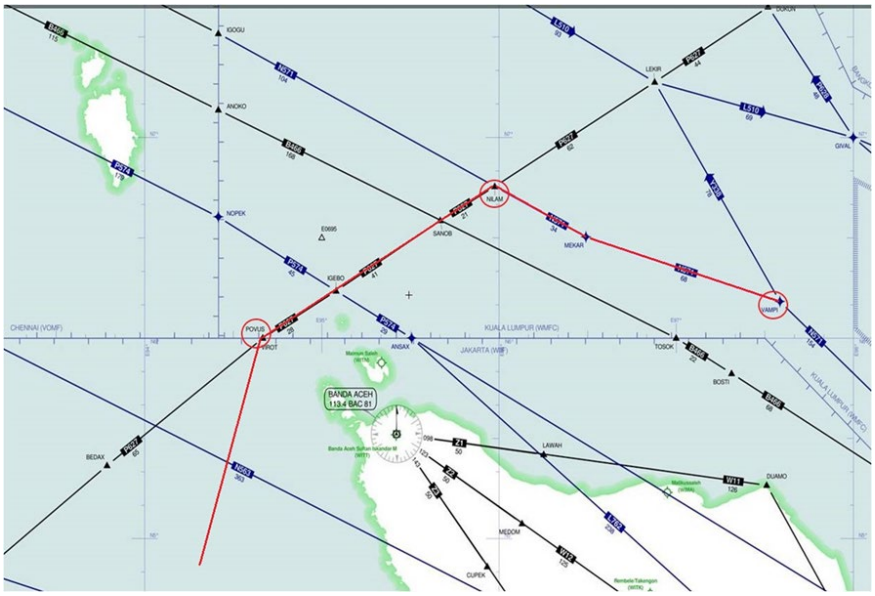

Figure 35: Malaysian Airspace including routes N571 and P627 with the intended route (Skyvector)

4.3 The « Final Major Turn[13] » (FMT)

Based on the Inmarsat BTOs and BFOs, the recalculated FMT presents a shape including unintended turns. In particular, the change from route N571 to route P627 was missed and the aircraft actually turned right first heading north towards waypoint NILAM before turning left to recover a direct route to waypoint POVUS. This manoeuvre - matching the Inmarsat data - appears to have been an unexpected turn and calls for a clear understanding of what could have happened in the cockpit. Overall, the FMT includes two parts; one around waypoint NILAM and a second one at waypoint POVUS. We dedicated specific effort to analyse this peculiar branch of the trajectory.

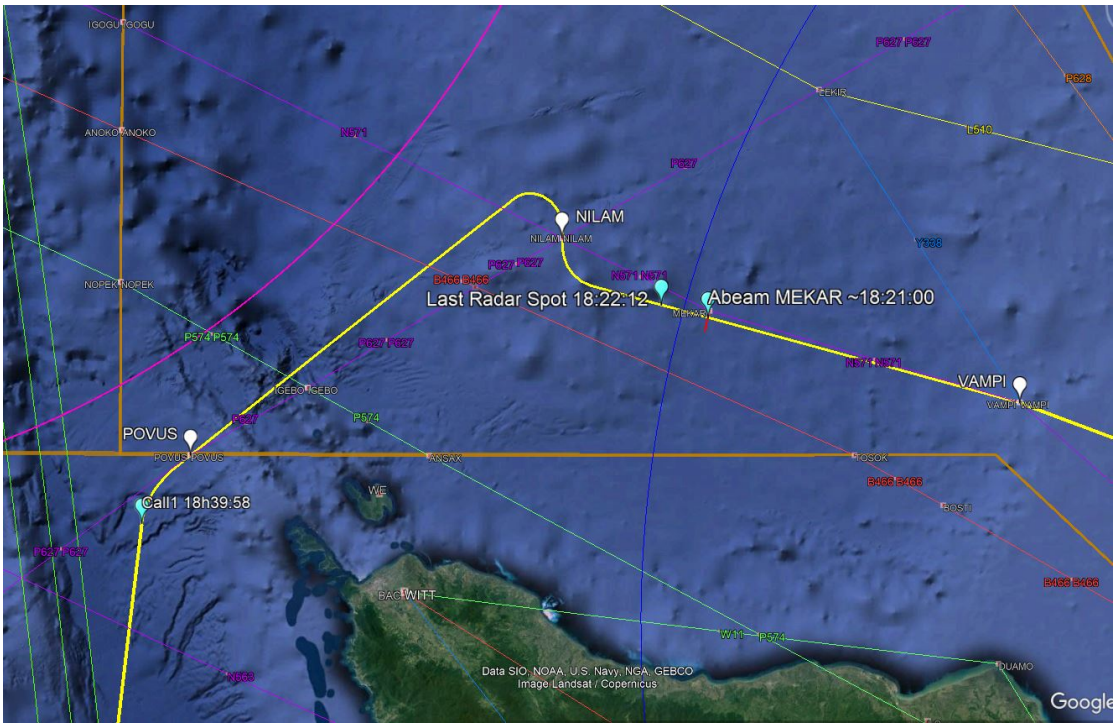

Figure 36: Recalculated FMT (Part1 around NILAM & part2 at POVUS)

In this section, the analysis focuses particularly on the leg starting at the last known position of the aircraft LSTRP at 18h22:12 UTC (c.f. Malaysian report [2]) until the beginning of an established southern route after the first unanswered phone call from the MAS Flight Operation office at 18:h39:58 UTC usually called “Phone call at 18h40”.

The FMT is the first part of what we call the MH370 recalculated unknown trajectory. Because of the nature of the Inmarsat data, the way to proceed is to make hypotheses, infer a trajectory and compare the related computed BTOs and BFOs with Inmarsat’s measured values.

Thanks to Inmarsat analysis in [3], it is established that the aircraft took a route towards a Southern direction globally. Subsequently and referring to the choice of route N571 then of P627, the aircraft

[13] *FMT: commonly used terminology to designate the manoeuvre to the south at large and considered as the last turn*

flew between the Andaman Islands and Sumatra Island avoiding the South-East India ADIZ and crossed the boundary between FIR Kuala Lumpur and FIR Jakarta at waypoint POVUS only.

4.3.1 Hypotheses at the Last Radar Plot

At waypoint LSTRP, the aircraft situation was the following:

- The aircraft was at 10Nm from waypoint MEKAR and was coming from somewhere in the South of abeam MEKAR on route at 285°
- As the segment from the south of Penang to MEKAR was flown at FL300 and as the last radar data indicates an altitude of 29,500 ft at the LSTRP, the aircraft had to descend at some point.
- From MEKAR to the LSTRP, the aircraft had accelerated because of this descent and reached an IAS of 325kt i.e. a ground speed of ~516 kt.
- Concerning the electrical power, all facts during the leg starting at waypoint IGARI concur to conclude that it was switched off voluntarily in a reversible way. This would have triggered the deployment of the RAM Air Turbine (RAT), which provides the minimum essential electrical power needs. Thus, the aircraft could have been piloted with the basics electrical systems only in parallel with the full hydraulic systems powered by the running engines.
- The person in command had probably spotted the lights of the Indigo 6E53 traffic coming ahead
- The cockpit may be still depressurised and the person in command may be still wearing an oxygen mask but it is possible that re-pressurising may have occurred earlier.

4.3.2 From Last Radar Plot to the electrical power restoration

The fictious waypoint LSTRP was not a particular location or a point in time for the person in command. It is just the mandatory starting point for any subsequent recalculated trajectory. Nevertheless, it corresponds to both the Butterworth radar range limit and the Penang VOR range limit.

In Section 4.3.1 above, the situation of the aircraft is detailed at that point as well as the working hypotheses. The next known waypoint to consider is the crossing of Inmarsat Arc1, which we call Arc1-Crossing. Its existence results from voluntary previous actions performed by the person in command.

The main action was the restoration of the full electrical power on the electrical network of the aircraft and in particular on the left part which powers the SATCOM provoking its logon to the Inmarsat satellite network at 18h25:27 UTC (Arc1) after its power-on self-test (POST). Considering our hypotheses, it is believed that this was done was restored by pressing the four push buttons controlling the generators located on the overhead panel.

After this, and since the aircraft was probably still depressurised, it is estimated that it was the right time also to subsequently press the pressurization button to the “auto” position (even though it could be possible to do it manually in a softer way). One should keep in mind that it would take a minimum of 20 minutes to restore and stabilise the aircraft interior pressure. So, the person in command was most likely still wearing an oxygen mask during the beginning of the FMT.

So far, the person in command took care to keep the aircraft “electromagnetically silent” including in particular the telecoms (ACARS, IFE, etc.) and lights. It is then possible the person in command was

then getting ready to manage the demanding restart of numerous systems normally available in cruise as well as to keep the aircraft "en-route" to Route P627.

4.3.2.1 The flown path

The path flown by the aircraft from abeam MEKAR is on track ~285/286° at a slight increasing ground speed of ~522kt and probably due to the slow descent which started earlier.

Considering the necessary SATCOM power-on self-test operations at cold start after such a long power interrupt, an estimated minimum time of 2 minutes was counted for this to be completed. As the SATCOM was operational at 18h25:27 UTC, the power restoration is estimated at around ~18h23:30 UTC or a little bit earlier. In addition, we assume that the heading remained most likely constant around ~285° since abeam waypoint MEKAR until shortly after the power restauration.

Consequently, the power restoration is estimated to at a location close to [6.575°N; 96.133°E] which is southeast of waypoint NILAM. At this point in time, the aircraft position relative to route N571 is key.

4.3.3 From the electrical power restoration to the Arc1-Crossing

The power restoration triggered a kind of countdown for the person in command to complete several necessary actions.

The following hypotheses are made:

- The highest priority for the person in command was to engage the A/P either with LNAV either with track/heading select to free himself and get time for other important tasks like stopping any telecommunication downlink as soon as possible.
- To do so, the person in command must ensure that the aircraft follows the intended route which was from MEKAR to NILAM. But as the systems' reboot took some time, the aircraft was flying away in the south of route N571. The aircraft was still on selected magnetic track 286° and arrived somewhere in the south of NILAM. In addition, the radar plot indicates that it was on track 285° thus it was further to the south.
- It is important to note that, at waypoint MEKAR, Route N571 includes a change of direction from 292° to 296° explaining this discrepancy. With the LNAV function engaged, the aircraft would have slightly turned to the right to precisely follow the route. This is an additional element to believe that the aircraft was not in automatic navigation.
- Additionally, because of the automatic setting of the speed during the power restoration which is very low at 200kt, the person in command had to set it at a much higher value and at least at the current speed or more. We estimate that it was about IAS 325kt selected i.e. 5 kt below the maximum operating speed.
- Simultaneously, at power restoration, the A/P kept the rate of climb/descent at its current value. According to the BFO at Arc1, the aircraft was descending at around -1000fpm, thus as we believe that the aircraft was already descending from the power restoration and reached FL270 somewhere close to or after NILAM.
- This descent could come from the rush (or from a lack of attention) of the person in command to perform the next actions paying no attention to correct it. It is also possible that at this stage the person in command was aware of the INDIGO aircraft coming ahead at FL330 with the risk of a potential traffic encounter in few minutes and commanded a voluntary descent below route N571 minimum en-route level at FL280 to cross the opposite traffic.

- Then, the person in command has engaged the LNAV function of the A/P in keying waypoint NILAM in the FMC followed by “Execute” and in pressing the LNAV button on the MCP dashboard. This made the aircraft automatically navigate towards waypoint NILAM.
- Subsequently, as the aircraft was in the south of NILAM it automatically turned right to this waypoint. It is considered that this turn is not accidental as there appears to be no reason for the aircraft to go this specific point in the middle of the Malacca Straight.
- Considering the path followed and the timing, NILAM appears to be overflown at the time of crossing Arc-1 by coincidence. Thus Arc-1 Crossing is considered to be at waypoint NILAM as illustrated in Figure 37.

4.3.3.1 *The flown path*

Based on these hypotheses, a corresponding path was recalculated and is presented in Yellow in Figure 37 with the approximate timing and location of the key events.

It should be noted that these path and timings were validated with our simulator in using the identified flight parameters. A video of this leg is available at www.mh”70-caption.net *(04-FMT-Final-Major-Turn.mp4)*.

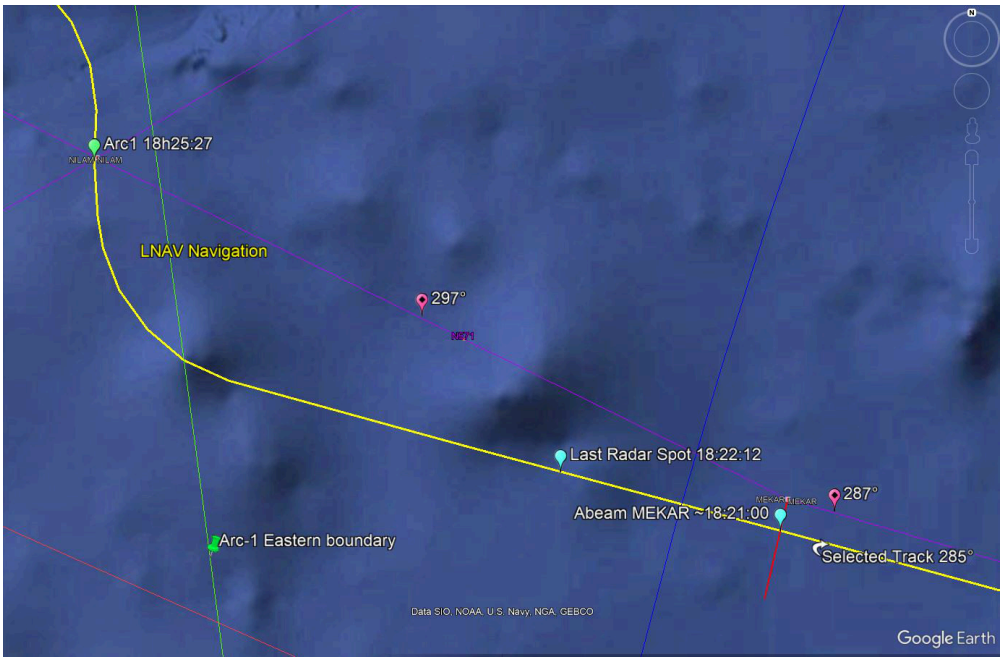

Figure 37: Recalculated and simulated flown path from waypoint MEKAR to Arc-1 crossing point

4.3.3.2 *Person in command’s workload in the cockpit*

For the person in command, the second priority was to be fast enough to stop any communication being broadcasted especially via the ACARS and the IFE through the SATCOM.

In addition, any means to identify the flight had also to be erased in the onboard systems. The Malaysian report [2] states that “when the Satcom link was re-established, no Flight-ID was present”.

The only way to complete both, is to perform a “data link system reset” manually first just after the power restoration via the “communication manager” master page followed by an “auto

message off" command. This instantaneously blocked any ACARS message to be sent and at the same time erased the flight and company information in the FMC, in particular the Flight ID. This is underlined in Red in Figure 38. These successive manipulations took some time, explaining why the aircraft, initially on "heading select", was in the south-east of waypoint NILAM without the person in command realising it.

As shown in Figure 39, the only occurrence of an automatic data link reset is after each flight and takes place between nine and ten minutes after the last engine is shut down and with any passenger entry door open. No reset occurs at power up. This is why the data link reset made after the electrical power restoration was manual.

In addition, the Flight ID information is kept in the FMS as long as the electrical power is available which is until the main battery power is exhausted. This means that the Flight ID is permanently stored during the flight. Thus, only one option remains to have the Flight ID erased: to perform a data link reset manually.

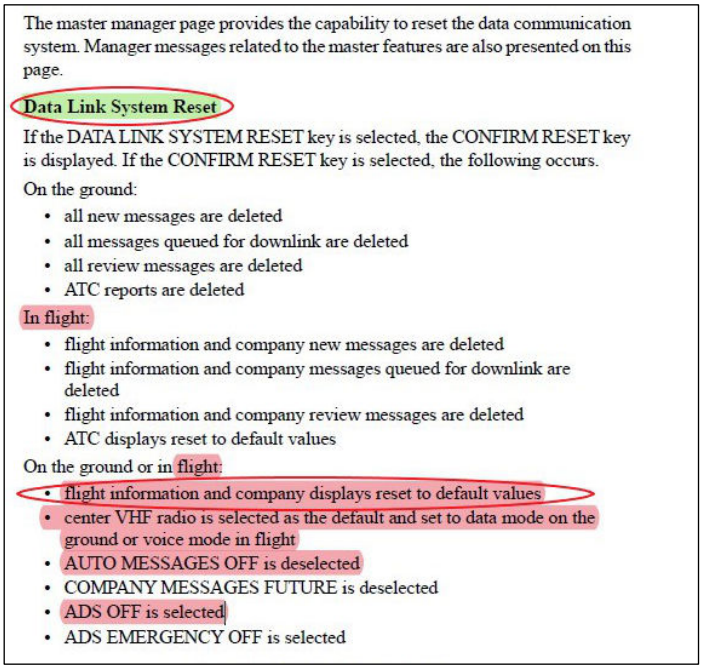

The master manager page provides the capability to reset the data communication system. Manager messages related to the master features are also presented on this page.

Data Link System Reset

If the DATA LINK SYSTEM RESET key is selected, the CONFIRM RESET key is displayed. If the CONFIRM RESET key is selected, the following occurs.

On the ground:

- all new messages are deleted
- all messages queued for downlink are deleted
- all review messages are deleted
- ATC reports are deleted

In flight:

- flight information and company new messages are deleted
- flight information and company messages queued for downlink are deleted
- flight information and company review messages are deleted
- ATC displays reset to default values

On the ground or in flight:

- flight information and company displays reset to default values
- center VHF radio is selected as the default and set to data mode on the ground or voice mode in flight
- AUTO MESSAGES OFF is deselected
- COMPANY MESSAGES FUTURE is deselected
- ADS OFF is selected
- ADS EMERGENCY OFF is selected

Figure 38: Data Link System Reset description (Source Company FCOM)

Master Manager

ATC	FLIGHT INFORMATION	COMPANY
REVIEW	MANAGER	NEW MESSAGES
1234Z	MASTER	
☑ DATA LINK SYSTEM RESET		☐ CONFIRM RESET
(Master Manager Messages)		

77710042

The master manager page provides the capability to reset the data communication system. Manager messages related to the master features are also presented on this page.

If the DATA LINK SYSTEM RESET key is selected, the CONFIRM RESET key is displayed. If the CONFIRM RESET key is selected, the following occurs:

- ATC connection is reset to NOT ESTABLISHED,
- Review messages are deleted,
- The center VHF radio is selected as the default,
- The VHF default radio set to the DATA mode on the ground; in the air, the default radio is set to VOICE,
- ACARS is set to the AUTO mode,
- Automatic messages are set to ON,
- The future company messages to printer feature is deselected,
- Downlink message parameters are initialized,
- Two seconds after selection, the CONFIRM RESET key is removed from the display and the DATA LINK SYSTEM RESET key is displayed as not selected.

This reset does not occur at power-up.

The data communication system is automatically reset after each flight. Reset occurs approximately 9 minutes after the last engine is shut down, and with any passenger entry door open.

Data link capability for the flight management system, FMS, and EICAS related maintenance functions, and cabin functions are not reset with this feature.

Figure 39: Extract from a company FCOM on Data Link Reset automatic occurrence

This explains why the logon-on request at 18h25:27 UTC includes only one signal unit while it should have included two as detailed in Table 13 which includes the very first logon request on the ground without the Flight ID, the last logon request on the ground with the Flight ID, the last ACARS report with the Flight ID and the first airborne logon request without the Flight ID.

Table 13: Log-on requests with and without Flight ID

Time	Channel	Type of signal Unit	Hexadecimal content	Request	Meaning
12:50:19	POR-R600-0-36D6	0x10 - Log-on Request (ISU)/Log-on Flight Information (SSU)	**1F** D0 10 75 00 8F 85 D0 FC 05 02 01 00 00 00 00 00 F4 6C	First Log-on on ground	1F: first log-on: No Flight identifier received by SDU as it had been erased at the end of previous flight MH371
15:59:55	IOR-R600-0-36F8	0x10 - Log-on Request (ISU)/ Log-on Flight Information (SSU)	**2F** D0 10 75 00 8F C5 D0 FC 05 82 09 00 00 00 00 00 97 1F	Last Log-on on ground-Part 1	2F+3F sequence = Flight identifier (MH370) received by SDU via ARINC 429
15:59:56	IOR-R600-0-36F8	0x10 - Log-on Request (ISU)/ Log-on Flight Information (SSU)	**3F** D0 10 75 00 8F C5 9A 82 A6 66 6E 60 40 41 00 00 93 88	Last Log-on on ground-Part2	Normal sequence after 2F
...					
17:07:39	IOR-T1200-0-3718	0x71 - User Data (ISU) - RLS	... DB 73 B3 C4 **CD C8 B0 B3 37 B0** 99 8C ...	Last ACARS report	... 3D**MH0370** ... Thus, Flight ID was present in the system memory at that time
18:25:27	IOR-R600-0-36E1	0x10 - Log-on Request (ISU)/ Log-on Flight Information (SSU)	**1F** D0 10 75 00 8F C5 D0 FC 05 82 09 00 00 00 00 00 B4 06	First Log-on in flight - Arc1	1F: similar to 12h50 log-on: No Flight identifier received by SDU (cf above)

Thus, from that moment, no identification of the flight nor any exchange of information was possible anymore. Nevertheless, the SATCOM was still powered and continued to respond with its terminal identification number only to the almost-hourly handshakes initiated by the Inmarsat ground segment.

4.3.4 From Arc1-Crossing to Arc1.2-Crossing… a manual turn

Once the person in command finished their head-down work, it would be realised that the aircraft had passed NILAM heading north. Immediately, the A/P would be disengaged, the descent stopped and a manual turn to the left initiated. The turn had to be sharp with a high banking to recover a direct track to waypoint POVUS quickly and to conform as closely as possible to route P627. In addition, being at ~FL270, the person in command also had to climb the aircraft to recover the planned flight cruise altitude i.e. FL300.

Considering the key points of FMT part1 and according to the information provided by the Inmarsat BTOs and BFOs in Table 12, the following conclusions are made:

- Around NILAM, the aircraft was heading north and descending. At 18h25:27 UTC Arc1 crossing took place nearby coincidently. The person in command had just finished switching off the communication functions.
- Realising the wrong course of the aircraft controlled by the engaged LNAV function, the A/P was disengaged and manual control taken back.
- First, the person in command turned left and then climbed before crossing Arc1.1 at 18h27:05 UTC with a rate of climb between ~1500-~2200fpm according to the calibrated BFO or to Inmarsat BFO.
- The turn ended at ~233°/234° in executing a direct to POVUS but still climbing
- At 18h28:06 UTC (Arc1-Boeing) and at 18h28:15 UTC (Arc1.2) the aircraft was still climbing at ~2000fpm on the same route.
- A short while later, having reached the targeted FL300, the climb ended. The route was maintained as a “direct to POVUS” with a high speed to get out of this zone as fast as possible.

The detailed data of this FMT part1 is provided in the summary Table 14 (further below) where the geodetic coordinates of the key locations where determined and/or verified by our simulations.

Figure 40 illustrates the FMT part1 from power restoration to Arc1.2 at 18h28:15 UTC. It shows that the reconstructed arc-crossings with a different colour each are well within their respective arc boundaries of the corresponding colour.

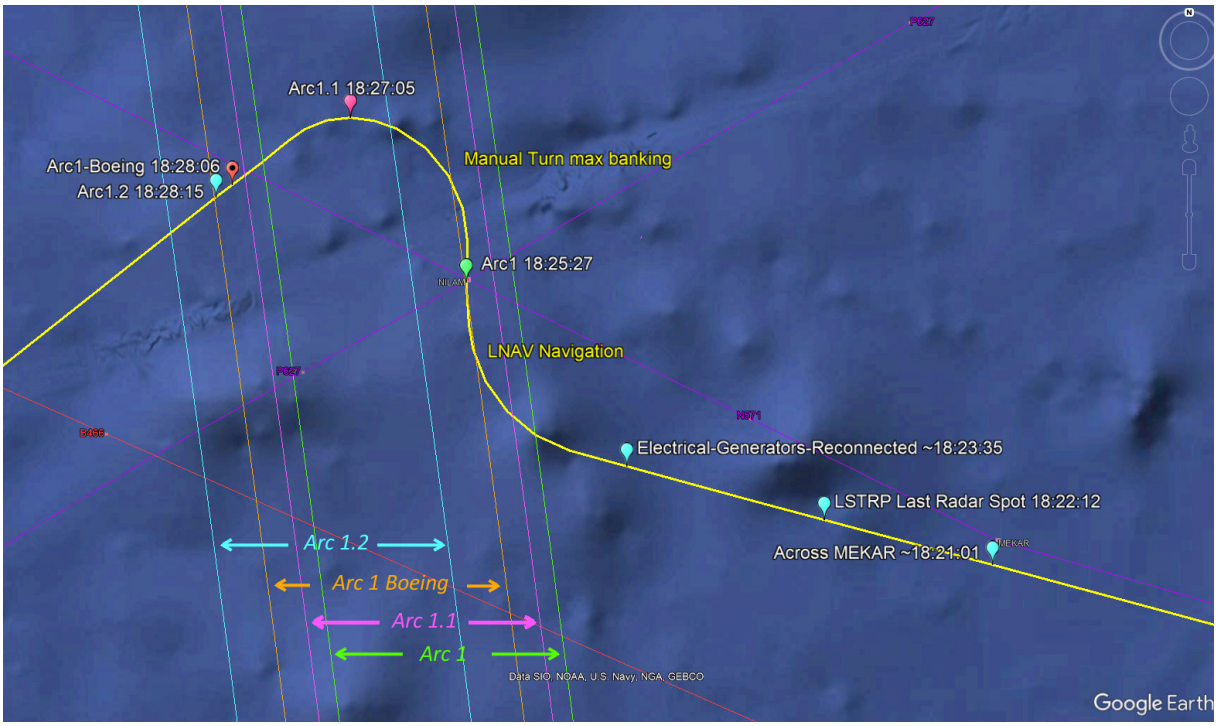

Figure 40: FMT part1 from power restoration to Arc1.2 at 18h28:15 UTC

The initial turn to the north is imposed by Inmarsat data. If the aircraft had flown on the same heading from MEKAR, its speed would not match the data as it would have been too slow.

4.3.5 From Arc1.2-Crossing to POVUS

This part 1 of the FMT turn could have been spotted as an erratic navigation to any potential ATC controller both from India or Indonesia who could have seen it. Thus, to avoid drawing their attention, the PIC had to go away as soon as possible from this zone. Consequently, speed was probably increased to Mach 0.850/ IAS 325kt just below the maximum operational speed of the aircraft.

At this stage, as the flight became stable and levelled, the most appropriate navigation way is to engage the autopilot and its LNAV function and execute a direct route to waypoint POVUS.

Why targeting waypoint POVUS in our opinion? Because it is a good way to avoid entering the South India ADIZ and the Indian Car Nicobar radar coverage. In addition, staying close to route P627 would have been the best way not to draw Indonesian controller's attention.

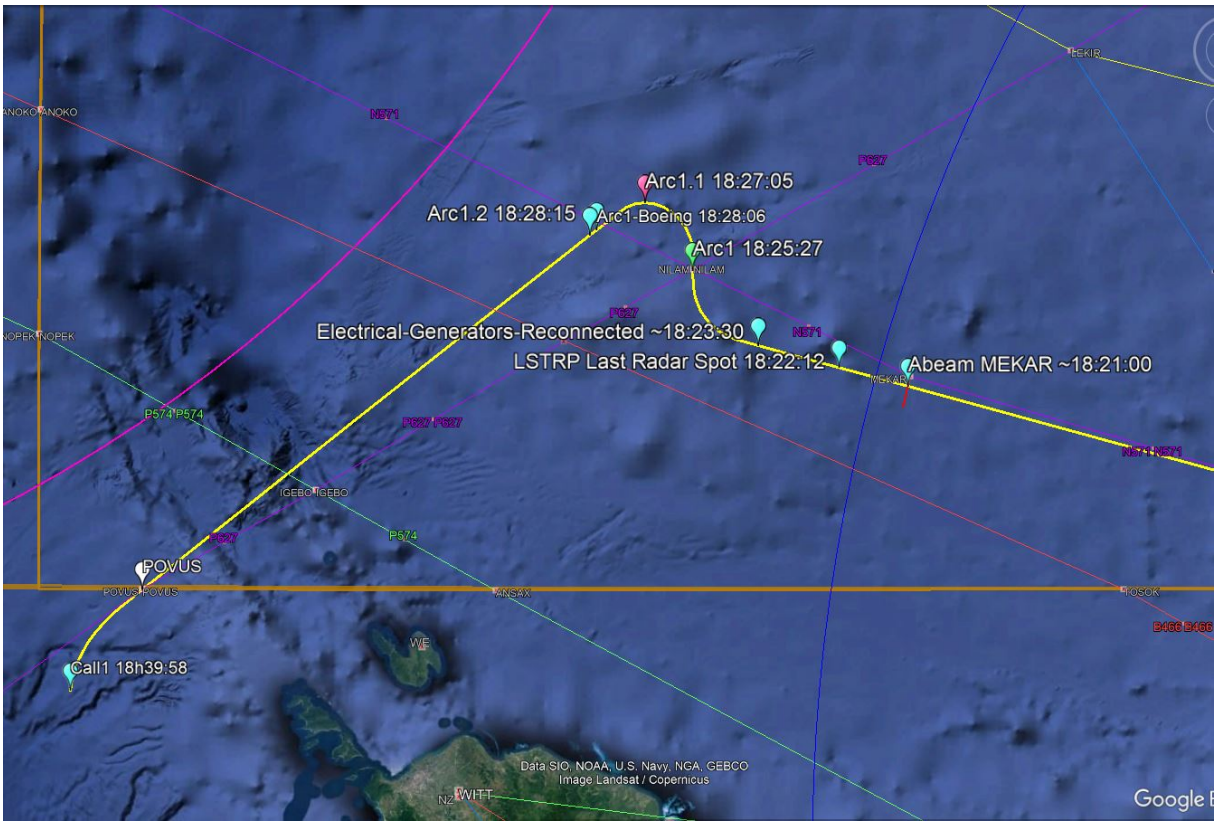

Figure 41: Final Major Turn Part1 (LSTRP-Arc1.2) and Part2 (POVUS-Phone Call1)

4.3.6 From POVUS to the Phone call-1 location

After waypoint POVUS, the PIC selected a southern trajectory. The initial selection of a magnetic track at 188° is justified by the presence of adverse cumulonimbus clouds development in the south-west of Banda Aceh as depicted in Figure 42 and underlined by the Red circles. In addition, this track ensures that the aircraft stayed away from the Sibolga military radar coverage. Choosing a more eastern direction would have been most probably too risky.

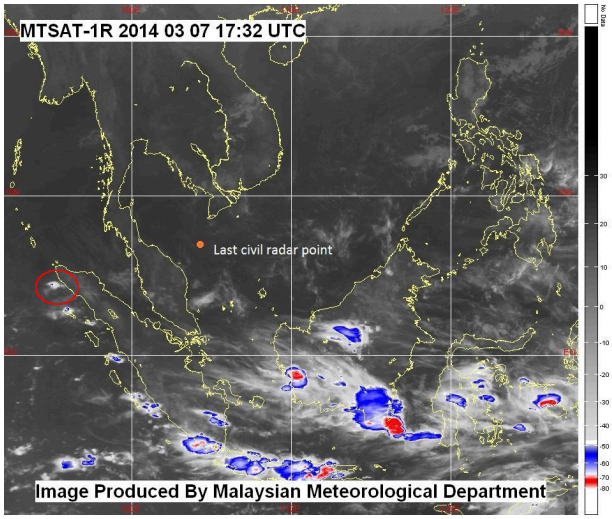

Fig. 42a: Cumulonimbus development at 17h32 UTC on March 7th

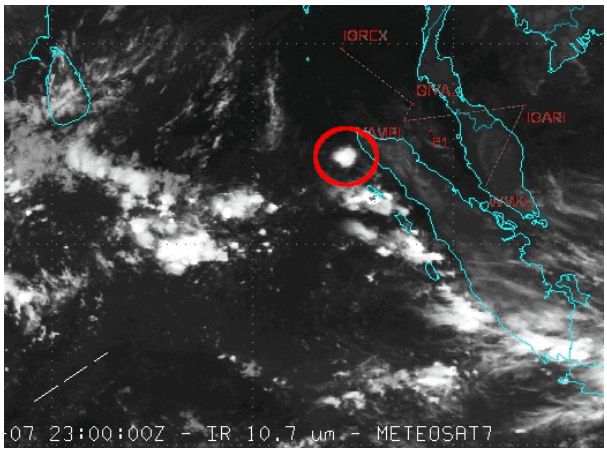

Fig. 42b: Cumulonimbus evolution at 23h00 UTC on March 7th

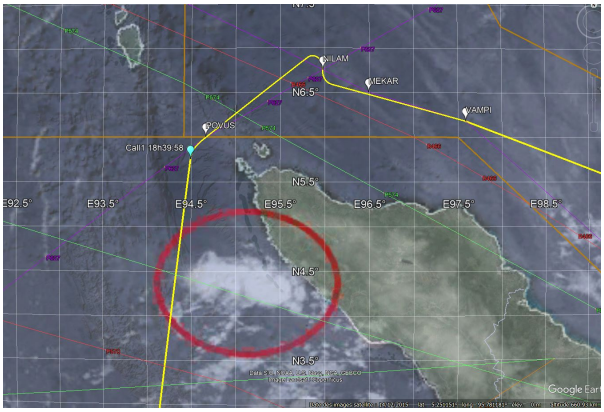

Fig. 42c: Path chosen to avoiding the cumulonimbus around 18h40 UTC

Figure 42: 188° Track selection to avoid meteorological adverse weather when exiting the FMT

At that time, the PIC chose the linear waiting speed recommended by the FAA/ICAO procedures at 30000ft which is IAS 265 kt as indicated in Figure 43.

ICAO Holding Airspeeds (Maximum)
FAA Holding Airspeeds (Maximum)

Altitude	Speed
Through 6,000 feet MSL	200 knots
6,001 feet MSL through 14,000 feet MSL	230 knots (210 knots Washington D. C. & New York FIRs)
14,001 feet MSL and above	265 knots

Figure 43: ICAO/ FAA maximum holding airspeeds (Source Company)

Thus, under the current weather conditions at that time, it corresponds to Mach 0.706. Subsequently, taking into account the wind, the ground speed was ~ 432kt. In fact, the usual way of the pilots to maintain speed is to adjust the Magenta IAS index indicator on the Primary Flight Display (PFD) scale using the Mach/speed button.

The hypothesis is made from this point onwards that the PIC maintained M0.706/IAS 265 kt for the rest of the flight at FL300 until Arc-6 crossing time.

Why did the person in command decide to fly at FL300 with the recommended linear waiting speed? The person in command had to make a trade-off between the fuel consumption, the time to stay airborne and the range. Climbing and/or choosing another speed would have consumed more fuel thus reducing available flight time and range. We think that at this point in time, the person in command was concerned about maintaining fuel in view to remain airborne as long as possible.

The justification of the selected Mach and flight level is provided later in section 4.4.1 below.

4.3.7 Compliance with Inmarsat data

The trajectory described above was reconstructed thanks to the Inmarsat data and validated by simulations. At all the key points and arc crossings, the estimated BTOs – when available – and BFOs are within the confidence intervals as defined by Inmarsat in [3] i.e. ±50µs and ±7Hz respectively. Table 14 summarises the computed BTOs and BFOs at these points with the comparison with Inmarsat measured values.

Table 14: BTO and BFO computed values at Key points during the FMT

BLELLY-MARCHAND Reconstructed Flight Path Results GDAS													
								Total Burst Freq. Offset Hz			Burst Time Offset (µs)		
	Time UTC	Lat°N	Lon°E	Altitude (100ft)	True Track (°ETN)	Speed (kt)	Vertical Speed (fpm)	Pred.	Meas.	Error	Pred.	Meas.	Error
Arc1	18:25:27	6.75	95.97	273	0	492	-1000	143	142	-1	12554	12520	-34
Arc1.1	18:27:04	6.91	95.86	273	269	488	2200	172	175	3	12516	12520	4
Arc1-Boeing	18:28:06	6.85	95.75	294	234	466	2000	144	144	0	12460	12500	40
Arc1.2	18:28:15	6.84	95.73	295	233	481	2000	143	143	0	12452	12480	28
Phone Call 1	18:39:58	5.76	94.49	300	187	432	0	88	88	0	11870	n/a	n/a

Note: At Arc1.1 the Calibrated CBFO is 156Hz. This value is matched with a rate of climb of 1500fpm. At this transitional point is between the descent and its subsequent climb, the instantaneous rate of climb at this stage of this demanding manual turn could have been within [0;3000] fpm. Thus both 1500 or 2200fmp are admissible as the aircraft rate of climb is very variable in manual piloting conditions.

4.3.8 Simulations

All characteristics determined above have been used for our simulation sessions.

Several sessions of simulations were performed with the Prepar3D simulator and its PMDG add-on according to the flight profile described above.

A video is available for this particular part of the recalculated FMT trajectory (MEKAR to Call1) at www.mh370-caption.net *(04-FMT-Final-Major-Turn.mp4)*.

The lesson learned from the simulations is that both manually piloting this trajectory and disabling the communications in the cockpit were performed by a qualified person only because of their complexity and need for detailed knowledge to handle the technical aspects.

4.3.9 Conclusions

The results of the analysis above show that considering a complex piloting from the last radar contact until the estimated location when the phone call 1 from the ground took place is a solid hypothesis. Different simulations were performed by airliner Captain's Blelly and have validated this hypothesis.

Concerning the fuel consumption, the only published data comes from Appendix 1.6E [5] of Boeing whose assumptions were based on ISA (International Standard Atmosphere) values and on a linear levelled trajectory with the corresponding speed. In our study, we calculated the actual true airspeed based on the GDAS data of the day. This is reflected in Table 15.

Table 15: Fuel estimation during the FMT

	Location	***IAS (kt)***	***Ground Speed (kt)***	***On-board Fuel (t)***	
				Calculated with GDAS weather	Boeing calculated at ISA
18h22:12	Last Radar Plot	IAS 325	517	34.7	34.2
18h28:06	Arc1-Boeing	IAS 290	466	34.1	33.5
18h34:00	En route to POVUS	M0.850/IAS325	522	33.2	n/a
18h39:58	Call-1	M0.706/IAS265	432	32.4	n/a

4.4 En-route at 188° from Phone Call 1 to Arc6

This chapter addresses the leg from the Call 1 location until the crossing of the 6th arc as illustrated in Figure 44.

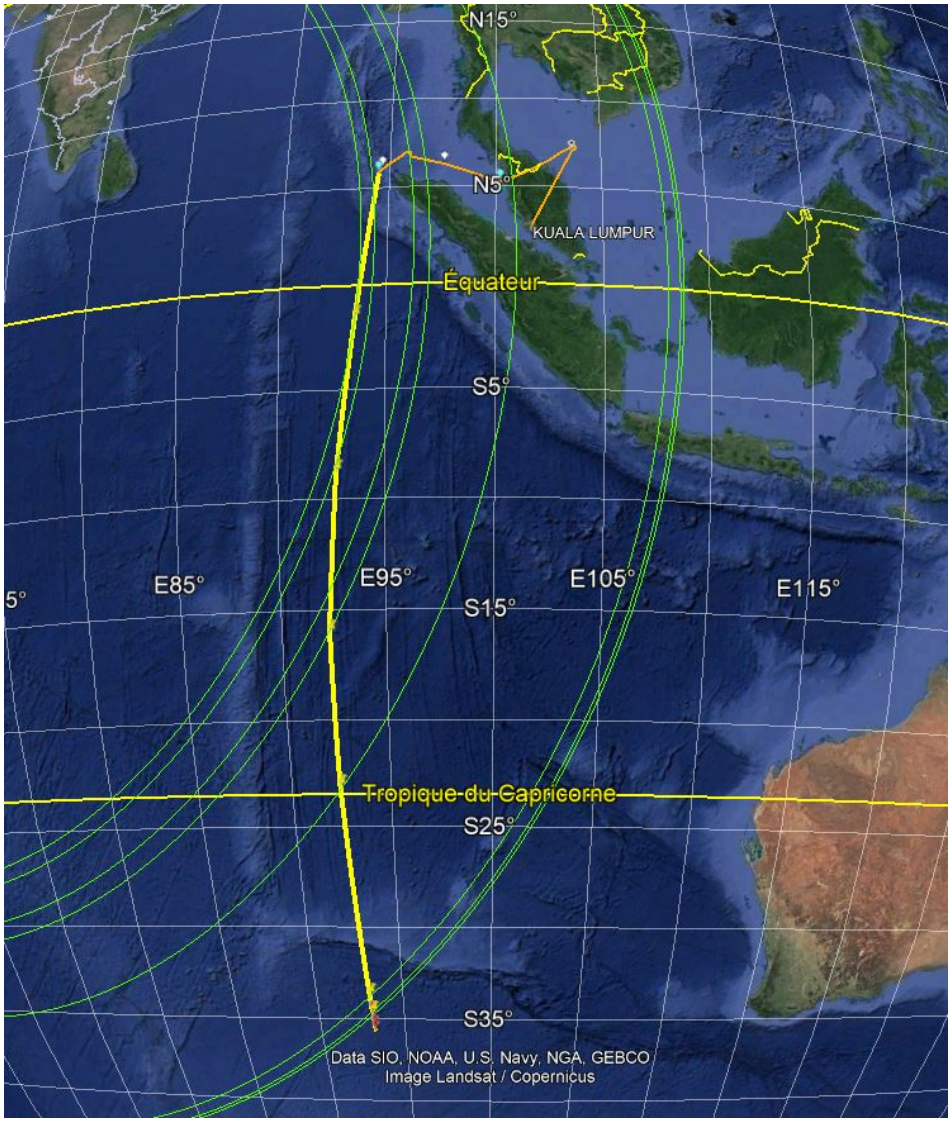

Figure 44: Southern part of the reconstructed unknown trajectory (Yellow)

4.4.1 Speed and Altitude Computation

The first point of the southern part of the trajectory (we will also call it "southern leg") is the location of the aircraft at 18h40' UTC where the 1st phone call took place. The chosen last point of this southern leg is the crossing point at Arc 6. As the latter is the starting point of the final leg, it is specifically analysed in more details in the next section 4.5 addressing the end of the flight.

In order to reconstruct the southern part of the trajectory (illustrated in Yellow in Figure 44), the following hypotheses were made and the following data was used:

1. At 18h40 UTC, the amount of fuel remaining on board is estimated at ~32.4 tons as presented in Table 15.
2. The flight level was maintained at FL300.
3. The Arcs have been precisely constructed at this flight level using Inmarsat official reported data.
4. For that day, GDAS measured meteorological data with ISA correction has been used for FL300.
5. "Performance in flight" data of the B777-200ER powered by R&R Trent-892 engines has been used.
6. Corrections for the overall fuel overconsumption were applied as follows: +1.5% of performance factor (aging of the engines) and +1.2% due to a high temperature on that day based on an estimation of a weighted average ISA +12° and following Boeing's recommendation to add +1% per 10° of extra ISA.
7. The flight time estimated by the ATSB between 18h40' UTC and the supposed flame out of the second engine – two minutes before the last logon request at 00h19'39 UTC – is 5h37'30" i.e. 5.625 decimal. *Note: This is a starting working hypothesis as in our actual End of Flight hypothesis the logon request came approximately ~30 seconds after the left engine manual shut down with the APU running.*

From these hypotheses and data, straightforward and coherent computations can be made:

1. The hourly consumption is equal to the average 32.4t /5.625h = 5760kg/h. This represents the actual hourly fuel consumption on that day including the +2.7% of overconsumption coming from the two factors identified above.
2. At mid-term of the southern route i.e. ~21h28' UTC, the aircraft **average** mass is estimated at approximately ~190 tons.
3. In Boeing's look-up table "performance Inflight Long Range" for the B777-200 ER, one has to look for the value 5760 kg/h for a reference weight of 190t. Unfortunately, neither this entry nor FL300 exists. Thus, a double cross-interpolation is required. A relevant extract of the lookup table is provided in Figure 45 with the corresponding details of the computation.
4. The double interpolation results in 5904kg/h for Mach 0.743 in Long Range Cruise (LRC) mode at FL300. In order to determine the Mach and the flight level corresponding to the value of 5760 kg/h for 190t, one must deduce 5% and then add +2.7% because of the overconsumption (c.f. above) since the look-up table is provided for brand new engines at ISA.
5. Figure 46 presents the curve "B777-200ER Cruise Mach, Fuel Flow, and Ratio of Specific Air Range to LRC Specific Air Range" provided by the IG in [10]. Considering the reduction of 5% of fuel computed above and reading the point "-5%" of fuel flow from the nominal point (1;1) on this curve, one can see that the corresponding Mach reduction is also 5%. Notably, on that curve at -5% fuel flow and -5% Mach, the air range is identical to LRC specific air range according to Boeing.

6. Thus, applying this reduction to the speed, one can conclude that for FL300 the Mach number becomes M 0.743([14]) – 5% = M 0.706. This Mach value offers a Maximum Air Range for FL300 as indicated by Boeing in table 4 of Appendix 1.6E [5]. Interestingly in the same table, M0.706 is given as the Mach of the Maximum Range Cruise (MRC) mode (in ISA) for this flight level.

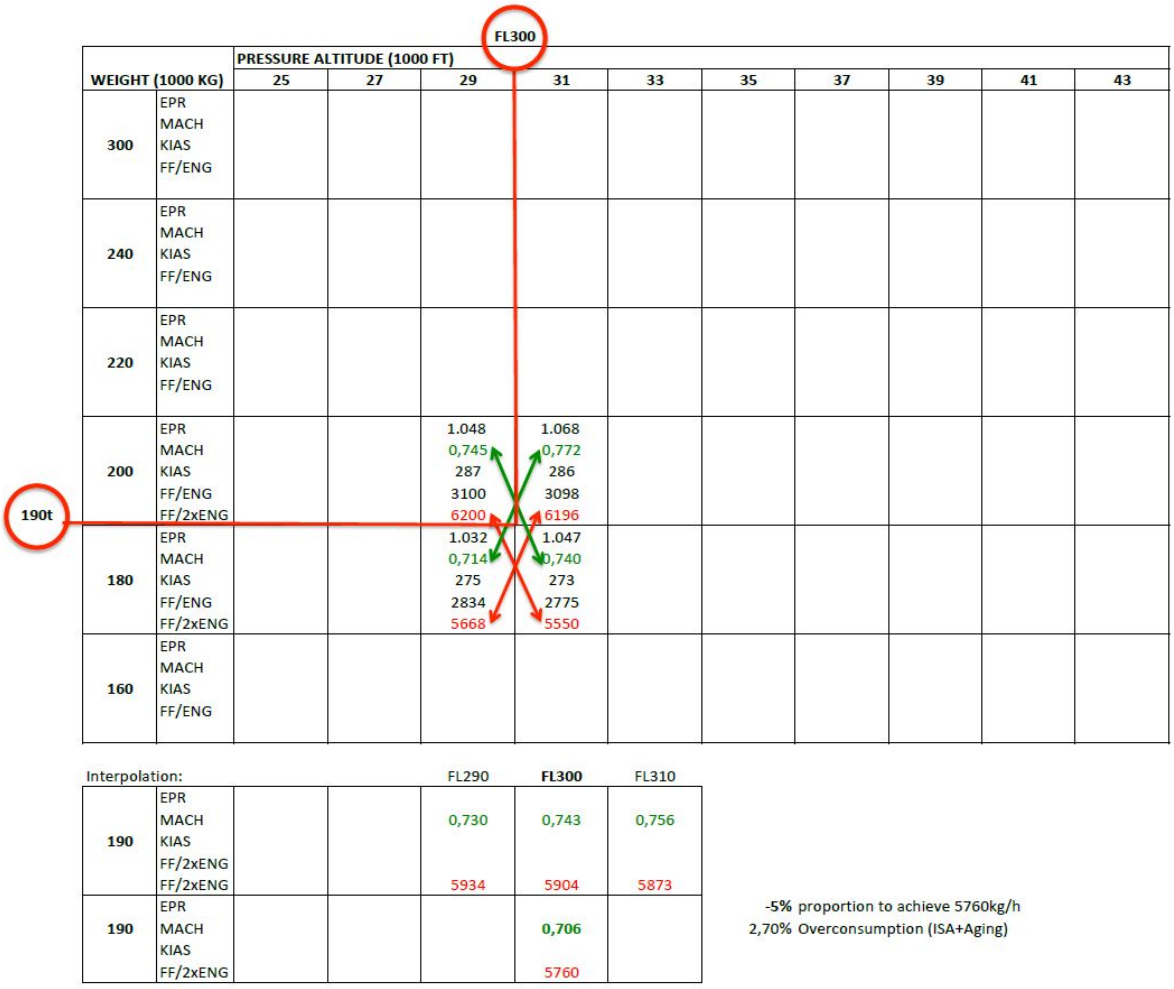

WEIGHT (1000 KG)		PRESSURE ALTITUDE (1000 FT) 25	27	29	31	33	35	37	39	41	43
300	EPR MACH KIAS FF/ENG										
240	EPR MACH KIAS FF/ENG										
220	EPR MACH KIAS FF/ENG										
200	EPR MACH KIAS FF/ENG FF/2xENG			1.048 0,745 287 3100 6200	1.068 0,772 286 3098 6196						
180	EPR MACH KIAS FF/ENG FF/2xENG			1.032 0,714 275 2834 5668	1.047 0,740 273 2775 5550						
160	EPR MACH KIAS FF/ENG										

Interpolation:				FL290	FL300	FL310
190	EPR MACH KIAS FF/2xENG FF/2xENG			0,730 5934	0,743 5904	0,756 5873
190	EPR MACH KIAS FF/2xENG				0,706 5760	

-5% proportion to achieve 5760kg/h
2,70% Overconsumption (ISA+Aging)

Figure 45: Extract of the look-up table from FCOM - Long Range Cruise Control Trent 892 (Source PMDG and Company FCOM)

[14] *LRC Mach is given as 0.743 after interpolation from the look up table and 0.742 in the graph. The impact of this difference is negligeable.*

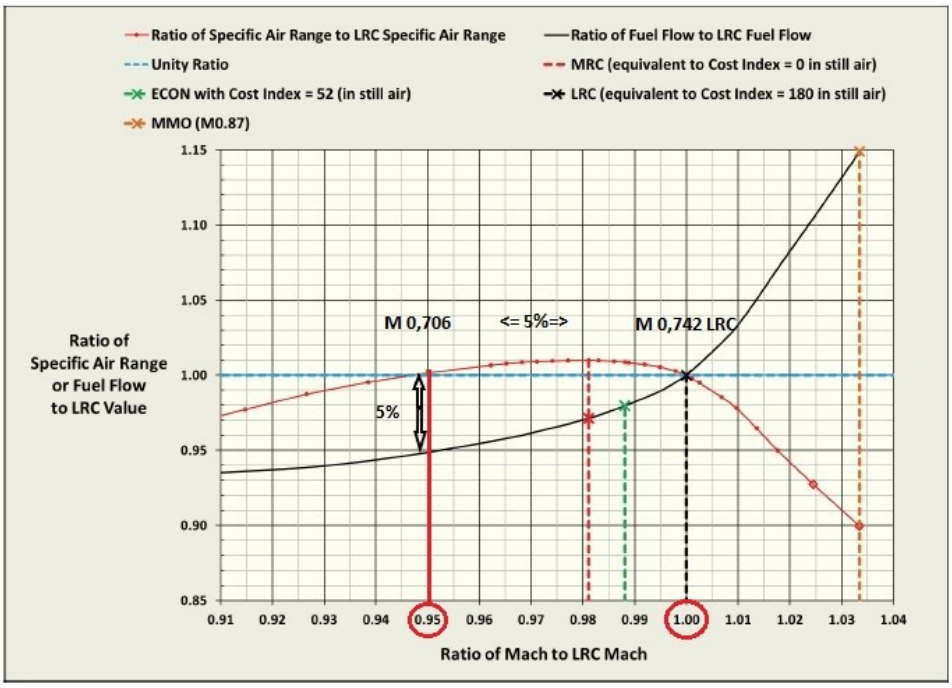

Figure A-1. B777-200ER Cruise Mach, Fuel Flow, and Specific Air Range

Figure 46: Specific consumption-distance for the B777-200ER (Source: Independent Group [10] p73)

Under these conditions, one can conclude that the flight level was indeed FL300 with a linear waiting speed at a Mach equal to M0.706 (i.e. IAS of 265kt) as deduced in section 4.3.6 with its Figure 43. During the southern leg of the trajectory, the average fuel consumption was indeed 5760kg/h which is confirmed by our simulator in Figure 47 taking into account the average aircraft weight.

Thus, from a pilot experience, it is believed that the chosen speed mode was “Mach Selected” which is adapted to a journey without any FMC route nor a specific targeted waypoint for the end of the flight.

In our fuel consumption considerations after the restoration of the electrical power, the assumption is made that the air conditioning packs were functioning. Thus, no subsequent fuel flow reduction is included in the computation nor accounted for. However, one or the other could have been switched off to reduce fuel consumption, but this is not known.

Figure 47: Fuel consumption modelled by our simulator at FL300 and at Mach 0.706.

4.4.2 Reconstructing the "Southern Leg"

Keeping this hypothesis of a levelled flight at a constant Mach, the southern leg can be reconstructed in using straight-line segments between the arcs taking into account the local meteorological conditions. This leads to (in UTC time):

1. From 18h40 to 19h41 (arc 2) = 61' => TAS[15] = 431 kt, GS = 434 kt and Distance = 442 Nm[16]. The great circle distance of 442Nm is "drawn" from the location of the 1st phone call at 18h40' to intercept arc 2.
2. From 19h41 to 20h41 (arc 3) = 60' => TAS = 430 kt, GS = 434 kt with distance = ~435 Nm[16]
3. From 20h41 to 21h41 (arc 4) = 60.3' => TAS = 430 kt, GS = 431 kt with distance = ~434Nm[16]
4. From 21h41 to 22h41 (arc 5) = 60' => TAS = 427 kt, GS = 426 kt with distance = ~425 Nm[16]
5. From 06h41 to 08h11 (arc 6) = 90' => TAS = 425 kt, GS = 425 kt with distance = ~635 Nm[16]

The detailed characteristics of the southern leg of the reconstructed trajectory are posted in Table 16. Figure 4 and Figure 44 graphically illustrate this southern leg.

Making an "aeronautical reading" of the data show that probably in the first place the person in command input a magnetic track reference at 188° on the MCP[17]. Then, somewhere in the south of the Tropic of Capricorn between 23°S and 25°S, the current true track of 178° was input as the reference to follow making the southern leg a quasi-straight line as illustrated in Figure 44. The magnetic declination became too large of approximately ~10°, thus the navigation mode was changed to use true north.

The initial selection of a 188° magnetic heading has been explained in Section 4.3.6 above.

---

[15] *TAS: True Air Speed*
[16] *Distance: computed with the exact time interval, it is not rounded thus a slight difference vis-à-vis the ground speed*
[17] *MCP: Mode Control Panel*

Table 16: Detailed characteristics of the "southern leg" from Blelly-Marchand

Arc UTC	Longitude °	Latitude °	Longitude °decimal	Latitude °decimal	True Direction °	Ground Distance Nm	Wind °/kt	Tempera-ture °C	ISA °C	Air Distance Nm	Delta Time h min s	Total Time min s	Mach	True Air Speed kt	Ground Speed kt
18h40'	94°29'00.34"E	5°45'00.21"N	94.493	5.756									0.706		
					187	442	(086/17)	-30	15	437	1h01'05"	1h01"		431	434
19h41' arc2	93°31'00.45"E	1°34'00.37"S	93.529	-1.577									0.706		
					186	435	(073/11)	-30	14	429	1h00'02"	2h01'		430	434
20h41' arc3	92°42'00.10"E	8°48'00.36"S	92.703	-8.810									0.706		
					184	434	(088/11)	-30	14	428	1h00'22"	3h01'		430	431
21h41' arc4	92°13'00.44"E	16°03'00.24"S	92.229	-16.057									0.706		
					179	425	(250/5)	-33	12	426	0h59'55"	4h01'		427	426
22h41' arc5	92°24'00.49"E	23°09'00.50"S	92.414	-23.164									0.706		
					178	635	(268/38)	-36	9	641	1h29'38"	5h31'		425	425
00h11' arc6	92°57'00.05"E	33°45'00.53"S	92.952	-33.765			252/34	-39	5				0.706		
FL195					178	59	248/25	-40	5	61	8'29"		0.700	421	412
00h19'29" arc7	92°59'00.34"E	34°45'00.24"S	92.993	-34.757				-41	4			5h39'36"	0.702	420	403
					178		245/34							411	396
00h19'38"	92°59'00.39"E	34°46'00.24"S	92.994	-34.773								5h39'45"	0.742	404	390

4.4.3 Validation of the "southern leg" with Inmarsat data

The next necessary step is to answer the question: how does the reconstructed trajectory compares to Inmarsat data? Table 17 presents the detailed characteristics of the full reconstructed trajectory. To ease the comparison, the same format has been used as in Table 9 of Inmarsat paper [3] in which an example of a possible trajectory is proposed (c.f. the red trajectory in Figure 49). This level of details offers the possibility to better understand the different components of the offsets (the BFOs[18] in particular). Extra elements have been included in our table like the BTOs[19] as well as additional waypoints allowing a more accurate comparison.

Please note that the same frequency bias δf = 150 Hz has been used as in Inmarsat report. In the same spirit, the same first four waypoints are posted to demonstrate the precision of our computation tools. The first tool is an Excel workbook initially created by Yap F. Fah, NTU, Singapore (Version 4) that we have enhanced gradually as our knowledge improved up to the current version 7. In particular, we have implemented an improved version of SK999-Satellite model which precisely fits Inmarsat ephemeris. The second tool, the Constraint Assessment Tool (CAT Version 3), is a specific homemade software developed in the frame of CAPTIO. It includes functions similar to the Excel workbook above enhanced with extra operational functions like the fuel consumption estimation, actual local meteorological data 4D interpolation, arcs generation at any altitude, great circle route computation, debris drift simulation etc.

In Table 17, one can see that the reconstructed trajectory complies with the two Inmarsat defined constraints: BTOs are within the error margin of +/-50µs and BFOs are within the error margin of +/-7Hz. Thus, this makes it an acceptable proposal for a piloted trajectory.

Please note that Table 17 does not include the BFO (-2Hz) of the last burst emitted by the SATCOM at 00h19:38 UTC. This peculiar case is addressed as a variant of the final descent presented in the next section. Details can be found in Annex 1: Variant 2 of the End of the Flight" of this report.

[18] *BFO: Burst Frequency Offset is a frequency shift due to an imperfect correction of the Doppler thus providing an instantaneous information on the speed and/or track of the aircraft*

[19] *BTO: Burst Time Offset provides an information on the instantaneous distance between the aircraft and the satellite at a given time*

Table 17: Blelly/ Marchand's Reconstructed Flight Path Results (same formatting as Table 9 in Inmarsat report)

Reconstructed Flight Path Results (ref. Inmarsat paper Table 9)																				
									Δ Fup						Total Burst Freq. Offset BFO (Hz)			Burst Time Offset BTO (µs)		
	Time UTC	Lat°N	Lon°E	Altitude (100ft)	True Track (°ETN)	Speed (kt)	Mach	Vertical Speed (fpm)	Aircraft (Hz)	Satellite (Hz)	Δ F down (Hz)	δ f comp (Hz)	δ Fsat + δ AFC (Hz)	δf bias (Hz)	Pred.	Meas.	Error	Pred.	Meas.	Error
Nominal-1-Inmarsat	16:30:00	2.75	101.72	0	0	0	-	0	0	-6	-84	0	29	150	89	88	-1	14910	14920	10
Nominal-2-Inmarsat	16:42:31	2.80	101.70	20	333	235	-	1200	218	-6	-80	-180	28	150	130	125	-5	14930	14900	-30
Nominal-3-Inmarsat	16:55:53	4.00	102.20	280	25	461	-	1500	-394	-4	-75	453	26	150	155	159	4	15210	15240	30
Nominal-4-Inmarsat	17:07:19	5.37	102.85	350	25	468	-	0	-459	-3	-71	490	24	150	131	132	1	15610	15660	50
Arc1	18:25:27	6.75	95.97	273	0	492	0.811	-1000	-138	-1	-37	159	10	150	143	142	-1	12554	12520	-34
Arc1.1	18:27:04	6.91	95.86	273	269	488	0.797	2200	870	-1	-36	-821	10	150	172	175	3	12516	12520	4
Arc1-Boeing	18:28:06	6.85	95.75	294	234	466	0.757	2000	742	-1	-36	-720	10	150	144	144	0	12460	12500	40
Arc1.2	18:28:15	6.84	95.73	295	233	463	0.754	2000	731	-1	-36	-709	10	150	144	143	-1	12452	12480	28
Phone Call 18h40	18:39:58	5.76	94.49	300	187	432	0.706	0	167	-2	-30	-205	8	150	88	88	0	11870	N/A	
A2	19:41:03	-1.58	93.53	300	187	434	0.706	0	10	-1	0	-50	-2	150	108	111	3	11485	11500	15
A3	20:41:05	-8.81	92.70	300	184	433	0.706	0	-180	6	29	142	-2	150	145	141	-4	11769	11740	-29
A4	21:41:27	-16.06	92.23	300	182	429	0.706	0	-348	17	56	315	-18	150	172	168	-4	12770	12780	10
A5	22:41:22	-23.16	92.41	300	178	425	0.706	0	-519	30	78	494	-29	150	205	204	-1	14499	14540	41
Phone Call 23h14	23:14:30	-27.02	92.69	300	178	427	0.706	0	-586	38	88	566	-33	150	224	217	-7*	15682	N/A	
A6	00:11:00	-33.76	92.95	300	178	423	0.706	0	-683	50	100	671	-37	150	252	252	0	17994	18040	46
A7	00:19:29	-34.76	92.99	195	178	420	0.670	-4000	-759	52	102	678	-38	150	186	182	-4	18373	18400	27

**: the data of the Phone Call at 23h14 is usually considered as statistically non-independent.*

Figure 48 replicates Figure 14 of Inmarsat paper [3] for comparison. The red plot represents Inmarsat data. The blue curve represents our computed estimation of the BFOs along the reconstructed trajectory. The matching is very good as the average BFO error is -1Hz and the standard deviation of the BFORs is σ ~2.5Hz. Furthermore, when considering the available extra BFOs (like the one we named Arc-1.2 for example) which are not usually considered by the other studies, the BFOR σ becomes ~3.0Hz with the same average BFO error of -1Hz.

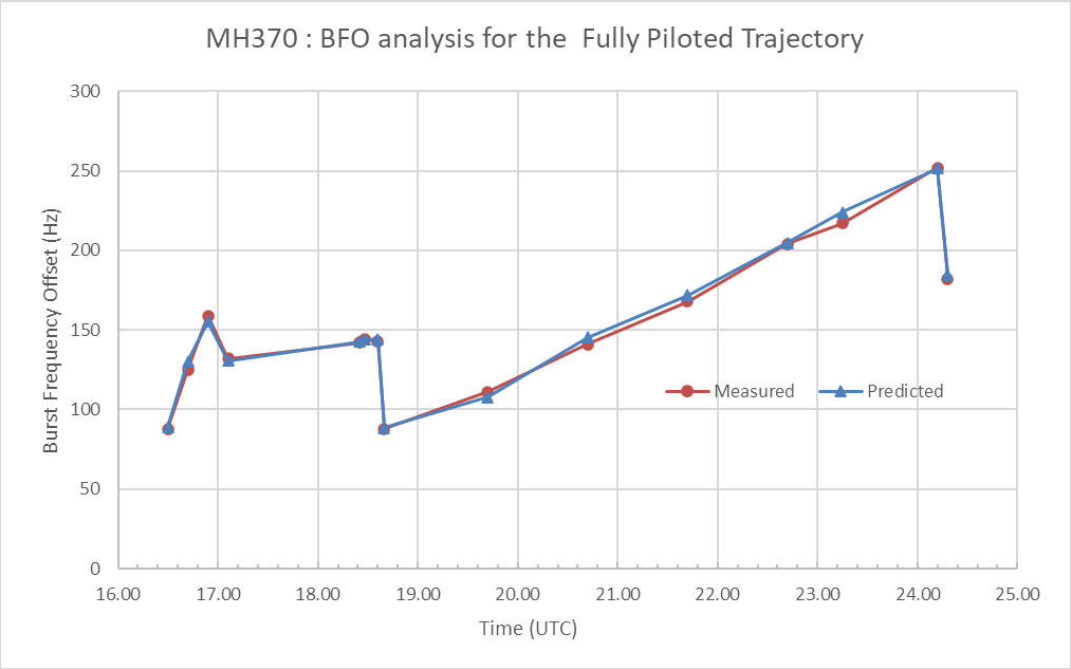

Figure 48: Comparison of Inmarsat BFO versus Captain's Blelly trajectory BFO (BFOR σ ~3.0Hz)

The comparison of the reconstructed trajectory with Inmarsat's example is presented in Figure 49. The similarity of the two paths between arc 2 and arc 6 is striking. Nevertheless, the arc crossing points are different except those at arc 7 which are very close i.e. less than a nautical mile apart.

However, Inmarsat's final major turn (FMT) is wider and is located ~75Nm further to the northwest compared to the FMT turn found here. The difference is explained by a greater average speed as well as a higher altitude in Inmarsat example in which the variable speed and the flight level have been considered closer to "standard" airline operational values.

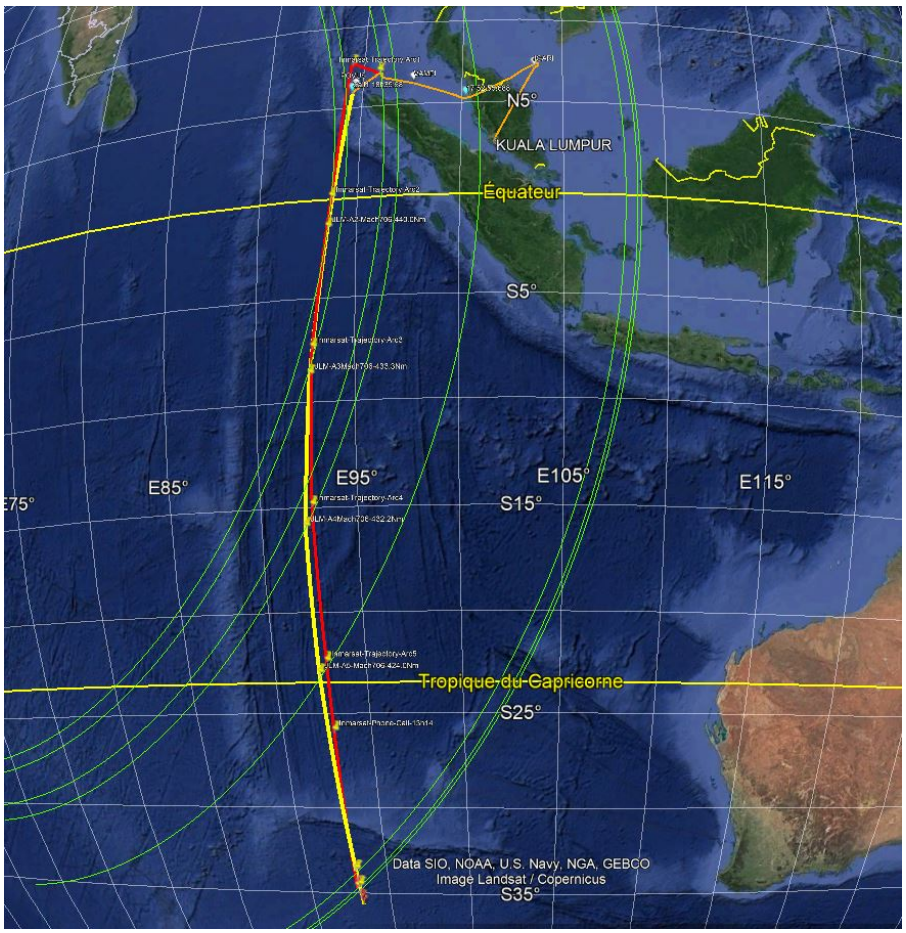

Figure 49: Trajectories comparison - the reconstructed trajectory (Yellow) and Inmarsat example (Red)

4.5 The Final Descent to the End of the Flight

The final descent is a phase which was – and still is – the object of numerous studies. A lot of them, as the official report for example, assumed that the aircraft was not piloted anymore when the descent started. Few studies made the hypothesis that the end of the flight was well controlled by a pilot carefully preparing a ditching. This hypothesis of a well mastered piloted descent from FL300 down to sea level ending in a controlled ditching is the basis of the work presented below.

The analysis was complex as numerous parameters had to be considered like the different horizontal speeds, the different average rates of descent, the remaining fuel at key points as well as the validation of this leg with the relevant measured BFOs and BTOs. An attempt to detail the method in a simple way follows:

4.5.1 Hypotheses and basic parameters:

1.1. At the arc6, the flight was level at FL300 and the Inmarsat handshake was complete and normal.
1.2. The ground speed was GS=410 kt at ISA +4° (which increased to ISA +8° at FL230 then decreased to ISA+5° at sea level)
1.3. The quantity of fuel is estimated at about ~800 kg.
1.4. The shortest straight-line ground distance flown by the aircraft in 8’30” between arc6 and arc7 is 59 Nm.
1.5. The wind decreased from 251°/33kt towards 220°/20kt at sea level

1.6. The top of descent was at FL300 at Mach M0.706 when the right engine flamed out due to fuel starvation.
1.7. The true track at 178° was kept from the top of descent to sea level
1.8. In this method, the computations consider the crossing point of arc 6 as the starting reference location for measuring the time and distances until the ditching.
1.9. Arc7 is where the logon request to the Inmarsat network took place within approximately ~30 seconds following the left engine manual switch-off. The electrical outage provoked a "break power transfer" to the APU electrical supply which was started just before. This triggered a reboot automatically followed by a logon request as described in the Boeing Maintenance Manuel. In this documentation, it is stated "When the ac (electrical alternative current) system changes from one power source to another ***in the air*** it does ***break power*** transfers" and "a (SATCOM) automatic log-on occurs when the system powers up". It is assumed that the oscillator oven (OCXO[20]) of the SATCOM did not cool down during such a short break power (few seconds) leading to a fast restart.
1.10. The hypothesis is made that the person in command in command managed to keep the necessary quantity of fuel for the APU until touch down keeping all flight control surfaces operational during a well-controlled gliding descent and ensuring a full flaps configuration for a controlled ditching.
1.11. It is important to realise that if with the two engines flamed out, the APU out and with the RAT only, it would be impossible to deploy the flaps for a ditching at reasonable speed. The impact would have been at high-speed producing numerous pieces of debris. The small number of found debris tends to support the conclusion on a low-speed ditching for MH370.

4.5.2 Profile of the descent

2. The different steps of the descent are sketched in Figure 50. By setting a reference initial time at T_0=00h11' UTC, these steps can be detailed as follows:

2.1. T_0= 00h11': at arc 6, both engines were running and the SATCOM answered the satellite interrogation (ping). The remaining fuel is estimated at ~800kg. It was not evenly distributed between the tanks because the right engine consumed more than the left one. At this point in time, the total fuel consumption of both engines was about 88kg/min i.e. 5280kg/h according to Boeing fuel performance table for the B777-200ER with a mass of 175t.
2.2. T_1= T_0+1': at about +1 min, the right engine flamed out because of a fuel shortage in the right tank. This is illustrated by the "N-1" tag in Figure 50. Thus, from this moment, all aircraft electrical systems were powered by the left engine only. The auto pilot and the flight director were still functioning and were available to the person in command who most likely kept the "Mach selected" mode active (it had been used in cruise until now). Thus, during the descent to come, the IAS progressively increased up to ~310kt which was maintained. The only setting input made by the person in command on the MCP to the A/P was a constant reference vertical speed value of around V/S ~ -1000fpm. This is the only situation where an aircraft with one engine off would accelerate during a descent in the mode "Mach selected". As a consequence, the TAS is estimated to be around ~434kt when the aircraft crossed FL230. This basically confirms that the aircraft did fly 59Nm in 8'30'' with an average ground speed of ~416kt taking the wind into account. At a rate of descent of ~-1000fpm, the consumption of the unique running engine is estimated at ~71kg/min i.e. ~4300kg/h.

[20] *OCXO: Oven Controlled Crystal Oscillator*

2.3. At the beginning of the descent after the right engine flamed-out, ***the person in command started the APU and opened the fuel cross-feed valves*** to be able to use all of the remaining fuel and to dry out the tanks (the aircraft was descending with a negative pitch with a small quantity of fuel). After being switched on, the APU takes approximately one minute to supply electrical power.

2.4. $T_2 = T_0$ +8'00": close to ~FL230 **the left engine was voluntarily manually stopped** as illustrated by the "N-2" tag in Figure 50. Thus, the aircraft started gliding with a slight increase of the pitch down. At this point, either by surprise or in a short period of inattention, a short lack of pitch control increased the vertical down speed during few seconds up to around -4000fpm as indicated by Inmarsat data.

2.5. $T_3 = T_0$ +8'29": The aircraft crossed flight level ~FL195. Logon request from the SATCOM producing an estimated BFO of 185Hz compared to Inmarsat measured 182Hz. Remember that following the left engine cut-off few seconds ago, no more power was available to the left AC bus which powers the SATCOM. Thus, the APU – the sole remaining source of power – took over from the left engine and powered the left AC bus in addition to the right AC bus it already powered. This left AC bus power Off/On sequence induced an electrical power break transfer leading to an automatic SATCOM power-off/power-up and subsequently to an automatic logon request initiated at T_3.

2.6. $T_4 = T_0$+8'38": within 9 seconds after T_3 the SATCOM logon to the network was properly completed according to the Inmarsat protocol. But, contrary to the previous logons, no other airborne system could logon subsequently and in particular the IFE[21]. This leads to conclude with confidence that the ELMS (Electrical Load Management System) shed the low priority utility buses and loads for dedicating the power to the high priority systems like the demanding pumps providing the hydraulic power to the flight control surfaces. One should keep in mind that the engines were stopped at this point in time and no hydraulic power was available anymore from them. This was an emergency configuration for the sole APU electrical generator powering the whole aircraft especially the electric pumps for the control surfaces.

At this point in time, the Inmarsat measured BFO of -2Hz raises questions. If this value is correct, it implies a rate of descent of at least -14500fpm meaning that the aircraft was diving just after the crossing of arc 7. No convincing technical explanation has been found for this "extraordinary" BFO. Nevertheless, we analyse it in Annex 1 of this report and present an alternate descent path including an explanation for this BFO. Since all searches of the wreckage in the Arc7 area were unsuccessful and since very few debris were found eventually, the best interpretation is operational: the person in command recovered from this unexplained dive and the aircraft continued its controlled gliding descent before a proper ditching.

2.7. $T_5 = T_0$+8'40" and later: In the gliding descent, the person in command could have used one of the two procedures they were probably aware of and maybe had even anticipated them:

2.7.1. Either a descent with the two engines inoperative at Boeing recommended IAS of 270kt called "drift down two engines inoperative". The estimated average ground speed would have been around 306kt with a rate of descent of about ~-2200fpm corresponding to a descent from FL195 in less than ~9 minutes. Thus, the maximum estimated distance flown from arc 7 would be ~45 Nm (without considering the reduction of speed induced by the full flap at 30° at the very end) ending with a ditching at $T_6 = \sim T_0$+ 17'20''.

[21] *IFE: In Flight Entertainment - a system that manages passengers communications (telephone, sms) and entertainment in the cabin*

2.7.2. Or a descent with the two engines inoperative at the minimum speed with the flaps at 0°. Therefore, its IAS would be Vref (function of the aircraft mass i.e. 175t) augmented by 80 kt which would mean an IAS = ~210kt in this case. This would have allowed flying in descent at no risk of stalling during approximately ~17 minutes. The aircraft glide ratio led to a rate of descent around ~ -1150 fpm and an average ground speed of ~236kt. The maximum estimated distance from arc 7 would be about ~ 67 Nm (without considering the reduction of speed induced by the full flap at 30° at the very end). Thus, the ditching would have occurred at $T_6 = \sim T_0$+25'30''.

4.5.3 Estimated point of ditching

Thus, based on the hypothesis of a constant true track, the estimated minimum and maximum flight distances lead to these points:

- The minimum ditching zone coordinates are: **-35.518° S and 93.025° E**
- The maximum ditching zone coordinates are: **-35.875° S and 93.039° E**

These are illustrated in Figure 51. But of course, other tracks and variable rates of descent could be envisaged for estimating the ditching location. This is taken into account in section 5 below where a new search zone is proposed.

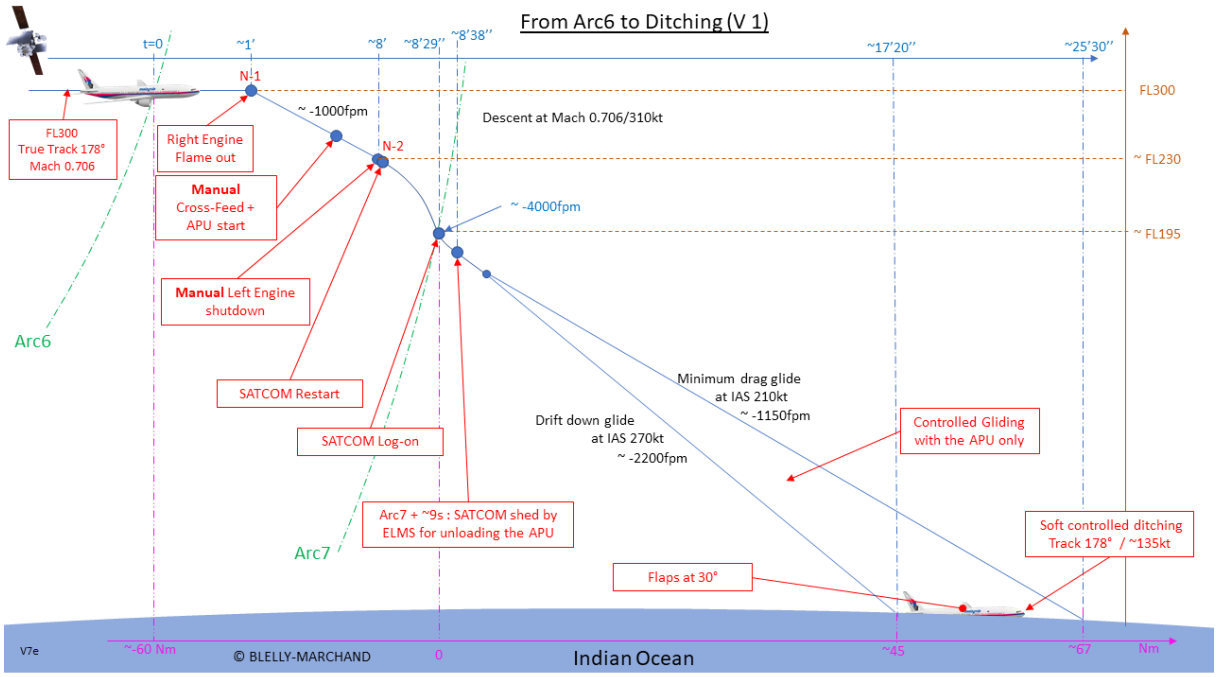

Figure 50: Considered end of the flight path (Blelly-Marchand) – Variant 1

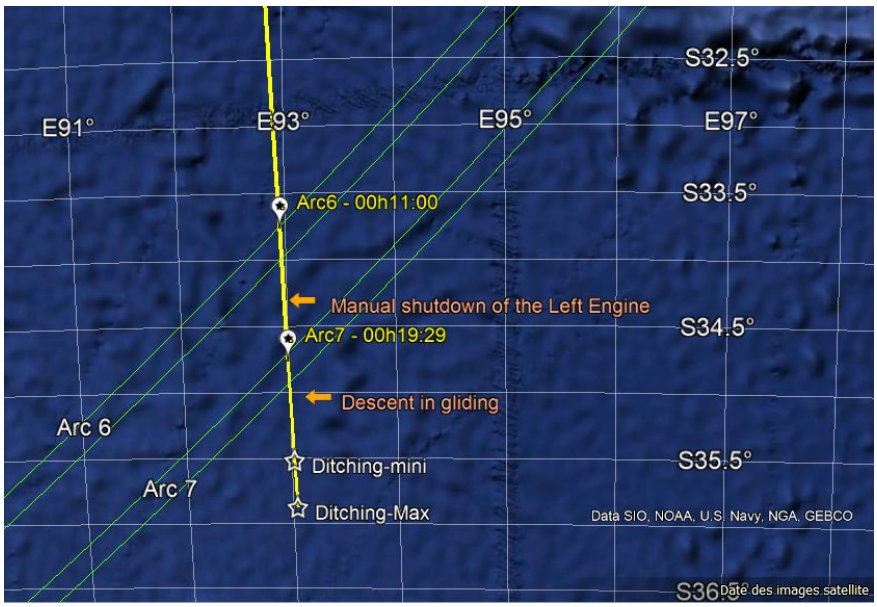

Figure 51: Estimated northern and southern possible locations of the controlled ditching (white stars)

4.5.4 Simulations

Two sets of simulations were performed for both variants of the final descent with the drift down (270kt) parameters and also with the minimum speed (210kt) parameters.

They confirmed the findings both in time, distance and fuel.

Two videos, one video sample per variant, are available at: www.mh370-caption.net :

- Variant 1 with descent at -4000fpm et minimum speed
  (06-last-descent-V1-210kt-MinDrag.mp4)

- Variant 2 with descent at -4000fpm / -14500fpm and then drift down at IAS 270kt
  (07-last-descent-V2-270kt-DriftDown.mp4)

5 The proposed new search zone

This concludes on the characteristics of the identified zone where to search the wreckage and which is proposed as a viable candidate for future underwater search campaigns.

In this region, two under-water search campaigns have been conducted until 2018. They covered areas on both sides of the arc 7 as illustrated in Figure 52 in Brown (Fugro) and in Blue (Ocean Infinity) based on the hypothesis that the plane crashed close to Arc7 after a quasi-vertical dive. They have been unsuccessful because we think that the very good gliding capability of the plane had not been considered nor was the possibility that a person in command was still in command. Considering the complexity of the known trajectory and its obvious realisation with somebody in command, we think that there is basically no reason for it to be different at the end of the flight.

The proposed new search zone is depicted in Green in Figure 52. It has a ~15 Nm wide trapeze shape prolongating the already scanned zone to the south by ~25 Nm. The zone includes a contingency margin of ~7.5Nm on each side of the true track of 178° to cover the case where the aircraft could have deviated slightly. This search zone is valid for both End of Flight variants presented in this report.

The proposed new search zone surface is estimated of ~350 Nm^2 approximately. It is small compared to the potential search zone of 10 000 Nm^2 envisaged by Ocean Infinity during a potential future 100-day campaign in 2023 or 2024. According to this daily rate, the proposed new search zone would be scanned in less than 5 days.

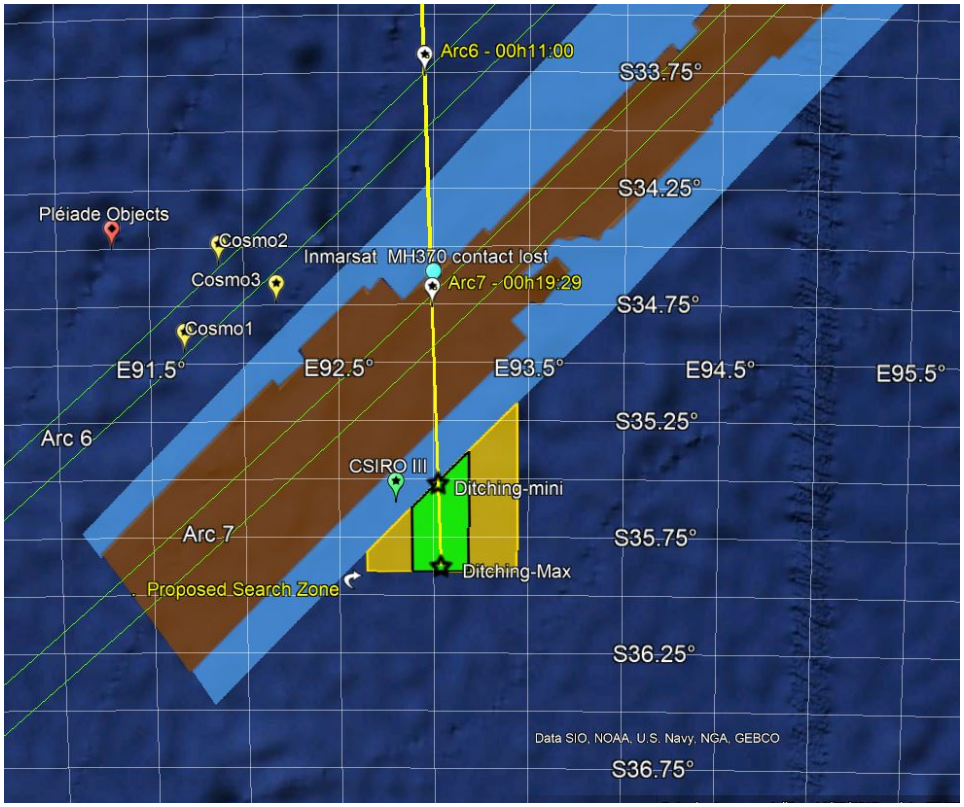

Figure 52: Proposed new search zone (Green area) potentially covered in less than 10 days

In order to take into account the possibility that the aircraft might have drifted to the left or to the right from the initial track at 178° due to different factors, an enlarged proposed new search zone is illustrated in Orange in Figure 53. It covers approximately 1200Nm^2.

Figure 53 shows also the AIS tracking of Ocean Infinity “Seabed Constructor” vessel during its 2018 campaign in Brown dots.

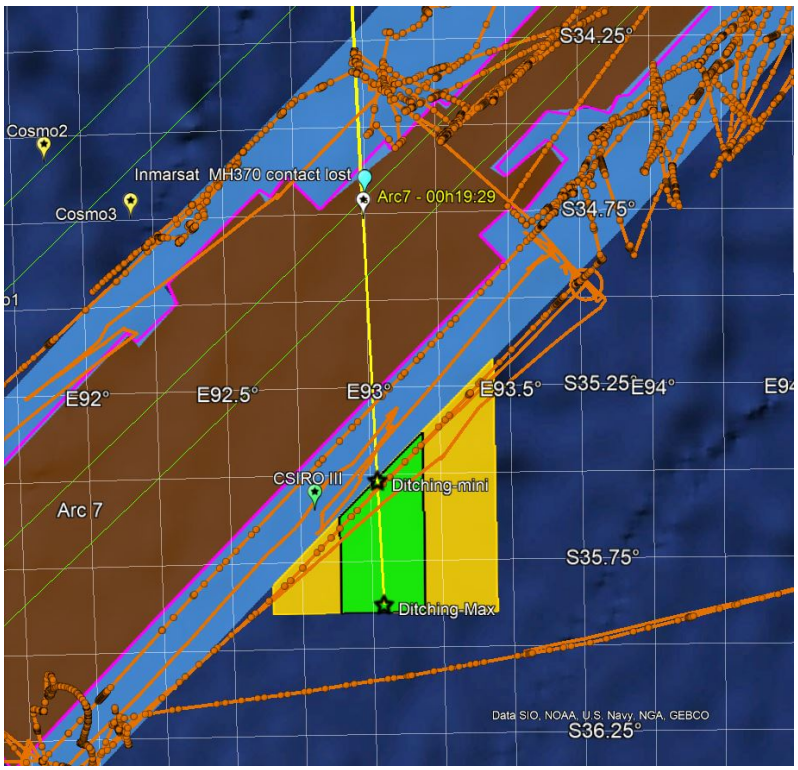

Figure 53: Extended proposed new search zone complementing the previously scanned areas

6 Conclusions

A complete reconstructed trajectory - validated by simulations - has been successfully presented in this report. It is based on the hypothesis that the aircraft was piloted all the way through until a kind of soft ditching producing only a few small pieces of debris. Due to a final descent while gliding, the identified point of impact is in a small zone around mid-point [-35.70°S; 93.03°E] located just outside of the area already searched until 2018.

All the elements presented above have been shown to be aeronautically and technically possible. They could be carried out and flown by a qualified person.

For each element described here, one can ask whether it was possible, justified and validated by simulation. The answer to all is “yes”. None of these elements can be eliminated as they all could have happened as described. They form a coherent and realistic piloted trajectory matching the Inmarsat measured data. Today we are not aware of any other possible trajectory with no gap like the one presented here.

But until the wreck is found, this trajectory remains a hypothesis.

Any contact for technical discussion or other exchange is possible via our mail addresses provided on page 1 of this report.

7 Additional elements of interest …

7.1 Visual detection of satellite images

Several relevant elements must be mentioned in relation to the geographical location of the ditching zone and the proposed search zone.

The first element comes from the report on the analysis of the "optical" images captured by the French satellite PLEIADES 1A on 23rd march 2014 [11]. From these images, a set of approximately 12 objects were identified as "possibly man-made". All of these objects include a top surface of 20 m^2 or larger. Their geographical location is pinpointed as "Pléiades objects" in Figure 52. This is in coherence with the results of one of the drift studies from the Australian organisation CSIRO (CSIRO report III) [13].

In addition, the Italian satellite "COSMO-Skymed" provided Synthetic Aperture Radar (SAR) data acquired on 21st March 2014. The geographical location of the objects identified as "possibly man-made" is illustrated by Cosmo Yellow tags in Figure 53.

7.2 How does our trajectory compare with Boeing Performance Analysis?

In Appendix-1.6E-Aircraft-Performance-Analysis-MH370-(9M-MRO) [25] to the Malaysian report [2], Boeing present the results of their performance analysis in which potential trajectories are defined based on different values of the true air speed.

Figure 54 presents the range computation made by Boeing considering first the flight level and then the TAS at standard ISA.

Table 4: Range Capability for Altitude/Speed Combinations (from Arc 1)

Flight Level	True Airspeed (knots)	Mach (*=MRC)	Time (hours)	Range (nm)
FL400	494	0.861	5.0	2491
FL400	475	0.828	5.9	2803
FL400	469	0.818*	6.0	2806
FL400	417	0.727	6.1	2538
FL350	500	0.867	4.7	2356
FL350	475	0.824	5.6	2657
FL350	466	0.824	5.9	2747
FL350	443	0.769*	6.2	2711
FL350	400	0.694	6.6	2624
FL300	500	0.848	4.5	2270
FL300	437	0.742	5.7	2523
FL300	416	0.706*	6.1	2552
FL300	323	0.548	6.8	2181
FL250	471	0.782	4.6	2151
FL250	383	0.642*	6.1	2363
FL250	291	0.483	6.8	1970
FL150	407	0.65	4.5	1835
FL150	333	0.532*	5.8	1923
FL150	250	0.399	6.75	1662
FL030	345	0.535	4.2	1446
FL030	284	0.437*	5.7	1534
FL030	235	0.359	6.2	1464

VMO-MMO
LRC
MRC
V Stall

Figure 54: Range computation by Boeing – FL300 is of interest – Arc1-Boeing is at 18h28:06 UTC (Source [25])

Based on these results they constructed possible flight paths as shown in Figure 55. In our case, the blue paths at FL300 are of particular interest.

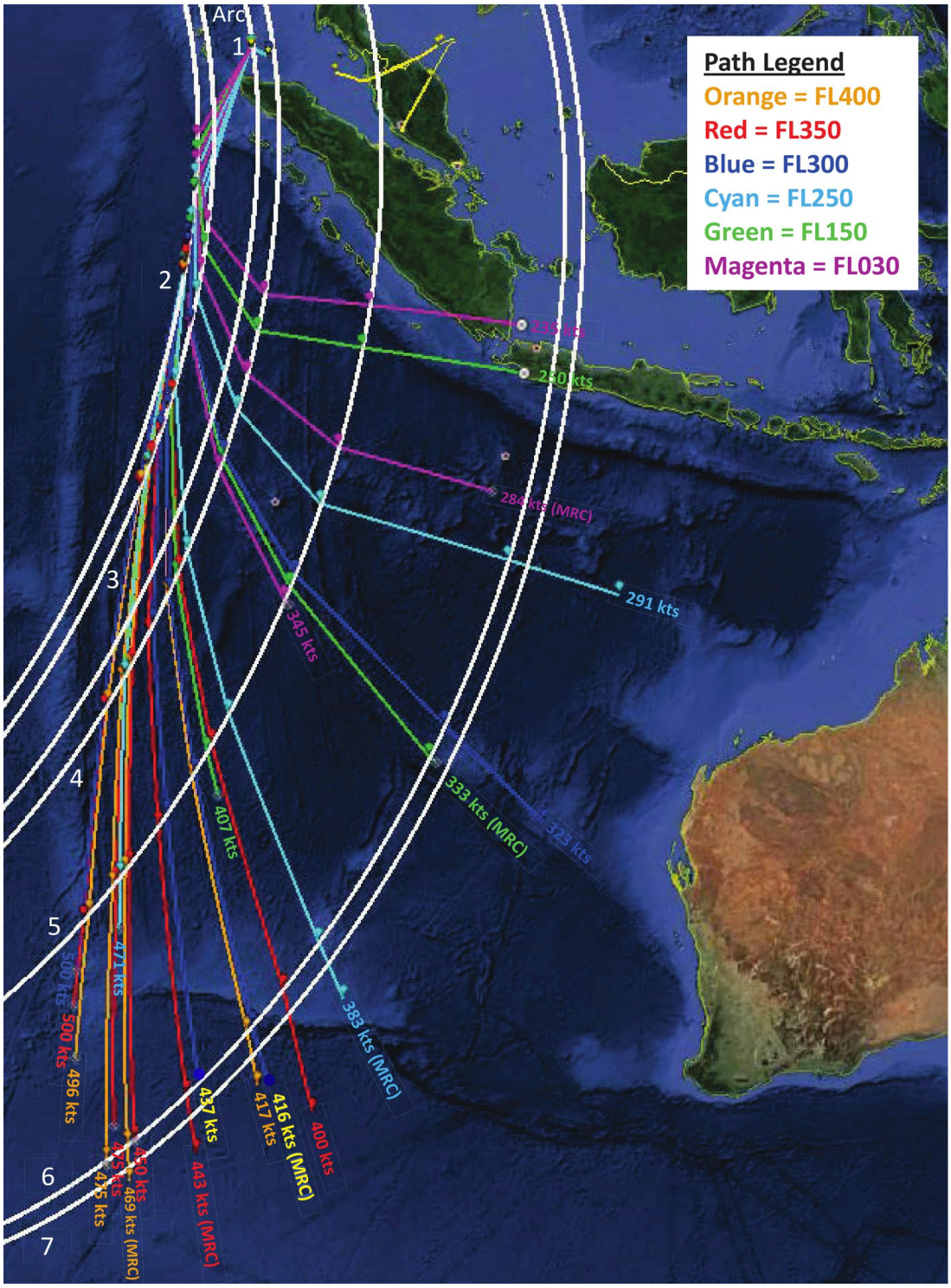

Figure 55 : Boeing calculated possible Flight Paths (Fig. 3 of [25])

Note: The blue paths TAS have been underlined in yellow for better contrast in the picture

The question addressed here is “how does our trajectory compare with these flight paths?”

Our trajectory is levelled at FL300, the average true air speed TAS is 431kt at ISA of the day (ISA+12) and the total distance flown from 18h28:06 (Arc1-Boeing) is 2522Nm. Thus, we focus our attention on the data given by Boeing for this flight level.

In Table 18 a line has been inserted including a flight path at TAS 431kt using the same computation from Boeing for determining the flight time and range (underlined in Red).

Table 18: Flight paths range including our trajectory

Flight Level	True Airspeed (knots)	Mach (ISA standard) (*=MRC)	Time (hours)	Range (Nm)
FL300	500	0.848	4.5	2270
FL300	437	0.742	5.7	2523
FL300	431	0.706 *(ISA +12)*	5.9	2544
FL300	416	0.706*	6.1	2552
FL300	323	0.548	6.8	2181

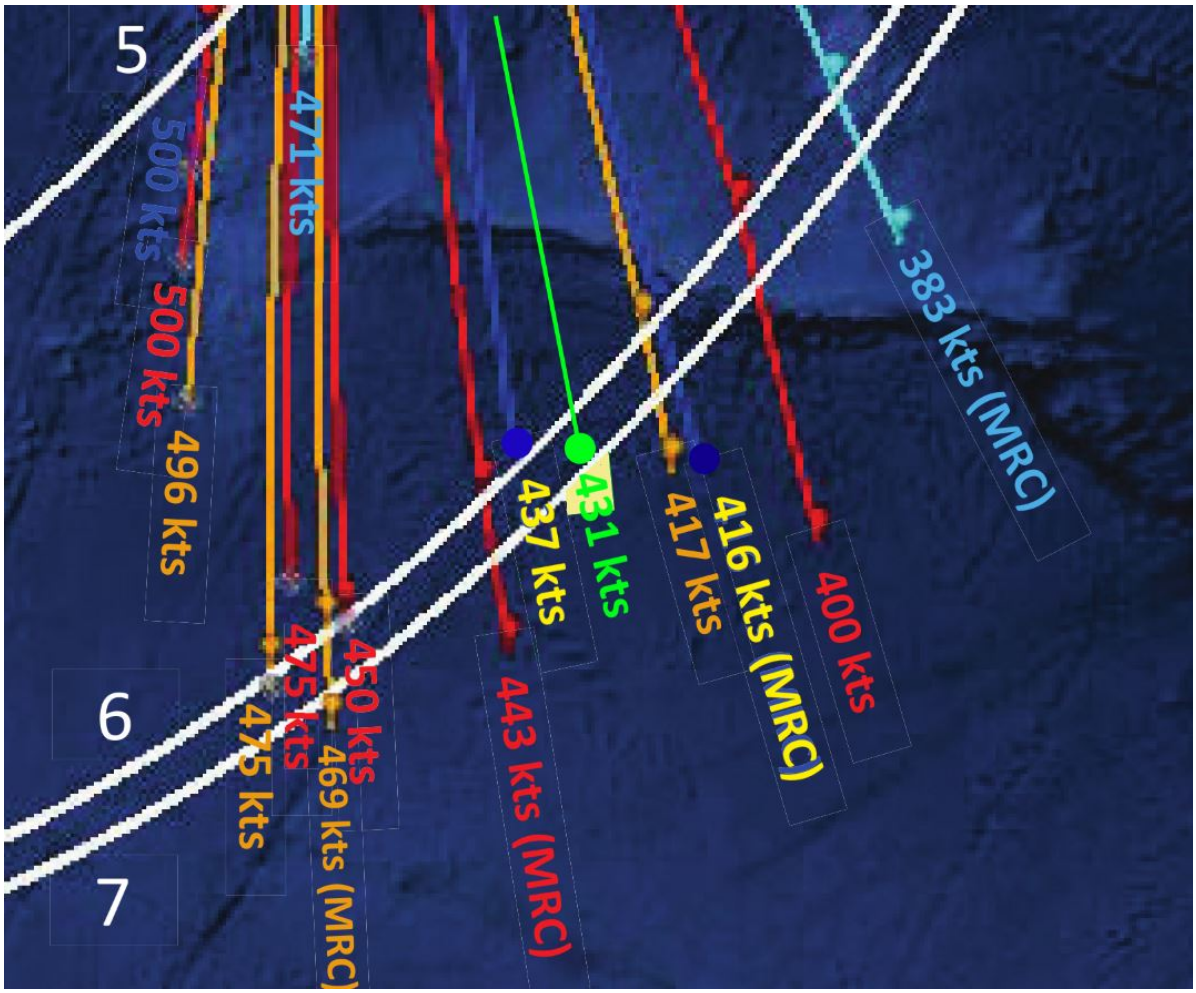

Figure 56: Range of our trajectory (Green) compared with Boeing possible paths at FL300

In interpolating the range and time in Table 18 with the ISA of the day (in average ISA+12°) we should match the corrected range of 2544Nm which is illustrated in Green in Figure 56. But actually, the path of our trajectory is 2522Nm long and was flown during 5.825 hours from 18h28:06 UTC.

The shortfall of 22Nm results most likely from the drag of the deployed RAT leading to a fuel overconsumption. From ARC1-Boeing at 18h28:06 UTC, we estimate this overconsumption at about ~300kg i.e. 0.9% of the fuel consumed during this southern leg.

Figure 57 illustrates a deployed RAT configuration where the turbine and its hatch are clearly justifying some fuel overconsumption.

Figure 57: Ram Air Turbine (RAT) and its hatch have been deployed

8 Annex 1: Variant 2 of the End of the Flight

At 00h19:29 UTC, arc 7 exists because the SATCOM of the aircraft sent a burst requesting a logon to the Inmarsat network. This provided the arc 7 BTO/BFO data. In the few seconds that followed, the logon procedure proceeded normally with the expected second burst from the SATCOM at 00h19:38 UTC but providing an unexpected measured BFO of -2Hz.

This BFO value is to be compared with the previous one equal to 182Hz. Professor Holland [12] analysed it and reported that in 9 seconds the aircraft could have accelerated because of a dive that increased its vertical speed from -4000fpm to -14500fpm. Subsequently, a lot of studies concluded that the aircraft was either in a free fall or in a high-speed vertical dive and smashed into the water … at the arc 7 or close to it.

If one considers a human presence in the cockpit, there is another possibility which is envisaged here and sketched in Figure 58. The small number of pieces of debris found and their type led to a conclusion that the aircraft did not violently crash into the water with a high speed. Otherwise, it would be similar to crashing into a concrete wall spreading thousands of pieces around. In our view, it is perfectly possible that after the start of the dive – it being voluntary or involuntary – the person in command recovered from this very quickly. The voluntary cut-off of the last running engine (the left one) and the management of the subsequent events in the cockpit might have triggered this temporary dive. For example, computations show that if the aircraft dived for 10 seconds shortly before the arc 7, the recovery manoeuvre sketched in Figure 58 would last 50 seconds with a flown distance of 6 Nm. Then a descent would take place similarly to the options described in Variant 1 and recalled in Figure 59.

The noticeable difference between the End of the Flight in Variants 1 and 2 is the estimation of the minimum and maximum distances flown by the aircraft. The minimum distance in Variant 1 would be ~45 Nm while the maximum would be ~67 Nm and ~42 Nm and ~59 Nm respectively in Variant 2 as posted in Figure 59.

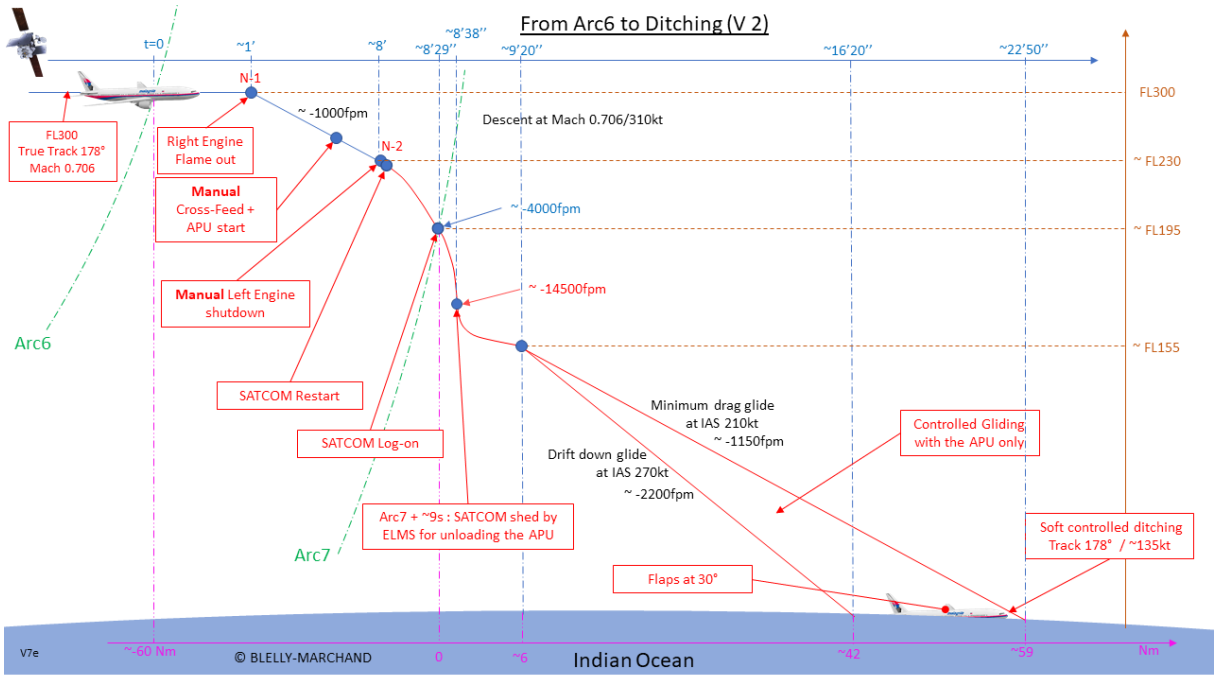

Figure 58: Variant 2 of the end of flight including a dive followed by a quick recovery (Blelly/Marchand)

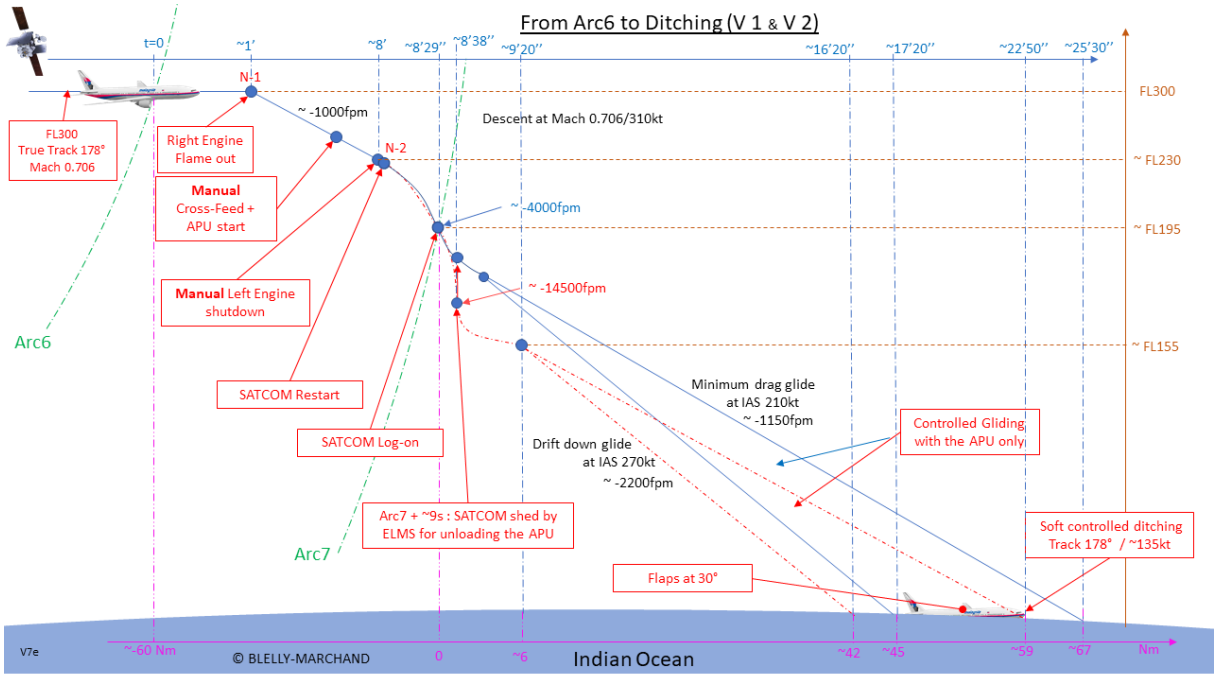

Figure 59: Synopsis of the End of Flight scenario (Variants 1 & 2)

9 References

[1] "MH370 La contre-enquête d'un pilote" by Captain P. Blelly – Ed. J-P. Otelli – 23rd Feb. 2022

[2] Safety Investigation Report, The Malaysian ICAO Annex 13 Safety Investigation Team for MH370, 02 July 2018

[3] The Search for MH370, Inmarsat, C. Ashton, A. Shuster Bruce, G. Colledge & M. Dickinson, Journal of Navigation, (2015) 68 1-22

[4] MH370 - Definition of Underwater Search Areas, ATSB Transport Safety Report, 26 June 2014, updated 18 Aug. 2014

[5] Malaysian Safety Investigation Report MH370 (9M-MRO) 2018, Appendix-1.6E-Boeing Performance-Analysis- Malaysian Airlines 777(9M-MRO) Missing Occurrence – 08 March 2014

[6] https://mh370.radiantphysics.com/2019/04/03/insights-from-new-mh370-tracking-data/ IG-D. Thompson-V. Iannello

[7] Meteorological data available at https://earth.nullschool.net https://earth.nullschool.net/#2014/03/07/1800Z/wind/isobaric/250hPa/equirectangular=-258.68,5.62,3000/loc=95.965,6.770

[8] Civilian Approach Radar data at Khota Bau and Penang, V. Iannello https://mh370.radiantphysics.com/2018/04/11/the-civilian-radar-data-for-mh370/

[9] MH370 SDU OCXO Transient analysis, B. Ulich, 07 Jan. 2018

[10] The final resting place of MH 370, Bobby Ulich, Richard Godfrey, Victor Iannello & Andrew Banks, 7th Mar 2020

[11] Summary of imagery analyses for non-natural objects in support of the search for Flight MH370, GA report, S.Minchin, N. Mueller, A. Lewis, G. Byrne, M. Tran, Record 2017/13 eCat 111041

[12] MH370 Burst Frequency Offset Analysis and Implications on Descent Rate at End-of-Flight, I. Holland, Defence Science and Technology Group, Edinburgh, AustraliaarXiv:1702.02432v3 [stat.OT] 15 Jan 2018

[13] The search for MH370 and Ocean surface drift – Part III, D. Griffin, P. Oke, Rep EP174155, 26 June 2017

[14] MH370 – L'impossible disparition, video documentary, RMCStory TV Channel, Simon Viguié, Nov. 2022

[15] Malaysian Safety Investigation Report MH370 (9M-MRO) 2018, Appendix 1.9A ACARS Traffic log – 08 March 2014

[16] ICAO International Standards and recommended Practices Annex 15 to the Convention of international Civil Aviation : Aeronautical Information Services

[17] MH370 – IGARI-MEKAR: the leg flown with the sole power of the RAT - Jean-Luc Marchand, CAPTION, in cooperation with Captain Blelly , Version 1.3 - updated 2nd March 2022.

[18] ENROUTE Chart – Malaysian Airspace, 2017

[19] Factual information – MH370 Safety Investigation, The Malaysian ICAO Annex 13 Safety Investigation Team for MH370, 08 March 2015

[20] Flight Crew Operational Manual FCOM 1 et 2. Table of « performance in flight » of the Boeing 777-200 ER with Trent 892 engines, PMDG and Airlines

[21] Comparison of Civil and Military Radar Tracks for MH370 (and its update with ADS-B), Steve Kent, sk999, 22nd Apr. 2018

[22] Some observations on the Radar data for MH370, V. Iannello, 18th, Aug. 2015

[23] Deriving MH370 Altitude and Speed Profiles from the January 2019 KB Civil PSR Data, Michael L. Exner, 13th March 2019

[24] skybrary.areo (for general aeronautics definitions)

[25] Boeing Performance Analysis, Appendix-1.6E-Aircraft-Performance-Analysis-MH370-(9M-MRO)

[26] Analysis of the geometry of the radar data at Kota Bharu and at Penang Island, Jean-Luc Marchand, Patrick Blelly, March 2023

10 Abbreviations and Index

A/P	Auto-Pilot	
ACARS	Aircraft Communication, Addressing and Reporting System	Digital link system for the transmission of messages between aircraft and ground stations.
ADIZ	Air Defence Identification Zone	National area where military authorities request specific rules to be obeyed before entry.
ADS-B	Automatic Dependence Surveillance-Broadcast	System in which the aircraft broadcast their current navigational situation allowing the ATC and the other airspace users to be aware of the current situation of their surroundings.
AIS	Automatic Identification System	VHF automatic surveillance system for marine vessels (similar system to the airborne ADS-B)
APU	Auxiliary Power Unit	Turbine located at the rear of the aircraft providing electrical power and pneumatic power
ATC	Air Traffic Control	Authority in charge of the control of the air traffic in a specific airspace volume.
ATHR	auto throttle	Automatic system for maintaining speed
ATSB	Air Transport Safety Board	Australian department in charge of the investigation on safety issues in Australian air transport.
BFO	Burst Frequency Offset	The BFO is the recorded value of the difference between the received signal frequency and the nominal frequency at the GES. It is a function of the Doppler effect between the aircraft and the satellite.
BTO	Burst Time Offset	The BTO is a measure of how long from the start of that time slot the transmission is received. This is essentially the delay between when the transmission was expected (given a nominal position of the aircraft) and when it actually arrives, and is a measure of twice the distance of the aircraft from the satellite.
Data link reset		reset of the data link function via the Communication Manager. When airborne, it erases the flight and company data
DME	Distance Measuring Equipment	Radio Navigation system measuring the distance between the aircraft and the terrestrial transmitter
ELMS	Electrical Load Management System	System providing load management and protection to ensure power is available to critical and essential equipment. It manages the balance between the available electrical power and the demand from the electrical loads. It could shed loads as necessary.
FCOM	Flight Crew Operating Manual	Document incorporating aircraft manufacturer guidance on how to use the systems on board the aircraft
FIR	Flight Information Region	The world has been cut out into a set of geographical areas like a jigsaw puzzle. Each area is called a FIR where the Air Traffic Control is under the responsibility of one authority only.
FL	Flight Level	Standard definition of the altitude when an aircraft is above the transition level with the altimeter set to 1013hp.
FMC	Flight Management Computer	Onboard computer managing the flight parameters and keeping the aircraft within the flight envelop.

FMT	Final Major Turn	Manoeuvre including several turns performed by the aircraft to circumvent Sumatra in the north
FsX	MS Flight Simulator X	PC simulator software from Microsoft Corp. Version 10.
GDAS	Global Data Assimilation System	Meteorological data combined and provided by US official meteorological institutions. In this study, a posteriori measurement data is used and is referred to as “actual” meteorological, ‘meteo’ or ‘met’ data.
IAS	Indicated Air Speed	
IFE	In Flight Entertainment	Onboard system offering entertainment to passengers including telecommunications and cabin comfort
IFR	Instrument Flight Rules	
IG	Independent Group	A group of experts who made secession from the ATSB because of a diverging opinion on where to search the wreckage and who are very active in studying the case.
ISA	International Standard Atmosphere	This standard is the foundation in building the reference atmosphere charts used in aeronautics. It always considers that the sea level temperature is 15°C.
kt	knot	Speed equals to 1 nautical mile per hour
LNAV	Lateral Navigation	Navigation function of the Auto Pilot with a specified precision
LRC	Long Range Cruise	This is the FMS mode which makes the aircraft fly a slightly shorter range than the maximum MRC at a more economical manner.
LSTPR	LaST Report Point	Virtual waypoint defined at the location of the last echo received by Butterworth radar
Mach		Speed of an aircraft relatively to the celerity of the sound. Usually used above flight level FL300.
MCDU	Multi-function Control Display Unit	Interface system for input and consultation of FMC information
MCP	Mode Control Panel	Panel to adjust settings for: speed, altitude, Rate of climb/descent for the A/P etc.
MFD	Multi function Display	Interface to some aircraft management functions
MRC	Maximum Range Cruise.	This is the FMS mode which makes the aircraft fly the longest range. Sometime it is called also the mode with Cost Index = 0.
ND	navigation display	Display for monitoring and controlling the navigation
Nm	Nautical Mile	Distance of 1852m
OCXO	Oscillator Cristal Oven	System maintaining the temperature of the oscillator for ensuring the required stable frequency
PFD	Primary Flight Display	Pilot's primary reference display for flight information
PIC	Pilot In Command	Usual term to designate the person currently piloting the aircraft and in full command of it.
Prepar3D		PC Simulator software from Lockheed-Martin.
PSR	Primary Surveillance Radar	Non-cooperative Radar system which sends radio pulses and listens for received echoes. This information is translated into a raw video ‘blip’ or processed ‘plot’ on the controller radar screen (no exchange of info with the aircraft).
QNH	Geographic Altitude Indication	The pressure set on the subscale of the altimeter so that the instrument indicates its heights above sea level

R&R	Rolls-Royce	MH370 engines manufacturer
RAT	Ram Air Turbine	Small windmill turbine generating electricity and pneumatic power as the last resort in emergency. It deploys underneath the aircraft's body.
SDU	Satellite Data Unit	Satellite communication system onboard the aircraft
SSR	Secondary Surveillance Radar	Cooperative Radar system which interrogates an aircraft transponder that collects and responds with current aircraft navigational parameters depending on its operating Mode (A, C, S).
TAS	True Air Speed	Speed of the aircraft relative to the surrounding air
True Track		Navigation function disregarding the magnetic declination
UTC	Universal Time Coordinated	Greenwich (UK) time taken as the universal reference.
VOR	VHF Omni Range	Radio Navigation system indicating the bearing of the terrestrial transmitter

THE JOURNAL OF NAVIGATION (2016), **69**, 1–23. © The Royal Institute of Navigation 2015
doi:10.1017/S0373463315000570

Reconstructing the Malaysian 370 Flight Trajectory by Optimal Search

Octavian Thor Pleter, Cristian Emil Constantinescu and Barna Istvan Jakab

(*University Politehnica of Bucharest, 060042 Bucharest, Romania*)
(E-mail: otp@brainbond.ro)

In the aftermath of the disappearance of the Malaysian 370 (MH370) flight in March 2014, new positioning methods were employed to establish the search area. In the absence of all other positioning technologies (Transponder, Radio communications, Radar), these innovative methods are based on the handshake signals between an INMARSAT satellite and the satellite transceiver on board the aircraft. The log of these signals was made public in order for the scientific community to engage in solving the mystery of the MH370 trajectory. The log indicates the delay between the interrogation and response signals, as well as the relative velocity indications, based on the shift of the carrier frequency due to the Doppler-Fizeau effect. This paper puts forward an original, independent and accurate positioning method and allows the calculation of the MH370 trajectory considering the wind vector field that day, the accurate satellite orbit and an accurate model of the Earth (the WGS-84 ellipsoid). The results were compared to other results published, indicating a different final position of the aircraft from the locations of the published search area.

KEYWORDS

1. MH370. 2. Trajectory. 3. Search and Rescue (SAR).

Submitted: 13 January 2015. Accepted: 1 July 2015. First published online: 30 July 2015.

1. INTRODUCTION. On 8 March 2014, the flight Malaysian 370 from Kuala Lumpur to Beijing disappeared without any trace. The aircraft was a Boeing 777-200ER (777-2H6ER, ICAO type designator B772) with the registration 9M-MRO. After 32 minutes of flight preparation, the aircraft took off and flew normally for 49 minutes. After the crucial point of IGARI at the border between Malaysian and Vietnamese airspace, the aircraft made abnormal manoeuvres for 1 hour and 17 minutes (turns, climbs, descents) then settled for a long range flight of 5 hours and 42 minutes. The total time flown abnormally was 7 hours, most probably until the fuel was exhausted. The long range en route flight of almost 6 hours was probably under automated guidance, very probably following a keyboard input flight plan changed earlier during the flight. Although all communication systems were shut down in a time window of 12 minutes (from 1709Z to 1721Z), the SATCOM satellite transponder continued to be functional and provided a number of very important clues

https://doi.org/10.1017/S0373463315000570 Published online by Cambridge University Press

Table 1. MH370 Flight Phases.

From	To	Phase	Duration	No
2014 March 8 00:00:13 (1600Z)	00:32:13 (1632Z)	Flight preparation	32′ 0″	1
---	---	*Start of flight*	**32′**	
00:32:14 (1632Z)	00:40:38 (1641Z)	Push-back, start and taxi	8′ 26″	2
00:40:38 (1641Z)	01:01:16 (1701Z)	Take-off and climb	20′ 38″	3
01:01:16 (1701Z)	01:21:04 (1721Z)	En route to IGARI	19′ 48″	4
---	---	*End of normal flight / Start of abnormal manoeuvers under military surveillance*	**49′**	
01:21:04 (1721Z)	02:22:00 (1822Z)	Manoeuvers under military surveillance	1 h 0′ 56″	5
---	---	*End of abnormal manoeuvers / Start of unknown flight*	**1 h 1′**	
02:22:00 (1822Z)	02:38:00 (1838Z) ?	Unknown continuation of the flight, including a turn onto a new flight track	Max 16′	6
02:38:00 (1838Z) ?	08:19:29 (0019Z)	Unknown en route flight	Min 5 h 42′	7
08:19:29 (0019Z) ?	08:28:29 (0028Z) ?	Glide descent with both engines out due to fuel starvation, until crash	≈ 9′	8
---	---	*End of flight*	**6 h 07′**	

about flight MH370. This paper is the result of the original work of the authors, calculating all trajectories of the aircraft consistent with a single turn after loss of ground radar contact. Also, an optimisation cycle was used to calculate the most probable trajectories, which fit best on all the data known. The results are surprising, because they indicate a position where the flight could have ended, which is different from the past and the current search areas. Besides its scientific relevance, the authors hope that their work will prove useful in the future search operations.

2. MH370 FLIGHT FACTS. Malaysian Airlines 370 took off with 239 Persons On Board (POB) (227 passengers out of the capacity of 282 and 12 members of crew). The initial flight plan was from Kuala Lumpur International (KLIA) to Beijing Capital International Airport (ZBAA). The ETA (Estimated Time of Arrival at planned destination (UTC)) was 2230Z and ETE (Estimated Time En route (estimated duration of flight in hours and minutes)) was 05:49. The fuel load was 49,100 kg, enough for over eight hours of flight. The MH370 flight phases are described in Table 1. Table 2 provides a detailed sequence of known facts about the flight, including the seven relevant ping exchanges between the INMARSAT-3 Indian Ocean Region (IOR) satellite and the SATCOM transceiver, which allow the calculation of the flight trajectory. The key moments of the flight are defined in Table 3.

The signal delay is called BTO (Burst Timing Offset) and it is caused by the time the radio waves take to travel from the satellite ground station to the satellite to the aircraft and back. Based on this, the instantaneous distance between the satellite and the aircraft (range) may be calculated for each ping exchange. The calculations presented in this paper rely mainly on these BTOs.

The locus of the points within a certain range is a sphere with the centre in the satellite position, with the range as the radius. This sphere may be intersected with the surface parallel to the ellipsoid or the geoid, at an altitude above the geoid, which

https://doi.org/10.1017/S0373463315000570 Published online by Cambridge University Press

Table 2. Sequence of Known Facts about MH370.

Time	Event of the Flight MH370	Reference
2014 March 8	INMARSAT I-3 IOR Log-On	Avionics Power Up
00:00:13 (1600Z)		
00:07:00 (1607Z)	First Air DATA-2 ACARS[1] message BFO 86–90 Hz BTO 14780–14900 μs	First ACARS
00:25:53 (1626Z)	"Delivery Malaysian Three Seven Zero good morning"	ATC Delivery contact
00:27:27 (1627Z)	"Ground Malaysian Three Seven Zero good morning Charlie One requesting push and start"	LUMPUR GND contact
00:29:00 (1629Z)	ACARS message BFO 98–100 Hz BTO 14920–14940 μs	
00:32:13 (1632Z)	"Malaysian Three Seven Zero request taxi"	
00:36:30 (1637Z)	"Tower Malaysian Three Seven Zero morning"	LUMPUR TWR contact
00:40:38 (1641Z)	TWR: "Three Seven Zero Three Two Right Cleared for take-off good night" MH370: "Three Two Right Cleared for take-off Malaysian Three Seven Zero thank you bye"	T/O clearance
00:41:43 (1642Z)	Take-Off RWY 32R KLIA	
00:42:05 (1642Z)	"Departure Malaysian Three Seven Zero"	LUMPUR APP contact
00:42:07 (1642Z)	Cleared to climb to FL180 Direct IGARI	
00:42:52 (1643Z)	Transferred from LUMPUR APP to LUMPUR RADAR	
00:46:51 (1647Z)	"Lumpur Control Malaysian Three Seven Zero"	LUMPUR ACC contact
00:46:51 (1647Z)	Cleared to climb to FL250	
00:50:06 (1650Z)	Cleared to climb to FL350	
00:55:00 (1655Z)	ACARS message BFO 155–156 Hz BTO 15200–15220 μs	
01:01:16 (1701Z)	Pilot reports maintaining FL350 (unnecessary, unsolicited) HDG 025 GS 471 kts	Strange human action
01:07:49 (1708Z)	Last Air DATA-2 ACARS message BFO 131 Hz BTO 15620 μs	Last ACARS
01:07:55 (1708Z)	Pilot reports maintaining FL350 (unnecessary, unsolicited, repeated)	Strange human action
01:09:00 (1709Z)	FMS flight plan changed from the keyboard	(unconfirmed)
01:19:24 (1719Z)	Transferred from LUMPUR RADAR[2] to HCM ATCC[3] on 120·9 MHz – Last transmission from cockpit: "Good Night Malaysian Three Seven Zero"	Last COM
01:21:04 (1721Z)	Fly over IGARI N06°55′15″ E103°34′43″ (as tracked by LUMPUR RADAR) FOB[4] for 8 hours of flight	Exit Malaysian airspace
01:21:13 (1721Z)	Transponder switched off or failed	Last XPDR[5]
01:22:00 (1722Z)	Turn Left HDG	PSR[6] data
01:30:00 (1730Z)	HCM ACC requests other aircraft to relay communications to MHA 370 – no answer	No COM
01:37:00 (1737Z)	Expected ACARS message not transmitted Climb to FL450 Descend to FL120 (or lower)	No ACARS PSR data PSR data
02:03:42 (1804Z)	No response to Air DATA-2 ACARS - ACARS failed or has been switched off between 01:07:49 and 02:03:41	Proof of no ACARS
02:22:00 (1822Z)	200 NM NW of Pinang – Last Military Primary Radar contact	Last PSR contact
02:25:28 (1825Z)	Ping Log-On request from aircraft BFO 142 Hz BTO 17120 μs	
02:25:34 (1825Z)	Ping handshake BFO 273 Hz BTO 51700 μs	
02:27:04 (1827Z)	Ping handshake BFO 175–176 Hz BTO 12560–12520 μs	
02:28:06 (1828Z)	Ping handshake BFO 144 Hz BTO 12500 μs	
02:28:15 (1828Z)	Ping handshake BFO 143 Hz BTO 12480 μs	

Continued

https://doi.org/10.1017/S0373463315000570 Published online by Cambridge University Press

Table 2. (*Continued*)

Time	Event of the Flight MH370	Reference
02:39:53 (1840Z)	Ground initiated Air Telephony call	
02:40:56 (1841Z)	No answer – Ping handshake BFO 88–90 Hz	Strange human action
02:41:00 (1841Z)	ACC Subang notifies about losing the flight	Aircraft on a new track
03:41:03 (1941Z)	Ping handshake BFO 111 Hz BTO 11500 μs	
04:41:05 (2041Z)	Ping handshake BFO 141 Hz BTO 11740 μs	
05:30:00 (2130Z)	Search and Rescue (SAR) operation activated by Kuala Lumpur Rescue Coordination Centre (KL RCC)	
05:41:27 (2141Z)	Ping handshake BFO 168 Hz BTO 12780 μs	
06:41:22 (2241Z)	Ping handshake BFO 204 Hz BTO 14540 μs	
07:13:58 (2314Z)	Ground initiated Air Telephony call	Last Telephony Call[7]
07:15:02 (2315Z)	No answer – Ping handshake BFO 216–219 Hz	
08:11:00 (0011Z)	Ping handshake BFO 252 Hz BTO 18040 μs	Last complete Ping
08:19:29 (0019Z)	Last incomplete ping requested by user BFO 182 Hz BTO 23000 μs	Last incomplete Ping / both engines out
08:30:00 (0030Z)	Flight time limit based on FOB at FL310 or above at normal cruise airspeed $TAS = 470$ kts	
09:10:00 (0110Z)	Expected Ping handshake did not arrive	Proof of avionics out

[1] ACARS: Aircraft Communications Addressing and Reporting System, automated bidirectional system for technical and operational messages between aircraft and a ground communication network or a satellite communication network
[2] ACC Subang, Malaysia
[3] ACC Ho Chi Mingh, Vietnam
[4] FOB: Fuel on Board
[5] XPRD: Secondary Surveillance Transponder
[6] PSR: Primary Surveillance Radar (military)
[7] Not answered, but the subsequent ping proved aircraft to be in operational status.

Table 3. Key moments of the MH370 flight.

Malaysian Time	UTC	Identifier	Description
00:00:13	1600Z	t_L	Avionics power up and satellite **L**og on
00:41:43	1642Z	t_T	**T**ake-Off RWY 32R KLIA
01:07:49	1708Z	t_A	Last Air DATA-2 **A**CARS message
01:19:24	1719Z	t_C	Last **C**OM "Good Night Malaysian Three Seven Zero"
01:21:04	1721Z	t_X	Last **X**PDR fly over IGARI N06°55′15″ E103°34′43″
02:22:00	1822Z	t_M	Last **M**ilitary PSR contact 200 NM NW of Pinang
02:25:28	1825Z	t_1	**1**st complete satellite ping considered in the literature
$t_M + TTT$	$t_M + TTT$	t_S	**S**tart turn on a new track
03:41:03	1941Z	t_2	**2**nd complete satellite ping, the first on the new track
04:41:05	2041Z	t_3	**3**rd complete satellite ping, the 2nd on the new track
05:41:27	2141Z	t_4	**4**th complete satellite ping, the third on the new track
06:41:22	2241Z	t_5	**5**th complete satellite ping, the fourth on the new track
08:11:00	0011Z	t_6	**6**th complete satellite ping, the fifth on the new track
08:19:29	0019Z	$t_7 = t_G$	7th incomplete user request ping – **E**nd of powered flight, start glide with both engines out
$t_G + TGE$	$t_G + TGE$	t_E	End of flight

corresponds with the presumed flight level of the aircraft. This is in fact the isobaric surface for level flight, corresponding to the local meteorological data. The intersection yields a curve very close to a circle. At the given moment of the ping, the position of the aircraft is somewhere on that quasi-circle.

https://doi.org/10.1017/S0373463315000570 Published online by Cambridge University Press

The shift in carrier frequency is called BFO (Burst Frequency Offset). It is caused by the Doppler-Fizeau effect due to the relative speed between the aircraft and the satellite. In the calculations below, the BFO values were not used, and this is a major difference between this method and other methods used until now and known to the authors (Ashton et al., 2014; Hradecky, 2014). The reason for avoiding the use of BFO values is that the problem of relative speed is geometrically ill conditioned in this case, especially in the first half of the flight.

3. CALCULATION OF QUASI-CIRCLES. This paper models the Earth as the WGS-84 ellipsoid. The ranges define quasi-circles at the intersection between the isobaric surface that the aircraft levels on, and the sphere with the centre in the satellite antenna position and the BTO-based range as the radius.

The INMARSAT-3 satellites are five satellites in 36,000 km high geostationary orbit (N0°), as follows: AOR-W at a longitude of W54°, AOR-E at W15·5°, I-3 at 25°E, IOR (the satellite used by MH370) at E64·5°, and POR at E178°. INMARSAT-3 IOR has an orbit inclined at 1·66°. This inclination gives a wobble movement with a period of T = 24 hours. The actual orbital altitude of IOR at t_6 was: 35,794 km, as compared to the target of 35,786 km Above Mean Sea Level (AMSL). Although geostationary, the actual position of the IOR satellite moved slightly during the MH370 flight.

In the Earth-Centred-Earth-Fixed (ECEF) frame, the system of equations used to calculate the seven quasi-circles (see Figure 8) are the WGS-84 rotation ellipsoid equations and the satellite-centred sphere equations:

$$n_\varphi = \frac{6378136{\cdot}6}{\sqrt{1 - e_2 \times (\sin\varphi)^2}} \tag{1}$$

$$\begin{cases} x = (n_\varphi + H)\cos\varphi\cos\lambda \\ y = (n_\varphi + H)\cos\varphi\sin\lambda \\ z = n_\varphi(1 - e_2) + H\sin\varphi \end{cases} \tag{2}$$

$$\sqrt{(x - x_{SAT})^2 + (y - y_{SAT})^2 + (z - z_{SAT})^2} - Range_{satellite\ to\ aircraft} = 0 \tag{3}$$

From (Ashton et al., 2014):

$$Range_{satellite\ to\ aircraft} = \frac{1}{2}c \cdot (BTO - bias) - Range_{satellite\ to\ Perth\ GES} \tag{4}$$

$$bias = -495679\ \mu s \tag{5}$$

The Equations (2) in *x, y, z* are substituted in Equation (3), providing a way to calculate longitude λ as a function of latitude φ. The seven quasi-circles correspond to the seven pings, illustrated in Figure 8, which occurred at the times t_1 to t_7 (see Table 3). However, the first complete satellite ping considered in the literature was not used in this paper, because the initialisation of the problem is uncertain, so less weight should be given to the starting point. Consequently, the work presented in this paper relies on the last six quasi-circles only. As a confirmation of this selection of quasi-circles, the contribution of the six pings to the total inconsistency of the trajectory is well balanced. The individual contribution of the first ping to the total inconsistency would have been disproportionately larger than the contributions of the other pings.

https://doi.org/10.1017/S0373463315000570 Published online by Cambridge University Press

4. SOLVING TRAJECTORY EQUATIONS. The authors independently calculated the MH370 trajectory based on the following data:

1. Flight trajectory until the last known position P_18_22 as recorded by the military primary radars (N 6° 36′ 15″ E 96° 33′ 14″) (Malaysian Gov., 2014; Hradecky, 2014).
2. The set of recorded INMARSAT (INMARSAT, 2014) satellite pings (signal handshake delays and carrier frequency drift) (Malaysian Gov., 2014, Hradecky, 2014).
3. The wind vector field, isobaric surface height and air temperature in the wider area at the moment of the flight, retrieved from the National Oceanic and Atmospheric Administration (NOAA) 2014). Interpolations in time, position, and flight levels were used for the best local current estimate of the wind velocity and the air temperature.
4. The Boeing 777-200ER flight performance and systems (Boeing, 1992a). A Boeing 777-200ER flight simulator based on a dynamic model was developed by the authors (Section 5).
5. The Boeing 777-200ER FMS (Flight Management System) specifications (Bulfer and Gifford, 1999).
6. The WGS-84 ellipsoid shape approximation of the Earth.
7. The INMARSAT-3 IOR satellite orbital data (Malaysian Gov., 2014).

The unknowns of this problem and the space of solutions are considered in the following subsections (see Figure 1).

4.1. *The Time to Turn Unknown (TTT).* It was assumed that the flight continued straight for a while (on the track of 291° true) from the moment it vanished from the military primary radars (t_M or P_18_22). The duration of this straight segment *TTT* (Time To Turn) is one of the unknowns of the problem. *TTT* search domain was initially considered 0–50 minutes, then reduced to 5–16·75 minutes, based on the following:

- In numerical search trials, for *TTT* over 17 minutes, the breakdown of the quadratic error (ε) on the six quasi-circles starts to show an abnormal error increase for the first two quasi-circles;
- In both the uncorrected (Hradecky, 2014), and the corrected *BFO* diagram (Ashton et al., 2014), the turn is marked by a significant drop in the frequency due to the Doppler-Fizeau effect between the moments 1820Z and 1830Z, i.e. in an 11 minutes time interval;
- The dynamic model simulation presented further provides an additional validation for the upper limitation of this time to 16·75 minutes; if the flight continued on the initial track for 17 minutes or more, the optimised trajectory solutions (*TK*, *FL* and *M*) would largely disagree with the dynamic simulation (the fuel would have been exhausted before the last complete ping due to the required thrust settings resulting from *FL* and *M*);
- No consistent solution emerged for *TTT* shorter than 5 minutes.

After *TTT*, a coordinated turn was simulated, using a dynamic model Boeing 777-200ER simulator (see Section 5). The search step was one minute, refined down to five seconds for the promising domains.

https://doi.org/10.1017/S0373463315000570 Published online by Cambridge University Press

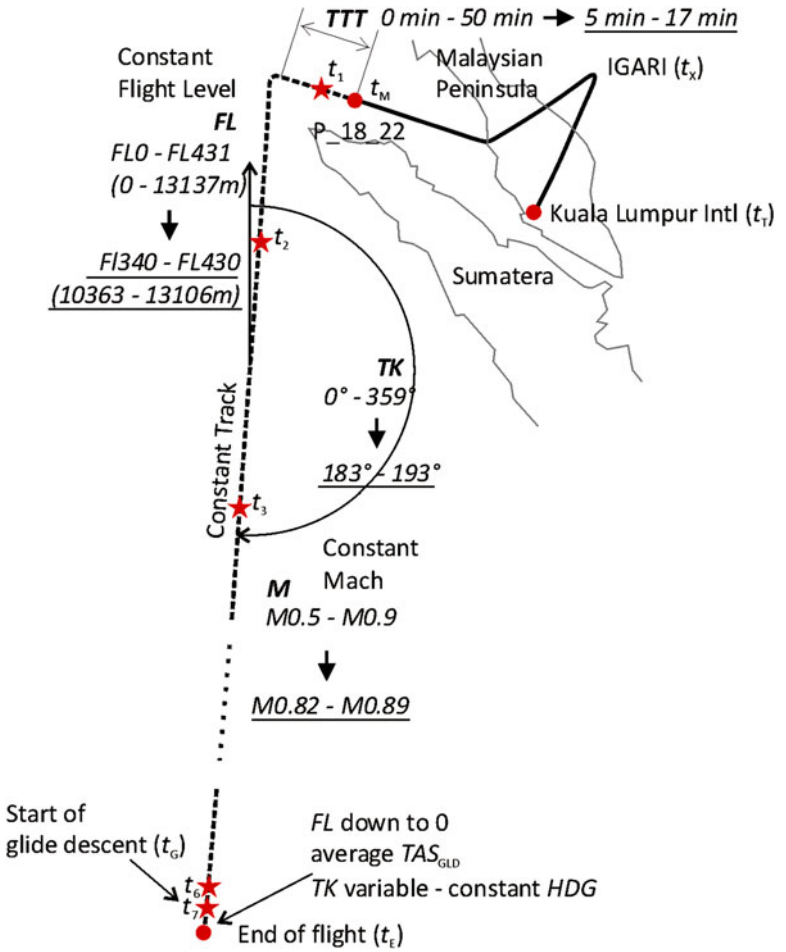

Figure 1. MH370 trajectory problem unknowns: *TTT*, *TK*, *FL*, and *M*.

This paper is based on the assumption that a single turn was made at the beginning of a long constant track segment. The *BFO* analysis (Figure 9 from Ashton et al., 2014) is consistent with a major turn between certain time moments: 1820Z and1830Z. After that turn, the *BFO* diagram indicates a linear variation of the Doppler-Fizeau frequency shift, i.e. no other turns. A notable fact is that one 360° turn at high *M* would typically last for 11·5 minutes, and the time window in the diagram is just too small for multiple turns concentrated at the beginning of the long constant track segment. On the other hand, multiple turns sparsely distributed over the entire voyage seem impossible given the same *BFO* diagram, because at each ping there is approximately the same *BFO*, the timing between pings is not always predictable (there are phone calls from the ground which spoil the one hour default time interval), and this is consistent with the hypothesis of an approximately constant ground speed vector. Another reason for the single turn assumption is the simplicity and the timing of the FMS programming. The programming of each additional turn into the FMS

https://doi.org/10.1017/S0373463315000570 Published online by Cambridge University Press

should have been based on *ad hoc* navigation points entered individually as *LAT-LONG*. Attempting such a scenario on a flight simulator indicated a significant duration of the operation, not consistent with the existing time window in this case.

One additional rationale of the single turn hypothesis comes from the speculation on the goal of the person who did program the FMS as such. The goal of this action could have been to hide evidence in a place as remote as possible. The choice of track coincides with such a strategy, to end the flight as far as possible from any populated or frequented area. Programming multiple turns into the FMS would have been pointless and detrimental to the goal of flying as far as possible. This is speculative, but it only supplements all the other non-speculative grounds of the single turn assumption.

4.2. *The Track Unknown (TK).* After *TTT* minutes, the aircraft took a turn to an unknown track *TK* (presumed constant), and from that moment it kept that track for the entire duration of the flight, until both engines became fuel starved. This is consistent with the variation of the frequency shift due to the Doppler-Fizeau effect on the carrier (the seven *BFO*s). Initially, all possible tracks were considered, (0°–359°), but a refined search was performed in the promising range of 170°–200° (the Southern range), and finally in the range 183°–193°, because all solutions obviously proved to be concentrated within these limits. The search step was 1°. The next best promising interval lays in the Northern range (around 336°) was not considered in the refined search for the following reasons:

- The Northern tracks lead to inconsistencies at least three times larger than the Southern tracks;
- In both the uncorrected (Hradecky, 2014), and the corrected BFO diagram (Ashton et al., 2014), the Southern variant matches very well the expected set of *BFO*s, in contrast with the Northern variant.

This constant track phase of the flight (Phase 7 in Table 1) was probably flown under automated guidance, until the airplane became fuel starved, glided down and crashed. Other authors considered a constant heading for the flight. Although the Boeing 777 autopilot has a function to maintain a constant heading (HDG HOLD on the Mode Control Panel–Boeing, 1992b), it is unlikely that this flight was not under FMS guidance (LNAV mode), and in this case *HDG* changes automatically to compensate for the crosswind. Thus, it is logical to assume a constant track flight (loxodrome or rhumb line) instead of a constant heading flight. A third hypothesis concerns a "DIRECT TO" a distant point flight, which would force navigation along the great circle (orthodrome). However, in the particular case of MH370, the difference between the orthodrome and the loxodrome routes is insignificant, and thus the constant track route covers both scenarios. A fourth hypothesis is a flight with the autopilot engaged in the "TRK HOLD" mode (constant track). This is also covered by the assumption made in this paper.

4.3. *The Flight Level Unknown (FL).* The flight level (*FL*) of the cruise flight is presumed constant. Initially, all possible flight levels from 0 ft to 43,100 ft were considered. The problem is not very sensitive to the geometric *FL* variable, except for the way the speed was formalised (see the Mach number below), where the temperature matters to a large extent. Also, the wind velocity changes from one level to the other, leading to significant differences between the flight levels. Very soon in the initial phase of the

https://doi.org/10.1017/S0373463315000570 Published online by Cambridge University Press

Table 4. The subspace of solutions for refined search.

Unknown	Significance	Units	Min	Max	Step	Layers
TTT	Time to turn	Minutes	5	16·75	0·25	48
TK	Track	°	183	193	1	11
FL	Flight level	×100 feet	340	430	10	10
M	Mach number	–	0·82	0·89	0·01	8
Total						42,240

optimisation process, it became obvious that flight levels below FL340 were impossible, for two reasons:

- The inconsistency of these solutions is unacceptably high;
- The dynamic model simulation indicated that achieving a time of flight until the last half ping (t_7) would require a lower density of air.

The fine phase of the optimisation was performed on a search range between FL340 (34,000 ft) and FL430 (43,000 ft), with a step of 1,000 ft.

The authors found no grounds to consider a variable flight level and Mach number along the cruise. Flying under FMS guidance would require a constant flight level selected for cruise, and the same value input in the altitude selector on the Mode Control Panel (Boeing, 1992b; Bulfer and Gifford, 1999).

4.4. *The Mach Number Unknown (M).* The Mach number (*M*) is presumed constant. The initial search domain was between M0·65 and M0·9, but the envelope was correlated with *FL* following the flight performance of the aircraft type. The reason for choosing Mach instead of True Airspeed (*TAS*), Indicated Airspeed (*IAS*), or Ground Speed (*GS*) is related to the operational logic of the Flight Management System, Auto-Pilot and Auto-Throttle System on board the Boeing 777 aircraft. There is a slight difference in the final result between maintaining a constant *M* and a constant *TAS*, and this comes from the outside temperature variations. The height of the isobaric surfaces, air temperatures and the wind velocity vectors along the route were taken from the NOAA archives (NOAA, 2014), as per the date and the hour of the flight. Interpolation in time, interpolation in the vertical profile of the wind vector field and interpolation in position data provide the best approximations of the real meteorological parameters. For the later stages of the optimisation, the Mach search range was reduced to M0·82–M0·89. Whereas the maximum Mach number was delivering many consistent solutions, the lower speeds proved to be constantly inconsistent and were discarded. The search step for the Mach number was 0·01.

4.5. *Assumptions for the Last Segment of the Flight.* The last incomplete user requested ping at t_7 is considered to mark the end of the powered flight, and the start of a powerless glide. The accurate simulation of the flight using a dynamic model (see Section 5) confirms this hypothesis, with a low error margin between the timing in the simulator and the timing of the ping signals (see Table 7).

The last segment of the flight was a glide with both engines out due to fuel starvation (Pleter and Constantinescu, 2014).

4.6. *Trajectory Equations.* Given the above considerations, the space of solutions was reduced from 34,056,000 initial possible solutions down to 42,240 possible trajectories, as summarised in Table 4 and illustrated in Figure 1 by underlined text.

https://doi.org/10.1017/S0373463315000570 Published online by Cambridge University Press

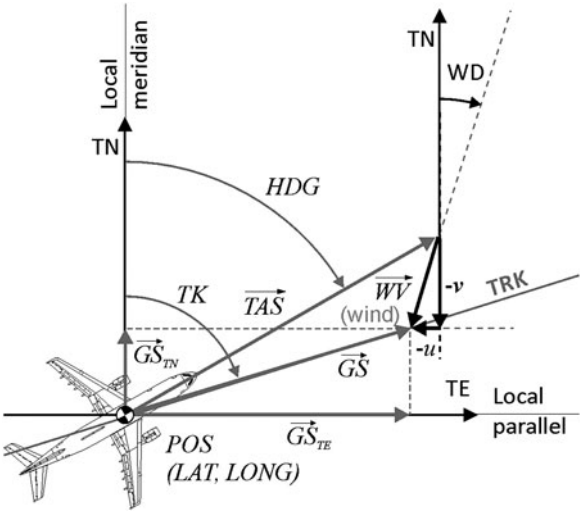

Figure 2. Local wind triangle solved at each time step in the course of flight simulation.

Considering the True North (u) and the True East (v) components of the local horizontal wind velocity vector retrieved from the NOAA records, the speed triangle system of trigonometric equations is the following (see Figure 2):

$$\begin{cases} TAS \cdot \cos HDG + v = GS \cdot \cos TK \\ TAS \cdot \sin HDG + u = GS \cdot \sin TK \end{cases} \tag{6}$$

The solution of the system is the following:

$$HDG = \mp 2 \tan^{-1}\left(\frac{\pm TAS \cdot \cos TK + \sqrt{TAS^2 - (u \cdot \cos TK - v \cdot \sin TK)^2}}{u \cdot \cos TK + (TAS - v) \cdot \sin TK}\right) \tag{7}$$

$$GS = v \cdot \cos TK + u \cdot \sin TK \mp \sqrt{TAS^2 - (u \cdot \cos TK - v \cdot \sin TK)^2} \tag{8}$$

The system of six equations that result from the data (the time delays BTO of the six relevant pings) is over determined, and it was solved so as to minimise the quadratic sum of errors, which was considered as the inconsistency of the solution (E). The inconsistency was calculated and used as an optimisation criterion to refine the search to the most plausible solution:

$$\varepsilon = \sqrt{\sum_1^6 d_i^2} = min \tag{9}$$

Each of the six errors d_i is the distance between the aircraft at the moment of each of the six pings, and the closest point belonging to the respective quasi-circle.

The flight was simulated using a Runge-Kutta IV method with a time step of 10 seconds, integrating the local speed triangle (Figure 2) and the dynamic flight

https://doi.org/10.1017/S0373463315000570 Published online by Cambridge University Press

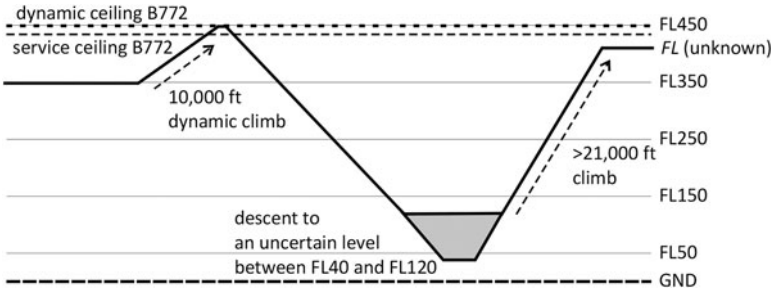

Figure 3. The flight profile of the MH370 under military primary radar surveillance.

simulator equations. At the moments of the pings, the position resulting from the simulation was compared to the position resulting from the radio transmission by calculating the distance d_i between the two. The quadratic sum of distances d_i was minimised using a complete search optimisation method. All calculations were done by a MATLAB application written by the authors.

The wind velocity and air temperature were retrieved from the NOAA world weather database (NOAA, 2014), with a granulation of 0·5° of latitude and longitude. Linear interpolation of latitude and longitude was used between the nodes. Vertically, the data are presented for the following isobaric surfaces: 10, 20, 30, 50, 70, 100, 150, 200, 250, 300, 350, 400, 450, 500, 550, 600, 650, 700, 750, 800, 850, 900, 925, 950, 975, and 1000 mbar. These isobars are converted into flight levels using the ISA model, and linear interpolation was used between the isobaric surfaces.

5. THE DYNAMIC MODEL FLIGHT SIMULATOR. For the purpose of this research, a Boeing 777-200ER flight simulator was developed. The simulator is based on a dynamic model i.e. considers the mass of the aircraft and calculates the fuel flow at each time step. The simulator served three separate goals:

- To integrate the flight trajectory, the current mass of the aircraft, and the fuel consumption. By comparing the fuel consumption to the known fuel on board in the first stage of the flight, one can determine the approximate moment of fuel exhaust. This is compared to t_G, which results from optimisation (see Table 7).
- To calculate the fuel consumption of a dynamic climb to FL450, a descent to FL120 or below, and a climb back to an unknown cruise *FL* (Figure 3). These manoeuvres were recorded by the military primary surveillance radars, so the exact levels or details of the manoeuvres are not known. Instead of a simulator based on a time step integration, the authors used a method based on energy and aircraft climb / descent efficiency to calculate the fuel consumed by it.
- To simulate the final glide descent portion, since the start of glide descent (t_G) until crash (t_E).

https://doi.org/10.1017/S0373463315000570 Published online by Cambridge University Press

Table 5. Aerodynamic Coefficients for Boeing 777 (Pereira, 2011).

$C_{L\alpha}$	C_{D0}	α_{CL0}	K_2
5·1	0·013	−2·8°	0·047

The equations of the simulator are the following:

$$TAS = M \cdot a \tag{10}$$

$$C_L = C_{L\alpha} \cdot (\alpha - \alpha_{CL0}) \tag{11}$$

$$C_D = C_{D0} + K_2 \cdot C_L^2 \tag{12}$$

$$L = \frac{\rho_0}{2} \cdot TAS^2 \cdot S \cdot C_L \tag{13}$$

$$D = \frac{\rho_0}{2} \cdot TAS^2 \cdot S \cdot C_D \tag{14}$$

$$T = \frac{D}{\cos(\alpha + \tau)} \tag{15}$$

$$T \cdot \sin(\alpha + \tau) + L = m \cdot g \cdot \cos(\phi) \tag{16}$$

The coefficients used for Boeing 777 are as presented in Table 5.

Simulation of the fuel consumption between the last ACARS message and last military primary radar contact was done with the following equations:

$$FF_{avg} \cdot (t_M - t_A) + FC_{\Delta E} = FC_{total} \tag{17}$$

$$FC_{\Delta E} = \frac{\Delta E_p + \Delta E_c}{s \cdot eff} \tag{18}$$

The efficiency *eff* of the engines was calibrated based on the FOB at engine start and FOB at the moment of the last ACARS message (A). The taxi fuel consumption was calculated using the following formula:

$$\frac{f}{\sqrt{T_{amb}}} = a_{taxi} + b_{taxi} \cdot t_{taxi} + c_{taxi} \cdot na \tag{19}$$

where $a_{taxi} = -0{\cdot}1223$ $b_{taxi} = 0{\cdot}0335$ $c_{taxi} = 0{\cdot}1385$ are the coefficients for a Boeing 777, na is the number of accelerations during taxi (it is considered to be at least two) and the ambient temperature in Kuala Lumpur in March during night was assumed to be $T_{amb} = 297{\cdot}15\ K$ (Khadilkar, 2011). The taxi fuel consumption which results from the above equation is $f = 457{\cdot}8\ kg$. The remaining FOB at take-off is 49100–457·8 = 48612 kg. Knowing the FOB broadcast by the last ACARS message (43,800 kg) and considering an average fuel flow of $FF_{avg} = 6406\ kg/h$ and the specific energy of Jet A-1, $s = 43{\cdot}02\ MJ/kg$, the resultant efficiency of the engines is 32·32%. In this case, both the kinematic and the potential energy of the aircraft change. Using the calibrated engine efficiency, the resulting fuel consumption between the last ACARS message (A) and last military primary surveillance radar contact (M) is approximately 10,000 kg, depending on the FL to which the aircraft is considered to have climbed for the long cruise flight towards the south. For example, if the aircraft climbs to FL390, the calculated fuel consumption for the

https://doi.org/10.1017/S0373463315000570 Published online by Cambridge University Press

Table 6. Equation (20) Coefficients.

$p_{0,0}$	$p_{1,0}$	$p_{0,1}$
31·47	0·004923	0·01895

last ACARS – last primary radar contact segment is $FC_{total} = 10065{\cdot}3\ kg$. In this case only the change in potential energy is considered (calculated with an average mass) and only at the climb regions. It is supposed that the fuel economy during the descending portions of the flight is balanced by the higher consumption in the dense air.

Simulation of fuel flow during the long cruise flight is based on Boeing (1992a) and Filippone (2006). Using the calculated thrust and the mass of the aircraft, the following polynomial equation was defined (coefficients are given in Table 6):

$$FF/ENG = p_{0,0} + p_{1,0} \cdot m + p_{0,1} \cdot T \tag{20}$$

Simulation of the final glide descent with both engines out in the time interval *TGD* presumed 9 minutes is presented in Pleter and Constantinescu (2014).

During the cruise flight, *TK* is kept constant by small turns, which compensate for crosswind. However, in the glide descent region, the simulation keeps a constant *HDG* instead of *TK*, and these turns are no longer performed, as illustrated in the inset in Figure 8. This is consistent with the expected behaviour of the automated systems. By keeping a constant *HDG*, the local crosswind slightly drifted the aircraft during the gliding descent.

6. ANALYSIS OF RESULTS. The multimodal optimisation using ε as a criterion (inconsistency to be minimised) yields the most probable trajectories and the most probable values of the unknowns *TTT*, *TK*, and *M*. The unknown *FL* is considered a parameter, because the problem is not sensitive with respect to the geometric *FL*. Just two *TK* ranges came out to be consistent: the Southern track around 190° (true) and the Northern track of around 336°. The Southern track fits better (a very low inconsistency, 38 solutions between 16 and 25 km), whereas the Northern track does not fit so well (zero solutions under 30 km).

The multimodal optimisation yields the set of all solutions with a certain minimum probability instead of a single most probable solution. Given the nature of the problem and the scarcity of data coming from a unique source, this approach adds more value than the initial search done by the same authors for the most probable trajectory (Pleter and Constantinescu, 2014). Thus all trajectories with an overall inconsistency lower than 25 km were considered as potential solutions, and they are represented in Tables 7 and 8, and in Figures 4 to 6. The threshold of 25 km is remarkably low as compared to the total length of the trajectory (almost 6,000 km). There are 38 consistent solutions (with $\varepsilon \leqslant 25$ km), and they are analysed in Table 7 and in the subsequent Figures. In Figure 4 all the 38 consistent solutions were represented as cylinders. The diameter of the cylinder is the inverse function of the inconsistency, i.e. consistency ($1/\varepsilon$).

The most consistent solutions presented in Table 7 have a remarkably low inconsistency, of $\varepsilon < 17$ km. Column "Fuel error" in Table 7 (second part) compares the top of descent (t_G) calculated with the optimisation method based on the satellite pings and

https://doi.org/10.1017/S0373463315000570 Published online by Cambridge University Press

https://doi.org/10.1017/S0373463315000570 Published online by Cambridge University Press

Table 7. Consistent MH370 trajectory solutions and the corresponding positions of the end of flight (E) – solutions in yellow are confirmed by the available fuel criterion, with a fuel error ≤ 1%.

Solution	ε (km)	TTT (min)	TK (°)	M (-)	FL (ft)	LAT_2 (°)	$LONG_2$ (°)	GS_2 (kts)	LAT_3 (°)	$LONG_3$ (°)	GS_3 (kts)	LAT_4 (°)	$LONG_4$ (°)	GS_4 (kts)	LAT_5 (°)	$LONG_5$ (°)	GS_5 (kts)
1	24·9	7:10	191	0·87	38,000	−2·58	93·51	501·9	−10·79	91·88	508·1	−19·13	90·22	493·5	−27·00	88·48	469·8
2	23·3	7:25	191	0·86	36,000	−2·59	93·49	503·3	−10·80	91·86	506·5	−19·14	90·19	499·6	−27·02	88·46	470·2
3	22·3	7:40	191	0·85	34,000	−2·61	93·47	505·1	−10·81	91·83	505·1	−19·16	90·17	505·9	−27·06	88·43	471·1
4	24·3	8:00	190	0·88	42,000	−2·25	93·61	492·6	−10·33	92·15	499·0	−18·57	90·65	493·9	−26·46	89·10	468·3
5	24·3	8:05	190	0·87	40,000	−2·28	93·61	494·2	−10·39	92·15	500·9	−18·65	90·65	490·9	−26·50	89·10	465·7
6	19·8	8:40	190	0·87	39,000	−2·24	93·54	498·3	−10·42	92·06	505·2	−18·75	90·56	491·7	−26·61	88·99	467·5
7	17·9	8:50	190	0·86	37,000	−2·27	93·52	499·2	−10·45	92·05	503·7	−18·77	90·55	495·4	−26·64	88·98	467·6
8	16·4	9:05	190	0·85	35,000	−2·28	93·50	500·4	−10·46	92·02	501·7	−18·78	90·52	500·9	−26·67	88·95	468·4
9	21·5	9:30	189	0·88	43,000	−1·92	93·63	489·6	−9·95	92·31	495·0	−18·14	90·97	494·7	−26·06	89·59	467·8
10	21·5	9:35	189	0·87	41,000	−1·94	93·63	490·8	−10·01	92·32	496·6	−18·23	90·98	492·6	−26·09	89·59	465·1
11	23·9	10:05	189	0·88	42,000	−1·88	93·56	493·4	−9·98	92·24	498·9	−18·23	90·89	496·3	−26·17	89·49	469·3
12	17·6	10:10	189	0·87	40,000	−1·88	93·54	494·7	−10·02	92·22	500·8	−18·30	90·88	494·0	−26·19	89·48	466·7
13	16·2	10:25	189	0·86	38,000	−1·91	93·53	495·9	−10·06	92·21	501·3	−18·36	90·87	493·8	−26·23	89·47	465·4
14	14·9	10:35	189	0·85	36,000	−1·94	93·52	496·3	−10·09	92·20	499·0	−18·38	90·85	497·3	−26·26	89·45	466·4
15	13·9	10:50	189	0·84	34,000	−1·96	93·49	497·2	−10·12	92·17	496·9	−18·40	90·82	501·1	−26·30	89·42	467·8
16	22·0	10:55	188	0·87	42,000	−1·64	93·66	487·4	−9·65	92·50	492·4	−17·82	91·31	491·9	−25·70	90·09	465·6
17	24·7	11:00	189	0·86	37,000	−1·88	93·45	499·2	−10·08	92·12	503·3	−18·42	90·77	498·0	−26·34	89·36	468·7
18	19·7	11:10	188	0·87	42,000	−1·59	93·63	487·6	−9·61	92·47	492·6	−17·77	91·29	492·0	−25·66	90·06	466·0
19	24·5	11:30	188	0·88	43,000	−1·55	93·57	490·2	−9·61	92·40	494·8	−17·81	91·21	495·3	−25·77	89·98	469·6
20	17·1	11:45	188	0·87	41,000	−1·55	93·55	491·4	−9·63	92·39	496·7	−17·86	91·20	494·6	−25·77	89·96	467·0
21	17·0	11:55	188	0·86	39,000	−1·57	93·55	492·8	−9·69	92·38	498·9	−17·96	91·19	493·5	−25·82	89·95	464·2
22	17·0	12:05	188	0·85	37,000	−1·60	93·53	493·0	−9·72	92·36	496·9	−17·98	91·18	495·1	−25·85	89·94	464·4
23	16·1	12:10	188	0·84	35,000	−1·63	93·51	493·3	−9·74	92·34	494·2	−17·99	91·15	497·6	−25·88	89·91	465·3
24	23·5	12:30	188	0·86	38,000	−1·53	93·46	496·1	−9·70	92·28	501·3	−18·02	91·09	496·7	−25·92	89·84	466·7

https://doi.org/10.1017/S0373463315000570 Published online by Cambridge University Press

25	18·0	12:40	187	0·87	43,000	−1·25	93·63	484·4	−9·22	92·62	488·1	−17·33	91·59	489·2	−25·24	90·53	467·9
26	23·6	12:40	188	0·85	36,000	−1·55	93·43	496·2	−9·72	92·26	498·5	−18·03	91·07	499·1	−25·95	89·82	467·6
27	24·2	12:45	187	0·86	41,000	−1·28	93·63	485·5	−9·27	92·62	490·5	−17·42	91·60	489·7	−25·28	90·53	464·1
28	17·1	13:15	187	0·87	42,000	−1·21	93·56	488·2	−9·24	92·54	492·5	−17·42	91·50	492·4	−25·35	90·43	468·5
29	17·8	13:25	187	0·86	40,000	−1·23	93·55	489·4	−9·29	92·53	495·0	−17·51	91·50	492·7	−25·39	90·42	465·0
30	21·5	13:35	187	0·85	38,000	−1·26	93·54	490·1	−9·34	92·52	495·6	−17·58	91·49	493·0	−25·43	90·41	462·9
31	21·6	13:40	187	0·84	36,000	−1·30	93·52	489·9	−9·38	92·51	492·5	−17·60	91·48	493·7	−25·47	90·40	463·3
32	22·0	13:50	187	0·83	34,000	−1·34	93·50	490·2	−9·43	92·49	489·7	−17·63	91·45	494·9	−25·53	90·38	464·3
33	23·9	14:00	187	0·86	39,000	−1·20	93·47	493·2	−9·33	92·45	499·4	−17·61	91·41	495·4	−25·52	90·32	465·9
34	20·7	14:45	186	0·87	43,000	−0·86	93·55	485·0	−8·85	92·68	487·6	−16·97	91·80	489·3	−24·91	90·89	470·2
35	19·4	14:55	186	0·86	41,000	−0·89	93·54	485·9	−8·90	92·68	490·4	−17·05	91·80	490·6	−24·95	90·88	466·1
36	24·6	15:05	186	0·85	39,000	−0·92	93·54	487·2	−8·96	92·67	493·9	−17·16	91·80	491·9	−25·01	90·88	461·7
37	23·6	15:45	185	0·86	43,000	−0·59	93·62	478·9	−8·49	92·90	480·7	−16·51	92·17	484·5	−24·39	91·43	467·2
38	22·5	16:20	185	0·86	42,000	−0·56	93·54	482·4	−8·52	92·82	484·8	−16·61	92·09	487·8	−24·51	91·34	467·4

Solution	ε (km)	*TTT* (min)	*TK* (°)	*M* (–)	*FL* (ft)	LAT_6 (°)	$LONG_6$ (°)	GS_6 (kts)	LAT_7 (°)	$LONG_7$ (°)	GS_7 (kts)	LAT_E (°)	$LONG_E$ (°)	*Fuel Error* (%)	(sec)	ε* *w/o wind* (km
1	24·9	7:10	191	0·87	38,000	−38·57	85·64	478·4	−39·66	85·34	475·1	−40·42	85·14	−2·6%	−681	195·8
2	23·3	7:25	191	0·86	36,000	−38·54	85·63	479·0	−39·64	85·34	474·0	−40·40	85·14	−4·6%	−1186	174·3
3	22·3	7:40	191	0·85	34,000	−38·55	85·62	480·0	−39·64	85·34	473·2	−40·41	85·15	−7·2%	−1859	154·6
4	24·3	8:00	190	0·88	42,000	−38·09	86·52	477·5	−39·18	86·25	474·8	−39·94	86·07	1·0%	251	188·9
5	24·3	8:05	190	0·87	40,000	−38·02	86·53	475·4	−39·12	86·26	472·1	−39·88	86·08	−0·4%	−95	187·0
6	19·8	8:40	190	0·87	39,000	−38·17	86·41	476·8	−39·26	86·14	473·6	−40·02	85·96	−1·5%	−392	194·7
7	17·9	8:50	190	0·86	37,000	−38·14	86·41	476·5	−39·24	86·15	472·8	−40·00	85·97	−3·2%	−836	178·4
8	16·4	9:05	190	0·85	35,000	−38·14	86·40	477·0	−39·23	86·14	472·7	−40·00	85·97	−5·5%	−1418	163·5
9	21·5	9:30	189	0·88	43,000	−37·70	87·28	476·8	−38·80	87·04	474·3	−39·56	86·88	1·6%	424	190·1
10	21·5	9:35	189	0·87	41,000	−37·63	87·29	474·9	−38·73	87·05	471·6	−39·49	86·88	0·6%	151	186·7
11	23·9	10:05	189	0·88	42,000	−37·83	87·17	478·3	−38·94	86·93	475·4	−39·70	86·77	1·0%	253	200·8
12	17·6	10:10	189	0·87	40,000	−37·75	87·17	476·5	−38·85	86·93	472·8	−39·62	86·76	−0·4%	−95	263·9
13	16·2	10:25	189	0·86	38,000	−37·71	87·16	475·3	−38·81	86·93	471·1	−39·57	86·76	−2·1%	−533	181·0
14	14·9	10:35	189	0·85	36,000	−37·71	87·16	474·7	−38·80	86·93	470·8	−39·57	86·77	−4·0%	−1028	164·9

Continued

https://doi.org/10.1017/S0373463315000570 Published online by Cambridge University Press

Table 7. (*Continued*)

Solution	ε (km)	*TTT* (min)	*TK* (°)	*M* (–)	*FL* (ft)	LAT_6 (°)	$LONG_6$ (°)	GS_6 (kts)	LAT_7 (°)	$LONG_7$ (°)	GS_7 (kts)	LAT_E (°)	$LONG_E$ (°)	*Fuel Error* (%)	(sec)	ε* *w/o wind* (km
15	13·9	10:50	189	0·84	34,000	–37·72	87·14	474·6	–38·82	86·92	470·9	–39·58	86·76	–6·5%	–1688	144·7
16	22·0	10:55	188	0·87	42,000	–37·25	88·05	473·9	–38·35	87·84	471·1	–39·11	87·70	1·4%	355	197·6
17	24·7	11:00	188	0·86	37,000	–37·88	87·05	477·2	–38·99	86·81	473·3	–39·75	86·65	–3·2%	–839	184·5
18	19·7	11:10	188	0·87	42,000	–37·21	88·03	474·1	–38·31	87·82	471·3	–39·07	87·68	1·4%	355	182·6
19	24·5	11:30	188	0·88	43,000	–37·44	87·92	477·5	–38·55	87·71	475·0	–39·31	87·58	1·7%	427	204·7
20	17·1	11:45	188	0·87	41,000	–37·34	87·92	475·8	–38·45	87·70	472·6	–39·21	87·56	0·6%	154	193·8
21	17·0	11:55	1E8	0·86	39,000	–37·28	87·91	474·4	–38·38	87·70	470·4	–39·15	87·56	–1·0%	–254	18E6
22	17·0	12·05	188	0·85	37,000	–37·27	87·91	473·2	–38·36	87·70	469·0	–39·13	87·56	–2·6%	–683	170·4
23	16·1	12:10	188	0·84	35,000	–37·28	87·89	472·3	–38·37	87·69	467·9	–39·13	87·55	–4·9%	–1256	155·8
24	23·5	12:30	188	0·86	38,000	–37·44	87·79	476·1	–38·54	87·58	472·1	–39·31	87·44	–2·1%	–533	189·6
25	18·0	12:40	187	0·87	43,000	–36·80	88·76	473·4	–37·90	88·58	470·5	–38·66	88·46	2·0%	517	184·7
26	23·6	12:40	188	0·85	36,000	–37·44	87·78	475·1	–38·54	87·58	471·0	–39·30	87·43	–4·0%	–1034	173·8
27	24·2	12:45	187	0·86	41,000	–36·73	88·76	471·6	–37·82	88·58	468·4	–38·59	88·46	1·0%	268	1810
28	17 1	13·15	187	0·87	42,000	–36·93	88·65	474 8	–38 03	88·47	472 0	–38 80	88·35	1·4%	358	194·7
29	17·8	13:25	187	0·86	40,000	–36·86	88·65	473·2	–37·96	88·47	469·9	–38·73	88·34	0·1%	34	185·4
30	21·5	13:35	187	0·85	38,000	–36·83	88·64	471·8	–37·92	88·46	467·9	–38·69	88·33	–1·5%	–386	174·3
31	21·6	13:40	187	0·84	36,000	–36·84	88·64	470·6	–37·93	88·46	465·8	–38·69	88·33	–3·4%	–869	158·3
32	22·0	13:50	187	0·83	34,000	–36·87	88·63	469·7	–37·96	88·45	464·0	–38·72	88·32	–5·9%	–1514	144·8
33	23·9	14:00	187	0·86	39,000	–37·01	88·54	474·9	–38·12	88·36	471·5	–38·88	88·23	–10%	–254	192·4
34	20·7	14:45	186	0·87	43,000	–36·51	89·37	474·6	–37·61	89·22	471·3	–38·37	89·12	2·0%	520	196·5
35	19·4	14:55	186	0·86	41,000	–36·44	89·37	472·5	–37·53	89·22	469·1	–38·30	89·11	1·0%	268	185·5
36	24·6	15:05	186	0·86	39,000	–3638	29·37	470·5	–37·48	89·21	467·1	–38·24	89·10	–0·5%	–116	177·7
37	23·6	15:45	185	0·86	43,000	–35·87	90·18	471·1	–36·97	90·05	466·7	–37·73	89·97	2·3%	604	185·9
38	22·5	16:20	185	0·86	42,000	–36·01	90·09	472·1	–37·11	89·96	467·9	–37·88	89·88	1·8%	461	186·8

https://doi.org/10.1017/S0373463315000570 Published online by Cambridge University Press

Table 8. Flight level distribution of the consistent MH370 trajectory solutions.

FL	340	350	360	370	380	390	400	410	420	430
Number of solution $\varepsilon < 25$ km	3	2	4	3	4	4	3	4	6	5
Average ε	19·41	16·22	20·87	19·86	21·54	21·32	18·73	20·53	21·57	21·65
ε	***3*** 22	***8*** 16·36	***2*** 23·31	***7*** 17·94	***1*** 24·93	***6*** 19·83	***5*** 20·79	***10*** 21·49	***4*** 24·33	***9*** 21·46
	15 13·92	***23*** 16·08	***14*** 14·93	***17*** 24·66	***13*** 16·24	***21*** 16·99	***12*** 17·64	***20*** 17·05	***11*** 23·88	***19*** 24·49
	32 22·01		***26*** 23·64	***22*** 16·98	***24*** 23·45	***33*** 23·88	***29*** 17·75	***27*** 24·18	***16*** 22·03	***25*** 18·01
			31 21·61		***30*** 21·54	***36*** 24·58		***35*** 19·41	***18*** 19·65	***34*** 20·67
									28 17·08	***37*** 23·63
									38 22·47	

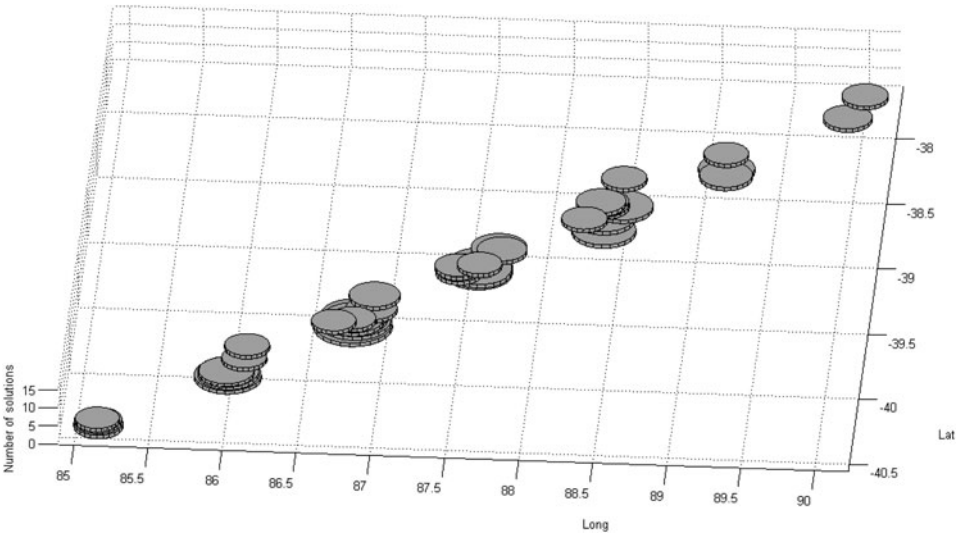

Figure 4. Position of the end of flight (E) for each of the 38 consistent solutions.

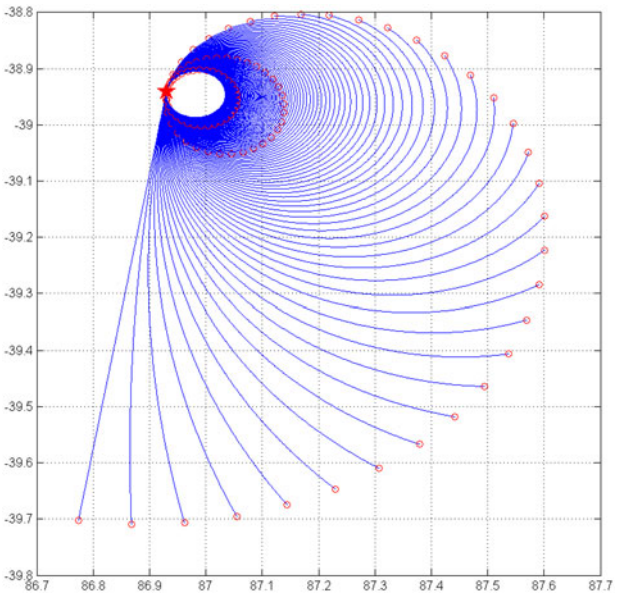

Figure 5. The locus of the end of flight positions (E^*) for solution ***11*** considering a constant angular velocity turn during glide descent; the circles represent the possible points of impact for each respective angular velocity.

https://doi.org/10.1017/S0373463315000570 Published online by Cambridge University Press

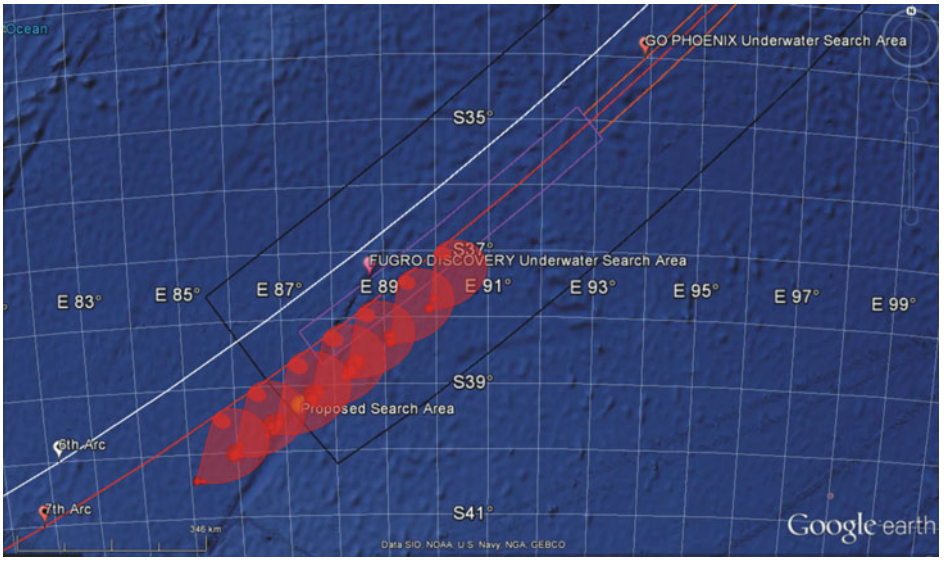

Figure 6. The end of flight point (*E*) for each of the 38 consistent solutions (discs); the weighted average of these points is represented by a light colour disc; the transparent areas resulting from the turning glide descent model (Figure 5) were positioned on the calculated end of flight points to give a probable area of impact; the ellipses on the 7th arc represent the most probable areas of impact.

the top of descent (t_{G*}) calculated with the integration of the fuel flow until the moment of fuel exhaust. The relative error ranges between −7·2% and +2·3%. For nine solutions (represented in yellow), the relative time error stays within ±1% (254 seconds of flight in absolute value), which is remarkable, given the inherent uncertainty caused by the manoeuvres before the last turn. Moreover, these small relative errors are symmetrically distributed in the range of the consistent solutions. Such a distribution appears to validate the results of the optimisation. The relative time error filter discards the lower *FL* solutions, such as solutions ***3***, ***15***, and ***32***. Also, this filter discards the lower *M* solutions, such as ***8*** and ***26***. Given the double validation, from the optimisation and the fuel burn simulation, solutions at the upper end of the *FL* and *M* scales stand out, e.g. solution ***11***.

The places where the flight might have ended in the 38 most probable scenarios are represented in Figures 4 and 5. The places seem clustered in seven isolated groups, but the gaps between these groups might be equally interesting for searching. The solution-clustering phenomenon is probably a consequence of selecting integer values for *TK*. In reality, *TK* could have very well been a rational number, in the case of the third hypothesis of the FMS programming presented above, a "DIRECT TO" a distant point given by *LAT* and *LONG*. Figure 8 illustrates the whole simulated trajectory, which corresponds to one of the solutions (***11***). The last portion of this trajectory is made visible at a better scale in the inset.

These 38 end of flight points were calculated assuming that the glide descent was flown with a constant heading (no turn). Since the probability of a turn due to the

https://doi.org/10.1017/S0373463315000570 Published online by Cambridge University Press

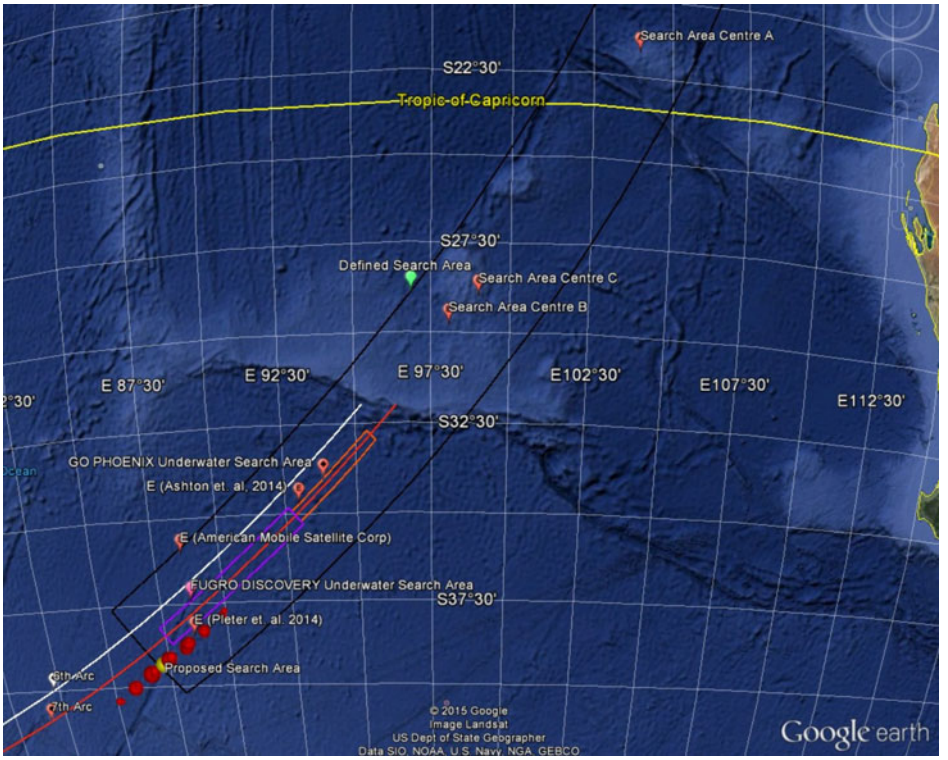

Figure 7. The end of flight point (*E*) for each of the 38 consistent solutions, compared to the current search areas and to other results published (CNN, 2014; Australian Government, 2014; Ashton et al., 2014; Pleter and Constantinescu, 2014).

initial thrust asymmetry is high (ATSB, 2014a; 2014b - MH370 - Definition of Underwater Search Areas), and the rate of turn (the angular velocity) is not known, a locus of all potential end of flight points (*E**) was developed and illustrated in Figure 5. All trajectories in Figure 5 correspond to the end of flight point of Solution ***11***, and are all turning trajectories with incremental angular velocities. The circles at the end of each same-length orthodrome trajectory represent potential points of impact with the water.

In reality, the turn could have been with variable angular velocity. The fixed angular velocity model in Figure 5 however includes in the envelope of the *E** points all possible impact points. In Figure 6, for each cluster of *E* solutions, the corresponding *E** envelope was represented as a transparent area. Out of this area, the ellipses on the seventh arch illustrate the spiral dive, which could be a higher probability impact area.

In Table 8 the same 38 solutions were placed on their *FL*s, making it obvious that the fuel burn criterion favours the higher *FL*s solutions (in yellow). Flying in a denser atmosphere, although geometrically consistent with the *BTO*s, would have fuel starved the engines much earlier than the moment t_G, which is known.

For the same solution ***11***, the simulated ground speed variation over the entire flight was represented in Figure 9. The ground speed is calculated as the vector addition

https://doi.org/10.1017/S0373463315000570 Published online by Cambridge University Press

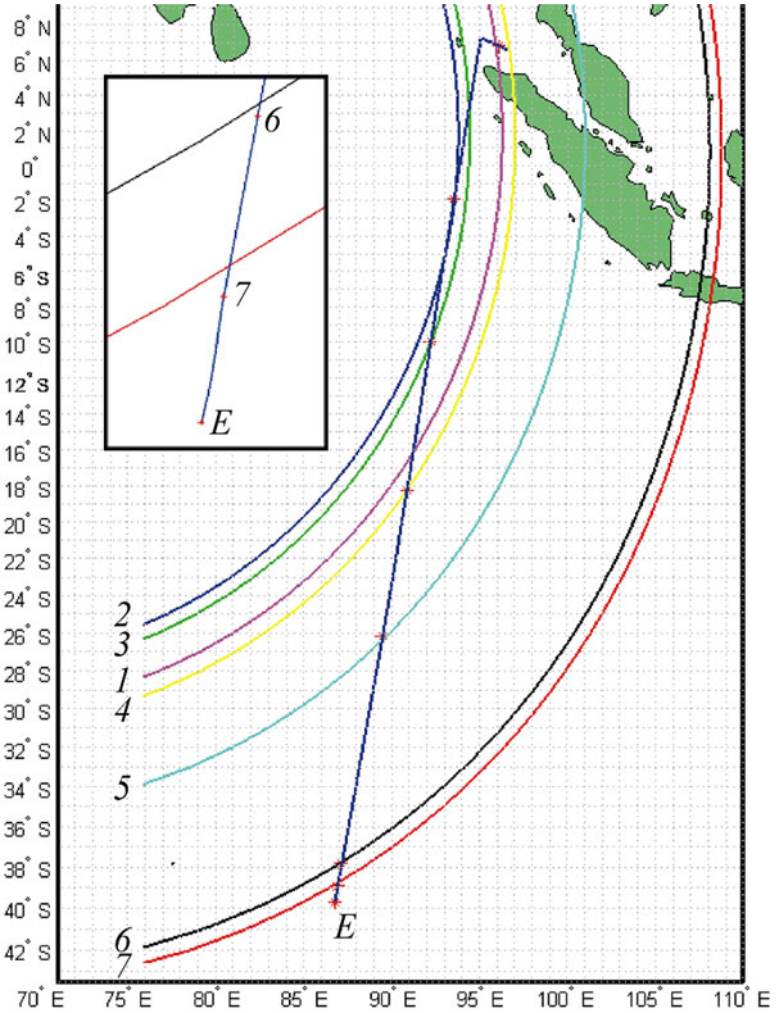

Figure 8. Quasi-circles of intersection between the satellite-centred spheres and the isobaric surface of the aircraft taken parallel to the WGS-84 rotation ellipsoid and the trajectory of MH370 as simulated for solution ***11***. Inset illustrates final segment with a slight drift both ways to the effect of the crosswind on the glide descent trajectory.

between the horizontal component of the true airspeed and the local wind velocity. For a possible validation of such a trajectory with a method based on *BFO*, Table 9 indicates the ground speed in the seven moments of the seven pings, decomposed in the ECEF framework.

The inclusion of the wind vector field in simulating the flight increased the relevance, as shown in Table 7. The inconsistency of the best-fit trajectories is between 6 and 15 times worse in cases where the wind vector field is not used. This validates the simulation and the use of the proper wind vector field, which is one of the few certain facts regarding this flight.

https://doi.org/10.1017/S0373463315000570 Published online by Cambridge University Press

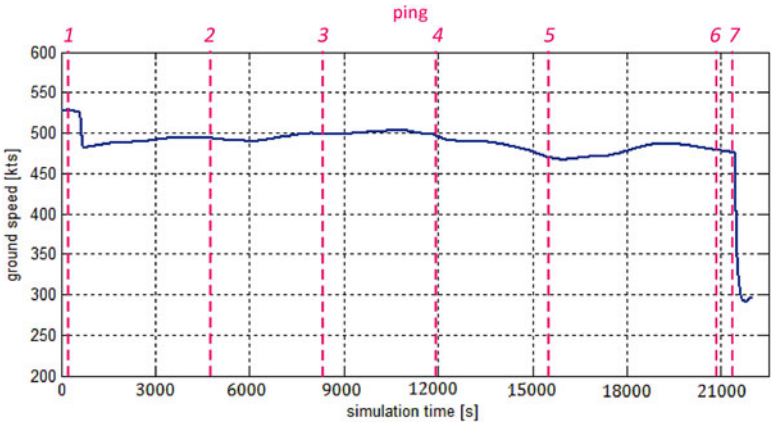

Figure 9. Simulated MH370 ground speed variation (solution ***11***).

Table 9. Solution **11** ground speed decomposed in ECEF reference for the seven quasi-circles.

ECEF	1	2	3	4	5	6	7
x′(m/s)	246·10194	41·08357	42·09721	41·21286	39·08501	33·95766	33·19933
y′ (m/s)	12·56416	−5·61979	−42·02263	−77·77739	−104·78226	−150·01248	−152·87285
z′ (m/s)	113·88568	−248·75327	−248·00685	−238·06273	−212·53179	−190·78845	−186·75045
t (s)	210	4743	8346	11967	15564	20940	21450
gs (kts)	528·3	493·4	498·9	496·3	469·3	478·3	475·4

7. CONCLUSIONS. The method presented uses the ranges determined by the last six pings along the unknown portion of the cruise flight, avoiding calculations based on the carrier frequency drift. Thus, an issue of geometric ill conditioning of the problem is avoided (since the relative aircraft-satellite speed vector is almost perpendicular to the aircraft ground speed vector). In a multimodal optimisation loop with complete search, the flight is simulated based on a dynamic model, determining the unknowns of the flight, which best fit the known facts. Thus, the method gives simultaneously the time from the last known position until the left turn, the track, and the Mach number of the cruise. The flight level can be used as a parameter of the optimisation.

All the 38 solutions found have a flight ending point *E* falling closely to each other, as illustrated in Figures 4, 6, and 7. The search area proposed by this paper may be approximated as a rectangle aligned with the 7th arch, with the following corners: S39°46′35″ E84°35′51″; S40°43′18″ E85°24′09″; S37°38′09″ E91°09′40″; S36°47′14″ E90°12′56″.

Figures 6 and 7 illustrate the most probable end of flight points calculated in this paper, in contrast to other published results (Ashton et al., 2014; Hradecky, 2014; CNN, 2014; Australian Government, 2014; Pleter and Constantinescu, 2014).

ACKNOWLEDGEMENTS

The authors wish to express their gratitude to the following contributors to their work: the reviewers of the Journal of Navigation, Capt. B787-B777 Dumitru Oprisiu, B777 Licensed Aircraft Engineer Adrian Matei, and Simon Hradecky (www.avherald.com).

https://doi.org/10.1017/S0373463315000570 Published online by Cambridge University Press

REFERENCES

Ashton, C., Schuster-Bruce, A., Colledge, G. and Dickinson, M. (2014). The Search for MH370. *The Journal of Navigation*, **68**(1), 1–22.

ATSB. (2014a). Australian Transport Safety Bureau, MH370 - Definition of Underwater Search Areas - 26 June 2014, Accessed 6 October 2014.http://atsb.gov.au/media/5243942/ae-2014-054_mh370_-_definition_of_underwater_search_areas_18aug2014.pdf

ATSB. (2014b). Australian Transport Safety Bureau, MH370 – Flight Path Analysis Update - 8 October 2014. http://atsb.gov.au/media/5163181/AE-2014-054_MH370%20-flightPathAnalysisUpdate.pdf Accessed 22 November 2014

Australian Government. (2014). Department of Infrastructure and Regional Development. (2014). http://www.jacc.gov.au/media/maps/index.aspx Accessed 21 August 2014.

Boeing. (1992a). *Boeing 777-200/-200ER Technical Characteristics*. http://www.boeing.com/boeing/commercial/777family/pf/pf_200product.page. Accessed 1 June 2014.

Boeing. (1992b). *Boeing 777 Flight Crew Training Manual*. Boeing.

Bulfer, B. and Gifford, R. (1999). *Big Boeing FMC User's Guide*. Leading Edge Publications.

CNN. (2014). *American Mobile Satellite Corp.* http://edition.cnn.com/2014/06/18/world/asia/malaysia-missing-plane/index.html Accessed 10August2014.

Filippone, A. (2006). *Flight Software - Sensitivity Analysis on Fuel Burn B777-300ER*, The University of Manchester. http://www.flight.mace.manchester.ac.uk/aircraft-performance-software/case-studies/by-aircraft-and-route/case-study-boeing-b777.html. Accessed 5 July 2014.

Hradecky, S. (2014). *Crash: Malaysia B772 over Gulf of Thailand on Mar 8th 2014, aircraft missing, data indicate flight MH-370 ended west of Australia*. www.avherald.com. Accessed 13 August 2014.

INMARSAT. (2014). MH370 Data communication logs, Accessed 15 August 2014. http://www.dca.gov.my/mainpage/MH370%20Data%20Communication%20Logs.pdf

Khadilkar, H. (2011). Estimation of Aircraft Taxi-out Fuel Burn using Flight Data Recorder Archives, Masters Dissertation, *Massachusetts Institute of Technology*.

Malaysian Government. (2014). Office Of The Chief Inspector Of Air Accidents Ministry Of Transport Malaysia, MH 370 Preliminary Report Serial 03/2014, Accessed 11 June 2014. http://www.dca.gov.my/MH370/Preliminary%20Report.pdf

NOAA. (2014). *NOAA National Operational Model Archive & Distribution System*. nomads.ncdc.noaa.gov/data.php?name=access#hires_weather_dataset. Accessed 1 June 2014.

Pereira, R. L. (2011). Validation of software for the calculation of aerodynamic coefficients, Degree Project. *Linköping University*.

Pleter, O. T. and Constantinescu, C. E. (2014). Possible Trajectories of Flight Malaysian 370 (plenary presentation), INCAS, *International Conference of Aerospace Sciences "AEROSPATIAL 2014"*. Bucharest 18–19 September 2014.

https://doi.org/10.1017/S0373463315000570 Published online by Cambridge University Press

Research Square

Preprints are preliminary reports that have not undergone peer review.
They should not be considered conclusive, used to inform clinical practice,
or referenced by the media as validated information.

MH370 Controlled Eastward Veering and Descent After the 6th Arc

Vincent Lyne (vincent.lyne@utas.edu.au)
Retired Scientist https://orcid.org/0000-0002-7718-4050

Research Article

Keywords: Burst Frequency Offset, Burst Timing Offset, MH370, Doppler Shift

Posted Date: December 27th, 2021

DOI: https://doi.org/10.21203/rs.3.rs-962332/v2

License: This work is licensed under a Creative Commons Attribution 4.0 International License.
Read Full License

MH370 Controlled Eastward Veering and Descent After the 6th Arc

Vincent Lyne [1*]

1 Retired Scientist. Hobart. Tasmania. Australia
* Correspondence: Vincent.lyne@utas.edu.au *(Note: UTas is not to be affiliated with this article)*

Abstract

Past expert analyses of communication signals from missing Malaysian Airlines MH370 reconciled Burst Frequency Offset (BFO) errors up to the 6th of 7 arcs for a southerly track. After the 6th arc, the Satellite Data Unit (SDU) power-up or reboot resulted in settling errors in the last two data points that were ignored (first search) and later bounded (second search). For the second search, investigators invoked a high-speed vertical descent to account for BFO errors for the south track fuel-starved scenario. Two searches disappointingly failed to find the implied violent-crash site. We report that interpretations were flawed in suggesting the plane dived vertically, as investigators did not recognize that BFO extrapolations implicitly implied mathematically that the plane was also cruising along the south track, but with no fuel. Our reanalysis used the "Penang Longitude" (PL) theory that predicted a similar southerly track to the 6th arc, and that MH370 subsequently veered eastwards and descended. Doppler Shifts from vertical motions were replaced with plausible horizontal veering and declination of a high-speed aircraft. Veering predicted by the PL theory plus controlled descent plausibly accounts for nominal 7th arc BFO discrepancies for the warm-reboot scenario. We conclude that the fuel-starvation scenario analyses wrongly implied a vertical high-speed crash that ignored the impossible implicit southerly cruise, with no fuel, assumption. Instead, MH370 was piloted to a precise glide landing under power, east of the 7th arc.

Keywords: Burst Frequency Offset, Burst Timing Offset, MH370, Doppler Shift

Introduction

Malaysian Airlines MH370, a Boeing 777-200ER equipped with the Inmarsat Classic Aero system, has not been found since it went missing on the 8th of March 2014 with 239 people on board [1]. Inmarsat engineers identified regular monitoring "Log-on Interrogation" communications after each hour of inactivity, and two phases of specific logon requests from the aircraft near 18:25 and 00:19 UTC [2]. Detailed complex analyses of the Burst Timing Offset (BTO – distance-based measurement) and the Burst Frequency Offset (BFO – relative speed-based measurement) from these communications resulted in seven BTO global arcs

along which the aircraft was located at different times, centred around the Inmarsat satellite located nominally above 0.5°N and 64.5°E [2].

Reconstructed potential flight paths, using the arc timings and BFO-estimated speeds/directions, generally supported a persistent southerly track down to the 6th arc [2,3]. At the 7th arc, anomalies in BFO remained after extrapolation of the BFO predicted from a good statistical fit to previous BFOs [3] and resolution of a wide variety of potential error sources [4]. Errors from the power-up settling anomalies from the Satellite Data Unit (SDU) were also bounded but discrepancies remained between a predicted BFO of 260 Hz and nominal observed BFOs of 182 Hz and -2 Hz respectively at the last two communications 8 seconds apart at the 7th arc [4]. Hypotheses on whether the SDU was started up from a power-off-on engine flame-out event (Hypothesis 1 – fuel-starvation scenario, long cold-start settling behaviour) or a warm reboot electronic event (Hypothesis 2 – electronic switching, short reboot settling behaviour) led to an extended BFO range error, and an extreme range which considered BFO noise [4]. The extreme range resulted in unrealistic descent rates, so mid-point values were used to determine that, if the southerly track continued to the 7th arc, anomalies could only be resolved from up-down motions, unaccounted for by the SDU which only compensated horizontal motions. This led Holland [4] to generally conclude that, discounting the unrealistic extreme range (primarily from the flame-out Hypothesis 1), a 0.68 g (g is Earth's surface gravitation acceleration constant) acceleration took place during the 8 seconds leading to a nominal high-speed descent of 10,800 fpm (feet per minute). These conclusions resulted in probable search locations of MH370 within bounds along the 7th arc which were supported by highly promising drift model analyses of recovered debris [5]. However, extensive, and extended, searches around these bounded locations along with previous aerial searches and satellite searches, were unsuccessful [1].

In early 2021, the fuel starvation theory which guided previous searches was challenged by the "Penang Longitude" (PL) theory [6] which not only reconciled the drift model analyses but also reconciled the pilot's home simulator tracks, satellite anomalies and hydroacoustic sounds heard at listening stations at Perth Canyon [7], Cape Leeuwin and Diego Garcia [8]; which were all abandoned previously as they could not be reconciled with a crash site along the 7th arc. The theory was predicated on the notion that there is one precise location for MH370, namely where the 33°S latitude intersects the longitude of Penang, where all evidence appears to plausibly intersect at an ultra-deep hole. The theory of a piloted glide landing was supported by expert investigations of debris damage by Vance [9] who has quietly suffered unfair unsubstantiated criticism of his excellent careful work. The explanation for what happened between the last two communications at the 7th arc may critically determine whether this theory is more plausible than the failed fuel-starvation theory.

As shown in Figure 1, the southerly track of MH370 approximately concords with this theory's intuitive explanation that the track taken was to stay outside of the western boundary of the Jindalee Over-the-Horizon Radar Network (JORN) from the Laverton station in Western Australia [10]. Note that the track shown in Figure 1 was changed from the original track outside JORN [6] by moving the southerly track to intersect the 6th arc at a bearing of about 6.7° east from due south. This change was made to align more closely with the estimated southerly track from the reconciled BFO analyses down to the 6th arc. We assume for this study that the aircraft is flying southerly at the 6th arc, as the primary interest is what caused the BFO changes after the 6th arc at the last two communications at the 7th arc: the first at 00:19:29 UTC, and the second at 00:19:37 UTC.

The 7th arc' BFO evidence and analyses to date suggesting an uncontrolled violent crash are at odds with this theory's prediction of a meticulously planned precise piloted powered glid landing, which was also suggested independently from the detailed careful interpretations

of debris "witness marks" by Vance [9] –implying that there was little or no randomness in the plan. Hence, our aim is to test whether alternate plausible explanations of the 7th arc BFOs are possible and in keeping with this theory's prediction of an eastward turn of MH370 once past the southern end of the JORN range located approximately at 32°S, with the actual turn taking place near 33°S latitude, at a waypoint, ultimately towards a secret deep hole.

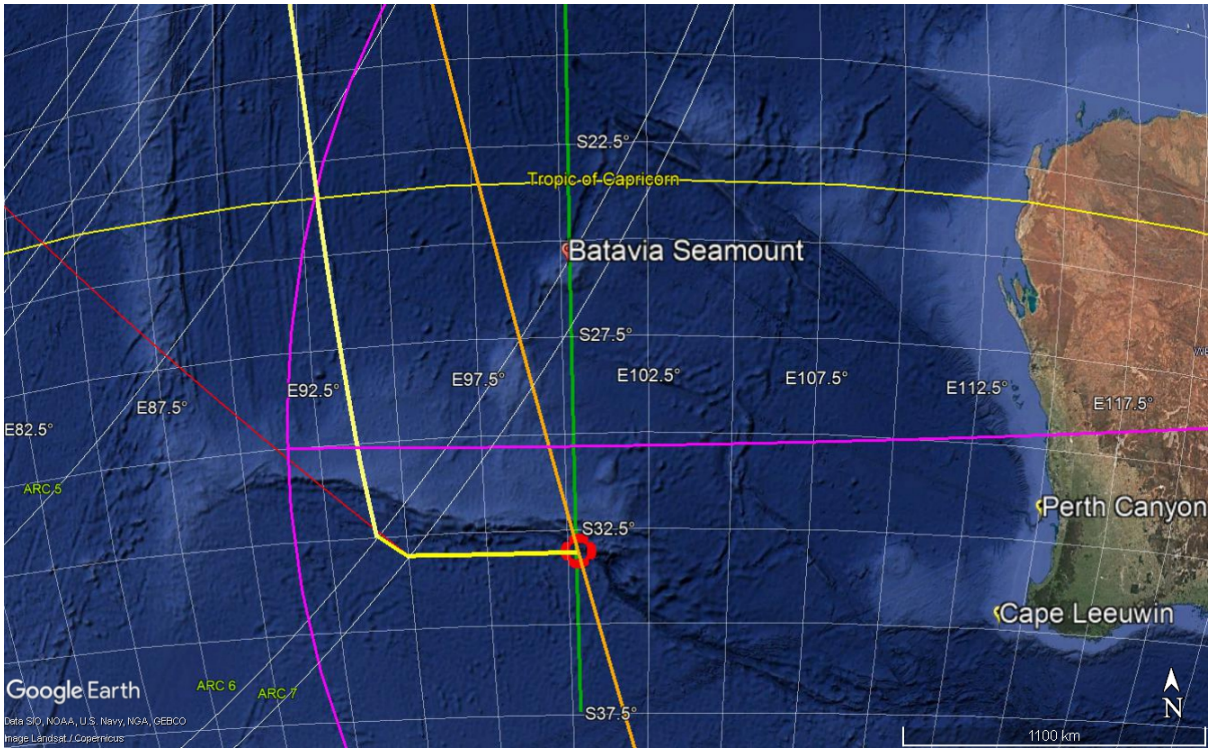

Figure 1 Main map features of the BFO analyses. The white curves are the 7 arcs. The purple curve is the Jindalee Over the Horizon Radar Network (JORN) range, and the purple line marks the southern limit of the range. One postulated example flight path of the Penang Longitude theory is in yellow showing an approximately southerly track that intersects the 6th arc (ARC 6) at 94°E, then veers to 33°S, 95°E at the 7th arc (ARC 7), and then proceeds to the postulated Penang Location (red circle) intersected by the Penang longitude (green vertical line). Note that this track is a modification of the original predicted southerly track outside the JORN range; this version cuts the southwest corner of JORN at a bearing of 6.7° east of a southerly track. Note for later purposes, the close alignment of the track running between the 6th and 7th arcs with the bearing to the satellite. The orange line running northeast is one of the simulation tracks from the pilot's home simulator [1] which passes precisely over the Penang Location. The depth at the Penang Location hole is just under 6000 m according to Google Earth Pro.

Much has been written about the BFO analyses, and since there is general acceptance of BFO interpretations of a southerly track up to the 6th arc, our focus, as per Holland [4], will be on the change between the two final 7th arc BFOs; in particular on alternate explanations for anomalies arising from Holland's calculated nominal range for the observed BFOs [4]. We focus on anomalies for the "warm start" Hypothesis 2, rather the extreme anomalies for Hypothesis 1 where fuel starvation leads to engine flame-out followed by a restart of the SDU using power from the Auxiliary Power Unit (APU) [4]. The "warm start" refers to a warm reboot from a power switching rather than a fuel-starved power outage, which is more compatible with the PL theory's prediction that the aircraft was undergoing preparations for its descent phase. In any case, the precedence for this power glitch assumption was established by a previous such event (at 18:25 UTC) when the aircraft clearly did not run out of fuel.

Method

The main difference between our proposed analysis and past analyses is that we allow the aircraft track to vary, and to veer eastwards from a southerly track at the 6th arc for a descent along the 33°S latitude to a destination at the PL location. This contrasts with the fuel-starvation theory which required the aircraft to maintain its southerly track – that was assumed to be compensated for by the SDU unit [2]. The other difference is that the up-down motions analysed by Holland [4] are implicitly incorporated into a flight descent model where the aircraft descends at a declination angle to the horizontal plane. For our analyses, we also ignore the 6.7° difference between the predicted track (Figure 1) and a southerly track required by the BFO analyses up to the 6th arc. We assume that the actual track is southerly at the 6th arc and only analyse differences from this at the last two communications at the 7th arc.

These changes are incorporated into the standard Doppler Shift model of equation (1) that defines the frequency change observed from a moving electromagnet source:

$$F_o = \frac{C * F}{(C - V)} \tag{1}$$

Where: speeds are in kilometres per hour (kph); frequencies are in Hertz (Hz); C is the speed of light (1.079e+9 kph); V is the speed component of the aircraft velocity vector (kph) that is aligned with the vector from the aircraft to the Inmarsat satellite (positive towards the satellite); F is the uplink frequency from the aircraft to the satellite (1646.6525 MHz); and F_o is the received Doppler-shifted frequency (assuming no compensation was applied).

The magnitude of velocity V was calculated from the aircraft track, heading and elevation to the Inmarsat satellite, and an assumed declination angle according to equation (2).

$$V = S * \cos(\theta_e - \theta_d) * \cos(\theta_s - \theta_a) \tag{2}$$

Where: heading and track angles are measured clockwise from North; S is the ground speed of the aircraft; θ_e is the aircraft to satellite elevation angle from horizontal (positive and set to 38.8°for the 7th arc following Holland [4]); θ_d is the aircraft declination angle (positive for descent); and θ_s and θ_a are heading angles at ground level for the satellite and aircraft respectively (so 0° is a track to the North and 180° is a South track).

The calculated velocity magnitude (V) is used in equation (1) following the appropriate sign conventions. The first cosine term in equation (2) accounts for the satellite elevation angle modulated by the aircraft declination, so that when these angles are the same the frequency offset is at an absolute maximum as the aircraft is proceeding directly to the satellite or away from it. Likewise, for the alignment of the satellite and aircraft headings in the second cosine term. The two equations represent the model we used to calculate expected uncompensated BFOs for various combinations of aircraft track angle (θ_a) and declination angle (θ_d). Other parameters were fixed as listed in Table 1.

Table 1 Ancillary parameters for the BFO calculations.

Parameter	Description	Value
Inmarsat Satellite Location [2]	Ground projected location of the Inmarsat Satellite at 00:19 UTC	0.5°N, 64.475°E
Inmarsat Satellite Elevation [4]	Elevation angle from the aircraft location to the satellite	38.8°

Aircraft Location and heading at 7th arc	Estimated by Ashton et al. (2015) [2]	Location: 34.7°S, 93.0°E Heading: 323.98° from North
Aircraft Location at 7th arc	According to the PL theory	Location: 33.0°S, 95.0°E Heading: 320.99°
Aircraft speed at 7th arc	In kph	829 kph [2]
First BFO at 7th arc: at 00:19:29 UTC [4]	Predicted for south track and observed	Predicted 260 Hz Observed 182 Hz
Second BFO at 7th arc: at 00:19:37 UTC [4]	Predicted for south track and observed	Predicted 260 Hz Observed -2 Hz

Our aim with the analyses was to investigate the change of BFO between the last two 7th arc communications. We had the choice of using the Ashton et al. (2014) [2] location (Table 1) or the PL theory location [6]. We chose the PL location since it is the focus of the analyses and the coincidence of the integer latitude and longitude crossing (33.0°S, 95.0°E) at the 7th arc seemed remarkable and was predicted by the PL theory as a waypoint (Figure 1).

The BFO error at the two times in Table 1represent the difference between predicted BFO for a frequency-compensated south track and measured SDU-frequency-compensated BFO. If the south track was correct, the SDU frequency compensation and predicted frequency compensation would match. In other words, a match of horizontal-motion-compensated BFOs would imply that the aircraft was indeed on a horizontal southerly track – as witnessed for arcs prior to the 7th arc. The 7th arc mismatch was interpreted by previous investigators as due to vertical motions not compensated by the SDU – leading to the high-speed descent conclusion [4]. By contrast, the PL theory suggests that the SDU was compensating for an eastward-veered track which would lead to a mismatch of frequency compensations between predicted and observed, in addition to any uncompensated vertical motions. It is this mismatch which we investigate using equations (1) and (2) to predict BFO errors expected between the south track and an assumed eastward-veered track (with positive values implying the aircraft was tracking more rapidly away from the satellite).

Results

For a level flight (no declination), the BFO difference between the south track (180° track) and other track angles are shown in Figure 2. At the south track reference, the difference is zero and increases as the track veers eastward towards angles smaller than 180°. Westward veering would lead to BFO changes of the wrong sign (increasing towards the satellite), and hence discounted.

The 80 Hz dashed line marks the approximate location of the mismatch at the first 7th arc communication (80 Hz = Predicted 260 Hz – Observed approximate 180 Hz). The mismatch would require a veering eastward of less than 8° from the south track, and it is in the right direction. This small angle change suggests also that the aircraft may have started to veer from a southerly track just before the first of the communications at the 7th arc. Implying that the path from the 6th arc to that point is less veered than suggested by the general PL path in Figure 1.

The second communication mismatch was nearly 260 Hz and the maximum veering (where the aircraft track is aligned to the satellite direction but moving away from the satellite) occurs at about 141° heading giving a value of 220 Hz. Implying that during the 8 seconds between communications, the aircraft would need to veer 39 degrees or at a rate of 4.875 degrees per second – compared to nominal aircraft turning rates of about 3 degrees per second.

Even though the bulk of the BFO mismatch is explainable, a significant amount (40 Hz) is not explainable by a veering model alone. Note that the heading required for maximum BFO is closely aligned coincidentally with the bearing to the satellite as noted in Figure 1. The totality of the required veering from the 6th arc is well matched in explaining much of the nominal BFO change.

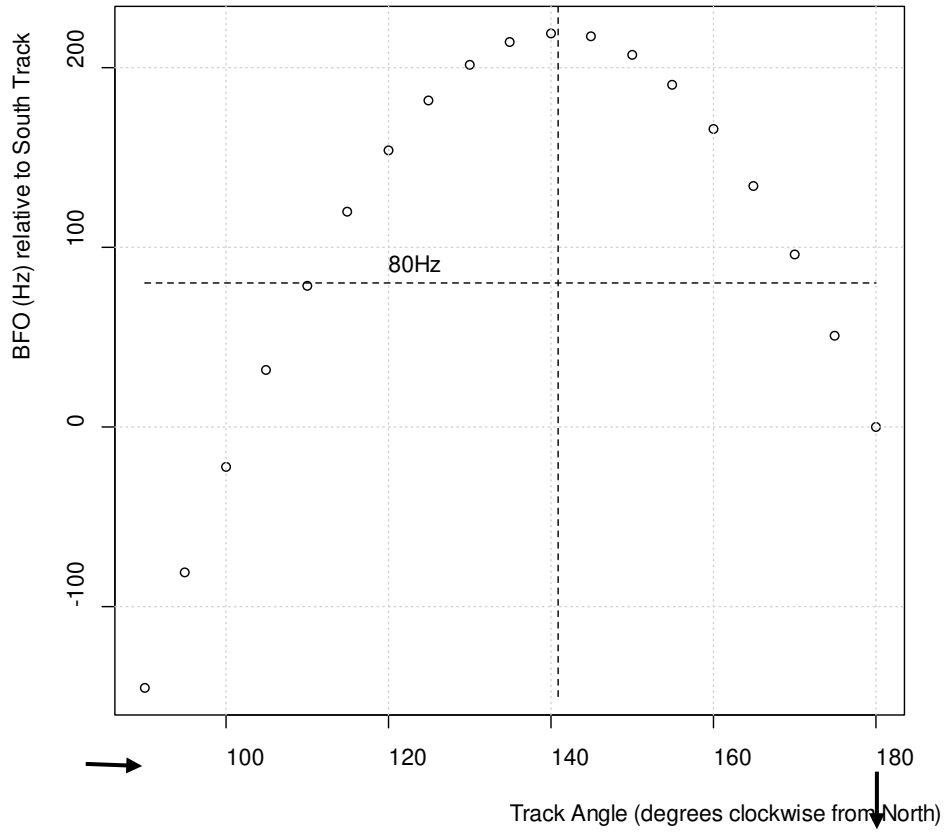

Figure 2 Variation of BFO (Hz) relative to a south track (180° track) with track angle measured in degrees clockwise from North. The dashed vertical line marks the approximate track which aligns with the aircraft to satellite direction. Note the directionality of the BFO change is such that if the aircraft is moving faster away from the satellite (as it will when it veers towards 141° heading), the SDU will compensate for the reducing frequency. So, a positive error as displayed means the error is defined as Predicted (BFO at 180°) – Measured (BFO at Track Angle).

For the indicated track range, the rate of decline of BFO with track angle as shown in Figure 3 is greatest at 180°, and zero when the track is aligned with the direction to the satellite. In other words, eastward veering produces the greatest BFO change rate at the south track, and the change with track angle is minimal when the track is aligned with the satellite direction. At the south track, one degree of track veering to the east, with no up-down motion, produces 10 Hz BFO decrease – a change that requires 588 fpm downward motion according to Holland's model.

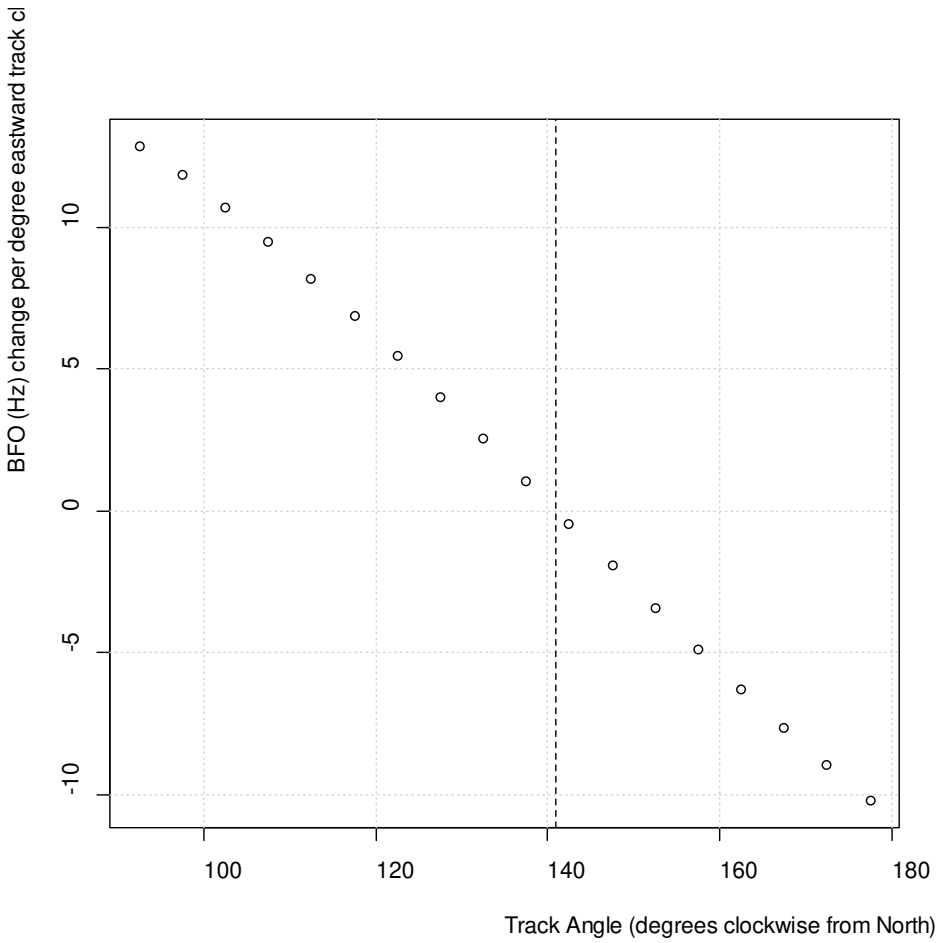

Figure 3 Variation of BFO change per degree of track angle change. The dashed vertical line marks the approximate track which aligns with the aircraft to satellite direction.

With declination included the range of BFO variation with track angle and declination angles are as contoured in Figure 4. For reference, the predicted 10,800 fpm high-speed descent of Holland corresponds to about 13.78° declination in Figure 2, with a maximum BFO mismatch of over 350 Hz explainable – compared to about 184 Hz for the up-down Holland model. The 260 Hz mismatch is now explainable using the approximate 250 Hz contour in Figure 4, which suggests a minimum declination required of about 3°. The contour displays the balance between veering and declination required to achieve a BFO mismatch. This angle is within normal aircraft descent angles near the satellite-aligned track, and achievable within the 8 second window. The minimum declination required also suggests that the aircraft was descending at the last signal.

At the south track, changes are near-maximal with veering and declination (Figure 4), whereas at the satellite-aligned track, declination is mainly responsible for changes. Of interest to note is that the veering to an easterly track was not achieved by the time of the second communication, implying that, if our interpretations are correct, the aircraft was still veering towards the final east track. The sensitivity to track change is also minimal at about 141° as shown in Figure 3, implying that the estimate of track angle at this point is not highly sensitive to BFO change. But there is high sensitivity in the opposite direction as the track veers further eastward, but we are unable to resolve this due to the lack of communications beyond the 7th arc.

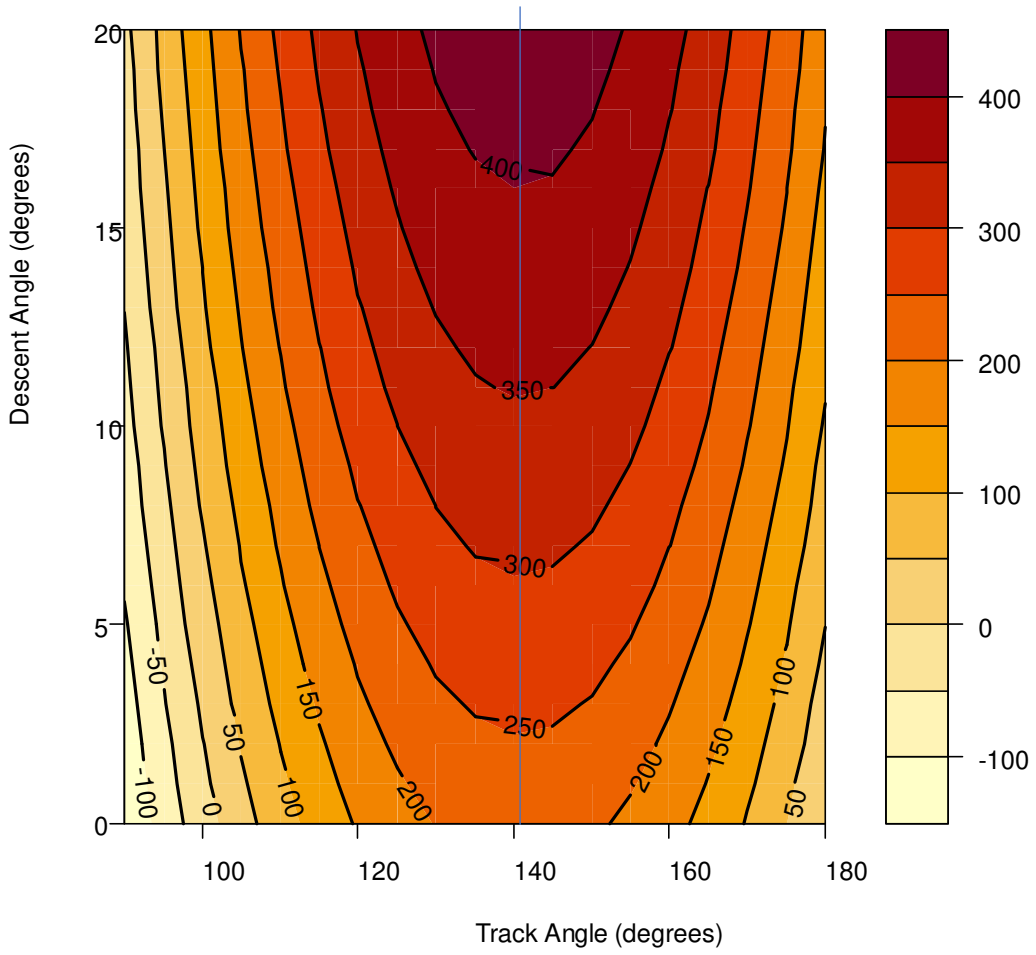

Figure 4 Contoured variation of BFO (Hz) with track angle and declination angle. The vertical line marks the approximate track which aligns with the aircraft to satellite direction.

Discussion

Brilliant past technical analyses of complex BFO changes deciphered from satellite and phone communications provided much needed clarification of MH370's southerly track to the southern Indian Ocean up to the 6th arc. However, later analyses of perplexing added BFO changes at the last two communications were apparently resolved through uncompensated up-down motions as there was no reason to assume a change from the fuel-starvation-theory southerly track. The south track was extrapolated to the 7th arc and vertical velocity shifts required to explain the remaining BFO changes led to the high-speed descent scenario and an assumed unobserved violent impact. Instead, the damage found on the recovered flaperon (and the limited amount of debris) was convincingly demonstrated, by finite-element simulations conducted by the MH370-Captio group [11], as well as careful detailed expert investigations by Vance [9], as most likely due to a piloted glided landing, and incompatible with a high-speed nosedive that would have crumpled the leading-edge nose [11] and obliterated the plane into many pieces within the blink of an eye [9].

Whilst the glided landing scenario is now more plausible, the notion that MH370 was in a vertical high-speed dive at the 7th arc is still prevalent in public media [12] and in acrimonius criticism of alternative theories. A glided landing at the 7th arc is also clearly at odds with the suggested uncontrolled high-speed descent demanded to explain the BFO changes. The failure of two comprehensive searches predicated on the theory of fuel-starvation-at-the-7th-arc has stymied plans for another search. The final location of MH370 must also explain all plausible evidence, one of which is the BFO interpretations at the 7th arc. No theory has succeeded in meeting these requirements till now.

Despite the reconciliation of all other evidence by the PL theory there were no previous analyses to support the predictions of this theory that MH370 veered eastward at the 7th arc to follow an easterly track at 33°S latitude. The theory is specific about when such a change should occur in relation to the JORN network range. The observation that such a change could be underway at 33°S, 95°E, which is on the 7th arc is either a remarkable coincidence, or a planned waypoint for a track change as predicted by the PL theory. These observations and the failures of the fuel-starvation theory led us to re-examine interpretations of the final BFOs from MH370.

Results of our veering model suggests that the first BFO is explainable with less than 8° eastward veering from the south track at the 7th arc where BFO changes are sensitive to track change. Reconciliation of the second BFO required a track change to about 141° heading (approximate south-eastward track), a declination angle of at least 3°, but with an aggressive turn rate. These parameters seem more reasonable and plausible, than an unverified high-speed descent. This disparity (of a small veering change and declination versus high-speed descent) is understandable as the Doppler Shift is due to the speed change in the direction of the satellite, regardless of whether it is from horizontal veering of an aircraft flying at high speed, or a presumed sudden diving down at high speed (whilst also maintaining its south track). But the two different interpretations give two very different and incompatible landing scenarios.

To resolve this, we suggest respectfully that past investigators forgot that the extrapolation of the BFO curve along the south track to the 7th arc implied that the plane was implicitly required to be flying south at its cruise speed; in addition to undergoing the high-speed vertical dive, with no fuel left. However, the official narrative for this scenario in media stories, which is inconsistent with the mathematics, is that the plane simply ran out of fuel and accelerated into a high-speed vertical dive. The mathematical narrative for this scenario is that the plane ran out of fuel but was still able to magically continue flying at cruise speed along the south track, and within 8 seconds also experienced an added (to the cruise speed) high-speed vertical dive of about 10,800 fpm. The two narratives are incompatible, implausible, and disappointing. The first does not explain the BFO changes, and the latter is clearly impossible. It's an honest mistake, that we should not unduly dwell upon, brought about by the complex assumptions in interpreting the BFO discrepancies. If we are to resume the search for MH370 we need to stop the misinformation on what happened at the second arc and show respect to investigators such as Vance [9] who have articulated a piloted glided landing scenario based on well-founded objective investigations of debris evidence.

Whilst details of the tracks predicted for the 6th arc and the first of the communications at the 7th arc aren't precise, results of the veering analyses can explain the 7th arc BFO changes. The analyses suggest that the turn to an easterly track was not complete and changes to the aircraft's flight were still underway. The overall changes in flight track align closely with the general predictions of the PL theory. We also note that the short disturbance to power to the SDU after the 6th arc (Hypothesis 2) may have been from preparation for the descent, predicted by the analyses to be underway by the end of the 7th arc. Whereas the fuel-starvation theory

assumes the power-up was from engines flaming out and the cold SDU restarting sometime later – the extreme Hypothesis 1 scenario.

Simply put, what we have demonstrated is that the Doppler Shifts observed at the 7th arc were not from implausible extreme combined vertical and horizontal motions, but were instead due to plausible horizontal veering of an aircraft travelling at high speed. Past analyses were hamstrung by wayward interpretations of complex analyses, by the south track fuel-starvation theory, and understandable lack of consideration of alternate scenarios which could have aided in optimizing the search strategy [13]. Still, given the uncertainties and disappointments to date in finding MH370, we caution that this and other predictions of the PL theory need to be subjected to further critical evaluation despite the theory being the only one that reconciles most if not all plausible evidence, which now includes the BFO changes at the 7th arc. This study should however be judged by its merits in explaining the BFO signals at the 7th arc.

Conclusions

The baffling BFO changes at the final two communications from MH370 at the 7th arc are more plausibly due to the aircraft veering eastward and in a controlled descent, as opposed to an uncontrolled high-speed vertical dive. These interpretations were predicted by the Penang Longitude theory which also predicts that MH370 proceeded to a precise piloted glide landing where the 33°S latitude intersects the longitude of Penang at an ultra-deep hole. These revised interpretations refute the high-speed descent demanded by the fuel-starvation southerly-track theory as that conclusion was based on incorrect interpretations of the BFO assumptions and analyses. We can state with greater certainty that MH370 veered eastward and was descending after its last known communication.

Acknowledgements

Many keen scientists indirectly contributed to this study which would not have been possible without their remarkable technical detective work on diverse aspects of finding MH370. We are all deeply indebted to all the brave folks who took part in the search for MH370 in one of the most inhospitable, but ecologically unique, ocean environments on the planet. Despite not finding MH370 your work has contributed to excluding vast areas of the ocean from further searches, and hopefully restored faith in humanity's kindness to those who lost loved ones. I am particularly indebted to Larry Vance for his independent expert thorough investigations of debris damage; a quiet voice of reason lost in the cacophony of contrived misinformation.

1. ATSB. *The Operational Search for MH370*; Canberra. Australia., 2017; p. 440pp.
2. Ashton, C.; Shuster Bruce, A.; Colledge, G.; Dickinson, M. The Search for MH370. *Journal of Navigation* **2014**, *68*, 1-22, doi:10.1017/s037346331400068x.
3. Davey, S.; Gordon, N.; Holland, I.; Rutten, M.; Williams, J. *Bayesian Methods in the Search for MH370*; Springer Singapore: 2016.
4. Holland, I.D. MH370 burst frequency offset analysis and implications on descent rate at end of flight. *IEEE Aerospace and Electronic Systems Magazine* **2018**, *33*, 24-33, doi:10.1109/maes.2018.170048.
5. Griffin, D.A.; Oke, P.R.; Jones, E.M. *The search for MH370 and ocean surface drift – Part II*; CSIRO Oceans and Atmosphere: Hobart. Australia, 2017; p. 26pp.

6. Lyne, V.; Lyne, M. Unravelled cryptic pathways of MH370-goodbye and travel-path secrecy reveals landing details and precise location. *Researchgate* **2021**, 36pp., doi:10.13140/RG.2.2.12116.94084/1.
7. Butler, D. Sound clue in hunt for MH370. *Nature* **2014**, *510*, 199-200.
8. Kadri, U. Effect of sea-bottom elasticity on the propagation of acoustic-gravity waves from impacting objects. *Sci Rep* **2019**, *9*, 912, doi:10.1038/s41598-018-37626-z.
9. Vance, L. *MH370 Mystery Solved*; Group of Three Publishing: 2018.
10. Wikipedia. Jindalee Operational Radar Network. Available online: https://en.wikipedia.org/wiki/Jindalee_Operational_Radar_Network (accessed on March 2021).
11. MH370-Captio. MH370: Was Air Traffic Control deliberately misled? Available online: https://www.youtube.com/watch?v=Qk1CxO9XGyQ (accessed on
12. Gregersen, E. Malaysia Airlines flight 370 disappearance. *https://www.britannica.com/event/Malaysia-Airlines-flight-370-disappearance* **2021**.
13. Wikipedia. Scenario optimization. Available online: https://en.wikipedia.org/wiki/Scenario_optimization (accessed on October 2021).

Malaysia Airlines Flight MH370: Water Entry of an Airliner

Goong Chen, Cong Gu, Philip J. Morris, Eric G. Paterson, Alexey Sergeev, Yi-Ching Wang, and Tomasz Wierzbicki

On March 8, 2014 Malaysia Airlines Flight MH370 disappeared less than an hour after take-off on a flight from Kuala Lumpur to Beijing. The Boeing 777-200ER carried twelve crew members and 227 passengers. On March 24 the Malaysian Prime Minister announced that "It is therefore with deep sadness and regret that I must inform you that …Flight MH370 ended in the Southern Indian Ocean." Though the exact fate of Flight MH370 remains undetermined, the available evidence indicates a crash into the ocean. However, disturbing as this is, not all emergency water landings, referred to as *"ditching"* when they are controlled, end in tragedy. In the "Miracle on the Hudson," on January 15, 2009, Capt. Chelsey B. "Sully" Sullenberger and his crew successfully ditched US Airways Flight 1549, an Airbus A320-200, in the Hudson River after a loss of power due to a bird strike on take-off from La Guardia Airport. There was no loss of life.

Figure 1 and the video animation referenced on the second page of this article show our "representation" of a commercial airliner, a Boeing 777 model, plunging into the ocean. (See our commentary in Box 1 in section "The Water Entry Problem Revisited".) Such simulations can help to understand the physical mechanisms at work and also to improve passenger safety. But these are highly challenging simulations that require the cooperation of engineers, mathematicians and computational scientists. Any scientific investigation of the mishap, apart from human factors of foul play and conspiracy, must consider factors of an *engineering nature*, such as machine and instrumentation breakdown, midair explosion, weather, navigation, etc. But this should not prevent mathematicians' curiosity—and our fascination with airplanes since childhood—from entering the fray to add and contribute something valuable regarding this investigation and recovery effort. The fact is, mathematics is closely intertwined with engineering and is not detached from the "real world" as some people may think. The statement made by the Malaysian Prime Minister that Flight MH370 "ended" in the Southern Indian Ocean was based on the assessment by the British company

Goong Chen is professor of mathematics at Texas A&M University (TAMU) and Texas A&M University at Qatar (TAMUQ). He is also a member of the Institute for Quantum Science and Engineering at TAMU. His email address is gchen@math.tamu.edu.

Cong Gu is a PhD student in the mathematics department of TAMU. His email address is gucong@math.tamu.edu.

Philip J. Morris is Boeing/AD Welliver Professor of Aerospace Engineering at The Pennsylvania State University. His email address is pjm@psu.edu.

DOI: http://dx.doi.org/10.1090/noti1236

Eric G. Paterson is Rolls Royce Commonwealth Professor of Marine Propulsion and department head of Aerospace and Ocean Engineering at Virginia Tech. His email address is egp@vt.edu.

Alexey Sergeev is postdoctoral fellow at the Qatar Environment and Energy Research Institute in Doha, Qatar. His email address is asergeev@asergeev.com.

Yi-Ching Wang is a PhD student in the mathematics department of TAMU. Her email address is ycwang@math.tamu.edu.

Tomasz Wierzbicki is professor of applied mechanics and Director of Impact and Crashworthiness Laboratory at MIT. His email address is wierz@mit.edu.

Page 879 of 1738

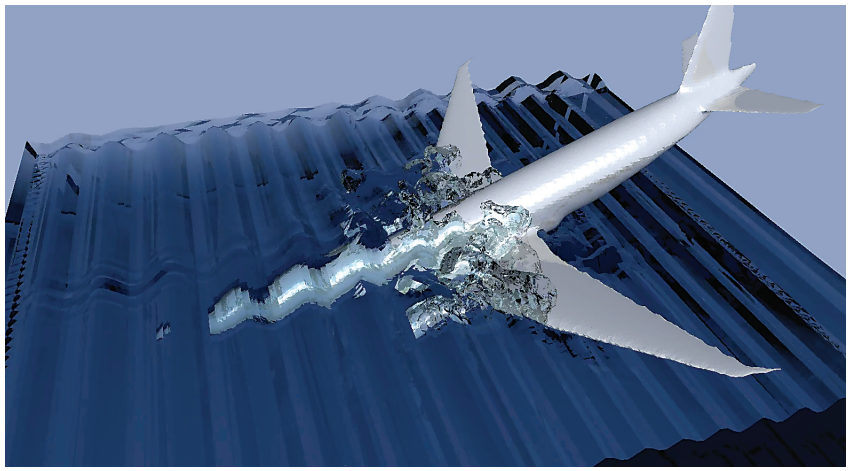

Figure 1. The aircraft is a Boeing 777 model flying into the ocean at the speed of 70m/sec, with pitch angle = −20°, at time t = 0.36 sec. A volume-of-fluid (VOF) scheme in OpenFOAM ([ope]) is used to simulate the two-phase flow for the fluid-aircraft body interaction. Please also use the link `https://www.dropbox.com/s/pbjhrovlqrqiizm/smooth-cin40.avi` to view the corresponding video animation of the dynamic motion.

Inmarsat. An article articulating how the radar signal backtracking made by Inmarsat works was published in SIAM News in [Zwe14], where John Zweck of the Math Department of the University of Texas–Dallas argued in support of Inmarsat by using the Doppler frequency shift, time and locations of ping, trigonometry and other mathematical methods, and MATLAB® software. Nevertheless, Inmarsat's radar tracking methodology and data analysis have not yet convinced everybody that they are ironclad; see some counter arguments by David Finkleman in [Fin14], for example. (Dr. Finkleman is Director of Studies and Analysis, and Senior Scientist, North American Aerospace Defense Command and US Space Command, at Peterson Air Force Base, Colorado.)

We discuss this air incident from a mathematical as well as an interdisciplinary perspective. We show how computational mathematics and mechanics can help us understand the physical nature of an aircraft emergency water landing, how to model and compute it, and how this knowledge is helping safe civil aviation and other aerospace-related undertakings. This kind of problems has become quite typical for the work of a mathematician as part of an interdisciplinary team in industry or government labs.

The problem under consideration is *dynamic* in nature and is best viewed with the aid of *video animation*. We encourage the reader to see such animations through the various URLs provided in the article by pasting and clicking them, using the online version of the paper in the *Notices* [not].

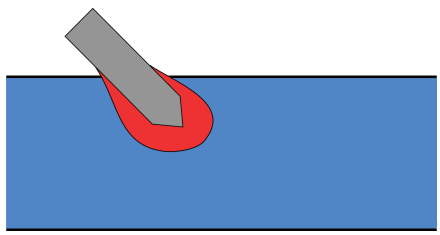

Figure 2. Von Karman's idea of "added mass" for the water entry problem, which is an idealization and simplification. Here the red region represents "added mass." This is the mass moving together with the mass of the wedge projectile. The portion of the (red) added mass lying above the still water surface is called the "pile up."

The Water Entry Problem Revisited

The *water entry problem* is a classical problem in applied mathematics and fluid dynamics. It considers the dynamic motion of an object upon its entry into the water. The problem was motivated by several applications: the landing of a hydroplane, the entry into water of a rocket or the Apollo module returning from space, and the ditching or crashing of aircraft.

A major contribution to this field was made by the celebrated applied mathematician and fluid dynamicist Theodore von Karman (1881–1963). He developed the idea of *"added mass"* (a mass of the fluid that is co-moving with the body) to study the problem [vK29]; see Figure 2. Von Karman inferred that the impact force on the body is related to the instantaneous change of total momentum of the body with its own mass but with an extra

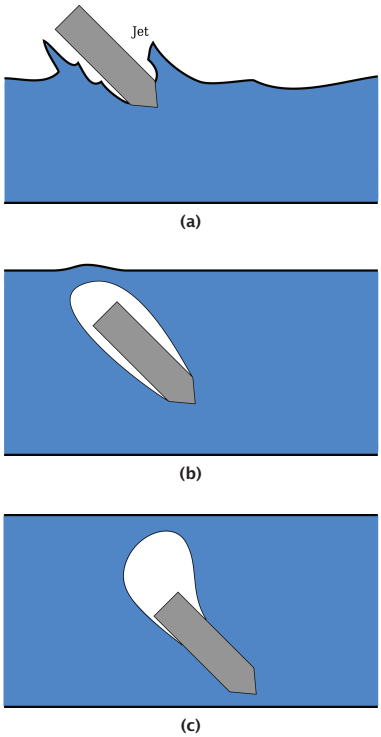

Figure 3. The several phases of a projectile entering water according to Mackey [Mac79]: (a) a cavity of air opens; (b) a cavity of air pocket encloses the projectile when it is totally submerged; and (c) the cavity begins to be detached from the projectile, leaving it totally surrounded by water. Some water vapor may exist in the cavity, and cavitation usually happens. (Adapted from [Abr11, p. 060803-2])

mass augmented by the "added mass" of the fluid around the submerged portion of the body. That is,

$$(1)\quad \frac{d}{dt}\left[(M+m(t))\dot{\zeta}(t)\right] = Mg - F_B - F_C - F_D$$

(cf. [Abr11, eq.(2.3)])

where M =mass of the projectile, $m(t)$ = "added mass," F_B = buoyancy force, F_C = capillary force, F_D = steady-state drag force, and $\zeta(t)$ = depth of penetration into fluid.

We note that the precise value of added mass $m(t)$ is not known. For small time or submerged depth upon entry of the body into the water, von Karman estimated the added mass to be half that of a flat plate with the same area as the instantaneous *still* water-plane of the body. Wagner [Wag31] further improved von Karman's work by including the effect of the *pile up* of the water and by associating the added mass with the *wetted* water-plane. Further work such as [Fab57] took account of the submerged geometry for the estimation of the added mass. The analysis and results from these simple approaches are found to compare favorably with experiments for simple geometries such as a wedge or a cone. They also helped the designs of air-to-subsea anti-submarine missiles, for example.

On the mathematical side, papers studying the water entry problem for a two-dimensional (2D) wedge were written by Shiffman and Spencer [SS51] for a normal incidence problem, and by Garabedian [Gar53] for oblique incidence, for example. These papers treated the case of 2D incompressible, irrotational, inviscid flow by complex variables and potential theory and offered rigorous analysis.

A comprehensive survey of water entry problems (up to the year 2011) can be found in [Abr11], where 476 references are listed, and where a dozen more mathematical (-oriented) papers can also be found.

The splashing and piling up of water waves surrounding the submerged part of the aircraft are close to realism, as the motion of the free (water) surface is modeled and computed by the *volume-of-fluid method*. We have also used the *level-set method* and obtained similar graphical results. However, several other physical factors and phenomena have not been taken into account:

(1) The *deceleration* of the aircraft motion, as its speed is maintained at 70m/sec. In addition, in general, the presence of water will cause *deflection* of the flight path.
(2) At the speed of 70 m/sec, *structural fracture and disintegration* of aircraft are likely to occur.
(3) Hydrodynamic force, fluid buoyancy, and drag force have not been incorporated into the model.

Box 1. Commentary on the water-entering motion of aircraft as shown in Figure 1 and its video animation.

The contributions made by von Karman, Wagner, and others were truly remarkable, and they continue to be used today. However, the physics of water entry is far more complex to model than the idea of "added mass" alone. In reality, there are several phases of water entry that have been observed in experiments [Mac79]: (1) cavity-opening and jet splashing; (2) cavity-closing and formation of an air pocket; and (3) cavity-detachment and cavitation; see Figure 3. A good way to capture the rich physics is through state-of-the-art *computational fluid dynamics (CFD)*. The CFD approach will enable us to simulate water entry for *complex, general geometries* rather than the simplified ones

such as cones, cylinders, and wedges treated in the early era by encompassing (1) naturally into the two-phase fluid-structure interaction models.

Simulation of the Ditching/Crashing of an Aircraft into Water as a Two-Phase Fluid-Structure Interaction Problem

Aircraft crashworthiness and human survivability are of utmost concerns in any emergency landing situation. The earth is covered 71 percent by water, and many major airports are situated oceanside. Therefore, the Federal Aviation Administration (FAA) requires all aircraft to be furnished with life vests and the pilots be given water-landing guidlines and manuals.

Assume that an aircraft such as MH370 did not have a midair explosion. Then all available signs indicate that it crashed somewhere in the Indian Ocean. This is an aircraft water-entry problem. Our objective in this section is to conduct numerical simulations for several hypothetical scenarios using CFD.

For a representative Boeing 777 aircraft, we use the values of parameters as given in Table 2.

The underpinning subject of this study is *continuum mechanics*, including the water-entry problem first as *fluid-structure interaction with a free fluid-gas interface* and the subsequent impact and structural failure analysis. Here, water and air are modeled as compressible flows using the Navier-Stokes equations; cf. Box 2. Our mathematical model is similar to that in Guo et al. [GLQW13].

Table 1. Parameter values for Boeing 777 used in CFD calculations.

Total weight	1.8×10^5 kg
Wing span	60.9 m
Fuselage cross section	29.6 m^2
Length	63.7 m
Roll Moment of Inertia	1.06×10^7 kg m^2
Pitch Moment of Inertia	2.37×10^7 kg m^2
Yaw Moment of Inertia	3.34×10^7 kg m^2

We are dealing with two fluids: air and water. Depending on the operating conditions (speed and altitude), we can regard air either as compressible or incompressible. For water, as a liquid, it is generally considered as *incompressible*. However, if we choose incompressibility as the model for water here, the CFD calculations will have *severe difficulty of convergence*. A likely cause is that, in water landing situations, local contact interface pressure can get *very high*, on the order of 10^6 Pascal, causing a compressed state of water. Therefore, we choose compressibility for both air and water as in [GLQW13].

Box 2. Modeling selections: compressible or incompressible?

The CFD software we have adopted here is *OpenFOAM*, which is open-source and is now widely used by industry and research communities. See an introductory article by several of us in [CXM+14]. In particular, we will be using `compressibleInterDyMFoam` for two-phase flow and RANS $k-\epsilon$ for *turbulence modeling*. (See some mathematical study on the $k-\epsilon$ turbulence modeling in [RL14, MP93], for example.) Computations were performed on the EOS supercomputer at Texas A&M University and the RAAD supercomputer at Texas A&M University at Qatar. For the computational work shown in the examples of this section, each run took one to several days on the campus supercomputers.

We assume that the aircraft is a *rigid body*. Except for the sample case shown in Figure 1, we did not include the under-wing engines in the Boeing 777 aircraft, with the understanding that the strut-mounted engine nacelles would likely be the first things to be torn off in a water-entry situation. (But, computationally, it is straightforward to include the engines in our CFD work as is shown in Figure 1.)

There are two distinct CFD features of this problem:

(a) Because of the *relative motion* between the aircraft and water, *dynamic mesh*, or a noninertial frame of reference, must be used. Here we have used a combination of `dynamicRefineFvMesh` and `dynamicMotionSolverFvMesh` in OpenFOAM for this purpose.

(b) The *free water surface* can be treated by using either the *volume of fluid method* (VOF), [HN81] the *level set method* [OS88, SSO94], a combination of these two methods [Son03], or the *cubic interpolated pseudoparticle method* [TNY85]. Because of the availability of the software for VOF in OpenFOAM, VOF is adopted here.

Table 2. Parameter values for fluid flow used in CFD calculations.

Atmospheric pressure	1×10^5 Pa
Lower bound for pressure	1×10^4 Pa
Kinematic viscosity of water	1×10^{-6} m^2/sec
Kinematic viscosity of air	1.589×10^{-5} m^2/sec
Water-air surface tension (γ)	0.07 N/m
Gravitational acceleration (g)	9.80665 m/sec^2
ρ_0 in Equation (6)	1000 kg/m^3
Compressibility of water (ψ_1 in Equation (6))	1×10^{-5} sec^2/m^2
Compressibility of air (ψ_2 in Equation (7))	1×10^{-5} sec^2/m^2
Constants in $k-\epsilon$ turbulence model	$C_\mu = 0.09, C_1 = 1.44, C_2 = 1.92, \sigma_\epsilon = 1.3$
Initial values for $k-\epsilon$ turbulence model	$k = 0.1$ m^2/sec^2, $\epsilon = 0.1$ m^2/sec^3
Initial aircraft speed relative to stationary water (V_0)	58 m/sec ($\approx$ 130 mph)

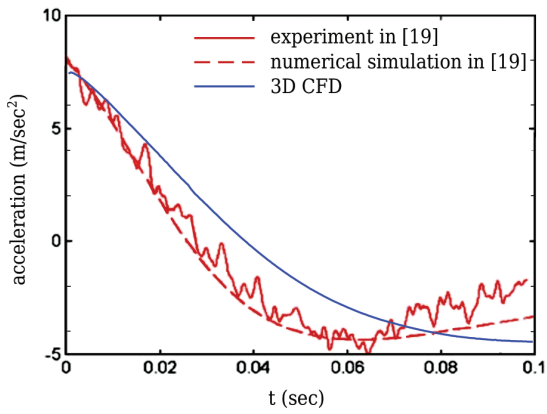

(a) deadrise angle is $\pi/4$, effective gravity is 8.0062 m/sec^2, mass of wedge is 13.522 kg, speed at water entry is 0.95623 m/sec.

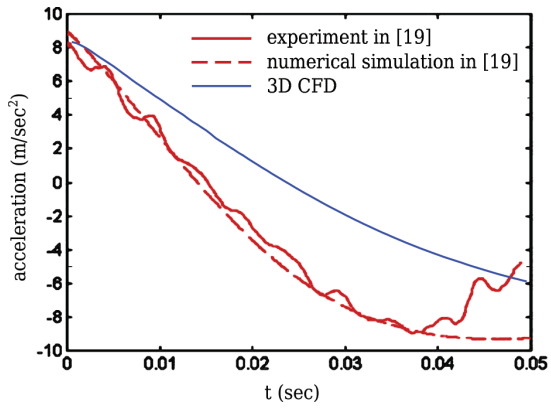

(b) deadrise angle is $\pi/4$, effective gravity is 8.9716 m/sec^2, mass of wedge is 30.188 kg, speed at water entry is 1.69673 m/sec.

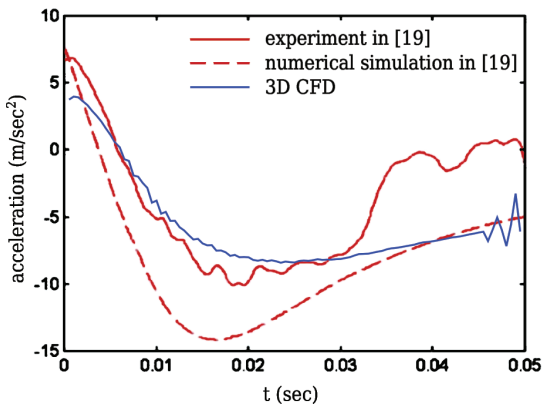

(c) deadrise angle is $\pi/9$, effective gravity is 7.8144 m/sec^2, mass of wedge is 12.952 kg, speed at water entry is 0.86165 m/sec.

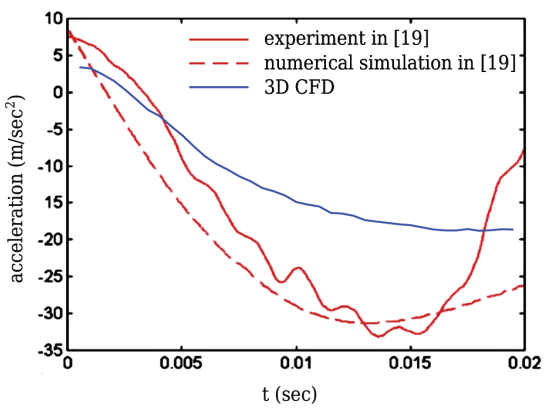

(d) deadrise angle is $\pi/9$, effective gravity is 8.6103 m/sec^2, mass of wedge is 29.618 kg, speed at water entry is 1.54405 m/sec.

Figure 4. Curves of acceleration versus time as benchmarks in comparisons with Wu et al. Graphs reprinted from [WSH04, p. 28], with permission from Elsevier. The curves obtained from experiment and numerical simulations are compared under different settings. The blue curves represent the data obtained by our computational methods in this paper.

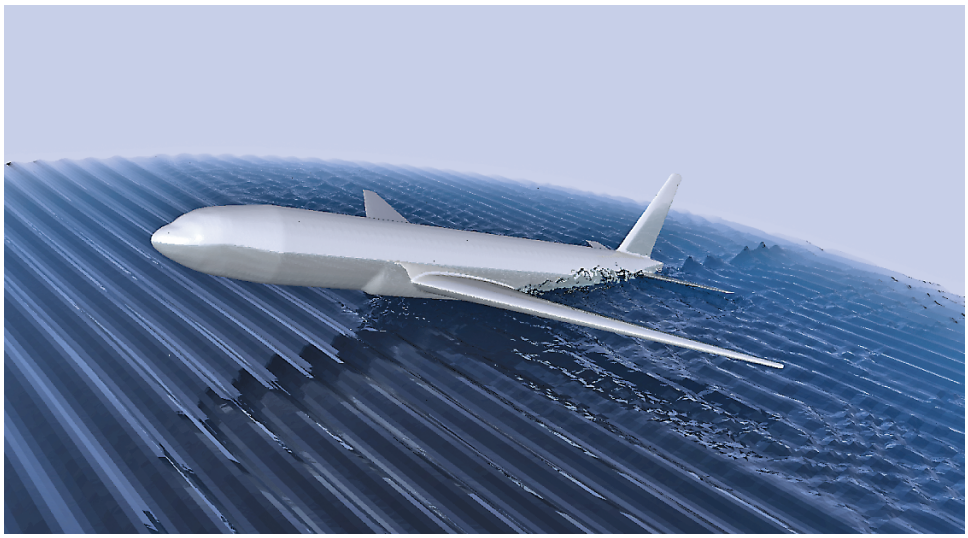

(a) gliding water entry

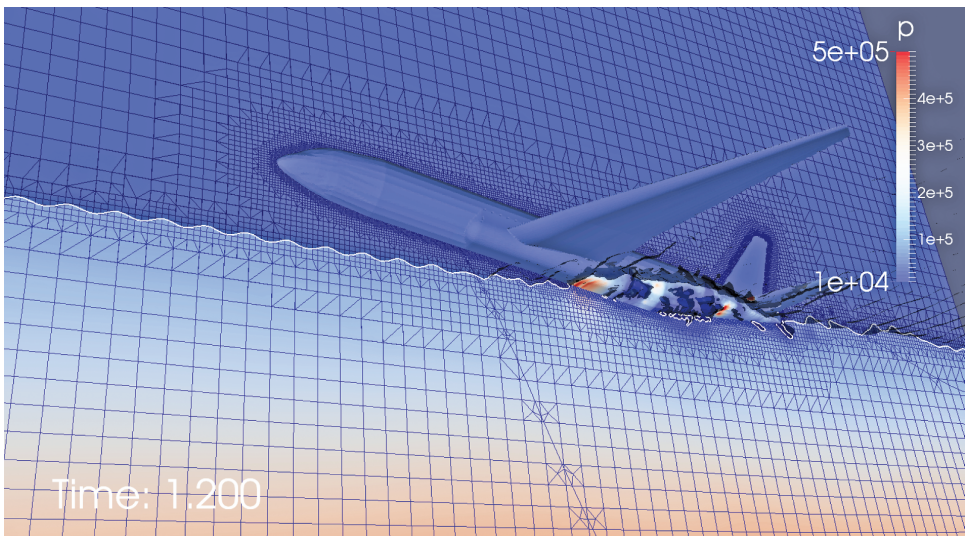

(b) pressure distribution and mesh

Figure 6. Pitch angle= 8°, angle of approach = 1°. This corresponds to Case 1; a video animation can be viewed at `https://www.dropbox.com/s/zpme04bmakien2h/comb8.mp4`. The animation has two parts: the first part shows the water flow pattern, while the second is intended to show the pressure distribution. (This is the same for all video animations corresponding to the remaining figures in this section.)

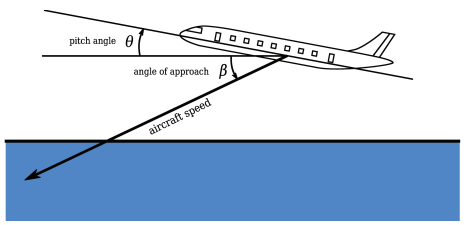

Figure 5. Angle θ here is the pitch angle signified in the computations of cases 1–5 and β is the angle of approach. The speed of the aircraft denotes the speed of its center of mass.

Equations for the volume of fluid two-phase problem are the following:

- Conservation of mass for each phase

$$\frac{\partial(\rho_i \alpha_i)}{\partial t} + \nabla \cdot (\rho_i \alpha_i \mathbf{u}) = 0, \tag{2}$$

where α_i, $i = 1, 2$, are volume fractions of each phase satisfying $\alpha_1 + \alpha_2 = 1$.

- Conservation of momentum

$$\frac{\partial(\rho \mathbf{u})}{\partial t} + \nabla \cdot (\rho \mathbf{u}\mathbf{u}) = -\nabla p + \nabla \cdot \boldsymbol{\mathcal{T}} + \rho \mathbf{g} + \gamma \kappa \nabla \alpha_1, \tag{3}$$

where $\boldsymbol{\mathcal{T}}$ is the deviatoric portion of the total stress tensor

$$\boldsymbol{\mathcal{T}} = \mu(\nabla \mathbf{u} + \nabla \mathbf{u}^{\intercal}) - \frac{2}{3}\mu \boldsymbol{\mathcal{I}} \nabla \cdot \mathbf{u} \tag{4}$$

with $\boldsymbol{\mathcal{I}}$ being the identity tensor. ρ and μ being effective density and viscosity fields for the mixture, respectively, γ being the surface tension, and κ being phase interface curvature

$$\kappa = -\nabla \cdot \left(\frac{\nabla \alpha_1}{|\nabla \alpha_1|} \right). \tag{5}$$

Note that the air-water interface condition is embedded in the $\nabla \alpha$ term in (3).

- Equation of State

$$\rho_1 = \rho_0 + \psi_1 p \quad \text{(for water)}, \tag{6}$$

$$\rho_2 = \psi_2 p \quad \text{(for air)}. \tag{7}$$

These equations model isothermal processes in air and water. The physical meaning of $\psi_j (j = 1, 2)$ here is $1/c_j^2$ where c_j is sound speed in the medium.

- Six degrees of freedom of motion

$$\boldsymbol{\sigma} = -p\boldsymbol{\mathcal{I}} + \boldsymbol{\mathcal{T}}, \tag{8}$$

$$\begin{aligned} \mathbf{F}(t) &= \text{force} = \int_{\partial\Omega(t)} \boldsymbol{\sigma} \hat{\mathbf{n}} \, dS, \\ \tau(t) &= \text{torque} = \int_{\partial\Omega(t)} \mathbf{r} \times \boldsymbol{\sigma} \hat{\mathbf{n}} \, dS. \end{aligned} \tag{9}$$

The exterior of the domain occupied by the aircraft is denoted as $\Omega(t)$ (depending on t due to aircraft motion), and $\partial\Omega(t)$ is its boundary. The boundary velocity $\mathbf{V}(\mathbf{x}, t)$ for $\mathbf{x} \in \partial\Omega(t)$ can be subsequently computed from (9) in rigid body dynamics.

- Moving boundary condition on aircraft skin

$$\mathbf{u}|_{\partial\Omega(t)} = \mathbf{V}(\mathbf{x}, t). \tag{10}$$

Note that at time $t = 0$, the velocity of the aircraft's center of mass is V_0 along various angles of approach; cf. Table 1. This, together with equations (2)-(9), constitute the complete initial-boundary value problem for the numerical computation. Various physical and computational parameter values are listed in Table 1.

Remark 1. Every CFD treatment needs to be validated. Why? CFD approaches have their roots in *theory, experiments, and computation*. Validation determines whether the computational results agree with physical reality—the experimental data. CFD codes must produce numerical results of desired accuracy so that they can be used with confidence. Here we use the experimental data available in [WSH04] for a simplified scenario, that is, a constrained free-falling "wedge" entering water. The wedge has only the vertical translational degree of freedom. The *acceleration(/deceleration)* of the wedge is measured throughout its impact with the water. The study in [WSH04] also employed a 2D potential flow model to study the problem numerically. In order to validate our CFD method, the setup for the experiment is replicated as a 3D mesh. Figure 4 shows the comparison of the acceleration time curves with a variety of parameters. (One of the varying parameters, the "deadrise angle", is defined as the angle formed between the angled side of the wedge with the horizon.) Although some differences of values are observed, our CFD simulation shows a strong qualitative match of the acceleration/deceleration curves. We also note that the numerical model in [WSH04] is a very simplified one, without the incorporation of several aero-hydrodynamic effects.

Aviation experts generally agree that *how the airliner enters the water determines its breakup*, which then yields major clues and directions of the search operations [syr]. Therefore, in the following, we provide *five scenarios* of water entry. In each case, we provide comments, schematics, snapshots, and a CFD animation. Each animation consists of two parts, with the first part showing visual effects and the second part showing pressure loading.

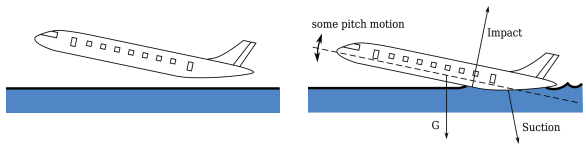

Figure 7. Schematics for the process of glided ditching. Major forces are illustrated. This corresponds to Case 1.

Case 1: pitch angle=8°, angle of approach=1°
This is what one might call *glided ditching*, similar to the US Airways Flight 1549 mentioned in the first section; see Figure 6 and the accompanying animation. The vertical component of the airline's velocity is found from (13) in the next section to be 1–2 m/sec. This is much smaller than the critical speed V_{cr} = 15–20 m/sec for structural failure in the next section and, thus, is good. See also Figure 7 for the interpretations of motion.

Case 2: pitch angle=−3°, angle of approach=3°
See Figure 8 and its animation. Here we see an interesting phenomenon; namely, even though the original pitch angle is *negative*, the aircraft will "bounce" on the water and make the pitch angle *positive*. See Figure 9. At the moment this happens, the bottom of the midsection (fuselage-water contact surface) of the aircraft undergoes high bending moment and surface pressure. This may cause the aircraft to break up in

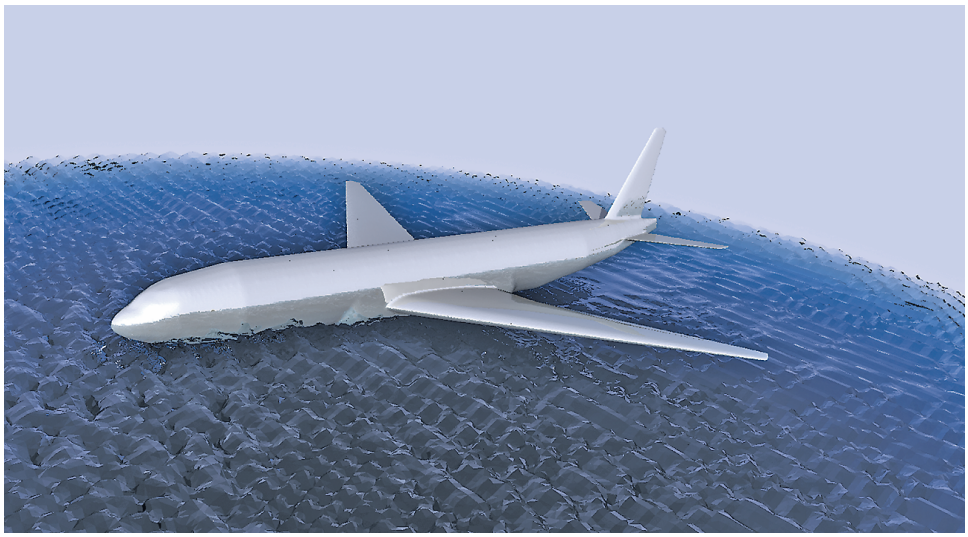

(a) gliding water entry (with a negative initial pitch)

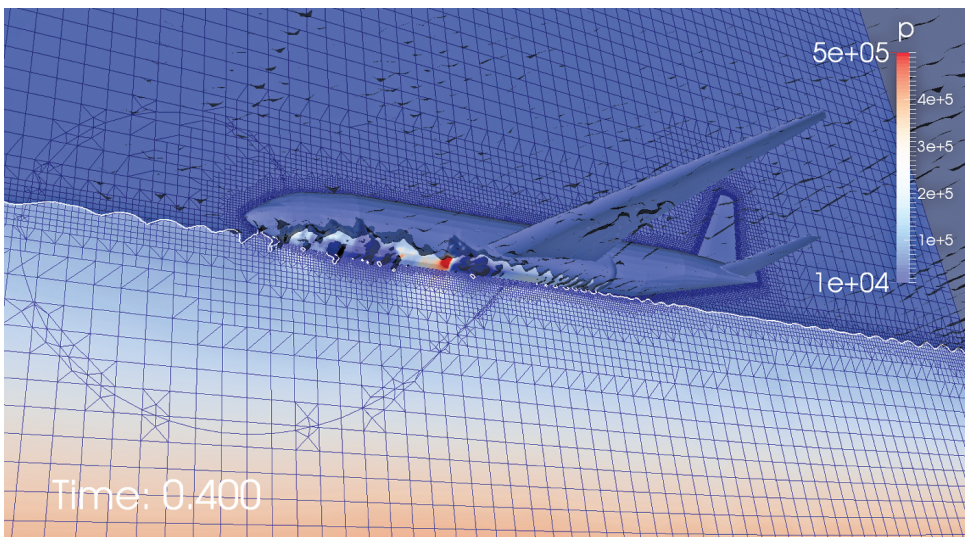

(b) pressure distribution and mesh

Figure 8. Pitch angle = −3°, angle of approach = 3°. This corresponds to Case 2. A video animation can be viewed at `https://www.dropbox.com/s/6zakw7js7kbcwed/comb-3.mp4`.

the middle section, a global failure to be described in the following section.

Case 3: pitch angle=−30°, angle of approach=30° See Figure 10 and its animation. Here we see that the aircraft nose is subject to high pressure throughout the time sequence. See also the schematics in Figure 11 in contrast to Figure 9. Once the wings enter the water, the leading edge of the wing is subject to high pressure loading up to 10^6 Pa.

Case 4: pitch angle = −90°, angle of approach = 93°

See Figure 12 and its animation. This is a *nose-dive* situation. Here we further assume that the ocean current flows from left to right at a velocity of 3 m/sec. Then, once the aircraft enters the water, the current gradually drives the aircraft toward the 5 o'clock direction. Eventually this could cause it to fall on the ocean floor *belly-up*. See Figure 13. Cf. more discussions in Box 3.

Case 5: pitch angle = −3° with *roll angle* = 20°, angle of approach=3°

See Figure 14 and its animation. Here, with a 20-degree roll, the left wing of the plane enters the water first. Almost inevitably, this would cause structural failure of the left wing. Read more in Box 4 about an air

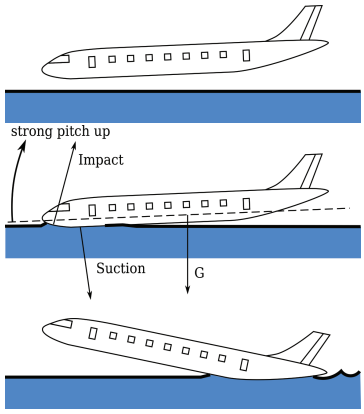

Figure 9. Schematics for the process of ditching with negative initial pitch. The plane is able to recover to the glided ditching attitude[1] similar to Figure 7. This corresponds to Case 2.

disaster on the seaside of Comoros Island, Africa.

Damage and Breakup

As described in the Introduction, not all emergency water landings end in disaster. The dramatic successful landing in the "Miracle on the Hudson" is such a case. The fact that no lives were lost is a testament to the experience and fast thinking under pressure of the captain and crew. The aircraft had a hole ripped open but was otherwise structurally virtually intact. The speed of the aircraft at ditching was estimated to be 150 mph (240 km/hr or 67 m/sec). It was deemed by NTSB as "the most successful ditching in aviation history." [23]

In addition to the Comoros Island air disaster in Box 4, we mention another ditching effort whose outcome was not as fortunate as the US Airways flight 1549. On August 6, 2005, a Tuninter Airlines Flight 1153 ATR-72 aircraft, flying from Bari International Airport, Bari, Italy, to Djerba-Zarzis Airport, in Djerba, Tunisia, ran out of fuel and ditched into the Mediterranean 43 km northeast of Palermo, Italy. Upon impact, the aircraft broke up into three pieces. Sixteen persons out of the thirty nine passengers and crew died. Eight of the deaths were actually attributed to drowning after the bodily injuries from impact.

In the numerical simulations provided in the preceding section, we have not included the effects of *rupture and structural disintegration*. But they are almost certain to happen upon the entry of the aircraft into water when the speed is sufficiently high. This happened even in the "Miracle on the Hudson" case with smooth gliding. The study of impact damage and breakup belongs to a field called *impact engineering*, which is based on the *plasticity* and *fracture* properties of solids that are totally different from the fluid dynamics issues we have been discussing up to this point.

Due to the limited scope of this article, we can't delve too much into the study of impact effects. Nevertheless, we can use another famous example, the disaster of the Space Shuttle Challenger, to understand what may happen, based on the analysis of one of the coauthors (Wierzbicki) in [WY86b, WY86a].

If an aircraft stalls in a climb, or if any control surfaces—ailerons, rudder, or stabilizers—malfunction, or if it runs out of fuel and the autopilot stops working (while the pilots are incapacitated or if the action is deliberate), it can fall into a steep nose-dive or even vertical drop (our Case 4 here).

What happens upon water-entry? Here, we directly quote [syr]:

"…The wings and tail would be torn away and the fuselage could reach a depth of 30 meters or 40 meters within seconds, then sink without resurfacing. Wing pieces and other heavy debris would descend soon afterward.

Whether buoyant debris from the passenger cabin—things like foam seat cushions, seatback tables and plastic drinking water bottles—would bob up to the surface would depend on whether the fuselage ruptured on impact, and how bad the damage was.

"It may have gone in almost complete somehow, and not left much on the surface," said Jason Middleton, an aviation professor at Australia's University of New South Wales…."

This may well offer a powerful clue as to why, so frustratingly, none of the debris of MH370 has been found so far.

Box 3. Does nose-dive have anything to do with the lack of debris?

The airframe of the Space Shuttle Challenger, an assemblage of ring and stringer-stiffened panels, was constructed essentially like a wide-body Boeing 747 airliner. This in turn is similar to a wide-body aircraft such as the example Boeing 777 under discussion here. Thus, we expect that much of the material and structural failure analysis performed in [WY86b, WY86a] for Challenger continues to hold.

There is a distinction between the following:

(i) *global failure* mode of fuselage, caused by *large contact forces* between water and structure;

(ii) *local failure* mode due to *excessive pressure*.

Both such contact forces and pressure vary spatially and temporally. They are obtained from the CFD part of the solution in the preceding section and used to assess the damage. In the

[1] *Note: "ditching attitude" is an academic term.*

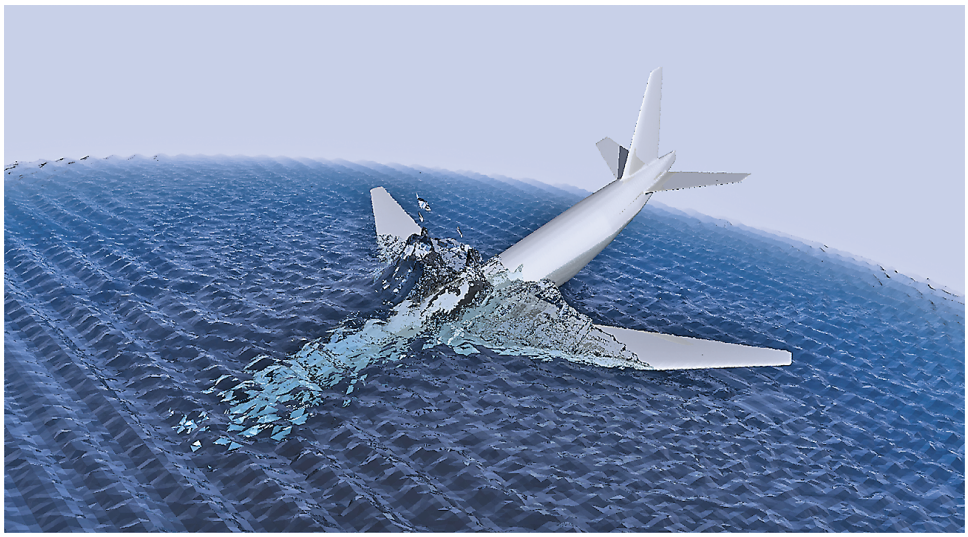

(a) diving water entry

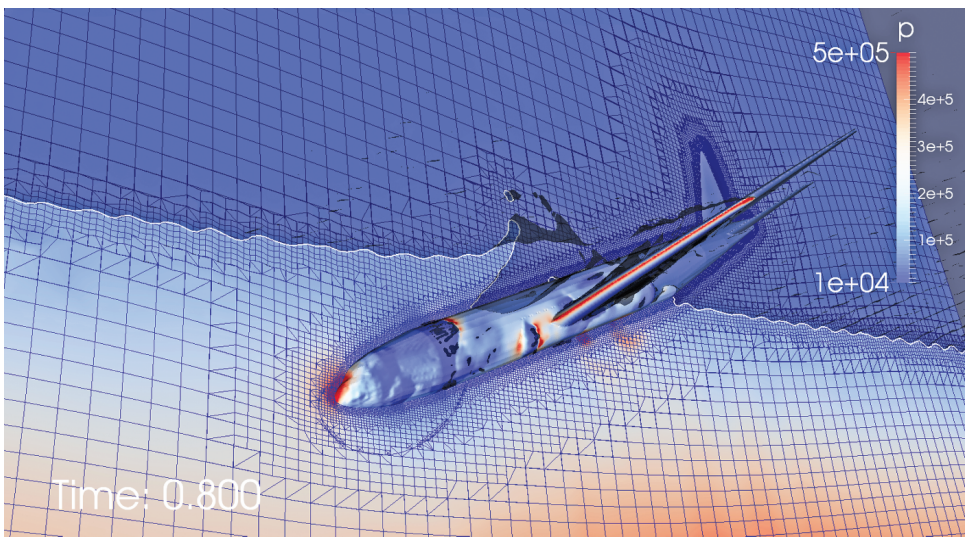

(b) pressure distribution and mesh

Figure 10. Pitch angle = −30°, angle of approach = 30°. This corresponds to Case 3. A video animation can be viewed at `https://www.dropbox.com/s/8iyj9xws4d90avk/comb-30.mp4`

analysis of global failure, simple structural models of *beams and rods* are used for the fuselage. In what follows, we give a quick review of how to study structural breakup upon impact, but defer the more technical study to a sequel.

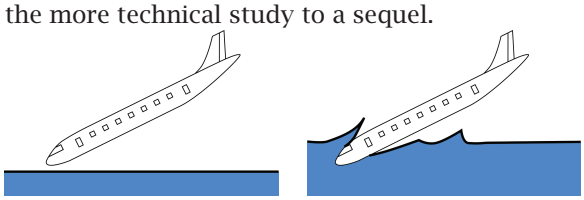

Figure 11. The pitch angle is too negative to recover to the glided ditching attitude. The plane's nose dives into the water with little bouncing motion. This corresponds to Case 3.

A flying aircraft was modeled in [WY86b] as a *free-free beam* with known spatial and temporal variation of external loading, where the distribution of bending moments can be uniquely found from the equations of dynamic equilibrium. Thence, the *maximum cross-sectional bending moment* can be compared with the fully plastic bending capacity of the fuselage. This will indicate the *onset* of structural collapse and break up.

The local failure mode is composed of tearing of fuselage skin as well as tensile and shear rupture of the system of stringers and ring frames; cf. Figure 15. Depending on the impact velocity, the local failure can involve progressive buckling and folding of the fuselage or fragmentation. Such

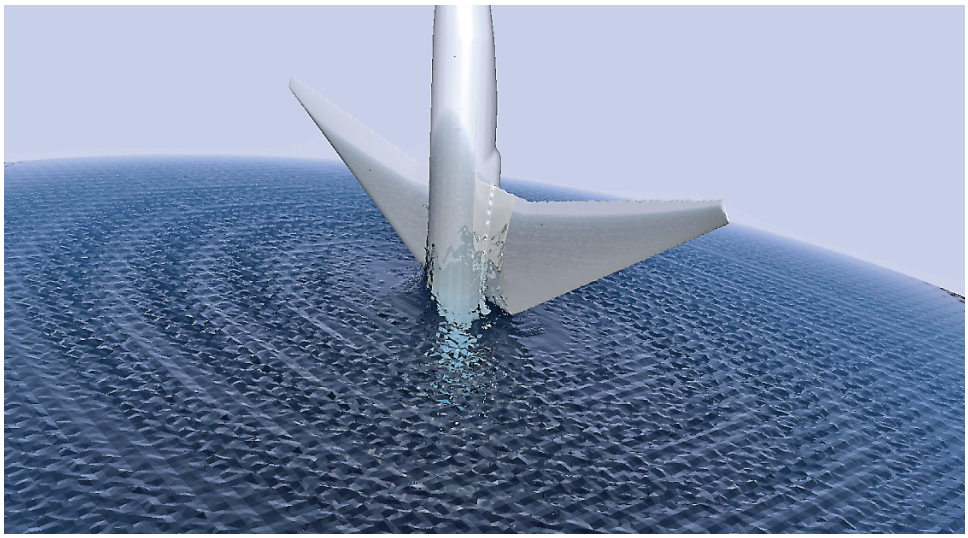

(a) nose-dive water entry

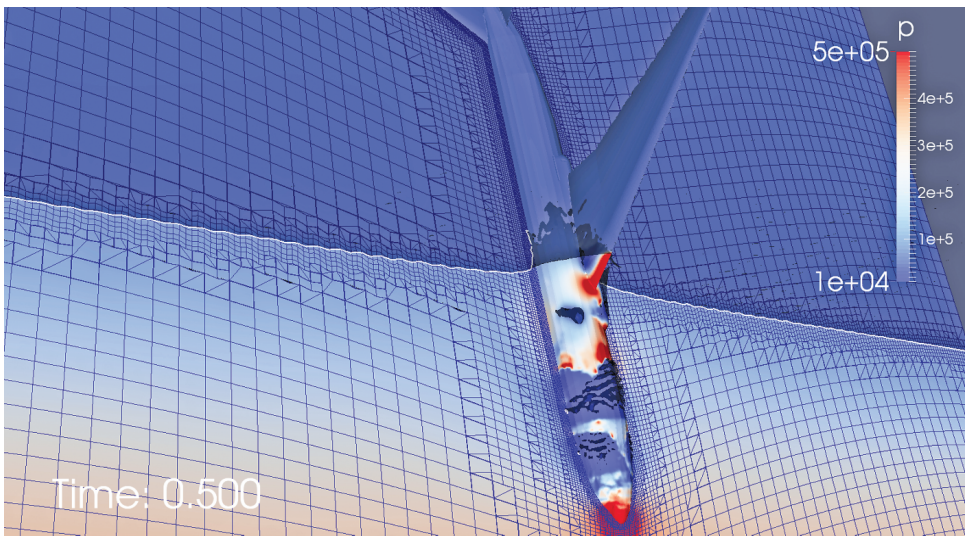

(b) pressure distribution and mesh

Figure 12. Pitch angle = −90°, angle of approach = 93°. This corresponds to Case 4. A video animation can be viewed at `https://www.dropbox.com/s/vaf0qenjw01k5yz/comb-90.mp4`.

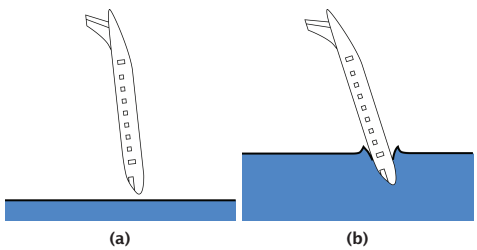

Figure 13. Schematics for nose-diving. The ocean current pushes the aircraft to the right, causing it possibly to finish belly-up on the ocean floor. This corresponds to Case 4.

failure modes occur at *low impact velocities*, as has been demonstrated with a real model of a retired aircraft in DYCAST (Dynamic Crash Analysis of Structures) by NASA [FWR87]. These findings were published nearly three decades ago but remain valid today.

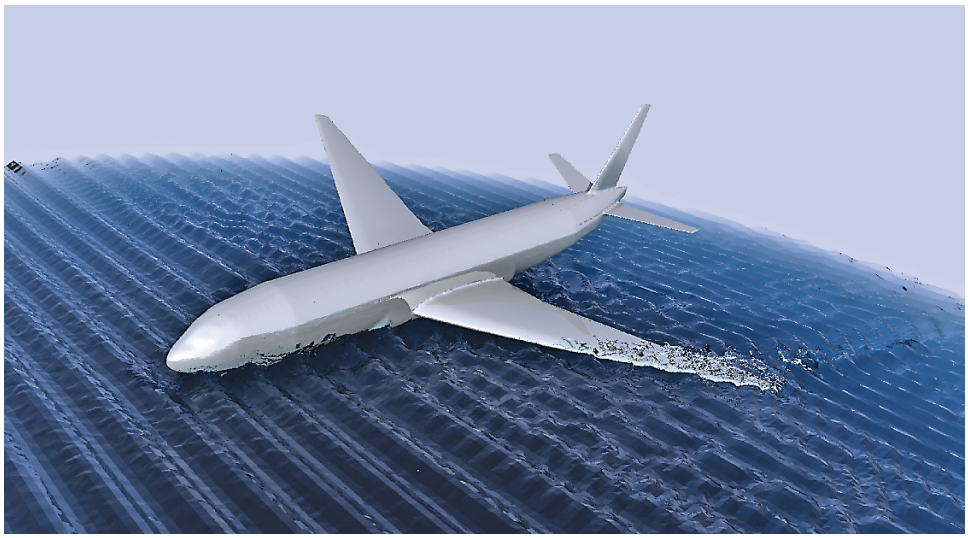

(a) rolling water entry

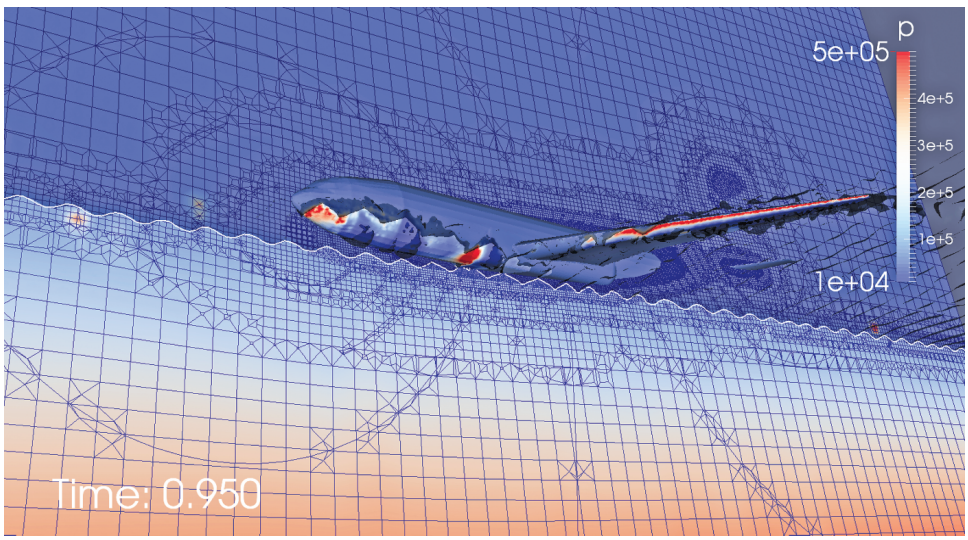

(b) pressure distribution and mesh

Figure 14. Pitch angle = −3°, angle of approach = 3°, but with a left-roll angle of 20°. This corresponds to Case 5. A video animation can be viewed at `https://www.dropbox.com/s/cgvn99okc4ao0i4/combSide.mp4`.

There is an incredible complete video recording of this air disaster, available for viewing at `www.youtube.com/watch?v=sKC9COHCNH8`.

The hijacked wide-body Boeing 767-260ER jetliner flew and rolled into the ocean with the left wing clipping water and getting torn off first. Immediately afterward, the same happened to the right wing. The fuselage went into cartwheeling and broke up. Only fifty of the 175 crew and passengers survived.

Debris spread over a wide area, and the light pieces could have floated for a long time.

Box 4. A rolling water-entry case: hijacked Ethiopian Airlines Flight 961 ditching by Comoros Island, Africa in 1996.

Fracture failure mode is estimated to happen when the vertical component of velocity exceeds certain critical value V_{cr}. Rupture of fuselage and wings as shear and tensile cracks will be initiated and then propagate through the stiffened shell, leading to global structural failure. This is a dynamic process whose analysis is very challenging. Nevertheless, a simple estimate on the onset of local failure can be given using the condition of dynamic continuity in uniaxial wave propagation along a rod based on the equation

$$[\sigma] = \rho c[u], \tag{11}$$

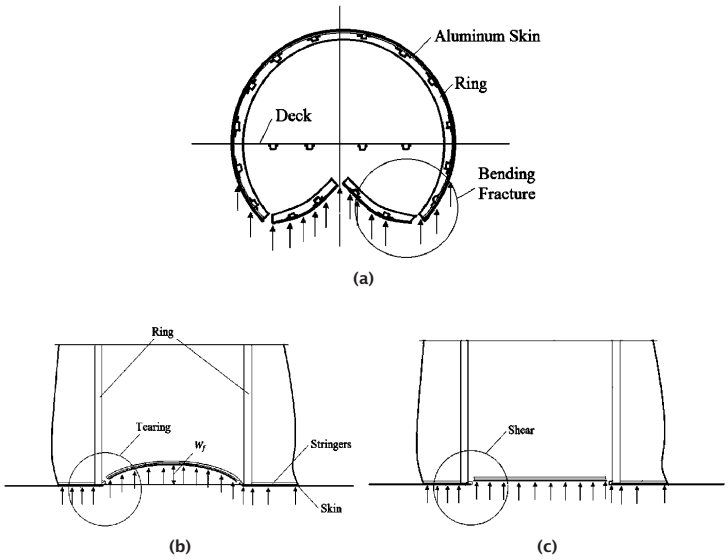

Figure 15. Three modes of structural failure for a wide-body airliner: (a) flexural failure of rings; (b) tearing fracture; and (c) shear of the longitudinally stiffened shell. (Adapted from [WY86b, p. 651])

where $[\sigma]$ and $[u]$ denote jump discontinuities across the water-structure interface, $\rho = 2.8$ g/cm^3 is the mass density of the aluminum fuselage, and $c = \sqrt{E/\rho}$ is the speed of the uniaxial wave propagation in an elastic rod with elastic modulus $E = 85$ GPa (i.e., 10^9 Pascal). The *critical impact velocity* V_{cr} (vertical component only) is reached when *the stress equals the yield stress* of the material σ_y. Thus, from (11) one gets the following estimate on V_{cr}:

$$V_{cr} = \frac{\sigma_y}{E} c. \tag{12}$$

Depending on the material, the critical descending speed of aircraft is normally in the range of $V_{cr} = 15$–20 m/sec. A common fuselage material is 2024 T351 aluminum alloy with the yield stress of $\sigma_y = 324$ MPa (10^6 Pascal). The critical impact velocity is thus $V_{cr} = 22$ m/sec, which is close to the value 18.8 m/sec predicted for the water ditching of the Space Shuttle Challenger, but using a different approach in [WY86b]. The vertical component V_{cr} of V_0, the aircraft speed at ditching, is related through the angle of approach β by

$$\sin\beta = \frac{V_{cr}}{V_0}. \tag{13}$$

Therefore, it is essential to keep the angle of approach small, especially when ditching with a high speed.

In addition to structural rupture and disintegration, the *acceleration due to free fall* and the *deceleration due to the impact of the structure* are important for human survival in a crash. In [WY86b], it was analyzed that if the vertical component of the terminal impact velocity lies in the range of *62.5 m/sec and 80.5 m/sec*, maximum decelerations could reach in the order of *100g to 150g* (g is the gravitational acceleration constant) over a short period of time, within a regime labeled "severe injuries" [WY86b, MHV59] by NASA.

Remark 2. According to the numerical simulation results in the preceding section, the airliner's skin will be subject to surface pressure in the order of 6 MPa, which is considerably smaller than the yield stress 324 MPa of the 2024 T351 aluminum alloy's. Thus, at the given (very low!) speed of ditching, 58 m/sec, there appears to be no local fracture due to yield stress. Any of the structural failures must happen at weak joints, strut-mounts, and stringer-stiffeners where the engine nascelles, wings, and fuselage are connected. These belong to the category of global failures.

The decelerations from computation indicate a maximum deceleration for all five cases to be about 6g, which is far smaller than the dangerous decelerations of 100g to 150g at the end of Remark 1. But the magnitude of decelerations could be far greater if the speed at ditching is large.

As a consequence of this, it now becomes clear that *the vertical component of the terminal water-entry velocity should be reduced as much as possible*, such as the glided water-landing approach taken by Captain Sullenberger for US Airways Flight 1549 on the Hudson River. That is, some "pitching attitudes" of the aircraft will yield a much higher probability of survival by averting structural damage and decelerations of the occupants [WY86a,

p. 34]. Indeed, according to Guo, et al. [GLQW13], it is recommended that, for a transport aircraft with a low horizontal tail, the pitch angle be chosen between 10° and 12° (with an angle of approach of 1°) for safer ditching, which is consistent with the prediction of (13). Such knowledge enhances air travel safety and, as shown here, can be obtained by CFD simulations.

Concluding Remarks

After viewing the five cases of simulation for an airliner's water entry and with some rudimentary knowledge about resulting damages in the preceding two sections, one naturally raises the question:

Which case is the most likely scenario for the final moments of Flight MH370?

Our assessment is **Case 4**; namely, the *nose-dive water-entry or a water-entry with a steep pitch angle*, is the most likely scenario. This particular assertion is speculative but forensic, based mainly on the observations of the computed data in the prior section, combined with the understanding of aviation precedents, atmospheric and ocean surface conditions, due to the following:

(a) So far, there is a total lack of floating debris. Similarly, oil spills have not been observed, hinting that the aircraft ran (almost) out of fuel before crashing.
(b) A smooth gliding water-entry as in **Case 1** (similar to US Airways Flight 1549) may result in only small rupture. But ditching a large airplane on the open Indian Ocean generally would involve waves of height several meters or more, easily causing breakup and the leak of debris.
(c) As already noted, **Case 2** suffers large bending moment, and buckling and breakup can ensue.
(d) For **Case 3**, rough waves may also cause breakup and the leak of debris.
(e) For **Case 5**, as we have seen from the video recording in Box 4, there is a high likelihood of breakup in some middle section of aircraft.

This leaves **Case 4** as the main possibility why no floating debris has been spotted. Again, this assessment is of a speculative character as our computer simulations have not included *all* aircraft speeds and ocean surface conditions, and the effects of bending moments. The mystery of the final moments of MH370 is likely to remain until someday when its black box is found and decoded.

The crash of an airliner into ocean is a profoundly tragic event. But on the mathematical and engineering side, there should be significant interest in its modeling and computation so that one can understand the physical mechanisms better in the hope of improving aircraft crashworthiness and survivability. The CFD approach is advantageous in saving long and expensive processes of laboratory setup and measurements. Now, with the availability of increased free and open-source computational tools and user-friendly software, it has become much easier for mathematicians to conduct interdisciplinary collaboration with engineers and physicists for the *modeling and computation of complex, "real world" problems*, just as this article has hoped to demonstrate. Many challenges remain. Regarding CFD for the study of aircraft ditching in water, see an excellent review and outlook paper in Liu et al. [LQG+14]. For an analysis-minded mathematician, it would be nice to formulate a list of problems dealing with the *rigor* of generality of approach, robustness, and stability issues, which are being considered.

A body of literature already exists for the computer simulation of *rupture and disintegration* of a crashing aircraft (*on land or into buildings*). The software by Abaqus [Aba], LS-DYNA [lsd] and others is known to be able to simulate the impact and breakup of solids in collisions. But this component of the problem is too technical and must be deferred to a sequel.

On any given day, there are hundreds of thousands of people traveling by air worldwide. Air travel has never been safer and continues to become even safer. According to Barnett [Bar10], in the 2000-2007 time period, the death risk per flight on a first-world airliner was 1 in every 2 million: and 2 million days is nearly 5,500 years! There are always bound to be unfortunate and tragic incidents. However, it is to be expected that data generated by numerical simulations will further improve passenger survival in emergency water landings.

Acknowledgment

We are indebted to Prof. Steven Krantz, Editor of the *Notices*, for advice on the style of presentation, and to Prof. V. Vuorinen of Aalto University, Finland, and anonymous reviewers for constructive comments. We thank the generous support from the Qatar National Research Funds grant National Priority Research Project #5-674-1-114 and Texas A&M University's internal grant for interdisciplinary research, CRI Scully funds, through the Institute for Quantum Science and Engineering. We also thank the staff at TAMU Supercomputing Facility and TASC at TAMUQ for software support and time allocation.

Page 892 of 1738

References

[Aba] Abaqus FEA. www.3ds.com/products-services/simulia

[Abr11] Serge Abrate, Hull slamming, *Applied Mechanics Reviews*, 64(6):060803, 2011.

[Bar10] Arnold Barnett, Cross-national differences in aviation safety records, *Transportation Science*, 44(3):322–332, 2010.

[CXM+14] Goong Chen, Qingang Xiong, Philip J. Morris, Eric G. Paterson, Alexey Sergeev, and Yi-Ching Wang, OpenFOAM for computational fluid dynamics, *Notices of the AMS* **61** (2014), no.4, 354–363.

[Fab57] Andrew G. Fabula, Ellipse-fitting approximation of two-dimensional, normal symmetric impact of rigid bodies on water, in *Proceedings of the 5th midwestern conference on fluid mechanics*, A. M. Kuethe, editor, Ann Arbor; The University of Michigan Press, 1957, pp. 299–315.

[Fin14] David Finkleman, A mathematical and engineering approach to the search of MH370, 2014, Powerpoint Presentation (unpublished).

[FWR87] Edwin L. Fasanella, E Widmayer, and Martha P. Robinson, Structural analysis of the controlled impact demonstration of a jet transport airplane, *Journal of Aircraft* **24** (1987), no. 4, 274–280.

[Gar53] P. R. Garabedian, Oblique water entry of a wedge, *Communications on Pure and Applied Mathematics* **6** (1953), no. 2, 157–165.

[GLQW13] Baodong Guo, Peiqing Liu, Qiulin Qu, and Jiawen Wang, Effect of pitch angle on initial stage of a transport airplane ditching. *Chinese Journal of Aeronautics* **26** (2013), no 1, 17–26.

[HN81] Cyril W Hirt and Billy D Nichols, Volume of fluid (vof) method for the dynamics of free boundaries. *Journal of Computational Physics* **39** (1981), no. 1, 201–225.

[LQG+14] Feiqing Liu, Qiulin Qu, Baodong Guo, Xing Jin, Jiali Wu, and Kai Zhang, Application of computational fluid dynamics in the planned ditching of a transport airplane. *Mechanics and Practices*, **36** (2014), 278–284. (in Chinese with English abstract).

[lsd] LS-DYNA. www.lstc.com/products/ls-dyna

[Mac79] A. M. Mackey, A mathematical model of water entry, *Admiralty Underwater Weapons Establishment TN*, (636/79), 1979. Publisher listed as PN.

[MHV59] John R McGehee, Melvin E Hathaway, and Victor L Vaughan, *Water-landing characteristics of a reentry capsule*, National Aeronautics and Space Administration, 1959.

[MP93] B. Mohammadi and Olivier Pironneau, *Analysis of the K-epsilon Turbulence Model*, Wiley-Masson Series Research in Applied Mathematics, 1994.

[not] *Notices of the American Mathematical Society.*

[ope] OpenFOAM. openfoam.org/

[OS88] Stanley Osher and James A Sethian, Fronts propagating with curvature-dependent speed: Algorithms based on Hamilton-Jacobi formulations, *Journal of Computational Physics*, **79** (1988), no. 1, 12–49.

[RL14] T. Chacón Rebollo and Roger Lewandowski, *Mathematical and Numerical Foundations of Turbulence Models and Applications*, Springer, 2014.

[Son03] Gihun Son, Efficient implementation of a coupled level-set and volume-of-fluid method for three-dimensional incompressible two-phase flows, *Numerical Heat Transfer: Part B: Fundamentals*, **43** (2003), no. 6, 549–565.

[SS51] M. Shiffman and D. C. Spencer, The force of impact on a cone striking a water surface (vertical entry), *Communications on Pure and Applied Mathematics*, **4** (1951), no. 4, 379–417.

[SSO94] Mark Sussman, Peter Smereka, and Stanley Osher, A level set approach for computing solutions to incompressible two-phase flow, *Journal of Computational Physics*, **114** (1994), no. 1, 146–159.

[syr] 4 possible ways Malaysia flight 370 hit the water and how each would affect the search, Associated Press, April 8, 2014.

[TNY85] H. Takewaki, A. Nishiguchi, and T. Yabe, Cubic interpolated pseudo-particle method (cip) for solving hyperbolic-type equations, *Journal of Computational Physics*, **61** (1985), no. 2, 261–268.

[23] US Airways Flight 1549. en.wikipedia.org/wiki/US_Airways_Flight_1549

[vK29] Theodore von Kármán, The impact on seaplane floats during landing, *NACA Technical Note* No. 321, 1929.

[Wag31] Herbert Wagner, Landing of seaplanes, *NACA Technical Memorandums*, No. 622, 1931.

[WSH04] G. X. Wu, H. Sun, and Y. S. He, Numerical simulation and experimental study of water entry of a wedge in free fall motion, *Journal of Fluids and Structures*, **19** (2004), no. 3, 277–289.

[WY86a] T. Wierzbicki and *D. K. Yue*, Spacecraft crashworthiness—towards reconstruction of the Challenger accident, *American Society of Mechanical Engineers, Applied Mechanics Division, AMD*, **79** (1986), 31–46.

[WY86b] Tomasz Wierzbicki and Dick K. Yue, Impact damage of the Challenger crew compartment, *Journal of Spacecraft and Rockets*, **23** (1986), no. 6, 646–654.

[Zwe14] John Zweck, How did Inmarsat deduce possible flight paths for MH370? *SIAM News*, May 1, 2014.

Page 893 of 1738

Australian Government
Australian Transport Safety Bureau

The Operational Search for MH370

3 October 2017

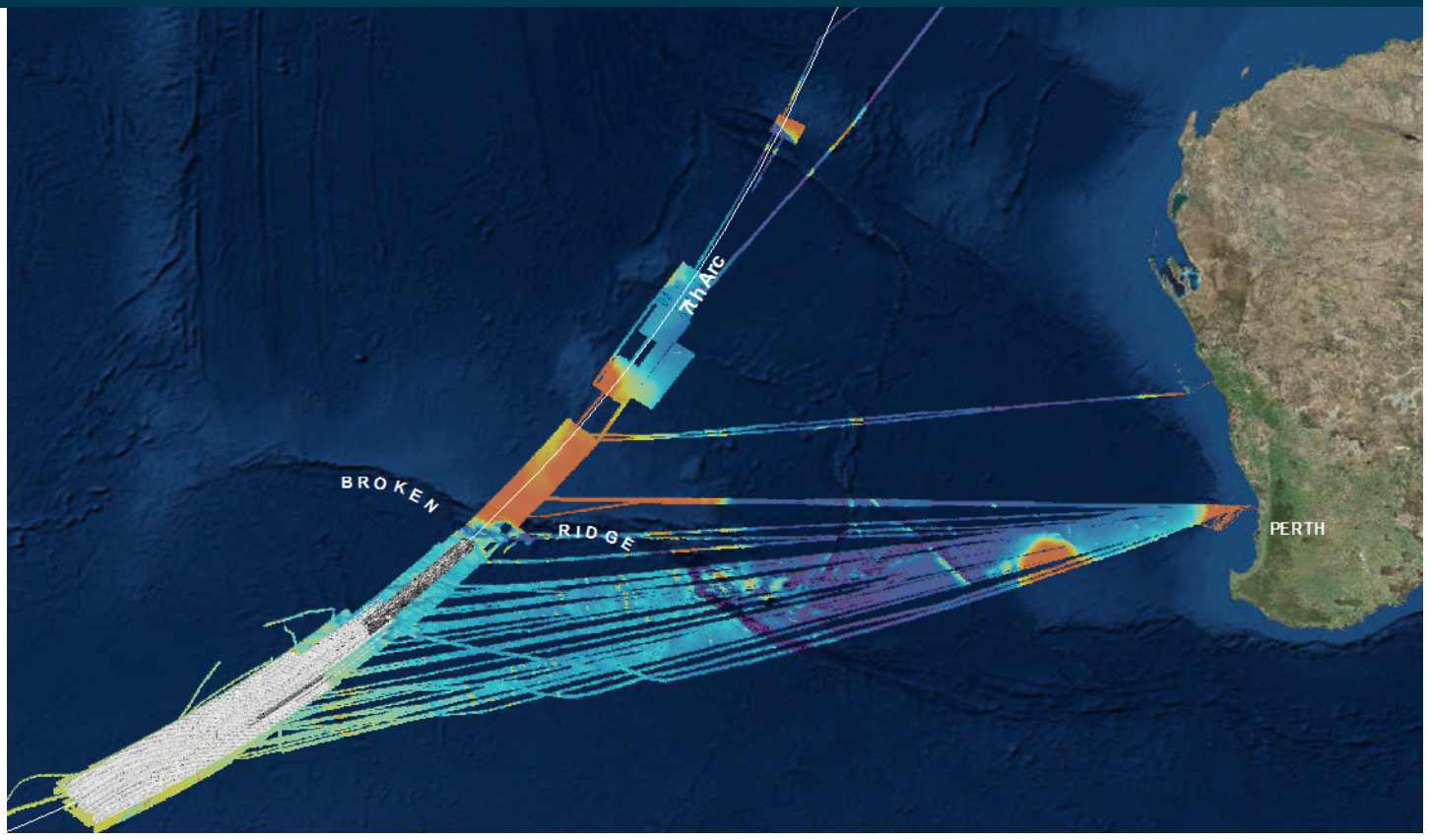

Investigation

ATSB Transport Safety Report
External Aviation Investigation
AE-2014-054
Final – 3 October 2017

Released in accordance with section 25 of the *Transport Safety Investigation Act 2003*

Publishing information

Published by: Australian Transport Safety Bureau
Postal address: PO Box 967, Civic Square ACT 2608
Office: 62 Northbourne Avenue Canberra, Australian Capital Territory 2601
Telephone: 1800 020 616, from overseas +61 2 6257 4150 (24 hours)
Accident and incident notification: 1800 011 034 (24 hours)
Facsimile: 02 6247 3117, from overseas +61 2 6247 3117
Email: atsbinfo@atsb.gov.au
Internet: www.atsb.gov.au

© Commonwealth of Australia 2017

Ownership of intellectual property rights in this publication
Unless otherwise noted, copyright (and any other intellectual property rights, if any) in this publication is owned by the Commonwealth of Australia.

Creative Commons licence
With the exception of the Coat of Arms, ATSB logo, and photos and graphics in which a third party holds copyright, this publication is licensed under a Creative Commons Attribution 3.0 Australia licence.

Creative Commons Attribution 3.0 Australia Licence is a standard form license agreement that allows you to copy, distribute, transmit and adapt this publication provided that you attribute the work.

The ATSB's preference is that you attribute this publication (and any material sourced from it) using the following wording: *Source:* Australian Transport Safety Bureau

Copyright in material obtained from other agencies, private individuals or organisations, belongs to those agencies, individuals or organisations. Where you want to use their material you will need to contact them directly.

Addendum

Page	Change	Date

Executive summary

On 8 March 2014, a Boeing 777 aircraft operated as Malaysia Airlines flight 370 (MH370) was lost during a flight from Kuala Lumpur in Malaysia to Beijing in the People's Republic of China carrying 12 crew and 227 passengers. The search for the missing aircraft commenced on 8 March 2014 and continued for 1,046 days until 17 January 2017 when it was suspended in accordance with a decision made by a tripartite of Governments, being Malaysia, Australia and the People's Republic of China.

The initial surface search and the subsequent underwater search for the missing aircraft have been the largest searches of their type in aviation history. The 52 days of the surface search involving aircraft and surface vessels covered an area of several million square kilometres. A sub surface search for the aircraft's underwater locator beacons was also conducted during the surface search.

The underwater search started with a bathymetry survey which continued as required throughout the underwater search and has mapped a total of 710,000 square kilometres of Indian Ocean seafloor, the largest ever single hydrographic survey. The high resolution sonar search covered an area in excess of 120,000 square kilometres, also the largest ever search or survey of its kind. Despite the extraordinary efforts of hundreds of people involved in the search from around the world, the aircraft has not been located.

Regardless of the cause of the loss of MH370, there were no transmissions received from the aircraft after the first 38 minutes of the flight. Systems designed to automatically transmit the aircraft's position including the transponder and the aircraft communications addressing and reporting system failed to transmit the aircraft's position after this time period. Subsequent analysis of radar and satellite communication data revealed the aircraft had actually continued to fly for a further seven hours. Its last position was positively fixed at the northern tip of Sumatra by the surveillance systems operating that night, six hours before it ended the flight in the southern Indian Ocean.

The challenge which faced those tasked with the search was to trace the whereabouts of the aircraft using only the very limited data that was available. This data consisted of aircraft performance information and satellite communication metadata initially, and then later during the underwater search, long-term drift studies to trace the origin of MH370 debris which had been adrift for more than a year, and in some cases, more than two years. The types of data, and the scientific methods used for its analysis, were never intended to be used to track an aircraft or pin point its final location.

On 28 April 2014, the surface search for MH370 coordinated by the Australian Maritime Safety Authority (AMSA) was concluded and the Australian Transport Safety Bureau (ATSB) assumed responsibility for conducting the underwater search for the aircraft. The underwater search area was initially defined at 60,000 square kilometres, and was increased in April 2015 when the Tripartite Governments (Malaysia, Australia and the People's Republic of China) agreed to expand the search area to 120,000 square kilometres. The primary objective of the underwater search was to establish whether or not the debris field of the missing aircraft was in the area of seafloor defined by expert analysis of the aircraft's flight path and other information. If a debris field was located, the search needed to confirm the debris was MH370 by optical imaging, and then map the debris field to enable planning for a subsequent recovery operation.

Once underwater search operations commenced in October 2014, the MH370 debris field could potentially have been located at any time. A recovery operation would need to have commenced as soon as possible after the debris field was located and the Tripartite governments had agreed on the next steps. The ATSB's role was therefore to also put in place the arrangements and plans necessary for a rapid recovery operation to occur at short notice.

The underwater search applied scientific principles to defining the most probable area to be searched through modelling the aircraft's flight path and behaviour at the end of the flight. The flight path modelling was based on unique and sophisticated analysis of the metadata associated with the periodic automated satellite communications to and from the aircraft in the final six hours of the flight. The end-of-flight behaviour of the aircraft, when MH370 was considered to have exhausted its fuel, has been analysed and simulated.

In 2015 and 2016, debris from MH370 was found on the shores of Indian Ocean islands and the east African coastline. The debris yielded significant new insights into how and where the aircraft ended its flight. It was established from the debris that the aircraft was not configured for a ditching at the end-of-flight. By studying the drift of the debris and combining these results with the analysis of the satellite communication data and the results of the surface and underwater searches, a specific area of the Indian Ocean was identified which was more likely to be where the aircraft ended the flight.

The understanding of where MH370 may be located is better now than it has ever been. The underwater search has eliminated most of the high probability areas yielded by reconstructing the aircraft's flight path and the debris drift studies conducted in the past 12 months have identified the most likely area with increasing precision. Re-analysis of satellite imagery taken on 23 March 2014 in an area close to the 7th arc has identified a range of objects which may be MH370 debris. This analysis complements the findings of the First Principles Review and identifies an area of less than 25,000 square kilometres which has the highest likelihood of containing MH370.

The ATSB's role coordinating the underwater search involved the procurement and management of a range of sophisticated and highly technical services. Management of the underwater search was aimed at ensuring high confidence in the acquisition and analysis of the sonar search data so that areas of the seafloor which had been searched could be eliminated. A comprehensive program was implemented to ensure the quality of the sonar coverage. A thorough sonar data review process was used to ensure areas of potential interest were identified and investigated.

During the early stages of the procurement, careful consideration was given to the methods available for conducting a large scale search of the seafloor. Water depths were known to be up to 6,000 m with unknown currents and unknown seafloor topography. Search operations would also have to be conducted in poor weather conditions and in a very remote area far from any land mass. Planning focused on selecting a safe, efficient and effective method to search the seafloor in an operation with an indeterminate timeframe.

The mapping of the seafloor in the search area revealed a challenging terrain for the underwater search which used underwater vehicles operating close to the seafloor. While the deep tow vehicles selected as the primary search method proved to be very effective, the seafloor terrain necessitated the use of a range of search methods including an autonomous underwater vehicle to complete the sonar coverage.

The underwater search area was located up to 2,800 km west of the coast of Western Australia and the prevailing weather conditions in this area for much of the year are challenging. Crews on the search vessels were working for months at a time in conditions which elevated the operational risks. The ATSB ensured that these risks to the safety of the search vessels and their crews were carefully managed.

At the time the underwater search was suspended in January 2017, more than 120,000 square kilometres of seafloor had been searched and eliminated with a high degree of confidence. In all, 661 areas of interest were identified in the sonar imagery of the seafloor. Of these areas, 82 with the most promise were investigated and eliminated as being related to MH370. Four shipwrecks were identified in the area searched.

The intention of this report is to document the search for MH370, in particular, the underwater search including; where the search was conducted (and why), how the search was conducted, the results of the search and the current analysis which defines an area where any future underwater

search should be conducted. The report also includes a safety analysis which is focused on the search rather than on discussing the range of factors which may have led to the loss of the aircraft.

The Government of Malaysia is continuing work on their investigation of the facts and circumstances surrounding the loss of MH370 aircraft consistent with their obligations as a member State of ICAO. The Malaysian investigation is being conducted in accordance with the provisions of ICAO Annex 13, Aircraft Accident and Incident Investigation.

The search, recovery and investigation of the loss of Air France flight AF447, in the South Atlantic Ocean in 2009, and the loss of MH370 have led to some important learnings related to locating missing aircraft on flights over deep ocean areas. Requirements and systems for tracking aircraft have been enhanced and will continue to be enhanced. Steps are being taken to advance other aircraft systems including emergency locator transponders and flight recorder locator beacons.

The ATSB acknowledges the extraordinary efforts of the hundreds of dedicated professionals from many organisations in Australia and around the world who have contributed their time and efforts unsparingly in the search for MH370.

The reasons for the loss of MH370 cannot be established with certainty until the aircraft is found. It is almost inconceivable and certainly societally unacceptable in the modern aviation era with 10 million passengers boarding commercial aircraft every day, for a large commercial aircraft to be missing and for the world not to know with certainty what became of the aircraft and those on board.

The ATSB expresses our deepest sympathies to the families of the passengers and crew on board MH370. We share your profound and prolonged grief, and deeply regret that we have not been able to locate the aircraft, nor those 239 souls on board that remain missing.

Contents

Executive summary ..... **i**
Contents ..... **iv**
Background **1**
The search program 2
Investigation 2
Search 3
Recovery 4
Governance 4
Communications and media 6
Search funding 7
Search actual costs 7
History of the flight **9**
Kuala Lumpur to waypoint IGARI 9
Waypoint IGARI to waypoint MEKAR 10
Waypoint MEKAR onwards 11
Aircraft Information 13
Airframe 13
Engines 14
Auxiliary Power Unit 14
Flight crew and passengers 14
The surface search **15**
Malaysian led surface search 15
East of the Malay Peninsula 15
West of the Malay Peninsula 16
Northern and southern corridors announced 17
Australian led surface search 19
Initial southern Indian Ocean surface search area 20
Satellite imagery debris detections 23
Refined surface search area 25
Second refinement surface search area 29
Debris sightings and recoveries 33
Surface search coverage and confidence 34
The acoustic search for the underwater locator beacons **36**
Underwater locator beacons 36
Acoustic detections 38
HMS Echo 38
Haixun 01 38
Ocean Shield 39
Analysis of acoustic detections 40
Marine animal tracking devices 41
Sonobuoys 41
Autonomous underwater vehicle search 41
The underwater search **43**
Defining the initial underwater search area 43
Initial priority search area 43
Mapping the seafloor in the search area 45
Bathymetric survey 45

Geology of the search area 48
Bathymetry processing 50
Backscatter analysis 51
Selecting the search method/systems 52
The search tender 53
Synthetic Aperture Sonar 59
Other search coverage considerations 59
Validating the search systems 60
Underwater search chronology 62
The priority search area refined southwards 63
Underwater search commences 64
Search area extension 69
Generalised flight dynamic model 71
Complete Bayesian analysis 72
Last refinement to underwater search area 75
ATSB contractor reports 77
Area searched 77
Search area probability density functions 77
Quality assurance of the sonar data 83
Sonar coverage 86
Data processing and information dissemination – a new approach 89
Sonar contacts 90
Confidence in the search results 95
Other search area considerations 98
Pilot in Command's flight simulator 98
Controlled glide or ditching 99
Aircraft debris 102
Marine ecology examinations 107
Australian beach searches 107
Debris drift analysis 112
Hydroacoustic analysis 114
Satellite imagery analysis 116
Contrails analysis 117
Reanalysis of satellite imagery 118
External contributions 119
Other search considerations – risk mitigation 121
Weather 121
Weather forecasting and recording 122
Real time weather records 124
Weather events impacting search operations 125
Mitigation of weather impact on search operations 128
Health, safety and environment 129
Operational safety 130
Remote area operations 130
Remote area risk mitigation 130
Incident recording and reporting 131
Significant HSE incidents 131
Significant equipment related incidents 132
Impact of fishing vessels in the search area 132

Recovery planning 134
Planning for recovery 134
The investigations 136
Disaster Victim Identification 136
Safety analysis 137
Introduction 137
Search, rescue, and recovery 138
Search, rescue, and recovery phases 139
Normal flight 139
Aircraft in distress 144
Surface search 144
Underwater locator beacon search 145
Sonar search 147
Summary 147
Records of previous searches 149
Related searches 149
Previous safety recommendations 150
Malaysian Air Accident Bureau 150
Bureau d'Enquêtes et d'Analyses pour la sécurité de l'aviation civile (BEA) 150
Aviation industry statements 151
Safety actions 151
International Civil Aviation Organization 151
Inmarsat 152
Malaysia Airlines 152
Airservices Australia 152
Joint committee 152
Conclusions 153
Flight tracking 153
Emergency locator transmitters 153
Drift measurements 154
Visual and radar search aids 154
Underwater locator beacons 154
Other considerations 155
ATSB safety recommendations 156
Search and rescue information 156
Aircraft tracking 156
Sources and submissions 157
Sources of information 157
References 158
Submissions 159
Appendices 161
Appendix A: Search vessels
Appendix B: Identification of the most probable final location of flight MH370 (Issue 2) – Joint Investigation Team paper - 26 April 2014
Appendix C: Burst Frequency Offset (BFO) Doppler Model Development
Appendix D: Fugro Survey Pty Ltd Search for Malaysian Airlines Flight MH370 All Vessels Reconnaissance Bathymetric Survey, Deep Tow Wide Area Survey and AUV Wide Area Survey Volume 7 – Summary Report
Appendix E: Phoenix International Holdings Inc. Malaysia Airlines Flight 370 (MH370) Search End of Contract Report

Appendix F: Chemical investigations on barnacles found attached to debris from the MH370 aircraft found in the Indian Ocean
Appendix G: Summary of Analyses Undertaken on Debris Recovered During the Search for Flight MH370
Appendix H: Analysis of Low Frequency Underwater Acoustic Signals Possibly Related to the Loss of Malaysian Airlines Flight MH370
Appendix I: Results of analysis of Scott Reef IMOS underwater sound recorder data for the time of the disappearance of Malaysian Airlines Flight MH370 on 8 March 2014
Appendix J: Seismic and hydroacoustic analysis relevant to MH370

Glossary **423**

Abbreviations **427**

Australian Transport Safety Bureau **429**
Purpose of safety investigations
Developing safety action

Background

On 8 March 2014, a Boeing 777-200ER aircraft, registered 9M-MRO and operated as Malaysia Airlines flight 370 (MH370) disappeared during a flight from Kuala Lumpur to Beijing, carrying 12 Malaysian crew members and 227 passengers.

At the request of the Malaysian Government, the Australian Government accepted responsibility for initial search operations in the southern part of the Indian Ocean on 17 March 2014. A surface search by aircraft and surface vessels in the Indian Ocean, coordinated by the Australian Maritime Safety Authority (AMSA), and an acoustic sub-surface search for the aircraft's flight recorder underwater locator beacons, found no debris nor signals associated with MH370.

The Malaysian Government, as the International Civil Aviation Organization (ICAO) Annex 13 state of registry for Malaysia Airlines, was responsible for the overall strategic approach to the search for MH370 and the associated investigation. The majority of the passengers on board MH370 were from Malaysia and the People's Republic of China, however due to the proximity of the search area to Australia, and the request from Malaysia to Australia to lead search operations, Malaysia, the People's Republic of China and Australia agreed to collaborate in relation to the overarching search strategy. This cooperation is referred to as the Tripartite arrangement.

On 30 March 2014, the then Prime Minister of Australia, the Hon Tony Abbott MP, established the Joint Agency Coordination Centre (JACC) to coordinate the Australian Government's support for the search for missing flight MH370. The JACC was the coordination point for whole-of-Australian Government information, messaging and international engagement, including keeping the families of those on board and the general public informed of the progress of the search.

At the conclusion of the surface search on 28 April 2014, the Australian Prime Minister offered that Australia could continue to lead search operations. Tripartite meetings in May 2014 agreed to this arrangement and the ATSB was tasked to lead an intensified and continuous underwater search of an initial area of 60,000 square kilometres (km^2). Subsequent Tripartite meetings in August 2014 agreed that Australia, through the ATSB, would also lead a recovery operation if and when the aircraft was located and a recovery was deemed suitable by the Tripartite.

A Memorandum of Understanding on Cooperation between the Governments of Australia and Malaysia in relation to MH370 (the MOU) provided a mechanism to formalise agreements on cooperation between the two governments. The then Australian Deputy Prime Minister and Minister for Infrastructure and Regional Development, the Hon Warren Truss MP, and Malaysian Minister for Transport Dato' Seri Liow Tiong Lai signed the MOU on 28 August 2014.

The MOU included a number of supplemental arrangements as annexures detailing the scope of work and responsibilities for specific areas of cooperation regarding MH370. The areas of cooperation included search, recovery, disaster victim identification, investigation, dealing with the debris site, and facilitating interactions with the next of kin. The MOU, and associated annexures, was deemed to have come into effect on 17 March 2014 for a period of three years.

On 16 April 2015, Tripartite Ministers met, considered next steps for the search and agreed that:

- If MH370 was not positively located in the initial 60,000 km^2 search area that the search would be expanded to an area of 120,000 km^2.
- When MH370 was located, a recovery operation would proceed with priorities for the recovery operation to include:
  - the aircraft's flight recorders
  - selected wreckage
  - where possible, human remains.

On 22 July 2016, Tripartite Ministers met and agreed that should the aircraft not be located in the search area, and in the absence of credible new evidence leading to the identification of a specific location of the aircraft, the search would be suspended, not ended, upon completion of the 120,000 km^2 search area. However, should credible new information emerge that can be used to identify the specific location of the aircraft, consideration would be given to determining next steps.

On 17 January 2017, in accordance with the decision made at the Ministerial Tripartite meeting in July 2016, the Tripartite countries issued a Joint Communiqué to announce the suspension of the underwater search following the completion of the 120,000 km^2 search area.

The search program

The operational search for MH370 (search program) was a large-scale complex international operation involving multiple assets in a dynamic environment. The search program encompassed a number of component activities, all of which were interdependent but with the unifying goal of ensuring the Australia (through the ATSB) fulfilled its obligations under Annex 13 of the Convention on International Civil Aviation (the Chicago Convention) and the MOU with Malaysia. Figure 1 depicts the search program objectives and the component activities.

Figure 1: Search program objectives

<table>
<tr><td>Program Goal</td><td colspan="5">To assist the Malaysian Government in its investigation to find answers to the disappearance on 8 March 2014 (0022 local time Malaysia) of the Boeing 777-200ER aircraft registered 9M-MRO and operated as Malaysia Airlines Flight 370 (MH370)

In accordance with Annex 13 to the Convention on International Civil Aviation (Annex 13) and the Memorandum of Understanding on Cooperation between the Government of Australia and the Government of Malaysia in relation to MH370 (the MOU)</td></tr>
<tr><td>Program Objectives</td><td>Assist the Malaysian Government with its Investigation into the disappearance of MH370</td><td colspan="3">To locate MH370 within the defined search area or determine to a high degree of confidence its absence from the defined search area

MOU Annexure 1: Search for MH370</td><td>To coordinate the recovery of MH370 and human remains in accordance with Tripartite directions

MOU Annexure 3: Recovery</td></tr>
<tr><td rowspan="3">Program Component Activities</td><td rowspan="2">Assist in the conduct of the Annex 13 Investigation</td><td>Define the search area</td><td>Map the search area to enable underwater search</td><td>Conduct the underwater search</td><td rowspan="2">Prepare for and coordinate the recovery of MH370</td></tr>
<tr><td colspan="3">Quality assurance and data management</td></tr>
<tr><td colspan="5">Program governance and assurance</td></tr>
<tr><td>Program End State</td><td colspan="5">ATSB has fulfilled its obligations under International Civil Aviation Organization (ICAO) Annex 13, the extant MOU and supplemental arrangements and agreements</td></tr>
</table>

Source: ATSB

Investigation

The primary goal of the ATSB search program was to assist the Malaysian Government's Annex 13 safety investigation into the circumstances surrounding the aircraft's disappearance. Recovery and analysis of the cockpit voice recorder (CVR) and flight data recorder (FDR) in particular, would assist in determining the events leading to the loss of MH370.

Investigations conducted in accordance with Annex 13 of the International Civil Aviation Organization's Chicago Convention are for the sole purpose of the prevention of accidents and incidents, not to apportion blame nor to provide a means of determining liability.

Australian assistance has been provided in accordance with Annex 13 protocols. The ATSB has provided assistance to the Malaysian Annex 13 investigation since the initial stages of the search for MH370. The appointment of an Australian accredited representative to the Malaysian ICAO Annex 13 safety investigation team for MH370 was formalised on 1 April 2014. The Malaysian Annex 13 investigation team also includes accredited representatives from aviation investigation agencies in the United States, the United Kingdom, the People's Republic of China, France, Indonesia and Singapore.

The final results of Malaysia's Annex 13 Investigation are yet to be published by the Ministry of Transport Malaysia.

Search

The underwater search consisted of three component activities as outlined in Figure 1, defining the search area, conducting underwater mapping of the search area to enable the underwater search and conducting the underwater search.

Definition of the search area

The key component objectives were to:

- review the available data to determine the most likely location of MH370
- define the search area, initially for an area of up to 60,000 km², extended to an area of up to 120,000 km² in April 2015, for the purpose of conducting an underwater search for MH370 within Australia's search and rescue region in the Indian Ocean.

This aspect of the underwater search was the most challenging with analysis to refine the underwater search area being performed concurrently with search activities for the entire period of the search.

The work of many organisations and individuals from Australia and around the world was coordinated by the ATSB. Of particular note was the contribution of members of the search strategy working group (SSWG) including; Inmarsat, Thales, Boeing, the Air Accidents Investigation Branch (AAIB) of the United Kingdom, the National Transportation Safety Board (NTSB) of the United States, the Defence Science and Technology Group[1] (DST Group) and the Department of Civil Aviation Malaysia. Other significant contributors were the Commonwealth Scientific and Industrial Research Organisation (CSIRO) and Geoscience Australia.

Underwater mapping of the search area

The key component objective was to obtain a topographic map of the search area detailing the contours, depths and composition of the seafloor to enable safe navigation of underwater search equipment and prioritisation of search zones.

The method chosen to map the seafloor was a bathymetric survey. A combination of vessels contracted by the ATSB and vessels provided by the Tripartite governments were used to conduct the bathymetric survey.

The majority of bathymetric survey data was acquired from June to December 2014. However, as the underwater search progressed and the area increased from an area of 60,000 km^2 to 120,000 km^2, further bathymetric data was acquired.

Early in the underwater search the ATSB established a National Collaboration Framework Head Agreement and Project Agreement for technical assistance with Geoscience Australia. This was a key relationship for the ATSB, used to facilitate many technical aspects of the underwater search. This included the analysis, quality assurance and storage of all underwater search data including the bathymetric survey data.

---

[1] Formerly the Defence Science and Technology Organisation

Underwater search

The key underwater search objectives were to:

- search for, locate and positively identify MH370 within the defined search area on the seafloor
- obtain optical imaging (photography or video) of the aircraft debris field if MH370 was located, and, if possible, recover the flight recorders

or

- positively eliminate areas searched within the defined search area for the presence of MH370 with a high degree of confidence.

Coordinating the underwater search involved the procurement of search services and overseeing all aspects of the underwater search from vessel tasking to data analysis, quality assurance and management. Fugro Survey Pty Ltd (Fugro Survey) was contracted by the ATSB to provide vessels, personnel and equipment, initially to conduct a bathymetric survey and later, underwater search services.

Phoenix International Holdings Inc. (Phoenix International) and their subcontractors Hydrospheric Solutions Inc., were initially contracted by the Malaysian Government (and later in the search by the ATSB) to provide search services including the synthetic aperture sonar equipped SLH PS-60 ProSAS (ProSAS) deep tow vehicle for underwater search operations.

Details of the vessels used in the search are included in appendix A.

Quality assurance and data management

Overseeing the acquisition, analysis and management of the search data was an essential component of the search program. Early in the search, the ATSB appointed a sonar data Quality Assurance Manager with significant experience in underwater search and recovery operations to provide advice on the procurement of search services and manage the acquisition and analysis of all search data.

Systems for monitoring the performance of the search contractors were implemented including stringent performance standards, testing of search systems and oversight of all operations by expert ATSB client representatives on each search vessel. Search data was subjected to multiple levels of independent analysis and review to ensure quality, coverage and identification of all seafloor anomalies of potential interest.

Recovery

A key program objective was to prepare for a recovery operation, pending the location and positive identification of the MH370 debris field, in accordance with decisions made by the Tripartite governments in August 2014 and May 2015.

This involved planning, preliminary procurement activity and the formulation of a range of agreements with Australian and Malaysian Government agencies, including the Australian Federal Police, Western Australia Police and the Royal Malaysian Police, in order to coordinate and facilitate the recovery of evidence relevant to the investigations into the disappearance of MH370.

Governance

Program governance and assurance was a component activity under the search program that covered all other components. The ATSB is an independent Commonwealth government agency accountable to the Minister for Infrastructure and Transport and forms part of the Infrastructure and Regional Development Portfolio.

The search program forms a temporary division within the ATSB organisational structure with a specific set of objectives and accountability for the efficient, effective and ethical use of the overall search program budget provided by the Tripartite governments. Whilst the Chief Commissioner of

the ATSB, who is also Chief Executive Officer, is ultimately accountable to the Minister of Infrastructure and Transport for the search program, management of the search program was delegated to a full time Program Director, reflecting the scale and complexity of this program.

Given the overall program budget of approximately $200 million, two program assurance mechanisms were implemented to provide assurance to the Chief Commissioner of effective program resource management.

- A program board, comprising the ATSB executive and representatives of key program stakeholders, provided guidance, advice and critical review of the search program. The program board was advisory rather than a decision making body due to the agile and dynamic nature of the operational environment, which required detailed technical decisions in short timeframes. The program board terms of reference were developed to support the role of the board.
- The ATSB's audit committee provided a review of program governance mechanisms through rolling audits of key program components, conducted by the ATSB's auditors. Details of the planned audits were outlined in the ATSB Internal Audit Annual Plans for each financial year. The ATSB's audit committee was focused on ensuring the program complied with all relevant legislation and policy and made efficient, effective and ethical use of public funds.

Figure 2 outlines the governance structure and lines of accountability for the search program as at January 2017.

Figure 2: Governance structure

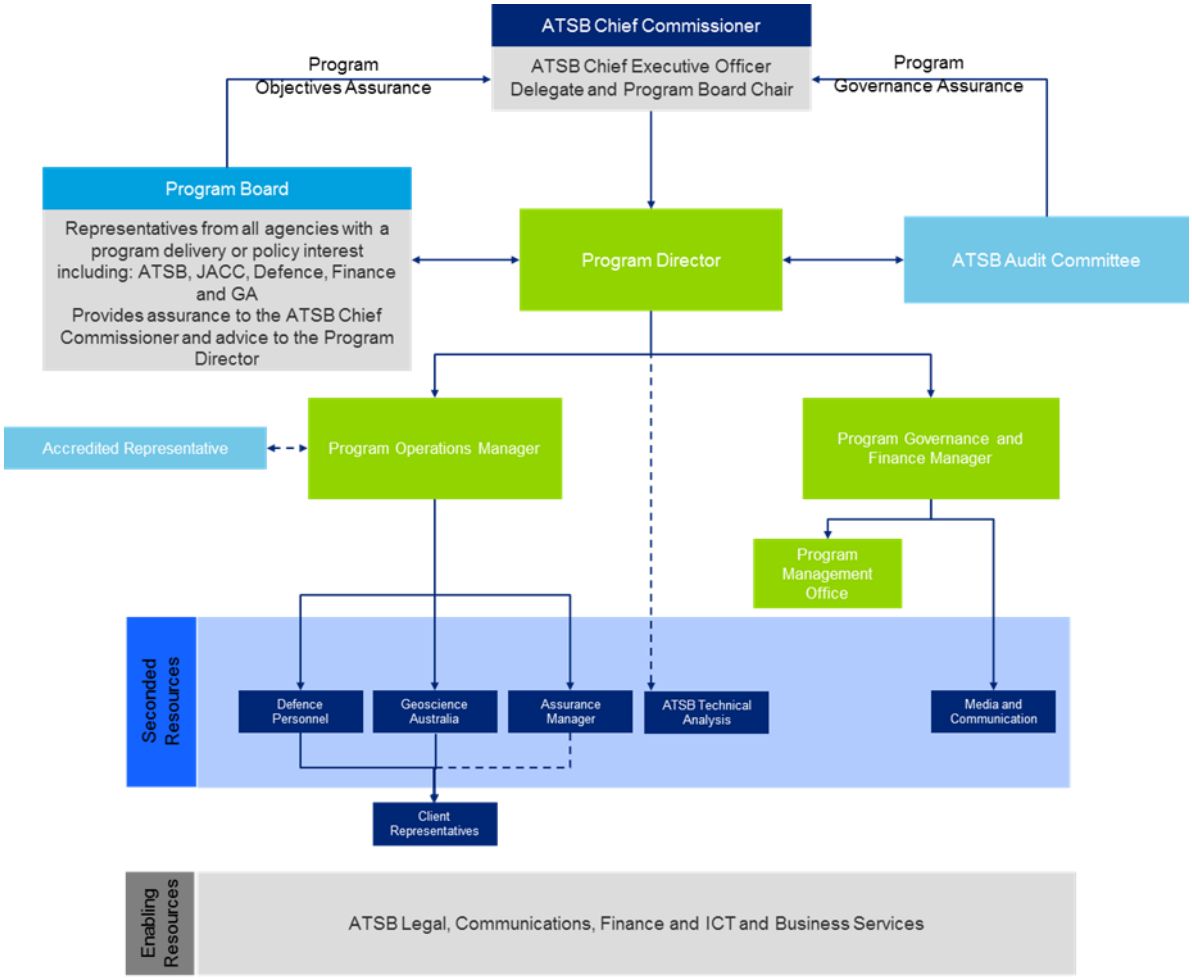

Source: ATSB

Communications and media

At times the ATSB's search program drew on the resources of the rest of the agency including the operational (investigation and technical resources), legal, finance, Information and Communications Technology and business services areas. Managing the significant volume of correspondence in relation to the search for MH370 required dedicated media and communications staff in the search team as the disappearance of MH370 has and continues to draw worldwide attention. The ATSB has received and processed over 3,500 pieces of correspondence, which include theories and queries from members of the public, scientists and academics, questions and requests for interviews and access from local and international press.

Website

When the ATSB assumed responsibility for coordinating the underwater search, a new MH370-specific section was added to the ATSB's website, www.atsb.gov.au/mh370. This section was designed to provide information and resources for all levels of interest. This included factsheets on various elements of the search, photographs and films, technical investigation reports and the archive of daily operational search updates.

Factsheets

The search for MH370 in the southern Indian Ocean involved a substantial amount of technical analysis and tasking, both to identify and refine the search area, and the practical elements of the conduct of the search itself. In an effort to provide the public with a clear understanding of the processes and resources, the ATSB published factsheets covering different elements of the search. These included:

- *MH370: Aircraft Debris and Drift Modelling*
- *MH370: Sonar Contacts*
- *Considerations on defining the search area – MH370*
- *Mapping the seafloor – Bathymetric survey – MH370*
- *The intensified underwater search for MH370*
- *MH370: Bathymetric Survey*
- *MH370: Multibeam Sonar*
- *MH370: Burst Timing Offset (BTO) Characteristics*
- *MH370: Update to Signalling Unit Logs*

The ATSB's website also provided links to works that collaborating agencies/bodies had published elsewhere:

- *The Search for MH370* (an article by Chris Ashton, Alan Shuster Bruce, Gary Colledge and Mark Dickinson of Inmarsat, published in The Journal of Navigation.)
- *MH370 – drift analysis: Trajectories of Global Drifter Program drifters* (an article by David Griffin of CSIRO)
- *The Use of Burst Frequency Offsets in the Search for MH370* (an article by Ian Holland of Defence Science and Technology Group.)
- *Bayesian Methods in the Search for MH370* (a book by Sam Davey, Neil Gordon, Ian Holland, Mark Rutten, and Jason Williams that encompassed the expert analysis of available data by the Defence Science and Technology Group.)

Technical Investigation Reports

As part of Australia's role in leading the search and as an accredited representative to Malaysia's Annex 13 investigation, the ATSB opened an external investigation, *AE-2014-054: Assistance to Malaysian Ministry of Transport in support of missing Malaysia Airlines flight MH370 on 7 March 2014 UTC.*

As part of that external investigation, the following reports have been published on the ATSB website:

- *MH370 – First Principles Review* (published 20 December 2016)
- *MH370 – Search and debris examination update* (published 2 November 2016, amended 2 December 2016)
- Debris examination reports 1, 2, 3, 4 and 5
- *MH370 – Definition of Underwater Search Areas* (published 3 December 2015, amended 10 December 2015)
- *MH370 – Flight Path Analysis Update* (published 8 October 2014)
- *MH370 – Definition of Underwater Search Areas* (published 26 June 2014, amended 18 August 2014, amended 30 July 2015).

The website also hosts the CSIRO reports; *The search for MH370 and ocean surface drift*, parts I, II and III and the Geoscience Australia report; *Summary of imagery analyses for non-natural objects in support of the search for Flight MH370*.

Search funding

Funding and resource contributions for the underwater search have been provided by the Governments of Malaysia, Australia and the People's Republic of China as outlined in Table 1.

Table 1: Resources available to the ATSB for search activities

Country	Contribution	Percentage of available resources
Malaysia[2]	A$115m	58%
Australia[3] [4] [5]	A$63m	32%
The People's Republic of China[6] [7]	A$~20m	10%
Overall Available Resources	**A$198m**	**100%**

Source: ATSB

Search actual costs

The estimated actual costs of the Australian led underwater search for MH370 to 30 June 2017 are detailed in Table 2. These costs cover the financial years 2013-14 through to 2016-17.

---

2 During 2014-15 Malaysia also directly funded the provision of a vessel (*GO Phoenix*) and search system as part of the underwater search. This vessel and equipment contributed to the search from September 2014 through to June 2015. The contract for the provision of these services was directly with Malaysia and the value of this contribution is not included in the figures above.

3 The funding contribution provided by Australia is outlined in Budget Measure 'Malaysia Airlines Flight MH370 – Search' as announced in the 2014-15 Budget. Details are provided in Budget Paper No. 2 2014-15 and the 2014-15 Portfolio Budget Statements for the Infrastructure and Regional Development Portfolio.

4 A funding measure was also provided by Australia and outlined in Budget Measure 'Malaysia Airlines Flight MH370 – International Contribution' as announced in the 2015-16 Budget. Details are provided in Budget Paper No. 2 2015-16 and the 2015-16 Portfolio Budget Statements for the Infrastructure and Regional Development Portfolio. The measure consisted of $43.9 million in 2014-15 and $50.0 million in 2015-16 with the cost of the measure fully offset by financial contributions to the search by the People's Republic of China and Malaysia.

5 A further funding contribution of $3 million provided by Australia outlined in Budget Measure 'Malaysia Airlines Flight MH370 - additional contribution - extension' in the 2016-17 Mid-Year Economic and Fiscal Outlook (MYEFO).

6 In November 2015 the People's Republic of China offered $20 million as a resource contribution to the search. This contribution included the search vessel, *Dong Hai Jiu 101*.

7 During the early part of the search the People's Republic of China provided the vessel *Zhu Kezhen* to undertake underwater mapping services. The value of this contribution is not included in the figures above.

Table 2: Estimated actual search costs to 30 June 2017

Search Phase	Cost area	Estimated actual cost to 30 June 2017
Underwater Search – ATSB Lead Program Components:	Underwater Search	A$170m
	Bathymetry (Underwater Mapping)	A$20m
	Program Management	A$7m
	Other sub-components (Definition of search area, Recovery preparation, Investigation Support)	A$1m
Total – Underwater Search Program Components:		**A$198m**

Source: ATSB

Costs for the search by Australian Government agencies (Commonwealth and State) over and above the funding provided in the Budget Measures have been absorbed by the respective agencies and are not included in the actual costs in Table 2.

History of the flight

Kuala Lumpur to waypoint IGARI

On 7 March 2014 at 1642 UTC[8], a Boeing 777-200ER aircraft, registered 9M-MRO and operating as Malaysia Airlines flight 370 (MH370), departed from runway 32R at Kuala Lumpur International Airport on an international scheduled passenger flight to Beijing, People's Republic of China. On board the aircraft were 239 persons, comprising 12 crew and 227 passengers.[9]

Following take-off, the aircraft was cleared by air traffic control (ATC) at Kuala Lumpur Air Traffic Control Centre to climb to 18,000 ft (FL180)[10]. The crew were approved to cancel the Standard Instrument Departure and track direct to the Instrument Flight Rules (IFR) waypoint IGARI (Figure 3).

Figure 3: History of recorded events

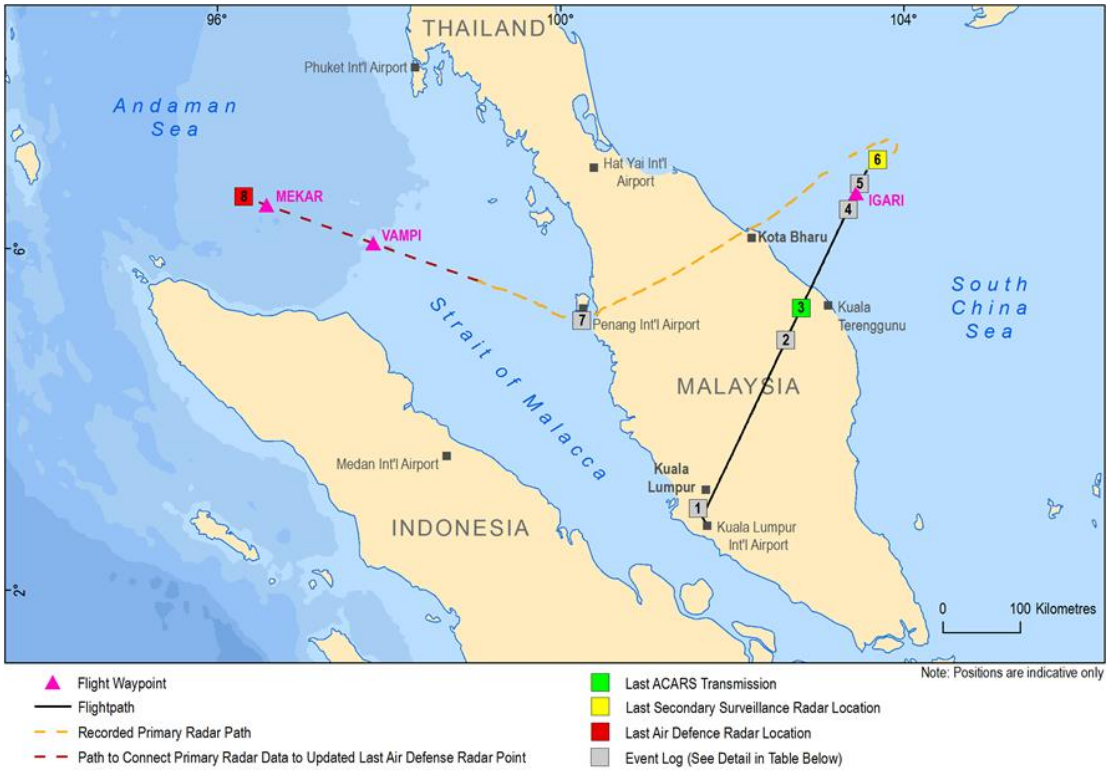

Source: ATSB, using Ministry of Transport Malaysia data

Subsequently, the aircraft was cleared to climb to FL250 and then to the planned cruising level of FL350. At 1701:17, the Pilot-in-Command (PIC) of MH370 reported maintaining FL350.

At 1707:29, the Aircraft Communications Addressing and Reporting System (ACARS) transmitted the flight's first 'B777 position report' via the aircraft's satellite communication system. Information in this report included the total fuel load of 43,800 kg, enough fuel for MH370 to remain airborne until approximately 0012. A position report was normally transmitted every 30 minutes, however the report at 1707:29 was the last ACARS report received from the aircraft.

Prior to the aircraft reaching waypoint IGARI, which denoted the border of the Vietnamese flight information region, Kuala Lumpur Air Traffic Control Centre instructed the crew to contact Ho Chi

---

8 Coordinated Universal Time (UTC) is used throughout this report. Malaysia time (MYT) was UTC +8 Hrs.

9 A more detailed history of the flight has been published by the Ministry of Transport Malaysia and is available here: www.mh370.gov.my/index.php/en/media2/transcript/category/13-mh370-safety-investigation-public

10 Flight levels give an approximate altitude in hundreds of feet. FL180 is approximately 18,000 ft.

Minh Air Traffic Control Centre (Vietnam) on a radio frequency of 120.9 MHz. At 1719:30, the PIC of MH370 acknowledged the instruction with 'Good night Malaysia Three Seven Zero.' This was the last recorded radio transmission from the aircraft.

Waypoint IGARI to waypoint MEKAR

The aircraft was fitted with a transponder that permitted ground-based secondary surveillance radars (SSR) to track it. A subsequent review of recorded ATC radar data revealed that the aircraft passed waypoint IGARI at 1720:31 and that the Mode S transponder symbol of the aircraft was not detected on Malaysian ATC radar after 1720:36. A matching SSR target captured by Vietnamese radar at Conson Island was no longer detected after 1720:33[11].

Some radars, called primary surveillance radars (PSR), can detect an aircraft without relying on a transponder, usually at a much shorter range than SSR. Recordings from a civilian PSR at Kota Baru in the north of Malaysia and a military PSR on Penang Island jointly showed a target that matched the time and location of MH370's last SSR position. While the recorded primary radar data was not continuous, the target could be followed with no ambiguity with other radar returns in the area. The limited fidelity of the PSR tracking data allowed the aircraft's speed, location, and altitude to be approximated from IGARI onwards.

From IGARI, the aircraft apparently made a 40° turn to the right and then a 180° turn to the left to track almost directly back across the Malay Peninsula, in the general direction of Penang Island. The aircraft passed over or near IFR waypoints ABTOK, KADAX and GOLUD (which are within 3 NM of each other) and later PUKAR.

The aircraft made a slow right turn south of Penang Island. A mobile telephone registered to the aircraft's first officer was detected by a mobile telecommunications tower at Bandar Baru Farlim Penang at 1752:27, when the aircraft was south of Penang. There was no record of communications having been made or attempted using this telephone.[12]

Radar data shows the aircraft then headed to the northwest, eventually aligning with published air route N571 from IFR waypoint VAMPI. The validity of this section of the radar data was verified using the track of a commercial flight that followed N571 about 33 NM behind MH370. The aircraft continued to the northwest until a final radar position for the aircraft was recorded approximately 10 NM beyond IFR waypoint MEKAR at 1822:12 (Figure 3). There were no reports of the aircraft being detected by any radar after this time. Key events are summarised in Table 3.

Table 3: Key recorded events

Recorded Event	Time (UTC)
Event 1: MH370 departed Kuala Lumpur International Airport	1642
Event 2: PIC reported maintaining FL350	1701:17
Event 3: ACARS report transmitted	1707:29
Event 4: Last radio transmission from MH370	1719:30
Event 5: Aircraft passed over waypoint IGARI	1720:31
Event 6: Last recorded secondary surveillance radar position	1721:13
Event 7: First officer's mobile phone detected by Penang communications system	1752:27
Event 8: Last primary surveillance radar position	1822:12

Source: Ministry of Transport Malaysia, Royal Malaysian Police

[11] From 1739:03 onwards, Malaysian and Vietnamese controllers attempted to contact the aircraft by radio without success. A distress phase was formally initiated by Malaysian ATC at 2232:00.

[12] This information was obtained by the Royal Malaysian Police and reported to the Ministry of Transport Malaysia. Though a formal report was not available to the ATSB, information relevant to the search was shared.

Waypoint MEKAR onwards

At 1825:27, about three minutes after the last primary radar return, the aircraft's satellite data unit (SDU) initiated a log-on sequence via the Inmarsat Indian Ocean Region I-3 satellite to the ground station in Perth, Western Australia. The log-on sequence and timings of subsequent SDU communications were recorded by the Inmarsat ground station, including several automated handshakes[13] initiated by either the ground station or the aircraft, and two unanswered ground-to-air satellite telephone call attempts (made by the aircraft operator in an attempt to contact the aircraft). This information showed that the flight continued for almost six hours after the last radar return (Table 4).

Table 4: Satellite communications after passing waypoint MEKAR

Recorded SDU communications	Time (UTC)
Handshake 1 initiated by the aircraft	1825:27
Unanswered ground to air telephone call	1839:52
Handshake 2 initiated by the ground station	1941:00
Handshake 3 initiated by the ground station	2041:02
Handshake 4 initiated by the ground station	2141:24
Handshake 5 initiated by the ground station	2241:19
Unanswered ground to air telephone call	2313:58
Handshake 6 initiated by the ground station	0010:58
Handshake 7 initiated by the aircraft	0019:29
Aircraft did not respond to log-on interrogation from the satellite earth ground station (failed handshake).	0115:56

Source: Inmarsat

As part of routine logging, Inmarsat recorded the burst timing offset (BTO) and burst frequency offset (BFO) information for each handshake. Though not intended for this purpose, the BTO could be used to find the distance between the aircraft and the satellite at the time of each handshake. A series of seven rings, joining points on the earth's surface equidistant from the satellite, shows the range of possible locations of the aircraft at the time of each handshake (Figure 4). By taking the maximum speed of the aircraft into account, the BTO derived rings could be reduced in length to arcs (there are some areas of the rings the aircraft simply could not have reached).

[13] In satellite communications, a handshake is a series of signalling messages that establish or maintain a communication channel.

Figure 4: BTO ring solutions for MH370

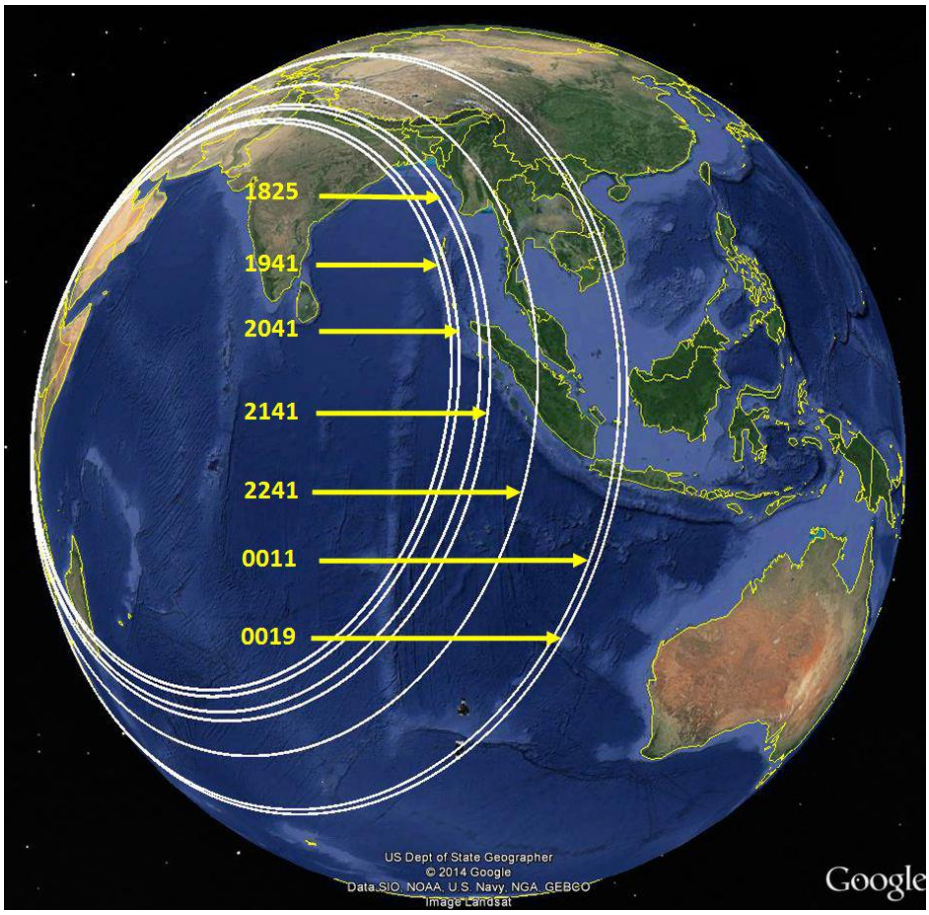

Source: Google earth, annotated by ATSB

The BFO was influenced by the speed of the aircraft relative to the satellite which is affected by the aircraft position, direction and speed of travel, and the satellite's own movement. Analysis of the BFO metadata revealed that the aircraft headed south from some point beyond waypoint MEKAR to a region in the southern Indian Ocean. This analysis was later supported by studying[14] the drift of MH370 debris which was found on the shorelines of eastern African nations in 2015 and 2016.

Analysis of the last satellite communication at 0019.29, which was an unscheduled log-on request from the aircraft, determined that it was probably the result of the aircraft having exhausted its fuel and then being powered by the auxiliary power unit. Based on the last transmitted fuel status and aircraft performance data the time that this occurred generally aligned with the expected time of fuel exhaustion. It was concluded that the aircraft probably impacted the ocean relatively close to the time this last transmission was made, which is referred to as the 7th arc.

The methodologies for calculating the aircraft's possible flight paths were outlined in the ATSB's reports:

- *MH370 – Definition of Underwater Search Areas* (released 26 June 2014, amended 18 August 2014, amended 30 July 2015)
- *MH370 – Flight Path Analysis Update* (released 8 October 2014)
- *MH370 – Definition of Underwater Search Areas* (released 3 December 2015, amended 10 December 2015)

[14] Refer to the CSIRO reports prepared for the ATSB: *The search for MH370 and ocean surface drift- parts I, II and III.*

- *MH370 – Search and debris examination update* (released 2 November 2016, amended 2 December 2016)
- *MH370 – First Principles Review* (released 20 December 2016)

Aircraft Information

The aircraft operating flight MH370 was a Boeing 777-2H6[15]ER model, powered by two Rolls-Royce Trent 800 Turbofan engines (Figure 5).

Figure 5: 9M-MRO, the aircraft operating Malaysia Airlines flight MH370 on 8 March 2014

Source: Seth Jaworski

Airframe

Manufacturer:	Boeing Company
Model:	777-2H6ER
Serial number:	28420
Registration:	9M-MRO
Date of manufacture:	29 May 2002
Date of delivery:	Delivered new on 31 May 2002
Certificate of airworthiness:	M.0938 valid to 2 June 2014
Certificate of registration:	M.1124 issued 23 August 2006 Replacement of Certificate issued 17 June 2002
Last maintenance check:	A1 Check on 23 February 2014 at 53,301:17 hours and 7,494 cycles
Total airframe hours/cycles:	53,471.6 hours/7,526 cycles (as of 7 March 2014)

Source: Malaysia Airlines

[15] H6 denotes the unique Boeing customer code for 737, 747 and 777 aircraft purchased by Malaysia Airlines.

Engines

Manufacturer:	Rolls-Royce	
Model:	RB211 Trent 892B-17	
	Engine 1 (Left)	**Engine 2 (Right)**
Serial number:	51463	51462
Date of construction:	November 2004	October 2004
Date installed:	8 May 2013	15 June 2010
Last Shop Visit:	6 September 2010 to 21 November 2010	5 February 2010 to 14 April 2010
Time in Service:	40,779 hours, 5,574 cycles (as of 7 March 2014)	40,046 hours, 5,508 cycles (as of 7 March 2014)

Source: Malaysia Airlines

Auxiliary Power Unit

Manufacturer:	Allied Signal
Model:	GTCP 331-500B
Serial number:	P1196
Auxiliary Power Unit hours:	22,093 (as of 7 March 2014)

Source: Malaysia Airlines

Flight crew and passengers

The passenger manifest for MH370, supplemented by information confirmed by INTERPOL, identifies the nationalities of passengers and crew on board the flight (Table 5).

Table 5: Nationalities of passengers and crew on board MH370

Nationality	Passengers	Crew
Chinese	153	
Malaysian	38	12
Indonesian	7	
Australian	6	
Indian	5	
French	4	
American	3	
New Zealander	2	
Ukrainian	2	
Canadian	2	
Russian	1	
Chinese Taipei	1	
Dutch	1	
Iranian	2 (travelling under stolen Austrian and Italian passports)	

Source: Malaysia Airlines flight MH370 flight manifest and INTERPOL

The surface search

The surface search for MH370 lasted from 8 March 2014 until 28 April 2014 and was initially a search and rescue operation. The intent was to locate the aircraft as quickly as possible in order to rescue any potential survivors. The areas searched were based on information from a range of sources and progressively refined analysis in relation to the aircraft's most likely flight path.

Early in the surface search the Malaysian Government convened the Joint Investigation Team (JIT) comprising experts from the People's Republic of China, France, Malaysia, United Kingdom, United States and Malaysian Government officials. Soon after, a satellite communications working group (SATCOM WG) was also formed and included experts from Inmarsat and Thales. These groups of experts worked together to provide advice to the Malaysian Government on the surface search areas.

By the end of the surface search an area of several million square kilometres had been searched by aircraft and surface vessels in the South China Sea, Andaman Sea, Bay of Bengal and Indian Ocean, however no items of debris from MH370 were recovered or positively identified.

The following section sets out the chronology of the surface search, the search assets used, the areas of focus at different times and the information or analysis used to define each area.

Malaysian led surface search

Search operations commenced on the day that MH370 went missing, 8 March 2014, and were led by Malaysian and Indonesian authorities in areas around Malaysia until 23 March 2014.

East of the Malay Peninsula

Initially search and rescue (SAR) operations were coordinated by Kuala Lumpur Aeronautical Rescue Coordination Centre (KL ARCC) and were conducted to the east of the Malay Peninsula in the South China Sea between 8 and 15 March 2014 (Table 6). This area was based largely on the last contact with the aircraft and where the SSR transponders ceased to operate.

Table 6: Initial surface search SAR operations east of Malaysia

Dates:	8–15 March 2014
Event:	Malaysia (KL ARCC) initial surface search area.
Search area location:	East of Malay Peninsula (South China Sea).
Search activity:	Aerial and surface search.
Guiding advice:	Malaysia Air Defense.
Data used in planning search area refinement:	Malaysia Air Defense secondary surveillance radar data. Track BD764 7 March 2014 1642:07–1728:37 UTC recorded at 10 second intervals.
Search equipment:	28 aircraft from the People's Republic of China (2), Japan (5), Malaysia (10), Singapore (4), Thailand (1), United States (2) and Vietnam (4). 34 vessels from the People's Republic of China (7) Malaysia (19), Singapore (3), United States (3) and Vietnam (2).
Search area:	573,000 km^2

Source: DCA Malaysia

The areas covered during the search operations in the South China Sea are shown in Figure 6.

Figure 6: Surface search east of the Malay Peninsula 8 to 15 March 2014

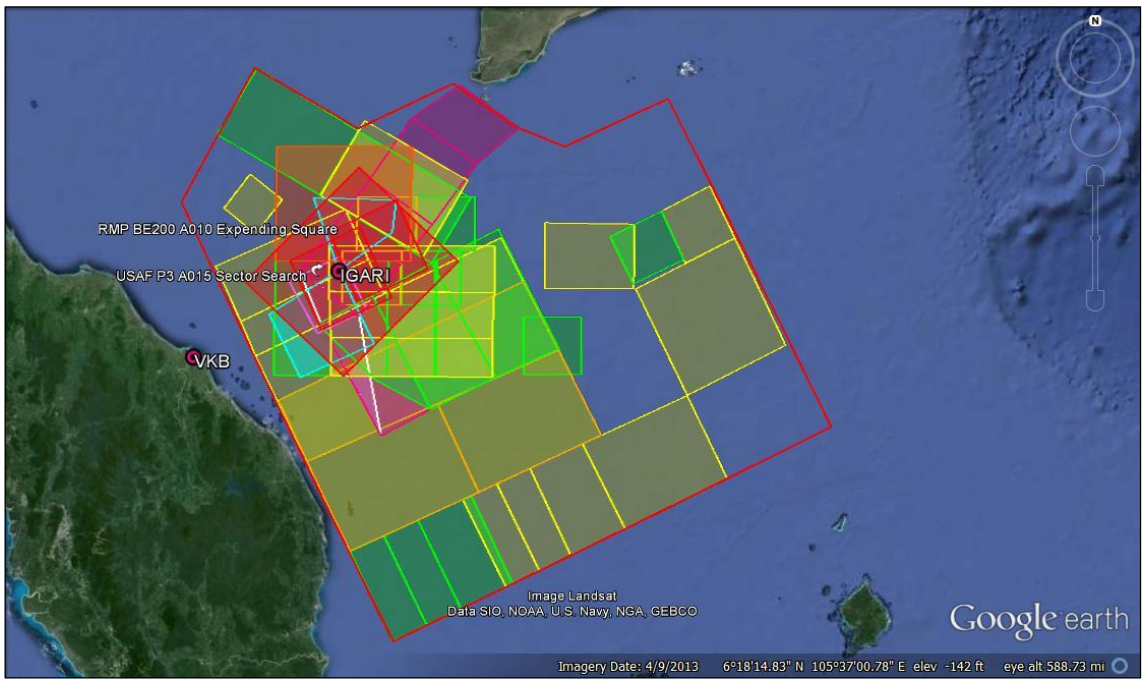

Source: Google earth, annotated by DCA Malaysia

West of the Malay Peninsula

From 8 to 15 March 2014, the same time as the surface search in the South China Sea east of the Malay Peninsula, SAR operations coordinated by the Royal Malaysia Air Force, were conducted to the west of the Malay Peninsula (Table 7).

Table 7: Initial surface search SAR operations west of Malaysia

Dates:	8–15 March 2014
Event:	Malaysia (Royal Malaysia Air Force) initial surface search area.
Search area location:	West of Malay Peninsula (Strait of Malacca, Andaman Sea and the Bay of Bengal) and West of Sumatra.
Search activity:	Aerial and surface search.
Guiding advice:	Malaysia Air Defense.
Data used in planning search area refinement:	Malaysia Air Defense primary radar data. Track BE144 7 March 2014 1729:09–1802:59 UTC recorded at 10 second intervals.
Search equipment:	36 aircraft and 35 vessels from Australia, Bangladesh, the People's Republic of China, India, Indonesia, Malaysia, New Zealand, Republic of Korea, Singapore, Thailand, United Arab Emirates and the United States.
Search area:	4,560,000 km^2

Source: DCA Malaysia

These search operations were undertaken in the Strait of Malacca, Andaman Sea, Bay of Bengal and west of Sumatra from 8 to 15 March 2014 (Figure 7, areas subject to search operations shown in white and blue). This area was searched based on the primary radar data which indicated an unidentified aircraft had flown up the Strait of Malacca, thought to be MH370.

Figure 7: Surface search areas west of the Malay Peninsula 8 to 15 March 2014

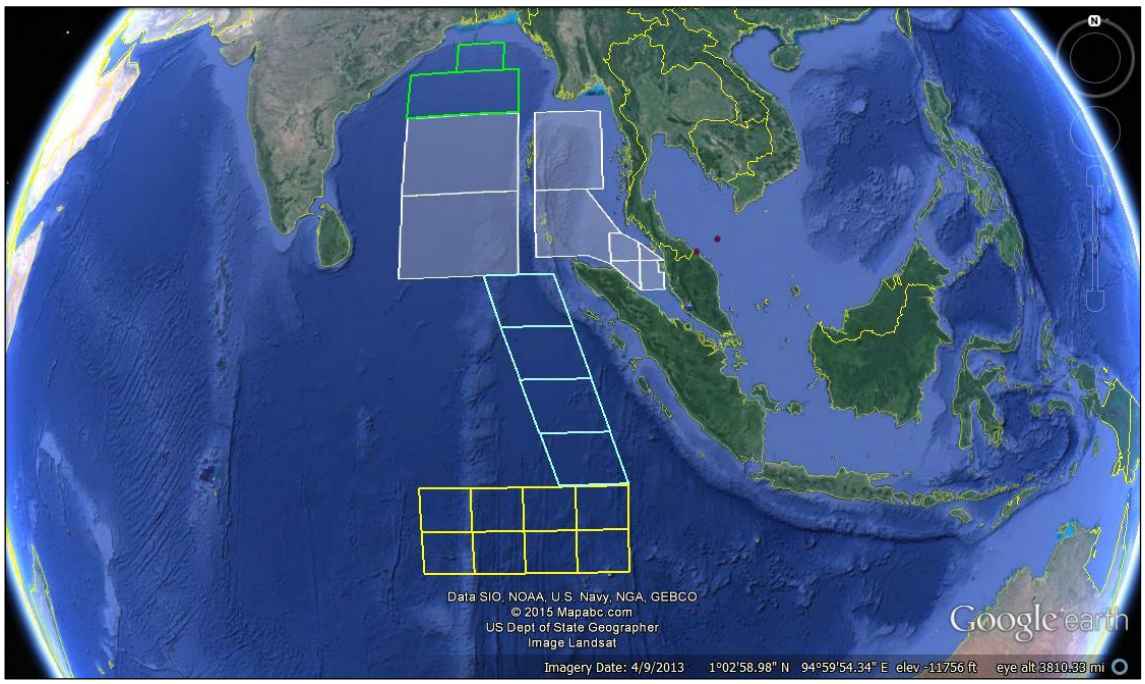

Source: Google earth, annotated by DCA Malaysia

Northern and southern corridors announced

In the first week of the surface search an analysis of Inmarsat satellite communication (SATCOM) data for MH370 indicated that the aircraft had flown for a further six hours after the final radar capture at the northern tip of Sumatra. The initial satellite data analysis indicated that the aircraft had flown along one of two corridors; one to the north in the direction of Kazakhstan or one to the south to the Indian Ocean. This new information led to the suspension of SAR operations to the east and west of the Malay Peninsula on 15 March 2014.

Figure 8: Southern corridor

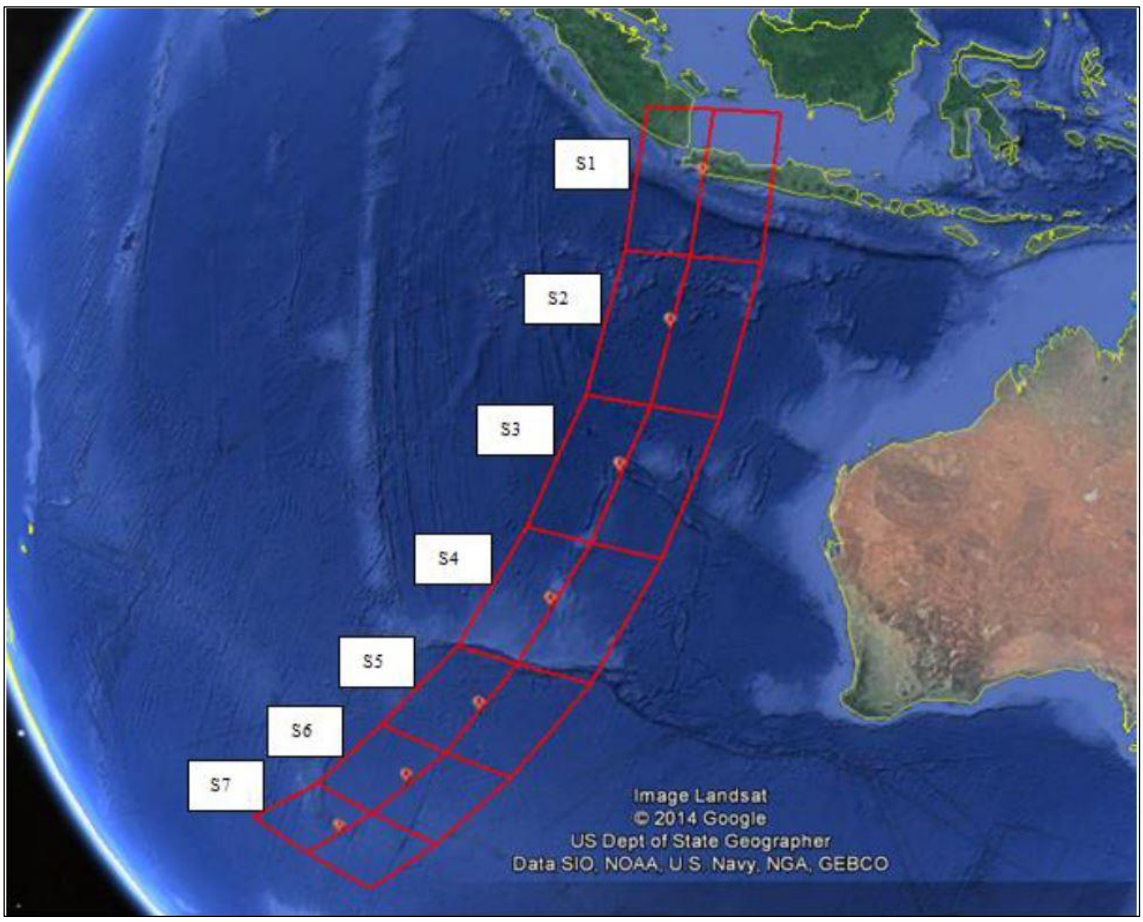

Source: Malaysia, ICAO Third Meeting of the Asia/Pacific Regional Search and Rescue Task Force (APSAR/TF/3) Working Paper 06, Maldives, 25 – 29 January 2015

An aerial search coordinated by KL ARCC and Badan SAR Nasional (BASARNAS), the Republic of Indonesia National Search and Rescue Agency, was conducted within the southern corridor indicated by the SATCOM data from 18 to 23 March 2014 (Table 8).

Table 8: SAR operations southern corridor

Dates:	18–23 March 2014
Event:	Malaysia (KL ARCC) and Indonesia (BASARNAS) refined surface search area.
Search area location:	Within S1-S3 (Malaysian designation – refer Figure 8 and Figure 9) of the southern corridor.
Search activity:	Aerial search
Guiding advice:	Timing information obtained from satellite data and aircraft performance data was used to identify a northern and southern corridor along which MH370 may have flown with probable final location close to the 6th arc.
Data used in planning search area refinement:	MH370 Inmarsat satellite data unit logs and advice from SATCOM WG and data compiled by the JIT.
Search equipment:	Eight aircraft from India, Japan, Malaysia, Republic of Korea, United Arab Emirates and the United States.
Search area:	1,630,000 km^2

Source: DCA Malaysia

By 24 March 2014, further analysis of the SATCOM data established that the data was only consistent with flight paths along the southern corridor ending in the southern Indian Ocean.

Figure 9: KL ARCC and BASARNAS S1, S2 and S3 search areas (18-23 March 2014)

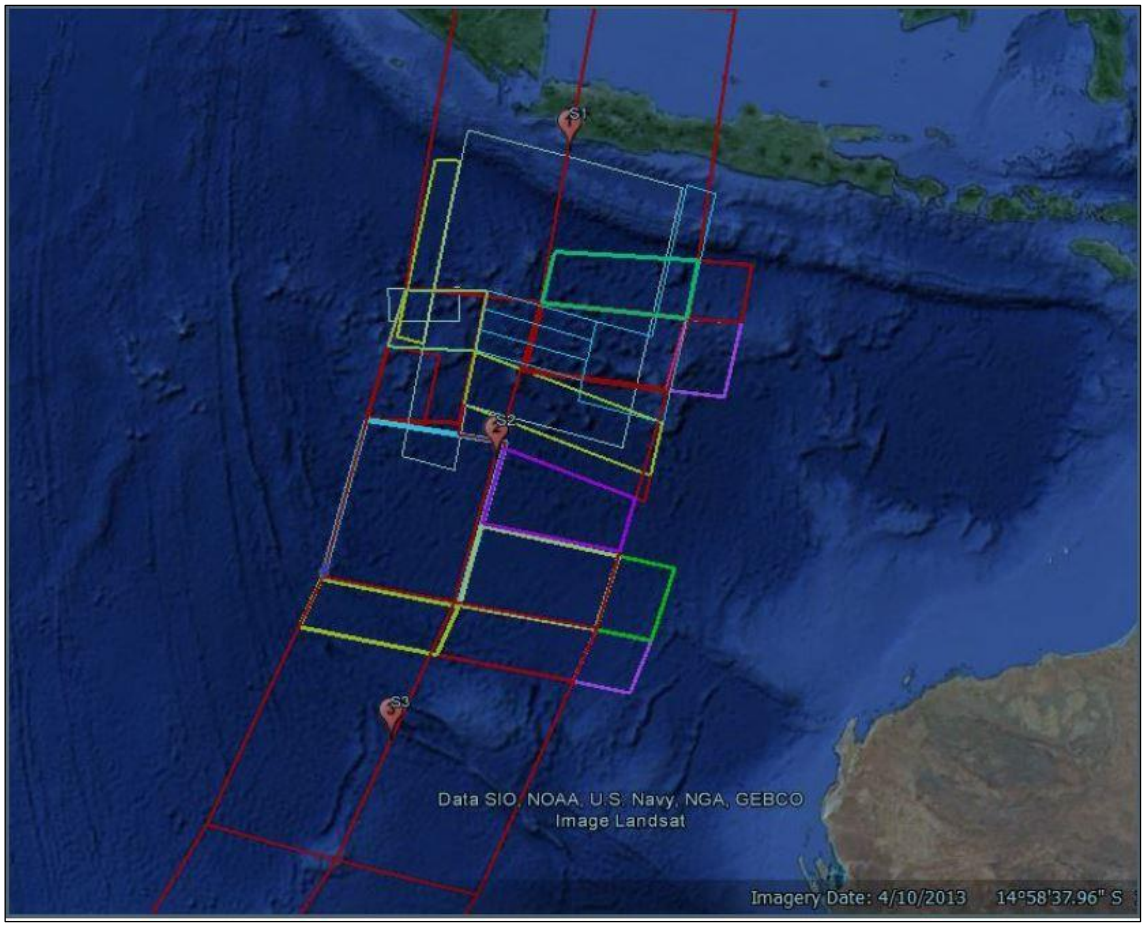

Source: Malaysia, ICAO Third Meeting of the Asia/Pacific Regional Search and Rescue Task Force (APSAR/TF/3) Working Paper 06, Maldives, 25 – 29 January 2015

Australian led surface search

On 17 March 2014, with the southern corridor extending into the Indian Ocean and the Australian search and rescue region, Australia assumed responsibility for coordinating the SAR operation for the aircraft, at Malaysia's request. The Australian Maritime Safety Authority (AMSA) was responsible for coordinating this activity using aircraft and surface vessels operating from Western Australia until 28 April 2014. AMSA continued to take advice on the areas to search from the JIT and SATCOM WG based on the progressive analysis of the Inmarsat satellite communication logs and other aircraft performance analysis.

The surface search was focused on the identification and recovery of any debris from the aircraft floating on the sea surface. When AMSA took over the coordination of the surface search nine days had passed since the aircraft went missing. It was therefore necessary to define the areas to be searched by aircraft and surface vessels based on the analysis indicating where the aircraft may have ended the flight and the calculated drift of a range of possible types of floating debris in the days after 8 March 2014.

A drift modelling working group was set up by AMSA, comprising a number of organisations including: CSIRO, Asia-Pacific Applied Science Associates, the United States Coastguard, the Bureau of Meteorology and Global Environmental Modelling and Monitoring Systems to ensure that best practice drift modelling was put in place for the surface search. The drift modelling was also informed by the deployment of self-locating datum marker buoys (SLDMB) from aircraft and

vessels throughout the surface search. A SLDMB is a drifting surface buoy fitted with a GPS that is used to measure surface ocean currents. The marker buoy has an expected lifetime of over 20 days once deployed in the ocean. Similarly, real-time wind and wave data from the search area was used to continuously update the drift models.

Initial southern Indian Ocean surface search area

The initial Australian led MH370 surface search area was determined to be a 600,000 km² area of the southern Indian Ocean approximately 2,500 km from Perth, Western Australia (Table 9). The area was determined by assuming the aircraft had made a southern turn shortly after the last radar capture at the northern tip of Sumatra and flew until fuel exhaustion.

Table 9: Initial southern Indian Ocean surface search SAR operations

Dates:	18–19 March 2014
Event:	Australia (AMSA) initial surface search area.
Search area location:	S1/S2[16]
Search activity:	Aerial visual and radar search.
Guiding advice:	MH370 Inmarsat satellite data unit logs and advice from SATCOM WG to AMSA. Data compiled by the JIT in conjunction with NTSB.
Data used in planning search area refinement:	The actual satellite location. Turn south occurred at the northern tip of Sumatra. Performance predictions based on speed and range only with no wind consideration. Only positional information from Malaysian primary radar data. Length of arc to the south constrained by maximum aircraft groundspeed Lateral navigation set to 'track' mode. Two speeds provided 'best fit` with longest and straightest tracks reaching the 6th arc. Assumed speed and altitude to last radar point were final ACARS values.
Search equipment:	Aircraft from Australia, New Zealand and the United States. Two merchant vessels responded to urgency broadcast and transited to and through search area.
Search area:	Refer to Table 10.

Source: ATSB

Search areas in the southern Indian Ocean designated S1, S2 and S3 (Figure 10) were defined from estimates of the aircraft's performance and endurance. In particular, two hypothetical speeds (469 and 475 knots) that resulted in the longest, straightest tracks that reached the 6th arc derived from the SATCOM data. These tracks intersected the arc in areas S1 and S2, so they were used to define the initial search area.

[16] JIT designation of search areas with S1 in the south (see Figure 10) as used by AMSA and ATSB

Figure 10: Possible southern final positions S1–S3 based on MH370 maximum range

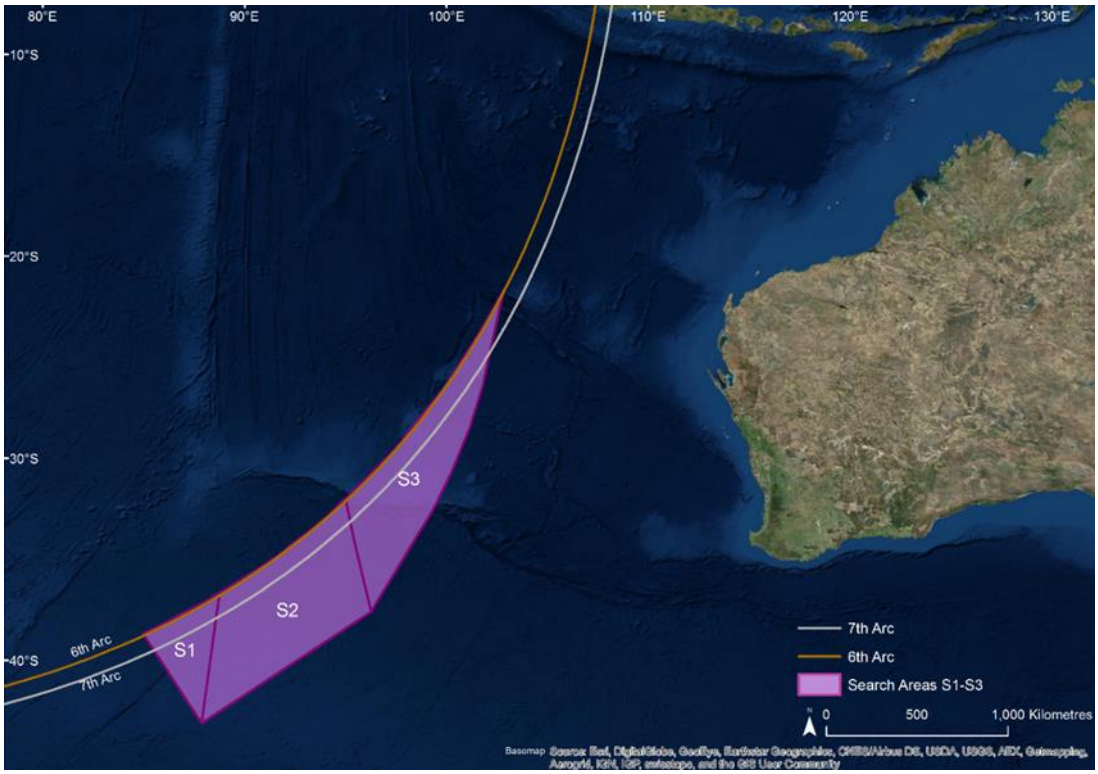

Source: ATSB, using JIT data

On 18 and 19 March 2014, areas S1 and S2 were corrected for drift which provided the surface search areas for those days (Figure 11 and Figure 12).

Figure 11: Area searched 18 March 2014

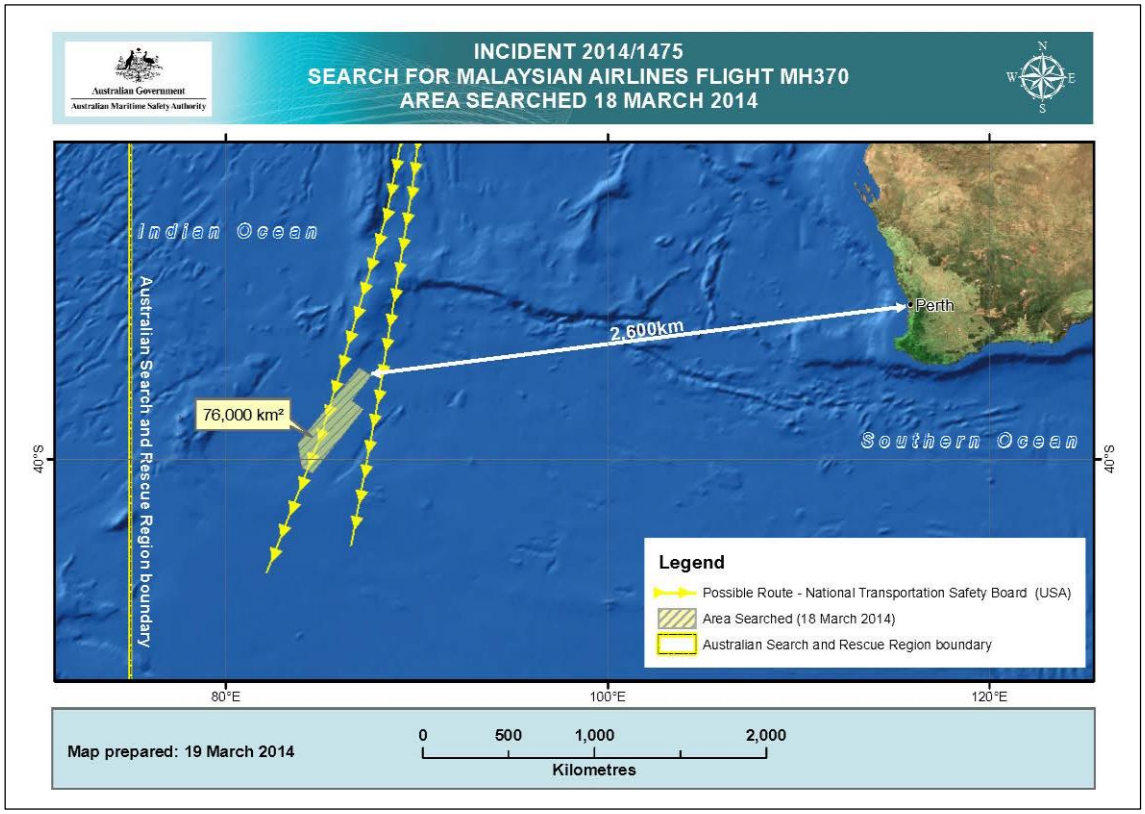

Source: AMSA

Figure 12: Area searched 19 March 2014

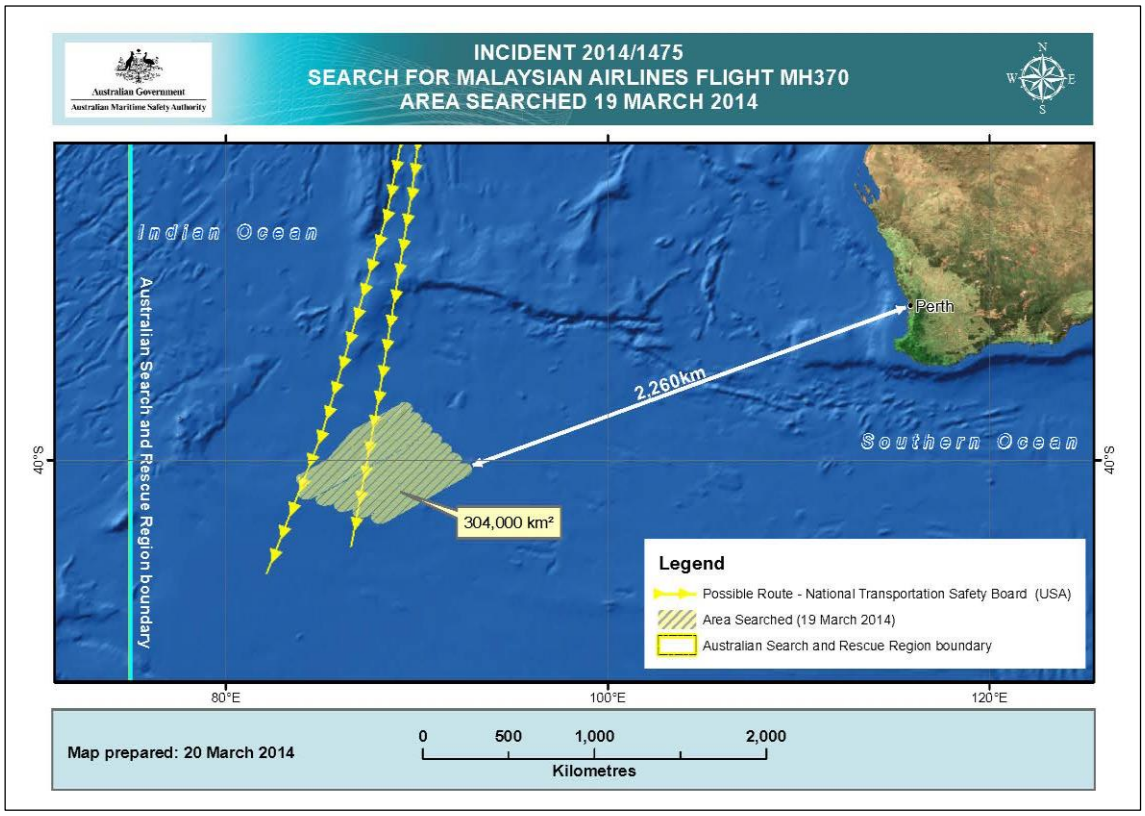

Source: AMSA

Table 10: Search area information 18 to 19 March 2014

Date	Drifted splash point area	Search Area (km²)	Track spacing (NM)	Aircraft	Vessels	SLDMB drop	Sightings
18-Mar-14	Initial JIT Analysis (S1/S2)	65,938	40	1	2		
19-Mar-14	Initial JIT Analysis (S1/S2)	320,855	40	4	1	1	

Source: AMSA

Satellite imagery debris detections

While the initial surface search activity in the southern Indian Ocean was based on the analysis of the aircraft's possible flight paths and maximum endurance, other information was being actively sought including satellite imagery. AMSA, working with the Australian Geospatial-Intelligence Organisation, had requested governments with low earth orbiting satellites to gather imagery in and around the MH370 search area (see section on Satellite imagery analysis). Imagery was analysed for possible aircraft debris and the information was passed to Australian Geospatial-Intelligence Organisation and AMSA.

From 16 to 27 March 2014, a number of potential debris sightings were made in satellite imagery including seven in the region of 43–45ºS, 90–97ºE. The objects were estimated to be between 5 m and 24 m in length. The surface search was refocused to this area to investigate these sightings and subsequent aerial sightings (Figure 13 and Table 11).

Search activity transitioned to a search and recovery operation from 25 March 2014.

Table 11: Satellite imagery search area

Dates:	20–27 March 2014
Event:	Australia (AMSA) satellite imagery search area.
Search area location:	Approximately 42ºS–46ºS
Search activity:	Satellite visual and radar search (multiple nations). Aerial and surface visual/ radar search. Datum marker buoys deployed by air to assist in future drift modelling.
Guiding advice:	MH370 Inmarsat satellite data unit logs and advice from SATCOM WG to AMSA Commercial satellite imagery of objects possibly related to MH370 received by AMSA.
Data used in planning search area refinement:	Assessment of commercial satellite imagery indicates possible debris approximately 148 km southeast of the initial search area.
Search equipment:	Aircraft from Australia, New Zealand, United States, Japan, the People's Republic of China and the Republic of Korea. Vessels from Royal Australian Navy (RAN) and the People's Republic of China.
Search area:	Refer to Table 12.

Source: ATSB

Figure 13: Cumulative area searched from 18 to 27 March 2014

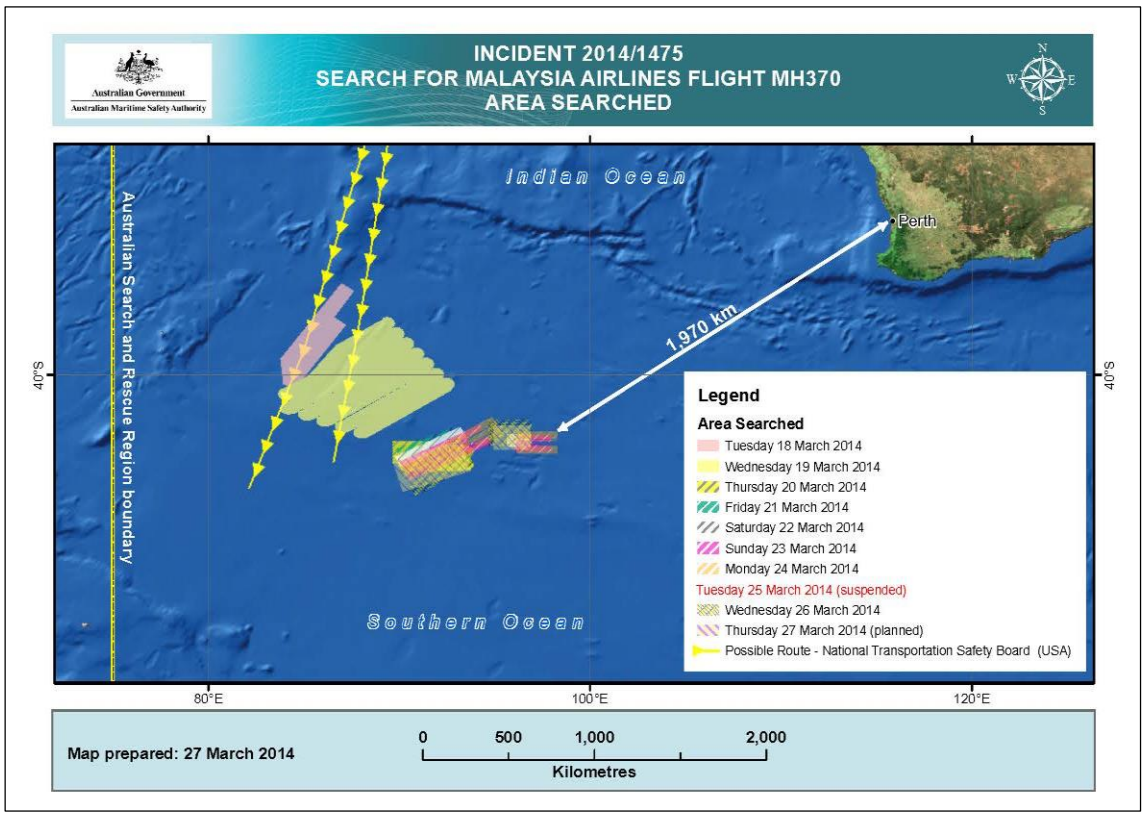

Source: AMSA

Table 12: Search area information 20 to 27 March 2014

Date	Drifted splash point area	Search Area (km^2)	Track spacing (NM)	Aircraft	Vessels	SLDMB drop	Sightings
20-Mar-14	Satellite imagery (SE of S1/S2)	67,827	40/9	5	1	3	4
21-Mar-14	Satellite imagery (SE of S1/S2)	22,869	2	6	1		1
22-Mar-14	Satellite imagery and aerial (SE of S1/S2)	40,178	3	7	3	1	6
23-Mar-14	Satellite imagery and aerial (SE of S1/S2)	59,138	3/4	9	1		9
24-Mar-14	Satellite imagery and aerial (SE of S1/S2)	72,501	3/4/5	10	1	1	6
25-Mar-14	Satellite imagery and aerial (SE of S1/S2)	0[17]	N/A	1	0	3	
26-Mar-14	Satellite imagery and aerial (SE of S1/S2)	74,420	2/3/4	11	5		3
27-Mar-14	Satellite imagery and aerial (SE of S1/S2)	0[18]	2/5	9	5		

Source: AMSA

[17] No aviation search due to weather.
[18] No aviation search due to weather.

There were also possible debris detections from 20 to 23 March 2014, by French satellites at a location 80 to 150 km west of the 7th arc (these are discussed further in the Satellite imagery analysis section).

Refined surface search area

By 27 March 2014, following further analysis, the JIT had more confidence in MH370's speeds derived by the primary radar data captured around Malaysia. The analysis indicated that the aircraft's rate of fuel burn was higher during this segment of the flight than first thought and therefore its maximum range was decreased. The most probable track moved north to the S3 area and two new search areas designated S4 and S5 were defined (Figure 14). The corresponding drifted areas during this period of the surface search were areas A and B (Figure 15).

The fuel analysis also provided more confidence that the 7th arc represented the point of fuel exhaustion for the aircraft so a recommendation was made to search in a north-easterly direction along the 7th arc from the S3/S4 area boundary (Table 13).

Table 13: Refined surface search area

Dates:	28 March – 3 April 2014
Event:	Australia (AMSA/ATSB) refined surface search area.
Search area location:	S3/S4 overlap drifted Area A, S3/S4 overlap, drifted Area B.
Search activity:	Aerial and surface visual and radar search of areas drifted from the 7th arc by drifting group comprising AMSA, Global Environmental Modelling and Monitoring Systems, CSIRO, Asia-Pacific Applied Science Associates and United States Coast Guard. Satellite search (multiple nations) of areas drifted from the 7th arc.
Guiding advice:	S3/S4 starting from southerly region of S4. MH370 Inmarsat satellite data unit logs and advice from SATCOM WG. Briefing by the JIT by telephone from Kuala Lumpur on 27 March 2014 to ATSB embedded team at AMSA.
Data used in planning search area refinement:	Greater confidence in increased speeds from primary radar thus increased fuel burn. More confidence that 7th arc was fuel exhaustion point.
Search equipment:	Aircraft from Australia, New Zealand, United States, Japan, the People's Republic of China, Republic of Korea and Malaysia. Vessels from the RAN and the People's Republic of China.
Search area:	Refer to Table 14.

Source: ATSB

Figure 14: Defined search areas 27 March 2014 (including 7th arc and maximum range cruise boundary)

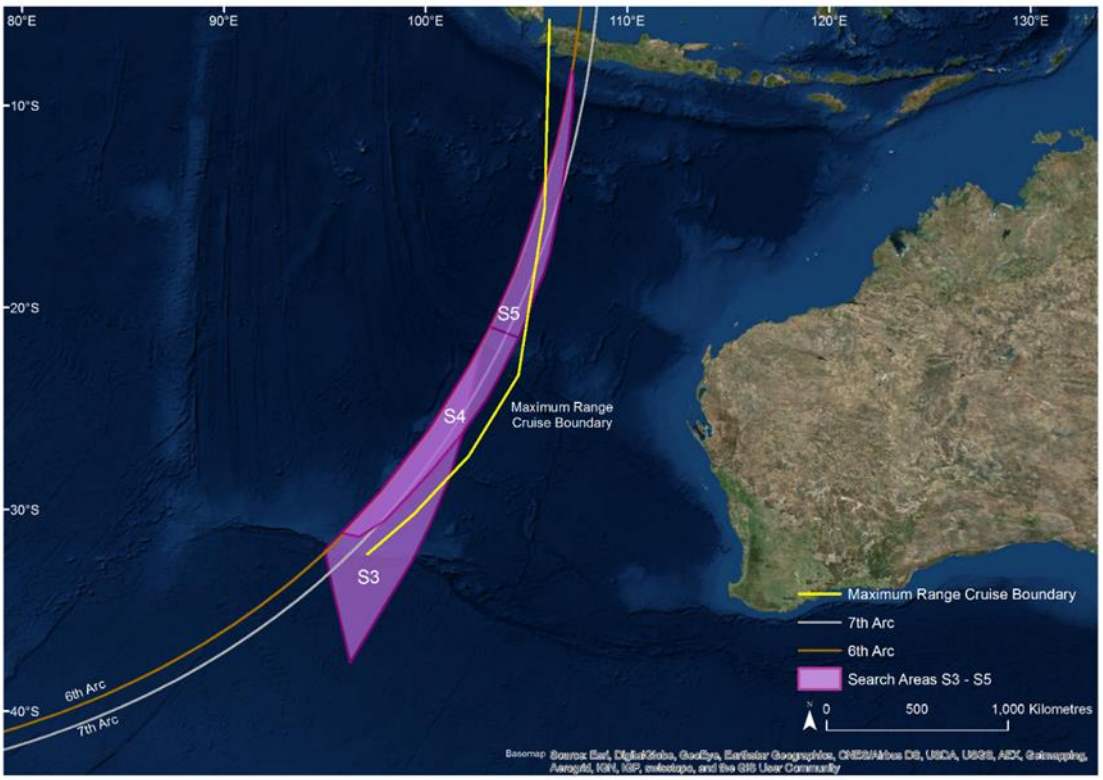

Source: ATSB, using JIT data

Figure 15: Original and drifted search areas 28 March 2014 to 28 April 2014

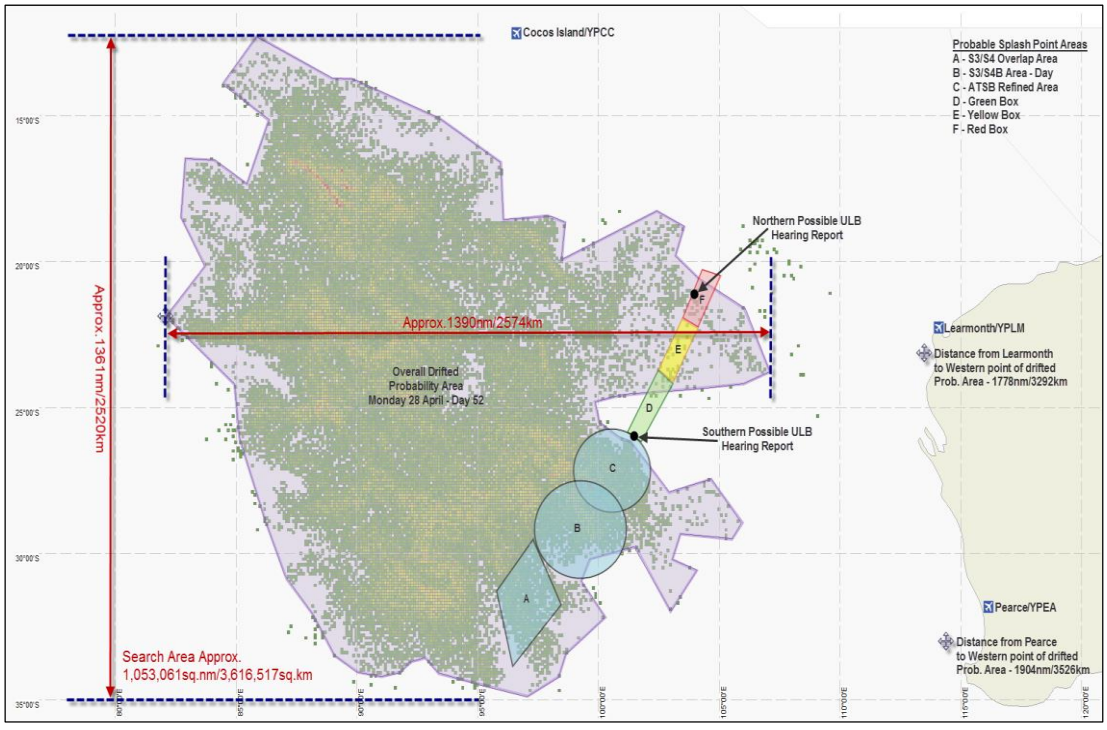

Source: AMSA

Figure 16: Move to refined area 28 March 2014 – planned and cumulative area searched

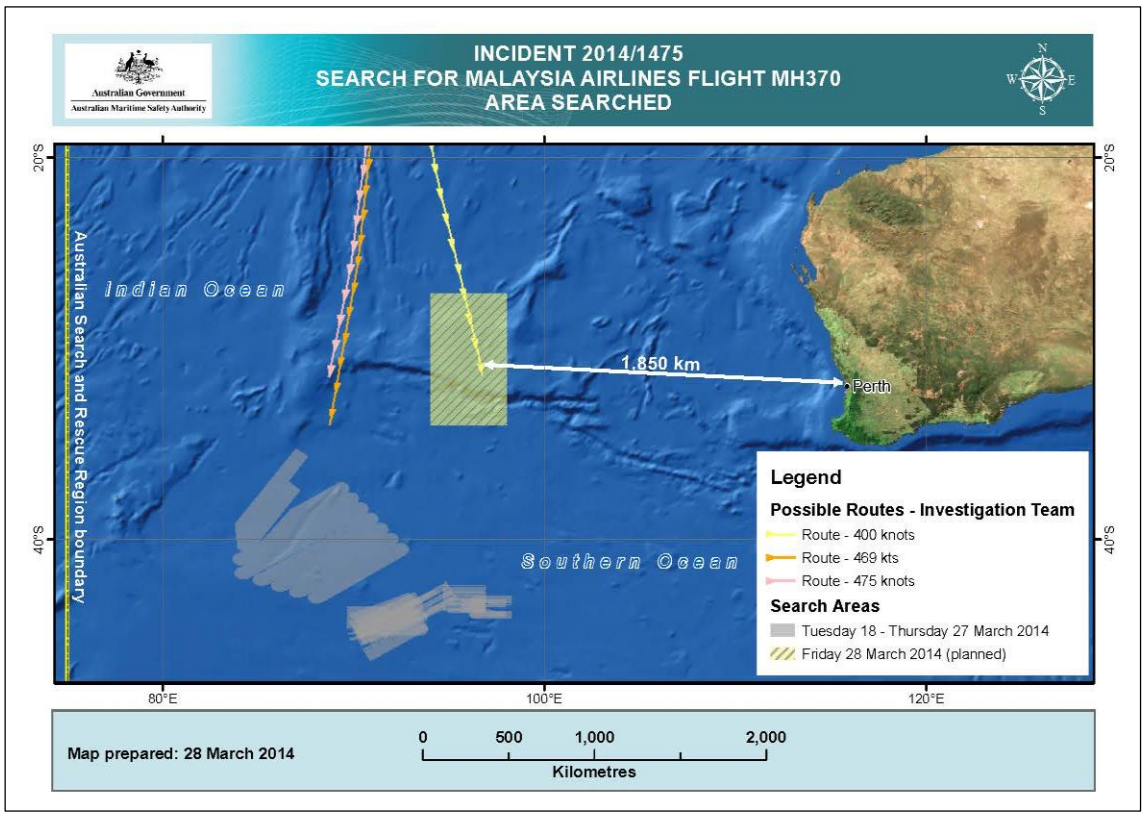

Source: AMSA

On 28 March 2014 a search of the drifted S3/S4 overlap area (Area A) was commenced. More than 50 objects were sighted and reported on that day (Table 14). Examination of images and recovery of items by surface vessels did not identify any items considered associated with MH370. A search of drifted Area B (Figure 15) within area S4 was undertaken on 2 and 3 April 2014.

Figure 17: Area searched and planned to 3 April 2014

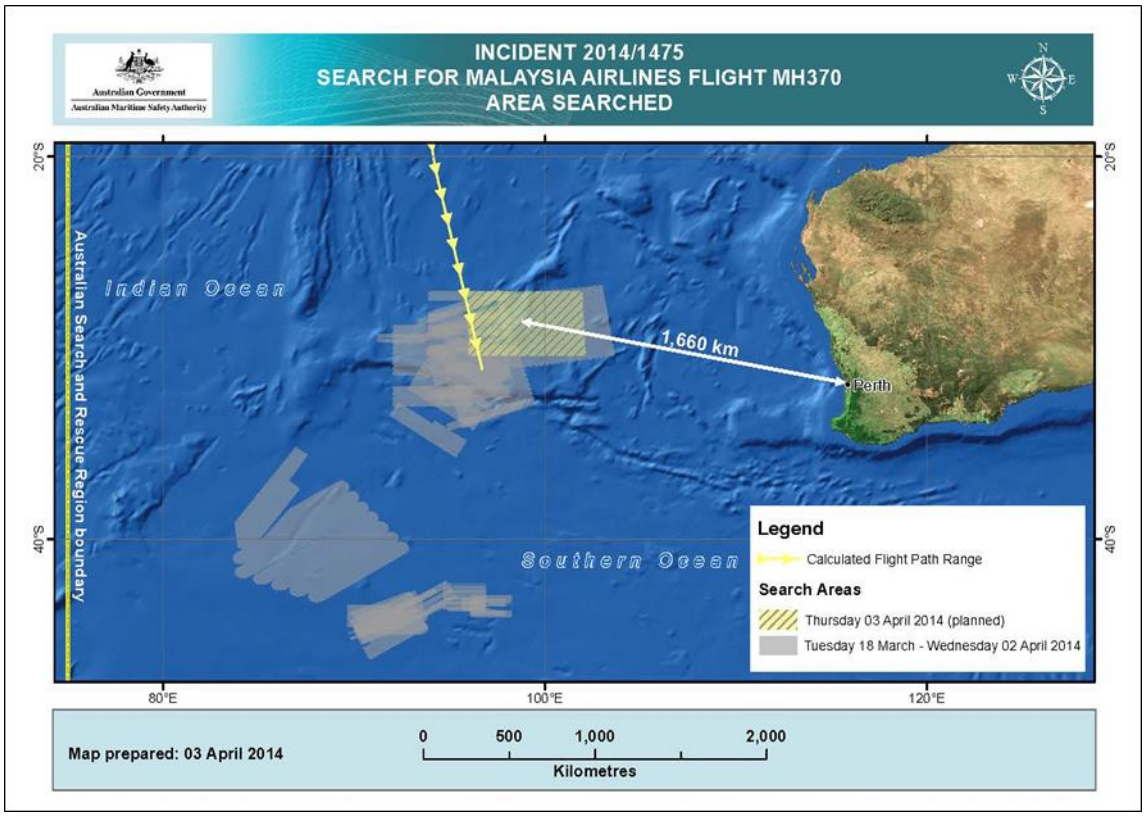

Source: AMSA

Table 14: Search area information 28 March 2014 to 3 April 2014

Date	Drifted splash point area	Search Area (km^2)	Track spacing (NM)	Aircraft	Vessels	SLDMB drop	Sightings
28-Mar-14	JIT 1A (S3/S4 overlap) Area A	298,636	14	10	6	3	50
29-Mar-14	JIT 1A (S3/S4 overlap) Area A	274,705	15	8	6	6	16
30-Mar-14	JIT 1A (S3/S4 overlap) Area A	251,009	12	10	8	1	5
31-Mar-14	JIT 1A (S3/S4 overlap) Area A	164,087	16	10	9	4	
1-Apr-14	JIT 1A (S3/S4 overlap) Area A	223,143	12	11	9	1	4
2-Apr-14	JIT 1A (S3/S4) Area B	236,966	15	9	9		
3-Apr-14	JIT 1A (S3/S4) Area B /JIT 1B - red box F	283,329	15/10/4	9	9	3	3

Source: AMSA

Second refinement surface search area

A second refinement to the SATCOM data analysis was provided by the JIT on 1 April 2014 which indicated the most probable aircraft path crossing at the S4/S5 area boundary. On 2 April 2014 further aircraft performance and flight path analysis starting further to the northwest of Sumatra had the effect of moving the most probable area to the northeast along the 7th arc into areas S4 and S5. Probable impact areas red, yellow and green were then defined (Figure 18). A 20,000 km² priority red area and lower probability yellow and green search areas extending to the southwest along the 7th arc were also defined.

Figure 18: Defined areas at 2 April 2014 showing red, yellow and green boxes, air route M641 and maximum range cruise boundary

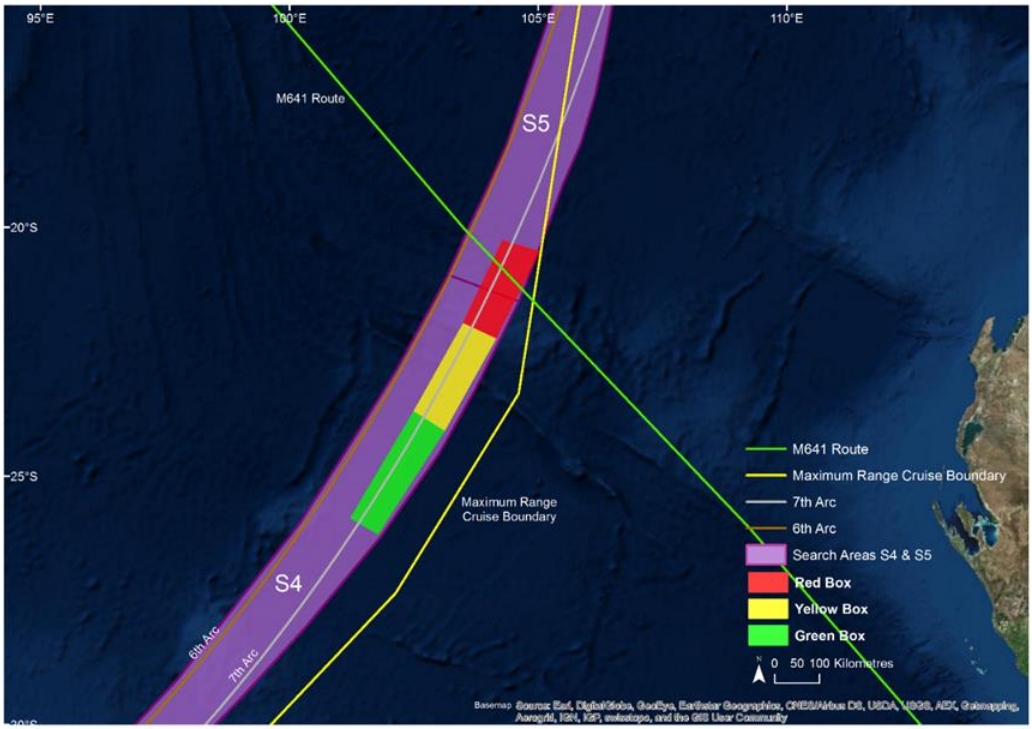

Source: ATSB, using JIT data

This analysis was used to guide the remainder of the surface search. Other areas of interest possibly indicating the location of MH370 were incorporated into the search as they became available. The S4/S5 drifted areas C, D, E and F were searched during this period (Figure 15 and Table 15).

Table 15: Second refinement to surface search area

Dates:	3–28 April 2014
Event:	Second refinement to surface search area.
Search area location:	S3/S4 overlap drifted Area A (3 April). S3/S4 overlap drifted Area B (3–7 April). Drifted red box (3–7 April). Drifted *Ocean Shield* flight recorder underwater locator beacon (ULB) hearing report (8–12 April). Drifted *Haixun 01* ULB hearing report (13–17 April). Drifted yellow box (18–20 April). Drifted S3/S4 ATSB refined area (21–28 April). S4/S5 starting at S4/S5 boundary and defined by red/ yellow/green areas.
Search activity:	Aerial and surface visual and radar search of areas drifted from 7th arc by expert drifting group of AMSA, Global Environmental Modelling and Monitoring Systems, CSIRO, Asia-Pacific Applied Science Associates and United States Coast Guard. Satellite search (multiple nations) of areas drifted from the 7th arc coordinated by Australian Geospatial-Intelligence Organisation with areas advised by AMSA/ATSB.

Guiding advice:	Areas S4 and S5 starting at S4/S5 boundary and defined by red/yellow/green areas. MH370 Inmarsat satellite data unit logs and advice from SATCOM WG. Briefing by the JIT on 2 April 2014 from United Kingdom, United States, Kuala Lumpur to AMSA (ATSB and NTSB embedded). Follow-up written briefing (refer JIT report at appendix B). Curtin University report (appendix H) on possible hydroacoustic event in search area (4 and 10 April 2014). Reported acoustic detections *Haixun 01* (4–5 April 2014). 5 April advice from JIT by email on effect of eclipse (resultant cooling and doppler correction) on Inmarsat's IOR-3 satellite on the signal frequency translation. This resulted in an increase to 425 knots groundspeed and shift to green zone. Reported ULB detections *Ocean Shield* (5-10 April 2014). MH370 PIC Microsoft flight simulator data analysis provided to AMSA/ ATSB by Australian Federal Police (19 April 2014).
Data used in planning search area refinement:	Based on the satellite timing data, the aircraft will be located near the 7th arc. Two scenarios were developed 1A and 1B based on the considered extents of the turn to the south. Scenario 1A had the aircraft fly south immediately after the first arc. Scenario 1B had the aircraft passing waypoint LAGOG before flying south. The 1B scenario had the aircraft passing close to a northwest point (8º 35.719'N, 92º35.145'E) at 1912. This was an initial qualitative assessment of the possible radar coverage from multiple data sources. This point was speculated and used as the furthest point west the aircraft was likely to have flown. The measured doppler profile closely matched that expected from an aircraft travelling in a southerly direction. One analysis showed that the best fit for the doppler frequency was at a ground speed of 400 knots, with slightly 'less' best fits at 375 and 425 knots. A Monte Carlo style analysis, using a number of different starting positions on the second arc also gave a best fit at 400 knots. A most probable speed range of 375 to 425 knots was selected. One analysis used a combination of aircraft performance and doppler data, obtained from the satellite, to generate a range of probable best fit tracks. This work was supported by a root mean square analysis. Flight planning carried out by Malaysia Airlines independently showed that there was sufficient fuel on board the aircraft to reach the positions determined by the analysis. The length of the 7th arc that defined the most probable area was obtained from the overlay of the results of all approaches. Given the probable battery life of the ULBs and the number of assets available to conduct the underwater search, it was decided to break the underwater search for the ULBs into three smaller areas (red, yellow and green). The width of the areas was defined by the probable position of the 7th arc, half of the glide range (40 NM) and the area the towed pinger locator (TPL) could cover before the ULB batteries expired. The area that was crossed by air route M641 was classified as red (Priority 1), the next two priorities, yellow and green, were then defined moving south along the arc from this position.
Search equipment:	Aircraft from Australia, New Zealand, United States, Japan, the People's Republic of China, the Republic of Korea and Malaysia. Vessels from the RAN, Royal Malaysian Navy, Royal Navy, United States Navy and the People's Republic of China.
Search area:	Refer to Table 16.

Source: ATSB

The S4/S5 area boundary on the 7th arc was considered the best starting point due to convergence of a number of candidate paths using independent techniques and because airways route M641 (Figure 16) passed through that location. The equivalent groundspeed of hypothetical flight paths ending in this region was about 363 knots. At this time, drifted Area B was being searched.

On 3 April 2014 the surface search (one mission) of a drifted red area was commenced. This continued until 6 April 2014 when further advice was received from the JIT regarding the cooling effect of an eclipse on the satellite, shifting the calculated groundspeed up to 425 knots and moving more probable paths to the green zone. The aerial search on that day was revised in response to that information.

Sonobuoys were deployed by Royal Australian Air Force P3 Orion aircraft to passively listen for underwater locator beacons. As information relating to the possible location of MH370 was provided to the ATSB, the location of the surface, satellite search and sonobuoy drops were adjusted.

The following items of interest influenced the search areas defined during this period:

- The People's Republic of China vessel *Haixun 01* reported possible underwater locator beacon (ULB) detections (4 to 5 April 2014) (See The acoustic search for the underwater locator beacons section).
- Curtin University reported a possible hydrophone detection (4 and 10 April 2014) (See Hydroacoustic analysis section).
- *Ocean Shield* reported possible ULB detections (6 to 10 April 2014) (See The acoustic search for the underwater locator beacons section).
- Five data points were recovered from the PIC's home flight simulator (19 April 2014) (See Pilot in Command's flight simulator section).

Table 16: Search area information 3 to 7 April 2014

Date	Drifted splash point area	Search Area (km^2)	Track spacing (NM)	Aircraft	Vessels	Sonobuoy drop area	SLDMB drop	Sightings
3-Apr-14	JIT 1A (S3/S4) Area B /JIT 1B - red box F	283,329	15/10/ 4	9	9		3	3
4-Apr-14	JIT 1B - yellow/red Box E and F	253,299	20/15/ 8	13	9		4	7
5-Apr-14	JIT 1B - yellow/red Box E and F	196,898	14/9	9	9			
6-Apr-14	JIT 1B - yellow/red Box E and F	216,309	15/10	10	11	For Defence To Provide		2
7-Apr-14	JIT 1B - yellow/red Box E and F	189,655	15/10	12	11	RSCU102 and RSCU104		1

Source: AMSA

Following the reported acoustic detections made by *Haixun 01* and *Ocean Shield* on 8 April 2014 the search areas were redefined (Table 17).

Table 17: Search area information 8 to 17 April 2014

Date	Drifted splash point area	Search Area (km^2)	Track spacing (NM)	Aircraft	Vessels	Sonobuoy drop area	SLDMB drop	Sightings
8-Apr-14	10 NM radius *Ocean Shield* ULB hearing report	77,333	4	11	13	RSCU105 approximately 360 NM to the south of the three main search areas.	1	8
9-Apr-14	10 NM radius *Ocean Shield* ULB hearing report	75,424	4	12	14	RSCU104 approximately 350 NM to the southeast of the three main search areas.	1	5
10-Apr-14	10 NM radius *Ocean Shield* ULB hearing report	57,923	4	11	13	RSCU102 and RSCU105 in the vicinity of *Ocean Shield* 250 NM east of the visual search area.		
11-Apr-14	10 NM radius *Ocean Shield* ULB hearing report	42,977	4/3	12	12	RSCU102, RSCU103 and RSCU105 in the vicinity of *Ocean Shield* approximately 260 NM east of the visual search area.		1
12-Apr-14	10 NM radius *Ocean Shield* ULB hearing report	41,393	4	7	13	RSCU103 in the vicinity of *Ocean Shield* approximately 315 NM east of the eastern search area.		1
13-Apr-14	10 NM radius *Haixun 01* ULB hearing report - green box D	57,466	5	9	13	RSCU102 and RSCU105 in the vicinity approximately 204 NM south east of the eastern search area.	1	14
14-Apr-14	10 NM radius *Haixun 01* ULB hearing report - green box D	47,706	5	9	11	RSCU102 and RSCU103 in the vicinity approximately 300 NM south east from the centre of the eastern search area.	1	
15-Apr-14	*Haixun 01* ULB hearing report - green box D	49,715	5	9	11	RSCU104 and RSCU105 approximately 600 NM north east from the centre of the eastern search area.		
16-Apr-14	*Haixun 01* ULB hearing report - green box D	33,199	5	14	11	RSCU102, RSCU103 and RSCU104 approximately 600 NM north east from the centre of the eastern search area.		13
17-Apr-14	*Haixun 01* ULB hearing report - green box D	41,579	5	12	12	RSCU103 and RSCU105 approximately 566 NM north east from the centre of the eastern search area.		

Source: AMSA

The search areas were again refined from 18 April 2014 following the completion of the search in acoustic detection areas to focus on other areas of interest (Table 18).

Table 18: Search area information 18 to 28 April 2014

Date	Drifted splash point area	Search Area (km^2)	Track spacing (NM)	Aircraft	Vessels	Sonobuoy drop	SLDMB drop	Sightings
18-Apr-14	Yellow box E	35,078	5	9	13			2
19-Apr-14	Yellow box E	48,190	7/5	8	12			
20-Apr-14	Yellow box E	41,229	5	8	11			
21-Apr-14	S3/S4 ATSB refined area C	49,492	4	8	11			12
22-Apr-14	S3/S4 ATSB refined area C	31,627	4	4	11			
23-Apr-14	S3/S4 ATSB refined area C	32,680	4	5	10			4
24-Apr-14	S3/S4 ATSB refined area C	51,923	4	8	11			
25-Apr-14	S3/S4 ATSB refined area C	49,241	4	6	11			
26-Apr-14	S3/S4 ATSB refined area C	56,206	4	7	11			15
27-Apr-14	S3/S4 ATSB refined area C	0	N/A	0	11			
28-Apr-14	S3/S4 ATSB refined area C	42,839	4	6	11			

Source: AMSA

Details of the daily surface search coverage up to 31 March 2014 can be found on the AMSA website.

On 31 March 2014, the search for MH370 transitioned to an investigation phase with the surface search still coordinated by AMSA as part of a larger interagency response which included ATSB, the Australian Departments of Defence, Foreign Affairs and Trade and Infrastructure and Regional Development headed by the Joint Agency Coordination Centre (JACC).

Search operations coordinated by AMSA were undertaken from 18 March to 29 April 2014 (42 days). A total of 21 aircraft and 19 vessels from Australia, the People's Republic of China, Japan, Malaysia, New Zealand, the Republic of Korea, United Kingdom and the United States were involved in the AMSA-led surface search.

An animation showing the daily progress of the aerial surface search areas is available for viewing on the ATSB YouTube Channel

Debris sightings and recoveries

During the surface search a number of floating objects in the drifted search areas were reported by aircraft, including wooden pallets and fishing equipment. None of these items were assessed as being associated with MH370. Over thirty items of debris were recovered by surface search vessels. All of these items were considered unlikely to be associated with MH370.

Surface search coverage and confidence

The area covered during the various phases of the AMSA-led surface search by air, sea and satellite up to 28 April 2014 is shown in Figure 19.

Daily coverage confidence was analysed by AMSA with consideration of reports of coverage and visibility conditions in the assigned search area. AMSA has extensive experience with search and rescue operations, enabling them to ascertain if the assigned area had been searched to a high level of confidence. Coverage confidence was low on some days due to poor weather or the large size of the search areas relative to the number of search assets available. On occasions, the postulated location of impact changed (as analysis of the aircraft's flight path accounted for new information) before the drifted search area was searched to high confidence.

Figure 19: Surface search coverage 18 March to 28 April 2014

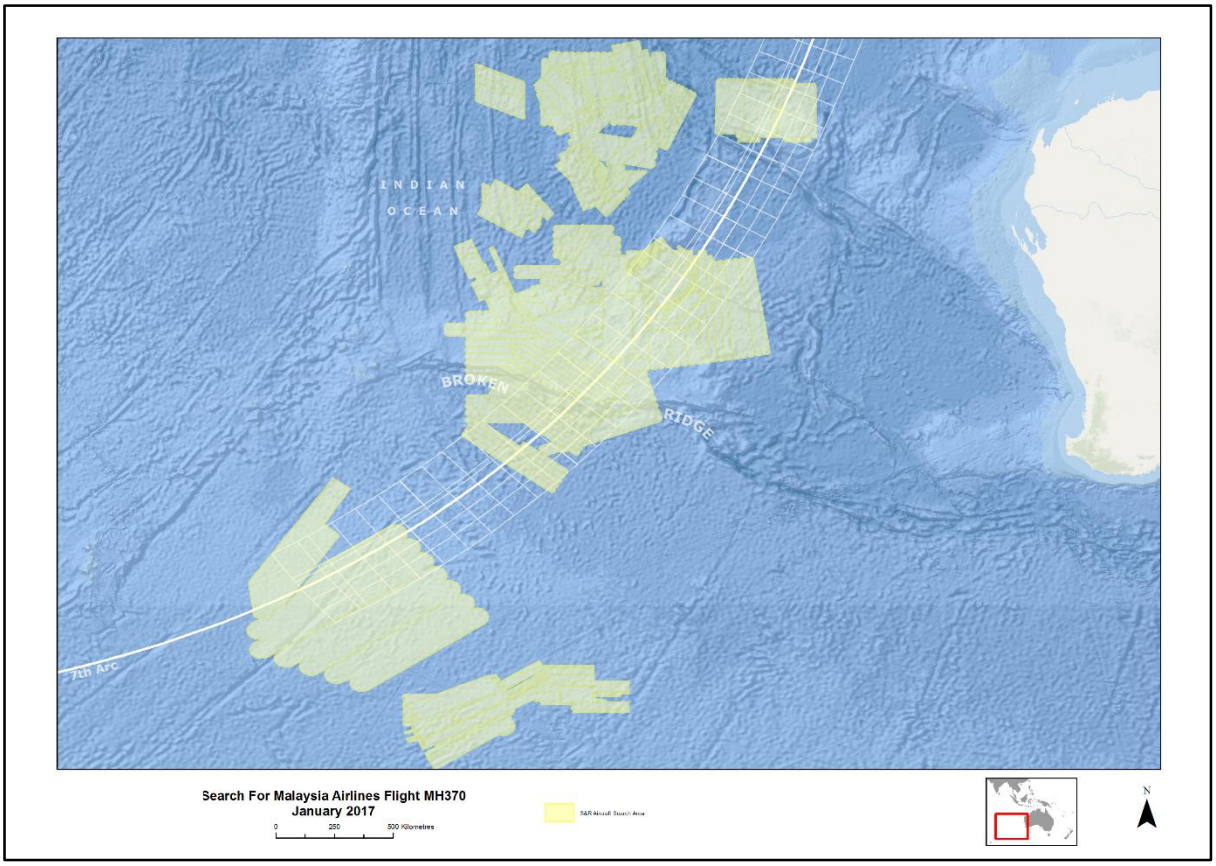

Source: ATSB, using AMSA data

CSIRO re-assessed the effectiveness of the surface search in terms of how it informed the underwater search. To do this, they re-assessed the degree of overlap of the drifted search areas with their updated estimates of where the debris field might have been, for a large number of potential impact sites distributed along the 7th arc from latitudes 21°S to 41°S and for items of debris with a range of susceptibility to the wind (leeway). For further details, see www.marine.csiro.au/~griffin/MH370/

Figure 20 shows that the first few days of the surface search was, with hindsight, fairly ineffective. This was because the number of search assets was low on the first day and because on following days the search was conducted much farther away from the 7th arc than the debris could have drifted, assuming now that the impact was within 25 NM of the 7th arc. In contrast, the northward move of the search on 28 March resulted in a high probability of detecting debris if the impact had been somewhere between about latitudes 26°S and 32.5°S. This phase of the surface search was therefore of high value to the underwater search because it adds to the weight of evidence suggesting that searching the seafloor north of about 32.5°S is unlikely to be successful.

Figure 20: Probability of detection for the surface search

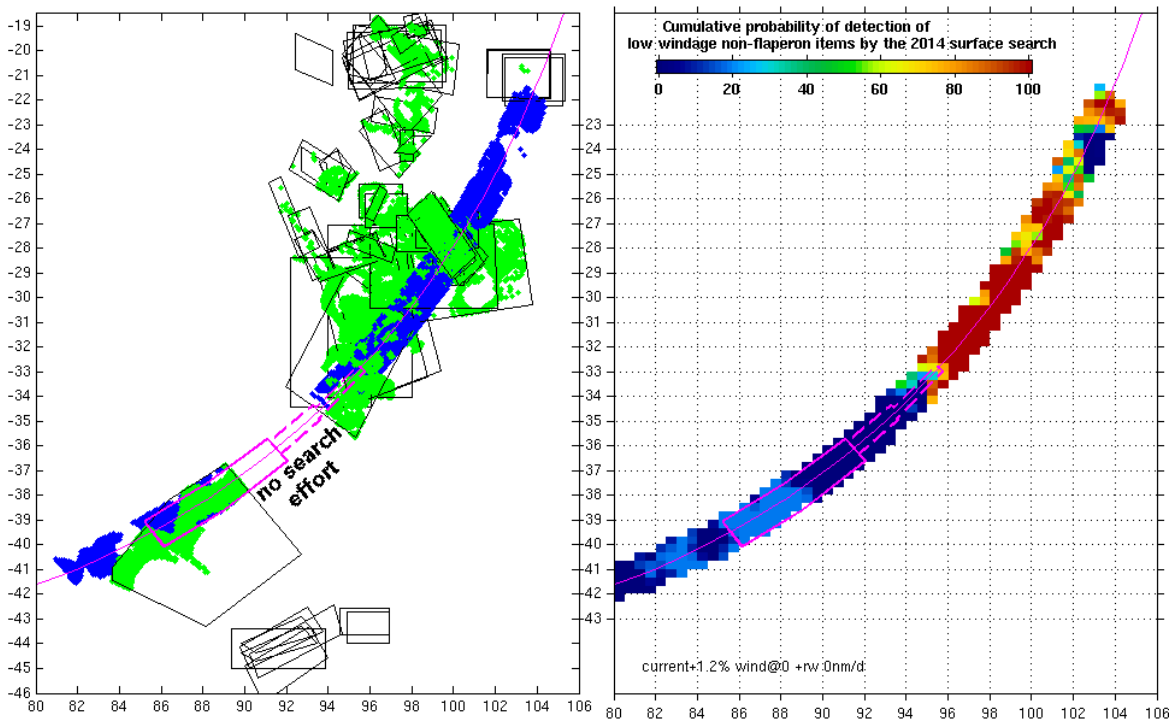

Source: CSIRO

The acoustic search for the underwater locator beacons

During the early stages of the AMSA-led surface search, efforts were also underway to mobilise a search for MH370's flight recorder underwater locator beacons (ULBs). United States Navy ULB detection equipment, including a towed pinger locator system and an autonomous underwater vehicle to investigate any detections, was shipped from the United States and mobilised on the Australian defence vessel *Ocean Shield.* The People's Republic of China vessel *Haixun 01*, equipped with a hand held hydrophone (underwater microphone) system and the United Kingdom defence vessel *HMS Echo* equipped with a hull-mounted hydrophone system were also used in the acoustic search. Later Royal Australian Air Force P-3C Orion aircraft also dropped sonobuoys in the search area to listen for MH370's ULBs.

The acoustic search started on 2 April and continued until 17 April 2014 (the date of the last sonobuoy drop) by which time it was considered that the ULB batteries would have been exhausted. The acoustic search for the ULBs also included a limited underwater search using the autonomous underwater vehicle on *Ocean Shield* which was completed on 28 May 2014.

Underwater locator beacons

An underwater locator beacon (ULB)[19] was attached to both the flight data recorder (FDR) and cockpit voice recorder (CVR) on board MH370. ULBs, also known as 'pingers', are battery operated acoustic transmitters which activate when immersed in water.

ULBs fitted to flight recorders (Figure 21) are designed to operate in water depths up to 6,000 m and emit a 10 millisecond sound pulse at a frequency of 37.5 kHz every second for a minimum of 30 days[20] when activated.

Figure 21: Typical crash protected recorder configuration with ULB

Source: ATSB

[19] The underwater locator beacons installed were Dukane Model DK100

[20] The ULB manufacturer predicted maximum life of the batteries once activated was 40 days

An activated ULB attached to a flight recorder enables a diver, or underwater vehicle, equipped with a hydrophone to detect and locate the recorders within a known underwater debris field. ULBs have also been used to locate an entire aircraft debris field as they can be detected from a distance of 2,000 m to 3,000 m, or further in favourable conditions. This is greater than the range of many mapping sonar systems (for example side scan sonar) which may be used to search for an aircraft debris field. This means an initial search for a ULB, rather than the aircraft debris field, can be an efficient way to search a large area quickly.

Many conditions influence the actual range and ability to detect a ULB. Underwater environmental factors such as thermoclines[21], high ambient noise or marine life in the area affect the detectability of a ULB. Impact damage can also affect the ULB housing, acoustic transducer, internal electronics, or battery functionality. The ULB could also be covered by sediment or shielded by surrounding debris on the seafloor. The surface support vessel can also be a source of noise which can affect ULB detection. Ships and their equipment are typically acoustically noisy and this can result in interference or false detections. Care is required to isolate any potential sources that may emit a similar acoustic sound or mask a real ULB signal.

The equipment used to detect a ULB signal is typically comprised of a hydrophone(s) with associated electronics to filter and amplify the acoustic pings allowing for either audible or visual detection by an operator. The detectability of a ULB signal is influenced by the hydrophone system being used to listen for it. Operators must ensure the hydrophone is operating correctly and potential sources of interference are monitored closely. Newer systems digitise and record the signal allowing for real time processing or post processing using specific software.

The method commonly used in shallow water is an immersed hydrophone mounted on a simple pole connected to a headset. The operator listens at defined locations as the hydrophone is rotated through different directions. This was the technique used by *Haixun 01*.

For deep water, a towed pinger locator (TPL) equipped with a hydrophone is towed behind a vessel close to the seafloor. A TPL system was used by *Ocean Shield* (Figure 22) which comprised the TPL, tow cable and winch and the electronics needed to process the acoustic data at the surface. Power to, and data from, the TPL was transmitted continuously via the tow cable. The TPL was also fitted with a test ULB which could be used to test the correct system operation, by emitting 10 seconds of pings, when the TPL was operating at depth.

[21] A distinct layer in a large body of water, such as an ocean or lake, in which temperature changes more rapidly with depth than it does in the layers above or below.

Figure 22: Towed pinger locator on board *Ocean Shield*

Source: RAN

Sonobuoys were also used in the search for MH370's ULBs. The sonobuoys were released from the search aircraft and left to drift to listen for a ULB. The sonobuoys are equipped with a hydrophone, which is streamed to a depth of 300 m below the buoy and a radio transmitter which allows acoustic data to be relayed back to the aircraft for processing when it is within range. This system was used by a P-3C Orion aircraft operated by the Royal Australian Air Force.

Acoustic detections

By 2 April 2014, search vessels equipped to listen for MH370's ULBs, including *Ocean Shield, HMS Echo* and *Haixun 01*, were en route to, or near the 7th arc. Flight path analysis at the time indicated that the most probable points at which MH370 crossed the 7th arc were the red/yellow/green areas (Figure 18). The search for the ULBs commenced at the boundary between areas S4 and S5 within the red box on the 7th arc.

HMS Echo

On 2 April 2014, *HMS Echo* reported a possible ULB detection close to the 7th arc and the S4/S5 boundary. The hull-mounted system on the vessel was designed to provide high accuracy deep water positioning of subsea transponders operating between 27 kHz and 30.5 kHz. The hydrophone system had been retuned to 37.5 kHz by the crew of *HMS Echo* to enable detection of a ULB. On 3 April 2014, following tests, this detection was discounted as being an artefact of the ship's sonar equipment.

Haixun 01

On 4 April 2014, crew from the People's Republic of China vessel *Haixun 01* reported detections at the southern end of the green zone at 25.975°S, 101.461°E. The crew were operating the hydrophone from one of the ship's rescue boats in an area where ocean depths were approximately 4,500 m. *Haixun 01*'s crew reported a pulsed signal with a frequency of 37.5 kHz for 15 minutes, repeating once per second. A second detection at the same frequency was made the next day, 3 km west of the first detection, for 90 seconds with a much weaker signal than the previous day.

On 6 and 8 April 2014, *HMS Echo* attempted to reacquire the detections reported by the crew of *Haixun 01*. However they were unsuccessful and concluded that the detections were unlikely to be MH370's ULBs due to the water depth, surface noise and the hydrophone equipment being used by the crew of *Haixun 01* which had a practical detection range of about 2,000 m according to the manufacturer. A submarine was also tasked to investigate the area and was also unable to identify any ULB transmissions.

Ocean Shield

Also on 4 April 2014, *Ocean Shield* commenced acoustic search operations in the red area (Figure 16) using two United States Navy TPLs (01D and 03S) operated by Phoenix International mission crew. The 01D TPL when initially deployed exhibited acoustic noise and was replaced with the 03S TPL. This TPL was deployed on 5 April and shortly after, whilst descending, detected an acoustic signal at a frequency of approximately 33 kHz for approximately 2 hours and 20 minutes. Two additional TPL search lines were run over this area with no further detections noted. However three additional detections were recorded at different locations, one on 5 April and two on 8 April. At these three distinct locations two frequencies were identified for each detection area, each around ~33 kHz and ~42 kHz. Additional TPL search lines were run over these areas with no further detections noted.

On 10 April 2014, a fifth detection[22] was recorded which consisted of three separate intermittent detections over a four hour period. However the operational log at the time notes the detections were a broad 32 kHz to 35 kHz signal and were suspected of originating from a malfunction within the TPL. For this reason, the TPL was recovered and no further search lines were run with either TPL system over this area. All five reported detections were made while using the 03S TPL and when the TPL was recovered following the fifth and final detection, the test ULB mounted on the 03S TPL was disconnected. Following the recovery the alternate 01D TPL system was then used for another four days with no further detections noted. An overview of the acoustic detections along with the TPL coverage is shown in Figure 23.

[22] The fifth detection was not reported at the time but was in subsequent reporting from the operator.

Figure 23: *Ocean Shield* TPL detections with distance between each and TPL coverage polygons

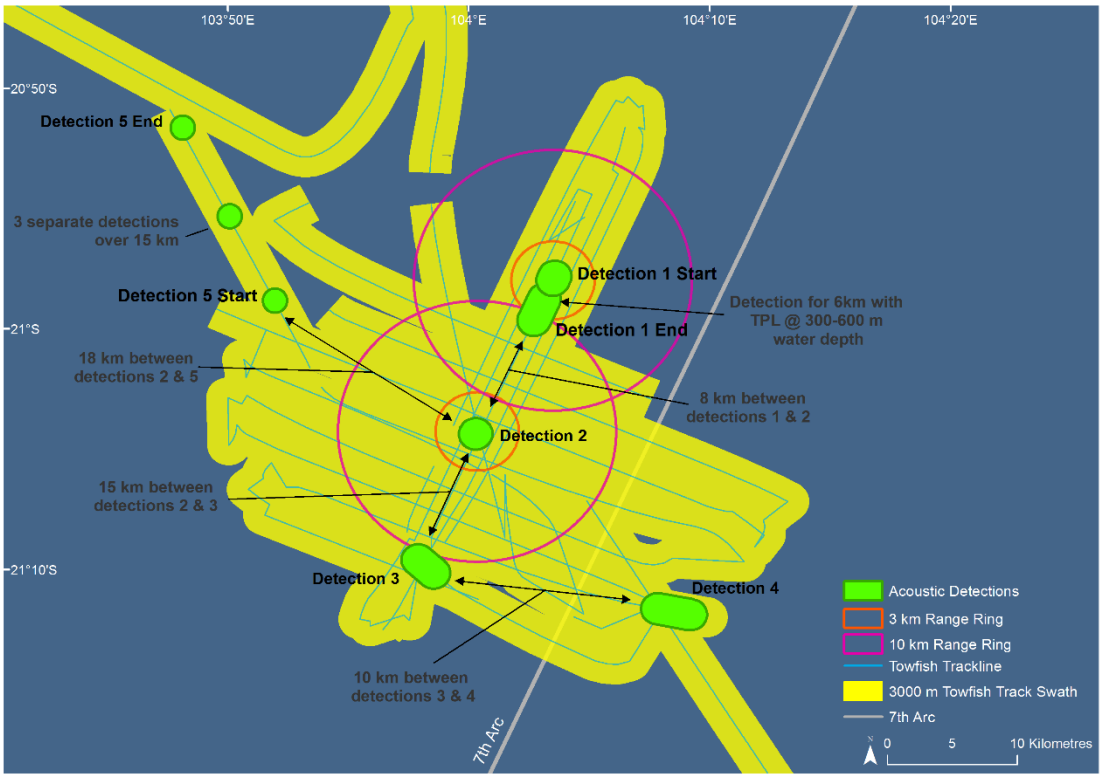

Source: ATSB, using Phoenix International data

Analysis of acoustic detections

A review of the *Ocean Shield* acoustic detections was undertaken independently by various specialists including the ULB manufacturer, DST Group, Air Accidents Investigation Branch (United Kingdom), NTSB, Curtin University and Australian Joint Acoustic Analysis Centre. The analyses determined that the signals recorded were not consistent with the nominal performance of a Dukane DK100 ULB. Some analysts noted that the acoustic signals detected may be consistent with a damaged ULB however the calculated offsets (by the manufacturer) to the frequency, pulse width, and pulse repetition rate, for a damaged ULB, did not fully match any of the recorded detections.

It was noted that if damage had occurred to both ULBs it would be highly unlikely that the resulting offset frequency would be the same for each. However it was also noted that environmental factors could affect both ULB's frequency equally. Given the uncertainty it was decided that a seafloor search using the autonomous underwater vehicle (AUV) on board *Ocean Shield* should be performed to fully investigate the detections by looking for an aircraft debris field on the seafloor. The second possible ULB detection was deemed to be the most promising and this was the area of focus for the AUV search.

After the TPL equipment had been demobilised from *Ocean Shield*, Phoenix International performed a full test on TPL system 03S to identify and/or eliminate any possible sources for the acoustic detections during the search for MH370's ULBs. One of the tests performed showed that a simulated faulty 'self-test' cable, with a high resistance short circuit, would activate the test ULB mounted on the TPL. The faulty 'self-test' cable also caused the output frequency from the test ULB to shift from 37.5 kHz to 33 kHz, caused broadband noise and altered the acoustic ping repetition rate. The resulting acoustic signal is similar to the detections on board *Ocean Shield* during the search for MH370's ULBs.

Phoenix International also verified during their lab testing that when this condition occurred a fully functional ULB operating at 37.5 kHz was still able to be detected by the TPL.

Phoenix International's engineering test report concluded:

> The fact that none of the recorded MH370 TPL search recorded acoustic detections were repeatable after numerous attempts, coupled with the significant geographical dispersion of the sounds will continue to challenge the theory that the detections were generated by an acoustic (ULB) source on the seafloor.

Marine animal tracking devices

Acoustic tracking

Acoustic tracking devices used by the Australian research community for tracking marine animals reportedly transmit at frequencies of 69 kHz or 180 kHz. These devices are monitored by hydrophones at fixed locations around Australia generally, on the continental shelf, and can only be detected up to a range of approximately 400 m. Based on the frequency of the acoustic detections on *Ocean Shield*, which ranged between 28-42 kHz, it was considered unlikely that they originated from marine animal tracking devices.

Satellite tracking

Satellite tags are another animal tracking technology commonly used. These tags are designed to transmit their data via satellite when the animal is on the surface. It was considered unlikely this type of tag would be detected by a hydrophone as the radio frequencies used are very high and quickly attenuated by water immersion. Since 2012 whale shark tracking has also largely been achieved by deploying archival tags that record but don't transmit data.

Sonobuoys

P-3C Orion sonobuoy acoustic search capability

When Australia joined the international effort to locate MH370, the Australian Defence Force and Australian Defence Industry worked together to enhance the search capabilities available to the authorities coordinating the search. They developed a capability to detect a ULB signal at a range of up to 4,000 m by deploying sonobuoys from a P-3C Orion aircraft with a single sortie capable of covering an area of approximately 3,000 km².

Sonobuoy drops were undertaken from 6-17 April 2014 in the region of the 7th arc, where depths were favourable, in areas where *Ocean Shield* and *Haixun 01* had possible ULB detections. Another area targeted was based on the bearing of an event recorded shortly after 0019 UTC on 8 March 2014 at the Comprehensive Nuclear Test Ban Treaty Organization hydrophone network (data from the H01 array off Cape Leeuwin, analysed by Curtin University) and the intersection with the 7th arc (See Hydroacoustic analysis section). No acoustic detections considered to be related to ULB transmissions were detected using sonobuoys.

Autonomous underwater vehicle search

An underwater search using an autonomous underwater vehicle (AUV) commenced on 14 April 2014 in the Zenith Plateau area based on the analysis of the acoustic detections from the TPL on board *Ocean Shield*. Thirty AUV missions conducted at depths from 3,800 m to ~5,000 m were completed.

Figure 24: Phoenix International *Artemis* AUV on board *Ocean Shield*

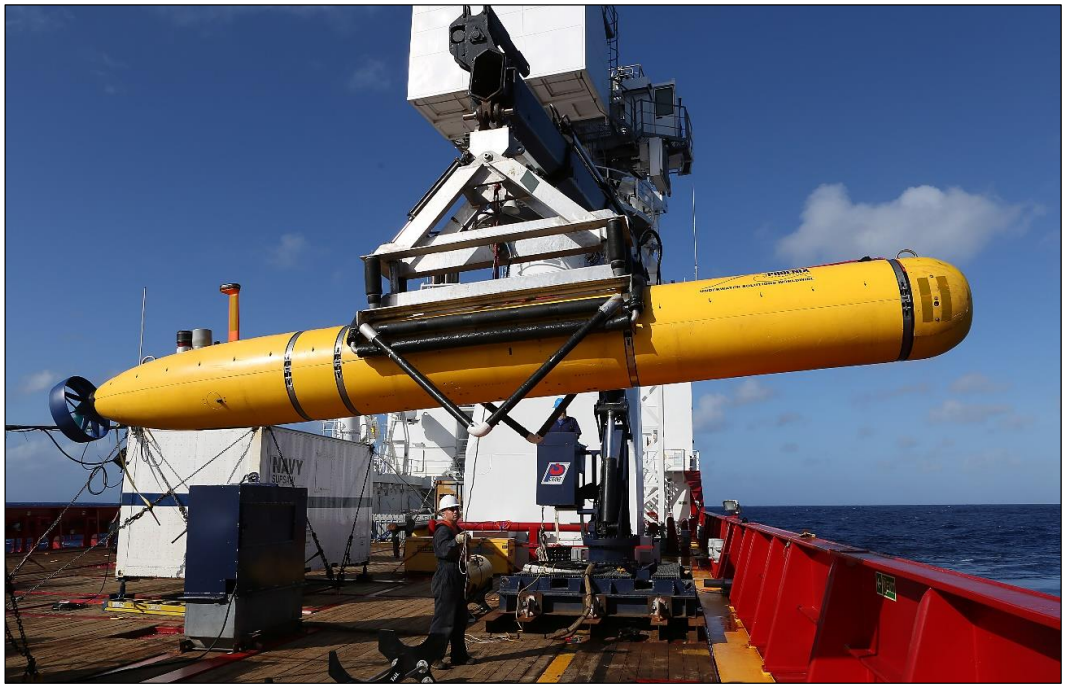

Source: RAN

The AUV (Figure 24) collected 120 kHz side scan sonar data using a 400 m range scale at an altitude of 45 m. The side scan sonar tasking focused on a 10 km radius around TPL detection number two and a 3 km radius area around TPL detections one, three and four. This search was completed on 28 May 2014 and covered 860 km^2 with no aircraft debris detected on the seafloor. The coverage achieved by the AUV relative to the positions of the acoustic detections is shown in Figure 25. An animation of the AUV search is available for viewing on the ATSB YouTube Channel.

Figure 25: *Ocean Shield* AUV coverage of acoustic detections

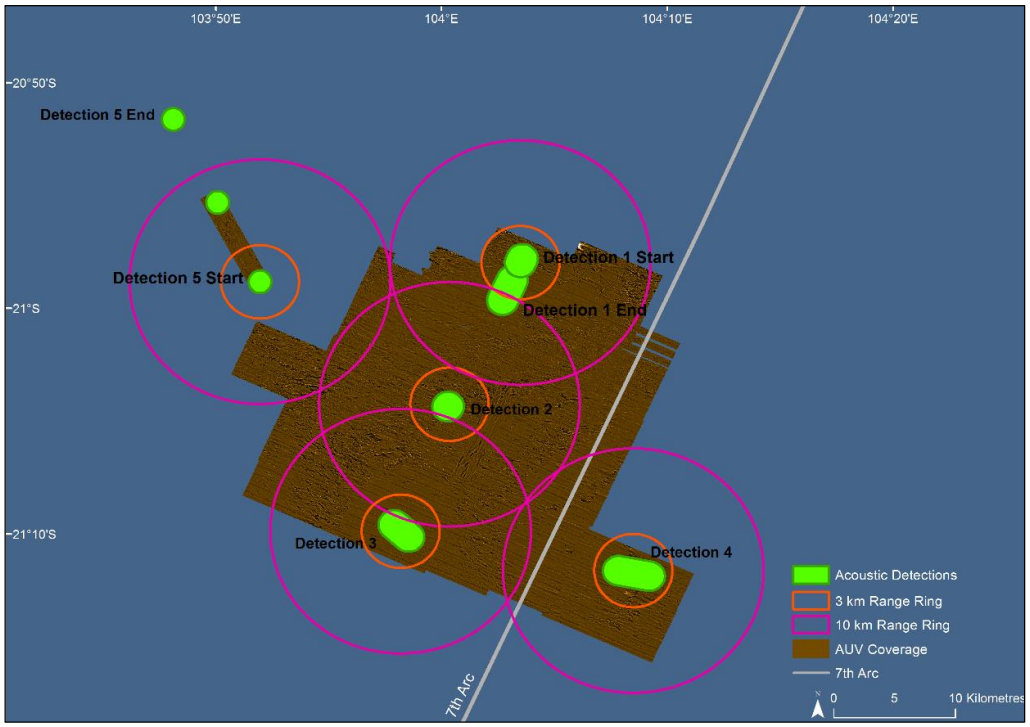

Source: ATSB, using Phoenix International data

The underwater search

Searching the seafloor for lost aircraft in deep water requires certain key components and thorough processes to maximise the chances of detection and success. The area to be searched must be identified with as much rigour and precision as the available information will allow. All sources of credible evidence as to how and why and where the aircraft may have ended the flight must be pursued and analysed to allow hypotheses to be formed and tested. While it is human nature to form a hypothesis and then attempt to 'fit' the evidence to that mental model, any hypothesis which is not in concert with all the evidence must be discarded, however reluctantly.

The significant challenge in finding MH370 has been defining the search area based on only limited SATCOM metadata for the final six hours of flight, and later, very long term drift studies when debris from the aircraft have been found. The total possible search area was in the order of 1,200,000 km² along the 7th arc when all possible flight paths and the potential glide range of the aircraft at the end-of-flight after fuel exhaustion are considered. To be practical, the underwater search area needed to be defined with as much precision as analysis of the available data would allow.

For the underwater search, seaworthy ships, well maintained underwater and surface equipment, and a robust program for ensuring the quality and analysis of the data collected are all critical components. All vessels used in the search for MH370 were built, crewed, operated and maintained in accordance with the appropriate international standards for international trading and/or special purpose vessels. The search equipment was tested and verified to meet the requirements stipulated by the ATSB for use in the underwater search.

During underwater search operations there were two particular areas of focus; maintaining a comprehensive program to ensure coverage of the area searched and a thorough review process for marking areas of interest, also referred to as sonar contacts. Sonar contacts were defined as any anomaly on the seafloor that appeared non-geologic in nature or unusual when compared to the surrounding seafloor. Contacts were marked to document specific points in the data which warranted further analysis or the need for additional data to be collected over the area.

Defining the initial underwater search area

Initial priority search area

On 28 April 2014, the Prime Minister of Australia announced that Australia, represented by the ATSB, would coordinate the underwater search for MH370. The ATSB subsequently formed and coordinated the Search Strategy Working Group (SSWG) to facilitate interaction with the Annex 13 investigation team flight path reconstruction group and satellite communications working group (SATCOM WG) to progress work on defining an initial underwater search area. The aim was to define underwater search areas along the 7th arc in the Indian Ocean where the SATCOM data indicated a power interruption close to the time of expected fuel exhaustion (Table 19).

An Inmarsat BFO model designated 'Differential Doppler Analysis ECLIPSE_2' was finalised in April 2014. This model incorporated all data frequency translations that Inmarsat were aware of at that time. The chronology and further information on doppler model development by Inmarsat is provided at appendix C.

Table 19: Initial priority search area

Dates:	14 June – 26 August 2014
Event:	Mapping of seafloor in proposed underwater search area of 60,000 km².
Search area location:	Priority and medium search areas; 27.4ºS to 32.1ºS along 7th arc, -20 NM, +30 NM across 7th arc.
Search activity:	Mapping of seafloor – bathymetry phase.
Guiding advice:	Initially Inmarsat's 'Differential Doppler Analysis Eclipse 2' BFO model was used to define priority, medium, wide search areas for 26 June 2014 report. The unified model released on 19 June 2014 and subsequent revisions were used in flight path modelling developments after this date.
Data used in planning search area refinement:	Effects of an eclipse on the satellite during a period of MH370 flight taken into consideration. Refined EAFC model. 1912 NW point (8º 35.719'N, 92º35.145'E) reassessed as invalid and no longer used by flight path reconstruction groups. Flight path from 2nd arc at 1941. Candidate paths with zero BTO tolerance. Candidate paths within BFO tolerance of 10Hz. Loss of control study, arc tolerance, balance of uncertainties and agreed area of 60,000km² results in width of +30 NM, -20 NM around 7th arc.
Search equipment	*Fugro Equator* (ATSB contract survey vessel, multibeam echo sounder (MBES)) *Zhu Kezhen* (the People's Republic of China hydrographic survey vessel, MBES)
Coverage details:	Approximately 38,000 km² completed in defined priority area 27.4ºS to 32.1ºS.
References	ATSB report: *MH370 – Definition of Underwater Search Areas* – 26 June 2014

Source: ATSB

Inmarsat techniques applied to the model indicated best fit agreement for a 400 knot ground speed flight crossing the 2nd arc at latitude 2°N, ending at 28.2°S, 99.6°E at 0019 UTC. The model provided reasonable matches for a range of ground speeds between 375 and 500 knots from the estimated 2nd arc starting location, with the end-of-flight between latitudes 25°S and 37°S on the 7th arc.

Further flight path reconstruction techniques using this model were undertaken in May and June 2014 to define the initial underwater search area. The proposed underwater search area at that time was defined in ATSB report MH370 – Definition of Underwater Search Areas released on 26 June 2014. The application of the 'Eclipse 2' BFO model by the flight path reconstruction group had resulted in a shift of the most probable aircraft paths southwest along the 7th arc from the red/yellow/green area (latitudes 20.2°S–26°S) to an orange priority area (latitudes 27.4°S–32.1°S).

The report defined priority, medium and wide search areas spanning increasing lengths along and widths across the 7th arc. The priority area for the underwater search defined in June was based on the area agreed by Tripartite governments of 60,000 km². This area was equal in size to the red/yellow/green search area defined during the surface search.

The underwater search areas were designated block numbers and width letters (Figure 26).The 'A' blocks were areas of 10,000 km² each. The priority search area was therefore defined as Blocks 1A–6A.

Figure 26: The underwater search area, June 2014

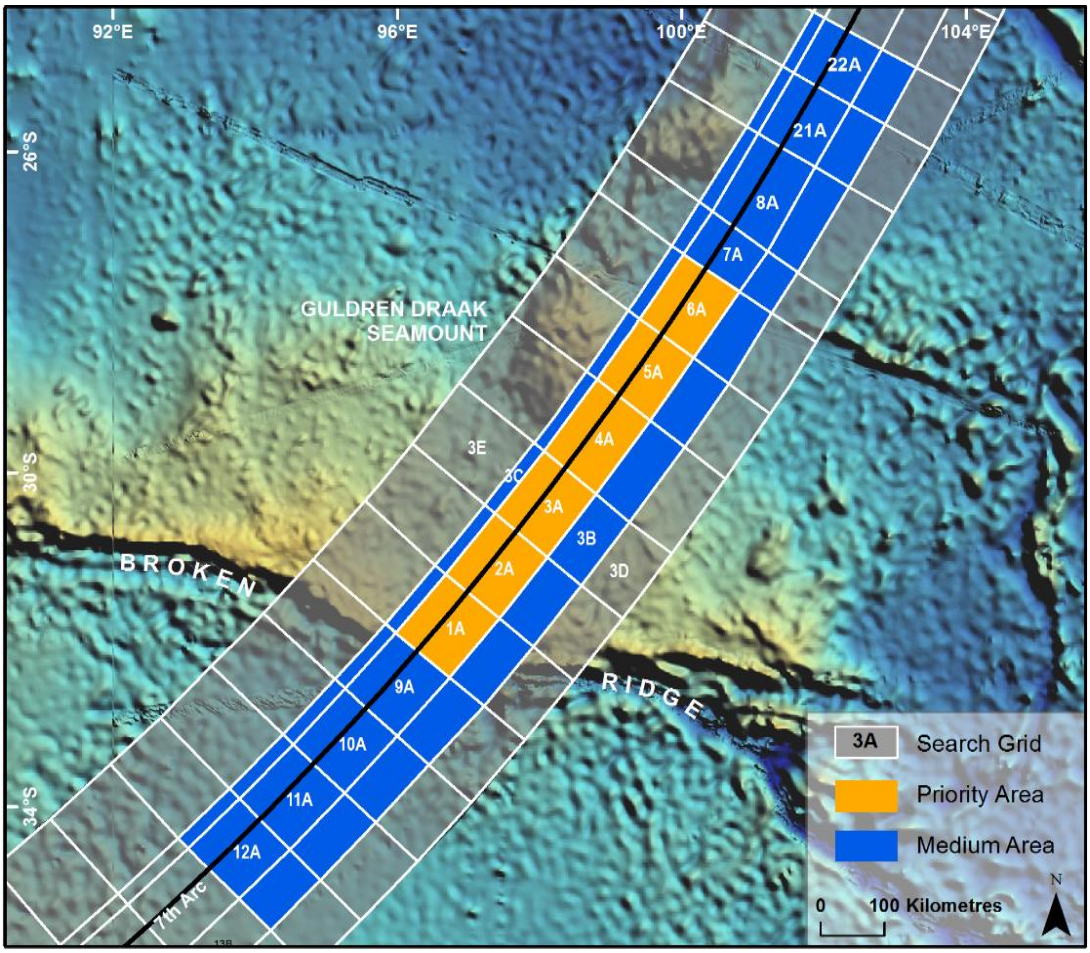

Source: ATSB

A reasonable search width for a 'loss of control' end-of-flight scenario was determined to be 30 NM in front and 20 NM behind the 7th arc. These were the limits of the A blocks. These widths allowed an approximate search area length of 650 km along the 7th arc (orange coloured area) for a total area of 60,000 km^2.

Mapping the seafloor in the search area

Bathymetric survey

The underwater search required a phased approach given the unknown composition and topography of the seafloor in the search area. Before the underwater search commenced, a bathymetric survey was conducted to ensure that high resolution maps were available for the safe and efficient navigation of underwater vehicles close to the seafloor. The bathymetric survey used hull-mounted multibeam sonar systems suitable for deep water wide area survey on the vessels *Fugro Equator*, *Fugro Supporter* and the People's Republic of China vessel *Zhu Kezhen*.

The majority of the bathymetric survey was conducted from May to December 2014. Supplementary bathymetry data was intermittently acquired to expand the search area as required from December 2014 to February 2017. The bathymetric survey commenced in the underwater search area defined in June 2014 (orange area in Figure 26).

In the search area 278,650 km^2 of high resolution multibeam bathymetry data was collected. In all, 710,000 km^2 of data was collected, which includes data acquired while search vessels transited to and from port to the search area (Figure 27).

Figure 27: The 710,000 km^2 bathymetric survey dataset is one of the largest marine surveys ever conducted

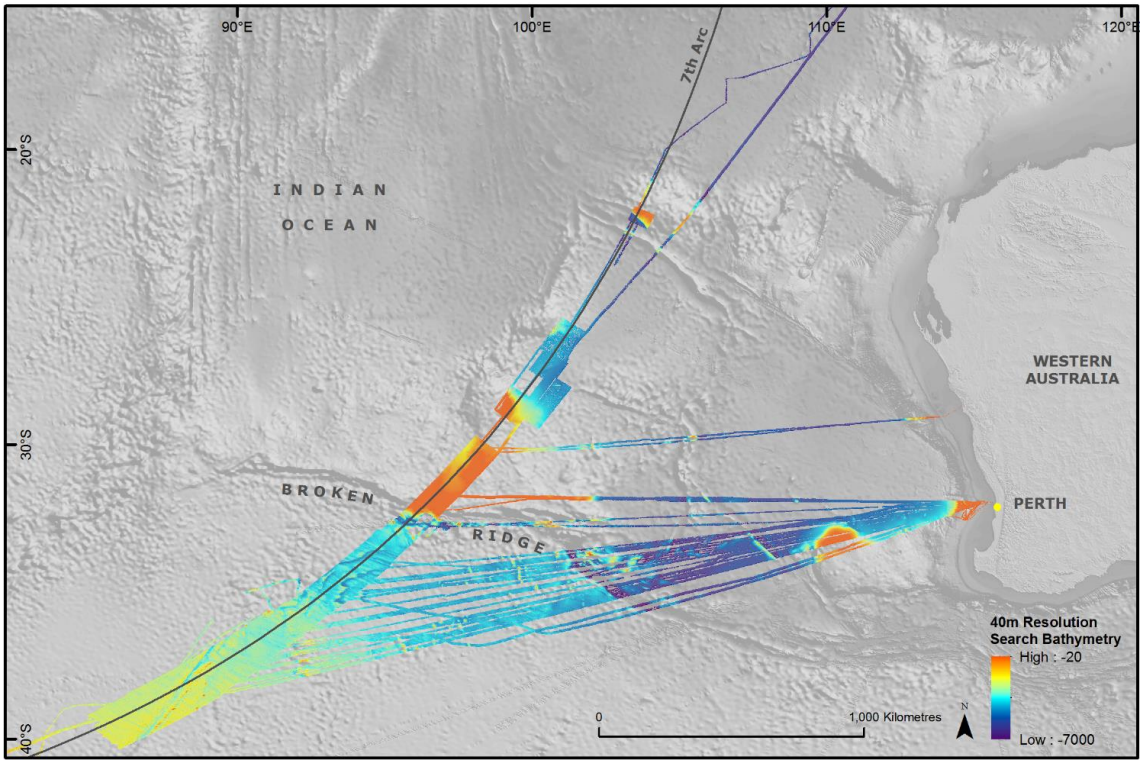

Source: ATSB

Previous maps of the seafloor in the search area were from satellite-derived gravity data and only indicated the depth of the ocean at a coarse resolution of approximately 5 km^2 per pixel. The bathymetric survey acquired for the underwater search collected data at 40 m^2 per pixel, allowing for finer scale awareness of topography as shown in Figure 28.

Figure 28: High resolution multibeam bathymetry data compared to low resolution satellite-derived bathymetry data

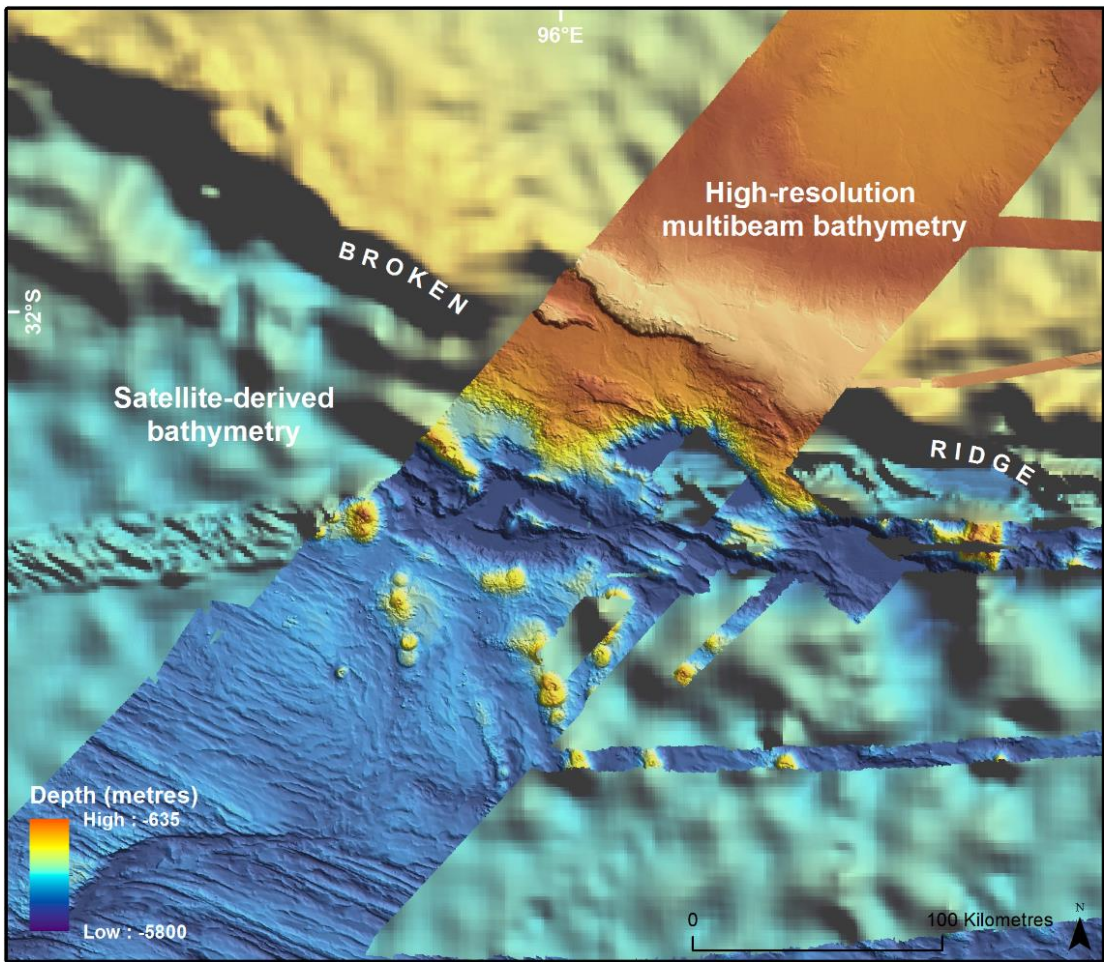

Source: ATSB

The underwater mapping revealed details about the seafloor which were not visible in the previous satellite-derived bathymetry including vast seamounts 1,500 m high and kilometres wide, deep canyons and underwater landslides of sediment that travel for kilometres along the seafloor (Figure 29 and Figure 30).

Figure 29: 2,200 m high volcano (vertical exaggeration is 3 times)

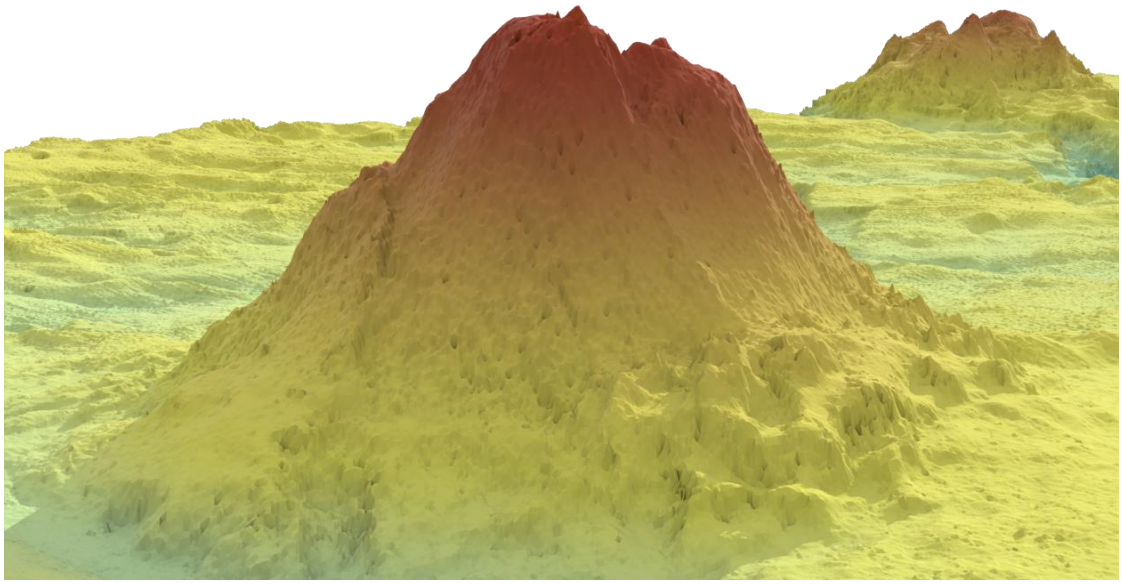

Source: Geoscience Australia

Figure 30: Geelvinck Fracture Zone, 4,500 m below sea level, fault depth 900 m (vertical exaggeration is 3 times)

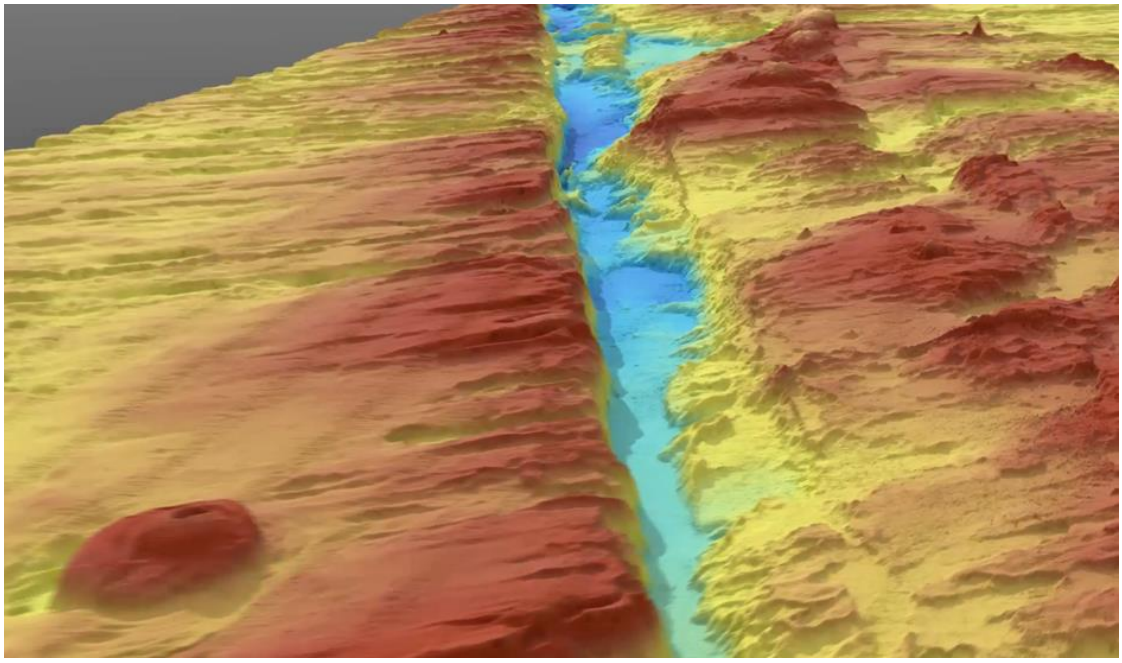

Source: Geoscience Australia

Geology of the search area [23]

The major geological feature of the seafloor in the search area is Broken Ridge. It is approximately 1,200 km long and was created by tectonic forces more than 40 million years ago.

[23] From Geoscience Australia - MH370 Phase One Data Release

Figure 31: North of Broken Ridge

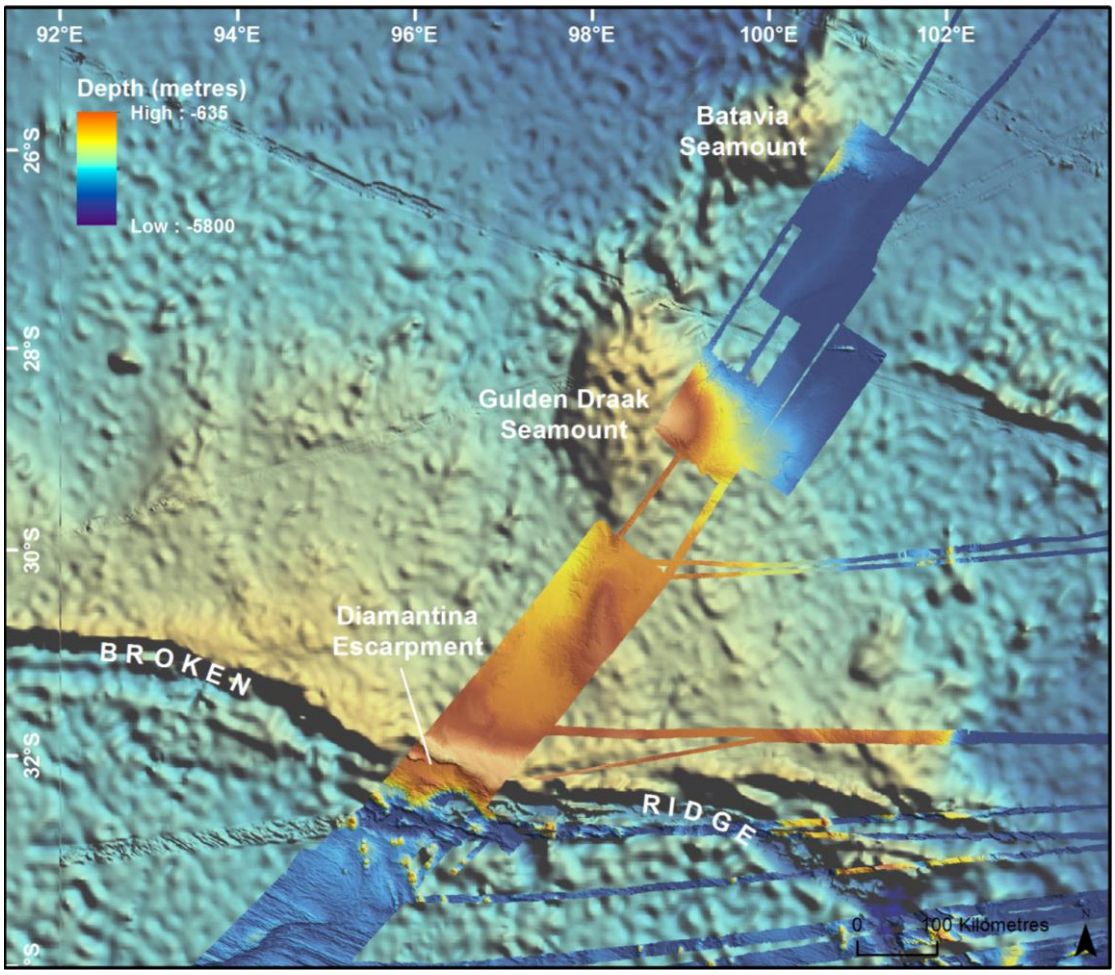

Source: ATSB

North of Broken Ridge

Here, water depths range between 635 m and 5,800 m. The seafloor north of Broken Ridge is more than 40 million years old, making it the oldest seafloor in the search area. The seafloor in this region is covered in a layer of sediment up to 300 m thick and is subject to extensive seafloor landslides, some of which are kilometres long. The Gulden Draak Seamount and the Batavia Seamount found in this part of the search area are significant due to their size (Figure 31).

Broken Ridge and the Diamantina Escarpment are a geological ‘breakup zone’, created approximately 40 million years ago as their tectonic plate broke apart.

Figure 32: South of Broken Ridge

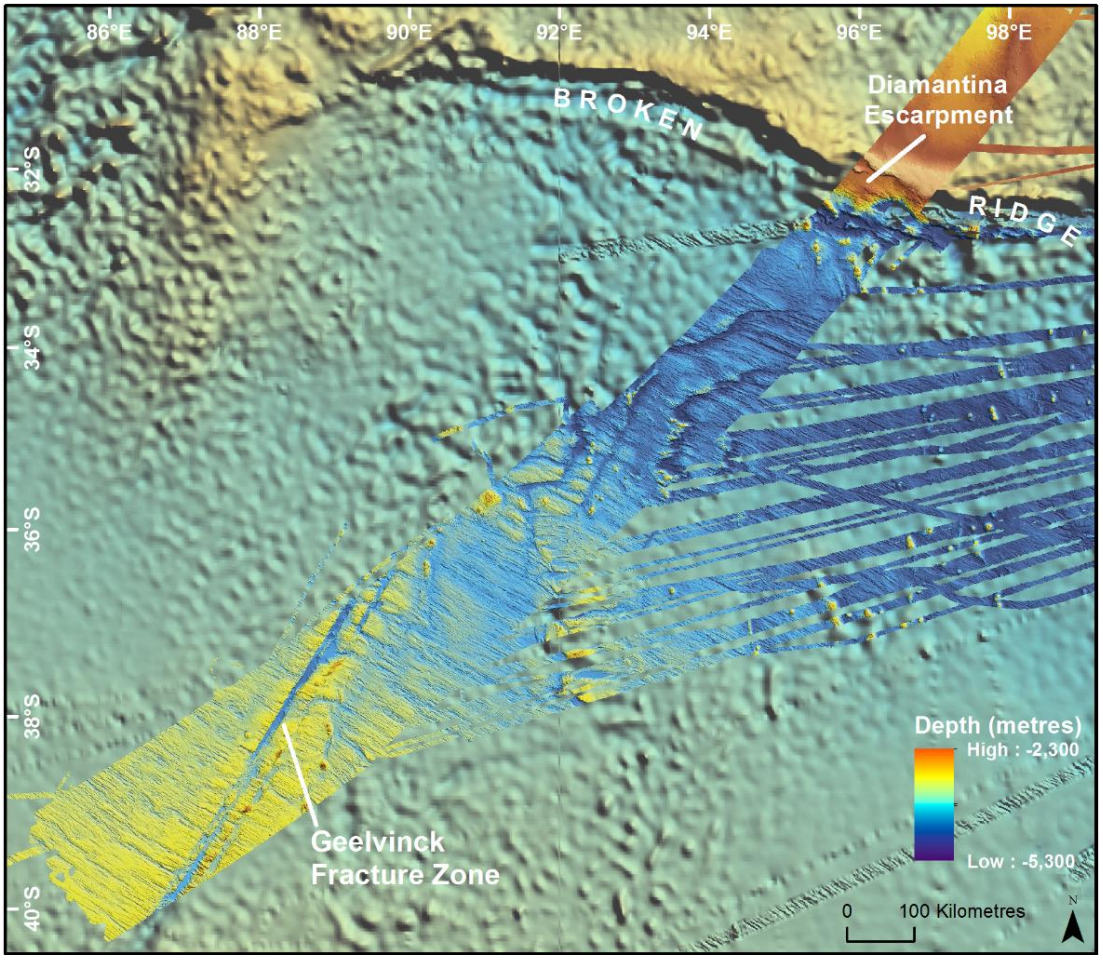

Source: ATSB

South of Broken Ridge

Here, water depths range between 2,300 m and 5,300 m. The seafloor south of the Diamantina Escarpment has the youngest geology within the search area. This region of the seafloor was formed by 'seafloor spreading' caused by tectonic plate movements. As a result, the seafloor is highly complex, including a series of ridges, volcanoes, and valleys. The Geelvinck Fracture Zone was the result of the same tectonic motion that created Broken Ridge. It is 900 m deep and 12 km wide (Figure 32).

Bathymetry processing

The data gathered during the bathymetric survey was analysed and processed by Geoscience Australia.

High resolution multibeam data was collected using a Simrad Kongsberg EM 302 (30 kHz, *Fugro Equator*), Simrad Kongsberg EM 122 (12 kHz, *Fugro Supporter*) and a modified Reson Seabat 7150 (12 kHz, *Zhu Kezhen*).

Raw data from the Fugro Survey vessels was post-processed, and processed data from the *Zhu Kezhen* were verified, using the CARIS Hydrographic Information Processing System (HIPS) and CARIS/Sonar Image Processing Software (SIPS) v.7.1.2 SP2. The processed data were exported as ASCII XYZ point cloud files. Bathymetry data were converted into 40 m and 110 m grid formats via LASTools and Python, and imported into ArcGIS v.10.0 for spatial analysis.

More information on bathymetric surveys can be found on the Geoscience Australia website at www.ga.gov.au/

Backscatter analysis

In addition to processing and mapping the bathymetric data, Geoscience Australia analysed the backscatter data from the hull-mounted multibeam sonar, looking for anomalies in the acoustic return.

The proportion of acoustic energy returned from a rough surface is determined by the impedance contrast, sometimes referred to as 'hardness' and apparent surface roughness scale (i.e. roughness scale relative to the acoustic wave length). In general, as the impedance contrast or roughness of a surface increases, so does the intensity of backscatter returned (Figure 33).

The surface scattering coefficient is a dimensionless quantity that accounts for the intensity (power) ratio of the incident and scattered waves determined per unit area at a reference distance of 1 m. When expressed in decibels, this quantity is commonly called the backscatter strength.

Hardness of the seafloor is measured by acquiring backscatter; the reflection of acoustic signal scattering from the seafloor back to the hull-mounted multibeam sonar transducer. Measured in intensity, backscatter ranges from 10 and -70 decibels, high to low, respectively (e.g. steep slopes to soft sediment).

Figure 33: Backscatter data at 30 m resolution showing volcano with hard rocky surface

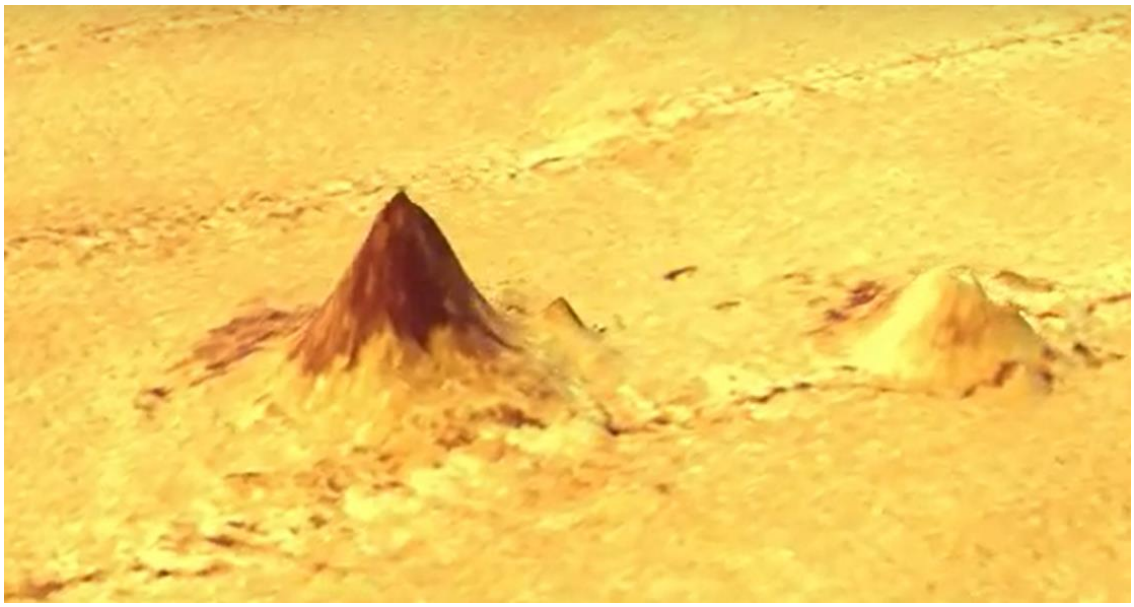

Source: Geoscience Australia

The backscatter analysis was used to identify anomalies on the seafloor. These anomalous areas were collected as a guide of potential areas of interest for the underwater search using side scan sonar.

Three classifications of area types were identified during the backscatter data analysis; navigation features, response uncertainty and potential targets (Table 20):

- Navigation features identifies areas that may be of interest for the navigation of underwater vehicles such as seafloor with high relief or large-scale irregular morphology, for example a canyon or seamount.
- Response uncertainty identifies areas of seafloor with relatively complex/highly reflective acoustic characteristics that could hinder the detection of aircraft debris.
- Potential targets identifies features that are of potential interest for further searching based on anomalies in backscatter intensity.

Table 20: Areas of interest identified in backscatter analysis

Navigation Features:	53
Response Uncertainty:	42
Potential Targets:	608

Source: Geoscience Australia

Potential targets were detected based on the anomalously high acoustic backscatter strength of small features. The identification of potential targets for fine-scale investigation was based on a line by line assessment of the backscatter strength and corresponding bathymetry data. For example, potential target areas of seafloor may have backscatter anomalies that are difficult to explain based on their corresponding geomorphology.

One potential target area is shown in Figure 34. Here, high backscatter values contrast with the surrounding seafloor of low backscatter strength. This potential target was located within the nadir region; a region in the backscatter data approximately 10 degrees to port and starboard of the ship's track, which changes in width systematically with depth. Results from this region were not considered due to the inherent reduced quality in backscatter response. Results were discounted at the time but later compared with the side scan sonar, revealing the potential target had coincided with a shipwreck.

Figure 34: Potential target with maps showing backscatter (A), side-scan sonar (B), and man-made feature (C)

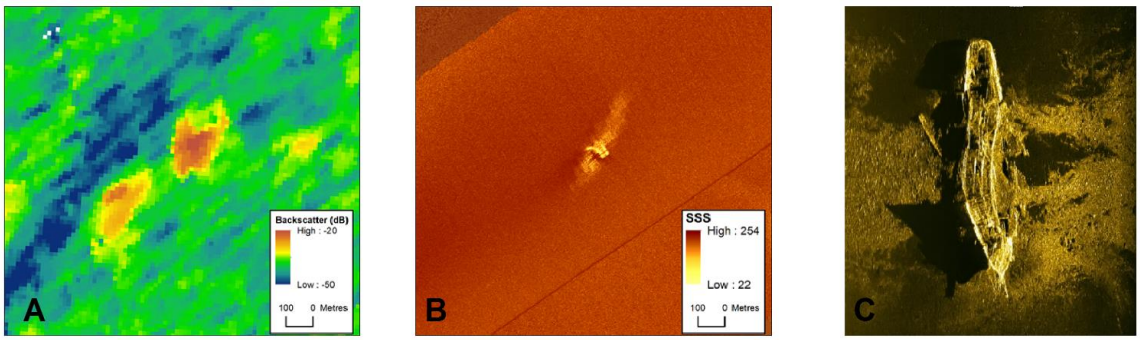

Source: Geoscience Australia (A), ATSB (B) and (C)

Selecting the search method/systems

When the surface search for MH370 concluded, it was agreed by the Tripartite governments that Australia, represented by the ATSB, would coordinate all aspects of the underwater search. This included the contracting of the necessary commercial services and also to manage the operations of all search vessels and equipment provided directly by the Governments of Malaysia and the People's Republic of China.

The initial area to be searched was very large at 60,000 km², and became larger in April 2015 when the Tripartite governments agreed to expand the search area to 120,000 km². The main objective of the search was to establish whether or not the debris field of the missing aircraft was in the area defined by expert analysis of the aircraft flight path. If a debris field was located, the search needed to confirm the debris was MH370 by optical imaging and then map the debris field to enable planning for a subsequent recovery operation.

Careful consideration was given to available equipment and methods for conducting a large scale search of the seafloor. Water depth was expected to be up to 6,000 m with unknown currents and unknown seafloor topography. Search operations would have to be often conducted in poor weather conditions in a very remote area. While the ATSB search team hoped the aircraft would be found quickly, planning focused on selecting an efficient and effective method to search the seafloor in an operation for an indeterminate period.

The search tender

The ATSB had not previously managed an underwater search operation in such deep water nor managed a procurement of this size or complexity. Initial market research was conducted which indicated that there was a small market of mostly international marine survey/salvage companies with the capacity and capability to undertake the underwater search.

When preparing the open tender for MH370 search services, the ATSB considered all of the technical and organisational requirements to conduct an efficient, effective, and safe underwater search operation in up to 6,000 m of water, in challenging conditions. The tender focused on the underwater search equipment, vessels, personnel, past experience with similar operations, the processing, storage, transmission and security of the search data and the organisational systems and plans to be put in place to manage the search with a particular focus on risk mitigation and the health and safety of the search crews.

The ATSB's tender was for seafloor search operations to localise, positively identify, map and obtain visual imaging of the MH370 debris field. The tender was divided into two primary areas; search for and locate MH370 debris within the defined search area on the seafloor and if located, map and optically image (photograph or video) the aircraft debris field.

The search for Air France 447 (AF447) off the coast of Brazil from 2009 to 2011 is the most analogous deep water search operation for an aircraft in recent times. The ATSB consulted extensively with France's air accident investigation organisation, the Bureau d'Enquêtes et d'Analyses pour la Sécurité de l'Aviation Civile (BEA) who were responsible for the AF447 search and recovery. Woods Hole Oceanographic Institute in the United States was also consulted on the underwater search as they provided equipment and expertise for the AF447 search operations.

AF447 was an Airbus A330 aircraft, a similar size to the B777 aircraft operating flight MH370, and the wreckage was recovered from a depth of water similar to that in the MH370 search area. It was also lost in a very remote location, midway between South America and Africa in the middle of the Atlantic Ocean. The AF447 debris field was approximately 600 m x 200 m in size at a depth of 3,980 m (Figure 35).

Figure 35: Air France 447 debris field overlaid to scale on a swath of MH370 deep tow vehicle sonar data

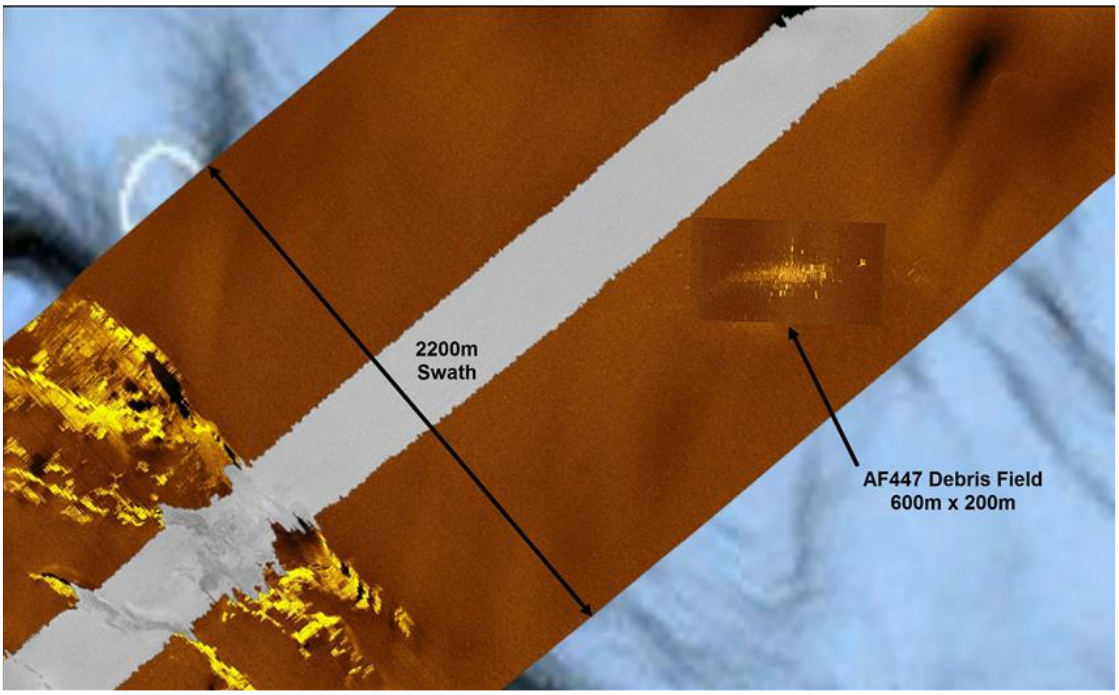

Source: ATSB, using BEA data

A key specification for the search equipment in the ATSB's tender was a feature detection capability, or resolution, of two cubic metres which was conservatively selected on the basis that this is the size of the core of B777 engines which are very robust and likely to survive a high energy impact relatively intact, as they did in the case of AF447 (Figure 36).

Figure 36: Air France 447 engines on the seafloor

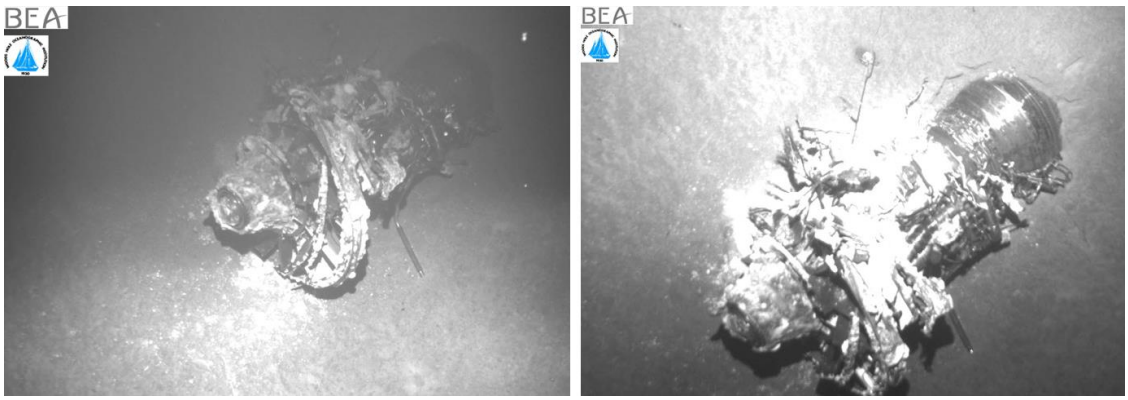

Source: BEA

The tender also specified a requirement to perform a fully functional test in deep water to demonstrate that the proposed search system would reliably detect targets of two cubic metres at the sonar range scales to be used in the search. Other key tender requirements specified the necessity to mobilise the search equipment quickly and complete the search of the initial 60,000 km² in a period of 300 days.

Tender responses broadly fell into two categories, those companies who offered towed side scan vehicles for primary search and detection with an alternate method to positively identify and map the debris field, usually a remotely operated vehicle (ROV) fitted with a camera. Other tenders offered autonomous underwater vehicles (AUVs) which could be used for both primary search and also positive identification and mapping using a camera. A few tenders offered both towed and autonomous search vehicles.

All tenders were assessed by a panel which included personnel who had experience in marine survey, marine salvage, marine operations, deep water search/survey and aircraft accident investigation. The tender assessment panel initially assessed each tender's compliance with the technical requirements set out in the request for tender and were not privy to the prices quoted by the tenderers. Once the tenders were ranked in merit order for the technical solutions they proposed, only then was the price considered. The intent was to ensure that the tender assessment process was weighted towards choosing the best overall technical solution.

Vehicles

There were only two choices of underwater vehicles to use in the underwater search for MH370, towed or autonomous, both had advantages and disadvantages and both types of vehicle were used in the search.

Towed vehicles are an efficient instrument platform when a search is to be conducted of a large area which can be performed in long continuous search lines where the seafloor terrain is relatively flat. Once launched from the support vessel, they can be towed for many weeks, including through periods of worse weather (than AUVs), without the need for recovery as power and data to and from the instruments on the vehicle are transmitted continuously via the tow cable. The deep tow system used in the search for MH370 is shown in Figure 37.

Figure 37: Deep tow vehicle operation

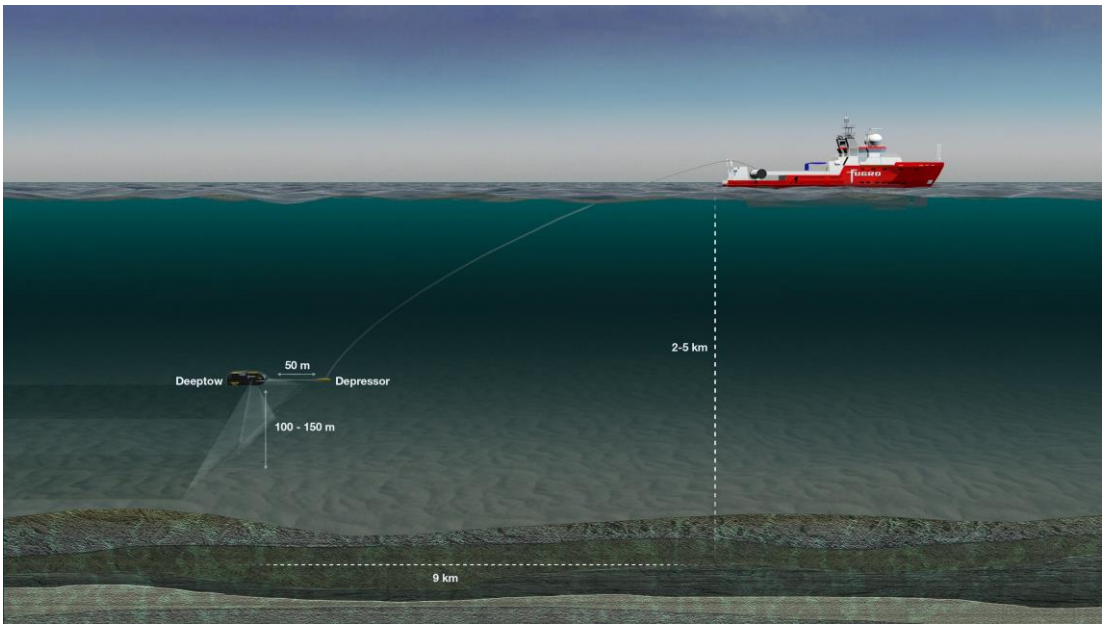

Source: Fugro Survey

Deep tow vehicles have disadvantages compared to AUVs including relatively little to no manoeuvrability and typically less accurate positioning, both of which can have an impact on the effective sonar coverage achieved in a wide are search/survey operation.

Deep tow vehicles must be positioned by changing the heading/speed/position of the tow vessel at the surface and the length of tow cable deployed. The depth of water dictates how much tow cable must be used to maintain the vehicle at a constant altitude above the seafloor for a given vessel speed. In 4,000 m of water there may be up to 8,000 m – 9,000 m of tow cable deployed which lies in a very long catenary behind the tow vessel. The response of the deep tow vehicle to changes in vessel speed, heading or position or the amount of tow cable deployed, is directly proportional to the rate each parameter is changed. The deep tow vehicle response may not be immediate but once the change begins it may happen relatively quickly and be very slow to reverse if needed.

Negotiating terrain features on the seafloor, for example a seamount where there is a steep gradient, requires the deep tow vehicle to be raised to clear the obstacle and then lowered after the obstacle is passed. This will often lead to sonar data degradation due to increased motion of the deep tow vehicle or a gap in the data termed a ‘terrain avoidance holiday’. Similarly, the very long tow cable means an end-of-line turn (through 180°) onto the next search line may take up to 12 hours.

Deep tow operations are limited by the weather as a proportion of the tow vessel’s pitch, heave and surge motions, in particular, are transmitted via the tow cable to the deep tow vehicle. While the very long catenary of the tow cable helps to damp these motions, any residual force at the end of the tow cable causes the deep tow vehicle to pitch and surge which can lead to sonar data quality degradation. A two body tow system (consisting of a heavy depressor connected to the end of the tow cable and a soft neutrally buoyant tether which connects the vehicle to the depressor) helps to mitigate this undesirable vehicle motion. However, depending on the weather which is forecast, decisions have to be made whether or not to recover the vehicle or continue deep tow operations based on the likely impact on the quality of the side scan sonar data and the increased risk to personnel and equipment as the sea states rise.

Accurately positioning an underwater vehicle in real time on a search line is critical to ensuring that the search is efficient and effective. Features identified in the sonar data must be able to be accurately georeferenced (using the vessel’s position to derive the deep tow vehicle’s position)

and there must be sufficient overlap in side scan sonar coverage to avoid data gaps (termed 'off-track holidays') between adjacent search lines. Accuracy in positioning a vehicle at depth generally diminishes as distance from the accurately known position of the vessel at the surface increases. For deep tow vehicles, factors like currents may result in the vehicle being significantly offset from the tow vessel's track and must be compensated for by manoeuvring the vessel to maintain the required deep tow vehicle track to ensure adequate overlap between search lines.

Deep tow vehicle positioning is most often derived using one or a combination of the following; cable lay back, seafloor feature matching methods, a bottom tracking doppler velocity log (DVL), and an inertial navigation system both fitted to the vehicle, ultrashort baseline (USBL) acoustic positioning or long baseline acoustic positioning. USBL systems provide a range and bearing from the vessel to the USBL beacon which is fitted to the vehicle, or for shorter range systems, an intermediate position on the tow cable. All of these methods have inherent inaccuracies with the most accurate available long range USBL systems when coupled with an inertial navigation system and DVL achieving vehicle position accuracy in practice of approximately 50 m at a range of approximately 8-9 km.

Autonomous underwater vehicles, once programmed and launched, can be completely independent of the support vessel and are highly manoeuvrable. They can search the seafloor effectively in any pattern, not just long continuous lines, and can closely follow dynamic seafloor terrain which often leads to better overall sonar coverage. They can also achieve higher resolution sonar data given they can safely fly closer to the seafloor than a typical deep tow vehicle. Similarly when the AUV's inertial navigation system is coupled with a DVL and USBL (or long baseline) acoustic tracking system at a relatively short range (4,000 to 5,000 m), with the support vessel tracking the AUV at the surface, or deploying a long baseline field, AUV positioning is generally more accurate than a deep tow system. Figure 38 shows an AUV operation (not to scale) with the support vessel gathering bathymetric data concurrently.

Figure 38: Autonomous underwater vehicle operation

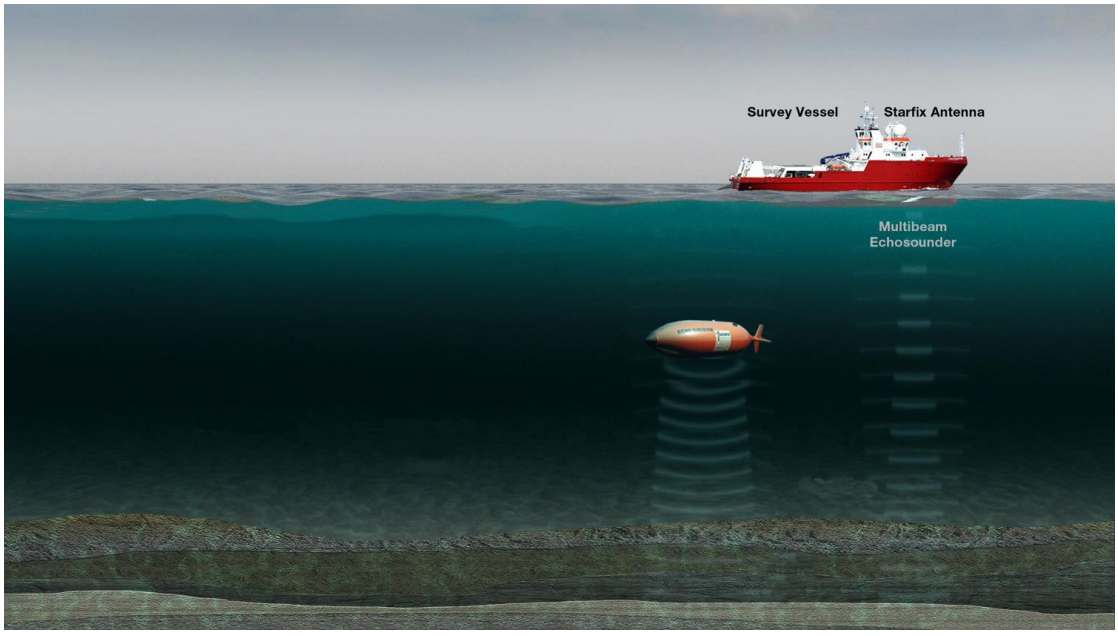

Source: Fugro Survey

The major disadvantages of AUV's are the need to safely launch and recover the vehicle before the batteries are exhausted, their limited duration on the seafloor per mission (typically less than 26 hours), the time to download the data which is stored on board the vehicle (or a data pod), and their relative high cost per km² compared to a deep tow vehicle equipped with the same instruments. At the time of the search tender there was also limited availability for 6,000 m rated AUVs, and multiple AUVs were needed to achieve the required search coverage rates.

In the MH370 search area, weather for much of the year is consistently beyond safe launch and recovery limits for effective AUV operations. The exception is the summer months, December to March, when there is a much higher proportion of better weather which allows for efficient AUV operations.

At the time the search tender responses were assessed, bathymetric mapping in the search area was not complete nor was the search area fully defined. There was ongoing analysis to define the most probable area along the 7th arc where the aircraft impacted the water. Research indicated that weather was likely to be challenging for much of the year in the most likely search area and that the prevailing weather was from the southwest.

The search was likely to be able to be conducted in long lines aligned with the 7th arc which would make deep tow vehicles the most effective search method for most of the area. The weather from the southwest would also mean that the search vessels would be towing the deep tow vehicles with the weather almost directly astern or ahead, a significant advantage for maintaining the tow vessel position accurately and therefore that of the deep tow vehicle.

The decision was therefore made that deep tow vehicles represented the most efficient systems to conduct the search offered in the tender. It was concluded that choosing deep tow vehicles as the primary search method would necessitate having an AUV or ROV readily available for positively identifying sonar contacts. It was also considered that AUVs would offer further advantages as these vehicles could also be used to perform infill search work (in areas where the deep tow vehicles could not search effectively) whereas an ROV could not. Fugro Survey's underwater vehicles used in the search for MH370 are show in Figure 39.

Figure 39: Fugro Survey search vehicles: Edgetech deep tow and Kongsberg Hugin 1000 AUV

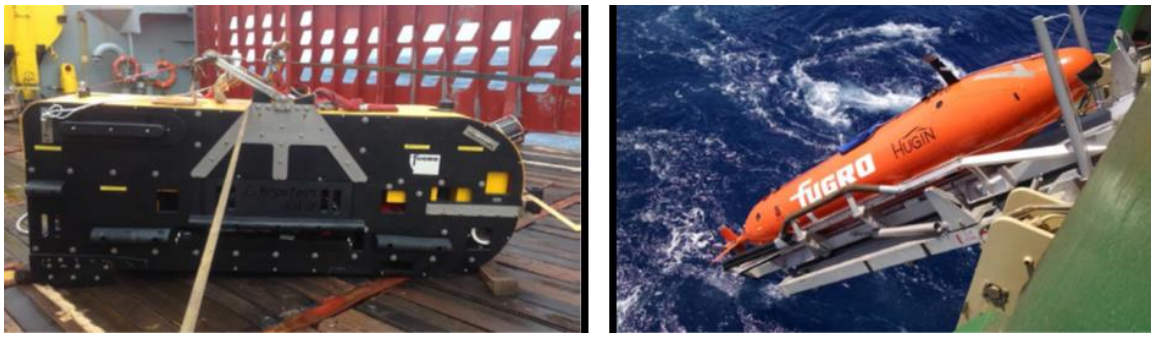

Source: Fugro Survey

Remotely Operated Vehicle

Phoenix International's *Remora III* ROV (Figure 40) was brought into the search in 2016, initially to recover the ProSAS deep tow system which was lost after a tow cable termination failure, and then later used to investigate a number of sonar contacts of potential interest. Unlike an AUV, the ROV remained tethered to, and controlled from, the support vessel. The ROV was rated to a depth of 6,000 m and was fitted with a video camera system, scanning sonar, manipulators (to gather samples), and a USBL positioning system. In good weather the ROV was able to be deployed, dive, survey and film the sonar target, return to the surface and be recovered by the vessel in 5 to 6 hours.

Figure 40: Phoenix International's *Remora III* remotely operated vehicle

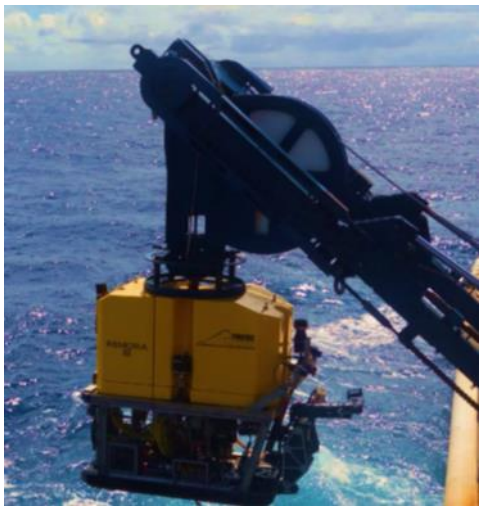

Source: Phoenix International

Sonar systems

The feature detection capability of a conventional side scan sonar system is a function of several factors and operational parameters. The frequency of the sonar signal, the transmit/receive cycle (range scale), acoustic energy levels and system noise levels all factor into detection capability.

Sonar coverage rates are a function of the sonar's effective range (swath) and the speed of the sonar system over the seafloor. Lower frequency systems typically have greater range capability however longer range scales also have longer transmit cycles between 'pings' and therefore fewer 'pings' reflect off an individual target than would occur with using shorter range scales. This essentially decreases the detection capability, especially for smaller objects. Using slower tow speeds can increase the number of 'pings' on a target however this directly impacts seafloor coverage rates.

Frequency, feature detection capability, resolution required, and rate of coverage of sonar systems are all related and need to be considered and carefully weighed based on the requirements of the survey (or search). For the search for MH370 with a basic requirement to detect an object two cubic metres in size, a frequency range and associated coverage rate was selected based on the feature detection capability of the sonar system.

Another important consideration for the sonar search systems was the side scan sonar 'blind spot' in the nadir area directly beneath the vehicle. This can significantly impact the amount of overlap required between adjacent search lines and therefore the overall seafloor coverage rate.

The deep tow vehicles offered in the tender were fitted with side scan sonar transducers with a range of frequencies, often more than one. The frequencies stipulated for wide area coverage ranged from 30 kHz through to 120 kHz with corresponding vessel speeds between 1.8 and 3.0 knots. While the lower frequency systems had generally longer maximum ranges (with side scan sonar swaths up to 6 km) these systems had to be operated at less than maximum range scales in order to meet the feature detection requirement. In addition, these vehicles often did not have any instrument to cover the nadir region below the vehicle and therefore relied on very large overlaps between search lines to achieve sonar coverage in the nadir area.

The frequency of the side scan sonar on the vehicles selected by the ATSB for the search was 75 kHz. The deep tow vehicles were operated at speeds between 2.5 and 3 knots with a validated swath width of 2,000 m (which was proven to meet the feature detection requirement over the sonar test range). Data was collected over a 2,200 m swath however the last 100 m of the range on each side of the sonar was only used for aiding in assessing overlap and feature matching for position validation. Test target detection was achieved in the outer range however it was not

consistent enough to meet the feature detection requirement and was therefore not included as valid sonar coverage. Search line spacing for most of the search was set at 1,700 m which allowed up to 300 m overlap between adjacent deep tow search lines. These systems achieved coverages in excess of 200 km² per operational day during the search excluding weather, equipment downtime and end-of-line turns.

The AUV used in the search was equipped with the same side scan sonar and transducers as the deep tow vehicles and was operated at generally lower range scales for infill work but at speeds up to 3.6 knots. The sonar system was validated up to a 2,000 m swath using the same feature detection requirements and testing as the deep tow vehicles. All the vehicles contracted by ATSB for the search (deep tow and AUV) had a multibeam echo sounder (MBES) to cover the nadir area and were equipped with inertial navigation, DVL, and USBL positioning system.

Synthetic Aperture Sonar

The ProSAS deep tow vehicle (Figure 41), built and operated by Hydrospheric Solutions Inc. (Hydrospheric Solutions) was initially mobilised on *Go Phoenix* and provided to the underwater search as Malaysian Government furnished equipment. The vehicle was the latest generation of deep water (6,000 m rated) towed sonar systems. It was equipped with a 60 kHz synthetic aperture sonar (SAS) system which was able to achieve higher resolutions at longer ranges compared to traditional side scan sonar systems. The SAS processing combines data from several individual sonar 'pings' in a sequence with a highly accurate inertial navigation solution to build a map of the seafloor with a consistent resolution of 10 cm over the entire swath width.

The ProSAS vehicle was operated at a speed of around 1.8 knots, achieving a swath of 2,000 m (range and speed are directly related for a SAS system). The ProSAS deep tow vehicle was also equipped with a MBES to cover the nadir area and an inertial navigation, DVL, and USBL positioning system.

Later in the search (January 2016) the ProSAS deep tow vehicle was mobilised on the vessel provided by the People's Republic of China, *Dong Hai Jiu 101*.

Figure 41: Hydrospheric Solutions ProSAS deep tow vehicle

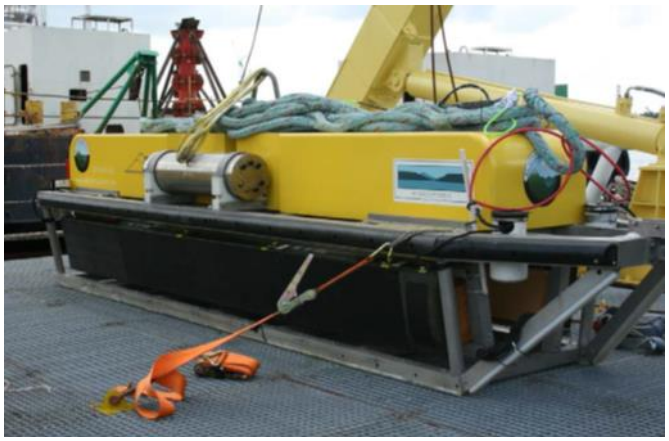

Source: Hydrospheric Solutions

Other search coverage considerations

The search for MH370 had to be conducted over a large area as a result of the limited data available with which to reconstruct the aircraft's flightpath or accurately determine where the aircraft may have impacted the water. A key consideration when selecting the search method was to complete the search in a reasonable time period within the constraints imposed by the weather and remoteness of the search area.

The overall rate of coverage is not only dependent on the coverage rate of the search systems when they are operational but also on the overall proportion of operational time in the search area

after discounting the time lost due to end-of-line turns (for deep tow vehicles), weather, equipment or other down time, and the time taken to transit to and from port for re-supply. The proportion of operational time in the search area is therefore maximised by extending the vessel endurance, minimising the transit time to and from the search area and minimising down time in the search area.

Operational tasking must be aimed at minimising end-of-line turns by tasking the deep tow vehicles to search on very long lines. Vessel and equipment downtime must be minimised by having well maintained and reliable vessels, equipment, sufficient spare parts and expertise on board to perform repairs while in the search area. Similarly the overall search organisation must take into account expected weather in the search area with search activity increased in the better weather months.

The request for tender, released in June 2014, stipulated a 300 day period to complete the search of the initial 60,000 km² area. At that time, the search was to be conducted in an area to the north of the underwater feature Broken Ridge. By the time the search commenced in October 2014, further search area analysis had been completed and the search area was moved 1,000 km south along the 7th arc to an area below Broken Ridge. This impacted the coverage performance targets required of the search contractor as there was additional transit time to and from port to be considered and significantly worse weather in the new search area.

To manage the coverage requirements, Fugro Survey, who were selected as prime contractor for the underwater search, decided on a deep tow vessel swing[24] length of 42 days to allow at least 30 possible operational days in the search area (transits were on average 5 days to and from Fremantle to the search area). The choice of industry standard Edgetech deep tow vehicles meant that spare parts and complete vehicles were also readily available. Fugro Survey maintained a complete spare deep tow system on board one of the search vessels, while a tow winch and spare tow cables were available in Perth. Equipment downtime amounted to 5.6 per cent of total time over the course of the two years of deep tow operations. Weather stand-by in the search area during deep tow operations on the Fugro Survey vessels amounted to 9.9 per cent of total time.

Validating the search systems

All underwater search systems used during the search were tested and evaluated on their object detection capabilities and overall system performance. Each system was tested at the purpose-built test range put in place by Fugro Survey off the coast of Perth. The range was in a water depth of 650 m and consisted of five steel objects ranging from 1.3 m x 1.3 m x 1.3 m to 2 m x 2 m x 2 m in size and placed on the seafloor over 1,150 m. The steel shapes consisted of two cubes, two crosses and a cylinder shape as shown in Figure 42.

[24] A swing is the time between port calls which includes the time to transit to and from the search area and the time in the search area.

Figure 42: Test range targets and spacing diagram

Source: Fugro Survey

After each underwater vehicle was mobilised and readied for offshore operations the vessel proceeded to the test range. Each underwater search vehicle was tested in full operation with all integrated systems expected to be used in the search area. All systems were tested and verified using their nominal operational settings. The test was concluded once the test targets were successfully detected and the sonar data quality met the requirements set out by the ATSB and was deemed fit for purpose by the ATSB's Quality Assurance Manager and/or the ATSB client representative on board the vessel.

Verification reports were created which documented the sonar's ability to detect the test targets through the entire swath of the SSS. Testing was performed to ensure repeatable and reliable detection of the test targets at the far range of the SSS as well as the how close to the nadir region the targets could be seen in the sonar record.

Figure 43 shows the test targets as detected with a SSS. Using a 1,000 m range scale the deep tow vehicles and AUV detected the test targets reliably. From 1,000 m to 1,100 m the test targets were seen intermittently, however there was still useful data in this far range. It was determined that the extra 100 m of range aided in feature matching used to verify overlap and coverage. However, it was maintained that only the first 1,000 m of data was accepted as fit for purpose and relied on for sonar contact detection.

The deep tow vehicle testing speed was 3 knots and the AUV speed was 3.6 knots. Testing included the MBES systems on each of the underwater vehicles. Verification of detection capability and the amount of the overlap between SSS and MBES systems was determined as the MBES was used to fill the SSS 'blind spot' in the nadir region directly below the deep tow vehicle and AUV. The camera on board the AUV was also tested. Figure 44 shows images of two of the

test targets on the seafloor photographed using the AUV's camera. Target position comparisons were made along with proper operation of the deck equipment (tow winch and cable) and the processing hardware and software were also tested and verified.

Verification testing was also performed if major repairs were carried out on the sonar systems or if the system was demobilised and mobilised again later.

Figure 43: Test range targets as imaged by deep tow vehicle side scan sonar on seafloor

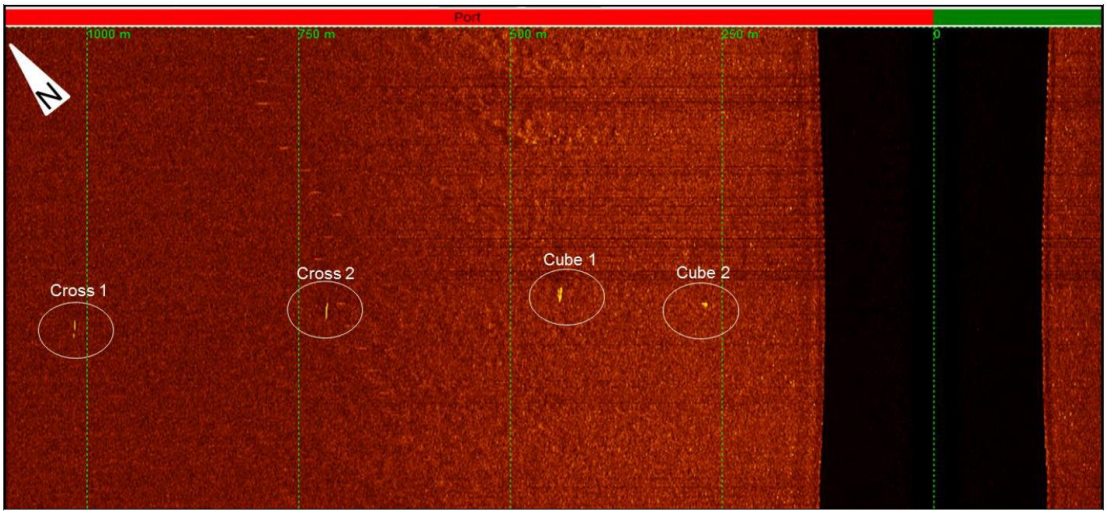

Source: ATSB

Figure 44: Test range targets as imaged by AUV camera on seafloor

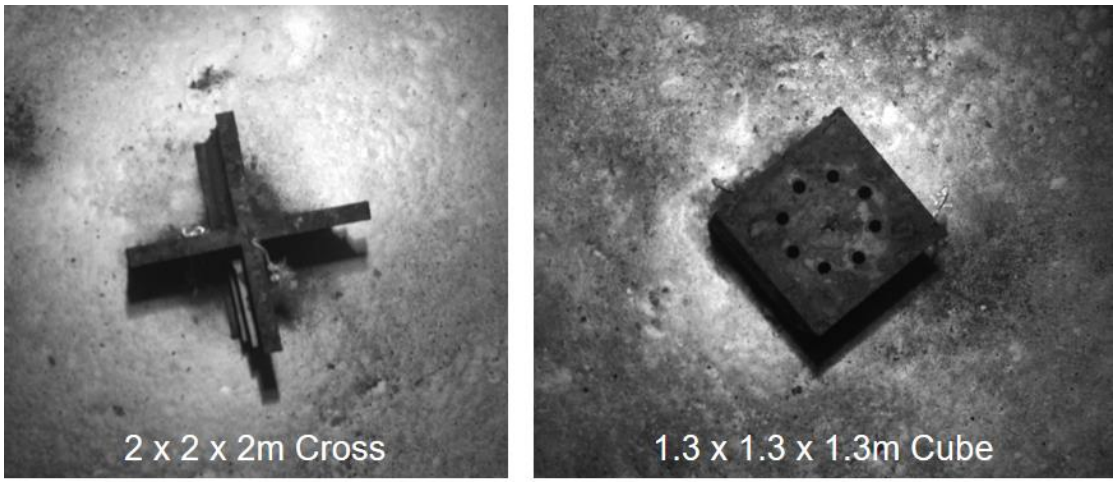

Source: ATSB

Underwater search chronology

Underwater search operations for MH370 lasted from 6 October 2014 until 17 January 2017. Before and during the underwater search, seafloor mapping was undertaken. The intent was to locate the aircraft debris field on the seafloor and then to commence a recovery operation. The areas searched were based on information from a range of sources, analysis which was progressively refined in relation to the aircraft's set of most likely flight paths and analysis relating to the aircraft's behaviour at the end-of-flight.

The SSWG formed by the ATSB at the end of the surface search brought together satellite, aircraft and data fusion specialists to progress work on defining the search area which would have the highest probability of containing MH370 to inform the underwater search. This group continued collaboration with the SATCOM WG and included experts from Inmarsat and Thales.

In June 2014 a search area of 60,000 km^2 was planned with an extension to the search area to 120,000 km^2 announced in April 2015. By the end of the underwater search an area in the order of 120,000 km² had been searched to a high confidence level by a combination of deep tow vehicles, an AUV and an ROV, however no item of debris from MH370 was located.

The following section sets out the chronology of the underwater search, the search assets used, where it was focused at different times and the information or analysis used to define those areas.

The priority search area refined southwards

While the bathymetric survey was being undertaken in the June 2014 priority search area, flight path analysis by the SSWG in July and August 2014 had focused on refinements to the 'Unified' BFO model and analysis of the BFO metadata related to the ground to air telephony call at 1839 UTC. A 'Unified 4x' BFO model (refer to appendix C) was approved by Inmarsat on 30 July 2014. This analysis redefined the priority search area of June 2014 and moved the search area south along the 7th arc (Table 21).

Table 21: Refined preparatory seafloor survey

Dates:	26 August – 26 September 2014
Event:	Mapping of seafloor in refined underwater search area of 60,000 km$^{2.}$
Search area location:	Underwater Search Area 1, 32.8ºS to 35ºS and -10 NM, +13 NM across 7th arc.
Search activity:	Mapping of seafloor – bathymetry phase
Guiding advice:	Inmarsat 'BFO Analysis Unified 4x' BFO Model. Flight path reconstruction group - 4 Analyses. SSWG's analysis techniques – Constrained autopilot dynamics (south) Data error optimisation (north)
Data used in planning search area refinement:	Attempt to cover approximately 80% of highest probability flight paths derived from both constrained autopilot dynamics and data error optimisation analysis techniques.
Search equipment:	*Fugro Equator* (ATSB contracted survey vessel MBES).
Coverage details:	32.8ºS to 35ºS bathymetry completed ≈ 14,000 km^2
References:	Press conference – Deputy Prime Minister on 26 August 2014. ATSB report: *MH370 – Flight Path Analysis Update* – 8 October 2014.

Source: SSWG, Fugro Survey, *Zhu Kezhen*, ATSB

As a consequence, on 26 August 2014 *Fugro Equator* was tasked to move bathymetric survey operations south along the 7th arc to an area below Broken Ridge (red area in Figure 45). The bathymetric survey continued through September in preparation for the arrival of the first search vessel, *Go Phoenix,* in the underwater search area.

Figure 45: Bathymetry survey June to September 2014, *Fugro Equator* and *Zhu Kezhen*

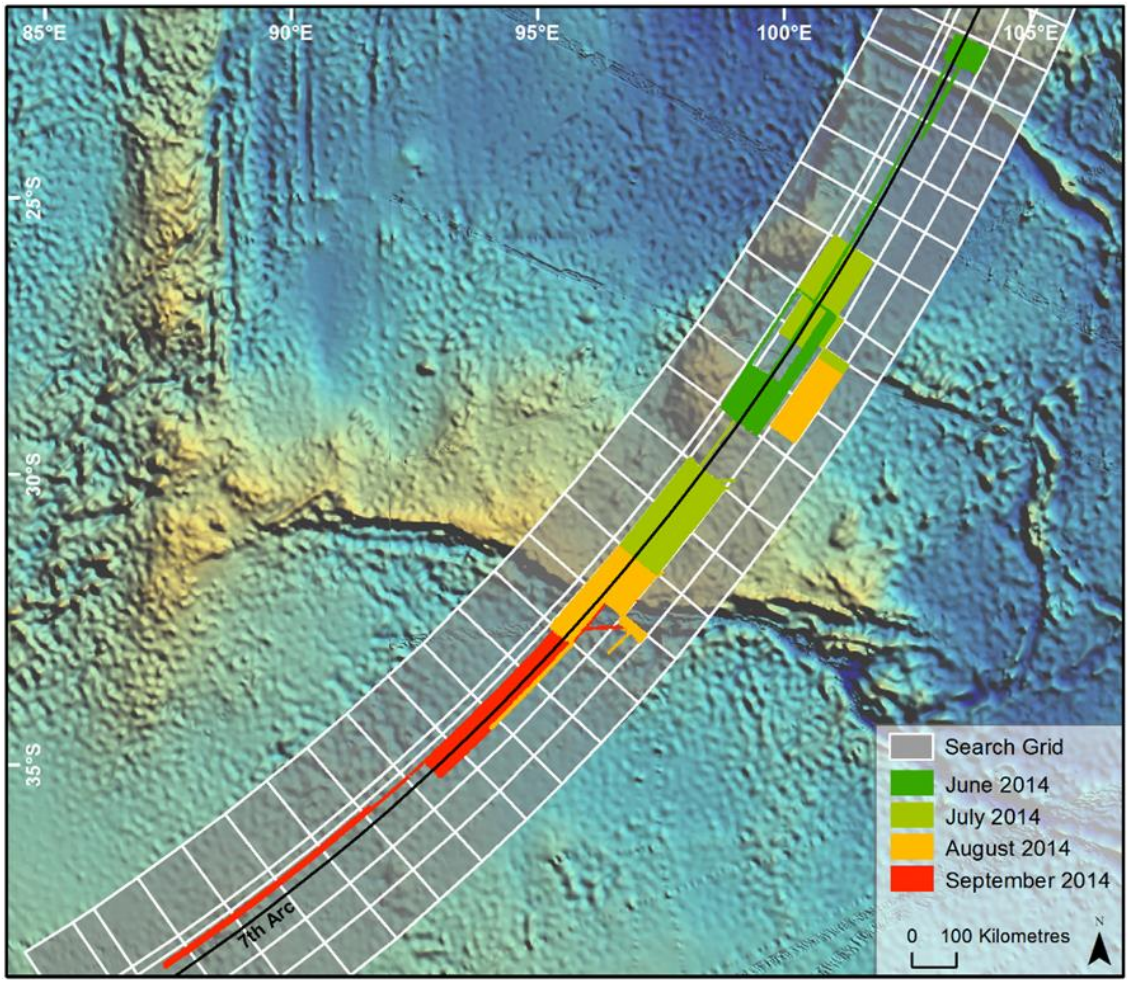

Source: ATSB

Underwater search commences

On 8 October 2014, the ATSB released the report '*MH370- Flight Path Analysis Update*' which detailed refinements to the BFO model and flight path analysis over the preceding months. The refined BFO model designated the 'Unified 4x' model had been developed and validated, and the various flight path reconstruction techniques had been applied to the model independently by the analysis groups. The analysis resulted in two probability distributions based on two different methods of calculating the statistical match of possible flight paths with the observed BTO and BFO values; 'data error optimisation' and 'constrained autopilot dynamics' refer to Figure 54.

Table 22: Underwater search commences

Dates:	26 September 2014 – 16 April 2015
Event:	Mapping of seafloor in refined underwater search area of 60,000 km^2. Underwater sonar search commenced in refined underwater search area.
Search area location:	Underwater Search Area 1 (*Go Phoenix*), 32.8ºS to 35ºS along 7th arc. Underwater Search Area 2 (Fugro Survey), 35ºS to 38.9ºS along 7th arc. -20 NM, +30 NM across 7th arc.
Search activity:	Mapping of seafloor – bathymetry. Underwater search using deep tow vehicles and an autonomous underwater vehicle.
Guiding advice:	Inmarsat 'BFO Analysis Unified 4x' BFO model.

	Flight path reconstruction group - four analyses. SSWG's analysis techniques – Constrained autopilot dynamics (south) Data error optimisation (north)
Data used in planning search area refinement:	Attempt to cover approximately 80% of highest probability flight paths derived from both constrained autopilot dynamics and data error optimisation analysis techniques.
Search equipment:	*Fugro Equator* (MBES bathymetry 26 September to 18 December 2014) *Go Phoenix* (ProSAS deep tow from 6 October 2014) *Fugro Discovery* (Edgetech deep tow from 22 October 2014) *Fugro Equator* (Edgetech deep tow from 15 January 2015) *Fugro Supporter* (Hugin AUV from 29 January 2015)
Coverage details:	32.8ºS to 38.9ºS bathymetry completed ≈ 46,000 km^2 32.8ºS to 38.9ºS underwater search completed ≈ 38,000 km^2
References:	ATSB report: *MH370 – Flight Path Analysis Update* – 8 October 2014

Source: Inmarsat, SSWG, Fugro Survey, Phoenix International, ATSB

With an agreed search area of 60,000 km^2 it was decided to search 80 per cent of the highest probability paths crossing the 7th arc for both analyses (Table 22). This required a search area length spanning from latitudes 33.5ºS to 38.3ºS[25]. An expanded priority search area south of Broken Ridge was created to accommodate this (Figure 46).

[25] The latitudes stated in this section are approximate and quoted at the crossing of the ATSB reference 7th arc (40,000 ft) unless otherwise stated.

Figure 46: Priority, expanded priority and medium search areas south of Broken Ridge, 19 October 2014

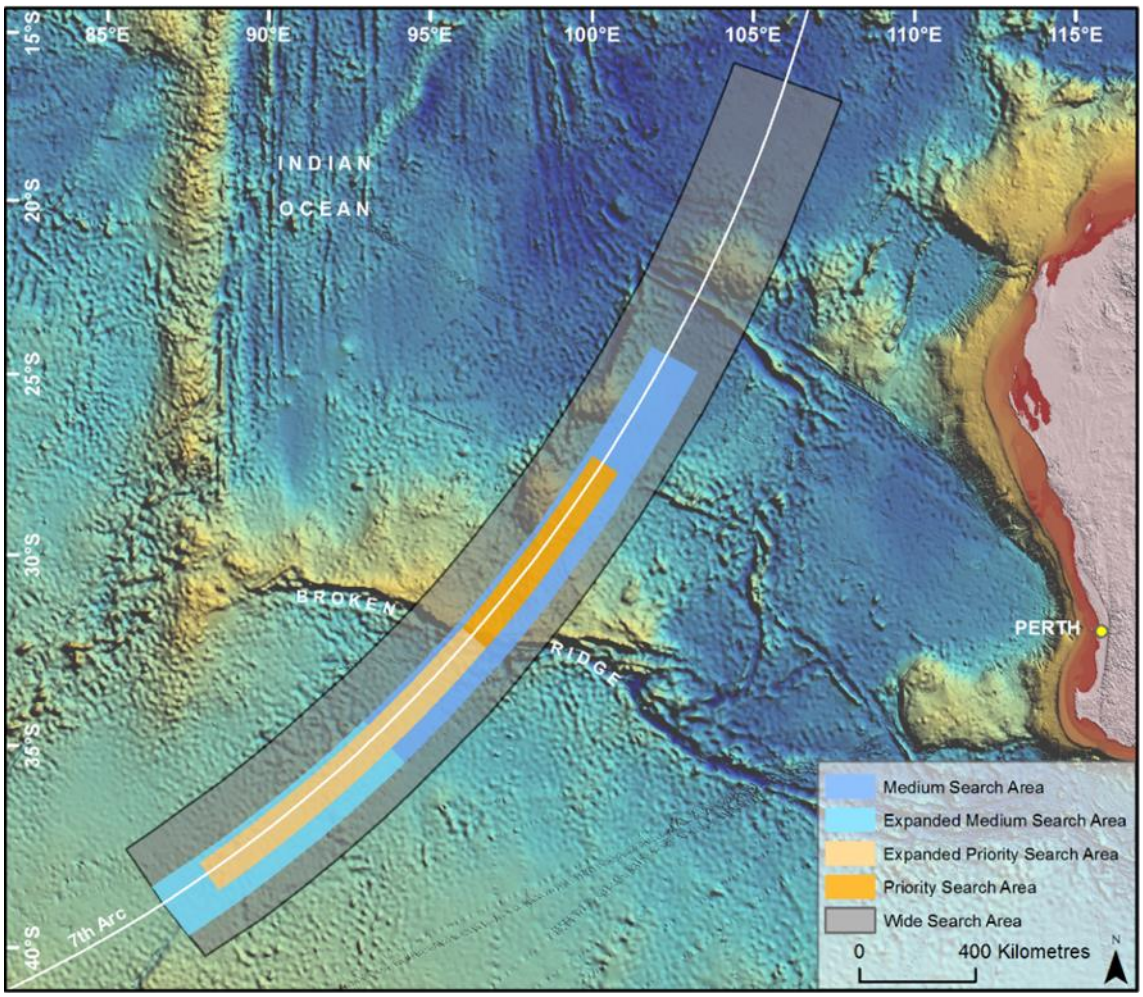

Source: ATSB

Go Phoenix commenced underwater search operations using the ProSAS deep tow vehicle on 6 October 2014. The vessel was assigned a search area from latitudes 32.8ºS to 35ºS where bathymetry had recently been completed by *Fugro Equator*. This area was designated Underwater Search Area 1 and was an area of approximately 14,000 km^2. Search lines were devised for *Go Phoenix* running parallel to the 7th arc.

Figure 47: Underwater Search Areas 1 and 2 based on completed bathymetry at start of *Go Phoenix and Fugro Discovery* arrivals in search area

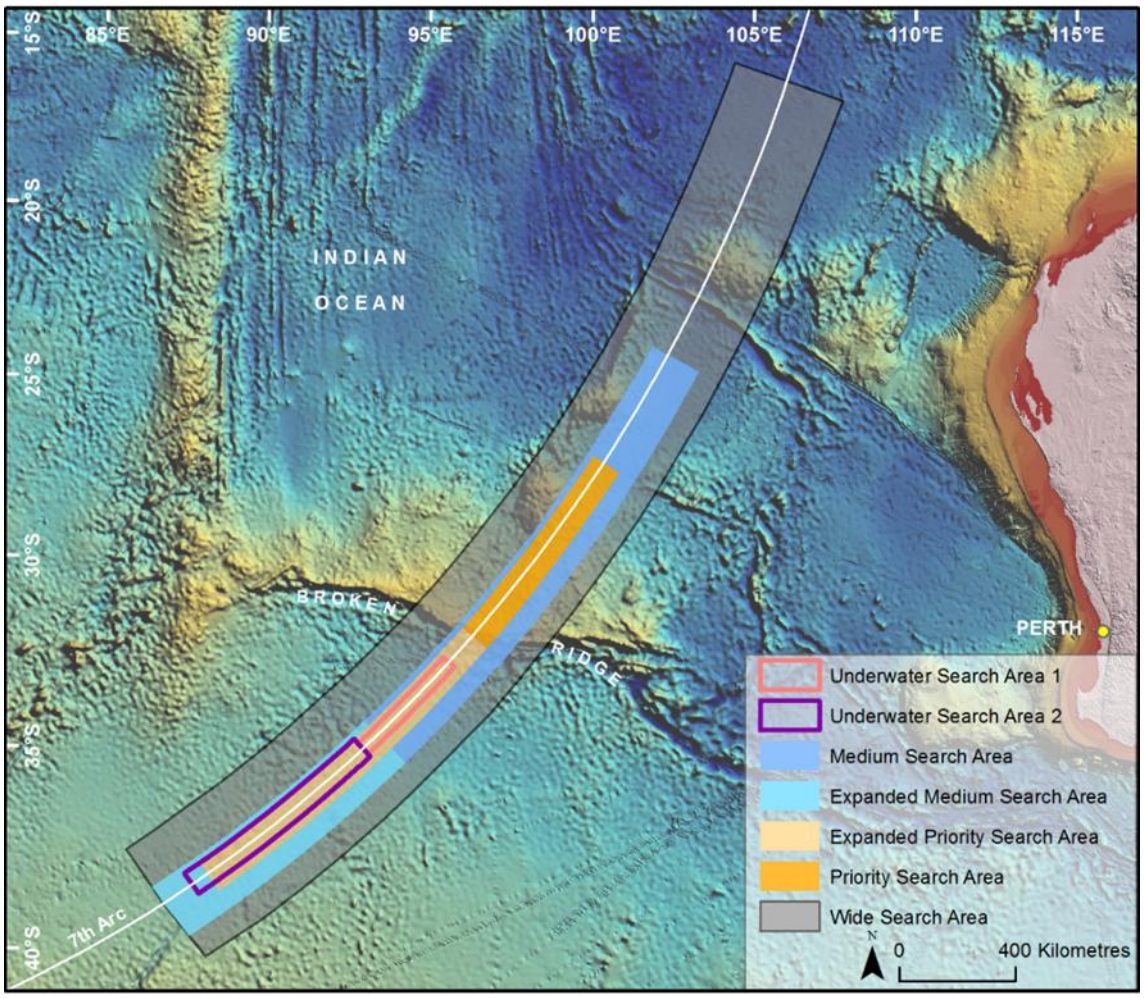

Source: ATSB

Fugro Equator completed the seafloor survey of Underwater Search Area 2 (an area of approximately 46,000 km^2) during its third and fourth bathymetric survey swings. This underwater search area, from latitudes 35ºS to 38.7ºS along the 7th arc was then assigned to the Fugro Survey vessels. *Fugro Discovery* subsequently commenced underwater search operations in this area on 22 October 2014.

It was planned that *Fugro Equator* would mobilise a deep tow vehicle and commence underwater search operations in November 2014. However, technical difficulties with the tow winch on the vessel necessitated a reassignment for a further bathymetry swing in November and December focused on the southern end of Underwater Search Area 2 extending the search area to latitude 38.9ºS (Figure 48).

Figure 48: Bathymetry coverage - *Fugro Equator* October to December 2014

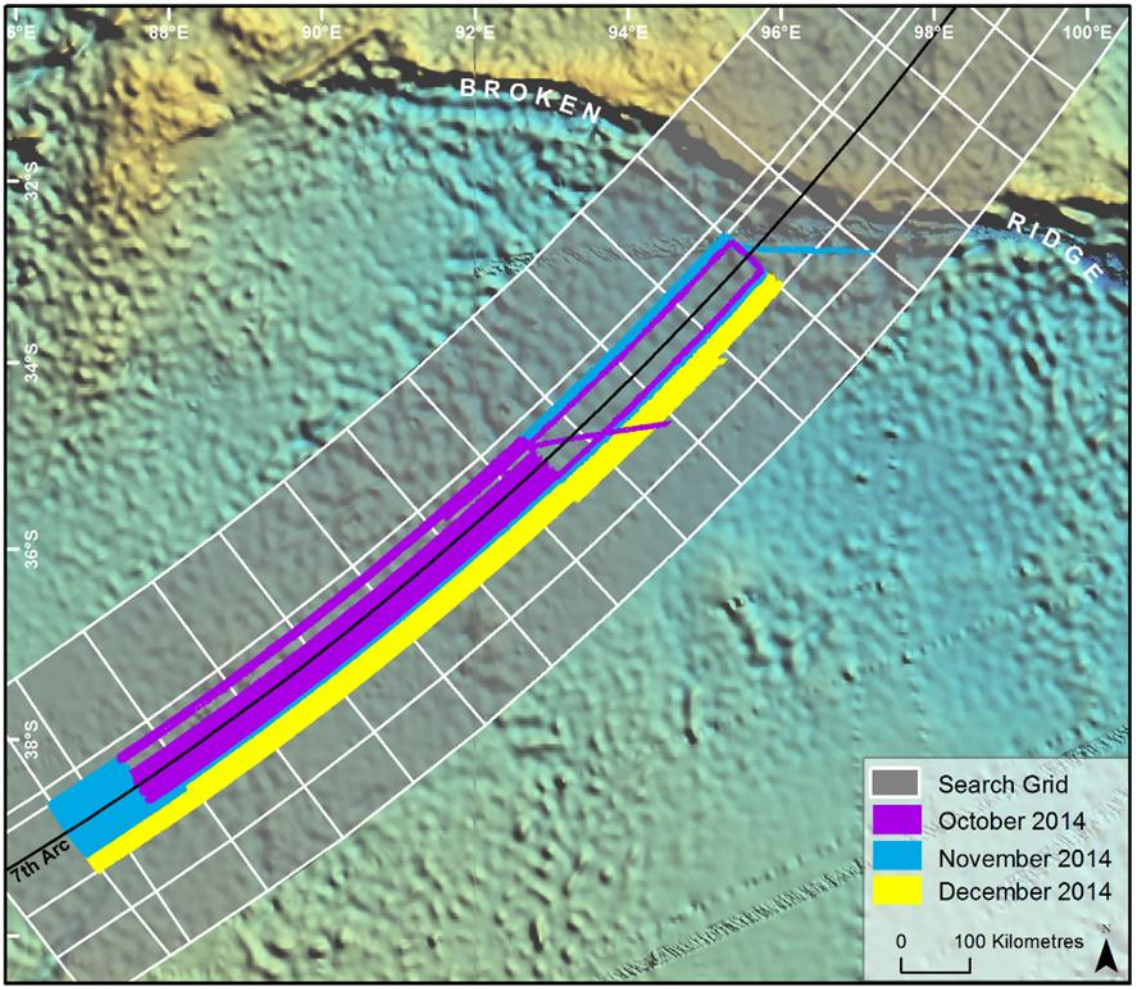

Source: ATSB

In January 2015, mobilisation of a deep tow search system on *Fugro Equator* was completed and the vessel commenced underwater search operations. In the same month *Fugro Supporter* entered the search equipped with an AUV to primarily search difficult seafloor terrain in the search area.

By 16 April 2015 an area of about 38,000 km^2 had been searched using three deep tow vehicles and the AUV system on board the four search vessels. *Go Phoenix* was close to completing its assigned area and the Fugro Survey vessels had focused on the area between latitudes 37.1ºS and 38.9ºS while the weather was favourable. Data gaps comprised approximately 5 per cent of the area searched (Figure 49).

During the period from November 2014 to April 2015 the four search vessels were affected by a number of tropical cyclones impinging on the search area which meant the vessels had to periodically suspend search operations to avoid storms and minimise potential damage.

Figure 49: Sonar coverage all vessels by April 2015

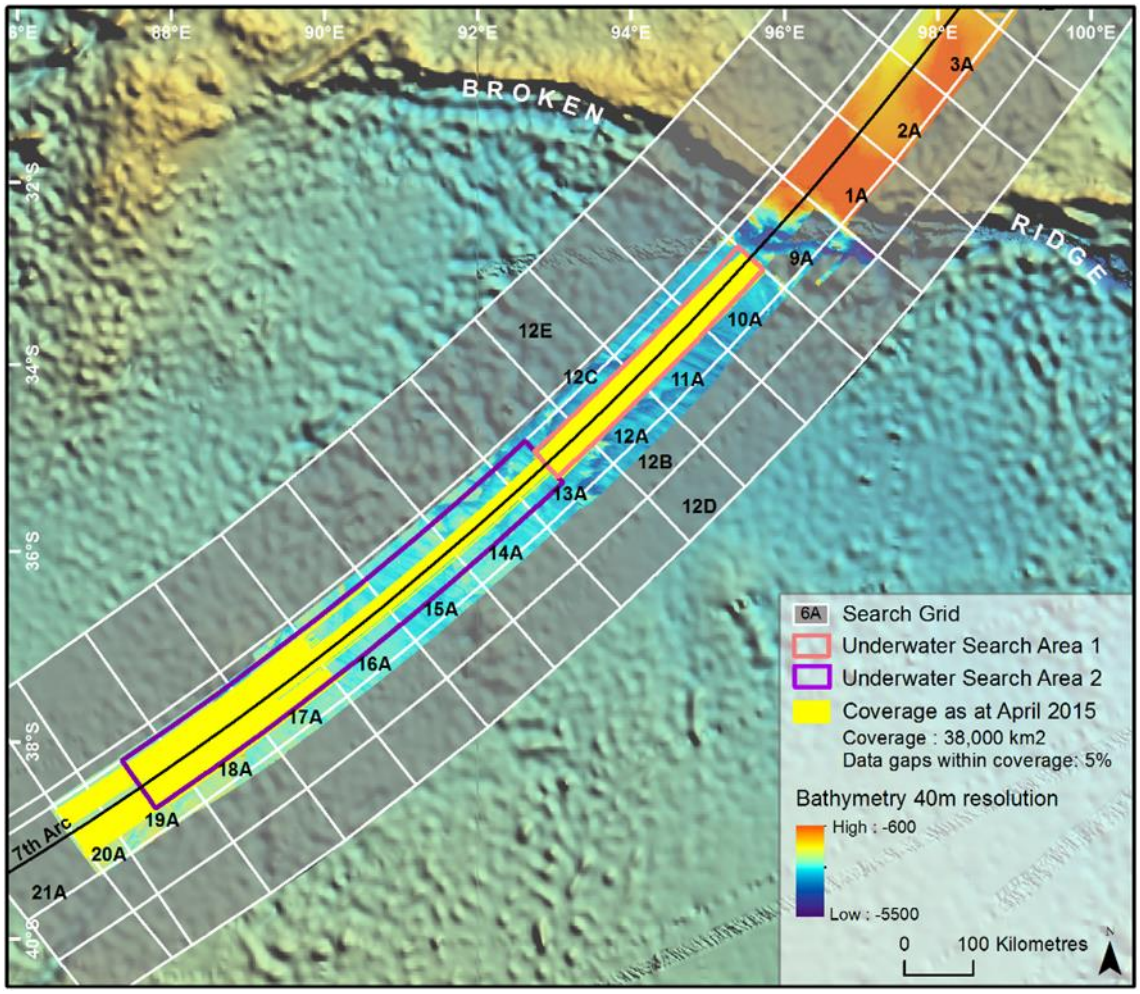

Source: ATSB

Search area extension

On 16 April 2015, the Governments of Malaysia, Australia and the People's Republic of China agreed to extend the underwater search area to 120,000 km^2 (Table 23). This allowed an additional area to the south to be included in the search area and a widening of the search area across the 7th arc to account for a greater range of possible aircraft end-of-flight behaviours.

The ATSB created a 120,000 km^2 indicative search area covering the highest probability paths of the then current flight path analysis from latitudes 32.5ºS to 39.1ºS with arrows indicating possible search area extension directions, depending on the outcome of further refinements to the flight path analysis (Figure 50).

Table 23: Underwater search area expanded

Dates:	16 April 2015 – 17 July 2015
Event:	Expanded underwater search area of 120,000 km^2 results in creation of indicative search area.
Search area location:	Underwater Search Area 1 (*Go Phoenix*). Indicative search area incorporating Underwater Search Area 2 (Fugro Survey). -20 NM, +30 NM across 7th arc
Search activity:	Underwater search using deep tow vehicles and autonomous underwater vehicle.

	Search area (reconnaissance) bathymetry undertaken at suitable operational times and during poor weather periods unsuitable for *Fugro Equator* deep tow vehicle operations to extend seafloor mapping to 120,000 km².
Guiding advice:	Tripartite governments agree to increase underwater search area to 120,000 km². Inmarsat 'BFO Analysis Unified 4x' BFO model. Flight Path Reconstruction Group – four analyses. SSWG's Analysis techniques – Constrained Autopilot dynamics (South) Data error optimisation (North)
Data used in planning search area refinement:	Attempt to cover approximately 80% of the highest probability flight paths derived from both constrained autopilot dynamics and data error optimisation analysis techniques.
Search equipment:	*Fugro Supporter* (Hugin AUV to 11 May 2015) *Go Phoenix* (ProSAS deep tow vehicle to 19 June 2015) *Fugro Discovery* (Edgetech deep tow vehicle) *Fugro Equator* (MBES bathymetry and Edgetech deep tow vehicle)
Coverage details:	Underwater search completed ≈ 56,750 km²
References:	Tripartite government press conference 16 April 2015. ATSB report: *MH370 – Flight Path Analysis Update* – 8 October 2014.

Source: Inmarsat, SSWG, Fugro Survey, Phoenix International, ATSB

Figure 50: 120,000 km² indicative search area and deep tow vehicle coverage, April 2015

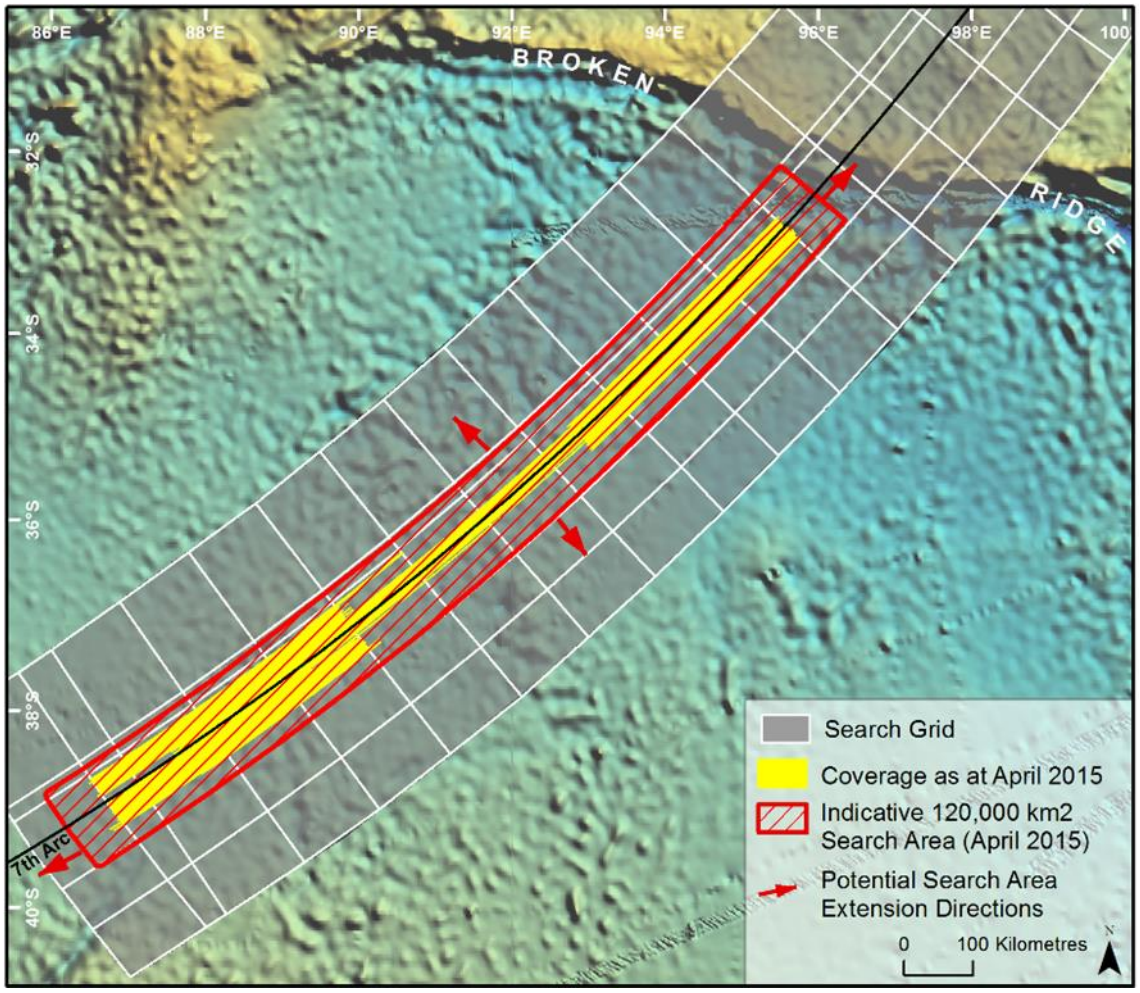

Source: ATSB

On 11 May 2015, after three swings of AUV operations, *Fugro Supporter* departed the search area for demobilisation in Fremantle.

On 19 June 2015, after eight swings of ProSAS deep tow vehicle operations, *Go Phoenix* departed the search area for demobilisation in Singapore following practical completion of Underwater Search Area 1.

Generalised flight dynamic model

On 17 July 2015, the decision was taken to extend deep tow search lines for *Fugro Equator* and *Fugro Discovery* to latitude 39.5ºS in response to the results of DST Group's analysis indicating high probability flight paths extending to that area (Table 24). As a result, the ATSB's indicative search area now extended from latitude 32.8ºS to 39.5ºS (Figure 51). Search operations continued to be from 20 NM behind to 30 NM in front of the 7th arc with *Fugro Equator* extending coverage to latitude 39.5ºS on its search lines to the east of the 7th arc.

Table 24: Generalised flight dynamics

Dates:	17 July – 30 November 2015
Event:	DST Group provide continued Bayesian analysis results which extends indicative search area to the south.
Search area location:	Extended indicative search area, -20 NM, +30 NM across 7th arc
Search activity:	Underwater search using deep tow vehicle sonar systems. Search area (reconnaissance) bathymetry undertaken at suitable operational times and during poor weather periods unsuitable for *Fugro Equator* deep tow vehicle operations to extend seafloor mapping to 120,000 $km^{2.}$
Guiding advice:	Inmarsat Differential Doppler Unified 4x BFO model. Flight path reconstruction group four analyses. SSWG analysis – Constrained autopilot dynamics (South) Data error optimisation (North) DST Group enhanced dynamic model results.
Data used in planning search area refinement:	DST Group developing Bayesian analysis. Consideration of possible ditching with minimal debris washed ashore.
Search equipment:	*Fugro Discovery* (Edgetech deep tow vehicle) *Fugro Equator* (MBES bathymetry and Edgetech deep tow vehicle)
Coverage details:	Underwater search area completed ≈ 75,850 km^2
References:	Tripartite governments press conference 16 April 2015. ATSB report: *MH370 – Flight Path Analysis Update* – 8 October 2014. DST Group analysis.

Source: DST Group, SSWG, Fugro Survey, ATSB

During *Fugro Discovery*'s tenth swing commencing on 29 October 2015, two separate medical evacuations of crew members were required shortly after the vessel's arrival in the search area. This meant over 22 days in transit to and from the search area were necessary with only 8 days of underwater search operations achieved for the swing (see Health, Safety and the Environment section).

Figure 51: 120,000 km^2 Indicative search area and deep tow vehicle coverage, 28 July 2015

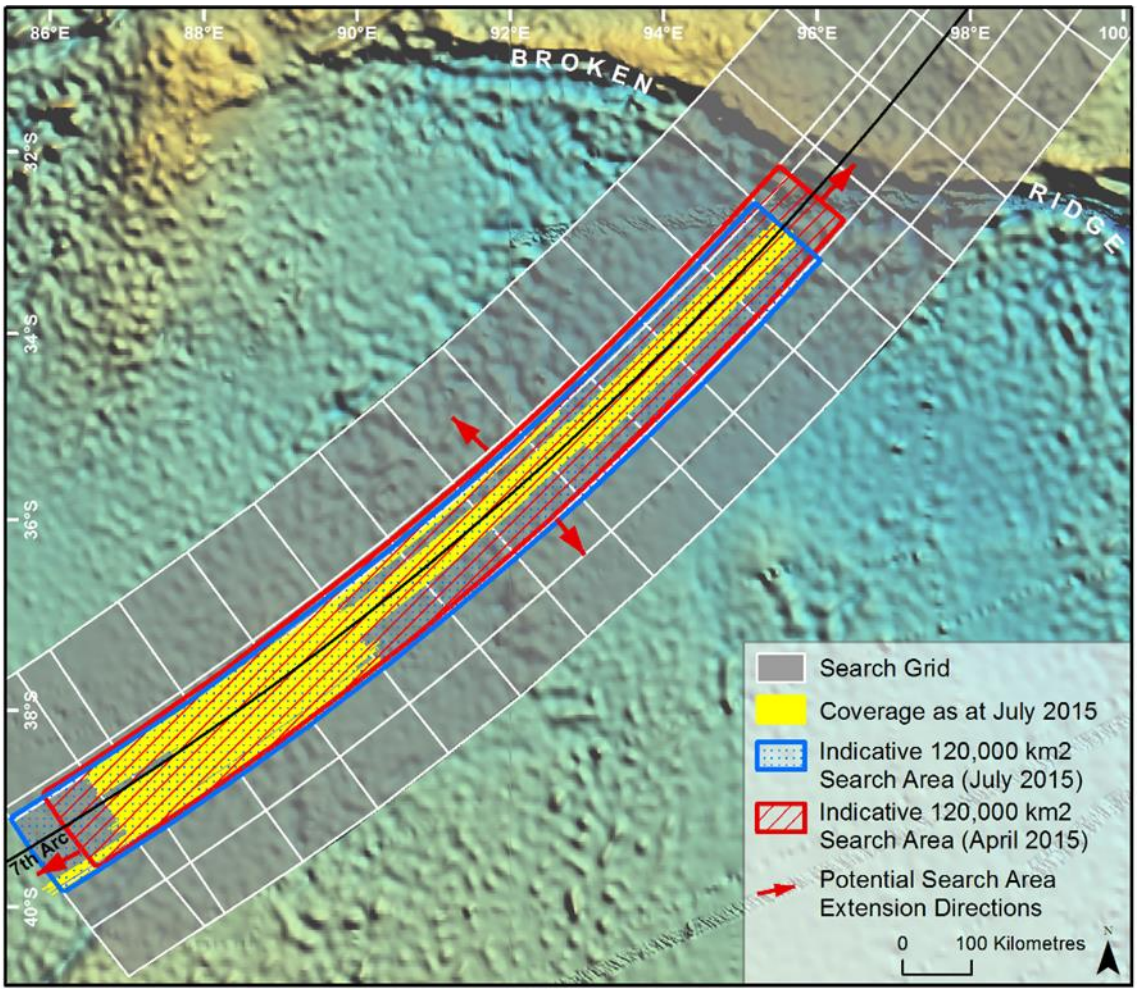

Source: ATSB

Complete Bayesian analysis

By 30 November 2015 an area of over 75,000 km^2 had been searched from latitudes 32.8ºS to 39.5ºS with about 3.8 per cent data gaps in the sonar coverage (Figure 52). *Fugro Equator* and *Fugro Discovery* were in the search area with their deep tow vehicles and *Havila Harmony* was being mobilised for AUV operations.

Figure 52: Underwater search coverage at 30 November 2015

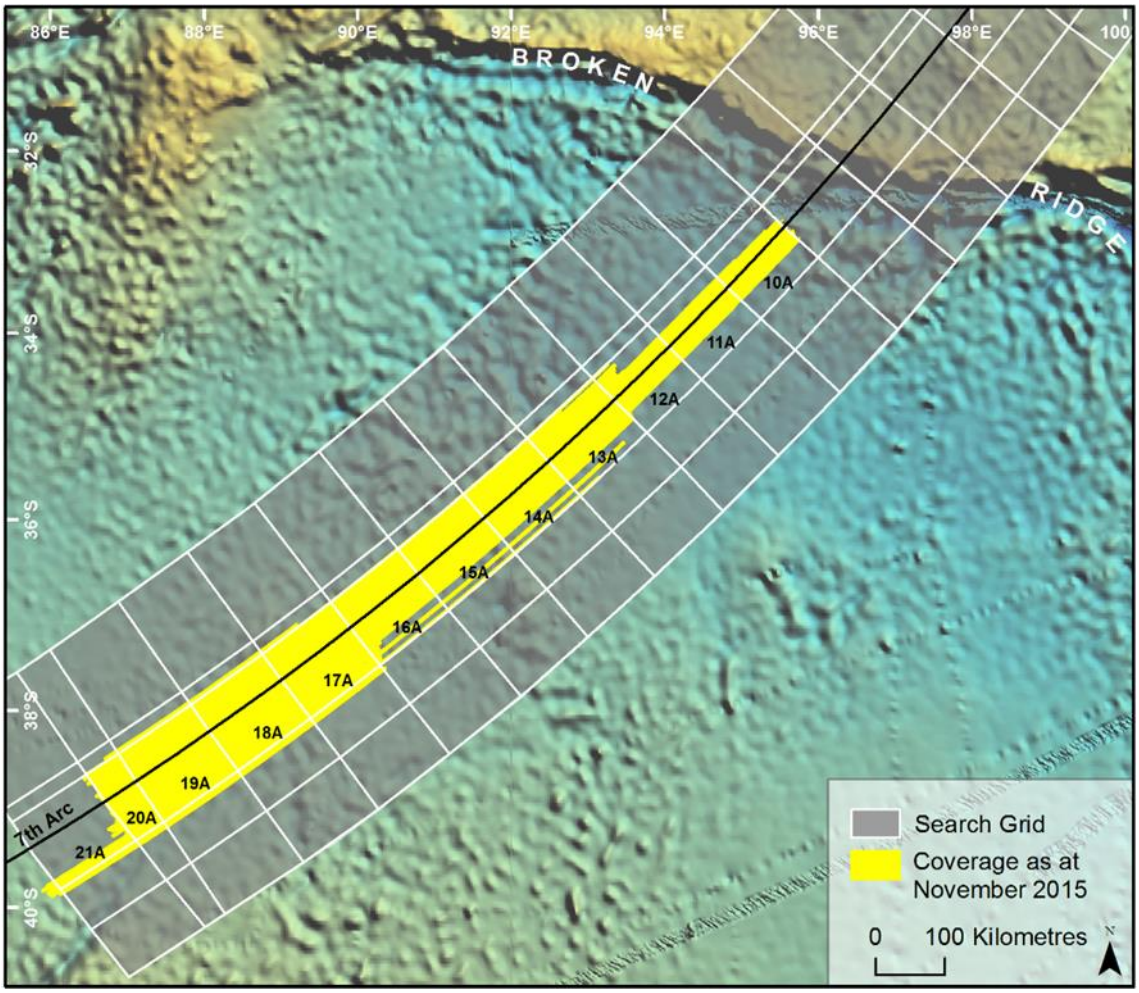

Source: ATSB

A refined analysis of the SATCOM data undertaken by DST Group and detailed in their pre-publication draft *Bayesian Methods in the Search for MH370* was used to define a new indicative search area and promulgated in the ATSB's report *MH370 – Definition of Underwater Search Areas* released on 3 December 2015 (Table 25). The indicative search area was refined by ATSB to latitudes between 36.1ºS and 39.5ºS to focus on the highest probability paths as shown in the heatmap generated using DST Group's analysis and the descent kernel defined by the ATSB (Figure 56). The search area remaining to complete 120,000 km² was chosen to cover 85-90 per cent of the probability density function (PDF) along the 7th arc defined by DST Group.

Table 25: Bayesian analysis released

Dates:	30 November 2015 – 31 August 2016
Event:	DST Group Analysis produces heatmap when descent kernel applied. Decision to search 85% of flight paths to the north and 90% of flight paths to the south.
Search area location:	Indicative Search Area extended and application of descent kernel to DST Group probability density function and -40 NM, +40 NM across 7th arc in the indicative search area.
Search activity:	Underwater search using deep tow vehicle sonar systems and AUV, ProSAS deep tow vehicle re-joins search on *Dong Hai Jiu 101*. Search area (reconnaissance) bathymetry undertaken at suitable operational times and during poor weather periods unsuitable for *Fugro Equator* deep tow vehicle operations.
Guiding advice:	DST Group analysis.

	ATSB descent kernel.
Data used in planning search area refinement:	DST Group analysis. ATSB descent kernel. Consideration of both controlled and uncontrolled end-of-flight scenarios.
Search equipment:	*Fugro* Discovery (Edgetech deep tow vehicle) *Fugro Equator* (Edgetech deep tow vehicle*)* *Havila Harmony* (Hugin AUV) *Dong Hai Jiu 101* (ProSAS deep tow vehicle)
Coverage details:	Underwater search area completed ≈ 115,640 km^2
References:	DST Group Bayesian analysis November 2015. ATSB report: *MH370 – Definition of Underwater Search Areas* – 3 December 2015. Tripartite government meeting 22 July 2016.

Source: DST Group, SSWG, Fugro Survey, Phoenix International, ATSB

Fugro Discovery and *Fugro Equator* continued the underwater search with deep tow vehicles and were joined in the search by *Havila Harmony* equipped with the AUV on 5 December 2015. Once again the AUV was used to search difficult areas of seafloor terrain inefficient for the deep tow vehicles to search. The vessels were tasked to complete the search of the new indicative area search area (Figure 53).

The three vessels were then joined by the People's Republic of China rescue and salvage vessel *Dong Hai Jiu 101* with an upgraded[26] ProSAS deep tow vehicle which arrived in the search area in March 2016.

[26] During the period between operations on *Go Phoenix* and *Dong Hai Jiu 101* the ProSAS system was upgraded by Hydrospheric Solutions with an added array. This was done to improve the coverage of the ProSAS system.

Figure 53: Underwater search coverage at June 2016 showing December 2015 indicative search area

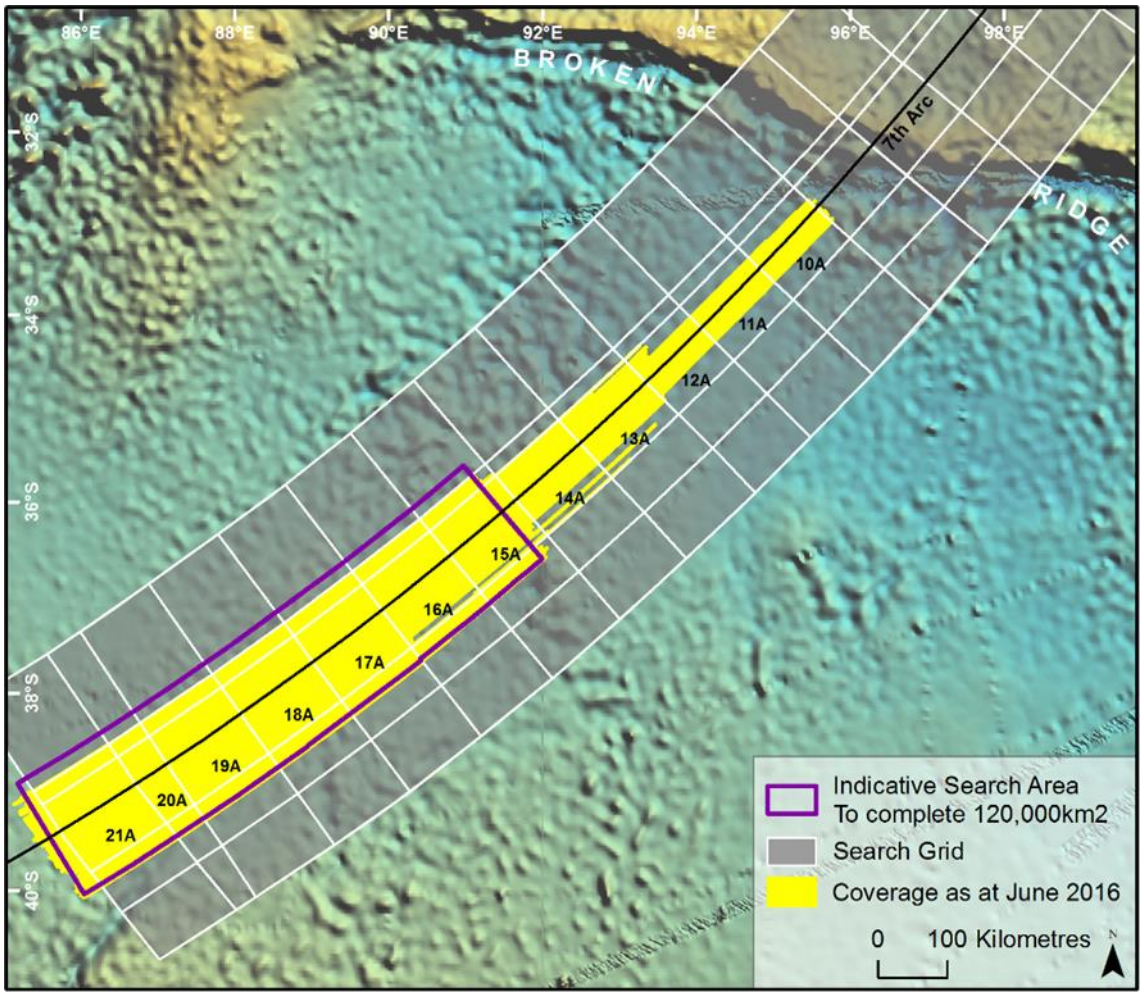

Source: ATSB

Last refinement to underwater search area

On 20 June 2016, the inboard section of MH370 right outboard wing flap was found on Pemba Island, East of Tanzania (refer to the Aircraft Debris section). This was an important development since evidence of flap extension at impact would indicate a controlled descent and thus increase the search width required in front of the arc. Conversely a retracted flap would indicate an uncontrolled end of flight scenario, close to the 7th arc.

From June to July 2016 discussions within the SSWG regarding end-of-flight 'controlled' or 'uncontrolled' descent scenarios continued and analysis using Boeing end-of-flight simulations again considered the distance beyond the 7th arc that was now a reasonable extent of an 'uncontrolled' descent. Further consideration of 7th arc BFO values was also underway by DST Group to see if the indicative rates of descent of the aircraft at the final arc could be ascertained.

The 7th arc width, tolerances and new simulations were incorporated into a revised descent kernel and probability map by ATSB and DST Group. The distance (prior to new simulations) recommended by the SSWG was 35 NM to the west of the 7th arc and for a 'controlled' scenario the search area would extend the most probable flight paths to the east of the 7th arc (Table 26).

In July 2016 *Fugro Discovery* departed Fremantle for her final swing in the search area and *Fugro Equator* commenced her penultimate deep tow swing. *Dong Hai Jiu 101* was in the search area with the ProSAS deep tow search system on board. The focus of the search was to cover gaps in

sonar data in the indicative search area, and to extend the area searched to the west of the 7th arc from 30 NM to 35 NM as recommended by the SSWG.

Table 26: Wing flap examination, BFO analysis and revised descent kernel

Dates:	August 2016 – January 2017
Event:	Examination of MH370 wing flap and DST Group BFO analysis. Analysis produces heatmap when descent kernel applied. Decision to search 85% north and 90% south of PDF.
Search area location:	Indicative Search Area extended and application of descent kernel to DST Group PDF.
Search activity:	*Fugro Equator* underwater search using Edgetech deep tow vehicle and AUV and *Dong Hai Jiu 101* mobilised with ROV. Search area (reconnaissance) bathymetry undertaken at suitable operational times and during poor weather periods unsuitable for *Fugro Equator* deep tow vehicle operations.
Guiding advice:	ATSB debris examination of wing flap. DST Group BFO analysis of final BFO sequence. ATSB revised descent kernel. DST Group revised heatmap.
Data used in planning search area refinement:	+25 NM and -25 NM from 7th arc across entire search area.
Search equipment:	*Fugro Equator* (Edgetech deep tow then Hugin AUV) *Dong Hai Jiu 101* (*Remora III* ROV)
Coverage details:	Underwater search area completed ≈ 120,000 km^2
References:	ATSB report: *MH370 Search and debris examination update* - 2 November 2016. First Principles Review, 2-4 November 2016. DST Group report: *The use of Burst Frequency Offsets in the search for MH370*, 7 Feb 2017. CSIRO report: *The search for MH370 and ocean surface drift* - 6 December 2016. ATSB report: *MH370 - First Principles Review* - 20 December 2016. Tripartite government press release 17 January 2017.

Source: DST Group, SSWG, Fugro Survey, Phoenix International, ATSB

On 22 July 2016 a Tripartite meeting (Malaysia, Australia and the People's Republic of China) agreed that the search would be suspended upon completion of the 120,000 km^2 search area, should the aircraft not be located and in the absence of credible new evidence leading to the identification of a specific location of the aircraft. The underwater search coverage at that time was 113,400 km^2.

Poor weather conditions in the search area over this period limited the search efforts in particular for *Dong Hai Jiu 101* and a decision was made to stand the vessel down and demobilise the ProSAS search system.

Following the completion of the wing flap examination indicating that it was probably housed at the time it separated from the aircraft and the completion of DST Group's BFO analysis indicating that the aircraft was probably in a high and increasing rate of descent the SSWG recommended the search be limited to a width of 25 NM either side of the 7th arc. This information was presented in the report *MH370 Search and debris examination update* on 2 November 2016.

In October *Dong Hai Jiu 101* was mobilised with Phoenix International's ROV and tasked to investigate a range of sonar contacts.

During its final deep tow swing in September and October 2016, *Fugro Equator* was tasked to fill areas of sonar data gaps within 25 NM of the 7th arc across the entire 120,000 km^2 and search some new area to the west of the 7th arc within the indicative area.

In December 2016, *Fugro Equator* mobilised the AUV which was used to fill sonar data gaps within 25 NM of the 7th arc and to search the area within 25 NM and to the west of the 7th arc between latitudes 34.7ºS and 36.1ºS.

On 17 January 2017, *Fugro Equator* completed AUV search operations and left the search area and the Tripartite Ministers jointly announced the suspension of the search for MH370.

An animation of the progressive search coverage over the entire underwater search is available for viewing on the ATSB YouTube Channel.

ATSB contractor reports

The final underwater operations reports provided to the ATSB by Fugro Survey and Phoenix International are provided in appendices D and E. These are the Fugro Survey summary report for four vessels *Fugro Equator*, *Fugro Discovery*, *Fugro Supporter* and *Havila Harmony* and Phoenix International's report for operations on *Dong Hai Jiu 101* in 2016.

Area searched

The search areas for MH370 were defined on the basis of probability. Following the final primary radar detection near the northern tip of Sumatra at 1822 UTC, the aircraft's location could not be determined with precision. For the final six hours of flight MH370's location was derived by modelling likely aircraft behaviour, under a range of assumptions, using a unique analysis of a few SATCOM metadata points. The output of this modelling was a probability density function for the aircraft's location at the time of the final SATCOM communication. This was derived using the primary radar detections, models of MH370's autopilot controlled flight dynamics, environmental information and the complete sequence of automated SATCOM communications.

Search area probability density functions

A probability density function (PDF) defines the likelihood that an event with an unknown outcome will take a particular value from within a range of possible values. The Bayesian approach to the MH370 search models the aircraft's flight path as an unknown event and then calculates the PDF of this unknown event based on the available information. For example, DST Group's PDF of November 2015 (Figure 55) indicated that it was ten times more likely that the aircraft crossed the 7th arc near 38°S than near 36°S.

When the results of the underwater sonar search are considered, if an area was searched to a high degree of confidence, the modelled flight paths which terminated at this location can be eliminated. This changes the PDF to make alternative flight paths and areas more likely to contain the aircraft. At any point in the underwater search the priority was to eliminate the highest probability areas defined by the PDF derived from the most up to date flight path analyses.

MH370 probability density functions evolution

Search area definition and analysis of available data was continuous throughout the entire search for MH370. Initial results assisted the surface search and later refinements formed the basis for the underwater search areas. The models used to define the search area and associated PDFs evolved during the search based on continuing analysis of the SATCOM data and efforts to identify the most likely behaviour of the aircraft at the end-of-flight.

In October 2014 the SSWG were using two methods to derive the flight paths and their associated probability:

1. **Constrained autopilot dynamics** –The aircraft is assumed to have been flown using one of the autopilot modes constant magnetic heading, constant true heading, constant magnetic

track, constant true track or lateral navigation. Starting points for the trajectories are defined by the primary radar detections. All autopilot modes were considered to be initially equally likely. The aircraft is assumed to have made one deliberate manoeuvre at some time after the primary radar detections. Candidate trajectories are created for a range of possible autopilot settings (e.g. Mach number, direction). Statistical consistency with the complete sequence of BTO and BFO measurements is used to score the trajectory.

2. **Data error optimisation** – Candidate trajectories are created for a range of values of constant ground speed. All points on the 1941 UTC BTO arc that are reachable by the aircraft from the time and position of the final primary radar detection are taken as the set of possible starting points for the trajectories. Each trajectory is broken up into segments at the time of successive recorded BTO values. At these times the trajectory is allowed to change direction and the average of the directions of the track before and after the change are used to evaluate a predicted BFO measurement. The Root Mean Square error between predicted and measured BFO values from 2041 UTC onwards is used to score the trajectory.

Figure 54 shows the top 100 constrained autopilot flightpaths and their intersection with the 6th arc at 0011 UTC for each of the two trajectory scoring methods.

Figure 54: Representation of probability density functions at the 6th arc for constrained autopilot dynamic trajectories scored by statistical consistency with SATCOM (red) and minimum Root Mean Square fit to BFO (green), October 2014

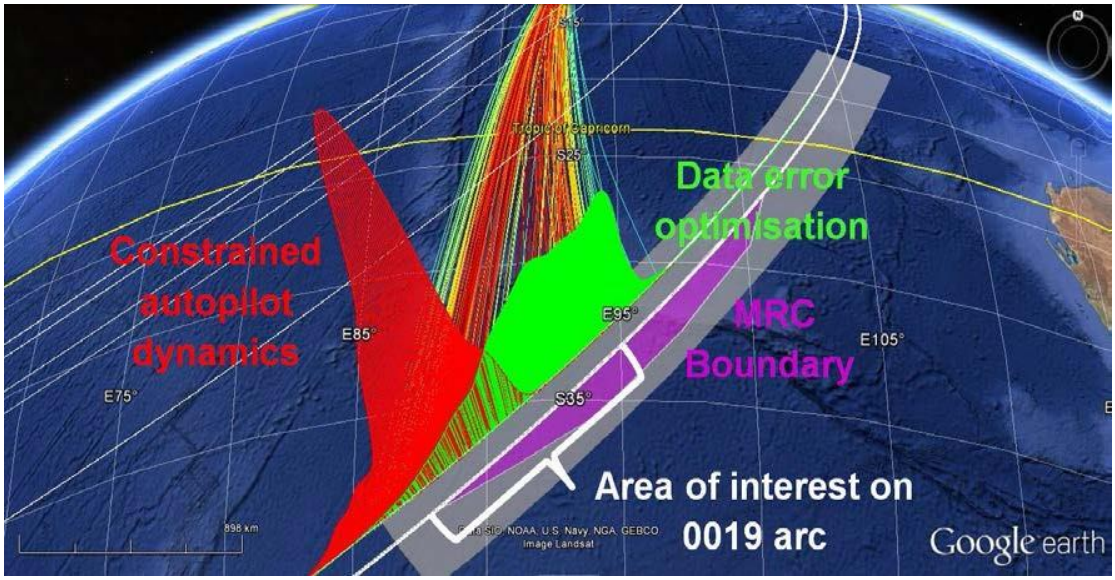

Source: Google earth, annotated by SSWG

There was an overlap of the two model PDFs located between latitudes between 35°S and 39°S on the 6th arc, with latitudes between 32.5°S and 38.1°S covering 80 per cent of the probable flight paths for both analyses.

More information about the models can be found in the ATSB report MH370-Flight Path Analysis Update of 8 October 2014.

During 2015, DST Group developed and validated a more comprehensive flight path model which allowed for the possibility of more than one deliberate manoeuvre after the time of the final primary radar detection. The PDF of flight paths was calculated using numerical Bayesian methods. The procedure was validated using examples of previous flights of the accident aircraft. The resulting PDF of MH370's flight path and location at the time of the final SATCOM communication is depicted in Figure 55. This single dimension PDF was then combined with an ATSB defined search area width based on the most likely end-of-flight behaviour of the aircraft (descent kernel) to produce a PDF in two dimensions referred to as a heatmap (Figure 56). ATSB's report MH370 -

Definition of Underwater Search Area Update of December 2015 and DST Group's Bayesian Methods in the Search for MH370 describe this work.

Figure 55: DST Group's flight path model probability density function (red line), November 2015

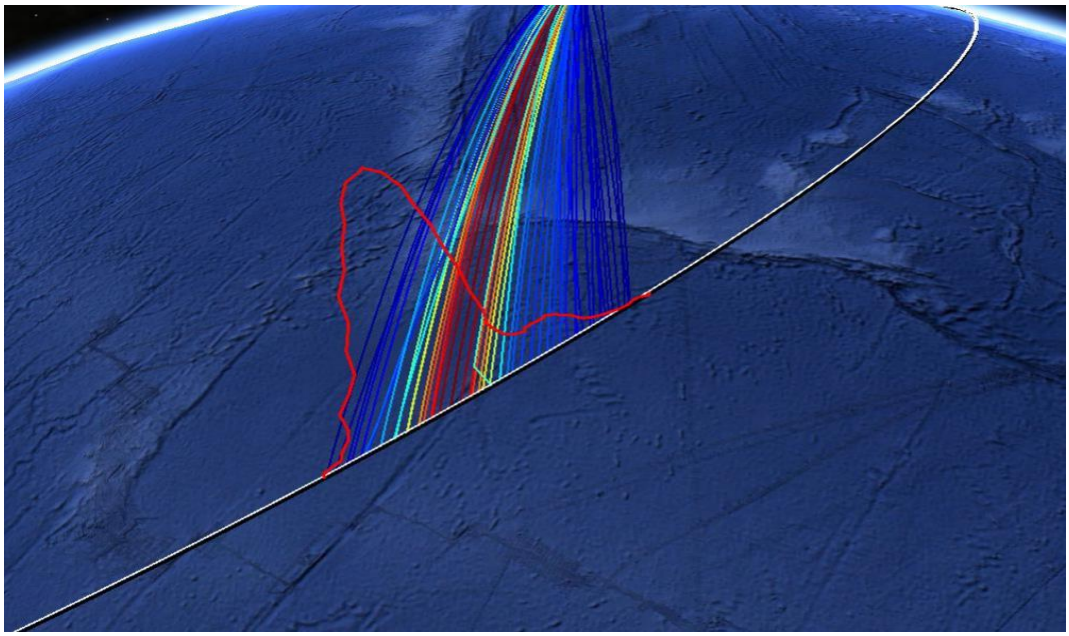

Source: Google earth, annotated by ATSB, using DST Group data

Figure 56: Two dimensional probability density function (heatmap), November 2015

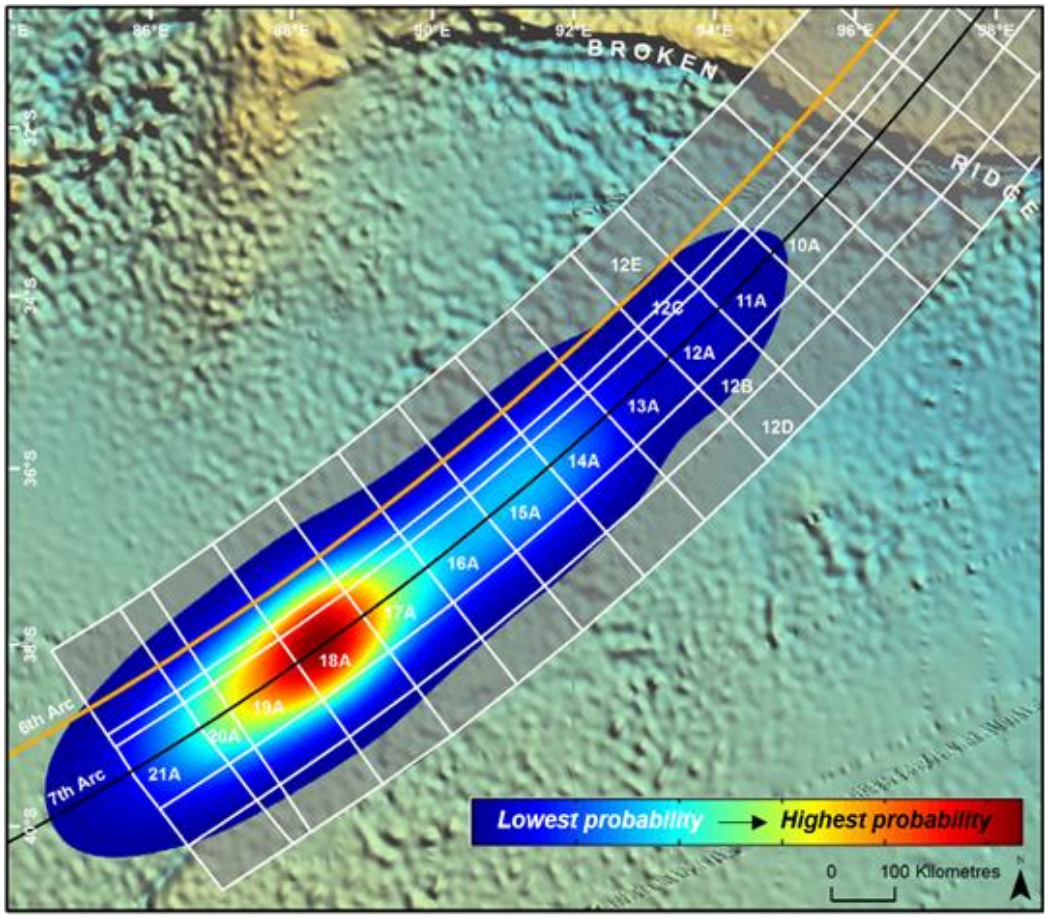

Source: ATSB, using DST Group data

Figure 56 is a graphical representation of the results of the DST Group analysis with the ATSB end-of-flight scenario, with the colours in the area representing the different location probabilities from lowest (blue) to highest (red) probability.

Revised probability density function – November 2016

In November 2016 experts from various organisations and agencies who had been closely involved in defining the MH370 search area met for a first principles review (the ATSB's report of the meeting can be found here: First Principles Review). The meeting was to reassess and validate existing evidence and analysis and to identify any new analysis that may assist in identifying the location of the missing aircraft. One of the main areas of focus was the effect of the sonar search results to that time on the previously defined most probable paths and therefore the location of MH370.

At the time of the first principles review an area of nearly 120,000 km² covering more than 85 per cent of the highest probability flight paths had been searched to a level of confidence greater than 95 per cent.

The results of new analysis indicated that the end-of-flight descent kernel defining the width of the search area could be reduced to approximately 25 NM either side of the 7th arc (ATSB report: MH370 - Search and Debris Update). This information was incorporated into the DST Group's two dimensional probability density function to produce a new heatmap (Figure 57).

Figure 57: Refined two dimensional probability density function with reduced search area width, November 2016

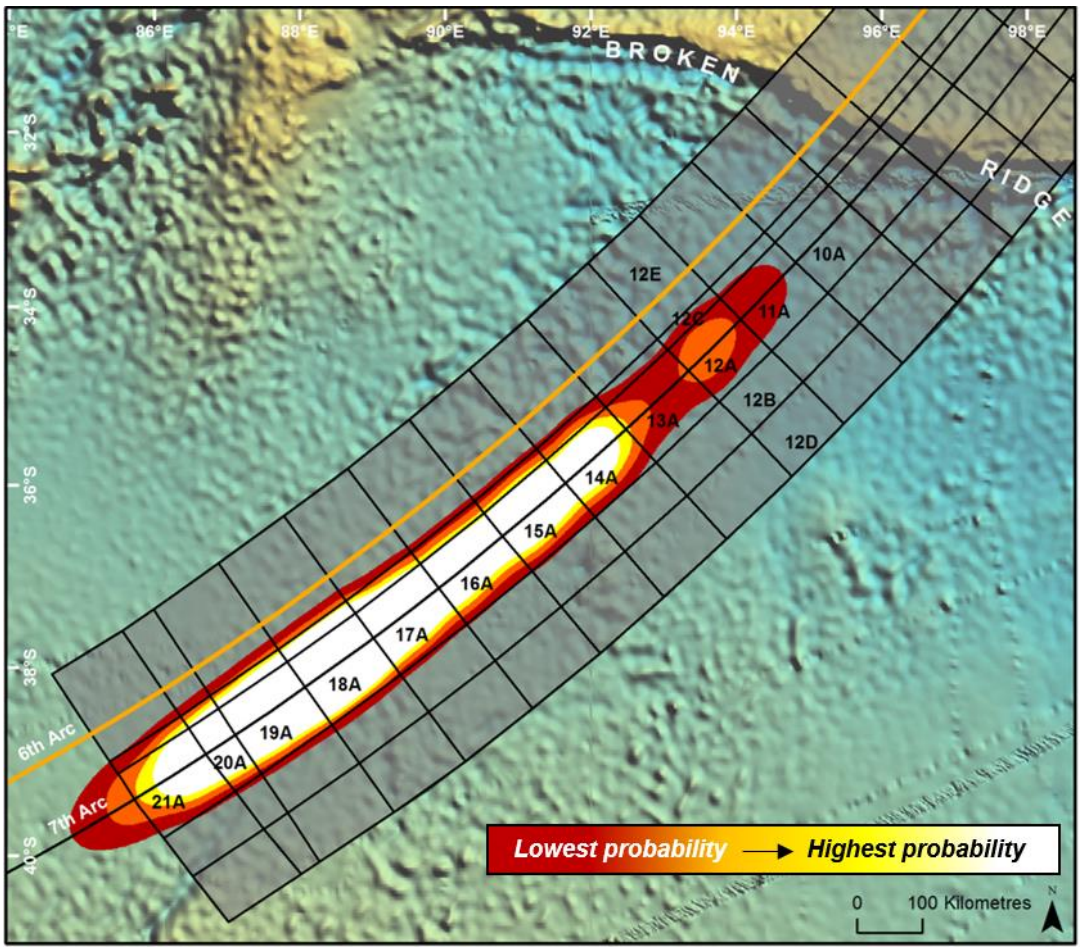

Source: ATSB, using DST Group data

Figure 57 is a graphical representation of the results of the DST Group analysis with the ATSB end-of-flight scenario taking into account search area width reduction to 25 NM. The colours in the area represent the different location probabilities from lowest (red) to highest (white) probability.

When the results of the underwater search were incorporated and considered as well as analysis from the CSIRO's drift study of MH370 debris (The search for MH370 and ocean surface drift), which identified a range of latitudes in the search area far more likely for the origin of debris which had been recovered from the aircraft, the PDF was modified again (Figure 58).

Figure 58: A residual probability density function updated with the area searched (mask), November 2016

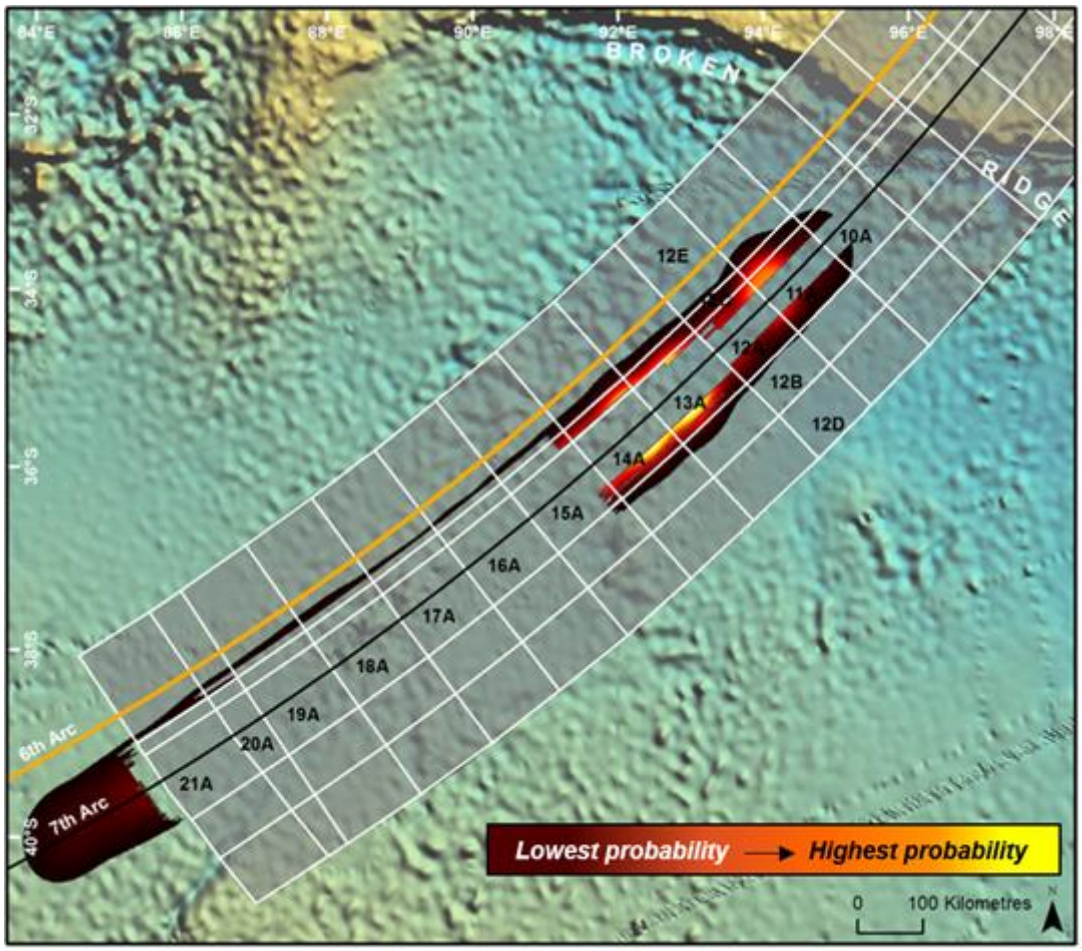

Source: ATSB, using DST Group data

Figure 58 is a graphical representation of the results of the DST Group analysis with the areas searched removed. The remaining residual probability is located in areas yet to be searched, with two clear areas of interest: north of the search area and south of the search area. The colours in the area represent the different location probabilities from lowest (brown) to highest (yellow) probability.

The effects of the completed sonar search on the PDF throughout the search can be displayed with a time sequenced animation, evolving trajectory probabilities and is available for viewing on the ATSB YouTube Channel. As sonar data was acquired, to a high level of confidence, the aircraft was not in the area searched and consequently the probability of locating the aircraft in the area covered diminishes. The sonar data coverage and associated confidence are modelled into the PDF. The DST Group PDF was visualised using trajectories of probable tracks, symbolised from more likely (red) to less likely (blue).

Analysis and quality assessment of the sonar data

Analysis and quality assessment of the sonar data from the underwater search began at the time of acquisition. Data from the deep tow vehicles was transmitted continuously to the tow vessel via the tow cable. The quality of the data, position, speed and altitude of the deep tow vehicles were monitored continuously in real time by the contractor's mission crew and independently by the ATSB client representative on each search vessel.

During the summer months the vessels using the AUV monitored the vehicle's performance continuously using an acoustic data link as the AUV was not physically connected to the surface vessel. During an AUV mission the operators continuously monitored the vehicle's performance, batteries, sensors, and sonar data acquisition. When the AUV was operating on the seafloor low resolution sonar data was transmitted back to the operators to ensure data collection was occurring. Once the AUV was recovered and back on the vessel full resolution data was downloaded from all relevant sensors.

After initial data collection was complete, the positioning data was post processed on board the vessel and verified for each underwater vehicle. Sonar data was processed and analysed in more detail for sonar contacts and quality by both the mission crew and the ATSB's client representative. Checks to ensure proper coverage of the seafloor were achieved to the standards specified for each system. Sonar contacts of interest were marked and sent ashore as daily Preliminary Contact Reports.

Fugro Survey vessels then sent the relevant processed search data daily via satellite to a Fugro Survey secure data cloud. This made the data accessible to all shore-based stakeholders. The Fugro Survey Perth office then processed and analysed the data again for quality, coverage, and contacts. In addition, final products such as mosaics, raster images, plots, and geospatial databases were created and provided to the ATSB. Fugro Survey's Perth office was staffed by sonar data specialists, geophysicists, geographic information system (GIS) analysts, data managers, vessel managers and support staff.

Phoenix International and Hydrospheric Solutions operating the ProSAS deep tow vehicle used a slightly different process. After initial sonar data collection and analysis, further processing occurred to ensure subsea positioning accuracy and overall quality of data. Another review for contacts of interest was also performed. Final products were created on board the vessel which included positioning plots, analysis of coverage, mosaics, and raster images of the relevant data sets. Specific databases captured contacts of interest and sonar coverage. Contact reporting, coverage mosaics and plots were provided daily via satellite. Raw and fully processed data were stored on board until the next port call when it was provided to the ATSB.

Once the data was supplied to the ATSB all relevant search data and databases were checked for quality, coverage and contacts by the GIS team based in the ATSB's Canberra office. Data analysis and quality control was also performed by the ATSB's Quality Assurance Manager (based in the United States) and by an independent highly experienced sonar data expert also based in the United States. Figure 59 shows the data flow from vessel to final archival storage.

Figure 59: Data flow diagram

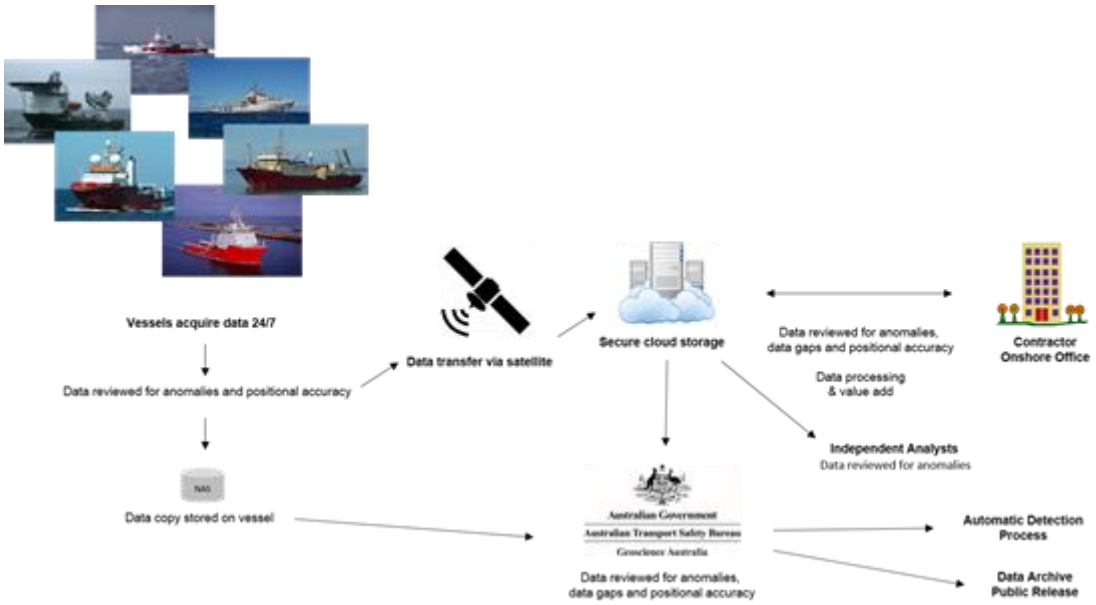

Source: ATSB

Results and assessments were compared and additional coverage maps were produced. Geoscience Australia produced bathymetric digital elevation models using the ship hull-mounted MBES data. Data was catalogued, backed up and prepared for archival storage.

Additionally, experts in the field of automatic target recognition (or detection) using sophisticated software algorithms to analyse the data were used. No new contacts have been identified to date using this technology however some existing contacts were flagged by the process. This work and process continues as the technology evolves.

Quality assurance of the sonar data

In addition to analysing the sonar data for areas of interest, there was a very careful focus on ensuring and quantifying seafloor coverage. This included proving sonar data overlap with adjacent sonar data and cataloging areas searched with systematic classifications and confidence ratings that an analyst would detect the MH370 debris field.

A historical study was conducted of available previously sonar mapped aircraft debris fields. Measurements of each field were made and aircraft size compared with any impact information available for each crash site. It was found that the area of a typical debris field for an aircraft the size of a B777, with any foreseeable crash scenario, in similar water depths similar to the MH370 search area, would be at least 100 m x 100 m and very likely to be greater than 200 m x 200 m.

The quality assurance program reviewed and monitored many aspects of the search. The following were some of the main areas of focus:

- data quality of the primary search sensors
- subsea positioning of the deep tow vehicle and AUV
- ensuring overlap between adjacent lines (or areas) of sonar data
- cataloguing all areas covered by the search systems
- reviewing the data for areas of interest (contacts)
- search methodology.

The process began with ensuring the data being collected was of the quality needed and specified by the ATSB. In short this was the ability to detect a two cubic metre object at the test range qualified range scale and vehicle altitude. Data quality was constantly monitored on board search

vessels by the equipment operators, data processors, and ATSB client representatives. It was further evaluated on shore by the data processing team, ATSB, and independent reviewer. If at any point the data quality was compromised the data coverage was reduced by narrowing the survey line spacing or the area was resurveyed. Typically any data quality or vehicle performance issues were addressed immediately on board the vessel and thus maintained operational efficiency and continuous coverage.

Ensuring the tracking system and accurate positioning of the deep tow vehicle and AUV was critical to ensuring complete sonar coverage, as this was the basis for the position being injected into all data files collected on the underwater vehicles. Figure 60 shows a typical track plot of the ship and the deep tow vehicle. This graphically represents how far the deep tow vehicle was off the planned line route and the position of the vessel relative to that planned line. Notice the 'steps' in the red vessel track, these were from the vessel shifting position to help 'steer' the deep tow vehicle down the planned route line. This allowed the operators to manipulate the deep tow vehicle position using the ship position. The graph also instantly highlighted areas where adequate overlap may be a concern with the adjacent search line.

Figure 60: Example vessel and deep tow vehicle position track plot

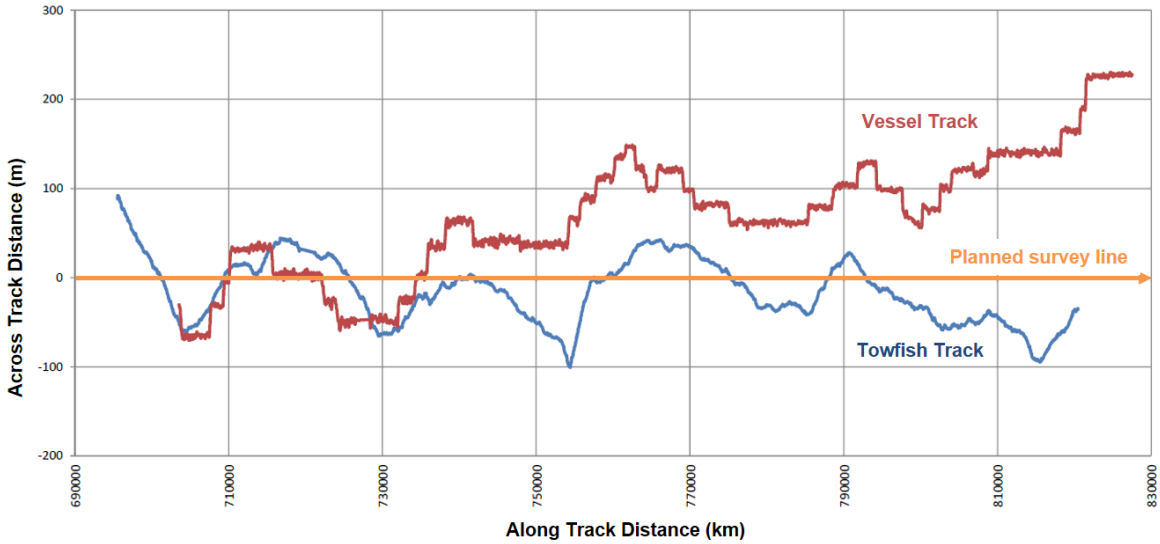

Source: ATSB

To verify the positioning of the deep tow vehicle two methods were used. The first method used the bathymetry data collected by the ship based MBES system to ground truth the sonar data. The bathymetry survey used precise motion tracking and GPS corrected positioning systems which provided reliable and accurate georeferenced MBES data to be collected in over 6,000 m of water depth. The three dimensional (3D) bathymetric maps created with the MBES data were primarily used to ensure the safe and efficient operation of the underwater vehicles, however the accuracy of the maps allowed them also to be used to verify the positioning of the sonar data.

Figure 61 shows an example of this process. The yellow area represents a depression in the seafloor, the red dots were digitised in GIS software to mark the edge of the depression within the SSS data, as indicated by the darker (blacker) coloured returns. This was a result of the SSS signal not being returned (reflected back) due to the seafloor sloping away. The SSS data was overlaid and draped onto the 3D bathymetric surface for comparison. If mismatched more than 50 m it was logged and the position of the SSS data was adjusted as required.

Figure 61: Example of matching side scan sonar data to a bathymetric feature

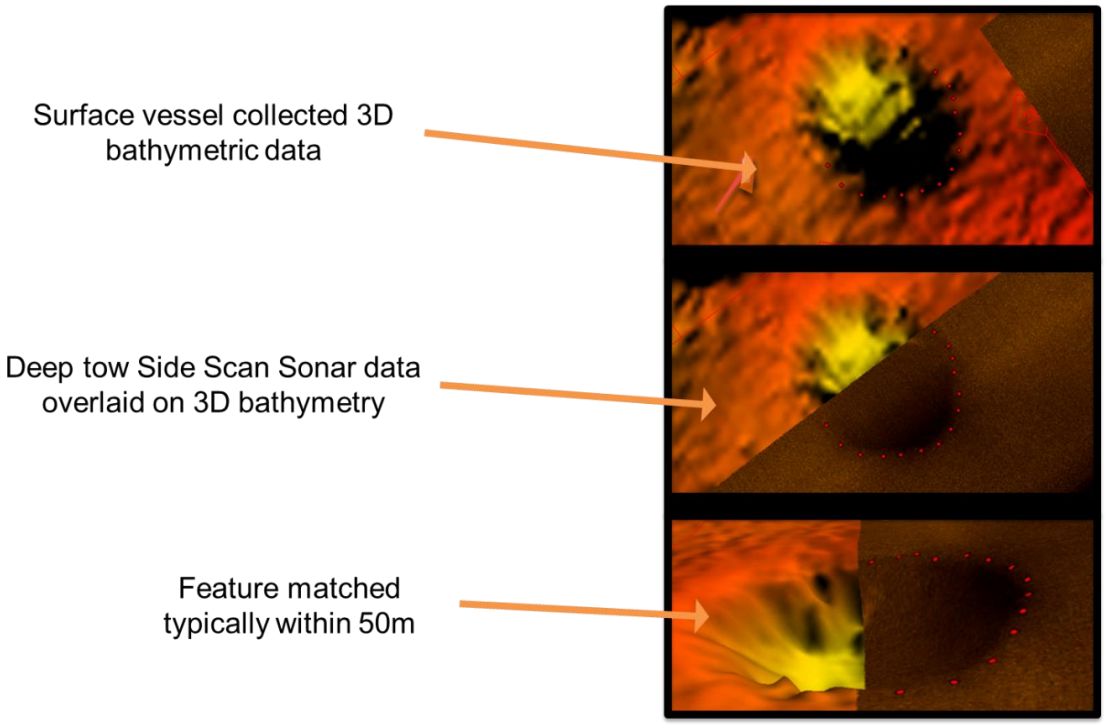

Source: ATSB

The second method used to verify the position of the deep tow vehicle was to match features between overlapping sonar data sets. This helped quantify errors in the positioning and provided a reliable 'check' of measurements for overlap between adjacent search lines. Figure 62 is an example of this. The feature circled in yellow was identified on two adjacent lines of sonar data. Selecting one discrete point within the feature allowed for a precise measurement between the lines of data using the same object. This measurement was further broken down and tabulated into along track and across track offsets. An accurate measurement was also made from the discrete point to the edge of the sonar range. This was combined with the adjacent line measurement which then gave an accurate overlap value for that point.

Figure 62: Example of adjacent line overlap, manual check for positional offsets

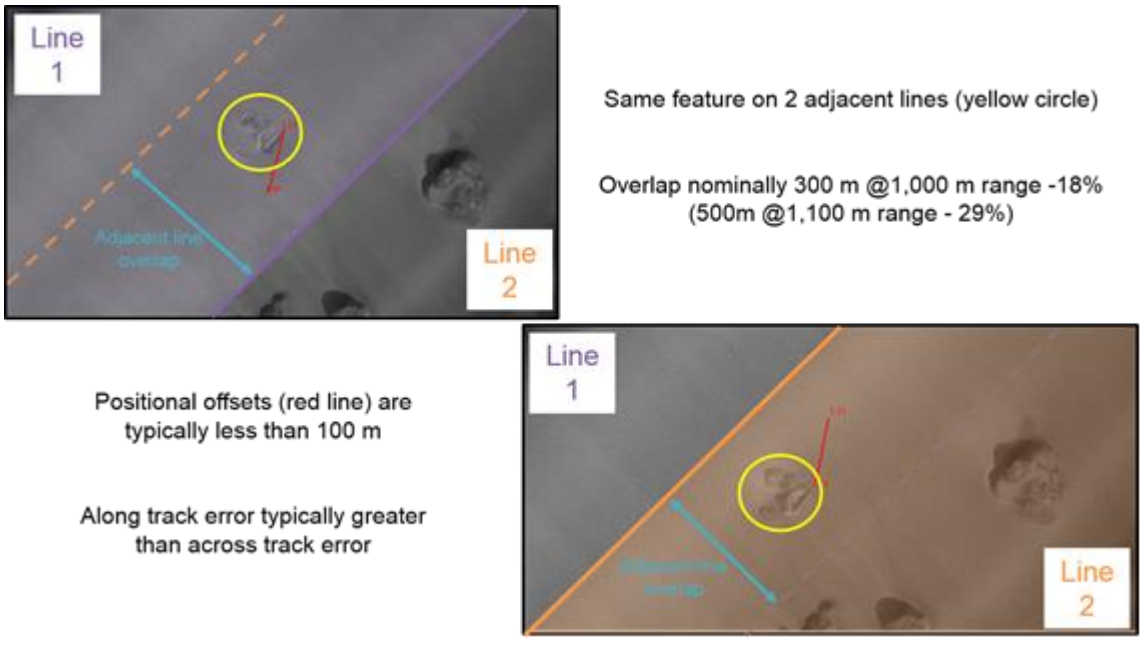

Source: ATSB

The final step in this process was to plot the findings of the overlap check, along with the actual deep tow vehicle tracks from the two adjacent lines. Figure 63 represents a plot of this process. The orange line was the planned track line. The green and red lines are two adjacent deep tow vehicle tracks, overlaid with matching distance along the track line. The blue line represents calculated overlap derived from plotting distances between the deep tow vehicle tracks. Nominally this would be 300 m using 1,000 m range scale and 1,700 m line spacing. In this example the overlap varies from 175 m to almost 400 m. In addition, the manual feature matches previously measured were plotted (purple points) and compared to the calculated overlap (blue line). Ideally these match, typical results proved to be within 50 m. This was within the ATSB's tolerance for the positioning systems and acceptable overlap coverage.

Figure 63: Example deep tow vehicle position track for two adjacent lines, overlap value and verification points plotted

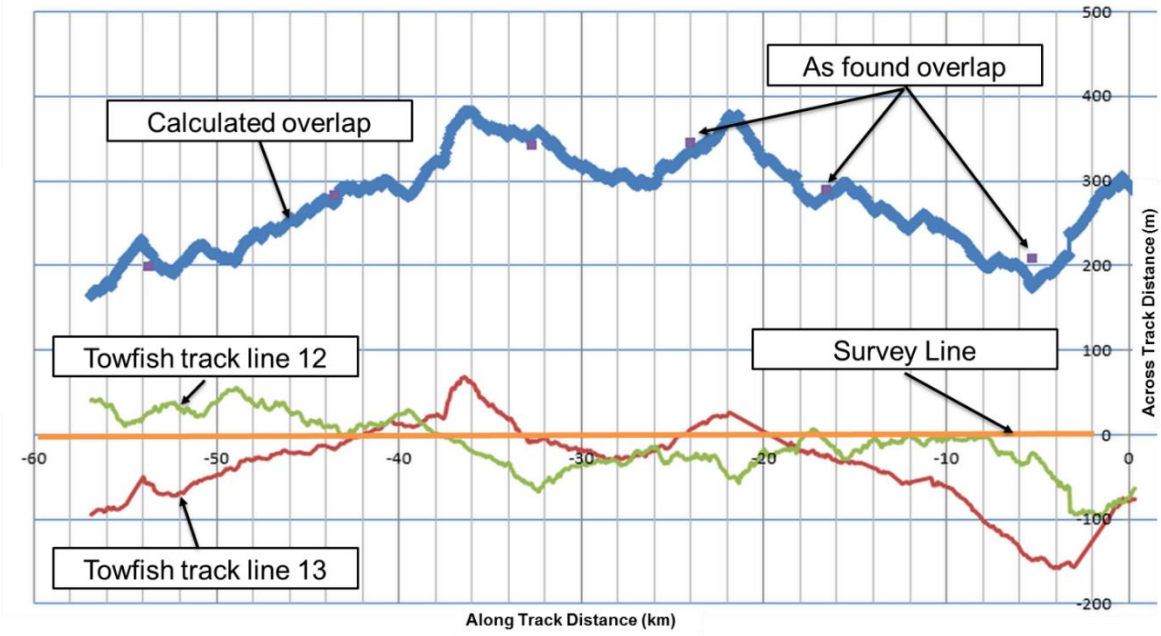

Source: ATSB

Using these techniques to verify the positioning of the deep tow vehicles established a high confidence in the position of the sonar data. With this confidence, coverage rates could be maximised allowing efficient operations while maintaining high confidence in the overall coverage. It is also the basis for accurately quantifying sonar data coverage, overlap, and seafloor areas with a lower chance of detection or no data.

Sonar coverage

The seafloor topography within the search area was such that the deep tow vehicles achieved approximately 98 per cent sonar coverage overall with a single pass. The remaining two per cent represented areas that had effectively no data. These areas were further categorised into four types of gaps in the sonar data (known as 'data holidays'), as described below:

- Terrain Avoidance Holiday
  - Areas where the deep tow vehicle had to be raised or lowered to negotiate or avoid seafloor terrain. This normally occurred around large seamounts or fracture zones. These were marked anywhere the underwater vehicle altitude was over 300 m.
- Shadow Holiday
  - Occurred when the seafloor terrain masked the area behind it. Typically caused by a geologic obstruction which blocks the sonar signal from going further, or a high down slope gradient where no return signal was detected.

- Off-track Holiday
  - A data gap between two adjacent lines of sonar data using a valid range of 1,000 m nominally. These were rare but sometimes occurred if the ship had large deviations from the planned line or subsea currents shifted the deep tow vehicle position.
- Equipment Failure Holiday
  - Area where valid data was not collected due to equipment malfunction.

A fifth category called Lower Probability of Detection (LPD) was used when valid sonar data was collected but the detection confidence was deemed less than nominal due to complex geology, environmental conditions, or data quality degradation. For example, a large rock field on the seafloor made it more difficult to detect the presence of aircraft debris. These areas were not considered data holidays because they still consisted of valid sonar data. LPDs accounted for about two per cent of the area covered by the deep tow vehicles.

Three types of sonar data were collected, traditional side scan sonar (SSS), synthetic aperture sonar (SAS), and multibeam echo sounder (MBES). Classification of search data and holiday type were maintained with each system used. It is noteworthy that the SAS system produced an overall higher resolution image providing a greater confidence of detection in areas with complex geology. This decreased the number of LPD areas substantially within that data set.

Figure 64 is a sample representation of these data categories marked within SSS data. Areas were manually digitised using GIS software and sonar processing software. Each polygon was categorised and placed in a geospatial database. This was initially performed by the search contractor(s) and then reviewed and verified by the ATSB quality assurance team to allow for accurate assessment of overall coverage and quantify the overall confidence in the data set.

Figure 64: Deep tow vehicle sonar data draped over 3D bathymetry data showing an area of complex seafloor topography in the search area and associated sonar coverage classifications

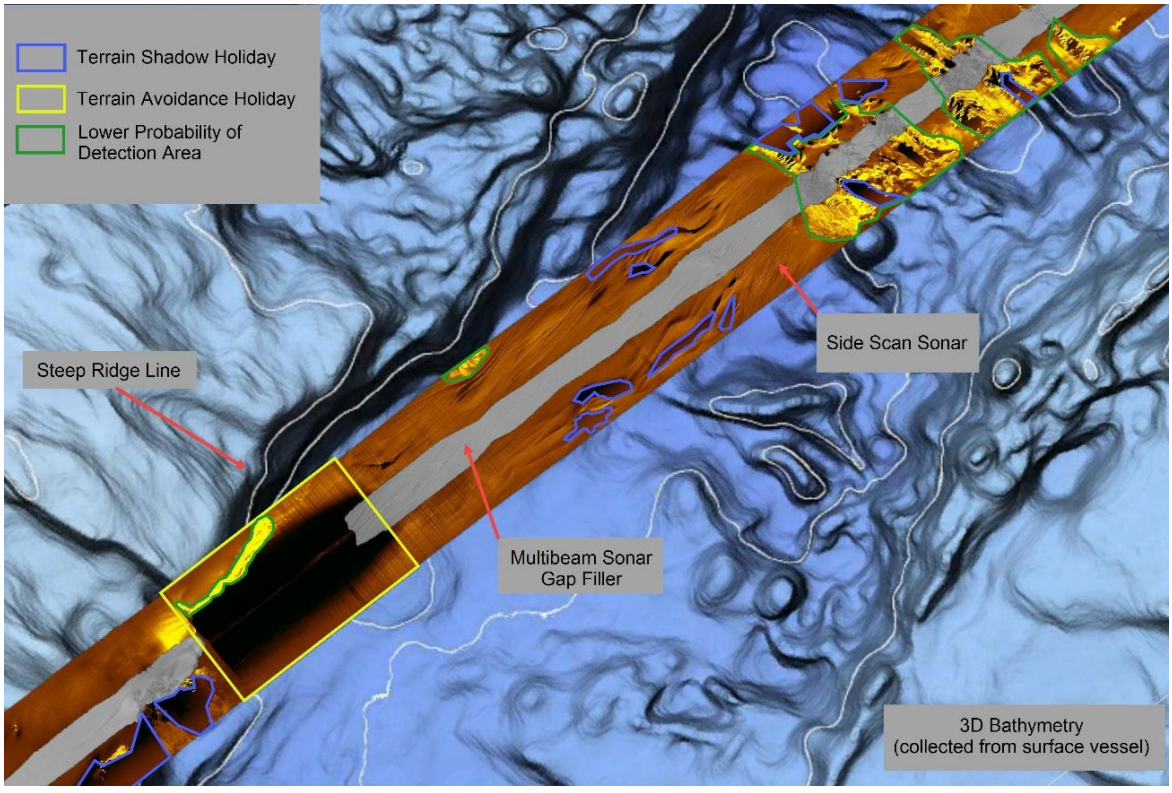

Source: ATSB

The sonar coverage geodatabase was further used to plan and execute missions performed by the AUV. With high confidence in the positioning of the search data, with each data holiday and LPD area digitised, the AUV was assigned discrete areas to infill (resurvey). Mission planning for the AUV was optimised as all areas needed to be infilled were known and precisely mapped. Data holidays were prioritised by size, grouping and proximity to the 7th arc to maximise coverage and minimise transit times between areas.

Areas designated as LPD were typically not resurveyed except in specific cases. One example was the Geelvinck Fracture Zone. This was a very large and steep ridge that transected the width of the search area and was also in a higher probability area within the search area. To ensure sufficient coverage was achieved the AUV and deep tow vehicle covered this area with multiple passes and alternate line plans.

Varying degrees of confidence were attached to LPD areas depending on interpretation of the complexity, texture, composition and topography of the seafloor. Nominally these areas were rated at 50-90 per cent likelihood that an analyst would detect the aircraft debris field. Approximately 48 per cent of LPD areas have been searched at least twice which added to the overall confidence of detection rating. Figure 65 shows an outline of all data collected by the AUV. Each colour represents one of three separate AUV campaigns over the course of the underwater search. The green area highlights a concentration of missions around the large fracture zone mentioned previously in the southern search area. A concentration of infill missions along the middle of the search area correlates with the position of the 7th arc.

Figure 65: Map showing coverage of AUV missions and statistics

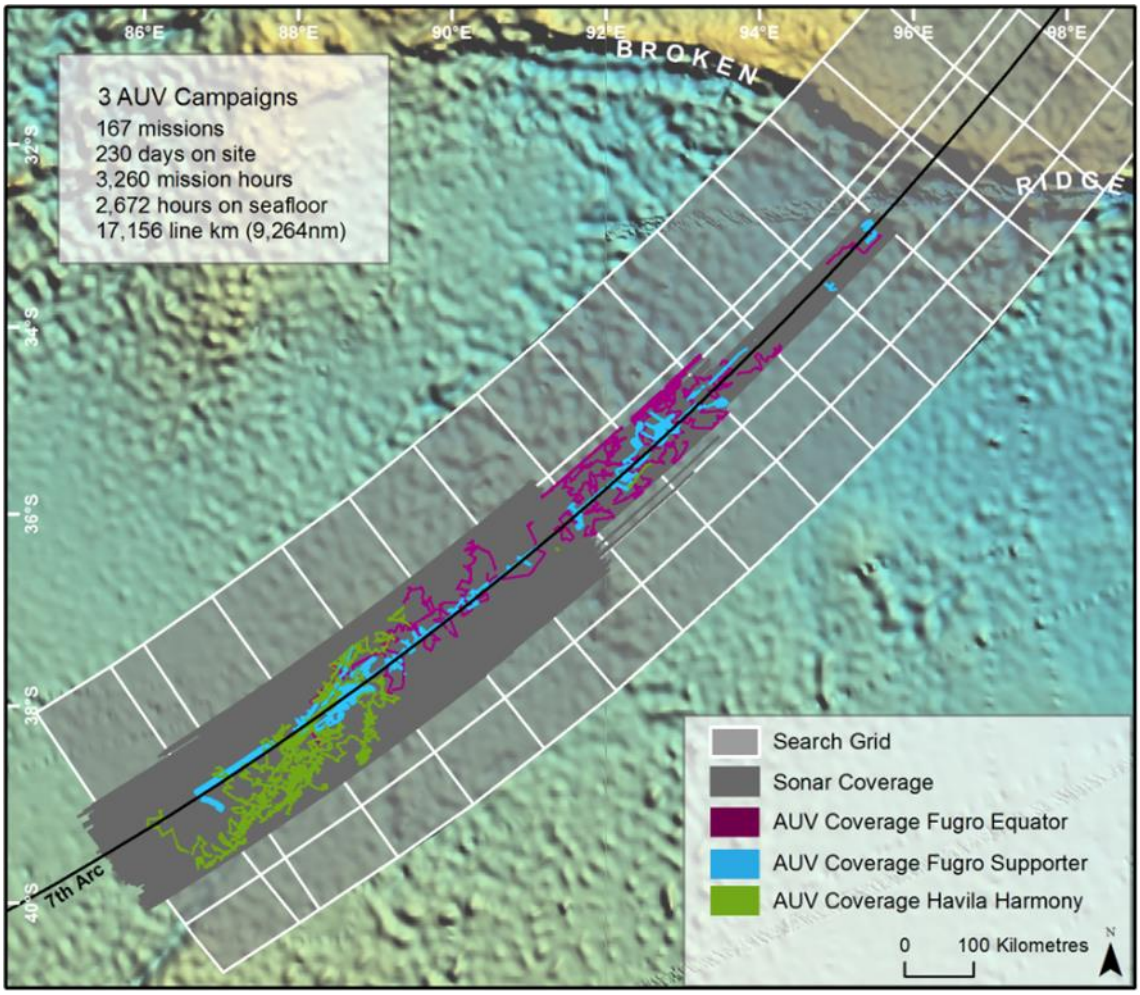

Source: ATSB

Data processing and information dissemination – a new approach

During the search for MH370 Fugro developed and deployed several new technologies to improve the analysis and transfer of the sonar search data. Due to the remoteness of the search area, and the requirement for multiple vessels operating in a coordinated manner, a system was implemented in which raw sonar data was packaged and transmitted via VSAT satellite communications systems from each vessel to a secure cloud facility (Fugro term this Back2Base). This permitted simultaneous data analysis and quality control by the shore-based analysts in Fugro Survey's Perth office, GIS specialists in the ATSB's Canberra office and the ATSB's Quality Assurance Manager based in the United States.

The large volume of data and its availability on a cloud server also created the opportunity for an automation step-change in the processing of positioning, SSS and MBES data. Fugro developed 'Roames', a cloud-based system, which allowed sonar data to be automatically processed in an efficient and consistent manner. This processing system employed algorithms which significantly improved the sonar signal processing, gain curves and accuracy of the bottom tracking of the first sonar return. Improved bottom tracking and the gains applied by Roames resulted in a better interpretation of sonar data, specifically within the near nadir region[27] to the mid-range, however the entire sonar record benefited out to the far field.

The products resulting from the Roames processing including geo-referenced sonar mosaics, sonar point clouds and conditioned SSS data files could then be visualised in near real-time from anywhere in the world via secure link. Conventional desktop-based processing using industry standard software packages was also undertaken in parallel with the Roames processing as check on the processing results. Bottom tracking from the port and starboard channels were cross-correlated to the downward looking multibeam echo sounder to ensure the validity of the bottom detection.

Tests were conducted over the first shipwreck site, Figure 67 and Figure 68, to validate the algorithms used by the Roames system. This site provided a well-suited test area, with low-lying objects less than 25 cm high and only a few pieces of debris near 1 m in height. The wreck was spread over an area 300 m by 250 m with three larger pieces of debris that could be used for reference.

Four test lines were run directly over the shipwreck site using the deep tow vehicle at altitudes of 125 m, 130 m, 165 m and 200 m. All runs used nominal operational settings for both the SSS and MBES sensors. MBES backscatter was used to verify the position of the debris field within the SSS nadir and the tests showed that a 200 m by 200 m low lying debris field could be detected in the SSS data at an altitude of up to 200 m with a high degree of confidence over a fairly benign seafloor.

This was an important finding as early in the search it was found that the optical fibres within the deep tow vehicle tow cables experienced increasing attenuation over the course of each six week search swing. Towards the end of a swing this resulted in some areas where the tow cable failed to communicate with the required gigabit Ethernet connection for MBES operations producing a long thin data gap typically 100 m to 150 m wide, depending on the vehicle altitude. The tow cable attenuation MBES communication problem was eventually overcome using a combination of modified operational practices, maintenance procedures and alternating tow cable cables every port call ('resting' the tow cables on alternate swings).

Following field testing of the Roames system at the shipwreck debris field many of these long thin data gaps were able to be discounted. This was based on the proven detection of at least a 200 m by 200 m debris field in the nadir of the SSS data when the towfish altitude was less than 200 m, which was mostly the case. Sub-bottom profiler data was also reviewed for these areas for

---

[27] The nadir region is defined in this report as the area directly beneath the deep tow vehicle and area adjacent to the first SSS signal return.

potential anomalies to gain further confidence that a debris field had not been missed in the nadir. Areas where the seafloor was geologically complex or dynamic remained classified as data gaps or were classified as LPD. In many cases these areas were later re-investigated using the AUV to ensure search integrity.

Using Fugro's cloud-based system visualisations of daily progress and data coverage were delivered through Google Earth (and other GIS applications) which provided the ATSB's search personnel with up-to-date information on the search without needing specific expertise in more complex GIS software packages. Other data delivered with the system included high resolution coverage maps, real time ship locations, line plans, track plots, weather maps, hill-shaded seafloor relief, MBES backscatter and various map layers which allowed operational decisions to be made in a timely and efficient manner. Throughout the search innovative technology was employed to improve cost-efficiency, search confidence and team safety. This technology is already being applied by Fugro to commercial and scientific marine operations across the world.

Sonar contacts

Sonar contacts (anomalous features) identified in the sonar data were classified in three ways: level 3 contacts were marked but assessed as unlikely to be related to the aircraft, level 2 contacts were marked but assessed as only possibly being related to the aircraft, and level 1 contacts were of high interest and warranted immediate further investigation. There were 618 level 3 contacts, 41 level 2 contacts, and two level 1 contacts identified and reported. The two level 1 contacts were investigated and found to be iron and coal remains of a wooden shipwreck and the other was a scattered rock field. In total, four shipwrecks were found.

Throughout the search 82 separate sonar contacts were investigated and eliminated (as being related to MH370) by the AUV, ROV, or deep tow vehicles. All investigations used either high frequency sonar or optical camera images to discount sonar contacts as related to MH370. Figure 66 shows the overall distribution and layout of the contacts that were marked and investigated.

Figure 66: Locations of contacts and secondary investigations

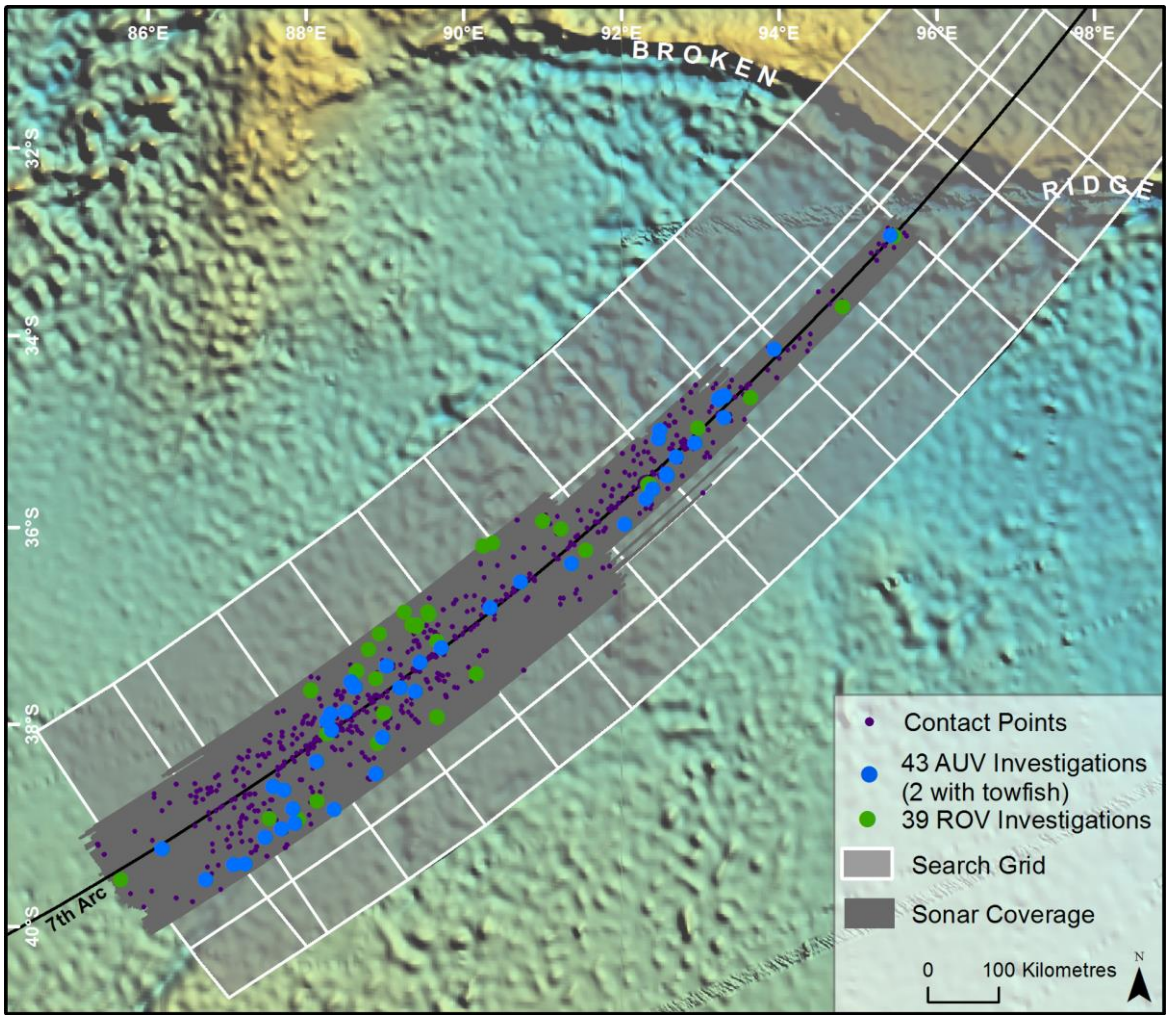

Source: ATSB

Overall these investigations and verifications provided increased confidence in the search area as they validated specific findings and provided assurance that the data analysis and interpretation were correct and accurate. This also verified the overall search methodology, providing confidence in the operations, sonar sensors and vehicles used.

The following example was a contact highlighted as a preliminary contact on board a search vessel. This data was reviewed by the contractor's processing team on shore, ATSB, and by independent analysis, after which it was decided to investigate further using the AUV. Figure 67 shows the first deep tow vehicle sonar line where the initial detection was made. Figure 68 shows the AUV mosaic created with several passes using 410 kHz high frequency SSS at 100 m range scale.

Figure 67: Initial deep tow vehicle sonar data, shipwreck #1 detection

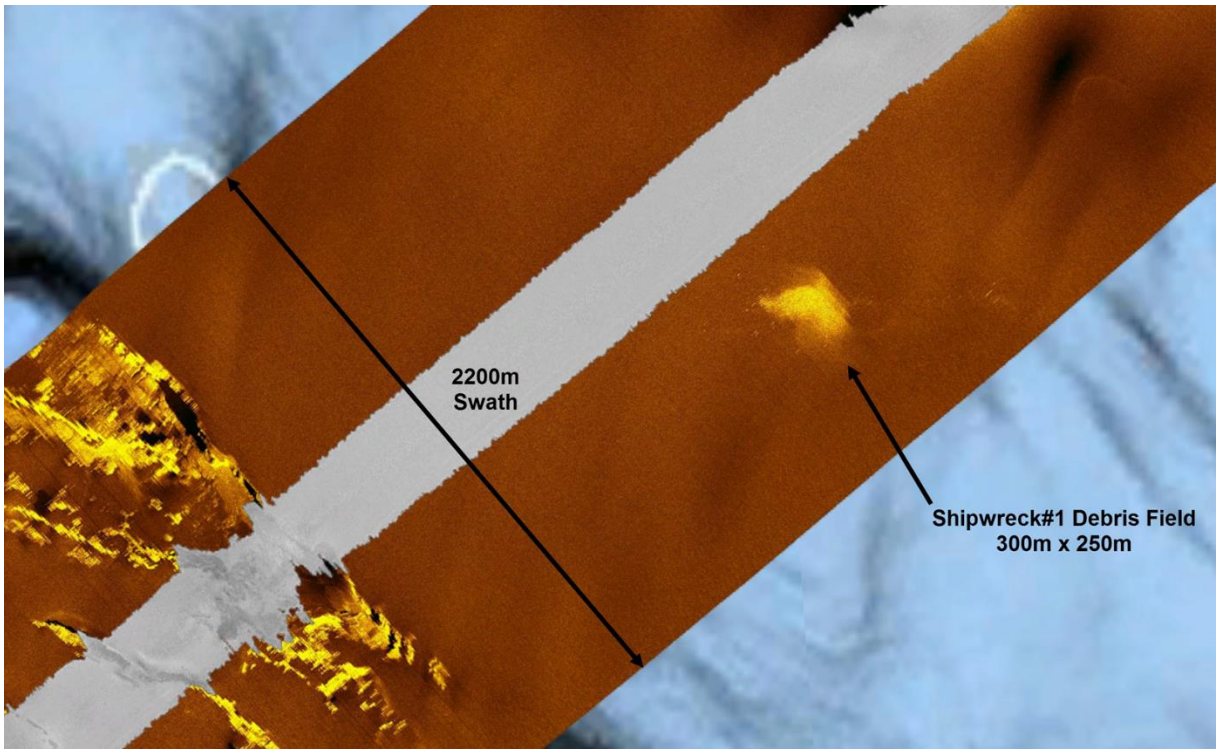

Source: ATSB

Figure 68: AUV side scan sonar mosaic of shipwreck #1 site

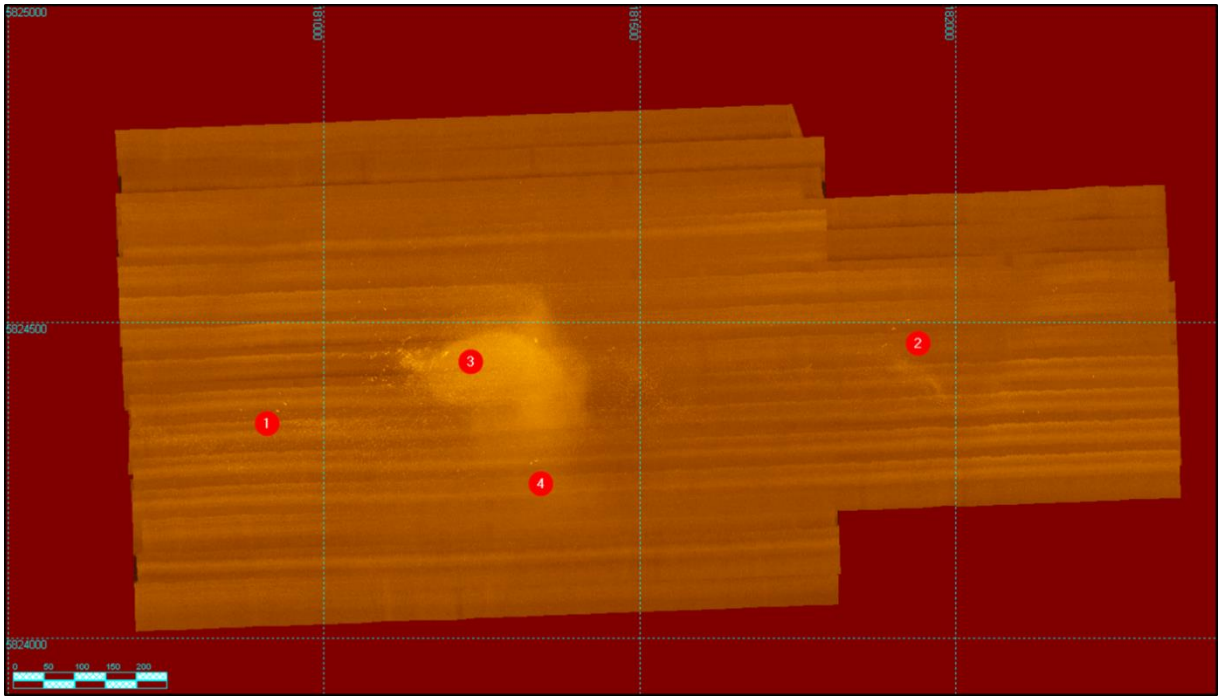

Source: ATSB

The sonar contact was suspected as being a shipwreck and confirmed by a follow-on AUV mission that collected black and white camera images. Figure 69 compares a camera image to a high frequency sonar image of an anchor highlighting the detail that was achieved using high frequency side scan sonar data and the correlation between data sets. Figure 70 is a photo mosaic created over a portion of the shipwreck site using multiple photographs taken by the AUV.

Figure 69: High resolution AUV sonar data and optical imagery of anchor

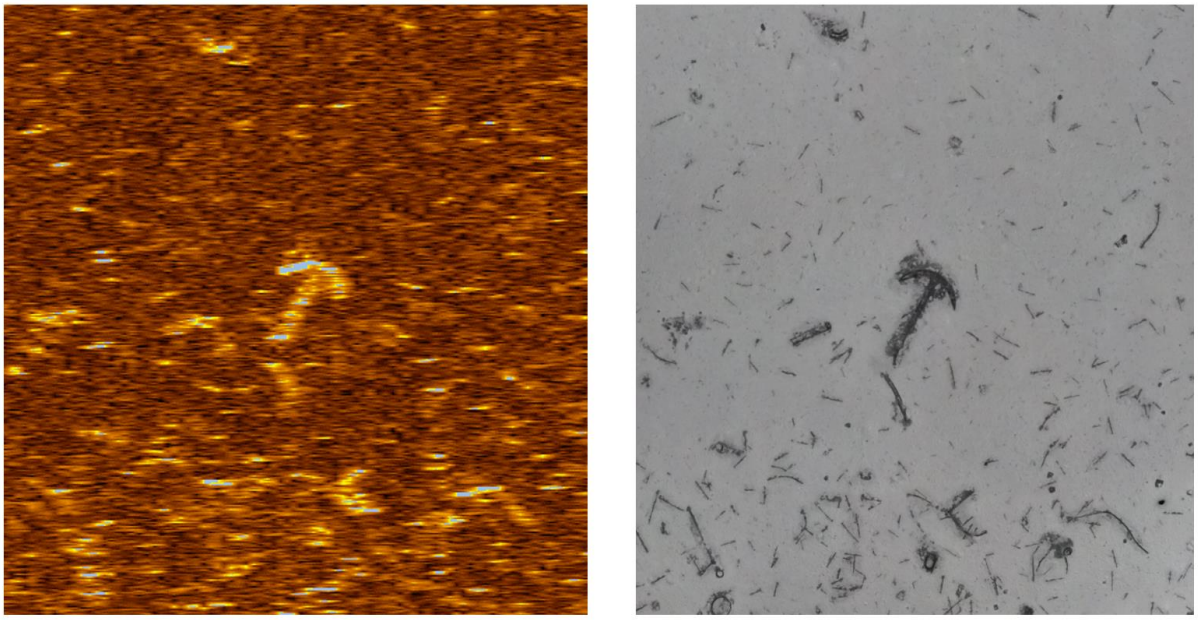

Source: ATSB

Figure 70: AUV photo mosaic subset of shipwreck #1 site

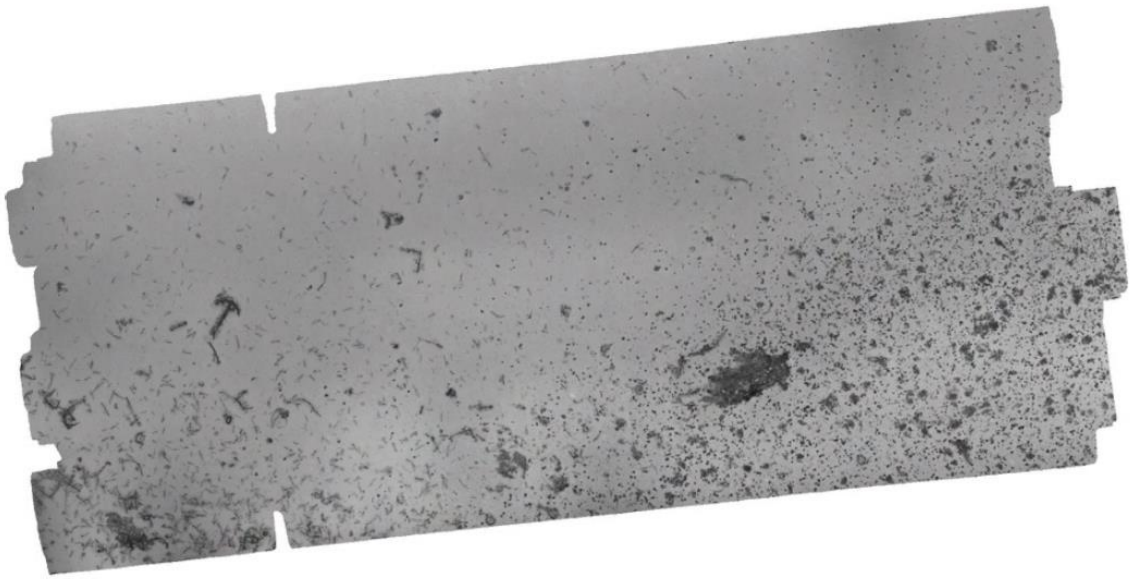

Source: ATSB

In addition to using the deep tow vehicles and the AUV to investigate areas of interest a ROV was also used. The ROV was deployed over specific sites to collect colour streaming video to confirm contacts were not related to MH370.

In total 39 discrete areas were investigated. Figure 71 shows a typical ROV track during a single investigation dive, which included a search of the immediate and surrounding area of a sonar contact. The ROV allowed for quick verification of sonar contacts, often completed in around five hours per location, with many of the contacts in difficult geologic areas within a complex and dynamic seafloor. The ROV also provided a safer alternative to using the AUV or deep tow vehicle in potentially hazardous (to the deep tow vehicle or AUV) seafloor environments. Figure 72 is a selection of man-made debris found using the ROV.

Figure 71: ROV track of typical contact investigation

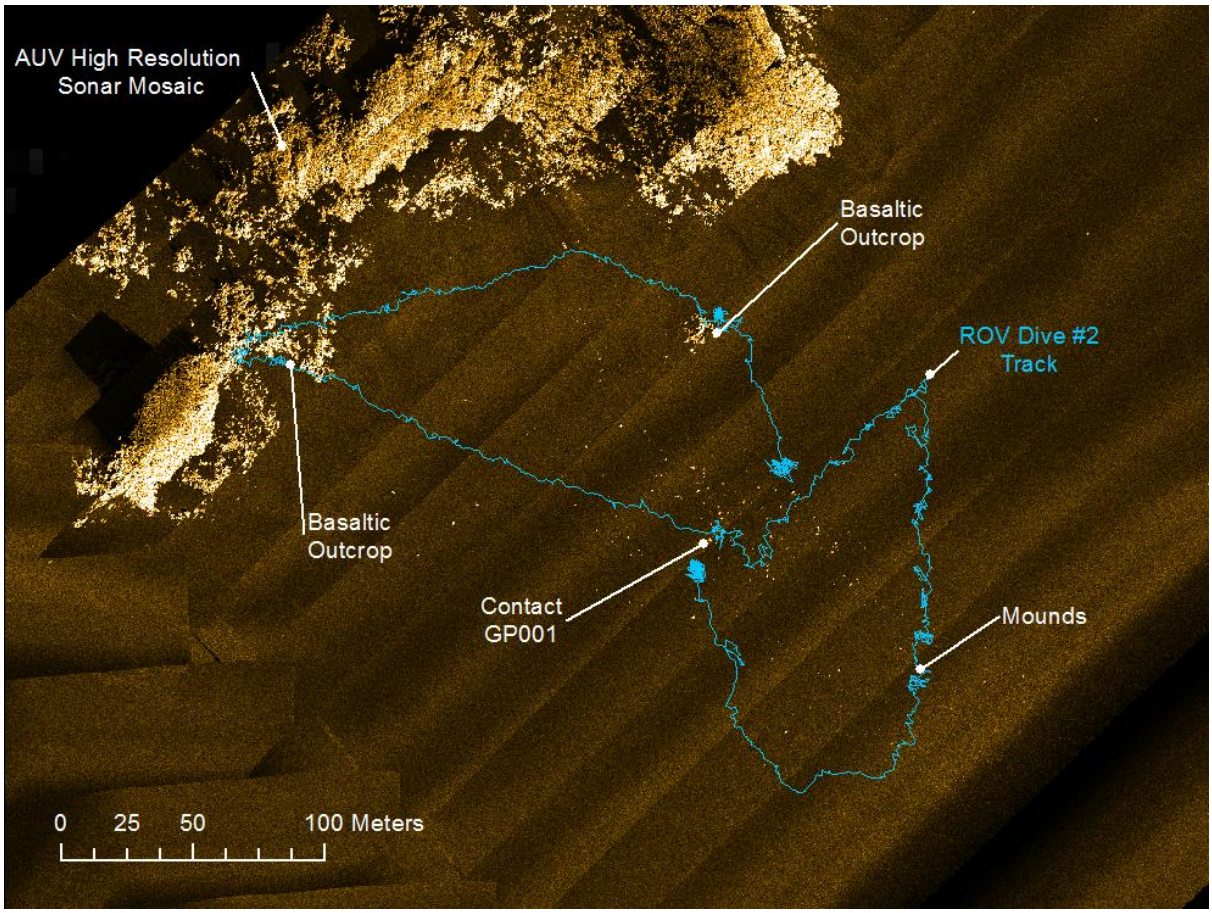

Source: ATSB

Figure 72: ROV images of man-made findings

Source: ATSB

Confidence in the search results

To quantify the confidence in the search results measurable parameters were tracked and catalogued. Separating search data into categories and assessing them individually decreased generalisations across the entire data set. In addition, contact investigations, proven object detection and verification, overlapping data and positioning repeatability all provide indicators when assessing the overall confidence of the underwater search.

As detailed within the sonar coverage section the sonar data and coverage were separated into different categories. The following designations were used with a confidence of detection rating assigned, zero per cent meaning there was no confidence of detection and 100 per cent meaning complete confidence the aircraft debris field would be detected within the collected sonar data.

- Shadow, off-track, and equipment failure data gaps were all given zero per cent confidence of detection.
- Terrain avoidance data gaps were also given zero per cent confidence of detection.
  - Normally some useable data was within these areas, however given the higher towing altitudes and increased deep tow vehicle motion often associated with this type of holiday a conservative value of zero per cent was chosen.
- Lower probability of detection areas, these varied in the level of detection confidence.
  - A range of 50-90 per cent was used to capture this category with an overall rating of 70 per cent as the nominal value. It is worth noting that 48 per cent of these areas were searched more than once, which positively contributed to the confidence rating.
- The remaining area had good quality sonar coverage resulting in a >95 per cent confidence of detection rating.

The statistics were further broken down into four areas based on the probability of the aircraft debris field lying in the area (based on the then flight path analysis, end-of-flight, PDF) during the search. The primary difference in the overall sonar coverage for these four discrete areas was the amount of AUV time used to fill in the data gaps and the more difficult seafloor topography within each region. A description of the four areas follows:

1. Red Area: ‘Indicative Search Area’ out to 27.5 NM to the northwest and 25 NM to the southeast of the 7th arc.
   - Consists of deep tow vehicle SSS data, SAS data, and AUV infill data.
2. Orange Area: North of the ‘Indicative Search Area’ out to 23 NM to the northwest and 17 NM to the southeast of the 7th arc.
   - Consists of mainly deep tow vehicle SSS data and AUV infill data.
3. Yellow Area: Furthest north of the ‘Indicative Search Area’ out to 10 NM to the northwest and 13 NM to the southeast of the 7th arc.
   - Consists of mainly deep tow vehicle SAS data and AUV infill data.
4. Purple Area: Outside 27.5 NM to 36 NM to the northwest and 25 NM to 41 NM to the southeast of the 7th arc.
   - Consists of mainly deep tow vehicle SSS data.

Figure 73 summarises the overall coverage percentages and corresponding confidence of detection ratings for each area, as well as for the total combined area searched based on cataloging all data gaps and LPD areas of 100 m by 100 m size and larger.

Figure 73: Coverage statistics and associated confidence of detection, using 100 m x 100 m data gap metric

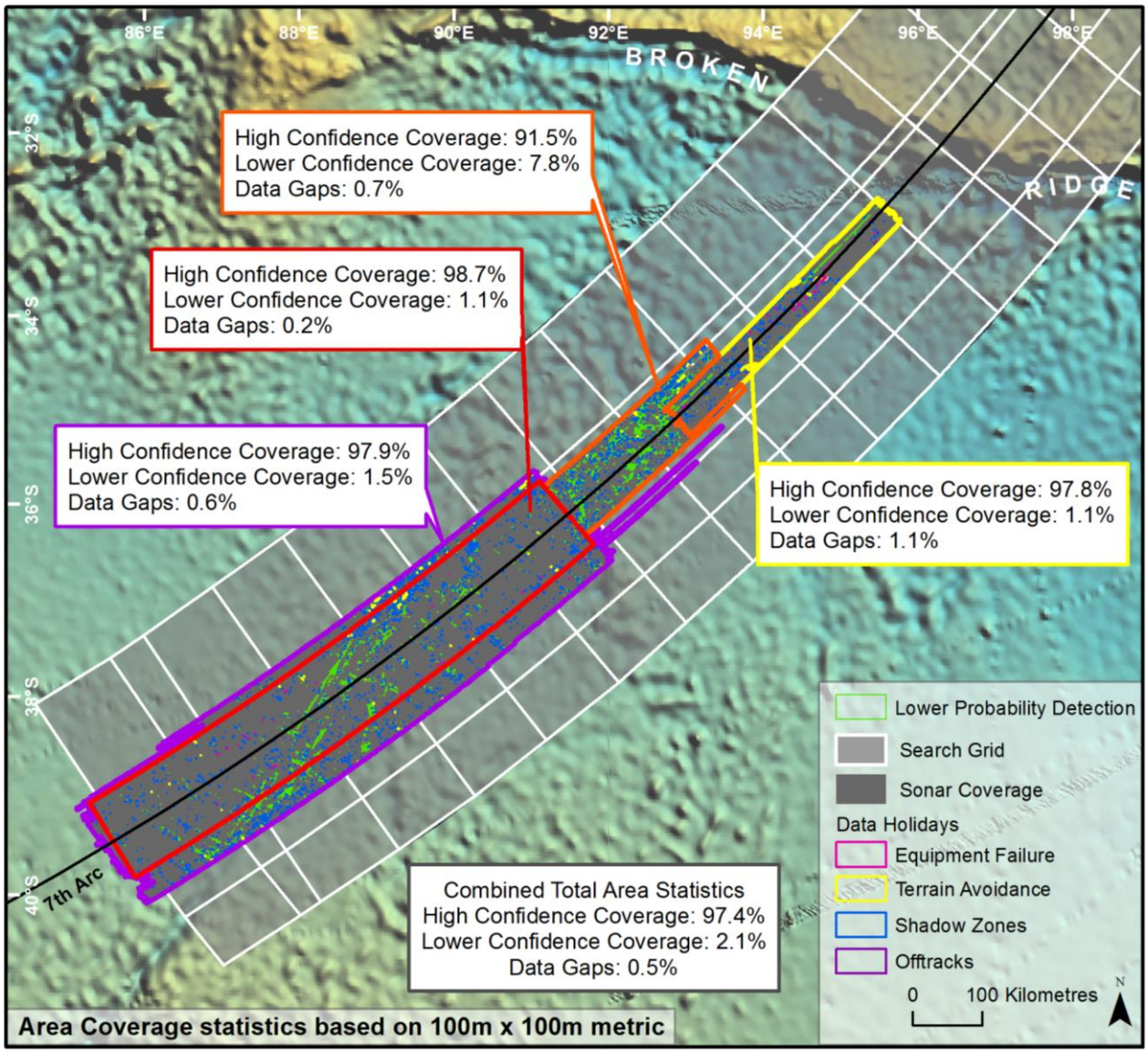

Source: ATSB

For reference, 'High Confidence Coverage' means a >95 per cent confidence of detection; 'Lower Confidence Coverage' means on average a 70 per cent confidence of detection, and 'Data Gaps' have a zero per cent confidence of detection.

For each area defined the final sonar data coverage value is determined by taking the total size of the area and subtracting out each data gap and LPD. Holidays are totaled by area (square kilometres) per individual polygon. This size attribute can be used to filter and further classify data gaps and LPDs.

It is worth noting that filtering out all data gaps and LPD areas less than 200 m by 200 m decreases the individual data gap count by 78 per cent, and LPD count by 60 per cent. Using this same metric but filtering by square kilometres reduces the total square kilometre area by 24 per cent and seven per cent respectively. This highlights that many of the data gaps and LPDs are smaller than 200 m by 200 m.

Historical analysis has shown that aircraft debris fields typically cover areas larger than 200 m by 200 m. Therefore, areas less than 200 m by 200 m can be discounted with a moderate to high degree of confidence as they are not large enough to fully contain the aircraft debris field.

However, this reduction only results in a small overall coverage increase of 0.1 per cent (data gaps) and 0.2 per cent (LPDs) respectively, hence the decision was made to maintain a conservative approach by using the 100 m by 100 m area metric.

Other search area considerations

During the course of the underwater search for MH370 the ATSB actively sought any information or analysis from credible sources which may have assisted in better understanding where the aircraft may be located. A range of information from disparate sources was carefully considered in the context of defining the most probable underwater search area. While some information and analysis did not yield any new insights or was considered and discounted on the basis of new or existing evidence or analysis, it was important to exhaust every avenue which could improve the chance of locating the aircraft.

Pilot in Command's flight simulator

Data from the Pilot-in-Command's (PIC) home flight simulator was recovered and analysed in March/April 2014. This information was provided to the ATSB on 19 April 2014, during the surface search and was subsequently also analysed for relevance to the underwater search.

The simulator data was a partial reconstruction of a flight simulator session from 2 February 2014. It comprised four complete and two partial data captures of various aircraft and simulator parameters at discrete points during the simulation. The aircraft simulated was a B777-200LR. Information on the data points is summarised below:

- The initial data point indicated an aircraft at Kuala Lumpur airport.
- No useful location or aircraft information apart from simulator time was able to be recovered for the second data point.
- The next two data points indicated an aircraft tracking to the northwest along the Strait of Malacca.
- The aircraft had climbed to an altitude of 40,000 ft by the fourth data point and was in a 20° left bank, 4° nose down, on a heading of 255°.
- The final two data points were close together in the southern Indian Ocean, 820 NM southwest of Cape Leeuwin. The data indicated that the simulated aircraft had exhausted its fuel. The fifth data point was at an altitude of 37,651 ft, the aircraft was in an 11° right bank and heading almost due south at 178°.
- The data for the sixth data point was incomplete. It was 2.5 NM from the previous data point and the aircraft right bank had reduced to 3°.The aircraft was pitched nose down 5° and was on a heading of 193°. At this time there was also a user input of an altitude of 4,000 ft.

The aircraft track from the simulator data points is shown in Figure 74. The track shows the aircraft flying up the Strait of Malacca before a left turn into the southern Indian Ocean. The aircraft then tracks southeast to the fifth data point (assuming that there is no intermediate data point not captured) to fuel exhaustion at the final point. By the last data point the aircraft had flown approximately 4,200 NM. This was further than was possible with the fuel loaded on board the aircraft for flight MH370. Similarly, the simulated aircraft track was not consistent with the aircraft tracks modelled using the MH370 satellite communications metadata.

Figure 74: Simulator data indicative track (and 7th arc)

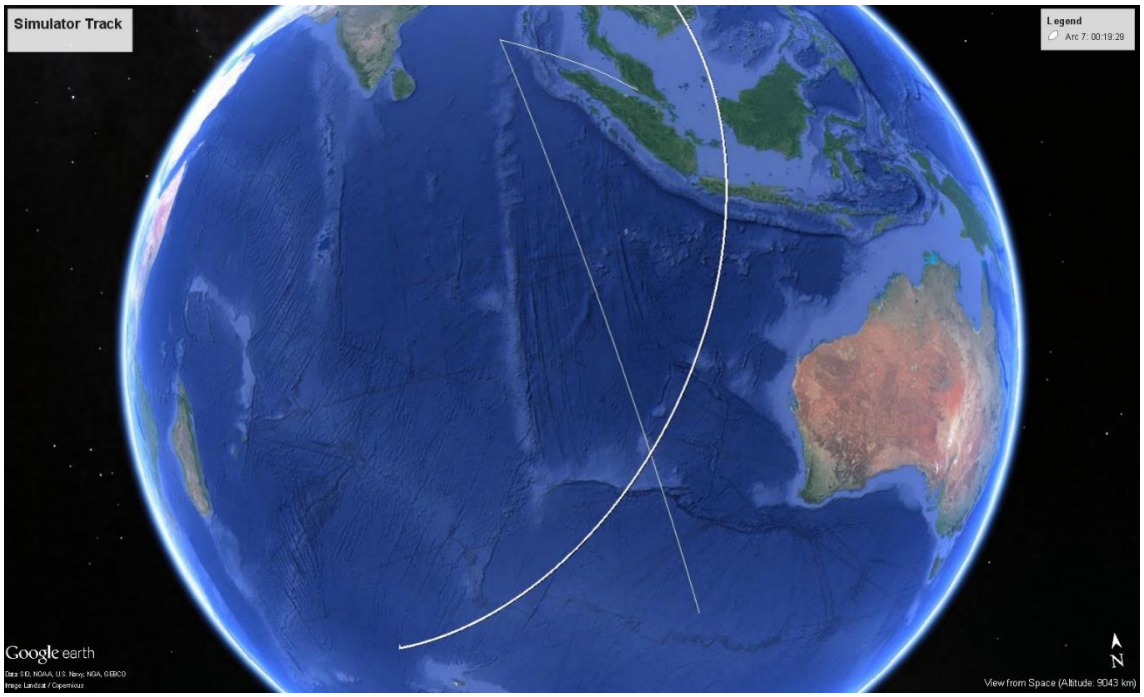

Source: Google earth, annotated by ATSB

On the day the simulation was conducted the PIC was on a rostered day of leave. The following day the PIC was rostered to fly from Kuala Lumpur to Denpasar, Bali and return the same day. On 4 February 2014 the PIC was rostered to fly from Kuala Lumpur to Jeddah, Saudi Arabia. The first three data points recovered from the simulator were consistent with the route from Kuala Lumpur to Jeddah. In the weeks between the Jeddah flight and the accident flight the PIC was rostered to fly return flights from Kuala Lumpur to; Denpasar, Beijing, Melbourne and then Denpasar again.

Six weeks before the accident flight the PIC had used his simulator to fly a route, initially similar to part of the route flown by MH370 up the Strait of Malacca, with a left-hand turn and track into the southern Indian Ocean. There were enough similarities to the flight path of MH370 for the ATSB to carefully consider the possible implications for the underwater search area. These considerations included the impact on the search area if the aircraft had been either glided after fuel exhaustion or ditched under power prior to fuel exhaustion with active control of the aircraft from the cockpit.

Controlled glide or ditching

The B777 aircraft can theoretically achieve an unpowered glide ratio of approximately 17:1. That is, for every 1,000 ft of altitude lost in an unpowered glide the aircraft can travel a distance of approximately 2.8 NM. If MH370 was at an altitude of 40,000 ft at the point of fuel exhaustion, the aircraft could be glided more than 100 NM with an average rate of descent between 2,500 and 3,000 ft/min. Simulations conducted in a B777 simulator early in the search, confirmed these results which were included in the ATSB's MH370-Definition of Underwater Search Areas report released in June 2014.

The possibility of a controlled ditching was carefully considered. Something occurred on board MH370 just before it reached the 7th arc which interrupted the power supply to the satellite data unit (SDU), (it takes a minute for the SDU to reboot after a short interruption of power). Since early in the search, analysis of the aircraft's fuel consumption and endurance, and the characteristics of the final series of SATCOM transmissions had yielded fuel exhaustion as the most likely explanation for the power interruption. However, it was considered that the SDU reboot could be explained in other ways, much less likely, if there was someone active in the cockpit and preparing the aircraft for a controlled ditching.

If the aircraft was being actively controlled during the final segment of the flight south into the Indian Ocean, a series of step climbs[28] (which must be initiated by someone active in the cockpit) could have resulted in enough fuel at the end of flight to perform a controlled ditching under power rather than an unpowered glide. At the time the 7th arc was generated by the aircraft logging back onto the SATCOM system, the aircraft could have been descending in a 'normal' landing configuration including full instrumentation and full hydraulic power available for all flight control surfaces including slats and flaps.

At normal rates of descent (around 2,000 ft/min) the aircraft could have flown approximately 120 NM from the top of descent (an assumed altitude of approximately 40,000 ft) to sea level. If the Boeing ditching procedure were being followed there would have been turns at lower altitudes, firstly to the southwest into the prevailing wind and finally a turn close to sea level to land the aircraft parallel to the prevailing seas.

On 8 March 2014 the sun was 6 degrees above the horizon at 0019:30 UTC as the aircraft reached the 7th arc. Sunrise had been 24.5 minutes earlier, at 2355 UTC. The surface of the ocean would have been visible in order to judge the touchdown on the sea surface. In addition, at the time the aircraft was close to fuel exhaustion, the lightest state it could be, and therefore it was possible to make a controlled ditching with the lowest possible approach speed, with flaps extended in accordance with the Boeing ditching procedure.

The most likely aircraft tracks (after the turn at the tip of Sumatra) derived from the DST Group modelling (summarised in the ATSB's MH370-Definition of Underwater Search Areas report released in December 2015) were considered at the time with a controlled descent starting just before the 7th arc, indicatively the areas of priority for searching to cover a controlled ditching (or a controlled glide) at the end of flight, as it was considered at the time, are shown in Figure 75.

[28] A step climb in aviation is a series of altitude gains that improve fuel economy by moving into thinner air as an aircraft becomes lighter (when fuel is burnt during the flight) and becomes capable of faster, more economical flight.

Figure 75: Indicative controlled ditch scenario search areas at July 2016

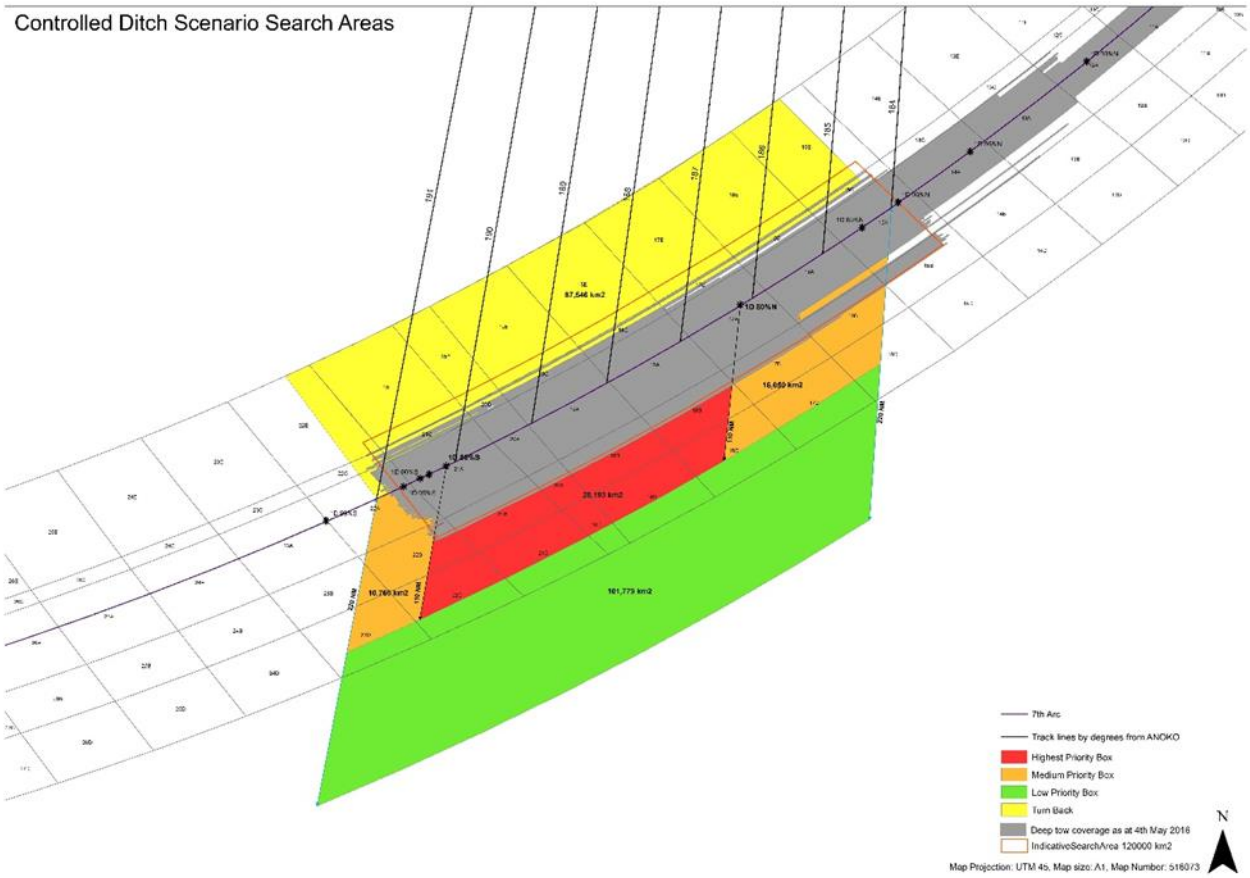

Source: ATSB

By June 2016 many pieces of aircraft debris (see following section on Aircraft debris) confirmed or very likely from MH370, had been recovered from east African shorelines. Some items were from within the fuselage. While no firm conclusions could be drawn given the limited amount of debris, the type, size and origin on the aircraft of these items generally indicated that there was a significant amount of energy at the time the aircraft impacted the water, not consistent with a successful controlled ditching.

Critically, a section of right outboard main flap (Figure 81) was found near Tanzania on 20 June 2016. The item was shipped to the ATSB for analysis. This analysis indicated that the flaps were most likely in a retracted position at the time they separated from the aircraft making a controlled ditching scenario very unlikely.

The ATSB's MH370-Search and Debris Examination Update on the flap analysis also contained the summary of the analysis The Use of Burst Frequency Offsets in the Search for MH370 performed by DST Group scientists on the final two satellite transmissions from the aircraft. This work quantified the range of possible rates of descent based on the burst frequency offsets of the SATCOM transmissions. In summary, the analysis concluded that the aircraft was descending at a rate of between 2,900 ft/min and 15,200 ft/min when the 7th arc was crossed. Eight seconds later the rate of descent had increased to between 13,800 ft/min and 25,300 ft/min[29]. These rates of descent ruled out a controlled unpowered glide with the intent to extend range.

[29] It should be noted that these descent rates were derived assuming the SDU was still receiving valid track and speed labels from the ADIRU at 0019:37 UTC for use in its doppler pre-compensation algorithm.

Aircraft debris

In the search for MH370, the recovery of debris from the aircraft has provided some of the most important evidence as to what may have happened to the aircraft at the end-of-flight and where it may be located.

Looking at past aircraft accidents, there is almost always some debris left floating after an aircraft crashes in water. The debris will often include items designed to float including seat cushions, life jackets, and escape slides, but also many items of cabin fit-out, like cabin linings and tray tables, which are made of low density synthetic materials. Similarly aircraft structural components, including flight surfaces, may entrap sufficient air to remain buoyant for long periods and have also been commonly found afloat following a crash.

The amount and type of debris varies but it is usually detected and recovered within the first few weeks of the accident before it has been significantly dispersed. Over time, all floating debris will eventually decompose, become water-logged and then sink. For some items of debris this may be relatively fast. For example, items which are buoyant due to entrapped air will sink when the air is released or void spaces become filled, a process which is hastened by the action of wind and waves. Other items constructed of materials which are less permeable, like seat cushions, will float for long periods but they too will eventually sink when the material degrades through chemical and/or mechanical decomposition. This decomposition may take a very long time in the case of some synthetic materials, plastics in particular, but is quicker for items which biodegrade.

The opportunity to locate and recover debris from the sea surface diminishes rapidly over the first few weeks from the time of a crash. Thereafter, there will be some less permeable items of debris which will remain afloat for a longer period but they will be increasingly dispersed. Dispersal is directly related to the surface drift experienced by the individual items of debris which in turn is related to their physical characteristics: size, shape and density. To be found ashore, an item of debris must remain afloat long enough and be subjected to the right combination of winds, waves and currents for it to make landfall.

Modern aircraft like the B777 have many structural and cabin fitout components manufactured of composite materials. These structures are typically of sandwich construction with hard outer layers, often of fibre reinforced plastic or alloy, which are bonded to a honeycomb core. They are light (buoyant), strong and highly resistant to decomposition and therefore may float for long periods before making landfall.

During the course of the underwater search for MH370 numerous items of debris were found and reported to the ATSB originating from a range of Australian and International sources. These items ranged from pieces of mechanical wreckage through to items of clothing, food wrappings and personal items.

When reports were received by the ATSB, contact would be made with the reporter to provide instructions including:

- Note the time and location (GPS position) of the find.
- Take photographs of the debris.
- Note any numbers or distinctive markings.
- Preserve any sea life that might be attached to the item.
- Check if the item floats (this helped to eliminate objects early on).
- Handle the item as little as possible and wrap it to preserve its condition.

Once photographic and other evidence was received, a process of assessment would take place in consultation with the Malaysian Annex 13 investigation team, Malaysia Airlines and Boeing as the aircraft manufacturer. If the item was considered to be potentially MH370 related then the member of the public was advised to hand it in to local authorities to await collection, usually by the Malaysian authorities. On several occasions debris was shipped directly to the ATSB

laboratories in Canberra and analysed at the request of the Malaysian Annex 13 investigation team.

The flaperon

On 29 July 2015, more than 500 days after the aircraft went missing, a large item of aircraft debris was recovered from a beach on La Réunion Island in the western Indian Ocean. A preliminary assessment confirmed that it was possibly a flaperon (a flight control surface which has the dual functions of an aileron and flap) from a B777 aircraft. The item was taken by the French authorities on the island and shipped to Toulouse in France for examination under the control of French judicial authorities.

The examination revealed a range of part and serial numbers marked on internal components of the item which were compared with the manufacturer's records to confirm that the item was the right flaperon from the B777 aircraft operating flight MH370. The flaperon was the first item of debris positively confirmed to have come from MH370.

A number of other tests and examinations were made in France on the flaperon, including marine specimen examinations (barnacles attached to the flaperon), failure analysis of metal and composite components and flotation testing. Details of all examinations were provided to the ATSB by the French judicial authorities to assist with the search for MH370 (the public release of any reports on the flaperon examination is the responsibility of the French judicial authorities). Figure 76 shows the flaperon buoyancy testing conducted in France.

Figure 76: The flaperon buoyancy test

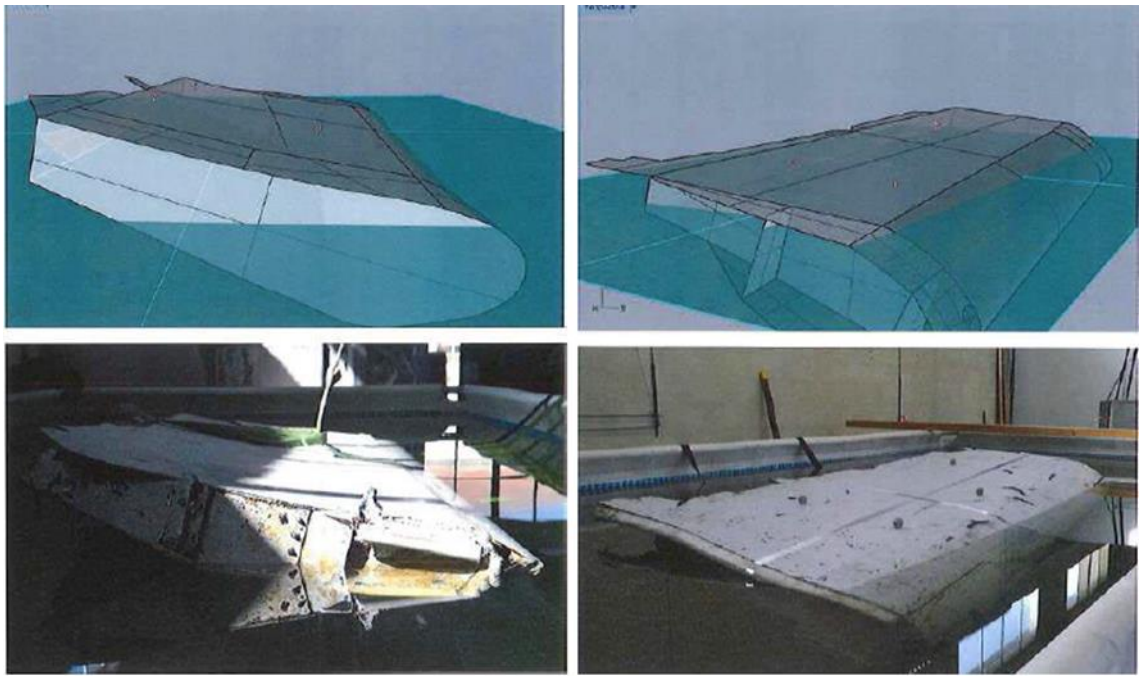

Source: Direction Générale de l'Armement Techniques Aéronautiques

Other parts recovered

Following the recovery of the flaperon, many more items of debris were found and recovered from beaches in Madagascar, Mauritius, Mozambique, South Africa and Tanzania late in 2015 and early 2016. Further debris items confirmed as originating from MH370 are shown in Figure 77, Figure 78, Figure 79, Figure 80 and Figure 81. Debris examination reports of these items are available on the ATSB website at www.atsb.gov.au.

Figure 77: Engine cowling section

Source: ATSB

Figure 78: Right wing flap track fairing section

Source: ATSB

Figure 79: Right horizontal stabilizer panel section

Source: ATSB

Figure 80: Internal cabin bulkhead panel section

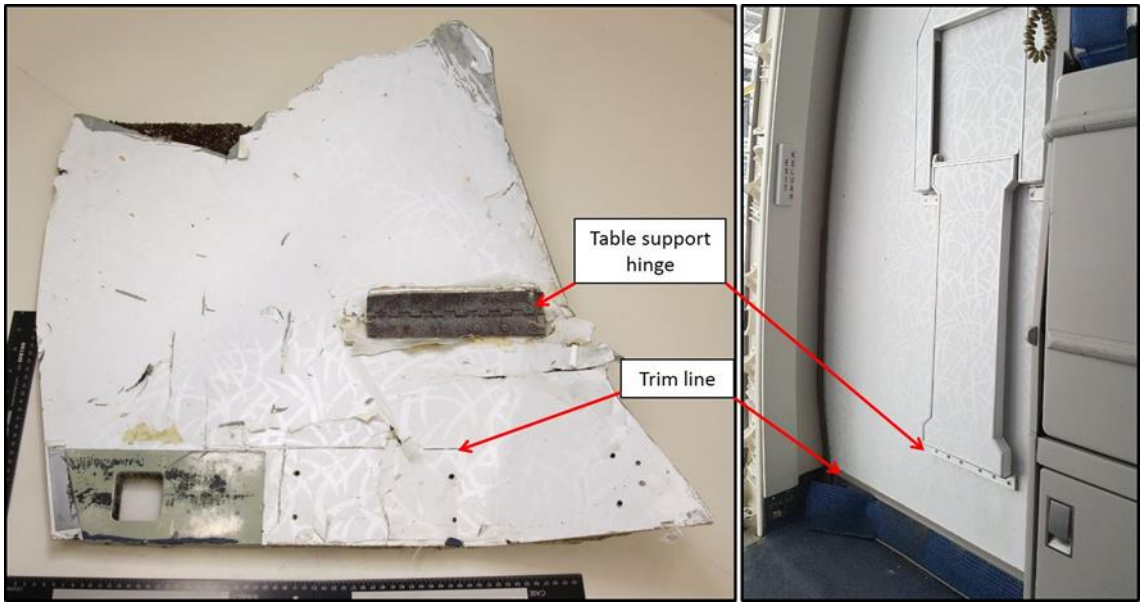

Source: ATSB and Ministry of Transport Malaysia

Figure 81: Right outboard flap section

Source: ATSB

Debris examination reports are available on the Ministry of Transport Malaysia website at www.mh370.gov.my. At the time of writing, 18 items were identified as being very likely or almost certain to originate from MH370, with another two assessed as probably from the accident aircraft. These are illustrated in Figure 82.

Figure 82: General locations of items recovered. Some parts could have come from different locations than shown

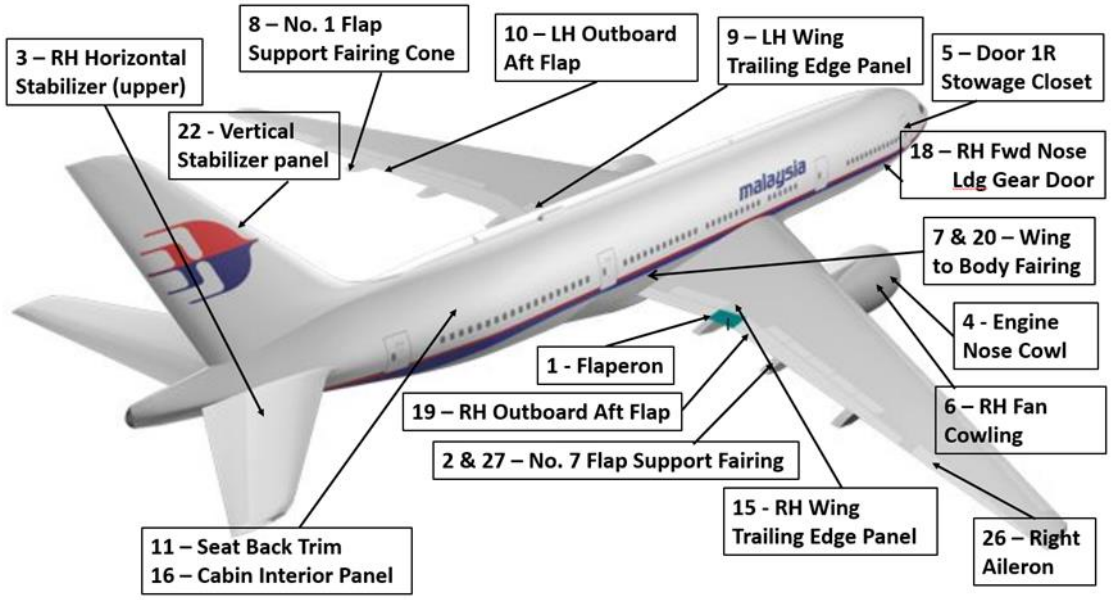

Source: Ministry of Transport Malaysia

Marine ecology examinations

When the flaperon was recovered from La Réunion Island there was a significant amount of marine growth attached to it. The majority of the marine organisms were a type of goose barnacle (Lepas (Anatifera) anatifera striata). After taking advice from an expert at the Western Australia Museum, who also identified the barnacle, the ATSB came to understand that the attachment and growth of the barnacles may reveal some evidence in relation to where the flaperon started its drift in the Indian Ocean and the passage that it took in the succeeding 500 days before it came ashore. Also, critically, that the chemical composition of the barnacle shells may yield some information about the temperature and salinity of the water where the various stages of the barnacle growth took place. For the oldest (and largest) barnacles it was thought that this may yield some evidence as to where MH370 may be located.

This advice was provided to the French investigation team who performed some analysis on the flaperon barnacles. Later the French investigation team provided some samples of the largest barnacles to Geoscience Australia who passed them onto a team at the Australian National University led by Dr Patrick De Deckker for further analysis. The results of the analysis were inconclusive, Dr De Deckker's report is reproduced at appendix F.

All suspected MH370 debris which were transported to the ATSB laboratories in Canberra underwent quarantine and processing at Geoscience Australia's Canberra facility en route. Processing involved photographing, examining, identifying (and removing) any organisms contained within, or attached to, the items of debris. Any items of particular interest were referred to relevant specialists for further analysis and advice. The scientific team from Geoscience Australia coordinated a range of identification and examinations which are included in appendix G.

Australian beach searches

Since the start of the search for MH370 the ATSB has been cognisant that any confirmed debris finds on the Australian coastline may be significant to the search. Initial drift modelling indicated that the most likely place for debris to come ashore in Australia in 2014-15, in particular, was the coast of Western Australia or South Australia. Various organisations and members of the public undertook searches along Australian coastlines which included actively looking for any form of debris that could possibly have originated from MH370. Australian beaches searched are depicted in Figure 83.

Figure 83: Australian beach search locations

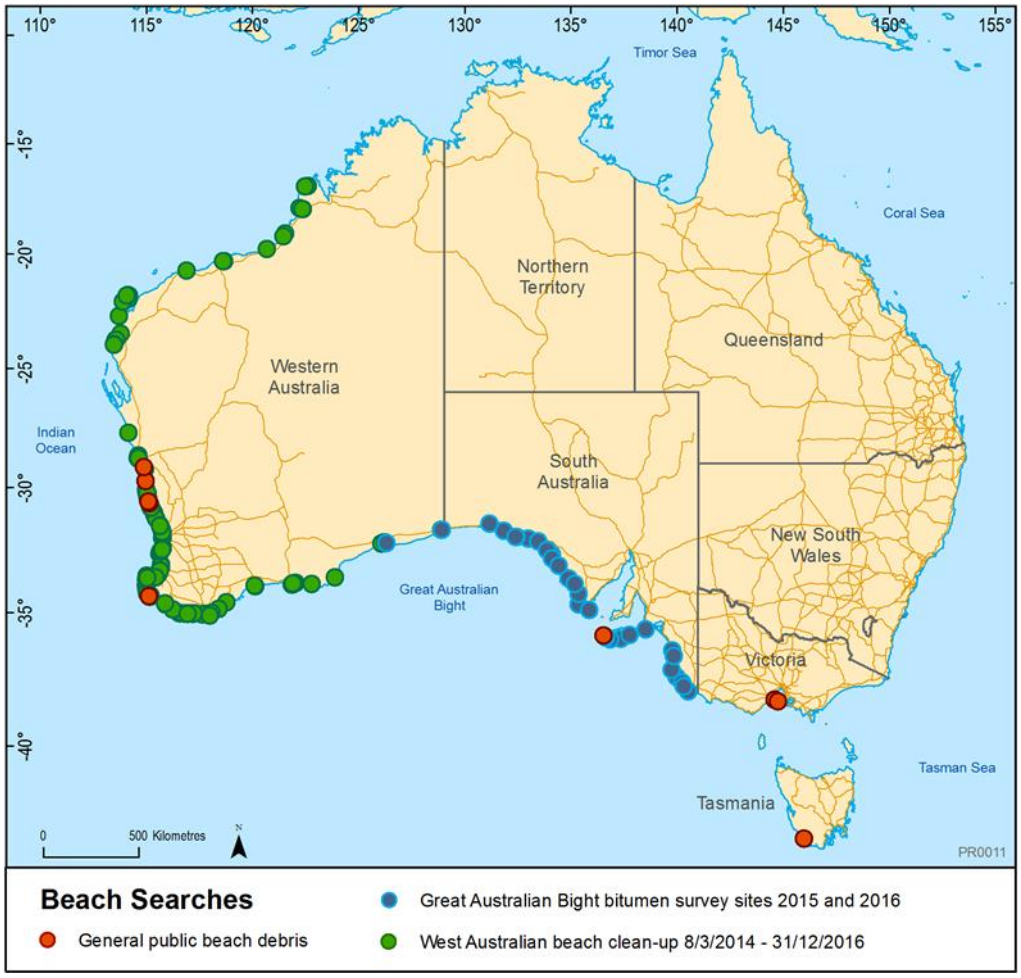

Source: ATSB. We acknowledge that the source of the West Australian beach clean-up data used in this image was the Tangaroa Blue Foundation Ltd Australian Marine Debris Initiative database with data being collected and provided by many individuals and organisations

Great Australian Bight

The University of Adelaide in conjunction with CSIRO conduct regular annual surveys of beaches sponsored by the petroleum industry stretching from the eastern coast of Western Australia, through South Australia to the western beaches of Victoria collecting bitumen from marine petroleum seeps which have drifted into the Great Australian Bight. Over time, specific beaches have been identified and targeted where the likelihood of finding bitumen washed up from global and local currents is likely. The origin of the bitumen ranges from either South East Asia, where they have drifted in the Leeuwin current down the western Australian coast, Southern Africa where they have drifted across the Indian Ocean or potentially from sedimentary basins in the Great Australian Bight. Known currents from historical research are depicted in Figure 84.

Figure 84: Known circulation of currents and bitumen samples from 40° south latitudes

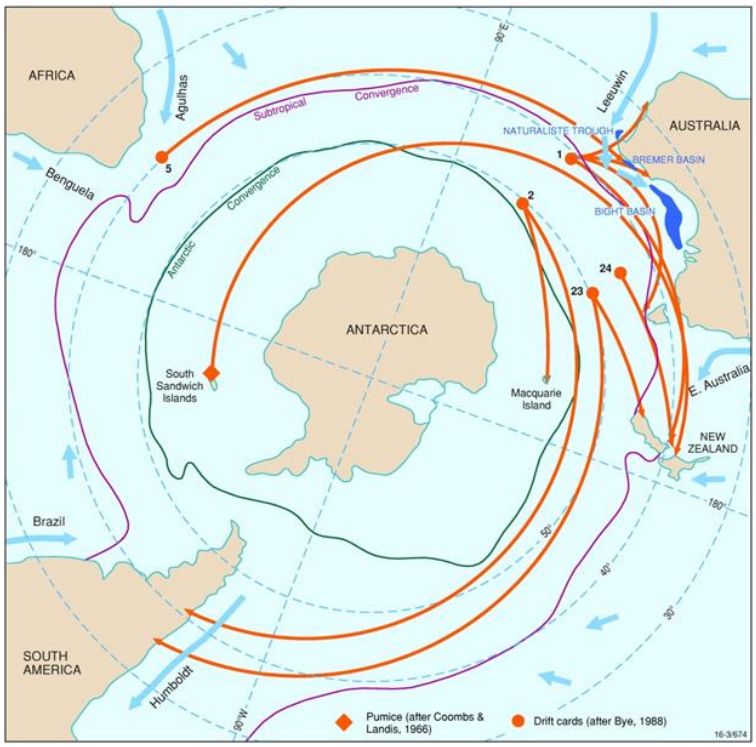

Source: Padley, D 1995, 'Petroleum geochemistry of the Otway Basin and the significance of coastal bitumen strandings on adjacent southern Australian beaches', PhD thesis, University of Adelaide

Bitumen surveys were conducted in September 2015 and October 2016 (Table 27). The surveys covered various beaches across the Great Australian Bight. The University of Adelaide and CSIRO were contacted through Geoscience Australia staff (involved with the MH370 search project) and were asked to assist the ATSB by also looking for anything that could conceivably be debris from MH370.

The following beaches were searched over the two years (2015 and 2016) and no debris from MH370 was located.

Table 27: Bitumen survey beaches

Area	Beach Name	Latitude	Longitude
Limestone Coast	28 Mile Crossing	S 36.437	E 139.772
Eyre Peninsula	Avoid Bay	S 34.669	E 135.345
Kangaroo Island	Bales Beach	S 35.992	E 137.346
Limestone Coast	Beachport Conservation Park	S 37.446	E 139.963
Eyre Peninsula	Cactus Beach	S 32.077	E 132.979
Eyre Peninsula	Cape Bauer	S 32.714	E 134.094
Great Australian Bight	Delisser Sandhills	S 31.716	E 128.896
Great Australian Bight	Dogfence Beach	S 31.769	E 131.842
Eyre Peninsula	Elliston	S 33.646	E 134.888
Limestone Coast	Evans Cave (Eves Cove)	S 37.182	E 139.744
Great Australian Bight	Eyre Bird Observatory	S 32.254	E 126.301
Great Australian Bight	Eyre Well	S 31.464	E 131.144
Eyre Peninsula	Fowlers Bay West	S 32.005	E 132.440
Eyre Peninsula	Gascoigne Bay West	S 32.529	E 133.893
Limestone Coast	Geltwood Beach	S 37.659	E 140.223

Eyre Peninsula	Hanson Bay	S 36.017	E 136.853
Eyre Peninsula	Mount Drummond Beach	S 34.258	E 135.343
Limestone Coast	Nene Valley	S 37.986	E 140.514
Limestone Coast	Number 1 and 2 Rocks (Channel Rocks)	S 37.796	E 140.321
Kangaroo Island	Pennington Bay	S 35.852	E 137.745
Eyre Peninsula	Point Peter	S 32.177	E 133.440
Kangaroo Island	Sandy River	S 35.951	E 136.634
Eyre Peninsula	Scott Bay	S 32.004	E 132.389
Eyre Peninsula	Sheringah Beach	S 33.873	E 135.174
Eyre Peninsula	Sleaford Bay	S 34.882	E 135.846
Eyre Peninsula	St Mary Bay	S 32.530	E 133.856
Eyre Peninsula	St Mary Bay South	S 32.536	E 133.857
Limestone Coast	The Granites	S 36.658	E 139.854
Eyre Peninsula	Tractor Beach	S 32.869	E 134.113
Eyre Peninsula	Tyringa Beach	S 33.147	E 134.418
Limestone Coast	Waitpinga Beach	S 35.635	E 138.499
Kangaroo Island	West Bay	S 35.888	E 136.553

Source: CSIRO and the University of Adelaide

Western Australia

The Tangaroa Blue Foundation and Celestial Vision conduct regular clean-ups of Australian coastlines.

The Tangaroa Blue Foundation

The Tangaroa Blue Foundation (Tangaroa Blue) is an Australia wide not for profit organisation dedicated to removal and prevention of marine debris entering the ocean systems. Further information is available at www.tangaroablue.org.

Tangaroa Blue organise volunteer beach and coastline clean-ups for the purpose of their marine debris research program. In 2014 and again in 2015 and 2016 organisers at Tangaroa Blue were contacted to be on the lookout for MH370 related debris on the Western Australian coastline.

Between the dates of 8 March 2014, and 8 April 2015 there were a total of 387 beach clean-ups reported to Tangaroa Blue along the Western Australian coastline between the South Australian and West Australian border and north to Kalbarri. These clean-ups involved 6,095 working hours with over 17 tonnes of marine debris and rubbish collected. In 2016 just under 1,800 volunteers at 138 beach locations removed more than 88,880 items of rubbish from the Western Australian coastline as part of the 2016 West Australian Beach Clean-up.

There were many items of possible MH370 debris reported by Tangaroa Blue during these beach clean ups, all of which were assessed but none of which were confirmed as originating from MH370.

Celestial Vision

The company proprietor of Celestial Vision undertakes photography for numerous publications and regularly visits coastal locations in mid to southern Western Australia. Celestial Vision is one of the many contributors to Tangaroa Blue and undertook an active search of beaches for MH370 debris.

The searches covered an area of almost 14 hectares, at 15 sites, along a 450 km section of the Western Australian coastline, between Myalup, and Drummond Cove (north of Geraldton). Some

beaches were visited more than once. Some items of possible interest in relation to MH370 were located and assessed but none were confirmed as originating from MH370.

Investigations of beach debris found by the general public

Media reporting of MH370 has been extensive which has prompted members of the public to look for and report items of debris found on Australian beaches. All reported finds were assessed but none were confirmed as originating from MH370. Two recent examples are included below, Figure 85 and Figure 86.

Debris from Kangaroo Island, South Australia (June 2016)

A member of the public notified ATSB in early June 2016 of an unusual piece of debris found on a beach on Kangaroo Island off the South Australian coast.

The item of interest was made of a similar composite material as those washed up on the African coastlines. There was little evidence of marine growth suggesting a short period in the water but the item was brought to Canberra by ATSB staff for examination.

Figure 85: Debris found on Kangaroo Island, South Australia

Source: South Australia Police

The item was marked with a stencil “No Step” in a font not used by Malaysia Airlines and although the item was a similar construction to aircraft components the colour of the paint differed enough to eliminate the origin of the item as being from MH370.

Debris from Queenscliff, Victoria (November 2016)

A member of the public notified the ATSB in early November 2016 of an unusual piece of debris found on a beach at Queenscliff, south of Melbourne on the Bellarine Peninsula at the entrance to Port Phillip in Victoria.

Figure 86: Debris found in Queenscliff, Victoria

Source: Victoria Police

The item was constructed with a carbon composite skin over an aluminium honeycomb core and had two square panels. The photographs of the item were assessed by Malaysia Airlines and Boeing and it was concluded it did not originate from MH370.

Debris drift analysis

Debris drift studies have been used extensively throughout the search for MH370. Early drift studies during the surface search in March and April 2014 aimed to inform the deployment of aircraft and vessels in the southern Indian Ocean searching for aircraft debris floating on the sea surface. Later drift studies in 2014 aimed to complement the search area definition analysis based on the SATCOM data by providing indications of likely timings and locations of debris landfall.

Following the release of the ATSB's *MH370 - Definition of Underwater Search Areas* report on 26 June 2014, a drift model was applied by one organisation (who had been a part of AMSA's drift modelling working group during the surface search) to the wide search area defined in the report. The drift modelling was run to provide an indication of when and where the first possible debris would make landfall. This modelling indicated that the first possible landfall was on the west coast of Sumatra, Indonesia and would have occurred in the first few weeks of July 2014. Indonesian search and rescue authorities were subsequently advised of the possibility of debris washing up on their shorelines.

In November 2014, the ATSB asked CSIRO to perform a drift study based on the revised search area defined in the *MH370 - Flight Path Analysis Update* report released on 8 October 2014. The CSIRO study indicated that there was an extremely low probability that any debris from MH370 would have made landfall at that time and the results were not consistent with the other organisation's study which indicated a Sumatra landfall (the study was later found to be erroneous). The ATSB fact sheet MH370: Aircraft Debris and Drift Modelling contains more information about the initial debris and drift modelling work.

A further drift study was performed by the CSIRO following the discovery in July 2015 of the first confirmed item of debris from MH370 (the flaperon) to identify the likely point of origin. The challenge associated with all the studies of MH370 debris is to trace the origin of debris which have been adrift for long periods of time and travelled thousands of kilometres in open ocean conditions.

In April 2016 the ATSB commissioned CSIRO to perform a comprehensive drift study to determine the likely origin of the significant numbers of MH370 debris items which had been found on African shorelines since December 2015. The discovery of many items of debris from MH370 confirmed the existence of a debris field, thereby discounting the possibility of an intact aircraft, and combined with the results of the seafloor search, narrowed the range of potential aircraft impact locations. The study differed from earlier drift modelling as all sources of evidence in relation to debris were considered and a number of modelled debris items were field tested to positively establish actual rates of drift in measured wind and wave conditions. The results of this study and subsequent complementary work are detailed in a series of reports jointly published by the CSIRO and ATSB.

The first CSIRO report, *The search for MH370 and ocean surface drift*, was released on 20 December 2016, and the analysis was based on:

- measuring the wind-driven drift rate of replica aircraft parts alongside oceanographic drifters (whose travel times across the Indian Ocean are well known)
- using an updated ocean surface current model, derived by accurate satellite measurements of small perturbations of sea level to yield estimates of surface currents, which were then validated using the global archive of oceanographic drifters.

The drift study also took into account other evidence including the:

- absence of debris findings on the Western Australian coastline
- absence of debris findings during the surface search
- July 2015 arrival time of the flaperon at La Réunion Island
- December 2015 and onwards arrival times of confirmed aircraft debris on shorelines in the western Indian Ocean.

The drift study concluded that latitudes from 36°S to 32°S, close to the 7th arc, were the most prospective as the likely point of origin of the recovered aircraft debris. The drift study identified an area near 35°S close to the 7th arc as particularly prospective, as this area was most consistent with all the evidence.

The drift study also concluded that:

- Debris originating north of 32°S, close to the 7th arc, would probably have been detected by the surface search, and that debris originating from this area would have probably arrived in Africa before December 2015.
- Debris originating south of 39°S, close to the 7th arc, would have been more likely to have arrived on the Australian coast than on eastern African coastlines.

The second CSIRO published report, *The search for MH370 and ocean surface drift – Part II*, was released on 21 April 2017. This drift study provided further validation that the area near 35°S on the 7th arc was the most prospective point of origin for the recovered aircraft debris. This result was based on the field testing of a genuine Boeing 777 flaperon cut down to match the flaperon recovered from MH370. The new field tests showed that the net drift of the actual flaperon due to its asymmetrical shape would have been at an angle to the prevailing winds and seas which explained the July 2015 arrival at La Réunion Island with more precision.

The third CSIRO published report, *The search for MH370 and ocean surface drift – Part III*, was released on 16 August 2017. This drift study tracks the point of origin of possible MH370 debris, identified by Geoscience Australia, in four French Pleiades satellite images captured on 23 March 2014 in an area to the west of the 7th arc (see section on Satellite imagery analysis). The study concluded:

- The most likely location of the aircraft point of impact is an area around 35.6°S, 92.8°E.
- Further possible yet lower likelihood aircraft impact locations are within about 50 km and parallel to the east of the 7th arc.

- A range of possible but lower likelihood aircraft impact locations are near 35.2°S 91.9°E on the western side of the 7th arc.

The discovery of MH370 debris in 2015 and 2016 has been the sole source of new evidence in the search for MH370 (since March 2014). The analysis of this debris, and particularly the drift studies, have yielded new insights about the likely location of the aircraft. The capture of possible debris in the French satellite imagery only two weeks after the aircraft was lost allows drift modelling results to be refined with considerable accuracy. While it cannot be concluded with certainty that the items identified in the satellite imagery are MH370 debris, the coincidence of the area identified in the drift study with all other search area analysis including the results of the surface and underwater searches is compelling.

Hydroacoustic analysis

At a depth of about 1,000 m there is a layer of water where sound travel is particularly efficient. This layer is called the Sound Fixing and Ranging Channel, or SOFAR channel. Hydroacoustic monitoring makes use of this channel, and the phenomenon of sound waves being 'trapped' in that layer and therefore propagating over a very large distance.

As part of the United Nations Comprehensive Nuclear-Test-Ban-Treaty Organization or the Integrated Marine Observing System (IMOS), there are a network of hydrophones installed in oceans around the world. There are two of these stations located in the Indian Ocean; one installed off the coast of Perth (HA01) and one installed at Diego Garcia (HA08).

Each station consists of an array of three hydrophones separated in space (Figure 87) and connected to a shore facility via a trunk cable.

Figure 87: Diagram of a hydrophone array showing three hydrophones and connection to a shore facility

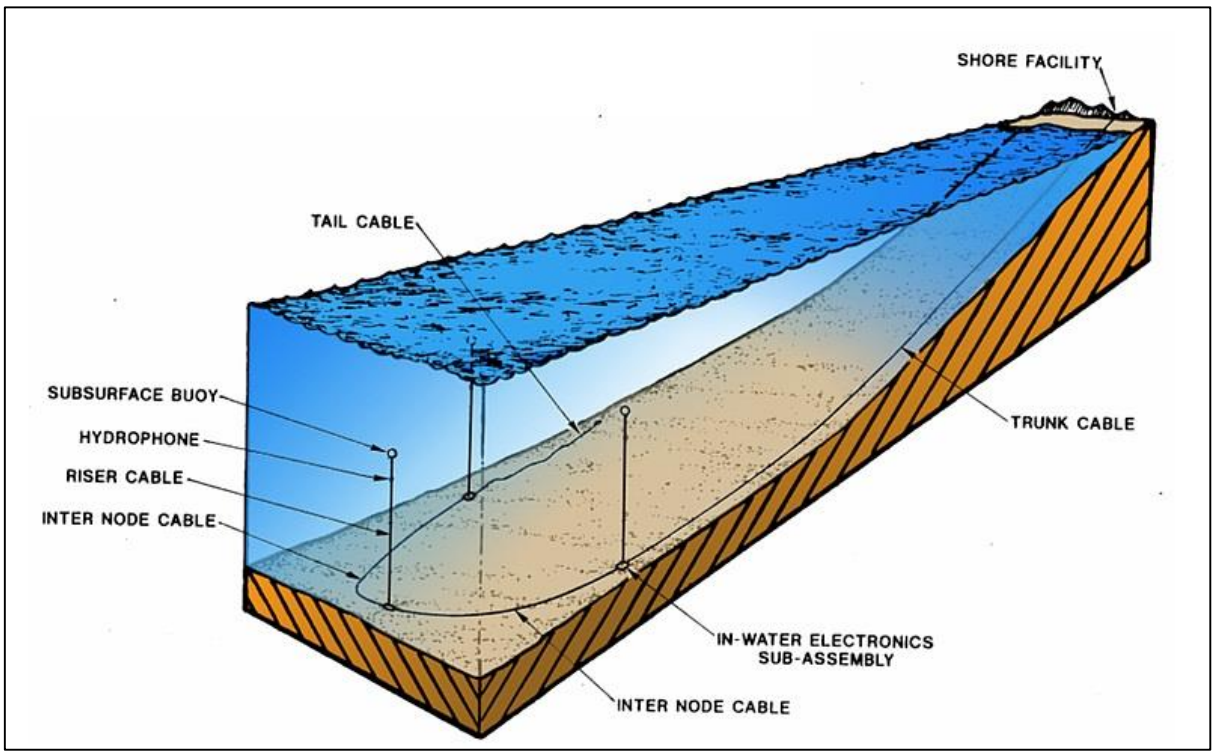

Source: Comprehensive Nuclear Test-Ban-Treaty Organization

For a given acoustic source origin, the configuration of the three hydrophone produces a different arrival time at each hydrophone. Analysis of these arrival times allows relatively accurate determination of the bearing to the sound source. The array can also give a coarse estimate of the distance from the hydrophone, however the tolerance in these calculations is large. In order to

accurately identify the origin of a signal, at least two stations are required to perform a triangulation on that signal.

After MH370 went missing, it was hypothesised that an impact with the water of a B777 could have created an acoustic source sufficiently large to propagate into the Sound Fixing and Ranging Channel and therefore to the hydrophone stations. As such, the hydroacoustic signals present in the Indian Ocean around the time of the aircraft's expected impact with water were examined to determine whether they could provide any information to help define the search area. Additional data was also received from recordings of low-frequency underwater acoustic signals from data loggers off the Western Australian coast owned by Curtin University's Centre for Marine Science and Technology (CMST).

The ATSB requested that CMST and DST Group analyse all available signals in an attempt to detect and localise underwater sounds that could be associated with the impact of the aircraft on the water or with the implosion of wreckage as the aircraft sank.

The CMST provided two reports to the ATSB:

- *Analysis of Low Frequency Underwater Acoustic Signals Possibly Related to the Loss of Malaysian Airlines Flight MH370*, CMST report 2014-30; 23 June 2014, (appendix H).
- *Results of analysis of Scott Reef IMOS underwater sound recorder data for the time of the disappearance of Malaysian Airlines Flight MH370 on 8th March 2014*; 4 September 2014, (appendix I).

The first report found one acoustic event of interest that occurred at a time that potentially linked it to MH370. This event was received on one of the Integrated Marine Observing System recorders near the Perth Canyon (RCS) and at the Comprehensive Nuclear-Test-Ban-Treaty Organization hydroacoustic station at Cape Leeuwin (HA01). A detailed analysis of these signals resulted in an estimated signal source that was compatible with the timing of the last satellite handshake with the aircraft, but incompatible with the satellite to aircraft range derived from this handshake.

The second report used data from a hydroacoustic logger from the Scott Reef to further examine the signal of interest. Based on this further data, the source was identified as being likely of geological origin and originating from the Carlsberg Ridge (source shown in Figure 88 as a red circle).

Figure 88: Locations of the hydroacoustic stations and the estimated signal source locations

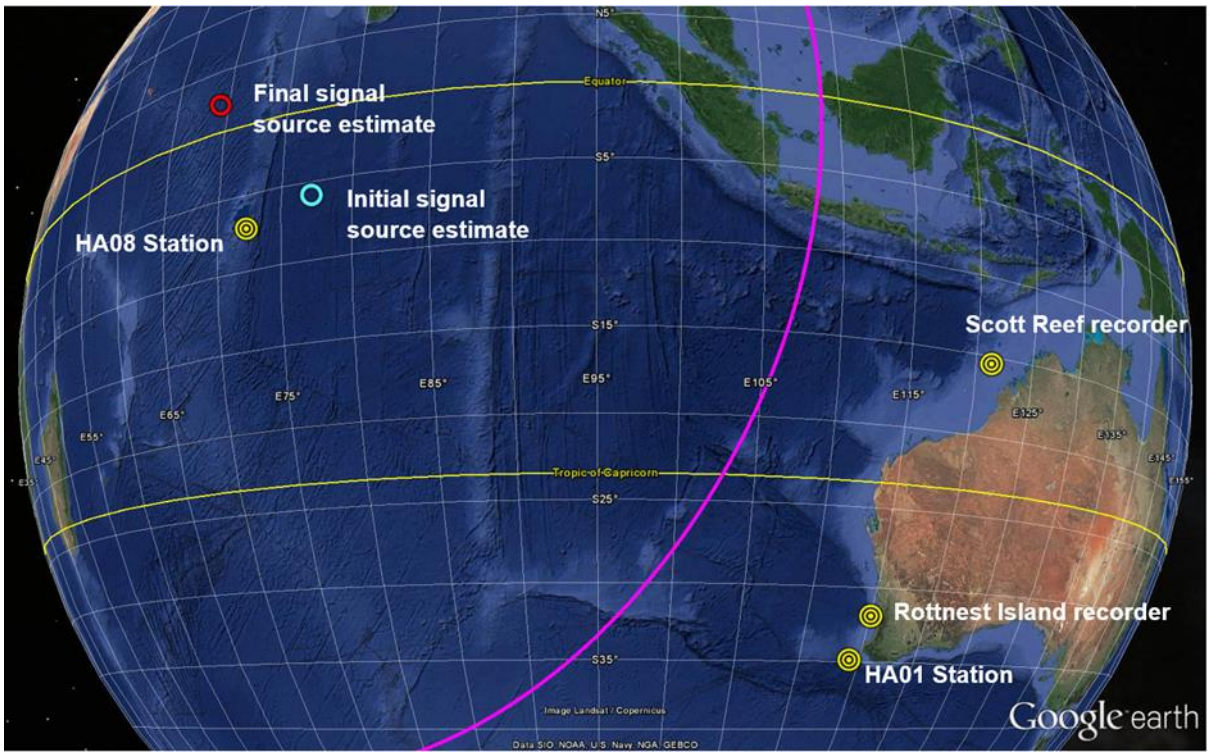

Source: Google earth, annotated by ATSB using Curtin University Centre for Marine Science and Technology data

The Los Alamos National Laboratory in the United States also published an analysis of the hydroacoustic signals (appendix J). The conclusions of this report were that there was a possible candidate arrival at HA01 that indicated the southern portion of the search area. The analysis highlighted that this signal was problematic due to its close proximity in time to the arrival at the station of an acoustic signal from an ice event from Antarctica.

CMST, acting as advisor to the ATSB, reviewed all the submitted and published analyses including the Los Alamos National Laboratory report. The result of this review did not identify any further signals of interest.

At the first principles review, the complete hydroacoustic data analysis results were presented. Meeting participants determined that hydroacoustic analysis did not contribute any useful new information to the search.

Satellite imagery analysis

During the initial stages of the search for MH370 there was a concerted effort to identify MH370, or a possible condensation trail from the aircraft, in any available satellite imagery captured over the Malay Peninsula and the Strait of Malacca. Available satellite imagery for the Indian Ocean was also later analysed for the time of the flight and some hours after. The aircraft was not identified in any of this imagery although some possible condensation trails were identified and analysed.

During the subsequent surface search in the Indian Ocean, AMSA, with the assistance of the Australian Geospatial-Intelligence Organisation, made requests of foreign governments including France, Italy, Germany, Thailand, the People's Republic of China and the United States to capture imagery (in various electromagnetic spectra including radar, optical and infrared) using their low earth orbiting satellites in the region of the MH370 search area. The intent was to cover as wide an area as possible with the satellites in the hope that aircraft debris floating on the ocean surface

could be identified in order to focus the aerial and surface vessel search. This request was made around 15 March 2014, a week after the aircraft went missing.

In the first week of the surface search satellite imagery was provided to AMSA in which possible debris had been identified. The area was in the region of 43-45°S, 90-97°E and this area was extensively searched by aircraft between 20 and 27 March 2014 without locating any MH370 related debris.

From 20 to 23 March 2014 possible debris was also detected in satellite imagery well to the north of the area being searched at the time. These satellite images of possible debris, both radar and optical, were captured much closer to the 7th arc in the region of 34-35.5°S, 90-92°E but the area was never searched by air. At the time of these detections, the surface search was focused elsewhere and there were two merchant vessels transiting through the area who had been warned to be on the lookout for debris. No reports of debris were received from these vessels.

Contrails analysis

In April 2014, scientists[30] from the National Aeronautics and Space Administration (NASA) in the United States analysed satellite imagery in the Indian Ocean looking for possible MH370 condensation trails (contrails). Their approach was to examine all available polar-orbiting satellite imagery available along possible MH370 flight tracks between 1900 UTC on 7 March 2014 and 0500 UTC on 8 March 2014. They also examined atmospheric temperature and moisture profiles to determine the potential for contrail formation at these times and locations.

One possible contrail was identified in NASA's Terra satellite Moderate Resolution Imaging Spectroradiometer (MODIS) instrument data at 0445 UTC on 8 March at 45.5°S, 84°E with an orientation from north-northeast to south-southwest, Figure 89. It was concluded that atmospheric conditions at the time were suitable for contrail formation. The position and orientation of the possible contrail, when cloud motion was accounted for over the previous four hours, were found to be broadly consistent with the assumptions about MH370's flight path at the time.

The possible contrail was analysed in the Terra MODIS data captured at several different wavelengths, and also using other satellite imagery captured around the same time in the area, and it was concluded that the possible contrail was probably a shadow from some other feature or a cloud edge.

[30] Dr Patrick Minnis, Kristopher Bedka, Doug Spangenberg and David Duda, NASA

Figure 89: Terra satellite MODIS image, 0445 UTC, 8 March 2014 at 45.5°S, 84°E

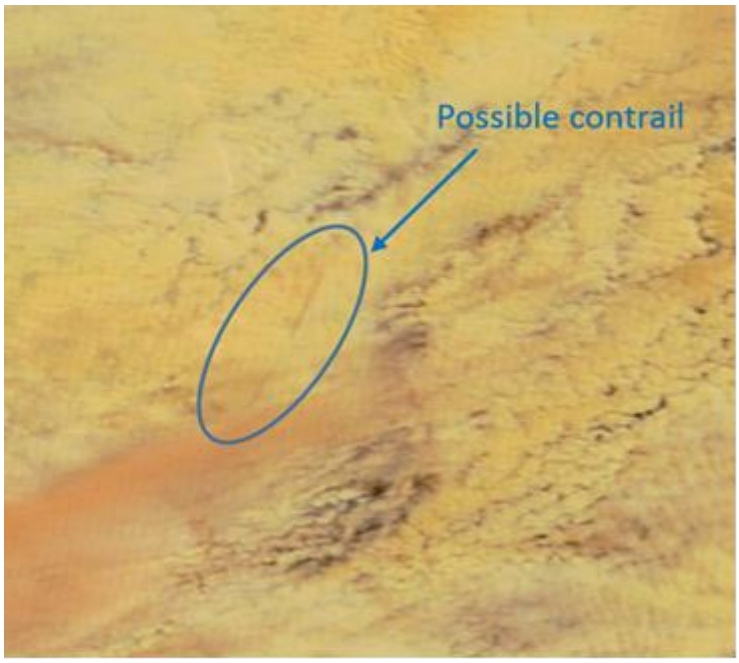

Source: NASA, annotated by ATSB

Later in the underwater search, the NASA scientists also provided an assessment of a third party analysis of possible condensation trails in satellite imagery captured at the northern tip of Sumatra around the time of the flight of MH370. They concluded after studying a range of satellite imagery for the area at the time that what had been identified as possible contrail was probably a nearly linear discontinuity in the stratocumulus cloud deck.

Reanalysis of satellite imagery

At the time the surface search commenced in the southern Indian Ocean on 18 March 2014, it was not known with certainty whether or not there was any debris still adrift in the search area nor the composition of that debris. The discovery of a range of MH370 debris on eastern African shorelines in 2015 and 2016 confirmed that debris was adrift at the time of the surface search, and importantly, the size, shape, colour and composition of some debris items. The discovery of this debris prompted the reanalysis of aerial surface search debris sightings and available satellite imagery based on the now known physical characteristics of some of the items.

Early in 2017 the French Ministry of Defence provided the ATSB with four native resolution optical satellite images from their Pleiades satellite constellation. The four images were captured on 23 March 2014 to the northwest of the 7th arc (Figure 90) in an area not searched by aircraft during the surface search. The area where the satellite images were captured was also significant as it was where MH370 debris was likely to have drifted, initially to the northwest, in the two weeks after MH370 was lost if the aircraft had impacted the water close to the 7th arc around latitude 35°S.

If debris could be identified within the satellite imagery it would provide very strong support to the range of other analyses indicating that the aircraft had impacted the water close to the 7th arc around latitude 35°S, specifically the CSIRO debris drift studies: *The search for MH370 and ocean surface drift* and *The search for MH370 and ocean surface drift-Part II*. The original French analysis in March 2014 had identified four possible objects which may be debris in the satellite images. The ATSB asked Geoscience Australia to reanalyse the images and determine whether the images included objects that were potentially man-made in origin.

Figure 90: Location of four Pleiades satellite images, surface and underwater search areas

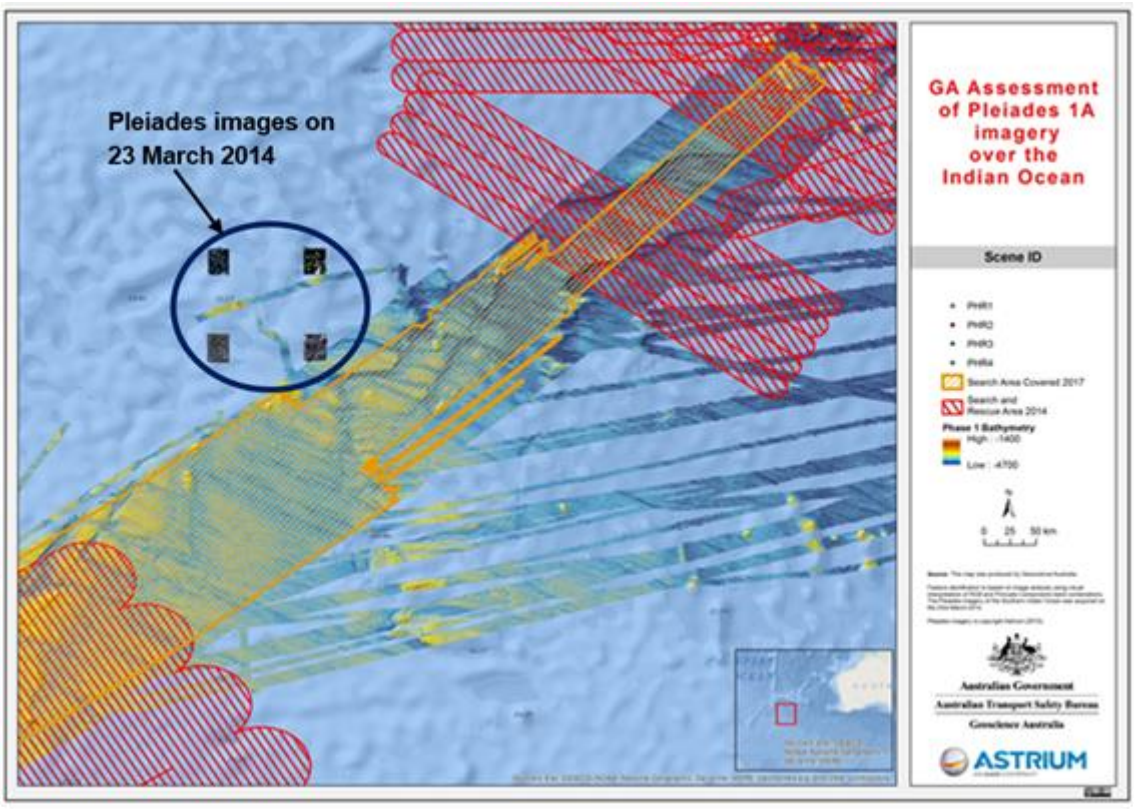

Source: Geoscience Australia, annotated by ATSB

Geoscience Australia's analyses included semi-automatic workflows and a comprehensive analysis using manual visual interpretation, with the optical data subjected to a principle components analysis to help distinguish potential objects from their surroundings. On 16 August 2017 the ATSB released Geoscience Australia's report: *Summary of imagery analyses for non-natural objects in support of the search for Flight MH370*, which concluded that the four satellite images contain at least 70 identifiable objects, with twelve being assessed as probably man-made and a further 28 objects assessed as possibly man-made. The resolution of the images at 0.5 m² was insufficient to conclude with certainty that any of the objects were debris from MH370 however some objects show geometric shapes that do not conform with wave patterns or other expected natural phenomena.

The ATSB passed the results of Geoscience Australia's analysis to CSIRO to perform a drift study to determine with greater precision where the objects identified in the imagery were likely to have been on 8 March 2014. CSIRO's report *The search for MH370 and ocean surface drift – Part III*, released with Geoscience Australia's report in August 2017, analyses the origin of the objects and concludes that if any of the objects identified in the satellite imagery are from MH370 that the most likely place the aircraft impacted the ocean was 35.6°S, 92.8°E (see section on Debris drift analysis).

External contributions

Over the course of the past three years the search for MH370 has prompted significant public interest and an extraordinary amount of correspondence with the ATSB from external sources. Individuals and groups with a variety of expertise submitted their considerations, theories and analysis supporting particular search locations. The ATSB has maintained a dialogue with various individuals and groups throughout the search, monitored online discussion forums and responded

to queries from MH370 researchers. The credible analyses provided by various external contributors were considered alongside the work of the search strategy working group.

The ATSB acknowledges the extensive contributions that many individuals and groups have made during the underwater search for MH370. Many contributors have provided credible, alternate and independent approaches and analysis of the limited data available. In particular, the 'MH370 Independent Group' comprised of scientists, researchers and individuals who have cooperated across continents to advance the search for MH370. The ATSB is grateful for their work collectively and individually including Duncan Steel, Mike Exner, Victor Iannello, Don Thompson, and Richard Godfrey. The ATSB also acknowledges the extensive and detailed contributions provided by Simon Hardy, Bobby Ulich and Robin Stevens.

The search for MH370 was significantly advanced after the first debris from the aircraft was found on La Reunion Island in July 2015. The subsequent efforts of Blaine Gibson in searching for and locating MH370 debris on east African coastlines did much to raise public awareness of the importance of the MH370 debris which led to many more items of debris being handed in. Mr Gibson met and communicated with ATSB during his 2015-2016 search expeditions and he is acknowledged for his outstanding efforts in communicating his debris finds to Malaysia, ATSB, the next of kin and the wider world.

Other search considerations – risk mitigation

The underwater search was conducted continuously over more than two and a half years in a remote area up to 1,500 NM off the west coast of Australia. The search was conducted in latitudes between 33°S and 39°S, an area where the weather is often poor depending on the season and seas are very often rough and, occasionally, extreme. There were significant risks to the search vessels and their crews associated with conducting the underwater search in these conditions which needed to be carefully managed.

Weather

Large weather systems consistently moved through or near the search area. The latitude of operations at different times in the search (both surface and underwater) was a major factor in the impact of these weather systems. During the surface search the vessels and aircraft experienced a wide range of weather conditions. Typically search operations could proceed however, in choppy sea surface conditions with breaking waves the ability to detect floating debris can be more difficult.

Most of the underwater search was conducted from latitudes 33°S to 39°S in the Indian Ocean adjacent to the 7th arc. The only underwater search outside of this area was the initial TPL search followed by AUV operations around potential detection locations up near latitude 21°S. The weather proved to be moderate in this northern area, resulting in minimal weather down time. However, the southern area where the underwater search had shifted was known for adverse weather conditions at any time of year, but especially during the cyclone season (November to April) and the winter months (June to August).

The search area, particularly towards the southern end, was subject to high winds, waves, and swell as a result of winter or cyclonic activity. Efforts were therefore made to better predict and understand weather impacts and to mitigate against any potential incidents. Figure 91 shows the back deck awash on *Go Phoenix* during a typical weather event in the search area.

Figure 91: A large amount of water flooding the back deck working area of *Go Phoenix*

Source: Hydrospheric Solutions

Weather forecasting and recording

A comprehensive understanding of the expected weather was required to better prepare the vessels for operations and for preparing the following day's operational schedule. Forecasting the weather and sea conditions was vital for deep water search operations. Typical deep tow vehicle recoveries took around six hours so the operators could not wait until the weather was upon them, they needed to react to the forecast weather prior to its arrival.

The ATSB, vessel operators and contractors sought forecasts from various commercial and public weather sources. The ATSB utilised the services of the Australian Defence Meteorological Support Unit (DMSU), a section of the Australian Bureau of Meteorology (BOM). Forecasting extended for five days, with an example report shown in Figure 92. The report used colour banding to reflect potential impacts to operations based on forecasted significant wave/swell height and wind speeds. DMSU also produced a series of wind and sea graphics that depicted the passage of weather systems, showing wind barbs and contoured charts for significant wave heights to be expected. This was transmitted to the search vessels, contractor operations staff and ATSB daily.

Figure 92: Example BOM Defence Meteorological Support Unit daily search area weather forecast report

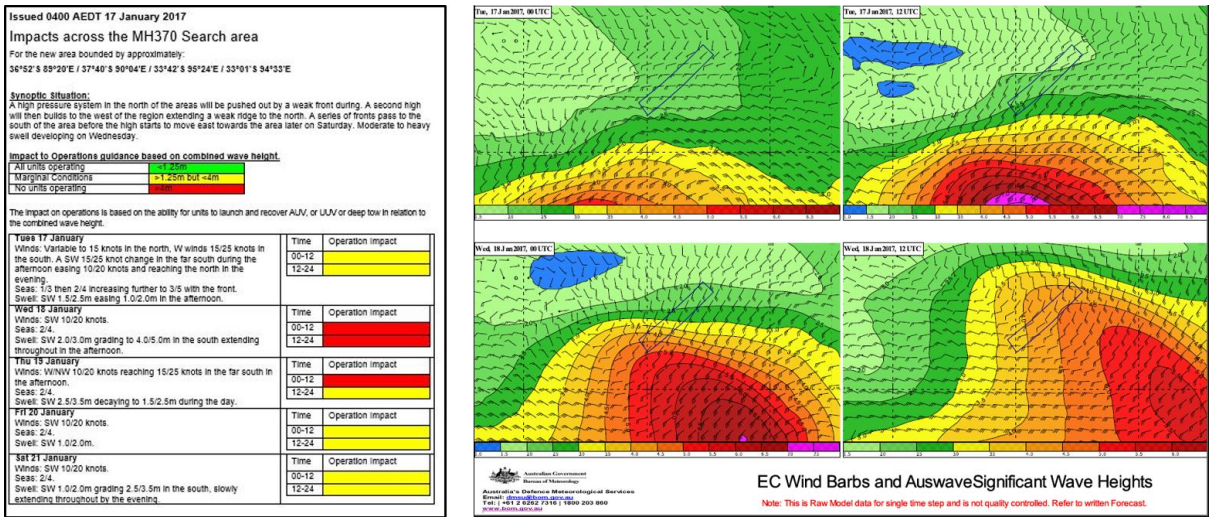

Issued 0400 AEDT 17 January 2017

Impacts across the MH370 Search area

For the new area bounded by approximately:

36°52'S 89°20'E / 37°40'S 90°04'E / 33°42'S 95°24'E / 33°01'S 84°33'E

Synoptic Situation:
A high pressure system in the north of the areas will be pushed out by a weak front during. A second high will then builds to the west of the region extending a weak ridge to the north. A series of fronts pass to the south of the area before the high starts to move east towards the area later on Saturday. Moderate to heavy swell developing on Wednesday.

Impact to Operations guidance based on combined wave height.

All units operating	<1.25m
Marginal Conditions	>1.25m but <4m
No units operating	>4m

The impact on operations is based on the ability for units to launch and recover AUV, or UUV or deep tow in relation to the combined wave height.

Tues 17 January Winds: Variable to 15 knots in the north, W winds 15/25 knots in the south. A SW 15/25 knot change in the far south during the afternoon easing 10/20 knots and reaching the north in the evening. Seas: 1/3 then 2/4 increasing further to 3/5 with the front. Swell: SW 1.5/2.5m easing 1.0/2.0m in the afternoon.	Time	Operation Impact
	00-12	
	12-24	
Wed 18 January Winds: SW 10/20 knots. Seas: 2/4. Swell: SW 2.0/3.0m grading to 4.0/5.0m in the south extending throughout in the afternoon.	Time	Operation Impact
	00-12	
	12-24	
Thu 19 January Winds: W/NW 10/20 knots reaching 15/25 knots in the far south in the afternoon. Seas: 2/4. Swell: SW 2.5/3.5m decaying to 1.5/2.5m during the day.	Time	Operation Impact
	00-12	
	12-24	
Fri 20 January Winds: SW 10/20 knots. Seas: 2/4. Swell: SW 1.0/2.0m.	Time	Operation Impact
	00-12	
	12-24	
Sat 21 January Winds: SW 10/20 knots. Seas: 2/4. Swell: SW 1.0/2.0m grading 2.5/3.5m in the south, slowly extending throughout by the evening.	Time	Operation Impact
	00-12	
	12-24	

Source: BOM Defence Meteorological Support Unit

Search vessel operators and contractors accessed their own weather forecasting services. Fugro Survey's GEOS weather service tabulated three hour interval predictions of wind, sea, swell and combined significant wave heights. This was also represented graphically as seen in Figure 93 and transmitted twice daily to the ATSB, contractor operations staff and search vessels.

Figure 93: Example Fugro GEOS weather service twice daily search area weather forecast report

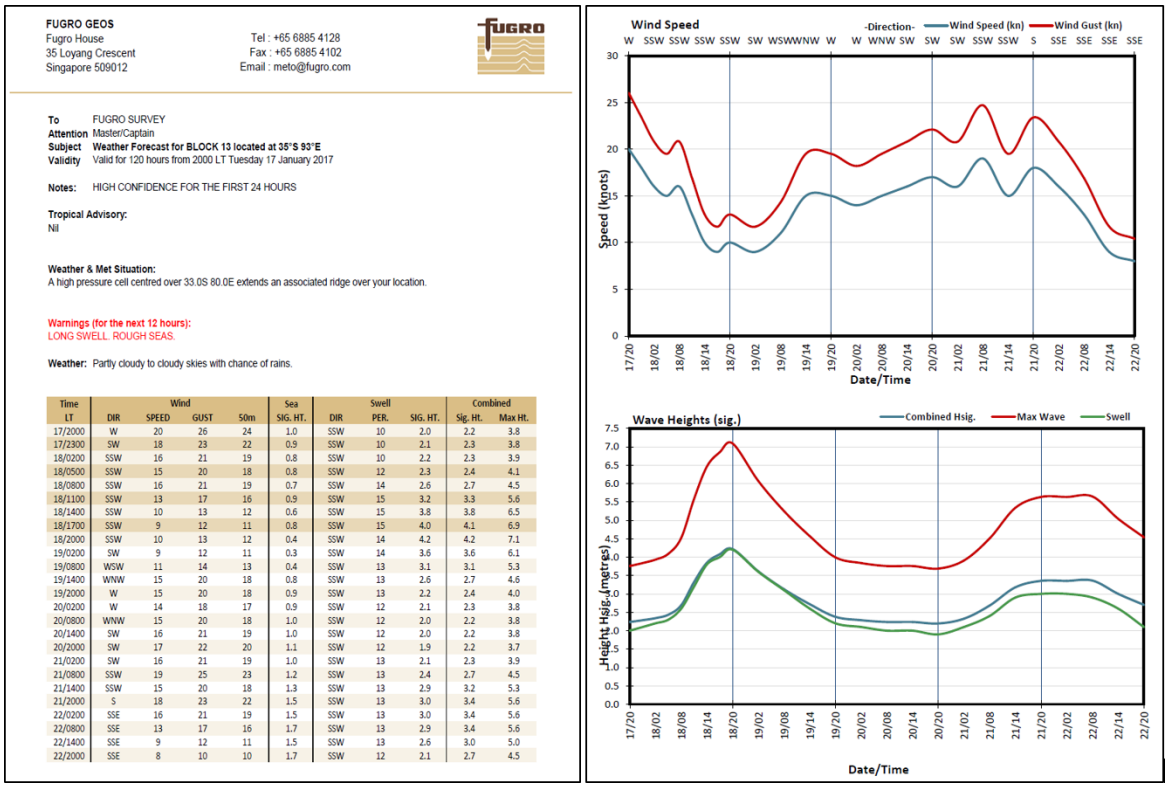

FUGRO GEOS
Fugro House
35 Loyang Crescent
Singapore 509012

Tel : +65 6885 4128
Fax : +65 6885 4102
Email : meto@fugro.com

To FUGRO SURVEY
Attention Master/Captain
Subject **Weather Forecast for BLOCK 13 located at 35°S 93°E**
Validity Valid for 120 hours from 2000 LT Tuesday 17 January 2017

Notes: HIGH CONFIDENCE FOR THE FIRST 24 HOURS

Tropical Advisory:
Nil

Weather & Met Situation:
A high pressure cell centred over 33.0S 80.0E extends an associated ridge over your location.

Warnings (for the next 12 hours):
LONG SWELL. ROUGH SEAS.

Weather: Partly cloudy to cloudy skies with chance of rains.

Time	Wind				Sea	Swell			Combined	
LT	DIR	SPEED	GUST	50m	SIG. HT.	DIR	PER.	SIG. HT.	Sig. Ht.	Max Ht.
17/2000	W	20	26	24	1.0	SSW	10	2.0	2.2	3.8
17/2300	SW	18	23	22	0.9	SSW	10	2.1	2.3	3.8
18/0200	SSW	16	21	19	0.8	SSW	10	2.2	2.3	3.9
18/0500	SSW	15	20	18	0.8	SSW	12	2.3	2.4	4.1
18/0800	SSW	16	21	19	0.7	SSW	14	2.6	2.7	4.5
18/1100	SSW	13	17	16	0.9	SSW	15	3.2	3.3	5.6
18/1400	SSW	10	13	12	0.6	SSW	15	3.8	3.8	6.5
18/1700	SSW	9	12	11	0.8	SSW	15	4.0	4.1	6.9
18/2000	SSW	10	13	12	0.4	SSW	14	4.2	4.2	7.1
19/0200	SW	9	12	11	0.3	SSW	14	3.6	3.6	6.1
19/0800	WSW	11	14	13	0.4	SSW	13	3.1	3.1	5.3
19/1400	WNW	15	20	18	0.8	SSW	13	2.6	2.7	4.6
19/2000	W	15	20	18	0.9	SSW	13	2.2	2.4	4.0
20/0200	W	14	18	17	0.9	SSW	12	2.1	2.3	3.8
20/0800	WNW	15	20	18	1.0	SSW	12	2.0	2.2	3.8
20/1400	SW	16	21	19	1.0	SSW	12	2.0	2.2	3.8
20/2000	SW	17	22	20	1.1	SSW	12	1.9	2.2	3.7
21/0200	SW	16	21	19	1.0	SSW	13	2.1	2.3	3.9
21/0800	SSW	19	25	23	1.2	SSW	13	2.4	2.7	4.5
21/1400	SSW	15	20	18	1.3	SSW	13	2.9	3.2	5.3
21/2000	S	18	23	22	1.5	SSW	13	3.0	3.4	5.6
22/0200	SSE	16	21	19	1.5	SSW	13	3.0	3.4	5.6
22/0800	SSE	13	17	16	1.7	SSW	13	2.9	3.4	5.6
22/1400	SSE	9	12	11	1.5	SSW	13	2.6	3.0	5.0
22/2000	SSE	8	10	10	1.7	SSW	12	2.1	2.7	4.5

Source: Fugro Survey

For long-term forecasts and trends in the southern Indian Ocean, climatological input was provided by the BOM and Fugro's Metocean Division. In 2014 Fugro Survey commissioned work to provide statistical meteorological data by using information from three available locations within the region. Operational wind and wave statistics were derived from data taken from the Fugro GEOS WorldWaves database, which in turn was derived from the European Centre for Medium-Range Weather Forecasts.

Fugro Survey provided the spreadsheet shown in Figure 94 which lists the percentage of time each month that the predicted significant wave height was expected. This aggregation of long term wave height averages for the search area was key to forward planning the search activities and considering weather downtime associated with deep tow, AUV or ROV operations. The higher the significant wave height, the riskier it was to safely launch and recover the respective search system being used. For example, for AUV operations the limit for the safe launch and recovery of the vehicle was significant wave heights no larger than 3.0 m, and if the intent was to work through the month of May, statistically 70.8 per cent downtime could be expected. This is determined by adding all the figures above the intercept of 3.0 m wave height in the month of May column. By comparison, a 3.0 m wave height limitation in January could statistically expect 13.7 per cent downtime.

Figure 94: Historical significant wave heights for each month as a percentage of time

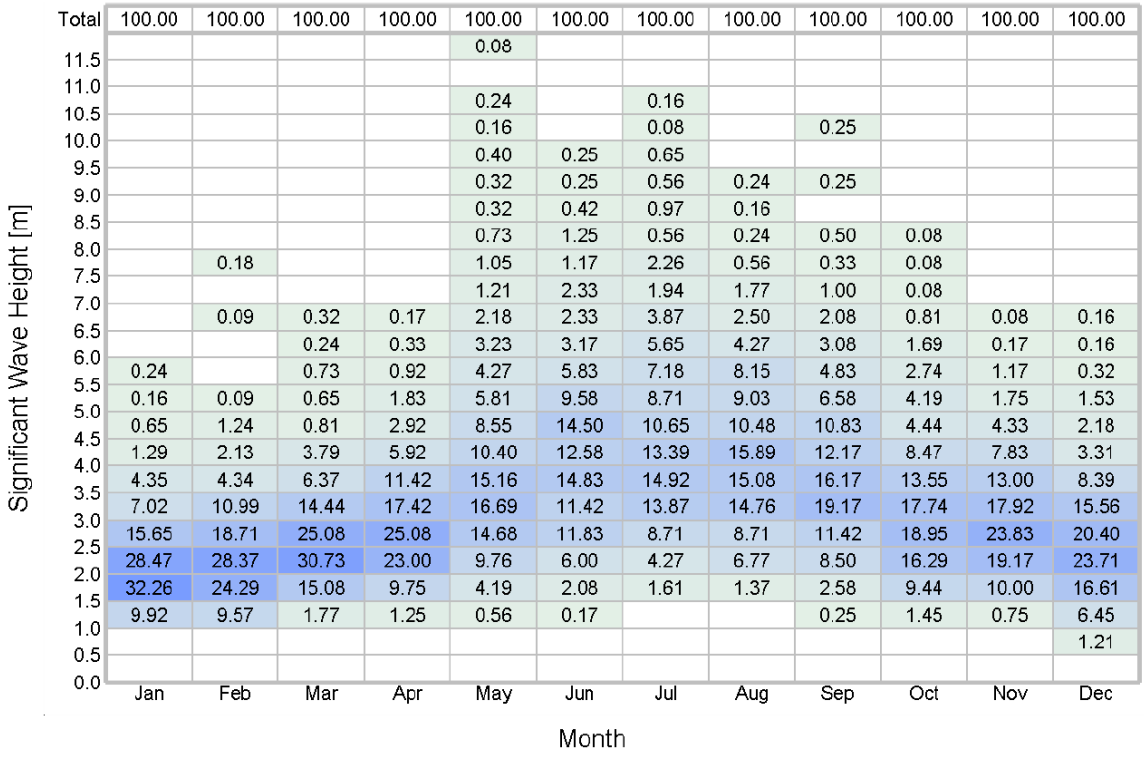

Source: Fugro Survey

Real time weather records

Real time weather observations were recorded as part of the daily reporting requirements for most search vessels while in the search area. This occurred every watch (four hours) with the observations provided to the BOM to ground truth the satellite weather observations and climate models used by world weather and climate agencies. These observations resulted in significant improvements to the models and forecasts as the search progressed.

Additionally, on board the Fugro Survey vessels real time weather observations were recorded from a weather station, positioning systems and motion sensors. Vessel position, heading, speed, pitch, roll, heave, wind speed, wind direction, atmospheric pressure and temperature were all recorded and available in real time. On *Fugro Equator* these parameters were recorded at one second intervals, and on *Fugro Discovery* every five seconds. These parameters were also recorded on *Fugro Supporter* and *Havila Harmony*. This not only assisted the operators with making operational decisions based on the weather conditions and vessel motion at any given time, but also documented a comprehensive historical account of the weather in the search area over a nearly three year period.

Plots of wind and heave data are included below. Figure 95 shows *Fugro Discovery*'s recorded heave in metres for both peak value (orange) and average value (blue) sampled over a 6-hour period. Figure 96 shows *Fugro Discovery*'s recorded wind speed in knots for both peak value (yellow) and average value (grey) sampled over a 6-hour period. Additionally, each plot has a 15 day rolling trend line (purple and black lines) to show the general monthly trends over the data collection period.

Figure 95: *Fugro Discovery* recorded heave in metres (Orange = max, Blue = average)

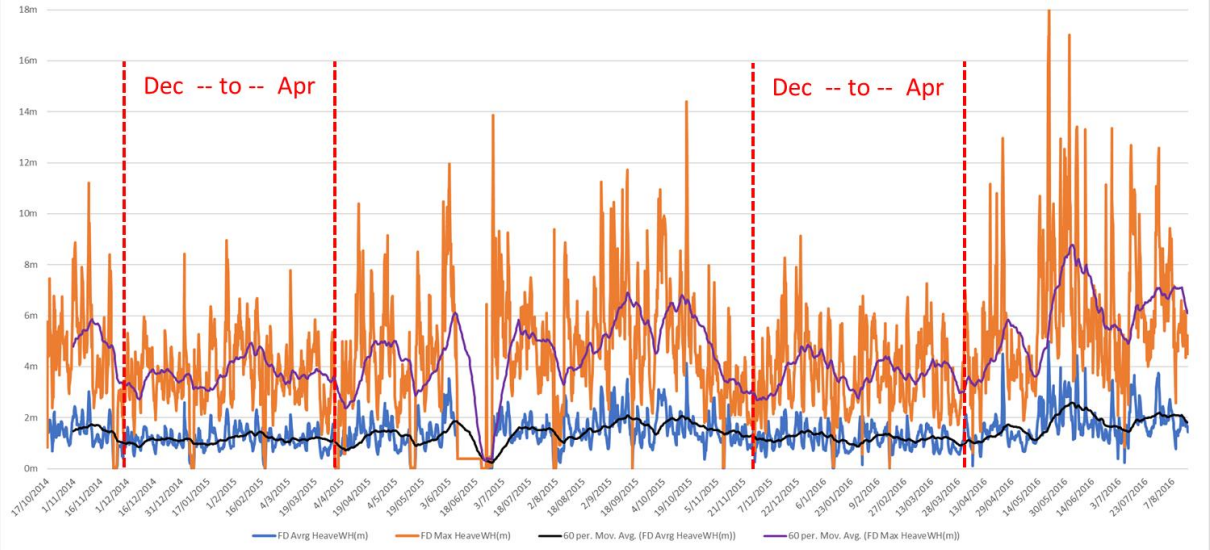

Source: ATSB

Figure 96: *Fugro Discovery* recorded wind speed in knots (Yellow = max, Grey = average)

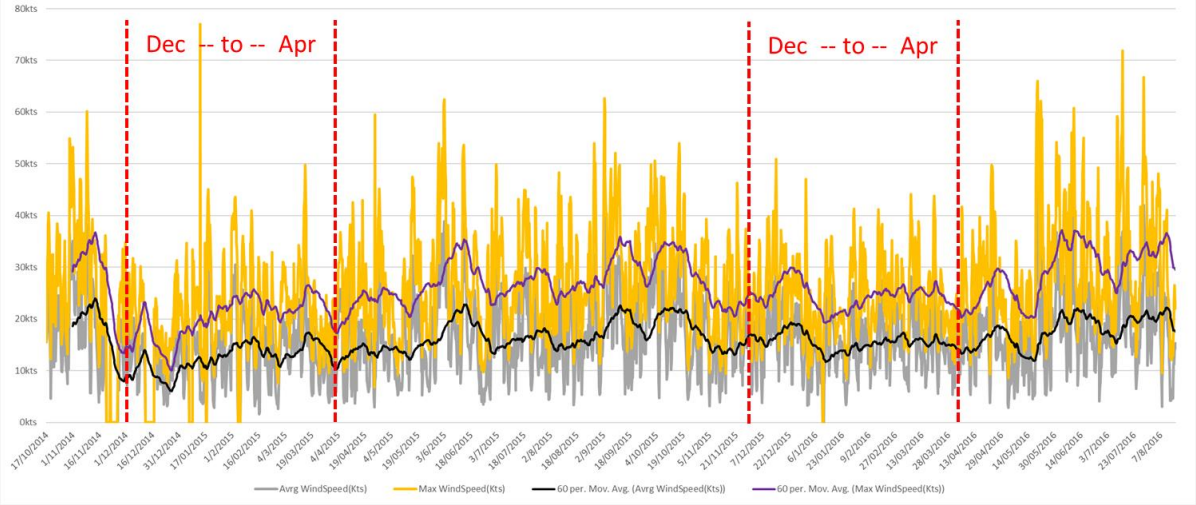

Source: ATSB

Weather events impacting search operations

The path of tropical cyclones and tropical storms had significant impacts on vessel operations at times during the search. The cyclone season in the southern Indian Ocean is from mid-November to the end of April the following year[31]. Tropical cyclones in the southern Indian Ocean normally form in the basin between Madagascar and the Maldives before departing for other areas of the Indian Ocean.

As part of an initial assessment of cyclone and storm activity, an examination was undertaken of data from the French meteorological service on La Réunion Island, which has responsibility for issuing advisories and tracking tropical cyclones in the southern Indian Ocean basin. Archive data (1998-2015) suggested an average of 4.8 cyclones and 4.1 tropical storms per year across the entire southern Indian Ocean region.

[31] For Seychelles and Mauritius the season ends mid-May

The 2014-15 cyclone season (Figure 97) was typical with five cyclones and six storms, whilst in 2015-16 (Figure 98) there were three cyclones and five storms reported. Even though few cyclones reached the search area the effects of a decaying cyclone or storm presented challenging conditions for the search vessels at times.

Figure 97: Tropical cyclone systems in the southern Indian Ocean 2014–15 cyclone season

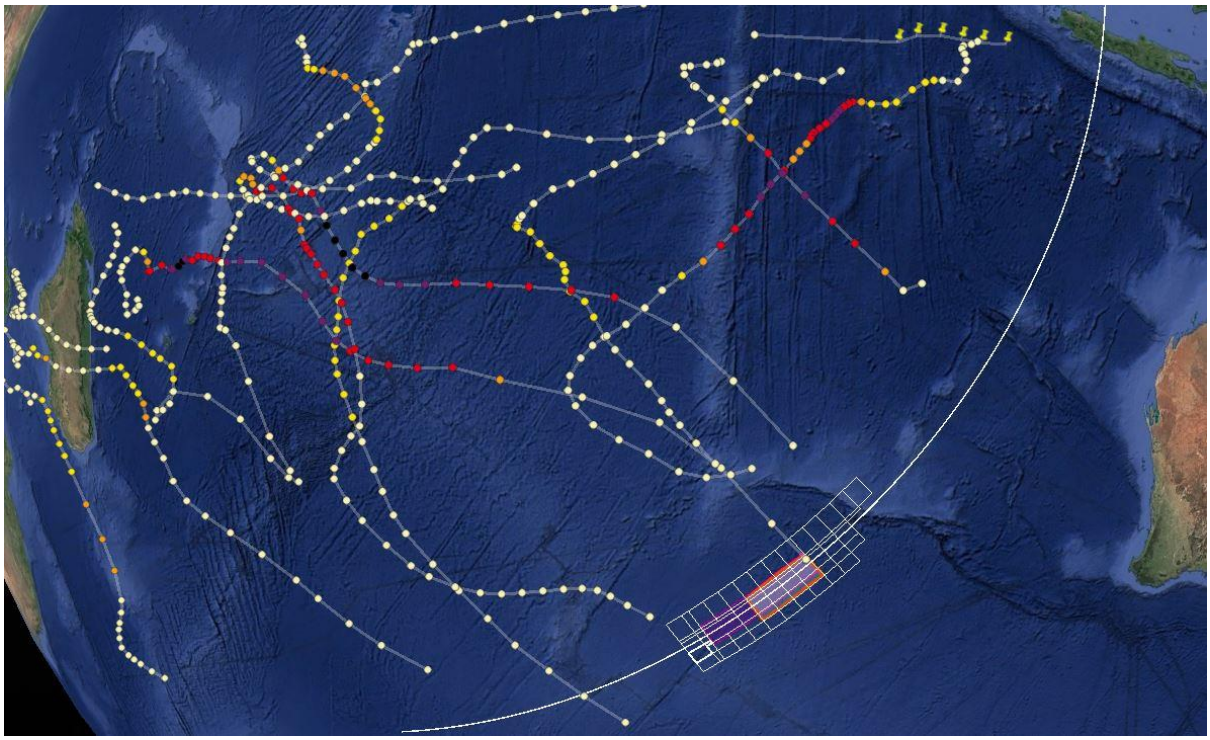

Source: Google earth, annotated by ATSB using Météo-France La Réunion data

During the 2014-15 cyclone season several systems severely affected search operations. During one period, all vessels departed the search area to seek calmer waters for several days. Vessels would often have to suspend search operations, recover the deep tow equipment and patiently ride out the severe sea conditions. In comparison, the 2015-16 cyclone season was relatively benign.

Figure 98: Tropical cyclone systems in the southern Indian Ocean 2015–16 cyclone season

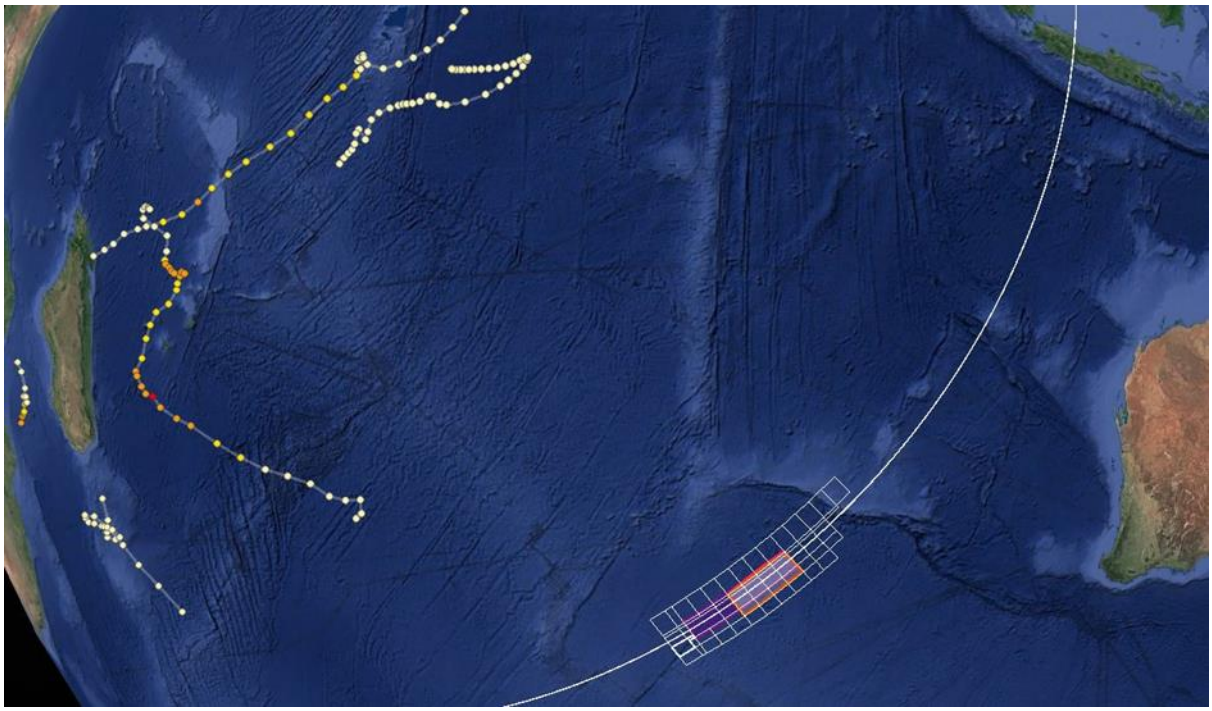

Source: Google earth, annotated by ATSB using Météo-France La Réunion data

Weather conditions in the winter months (June to August) also had significant impacts on vessel operations at times during the search. The onset of winter conditions coincided with the initial phase of bathymetric data collection from late May 2014. The survey vessels experienced periods of poor weather however were typically able to continue collecting data. During periods of higher significant wave heights the survey coverage rate was reduced to maintain data quality. Winter weather conditions in 2014 did not impact underwater search operations, as these commenced in latitudes between 33°S and 39°S in October 2014.

After the severe weather impacts of the 2014-15 cyclone season, winter conditions continued to bring adverse weather, although July 2015 brought unseasonal fair weather conditions resulting in better than expected underwater search coverage rates for the month.

After a relatively benign cyclone season in 2015-16, the vessels encountered consistent severe winter weather conditions. From 8 May 2016 to 16 June 2016 no underwater search operations could be performed. Surface bathymetric data could be collected successfully by *Fugro Equator* for brief periods when conditions allowed. Severe weather conditions continued with significant wave heights above the limitations for the launch and recovery of the deep tow vehicle on *Dong Hai Jiu 101*, resulting in the decision to suspend *Dong Hai Jiu 101* search operations in August after two swings with minimal underwater search time. The ProSAS search system was demobilised and the vessel went to standby at anchor off Fremantle until the weather improved in October 2016.

Fugro Equator and *Fugro Discovery* had both been subject to ‘winterisation’ modifications to improve the safety and operability of the vessels and equipment in the extreme conditions. One major improvement was to their launch and recovery systems for their deep tow vehicles which enabled them to work in higher sea states safely and effectively. Fugro Survey also designed and implemented an optional secondary recovery system for their AUV, this allowed recovery of the AUV in higher sea states. This system was transferrable and used for both *Havila Harmony* and *Fugro Equator* AUV operations.

As an example of conditions experience in the search area, on 13 July 2016 *Fugro Equator* recorded a combined wave and swell measurement of 24.03 m (trough to peak). This occurred in

a 12 hour period where four other waves over 20 m were experienced, all on a 65 m vessel whilst operating at a latitude of 38°S. Figure 99 shows *Fugro Discovery* in typical sea conditions.

Towards the end of 2016 and early 2017 the weather improved in the search area with the coming of summer. However, operations were still impacted with passing weather systems. By this time *Dong Hai Jiu 101* had mobilised an ROV and successfully completed 30 dives but there was still 47 per cent weather standby time. During this period *Fugro Equator* demobilised the deep tow system and mobilised the AUV which was able to complete all of its tasking with only 11 per cent of the time on weather standby.

The Fugro Survey vessels operated over the entire search period and in all regions of the search area with an overall weather standby time for all vessels for both AUV and deep tow vehicle operations accounting for 9.4 per cent of their total time on the search.

Figure 99: *Fugro Discovery* in the search area in typical conditions and a rare calm day

Source: Fugro Survey

Mitigation of weather impact on search operations

Aside from comprehensive weather forecasting the following actions were taken to mitigate the weather risk to search operations:

Weather avoidance

As per normal practices on board a vessel, the Captain was responsible for the safety of the vessel and the crew. The decision to depart the search area for calmer waters always lay with the vessel master and the operator.

Vessel equipment improvements

Winterisation of the search vessels meant making changes to equipment or procedures to promote safer operations in higher sea states and was implemented by Fugro Survey. This was a significant factor when working on deck but also a factor in day to day living within the vessel accommodation areas.

Variable tasking

Both *Fugro Supporter* and *Fugro Equator* were fitted with hull-mounted multibeam echo sounder systems capable of bathymetric survey in the search area and therefore had dual roles at times during the search. Both vessels were tasked to conduct bathymetric survey operations (in areas planned to be searched) whenever the sea conditions were deemed unsafe to conduct their primary tasking of underwater search operations using their deep tow or AUV systems.

Line Planning

For safety and efficiency the deep tow lines ran nearly perpendicular to the typical swell and wind direction for the search area. This allowed the vessels to steer directly into or with the seas as opposed to running parallel to them. As sea states increase running parallel to the seas will cause the vessel to roll considerably and is much harder to maintain straight track lines needed for deep tow operations.

Further mitigation actions for risks to crew safety associated with operating in such a remote area are outlined in the following Health, Safety and Environment section.

Health, safety and environment

The underwater search for MH370 presented some significant risks to the health and safety of the crews on board the search vessels. As Australia's transport safety investigator the ATSB was particularly aware of the need to ensure these risks were carefully managed and that the standard for all operations carried out by the search contractors were industry best practice. Contractors were advised that at all times the safety of the vessels and their crews must never be compromised during search operations and this was reiterated throughout the duration of the search.

The ATSB took an end-to-end approach to ensure search operations were conducted safely and contractors had appropriate systems in place to manage the safety of their staff. It started with specifying the health, safety and environment (HSE) standards which potential search contractors needed to meet. These became contracted obligations when search contracts were awarded. Finally, during search operations the contractor's compliance with the HSE standards was monitored with a comprehensive reporting system and ATSB staff on each search vessel who (amongst other things) monitored the management of safety on board the vessel.

Requirements stipulated in the request for tender for search services included that all search vessels must comply with all International Maritime Organisation instruments including the Safety of Life at Sea Convention, the International Convention for the Prevention of Pollution from Ships, and International Safety Management Code[32]. The contractor was also required to operate risk management and safety management systems covering all their assets, operations and personnel which were subject to regular inspection and audit by relevant regulatory authorities. In addition, if the contractor was proposing to charter search vessels from a third party, that the vessel's safety management system was appropriately bridged to the contractor's safety management system.

Search contractors were required to include full details of their safety management systems and the implementation of these systems in the context of the underwater search, in a project execution plan. All personnel embarking on search vessel operations were required to have medical fitness certificates as well as (at least) Basic Offshore Safety Induction and Emergency Training. Contractors were also required to provide effective reporting of health, safety and environment matters in their daily operational reporting to the ATSB and provide timely notice and when any incidents occurred.

Consideration was also given to managing emergencies at sea, in a remote area, due to a serious injury or illness to the contractor's personnel, vessel crew or the ATSB's client representative. Risk mitigation strategies were put in place including a requirement for qualified medical personnel to be carried on each vessel together with additional medical supplies and equipment.

Fugro Survey operated a mature whole-of-organisation quality, risk and safety management system. The system included appropriate policy and procedures and was designed to inculcate an organisational culture in which staff actively recognised and responded appropriately to risk within a supportive management framework. Responsibility for maintaining HSE standards was assigned to all employees and sub-contractors, ensuring ownership and accountability remained with every person in the organisation.

Phoenix International also operated a mature health, safety and environmental management system containing a comprehensive suite of policies and procedures. There was a particular focus on safe methods of work and the identification and mitigation of risks associated with operational tasks.

---

[32] For international trading vessels the International Safety Management Code sets out the requirements for vessel safety management systems and compliance is audited by Classification Societies, Flag and Coastal State Authorities.

Operational safety

Both Fugro Survey and Phoenix International operated safety management systems which included a hazard analysis and job safety environmental analysis for all high risk operations on their vessels (for example launch and recovery of underwater search vehicles). Over the course of the search, Fugro Survey, in particular, implemented significant improvements to equipment and procedures used for some of these safety critical operations.

Daily meetings were conducted on each search vessel to discuss operational activities for the next 24 hours including weather updates and any deviation from agreed and approved operations. Shorter focus meetings, 'toolbox talks', were held with relevant crew prior to undertaking any operational task. Toolbox talks also facilitated the handover to the next shift of any incomplete work or new hazards identified.

Weekly safety meetings reviewed any HSE issues raised since the previous meeting, any incident reports and reviewed any proposed amendments to procedures based on job safety or hazard analysis. All personnel were encouraged to note safety observations throughout the week and the weekly safety meetings enabled a forum to discuss what worked well and highlighted areas for improvement.

Emergency drills were conducted within 24 hours of leaving port and then at least once a week during search operations, involving all crew. These drills included fire and abandon ship, man overboard, and emergency helivac. Periodic safety audits were also performed throughout the course of the search and provided confirmation of safety practices on each vessel.

Remote area operations

The weather in the search area for much of the search was poor, the search area was 5-6 days transit from the coast of Western Australia and the vessels were in the search area for protracted periods (42 day swings for Fugro Survey's deep tow vessels). The crews on board the search vessels were exposed to a level of risk not normally experienced in the marine industry. Poor weather increases the risk of a serious injury during vessel operations especially when exposure to the risk is over many weeks. Similarly the protracted period in the search area increases the chance that a serious illness may develop which may have been undiagnosed at the time the vessel departed port. Additionally, the risk of a poor outcome for the injured or ill crew member is significantly increased as a result of the protracted time needed to transport them from the search area to comprehensive medical facilities ashore.

When making operational decisions and tasking requests the ATSB and search contractors continually considered ways to mitigate the risks associated with the weather and the remoteness of the search area. Shore staff and vessel crews worked continuously to improve the safety of any operation performed at sea and while underway to and from the search area. On board the vessels safety meetings and risk assessments occurred daily or as needed during operational periods. A close working relationship between the search equipment operators (mission crew) and vessel crew helped to ensure the safety of all personnel especially during periods of rough weather.

Remote area risk mitigation

Upgraded medical support

In addition to a comprehensive medical required for all vessel crew the medical facilities on board the search vessels were upgraded. The remote and through-winter operations meant that standard medical facilities and support carried typically on the vessels as part of their normal surveys/tasks was inadequate. Doctors were embarked on all search vessels and the medical kit carried by the vessels was significantly upgraded.

Vessel scheduling

In case of an emergency in the search area mutual vessel support could be vital. Whilst vessel schedules and tasking were not routinely adjusted to guarantee there were at least two vessels working in the search area, it was always a consideration in planning tasking for the vessels. The sheer size of the search area, the patchwork of tasks outstanding as the search progressed and the operational and contractual management of the vessels meant that dual operations in close proximity could not always be achieved. However, it was strived for and achieved whenever possible.

Incident recording and reporting

The ATSB was informed of any incidents on board the search vessels via telephone or email or via daily operations reports. A register was developed to ensure all incidents which occurred during search operations were recorded and followed with the search contractors. Open incidents were followed up with the vessel project managers and while most were resolved quickly, a few remained unresolved for longer periods, pending outcomes of internal investigations or awaiting approval for procedural changes.

A summary of HSE incidents was included in both the contractor weekly operations reports and the ATSB client representative weekly reports. These provided a good way to confirm all parties were recording the same information and reconciled the activities reported on the daily operations reports, for the same reporting period.

Lagging indicators are normally seen to identify trends in past performance, assess outcomes and occurrences. These include possible near misses, crew injury and illness, equipment damage or loss, or an environmental incident. Leading indicators can reveal areas of possible weakness, be utilised to identify hazards, assist risk assessments and define risk management policy, such as vessel inductions, permits to work and safety drills.

Both Fugro Survey and Phoenix International provided a table of leading and lagging indicators, with incident narration, in their respective operational reports. These provided an overall summary of health, safety and environmental incidents throughout the underwater search (including the mapping of the seafloor), as shown in Table 28.

Table 28: Summary of MH370 HSE Lagging and Leading Indicators

Lagging Indicators	TOTAL	Leading Indicators	TOTAL
Near miss	39	JSEA[33]s and inductions	687
Injury or Accident	9	Safety meetings	5442
Medical Treatment	13	Emergency drills	392
Equipment damage or Loss	60	Safety observations	395
Environmental incident	1	Safety inspections	344
		Marine fauna observations	29
TOTAL	**122**	**TOTAL**	**7289**

Source: Fugro Survey and Phoenix International

Significant HSE incidents

Although Table 28 shows 122 separate incidents across all vessels, most had little or no impact on search operations. HSE incidents which did impact on search operations during the course of the underwater search were three medical evacuations of ill or injured crew members on search vessels:

[33] Job Safety and Environmental Analysis

- On 4 November 2015 a crew member on *Fugro Discovery* advised the doctor on board that he had abdominal pains. After consulting with International SOS (travel medical service) possible appendicitis was suspected. Search operations were suspended and the vessel commenced transit to Fremantle. A medical examination on shore ruled out appendicitis and the patient made a full recovery.
- On 16 November 2015 a crew member on *Fugro Discovery* presented to the doctor on board with visual disturbance, headache, nausea and unequal pupil size. The doctor contacted International SOS who advised 'a life threatening condition could not be ruled out'. A medivac was recommended as further tests were needed in a hospital, including CT scan, MRI and bloods. The vessel transited to Fremantle where the patient was hospitalised. After testing and a few days of rest, he was granted a permit to fly home.
- On 26 June 2016 a crew member on aboard *Dong Hai Jiu 101* fell from a top bunk and injured his right shoulder and right thigh. Although the patient's shoulder was in a satisfactory condition after treatment, a deep cut was found in his thigh which required stitches. Further consultation on board determined the vessel's medical facilities were not sufficient to treat a severe infection and the vessel returned to Fremantle. The patient was transferred ashore from the anchorage for further treatment and was cleared to travel home two days later.

From the mobilisation of *Fugro Equator* on 2 June 2014 (in Singapore) to undertake the bathymetry survey until the demobilisation of *Fugro Equator* on 23 January 2017 (following the final AUV campaign), underwater search operations occurred for a total of 966 days. The search operations involved two major contracted companies, six different vessels which completed a combined 59 swings (from port to search area and return to port) with rotating personnel totalling in the hundreds (including marine and survey crew, client representatives, interpreters, doctors, and equipment specialists).

Considering the remote and dangerous weather conditions encountered during the underwater search, high praise should go to the captains and marine crew for the extraordinary management of each vessel which resulted in minimum incidents involving personnel and equipment. The low number of HSE incidents over close to 1,000 days of search operations is a testament to the cooperation, resilience and good practice by all involved in the underwater search.

Significant equipment related incidents

The loss of two separate deep tow vehicles, within months of each other, significantly impacted search operations. On 24 January 2016, while running a deep tow survey line, *Fugro Discovery* lost its deep tow vehicle, when it collided with a volcano about 2,500 m below sea level. Only 4,500 m of the 10,000 m tow cable was recovered. The crew marked the approximate location of the deep tow vehicle and returned to port where the tow cable, reel and deep tow vehicle were replaced. The vessel then returned to the search area and continued normal survey operations. *Havila Harmony*, having completed its first AUV swing for the summer campaign, mobilised a remotely operated vehicle during its port call. On returning to the search area *Havila Harmony*'s crew successfully located and recovered *Fugro Discovery*'s lost deep tow vehicle by 3 February 2016.

On 21 March 2016 the ProSAS deep tow vehicle on aboard *Dong Hai Jiu 101* was lost while it was being hauled in for recovery. The tow cable termination attached to the depressor had failed. The last known position of the deep tow vehicle was marked by the mission crew and the vessel returned to Fremantle. A remotely operated vehicle was mobilised on *Dong Hai Jiu 101* in Fremantle and the vessel returned to the search area where the deep tow vehicle was located and recovered from the seafloor on 18 April 2016.

Impact of fishing vessels in the search area

Despite the remote location of the underwater search, fishing vessels were regularly encountered by the search vessels in the search area during the summer months. It was considered that

search operations could be impacted as most of the fishing vessels appeared to be working with long lines. Fishing long lines are very strong synthetic monofilament main lines tens of kilometres long which may carry thousands of baited hooks on branch lines (snoods). Once set, they are free to drift for many hours with the prevailing currents before being recovered by the fishing vessel. If a fishing line were to become entangled with a search vessel tow cable there was a real risk that a deep tow vehicle could be lost and so steps were taken by the search vessels to make contact with, identify and warn the crews of the fishing vessels. These efforts met with limited success.

After several encounters between search vessels and fishing vessels measures were taken by ATSB in an attempt to reduce the likelihood of encounters. This including the issue of NAVAREA warnings (a marine safety information or warning notice for an area issued by maritime safety authorities, in this instance the Australian Maritime Safety Authority) and direct contact with fishing vessel owners when the vessels could be identified. This too resulted in almost no success and so when fishing vessels were encountered in close proximity, the search vessels either recovered their equipment until it was safe to redeploy, or diverted their course to avoid contact (when they were performing AUV operations).

***Havila Harmony*'s encounter with fishing gear**

On 8 January 2016 *Havila Harmony* (Figure 100) was undertaking AUV operations in the search area. During the afternoon fishing vessels had been sighted within 200 m of the vessel and a notification was sent to other search vessel in the area and the ATSB. The AUV was performing a dive with the ship tracking the position of the AUV from the surface using the USBL system fitted to a pole which is hydraulically extended several metres below the hull when it is operating.

It was noted by the crew that the USBL positioning data had become inconsistent during the AUV mission. When the AUV was recovered, the crew attempted to recover the USBL pole for further inspection but were only able to raise it 11 cm before it became stuck. Unable to resolve this issue, the vessel had to return to port where it was found that the USBL pole was bent with a large amount of fishing line wrapped around it (Figure 100). The damage required *Havila Harmony* to be dry docked so the USBL pole could be replaced.

Figure 100: *Havila Harmony* and fishing line wrapped around the vessel's USBL pole

Source: Fugro Survey

Recovery planning

Once underwater search operations commenced in October 2014, the MH370 debris field could potentially have been located at any time. A recovery operation would need to commence as soon as possible after the debris field was located and the Tripartite governments had agreed on the next steps. The ATSB therefore needed to put in place the arrangements and plans necessary for a rapid recovery operation to occur at short notice.

Planning for recovery

The Governments of Malaysia, Australia and the People's Republic of China had decided that they would meet if MH370 was found, to consider issues relating to any recovery. It was decided that the ATSB would coordinate the on-water component of recovery operations, in consultation with other involved agencies. The ATSB would be responsible for overall coordination including:

- procuring recovery services (vessel(s), recovery equipment and subsea assets)
- planning operations including the tasking of vessels, assets and personnel
- liaising with the recovery contractor and their staff
- assuring the overall quality of the recovery operation services.

Considerations for the recovery of MH370 had commenced during March 2014, with a request to the French BEA to share information relating to the technical and operational support required during the recovery of AF447. Like the underwater search operation, the recovery operation for AF447 provided an example of operational challenges likely to be similar for an MH370 recovery, including the depth of water and the remoteness of the area.

The recovery of aircraft debris in deep water is generally accomplished by using a ROV (Figure 101) to either rig large items to lifting equipment or place small items in baskets or cages lowered to the seafloor and then lifting the baskets by winch or crane from the seafloor to the recovery vessel. A recovery vessel is required to have a dynamic positioning system capable of positioning the vessel for extended periods while the ROV is operating on the seafloor. For the MH370 recovery planning, weather was also a key consideration as the search area is prone to poor weather conditions for much of the year, often beyond the significant wave height limits for safe ROV operations.

Figure 101: A remotely operated vehicle on the seafloor

Source: Fugro Survey

Early in 2015 the ATSB called for expressions of interest for the MH370 recovery operation. The objective of the request for expressions of interest was to establish a shortlist of pre-qualified suppliers who could be rapidly contracted to undertake the recovery. A range of requirements were stipulated including specifications for the vessel and recovery systems (which included two ROVs).

Requirements were designed around the need to support the range of activities involved in a recovery for up to 30 days at a time in a remote area offshore, working in water depths up to 6,000 m in often poor weather. The goal was to recover evidentiary material to support the Annex 13 and Royal Malaysian Police (RMP) investigations and the recovery of human remains. The large number of people required to be involved in the operation, and the requirements to process and store recovered items, also posed some logistical challenges.

The potential services included:

- mapping and capturing optical imaging of the MH370 debris field
- recovering human remains and debris from the MH370 debris field
- providing deck space and support services on board the recovery vessel for recovery equipment supplied to preserve human remains and aircraft debris
- providing accommodation on board the recovery vessel for all involved personnel
- providing data storage services and communication services to relay information to the Australian mainland.

To be prepared for the recovery operation the ATSB developed, in consultation with Malaysia and the People's Republic of China, a detailed *MH370 Recovery Operational Plan* that would be implemented once MH370 was positively identified. To facilitate all aspects of the potential recovery operation, the ATSB also drafted a collaborative head agreement and specific project agreement with the Australian Federal Police (AFP) under the Commonwealth National Collaboration Framework, to define roles and responsibilities. The ATSB also arranged a MoU with the Australian Department of Defence to collaborate in any potential recovery operation. These arrangements were designed to assist the ATSB to coordinate the range of specialist input required for a complex deep water recovery operation as outlined in Figure 102.

Figure 102: Recovery coordination structure

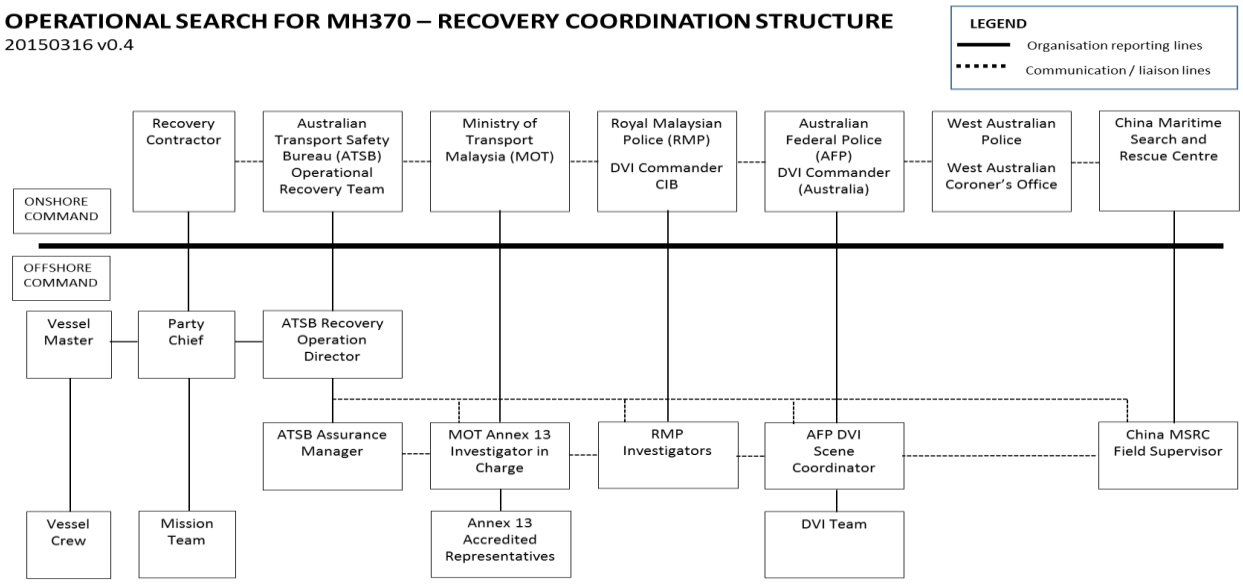

Source: ATSB

The ATSB also planned for a range of other activities associated with the recovery operation and included them in the *MH370 Recovery Operational Plan*. These activities included the medical certification and premobilisation training for personnel who would be on board the recovery vessel including survival at sea and critical incident stress.

The investigations

Information about the debris field itself would only be available when MH370 was found. Part of the requirements for the underwater search were for the contractor to positively identify the debris field, map the debris field and produce a photographic mosaic of the entire field. Using this photomosaic, and prior to the commencement of a recovery operation, areas of particular interest could be identified which would form the basis for the initial priorities of the recovery operation.

During recovery operations investigation personnel are required to oversight the aircraft component recovery and legal aspects of the recovery operations. It was foreseen that investigators and representatives from the Malaysian Annex 13 investigation team, supported by representatives from Boeing, would need to be on board the recovery vessel to lead all aspects of the Annex 13 investigation. It was agreed that aircraft debris preservation procedures were to be in accordance with ICAO guidelines.

Similarly, officers from the RMP would be on board the recovery vessel to oversee the collection, processing and storage of evidence for their investigation.

The priority items for the investigations were the flight recorders (FDR and CVR) and quick access recorder. Further priority items included other potential sources of non-volatile memory such as avionics components or personal electronic devices and specific items of the aircraft structure or interior.

The initial prioritisation of debris would then be reviewed once the recovery vessel was on site, with opinions from all investigation parties considered with a view to the overall investigation. The early recovery, and initial analysis of the FDR, CVR and quick access recorder may assist the selection process. A potential expedited transfer of the FDR, CVR and quick access recorder from the recovery vessel to ATSB Canberra offices for analysis was also considered.

Disaster Victim Identification

Specialist personnel were required to oversight the recovery and repatriation of human remains in accordance with the INTERPOL Disaster Victim Identification process. Recovery of human remains would involve a multi-national and multi-jurisdictional operation led by the RMP and supported by the AFP.

Recovery planning identified that AFP Disaster Victim Identification professionals, in collaboration with Western Australia Police, PathWest Laboratory Medicine WA (Western Australian Government Pathology), Western Australia State Coroner, and RMP, would be on board the recovery vessel to coordinate the recovery of human remains, including recording and photography at the point of recovery, and appropriate transport to Western Australia.

The AFP, in collaboration with its partner agencies, planned to establish a temporary mortuary in Perth, Western Australia, to coordinate autopsies and post-mortem information.

The RMP, with the support of the AFP, would coordinate the collection of ante-mortem information, reconciliation of ante-mortem and post-mortem information, and repatriation of human remains once identified.

Safety analysis

Introduction

The disappearance of MH370 and the scale of the search for the aircraft is unprecedented in commercial aviation history. The aircraft continued to fly for almost six hours after the last time its positon was positively fixed at the northern tip of Sumatra by the surveillance systems operating on the night. Whether or not the loss of MH370 was the result of deliberate action by one or more individuals, or the result of a series of unforeseen events or technical failures, it is almost inconceivable and certainly societally unacceptable in this modern aviation age with 10 million passengers boarding commercial aircraft every day, for a large commercial aircraft to be lost and for the families of those on board not to know with certainty what became of the aircraft nor those on board.

The function of the ATSB as described in the *Transport Safety Investigation Act 2003* is to improve transport safety. The ATSB considers, in relation to MH370, that it is difficult to fulfil this remit without locating the aircraft and determining the reasons for its disappearance.

MH370 was equipped with a variety of systems designed to communicate the aircraft's position during normal operations and in emergencies. These included the transponder system, the ACARS communication system, the emergency locator transmitters, and the underwater location beacons fitted to the flight recorders. All these systems complied with industry standards and were the state of the art at the time that the Boeing 777 was designed and certified and at the time the aircraft was delivered in 2002. Unfortunately, none of these systems succeeded in transmitting the aircraft's position at the end of its flight.

The search for MH370 commenced more than three years ago, on 8 March 2014. The initial surface search and the subsequent underwater search have been the largest in aviation history. The significant challenge has been to trace the whereabouts of the aircraft using the very limited available data: satellite communications metadata for the final six hours of flight – a method never intended to be used for this purpose – and long-term debris drift modelling to trace the origin of MH370 debris which had been adrift for more than a year and in some cases almost two years.

Improvements in international civil aviation regulation must be sought to ensure that this type of event is identified as soon as possible and mechanisms are in place to track and locate a commercial aircraft that is in distress or not following its filed flight plan.

The International Civil Aviation Organization (ICAO) is responsible for setting the international standards for civil aviation safety which are applied, in law, by all contracting States. The Annexes to the Convention on International Civil Aviation (the Chicago Convention) set out provisions for the safe and effective conduct of aviation activities. Among them, Annex 12 is applicable to search and rescue (SAR), though many of the factors that can determine the success of a SAR are contained in other Annexes, in particular, those for the operation of aircraft (Annex 6), aeronautical telecommunications (Annex 10) and air traffic services (Annex 11). Additionally, the outcomes of a search directly impact the effectiveness of an Annex 13 safety investigation. This in turn influences ongoing aviation safety.

Hundreds of millions of passengers are flown across transoceanic routes each year. More than 7 trillion commercial passenger-kilometres were flown in 2016, about a third of which were over major oceans (Figure 103[34]). This safety analysis aims to broadly determine possible improvements in these areas in order to increase the efficiency and effectiveness of searches of aircraft lost in international waters.

---

[34] IATA World Air Transport Statistics, 60th Edition. A passenger-kilometre is equivalent to one passenger flown for one kilometre. It can be used as a measure of civil aviation activity and, to some extent, exposure to risk.

Figure 103: Proportion of passenger-kilometres on international, scheduled routes, 2016

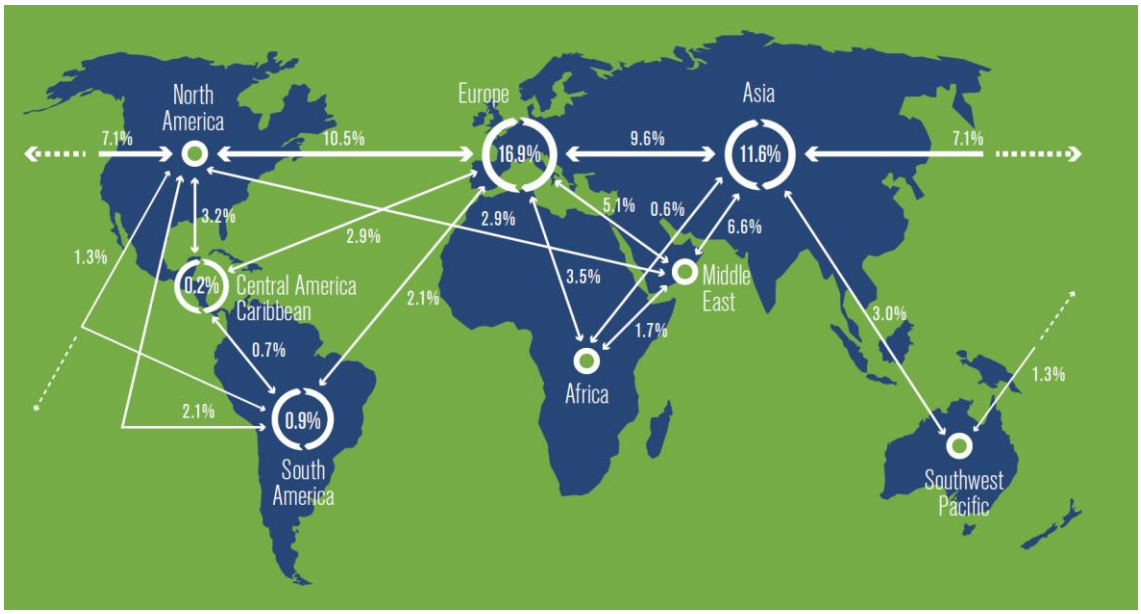

Source: International Air Transport Association

Search, rescue, and recovery

The main objectives of search, rescue and recovery operations performed when a commercial aircraft has been subject to an accident are to:

- Locate, rescue and retrieve survivors and casualties.
- Provide evidence for an investigation to determine what happened:
  - to permit safety improvement
  - for the benefit of grieving families, friends, and communities.

There have been many occasions where people have survived major passenger aircraft accidents, including impacts into the sea. While survival appears most likely if an accident occurs during take-off or landing, when a rapid response is to be expected, some of these accidents occurred in relatively remote locations. In such cases, timeliness is critical because the occupants are likely to have injuries and be exposed to harsh environmental conditions. The sooner medical attention can be administered, the greater their chances of survival beyond the first few hours or days.

The purpose of an accident investigation as detailed in Para 3.1 of ICAO Annex 13 is:

> The sole objective of the investigation of an accident or incident shall be the prevention of accidents and incidents.

If an aircraft is lost or missing for an extended period of time, then the amount of information available to achieve the objectives of the investigation is diminished and safety issues may not be identified and resolved as quickly.

An Annex 13 investigation authority's role is to bring about positive safety change in an objective way. It is also important to understand and consider the emotional impact of an accident that affects individuals, groups, and communities. Recovery of accident casualties is also important from a cultural perspective. A successful search and investigation provides answers that may contribute to the alleviation of grief, and in a broader sense, confidence in the safety of the global aviation industry is maintained when an accident is well understood. A rapid, successful search helps make these things possible.

Search, rescue, and recovery phases

A search consists of a number of stages that differ depending on whether the accident is over water or land. Since a search relies heavily on the information available prior to the accident, the ATSB has included consideration of pre-accident factors in this analysis.

The ATSB has divided the process into phases as summarised in Table 29.

Table 29: Search phases associated with different accident locations, and example activities associated with each phase

Phase	Accident over water	Accident over land
Normal flight	Scheduled, triggered, or continuous monitoring of aircraft position and status	Scheduled, triggered, or continuous monitoring of aircraft position and status
Aircraft in distress	Triggered monitoring of aircraft position and status following an abnormal event	Triggered monitoring of aircraft position and status following an abnormal event
Primary search	Search for survivors, casualties, and floating debris	Search for survivors, casualties, and main wreckage
Underwater locator beacon search	Wide search for submerged wreckage and ULB signals (general area)	Not applicable
Sonar search	Narrow search for submerged wreckage and casualties ('pinpointing')	Not applicable
Recovery	Recovery of casualties, wreckage and recorders.	Not applicable

Source: ATSB

Normal flight

Position tracking

Position reports (made by crew over radio, or automated data transmissions) are often the best information available to SAR authorities to define a search area. Their usefulness diminishes with time elapsed from the last report, and to some extent, whether that report was routine or indicated an emergency (this is discussed more in the following section). Knowing the maximum time from the last report to the time of the aircraft impact is critical in determining the area for the initial search. The potential search area becomes much larger when there is more uncertainty.

In cruise, an airliner travels about 8 NM per minute. In 15 minutes, an aircraft could be at any location within a 125 NM radius circle, with an area of about 170,000 km^2.

If the aircraft's track at the time of the last position report is known or can be estimated, and assuming that the aircraft is unlikely to turn more than about 45º either side of that track, this area can be reduced to a quadrant with an area of approximately 42,000 km^2. An indication of the effect of time uncertainty on the likely impact area is given in Table 30 and Figure 104.

Table 30: Search areas associated with time uncertainty, assuming 500 knot groundspeed

Time between position reports (mm:ss)	Radius (NM)	Maximum area (km²)	Typical highest likelihood area (km²)
15:00	125	168,365	42,000
10:00	83	74,829	19,000
5:00	42	18,707	4,700
1:00	8	748	190
0:30	4	187	47
0:15	2	47	12

Source: ATSB

Figure 104: Example visual representation of search areas associated with time uncertainty, assuming 500 knot groundspeed

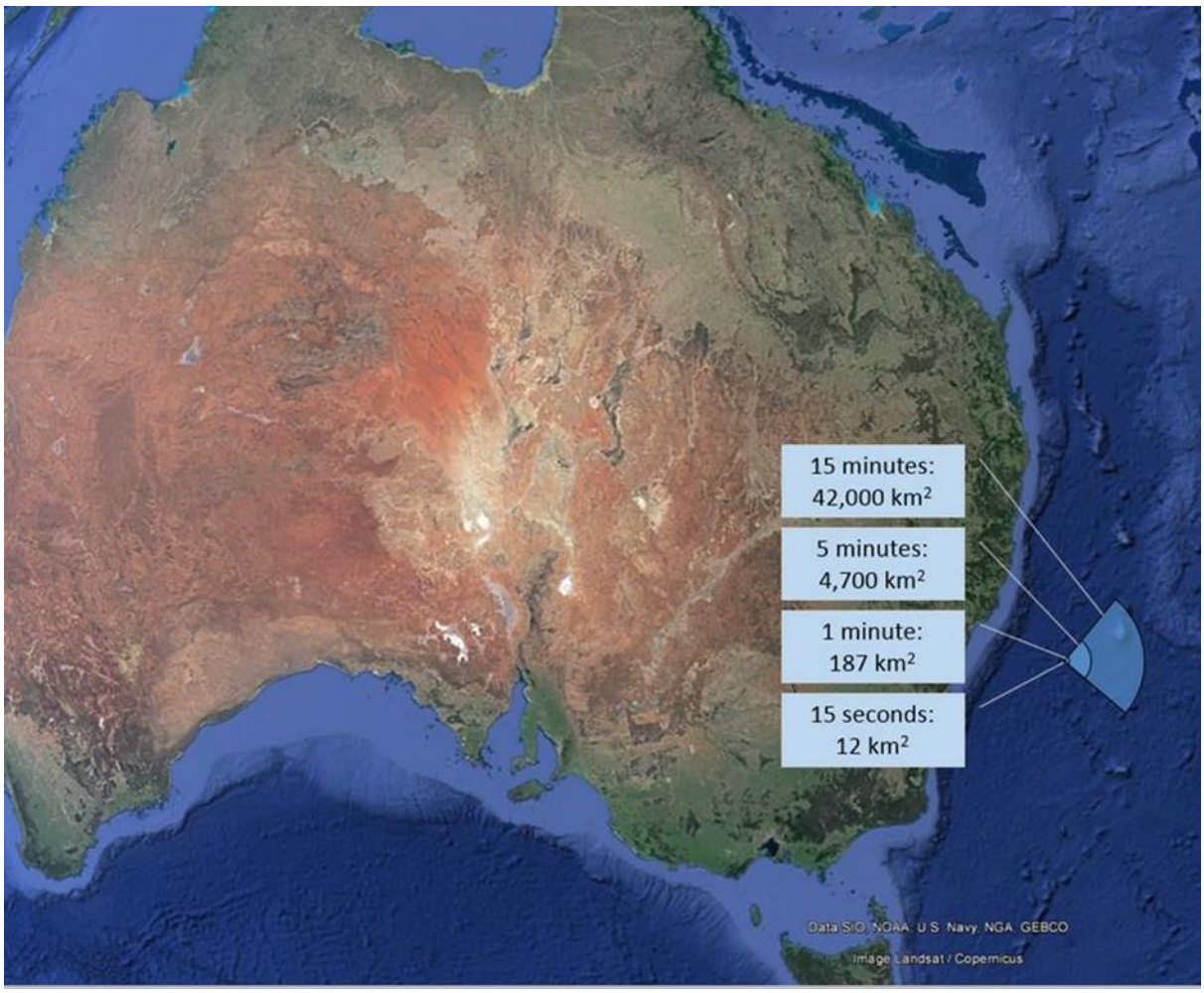

Source: Google earth, annotated by ATSB

In the accident involving AF447, the aircraft was programmed to transmit ACARS reports (including position information) every 10 minutes. AF447 also sent an unscheduled, triggered report during the event sequence. The searchers therefore had an indication that impact with water would have been within a few minutes and almost certainly within 10 minutes. The initial search area for AF447 was 17,000 km^2 with the main wreckage not found until almost two years later. The investigation found that impact with water was about four minutes after the final triggered position report. As with MH370, the duration of the search was a function, to a large extent, of the level of uncertainty about the aircraft's position at impact.

A BEA review (BEA 2011) concluded that when the aircraft position could be determined one minute prior to the accident, 95 per cent of accidents were within a 6 NM radius of that position, and 85 per cent were within 4 NM. When the aircraft position could be determined ten minutes prior to impact, none were within 20 NM. This indicates that a 10 minute interval between position reports would result in a potential search area of at least 4,300 km^2 in most cases.

To reduce the potential search area, position reports could either be sent at shorter intervals, or triggered by abnormal aircraft events to increase the likelihood that the most recent position report would be nearer to the accident site.

The information available for the search for MH370 was atypical because the normal aircraft position messages were not reported for the majority of the flight. MH370 was fitted with a system that would normally provide position reports via satellite every 30 minutes. During MH370 only basic handshake data and not position information was transmitted. The search area was established by a series of complex analyses of that data and refinements during the search using data not intended for that purpose.

Initially, MH370 was thought to be in the seas around the Malaysian peninsula. The search did not commence in the Indian Ocean until 10 days after the flight. The delay and resulting oceanic drift led to large search areas and wide debris dispersal. By then, any debris left afloat would have drifted well over 100 km. Furthermore, unlike for most other searches, there was no single starting point. The position of MH370 at the time of the last satellite transmission could not be calculated as a particular point but lay somewhere along an arc more than 3,000 km long. The wide underwater search area, allowing for uncertainties and potential glide distance, was in the order of 1,200,000 km^2.

The aircraft's ACARS system had the ability to provide position reports and was configured by Malaysia Airlines to transmit position reports every 30 minutes. These were not sent for the majority of the flight. More recent position reports would have reduced this search area even if they had occurred a few hours before the end of the flight. Position reporting systems need to be both reliable and secure. Multiple sources and mechanisms to transmit position information can also be beneficial for redundancy.

Position tracking technologies

Around areas with high population density, controllers continuously track aircraft using secondary surveillance radar and Automatic Dependent Surveillance – Broadcast (ADS-B). Both of these technologies rely on aircraft and ground equipment, and only work when the aircraft is within range of the ground stations (Figure 105 and Figure 106). Aircraft-to-ground voice communications is generally accomplished over Very High Frequency (VHF) radio, which also has a limited range and is not available in oceanic areas.

Figure 105: Secondary surveillance radar (cyan) and ADS-B (blue) coverage in Australia

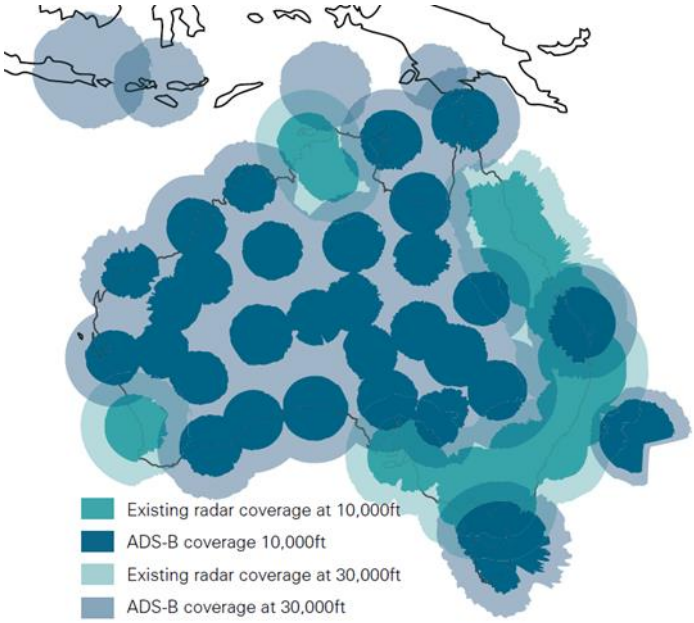

Source: Civil Aviation Safety Authority, modified by ATSB

Figure 106: Coverage of an ADS-B network

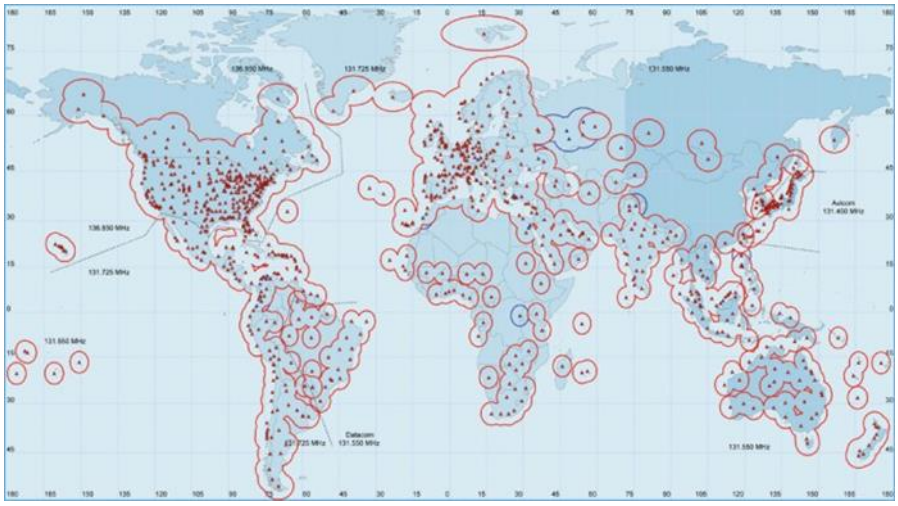

Source: SITA

If certain aircraft systems are not operational, the only way to track an aircraft outside of visual range is through the use of primary surveillance radar. Compared with secondary surveillance radar, these systems have reduced coverage, cannot positively identify an aircraft, and provide significantly degraded location and speed information.

Over less populated areas and oceans, aircraft can send triggered, on-demand or scheduled position reports via satellite or long-range High Frequency radio with near-global coverage (Figure 107 and Figure 108). Both of these technologies need the equipment on board the aircraft to be operational.

Figure 107: Primary (green) and secondary (blue) coverage of a High Frequency network

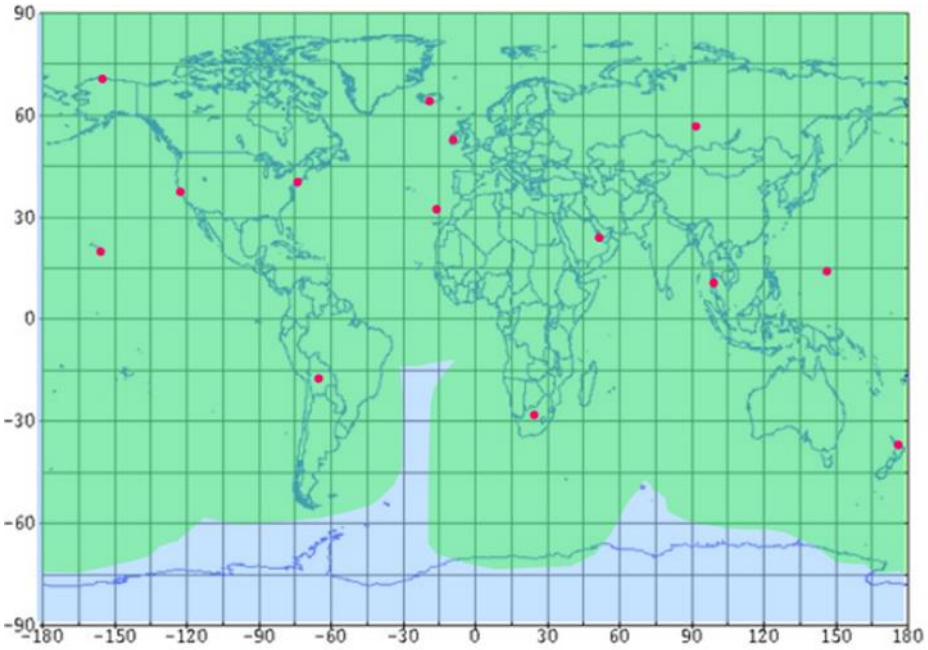

Source: ARINC

Figure 108: Coverage of the Inmarsat Swift-Broadband satellite constellation

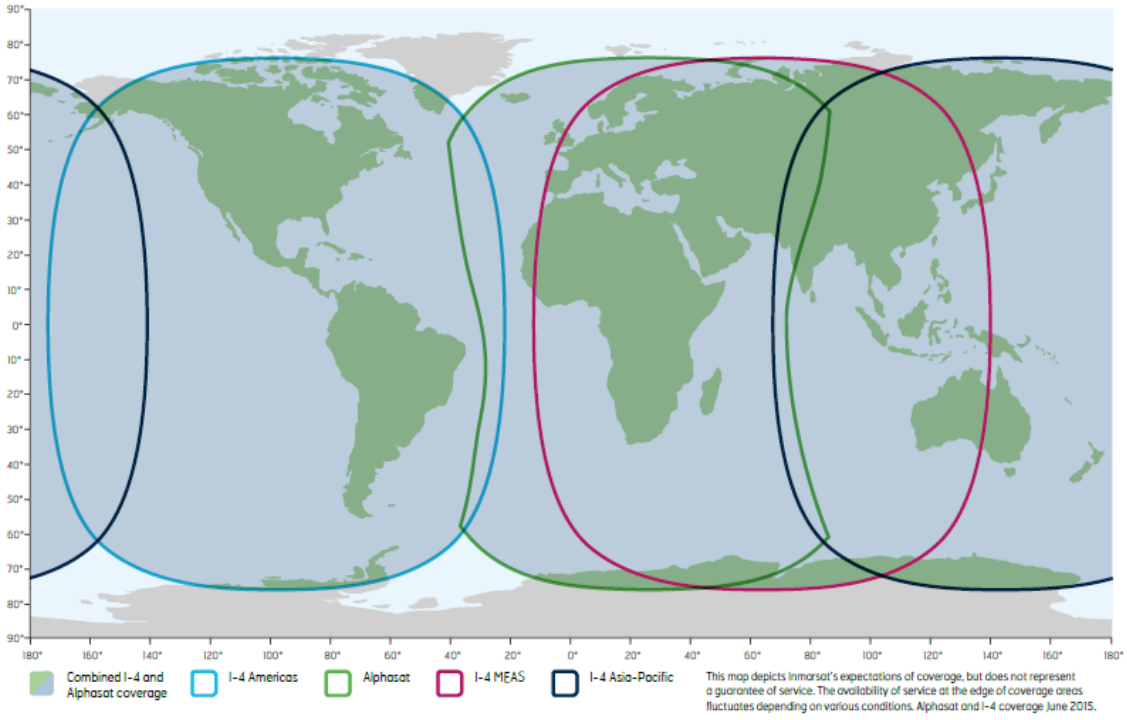

Source: Inmarsat

MH370 was within radar (both primary and secondary) and VHF range for the first part of the flight. For most of the flight over the Indian Ocean, the only available mechanisms to communicate with or locate it – that is, satellite and High Frequency radio – relied on the aircraft systems being both operational and switched on.

Aircraft in distress

Timeliness of accident detection is important in terms of narrowing the search area, and in some circumstances may also provide opportunities for positive intervention. In the case of MH370 the alert was not raised until some hours after the aircraft diverted from its planned route despite the expected handover to a different air traffic control authority and absence of scheduled ACARS reports.

However, this situation is very unusual. In general, an emergency situation in controlled airspace, particularly within range of radar or other tracking technology, is likely to be detected relatively quickly. Outside of these areas, the remote detection of abnormal conditions depends on information being transmitted from the aircraft to ground-based monitoring systems. There is often a very high pilot workload during an emergency and crews may not be willing or able to make a distress call or activate a distress signal.

The same technologies used for aircraft tracking in normal flight can also be used to detect and respond to abnormal events, such as deviation from a flight path or unusual aircraft behaviour. Currently, some aircraft can automatically transmit when certain events occur such as a change in climb or descent rate, or when there is an aircraft fault. This is likely to significantly reduce search area because a manually – or automatically – triggered position report is more likely to occur closer to the point of impact than a scheduled position report.

If there are adequate processes and assets in place to monitor this information, a timely response can be initiated. The response can be made more effective when there is more information available to draw upon, particularly the aircraft position as close as possible to the time of the accident, and information about the nature of the problem. Currently, the content and rate of automatic and manual reports, and the extent to which they are monitored for signs of abnormal events, is probably very variable.

There are significant technological hurdles that need to be overcome for all civil aircraft to continuously transmit detailed flight data and there is also a cost associated with such a systems. Nevertheless, the automatic streaming (continuous transmission) of detailed flight data may provide information of great value for both the search and investigation, possibly to an extent that recovery of the flight data recorders becomes significantly less important.

Furthermore, such data streamed from an aircraft in a distress situation or continuously throughout the flight may allow early detection and mitigation of factors that might lead to an accident. Such technology is evolving and already exists to some degree on some airframes. Initially, it may be feasible to only stream data in emergencies due to data capacity and rate limitations, but as the performance of datalink technology improves, these practices are expected to be more widely adopted in normal flight due to the potential economic and safety benefits that result from the availability of near real time flight data.

MH370's systems were capable of sending limited status data, automatically triggered by certain types of fault, via satellite or VHF radio. However, those transmission systems were not operating normally (and the aircraft was also out of range of VHF stations) for most of the flight.

Surface search

Once an aircraft is known or suspected to be subject to abnormal operations, and its exact location is not immediately apparent, a visual search is initiated. This is primarily conducted by aircraft and, if applicable, surface vessels. The purpose of this stage of the search is to find survivors and (if over water) floating debris. The size of the area to be searched is highly dependent on the information available about the aircraft's last positon at this point in time.

Locating an aircraft which has impacted on land is less problematic than one in water. The wreckage doesn't sink or drift and impact usually leaves ground marks and smoke from a post-impact fire. The aircraft is more likely to have been seen if near a populated area. Weather,

terrain, and heavy foliage can be an issue, however, particularly for accidents involving small aircraft.

Accidents over water pose a different set of challenges. The aircraft usually breaks up on impact and most of it is likely to sink. Floating debris immediately begins to disperse with wind and waves and their distribution becomes wider over time. The first floating debris from AF447 was 70 km from the aircraft's last known position after 5 days. If the area is remote it may not be possible to deploy search resources quickly enough to avoid a search area that is tens of thousands of square kilometres. It is therefore imperative to obtain the best possible information about the impact location and to deploy effective search assets to the area as soon as possible to minimise the search area and maximise the likelihood of finding survivors and floating debris.

Aircraft are fitted with emergency locator transmitters (ELTs) to aid in locating an accident site. If effective, they provide accurate impact position information to monitoring satellites or nearby aircraft or surface craft. ELTs are designed to transmit locating signals on impact, and some can be manually triggered. This occurs very rarely, probably because crews understandably focus on resolving an emergency and preventing an accident rather than activating a device that cannot directly help them. ELTs that are activated on impact can often be damaged or shielded by wreckage or terrain, rendering them ineffective. Studies have indicated that ELT failure rates are in the region of 25-75 per cent though data is limited (ATSB 2013; Defence Research and Development Canada 2009; Stimson 2015).

Current-generation ELTs are not suitable for accidents on water, because they or their attached antennas are usually rendered ineffective by submersion and/or impact. It would be of significant benefit if an ELT transmission was automatically triggered whenever flight or fault conditions become significantly unsafe, prior to impact. A triggered ELT transmission provides similar benefits to triggered position reports with the additional benefit of a more rapid response because global monitoring and response systems are already proven and in operation.

An additional consideration is an ELT or similar device that is designed to float free following a water impact. This would generally drift with other debris permitting determination of the point of impact and the movement of floating debris after the impact.

There were four ELTs on board MH370. One was a fixed unit (located in the fuselage crown over the aft passenger cabin) and could have been either manually activated or automatically activated by a significant deceleration force. If activated, this unit would have transmitted a 406 MHz signal to specialised SAR satellites, and signals detectable by nearby aircraft or surface craft monitoring the relevant distress frequencies (243 MHz and 121.5 MHz).

A second ELT was portable with manual activation only, but otherwise had similar capabilities as the fixed unit, and was stowed in the forward cabin in a locker.

The other two ELTs were located in the emergency escape slides (which could be detached for use as a life raft) at door 1 left and at door 4 right. These ELTs were of a type that automatically activated on contact with water and transmitted only the 243 MHz and 121.5 MHz homing signals that are no longer monitored by satellite.

Despite the number of ELTs on board MH370, no distress transmissions were received by SAR authorities at any time during the fight. This suggests that the ELTs on board the aircraft did not transmit an emergency signal either by automatic or manual activation or by water immersion. This highlights the potential benefit of reliable, deployable and accident-resistant emergency beacon technology.

Underwater locator beacon search

The majority of aircraft wreckage usually sinks shortly after impact with the sea surface. This means that the technology with the greatest potential to assist searchers locate the main aircraft wreckage are the underwater locator beacons (ULBs) fitted to the flight recorders which commence transmitting on contact with water. The time available for searchers to locate the

aircraft debris field and the flight recorders on the seafloor is therefore limited by the battery life of the ULBs.

There are many factors which may delay the search for an aircraft's ULBs including: the accuracy of the last aircraft position data, the remoteness of the area, an initial search focused on rescuing survivors, the availability of suitable ULB detection equipment and a suitable vessel, time to mobilise the vessel, equipment and personnel and transit to the search area, and the weather in the area. All of these factors will reduce the window of opportunity to locate the ULBs before their batteries expire and limit the area that can be searched before this occurs.

As noted previously, a 10-minute position reporting interval would result in a search area of more than 4,300 km^2. By way of comparison, ICAO estimates that a ULB search can typically be conducted at a rate of about 100 km^2/day and that a maximum of about 2,300 km^2 can be searched within the currently-mandated 30-day battery life (ICAO 2016).

Current generation ULBs transmit on a frequency of 37.5 kHz with a range of detection between 2 km and 3 km. This range depends on factors which affect the propagation of the ULB's acoustic transmissions through the water which include; depth, pressure, temperature and salinity and also the sensitivity of the detection equipment. Surface hydrophones are only effective in water depths up to approximately 2 km. In very deep water, a towed pinger locator (TPL) system must be used. These systems are not readily available and therefore take time to source, mobilise and transit to a search area on a suitable vessel. Furthermore, once a ULB is detected, multiple search passes with a TPL are needed to adequately triangulate the position of the ULB.

A significant complication in ULB searches is the reliability of detection, which can be affected by background noise, as well as potential for false positives from equipment on the search vessel or other transmitters such as marine science tracking devices.

The duration of the ULB search phase is influenced by how broad the search area is and how quickly the search equipment can be mobilised to the area. In the case of Air Asia 8501, the aircraft's last location was captured on radar, allowing early discovery of floating debris and an initial underwater search area of 9 km^2 (Kurniadi & Ng 2015). The underwater wreckage was located within days of the underwater search commencing. If the search had relied only on the position of floating debris, the underwater search may have taken considerably longer – the first floating debris found was over 50 km away (Komite Nasional Keselamatan Transportasi 2015).

ULBs can be difficult to locate due to extreme depths, or to a lesser extent, challenging underwater terrain. In this case wreckage might not be found within the limited battery life. The acoustic search for AF447's ULBs did not detect them even though vessels passed within expected detection range of the aircraft site; this may indicate that the beacons were not operational or that the signals were shielded by wreckage or silt.

In 2016, EgyptAir flight 804 impacted the Mediterranean Sea in an area with challenging underwater terrain. Due to an unusual circumstance the ELT was triggered prior to impact. With the aircraft's position known within about 5 km, and both ULBs being operational, the underwater wreckage took about a month to locate. The search came close to extending beyond the expected battery life even though it had the benefit of unusually good position information.

These accidents demonstrate that even precise impact position information may not be sufficient to provide a high level of confidence that a current-generation ULB will be located, particularly in deep or difficult waters. The benefits of having ULB devices that are as reliable, long-range and long-duration as practicalities permit are numerous. With greater battery life, the search can be extended. With greater range (using a lower frequency), more area can be searched in a given period of time. For accidents in deep waters, an extended-range ULB can also be detected by surface search equipment that is much more rapidly mobilised than a TPL or underwater vehicles.

MH370 was fitted with current-generation ULBs operating on 37.5 kHz with an expected battery life of between 30 and 40 days. Due to the very limited information available about the aircraft's location the ULB search along the 7th arc did not commence until 25 days after the flight, allowing

between 5 and 15 days to locate the beacons. Several false detections led to inefficient coverage of the search area. The search for the ULB's continued until 17 April 2014, 40 days after the flight. Subsequent refinements of the satellite data and other analyses indicated that this part of the search was concentrated too far north and well beyond the range of any current or proposed ULB type.

Sonar search

The final stage of the search is to determine the exact location of the aircraft debris field on the seafloor using sonar then optical imaging for positive identification. If a ULB is detected and its approximate location can be triangulated, this phase of the search can be relatively brief. For example, the wreckage of EgyptAir flight 804 was found about two weeks after the first ULB detection. If the location of the aircraft debris field has not been narrowed down with any other method a sonar search can take a long time and be very expensive.

The searches for AF447 and MH370 both demonstrate the extent of this effect. In the case of AF447, the aircraft's location was known to within a few minutes' flying time, with additional information available to prioritise the search area, yet an unsuccessful ULB search led to a sonar search that took four months over nearly two calendar years and at a cost of about €21 million (BEA 2012).

The sonar search for MH370 was based on even more limited information. Since there was very little information available about the aircraft's position (which partly led to the subsequent ULB search being unsuccessful) the sonar search area had to be several times greater than that for AF447. Primarily as a result of these issues, the sonar search has been unable to locate MH370 at a cost of up to A$200 million.

Summary

The preceding sections illustrate that issues arising early in a search can have a cumulative effect on the eventual outcome. Figure 109 illustrates the progression through each stage of a sea search, with some of the factors that help and hinder.

If an aircraft's initial position is not known with sufficient accuracy or there is a delay in responding, the area of floating debris will have drifted further from the impact point and dispersed, increasing the size required for a surface search. Debris drift modelling becomes less accurate over time and the potential location of an underwater debris field and ULBs becomes more uncertain. ULBs may not be detected before batteries become exhausted, resulting in a sonar search that needs to cover a wide area. Ultimately, every stage of the search becomes increasingly more difficult and costly.

Alternatively if the appropriate equipment, monitoring and response mechanisms are in place to capitalise on each opportunity to narrow the search area, the total search effort becomes far more manageable and has a much greater likelihood of success.

Figure 109: Factors affecting a sea search

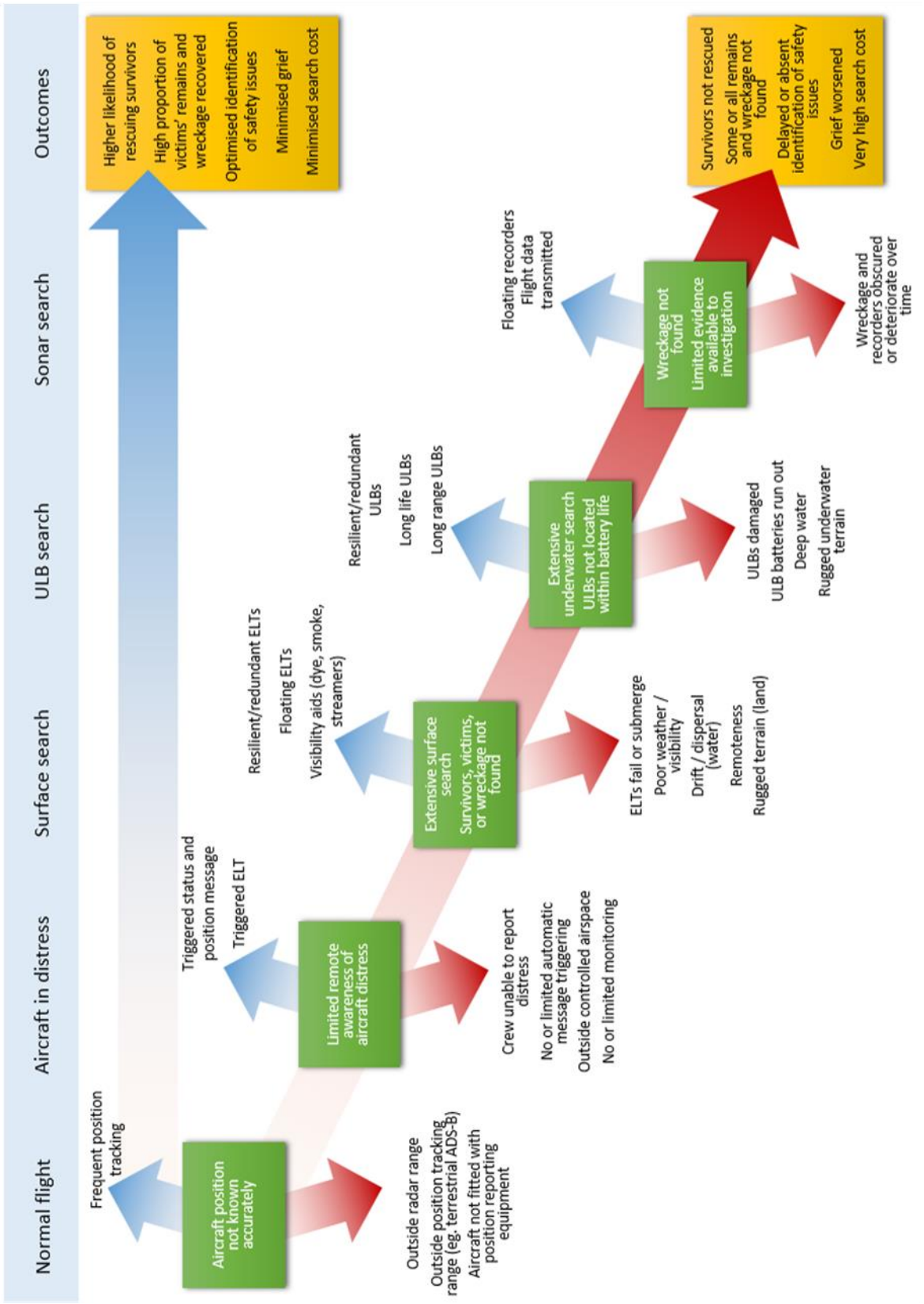

Source: ATSB

Records of previous searches

The detailed search reports previously published by the BEA, and search information provided in some Annex 13 investigation reports such as for Asiana Airlines cargo flight 991 (Aviation and Railway Accident Investigation Board 2015) provide useful information for the benefit of planning and conducting future searches, and for pre-emptively improving search results as outlined in this report.

There is relatively limited public and official information available about the process and outcomes of some searches. It is not an explicit part of the Annex 13 guidelines for inclusion in an accident investigation report, so some reports do not address the search itself, or do so only in general terms. There is no Annex 12 requirement to publish or analyse search information. This limits the ability for researchers to determine the factors that help or hinder a search, and provide focus on factors that can be controlled.

The ATSB therefore considers it would be beneficial to include relevant and useful SAR information after an investigation. Examples of information that would be useful for future analysis include:

- last confirmed time, position, altitude, and position accuracy
- initial alert time and mechanism
- impact time and location
- initial search area and type, and search assets deployed
- underwater search area and type
- water depth, topography, and type of seafloor (such as rock, silt, sand, mixed)
- time and location of rescues
- time, location, and mechanism (such as visual, sonar, beacon detector) of important finds, including major floating debris, main wreckage, all flight recorders, and ULBs
- effectiveness of ELTs and ULBs when found (such as operational, non-operational, disconnected antenna) and other search and rescue aids.

Brief information could be included in the Annex 13 investigation report. More detailed information can be included in appendices, or separate reports, either published or held by ICAO for access by contracting States.

Related searches

In December 2009, a working group led by the BEA published a report that included details of 26 searches for aircraft lost at sea from 1980 – 2009 (BEA 2009). Since then, four more civil aircraft searches have occurred (Table 31).

Table 31: Related occurrences since December 2009

Date	Flight number	Location	Initial alert	ULB detected	Main wreckage found
19 May 2016	EgyptAir flight 804	Mediterranean Sea	ELT (triggered by electrical fault)	13 days	27 days
28 December 2015	Air Asia X flight 8501	Java Sea	Lost radar contact	Within 5 days	5 days
8 March 2014	Malaysia Airlines flight 370	Indian Ocean	Lost radio contact	No	No
28 July 2011	Asiana Airlines cargo flight 991	Korea Strait	Declared emergency over radio	No	5 days

Source: ATSB

Previous safety recommendations

Malaysian Air Accident Bureau

On 9 April 2014, the Malaysian Air Accident Bureau recommended that ICAO examine the safety benefits of introducing a standard for real-time tracking of commercial transport aircraft. At the time of writing, the Malaysian ICAO Annex 13 Safety Investigation Team advised that it had not received a formal response from ICAO to this recommendation.

Bureau d'Enquêtes et d'Analyses pour la sécurité de l'aviation civile (BEA)

Data transmission and emergency locator transmitters

The BEA directed an international working group on triggered transmission of flight data and in 2009 issued two recommendations (BEA 2009b) requesting that the European Aviation Safety Agency (EASA) and ICAO:

> … study the possibility of making it mandatory for airplanes performing public transport flights to regularly transmit basic flight parameters (for example position, altitude, speed, heading).
>
> … study the possibility of making mandatory, for airplanes making public transport flights with passengers over maritime or remote areas, the activation of the emergency locator transmitter (ELT), as soon as an emergency situation is detected on board.

In 2011, in a further update to the AF447 investigation (BEA 2011a), the BEA recommended that EASA and ICAO:

> … make mandatory as quickly as possible, for airplanes making public transport flights with passengers over maritime or remote areas, triggering of data transmission to facilitate localisation as soon as an emergency situation is detected on board.

The BEA published a report by the Triggered Transmission Working Group (BEA 2011b) which advised that:

> … it is technically feasible to significantly reduce the search area for wreckage by:
>
> - Triggering transmission of appropriate data via SatCom prior to impact, and/or
> - Automatically activating next generation ELTs prior to impact, and/or
> - Increasing the frequency of position reports.
>
> The working group also suggests that the location radius of 4 NM is a realistic aim for 2020.

Underwater locator beacons

On 17 December 2009, the BEA recommended (BEA 2009b) that EASA and ICAO

> …extend as rapidly as possible to 90 days the regulatory transmission time for ULBs installed on flight recorders on airplanes performing public transport flights over maritime areas.
>
> …make it mandatory, as rapidly as possible, for airplanes performing public transport flights over maritime areas to be equipped with an additional ULB capable of transmitting on a frequency (for example between 8.5 kHz and 9.5 kHz) and for a duration adapted to the pre-localisation of wreckage.

In 2012, the BEA advised (BEA 2012b)

> During the acoustic searches undertaken during the first phase, the raw acoustic data from the towed pinger locators (TPL) was not recorded. Use of post-readout software would have made it possible to check if the ULB signals were present in the background noise. For future passive acoustic search systems, it appears to be essential to record this raw acoustic data.

Drift measurement buoys

On 5 July 2012, BEA issued numerous recommendations resulting from the AF447 investigation (BEA 2012), addressing several matters relevant to SAR. A recommendation addressed to ICAO recommended the amendment of ICAO Annex 12 to encourage contracting States to equip their search aircraft with buoys to measure drift and to drop them, when these units are involved in the search for persons lost at sea.

Aviation industry statements

International Air Transport Association

In an 11 November 2014 report on issues surrounding flight tracking and search activities, the IATA Aircraft Tracking Task Force (ATTF) made seven recommendations addressing aircraft tracking and coordinating responses to aircraft incidents (International Air Transport Association Aircraft Tracking Task Force 2014).

British Airline Pilots Association

On 8 March 2017, the British Airline Pilots Association (BALPA) issued a media release urging improved position tracking, including retrofitting advanced position tracking technology onto older aircraft (British Airline Pilots' Association 2017).

Safety actions

The key developments related to aircraft search in recent years are summarised here, and it is likely that other organisations have implemented additional local safety measures. It should be noted that the pace of change in aviation can be slow, especially when changes are far reaching. In addition to the time taken to determine and agree on the best approaches at an international level, it is necessary to provide state regulators, manufacturers and operators time to prepare and implement them.

International Civil Aviation Organization

In recent years, ICAO have convened several working groups and meetings to discuss issues related to aircraft tracking and search activities. Some are ongoing at the time of writing, with the following changes to ICAO Standards and Recommended Practices implemented from 2014 through 2016:

- Annex 6 Amendments 38 and 40-A introduced provisions for automatic deployable flight recorders (ADFR). These are deployable, buoyant flight data recorders that have an integrated ELT instead of a ULB.
- Annex 6 Amendment 38 also requires recorder-mounted ULBs to have increased battery life of 90 days from 1 January 2018. From the same date, most large aircraft operated on remote

oceanic routes are to be equipped with an additional airframe-mounted, long-range, 30-day ULB to supplement those fitted to the flight recorders.

- Annex 6 Amendment 40-A also introduced requirements for responding to distress alerts, and clarifications related to the use of emergency location equipment. Complementary to Amendment 40-A, ICAO Document 10054, *Manual on Location of Aircraft in Distress and Flight Recorder Data Recovery* is in development at the time of writing.

Annex 6 Amendment 39 specified aircraft to be fitted with tracking equipment from 8 November 2018, with 15-minute tracking intervals (recommended for all commercial aircraft over 27 t and mandated for aircraft over 45.5 t[35]). This interval is to be decreased to every minute for an aircraft in distress[36], for aircraft certified after 1 January 2021 (recommended for new aircraft designs over 5.7 t and mandated for aircraft over 27 t). This is to provide 'a high probability of locating an accident site to within a 6 NM radius'. In recent years the two largest regulators of aircraft manufacturers, EASA and the United States Federal Aviation Administration (FAA), implemented similar new rules governing the fitment and specification of ULBs.

Inmarsat

On 12 May 2014 Inmarsat announced the proactive provision of free ADS position reporting at 15-minute intervals to all aircraft equipped with its Classic Aero system (the system installed on MH370) which represents most long-haul commercial aircraft. Inmarsat's more recent Swift Broadband service, which has been operational for over five years and is currently installed on more than 1,000 commercial passenger aircraft, automatically records the location of all aircraft in flight every two minutes for system optimisation purposes at no cost.

Malaysia Airlines

Malaysia Airlines plans to implement satellite-based ADS-B data monitoring and automated alerting to its existing fleet when the Aireon satellite constellation is operational in 2018. It was reported that this will not require the installation of any new equipment and will be capable of minute-by-minute reporting (Aireon 2017).

Airservices Australia

Among many other air traffic services providers worldwide, Airservices Australia have implemented a satellite ADS-C service. This enables aircraft to be tracked at 14-minute intervals in Australian airspace. According to Airservices Australia, controllers can now observe and react to any unusual flight behaviour and notify SAR agencies sooner. In the event of an abnormal situation, the reporting rate automatically increases to every five minutes. Air traffic controllers are also able to set the rate to near real-time for individual aircraft if required.

Joint committee

In 2013 the Radio Technical Commission for Aeronautics (RTCA) and European Organisation for Civil Aviation Equipment (EUROCAE) convened a joint committee (SC-229 and WG 98) to update standards addressing the latest design, performance, installation and operational issues for 406 MHz emergency beacons. In part, the committees' scope includes the study of in-flight triggering and crashworthiness (Radio Technical Commission for Aeronautics 2016).

---

[35] As a guide, the latter category includes aircraft about the size of a Fokker 100 or larger.

[36] Triggering criteria is provided in EUROCAE ED-237, *Minimum Aviation System Performance Specification for Criteria to Detect In-Flight Aircraft Distress Events to Trigger Transmission of Flight Information*.

Conclusions

Flight tracking

Some of the most significant safety actions to date include:

- ICAO mandated that new aircraft types must be capable of detecting unsafe conditions, which triggers near-continuous data and position reports that can be remotely monitored.
- ICAO mandated that operators will need to track aircraft position at 15-minute intervals in normal flight.
- Airservices Australia now tracks aircraft position at 14-minute intervals within Australian airspace, and the reporting rate can be increased in response to abnormal situations.
- Inmarsat and Malaysia Airlines have voluntarily implemented a secondary means of position tracking that exploits a previously-unused capacity of existing technology.

There are some limitations to the improvements. The 15-minute position tracking interval may not reduce the search area enough to ensure that survivors and wreckage are located within a reasonable timeframe. This should be alleviated in new aircraft by the use of ADFRs and triggered, and subsequently near-continuous position reports but the former may not be widespread and the latter may not be effective when there are multiple aircraft system failures. Furthermore, until either capability is retrofitted to existing aircraft, the tracking interval would remain at 15 minutes and, with several new types already in service, there may be no significant change for many years. ATSB considers it highly desirable to find ways of implementing similar measures to existing aircraft. This can be done by increasing the rate of position reports, by implementing triggered transmissions, or recognising that there may be technical limitations of existing equipment, some combination of both.

Inmarsat and Malaysia Airlines have demonstrated that improvements to current – and previous – generation aircraft can be made with a relatively small initial outlay and minimal ongoing cost. While this approach may not provide the same level of functionality as mandated for newer aircraft, it should be applied to the existing fleets and aircraft designs that will constitute the bulk of air transport for the foreseeable future.

Given that many emergencies involve aircraft system failures and high crew workload, airborne locating systems must be designed to be automated as much as possible and resilient to failure of other systems (such as power), impact, fire, and immersion in water. For security reasons they should also be resistant to tampering and remote interference.

Emergency locator transmitters

The use of automatic deployable flight recorders (ADFR) is likely to significantly improve the information available for a search. An ADFR would have an integrated ELT that is more likely to remain operational after accidents over land and sea, and can also be used to monitor debris drift. However, partly due to technical challenges in ADFR design, there may be significant costs in developing and installing them and there are currently no rules requiring that they be installed. For this reason, other avenues should be explored to enhance ELT effectiveness in existing and future fleets.

Following the search and investigation into the loss of AF447, the BEA issued a recommendation to EASA and ICAO in regard to the activation of ELTs as soon as an emergency situation is detected on-board the aircraft. This is broadly similar in concept to the increase in position reporting rates for aircraft certified from 2021 onwards, but has the advantage of potentially being more readily retrofitted to existing fleets, and would also be more resilient to multiple aircraft system failures. International groups have been studying ways to improve ELT effectiveness.

Drift measurements

The surface search drift modelling was informed by the deployment of self-locating datum marker buoys from aircraft and vessels. Standard SAR marker buoys have an expected lifetime of around 20 days once deployed in the ocean and are fitted with a drogue. Their design attempts to minimise the effects of wind and surface waves so the buoy drifts primarily with the surface layer (top one to two metres of water) in a way analogous to a human being treading water.

Using standard SAR marker buoys to track the potential path of MH370 debris over long periods had some limitations. Their battery life needed to be longer, preferably several months at least, and the buoys needed to be designed to drift in a way similar to the debris which was recovered, on the surface and subject to the effects of both wind and surface waves.

Visual and radar search aids

Consideration could be given to installing automatically-deployed, floating search aids such as streamers or radar reflectors, particularly if it is feasible to install several, because they will tend to drift together with other debris. These could be incorporated as part of seat cushion design, or placed in frangible containers in cargo compartments and empty spaces throughout the airframe, to break loose during an impact sequence and can ultimately aid in the search for survivors, bodies, and floating wreckage. Water marking dye and smoke could also be considered, but less likely to be feasible because of their limited useful duration, and because smoke devices can themselves be hazardous.

Underwater locator beacons

Previous searches illustrate the benefit of having ULB devices that are as reliable, long-range and long-duration as practicalities permit. With greater battery life, a search can be extended if needed. With greater range, more area can be searched in a given period of time.

ICAO have mandated the introduction of ULBs that have a longer battery life and, for remote oceanic flights, have a much greater effective signal distance. The latter means that a greater area can be searched in a given period of time, and also that more assets can be deployed to searches in deeper waters where more specialised equipment was previously needed. These improvements to airborne equipment should greatly improve the likelihood of a successful underwater search.

Further improvements can be made by addressing the ways that a search is conducted. It is imperative to differentiate between ULB signals and others, and to make the most of available equipment to ensure that even very faint signals are detected. Examples of ways to accomplish both of these things are to record all measurements so that they can be reviewed later, and wherever possible, to use signal processing techniques to evaluate the validity of signal detections and maximise the detection sensitivity.

The BEA previously advised search authorities to record all acoustic data for later analysis if needed, in case a faint, ambiguous or obscured signal was not initially identified. In the case of the search for MH370, some recorded acoustic data was later analysed by several agencies to establish the validity of potential detections. Other potential detections could not be re-analysed because the data was not recorded; this meant that a search asset was diverted to the area for another scan, reducing the total area that could be acoustically searched in the limited time available. Though it made no difference to the outcome on this occasion, this kind of difficulty can be readily overcome if all search data is continuously recorded.

During the search for MH370, ATSB found that military sonobuoys can provide a rapidly-deployed and effective means to listen for ULBs over a wide area. One sortie was capable of searching an area of approximately 3,000 km^2. It is therefore beneficial to use this type of asset when possible.

Other considerations

As mentioned previously, the pace of change in aviation can be slow. Depending on the nature of the, as yet, undetermined reasons for the loss of MH370, it is possible that timely fulfilment of the BEA's 2009 and 2011 recommendations on transmission of flight data might have assisted in the search for MH370. On the other hand Inmarsat's voluntary and proactive inclusion of rudimentary tracking information into its satellite communications system has proven invaluable. This demonstrates how beneficial advancements can be found and implemented before the formal process is complete, and that those solutions can be simple and low-cost.

The equipment fit of current aircraft is far from uniform, and every operation is different. For example, there is less benefit in having frequent position reports if an effective distress or diversion alerting system is in place, or an aircraft is fitted with an ADFR, or if it only flies in radar-controlled airspace. Operators and manufacturers will need to find innovative ways of improving existing fleets in a way that suits their individual needs and capabilities. Regulators should support this approach.

To maximise effectiveness, an approach similar to that made for flight safety can be applied to the fitment of tracking and emergency location equipment. It is beneficial to have a level of functional overlap between systems to maximise reliability in the event of malfunction, and to reduce interdependencies for important systems.

Finally, though there are many uncontrollable factors that hinder a search, such as weather, remoteness and water depth, these factors can be managed. It is therefore critical to plan for an emergency response. Above all, a quick response can greatly assist in delivering a successful outcome. This means having the technology in place for alerting and information transfer, and the ground-based resources and processes to monitor and respond to them. Each system will be different depending on the requirements and capabilities of the operation, but the most important consideration is that the system needs to be viewed in its entirety from normal flight to finding underwater wreckage. This will make the process both effective and efficient.

ATSB safety recommendations

Malaysia is the responsible State for the ICAO Annex 13 investigation into the occurrence involving Boeing 777-200ER registered 9M-MRO and operating as Malaysia Airlines flight 370 (MH370). As a State that has participated in the investigation, Australia may also issue safety recommendations under Annex 13.

Search and rescue information

There is relatively limited public and official information available about the process and outcomes of some searches. It is not an explicit part of the ICAO Annex 13 guidelines for inclusion in an accident investigation report. Similarly there is no Annex 12 requirement to publish or analyse search information. This limits the ability for researchers to determine the factors that help or hinder a search.

Therefore the ATSB recommends that:

- ICAO encourages or mandates the publication of relevant information about search, rescue and recovery operations for the benefit of future research.
- ICAO Annex 13 investigation bodies should endeavour to publish relevant information about search, rescue and recovery operations for the benefit of future research.

Aircraft tracking

While there has been significant enhancements in the tracking of commercial aircraft in recent years there are some limitations to the improvements. The ICAO mandated 15-minute position tracking interval for existing aircraft may not reduce a potential search area enough to ensure that survivors and wreckage are located within a reasonable timeframe.

Therefore the ATSB recommends that:

- States ensure that sufficient mechanisms are in place to ensure a rapid detection of, and appropriate response to, the loss of aircraft position or contact throughout all areas of operation.
- Aircraft operators, aircraft manufacturers, and aircraft equipment manufacturers investigate ways to provide high-rate and/or automatically triggered global position tracking in existing and future fleets.

Sources and submissions

Sources of information

The sources of information used in the preparation of the report included the:

- Air Accidents Investigation Branch of the United Kingdom
- Annexes to the Convention on International Civil Aviation (Chicago, 1944)
- Australian Geospatial-Intelligence Organisation
- Australian Maritime Safety Authority
- Australian National University
- Boeing
- Bureau of Meteorology Defence Meteorological Support Unit
- Commonwealth Scientific and Industrial Research Organisation
- Curtin University Centre for Marine Science and Technology
- Defence Science and Technology Group
- Department of Civil Aviation Malaysia
- Dukane
- External contributors including members of the public reporting items of debris
- French Civil Aviation Safety Investigation Authority, BEA
- French Judicial Authorities
- French meteorological service on La Réunion Island
- French Ministry of Defence
- Fugro Survey Pty Ltd
- Geoscience Australia
- Hydrospheric Solutions Inc.
- Inmarsat
- Joint Agency Coordination Centre
- Joint Investigation Team
- Los Alamos National Laboratory (United States)
- Malaysia Airlines
- Ministry of Transport Malaysia
- National Aeronautics and Space Administration
- National Transportation Safety Board of the United States
- People’s Republic of China government agencies
- Phoenix International Holdings Inc.
- Royal Australian Air Force
- Royal Australian Navy
- Royal Navy
- Scientific experts at Australian and international universities, museums and institutions
- Tangaroa Blue Foundation Ltd and Celestial Vision
- Thales
- University of Adelaide.

References

Aireon 2017, *Malaysia Airlines Enlists SITAONAIR, Aireon and FlightAware for 100% Global Flight Tracking*, media release, Aireon, Virginia, 18 April.

Australian Transport Safety Bureau 2013, *A review of the effectiveness of emergency locator transmitters in aviation accidents*, ATSB Transport Safety Report AR-2012-128, ATSB, Canberra.

Aviation and Railway Accident Investigation Board 2015, *Crash Into The Sea After An In-Flight Fire, Asiana Airlines, Boeing 747-400F, HL7604, International Waters 130 km West Of Jeju International Airport, 28 July 2011*, Aircraft Accident Report ARAIB/AAR1105, Aviation and Railway Accident Investigation Board, Sejong Special Self-governing City, Republic of Korea.

British Airline Pilots' Association 2017, *Pilots renew call for improved tracking on all aircraft on MH370 three-year anniversary*, media release, BALPA, London, 8 March.

Bureau d'Enquêtes et d'Analyses pour la sécurité de l'aviation civile 2009a, *Flight Data Recovery Working Group Report*, Technical document, BEA, Paris.

Bureau d'Enquêtes et d'Analyses pour la sécurité de l'aviation civile 2009b, *Interim Report n°2 on the accident on 1st June 2009 to the Airbus A330-203 registered F-GZCP operated by Air France flight AF 447 Rio de Janeiro – Paris*, BEA, Paris.

Bureau d'Enquêtes et d'Analyses pour la sécurité de l'aviation civile 2011a, *Interim Report n°3 On the accident on 1st June 2009 to the Airbus A330-203 registered F-GZCP operated by Air France flight AF 447 Rio de Janeiro – Paris*, BEA, Paris.

Bureau d'Enquêtes et d'Analyses pour la sécurité de l'aviation civile 2011b, *Triggered Transmission of Flight Data Working Group Report*, Technical document, BEA, Paris.

Bureau d'Enquêtes et d'Analyses pour la sécurité de l'aviation civile 2012a, *Final Report On the accident on 1st June 2009 to the Airbus A330-203 registered F-GZCP operated by Air France flight AF 447 Rio de Janeiro – Paris*, update 27 July 2012, BEA, Paris.

Bureau d'Enquêtes et d'Analyses pour la sécurité de l'aviation civile 2012b, *Sea Search Operations*, BEA, Paris.

Defence Research and Development Canada 2009, *Emergency Locator Transmitter (ELT) Performance in Canada from 2003 to 2008: Statistics and Human Factors Issues*, report prepared by J Keillor, G Newbold, A Rebane, S Roberts & J Armstrong, Technical Report DRDC Toronto TR 2009-101, Defence Research and Development Canada, Toronto.

International Air Transport Association Aircraft Tracking Task Force 2014, *Aircraft Tracking Task Force Report and Recommendations*, IATA, Montréal.

Inmarsat 2014, *Inmarsat to provide free global airline tracking service*, media release, Inmarsat, London, 12 May.

International Civil Aviation Organization 2016, *Annex 6 to the Convention on International Civil Aviation – Operation of Aircraft Part I – International Commercial Air Transport – Aeroplanes*, 10th edn, ICAO, Montréal, ATT K-1.

Komite Nasional Keselamatan Transportasi 2015, *PT. Indonesia Air Asia Airbus A320-216; PK-AXC Karimata Strait Coordinate 3º37'19"S – 109º42'41"E Republic of Indonesia 28 December 2014*, Aircraft Accident Investigation Report KNKT.14.12.29.04, KNKT, Jakarta.

Kurniadi T & Ng J 2015, 'Challenges of Sea Search and Recovery Operations - Sharing of Experience from a Recent Joint Operation', paper presented to the International Society of Air Safety Investigators Annual Seminar, Augsburg, Germany, 24-27 August.

Radio Technical Commission for Aeronautics 2016, 'Special Committee (SC) 229 – 406 MHz Emergency Locator Transmitters (ELTs) Terms of Reference', Revision 2, RTCA Paper No. 151-16/PMC-1506.

Stimson CM 2015, '2nd Generation ELT Performance Specification Development', visual presentation presented to the International SAR 2015 Conference and Exhibition, Brighton, United Kingdom, 12-13 May.

Submissions

Under Part 4, Division 2 (Investigation Reports), Section 26 of the *Transport Safety Investigation Act 2003* (the Act), the Australian Transport Safety Bureau (ATSB) may provide a draft report, on a confidential basis, to any person whom the ATSB considers appropriate. Section 26 (1) (a) of the Act allows a person receiving a draft report to make submissions to the ATSB about the draft report.

A draft of this report was provided to:

Air Accidents Investigation Branch of the United Kingdom

Australian Department of Defence

Australian Department of Finance

Australian Department of Infrastructure and Regional Development

Australian Maritime Safety Authority

Australian National University

Boeing

Bureau d'Enquêtes et d'Analyses pour la Sécurité de l'Aviation civile (France)

Chinese Maritime Safety Administration

Civil Aviation Administration of China

Commonwealth Scientific and Industrial Research Organisation

Curtin University Centre for Marine Science and Technology

Defence Science and Technology Group

Department of Civil Aviation Malaysia

Fugro Survey Pty Ltd

Geoscience Australia

Hydrospheric Solutions Inc.

Inmarsat

Joint Agency Coordination Centre

Komite Nasional Keselamatan Transportasi, Indonesia

Los Alamos National Laboratory (United States)

Malaysia Airlines Berhad

Ministry of Transport Malaysia

National Transportation Safety Board of the United States

Phoenix International Holdings Inc.

Thales

Transport Safety Investigation Bureau of Singapore

Submissions were received from:

Air Accidents Investigation Branch of the United Kingdom

Australian Department of Finance

Australian National University

Boeing

Commonwealth Scientific and Industrial Research Organisation

Defence Science and Technology Group

Fugro Survey Pty Ltd

Inmarsat

Malaysia Airlines Berhad

Ministry of Transport Malaysia

The submissions were reviewed and where considered appropriate, the text of the report was amended accordingly.

Appendices

Appendix A: Search vessels

Search vessels

Fugro Equator

At the time of involvement in the underwater search, the purpose built survey vessel, *Fugro Equator*, was operated by Fugro Survey Pty. Ltd., Australia. The ATSB contracted Fugro Survey Pty. Ltd. to provide the vessel, marine crew, survey crew and subsea equipment for search services in support of the ATSB led search operations to locate MH370. With a low acoustic signature, the vessel is fitted with a hull-mounted Kongsberg EM302 deep water multibeam echo sounder to undertake seabed mapping.

Fugro Equator involvement in the underwater search spanned from June 2014 to February 2017.

Figure 1: *Fugro Equator*

Source: Steph Turner

Ship details

Name:	*Fugro Equator*
IMO number:	9627411
Call sign:	C6ZT5
Flag:	Bahamas
Classification society:	Germanischer Lloyd
Ship type:	Research Survey Vessel
Year built:	2012
Owner(s):	Fugro Equator Inc.
Manager:	Fugro Survey Pte Ltd
Gross tonnage:	1,929 t
Deadweight:	564 t
Length overall:	65.74 m
Main engine(s):	3 x Mitsubishi S12R-MPTA
Maximum power:	3,420 kW
Service speed:	10 knots

GO Phoenix

At the time of involvement in the underwater search, the anchor handling tug supply (AHTS) vessel, *GO Phoenix*, was owned and managed by GO Marine Group Pty Ltd (GO Marine), Australia. The vessel was under charter to Phoenix International Holdings Inc. (Phoenix) who were contracted by DEFTECH, on behalf of the Malaysian Government, to provide Government Furnished Equipment (GFE) in support of the ATSB led search operations to locate MH370.

GO Marine provided the marine crew, and Phoenix provided the survey crew and subsea equipment. Phoenix subcontracted Hydrospheric Solutions Inc. (SLH) to provide survey crew and the ProSAS SLH PS-60 synthetic aperture sonar (SAS) system.

Go Phoenix involvement in the underwater search spanned from September 2014 to June 2015.

Figure 2: *GO Phoenix*

Source: ATSB Client Representative

Ship details

Name:	*GO Phoenix*
IMO number:	9495208
Call sign:	V7AW9
Flag:	Marshall Islands
Classification society:	Det Norske Veritas
Ship type:	Anchor Handling Tug Supply Vessel
Year built:	2013
Owner(s):	Hai Jiao 1207 Ltd
Manager:	Go Offshore Asia Pte Ltd
Gross tonnage:	7,534 t
Deadweight:	4,500 t
Length overall:	91.0 m
Main engine(s):	2 x MaK 16M32C
Maximum power:	16,000 kW
Service speed:	13 knots

Fugro Discovery

At the time of involvement in the underwater search, the survey vessel *Fugro Discovery* was operated by Fugro Survey Pty. Ltd., Australia. The ATSB contracted Fugro Survey Pty. Ltd. to provide the vessel, marine crew, survey crew and subsea equipment for search services in support of the ATSB led search operations to locate MH370.

Originally purpose built as a Norwegian Navy patrol boat, the vessel underwent a conversion before joining the Fugro fleet as a multi-role geophysical and hydrographic survey vessel.

Fugro Discovery involvement in the underwater search spanned from October 2014 to August 2016.

Figure 3: *Fugro Discovery*

Source: Fugro Survey/Oliver Edwards

Ship details

Name:	*Fugro Discovery*
IMO number:	9152882
Call sign:	3EKE6
Flag:	Panama
Classification society:	Det Norske Veritas
Ship type:	Research Survey Vessel
Year built:	1997
Owner(s):	Fugro Discovery Inc.
Manager:	Fugro Marine Services BV
Gross tonnage:	1,991 t
Deadweight:	1,350 t
Length overall:	70.0 m
Main engine(s):	1 x MaK 6M32
Maximum power:	2,638 kW
Service speed:	10 knots

Fugro Supporter

At the time of involvement in the underwater search, the survey vessel *Fugro Supporter* was operated by Fugro Survey Pty. Ltd., Australia. The ATSB contracted Fugro Survey Pty. Ltd. to provide the vessel, marine crew, survey crew and subsea equipment (AUV system) for search services in support of the ATSB led search operations to locate MH370.

Originally built as a Buoy and Lighthouse Tender, the vessel underwent a conversion before joining the Fugro fleet as a multi-purpose geophysical and hydrographic survey vessel.

Fugro Supporter involvement in the underwater search spanned from January 2015 to May 2015.

Figure 4: *Fugro Supporter*

Source: ATSB

Ship details

Name:	*Fugro Supporter*
IMO number:	8518364
Call sign:	JZKY
Flag:	Indonesia
Classification society:	Biro Klasifikasi Indonesia
Ship type:	Research Survey Vessel
Year built:	1994
Owner(s):	Suar Samudera Abadi PT
Manager:	Suar Samudera Abadi PT
Gross tonnage:	2,065 t
Deadweight:	1,152 t
Length overall:	75.39 m
Main engine(s):	3 x Caterpillar 3516TA
Maximum power:	2,760 kW
Service speed:	12 knots

Havila Harmony

At the time of involvement in the underwater search, the survey vessel *Havila Harmony* was operated by Fugro NV. The ATSB contracted Fugro Survey Pty. Ltd. to provide the vessel, marine crew, survey crew and subsea equipment (AUV system) for search services in support of the ATSB led search operations to locate MH370.

Originally built as an Offshore Supply Vessel, the vessel underwent a conversion before joining the Fugro fleet as a multi-purpose geophysical and hydrographic survey vessel, fitted with dynamic positioning (DP2).

Havila Harmony involvement in the underwater search spanned from November 2015 to March 2016.

Figure 5: *Havila Harmony*

Source: Fugro

Ship details

Name:	*Havila Harmony*
IMO number:	9343596
Call sign:	LAYW7
Flag:	NIS (Norway)
Classification society:	Det Norske Veritas
Ship type:	Offshore Support Vessel
Year built:	2005
Owner(s):	Havila Offshore Labuan Ltd
Manager:	Havila Shipping ASA
Gross tonnage:	4,724 t
Deadweight:	3,000 t
Length overall:	92.95 m
Main engine(s):	4 x Cummins QSK60-M
Maximum power:	7,600 kW
Service speed:	13.5 knots

Dong Hai Jiu 101

At the time of involvement in the underwater search, the search and rescue vessel, *Dong Hai Jiu 101*, was operated by the Dong Hai Rescue Bureau, China. The vessel and marine crew was made available by the Chinese Government to support the ATSB led search operations to locate MH370. Dong Hai Jiu translates to East China Sea.

The ATSB contracted Phoenix to provide the survey crew and subsea equipment. Phoenix subcontracted SLH to provide survey crew and the ProSAS SLH PS-60 synthetic aperture sonar (SAS) system. Phoenix also provided an ROV system.

Dong Hai Jiu 101 involvement in the underwater search spanned from January to December 2016.

Figure 6: *Dong Hai Jiu 101*

Source: ATSB

Ship details

Name:	*Dong Hai Jiu 101*
IMO number:	9654816
Call sign:	BSIN
Flag:	China
Classification society:	China Classification Society
Ship type:	Search and Rescue Vessel
Year built:	2012
Owner(s):	China Government Dong Hai Rescue Bureau
Manager:	China Government Dong Hai Rescue Bureau
Gross tonnage:	4,747 t
Deadweight:	1,759 t
Length overall:	116.95 m
Main engine(s):	2 x MAN-B&W 6L48/60CR
Maximum power:	14,400 kW
Service speed:	21 knots

Appendix B – Identification of the most probable final location of flight MH370 (Issue 2) – Joint Investigation Team paper - 26 April 2014

Note: This appendix provides a copy of the analysis as provided post a Joint Investigation Team (JIT) briefing to AMSA on 2 April 2014. The paper therefore describes the analysis and advice to 2 April 2014 and represents only a snapshot of the JIT on-going analysis to early April 2014.

The paper provides the background on BTO and BFO analysis during the Australian-led surface search in March-April 2014. The reader should consider the contents of this paper in this context only. Later published technical analysis of BTO and BFO referred to in the main report links provides the refined BTO and BFO analysis used to define underwater search areas.

At the time this paper was written the aircraft manufacturer, was providing assistance to Malaysia and the ATSB in establishing:

- possible reasons for the total communication loss between 1707 UTC and 1825 UTC (page 3)
- end-of-flight scenario theories based on the final arc as it related to possible fuel exhaustion (page 16).

No current investigations or assessments are currently being undertaken by Boeing into this.

The JIT paper analysis provided in this appendix showing a 400 knots best fit path was revised on 5 April 2014 for 425 knots as the best fit. (See Table 15 of the main report).

IDENTIFICATION OF THE MOST PROBABLE FINAL LOCATION OF FLIGHT MH 370 (ISSUE 2)

INTRODUCTION

This document records the development of a process, up to 2 April 14, to determine the most probable final location of Flight MH 370. Issue 2 was issued on 26 April 14 with some minor changes to ensure that the terminology for handshake is consistent with earlier communications. There are no changes in the resultant search areas.

Timing information obtained from satellite data and aircraft performance data was used to identify a Northern and Southern corridor along which Flight MH 370 may have flown. Doppler information from the satellite data, combined with aircraft performance data was then used to further refine the most probable final location. Finally, consideration was given to the navigation of the aircraft and the mode that it may have flown in utilising the stored routes and waypoints in its Flight Management System. This work concluded that Flight MH 370 probably ended in an area 375 nautical miles long and 40 nautical miles wide, centred approximately 900 nautical miles off the west coast of Australia, with the most probable location in the northern part of this area.

At the time of this report, further work is being carried out using the satellite data in order to further refine this position.

Timings. All timings are UTC. Malaysian time (MYT) is UTC + 8 hours.

BACKGROUND INFORMATION ON SATELLITE COMMUNICATIONS

Functions

Satellite Communications (SATCOM) provides the satellite link for the following functions:

- Audio and text communication.
- Interface with ACARS.
- In-flight Entertainment Equipment.

Technical information

The aircraft satellite communication system operates on L Band, transmits at 1.6 GHz and receives at 1.5 GHz. The Earth Station uses C Band, transmits at 6 GHz and receives at 4 GHz. During the flight of MH 370, the aircraft communicated through the Inmarsat Indian Ocean Region (IOR) I-3 satellite and the Earth Station in Perth Australia.

There are a number of channels available for messages to be sent between the satellite and Earth Station. One of the channels is called the 'common access channel', which aircraft will listen to when not engaged in a call on another channel.

If the ground station has not heard from an aircraft for an hour since the last communication then it transmits a 'log on / log off' ("ping") message on the common access frequency using the aircraft's unique identifier. If the aircraft receives its 'unique identifier' it returns a short message that it is still logged onto the network. This process has been described as a handshake.

The following timing information is recorded at the satellite Earth Station for each handshake:

- Earth Station to the Satellite,
- Satellite to the Aircraft,
- Aircraft to the Satellite,
- Satellite to the Earth Station.

During the flight of MH 370, the satellite reached its most northerly point of the inclination orbital path at approximately 19:30 hrs, after which it moved in a southerly direction increasing in velocity until it crossed the equatorial plane at 01:30 hrs. For an aircraft in the southern hemisphere the satellite appears to be moving towards it during this period and hence the Doppler frequency increases as the satellite velocity increases. For an aircraft in the northern hemisphere the satellite will appear to be moving away from it and the Doppler will decrease as the satellite's velocity increase.

INITIAL PREDICTIONS OF THE AIRCRAFT FLIGHT PATH

Initial information

MH 370 departed Kuala Lumpur international airport (KLIA) at 16:41 hrs on 7 March 14. On 8 March 14, Malaysian Airlines (MAS) established that the aircraft SATCOM had completed a handshake with the

Inmarsat satellite at 00:19 hrs. At this time MAS also estimated that there was sufficient fuel on the aircraft for it to remain airborne until 00:12 hrs.

Final seven handshakes

Apart from a period between the last ACARS message at 17:07 hrs and the handshake at 18:25 hrs on the 7 March 14, the SATCOM link was available during the flight. This interruption of the SATCOM link occurred after ACARS had stopped transmitting messages and may have occurred for a number of reasons such as cycling of the electrical power, the aircraft's antenna losing sight with the satellite or the resetting of the aircraft's Satellite Display Unit (SDU). There is no record in the satellite Earth Station log of the link having been logged-off from the cockpit through the Control Display Unit (CDU); such an activity would have been automatically captured in the Earth Station log. The reason for the loss of the SATCOM link is currently being investigated by the aircraft and equipment manufacturers.

Data from the last seven handshakes[1] was used to help establish the most probable location of the aircraft. Initially only six of these handshakes, which had been initiated by the Earth Station, were considered to be complete. The seventh and last handshake, which had been automatically initiated by the aircraft, was originally assessed as a partial handshake and was not used in the analysis. Two unanswered ground to air telephone calls had the effect of resetting the activity log and hence increased the period between the ground initiated handshakes. The significant timings used to identify the most probable final location of the aircraft are as follows:

Aircraft departs KLIA	16:41 hrs
Last ACARS transmission	17:07:48 hrs
1st – handshake initiated by the ground station	18:28:27 hrs
Unanswered ground to air telephone call	18:39:52 hrs
2nd – handshake initiated by the ground station	19:41:00 hrs
3rd – handshake initiated by the ground station	20:41:02 hrs
4th – handshake initiated by the ground station	21:41:24 hrs
5th – handshake initiated by the ground station	22:41:19 hrs
Unanswered ground to air telephone call	23:13:58 hrs
6th – handshake initiated by the ground station	00:10:58 hrs
7th – handshake initiated by the aircraft	00:19:29 hrs
Aircraft did not respond to handshake from the satellite earth ground station.	01:15:56 hrs

[1] Since the 2 April 14 the seven handshakes have been redefined such that only five meet the definition originally given in this paper. This change makes no difference to the final location of the aircraft. In order to be consistent with information previously released by the Malaysian authorities, Issue 2 of this paper continues to call all seven contacts 'handshakes'.

Construction of the seven arcs

From the time that it took the signals to be sent and received by the Earth Station it was possible to determine the elevation between the aircraft and satellite at each handshake and the previous ACARS exchanges. This elevation data is plotted in Figure 1.

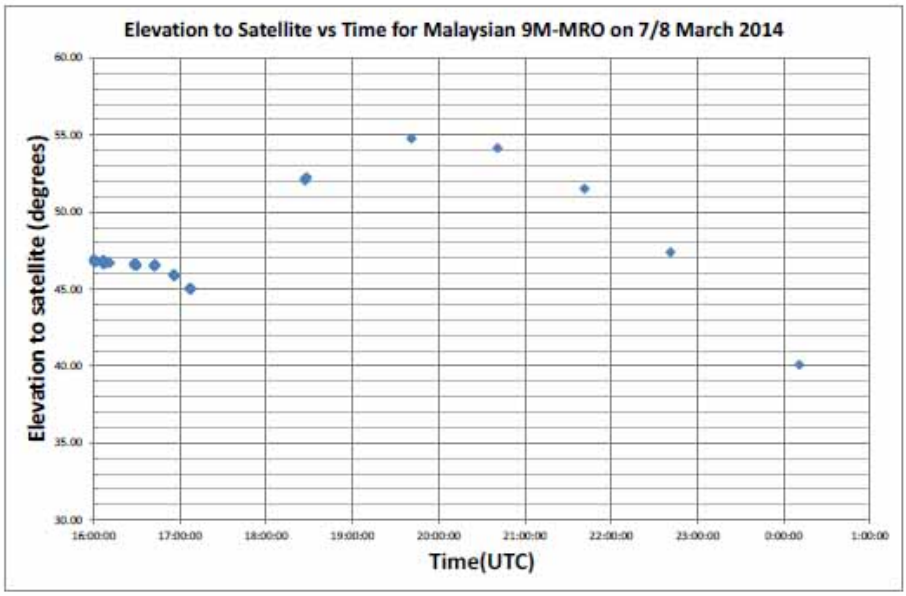

Figure 1 – Plot of the elevation of the aircraft to the satellite

This initial analysis assumed a fixed satellite location. The analysis was subsequently updated to incorporate the inclined orbit of the satellite, which reached approximately 1,200 km above and below (z-axis) the equatorial plane over a 24 hour period. On the 7 March 14, the satellite was at the most northerly point of its orbit at approximately 19:30 hrs.

The time that the seven handshakes occurred and the exact knowledge of the satellite location enabled a number of arcs to be drawn on the earth's surface at a fixed distance from the satellite - the altitude of the aircraft was not taken into account. The length of these arcs was constrained by the maximum speed of the aircraft, which was initially set at a ground speed of 652 kt. The arcs for the seven handshakes are shown at Figure 2.

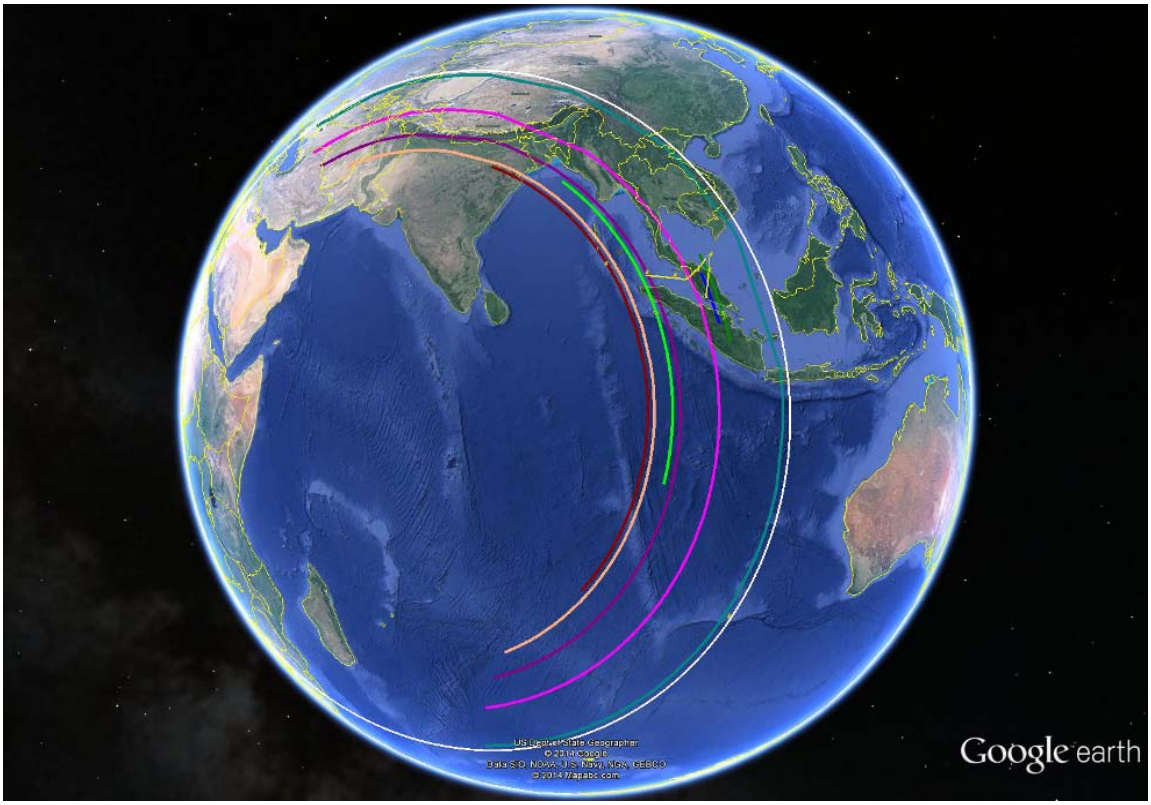

Figure 2 - Position of the arcs obtained from the 7 handshakes

Development of Northern and Southern routes

Primary radar data provided by the Royal Malaysian Air Force detected an aircraft believed to be MH 370, flying through the Straits of Malacca. At this time only the location data was used in the final location analysis as the accuracy of the speed and altitude information was not known. Therefore, for the initial calculations, the altitude and speed of the aircraft was obtained from the data in the cruise report, timed at '17:06:43 hrs' ('latitude 5.299º S and longitude 102.813º E') that had been transmitted via ACARS. The altitude was recorded as 35,000 feet and from the other recorded parameters Boeing calculated a ground speed of 473 kts. The cruise report also stated that the total fuel weight (TOTFW) at this time was 43,800 kg.

The aircraft had to cross each of the seven arcs at the time of the handshake. Using the assumption that the aircraft altitude and speed remained the same, it was possible to estimate where the aircraft would have crossed the 1st arc. This approach produced two solutions, one heading in a northerly direction and the second in a southerly direction.

Boeing undertook a number of performance calculations varying the speed and altitude to determine the range of the aircraft. The speed chosen affected where the aircraft crossed each of the arcs. This resulted in a family of solutions along the arc generated by the satellite data from the 6th handshake. These

northern and southern solutions are shown in Figure 3 and are bounded by the low and high speed flight paths which terminate on the final position arcs (6th arc).

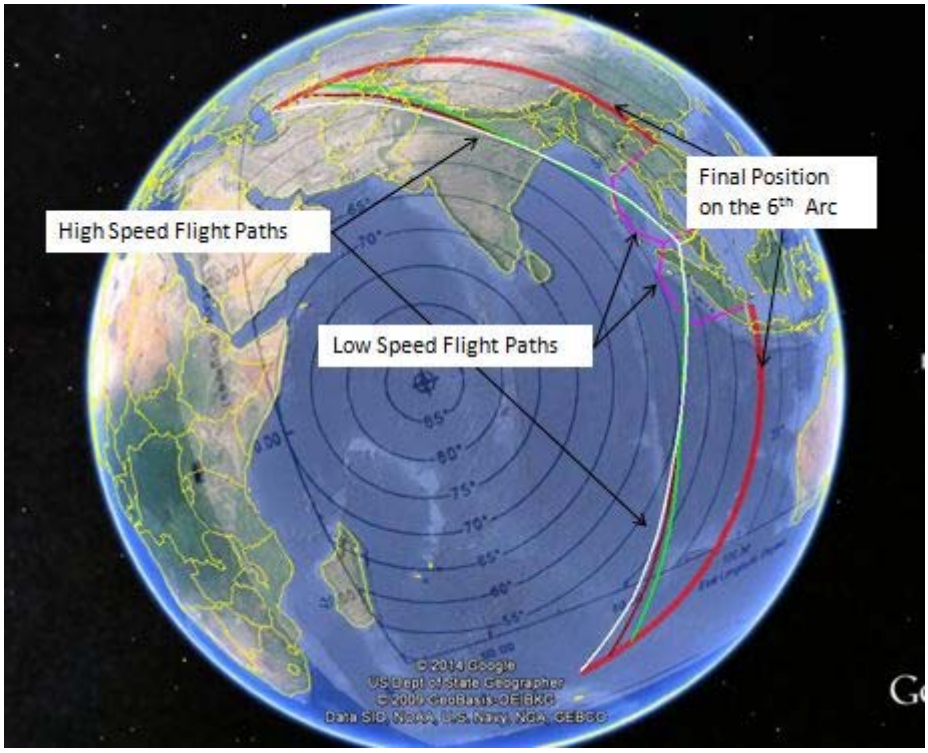

Figure 3 - Northern and southern final position arcs

PREDICTIONS BASED ON THE OFFSET BURST FREQUENCY

In order to determine if the aircraft flew the northern or southern route a second technique was developed by Inmarsat, which considered the relative velocity of the satellite to the aircraft. This technique considered the difference in frequency of the pulse sent and received by the earth station, which was defined as the Offset Burst frequency (OBF).

Use of Doppler data to help locate the aircraft

The OBF results from the position and movement of the satellite relative to the aircraft. The aircraft attempts to compensate for the Doppler generated by the aircraft's movement and the Earth Station for the movement of the satellite. The contribution to the OBF from the various Doppler contributions is shown in Figure 4.

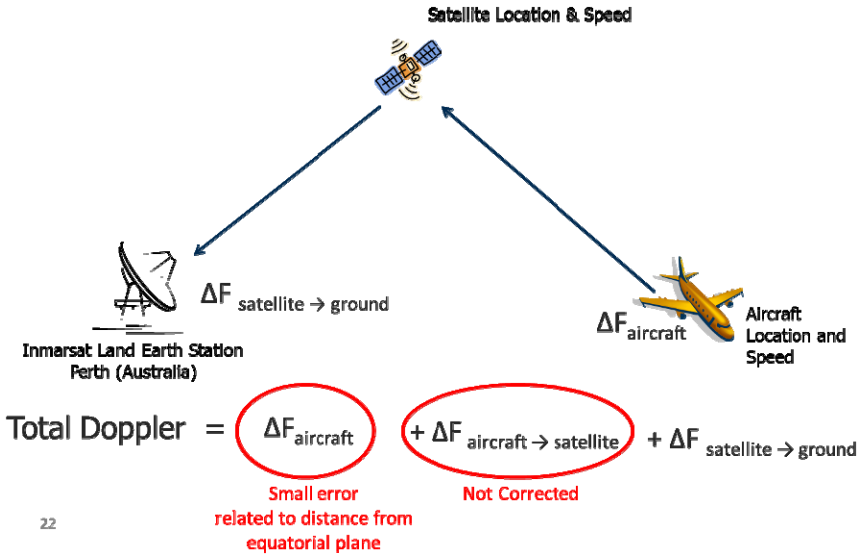

Figure 4 - Doppler contributions to OBF

The Doppler is comprised of the following components:

- The $\Delta F_{aircraft}$ component is the correction applied by the terminal for the aircraft velocity and assumes a fixed satellite position. When the satellite is furthest from the assumed position the applied frequency offset error, while not large, will be its largest. As the satellite moves towards the equatorial plane the assumed satellite position becomes closer to reality and the correction applied by the terminal become more accurate and the $\Delta F_{aircraft}$ error becomes insignificant.

- The $\Delta F_{aircraft \rightarrow satellite}$ component is at its lowest when the satellite is turning from a northerly to southerly direction. The satellite will accelerate as it heads towards the equatorial plane so the $\Delta F_{aircraft \rightarrow satellite}$ component becomes larger with time. For an object in the southern hemisphere the satellite will now be moving towards it and hence the Doppler will increase. This is what the data shows for MH 370 indicating that it had flown to the south.

The overall Doppler is therefore a combination of $\Delta F_{aircraft}$, which is largest earlier in the flight and decreases over time, and $\Delta F_{aircraft \rightarrow satellite,}$ which is lowest earlier in the flight and increases over time. The maximum error for $\Delta F_{aircraft}$ is still quite small and is of the same order of magnitude as $\Delta F_{aircraft \rightarrow satellite}$ during the first few hours after the last known ACARS transmission.

The theory is that the frequency shift will be different depending where you are on the arc, the direction of travel and the speed of the aircraft. This theory has been checked against 11 other Boeing 777 aircraft, flying in various northern and southern directions.

While on the ground at Kuala Lumpur airport and during the early stage of the flight MH 370 transmitted 17 messages. At this stage the location of the aircraft and the satellite were known; therefore it was possible to calculate the system time delay for the aircraft, satellite and ground station. The OBF was calculated at each handshake and knowing the time and position of the satellite it was possible, considering the aircraft performance, to determine where on each arc the OBF would fit best.

The position that the aircraft crossed the 6th arc was dependent on the aircraft speed and the position where the aircraft turned south after flying north along the Straits of Malacca. The assumption was that the turn south occurred at the northern end of Sumatra. The analysis showed poor correlation on the northern track, but good correlation on the southern track. The analysis also indicated that using these assumptions, speeds of approximately 450 kts and 400 kts resulted in the best fit. This can be seen in Figure 5.

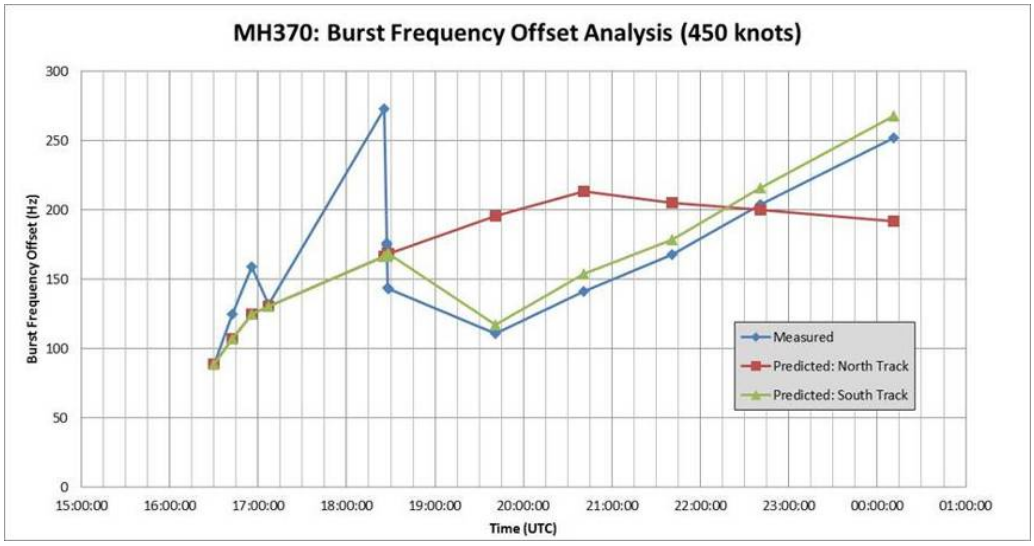

Figure 5 - Best fit OBF at 450 kts

The yellow track shown in Figure 6 is an example of a quick turn south after the final military radar contact coupled with a high speed track of 450 kts. The red track represents a more northern track after the final military radar contact followed by a 400 kts southern track. This shows a good correlation between the southern track prediction and the aircraft performance.

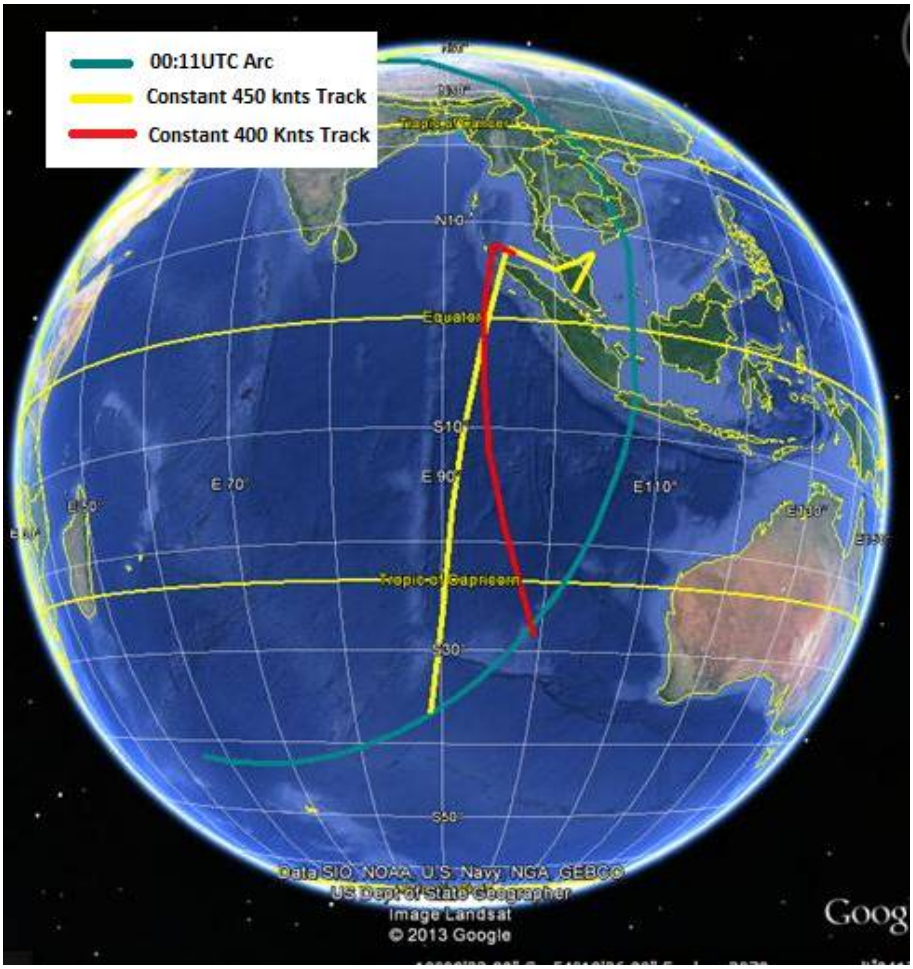

Figure 6 - Examples of southern solutions from Inmarsat analysis

It was possible to assess the accuracy of the analysis using the timing from the 17 messages transmitted from the aircraft while it was on the ground at Kuala Lumpur airport. The maximum positional error from the analysis was approximately 17 km. Inmarsat advised that the positional error of the 6th and 7th arcs would be of the same order.

No response was received from the aircraft at 01:15:56 hrs when the ground earth station sent the next log on / log off message, indicating that the aircraft was no longer logged onto the network.

This analysis established that the aircraft had not flown along the northern corridor and it was unlikely that the flight ended in the north part of the southern corridor. However the flight had to have crossed the 6th arc at 00:10:58 hrs and the 7th arc at 00:19:29 hrs. The estimation of the final position had yet to be determined.

FIRST PROPOSED SEARCH AREAS

Performance based analysis

The first proposed search areas were established by using Boeing's performance predictions and the criteria that for a track to be valid it must reach the 6th arc. The flight tracks shown in Figure 7 represent the maximum distances based on the crossing of the arcs and the speed of the aircraft. The lower boundary defined by S1 to S5 represents the maximum range of the aircraft. As the S1 and S2 areas were created by the longest and straightest tracks they initially generated the greatest interest.

First assumption on lateral navigation mode

By setting a heading for the aircraft to fly, the track would change with the increase in magnetic variation the further south the flight progressed. It was concluded that in order to be assured of flying a required track, the aircraft lateral navigation would probably have been selected to the 'track' mode. This would maintain the desired track with the increasing magnetic variation being compensated for.

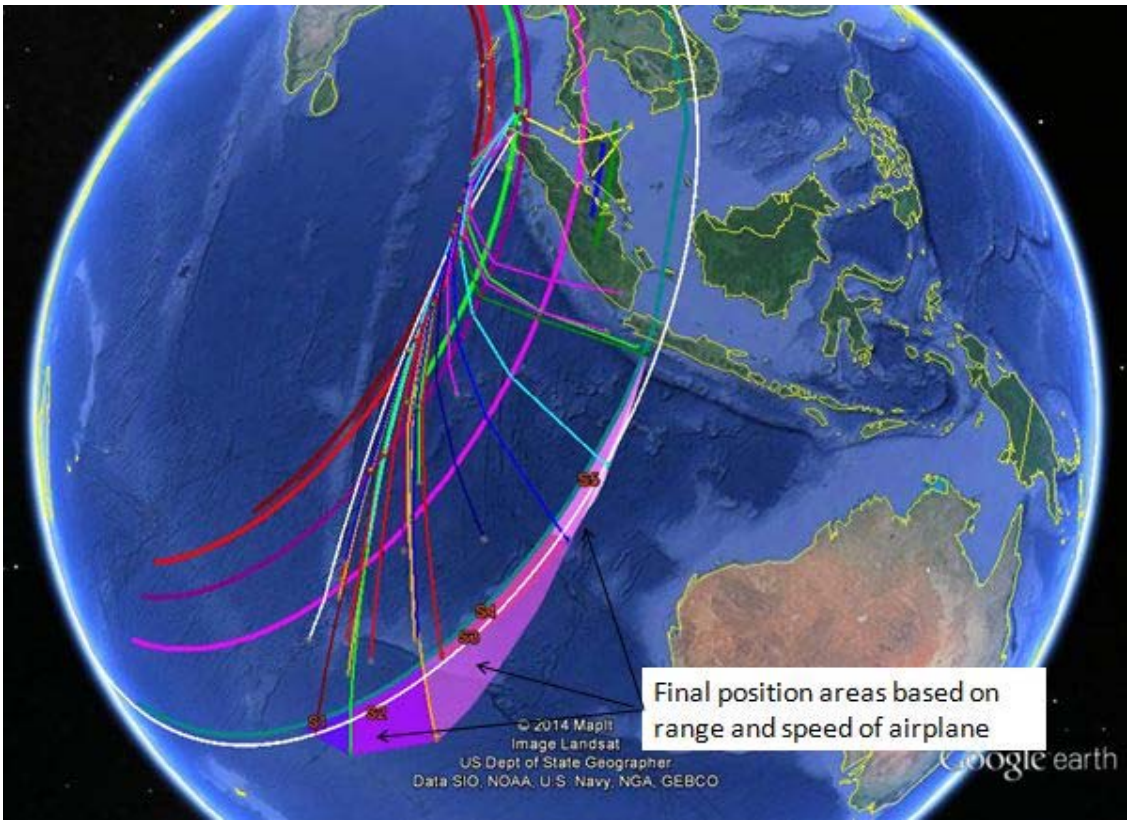

Figure 7 - Early final position locations based on aircraft performance

REFINEMENT OF INITIAL ASSUMPTIONS

Boeing's analysis of the aircraft's movement from the last ACARS reporting position and the end of the primary radar coverage showed that the aircraft had accelerated from 473 kts to 500 kts as it transited across the Malaysia Peninsular and along the Straits of Malacca. This was confirmed by the last two Royal Malaysian Air Force air defence radar returns.

Moving the aircraft's turn south to a position slightly north of Sumatra resulted in a closer fit of the Doppler at the arc defined by the first handshake. This change resulted in a decrease in range for the longest flight paths that had helped to define S1 and S2 and which now no longer reached the 6th arc. Consequently S1 and S2 were no longer considered to be locations where the flight could have ended. See Figure 8.

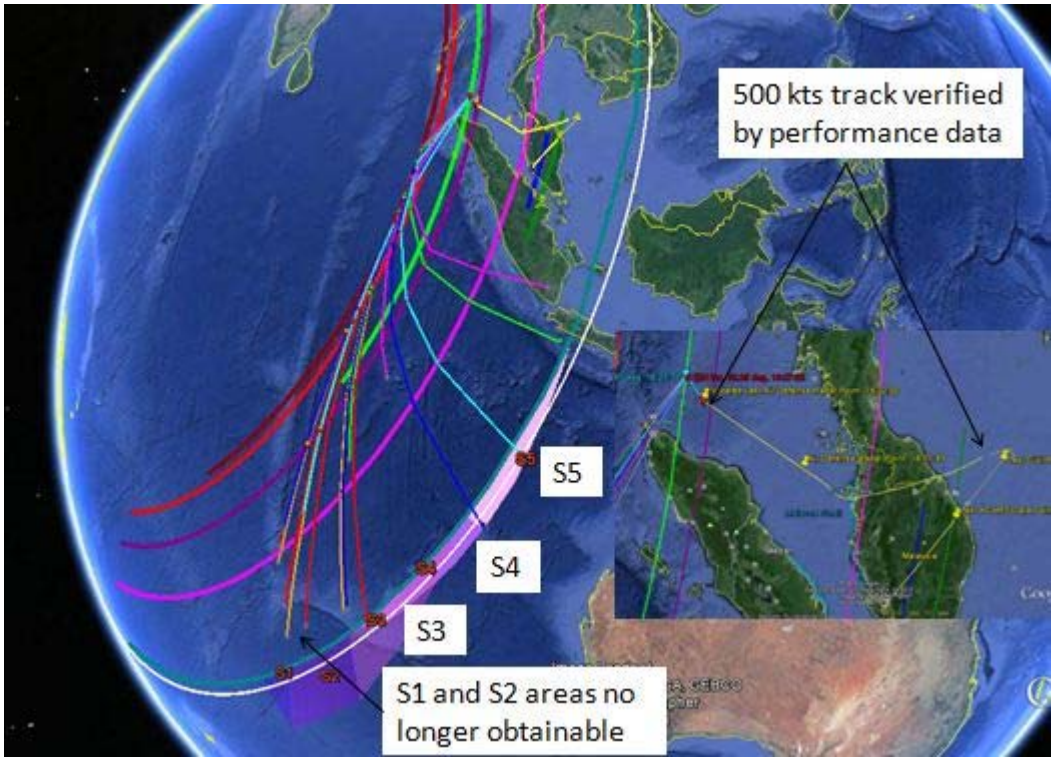

Figure 8 - Valid tracks based on Boeing analysis using Doppler and performance

THE SEVENTH HANDSHAKE

The timing offset used in the 7th handshake at 00:19:29 hrs, which had been initiated from the aircraft, was now better understood and allowed the position of the 7th arc to be defined. However, analysis of the

Doppler frequency revealed a significant difference to that predicted; actual was 2 Hz and predicted was 250 Hz.

From an analysis of the most probable reason why the aircraft had initiated the message, the working assumption was made that the 7th arc was the point at which Flight MH 370 ran out of fuel. The Doppler and performance calculations were then used to refine the final position along the arc.

SCENARIO ROUTE 1A AND 1B

In carrying out the Doppler and performance analysis, two scenarios, 1A and 1B, were developed. Scenario 1A required the aircraft to fly in a southern direction after it crossed the 1st arc. Scenario 1B required the aircraft to fly a northern route through waypoint IGREX and waypoint LAGOG, before flying south. The LAGOG waypoint was included as it was close to a supplied, high confidence position labelled '19:12Z'. The 1B scenario resulted in a reduced number of possibilities for the final position on the southern end of the 7th arc.

REFINEMENT OF INMARSAT ANALYSIS - 31 MARCH 14

Inmarsat reran their analysis using the 19:12Z position as a starting point. The analysis used ten evenly spaced points on the 2nd arc between the northern and southern limits where the aircraft could have crossed this arc. In each case the aircraft's speed across a range of 350 to 500 kts was analysed. The aircraft was also constrained to cross the arcs at the appropriate time and to travel in a straight line between the arcs, crossings at the designated speed.

The results were evaluated against the Differential Doppler predictions at the crossing of the last three arcs: handshakes 5, 6 and 7. The best fit for the aircraft tracks was found to be at 400 kts and this was independent of whether the analysis started from the new position or from the best point determined by the crossing of the 1st arc. This analysis assumed a constant speed after the 19:12Z point with the aircraft moving in a straight line between the arcs: the heading can change when the aircraft crosses an arc, but it must cross the next arc at the correct time.

Starting from position 19:12Z, the best fit is shown in Figure 9. It is within 1 Hz of the prediction for the final three data points, and results in a crossing of the 7th arc at Latitude 23.4°S, Longitude 102.8°E.

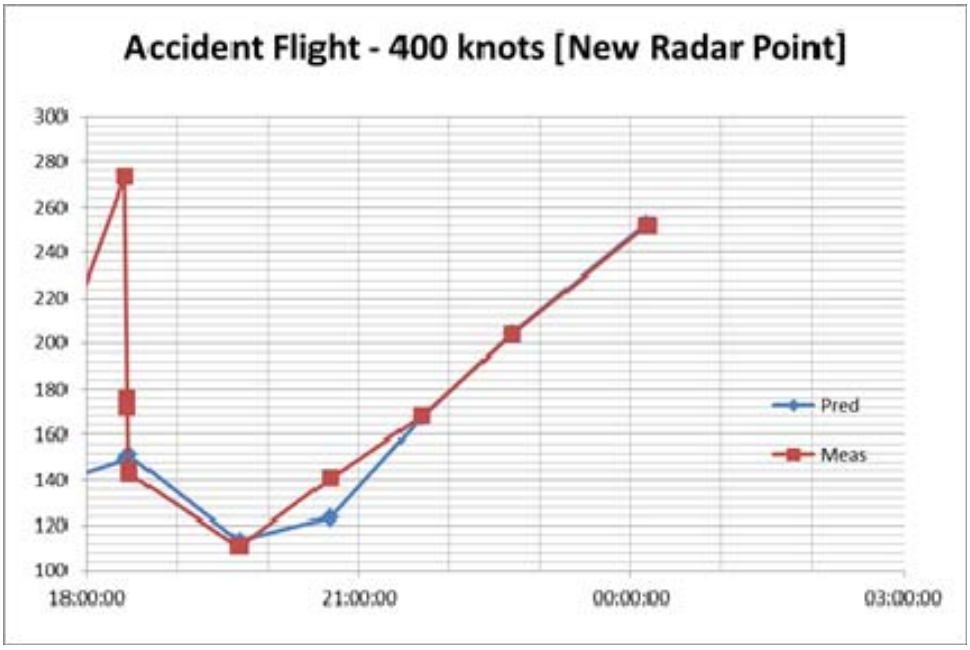

Figure 9 - Best fit for Inmarsat Doppler analysis

The higher accuracy of the satellite timing data means that the location of the arc itself is accurately known and the main error in the analysis occurs with the position of the aircraft. The analysis established that the mismatch between the measured and predicted frequency at the last handshake (7th arc) at speeds of 375 kts and 425 kts was as follows:

375 knots	20.6°S	104.2°E	[mismatch 6 Hz]
400 knots	23.4°S	102.8°E	[mismatch 1 Hz] <- best fit
425 knots	25.9°S	101.2°E	[mismatch 4 Hz]

Figure 10 shows these positions on the 7th arc.

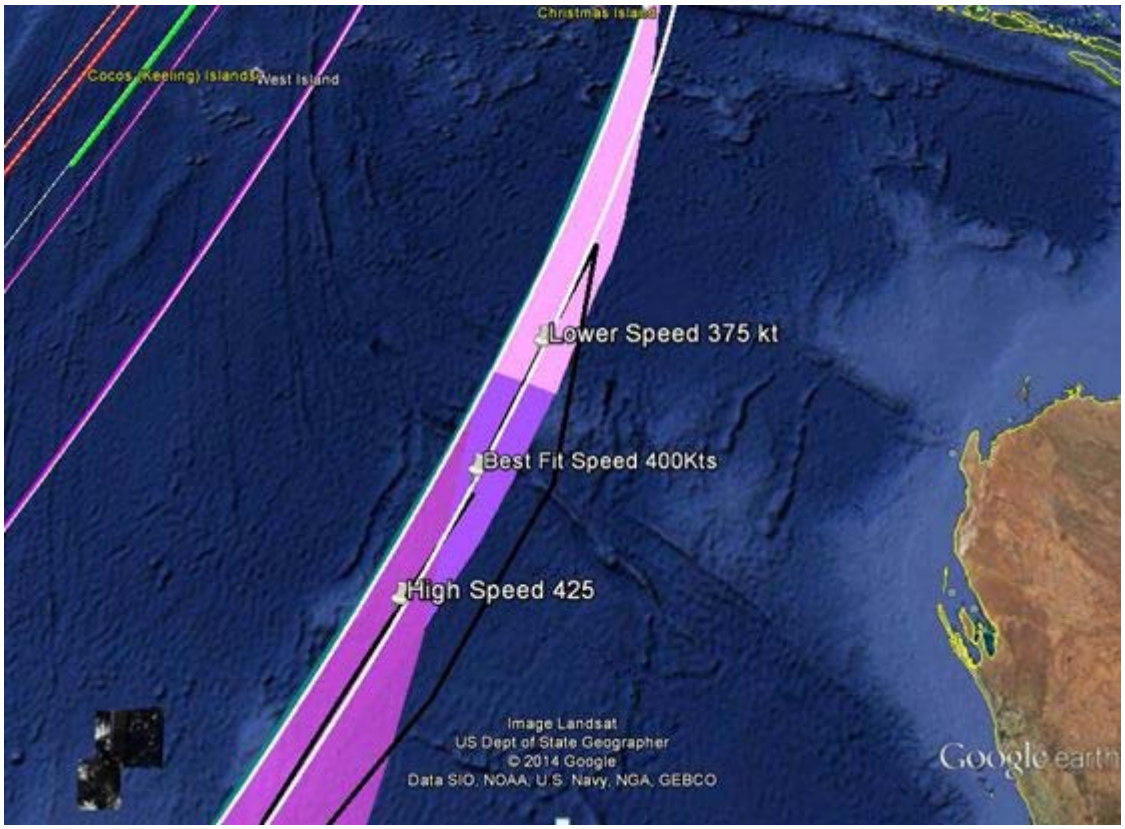

Figure 10 - Segment of the 7th arc over which Inmarsat Doppler information fits best.

As it is not known when the aircraft turned south, Inmarsat carried out an analysis using the 2nd arc crossing as the start location for a Monte Carlo style analysis. Ten different start locations on the 2nd arc were tested (equally spaced between 6°N and 4°S), at speeds ranging from 350 to 500 kts in 25 kt steps. The match with the differential Doppler curve at the final three points was used to evaluate the results.

In this analysis the track starting at the 6°N, 93.5°E crossing at the 2nd arc (19:41 hrs handshake) and terminating at 23.4°S 102.8°E crossing of the 7th arc, with a velocity of 400 kts, was the best fit. The sum of the mismatch across the last 3 arcs was 1 Hz. See Figure 11.

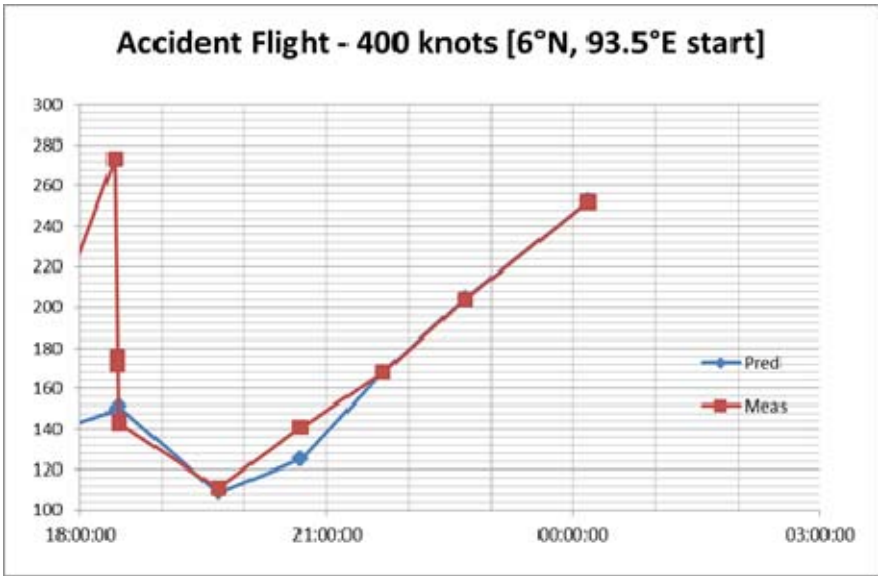

Figure 11 - Results of Inmarsat Monte Carlo style analysis

REFINEMENT OF BOEING ANALYSIS

In this refinement Boeing used the performance based flight tracks, previously identified, and compared the Doppler that these tracks generated with the Doppler information obtained from the OBF. The difference between the Doppler values was then classified as red, yellow, green or blue, with red being the 'best fit'. This further refinement identified a higher probability of final position solutions identified by the area bounded by the black line in Figure 12. The thickness of this bounded area was determined by maximum range calculations.

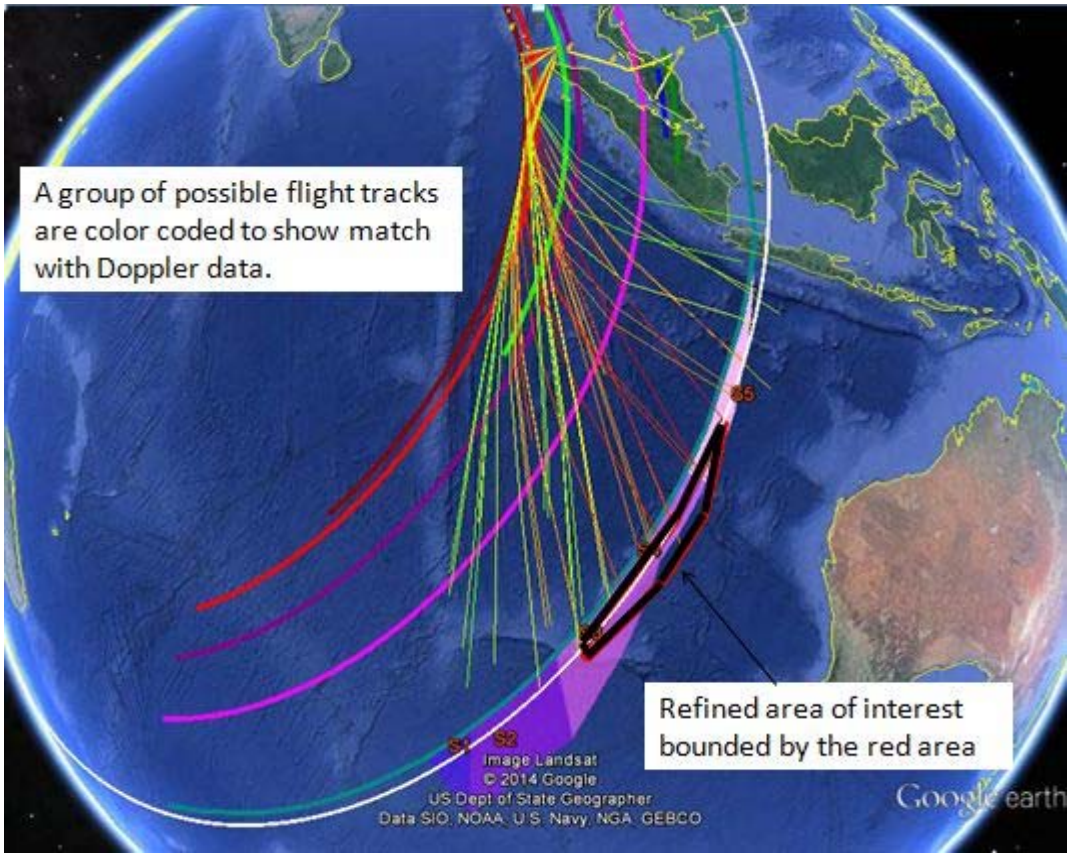

Figure 12 - Boeing combined Doppler and performance tracks

STATUS OF FLIGHT MH 370 AT SEVENTH ARC

The status of the airplane at the 7th and last arc (0:19:29 hrs), is still being assessed by Boeing. The exchange of information between the aircraft and the satellite was initiated by the aircraft's SATCOM system and does not contain the same characteristics as the previous six handshakes. There are a number of possibilities as to why the aircraft might have initiated this message.

AIR ROUTES

The track following the initial left turn off the planned route was towards Penang, from there the aircraft appeared to follow air routes to the 19:12Z position. The use of stored waypoints in the aircraft Flight Management System (FMS) suggests that the navigation was carried out using the Automatic Flight Control System (AFCS) in the lateral navigation mode. When the aircraft departed LAGOG the next major waypoint to the south was COCOS, which could be linked to the M641 air route. This would have taken the aircraft towards Perth. Once this route was set it would need no further input from the pilot for the aircraft to maintain altitude and route using the AFCS and auto throttle system. The fuel endurance would depend on the indicated airspeed selected and the flight level flown. This process allowed a

possible fixed point to be identified where both engines had flamed out at the 7th handshake. This would have been where the air route centreline crossed the 7th arc.

SIZING THE UNDERWATER SEARCH AREA

The final refinement to the underwater search area was obtained by overlaying the results of the refined Inmarsat Doppler analysis, Boeing refined Doppler and range analysis, and air route M641. The width of the area was determined by considering the error in the position of the 7th arc, the gliding range of an unpowered Boeing 777 from an altitude of approximately 30,000 feet. Consideration was also taken regarding the area that the towed underwater detector could cover before the predicted life of the batteries in the Dukane beacon expired.

The Joint Investigation Team had been advised that there were three assets available that could conduct underwater acoustic detection. Therefore the area was divided into three equal size segments along the arc with the highest priority given to the area where the air route M641 crossed the 7th arc. The proposed underwater search area, shown at Figure 13, is approximately 375 nautical miles long and 40 nautical miles wide and is defined by the following points:

U1	20° 16’ 2.71” S 104° 17’ 4.86” E	red, upper north west
U2	20° 29’ 10.22” S 105° 01’ 14.01” E	red, upper south east
U3	21° 55’ 50.84” S 103° 29’ 13.66” E	red/yellow, boundary north west
U4	22° 14’ 21.49” S 104° 08’ 34.81” E	red/yellow, boundary south east
U5	23° 42’ 18.69” S 102° 29’ 26.29” E	yellow/green, boundary north west
U6	24° 05’ 31.73” S 103° 06’ 27.22” E	yellow/green, boundary south east
U7	25° 49’ 56.65” S 101° 12’ 52.20” E	green, lower north west
U8	26° 09’ 59.47” S 101° 46’ 22.04” E	green, lower south east

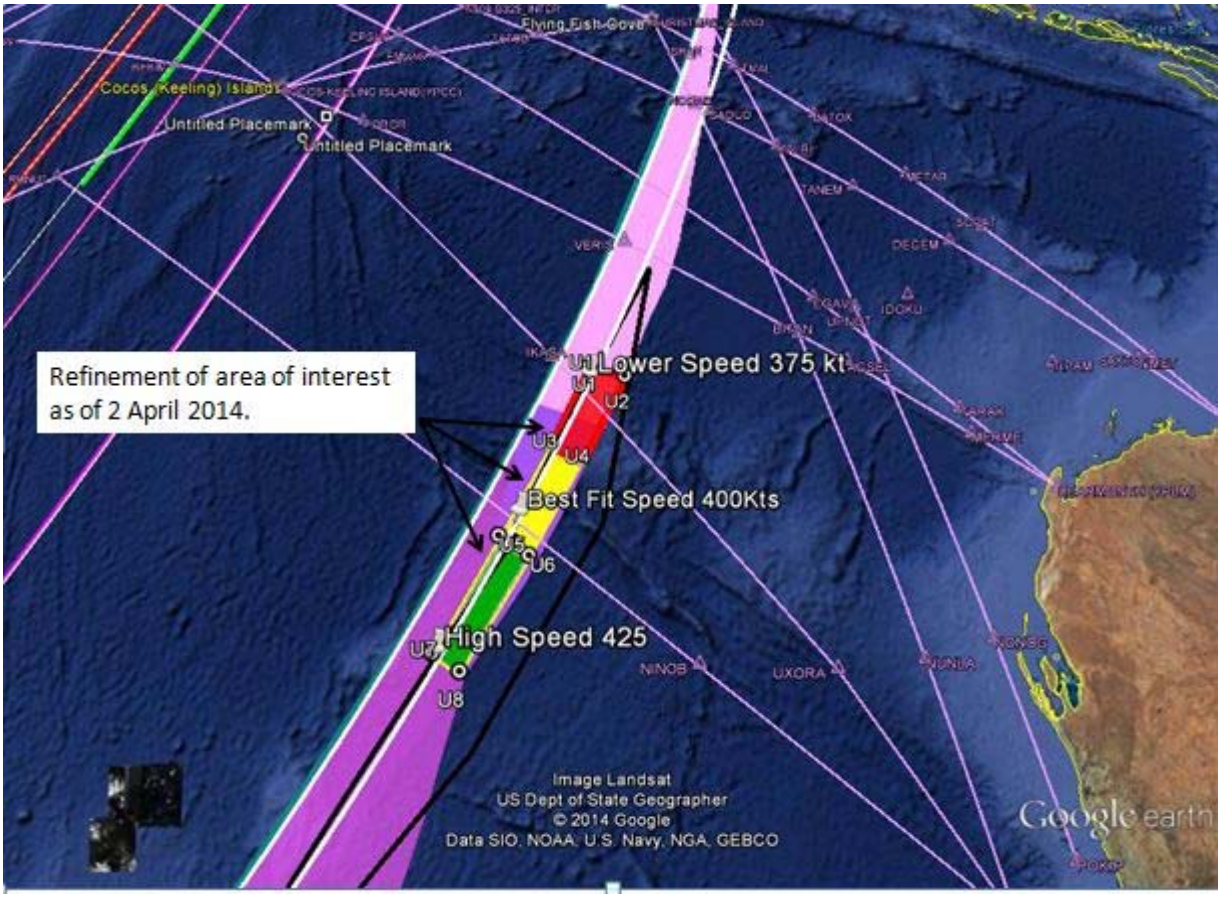

Figure 13 - Underwater search area as defined by the Joint Investigation Team on 2 April 2014

SUMMARY OF THE FACTORS USED TO DETERMINE THE UNDERWATER SEARCH AREAS

The following factors were used to determine the underwater search area.

- The flight ended after the 7th handshake, which occurred at 00:19:29 hrs on 8 March 2014.
- Based on the satellite timing data, the aircraft will be located near the 7th arc.
- The aircraft passed close to the point identified as 19:12Z.
- The measured Doppler profile closely matched that expected from an aircraft travelling in a southerly direction.
- Inmarsat analysis showed that the best fit for the Doppler frequency was at a ground speed of 400 kts, with slightly 'less' best fits at 375 and 425 kts. A Monte Carlo style analysis, using a number of different starting positions on the 2nd arc also gave a best fit at 400 kts. From this approach a most probable speed range of 375 to 425 kts was selected.

- Boeing analysis using a combination of aircraft performance and Doppler data, obtained from the satellite, to generate a range of probable best fit tracks. This work was supported by a Root Mean Square analysis that took account of a number of variables.
- Flight planning carried out by MAS independently showed that there was sufficient fuel onboard the aircraft to reach the positions determine by the Inmarsat and Boeing analysis.
- The length of the arc that defined the most probable area was obtained from the overlay of the results of the Inmarsat and Boeing approaches.
- Given the probable battery life of the Dukane beacon, and the number of assets available to conduct the underwater search, it was decided to break the underwater search area into three smaller areas.
- The width of the areas was defined by the probable position of the 7th arc, half of the glide range (40 nautical miles) and the area the towed detector could cover before the Dukane battery expired.
- The area that was crossed by air route M641 was classified as red (Priority 1), the next two priorities, yellow and green, were then defined moving south along the arc from this position.

The position and sizing of the underwater search area was based on the facts available on the 2 April 14. The analysis and underlying assumptions were constantly being reviewed and it was possible that further adjustments may be necessary.

CAUTION

The Doppler technique used as a method for determining the likely aircraft speed is sensitive to input variables and in particular the frequency compensation applied at the satellite earth ground station. As of the 2 April 14, work was still being carried out to understand these variables and the effect of the temperature variation as a result of the satellite experiencing an eclipse during the early part of the flight. Any further refinements would probably adjust the search area along the 7th arc.

Appendix C – Burst Frequency Offset (BFO) Doppler Model Development

Burst Frequency Offset (BFO) doppler model development[1]

BFO doppler model summary

Inmarsat commenced work on BFO doppler modelling in the days after the aircraft went missing, with effort being ramped up once the timing analysis was essentially complete. Three significant model variants were generated, although many others were developed on the way to these three.

'Differential Doppler Analysis Release 2 (OAMS)'.

This model was finalised on 22 March 2014 and was used to generate the curves that were released to the public at that time indicating that the aircraft took a southerly route. The Differential Doppler Analysis Release 2 (OAMS) modelled:

- doppler shift associated with aircraft and satellite movement;
- Perth GES translation error based on sinusoidal model;
- satellite frequency shift during eclipse period based on pilot signal measurements.

'Differential Doppler Analysis ECLIPSE_2'.

This model was distributed to the Satcom Subgroup on 8 April 2014 and incorporated:

- Better curve fitting and smoothing of data associated with Perth and satellite frequency translation;
- all data frequency translations that Inmarsat were aware of at the time, having a good understanding and justification for them all.

This model was used for the analysis to define the initial underwater search area. [2]

'*Differential Doppler Analysis UNIFIED_2x*'.

This was distributed to the Satcom Subgroup on 19 June 2014. The Differential Doppler Analysis UNIFIED_2x':

- corrected minor timing error in OAMS data (2 min 55 seconds);
- accurately modelled Perth and Satellite frequency translation based on measured data.
- was used for the explanatory notes at Appendix G of the ATSB report released on 26 June 2014.[3]

[1] This appendix should be read in conjunction with the Inmarsat paper *'The search for MH370'* published in Oct 2014 that presents analysis of the satellite signals that resulted in the definition of the MH370 search area. This paper is available via a link on the ATSB website at http://www.atsb.gov.au/mh370-pages/resources/fact-sheets/

[2] As shown in Table 2 and Appendix F of *'MH370 – Definition of Underwater Search Areas'* published on 26 June 2014. Available on the ATSB website at http://www.atsb.gov.au/mh370-pages/updates/reports/

[3] *'MH370 – Definition of Underwater Search Areas'* published on 26 June 2014 is available on the ATSB website at http://www.atsb.gov.au/mh370-pages/updates/reports/

BFO doppler model chronology

21 Mar 2014 *Differential Doppler Analysis*

First (internal to Inmarsat) release of fully worked out Doppler analysis, including AES velocity, satellite velocity, AES frequency correction, Perth GES frequency correction.

- No allowance made for satellite translation frequency variation;
- Perth GES frequency correction based on sinusoidal correction reported by GES staff.

Resultant curve indicated better fit for southern routes:

Figure 1: Differential Doppler Analysis BFO versus time (21 March 2014)

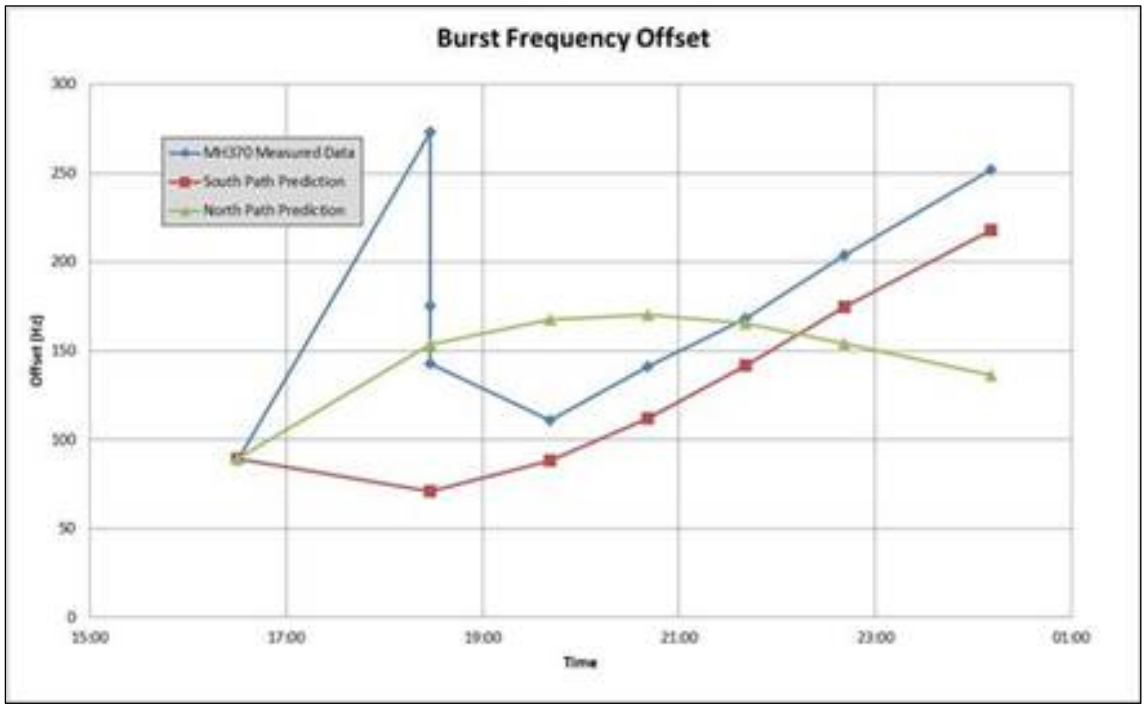

Source: Inmarsat

22 Mar 2014 *Differential Doppler Analysis Release 2 (OAMS)*

Updated analysis using measured data from Inmarsat's Off Air Monitoring System (OAMS) to improve the estimation of the Perth GES frequency correction. The OAMS measured data showed the receive frequency of a pilot signal after it had passed through the Perth receive system, and as well as showing the sinusoidal variation in frequency it showed the 'kink' caused by the satellite going through eclipse.

Figure 2: Measured pilot frequency error in Perth

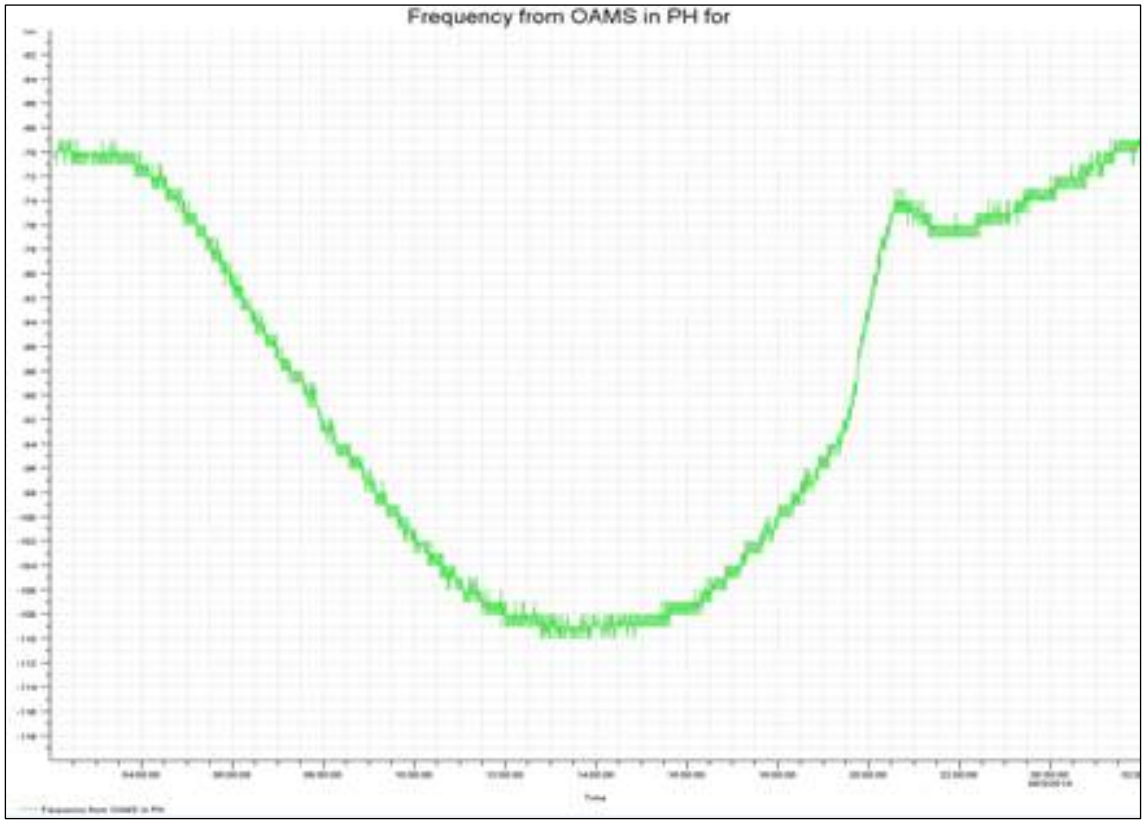

Source: Inmarsat

The OAMS data was inverted and scaled to give a more representative indication of the overall frequency correction due to satellite eclipse (the kink in the curve) and the Perth GES correction (the 24 hour sinusoidal shape). The scaling/inversion mapped the 24 hour frequency variation to the 24 hour frequency variation measured/reported by the Perth staff in the previous model. The effect of eclipse on the satellite translation frequency was determined by the scaled version of the kink in the curve.

- Satellite translation frequency variation outside of the eclipse effects were not modelled by this approach, but were assumed to be small.

The model gave good results when applied to a number of 'calibration' flights and it formed the basis for the statement by the Prime Minister of Malaysia and the release of the BFO chart on 24 Mar 2014. Whilst satellite translation frequency uncertainty was known to be present, the difference between the North and South paths was significantly larger than these errors, as determined by the calibration flights.

25 Mar 2014 *Differential Doppler Analysis EXT*

A tidied up version of the previous analysis, which removed unnecessary and obsolete calculations. This was released to the wider Satcom Group for peer review and checking, and to form the basis for subsequent flight path reconstruction work.

3 Apr 2014 *Differential Doppler Analysis ADJ_EXT*

Internal Inmarsat model where Eclipse and diurnal (sinusoidal) contributions to frequency translation were separated.

8 Apr 2014 *Differential Doppler Analysis ECLIPSE_1*

Formal release of previous model.

8 Apr 2014 *Differential Doppler Analysis ECLIPSE_2*

A tidied up version of the previous model distributed to the wider Satcom Group. The model incorporated all the frequency translations that Inmarsat were aware of, and they considered they had a good understanding and justification for all of them. The model indicated best fit agreement for a 400

kt [4]ground speed flight which crossed the 19:41 arc at 2°N. This showed the predicted and measured frequencies agreeing to within an average of 2 Hz for all five measurement points between 20:41 and 00:11 UTC. The track was on a constant heading of 165.3°ETN for the first three hours, then swings slightly to the East, ending at 28.2°S, 99.6°E at 00:19 UTC. It should be noted that the model provided reasonably good matches for a range of ground speeds between 375 and 500 knots from this starting location.

Figure 3: BFO vs time. AFC/ Eclipse corrected best fit - 400 knots (ends 28.2°S, 99.6°E)

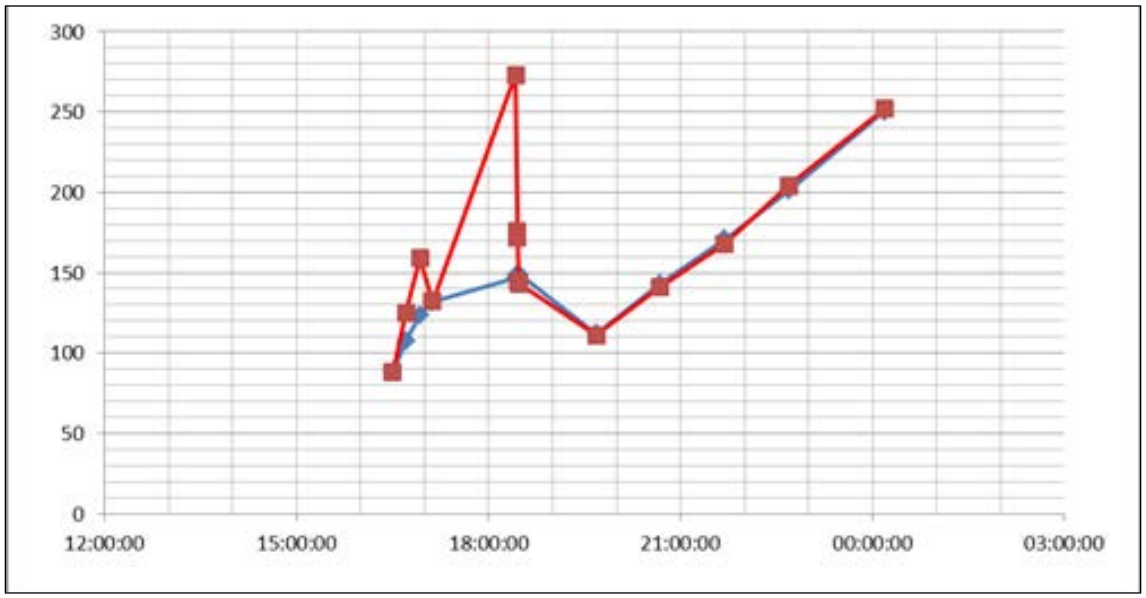

Source: Inmarsat

Eclipse 2 Sensitivity

The optimal fit was determined by starting from the 19:41 arc at different latitudes (in 1° steps from 4°S to 10°N). The best fit was clearly associated with the 2°N starting point. Ground speeds were varied in 25 knot steps from 350 knots to 500 knots, but were kept constant for each track analysed. Aircraft heading was kept constant between arc crossings, but was allowed to change as the ground track crossed each arc.

From the same starting point there were visible differences in quality of match for different ground speeds. For the (optimum) 2°N start point the match remained good across a range of ground speeds, but the gradient of the predicted (blue) and measured (red) lines diverge, indicating a 'sweet spot' in the range 375 to 500 knots, with end of flight between 25°S and 37°S:

Eclipse 2 Model Reference Data

The following reference data was used in the model:

- AES Frequency Compensation: used same algorithm as aircraft;
- AES induced Doppler: used location, ground speed & heading of AES and signal frequency and true satellite location;
- Satellite induced Doppler: used true satellite location/velocity and true AES and Perth GES location and frequency;
- Perth GES Frequency Compensation: calculated by comparing calculated pilot signal Doppler variation (known frequency, location and satellite velocity/location) with its variation after Perth GES frequency compensation applied;

[4] On 5 April 2014 the best fit speed was revised to 425 kts and the most probable path was adjusted

- Satellite eclipse frequency shift: measured from deviation of measured pilot frequency from residual Doppler related variations after GES frequency compensation applied (13 Hz variation measured, peaking around 19:40 UTC).

Verification

The model was verified using Malaysia Airlines Boeing 777 flight MH0093 from Narita to Kuala Lumpur on 7th March, which was in the air at the same time as MH370. It indicated a good match, but subject to errors of up to 3 Hz for individual measurement points.

Figure 4: BFO vs time. Eclipse 2 calibration

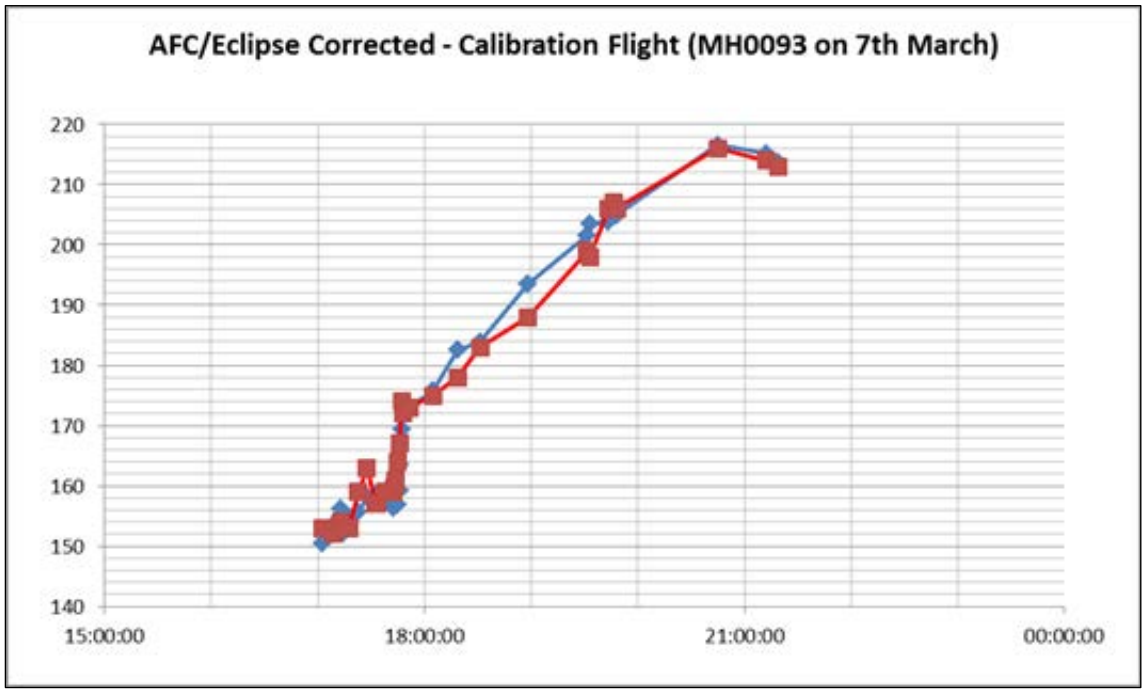

Source: Inmarsat

23 May 2014 Differential Doppler Analysis ECLIPSE_3

Internal Inmarsat model, refining curve fitting aspects of the ECLIPSE_2 model. Never released.

19 Jun 2014 BFO Analysis UNIFIED

The Unified model was developed when Inmarsat found out more about how the Miteq tracking receiver, used in the Perth GES, worked. The model avoided assumptions about the performance of the tracking receiver by processing the OAMS measured data in a different way to accurately measure the combined frequency shift of the Perth GES and the satellite, rather than trying to handle them separately. It fully modelled the pilot signal which forms the OAMS measured data to do this. The signal is transmitted at a constant frequency from the Burum GES (in the Netherlands) and is subject to Doppler shift due to satellite motion relative to both Burum (on the signal uplink) and Perth (on the signal downlink) which can be accurately predicted and removed from the OAMS measurement, leaving only the frequency variation related to the satellite frequency translation variation and the Perth GES translation frequency variation. This accurately calibrated out all frequency translations in the signal path and so was much more accurate than the previous ECLIPSE variants of analysis.

Figure 5: BFO vs time. Unified best fit 450 knots ends at 7th arc 32.7°S

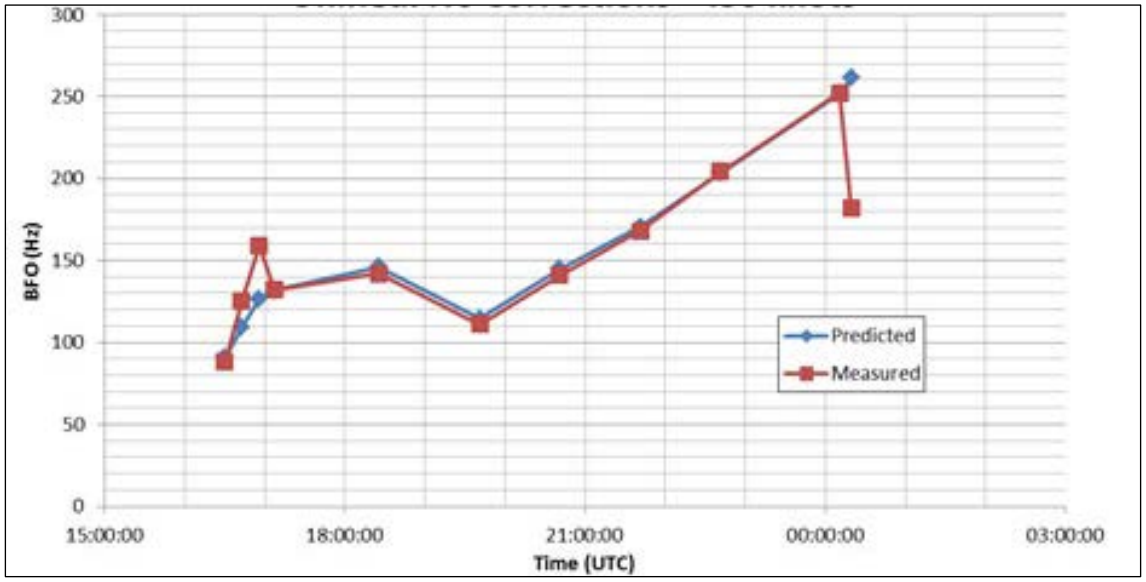

Source: Inmarsat

The UNIFIED model was briefed to the Search Strategy WG on 19 June 2014, explaining why it was more accurate than the previous ECLIPSE variants, and the spreadsheet containing the model was distributed.

20 Jun 2014 *BFO Analysis UNIFIED 2x*

A timing error of 2 minutes 55 seconds associated with the labelling of OAMS data records was corrected in this model, which was otherwise identical to the original UNIFIED model. It was distributed to the Search Strategy WG later on the same day as the original model was sent out.

21 Jul 2014 *BFO Analysis UNIFIED 3x*

Internal Inmarsat minor refinement of UNIFIED 2x model. Not distributed.

30 Jul 2014 *BFO Analysis UNIFIED 4x*

Formal release version of UNIFIED 2x model but with more streamlined lookup tables.

Appendix D – Fugro Survey Pty Ltd Search for Malaysian Airlines Flight MH370 All Vessels Reconnaissance Bathymetric Survey, Deep Tow Wide Area Survey and AUV Wide Area Survey Volume 7 – Summary Report

FUGRO SURVEY PTY LTD

Search for Malaysian Airlines Flight MH370

All Vessels

Reconnaissance Bathymetric Survey, Deep Tow Wide Area Survey and AUV Wide Area Survey

Volume 7 – Summary Report

Survey Period: 2 June 2014 – 24 January 2017
Fugro Document No: FRPT GP1500-SUM_Vol7_Summary Report

Australian Transport Safety Bureau

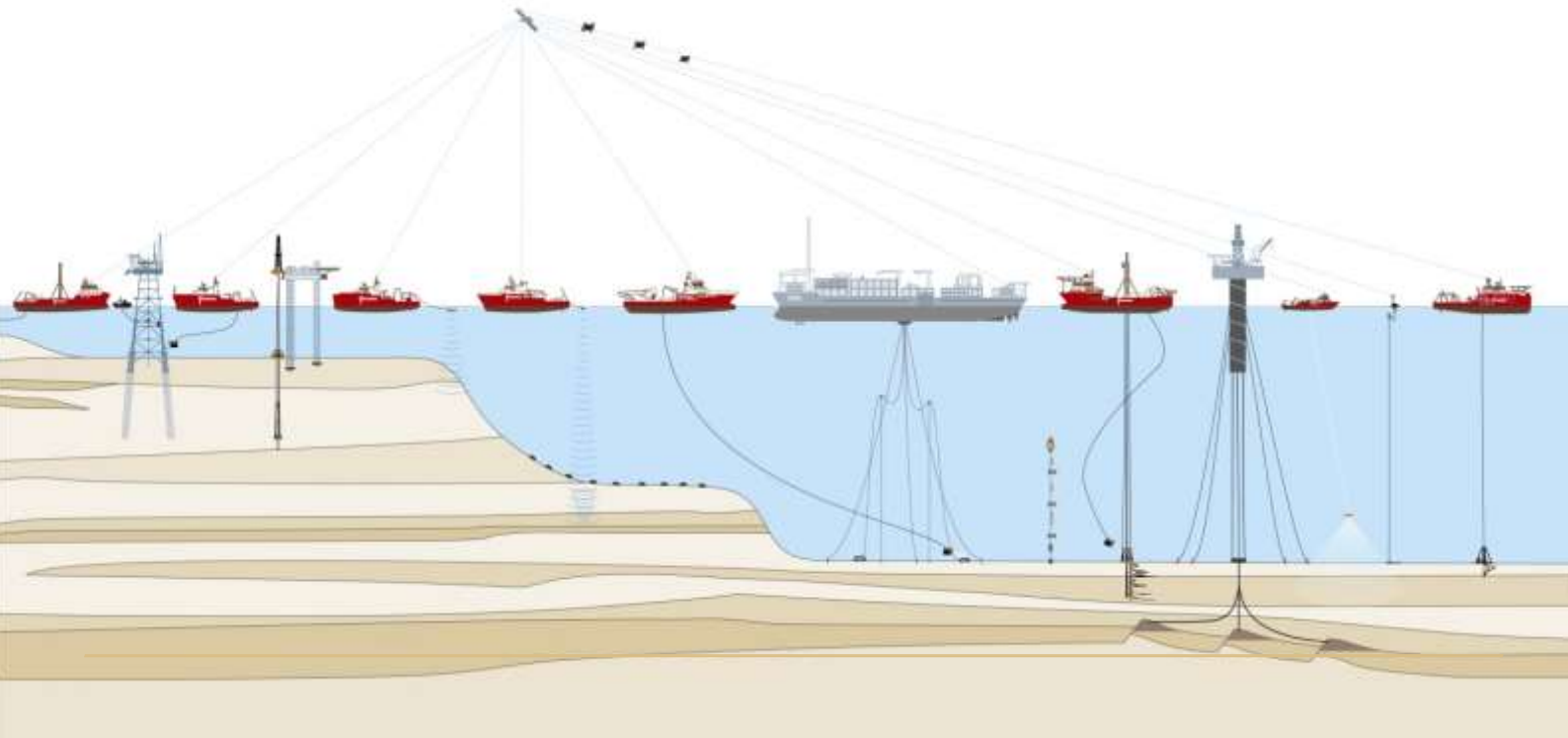

FUGRO SURVEY PTY LTD ABN 81 009 172 990

All Vessels

Reconnaissance Bathymetric Survey, Deep Tow Wide Area Survey and AUV Wide Area Survey

Volume 7 – Summary Report

Survey Period: 2 June 2014 – 24 January 2017

Fugro Document No: FRPT GP1500-SUM_Vol7_Summary Report

Prepared For:

Australian Transport Safety Bureau
62 Northbourne Avenue
Canberra, 2601
ACT

0	Draft final with client's comments addressed	H. Ballantyne	M. Watson	M. Roberts	30 May 2017
A	Draft final for client's comments	H. Ballantyne	M. Watson	M. Roberts	18 April 2017
Rev	**Description**	**Prepared**	**Checked**	**Approved**	**Date**

CONTENTS

1.	**INTRODUCTION**	**1**
1.1	Project Description	1
1.2	Project Objectives	3
1.3	Scope of Work	3
1.4	Survey Operations	4
1.5	Report Structure	5
2.	**HEALTH, SAFETY AND ENVIRONMENTAL MANAGEMENT**	**6**
2.1	Health, Safety and Environmental Performance (HSE)	6
3.	**SURVEY OPERATIONS**	**9**
3.1	Sequence of Events	9
3.2	Vessel Swings	10
3.3	Mobilisations	11
3.4	Production Summary	12
3.5	Project Time Allocation	17
3.6	Survey Coverage	17
	3.6.1 Port Calls	19
3.7	Processing and Reporting	19
3.8	Data Transfer Ashore	20
3.9	Demobilisation	21
4.	**STATISTICAL SUMMARIES**	**22**
4.1	Data Holiday Types and Extents	22
	4.1.1 Remaining Holidays	22
4.2	Contact Summary	24
4.3	Findings	25
	4.3.1 Shipwreck #1	25
	4.3.2 Shipwreck #2	28
	4.3.3 Shipwreck #3	30
	4.3.4 Shipwreck #4	31
	4.3.5 Small Target Detection	32
4.4	Sound Velocity Profiles	33
4.5	Seabed Features	35
4.6	Transit Distance	36
4.7	Personnel Hours	36
4.8	Equipment – Deep Tow and AUV	37
4.9	MBES Coverage	39

4.10 Extreme Sea Condition 41
4.11 Time Spent On Line Turns 42
4.12 Fuel Consumption 43

5. SURVEY PARAMETERS 44
5.1 Geodetic and Projection Parameters 44
5.2 Vertical Control 45

6. SURVEY EQUIPMENT, VESSEL AND PERSONNEL 46
6.1 Vessels 46
6.1.1 Fugro Equator 46
6.1.2 Fugro Discovery 47
6.1.3 Fugro Supporter 48
6.1.4 Havila Harmony 48
6.2 Personnel 49

7. DATA HANDLING 50

8. DISTRIBUTION 52

APPENDIX

A. SOUND VELOCITY PROFILES

TABLES IN THE MAIN TEXT

Table 1.1: Report Structure 5
Table 2.1: Safety Performance Summary – Leading Indicators All Vessels 6
Table 2.2: Safety Performance Summary – Lagging Indicators All Vessels 8
Table 3.1: Dates of Vessels in Field 9
Table 3.2: Fugro Discovery – Dates of Individual Swings 10
Table 3.3: Fugro Supporter – Dates of Individual Swings 10
Table 3.4: Havila Harmony – Dates of Individual Swings 11
Table 3.5: Fugro Equator – Dates of Individual Swings 11
Table 3.6: Total Line km per Phase (DOR) 14
Table 3.7: Equator v Discovery km^2 16
Table 3.8: Number of Port Calls – All Phases 19
Table 4.1: Data Holiday and LPD Count 22
Table 4.2: Data Holiday and LPD Infill Statistics for the three AUV Campaigns 23
Table 4.3: Personal Hours All Vessels 36

Table 4.4: '*Spero*' Deep Tow Sensors 37
Table 4.5: 'Dragon' DT-1 and '*Intrepid*' DT-2 Sensors 38
Table 4.6: Hugin ES7 1000 AUV 38
Table 4.7: Total Bathymetric Coverage Compared to Countries and States 39
Table 4.8: Reconnaissance Bathymetric Coverage Compared to Countries and States 39
Table 4.9: Depth Range Histogram 40
Table 4.10: Fuel Used by Each Vessel During Each Phase 43
Table 5.1: Project Geodetic and Projection Parameters 44

FIGURES IN THE MAIN TEXT

Figure 1.1: General location diagram 2
Figure 2.1: Leading indicators (%) – all vessels 7
Figure 2.2: Lagging indicators (%) – all vessels 8
Figure 3.1: Dates and durations of vessels in field 9
Figure 3.2: Example line statistics showing Distance Cross Course (DCC) and Altitude at KP values 13
Figure 3.3: Total Line km (%) all phases (DOR) 15
Figure 3.4: Total line kms by all vessels by end of swing date 15
Figure 3.5: Equator v Discovery km^2 **(%)** 16
Figure 3.6: Time allocations for the Fugro Equator Deep Tow 17
Figure 3.7: Combined Deep Tow and AUV coverage overlain over the Reconnaissance Bathymetric Survey 18
Figure 3.8: Deep Tow coverage overlain over the Reconnaissance Bathymetric Survey 18
Figure 3.9: AUV trackplots from data holiday infills overlain over the Reconnaissance Bathymetric Survey 19
Figure 3.10: Typical directory structure for data upload 20
Figure 4.1: Area of remaining Fugro data holidays 22
Figure 4.2: Data holiday and LPD infill statistics for AUV campaigns 23
Figure 4.3: Remaining data holidays for Fugro v non-Fugro vessels 24
Figure 4.4: Number of contacts per phase 24
Figure 4.5: Sidescan sonar over shipwreck #1 25
Figure 4.6: Shipwreck #1 – anchor 26
Figure 4.7: Shipwreck #1 – ship's capstan 26
Figure 4.8: Shipwreck #1 – possible water tank 27
Figure 4.9: Shipwreck #1 – chain 27
Figure 4.10: Shipwreck #1 – angular item 28
Figure 4.11: Shipwreck #2 – original Deep Tow image 28
Figure 4.12: Shipwreck #2 – bow on sidescan sonar image 29
Figure 4.13: Shipwreck #2 – side on image 29

Figure 4.14: Shipwreck #3 – sidescan sonar image 30
Figure 4.15: Shipwreck #3 – showing deck railing and nets 30
Figure 4.16: Shipwreck #4 – port bow 31
Figure 4.17: Shipwreck #4 – starboard bow damage 31
Figure 4.18: 200 litre drum – original Deep Tow sidescan sonar data, 690 m range 32
Figure 4.19: 200 litre drum – original Deep Tow sidescan sonar data, 1100 m range 32
Figure 4.20: 200 litre drum – ROV photo 33
Figure 4.21: Location of sound velocity profiles at the search area site 34
Figure 4.22: Location of sound velocity profiles at the trial site 34
Figure 4.23: The Geelvink fracture zone 35
Figure 4.24: Cross-section of Geelvink Fracture Zone (452 m Petronas Towers for scale) 35
Figure 4.25: 2500 km range ring from Fremantle 36
Figure 4.26: Personal hours all vessels 37
Figure 4.27: Cross-section through Diamantina Fracture Zone 40
Figure 4.28: Reconnaissance bathymetric survey by depths (%) 41
Figure 4.29: Maximum vessel heave recorded during the survey 42
Figure 4.30: Cumulative fuel consumption for each vessel for each swing 43
Figure 6.1: Fugro Equator 46
Figure 6.2: Fugro Discovery 47
Figure 6.3: Fugro Supporter 48
Figure 6.4: Havila Harmony 49
Figure 7.1: Vessel and Deep Tow raw and processed data formats 50

ABBREVIATIONS

AINS	Aided Inertial Navigation System
APOS	Acoustic Processor Operating Station
ATSB	Australian Transport Safety Bureau
AUSat	Australian Satellite
AUV	Autonomous Underwater Vehicle
CAT	Customer Acceptance Test
DGNSS	Differential Global Navigation Satellite System
DP	Dynamic Positioning
DVL	Doppler Velocity Log
Fugro	Fugro Survey Pty Ltd
GPS	Global Positioning System
GLONASS	Global Navigation Satellite System
HARS	HUGIN Alternative Recovery System
HDD	Hard Disc Drive
HiPAP	High Precision Acoustic Positioning System
HOC	Hazard Observation Card
HOS	Hugin Operating System
HSE	Health, Safety and Environment
IOR	Indian Ocean Region
JHA	Job Hazard Analysis
LARS	Launch and Recovery System
LPD	Low Probability Detection Zone
MBES	Multibeam Echo Sounder
NAS	Network Attached System
NCR	Non-Conformance Report
PP	Payload Processor
QC	Quality Control
SBP	Sub-Bottom Profiler
SSS	Sidescan Sonar
SVP	Sound Velocity Profile
TFI	Tile Fish Imagery
TRA	Task Risk Assessment
USBL	Ultra Short Baseline
UTC	Coordinated Universal Time
UTM	Universal Transverse Mercator
WGS84	World Geodetic System (1984)

1. INTRODUCTION

1.1 Project Description

Fugro Survey Pty Ltd (Fugro) has been contracted by the Australian Transport Safety Bureau (ATSB) on behalf of the Commonwealth of Australia to supply seafloor survey vessels, equipment and services to undertake a search for the wreckage of the Boeing 777 aircraft operated as Malaysia Airlines Flight 370 (MH370). The contract covers operations to locate, positively identify, map and obtain visual imagery of the wreckage.

Flight MH370 carrying a total of 239 persons onboard, disappeared on 8 March 2014, whilst en route from Kuala Lumpur, Malaysia to Beijing, China. Subsequent analysis of available satellite, radar and other data has determined that the aircraft most likely ended its flight in the southern Indian Ocean, on or adjacent to what is termed the “7th arc” within Australia’s search and rescue zone. The initial search area was an area of 30,000 km^2 on or adjacent to the 7th arc as advised by the ATSB.

The search area was extended several times including widening the search area adjacent to the 7th arc in the south, as well as the addition of blocks to the south of the search area. By the end of the search, in January 2017, the area covered was over 120,000 $km^{2.}$

A general location diagram highlighting the potential search areas is provided as Figure 1.1.

All survey services were conducted from the Fugro owned and operated vessels the Fugro Discovery and the Fugro Equator, both of which have been equipped and crewed as dedicated survey vessels. Each vessel was mobilised with an Edgetech DT-1 or DT-2 Deep Tow (DT) system comprising of a 6000 m rated Deep Tow, sidescan sonar (SSS), multibeam echo sounder (MBES), sub-bottom profiler (SBP), high definition camera and an aided inertial navigation system (AINS).

The Fugro Supporter equipped with a Hugin Echo Surveyor 7 autonomous underwater vehicle (AUV) joined the search in January 2015 and left the search in May 2015. The Havila Harmony replaced the Fugro Supporter until March 2016. Upon completion of Deep Tow operations the Fugro Equator was remobilised to operate the AUV. The AUV was rated to a depth of 4500 m and was equipped with full suite of survey sensors including sidescan sonar, multibeam echo sounder, sub-bottom profiler, high definition camera and an aided inertial navigation system (AINS). The AUV had a two-fold tasking; firstly, to search areas too difficult for the Deep Tow systems to safely or efficently investigate, and secondly to carry out detailed investigations of sonar contacts that may represent debris from the lost aircraft.

This Summary Report summarises some of the significant statistical achievements from the search for MH370 in terms of the people and vessels involved and the data collected.

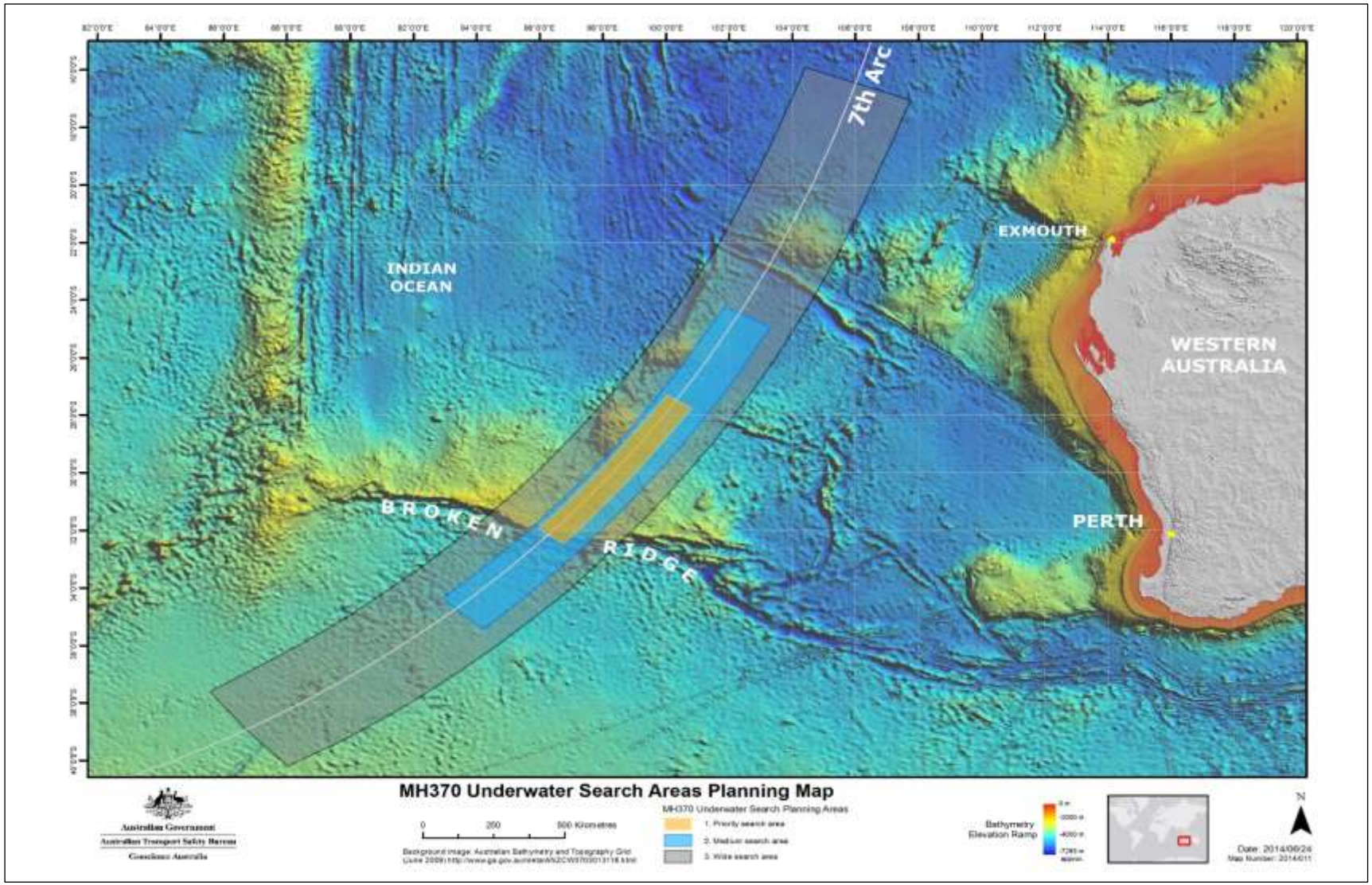

Figure 1.1: General location diagram

1.2 Project Objectives

The objective of the wide area search phase was to investigate the search area for all seafloor anomalies and discount natural geological or environmental features. In order to satisfy the ATSB requirements, Fugro was required, according to the Contract (570-04) to complete the following:

i. Search for, locate and positively identify MH370 within the defined search area on the seafloor;
ii. If MH370 is located, obtain optical imaging (photograph or video) of the aircraft debris field and, if possible, recover the flight data recorders; and,
iii. Discount any area searched for the presence of MH370 with a high degree of confidence.

All search activities were conducted in an effective and cooperative manner which ensured the safety of the search vessels and the personnel onboard was paramount.

1.3 Scope of Work

For the Fugro Equator and the Fugro Discovery the wide area search for MH370 was carried out within the search areas defined by the ATSB around the 7th arc using a Deep Tow system.

The Deep Tow system was positioned using USBL aided INS and completed the seafloor investigation using the following main instrumentation:

- Edgetech 75 kHz and 410 kHz chirp sidescan sonar, to provide primary object detection over a large [2 km] swath;
- Kongsberg EM2040 multibeam, used to provide high resolution bathymetry and object detection coverage across the sidescan sonar nadir gap;
- HD camera system, to further confirm the object identification;
- Subsea fluorometer for polycyclic aromatic hydrocarbons sensing.

The primary purpose of the AUV survey onboard the Fugro Supporter, Havila Harmony and Fugro Equator was to carry out a wide area search using the low frequency sidescan sonar in areas where the Deep Tow systems had not been able to acquire data due to seabed terrain shadows and terrain avoidance. These areas where there was insufficient Deep Tow sonar coverage have been classed as "data holidays". The data holidays were collated and grouped together into polygons to provide defined areas for the AUV to acquire data.

Data holidays include the following:

- Shadow zones which were created by the topographical relief where the sidescan sonar signal could not reach the seafloor (acoustic shadow);
- Off-tracks, where the tow fish deviated from the line plan resulting in data gaps between adjacent lines;
- Equipment failure, where no data were recorded in certain areas;
- Terrain avoidance, where the Deep Tow sensor altitude was over 300 m, typically caused by large seafloor gradients.

In addition to these holidays another category was mapped, but not classified as data holidays:

- Lower probability detection zones (LPDs), which were generally areas of complex geology where the ability to detect plane debris was limited.

The second purpose of the AUV survey was to reinvestigate contacts using a high frequency sidescan sonar to provide a higher resolution image and where necessary, to then carry out an optical imaging mission in order to obtain photographs of the contacts in question.

1.4 Survey Operations

Prior to commencement of Deep Tow operations the Fugro Equator conducted five Swings of reconnaissance MBES. The existing bathymetry derived from scattered surveys and satellite bathymetry was not of a high enough resolution to allow for safe Deep Tow and AUV operation. Reconnaissance survey operations were conducted between 2 June and 22 December 2014, and also at periodic times up to demobilisation when weather did not permit Deep Tow or AUV operations or when tasked to do so by the ATSB. The data was initially processed using VBAProc onboard the Fugro Equator to ensure coverage and then sent to Geoscience Australia for final processing.

The Fugro Equator was then remobilised and then began Deep Tow operations from 5 January 2015, until 15 October 2016. After this the Equator was remobilised again to conduct AUV operations between 22 October 2016 and 23 January 2017 (arrival in Fremantle), before being fully demobilised upon return to Singapore on 7 February 2017.

The Fugro Discovery was mobilised on 5 October 2014, and after completing Deep Tow operations on 11 August 2015, was demobilised.

The Fugro Supporter was mobilised with the AUV in Bali, Indonesia on 4 January 2015, and conducted AUV operations until 17 May 2015.

The Havila Harmony replaced the Fugro Supporter conducting AUV operations from 23 November 2015, until 26 March 2016. The AUV was then taken ashore and mobilised on the Fugro Equator October 2016.

1.5 Report Structure

The report for the reconnaissance bathymetric survey and wide area search phase is presented in eight volumes outlined in Table 1.1.

Table 1.1: Report Structure

Fugro Report No.	Volume	Report Title
FRPT GP1500-1_FD_Vol1_ Operations Report	1	Fugro Discovery Deep Tow Wide Area Survey Survey Operations
FRPT GP1483_GP1500-2_FE_Vol2_ Operations Report	2	Fugro Equator Reconnaissance Bathymetric Survey and Deep Tow Wide Area Survey Survey Operations
FRPT GP1500-5_FS_Vol3_ Operations Report	3	Fugro Supporter AUV Wide Area Survey Survey Operations
FRPT GP1500-6 HH_Vol4_ Operations Report	4	Havila Harmony AUV Wide Area Survey Survey Operations
FRPT GP1500-6_FE_Vol5_ Operations Report	5	Fugro Equator AUV Wide Area Survey Survey Operations
FRPT GP1500-3_Vol6_ Processing, Interpretation and Results Report	6	Reconnaissance Bathymetric Survey, Deep Tow Wide Area Survey and AUV Wide Area Survey Processing, Interpretation and Results Report
FRPT GP1500_SUM_Vol7_ Summary Report	**7**	**Summary Report (this report)**
FRPT GP1483_GP1500_LL_Vol 8_ Lessons Learnt	8	Reconnaissance Bathymetric Survey, Deep Tow Wide Area Survey and AUV Wide Area Survey Lessons Learnt

2. HEALTH, SAFETY AND ENVIRONMENTAL MANAGEMENT

2.1 Health, Safety and Environmental Performance (HSE)

The total working personnel hours for all phases of this project, based on 24 man hours per day, was 625,488.

To better understand HSE during the course of the survey the events were split into two groups: Lagging Indicators and Leading Indicators. Lagging indicators are negative HSE events that occurred over the course of the project such as illness or first aid cases. Leading indicators are positive and proactive HSE events, such as Toolbox Talks and Marine Fauna Observations. Table 2.1 shows the leading indicators numbers from all vessels and Figure 2.1 shows the same data graphically as percentages.

Table 2.1: Safety Performance Summary – Leading Indicators All Vessels

Leading Indicator	Total
Toolbox Talks	4807
Permit to Work	852
HOC Unsafe Conditions	754
Vessel Inductions	433
Emergency Exercises/Drills	350
RA Reviewed	350
HOC Safe Act/Suggestions	343
Inspection/Reviews	342
Management Visits	326
HSE Meetings	154
HOC Unsafe Acts	118
Safety Training Conducted	75
Audits	41
RA Developed	36
Hazard Hunts	34
Marine Fauna Observations	29
GroSAFE Observations	14
Stop Work Exercised	13

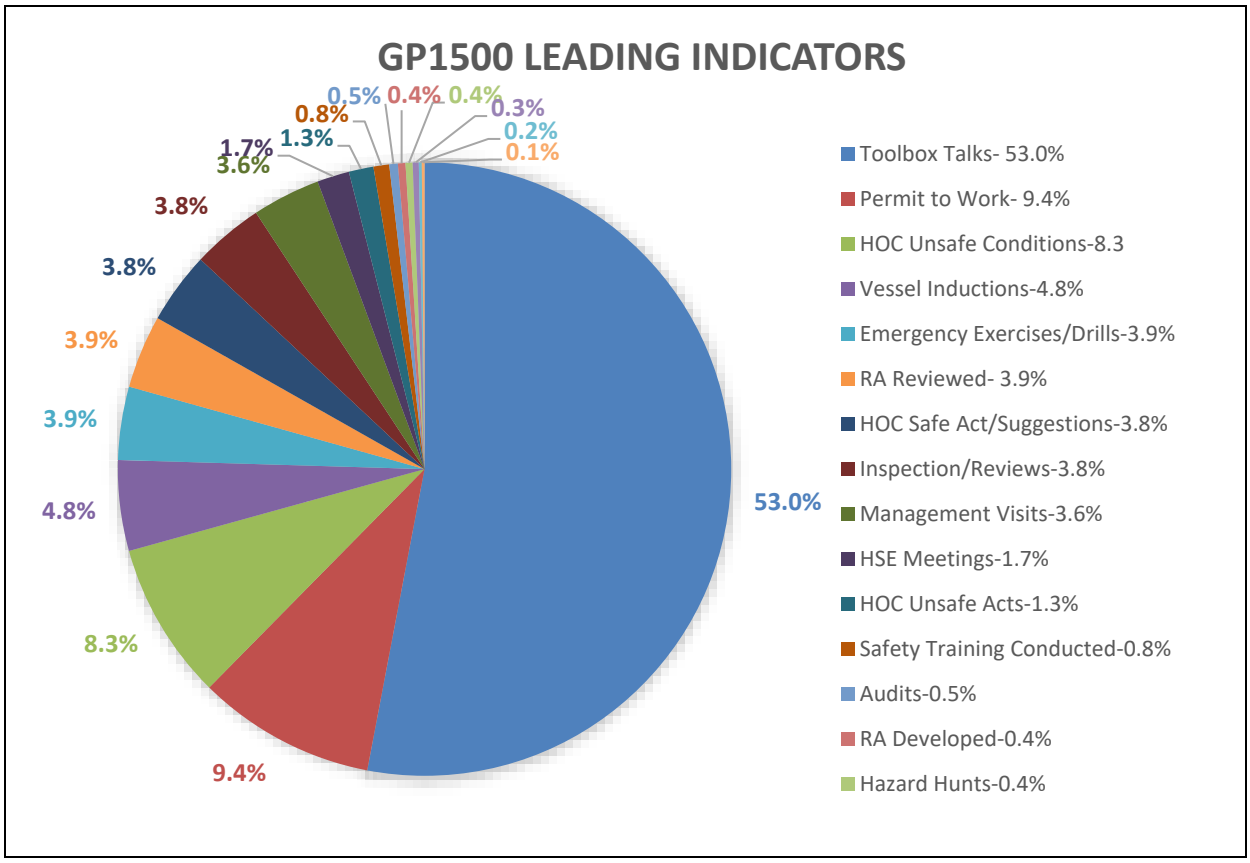

Figure 2.1: Leading indicators (%) – all vessels

Table 2.2 shows the lagging indicators numbers from all vessels and Figure 2.2 shows the same data graphically as percentages.

Table 2.2: Safety Performance Summary – Lagging Indicators All Vessels

Lagging Indicators	Total
Equipment Damage/Loss	46
Near Miss	35
Crew Boat Transfers	11
First Aid Case	6
Medical Treatment	6
Hi Potential Incident	3
NWR – Medical treatment	3
Environmental Incident	1
MOB Deployments	1
NWR – Injury/Illness	1
Occupational Illness	1
Restricted Work Case	1
EP Non-Compliance	0
Fatality	0
Lost Work Day Case	0
NWR – First Aid Case	0
Open Action Items	0
Overdue Action Items	0

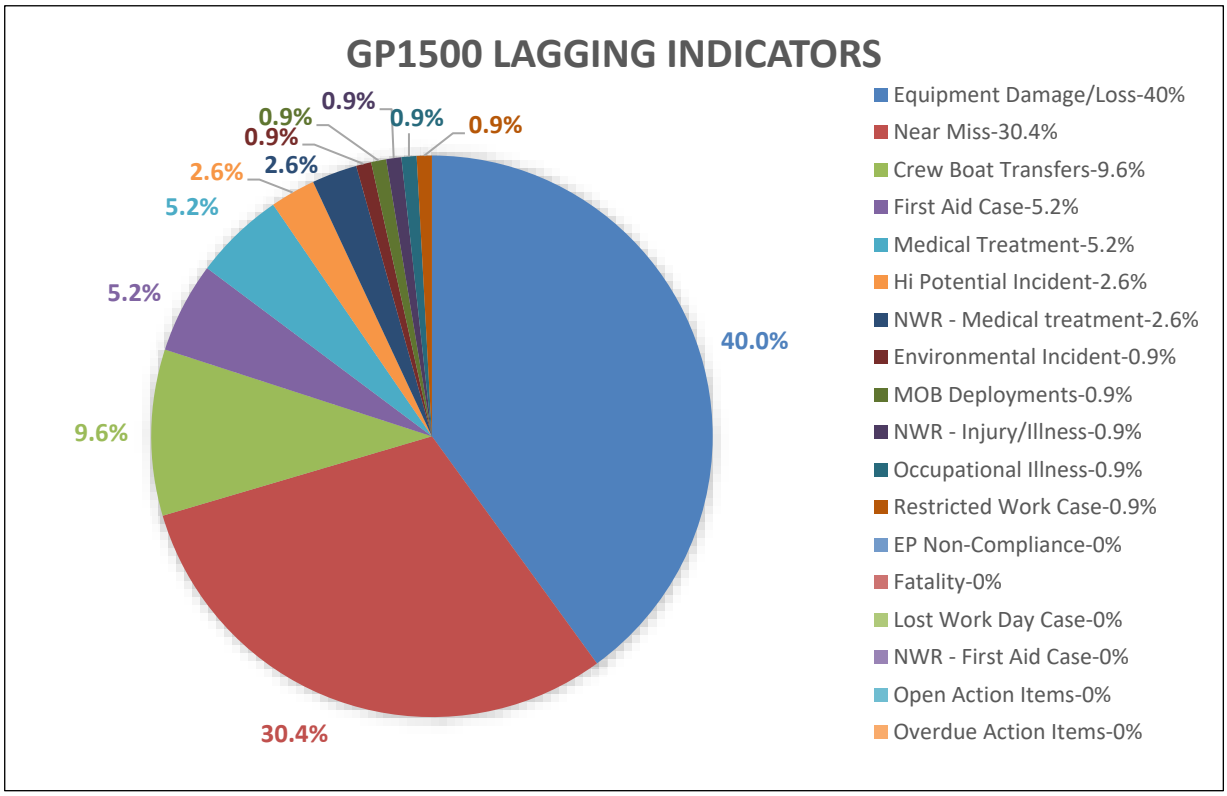

Figure 2.2: Lagging indicators (%) – all vessels

3. SURVEY OPERATIONS

Overall, survey operations were conducted successfully and the acquired data was of good quality.

3.1 Sequence of Events

The offshore phase of the Wide Area Search was undertaken between 2 June 2014, and 7 February 2017, when the vessel demobilised in Singapore.

A brief summary of significant survey events is presented in Table 3.1 and in Figure 3.1. The figures include time spent mobilising and in transit to and from the survey site. For more detail, refer the individual volumes for each vessel.

Table 3.1: Dates of Vessels in Field

Vessel	Dates in Field
Fugro Equator (Reconnaissance MBES)	2 June 2014 – 01 November 2014 and, 16 November 2014 – 22 December 2014
Fugro Discovery (Deep Tow)	05 October 2014 – 24 August 2016
Fugro Equator (Deep Tow)	01 November 2014 – 15 November 2014 and, 29 December 2014 – 21 October 2016
Fugro Supporter (AUV)	04 January 2015 – 17 May 2015
Havila Harmony (AUV)	23 November 2015 – 26 March 2016
Fugro Equator (AUV)	22 October 2016 – 23 January 2017
Fugro Equator (Final transit to Singapore)	24 January – 07 February 2017

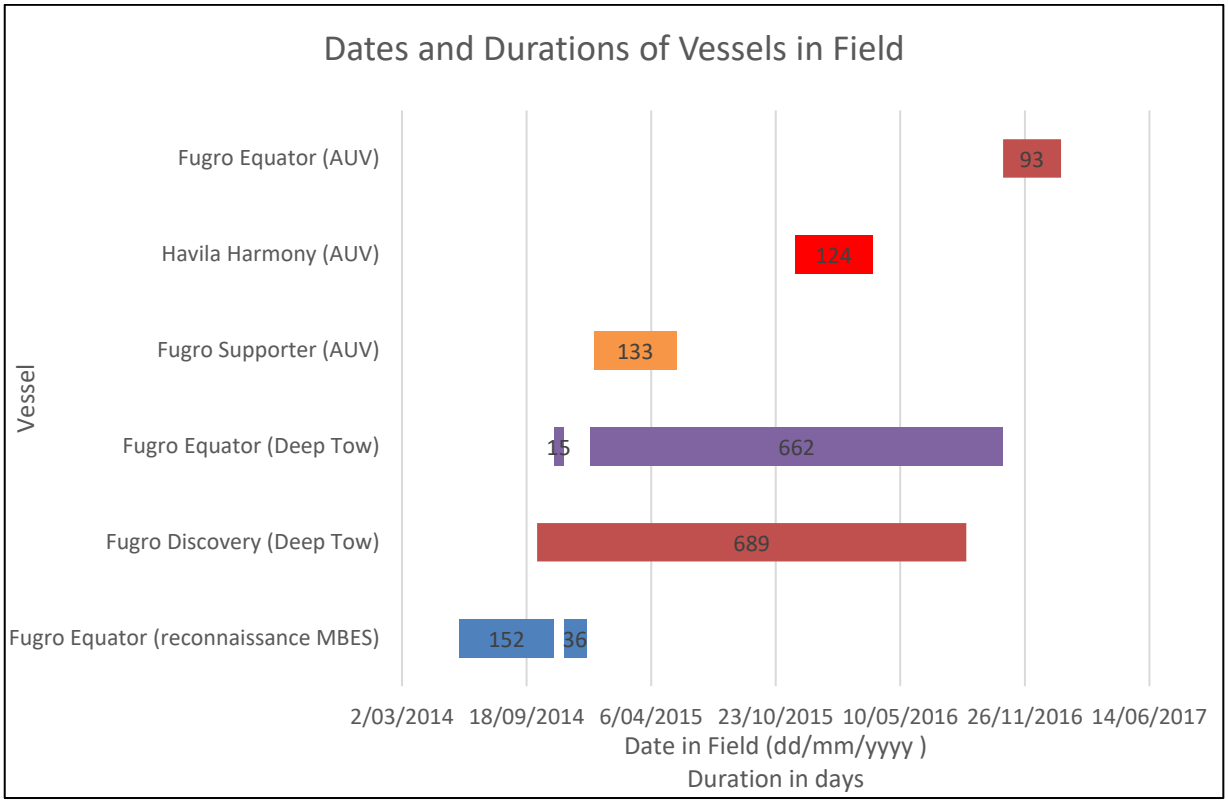

Figure 3.1: Dates and durations of vessels in field

3.2 Vessel Swings

Dates of the 16 swings carried out by the Fugro Discovery are shown in Table 3.2.

Table 3.2: Fugro Discovery – Dates of Individual Swings

Fugro Discovery Swing	Port to Port Dates	On Site
1	17 October 2014 – 24 November 2014	22 October 2014 – 17 November2014
2	27 November 2014 – 06 January 2015	04 December 2014 – 30 December 2014
3	09 January 2015 – 18 February 2015	15 January 2015 – 11 February 2015
4	20 February 2015 – 30 March 2015	25 February 2015 – 24 March 2015
5	04 April 2015 – 13 May 2015	10 April 2015 – 08 May 2015
6	15 May 2015 – 23 June 2015	22 May 2015 – 18 June 2015
7	27 June 2015 – 01 August 2015	04 July 2015 – 24 July 2015
8	05 August 2015 – 16 September 2015	11 August 2015 – 15 September 2015
9	16 September 2015 – 27 October 2015	21 September 2015 – 22 October 2015
10	28 October 2015 – 28 November 2015	4 November 2015 and 14 – 22 November 2015[1]
11	29 November 2015 – 11 January 2016	03 December 2015 – 06 January 2016
12	13 January 2016 – 15 February 2016	20 – 24 January 2016 and 06 – 10 February 2016[2]
13	18 February 2016 – 05 April 2016	25 February 2016 – 30 March 2016
14	07 April 2016 – 16 May 2016	12 April 2016 – 11 May 2016
15	17 May 2016 – 29 June 2016	24 May 2016 – 23 June 2016[3]
16	11 July 2016 – 22 August 2016	21 July 2016 – 11 August 2016

[1] On Swing 10 the Fugro Discovery had to return to port twice to relieve crew members for medical reasons
[2] On Swing 12 the Fugro Discovery had to return to port twice. Initially due to loss of towfish on 24 January 2016,then due to tow cable break on 9 February 2016
[3] The port call between Swing 15 and Swing 16 was extended due to necessary maintenance

Dates of the three swings carried out by the Fugro Supporter are shown in Table 3.3.

Table 3.3: Fugro Supporter – Dates of Individual Swings

Fugro Supporter Swing	Port to Port Dates	On Site
1	18 January 2015 – 20 February 2015	29 January 2015 – 11 February 2015
2	23 February 2015 – 08 April 2015	28 February 2015 – 01 April 2015
3	10 April 2015 – 18 May 2015	18 April 2015 – 11 May 2015

Dates of the two swings carried out by the Havila Harmony are shown in Table 3.4.

Table 3.4: Havila Harmony – Dates of Individual Swings

Havila Harmony Swing	Port to Port Dates	On Site
1	30 November 2015 – 21 January 2016	05 December 2015 – 15 January 2016
2	25 January 2016 – 26 March 2016	03 February 2016 – 20 March 2016

Dates of the 20 swings carried out by the Fugro Equator are shown in Table 3.5.

Table 3.5: Fugro Equator – Dates of Individual Swings

Fugro Equator Swing	Port to Port Dates	On Site
1 GP1483	02 June 2014 – 08 July 2014	14 June 2014 – 03 July 2014
2 GP1483	09 July 2014 – 12 August 2014	13 July 2014 – 07 August 2014
3 GP1483	13 Aug 2014 – 18 September 2014	17 Aug 2014 – 13 September 2014
4 GP1483	19 Sept 2014- 31 October 2014	24 Sept 2014- 25 October 2014
5 GP1483*	16 Nov 2014 – 22 December 2014	21 Nov 2015 – 18 December 2014
1	05 January 2015 – 17 February 2015	15 January 2015 – 10 February 2015
2	20 February 2015 – 08 April 2015	27 February 2015 – 28 March 2015
3	09 April 2015 – 19 May 2015	16 April 2015 – 13 May 2015
4	23 May 2015 – 29 June 2015	28 May 2015 – 23 June 2015
5	30 June 2015 – 12 August 2015	06 July 2015 – 06 August 2015
6	12 August 2015 – 23 September 2015	19 August 2015 – 17 September 2015
7	25 September 2015 – 09 November 2015	05 October 2015 – 03 November 2015
8	10 November 2015 – 21 December 2015	15 November 2015 – 16 December 2015
9	28 December 2015 – 09 February 2016	03 January 2016 – 02 February 2016
10	10 February 2016 – 23 March 2016	16 February 2016 – 17 March 2016
11	24 March 2016 – 05 May 2016	30 March 2016 – 29 April 2016
12	06 May 2016 – 15 June 2016	14 May 2016 – 09 June 2016
13	15 June 2016 – 27 July 2016	21 June 2016 – 22 July 2016
14	28 July 2016 – 07 September 2016	04 August 2016 – 02 September 2016
15	08 September 2016 – 21 October 2016	15 September 2016 – 15 October 2016
16	28 October 2016 – 12 December 2016	02 November 2016 – 06 December 2016
17	12 December 2016 – 24 January 2017	19 December 2016 – 17 January 2017

* This swing was originally designated Fugro job number GP1500-4, and this appears in the DORs until 26 November 2014, but was retrospectively changed back to GP1483

3.3 Mobilisations

The Fugro Equator was initially mobilised in Benoa, Bali between 7 and 9 July 2014, where a patch test was undertaken before transit to the trial site for operations.

Mobilisation of the Fugro Discovery took place between 5 and 10 October 2014, whilst the vessel was alongside at Fremantle.

The original mobilisation of the Fugro Equator for Deep Tow operations took place alongside at the Port of Fremantle, Western Australia, between 1 and 8 November 2014. Problems were encountered with the installed winch which meant that a replacement had to be found. While the replacement winch was being sourced the Fugro Equator returned to site to conduct more reconnaissance MBES. On 28 December 2014, the Fugro Equator returned to Fremantle to complete Deep Tow mobilisation and commence Deep Tow operations.

The Fugro Supporter was mobilised with the Hugin 1000 AUV Echo Surveyor 7 in Benoa, Bali, Indonesia between 4 and 18 January 2015.

The Havila Harmony was mobilised between 23 and 26 November 2015, alongside the BAE Henderson, just south of Fremantle.

On 22 October 2016, the Equator was remobilised for ES7 AUV alongside the AMC4 Wharf, Henderson.

3.4 Production Summary

The survey work scope for each swing was defined by Tasking Requests issued by the ATSB which detailed the preferred order of survey lines to be run and whether Deep Tow or MBES reconnaissance operations were to be carried out. Similar Tasking Requests were issued to the AUV vessels for missions, although there was a great deal of input from the Mission Planners onboard each vessel as well.

The Deep Tow survey line spacing was initially set at 2000 m with a sidescan sonar range of 1250 m in order to acquire data efficiently. This was the case for lines 01-NW, 02-NW and 03-NW. Subsequently the line spacing was reduced to 1800 m with a sidescan sonar range of 1110 m in order to ensure data quality over the full scan range. This was the case up until completion of 05-SE. After this lines were acquired with 1700 m line spacing and sidescan sonar range 1110 m to reduce offtrack holidays (only the first 1000 m of the data was considered acceptable for object detection). This was the case for the remainder of the project, unless there were towfish positioning issues such as the USBL system dropping out. If this occurred the line spacing was reduced to 1600 m.

The survey required 100 % seafloor coverage by the sidescan sonar with the nadir gaps being filled by processed multibeam backscatter data. The online surveyor attempted to maintain the towfish within 100 m of the line being surveyed, with a maximum excursion of 150 m being acceptable to ensure data overlap and 100 % coverage of the seabed. On the completion of each line, statistics were produced to provide a summary of line keeping and towfish altitude for that line (see Figure 3.2).

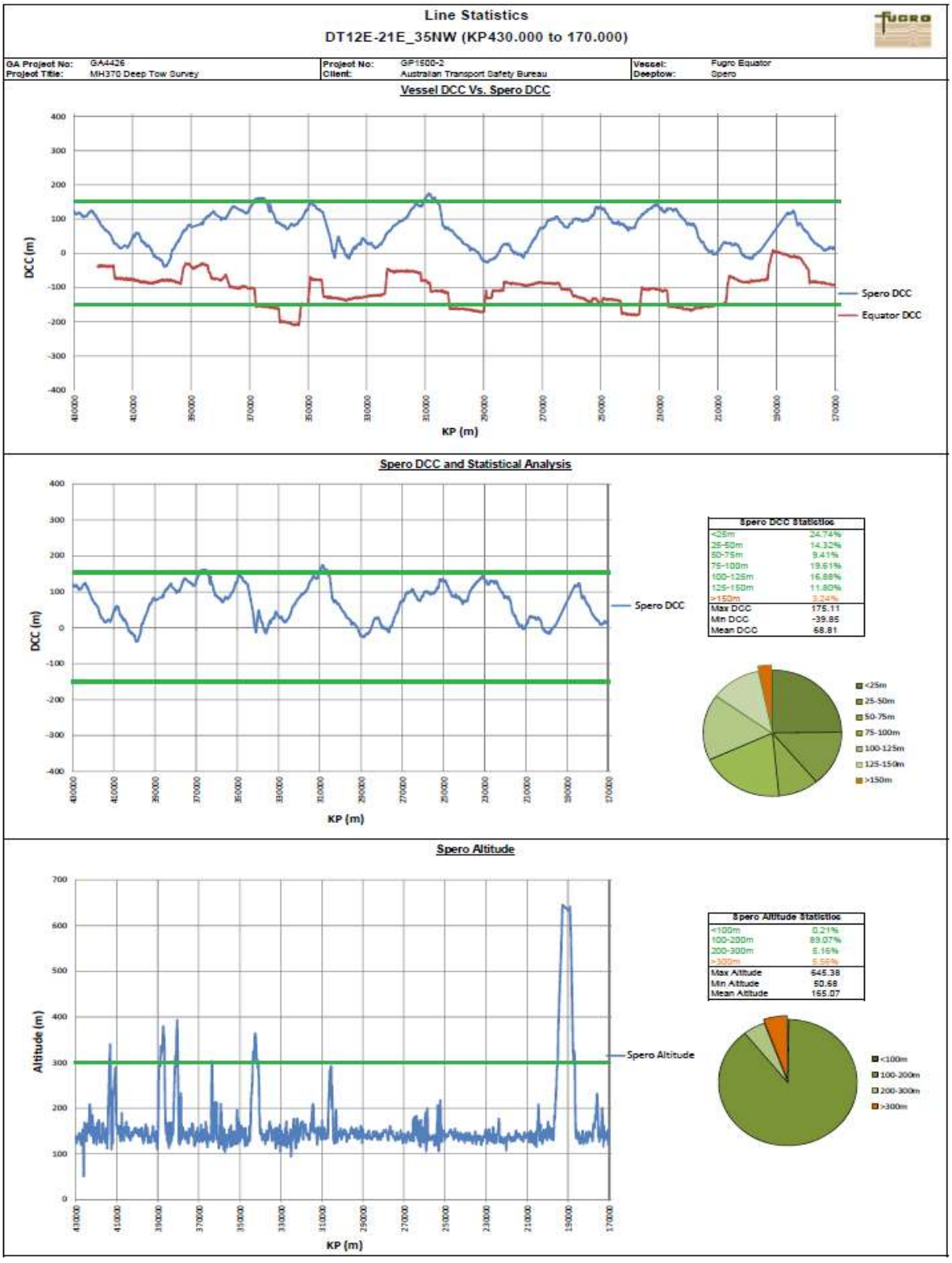

Figure 3.2: Example line statistics showing Distance Cross Course (DCC) and Altitude at KP values

Although each port to port swing was of six weeks duration for Deep Tow operations and eight weeks for swings onboard the Havila Harmony, the long transit of over 1000 Nm to and from the search area resulted in approximately 30 days on site each swing and 41 days for the Havila Harmony.

Operations to safely launch and recover the Deep Tow and AUV were restricted by the weather conditions, particularly during the winter months, and productivity was reduced as a result.

Daily weather forecasts were obtained from Fugro GEOS and from the Bureau of Meteorology (BOM) Defence Meteorological Support Unit (DMSU) and this allowed onsite planning of operations to maximise Deep Tow productivity. As the search area was in excess of 800 kms in length it was often possible to work in the north of the search area when weather conditions prevented safe operations in the south, and vice versa.

The Fugro Equator and Fugro Supporter also had the option to undertake reconnaissance MBES work when the weather was unsuitable for Deep Tow operations or it was tasked to do so by the ATSB. The vessels were able to continue acquisition of acceptable MBES data in often very poor weather conditions, although data quality was dictated by the relative direction of the surveyed line and prevailing weather conditions.

On completion of each swing a summary report was produced highlighting, amongst other things, the productivity achieved for that particular swing.

The combined Deep Tow sidescan sonar virgin territory coverage from both the Fugro Equator (Deep Tow and AUV) and, Fugro Discovery amounted to 104,033 km^2. The Fugro Supporter and Havila Harmony AUV covered 700 km^2. When combined with the data acquired by the DJ101 and the GO Phoenix, the total sidescan sonar coverage for the entire project amounted to 121,502 km^2.

Table 3.6 shows the total line kilometres for each phase with figures taken from the Daily Operation Reports submitted each day from each vessel.

Table 3.6: Total Line km per Phase (DOR)

Total Line km per Vessel (DOR)	
Vessel	**[kms]**
GP1483 – Equator Vessel MBES	33340
GP1500-2 – Equator Deep Tow	29635
GP1500-2 – Equator Vessel MBES	9488
GP1500-1 – Discovery Deep Tow	29884
GP1500-5 – Supporter AUV	5491
GP1500-5 – Supporter Vessel MBES	2733
GP1500-6 – Harmony AUV	7431
GP1500-6 – Equator AUV	5234
GP1500-6 – Equator Vessel MBES	2789
Total	**126025**

These kilometres are represented as pie chart percentages in Figure 3.3 and for all the Deep Tow and AUV swings as kilometres against dates in Figure 3.4.

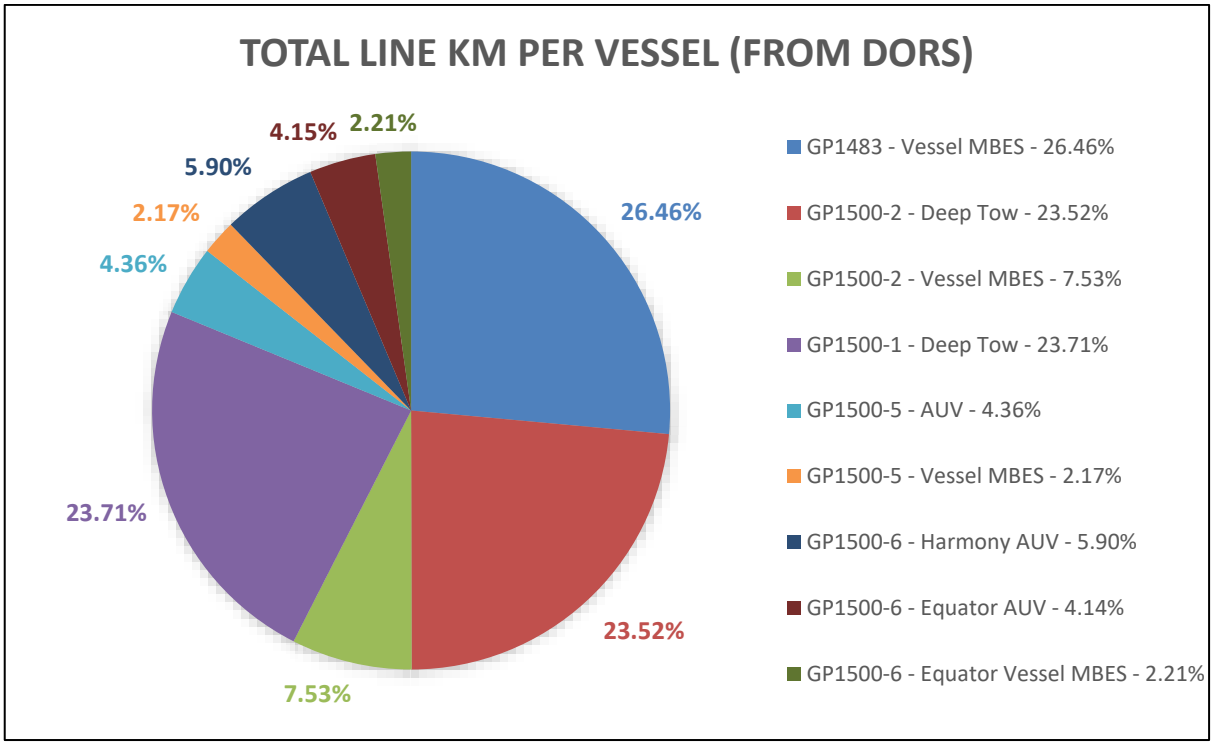

Figure 3.3: Total Line km (%) all phases (DOR)

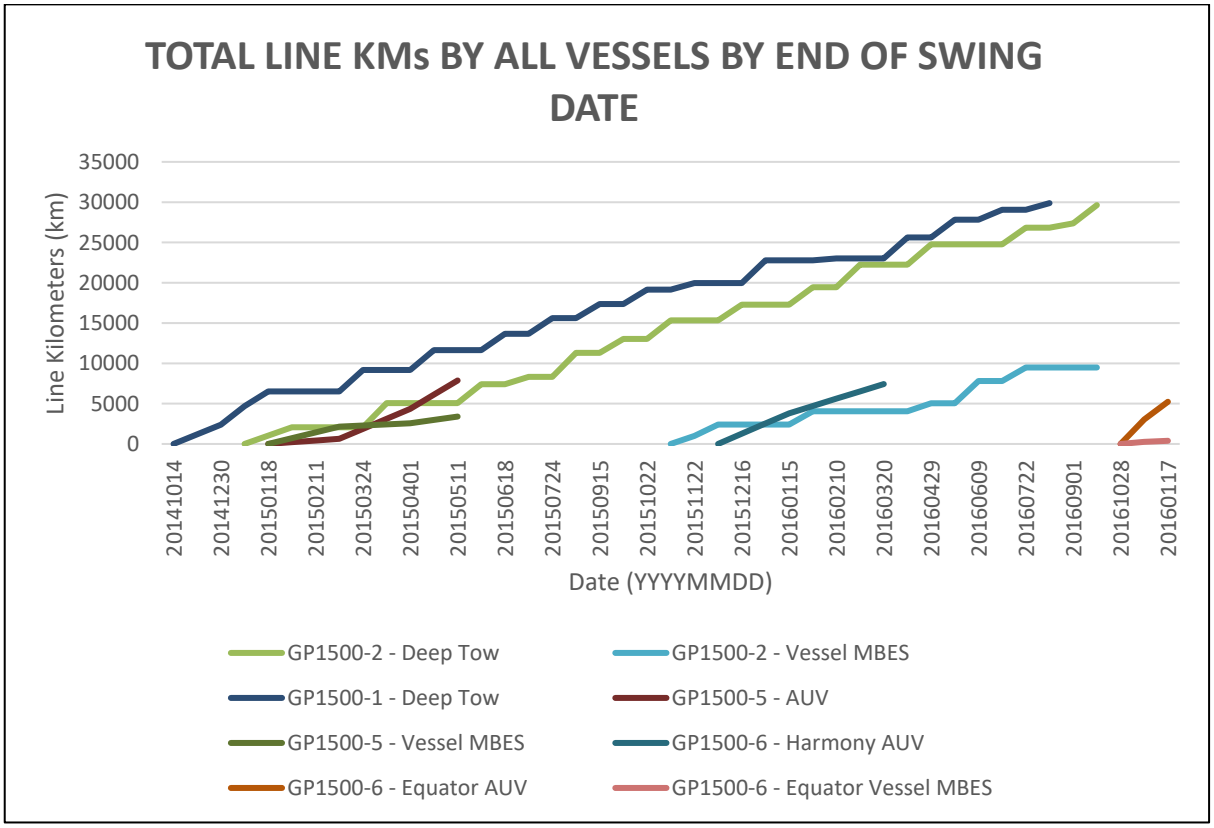

Figure 3.4: Total line kms by all vessels by end of swing date

After two years of Deep Tow acquisition between the Fugro Discovery and Fugro Equator the square kilometres survey by each were almost identical, the Fugro Discovery completing just 432 km (0.42 %) more than the Fugro Equator (see Table 3.7 and Figure 3.5).

Table 3.7: Equator v Discovery km²

Vessel	[km²]	[%[
Equator DT	51389.6	49.79
Discovery DT	51821.9	50.21
Total DT km²	**103211.5**	

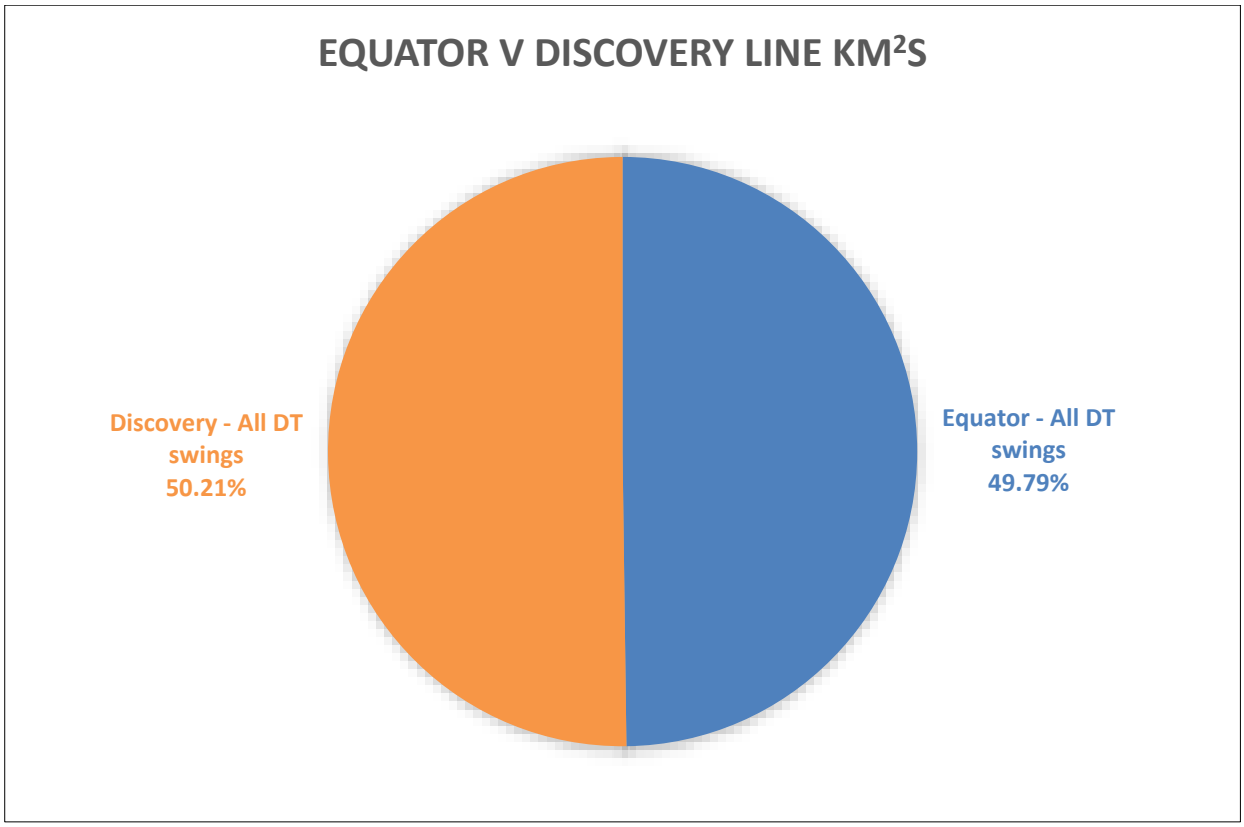

Figure 3.5: Equator v Discovery km² (%)

3.5 Project Time Allocation

Overall the project was conducted in an efficient manner with minimal amounts of down time attributable to equipment problems. A summary of the project time allocations, abstracted from the Daily Operations Report, is presented in Figure 3.6. In total there were 2099 Daily Operations Reports issued for all vessels involved in the search.

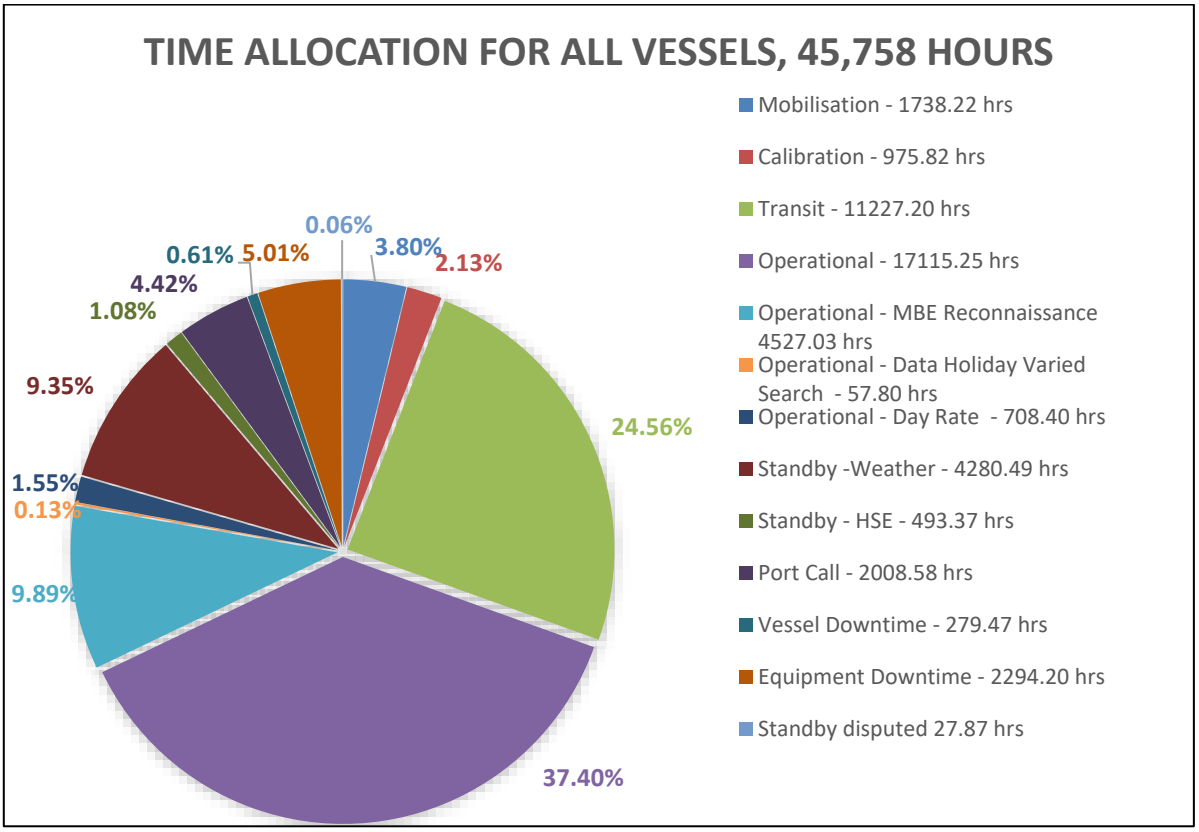

Figure 3.6: Time allocations for the Fugro Equator Deep Tow

The location of the MH370 search area, being more than 1000 Nm west of Fremantle, is reflected in the large percentage ≈25 % of project time devoted to vessel transit. Weather conditions on site varied throughout the year and a total of 10 % of time was lost to weather, particularly during the winter months. There was no production at all during Swing 12 of the Fugro Equator (May 2016 – June 2016) as the adverse weather prevented launch of the Deep Tow.

3.6 Survey Coverage

The Reconnaissance Bathymetric phase of the survey covered a much larger area than was achieved with all subsequent Deep Tow, AUV and ROV surveys combined. This is shown in Figure 3.7 which has the combined Deep Tow and AUV coverage, in purple, overlying the Reconnaissance Bathymetric area as a backdrop. The coverage achieved by just the Fugro Equator and Fugro Discovery Deep Tow operations is shown in Figure 3.8. The AUV tracks for the data holiday infill survey, the primary task during the three AUV phases, are shown in Figure 3.9.

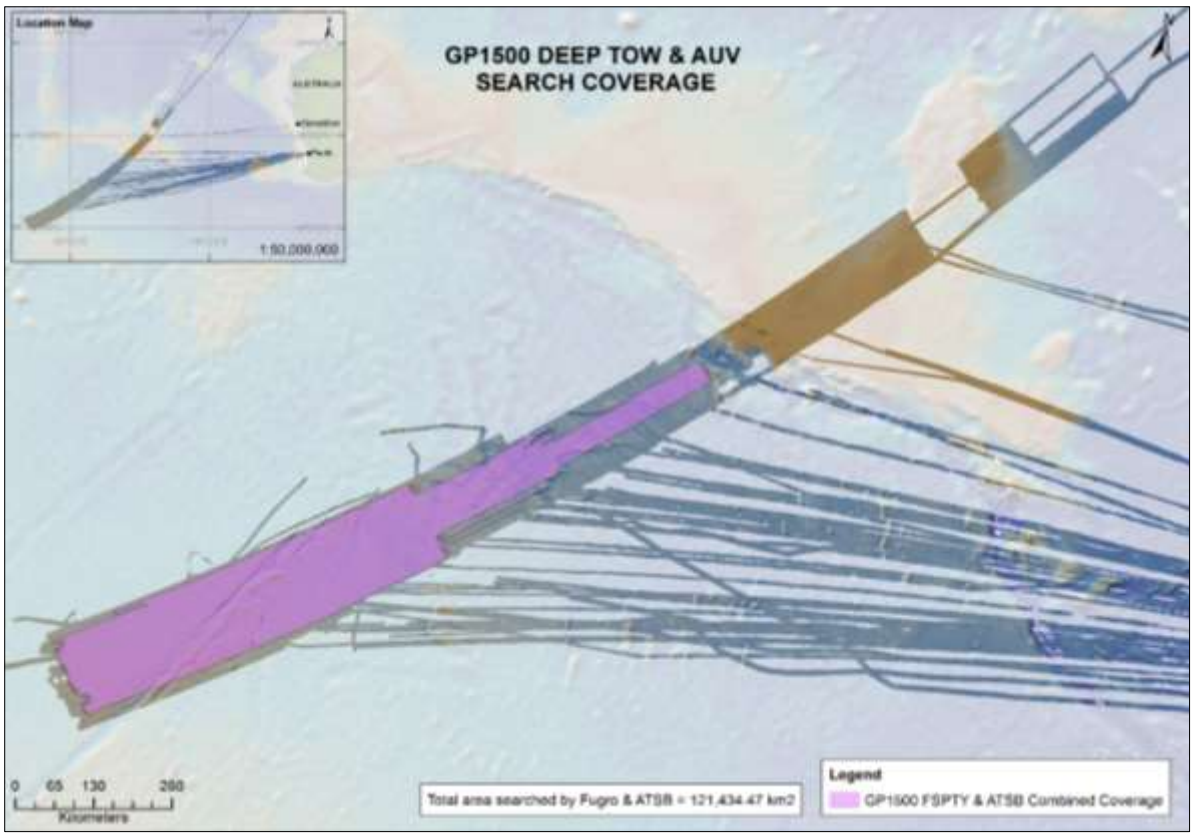

Figure 3.7: Combined Deep Tow and AUV coverage overlain over the Reconnaissance Bathymetric Survey

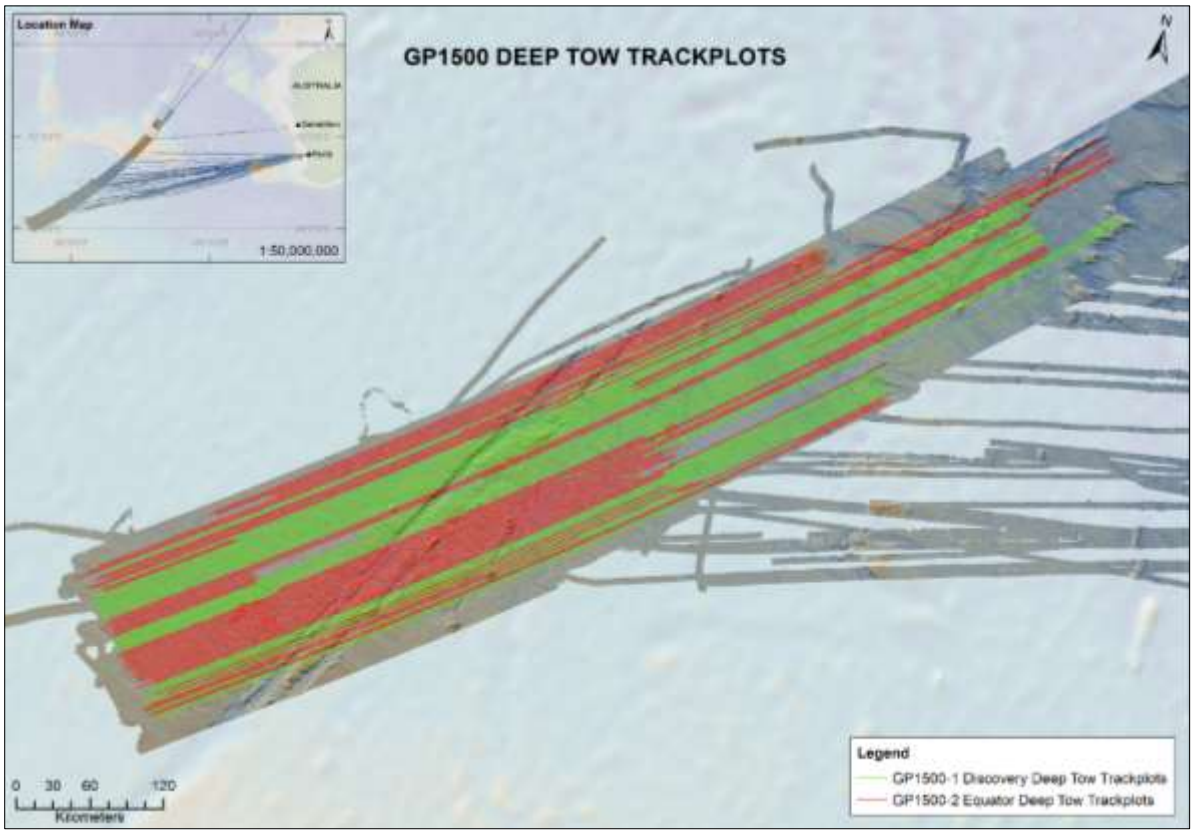

Figure 3.8: Deep Tow coverage overlain over the Reconnaissance Bathymetric Survey

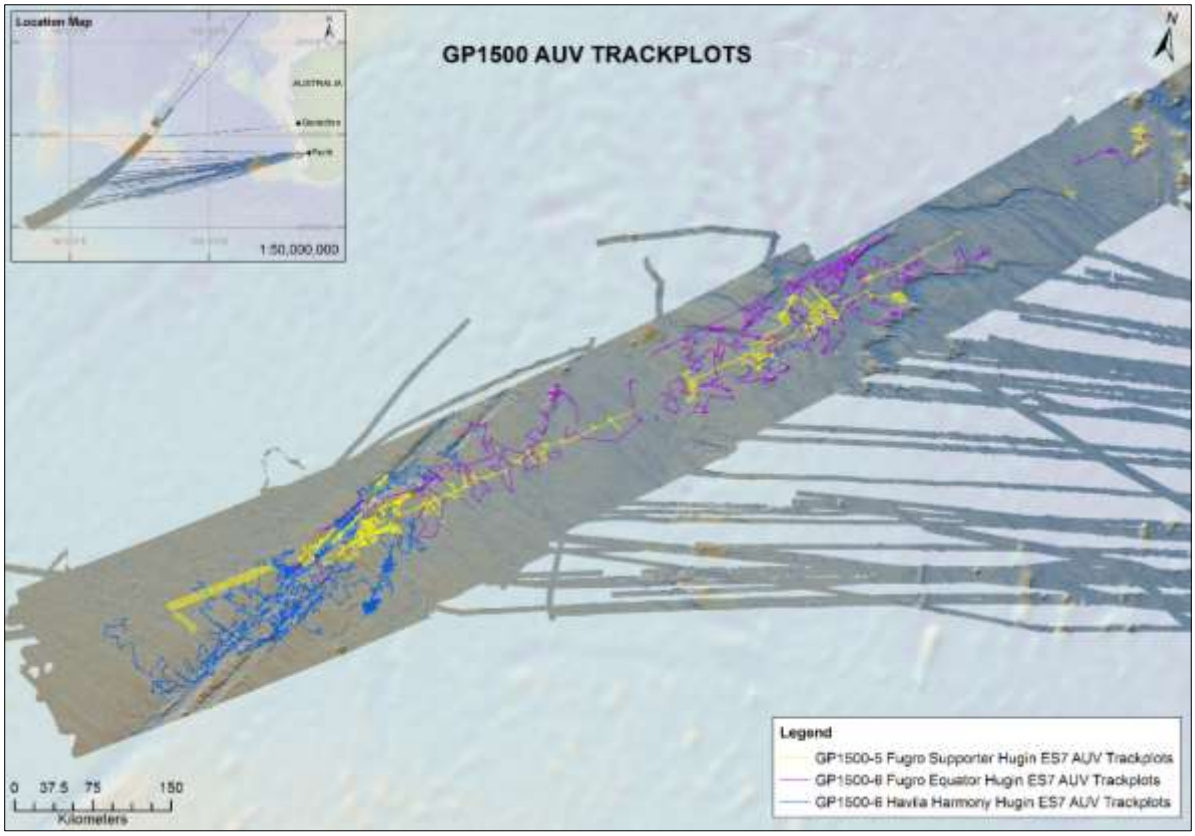

Figure 3.9: AUV trackplots from data holiday infills overlain over the Reconnaissance Bathymetric Survey

3.6.1 Port Calls

A total of 50 port calls were conducted over the course of the project at five different ports, as shown in Table 3.8.

Table 3.8: Number of Port Calls – All Phases

Port	Number of Port Calls
Bali – Indonesia	2
Geraldton – Australia	1
Fremantle – Australia	40
Henderson – Australia	5
Singapore	2
Total	**50**

3.7 Processing and Reporting

Multibeam data processing was undertaken onboard the vessels after each day of survey by the dedicated multibeam processor using CARIS processing software (see Section 7.2). A geophysical data processing work station was located in the geophysical laboratory to enable interactive data QC during the field work. The onboard geophysicist was able to complete QC of the sidescan sonar data whilst offshore. In addition the onboard geophysicist uploaded all processed geophysical data to Fugro's server in Perth so that the data was available onshore for more thorough analysis. As the job progressed, the onboard geophysicist sent a brief Preliminary Contact Report ashore each day prior to analysis

onshore. A dedicated onshore team was then able to produce contact reports after reviews by three different people. Each contact report contained a picture of the data, where the contact was identified, and categorised the contact into one of three classifications:

- Classification 1: Marked with high interest and warrants further investigation;
- Classification 2: Marked with some interest but has low probability;
- Classification 3: Marked but not probable.

The onboard QC and onshore interpretation allowed the data quality to be confirmed and survey coverage to be monitored, thus ensuring that the survey objectives had been met prior to each port call and eventually demobilisation.

All onboard data (raw and processed) were regularly backed up to the vessel's server and to removable storage media throughout the project. A copy of the agreed data deliverables was issued to the ATSB on an external hard drive after each swing. Data processed in the office and uploaded to the ATSB during each swing was also added to this hard drive.

Further details of the sequence of processing is contained in Volume 6 – Processing, Interpretation and Results Report.

3.8 Data Transfer Ashore

Survey data from the vessels was transmitted ashore using the vessel's upgraded C-Band VSat system. Initial processing of the data was conducted onboard and a set of deliverables created for each 24 hour period. This data was uploaded to the Fugro Aspera Shares site in the Unites States on a daily basis.

The type of data uploaded depended on the operations being conducted on the vessel. Figure 3.10 illustrates the different directory structures for Deep Tow, Reconnaissance MBES and AUV operations. Only data directly relevant to the search and the identification of anomalies was transmitted ashore for final processing. All auxiliary data such as sub-bottom profile data and MBES water column data was retained onboard and copied to hard drive for delivery to the office at each port call.

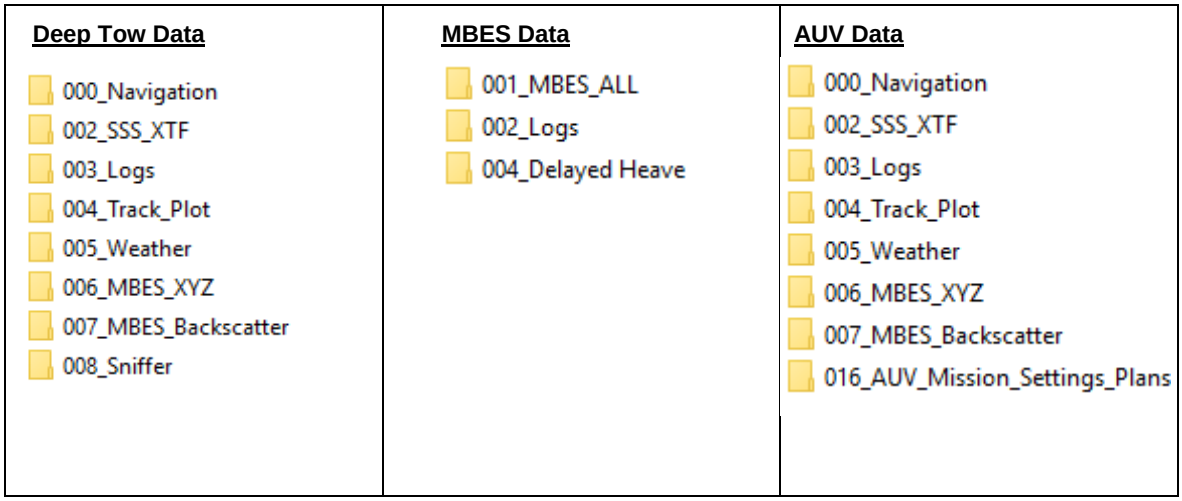

Figure 3.10: Typical directory structure for data upload

3.9 Demobilisation

The Fugro Supporter was demobilised in Fremantle on 17 May 2015, the AUV removed and then departed for Benoa, Bali.

The Havila Harmony was demobilised on 26 March 2016, in Fremantle.

The Fugro Discovery finished Deep Tow operations on 11 August 2016, and began transit to Singapore, arriving on 22 August 2016 for demobilising and preparation for dry docking.

On 16 October 2016, following completion of the Swing 15 Task Request, the Fugro Equator departed the search area and transited to Fremantle for demobilisation of the Deep Tow equipment, arriving alongside the Australian Maritime Complex in Henderson, Western Australia, on 21 October 2016. Preparation for the demobilisation was undertaken during transit to port and, on arrival, the Dynacon traction winch, HPU diesel generator and EdgeTech Deep Tow-2 towfish were quickly demobilised from the vessel.

The Fugro Equator was scheduled to continue working on the project, and mobilisation of Fugro EchoSurveyor VII Hugin 1000 AUV commenced immediately to make the vessel ready for AUV operations. After completion of its AUV campaign the Fugro Equator returned to Fremantle and was demobilised between 22 and 27 January 2017, before transiting to Singapore for dry docking.

4. STATISTICAL SUMMARIES

4.1 Data Holiday Types and Extents

4.1.1 Remaining Holidays

Table 4.1 shows the number and size of the remaining data holidays as well as the percentage of the total remaining holidays that resulted from the surveys carried out by Fugro. The table shows the effectiveness of survey operations conducted by Fugro. Equipment failure and offtracks are particularly low, especially considering the time spent surveying was over two years.

Table 4.1: Data Holiday and LPD Count

	Remaining Data Holidays and LPDs*		Remaining Fugro Data Holidays and LPDs		
	Polygon Count	**Area [km²]**	**Polygon Count**	**Area [km²]**	**[%] of Total Remaining**
Equipment Failure	88	17.1	40	3.49	20.41
Offtracks	8	19.2	2	0.07	0.36
Shadow Zones	5026	312.94	4521	264.09	84.39
Terrain Avoidance	146	218.79	120	116.34	53.17
Lower Probability of Detection	7440	2510.09	7285	2379.72	94.81
*Includes Go Phoenix and DJ101					

Figure 4.1 shows the individual Fugro data holidays (not LPDs) in area (km2) as percentages of the total remaining data holidays.

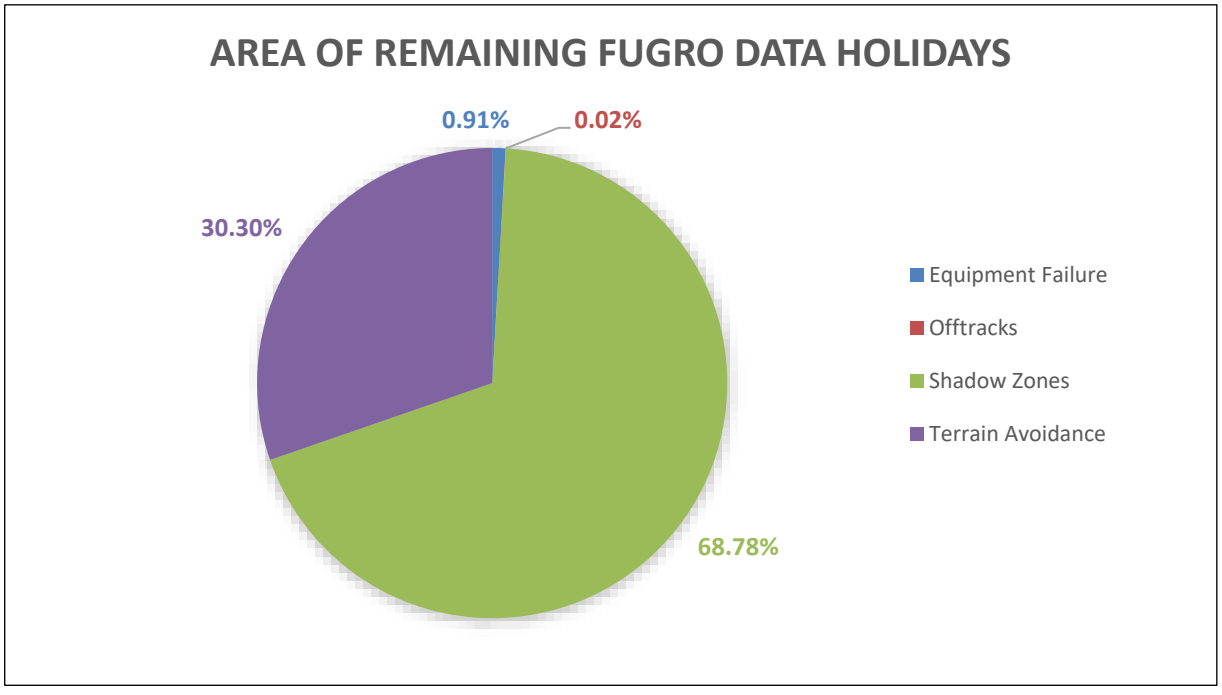

Figure 4.1: Area of remaining Fugro data holidays

The prime reason for the AUV phase of the survey was to fill in data holidays, though the AUV was used on a few occasions to cover virgin territory in the same manner as the Deep Tow was tasked.

Table 4.2 shows the infill statistics from the three AUV phases of the search. Between 73.5 % for the Havila Harmony and 85.4 % for the Fugro Supporter, of data holidays were successfully infilled by good AUV data. The next highest percentage is LPD, between 11.58 % for the Fugro Supporter and 24.05 % for the Havila Harmony. It should be noted LPDs, when resurveyed by the AUV, generally confirmed that the terrain consisted of complex geology and/or a dynamic sea floor environment which typically decreases the confidence of detection for delineating man made debris from geology.

Table 4.2: Data Holiday and LPD Infill Statistics for the three AUV Campaigns

	Fugro Supporter		Havila Harmony		Fugro Equator	
	Area [km²]	[%]	Area [km²]	[%]	Area [km²]	[%]
No Change[1]	5.85	1.35	13.89	2.41	19.00	5.33
Filled[2]	368.95	85.37	423.98	73.49	266.94	74.85
LPD[3]	50.04	11.58	138.76	24.05	70.59	19.79
<100 m[4]	7.35	1.70	0.29	0.05	0.10	0.03
[1]Data holiday has not been filled in by good AUV data						
[2]Data holiday has successfully been filled in by good AUV data						
[3]Data holiday has turned into a LPD as a result of AUV data						
[4]Data holiday has been cut down to a size which no longer classifies it as a holiday						

Figure 4.2 shows the overall data holiday and LPD statistics for all three AUV campaigns in percentage terms.

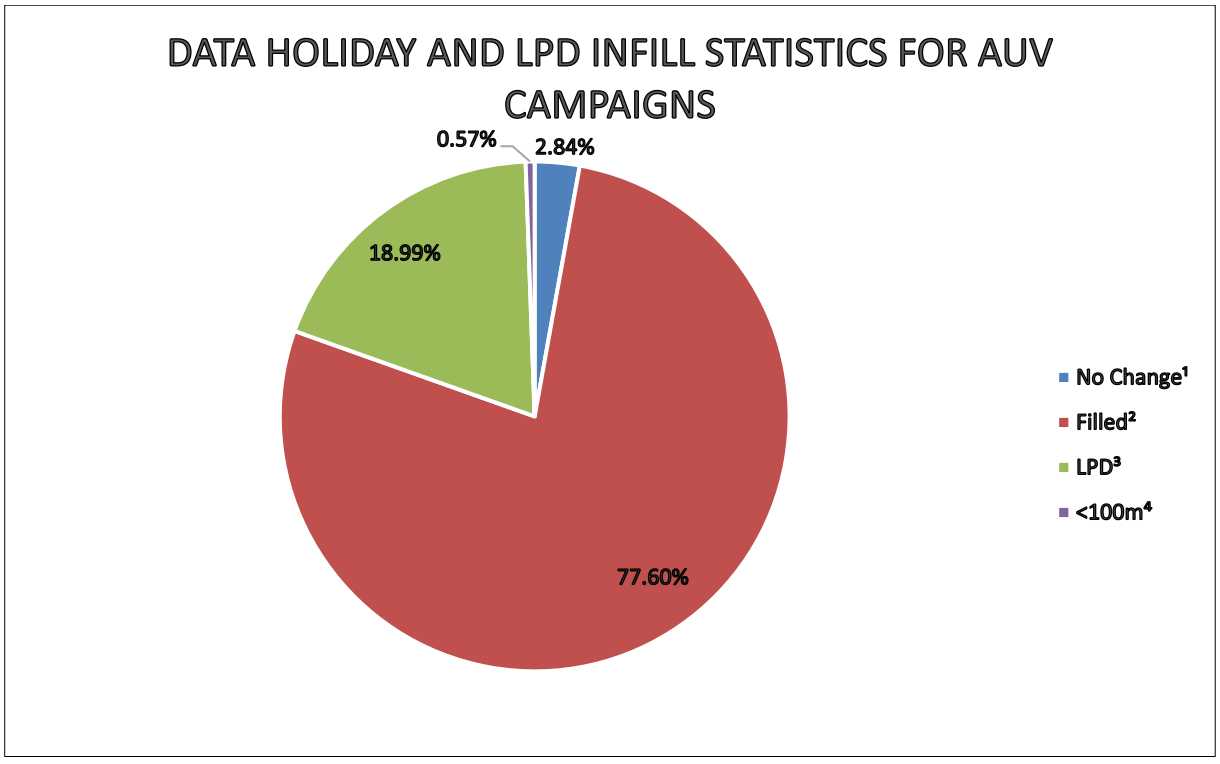

Figure 4.2: Data holiday and LPD infill statistics for AUV campaigns

Figure 4.3 shows the areas of all remaining data holidays for Fugro v non-Fugro vessels.

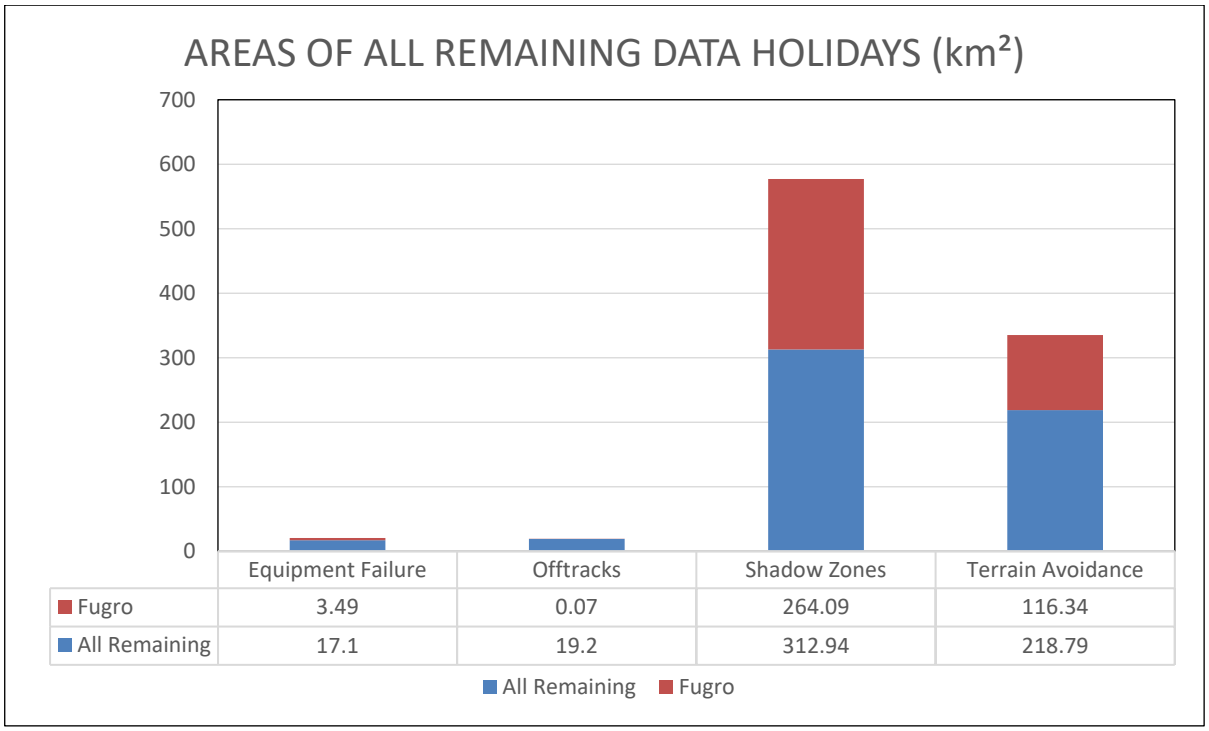

Figure 4.3: Remaining data holidays for Fugro v non-Fugro vessels

4.2 Contact Summary

A summary of the contacts for each phase of the survey picked by the two onshore based reviewers, those contacts that were subsequently forwarded to the ATSB and then the number of these contacts that were picked by both onshore reviewers is shown in Figure 4.4.

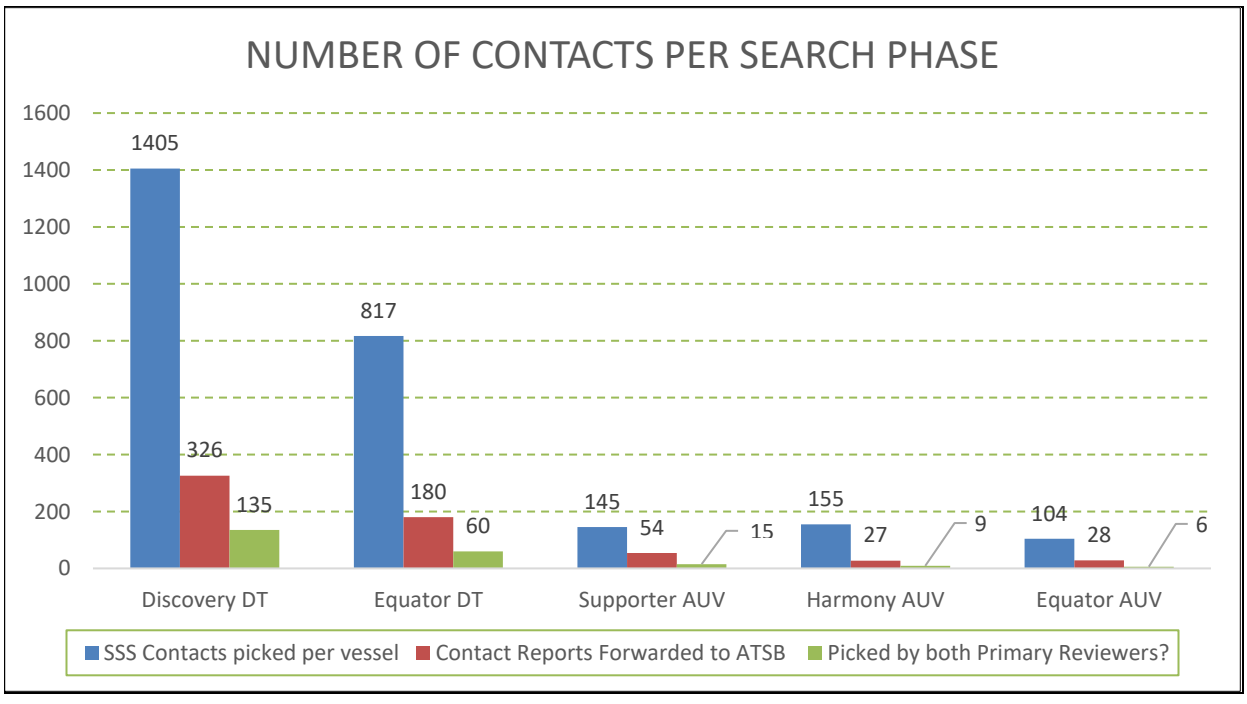

Figure 4.4: Number of contacts per phase

This graph demonstrates the process of narrowing down all possible contacts that were deemed interesting enough to warrant further investigation. All data were reviewed multiple times both offshore and onshore to identify all possible contacts and then reviewed again to ensure nothing of interest could be missed.

4.3 Findings

A number of contacts upon investigation by the AUV or ROV turned out to be shipwrecks.

4.3.1 Shipwreck #1

The sidescan sonar over the first shipwreck (designated Shipwreck #1) discovered on the search is shown in Figure 4.5. It shows the many bright and large returns that suggested that there might be something of interest to investigate.

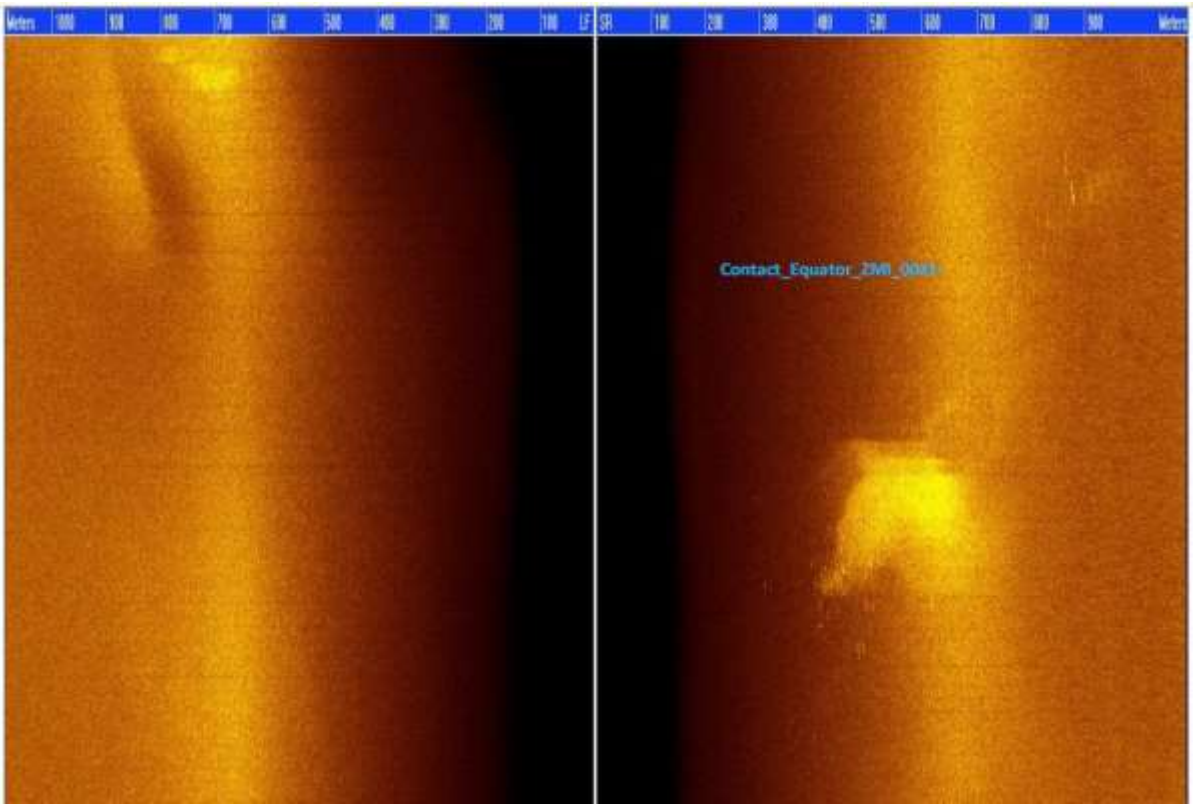

Figure 4.5: Sidescan sonar over shipwreck #1

Shipwreck #1 was in 3800 m of water and when investigated further by a camera survey from the AUV, very detailed images emerged of debris associated with the wreck.

Figure 4.6 to Figure 4.10 clearly shows identifiable images of an anchor, a capstan, a chest, a chain and many items of debris.

Figure 4.6: Shipwreck #1 – anchor

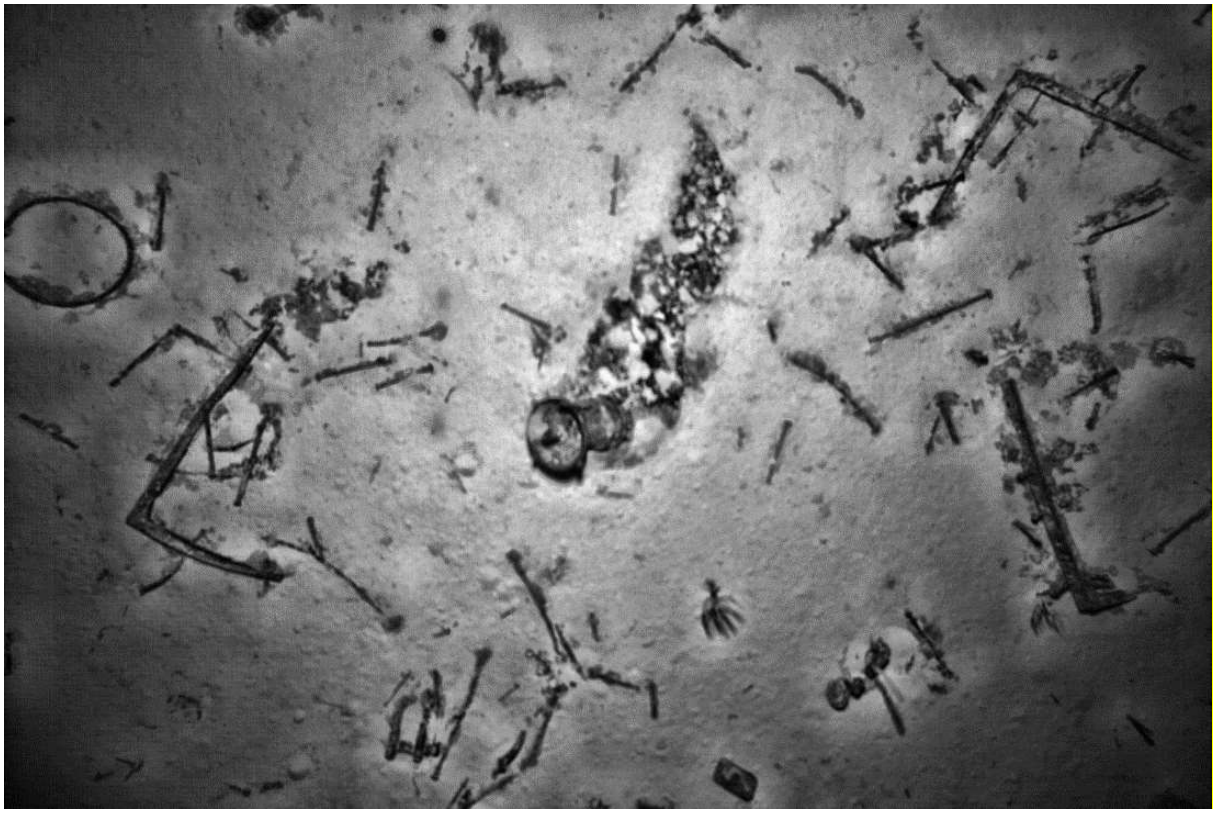

Figure 4.7: Shipwreck #1 – ship's capstan

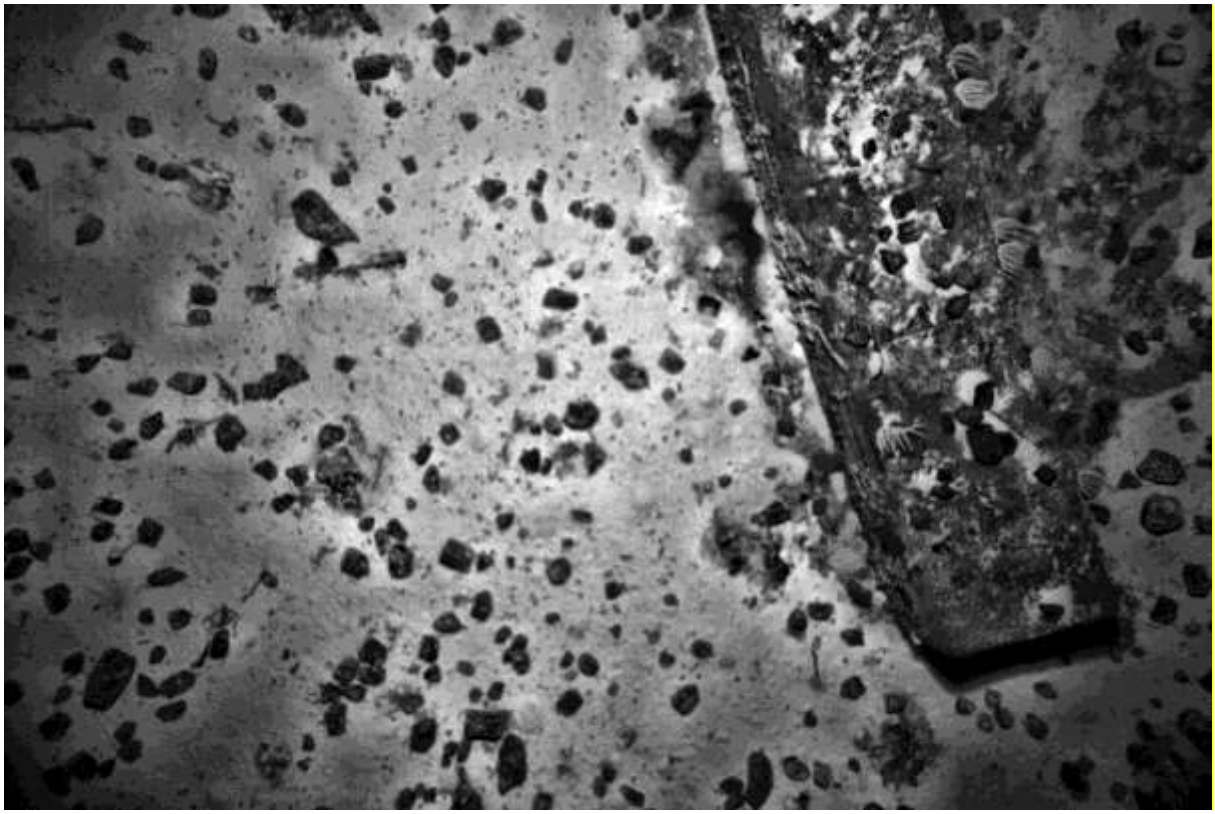

Figure 4.8: Shipwreck #1 – possible water tank

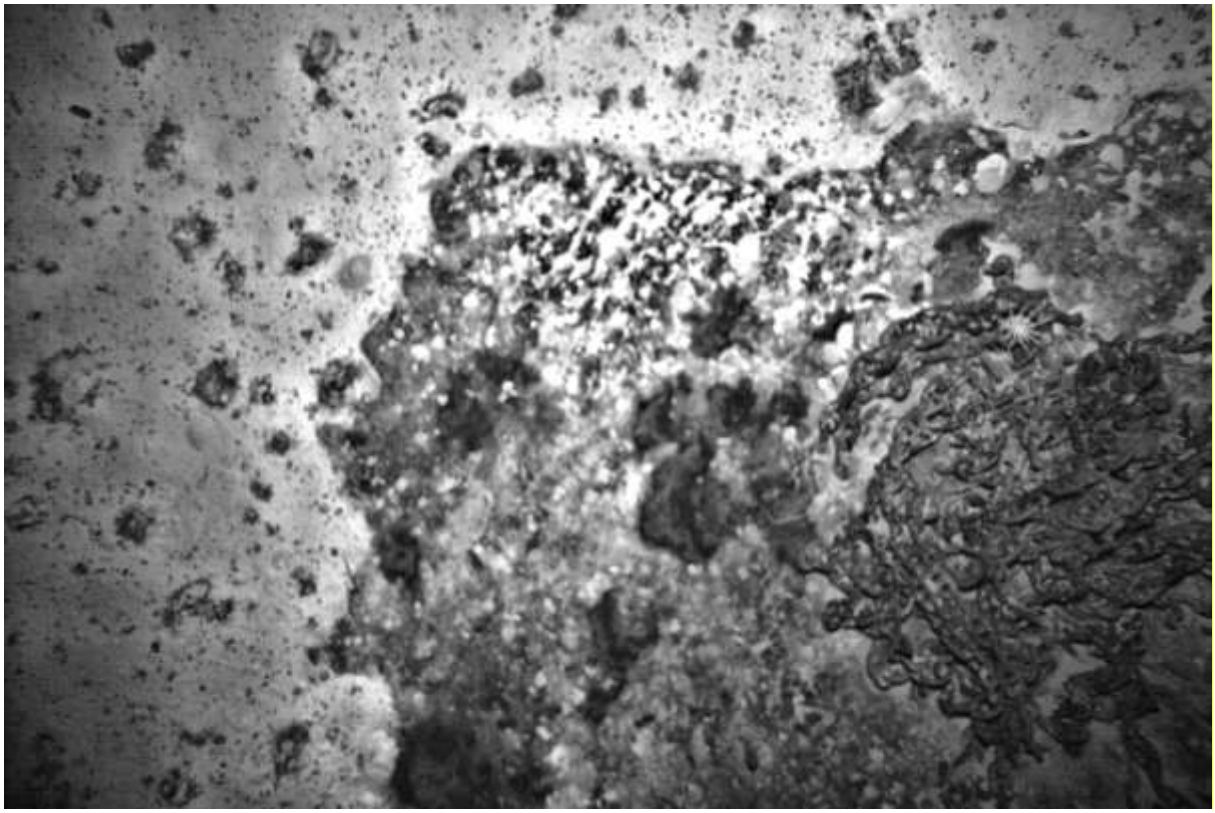

Figure 4.9: Shipwreck #1 – chain

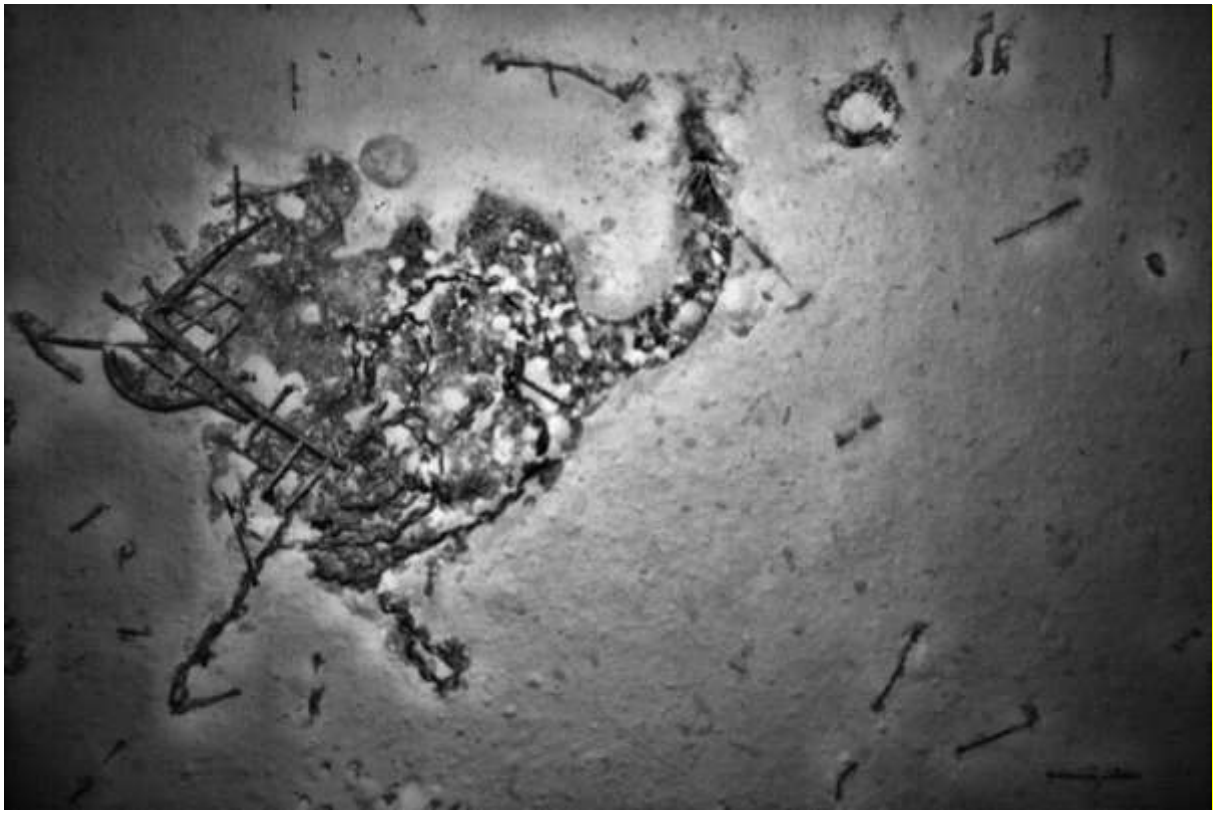

Figure 4.10: Shipwreck #1 – angular item

4.3.2 Shipwreck #2

The sidescan sonar from the Deep Tow over the second shipwreck (designated Shipwreck #2) is shown in Figure 4.11. It originally showed up as a bright patch centred on a brighter symmetrical body which had shadows, indicating it had a visible vertical dimension.

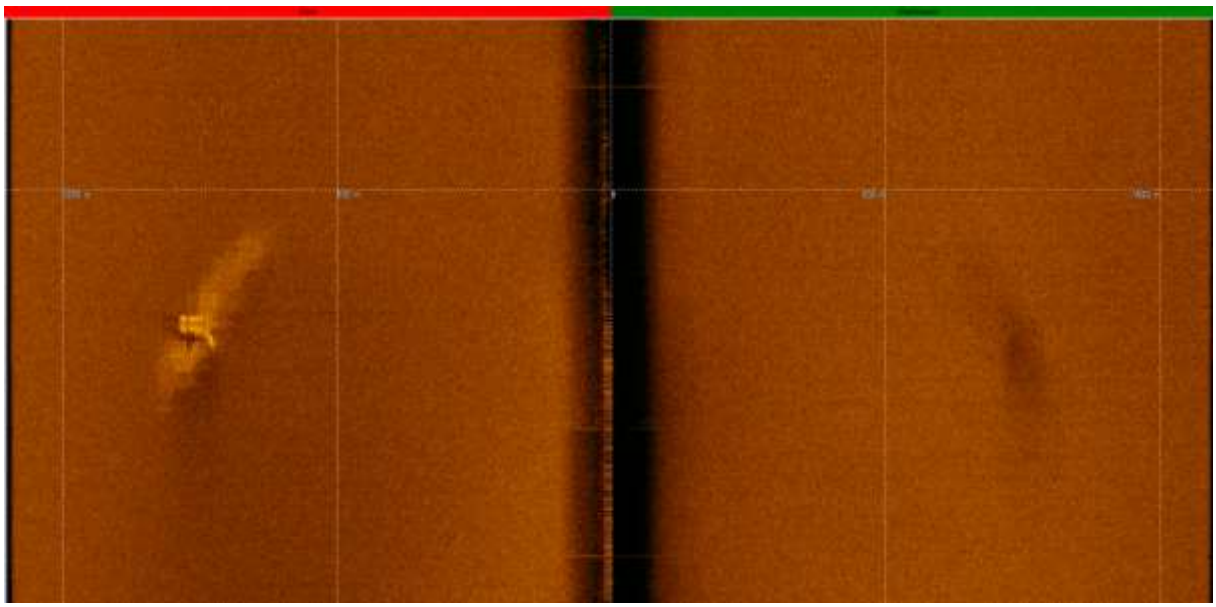

Figure 4.11: Shipwreck #2 – original Deep Tow image

Further investigation by the Deep Tow, flying at an altitude of approximately 35 m above the seabed revealed a complete steel hulled shipwreck sitting upright on the seabed (Figure 4.12 and Figure 4.13).

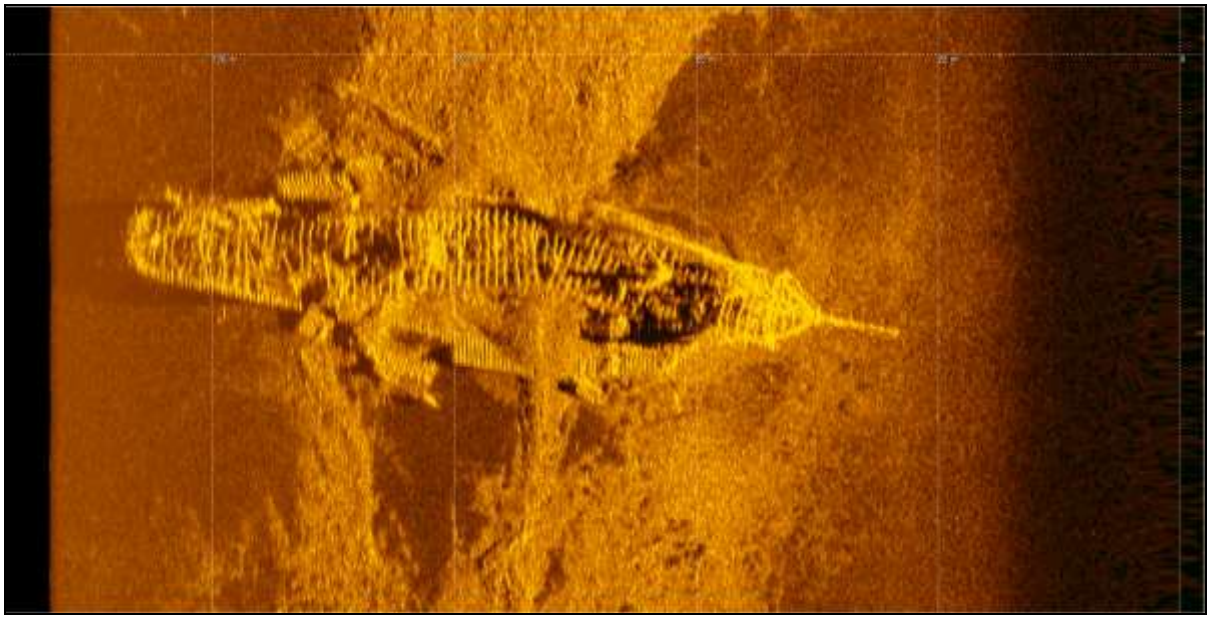

Figure 4.12: Shipwreck #2 – bow on sidescan sonar image

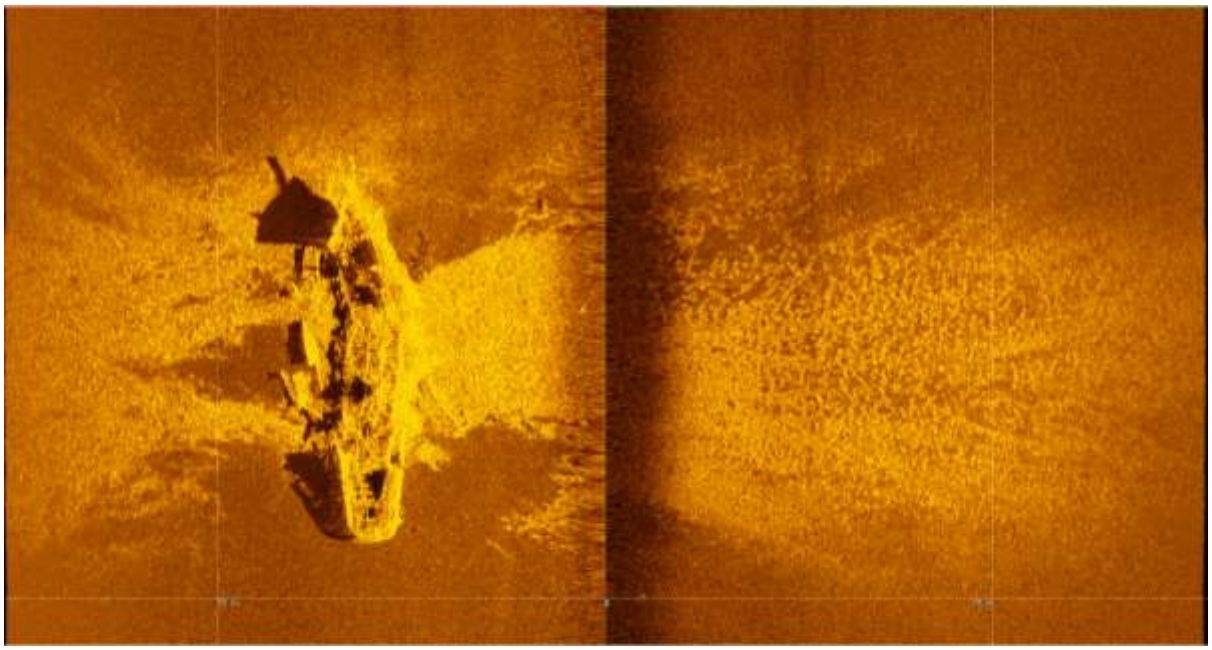

Figure 4.13: Shipwreck #2 – side on image

4.3.3 Shipwreck #3

Shipwreck #3 was a recent steel fishing vessel, found upright, intact and complete with nets, as shown in Figure 4.14 and Figure 4.15.

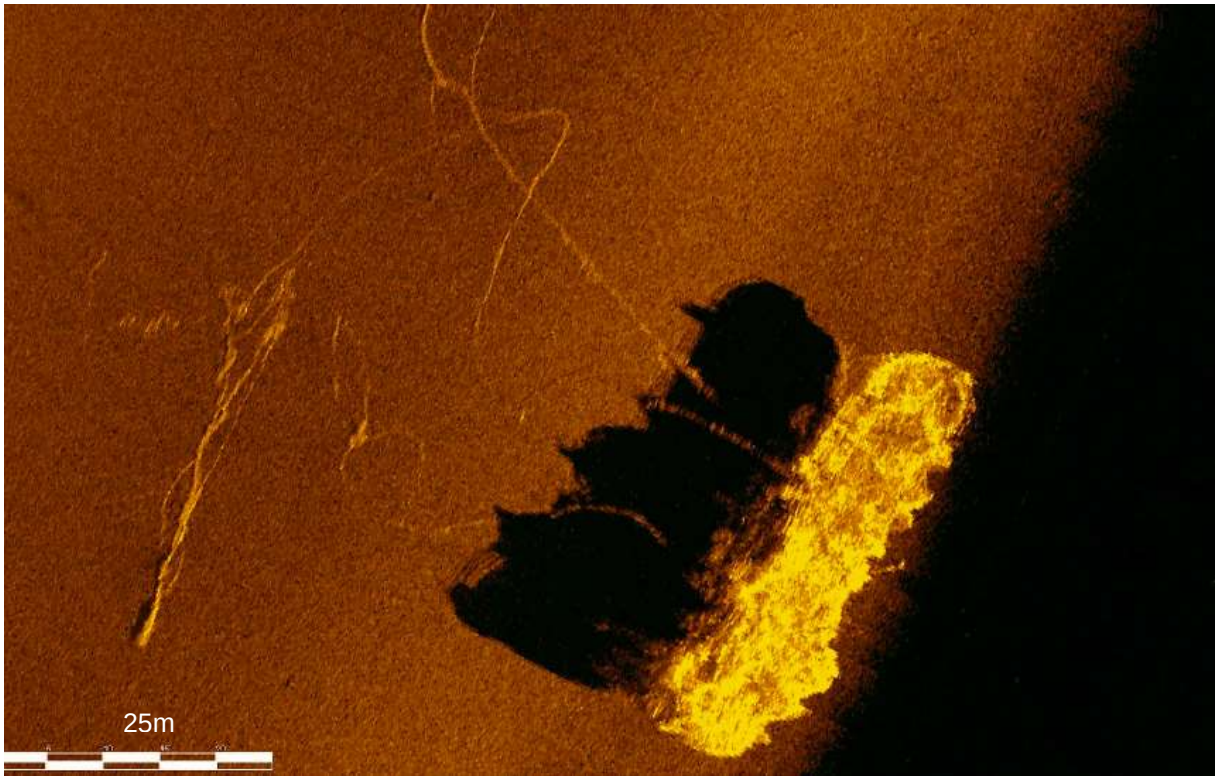

Figure 4.14: Shipwreck #3 – sidescan sonar image

Figure 4.15: Shipwreck #3 – showing deck railing and nets

4.3.4 Shipwreck #4

Shipwreck #4 was a small wooden fishing vessel with substantial damage to the bow as shown in Figure 4.16 and Figure 4.17.

Figure 4.16: Shipwreck #4 – port bow

Figure 4.17: Shipwreck #4 – starboard bow damage

4.3.5 Small Target Detection

Probably the clearest demonstration of the Deep Tow systems capability was the detection of a 44 gallon (200 litre) drum at a range of 690 m (see Figure 4.18). Clearly it helped that the seabed was smooth and free from outcrops. The drum was photographed during an ROV mission.

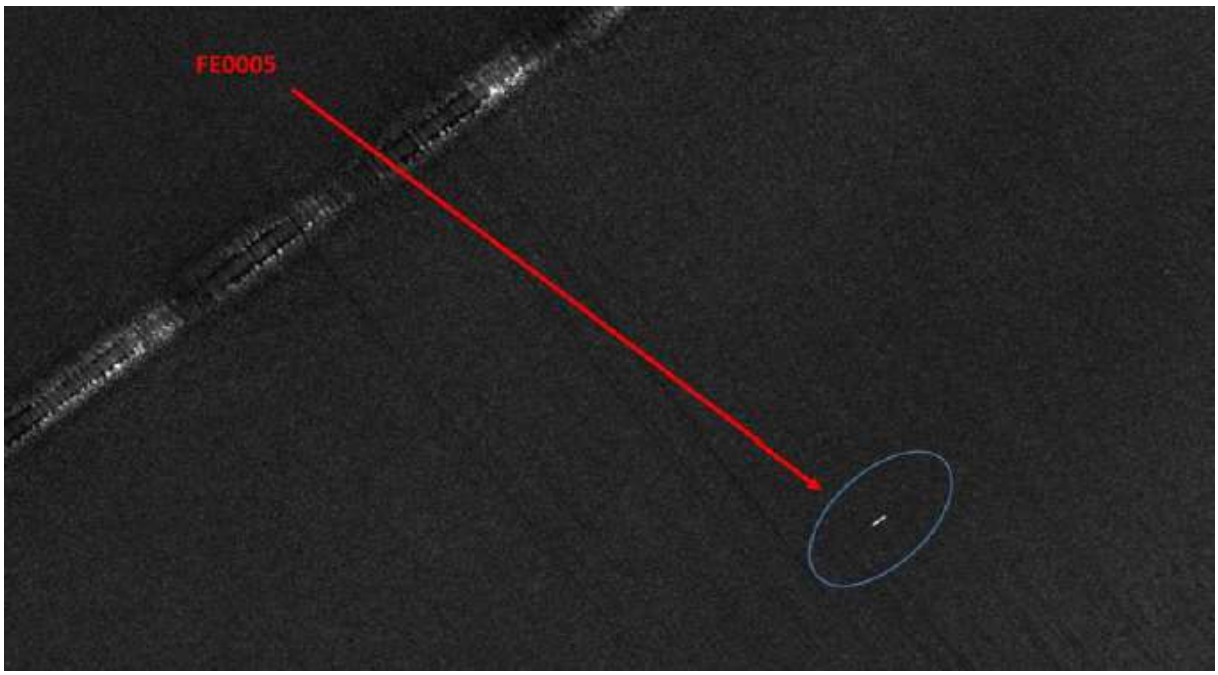

Figure 4.18: 200 litre drum – original Deep Tow sidescan sonar data, 690 m range

The drum was also observed on the adjacent line at 1100 m range as seen in Figure 4.19.

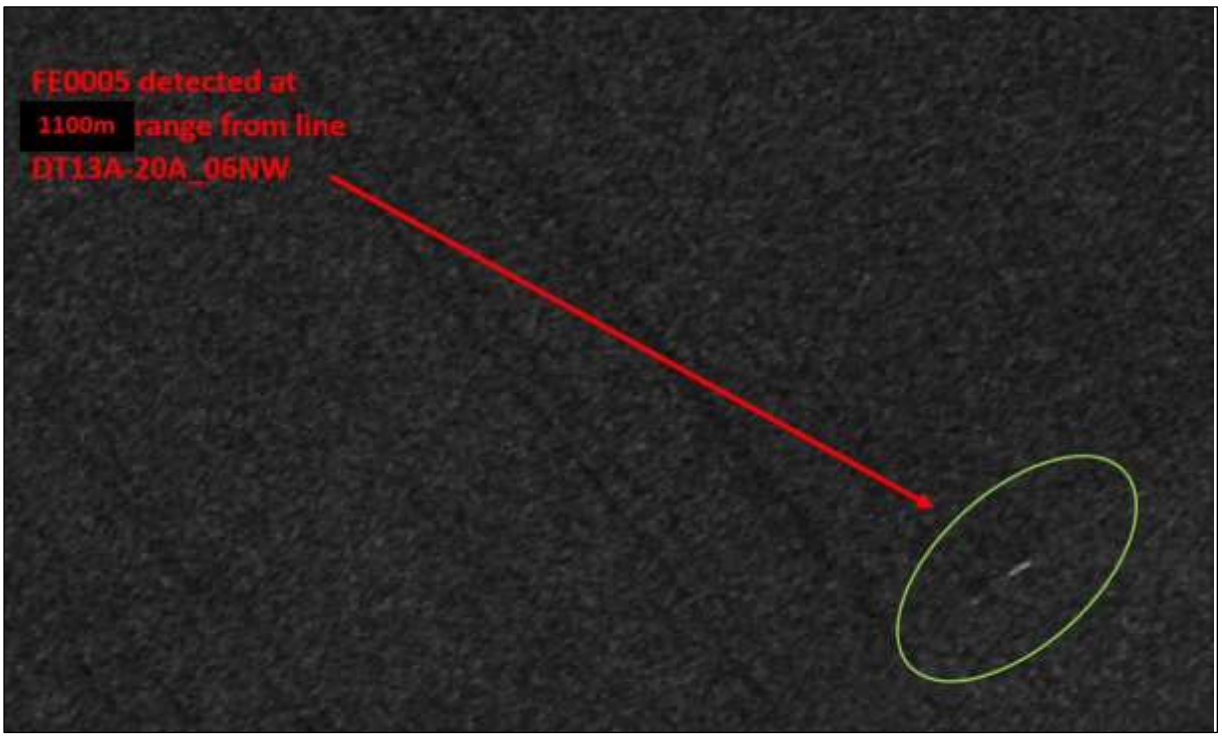

Figure 4.19: 200 litre drum – original Deep Tow sidescan sonar data, 1100 m range

The photograph of the drum taken from the ROV is shown in Figure 4.20.

Figure 4.20: 200 litre drum – ROV photo

4.4 Sound Velocity Profiles

Sound velocity profiles (SVPs) were required to accurately gather vessel based MBES data and to conduct USBL positioning of both the Deep Tow and AUV systems.

For the initial sound velocity profiles completed during the Reconnaissance phase a MIDAS SVX2 sound velocity sensor was lowered over the side of the Fugro Equator to near the sea floor. In total 29 SVPs were taken, all subsequent SVPs were taken from sensors mounted on the Deep Tow and AUV systems as they were raised and lowered.

It was important to conduct multiple sound velocity profiles as the speed of sound in water varied based on location and time of year and to this end results were shared between vessels so that all of the survey area was covered.

The tables provided in Appendix A, give a summary of the collected sound velocity profiles for each phase of the search.

In all, 195 SVPs were taken on the search area site, the spread of which is shown in Figure 4.21.

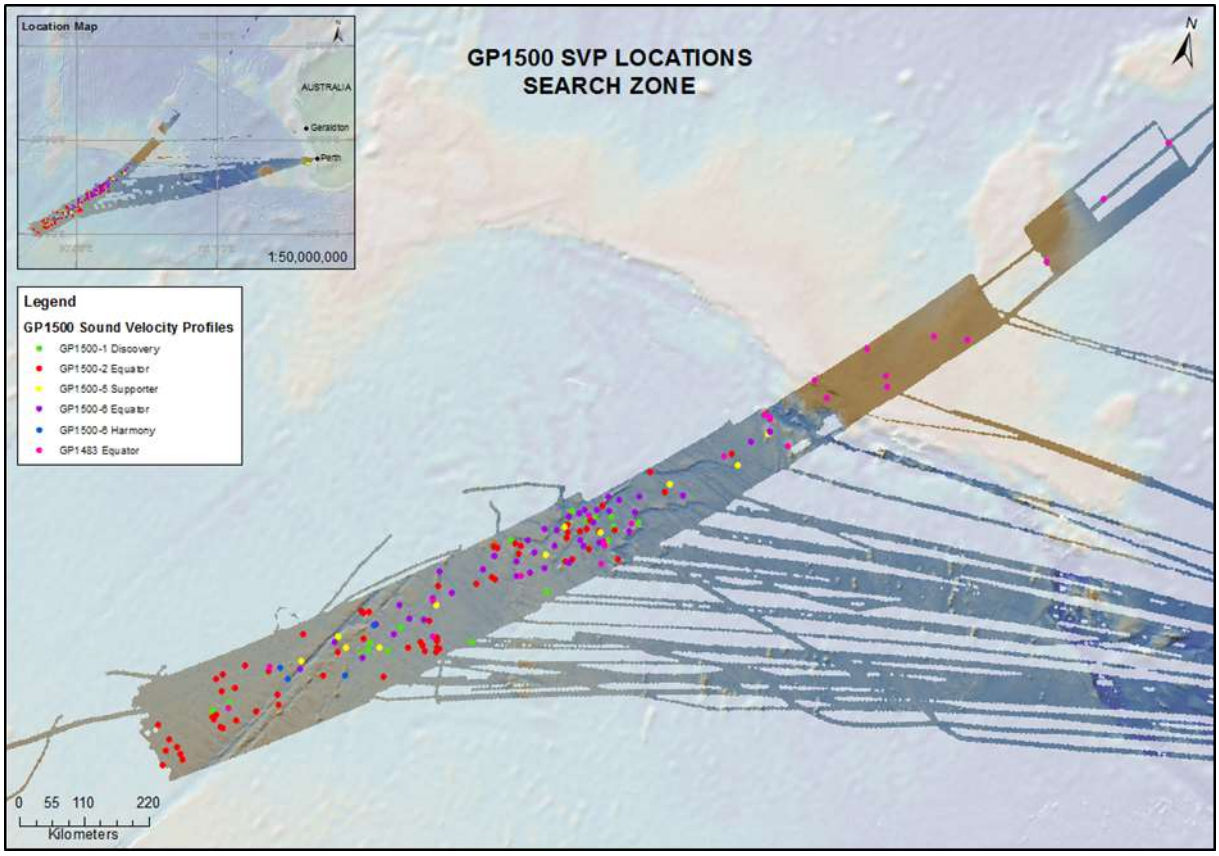

Figure 4.21: Location of sound velocity profiles at the search area site

There were also a number of sound velocity profiles carried out on the trials site off the coast of Fremantle, these are shown in Figure 4.22.

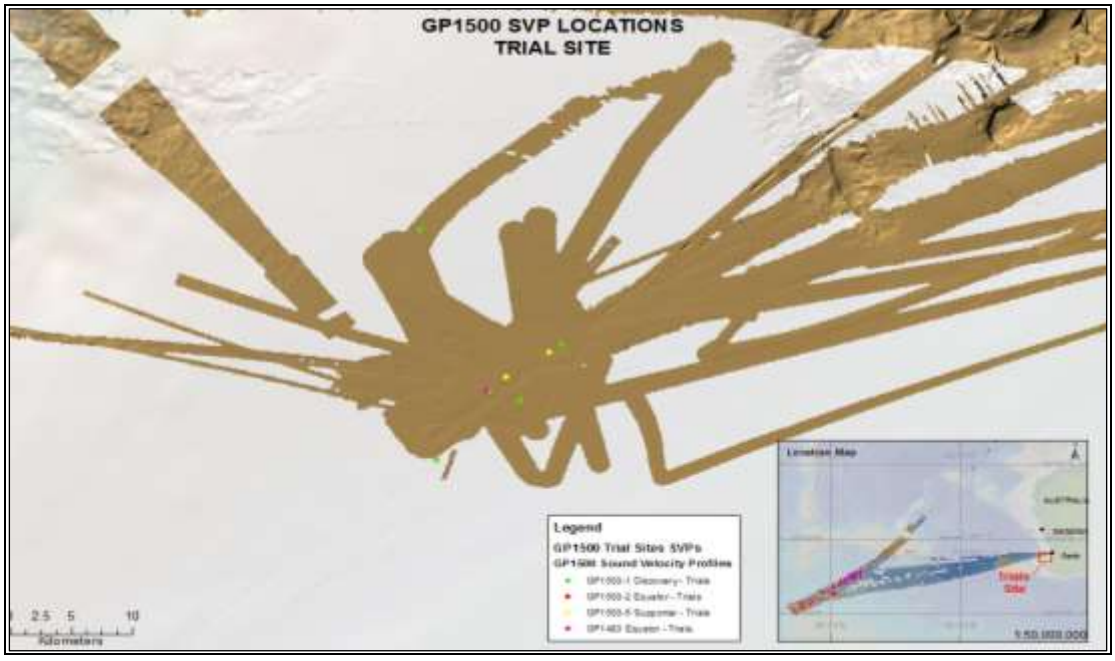

Figure 4.22: Location of sound velocity profiles at the trial site

4.5 Seabed Features

The reconnaissance bathymetric survey highlighted some significant seabed features the most significant being the Geelvink Fracture Zone, part of which is seen as a large canyon, shown in Figure 4.23.

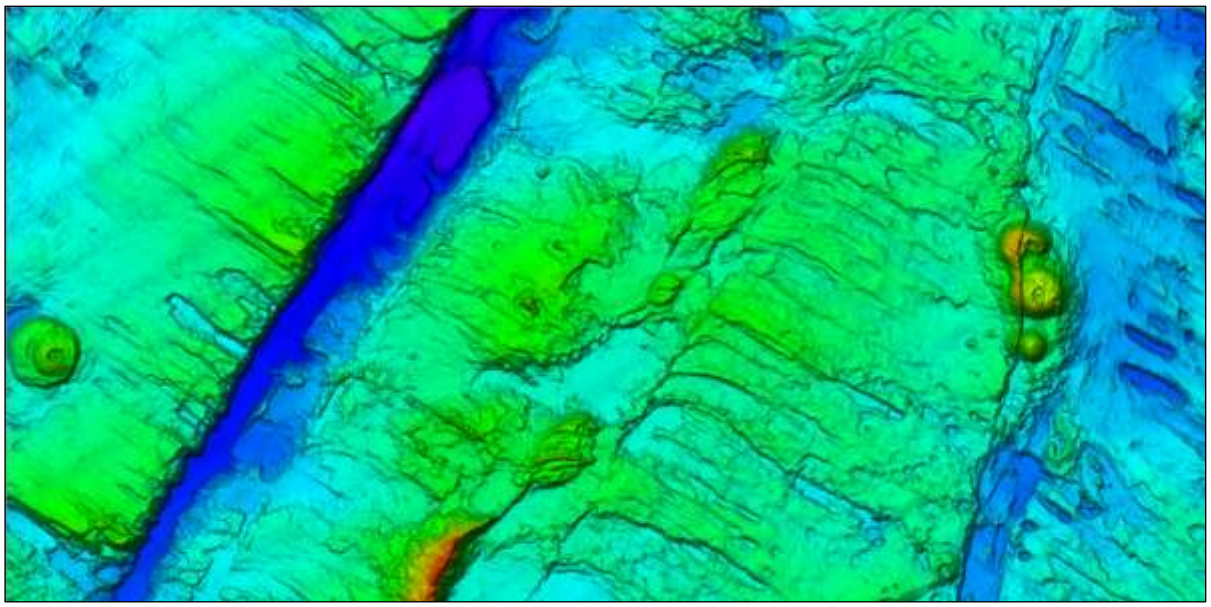

Figure 4.23: The Geelvink fracture zone

The Geelvink Fracture Zone could be a detachment fault associated with large scale extensional tectonic movement in the area. The presence of seamounts in the vicinity confirm volcanic activity which could be associated with very thin oceanic crust. On some of the sidescan files structures resembling pillow basalts can be seen. These clues hint at the possibility that the escarpment could represent an area of incipient oceanic crust. Close examination of the walls of the fault shows smaller faults which are shooting off perpendicular to the main fault strike. These are likely to be caused by brittle deformation whereby the crust is being stretched over the spherical surface of the earth and failing. There is some evidence for lateral displacement on the north-west/south-east striking faults suggesting a strike-slip component to the major fault movement.

The scale of the Geelvink Fracture Zone is shown in Figure 4.24, with the 452 Petronas Towers at 452 m for scale. In places it is up to 800 m deep.

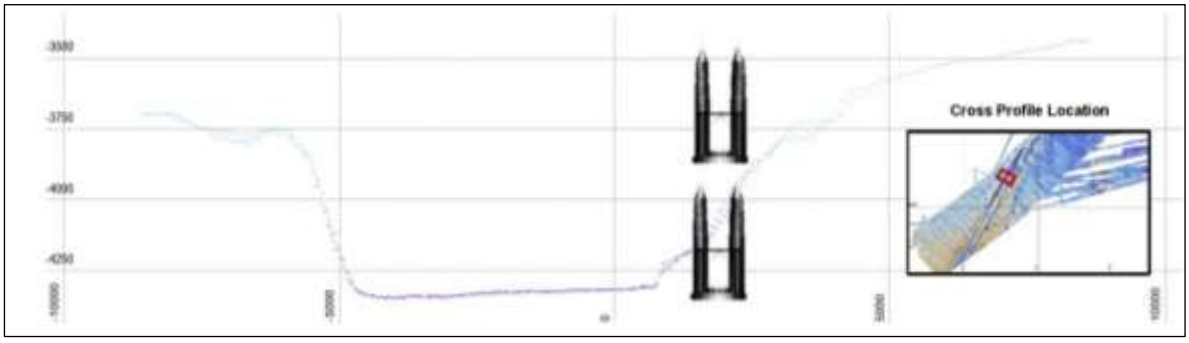

Figure 4.24: Cross-section of Geelvink Fracture Zone (452 m Petronas Towers for scale)

4.6 Transit Distance

The remoteness of the survey area from Australia is shown in Figure 4.25. The red ring is 2500 km radius centred on Fremantle. At approximately 9 knts it generally took the search vessels approximately six days to reach site, depending where on site search operations were to begin for each swing. Usually operations where practical started and ended with minimal transit (five days) to maximise operational time.

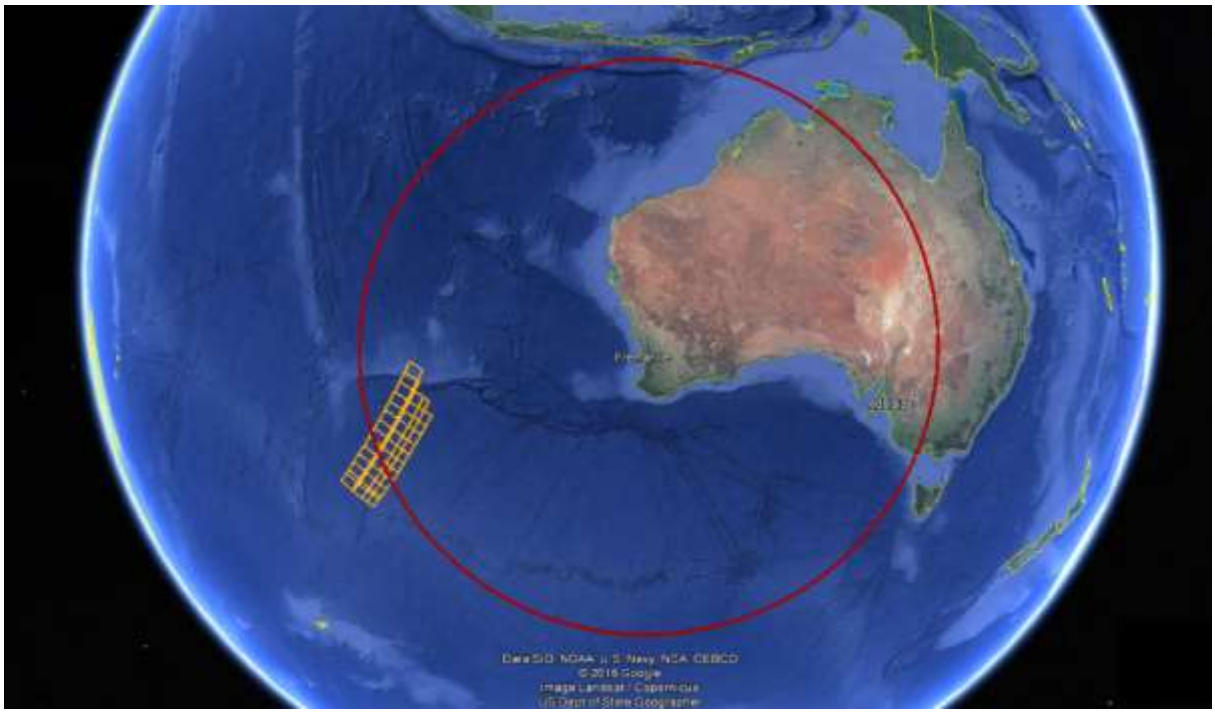

Figure 4.25: 2500 km range ring from Fremantle

Considering just the transit distance the search vessels combined completed 213,260 kms or 5.3 laps around the earth as measured at the equator (this distance was derived from transit multibeam data acquired. The Fugro Discovery and the Havila Harmony did not acquire data on their transits distances so their values were estimated). The distance covered by vessels on site was not factored into this equation as there was no detailed log for the vessels kilometres covered.

4.7 Personnel Hours

Table 4.3 and Figure 4.26 show how many billing hours each of the Fugro Operating Companies accrued during the entire duration of the search across all vessels.

Table 4.3: Personal Hours All Vessels

Personal Hours for all Vessels	
Operating Company	**Hours**
Fugro Survey Ltd	160860
Fugro Survey Pty Ltd	43392
Fugro Survey PTE Ltd	36648
ATSB	23712
Fugro Marine	326280
Contractors	23496
ISOS	11196

Personal Hours for all Vessels	
PT Fugro Indonesia	4692
Fugro GeoServices, Inc	17592
Fugro BTW Ltd	1596
Imtecc (Port Call only)	24
Fugro TSM	4320
Other (Harmony)	6912
Total	**660720**

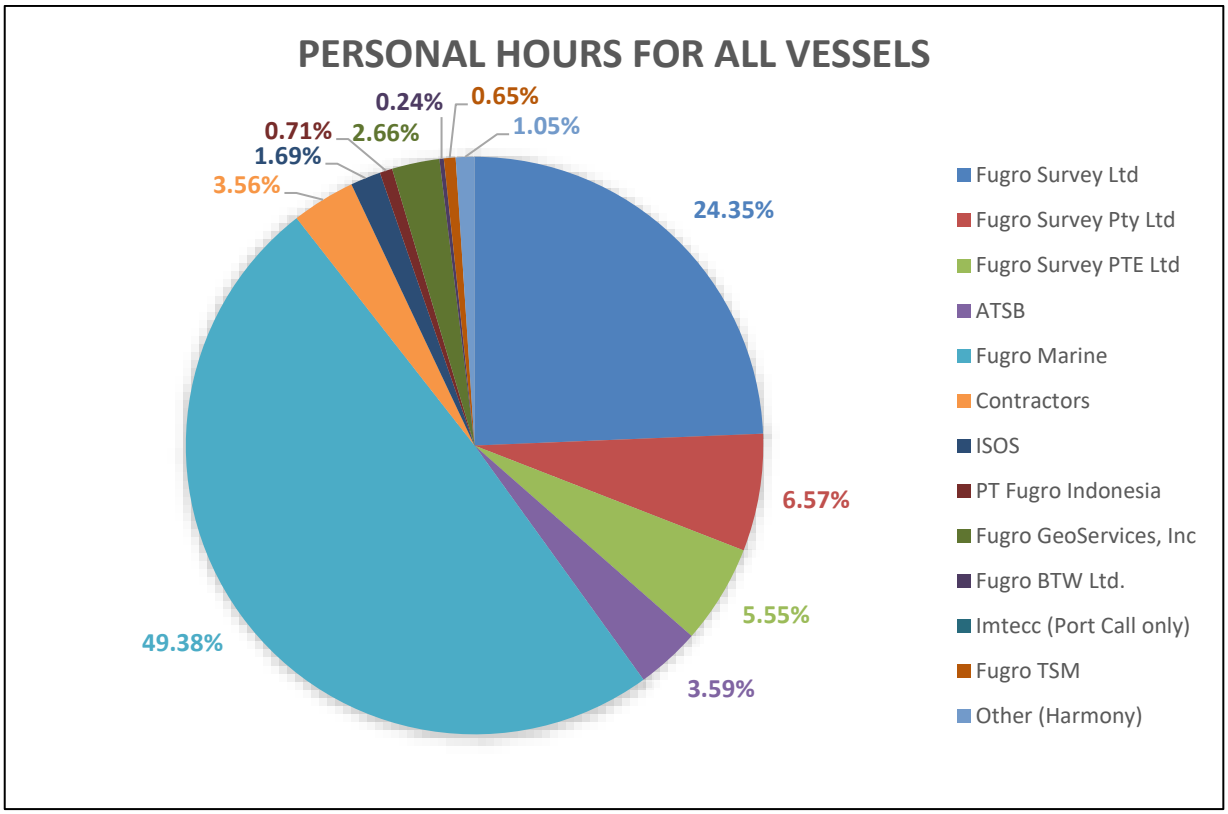

Figure 4.26: Personal hours all vessels

4.8 Equipment – Deep Tow and AUV

The Deep Tow system onboard the Fugro Equator is shown in Table 4.4.

Table 4.4: '*Spero*' Deep Tow Sensors

Acoustic Navigation	
System	Hydroacoustic Aided Inertial Navigation (HAIN)
USBL	Kongsberg HiPAP 101, cNODE Maxi Transponder
Inertial measurement unit	Teledyne CDL MiniRLG
Doppler velocity log	RDI Teledyne Workhorse 300 kHz
Geophysical Sensors	
Multibeam	EM2040 200kHz
Sidescan sonar	EdgeTech Chirp FS 75 kHz and 410 kHz
Sub-bottom profiler	EdgeTech 2200-M, FS Chirp 1 kHz – 10 kHz
Communications	
Emergency communication system	Xeos Iridium Micro Beacon

Additional Sensors	
Speed of sound	Valeport Midas Bathypack
Altimeter	Valeport Midas Bathypack
HD camera	Kongsberg OE14-408-055 Camera
Hydrocarbon detection system	HydroC Subsea Fluorometer

The Deep Tow system onboard the Fugro Discovery is shown in Table 4.5.

Table 4.5: 'Dragon' DT-1 and '*Intrepid*' DT-2 Sensors

Acoustic Navigation	**Deep Tow-1**	**Deep Tow-2**
System	Hydroacoustic Aided Inertial Navigation (HAIN)	
USBL	Kongsberg HiPAP 101, cNODE Maxi Transponder	
Inertial measurement unit	Teledyne CDL MiniRLG2	
Doppler velocity log	RDI Teledyne Workhorse	
Geophysical Sensors		
Multibeam	EM2040 200 kHz	
Sidescan sonar	Edgetech chirp FS 75 kHz and 410 kHz	
Sub-bottom profiler	Edgetech 2200-M, FS chirp 1 kHz to 10 kHz	
Communications		
Emergency communication system	Xeos Iridium Micro Beacon	Metocean AS-900A
Flashers	-	Metocean ST-400A
Additional Sensors		
Speed of sound	Valeport Midas Bathypack	
Altimeter	Valeport VA500 Altimeter	
HD camera	Kongsberg OE14-502-055 Camera	Kongsberg OE14-408-055 Camera
Hydrocarbon detection system	HydroC Subsea Fluorometer	

The systems onboard the Hugin Echo Surveyor 7 1000 AUV is shown in Table 4.6.

Table 4.6: Hugin ES7 1000 AUV

Acoustic Navigation	
System	Hydroacoustic Aided Inertial Navigation
USBL	Kongsberg HiPAP 501 system
Inertial measurement unit	Honeywell HG9900 inertial navigation system
Doppler velocity log	RDI Teledyne workhorse 300 kHz
Geophysical Sensors	
Multibeam	EM2040 200 kHz
Sidescan sonar	EdgeTech2400 75/410 kHz chirp
Sub-bottom profiler	EdgeTech 2200-DW 2 kHz – 16 kHz
Communications	
Emergency communication system	Xeos Iridium Micro Beacon
Additional Sensors	
Speed of sound	Valeport Midas Bathypack
Altimeter	Kongsberg Mesotech 1007 200 kHz Digital Altimeter
HD camera	Kongsberg NEO 11 megapixel 35 mm monochrome +
Hydrocarbon detection system	HydroC Subsea Fluorometer

4.9 MBES Coverage

The total area covered by search was 728,243 km^2. This figure is made up of Reconnaissance MBES data, while on weather standby, all transit data gathered while the vessels transited to and from the five ports of call, and while the Fugro Equator transited to and from Singapore when mobilising and demobilising for the search. To put this in perspective Table 4.7 gives comparable sizes of countries and states by area.

Table 4.7: Total Bathymetric Coverage Compared to Countries and States

MBES Coverage [728,243 km^2]		
Country/*State*[1]	**Area [km^2]**	**Total Coverage Compared to Country/State**
New Zealand	270,467	x 2.69
Australia	7,692,024	x 0.09
Malaysia – East and West	330,803	x 2.20
Chile	756,102	x 0.96
France	640,679	x 1.14
United Kingdom	242,495	x 3.00
Netherlands	41,850	x 17.40
Texas	695,662	x 1.05

[1] **Figures derived from Wikipedia**

For the Reconnaissance Bathymetric Survey a total of 277,082 km^2 was covered. To put this in perspective Table 4.8 gives comparable sizes of countries and States by area.

Table 4.8: Reconnaissance Bathymetric Coverage Compared to Countries and States

Reconnaissance MBES coverage [277,082 km^2]		
Country/*State*[1]	**Area [km^2]**	**Total Coverage Compared to Country/State**
New Zealand	270,467	x 1.02
Australia	7,692,024	x 0.04
Malaysia – East and West	330,803	x 0.84
Laos	236,800	x 1.17
United Kingdom	242,495	x 1.14
Netherlands	41,850	x 6.62
Minnesota	225,163	x 1.23

The maximum depth recorded was 6950 m during transit to site, over the Diamantina Fracture Zone. Figure 4.277 shows a cross-section through this deep transit data and a rapid 3165 m change in depth over 10 kms.

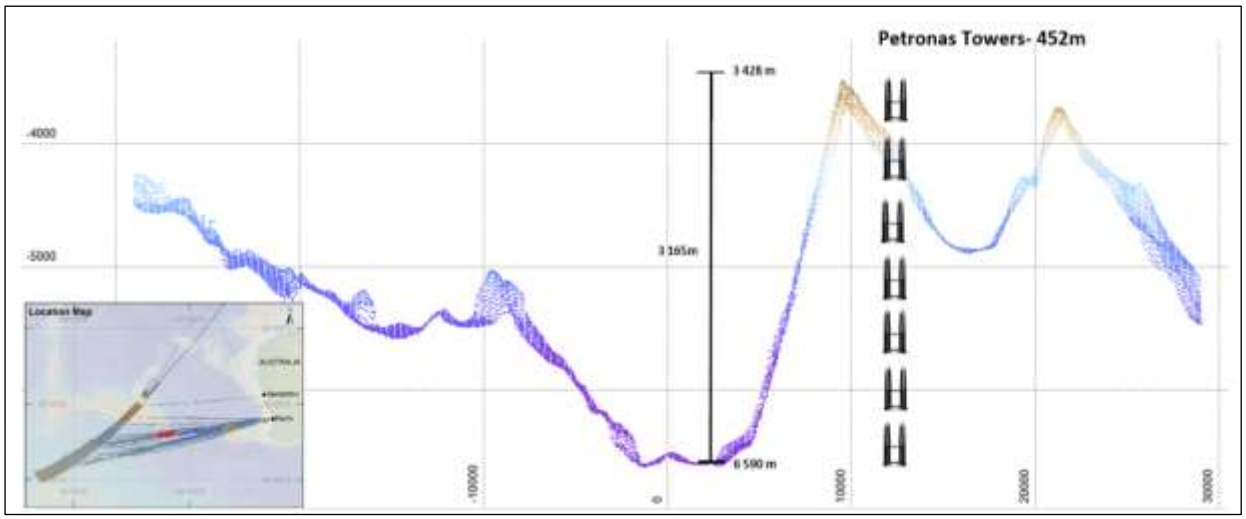

Figure 4.27: Cross-section through Diamantina Fracture Zone

The Reconnaissance Bathymetric Survey ranged in depths from 623 m to 5525 m.

Table 4.9 and Figure 4.28 show the variation in depths found within the search site. Both the table and the figure illustrate just how deep the majority of the search site was – 72 % of the area was deeper than 3500 m.

Table 4.9: Depth Range Histogram

Depth Range [m]	Depth Range [%]
500 – 1000	0.04
1000 – 1500	1.02
1500 – 2000	2.89
2000 – 2500	5.14
2500 – 3000	6.34
3000 – 3500	12.42
3500 – 4000	41.21
4000 – 4500	24.95
4500 – 5000	5.63
>5000	0.35

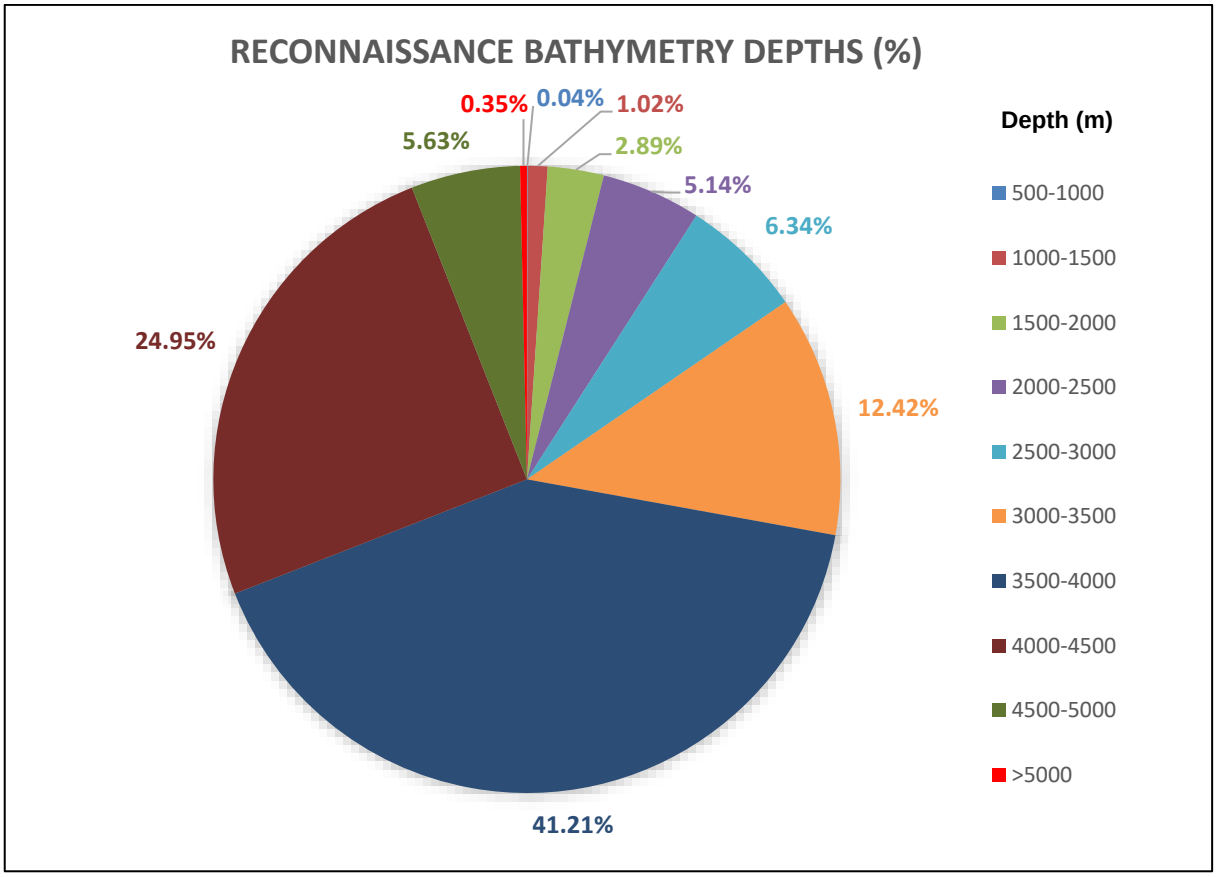

Figure 4.28: Reconnaissance bathymetric survey by depths (%)

4.10 Extreme Sea Condition

Sea state on site was the predominant factor in weather downtime during the survey. Launch or recovery of either the Deep Tow or AUV was determined by sea state, and planning for conditions when it was possible to recover and launch meant that weather forecasts were crucial.

During one whole swing of the Equator Deep Tow survey, Swing 12, between 6 May and 15 June 2015, the weather was so bad that the Deep Tow was unable to be launched at all.

The most extreme sea state measured by any of the vessels was recorded on the Fugro Equator on 13 July 2016, and measured at 23.99 m in height, from peak to trough over a period of 8 to 9 seconds. The heave was calculated from a motion sensor located above the MBES and tracked the actual movement of the boat from that position not the actual swell height, which could have been higher or lower than this. The graph of this particular heave is shown in Figure 4.29.

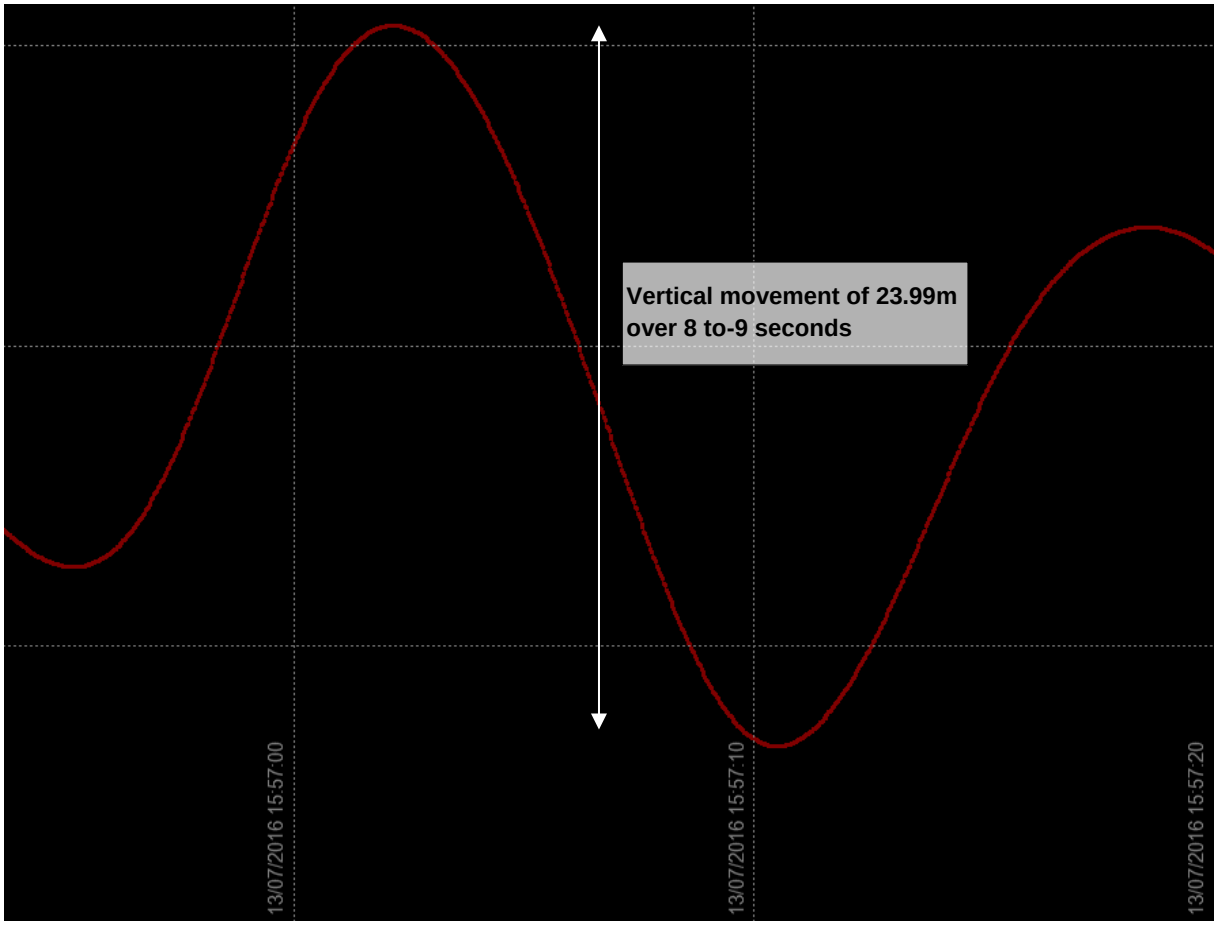

Figure 4.29: Maximum vessel heave recorded during the survey

4.11 Time Spent On Line Turns

Due to the extensive cable out for the Deep Tow survey, up to 9.5 km, depending on depth of the seabed, the vessel needed to go well beyond the end point of a survey line and ensure there was enough run in to the start of lines to enable the Deep Tow to get on line. This often meant elevating the Deep Tow to a safe height above the seafloor by pulling in cable in areas where there was no Reconnaissance Survey data. It also meant that there were more kilometres involved in line turns that there was cable out to the Deep Tow. Consequently line turns were very time consuming averaging, for instance, 10.2 hours over 60 Deep Tow line turns made by the Fugro Equator from Swing 1 through to Swing 15.

There are many factors that can determine the duration of a turn including; the difference between end KP and start KP between lines, the cross-track distance between lines, water depth, type of turn, equipment issues and weather.

4.12 Fuel Consumption

In total 9268 m3 was used by all five Fugro vessels during the survey, as set out in Table 4.10.

Table 4.10: Fuel Used by Each Vessel During Each Phase

Vessel	Phase (Fugro Job #)	Fuel [m³]
Fugro Equator	Reconnaissance (GP1483)	988.6
Fugro Discovery	Deep Tow (GP1500-1)	2890.3
Fugro Equator	Deep Tow (GP1500-2)	3295.6
Southern Supporter	AUV (GP1500-5)	644.8
Havila Harmony	AUV (GP1500-6)	1044.0
Fugro Equator	AUV (GP1500-6)	404.7
Total		**9268.0**

The cumulative breakdown of fuel consumption for each vessel for each swing is shown in Figure 4.30. (These figures do not include fuel figures to and from ports prior to mobilisation and after demobilisation).

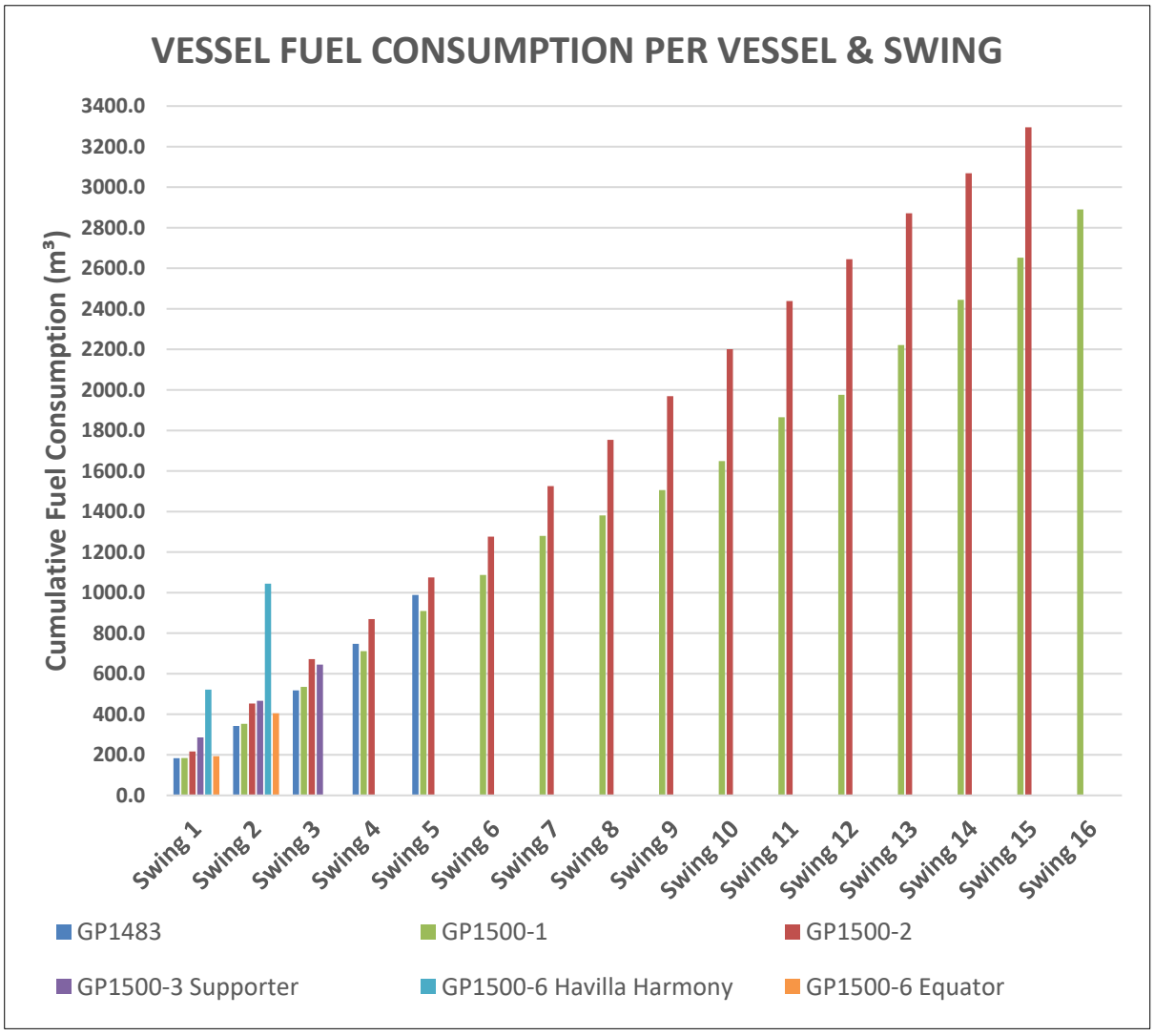

Figure 4.30: Cumulative fuel consumption for each vessel for each swing

5. SURVEY PARAMETERS

5.1 Geodetic and Projection Parameters

The search area covered Blocks 12 to 21 which traversed two projected Universal Transverse Mercator (UTM) Zones – 45 S (CM 87 °E) to 46 S (CM 93 °E). In addition the Fugro Equator was tasked to carry out Reconnaissance Surveys between Block 12 in the south to Block 7 in the north, adding another UTM Zones – 47 S (CM 99 °E). Having to log data over three projected coordinate zones was logistically untenable as it would have meant changing UTM zones at the UTM boundary whilst still surveying. As the projected coordinates were not a crucial issue in that real positions could be related to any coordinate system it was decided to adopt the westernmost Zone – 45 S – throughout. This had the advantage of never having negative eastings and the vessels would not have the problems associated with changing projections during a survey line.

The geodetic parameters used during this project are shown in Table 5.1.

Table 5.1: Project Geodetic and Projection Parameters

Global Navigation Satellite System (GNSS) Geodetic Parameters 1)		
Datum:	International Terrestrial Reference Frame 2008	
Ellipsoid:	Geodetic Reference System 1980 (GRS80)	
Semi-major Axis:	a = 6 378 137.000 m	
Inverse Flattening:	$^1/_f$ = 298.257 223 101	
Local Datum Geodetic Parameters 2)		
Datum:	World Geodetic System 1984 (WGS84)	
Ellipsoid:	WGS84	
Semi-major Axis:	a = 6 378 137.000 m	
Inverse Flattening:	$^1/_f$ = 298.257 223 563	
Datum Transformation Parameters 3) from ITRF2008 to GDA94		
Shift dX: 0.00000 m	Rotation rX: 0.00000arcsec	Scale Factor: 0.00000000 ppm
Shift dY: 0.00000 m	Rotation rY: 0.00000arcsec	
Shift dZ: 0.00000 m	Rotation rZ: 0.00000arcsec	
Project Projection Parameters		
Map Projection:	Transverse Mercator	
Grid System:	UTM Zone 45 South	
Central Meridian:	87° East	
Latitude of Origin:	0° (Equator)	
False Easting:	500 000 m	
False Northing:	10 000 000 m	
Scale Factor on Central Meridian:	0.9996	
Units:	Metres	

Notes:
1. The geodetic datum of Fugro's global GNSS correction data is ITRF2008.
2. Source: Client and Fugro.
3. WGS84 has been refined on several occasions since its inception, the most recent update (G1762) aligns WGS84 with ITRF with an accuracy better than one cm-per-component, resulting in an overall difference of less than one cm.

5.2 Vertical Control

Bathymetry data has not been tidally corrected since reducing water depths of between 2500 m and 4600 m to a particular datum was considered to be academic in terms of the purpose of this survey.

6. SURVEY EQUIPMENT, VESSEL AND PERSONNEL

6.1 Vessels

6.1.1 Fugro Equator

The survey vessel which was in the field longest was the Fugro Equator (Figure 6.1). The vessel is managed by Fugro Marine Services (FMS) and was built in 2012 specifically for survey operations. It is 65.7 m long, 14.0 m wide, with a draft of 4.2 m and can accommodate 42 people.

The vessel has a multi-role capability and can undertake pipeline and cable route surveys, high resolution seismic acquisition surveys, geotechnical surveys and environmental surveys. In addition, AUV and ROV systems can be mobilised to the vessel as required. The vessel is permanently fitted with a full suite of modern analogue and digital geophysical equipment, Fugro Starfix high precision DGNSS positioning and through hull USBL for acoustic positioning. Deck equipment includes a variety of survey and oceanographic winches, port and starboard 2.5 T boom cranes and a 12.5 T hydraulic A-frame.

Figure 6.1: Fugro Equator

6.1.2 Fugro Discovery

The vessel which had the second longest duration was the Fugro Discovery (Figure 6.2). The vessel was originally built for the Norwegian Navy and is an Ice-Class vessel. It is 70 m long, 12.6 m wide, with a draft of 6.0 m and can accommodate 35 persons.

Figure 6.2: Fugro Discovery

The vessel is well appointed with a multi-role capability; ROV inspection, pipeline and cable route surveys, high resolution seismic acquisition surveys, geotechnical surveys and environmental surveys. The vessel is fitted with an auto positioning system, a full suite of modern analogue and digital geophysical equipment, and a comprehensive suite of deck equipment which includes a 16 tonne A-frame.

6.1.3 Fugro Supporter

The first Fugro vessel in the field with AUV capability was the Fugro Supporter (Figure 6.3) which carried the Echo Surveyor 7 AUV for three swings. The vessel is a 72 m multipurpose vessel owned and operated by Fugro Marine Services.

Figure 6.3: Fugro Supporter

The vessel is fitted with state-of-the-art geophysical and geotechnical equipment, this full-ocean depth vessel specialises in cable route surveys and is a versatile platform capable of deploying work class ROVs, AUVs, and both 2-D and 3-D High Resolution seismic spreads.

The vessel offers excellent deck handling facilities including a 15 tonne A-frame and 12 tonne deck crane. It has comfortable accommodations for 47 personnel with all cabins offering en-suite facilities, plus an extensive survey laboratory and client office space.

6.1.4 Havila Harmony

The second Fugro vessel in the field with AUV capability was the Havila Harmony (Figure 6.4) which carried the Echo Surveyor 7 AUV for two swings. The vessel is a 93 m multipurpose vessel owned and operated by Fugro-TSM. It can be used for construction support, ROV survey and inspection, geophysical surveys and AUV surveys.

It carries a 150 Te heave compensated crane, moonpool, helideck and extended accommodation for 86 people.

Figure 6.4: Havila Harmony

6.2 Personnel

The project extended from June 2014 to January 2017, with regular, six weekly, crew changes being conducted at the Port of Fremantle. The only exceptions were a crew change in Geraldton and two seven to eight week swings on the Havila Harmony.

The total number of Fugro personnel involved in the project was 390 from over 20 nationalities.

7. DATA HANDLING

From the beginning of the project it was identified that, due to the huge amount of data being logged each day, good data management was of paramount importance.

The Deep Tow system comprised a number of survey sensors and data is recorded in a variety of file formats. To help manage this aspect of the project a Data Management Plan was created (FDMP GP1500) as part of the project documentation.

In addition, a work instruction was developed offshore (GP1500_WI_000_General Project Data Management and Requirements) to provide a detailed description of the requirements for data logging and storage.

Figure 7.1 provides a summary of the directory structure used for data management and the raw and processed file types created from the Deep Tow vessels.

Figure 7.1: Vessel and Deep Tow raw and processed data formats

All raw data logged onboard the vessel was backed up to a central project directory located on one of the vessel's three data servers. The project directory was also backed up to a second data server at least once every 24 hours. To provide multiple redundancy against any potential data loss the project data was also backed up to duplicate external hard drives, with progressive backups being completed on a daily basis.

At each port call two duplicate hard drives were removed from the vessel and transferred to Fugro's Perth office for data processing and archiving. An additional hard drive containing raw data and data uploaded from the Fugro office to the ATSB during the swing was supplied to the ATSB after each port call.

All survey data relevant to the seafloor search was initially processed offshore in order to assess data quality, coverage, and preliminary feature detection. Data directly relevant to the seabed search and identification of anomalies was transmitted to Fugro's Perth based processing centre using Aspera FTP software.

8. DISTRIBUTION

A copy of this report has been distributed as follows:

Australian Transport Safety Bureau

Attn: Mr Duncan Bosworth : 1 electronic copy

APPENDIX

A. SOUND VELOCITY PROFILES

A. SOUND VELOCITY PROFILES

FUGRO SURVEY PTY LTD
SUMMARY OF SOUND VELOCITY PROFILES

CLIENT: ATSB	LOCATION: Indian Ocean			
PROJECT: MH370			Job No.	GP1483/GP1500

GP1483 Equator

SVP No.	Time Date [UTC +8]	Latitude [S]	Longitude [E])	Sound Velocity [m/s]		
				Min	Max	Mean
1	17:24 on 07/06/2014	08° 59' 30"	115° 05' 01"	1485.41	1537.14	1494.28
2	16:04 on 08/06/2014	09° 30' 23"	115° 03' 59"	1485.55	1538.99	1495.53
3	10:00 on 16/06/2014	26° 55' 48"	100° 36' 27"	1484.4	1526.52	1501.88
4	15:02 on 18/06/2014	28° 02' 11"	99° 50' 40"	1484.23	1525.12	1496.4
5	15:52 on 25/06/2014	29° 11' 55"	99° 15' 27"	1483.99	1522.18	1495.36
6	01:35 on 14/07/2014	30° 41' 00"	098° 21' 24"	1484.95	1521.13	1496.21
7	10:44 on 18/07/2014	30° 47' 41"	97° 46' 46"	1484.45	1518.38	1494.35
8	10:44 on 23/07/2014	31° 16' 47"	96° 42' 32"	1484.31	1513.54	1493.46
9	19:07 on 27/07/2014	31° 35' 19"	97° 09' 41"	1484.56	1515.12	1494.4
10	19:07 on 01/08/2014	31° 57' 19"	95° 58' 21"	1484.12	1514.2	1492.58
11	12:58 on 17/08/2014	31° 43' 57"	97° 15' 16"	1485.54	1514.11	1491.48
12	15:36 on 23/08/2014	32° 09' 53"	96° 16' 13"	1484.76	1512.97	1492.59
13	20:47 on 26/08/2014	32° 41' 06"	95° 16' 57"	1484.17	1509.07	1494.65
14	16:16 on 01/09/2014	34° 50' 43"	93° 29' 07"	1484.59	1523.95	1500.72
15	11:46 on 09/09/2014	33° 27' 50"	94° 47' 27"	1485.71	1524.53	1501.21
16	08:29 on 23/09/2014	32° 41' 52"	95° 23' 38"	1484.84	1523.04	1500.31
17	04:36 on 29/09/2014	38° 18' 34"	87° 26' 59"	1486.16	1514.37	1497.98
18	16:28 on 01/10/2014	34° 54' 09"	92° 41' 05"	1484.5	1527.11	1501.35
19	18:45 on 08/10/2014	36° 45' 06"	90° 13' 47"	1485.27	1518.07	1498.63
21	15:52 on 19/10/2014	36° 03' 52"	91° 44' 06"	1485.57	1526.92	1501.55
22	17:39 on 23/10/2014	35° 13' 21"	93° 03' 56"	1484.63	1522.04	1499.79
Trial	0:54 on 06/11/2014	32° 31' 10"	114° 42' 25"	1484.28	1522.87	1501.23
24	04:42 on 21/11/2014	32° 44' 03"	95° 23' 54"	1484.31	1523.79	1501.38
25	13:56 on 24/11/2014	35° 16' 13"	93° 07' 13"	1485.15	1509.06	1493.02
26	14:00 on 27/11/2014	39° 03' 26"	86° 49' 26"	1484.39	1514.18	1496.65
27	10:05 on 04/12/2014	37° 17' 03"	90° 23' 12"	1484.59	1505.7	1492.44
28	04:00 on 09/12/2014	33° 02' 53"	95° 51' 20"	1485	1515.08	1494.04
29	16:00 on 16/12/2014	35° 33' 52"	93° 08' 19"	1485.4	1506.6	1493.45

GP1500-1 Discovery

SVP No.	Time Date [UTC +8]	Latitude [S]	Longitude [E])	Sound Velocity [m/s]		
				Min	Max	Mean
1	07:25 on 13/10/2014	32° 35' 03"	114° 42' 04"	1495.41	1521.98	1508.93
2	09:16 on 22/10/2014	34° 49' 43"	93° 5' 25.4"	1484.26	1528.29	1512.82
3	00:00 on 17/12/2014	37° 16' 17"	89° 44' 32"	1484.4	1669	1495.84
4	17:30 on 15/01/2015	34° 57' 18"	93° 10' 44"	1484.74	1524.02	1499.95
5	17:30 on 31/01/2015	39° 08' 12"	86° 31' 33.3"	1484.94	1514.5	1497.33
6	00:00 on 25/02/2015	37° 37' 22"	89° 15' 32"	1485.93	1518.12	1500.7

FUGRO SURVEY PTY LTD
SUMMARY OF SOUND VELOCITY PROFILES

CLIENT: ATSB		LOCATION: Indian Ocean				
PROJECT: MH370				Job No.	GP1483/GP1500	
7	02:45 on 03/04/2015	32° 30' 55"	114° 44' 09"	1488.76	1530.25	1510.78
8	08:30 on 10/04/2015	37° 38' 13"	88° 37' 54"	1485.7	1517.77	1502.67
9	22:03 on 21/05/2015	35° 03' 29"	92° 20' 31"	1497.74	1519.53	1507.31
10	13:43 on 07/05/2015	34° 53' 51"	92° 21' 14"	1498.58	1507.15	1501.38
11	08:42 on 03/08/2015	32° 31' 07"	114° 42' 35"	1502.74	1524.85	1507.93
12	00:20 on 02/08/2015	34° 54' 38"	92° 48' 08"	1483.95	1528.56	1501.51
13	09:00 on 29/08/2015	34° 58' 51"	92° 39' 41"	1484.22	1529.43	1501.98
14	07:25 on 21/09/2015	35° 11' 07"	93° 08' 53"	1484.58	1526.92	1508.59
15	07:25 on 22/09/2015	35° 11' 07"	93° 08' 53"	1481.69	1523.33	1501.12
16	00:32 on 05/10/2015	34° 47' 38"	93° 36' 25"	1484.94	1533.03	1503.87
17	23:00 on 30/10/2015	32° 27' 46"	114° 44' 29"	1491.02	1521.01	1510.29
18	03:30 on 14/11/2015	36° 11' 02"	92° 17' 04"	1485.07	1558.2	1498.45
19	16:30 on 22/12/2015	38° 58' 00"	86° 48' 46"	1485.75	1537.71	1501.48
20	12:00 on 14/01/2016	32° 25' 39"	114° 35' 24"	1486.7	1528.08	1502.81
21	12:00 on 20/01/2016	37° 43' 25"	89° 14' 33"	1484.53	1519.3	1515.27
22	04:00 on 08/02/2016	37° 40' 15"	89° 37' 31"	1484.81	1522.1	1499.88
23	12:00 on 25/02/2016	37° 48' 36"	89° 07' 11"	1484.42	1517.99	1498.35
24	07:00 on 12/04/2016	37° 13' 54"	91° 08' 15"	1484.94	1533.03	1503.87
25	19:23 on 06/06/2016	35° 34' 03"	91° 23' 11"	1485.61	1517.32	1499.73

GP1500-2 Discovery

SVP No.	Time Date [UTC +8]	Latitude [S]	Longitude [E])	Sound Velocity [m/s]		
				Min	Max	Mean
3	18:45 on 15/01/2015	35° 06' 39"	92° 42' 49"	1485.81	1519.99	1494.64
4	14:09 on 18/01/2015	36° 11' 27"	91° 13' 05"	1485.21	1519.02	1500.48
5	22:19 on 20/01/2015	36° 21' 17"	90° 57' 29"	1485.41	1517	1497.95
6	02:49 on 01/02/2015	35° 18' 34"	92° 23' 19"	1485.23	1519.77	1498.75
7	01:17 on 05/02/2015	35° 03' 29"	92° 20' 31"	1484.7	1518.29	1498.95
8	14:13 on 10/02/2015	38° 50' 03"	86° 37' 57"	1485.21	1514.96	1497.03
9	09:07 on 27/02/2015	37° 04' 46"	90° 15' 15"	1485.13	1514.93	1497.47
10	09:15 on 14/03/2015	39° 12' 00"	86° 36' 08"	1484.59	1512.56	1495.99
11	19:22 on 16/03/2015	39° 14' 49"	86° 33' 08"	1485.54	1511.39	1497.05
12	15:19 on 23/03/2015	39° 15' 54"	86° 35' 19"	1485.71	1511.64	1496.87
13	09:30 on 29/03/2015	38° 42'16"	87° 42' 16"	1484.94	1520.18	1495.24
14	11:25 on 16/04/2015	38° 15'48"	88° 29' 36"	1485.56	1509.97	1498.04
15	20:00 on 28/05/2015	39° 14' 36"	86° 32' 48"	1485.65	1509.97	1496.09
16	12:30 on 30/05/2015	39° 01' 05"	87° 21' 45"	1485.83	1512.82	1498.46
17	15:30 on 06/06/2015	38° 22' 21"	87° 26' 54"	1485.37	1512.08	1496.4
18	18:44 on 11/06/2015	39° 22' 30"	86° 44' 10"	1484.52	1510.62	1496.51
19	14:06 on 14/06/2015	37° 33' 12"	89° 59' 01"	1484.23	1515.63	1497.63
20	22:46 on 17/06/2015	37° 25' 13"	90° 11' 25"	1484.05	1514.35	1497.28

FUGRO SURVEY PTY LTD
SUMMARY OF SOUND VELOCITY PROFILES

CLIENT: ATSB		LOCATION: Indian Ocean				
PROJECT: MH370				Job No.	GP1483/GP1500	
21	22:19 on 19/06/2015	39° 13' 51"	87° 00' 57"	1484.93	1510	1496.5
22	07:13 on 20/06/2015	39° 23' 12"	86° 48' 01"	1484.98	1510.28	1496.6
23	03:10 on 21/06/2015	38° 51' 30"	87° 46' 13"	1485.17	1508.89	1495.91
24	08:10 on 07/07/2015	36° 30' 59"	90° 16' 06"	1484.47	1518.54	1499.74
25	12:03 on 09/07/2015	35° 36' 51"	91° 36' 23"	1485.12	1515.82	1498.52
26	02:12 on 11/07/2015	34° 41' 54"	92° 52' 19"	1483.43	1522.13	1501.11
27	02:52 on 14/07/2015	37° 18' 42"	90° 27' 46"	1483.92	1515.07	1496.8
28	04:21 on 18/07/2015	39° 53' 45"	85° 45' 50"	1487.12	1511.51	1506.01
29	00:29 on 22/07/2015	37° 28' 13"	90° 14' 33"	1484.17	1512.96	1496.97
30	08:57 on 22/07/2015	37° 20' 22"	90° 29' 02"	1483.84	1518.29	1498.25
31	02:45 on 26/07/2015	39° 48' 47"	85° 58' 29"	1484.61	1509.68	1496.31
32	02:29 on 30/07/2015	37° 32' 37"	90° 18' 43"	1484.18	1515.85	1498.16
33	11:27 on 30/07/2015	37° 18' 03"	90° 28' 38"	1484.06	1502.57	1492.94
34	16:53 on 31/07/2015	37° 09' 13"	88° 56' 37"	1484.13	1524.13	1500.98
35	09:14 on 19/08/2015	35° 00' 43"	93° 13' 34"	1480.97	1525.8	1498.74
36	23:32 on 04/09/2015	35° 24' 00"	92° 50' 50"	1480.43	1519.37	1497.66
38	08:12 on 12/09/2015	35° 39' 49"	92° 29' 32"	1481.7	1522.43	1499.11
39	11:53 on 17/09/2015	35° 36' 17"	92° 36' 05"	1480.53	1519.04	1497.25
40	12:03 on 05/10/2015	34° 21' 03"	93° 34' 12"	1485.12	1526.98	1501.48
41	12:34 on 06/10/2015	34° 58' 07"	92° 45' 29"	1490.33	1525.44	1506.53
42	14:13 on 07/10/2015	35° 13' 50"	92° 23' 03"	1481.37	1529.72	1500.25
43	19:41 on 08/10/2015	35° 25' 28"	93° 25' 52"	1485.06	1514.21	1496.91
44	23:07 on 09/10/2015	34° 56' 56"	92° 43' 50"	1481.93	1523.06	1498.13
45	19:46 on 12/10/2015	35° 07' 21"	92° 20' 27"	1482.35	1524.46	1500.7
46	19:06 on 26/10/2015	38° 34' 26"	86° 33' 56"	1485	1514.52	1498.24
47	07:37 on 17/11/2015	37° 26' 42"	90° 32' 10"	1484.58	1516.14	1498.05
48	02:04 on 21/11/2015	39° 53' 41"	86° 04' 06"	1483.06	1508.91	1494.57
49	22:05 on 26/11/2015	38° 43' 54"	86° 51' 35"	1485.03	1511.77	1497.1
50	04:21 on 09/12/2015	39° 31' 45"	85° 30' 33"	1482.91	1510.41	1495.17
51	08:37 on 10/12/2015	40° 06' 54"	85° 45' 16"	1483.07	1511.48	1497.31
52	08:16 on 13/12/2015	38° 04' 45"	89° 38' 41"	1486.19	1514.11	1499.04
53	18:27 on 06/01/2016	35° 44' 10"	91° 36' 01"	1484.38	1522.37	1498.11
54	19:00 on 16/01/2016	39° 42' 50"	85° 47' 40"	1483.11	1525.18	1499.37
55	06:26 on 27/01/2016	39° 58' 30"	86° 07' 20"	1482.95	1512.73	1494.19
56	08:59 on 16/02/2016	37° 27' 08"	90° 34' 52"	1484.21	1516.72	1497.85
57	16:11 on 17/03/2016	37° 30' 50"	90° 31' 01"	1485.92	1520.32	1499.86
58	01:19 on 04/04/2016	37° 11' 26"	88° 59' 27"	1484.54	1524.1	1499.81
59	08:51 on 19/04/2016	38° 39' 23"	86° 27' 29"	1483.51	1505.53	1492.43
60	01:59 on 22/04/2016	38° 21' 46"	86° 58' 06"	1480.64	1516.89	1496.39
61	21:52 on 28/04/2016	35° 43' 25"	91° 06' 16"	1485	1510.9	1496.52
62	20:55 on 21/06/2016	35° 43' 47"	91° 07' 30"	1487.67	1515.43	1501.2

FUGRO SURVEY PTY LTD
SUMMARY OF SOUND VELOCITY PROFILES

CLIENT: ATSB		LOCATION: Indian Ocean				
PROJECT: MH370				Job No.	GP1483/GP1500	
63	23:47 on 07/08/2016	35° 44' 07"	91° 10' 24"	1486.48	1517.42	1499.34
64	20:00 on 10/08/2016	37° 43' 06"	87° 57' 13"	1486.48	1515.19	1498.19
65	08:50 on 17/08/2016	37° 09' 15"	89° 05' 44"	1486.49	1517.01	1499.25
66	13:56 on 19/08/2016	35° 36' 05"	91° 28' 58"	1484.39	1515.29	1497.13
67	14:47 on 21/08/2016	35° 05' 38"	92° 56' 38"	1484.99	1518.62	1498.71
68	08:02 on 26/08/2016	37° 34' 45"	89° 06' 43"	1486.43	1513.21	1498.08
69	07:37 on 28/08/2016	36° 12' 39"	91° 17' 11"	1485.44	1519.02	1499.18
70	16:30 on 29/08/2016	34° 14' 23"	93° 55' 38"	1486.24	1526.83	1502.58
71	23:10 on 01/09/2016	33° 24' 08"	94° 55' 24"	1485.43	1524.06	1500.79
72	14:45 on 15/09/2016	37° 51' 48"	88° 40' 43"	1484.83	1513.64	1498.666

GP1500-5 Supporter

SVP No.	Time Date [UTC +8]	Latitude [S]	Longitude [E]	Sound Velocity [m/s]		
				Min	Max	Mean
1	17:08 on 05/01/2015	08° 56' 59.6"	115° 10' 02.6"	1495.28	1543.68	1516.31
2	08:25 on 07/01/2015	08° 57' 26.58"	115° 11' 3.48"	1491.29	1543.5	1512.28
3	02:30 on 08/01/2015	08° 59' 12"	115° 08' 25"	1485.36	1543.27	1498.37
4	10:40 on 10/01/2015	08° 56' 38.21"	115° 10' 38.35"	1497.24	1543.69	1521.24
5	00:34 on 12/01/2015	08° 58' 57"	115° 08' 25"	1484.41	1543.45	1498.14
6	12:01 on 13/01/2015	09° 49' 09"	114° 48' 13"	1486.32	1543.75	1497
7	07:01 on 18/02/2015	36° 48' 33"	90° 18' 05"	1485.61	1514.13	1497.6
8	11:50 on 22/02/2015	32° 28' 22"	114° 44' 06"	1485.17	1515.54	1497.97
9	08:50 on 28/02/2015	35° 09' 29"	92° 17' 48"	1488.77	1529.62	1503.76
10	03:30 on 11/03/2015	35°38' 42"	92° 05' 00"	1485.72	1523.42	1499.24
11	16:25 on 18/03/2015	36°48' 33"	90°18'04"	1485.96	1523.44	1502.82
12	18:29 on 27/03/2015	37°46' 32"	88°48'56"	1486.34	1520.18	1507.64
13	16:25 on 01/04/2015	38°07' 02"	88°00'53"	1486.29	1526.94	1510.94
14	07:59 on 11/04/2015	32° 30' 12"	114° 42' 55"	1482.76	1530.85	1509.18
15	10:49 on 24/04/2015	37°37' 32"	88°36'51"	1486.85	1527.83	1510.01
16	16:15 on 30/04/2015	32° 56' 42"	95° 25' 30"	1483.57	1528.7	1502.3
17	12:53 on 02/05/2015	33° 32' 16"	95° 04' 26"	1481.02	1528.01	1502.22
18	01:59 on 04/04/2015	34° 06' 52"	93° 57' 54"	1481.02	1528.01	1502.22
19	14:08 on 05/04/2015	34° 06' 54"	93° 57' 53"	1485.56	1529.79	1509.69
20	01:56 on 06/05/2015	35° 05' 37"	92° 57' 51"	1486.25	1529.8	1508.75
21	16:12 on 08/05/2015	37° 38' 51"	89° 25' 44"	1487.09	1521.35	1501.62

GP1500-6 Havila Harmony

SVP No.	Time Date [UTC +8]	Latitude [S]	Longitude [E])	Sound Velocity [m/s]		
				Min	Max	Mean
1	12:00 on 07/12/2015	37 20'34.595"	89 13'45.937"	1485.96	1514.28	1497.19
2	10:43 on 20/12/2015	38 11'16.789"	88 54'50.508"	1485.96	1514.28	1497.19

FUGRO SURVEY PTY LTD
SUMMARY OF SOUND VELOCITY PROFILES

CLIENT: ATSB		LOCATION: Indian Ocean				
PROJECT: MH370				Job No.	GP1483/GP1500	
3	11:00 on 27/12/2015	38 11'16.789"	88 54'50.508"	1486.16	1512.8	1495.9
4	02:40 on 02/01/2016	38 16'56.348"	87 38'49.186"	1486.52	1503.37	1496.71

GP1500-6 Equator

SVP No.	Time Date [UTC +8]	Latitude [S]	Longitude [E]	Sound Velocity [m/s]		
				Min	Max	Mean
1	04:47 on 02/11/2016	32° 53' 55"	95° 28' 02"	1476.63	1510.7	1495.71
2	23:40 on 02/11/2016	32° 53' 55"	95° 28' 02"	1476.31	1514.84	1498.15
3	19:17 on 04/11/2016	33° 07' 47"	95° 10' 45"	1477.07	1519.19	1495.68
4	19:09 on 05/11/2016	34° 12' 59"	94° 15' 27"	1483.4	1529.99	1506.08
5	04:01 on 07/11/2016	34° 24' 59"	93° 29' 04"	1485.04	529.89	504.28
6	10:41 on 08/11/2016	34° 40' 11"	93° 28' 54"	1484.82	1530.25	1505.97
7	11:03 on 09/11/2016	34° 32' 21"	93° 09' 18"	1485.42	1530.51	1504.86
8	04:12 on 10/11/2016	34° 44' 58"	93° 01' 51"	1505.57	1485.46	1530.61
9	06:25 on 11/11/2016	34° 58' 04"	93° 28' 27"	1485.44	1530.05	1504.99
10	08:36 on 12/11/2016	34° 59' 03"	92° 48' 26"	1486.19	1530.47	1504.85
11	16:38 on 15/11/2016	34° 47' 21"	92° 48' 05"	1485.9	1530.06	1505.95
12	06:01 on 19/11/2016	35° 17' 46"	92° 38' 53"	1486.42	1530.59	1508.96
13	11:14 on 20/11/2016	35° 14' 37"	93° 00' 11"	1486.05	1529.8	1506.28
14	17:39 on 21/11/2016	35° 21' 57"	92° 43' 56"	1486.19	1527.68	1507.28
15	22:18 on 22/11/2016	35° 40' 11"	92° 32' 40"	1486.52	1522.75	1503.16
16	11:26 on 23/11/2016	35° 40' 08"	92° 33' 01"	1486.52	1527	1505.67
17	16:14 on 24/11/2016	35° 50' 47"	92° 07' 34"	1486.14	1526.76	1505.2
18	05:23 on 26/11/2016	35° 28' 36"	92° 11' 36"	1485.86	1529.88	1507.27
19	10:23 on 27/11/2016	35° 14' 48"	92° 09' 57"	1486.02	1530.98	1506.97
20	15:24 on 28/11/2016	35° 30' 10"	91° 41' 31"	1485.54	1529.79	1504.85
21	01:27 on 30/11/2016	35° 51' 24"	91° 35' 18"	1485.58	1527.89	1507.49
22	12:32 on 01/12/2016	35° 39' 28"	91° 52' 21"	1485.32	1519.51	1500.29
23	16:34 on 02/12/2016	35° 57' 56"	91° 53' 33"	1486.1	1523.15	1503.51
24	20:51 on 03/12/2016	36° 04' 40"	91° 39' 16"	1486.6	1526.6	1503.94
25	23:23 on 04/12/2016	36° 05' 52"	91° 00' 37"	1486.24	1525.64	1504.47
26	14:10 on 19/12/2016	36° 34' 09"	90° 33' 11"	1486.24	1512.87	1497.13
27	07:29 on 24/12/2016	36° 18' 19"	90° 13' 36"	1486.38	1524.98	1504.89
28	15:23 on 25/12/2016	36° 43' 32"	90° 12' 36"	1486.05	1511.21	1497.45
29	16:49 on 26/12/2016	37° 04' 05"	90° 08' 35"	1485.79	1524.17	1505.49
30	19:27 on 27/12/2016	37° 06' 40"	89° 52' 27"	1477.38	1525.79	1504.38
31	22:10 on 28/12/2016	36° 56' 58"	89° 37' 58"	1485.84	1524.78	1506.2
32	00:04 on 30/12/2016	37° 23' 52"	89° 38' 56"	1485.74	1524.35	1504.33
33	01:44 on 31/12/2016	37° 19' 06"	89° 15' 39"	1485.85	1526.38	1505.54
34	08:19 on 01/01/2017	37° 52' 00"	89° 10' 17"	1485.8	1521.72	1502.35
35	09:47 on 02/01/2017	37° 43' 06"	88° 34' 34"	1485.45	1528.46	1510.22

FUGRO SURVEY PTY LTD
SUMMARY OF SOUND VELOCITY PROFILES

CLIENT: ATSB		LOCATION: Indian Ocean				
PROJECT: MH370				Job No.	GP1483/GP1500	
36	08:29 on 03/01/2017	38° 14' 32"	88° 01' 32"	1485.13	1524.21	1502.62
37	07:37 on 06/01/2017	35° 51' 55"	91° 09' 49"	1486.01	1516.57	1494.4
38	14:15 on 06/01/2017	35° 51' 55"	91° 09' 49"	1485.94	1529.99	1510.32
39	17:38 on 07/01/2017	34° 59' 08"	92° 19' 48"	1485.3	1530.47	1504.81
40	21:45 on 08/01/2017	35° 16' 09"	91° 56' 39"	1485.8	1529.71	1506.68
41	18:12 on 09/01/2017	34° 59' 08"	92° 19' 45"	1485.09	1530.57	1506.76
42	14:27 on 10/01/2017	34° 32' 28"	92° 56' 27"	1483.56	1530.69	1509.09
43	05:46 on 12/01/2017	34° 54' 02"	92° 29' 48"	1485.07	1530.21	1507.88
44	10:23 on 16/01/2017	34° 50' 05"	92° 35' 01"	1484.28	1530.21	1506.08

Appendix E – Phoenix International Holdings Inc. Malaysia Airlines Flight 370 (MH370) Search End of Contract Report

MALAYSIA AIRLINES FLIGHT 370 (MH370) SEARCH

END OF CONTRACT REPORT

10 May 2017

Submitted to
AUSTRALIAN TRANSPORT SAFETY BUREAU
Attn: Mr. Duncan Bosworth
62 Northbourne Avenue
Canberra ACT 2601
Australia

By
PHOENIX INTERNATIONAL HOLDINGS, INC.
9301 Largo Drive
Largo, MD 20774
+1.301.341.7800
www.phnx-international.com

TABLE OF CONTENTS

1.0 INTRODUCTION 1
2.0 BACKGROUND 1
3.0 MOBILIZATION AND ACCEPTANCE TRIALS 5
4.0 DEEP TOW SAS SEARCH ABOARD *DONG HAI JIU 101* 7
4.1 Swing 1 7
4.1.1 ProSAS Loss 8
4.1.2 ProSAS Recovery 9
4.1.3 ProSAS Repairs and Testing 10
4.2 Swing 2 10
4.3 Swing 3 11
4.4 Operational Stand Down 12
4.5 Swing 4 12
5.0 LESSONS LEARNED 14
5.1 Mobilization/Operation/Demobilization from a Vessel of Opportunity 14
5.1.1 Lesson Learned 14
5.2 Problem Encountered: ProSAS Umbilical Failure 14
5.2.1 Lesson Learned 14
5.3 Problem Encountered: ROV Load Release Shear Pin Failure 15
5.3.1 Lesson Learned 15
5.4 Problem Encountered: ProSAS-60 Cable Damage 15
5.4.1 Lesson Learned 15
5.5 Problem Encountered: Sonardyne iUSBL Failure 15
5.5.1 Lesson Learned 16
5.6 Problem Encountered: ROV Fiber Link Lost 16
5.6.1 Lesson Learned 16
6.0 CONCLUSION 17

1.0 INTRODUCTION

This End of Contract Report details Phoenix International Holdings, Inc. (Phoenix) operational search for Malaysia Airlines Flight 370 (MH 370) and Lessons Learned aboard the People's Republic of China (PRC) Rescue Salvage Bureau (RSB) vessel *Dong Hai Jiu 101*. Phoenix was contracted by the Commonwealth of Australia under the direction of Australian Transport Safety Bureau (ATSB) to provide deepwater towed side scan sonar and Remotely Operated Vehicle (ROV) services in support of continuing the underwater search for Malaysia Airlines Flight 370 (MH370).

The findings in this report are derived from Daily, Weekly, and Swing reports filed by the Project Manager deployed aboard *Dong Hai Jiu 101*. This End of Contract Report includes a summary of the key project events, i.e. engineering activities and vessel preparations in advance of project operations, mobilization/demobilization, operational swing reports, vessel, and lessons learned.

During the timeframe February – August 2016 Phoenix and teammate Hydrospheric Solutions, Inc. (HSI) conducted side scan sonar operations using the highly capable and technologically advanced SLH PS-60 (ProSAS-60), a 6,000 meter depth-rated synthetic aperture sonar (SAS) towed system onboard the Chinese Rescue Salvage Bureau (RSB) vessel *Dong Hai Jiu 101* (DJ101).

During the timeframe October – December 2016 Phoenix conducted Remotely Operated Vehicle (ROV) search operations using the Phoenix 6,000 meter depth-rated Remora III ROV onboard the *Dong Hai Jiu 101* (DJ101).

2.0 BACKGROUND

The Commonwealth of Australia (Commonwealth), as represented by the Australian Transport Safety Bureau (ATSB) and Phoenix International Holdings, Inc. (Phoenix) signed Contract 570-19 on 12 January 2016, for the provision of equipment and services for the search for Malaysia Airlines Flight 370 (MH370). Contract 570-19 supported the Commonwealth 's efforts to carry out seafloor search operations to localize, positively identify, map and obtain visual imaging of the wreckage of MH370 which is believed to have gone missing in the Indian Ocean on or around 08 March 2014. Objectives under the Contract were to search for, locate and identify MH370 within the defined Search Area on the sea floor.

The contract required Phoenix to provide the following key search equipment, with availability as noted in the table below:

SEARCH KEY EQUIPMENT		
Equipment	**Description**	**Availability**
ProSAS Deep Tow System	The deep tow systems comprise Key Equipment and Subsurface Equipment which includes; the towfish and its systems including SAS, MBES, the depressor, winch and wire and the towfish positioning equipment including	The ProSAS Deep Tow System will be mobilized and made available on board the Third Party Supplied Vessel in accordance with the directions of the Commonwealth Contract Authority.

	the USBL. Sonardyne positioning system.	
Remora 3 Remotely Operated Vehicle (ROV)	The ROV systems comprise Key Equipment and Subsurface Equipment which includes; the ROV and its launch and recovery system including colour video camera, winch and wire and the ROV positioning equipment including the USBL positioning system.	The Commonwealth Contract Authority may request in writing that the ROV and the Contractor will use its best endeavors to mobilize and make the ROV available on board the Third Party Supplied Vessel in accordance with the request.
Artemis Autonomous Underwater Vehicle (AUV)	The AUV systems comprise Key Equipment and Subsurface Equipment which includes; the AUV and its launch and recovery systems including SSS, MBES, black and white still photography camera, and the AUV positioning equipment.	The Commonwealth Contract Authority may request in writing that the AUV and the Contractor will use its best endeavors to mobilize and make the AUV available on board the Third Party Supplied Vessel in accordance with the request.

The People's Republic of China provided a crewed vessel *Dong Hai Jiu 101*, coordinated by the Commonwealth, as part of the search.

In advance of the contract signing, the ATSB and Phoenix participated in meetings with the Donghai Rescue Bureau/Ministry of Transport, and conducted a ship-check of the Chinese vessel *Dong Hai Jiu 101* during the period 19-20 November 2015 in Shanghai China. The ship-check was conducted on the 19th of November 2015, and follow-on meetings and briefings with the ATSB and senior level Chinese officials were conducted on the 20th of November 2015.

Meetings and discussions during this visit focused on three areas of interest, i.e. Vessel Ship-Check, Operational Considerations, and Mobilization Coordination issues/or concerns. Additional areas of interest included vessel GA drawing requirements, DP 24/7 operations and vessel ship handling, messing/berthing accommodation arrangement options, food requirements, non-smoking requirements, power supply/cable lengths and VFD location, ROV/AUV/ProSAS deck lay-out installation options, deck timber removal concerns/options, locator pole installation options, equipment stowage and data processing room options, vessel communications capabilities (512kb upload/1024Kb download), IMO/SILOS certifications, Communications (e.g. English-Chinese translation requirements), etc.

19-20 November 2015 Visit - Summary Findings

- *Dong Hai Jiu 101* was built in 2012, and was found to be very clean and well-maintained.
- The ship is a well-equipped, DP-2 towing/salvage vessel, with ~600m2 total deck area (~328m^2 working deck area aft). Engine rooms were clean and well-lighted.
- Ship's power is adequate to support search equipment demands. China agreed to procure/install a Variable Frequency Drive (VFD) unit. Exact location of the VFD is TBD.
- Ship follows China Ship Class (CSC) rules.
- The ship does not have an A-frame, but agreed to fabricate an A-frame (20-ton capability) based on a Phoenix design and installation drawing.
- Deck area (aft deck and helicopter deck) is adequate to support installation of ProSAS, Remora III (optional), and Artemis (optional). Vessel deck area was adequate to support 10 tons/m2 aft of frame 20, and approximately 6 tons/m2 forward of frame 20.
- Phoenix tasking included the following:
    - A-Frame design/installation drawing (fabrication work in China).
    - Basic installation concept drawing(s).
    - Provide ATSB with ROM estimate on design/engineering services work to support mobilization effort.
    - Installation drawings/plan for CSC review and approval by surveyor. Separate installation drawings will be initiated for each system, i.e. ProSAS, Remora III, and Artemis.
    - List of computers and equipment (and power requirements) for data center room.
    - Mobilization and Demobilization cost estimate and timeline estimate to ATSB. Include engineering support (e.g. design effort, etc) in mobilization cost.
    - Stand-alone communications VSAT day-rate estimate to support corporate related message traffic.
    - Review/comment on indicative draft contract.

On 13 December 2015 Phoenix again met with the Chinese Rescue Salvage Bureau (RSB), Dong Hai Jiu 101 officers/crew, and the Shanghai Merchant Ship Design & Research Institute. Meeting participants (approximately 20-25 participants) included Mr. Wang (Deputy Director-General China Rescue Salvage/RSB), Mr. Guo (Deputy Director Rescue Bureau), Mr. Xu (Senior Engineer, RSB), Mr. Hueng (Deputy Director Rescue Bureau), Mr. Liu (Deputy Department Leader Rescue Bureau), Dong Hai Jiu 101 Captain/Chief Engineer/crew Han Qiang (Shanghai Merchant Ship Design & Research Institute), Shanghai Merchant Ship Design & Research Institute staff, and Robert Lohe and Jim Gibson (Phoenix).

13-15 December 2015 Visit - Summary Findings

- A-Frame. RSB provided a detailed engineering design status update. China purchased an existing (30 Ton) A-Frame from a commercial company. Engineering design drawing package was submitted to the CSC (vessel surveyor/classification society) for approval.
- Reviewed Power Supply System options for A-Frame and Winch
- Reviewed proposed Deck Lay-out (includes ProSAS plus Remora III ROV (option))
- Conducted Engineering Design Review, including A-Frame, locator pole, ROV platform drawing packages.
- Reviewed status of fabrication efforts, e.g. Locator Pole, ROV platform, deck risers, etc.
- A-Frame Padeyes. Phoenix provided lift padeye and towing padeye details.
- Storage Winch/Traction Winch. Phoenix provided additional details on traction winch and storage winch placement.
- Design Documentation. Phoenix provided additional engineering design documentation to include drawings and calculations.
- Locator Pole. Phoenix provided additional details on locator pole placement, fabrication, and installation.
- Van Placement. Phoenix – RSB conducted detailed discussion on placement of ProSAS/Remora III Ops and Maintenance Vans. Installation drawings will reflect the inclusion and placement of Remora III ROV Ops/Maintenance Vans.
- Equipment Foundation Elements. Phoenix – RSB reviewed details of equipment foundation elements, fabrication, and installation.
- Phoenix provided detailed presentation providing answers/or discussion points based on RSB list of clarification questions.
- RSB expressed interest in the mobilization schedule and delivery timeline for ProSAS. Phoenix took an action to provide a notional (~4 week) schedule for the delivery of ProSAS in Singapore.
- Reviewed 7 day installation/test schedule in Singapore.
- *Dong Hai Jiu 101* inspection/assessment. Conducted another detailed tour of fantail/deck areas affected by new installation plan.
- Discussed Singapore mobilization roles and responsibilities, to include work assignments and areas of responsibility, and logistics coordination, e.g. crane/welding services, etc.
- Discussed the timing on the arrival of ProSAS and arrival of *Dong Hai Jiu 101* in Singapore. Ship is reporting a projected SOA of ~17 kts during (6-day) transit to Singapore.
- Reviewed the timing on Remora III ROV platform fabrication/installation in Shanghai.
- Reviewed A-Frame static and dynamic load factors.

- Assigned Actions
  - **Rescue Salvage Bureau (RSB) Actions**
    a. Engineering Design Drawings. The RSB was tasked to complete all engineering design fabrication and installation drawings. RSB assumed ownership and responsibility for all engineering drawing development and delivery of the final drawing package.
    b. ROV Platform Fabrication and Installation. The RSB agreed to take an action to discuss further with Peter Foley (ATSB Program Director, Operational Search for MH370). Phoenix recommended completing the fabrication and installation of the ROV platform in Shanghai, even if the ROV was still being considered as an option. RSB completed the ROV platform fabrication design and installation drawings. Phoenix shared additional ROV platform drawings and calculations with the RSB.
    c. The RSB was tasked to comment on Singapore Mobilization Roles/Responsibilities.
  - **Phoenix Actions**
    a. Notional Mobilization Timeline. Phoenix was tasked to develop a notional timeline/schedule for the delivery of ProSAS to Singapore.
    b. Engineering Design Support. Phoenix was requested to continue to provide engineering design support as required by the RSB.
    c. Phoenix was asked to stop (as requested by Mr. Wang) all engineering design efforts and installation drawing work, to include modeling, load case studies, and fabrication and installation drawings, etc.

Phoenix met with the RSB and Shanghai Merchant Ship Design & Research Institute staff again on Tuesday, 15 December to continue the review and discussion on the drawing packages currently under development, and worked towards finalizing Singapore-based mobilization roles/responsibilities.

3.0 MOBILIZATION AND ACCEPTANCE TRIALS

Phoenix and HSI crew departed the United States on 21 January 2016 and arrived in Singapore on 23 January 2016 to begin mobilizing the *Dong Hai Jiu 101*. Mobilization of the equipment onto the vessel began on 25 January 2016 at Berth 12 in Singapore. During the mobilization period, HSI added a fourth array panel to the ProSAS system and updated the software on the system to allow operation with 4 panels per side vice the normal 3 panel configuration. The advantage of adding a fourth array panel enabled greater coverage (range scale) at the same tow speed (2 knots). The three panel array provided a 1000 meter range scale at 2 knots. The four panel array provided a 1300 meter range scale at 2 knots.

The vessel shifted to dry dock on 27 January 2016 and remained there until 29 January 2016 to have its hull cleaned, a shaft seal repaired and propeller work completed. Mobilization and equipment testing continued during this time.

*Dong Hai Jiu 101*returned to Berth 12 on 29 January 2016 and completed mobilization and equipment testing on 31 January 2016 when the vessel departed for Fremantle Western Australia .

During the transit to Fremantle Western Australia , the *Dong Hai Jiu 101*conducted launch and recovery practice, equipment testing, buoyancy and trim checks, INS alignment, data collection and Multibeam Echo Sounder calibration. *Dong Hai Jiu 101*arrived at Fremantle Western Australia's outer anchorage on 08 February, boarded the ATSB Data Quality Manager, and proceeded to the test range for acceptance trials.

The ProSAS-60 vehicle dove on the test range on 09 February 2016 and failed the acceptance test because of excessive noise in the data. The vessel returned to Fremantle Western Australia and moored at Berth E to take on fuel and troubleshoot the system.

Vehicle repairs and troubleshooting were completed and the *Dong Hai Jiu 101*departed for the test range on 15 February 2016. Acceptance trials were completed on 17 February 2016 and the vehicle data was accepted, however, the vehicle frame was damaged during the recovery and the vessel returned to Fremantle Western Australia, Berth E to conduct repairs on the vehicle frame.

*Dong Hai Jiu 101*arrived Fremantle Western Australia on 18 February 2016 and the vehicle frame was transported to a local metal shop for repairs. The repairs were completed and the frame returned to the ship on 21 February 2016. The vessel got underway to return to the test range to insure the data was still acceptable. Trials were conducted on 21 February 2016 and the vehicle data was still of an acceptable quality.

The vessel proceeded to the Operations Area and arrived for dive operations on 25 February 2016 to begin Swing 1.

4.0 DEEP TOW SAS SEARCH ABOARD *DONG HAI JIU 101*

Phoenix International Holdings, Inc. (Phoenix) was contracted by the Commonwealth of Australia under the direction of Australian Transport Safety Bureau (ATSB) to provide deepwater towed side scan sonar services in support of continuing the underwater search for Malaysia Airlines Flight 370 (MH370). Phoenix and teammate Hydrospheric Solutions, Inc. (HSI) conducted side scan sonar operations using the highly capable and technologically advanced SLH PS-60 (ProSAS-60), a 6,000 meter depth-rated synthetic aperture sonar (SAS) towed system.

Team Phoenix mobilized aboard the Chinese Rescue Salvage Bureau (RSB) vessel *Dong Hai Jiu 101* in Singapore in late January 2016. Following a brief port call in Fremantle Western Australia, Phoenix commenced ProSAS-60 search operations in late February 2016.

Dong Hai Jiu 101 and the Phoenix/HSI crew were tasked by the ATSB to conduct a wide area search east of the 7th arc. Lines DT13A-21A_19SE thru DT13A-21A_25SE were assigned and bounded approximately between KP170 to KP355. ProSAS data was collected at the 1100m range scale to maintain at least a nominal 200m overlap, however overlap greater than 500m was consistently achieved throughout the operation.

Dong Hai Jiu 101

4.1 Swing 1

Swing 1 commenced 25 February 2016 with the first dive in the Operations Area and lasted until the *Dong Hai Jiu 101*returned to Fremantle Western Australia on 26 March 2016.

The towfish was first launched on 25 February 2016, but during descent the depth sensor failed and a recovery was conducted to change out the sensor. A second launch was conducted and the towfish began collecting data on line DT13A-21A_19SE on 26 February 2016, followed by line DT13A-21A_20SE a few days later.

During deep tow operation on line 13A-21A_21SE a fishing vessel was encountered. The vessel was on an intercept course based on the tow (search) direction. After repeated unacknowledged hails on the radio and flashing the vessel with the search light, the *Dong Hai Jiu 101* had to divert its heading slightly to avoid collision with the fishing vessel. Data collection during this encounter was not affected.

On 27 February 2016 the iUSBL transceiver experienced water intrusion and the connector pins were damaged beyond repair. The operators followed the recommendations of the manufacturer and did not use an O-ring in the connector which allowed water intrusion at depth. There were no spare connectors onboard and the operators used a layback calculation for positioning until a spare unit was received. The manufacturer later rescinded that recommendation and an O-ring was used on future operations.

On 07 March 2016 the vessel was unable to safely maintain speed and heading down line DT13A-21A_22SE due to high sea state and the ProSAS-60 was hauled back to 600 meters of cable out and laid to in the seas for a weather standby until 09 March 2016 when wide area search operations resumed on line DT13A-21A_22SE.

After completing line DT13A-21A_22SE, a decision was made to move onto line 13A-21A_24SE skipping over line DT13A-21A_23SE which would be completed after line DT13A-21A_25SE. This decision was made in an effort to maximize time on bottom collecting data and minimize time in turns and transit due to lines 24SE and 25SE being longer then line 23SE.

On 14 March 2016 the ProSAS-60 multibeam system experienced a synchronization failure which required a reboot of the system which took several minutes and caused a loss of data collection creating a 2km nadir gap. Due to this loss of data the towfish was hauled in to 300m of cable out and the vessel turned back to several kilometers before the data gap to acquire the missing data. After completing line DT13A-21A_25SE a turn was conducted onto the previously skipped line DT13A-21A_23SE to collect data along this line.

On 18 March 2016, during tow operations down line DT13A-21A_23SE, the ATSB sent an amended task request with instructions to conduct SAS imaging of shipwreck #1 at a 1300m range scale, followed by an LPD test line and concluding with infill lines. This amended task was to commence upon completion of Line 23SE. The shipwreck was imaged on 19 March 2016 followed by the LDP line SAS_DJ101_LPD_01 on 20 March 2016.

After completing data collection on the first infill line, DT13A-21A_02NW_125m_SE, on 21 March 2016, the towfish was being hauled in to approximately 300m cable out to conduct a turn onto the next assigned line. During the haul back, when the cable was at 608m of cable out and at a depth of 447m, the mechanical termination failed at 11:19 UTC. This failure caused the depressor to separate from the cable and descend uncontrolled to the bottom at a depth of water of approximately 3600m with the ProSAS in tow. The position was well logged and the decision was made to head to port to plan and refit for a recovery of the ProSAS-60. The vessel arrived in Fremantle Western Australia on 26 March 2016 ending Swing 1.

4.1.1 ProSAS Loss

At 1119 (UTC) on 21 March 2016, after completing line DT13A-21A_02NW_125m_SE, communication was lost to the ProSAS-60 vehicle and the vehicle tow cable tension went from over 2,000 lbs to approximately 700 lbs. The navigational position of this event was recorded immediately. The topside power reading was checked and found to be consistent with exposed power conductors on the tow cable, indicating a potential break or separation in the tow cable.

Phoenix recovered the tow cable to the surface and reported the ProSAS vehicle was disconnected and noted the exposed cable was pulled out of the depressor.

An accident/incident report was initiated and the accident reported to the ATSB. The following information was noted regarding the incident:

- Sea conditions at the time of loss recorded winds at 18-20 knots out of the SE and seas of approximately 3 meters.
- The winch speed at the time of the accident was approximately 30 m/s and the vessel speed was approximately 2.35 knots.
- The termination which failed was deployed for a total of 25 days, 2 hours, and 30 minutes. These values were determined from the daily search situational reports (SITREPS).
- The umbilical cable is a Tyco Electronics, Rochester Corporation electro-optical-mechanical steel armored cable. The umbilical is 0.681 inch nominal diameter cable.
- The weight of the depressor is between 1,800 and 2,000 pounds.
- The connection of the umbilical termination to the depressor is made with a shackle from the depressor padeye to a steel endless loop which is captured in the PMI EVERGRIP Termination by a pin.

The ProSAS had been in the water since 25 February 2016. The depressor had been recovered several times to inspect the cable and mechanical termination. Visual checks of the termination on ProSAS-60 were conducted on two previous occasions during the deployment prior to the loss. These previous observations occurred on 10 March 2016 at 0902 UTC (about 11 days prior) and on 14 March 2016 at 0926 UTC (about 7 days prior). No wear of the PMI EVERGRIP termination was observed during either of these inspections. There were no visible signs of damage or slippage of the termination noted.

4.1.1.1 Findings

The failure of the termination was the result of fatigue failures of all but two of the grip rods. The rod failure location corresponded approximately to the nose of the PMI EVERGRIP™ termination housing. The two intact rods had apparently pulled out of the housing after failure of the other rods.

The ends of the failed rods were examined under low power magnification. The broken rod ends exhibited classic fatigue failures, most likely caused by cable strumming also known as vortex-induced vibration.

The cable strength loss was likely due to the general corrosion observed on the outer armor wires, it was noted that the inner two armor layers had little to no corrosion present. This is consistent with vortex-induced vibration where the outer armor wires break and the adjacent inner wires will be called upon to carry more tension. During this process the cable will become less well torque balanced. Eventually, there could be a cascade effect that results in the failure of the outer wires.

4.1.2 ProSAS Recovery

In response to the loss of ProSAS, Phoenix began mobilizing the *Remora III* Remotely Operated Vehicle (ROV) aboard *Dong Hai Jiu 101* on 05 April 2016 for ProSAS recovery efforts. Mobilization was completed on 10 April 2016 and the vessel proceeded to the ProSAS-60 loss

location. *Dong Hai Jiu 101* arrived at the loss location on 14 April 2016 and conducted ROV test dives.

Between 15 April 2016 and 18 April 2016, the ProSAS-60 vehicle and depressor weight were located on the seafloor and after several attempts between weather fronts and rigging, both the vehicle and depressor weight were recovered to deck and secured for transit to Fremantle Western Australia.

Dong Hai Jiu 101 arrived in Fremantle Western Australia on 22 April 2016 and repairs to the vehicle began and the cable was re-terminated.

4.1.3 ProSAS Repairs and Testing

The ProSAS vehicle was disassembled and inspected for mechanical and electrical problems associated with the cable detachment and descent to the seafloor. This repair period took place in Fremantle Western Australia from 22 April 2016 until 05 May 2016. The primary corrective actions were focused on stabilizing the INS power supply and reducing the noise levels in the arrays. Vehicle repairs were completed by 05 May 2016 and the vessel departed for the test range to validate the data quality.

The vessel conducted multiple dives on the test range between 05 May 2016 and 08 May 2016. The data was accepted by the ATSB representative and the vessel returned to Fremantle Western Australia on 09 May 2016, disembarked the test crew and began transiting to the Operations Area.

4.2 Swing 2

Swing 2 commenced 09 May 2016 with the transit to the Operations Area and concluded on 21 June 2016 in Fremantle Western Australia . Swing 2 experienced very rough working conditions throughout. On 16 May 2016, the ProSAS-60 launch was aborted due to conditions above safe working limits.

After a prolonged weather standby period, Phoenix received an amended tasking from the ATSB on 19 May 2016 to identify contact FE0133 with REMORA III. Prior to arrival at FE0133, the vessel Master received a directive from RSB that no ROV operations are to be performed from the *Dong Hai Jiu 101* and the ROV dive was not conducted.

Attempts were made again to find an operable weather window for towed ProSAS operations by working in areas north or south of where the weather was the strongest. A negative ProSAS-60 launch assessment was made on 03 June 2016 and the weather standby continued. Finally the ProSAS-60 launched the morning of 12 June 2016 and during the early cable pay out the topside tow fish power tripped a breaker. The cause was found to be water intrusion into the rotating junction box and slip ring attributed to the heavy sea conditions. These components were cleaned and the unit resealed and operated nominally.

During the same descent, the cable pay out continued until 1950 m depth when the depth sensor failed and array P1 array began showing intermittent problems. The failed depth sensor was bypassed using depth from the iUSBL. The lead-in to line DT13A-20A_27SE was too short to continue cable payout so the cable was recovered to 1,000 meters for a racetrack turn to bring the vehicle onto the survey line to avoid a data gap.

During the transit to the final approach turn site, the tow fish was deployed to the seafloor for sample data collection and confirmed that only 7 of the 8 arrays were operable. The ATSB through their onboard Commonwealth Representative gave approval for operations with only 7 of 8 arrays functioning on line DT13A-20A_31SE. Towed ProSAS operations continued through 14 June 2016 when the failed slip-ring was replaced to insure continued operations which required a turn back up line to avoid any data gaps.

The search continued along line DT13A-20A_31SE until 15 June at KP 260 when the weather conditions quickly deteriorated. The ProSAS-60 was towed in the water with 2000 m cable out until 17 June when it was possible to recover to deck. After recovery the vessel began a transit to Fremantle Western Australia anchorage.

The vessel arrived at the Fremantle Western Australia anchorage on the morning of 21 June at 0220 UTC ending Swing 2.

4.3 Swing 3

Swing 3 commenced 26 June 2016 with the *Dong Hai Jiu 101* transit to the Operations Area and concluded on 07 August 2016 in Fremantle Western Australia . During the transit, launch and recovery training was conducted with the new crew, and the ProSAS-60 was also wet tested. After evolutions were completed, the vessel resumed transit to the search area.

On 27 June 2016, a crew member sleeping in an upper bunk fell from his bed and onto furniture below when the vessel rolled in heavy weather. The crew member received medical treatment from the ship's doctor for a laceration and bruised shoulder. A decision was made to return to Fremantle Western Australia and transfer the injured crew member to shore for further assessment and care.

Dong Hai Jiu 101 commenced the transit to Fremantle Western Australia on the morning of 28 June 2016. Arrangements were made to provide replacement crew member. *Dong Hai Jiu 101* departed Fremantle Western Australia on 01 July 2016 with the new crewmember onboard.

Upon arrival to search area on 06 July 2016, the vessel was met by adverse weather conditions. The weather continued deteriorating until the vessel departed search area to seek safer conditions. During the evening on 13 July 2016, severe weather caused water intrusion into the PDU supply for the deck equipment. Power was secured eliminating the internet connection and was not restored until 18 July 2016.

Once the weather subsided to safe working limits, the ProSAS-60 was launched on 22 July 2016. The tow cable was damaged during launch requiring recovery of the ProSAS-60. The cable was repaired and the vehicle was launched on 23 July 2016 then immediately recovered due to a problem with the projectors. Repairs were conducted and on 25 July 2016, the ProSAS-60 was launched for dive 14. The search survey continued until the vehicle was recovered on 25 July 2016.

Adverse weather returned and the *Dong Hai Jiu 101* began transit to an area with workable conditions (Block 10A) to conduct holiday infill. The ProSAS-60 was able to complete infill on the larger holiday areas before recovery in this region due to adverse weather. Weather standby conditions continued until ATSB direction was received to return to Fremantle Western Australia on 01 August 2016.

During the transit to Fremantle Western Australia, the depressor was launched to perform adjustments to the level wind system on the Dynacon winch. *Dong Hai Jiu 101* arrived in Fremantle Western Australia on 06 August 2016. On 08 August 2017, the ATSB directed Phoenix to demobilize the ProSAS-60 system, place the Remora III ROV system in storage, and stand down all operations until the weather improved.

4.4 Operational Stand Down

Equipment demobilization and storage preparations commenced on 09 August 2016 and continued until 13 August when the crew began their travel home. The operation stand down continued until 14 October 2016 when the crew began travel back to Fremantle Western Australia to begin the remobilization of equipment for Remora III ROV operations to investigate targets located during the sonar search.

4.5 Swing 4

The Remora III ROV equipment was mobilized onto the *Dong Hai Jiu 101*, and re-activated and tested between 17 October 2016 and 20 October 2016. *Dong Hai Jiu 101* was underway on 20 October 2016 and proceeded to a 1,000 meter water depth, where ROV test operations were successfully conducted.

The vessel arrived at the first target location on 24 October 2016 and conducted a dive on contact GP-001. Weather conditions remained an issue. *Dong Hai Jiu 101* continued to chart a course to investigate the list of targets, deploying the ROV on contacts GP-038, GP-042, FS0052A, FE0151, and FE0152. Occasionally weather conditions would increase delaying dives on average by 24 hours.

A problem was discovered during the first group of dives with the ROV umbilical. The cable was not conditioned to the current operating depth, which resulted in loss of two floats and re-terminations of the umbilical had to be performed.

On 30 October 2016 the vessel commenced a transit to a water of depth 4,900 meters to condition the ROV cable. The umbilical was paid out with a weight replacing the ROV to remove the turns in the cable which resolved the twist in the cable. The cable was recovered and the ROV re-terminated to the umbilical. *Dong Hai Jiu 101* then transited to the next target and successfully resumed ROV dive operations on 01 November 2016.

04 November 2016 weather conditions again deteriorated to the point of being not safe while diving on contact FD0268. The operation went into a standby weather condition until 06 November 2016 when ROV dive operations were resumed.

Operations continued on contacts FD0292 and FE0150 with no interruptions. Contacts FE0162, FE0164 and FD0319 were investigated with small weather delays. On 07 November 2016, after the investigation of contact FD0319 was completed, the weather conditions began deteriorating to an unsafe working condition and operations went to another weather standby condition. Once the weather improved, *Dong Hai Jiu 101* initiated a slow transit to contact RMSFD002 on 11 November 2016.

Poor weather conditions continued until 19 November 2016 when the ROV was finally deployed to investigate contacts RMSFD002 and HH0009A. Weather conditions deteriorated after recovery and operations were in a standby weather condition until 22 November 2016 while the ship held station at contact FE0154. The vehicle was deployed to investigate contacts FE0154A,

FE0154B, and HH0029 when the vehicle experienced water intrusion into the ROV motor causing a motor failure while simultaneously the light control board on the ROV failed and required replacement. The ROV was recovered, and the motor and light control board replaced with spares. Dive operations resumed on 23 November 2016.

During dive operations on 24 November 2016, the ROV camera began experiencing oil intrusion into the camera lens while working at depth. The camera was removed and drained during the transit between targets. Also on this day, the ROV transponder flooded and was not repairable. No further USBL tracking was available after this point. No spare was available. Weather conditions deteriorated and the operation went to a standby weather condition.

ROV dive operations resumed on 26 November 2016 when the weather subsided. During the dive operations the color camera connector failed and the camera had to be removed from service. The camera was replaced with a spare that did not have a zoom capability.

ROV operations concluded on 02 December 2016 and *Dong Hai Jiu 101* commenced the transit to Fremantle Western Australia for demobilization. *Dong Hai Jiu 101* arrived in Fremantle Western Australia on 07 December 2016 and system demobilization commenced immediately. Demobilization was completed on 10 December 2016 and the crew departed for home.

Overall, Remora III conducted a total of 33 dives to inspect targets of interest identified during previously completed side scan sonar search operations. The Remora III operated in depths down to 4,800 meters of seawater (msw) and provided investigators with clear imagery of the targets of interest, which were ultimately identified as a combination of seafloor geology and manmade objects, such as shipwrecks, a pile of wire rope, and a 55 gallon drum.

5.0 LESSONS LEARNED

This section discusses lessons learned while performing ProSAS-60 side scan sonar search operations and Remotely Operated Vehicle (ROV) operations onboard the Chinese Rescue Salvage Bureau (RSB) vessel *Dong Hai Jiu 101 (DJ101)*. The objective is to promote awareness and understanding and preclude the recurrence of any undesirable outcomes on future projects.

5.1 Mobilization/Operation/Demobilization from a Vessel of Opportunity

Phoenix operated from the vessel *Dong Hai Jiu 101 (DJ101)* from January 2016 until December 2016.

5.1.1 Lesson Learned

Well-coordinated and executed pre-planning activities well in advance of mobilization and operations onboard a Vessel of Opportunity is critical to the success of any at-sea operation. The ATSB/ Donghai Rescue Bureau/Ministry of Transport support and guidance in the conduct of the pre-mobilization ship-check of the Chinese vessel *Dong Hai Jiu 101*, and participation in the associated follow-on meetings and briefings was key to the transparency and efficiency, and safe execution of all key operational project events, to include vessel mobilization and at-sea operations.

Pre-planning activities provided a well-structured process for the review of several very important key project requirements, to include: vessel GA drawings, DP 24/7 operations and vessel ship handling, messing/berthing accommodation arrangement options, food requirements, non-smoking requirements, power supply/cable lengths and VFD location, ROV/AUV/ProSAS deck lay-out installation options, deck timber removal concerns/options, locator pole installation options, equipment stowage and data processing room options, vessel communications capabilities (512kb upload/1024Kb download), IMO/SILOS certifications, Communications (e.g. English-Chinese translation requirements), etc.

5.2 Problem Encountered: ProSAS Umbilical Failure

At 1119 (UTC) on 21 March 2016, after completing line DT13A-21A_02NW_125m_SE, communication was lost to the ProSAS-60 vehicle and the vehicle tow cable tension went from over 2,000 lbs to approximately 700 lbs. The navigational position of this event was recorded immediately. The topside power reading was checked and found to be consistent with exposed power conductors on the tow cable, indicating a potential break or separation in the tow cable.

5.2.1 Lesson Learned

1. Use of the PMI Everflex BSR (Bending Strain Relief) (http://pmiind.com/rugged-cable-hardware/everflex-bsr-bending-strain-relief/) will significantly deter the potential failure rate of the helical cable from 5,000 cycles to 5 million cycles.
2. PMI reports that high loads and large angles of deflection can induce strain near the rigid termination attachment point. During adverse weather conditions the ProSAS vehicle was put on a short tow and the vessel increased speed to maintain steerage way operating in a racetrack course to stay close to the last line surveyed. These actions induced higher loads and increased harmonic frequencies on the cable at the rigid termination point increasing the rate of cyclical fatigue. Phoenix made the following recommendations for operational changes during these conditions:

a. During turns, only bring in enough cable to be above minimum water depth plus a safety margin to leave sufficient catenary in the wire to dampen any resultant forces.

b. During recovery, reduce speed to bare steerage way so that the vessel can maintain the proper sea/wind aspect and haul in the cable at a reduced speed to minimize the loading on the cable.

2. HSI reported that the ProSAS vehicle was 15 pounds buoyant, however, when the vehicle was recovered from the seafloor it took over 100 pounds of weight to sink the vehicle during the recovery. Phoenix recommended that the buoyancy be verified to more properly align with the ProSAS-60 designed flight profile.
3. As an added measure of safety, a keeper line was installed on the tow cable to avoid any potential future loss of the ProSAS and depressor weight as a result of the cable failure. Phoenix recommended the installation of a second torque grip up the tow cable with a safety wire going directly to the depressor weight. The safety cable was left slack and tie-wrapped to the tow cable to secure it so it fit through the sheave on a normal recovery.
4. Phoenix recommended the re-installation of a passive pinger on the ProSAS-60 vehicle to help locate the vehicle if it was lost again.
5. Phoenix recommended the installation of a remotely activated guillotine cutter on the ProSAS which when activated would allow the vehicle to float to the surface.

5.3 Problem Encountered: ROV Load Release Shear Pin Failure

The ROV load release shear pin is a fuse-able link that protects the umbilical from parting when load conditions exceed a limit.

5.3.1 Lesson Learned

The shear pin failed as designed when the dynamic loading conditions during the ROV recovery exceeded that limit. During the recovery in a moderate sea state, the swell action and ship motion created a dynamic load that momentarily exceeded the breaking strength of the shear pin and it released the load. The shear pin performed as designed and saved parting the cable or causing vehicle damage due to excessive load conditions. Recommend delaying heavy lift activities during excessive sea states to mitigate recurrence.

5.4 Problem Encountered: ProSAS-60 Cable Damage

While deploying the ProSAS-60, slack in the cable caused the cable in the traction sheaves to fall out of the grooves. When the winch operator started hauling in cable, the slack on the traction winch pulled tight onto the motor shafts for the sheaves causing damage to the cable outer armor.

5.4.1 Lesson Learned

The Project Team modified launch procedures by assigning a dedicated watch to the portions of the winch obscured to the winch operators line of sight to reduce risk of a recurrence.

5.5 Problem Encountered: Sonardyne iUSBL Failure

Sonardyne iUSBL failed due to a connector flooding and caused positioning loss for the ProSAS.

5.5.1 Lesson Learned

The Sonardyne iUSBL was rented from Seatronics. The unit was inspected upon receipt and found to not have an O-ring in the connector. Sonardyne (OEM) was contacted and queried about the need for an O-ring in this connector. Sonardyne stated that an O-ring was not needed for this type of connector. However, the Project Team discovered when the unit was submerged for an extended period of time water intruded this connection causing a ground fault and shorted out the iUSBL unit. Spares inventory should be confirmed to avoid single points of failure. System sparing and redundancy must be a top priority.

5.6 Problem Encountered: ROV Fiber Link Lost

During ROV dive #2 the fiber link to the ROV was lost at a depth of 3,300 msw requiring a dead vehicle recovery. The vehicle was kept outboard of the vessel and out of harm's way by correctly positioning the ship and adjusting the winch recovery rate. The fiber break was a result of the umbilical twisting and tangling the third and sixth floats together.

5.6.1 Lesson Learned

This was a new umbilical which was spooled onto the storage drum in Fremantle Western Australia by Green Monster according to manufacturer tensioning specifications. While all procedures were followed, experience has shown that new umbilical lines need to be conditioned using a swivel and weight in deep water at maximum depth to allow all the twists to come out of the cable. Operational schedules should be adjusted (if feasible) in coordination with the client to allow time for cable conditioning.

6.0 CONCLUSION

Phoenix's work aboard the *Dong Hai Jiu 101* was Phoenix's third effort to support the search for Malaysia Airlines Flight 370 (MH370). Phoenix was involved in the search for MH370 from March 2014 – December 2016. During this time Phoenix used a wide variety of underwater systems, including the U.S. Navy Towed Pinger Locator (TPL-25), the Phoenix 5,000 meter depth-rated AUV *Artemis*, Hydrospheric Solutions' 6,000 meter depth-rated ProSAS-60 towed synthetic aperture sonar system, and the Phoenix 6,000 meter depth-rated Remora III ROV.

During the course of this extensive search effort, Phoenix conducted operations on three different ships: the Australian Defence Vessel (ADV) *Ocean Shield*, the M/V *GO Phoenix*, and the Chinese Rescue Salvage Bureau (RSB) vessel *Dong Hai Jiu* 101.

In total, Phoenix completed 13 "swings" to the MH370 search area, which was approximately 1,500 nautical miles west of Fremantle Western Australia, Western Australia. Each swing consisted of a five-day transit to the search area, 30 days or more of search operations, and a five-day transit back to Fremantle Western Australia, Western Australia.

Phoenix proudly recognizes the dedication and professionalism of the many countries, Governmental Agencies, vessel crew, and private industry that have spent years in the search for MH370. Phoenix stands ready to assist and remains fully committed to supporting any future search effort to one day locate Malaysia Airlines Flight 370 (MH370).

Appendix F – Chemical investigations on barnacles found attached to debris from the MH370 aircraft found in the Indian Ocean

Chemical investigations on barnacles found attached to debris from the MH370 aircraft found in the Indian Ocean

Patrick De Deckker
Research School of Earth Sciences
The Australian National University
Canberra ACT 2601

Summary

Trace element analyses were conducted on calcified scuta plates of sessile pedunculate barnacles, belonging to the species *Lepas (Anatifera) anatifera striata*, found attached to debris of the MH370 aircraft. The Laser Ablation Inductively Coupled Plasma Spectrometer [LA-ICPMS] technique was used at the Australian National University to reconstruct the magnesium to calcium ratio [Mg/Ca] across the growth lines of several scutum plates in an attempt to reconstruct the water temperature [SST] at the sea-surface in which the barnacles grew during their drifting at sea while attached to the aircraft debris.

The reconstruction of the sea-surface temperature of the seawater in which the barnacles grew is hindered by a number of factors:

(1) the correlation between SST and the Mg/Ca of the water in which barnacles grew is based on too few analyses carried out over sixty years ago by Chave (1954);
(2) there is a large amount of organic matter in the scuta plates of the barnacles and it was found that this organic matter is rich in magnesium, thus preventing us from using the Mg/Ca in the calcite matrix of the scuta plates to reconstruct SST at the time of formation of the plates.

In addition, as so few observations have so far made on barnacles growth, we are unable to establish if rates of growth and calcification are controlled by temperature or food supply, or both. In addition, we are also unable to tell if the barnacles we examined grew continuously once attached to the aircraft debris or stopped growing at some stage for several possible reasons such as lack of food supply and/or temperatures unsuitable for growth, or exposure outside water.

We carried out chemical analyses on the same scuta specimens analysed by our French colleagues [see Blamart & Bassinot, 2016] following parallel lines to their sampling and our attempts at reconstructing past SST do not match the reconstructions based on oxygen isotope analyses, thus further suggesting the organic matter contamination in the scuta shells is hindering any possible reconstruction of water temperatures.

1. Introduction

Darwin (1851), in an extensive monograph, was first to establish the morphological nomenclature and systematics of barnacles which belong to the Crustacea in a very diverse class called Cirripedia. Crustaceans encompass prawns, shrimps and lobsters among others. The barnacle specimens found attached to the MH370 debris are sessile and use a peduncle to remain attached to material floating at sea such as wood and pumice, as well as other debris, such as those discussed here. During their life cycle, barnacles undergo metamorphosis, starting from an egg developing into a minuscule swimming larva, referred to as the cyprid larva, that eventually attaches itself to floating objects and, in the case of the specimens examined here, become securely attached with a fleshy peduncle. Pedunculate barnacles feed on the neuston, being floating particulate matter often found at the sea surface. Thus, the specimens examined here

are referred to as neustonic pedunculate barnacles or as epipelagic goose barnacles [*sensu* Schiffer & Herbig, 2016]. Several calcified plates made of calcite [= calcium carbonate: $CaCO_3$] progressively grow on the outside of the animals and thus cover and protect the soft appendages and organs. Rates of growth are thought to be dependant on water temperature, food supply and the conditions experienced while drifting with their 'substratum', but ecological observations on peduncular barnacles are unfortunately very few (de Graaf, 1952; Evans, 1958; Skerman, 1958; Patel, 1959; Thiel & Gutow, 2005; Inatsuchi et al., 2009).

2. The hard calcified plates of the barnacles

Pedunculate barnacles are commonly found on Australian beaches as they attach themselves to floating debris, such as wood, and also pumice. The fleshy peduncle is quite solid and even after death of the organisms - often as a result of 'beaching' – will permit the barnacle shell to remain attached for quite some time (
see figure 1).

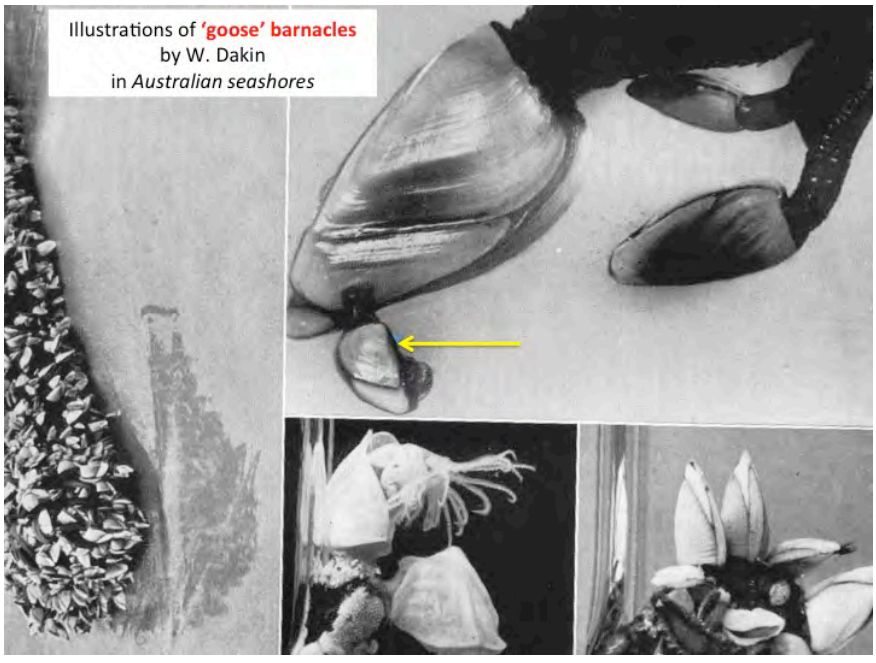

Figure 1. Photographs modified from the book "Australian Seashores'" by Dakin (1973, plate 45) showing on left how barnacles accumulate on debris, in this case a drifting wooden log, on top right corner four generations of *Lepas anatifera* with their characteristic fleshy peduncle; [the arrow shows the youngest specimen], and on the bottom, in the middle image the appendages are clearly visible, and bottom right specimens of a different species of *Lepas* being the short – stalked *L. anserifera*.

We propose to use the terminology of the calcified plates first employed by Darwin (1851), an original sketch of which is presented in Figure 2.

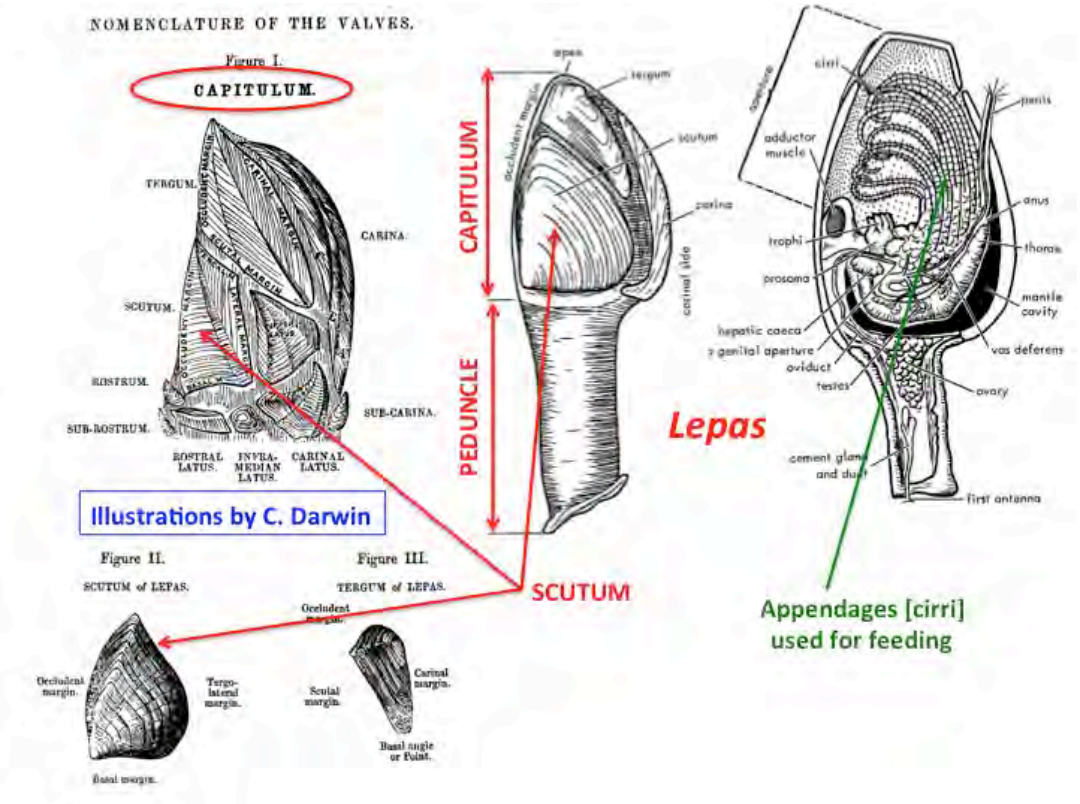

Figure 2. On left, copy of the original illustrations (1-3) of a pedunculate barnacle made by Darwin (1851) detailing the terminology used in this report. On the right are illustrations of the pedunculate barnacle *Lepas* showing the hard parts and peduncle, and next to it is a specimen showing the appendages which are used for feeding and aerating the inside of the shell. Illustrations modified from The Treatise of Invertebrate Paleontology Part R (1969).

The scutum plates which adorn the organism are the largest ones and therefore were used for chemical analyses. In fact, we received 3 scutum plates from Drs Dominique Blamart and Franck Bassinot from the Laboratoire des Sciences du Climat et de l'Environnement in Gif-sur-Yvette near Paris, one from La Réunion Island which had previously been "microdrilled" for stable isotope analyses. This specimen labelled A2 G1 is illustrated in Figure 3 and the location of the microdrilling is very obvious. Microdrilling involves extraction of the upper surface of the scutum plate and the resulting powder is then analysed for its isotopic composition [see report by Blamart & Bassinot, 2016]. The scutum plates of 2 barnacles recovered from Rodrigues Island [19° 44' 26.49"S] were also analysed, one being large and the other representing a much smaller specimen. Because these 2 specimens were not dissected - for fear of breaking them - we are unaware if they are juveniles or adults.

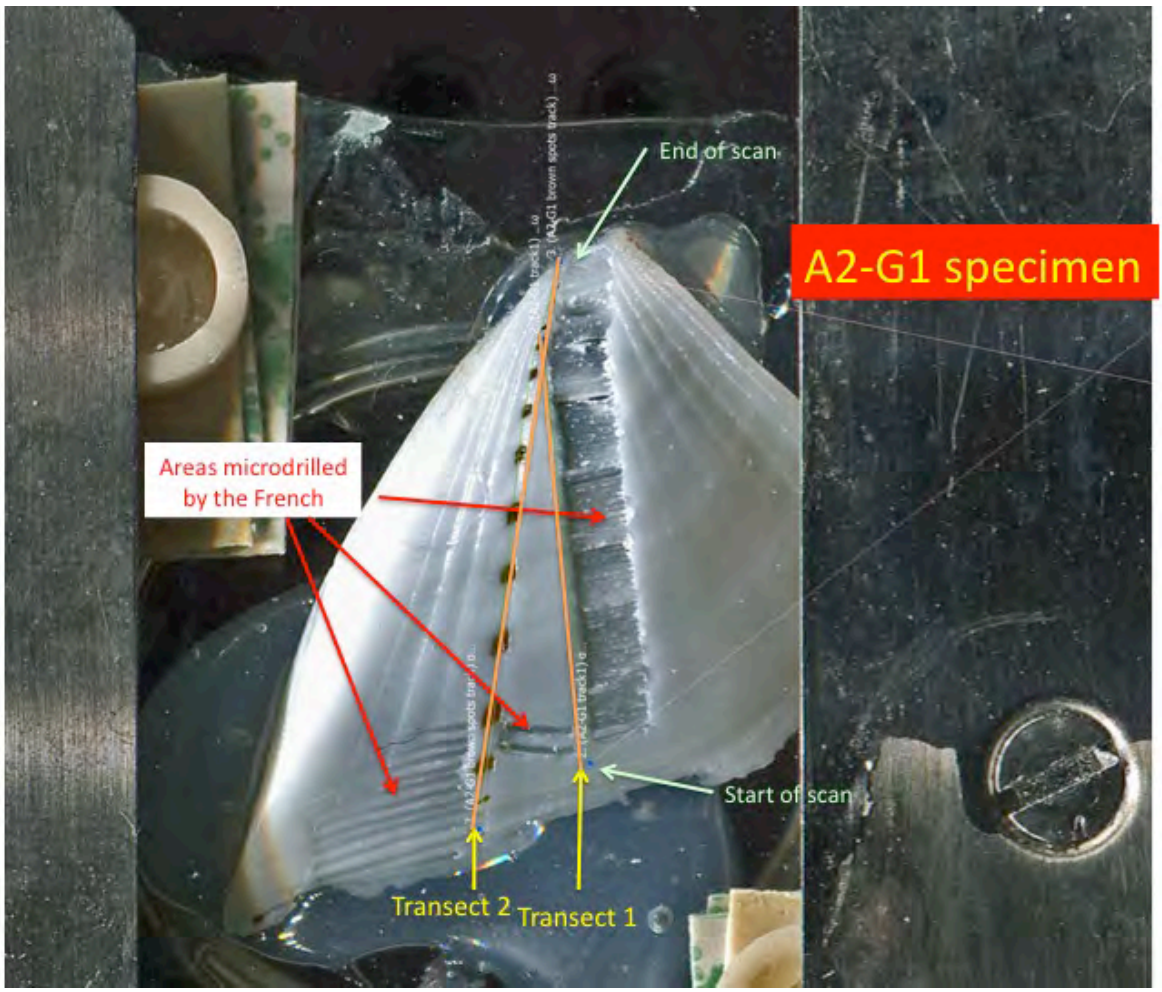

Figure 3. Photograph of the scutum plate of specimen A2-G1 collected at La Réunion and which was originally attached to the fragment of the aircaft.
The red arrows indicate the parts which had been microdrilled by our French colleagues. The orange lines show the tracks followed by the laser ablation at the ANU. Transect 1 lies just outside the area microdrilled in France for oxygen isotope analyses. Transect 2 goes from the tip of the scutum at the top (which was formed in the early stage of growth) and ends near the last part of growth of the scutum. Note that transect 2 was arranged to pass over the brown spots that are almost equidistantly located. The dark part on either sides of the scutum plate belong to the metal holder in which the specimen was fixed.

The barnacle plates are made of low Mg calcite [viz. <5% Mg in $CaCO_3$] which allow them to remain intact in sea water. All the elements such as Ca and Mg are taken by the organism directly from seawater and possibly from the food it eats. As Ca is a bivalent cation, other bivalent cations (e.g. Mg^{2+}, Sr^{2+}, Ba^{2+} and Cd^{2+}) can take its place and fit within the $CaCO_3$ lattice. Such elements can be It is now clear from observations made at the ANU that the calcite lattice contains numerous microlayers of organic matter that are visible under a powerful microscope. These layers are coloured pale brown and follow the obvious growth lines seen externally (See Figures 3-4).

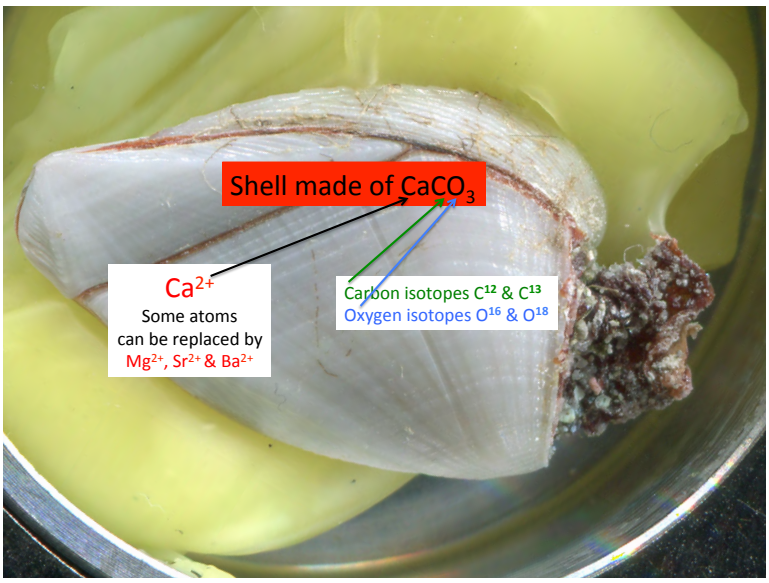

Figure 4. Photograph of an entire barnacle from Rodrigues Island showing the large scutum plate lying inside a metal holder and resting on (yellow) parafilm material for stable mounting of the sample while ablating the specimen. Note the broken piece of peduncle on the right hand side which is coloured brown and has shrunk substantially due to dehydration. Note the faintly visible microlayers that are almost parallel to the boundary between the scutum plate and the tergum (see Fig. 1) and which are representative of growth lines. Such lines are more obvious when the specimen is examined at high magnification.

3. Carbonate chemistry of barnacle plates

Chave (1954) was the first to systematically assess the Mg content in biogenic carbonates of many different phylogenies. His aim was to determine whether there is a link between ambient water temperature and the Mg composition of carbonates. Concerning barnacles, he used spectrography to determine the percentage of $MgCO_3$ in the calcite lattice and 2 of the data points he used came from Clarke and Wheeler (1917). All the samples had less than 5% magnesium carbonate, and Chave (1954) showed an obvious relationship between water temperature and the weight per cent $MgCO_3$ of barnacle valves (Chave, 1954). Note, however, that in his figure 12 Chave presented results for 6 samples of mixed barnacles. In our plot of Chave (1954)'s data (Figure 5-6), we eliminated 3 data points as they clearly represented outliers, especially since the fragments came from low temperatures; 2 samples were associated with 5.2°C from Adak Island in Alaska and the other from Mount Desert being a large island offshore Maine, USA. It also appears that there is a better relationship between water temperature and the Mg/Ca of barnacle shells by using a logarithmic correlation curve (red line in Fig. 6).

There is however an important observation to make as we do not know if the temperature values tabled by Chave (1954) represent an annual mean, or the temperature at the time of collection. Note also that 7 out of 9 specimens Chave (1954) listed were barnacle fragments.

4. Information on the growth of *Lepas anatifera*

Very little information is available in the scientific literature about the ecology of *Lepas anatifera*. Evans (1958) examined colonies of *Lepas hillii* and *L. anatifera* barnacles that had settled on the side of the yacht *Petula* between Dakar and Barbados during the winter season of 1953-54. It seems that none of the barnacles listed above had settled on the ship while in Dakar Harbour. On the way to Barbados, thirty days later, a sample of 20 of the largest *Lepas* barnacles growing on the topside of the yacht was collected

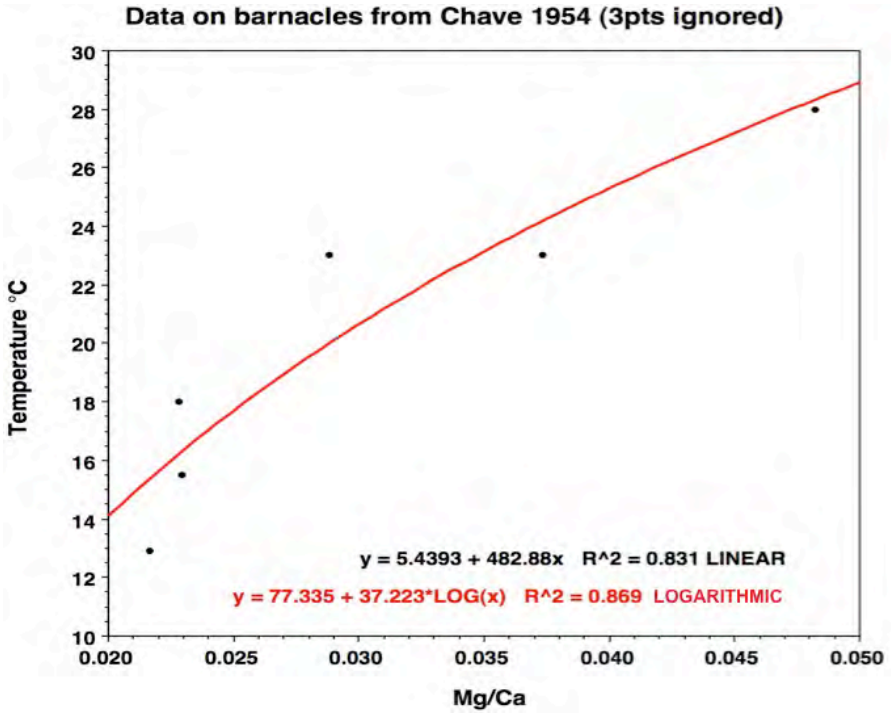

Figure 5. Plot of the Mg/Ca of complete barnacle shells against water temperature in which the barnacles grew. Data from Chave (1954) for which 3 outlier points were omitted [see text for explanation]. In red is the logarithmic correlation and the linear correlation value appears in black.

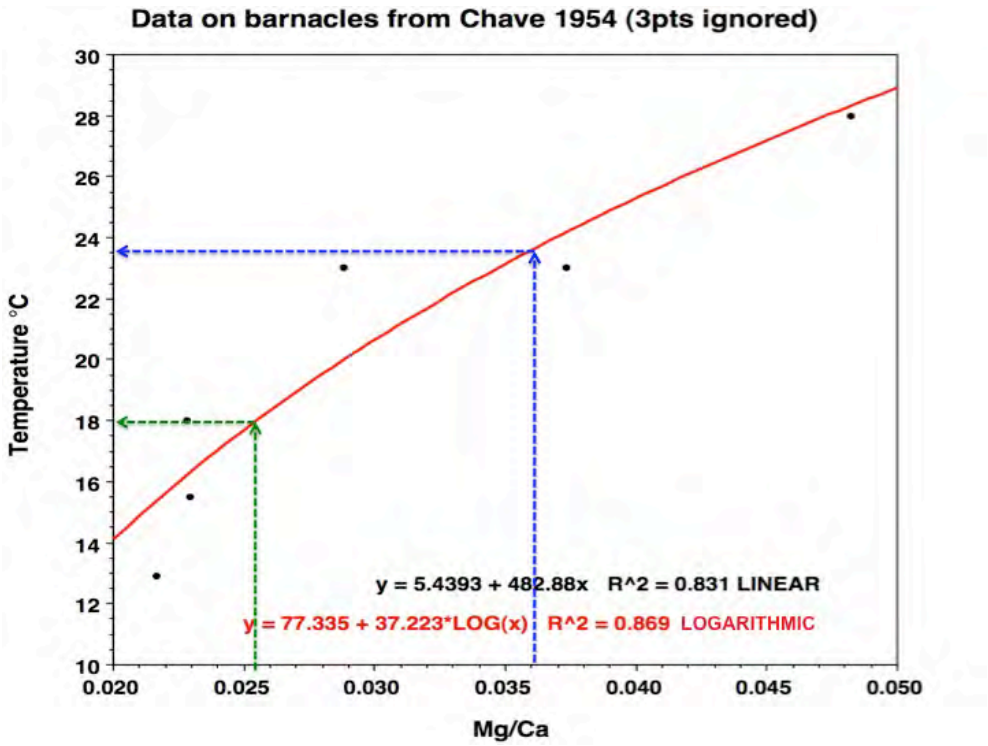

Figure 6. Copy of figure 4 showing how water temperature can be obtained from the Mg/Ca composition of the barnacle shell based on Chave (1954)'s data. Using the logrithmic correlation, a Mg/Ca ratio of 0.0361 would represent a temperature of 23.6°C [blue lines] whereas a Mg/Ca of 0.0254 would dictate a temperature of 18°C [green lines].

and preserved. A further collection of 60 of the largest specimens from an adjacent position on the ship was taken after 60 days. Evans (1958) estimated that average daily size increase was about 0.5mm in the first month and may have continued as such during ontogeny, generally on the 30th to 34th day. Afterwards, the growth rates near 0.3mm/day were interpolated. Apparently, the sea-surface temperature during the voyage ranged between 24.4° and 26.1°C. In addition, Evans (1958) cautioned about extrapolating growth rate and length of the barnacle juvenile phase in cooler waters.

In a second study, MacIntyre (1966) collected *L. anatifera* barnacles after a [originally clean] buoy was recovered 17 days later in the Tasman Sea off the eastern coast of Australia in December 1960. Maximum lengths of the capitulum of the barnacles were recorded. Only 2 specimens had mature ovaries and these specimens were 23mm long (Figure 7) whereas a large range of sizes were recorded as shown in that figure. Hence, as indicated by MacIntyre (1966) 'it would be unwise to generalise about barnacle growth rates and their dependence on temperature'. Nevertheless, if we were to assume that the mature barnacles had grown over 17 days at the most, growth rate could be estimated to have been ~1.35 mm/day and the temperature range around the buoy was 25-28°C. Another study examining *L. anatifera* adhered to beacons in Hawke Bay on the east coast of the North Island of New Zealand looked at growth of the barnacles, this time at lower temperatures than for the Tasman Sea study (Figure 8 and comments). More recently, Magni et al. (2015) who attempted to evaluate the floating time of a corpse recovered in the Tyrrhenian Sea based on *L. anatifera* barnacles found attached to the body estimated a growth rate of 0.2mm/day, with temperatures having possibly ranged between 13° and 19°C, or less depending on when barnacles started growing on the body. Further, Magni et al (2015) estimated that within that temperature range, a capitulum may reach 12 mm after approximately 60 days. Hence, it seems likely that size is related to water temperature. However, once again, caution has to be exercised because other factors may contribute to growth, such as food availability. This issue was already partly addressed by Inatsuchi et al (2010) both in the ocean and in the laboratory, who concluded that both high temperature and high food availability contributed to greater growth.

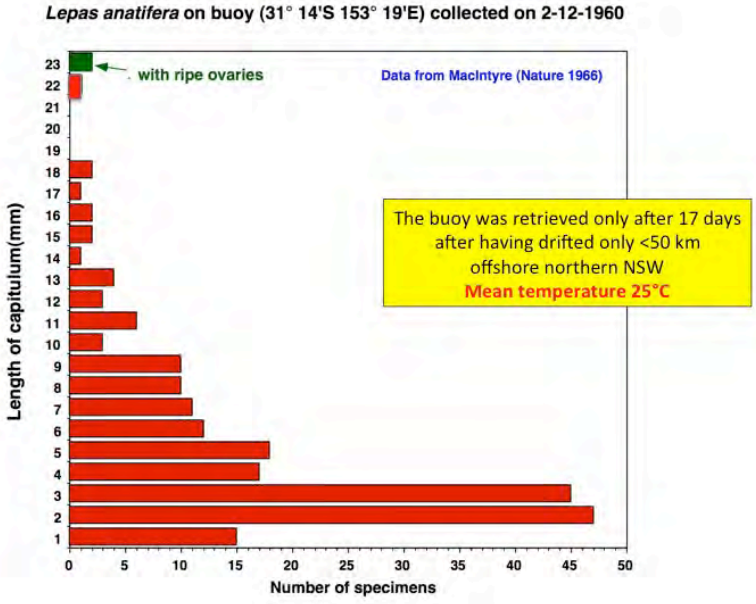

Figure 7. Histogram plot of the size of *L. anatifera* specimens found attached to a buoy offshore eastern Australia only after 17 days. Note that we do not know when the juvenile barnacles settled on the buoy within that 17 days period. Hence, growth rates may even be higher, but it is not possible to find out.

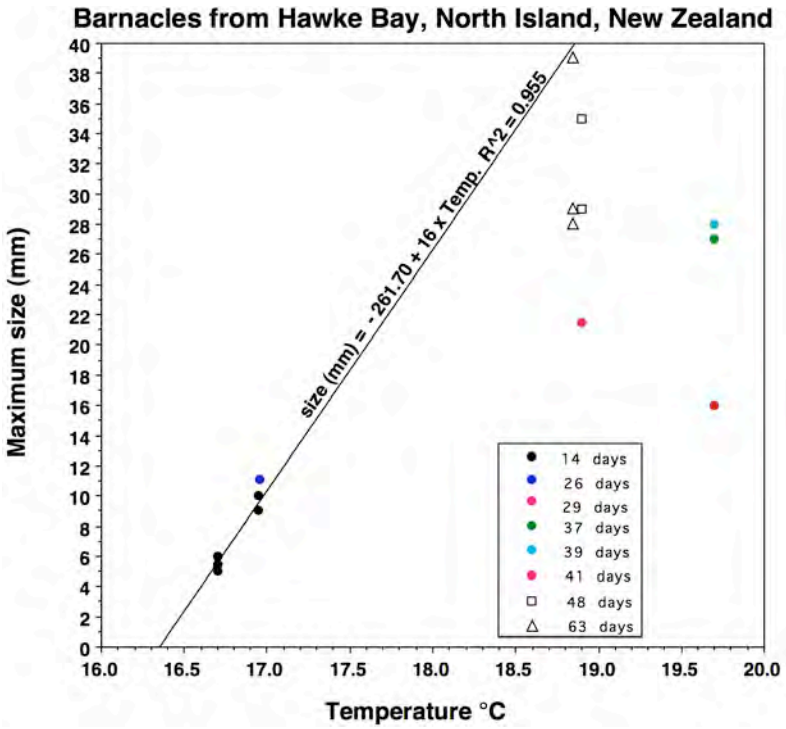

Figure 8. Plot of all maximum sizes of barnacles collected from beacons immersed in Hawke Bay along the North Island of New Zealand over the 1954-55 period (refer to Skerman, 1956 for more details). A regression line is provided here only for the barnacles that were collected from the beacons after 14 days. This indicates a substantial growth rate, viz ~1cm over 14 days at about 17°C. At slightly higher temperatures and over longer time periods, the growth rate appears to be slightly lower. Compare the data presented here with that of McIntyre in figure 7 which shows one barnacle having reached 22mm over 17 days when temperature was much higher, viz. 25°C.

5. Microanalytical techniques

We used a laser ablation inductively coupled mass spectrometer [LA-ICPMS] at the Research School of Earth Sciences at The Australian National University (Figure 9). We performed linear transects along the surface of the shells following the initially developed technique to analyse planktic foraminifera tests (Eggins et al., 2003), to investigate the nature and extent of the compositional variation along the growth lines of the barnacle scuta.

It proved unnecessary to clean the specimens and therefore, on each occasion and for every new profile, laser ablation was performed to clean the outer surface of the shells by “shaving off” the upper few microns of the outer surface.

More information on the technique is available in Eggins et al. (1998).

Nevertheless, below are some specifications of the technique we used. These were:

- Before proper analyses could be performed, a thorough cleaning of the outer surface of the shells had to be performed. As a result 50µm spots at 5 pulses per second were drilled, thus resulting in a 20-40µm deep groove. Following that procedure, analyses were performed in the groove.
- Continuous ablation at 20 microns per second, 10 Hertz at 20 kvolts;
- Elements and their respective isotopes being recorded: Be^{11}, Mg^{24}, Mg^{25}, Ca^{43}, Ca^{44}, Sr^{86}, Sr^{88}, Ba^{138};
- Results were reported as ratios to calcium in the calcitic shells;
- Consequently, about 1400 continuous analyses covered approximately a 1.4 cm long transect.

- Hence, because so many analyses were performed for a single transect, there was a need to smooth the data at times due to ‘analytical noise’, we used 14 point smoothing.

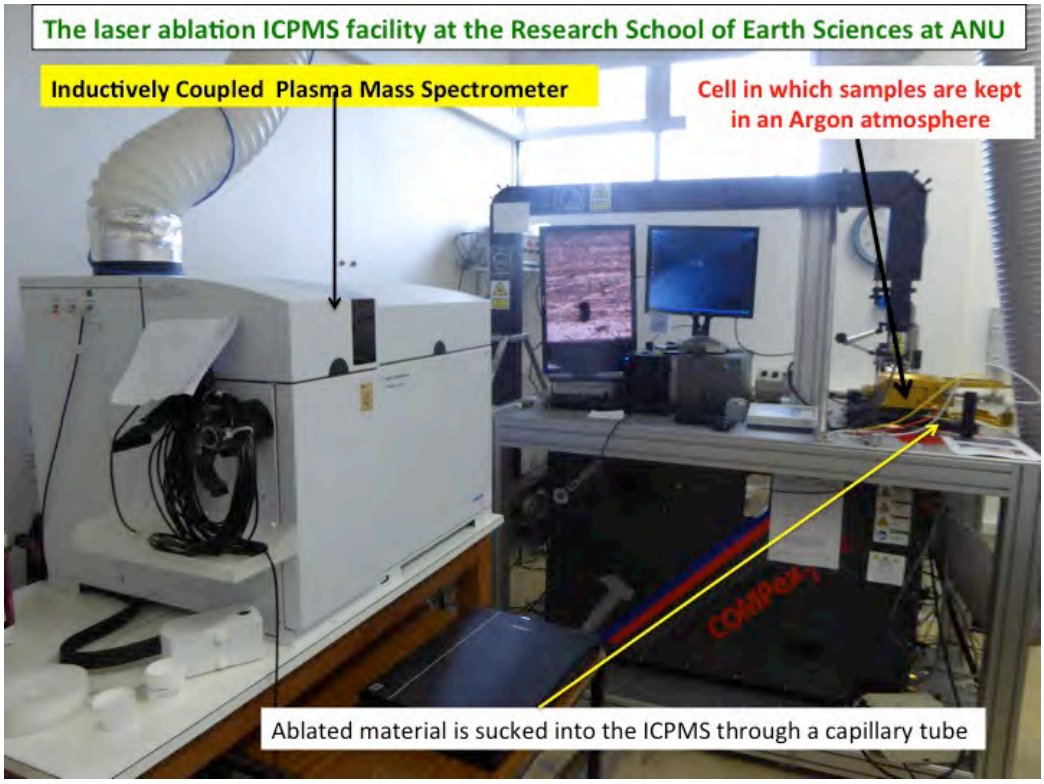

Figure 9. Photograph of the equipment used at the Research School of Earth Sciences.

6. LA-ICPMS results

It was decided to plot all the results in the figures presented below, having ‘translated’ the Mg/Ca into temperature values, using the correlation obtained from Chave (1954)’s data point shown in figures 5 and 6. This is to better visualise the results as sea-surface temperatures instead but, more importantly, for the reader to assess the veracity of the reconstructed temperatures.

Below is a presentation of the results form the laser ablation analyses, and their interpretation will be provided in section 7.

6.1 *Specimens retrieved from La Réunion Island*

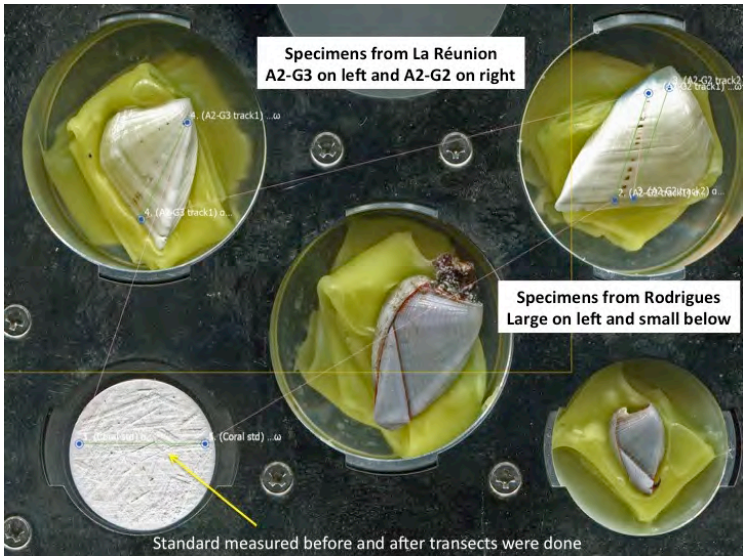

Figure 10. Photograph of the metal holder showing cavities in which the barnacle specimens were placed prior to the laser ablations. The yellow material on which the barnacles rest is made of parafilm which was partly heated with a hair drier to soften it before allowing to cool so as to maintain the barnacles in a stable position. The yellow lines show the transect followed by the equipment before ablation could proceed. The surface of the coral standard displays numerous grooves related to previous ablations.

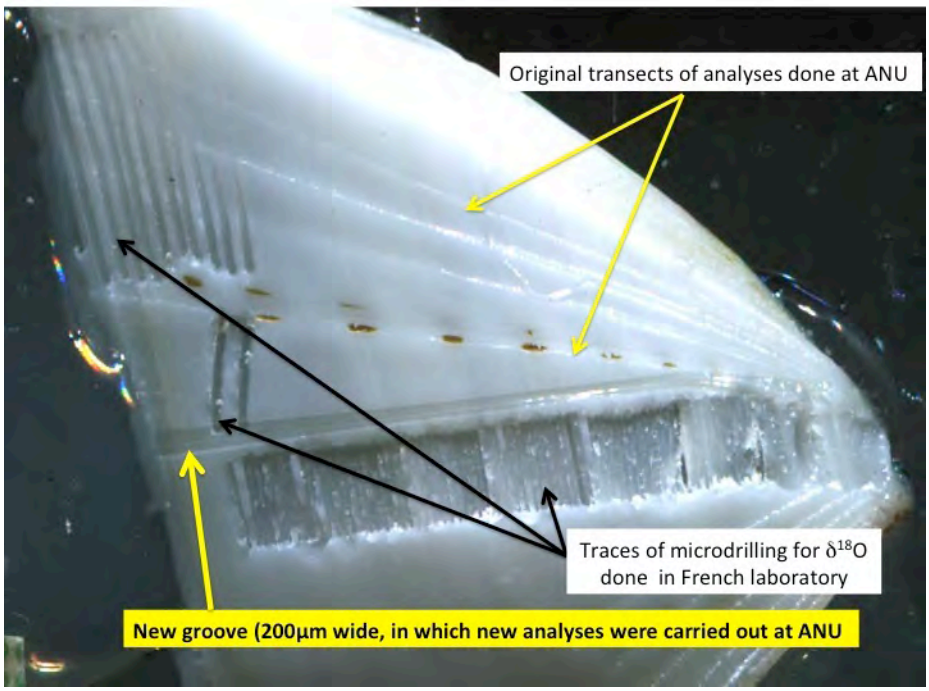

Figure 11. Photograph of the scutum of barnacle A2-G1 which shows the location of the microdrilling (indicated by black arrows) done in France (for oxygen isotope analysis) as well as the fine transects performed by the laser. Note that the middle transect passed over the brown 'spots' and consequently partly ablated them. These 'spots' coincide to sites of high Mg/Ca values (see Figure 12 and text for more explanation).
The lowest and much wider 'groove', that partly ablated the brown spots, was performed before a new ablation of the calcite could be done. The results of the original ablation are presented in figure 12.

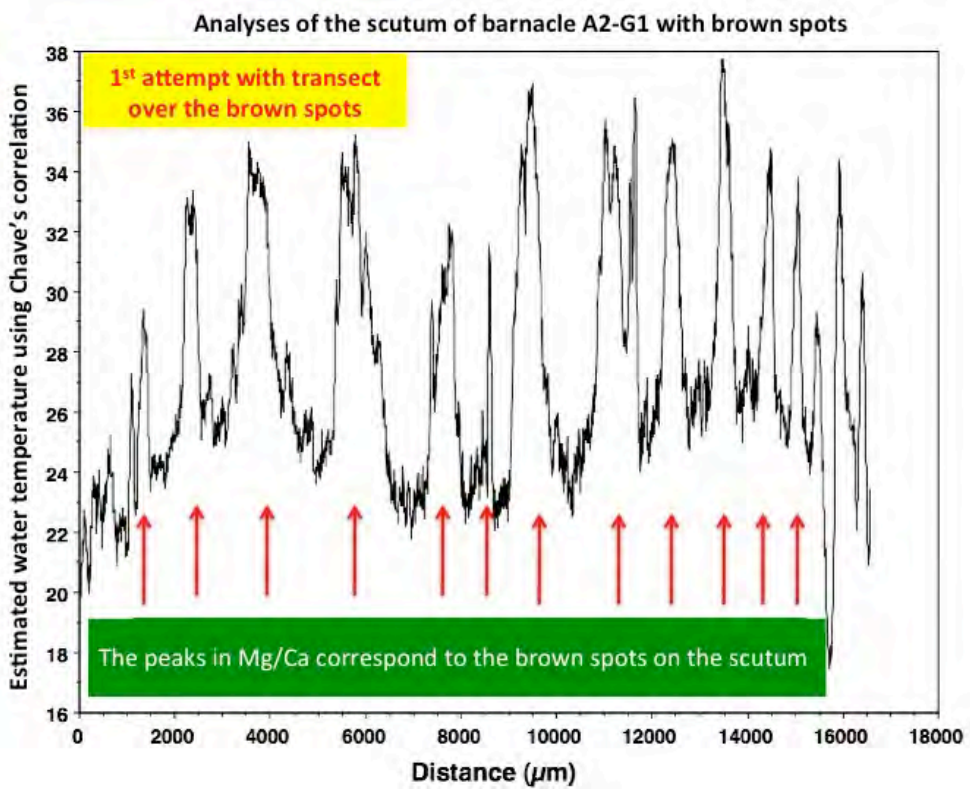

Figure 12. Plot of the analyses performed along the groove that passed over the brown spots on barnacle A2-G1 (shown in figure 11). The data was obtained as Mg/Ca ratios, but transformed into estimated temperatures based on the Chave (1954) correlation. This procedure is used to simply demonstrate the obviously implausible temperature reconstructions. The transect is almost 1.7cm in length.

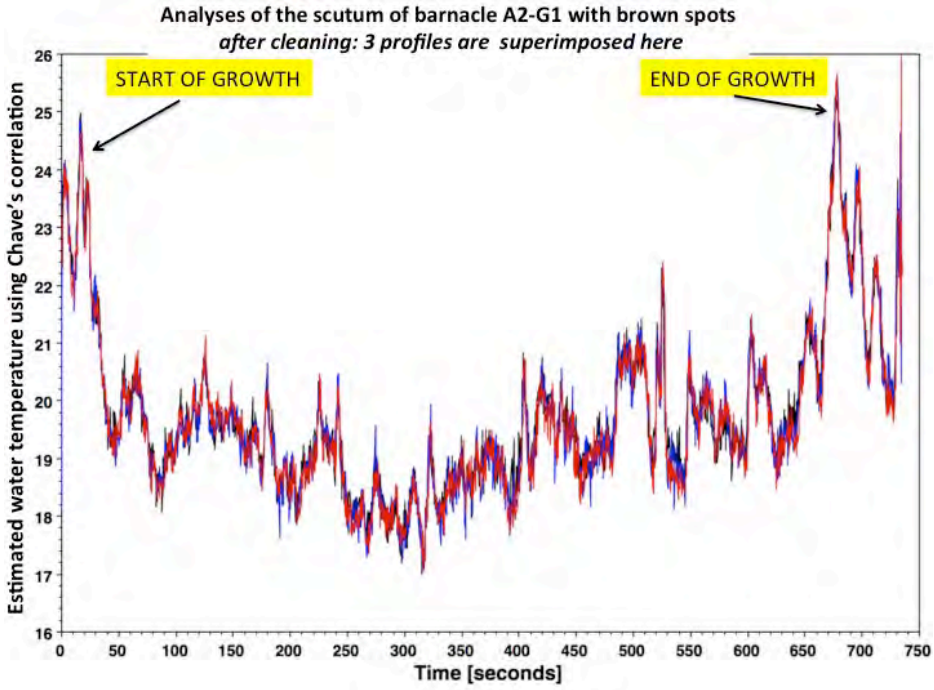

Figure 13. Plot of three sets of analyses performed along the groove that passed over the brown spots on barnacle A2-G1 after surface cleaning was performed by ablation. Once again the Mg/Ca data were translated into an estimates of water temperature based on the Chave (1954) correlation presented in figure 6. Note the horizontal axis gives the time used to obtain the profile.

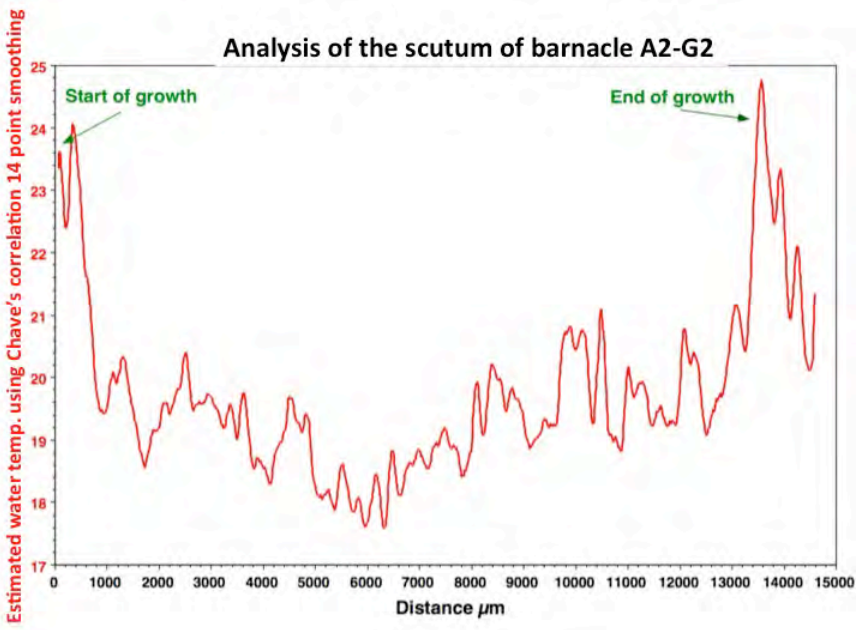

Figure 14. Plot of one set of analyses performed along the groove that passed over the brown spots on barnacle A2-G1 after cleaning was performed by a substantial amount of ablation was performed. Once again the Mg/Ca data were translated into an estimation of water temperature using Chave (1954)'s formula presented in figure 6. This time 14-point data smoothing was performed to clearly evaluate the temperature trends. Note that both the start and end of growth of the scutum 'report' higher temperature estimates.

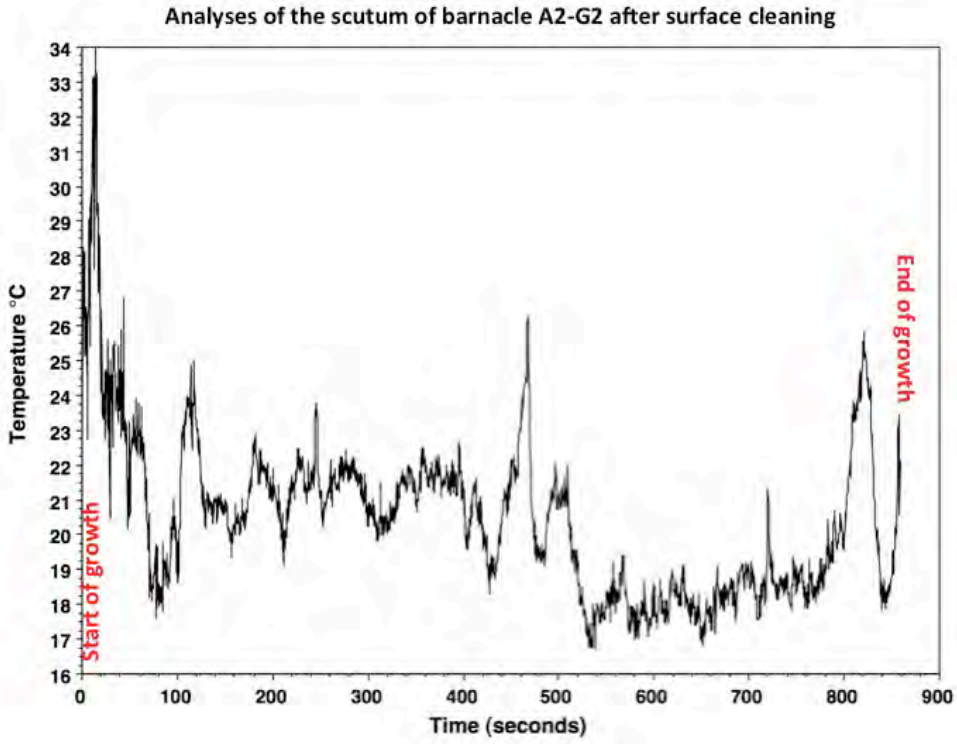

Figure 15. Plot of the analyses performed along the transect on barnacle A2-G2 after the strong cleaning procedure was performed with deep and wide ablation of the outer surface of the scutum shell. Once again the Mg/Ca values were translated into estimated water temperatures based on the Chave (1954) correlation shown in figure 6. Note the horizontal axis gives the time used to obtain the profile.

6.2 *Specimens retrieved from Rodrigues Island*

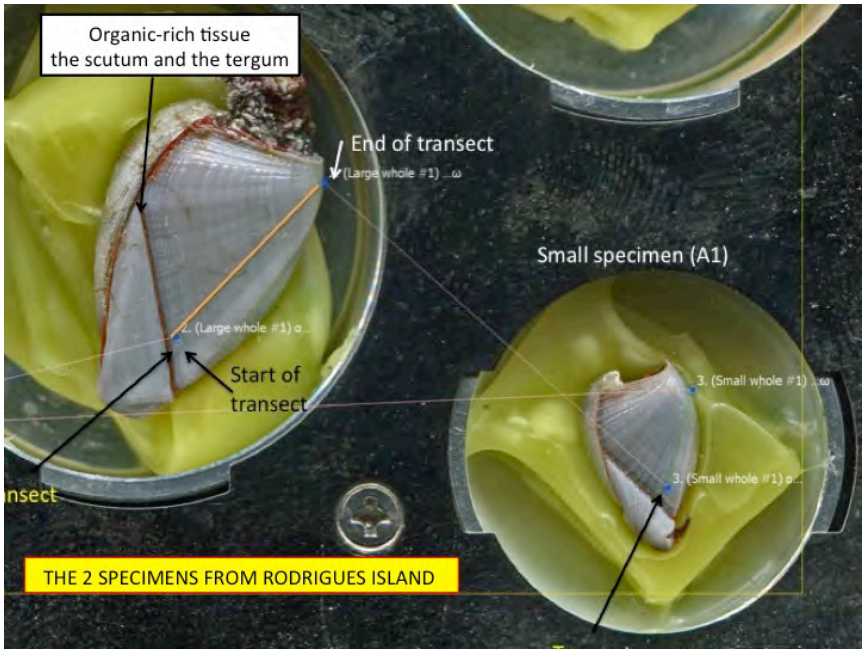

Figure 16. Photograph of the 2 entire barnacles collected on Rodrigues Island, mounted and kept inside the metal holder used of the LA-ICPMS analyses. The orange lines show the location of the transects performed on the scuta after strong ablation was performed before the analyses were performed. The results of the analyses are displayed in the following two figures.

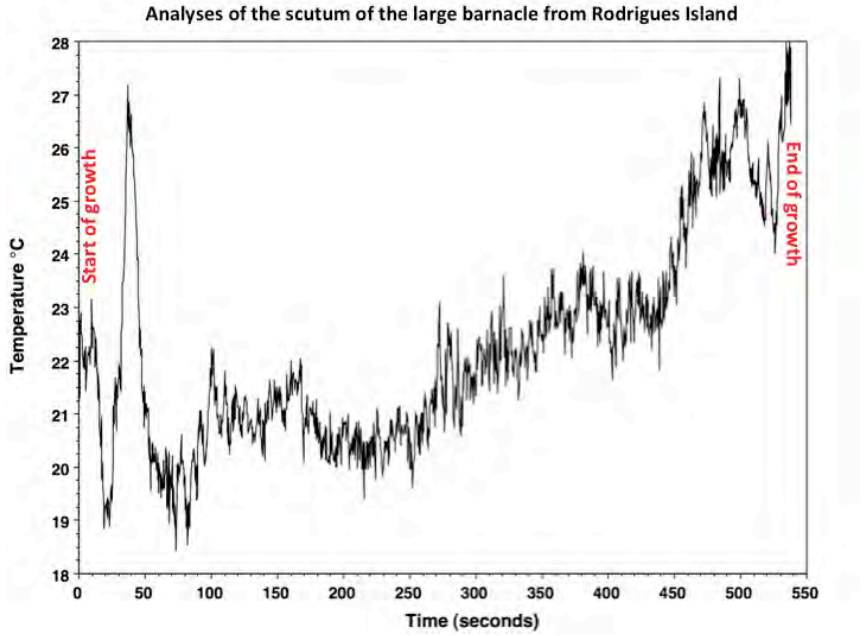

Figure 17. Plot of the analyses performed along the **large** barnacle collected on Rodrigues Island after the strong cleaning procedure was performed with deep and wide ablation of the outer surface of the scutum shell. Once again the Mg/Ca values were translated into estimated water temperatures based on Chave (1954)' correlation shown on figure 6. Note the horizontal axis gives the time used to obtain the profile.

7. Discussion and interpretation of the results

7.1 Growth rates of Lepas anatifera

Based on the limited data available in the scientific literature, it is very hard to come up with an age of the barnacles that were found attached to the aircraft debris from either islands. The prime factor that seems to determine rate of growth is temperature (as shown in figure 8). However, as mentioned in the study of Inatsuchi et al. (2010), nutrients can also intervene in growth rate. The study of MacIntyre (1965) demonstrates a very obvious point: barnacles may take time before settling on floating material, and therefore we are unable to tell when the barnacles that adhered to the aircraft debris 'anchored' themselves. It is unknown whether they grow continuously after settlement.

If we follow the findings of Inatsuchi et al. (2010) barnacles that were living in the ocean within the range of 19 to 29°C reached a capitulum size of 12 mm within 15 days, ca. 0.7-1 mm/day. It could be assumed the specimens analysed here were quite young, perhaps less than one month, considering that some of the scuta we analysed would have been part of much larger capitula, but not more than~ 20mm.

7.2 Reconstructed water temperatures based on barnacle shell chemistry

Significant difficulties were encountered in attempting to reconstruct the temperatures of the waters in which the barnacles grew for several reasons; including

1. The data on the Mg content of barnacles published by Chave in 1954 is limited to only 9 samples, of which and we decided to eliminate three were eliminated as outliers. Hence, with only too few samples analysed, we have to be cautious due to large uncertainties surrounding the formed uncertainty of the relationship between Mg/Ca and temperature.
2. Large amounts of organic matter/tissue occur in specific regions of scutum shells [i.e. the brown spots visible in figure 3] and throughout the shell. These regions associated with organic matter are enriched in magnesium.
3. After ablating the outer surface of scuta (see figures 11, 12), we are unsure if some organic layers remained in the calcite even after ablation to obtain Mg/Ca of the calcite.
4. It is also obvious that the extermities of the scuta are the sites of early growth and final growth, are characteristically coloured brown [figures 4, 10 and 16], indicating the presence of organic matter. These areas contain higher measured Mg/Ca and their higher estimated temperatures compared to the rest of the scuta [see figures 13-15, 16-17]. We do not know if these temperature values are accurate due to the presence of organic matter.
5. The observations made in several previous studies [Evans,1958; Skerman, 1958; Patel et al., 1959; McIntyre, 1965; Inatsuchi et al., 2009; Magni et al., 2015] indicate that the rate of growth of *Lepas anatifera* barnacles is affected by temperature and other factors such as nutrient availability. The rate of growth may also determine incorporation of Mg into the $CaCO_3$ precipitated by the barnacle as in other crustaceans which also secrete low-magnesium calcite (e.g. ostracods). Chivas et al. (1983) who grew ostracods in the laboratory under controlled conditions [temperature and salinity] identified that the early stages of growth of the organisms [when shell growth is very rapid] yielded higher Mg concentration compared to when the shells reached a stable weight and size. Thus, in general, faster growth results in higher Mg/Ca. Consequenly, if barnacle growth rate changed with life stage or with nutrient availability, the Mg/Ca of the barnacle shell may change accordingly. We were unable to assess the impact of growth rate on barnacle shell chemistry.
6. Further difficulty at assessing the results of the analyses on the shells is that we are unaware as to (1) when the barnacles first adhered to the aircraft debris, (2) if

they did possibly undergo a period of reduced or no growth during their life, and (3) if all the barnacles on a single debris grew synchronously. Comparison of the profiles for two barnacle scuta collected on the same aircraft debris provided different estimated temperature profiles, thus confusing our possible interpretation of the path in the Indian Ocean where the barnacles may have grown.

7. Reference to the distribution of the monthly average sea surface temperatures in the Indian Ocean obtained from the NOAA web site that span several years (see figure 19 below), indicates that if the aircraft had impacted the ocean at a high latitude in the lower half of the grey rectangle shown on the map, the estimated temperature should have been within the vicinity of 16 to 18°C in March. As circulation as the surface of the Indian Ocean follows an anticlockwise gyre on the eastern side of the Indian Ocean, temperatures at which the barnacle shells grew might be expected to increase (along the flow path) and eventually reach values of 24 to 27°C depending on the time when the debris reached the islands. If, on the other hand, the aircraft had impacted the ocean at a lower latitude, the profile of estimated temperature ought to have shown little variation.
8. Finally, we still do not know the timing of barnacle adherence to the debris, or the respective ages of the barnacle.

.

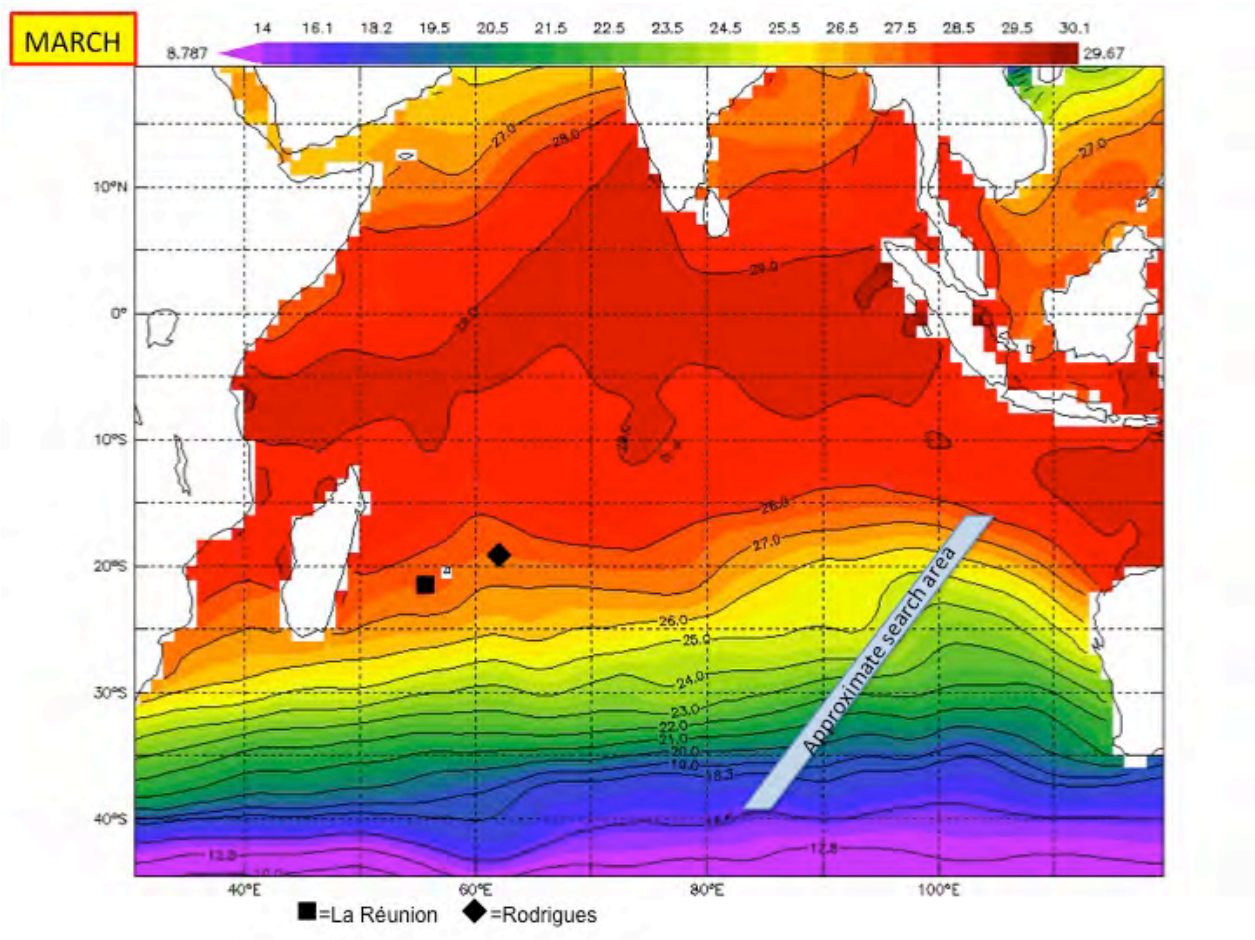

Figure 18. Average sea-surface temperature [SST] map for March for the Indian Ocean obtained from http://ferret.pmel.noaa.gov. The location of the 2 islands [La Réunion and Rodrigues] on which barnacles recovered from the aircraft debris were found. The approximate area of the search for the aircraft is shown in grey (although in reality it is arcuate in shape]. Note also the colour schemes for the SSTs varies slightly between this figure and figure 19 below.

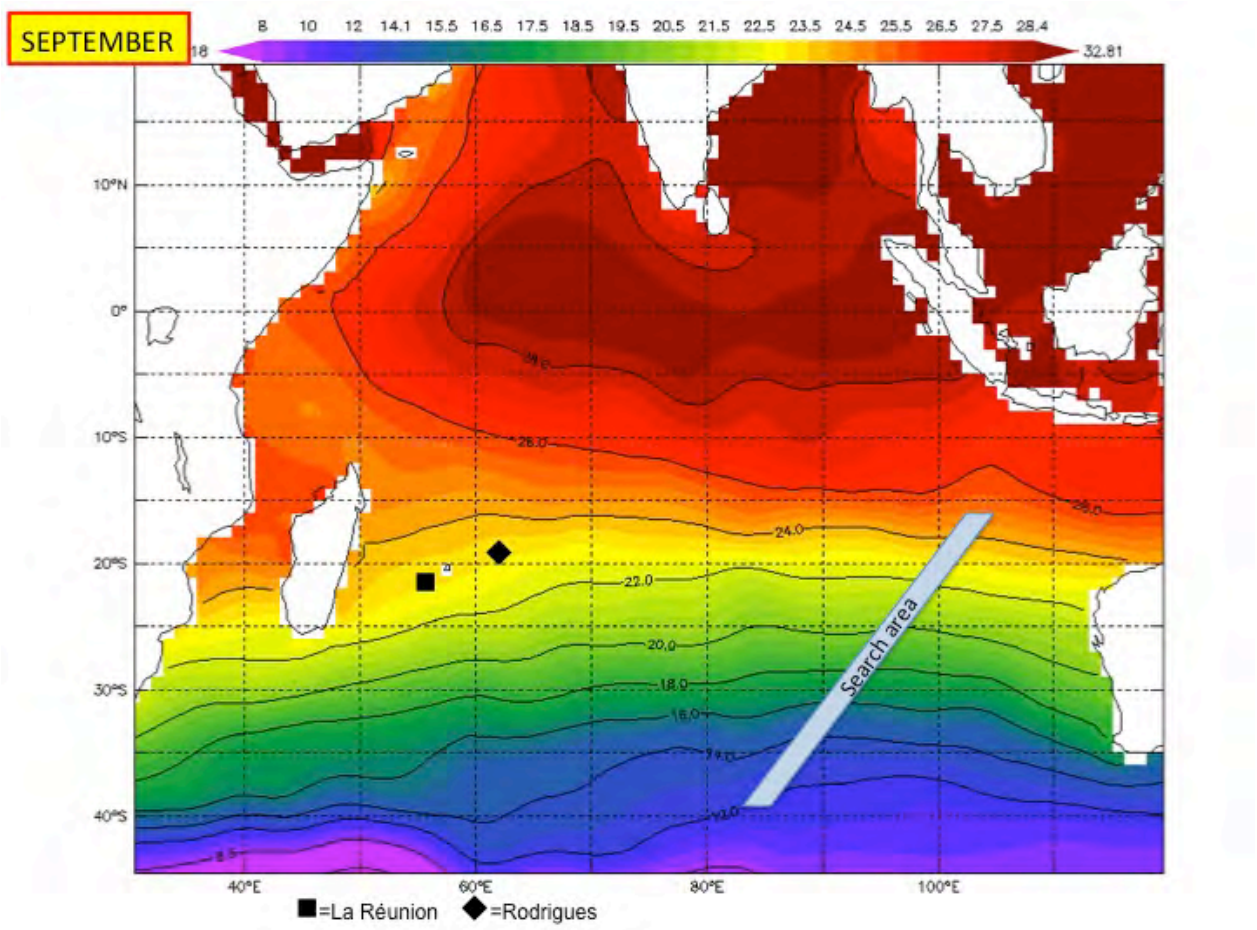

Figure 19. Average sea-surface temperature [SST] map for September for the Indian Ocean obtained from http://ferret.pmel.noaa.gov. This is displayed to identify the seasonality in SSTs between March and September. The location of the 2 islands [La Réunion and Rodrigues] on which barnacles recovered from the aircraft debris were found. The approximate area of the search for the aircraft is shown in grey (although in reality it is arcuate in shape]. Note also the colour schemes for the SSTs varies slightly between this figure and figure 18 above.

8. Conclusions

If the aircraft had crushed at high latitude in the vicinity of the grey rectangle, and if the barnacle shells had commenced adhering to the plan debris soon after reaching the sea surface at that time, temperatures of the order of ~18°C should have been recorded by the shells. If on the other hand, the aircraft had impacted the ocean at a lower latitude in the rectangle, temperatures of ~27-28°C should have been recorded.

Note that seasonal changes of sea surface temperatures around La Réunion and Rodrigues Islands range between within a single year. So, if the barnacles had only started adhering to the aircraft debris in that region, the Mg/Ca of their shells ought to indicate values ranging between ~23° [for September; see figure 19] and ~27.5°C [for March; see figure 18].

Acknowledgements

I wish to thank Professor Stephen Eggins, Director of the Research School of Earth Sciences at the ANU for his permission to use ANU facilities. Mr Les Kinsley and Dr Pete Tollan also at ANU for expert help at using the Laser Ablation facility and processing the raw data.

Mr Joe Hattley from ATSB and Maggie Tran and John Pugh from Geoscience Australia, are all thanked for facilitating access to the barnacles and information on the missing

aircraft search. In addition, I wish to acknowledge the help of Professor Franck Bassinot and Dr Dominique Blamart of the Laboratoire des Sciences de l'Environnement et du Climat in Gif-sur-Yvette, France for providing barnacle specimens they also analysed and the many long phone conversations at night and on weekends concerning the interpretation of the results presented here.

The interpretation of the results are my own responsibility.

References

Blamart, D. Bassinot, F. 2016. Rapport d'expertise: Estimation des températures de croissance des valves de cirripèdes fixes sur le flaperon du vol MH370 à partir de l'analyse de leur composition isotopique $^{18}O/^{16}O$. *Submitted to the 'Tribunal de Grande Instance de Paris' [unpublished].*

Chave, K.E. 1954. Aspects of the Biogeochemistry of Magnesium 1. Calcareous Organisms. *The Journal of Geology* 62, 266-283.

Chivas, A.R., De Deckker, P., Shelley, J.M.G. 1983. Magnesium, strontium, and barium partitioning in nonmarine ostracode shells and their use in paleoenvironmental reconstructions – a preliminary study. In *Applications of Ostracoda* (R. F. Maddocks, ed.), University of Houston Geoscience, pp. 238-249.

Clarke, F.W., Wheeler, W.C. 1917. The inorganic constituents of marine invertebrates. U.S. Geological Survey Professional Paper 124.

Dakin, W.J. 1973. *Australian Seashores*. Revised edition, assisted by I. Bennett & E. Pope. Angus & Robertson Publishers, Sydney.

Darwin, C. 1852. *A monograph of the subclass Cirripedia, with figures of all species. The Lepadidae, or pedunculated cirripedes.* Volume 1. The Ray Society, London, 400 pp.

Eggins, S.M., De Deckker, P., Marshall, J. 2003. Mg/Ca variation in planktonic foraminifera tests: implications for reconstructing palaeo-seawater temperature and habitat migration. *Earth and Planetary Science Letters* 212, 291-306.

Eggins, S.M., Kinsley, L.K., Shelley, J.M.G. 1998. Deposition and element fractionation processes occurring during atmospheric pressure laser sampling for analysis by ICPMS. *Applied Surface Science* 127-129 278-286.

Evans, F. 1958. Growth and maturity of the barnacles *Lepas hilii* and *Lepas anatifera*. *Nature* 182, 1245-1246.

Inatsuchi, A., Yamato, S., Yusa, Y. 2009. Effects of temperature and food availability on growth and reproduction in the neustonic pedunculate barnacle *Lepas anserifera. Marine Biology* 157, 899-905.

Killingley, J. S. & Newman, W. A. 1982. O^{18} fractionation in barnacle calcite – a barnacle paleotemperature equation. *Journal of Marine Research* 40, 893-901.

Magni, P.A., Venn, C., Aquila, I., Pepe, F., Ricci, P., Di Nunzio, C., Ausania, F., Dadour, I.R. 2015. Evaluation of the floating time of a corpse found in a marine environment using the barnacle *Lepas anatifera* L. (Crustacea: Cirripedia: Peduncalata). *Forensic Science International* 24 (doi.org/10.1016/j.forsciint.2014.11.016).

McIntyre, R.J. 1966. Rapid growth in stalked barnacles. *Nature* 212, 637-638.

Patel, B. 1959. The influence of temperature on the reproduction and moulting of *Lepas anatifera* L. under laboratory conditions. *Journal of the Marine Biological Association of the United Kingdom* 38, 589-597.

Shiffer, P.H., Herbig, H-G. 2016. Endorsing Darwin: global biogeography of the epipelagic goose barnacle *Lepas* spp. (Cirriperdia, Lepadomorpha) proves cryptic speciation. *Zoological Journal of the Linnean Society* doi: 10.1111/zoj.12373.

Skerman, T.M. 1958. Rates of growth in two species of *Lepas* (Cirripedia). *New Zealand Journal of Science* 1, 402-411.

Treatise of Invertebrate Paleontology (1969) Part R. Arthropoda 4, volume 1. The Geological Society of America Inc & The university of Texas.

Appendix G – Summary of Analyses Undertaken on Debris Recovered During the Search for Flight MH370

Note: When the samples were originally created for analysis, there was discussion about providing one of the samples to Boeing for analysis. However, the ATSB and Geoscience Australia later determined that no analysis by Boeing was necessary and retained the samples. (Page 44)

Australian Government
Geoscience Australia

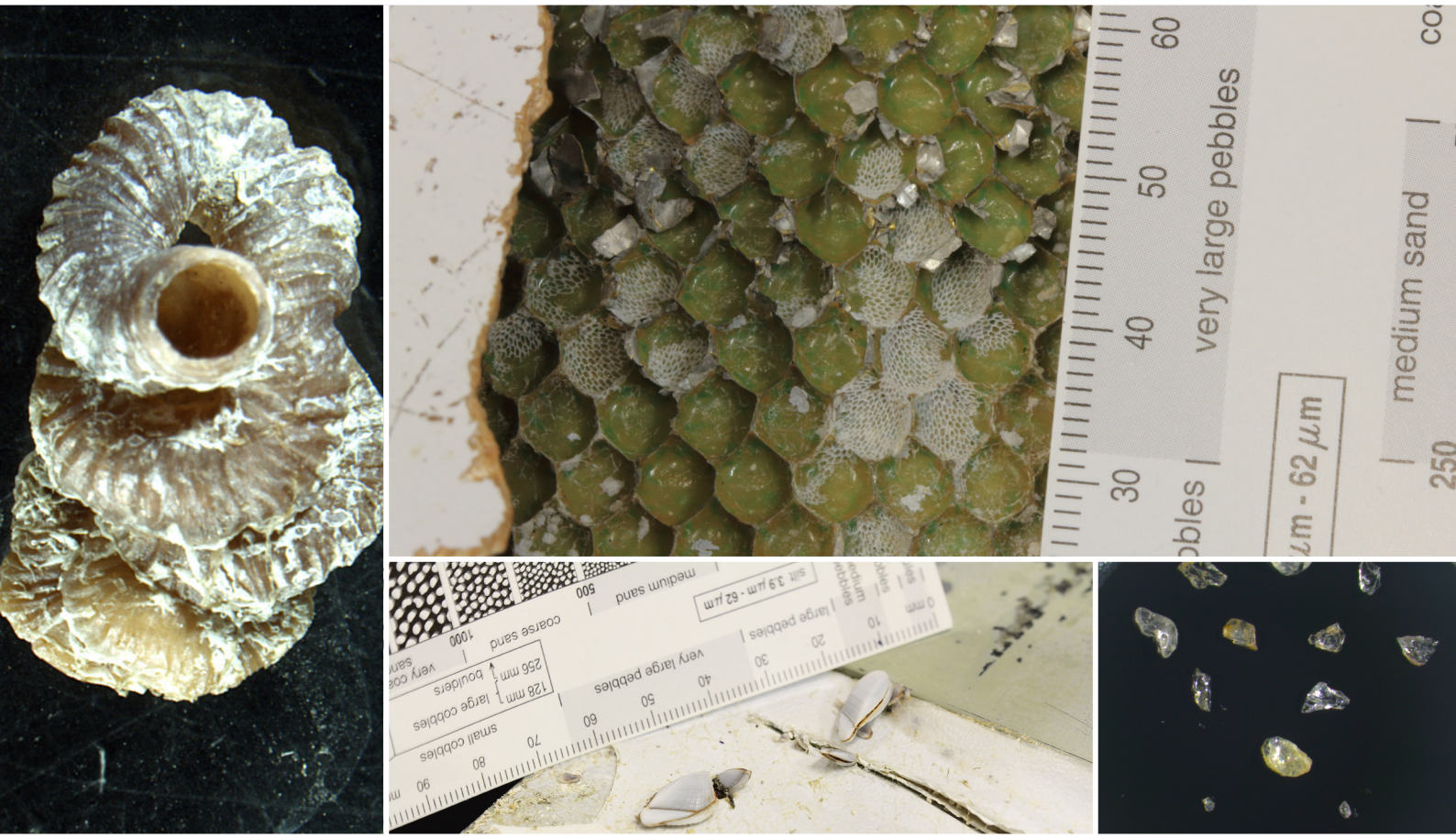

Record 2017/11 | **eCat** 110564

Summary of Analyses Undertaken on Debris Recovered During the Search for Flight MH370

A collation of reports describing quarantine and parts analysis undertaken by Geoscience Australia

M. Tran, W.A. Nicholas, J. Chen, Z. Hong, J. Sohn, T. Whiteway, J. Pugh, and C. Thun

Summary of Analyses Undertaken on Debris Recovered During the Search for Flight MH370

A collation of reports describing quarantine and parts analysis undertaken by Geoscience Australia

GEOSCIENCE AUSTRALIA
RECORD 2017/11

M. Tran, W.A. Nicholas, J. Chen, Z. Hong, J. Sohn, T. Whiteway, J. Pugh, and C. Thun

Department of Industry, Innovation and Science
Minister for Resources and Northern Australia: Senator the Hon Matthew Canavan
Assistant Minister for Industry, Innovation and Science: The Hon Craig Laundy MP
Secretary: Ms Glenys Beauchamp PSM

Geoscience Australia
Chief Executive Officer: Dr James Johnson
This paper is published with the permission of the CEO, Geoscience Australia

© Commonwealth of Australia (Geoscience Australia) 2017

With the exception of the Commonwealth Coat of Arms and where otherwise noted, this product is provided under a Creative Commons Attribution 4.0 International Licence. (http://creativecommons.org/licenses/by/4.0/legalcode)

Geoscience Australia has tried to make the information in this product as accurate as possible. However, it does not guarantee that the information is totally accurate or complete. Therefore, you should not solely rely on this information when making a commercial decision.

Geoscience Australia is committed to providing web accessible content wherever possible. If you are having difficulties with accessing this document please email clientservices@ga.gov.au.

ISSN 2201-702X (PDF) 110564
ISBN 978-1-925297-48-5 (PDF)
eCat 110564

Bibliographic reference: Tran, M., Nicholas, W.A., Chen, J., Hong, Z., Sohn, J., Whiteway, T., Pugh, J. & Thun, C. 2017. Summary of analyses undertaken on debris recovered during the search for flight MH370: a collation of reports describing quarantine and parts analysis undertaken by Geoscience Australia. Record 2017/11. Geoscience Australia, Canberra.
http://dx.doi.org/10.11636/Record.2017.011

Version: 1701

Abbreviations

AM	Australian Museum
ANU	Australian National University
ATSB	Australian Transport Safety Bureau
GA	Geoscience Australia
µm	micrometre
m	metres
MAGNT	Museum and Art Gallery of the Northern Territory
MTQ	Museum of Tropical Queensland
NIWA	National Institute of Water and Atmospheric Research (New Zealand)
SEM-EDS	Scanning Electron Microscope-Energy Dispersive Spectroscopy
WAM	Western Australian Museum

Acknowledgements

The authors thank the following people for their generous contributions to this report through advice, research, time and expertise. Peter Foley, Joe Hattley, Jason Mcguire, Rob Smith, Seb Davey (Australian Transport and Safety Bureau); Andy Sherrell (Sherrell Ocean Services); Diana Jones (Western Australian Museum); Richard Willan and Chris Glasby (MAGNT); Dennis Gordon (National Institute of Water and Atmospheric Research); Robyn Cumming (Museum of Tropical Queensland); Elena Kupriyanova (Australian Museum); Megan McCabe, Andrew Carroll, Rachel Przeslawski, Christian Thun, Abby Loiterton, Ian Long, Billie Poignand, Simon Webber, Keith Sircombe, Bruce Kilgour (Geoscience Australia); Patrick De Deckker (Australian National University); the crew from Fugro Equator, Fugro Supporter, Fugro Discovery, Go Phoenix, Havila Harmony, Dong Hai Jiu and onshore staff of Fugro; Aslam Basha Khan bin Zakaria Maricar, Mohan Sippiah, Dato Kok Soo Chon (Malaysian Ministry of Transport). We also thank Drs Stephanie McLennan and Scott Nichol for reviewing this report.

Contents

Abbreviations iii
Acknowledgements iv
Contents v
1 Executive Summary 7
2 Review of Sediment on Aircraft Pieces from Mozambique, Mossel Bay and Mauritius (Items 2 to 5) 9
2.1 Summary 9
2.2 Methods 9
2.2.1 Establishing Geological Context 9
2.2.2 Sediment Analysis 10
2.3 Results for Items 2 and 3 10
2.3.1 Geological Context: Mozambique 10
2.3.2 Sediment Analysis Results 12
2.3.3 Discussion 15
2.3.4 Conclusion 16
2.4 Item 4 17
2.4.1 Geological Context: Mossel Bay, South Africa 17
2.4.2 Sediment Analysis Results 17
2.4.3 Discussion 17
2.4.4 Conclusion 17
2.5 Item 5 18
2.5.1 Geological Context: Rodrigues Island 18
2.5.2 Sediment Analysis Results 19
2.5.3 Discussion 19
2.5.4 Conclusions 20
2.6 References 21
3 Review of Macrofauna on Pieces from Mozambique (Item 2 and 3) 24
3.1 Summary 24
3.2 Method 25
3.3 Results 25
3.3.1 Item 2: Recovered From Daghatane Beach, Mozambique 25
3.3.2 Item 3 (Right Horizontal Stabilizer Panel): Recovered From a Beach in the Mozambique Channel 28
3.4 References 39
4 Stable Isotope Analyses of Paints on Aircraft Pieces From Mozambique (Items 2 and 3) and Mauritius (Item 5) 40
4.1 Summary 40
4.2 Method 40
4.2.1 Sub-Sampling Items 2 and 3 40
4.2.2 Sub-sampling Item 5 and Control Sample 41
4.2.3 Isotopic Analysis of Items 2, 3 and 5 and the Control Sample 41
4.3 Results 42

5 Analyses of Organic Compounds on Aircraft Pieces From Mozambique (Item 2) 44
5.1 Summary 44
5.2 Methodology 44
5.3 Results 44
5.4 References: 48
6 Review of Macrofauna on Aircraft Pieces Found on Mauritius and South Africa (Item 5) 49
6.1 Summary 49
6.2 Method 50
6.3 Results 54
6.3.1 Item 4 (External Engine Cowling) 54
6.3.2 Item 5 (Door R1 Stowage Closet) 54
6.4 References 56

1 Executive Summary

On 8 March 2014, the Boeing 777-200ER aircraft registered as Malaysia Airlines 9M-MRO and operating as flight MH370 (MH370) disappeared from air traffic control radar after taking off from Kuala Lumpur, Malaysia on a scheduled passenger service to Beijing, China with 227 passengers and 12 crew on board.

After analysis of satellite data it was discovered that MH370 continued to fly for over six hours after contact was lost. All the available data indicates the aircraft entered the sea close to a long but narrow arc of the southern Indian Ocean.

On 31 March 2014, following an extensive sea and air search, the Malaysian Government accepted the Australian Government's offer to lead the search and recovery operation in the southern Indian Ocean in support of the Malaysian accident investigation.

On behalf of Australia, the Australian Transport Safety Bureau (ATSB) coordinated and lead the search operations for MH370 in the southern Indian Ocean. Geoscience Australia (GA) provided advice, expertise and support to the ATSB in sea floor mapping (bathymetric survey) and the underwater search. Geoscience Australia has also provided quarantine facilities for receipt of possible debris, and has undertaken laboratory analyses for a number of these pieces.

Over twenty debris items of interest to the ATSB investigation team have washed up on the east and south coast of Africa, the east coast of Madagascar and the Islands of Mauritius, Reunion and Rodrigues in the Indian Ocean. Of these, a number of items were sent to Australia for identification and examination. Items transported to Australia were received through Geoscience Australia's Quarantine Approved Premise prior to analysis and ATSB investigation (Table 1).

This record compiles reports produced during the course of the laboratory analyses and investigation. The record is divided into five sections (reports) and covers the results of each analytical technique that Geoscience Australia has applied to the debris items:

1. Analysis of sediment to identify if the items had beached at any other locations prior to their discovery, and
2. Analysis of marine fauna found on the items to assess:
    a) the length of time the items were in the water (based on the age and growth rates of particular species present),
    b) the possible location of the aircraft crash site (based on age and growth rates of marine fauna endemic to particular ocean areas),
3. Analysis of stable isotopes and organic compounds to identify if there were any unusual chemical signatures on the items.

Results from these analyses show that:

- The constituents of sediment found on Items 2 to 5 match the location at which the items were recovered and were comprised natural and loose aircraft material.
- Macrofaunal analyses of Items 2 and 3 showed that these aircraft pieces were colonized with opportunistic and cosmopolitan species originating from the tropical Indo-Pacific Ocean. No evidence of cool or cold-temperate molluscs or annelids was found.

- Stable isotope analysis of the paint on the aircraft items analyzed indicated that all samples tested might have come from the same source.
- Organic compound analyses on aircraft pieces indicated that results were consistent with organic compounds of grease, lubricants or lubricant additives and possibly derived from higher plant origin petroleum.

Table 1. Summary of analyses on pieces of debris undertaken by Geoscience Australia

Item Reference Number*	Date Received at GA	Analyses undertaken	Relevant Reports
2	21/03/2016	Sedimentology	Review of sediment on pieces from Mozambique, Mossel Bay and Mauritius (Items 2 to 5)
		Macroecology	Review of macrofauna on pieces from Mozambique (Items 2 & 3)
		Isotopes	Stable isotope analyses of paints on pieces from Mozambique (Items 2 & 3) and Mauritius (Item 5)
		Geochemistry	Analyses of organic compounds on the MH370 pieces from Mozambique (Item 2)
3	21/03/2016	Sedimentology	Review of sediment on pieces from Mozambique, Mossel Bay and Mauritius (Items 2 to 5)
		Macroecology	Review of macrofauna on pieces from Mozambique (Items 2 & 5)
4	14/04/2016	Sedimentology	Review of sediment on pieces from Mozambique, Mossel Bay and Mauritius (Item 2 to 5)
		Isotopes	Stable isotope analyses of paints on pieces from Mozambique (Items 2 & 5) and Mauritius (Part 5)
		Macroecology	Review of macrofauna on possible MH370 Aircraft pieces found on Mauritius and Mozambique (Items 4 to 5)
5	14/4/2016	Sedimentology	Review of sediment on pieces from Mozambique, Mossel Bay and Mauritius (Items 2 to 5)
		Macroecology	Review of macrofauna on possible MH370 Aircraft pieces found on Mauritius and Mozambique (Items 4 to 5)
		Isotopes	Stable isotope analyses of paints on pieces from Mozambique (Items 2 & 3) and Mauritius (Item 5)

* Item reference numbers are consistent with the Malaysian Ministry of Transport and further information on each of these items can be found at:

http://www.mh370.gov.my/phocadownload/3rd_IS/Summary%20of%20Debris%20Recovered%20-%2028022017.pdf

2 Review of Sediment on Aircraft Pieces from Mozambique, Mossel Bay and Mauritius (Items 2 to 5)

2.1 Summary

This report provides a review of the sediment found on aircraft pieces recovered from Daghatane Beach, Mozambique (Item 2), Mozambique Channel (Item 3), Mossel Bay (Item 4) and Rodrigues Island, Mauritius (Item 5). For consistency, the four pieces are labelled as Right wing No. 7 Flap Track Fairing (Item 2), Right Horizontal stabiliser panel piece (Item 3), Engine Nose Cowl (Item 4) and Door R1 Stowage Closet (Item 5). This report is structured into three sections to address the different locations of debris discovery. The key findings from the study are:

- Each of the sediment samples analysed was observed to have constituents that closely match either published evidence, or in the case of the sample from Rodrigues Island, to match what would broadly be expected at the location at which the piece was recovered.
- No material was observed that would indicate a source distal to the location from which the aircraft pieces were found.
- Each sediment sample examined had a minor component of honeycomb material from the aircraft. The presence of loose honeycomb material suggests that natural sediment and other material could have been transported within the aircraft pieces, but this was not able to be confirmed.
- Sediment grains from the Rodrigues sediment sample were examined by scanning electron microscope-energy dispersive spectroscopy (SEM-EDS) to determine if the grains were natural or man-made, with results confirming that only natural material was present in the sample.

Caveats: Some criteria were applied to the acceptance of samples analysed, these include:

- Any sediment within voids that could not be accessed without destructively breaking apart the pieces was not sampled, and
- Any sediment < 100 µm was not analysed.

2.2 Methods

The following procedures were followed for inspection of sediment samples from all aircraft items numbered 2 to 5 provided to Geoscience Australia.

2.2.1 Establishing Geological Context

The locations where the aircraft pieces were recovered are not locations normally studied at Geoscience Australia. Thus the first part of this investigation was to establish geological context for the material being studied. Once the geological background was broadly established, insight was gained by intensively analysing the first two samples. Once this baseline understanding of the sediment from the aircraft parts, and the sediment from locations where they were found was thoroughly understood, it was possible to more rapidly investigate the other samples.

2.2.2 Sediment Analysis

Two samples were sieved into three grain-size intervals (100-500 µm, 500-1000 µm and > 1000 µm) and inspected using a binocular microscope at Geoscience Australia. To compare the characteristics of the sediment with descriptions of the environment in which they were found a detailed assessment of the components of each sediment sample was made. Sand grains were identified and counted using standard point-counting techniques. A minimum of 300 grains were used to make inferences on sediment sample composition and history. The principal constituents of each sample were counted, both for the mineral grains, and for the total mineral and biogenic carbonate assemblage. Grain counts were limited to 10 identifiable components.

2.3 Results for Items 2 and 3

2.3.1 Geological Context: Mozambique

The coastal locations at which the pieces were found in Mozambique are situated within the adjacent Gaza and Inhambane provinces, set within an expansive coastal plain that stretches across south and central Mozambique. Two prominent rivers discharge on the Gaza-Inhambane coast. These are the Limpopo at Xai Xai, and the Save, which discharges at Nova Mambone (Figure 1). Additionally, 270 km north of the Save delta, the Zambesi river, the largest river in southeastern Africa, enters the Mozambique Channel south of Quelimane. Both the Zambesi and the Limpopo rivers incise Precambrian igneous, and to a lesser extent, metamorphic terranes and discharge large volumes of sediment to the continental shelf and Mozambique Channel. The Zambesi discharges northeast from its delta, away from the locations where aircraft pieces were found (Schultz et al., 2011). The precise route of sediment dispersal once it reaches the coast from the Limpopo River is uncertain. However, based on the evidence from sediment bedforms at Maputo, and the general form of the coastal geomorphology, it is likely the Limpopo discharges northwards, potentially in the same direction as the longshore drift. Thus, the locations of Items 2 to 3 lie along this northward route of Limpopo sediment transport (Figure 1).

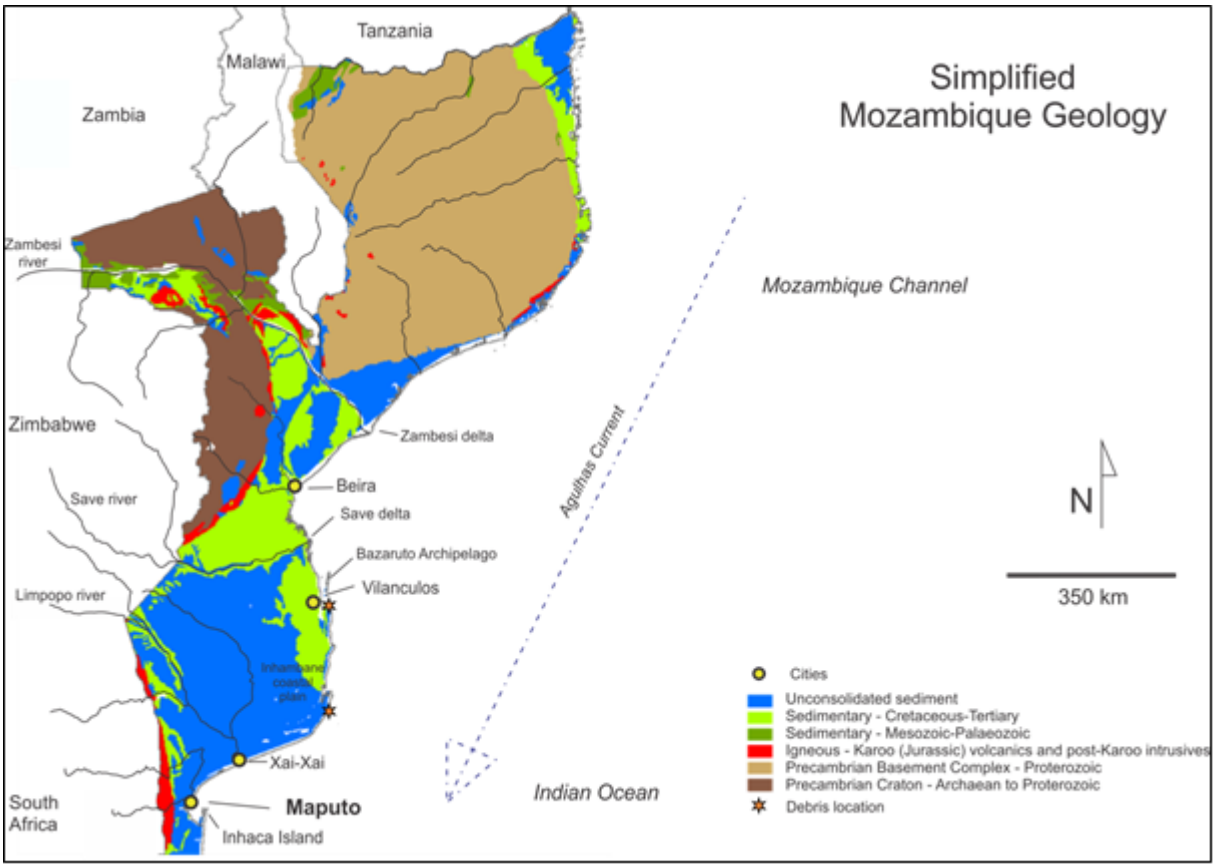

Figure1. Geological context of the locations where aircraft pieces were found on the Mozambique coast. Map adapted from http://earthwise.bgs.ac.uk/index.php/Hydrogeology_of_Mozambique

Between the city of Maputo, southwest of the Limpopo estuary, and the Save delta, the coast is dominated by modern and Pleistocene age coastal dunes, underlain by Quaternary, Paleogene and Neogene sedimentary strata (Rutten et al., 2008). The principal landforms along this coast are parabolic dunes that in many instances are 1-2 km or more in length. These dunes also form the islands of the Bazaruto Archipelago, located approximately 12 km offshore from Vilankulos south of the Save delta, and where one aircraft piece was reported to be found at the southern end of the archipelago. The modern coastal parabolic dunes on Bazaruto Island are underlain by older unconsolidated reddish-yellow sands and aeolianite, suggesting long-term deposition, reworking and aeolian dune formation (Armitage et al., 2006). Bazaruto Island appears typical of the coastal sediments between Maputo and the Save river delta, and its geomorphology suggests considerable erosion of the coastal margin and redeposition of sediment inland has occurred in the past. Dune sands on the mainland coast opposite Bazaruto Archipelago are fine to medium grained (Avis et al., 2015). To the south, at the Mozambique-South Africa border, aeolian dunes rise up to 143 m above sea-level (Botha et al., 2003), and along the Inhambane coast active coastal dunes have been reported to be up to 191 m above sea-level (Tinley, 1985). Inland from the coast, between Maputo and the Save delta, calcrete is ubiquitous. In contrast, the coastal strata appear uncalcified, and the presence of several generations of dunes strongly suggests a long history of aeolian reworking of coastal sands. These reworked mineral grains tend to be fine to medium grained and rounded in shape.

At the location where Item 2 was found (Vilanculos), the Mozambique coast is characterised by dunes, mangrove swamps and shallow lakes, with seagrass meadows and coral reefs offshore. The Quaternary geology of the Bazaruto islands appears similar in composition and age to Inhaca Island, at Maputo (Armitage et al., 2006). Inhaca Island sedimentology, morphology, age and composition is well documented (Perry, 2005; Perry and Beavington-Penney, 2005; Peche, 2012).

Sediments comprise fine to medium quartz sand (monocrystalline) that is typically angular to rounded when observed in thin section (Peche, 2012). Accessory minerals include ilmenite and peridot (olivine). Similarly, tidal flats are characterised by sub-rounded to rounded quartz that comprises up to 90% of sediment.

On the inner to mid continental shelf, south of Maputo, seabed sediments comprise fine to medium-grained quartzose sand in the 20-50 m depth range (Green, 2009). Further south, surficial sands such as those to the south in Lake Sibaya, consist of well sorted, fine to medium grained quartz sand (Wright et al., 2000), that may be equivalent to those at Inhaca Island and Maputo. The key point here is that there appears to be a significant amount of terrestrial quartz within this part of the Mozambique coast and shelf, but detailed petrographic descriptions of these units are limited to those from Inhaca Island (Peche, 2012; Perry, 2005; Perry and Beavington-Penney, 2005). Maputo is ~ 50 km from the Limbombos Mountains to the west, where rhyolites and basalts are presently being eroded by numerous small creeks and streams that feed into the rivers discharging into Maputo Bay. It is highly likely that much of the quartz sediment present in Maputo Bay is sourced from the Limbombos mountains igneous units that are part of the regionally important Jurassic Karoo flood basalt province (Manninen et al., 2008). The Limpopo, Save and Zambezi rivers also incise the Karoo flood basalt province strata, and older igneous strata. Sediment chemistry indicate the Limpopo and its offshoot, the Olifants River, are both sourced from mafic (cf. basaltic) source rock while the Zambezi river to the north is largely sourced from felsic (cf. granitic) rock (Garzanti et al., 2014). Additionally, the Olifants River drains the huge Paleoproterozoic layered mafic intrusion of the Bushveld Complex and similarly incises through the Karoo Flood Basalts (Von Gruenewaldt et al., 1985; Garzanti et al., 2014).

2.3.2 Sediment Analysis Results

Both samples from Item 2 and Item 3 are dominated by low sphericity, angular to sub-rounded, clear, glassy, crystalline grains, most of which are quartz (Table 1). No clay or silt particles (silt + clay = mud) were observed in these samples, nor was mud observed on the aircraft pieces (from photographs). There are rare mineral grains that are clear, glassy, and crystalline and have one or two apparent cleavages. These are most likely zeolites (formed by chemical processes from original igneous minerals), but have been included in the quartz fraction for simplicity. In addition to these, a small proportion of rounded, anhedral yellow crystalline grains are present, many of which are likely reworked or secondary quartz. Also identified in the sample were rare grains of a pink crystalline mineral, a prismatic ilmenite, and olivine (anhedral), and an unidentified aquamarine coloured mineral (tentatively identified as the mineral aquamarine).

Table 1. Mineral grain counts from Items 2 & 3.

Sample and sieve size (µm)	Total count	Quartz clear, very angular to angular (%)	Quartz, clear, sub-angular to sub-rounded (%)	Quartz, clear, rounded to very rounded (%)	Yellow minerals Angular (%)	Yellow minerals rounded (%)	Green minerals angular (%)	Green minerals Rounded (%)	White Quartz (%)	Pink Minerals angular (%)	Pink minerals rounded (%)
1-1000	21	19.0	4.8	47.6	4.8	9.5	0.0	0.0	28.6	0.0	0.0
1-500	530	29.6	40.2	21.3	1.3	4.5	0.2	0.0	1.1	0.6	1.1
1-100	555	74.1	18.7	4.0	3.2	1.8	0.0	0.0	0.9	2.2	0.2
2-1000	13	7.7	30.8	38.5	7.7	15.4	0.0	0.0	0.0	0.0	0.0
2-500	315	36.5	47.0	15.9	0.6	1.3	0.0	0.0	0.6	0.0	0.0
2-100	516	59.9	27.9	7.0	0.4	0.6	1.0	0.6	0.6	2.7	0.4

Apart from minerals, the dominant constituent of the sediment samples, particularly from Item 3 (Table 2, Figure 2) is broken bryozoan pieces, which do not have any significant degradation. There are also trace amounts of benthic foraminifera and planktonic forams in both samples.. In the fine-grained sediment of Item 3 (100 µm sieve) microscopic articulated bivalve molluscs were observed. A single juvenile (3 mm length) Goose Barnacle (Lepas sp) was present in the > 1000 µm sediment from Item 3. Broken specimens (n = 3) of the agglutinated foraminifera *Textularia hauerii* (Makled and Langer, 2010) are present in the 500-1000 µm subsample from both Item 2 and 3.

Table 2. Total assemblage counts for all pieces in representative sediment aliquots.

Sample and sieve size	Total # grains	Mineral grains (%)	Shells, unmodified, to sharp edges (%)	Shells, rounded, degraded (%)	Benthic Foraminifera (%)	Planktonic Foraminifera (%)	Ostracods, articulated (%)	Ostracods, disarticulated (%)	Bryozoan pieces (%)	Sponge spicules (%)	Echinoid spine pieces (%)
1-1000	24	16.7	4.2	41.7	4.2	8.3	0	0	25	0	0
1-500	542	90.2	0.7	8.7	0.2	0	0	0	0.4	0	0
1-100	413	98.8	0.2	1.0	0	0	0	0	0	0	0
2-1000	301	7.7	3.0	8.3	0.3	0	0	0	81	0	0
2-500	439	49.1	1.4	4.9	1.9	0.2	0	0	43.7	0.5	0.5
2-100	516	90.9	0.2	0	0.8	0	1.2	0.2	4.4	4.6	0

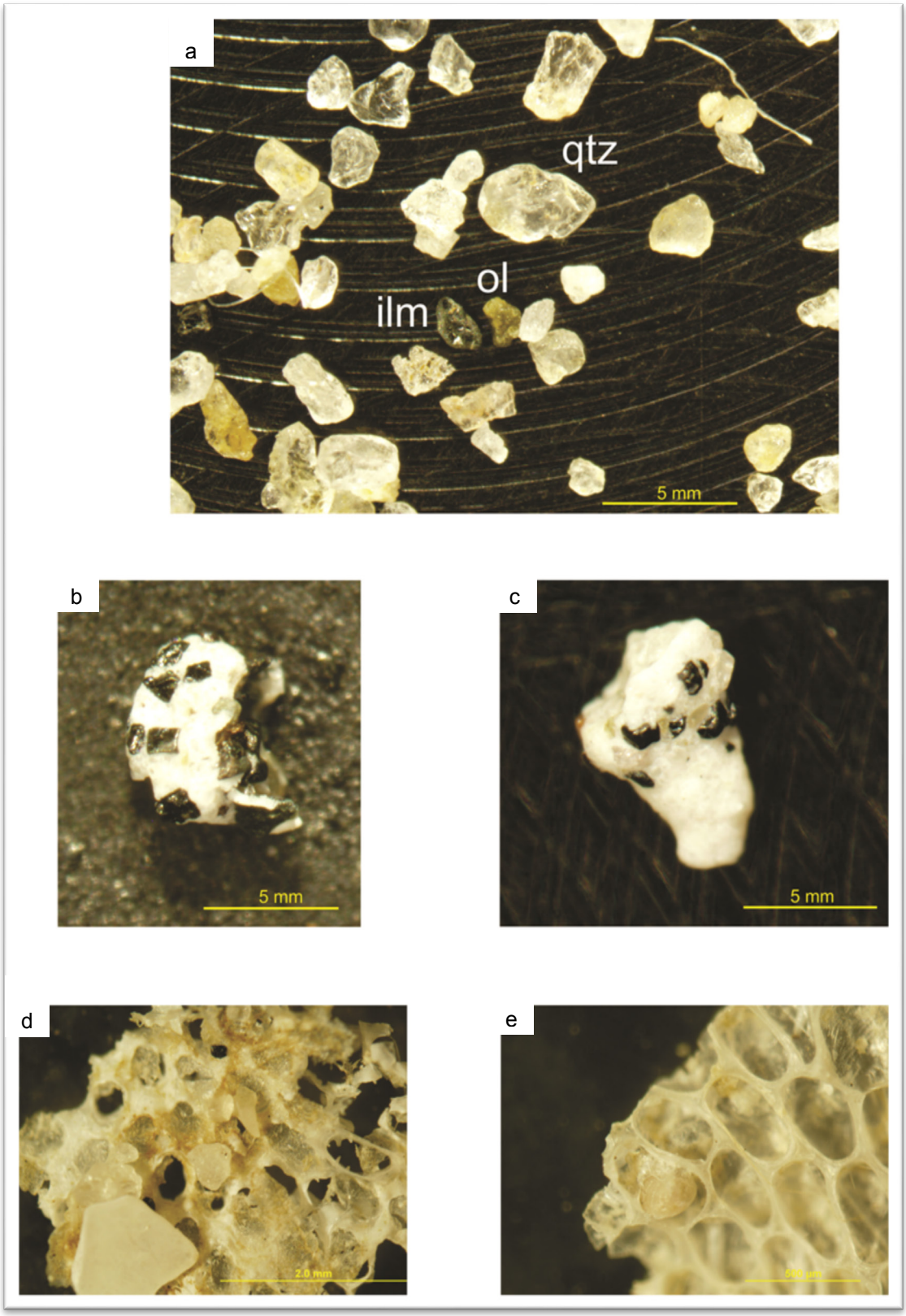

Figure 2. a) Example of clear crystalline grains of quartz (qtz), olivine (ol) and possible ilmenite (ilm); b) and c) examples of broken tests of agglutinated foraminifera that are possibly Textularia hauerii d'Orbigny with silt grains attached; d) and e) sediment grains attached underneath a bryozoan fragment and a benthic rotallid foraminifera overgrown by an enclosing bryozoan colony.

2.3.3 Discussion

The majority of quartz grains in samples from Item 2 and Item 3 appear young, unaltered, and angular to slightly rounded. The dominant proportion of minerals in the fine sediment fraction (100 µm sieve) are angular. The presence of minor amounts of ilmenite and olivine together with the juvenile nature of the quartz suggest the assemblage of minerals may potentially be from similar source material. The presence of pristine, angular mineral grains would require a crystalline, magmatic or high-grade metamorphic source rock, and either a proximal terrestrial source (e.g. volcanic rock or granites close to shore), or large rivers to deliver relatively unrounded sediment derived directly from the crystalline source rock, to the coast. All the rivers in the region where the debris pieces were recovered derive sediment from old igneous and metamorphic terrains, with the igneous Karoo Flood Basalt lavas and related igneous intrusive rocks west of Maputo for example, being closest to the coast.

The dominance of very angular to angular, juvenile quartz grains in fine sand-sized sediment is possible where the source rock is unaltered, where the transport distance is relatively short, and transport only occurs in water rather than in air. Ilmenite occurs in a wide variety of igneous and metamorphic rocks as a high-temperature accessory mineral (Wechsler and Prewitt, 1984) and is commonly found in placer deposits worldwide, because of its resistance to physical and chemical degradation (Riffel et al., 2016). In stark contrast, olivine is rapidly weathered to form clay minerals. Their presence together in the debris samples suggests they have either come from the same source via the same or similar pathways, or they are mixed from different sources. Both ilmenite and olivine are common to the basalt-rich igneous terrains of South Africa and Mozambique, but also to island basalt sources including Grand Comoros in the north of the Mozambique Channel, as well as La Reunion and Mauritius. Similar to the quartz sand at Maputo, igneous rock is the most likely source of any clear monocrystalline quartz along this coast, including any grains that remain angular. This is because comparatively little rounding and frosting of igneous silicic and lithic grains occurs while they are being transported in water (Haines and Mazzullo, 1988). In contrast, rounding, frosting and pitting and other degradation of quartz and similar minerals tends to be very rapid under aeolian conditions.

Skeletal carbonate in the samples from Items 2 and 3 is composed primarily of bryozoans and foraminifera. In the larger grained samples, quartz grains were trapped within some open bryozoan opercula, and underneath (on the base of) bryozoan pieces. One quartz grain was trapped by bryozoan mineralisation, indicating that the bryozoan had grown around the quartz grain. Some foraminifera are also encased by bryozoan mineralisation, indicating that the foraminifera were present before the mineralisation by bryozoans. The timing of bryozoan growth is not known, thus the foraminifera and quartz grains trapped may have been transported in a marine setting, or have been incorporated into the bryozoan structure within the aircraft piece at the shoreline where it was found. It is important to note however that the trapped foraminifera appear to be shallow-water benthic rotallids, with shallow water genera such as *Elphidium* present in the recovered sediment. Although occasional planktonic foraminifera are present, the trapped foraminifera are not planktonic. It would be possible for planktonic foraminifera to be trapped at any stage of the transport path of the aircraft pieces, but wherever the benthic foraminifera are sourced from must be shallow seabed. Thus at least some bryozoan growth occurred after the aircraft piece had passed through a shallow water setting.

The few foraminifera present are generally white in colour, commonly abraded, and are likely reworked benthic forms. These include genera such as *Elphidium* and *Amphistegina*. However, in these sediment samples foraminifera are few in number. Apart from one specific species, it is not possible to directly relate the examples found to a locality, as they are found globally. Additionally, it is commonly accepted that a relatively large number of microfossils are required to characterise an assemblage (≥300). As such it is not possible to infer whether one or more species are from locations distant to the locations at which the aircraft piece was recovered. However, foraminifera are marine organisms, and low numbers of foraminifera can be

present in areas of low salinity water, including estuaries and lagoons, either present as extant species or reworked from more marine settings.

In both samples (Item 2 and Item 3) fragments of an agglutinated foraminifera (*Textularia hauerii;* Makled and Langer, 2010) was observed, with ilmenite grains embedded within its test. This particular example of an agglutinated species with ilmenite grains attached has only been reported from the Bazaruto Archipelago, Mozambique (Makled and Langer, 2010). The presence of broken examples of *Textularia hauerrii* may suggest transport from a zone where this species inhabits, either as part of the inspected sediment sample, or independent of it with post-transport incorporation into these samples. Onshore, to the south of Bazaruto Archipelago, a large ilmenite-rich placer deposit has recently been identified in surface (dredged) sediments at Mutamba (Riotinto.com) as well as extensive buried sands at Jangamo. This suggests that heavy minerals including ilmenite are readily available along the coast for agglutinated foraminifera to incorporate into their test structure because these dune sands are being eroded along the coast, and are incised into by local creeks and rivers.

The presence of rare planktonic foraminifera in these samples is of interest because benthic and planktonic foraminifera are not normally found together in shallow coastal sediments, unless the coasts are directly influenced by offshore water masses. Thus, their presence may indicate either that the coastal waters in which the aircraft pieces were recovered are influenced by offshore water masses and probably located close to open oceanic conditions, or that they are sourced and transported from a different area than where the debris was found.

The microscopic articulated bivalve molluscs in Item 3 are most likely derived from the coastal region of Mozambique because the post-mortem transport of these particularly fragile biogenic skeletal carbonate, very rapidly results in disarticulation and breakage. It may also be the case (although highly unlikely), that they have been transported to the Mozambique coast along with the aircraft pieces. If some of the biogenic carbonate material (foraminifera, ostracods, and bryozoans) represent material transported across an ocean, it indicates a transport pathway above the carbonate compensation depth (est -3000 m), below which $CaCO_3$ is dissolved. In the larger grain size samples, particularly Item 3 (1000 µm sub-sample), many mineral grains are attached, wrapped and partially encapsulated by a clear to translucent membrane. These agglomerated pieces are also attached to fibrous material that may be aircraft debris. The membrane in which the grains are fixed appears to be organic.

Fragments with metallic lustre and composed of plastic/polycarbonate of the same size as the mineral grains were also present. These had been variously torn, broken and twisted. The plastic/polycarbonate has low density (low specific gravity). These are believed to be pieces of aircraft, trapped within the large debris pieces. The colour and shape of these appear to be the same as the honeycomb structures that are present within the debris structure. The presence of these pieces, having been transported within the aircraft debris, suggests that sediment may also be transported from outside the locations at which the aircraft debris was found. Because of their similar geological composition, sediment from the Comoros Islands, Madagascar, and the Mascarene Islands could be present as part of the sediment recovered from the aircraft debris pieces. However, the weight of evidence suggests that the sediment recovered is derived from locations proximal to the recovery locations of the aircraft pieces.

2.3.4 Conclusion

There is insufficient evidence to identify a specific source for the sediment recovered from the two aircraft pieces. However, the Mozambique coast is logically the strongest candidate as the source of sediment in both cases. This is because the sediment petrology indicates a similarity between mineral grains in the recovered sediment, and the coastal sediment transported by large rivers from the Karoo Flood Basalts and

older igneous rock inland in Mozambique and South Africa. However, similar igneous rock is also present on La Reunion, the Comoros Islands, and Mauritius.

The evidence from biogenic carbonate is largely inconclusive, except that fragments of agglutinated benthic foraminifera (*Textularia hauerii)* were identified in the sediment from each piece of aircraft debris, with ilmenite grains embedded in the foram body wall. This association of ilmenite grains and agglutinated foraminifera is only known from one location, the Bazaruto Archipelago, on the southern Mozambique coast. Inland of Bazaruto Archipelago, an ilmenite placer deposit is present in surficial Cenozoic sediment, so it is likely these grains are locally derived at the site where the debris was recovered.

2.4 Item 4

2.4.1 Geological Context: Mossel Bay, South Africa

Mossel Bay is located near the eastern margin of the Southern Coastal Plain, South Africa (Cawthra, 2014; Cawthra et al., 2016). The coastal plain is relatively low-relief, bordered at its landward limit by the Cape Fold Belt (Locke, 1978), and at the seaward margin by the Indian Ocean. The coastal sediments along the Southern Coastal Plain are predominantly derived from the Cape Fold Belt mixed with marine carbonate and related cement formed at the coast during the Quaternary. Further landward of the Cape Fold Belt is the expansive Karoo Basin, where several of the large rivers that discharge to the Indian Ocean have their headwaters. Thus, the mineralogy of coastal sediments at Mossel Bay would potentially be similar to the coastal sediment of the southern Mozambique regions because they are ultimately sourced from very similar geology.

2.4.2 Sediment Analysis Results

The sediment in the sample from Item 4 is dominated by clear monocrystalline grains, most likely quartz, with some rounded yellowed grains, minor counts of foraminifera and a moderate proportion of multi-crystalline grains that are dominated by quartz. Shell and other bioclastic carbonate pieces were not common, except as broken, rounded grains that were commonly yellow (i.e. discoloured). In white light (i.e. normal daylight) the sample appears slightly yellow-brown. Under the microscope it is evident that because of the transparency of the clear grains the yellow colour of older and discoloured grains dominates the gross colour of the sample. This is similar to the samples from Mozambique.

2.4.3 Discussion

The angularity of sediment grains is very similar to those from the Mozambique coast, and the general composition (quartz rich with minor heavy minerals and low proportions of bioclastic carbonate) is also similar. The very low carbonate (i.e. lack of shelly sediment) is consistent with the general setting of Mossel Bay, and the position at which the aircraft piece was recovered (close to a river). Based on the composition and angularity of grains, this sediment sample resembles most closely the foreshore sample at the same location described by Cawthra (2014).

2.4.4 Conclusion

The sample of sediment from Mossel Bay is composed of very similar minerals and grains to that described in Cawthra (2014), a thesis describing the sediments, sedimentology and marine geology of Mossel Bay, South Africa. There is no evidence for any material from outside this location being present.

2.5 Item 5

2.5.1 Geological Context: Rodrigues Island

Rodrigues Island is the most isolated and easterly island of the Mascarene Island Group, which includes Mauritius and Reunion islands some 600 and 800 km to the east and southeast, respectively (Figure 3) (O'Leary and Perry, 2010). Rodrigues Island is a volcanic pedestal platform, with approximately 110 km^2 of land and a 240 km^2, 8 km wide lagoon. Lagoon water depths are typically less than 3 m and the lagoon is fringed by a near-continuous, 0.5-0.75 km wide, 90 km long barrier reef (O'Leary and Perry, 2010).

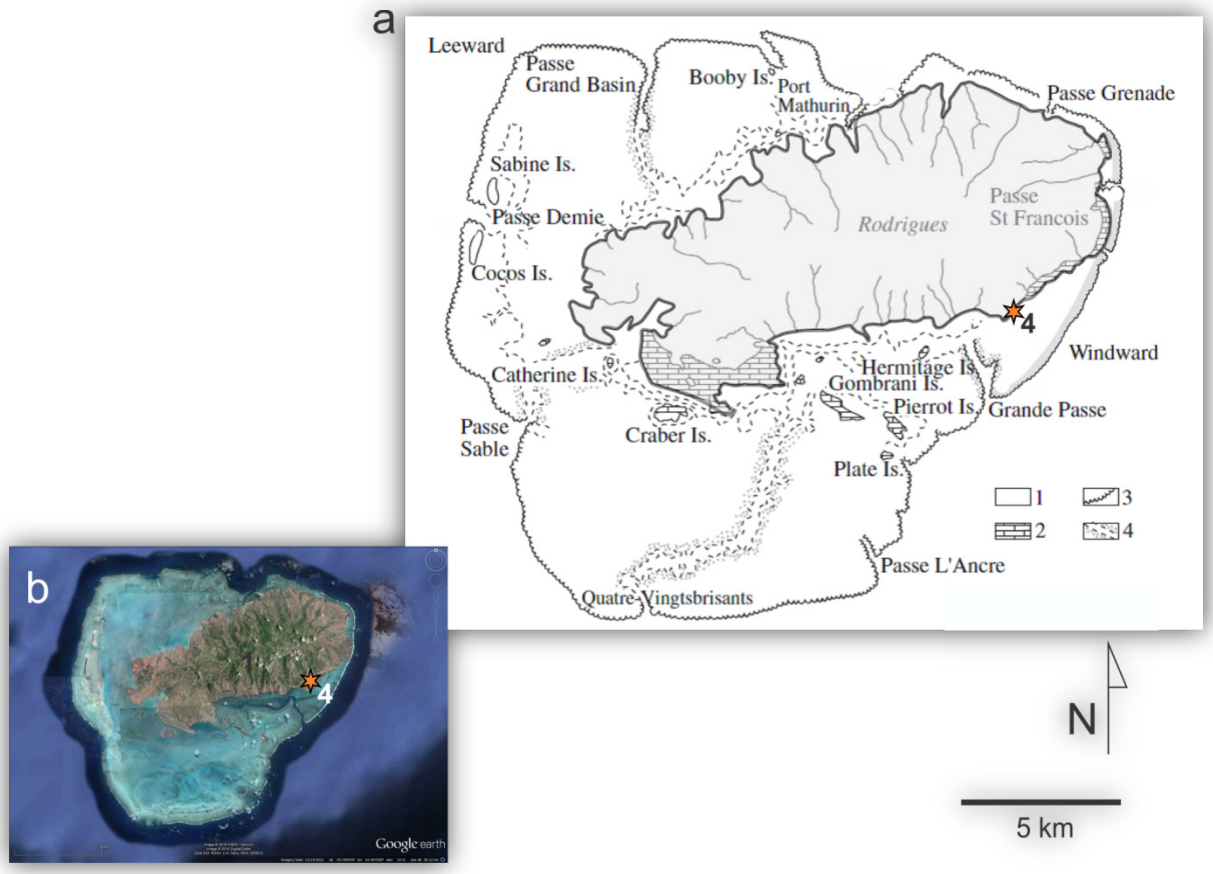

Figure 3. a) Map of Rodrigues Island, adapted from Rees et al., 2005, and b) Google Earth image of same. Location of debris (Item 5) is on the windward side of the island is shown.

Currents in the lagoon are wind-driven, flowing in a general clockwise direction (i.e. westerly to northwesterly) (O'Leary and Perry, 2010). At Port Mathurin, on the northern coast close to the reef margin, tidal amplitudes are up to 1.5 m, while at Mourouk, close to where the piece of debris was recovered, tidal amplitudes are broadly similar to Port Mathurin (Lowry, et al., 2008). Regionally, the South Equatorial Counter Current (SECC) flows east to west across the Mascarene plateau (Vianello, 2015; Badal et al., 2009; New et al., 2005). The southeast trade winds occur between June and October, and typically have accompanying swells of up to 2 m in amplitude (Naim et al., 2000, in Reese et al., 2004). For the rest of the year, winds are generally lighter, and produce swells less than 0.5 m amplitude. On nearby Mauritius, climate can be broadly divided into two seasons. These are the southeast lesser monsoon season, occurring between late June and late October, as on Rodrigues, and the northwest monsoon and cyclone season that extends from early December to May (Senapathi et al., 2010). Thus, because of their proximity, it would be

expected that Rodrigues Island also experiences a northwest monsoon and cyclone season during approximately the same season as Mauritius.

Large amplitude internal waves may be generated around the Mascarene Plateau (Lowry et al., 2008). Rodrigues Island is also affected by long wavelength swells from the southern ocean. Though the island is largely composed of basaltic rock, large areas of the southern and eastern coasts are covered with aeolian calcarenite, and these locations have many features typical of karst environments (Rees, et al., 2005; Burney et al., 2015).

2.5.2 Sediment Analysis Results

Approximately 60% of the sediment sample from Item 5 is composed of biogenic carbonate material, and most of this was broken and degraded. Most of the remainder consisted of sand-sized pieces of crystalline rock, commonly dark in colour and rounded, or sand-sized rock particles composed of a large proportion of variably rounded quartz-like minerals. This latter material is most likely to be aeolianite – a type of rock composed of carbonate cement and wind-blown sand grains. Of the biogenic components, only small barnacles were complete, unbroken, unaltered and intact.

Several grains were analysed to determine whether they are glass (i.e. man-made) or natural minerals. The results indicate all are natural, and all would potentially be associated with basalt or basalt-related igneous processes. In particular, the glass-like mineral grains were identified by the SEM-EDS analyser as zeolite – a chemical alteration mineral commonly formed by the interaction of basaltic minerals with seawater and/or groundwater (Figure 4).

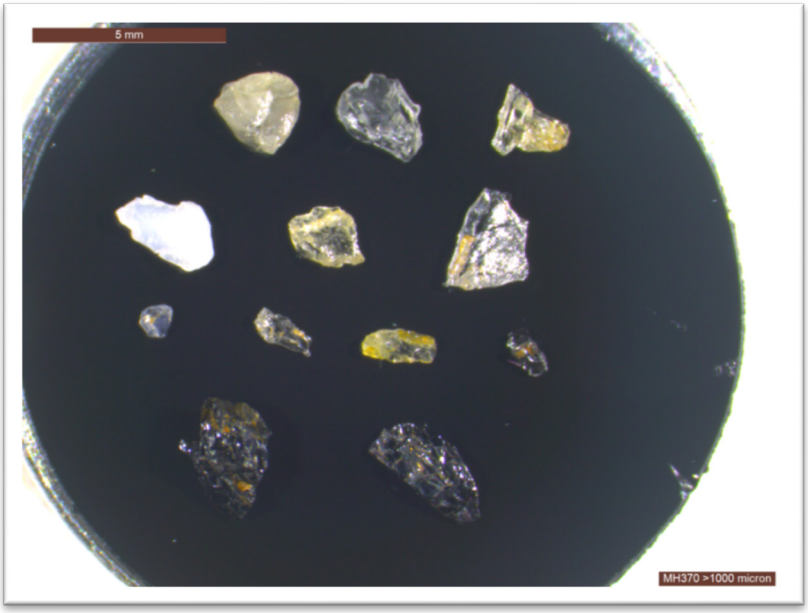

Figure 4. Photograph of mineral grains examined by SEM-EDS from the >1000 µm fraction from Item 5, Rodrigues Island.

2.5.3 Discussion

All the observed mineral grains and fine-grained pieces of rock (sand-sized sediment) are what would be expected at this location. No detailed sedimentological information was found in a literature search that would enable a direct comparison with the sediment sample examined.

2.5.4 Conclusions

The minerals and rock fragments in sediment from Item 5 are consistent with a source from Rodrigues Island. There are no minerals or biological material in the sample to indicate any other source of sediment.

2.6 References

Armitage, S. J., Botha, G. A., Duller, G. A. T., Wintle, A. G., Rebêlo, L. P., Momade, F. J. 2006. The formation and evolution of the barrier islands of Inhaca and Bazaruto, Mozambique. Geomorphology, 82, 295-308.

Armitage, S. J. 2003. Testing and application of luminsescence techniques using sediment fromthe southeast African coast. PhD Thesis, University of Aberystwyth. 307 pp.

Avis, T., Martin, T., Massingue, A. Buque, L. 2015. Nhangonzo coastal stream critical habitat biodiversity assessment: vegetation and floristic baseline survey. Sasol PSA development and LPG project, Inhambane province, Mozambique. Report No. 1521646-13550-24, EOH Coastal and Environmental Services. 57 pp.

Badal, M. R., Rughoopupth, S. D. D. V., Rydberg, L., Robinson, I. S., Patiaratchi, C. 2009. Eddy formation around south west Mascarene Plateau (Indian Ocean) as evidenced by satellite 'global ocean colour' data. Western Indian Ocean Journal of Marine Science, 8**,** 139-145.

Botha, G. A., Bristow, C. S., Porat, N., Duller, G., Armitage, S. J., Roberts, H. M., Clarke, B. M., Kota, M. W., Schoeman, P. 2003. Evidence for dune reactivation from GPR profiles on the Maputaland coastal plain, South Africa. In: Bristow, C. S. and Jol, H. M. (eds): Ground penetrating radar in sediments. Geological Society, London, Special Publications, 211, 29-46.

Burney, D. A., Hume, J. P., Middleton, G. J., Steel, L., Burney, L. P., Porch, N. 2015. Stratigraphy and chronology of karst features on Rodrigues Island, southwestern Indian Ocean. Journal of Cave and Karst Studies, 77**,** 37-51.

Cawthra, H. C. 2014. The Marine Geology of Mossel Bay, South Africa. PhD Thesis, University of Cape Town. 256 pp.

Cawthra, H. C., Compton, J. S., Fisher, E. C., MacHutchon, M. R., Marean, W. C. 2016. Submerged shorelines and landscape features offshore of Mossel Bay, South Africa. In: Harff, J., Bailey, G. & Luth, F. (eds.) Geology and Archaeology: submerged landscapes of the continental shelf. London: Geological Society.

Garzanti, E., Padoan, M., Setti, M., Lopez-Galindo, A., Villa, I. M. 2014. Provenance versus weathering control on the composition of tropical river mud (southern Africa). Chemical Geology, 366, 61-74.

Green, A. 2009. Sediment dynamics on the narrow, canyon-incised and current-swept shelf of the northern KwaZulu-Natal continental shelf, South Africa. Geo-Marine Letters, 29**,** 201-219.

Haines, J. & Mazzullo, J. 1988. The original shapes of quartz silt grains: a test of the validity of the use of quartz grain shape analysis to determine the sources of terrigenous silt in marine sedimentary deposits. Marine Geology, 78**,** 227-240.

Locke, B. E. 1978. The Cape Fold Belt of South Africa: tectonic control of sedimentation. Proceedings of the Geological Association, 89**,** 263-281.

Lowry, R., Pugh, D. T. & Wijeratne, E. M. S. 2008. Observations of seiching and tides around the islands of Mauritius and Rodrigues. Western Indian Ocean Journal of Marine Science, 7**,** 15-28.

Makled, W. A. & Langer, M. R. 2010. Preferential selection of titanium-bearing minerals in agglutinated Foraminifera: Ilmenite (FeTiO3) in Textularia hauerii d'Orbigny from the Bazaruto Archipelago, Mozambique. Revue de micropaleontologie, 53**,** 163-173.

Manninen, T., Eerola, T., Mäkitie, H., Vuori, S., Luttinen, A., Sénvano, A., Manhiça, V. 2008. The Karoo volcanic rocks and related intrusions in southern and central Mozambique. Geological Survey of Finland Special Paper 48, 211-250.

New, A. L., Stansfield, K., Smythe-Wright, D., Smeed, D. A., Evans, A. J., Alderson, S. G. 2005. Physical and biochemical aspects of the flow across the Mascarene Plateau in the Indian Ocean. Philosophical Transactions of The Royal Society A: Mathematical, Physical & Engineering Sciences, 363**,** 151-168.

O'Leary, M. J., Perry, C. T. 2010. Holocene reef accretion on the Rodrigues carbonate platform: an alternative to the classic "bucket-fill" model. Geology, 38**,** 855-858.

Parker, J. H. & Gischler, E. 2011. Modern foraminiferal distribution and diversity in two atolls from the Maldives, Indian Ocean. Marine Micropaleontology, 78**,** 30-49.

Peche, M. 2012. Geology of the KaNyaka barrier island system, Maputo Bay, Mozambique. MSc Thesis, Univeristy of Johannesburg. 247 pp.

Perry, C. T. 2005. Structure and development of detritial reef deposits in turbid nearshore environments, Inhaca Island, Mozambique. Marine Geology, 214**,** 143-161.

Perry, C. T., Beavington-Penney, S. J. 2005. Epiphytic calcium carbonate production and facies development within sub-tropical seagrass beds, Inhaca Island, Mozambique. Sedimentary Geology, 174**,** 161-176.

Rees, S. A., Opdyke, B. N., Wilson, P. A., Fifield, L. K. 2005. Coral reef sedimentation on Rodrigues and the Western Indian Ocean and its impact on the carbon cycle. Philosophical Transactions of The Royal Society A: Mathematical, Physical & Engineering Sciences, 363**,** 101-120.

Riffel, S. B., Vasconcelos, P. M., Carmo, I. O., Farley, K. A. 2016. Goethite (U-Th)/He geochronology and precipitation mechanisms during weathering of basalts. Chemical Geology, doi:10.1016/j.chemgeo.2016.03.033

RioTinto.com http://www.riotinto.com/documents/ReportsPublications/Titanium_mineral_sands_exploration_target_in_Mozambique.pdf (last accessed 14 April 2016)

Rutten, R., Mäkitie, H., Vuori, S., Marques, J. M. 2008. Sedimentary rocks of the Mapai Formation in the Massingir-Mapai region, Gaza Province, Mozambique. Geological Survey of Finland Special Paper 48, 251-262.

Schultz, H., Lückge, A., Emeis, K-C., Mackensen, A. 2011. Variability of Holocene to Late Pleistocene Zambezi riverine sedimentation at the upper continental slope off Mozambique, 15°-21° S. Marine Geology, 286, 21-34.

Senapathi, D., Underwood, F., Black, E., Nicoll, M. A. C., Norris, K. 2010. Evidence for long-term regional changes in precipitation on the East Coast Mountains in Mauritius. International Journal of Climatology, 30**,** 1164-1177.

Vianello, P. 2015. A Qualitative and physical analysis of processes around the Mascarene Plateau. Doctor of Philosophy, University of Cape Town, South Africa.

Von Gruenewaldt, G., Sharpe, M. R., Hatton, C. J. 1985. The Bushveld Complex: introduction and review. Economic Geology, 80, 803-812.

Wechsler, B. A., Prewitt, C. T. 1984. Crystal structure of ilmenite ($FeTiO_3$) at high temperature and high pressure. American Mineralogist, 69, 176-185.

Wright, C. I., Miller, W. R., Cooper, J. A. G. 2000. The late Cenozoic evolution of coastal water bodies in Northern Kwazulu-Natal, South Africa. Marine Geology, 167, 207-229.

Page 1227 of 1738

3 Review of Macrofauna on Pieces from Mozambique (Item 2 and 3)

3.1 Summary

This report provides a brief review of the macrofauna found on the aircraft pieces from Mozambique, Daghatane Beach (Item 2) and Mozambique Channel (Item 3). For consistency, the two pieces are labelled Right wing No. 7 flap track fairing (Item 2) and Right horizontal stabilizer panel piece (Item 3). This report includes evaluation of external macrofauna collected off the pieces as well as the sieved fractions.

- Items 2 and 3 had evidence of barnacle peduncle attachment and other areas of sessile species attachment. Based on the visual similarities of the barnacle peduncle attachment, and from the samples from the peduncle attachment on the door R1 Stowage closet (Item 5), many samples that were collected from Items 2 and 3, could possibly be from barnacle pedunculated cement. The interior honeycomb of Item 2 was heavily colonised by encrusting bryozoans (*Jellyella tuberculata*).
- Identified mollusc species on Item 3 suggest that the item originated from, or picked up, macrofauna from the tropical Indo-Pacific Ocean. Most mollusc specimens found were recently dead or long-dead and possibly lodged into the item at the location where the item was found. Based on the species assemblage, the only taxon that could be significant in determining the oceanic waters that the aircraft piece had been in was *Petaloconchus renisectus*. This specimen is estimated to be 8-12 months old and has a distribution that spans the tropical Indo-Pacific Ocean.
- From the species assemblage recovered and identified, there is no evidence of any cool- or cold-temperate mollusc or annelid in these samples that might suggest the aircraft pieces had been in the cold waters of the Southern Indian Ocean.
- One third of the identified molluscs on Item 3 are sufficiently opportunistic to grow on floating debris, and represent juveniles at approximately two months old.

Caveats: The aircraft pieces were retained over lengthy time frames (months), and under conditions that may not be conducive for faunal preservation. Therefore, some criteria were applied to the acceptance of samples analysed, these include:

- Any macrofauna within voids that could not be accessed without destructively breaking apart the pieces was not sampled
- Broken shells were not identified (only whole shells were identified)
- Any animals < 100 µm were not analysed
- Conclusions were based on the macrofauna found on the pieces

3.2 Method

1. The two pieces of aircraft were received on the 21st March 2016 and stored in Geoscience Australia Quarantine Approved Premises.
2. The pieces were visually examined for any obvious macrofauna then photographed with an SLR Canon 60D with a macrolens (EF 100mm).
3. Items were removed or scraped off and any biota collected was preserved in 75% ethanol.
4. The pieces were then washed and agitated in water to ensure any animals within cavities were flushed out. The resultant water was then passed through 3 sieves of sizes 100 µm, 500 µm and 1000 µm to ensure no spillage occurred in case of any obstruction. All material on each sieve was then carefully washed into a petri dish and then sorted under a microscope for any biological material. Any biota was then photographed with a Leica IC80 HD camera.
5. All waste material and liquids were disposed of via irradiation or a quarantine approved procedure.
6. Expert taxonomists from Australia were contacted via email and phone to ascertain species present in the images, including:
    a. Dr Diana Jones for barnacles /other species (Western Australian Museum)
    b. Dr Richard Willan for molluscs (Museum and Art Gallery of the Northern Territory; MAGNT)
    c. Dr Chris Glasby for worms (MAGNT) and Dr Elena Kupriyanova (Australian Museum), Dr Katherine Yoo for photography of specimens (MAGNT), and Mr Neil Wright for assistance with post-production of images (MAGNT).
    d. Dr Robyn Cumming and Dr Dennis Gordon for bryozoans (Museum of Tropical Queensland)

3.3 Results

3.3.1 Item 2: Recovered From Daghatane Beach, Mozambique

There was not a large amount of fauna found within the sieved fractions or attached to the surface of Item 2. However, evidence of barnacle peduncle and other sessile species attachment was clear on the bottom of the external rounded section (Figure 1). Based on the visual similarities of the barnacle peduncle attachment and physical evidence from the samples on the internal partition (Item 5) of the peduncle attachment, many samples collected on Item 2 and 3, are possibly barnacle pedunculated cement (Jones 2016; pers. obs; Table 1).At the time of writing this report, the species of barnacles could not be determined.

Crustacea:

One small juvenile barnacle (*Lepas anatifa anatifera*) was found within the sieved fractions attached to possible peduncle material (Table 1). *L. anatifera* is a species that commonly settles on floating animate or inanimate items in open water. It is a neustonic species (floating organism), which means

that only surface temperatures would need to be used to evaluate possible ages. *L. anatifera* has a cosmopolitan geographical range across the open water.

Mollusc:

One juvenile molluscan taxon was identified from Item 2; Mollusca: Bivalvia: Pteriidae: *Pinctada radiata* (Table 1 & 3). This mollusc is also known as the Atlantic pearl-oyster and is generally found throughout the Indo-Pacific at all depths but more commonly between 5-25 m. This species is also opportunistic and settles from plankton to grow on floating objects but detaches and falls off with age. This species is tolerant of a wide temperature range (13-30°C).

Bryozoa:

Bryozoa species found encrusting internal exposed honeycomb material are possibly colonies of *Jellyella tuberculate* (Table 1). This is a species that commonly settles on pumice, plastics and other floating substrata. It has been referred to as a 'pseudoplanktonic species'. These are small colonies that would achieve their size in a matter of weeks so it is difficult to ascertain how long the floating components were on the sea floor or at the sea surface based on bryozoan size alone (Gordon, 2016) (Table 1).

Figure1 – Overview images of Item 2 (Right wing No. 7 flap track fairing); a) the external side of Item 2; b) internal side of Item 2; c) close up of bottom external side of Item 2; d) close up of possible remnants of barnacle cement.

Table 1: Images of species identified from Item 2 (Right Wing No. 7 Flap Track Fairing) originating from Mozambique.

Species	Image
Mollusca: Bivalvia: Pteriidae: *Pinctada radiata*	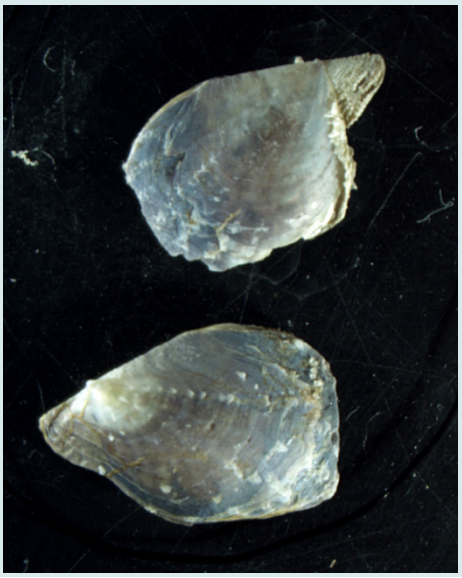
Crustacea: Cirripedia: Lepadidae: *Lepas Anatifa anatifera*	
Bryozoa: Gymnolaemata: Cheilostomata: Menbraniporidae: *Jellyella tuberculate* On Item 2 (left) and 3 (right) image	

Images of likely peduncle attachment images sent to Diana Jones (WA Museum) for analysis	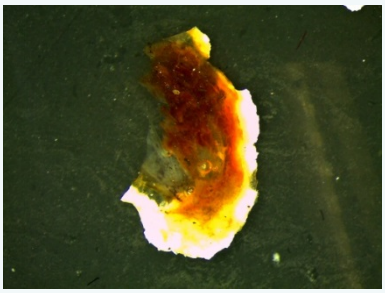 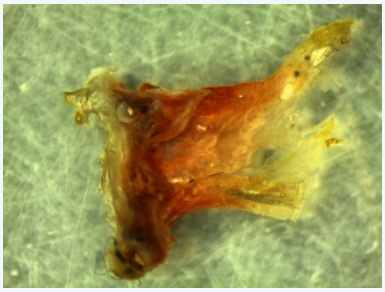 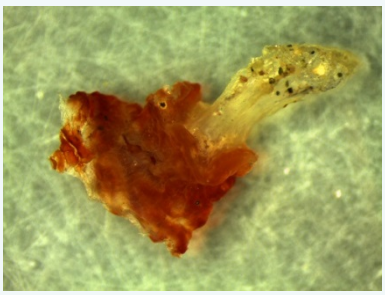

3.3.2 Item 3 (Right Horizontal Stabilizer Panel): Recovered From a Beach in the Mozambique Channel

Item 3 had evidence of attached and unattached macrofauna within the sieved sections, and similar to Item 2, had evidence of barnacle peduncle and other sessile species attachment on the external facing section of the piece (Figure 2).

Molluscs and Annelids:

A total of 20 taxa (18 mollusc species and 2 annelid species) were identified from the sieved fractions, or attached on the surface of the aircraft piece. The majority of taxa (17 mollusc and 2 annelid species) were identified from Item 3.

Judging by its size and hence age, and by tendency to attach to floating objects, the only taxon that could be of possible significance in determining the oceanic waters that the aircraft piece had been in

is *Petaloconchus renisectus* (Table 2 & 3). This mollusc from the family Vermetidae is estimated to be 8–12 months old and is a species whose distribution encompasses the tropical Indo-Pacific Ocean. It is believed to have been living attached to the aircraft part prior to beaching at the discovery site because it has remnants of encrusting bryozoans on the under-surface consistent with those fouling the aircraft debris. Being a tropical species, it provides the only macrofaunal evidence that the debris had been in tropical waters at some early stage in its drift.

From the species identified on Item 3, there is no evidence of any cool- or cold-temperate mollusc or annelid that might suggest the aircraft debris had been in the cold waters of the Southern Indian Ocean. However, this does not rule out the possibility that the pieces did not travel through the Southern Indian Ocean, only that no species were retained on the piece after collection from Mozambique.

About two-thirds of the molluscs recovered from Items 2 and 3 must have been lodged onto the aircraft part(s) by waves when /they drifted ashore or were cast up on the beach(es) or by accidental human contamination [as in dragging the wreckage across the beach during its recovery]. Any handful of sediment, even a small one, from a tropical locality in the Indian Ocean would contain a very high diversity [hundreds] of dead shells of such species.. The natural habitat of the recovered molluscs is shallow water, on clean coral sand or in seagrass meadows. None of them could or would ever attach to drifting debris. These species are *Donax* cf. *nitidus, Ervilia* cf. *scaliola*, *Voorwindia* cf. *tiberiana*, *Nucinella* sp. 1, *Antosolarium* sp. 1, *Smaragdia souverbiana*, *Sigatica* sp. 1, *Hypermastus* sp. 1, *Pleuromeris* sp. 1 and *Spectamen* sp. 1 (Table 2 & 3) (Willan and Glasby, 2016).

About one-third of the molluscs and both the species of annelids in these samples are sufficiently opportunistic to settle out from the plankton and grow amongst fouling communities on floating objects. Some of them – the micromolluscs and *Neodexiospira* annelids – could grow to maturity (in six months or less) and reproduce on these floating objects. All of these species are only represented as juveniles in these samples, so they are assumed to be less than two months old. These species are *Cyclostrema* cf. *placens*, *Nozeba* sp. 1, *Iravadia* sp. 1, *Iravadia* sp. 2, *Diala semistriata*, "*Serpula* sp. 1" and *Neodexiospira* sp. 1. Again, partitioning these species into the opportunistic category does not negate their accidental lodgement onto the aircraft part(s) when it/they drifted ashore or were cast up on the beach(es) (Table 2 & 3) (Willan and Glasby, 2016).

One annelid tube from Item 3 belongs to a species of the genus *Vermiliopsis* (Saint-Joseph, 1894). The genus has a world-wide distribution and is found from subtidal to bathyal depths, mostly in tropical and subtropical areas, but this is typical for serpulid polychaetes in general. Species within the genus Vermiliopsis are morphologically recognised mainly based on the structure on the operculum (the specialised tube plugs). Thus, the animal, not just an empty tube is needed for positive identification. The tube, however, with its distinct longitudinal and transverse sculptural elements is quite typical for the genus. It resembles the tubes of species Vermiliopsis monodiscus Zibrowius, 1968 or rather *Vermiliopsis* ex gr *monodiscus* (one of the species from this group). *Vermiliopsis monodiscus* was described from the Mediterranean Sea, but then this identification seems unlikely given the region where the tube was found, so it might belong to one of the Indo-Pacific species.

Reproduction in this genus is also poorly known. Based on scarce egg size data, the larval development in *Vermiliopsis* appears to be lecithotrophic (= larvae rely on yolk provided in the egg at the time of spawning, do not feed independently on unicellular algae suspended in water column). Thus, larval growth is independent of food supply (algae), but the rate of larval growth and maturation mostly depends on water temperature. The sperm structure of *Vermiliopsis* suggests that fertilisation is external and larvae develop in the water column. Larvae have some limited swimming abilities, but mostly are distributed by water currents. Nothing is known about any substrate preferences by settling

larvae of *Vermiliopsis.* Most likely they are capable on settling on any available hard substrate, like many other serpulids. Life span (longevity) depends on body size: small serpulids have shorter life spans that large ones (the largest are estimated to live for 10-12 years). For a serpulid that inhabited the examined tube the life span is likely to be 2-3 years and the age of the animal is likely 6-8 months.

Crustacea:

One barnacle was found (*Lepas anatifa anatifera*) in the sieved sections. *L. anatifera* is a species that commonly settles on floating animate or inanimate items in open water. It is a neustonic species, which means that only surface temperatures would need to be used to evaluate possible ages. *L. anatifera* has a cosmopolitan geographical range across the open water (Table 2) (Jones, 2016).

Bryozoa:

Bryozoa species found encrusting on internal exposed honeycomb material are possibly colonies of *Jellyella tuberculata*. This is a species that commonly settles on pumice, plastics and other floating materials. It has even been dubbed a 'pseudoplanktonic species'. These are small colonies that would achieve their size in a matter of weeks so it is difficult to ascertain how long the floating components were on the sea floor or at the sea surface based on bryozoan size alone (Gordon, 2016) (Table 2).

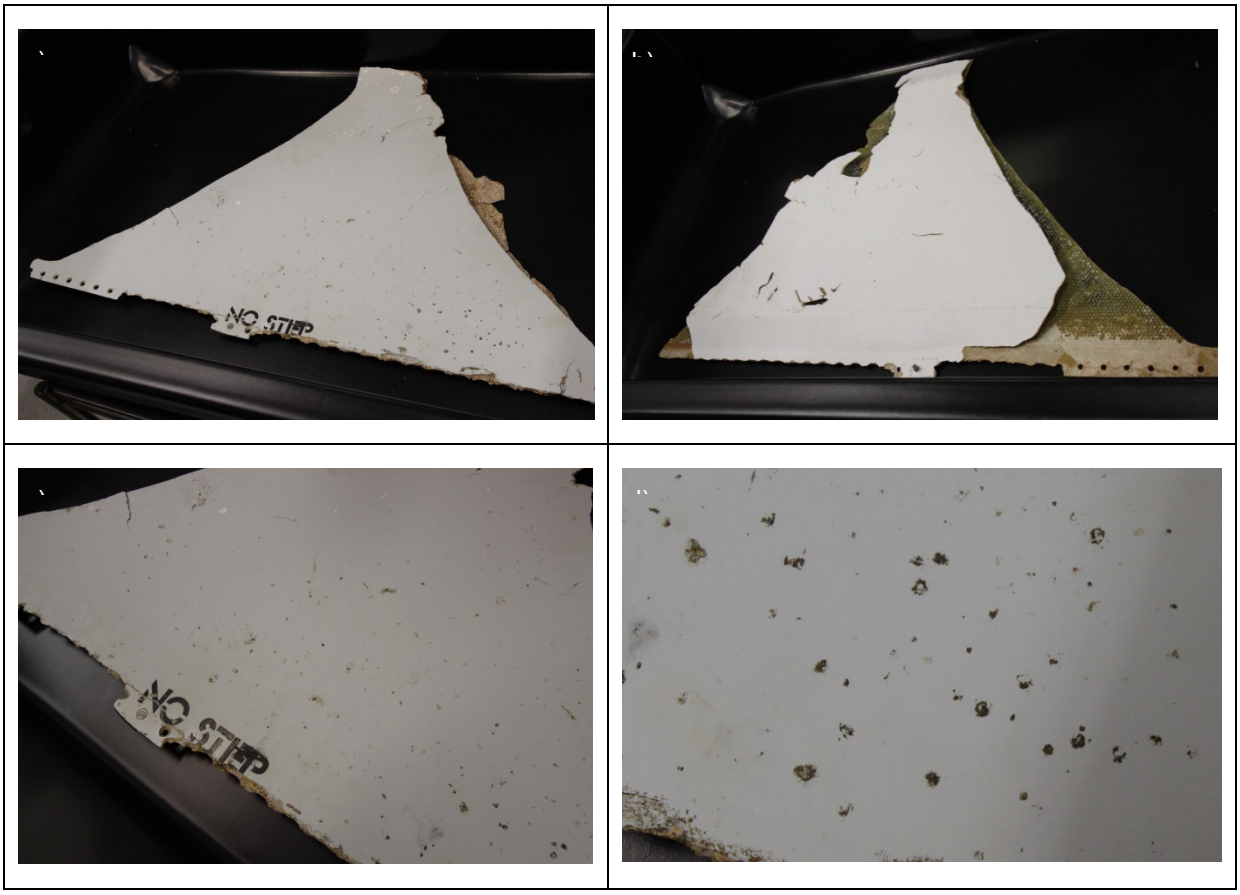

Figure 2 – Overview images of Item 3 (Right horizontal stabiliser panel piece)); a) the external side of Item 3 indicating evidence of cementing structures; b) internal side of Item 3; c) close up of bottom external side of item 3; d) close up of possible remnants of barnacle cement.

Table 2: Images of species identified from Item 2 and 3 originating from Mozambique. Images are sourced from Drs Richard Willan and Katherine Yoo, and Neil Wright from the Museum and Art Gallery of the Northern Territory.

Species	Image
Mollusca: Bivalvia: Donacidae: *Donax* cf. *nitidus*	
Mollusca: Gastropoda: Vermetidae: *Petaloconchus renisectus*	
Mollusca: Gastropoda: Liotiidae: *Cyclostrema* cf. *placens*	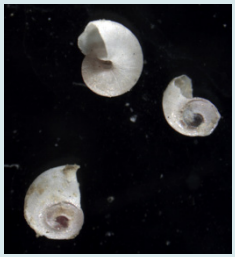
Mollusca: Bivalvia: Semelidae: *Ervilia* cf. *scaliola* Found: HSP	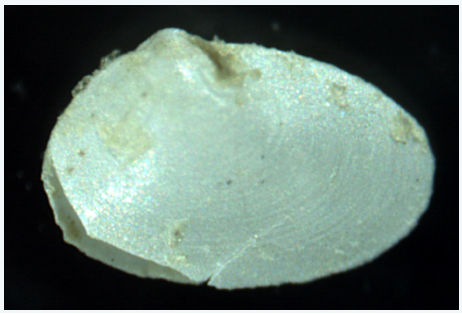
Mollusca: Gastropoda: Rissoidae: *Voorwindia* cf. *tiberiana* Found: HSP	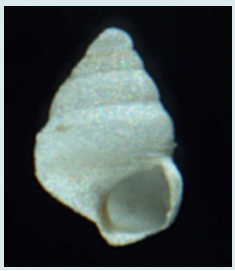

Mollusca: Gastropoda: Iravadiidae: *Nozeba* sp. 1	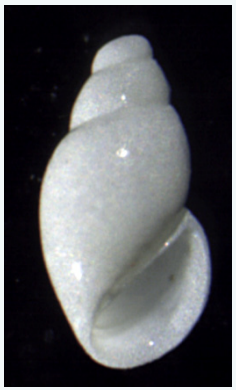
Mollusca: Bivalvia: Nucinellidae: *Nucinella* sp. 1	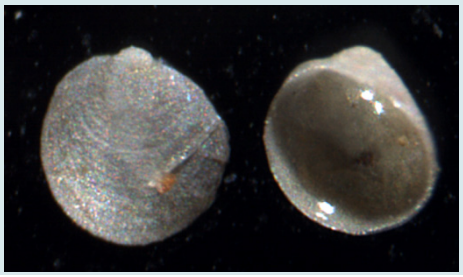
Mollusca: Gastropoda: Trochidae: *Antisolarium* sp. 1	
Annelida: Polychaeta: Serpulidae: *Neodexiospira* sp. 1	
Mollusca: Gastropoda: Iravadiidae: *Iravadia* sp. 2	
Mollusca: Bivalvia: Semelidae: *Ervilia* cf. *scaliola*	

Mollusca: Gastropoda: Iravadiidae: *Iravadia* sp. 1	
Mollusca: Gastropoda: Dialidae: *Diala semistriata*	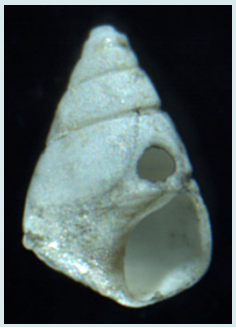
Mollusca: Gastropoda: Liotiidae: *Cyclostrema* cf. *placens*	
Mollusca: Bivalvia: Donacidae: *Donax* cf. *nitidus*	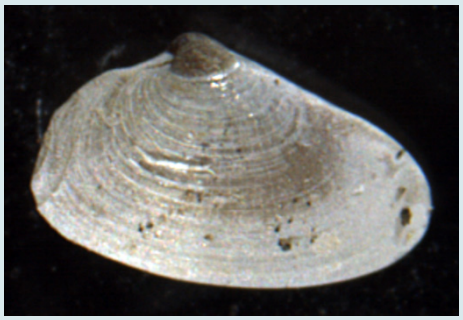
Mollusca: Gastropoda: Haminoeidae: *Haminoea* sp. 1	

Mollusca: Gastropoda: Neritidae: *Smaragdia souverbiana*	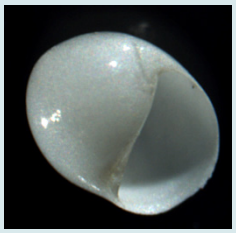
Mollusca: Gastropoda: Naticidae: *Sigatica* sp. 1	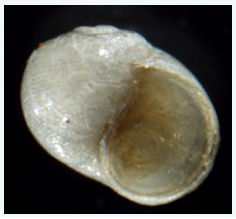
Mollusca: Gastropoda: Eulimidae: *Hypermastus* sp. 1	
Annelida: Polychaeta: Serpulidae: *Neodexiospira* sp. 1	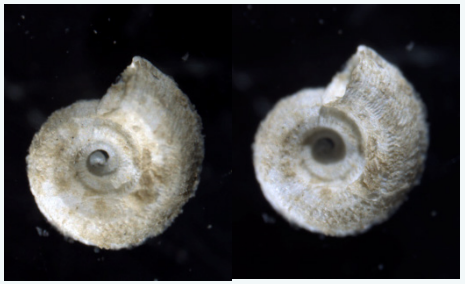
Mollusca: Bivalvia: Carditidae: *Pleuromeris* sp. 1	
Mollusca: Gastropoda: Solariellidae: *Spectamen* sp. 1	

Mollusca: Gastropoda: Dialidae: *Diala semistriata*	
Crustacea: Cirripedia: Lepadidae: *Lepas Anatifa anatifera*	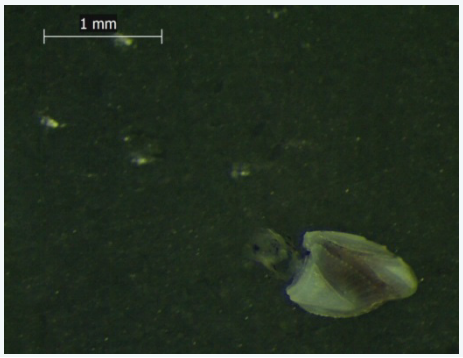
Bryozoa: Gymnolaemata: Cheilostomata: Menbraniporidae: *Jellyella tuberculate*	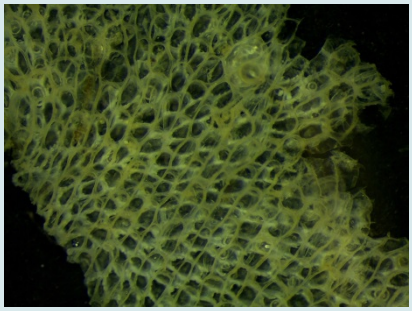 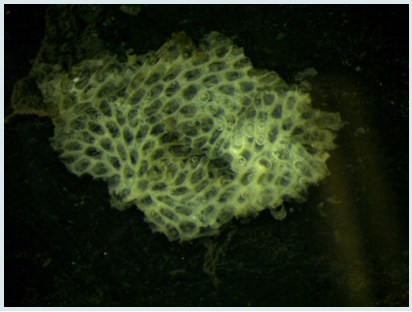
Annelida: Polychaeta: Sabellida: Serpulidae: *Vermiliopsis* cf. *monodiscus*	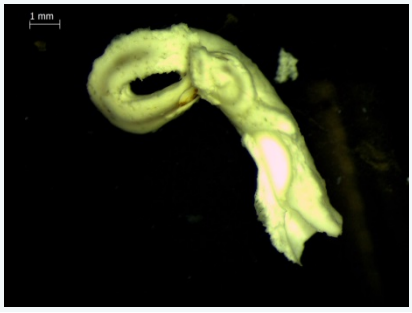

Table 3 Identified mollusc and annelid species from Item 1 and Item 2.

Sample ID	Part	Identification	Comment	Significance for determining crash site	Habitat
HSP01	Horizontal Stabilizer Panel	Mollusca: Bivalvia: Donacidae: Donax cf. nitidus	One half valve from adult individual; long dead.	None	Tropical Indian Ocean. Shallow water, in clean coral sand or seagrass meadows
HSP02	Horizontal Stabilizer Panel	Mollusca: Gastropoda: Vermetidae: Petaloconchus renisectus	One adult or near-adult individual; freshly dead	Possible	Tropical Indo-Pacific Ocean. Shallow water, permanently attached to corals and rocks. Occasionally also grows on floating structures.
HSP03	Horizontal Stabilizer Panel	Annelida: Polychaeta: Serpulidae: "Vermiliopsis cf. monodiscus"	Specimen sent for precise determination and further comment to Elena Kupriyanova	Possible	Possible Indo-Pacific species, generally described from Mediterranean Sea. Generally found subtidal to bathyal depths, mostly in tropical and subtropical areas.
HSP100um 01	Horizontal Stabilizer Panel	Mollusca: Gastropoda: Liotiidae: Cyclostrema cf. placens	Three adult shells, all juveniles; freshly dead.	None	Tropical Indian Ocean. Shallow water, in clean coral sand or seagrass meadows.
HSP100um 02	Horizontal Stabilizer Panel	Mollusca: Bivalvia: Semelidae: Ervilia cf. scaliola	One half valve form adult individual; long dead.	None	Tropical Indian Ocean. Intertidal and shallow subtidal, on clean coral sand or seagrass meadows.
HSP100um 03	Horizontal Stabilizer Panel	Mollusca: Gastropoda: Liotiidae: Cyclostrema cf. placens	One subadult individual; long dead.	None	Tropical Indian Ocean. Intertidal and shallow subtidal, on clean coral sand or seagrass meadows.
HSP100um 04	Horizontal Stabilizer Panel	Mollusca: Gastropoda: Rissoidae: Voorwindia cf. tiberiana	One juvenile individual; freshly dead.	None	Tropical Indian Ocean. Intertidal and shallow subtidal, on clean sand or seagrass meadows.
HSP100um 05	Horizontal Stabilizer Panel	Mollusca: Gastropoda: Iravadiidae: Nozeba sp. 1	One adult individual; freshly dead.	None	Tropical Indian Ocean. Intertidal and shallow subtidal, on clean coral sand or seagrass meadows.
HSP100um 06	Horizontal Stabilizer Panel	Mollusca: Bivalvia: Nucinellidae: Nucinella sp. 1	One juvenile individual; freshly dead.	None	Tropical Indian Ocean. Intertidal and shallow subtidal, on clean coral sand or seagrass meadows.
HSP500um 01	Horizontal Stabilizer Panel	Mollusca: Gastropoda: Trochidae: Antisolarium sp. 1	One juvenile individual; freshly dead.	None	Tropical Indian Ocean. Intertidal and shallow subtidal, on clean coral sand or seagrass meadows.

Sample ID	Part	Identification	Comment	Significance for determining crash site	Habitat
HSP500um 02	Horizontal Stabilizer Panel	Annelida: Polychaeta: Serpulidae: Neodexiospira sp. 1	One adult individual; freshly dead.	None	Cosmopolitan genus, well represented in tropical Indo-Pacific Ocean. Opportunistic, settling on a multitude of hard substrates.
HSP500um 03	Horizontal Stabilizer Panel	Mollusca: Gastropoda: Iravadiidae: Iravadia sp. 2	One adult individual; freshly dead.	None	Tropical Indian Ocean. Intertidal and shallow subtidal, on clean coral sand or seagrass meadows.
HSP500um 04	Horizontal Stabilizer Panel	Mollusca: Bivalvia: Semelidae: Ervilia cf. scaliola	One juvenile individual; freshly dead.	None	Tropical Indian Ocean. Intertidal and shallow subtidal, on clean coral sand or seagrass meadows.
HSP500um 05	Horizontal Stabilizer Panel	Mollusca: Gastropoda: Iravadiidae: Iravadia sp. 1	One adult individual; freshly dead.	None	Tropical Indian Ocean. Shallow water, in clean coral sand or seagrass meadows.
HSP500um 06	Horizontal Stabilizer Panel	Mollusca: Gastropoda: Dialidae: Diala semistriata	One subadult individual; long dead.	None	Tropical Indo-Pacific Ocean. Shallow water, in clean coral sand or seagrass meadows.
HSP500um_07	Horizontal Stabilizer Panel	Mollusca: Gastropoda: Liotiidae: Cyclostrema cf. placens	One adult individual; freshly dead.	None	Tropical Indian Ocean. Intertidal and shallow subtidal, on clean coral sand or seagrass meadows.
HSP500um_08	Horizontal Stabilizer Panel	Mollusca: Bivalvia: Semelidae: Ervilia cf. scaliola	One juvenile individual; freshly dead.	None	Tropical Indian Ocean. Intertidal and shallow subtidal, on clean coral sand or seagrass meadows.
HSP500um_09	Horizontal Stabilizer Panel	White inorganic particle - probable contaminant		None	Tropical Indian Ocean. Shallow water, in clean coral sand or seagrass meadows
HSP500um_10	Horizontal Stabilizer Panel	Mollusca: Bivalvia: Donacidae: Donax cf. nitidus	One juvenile individual; freshly dead.	None	Tropical Indian Ocean. Shallow water, in clean coral sand or seagrass meadows
HSP500um_11	Horizontal Stabilizer Panel	Mollusca: Gastropoda: Haminoeidae: Haminoea sp. 1	One juvenile individual; freshly dead.	None	Tropical Indian Ocean. Shallow water, amongst fine filamentous algae on clean coral sand or seagrass meadows
HSP500um_12	Horizontal Stabilizer Panel	Mollusca: Gastropoda: Neritidae: Smaragdia souverbiana	One juvenile individual; long dead.	None	Tropical Indian Ocean. Shallow water, in seagrass meadows

Sample ID	Part	Identification	Comment	Significance for determining crash site	Habitat
HSP500um_13	Horizontal Stabilizer Panel	Mollusca: Gastropoda: Naticidae: Sigatica sp. 1	One juvenile individual; live	None	Tropical Indo-Pacific Ocean. Shallow water, in clean coral sand or seagrass meadows
HSP500um_14	Horizontal Stabilizer Panel	Mollusca: Gastropoda: Eulimidae: Hypermastus sp. 1	One juvenile individual; freshly dead.	None	Tropical Indo-Pacific Ocean. Shallow water, in clean coral sand or seagrass meadows
HSP1000um 01	Horizontal Stabilizer Panel	Annelida: Polychaeta: Serpulidae: Neodexiospira sp. 1	One adult individual; freshly dead.	None	Cosmopolitan genus, well represented in tropical Indo-Pacific Ocean. Opportunistic, settling on a multitude of hard substrates.
HSP1000um 02	Horizontal Stabilizer Panel	Mollusca: Bivalvia: Carditidae: Pleuromeris sp. 1	One half valve from adult individual; freshly dead.	None	Tropical Indo-Pacific Ocean. Shallow water, in clean coral sand or seagrass meadows
HSP1000um 03	Horizontal Stabilizer Panel	Mollusca: Gastropoda: Solariellidae: Spectamen sp. 1	One adult individual; freshly dead.	None	Tropical Indian Ocean. Shallow water, in clean coral sand or seagrass meadows
HSP1000um 04	Horizontal Stabilizer Panel	Mollusca: Gastropoda: Dialidae: Diala semistriata	One adult individual; long dead.	None	Tropical Indo-Pacific Ocean. Shallow water, in clean coral sand or seagrass meadows.
CF01	Right Wing No. 7 Flap Track Fairing	Mollusca: Bivalvia: Pteriidae: Pinctada radiata	One juvenile individual; probably live when washed ashore	None	Tropical Indo-Pacific Ocean. Shallow water, permanently attached to corals and rocks. Juveniles occasionally grow on floating structures.

3.4 References

Gordon, D. 2016. Personal communication.

Hove, H.A. ten and Kupriyanova, E. K. 2009. Taxonomy of Serpulidae (Annelida, Polychaeta): the state of affairs. *Zootaxa* 2036: 1-126.

Jones, D.S. 2016. Personal communication.

Kupriyanova, E.K., E. Nishi, H.A. ten Hove, & A.V. Rzhavsky 2001. A review of life history in serpulimorph polychaetes: ecological and evolutionary perspectives. *Oceanography and Marine Biology: an Annual Review* 39:1-101.

Saint-Joseph, A. de 1894. Les annélides polychètes des côtes de Dinard, III. Annales des Sciences naturelles, Paris 17: 1-395.

Zibrowius, H., 1968b. Description de Vermiliopsis monodiscus. n.sp., espece Mediterranene nouvelle de Serpulidae (Polychaeta Sedentaria). *Bulletin du Muséum d'Histoire Naturelle, Marseille* 39: 1202–1210.

Willan, R. and Glasby, C. 2016. Personal communication.

4 Stable Isotope Analyses of Paints on Aircraft Pieces From Mozambique (Items 2 and 3) and Mauritius (Item 5)

4.1 Summary

This report provides the results of stable carbon isotope analysis for the paint samples collected from the three pieces from Mozambique, Daghatane Beach (Item 2), Mozambique Channel (Item 3) and Rodrigues Island, Mauritius (Item 5). This report also includes evaluation of control samples received from the Australian Transport Safety Bureau (ATSB).

- All the samples have similar δ13C values, in the range of -29.5‰ to -30.6‰. The similar carbon isotopic compositions indicate that the paint samples may have come from the same source, and hence, Items 2 and 3 may also be from the same source.
- The decorative panel coating from Item 5 has a δ13C value of -25.84‰, which is very close to the δ13C value of the control sample, which is -25.151‰. The similar carbon isotope values indicate they may have come from the same source.

4.2 Method

Three pieces of debris Items 2 and 3 (from the Mozambique coastline) and Item 5 (from the Rodrigues Island, Mauritius) were supplied to Geoscience Australia Laboratory on the 21st March 2016 and the 14th of April 2016 (respectively) for geochemical analyses.

Stable isotopic analysis was undertaken on samples from all three items and on two ‘control’ samples which were supplied by the ATSB for analytical comparison. The control samples included painted plates and a sample of a new decorative panel.

4.2.1 Sub-Sampling Items 2 and 3

1. Paint samples from Items 2 and 3 were removed for analysis using an unused scalpel, and weighed into 8 capsules for analysis.
2. The prepared samples were loaded into 5 mm tin capsules on a Sartorius MC 5 micro balance using a thin metal spatula.
3. Weights of sample were recorded to ± 1µg.
4. The paint samples were cleaned with mild detergent solution (HAEMO-SOL cleaner, Baltimore, USA) to remove obvious external dirt particles, potential grease and other contaminants, then rinsed well with deionised water and dried at room temperature.

4.2.2 Sub-sampling Item 5 and Control Sample

1. Scissors were used to prepare the following top coating layer samples:
   a. One piece of top coating from the decorative panel of the inner cabin from Item 5.
   b. One piece of Tedlar Polyvinyl fluoride (PVF) was collected from Item 5.
   c. One piece of top coating from the decorative panel of the inner cabin from the control sample. The top coating was peeled off after immersing the part in dichloromethane (DCM).
2. The coating sample was rinsed with DCM before the analyses.

4.2.3 Isotopic Analysis of Items 2, 3 and 5 and the Control Sample

1. Bulk stable carbon isotopic analysis was performed using a Thermo Finnigan Elemental Analyser (Flash EA 1112) linked to Thermo Scientific MAT 253 Isotope-Ratio Mass Spectrometry (IRMS) with a Thermo Scientific ConFlo IV as an interface.
2. Approximately 0.3 mg of sample was weighed into tin capsules (SerCon) and introduced via an autosampler.
3. The Flash EA reactor tubes were comprised of two quartz glass tubes filled with chromium (III) oxide and copper oxide, held at 900 °C for combustion and a reduction reactor filled with reduced copper, held at 650 °C.
4. A post-reactor gas chromatography (GC) column was kept at 40°C. Measured $^{13}C/^{12}C$ isotope ratios are expressed in the δ notation [‰], relative to the international standard Vienna PeeDee Belemnite (VPDB).

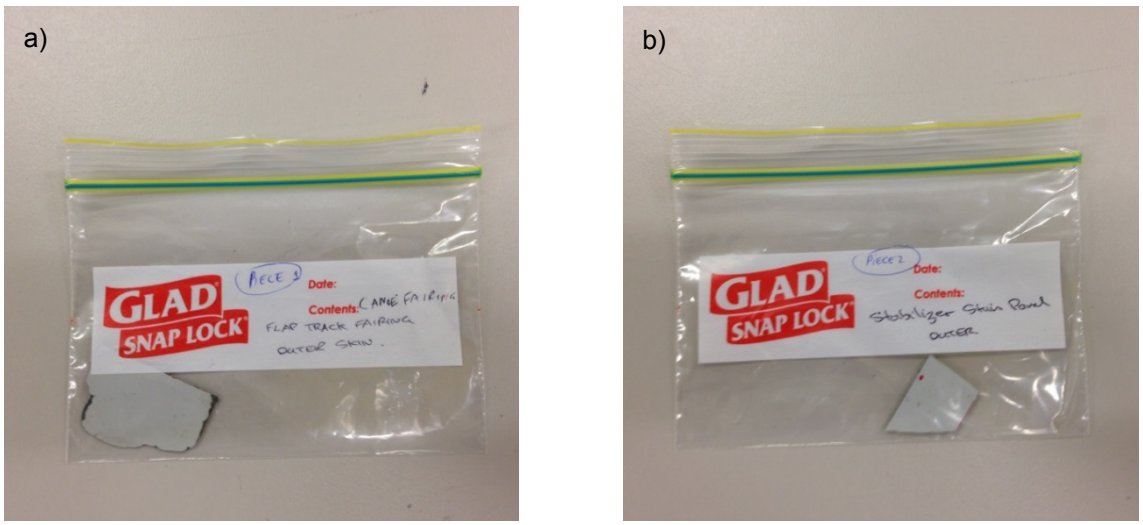

Fig. 1: a. Item 2. Right wing No. 7 Flap Track and b. Item 3. Right Horizontal stabiliser panel, Outer Fairing, Outer Skin.

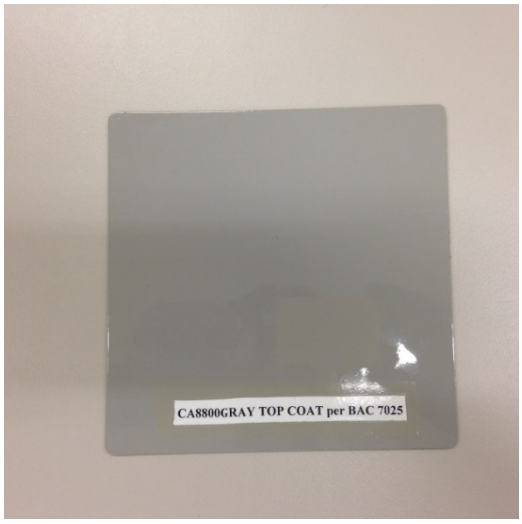

Fig. 2: Item 2. CA8800GRAY TOP COAT per BAC 7025 (from control sample)

Fig. 3: Item 3. CA8800GRAY TOP COAT per BAC 707 (from control sample)

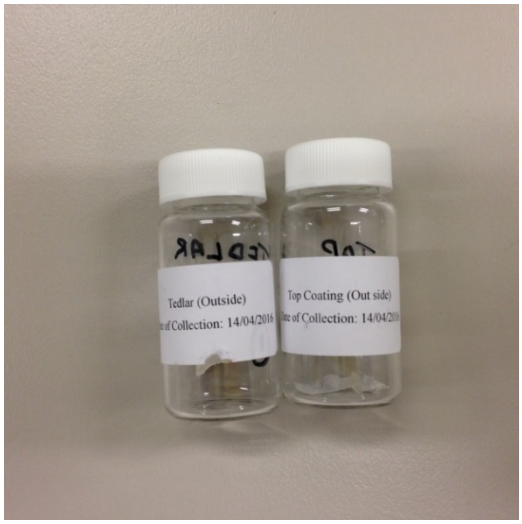

Fig. 4: Sample of Tedlar and top coating from Item 5

Fig. 5: A roll of decorative panel used as a control

4.3 Results

a. The stable carbon isotopic compositions of paint samples are listed in Table 1. All the samples have similar δ13C values, in the range of -29.5‰ to -30.6‰. The similar carbon isotopic compositions indicate that the paint samples may have come from the same source.

b. The stable carbon isotopic results of decorative panel coating collected from Item 5, and from the control sample are displayed in Table 2. The sample from Item 5 has a δ13C value of -

25.840‰, which is close to the δ13C value of control sample,of -25.151‰. Similar carbon isotope values indicate they may have come from the same source.

c. The sample of Tedlar from Item 5 has a δ13C value of -24.778‰. The control sample for the Tedlar piece is unavailable for comparison.

Table 1. Stable carbon isotopic results of paint samples from two pieces of the Right Wing No. 7 Flap Track Fairing from Mozambique and control samples

Samples	$\delta^{13}C$ (‰)	Stdev (‰)	Comments
Item 2. CA8800GRAY TOP COAT per BAC 7025	-30.582	0.009	From control sample
Item 3. CA8800GRAY TOP COAT per BAC 707	-30.642	0.001	From control sample
Item 2. Flap Track Fairing, Outer Skin	-29.507	0.071	
Item 3. Stabiliser Stain Panel, Outer	-30.209	0.088	

Table 2. Stable carbon isotopic results of decorative panel coating for Item 5 and the control sample.

Samples	$\delta^{13}C$ (‰)	Stdev (‰)	Comments
Top Coating Outside	-25.840	0.092	
Top Coating Control	-25.151	0.118	
Tedlar (outside)	-24.778	0.199	No control supplied

5 Analyses of Organic Compounds on Aircraft Pieces From Mozambique (Item 2)

5.1 Summary

This report provides an analysis of the organic compounds detected on Item 2 (Right wing No. 7 Flap Track Fairing) of aircraft debris found in Mozambique.

- Higher n-alkanes (straight-chain alkanes; C21-C35) were detected in both debris samples (with and without solvent). These compounds are wax separated from petroleum and used as major constitutes of grease and lubricants and indicate a possible source of higher plant origin petroleum.
- Four ester compounds were found with higher concentrations in the sample acquired with the application of organic solvent during sample collection (Table 1). These compounds contained grease, lubricants or lubricant additives.

5.2 Methodology

Cotton wool (pre-extracted with organic solvent to remove fat and grease and other organic materials) was used to collect the dust particles by wiping the surface of debris piece (Right Wing No. 7 Flap Track Fairing). Two samples were collected, the first (Sample #1) was the sample collected with dry cotton; the second (Sample #2) was collected with cotton soaked with organic solvent (mixture of dichloromethane and methanol 50:50). It was observed that more particles were collected with cotton soaked in solvent. The samples then were subsampled: one set was kept by Boeing for further analysis, and the other set was used for further analyses in the Geoscience Australia organic laboratory. Each sample was kept in individual 20 ml glass vials. The sample was covered with 10 ml hexane and extracted with sonication for 5 minutes. The hexane solution was transferred into a new 20 ml vial. The cotton was rinsed with 3 ml hexane and the solution was transferred into the same solution vial and performed 3 times. The total solution was concentrated to 4 ml with a nitrogen gas stream. A 2 mL aliquot was taken and concentrated further to approximately 100 µl which was then subjected to gas chromatography-mass spectrometry (GCMS) analyses with an injection volume of 0.5 µl. A full-scan was performed to measure the relative abundance and nature of detected compounds. Two blank samples (cotton wool with and without solvent) also underwent the same analytical procedures to trace any sources of contamination.

5.3 Results

Higher n-alkanes (straight-chain alkanes; C21-C35) were detected in both debris samples with much higher concentration (about 30 times) in Sample #2 (with solvent). The identifications are based on the comparison of GA's petroleum standard. These compounds are wax separated from petroleum and used as major constitutes of grease and lubricants. The C27 is the most abundant compound among

the n-alkanes. The n-alkanes demonstrate the pattern of ‘odd-over-even’ in the range of n-C27 to n-C35, indicating a possible source of higher plant origin petroleum.

Four ester compounds are detected in Sample #2 (with solvent) (Table 1). The identification of these ester compounds are based on the NIST mass spectrometry library search and comparison. These compounds have higher concentrations compared to n-alkanes. Some properties and usage of these esters are collected in Table 1 for reference. Please note that Compound ‘D’ (Nonanedioic acid, bis (2-ethylhexyl) ester) is used as grease and lubricant or as a lubricant addictive. Other compounds, Phosphoric acid, dibutyl phenyl ester (‘A’) and 1,2-Benzenedicarboxylic acid, diisooctyl ester (‘C’) is toxic and can cause fire hazards.

These ester compounds are not detected in samples #1 (without solvent). This is possibly due to the use of organic solvents to sample the compounds from the surface of the debris, as physical sampling without solvent was not able to extract these compounds.

The results found on the aircraft items indicated that the higher n-alkanes indicate a possible source of higher plant origin petroleum and the ester results were consistent with organic compounds of grease, lubricants or lubricant additives.

Table 1. Some compounds detected in the sample #2.

Peak	Name	Structure	Chemical Formula	CAS Number	Synonyms	Molecular Weight	Properties and Usage (Refer to references)
A	Phosphoric acid, dibutyl phenyl ester	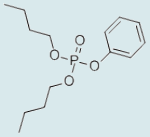	C14H23O4P	2528-36-1	Dibutyl phenyl phosphate	286	Clear colourless liquid. Insoluble in water; Organophosphates, such as dibutyl phenyl phosphate, are susceptible to the formation of highly toxic and flammable phosphine gas in the presence of strong reducing agents such as hydrides. Partial oxidation by oxidizing agents may result in the release of toxic phosphorus oxides.
B	Phosphoric acid, dibutyl phenyl ester	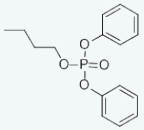	C16H19O4P	2752-95-6	butyl diphenyl phosphate; Phosphoric acid, butyl diphenyl ester; butyl diphenyl phosphate	306	Liquid; Industrial use: Flame retardants; Functional fluids
C	1,2-Benzenedicarboxylic acid, diisooctyl ester	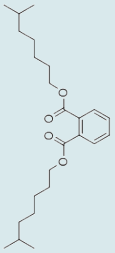	C24H38O4	27554-26-3	1,2-Benzenedicarboxylic acid diisooctyl ester;DIISOOCTYL PHTHALATE;alkylphthalates;Bis(6-methylheptyl) phthalate;Corflex 880;Flexol plasticizer diop;Hexaplas M/O;Isooctyl phthalate	390	Oily colourless liquid with a slight ester odour. Denser than water. Insoluble in water. Diisooctyl phthalate reacts exothermically with acids to generate isooctyl alcohol and phthalic acid. Strong oxidizing acids may cause a vigorous reaction that is sufficiently exothermic to ignite the reaction products. Heat is also generated by interaction with caustic solutions. Flammable hydrogen is generated by mixing with alkali metals and hydrides. Can generate electrostatic charges. [Handling Chemicals Safely, 1980. P. 250].

D	Nonanedioic acid, bis(2-ethylhexyl) ester		C25H48O4	103-24-2	BIS(2-ETHYLHEXYL) AZELATE;BIS(2-ETHYLHEXYL) NONANEDIOATE;AZELAIC ACID DIOCTYL ESTER;AZELAIC ACID BIS(2-ETHYLHEXYL) ESTER;AZELAIC ACID DI(2-ETHYLHEXYL) ESTER;DI(2-ETHYLHEXYL) AZELATE;DIOCTYL AZELATE;DIISOOCYL AZELATE	412	Industry use: Lubricants and lubricant additives; Consumer Use: Lubricants and Greases

5.4 References:

Dibutyl Phenol Phosphate Chemical Description:
http://www.chemicalbook.com/ChemicalProductProperty_EN_CB9915709.htm

Butyl Diphenyl Phosphate Chemical Description:
https://pubchem.ncbi.nlm.nih.gov/compound/butyl_diphenyl_phosphate#section=Use-and-Manufacturing

Bis(2-Ethylhexyl Azelate Chemical Description:
https://pubchem.ncbi.nlm.nih.gov/compound/Bis_2-ethylhexyl__azelate#section=Use-and-Manufacturing

Dirthyl Phthalate Chemical Description:
https://pubchem.ncbi.nlm.nih.gov/compound/6781#section=Wikipedia

6 Review of Macrofauna on Aircraft Pieces Found on Mauritius and South Africa (Item 5)

6.1 Summary

This report provides a review of the macrofauna removed from aircraft pieces found on the coast of Mauritius and South Africa. For consistency, the two pieces are labelled as Engine Nose Cowling (Item 5) and Door R1 Stowage Closet (Item 5). This report only covers external macrofauna collected directly off the pieces, and not the sieved fractions.

The key points from investigations of Items 4 and 5 are:

- The smooth exterior engine cowling from Item 4 was not heavily colonised by macrofauna. Evidence of possible cementing structures was generally found on the external facing section of the piece. Macrofauna present suggest animals that are either cosmopolitan or resultant from terrestrial species from South Africa (grass stolons).
- Item 5 (Door R1 Stowage Closet) was heavily colonised by the *Lepas anatifa anatifera* barnacle, with evidence of cementing structures on the smoother sections of the part. Size plays an important role in age determination for *Lepas* sp.. The largest specimens were used to determine possible time periods, with evidence suggesting that Item 5 had active growth at a minimum of **45** to **105** days, but likely between **45** to **50** days due to surrounding sea surface temperature.
- The external facing section of Item 5 was colonised by more barnacles than the internal facing section.
- Based on the visual similarities of the peduncle (stalk-like) attachment and certainty from the samples on the Door R1 Stowage Closet from the peduncle attachment, many samples that were collected on Item 2 and 3 (Right wing No. 7 Flap Track Fairing and Right Horizontal stabiliser panel piece), could possibly be from barnacle pedunculated cement. Most of the barnacles were attached to exposed internal honeycomb, whereas only larger barnacles were found attached to smooth exposed materials.

Caveats: The sampling procedure to acquire macrofauna attached to the pieces highlights some possible deficiencies. The pieces were retained over different time frames, and under conditions that may not be conducive for faunal preservation, therefore, some criteria were applied to the acceptance of samples analysed, these include:

- Any macrofauna within voids that could not be accessed without destructively breaking apart the pieces was not sampled
- Broken shells were not identified
- Broken barnacle shells were not counted or measured
- Any animals < 100 µm were not analysed

6.2 Method

The two pieces (Items 4 and 5) were received on the 14th April 2016 and examined in Geoscience Australia's Quarantine Approved facilities.

The pieces were photographed with an SLR Canon 60D with a macrolens (EF 100mm) and visually examined for any obvious macrofauna.

The pieces were then washed and agitated in water to ensure any animals within cavities were flushed out. The resultant water was then passed through 3 sieves of sizes 100µm, 500µm and 1000µm to ensure no spillage occurred in case of any obstruction. All material on each sieve was then carefully washed into a petri dish and sorted under microscope for any biological material. The biota was photographed with a Leica IC80 HD camera.

For Item 5 (Door R1 Stowage Closet), due to the large number of barnacles present on internal and external parts, barnacle counts were separated into 6 grids. An examination of where the barnacles had colonised the item were recorded and the results separated into:

- Grids A1, A2, B1, B2, C1 and C2 (internal and external),
- Unattached barnacles (these had fallen off either through transit, transportation or physical movement), and
- Barnacles collected around the edges within honeycomb (Figure 3).

Barnacles were then measured with digital callipers and counted per grid.

Biological items were scraped off and any biota was preserved in 75% ethanol[1]. Barnacles were stored in 100% ethanol for DNA preservation. Barnacles were removed manually and stored in allocated containers, however not all barnacles were stored in ethanol due to possible future analyses requiring different preservation techniques[2].

Sea surface temperature values around Mauritius were determined using monthly means available from the NASA MODIS ocean data website (NASA, 2016; Savtchenko et al., 2004).

[1] Expert taxonomists from Australia were contacted via email and phone to ascertain species present in the images. These specialists included: Dr Diana Jones for barnacles, barnacle cement remnants and other species (Western Australian Museum) Dr Robyn Cumming and Dr Dennis Gordon for bryozoans (Museum of Tropical Queensland)

[2] All waste material and liquids will be disposed of via irradiation or a quarantine approved procedure.

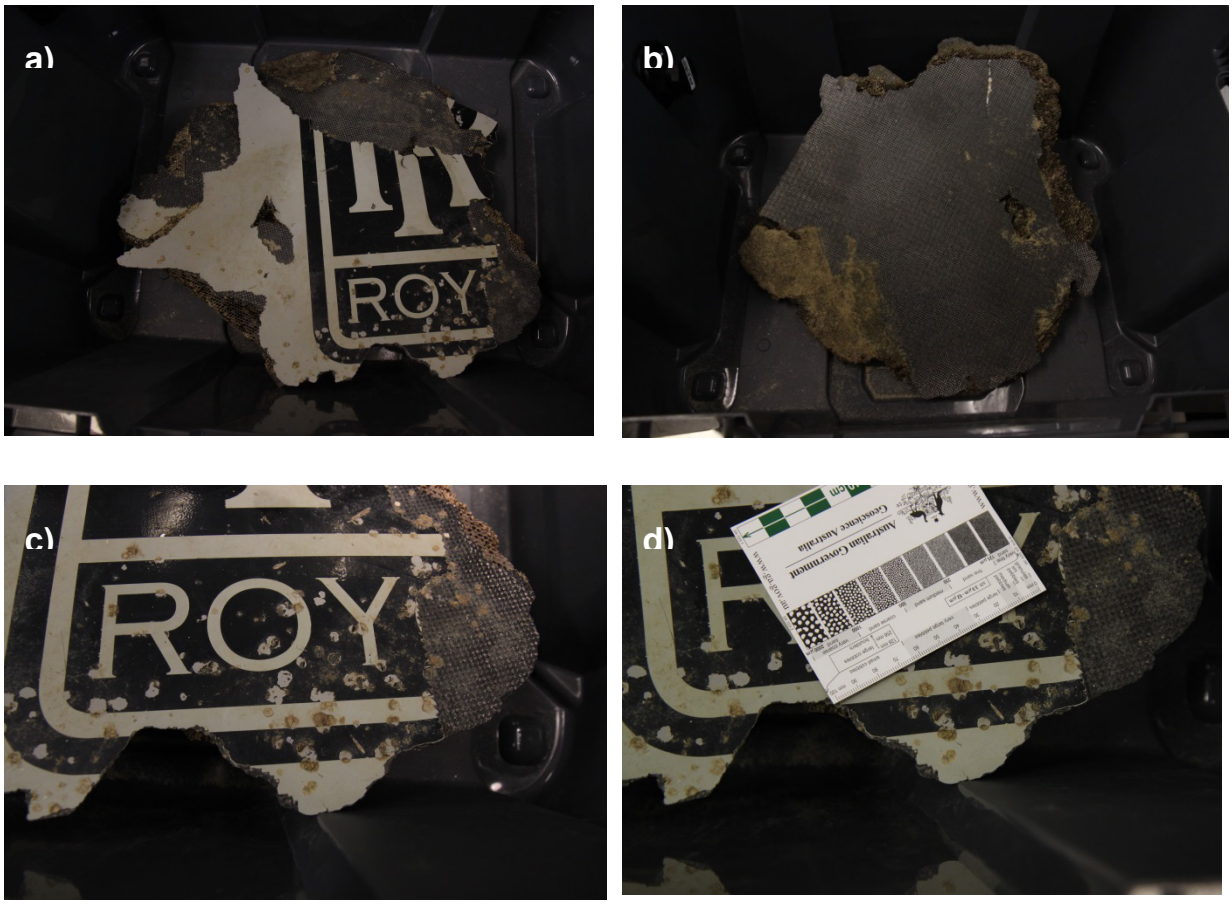

Figure 1 Overview images of Item 4 (Engine Nose Cowl); a) the external side of Item 4 indicating evidence of cementing structures; b) internal side of Item 4; c and d) close up of bottom external side of item 4

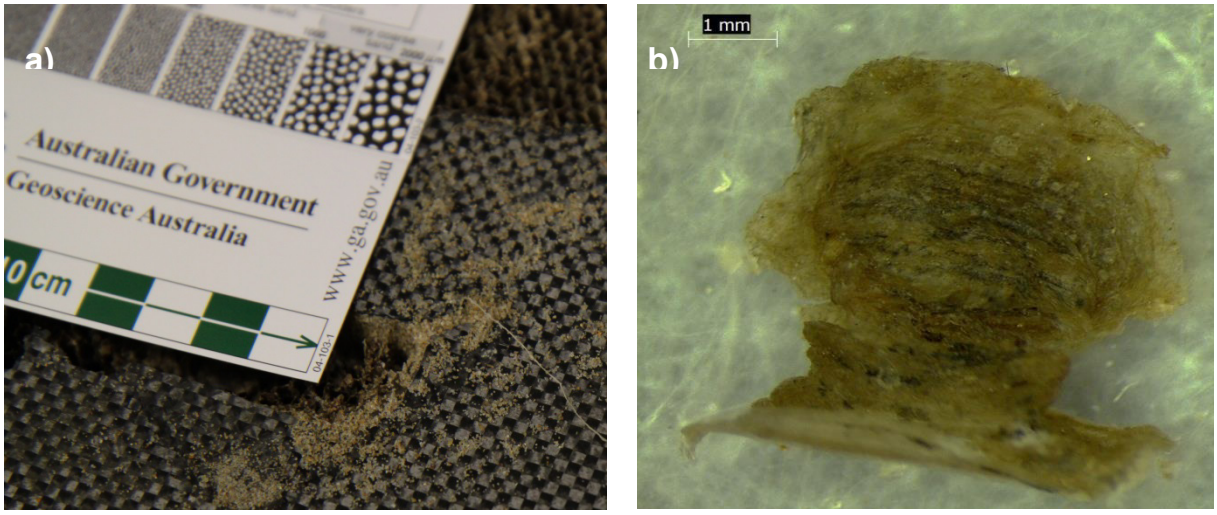

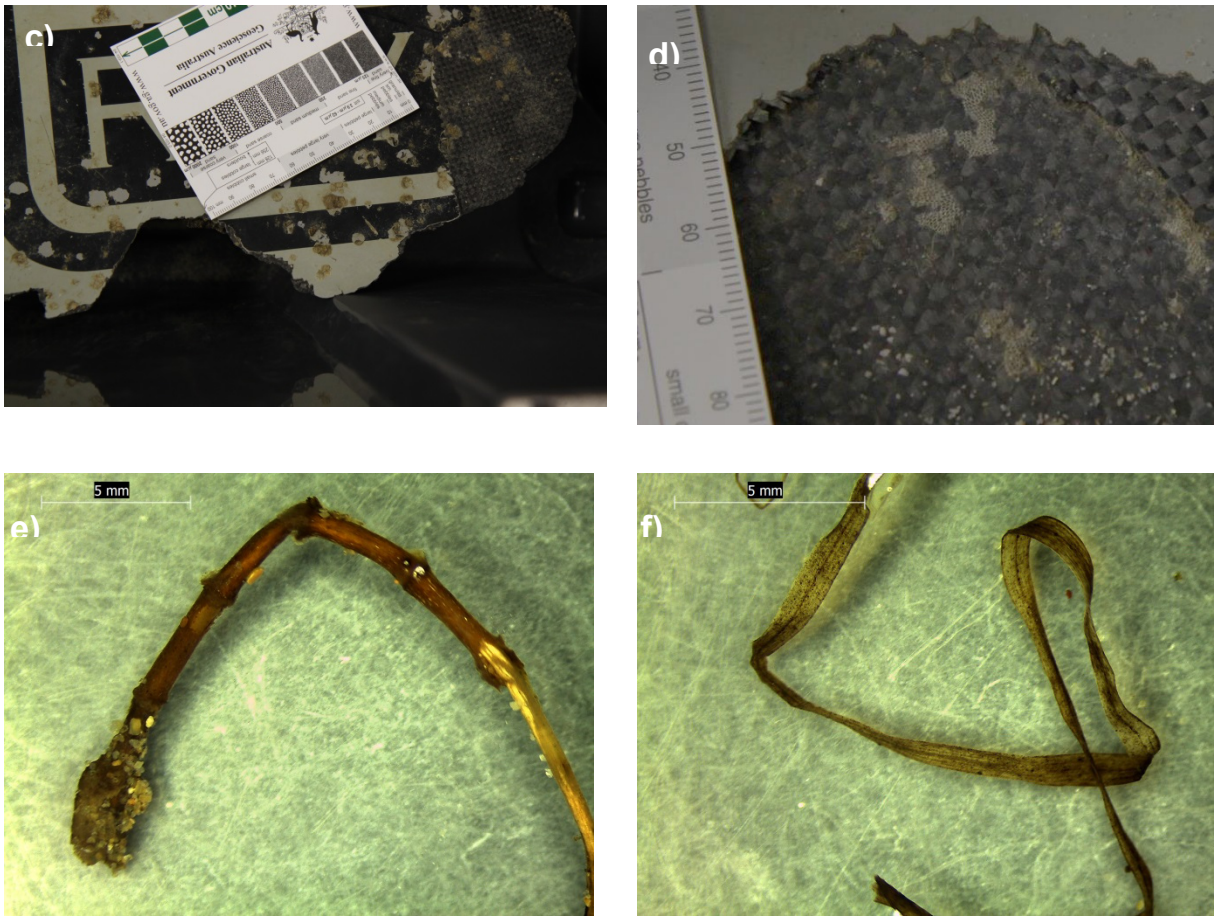

Figure 2 Examples of biota found on Item 4; a) unknown; b) possible remnant barnacle peduncle attached to the honeycomb from the exterior section; c) remnant barnacle scars on external facing section; d) possible Jellyella tuberculata colonies on internal facing section; e) stolon of terrestrial grass species; f) leaves of the terrestrial grass species.

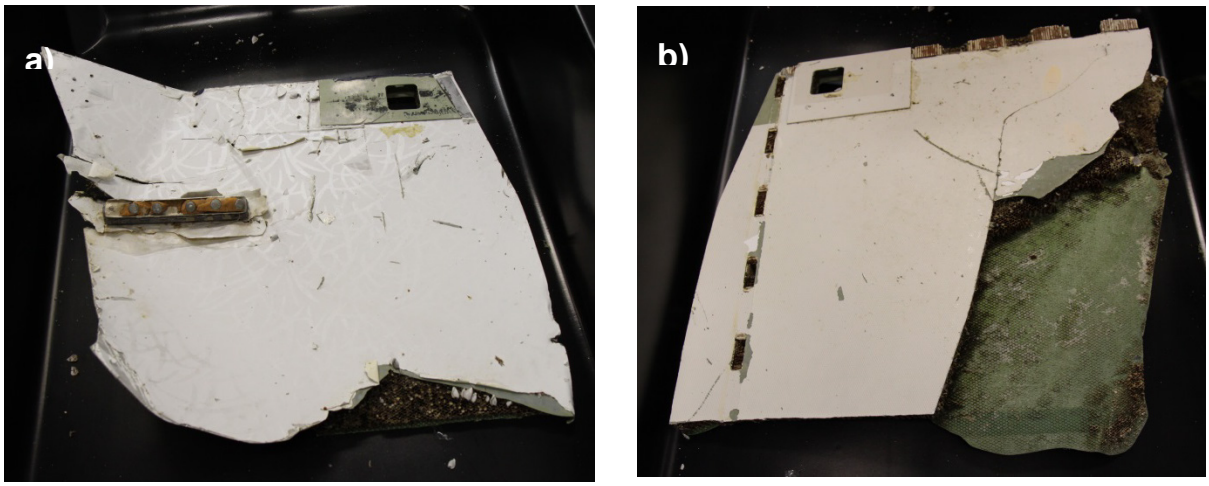

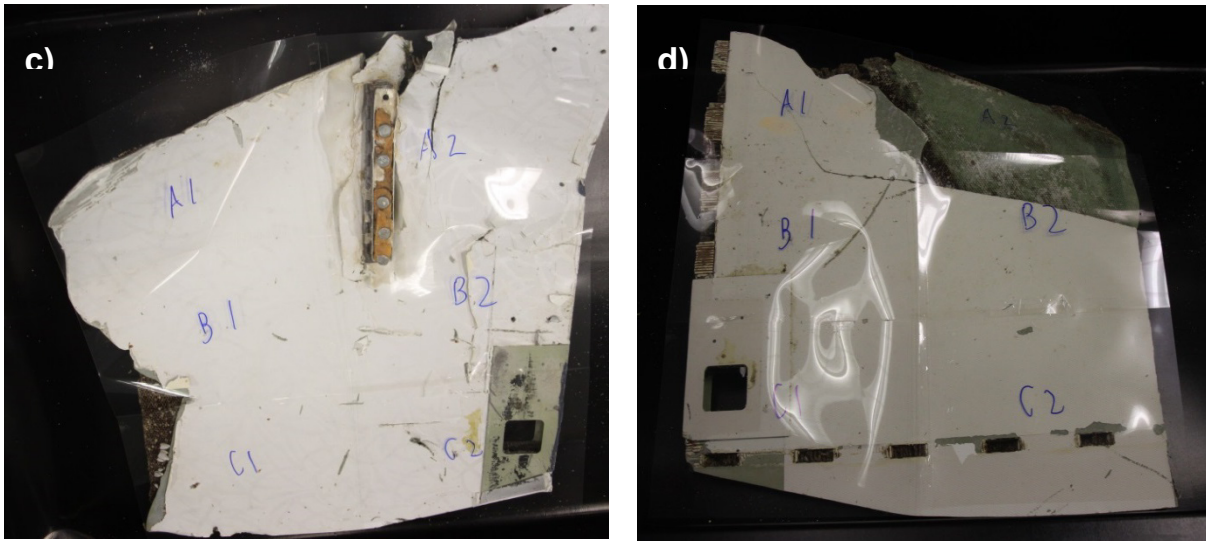

Figure 3 Images of Item 5; a) internal facing section of Item 5, b) external facing section of Item 5, c) grid of labels overlaid on the internal d) and external facing section of Item 5.

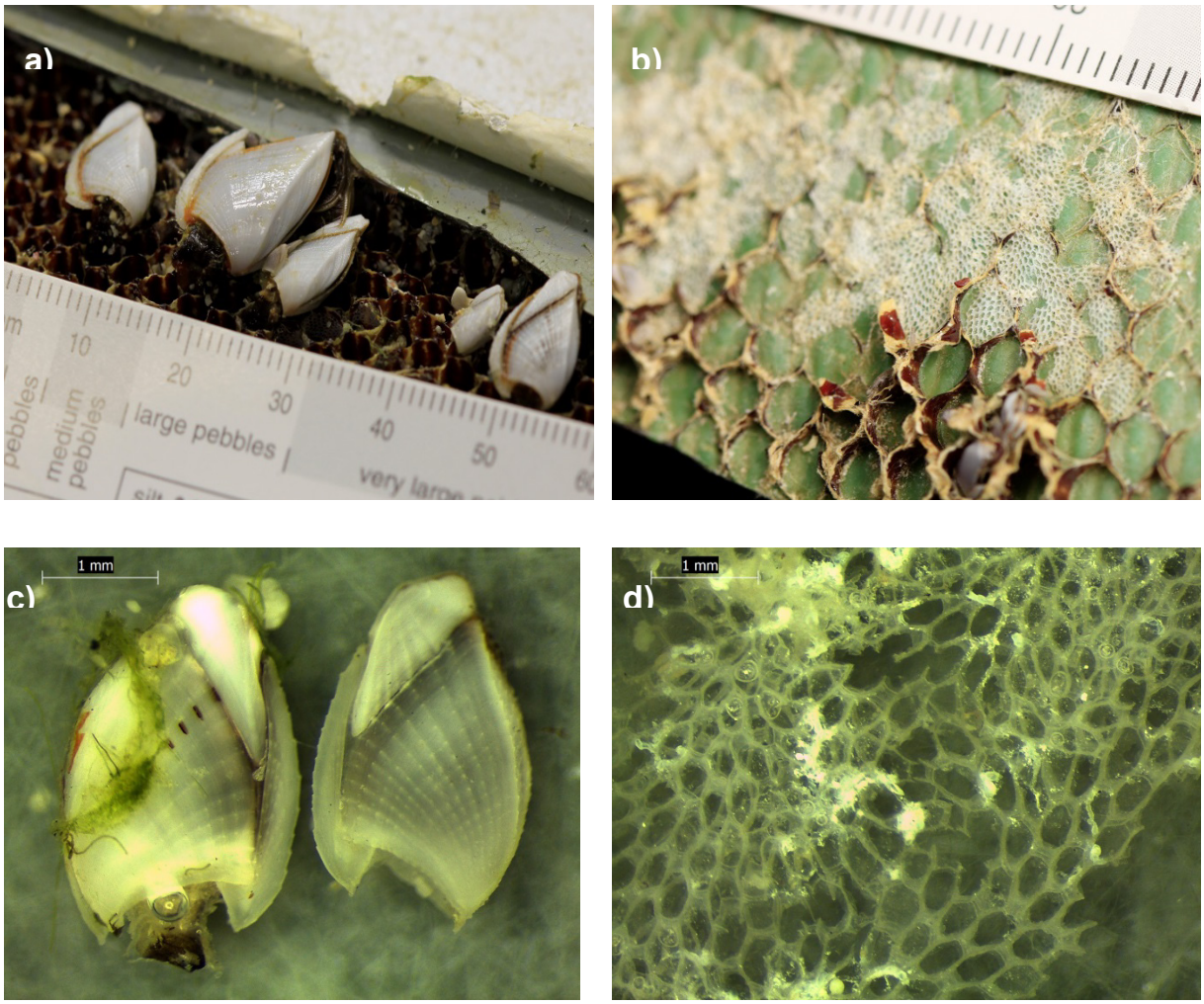

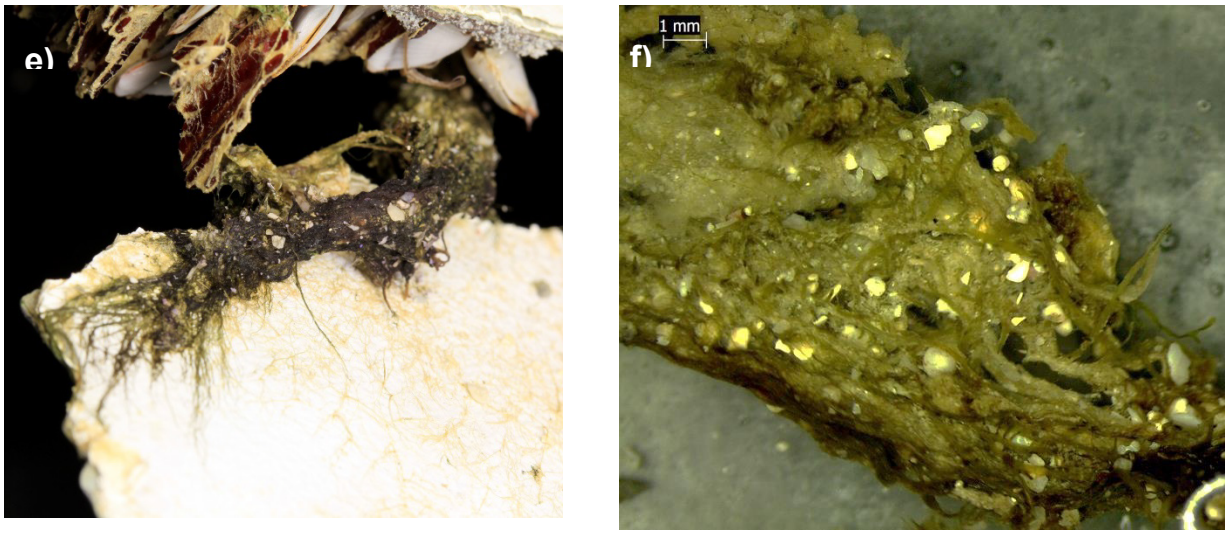

Figure 4 Examples of biota found on Item 5; a) colonies of barnacles attached to the more complex honeycomb of the Door R1 Stowage Closet); b) bryozoan colonies (possibly colonies of Jellyella tuberculata) on internal honeycomb structure; c) barnacle of Lepas anatifa anatifera; d) close up image of possible Jellyella tuberculata colonies; e) possible dried and matted filamentous green algae; f) close up image of dried and matted filamentous green algae entwined with Caulerpa sp.

6.3 Results

6.3.1 Item 4 (External Engine Cowling)

The Engine Nose Cowl (with the RR insignia) of Item 4 had evidence of many possible areas of attachment on the lower section. These include remnant scars with biological material (66) and remnant scars without any remnant material (15) (Figure 1). These areas are possibly related to peduncle attachment from barnacles. However, without any evidence of barnacle shells for size and identification, the species cannot be resolved.

In contrast, the internal facing section of Item 4 was relatively barren. Bryozoan colonies, possibly of species *Jellyella tuberculata* were found encrusted on the internal honeycomb and the black exterior of Item 4 (Figure 2).

6.3.2 Item 5 (Door R1 Stowage Closet)

A larger number of barnacles were found on the external section of the Door R1 Stowage Closet ranging between 1.39 mm to 20.05 mm in size (Figure 3; Table 1). Based on visual analysis:

- The barnacle species present on the Door R1 Stowage Closet is *Lepas anatifa anatifera* (Figure 4)
- Eleven ‘adult’ barnacles were found (between 13-23 mm capitulum length) (3% of collected barnacles)
- The size of the largest barnacle present corresponds to a growth period of approximately **45-50 days**, based on data by Evans (1958) for a growth rate of *Lepas (L. anatifera),* or **105 days** (based on the lower end 19 to 25°C sea surface temperature for optimum growth at 0.2 mm/day for the species) (Magni et al., 2015). However, it is likely that the higher growth rate of

age 45-50 days at approximately 0.44-0.55 mm/day can be assumed as sea surface temperatures surrounding Mauritius fluctuated between 26°C to 30°C during March 2016, 25°C to 30°C during February 2016 and 23°C to 29°C during January 2016 (NASA, 2016)

- Assumed minimum time for attachment of approximately 5 days for *Lepas* attachment to the debris (Magni et al., 2015)

Lepas anatifa anatifera is a species that commonly settles on floating animate or inanimate items in open water. It is a neustonic species (living on top of the water or right below the surface (Jones, 2016)), which means that only surface temperatures need to be used to evaluate possible ages. *L. anatifera* has a cosmopolitan geographical range across the open water. An understanding of growth rates of this species is summarised by Jones (2016), as follows:

> "There are few studies on the growth rate of *Lepas anatifera* as the species lives in open marine environments and is difficult to culture under laboratory conditions. Whilst there are many qualitative observations that indicate fast growth in *Lepas* species, quantitative growth estimates are few or are based on laboratory experiments. In most *Lepas* species, growth is rapid and individuals achieve sexual maturity within a few weeks after settlement"

> "The growth of barnacles varies with several factors, such as water temperature (mainly water surface), latitude, speed of movement of the item on which the barnacles are settling (Dalley & Crisp 1981) and the availability of food. In general, the growth rate of barnacles increases with increased temperature and current flow. However, this growth rate can be restricted with increased population density, competition from other species and adverse local environmental conditions (Bertness et al. 1991, Sorg et al. 1997)." (Jones, 2016)

Bryozoa species found encrusted on internal exposed honeycomb material are possibly colonies of *Jellyella tuberculata*. This is a species that commonly settles on pumice, plastics and other floating substrata. It has even been dubbed a 'pseudoplanktonic species'. These are small colonies that would achieve their size in a matter of weeks, and as such it is difficult to ascertain how long the floating components were on the sea floor or at the sea surface based on bryozoan size alone (Gordon, 2016).

Algae species found on Item 5 are possibly from the genus *Caulerpa sp.*, which is a common species found on Rodrigues Island (Coppejans et al., 2004), and filamentous green algae.

*Table 1 Summary table highlighting statistics on macrofauna (barnacles) identified on Item 5 (Door R1 Stowage Closet). *I after the sample name indicates that the sample is from the internal facing components of the item (section with decorative decal), whereas E indicates external section of the item.*

Sample location	Total Count	Minimum (mm)	Maximum (mm)	Median (mm)	Adult count
A1I*	1	11.53	11.53		0
A2I	6	2.41	9.03	3.655	0
B1I	0	N/A	N/A	N/A	0
B2I	17	1.95	15.84	4.27	2
C1I	26	1.39	15.95	5.7	3
C2I	13	1.91	4.63	2.62	0
Internal	**63**	**1.39**	**15.95**	**4.27**	**5**
A1E	117	2.27	20.05	5.23	3
A2E	48	1.88	7.76	3.56	0

Sample location	Total Count	Minimum (mm)	Maximum (mm)	Median (mm)	Adult count
B1E	33	1.82	10.67	3.56	0
B2E	NA	NA	NA	NA	0
C1E	4	3.88	11.26	4.71	0
C2E	NA	NA	NA	NA	0
External	**202**	**1.82**	**20.05**	**4.135**	**3**
Unattached	**30**	**2.9**	**16.34**	**6.19**	**3**
Exterior Honeycomb	**91**	**2.06**	**11.72**	**3.6**	**0**
Total	***386***	***1.39***	***20.05***	***4.203***	***11***

6.4 References

Bertness, M.D., Gaines, S.D., Bermudez, D. & Sanford, E. (1991). Extreme spatial variation in the growth and reproductive output of the acorn barnacle *Semibalanus balanoides. Marine Ecology Progress Series* **75**: 91-100.

Coppejans, E., Leilaert, F., Verbruggen, H., De Clerck, O., Schils, T., De vriese, T. and Marie, D. (2004). The marine green and brown algae of Rodrigues (Mauritius, Indian Ocean). *Journal of Natural History* **38**: 2959-3020.

Dalley, R. & Crisp, D.J. (1981). *Conchoderma*: a fouling hazard to ships underway. *Marine Biology Letters* **2**: 141-152.

Evans, F. (1958). Growth and maturity of the Barnacles *Lepas hillii* and *Lepas anatifera*. *Nature* **182**: 1245-1246

Gordon, D. 2016. Personal communication.

Jones, D.S. 2016. Personal communication.

Magni, P.A., Venn, C., Aquila, I., Pepe, F., Ricci, P., Di Nunzio, C. et al. (2015). Evaluation of the floating time of a corpse found in a marine environment using the barnacle *Lepas anatifera* L. (Crustacea: Cirripedia: Pedunculata). *Forensic Science International* **247**: e6-e10.

NASA Earth Observations. (2016). Sea surface temperature (1 month – AQUA/MODIS). Retrieved from http://neo.sci.gsfc.nasa.gov/view.php?datasetId=MYD28M

Savtchenko, A., Ouzounov, D., Ahmad, S., Acker, J., Leptoukh, G., Koziana, J., Nickless, D. 2004. Terra and Aqua MODIS products available from NASA GES DAAC. *Advances in Space Research*. **34**: 710-714

Sorg, M.H., Deaborn, J.H., Monahan, E.I., Ryan, H.F., Sweeney, K.G. & David, E. (1997). Forensic taphonomy in a marine context. In: Haglund, W.D. & Sorg, M.H. (eds), *Forensic taphonomy. The post mortem fate of human remains*. Pp 567-604. (CRC, Boca Ranton.)

Appendix H – Analysis of Low Frequency Underwater Acoustic Signals Possibly Related to the Loss of Malaysian Airlines Flight MH370

Centre for Marine Science and Technology

Analysis of Low Frequency Underwater Acoustic Signals Possibly Related to the Loss of Malaysian Airlines Flight MH370

Prepared for:
Australian Transport Safety Bureau

Prepared by:
Dr Alec J Duncan, Dr Alexander Gavrilov, Dr Rob McCauley

PROJECT CMST 1308
REPORT 2014-30

June 23rd 2014

Executive Summary

Malaysian Airlines flight MH370 disappeared in the early hours of 8th March 2014 and its whereabouts remain unknown. Current search efforts are based on position information derived from a satellite communication system and are focussed on the Indian Ocean, within Australia's search and rescue zone. The Australian Transport Safety Bureau (ATSB) has asked the Centre for Marine Science and Technology (CMST) to analyse signals received on underwater sound recorders operated by CMST that form part of the Australian Government funded Integrated Marine Observing System (IMOS), and on hydroacoustic stations operated by the Comprehensive Nuclear Test Ban Treaty Organisation (CTBTO) in an attempt to detect and localise underwater sounds that could be associated with the impact of the aircraft on the water or with the implosion of wreckage as the aircraft sank.

One acoustic event of particular interest has been identified that occurred at a time that could potentially link it to MH370 and appears to have been received on one of the IMOS recorders near the Perth Canyon (RCS) and at the CTBTO hydroacoustic station at Cape Leeuwin (HA01).

A detailed analysis of these signals has resulted in an approximate localisation for the source that is compatible with the time of the last satellite handshake with the aircraft, but incompatible with the satellite to aircraft range derived from this handshake. There appear to be three possible explanations for this discrepancy:

1. The signals received at HA01 and RCS are from the same acoustic event, but the source of the signals is unrelated to MH370.
2. The signals received at HA01 and RCS are from different acoustic events, which may or may not be related to MH370.
3. The signals received at HA01 and RCS are from the same acoustic event, and the source of the signals is related to MH370, but there is a problem with the position line determined from the satellite handshake data.

Of these, the first explanation seems the most likely as the characteristics of the signals are not unusual, it is only their arrival time and to some extent the direction from which they came that make them of interest.

If the second explanation was correct then there would still be some prospect that the signal received at HA01 could be related to the aircraft, in which case the combination of the HA01 bearing and the position arc derived from the satellite handshake data would provide an accurate location on which to base a search. However, the analysis carried out here indicates that, while not impossible, this explanation is unlikely.

The third explanation also seems unlikely because of the intense scrutiny the satellite handshake data has been subjected to. However, should the arc defined by the handshake data be called into question, the various timing and acoustic considerations discussed here would suggest that a reasonable place to look for the aircraft would be near where the position line defined by a bearing of 301.6° from HA01 crosses the Chagos-Laccadive Ridge, at approximately 2.3°S, 73.7°E. If the source of the detected signals was the aircraft impacting the sea surface then this would most likely have occurred in water depths less than 2000m and where the seabed slopes downwards towards the east or southeast. These considerations could be used to further refine the search area. If, instead, the received sounds were due to debris imploding at depth it is much less certain where along the position line from HA01 this would have occurred.

Contents

1 Introduction 5
2 Signal descriptions and analysis 6
3 Automated signal detection algorithm 11
3.1 General description 11
3.2 Mathematical derivation 12
3.3 Results 13
4 Independent time calibration check 14
5 Estimate of the probability that events at HA01 and RCS are from the same source 17
6 Analysis of data from HA08S 20
7 Discussion 25
8 Conclusions 31

1 Introduction

Malaysian Airlines flight MH370 disappeared in the early hours of 8th March 2014 and its whereabouts remain unknown. Current search efforts are based on position information derived from a satellite communication system and are focussed on the Indian Ocean, within Australia's search and rescue zone. The Australian Transport Safety Bureau (ATSB) has asked the Centre for Marine Science and Technology (CMST) to analyse signals received on underwater sound recorders operated by CMST as part of the Integrated Marine Observing System (IMOS) and on hydroacoustic stations operated by the Comprehensive Nuclear Test Ban Treaty Organisation (CTBTO) in an attempt to detect and localise underwater sounds that could be associated with the impact of the aircraft on the water or with the implosion of wreckage as the aircraft sank. This report collects together the results of various analyses that have been carried out by CMST, several of which have previously been reported to ATSB in summary reports.

One acoustic event of particular interest has been identified that occurred at a time that could potentially link it to MH370 and appears to have been received on CMST's acoustic recorders near the Perth Canyon (RCS), and at the CTBTO hydroacoustic station at Cape Leeuwin (HA01). Section 2 describes the signals associated with this event and the attempt made to localise it. Section 3 details an automatic detection algorithm that was developed to search for the same event in data from HA08S and was also used to characterise all events arriving at HA01 within an eight hour time period. HA08S and HA01 were the only operational CTBTO hydroacoustic stations in the Indian ocean at the time, The use of two of the separate events to check the calibration of the clock offset between RCS and HA01 is described in Section 4, while Section 5 details an initial attempt to estimate the probability that the signals at RCS and HA01 originated from the same source. Section 6 details the results of a search for the same event in data from HA08S, Section 7 provides a discussion that attempts to draw these various strands together, and the conclusions that can be drawn from this work are detailed in Section 8.

2 Signal descriptions and analysis

An underwater sound recorder operated by the Centre for Marine Science and Technology as part of IMOS and located at the seabed in 450 m water depth in the Perth Canyon (Rottnest Trench) received a transient signal at approximately 01:34:00 UTC on 8th March 2014. (This receiver is referred to as RCS in what follows.) After correction for clock drift the time of arrival of the peak energy in this signal has been calculated to be 01:33:44 UTC +/- 4 seconds. The signal and its spectrogram are shown in Figure 1.

A search of data from the Comprehensive Test ban Treaty Organisation's hydroacoustic station off Cape Leeuwin, Western Australia (HA01) carried out by the authors has revealed a signal believed to be from the same source, with a peak energy arrival time of 01:34:50 UTC +/- 3seconds. The signals and their spectrograms are shown in Figure 2.

Although the signal to noise ratio was poor on a single HA01 hydrophone, the signal at HA01 was strongly correlated between the station's three hydrophones which allowed the bearing of the source to be calculated with considerable accuracy. The result was a bearing of 301.6° +/- 0.75°.

Projecting this bearing back from HA01 towards the source, computing the expected time difference between signals arriving at the two receiving stations as a function of distance along the track, and matching this to the measured time difference results in a most probable position for the sound source of 5.93°S, 77.22°E (see Figure 3). Calculations were carried out using Matlab's mapping toolbox and the WGS84 elipsoid. Further details of this result are given in Table 1.

Uncertainties of +/- 0.75° in bearing from HA01 and +/- 4 s in travel time difference result in the bounding box shown in Figure 3 and uncertainties of +/- 1° in bearing and +/- 7 s in time difference result in the somewhat larger bounding box shown in Figure 4.

Calculated latitudes and longitudes of the vertices of the bounding box are given in Table 2. The bounding box is very elongated along the bearing from HA01 which is a result of the hyperbolic position line obtained from the arrival time difference being almost parallel to the bearing from HA01 at that range.

If the source was at the most probable position, then the signal would have been emitted at approximately 00:39:11 UTC.

The travel time differences have been calculated using acoustic group velocities estimated from numerical waveform modelling using an adiabatic normal mode model and climatological sound speed profiles for the appropriate time of year from the World Ocean Atlas 2005, (NOAA 2005). This gave a mean group velocity of 1486.20 m/s along the path from the most probable source location to HA01 and 1486.35 m/s along the path from the most probable source location to RCS.

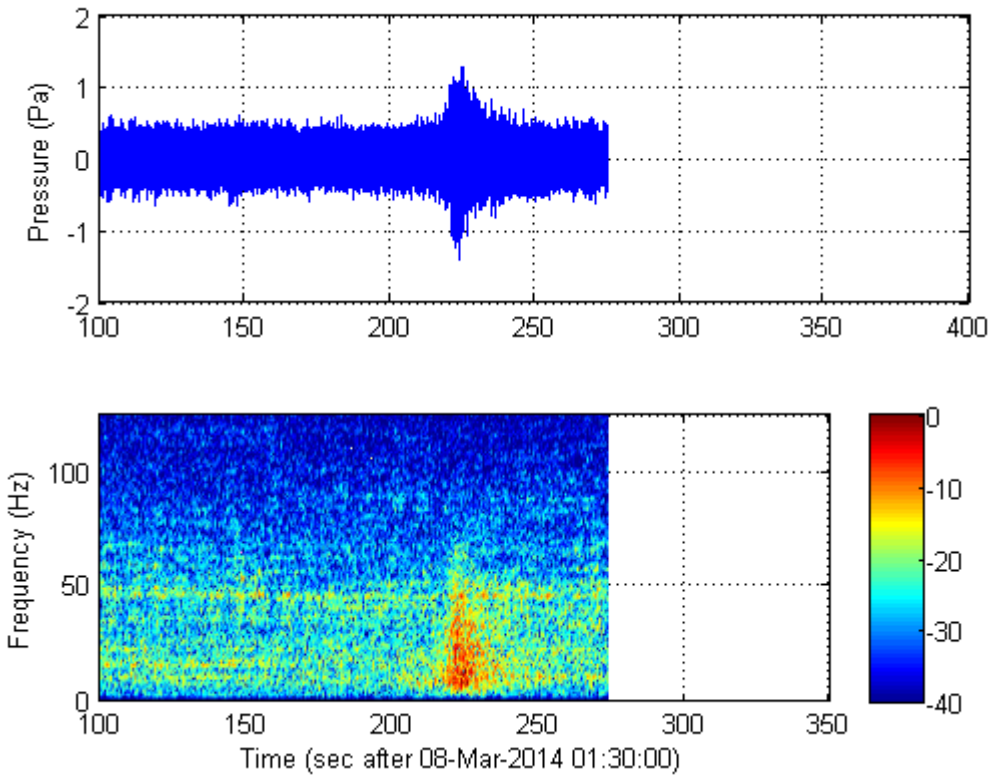

Figure 1. Time series (top) and spectrogram (bottom) showing the signal received at the Perth Canyon logger at 01:33:44 UTC on 8th March 2014. The spectrogram colour scale is in dB relative to the largest value in the spectrogram.

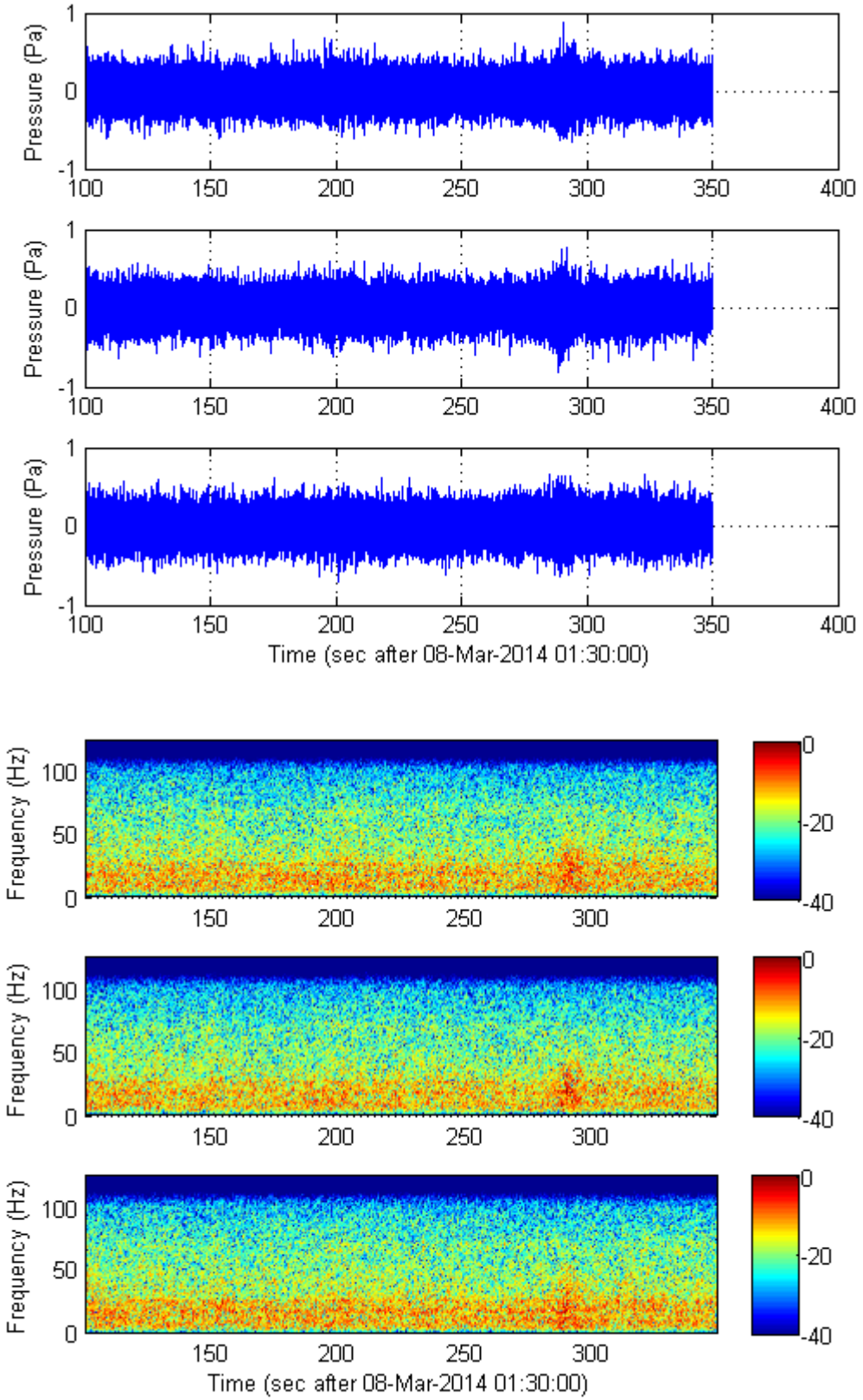

Figure 2. Time series (top) and spectrograms (bottom) showing the signals received at the three hydrophones of HA01 at 01:34:50 UTC on 8th March 2014. The spectrogram colour scales are in dB relative to the largest value in each spectrogram. Times scales are the same as for Figure 1.

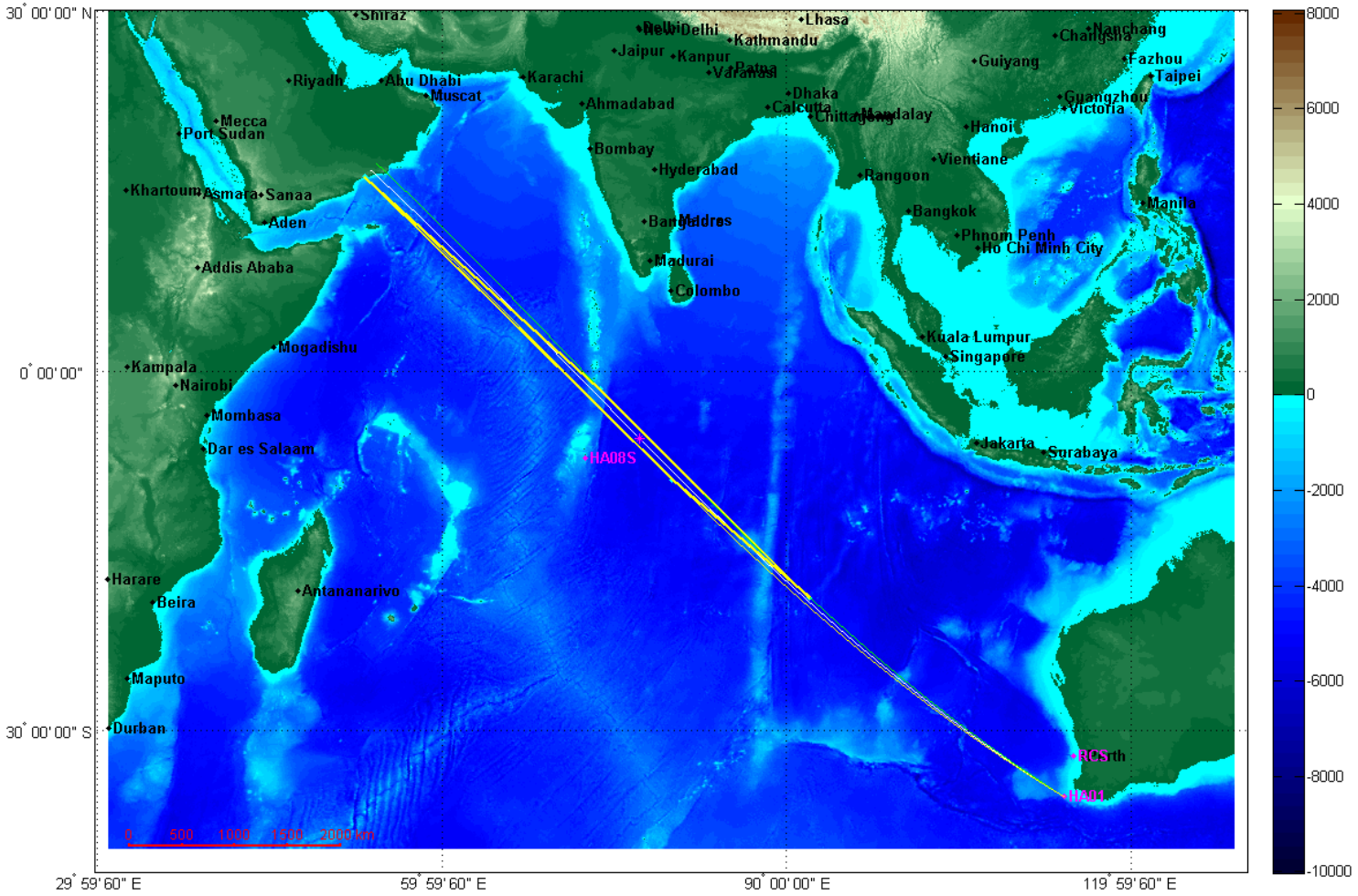

Figure 3.Map showing most probable location for the source of the received sound signals (magenta asterisk) and the uncertainty region (yellow polygon) based on an uncertainty of +/- 0.75° in the bearing from HA01 and a +/- 4s uncertainty in the difference between signal arrival times at RCS and HA01.

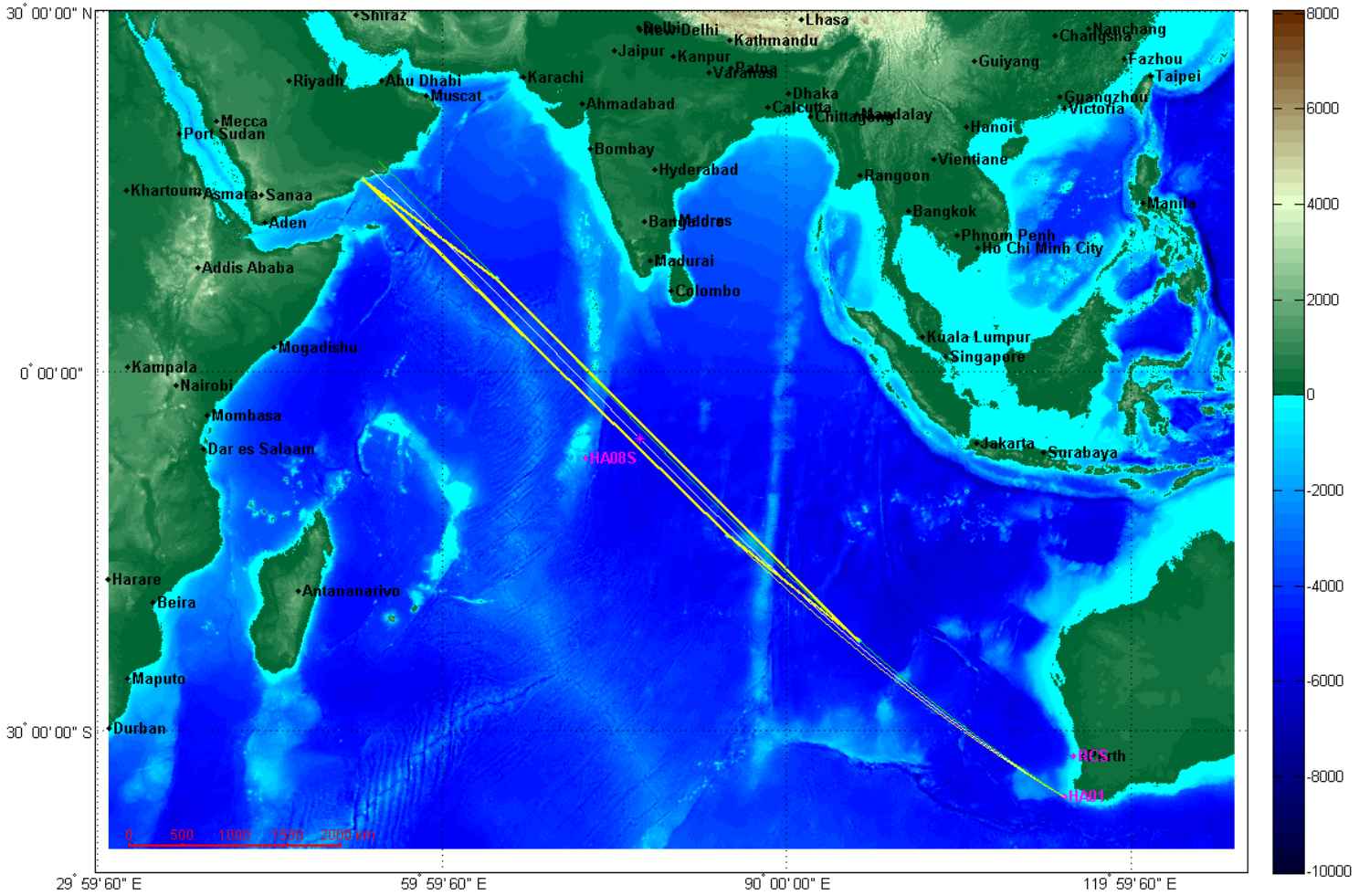

Figure 4. As for Figure 3 except the uncertainty region is based on +/- 1° in bearing and +/- 7s in arrival time difference.

Table 1.Details of most probable position.

Position	5.93°S, 77.22°E
Distance to HA01 (km)	4961.6
Distance to RCS (km)	4864.0
Signal travel time to HA01 (s)	3338.4
Signal travel time to RCS (s)	3272.4
Calculated arrival time difference (s)	66.0
Measured arrival time difference (s)	66.0

Table 2. Uncertainty box bounds

Vertex	Position with +/-0.75° bearing error and +/-4 s timing error	Position with +/-1° bearing error and +/-7 s timing error
Northwest	16.8°N, 53.3°E	16.6°N, 53.1°E
Northeast	1.6°S, 73.8°E	8.1°N. 64.7°E
Southwest	9.5°S, 80.1°E	14.2°S, 84.9°E
Southeast	19.5°S, 92.0°E	23.0°S, 96.3°E

3 Automated signal detection algorithm

3.1 General description

To provide an efficient means of searching for other arrivals a Matlab program was written that breaks the signals received at a CTBTO hydroacoustic station into short blocks and then iteratively calculates the bearing to any sources. A 95% block overlap was used so that any genuine signal should appear as a detection in multiple blocks.

Each block was processed by computing the bearing to the strongest source using the conventional plane-wave fitting method (Menke, 1984, del Pezzo and Giudicepietro, 2002), estimating that signal using a least squares process, subtracting the estimated signal from the received signals (with appropriate time adjustments) to produce modified signals, and then applying the plane wave fitting method to the modified signals. This process can be repeated an arbitrary number of times, but it was found that there was little point in proceeding beyond three iterations.

At each stage the integrity of the fitted bearing was checked by requiring a discrepancy in the arrival time differences of no more than 10 ms, a fitted group velocity in the range 1420m/s to 1550m/s, and at least one neighbouring detection with a bearing within +/- 0.5°. The last criterion is based on the expectation that, because of the 95% block overlap, any genuine detection would occur in multiple adjacent blocks.

3.2 Mathematical derivation

Working in the horizontal (X,Y) plane, assume the incoming signal is made up of N plane waves coming from different directions. Then the received signal at time t at receiver $m \in \{1 \cdots M\}$, located at x_m, y_m can be written:

$$p_1(x_m, y_m, t) = \sum_{n=1}^{N} s_n\left(t - \nu_{xn} x_m - \nu_{yn} y_m\right) + \varepsilon(x_m, y_m, t) \qquad (1)$$

where

$\nu_{xn} = \frac{1}{c_{gn}} \cos\theta_n$ is the X-component of the slowness (inverse sound speed),

$\nu_{yn} = \frac{1}{c_{gn}} \sin\theta_n$ is the Y-component of the slowness,

c_{gn} is the plane wave group velocity,

θ_n is the direction in which the wave is travelling

$s_n(\cdot)$ is the waveform of signal n, and

$\varepsilon(x, y, t)$ is random noise that is assumed uncorrelated between receivers.

If the signals are ordered such that $|s_1| >> |s_2| >> |s_3|$ etc. then ν_{x1} and ν_{y1} can be estimated using the plane-wave fitting method (Menke, 1984, del Pezzo and Giudicepietro, 2002) and can therefore be considered known. We can write:

$$p_1(x_m, y_m, t) = s_1(t - \nu_{x1} x_m - \nu_{y1} y_m) + p_2(x_m, y_m, t) \quad (2)$$

where $p_k(x_m, y_m, t) = \sum_{n=k}^{N} s_n(t - \nu_{xn} x_m - \nu_{yn} y_m) + \varepsilon(x_m, y_m, t)$.

So:

$$p_1(x_m, y_m, t + \nu_{x1} x_m + \nu_{y1} y_m) = s_1(t) + p_2(x_m, y_m, t + \nu_{x1} x_m + \nu_{y1} y_m). \quad (3)$$

Defining $t'_{mn} = t + \nu_{xn} x_m + \nu_{yn} y_m$ we can rewrite (3) as:

$$p_1(x_m, y_m, t'_{m1}) = s_1(t) + p_2(x_m, y_m, t'_{m1}). \quad (4)$$

If the $p_2(x_m, y_m, t'_{m1})$ are treated as noise that is uncorrelated between sensors then equation (4) defines a set of three equations in terms of the unknown $s_1(t)$. The assumption that the $p_2(x_m, y_m, t'_{m1})$ are uncorrelated between sensors is justified because, by definition, all signal components that are correlated between sensors when the time delays associated with t'_{m1} are applied are included in $s_1(t)$. The least squares estimate of $s_1(t)$ is simply the average over the appropriately delayed sensor outputs:

$$\hat{s}_1(t) = \frac{1}{3} \sum_{m=1}^{M} p_1(x_m, y_m, t'_{m1}) \quad (5)$$

Once $\hat{s}_1(t)$ has been estimated, the residual signals can be calculated using a rearrangement of (2):

$$p_2(x_m, y_m, t) = p_1(x_m, y_m, t) - \hat{s}_1(t - \nu_{x1} x_m - \nu_{y1} y_m) \quad (6)$$

The plane-wave fitting algorithm can then be applied to $p_2(x_m, y_m, t)$ and the process repeated to estimate $\hat{s}_2(t)$, and so on.

3.3 Results

The results of applying two iterations of this algorithm to the HA01 data from 00:10:00 UTC on the 8th March to 08:00:00 UTC on the same day are shown in Figure 1. These

results were obtained a block duration of 20s and a block overlap of 19s. A zero-phase high pass filter with a cut-off frequency of 3 Hz was applied to the data prior to processing to remove very low frequency flow noise.

The vast majority of the detections originated from the Antarctic sector, which extends from 158° to 209°, or from just outside it. The majority of these are likely to be ice cracking events, although some may be some seismic events along a seafloor spreading ridge between Australia and Antarctica.

The 01:34:50 arrival (indicated by the orange arrow) stands out as being the only signal over this time period that originated from a northerly direction.

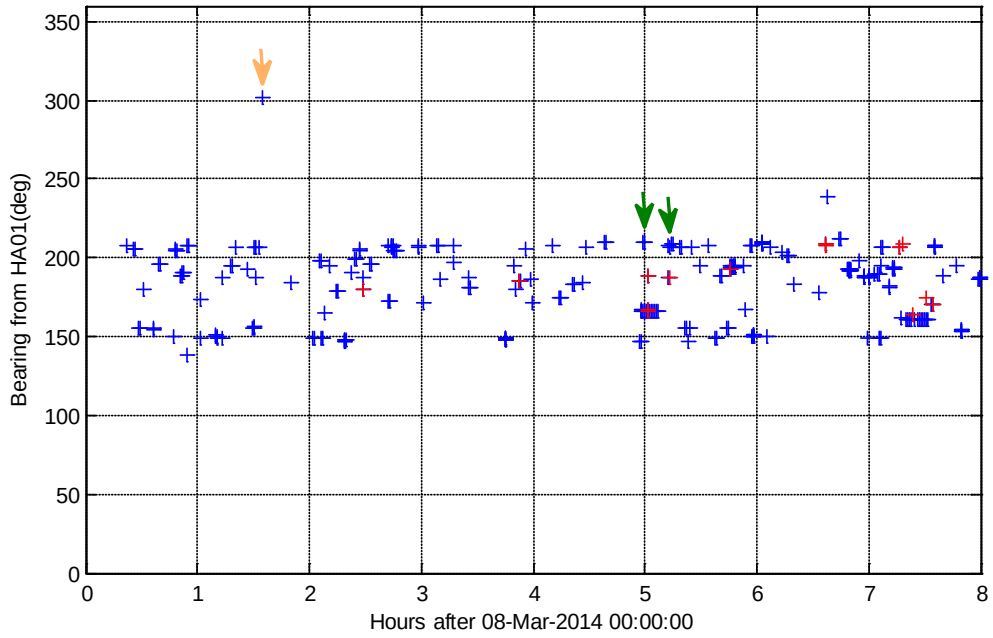

Figure 5.All automatic detections at HA01 between 00:00:10 and 08:00:00 UTC on 8th March 2014. The detection possibly associated with MH370 is indicated by the orange arrow. Blue crosses indicate detections made on the first iteration, red crosses are detections made on the second iteration. The dark green arrows indicate the two detections used for cross-checking the clock drift calibration.

4 Independent time calibration check

The estimate of the range of the source from HA01 is strongly dependent on the measured difference between the signal arrival times at RCS and HA01. The RCS recorder was deployed for a period of approximately three months during which its internal clock, which was set to UTC time prior to deployment and checked against UTC time after

deployment, gained 31.76 seconds (this is done in the noise logger hardware software using and external GPS and its UTC transmitted time). The time reference in both cases was the 1 pulse per second output from a GPS receiver. Assuming this drift rate was constant throughout the deployment, early on the 8th March 25.8 seconds must be subtracted from times according to the recorder clock in order to convert them to UTC.

An independent check of the accuracy of the drift correction of RCS compared with HA01 was carried out using two events other than the primary signal of interest, that resulted in signals that were received at both HA01 and RCS. The first of these resulted in a signal that was received at HA01 at 04:59:21 UTC on 8th March 2014 (17961 seconds after midnight) and came from a bearing of 210.2°. The corresponding signal arrived at RCS at 05:03:01 (18181 seconds after midnight). Both signals had high signal to noise ratio.

The second event was of much lower amplitude but came from a similar direction, and resulted in a signal that was received at HA01 at 05:14:28 UTC (18868 seconds after midnight) on the same day from a bearing of 208.5°. The corresponding signal was received at RCS at 05:18:13(19093 seconds after midnight).

For each event, the arrival times and bearings at HA01 were used to compute a predicted arrival time at RCS, which was then compared to the measured arrival time. The results were computed using an assumed source range of 5000 km and an assumed group velocity of 1484 m/s and are given in Table 3.

Both arrivals came from a direction that is only about 15° from the direction of the line joining RCS and HA01, so the predicted arrival times at RCS depend only weakly on the source range assumption. A sensitivity study showed a 2 second increase in predicted arrival time if the assumed source range from HA01 was reduced to 1,000km, and a 0.2 second decrease if the source range was increased to 10,000km.

The assumed group velocity of 1484 m/s was obtained from numerical propagation modelling for a signal arriving from this direction and is considered accurate to within +/- 5 m/s. The effect of this uncertainty is considered along with other sources of error in the following analysis.

The uncertainties in the predicted arrival times at RCS were estimated based on a local plane geometry approximation to the ellipsoidal Earth in the vicinity of HA01 and RCS,

and the assumption that the source is an infinite distance away from the two stations. Note that this approximation has only been used to estimate the uncertainties. The actual arrival time calculations are based on ellipsoidal geometry and were carried out using Matlab's Mapping Toolbox.

With this approximation the arrival time at RCS is given by:

$$t_{RCS} = t_{HA01} + \frac{d\cos(\theta - \alpha)}{c_g}$$

where t_{HA01} is the arrival time at HA01 (seconds), d is the distance between HA01 and RCS (m), θ is the bearing of the source from HA01, α is the bearing of RCS from HA01 (13.65°), and c_g is the group velocity of the sound. The uncertainty in the predicted arrival time is given by:

$$\delta t_{RCS} = \left|\frac{\partial t_{RCS}}{\partial t_{HA01}}\right| \delta t_{HA01} + \left|\frac{\partial t_{RCS}}{\partial c_g}\right| \delta c_g + \left|\frac{\partial t_{RCS}}{\partial \theta}\right| \delta\theta$$

where $\delta\theta$ is the uncertainty in the bearing to the source (radians) etc. This leads to:

$$\delta t_{RCS} = \delta t_{HA01} + \Delta\frac{\delta c_g}{c_g} + \Delta\tan(\theta - \alpha)\delta\theta$$

where $\Delta = \left|\frac{d\cos(\theta - \alpha)}{c_g}\right|$ is the absolute value of the time delay between the signal arriving at HA01 and at RCS in seconds.

In both cases the predicted and actual arrival times agree within uncertainties, with the maximum discrepancy being 3.2 seconds. This provides strong evidence that the clock synchronisation between HA01 and RCS is at least this accurate.

Table 3. Times are in seconds after 00:00:00 UTC on 8th March 2014.

Arrival time at HA01 (seconds)	Source bearing from HA01 (degrees)	Predicted arrival time difference (seconds)	Predicted arrival time at RCS (seconds)	Actual arrival time at RCS (seconds)	Predicted - actual (seconds)
17961 +/-2	210.2 +/-1	223.2 +/-2	18184.2 +/-4	18181 +/-2	3.2 +/-6
18868 +/-3	208.5 +/-1	225.0 +/-2	19093.0 +/-5	19093 +/-2	0 +/-7

5 Estimate of the probability that events at HA01 and RCS are from the same source

The estimate of the range of the source from HA01 depends on the assumption that the signals received at HA01 and RCS were generated by the same source and at the same time. An estimate has therefore been made of the probability that two signals arriving within a time window that would result in a valid fix, did so purely by chance. It should be noted that this estimate is based on very limited data and should therefore be treated as indicative only.

Let $P(A)$ be the *a-priori* probability that the HA01 and RCS arrivals are from the same source, and $P(B)$ be the *a-priori* probability that an arrival is observed at the RCS within a time interval of the arrival at HA01 that results in a valid fix.

Then $P(\overline{A}) = 1 - P(A)$ is the *a-priori* probability that the arrivals are from different sources and $P(\overline{B}) = 1 - P(B)$ is the a-priori probability that there was no arrival in the time interval required for a valid fix.

We want to calculate the *a-posteriori* probability that the arrivals are signals from the same source, given that the arrival at RCS occurred within the required time interval for a valid fix, i.e. $P(A \mid B)$, based on estimates of the probability of observing an arrival in the required time interval given that the signals are from the same source, i.e. $P(B \mid A)$, and

the probability of observing an arrival in the required time interval given that the signals are not from the same source, $P(B \mid \overline{A})$.

This can be done using Bayes Theorem (Walpole & Myers, 1985) :

$$P(A \mid B) = \frac{P(A)P(B \mid A)}{P(B)} \tag{7}$$

which can also be written:

$$P(A \mid B) = \frac{P(A)P(B \mid A)}{P(A)P(B \mid A) + P(\overline{A})P(B \mid \overline{A})} \tag{8}$$

So the problem reduces to estimating the various probabilities on the right hand side of Eq. (8).

If the signals are from the same source, then the RCS arrival must occur within the valid time interval, so $P(B \mid A) = 1$.

$P(B \mid \overline{A})$ can be estimated by looking at the statistics of similar arrivals at RCS over a long period of time. So far we have only looked at five hours of data, which is only enough for a very rough estimate, however even this is potentially useful as a starting point. There were two arrivals at RCS in that five hour period with broadly similar characteristics (duration and bandwidth) to the HA01 arrival – the one within the feasible time interval and another about 3 hours later. (The second arrival was actually a bit different in that it had a different pulse shape and a somewhat broader bandwidth, but for the purposes of this analysis we'll consider them as two events from the same process.) If we assume these pulses originate from a Poisson process, then an estimate of the process's rate parameter is $\lambda = 2/(5 \times 3600) = 1.11 \times 10^{-4}$ events per second. The probability of receiving k arrivals within a given time interval T is then given by the Poisson probability mass function:

$$P(X = k) = \frac{(\lambda T)^k}{k!} e^{-\lambda T} \tag{9}$$

The probability of receiving one arrival within the feasible time interval is then:

$$P(B \mid \overline{A}) = P(X = 1) = \lambda T e^{-\lambda T} \tag{10}$$

where T is the duration of the feasible time interval and can be determined from the geometry. Valid arrival time differences range from -200 s (for a source 40km from HA01, negative indicates the signal arrives at HA01 first) to +80 s for a source at 15,000km range, giving an interval duration of T =280 s. Substituting this into Eq. (10) with the previously calculated value of λ gives $P\left(B \mid \overline{A}\right) = 0.030$.

The other term required in order to evaluate Equation (8) is $P(A)$, the *a-priori* probability that the HA01 and RCS arrivals are from the same source. This can be interpreted to mean the probability that one would assign given only information about the characteristics of the two signals and without any knowledge of their relative arrival times. The arrivals at HA01 and RCS have very similar durations and spectra that are unlike the majority of other signals received at HA01, and the ratio of their amplitudes is consistent with model predictions. $P(A)$ should therefore be reasonably high, however as it is unclear (at least to the author) how this could be determined from the available data, results are plotted below in Figure 1 with $P(A)$ as a parameter.

It can be seen that providing $P(A)$ is greater than 0.03, $P(A \mid B)$ will be greater than 0.5. Furthermore, if $P(A) > 0.5$, then $P(A \mid B) > 0.97$.

Although the dependence of the final result on the difficult to determine *a-priori* probability, and the small amount of data used to estimate $P(B \mid \overline{A})$ make this analysis somewhat unsatisfactory, it does indicate that it is quite likely that the signals received at HA01 and RCS are from the same source. Analysis of considerably more data from both HA01 and RCS would provide a more robust result, but this has not been attempted.

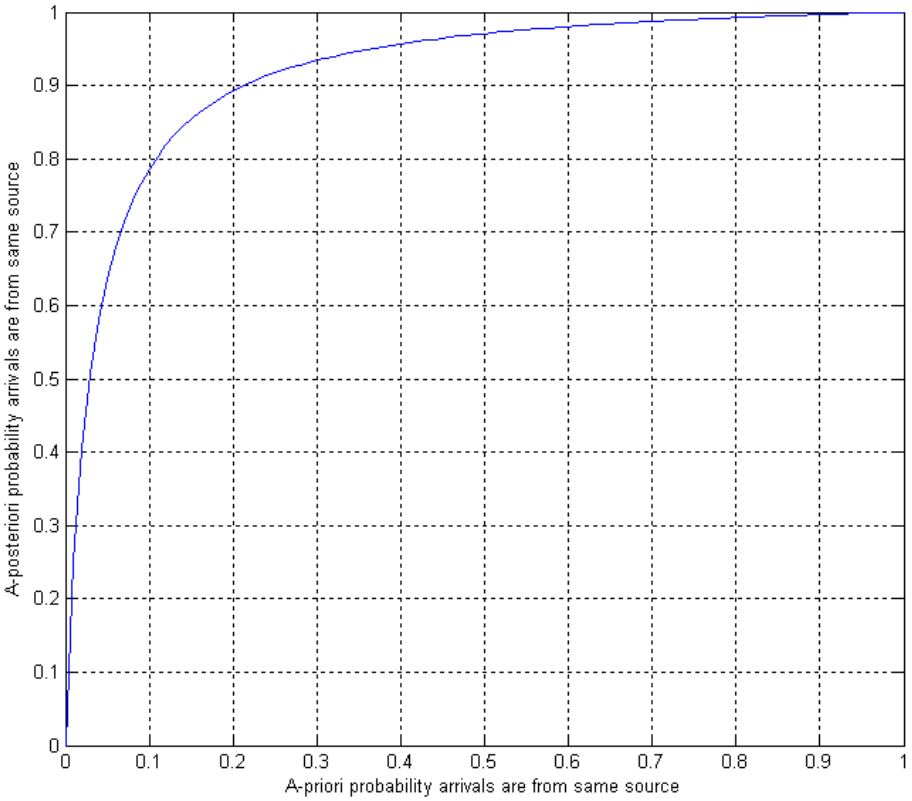

Figure 6.Plot of the a-posteriori probability against the a-priori probability that the arrivals at the two stations are from the same source.

6 Analysis of data from HA08S

Figure 6 shows the automatically calculated arrival bearings as a function of arrival time for all detections at HA08S. These results are summarised in Table 1. The two lines of detections that occur at almost constant bearings of 35° and 113° have characteristics consistent with offshore seismic surveys, which appear to have been taking place off Sri Lanka or in the Bay of Bengal, and off the northwest coast of Australia respectively. There were two other detections, one at about 700 seconds from a bearing of 168.1° and one at 7135 seconds from a bearing of 93°. Position lines corresponding to these various detections are shown in Figure 8.

A curve showing the expected arrival bearing at HA08S as a function of arrival time for the signal detected at HA01 at 01:34:50 on 8/3/2014 UTC is overlaid on Figure 6 It can be seen that neither of the discreet detections is consistent with the HA01 data.

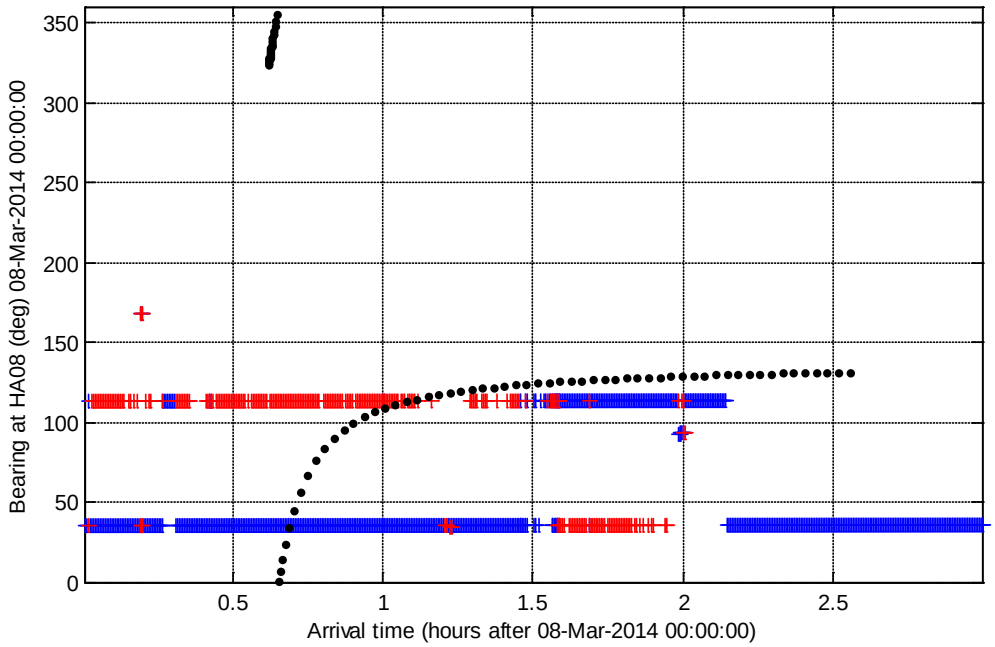

Figure 7. All automatic detections at HA08S between 00:00:00 and 03:00:00 UTC on 8th March 2014. The black dotted line shows the expected arrival bearing at HA08S as a function of arrival time for the signal detected at HA01 at 01:34:50 on 8/3/2014 UTC.

Table 4 Summary of HA08S detections

Time range (hours after 00:00:00 on 8/3/2014 UTC))	**Bearing range (deg)**	**Figure 7 line colour**	**Likely source**
0 to 3.00	34.9 - 35.4	Yellow	Seismic survey off Sri Lanka or in Bay of Bengal
0 to 2.14	113.0 - 113.6	Green	Seismic survey off NW Australia
0.19 to 0.20	168.05	White	Unknown. Possibly ice cracking noise or a small seismic event.
1.98 to 2.00	92.5 to 93.5	Red	Small earthquake in the Java Trench

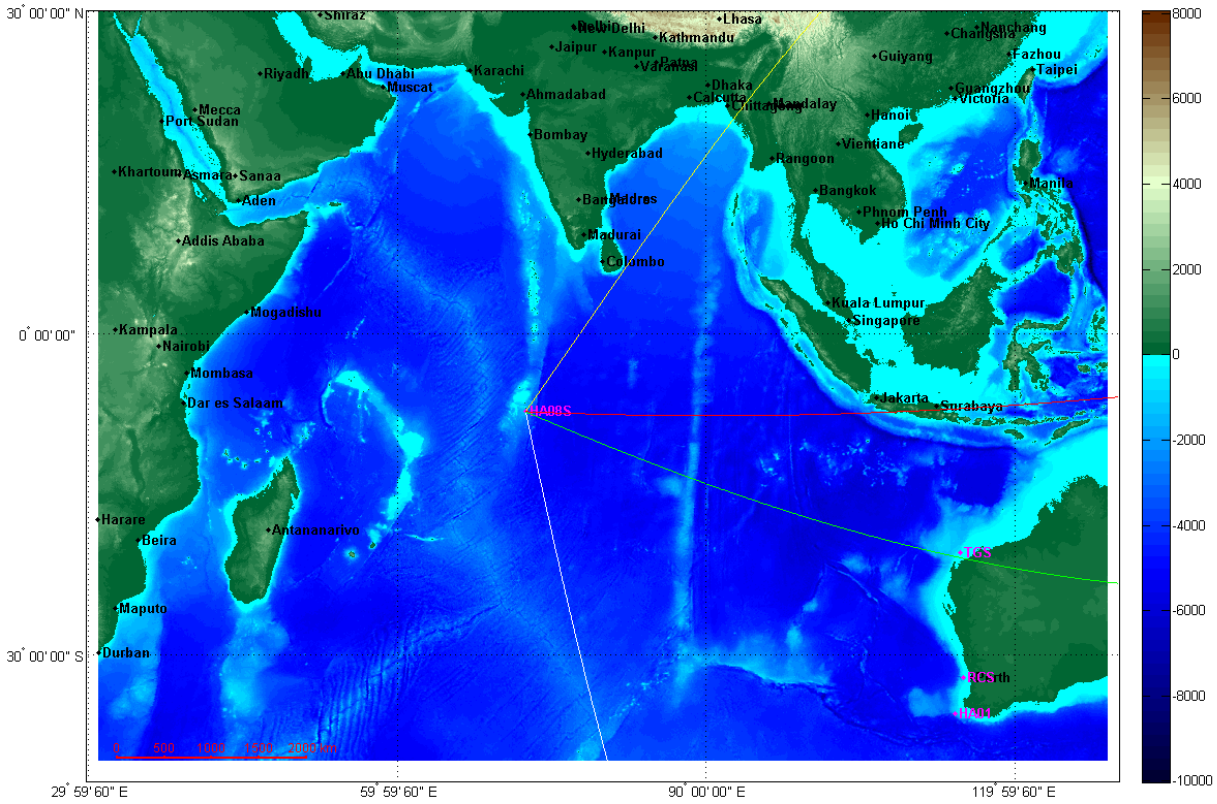

Figure 8. Map showing position lines for the HA08S detections listed in Figure 4. The location of the TGS seismic survey is shown by the magenta dot labelled "TGS".

Enquiries with industry contacts revealed that at the time MH370 is thought to have crashed, two seismic surveys were taking place off the northwest coast of Australia, close to the position line based on the 113° bearing from HA08S. These were the Woodside Centaurus 3D Survey and the TGS Huzzas 3D Survey. Both operators have provided the navigation data from the relevant survey lines, which are plotted in Figure 8.

The Woodside survey line was over a fairly flat seabed in just over 1000 m of water, whereas the TGS survey was over the continental slope in about 260 m of water. The time of reception of the last shot and the change in bearing with time both clearly indicate that the signals received at HA08S were from the TGS survey. The Woodside survey was not detected. This is consistent with the physics of acoustic propagation which requires a shallow sound source, such as a seismic survey airgun array, to be over a favourably sloping seabed in order to efficiently couple the sound into the Deep Sound Channel and achieve very long range propagation.

The navigation data provided by TGS allowed a check to be made of the bearing accuracy of HA08S. The results are plotted in Figure 9 and show a mean bearing offset of 0.6°. The resolution of the bearing measurement is sufficient to clearly track the northeast to southwest motion of the survey vessel.

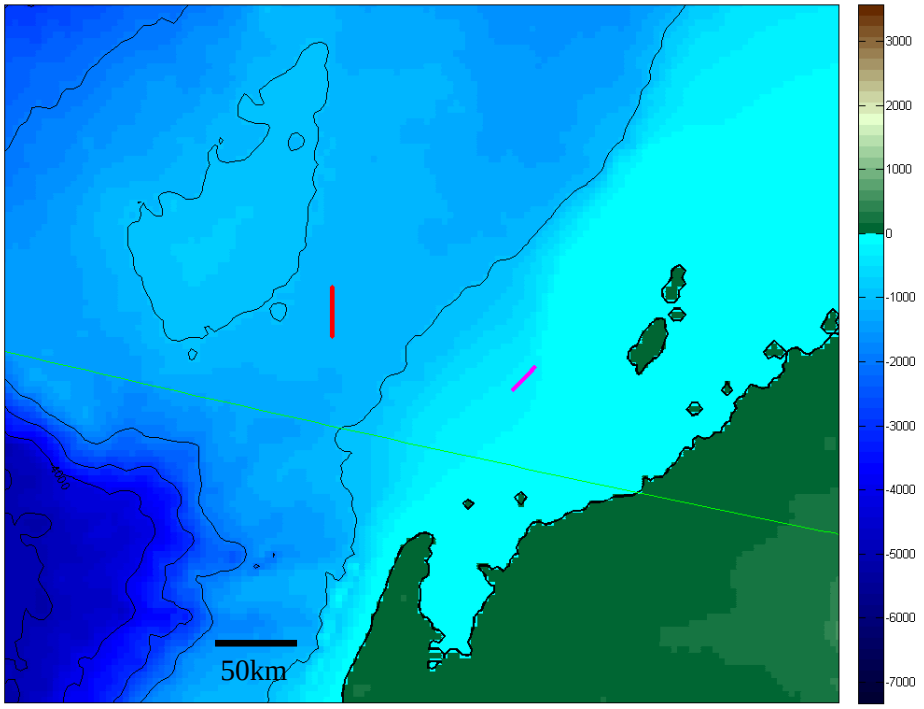

Figure 9. Map of Northwest Cape region, Australia, showing seismic survey lines being shot by Woodside (red) and TGS (magenta) around the time MH370 is thought to have crashed. The green line is the position line from HA08S

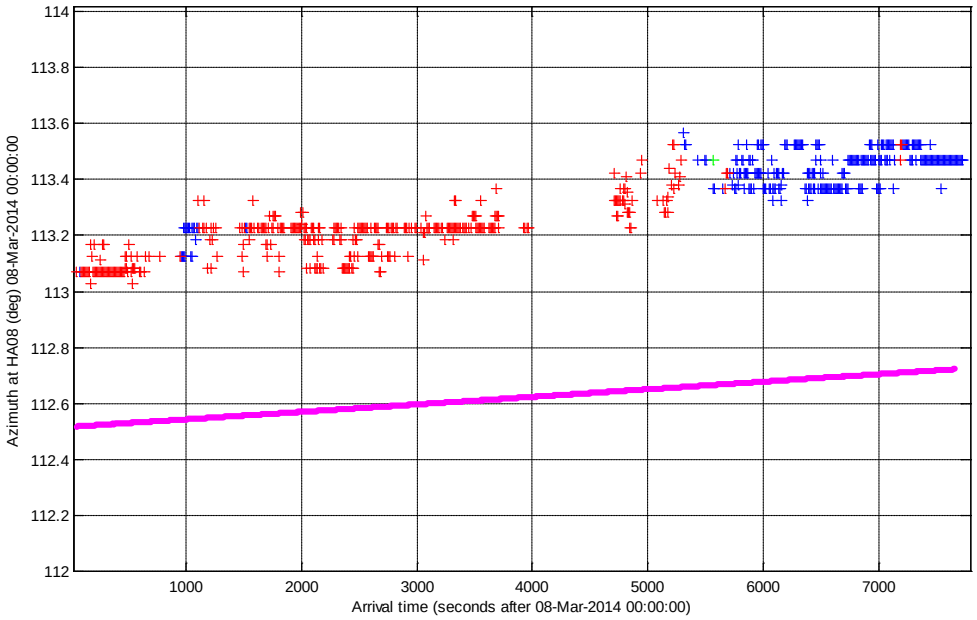

Figure 10.Plot of bearing vs. time for detections at HA08S that correspond to the TGS Huzzas 3D seismic survey (crosses). The magenta line is the calculated bearing based on the survey navigation data provided by TGS.

7 Discussion

Even with the largest likely uncertainties of +/- 1° in the bearing from HA01 and +/- 7s in the difference between the times of arrival of the signals at HA01 and RCS, the uncertainty region for the source location does not intersect the arc defined by the last satellite handshake (see Figure 11). An investigation of the timing error required to place the source location on the satellite handshake arc indicated that the arrival time difference would have to be 17 seconds less than measured, which is well outside uncertainties. Our estimate of the time of arrival of the signal at HA01 has been confirmed by Mark Prior from the CTBTO in Vienna, and the correction for clock drift in the RCS recorder has been checked and rechecked. Furthermore, the time calibration checks described in Section 4 provide independent confirmation that time of arrival measurements made at the two stations are consistent once the clock drift correction has been applied.

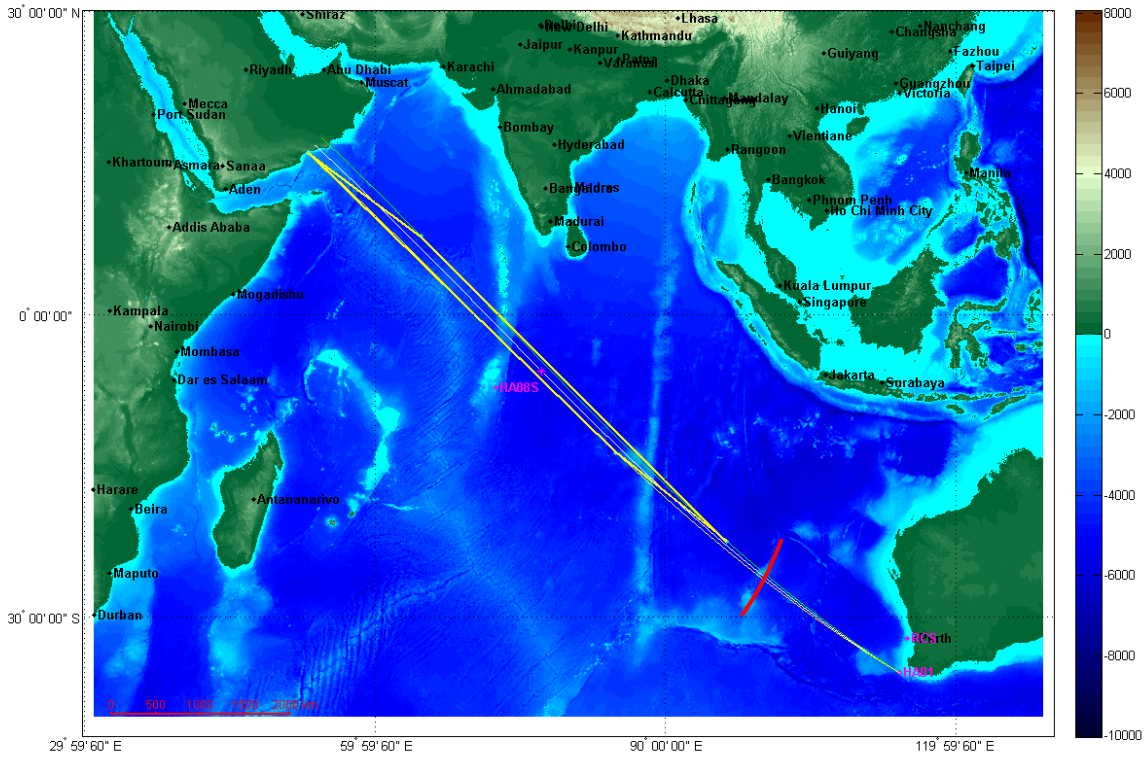

Figure 11. Map showing the uncertainty region (yellow polygon) based on an uncertainty of +/- 1° in the bearing from HA01 and +/- 7s in the arrival time difference, with the approximate location of the arc defined by the satellite handshake data superimposed (red line).

It is therefore apparent that the acoustic measurements are inconsistent with the satellite handshake data. We consider three possible explanations for this:

1. The signals received at HA01 and RCS are from the same acoustic event, but the source of the signals is unrelated to MH370.

This seems the most likely explanation as the characteristics of the received signals are similar to those of some natural events. The origin of these events is not certain, but they are thought to be of natural seismic origin. Events from this particular direction are not particularly common, but do occur. An analysis of five years of historical data from HA01 that was available to the authors indicated that over that period there was an average of about one event per day from this direction. However, on closer inspection it became apparent that most of these events occurred on one day, and then became progressively less frequent. (This is a common pattern with natural seismic events.) It would be useful to analyse data from the year or so leading up to 8th March 2014 in order to obtain a better estimate of the statistics relevant to that date, but this has not been done.

2. The signals received at HAO1 and RCS are from different acoustic events, which may or may not be related to MH370.

If this were the case then the distance determination would be invalid and the source of the signal received at HA01 could be anywhere along the position line defined by the measured bearing from HA01, including on the satellite handshake arc. However, the analysis carried out in Section 5, while imperfect, indicates that it is more likely that the signals received at the two stations are from the same event. Also, if the sound source was on the satellite arc the signal would have been generated at 01:16:19 UTC on 8th March, some 25 minutes after the latest time it is thought that MH370 could have hit the water (00:51:00 UTC according to ATSB). The signal could, however, have been generated by the implosion of sinking debris if this occurred well after the initial impact, although this would be expected to be within a few km of the surface impact site.

3. The signals received at HA01 and RCS are from the same acoustic event, and the source of the signals is related to MH370, but there is a problem with the position line determined from the satellite handshake data.

If this were the case then the location of the aircraft would be much further from the Australian coast than the satellite handshake data would indicate. This explanation seems unlikely given the intense scrutiny that the satellite handshake data has been subjected to, however it is worth noting that the time at which the signal was received at HA01 is consistent with the time the aircraft is thought to have crashed if the impact occurred in the central portion of the uncertainty box plotted in Figure 3. To make this explicit, Figure 12 plots the source locations for a signal generated at the earliest possible impact time (00:19:49 UTC - north-western triangle), at the latest possible impact time (00:51:00 UTC - south-eastern triangle) and following the arc given by the signal received at HA01, based on the computed acoustic travel time to HA01 assuming a mean group velocity of 1486 m/s. These extreme locations can be seen to bracket the most probable position obtained solely from the acoustic data.

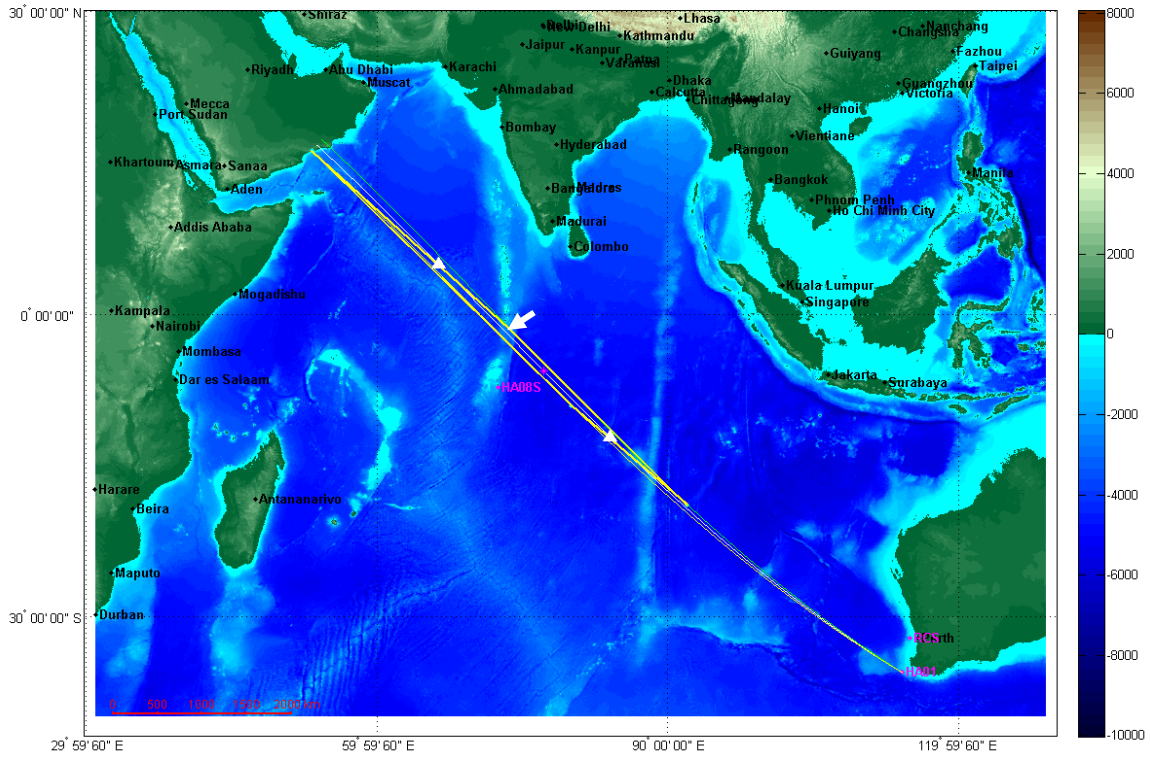

Figure 12. Map showing the smaller uncertainty box with range limits based on the earliest and latest times it is thought the aircraft could have hit the water superimposed (white triangles), assuming the aircraft crash was along the arc from HA01 given by the signal of interest. The arrow indicates the only area between these range limits that also satisfies the requirements for efficient coupling of sound from a near-surface source into the Deep Sound Channel.

Another consideration is that for sound from a near-surface sound source to be detectible at ranges of thousands of kilometres it must couple into the Deep Sound Channel well. A near surface source will generate sound in the water mostly at steep angles and will not efficiently couple into the Deep Sound Channel unless the seabed bathymetry is favourable. For the signal sound energy to couple into the Deep Sound Channel it is necessary for the seafloor at the source location to be sloping downwards towards the receiver. This allows sound reflected from the seabed to be directed into the Deep Sound Channel where it can propagate with very little attenuation. This process is most effective when the water depth is also shallow enough that the seabed intersects the Deep Sound Channel, the axis of which lies somewhere between 800-1200 m depth depending on latitude.

The only area between the locations defined by the earliest and latest impact times along the arc form HA01 given by the signal of interest that satisfies this criterion is on the Chagos-Laccadive Ridge, the submarine ridge that extends northwards from HA08S. The bearing from HA01 crosses this ridge at approximately 2.3°S, 73.7°E, just south of the Maldives, as indicated by the arrow in Figure 12.

The water depths along this bearing of 301.6°, and bearings 0.75° either side of it are plotted as a function of range from HA01 in Figure, along with plots of the computed acoustic transmission loss between a 20 Hz sound source, 30 m below the water surface, and HA01. Note that the way the transmission loss is plotted, an upward excursion corresponds to a reduction in transmission loss, which corresponds to an increase in the received signal. The transmission loss was computed using the Parabolic Equation acoustic propagation model RamGeo (Collins 1993), using range-dependent sound speed profiles from the World Ocean Atlas, 2005 (NOAA 2005), and assuming a low reflectivity, silt seabed with geoacoustic parameters from Jensen (2011). The effect would be enhanced if the seabed were harder and more reflective. Transmission loss calculations were also carried out for frequencies of 10 Hz and 40 Hz and produced similar results.

As expected, oceanographic features that result in sharp reductions in water depth give rise to corresponding reductions in transmission loss, which would correspond to an improved likelihood of detecting a signal for a source at that location. The effect does, however, depend critically on water depth. It can be seen that the Chagos-

Laccadive Ridge is too deep to have much effect along a bearing of 301.6° where it reaches a minimum depth of about 2200 m, but reduces the transmission loss by 20 dB along 302.36° where it rises to a minimum depth of just over 1000m.

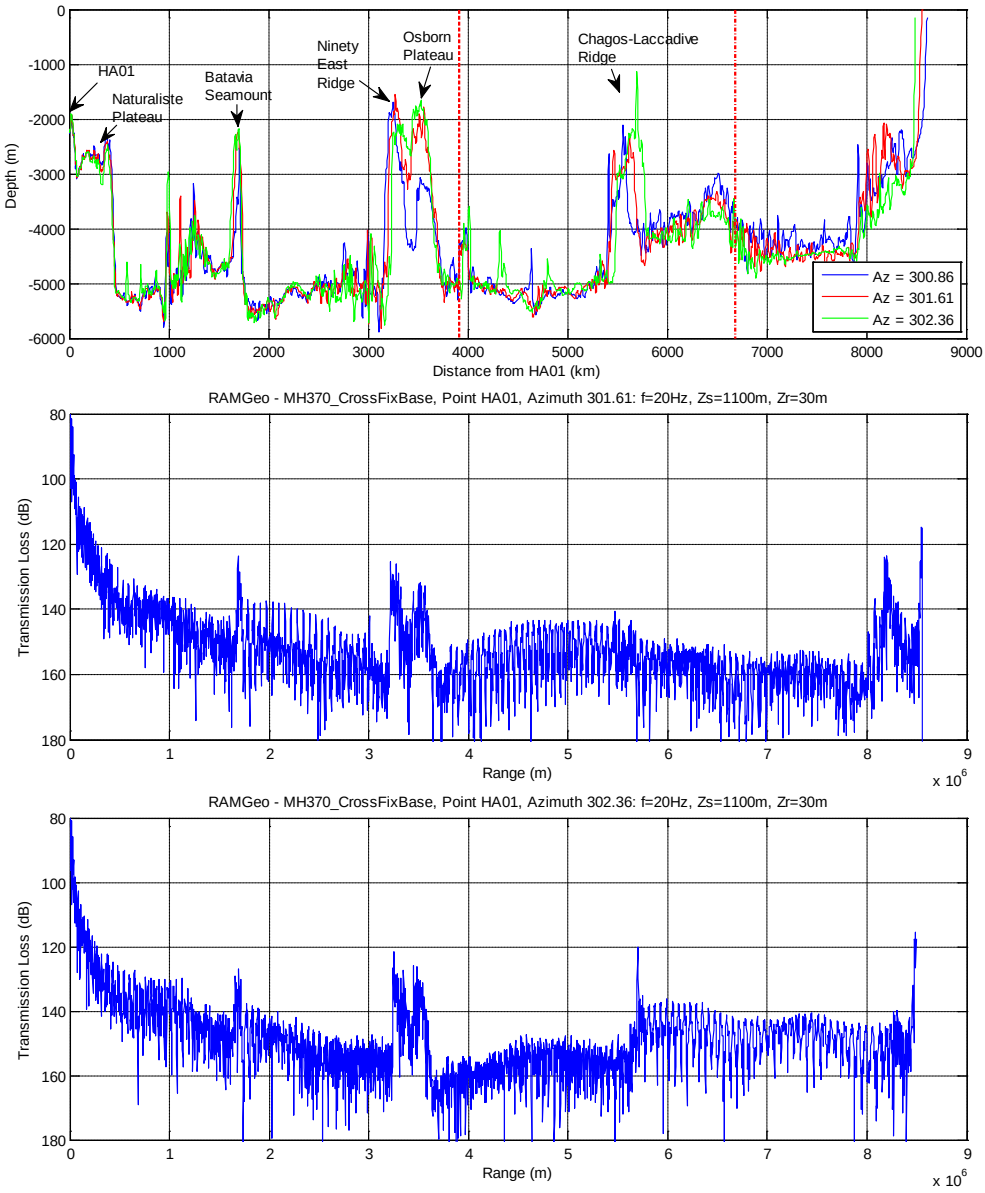

Figure 13. Top panel shows the bathymetry along the position line defined by a bearing of 301.61° from HA01, and bearings 0.75° either side of this as a function of distance from HA01. Red vertical lines indicate the range limits computed from the earliest and latest possible impact times. Various oceanographic features are indicated. The middle and lower panels show the computed transmission loss between a 20Hz acoustic source, 30m below the water surface, and HA01 as a function of range from HA01. Middle panel is for a bearing of 301.61°, lower panel is for 302.36°.

The above argument applies only if the source of the sound was the impact of the plane on the water surface. If it was the implosion of sinking debris, some time after

the impact, then the location could be closer to HA01 than the range limits based on the impact time would indicate. If the implosion occurred in the upper one hundred metres or so of the water column then the same considerations regarding bathymetry would apply, and other possible locations for the aircraft would include the Ninety East Ridge and the Osborn Plateau. However, if an implosion occurred deeper, then efficient deep sound channel propagation would be possible irrespective of the bathymetry. This effect is illustrated in Figure 14, which plots the transmission loss as a function of the distance of the source from HA01, and the source depth.

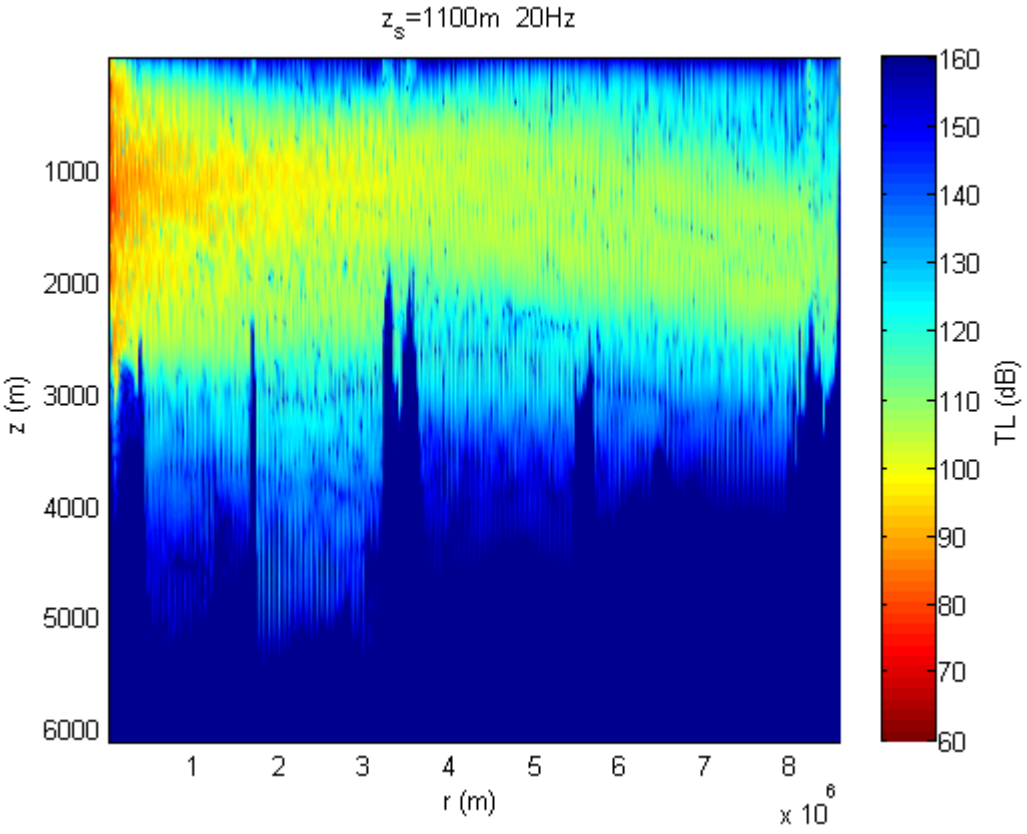

Figure 14.Transmission loss for 20 Hz acoustic signals arriving at HA01 at a bearing of 301.61° as a function of the distance of the source from HA01 and the depth of the source.

CMST are attempting to obtain other sources of acoustic data from the Indian Ocean which may contain the signals discussed here and may allow a better definition of the acoustic data discussed here. These sources are:

1. IMOS passive acoustic recorder located west of Dampier, North Western Australia (19º 23.06' S, 115º 54.92). This mooring is expected to be recovered in early August 2014. This receiver is on a 33% duty cycle.
2. IMOS passive acoustic recorder located north of Broome, North Western Australia (15º 29.002' S, 121º 15.06' E). This mooring is expected to be recovered in early August 2014. This receiver is on a 33% duty cycle.
3. Marine seismic survey recordings operating in the northern Indian Ocean over the time frame of aircraft impact. We have had an excellent response from the marine seismic community with regard to searching for seismic surveys operating in this area over the time frame of interest. If we can locate seismic surveys which were operating over the time frame of interest in areas where it is possible they may have received the signals disucssed here we will request their streamer data to check for signals of interest. Marine seismic surveys tyically collect data at a 60-80% duty cycle although analysis would be complicated by the presence of the intense marine seismic source signals.

8 Conclusions

Analysis of the low frequency acoustic signals that were received at RCS and HA01 around the time that MH370 disappeared has identified one acoustic event that could possibly be linked to the loss of the aircraft. It is also possible that this was a natural event and unrelated to the aircraft.

A detailed analysis of these signals has resulted in an approximate localisation for the source of the signals that is compatible with the time of the last satellite handshake with the aircraft, but not compatible with the satellite to aircraft range derived from this handshake which is being used to guide the search. There appear to be three possible explanations for this discrepancy:

1. The signals received at HA01 and RCS are from the same acoustic event, but the source of the signals is unrelated to MH370.
2. The signals received at HAO1 and RCS are from different acoustic events, which may or may not be related to MH370.

3. The signals received at HA01 and RCS are from the same acoustic event, and the source of the signals is related to MH370, but there is a problem with the position line determined from the satellite handshake data.

Of these, the first explanation seems the most likely as the characteristics of the signals are not unusual, it is only their arrival time and to some extent the direction from which they came that make them of interest.

If the second explanation was correct then there would still be some prospect that the signal received at HA01 could be related to the aircraft, in which case the combination of the HA01 bearing and the position arc derived from the satellite handshake data would provide an accurate location on which to base a search. However, the analysis carried out here indicates that, while not impossible, this explanation is unlikely.

The third explanation also seems unlikely because of the intense scrutiny the satellite handshake data has been subjected to, however, should the arc defined by the handshake data be called into question, the various acoustic considerations discussed here would suggest that a reasonable place to look for the aircraft would be near where the position line defined by a bearing of 301.6° from HA01 crosses the Chagos-Laccadive Ridge, at approximately 2.3°S, 73.7°E. If the source of the detected signals was the aircraft impacting the sea surface then this would most likely have occurred in water depths less than 2000 m and where the seabed slopes downwards towards the east or southeast. This consideration could be used to further refine the search area. If, instead, the received sounds were due to debris imploding at depth it is much less certain where along the position line from HA01 this would have occurred.

The CMST are still to receive further passive acoustic data which may improve the location estimate provided here and allow a better definition of the signal source.

References

Collins, M. D. (1993), A split-step Pade solution for the parabolic equation method. *The Journal of the Acoustical Society of America*, 93(4), 1736-1742.

del Pezzo, E., and Giudicepietro, F. (2002), Plane wave fitting method for a plane, small aperture, short period seismic array: a MATHCAD program, *Computers & Geosciences,* Vol. 28, pp 59-64.

Jensen, F. B., Kuperman, W. A., Porter, M. B., & Schmidt, H. (2011). *Computational Ocean Acoustics,* Springer, ISBN 978-1-4419-8677-1.

Menke W., (1984), *Geophysical Data Analysis: Discrete Inverse Theory,* Academic Press, New York.

Walpole, R. E., and Meyers, R. H. (1985),*Probability and Statistics for Engineers*, Macmillan, ISBN 0-02-946950-3.

NOAA. (2005), *World Ocean Atlas*, National Oceanic and Atmospheric Administration, National Environmental Satellite, Data, and Information Service 61-62, U.S. Government Printing Office, Washington, D.C., 182 pp., CD-ROM

Appendix I – Results of analysis of Scott Reef IMOS underwater sound recorder data for the time of the disappearance of Malaysian Airlines Flight MH370 on 8th March 2014

Results of analysis of Scott Reef IMOS underwater sound recorder data for the time of the disappearance of Malaysian Airlines Flight MH370 on 8th March 2014.

Alec Duncan, Rob McCauley, Alexander Gavrilov
Centre for Marine Science and Technology, Curtin University
4th September 2014

Introduction

An underwater sound recorder that forms part of the Integrated Marine Observing System System (IMOS) and was located off Scott Reef, Western Australia has recently been recovered. Data from the recorder was downloaded on 3rd September 2014. The recorder was located at 15° 29.002' S, 121° 15.060' E. This data set is of interest because the recorder was operational at the time that Malaysian Airlines Flight MH370 went missing on 8th March 2014.

Results

Signals and their spectrograms recorded between 01:00:00 UTC and 02:20:00 UTC on 8th March 2014 are plotted in the Appendix. Each recording is of five minutes duration and recordings started every 15 minutes, commencing approximately 15 seconds before the hour. The 15 second offset was due to drift of the noise recorder's internal clock relative to UTC. Drift was corrected by comparing the noise recorder's clock to UTC from a GPS receiver before deployment and after recovery, and assuming a constant drift rate during deployment.

The recordings are dominated by Bryde's whale calls in the 25Hz to 50 Hz frequency range, and also contain a number of short, impulsive signals of unknown but probably local origin. Of particular interest is a signal with considerable energy below 20 Hz commencing at 01:32:49 UTC. This signal and its spectrogram are shown in Fig. 1. The structure of the low frequency arrival is shown more clearly in Fig. 2, which is the same data after filtering with a 15 Hz, 4th order, low pass Butterworth filter to remove the whale calls and other higher frequency signals. It appears to consist of an initial high amplitude arrival of about ten seconds duration followed by a lower amplitude tail that lasts for at least another 100 seconds (the logger stopped recording before the end of the signal). The duration and frequency content of the initial high amplitude arrival are consistent with the signals received at the Comprehensive Nuclear Test-ban Treaty hydroacoustic station, HA01 at 01:34:50 UTC, and with the corresponding signal received at the IMOS underwater recorder off Rottnest Island (Duncan et. al. 2014).

The arrival time of this signal at the Scott Reef recorder is also within the range of possible times of arrival of signals from the event that generated the signal received at HA01, at 01:34:50 UTC.

A least squares fix was calculated based on the signal arrival time and arrival direction at HA01 and the arrival times at the Rottnest and Scott Reef IMOS recorders. The results are given in Table 1 and plotted in Fig. 3. The estimated position is close to the

Carlsberg Ridge, a geologically active mid-ocean spreading ridge, and is about 400km southeast of the position obtained by Dall'Osto and Dahl (2014) based on a low frequency arrival at HA08S, and the HA01 direction and arrival time data.

Conclusions

It is impossible to be certain that the Scott Reef IMOS recorder arrival at 01:32:49 UTC is from the same event as the arrivals at HA01 and the Rottnest IMOS recorder that have been analysed previously, however they share enough characteristics that it seems plausible that they are from the same event. Assuming this is the case results in an event location that is near the geologically active Carlsberg Ridge southwest of India. This location, together with the lower amplitude tail that appears to extend at least 100 seconds after the initial onset makes it likely that the event is of geological origin.

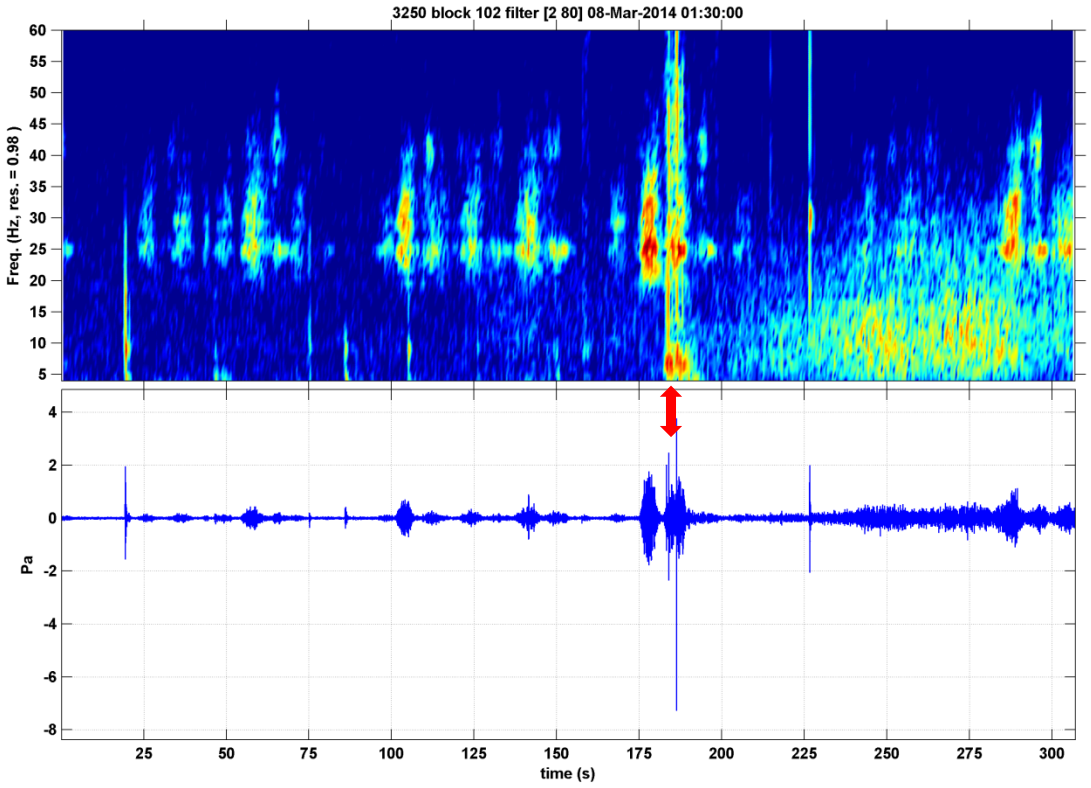

Fig. 1. Signal and spectrogram of the recording commencing at 01:29:45.9 UTC (drift corrected). The beginning of the 01:32:49 arrival is marked by the red arrow at about 180 seconds.

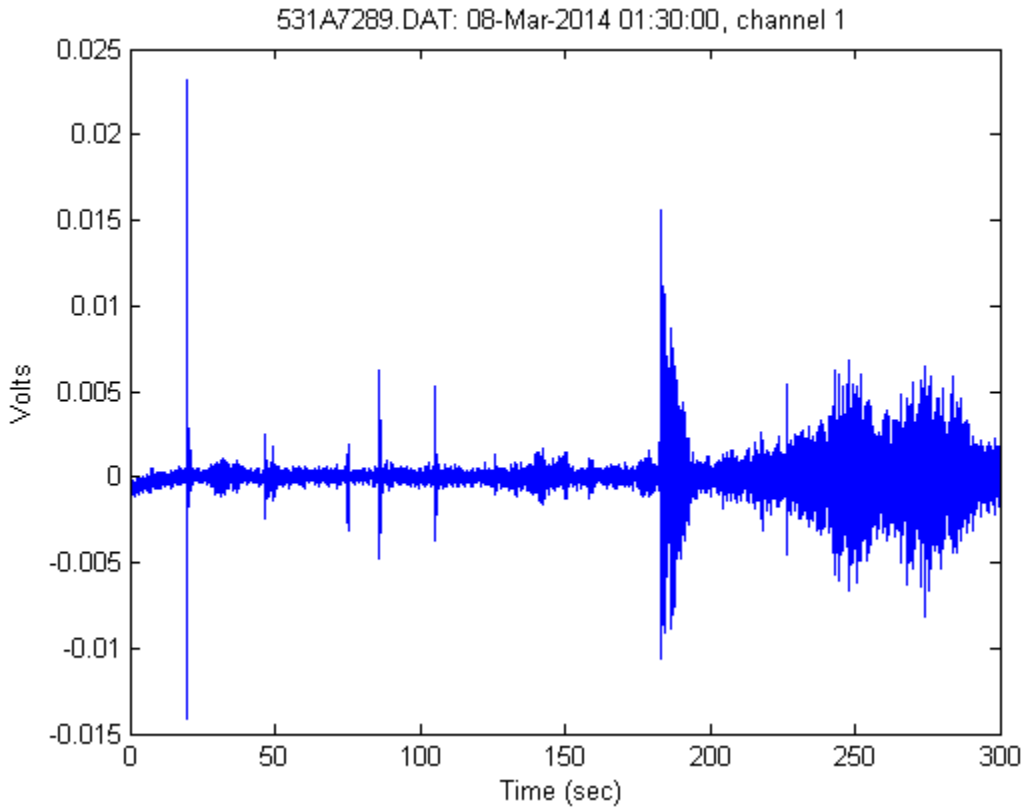

Fig. 2. The same signal after filtering with a 4th order low pass Butterworth filter with a 15Hz cutoff frequency. Times are relative to 01:29:45.9 UTC (drift corrected).

Table 1. Least squares fix results

Estimated event position (WGS84)	2.11°N, 69.31°E
Standard deviation in estimated latitude, longitude	0.67°, 0.96°
Covariance between latitude and longitude estimates	-0.63 $(°)^2$
Estimated event time	00:25:13.3 UTC on 8th March 2014
Standard deviation in estimated event time	85 s
HA01 angle measurement residual	0.06°
HA01 time measurement residual	-0.2 s
Rottnest time measurement residual	1.7 s
Scott Reef time measurement residual	-0.04 s

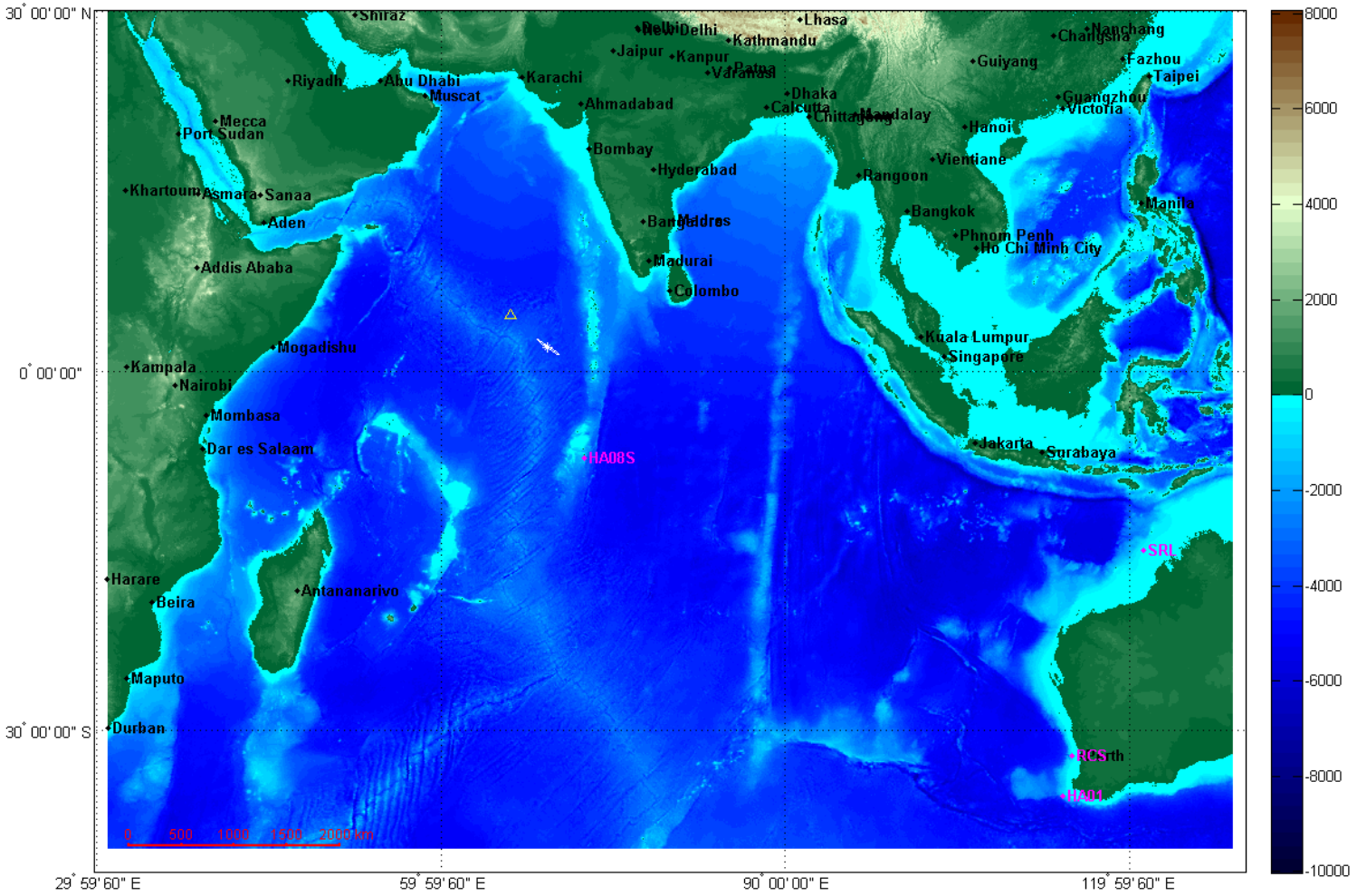

Fig. 3. Map showing least squares fix location (white asterisk) based on the signal arrival time and arrival direction at HA01 and the arrival times at the Rottnest and Scott Reef IMOS recorders. The white ellipse is the nominal 95% confidence area. The yellow triangle is the position obtained by Dall'Osto and Dahl (2014) based on a low frequency arrival at HA08S, and the HA01 direction and arrival time data.

APPENDIX: All Scott Reef Logger Recordings from 01:00:00 UTC to 02:20:00 UTC on 8th March 2014

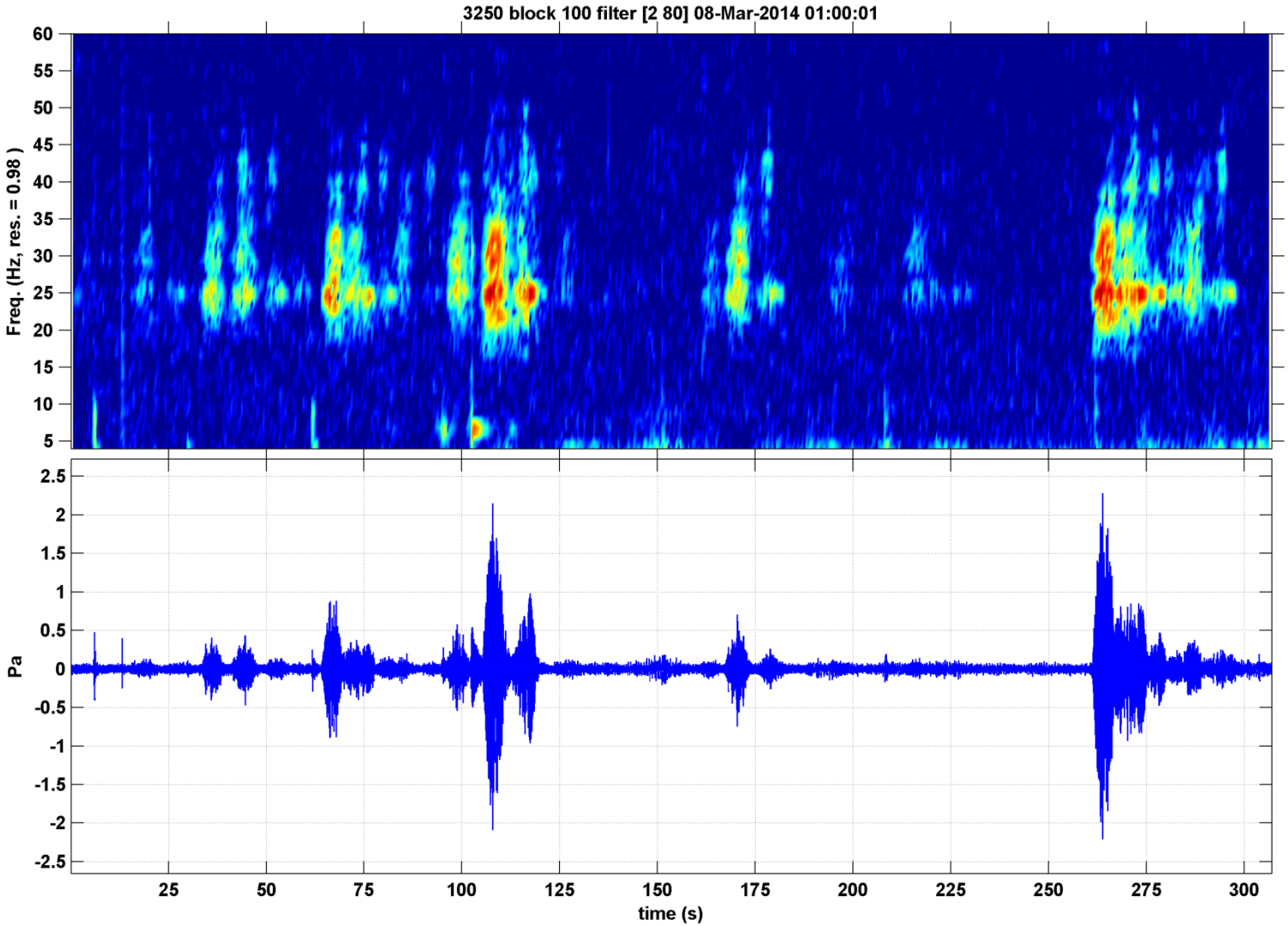

Block 100. Times are relative to 8-03-2014 0:59:46.3 UTC (drift corrected)

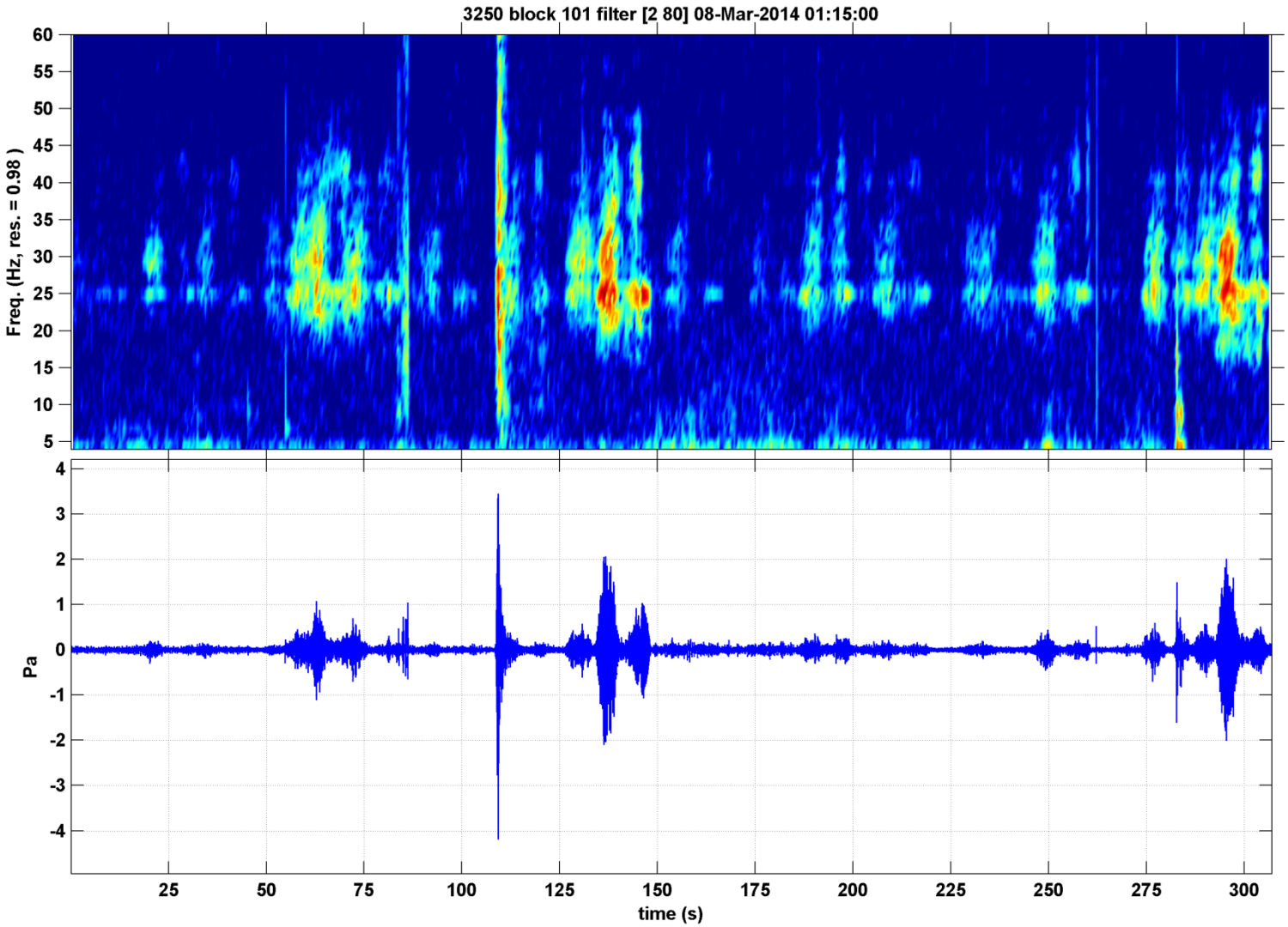

Block 101. Times are relative to 8-03-2014 1:14:45.8 UTC (drift corrected)

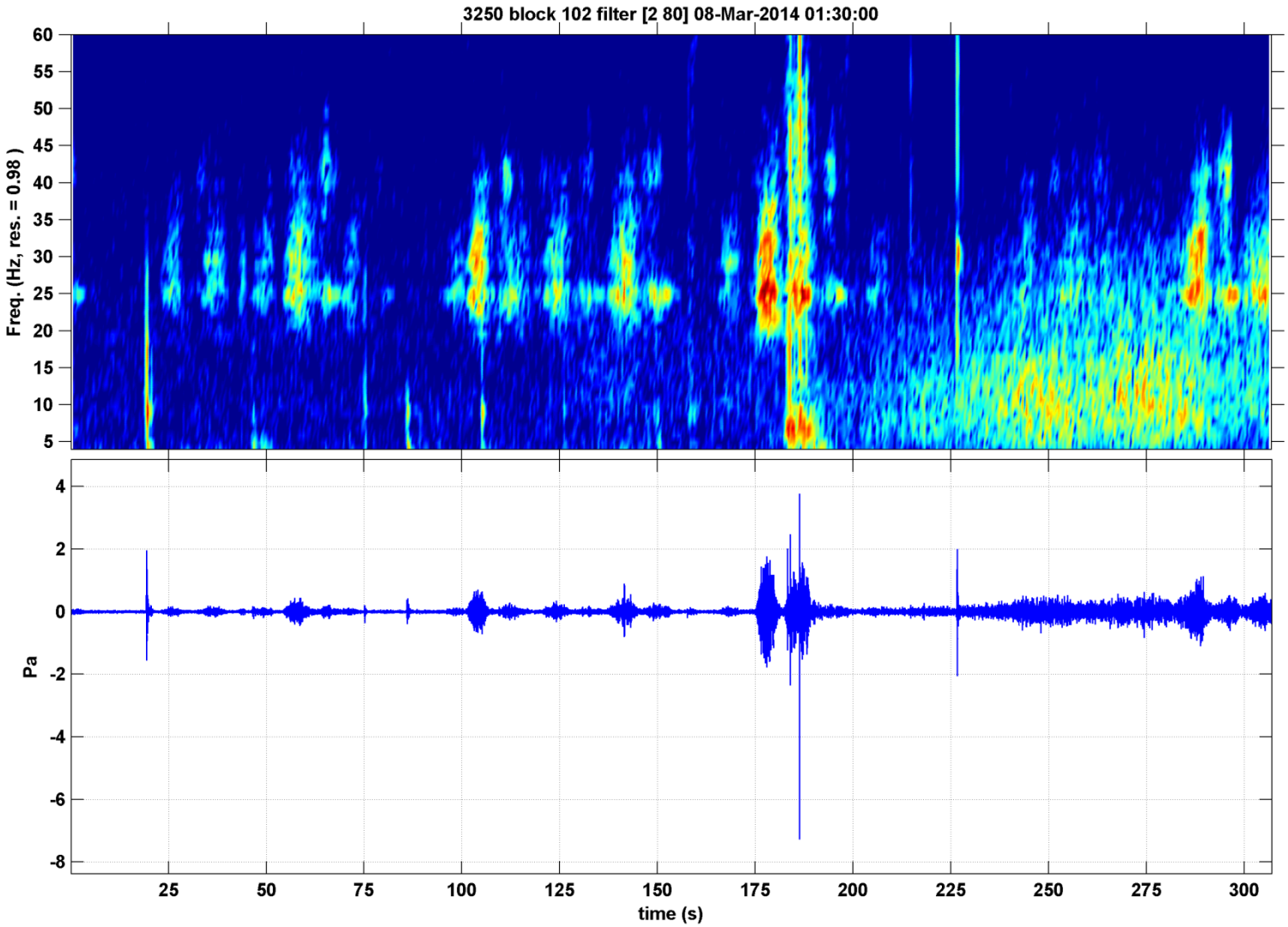

Block 102. Times are relative to 8-03-2014 1:29:45.9 UTC (drift corrected)

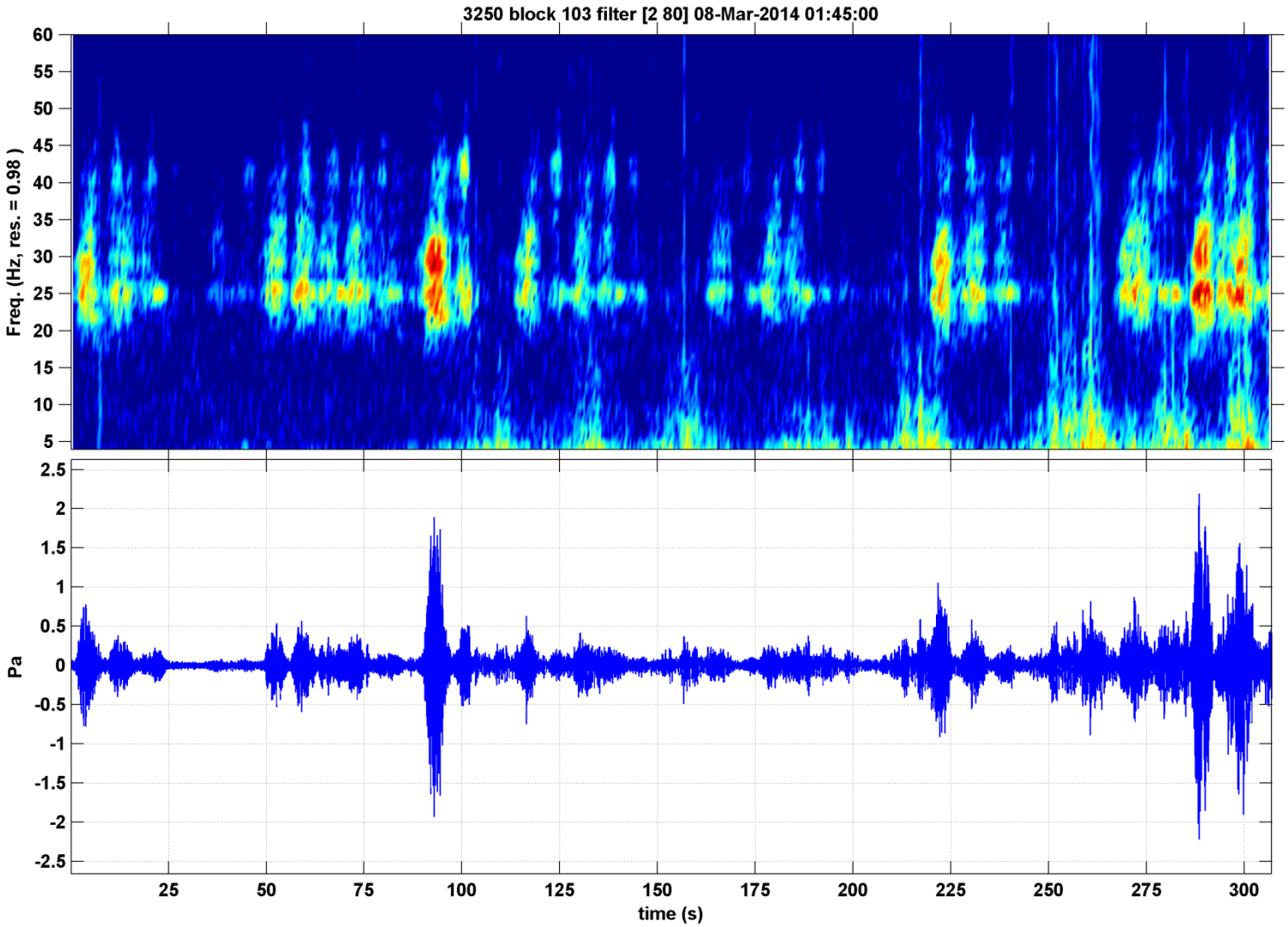

Block 103. Times are relative to 8-03-2014 1:44:45.7 UTC (drift corrected)

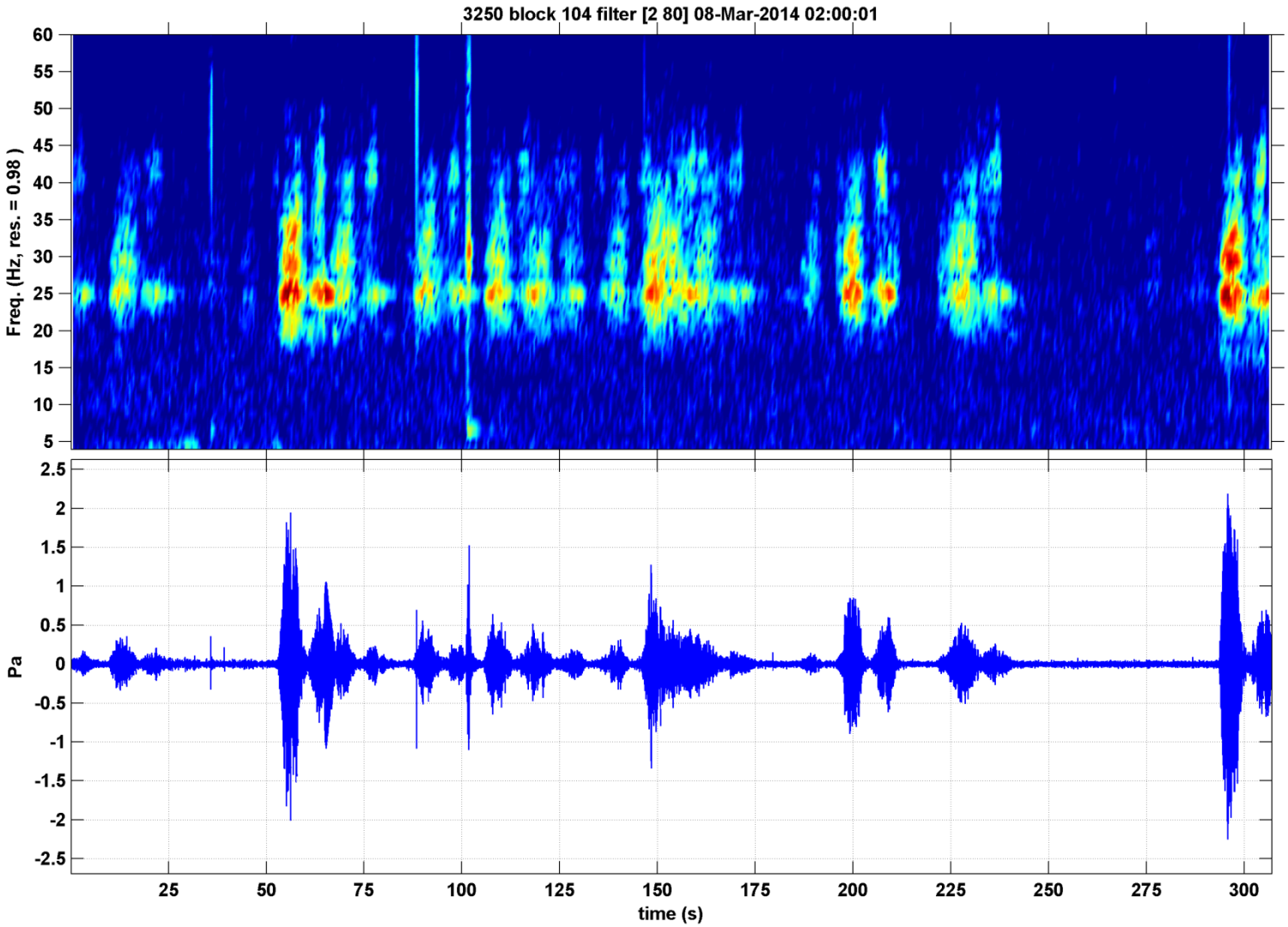

Block 104. Times are relative to 8-03-2014 1:59:46.1 UTC (drift corrected)

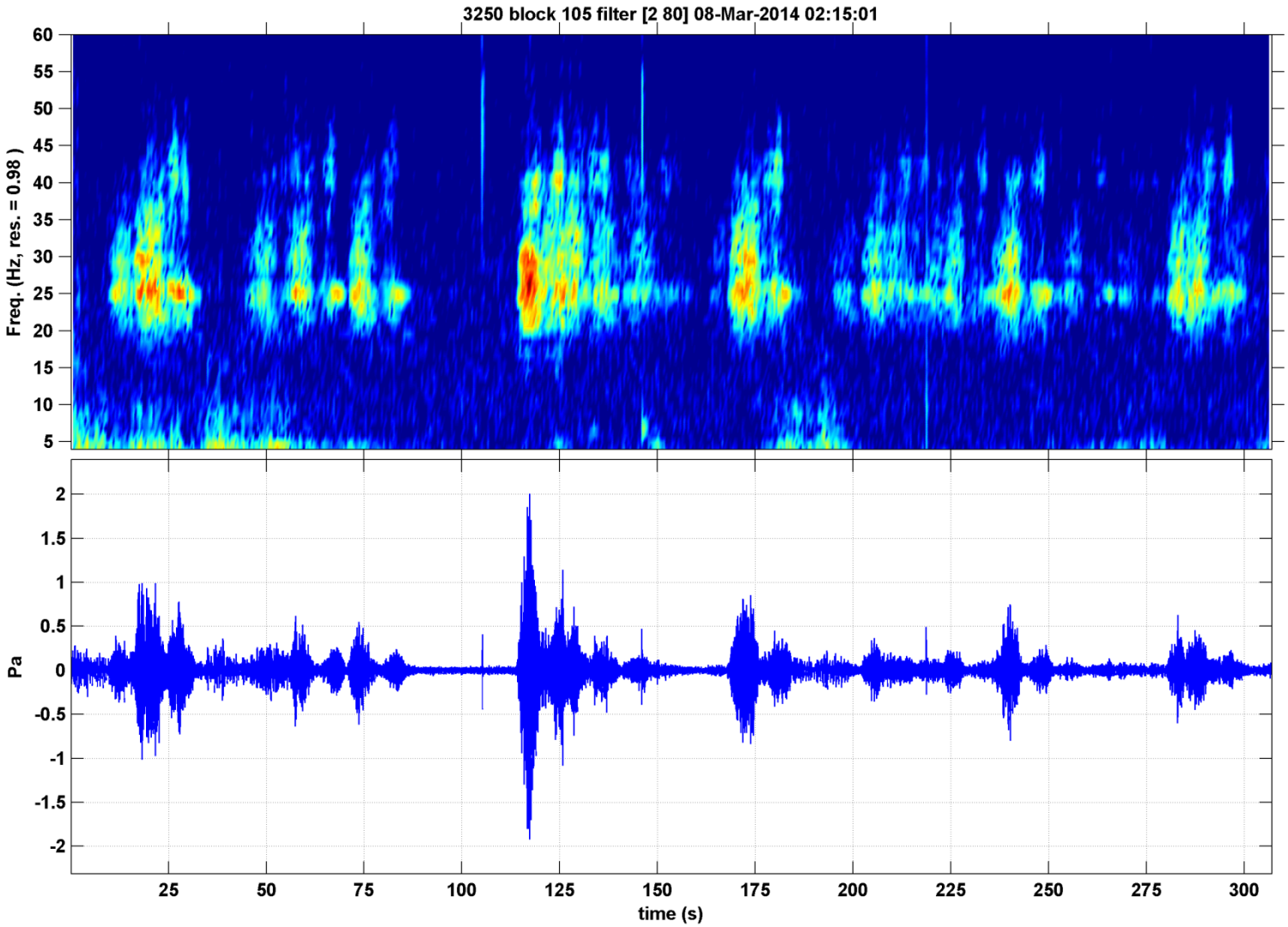

Block 105. Times are relative to 8-03-2014 2:14:46.4 UTC (drift corrected)

References

Dall'Osto, D. R., and Dahl, P. H. "Analysis of hydroacoustic signals from Diego Garcia South CTBTO station in support of Curtin University analysis of Cape Leeuwin CTBTO data regarding possible location of MH370 crash", Applied Physics Laboratory, University of Washington, Seattle, July 2014.

Duncan, A. J., Gavrilov, A. N., McCauley, R. D., "Analysis of Low Frequency Underwater Acoustic Signals Possibly Related to the Loss of Malaysian Airlines Flight MH370", Centre for Marine Science and Technology Report 2014-30, June 2014.

Appendix J – Seismic and hydroacoustic analysis relevant to MH370

LA-UR-14-24972
Approved for public release; distribution is unlimited.

Title: Seismic and hydroacoustic analysis relevant to MH370

Author(s): Stead, Richard J.

Intended for: Report

Issued: 2014-07-03

Disclaimer:
Los Alamos National Laboratory, an affirmative action/equal opportunity employer,is operated by the Los Alamos National Security, LLC for the National NuclearSecurity Administration of the U.S. Department of Energy under contract DE-AC52-06NA25396. By approving this article, the publisher recognizes that the U.S. Government retains nonexclusive, royalty-free license to publish or reproduce the published form of this contribution, or to allow others to do so, for U.S. Government purposes. Los Alamos National Laboratory requests that the publisher identify this article as work performed under the auspices of the U.S. Departmentof Energy. Los Alamos National Laboratory strongly supports academic freedom and a researcher's right to publish; as an institution, however, the Laboratory does not endorse the viewpoint of a publication or guarantee its technical correctness.

Seismic and hydroacoustic analysis relevant to MH370

Abstract

The vicinity of the Indian Ocean is searched for open and readily available seismic and/or hydroacoustic stations that might have recorded a possible impact of MH370 with the ocean surface. Only three stations are identified: the IMS hydrophone arrays H01 and H08, and the Geoscope seismic station AIS. Analysis of the data from these stations shows an interesting arrival on H01 that has some interference from an Antarctic ice event, large amplitude repeating signals at H08 that obscure any possible arrivals, and large amplitude chaotic noise at AIS that obscures any arrivals at lower frequencies while the low sample rate at AIS precludes any analysis at higher frequencies of interest. The results are therefore rather inconclusive but may point to a more southerly impact location within the overall Indian Ocean search region. The results would be more useful if they can be combined with any other data that are not readily available.

Introduction

MH370 is a Malaysian Airlines flight that was lost over the Indian Ocean, and assumed to have crashed sometime shortly after 00:00 UTC on 2014/03/08. The impact of a large passenger jet with the ocean surface should create a signal that could be observed on hydrophones or nearby seismic stations. The study discussed here is an analysis of the hydroacoustic and seismic data readily available, in an effort to determine is such signals are present and if they can provide any information regarding the hypothesized impact event.

Data

The Indian Ocean is a relatively poorly monitored region of the globe. For sources near the ocean surface, the best records would be hydrophone stations, followed by near-shore seismic stations (to look for signals that result from the conversion of hydroacoustic energy to seismic energy, known collectively as T phases). In the southern Indian Ocean, there are only 2 hydrophone stations readily available, both from the CTBT IMS network: Cape Leeuwin, Australia, having the code H01, and Diego Garcia, an island in the British Indian Ocean Territory (BIOT), Chagos Archipelago, having the code H08. Both hydrophone stations have 3-element triangular arrays of hydrophones installed well offshore and positioned in the SOFAR channel. Other hydrophone stations in the Atlantic and Pacific are generally blocked from this source region. There is only one nearby seismic station for the expected region of impact, and that is Amsterdam Island, code AIS, a Geoscope station (Geoscope is a French international seismic network). This station has a

three-component broadband seismometer. The IMS data are available from the CTBTO located in Vienna, Austria. The data from AIS are available at the IRIS DMC located in Seattle, Washington, USA.

Analysis

H01

H01 is the closest hydrophone station, and as such has the highest likelihood of recording any signal that may have been generated by the expected impact event. H01 consists of a single 3-element array.

We started with a scan of the raw, broadband hydrophone data, for approximately 2 hours around the expected time of impact, adjusted for some travel time from the point of impact to the station. This scan revealed only one set of signals that was significantly above the background noise, including various small signals. These signals were observed at approximately 00:52 UTC, and shown in Figure 1. We focus all further analysis on these signals.

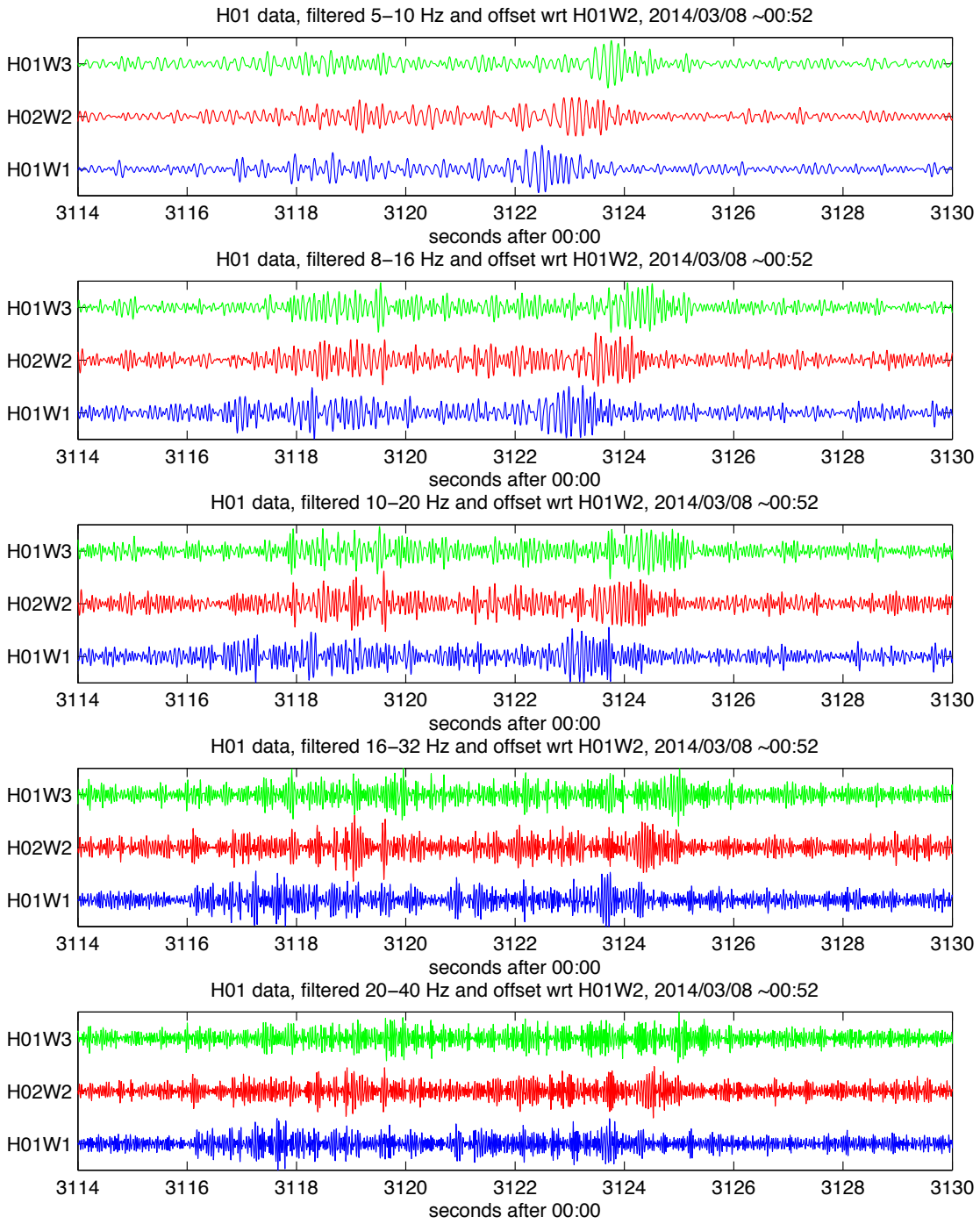

Figure 1: Filtered waveforms from all three elements of H01 around the time 00:52 UTC on 2014/03/08. The filters are 1-octave bands as indicated above each subimage. The features and alignment of the traces will be discussed later in the text.

The signals visible in figure 1 comprise two groups. The largest is the latter group showing large amplitudes and significant dispersion. We begin our analysis with that group. Using a time window relatively tight to just the late signals, we perform

a cross-correlation analysis to find the correct alignment of this group. The results are shown in figure 2. All further analysis of these signals is performed in the 10-20 Hz band. Figure 1 shows that the latter signal dominates the waveform at lower frequencies, and the signal-to-noise ratio is poor at higher frequencies. Thus 10-20 Hz is the best band in which to analyze all of the signals present.

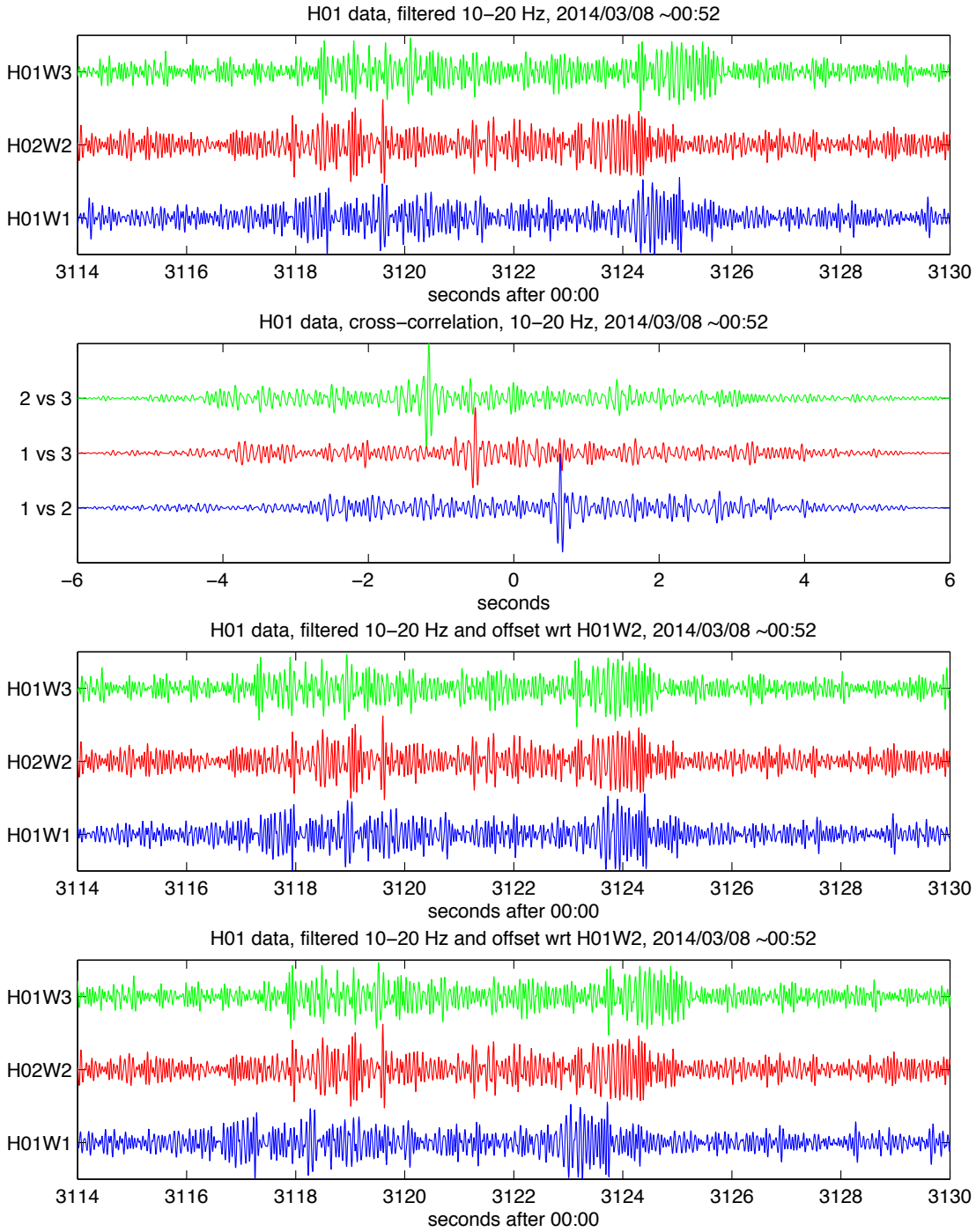

Figure 2: Cross-correlation analysis of the signals at H01. The first subimage shows all 3 elements, filtered 10-20 Hz and aligned on true time. The second shows the

cross-correlation analysis of just the 6 seconds surrounding the latter, large, dispersive signal, also performed in the 10-20 Hz band. The third subimage is aligned using the results of the cross-correlation analysis. Note the excellent alignment of the latter signal, particularly frequency dispersion, but the lack of alignment of earlier features. The alignment of the fourth subimage is discussed later in the text.

The cross-correlation analysis works very well on the latter, large-amplitude, dispersive signal. But it does not work well on the earlier signals. This leads us to conclude that the two sets of signals may originate from different sources. Other characteristics seem to support this conclusion, since the earlier signals seem to lack significant dispersion and also lack significant energy in the lower frequencies, such as 5-10 Hz, as can be seen in Figure 1. Using the offsets for the latter phase, we compute the direction of arrival (DOA, always given here as a 2D horizontal DOA measured in degrees clockwise from north) and observed phase velocity for that phase. DOA is 190.5°, and the phase velocity (inverse of apparent slowness) is 1.46 km/s, quite consistent with expected SOFAR channel phase velocities. For that direction, it is most likely that this signal originated in an ice-related event in the vicinity of Antarctica.

Cross-correlation was attempted on the earlier signals, without success – there were no significant peaks found, unlike the clear peaks shown in figure 2 for the latter signal. This is not surprising, since the separation of the array elements, which is on the order of 2 km, represents multiple wavelengths at this phase velocity and frequency. Most signals would not be expected to have strong coherence between the elements, especially those that are more impulsive and not dispersed. Instead of cross-correlation, we rely on a manual alignment of key features. Beginning with elements W2 and W3, which seem the most coherent for the earlier energy, we align 4 prominent peaks in the energy observed in the signals. This is shown in the lower part of figure 2. The third element of the array, W1, is then aligned by constraining the phase velocity to be that observed for the ice signal, 1.46 km/s. Geometrical constraints and the assumed phase velocity then determine uniquely the offset for W1. W1 is clearly not very coherent with either W2 or W3 for this signal, but in general, the bulk of the energy for this arrival appears in the same time window as it does on W2 and W3, with the exception of an early pulse of energy, which could be unrelated. Note that figure 1 is also created with this alignment, and the 8-16 Hz band shows good alignment for the timing of the bulk of the energy, again with the exception of spurious energy early on W1. Attempts to align the early energy on W1 result in unphysical phase velocities, which also leads us to conclude that this early energy on W1 is unrelated. The final alignment of the first arrivals produces a DOA of 246.9° (with the phase velocity fixed at 1.46 km/s). The source for this arrival would then be WSW of the array, in the general direction of the region in which MH370 may have impacted the ocean, and has an arrival time that could be consistent as well. Although the arrival is weak and is interfered by a strong ice source arrival, there is evidence that this could be an arrival from an impact of MH370 with the ocean surface. Figures 3 and 4 show spectrograms aligned with the

computed cross-correlation for the latter arrival and the manual alignment of the first arrival. The alignment of energy in these figures also supports the direction of arrival conclusions.

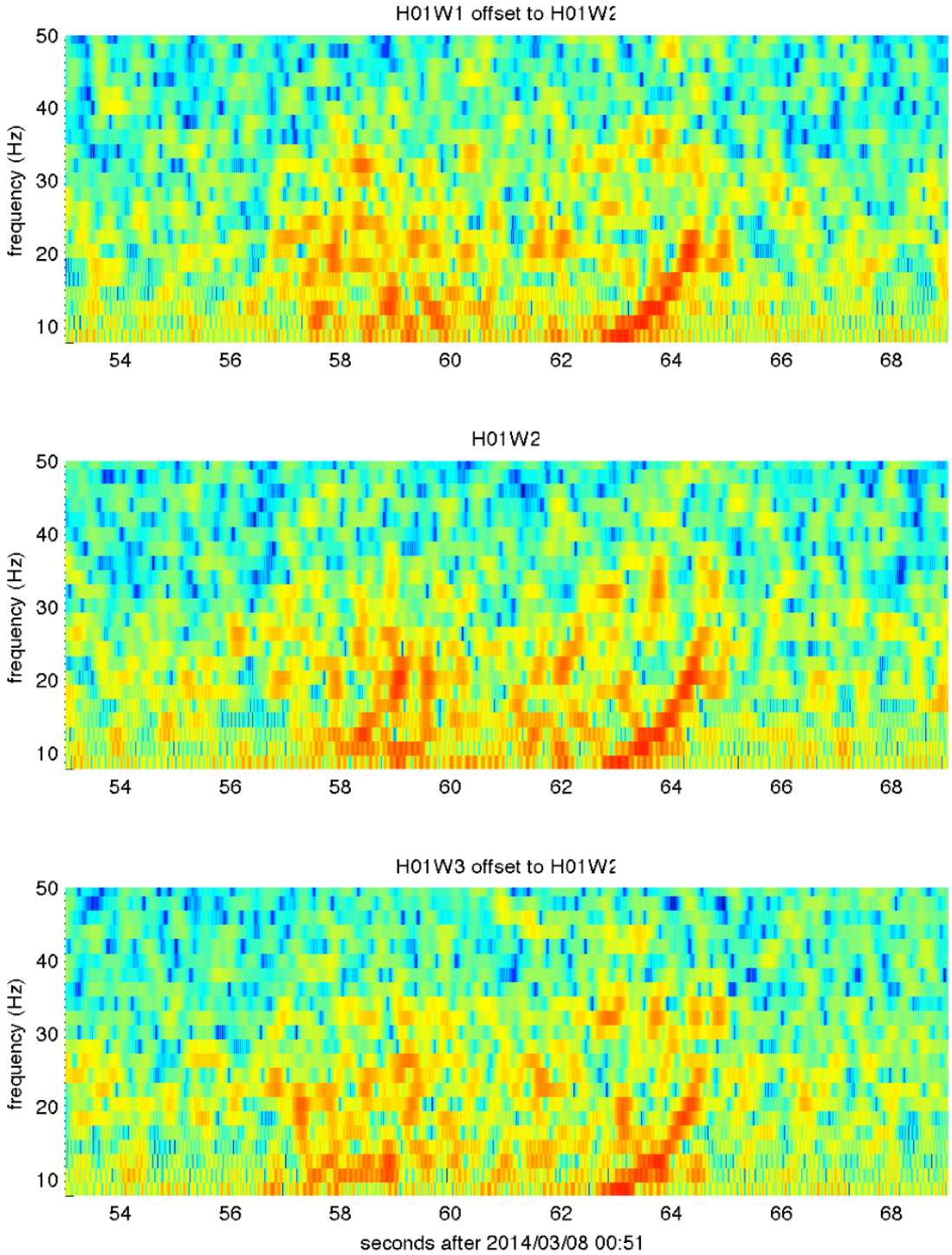

Figure 3. Spectrograms, 8-60 Hz, around 2014/03/08 00:52 UTC for hydroacoustic array H01. The spectrograms for the three elements of the array are aligned on the computed cross-correlation offsets for the latter arrival (the large-amplitude highly

dispersed arrival between about 63 and 65 seconds after 00:51). Note the apparent lack of alignment for the earlier energy.

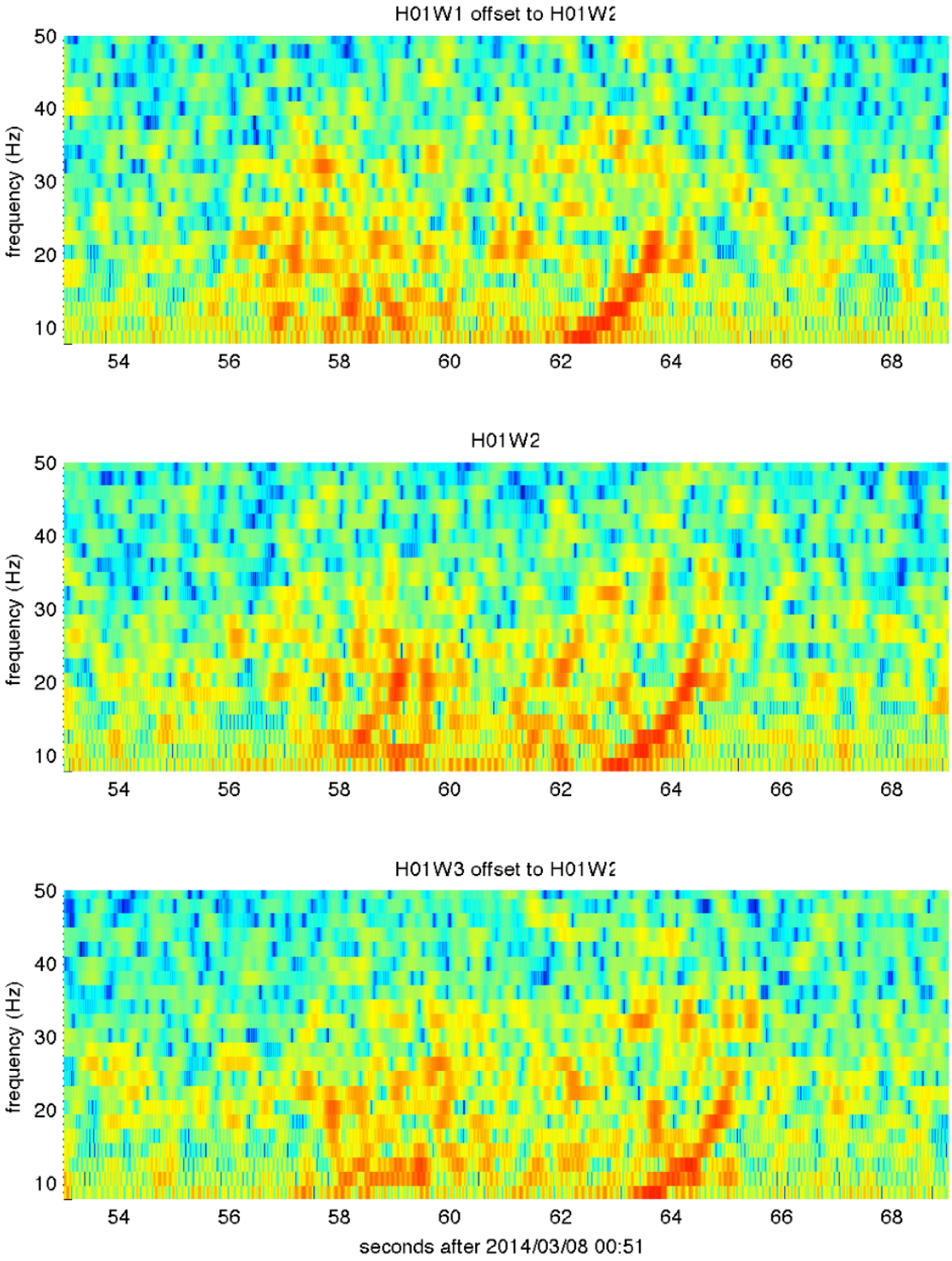

Figure 4: Spectrograms aligned according to manual alignment of early features. Apart from some early energy on H01, features of the earlier energy appear better aligned, particularly between W2 and W3 elements. All elements now show

features between 57.8 and 58.5 and again between 59 and 60 that appear to be well aligned. A feature between 58 and 58.5 may show some evidence of identical dispersion on elements W2 and W3.

H08

H08 is a hydrophone station that is quite a bit further from the potential impact region than H01. We started with the same type of time scan as we did on H01, applied to the southern 3-element array form H08. However, this analysis revealed a long set of two large-amplitude, broadband, repeating signals, one at approximately 10-second intervals and one at approximately 8-second intervals, that dominate the record throughout. These signals continue for hours both before and after the time of interest, and, as can be seen in the figure, are very broadband. In addition, they are larger in amplitude, relative to background, than the signals of interest observed on H01. These signals preclude any possibility of identifying any signal from the impact that might have arrived at H08. The signals arrive from two separate directions. They are both coming from the sea so they are either anthropogenic (airgun surveys or something similar) or biogenic (whales, for example).

A sample of H08 data is shown in figure 5. The same 5 filters are used as were used for H01 data in figure 1. The large amplitude signals appear at approximately 10-second intervals. The smaller amplitude signals are at about 8-second intervals and can be seen progressively interfering with the larger signals. To see this most clearly, look at element S2 at 10-20 Hz. The small signal clearly follows the large one at about 3707 (seconds after 2014/03/08 00:00), has about the same arrival time as the large one at 3715, arrives before the larger signal at 3723 and is almost completely before the larger signal at 3731, and these are 8-second intervals (the large arrivals are at 3704, 3714, 3724, 3734, which are 10-second intervals). The traces in figure 5 are aligned on the expected direction of arrival (and a fixed phase velocity of 1.46 km/s, as observed at H01) for a source in the vicinity of the MH370 expected impact. It is readily apparent that neither of the repeating signals arrivals are from that direction, and that they arrive from 2 different directions. The DOA for the larger 10-second signal is 29.8°, and the observed phase velocity is 1.485 km/s. For the smaller 8-second phase, the DOA is approximately 117° (determination is less reliable due to interference from larger signal). Therefore, H01 will not be useful for investigation of potential arrivals from an MH370 impact. H08 also has a northern array, but it would be blocked by Diego Garcia Island for any arrivals coming from the vicinity of the expected impact site.

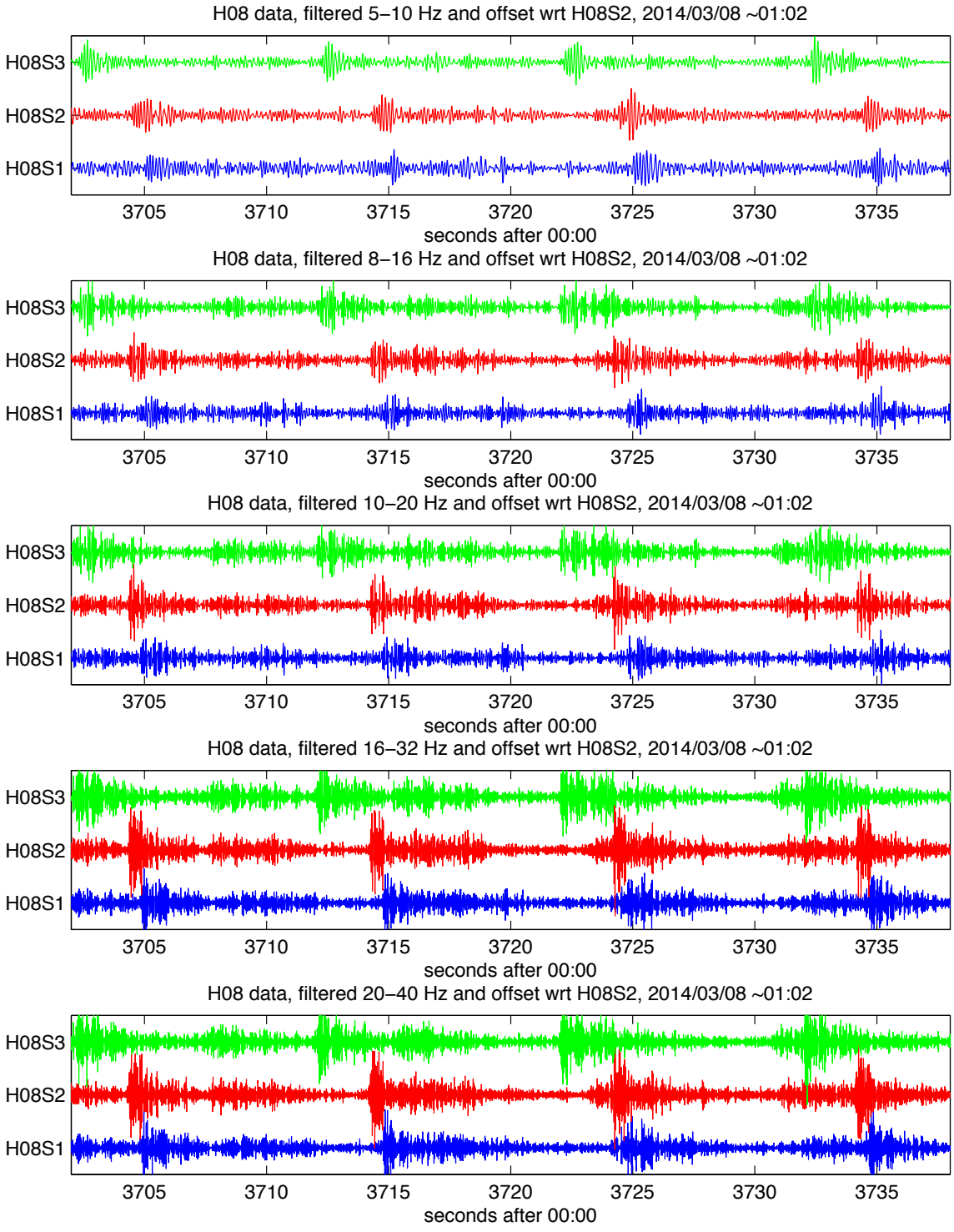

Figure 5: H08 data near expected arrival time. Data are shown filtered into 5 1-octave bands, same filters as figure 1. Note large amplitude signals repeating at 10-second intervals and smaller amplitude signals at 8-second intervals. Also note the broadband nature of the signals, having significant signal-to-noise ration in all bands from 5 to 40 Hz here. These signals completely obscure any other signals that may be present.

AIS

As expected, AIS is a noisy site. It is close to shore on an island often buffeted by large breakers and exposed to strong winds. We again scanned the waveforms, looking for any signals that might stand out from the noise in any characteristic; however none could be found. Part of the problem is that the station has a low sample rate (20 samples per second) that precludes examining the waveforms in the band of interest, 10-20 Hz (as indicated by the signal of interest observed at H01), since the Nyquist is only at 10 Hz. One could well expect that if the suspected impact signal is not above the noise below 10 Hz at the hydrophones of H01, it then could not be above the noise when converted to a T phase, even without the excessive noise at these frequencies at AIS. As for higher frequencies, since AIS is likely closer to a potential impact site, then frequencies above 20 Hz may be above noise here that are not above noise at H01. But again, the low Nyquist frequency precludes any opportunity to investigate that possibility.

Figure 6 shows a sample of the waveforms around the time of the expected arrival. It was chosen to show one of the common noise bursts (at about 00:36) observed at this station. Several of these appear in the record every hour, so this is not unique and likely represents a local nature noise source, such as large waves crashing on a nearby shore or something similar. The waveforms were filtered at 2-9 Hz to eliminate most of the longer period ocean noise while retaining all available data above 2 Hz (and below the effects of the anti-aliasing filters at the station). We performed a polarization analysis on the data to look for any signals that might appear both above noise and with the correct DOA. The expected DOA here is approximately 137°. The polarization results for approximately the same time intervals as the waveforms in figure 6 are shown in figure 7. As can be seen, the large noise burst has a DOA (labeled ‘az’ on the figure) of approximately 40 degrees, which is about 100 degrees off from that expected. It is also similar to most of the background noise. Rectilinearity (labeled ‘rect’ on the figure, a measure of how closely the particle motion conforms to a plane wave, on a scale of 0-1, with 1 being a perfect plane wave) is slightly elevated for this phase, but not particularly distinct from the background noise. The incidence angle (labeled ‘inc’ on the figure, and is the angle the 3D DOA vector makes with respect to horizontal plane in a vertical plane that includes the vector) is also not distinct from the background noise. In all three measures, the polarization is not distinct from the background noise, indicating that this noise burst is merely a large-amplitude version of the background.

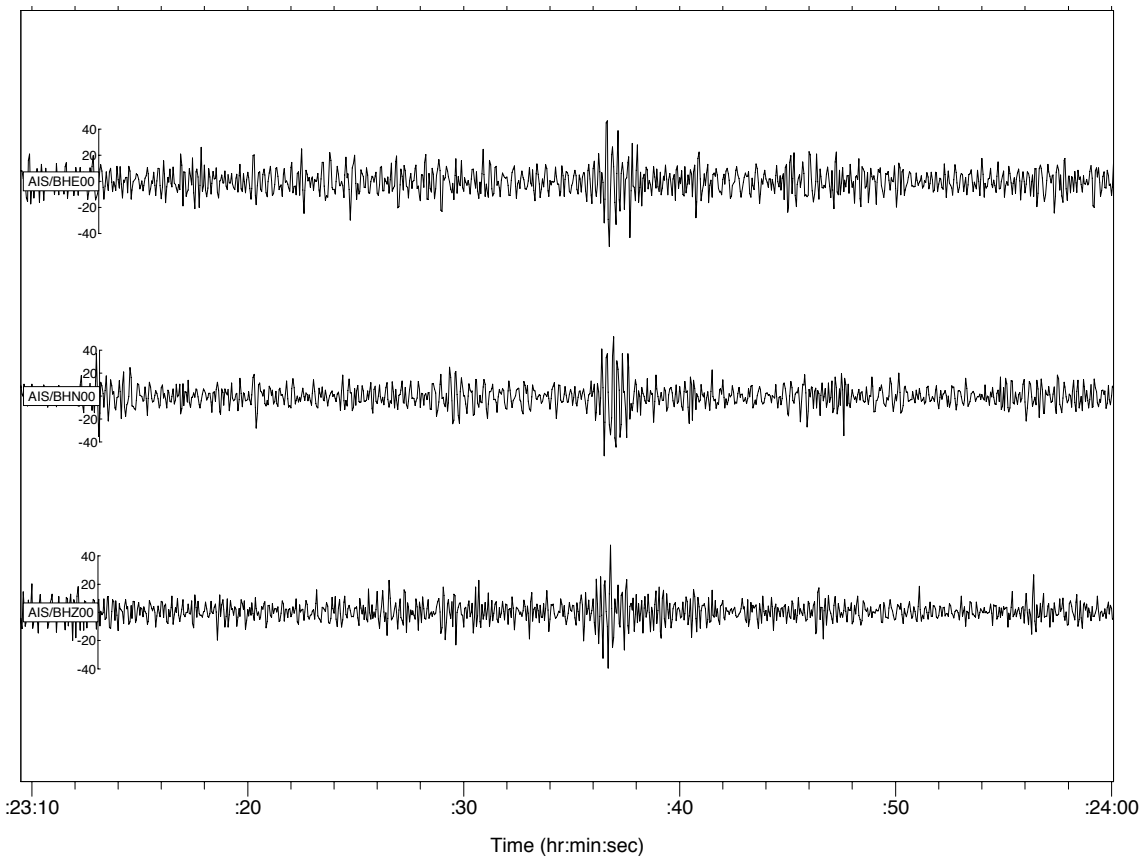

Figure 6: Waveforms from the seismic station at Amsterdam Island (AIS), filter at 2-9 Hz. For the channel names, "BH" indicates a broadband seismometer recorded at high gain, the "00" indicates that these are all components of a single instrument designated "00", and the "E, N and Z" indicate the component of motion: E is positive east, N is positive north and Z is positive down. Time is given as hour:minute:second after 2014/03/08 00:00 UTC.

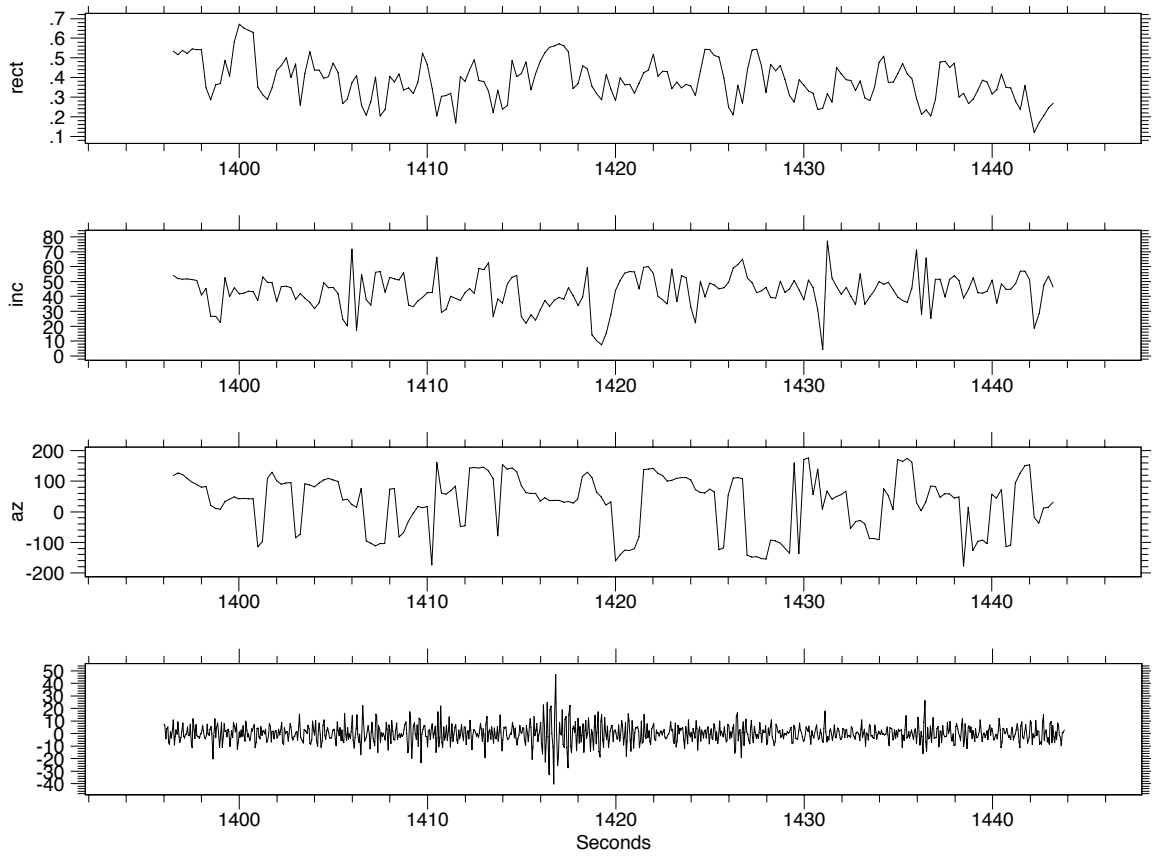

Figure 7: Polarization analysis of Amsterdam Island (AIS) seismic data. Data have been pre-filter to 2-9 Hz. The plots, in order from top to bottm, show rectilinearity, incidence angle, DOA and the seismogram from the vertical component. Time is given in seconds from 2014/03/08 00:00 UTC.

Given that no reasonable signals seem to be present above the noise and from the roughly expected azimuth, it is worth examining the orientation of the station to confirm that it is correctly oriented and would provide accurate azimuths. To do this we chose a large teleseism that is close to the day in question for an analysis to confirm the orientation of the instrument. We chose a M6.5 event near Japan, in the subducting slab of the Philippine Sea plate NW of Okinawa in the Ryukyu Islands. This event occurred on 2014/03/02 at 20:11:23 UTC at the geographic coordinates 27.431°N 127.367°E and a depth of 119.0km (magnitude, location and time from the USGS National Earthquake Information Center).

The P-wave from this quake would be expected to be strong in approximately 1-5 Hz at this range. We observed an arrival around 1-2 Hz at the expected P wave time of approximately 20:23:21, but signal-to-noise ration was only about 2, which is insufficient to get a good horizontal polarization, especially for near-vertical incidence as this arrival would be. However, The dominant crustal surface waves near 20 seconds (0.05 Hz) would be well excited by this event and are also well below the microseism frequency band that creates so much noise at AIS. A plot of the waveforms with a 1-octave filter across 20 Hz is shown in figure 8. As can be

seen in the figure the north and east components show clear Love and Rayleigh waves well above the noise. The amplitudes on both horizontal components for both waves are roughly equivalent as would be expected for an approximately 45° DOA, clockwise from north. In addition, the motion of the Love wave is NW-SE as expected, and the horizontal motion of the Rayleigh wave is NE-SW, also as expected. This confirms the orientation of the station.

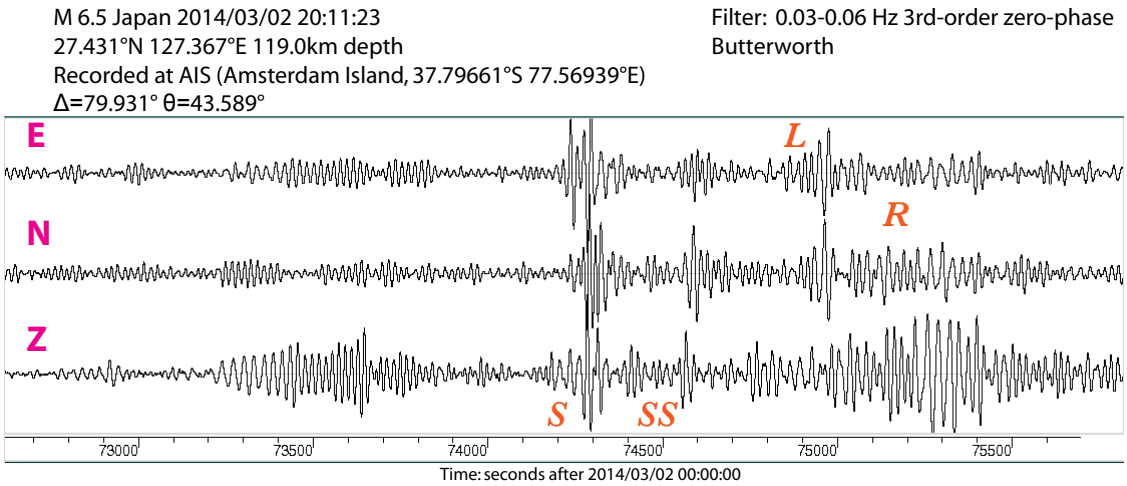

Figure 8. Orientation analysis of AIS using the M6.5 Japan quake from 2014/03/02. E, N, and Z label the 3 components of the instrument. S and SS are body-wave shear arrivals. L and R are the Love and Rayleigh surface waves, respectively. Waveforms have been filtered in a 1-octave band around 20 Hz.

Further information regarding possible flight paths indicated that a time of arrival at AIS of approximately 00:26:30 might be possible. For completeness, we looked at this time in more detail as well. We applied the same tools, including polarization, and careful review as we have done above. No useful signals were discovered; the time includes only the common noise found at this site. Figure 9 shows approximately 1 full minute of data around 00:26:30, filter in 4 bands. The 4 bands from top to bottom are octave bands 2-4, 3-6, 4-8 and 5-10 Hz. The Nyquist frequency is 10 Hz, so it is unnecessary to attempt any higher bands. The figure shows the relatively constant background at 2-4 Hz that is similar to what is seen at all lower frequencies as well. As the frequencies get higher, the more impulsive signals from wave strikes and similar weather-driven phenomena become more prominent. But none of this energy corresponds to seismic body waves that would be expected from the conversion of hydroacoustic energy in the SOFAR channel to seismic energy at the island's offshore slope. Very likely, small signals from converted hydroacoustic phases will be completely obscured in this much noise. The only signal that is not noise in the figure is a seismic surface wave, Rg, visible at about 00:26:25, identified as a surface wave from its dispersion. This would be from

some small seismic source on the island, and not from a more distant ocean surface impact.

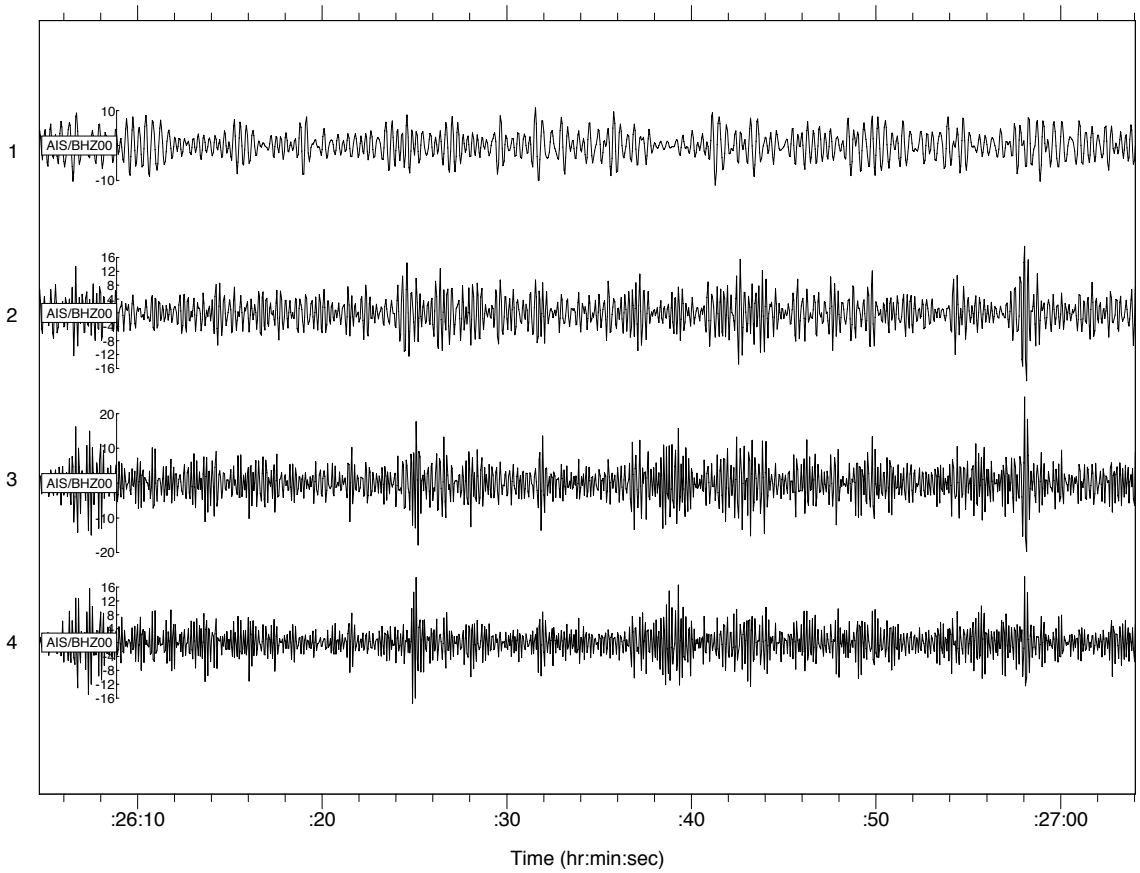

Figure 9. This figure shows a closer look as the seismic waveforms from around the time 00:26:30 at AIS. The vertical component is shown filtered to 4 1-octave overlapping bands. The time interval displays a variety of large-amplitude noise.

Conclusions

The seismic and hydroacoustic data readily and openly available for analysis are quite limited. Only Three potentially applicable station were identified: H01, H08 and AIS. Of these, H01 has a very interesting and potential applicable arrival. H08 is contaminated by a long series of large-amplitude repeating and interfering signals that completely obscure any possible applicable arrival. AIS is contaminated by natural noise sources and has a sample rate sufficiently low as to likely exclude any signals of interest. Thus, at most, we were able to identify a candidate arrival from only a single station. This arrival also has problems in analysis, since it is interfered with by a large-amplitude arrival that follows it with only a small delay. That arrival is clearly associated with some sort of ice event from Antarctica. Continued analysis and further confirmation of the arrival at H01 would only be possible if there are additional sources of data that are either not open or not readily available. The

arrival at H01, if it is indeed from the impact of MH370, would indicate that the impact is toward the southern portion of the broad search area previously declared and likely south of the area in which possible pings were briefly recorded.

In addition it is concluded that the southern Indian Ocean is insufficiently monitored for events of any type, including events of interest for the CTBT. Relatively small but significant explosions could prove to be difficult to detect, locate and identify in this region due to the shortage of useful stations and the likelihood that one or more stations could be rendered useless for monitoring purposes by various types of common noise sources in their vicinity.

Glossary

Accredited Representative

A person designated by a State, on the basis of his or her qualifications, for the purpose of participating in an investigation conducted by another State. Where the State has been established an accident investigation authority, the designated accredited representative would normally be from that authority.

Air-ground communication

Two-way communication between aircraft and stations or locations on the surface of the earth.

Airspace

Any part of the earth's atmosphere that can be used by an aircraft. It is a three-dimensional space where aircraft can operate.

Annex 13

Annex 13 of the Convention on International Civil Aviation (Chicago, 1944) provides the international Standards and Recommended Practices for Aircraft Accident Inquiries and was developed by ICAO. These practices are the basis for aviation accident, serious incident and incident investigations, accident prevention and accident and serious incident reporting.

Australian Search and Rescue Region Region

Australia, as signatory to the Convention on International Civil Aviation, 1944; the International Convention for the Safety of Life at Sea, 1974; and the International Convention on Maritime Search and Rescue, 1979, is responsible for search and rescue over a vast area (52.8 million square kilometres) made up of the East Indian, South-west Pacific and Southern oceans. Australia has the same boundaries for aviation and maritime search and rescue.

Autonomous Underwater Vehicle

An autonomous underwater vehicle (AUV) is a battery-powered self-propelled underwater vehicle that can be launched and retrieved from a search vessel and is pre-programmed with a search mission. The vehicle may be fitted with instruments including sonar and optical imaging systems.

Bathymetry

The study and mapping of seafloor topography. It involves obtaining measurements of the ocean depth and is equivalent to mapping topography on land.

Beaufort Scale

A scale of wind force, developed in 1805 by Admiral Sir Francis Beaufort, which uses observations of the effects of wind on the sea surface to estimate wind speed. Measurements range from 0 (calm) through to 12+ (hurricane).

Burst Frequency Offset

BFO is a measure of the difference between the expected frequency of a satellite transmission and the frequency received at the ground station.

Burst Timing Offset

BTO is a measure of the time taken for a satellite transmission round trip (ground station to satellite to aircraft and back) and allows a calculation of the distance between the satellite and the aircraft.

Controlled air space

Airspace that is actively monitored and managed by air traffic controllers. To enter controlled airspace, an aircraft must first gain a clearance from an air traffic controller.

Cockpit Voice Recorder

A CVR is a recorder placed in an aircraft for the purpose of facilitating the investigation of an aircraft accident or incident. It records the total audio environment of the cockpit area.

Coordinated Universal Time (UTC)

Coordinated Universal Time (UTC) or Universal Time Coordinated. UTC is the worldwide standard for time and date.

Depressor

A steel weight that is towed behind a search vessel on a long cable in front of the tow vehicle, to help stabilise it. This allows the tow vehicle to 'fly' with less motion above the seafloor, while gathering detailed imagery.

Flight Data Recorder

An FDR is a recorder placed in an aircraft for the purpose of facilitating the investigation of an aircraft accident or incident. It records flight parameters such as indicated airspeed.

Ground earth station

A satellite ground station sends or receives data from orbiting satellites.

Handshake

Satellite log-on interrogation messages that originate at the ground earth station and are transmitted through the satellite to the aircraft's satellite communication system.

Hydrophone

A microphone designed to be used underwater for recording or listening to underwater sound.

Joint Investigation Team

Convened by the Government of Malaysia, the group of international academics and government officials worked towards defining the most probable position of MH370 from early in the surface search until 2 April 2014.

Knot

A unit of speed that is equal to one nautical mile (1.852km) per hour.

Nadir

In sonar systems, a nadir is the region directly below a deep tow vehicle or AUV which is not covered by side scan sonar.

National Collaboration Framework

The National Collaboration Framework was created to assist Commonwealth entities, State, Territory and local jurisdictions to work collaboratively to achieve government objectives.

Nautical mile

A unit of distance based on the circumference of the earth, used for marine charting and navigating. One nautical mile (NM) is equal to 1.852 km.

Pilot-in-Command

The pilot responsible for the operation and the safety of the aircraft during flight time.

Ping

A pulse of sonar sound.

Primary surveillance radar

Primary (or terminal area) radar relies on radio waves reflecting off metallic objects and is effective within a short range from the radar head, which is usually located at an airport.

Remotely Operated Vehicle

A remotely operated vehicle (ROV) is an underwater vehicle which is tethered to a search vessel by a cable and operated remotely by an operator on a search vessel. ROVs are equipped with a range of cameras, lights and manipulator arms to cut and lift objects on the seafloor.

Satellite Communications Working Group

Convened by the Government of Malaysia from early in the surface search, the group of international satellite communications specialists, including Inmarsat and Thales, worked towards defining the most probable position of MH370.

Sea state

A description of sea conditions, recorded using the World Meteorological Organization Sea State Codes. Measurements range from 0 (calm) through to 9 (phenomenal).

Search Strategy Working Group

Coordinated by the ATSB since the completion of the surface search, the group of international satellite and aircraft specialists worked towards defining the most probable position of MH370, at the time of the last satellite communications.

Secondary surveillance radar

Secondary (or en route) radar returns are dependent on a transponder in the aircraft to reply to an interrogation from a radar ground station.

Self-Locating Datum Marker Buoy

A floating buoy equipped with a global positioning system and satellite communication system to periodically transmit its location to primarily aid in search and rescue missions.

Seventh arc

Independent analysis of satellite communications and aircraft performance confirms MH370 will be found in close proximity to the arc labelled as the 7th arc. The arc extends from approximately latitude 20 degrees south to approximately latitude 44 degrees south. At the time MH370 reached this arc the aircraft is considered to have exhausted its fuel and to have been descending.

Side Scan Sonar

A sonar system which uses acoustic pings to form an image of the seafloor. Typically, a side scan sonar consists of two transducers, located in either side of a tow vehicle, AUV or ROV, each of which generates a fan-shaped sonar ping perpendicular to the vessel track.

A sonar system which uses sophisticated post-processing of sonar data to combine a number of sonar pings to form an image with higher resolution than conventional sonar.

Sonar contact

Any anomaly on the seafloor identified in sonar data that looks non-geologic in nature or unusual when compared to the surrounding seafloor.

Sonobuoy

A floating buoy equipped with a hydrophone and a radio transmitter to transmit the underwater sounds to overflying aircraft.

State of Registry

The State on whose register the aircraft is entered.

Note: In the case of the registration of aircraft of an international operating agency on other than a national basis, the States constituting the agency are jointly and severally bound to assume the obligations which, under the Chicago Convention, attach to a State of Registry. See, in this regard, the Council Resolution of 14 December 1967 on Nationality and Registration of Aircraft Operated by International Operating Agencies which can be found in Policy and Guidance Material on the Economic Regulation of International Air Transport (Doc 9587).

Surface search

A surface search for MH370 was conducted from 18 March to 28 April 2014. Coordinated by AMSA and the JACC, it was carried out by an international fleet of aircraft and ships along the seventh arc.

Swath

The effective range of a sonar system.

Swing

The amount of time it takes a vessel to go from its port of departure, out to sea and return to port.

Synthetic Aperture Sonar

A sonar system which uses sophisticated post-processing of sonar data to combine a number of sonar pings to form an image with higher resolution than conventional sonar.

Towed Pinger Locator

A TPL is a device that is towed behind a vessel for detecting the signals being emitted from an underwater locator beacon fitted to an aircraft's Flight Data Recorder and Cockpit Voice Recorder.

Tow Vehicle

A vehicle which is towed behind a search vessel. The vehicle may be fitted with instruments including sonar and optical imaging systems.

Transponder

A device that emits an identifying signal in response to an interrogating received signal from a communications satellite or ground station.

Tripartite

Shared by or involving three parties. Tripartite meetings that make decisions with regard to MH370 involve the Governments of Australia, Malaysia and the People's Republic of China.

Underwater Locator Beacon

A device attached to aviation flight recorders that when immersed in water emits an acoustic signal, to assist with locating an aircraft's Flight Data Recorder and Cockpit Voice Recorder.

Uncontrolled air space

Airspace that has no supervision by air traffic control, so no clearance is required.

Waypoint

A predetermined geographical position that is defined in terms of latitude and longitude coordinates, used for navigation.

Abbreviations

3D	Three Dimensional
ACARS	Aircraft Communications Addressing and Reporting System
ADFR	Automatic Deployable Flight Recorder
ADS-B	Automatic Dependent Surveillance – Broadcast
AF447	Air France flight 447
AFP	Australian Federal Police
AMSA	Australian Maritime Safety Authority
Annex 13	Annex 13 of the Convention on International Civil Aviation (Chicago, 1944)
ATC	Air Traffic Control
ATSB	Australian Transport Safety Bureau
AUV	Autonomous Underwater Vehicle
BASARNAS	Badan SAR Nasional, National Search and Rescue Agency Republic of Indonesia
BEA	Bureau d'Enquêtes et d'Analyses pour la Sécurité de l'Aviation civile (France)
BFO	Burst Frequency Offset
BOM	Bureau of Meteorology
BTO	Burst Timing Offset
CMST	Centre for Marine Science and Technology at Curtin University
CSIRO	Commonwealth Scientific and Industrial Research Organisation
CVR	Cockpit Voice Recorder
DCA	Department of Civil Aviation (Malaysia)
DST Group	Defence Science and Technology Group
DVL	Doppler Velocity Log
EASA	European Aviation Safety Agency
ELT	Emergency Locator Transmitter
FDR	Flight Data Recorder
FL	Flight Level
ft	Feet (dimensional unit)
GIS	Geographic Information System
GPS	Global Positioning System
HSE	Health, Safety and Environment
ICAO	International Civil Aviation Organization
ICT	Information and Communications Technology
IFR	Instrument Flight Rules
JACC	Joint Agency Coordination Centre
JIT	Joint Investigation Team

kHz	Kilo Hertz
KL ARCC	Kuala Lumpur Aeronautical Rescue Coordination Centre
km	Kilometre
km^2	Square kilometre
LPD	Lower Probability of Detection
MBES	Multibeam Echo Sounder
MH370	Malaysia Airlines flight 370
MHz	Mega Hertz
MOU	Memorandum of Understanding
NASA	National Aeronautics and Space Administration
NM	Nautical Mile
NTSB	National Transportation Safety Board (United States)
PDF	Probability Density Function
PIC	Pilot-in-Command
PSR	Primary Surveillance Radar
RAN	Royal Australian Navy
RMP	Royal Malaysia Police
ROV	Remotely Operated Vehicle
SAR	Search and Rescue
SAS	Synthetic Aperture Sonar
SATCOM	Satellite Communications
SATCOM WG	Satellite Communications Working Group
SDU	Satellite Data Unit
SLDMB	Self-Locating Datum Marker Buoy
SSR	Secondary Surveillance Radar
SSS	Side Scan Sonar
SSWG	Search Strategy Working Group
t	Tonne
TPL	Towed Pinger Locator
ULB	Underwater Locator Beacon
USBL	Ultra-Short Base Line
UTC	Coordinated Universal Time
VHF	Very High Frequency

Australian Transport Safety Bureau

The Australian Transport Safety Bureau (ATSB) is an independent Commonwealth Government statutory agency. The ATSB is governed by a Commission and is entirely separate from transport regulators, policy makers and service providers. The ATSB's function is to improve safety and public confidence in the aviation, marine and rail modes of transport through excellence in: independent investigation of transport accidents and other safety occurrences; safety data recording, analysis and research; fostering safety awareness, knowledge and action.

The ATSB is responsible for investigating accidents and other transport safety matters involving civil aviation, marine and rail operations in Australia that fall within Commonwealth jurisdiction, as well as participating in overseas investigations involving Australian registered aircraft and ships. A primary concern is the safety of commercial transport, with particular regard to operations involving the travelling public.

The ATSB performs its functions in accordance with the provisions of the *Transport Safety Investigation Act 2003* and Regulations and, where applicable, relevant international agreements.

Purpose of safety investigations

The object of a safety investigation is to identify and reduce safety-related risk. ATSB investigations determine and communicate the factors related to the transport safety matter being investigated.

It is not a function of the ATSB to apportion blame or determine liability. At the same time, an investigation report must include factual material of sufficient weight to support the analysis and findings. At all times the ATSB endeavours to balance the use of material that could imply adverse comment with the need to properly explain what happened, and why, in a fair and unbiased manner.

Developing safety action

Central to the ATSB's investigation of transport safety matters is the early identification of safety issues in the transport environment. The ATSB prefers to encourage the relevant organisation(s) to initiate proactive safety action that addresses safety issues. Nevertheless, the ATSB may use its power to make a formal safety recommendation either during or at the end of an investigation, depending on the level of risk associated with a safety issue and the extent of corrective action undertaken by the relevant organisation.

When safety recommendations are issued, they focus on clearly describing the safety issue of concern, rather than providing instructions or opinions on a preferred method of corrective action. As with equivalent overseas organisations, the ATSB has no power to enforce the implementation of its recommendations. It is a matter for the body to which an ATSB recommendation is directed to assess the costs and benefits of any particular means of addressing a safety issue.

When the ATSB issues a safety recommendation to a person, organisation or agency, they must provide a written response within 90 days. That response must indicate whether they accept the recommendation, any reasons for not accepting part or all of the recommendation, and details of any proposed safety action to give effect to the recommendation.

The ATSB can also issue safety advisory notices suggesting that an organisation or an industry sector consider a safety issue and take action where it believes it appropriate. There is no requirement for a formal response to an advisory notice, although the ATSB will publish any response it receives.

Australian Transport Safety Bureau

Enquiries 1800 020 616
Notifications 1800 011 034
REPCON 1800 020 505
Web www.atsb.gov.au
Twitter @ATSBinfo
Email atsbinfo@atsb.gov.au
Facebook atsbgovau

Investigation

ATSB Transport Safety Report
External Aviation Investigation
The Operational Search for MH370

AE-2014-054
Final – 3 October 2017

APSAR/TF/3−WP05
25 – 29/01/2015

International Civil Aviation Organization

Third Meeting of the Asia/Pacific Regional Search and Rescue Task Force (APSAR/TF/3)

Maldives, 25 – 29 January 2015

Agenda Item 4: Asia/Pacific and inter-regional SAR planning, coordination and cooperation

ICAO BRIEF ON THE SAR RESPONSE TO MH370

(Presented by the Secretariat)

SUMMARY

This paper presents a brief on the events noted by the ICAO Regional Office at the time of the MH370 event, which may reveal some areas of improvement for consideration by the APSAR/TF for inclusion in the Asia/Pacific SAR Plan, global SAR documents and action by States concerned.

1. INTRODUCTION

1.1 Malaysia Airlines Flight 370 (MH370) disappeared on Saturday, 8 March 2014, while flying from Kuala Lumpur, Malaysia to Beijing, China with 239 people on board (227 passengers and 12 crew). After ten months the whereabouts of the B777-200ER aircraft remained a mystery, with current search efforts focused on the Southern Indian Ocean.

2. DISCUSSION

Purpose of Brief

2.1 The purpose of this brief is to provide feedback from the ICAO Regional Office on aspects of events, coordination, advice, challenges noted and possible improvement suggestions as a result of the MH370 tragedy that could be incorporated into the Asia/Pacific Plan.

2.2 The purpose is not to assign blame, but for all States to examine their own systems in terms of the lessons learnt from this tragedy.

Timeline

2.3 The following is a summary of key events that the Asia/Pacific Regional Office's Air Traffic Management (ATM) Section was aware of, or became involved in.

Saturday 08 March 2014

a) MH370 last made voice contact with Kuala Lumpur Air Traffic Control (ATC) at 17:19 UTC, 07 March (01:19 Malaysian time, 08 March) less than an hour after takeoff.

b) MH370 disappeared from Malaysian ATC Secondary Surveillance Radar (SSR) screens at 17:21 UTC.

c) MH370's estimated time at the transfer of control point boundary between the Kuala Lumpur Area Control Centre (ACC) and the Ho Chi Minh ACC at position IGARI was 17:22.

d) Based on radar data records, Ho Chi Minh ACC received radar symbol (Secondary Surveillance response) of MAS 370 on ATS route R208 (South of IGARI) and this symbol disappeared when aircraft approached near IGARI.

e) At 17:38:54 UTC (IGARI plus **16:54 minutes**), after a number of attempts to communicate on main and emergency frequencies directly and through indirect contacts (via other aircraft) with MH370, Ho Chi Minh ACC informed Kuala Lumpur that they had no radio and no radar contact with the aircraft.

f) At 18:00 UTC (IGARI plus **38 minutes**), Ho Chi Minh ACC informed the Ho Chi Minh Rescue Coordination Centre (RCC) and the Aviation RCC (Ha Noi) of an INCERFA SAR Phase, as well as informing the Phnom Penh ACC. The Aviation RCC reported to the National SAR Agency Committee and Maritime RCC and other relevant units (note: excerpts from Annex 11 and Doc 4444 regarding alerting Standards and Recommended Practices are in **Appendix 1**).

g) Malaysian military (Primary Surveillance Radar (PSR) continued to track an unknown aircraft now presumed to be MH370 as it deviated from its planned flight path and crossed over the Malay Peninsula via Malaysia and the southern provinces of Thailand. It was reported that Thai PSR also tracked MH370 as it flew west, then northwest over the Andaman Sea. The last target was seen on Malaysian military radar at 18:15 UTC approximately 200 nautical miles (370 km) west of Penang, 54 minutes after the aircraft had disappeared from civilian SSR screens.

h) Within 60 minutes of the disappearance of MH370, Ho Chi Minh ACC also informed Sanya and Hanoi ACCs.

i) At 00:43 UTC (IGARI plus **7 hours 21 minutes**) Ho Chi Minh ACC issued an ALERFA/DETRESFA message.

j) The Regional Office (RO) wrote to the Civil Aviation Authority of Viet Nam and the Kuala Lumpur RCC, offering assistance should it be required. Meanwhile, the RO engaged in informal coordination and information sharing of on-going events with ICAO HQ, the Chair of the ICAO-IMO Joint Working Group (JWG), IMO and the Chair of the Asia/Pacific SAR Task Force (APSAR/TF).

Wednesday 12 March 2014

k) In response to enquiries from the RO, the International Air Transport Association (IATA) advised that '*All onboard surveillance and surveillance sources e.g. ADS-B/X'PDR/FMS can be turn off inflight by switches or via circuit breakers. The aircraft Emergency Locater Transmitter that is installed on all B777 (a recent mandate) failed to provide a signal. Apparently this can also be deactivated if the switch is left in 'reset' position by the crew. It is normally set to ARM during the crew pre-flight checks'* (**Figure 1**).

Fuselage Mounted Emergency Locator Transmitter

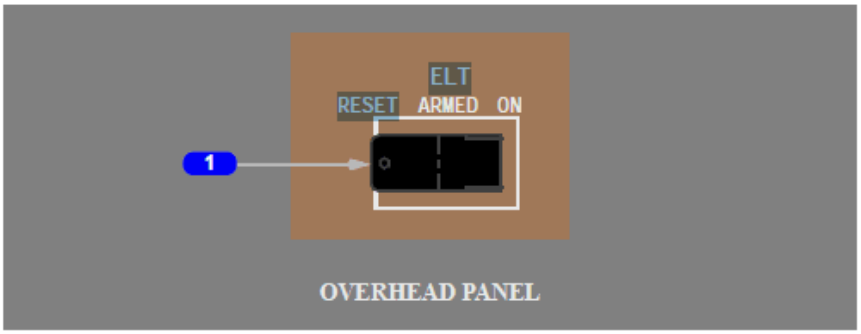

1 Emergency Locator Transmitter (ELT) Switch

RESET (spring-loaded) – ends transmission of emergency locator signal.

ARMED (guarded position) – transmits emergency locator signal if activated by high deceleration forces.

ON – transmits emergency locator signal.

Figure 1: ELT switch

Thursday 13 March 2014

l) The RO noted that ICAO HQ Chief Accident Investigation Section (AIG) had confirmed by letter to Malaysia that Malaysia as the State of Registry was responsible for instituting an investigation when the location of accident or the serious incident cannot be definitely established.

Friday 14 March 2014

m) The RO received communication from Phoenix International Holdings, Inc., regarding their expertise in the field of aircraft search and recovery, which was checked and passed onto Malaysia for their information (Phoenix systems were subsequently employed in the search).

Saturday 15 March 2014

n) The RO had communication with the RCCs in Kuala Lumpur and Canberra, which expressed concern about the management of aircraft within the Australian Search and Rescue Region (SRR). The search aircraft appeared to be under the direction of high Malaysian officials, and not the RCCs. It was not clear that the States involved were actively searching within their airspace under the provisions of Annex 12 paragraph 5.3.1 i). Moreover, the RCCs were reportedly receiving information only from journalists or via 'diplomatic channels'.

Sunday 16 March 2014

o) The RO sent a message to the Malaysian Director of Civil Aviation Dato' Azharuddin Abdul Rahman extending its sincere sympathy to all those affected in Malaysia by the MH370 disappearance. The correspondence also stressed: *As the SAR activity now involves several States, the expectation from the ICAO APAC Regional Office is that all SAR actors to this unfolding situation comply with the provisions of Annex 12 and the spirit of international cooperation enshrined in the IAMSAR (International Aeronautical and Maritime SAR Manual), setting aside all other priorities to the greatest extent possible in the urgent pursuit of an effective SAR response to MH370's disappearance*.

Monday, 17 March 2014

p) The RO sent an urgent email message to Malaysia and Australia, emphasizing the need for clarity in the SAR response, as it appeared that there was a lack of understanding as to who was responsible for managing the SAR response to MH370's disappearance and deploying SAR assets. The root cause of the problem appeared to be confusion between the provisions of Annex 12 (SAR) and Annex 13 (Air Safety Investigation), and political involvement at the highest levels in the search direction. It was noted that Annex 12 was not 100% clear as there was no mention of the transition process between any Annex 12 and Annex 13 action, apart from a brief reference to the need to 'cooperate' with air safety investigators in 3.2.3 (and a later reference to including investigators in Search and Rescue Units - SRUs).

The RO noted that normally, an event moved time sequentially from an Annex 12 SAR response to an Annex 13 investigation, but in this case there was a high profile concurrent investigation guiding parts of the SAR response. In the case of MH370, the investigation (whether it was formally declared as such or not) was providing potentially valuable clues for the SAR response, but that did not mean that the investigation took over from the SAR response.

The RO message clarified that until there was little prospect of survival, the provisions of Annex 12 should take precedence so Australia should direct operations within their SRR (however this was not explicitly clear in Annex 12 and 13). This was because the people who have the necessary expertise to act on any information and direct SRUs accurately with the appropriate knowledge of crucial things like ocean currents were the RCCs.

The RO noted that what seemed to be causing confusion was the provision in Annex 13 which dictated that 'should an accident happen over the high seas the State of Registry would be responsible for instituting and conducting the investigation of the occurrence'. However this provision only dictated who was responsible for the investigation, and not the SAR response.

q) Australia advised that a high level meeting of the Inter-Governmental Coordination Group was meeting, then subsequently the RO was advised that the Australian Prime Minister had accepted a request from Malaysia to take charge of the 'southern vector' of the search, and offered additional surveillance resources.

r) The RO advised ICAO HQ that the MH370 event had exposed several potential problem areas in Annex 12:

- it was not 100% clear in terms of which RCC should be managing the SAR response, as 5.2.4 b) only gave four choices, whereas the second choice was closest. However this did not take into account the scenario of MH370 with several SRRs being involved not on the original flight path of the aircraft and included the anomalous words 'was on the line separating two search and rescue regions'; and

- the potential confusion caused by multiple overlapping SRRs, was not helping a complex search situation with many permutations involving several SRRs. A major root cause of this was noted as being the SRRs being designated by States themselves under the provision of Annex 12. Despite the requirements of the paragraph 2.2.1: *Such regions shall not overlap and neighbouring regions shall be contiguous'*, this was not always followed.

  ICAO HQ noted that SRR were currently in regional ANPs and could only be amended by regional air navigation agreement. Moreover, ICAO HQ did not have the resources to consider such a change to ensure the ICAO Council were able to make decisions on SRR boundaries, recommending that regions could try to sort out the inconsistencies but HQ was not recommending this. ICAO HQ noted that there was more critical work to be done and they were only putting limited efforts into SAR.

s) The RO received the first Situation Report (SITREP) from the Australian RCC. By 02 April, 17 SITREPs had been received.

Wednesday 19 March 2014

t) The ICAO/IMO JWG Chair advised that the JWG planned for September 2014 had been moved from Bangkok to London, which meant the opportunity for JWG to review the outcomes of investigations into MH370's SAR response could not be conducted with all the Asia/Pacific States concerned.

Tuesday 25 March 2014

u) Australia advised that they were having difficulty obtaining the updated analysis of Inmarsat data announced by the Malaysian Prime Minister which had been stated as confirming the southern route of MH370 inside the Australian SRR. Australia wanted to obtain this as a contributory source of data for the search in their SRR, and asked to obtain this information through RCC Kuala Lumpur without success. They understood that this Inmarsat information went to the 'Steering Committee' (DG DCA, MAS, military) who then passed it upwards to the Prime Minister's office, with the Kuala Lumpur RCC only supplied with the last known position by the Director General DCA Malaysia.

  Australia had unsuccessfully approached Inmarsat and had made a written request to their Australian Safety Transport Bureau, which had made contact with the investigators in Kuala Lumpur seeking the information. In addition, Australia noted that they had experienced difficulty obtaining the MH370 cargo manifest which would be useful for identification against debris recovered.

v) Tuesday 25 March 2014: The RO contacted the Director General DCA Malaysia to urge release of the requested data. The information was duly provided to Australia.

Key SAR Issues

2.4 The following issues are highlighted:

a) There was a time lapse of more than 16 minutes between the transfer of control point at IGARI and the advisory to the last ATC unit (Kuala Lumpur ACC) that MH370 had disappeared.

b) There was a time lapse of at least 38 minutes between the disappearance of MH370 before IGARI and the issuance of an INCERFA SAR phase.

c) There was a time lapse of 7 hours and 21 minutes between the disappearance of MH370 and the issuance of an ALERFA/DETRESFA SAR phase.

d) Annex 11/12 Alerting Service phases that were designed to meet the needs of a procedural (non-surveillance) environment had been relatively unchanged for decades. Thus the SAR alerting phases do not take into account the logical actions that should be possible within a modern ATS surveillance environment.

e) PSR information from Malaysian military PSR and the two PSRs in Thailand at Hat Yai (near the Thai-Malaysian border) and Phuket (Bang Duk Hill) that could have observed the westbound track of MH370 were not provided to civilian authorities during the immediate period following the disappearance. The Malaysian military PSR information was not publically released for approximately a week after the disappearance.

f) Poor and ad hoc coordination post-incident between States was evident, with a lack of flow of information between RCCs and third parties such as political entities being involved in the operational decision-making process, which required several 'interventions' and clarifications by the RO.

The weaknesses in Asia/Pacific SAR preparedness, particularly in respect of a lack of SAR Agreements and testing of systems using SAREX, had been identified previously by the APSAR/TF. An APANPIRG Conclusion (24/22) *Search and Rescue Agreements* urging States to make arrangements for senior civil and military decision-makers to facilitate the implementation and maintenance of SAR Agreements as early as possible had not resulted in a noticeable improvement.

g) Annex 12 and Annex 13 were largely silent on the transition procedures between the two Annexes, particularly concerning who was responsible during concurrent activities (note: the enquiry from Malaysia to ICAO HQ to clarify Annex 13 responsibilities without also referring to Annex 12 may have contributed to the subsequent confusion of responsibilities in the period prior to 17 March 2014).

Annex 12 had no reference in paragraph 5.2.4 as to responsibility when more than two SRRs are involved, especially if the airspace concerned was not part of the original flight plan.

SRR designation by States instead of the Council had led to many areas having a confusing disposition of SAR responsibilities.

Possible Actions

2.5 The following actions are not presented as recommendations because this Brief had been prepared on the basis of incomplete information. However, due to the need to urgently address the potential issues, the following possible actions are suggested for consideration.

a) The time lapses of more than 16 minutes between the transfer of control point at IGARI and the advisory to Kuala Lumpur ACC that MH370 had disappeared, 38 minutes for the issuance of an INCERFA SAR phase and 7 hours and 21 minutes for the issuance of an ALERFA/DETRESFA SAR phase by Viet Nam indicates there was probably not enough resources utilized and/or urgency in responding.

b) It is apparent that a higher degree of Malaysian civil/military coordination may have revealed the possibility of the MH370 course reversal much earlier after the initial alert advice from Viet Nam, and as the hypothesized track also crossed Thailand's PSR coverage, advice to Thailand may have also proved beneficial. In essence, a week or more was lost in the initial search because of poor civil/military cooperation.

c) Annex 12 SAR phases and actions need to be revised to take into account the expectations and capabilities of an ATS surveillance environment. The SAR actions should include the need for civil/military coordination where appropriate, and advisories to all neighbouring ACCs in the case of uncertainty of the aircraft's track.

d) Poor SAR preparedness and ad hoc SAR coordination between States, including the intervention by political decision-makers needs to be addressed if an optimal operational response is to be possible. Past APANPIRG Conclusions meant to address SAR coordination weaknesses have been largely ignored. In some cases SAR Agreements are hindered by political barriers whereby States can take many years to progress documents through government ministries. This requires a high level political agreement (above APANPIRG - ASEAN, SAARC, etc.) to change the manner in which SAR agreements and operational coordination is prioritized and managed. In addition, the region needs to conduct properly organized SAREX* on a regular basis and reported to APANPIRG, instead of this being done on an ad hoc basis between States.

e) Annex 12 and Annex 13 need to be updated to include SARPs on transition procedures between the two Annexes, particularly regarding who is responsible during concurrent Annex 12 and Annex 13 activities.

f) Annex 12 had no reference in paragraph 5.2.4 as to responsibility when more than two SRRs are involved, especially if the airspace concerned was not part of the original flight plan.

g) Aeronautical SRR designation by States instead of the ICAO Council was not optimal, but this would require changes to SARPs and a complete review of the current situation to resolve and optimize the SRRs.

h) Lack of ICAO HQ SAR resource and oversight, as identified in an APSAR/TF/2 Draft Conclusion that was formulated on 30 January 2014 would need to be addressed urgently if the lessons learnt in the MH370 accident were able to result in the necessary changes to ICAO SARPs.

*Note – many SAREX in the Asia/Pacific are in fact airport emergency plan and crash response displays for dignitaries with no actual search element, or real testing of the system because everyone knows prior to the SAREX what will happen.

3. ACTION BY THE MEETING

3.1 The meeting is invited to:

a) note the information contained in this paper;

b) comment on the Key SAR Issues and Possible Actions; and

c) discuss any relevant matters as appropriate.

…….

Appendix 1: ICAO SARPS

Annex 11

5.2.1 Without prejudice to any other circumstances that may render such notification advisable, air traffic services units shall, except as prescribed in 5.5.1, notify rescue coordination centres immediately an aircraft is considered to be in a state of emergency in accordance with the following:

a) *Uncertainty phase* when:

1) no communication has been received from an aircraft within a period of thirty minutes after the time a communication should have been received, or from the time an unsuccessful attempt to establish communication with such aircraft was first made, whichever is the earlier, or when

2) an aircraft fails to arrive within thirty minutes of the estimated time of arrival last notified to or estimated by air traffic services units, whichever is the later, except when no doubt exists as to the safety of the aircraft and its occupants.

b) *Alert phase* when:

1) following the uncertainty phase, subsequent attempts to establish communication with the aircraft or inquiries to other relevant sources have failed to reveal any news of the aircraft, or when 2) an aircraft has been cleared to land and fails to land within five minutes of the estimated time of landing and communication has not been re-established with the aircraft, or when

3) information has been received which indicates that the operating efficiency of the aircraft has been impaired, but not to the extent that a forced landing is likely, except when evidence exists that would allay apprehension as to the safety of the aircraft and its occupants, or when

4) an aircraft is known or believed to be the subject of unlawful interference.

c) *Distress phase* when:

1) following the alert phase, further unsuccessful attempts to establish communication with the aircraft and more widespread unsuccessful inquiries point to the probability that the aircraft is in distress, or when

2) the fuel on board is considered to be exhausted, or to be insufficient to enable the aircraft to reach safety, or when

3) information is received which indicates that the operating efficiency of the aircraft has been impaired to the extent that a forced landing is likely, or when

4) information is received or it is reasonably certain that the aircraft is about to make or has made a forced landing, except when there is reasonable certainty that the aircraft and its occupants are not threatened by grave and imminent danger and do not require immediate assistance.

PANS ATM

9.2.2.2 When alerting service is required in respect of a flight operated through more than one FIR or control area, and when the position of the aircraft is in doubt, responsibility for coordinating such service shall rest with the ATS unit of the FIR or control area:

a) within which the aircraft was flying at the time of last air-ground radio contact;

b) that the aircraft was about to enter when last air-ground contact was established at or close to the boundary of two FIRs or control areas;

c) within which the aircraft's intermediate stop or final destination point is located:

1) if the aircraft was not equipped with suitable two-way radio-communication equipment; or

2) was not under obligation to transmit position reports.

9.2.2.3 The unit responsible for alerting service, in accordance with 9.2.2.2, shall:

a) notify units providing alerting service in other affected FIRs or control areas of the emergency phase or phases, in addition to notifying the rescue coordination centre associated with it;

b) request those units to assist in the search for any useful information pertaining to the aircraft presumed to be in an emergency, by all appropriate means and especially those indicated in 5.3 of Annex 11 (Use of communication facilities);

c) collect the information gathered during each phase of the emergency and, after verifying it as necessary, transmit it to the rescue coordination centre;

d) announce the termination of the state of emergency as circumstances dictate.

9.2.2.4 In obtaining the necessary information as required under 5.2.2.1 of Annex 11, attention shall particularly be given to informing the relevant rescue coordination centre of the distress frequencies available to survivors, as listed in Item 19 of the flight plan but not normally transmitted.

THE JOURNAL OF NAVIGATION (2015), **68**, 1–22. © The Royal Institute of Navigation 2014
This is an Open Access article, distributed under the terms of the Creative Commons Attribution licence <http://creativecommons.org/licenses/by/3.0/>, which permits unrestricted re-use, distribution, and reproduction in any medium, provided the original work is properly cited.
doi:10.1017/S037346331400068X

The Search for MH370

Chris Ashton, Alan Shuster Bruce, Gary Colledge and Mark Dickinson

(*Inmarsat*)
(Email: chris.ashton@inmarsat.com)

At 17:22 UTC on 7th March 2014 Malaysian Airlines flight MH370 carrying 239 passengers and crew from Kuala Lumpur to Beijing lost contact with Air Traffic Control and was subsequently reported missing. Over the following days an extensive air and sea search was made around the last reported location of the aircraft in the Gulf of Thailand without success. Subsequent analysis of signals transmitted by the aircraft's satellite communications terminal to Inmarsat's 3F1 Indian Ocean Region satellite indicated that the aircraft continued to fly for several hours after loss of contact, resulting in the search moving to the southern Indian Ocean. This paper presents an analysis of the satellite signals that resulted in the change of search area.

KEY WORDS

1. MH370. 2. Air Accident. 3. Satellite Communications.

Submitted: 4 September 2014. Accepted: 14 September 2014. First published online: 7 October 2014.

1. INTRODUCTION. During the search for MH370 information derived from the analysis of satellite signals was released over a period of weeks as the investigation progressed. In some cases this information may have appeared confusing or contradictory, however in a situation where time is critical the early release of preliminary results followed by more detailed refinements is generally more useful than waiting for the completion of a comprehensive analysis. Satellite navigation systems rely on multiple satellites which are designed for accurate navigation and positioning: in this case only a few data points from a single communication satellite were available and an approximate track and final position were determined using techniques developed after the loss of the aircraft. This paper aims to shed some light on the way the analysis progressed over time, narrowing down the target search area at each iteration.

2. SATELLITE SYSTEM OVERVIEW. MH370, a Boeing 777-200ER aircraft registration 9M-MRO, was equipped with a satellite communications terminal that used the Inmarsat Classic Aero system. This system has been operational since 1990 and provides voice and data services to both cockpit and cabin through a

https://doi.org/10.1017/S037346331400068X Published online by Cambridge University Press

network of seven geostationary satellites. Each satellite communicates with aircraft terminals, or Aircraft Earth Stations (AESs), through a single 'global coverage' beam, which links to a Ground Earth Station (GES) where calls are connected to their destination. Because the Classic Aero system uses a global beam it is not necessary for the aircraft to report its position to the GES for the system to work: in contrast aircraft using Inmarsat's SwiftBroadband system use a number of smaller spot beams, and have to report their location regularly to allow the network to use the appropriate beam.

Each aircraft terminal must logon to the network before calls can be made or received; this tells the network which satellite the aircraft is connected to, allowing calls to be routed appropriately. Once logged on the terminal monitors a signalling channel that is used to alert it to incoming calls and messages. If a terminal does not send any data for an hour the network checks that it is still connected by sending it a 'Log-on Interrogation' (LOI) message asking for a response. If no response is received the network will assume that the terminal has been switched off, and remove it from its list of active terminals. This one hour timer has since been reduced to 15 minutes.

After contact with MH370 was lost at 17:22 UTC, its satellite terminal continued to exchange signalling messages with the GES and it is these messages that were analysed to determine the likely location of the aircraft. Two key parameters associated with these messages were used in the analysis: the Burst Timing Offset (BTO) and the Burst Frequency Offset (BFO).

The aircraft satellite communication system operates at L Band, transmitting signals to the satellite at 1·6 GHz and receiving signals from the satellite at 1·5 GHz. The GES to satellite link uses C Band, transmitting at 6 GHz and receiving at 4 GHz. Several channels are used within these bands for message transmissions. One of the channels is called the P-Channel, which the aircraft continually listens to and is used for signalling and data transmissions from the ground to the aircraft. The R-Channel is used for signalling and short data transmissions from the aircraft to the ground.

For system efficiency and for the satellite communication to remain reliable, aircraft R-Channel transmissions are in time slots referenced to the P-Channel as received by the aircraft using the slotted aloha protocol. The BTO is a measure of how long from the start of that time slot the transmission is received. This is essentially the delay between when the transmission was expected (given a nominal position of the aircraft) and when it actually arrives, and is a measure of twice the distance of the aircraft from the satellite. This is illustrated in Figure 1. The BTO was only a relatively recent addition to the ground stations' data set, being added following the Air France 447 accident in 2009 to assist in geo-locating an aircraft.

There is a limit to the number of aircraft that are able to share a single frequency, and so the Classic Aero system uses several different frequencies to carry traffic. The spacing between these frequencies is determined by the data rate plus an allowance for frequency errors due to aircraft oscillator and other tolerances. The BFO is the recorded value of the difference between the received signal frequency and the nominal frequency at the GES. It is determined by several factors including the aircraft's location and ground velocity, providing us with additional information in our search for MH370. This is further explained in Section 4. Table 1 presents these measurements for the MH370 flight.

https://doi.org/10.1017/S037346331400068X Published online by Cambridge University Press

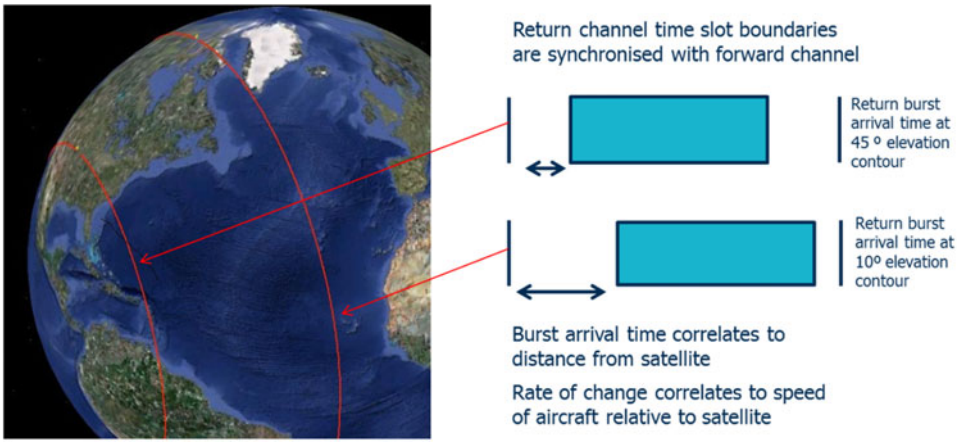

Figure 1. Burst Time Offset Principle.

Table 1. Signalling Message Parameters from Flight MH370 (Malaysian Government, 2014).

Time (UTC)	SU Type	Channel	Channel Unit	Rx Power (dBm)	BFO (Hz)	BTO (μs)
16:42:32	0×62 - Acknowledge User Data (R-channel)	IOR-R1200-0-36ED	4	−57·6	125	14900
16:55:53	0×22 - Access Request (R/T-Channel)	IOR-R1200-0-36ED	4	−56·2	159	15240
17:07:19	0×22 - Access Request (R/T-Channel)	IOR-R1200-0-36ED	4	−55·7	132	15660
18:25:27	0×10 - Log-on Request (ISU)/Log-on Flight Information (SSU)	IOR-R600-0-36E1	8	−52·3	142	17120
18:25:34	0×15 - Log-on/Log-off Acknowledge	IOR-R1200-0-36ED	4	−54·6	273	51700
18:27:04	Eleven Octet User Data	IOR-R1200-0-36ED	4	−54·2	176	12560
18:27:04	Four Octet User Data	IOR-R1200-0-36ED	4	−54·7	175	12520
18:27:08	0×62 - Acknowledge User Data (R-channel)	IOR-R1200-0-36ED	4	−54·9	172	12520
18:28:06	0×22 - Access Request (R/T-Channel)	IOR-R1200-0-36ED	4	−54·5	144	12500
18:28:15	0×62 - Acknowledge User Data (R-channel)	IOR-R1200-0-36ED	4	−54·5	143	12480
19:41:03	0×15 - Log-on/Log-off Acknowledge	IOR-R1200-0-36ED	4	−54·5	111	11500
20:41:05	0×15 - Log-on/Log-off Acknowledge	IOR-R1200-0-36ED	4	−55·5	141	11740
21:41:27	0×15 - Log-on/Log-off Acknowledge	IOR-R1200-0-36ED	4	−54·1	168	12780
22:41:22	0×15 - Log-on/Log-off Acknowledge	IOR-R1200-0-36ED	4	−53·0	204	14540
00:11:00	0×15 - Log-on/Log-off Acknowledge	IOR-R1200-0-36ED	4	−53·3	252	18040
00:19:29	0×10 - Log-on Request (ISU)/Log-on Flight Information (SSU)	IOR-R600-0-36F8	10	−51·0	182	23000
00:19:37	0×15 - Log-on/Log-off Acknowledge	IOR-R1200-0-36F6	10	−53·7	−2	49660

https://doi.org/10.1017/S037346331400068X Published online by Cambridge University Press

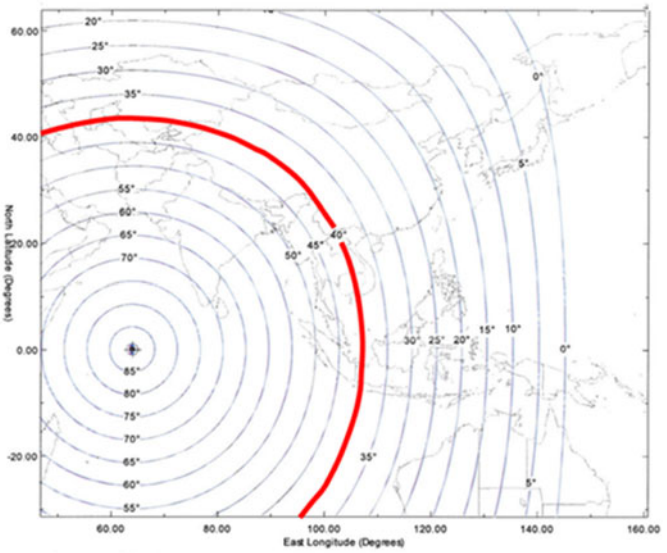

Time (UTC)	Elevation (degrees)
16:42:32	46.5
16:55:53	46.0
17:07:19	45.0
18:25:34	-
18:27:04	52.0
18:27:04	52.0
18:27:08	52.0
18:28:06	52.0
18:28:15	52.0
19:41:03	55.0
20:41:05	54.0
21:41:27	51.5
22:41:22	47.2
00:11:00	40.0
00:19:37	-

Figure 2. Initial BTO Analysis (00:11 UTC Arc Highlighted).

3. ARCS AND PROBABLE TRACKS. The first deduction that can be made from the signalling data is that the aircraft remained operational for at least seven hours after the loss of contact, as the satellite terminal continued to transmit messages during this period. It may further be deduced that the aircraft navigation system was operational, since the terminal needs information on location and track to keep its antenna pointing towards the satellite. Finally the varying BTO measurements indicate that the aircraft was moving (at speed) during this period. The terminal did not respond to the LOI message at 01:16 UTC on 8 March.

3.1. *Initial BTO Analysis.* The initial analysis related BTO measurement to the elevation angle from the aircraft to the satellite, based on work performed following the Air France 447 investigation. This achieved an approximate elevation angle accuracy of 1°, and showed the aircraft to lie close to the 40° elevation angle contour at 00:11 UTC (Figure 2). BTO measurements at 18:25 and 00:19 were excluded from the initial analysis as they gave anomalous results: these anomalies were subsequently resolved and will be covered later in this paper.

3.2. *Refined BTO Analysis.* While the initial BTO analysis provided a rapid and reasonably accurate assessment of the aircraft location at specific measurement times it made the approximation that the satellite was at its nominal orbital location above the equator. In fact the satellite orbit is slightly inclined, resulting in a north-south movement of 2,412 km each day. To correct for this a more precise analysis was performed taking account of the actual location of the satellite at each measurement point.

The BTO measurement comprises two components: a bias component caused by fixed delays in the system, plus a variable component caused by the time taken for the outbound radio wave to pass from the GES to the aircraft and the inbound radio wave

https://doi.org/10.1017/S037346331400068X Published online by Cambridge University Press

Table 2. BTO Calibration Geometry.

	Location (km)				
Terminal	x	y	z	Lat °N	Lon °E
GES (Perth)	−2368·8	4881·1	−3342·0	−31·8	115·9
AES (KLIA)	−1293·0	6238·3	303·5	2·7	101·7

	Satellite Location (km)			Dist to Satellite	
Time (UTC)	x	y	z	GES (km)	AES (km)
16:00:00	18118·9	38081·8	706·7	39222·7	37296·0
16:05:00	18119·6	38081·5	727·9	39225·0	37296·4
16:10:00	18120·3	38081·2	748·7	39227·3	37296·7
16:15:00	18120·9	38080·9	769·2	39229·6	37297·1
16:20:00	18121·6	38080·6	789·4	39231·8	37297·4
16:25:00	18122·2	38080·3	809·1	39233·9	37297·8
16:30:00	18122·9	38080·0	828·5	39236·1	37298·1

to make the return journey. This allows a simple equation to be developed relating satellite to aircraft distance to timing delay.

$$Range_{(satellite\ to\ aircraft)} = \frac{c.(BTO - bias)}{2} - Range_{(satellite\ to\ Perth\ GES)} \quad (1)$$

where *bias* is a fixed (and constant) delay due to GES and AES processing and c is the speed of light.

To determine the bias value, and obtain an indication of the accuracy of the technique, signals exchanged between the GES and aircraft in the 30 minutes prior to take off were processed. During this 30 minute period the satellite moved 122 km. Table 2 shows the location of the satellite, aircraft and GES over this period, expressed in an Earth Centred Earth Fixed (ECEF) coordinate system where the centre of the earth is the origin, the z-axis is due North and the x and y axes are in the equatorial plane with 0° and 90° longitude respectively (note: throughout this paper we use an ellipsoid Earth model).

Seventeen measurements were taken during this 30 minute period, and these were processed to estimate the fixed timing bias. The mean bias of −495,679 μs was then used to predict the path length from the measured data (Table 3 right hand columns), showing a high degree of consistency. The peak error out of all 17 measurements is 17·7 km in the distance from GES to AES and back, equivalent to less than 9 km in the distance between the satellite and the AES.

With the bias value determined from the ground measurements, the in-flight measurements were processed to determine the satellite to aircraft distance at each measurement point. The locus of points on the earth of constant distance to the satellite is a ring (for a spherical earth these would be circles) centred on the sub-satellite point. These results were then converted to a set of rings at an assumed cruising altitude of 10,000 m, where the distance from the satellite matched the measurement. The rings were then reduced to arcs by excluding locations that were too

https://doi.org/10.1017/S037346331400068X Published online by Cambridge University Press

Table 3. BTO Calibration (Kuala Lumpur International Airport).

Time (UTC)	BTO (μs)	Path (km)	Transmission Delay (μs)	Bias (μs)	Predicted Path (km)	Error (km)
16:00:13	14820	153037	510478	−495658	153044	−6·3
16:00:17	14740	153037	510478	−495738	153020	17·7
16:00:18	14780	153037	510478	−495698	153032	5·7
16:00:18	14820	153037	510478	−495658	153044	−6·3
16:00:23	14740	153037	510478	−495738	153020	17·7
16:00:23	14820	153037	510478	−495658	153044	−6·3
16:00:32	14820	153037	510478	−495658	153044	−6·3
16:09:37	14840	153048	510514	−495674	153050	−1·7
16:09:47	14840	153048	510514	−495674	153050	−1·7
16:11:04	14840	153048	510514	−495674	153050	−1·7
16:11:13	14860	153048	510514	−495654	153056	−7·7
16:27:59	14920	153068	510581	−495661	153074	−5·5
16:28:16	14860	153068	510581	−495721	153056	12·5
16:29:17	14860	153068	510581	−495721	153056	12·5
16:29:42	14920	153068	510581	−495661	153074	−5·5
16:29:50	14940	153068	510581	−495641	153080	−11·5
16:29:52	14920	153068	510581	−495661	153074	−5·5
			Average:	−495679		

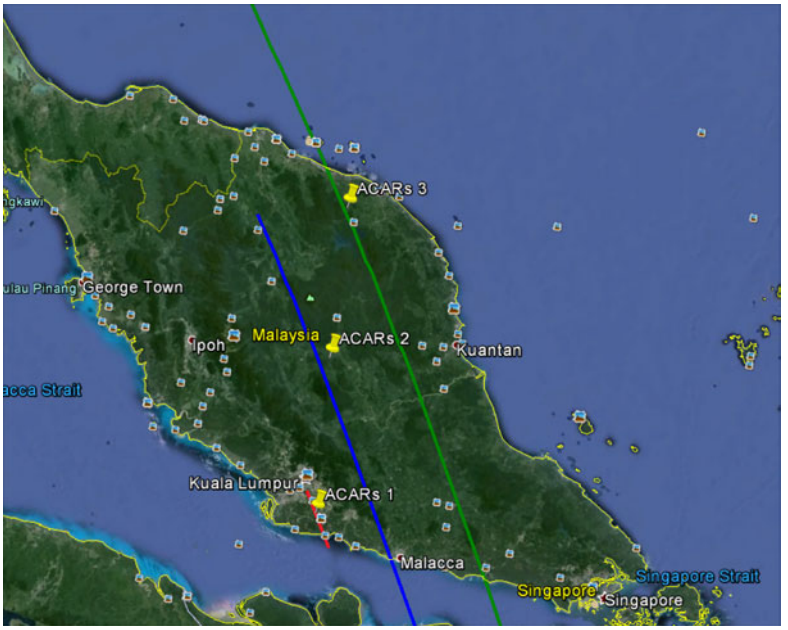

Figure 3. 16:42, 16:56 and 17:07 Arcs with Mode S Positions Shown.

far away from the original location for the aircraft to reach at its highest speed. Figure 3 shows the first three arcs produced by this technique, with the true aircraft location (as reported by the Mode S transponder) overlaid, illustrating the accuracy achieved.

https://doi.org/10.1017/S037346331400068X Published online by Cambridge University Press

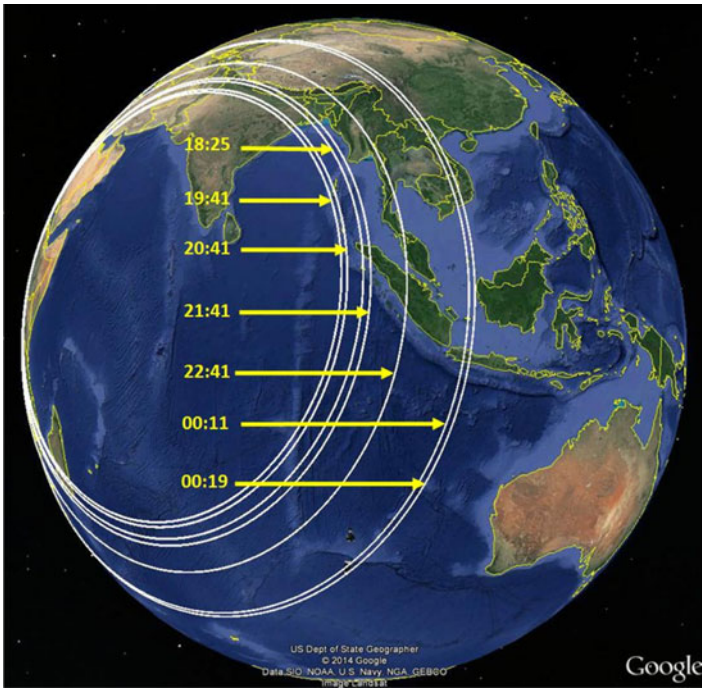

Figure 4. BTO Rings during Later Stages of Flight (ATSB, 2014).

3.3. *Log-on Sequence BTO Measurements.* The BTO readings for the signals at 18:25:27 and 00:19:37 UTC are much larger than the other readings, and were not included in the original analysis. However the final signal has special significance as it appears to have been triggered by the aircraft terminal being power cycled, and may indicate the aircraft running out of fuel. The signals at 18:25:27 and 00:19:37 were both generated as part of a logon sequence, contrasting with the other messages which were generated as part of a standard LOI exchange. Each power up sequence starts with a Logon Request message that has been found to have a fixed offset of 4600 μs relative to the LOI message exchange by inspecting historical data for this aircraft terminal. The subsequent messages during the logon sequence were found to have unreliable delay and are believed to be an artefact of the terminal switching channel and frequency during logon and so are not used in this analysis. This means that the BTO data for 18:25:34 and 00:19:37 should be ignored, but that corrected BTO values of 12520 and 18400 μs may be derived from the Logon Request messages at 18:25:27 and 00:19:29 UTC respectively. This results in the rings shown in Figure 4 for the later stages of the flight.

3.4. *Initial Flight Path Reconstruction.* The BTO analysis provides us with a series of arcs that the aircraft must cross at specific times. Combining this with the last known location and the viable aircraft speeds allows us to identify a number of flight paths. Each path must cross the arcs at the appropriate time, and it must be possible to travel from one arc crossing point to the next in the available time as illustrated in Figure 5. However we do not know the track or speed of the aircraft, nor whether these are going to change with time, which results in a large number of potential flight paths. While the aircraft could have flown in a relatively straight line travelling as far

https://doi.org/10.1017/S037346331400068X Published online by Cambridge University Press

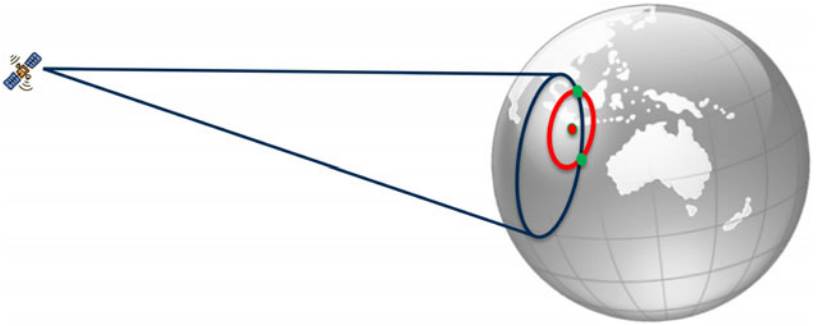

Figure 5. Flight Path Reconstruction Technique.

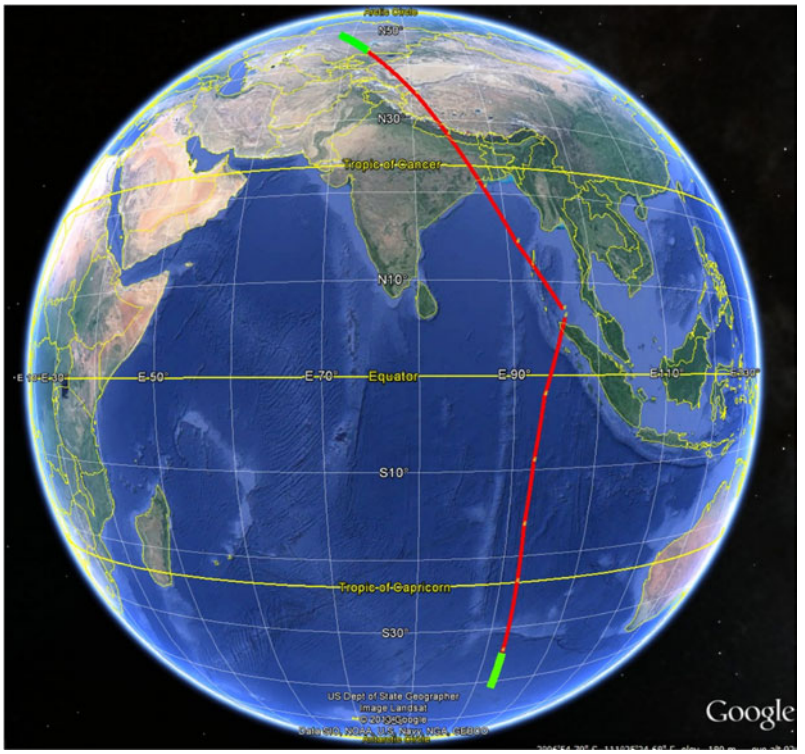

Figure 6. Initial Flight Path Reconstructions.

north as Kazakhstan or deep into the southern Indian Ocean, it could also have flown around in circles and ended up almost anywhere on the final arc.

Initial flight path reconstruction attempts were based on the aircraft flying at a steady speed on a relatively constant track consistent with an aircraft operating without human control. It was initially thought that for the fuel to have lasted until 00:19 UTC the aircraft would have needed to be flying at high altitude, where the air is thinner and drag is reduced, which would have resulted in its flying at close to its maximum speed of just over 500 knots (926 kph). This gave two solutions, one in a northerly and the other in a southerly direction, as illustrated in Figure 6, where the

https://doi.org/10.1017/S037346331400068X Published online by Cambridge University Press

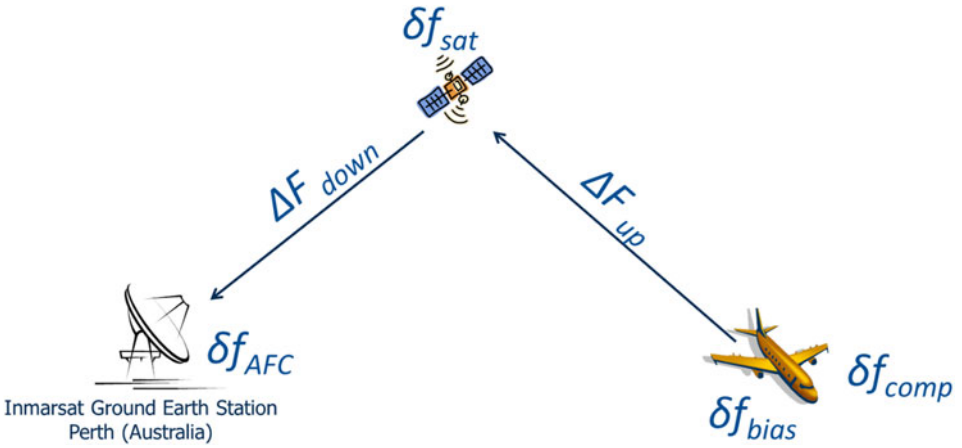

Figure 7. Basis of Frequency Calculation.

red lines indicate the flight paths prior to 00:19 UTC and the green lines indicate the potential additional flight paths between the last signal at 00:19 UTC and the failure to respond to the LOI message sent by the GES at 01:15 UTC.

It is important to remember that these initial flight paths, while consistent with the BTO timing data and the aircraft performance, were based on a number of assumptions: that the aircraft travelled at a steady and high speed and did not make any manoeuvres beyond a turn to the north or south shortly after its last radar detection.

4. FREQUENCY CALCULATION. While the timing work derived a series of high-resolution location arcs, these gave many different flight path solutions resulting in an extremely large search area. Even discriminating between southern and northern routes was impossible, although the northern route appeared less likely given the large number of civil and military radar installations it passed over. The possibility also remained of a circular flight path ending in China, Vietnam, Borneo or Indonesia. To try and resolve this ambiguity an analysis of the BFO data was undertaken, in the hope that the Doppler components of the two routes would be sufficiently different to discriminate between them.

4.1. *Theory*. Unlike the timing calculation, which predicts the location of the aircraft relative to the satellite from the BTO measurement, the frequency calculation works backwards, taking the aircraft location and velocity at a given time and calculating the BFO that this would generate. This enables the likelihood of potential flight paths to be evaluated, depending on how well the calculated BFO values align with the measured values during the flight.

The BFO may be calculated by combining the contributions of several factors illustrated in Figure 7:

$$BFO = \Delta F_{up} + \Delta F_{down} + \delta f_{comp} + \delta f_{sat} + \delta f_{AFC} + \delta f_{bias} \quad (2)$$

where ΔF_{up} is the Doppler on the signal passing from the aircraft to the satellite, ΔF_{down} is the Doppler on the signal passing from the satellite to the GES, δf_{comp} is the frequency compensation applied by the aircraft, δf_{sat} is the variation in satellite

https://doi.org/10.1017/S037346331400068X Published online by Cambridge University Press

Table 4. Satellite Location and Velocity (ECEF).

	Satellite Location (km)			Satellite Velocity (km/s)		
Time (UTC)	x	y	z	x′	y′	z′
16:30:00	18122·9	38080·0	828·5	0·00216	−0·00107	0·06390
16:45:00	18124·8	38079·0	884·2	0·00212	−0·00114	0·05980
16:55:00	18126·1	38078·3	919·2	0·00209	−0·00118	0·05693
17:05:00	18127·3	38077·6	952·5	0·00206	−0·00120	0·05395
18:25:00	18136·7	38071·8	1148·5	0·00188	−0·00117	0·02690
19:40:00	18145·1	38067·0	1206·3	0·00189	−0·00092	−0·00148
20:40:00	18152·1	38064·0	1159·7	0·00200	−0·00077	−0·02422
21:40:00	18159·5	38061·3	1033·8	0·00212	−0·00076	−0·04531
22:40:00	18167·2	38058·3	837·2	0·00211	−0·00096	−0·06331
00:10:00	18177·5	38051·7	440·0	0·00160	−0·00151	−0·08188
00:20:00	18178·4	38050·8	390·5	0·00150	−0·00158	−0·08321

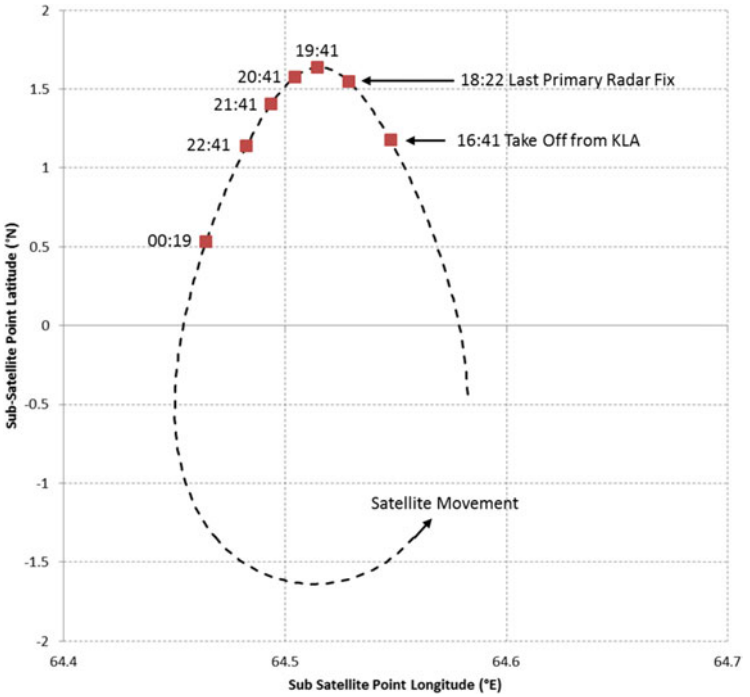

Figure 8. 3F1 Sub-Satellite Point Locations during MH370 Flight.

translation frequency, δf_{AFC} is the frequency compensation applied by the GES receive chain and δf_{bias} is a fixed offset due to errors in the aircraft and satellite oscillators.

The uplink and downlink Doppler may be calculated from the relative movement of the aircraft, satellite and GES using the signal frequencies of 1646·6525 MHz (uplink) and 3615·1525 MHz (downlink). The satellite location and velocity are accurately determined by Inmarsat for satellite station keeping and collision avoidance activities, and are shown in Table 4 for the key times used in the analysis. For the purpose of illustration Figure 8 shows the locus of the sub-satellite point (the point on the earth's

https://doi.org/10.1017/S037346331400068X Published online by Cambridge University Press

surface directly below the satellite) highlighting the location at key times during the MH370 flight.

The aircraft terminal adjusts its transmit frequency to compensate for the Doppler induced on the uplink signals by the aircraft velocity. Aircraft latitude, longitude, track and ground speed are used to calculate the Doppler shift the signal would experience if the satellite was at its nominal location over the equator. This only partially compensates for the Doppler associated with the aircraft's velocity as it does not allow for vertical movement (which introduces discrepancies when the aircraft is climbing/descending) and the satellite is rarely at its nominal location: these small errors are immaterial to the communications performance, but do affect the BFO. This is δf_{comp} in Equation (2).

Signals received by the satellite are translated in frequency, amplified and relayed to the GES. The satellite translation frequency is derived from an oscillator that is maintained in a temperature-controlled enclosure to improve its stability. During eclipse periods when the satellite passes through the earth's shadow, the satellite temperature drops resulting in a small variation in translation frequency. Such an eclipse occurred during the flight of MH370 starting at 19:19 UTC and ending at 20:26 UTC, affecting the 19:40 and 20:40 measurements. The temperature of the oscillator is also affected by the rotation of the satellite relative to the sun every 24 hours which gives a regular daily temperature variation to the equipment, further complicated by heaters which are switched on if the equipment drops out of pre-defined temperature limits. All of these thermal effects impact on the satellite translation frequency. This is δf_{sat} in Equation (2).

The GES translates the frequencies it receives from the satellite to an Intermediate Frequency (IF) before passing them to the equipment that demodulates and processes them. The translation frequency applied is controlled by an Automatic Frequency Control (AFC) loop to compensate for the downlink Doppler. The AFC loop works by monitoring the absolute frequency of a reference signal transmitted through the satellite, and using these measurements to determine the appropriate translation frequency to apply over a 24-hour period. For operational reasons associated with the hardware used to implement this AFC loop in the Perth GES it only partially compensates for the downlink Doppler. This is δf_{AFC} in Equation (2).

The final component in the frequency calculation is a fixed bias component related to the aircraft and satellite oscillator errors such as those associated with long term drift and ageing. While manufactured to high tolerances, the oscillators on the aircraft and the satellite exhibit small fixed frequency errors that result in a bias value appearing in the BFO associated with any particular terminal. As the value is constant it can be determined through calibration measurements when the aircraft location and velocity are known. This is δf_{bias} in Equation (2). Table 5 shows how the frequency bias for flight MH370 was determined, based on measurements taken prior to take off.

4.2. *Initial Results*. Applying the BFO calculation to the original northern and southern routes produced the curves shown in Figure 9, which were published by the Malaysian authorities on 25 March 2014 and used to justify the southern route and the loss of the aircraft. It is noted that the discrepancies in the early measurements were (correctly) ascribed to the effect of the aircraft climbing. The spike in the measured data at 18:28 is not fully understood and was originally ascribed to a possible manoeuvre of the aircraft: although it could be related to frequency changes during the logon sequence described in Section 3.3.

https://doi.org/10.1017/S037346331400068X Published online by Cambridge University Press

Table 5. Frequency Bias Calibration.

Parameter	Value	Unit	Notes
Time	16:30	UTC	
Aircraft Latitude:	2·75	°N	
Aircraft Longitude:	101·71	°E	
Aircraft Ground Speed:	0	kph	
Aircraft True Track:	N/A	°ETN	
Aircraft Freq. Compensation:	0	Hz	Stationary aircraft
Uplink Doppler:	−6	Hz	Satellite movement
Satellite & GES AFC Offset:	29	Hz	Measured
Downlink Doppler:	−85	Hz	Satellite movement
BFO (measured):	88	Hz	Measured
Bias Component:	150	Hz	Calculated

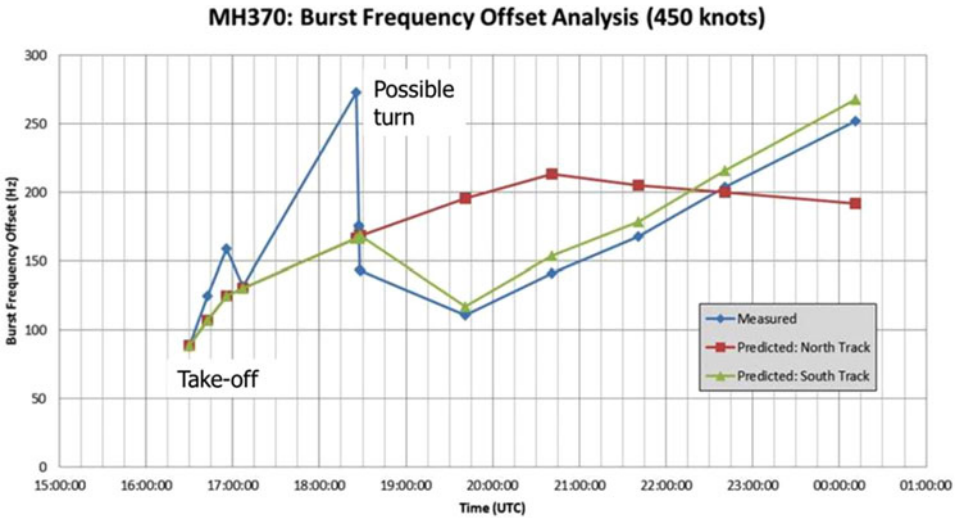

Figure 9. Initial BFO Results indicating Southern Route.

While not providing an exact match, the measured BFO data much more closely resembled the southern route after 18:30 UTC, indicating that the aircraft was most likely to have been travelling in a southerly direction. This information was double checked, validated against flights made by other aircraft and reported to the authorities to assist in the on-going search. Work then continued on identifying a southern route that better matched both timing arcs and BFO curve and on refining the BFO model which (at this stage) did not include second order effects associated with satellite eclipse or accurate measurements of the GES frequency compensation loop.

5. REFINED FREQUENCY CALCULATION. Following the initial work considerable effort went into refining the BFO model and characterising the various components within it. At the same time improvements were made in the

https://doi.org/10.1017/S037346331400068X Published online by Cambridge University Press

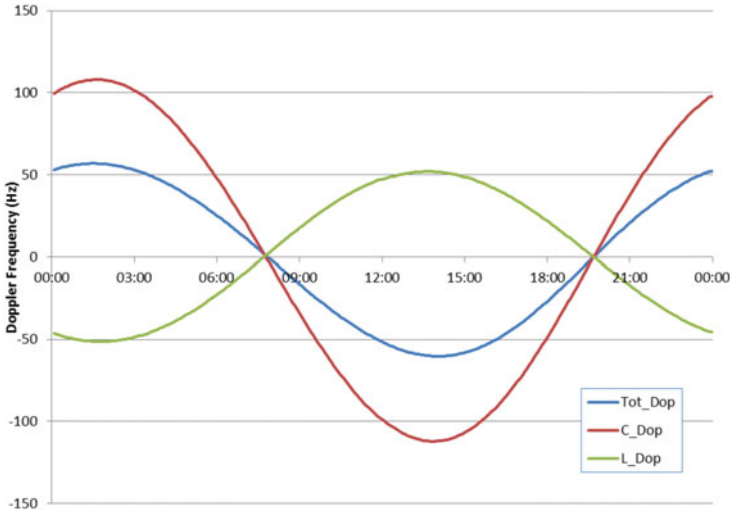

Figure 10. Calculated Pilot Frequency Doppler Offset.

understanding of the measurement data and identifying which points were reliable and which were not.

5.1. *GES AFC Compensation*. The Perth GES partially compensates for C Band Doppler effects by adjusting the translation frequency it applies to receive signals. This frequency adjustment is controlled by an AFC receiver, which measures the absolute downlink frequency of a constant uplink frequency (Pilot) signal that is transmitted to the satellite from Inmarsat's Burum facility in the Netherlands. The receiver maintains a moving average of the received frequency over 24 hours and treats the difference between the received frequency and this average as being due to Doppler. Based on knowledge of the Pilot transmitter location and frequency and the GES location it determines the component of this Doppler attributable to the C Band downlink and adjusts the receive translation frequency to correct for this.

The AFC receiver was not designed to handle a GES located south of the equator, and so to make it work it was configured with a positive GES latitude rather than a negative one. This means that the receiver did not behave as intended, and that its Doppler compensation algorithm did not accurately remove the C Band component of Doppler present in the signal. Fortunately Inmarsat monitors the received frequency of the Pilot signal after it has passed through the frequency conversion at the GES and it is possible to calculate the frequency conversion applied by the receive chain so that it can be calibrated out in the BFO calculation.

Figure 10 shows the calculated Doppler induced frequency shift on the Pilot signal for 7 March 2014. The L Band uplink component is smaller than the C Band downlink component as Doppler shift is proportional to signal frequency. It is interesting to note that when the C Band value is positive the L Band value is negative, as the Pilot is transmitted from north and received from south of the equator, so when the satellite is moving towards the GES it is moving away from the Pilot transmitter.

After AFC controlled frequency conversion the Pilot frequency should lose the Doppler variation attributable to the C Band downlink, but retain the contribution due to the L Band uplink. That is to say the output signal should exhibit a 24 hour

https://doi.org/10.1017/S037346331400068X Published online by Cambridge University Press

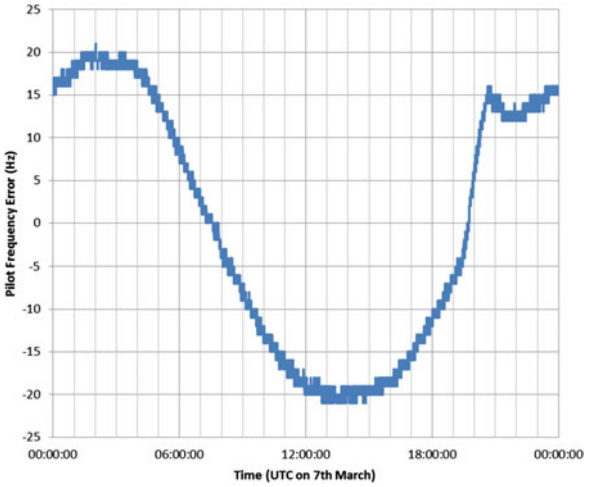

Figure 11. Measured Pilot Frequency Error (After Conversion).

frequency variation of ±52 Hz with the highest frequency occurring at around 14:00 UTC. However the output frequency actually exhibits a 24 hour variation of ± 20 Hz, with the lowest frequency occurring around 14:00. It also shows a distinct kink between 19:30 and 22:30, as illustrated in Figure 11.

This difference in the measured frequency can be explained by the fact that the AFC receiver expects the L Band and C Band Doppler components to add, and so interprets the ±60 Hz input signal variation as being due to the sum, rather than the difference, of the L and C Band components and so removes two thirds of the variation which would be the C Band contribution in such a case.

5.2. *Satellite Thermal Modelling*. The kink in the measured Pilot frequency characteristic was unexplained until it was noticed that it coincided with the satellite eclipse which took place between 19:19 and 20:26 UTC, and so was probably due to satellite oscillator errors due to thermal variations caused by the eclipse. However if we see such marked variations in translation frequency during the satellite eclipse period, it is likely that we will see smaller level variations due to thermal cycling of the satellite oscillator throughout the day that would reduce the accuracy of the BFO calculation.

By modelling the performance of the AFC receiver over several days it is possible to deduce the input signal frequency that it receives and compare the frequency variations of this reconstructed signal with the calculated Doppler to determine the frequency variations due to the satellite oscillator. These are shown in Figure 12 for the day of the MH370 flight, and align well with the temperature of the oscillator that is monitored through routine satellite telemetry (see Figure 13).

While the agreement between satellite thermal effects and residual Pilot frequency error demonstrates the physical source of the variation, it is not necessary to separate the AFC and satellite effects when performing the BFO calculation as their combined effect is directly determined by subtracting the output signal frequency variation shown in Figure 11 with the signal frequency variation due to Doppler shown in Figure 10.

https://doi.org/10.1017/S037346331400068X Published online by Cambridge University Press

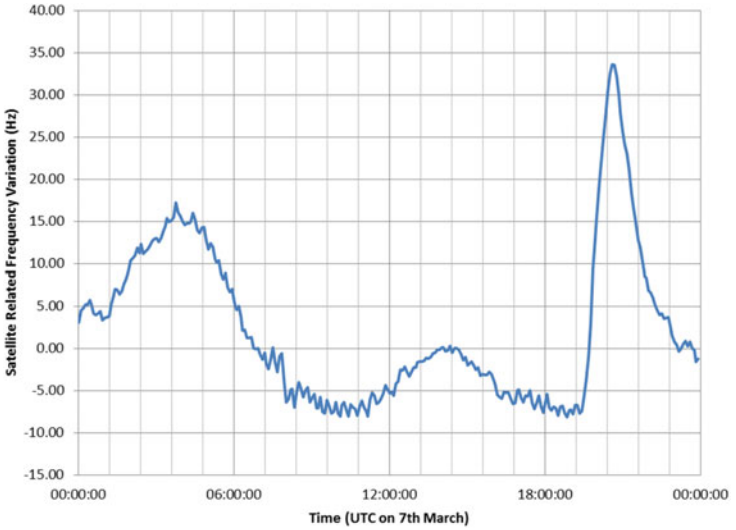

Figure 12. Satellite Translation Frequency Variation.

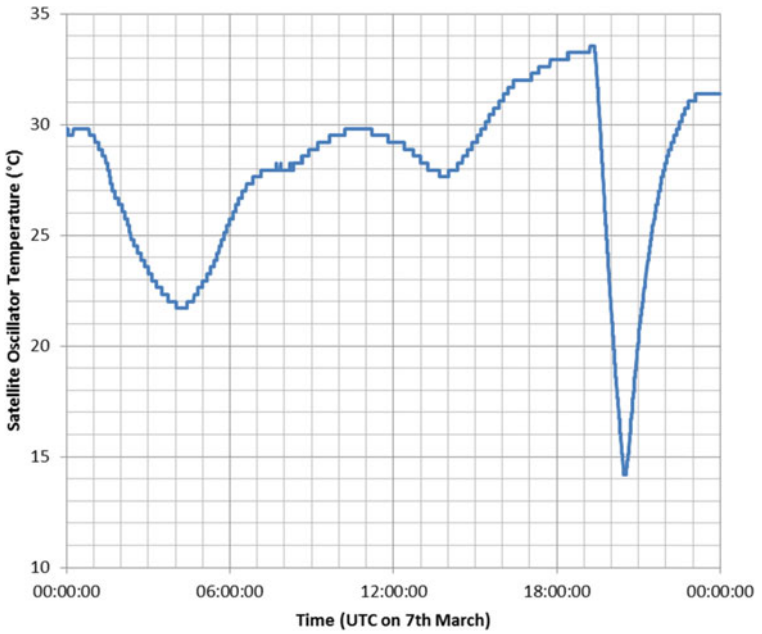

Figure 13. Satellite Oscillator External Temperature Variation.

5.3. *Refinement of BFO Samples.* Detailed analysis of BFO samples taken from other flights showed a high degree of consistency for the signalling message frequencies, with the exception of those that were performed immediately after the initial logon process. This called into question the BFO measurements after the log-on sequences at 18:25 and 00:19. However it was also determined (by the same method) that the first message transmitted by the aircraft in the logon sequence, the Logon Request message, did provide a consistent and accurate BFO measurement. This

https://doi.org/10.1017/S037346331400068X Published online by Cambridge University Press

Table 6. Refined Signalling Message Parameters from Flight MH370.

Time (UTC)	SU Type	Channel	BFO (Hz)	BTO (μs)	Note
16:42:32	0×62 - Acknowledge User Data (R-channel)	IOR-R1200-0-36ED	125	14900	
16:55:53	0×22 - Access Request (R/T-Channel)	IOR-R1200-0-36ED	159	15240	
17:07:19	0×22 - Access Request (R/T-Channel)	IOR-R1200-0-36ED	132	15660	
18:25:27	0×10 - Log-on Request (ISU)/Log-on Flight Information (SSU)	IOR-R600-0-36E1	142	12520	(1)
18:39:58	0×60 - Telephony Acknowledge	IOR-373E-21000	88	–	(2)
19:41:03	0×15 - Log-on/Log-off Acknowledge	IOR-R1200-0-36ED	111	11500	
20:41:05	0×15 - Log-on/Log-off Acknowledge	IOR-R1200-0-36ED	141	11740	
21:41:27	0×15 - Log-on/Log-off Acknowledge	IOR-R1200-0-36ED	168	12780	
22:41:22	0×15 - Log-on/Log-off Acknowledge	IOR-R1200-0-36ED	204	14540	
23:14:03	0×60 - Telephony Acknowledge	IOR-3737-21000	217	–	(3)
00:11:00	0×15 - Log-on/Log-off Acknowledge	IOR-R1200-0-36ED	252	18040	
00:19:29	0×10 - Log-on Request (ISU)/Log-on Flight Information (SSU)	IOR-R600-0-36F8	182	18400	(1)

(1) Modified value, determined by subtracting 4600 μs from measured
(2) Average of 51 values ranging from 86 to 90 Hz. No BTO value available for voice channels
(3) Average of 29 values ranging from 216 to 222 Hz. No BTO value available for voice channels

means that we can use the Logon Request message information from 18:25:27 and 00:19:29, but it is prudent to discount the measurements between 18:25:34 and 18:28:15 inclusive, and the one at 00:19:37.

In addition to the LOI related signals presented in Table 1, MH370 also exchanged signalling messages with the Perth GES at 18:40 and 23:14 UTC related to unanswered ground to air telephone calls. The signalling associated with these calls does not result in a BTO measurement, but did give BFO measurements of 88 and 217 Hz respectively which may be used. This results in a refined set of BTO/BFO measurement data presented in Table 6 for the flight path reconstruction work.

The fit to the originally postulated northern and southern paths is illustrated in Figure 14 that fits the northern path until 18:25, but switches to the southern path by 18:40. The divergence between the measured data and the southern path suggest that a better match may be possible if we make some minor adjustments to the flight path.

5.4. *Validation of BFO Equation.* The technique was validated by applying it to measurements taken from other aircraft whose location and velocity were known, and was found to work well. Validation was performed against several aircraft that were in flight at the same time as MH370, and for the MH370 aircraft in the days leading up to the accident, and good agreement between predicted and measured BFO was seen. Figure 15 shows the measured BFO for flight MH21 that travelled from Kuala Lumpur to Amsterdam at the same time as the MH370's final flight, overlaid with the upper and lower BFO predictions (± 7 Hz) using the refined BFO model. This suggests that ±7Hz is a conservative estimate of the typical accuracy BFO calculation achieves, as well as illustrating the BFO versus time characteristics for a flight moving along a path close to the Northern route. While the validation demonstrates the general accuracy of the BFO technique, it is important to note that agreement is only achieved with ±7 Hz accuracy during this flight, and to assume better accuracy for the measurements taken on MH370 would be unrealistic.

https://doi.org/10.1017/S037346331400068X Published online by Cambridge University Press

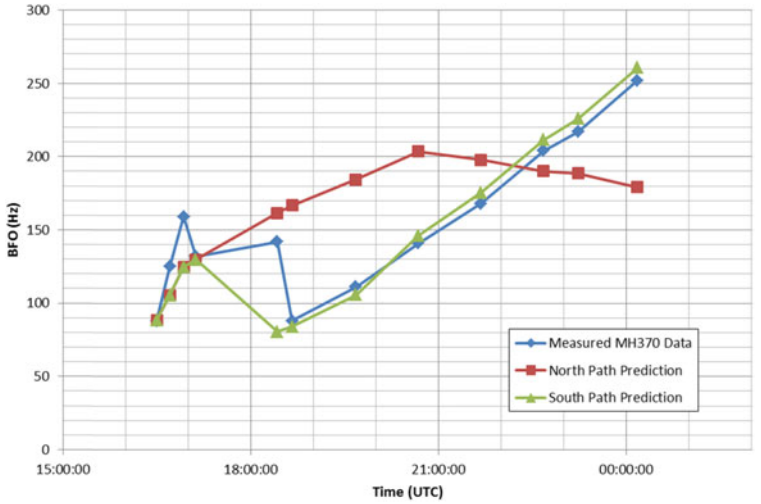

Figure 14. BFO Results using Refined Model.

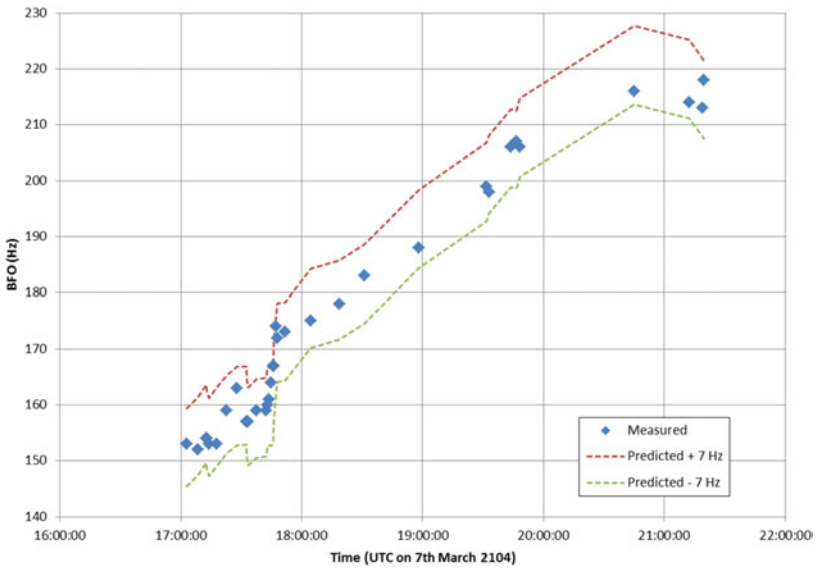

Figure 15. Burst Frequency Offset Validation (Amsterdam Flight).

5.5. *BFO Calculation Sensitivity*. Tables 7 and 8 present the BFO calculation during the early phase of flight MH370 when the aircraft location, ground speed and track are known. They illustrate the sensitivity of the BFO frequency calculation to track and latitude errors, showing that the calculation works and that it is reasonably sensitive to errors in aircraft location and track.

Combining the sensitivity data with the measurement accuracy of ±7 Hz indicates that inaccuracy in each individual BFO measurement would correspond to ±28° heading uncertainty and ±9° of latitude uncertainty.

https://doi.org/10.1017/S037346331400068X Published online by Cambridge University Press

Table 7. BFO Sensitivity to Aircraft Track Errors.

	Heading				
Measurement Parameter	−25°	True	+25°	Unit	Notes
Time	17:07	17:07	17:07	UTC	
Aircraft Latitude:	5·27	5·27	5·27	°N	
Aircraft Longitude:	102·79	102·79	102·79	°E	
Aircraft Ground Speed:	867	867	867	kph	
Aircraft True Track:	0	25	50	°ETN	
Bias Component:	150·0	150·0	150·0	Hz	From Calibration
Aircraft Freq. Compensation:	108·0	490·4	779·0	Hz	Calculated (for 64·5°E satellite)
Uplink Doppler:	−77·7	−463·1	−760·2	Hz	Satellite and aircraft movement
Downlink Doppler:	−71·9	−71·9	−71·9	Hz	Satellite movement
Satellite & EAFC Effect	24·2	24·2	24·2	Hz	Measured
BFO (predicted):	132·6	129·7	121·1	Hz	
Measured BFO:	132·0	132·0	132·0	Hz	Measured
Error:	0·6	−2·3	−10·9	Hz	0·25 Hz/degree sensitivity

Table 8. BFO Sensitivity to Aircraft Latitude Errors.

	Latitude				
Measurement Parameter	−5°	True	+5°	Unit	Notes
Time	17:07	17:07	17:07	UTC	
Aircraft Latitude:	0·27	5·27	10·27	°N	
Aircraft Longitude:	102·79	102·79	102·79	°E	
Aircraft Ground Speed:	867	867	867	kph	
Aircraft True Track:	25	25	25	°ETN	
Bias Component:	150·0	150·0	150·0	Hz	From Calibration
Aircraft Freq. Compensation:	398·0	490·4	581·3	Hz	Calculated (for 64·5°E satellite)
Uplink Doppler:	−374·7	−463·1	−550·2	Hz	Satellite and aircraft movement
Downlink Doppler:	−71·9	−71·9	−71·9	Hz	Satellite movement
Satellite & EAFC Effect	24·2	24·2	24·2	Hz	Measured
BFO (predicted):	125·7	129·7	133·4	Hz	
Measured BFO:	132·0	132·0	132·0	Hz	Measured
Error:	−6·3	−2·3	1·4	Hz	0·8 Hz/degree sensitivity

6. HYPOTHETICAL FLIGHT PATH RECONSTRUCTION.

Many techniques may be used to generate an aircraft flight path consistent with the BTO and BFO measurements, bounded by the physical capabilities of the aircraft and its assumed operating mode. Several different agencies worked on this issue in parallel, both independently and collaboratively. What we present here is a simplified flight path reconstruction technique to illustrate how the measurements may be transformed into a reasonable flight path. It should be emphasised that other members of the international investigation team developed far more sophisticated models factoring in aircraft and avionics performance characteristics to determine the final underwater search area.

6.1. *Early Flight Path.* The last published primary radar location of the aircraft was at 18:22 UTC when it passed close to the MEKAR waypoint at N06 30, E096 30.

https://doi.org/10.1017/S037346331400068X Published online by Cambridge University Press

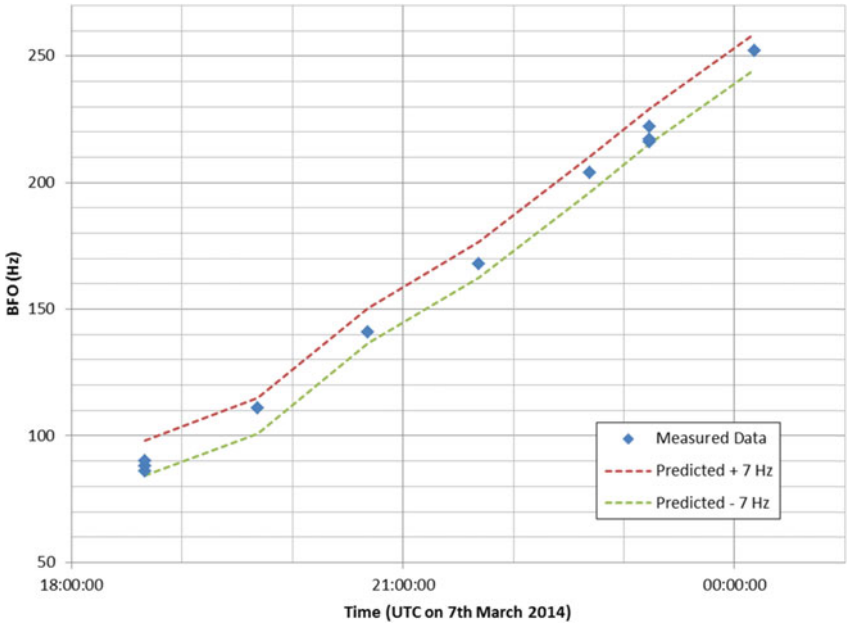

Figure 16. BFO Results for Example Flight Path.

Five minutes later it crossed the 18:27 arc generating a BFO of 142 Hz. Due to the close proximity of the arc crossing to the last radar fix we have limited uncertainty in the arc crossing points and so the main variables we have to align the predicted BFO with the measured value are the aircraft ground speed and track. Trial and error shows that we obtain the best BFO match for an aircraft track of 300°, which is consistent with the aircraft travelling along airway N571 towards the IGOGU waypoint at N07 31, E094 25 at a ground speed of 480 knots. Such a flight path would be consistent with the route determined by radar prior to 18:22 UTC where the aircraft appears to be moving between waypoints.

6.2. *Late Flight Path*. The technique presented here to reconstruct the end of the flight path uses a constant ground speed model. Constant ground speed is capable of being programmed into an autopilot, and flight paths consistent with these are relatively straightforward to generate and evaluate.

At some time between 18:27 and 19:41 MH370 turned south, however rather than trying to predict when (and where) the aircraft turned this analysis takes the 19:41 arc as its starting point. It models a large number of routes that started on the 19:41 arc between 6°N and 4°S, travelled at ground speeds ranging from 375 to 500 knots and crossed the timing arcs at the appropriate times. The track of each route was allowed to change as it crossed each arc, with the mean of the approach and departure tracks being used to calculate the BFO. Each route was analysed and the error between predicted and measured BFO evaluated to identify the route with the best match.

The ±7 Hz tolerance between measured and predicted BFO (see Figure 15) results in many candidate routes meeting the BFO constraints, giving a probability distribution of locations for the 00:19 arc crossing. The BFO predictions for one example route are plotted in Figure 16 between the upper and lower BFO measurement bounds. This route crossed the 19:41 arc at 0°N and travelled south at a constant

https://doi.org/10.1017/S037346331400068X Published online by Cambridge University Press

https://doi.org/10.1017/S037346331400068X Published online by Cambridge University Press

Table 9. Example Reconstructed Flight Path Results.

Time UTC	Lat °N	Lon ° E	True Track °ETN	Speed kph	Δ *F up* Aircraft (Hz)	Δ *F up* Satellite (Hz)	Δ *F down* (Hz)	*δ f comp* (Hz)	*δF sat* + *δF AFC* (Hz)	*δf bias* (Hz)	Total Offset (Hz) Pred	Meas	Error.
16:30:00	2·7	101·7	0	0	0	−6	−85	0	29	150	88	88	0
16:42:31	2·8	101·7	333	435	194	−6	−79	−180	27	150	105	125	20
16:55:53	4·0	102·2	25	848	−424	−4	−76	453	26	150	125	159	34
17:07:19	5·3	102·8	25	867	−460	−3	−72	490	24	150	130	132	2
18:25:27	6·9	95·8	300	800	575	−1	−37	−556	11	150	141	142	1
18:39:58	7·5	94·4	200	800	353	−1	−30	−389	8	150	91	88	−3
19:41:03	0·0	93·7	186	800	32	−1	0	−72	−1	150	108	111	3
20:41:05	−7·5	92·9	182	829	−182	5	29	143	−1	150	143	141	−2
21:41:27	−15·0	92·7	180	829	−365	16	55	331	−18	150	170	168	−2
22:41:22	−22·5	92·9	179	829	−522	29	78	497	−29	150	203	204	1
23:14:00	−26·6	93·0	179	829	−595	37	88	575	−33	150	222	217	−5
00:11:00	−33·7	93·0	180	829	−702	50	101	691	−38	150	252	252	0
00:19:29	−34·7	93·0	180	829	−717	52	102	708	−38	150	256	182	−74

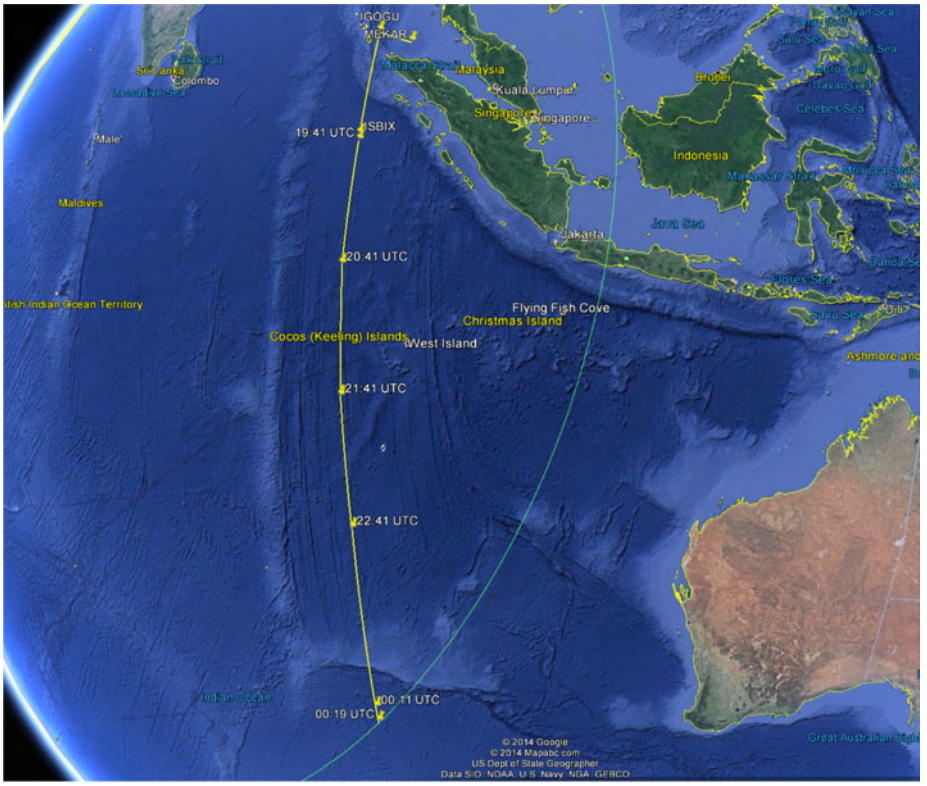

Figure 17. Example Flight Path.

ground speed of 450 knots, matching the BFO measurements to within 2 Hz at each of the five signalling data points between 19:41 and 00:11 UTC and within 6 Hz of the two voice call data points at 18:39 and 23:14. While the route is no more valid than many other potential routes it is interesting as it gives a good match to the measured data at a relatively constant track and ground speed.

6.3. *Consolidated Flight Path.* It is possible to join the early and late flight paths of the previous two sections to generate a hypothetical route that is consistent with the measured data, by assuming that MH370 flew from the last primary radar fix to the IGOGU air waypoint from where it turned south towards the ISBIX waypoint (N00 22, E093 40·5) and then continued in a southerly direction with its true track drifting from the initial 186° (IGOGU to ISBIX) to 180° by the end of the flight.

Table 9 presents the results of the BFO calculation for the reconstructed flight path, breaking out the different contributors to the frequency offset. The uplink Doppler contribution (ΔF_{up}) is split into two components: aircraft velocity in the direction of the satellite and satellite velocity in the direction of the aircraft. The errors at 16:42, 16:55 and 00:19 are thought to be due to vertical movement of the aircraft that is not included in this model. The values at 18:39 and 23:14 are based on the telephone call attempts, where BFO is recorded but BTO is not: the values in the table are the average of all the measurements associated with the call attempts, which spanned from 86 to 90 Hz at 18:39 and from 216 to 222 Hz at 23:14. Figure 17 illustrates the route.

https://doi.org/10.1017/S037346331400068X Published online by Cambridge University Press

7. CONCLUSIONS. The analysis presented in this paper indicates that MH370 changed course shortly after it passed the Northern tip of Sumatra and travelled in a southerly direction until it ran out of fuel in the southern Indian Ocean west of Australia. A potential flight path has been reconstructed that is consistent with the satellite data, indicating a last contact location of 34·7°S and 93·0°E, but it is stressed that the sensitivity of the reconstructed flight path to frequency errors is such that there remains significant uncertainty in the final location.

ACKNOWLEDGEMENTS

This material is based on work performed by Inmarsat in its role as Technical Advisor to the UK Air Accidents Investigation Branch (AAIB). We would like to thank our colleagues in the wider Flight Path Reconstruction group including Thales, the US National Transportation Safety Board (NTSB), Boeing and Australia's Defence Science and Technology Organisation (DSTO), who all independently verified and calibrated the frequency model, Thales and Honeywell who provided expert knowledge on the AES terminal performance, and SED and Square Peg Communications who provided expert knowledge on the GES equipment. The group has been expertly led by the Australian Transport Safety Bureau (ATSB) along with Malaysia's Department of Civil Aviation (DCA).

Inmarsat and the Flight Path Reconstruction group are committed in their continued support in the search for MH370 to help find closure for the families involved.

REFERENCES

ATSB. (2014). Australian Transport Safety Bureau (August 2014) Transport Safety Report AE-2014-054, "MH370—definition of underwater search areas" http://www.atsb.gov.au/media/5243942/ae-2014-054_mh370_-_definition_of_underwater_search_areas_18aug2014.pdf

Malaysian Government. (2014). Malaysian Government Department of Civil Aviation (May 2014) "MH370 data communication logs" http://www.dca.gov.my/mainpage/MH370%20Data%20Communication%20Logs.pdf

https://doi.org/10.1017/S037346331400068X Published online by Cambridge University Press

Australian Government
Australian Transport Safety Bureau

MH370 – Search and debris examination update

ATSB Transport Safety Report
Aviation External Investigation
AE-2014-054
2 November 2016

Released in accordance with section 25 of the *Transport Safety Investigation Act 2003*

Publishing information

Published by: Australian Transport Safety Bureau
Postal address: PO Box 967, Civic Square ACT 2608
Office: 62 Northbourne Avenue Canberra, Australian Capital Territory 2601
Telephone: 1800 020 616, from overseas +61 2 6257 4150 (24 hours)
Accident and incident notification: 1800 011 034 (24 hours)
Facsimile: 02 6247 3117, from overseas +61 2 6247 3117
Email: atsbinfo@atsb.gov.au
Internet: www.atsb.gov.au

© Commonwealth of Australia 2017

Ownership of intellectual property rights in this publication
Unless otherwise noted, copyright (and any other intellectual property rights, if any) in this publication is owned by the Commonwealth of Australia.

Creative Commons licence
With the exception of the Coat of Arms, ATSB logo, and photos and graphics in which a third party holds copyright, this publication is licensed under a Creative Commons Attribution 3.0 Australia licence.

Creative Commons Attribution 3.0 Australia Licence is a standard form license agreement that allows you to copy, distribute, transmit and adapt this publication provided that you attribute the work.

The ATSB's preference is that you attribute this publication (and any material sourced from it) using the following wording: *Source:* Australian Transport Safety Bureau

Copyright in material obtained from other agencies, private individuals or organisations, belongs to those agencies, individuals or organisations. Where you want to use their material you will need to contact them directly.

Addendum

Page	Change	Date
18	Correction to Figure 11 caption to remove inconsistency with report text on Page 17.	2 Dec 2016
All	Corrected erroneous page numbers.	18 Aug 2017

Executive summary

This report provides an update to the MH370 search area definition described in previous ATSB reports. It comprises further analysis of satellite data, additional end of flight simulations, a summary of the analysis of the right outboard wing flap, and preliminary results from the enhanced debris drift modelling.

For background information, please refer to the ATSB publications available online at www.atsb.gov.au/mh370:

- Definition of underwater search areas, 18 August 2014
- Flight Path Analysis Update, 8 October 2014
- Definition of Underwater Search Area Update, 3 December 2015.

The Australian Defence Science and Technology (DST) Group[1] conducted a comprehensive analysis of the Inmarsat satellite communications (SATCOM) data and a model of aircraft dynamics. The output of the DST Group analysis was a probability density function (PDF) defining the probable location of the aircraft's crossing of the 7th arc.

Details of this analysis and the validation experiments are available in the open source published book here: http://link.springer.com/book/10.1007/978-981-10-0379-0.

Additional analysis of the burst frequency offsets associated with the final satellite communications to and from the aircraft is consistent with the aircraft being in a high and increasing rate of descent at that time. Additionally, the wing flap debris analysis reduced the likelihood of end-of-flight scenarios involving flap deployment.

Preliminary results of the CSIRO's drift analysis indicated it was unlikely that debris originated from south of the current search area. The northernmost simulated regions were also found to be less likely. Drift analysis work is ongoing and is expected to refine these results.

[1] Formerly the Defence Science and Technology Organisation (DSTO).

Contents

7th arc burst frequency offset (BFO) analysis 1
BFO tolerance or error 3
Direction of flight 3
Oscillator warm-up drift 3
Descent rate 4
Results of analysis 4
End of flight simulations 7
Drift modelling update 9
Debris summary and analysis 13
Flap position 15
Contact damage between the flaperon and outboard flap 17
Analysis 20
Acknowledgements 21

7th arc burst frequency offset (BFO) analysis

The final satellite communication (Satcom) transmissions between the Inmarsat Ground station and 9M-MRO occurred at 00:19 on the 8th March 2014. These transmissions were the aircraft logging on to the Satcom system, likely after an interruption to the power that supplies the satellite data unit (SDU) – an integral part of the Satcom system.

The ground station Satcom logs recorded the burst timing offset (BTO) and the burst frequency offset (BFO) for each received message. A complete explanation of the BTO and BFO is provided in the ATSB publication, *MH370 – Definition of Underwater Search Areas, August 2014*.

The BFO is a function of the Doppler shifts imparted on the communication signal due to the motion of the satellite and the aircraft. The relationship is more complicated than a direct Doppler calculation because the aircraft software contains Doppler compensation that offsets the Doppler shift due to the aircraft motion. Although the aircraft attempts to compensate for its own motion, it does this under the assumption that the communications satellite is in notional geostationary orbit and it does not include the vertical component of the aircraft velocity.

Analysis of the BFO value can provide information about the relative motion between the satellite and the aircraft. Figure 1 shows all the BFO recordings from 9M-MRO. The comprehensive analysis provided by the Defence Science and Technology (DST) Group (*Bayesian Methods in the Search for MH370*) indicated that the aircraft was likely on a southerly heading at 18:39. From that point until 00:11, all the solutions of the analysis showed a continuing southerly track.

Figure 1: Recorded BFO values throughout the flight

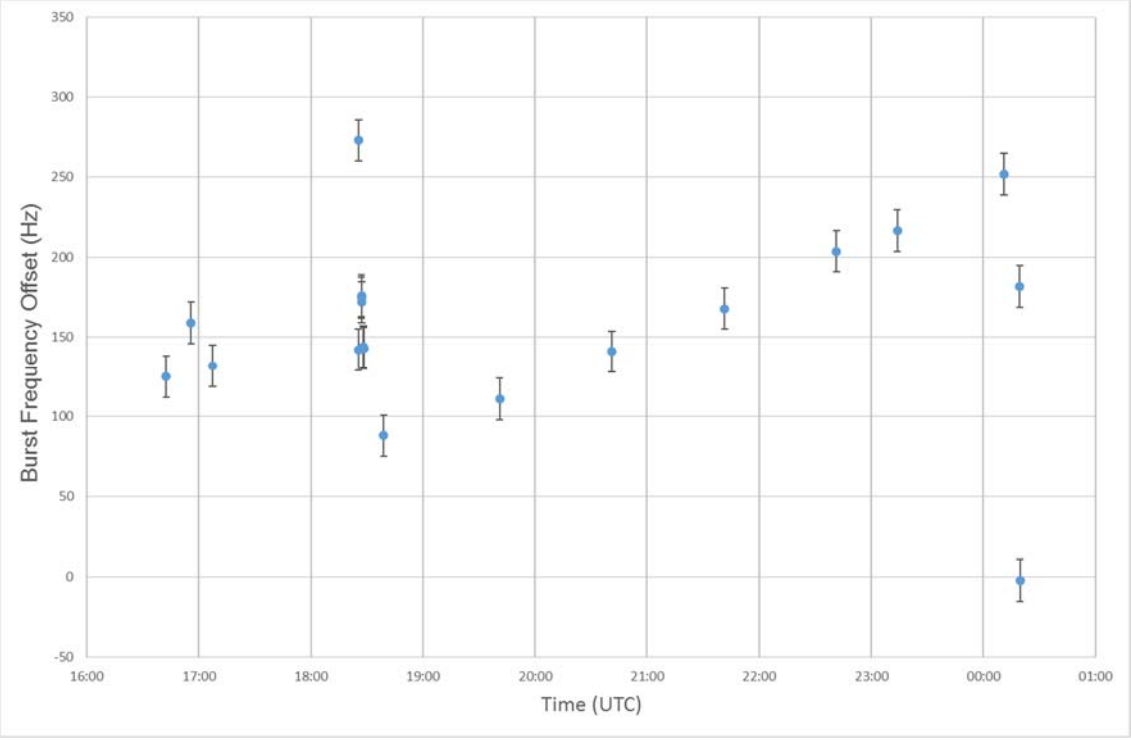

Source: ATSB

This graph illustrates the measured BFO recordings throughout the flight with the appropriate error bars on the measurements. After 18:39 the BFO values follow an approximately linear trend until the final two values at 00:19.

The trend of the BFO values from 18:39 until the 6th arc (00:11) is due to the change in location of the aircraft and can be linearly approximated (Figure 2). If this linear approximation is extrapolated to 00:19, and if neither the Satcom system nor the aircraft flight path were altered after 00:11, a BFO value of approximately 260 Hz would have been expected.

Figure 2: Linear approximation of the BFO values between 18:39 and 00:11

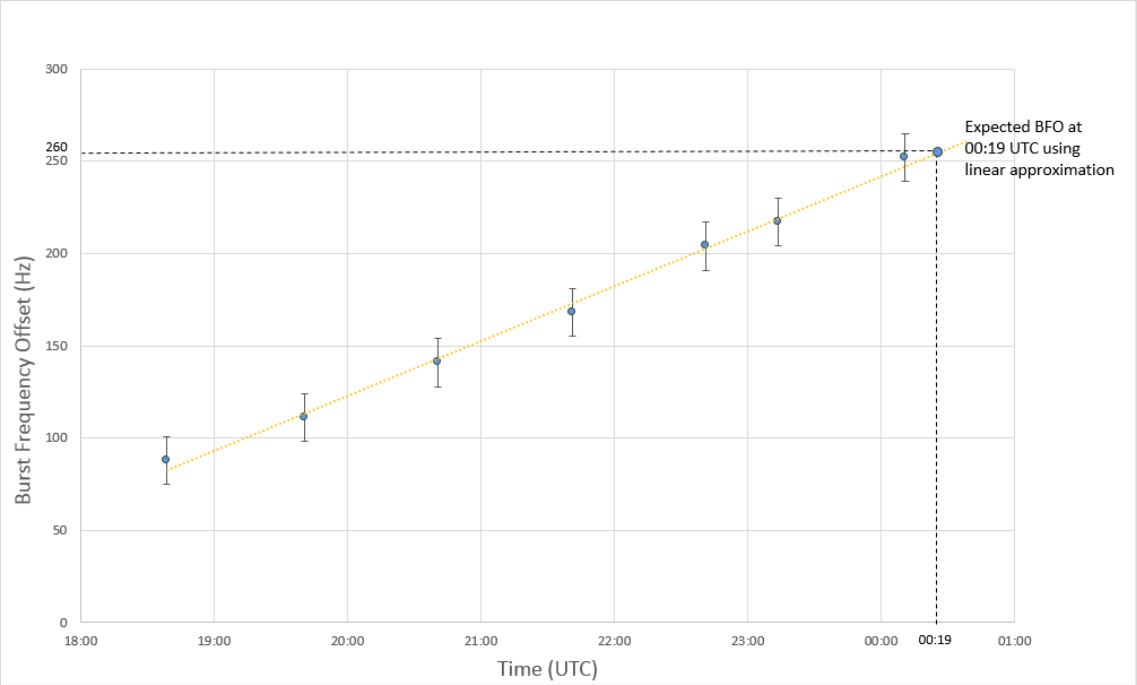

Source: ATSB

This graph illustrates 5 BFO values recorded between 18:39 and 00:11 and the linear approximation of the BFO at 00:19. The first 5 values correspond to the 2nd-6th arcs. During this time the aircraft is likely to be following a relatively constant southerly track. Continuing this linear trend to 00:19, a value of 260 Hz would be expected.

The recorded values of the BFO for the two messages at 00:19 were the following:

Table 1: Recorded BFO values at 00:19

Time	Burst Frequency Offset
00:19:29	182 Hz
00:19:37	-2 Hz

To explain this difference between the expected BFO value (260 Hz) and the recorded BFO values (Table 1), an examination was undertaken of the elements that contribute to the BFO.

This analysis includes a number of approximations, and the results should be interpreted as an approximate guide on the range of possible descent rates at the time of the last two SATCOM messages that were sent from 9M-MRO. DST Group intend to publish a more detailed version of the analysis in the near future. It should be noted that small refinements in the analysis may result in descent rate calculations that differ slightly from the values published here.

In the analysis it is assumed that there were no major changes to the satellite system between 00:11 and 00:19. Therefore the contributing elements consist of the:

- tolerance or error of the BFO
- direction of travel of the aircraft
- oven-controlled oscillator warm-up drift
- descent rate of the aircraft.

BFO tolerance or error

A statistical analysis of the BFO error from all the 20 previous flights of 9M-MRO identified that the distribution was approximately Gaussian (see DST Group book – link above) with a standard deviation of 4.3 Hz. ±3 standard deviations (12.9 Hz) is a conservative choice for the error.

Direction of flight

For any given speed, the estimated BFO differences can be plotted against the predicted heading of the aircraft (Figure 3). The maximum variation in the BFO differences based solely on change in direction is approximately 20 Hz.

Figure 3: Variation in estimated BFO differences at 00:19 for given track angles and groundspeed

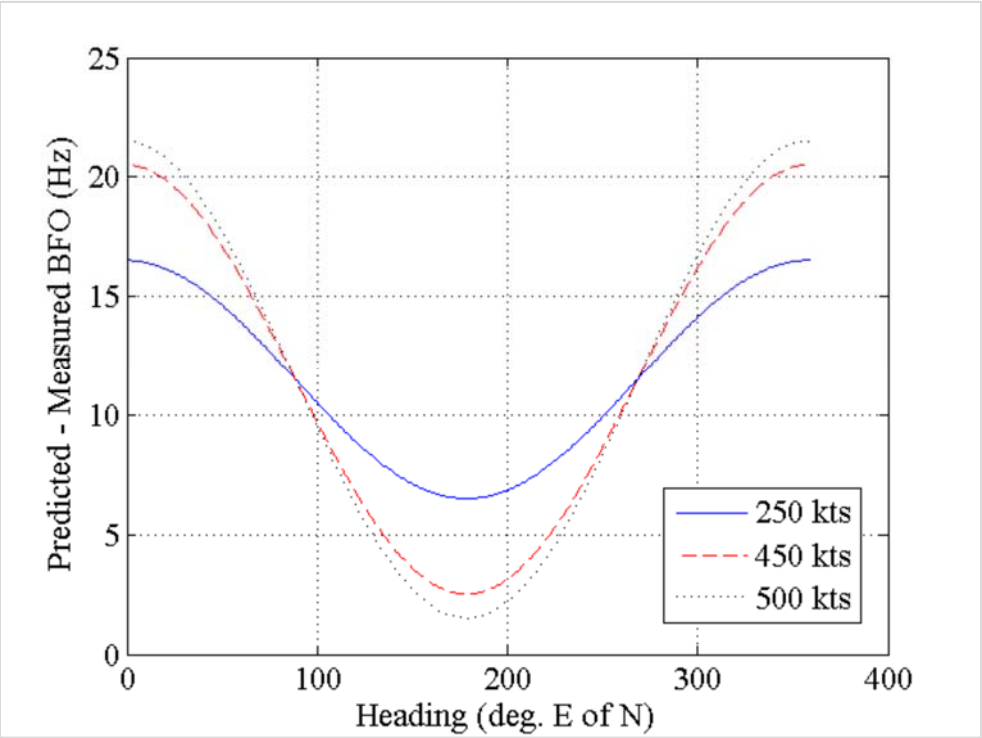

Source: DST Group

This graph indicates that the lowest BFO differences, and therefore the closest to our measured values, would be attained for any given speed by continuing in a southerly direction.

Oscillator warm-up drift

The oven-controlled crystal oscillator (OCXO) maintains the oscillator in the satellite data unit (SDU) at the design temperature. The performance of the OCXO in maintaining the correct temperature directly affects the transmitted frequency. When power is first applied to the SDU, the transient temperature variation associated with the OCXO warming-up causes a variation in the output frequency. This is referred to as warm-up drift.

To further understand this behaviour, the manufacturer of the SDU performed multiple power-up tests on several SDUs. It was observed that individual SDUs exhibit different warm-up drift characteristics. The differences were the magnitude of the frequency deviation, the time to reach steady state as well as the general shape of the curve.

Variations in the time in which the SDU (and OCXO) was not powered, prior to powering on, affected both the magnitude of the drift and the time taken for the frequency to stabilise, however the characteristic (or general shape of the curve) was not affected.

All available information indicated that, after power-up, the SDU in 9M-MRO exhibited a decay characteristic, represented in Figure 4. The values recorded shortly after power up would therefore be greater than the steady state value.

Figure 4: Representation of 9M-MRO SDU decaying warm-up characteristic (not to scale)

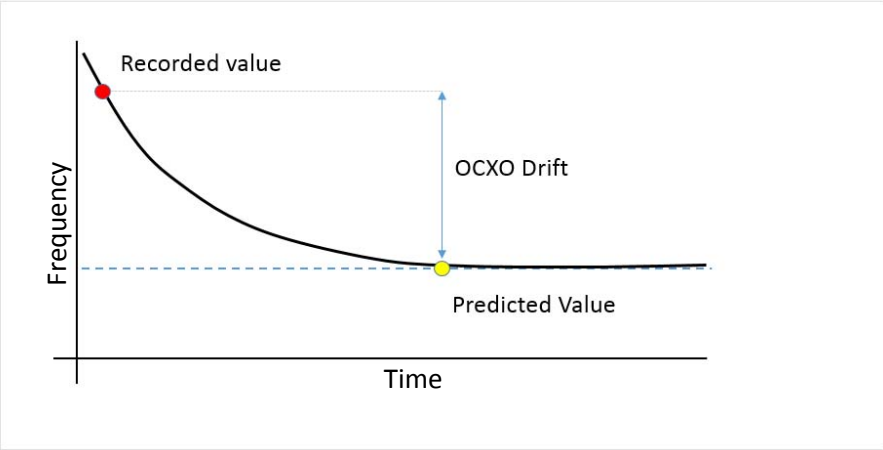

Source: ATSB

This graph illustrates the warm-up characteristic of the 9M-MRO SDU. After power is restored to the SDU, the OCXO drift results in BFO value being above the steady state value until the OCXO has stabilised.

The maximum OCXO drift value observed in the previous data of 9M-MRO was around 130 Hz and if the power interruption was sufficiently short, the OCXO drift could be negligible.

Descent rate

The remaining element to explain the difference in the predicted BFO value and the recorded BFO value is the descent rate of the aircraft. Analysis shows that at locations consistent with the search area and at the time of the last transmission, the descent rate affects the BFO value at -1.7 Hz per 100 ft/min.

Results of analysis

Due to the uncertainties associated with the end-of-flight scenario, it is not possible to define a specific descent rate from the recorded BFO values. Instead, using the limits of each contributing element, a range of possible descent rates, consistent with the recorded BFO values can be determined.

Case A and Case B below represent the boundary cases for the minimum descent rate and the maximum descent rate respectively. For each transmission at 00:19, Case A applies assumptions that reduce the required rate of descent to match the recorded BFO. Case B does the opposite and applies assumptions which increase the required rate of descent.

A. Minimum Descent Rate

   i. Southerly direction,

   ii. Maximum positive error of measured BFO for 00:19:29 and 00:19:37 (~ 13 Hz),

   iii. No OCXO drift – very short duration power interruption.

B. Maximum Descent Rate

i. Northerly direction,

ii. Maximum negative error on measured BFO at 00:19:29 and 00:19:37 (~ -13 Hz),

iii. Maximum OCXO drift – 130 Hz (as observed in other power-up logons of 9M-MRO).

Table 2 and Figure 5 following provide the resulting descent rates based on cases above for the log-on request at 00:19:29 and the log-on acknowledge at 00:19:37.

Table 2: Derived descent rate boundary cases

00:19:29 log-on request	**Case A (minimum)**	**Case B (maximum)**
Predicted BFO level flight	260 Hz	280 Hz
Measured BFO	182 Hz	182 Hz
Possible error (3 std dev.)	13 Hz	-13 Hz
OCXO Drift	0 Hz	130 Hz
Derived descent rate	260- (182+13) = 65 Hz (65 / 1.7) *100 ≈ 3,800 ft/min	280 - (182 - 13 - 130) = 241 Hz (241 / 1.7) *100 ≈ 14,200 ft/min

00:19:37 log-on ACK	**Case A (minimum)**	**Case B (maximum)**
Predicted BFO level flight	260 Hz	280 Hz
Measured BFO	-2 Hz	-2 Hz
Possible error (3 std dev.)	13 Hz	-13 Hz
OCXO Drift	0 Hz	130 Hz
Derived descent rate	260-(-2+13) = 249 Hz (249 / 1.7) *100 ≈ 14,600 ft/min	280 - (-2 - 13 - 130) = 425 Hz (425 / 1.7) *100 ≈ 25,000 ft/min

Figure 5: Association of BFO differences to descent at 00:19

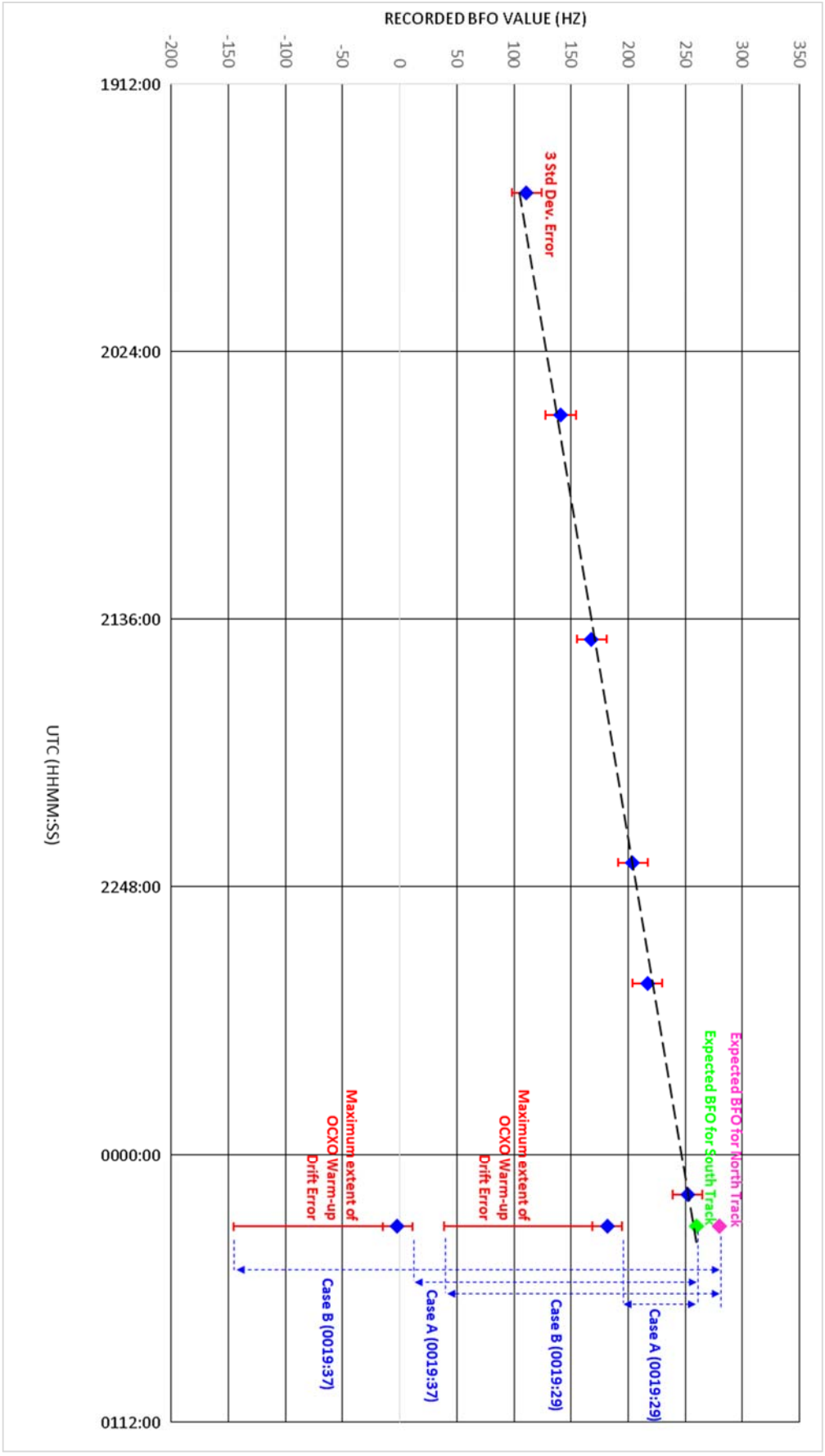

Source: ATSB

End of flight simulations

The ATSB report *MH370 – Definition of Underwater Search Areas, December 2015* outlined the previous simulations that the manufacturer had undertaken to assist in determining the aircraft's behaviour at the end of the accident flight.

In April 2016, the ATSB defined a range of additional scenarios for the manufacturer to simulate in their engineering simulator. Reasonable values were selected for the aircraft's speed, fuel, electrical configuration and altitude, along with the turbulence level.

The results of the simulation are presented in Figure 6. The results have all been aligned to the point two minutes after the loss of power from the engines. This is the theorised time at which the 7th arc transmissions would have been sent.

Figure 6: Results from simulated scenarios

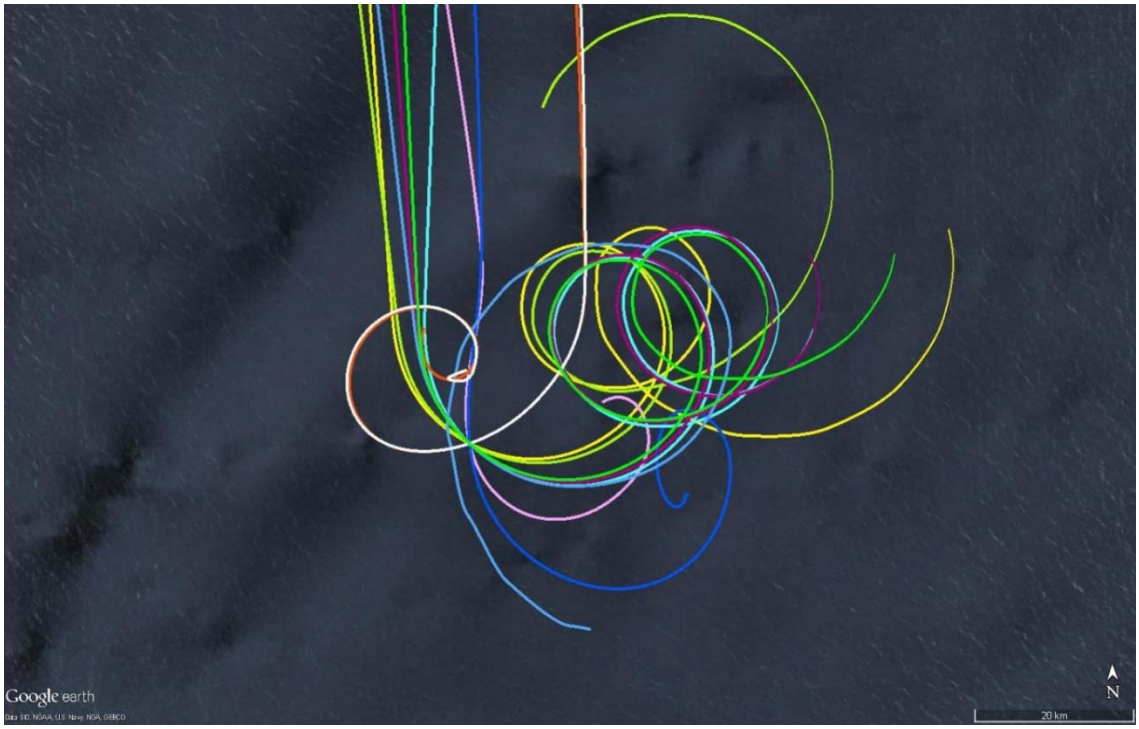

Source: ATSB

This figure illustrates the resulting flight paths from the simulations performed by the manufacturer and aligned at a point consistent with when the final BTO transmission may have occurred.

The simulations were completed in the manufacturer's engineering simulator. The engineering simulator uses the same aerodynamic model as a Level D simulator used by the airlines. The simulator is not a full motion simulator but instead is used when a high level of system fidelity is required. The appropriate firmware and software applicable to the accident aircraft can be loaded.

The results of the simulations were that:

- The aircraft was capable of travelling rearwards (from the direction of travel) approximately 21 NM.
- Simulations that experienced a descent rate consistent with the ranges and timing from the BFO analysis generally impacted the water within 15 NM of the arc.
- In some instances, the aircraft remained airborne approximately 20 minutes after the second engine flameout.

- In an electrical configuration where the loss of engine power from one engine resulted in the loss of autopilot (AP), the aircraft descended in both clockwise and anti-clockwise directions.
- In some simulations, the aircraft exhibited phugoid motion[2] throughout the descent.
- Simulations that exhibited less stable flight resulted in higher descent rates and impact with water closer to the engine flameout location. In some simulations, the aircraft's motion was outside the simulation database. The manufacturer advised that data beyond this time should be treated with caution.
- Some of the simulated scenarios recorded descent rates that equalled or exceeded values derived from the final SATCOM transmission. Similarly, the increase in descent rates across an 8 second period (as per the two final BFO values) equalled or exceeded those derived from the SATCOM transmissions. Some simulated scenarios also recorded descent rates that were outside the aircraft's certified flight envelope.
- The results of the scenarios, combined with the possible errors associated with the BTO values indicate that the previously defined search area width of ±40 NM is an appropriate width to encompass all uncontrolled descent scenarios from the simulations.

The simulated scenarios do not represent all possible scenarios, nor do they represent the exact response of the accident aircraft. Rather, they provide an indication as to what response the accident aircraft may have exhibited in a particular scenario. As such, the results are treated with caution, and necessary error margins (or safety factors) should be added to the results.

It was not possible to simulate all likely scenario conditions due to the limitations of the simulator. Specifically, flight simulators are unable to accurately model the dynamics of the aircraft's fuel tanks. In the simulator, when the fuel tank is empty, zero fuel is available to all systems fed from the tank. However, in a real aircraft, various aircraft attitudes may result in unusable fuel (usually below engine/APU inlets) becoming available to the fuel inlets for the APU/engines. If this resulted in APU start-up, it would re-energise the AC buses and some hydraulic systems. This could affect the trajectory of the aircraft. Similarly, the left and right engines may also briefly restart, affecting the trajectory.

[2] A long-period oscillation of pitch axis, perpetually hunting about level attitude and trimmed speed.

Drift modelling update

To assist with the underwater search for 9M-MRO, the Commonwealth Scientific and Industrial Research Organisation (CSIRO) undertook an analysis of existing ocean data from the Global Drifter Program[3]. The analysis used the behaviour of drogued and undrogued drifters[4], as well as numerical simulations using ocean models. The purpose of this work was to trace any recovered debris to its likely point of origin. However, a drifter's geometry and buoyancy is not generally representative of aircraft debris and it was considered that the drift characteristics might also be different. To account for this difference, the CSIRO engaged in field work, studying how aircraft debris moves through the water compared to drifters, with regard to wind and ocean currents. This data was incorporated into numerical simulations in order to predict the drift behaviour of aircraft debris with more confidence.

As part of the ongoing field testing, the drift behaviour of replica flaperons and other recovered aircraft parts is being assessed. Replica flaperons were constructed with dimensions and buoyancy approximately equal to that of the recovered flaperon (Figure 7), which was float-tested during the detailed examinations in France. The replica flaperons were deployed into a bay for short term tests during various weather conditions. Longer term tests were then performed in the open ocean. For comparison, undrogued drifters were deployed alongside the flaperons. Drogued drifters were also used, because they move predominantly with the currents, as opposed to wind and waves. Data for currents was then able to be subtracted from the flaperons' drift data so that wind and wave behaviour could be assessed in isolation.

Figure 7: Flaperon recovered from Reunion Island on 29 July 2015

Source: Bureau d'Enquetes et d'Analyses (BEA)

Field tests demonstrated that the replica flaperons drift similarly to undrogued drifters:

- In low wind conditions, the flaperons move slightly faster than undrogued drifters due to the energy absorbed from waves.

---

3 Visit www.aoml.noaa.gov/phod/dac/ for further details.

4 A drifter is a satellite-tracked buoy which either has a subsurface sea anchor attached (drogued) or not (undrogued).

- In higher winds, the energy absorbed from waves was less significant, and the flaperons' behaviour was analogous to the undrogued drifters'.

The replica flaperons presented their raised trailing edge to the wind, allowing waves to propel them in the wind direction. If waves tipped or turned the flaperons, the wind quickly reoriented them, so the direction of movement remained consistent.

Replicas of two other recovered items of debris drifted at a rate that was practically indistinguishable from undrogued oceanographic drifters in all wind conditions. Therefore, the trajectories of undrogued oceanographic drifters were valid for use in the analysis.

Preliminary results from the updated drift analysis indicated that the current search area was a possible origin for the recovered debris.

Using the collected field data, a new forward-tracking numerical simulation was performed. Within the simulation, flaperons were deployed on and around the current search area and allowed to drift freely. Results after 500 days of simulated drift are presented in Figure 8. For comparison, Figure 9 shows the results of a simulation where the original undrogued drifter model was used. By comparing the two figures, it can be seen that the flaperons generally moved further west within 500 days due to the extra speed at low winds.

Figure 8: Simulated location of flaperon-type drifters after 500 days

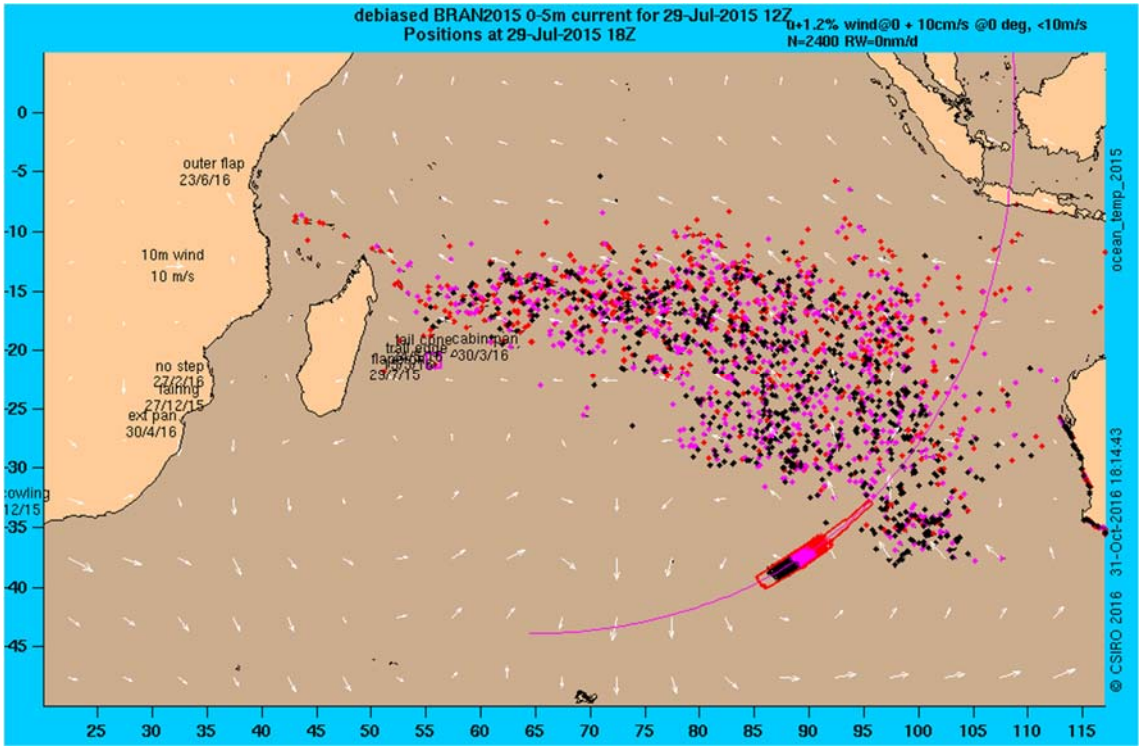

Source: CSIRO

Figure 9: Simulated location of undrogued drifters after 500 days

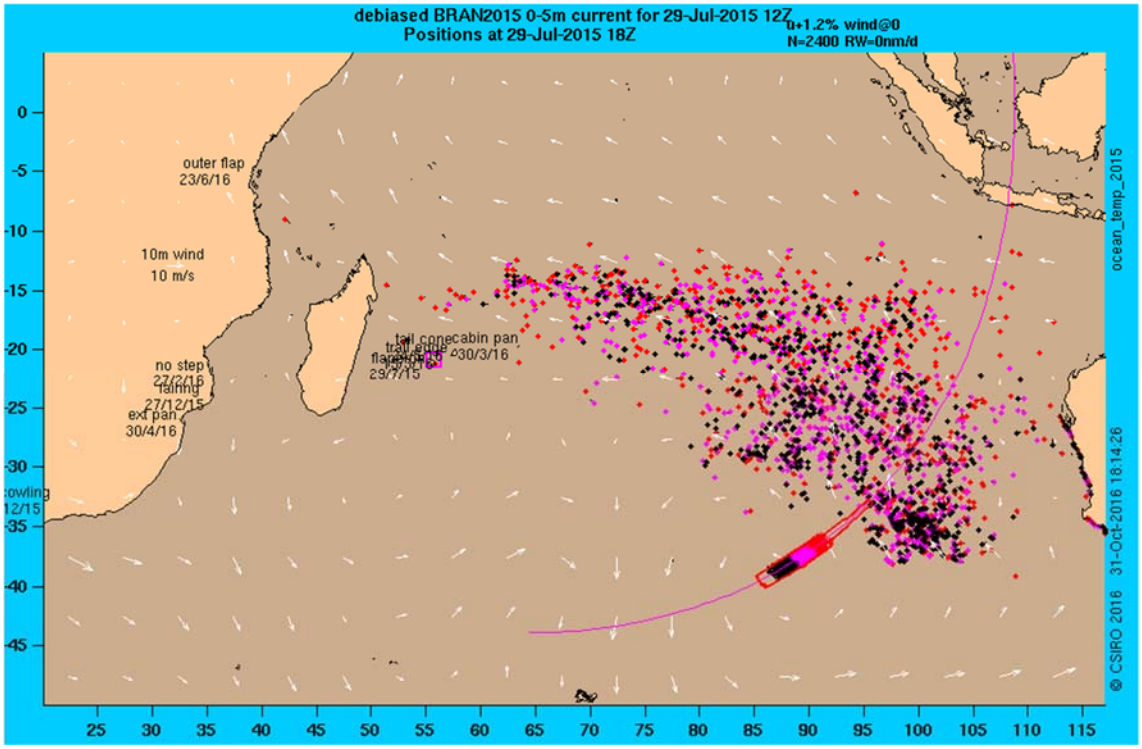

Source: CSIRO

Small errors in the simulation can result in large divergences over time. As such, an examination of the debris behaviour in the first months after the accident was conducted.

Figure 10 illustrates the starting location of the simulated drifters along the 7th arc. After eight months of simulated drift (Figure 11), some initial conclusions can be drawn about the drifter's path with respect to debris discovered to date. A significant number of drifters arrived on the coast of Western Australia. Similarly, a number of drifters had arrived on the coast of Africa. The colour of each drifter identifies its starting location as marked along the arc.

- Drifters starting in the southern half of the current search area or below (dark blue, green, light blue) can be observed on and around the coast of Western Australia, with many drifting towards Tasmania. No debris has been discovered on the Australian coast. This indicates that a starting location within the current search area, or further north, is more likely.
- A significant number of red drifters have already reached the coast of Madagascar and mainland Africa. This is not consistent with the time at which debris was discovered. The first item of debris was not discovered on Reunion Island until 16 months after the accident. This suggests a reduced likelihood of debris originating from the northernmost areas shown in Figure 10 (red and white coloured regions).

Refinement of the drift analysis is continuing. Flaperon replicas are currently deployed in the open ocean along with drogued and undrogued drifters, and replicas of smaller debris. This is to study the longer-term drift behaviour of the parts in conditions similar to those expected in the Indian Ocean. The long-term tests may provide additional improvement to the simulations and confidence in the backtracking results.

Figure 10: Simulated starting location of undrogued drifters

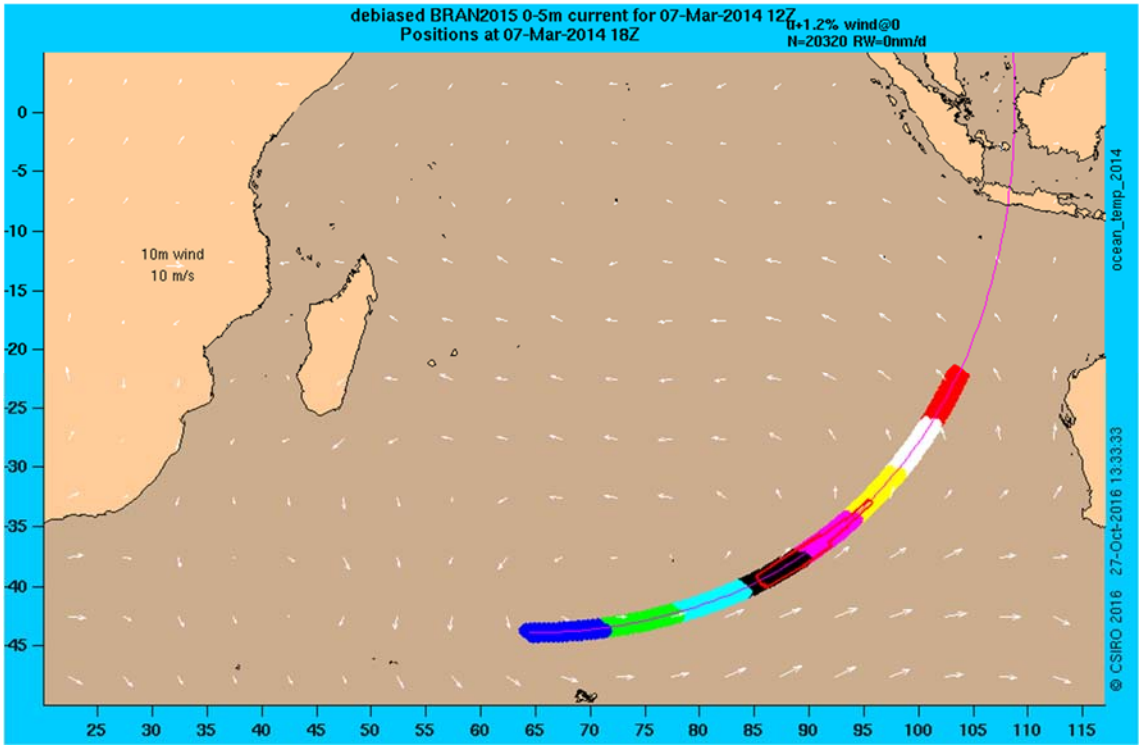

Source: CSIRO

Figure 11: Simulated location of undrogued drifters after 8 months

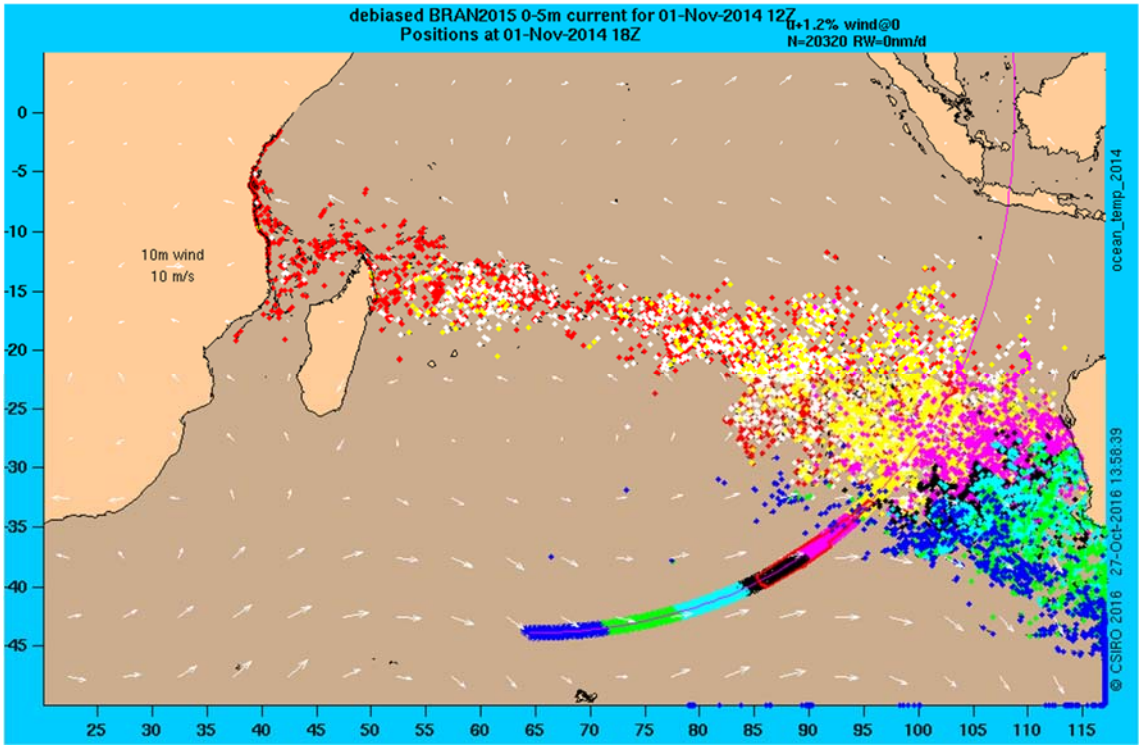

Source: CSIRO

A significant number of drifters from the light blue and green areas have made landfall on the West Australian coast. Similarly, drifters from the red and white areas have begun to make landfall on the African coastline. Neither are consistent with times and/or locations at which MH370 debris was discovered, therefore reducing the likelihood of debris originating from these locations.

Debris summary and analysis

Currently, more than 20 items of debris have been brought to the attention of and are of interest to the investigation team. The items have been located along the east and south coast of Africa, the east coast of Madagascar and the Islands of Mauritius, Reunion and Rodrigues in the Indian Ocean. A list of items recovered was published by the Malaysian investigation team and can be found at www.mh370.gov.my/index.php/en/.

The right flaperon has been examined by the French Judiciary and confirmed to have originated from 9M-MRO. Six further items of debris have previously been examined by the ATSB, comprising a:

- section of the right outboard flap fairing
- panel section from the right horizontal stabiliser
- piece of engine cowling
- closet panel section from the closet adjacent to door R1
- inboard section of the right outboard flap
- trailing edge section of the left outboard flap.

Both flap sections had unique identification numbers that were able to be linked, through manufacturing records, to 9M-MRO. The remaining examined items were confirmed as Boeing 777 parts and had identifying features linking them to a Malaysian Airlines origin, however there were no unique identifiers to link the parts directly to 9M-MRO. The parts were therefore determined to have *almost certainly* originated from 9M-MRO, given that the likelihood of originating from another source is very remote. The ATSB debris examination reports are available at www.atsb.gov.au/mh370-pages/updates/reports/.

Outboard flap failure analysis

The recovered right, outboard wing flap section (Figures 12, 13 and 14) was examined for any evidence of interaction with mechanisms, supports and surrounding components that may indicate the state of flap operation at the time of fracture and separation from the wing. The purpose of the examination was to inform the end-of-flight scenarios being considered by the search team. The most significant items of evidence in relation to this are documented below.

Figure 12: Location of recovered outboard flap section

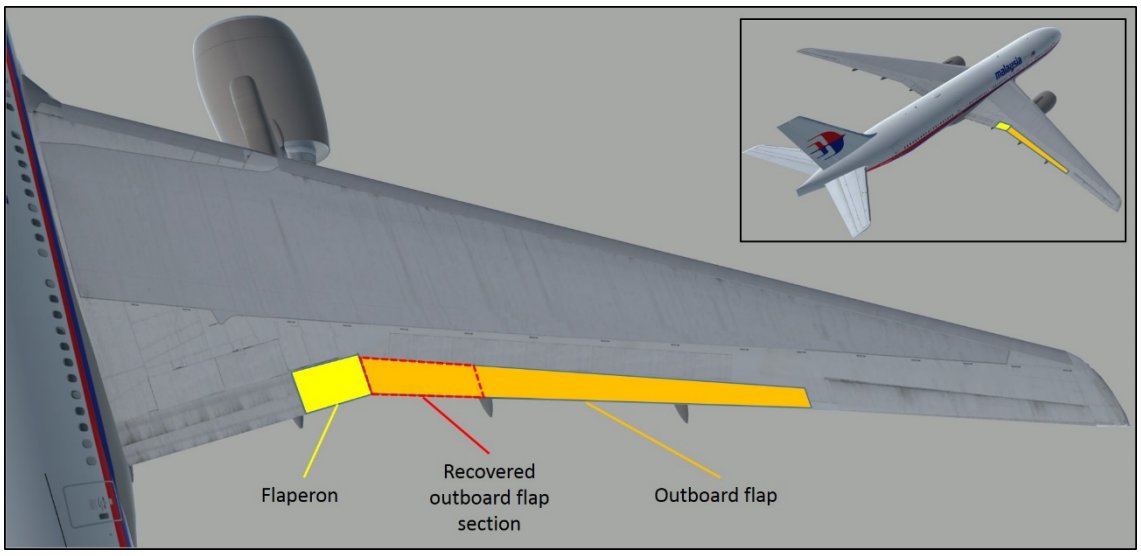

Source: DST Group (Modified by ATSB)

Figure 13: Inboard section of outboard flap

Source: ATSB

Figure 14: Inboard section of outboard flap (inverted)

Source: ATSB

Flap position

The trailing edge outboard wing flaps form part of the aircraft's high-lift control system and are deployed to alter the shape of the aircraft wing, improving lift at lower aircraft speeds during takeoff, approach and landing. The outboard wing flaps have defined stages of flap deployment between 'up' (retracted / cruise position) and 30-units of extension (landing position).

A fibreglass and aluminium seal pan is located at the inboard end of the outboard flap. It houses the inboard auxiliary support, comprising a deflection control track (support track) and carriage assembly. The support track is affixed to the rear of the wing. Using rollers in the carriage assembly, the inboard end of the flap is guided along the support track as the flap moves through its deflection range. The track is fully inserted into the flap in the 'up' position and progressively withdrawn from the flap as the flaps are deployed (Figure 15). The inboard auxiliary support track and carriage assembly were not present with the recovered debris.

Two adjacent aluminium stiffeners within the inboard seal pan area exhibited impact damage. The damage was significant because it was indicative of impact damage and the only component in the vicinity of the stiffeners, capable of independent movement within the seal pan, was the support track. Measurements of the support track position at the various stages of flap deployment, indicated that the track would have to be fully inserted into the flap in the retracted position to be adjacent to the damaged stiffeners (Figures 16, 17 and 18).

An outwards-fracture of the fibreglass seal pan initiated at a location adjacent to the damaged aluminium stiffeners (Figure 19). The damage was most likely also caused by impact from the support track. That damage provided further evidence of the support track position within the flap seal pan cavity, indicating that the flaps were retracted at the point of fracture and separation from the wing.

Figure 15: Outboard flap, inboard auxiliary support

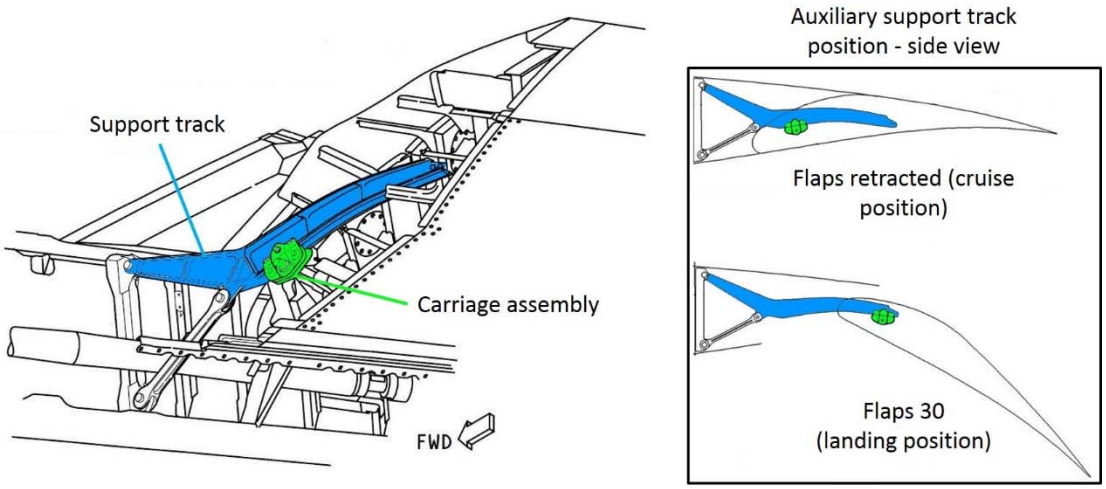

Source: Boeing (modified by ATSB)

Figure 16: Outboard flap location of damaged stiffeners within the seal pan cavity

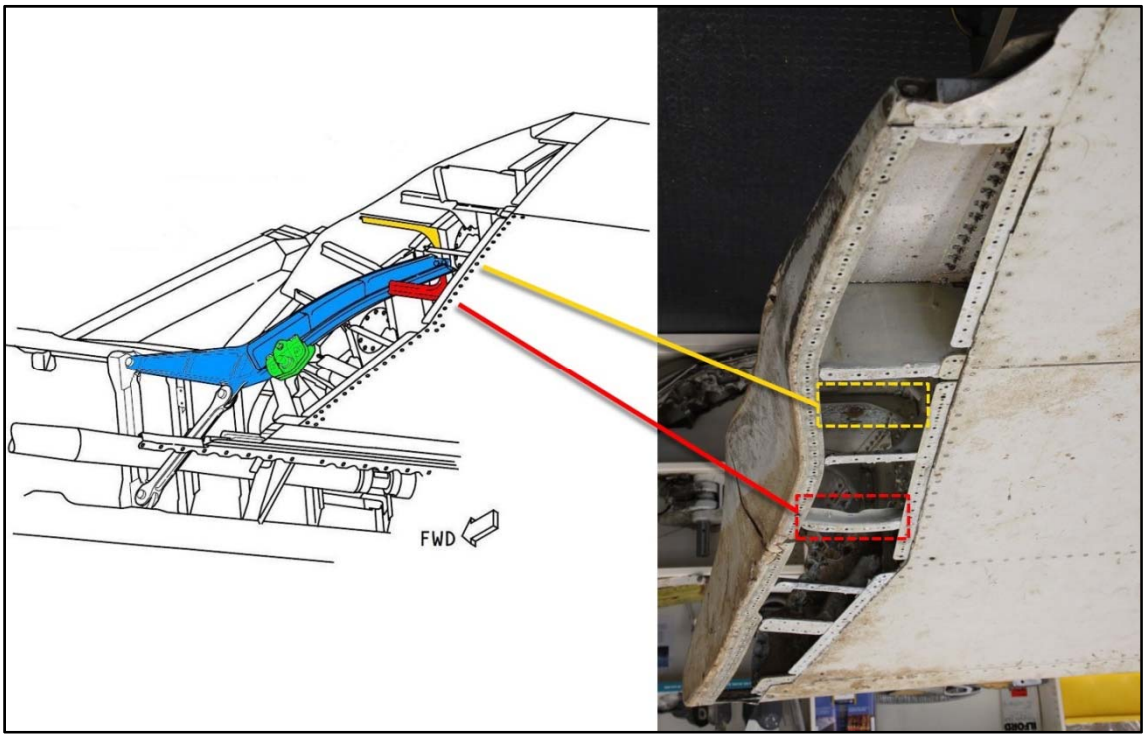

Source: Boeing (modified by ATSB) / ATSB

Figure 17: Outboard flap, damaged stiffeners within the seal pan cavity

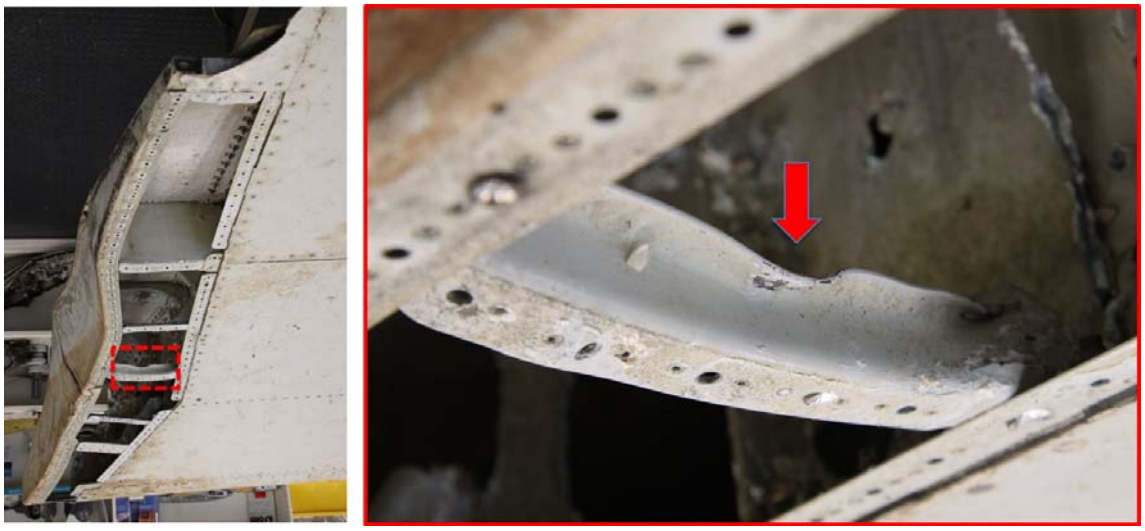

Source: ATSB

Figure 18: Outboard flap, damaged stiffeners within the seal pan cavity

Source: ATSB

Figure 19: Outboard flap, fractured seal pan (forward)

Source: ATSB

Contact damage between the flaperon and outboard flap

The flap seal pan was also fractured adjacent to the rear spar. The fracture resulted from external impact, puncturing the fibreglass and plastically deforming the supporting aluminium structure within the seal pan cavity (Figure 20). Comparable damage was noted at the outboard, rear spar and surrounding structure of the adjacent flaperon (Figure 21). It was noted that the two areas in question are aligned when the flaps are in the retracted position, with a significant offset existing at other stages of flap extension (Figure 22).

Figure 20: Outboard flap, fractured seal pan (aft)

Source: ATSB

Figure 21: Flaperon, outboard side damage

Source: Direction générale de l'armement / Techniques aéronautiques (modified by ATSB)

Figure 22: Flaperon and outboard flap from below, showing relative alignment of rear spar rivet line (highlighted) in the flaps retracted (left) and extended position (right)

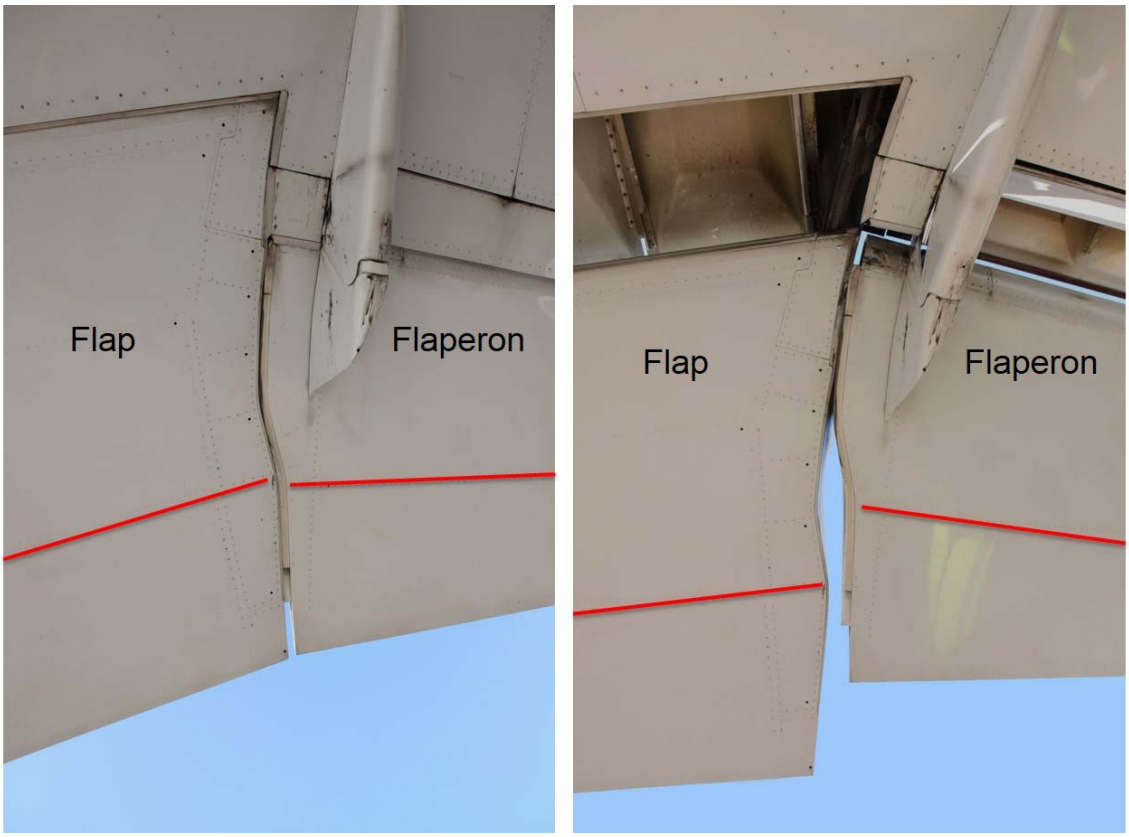

Source: ATSB

Analysis

Damage to the internal seal pan components at the inboard end of the outboard flap was possible with the auxiliary support track fully inserted into the flap. That damage was consistent with contact between the support track and flap, with the flap in the retracted position. The possibility of the damage originating from a more complex failure sequence, commencing with the flaps extended, was considered much less likely.

With the flap in the retracted position, alignment of the flap and flaperon rear spar lines, along with the close proximity of the two parts, indicated a probable relationship between two areas of damage around the rear spars of the parts. This was consistent with contact between the two parts during the aircraft breakup sequence, indicating that the flaperon was probably aligned with the flap, at or close to the neutral (faired) position.

Numerous other discrete areas of flap damage were analysed. Some of the damage was consistent with the flaps in the retracted position, while other areas did not provide any useful indication of the likely flap position. It was therefore concluded that:

- The right outboard flap was most likely in the retracted position at the time it separated from the wing.
- The right flaperon was probably at, or close to, the neutral position at the time it separated from the wing.

Acknowledgements

The ATSB would like to acknowledge the following organisations for their input and continued assistance with the analysis:

- Air Accidents Investigation Branch (UK)
- Australian Bureau of Meteorology
- Australian Defence Science and Technology Group
- Boeing
- Commonwealth Scientific and Industrial Research Organisation
- Department of Civil Aviation, Malaysia
- Inmarsat
- Malaysian Airlines Berhad
- Malaysian Ministry of Transport
- National Transportation Safety Board (US)
- Thales.

Those involved have dedicated many hours outside of normal duties to advance the collective understanding of the event. The main focus has always been in finding the aircraft to assist the Malaysian investigation team and to bring closure to the families of the passengers and crew of MH370.

Nat. Hazards Earth Syst. Sci., 16, 1623–1628, 2016
www.nat-hazards-earth-syst-sci.net/16/1623/2016/
doi:10.5194/nhess-16-1623-2016
© Author(s) 2016. CC Attribution 3.0 License.

Natural Hazards and Earth System Sciences
Open Access
EGU

Drift simulation of MH370 debris using superensemble techniques

Eric Jansen[1], **Giovanni Coppini**[1], **and Nadia Pinardi**[2,1]

[1]Euro-Mediterranean Center on Climate Change (CMCC), Lecce, Italy
[2]Department of Physics and Astronomy, Alma Mater Studiorum University of Bologna, Bologna, Italy

Correspondence to: Eric Jansen (eric.jansen@cmcc.it)

Received: 17 March 2016 – Published in Nat. Hazards Earth Syst. Sci. Discuss.: 30 March 2016
Accepted: 5 July 2016 – Published: 27 July 2016

Abstract. On 7 March 2014 (UTC), Malaysia Airlines flight 370 vanished without a trace. The aircraft is believed to have crashed in the southern Indian Ocean, but despite extensive search operations the location of the wreckage is still unknown. The first tangible evidence of the accident was discovered almost 17 months after the disappearance. On 29 July 2015, a small piece of the right wing of the aircraft was found washed up on the island of Réunion, approximately 4000 km from the assumed crash site. Since then a number of other parts have been found in Mozambique, South Africa and on Rodrigues Island.

This paper presents a numerical simulation using high-resolution oceanographic and meteorological data to predict the movement of floating debris from the accident. Multiple model realisations are used with different starting locations and wind drag parameters. The model realisations are combined into a superensemble, adjusting the model weights to best represent the discovered debris. The superensemble is then used to predict the distribution of marine debris at various moments in time. This approach can be easily generalised to other drift simulations where observations are available to constrain unknown input parameters.

The distribution at the time of the accident shows that the discovered debris most likely originated from the wide search area between 28 and 35° S. This partially overlaps with the current underwater search area, but extends further towards the north. Results at later times show that the most probable locations to discover washed-up debris are along the African east coast, especially in the area around Madagascar. The debris remaining at sea in 2016 is spread out over a wide area and its distribution changes only slowly.

1 Introduction

Modern sea situational awareness technologies make use of both real-time information and advanced, long-term reconstructions of the ocean state. Among many other applications, the ocean reconstructions allow the study of transport and dispersal scenarios for objects and pollutants at sea. Such studies are key to preparing better emergency response management plans and performing post-crisis assessments. The use of numerical simulations for search-and-rescue modelling dates back to the early 1970s, when the US Coast Guard introduced its Computer-Assisted Search Planning system (Frost and Stone, 2001). Developments in meteorology, oceanography and computer technology have since led to large improvements in the performance and accuracy of the numerical models. However, the basic methodology of drift modelling has remained the same, using an ensemble of particles that respond linearly to the wind speed (Hackett et al., 2006; Breivik et al., 2012). The relationship between drift and wind speed has been the subject of several decades worth of field experiments, ultimately leading to a system of standardised coefficients or leeway factors (Allen and Plourde, 1999).

The use of superensembles, a weighted combination of multiple models, was first introduced in meteorology by Krishnamurti et al. (1999) as a method to create multi-model forecasts. Applications in oceanography and more specifically in surface drift modelling (Rixen and Ferreira-Coelho, 2007; Rixen et al., 2008) have so far focused on improving the forcing fields used as input to the drift model. This paper presents a different approach, applying the superensemble technique to multiple realisations of the drift model itself. Using long-term global ocean and weather reconstructions, the superensemble drift model is used to produce probability

Published by Copernicus Publications on behalf of the European Geosciences Union.

distributions for the surface drift of aircraft debris originating from an accident in the southern Indian Ocean.

Malaysia Airlines flight 370 (MH370) was a scheduled passenger flight from Kuala Lumpur, Malaysia, to Beijing, China. The Boeing 777-200 ER aircraft carrying 239 passengers and crew disappeared less than an hour after take-off. Air traffic control (ATC) lost voice and radar contact with the flight at 17:22 UTC on 7 March 2014, while the aircraft was over the Gulf of Thailand. Initially it was assumed that the flight had crashed, but analysis of military radar data showed that the plane had deviated from its planned flight path and returned towards Malaysia. The aircraft continued flying in a westward direction and eventually exited the radar coverage at 18:22 UTC (Safety Investigation Team for MH370, 2015).

While most on-board communication equipment was inoperable, minimal communication between the aircraft's satellite terminal and the satellite network continued until 00:19 UTC. Analysis of this communication (Ashton et al., 2015) concluded that the aircraft changed course towards the south and continued in this direction until fuel ran out. Based on this information, various search areas have been defined in the southern Indian Ocean in an effort to locate the wreckage (ATSB, 2015). These areas straddle the arc of constant distance to the satellite at the time of the final communication. The most important areas are shown in Fig. 1. The *wide search area* is the envelope of possible locations, but due to its size a full search of this area is not feasible. Motivated by the most probable flight path, underwater searches for the wreckage have concentrated in the southern part of this area. However, the main wreckage has not been located. The only parts of the aircraft that have been recovered so far are the following:

- a *flaperon*, part of the right wing of the aircraft, found on the beach of Réunion on 29 July 2015;
- a *flap fairing* from the right wing, found in Mozambique in December 2015, but only reported to the authorities in March 2016 after media coverage of other debris (ATSB, 2016a);
- part of an engine cowling, discovered in South Africa in March 2016, but later found to be photographed already on 23 December 2015 (ATSB, 2016b);
- part of the horizontal stabiliser, found on a sandbank off the coast of Mozambique on 27 February 2015 (ATSB, 2016a);
- a cabin interior panel, discovered on Rodrigues Island, Mauritius, on 30 March 2016 (ATSB, 2016b).

The following sections will present a numerical simulation that uses all available information about the crash site and the discoveries of washed-up debris to predict the distribution of floating debris from the accident. The paper is organised as follows: in Sect. 2 the drift modelling and the treatment of unknown initial conditions is discussed; Sect. 3 shows the predictions of the model in terms of a time series of debris probability maps; and finally, Sect. 4 presents the conclusions of this study.

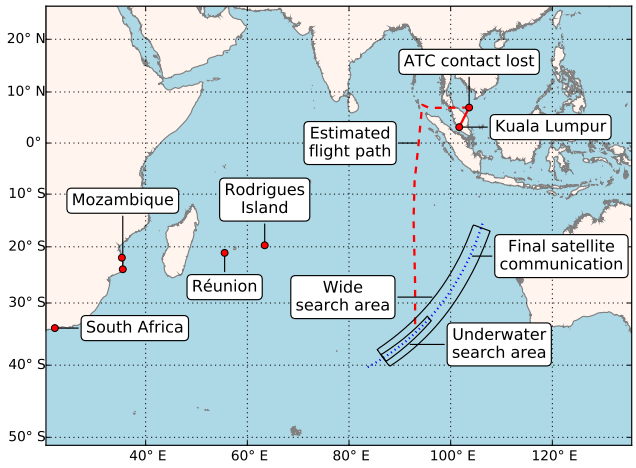

Figure 1. Estimated flight path of flight MH370 based on military radar and satellite data analysis. Also indicated are the search areas and the locations where washed-up debris was discovered.

2 Modelling

2.1 Drift trajectories

Drift trajectories are modelled using an ensemble of particles drifting on the ocean surface. Due to differences in their initial positions and due to random motion these particles will slowly diverge over time. Each trajectory represents a possible path of the object being studied.

In this model the displacement $\mathrm{d}\boldsymbol{x}_i$ of particle i in an infinitesimal time interval $\mathrm{d}t$ is given by

$$\mathrm{d}\boldsymbol{x}_i = [\boldsymbol{c}(\boldsymbol{x}_i, t) + L\boldsymbol{w}(\boldsymbol{x}_i, t)]\,\mathrm{d}t + \boldsymbol{n}. \quad (1)$$

Here $\boldsymbol{c}(\boldsymbol{x}_i, t)$ and $\boldsymbol{w}(\boldsymbol{x}_i, t)$ are the ocean current and wind forcing fields, interpolated at position $\boldsymbol{x}_i$ and time t. The constant L is the wind drag coefficient, or downwind leeway (Allen and Plourde, 1999) of the particle. It accounts for both direct and indirect (e.g. Stokes drift) wind-induced motion. The term $\boldsymbol{n}$ parameterises the incoherent turbulent motion of the particle. Its components n_j are random variables, distributed according to

$$n_j \sim \mathcal{N}\left(0, \sqrt{2K_h \Delta t}\right) \quad (2)$$

$$K_h = 2\ \mathrm{m}^2\ \mathrm{s}^{-1}, \quad (3)$$

where $\mathcal{N}(\mu, \sigma)$ is the normal distribution and Δt the length of an integration time step. The constant K_h is the turbulent diffusion coefficient. The value of this coefficient is taken from De Dominicis et al. (2013).

The particles in the model are advected by integrating Eq. (1) numerically using the fourth-order Runge–Kutta method.

2.2 Superensemble

To account for the fact that the location of the wreckage and the wind drag coefficient are not accurately known, the results presented here use multiple realisations of the model, with varying initial conditions and parameters. The different realisations are then combined into a superensemble.

The superensemble probability $P(\boldsymbol{x}, t)$ of finding aircraft debris in a location $\boldsymbol{x}$ at time t is expressed as a sum over all model realisations k and their individual probabilities P_k as

$$P(\boldsymbol{x}, t) = \sum_k \alpha_k P_k(\boldsymbol{x}, t), \tag{4}$$

where α_k is the model weight coefficient. The probability predicted by the kth model realisation can be defined as

$$P_k(\boldsymbol{x}, t) = \frac{1}{N_k} \sum_{i=1}^{N_k} \delta(\boldsymbol{x} - \boldsymbol{x}_{k,i}(t)), \tag{5}$$

where N_k is the total number of particles and δ a function that equals 1 below a certain distance and 0 otherwise. For all debris discoveries this distance is set to 100 km.

2.2.1 Model coefficients

In order to obtain meaningful results from the superensemble, the coefficients α_k are chosen to represent the likelihood of a particular model realisation M_k, given the observed debris D. Using Bayesian inference α_k can be expressed as

$$\alpha_k = \mathcal{P}(M_k|D) \propto \mathcal{P}(D|M_k) \times \mathcal{P}(M_k). \tag{6}$$

Here $\mathcal{P}(\mathrm{D}|M_k)$ can be obtained as a product of probabilities of the individual debris discoveries l using Eq. (5):

$$\mathcal{P}(D|M_k) = \prod_l P_k(\boldsymbol{x}_l, t_l). \tag{7}$$

The prior model likelihood $\mathcal{P}(M_k)$ is chosen inversely proportional to the model variance:

$$\mathcal{P}(M_k) = \frac{1/\sigma_{x,k}^2}{\sum_n 1/\sigma_{x,n}^2}. \tag{8}$$

The variance is evaluated at time $t = 90$ days to capture the variability of the different model realisations without particles stranding on the coastline.

2.2.2 Initial conditions and parameters

The superensemble is initialised with 30 model realisations, each containing 5000 particles. The realisations contain all possible combinations of six different wind drag coefficients and five starting locations. The wind drag coefficients range from 0 to 2.5 % in increments of 0.5 %, spanning roughly the range from no wind drag at all to a drag similar to that of a small boat (Allen and Plourde, 1999). The starting locations are obtained by dividing the wide search area (see Fig. 1) in five sections of equal size, along the arc of the final satellite communication.

2.3 Forcing field data

The oceanographic and meteorological data for the simulation are provided by the European Copernicus Marine Environment Monitoring Service[1]. The ocean currents at the surface level are extracted from the global ocean analysis[2] data, which provide a three-dimensional ocean reconstruction with global coverage at a spatial resolution of $1/12°$. The temporal resolution for the period of the simulation is 2-hourly, except for the period of 8–18 March 2014, where the daily average is used. The wind forcing uses the global near-real-time ocean wind observations[3], which consist of satellite scatterometer observations combined with the operational wind analysis from the European Centre for Medium-Range Weather Forecasts (ECMWF). The wind fields are measured as a 6 h time average with a spatial resolution of $1/4°$. The wind speed is defined at a reference height of 10 m.

3 Results

3.1 First debris discovery

Figure 2 shows the distributions for floating MH370 debris in the southern Indian Ocean, using only the first observation in July 2015 to calculate the weights. The amount of debris predicted in a certain location is expressed as the number of simulated drifting particles in an area of $1° \times 1°$. The number of particles is normalised to that used in a single model realisation, i.e. $\sum_k \alpha_k = 1$. Areas containing fewer than two particles per square degree are not shown.

The distribution at the time of the discovery in Réunion is shown in Fig. 2a. In addition to Réunion and the neighbouring islands, it shows a high probability of debris washed up in the northeast of Madagascar and on the African mainland in Tanzania and Mozambique. It also shows the probability of debris drifting east from the search area, ending up on the coast of southwest Australia.

In February 2016 (see Fig. 2b) the debris had spread further south along the African coast, reaching as far as South Africa. This distribution shows good agreement with the debris that was discovered roughly around this time on Rodrigues Island and in Mozambique. The engine cowling frag-

[1] http://marine.copernicus.eu.

[2] Dataset global-analysis-forecast-phys-001-002.

[3] Dataset wind-glo-wind-l4-nrt-observations-012-004.

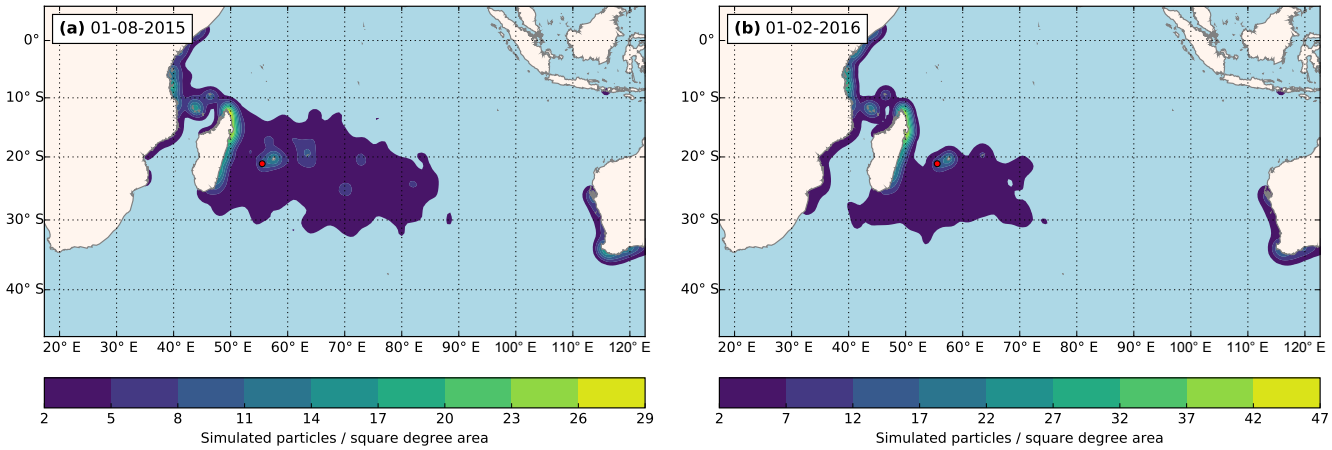

Figure 2. Floating aircraft debris probability density in **(a)** August 2015 and **(b)** February 2016, based only on the first observed debris at the end of July 2015. The location of this observation is indicated by the circular red marker.

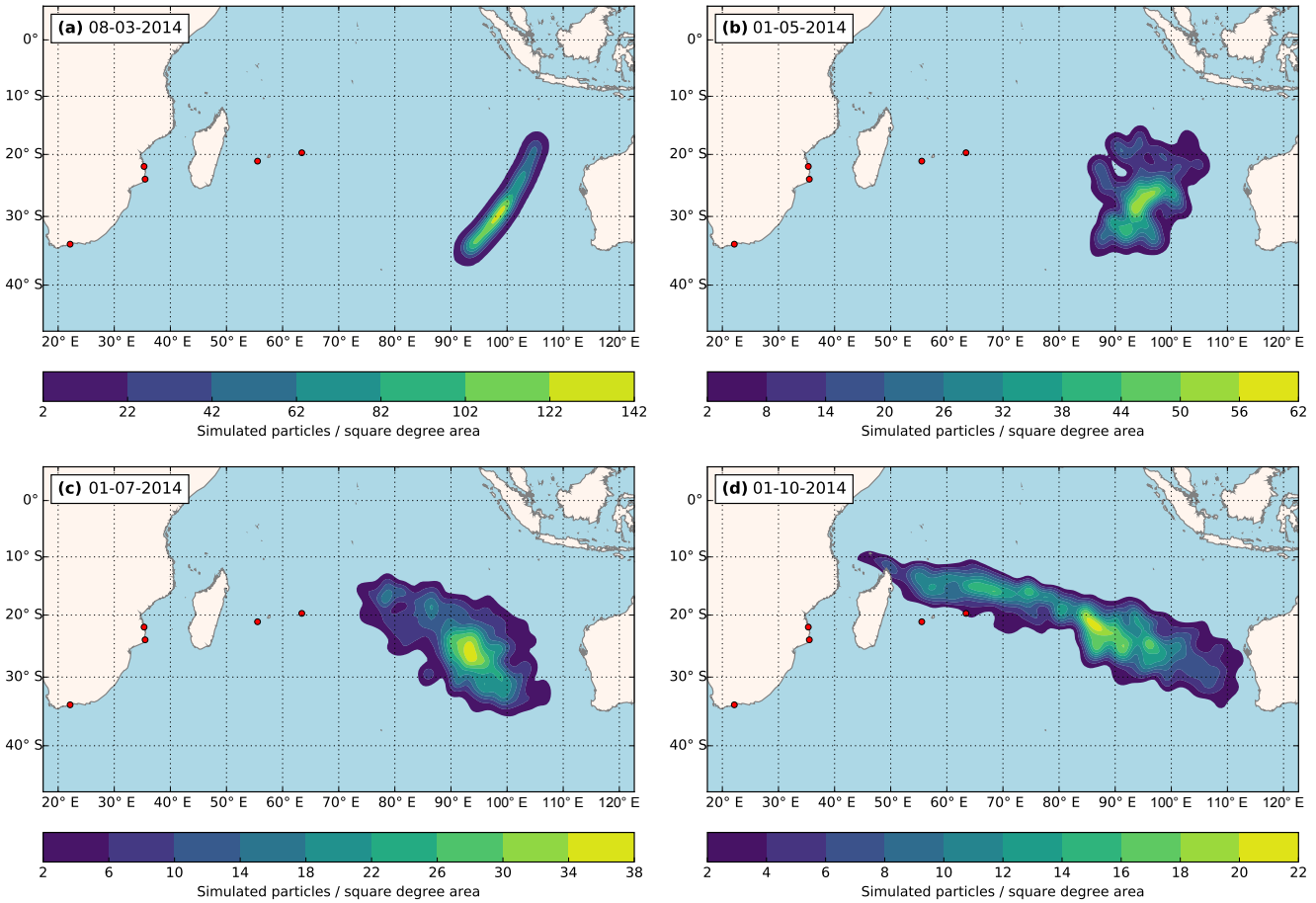

Figure 3. Floating aircraft debris probability density between March and October 2014. The superensemble weights are calculated based on all five debris observations. The locations of the observations are indicated by the circular red markers.

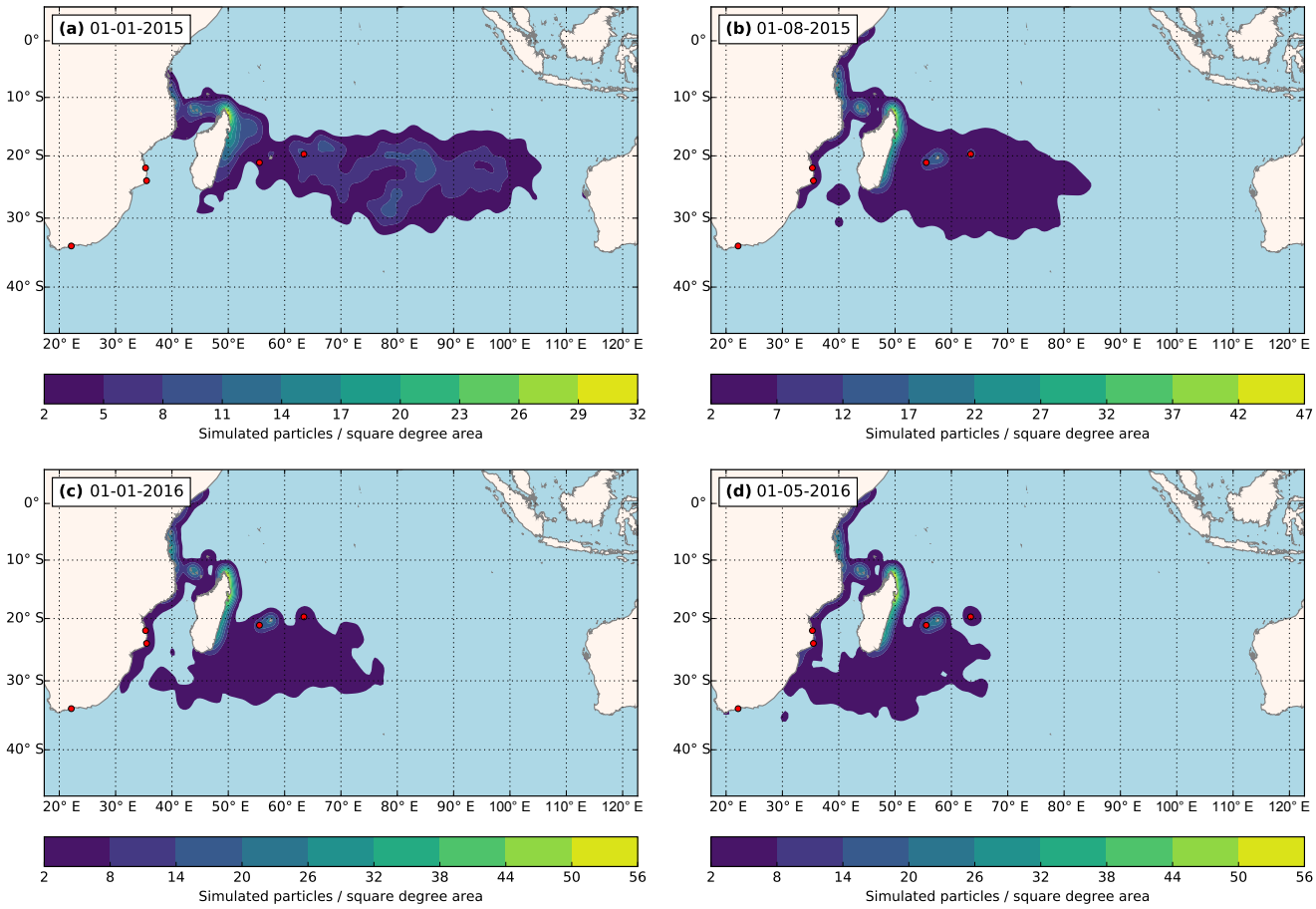

Figure 4. Floating aircraft debris probability density between January 2015 and May 2016. The superensemble weights are calculated based on all five debris observations. The locations of the observations are indicated by the circular red markers.

ment was discovered further south in South Africa, in a region where the simulation predicts fewer than two particles per square degree area.

3.2 Including further discoveries

The new debris discoveries can be included into the simulation by recalculating the model weights α_k, resulting in the most likely distribution of debris that is compatible with all five observations. The time evolution of this distribution is shown in Figs. 3–4.

One density distribution that is of particular interest is the distribution at the time of the accident, shown in Fig. 3a. It shows that the most likely origin for the discovered debris ($>$ 100 simulated particles per square degree) coincides with the northern half of the underwater search area, but extends further north until approximately 28° S. Debris originating from the southern part of the underwater search area, below 35° S, is found to be poorly compatible with the observed debris in Mozambique and South Africa.

Figure 3b–d clearly show the anticlockwise pattern of the Indian Ocean gyre, with the West Australian Current moving north along the Australian coast and the westward South Equatorial Current around 20° S. Figure 3d shows that the first debris may have arrived on Rodrigues Island and the northern part of Madagascar as early as October 2014.

In January 2015 (Fig. 4a) the first debris may have reached Réunion. At roughly the same time debris is also predicted to have reached the African mainland, mostly on the coast of Tanzania and Mozambique. From this point on the debris entered the Agulhas Current that flows south along the African coast, possibly carrying debris as far as South Africa at the beginning of 2016 (Fig. 4c). The debris that remains at sea in 2016 (Fig. 4d) is spread out over a large area, and its distribution changes only slowly.

While debris may wash up on shore in various locations, it is important to note that there are many other factors that determine whether the debris will be found, recognised and reported to the proper authorities. In sparsely populated areas it may take a long time before debris is discovered, while in developing countries a discovered piece of debris may be

discarded because people are not aware of the missing aircraft. It is therefore not unlikely that debris has washed up in other locations but has remained unreported.

4 Conclusions

The availability of high-resolution oceanographic and meteorological data is key to adequately responding to accidents and emergencies at sea. The case of MH370 especially underlines the importance of data that provide global coverage. With the operational range of modern airliners in excess of 10 000 km, accidents may happen in remote areas that are deprived of most means of communication. In such cases the meteo-oceanographic data might be the only source of information on the circumstances of the accident and the conditions afterwards.

The results presented in this paper show that the aircraft debris discovered so far in Réunion, Mozambique, South Africa and Rodrigues Island most likely originated from the wide search area between 28 and 35° S. This is in agreement with the estimated flight path of Ashton et al. (2015) and partially overlaps with the underwater search area between 32 and 35° S. However, this area extends further north than the current underwater search area, suggesting that if the current search proves unsuccessful, a northward extension of the search area should be considered.

Based on the particle distribution, the most probable locations to discover further washed-up debris from flight MH370 are Tanzania, Mozambique, Madagascar and surrounding islands such as Réunion, Mauritius and the Comoros. The time evolution shows that from 2016 onwards the floating debris that remains at sea is spread out, and its distribution changes only slowly. The probability of new debris washing up in the future is therefore quite low.

The results obtained for MH370 show that the superensemble method described in this paper is well-suited for drift simulations where additional observations are available to refine the result. By adjusting the weight of the superensemble members it is straightforward to incorporate information such as the discovered debris into the simulation. Moreover, as this weighting procedure is computationally inexpensive, the method could also be used to provide real-time operational forecasts during an emergency at sea.

Acknowledgements. This work was performed in the framework of the TESSA Project (Sviluppo di TEcnologie per la Situational Sea Awareness) supported by PON (Ricerca & Competitività 2007–2013), cofunded by EU (European Regional Development Fund), MIUR (Ministero Italiano dell'Università e della Ricerca) and MSE (Ministero dello Sviluppo Economico). This study has been conducted using EU Copernicus Marine Service Information.

Edited by: R. Archetti
Reviewed by: two anonymous referees

References

Allen, A. A. and Plourde, J. V.: Review of leeway: field experiments and implementation, Tech. Rep. CG-D-08-99, US Coast Guard Research and Development Center, Groton, CT, USA, 1999.

Ashton, C., Shuster Bruce, A., Colledge, G., and Dickinson, M.: The search for MH370, J. Navigat., 68, 1–22, doi:10.1017/S037346331400068X, 2015.

ATSB: MH370 – Definition of underwater search areas, Tech. Rep. AE-2014-054, Australian Transportation Safety Bureau, Canberra, ACT, Australia, 2015.

ATSB: Debris examination – update No. 1, Tech. Rep. AE-2014-054, Australian Transportation Safety Bureau, Canberra, ACT, Australia, 2016a.

ATSB: Debris examination – update No. 2, Tech. Rep. AE-2014-054, Australian Transportation Safety Bureau, Canberra, ACT, Australia, 2016b.

Breivik, Ø., Allen, A. A., Maisondieu, C., and Olagnon, M.: Advances in search and rescue at sea, Ocean Dynam., 63, 83–88, doi:10.1007/s10236-012-0581-1, 2012.

De Dominicis, M., Pinardi, N., Zodiatis, G., and Lardner, R.: MEDSLIK-II, a Lagrangian marine surface oil spill model for short-term forecasting – Part 1: Theory, Geosci. Model Dev., 6, 1851–1869, doi:10.5194/gmd-6-1851-2013, 2013.

Frost, J. and Stone, L.: Review of search theory: advances and applications to search and rescue decision support, Tech. Rep. CG-D-15-01, US Coast Guard Research and Development Center, Canberra, ACT, Australia, 2001.

Hackett, B., Breivik, Ø., and Wettre, C.: Forecasting the drift of objects and substances in the ocean, in: Ocean weather forecasting, vol. 5, chap. 23, edited by: Chassignet, E. P. and Verron, J., Springer Netherlands, 507–523, doi:10.1007/1-4020-4028-8_23, 2006.

Krishnamurti, T. N., Kishtawal, C. M., LaRow, T. E., Bachiochi, D. R., Zhang, Z., Williford, C. E., Gadgil, S., and Surendran, S.: Improved weather and seasonal climate forecasts from multimodel superensemble, Science, 285, 1548–1550, doi:10.1126/science.285.5433.1548, 1999.

Rixen, M. and Ferreira-Coelho, E.: Operational surface drift prediction using linear and non-linear hyper-ensemble statistics on atmospheric and ocean models, J. Mar. Syst., 65, 105–121, doi:10.1016/j.jmarsys.2004.12.005, 2007.

Rixen, M., Ferreira-Coelho, E., and Signell, R.: Surface drift prediction in the Adriatic Sea using hyper-ensemble statistics on atmospheric, ocean and wave models: uncertainties and probability distribution areas, J. Mar. Syst., 69, 86–98, doi:10.1016/j.jmarsys.2007.02.015, 2008.

Safety Investigation Team for MH370: factual information – safety investigation for MH370, Tech. Rep. MH370/01/15, Ministry of Transport, Malaysia, 2015.

Search strategy in a complex and dynamic environment: the MH370 case

Stefan Ivić, Bojan Crnković, Hassan Arbabi, Sophie Loire, Patrick Clary, Igor Mezić

arXiv:2004.14110v1 [math.OC] 29 Apr 2020

***Abstract*—Search and detection of objects on the ocean surface is a challenging task due to the complexity of the drift dynamics and lack of known optimal solutions for the path of the search agents. This challenge was highlighted by the unsuccessful search for Malaysian Flight 370 (MH370) which disappeared on March 8, 2014. In this paper, we propose an improvement of a search algorithm rooted in the ergodic theory of dynamical systems which can accommodate complex geometries and uncertainties of the drifting search areas on the ocean surface. We illustrate the effectiveness of this algorithm in a computational replication of the conducted search for MH370. In comparison to conventional search methods, the proposed algorithm leads to an order of magnitude improvement in success rate over the time period of the actual search operation. Simulations of the proposed search control also indicate that the initial success rate of finding debris increases in the event of delayed search commencement. This is due to the existence of convergence zones in the search area which leads to local aggregation of debris in those zones and hence reduction of the effective size of the area to be searched.**

***Index Terms*—complex and dynamic environments, MH370, oceanic search, search theory, dynamic spectral multi-scale coverage, multi-agent search, motion control**

I. Introduction

The problem of search and detection is a crucial part of aerial and maritime operations. The importance of this task was accentuated by the tragic mystery of the missing Malaysian Airline Flight, known as MH370 [27]. The surface search operation that began in the aftermath of the disappearance involved as many as 40 ships and aircraft sweeping an area of over 4,600,000 square kilometers in the Indian Ocean but ended without finding any conclusive traces of the passengers or the plane wreckage [4].

There are two significant sources of difficulty in designing search operations on the surface of the ocean. First is the high level of uncertainty associated with the assessment of the search target area. In the case of MH370, the target areas were continuously reassigned due to a stream of incoming information from satellite data analysis, suspicious debris sightings, and detection of signals suspected to be from the underwater locator beacon. This type of uncertainty is further compounded by the complex drift dynamics on the surface of the ocean. The unsteady nature of ocean currents amplifies the errors in the estimation of the splash location in the days lapsed between the splash and the start of the search operation. In addition, given that drift models also have inaccuracies, the final computational estimates for the search targets typically have a considerable amount of uncertainty. A more detailed studies are published on topics of complexity and uncertainties of MH370 path and splash estimation [2], [5], and debris drift affected by the stirring of the ocean [7], [13], [40], [31].

The second source of difficulty is that even when the target area for search is known and the associated uncertainty is well-characterized, e.g. in the form of a probability distribution, the problem of the design of the search agents' paths generally does not have a known optimal solution. The conventional approach is to divide the target area into subdomains and assign them to different agents which will sweep each subdomain in organized paths, e.g., parallel lines. This so-called "lawnmower" strategy is easy to plan and implement for simple geometries, but it cannot be readily extended to complex geometries that arise from the surface drifts or areas with non-uniform distribution of likelihood for finding targets. The lawnmower technique also lacks the flexibility required for real-world operations: for example, it would require reassignment of search areas and agents in case of an agent going astray.

We propose a multi-agent motion control method called modified Dynamic Spectral Multi-scale Coverage (mDSMC), for search and detection of objects in dynamically evolving environments such as the ocean surface. This algorithm combines the classical theory of optimal search [17][37] with concepts from ergodic theory and is capable of accommodating complex geometries, non-uniform distributions and the instantaneous drift of targets during the search. The algorithm is particularly designed to downplay the role of small spatial characteristics of the target area which leads to a significant increase in the success rate of the search operation. To show the promise of this algorithm for real-world applications, we compare its performance with conventional search techniques in a computational replication of the surface search for MH370.

II. Related research

The design of search agents' path is a multi-agent control problem whose objective function involves the estimation of a time evolving probability distribution. Although considering the dynamics is a key feature of successful oceanic search, there are a lot of relevant and interesting details that can be

S. Ivić is with Faculty of Engineering, University of Rijeka, Rijeka, Croatia, e-mail: stefan.ivic@riteh.hr.

B. Crnković is with Department of Mathematics, University of Rijeka, Rijeka, Croatia.

H. Arbabi is with Department of Mechanical Engineering, Massachusetts Institute of Technology, Cambridge, USA.

S. Loire is with Bruker Nano Surfaces, Santa Barbara, USA.

P. Clary is with Oregon State University, Corvallis, USA.

I. Mezić is with Department of Mechanical Engineering and The Center for Control, Dynamical Systems and Computation, University of California, Santa Barbara, USA.

found in papers discussing both static and dynamic search problems. The following overview of related literature presents the relevant publications grouped to approaches considering static targets and the ones where targets are dynamic.

A. Stationary targets

In [43] a route planning for Unmanned Aerial Vehicle (UAV) in stationary target search mission over a river region is considered. Sub-regions along the river are extracted using a Gaussian mixture model (GMM) and prioritized heuristically with an approximation insertion (AI) approach. The optimal routes are obtained maximizing stationary target detection in a given time window. This approach is extended to the search with multiple UAVs in [42] where Receding Horizon Control (RHC, also known as Model Predictive Control or MPC) is employed for finding the optimal paths. In [30] RHC is employed to solve ergodic exploration of distributed information. It is shown that optimization-based approach is suitable for both local and global search density i.e. whether the information is localized or diffused. The optimization-based path-planner, presented by Gramajo and Shankar [8], optimizes the search for given energy consumption and maneuverability constraints.

An advanced lawnmower-type control algorithm presented in [14] considers the dynamics of the UAV, the spatial scope and the quality of the sensor. Another lawnmower-based search improvement [21] finds paths that approximate the payoff of an optimal solution based on partial detection in the form of a task difficulty map. The algorithm uses the mode goodness ratio heuristic that uses a Gaussian mixture model to prioritize search subregions.

Target search sometimes appears as an objective of reconnaissance mission. A reconnaissance mission control presented by Wang et al. [41] focuses on particle swarm optimization for UAV swarm path planning. The optimization considers different search strategies and optimization objectives, and constraints regarding the mobility and communication of the UAV swarm.

Ni et al. [32] model the search with the use of potential game theory, and solves collaborative control and search area coverage problem utilizing a modification of binary log-linear learning (BLLL) algorithm [22].

A machine learning approach for the search and rescue in indoor environments using UAVs has been investigated in [18]. The reinforced learning is used to locate the trapped victim by sensing the RF signals emitted from the victim's smart device.

A heat equation driven area coverage (HEDAC) control method [12] has been employed for heterogenous multi-agent search in uncertainty conditions [11]. An exact probabilistic model and state-of-the-art control method ensures a near-optimal performance for stationary targets.

An algorithm called layered search and rescue (LSAR) is employed in [1] for multi-agent search and rescue missions in order to minimize the search time while finding the maximum number of victims.

The proposed system allows an autonomous control of rescue mission considering the terrain and avalanche environmental conditions. In [3], active visual search is solved using a probabilistic model of the search environment which allows for prioritizing the search effort for certain regions on a building floor.

B. Non-stationary targets

An Ant Colony Optimization (ACO) is used in [33] to determine paths of multiple UAVs that ensure minimal time needed to find moving targets. A specialized multi-UAV sea area search map is presented in [47], where the target probability map (TPM) was designed to handle uncertainties caused by dynamic targets. The TPM is used as a pheromone map in an improved multi-ant colony algorithm - a derivation of ACO algorithm. The main drawback of this heuristic approach is that the resulting paths are straight-segmented due to the discrete nature of the method. Another heuristic approach is presented in [6] where several algorithms are combined in a multi-UAV search procedure for missing persons with the time-varying distribution of target location probabilities. The algorithm used for evolving a population of main solutions is a hybrid evolutionary optimization method, while each UAV path is finely optimized using Tabu Search method.

A distributed cooperative multi-UAV search based on the prediction of non-stationary targets is proposed in [35]. Target existence probability is updated using detection information of on-board sensors while the UAV's are directed using RHC for maximizing search performance. Ergodic exploration using RHC, presented in [26], plans a real-time motion that locally optimize ergodicity with respect to the dynamic information density. RHC is also utilized in [9] where targets are partially aware of the UAVs locations and are trying to escape them. Although this is not the case in MH370 search, it provides an interesting game-theoretic view of the search problem [20].

A mission planner for locating and tracking harmful ocean debris with UAVs is presented in [36]. Actual weather data and predicted icing conditions and their impact on the UAV performance are taken into account in the search simulations. Market-based cooperation strategies for multiple UAVs and evolutionary computation techniques are utilized for conducting low-cost oceanic search missions.

A path planning algorithm [39] governs the coordinated search using unmanned aerial vehicles and autonomous underwater vehicles. The proposed control framework is tested on lawnmower-style multi-agent search simulations. A search control for autonomous underwater vehicles is studied in [10] where non-stationary targets driven by ocean current are considered. A search for multiple target locations in an unsteady ocean environment is achieved with a self-organizing map (SOM) neural network. Considering target movement due to ocean currents, an optimal search agent path is found using a velocity synthesis approach.

Yau and Chung [44] investigate the application of linear search and discrete myopic search, coupled with surrogate ocean models, for locating a drifting object.

Perez et al. [34] propose a motion and camera control algorithm for multiple UAVs which minimizes the expected detection time of a nondeterministically moving target of an uncertain initial position. The method is tested on 3 real-world inspired scenarios including a drifting boat by the coast.

A multi-objective path planning (MOPP) framework [45] is utilized for finding a suitable UAV path in a dynamic urban environment. Ensuring the safety of UAV is done twofold using safety index maps: considering known static obstacles and unexpected obstacles.

Multi-UAV search for moving targets in an unknown environment is established in [46] using a reinforced learning scheme. The technique is applied in a search of moving ships at the sea.

The integration of different flight and search features such as autonomous take-off, collision avoidance, communication failure, target search, task assignment, and tracking using multiple fixed-wing UAVs in urban environments in presented in [28]. The targets are grouped into convoys that are moving on the known roads.

III. Search in dynamic environments

We will consider a rectangular domain $S \subset \mathbb{R}^2$ with boundary ∂S which is large enough to contain all potential debris floating in the sea and agent trajectories for the entire search period. The algorithm that we use here is a new variant of the Spectral Multi-scale Coverage (SMC) algorithm which was proposed in [24]. This algorithm was extended to dynamic environments in [25] (called DSMC) and its practical feasibility was shown in [23]. We give a short introduction to DSMC algorithm and emphasize the alterations and that leads to the algorithm introduced in this paper called modified DSMC (mDSMC).

From a mathematical viewpoint, a search problem is formulated around two central concepts. First is the probability distribution function of the search targets (i.e. survivors, debris, etc.) which denotes the likelihood of finding targets in each subset of the domain. This distribution, denoted here by p^t, is dynamic and evolves in time according to the drift equation in an incompressible flow:

$$\frac{\partial p^t}{\partial t} + v\nabla p^t = 0, \qquad \forall x \in S, \tag{1}$$

where v is the ocean surface velocity and the initial distribution p^{t_0} specifies the estimated splash location and the uncertainties therein at the estimated time of the splash t_0.

We denote a flow map $\mathcal{T}^{t_1,t_2} : \mathbb{R}^2 \mapsto \mathbb{R}^2$, which maps a location of a sample (or a target) at time t_1 to its location at time t_2 using the unsteady velocity field v. The flow map $\mathcal{T}$ describes the evolution of target and sample positions on the ocean surface which is a basis for the use of Lagrangian methods. The advection of samples placed on the initial splash location through flow map composition yields numerical solutions almost devoid of artificial diffusion and allows for direct parallelization.

The second concept is the coverage distribution c^t, which reflects the spatial distribution of the conducted search time up to time t. In other words, regions with higher coverage have been traversed by search agents more often. Assuming N search agents are dispatched at time 0 for a ceaseless search operation, and the path of each agent is denoted by z_i^t with $i = 1, 2, \ldots, N$, the coverage distribution is given by

$$c^t = \sum_{i=1}^{N} \int_0^t \delta(x - \mathcal{T}^{\tau,t}(z_i^\tau))\,\mathrm{d}\tau, \tag{2}$$

where δ is the Dirac delta function. The coverage can be thought of as a distribution with support on the points visited by the agents, but evolved forward in time by drift dynamics of the ocean surface. Note that the total search coverage at time t can be computed by integrating the above density over the whole area of search S,

$$\int_S c^t\,\mathrm{d}x = Nt. \tag{3}$$

When considering the concept of coverage, it is useful to model the search process by taking into account the properties of the detection system used in the search. The agent is able to detect targets near the current location but the detection ability decreases as the distance between the agent and the target increases. A simple model of this detection process and data acquisition can be described using a positive smooth compact support Radial Basis Functions (RBF) ϕ and ϕ_σ that satisfy:

$$\phi_\sigma(x) = \sigma^{-2}\phi\left(\frac{x}{\sigma}\right),$$

$$\int_{\mathbb{R}^2} \phi(x)\,\mathrm{d}x = 1,$$

where σ is a positive scaling factor that controls the visual detection range. The RBF models the measurement density of the visual detection system. To incorporate the RBF model we must also modify the coverage and define a smooth modified coverage function which represents the approximation of total measurement density in the domain up to time t:

$$c_\sigma^t(x) = \phi_\sigma(x) * c^t, \tag{4}$$

which also satisfies the condition:

$$\int_S c_\sigma^t\,\mathrm{d}x = Nt. \tag{5}$$

Furthermore, one can observe that these two definitions are consistent by passing to the limit:

$$\lim_{\sigma\to 0^+} c_\sigma^t(x) = c^t.$$

If the coverage (4) is integrated over S and the support of the RBF function is outside S, one must rescale the coverage to keep growth of total coveage linear in time.

This modification of coverage is not an exact model of coverage drift since it does not allow for the stretch and contraction of coverage support during the drift (i.e. $supp(c_\sigma^t) \subset supp(c^t) + supp(\phi_\sigma)$, where $+$ denotes the Minkowski addition) but it models the search process more faithfully compared to (2). Furthermore, it makes implementation straightforward and allows for real-time computation.

The goal of the search operation planning is to design the paths of the search agents such that the probability of detecting targets is maximized over a given time window. From [16], the probability of the target being detected by time t is

$$P_d = \int_S p^t \mathcal{F}(c_\sigma^t(x))\,\mathrm{d}x \tag{6}$$

where $\mathcal{F}$ is called the detection function. To be more precise, $\mathcal{F}(c_\sigma^t(x))$ denotes the (conditional) probability of the target being detected given the target is at x. The prevalent choice of detection function, which comes from the assumption of locally random search [15][38], is the exponential saturation. Mathematically speaking, this law is stated as

$$\mathcal{F}(c) = 1 - e^{-c}.$$

This means that if the agent and the target visit the same location at the same time, there is still some probability that the agent misses the target, but this probability decays exponentially with each visit.

The optimal coverage distribution that maximizes the probability in (6), regardless of how the motion of agents should construct such distribution, is given in the seminal paper of Koopman [16]. Assume for now that the target distribution p is stationary. Koopman showed that the optimal coverage distribution up to time t is

$$c_{opt}^t = \max\left[\ln p - \alpha^t, 0\right], \tag{7}$$

where α^t satisfies

$$Nt = \int_S \max\left[\ln p - \alpha^t, 0\right] \mathrm{d}x.$$

From (3) and (5) it is clear that the total coverage is a linear function in time. Therefore, the total amount of available coverage in a time interval of size Δt is equal to $N\Delta t$. Koopman also showed that the optimal solution can be achieved by incremental planning, i.e., if after spending Nt of coverage, the target has not been found but some extra amount of coverage, $N\Delta t$, becomes available then we can use the same procedure, using the posterior probability of targets, to compute the optimal distribution for the next stage of the search, and yet the probability of detection would have been the same if we had allocated $N(t + \Delta t)$ from the beginning.

Although the optimal coverage distribution in (7) can be readily computed, it is not known how to design the search agent paths to achieve this optimal distribution while satisfying physical constraints like the continuity of the paths. In fact, given any special form of coverage distribution, such as (2) or (4), achieving the optimal distribution might be infeasible. On the other hand, direct maximization of (6) over the space of agent paths leads to a nonconvex problem which is highly dependent on the initial guess, and therefore too costly for real-time applications. In order to make this problem feasible, we reformulate the optimal search problem as follows.

Assume that during the time interval $[0, t]$, N agents have searched the area but the search target has not been detected yet. The current coverage distribution is given by c^t, which is not necessarily the optimal coverage. Now for the next stage of the search over the horizon $[t, t + \Delta t]$, there are N_1 agents available and the amount of available coverage is $N_1\Delta t$. If we assume that during the time period Δt the drift of distribution p^t is negligible when compared with dynamics of the search, the optimal coverage at time $t + \Delta t$ according to Koopman theory of search is given by (7), but this time α satisfies

$$\int_S c_\sigma^t \,\mathrm{d}x + N_1\Delta t = \int_S \max\left[\ln p^t - \alpha^t, 0\right] \mathrm{d}x. \tag{8}$$

Given that achieving this optimal coverage may be infeasible, *we only strive to minimize the mismatch between the current distribution and the optimal distribution locally in time*. Therefore, the mDSMC algorithm uses a mismatch distribution which follows naturally from the Koopman search theory:

$$s_\sigma^t = \max\left[\ln p^t - \alpha^t - c_\sigma^t, 0\right]. \tag{9}$$

and we seek the next direction of motion for each agent that minimizes the scalar quantity

$$\Phi^t = \|s_\sigma^t\| \tag{10}$$

On the other hand, the DSMC algorithm mismatch distribution used in [25] has a much simpler form:

$$s^t = p^t - \frac{c^t}{Nt}, \tag{11}$$

and we seek to minimize $\|s^t\|$.

There are some important advantages of using (10) instead of (11). The mDSMC mismatch excludes the "over-searched" areas i.e. when $c_\sigma^t > \ln p^t - \alpha^t$. which improves search results significantly and removes some instabilities which are often present with DSMC algorithm.

IV. Spectral Multi-scale Coverage path planning

The key feature of spectral multi-scale algorithms is that they use a special class of function norms, called the Sobolev-space norm of negative index, to quantify the mismatch of current and optimal coverage. This norm for the mismatch distribution defined above is

$$\Phi^t = \sum_{k \in Z^2} \Lambda_k s_k^t, \tag{12}$$

where s_k^t is the coefficients of Fourier expansion of s^t, given by

$$s_k^t = \int_A f_k s^t \,\mathrm{d}x$$

where $f_k(x)$ are the Fourier basis functions. For a two dimensional implementation, Fourier basis functions are calculated on a rectangular domain $[0, L_1] \times [0, L_2]$ as:

$$f_k(x) = \frac{1}{h_k} \cos\left(\frac{k_1\pi x_1}{L_1}\right) \cos\left(\frac{k_2\pi x_2}{L_2}\right),$$
$$h_k = \int_0^{L_1}\int_0^{L_2} \cos^2\left(\frac{k_1\pi x_1}{L_1}\right) \cos^2\left(\frac{k_2\pi x_2}{L_2}\right) \mathrm{d}x_1\,\mathrm{d}x_2 \tag{13}$$

where $k = (k_1, k_2)$ is the wave-number vector.

The norm coefficients in (12) are given by

$$\Lambda_k = \left(1 + \|k\|^2\right)^\beta,$$

where β is the index of the norm and takes a negative value. This type of coefficient makes the contribution of components with smaller spatial scale (represented by larger k) proportionally smaller. Therefore, any algorithm that minimizes the mismatch function Φ^t automatically puts more weight on the large-scale spatial features of the target distribution. For the mDSMC algorithm $\beta = -\frac{1}{2}$ is used while for the DSMC $\beta \leq -\frac{3}{2}$ (in all calculations we used $\beta = -3/2$). Lower

exponent β in mDSMC algorithm reduces smoothing of the mismatch function which becomes important later in the search when smaller spatial scale features are explored.

DSMC and mDSMC algorithm minimize the mismatch distribution by implementing the instantaneous corrections to the agent paths that result in the fastest descend in the value of Φ at any time. Our modified algorithm can be extended to agents with second-order dynamics similar to [25] but here we assume that the agents have first-order dynamics with constant velocity. As shown in [25], we first need to define the potential field

$$u^t(z_i^t) = \sum_{k \in Z^2} \Lambda_k s_k^t f_k(x).$$

Then the velocity vector for each agent is given by

$$v_i^t = \frac{\nabla u^t(z_i^t)}{\|\nabla u^t(z_i^t)\|} v_{mag,i}$$

where $v_{mag,i}$ is the constant velocity magnitude of the i-th agent.

Finally, the movement of the search agents is governed by the first order motion law:

$$\frac{\mathrm{d}z_i^t}{\mathrm{d}t} = v_i^t.$$

To summarize, the mDSMC in contrast to DSMC uses a new type of objective function, described in (9) and minimizes the Sobolev norm with index $\beta = -1/2$, which is better suited to search problems.

In this specific application of mDSMC algorithm for the RBF, we used a compact support approximation of normal distribution centered at the agent location with a standard deviation of $\sigma = 3$km and 1-hour window to determine the amount of available coverage in (8).

V. Search for MH370 (Results)

The search and rescue operation for MH370 began on March 9, 2014, one day after the loss of communications between the plane and ground stations. The surface search lasted for 50 days and included areas near the Malay Peninsula and the Southern Indian Ocean. The estimated splash location was constantly updated due to a stream of incoming information and the drifted image of the most probable splash area was drifted under the ocean model to obtain the target area for each stage of the search. We consider three probable splash areas:

- Area A: the drifted image of this area was searched from March 28 to April 1,
- Area B: the drifted image of this area was searched on April 2 and 3,
- Area P: this area, in its totality, was not searched in the surface search. However, after the conclusion of the surface search, area P was recognized as the most probable splash area and marked as the priority location for underwater search [4].

In the actual search for MH370, the probable splash areas (including A and B above) were drifted using the knowledge of the ocean currents and wind effects, over the time lapse between the splash and commencement of the search. A precise description of the used drift model is not disclosed; however, the coordinates of the splash areas and some of the drifted images (including images of A and B) are publicly available. In our computational model, we use the surface velocity data obtained from the HYbrid Coordinate Ocean Model (HYCOM) to drift the splash areas. Moreover, we assume that the initial target distribution is uniform over each area.

We simulate the following scenarios:

1) *Lawnmower scenario 1*: the reported search areas are searched using the lawnmower algorithm representing the strategy that occurred in the actual MH370 search.
2) *Lawnmower scenario 2*: the splash areas are drifted using our drift model, and then convex-hull of target distribution is searched using the lawnmower algorithm.
3) *DSMC*: the splash areas are drifted using our drift model, and then searched using the DSMC algorithm.
4) *mDSMC*: The splash areas are drifted using our drift model, and then searched using the mDSMC algorithm.

Note that scenario 1 is a replication of the actual search. Contrasting scenario 2 and 3 provides a comparison of the search algorithms independent of the drift model, while contrasting scenario 1 and 3 distinguishes the combined effect of our drift model and search algorithm. Comparing scenario 3 and 4 shows the advantages gained by modifying DSMC.

A. Problem Definition of Search for MH370

The search parameters used in this study are based on two main sources: The coordinates of the probable splash areas are extracted from a series of reports on MH370 search operation by the Australian Transport Safety Bureau (ATSB) [4], and the information on search agents and the searched areas are collected from media releases and daily briefings by the Joint Agency Coordination Centre (JACC) for MH370 search. The target areas of search by JACC were determined by drifting the splash areas using models of the surface currents complemented with the real-time wind and wave data, however, the details of the drifting model are not publicly available. The search areas specified by JACC are used in scenario 1. In scenario 2, we have used the splash areas reported by ATSB and drifted them using our model. The search area for lawnmower was then computed as the smallest convex bounding polygon around the area with a nonzero probability of targets.

Up to 21 aircraft and 19 ships were deployed in the search operation. In our study, we have only used the aircrafts as search agents, due to the lack of data on the technical specifications of the ships. The number and type of the deployed aircraft vary with the search day (see Table I). but we have chosen the speed of every agent to be 380 km/h which represents the typical loiter speed of the military aircraft involved in the search. We also assume that the scanning of the search areas on each day started at 2:00 pm and ended at 5:00 pm (UTC).

A simplified stochastic model is used to emulate the target detection by the search observers aboard the aircraft. In

TABLE I
THE PARAMETERS OF MH370 SEARCH OPERATION.

Search Area	Seach Period	Number of search aircraft
Area A	March 28 - April 1	10, 8, 10, 10, 11
Area B	April 2 - 3	9, 9
Area P	March 8-17, March 13-22, March 18-27	10, 10, 10, 10, 10, 10, 10, 10, 10, 10

this model, if the target remains within the 1.5-km radius of an agent for time t, then it will be detected with the probability $P = 1 - \exp(-t/T)$, where $T = 2$ seconds is the expected detection time. A machine vision system for a low-cost fixed-wing UAV has been investigated in [19] where thermal imaging camera and onboard processing unit are used for performing real-time detection, classification, and tracking of objects floating on the ocean surface. Bearing in mind that mainly an eye vision is used in MH370 search, the authors believe the expected detection time of 2 seconds used in simulations is a reasonable estimate.

B. Drift model

Our drift model is based on the surface velocity data computed by the US Navy, using the HYbrid Coordinate Ocean Model (HYCOM). The data consists of 3-hourly longitudinal and latitudinal velocity components with a spatial resolution of 1/25 degrees in each direction. The drift model is used to compute the flow map $\mathcal{T}$ i.e. the paths of the search targets as well as the trace of search agent paths in (2). The location of the targets in the splash area is initialized at 0:30 UTC on March 8 using the Halton sequence and then updated through a 4th-order adaptive Runge-Kutta method with linear interpolations of the surface velocity in time and space. The evolution of the target distribution is simulated using a semi-Lagrangian method: we uniformly sampled the probable splash areas with a high number of tracers (10^5 tracers per area) and drifted those tracers using the above drift model. By computing the local density of tracers, we assemble the distribution at future times. This method does not require a numerical mesh and eliminates the artificial diffusion associated with Eulerian schemes for solving (1).

Figure 1 shows the drift of the area A. During the 19-day lapse between the estimated splash time and the start of the search in this area, the probability distribution of the search targets undergoes substantial change, and a potential search target moves several hundred kilometers away from its initial position (purple diamond). The reported areas of actual search are mainly covering the drifted target probability, but it is evident that a lot of search effort is spent on regions where target probability is zero. For area B, a similar visualization is shown in Figure 2. Seemingly, the conducted search regions are well placed, but a large part of the target probability in the west is not covered at all. The stretching and folding of the support of the target distribution in Figures 1 and 2 is typical of unsteady geophysical flows with strong mixing behavior [29]. Therefore, using a lawn-mower search algorithm, which is suited to regular shapes, would be inefficient in such situations. In contrast, the paths of the mDSMC would naturally adapt to the shape of the drifted area.

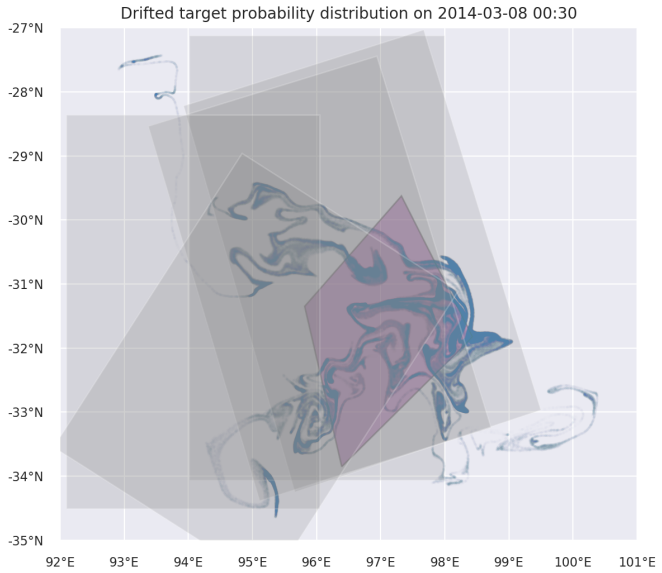

Fig. 1. The estimated splash area A (purple diamond) and the drifted probability distribution of search targets on the first day of actual search (March 28). Gray polygons represent regions of actual search which is simulated in Lawnmower scenario 1 which was conducted from March 28 to April 1.

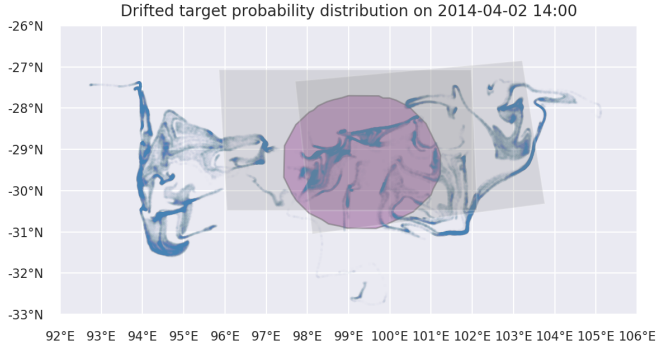

Fig. 2. The estimated splash area B (purple circle) and the drifted probability distribution of search targets on the first day of actual search (April 2). Gray polygons represent regions of actual search which is simulated in Lawnmower scenario 1 which happened on April 2 and April 3.

C. The search

The visualization of all four considered scenarios for area A search is shown in Figure 3. The lawnmower areas of actual MH370 search yield the trajectories shown in 3.A, while 3.B show trajectories of lawnmower strategy which relies on our drift model. Both sets of trajectories fails to achieve acceptable results in terms of detection rate (33.7% and 43.8%, respectively) which is indicated with green crosses representing detected targets.

The DSMC and mDSMC search strategies (Figures 3.C and 3.D, respectively) are guided by the drifted target probability distributions and, as result of that, accomplished trajectories are passing through the regions of high probability and consequentially produce better target detection rate. The improvements made in mDSMC, in contrast to DSMC, are recognizable in a better local search and in the elimination of wide and unnecessary paths. It is rather interesting to observe how mDSMC covers thin ribbons of the target probability distribution, especially the one in the north of the search domain.

Figure 4 displays the results of search simulations for area B. In lawnmower strategies, an unexpected anomaly can be observed: the lawnmower scenario 2, shown in Figure 4.B, although taking into account probability distribution drifted with the same drift model as targets, is apparently not better than the "naive" lawnmower scenario 1 (Figure 4.A) if the number of detected targets is compared. Even though the lawnmower scenario 1 strategy missed a big portion (approx. 1/4) of targets on the west part of the domain, due to the density of lawnmower trajectories in remaining regions, it outperforms the scenario 2 which sparsely covers whole target distribution. Similar to area A results, both DSMC and mDSMC (Figures 4.C and 4.D, respectively) achieved better results than lawnmower strategies. Due to the highly indented and complex shape of the target probability distribution, DSMC's tendency to global search prevents more accurate search.

To evaluate the success of different search scenarios, we have performed the following experiment: For each case, we have seeded the splash area on the day of the splash with 1000 randomly positioned targets and drifted the targets with the surface flow. On each day of the search, the search algorithms are executed while the targets are drifting during the search, and the success rate of each algorithm is computed as the fraction of targets detected by the agents. The detection is modeled as a stochastic process with the law of exponential saturation. The described procedure of a search simulation is repeated 100 times for each scenario using randomly varying initial positions for the targets and agents, and the ensemble average of the success rates are reported here.

Figures 5 and 6 summarize the results of the above experiment for area A and area B, respectively. Note that the execution of the search algorithms is limited to a 3-hour period each day to account for the travel time of the agents between the closest airbase and the search area. The performance of DSMC and mDSMC algorithms is remarkably different from the lawnmower technique: the lawnmower scenarios have uniform daily progress which is expected since the lawnmower covered area progresses linearly with time. The DSMC generates trajectories that roughly follow the target distribution - addressing the broad non-local search which is improved in mDSMC. In the case where mDSMC algorithm is used, however, the search agents perform large sweeps of the area first, which results in capturing about %50 of the targets on the first day. In the subsequent two days, the agents perform increasingly localized search to find the remaining targets. The results for both areas A and B show that mDSMC algorithm would have significantly improved the chances of finding floating debris from the MH370 airplane.

The dynamics and comparison of the search for area A and B can be found in Video 1 and Video 2 included in supplementary materials.

VI. Effect of delayed search on the success rate

An unfortunate circumstance of the MH370 search was that a reliable estimate of the splash location was not known immediately after the plane's disappearance. The day after the plane went missing, the search started by focusing on the vicinity of the Malay Peninsula. In the meantime, the analysis of satellite data indicated that the plane had continued to fly for six hours after the last communication, and two preliminary corridors, one pointing north toward Kazakhstan and one to the south toward the Indian Ocean, were speculated as to the probable flight paths. By March 24, a consensus was formed around the hypothesis that the plane had crashed on the ocean surface in the southern Indian Ocean.

An important question that arose in these circumstances is how the dispersion of the debris until the start of the search would have affected the success of the search performance. To answer this question, we have simulated the mDSMC search on the area P starting 0, 5 and 10 days after the day of the splash. Figure 7 illustrates the dynamics of ocean surface mixing and the complexity of drifted target distribution. The initially estimated splash area and its drifted image after 20 days is shown in (Fig. 7.A). The drifted target probability distribution and the accomplishment of the search started on the day of the splash, 5 and 10 days later are shown in figures 7.B, 7.C and 7.D, respectively. As time goes by, the target distribution is accumulated in certain parts of the search domain and, since it is aware of the target distribution, mDSMC control method guided agents towards parts with higher target probability. At the start of the search (Figure 7 show searches after a day of the search) trajectories are more accumulated as the later search start time.

Figure 8.A shows the daily progress of the search algorithm starting with 0-day (immediately after the splash), 5-day and 10-day delay, while Figure 8.B depicts the variations thereupon for the search operations starting 5 or 10 days later. The results, surprisingly, indicate that the chances of finding debris in a 5-day search are greater if the search is started later. The consistency of the detection rate over 100 runs indicates the robustness of the mDSMC method.

The above observation can be explained by inspecting the surface mixing in the search area. To do so, we employ the so-called hypergraph analysis introduced in [29]. The hypergraphs provide qualitative maps of finite-time motion for small objects carried by unsteady flows. Based on determinant $\det\left(\nabla \mathcal{T}^{t_1,t_2}/(t_2,t_1)\right)$ the flow domain is partitioned into two qualitative classes of behavior: mesoelliptic regions where the motion is dominated by rotation, and mesohyperbolic regions where motion is dominated by stretching in one direction and contraction in the other. The hypergraph of the area P for mixing over the 12-day interval starting at the splash day is shown in Figure 9, with hyperbolic behavior, marked in red and elliptic in blue. The key observation in [29] was that

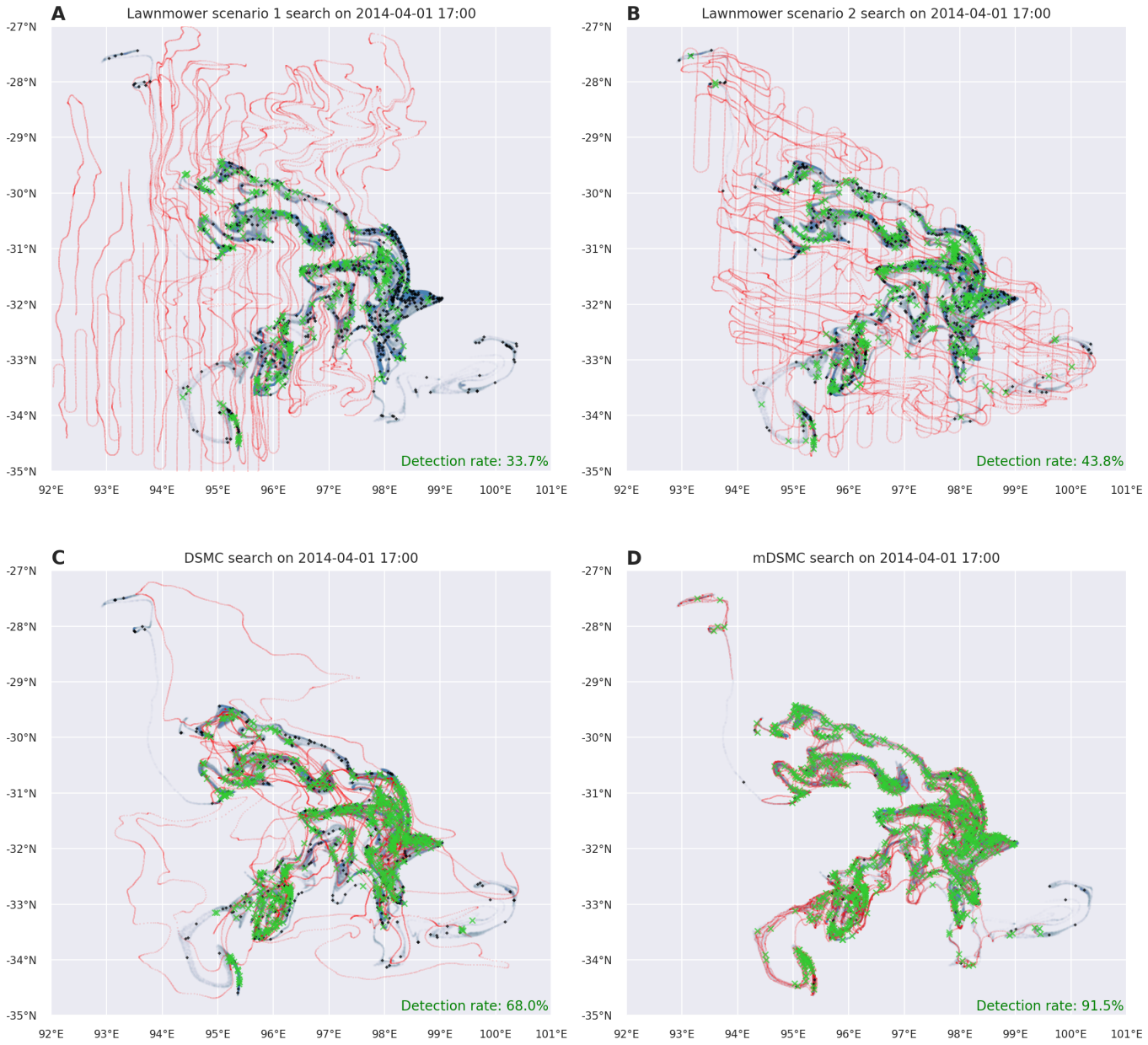

Fig. 3. Path of agents in different search scenarios for MH370: (A) The estimated splash area A at March 9 (diamond) and the drifted probability distribution of search targets on the first day of actual search (March 28). (B) The paths of search agents in the mDSMC search on the drifted image (scenario 3) (C) The lawnmower path of search agents in the reported search (scenario 1). (D). The path of search agents in lawnmower search on the drifted image (scenario 2).

hyperbolic regions reveal the convergence zones for floating objects on the surface. As shown in the figure, the majority of the search targets would accumulate around these regions over the first few days after the splash. As a result, the delayed search operations would initially encounter a higher concentration of targets in those areas and therefore yield higher success rates at the beginning.

VII. Conclusion

The mDSMC algorithm is shown to be a viable and efficient algorithm for real-time planning of search operations in a dynamic and large environment such as ocean surface. This algorithm is based on a feasible formulation of the classic optimal search theory and is capable of addressing complex geometries with large uncertainty that arise in complex and unsteady environmental dynamics. Important features of mDSMC are the awareness of search agents of the large-scale spatial structure of the target area, the continuous balance of search load between agents and the ability to concentrate the search on most feasible areas. mDSMC brings an improvement over DSMC in local search, where high- detailed structures of the probability distribution are explored. The application of this algorithm to the MH370 case showed that these features lead to a several-fold improvement in the success rate of the search compared to the conventional lawnmower method. This suggests that using this algorithm could lead to a

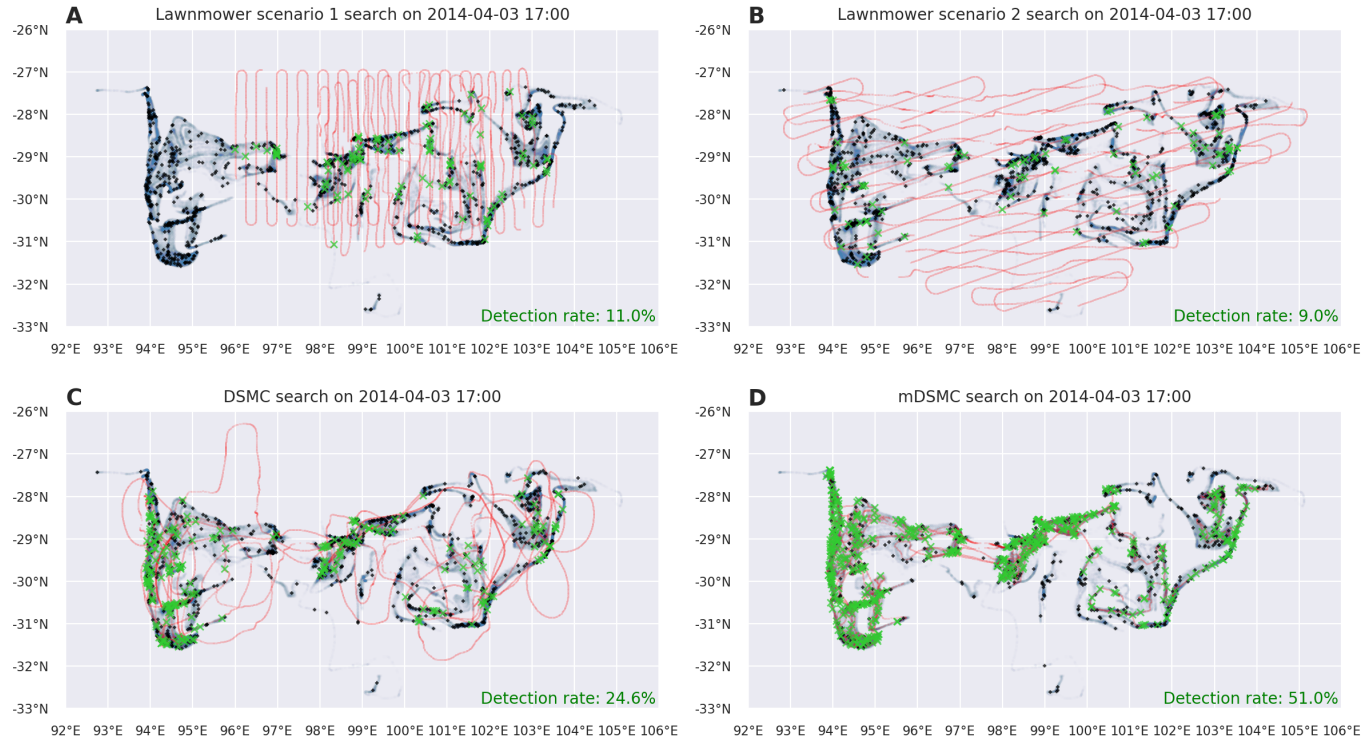

Fig. 4. Path of agents in different search scenarios for MH370: (A) The estimated splash area B at March 9 (diamond) and the drifted probability distribution of search targets on the first day of actual search (April 2). (B) The paths of search agents in the mDSMC search on the drifted image (scenario 3) (C) The lawnmower path of search agents in the reported search (scenario 1). (D). The path of search agents in lawnmower search on the drifted image (scenario 2).

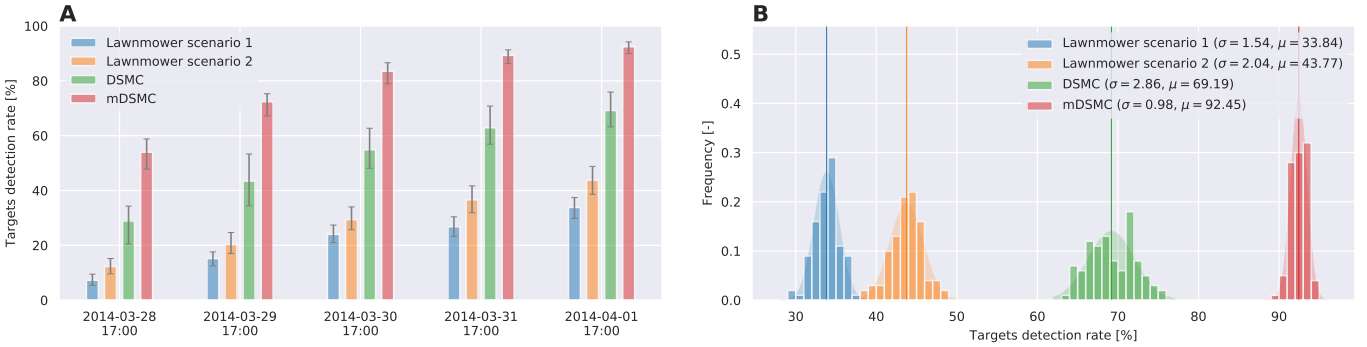

Fig. 5. Success rate of search scenarios for MH370: (A) The progress of the search scenarios vs time for drifting area A. The target detection only moves upward in the time interval of 14:00-17:00 on each day. This constraint is posed by the fact that the search area is about 700 km away from the operation base. (B) Histogram of the success rate for search scenarios in 100 realizations of each scenario with random initial conditions.

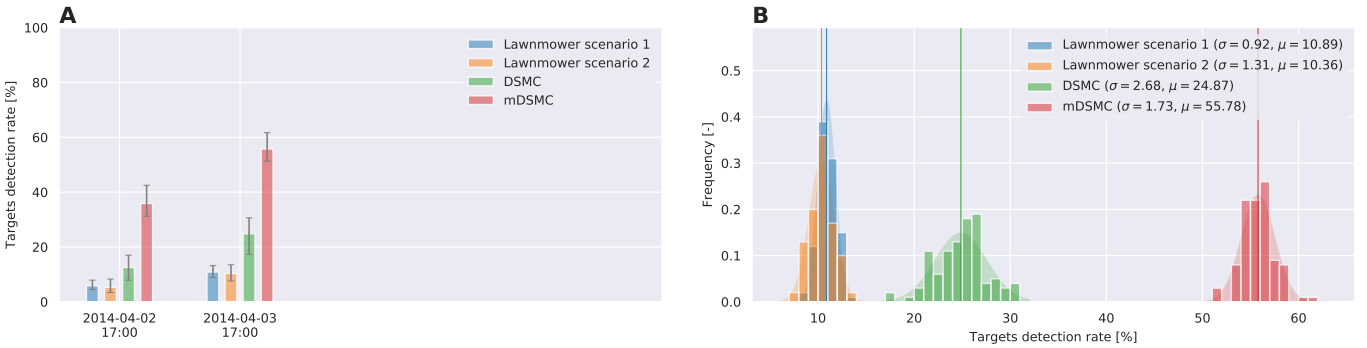

Fig. 6. Success rate of search scenarios for MH370: (A) The progress of the search scenarios vs time for drifting area B. The target detection only moves upward in the time interval of 14:00-17:00 on each day. This constraint is posed by the fact that the search area is about 2700 km away from the operation base. (B) Histogram of the success rate for search scenarios in 100 realizations of each scenario with random initial conditions.

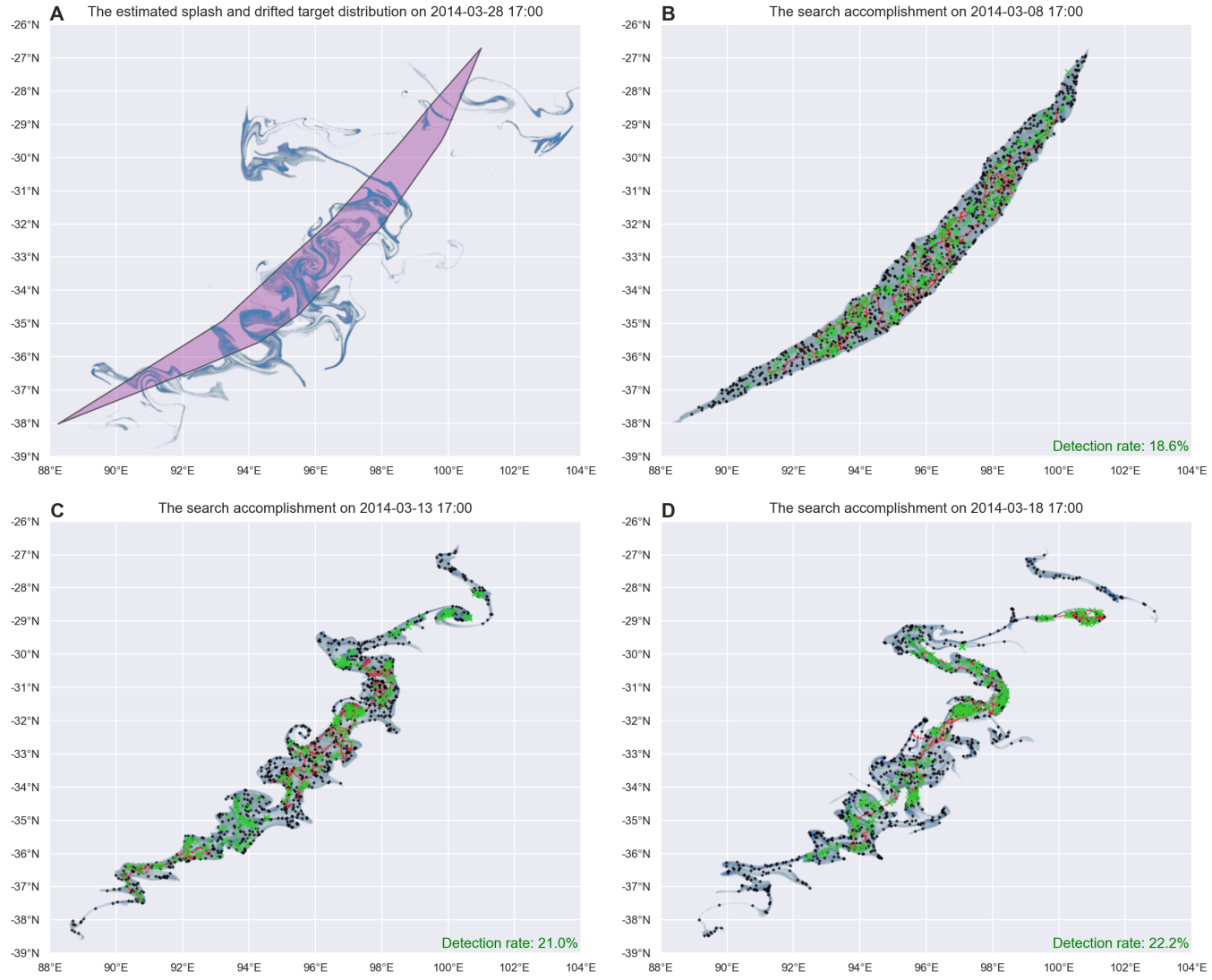

Fig. 7. (A) The estimated splash area P (purple region) and the drifted area P for March 28. (B, C, D) show drifted target distribution, the agent paths and target detection at the end of the first search days as a result of search simulation starting on the day of the splash, 5 and 10 days after, respectively.

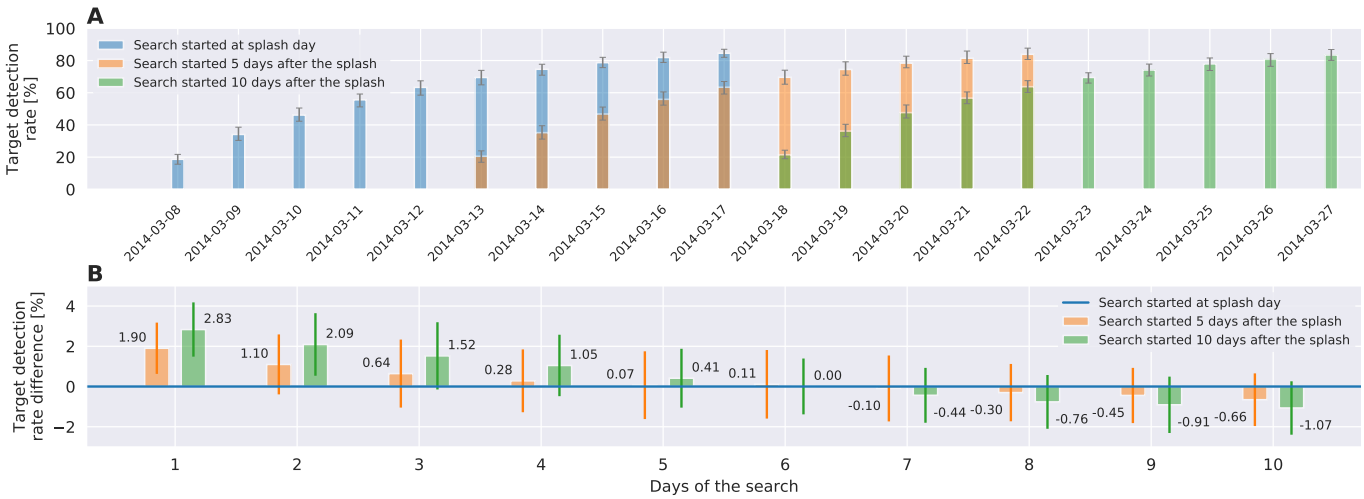

Fig. 8. Effect of delayed search on the success rate of mDSMC algorithm: (A) The progress of the mDSMC search algorithm on area P. (B) Variations in the success rate of daily search due to a 5-day or 10-day delay in the commencement of search.

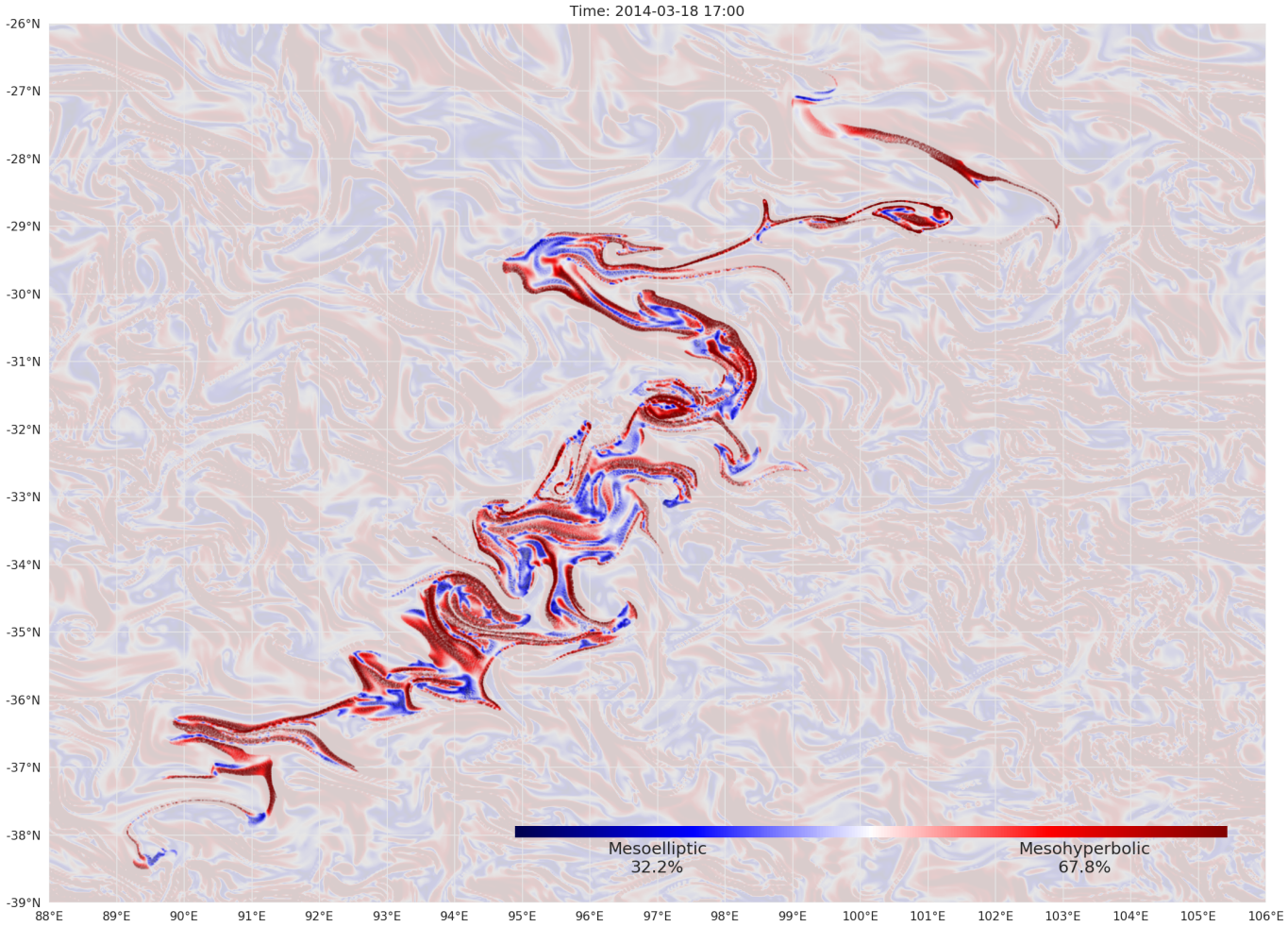

Fig. 9. Finite-time mixing analysis of the search area: The colors depict the finite-time Lagrangian behavior in the drifted area A. Dominant rotational behavior is marked in blue and stretching behavior in red. The search targets accumulate around red ridges which reduces the effective size of the search area.

critical improvement in the survivor rescue operations and/or finding critical evidence in similar incidents. The mDSMC algorithm can also be employed in other forms of operations that involve mobile agents (planes, drones, land patrols, etc.) and moving targets (individuals, animals, debris, black box, etc.). Examples of such operations include geographical and zoological surveys, underwater sonar mapping and search, the rescue of/from wildlife, contamination removal and spill containment in natural reserves and oceans.

A surprising conclusion of our study was that delaying the search operation in dynamic environments can lead to higher success rates in finding the debris in the initial stages of the search. In the case of MH370, this is caused by the convergence zones within the initial uncertainty distribution. Over the first few days, these zones attract and accumulate the target probability density on the surface. A search operation at the right time can exploit this accumulation of density and lead to a higher success rate given the same amount of coverage. The convergence property is typical of a dynamic environment that shows regular patterns for the accumulation of targets (e.g. shrinkage of area, or existence of attracting regions), and it can be exploited in other problems to increase the efficiency of search and sampling in terms of search time and the number of agents.

ACKNOWLEDGEMENTS

The authors are grateful to Pat Hogan and Ole Martin Smedstad for providing the Global Ocean Prediction data for the drift model. Funding: B.C.'s research is fully supported by the Croatian Science Foundation under the project IP-2019-04-1239. S. I.'s contribution is supported by the University of Rijeka under the project number 17.10.2.1.04. I.M's research is supported by ARO-MURI grant W911NF-17-1-0306. Author Contribution: I.M. conceived the idea for the article. S.L. and P.C. verified the data sets and prototyped the search algorithm. S.I. and B.C. proposed the modifications to the search algorithms and simulated the experiments. H.A. collected the search parameters, formulated the search problem, and wrote the initial manuscript.

VIDEO CAPTIONS

Video 1: Simulation of area A search
Video 2: Simulation of area B search

REFERENCES

[1] Ebtehal Turki Alotaibi, Shahad Saleh Alqefari, and Anis Koubaa. Lsar: Multi-uav collaboration for search and rescue missions. *IEEE Access*, 7:55817–55832, 2019.

[2] Chris Ashton, Alan Shuster Bruce, Gary Colledge, and Mark Dickinson. The search for mh370. *The Journal of Navigation*, 68(1):1–22, 2015.

[3] Alper Aydemir, Andrzej Pronobis, Moritz Göbelbecker, and Patric Jensfelt. Active visual object search in unknown environments using uncertain semantics. *IEEE Transactions on Robotics*, 29(4):986–1002, 2013.

[4] Australian Transport Safety Bureau. The operational search for MH370. *Canberra, Australian Capital Territory, Commonwealth of Australia, Tech. Rep. AE-2014-054*, 2017.

[5] Sam Davey, Neil Gordon, Ian Holland, Mark Rutten, and Jason Williams. *Bayesian Methods in the Search for MH370*. Springer Singapore, 2016.

[6] Yi-Chen Du, Min-Xia Zhang, Hai-Feng Ling, and Yu-Jun Zheng. Evolutionary planning of multi-uav search for missing tourists. *IEEE Access*, 7:73480–73492, 2019.

[7] VJ García-Garrido, AM Mancho, S Wiggins, and C Mendoza. A dynamical systems approach to the surface search for debris associated with the disappearance of flight mh370. *Nonlin. Processes Geophys*, 22:701–712, 2015.

[8] German Gramajo and Praveen Shankar. An efficient energy constraint based uav path planning for search and coverage. *International Journal of Aerospace Engineering*, 2017, 2017.

[9] Xiaoxuan Hu, Yanhong Liu, and Guoqiang Wang. Optimal search for moving targets with sensing capabilities using multiple uavs. *Journal of Systems Engineering and Electronics*, 28(3):526–535, 2017.

[10] Huan Huang, Daqi Zhu, and Feng Ding. Dynamic task assignment and path planning for multi-auv system in variable ocean current environment. *Journal of intelligent & robotic systems*, 74(3-4):999–1012, 2014.

[11] Stefan Ivić. Motion control for autonomous heterogeneous multi-agent area search in uncertain conditions. *arXiv preprint arXiv:1911.09137*, 2019.

[12] Stefan Ivić, Bojan Crnković, and Igor Mezić. Ergodicity-based cooperative multiagent area coverage via a potential field. *IEEE transactions on cybernetics*, 47(8):1983, 2017.

[13] Eric Jansen, Giovanni Coppini, and Nadia Pinardi. Drift simulation of mh370 debris using superensemble techniques. *Natural Hazards and Earth System Sciences*, 16(7):1623–1628, 2016.

[14] Derek Kingston, Steven Rasmussen, and Laura Humphrey. Automated uav tasks for search and surveillance. In *2016 IEEE Conference on Control Applications (CCA)*, pages 1–8. IEEE, 2016.

[15] Bernard O Koopman. The theory of search. ii. target detection. *Operations research*, 4(5):503–531, 1956.

[16] Bernard O Koopman. The theory of search: Iii. the optimum distribution of searching effort. *Operations research*, 5(5):613–626, 1957.

[17] Bernard Osgood Koopman. Search and screening. *OEG Rep.*, 1946.

[18] Shriyanti Kulkarni, Vedashree Chaphekar, Md Moin Uddin Chowdhury, Fatih Erden, and Ismail Guvenc. Uav aided search and rescue operation using reinforcement learning. *arXiv preprint arXiv:2002.08415*, 2020.

[19] Frederik S Leira, Tor Arne Johansen, and Thor I Fossen. Automatic detection, classification and tracking of objects in the ocean surface from uavs using a thermal camera. In *2015 IEEE aerospace conference*, pages 1–10. IEEE, 2015.

[20] Pei Li and Haibin Duan. A potential game approach to multiple uav cooperative search and surveillance. *Aerospace Science and Technology*, 68:403–415, 2017.

[21] Lanny Lin and Michael A Goodrich. Hierarchical heuristic search using a gaussian mixture model for uav coverage planning. *IEEE Transactions on Cybernetics*, 44(12):2532–2544, 2014.

[22] Jason R Marden, Gürdal Arslan, and Jeff S Shamma. Cooperative control and potential games. *IEEE Transactions on Systems, Man, and Cybernetics, Part B (Cybernetics)*, 39(6):1393–1407, 2009.

[23] George Mathew, Suresh Kannan, Amit Surana, Sanjay Bajekal, and Konda R Chevva. Experimental implementation of spectral multiscale coverage and search algorithms for autonomous uavs. In *AIAA Guidance, Navigation, and Control (GNC) Conference*, page 5182, 2013.

[24] George Mathew and Igor Mezić. Metrics for ergodicity and design of ergodic dynamics for multi-agent systems. *Physica D: Nonlinear Phenomena*, 240(4-5):432–442, 2011.

[25] George Mathew, Amit Surana, and Igor Mezić. Uniform coverage control of mobile sensor networks for dynamic target detection. In *49th IEEE Conference on Decision and Control (CDC)*, pages 7292–7299. IEEE, 2010.

[26] Anastasia Mavrommati, Emmanouil Tzorakoleftherakis, Ian Abraham, and Todd D Murphey. Real-time area coverage and target localization using receding-horizon ergodic exploration. *IEEE Transactions on Robotics*, 34(1):62–80, 2017.

[27] Marcia McNutt. The hunt for mh370. *Science*, 344(6187):947–947, 2014.

[28] Wei Meng, Zhirong He, Rong Su, Pradeep K Yadav, Rodney Teo, and Lihua Xie. Decentralized multi-uav flight autonomy for moving convoys search and track. *IEEE Transactions on Control Systems Technology*, 25(4):1480–1487, 2016.

[29] Igor Mezić, S Loire, Vladimir A Fonoberov, and P Hogan. A new mixing diagnostic and gulf oil spill movement. *Science*, 330(6003):486–489, 2010.

[30] Lauren M Miller, Yonatan Silverman, Malcolm A MacIver, and Todd D Murphey. Ergodic exploration of distributed information. *IEEE Transactions on Robotics*, 32(1):36–52, 2015.

[31] Oleksandr Nesterov. Consideration of various aspects in a drift study of mh370 debris. *Ocean Science*, 14(3), 2018.

[32] Jianjun Ni, Guangyi Tang, Zhengpei Mo, Weidong Cao, and Simon X Yang. An improved potential game theory based method for multi-uav cooperative search. *IEEE Access*, 2020.

[33] Sara Perez-Carabaza, Eva Besada-Portas, Jose A Lopez-Orozco, and M Jesus. Ant colony optimization for multi-uav minimum time search in uncertain domains. *Applied Soft Computing*, 62:789–806, 2018.

[34] Sara Pérez-Carabaza, Eva Besada-Portas, José Antonio Lopez-Orozco, and Gonzalo Pajares. Minimum time search in real-world scenarios using multiple uavs with onboard orientable cameras. *Journal of Sensors*, 2019, 2019.

[35] Chang-jian Ru, Xiao-ming Qi, and Xu-ning Guan. Distributed cooperative search control method of multiple uavs for moving target. *International Journal of Aerospace Engineering*, 2015, 2015.

[36] Juan Carlos Rubio, Juris Vagners, and Rolf Rysdyk. Adaptive path planning for autonomous uav oceanic search missions. In *AIAA 1st Intelligent Systems Technical Conference*, page 6228, 2004.

[37] Lawrence D Stone. *Theory of optimal search*, volume 118. Elsevier, 1976.

[38] Lawrence D Stone, Johannes O Royset, and Alan R Washburn. Search for moving targets in continuous space. In *Optimal Search for Moving Targets*, pages 121–153. Springer, 2016.

[39] PB Sujit, Joao Sousa, and FL Pereira. Coordination strategies between uav and auvs for ocean exploration. In *2009 European Control Conference (ECC)*, pages 115–120. IEEE, 2009.

[40] Joaquin A Trinanes, M Josefina Olascoaga, Gustavo J Goni, Nikolai A Maximenko, David A Griffin, and Jan Hafner. Analysis of flight mh370 potential debris trajectories using ocean observations and numerical model results. *Journal of Operational Oceanography*, 9(2):126–138, 2016.

[41] Yubing Wang, Peng Bai, Xiaolong Liang, Weijia Wang, Jiaqiang Zhang, and Qixi Fu. Reconnaissance mission conducted by uav swarms based on distributed pso path planning algorithms. *IEEE Access*, 7:105086–105099, 2019.

[42] Peng Yao, Honglun Wang, and Hongxia Ji. Gaussian mixture model and receding horizon control for multiple uav search in complex environment. *Nonlinear Dynamics*, 88(2):903–919, 2017.

[43] Peng Yao, Zexiao Xie, and Ping Ren. Optimal uav route planning for coverage search of stationary target in river. *IEEE Transactions on Control Systems Technology*, 27(2):822–829, 2017.

[44] Joses Yau and Timothy H Chung. Search-theoretic and ocean models for localizing drifting objects. In *2012 IEEE/RSJ International Conference on Intelligent Robots and Systems*, pages 4749–4755. IEEE, 2012.

[45] Chao Yin, Zhenyu Xiao, Xianbin Cao, Xing Xi, Peng Yang, and Dapeng Wu. Offline and online search: Uav multiobjective path planning under dynamic urban environment. *IEEE Internet of Things Journal*, 5(2):546–558, 2017.

[46] Wei Yue, Xianhe Guan, and Liyuan Wang. A novel searching method using reinforcement learning scheme for multi-uavs in unknown environments. *Applied Sciences*, 9(22):4964, 2019.

[47] Wei Yue, Yun Xi, and Xianhe Guan. A new searching approach using improved multi-ant colony scheme for multi-uavs in unknown environments. *IEEE Access*, 7:161094–161102, 2019.

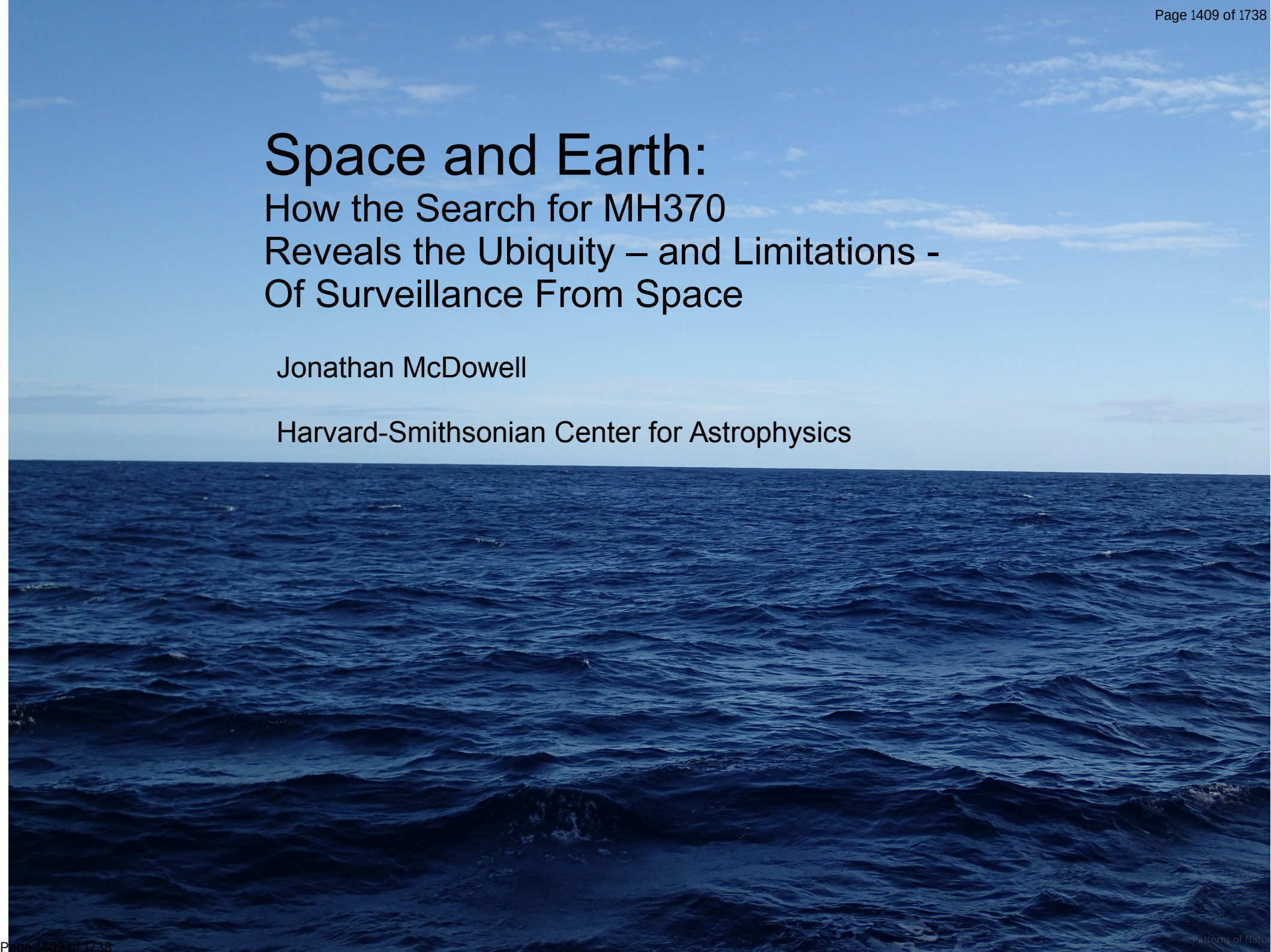

Space and Earth:
How the Search for MH370 Reveals the Ubiquity – and Limitations - Of Surveillance From Space

Jonathan McDowell

Harvard-Smithsonian Center for Astrophysics

Part 1: MH370 goes missing - and INMARSAT finds a clue

Ocean pic credit:
patternsofnatureblog.com B.Ellis

2014 Mar 7: Boeing 777-200ER aircraft, flight MH370 from KUL (Kuala Lumpur, Malaysia) to PEK (Beijing) loses contact at 1719 UTC, 40 min into a 6 hr flight

The plane, with 239 people aboard, has not been seen since

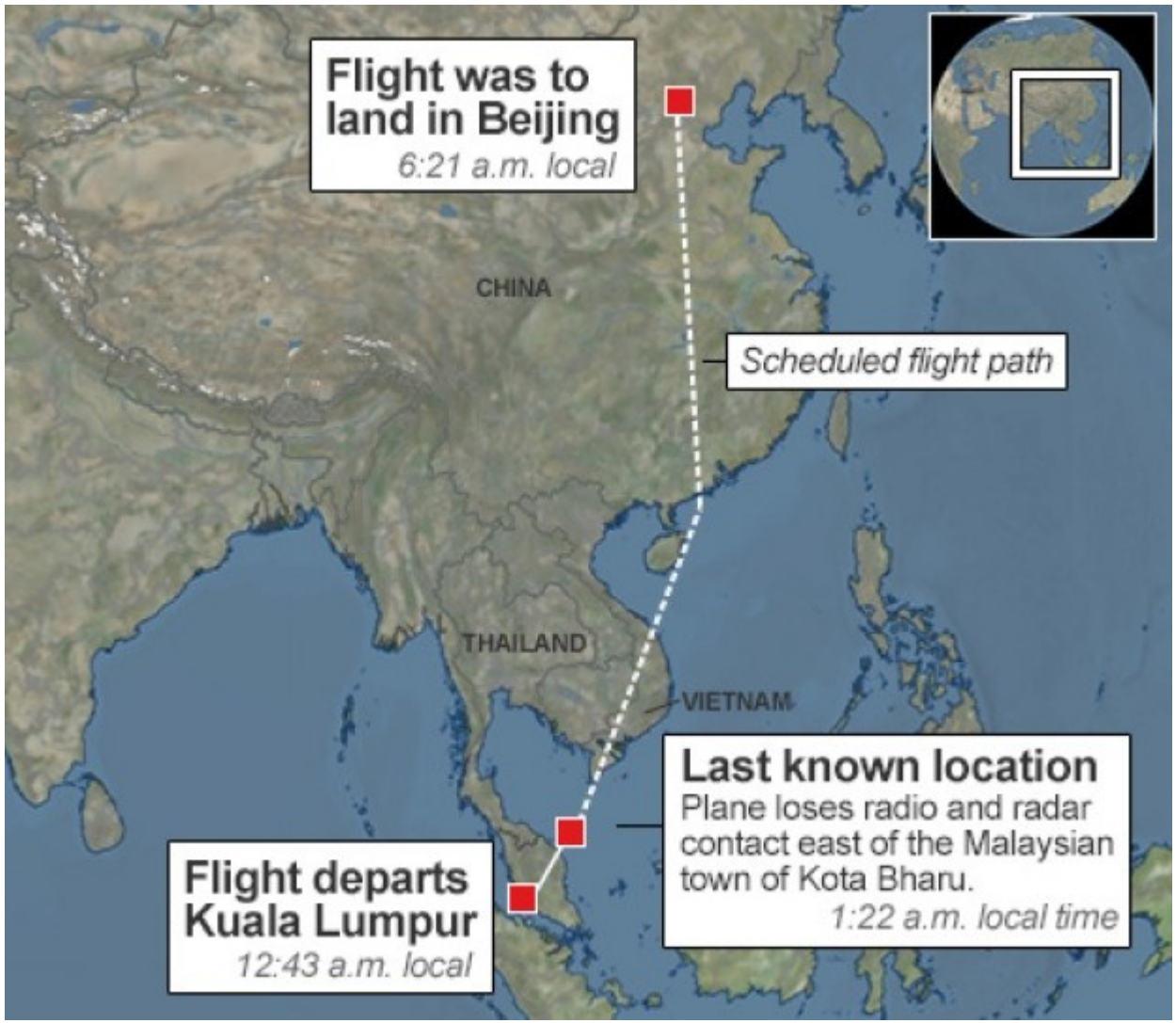

Credit: Canadian Broadcasting Corp

AHeenen via Wikipedia

No radio contact
Nothing on radar
A complete mystery

… then came a surprising breakthrough

Communications satellites!

Hackney, London: (1 km N of St Paul's Cathedral)
INMARSAT headquarters

INMARSAT was the International Maritime Satellite Organization
until it was privatized in 1999

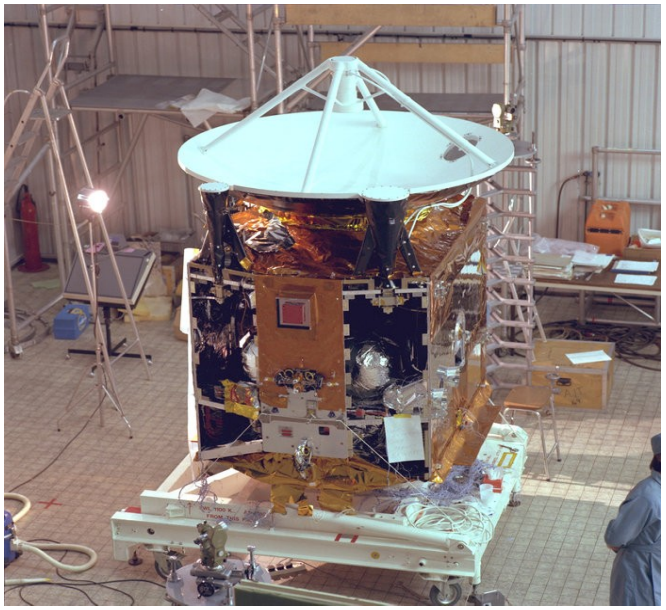

MARECS A under assembly in Stevenage, UK in 1981 – first maritime comms satellite for INMARSAT

US-built INMARSAT 3 F1 satellite
L-band communications payload (MMS-UK)
Launched from Cape Canaveral, Apr 1996
Stationed over Indian Ocean at 64 E, May 1996

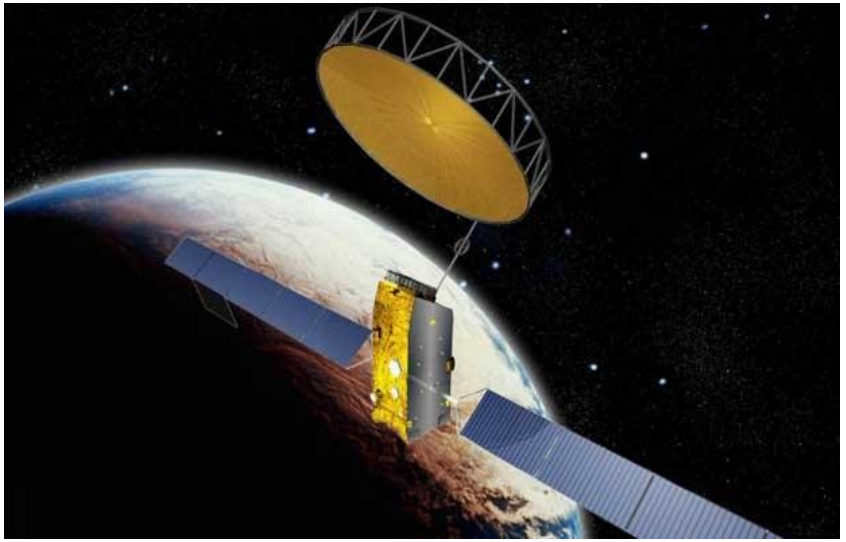

Newer generation INMARSAT-4 satellite
4 in orbit 2005-2013

Inmarsat hosts Rockwell Collins ARINC system “ACARS”
Aircraft Communications Addressing and Reporting System

The discussion that follows reports the work of the INMARSAT investigation team:

Chris Ashton, Alan Shuster Bruce, Gary Colledge, Mark Dickinson
The Search for MH370
Journal of Navigation, 2014
doi:10.1017/S037346331400068X

supplemented by the work of the Australian Transport Safety Bureau (ATSB)
MH370 – Flight Path Analysis Update
ATSB Transport Safety Report, AE-2014-054, 8 Oct 2014

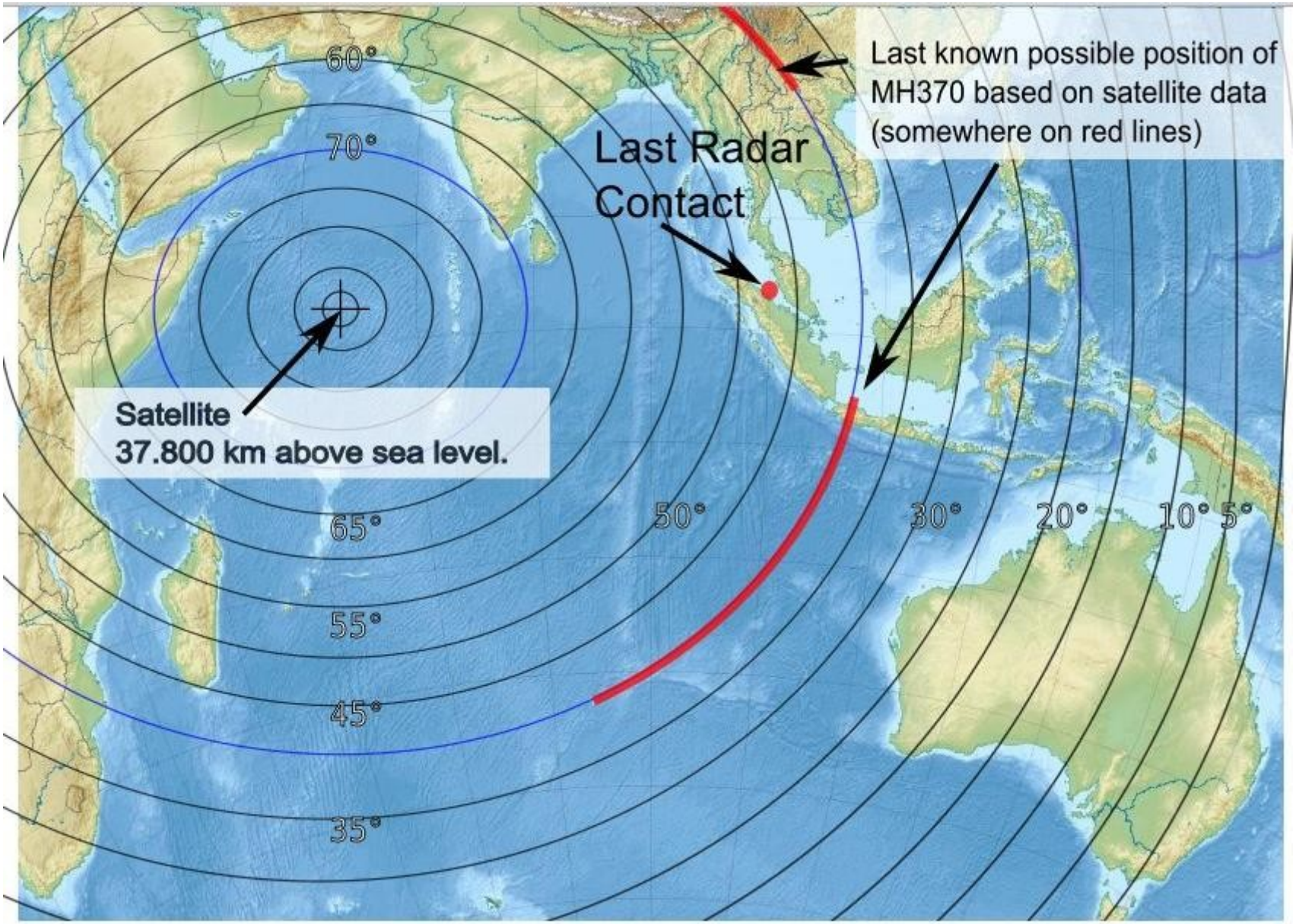

ACARS “switched off” by crew (or failed off?) but system stayed logged on to satellite – hourly 'pings' give the round trip travel time satellite-aircraft-satellite

Time	Channel Name	Ocean Region	GES ID (octal)	Channel Unit ID	Channel Type	SU Type	Burst Frequency Offset (Hz) BFO	Burst Timing Offset (microseconds) BTO
.....								
48 C-Channel and 1 P-Channel messages moved into separate below table (see appendix 2) to ease the reading of key events. C-Channel messages have no BTO values								
.....								
7/03/2014 23:15:02.032	IOR-3737-21000	IOR	305	6	C-Channel RX	0x30 - Call Progress - Channel Release	219	
00:10:58 - Handshake Request, with response								
8/03/2014 00:10:58.000	IOR-P10500-0-386B	IOR	305	10	P-Channel TX	0x14 - Log Control - Log-on Interrogation		
8/03/2014 00:10:59.928	IOR-R1200-0-36ED	IOR	305	4	R-Channel RX	0x15 - Log-on/Log-off Acknowledge	252	18040
00:19:29 - Log-On Request (reported as a Partial Handshake), initiated from the aircraft terminal								
8/03/2014 00:19:29.416	IOR-R600-0-36F8	IOR	305	10	R-Channel RX	0x10 - Log-on Request (ISU)/Log-on Flight Information (SSU)	182	23000
8/03/2014 00:19:31.572	IOR-P600-0-36FC	IOR	305	10	P-Channel TX	0x11 - Log-on Confirm		
8/03/2014 00:19:32.212	IOR-P600-0-36FC	IOR	305	10	P-Channel TX	0x40 - P-/R-Channel Control (ISU)		
8/03/2014 00:19:32.212	IOR-P600-0-36FC	IOR	305	10	P-Channel TX	Subsequent Signalling Unit		
8/03/2014 00:19:32.852	IOR-P600-0-36FC	IOR	305	10	P-Channel TX	0x41 - T-Channel Control (ISU)		
8/03/2014 00:19:32.852	IOR-P600-0-36FC	IOR	305	10	P-Channel TX	Subsequent Signalling Unit		
00:19:37 - Note that the following R-Channel burst at 00:19:37.443 is the last transmission received from the aircraft terminal								
8/03/2014 00:19:37.443	IOR-R1200-0-36F6	IOR	305	10	R-Channel RX	0x15 - Log-on/Log-off Acknowledge	-2	49660
8/03/2014 00:19:38.407	IOR-P10500-0-386B	IOR	305	10	P-Channel TX	0x15 - Log-on/Log-off Acknowledge		
01:15:56 – Handshake Request - No Response from Aircraft Terminal								
8/03/2014 01:15:56.000	IOR-P10500-0-386B	IOR	305	10	P-Channel TX	0x14 - Log Control - Log-on Interrogation		
01:16:06 - Handshake Request - No Response from Aircraft Terminal								
8/03/2014 01:16:06.000	IOR-P10500-0-386B	IOR	305	10	P-Channel TX	0x14 - Log Control - Log-on Interrogation		
01:16:15 - Handshake Request - No Response from Aircraft Terminal								
8/03/2014 01:16:15.000	IOR-P10500-0-386B	IOR	305	10	P-Channel TX	0x14 - Log Control - Log-on Interrogation		

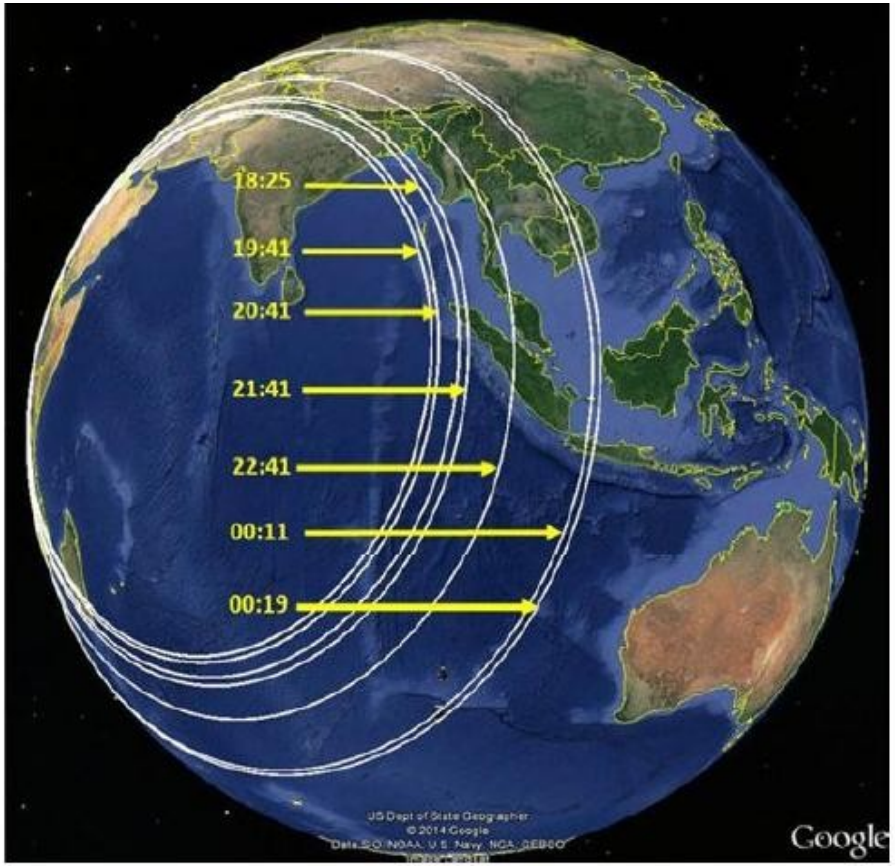

ATSB

Each 'ping' between aircraft and satellite gives a distance to the aircraft corresponding to a ring on the Earth's surface centered on the subsatellite point in the Indian Ocean

The investigative team modelled the motion of the aircraft at constant speed, constant heading with the constraint of intersecting these rings at given times. Lack of angular data and symmetry of problem → 2 solutions

Example Southern Tracks

(tracks ends at 00:11 UTC)

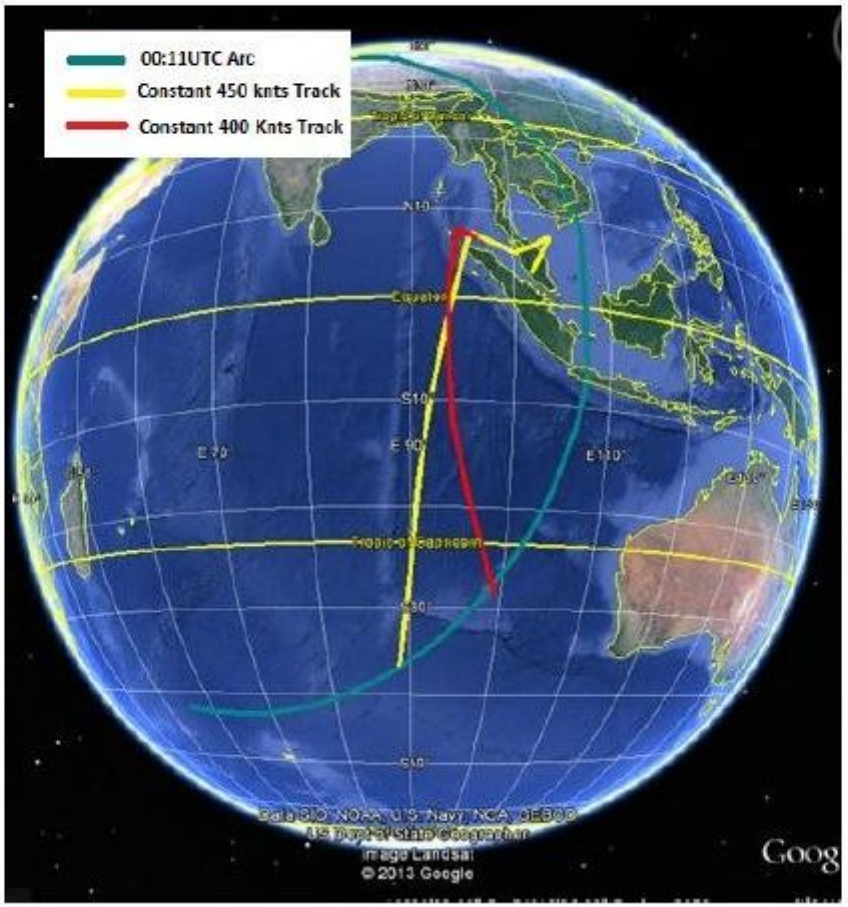

3

Complications:

- calibration errors
- altitude changes by plane
- exact time of turn south
- movement of satellite
- modelling of maximum range cruise (MRC): how far the A/C gets before fuel runs out

Source: INMARSAT

Data: range and range rate versus time
Model: Moving on great circle at constant speed v on heading theta
Fit data to model assuming a given value of v, get theta and final position
Figure shows v = 400 knots (red) and v = 450 knots (yellow)

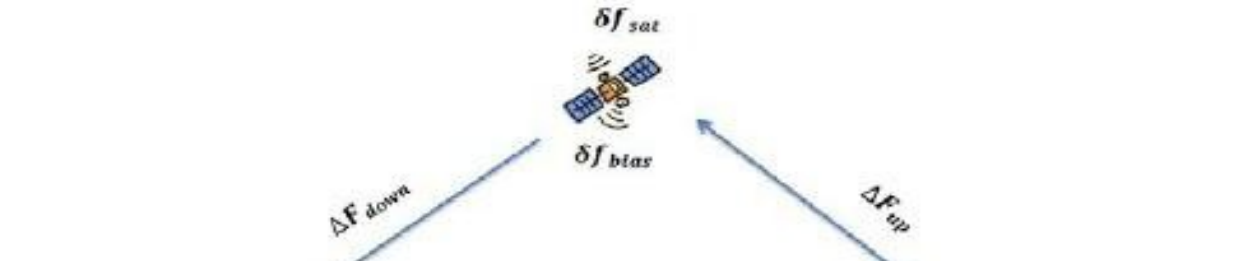

$$BFO = \Delta F_{up} + \Delta F_{down} + \delta f_{comp} + \delta f_{sat} + \delta f_{AFC} + \delta f_{bias}$$

ΔF_{up}	*Doppler on the signal passing from the aircraft to the satellite*
ΔF_{down}	*Doppler on the signal passing from the satellite to the ground station*
δf_{comp}	*Frequency compensation applied by the aircraft, assuming level flight and a fixed satellite location*
δf_{sat}	*Variation in satellite translation frequency*
δf_{AFC}	*Frequency compensation applied by the ground station receive chain*
δf_{bias}	*Fixed offset due to errors in the aircraft and satellite oscillators*

BTO Burst Timing Offset – records difference in expected and actual signal round trip time satellite-aircraft-satellite
Gives satellite-aircraft range

Source: SATCOM Working Group, INMARSAT

BFO Burst Frequency Offset
Compares received frequency to expected frequency after Doppler and electronics corrections (error ~ 7 Hz ~ 5kph)
Gives satellite-aircraft radial velocity

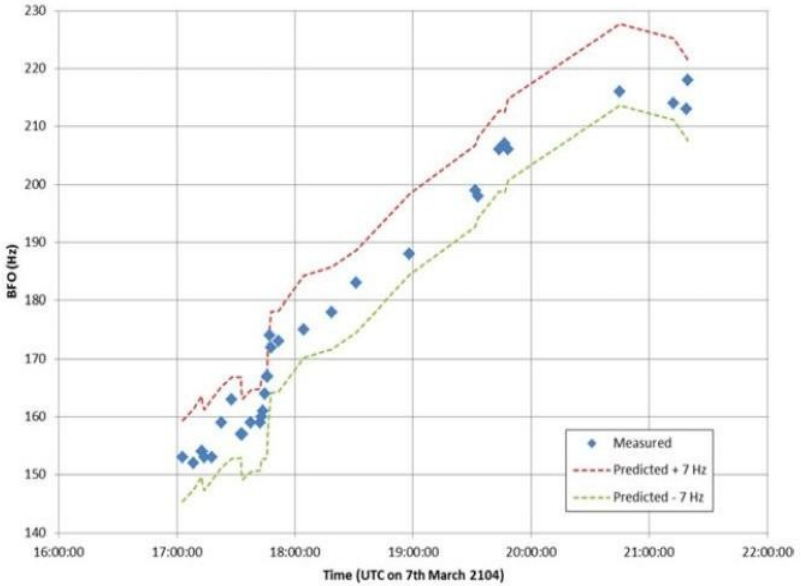

Figure 15. Burst Frequency Offset Validation (Amsterdam Flight).

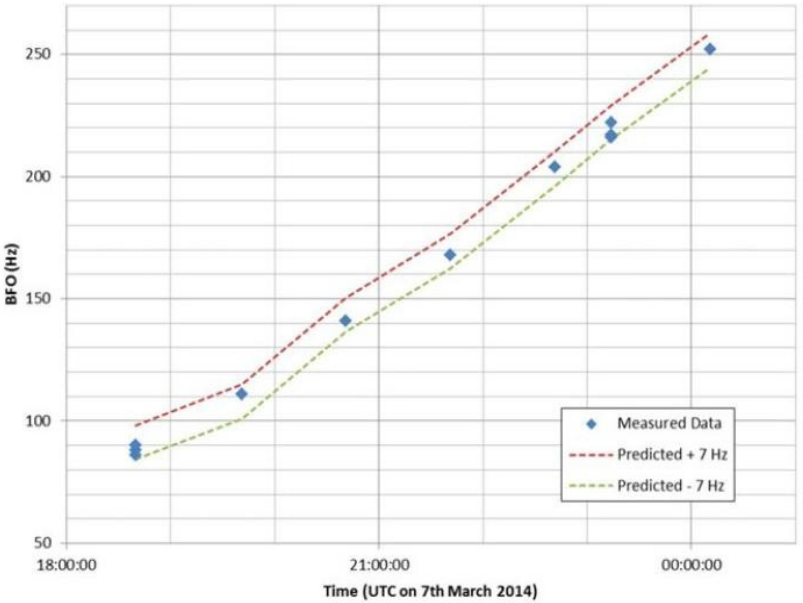

Figure 16. BFO Results for Example Flight Path.

Predicted Doppler versus time for known flight path
MH21 Kuala Lumpur-Amsterdam same day as MH370

Example model ground track for MH370, +/- 7Hz errors, compared to MH370 data points- for later part of flight

MH370 measured data against predicted tracks

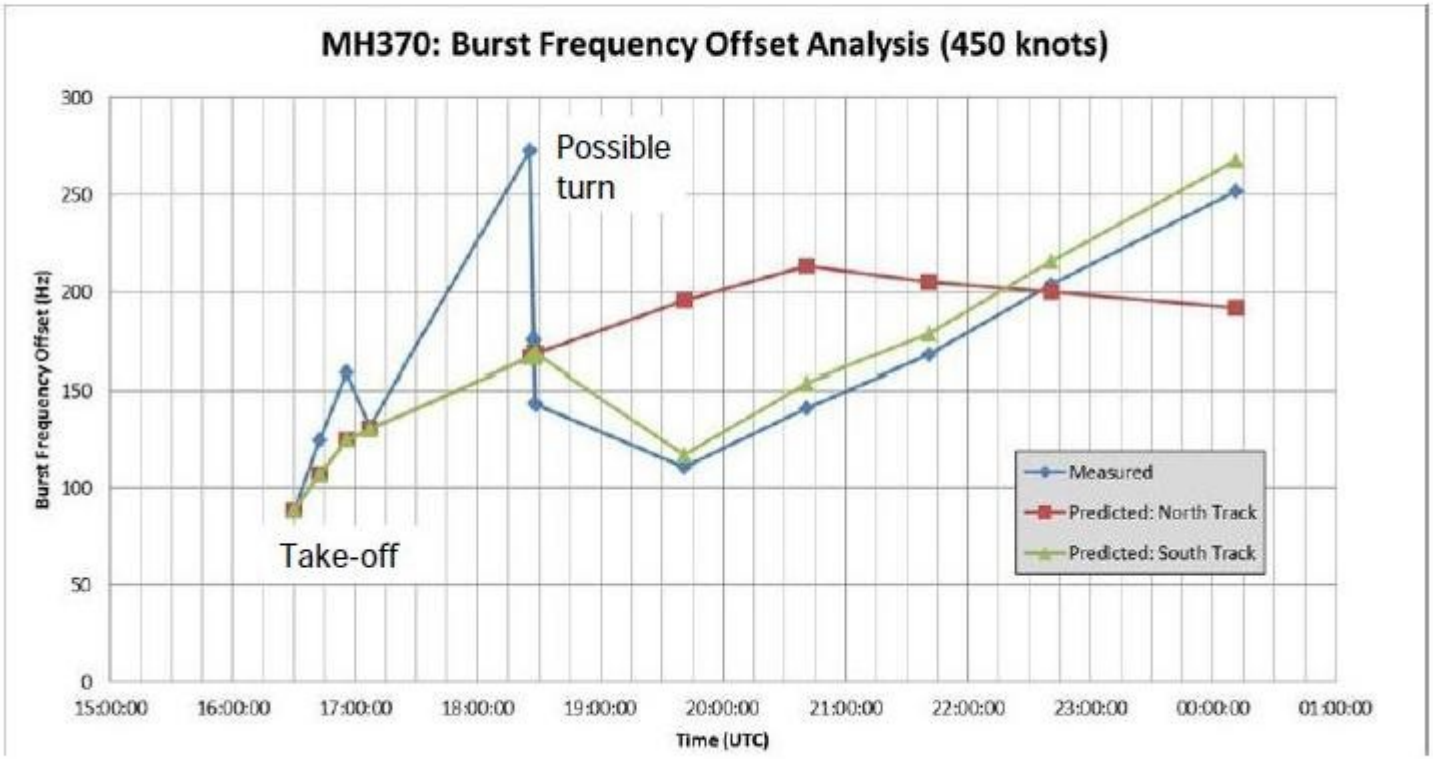

2

Source: INMARSAT - as released in spring 2014

Blue points are the actual data (Doppler shift in Hz of MH370 rel to sat)
Includes earlier times than previous plot
Green points are the fit using v=450 knots
(Get two solutions for each v, a northern and southern one;
southern one clearly fits better)

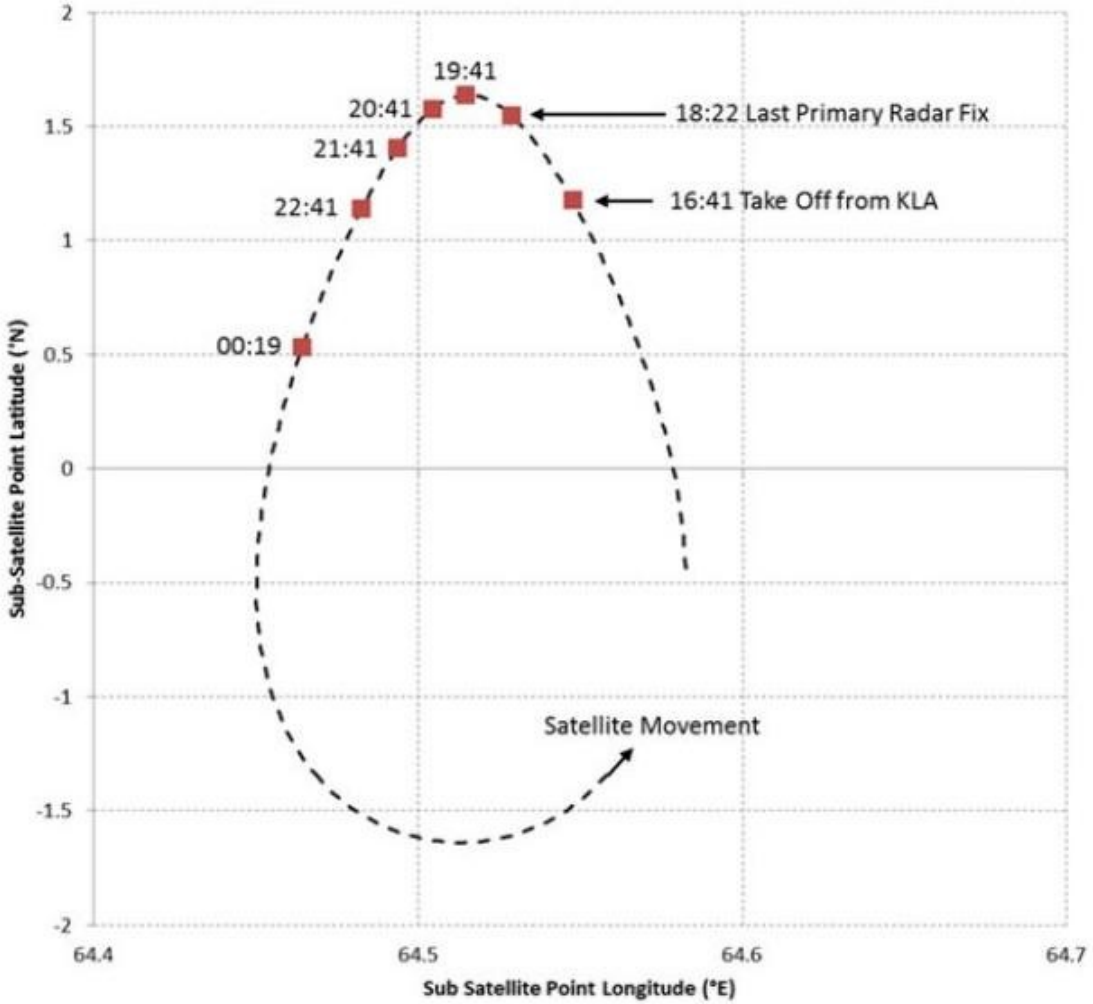

Satellite moves +/- 1.5 deg N/S of equator (Ashton et al 2014)
This must be taken into account

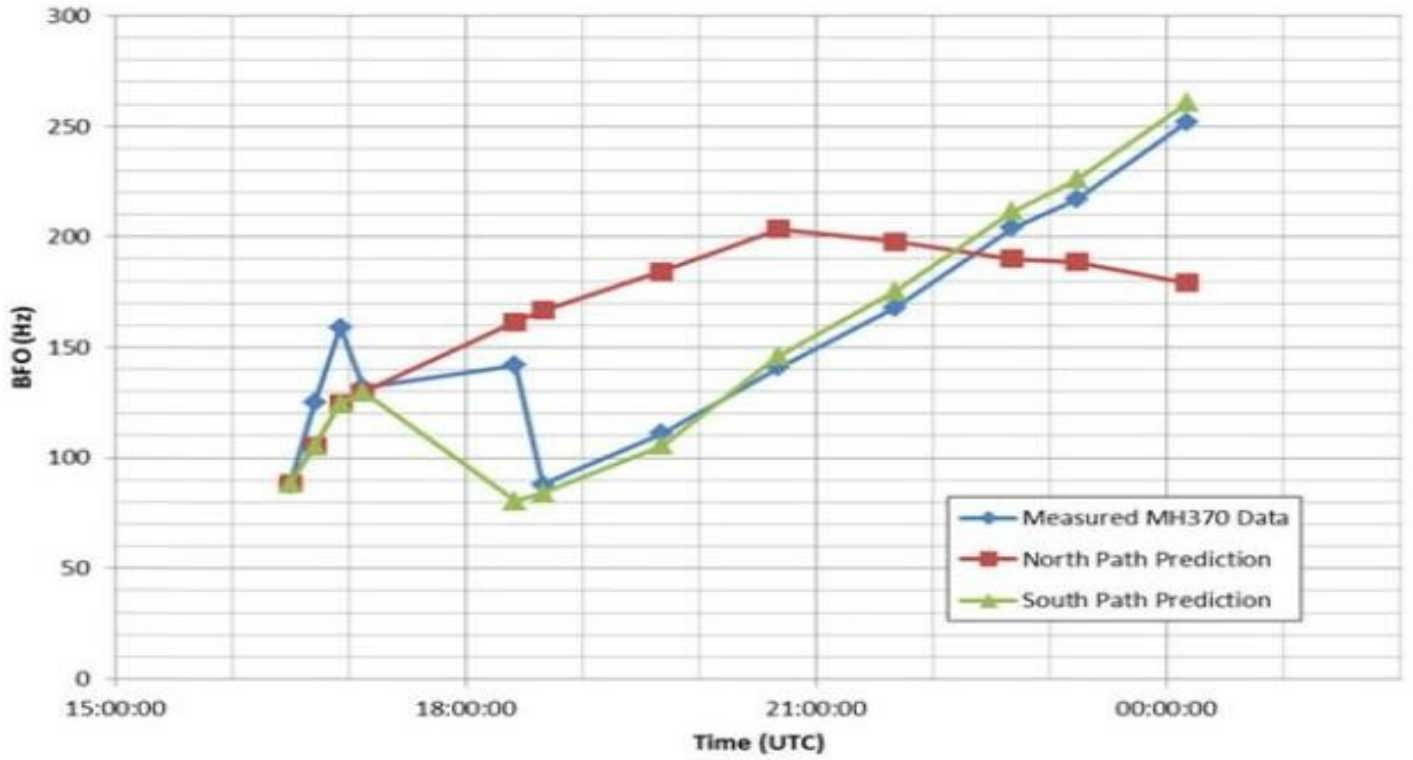

Figure 14. BFO Results using Refined Model.

Source: INMARSAT - as updated in paper, fall 2014
- better satellite motion model, correction for satellite eclipse thermal effects, improved calibration of ground station electronics

Blue points are the actual data (Doppler shift in Hz of MH370 rel to sat)
Green points are the fit using v=450 knots
(Get two solutions for each v, a northern and southern one;
southern one clearly fits better)

Sensitivity of final location to assumed aircraft altitude

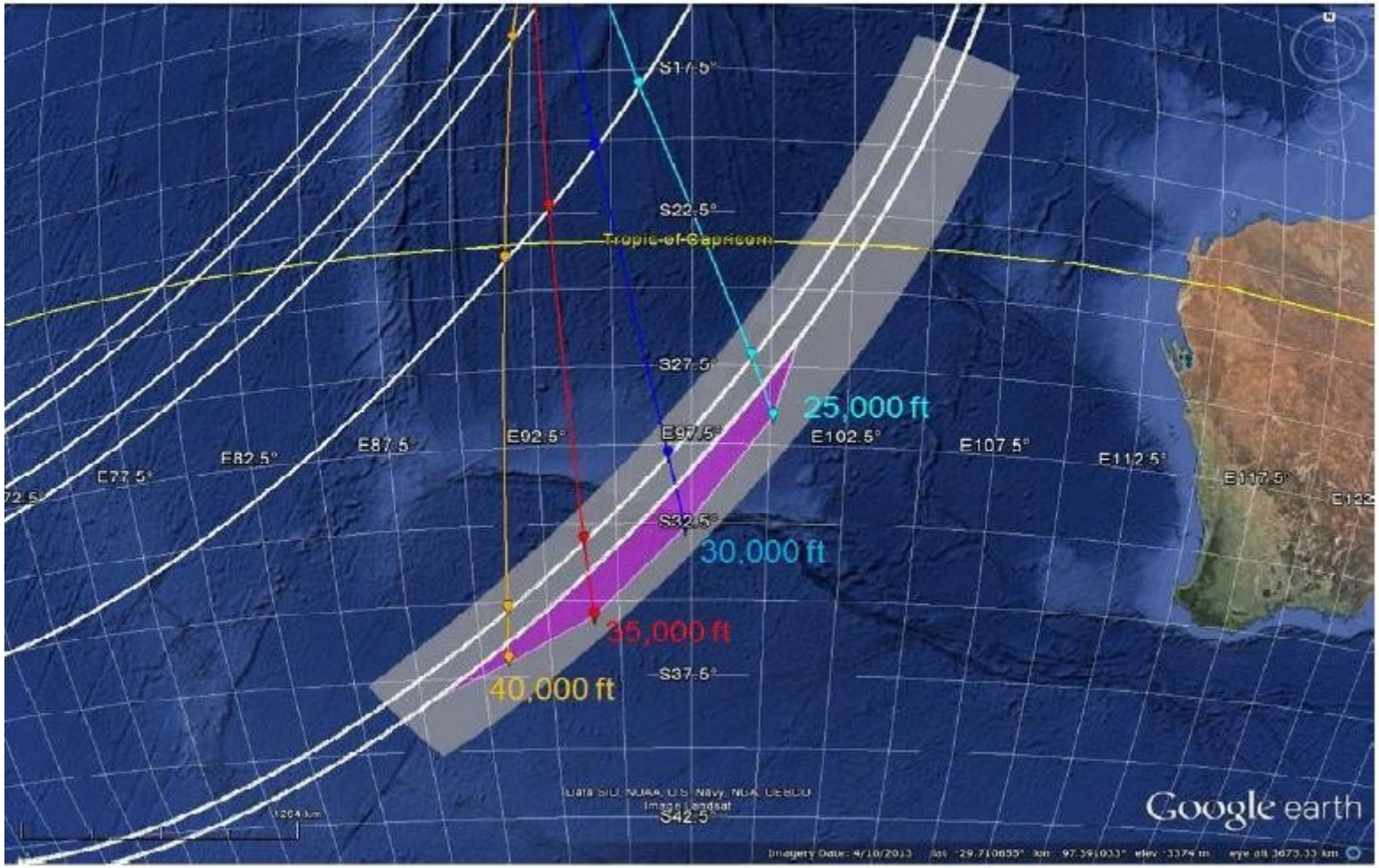

ATSB update, Oct 2014

Future developments

Aug 2014:
EUTELSAT announces that the new EUTELSAT 172B satellite to be launched over the Pacific in 2017 will be the first to carry a Ku-band payload dedicated to airplane connectivity with coverage beams targeted on busy Asia/Pacific air corridors

Space-Based ADS-B: Automatic Dependent Surveillance, satellite based data relay from airplanes
- **to be provided on Globalstar-2 satellites now in orbit**
- **ITU expected to approve 1090MHz air-to-space ADS-B signal in Nov 2015**
- **Iridium 2nd generation satellites to carry Aireon ADS-B receivers (launch 2015 on Falcon 9)**
- **Aalborg University (Denmark)/GomSpace GATOSS ADS-B demo cubesat satellite launched 2013 for tests**
- **Worldwide coverage by 2017?**

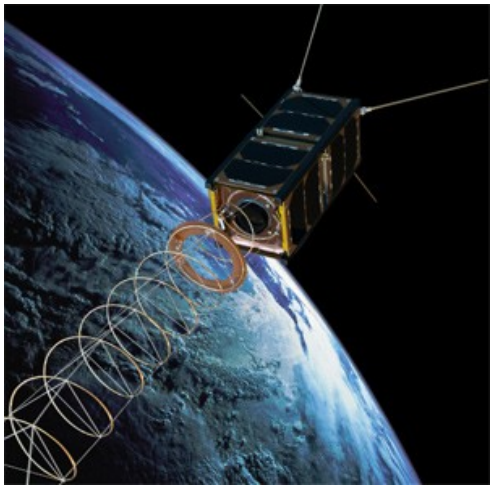

Part 2: The (imaging) search from space

Missile Early Warning systems – large infrared telescopes, usually at GEO altitude

USAF/TRW Defense Support Program (DSP) and its successor
USAF/Lockheed Martin Space-Based Infrared System (SBIRS)
PVO (Russia) /Lavochkin Upravlaemiy-Sputnik-K 'Oko" (Eye) satellites

- able to see Scud missile launches in Middle East conflicts
- should have seen an exploding airliner if there was one?
- US DoD implies not seen

DSP

SBIRS

Oko

Signals Intelligence Satellites

The most highly secret space systems. Includes large radio telescopes in GEO pointing down... dishes possibly up to 75 metre dia!
Include COMINT (communications intelligence) capability
But probably not usually targeting commercial airliners
If they detected any transmissions, they are not saying!

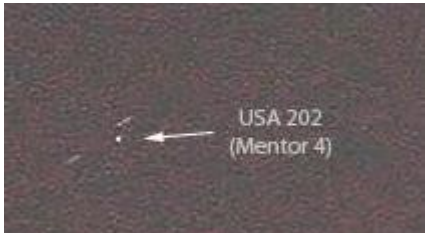

mag 8 apparent magnitude in GEO (bright!)

Marco Langbroek

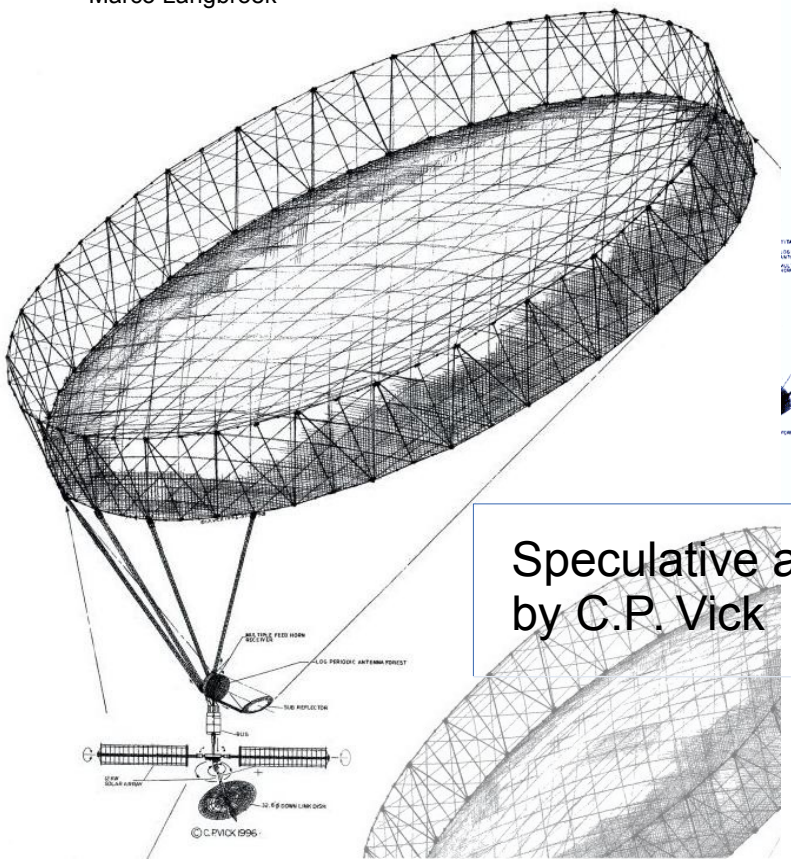

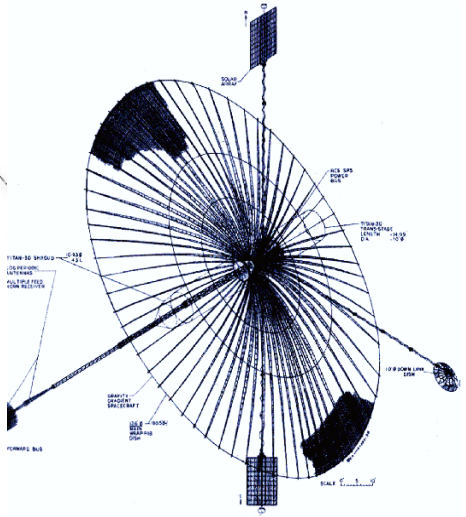

Speculative art by C.P. Vick

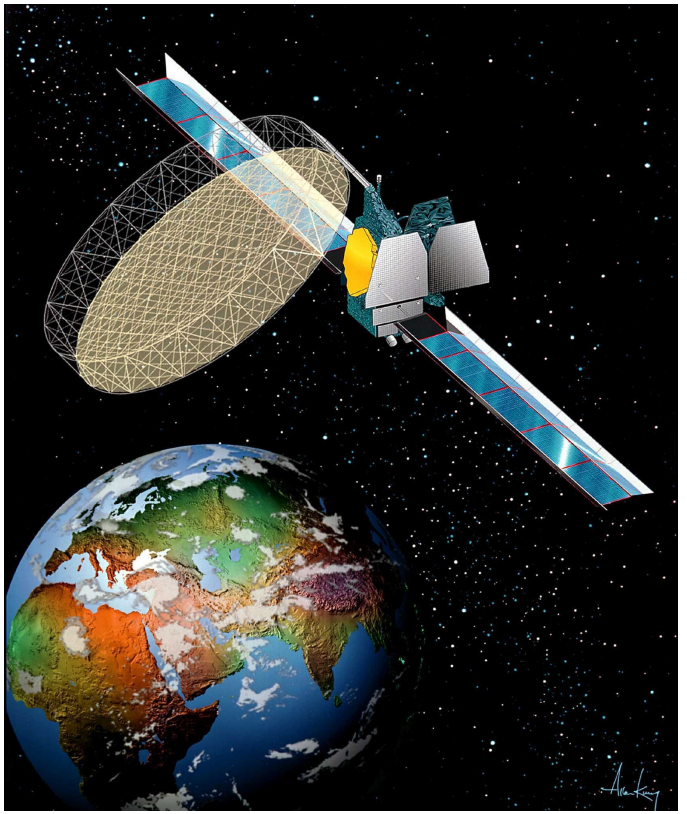

Civilian cellphone satellite with 12 metre antenna

MH370 debris candidates in satellite imagery

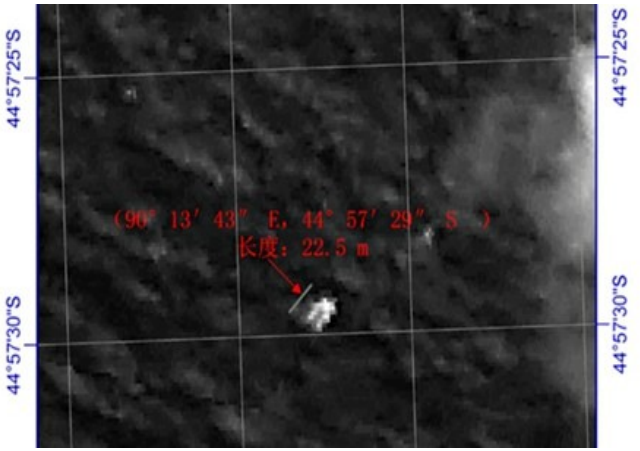

Gao Fen 1 (China)

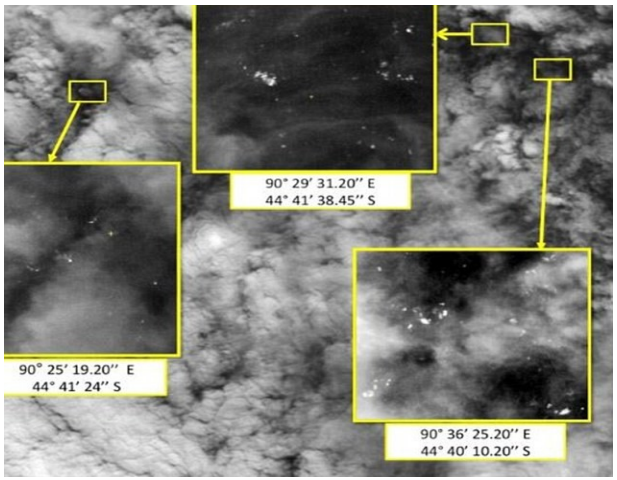

SPOT-6 (France)

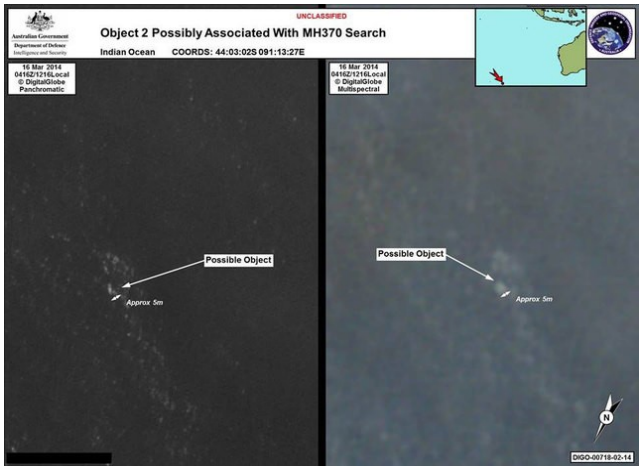

Worldview-2

DigitalGlobe, USA

THAICHOTE imagery acquired on March 24, 2014 03:07 (UTC) In the Indian Ocean

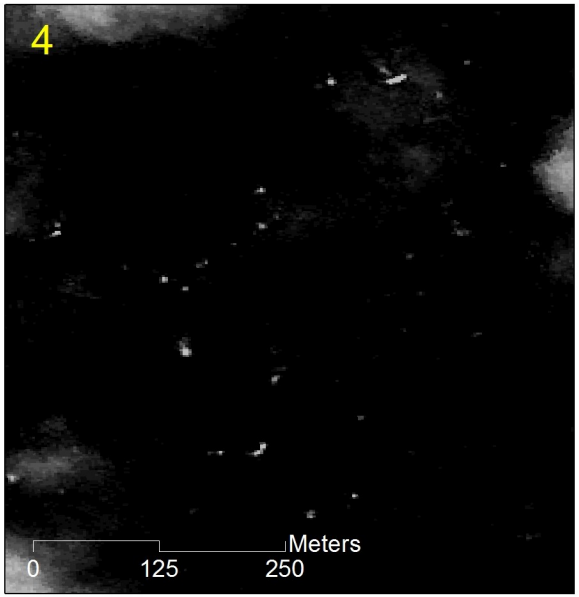

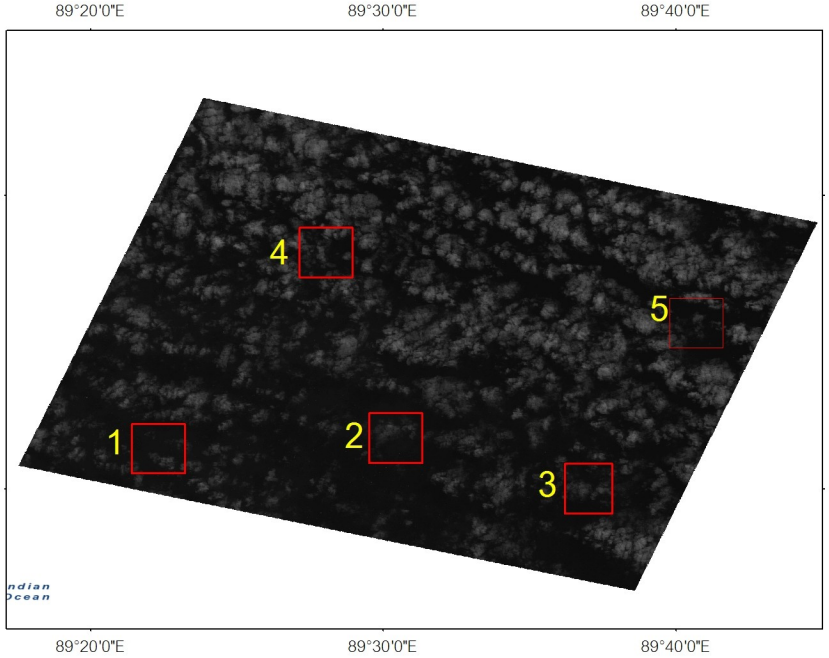

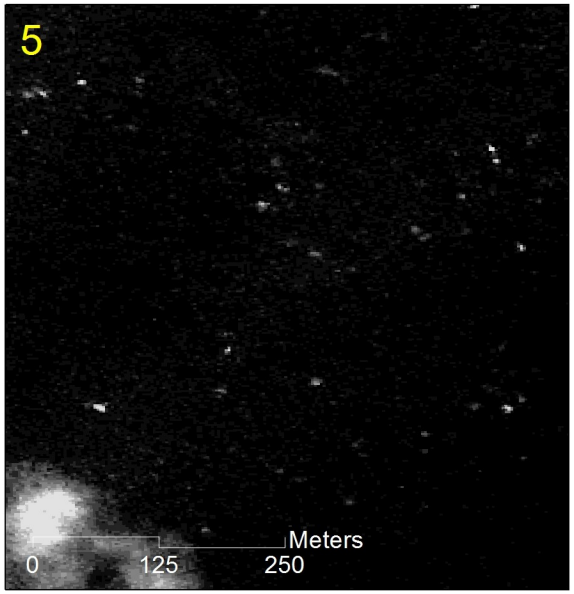

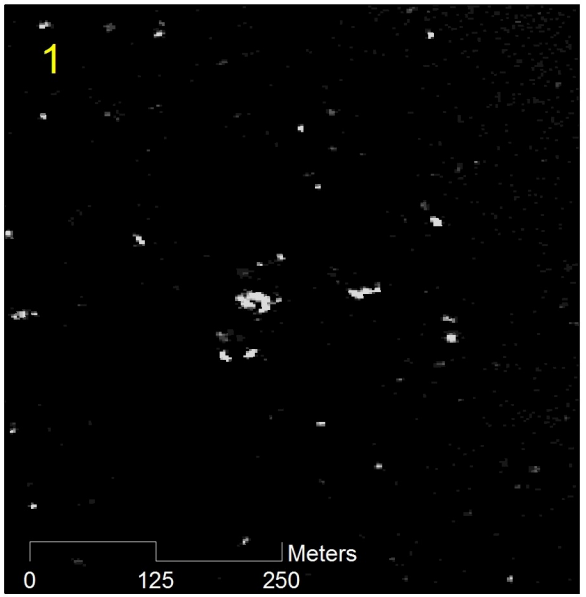

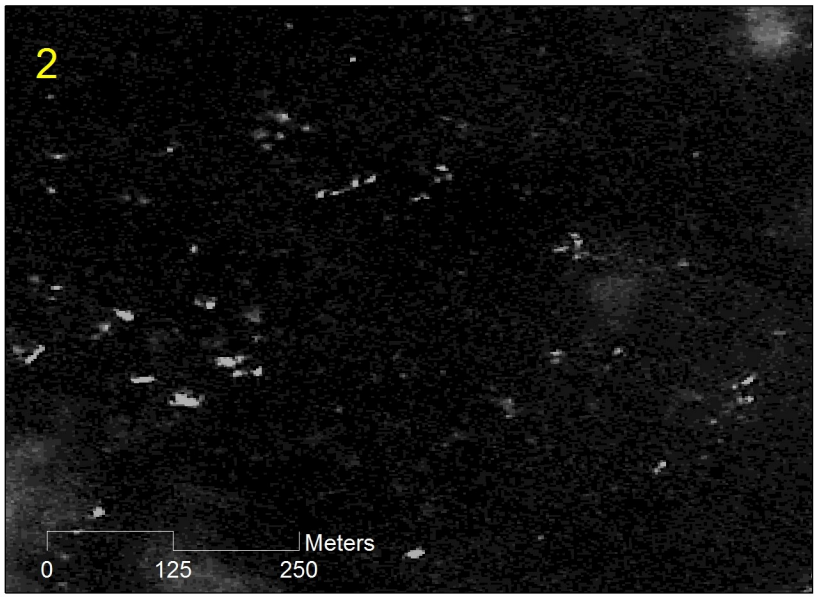

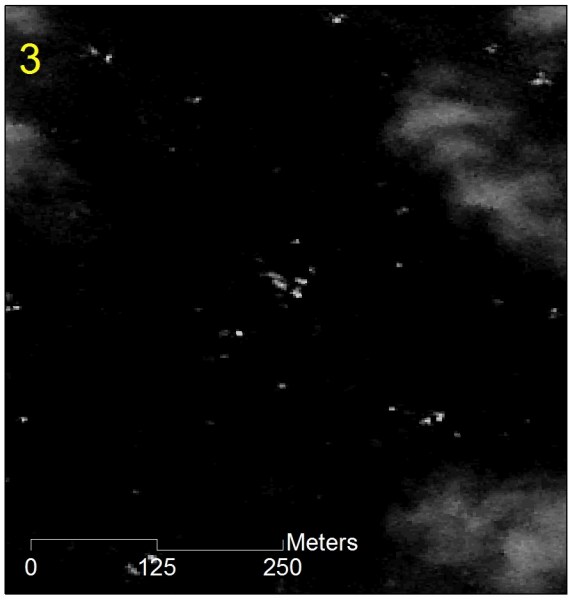

SATELLITE NAME: THAICHOTE (GISTDA,THAILAND)
MODE: PANCHROMATIC (2 Meters Resolution)
DATE: 2014-03-24
TIME: 03:07:56.153985 (UTC)
SATELLITE INCIDENCE ANGLE: 26.982451

ELLIPSOID.....WORLD GEODETIC SYSTEM 1984
GRID.....GEOGRAPHIC COORDINATE SYSTEM
VERTICAL DATUM.....MEAN SEA LEVEL
HORIZONTAL DATUM.....WORLD GEODETIC SYSTEM 1984
PRINTED BY.....GISTDA

GEO-INFORMATICS AND SPACE TECHNOLOGY DEVELOPMENT AGENCY (PUBLIC ORGANIZATION)

MINISTRY OF SCIENCE AND TECHNOLOGY, THAILAND

“Thaichote”? Really?

Many developing countries now have imaging satellites
Surrey Satellite in England started selling 100 kg imaging satellites to developing countries in the 1990s

Other European satellite manufacturers now in the game – Thaichote was built by Astrium-Toulouse for the Geo-Informatics and Space Technology Development Agency of Bangkok

Alsat (Algeria) 2002

Tiungsat (Malaysia) 2000

Fasat (Chile) 1998

Posat
(Portugal)
1993

Bilsat (Turkey) 2003

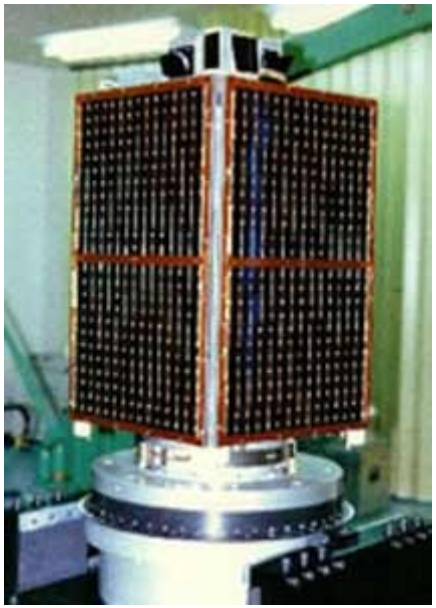

Uribyol
S Korea 1992

Nigeriasat-2 2011

What was the result of the searches by imaging satellites?

There is a LOT of debris and garbage floating around the Indian Ocean...

… but apparently none of it is from MH370

Why was nothing seen?

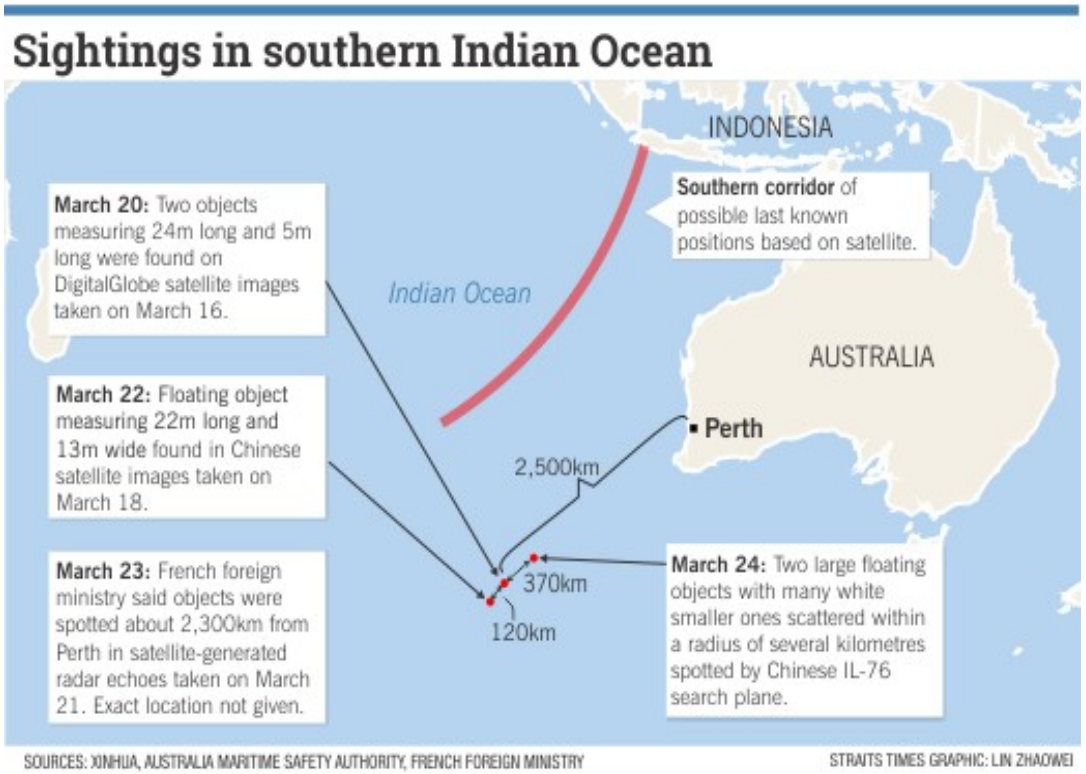

Part 3: Imaging satellites in 2014 and the myth of global imaging surveillance

Global coverage - low resolution

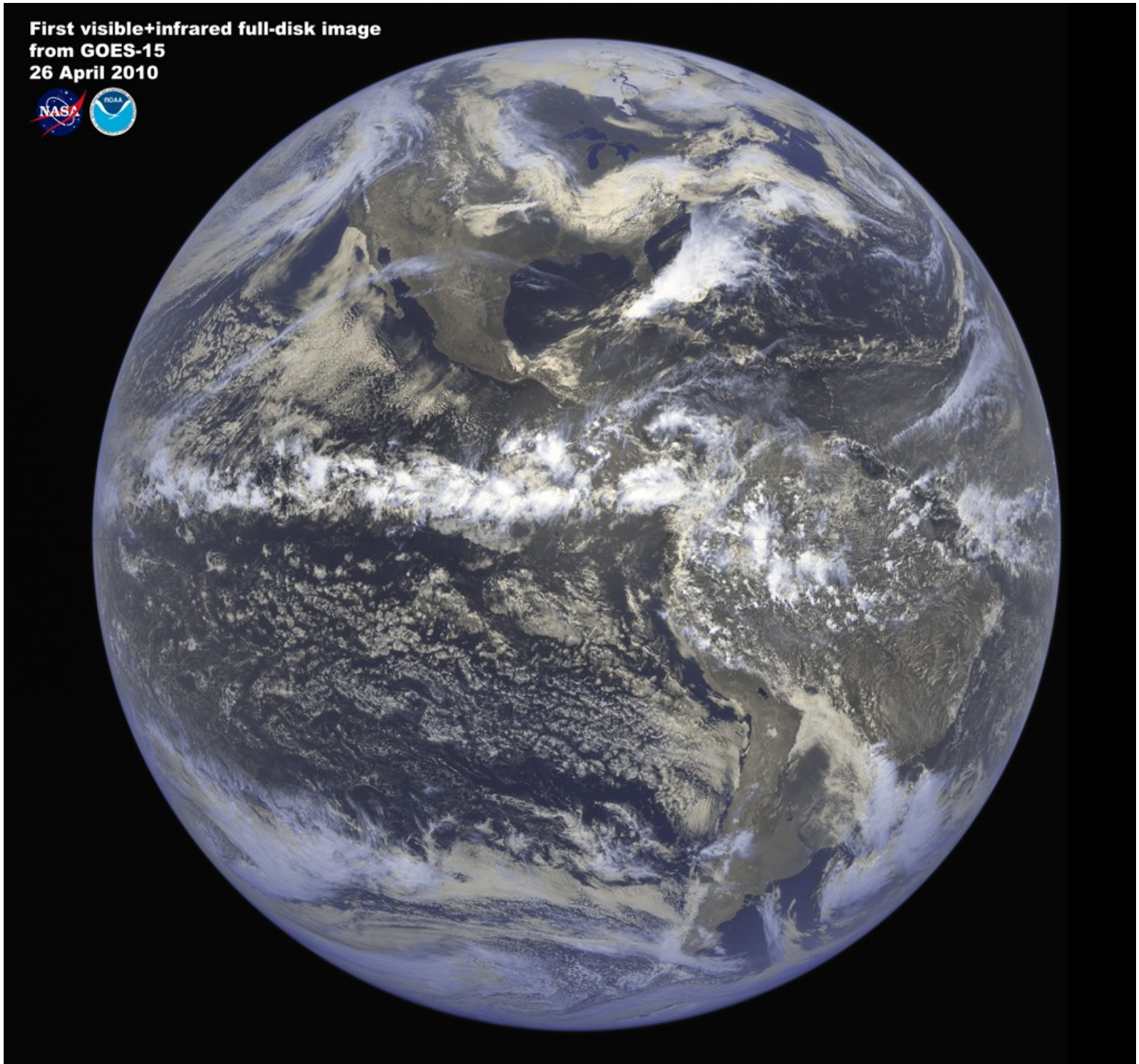

Small area, high resolution: 40cm image from Worldview-3
Top of the line DigitalGlobe civilian imaging satellite

(c) DigitalGlobe

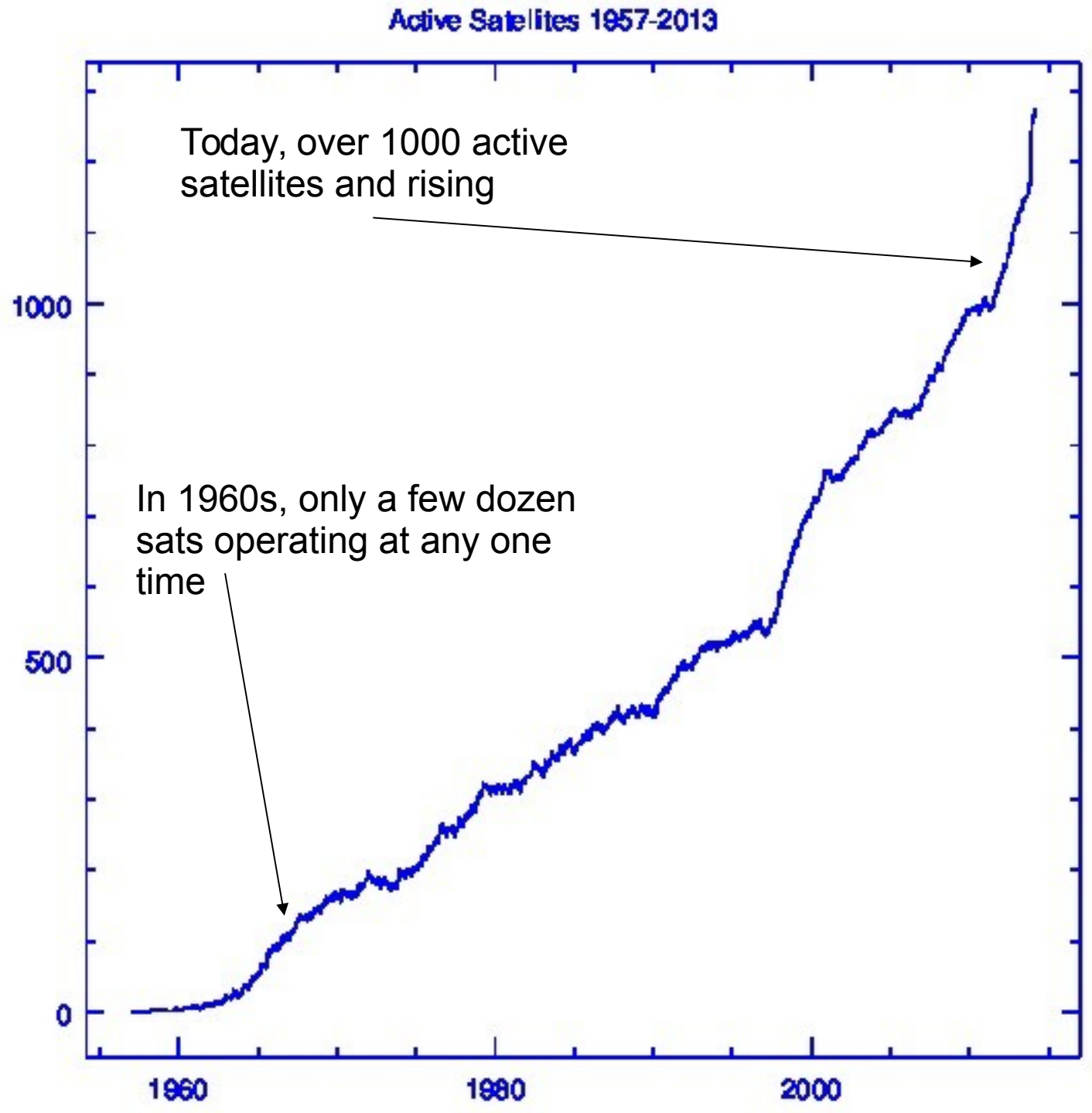

McDowell 2014: http://planet4589.org/space/log/stats.html

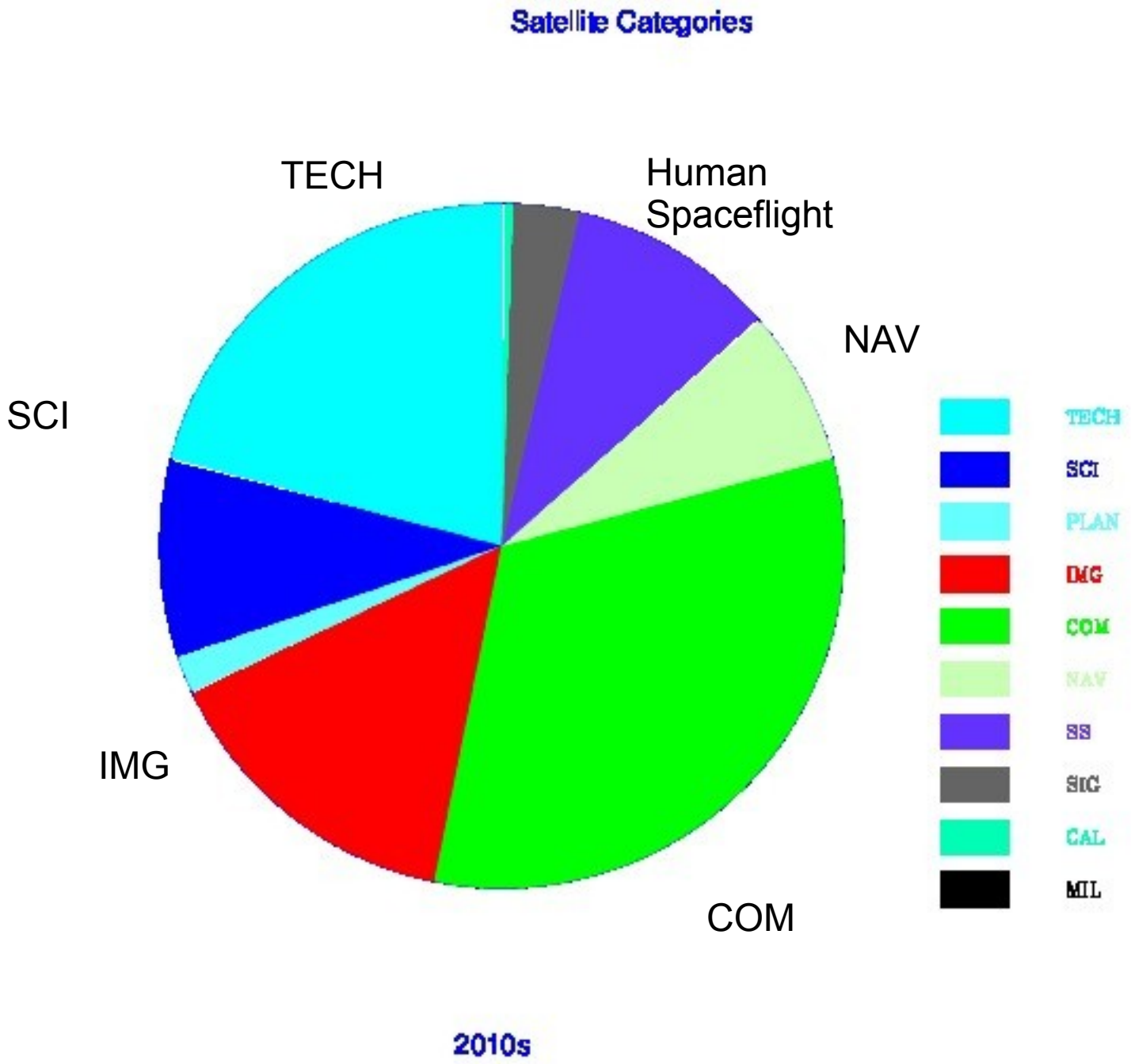

In the 2010s, most sats are either communications or imaging; technology development (including student satellites) also a big sector

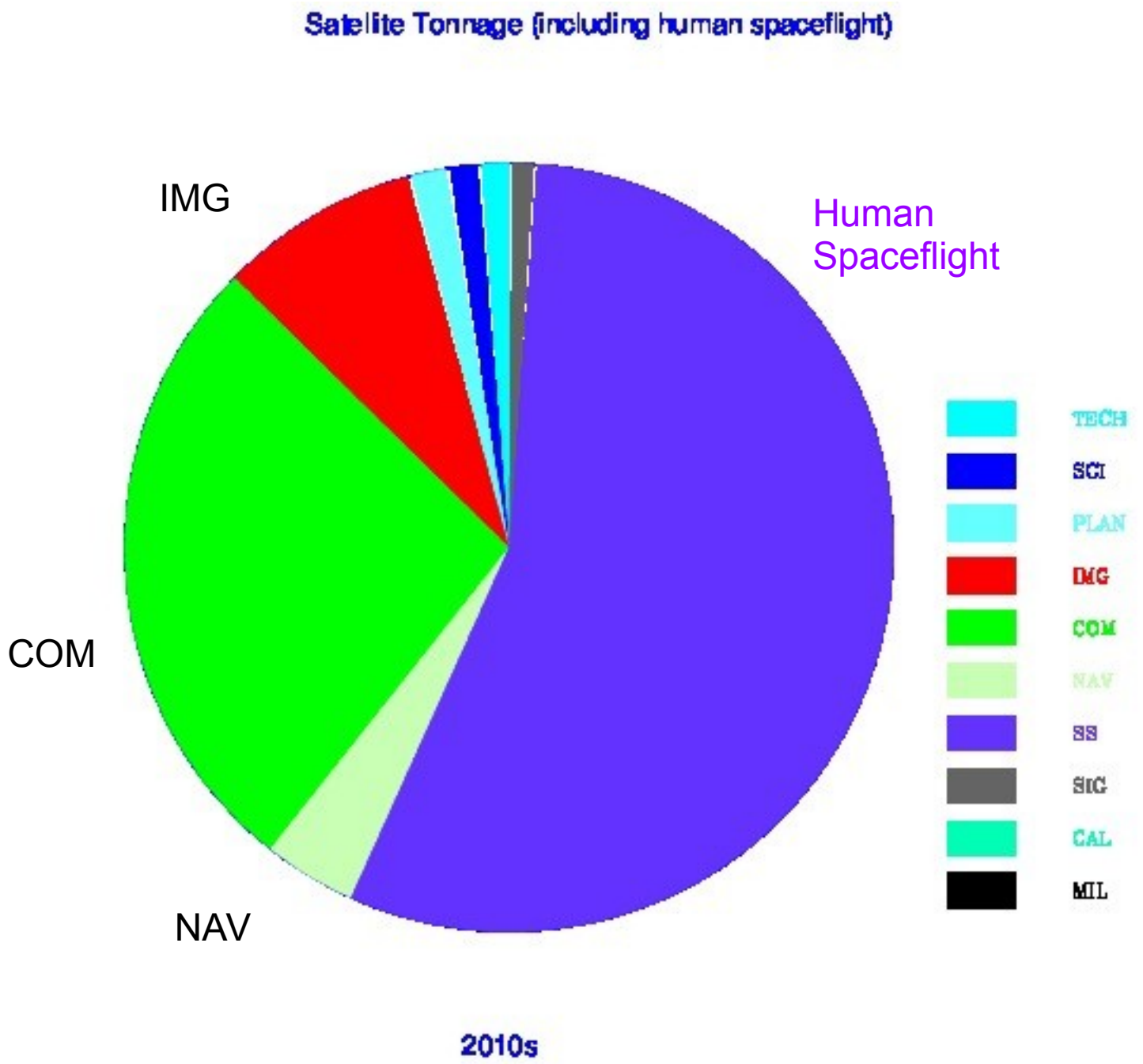

By mass however, human spaceflight dominates – comms still next
Tech/student satellites vanish, they are mostly little cubesats which don't weigh much

4-yr total 900 t robotic, 1100 t 6 x Shuttle + ISS/PRC

Decade by decade:

Red:
Imaging (spy sats) dominated in cold war

Purple:
Human spaceflight tonnage huge in 1990s (100 tonnes for each Shuttle)

Green:
Steady growth of communications sector

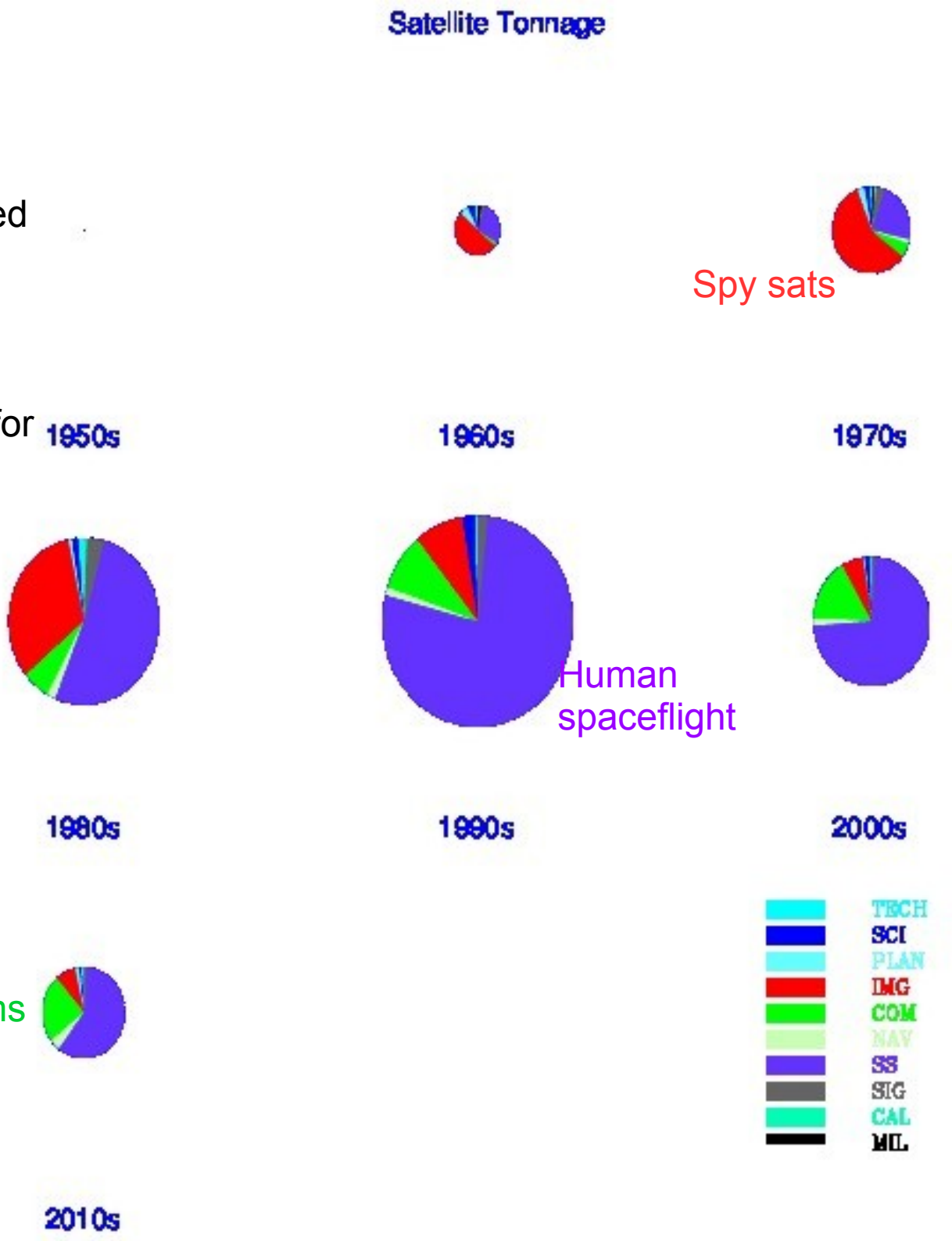

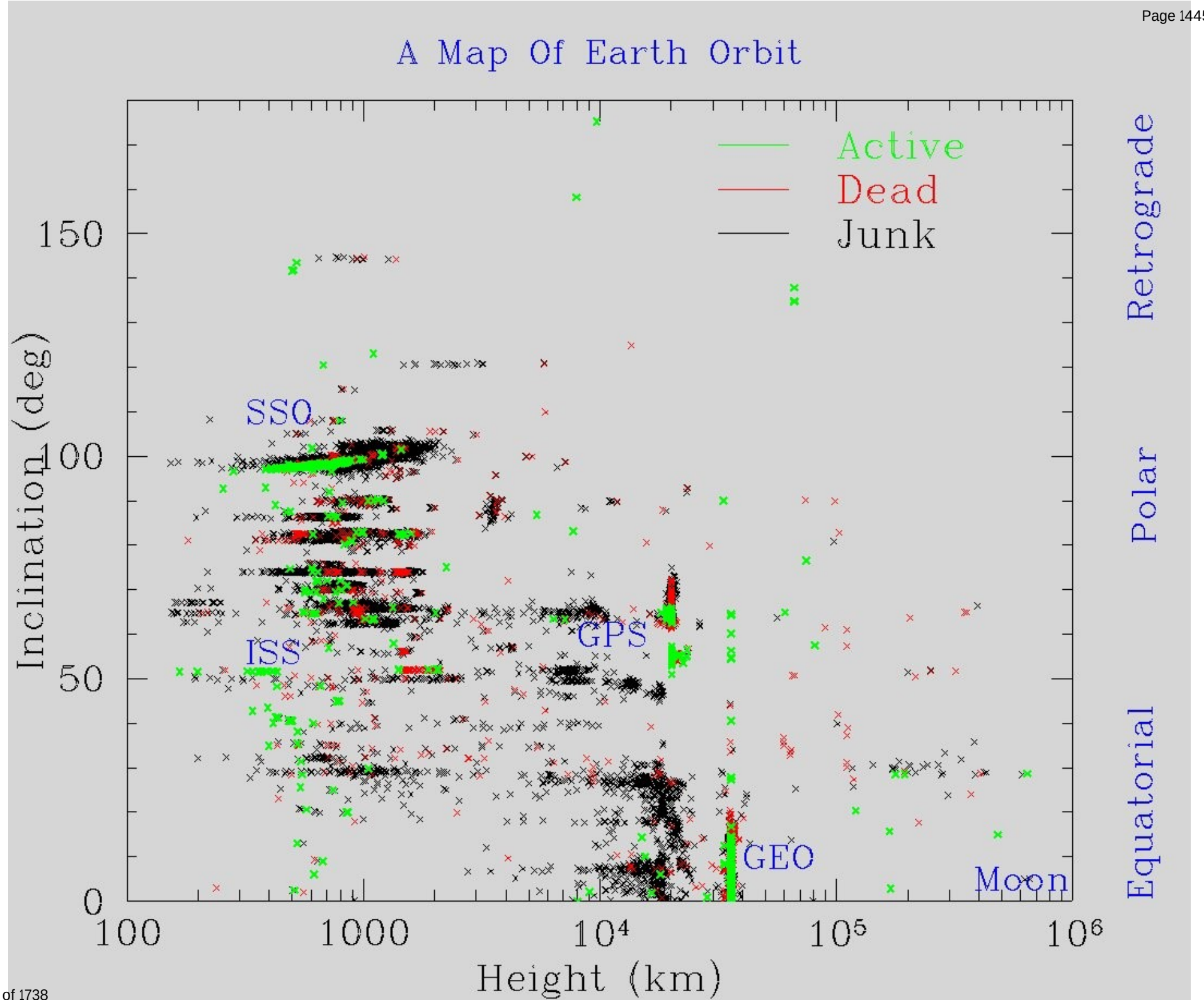
A Map Of Earth Orbit
Active
Dead
Junk
SSO
ISS
GPS
GEO
Moon
Retrograde
Polar
Equatorial
Inclination (deg)
Height (km)
0
50
100
150
100
1000
10^4
10^5
10^6

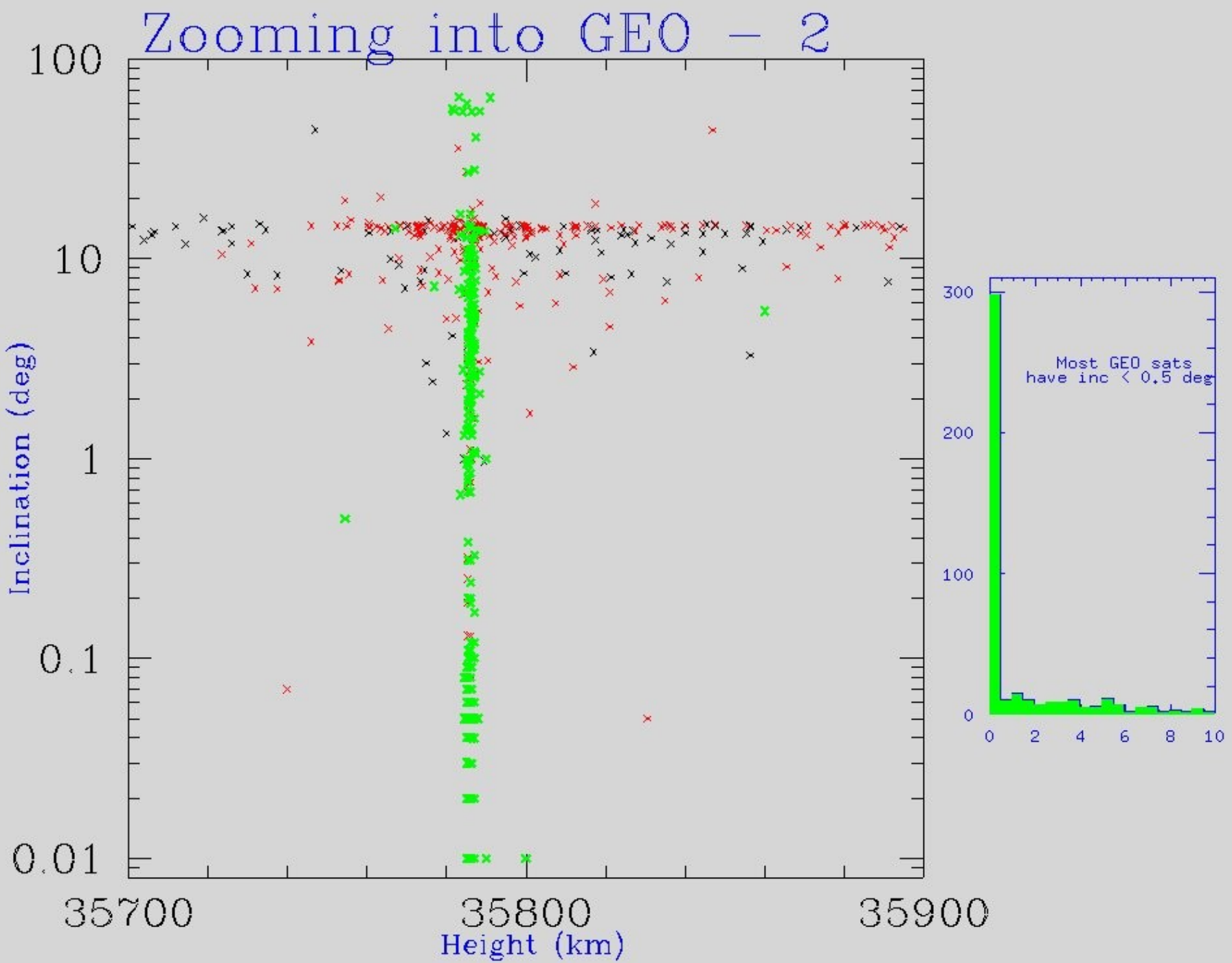
Zooming into GEO – 2
100
10
1
0.1
0.01
Inclination (deg)
35700
35800
35900
Height (km)
300
200
100
0
0
2
4
6
8
10
Most GEO sats
have inc < 0.5 deg

SSO: Sun Synchronous Orbit

Actually we left something out of our math: the Earth is NOT ROUND!
It's a little squashed at the poles (polar radius is 22 km smaller than at equator)
Every time a sat goes over the poles, it gets less of a tug; over the equator it gets more.
This twists the orbit – makes it rotate in space.
We consider the first term (J2) in the spherical harmonic expansion of the potential
This gives first order corrections to the orbital elements (node, arg of peri.)
- varying linearly in time
By picking the orbit cleverly you can make the twist do something useful.

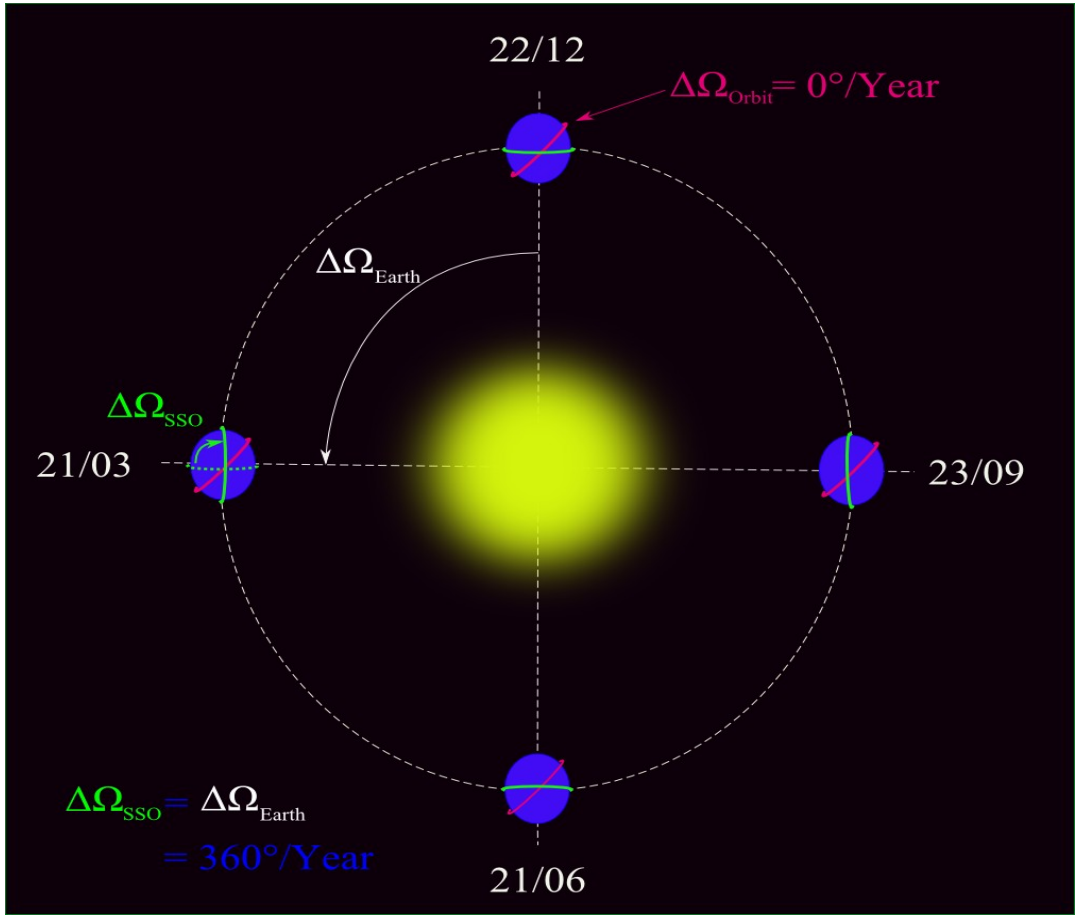

Source: wikipedia

The magenta colored orbit is what you get for a perfect sphere Earth

It stays fixed in space so in August (in this particular case) it is facing the sun – the satellite orbits over the dawn/dusk line
- but in May the orbit is edge on to the sun, orbiting noon to midnight.

The green colored orbit is SSO, turning so it's always facing the Sun

Zooming into SSO

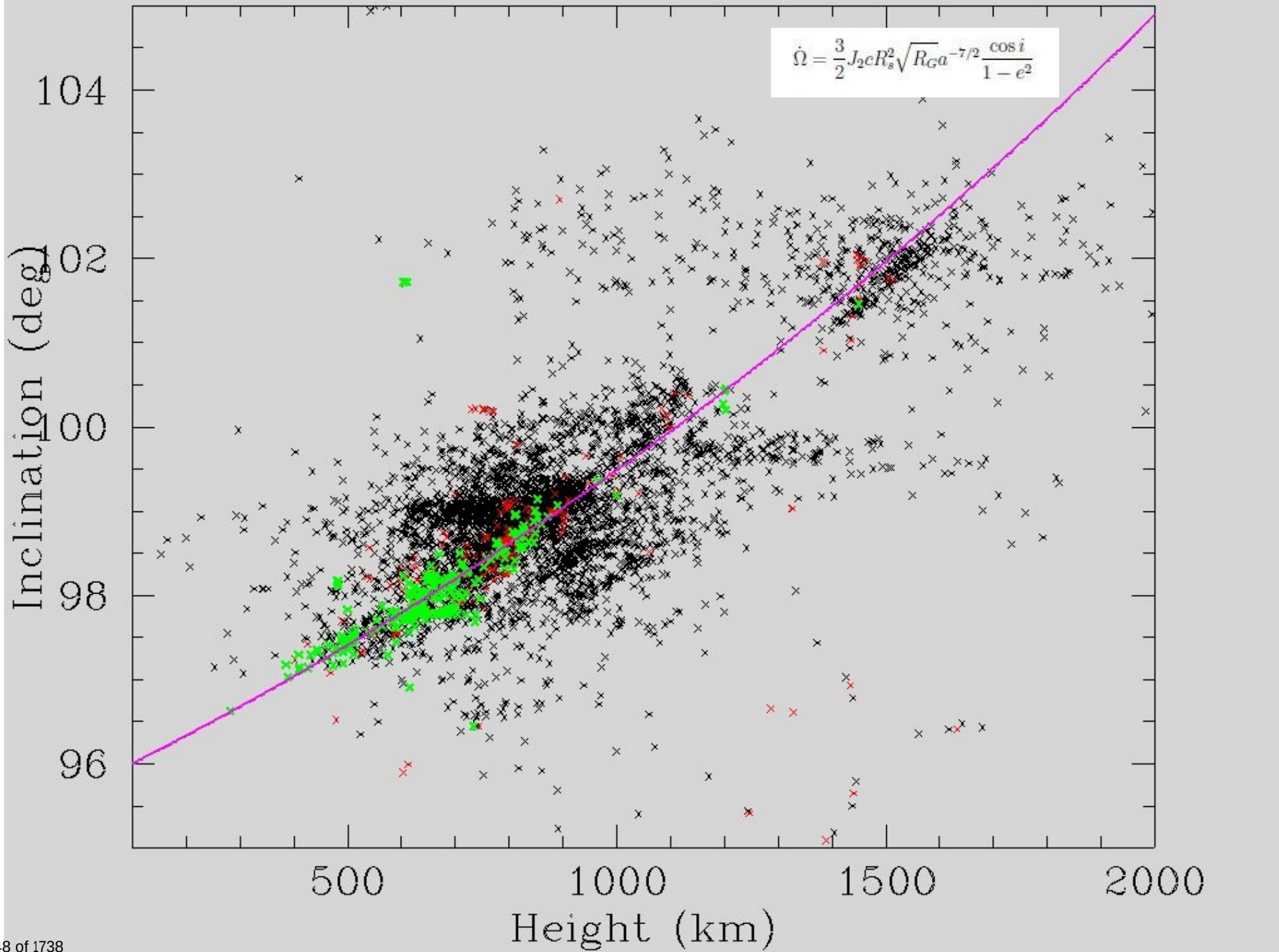

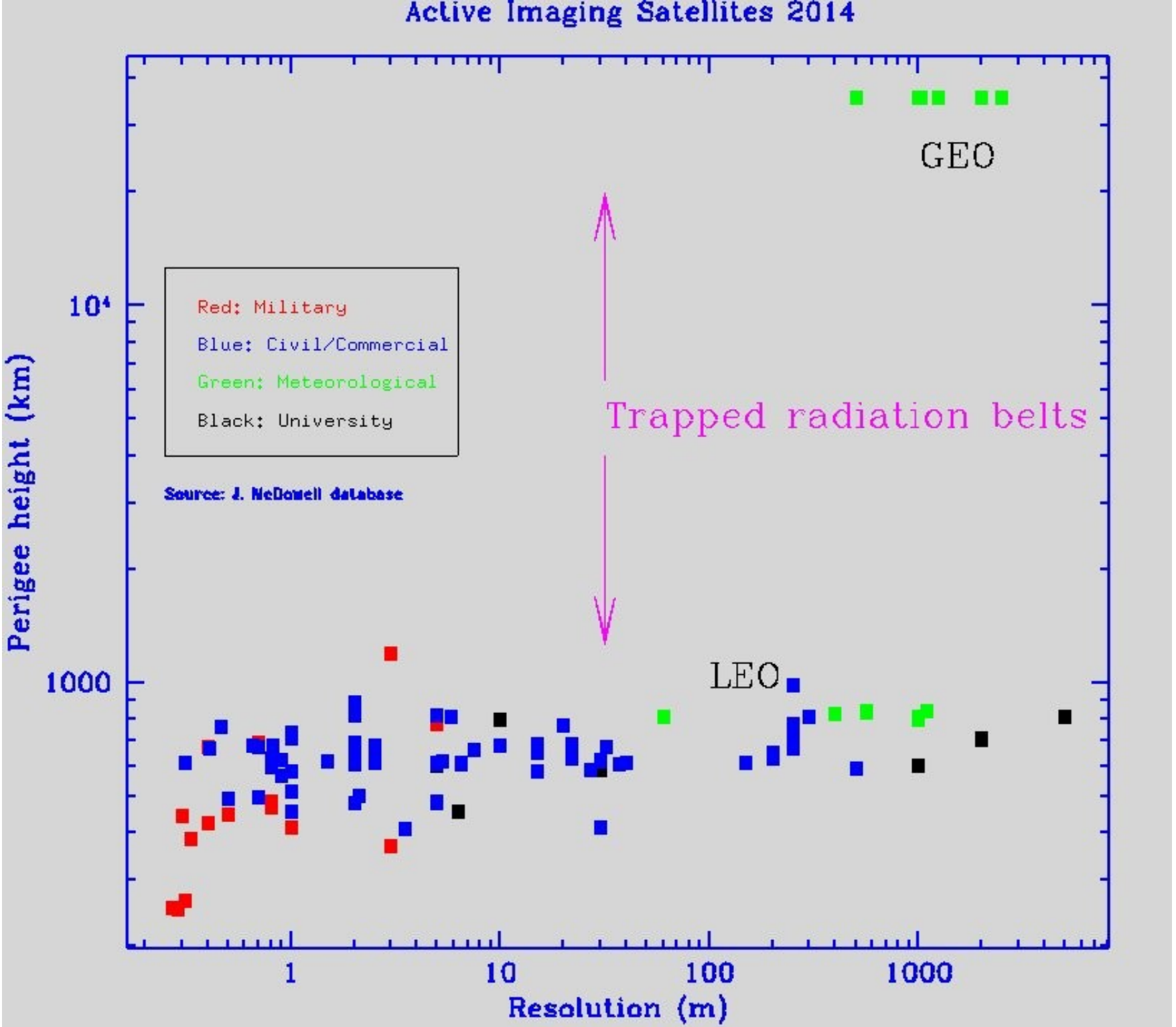

Total:
161 sats

IMAGING SATELLITE LIMITATIONS

Ground resolved distance vs. swath (image width in km)

- Traditionally, large swath, low resolution, high altitude (e.g. weather sats)
  small(er) swath, high res, low altitude (spy sats)

Latency vs bandwidth
- How much data per day?
- How soon do you get the data?

Old film return spy sats: high bandwidth, very low latency

You can get a LOT of megabyte-equivalents in a film canister but you have to wait weeks or months to get it...

Modern imaging satellites:

Spy satellites use GEO data relay sats for immediate availability of raw data
Civilian satellites use ground stations – latency of a few hours to days, and limited time (=> bandwidth) to download during a pass

Additional latency for ground software to process raw telemetry to processed, value-added data products often dominates

Low Earth Orbit

- a brief polemical digression

Earth surface has $R = 6378$ km and $R_G = 4.4$ mm
ISS has height h = 400 km so $r = R + h = 6778$ km
Then

$$\sqrt{R_G/r} = 1/39250$$

corresponding to $v = 7.67$km/s = 17158mph and orbital period T of 92.5 min.

The constant 'big G' is evil and has confusing units. By using

$$R_G = \frac{GM}{c^2}$$

instead we make the dimensionality more obvious as well as easily seeing how far we are from being in the GR limit:
Consider orbits around an object of mass M, radius R_s and gravitational radius R_G (where we will consider only the case $R_s \gg R_G$!). From Newton's law of gravitation, the potential is

$$V = mc^2 \left(\frac{r}{R_G}\right)^{-1}$$

it follows trivially that circular orbits of radius r will have

$$v/c = \sqrt{R_G/r}$$

The orbital period T is then given by

$$T = \frac{2\pi r}{c}\sqrt{r/R_G}$$

In other words, the orbital period is
the time it would take to go round the orbit at the speed of light
times root of
the ratio of the orbit size to the size of an Earth-mass black hole.
This is Kepler's third law.

Now consider an imaging satellite orbiting at height h
with angular field of view α resulting in a nadir swath width

$$s = h\alpha$$

In time t the satellite will see an area A = svt
so for typical LEO values and s ~ 100 km, A~ 3 million sq km / hr

In one orbit you see $2\pi Rs$ (where R is Earth radius)
In LEO, the next orbit crosses the equator ~22 deg W of the previous one because of Earth rotation, which given actual values of s for current satellites means that the swaths do not overlap there..

so it takes you $N = 4\pi R^2/2\pi Rs = 2R/s$ orbits to cover
the surface area of the Earth
- *except of course that the swaths overlap at the poles, we will neglect that.*

The fraction of the Earth's surface seen in unit time is

$$f = (csR_G^{0.5}/4\pi R)(R+h)^{-1.5} = 0.11\,(s/100\text{ km})(1+h/6378\text{ km})^{-1.5}\text{ per day}$$

… *if only the satellite had high def video streaming* (which they don't)
… *if only they could see in the dark* (I am considering visible light imagers, not radar satellites)

In fact the observing efficiency relative to this calculation can be about 10 %.

Largest US commercial imagery operator: DigitalGlobe

5 main satellites:

	Resolution m	Swath km	Orbit ht km	f	eff %	coverage mplanet/d
Ikonos	0.82	11.3	681	0.010	5	0.47
GeoEye-1	0.41	15.2	671	0.014	5	0.68
WorldView-1	0.50	17.6	496	0.017	9	1.47
WorldView-2	0.46	16.4	764	0.015	13	1.91
WorldView-3	0.31	13.1	617	0.012	11	1.33

Total capacity 3 million sq km / day
Compare Earth surface area: 511 million sq km
So a constellation of 5 top-end satellites covers 6 milliplanets per day
Would need 4000 such satellites for hourly global coverage
How many are there?

Sources: DigitalGlobe (actual claimed coverage)
Herb Kramer/eoportal.org (sensor parameters)
USAF/space-track.org (orbit data)

WV-1

WV-2

WV-3

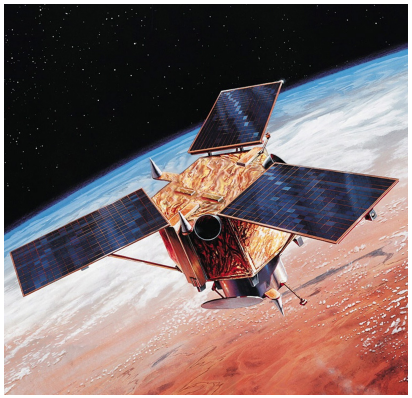

Ikonos

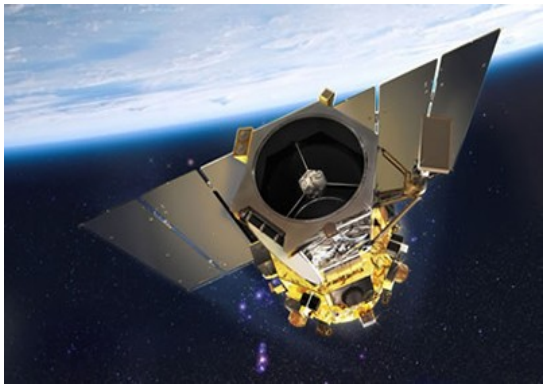

GeoEye-1

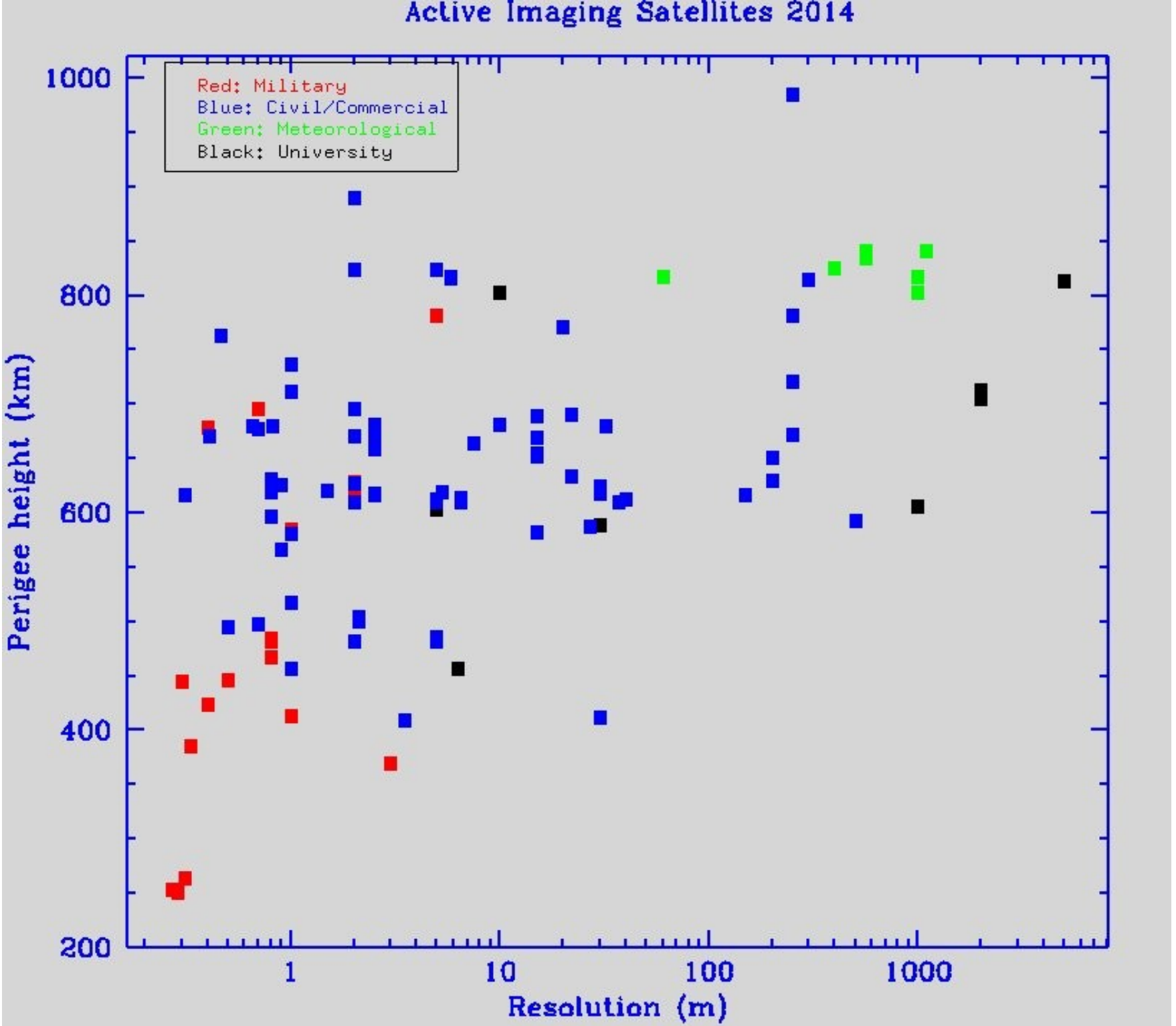
Active Imaging Satellites 2014
Red: Military
Blue: Civil/Commercial
Green: Meteorological
Black: University
Perigee height (km)
1000
800
600
400
200
1
10
100
1000
Resolution (m)

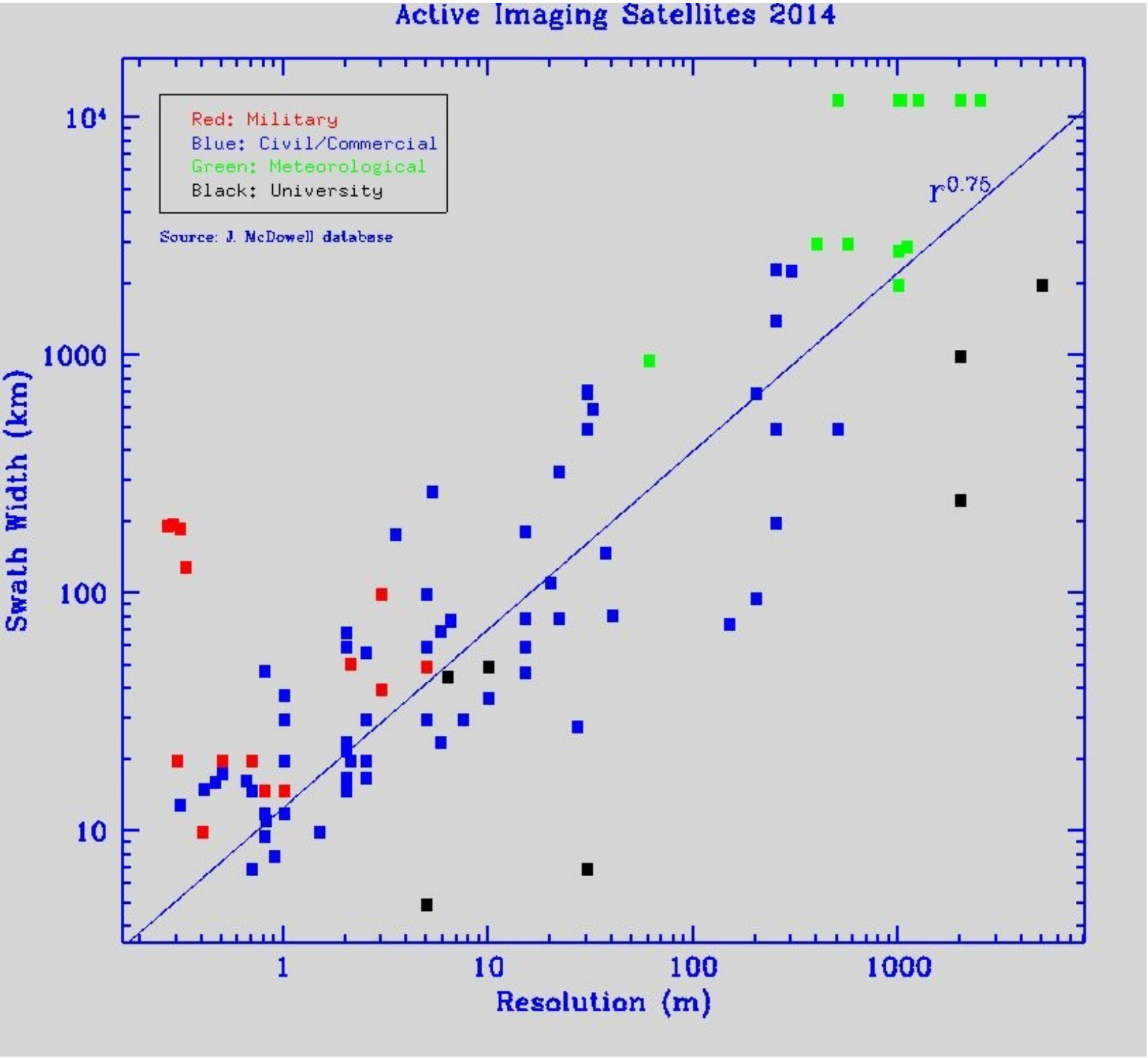

Active Earth visible-light imaging satellites: 161

With resolution <= 10m: 100

Active Imaging Satellites 2014

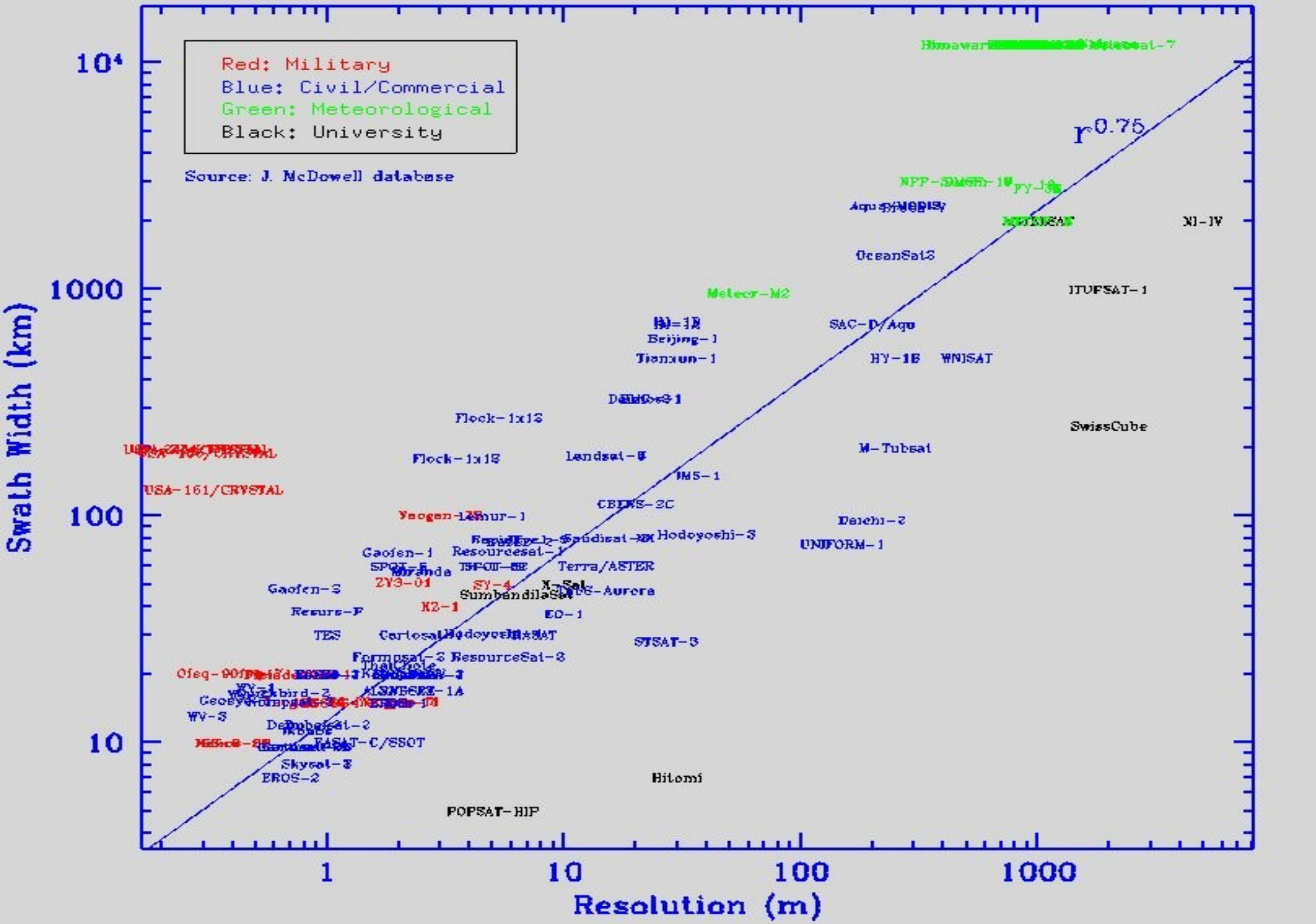

Active Imaging Satellites 2014

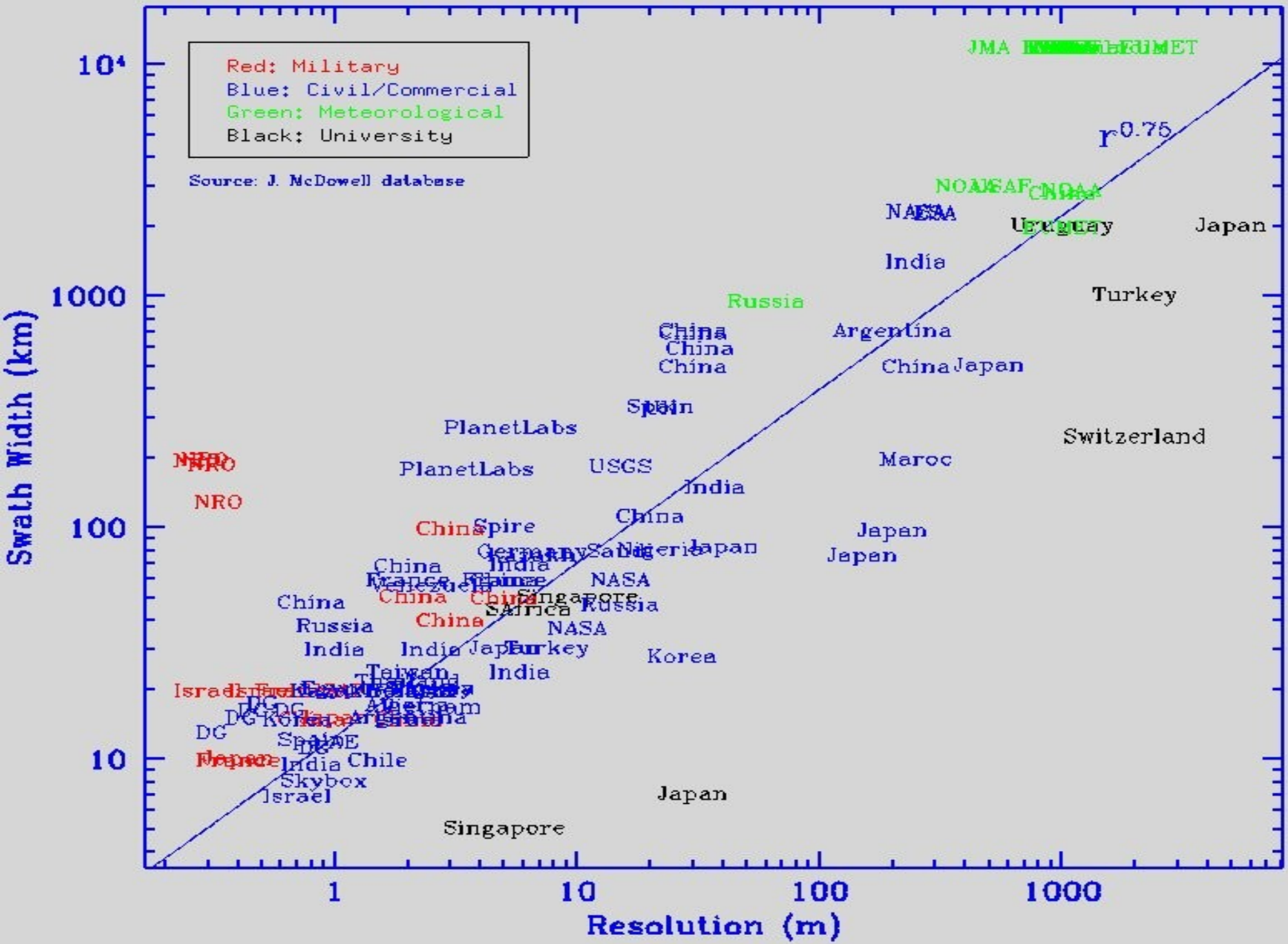

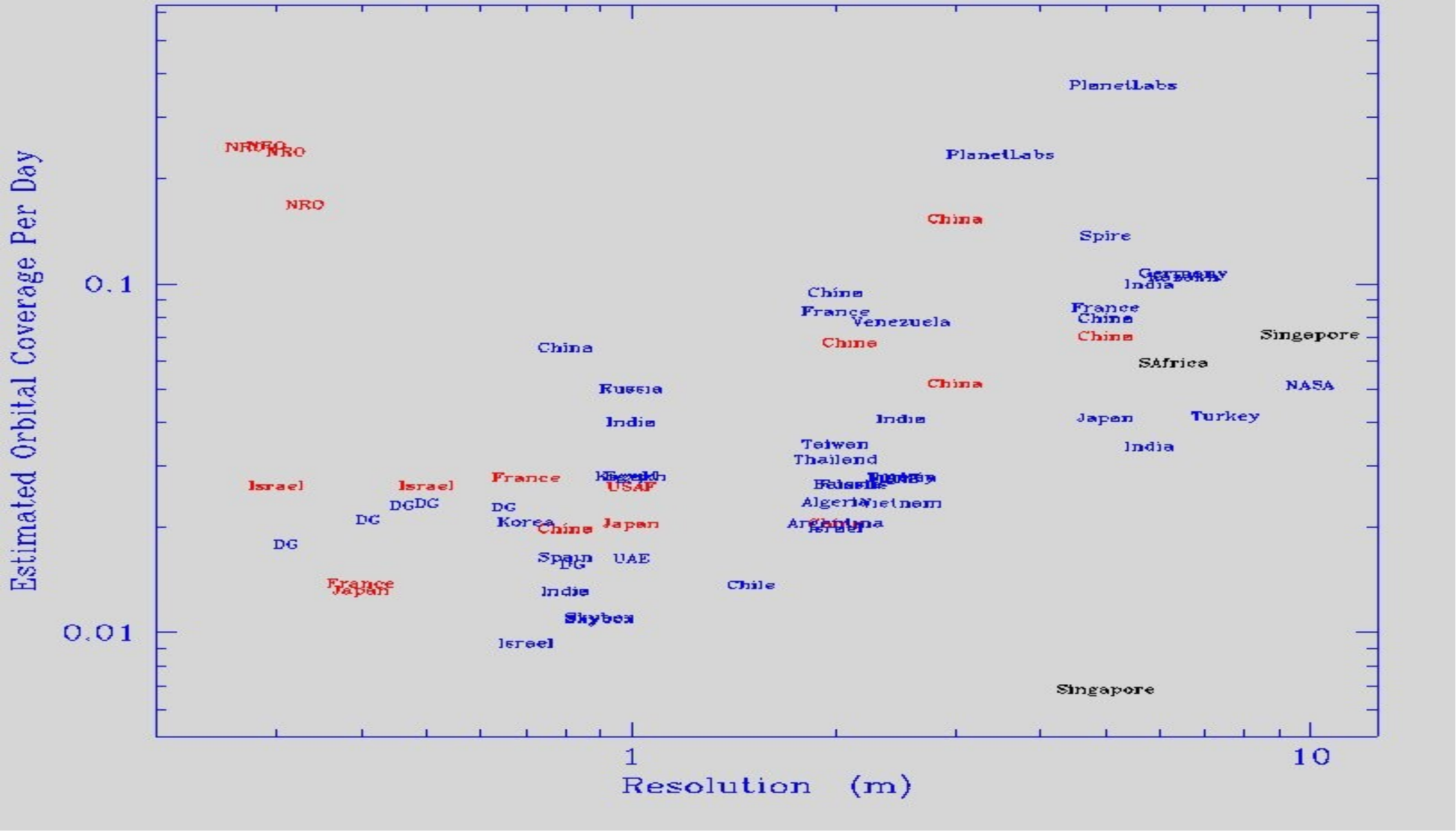

When corrected for estimated 10% efficiency,
total coverage is 0.44 planet/day (0.19 from spy sats, incl. 0.09 from NRO alone)
Of this, 0.16 is from high res (<1 m) satellites.
Note: Spy satellite swaths and efficiencies uncertain by factor 2 or so

CONCLUSIONS

Imaging spy satellites are watching us – but not ALL the time. Yet.

The real near-ubiquitous surveillance is more subtle: communications satellite technology provides a hidden infrastructure that can be used in surprising ways

We still don't know what happened to MH370, but time-delay and Doppler evidence hidden in network communications metadata allow its location to be constrained.

Increased, cheaper satellite broadband capacity will allow us to stream internet video in coach class – this and deployment of space-based ADS-B will ensure airliners stay in touch with data centers during transoceanic flights.

More fun with orbit databases

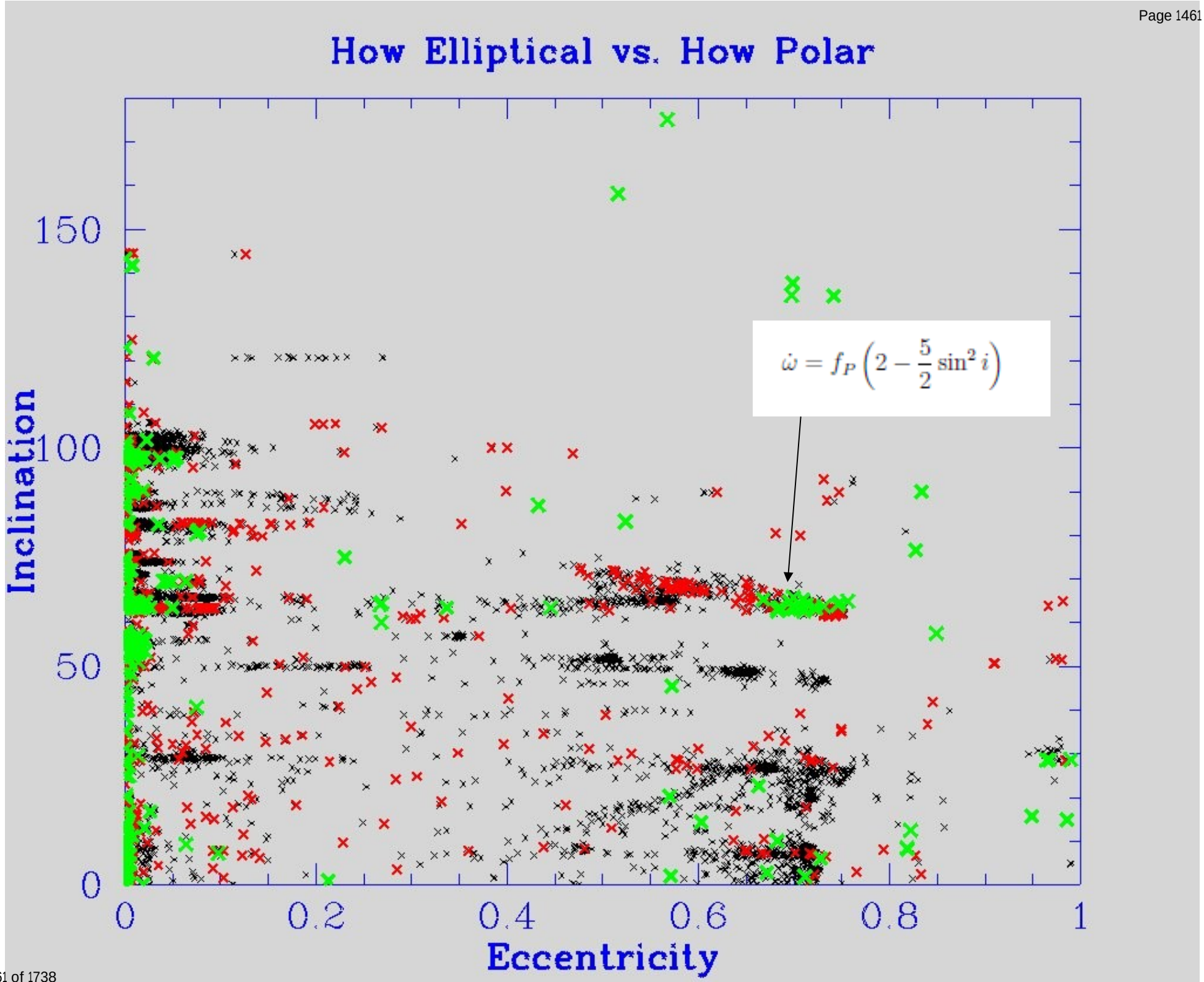
How Elliptical vs. How Polar
150
100
50
0
Inclination
0
0.2
0.4
0.6
0.8
1
Eccentricity
$\dot{\omega} = f_P \left(2 - \frac{5}{2}\sin^2 i\right)$

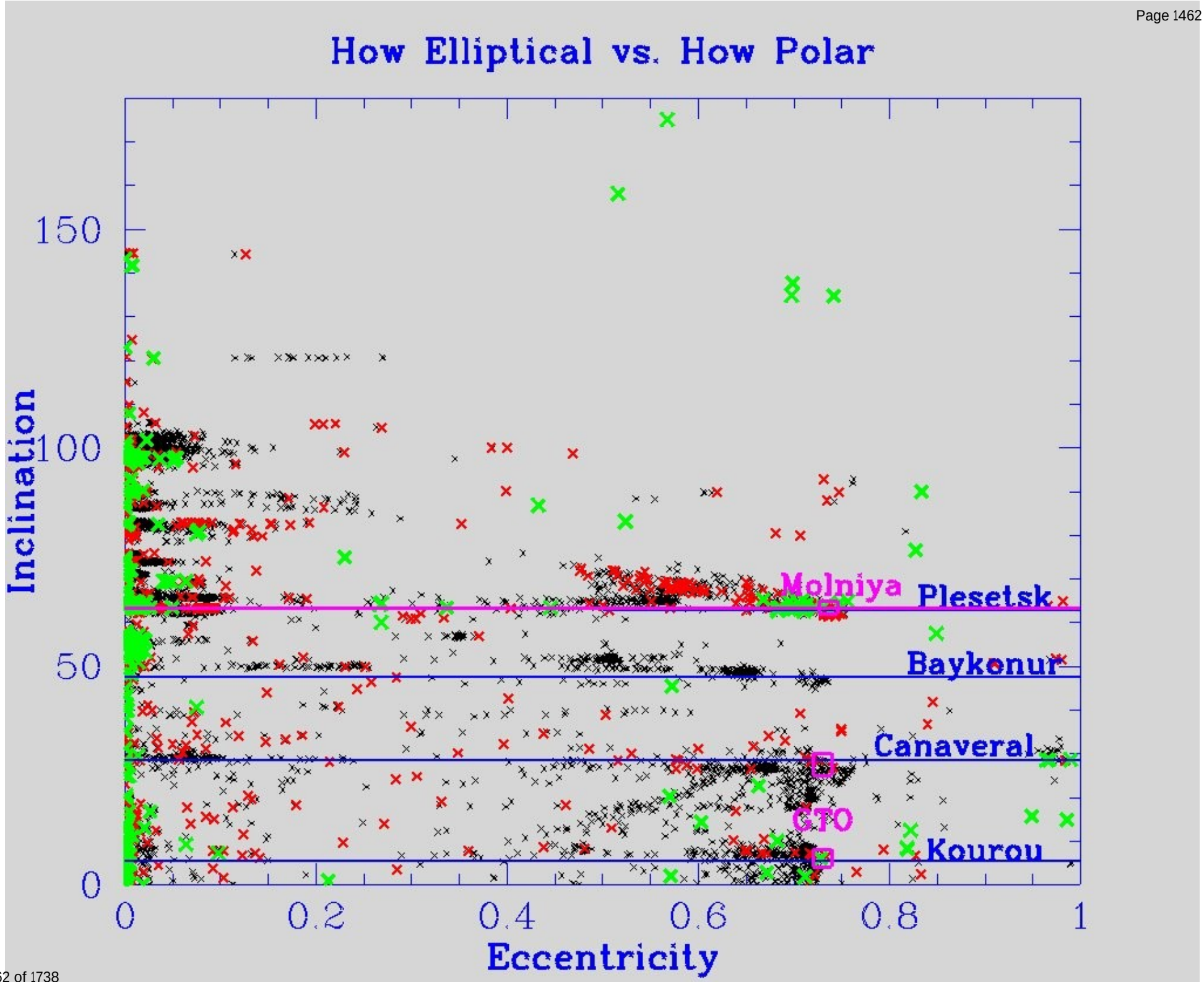
How Elliptical vs. How Polar
Inclination
150
100
50
0
0
0.2
0.4
0.6
0.8
1
Eccentricity
Molniya
Plesetsk
Baykonur
Canaveral
GTO
Kourou

The Growth of Space Junk

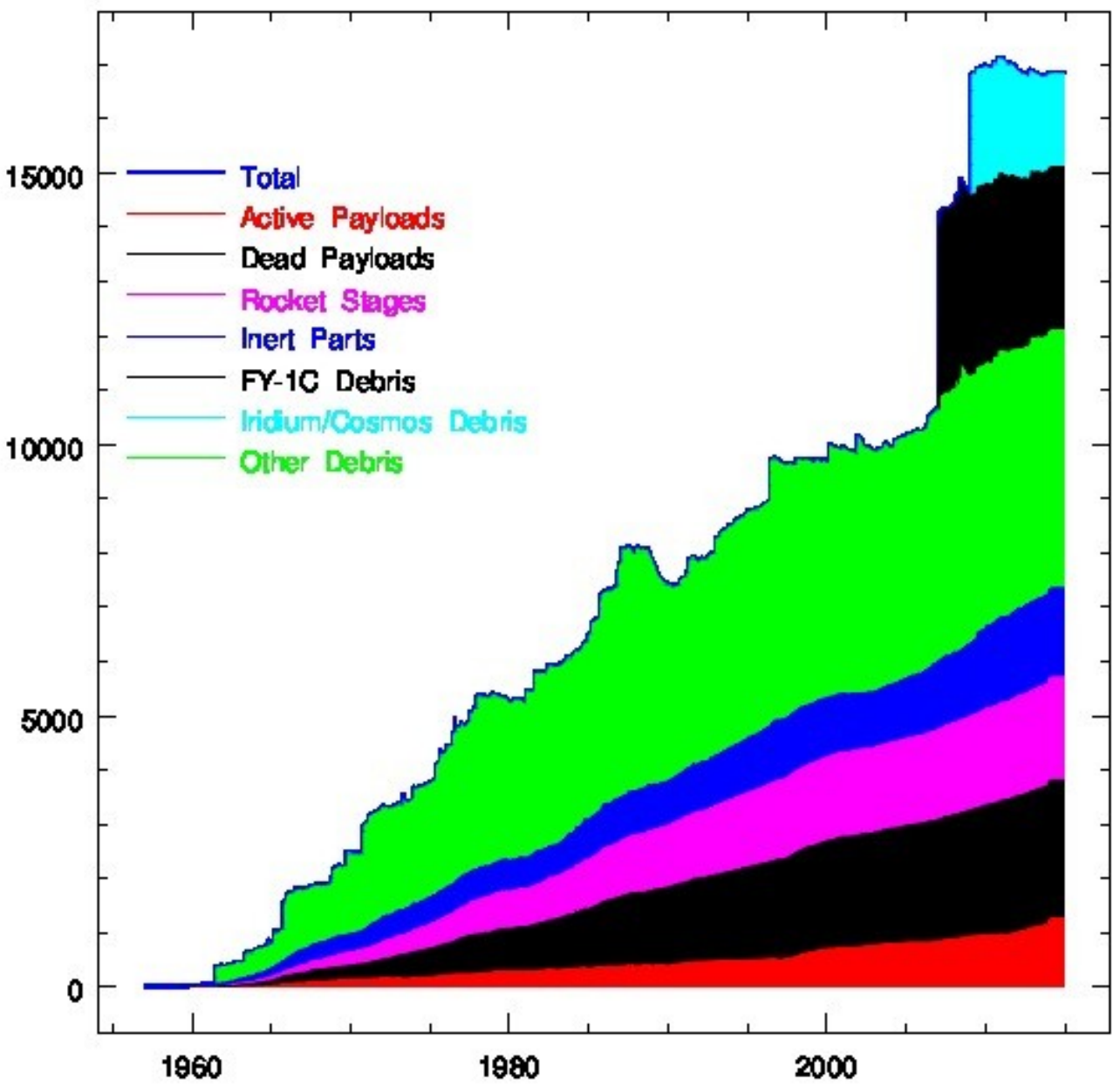

Space Junk - mass in metric tons

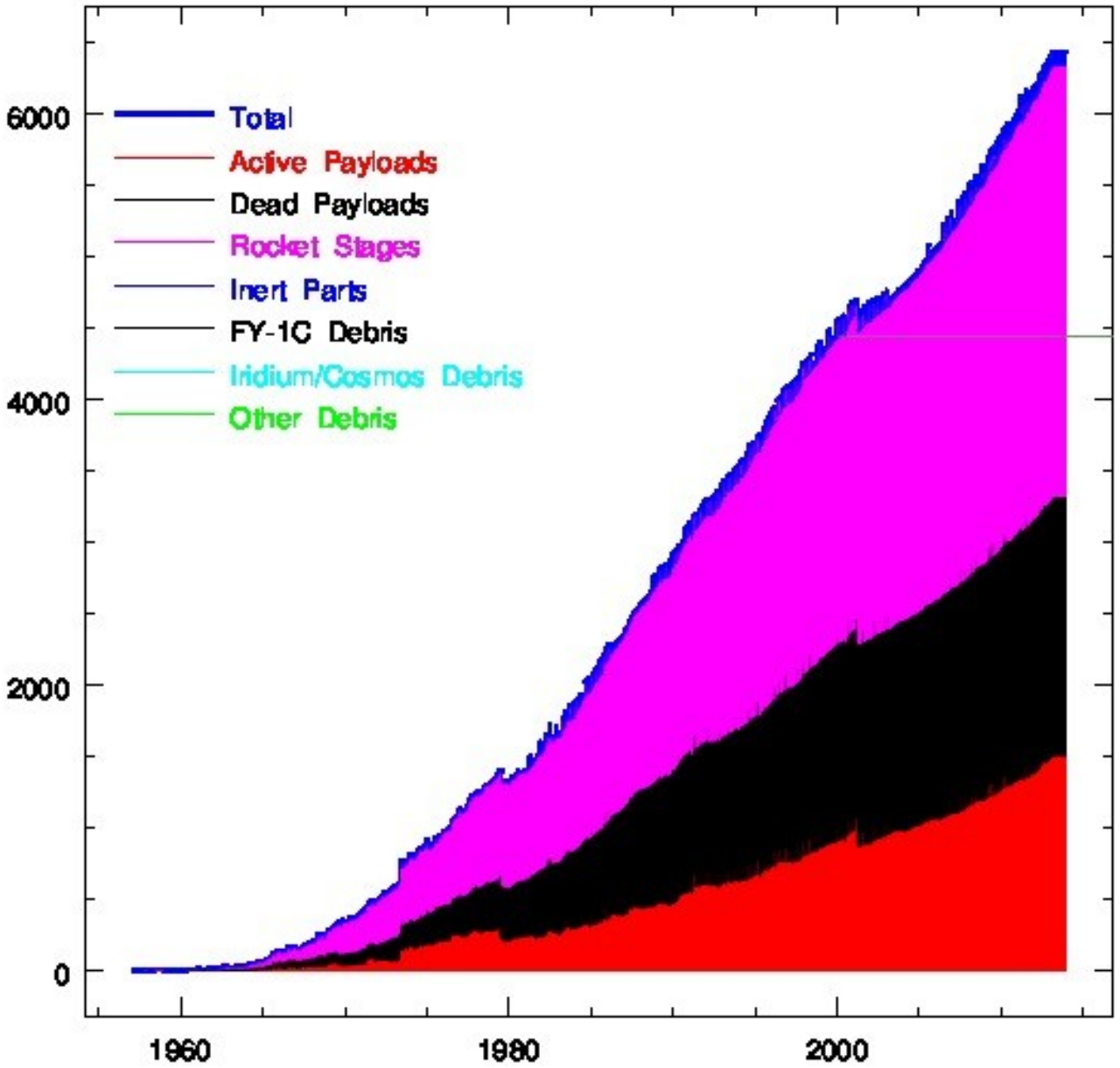

MH370 Flight Path

Flight path pieced together from primary and secondary radar, the INMARSAT connections, and the WSPR analysis.

Timeline

[A]: Takeoff (16:42)
[B]: Loss on Secondary Radar (17:21)
[C]: Loss on Primary radar (18:22)
[D]: SATCOM Log-On Request (18:25)
[E]: First Handshake (19:41)
[F]: Second Handshake (20:41)
[G]: Third Handshake (21:41)
[H]: Fourth Handshake (22:41)
[I]: Fifth Handshake (00:11)
[J]: Partial Handshake and Final Transmission (00:19)

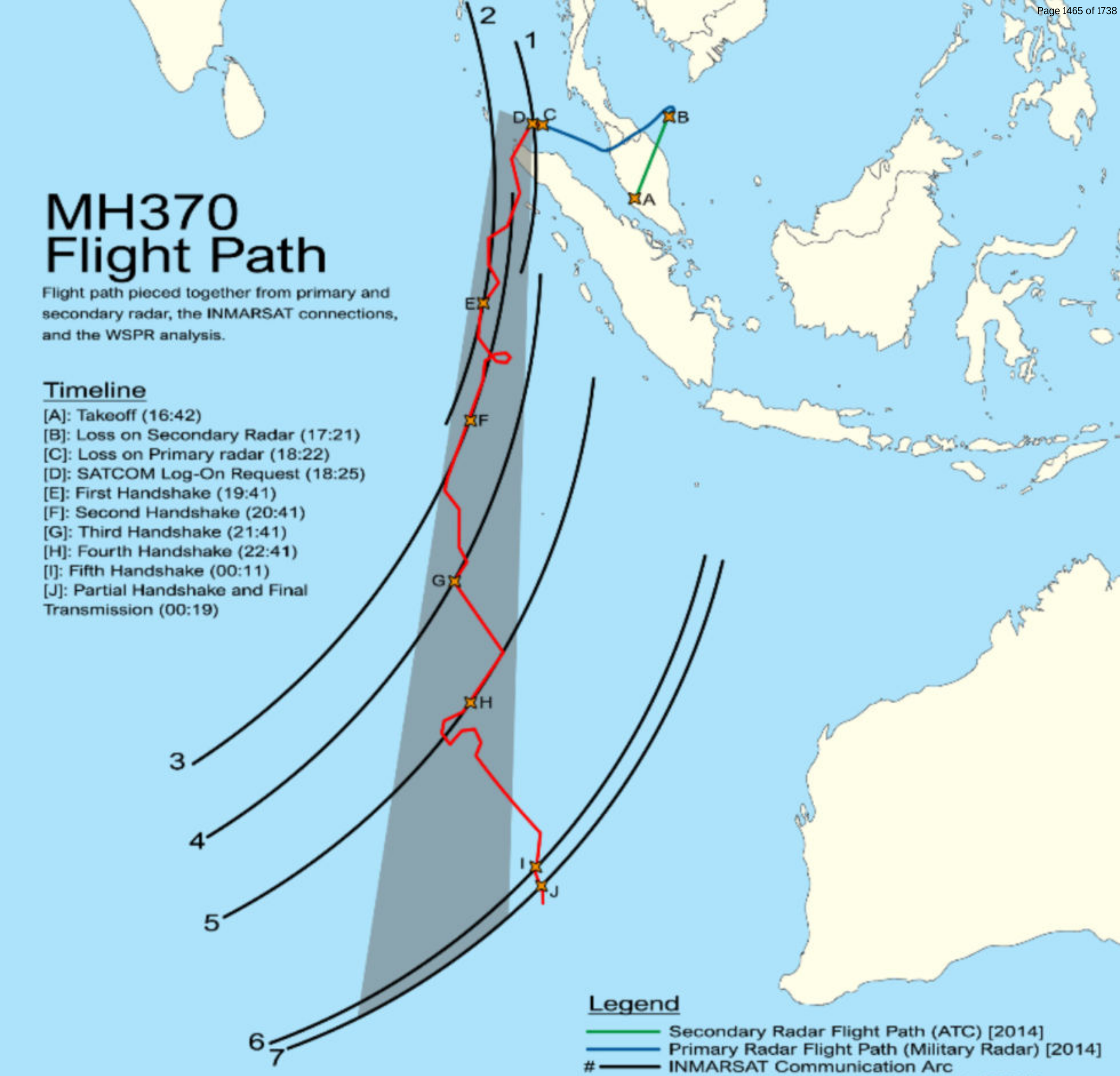

Legend

- Secondary Radar Flight Path (ATC) [2014]
- Primary Radar Flight Path (Military Radar) [2014]
- # INMARSAT Communication Arc
- INMARSAT Flight Path Uncertainty [2014]
- WSPR Flight Path [2022]
- Key Point

Analysis of Flight MH370

From waypoint VAMPI until the estimated touch down

Captain Patrick Blelly, Jean-Luc Marchand
patrick.blelly@protonmail.com, jean-luc.marchand@mh370-caption.net
Version 4a - May 13th, 2022 - updated June 24th, 2022

Note: Part of this document may be used or copied with no restriction under the condition that its full title, its version number and date and the author's name are included on all such copies and derivative work.

Executive Summary:

Reconstructing the proposed probable trajectory took four years and was possible thanks to publicly available material and information. The main findings of this study and some complementary aspects have been recently published in a book [1]. This paper presents the methods, the computations and their justification and the results in more details.

The following elements have been addressed:

1. The reconstructed trajectory using proven aeronautical computations based on:
   a. The fuel quantity at 02h28 MYT[1] estimated and reported by Boeing in the Appendix 1.6E of the official report in 2018 [2].
   b. Inmarsat satellite arcs which are considered trustworthy.
   c. Meteo information of the day used by pilots (wind maps, temperature reports etc.)
   d. In Flight Performance tables for the B777-200ER with Rolls-Royce Trent 892 engines.
   e. Specific technical data to 9M-MRO like the "performance factor" of the fuel consumption

2. BTO and BFO[2] values computed along our trajectory match the official reported measured values since they are within Inmarsat defined margins of +/-50 µs and +/- 7 Hz respectively.

The following conclusions were drawn:

1. The reconstructed trajectory is similar to Inmarsat's example published in the report "the Search for MH370" [3]. Figure 1 below allows comparing the reconstructed trajectory in yellow with Inmarsat's example in red.

2. Inmarsat "loss of contact point" is very close to the reconstructed trajectory path and coincides well with our estimated location where the second engine was voluntarily shut down (cf Figure 3).

3. The northernmost probable point of impact (POI) identified in this study is located at [35°39'S ; 93°01'E]. It is very close to the POI computed by CSIRO forward drift analysis reported in their report n°III of 26 June 2017. In addition, potential debris have been photographed by the French CNES Pléiades 1A satellite in this area.

4. For the end of flight, two slightly different possible scenarios have been elaborated. Both include a gliding phase with a final controlled ditching producing little debris. Scenario 1 is illustrated in figure 2.

5. From these scenarios, a zone for a new search of the wreckage is proposed (yellow area in figure 3) which extends the already searched area in 2018 to the south by about 38Nm. Its width is ~16Nm. The estimated duration to scan this area of ~600Nm2 is approximately 10 days according to recent information provided by Ocean Infinity which was the last company searching in the field in 2018.

[1] *MYT: Malaysian Time*
[2] *BTO: Burst Time Offset ; BFO: Burst Frequency Offset*

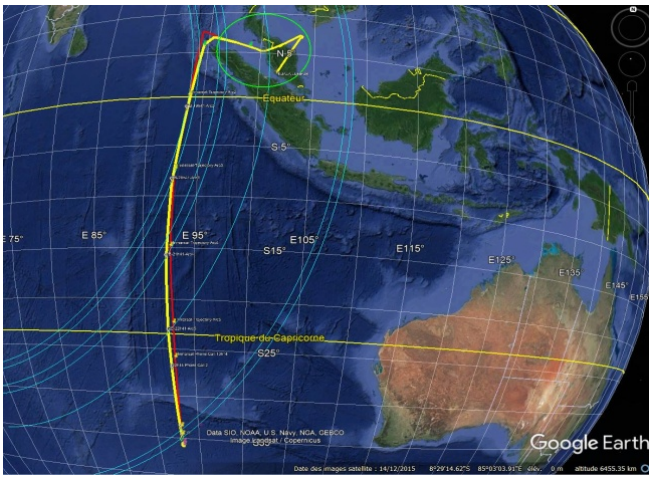

Figure 1: Reconstructed trajectory (Yellow) and Inmarsat example (Red)

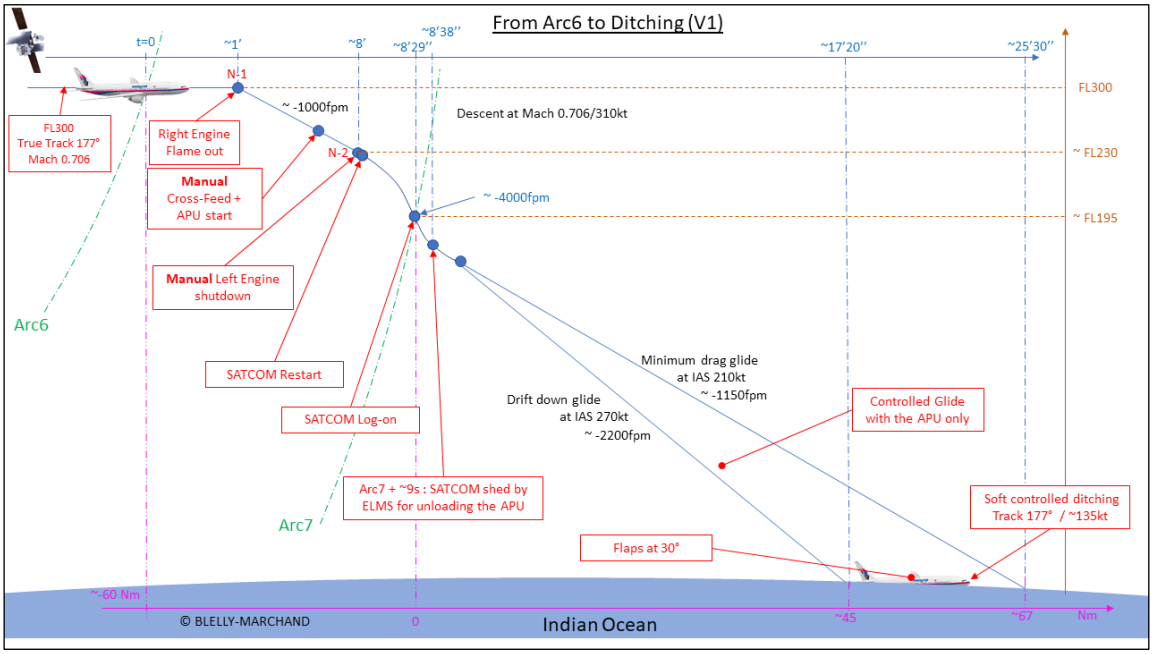

Figure 2: Scenario 1 of the probable final descent of MH370 with a glide

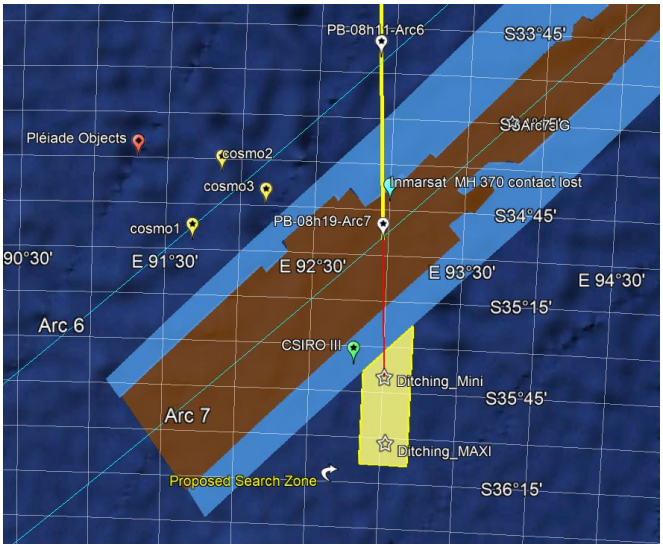

Figure 3: Proposed search zone (Yellow, ~600Nm^2) and CSIRO III estimated Point of Impact

Table of Contents

1 Introduction 3
2 The « Final Major Turn » (FMT) 4
3 The Southern Part of the Trajectory 7
3.1 Speed and Altitude Computation 7
3.2 Reconstructing the “Southern Leg” 10
3.3 Validation of the “southern leg” with Inmarsat data 12
4 The Final Descent to the End of Flight 15
5 The proposed new search zone 18
6 Additional elements of interest … 19
Annex 1: Variant 2 of the End of Flight 20
References 21

1 Introduction

This paper presents the findings of a study focused on reconstructing the portion of the trajectory, which starts shortly before 02h22 MYT when the aircraft exited the Malaysian radar coverage. The previous portion of the trajectory does not need a specific aeronautical analysis. Thanks to the radar data it is almost certain that the aircraft overflew waypoint *VAMPI* located in the north-west of Sumatra. Then its radar blip was lost few minutes later after passing close to waypoint *MEKAR*.

Thus, to ease the understanding, the starting point of this analysis was chosen to be waypoint *VAMPI* as it is the last precisely known location of the aircraft with its timing at 02h13’ MYT on March 8th, 2014:

1. Section one addresses the leg from passing waypoint *VAMPI* until the phone call of the ground at 02h40’. It includes a slow turning manoeuvre to the south which is commonly called FMT (Final Major Turn).
2. Section two details the reconstructed trajectory after the FMT which is almost a straight line to the south. The selected flight settings and characteristics are provided here.
3. Section three aims to identify the scenario of the final descent and the related actions performed by the pilot in command leading to a probable soft ditching creating a minimum number of pieces of debris.
4. Section four concludes on the characteristics of the identified zone where to search the wreckage and which is proposed as a viable candidate for future underwater search campaigns.
5. Finally, complementary and relevant elements are brought to attention in Section 5.

One should keep in mind that what is presented in this report is a highly probable reconstructed trajectory. But until such a moment when the wreckage is found, it remains a hypothesis still.

2 The « Final Major Turn[3] » (FMT)

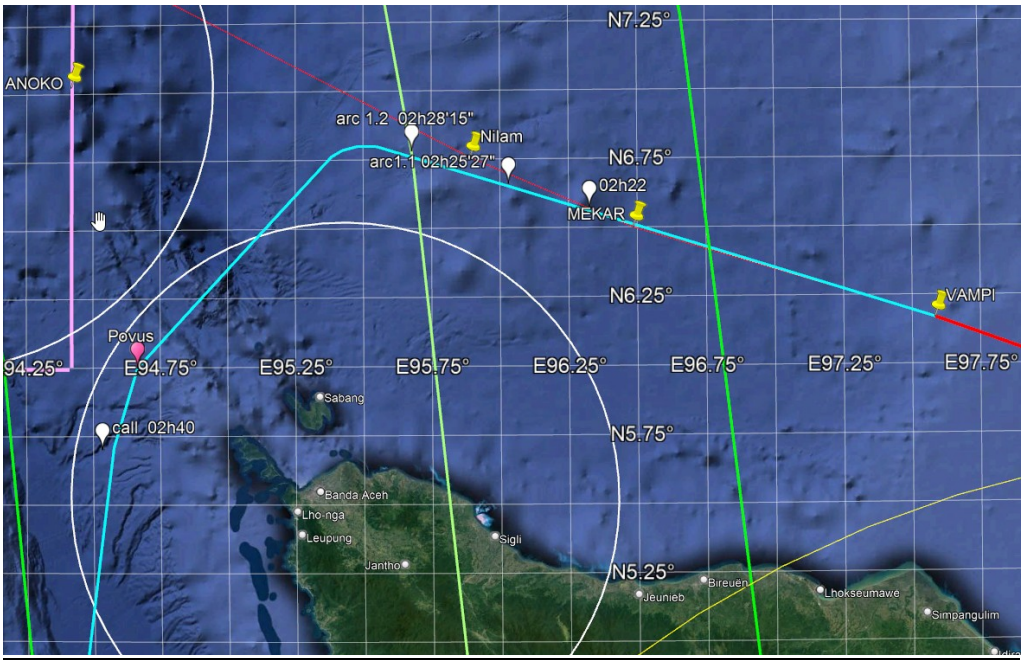

Figure 4: The Final Major Turn (FMT) in the north-west of Sumatra: a succession of 2 light turns

Preamble

- Back to the first part of the flight and just after the U-Turn after IGARI, one should remember that the pilot in command (PiC) most probably performed several actions affecting the aircraft trajectory. The main actions would be: a probable descent to FL300 (~30000ft) and, following the loss of the electrical power, to leave the throttles untouched resting in their current position. This is in line with Boeing report [2]. Together, these actions led to a progressive increase of the ground speed up to 516kt. At ISA +14°, the Indicated Air Speed (IAS) would have been at ~310kt with possible peaks at 330kt.
- The PiC changed flight level down to FL300 because he knew that usually at this late time in the night in this region this level was not much used. In addition, this induced a higher ground speed as well as a less cold temperature inside the cockpit [1].
- In addition, the current high speed would have allowed him to exit the Malaysian radar coverage quickly in the vicinity of waypoint *MEKAR* after overflying *VAMPI*.

<u>From *VAMPI* to the 1st Phone call from the ground at 02h40' MYT (cf figure 4):</u>

- It appears that after overflying waypoint *IGARI*, *VAMPI* has been the last waypoint exactly overflown by the MH370. This implies a well-controlled navigation by the pilot in command to turn around FIR Jakarta (Sumatra Island) while staying outside the alert surveillance zone.
- From waypoint *VAMPI*, the route is found constant at 287° until about 02h29' MYT i.e. shortly after the bursts at 02h28' MYT. The identified trajectory passes slightly north of waypoint *MEKAR*. This is in accordance with the famous picture presented to the families at the Lido Hotel by the Malaysian authorities. Until about 10Nm after MEKAR, at 02h22' MYT, the

[3] *FMT: commonly used terminology to designate the manoeuvre to the south considered as the last turn*

estimated ground speed was ~516kt. This corresponds well with the loss of contact by Western Hill radar. Figure 4 sketches this manoeuvre.

- Clearly, the pilot in command aimed to turn around Sumatra as fast as possible and as discreetly as possible at the limit of mid-range radar coverage.
- Considering Inmarsat findings [3], a left turn has probably been executed at 02h29' (or just after) towards waypoint POVUS approximately, possibly at the limits of Banda Aceh radar and avoiding entering Indian FIR Chennai. After the turn and considering the wind, the estimated ground speed would have slightly decreased down to ~503kt and still at ~310kt IAS. This gradual decrease of speed was probably due to a transition phase towards a stable flight at a constant Mach.
- At 02h40' MYT which is the time of the first phone call from the ground to the aircraft, in the vicinity of waypoint POVUS, the ground speed (GS) is estimated at ~456kt.
- This helps identifying the approximate location of the aircraft at the time of this unsuccessful phone call (Cf. Table 4).
- From that moment, computations show that the estimated speed was basically constant all the way long to the south at a constant Mach of 0.706. The analysis presented in [1] demonstrates that this corresponds to an indicated speed (IAS) equal to 265kt at FL300. This could appear as a paradox, but it is not. Mach 0.706 is 5% lower that the Long-Range Mach and also well below the Maxi Range Mach. But most probably, by experience, the PiC took advantage of the correlation between the decrease of speed and the subsequent decrease of fuel consumption of the same amount (-5%). These effects produce a net result of the same flown distance as in the Long-Range mode but in a slightly longer time at no extra fuel cost in the absence of climb. During this particular flight and contrary to normal operational practices, the fuel was practically fully consumed at cruise level and no consideration of the descent is necessary as it glided. From a pilot experience, it is believed that the chosen mode was "Mach Selected" as no route input was possible in the FMC.
- Concerning the electrical power status, all facts during the leg starting at waypoint IGARI concur to conclude that it was switched off voluntarily in a reversible way. This would have triggered the deployment of the RAM Air Turbine (RAT) which satisfied the essential electrical power needs. Thus, the aircraft could have been piloted with the basics systems alone but with the full hydraulic power - still available at that time - from the running engines.
- In order to recover the full functionality of the systems, the PIC switched the electrical power back on at about 02h23' MYT triggering the reboot of the SATCOM and its Logon request at 02h25'27 MYT according to the Inmarsat data. In order to maintain the aircraft "invisibility" and to avoid to be recognised by the ground, a "data link reset" has been completed just after the power was switched back On via the "com manager" followed by an "auto message off" command. These actions erased the Flight ID (which was missing in due places in the subsequent bursts) and also instantaneously blocked the sending of ACARS messages. Thus, no identification nor any exchange of information were possible anymore. Nevertheless, the SATCOM was still powered and continued to respond to the (almost) hourly handshakes initiated by the ground.

The details of the FMT are posted in Table 4.

Table 4: Detailed characteristics of the reconstructed trajectory during the FMT

Waypoint	longitude °	latitude °	longitude °	latitude °	True Track °	Ground Distance Nm	Wind kt	temperature °C	ISA °C	Air Distance Nm	Delta Time min s	Total Duration min s	Mach	True Airspeed kt	Ground Speed kt
VAMPI	97°35'01.00"E	6°10'09.00"N	97.5836	6.1692									0.845		
					287	68.5	14	-31	14	67	8'	-		502	516
MEKAR	96°29'05.00"E	6°30'02.00"N	96.4847	6.5006									0.832		
					287	10	14	-31	14	10	1'10"	-		502	516
02h22' *	96°19'46.41"E	6°33'31.83"N	96.3296	6.5588									0.832		
					287	18	9	-31	14	24.7	3'	3		494	503
Arc1 02h25'27"	96°02'24.37"E	6°39'01.23"N	96.0401	6.6503									0.814		
					287	22	9	-31	14	24.7	3'	6		494	503
Arc1.2 02h28'15"	95°41'13.35"E	6°45'22.48"N	95.6870	6.7562									0.814		
					287/223	81	9	-31	14	78.2	9'30"	15"30"		494	503
POVUS	94°39'55.80"E	6° 00'02.40"N	94.6655	6.0007									0.734		
					197	18	10	-31	14	18.6	2'30"	18"		446	456
Phone Call 1 02h40'	94°37'37.44"E	5°42'34.56"N	94.5771	5.7096	187								0.706		

* Time is given in Malaysian time (MYT)

3 The Southern Part of the Trajectory

3.1 Speed and Altitude Computation

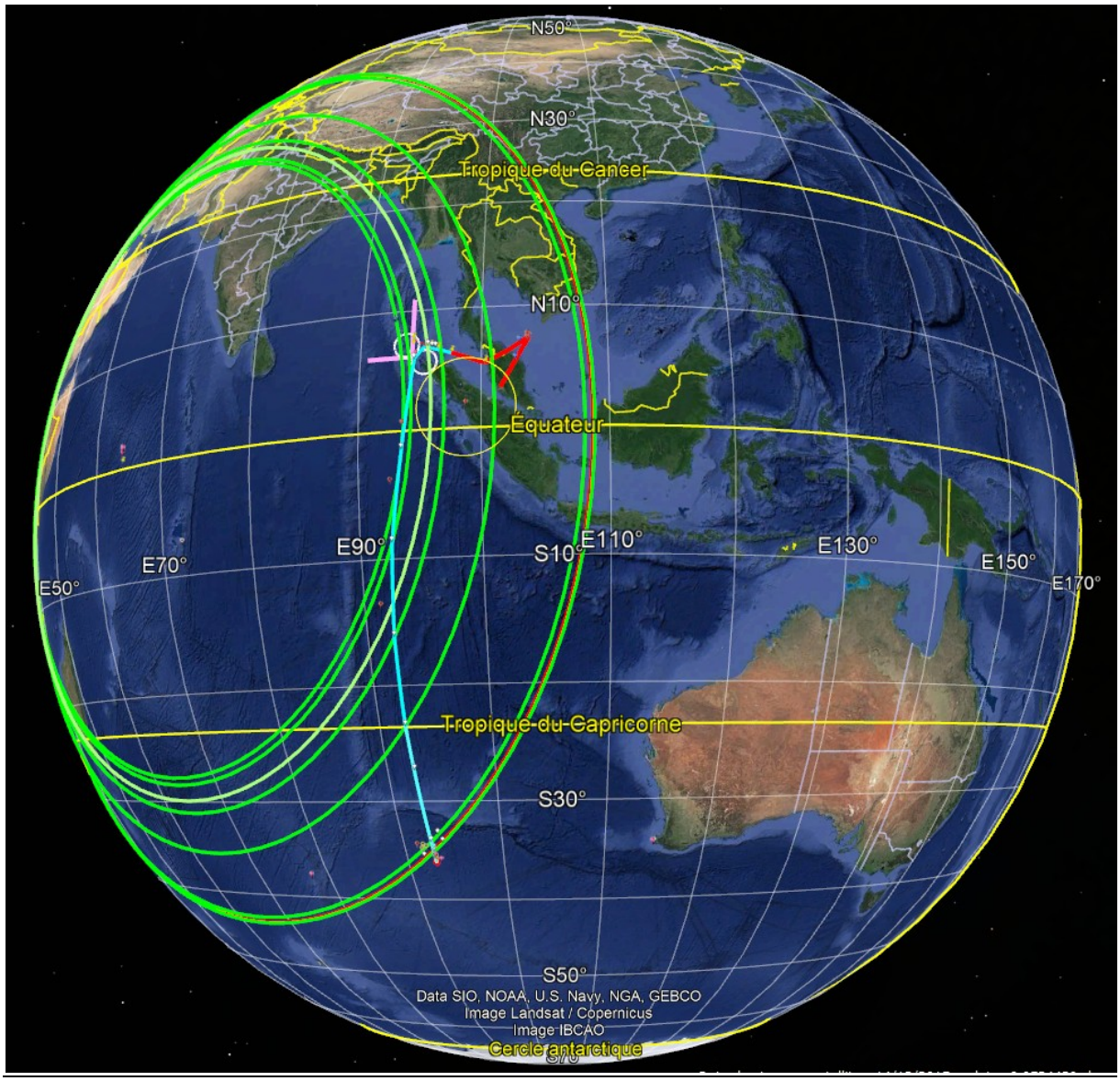

Figure 5: Southern part of the reconstructed trajectory (Cyan)

The first point of the southern part of the trajectory (we will also call it “Southern leg”) is the location of the aircraft at 02h40’ MYT when the 1st phone call took place. The last point is taken as the crossing point at Arc 6. This last point is specifically addressed in the next section where it is considered as the starting point of the final leg.

In order to reconstruct the southern part of the trajectory (illustrated in Cyan in figure 5), the following hypotheses were made and the following data was used:

1. At 02h28' MYT, the amount of fuel remaining on board has been officially evaluated by Boeing at 33524 kg.
2. An assumption is made here that a speed decrease took place (justified below in this report) from M0.814 at ISA +14° (M0.838 at ISA cf Boeing in [2]) within approximately 12 minutes before the phone call. During this time about ~1120kg of fuel was burnt when considering an averaged Mach and the fact that the engines were idle during approximately 1.5 minutes as experimented during simulations.
3. Thus, at 02h40 MYT, the amount of fuel remaining on board is estimated at ~32400kg.
4. Arcs have been precisely constructed per altitude using Inmarsat official reported data.
5. For that day, Meteo and wind data and temperature data for ISA correction have been used for FL300.
6. "Performance in flight" data of the B777-200ER powered by R&R Trent-892 engines has been used.
7. Corrections for the overall fuel overconsumption were applied as follows: +1.5% of perf factor (aging of the engines) and +1.2% due to a high temperature on that day based on an estimation of an average ISA +12° and following Boeing's recommendation to add +1% per 10° of extra ISA.
8. The flight time estimated by the ATSB between 02h40' MYT and the supposed flame out of the second engine – two minutes before the last logon request at 08h19'39 MYT – is 5h37'30"" i.e. 5.625 decimal. *Note: This is a starting working hypothesis as in our actual End of Flight scenario the logon request comes approximately ~30 seconds after the left engine manual shut down with the APU operating.*

From these hypotheses and data, straightforward, coherent computations can be made:

1. The hourly consumption is equal to the average (33524kg – 1120kg) /5.625h = 5760kg/h. This represents the actual hourly fuel consumption on that day including the +2.7% of overconsumption coming from the two factors identified above.
2. At mid-term of the southern route i.e. ~05h28' MYT, the aircraft **average** mass is estimated at ~190.6 tonnes. For the sake of simplification, we will truncate this value down to 190t. The actual impact on the final result of the following computation is negligeable.
3. In Boeing's look-up table "performance Inflight Long Range" for the B777-200 ER, one has to look for the value 5760 kg/h for reference weight of 190t. Unfortunately, this entry does not exist nor does FL300 exist. Thus, a double cross-interpolation is required. A relevant extract of the lookup table is provided in figure 6 along with the details of the computation.
4. The interpolation results in 5904kg/h for Mach 0.743 in Long Range mode at FL300. In order to match the value of 5760 kg/h for 190t, one must deduce 5% and then add +2.7% because of the overconsumption (cf above) since the look-up table is provided for brand new engines at ISA.
5. Considering this result and reading the point -5% of fuel flow from the nominal point (1;1) on the curve "B777-200ER Cruise Mach, Fuel Flow, and Ratio of Specific Air Range to LRC Specific Air Range" given in figure 7, one can see that the ratio is also 1 at this other point. Thus at -5% fuel flow, the air range is identical to LRC range according to Boeing. On the abscise axis, one can read that the ratio of Mach to LRC Mach is 0.95 i.e. a 5% reduction.
6. Thus, applying this reduction to the speed, one can conclude that for FL300 the Mach number becomes M 0.743([4]) – 5% = M 0.706. It must be noted here that the corresponding computed air range value is in adequacy with the Mach of the MRC mode indicated par Boeing in table 4 of Appendix 1.6E [2].

[4] *LRC Mach is given as 0.743 after interpolation from the look up table and 0.742 in the graph. The impact of this difference is negligeable.*

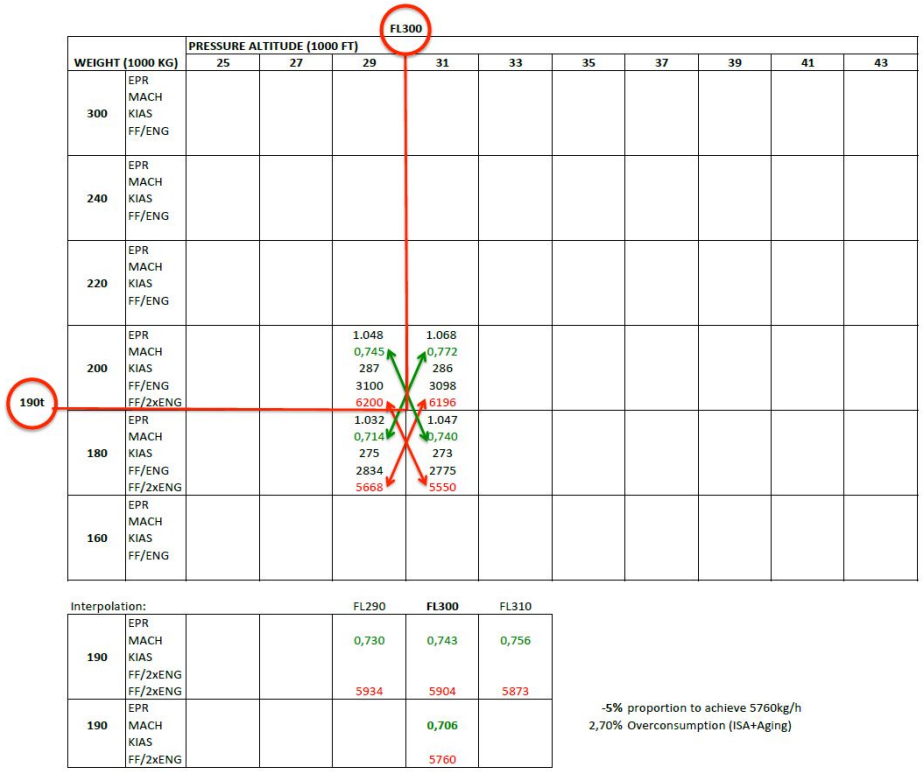

WEIGHT (1000 KG)		PRESSURE ALTITUDE (1000 FT) 25	27	29	31	33	35	37	39	41	43
300	EPR MACH KIAS FF/ENG										
240	EPR MACH KIAS FF/ENG										
220	EPR MACH KIAS FF/ENG										
200	EPR MACH KIAS FF/ENG FF/2xENG			1.048 0,745 287 3100 6200	1.068 0,772 286 3098 6196						
180	EPR MACH KIAS FF/ENG FF/2xENG			1.032 0,714 275 2834 5668	1.047 0,740 273 2775 5550						
160	EPR MACH KIAS FF/ENG										

Interpolation:				FL290	FL300	FL310
190	EPR MACH KIAS FF/2xENG FF/2xENG			0,730 5934	0,743 5904	0,756 5873
190	EPR MACH KIAS FF/2xENG				0,706 5760	

-5% proportion to achieve 5760kg/h
2,70% Overconsumption (ISA+Aging)

Figure 6: Extract of the look-up table from the FCOM - Long Range Cruise Control Trent 892 (Source PMDG and Airlines [5])

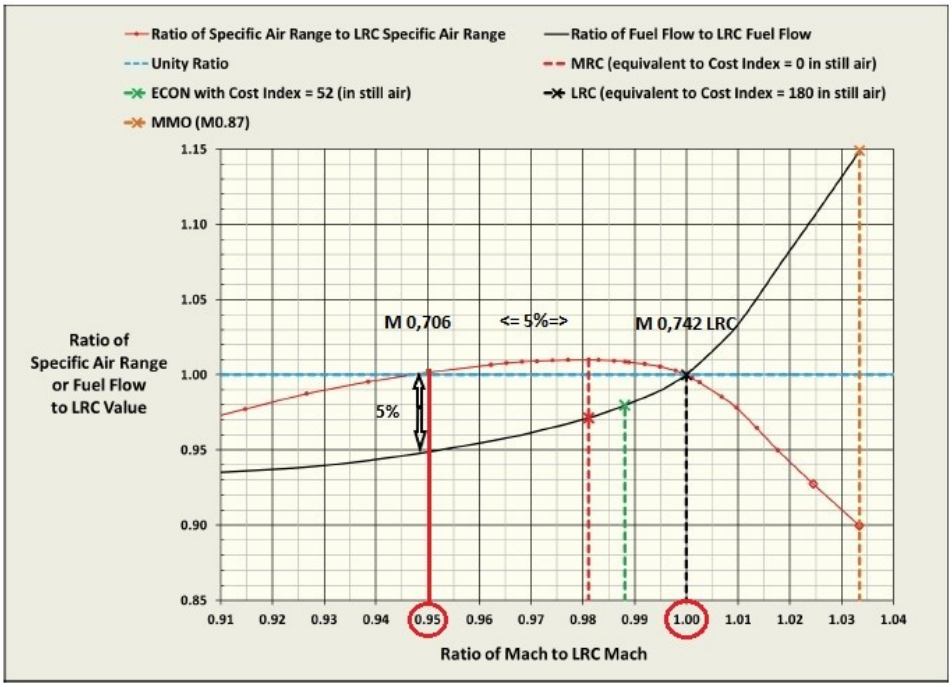

Figure A-1. B777-200ER Cruise Mach, Fuel Flow, and Specific Air Range

Figure 7: Specific consumption-distance for the B777-200ER (Source: Independent Group [6])

Under these conditions, one can conclude that the flight level was indeed FL300 with a Mach equal to 0.706 (i.e. IAS of 265kt) and that, during the southern leg of the trajectory, the hourly fuel consumption was indeed 5760kg/h in average.

3.2 Reconstructing the "Southern Leg"

Keeping the hypothesis of a levelled flight at a constant Mach, the southern leg can be reconstructed in using straight line segments between the arcs taking into account the local meteo conditions. This leads to (in MYT time):

1. From 02h40 to 03h41 (arc 2) = 61' => TAS[5] = 429 kt, GS = 435 kt and Distance = 442 Nm. The great circle distance of 442Nm is "drawn" from the location of the 1st phone call at 02h40' to intercept arc 2.
2. From 03h41 to 04h41 (arc 3) = 60' => TAS = 429 kt, GS = 436 kt with distance = 436 Nm
3. From 04h41 to 05h41 (arc 4) = 60' => TAS = 429 kt, GS = 440 kt with distance = 440 Nm
4. From 05h41 to 06h41 (arc 5) = 60' => TAS = 428 kt, GS = 437 kt with distance = 437 Nm
5. From 06h41 to 08h11 (arc 6) = 90' => TAS = 426 kt, GS = 419 kt with distance = 629 Nm

The detailed characteristics of the southern leg of the reconstructed trajectory are posted in table 9. Figures 1 and 5 graphically illustrate this southern leg.

Making an "aeronautical reading" of the data show that probably in the first place the pilot input a magnetic track reference at 187° on the MCP[6] and that later, somewhere south of the Tropic of Capricorn between 23°S and 25°S, he input a true track reference at 177° making the southern leg a quasi-straight line.

The initial selection of 187° magnetic heading is justified by the presence of adverse cumulonimbus clouds off the north-west coast of Sumatra as depicted in Figure 8.

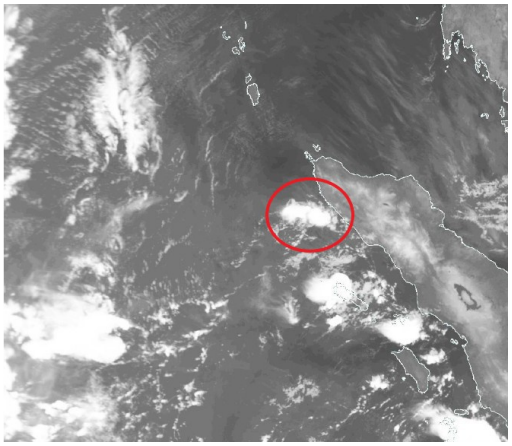

Fig. 8a

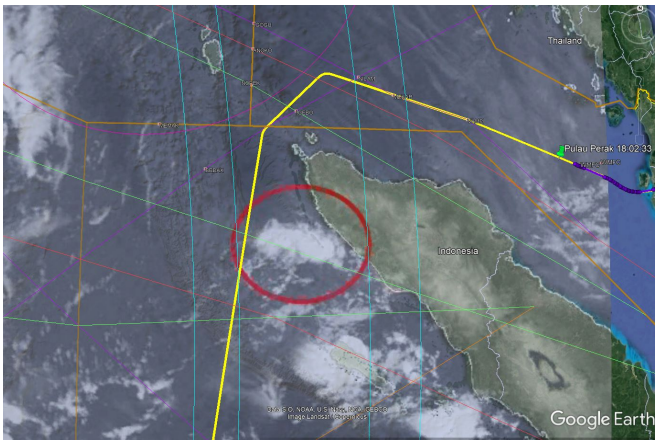

Fig. 8b

Figure 8 : Heading selection to avoid meteo obstacles when exiting the FMT

[5] *TAS: True Air Speed*

[6] *MCP: Mode Control Panel*

Table 9: Detailed characteristics of the "southern leg"

Arc MYT	Longitude °	Latitude °	Longitude °decimal	Latitude °decimal	True Direction °	Ground Distance Nm	Wind °/kt	Tempera-ture °C	ISA °C	Air Distance Nm	Delta Time h min s	Total Time min s	Mach	True Air Speed kt	Ground Speed kt
02h40'	94°34'37.44"E	5°42'34.56"N	94.5771	5.7096									0.706		
					187	442	023/6	-31	14	436	1h01'	1h01"		429	435
03h41' arc2	93°37'28.56"E	1°31'17.76"S	93.6246	-1.5216									0.706		
					187	436	050/10	-31	14	429	1h00'	2h01'		429	436
04h41' arc3	92°40'37.20"E	8°45'28.80"S	92.6770	-8.7580									0.706		
					183	440	000/11	-31	14	429	1h00'	3h01'		429	440
05h41' arc4	92°18'41.76"E	16° 7'25.32"S	92.3116	-16.1237									0.706		
					180	437	052/15	-32	13	428	1h00'	4h01'		428	437
06h41' arc5	92°22'33.60"E	23°24'29.88"S	92.3760	-23.4083									0.706		
					177	629	260/40	-34	11	639	1h30'	5h31'		426	419
08h11' arc6	92°54'2.16"E	33°54'50.04"S	92.9006	-33.9139									0.706		
					177	60	260/25	-41	8	60.5	8'30"			430	423
08h19'29" arc7	92°57'53.65"E	34°54'53.58"S	92.9649	-34.9149								5h39'30"	0.702		
					177									440	436
08h19'38"	92°58'07.22"E	34°56'29.49"S	92.9687	-34.9415									0.7		

3.3 Validation of the "southern leg" with Inmarsat data

The next necessary step is to answer the question: how does the reconstructed trajectory compares to Inmarsat data? Table 10 presents the detailed characteristics of the full reconstructed trajectory. To ease the comparison, the same format has been used as in Table 9 of Inmarsat paper [3] when presenting their example of possible trajectory. This level of details offers the possibility to better understand the different components of the offsets (the BFOs[7] in particular). Extra elements have been also included like the BTOs[8] as additional waypoints allowing a more accurate comparison.

Please note that the same frequency bias δf = 150 Hz has been as in Inmarsat report. In the same spirit, the same first four waypoints are posted to demonstrate the precision of our computation tools. The first tool is an Excel workbook initially created by Yap F. Fah, NTU, Singapore (Version 4) that we have enhanced gradually as our knowledge improved up to the current version 7. In particular, we have implemented an improved version of SK999-Satellite model which precisely fits Inmarsat ephemeris. The second tool, the Constraint Assessment Tool (CAT), is a specific homemade software developed in the frame of CAPTIO. It includes functions similar to the Excel workbook above enhanced with extra operational functions like the fuel consumption estimation, actual local meteo data 4D interpolation, arcs generation at any altitude, great circle route computation, debris drift simulation etc.

In Table 10, one can see that the reconstructed trajectory complies with the two Inmarsat defined constraints: its BTOs are within the error margin of +/-50µs and its BFOs are within the error margin of +/- 7Hz. Thus, this makes it an acceptable candidate.

Please note that Table 10 does not include the BFO (-2Hz) of the last burst emitted by the SATCOM at 08h19:38 MYT. This peculiar case is addressed as a variant of the scenario presented in the next section. Its details can be found in Annex 1 of this report.

[7] BFO: Burst Frequency Offset is a frequency shift due to an imperfect correction of the Doppler thus providing an instantaneous information on the speed and/or track of the aircraft

[8] BTO: Burst Time Offset provides an information on the instantaneous distance between the aircraft and the satellite at a given time

Table 10: Captain Blelly/Jean- luc Marchand's Reconstructed Flight Path Results (same formatting as Table 9 in Inmarsat report)

Reconstructed Flight Path Results (ref. Inmarsat paper Table 9)																Total Burst Freq. Offset BFO (Hz)			Burst Time Offset BTO (µs)		
									Δ Fup												
	Time UTC *	Lat°N	Lon°E	Altitude (100ft)	True Track (°ETN)	Speed (kt)	Speed (km/h)	Vertical Speed (fpm)	Aircraft (Hz)	Satellite (Hz)	Δ F down (Hz)	δ f comp (Hz)	δ Fsat + δ AFC (Hz)	δf bias (Hz)	Pred.	Meas.	Error	Pred.	Meas.	Error
Nominal-1-Inmarsat	16:30:00	2.70	101.70	0	0	0	0	0	0	-6	-84	0	29	150	88	88	0	14893	14920	27
Nominal-2-Inmarsat	16:42:31	2.80	101.70	20	333	235	435	1200	194	-6	-80	-180	27	150	130	125	-5	14931	14900	-31
Nominal-3-Inmarsat	16:55:53	4.00	102.20	280	25	461	854	1500	-424	-4	-75	453	25	150	155	159	4	15212	15240	28
Nominal-4-Inmarsat	17:07:19	5.30	102.80	350	25	468	867	0	-461		-71	488	24	150	130	132	2	15587	15660	73
Arc1	18:25:27	6.65	96.00	300	287	503	932	0	774	-1	-37	-761	10	150	136	142	6	12560	12520	-40
Arc1.2	18:28:15	6.76	95.69	300	287	503	932	0	769	-1	-36	-755	10	150	137	143	6	12430	12480	50
Phone Call 1	18:40:33	5.71	94.58	300	187	428	793	0	165	-2	-30	-203	8	150	89	88	-1	11910	N/A	N/A
Arc 2	19:41:03	-1.52	93.62	300	187	435	806	0	11	-1	0	-51	-2	150	108	111	3	11520	11500	-20
Arc 3	20:41:05	-8.76	92.68	300	185	436	807	0	-169	6	29	130	-2	150	145	141	-4	11750	11740	-10
Arc 4	21:41:27	-16.12	92.31	300	182	440	815	0	-364	17	56	331	-18	150	171	168	-3	12820	12780	-40
Arc 5	22:41:22	-23.41	92.38	300	179	437	809	0	-533	30	78	508	-29	150	204	204	0	14560	14540	-20
Call 23h14	23:14:30	-27.22	92.55	300	177	419	776	0	-590	38	88	570	-33	150	224	217	-7	15700	N/A	N/A
Arc 6	00:11:00	-33.91	92.90	300	177	413	765	0	-681	50	100	670	-37	150	252	252	0	18040	18040	0
Arc 7	00:19:29	-34.91	92.96	195	177	433	783	-4000	-782	52	102	701	-38	150	186	182	-4	18430	18400	-30

* UTC = Malaysian Time – 8h

Figure 11 replicates Figure 9 of Inmarsat paper [3] for comparison. The red plot represent Inmarsat data as provided by Inmarsat in [3]. The blue curve represents the computed estimation of the BFOs of the reconstructed trajectory. The matching is very good as the standard deviation of the BFORs is σ ~3.9Hz. Furthermore, when considering the available extra BFOs (like the one we name Arc-1.2 for example) which are not usually considered by the other studies the BFOR σ becomes ~4.3Hz.

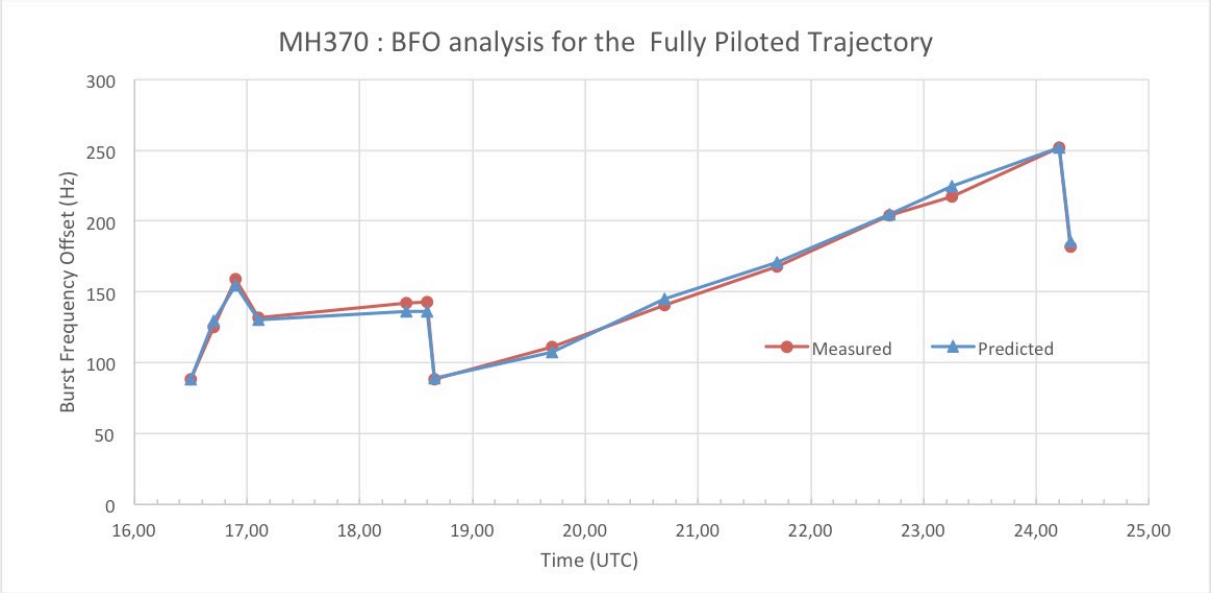

Figure 11: Comparison of Inmarsat BFO versus Captain's Blelly trajectory BFO (BFOR σ ~3.9Hz)

The comparison of the reconstructed trajectory with Inmarsat's example is presented in figure 12. Their similarity between arc 2 and arc 6 is striking. Nevertheless, the arc crossing points are different except those at arc 7 which are very close i.e. only 10Nm apart.

However, Inmarsat's final major turn (FMT) is wider and is located ~75Nm further to the northwest compared to the turn found here. The difference is explained by a greater average speed as well as a higher altitude in Inmarsat example.

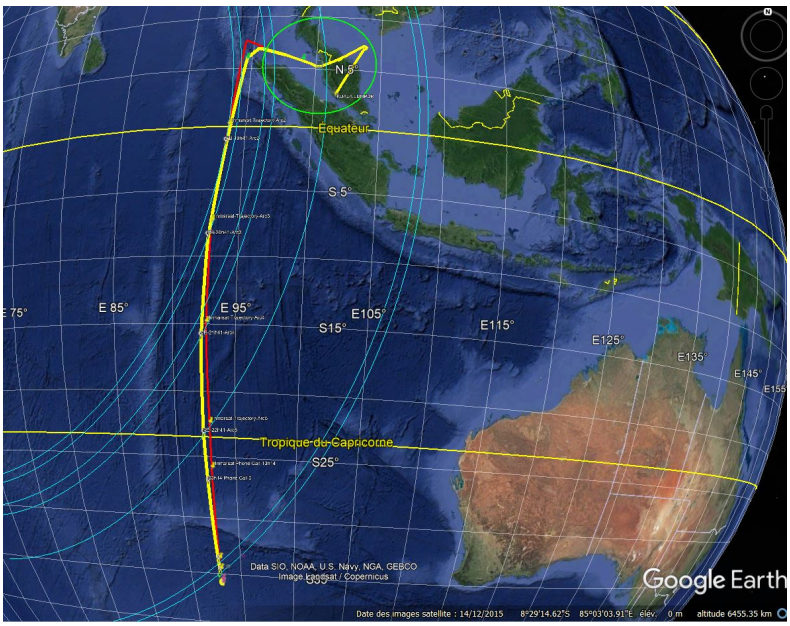

Figure 12: Trajectories comparison - the reconstructed trajectory (Yellow) and Inmarsat example (Red) (source Inmarsat)

4 The Final Descent to the End of Flight

The final descent is a phase which was – and still is – the object of numerous studies. A lot of them assumed that the aircraft was not piloted anymore when the descent started. Few made the hypothesis that the end of flight was well controlled by a pilot carefully preparing a ditching. This hypothesis of a well mastered descent from FL300 down to sea level ending in a controlled ditching is the basis of the work presented here.

The analysis was complex as numerous parameters had to be considered like the different horizontal speeds, the different average rates of descent, the remaining fuel at key points as well as the validation of this leg with the relevant measured BFO and BTO. Here is an attempt to detail the method in a simple way:

1. The hypotheses and the required basic parameters are:
   1.1. The shortest straight-line ground distance between arc 6 and arc 7 is 60 Nm flown by the aircraft in 8'30".
   1.2. The top of descent was at FL300 at Mach 0.706 with both engines running
   1.3. At the arc 6, the Inmarsat handshake was complete and normal.
   1.4. At the arc 6, the ground speed was GS=413 kt at ISA +4° (which increased to ISA +8° at sea level)
   1.5. The wind decreased from 260°/40kt towards 235°/25kt at lower flight levels
   1.6. At the arc 6, the quantity of fuel is estimated at about ~800 kg.
   1.7. The true track at 177° was kept from the top of descent to sea level
   1.8. In this method, the computations actually consider the crossing point of arc 7 as the starting reference location for measuring distances. This is where the logon request to the Inmarsat network was made within approximately 30 seconds following the power switch off. It occurred due to a "break power transfer" which automatically triggered a reboot followed by a logon request. It is assumed that the OCXO[9] of the SATCOM did not cool down in such a short time.
   1.9. Going backwards from the arc 7 to the arc 6, the average speed could be computed taking into account the auto pilot automation and the management of the remaining fuel.
   1.10. The hypothesis is made that ***the pilot in command managed to keep the necessary quantity of fuel for the APU until touch down thus keeping all control surfaces operational for a well-controlled gliding descent*** and ensuring a full flaps configuration for a controlled ditching.

2. The different steps of the descent are sketched in figure 13. By setting a reference initial time at T_0=08h11' MYT, they can be detailed as follows:
   2.1. T_0= 0': at arc 6, both engines were running and the SATCOM answered the satellite ping. The remaining fuel is estimated at ~800kg. It was not evenly balanced between the tanks because the right engine was more consuming than the right one. At this point in time, the total fuel consumption of both engines was about 88kg/min i.e. 5280kg/h according to Boeing fuel performance table for the B777-200ER with a mass of 175t.
   2.2. T_1=+1': at about +1 min, the right engine flamed out because of a shortage of fuel in the right tank. This is illustrated by the "N-1" tag in figure 13. Thus, from this moment and for all aircraft systems, the power was supplied by the left engine only. Subsequently the auto pilot and the flight director were still functioning and available to the pilot who most likely kept the "Mach selected" mode active (it was being used in cruise until now). Thus, during the coming descent, the IAS will progressively increase and stay at 310kt which is the speed limit imposed by the flight envelop. The only reference setting input made by the pilot on the MCP for the A/P was a constant reference vertical speed value of V/S=-1000fpm. As a consequence, the TAS is estimated around ~430kt when the aircraft crossed FL210. This basically confirms that the aircraft did fly 60Nm in 8'30'' with an average ground speed of 423kt, wind considered. A key element to keep in mind is that the aircraft accelerated, which is only

[9] *OCXO: Oven Controlled Crystal Oscillator*

possible if the "Mach selected" mode is active. At a rate of descent of ~-1000fpm, the consumption of the unique running engine is estimated at ~71kg/min i.e. ~4300kg/h.

2.3. At the beginning of the descent after the right engine flame-out, ***the pilot started the APU and opened the fuel cross-feed valves*** to be able to use all of the remaining fuel and to dry out the tanks (the aircraft was descending with a negative pitch with a small quantity of fuel).

2.4. T_2 = +8'00": close to FL230/FL225 **the left engine was voluntarily manually stopped** as illustrated by the "N-1" tag in figure 13. Thus, the aircraft started gliding with a slight increase of the pitch. At this point, either by surprise or in a short period of inattention, a short lack of pitch control increased the vertical down speed during few seconds up to ~-4000fpm. This would have led the aircraft down to ~FL195 (19500ft).

2.5. T_3 = +8'29": Logon request from the SATCOM producing an estimated BFO of 186Hz compared to Inmarsat measured 182Hz. Remember that following the left engine cut-off few seconds ago, no more power was available to the left AC bus which powers the SATCOM. Thus, the APU – the sole remaining source of power – took over from the left engine and powered the left AC bus in addition to the right AC bus. This left AC bus power Off/On sequence induced a power-off/power-up of the SATCOM automatically leading to a logon request initiated at T_3.

2.6. T_4 = +8'38": within the 9 seconds after T_3 the SATCOM logon to the network was properly completed according to the protocol. But, contrary to the previous logons, no other airborne system could logon subsequently and in particular the IFE[10]. This leads to conclude with confidence that the ELMS (Electrical Load Management System) shed the low priority utility buses and loads for dedicating the power to the high priority systems like the demanding pumps providing the hydraulic power to the control surfaces. Subsequently the SATCOM was shed to avoid overloading the APU which was the sole source of power operating at that time.

At this point in time, the Inmarsat measured BFO of -2Hz raises questions. If this value is correct, it implies a rate of descent of -14500fpm meaning that the aircraft was diving just after the crossing of arc 7. No convincing technical explanation has been found for this "extraordinary" BFO. Nevertheless, we analyse it in Annex 1 of this report. Since all searches of the wreckage in this zone were unsuccessful and since very few debris were eventually found, the best interpretation is operational: the pilot recovered from this unexplained dive and the aircraft continued its controlled gliding descent before a proper ditching.

2.7. T_5 = +8'40" and later: The pilot could have used one of the two procedures he had been probably trained for:

2.7.1. Either a descent with the two engines inoperative at Boeing recommended IAS of 270kt called "drift down two engines inoperative". The estimated average ground speed would have been 306kt with a rate of descent of about ~-2200fpm corresponding to a descent from FL195 in less than ~9 minutes. Thus, the maximum estimated distance flown from arc 7 would be ~45 Nm (without considering the reduction of speed induced by the full flap at 30° at the very end) ending with a ditching at T_6 = ~ 17'20''.

2.7.2. Or a descent with the two engines inoperative at the minimum speed with the flaps at 0°. Therefore, its IAS would be Vref (function of the aircraft mass i.e. 175t) augmented by 80 kt which would mean an IAS = 210kt in this case. This would have allowed flying at no risk of stalling during approximately ~17 minutes in descent. The aircraft glide ratio led to a rate of descent around ~ -1150 fpm and an average ground speed of ~236kt. The maximum estimated distance from arc 7 would be about ~ 67 Nm (without considering the reduction of speed induced by the full flap at 30° at the very end). Thus, the ditching would have occurred at T_6 = ~25'30''.

2.8. The minimum crash zone coordinates are: **-35.6650° S and 93.0130° E**

2.9. The maximum crash zone coordinates are: **-36.0269° S and 93.0364° E**

[10] IFE: In Flight Entertainment - a system that manages the passengers communications (telephone, sms) and entertainment in the cabin

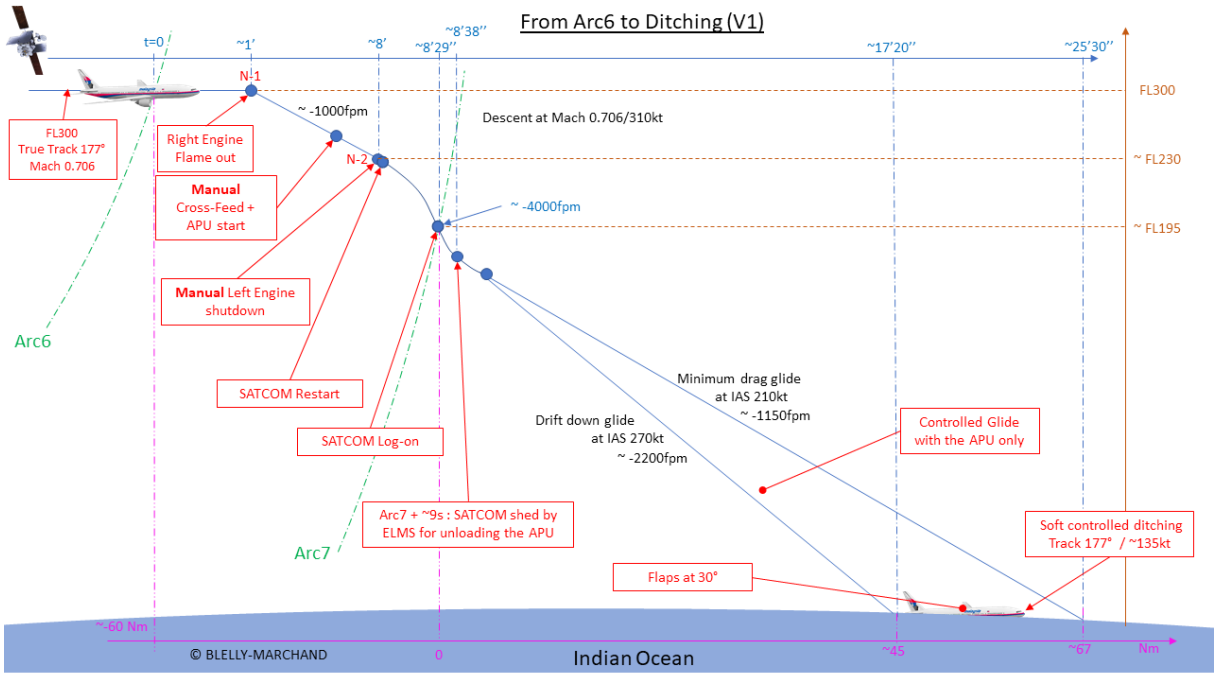

Figure 13: Considered end of flight scenario (Blelly-Marchand) – Variant 1

Figure 14 sketches the location of the northern and southern points which have been determined in function of the arc 6 and the arc 7.

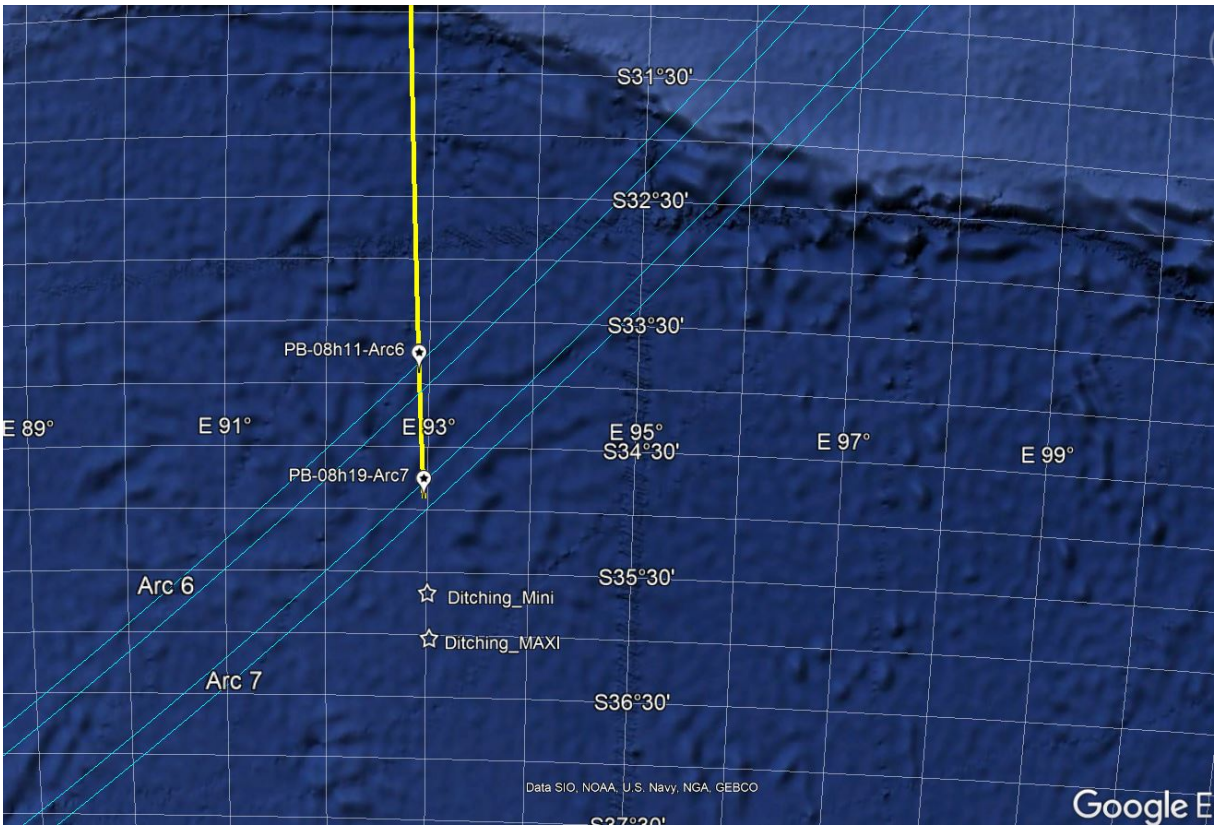

Figure 14: Estimated northern and southern locations of a controlled ditching (white stars)

5 The proposed new search zone

Not far from the identified locations of the potential ditching, two under-water search campaigns have covered areas on both sides of the arc 7 as illustrated in figure 15 in Brown (Fugro) and in Blue (Ocean Infinity). They have been unsuccessful because we think that the very good gliding capability of the plane had not been considered nor the possibility that a pilot was still in command.

The proposed new search zone is depicted in Yellow in figure 15. It is 14 Nm wide trapeze shape prolongating the already scanned zone to the south by ~37 Nm. The zone includes a contingency margin of ~7Nm on each side of the true track of 177° and on the southern limit to cover the case where the aircraft could have deviated slightly. This search zone is valid for both End of Flight scenarios presented in this report.

The proposed new search zone surface is estimated of ~600 Nm^2 approximately. It is small compared to the potential search zone of 10 000 Nm^2 envisaged by Ocean Infinity (sketched by the two Orange rectangles in figure 15) during a future 100-day campaign in 2023 or 2024. According to this daily rate, the proposed search zone would be scanned in less than 10 days.

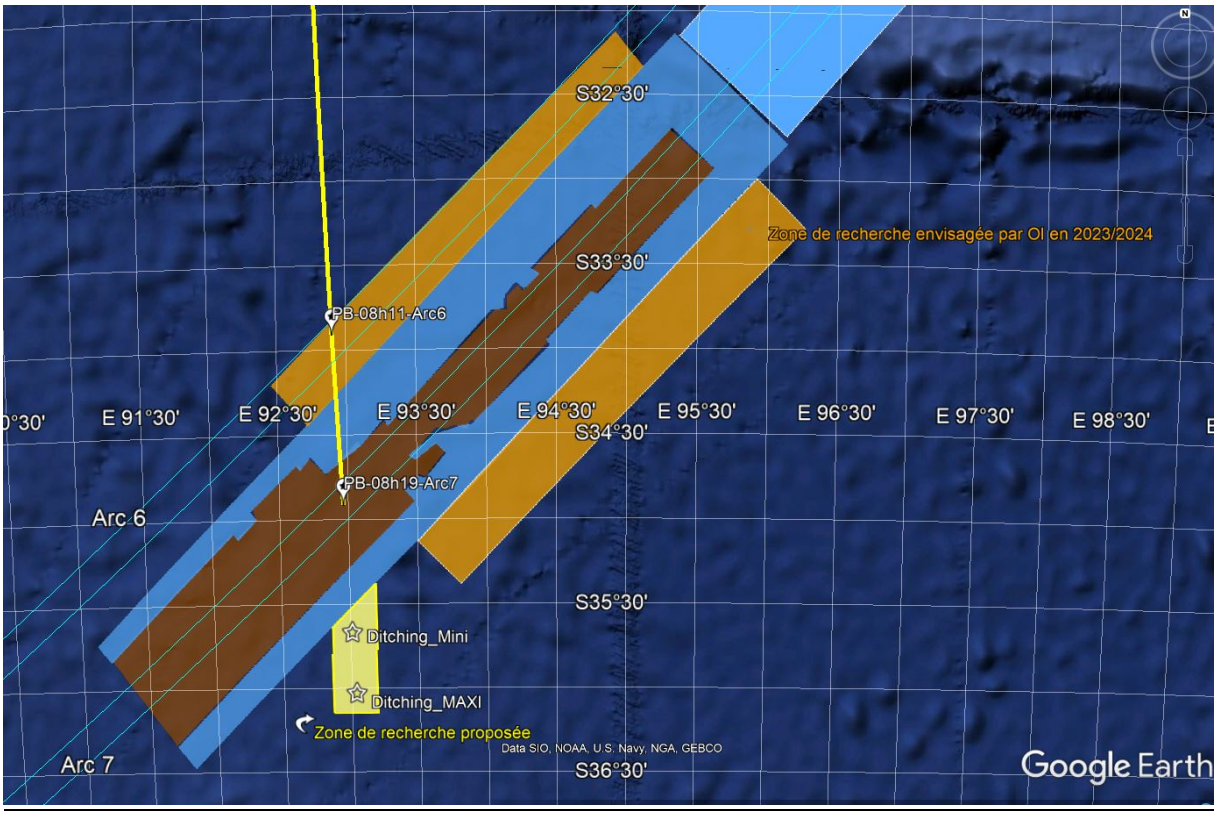

Figure 15: Proposed new search zone (Yellow area) potentially covered in less than 10 days

6 Additional elements of interest …

Several relevant elements must be mentioned in relation to the geographical location of the ditching zone and the proposed search zone.

The first element comes from the report on the analysis of the “optical” images captured by the French satellite PLEIADES 1A on 23 march 2014 [4]. From these images, a set of approximately 12 objects were identified as “possibly man-made”. All of these objects include a top surface of 20 m^2 or larger. Their geographical location is pinpointed as “Pléiades objects” in figure 16. This is in coherence with the results of one of the drift studies from the Australian organisation CSIRO (CSIRO report III).

In addition, Italian satellite COSMO-Skymed provided Synthetic Aperture Radar (SAR) data acquired on 21 March 2014. The geographical location of the objects identified as “possibly man-made” is illustrated by CosmoX tags in figure 16.

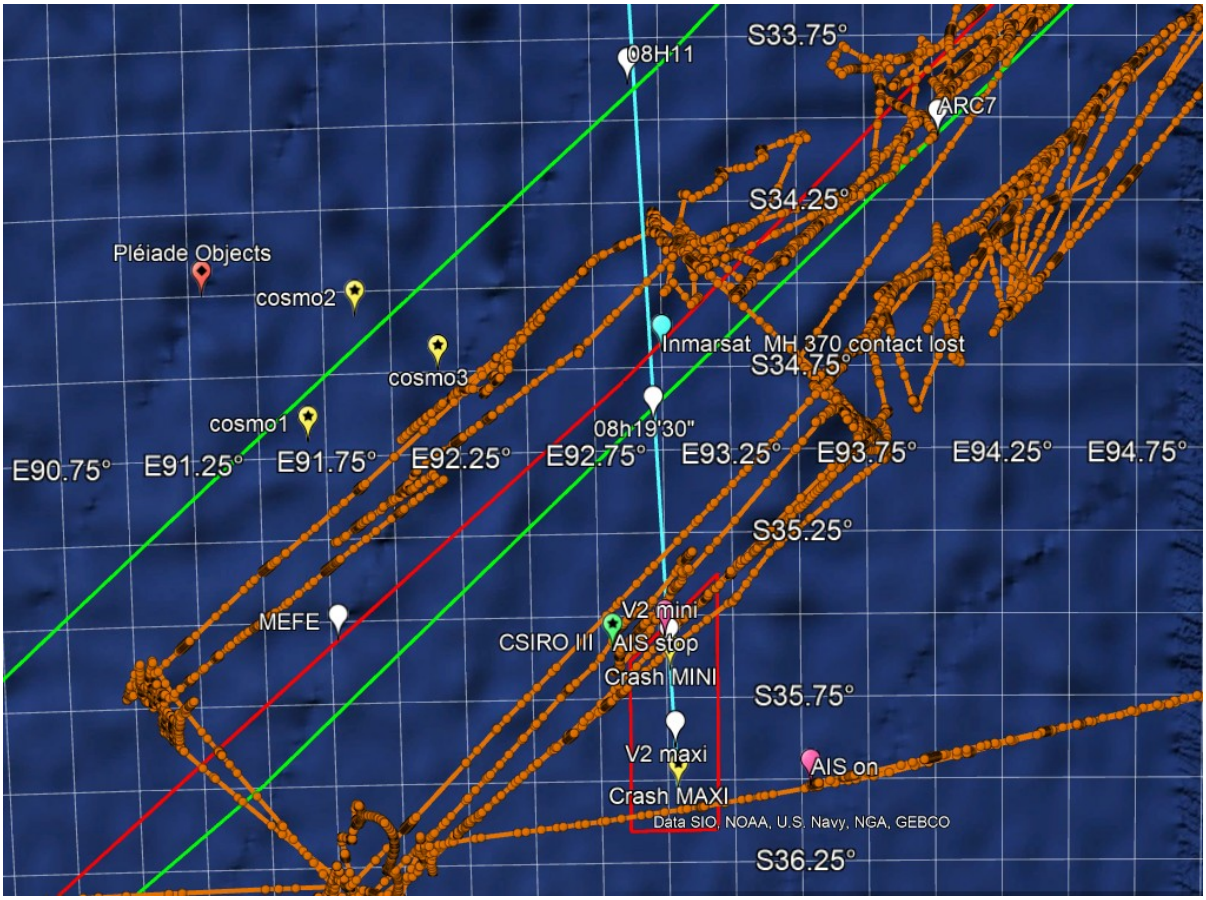

Figure 16: Additional elements of consideration in the vicinity of the ditching location (Pléiades, Cosmo, CSIRO, AIS …)

Annex 1: Variant 2 of the End of Flight

At 08h19:29 MYT the arc 7 exists because the SATCOM of the aircraft sent a burst requesting the logon to the Inmarsat network. This provided the arc 7 BTO/BFO doublet. In the few seconds that followed, the logon procedure proceeded normally with the expected second burst from the SATCOM at 08h19:38 MYT but providing a measured BFO of -2Hz.

This BFO value is to be compared with the previous one at 182Hz. Professor Holland [7] analysed it and reported that in 9 seconds the aircraft could have accelerated because of a dive that increased its vertical speed from -4000fpm to -14500fpm. Subsequently, a lot of studies concluded that the aircraft was either in a free fall or in a high-speed vertical dive and smashed into the water … at the arc 7 or close to it.

If one considers a human presence in the cockpit, there is another possibility which is envisaged here and sketched in Figure 17. The small number of found debris and their type lead to conclude that the aircraft did not violently crashed into the water at a high speed. Otherwise, it would be similar to crashing into a concrete wall spreading thousands of pieces around. In our view, it is perfectly possible that after the start of a dive – being it voluntarily or involuntarily – the pilot recovered very quickly. The voluntary cut-off of the last running engine (the left one) and the management of the subsequent events in the cockpit might have triggered this temporary dive. For example, computations show that if the aircraft dove during 10 seconds shortly before the arc 7, the recovery manoeuvre sketched in figure 17 would last 50 seconds with a flown distance of 6 Nm. Then a descent would take place similarly to the one described in Variant 1 and recalled in figure 18.

The noticeable difference between the End of Flight Variants 1 and 2 is the estimation of the minimum and maximum distances flown by the aircraft. The minimum distance in Variant 2 would be ~42 Nm while the maximum would be ~59 Nm. These would be ~45 Nm and ~67 Nm respectively in Variant 1 as posted in figure 18.

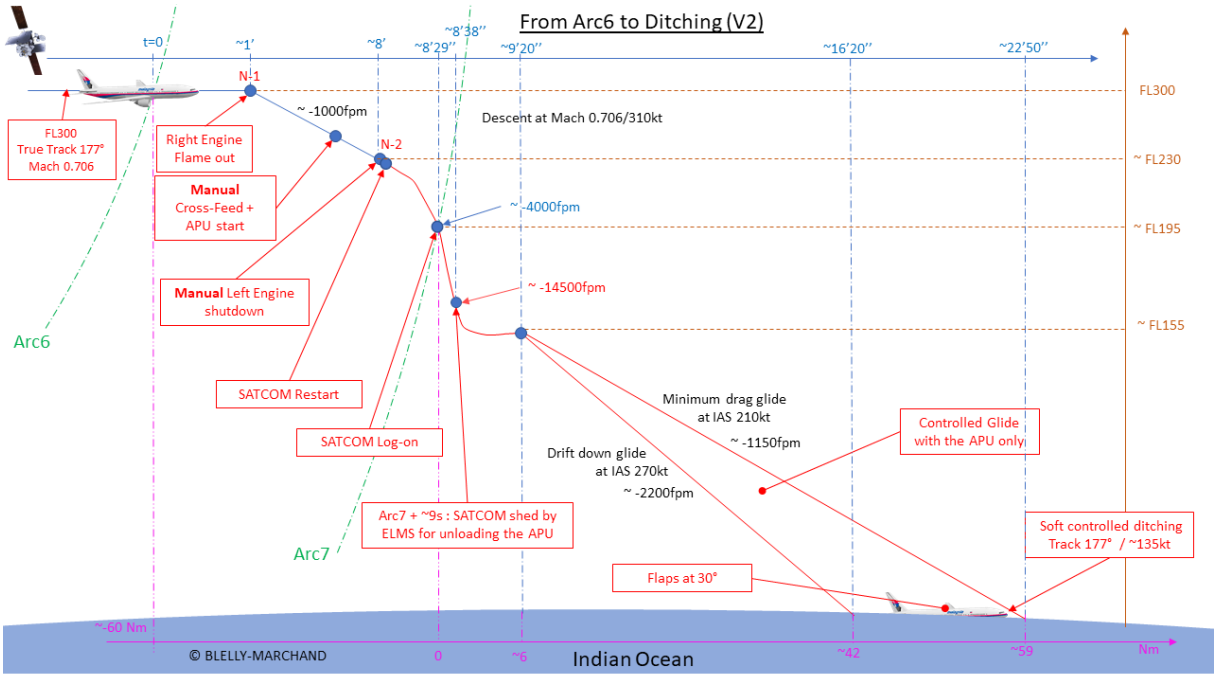

Figure 17: Variant 2 of the end of flight including a dive followed by a quick recovery (Blelly/Marchand)

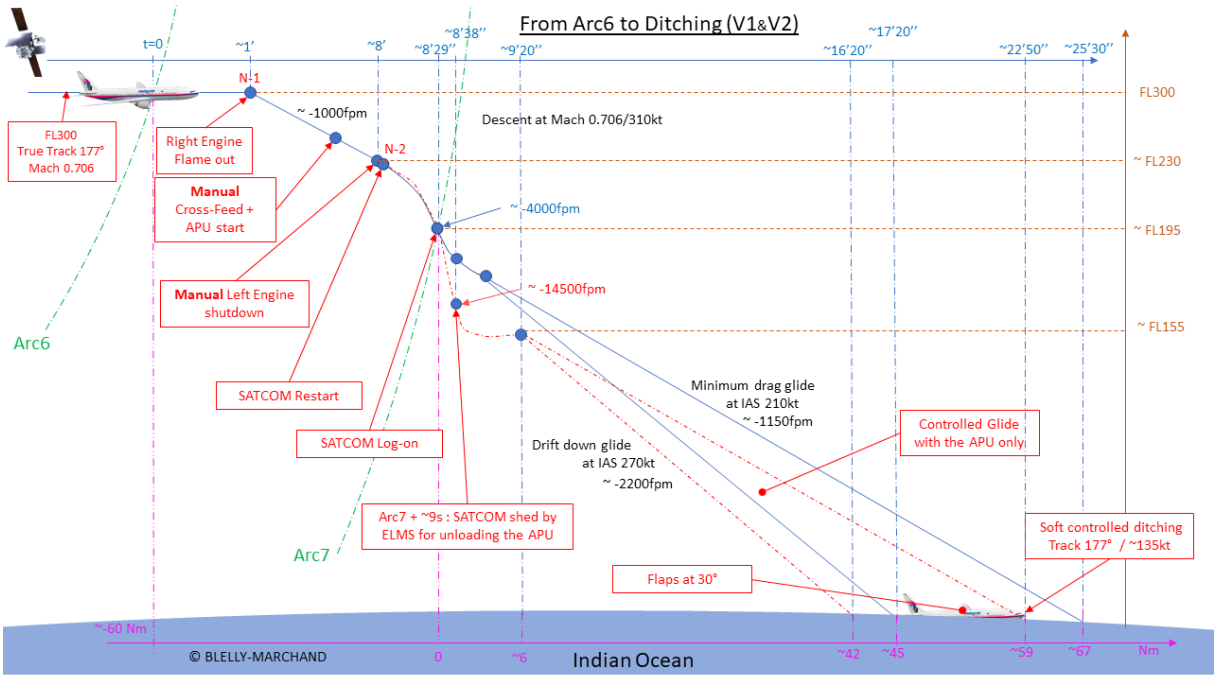

Figure 18: Synopsis of the End of Flight scenario (Variants 1 & 2)

References

[1] "MH370 La contre-enquête d'un pilote" by Captain P. Blelly – Ed. J-P. Otelli – 23 Feb. 2022

[2] Malaysian Safety Investigation Report MH370 (9M-MRO) 2018, Appendix-1.6E-Boeing Performance-Analysis- Malaysian Airlines 777(9M-MRO) Missing Occurrence – 08 March 2014

[3] The Search for MH370, Inmarsat, C. Ashton, A. Shuster Bruce, G. Colledge & M. Dickinson, Journal of Navigation, (2015) 68 1-22

[4] Summary of imagery analyses for non-natural objects in support of the search for Flight MH370, GA report, S.Minchin, N. Mueller, A. Lewis, G. Byrne, M. Tran, Record 2017/13 eCat 111041

[5] Flight Crew Operational Manual FCOM 1 et 2 from Boeing. Table of « performance in flight » of the Boeing 777-200 ER with Trent 892 engines, PMDG and Airlines

[6] The final resting place of MH 370, Bobby Ulich, Richard Godfrey, Victor Iannello & Andrew Banks, 7th Mar 2020

[7] MH370 Burst Frequency Offset Analysis and Implications on Descent Rate at End-of-Flight, I. Holland, Defence Science and Technology Group, Edinburgh, AustraliaarXiv:1702.02432v3 [stat.OT] 15 Jan 2018

[8] The search for MH370 and Ocean surface drift – Part III, D. Griffin, P. Oke, Rep EP174155, 26 June 2017

MH370 Burst Frequency Offset Analysis and Implications on Descent Rate at End-of-Flight

Ian D. Holland
Defence Science and Technology Group, Edinburgh, Australia

arXiv:1702.02432v3 [stat.OT] 15 Jan 2018

I. Introduction

ON 7 March 2014 at 16:41:43Z[1], Malaysian Airlines flight MH370 departed Kuala Lumpur (KL) International Airport bound for Beijing. Less than an hour later, following the last recorded radio transmission from MH370 at 17:19:30Z, the plane's secondary radar transponder went offline. As evidenced by Malaysian military radar, the plane (registration number 9M-MRO) then veered off course unexpectedly, backtracked across the Malaysian Peninsula, and was then tracked heading northwest from Penang through the Malacca Straits. After disappearing from radar at 18:22:12Z, it re-established a satellite communications (SATCOM) link with the Inmarsat satellite I-3F1 at 18:25:27Z. By analyzing a series of automated messages exchanged via that satellite between the plane and an Inmarsat ground station in Perth, Australia, it was determined that the plane continued to fly for six hours, before finally ceasing message exchange with the ground station at 00:19:37Z on 8 March 2014. This article discusses specifically the analysis of burst frequency offset (BFO) metadata from the SATCOM messages. Importantly, it is shown that the BFOs corresponding to the last two SATCOM messages from the plane at 00:19:29Z and 00:19:37Z suggest that flight MH370 was rapidly descending and accelerating downwards when message exchange with the ground station ceased.

An initial analysis by Inmarsat of the SATCOM metadata for MH370 in the last six hours of flight suggested that MH370 had flown into the Southern Indian Ocean before SATCOM was ultimately lost (see [1] for further details). As summarized in [2] an intensive aerial and surface search was undertaken in the Southern Indian Ocean by an international search team during March and April 2014, with no MH370 related debris found. On 28 April 2014, the aerial search concluded and the search transitioned to an underwater phase [2]. The Australian Transport Safety Bureau (ATSB) took responsibility for the definition of the underwater search zone. It convened an international flight path prediction working group bringing together experts in satellite communications, statistical data processing and aviation, in order to estimate the most likely final location of flight MH370. The group consisted of representatives from the Australian Defence Science and Technology (DST) Group and the other organizations listed in the Acknowledgment section of this article.

New methods of analyzing the Inmarsat data were developed by the group, resulting in the release of reports concerning the likely final location of flight MH370 from the ATSB in August 2014 [3], October 2014 [4], and December 2015 [5]. Inmarsat also published an article regarding their contribution to the flight path reconstruction effort [1]. The DST Group contribution that assisted in the definition of an extended priority search area in December 2015 [5] has been detailed in [2]. This demonstrated how Bayesian analysis was used to identify a high probability region of where the plane was believed to be at the time of last SATCOM transmission (00:19:37Z 8 March 2014). The DST Group Bayesian method used a prior probability distribution defined by the Malaysian military radar, a likelihood function describing the relationship between SATCOM measurements and the aircraft position and velocity during the flight, and a model of the aircraft dynamics.

It should be noted that this article does not cover the Bayesian method used in defining the underwater search area. For details on that method, the reader is referred to [2]. Instead, this article focuses on:

1) A brief review of the statistical analysis of BFOs for several previous flights of 9M-MRO.
2) Examination of the effects of the plane's vertical velocity on the BFO.
3) An analysis of the effect of the track angle of the plane on the BFO towards the end-of-flight.
4) The establishment of a BFO trend throughout the last 6 hours of flight so as to determine an expected BFO at end-of-flight.
5) An analysis of the behavior of the frequency oscillator in the plane's satellite data unit (SDU) after power outage events such as those believed to have occurred twice during flight MH370, and how this affects the BFO.
6) An analysis that shows that the final two BFO's are consistent with MH370 being in a rapid descent and accelerating downwards.

The remainder of this article is structured as follows. Section II presents a brief timeline of key events during the MH370 accident flight. In Section III, a review of the SATCOM model is provided, along with a brief review of the BFO statistics. This serves as a summary of work previously presented in [2]. Section IV describes the effects of aircraft position and velocity on the BFO. The settling behavior of the SDU's frequency oscillator for 9M-MRO after power-up is then detailed in Section V. This is important because the SDU is believed to have undergone a power outage between 00:11Z and 00:19Z on 8 Mar 2014, immediately preceding the last two SATCOM transmissions from MH370. The effect of oscillator

Copyright © 2018 Commonwealth of Australia.

[1]All times given in this article are in UTC or "Zulu" time, denoted by "Z".

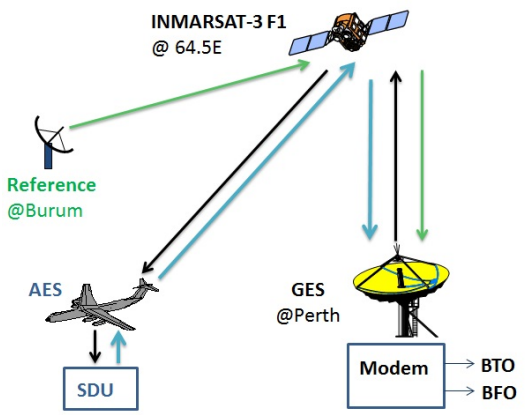

Fig. 1. System model of the satellite communication system [2].

warm-up on the BFO after power-up can be used in bounding the descent rates for MH370 at 00:19:29Z and 00:19:37Z. In Section VI an analysis of the descent rate of MH370 based on the last two BFO values is presented. This analysis derives lower and upper bounds on the descent rate at 00:19:29Z and 00:19:37Z. Conclusions are presented in Section VII.

II. Timeline of Events During the Accident Flight

A comprehensive description of the events occurring during the MH370 accident flight is provided in [6]. A summary of salient events to this article is provided in Table I.

III. Review of SATCOM Model

The accident aircraft was fitted with a SATCOM terminal that used the Inmarsat Classic Aero system [1], which uses geosynchronous satellites to relay messages between aircraft and ground stations. During the flight, messages were passed between the aircraft and a ground receiving station located in Perth, Australia, via the Inmarsat-3F1 satellite. Figure 1 illustrates the SATCOM system in use during the flight. The aircraft is referred to as the Aircraft Earth Station (AES) and the ground receiving unit is referred to as the Ground Earth Station (GES). Inmarsat-3F1 is a satellite in geosynchronous orbit at 64.5° East longitude and it was used exclusively for the duration of the flight.

An AES is equipped with an SDU comprising a satellite modem with auxiliary hardware and software. Transmission of data over the satellite is via bursts which are scheduled to arrive at the GES at a specified time and a given frequency. As explained in [2], [1], communications from multiple users are coordinated by the allocation of different time and frequency slots to each user. This is done without knowledge of individual AES locations or precise knowledge of the satellite location. Therefore, messages from a given AES might not arrive at the GES at exactly the expected time, and generally would arrive slightly later. The difference between the expected time of arrival (based on a nominal assumed position for the satellite and the AES) and the actual time of arrival is referred to as the Burst Timing Offset (BTO). The BTO is a measure of how far the aircraft is from the sub-satellite position[2].

The relative velocity between the satellite and the AES, as well as between the satellite and the GES, leads to a Doppler frequency offset on the signals received at the GES. Coupled with small frequency offsets inherent in the reference frequency oscillators in the AES, satellite and GES, this results in a net difference between the expected and actual frequency of the signal presented to the modem in the GES for a given user. Frequency compensations applied onboard the aircraft (aircraft induced Doppler pre-compensation) and at the ground station (Enhanced Automatic Frequency Correction, which utilizes the reference signal transmitted from a reference station in Burum, Netherlands), [2], [1] serve to reduce the possible difference between the expected and actual frequency of the messages received from the aircraft. The residual difference between the expected frequency of each communications burst and the actual received frequency is referred to as the BFO.

A. Review of BFO Statistics

Based on 20 previous flights of 9M-MRO in the week leading up to the accident flight (see [2] for further details), a histogram was produced for the difference between the predicted BFO (based on known details of the plane and the satellite's position and velocity) and the measured BFO (based on Inmarsat ground station logs). This difference (i.e. predicted minus measured) is referred to as the BFO error. The histogram of the BFO error is shown in Fig. 2, along with a Gaussian distribution fit line. It can be seen that the distribution is somewhat Gaussian. The standard deviation of the BFO error was found in [2] to be 4.3 Hz. Whilst it is reasonable to apply bounds on the possible BFO error based on ± 3 standard deviations as was done for the approximate analysis described in [7], for the purpose of the descent analysis presented later in Sec. VI, it is assumed the BFO error is strictly bounded on the larger interval $[-28, +18]$ Hz, which corresponds to the bounds of all 2501 observed valid[3] in-flight BFO error values available from the preceding 20 flights of 9M-MRO.

IV. Effects of Aircraft Position and Velocity on the Burst Frequency Offset

A. Mathematical Description of the BFO

In [2], the BFO is defined mathematically at time step k as the sum of a noiseless component h_k^{BFO} and a scalar w_k^{BFO} that represents the BFO noise. The noiseless component of the BFO is defined in [2] as the sum:

$$\begin{aligned} h_k^{\mathsf{BFO}}(\mathbf{x}_k, \mathbf{s}_k) \;=\; & \Delta F_k^{\mathsf{up}}(\mathbf{x}_k, \mathbf{s}_k) + \Delta F_k^{\mathsf{down}}(\mathbf{s}_k) \\ & + \delta f_k^{\mathsf{comp}}(\mathbf{x}_k) + \delta f_k^{\mathsf{sat}}(\mathbf{s}_k) \\ & + \delta f_k^{\mathsf{AFC}}(\mathbf{s}_k) + \delta f_k^{\mathsf{bias}}(\mathbf{x}_k, \mathbf{s}_k), \end{aligned} \quad (1)$$

where

- $\mathbf{x}_k$ denotes the state vector of the aircraft;
- $\mathbf{s}_k$ denotes the state vector of the satellite;

[2]The sub-satellite position is the point on the earth directly below the satellite.

[3]One outlier was removed as explained in Sec. V.

TABLE I
TIMELINE OF EVENTS DURING MH370

Date and Timestamp(s)	Description	Comments
7 Mar. 2014 16:42Z	MH370 departs Kuala Lumpa Airport	Normal take-off
Last ACARS transmission	7 Mar. 2014 17:07Z	Everything normal, on path to Beijing
Loss of secondary radar	7 Mar. 2014 17:21:13Z	Onboard transponder goes inactive; last civilian radar
7 Mar. 2014 18:22:12Z	Last Malaysian military radar contact	MH370 shown tracking NW through Malacca Straits
7 Mar. 2014 18:25Z-18:28Z	Satellite Data Unit (SDU) log-on sequence	If flying level, MH370 still tracking NW
7 Mar. 2014 18:39-18:41Z	Unanswered ground-to-air phone call	If flying level, MH370 tracking southwards
7 Mar. 2014 19:41Z to 8 Mar. 2014 00:11Z	SATCOM metadata approx. hourly from MH370	[1], [2] suggest flight into Southern Indian Ocean
8 Mar. 2014 00:19:29Z-00:19:37Z	Partial SDU log-on sequence	Implies rapid descent

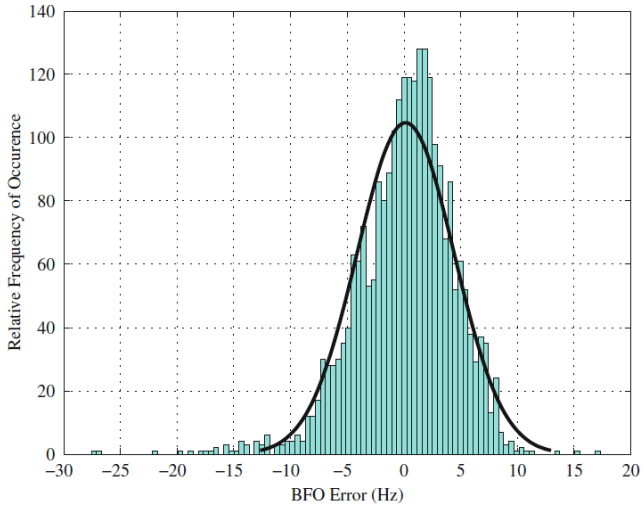

Fig. 2. Histogram of BFO errors for 20 flights of 9M-MRO prior to MH370 (reproduced from Fig. 5.5 of [2]). The mean and standard deviation for the distribution are 0.18 Hz and 4.3 Hz, respectively [2].

- $\Delta F_k^{\mathsf{up}}(\mathbf{x}_k, \mathbf{s}_k)$ is the uplink (aircraft to satellite) Doppler shift;
- $\Delta F_k^{\mathsf{down}}(\mathbf{s}_k)$ is the downlink (satellite to ground station) Doppler shift;
- $\delta f_k^{\mathsf{comp}}(\mathbf{x}_k)$ is the frequency compensation applied by the aircraft;
- $\delta f_k^{\mathsf{sat}}(\mathbf{s}_k)$ is the variation in satellite translation frequency;
- $\delta f_k^{\mathsf{AFC}}(\mathbf{s}_k)$ is the frequency compensation applied by the ground station receive chain;
- $\delta f_k^{\mathsf{bias}}(\mathbf{x}_k, \mathbf{s}_k)$ is a slowly varying bias due to errors in the aircraft and satellite oscillators and processing in the SDU.

By treating the bias $\delta f_k^{\mathsf{bias}}(\mathbf{x}_k, \mathbf{s}_k)$ as a constant determined at the source tarmac for any particular flight, as was done in [2] for MH370, any small time-varying component of the bias during a particular flight can be considered as part of the BFO noise (indeed this was done when compiling the results used to obtain the BFO error histogram shown in Fig. 2). Details regarding the terms $\delta f_k^{\mathsf{sat}}(\mathbf{s}_k)$ and $\delta f_k^{\mathsf{AFC}}(\mathbf{s}_k)$ are provided in [1]. Tabulated values of the sum of these two terms were provided by Inmarsat to the MH370 Flight Path Reconstruction Group to use in estimating the likely trajectory flown. These two terms depend on the satellite state $\mathbf{s}_k$ only, and not on the aircraft state $\mathbf{x}_k$. Moreover, the downlink Doppler $\Delta F_k^{\mathsf{down}}(\mathbf{s}_k)$ does not depend on the location or velocity of the aircraft, and can be calculated given the known frequency of the downlink and the known satellite state at any given time.

Equation (1) can be then be simplified to:

$$h_k^{\mathsf{BFO}}(\mathbf{x}_k, \mathbf{s}_k) = \Delta F_k^{\mathsf{up}}(\mathbf{x}_k, \mathbf{s}_k) + \delta f_k^{\mathsf{comp}}(\mathbf{x}_k) + \delta f_k^{\mathsf{det}}(\mathbf{s}_k), \tag{2}$$

where $\delta f_k^{\mathsf{det}}(\mathbf{s}_k)$ is effectively a known deterministic value for any time step k. The other terms in (2) couple the aircraft state $\mathbf{x}_k$ by way of the aircraft position and velocity to the BFO as per the following equations adapted from [2][4]:

$$\Delta F_k^{\mathsf{up}}(\mathbf{x}_k, \mathbf{s}_k) = \frac{F^{\mathsf{up}}}{c} \frac{(\mathbf{v}_{\mathsf{s}} - \mathbf{v}_{\mathsf{x}})^{\mathsf{T}} (\mathbf{p}_{\mathsf{x}} - \mathbf{p}_{\mathsf{s}})}{|\mathbf{p}_{\mathsf{x}} - \mathbf{p}_{\mathsf{s}}|}, \tag{3}$$

$$\delta f_k^{\mathsf{comp}}(\mathbf{x}_k) = \frac{F^{\mathsf{up}}}{c} \frac{(\hat{\mathbf{v}}_{\mathsf{x}})^{\mathsf{T}} (\hat{\mathbf{p}}_{\mathsf{x}} - \hat{\mathbf{p}}_{\mathsf{s}})}{|\hat{\mathbf{p}}_{\mathsf{x}} - \hat{\mathbf{p}}_{\mathsf{s}}|}, \tag{4}$$

where the dependence on the time step k on the right hand side of the equations has been removed for simplicity of notation. In equations (3) and (4), $|\cdot|$ is the three dimensional Cartesian distance, and:

- F^{up} is the uplink carrier frequency;
- c is the speed of light;
- $\mathbf{v}_{\mathsf{s}}$ is the velocity vector of the satellite;
- $\mathbf{v}_{\mathsf{x}}$ is the velocity vector of the plane;
- $\mathbf{p}_{\mathsf{s}}$ is the position vector of the satellite;
- $\mathbf{p}_{\mathsf{x}}$ is the position vector of the plane;
- $\hat{\mathbf{v}}_{\mathsf{x}}$ is the SDU's estimate of the plane's velocity vector, which is obtained using the plane's track angle and ground speed, whilst assuming the vertical speed is zero;
- $\hat{\mathbf{p}}_{\mathsf{s}}$ is the SDU's estimate of the position vector of the satellite, which assumes the satellite is at its nominal orbital slot of 0 degrees North and 64.5 degrees East;
- $\hat{\mathbf{p}}_{\mathsf{x}}$ is the SDU's estimate of the position vector of the plane, which is obtained using the plane's latitude and longitude, whilst assuming the plane is at sea level.

B. Effect of uncompensated vertical velocity

The vertical speed of the plane is not used in the SDU Doppler compensation. As such, there is a direct contribution

[4]Note that the sign convention used in [2] is opposite to that used in (3)

of Doppler due to the proportion of the vertical velocity vector projected onto the radial direction from the aircraft to the satellite. It is straightforward to understand that if the plane was directly below the satellite, the vertical velocity vector would be fully towards or away from the satellite if the plane was climbing or descending. The direct contribution of the Doppler to the BFO in that case would be governed by the following standard Doppler equation.

$$\Delta F_k^{\mathsf{up}}\left(\mathbf{x}_k, \mathbf{s}_k\right) \quad = \quad \frac{v_z \cdot F^{\mathsf{up}}}{c}, \tag{5}$$

where F^{up} and c are as previously defined, and v_z is the vertical speed of the plane. Substituting an uplink frequency of 1646.6525 MHz (the uplink frequency stated in [1]) and a vertical velocity of 100 feet per minute (fpm), equivalent to 0.508 meters per second, equation (5) implies that the predicted BFO would increase by 2.8 Hz per 100 fpm of climb rate or decrease by 2.8 Hz per 100 fpm of descent rate if the plane were directly below the satellite. This is the maximum possible contribution of the plane's climb or descent rate to the BFO. In the more general case, equation (5) is moderated by the sine of the elevation angle θ from the aircraft to the satellite. This is expressed as

$$\Delta F_k^{\mathsf{up}}\left(\mathbf{x}_k, \mathbf{s}_k\right) \quad = \quad \frac{v_z \cdot F^{\mathsf{up}} \sin(\theta)}{c}. \tag{6}$$

As such, at 00:19Z (the time at which the plane crosses the 7th arc provided by Fig. 3)[5], where the elevation to the satellite is 38.8 degrees, the contribution to the BFO of climb or descent rate is reduced to approximately $+1.7$ Hz or -1.7 Hz per 100 fpm respectively.

C. Effect of track angle on BFO towards end-of-flight

Another factor that needs to be considered in interpreting the BFOs at 00:19Z is the track angle of the aircraft. In [2], Fig. 5.6, a set of curves were shown illustrating the relationship of the BFO error and the aircraft track angle at 18:39Z. That was done to illustrate that under the assumption of level flight during the unanswered telephone call period of 18:39Z-18:41Z, MH370 would have been tracking in a southerly direction. The same model can be used to examine the relationship between the BFO error and the track angle at 00:11Z, when MH370 crossed the 6th arc, just 8 minutes prior to the last messages were received from MH370.[6] To generate the curve of BFO error vs. track angle, it is assumed that the aircraft crossed this arc at 38.67S, 85.11E. A previous sensitivity analysis has revealed the curve is relatively insensitive to the actual crossing point. Also, calculations revealed that (as shown in Fig. 5.6 of [2] at 18:40Z) the track angle of the aircraft influences the BFO to a greater degree for a faster assumed ground speed. To assess the maximum possible effect of track angle on the BFO at 00:19Z, a ground speed of 500 kts is assumed, and the BFO error vs. track angle is then

[5]The arcs referred to in this paper and other MH370 literature are segments of the rings in Fig. 3.

[6]Note that the 6th arc crossing is considered here to isolate effects of ground track angle variation as opposed to vertical velocity, since the measured BFO at the 6th arc is still consistent with level flight.

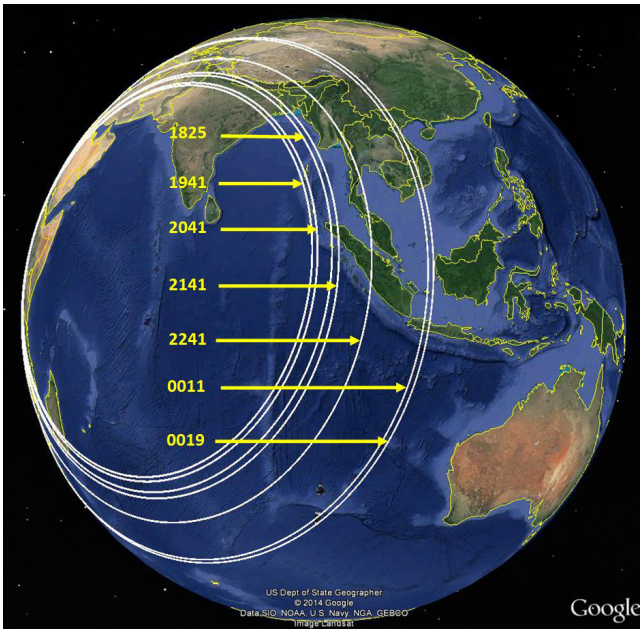

Fig. 3. BTO rings during the MH370 flight [3]. Note that the latitude of the arrows shown for each ring is arbitrary.

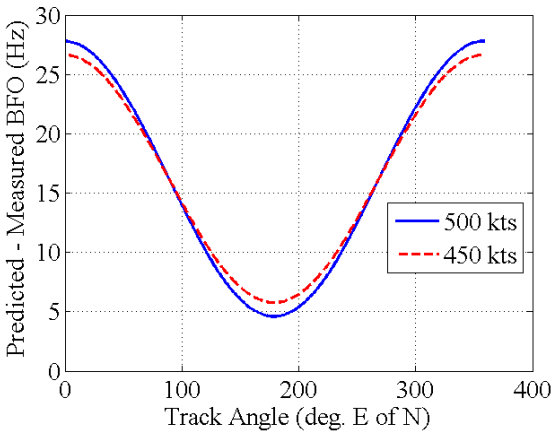

Fig. 4. BFO errors as a function of track angle at 00:11Z.

as shown in Fig. 4. Another curve assuming 450 kts ground speed is shown for comparative purposes. It is noted that the peak-to-peak variation of the BFO difference is similar for both considered ground-speeds.

D. BFO Trend During the MH370 Flight

The measured BFOs from 19:41Z to 00:11Z are shown in Fig. 5 together with a line-of-best-fit. This line is extended forward to the time of the 00:19Z log-on resulting in an expected BFO of roughly 254 Hz[7]. With reference to the track angle curves presented in Fig. 4, the 00:11Z BFO error value for the southern-most track is roughly 6 Hz, meaning the measured BFO of 252 Hz was 6 Hz lower than the lowest value it could have been (assuming roughly level flight at

[7]Note the BFOs observed at 00:19Z were much lower than the expected value.

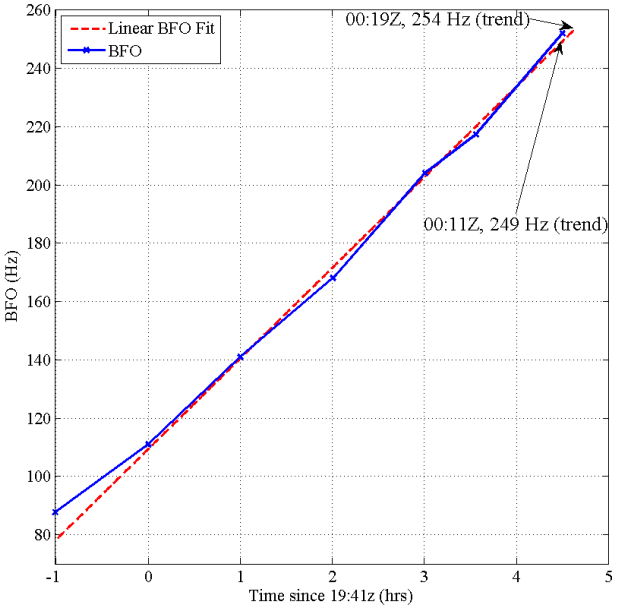

Fig. 5. Measured BFOs during the MH370 flight with trend-line extrapolated back to 18:40Z and forward to 00:19Z.

approximately 450 kts). If we assume the same error value at 00:19Z, and use the extrapolated BFO, assuming a south track with level flight and similar ground speed, the expected BFO value is 260 Hz.

The linear trend-line in Fig. 5 is also extended back by 1 hour to the time of the first unanswered satellite telephone call to MH370. The mean of the measured BFOs during that call attempt is also shown. Since the mean of the measured BFOs from the 18:39-18:41Z call attempt are in broad agreement with the linear trend observed in the BFOs from 19:41Z to 00:11Z (for which the BTOs themselves were consistent with straight and level flight [2]), this supports the finding in [2] that there were most-likely no major turns after the unanswered call attempt (see ([2], Fig. 10.5)).

V. Effect of SDU Startup on the BFO

The BFOs logged for messages from the plane received at the Perth GES at 00:19:29Z and 00:19:37Z 8 March 2014 were much lower than the expected value of 260 Hz. In the absence of any other factors affecting the BFOs at these times, this suggests a large uncompensated negative vertical velocity component in the BFOs. In determining how to interpret this data, it is important therefore to carefully consider any known other factors that could effect these BFOs. One potential factor is an SDU oscillator startup transient. This section analyses the range of expected effect on the BFO caused by a period of power outage followed by a restart of the SDU, as was a possibility between 00:11Z and 00:19Z on 8 March 2014 (see [3] for further details).

A. Detailed Analysis of SDU Startup Effects on the BFO

At 18:25:27Z 7 March 2014, the Inmarsat GES in Perth received a SATCOM log-on request from 9M-MRO. A series of messages were exchanged in the following few minutes

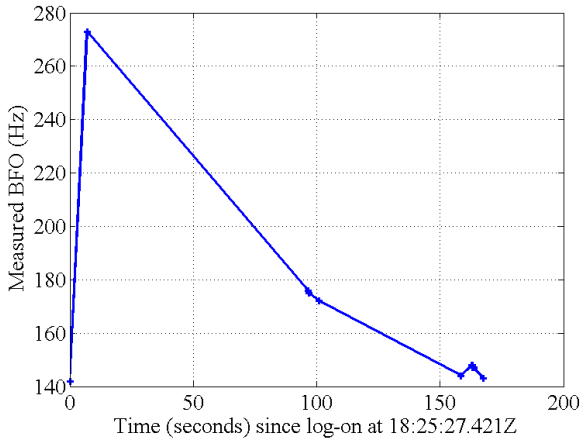

Fig. 6. Measured BFOs following the 18:25:27Z log-on message from MH370.

as part of a standard log-on sequence. The BFOs over those minutes displayed somewhat unusual behavior in that (barring the first BFO) the BFO appeared to be exhibiting a transient settling behavior. This is shown in Fig. 6. It was noted in [1] that the spike in BFO observed at this time[8] was not fully understood and whilst originally attributed to a possible aircraft maneuver it could also be related to actual frequency changes occurring during the logon sequence. A subsequent study [8] by the SATCOM sub-group of the MH370 Flight Path Reconstruction Group revealed this was most likely due to power-on frequency drift and subsequent stabilization of the oven-controlled crystal oscillator (OCXO) in the SDU. In [8], a number of different SDUs were tested to investigate the effects of power outages on the BFO during SDU power on, triggering a SATCOM logon such as that which occurred for MH370 at 18:25:27Z. It was found that whilst the frequency settling behavior was different for each individual SDU, any given SDU displayed repeatable behavior for a fixed outage duration, and similar settling characteristics for outages of different duration.

Based on sequences of Inmarsat BFO logs for 9M-MRO concerning four log-ons after periods of SATCOM outage in the week leading up to the accident flight, it was found (in [8]) that the SDU in 9M-MRO resulted in a BFO that was initially too high at the time of log-on, followed by a simple decay over the next few minutes to a steady-state value. Regarding the log-on event at 18:25:27Z for MH370, it was noted that there was a non-zero bit error rate (BER) associated with the log-on request at that time. The associated received signal level and carrier-to-noise density ratio (C/N_0) were also unusually low. As such, the first BFO was deemed untrustworthy.[9] Note that this is not the only time such a behavior was observed for the SDU in 9M-MRO. In the analysis of BFOs presented in [2], there was an outlier in the BFO (with an error of

[8]When viewed on a time-scale of hours as shown in Fig. 9 of [1], this behavior looks like a spike in BFO between 18:25Z and 18:28Z.

[9]An alternative explanation for this outlier BFO could be the unknown conditions of the aircraft between 17:22Z and 18:25Z, for instance the temperature of the SDU might have been much lower than the expected ambient temperature.

-170 Hz) found to have occurred for a SATCOM message associated with 9M-MRO in one of the 20 previous flights of 9M-MRO. This was discarded as an outlier and not presented in [2]. It too had a non-zero BER and a low C/N_0 (37.6 dBHz compared to surrounding values between 41.5 and 42 dBHz). With the removal of the untrustworthy BFO logged for the first message in the sequence shown in Fig. 6, the 18:25Z log-on from MH370 was also determined to follow the simple decay trend observed in other instances.

It was noted by DST Group that if the simple BFO decay trend established after SDU power-up [8] also occurred during the MH370 SATCOM log-on event beginning at 00:19:29Z, then it would allow bounds to be established on the BFO that would have been expected for MH370 if the plane was flying level at that time. This in turn would allow the determination of bounds on the possible descent rates of MH370 during that final log-on event. In order to build confidence that the simple BFO decay trend would hold for the 00:19Z log-on event, DST Group reviewed additional Inmarsat logs for 9M-MRO, corresponding to the period 22 February to 28 February 2014. Two additional cases were identified in which 9M-MRO logged back onto an Inmarsat satellite after a sustained period of SATCOM outage. The sequence of BFOs observed in these two cases, along with the five already considered by the SATCOM working group in [8], are shown in Fig. 7, and details about each of the log-ons are given in Table II.

The periods of SATCOM outages followed by log-on events were identified from Inmarsat-provided ground-station logs by identifying sequences of three or more unsuccessful log-on interrogations to 9M-MRO (suggesting the SDU was likely powered off) followed by a log-on to the satellite system initiated from 9M-MRO at some later time. The exact duration of the power-off period for the SDU was unable to be determined from the logs, however the timestamps associated with the unsuccessful log-on interrogations and subsequent 9M-MRO initiated log-ons were used to determine bounds on the outage time as shown in the 3rd column of Table II.[10] Additional comments about each log-on sequence are given in the final column. Whilst some of the BERs for log-ons 1 and 6 were non-zero, the BFOs did not appear to be outliers, and were therefore considered valid. The uncertainty window in the length of the outage durations shown is roughly 60 minutes; this relates to timers in the Inmarsat satellite ground stations that result in a log-on interrogation being sent to the plane after roughly 60 minutes of SATCOM inactivity. Indeed, it is this same timing responsible for the roughly 60 minute separation between the four BTO arcs from 19:41Z to 22:41Z (e.g. [3], [1]). It is also of note that based on other evidence related to MH370 (e.g. secondary radar transponder loss of signal at 17:22Z) that SDU power was probably first lost at 17:22Z, in which case the SDU power outage duration for log-on 7 would be approximately 63 minutes.

For log-ons 3 and 5, there were some points available about half an hour after the log-on in each case (noting the plane was

[10]Note that the bounds shown are derived under the assumption that the SATCOM outage was exclusively due to a power outage. It is also possible that the first part of some outages was due to a blocked line of sight to the Inmarsat satellites.

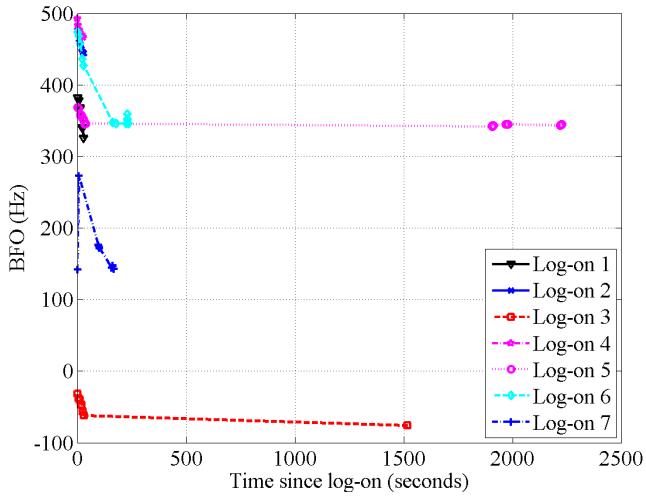

Fig. 7. Measured BFOs for 7 log-ons of 9M-MRO.

on the tarmac for the whole time) that demonstrate the BFO appears to have fully settled to a steady-state value. Log-ons 1 to 5 only lasted for less than 1 minute after the log-on request message. The results for log-ons 6 and 7, which had log-on sequences lasting a few minutes suggest a settling behavior of approximately 3 minutes duration. For all observed log-on sequences, there seems to be a simple decay of BFO over a few minutes after SDU startup and log-on request (see also Fig. 8). It is therefore possible a similar decay was occurring during the SDU log-on sequence beginning at 00:19:29Z.

In order to establish what the likely range of steady-state equivalent BFOs would have been at 00:19Z, it is useful to re-plot the curves from Fig. 7 translated vertically such that the log-on acknowledgment has 0 Hz offset. This is done in Fig. 8, which has also been zoomed in the time-axis for clarity.

For log-ons 1 to 6, the aircraft was on the ground at an airport. It has been established that the most common scenario for an on-ground-at-airport log-on after sustained power outage of the SDU is for the AES to use a different self-Doppler compensation method than was in use for log-on 7 and the log-on at 00:19Z. This is due to a lack of navigational input data from the aircraft's inertial navigation unit in the few minutes after power-up, and is referred to as the closed-loop Doppler compensation approach.[11]

The standard AES Doppler compensation mode when navigational data is available to the SDU is the mode used for log-on 7 and the log-on at 00:19Z. This approach was briefly described in Sec. IV-A. It used the aircraft's own estimates of its position and horizontal velocity to predict and correct the AES contributed Doppler shift. This is referred to as open-loop Doppler compensation.

For log-ons 1 to 6, we work on the premise that closed-loop Doppler compensation was used.[12] In that approach, the frequency of broadcast P-channel transmissions received by 9M-

[11]The use of closed-loop Doppler compensation in this circumstance was established in consultation with members of the MH370 Flight Path Reconstruction Group, including representatives from Thales and Inmarsat.

[12]Previous analysis had not considered the difference in Doppler compensation mode, yet still resulted in similar descent rates to those presented in this paper.

TABLE II
DETAILS OF LOG-ON SEQUENCES USED FOR ANALYSIS

Identifier	Date and Timestamp of Log-on	Duration of Preceding Power Outage	Any Other Comments
Log-on 1	23rd Feb. 23:57Z	Between 381 and 442 minutes	After scheduled A1 maintenance check, some non-zero BERs
Log-on 2	26th Feb. 14:11Z	Between 295 and 354 minutes	
Log-on 3	5th Mar. 03:06Z	Between 35 and 95 minutes	
Log-on 4	6th Mar. 13:29Z	Between 43 and 103 minutes	
Log-on 5	6th Mar. 15:02Z	Between 35 and 92 minutes	
Log-on 6	7th Mar. 12:50Z	Between 228 and 288 minutes	Some non-zero BERs
Log-on 7	7th Mar. 18:25Z	Between 20 and 78 minutes	First point untrustworthy

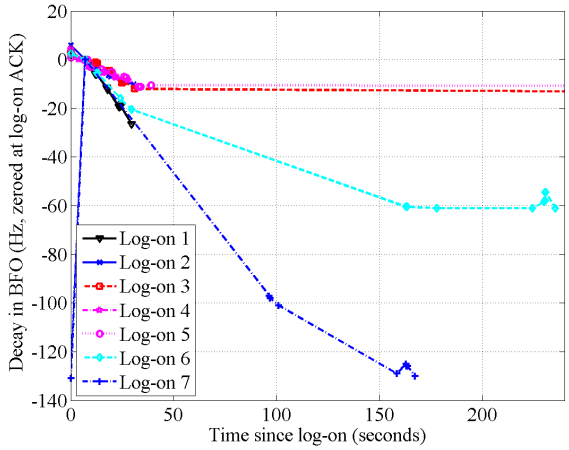

Fig. 8. Decay in measured BFOs for 7 log-ons of 9M-MRO. The decay rates for log-ons 1 to 6 have been adjusted to account for the different AES Doppler compensation mode used during these log-ons.

MRO were used to determine the AES Doppler contribution. In this approach, all of the difference between the received and expected P-channel frequency is attributed by the SDU to be caused by AES motion induced Doppler. As such, if the OCXO frequency is higher than its nominal settled value, due to incomplete temperature stabilization, the received frequency will appear lower than expected by the corresponding amount. When applying the AES Doppler compensation in this case, the transmit frequency is increased by the difference between the stable and pre-stabilized oscillator frequency (scaled to account for the difference between P-channel frequency and the R-channel transmit frequency). Moreover, the transmit frequency itself (prior to AES Doppler compensation) will already be too high by the same amount due to the incomplete temperature stabilization. The net combined effect to the BFO decay observed due the OCXO settling will therefore be doubled compared to the case where open-loop AES Doppler pre-compensation is used. Hence, the BFO decay results for log-ons 1 to 6 shown in Fig. 8 have been halved for the analysis when compared to those inferred from the raw measured BFOs presented in Fig. 7.

Recall that the two messages at 00:19:29Z and 00:19:37Z are a log-on and log-on acknowledgment respectively. From the data used to plot Fig. 8, it can be determined that the log-on acknowledgment BFOs are in the range of [0,6] Hz lower than the log-on BFOs. Also the maximum difference between the log-on BFO and the settled BFO value is in the range [17,136] Hz. The only log-on that doesn't appear to be approaching a settled value in this range is log-on 1, for which it is anticipated that if more data points were available several minutes later, as was the case for log-ons 3, 5, 6 and 7, the settling behavior would be similar to that for log-ons 6 and 7, bearing in mind the outage duration for log-on 1 is probably at least 381 minutes, and the BFO already dropped substantially in the first 30 seconds after log-on.

B. Summary of SDU Startup Effects on the BFO

It is likely that the SDU in 9M-MRO lost power sometime after 00:11Z, and then regained power (presumably due to Auxiliary Power Unit (APU) startup) prior to 00:19Z, leading to the SDU making the log-on attempt at 00:19:29Z. Previous such events for 9M-MRO have shown that this results in an initially too-high BFO for the log-on message, followed by a simple decay characteristic to reach a steady-state BFO after several minutes. In order to establish the relevance of the BFOs at 00:19:29Z and 00:19:37Z to the motion (including descent rate) of MH370 at those times, this section has established bounds for the likely range of steady-state equivalent BFOs at those times. This was done by analyzing BFOs from seven previous SDU start-up events for a period of several minutes. The specific results obtained suggest that:

1) The recorded BFO for the 00:19:29Z log-on was between 17 and 136 Hz higher than it would have been if the OCXO in the SDU was in a steady state at that time;
2) The recorded BFO for the 00:19:37Z log-on acknowledge message was between 17 and 130 Hz higher than it would have been if the OCXO in the SDU was in a steady state at that time.

VI. BOUNDING THE DESCENT RATES OF MH370

The results from Sections IV and V can be combined to provide bounds on the descent rate of MH370 implied by the BFOs from the two last SATCOM messages for the flight. In this section, it is shown how this is done for two different possibilities that could explain the attempted SATCOM log-on from 9M-MRO at 00:19Z. In [3] the most likely cause of this log-on was stated to be a power interruption resulting from insufficient fuel and subsequent engine flameout. It could

also have been due to a temporary software failure, a loss of systems providing critical input to the SDU, or a loss of the SATCOM link due to aircraft attitude being such that the line-of-sight to the satellite is blocked. If it was indeed a power interruption to the SDU caused by loss of fuel and subsequent reboot using the APU, the SDU would be without power for about one minute. In this case, the results of Sec. V-B need to be considered when interpreting the last two BFOs.[13] If on the other hand, the power loss was momentary (resulting in a reset of the SDU) or if the temporary SATCOM outage leading to the log-on request was due to one of the other listed reasons, there would be no "warm-up drift" to consider, so the results of Sec. V would not need to be applied. Both cases are considered separately in the following two sub-sections, and then combined overall bounds are presented.

A. Hypothesis 1: SATCOM outage due to insufficient fuel

In the event that the SDU log-on at 00:19:29Z was due to engine flame-out, followed by a restart of the SDU using power from the APU, the SDU outage preceding the log-on would have lasted about one minute. This would result in some cooling of the OCXO in the SDU. The likely effect of the SDU startup and consequent 'warm-up drift' of the OCXO is summarized in Sec. V-B. Table III presents the recorded BFOs and bounds on the adjusted BFOs to remove these effects of warm-up drift. In the last column of the table, the bounds are extended taking into account the BFO noise bounds of $[-28, +18]$ Hz established in Sec. III-A.

As established in Sec. IV-B, the recorded BFO would be roughly 1.7 Hz lower for every 100 fpm of descent rate. As such, depending on whether the plane was tracking South or North (minimum or maximum expected BFOs, respectively, see Sec. IV-C), bounds on the descent rate of MH370 at the times of transmission corresponding to the last 2 BFOs can be determined by subtracting the values given in the rightmost column of Table III from the expected BFO values for level flight tracking South or North, dividing the result by 1.7 Hz and multiplying by 100 fpm. The expected BFO for a south track is approximately 260 Hz, whilst for a north track it is close to 280 Hz. Using these numbers, it is straightforward to obtain the bounds shown in Table IV. Note that the bounds have been rounded to the nearest 100 fpm. Looking at all values in the table, it can be concluded that irrespective of ground track angle and for assumed ground speeds less than approximately 500 kts, under Hypothesis 1, MH370 would have been descending at between 3,900 and 14,800 fpm at 00:19:29Z, and just 8 seconds later at between 14,800 and 25,300 fpm. These descent rates are consistent with simulations of an uncontrolled phugoid descent reported in [7].

B. Hypothesis 2: SATCOM outage due to some other reason

It is still of interest to determine bounds on the descent rates under the alternate hypothesis that something else not associated with a power outage led to the SDU-initiated log-on event at 00:19Z. In this case, the warm-up drift would not apply. Therefore, the recorded BFOs can be treated normally (though still subject to BFO noise). In this case, the BFO bounds are as set out in Table V. Using these bounds, the lower and upper descent rates can be calculated again, resulting in the bounds presented in Table VI. It can be concluded from the table that the recorded BFOs indicate that at 00:19:29Z the plane was descending at between 2,900 fpm and 6,800 fpm. At the time of the last SATCOM message, it can be concluded under Hypothesis 2 that the descent rate would have been between 13,800 fpm and 17,600 fpm.

[13]Given the relatively short duration of the power-loss under Hypothesis 1, it is possible that the extent of BFO decay due to OCXO warm-up would be less than shown for log-ons 1 to 7. This is essentially covered within Hypothesis 2, which considers a momentary SATCOM outage.

C. Summary of Descent Rate Bounds

Combining the descent rate bounds for Hypotheses 1 and 2, outer bounds can be established for the descent rate of MH370 at 00:19:29Z and 00:19:37Z. Specifically, regardless of ground track angle and for ground speeds less than approximately 500 kts, accounting for possible BFO noise, and regardless of whether the SATCOM outage between 00:11Z and 00:19Z was due to an SDU power outage or another reason, the outer bounds on the possible descent rates at the times of the last two SATCOM messages from MH370 are given in Table VII.

D. Estimated Downwards Acceleration

When interpreting the bounds presented in Table VII, the different conditions under which each bound was derived need to be considered. For instance the lowest rate at 00:19:29Z was derived assuming no period of SDU outage and a southwards track, whereas the highest descent rate for 00:19:37Z was derived assuming a one minute outage of the SDU with the maximum BFO decay observed in the previous 7 SDU outage events for 9M-MRO. Hence, it would not be reasonable to say that the plane could have been descending at 2,900 fpm at 00:19:29Z and 25,300 fpm 8 seconds later, which would imply a downwards acceleration on the order of 2,800 fpm per second. Whilst it is not possible to determine a precise acceleration value, a rough approximation of the average descent rate over those 8 seconds could for instance be taken using the mid-points of the bounds at each time, which would result in an average downwards acceleration of 10,700 fpm in 8 seconds or around 1,300 fpm per second, which equates to around 6.7 ms^{-2} or $0.68g$, where g denotes Earth's gravitational constant, which is approximately 9.8 ms^{-2}. It is straightforward to see that other reasonable methods of estimating the downward acceleration (such as taking the difference between the two minimum descent rates or the two maximum descent rates at 00:19:29Z and 00:19:37Z) would yield similar acceleration values.

VII. Conclusion

This article has discussed in detail all known factors that could have influenced the BFOs associated with the last two SATCOM messages received from MH370 at 00:19Z. Lower and upper bounds on its descent rate at this time

TABLE III
THE LAST TWO BFOS FOR MH370 UNDER HYPOTHESIS 1

Timestamp	Recorded BFO (Hz)	BFO Range if Start-Up Drift Removed (Hz)	Extended Range Considering BFO Noise (Hz)
00:19:29Z	182	$[46, 165]$	$[28, 193]$
00:19:37Z	-2	$[-132, -19]$	$[-150, 9]$

TABLE IV
MH370 DESCENT RATES AT 00:19Z 8 MARCH 2014 UNDER HYPOTHESIS 1

Timestamp	Min. Desc. Rate, South Track	Min. Desc. Rate, North Track	Max. Desc. Rate, South Track	Max. Desc. Rate, North Track
00:19:29Z	3,900 fpm	5,100 fpm	13,600 fpm	14,800 fpm
00:19:37Z	14,800 fpm	15,900 fpm	24,100 fpm	25,300 fpm

TABLE V
THE LAST TWO BFOS FOR MH370 UNDER HYPOTHESIS 2

Timestamp	Recorded BFO (Hz)	BFO Bounds With Noise (Hz)
00:19:29Z	182	$[164, 210]$
00:19:37Z	-2	$[-20, 26]$

were then derived.[14] The downwards acceleration over the 8 second interval between these two messages was found to be approximately $0.68g$. The derived bounds and approximate downwards acceleration rate are consistent with simulations of an uncontrolled descent near the 7th arc as reported in [7]. This suggests that 9M-MRO should lie relatively close to the 7th BTO arc.

At the time of submission of this paper, MH370 had not been located. The search was in indefinite suspension pending 'credible new evidence pointing to a specific location for the plane'. Further efforts in data analysis and in drift modeling of located MH370 debris have been conducted and reported (e.g. [9], [10], [7]). Note that the descent analysis from this paper was used in [7] when considering the width of any potential future search area. Some recent news reports have suggested a US underwater exploration firm named Ocean Infinity may soon be launching a renewed search effort for MH370. The reader should refer to the Australian Transport Safety Bureau website [11] and the general media for updates.

ACKNOWLEDGMENT

The author would like to thank his Defence Science and Technology Group colleagues Dr. Neil Gordon, Dr. Samuel Davey, Dr. Jason Williams, and Dr. Mark Rutten who worked alongside him as part of the MH370 Flight Path Reconstruction Group, as well as Mr. Balachander Ramamurthy for his support to the satellite data analysis. Special thanks goes to Dr. Gerald Bolding, both for his support to the satellite data analysis and his extensive efforts in reviewing and improving this article. The author also thanks the many other members of the MH370 Flight Path Reconstruction Group, which comprised representatives from Inmarsat, Thales, Boeing, US National Transportation Safety Board (NTSB), UK Air Accidents Investigation Branch (AAIB), Honeywell, SED, Square Peg Communications Inc., and Panasonic. The group has been expertly led by the Australian Transport Safety Bureau (ATSB).

[14]The conclusions regarding descent rate have been made taking into account BFO noise bounds, all reasonably feasible ground tracks and speeds, and possible OCXO warm-up drift. It has been implicitly assumed that there were no otherwise unknown factors that could have affected the last two BFOs.

REFERENCES

[1] C. Ashton, A. Shuster Bruce, G. Colledge, and M. Dickinson, "The search for MH370," The Journal of Navigation, vol. 68, no. 1, pp. 1–22, Oct. 2014. [Online]. Available: http://dx.doi.org/10.1017/S037346331400068X
[2] S. Davey, N. Gordon, I. Holland, M. Rutten, and J. Williams, Bayesian Methods in the Search for MH370. SpringerOpen, Aug. 2016.
[3] ATSB, "MH370 Definition of Underwater Search Areas," Australian Transport Safety Bureau, ATSB Transport Safety Report, External Aviation Investigation AE-2014-054, Aug. 2014.
[4] ——, "MH370 flight path analysis update," Australian Transport Safety Bureau, ATSB Transport Safety Report, External Aviation Investigation AE-2014-054, Oct. 2014.
[5] ——, "MH370 search area definition update," Australian Transport Safety Bureau, ATSB Transport Safety Report, External Aviation Investigation AE-2014-054, Dec. 2015.
[6] Safety Investigation Team for MH370, "Factual Information : Safety Investigation for MH370," Ministry of Transport, Malaysia, Tech. Rep. MH370/01/15, 2015. [Online]. Available: http://mh370.mot.gov.my/download/FactualInformation.pdf
[7] ATSB, "MH370 - Search and debris examination update," Australian Transport Safety Bureau, ATSB Transport Safety Report, External Aviation Investigation AE-2014-054, Nov. 2016.
[8] "Internal study regarding SATCOM ground-station logs," MH370 Flight Path Reconstruction Group - SATCOM Subgroup.
[9] D. Griffin, P. Oke, and E. Jones, "The search for MH370 and ocean surface drift," CSIRO, Tech. Rep. EP167888, Dec. 2016.
[10] ——, "The search for MH370 and ocean surface drift - Part II," CSIRO, Tech. Rep. EP172633, Apr. 2017.
[11] "ATSB website." [Online]. Available: http://www.atsb.gov.au

Ian D. Holland received the Bachelor of Electronic and Communication Engineering in 2000 and a Ph.D. in wireless telecommunications in 2005, both from Curtin University of Technology, Western Australia. Since then he has held positions in the University of Western Australia, the Institute for Telecommunications Research at the University of South Australia, EMS Satcom Pacific and Lockheed Martin Australia. Since January 2011, Ian has been working as a Research Scientist in Protected Satellite Communications at the Defence Science and Technology Group, Australia.

TABLE VI
MH370 DESCENT RATES AT 00:19Z 8 MARCH 2014 UNDER HYPOTHESIS 2

Timestamp	Min. Desc. Rate, South Track	Min. Desc. Rate, North Track	Max. Desc. Rate, South Track	Max. Desc. Rate, North Track
00:19:29Z	2,900 fpm	4,100 fpm	5,600 fpm	6,800 fpm
00:19:37Z	13,800 fpm	14,900 fpm	16,500 fpm	17,600 fpm

TABLE VII
RANGE OF POSSIBLE MH370 DESCENT RATES AT 00:19Z 8 MARCH 2014

Timestamp	Min. Desc. Rate	Max. Desc. Rate
00:19:29Z	2,900 fpm	14,800 fpm
00:19:37Z	13,800 fpm	25,300 fpm

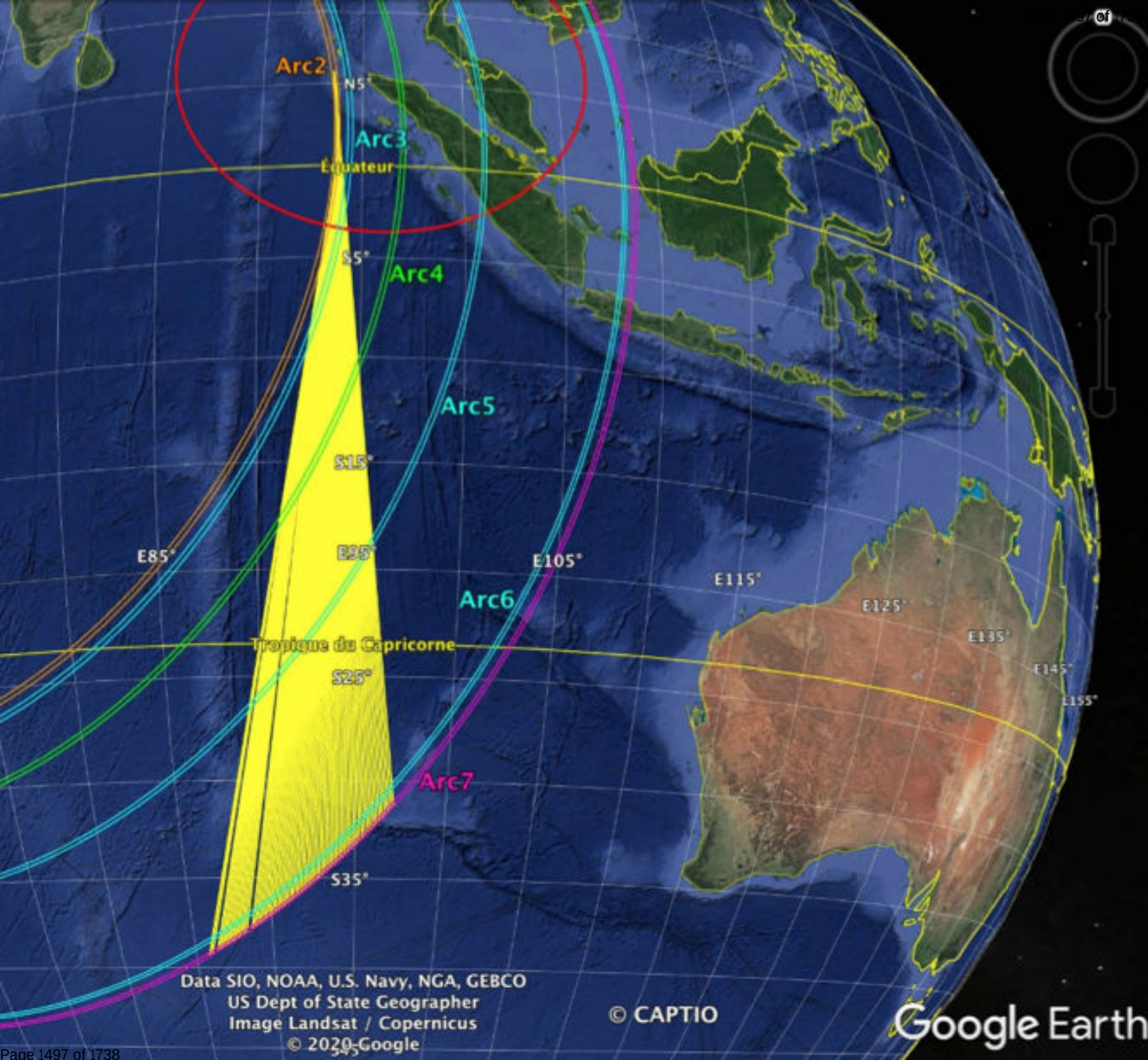
Arc2
N5°
Arc3
Équateur
S5°
Arc4
Arc5
S15°
E85°
E95°
E105°
E115°
Arc6
E125°
Tropique du Capricorne
S25°
E135°
E145°
E155°
Arc7
S35°
Data SIO, NOAA, U.S. Navy, NGA, GEBCO
US Dept of State Geographer
Image Landsat / Copernicus
© 2020 Google
© CAPTIO
Google Earth

IDC infrasound search for missing flight Malaysian Airlines MH370

Summary

This brief report summarizes the analysis and findings using IMS infrasound data and IDC bulletins on the search for the missing flight MH370 from Malaysian Airlines. The flight MH370 took-off from Kuala Lumpur airport, Malaysia, on Friday 7 March at 16:41 GMT and was on route for Beijing, China. It went missing within the first hour of flight (source: BBC).

Infrasound recordings from the IMS infrasound network and IDC bulletins are then searched for potentially related information. The IMS infrasound network routinely detects commercial flight taking off and landing from local airports.
However it should be noted that:

- Commercial planes in normal flight conditions are usually detected by IMS infrasound stations only at close range (within about 100km from stations).
- The only reported commercial plane that could be tracked over large distances (across the Atlantic) with an infrasound station was the Concorde as it was travelling as supersonic speed. The Concorde was discontinued 10 years ago.
- For flight MH370 to be picked up by IMS infrasound network at regional or global distances, it could mean that it crashed, exploded or disintegrated. However it would likely not be possible to draw any definitive conclusion based on remote infrasound recordings alone.

The geographical situation of Kuala Lumpur and the flight route with the infrasound network is not favourable as the closest station to Kuala Lumpur is I06AU, Cocos Island, and located 1700km away. On the northern part of the flight path, the installation of the 2 Chinese stations is still to be completed. The next closest certified stations are at ranges over 3500km.
The infrasound atmospheric propagation in regions close to the Equator is often complex given the relatively quiet upper atmospheric winds. This implies that long distance infrasound wave propagation is less favourable than at higher (and lower) latitudes. The infrasound network performance (using state-of-the-art meteorological models and background noise levels at IMS station for this specific time – Friday 7 March at 18:00 GMT) exhibits relatively fair to weak detection capabilities for the area surrounding Malaysia and Vietnam.
IDC bulletins and interactive review analysis results for all stations located within 5000km from the search area did not provide any detection or trace of signals related to the missing flight MH370.

Background information about Malaysian Airlines MH370

MH370 flight took off from Kuala Lumpur airport on 7 March 2014 at 16:41 GMT. According to the BBC (http://www.bbc.com/news/world-asia-26503141), the air traffic controllers lost contact with the plane within 50mn and the last reported location is 200km north of Kuala Lumpur (source: Flight Aware).

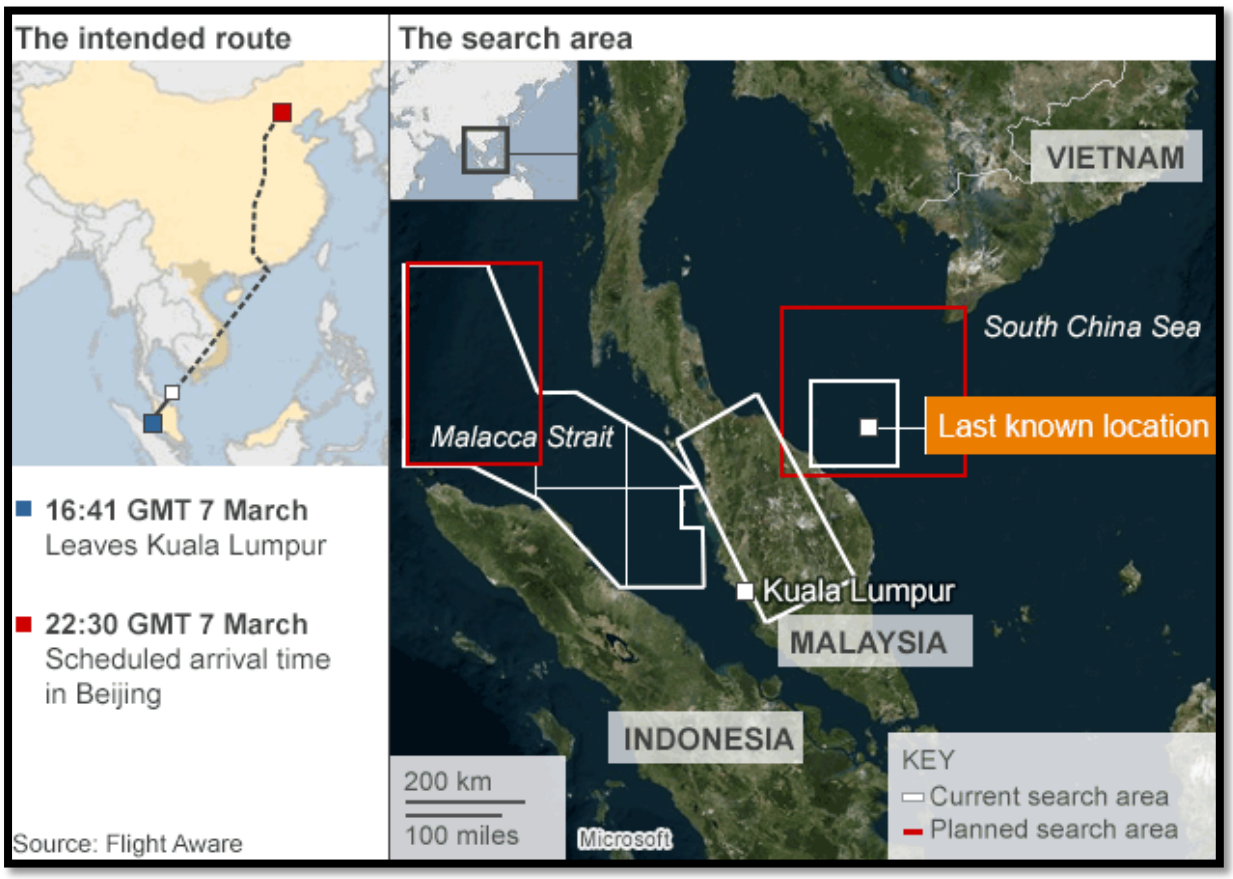

Figure 1: BBC summary of the situation for missing flight MH370 (Source: BBC.co.uk)

The media reports that the search areas are focusing within less than 800km in the north of Kuala Lumpur as of Monday 10 March.

IMS infrasound network

In the region around Kuala Lumpur, Malaysia the only certified station within 2000k is IS06 (Cocos Island, Australia). The 2 next stations located about 3500km are IS52 (Diego Garcia, UK) and IS39 (Palau). Other regional stations are beyond 4300km in Australia (IS04 and IS07) and beyond 5000km in Mongolia (IS34) and Japan (IS30) – see figure 2.

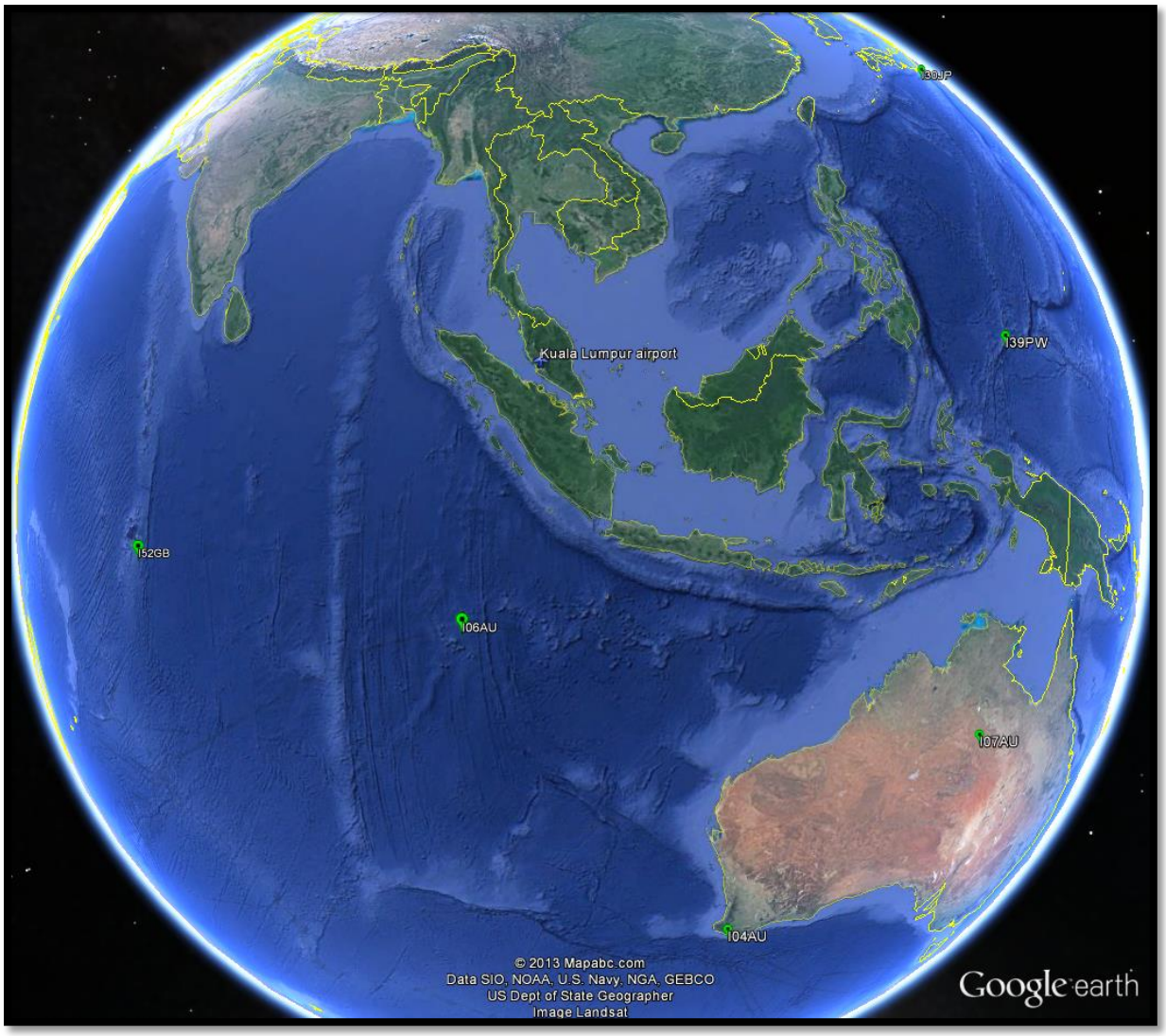

Figure 2: Situation of IMS infrasound network around Malaysia

IDC automatic bulletin review

Looking into the IDC automatic bulletins (SEL3), no matching event is reported within the first 15mn of the flight (see figure 3 with predicted and matching detections). The bulletins for the 7 closest stations only show 1 station (IS3), Isumi, Japan) with detections potentially originating from the Malaysian and Vietnamese area, but located at over 5300km.

Looking at the daily infrasound detection bulletin for the day (figure 4), it appears that this azimuth is rather common and could either be related to volcanic activity in Kyushu and Tanegashima islands (two well-known active volcanoes: Sakura-jima and Suwanose-jima) or microbarom-like activity in the seas south-west of the station.

CTBTO preparatory commission for the comprehensive nuclear-test-ban treaty organization

Distance/Azimuth

Source information
Latitude=3.125 **Longitude**=101.550 **Origin time**=2014/03/07 16:41:00

Search criteria *(SEL3.arrival@odb)*
Infra arrivaltime +/- 900 s **Infra Backaz** +/- 15.0 deg **Seismic Origintime** + 1200 s **Seismic Backaz** +/- 50.0 deg

Predicted arrivals at receivers (using iasp91 infra celerities)

	Station	Latitude	Longitude	Range (deg)	Range (km)	Back Az. (deg)	Azimuth (deg)	Prop.time	Arrival time
	I06AU	-12.15	96.82	15.88	1766	17.5	197.1	01:34:56	18:15:56
	I52GB	-7.38	72.48	30.82	3427	71.2	250.1	03:08:31	19:49:31
	I39PW	7.54	134.55	33.13	3684	264.2	81.0	03:22:39	20:03:39
	I07AU	-19.93	134.33	39.51	4393	301.8	126.8	04:01:39	20:42:39
	I04AU	-34.60	116.36	40.02	4450	336.6	160.9	04:04:47	20:45:47
	I34MN	47.80	106.41	44.70	4970	186.9	4.7	04:33:24	21:14:24
I	I30JP	35.31	140.31	48.09	5347	237.1	43.5	04:54:07	21:35:07

Figure 3: Infrasound tool for searching event matching arrivals in IDC bulletins. The source is Kuala Lumpur airport at the time of take-off and the receivers are all stations within 50 degrees.

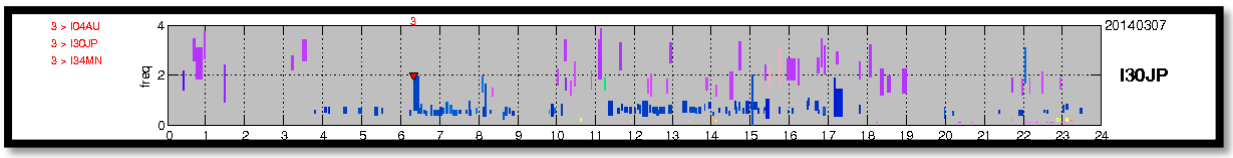

Figure 4: Daily IDC bulletins for IS30 (Japan) station showing detections from Kyushu volcanoes (dark blue) mixed with microbaroms (dark to light blue) and local activity in the bay of Tokyo (purple).

Infrasound propagation status

Before investigating station by station if traces of signal could be found, the infrasound network performance are a useful indicator on station that have higher likelihood of recording related signals. The infrasound threshold monitoring software (DTK-NetPerf) summarizes the performances combining the station background noise computed by IDC and the atmospheric characteristics (in the stratosphere) for the specific period of time.

From the figure 5, it appears that Kuala Lumpur is at the edge of Equatorial wind shift between southern and northern hemisphere. This region is usually not favorable for long propagation of infrasound waves. The Malaysia – Vietnam region is also exhibiting rather fair to poor network performances, for this specific period, due to the distance to the closest station (IS06 at over 1600km) and the relatively high level of noise at this station (typical for station on islands).

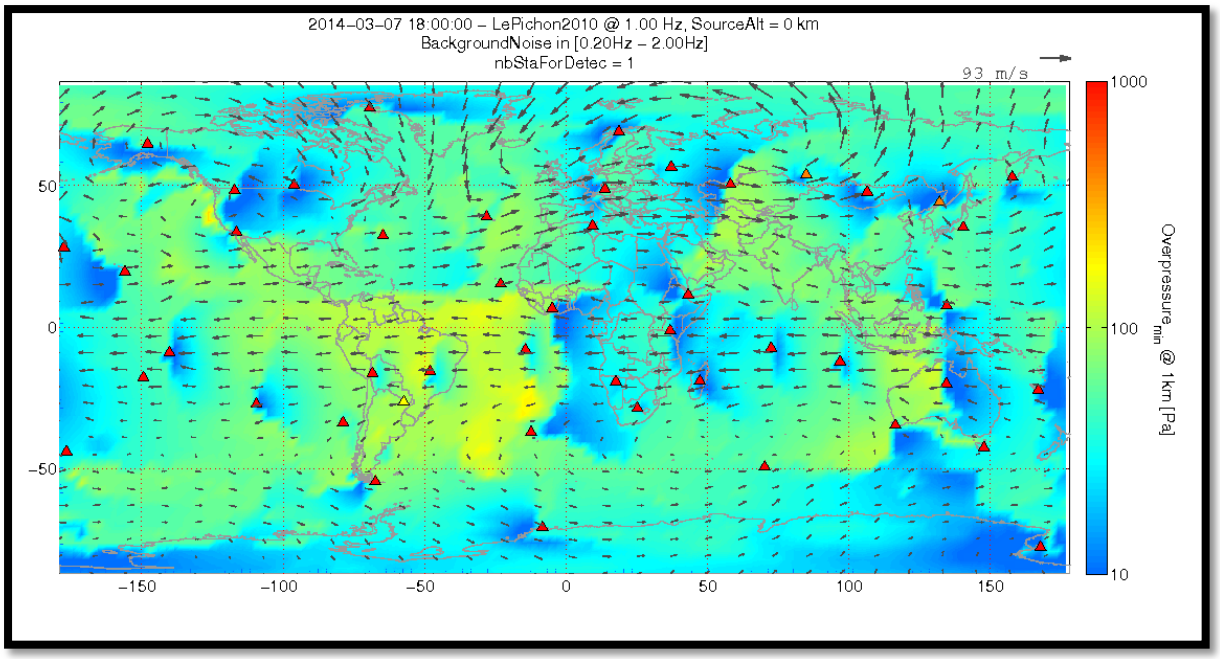

Figure 5: infrasound threshold monitoring results with DTK-Netperf for Friday

An Analysis of MH370's Flight Path Between Waypoints IGARI and VAMPI, a Review of Potential Vulnerabilities Specific to Airplane 9M-MRO and a Hypothesis Regarding Possible In Flight Events and an End-of-Flight Scenario

Mick Gilbert

V3.4 22 October 2016

Introduction

The purpose of this paper is to outline the findings of research into the flight path of Malaysia Airlines flight MH370 between waypoints IGARI and VAMPI and into potential vulnerabilities of the operating airplane, B777-200ER Registration 9M-MRO. Some of the findings support a hypothesis as to the cause of the loss of Malaysia Airlines flight MH370. Other findings contradict or undermine elements of the theory that deliberate and malicious direct action by a member of the flight crew, a "rogue pilot", was responsible for the disappearance of MH370.

Summary of Findings

1. There is no evidence to support the contentions that MH370 flew anything other than a direct route to Penang subsequent to the initial deviation from its planned flight path just past IGARI.

2. 9M-MRO, the Malaysia Airlines' B777 that operated as MH370, was at a significantly increased risk of experiencing a windshield heater fire or failure.

3. The crew oxygen system on 9M-MRO may have been leaking.

4. The initial deviation from the flight plan just past IGARI was consistent with the response to an inflight emergency such as a windshield heater fire.

5. A windshield heater fire can explain both the loss of the transponder signal and the interruption to the satellite communications link.

Discussion

1. There is no evidence to support the contentions that MH370 flew anything other than a direct route to Penang subsequent to the initial deviation from its planned flight path just past IGARI.

Considerable misinformation abounds regarding the course that MH370 flew after turning back towards the Malay Peninsula. This misinformation together with associated misrepresentations have, to a large extent, guided thinking towards the "rogue pilot" theory.

There is a common misconception that MH370 flew along air space boundaries and navigated from one waypoint to another after departing from its planned flight path. This is not supported by the evidence as detailed in the Factual Information Report released by the Malaysian ICAO Annex 13 Safety Investigation Team in 2015. Many people believe that MH370 was tracked continuously on primary radar from when it turned back just past waypoint IGARI to when it was lost from radar at the top of the Strait of Malacca. That is not the case.

The inferred 750 odd kilometre flight path of MH370 after the turn back just past IGARI until radar contact is lost north west of MEKAR is based on seven separate primary radar traces. The longest continuous radar trace by the same radar station was the final 120 kilometres over the Malacca Strait from near VAMPI to past MEKAR. The only waypoint that MH370 *may* have overflown was VAMPI. As detailed in the Factual Information Report, page 7, point 9, MH370 flew about 16 kilometres to the north of MEKAR (although contrary to what is stated, MH370 most certainly did not join Airway RNAV Route N571; if it had of it would have tracked directly to MEKAR from VAMPI). Radar contact was lost well before the airplane approached NILAM however a track from VAMPI to 16 kilometres north of MEKAR will pass about 12 kilometres to the north of NILAM.

Further, and also contrary to popular belief, MH370 did not track or "zig zag" along air space boundaries. After departing from its planned flight path MH370 flew on a heading that took it over, not along, a stretch of about 120 kilometers of the Bangkok (Thailand)-Kuala Lumpur (Malaysia) boundary that traces the Golong River. Subsequently, MH370 remained firmly in the Kuala Lumpur FIR (Malaysian airspace) at all times until it was lost from radar.

The map below illustrates the very simple course that MH370 flew; an initial right turn at IGARI towards BITOD followed almost immediately by a left turn back towards Penang on a heading of 240°. Then from south of Penang a right turn to 290°; this track would take MH370 over VAMPI and to the north of MEKAR.

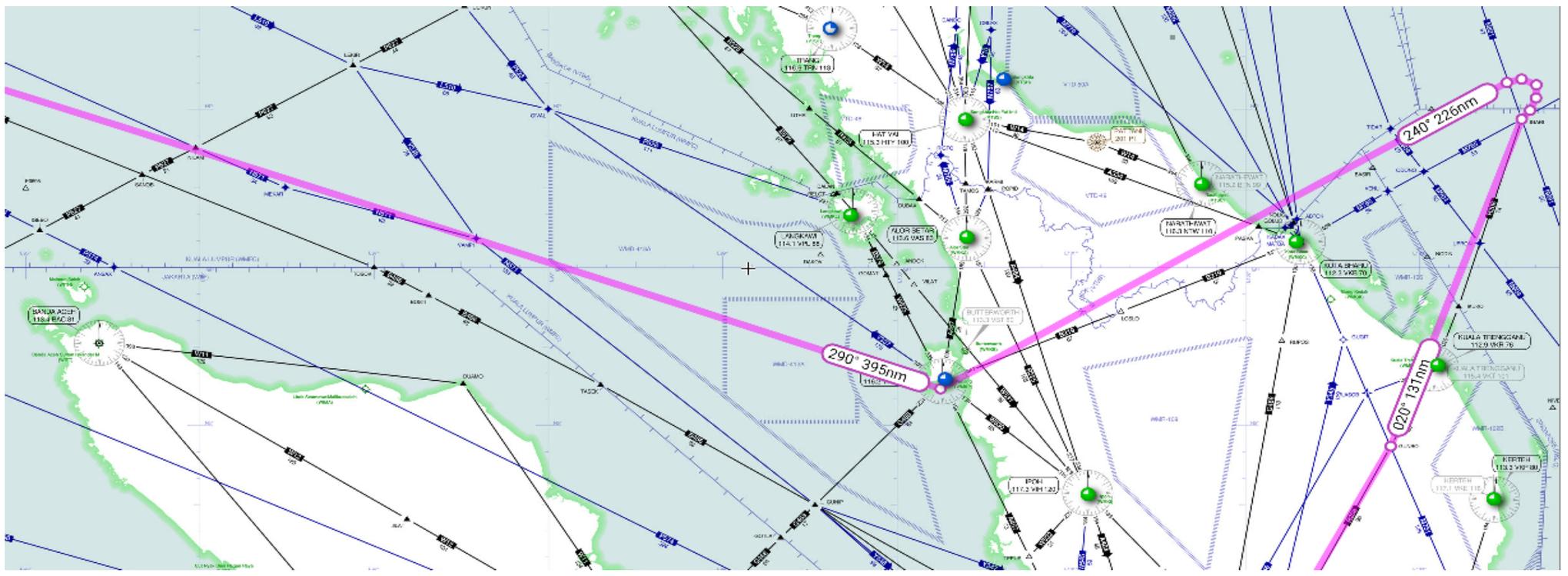

In short, the evidence indicates that MH370 may have tracked via one waypoint, VAMPI and I would content that this was coincidental.

2

Importantly, the flight path above does not require programming into the Flight Management System computer (in fact it would be quite laborious to do so), it can be flown very simply using the basic Mode Control Panel autopilot function in Heading or Track Select/Hold.

There have also been a range of misrepresentations about the altitudes flown by MH370 after the turn, ranging from the physically impossible climb to 45,000 feet to a low level, radar-evading run at 5,000 feet across the Malay Peninsula. Of course, none of that is true.

To determine what is true we again go to the primary radar data. Of the seven primary radar traces only three contain altitude data:

- 1730:35 UTC - 1735 UTC, the radar return was at a registered height of 35,700 ft.
- 1736 UTC - 1736:40 UTC, the radar return was at a registered height of between 31,100 and 33,000 ft.
- 1739:59 UTC, the radar return was at a registered height of 32,800 ft.

Allowing for the vagaries of primary radar with regards to determining altitude, that data suggests an altitude below the previously established cruise of 35,000 feet.

Going beyond the radar altitude data, if we assume some consistency with regards to MH370's altitude and air speed from when it turned back until when it disappeared off radar, then we can use the distance flown and the time taken to fly it to do some calculations. Given the known weather conditions, a constant true air speed of 498 knots satisfies the time and distance involved. Based on the known conditions if we convert a TAS of 498 knots to a Mach number we get M = 0.840 at FL340 (34,000 feet). M0.84 is not only the last reported speed for MH370 prior to the loss of the transponder signal it is also the typical cruising speed for a B777-200ER. Moreover, if you compare M0.84 at FL340 to the actual radar traces with regards to distance and time you also get a very good fit.

I should point out that ground speed conversion calculations are not mine, they were first published by Victor Iannello of Duncan Steel's Independent Group (http://www.duncansteel.com/archives/1969)

After the initial turn back there were no en route deviations, no zigzagging, no tracking along airspace boundaries, no changes of altitude apart from the initial descent to FL340 (the correct flight level for the westerly heading), and no changes to speed. In short, there were no attempts to evade radar detection or confuse observers.

2. 9M-MRO was at a significantly increased risk of experiencing a windshield heater fire or failure.

The Boeing B757, B767 and B777 all use the same forward windshields; there are two per airplane - left (Captain's) and right (First Officer's). They are manufactured by PPG Aerospace Transparencies of Huntsville, Alabama in the United States.

As illustrated below, the windshield is made up of two inner panes of Herculite (chemically strengthened) glass and an outer pane of tempered glass bound together with urethane interlayers. On either side of the middle pane of Herculite and adjacent to the inner and outer panes are layers of Nesatron film. Nesatron is transparent but electrically conductive and heats up when a current is passed through it - the layers of Nesatron are the windshield heaters. The inner heater prevents fogging of the inner pane and the outer heater prevents both icing and contracting of the outer pane due to exposure to sub-zero air temperatures at altitude. If the outer pane wasn't heated it would suffer a "thermal break" and shatter which would then expose the middle pane.

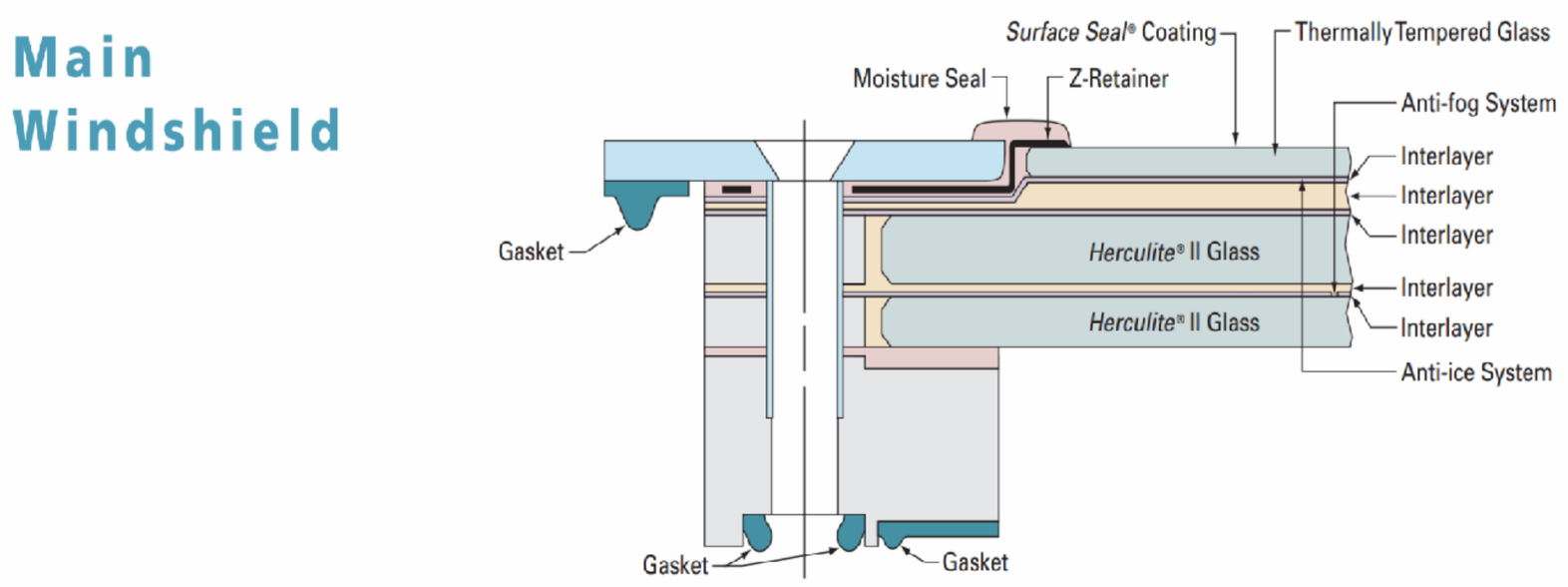

In 2007, the cost of each windshield was around $US100,000.

In the late 1990s and early 2000s, Boeing started to experience problems with windshield heaters either failing or shorting and catching on fire. The problems were encountered initially on the B757 and B767 but eventually the problem manifested itself in the B777 fleet as well. On 17 October 2002, an Air France B777 flying as flight AF062 from Paris to Los Angeles experienced a fire in the immediate area surrounding the windshield heater of the Captain's windshield. It took two fire extinguishers to put the fire out. The outer pane had cracked in a number of places. The crew initiated an emergency diversion and completed a successful landing at Churchill Airport, Canada.

Ten months after the Air France AF062 incident, on 24 July 2003, an Alitalia B777 flying as flight AZ610 from Rome to New York also had an inflight windshield fire that started with the Captain’s windshield heater. The fire was extinguished but the outer pane of the Captain's windshield shattered and the crew initiated an emergency diversion to Shannon International Airport, Ireland.

In an attempt to address the problem Boeing had PPG redesign the windshield heater terminal connections, replacing the original screw-in connections with pin-and-plug connectors. In April 2004, Boeing issued a number of service bulletins for the various airplane models impacted - Service Bulletin 777-30-0012 related to the B777 windshield heaters. The bulletin recommended that airlines inspect the electrical connections of the windshield heaters and adjust the connections if necessary or replace the entire windshield assembly with the new design with the improved electrical connections. The bulletin covered all 440-odd B777-200/300 aircraft produced up until 2004. Aircraft built after that time were fitted with the new windshields during production.

It was not until 2007, after investigating American Airlines flight AA1477, a B757 that had declared an emergency on departure from the Dallas-Fort Worth International Airport

because of smoke and a fire near the Captain's windshield heater terminal that the US National Transport Safety Board issued Safety Recommendation A-07-050. That recommendation asked that Boeing and the Federal Aviation Administration require operators to replace the windshield terminal blocks rather than just inspecting them. However, later that year when the FAA issued Airworthiness Directive FAA–2008–0274, which covered B757, B767 and B777 airplanes, it only required operators to comply with Boeing's Service Bulletin(s) with regards to the inspections and adjustments; replacement of the windshields was not required.

Boeing's service bulletins and the FAA's directive were temporarily effective – the incidence of windshield heater related issues fell to zero in the Boeing B777 fleet. But then in 2011, the problem re-surfaced, with two incidents involving B777s in 7 months. On 5 September 2011, an Air France B777 performing flight AF900 from Paris Charles de Gaulle to Yaounde, Cameroon was enroute at FL350 about 270 kilometres south of Paris when the crew experienced a windshield heater failure that led to windshield cracking. Then on 13 April 2012, an Alitalia B777 flying as flight AZ8320 from Rome to Dubai suffered cracking to the First Officer's windshield when the heater failed.

There were also renewed problems with the windshield heaters on B757 and B767. These included a 2008 incident involving an American Airlines B757 operating as flight AA1738 where the inner pane on the First Officer's windshield shattered spraying him with shards of glass and a 2010 incident involving a United Airlines B757 operating as flight UA057 where the Captain's windshield heater caught fire - the Captain emptied two extinguishers onto the fire to put it out, in the process he had his oxygen mask torn from his face twice while retrieving fire extinguishers (the hoses simply aren't long enough for the wearer to move far from their seat with the mask on).

There were at least 39 windshield heater related incidents between 2002 and 2014, eight involving B777s. I say "at least" because, alarmingly, not all incidents are reported through official channels. Boeing concedes that there have been 39 incidents but a review of NASA's Aviation Safety Reporting System database (the ASRS is an external to "official" channels, confidential, voluntary safety reporting system open to flight crew, cabin crew and ground staff) shows a number of incidents that do not tally with NTSB records (a matter that the NTSB acknowledges). The chain of correspondence between the NTSB and the FAA while all of this was unfolding highlights the NTSB's palpable frustration with the slowness of the FAA's initial response and the lack of firm direction regarding windshield replacement.

Analysis of the B777 windshield heater incidents is instructive. The airplane involved in the first incident, Air France F-GSPZ, was production line number 401; the Alitalia B777 involved in the second incident (I-DISU) was number 425. When windshield heater fires re-emerged, the Air France (F-GSPY) and Alitalia (EI-ISB) B777s were line numbers 395 and 426 respectively. All four airplanes – **395**, **401**, **425** and **426** – came off the Boeing production line in a nine month period from late March to mid-December 2002. Together, that small cohort represents half of the B777s that have experienced windshield heater related incidents.

There was also a 30 July 2008 incident involving an Emirates Boeing B777, registration A6-EMS operating as flight EK006 from London to Dubai where the crew reported smoke in the cockpit and carried out an emergency landing at Budapest Ferihegy airport but I have been unable to confirm that the source of the smoke was a windshield heater. A6-EMS was line number **408**.

An inferential statistical analysis of the confirmed windshield heater related incidents involving B777s highlights that 50% of the incidents occurred in less than 5% of the fleet. When adjusted for years of service, the rate of incidence of windshield heater fires/failures by years of service for B777s produced in 2002 is more than 12 times higher than the incidence rate for the entire B777 fleet and more than 30 times higher when compared to the remainder of the fleet (ie the fleet excluding the 2002 sub-group).

9M-MRO was manufactured on 14 May 2002, production line number **404**.

If Malaysia Airlines were complying with Airworthiness Directive FAA–2008–0274 and were following the Boeing phased-A check schedule, the flight compartment windows would have been inspected for condition in accordance with the Aircraft Maintenance Manual at every A2 Check. 9M-MRO's last A2 Check was 4 November 2013 and her next A2 Check would have fallen around the end of March-early April 2014.

9M-MRO belonged to a cohort of B777s that were statistically significantly over-represented in windshield heater related incidents and it is probable that 9M-MRO's windshield heaters were inspected for condition some 4 months before it flew as MH370.

3. The crew oxygen system on 9M-MRO may have been leaking.

The crew oxygen system provides pressurised oxygen to four masks on the flight deck for use in the event of an emergency. Malaysia Airlines B777s are fitted with two cylinders that hold 3150 litres of oxygen each at 1850 psi. This is sufficient capacity to provide 100% pressurised oxygen on demand to two flight crew for 13.5 hours.

Oxygen is drawn off from the system as part of the daily maintenance check; typically this check consists of a 5 second pressure check per mask. Additionally, before each flight, flight crew members check the flow of oxygen to their mask and the function of their mask microphone; these checks are combined into one 5 second test - the mask microphone is selected to INT (for intercom) and the oxygen flow test button is depressed, the oxygen flow can be heard on the flight deck speakers. Further, on the start of the first engine, 25 seconds of oxygen is automatically bled off so that the airplane’s sensors can confirm both flow and pressure.

The following information has been sourced from the Factual Information Report, FAA Airworthiness Directives, Boeing Service Bulletins and the operational records for 9M-MRO:

- On 14 January 2014, the crew oxygen system was serviced and topped up to 1800-1850 psi.

- On 17 January 2014, maintenance work was carried out on the crew oxygen system. That work was associated with an FAA Air Worthiness Directive, FAA AD 2012-13-05 (Replacement of Low Pressure Oxygen hose). According to the relevant Boeing Service Bulletin, the replacement job consists of 17.75 task hours and takes 11.2 hours elapsed time for two technicians to complete (that elapsed time does not include set-up, clean-up or independent inspection times). All the work is carried out on the flight deck on the low pressure side of the crew oxygen system and concludes with a simple flow check at the end of the job. The First Officer's seat need to be removed to access the flight deck oxygen system connections.

- 9M-MRO came out of an A4 Check on 16 January and was scheduled to fly from Kuala Lumpur to Melbourne on 17 January 2014 as MH149 departing at 11:45pm MYT. Thus, there was an operational requirement to have 9M-MRO out of maintenance and back on the line by no later than around 8.30-9.00pm local time. Work on the AD task would have occupied much of the day and early evening of 17 January. Given the requirement to first remove and lastly replace the First Officer's seat, the task is not one that can be easily rushed or curtailed.

- FAA AD 2012-13-05 had to be completed before the mandatory completion date of 12 February 2014. 17 January represented the last scheduled opportunity for the AD to be completed on 9M-MRO before the mandatory completion date.

- On 20 January 2014, three days after the work was performed, the First Officer's seat's forward/aft power adjustment was reported as inoperative.

- On 7 March 2014, the afternoon prior to flying as MH370, the crew oxygen system pressure read 1120 psi and was topped up to 1800 psi.

- Between 14 January and 7 March 9M-MRO flew 100 flights and accumulated around 550 airframe hours.

In aggregate, the daily and pre-flight mask checks together with the pressure check bleeds on engine start should have accounted for 5540 seconds or around 315 psi. The drop of 680-730 psi between 14 January to 7 March was about 2-2.5 times higher than what would be expected from the mask checks and start-up pressure check bleeds associated with 100 flights over 52 days.

Based on the above I'm led to believe that 9M-MRO had an oxygen leak, probably from one of the cockpit mask hoses given the nature of the work performed on 17 January. The leak may have resulted from the work associated with AD 2012-13-05 being rushed. The task may have been rushed because the maintenance crew would have been under pressure to complete the AD task on 17 January and operational requirements meant that they were afforded virtually no extra time to complete the task in the event of unforeseen delays or difficulties. The subsequent failure of the First Officer's seat's power adjustment may have been the result of the seat being hurriedly replaced.

Dangers associated with oxygen-enriched atmospheres

While oxygen itself is not flammable when the concentration of oxygen in the atmosphere rises by just 2%, from the usual 21% to 23%, the chemistry of fire changes and it changes dramatically; materials that do not normally burn become flammable and normally flammable materials ignite at lower temperatures and burn faster and hotter. Fires in oxygen-enriched atmospheres are extraordinarily difficult to extinguish.

The photograph below is of the flight deck of an EgyptAir B777 that suffered an oxygen fire whilst on the ground at Cairo International Airport on 29 July 2011. It took less than 4 minutes for the fire to cause that damage. (As a matter of happenstance, the work that was done on 9M-MRO's crew oxygen system under FAA AD 2012-13-05 was a result of the findings and recommendations arising from the Egyptair B777 oxygen fire.)

A contributory factor, perhaps the major one, to an oxygen-enriched atmosphere may well have been a flight crew mask. The crew's initial reaction to a windshield issue or smoke, fire or fumes in the cockpit is to don their oxygen masks, select 100% oxygen and select emergency mode on their mask. The combination of 100% oxygen and emergency mode ensures that oxygen is delivered continuously to the mask at a positive pressure to ambient; this is to ensure that smoke or fumes cannot be drawn into the mask. The cockpit fire extinguisher is behind the Captain's seat and while it can be reached by the Captain while seated it is easier for the Captain to retrieve it and use it by getting out of his seat. However, doing so would tear the mask from the Captain's face in much the same fashion as the UA057 incident mentioned above or, if the hose hadn't been fitted properly, it may have torn the hose from its mount. If the mask came off, 100% oxygen would flow into the flight deck at the rate of 30 litres per minute at around 14-15 psi. However, if the hose had been torn from its mount, 100% oxygen would flow into the flight deck at the rate of more than than 30 litres per second at 70 psi.

In either case, the air flow on the flight deck is such that oxygen venting from the mask or its hose would most likely be drawn towards the forward instrument panel and the fire.

4. The initial deviation from the flight plan just past IGARI was consistent with the response to an inflight emergency such as a windshield heater fire.

In the event of an inflight emergency such as windshield cracking or a windshield heater fire, the crew would divert to the nearest airport. A list of the four nearest airports in

terms of ETA can be quickly accessed via the Flight Management Computer. If an emergency were to present itself approaching or just past IGARI the two nearest airports were Kota Bharu (about 10 minutes flying time away) and Penang (about 30 minutes flying time away). However, Kota Bharu is not a 24 hour airport and was closed when MH370 was flying; its runway is also on the short side for a B777 at MH370's weight. A diversion to Penang, however, would have taken MH370 past Kota Bharu therefore providing an option if the emergency progressed rapidly to the point where an immediate landing was required.

MH370's change of direction back towards Penang on a heading of about 240° and its descent to FL340 just past IGARI were entirely consistent with a response to an inflight emergency.

5. A windshield heater fire can explain both the loss of the transponder signal and the interruption in the satellite communications link.

There are two transponders on the B777; left and right. In normal operations one transponder is active and the other is in standby mode. If the active transponder fails there is no automatic fail-over to the standby transponder, it needs to be selected manually. I have not been able to determine what Malaysia Airlines' procedures are for selecting the active transponder when crew are undergoing training but under normal circumstances the left transponder is active and the right is on standby.

The circuit breakers in airplanes are thermal-magnetic; they are designed to respond to the heat generated by an electrical overload or the magnetic flux associated with a short circuit. Because they are sensitive to heat, external heat will trip a thermal-magnetic circuit breaker.

There are two overhead circuit breaker panels on the flight deck that hold, amongst others, the circuit breakers for the transponders. Heat rises and, in the case of a windshield heater fire, would roll across the flight deck ceiling and over the circuit breaker panels. Heat from a windshield heater fire, particularly if it was in an oxygen-enriched atmosphere, may have started tripping some of the lower rated thermal-magnetic circuit breakers in the overhead panels. The right and left transponder circuit breakers are rated at only 5 amps. Further, the left transponder circuit breaker is located at the A3 position on the left panel, placing it closest (bar two) to the potential heat source, the Captain's windshield.

With regards to the failure of MH370's satellite communications, the Satellite Data Unit is powered by the left AC bus. In the event of a fire, smoke or fumes in the cockpit, the B777 Quick Reference Handbook checklist states the objectives are; To remove power from the ignition source, and To land the airplane as soon as possible, if needed. The checklist states that if the source of the fire is obvious, power should be removed from any affected equipment. If the fire originated in the Captain's windshield heater the approach to removing power from it would be to first turn off the windshield heaters and then fully isolate the Left AC bus. The latter is accomplished by selecting the Left Bus Tie Breaker to ISLN, selecting the Left Backup Generator to OFF, and selecting the Left Generator to OFF. This would have the effect of cutting power to the SDU.

Hypothesis

While the following is speculation on my part it is to a large degree based on research and precedent accidents.

As alluded to above, I believe that MH370 suffered a windshield heater related incident involving the Captain's windshield shortly before arriving at waypoint IGARI. At the first sign of smoke, a burning smell or a fire, the crew's initial reaction would have been to don their oxygen masks. In keeping with prior windshield heater fire incidents the fire most likely would have broken out around the frame of the Captain's windshield. The Captain would have ordered the First Officer to identify the nearest airport and initiate a diversion. There would almost certainly have been some initial confusion/discussion regarding the choice of diversion - Kota Bharu, which was closer but closed, versus Penang, which was further but open. That delay may well account for the initial right turn at IGARI as the Flight Management System would have commanded a right turn to 059° to track towards their next waypoint, BITOD. Having decided on Penang the First Officer would have taken the autopilot out of LNAV mode and into Mode Control Panel Track Select and selected 240° to take them back to Penang; the airplane would have stopped the right turn and then turned left. The First Officer would have also commanded a 1,000 descent to Flight Level 340 to put them on the correct level for a westerly heading.

I suspect that the Captain got out of his seat to retrieve the cockpit fire extinguisher and fight the fire (a small fire burning directly in front of him may have also prompted him to leave his seat). That would have meant either taking his mask off or having it torn off when the hose reached full extension. He would have then either donned the PBE (which was right beside the fire extinguisher and designed for just such a situation) or donned one of the observer's oxygen masks at the rear of the flight deck.

If the Captain had donned the PBE he was now out of communication with the First Officer; this would have left the First Officer to work the Smoke, Fire or Fumes checklist. A mayday call does not appear on the checklist and, moreover, as the Captain had been handling the radios for the flight up till this point, making a mayday call may not have been front of mind for the First Officer. Having identified the source of the fire as the Captain's windshield the First Officer would have first turned the windshield heat off on the overhead panel and then isolated the Left AC Bus; in doing so power to the SATCOM would have been cut. The oxygenation of the flight deck would cause the fire to flare, tripping the transponder circuit breaker and possibly injuring either or both the pilots.

The fire would have then propagated rapidly possibly forcing one or both pilots from the flight deck. However, it would have only burned for only a few minutes and then the Captain's windshield would have failed causing a rapid depressurisation. If the flight deck door was closed the sudden change in pressure would cause it to unlatch and the rapidly escalating pressure differential between the flight deck and the main cabin would force it to open - this safety feature is designed to prevent the bulkhead between the flight deck and the main cabin from collapsing in the event of a flight deck depressurisation. Given the sustained rapid outflow of air anyone on the flight deck who was unrestrained risked being forced towards and possibly through the failed windshield.

The rapid outflow of air and the sudden cooling caused by the depressurisation would have extinguished the fire.

The basic autopilot function is highly protected and runs on redundant systems and would have kept MH370 tracking towards Penang on 240° at FL340.

Within 20-25 minutes of the depressurisation event, 5-10 minutes before reaching Penang, almost everyone on board would have been dead. The passenger oxygen system uses chemical oxygen generators and continuous flow masks that have inhalation and exhalation check valves. Because the inhalation check valves on the masks dilute the supplied oxygen with the ambient atmosphere, at 34,000 feet the passenger oxygen generators cannot provide sufficient partial pressure of oxygen in the lungs to maintain consciousness without considerable conscious respiratory effort. People unfamiliar with hypoxia would have simply lost consciousness and died after 20-22 minutes when the oxygen generators burned out. A flight or cabin crew member may have recognised the early symptoms of hypoxia and started deep, forceful breathing and remained conscious. The PBE, which provides unpressurised but undiluted 100% oxygen to the wearer, would have offered the best chance of remaining conscious after the depressurisation.

I believe that one of the flight crew survived the fire and depressurisation event, possibly because they had donned the cockpit PBE, possibly because they were out of the cockpit retrieving an extra fire extinguisher when the windshield failed, possibly both.

The cockpit would have been reduced to something akin to the EgyptAir B777 photograph with the additional problems of being both incredibly noisy and extremely cold (around -30°C). The cockpit displays are liquid crystal and quite vulnerable to heat damage, in all likelihood they would have all been destroyed. There are no analogue back-up instruments. Moulded plastics such as keypads and switches together with oxygen masks and hoses, headsets and microphones would have been burned or melted. Unused crew oxygen masks at the observers' stations would probably have still been usable but with two destroyed masks venting oxygen uncontrollably the supply would be depleted very quickly. There would be effectively no visibility from the cockpit - it would be almost impossible to look through the open section left by the failed windshield and all the other windows would have been covered with soot from the fire and would also be rapidly accumulating frost.

For someone to get back to the cockpit would have taken considerable effort. First of all, they would have needed to retrieve one of the portable walk-around oxygen bottles - one bottle would give them 15 minutes of oxygen - or one of the extra PBEs. Then they would need to brave the cold and the noise.

On approaching Penang the surviving pilot would have come to the realisation that he had no means of communication; radio communication panel keypads, microphones and headsets would have been burned or melted by the fire. He may have tried using the emergency locator beacon stowed in the cabin but the airplane fuselage would act like a Faraday cage and shield the signal; trying to get line of sight to a satellite through a window would be highly problematic and the battery would have been short-lived given the freezing temperature (the batteries are not rated to function in temperatures below -20°C). He may have tried mobile phones but the altitude would have made a connection improbable and the batteries would have quickly succumbed to the cold.

The pilot would have also realised that they was no reasonable chance of manually flying the airplane; he had no instruments, it was night, there was no moon, he could only occupy the cockpit for short periods of time and oxygen supplies were dwindling. Any attempt to take manual control of the airplane would almost invariably end with loss of control and there could be no guarantee that he could re-engage the autopilot if he disengaged it.

Just off the starboard wing was Penang; population 1.65 million. Immediately ahead and stretching 900 kilometres from the north-west to the south-east was the world's second

busiest shipping lane, the Strait of Malacca, the conduit for trade from Europe and the Middle East to South East Asia. There would have been ships - tankers, chemical ships, container ships, bulk carriers and cruise liners - about every 5-6 kilometres along the Strait. 20 minutes ahead lay nearly five million people, the inhabitants of the North Sumatra province of Indonesia and that country's third largest city, Medan.

Given the situation I believe that the pilot then elected to do what many pilots in stricken airplanes have done in the past; steer it clear of populated areas. He turned up the Strait of Malacca running parallel to but to the north of the shipping lane. On this leg the pilot may have made some attempts to establish communications or to regain some additional flight functions by reconnecting the Left AC Bus, resetting the Right AC Bus or both. Reconnecting the Left AC Bus would have had the effect of reconnecting power to the SATCOM which then rebooted and started the sequence of satellite handshakes that allowed MH370 to be eventually tracked to the Southern Indian Ocean.

On reaching the top of the Strait the pilot would have been exposed to -30°C temperatures for over an hour and would have been suffering from hypothermia. The crew oxygen system would by now be largely, if not completely, depleted. Given these circumstances and with the densely populated southern coast of India less than 2 hours directly ahead, I believe that the pilot simply pointed the airplane in the safest possible direction, due south using Track Select onto 180°.

Moving to the end of flight, I believe that MH370 ran out of fuel on the 7th arc and came down near 34° 12' S, 94° 30' E, about 695 kilometres north east of the ATSB hot spot and about 200 kilometres outside the current search area. The ATSB modelling assumed an undamaged, intact airplane and favours flight paths to the 7th arc that are consistent with a normal fuel burn. Factoring in the additional drag from the failed windshield makes shorter paths that use more fuel over the same period of time more likely. A southerly track on 180° gives a total flying distance from IGARI to fuel exhaustion that is 360 kilometres (or roughly 7.5%) shorter than that modelled as most likely by the ATSB.

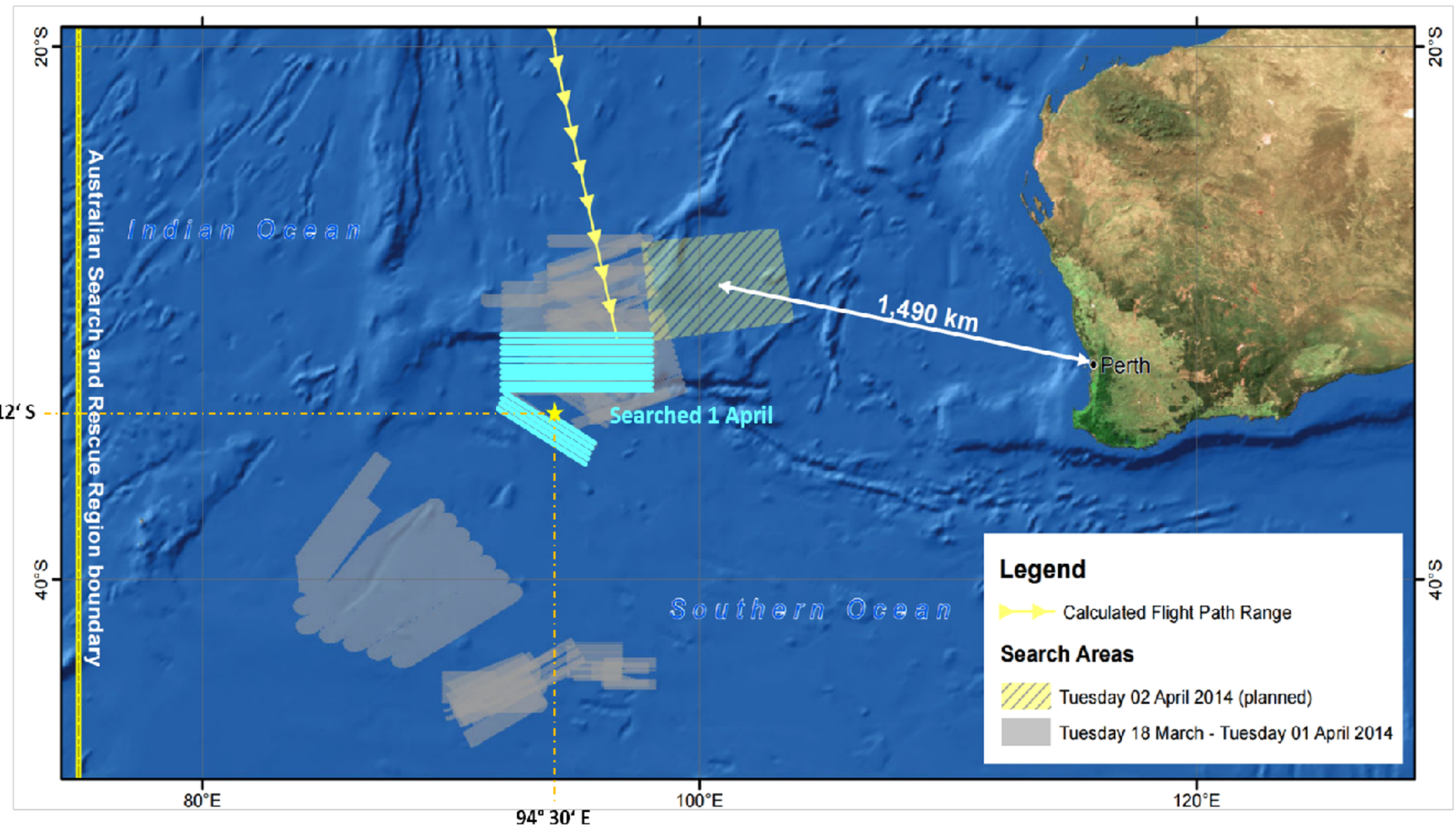

34° 12' S, 94° 30' E is interesting in another regard also; as illustrated on the map above it sits right in a gap in the aerial search zone of 1 April 2014 (the calculated flight path shown

12

on the map was the best guest as of 30 March 2014). A debris field would have drifted north-west by the time the aerial search reached that location on 1 April. On 2 April the search was moved a few hundred kilometres to the north east. Then, on 4 April 2014 all the search assets were redirected about 1,500 kilometres to the north chasing what turned out to spurious underwater acoustic signals.

13

MH370 Flight Route - Southern Indian Ocean

based on Satellite Data

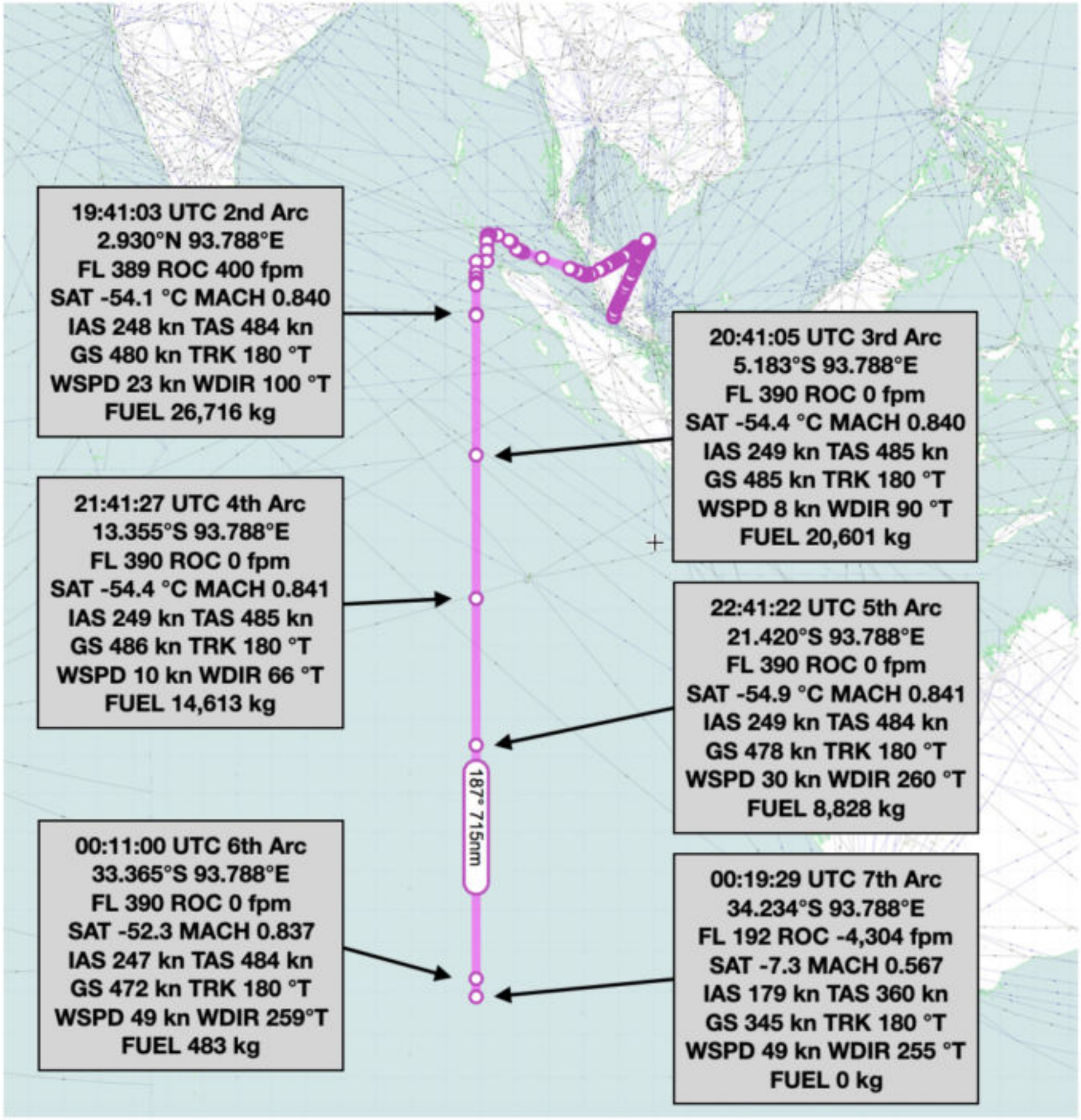

Eos, Vol. 95, No. 21, 27 May 2014

EOS
EOS, TRANSACTIONS, AMERICAN GEOPHYSICAL UNION

VOLUME 95 NUMBER 21
27 May 2014
PAGES 173–180

Seafloor in the Malaysia Airlines Flight MH370 Search Area

PAGES 173–174

On the morning of 8 March 2014, Malaysia Airlines flight MH370, from Kuala Lumpur to Beijing, lost contact with air traffic control shortly after takeoff and vanished. While the world waited for any sign of the missing aircraft and the 239 people on board, authorities and scientists began to investigate what little information was known about the plane's actual movements.

As days and weeks passed, the search began to focus on the Indian Ocean to the west of Australia—far from the flight's intended path. Clues to how the plane got so far off course may be in the plane's "black boxes"—its flight data and cockpit voice recorders. Finding the recorders is therefore a top priority.

Little is known about the seafloor from ship-borne echo sounder measurements in the region where flight MH370 is believed to have crashed. Available depth measurements cover only 5% of the 2000 by 1400 kilometer area in Figure 1 (a high-resolution copy of this figure may be found in the additional supporting information in the online version of this article), and only a very few of them were acquired with modern acoustic and navigational systems. This lack of data makes the search for MH370 all the more difficult. It also highlights how most seafloor features are very poorly resolved. However, satellite altimeter measurements provide global bathymetry estimates at a resolution of about 20 kilometers [*Smith and Sandwell,* 1997], making it at least possible to map the major seafloor features in the search area.

Constraining the Search Area

When MH370 went missing, the search initially focused in the Gulf of Thailand and the South China Sea, along the intended flight path from Kuala Lumpur to Beijing. After a few days, reports of possible radar contacts caused the search to expand westward, across the Malay Peninsula to the Strait of Malacca and the Andaman Sea.

Later, the search was extended even farther west into the Indian Ocean, when it was realized that the aircraft's satellite communications system had remained operating for several hours. Although the aircraft was not actively transmitting information about its health and position, it was automatically replying to brief queries from a ground station in a process known as a handshake. These handshakes, which took place approximately hourly, were relayed through an Inmarsat telecom satellite in geostationary orbit over the central Indian Ocean. The round-trip travel time of each handshake gave a crude estimate of the distance between the aircraft and the satellite while Doppler shifts in the handshake allowed a rough estimate of the aircraft's velocity away from the satellite.

This analysis, completed about 10 days after the disappearance, was combined with estimates of when the plane might have run out of fuel. Together they suggested that the aircraft might be anywhere in a large area of the Indian Ocean west of Australia.

MH370's black boxes were equipped with "pingers" programmed to emit acoustic signals if the boxes fell into the sea. The expected battery life of these pingers was approximately 1 month, so there were only a few days of expected pings left when it was reported that the Chinese vessel *Haixun 01* had detected pings on 4 and 5 April in the water above the east flank of the Batavia Plateau (see black circle in Figure 1). Over the next 3 days the Australian vessel *Ocean Shield* reported three other contacts, one contact apparently hearing pings emitted by two distinct devices, in an area above the north flank of the Zenith Plateau (see red circle in Figure 1).

The Batavia and Zenith contact locations are approximately 600 kilometers apart, and it seems unlikely that pingers at the end of their battery life could be heard over such distances, yet sound propagation in the ocean is quite complex. Nonetheless, Chinese and Australian authorities seemed confident that the carrier frequency, duration, and pulse repetition interval of the pings heard were likely those of an aircraft black box pinger rather than those mounted on commercial fishing gear or on whales to track their migration.

The dashed lines in Figure 1 roughly parallel the estimated flight paths suggested by the Doppler handshake analysis and encompass the areas of the various reported acoustic contacts. Here the swath defined by these dashed lines is referred to as the acoustic search zone.

Seafloor Data From Ship Surveys

Data collected by research vessels *Vema* and *Robert D. Conrad* provide the only available depth surveys [*International Hydrographic Organization Data Center for Digital Bathymetry* (*IHO DCDB*), 2014] over the Batavia and Zenith plateaus (see Figure 1, B and Z). The Batavia Plateau was crossed by *Vema* in 1962 and by *Conrad* in 1965; both dates are prior to when the U.S. Navy–run Transit satellite navigation system became standard for remote ocean navigation. *Vema* also crossed the Zenith Plateau in 1977, when Transit was available.

Navigation on all these expeditions was by dead reckoning between sparse navigation points. In the Transit era these points could be obtained once every few hours and had accuracies of a few kilometers. Prior to Transit, these points would be celestially determined, perhaps days apart in bad weather. Both expeditions occurred prior to the use of modern multibeam echo sounders (MBES), so depth measurements were collected by single, wide-beam echo sounders that recorded on analog paper scrolls, the digitizing of which is often in error by hundreds of meters [*Smith,* 1993].

Of the publicly available data, ships carrying MBES and navigating by GPS have passed through the area only twice; the R/V *Melville* and the R/V *Knorr* each made a passage in 1996, but neither surveyed any of the major topographic features. Apart from those two transits, all other data publicly available in the area are analog, low-tech soundings, and most predate the era of GPS navigation.

The estimate that 5% of the seafloor in the area has been mapped comes from inspection of the data in *IHO DCDB* [2014], the *General Bathymetric Chart of the Oceans* (*GEBCO*) [2010], and versions 15 and 16 of the bathymetric model by *Smith and Sandwell* [1994, 1997]. Some additional data may exist but not reside in openly available databases. For example, the Zenith Plateau was named

By W. H. F. Smith and K. M. Marks

This paper is not subject to U.S. copyright. Published in 2014 by the American Geophysical Union.

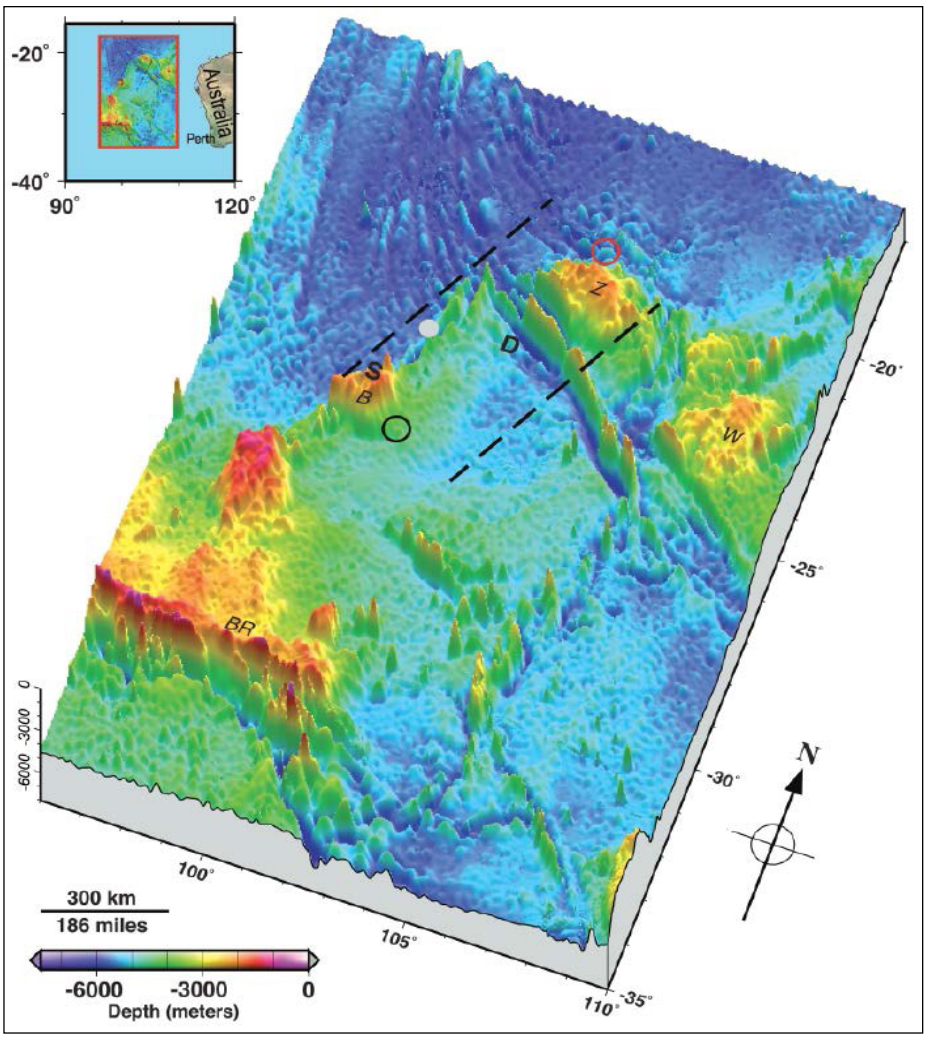

Fig. 1. Seafloor topography in the Malaysia Airlines flight MH370 search area. Dashed lines approximate the search zone for sonar pings emitted by the flight data recorder and cockpit voice recorder popularly called black boxes. The first sonar contact (black circle) was reportedly made by a Chinese vessel on the east flank of Batavia Plateau (B), where the shallowest point in the area (S) is at an estimated depth of 1637 meters. The next reported sonar contact (red circle) was made by an Australian vessel on the north flank of Zenith Plateau (Z). The deepest point in the area (D) lies in the Wallaby-Zenith Fracture Zone at an estimated depth of 7883 meters. The Wallaby Plateau (W) lies to the east of the Zenith Plateau. The shallowest point in the entire area shown here is on Broken Ridge (BR). Deep Sea Drilling Project (DSDP) site 256 is marked by a gray dot. The inset in the top left shows the area's location to the west of Australia. Seafloor depths are from the General Bathymetric Chart of the Oceans *[2010].*

for R/V *Zenith* (see GEBCO Undersea Feature Names Gazetteer, http://www.ngdc.noaa.gov/gazetteer), which apparently discovered it in the 1930s; *Veevers et al.* [1985] allude to a crossing of the Zenith Plateau by Royal Australian Navy vessel *Cook* in 1983. *Williams et al.* [2013b] report that R/V *Southern Surveyor* obtained some data over the Batavia Plateau in 2011, although the abyssal depths in the region adjacent to the plateau exceeded the designed operating range of its MBES system. Data from the *Zenith, Cook,* and *Southern Surveyor* expeditions could not be found in digital form in open source databases, and they are not used in the Smith and Sandwell or GEBCO compilations.

Another confounding factor is that the feature names in this area are not universally agreed upon. Google Earth™ uses the name Wallaby Plateau for the Zenith Plateau because Google Earth™ displays names used by the U.S. Board on Geographic Names. However, the international community uses Zenith Plateau to avoid confusion with another Wallaby Plateau [*Sayers et al.,* 2002] that lies closer to the coast of Australia (Figure 1). Greater standardization of nomenclature and sharing of data could improve ocean mapping.

Satellite Interpolation of Seafloor Data Gaps

The depths in Figure 1 are from *GEBCO* [2010], which uses satellite altimetry to interpolate gaps between ship survey data publicly available in open sources [*Smith and Sandwell,* 1994, 1997]. The accuracy of the positions and depths in these survey data limits the accuracy of the satellite estimates. In addition, depth estimates from satellite altimetry are most accurate where the seafloor topography is moderate and composed of oceanic crust overlain by less than 200 meters of sediment [*Smith and Sandwell,* 1994]. *Whittaker et al.* [2013] estimate sediment thicknesses in the area varying from 12 meters to 1.5 kilometers, and Deep Sea Drilling Project site 256 (gray dot in Figure 1) found 251 meters of sediment [*Davies et al.,* 1974].

The seabed in the MH370 search area records a complex geologic history of the breakup of Australia, India, and Antarctica approximately 130 million years ago [*Williams et al.,* 2013a]. The shallowest depth in the area shown in Figure 1 is about 237 meters on Broken Ridge, a structure related to the separation of Australia and Antarctica whose conjugate, the Kerguelen Plateau, lies on the Antarctic plate. Within the acoustic search zone of Figure 1, the shallowest depth is about 1637 meters at the summit of Batavia Plateau. The deepest point in the area shown also lies within the acoustic search zone, where the trough of the Wallaby-Zenith Fracture Zone plunges to an estimated 7883 meters, just south of the Zenith Plateau. These plateaus are fragments of continental crust, leftovers of Indo-Australian continental breakup [*Williams et al.,* 2013b], and are embedded in old, deep seafloor.

Unknown Seafloor Depths Complicate the Search

The search for airplane debris in the open ocean is not without precedent: On 1 June 2009, Air France flight AF447 disappeared over the Atlantic Ocean. However, the present search for missing Malaysia Airlines flight MH370 takes place under very different circumstances.

When AF447 disappeared, there was little doubt about where it would be found. The flight had not deviated significantly from its intended path from Rio de Janeiro to Paris, and the aircraft was routinely sending messages monitoring the health of its flight systems along with its position. Warning and failure messages generated by these systems in the last few minutes of flight helped to locate the crash site, and a surface search there found floating debris and fuel slicks the very next day.

In addition, the AF447 crash site was in an area already 100% covered by a previous state-of-the-art bathymetric survey (MBES and GPS), and this knowledge of the undersea terrain helped searchers select and program autonomous underwater vehicles (AUVs) to search for the black boxes. Even so, they were not recovered until nearly 2 years after the crash.

In comparison, the MH370 crash site is very poorly known. There are no measured depths in public databases at the locations where ping contacts were reported. Satellite altimetry estimates that depths at the Chinese and Australian contact locations are about 4300

This paper is not subject to U.S. copyright. Published in 2014 by the American Geophysical Union.

23249250, 2014, 21, Downloaded from https://agupubs.onlinelibrary.wiley.com/doi/10.1002/2014EO210001, Wiley Online Library on [22/05/2024]. See the Terms and Conditions (https://onlinelibrary.wiley.com/terms-and-conditions) on Wiley Online Library for rules of use; OA articles are governed by the applicable Creative Commons License

and 5160 meters, respectively, but these estimates are quite uncertain and might be in error by approximately 250 meters or more. Selecting an appropriate AUV and programming its search path require knowledge of the terrain. A Bluefin 21 AUV initially deployed over Zenith Plateau to search for debris, for example, was not designed to operate at depths below 4500 meters.

Lack of knowledge of seafloor topography has other consequences. Bottom topography steers surface currents [*Gille et al.,* 2004] while bottom roughness controls ocean mixing rates [*Kunze and Llewellyn Smith,* 2004], and poor knowledge of these characteristics limits the accuracy of forecasts of everything from the path of floating debris to the path of tsunamis [*Mofjeld et al.,* 2004] and the future of climate [*Jayne et al.,* 2004].

Seafloor Features: Not as Well Resolved as Martian Topography

The state of knowledge of the seafloor in the MH370 search area, although poor, is typical of that in most of Earth's oceans, particularly in the Southern Hemisphere. In many remote ocean basins the majority of available data are celestially navigated analog measurements [*Smith,* 1993] because systematic exploration of the oceans seems to have ceased in the early 1970s [*Smith,* 1993, 1998; *Wessel and Chandler,* 2011], leaving the ocean floors about as sparsely covered as the interstate highway system covers the United States [see *Smith and Sandwell,* 2004, Figure 2]. When these sparse soundings are interpolated by satellite altimetry, as in Figure 1, the resulting knowledge of seafloor topography is 15 times worse in the horizontal and 250 times worse in the vertical than our knowledge of Martian topography [*Smith,* 2004].

Although a new bathymetric satellite altimeter mission could improve this situation significantly [*Smith and Sandwell,* 2004], ships with echo sounders remain the best technology for ocean mapping. The global ocean deeper than 500 meters (that is, deeper than the continental shelves) could be fully surveyed with state-of-the art navigation and acoustic multibeam systems with a total effort of about 200 ship-years of vessel activity at a total cost less than that of a typical planetary exploration mission [*Carron et al.,* 2001].

Until there is such an effort, knowledge of Earth's ocean floors will remain limited to the resolution available from satellite altimetry, which is vastly poorer than our knowledge of the topographies of Earth's Moon, Mars, and Venus. Perhaps the data collected during the search for MH370 will be contributed to public databanks and will be a start of greater efforts to map Earth's ocean floor.

Acknowledgments

Reviews by S. Stein and additional suggestions from E. W. Leuliette improved the manuscript. W.H.F.S. was formerly and K.M.M. is currently chair of the Technical Sub-Committee on Ocean Mapping of the United Nations Intergovernmental Oceanographic Commission (IOC) and IHO joint committee for GEBCO. The paper's contents are solely the opinions of the authors and should not be construed as an official statement of policy, decision, or position on behalf of the National Oceanic and Atmospheric Administration (NOAA), the U.S. government, GEBCO, the IOC, or the IHO.

References

Carron, M. J., P. R. Vogt, and W.-Y. Jung (2001), A proposed international long-term project to systematically map the world's ocean floors from beach to trench: GOMaP (Global Ocean Mapping Program), *Int. Hydrogr. Rev., 2*(3), 49–55.

Davies, T. A., et al. (1974), Site 256, *Initial Rep. Deep Sea Drilling Proj., 26,* 295–325.

General Bathymetric Chart of the Oceans (GEBCO) (2010), GEBCO_08 grid, version 20100927, http://www.gebco.net/data_and_products/gridded_bathymetry_data/, Br. Oceanogr. Data Cent., Liverpool, U. K.

Gille, S. T., E. J. Metzger, and R. Tokmakian (2004), Seafloor topography and ocean circulation, *Oceanography, 17*(1), 47–54, doi:10.5670/oceanog.2004.66.

International Hydrographic Organization Data Center for Digital Bathymetry (IHO DCDB) (2014), Marine Trackline Geophysical Data, http://ngdc.noaa.gov/mgg/geodas/trackline.html, Natl. Geophys. Data Cent., Boulder, Colo.

Jayne, S. R., L. C. St. Laurent, and S. T. Gille (2004), Connections between ocean bottom topography and Earth's climate, *Oceanography, 17*(1), 65–74, doi:10.5670/oceanog.2004.68.

Kunze, E., and S. G. Llewellyn Smith (2004), The role of small-scale topography in turbulent mixing of the global ocean, *Oceanography, 17*(1), 55–64, doi:10.5670/oceanog.2004.67.

Mofjeld, H. O., C. Massell Symons, P. Lonsdale, F. I. González, and V. V. Titov (2004), Tsunami scattering and earthquake faults in the deep Pacific Ocean, *Oceanography, 17*(1), 38–46, doi:10.5670/oceanog.2004.65.

Sayers, J., I. Borissova, D. Ramsay, and P. A. Symonds (2002), *Geological Framework of the Wallaby Plateau and Adjacent Areas, Geosci. Aust. Record,* vol. 2002/21, 133 pp., Geosci. Aust., Canberra.

Smith, W. H. F. (1993), On the accuracy of digital bathymetric data, *J. Geophys. Res., 98*(B6), 9591–9603, doi:10.1029/93jb00716.

Smith, W. H. F. (1998), Seafloor tectonic fabric from satellite altimetry, *Annu. Rev. Earth Planet. Sci., 26,* 697–747, doi:10.1146/annurev.earth.26.1.697.

Smith, W. H. F. (2004), Introduction to this special issue on bathymetry from space, *Oceanography, 17*(1), 6–7, doi:10.5670/oceanog.2004.62.

Smith, W. H. F., and D. T. Sandwell (1994), Bathymetric prediction from dense satellite altimetry and sparse shipboard bathymetry, *J. Geophys. Res., 99*(B11), 21,803–21,824, doi:10.1029/94jb00988.

Smith, W. H. F., and D. T. Sandwell (1997), Global sea floor topography from satellite altimetry and ship depth soundings, *Science, 277*(5334), 1956–1962, doi:10.1126/science.277.5334.1956.

Smith, W. H. F., and D. T. Sandwell (2004), Conventional bathymetry, bathymetry from space, and geodetic altimetry, *Oceanography, 17*(1), 8–23, doi:10.5670/oceanog.2004.63.

Veevers, J. J., J. W. Tayton, B. D. Johnson, and L. Hansen (1985), Magnetic expression of the continent-ocean boundary between the western margin of Australia and the eastern Indian Ocean, *Z. Geophys., 56,* 106–120.

Wessel, P., and M. T. Chandler (2011), The spatial and temporal distribution of marine geophysical surveys, *Acta Geophys., 59*(1), 55–71, doi:10.2478/s11600-010-0038-1.

Whittaker, J., A. Goncharov, S. Williams, R. D. Müller, and G. Leitchenkov (2013), Global sediment thickness data set updated for the Australian-Antarctic Southern Ocean, *Geochem. Geophys. Geosyst., 14*(8), 3297–3305, doi:10.1002/ggge.20181.

Williams, S. E., J. M. Whittaker, R. Granot, and D. R. Muller (2013a), Early India-Australia spreading history revealed by newly detected Mesozoic magnetic anomalies in the Perth Abyssal Plain, *J. Geophys. Res. Solid Earth, 118*(7), 3275–3284, doi:10.1002/jgrb.50239.

Williams, S. E., J. M. Whittaker, and R. D. Müller (2013b), Newly-recognised continental fragments rifted from the West Australian margin, paper presented at the West Australian Basins Symposium 2013, Pet. Explor. Soc. of Aust., Perth, Western Australia, Australia, 18–21 Aug.

Author Information

WALTER H. F. SMITH and KAREN M. MARKS, Laboratory for Satellite Altimetry, National Oceanic and Atmospheric Administration, College Park, Md.; email: Walter.HFSmith@noaa.gov

This paper is not subject to U.S. copyright. Published in 2014 by the American Geophysical Union.

23249250, 2014, 21, Downloaded from https://agupubs.onlinelibrary.wiley.com/doi/10.1002/2014EO210001, Wiley Online Library on [22/05/2024]. See the Terms and Conditions (https://onlinelibrary.wiley.com/terms-and-conditions) on Wiley Online Library for rules of use; OA articles are governed by the applicable Creative Commons License

Preprints (www.preprints.org) | NOT PEER-REVIEWED | Posted: 21 November 2018 doi:10.20944/preprints201811.0515.v1

Manuscript type: Article

Using Landsat 8 images along with Google Earth Engine for investigation the location of the crashed aircrafts

Azad Rasul [1, *]

1 Department of Geography, Soran University, Kawa Street, Soran 44008, Erbil, Iraq

* Correspondence: azad.rasul@soran.edu.iq or aor4@alumni.le.ac.uk; Tel.: +964-(0)750-735-8574

Abstract

Remote sensing data and techniques utilized for various purposes including natural disasters such as earthquake as well as flood. The research aims to consume liberates Landsat 8 images for investigating crashed airplanes such as MH370. Overall approximately 300 Landsat images with less than 10% clouds utilized in addition processed through Google Engine Platform. Due to the materials as well as the color of airplane body different from the area which is a plane crashed there, moreover, it should be the characteristics of the plane shapefile different in terms of albedo, temperature as well as vegetation index value. The research observed Landsat 8 data as well as methods utilized in this research, especially, NDVI, albedo in addition to band 4, capable to distinguish between the plane and its surrounding green area. Therefore, our result confirms during the research period, there was no plane on the location as well as MH370 not crashed in this site.

Keywords: crashed aircraft; NDVI; albedo; MH370; remote sensing; Landsat 8; disaster; Boeing 777; panchromatic band; thermal band

1. Introduction

Remote sensing as a valuable source applied successfully in several natural disaster events around the world [1]. Due to it is capable of assist to identify natural disaster's damages as well as furnish maps of the near actual time of the disaster [2]. For instance, it is data and techniques such as SAR, optical and thermal, LiDAR detection, applied for landslides, volcanic activity, earthquakes and faulting, flooding, wildfire [3–7]. There is a possibility to use it for disappeared aircraft more broadly.

A Malaysian Airlines Flight MH370 disappeared on the morning of 8th of March 2014 with 227 passengers besides 12 crew members [8,9]. The type of aircraft is Boing 777 which is one of the world's largest aircraft. It has the capacity to travel a range of 9,695 to 17,372 km. MH370 was on a routine flight from Kuala Lumpur to Beijing [10]. Rolls-Royce's (the engine manufacturing company), confirmed that they had received a health report for five hours. It means that the aircraft had remain flying for four hours [11].

Besides a long, wide as well as expensive search for MH370, the story of missing it remain a mystery. According to Malaysian Safety Investigation Team for MH370, by now (2018), 27 suspected and confirmed fragments were found [9]. Discovered debris up to now in South Africa, Reunion, Mozambique as well as Rodrigues Island presumably derived from the wide search

© 2018 by the author(s). Distributed under a Creative Commons CC BY license.

area between latitude 28 and 35 South [8]. To determined location of MH370, drift studies focused on the spatial distribution of the derbies or on the aerial search [9,12]. During September of 2018, after four years and half of missing MH370, British photographer Ian Wilson confirmed what a YouTube video claimed in 2014 which is a plane appeared on Google Earth inside a jungle in Cambodia believing it is MH370. Before going to the field, remote sensing has capabilities to obtain more information regarding these locations and allegations.

Generally, remote sensing has high ability to find change detection as well as investigate disasters even in remote and not easily reachable locations such as dense jungles through compare images of before and after events. One of its advantages is it is capable of consuming several techniques, band compassion and indices and it is not only relying on visible images. However, several factors have a role in remote sensing capacity to investigation objects such as the resolution of the images as well as cloud situation.

In remote sensing, quickly and accurately airport and aircraft detection are substantial for several civilian as well as military purposes [13]. As a reason of simple sky background, detection of flying airplanes is easy in comparison to airplanes on the ground due to the intervention of the surrounding area and color features. Usually, the first step of airplane detection methods are location candidate regions and the second is classifying objects [13]. Aircraft detection consumes templates matching which is an approach to finding diminutive objects in digital image processes [14]. In previous years, methods of an airport as well as airplane detection developed considerably [15–19]. However, these researches usually utilized Google Earth or visible bands of high-resolution satellite images.

In 2013, Landsat 8 was launched with two sensors, the Operational Land Imager (OLI) and the Thermal Infrared Sensor (TIRS). To monitor terrestrial change detection, Landsat data are crucial [20]. Landsat 8 data utilized for different research fields, for instance, urban expansion, a variation of land surface temperature, global land change, land cover classification, mapping of ice flow [21–24]. To the best of our knowledge, Landsat 8, not used for study missing aircraft before thus this study selected it for this purpose. While Landsat is a medium resolution optical satellite, it has several advantages, for instance, Landsat data freely available for a long period and it has multi-spectral bands.

Generally, remote sensing is engaging effectively in the search for the MH370 [10]. For instance, the final route of MH370 determined above the Southern Indian Ocean by the International Maritime Satellite Organization (Inmarsat) based on automatic communication between one of its satellites and the airplane [9,10]. Moreover, during the research operation for MH370 on the sea surface, radar as well as infrared sensors equipment utilized by the Lockheed Martin P-3 Orion [10]. However, there is other remote sensing data and techniques can play a greater role in this disaster.

While remote sensing images and techniques utilized for different natural as well as human disasters, in literature we have not observed scientific research used Landsat images for investigating disappeared or crashed airplane. The objective of this study is to prove the ability of Landsat 8 as freely available satellite image to discover a missing plane landed inside the

dense jungle. Moreover, it attempts to consume remote sensing to contribute in search of MH370 through the experiment is there airplane on the claimed crash site of the plane or it is just routine flying of the plane during satellite image acquisition.

2. Materials and methods

2.1. Study sites

The research was conducted in three locations which situated in different countries. For each case the shapefile of the plane in addition to one site selected as a reference to compare with the location of the aircraft.

2.1.1. The claimed crash site of MH370 in Cambodia:

The study site in Cambodian Jungle located in 12°05'20"N latitude and 104°09'06"E longitude inside Pursat province. The reference site is forest area which is located in the east direction and it is close to the mentioned location of the plane (Figure 1). The area is part of Phnom Aural Wildlife Sanctuaries which is established in 1993 and it is located in the South of Chrak Loieng Waterfall. The area is dominated by evergreen forest. In high elevation evergreen forest, in the area, dominate trees type are 'conifer-oak' and/or 'oak-laural.' Fagaceae, Lauraceae, Myrtaceae, and Podocapaceae [25]. Regarding the climate, the average temperature of the province is 32.5 °C and the annual rainfall is 1,487.42 mm/year [26].

2.1.2. Heathrow Airplane site in the UK:

Heathrow Airport located in 23km to the west of center in the district of Longford, Hounslow, in Greater London. It is latitude is 51°28′39″N and it is longitude is 000°27′41″W with the elevation of 25 m above sea level. Regarding the climate, annual rainfall of the airport is 601.7mm and the annual maximum temperature is 15.2 °C and the annual minimum temperature is 7.5 °C. Average annual sunshine hours is 1632.6 [27]. For the study site, only one aircraft stand selected as a shapefile of the plane and the reference site selected outside the airport in the green area located in the west of the airport (Figure 1).

2.1.3. Airplane Home site in the US:

A Boeing 727-200 converted into a residence located in 15270 SW Holly Hill Rd, Hillsboro, Oregon, USA. It is latitude is 45°24′29.1″N and it is longitude is 123°00′28″W (Figure 1). The elevation of Hillsboro is 59 m above sea level. The area is rolling hill and the landscape covered by orchards. The airplane is surrounded by high pines. Regarding the climate, average annual rainfall in Hillsboro is 954 mm and the average temperatures range between 5.61 °C and 17.2 °C [28]. The reference site is selected inside the tree area in the North West of the Airplane Home and it is approximately 1 km far from it. The location of the reference site is 45°24′49″N latitude and 123°01′13.4″W longitude.

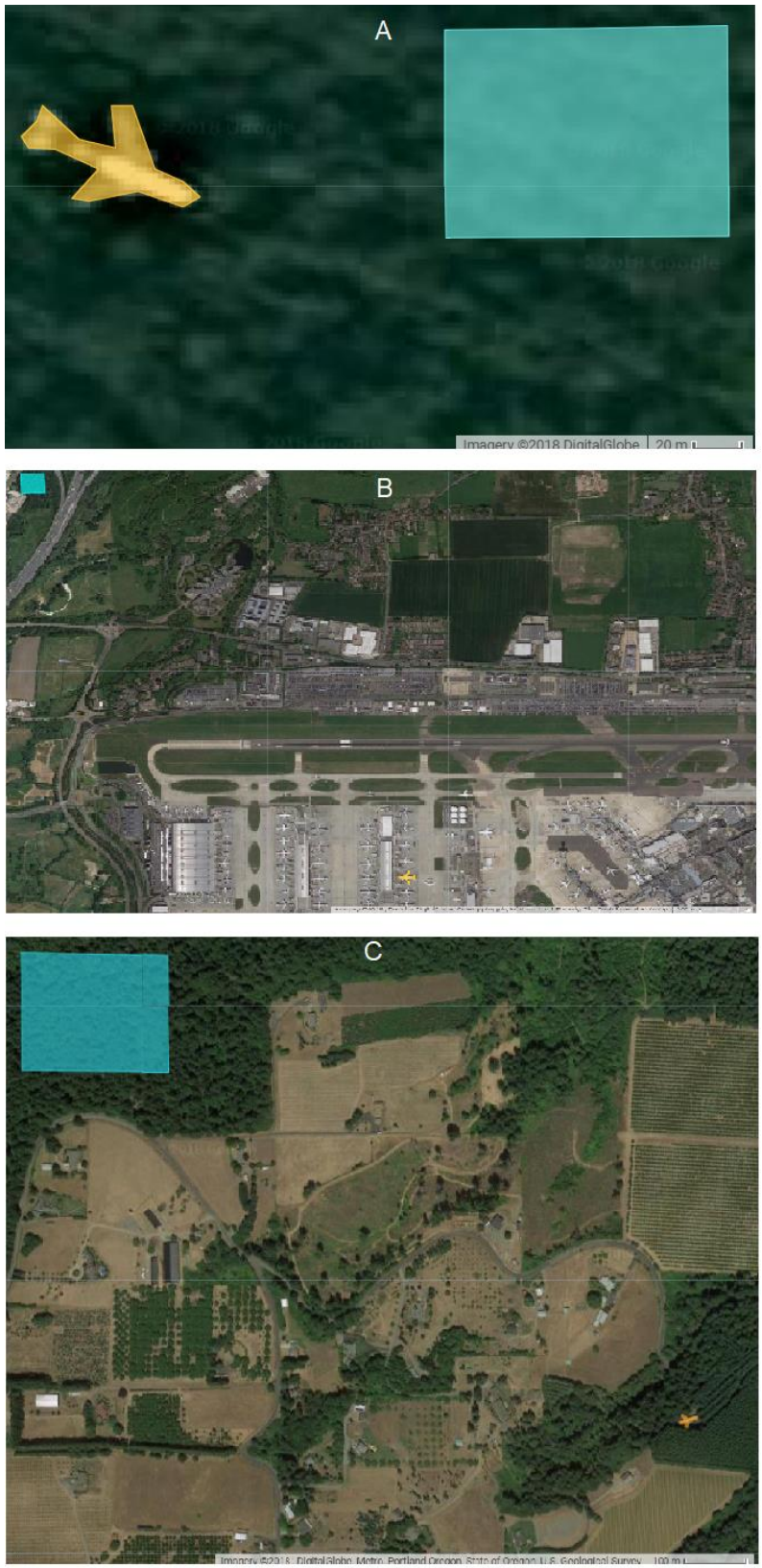

Figure 1: Study sites. A: Cambodian Jungle, B: Heathrow Airport in the UK, C: Airplane Home in the US.

2.2. Data

Overall approximately 300 of freely available Landsat 8 data from 2013 to 2018 for the study sites utilized in this research (Appendix 1).

2.3. Methodology

In order to achieve objects of this research as well as evaluate the capacity of the free satellite image of Landsat 8, overall approximately 300 Landsat images with less than 10% clouds used and processed through Google Engine Platform [29]. As an experiment case of using albedo, NDVI, spectral, panchromatic as well as thermal bands method for the difference between plane area and sample background, samples of Heathrow in the UK and Airplane Home in the US selected. Then as validation, these methods applied with Cambodian Jungle case.

2.3.1. Albedo

The surface albedo is the fraction of reflected solar radiation by the surface to the received radiation [30]. In the investigation of missing airplane, the albedo of materials has a great role. Usually, civilian airplanes are made of aluminum and painted with white color. The albedo of white painted aluminum material is 0.80 while for instance, the albedo value of the coniferous forest is between 0.09 to 0.15 and the albedo of pennaceous forests is between 0.15 to 0.18 [31,32]. Therefore, a plane should have higher albedo, especially if it is crashed in a vegetated area like the claimed crash site of MH370 in the Cambodian jungle. Due to cloudy pixels usually have a high albedo, only images with less than 1% of cloud used. As a result of having a cloud above the study site, Landsat 8 images of 2014 excluded while 62 transparent satellite images from 2015 to 2017 used. According to [33], Eq. 1 used for retrieval the land surface albedo.

$$Albedo = ((0.356 * blue) + (0.130 * red) + (0.373 * nir) + (0.085 * swir1) + (0.072 * swir2) - 0.018)/ 1.016 \quad (1)$$

where *blue* is B2, *red* is reflectance B4, *nir* is B5, *swir1* is B6, *swir2* is B7. For mentioned bands TOA reflectance used.

2.3.2. NDVI

NDVI is the simple as well as widely used vegetation index. It is a ratio-based index using two bands (red and near infrared) to recognize healthy flora and green biomass differences due to vegetation has a strong assimilation in the red band and a strong reflection of the solar radiation in the NIR band [34]. For NDVI comparison, less than 10% cloud images from 2013 to 2016 used. For NDVI comparison overall 88 satellite images used. NDVI is calculated as follows:

$$NDVI = \frac{(\rho NIR - \rho RED)}{(\rho NIR + \rho RED)} \quad (2)$$

where *NDVI* is normalized difference vegetation index, ρNIR is the surface reflectance of band 5 and ρRED is the surface reflectance of band 4 in Landsat 8. NDVI values range from -1.0 to +1.0. High NDVI values (about 0.6 to 0.9) related to dense vegetation such as temperate and tropical forests [35]. While NDVI value of inanimate elements such bare soil is quite low.

Therefore, the NDVI value of vegetated background should be higher than the NDVI value of airplane shapefile.

2.3.3. Spectral difference

Spectral characterization of the Operational Land Imager (OLI) is disclosed in Appendix 1. In Landsat 8, Costal, Blue, Green and Red bands, aluminum has higher reflectance than vegetation (Appendix 2). For spectral comparison overall 22 satellite images with less than 10% cloud for 2014 used.

2.3.4. Panchromatic difference

The bandwidth of the panchromatic band Landsat 8 has covered the red, green and blue bands in the grayscale image [37]. Panchromatic band in Landsat OLI is band 8 and it has the highest spatial resolution (15 m). For panchromatic comparison overall 31 satellite images with less than 10% cloud for 2014 used. The value of the airplane in panchromatic band anticipates being higher than its value on the vegetated background.

2.3.5. Thermal band difference

Differences between thermal characteristics of objects are capable of being measured by means of thermal sensors. For thermal band comparison overall 96 Landsat 8 images with less than 10% cloud from 2014 to 2017 used. Bands 10 and 11 of Landsat 8 Thermal Infrared Sensor (TIRS) instrument are the thermal band, however, in this study, Band 10 used due to it is retrieval LST more accurately.

3. Results

As a result of using free Landsat 8 images from 2013 to 2018 besides using multi techniques, the research disappeared there is not a plane in the study site due to not any significant changes occurred in visible true and false color, thermal, panchromatic, NDVI and albedo values in the location.

3.1. Albedo:

In Heathrow case study, the average albedo of the plane area was 0.17±0.03 while average albedo of the green reference was 0.013±0.02 (Figure 2). It means albedo of the plane shapefile was 0.04 higher than the albedo of the reference. In a sample of Airplane Home, the average albedo of the plane shapefile was 0.13±0.09 while average albedo of the reference was 0.09±0.02 and it is albedo 0.036 less than albedo of the plane. Experiment case samples suggest that albedo is effective for differentiating between plane and green background reference.

In the Cambodian Jungle case, an average of claimed airplane shapefile was 0.117±0.016 and average albedo of forest reference sample was 0.12±0.017. It means no significant difference found between them in addition albedo of reference is 0.003 higher than albedo of the plane. While, logically if the plane is located in the location, it's albedo should be higher than albedo of the background forest.

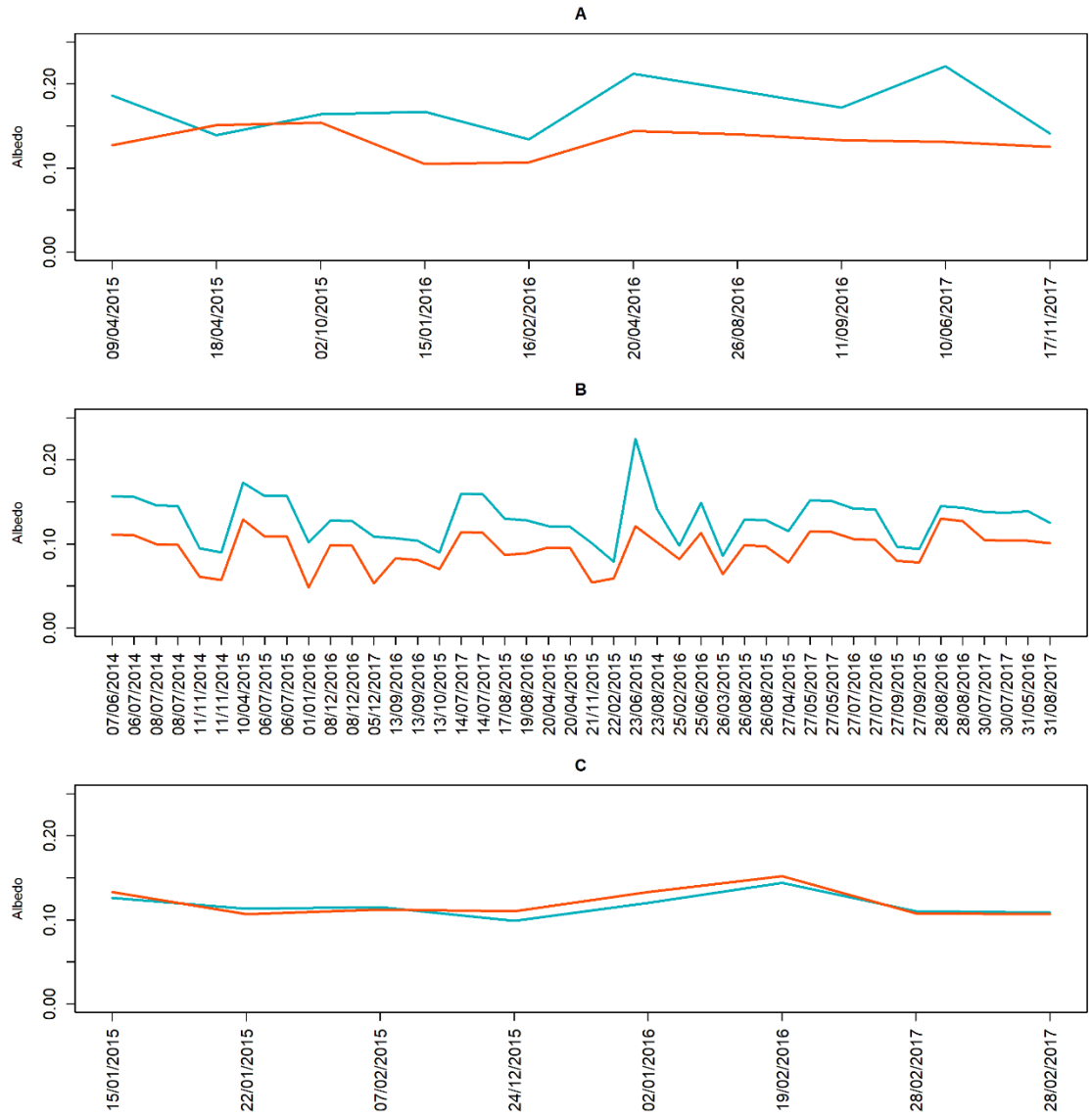

Figure 2: Albedo difference between the plane and reference site from Landsat 8. A: Heathrow Airplane, B: Airplane Home in the US, C: Cambodian Jungle. Blue is airplane shapefile and orange is a reference.

3.2. NDVI:

In Heathrow Airport case study, average NDVI of the plane site was 0.018±0.02 while NDVI of green reference area was 0.68±0.14 (Figure 3). It means NDVI of the plane site is 0.67 higher. In the Airplane Home case study, average NDVI of the plane was 0.77±0.09 besides it is less than NDVI of the reference by 0.09. Usually, NDVI of the reference higher, however, sometimes NDVI of the reference less than NDVI of the plane site. It means using average is facilitating while using only NDVI of one satellite image not valuable for differentiating between a plane and its reference background.

Regarding the Cambodian Jungle case study, there is not a significant difference between the claimed crash site of the airplane and the green reference. Average NDVI of the plane site was 0.885±0.03 and NDVI of the reference was 0.887±0.03. It suggests that during the study period there was no a plane in the location of the claimed of discovered MH370 in Cambodia.

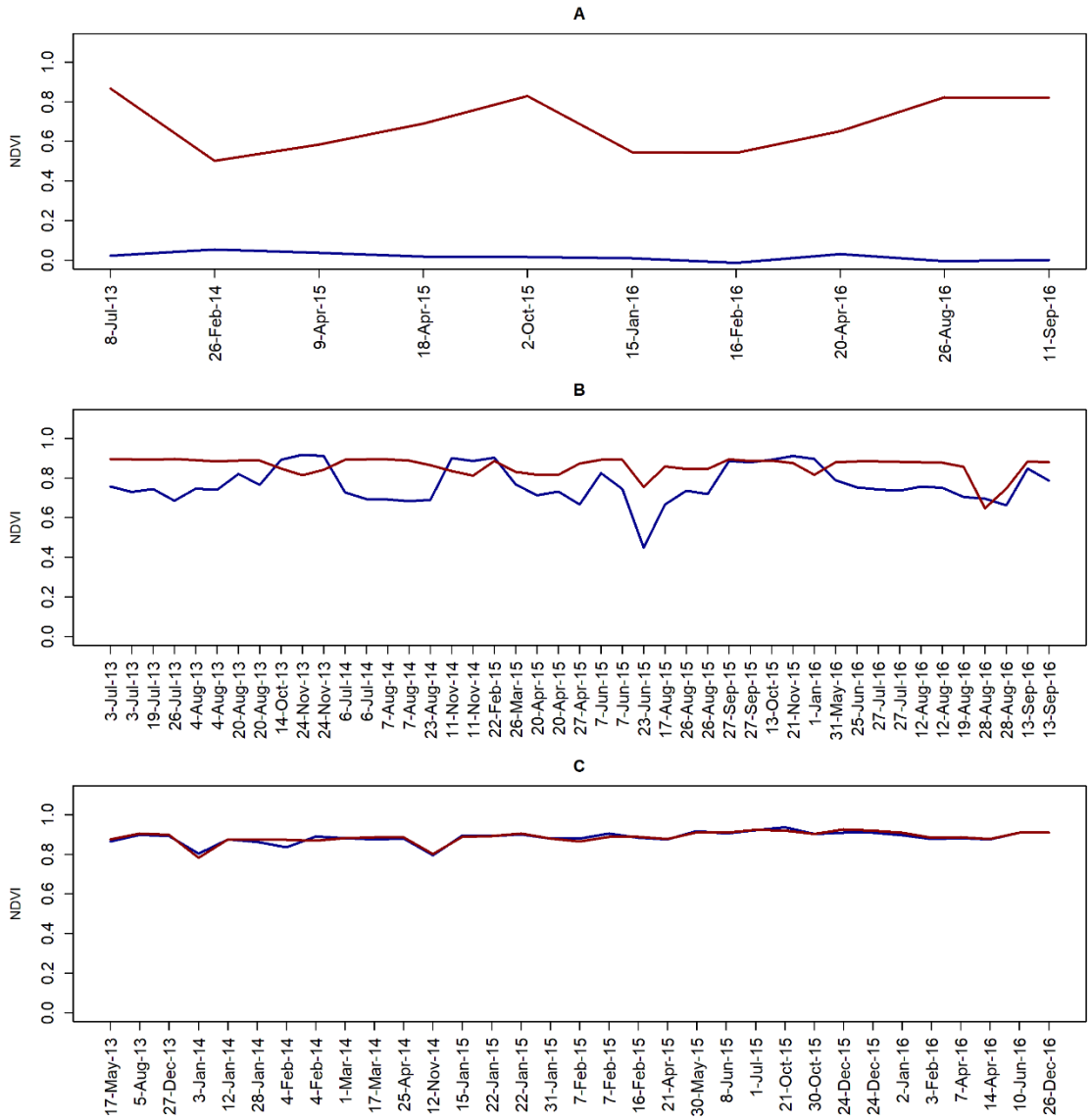

Figure 3: NDVI difference between the plane and reference sites from Landsat 8. A: Heathrow Airplane, B: Airplane Home in the US, C: Cambodian Jungle. Blue is airplane shapefile and red is a reference.

Preprints (www.preprints.org) | NOT PEER-REVIEWED | Posted: 21 November 2018 doi:10.20944/preprints201811.0515.v1

3.3. Spectral Difference:

In Heathrow Airport case study, plane shapefile has higher reflectance than the reflectance of the reference site in bands 1, 2, 3, 4 and 8 (Figure 4). In bands 5, 6, 7 and 9 the values have fluctuated. The largest spectral difference observed in band 4 with 0.27±0.14 and 0.09±0.02 reflectance of the plane shapefile and reference, respectively. In case of Airplane Home, in bands 1 to 8, the reflectance of airplane site was higher than the reflectance of the reference site and in the band 5, the spectral difference reaches highest when the reflectance was 0.27±0.06 and 0.23±0.08 for both the airplane and reference sites, respectively. It means the reflectance of the plane is 0.4 higher. The experiment case samples suggest that we are capable of consuming spectral differences from bands 1 to 5 of Landsat 8 to differentiate between an airplane and vegetated reference sites.

Whereas in the case of Cambodian Jungle, from band 1 to 9, there are only neglectable differences between airplane shapefile and reference. The result confirms that the pixels of both areas of claimed crashed MH370 and the reference dominated by tree and vegetation. For instance, the average reflectance of airplane shapefile in band 5 was 0.272±0.039 and reflectance of reference was 0.27±0.037.

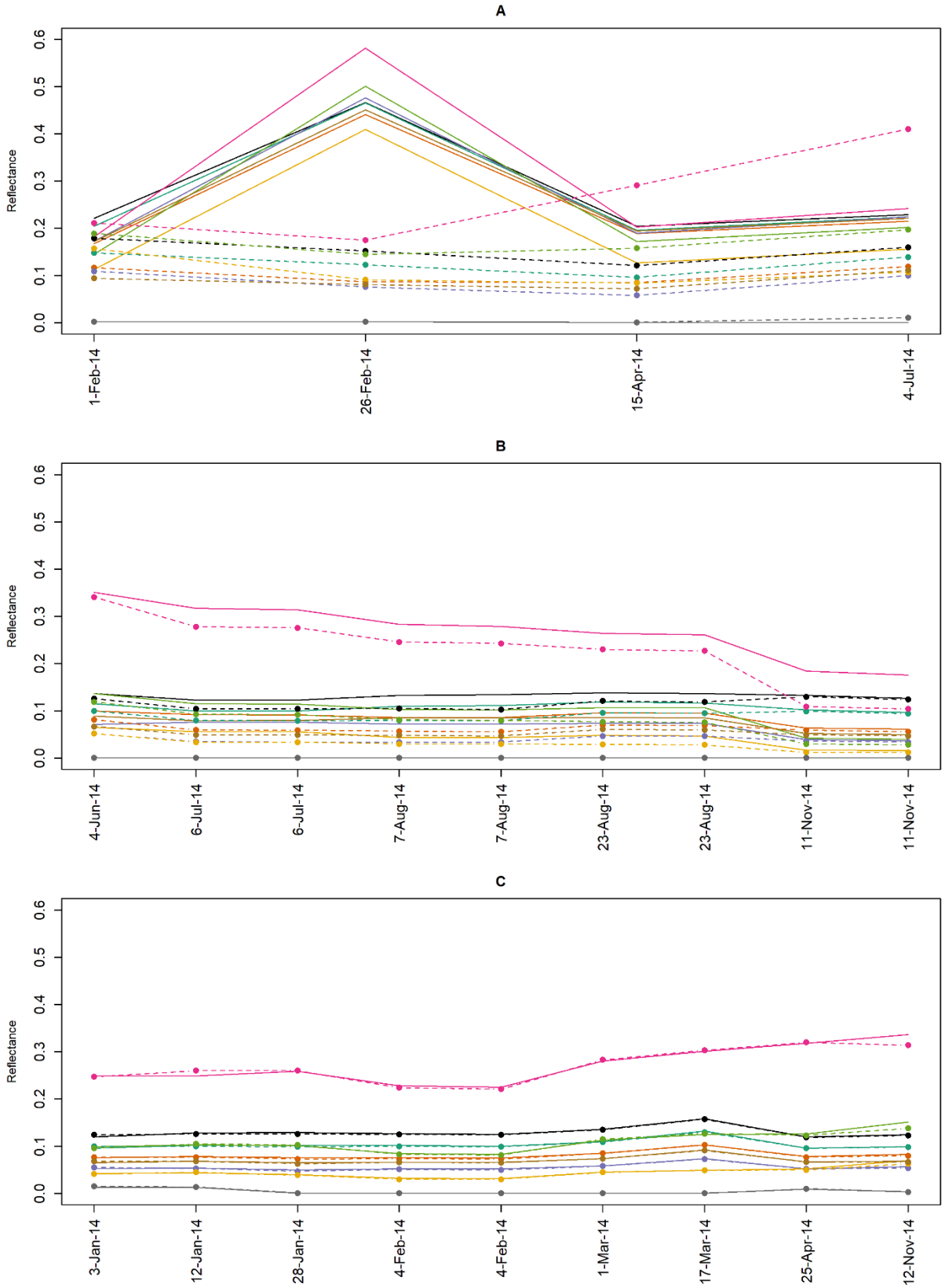
A
Reflectance
0.0
0.1
0.2
0.3
0.4
0.5
0.6
1-Feb-14
26-Feb-14
15-Apr-14
4-Jul-14
B
Reflectance
0.0
0.1
0.2
0.3
0.4
0.5
0.6
4-Jun-14
6-Jul-14
6-Jul-14
7-Aug-14
7-Aug-14
23-Aug-14
23-Aug-14
11-Nov-14
11-Nov-14
C
Reflectance
0.0
0.1
0.2
0.3
0.4
0.5
0.6
3-Jan-14
12-Jan-14
28-Jan-14
4-Feb-14
4-Feb-14
1-Mar-14
17-Mar-14
25-Apr-14
12-Nov-14

Figure 4: The Spectral difference between the plane and the reference sites from Landsat 8. A: Heathrow Airplane, B: Airplane Home in the US, C: Cambodian Jungle. Solid line: airplane shapefile, dashed: reference. Black: B1, green: B2, tenne: B3, blue: B4, cerise: B5, christi: B6, gamboge: B7, hot toddy: B8, gray: B9.

3.4. The Panchromatic difference

In both the Heathrow Airport and Airplane Home case, in the panchromatic band (band 8), the reflectance of plane site higher than the reflectance of references. The reflectance of the planes was 0.25±0.13 and 0.09±0.02 for Heathrow and Airplane Home, respectively (Figure 5). While the reflectance of the reference sites in the first case was 0.09±0.02 and in the second case was 0.05±0.01. It suggests that panchromatic band of Landsat 8 capable to distinguish between the plane site and the vegetated reference location. In contrast, in the case of Cambodian Jungle, the reflectance of the plane shapefile was 0.11±0.13 and reflectance of the reference site was 0.11±0.14. It means there is no difference between them as well as there is no plane in the claimed crashed site and both areas are dominated by the tree.

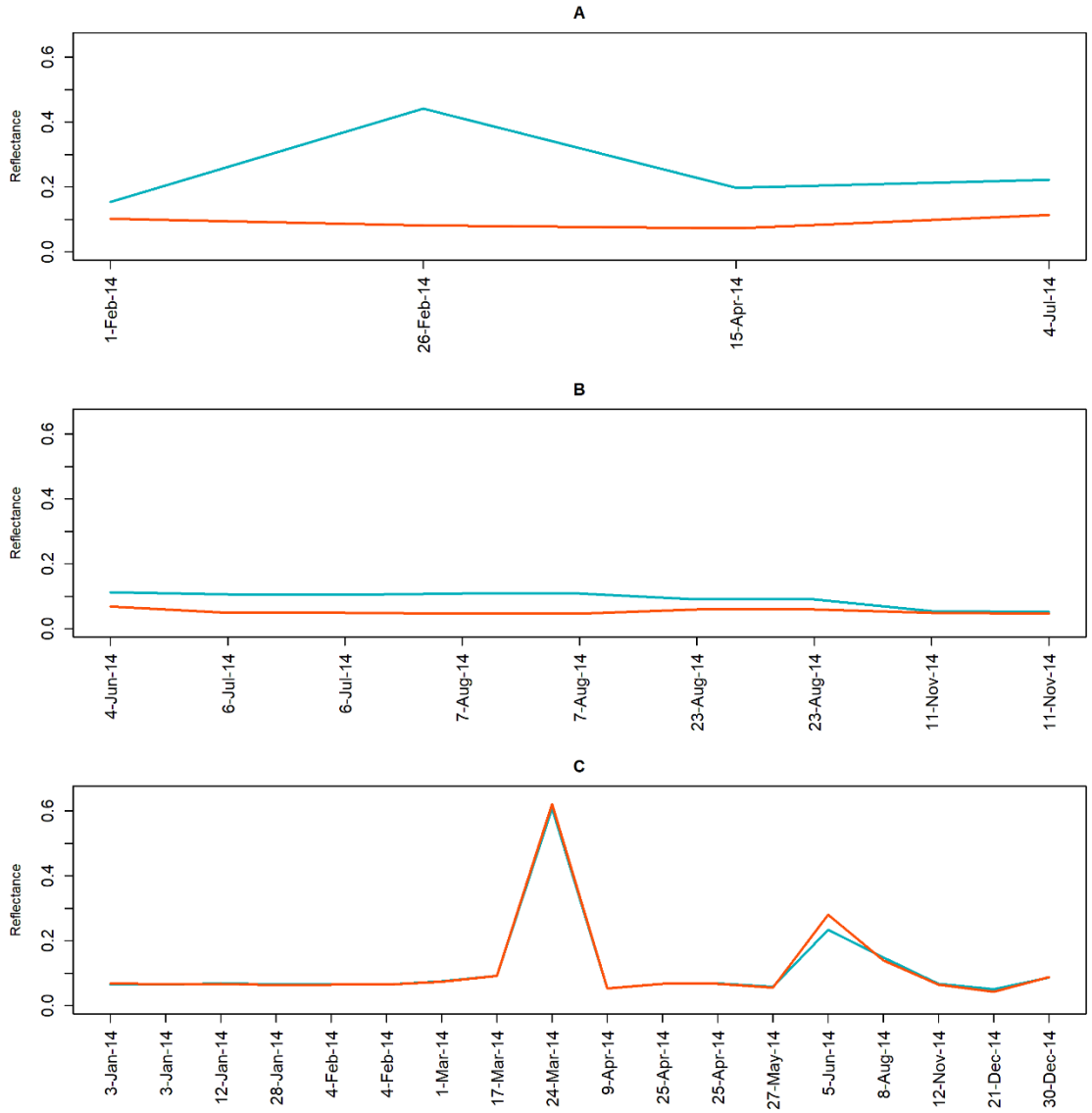

Figure 5: The Panchromatic difference between the plane and the reference sites from Landsat 8. A: Heathrow Airplane, B: Airplane Home in the US, C: Cambodian Jungle. Blue is airplane shapefile and orange is a reference site.

3.5. Thermal band difference

In the study site of Heathrow Airport, there is a seasonal fluctuation between top-of-atmosphere (TOA) LST of the aircraft and the reference sites. However, in Airplane Home case, average TOA LST of shapefile in both b10 from 2014 to 2017 was higher than average TOA LST of the vegetated reference site (Figure 6). LST of the plane was 292.31±9.47 K whereas LST of the reference was 290.91±7.99 K. It means LST of the plane was 1.41 K higher.

Regarding the Cambodian Jungle sample, generally, there is no difference between LST of the aircraft site (294.58±2.95 K) and LST of the reference (294.54±2.99 K). For instance, on 25th April of 2014, after missing MH370, LST of the claimed aircraft site was 294.28 K and LST of the reference site was 294.33 K. It means no difference observed between locations in the thermal band, therefore, it suggests there is no aircraft in the location.

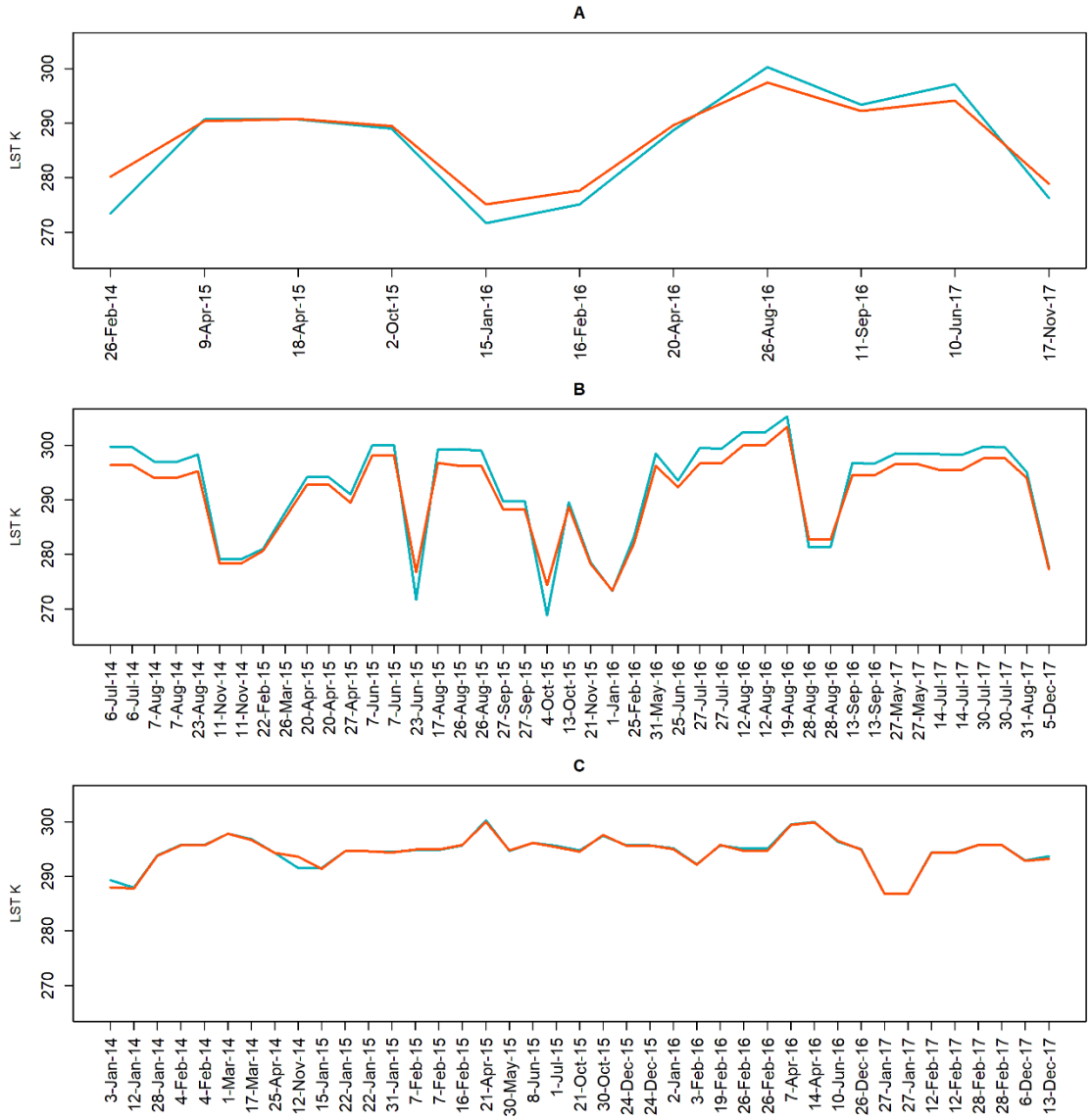

Figure 6: The Thermal difference between the plane and the reference sites from Landsat 8. A: Heathrow Airplane, B: Airplane Home in the US, C: Cambodian Jungle. Blue is airplane shapefile and orange is a reference site.

4. Discussion

Crashing as well as disappearing aircraft, usually, cause human and finance damage. In case of crash down the plane in the remote and bumpy area such as jungle, like what occurs with MH370, remain a mystery for a long time. Disclose these mysteries require great effort and costly research. At that time, perhaps several individuals claim they discovered it in different locations only based on visual view on satellite image like Google Earth software. Whereas using remote sensing techniques such as different indices, composition, and bands is the necessary and scientific approach.

Landsat 8 images even it has less resolution compared with commercial high-resolution satellite images, however, its advantage is having several bands and the possibility of using it for various scientific purposes as well as Landsat data freely available for the long period. Landsat 8 pixels have 15, 30 and 100m resolution for panchromatic, visible and thermal bands, respectively. Even if the plane body does not cover all size of the pixel, due to the digital number of the pixels considered as the average of the entire area of the pixel, having the plane body even in part of the pixel is capable to change the value of the pixels compared to its surrounding pixels.

One benefit of this research is the possibility of distinguishing between the fly plane during the satellite image acquired and the plane actually on the ground. Especially, this research assists in investigate of the plane in a jungle. Moreover, these results subseries the relative of victims of the airplane crash, airline company and component authorities for the missed airplane.

5. Conclusion

Remote sensing data besides techniques used for various purposes including natural disasters such as earthquake and flood. The research aims to consume freely available Landsat 8 images for investigating crashed airplanes such as MH370. Due to the materials and color of aircraft body different from the site of a crashed aircraft, moreover, it should be the characteristics of the aircraft shapefile different in terms of albedo, temperature and vegetation index degree.

The result of this research realized that in albedo, panchromatic, average of the thermal band, bands 1 to 5, plane sites have a higher value compared to the value of green background area. In contrast, the reference samples have higher NDVI compared to NDVI of plane sites. The research observed Landsat 8 data as well as methods used in this research, especially, NDVI, albedo and band 4, able to distinguish between the plane and its surrounding green area.

Regarding the case of Cambodian Jungle, in albedo, NDVI, spectral difference, panchromatic and thermal band, in other words, in all used methods in this study, there was no significant difference between the claimed crash site (12°05'20"N 104°09'06"E) and the sample of reference. Therefore, our result suggests that during the research period, there was no plane on the location, in addition, MH370 not crashed in this site.

Even remote sensing may have the ability to differentiate between various land cover background and airplane, this research only limited to green background area such as a forest. The result of the study suggests there is no an airplane on the claimed crashed site, not entire Cambodian Jungle which is a wide as well as a dense jungle. To confirm as well as complement the ability of remote sensing data and techniques to investigate disappeared airplane, we suggest

performing further research besides using different remote sensing data in different study site within the various land cover.

Reference

1. Karen E. Joyce, Stella E. Belliss, Sergey V. Samsonov, Stephen J. McNeill, Phil J. Glassey, S. E. B. A review of the status of satellite remote sensing and image processing techniques for mapping natural hazards and disasters. (2009). Available at: https://journals.sagepub.com/doi/abs/10.1177/0309133309339563. (Accessed: 13th November 2018)
2. Stefanov, W. L. & Evans, C. A. Data Collection for Disaster Response from the International Space Station. *ISPRS - Int. Arch. Photogramm. Remote Sens. Spat. Inf. Sci.* **XL-7/W3**, 851–855 (2015).
3. Rosen, P. A. *et al.* Synthetic aperture radar interferometry. *Proc. IEEE* **88**, 333–382 (2000).
4. Kwoun, O.-I., Lu, Z., Neal, C. & Wicks, C. Quiescent deformation of the Aniakchak Caldera, Alaska, mapped by InSAR. *Geology* **34**, 5–8 (2006).
5. Torres, R. *et al.* Monitoring the evolution of the Pasig–Potrero alluvial fan, Pinatubo Volcano, using a decade of remote sensing data. *J. Volcanol. Geotherm. Res.* **138**, 371–392 (2004).
6. Tansey, K. *et al.* A new, global, multi-annual (2000–2007) burnt area product at 1 km resolution. *Geophys. Res. Lett.* **35**, (2008).
7. Mojaddadi, H., Pradhan, B., Nampak, H., Ahmad, N. & Ghazali, A. H. bin. Ensemble machine-learning-based geospatial approach for flood risk assessment using multi-sensor remote-sensing data and GIS. *Geomat. Nat. Hazards Risk* **8**, 1080–1102 (2017).
8. Jansen, E., Coppini, G. & Pinardi, N. Drift simulation of MH370 debris using superensemble techniques. *Nat. Hazards Earth Syst. Sci.* **16**, 1623–1628 (2016).

Preprints (www.preprints.org) | NOT PEER-REVIEWED | Posted: 21 November 2018 doi:10.20944/preprints201811.0515.v1

9. Nesterov, O. Consideration of various aspects in a drift study of MH370 debris. *Ocean Sci.* **14**, 387–402 (2018).

10. Okolia, E. J., Enegbumab, W. I. & Bahru, U. J. OVERVIEW OF REMOTE SENSING APPLICATION FOR SEARCH OF MH370. *J. Teknol.* **77**, 63–68 (2015).

11. AlBattat, D. A. Biometric Technologies and Airline Security: A Case Study of Flight MH370.

12. García Garrido, V., Mancho, A. M., Wiggins, S. & Mendoza Parra, C. A. A dynamical systems perspective on the absence of debris associated with the disappearance of flight MH370. *Nonlinear Process. Geophys. Discuss.* **22**, 701–712 (2015).

13. Xu, Y. *et al.* Rapid Airplane Detection in Remote Sensing Images Based on Multilayer Feature Fusion in Fully Convolutional Neural Networks. *Sensors* **18**, 2335 (2018).

14. Hemalatha, P. C. & ME, M. M. A. Aircraft Recognition in High Resolution Satellite Images. *Int. J. Eng. Sci. IJES* **3**, 21–25 (2014).

15. Aytekin, Ö., Zöngür, U. & Halici, U. Texture-based airport runway detection. *IEEE Geosci. Remote Sens. Lett.* **10**, 471–475 (2013).

16. Yao, X., Han, J., Guo, L., Bu, S. & Liu, Z. A coarse-to-fine model for airport detection from remote sensing images using target-oriented visual saliency and CRF. *Neurocomputing* **164**, 162–172 (2015).

17. Liu, L. & Shi, Z. Airplane detection based on rotation invariant and sparse coding in remote sensing images. *Opt.-Int. J. Light Electron Opt.* **125**, 5327–5333 (2014).

18. Zhang, W., Sun, X., Wang, H. & Fu, K. A generic discriminative part-based model for geospatial object detection in optical remote sensing images. *ISPRS J. Photogramm. Remote Sens.* **99**, 30–44 (2015).

Preprints (www.preprints.org) | NOT PEER-REVIEWED | Posted: 21 November 2018 doi:10.20944/preprints201811.0515.v1

19. Cheng, G. & Han, J. A survey on object detection in optical remote sensing images. *ISPRS J. Photogramm. Remote Sens.* **117**, 11–28 (2016).

20. Rasul, A. *et al.* Applying Built-Up and Bare-Soil Indices from Landsat 8 to Cities in Dry Climates. *Land* **7**, 81 (2018).

21. Roy, D. P. *et al.* Landsat-8: Science and product vision for terrestrial global change research. *Remote Sens. Environ.* **145**, 154–172 (2014).

22. Jia, K. *et al.* Land cover classification using Landsat 8 Operational Land Imager data in Beijing, China. *Geocarto Int.* **29**, 941–951 (2014).

23. Fahnestock, M. *et al.* Rapid large-area mapping of ice flow using Landsat 8. *Remote Sens. Environ.* **185**, 84–94 (2016).

24. Rasul, A., Balzter, H. & Smith, C. Applying a normalized ratio scale technique to assess influences of urban expansion on land surface temperature of the semi-arid city of Erbil. *Int. J. Remote Sens.* **38**, 3960–3980 (2017).

25. Webb, C. O. Vegetation mapping in Phnom Samkos and Phnom Aural Wildlife Sanctuaries, Cardamom Mountains, Cambodia. *Unpubl. Rep. Fauna Flora Int. Phnom Penh* (2005).

26. Council for the Development of Cambodia. *Cambodia Municipality and Province Investment Information*. (2013).

27. Office, M. London Heathrow Airport climate. Available at: https://www.metoffice.gov.uk/public/weather/climate/gcpsvf37b. (Accessed: 16th November 2018)

28. About Hillsboro. *Hillsboro Chamber of Commerce*

Preprints (www.preprints.org) | NOT PEER-REVIEWED | Posted: 21 November 2018 doi:10.20944/preprints201811.0515.v1

29. Google Earth Engine. Available at: https://earthengine.google.com. (Accessed: 19th November 2018)

30. Coakley, J. A. REFLECTANCE AND ALBEDO, SURFACE. in *Encyclopedia of Atmospheric Sciences* 1914–1923 (Elsevier, 2003). doi:10.1016/B0-12-227090-8/00069-5

31. Santamouris, M. Heat Island Research in Europe: The State of the Art. *Advances in Building Energy Research* (2013). doi:10.4324/9781849770378-12

32. Barry, R. & Chorley, R. *Atmosphere, Weather and Climate*. (Routledge, 2002).

33. Waters, R., Allen, R., Bastiaanssen, W., Tasumi, M. & Trezza, R. Surface energy balance algorithms for land, Idaho implementation, advanced training and users manual. *NASA USA* (2002).

34. Karnieli, A. *et al.* Use of NDVI and Land Surface Temperature for Drought Assessment: Merits and Limitations. *J. Clim.* **23**, 618–633 (2010).

35. Remote Sensing Phenology NDVI the Foundation. Available at: https://phenology.cr.usgs.gov/ndvi_foundation.php. (Accessed: 16th November 2018)

36. Kokaly, R. F. *et al. USGS Spectral Library Version 7*. 68 (U.S. Geological Survey, 2017).

37. Li, Z. *et al.* Landsat 15-m Panchromatic-Assisted Downscaling (LPAD) of the 30-m Reflective Wavelength Bands to Sentinel-2 20-m Resolution. *Remote Sens.* **9**, 755 (2017).

Acknowledgments

The author would like to thank the Google Earth Engine program. Furthermore, much gratitude goes to the USGS, for providing the research with liberates Landsat 8 images.

Author Contributions

Data curation, A.R.; Formal analysis, A.R.; Investigation, A.R.; Methodology, A.R.; Resources, A.R.; Validation, A.R.; Visualization, A.R.; Writing—original draft, A.R.; Writing—review &

editing, A.R..

Appendixes

Appendix 1: Characteristics of Landsat 8.

Bands	Bands Name	Wavelength (micrometers)	Resolution (meters)
1	Coastal/Aerosol (CA)	0.435 - 0.451	30
2	Blue	0.452 - 0.512	30
3	Green	0.533 - 0.590	30
4	RED	0.636 - 0.673	30
5	NIR	0.851 - 0.879	30
6	SWIR1	1.566 - 1.651	30
7	SWIR2	2.107 - 2.294	30
8	Panchromatic	0.503 - 0.676	15
9	Cirrus	1.363 - 1.384	30

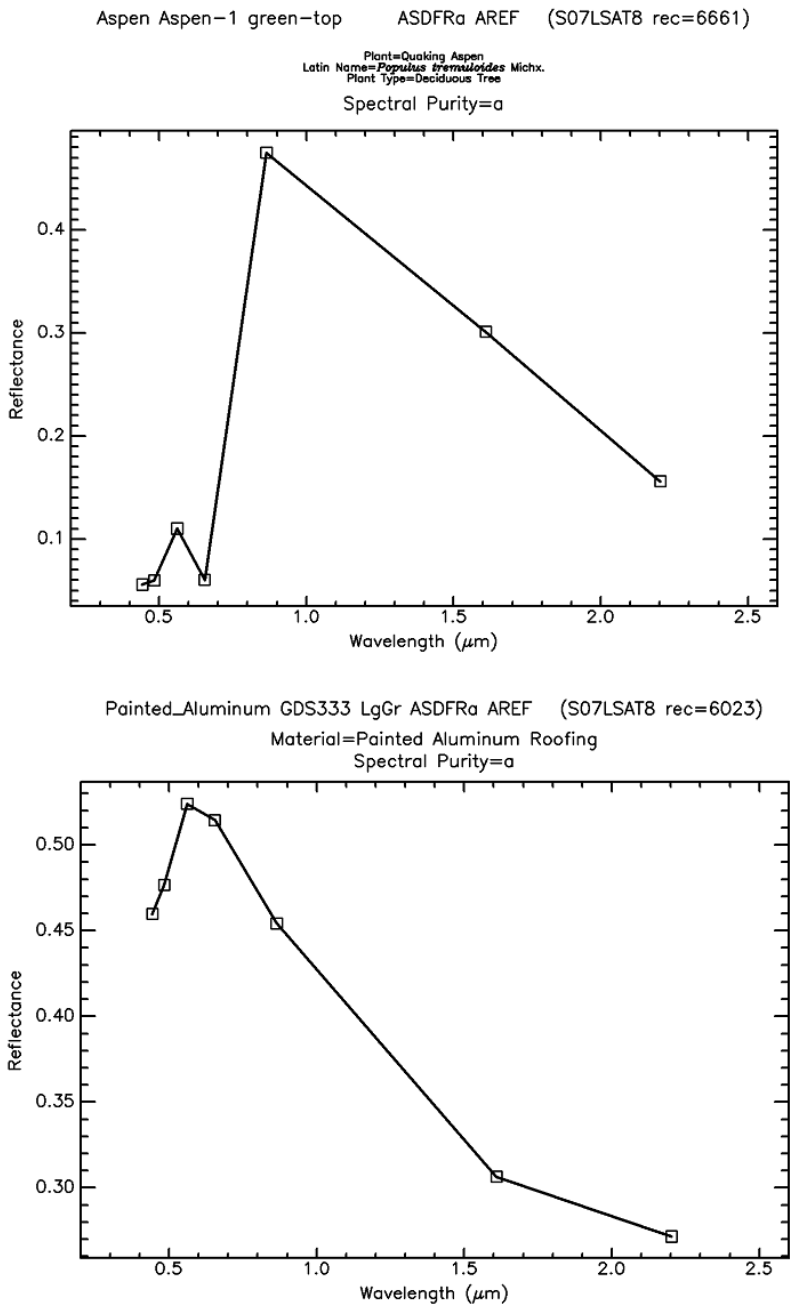

Appendix 2: the Spectral difference between painted aluminum and aspen tree in Landsat 8 from USGS Spectral Library Version 7 [36].

ANALYSIS OF METHODS USED TO RECONSTRUCT THE FLIGHT PATH OF MALAYSIA AIRLINES FLIGHT 370

JOHN ZWECK*

1. Introduction. In the early hours of March 8, 2014, a Malaysia Airlines Boeing 777 disappeared en route from Kuala Lumpur to Beijing with 239 people on board [14]. At the time of writing this article there has been no confirmation of any debris from the aircraft and no survivors have been found.[1] If the crash site is not discovered, this tragedy may become one of the great aviation mysteries.

The disappearance of MH370 is all the more mysterious in the age of highly accurate global navigation and communications systems. During flight, commercial aircraft use satellite communications links to exchange information with ground stations via the Aircraft Communications Addressing and Reporting System (ACARS) [7]. Although most of the functionality of ACARS was disabled early in the flight, for six hours after the last radar contact the aircraft and ground station exchanged a series of short messages, which we will refer to as **pings**. These messages were relayed to a ground station in Perth, Australia, by the Inmarsat 3-F1 satellite which was in a geosynchronous orbit over the equator at longitude 64.5°E.

A team of engineers at the British satellite company Inmarsat discovered that for each ping, ACARS recorded three pieces of data: the ping time, the Burst Timing Offset (BTO), and the Burst Frequency Offset (BFO). The BFO, which is discussed in Section 3 below, is a quantity that is related to the Doppler shift due to the motion of the aircraft relative to the satellite. The BTO is a time delay measured at the ground station which the satellite engineers used to accurately determine the distance between the aircraft and the satellite at each ping time [2]. As we see in Figure 1.1, the set of all points on a sphere (the earth) that are at a fixed distance from a given point (the satellite) forms a circle. Therefore, factoring in the speed and fuel constraints of the aircraft, the satellite engineers determined that at each ping time the aircraft was located somewhere on a segment of a circle, which we call a **ping arc**. Each such circle is characterized by a **ping arc angle**, which is the angle between the aircraft and the satellite, as measured from the center of the earth (see Figure 1.1). Consequently, they were able to deduce that at the last ping time, the aircraft was located somewhere on a ping arc that extended from the latitude of the Roaring Forties in the southern Indian Ocean to the steppes of Central Asia. We show the ping circles in Figure 1.2 (A), and in Table 1.1 we show the ping times, the ping arc angles (which can be computed from the BTO data [2]), and the BFO data.

The Doppler effect is a property of an electromagnetic signal that is due to the relative motion between a source (the aircraft) and a receiver (the satellite). If the distance between the aircraft and the satellite is decreasing then the frequency of the received signal will be higher than that of the transmitted signal, and if the distance is increasing the received frequency will be lower. This change in frequency is called the Doppler shift. The Doppler shift is proportional to the component of the relative

*Department of Mathematical Sciences, University of Texas at Dallas, 800 West Campbell Road, Richardson, TX 75080-3021 (zweck@utdallas.edu).

[1] On July 29, 2015, while this article was under revision, a flaperon from the wing of a Boeing 777 was discovered on Reunion Island, which is located east of Madagascar in the Indian Ocean. On September 4th, 2015, French investigators used serial numbers on the flaperon to confirm that the debris is from MH370.

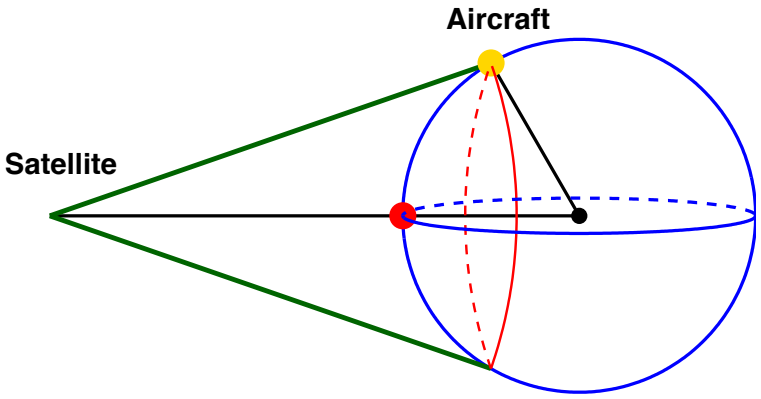

FIG. 1.1 *Sketch illustrating the circle (shown in red) whose points are at the same altitude above the surface of the earth and at the same distance from the satellite as the aircraft (shown with a yellow dot). The distance of the satellite from the center of the earth is 6.6 times the radius of the earth, whereas the altitude of the aircraft was approximately 10 km. (The radius is the earth is 6,370 km.) The red dot is the projection of the satellite onto the sphere of radius 6380 km.*

velocity vector of the two moving objects that is in the direction of the displacement vector between them. Taken together, the BTO and BFO data provide partial position and velocity information for the aircraft at each of the ping times.

Although the ping data recorded by the ACARS system was not specifically designed to be used for tracking aircraft, the Inmarsat engineers rapidly developed mathematical methods to determine flight paths that best fit the BTO and BFO data. These flight paths were then used to identify search areas located on the last ping arc in the southeast Indian Ocean.[2] Because of the urgency of the search for the aircraft's black boxes, the initial search areas were based on preliminary analyses of the satellite data. Since it took time to understand and analyze the satellite data and other relevant information, the search area was changed several times between March 9th and June 26th. While these changes in the search area presented a public relations challenge, they also gave the general public a rare opportunity to witness an engineering team attempt to solve a high-profile research problem.

In this article, we describe mathematical models similar to those used by the government-appointed Satellite Working Group (SWG) to reconstruct the flight path of MH370 and presented in a June 26th, 2014 report by the Australian Transport Safety Bureau (ATSB) [2]. We will validate these models using data from simulated flight paths and by comparing the results we obtained for MH370 to those found by the SWG. We work analytically as much as possible and only resort to numerical methods when necessary. The exposition is aimed at students with a background in vector calculus, matrix analysis, and numerical analysis and who are at the transition between an undergraduate education in mathematics and a graduate education in mathematics or engineering. At the end of each section we have included a range of

[2] An article by Chen *et al.* in the Notices of the American Mathematical Society discusses several water-entry scenarios for a Boeing 777 aircraft [4]. Since no debris field has been found for MH370, the authors conclude that the most likely scenario is that MH370 underwent a nose-dive water-entry or a water-entry with a steep pitch angle.

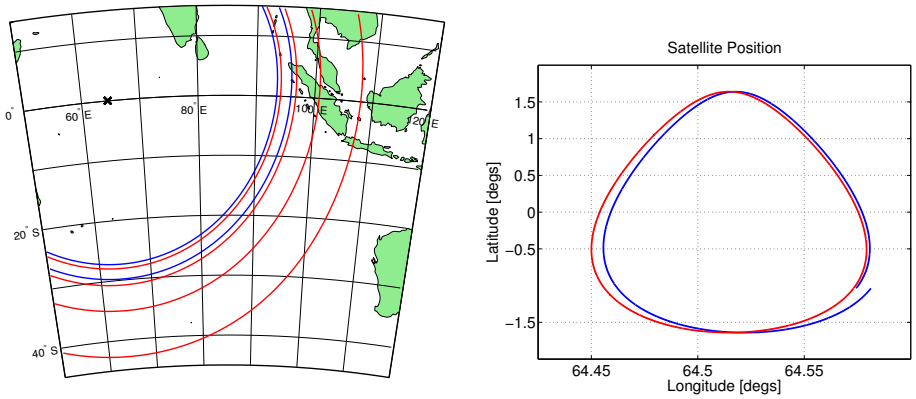

(A) (B)

FIG. 1.2 *(A) The ping arcs (blue and red curves) and the nominal location of the projection of the satellite onto the surface of the earth (black cross). The aircraft first crossed the two blue arcs traveling towards the black cross and then crossed the four red arcs traveling away from it. (B) The projection of the geosynchronous orbit of the Inmarsat 3-F1 satellite onto the surface of the earth. Red curve: model (see Section 4). Blue curve: data.*

modeling, analytical, and numerical problems, some of which are open-ended.[3]

We will develop a series of three progressively more realistic models. In Model I, we assume a known constant ground speed for the aircraft and we approximate the flight path by a concatenation of segments of great circles. With Model I, the satellite is assumed to be in a **geostationary orbit**, which means that from the point of view of an observer on the earth the satellite is always located at a fixed point in the sky above the equator [13]. This model, which does not make use of the BFO data, is similar to that used between March 17th and April 1st to determine search areas for the missing aircraft [2]. A preliminary version of this model was discussed in [15]. In Model II, the flight path is approximated by a concatenation of segments of constant-speed great circles for which the different segments have *a priori* unknown speeds. This semi-analytical model makes use of aircraft-satellite Doppler shift data at the ping times. With Model II, the satellite is assumed to be in a **geosynchronous** orbit, which means that from the point of view of an observer on the earth the satellite returns to the same point in the sky at the same time each day. In particular, if the orbit is a constant-speed, perfect circle in a plane that is slightly tilted with respect to the equator, then the motion of the satellite over the surface of the earth takes the form of a figure-eight curve [8]. However, in Section 4 we will see that in reality the Inmarsat 3-F1 satellite traces out a curve on the earth that looks more like a very narrow teardrop-shaped curve (see Figure 1.2 (B)). Finally, in Model III we develop a fully numerical model based on segments of small circles and which uses the recorded BFO data. For all three models, we assume that the earth is a perfect sphere and that the aircraft flies at a constant altitude, which we took to be 35,000 feet (10.7 km).

2. Model I: The Known-Speed, Concatenation-of-Geodesics Model. Inmarsat's initial attempts to reconstruct the flight path of MH370 from the ping data

[3]Solutions to selected starred problems$^{(*)}$ are provided in an Appendix in the online supplementary material.

TABLE 1.1 *The relevant satellite data [2], [5]. Times are given in Coordinated Universal Time (UTC) which is the successor to Greenwich Mean Time. At the time of last radar contact (18:15 UTC) the aircraft was located at* $97.72°\,E$, $6.82°\,N$.

Ping Time (UTC)	18:28	19:41	20:41	21:41	22:41	24:11
Ping Arc Angle, Φ [deg]	31.42	29.01	29.67	32.27	36.30	43.44
BFO [Hz]	143	111	141	168	204	252

used the last known location of the aircraft, viable aircraft speeds, and trigonometry to identify flight paths that crossed each of the ping arcs at the appropriate time. For these calculations, they assumed that the aircraft was "flying at a steady speed on a relatively constant track consistent with an aircraft operating without human control" [1]. The flight paths reconstructed by Inmarsat were then used by the ATSB to define initial search areas for the aircraft in the southern Indian Ocean. In this section, we describe a model that incorporates the main assumptions and ideas used by the Inmarsat engineering team.

In this model, we assume that the altitude of the aircraft is a known constant. Therefore, the flight path of the aircraft is constrained to lie on a sphere whose center is the center of mass of the earth and whose radius, R_A, is determined by the altitude of the aircraft. This sphere is depicted in Figure 2.1 (A). We also assume that the ground speed of the aircraft is a known constant, and we approximate the flight path by a concatenation of segments of great circles on the sphere. A **great circle** is the intersection of a sphere with a plane through the center of the sphere. The equator and circles of longitude are examples of great circles on the surface of the earth. The yellow and green curves in Figure 2.1 (A) are great circles. Segments of great circles on the sphere and straight lines in the plane are examples of **geodesics**, which are the constant-speed curves on a surface (or more generally on a Riemannian manifold) that locally minimize the distance between two points on the surface [6].

The speed and initial position of the aircraft are input parameters to the model. Starting at a given initial position on the first ping arc, we need to find a great circle segment that ends on the second ping arc at the second ping time. Then, starting from the position we just reached on the second ping arc, we repeat the process—using a segment of a possibly different great circle—to reach the third ping arc at the third ping time, and so on. Note that with this model we make no attempt to match the Doppler shift (or BFO) data recorded at the ping times. For simplicity, we assume that the satellite is in a geostationary orbit at an altitude of 35,786 km above the point on the equator at longitude 64.5°E. Since a great circle through a given initial point is uniquely determined by its initial velocity [6], and since we are given a value for the aircraft speed, we just need to determine the direction in which the aircraft is heading when it crosses each ping arc. To determine the heading direction we derive an equation that enforces the condition that the aircraft arrives at the next ping arc at the next ping time. We refer to this equation as the **ping arc equation**.

To study the ping arcs, we use a special **satellite coordinate system**, which is a rectangular coordinate system so that the origin is at the center of mass of the earth and the satellite is located on the positive x-axis (see Figure 2.1 (B)). Let $\{\mathbf{i}_S, \mathbf{j}_S, \mathbf{k}_S\}$ be the orthonormal basis for $\mathbf{R}^3$ whose elements are in the directions of the positive coordinate axes of such a coordinate system. We then define the **spherical satellite**

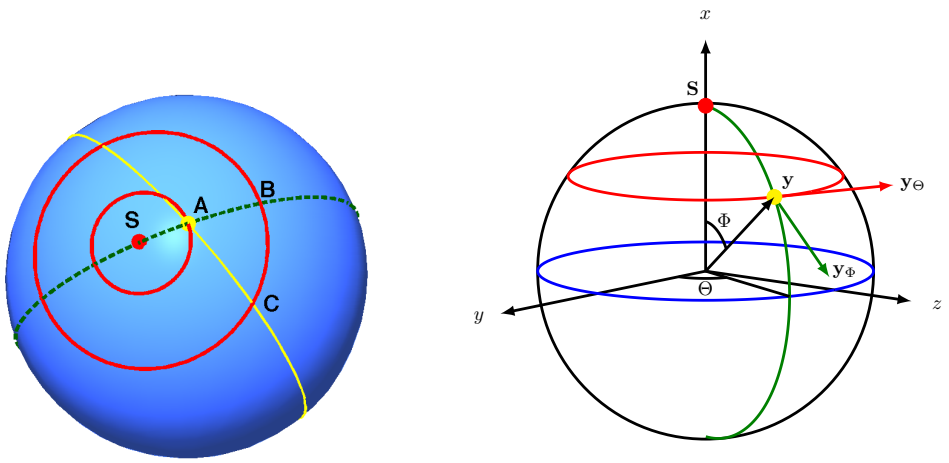

(A) (B)

FIG. 2.1 *(A) The spherical right triangle ABC used in the derivation of the ping arc equation. The red dot, S, is the projection of the satellite onto the blue sphere of radius, R_A. The two red curves are ping arcs, which are circles of latitude in the satellite coordinate system, and the dotted green curve is a circle of longitude. The flight path is the segment, AC, of the solid yellow great circle that forms the hypotenuse of the spherical right triangle. (B) The satellite coordinate system. The projection of the satellite onto the unit sphere is shown with a red dot. The unit vector, $\mathbf{y} = \mathbf{y}(\Phi, \Theta)$, in Equation 2.1 is shown with a yellow dot. The unit tangent vectors, $\mathbf{y}_\Phi$ and $\mathbf{y}_\Theta$, in Equation 2.4 are shown with green and red arrows, respectively. The orthonormal basis $\{\mathbf{y}, \mathbf{y}_\Phi, \mathbf{y}_\Theta\}$ is a rotation of the standard (right-handed) basis $\{\mathbf{i}_S, \mathbf{j}_S, \mathbf{k}_S\}$.*

coordinates, (Φ, Θ), of a unit vector, $\mathbf{y}$, by the equation

$$\mathbf{y} \;=\; \mathbf{y}(\Phi, \Theta) \;=\; \cos\Phi\,\mathbf{i}_S + \cos\Theta\sin\Phi\,\mathbf{j}_S + \sin\Theta\sin\Phi\,\mathbf{k}_S. \tag{2.1}$$

Since all points on the same circle of latitude in the satellite coordinate system are at the same distance from the satellite (see Figure 1.1), the ping arcs are circles of latitude, $\Phi = c$, on the sphere of radius R_A. The red circles in Figure 2.1 are ping arcs.

Using the satellite coordinate system, the ping arc equation can be derived using trigonometry. However, rather than using a triangle in the plane whose sides are segments of straight lines, we will use a triangle on the sphere of radius, R_A, whose sides are segments of circles. This spherical triangle is the triangle ABC depicted in Figure 2.1 (A). The projection, S, of the satellite onto the sphere is shown with a red dot. The two solid red circles represent two ping arcs, which are circles of latitude in the satellite coordinate system. The dashed green curve is a circle of longitude in the satellite coordinate system that intersects the solid red circles of latitude at right angles. The initial position of the aircraft on the first ping arc is shown with a yellow dot. The flight path of the aircraft is the yellow great circle which forms the hypotenuse of the triangle. Since we know the distance, L, the aircraft travels between the two ping times, we just need to rotate the yellow great circle flight path about the initial position, A, until the length of the hypotenuse AC is L. Of course, if the distance, L, the aircraft travels is less than the geodesic distance, $|AB|$, between the two ping arcs, then the problem has no solution.

At the n-th ping time, t_n, the position, $\mathbf{r}_n$, of the aircraft can be expressed as

$$\mathbf{r}_n \;=\; R_A\mathbf{y}_n \;:=\; R_A\mathbf{y}(\Phi_n,\Theta_n), \tag{2.2}$$

where R_A is the radius of the sphere on which the aircraft is flying and (Φ_n,Θ_n) are the spherical satellite coordinates of the aircraft. For each $n\in\{1,2,\cdots,N\}$, the **ping arc angle**, Φ_n, of the n-th ping arc can be calculated from the recorded BTO data, and by assumption Θ_1 is known. Our goal is to solve for $\Theta_2,\cdots,\Theta_N$ in succession. To that end, we observe that the great circle flight path, which at time, t_n, has position, $\mathbf{r}_n$, and velocity, $\mathbf{v}_n$, is parametrized by

$$\mathbf{r}_A(t) \;=\; \cos\left[\frac{v(t-t_n)}{R_A}\right]\mathbf{r}_n \;+\; \frac{R_A}{v}\sin\left[\frac{v(t-t_n)}{R_A}\right]\mathbf{v}_n, \tag{2.3}$$

where R_A is the radius of the sphere on which the great circle lies, and $v=|\mathbf{v}_n|$ is the known constant ground speed of the aircraft. Since the velocity vector, $\mathbf{v}_n$, is tangent to the sphere at the point, $\mathbf{r}_n=R_A\mathbf{y}_n$, it can be expressed in the form

$$\mathbf{v}_n \;=\; v\cos\beta_n\,\mathbf{y}_{\Theta,n} \;+\; v\sin\beta_n\,\mathbf{y}_{\Phi,n}, \tag{2.4}$$

where the angle, β_n, is the unknown **heading direction** of the aircraft. Here $\mathbf{y}_{\Theta,n}$ and $\mathbf{y}_{\Phi,n}$ are unit vectors tangent to the coordinate curves, $\Phi=\Phi_n$ and $\Theta=\Theta_n$, respectively (see Figure 2.1 (B)).

The **ping arc equation**, which enforces the condition that the aircraft crosses the $(n+1)$-st ping arc at time t_{n+1} is therefore given by the vector equation

$$\mathbf{r}_A(t_{n+1}) \;=\; R_A\mathbf{y}(\Phi_{n+1},\Theta_{n+1}). \tag{2.5}$$

Since both sides are tangent to the sphere of radius, R_A, Equation (2.5) is really two independent equations in the two unknowns, β_n and Θ_{n+1}. As can be seen in Figure 2.1 (B), we can rotate the satellite coordinate system about the x-axis so that $\mathbf{r}_n$ is in the xy-plane (*i.e.*, $\Theta_n=0$). Then, since the $\mathbf{i}_S$-component of $\mathbf{y}(\Phi_{n+1},\Theta_{n+1})$ is independent of Θ_{n+1} (see Equation (2.1)), we can eliminate Θ_{n+1} by taking the inner product of Equation (2.5) with the vector $\mathbf{i}_S$. Solving for the heading direction, β_n, we obtain

$$\sin\beta_n \;=\; \frac{\cos\left(\frac{v\Delta t_n}{R_A}\right)\cos\Phi_n \;-\; \cos\Phi_{n+1}}{\sin\left(\frac{v\Delta t_n}{R_A}\right)\sin\Phi_n}. \tag{2.6}$$

If $\beta_n\neq\pm\pi/2$ then there are two distinct solutions, $\beta_n^{\pm}$, of Equation (2.6), one with $\cos\beta_n^{+}>0$ and the other with $\cos\beta_n^{-}<0$.

In Figure 2.2 (A), we show three constant-speed flight paths for MH370 that were computed using Model I. These flight paths are very similar to flight paths that were found by the Satellite Working Group and that were used between March 17th and April 1st to define a series of search areas for the missing aircraft [2].

2.1. Problems.

1. Provide geometric and algebraic justifications for Equation (2.3).$^{(*)}$
2. Make a sketch illustrating the geometric relationship between β_n and the circles of longitude and latitude in the spherical satellite coordinate system.
3. Fill in the details of the derivation of Equation (2.6).$^{(*)}$

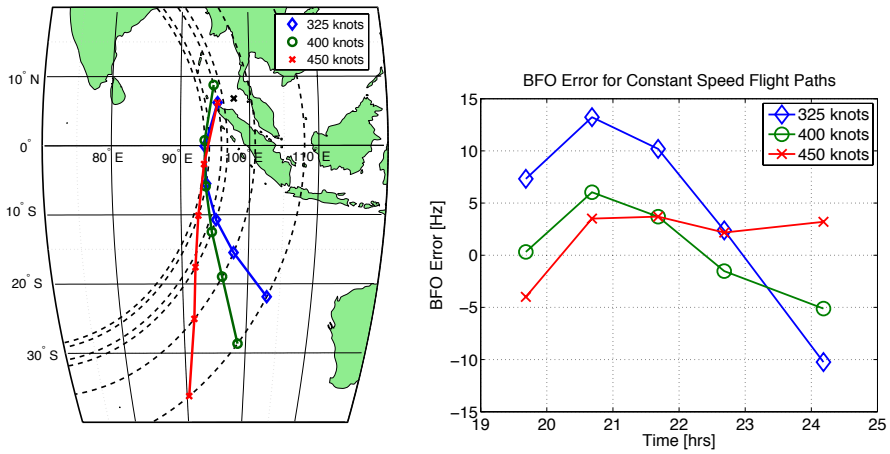

(A) (B)

FIG. 2.2 *(A) Three constant-speed flight paths for MH370 computed using Model I. The ground speeds for these flight paths are 325 knots (602 km/hr), 400 knots (741 km/hr), and 450 knots (833 km/hr). The position of MH370 at last radar contact is shown with the black cross. (B) The differences between the BFO values of each of the three flight paths shown on the left and the recorded BFO values given in Table 1.1. The BFO errors at 18:28 UTC, which are not shown, are approximately −50 Hz.*

4. For all ping times except the first, you can usually make a reasonable guess for which of the two solutions, $\beta_n^{\pm}$, of Equation (2.6) to choose. How? Why only usually? As a result, we can usually obtain two plausible flight paths, one with $\beta_1 = \beta_1^+$ and the other with $\beta_1 = \beta_1^-$. We will refer to these as the **positive and negative flight paths**.
5. Recall that our goal was to solve for Θ_{n+1}. How do you do that?
6. In Section 7, we will see that there is some uncertainty in the initial position, Θ_1, of MH370. With Model I, if you rotate the initial position, Θ_1, of the aircraft on the first ping arc by $\Delta\Theta_1$, what happens to final position, Θ_N? Discuss possible implications for the problem of determining search areas for MH370.
7. Write a computer program that implements Model I and validate it by comparison with ping arc data obtained from simulated flight paths.
8. Assuming that the position, $\mathbf{r}_n = R_A\mathbf{y}(\Phi_n, \Theta_n)$, of the aircraft on the n-th ping arc is known, numerically and/or analytically quantify the uncertainty in the position, $\mathbf{r}_{n+1}$, of the aircraft at the next ping time, t_{n+1}, due to uncertainty in either (a) the speed, v, of the aircraft, (b) the altitude of the aircraft, or (c) the ping arc angle, Φ_{n+1}. To what degree do these uncertainties in $\mathbf{r}_{n+1}$ depend on the choice of Φ_n?

3. The Doppler shift and Burst Frequency Offset. As discussed in the Introduction, the Doppler shift is a frequency shift in an electromagnetic signal that is transmitted by one object (the aircraft) and received by another object (the satellite). The Doppler shift can be expressed in terms of the relative velocity vector, $\mathbf{v} = \mathbf{v}_A - \mathbf{v}_S$, and the unit displacement vector $\widehat{\mathbf{u}} = (\mathbf{r}_A - \mathbf{r}_S)/\|\mathbf{r}_A - \mathbf{r}_S\|$ of the aircraft with respect to the satellite. Specifically, the Doppler shift, Δf, is proportional to

the component of $\mathbf{v}$ in the line of sight direction, $\widehat{\mathbf{u}}$:

$$\frac{\Delta f}{f} \;=\; -\frac{1}{c}\,\widehat{\mathbf{u}}\cdot\mathbf{v}. \tag{3.1}$$

Here f is the frequency of the transmitted signal and c is the speed of light.

We now derive a formula for the aircraft-satellite Doppler shift at each ping time under the assumption that the satellite is in a geostationary orbit. In Section 5, we will extend this formula to the more realistic case of a geosynchronous satellite orbit. In terms of the orthonormal basis, $\{\mathbf{i}_S, \mathbf{j}_S, \mathbf{k}_S\}$, associated with the satellite coordinate system discussed in Section 2, the position of the geostationary satellite is of the form $\mathbf{r}_S = R_S\mathbf{i}_S$, where R_S is the radius of the satellite orbit as measured from the center of mass of the earth. In addition, the position of the aircraft at the n-th ping time is given by $\mathbf{r}_A(t_n) = R_A\mathbf{y}(\Phi_n, \Theta_n)$, and the velocity of the aircraft is given by

$$\mathbf{v}_A(t_n) \;=\; \mathbf{v}_n \;=\; v_{\Theta,n}\mathbf{y}_{\Theta,n} \;+\; v_{\Phi,n}\mathbf{y}_{\Phi,n}. \tag{3.2}$$

Here $v_{\Theta,n}$ and $v_{\Phi,n}$ are the components of the aircraft velocity that are respectively parallel and perpendicular to the n-th ping arc.[4] Since $\widehat{\mathbf{u}}(t_n)\cdot\mathbf{y}_{\Theta,n} = 0$, we find that for a geostationary satellite, the aircraft-satellite Doppler shift, Δf_n, at the n-th ping arc is related to the component, $v_{\Phi,n}$, of the aircraft velocity that is perpendicular to the ping arc by

$$\Delta f_n \;=\; -\frac{f}{c}\frac{R_S}{D_{\mathrm{SA},n}}\,v_{\Phi,n}\sin\Phi_n, \tag{3.3}$$

where the distance between the satellite and aircraft is given by

$$D_{\mathrm{SA},n} \;=\; \sqrt{R_S^2 - 2R_SR_A\cos\Phi_n + R_A^2}. \tag{3.4}$$

The Inmarsat communications system is not able to directly record the aircraft-satellite Doppler shift. However, the values of a closely related quantity—the Burst Frequency Offset (BFO)—were logged by the satellite ground station in Perth. The BFO can be regarded as the difference between the frequency actually received by the ground-station and the frequency it is designed to receive. To optimize performance, satellite communications systems are designed to keep the BFO small. One of the main contributions to the BFO is the Doppler shift, Δf_{AS}, between the aircraft and the satellite, which is in a geosynchronous orbit, and is thus moving relative to the earth. To prevent the BFO from becoming too large, the aircraft uses knowledge of its current position to partially compensate for Δf_{AS} by shifting the frequency it transmits by the Doppler shift, $\Delta f_{\mathrm{AS\text{-}Comp}}$, due to the relative motion of the aircraft and an imaginary geostationary satellite, located at an altitude of 35,786 km above the point on the equator at longitude 64.5°E. Overall, the BFO is given by [2]

$$\mathrm{BFO} \;=\; \Delta f_{\mathrm{AS}} - \Delta f_{\mathrm{AS\text{-}Comp}} + \Delta f_{\mathrm{SG}} + \delta f_{\mathrm{AI}} + \delta f_{\mathrm{Bias}}, \tag{3.5}$$

where Δf_{SG} is the Doppler shift between the geosynchronous satellite and the ground station, δf_{AI} is a known time-dependent aircraft-independent frequency shift [2], and δf_{Bias} is a time-independent frequency shift.

[4] For convenience from now on we choose to work with $v_{\Theta,n}$ and $v_{\Phi,n}$ rather than with the variables v_n and β_n in Equation (2.4).

In Figure 2.2 (B), we show the difference in the BFO between the model and the data in Table 1.1, for each of the flight paths in Figure 2.2 (A). For these results we used the nominal value of $\delta f_{\text{Bias}} = 150$ Hz for the time-independent frequency shift. The reported uncertainty in δf_{Bias} is ± 5 Hz [2]. The small differences between the BFO values of these three reconstructed flight paths together with the large uncertainty in δf_{Bias} demonstrate the significant challenges the Satellite Working Group faced in narrowing the search area.

3.1. Problems.

1. Give a geometric explanation and an algebraic proof for why $\widehat{\mathbf{u}}(t_n) \cdot \mathbf{y}_{\Theta,n} = 0$, and hence derive Equation (3.3).$^{(*)}$
2. With a geostationary satellite model, it is impossible to use Doppler shift data to break the symmetry (*i.e.*, distinguish) between the positive and negative flight paths. Why?
3. Show that with a geostationary satellite model, it is impossible to use ping arc angle and Doppler shift data to distinguish between two flight paths that are rotations of each other about the x-axis of the satellite coordinate system.

4. A Model of the Satellite Motion. In Section 2, we determined the velocity, $\mathbf{v}_n$, by assuming knowledge of the speed, v, and using Equation (2.6) to solve for the heading, β_n. However, by now you may have realized that we could instead determine the velocity, $\mathbf{v}_n$, by using Equation (3.3) to solve for $v_{\Phi,n}$ in terms of the Doppler-shift data, Δf_n, and then reformulating Equation (2.5) to solve for $v_{\Theta,n}$. This observation forms the basis of Model II, described in Section 5 below. However, to break the symmetry between the positive and negative flight paths, in this section we replace the geostationary satellite model used in Section 2 with a more realistic geosynchronous satellite model to be used in Section 5. Specifically, we derive a formula for the position and velocity of the Inmarsat 3-F1 satellite in a coordinate system that rotates with the earth. We will develop this formula using publicly available data that gives the position and velocity of the satellite at 1 second intervals on the day that MH370 disappeared.[5] Although it may be more accurate to use this data directly, we include the satellite model presented in this section to provide the reader with a better understanding of the nature of the satellite orbit.

If we assume that the motion of the satellite is determined solely by the gravitational force exerted by the earth, then the satellite will move in a nearly-circular elliptical orbit whose center is at the center of mass of the earth. Ideally, the orbit of a communications satellite should be geostationary. Assuming that the orbit is a perfect circle in the equatorial plane, the radius of such an orbit is 42,157 kilometers, which is about 6.6 times the radius of the earth. However, it is not possible to achieve a perfect geostationary orbit due to the gravitational effects of the moon and sun, together with the flattening of the earth at the poles [13]. Instead, over time the orbital plane of the satellite tilts slightly with respect to the equatorial plane of the earth. Consequently, the satellite orbit is at best geosynchronous, *i.e.*, the satellite returns to the same point in the sky at the same time each day. In general, the projection onto the surface of the earth of the path of a geosynchronous satellite is a curve called an analemma, which depending on the values of the parameters of the orbit, can be a figure-eight or tear-drop shaped curve [8]. In particular, as we see in Figure 1.2 (B), the Inmarsat 3-F1 satellite traces out a curve on the earth that looks like a very narrow teardrop-shaped curve.

[5] A copy of this data was sent to the author and is included in the supplementary material.

The motion of a satellite about the earth is most readily described using an Earth-Centered Inertial (ECI) coordinate system in which the origin is at the center of mass of the earth and with respect to which the earth and the satellite rotate [10]. However, the motion of an aircraft relative to a satellite is best described using a coordinate system that rotates with the earth. A standard choice for such a coordinate system is the Earth-Centered Earth-Fixed (ECEF) coordinate system [12] which places the origin at the center of mass of the earth and for which the z-axis is aligned with a reference north pole and the xz-plane is aligned with a reference prime meridian (i.e, a great circle with 0° longitude). For simplicity, we assume that the axis of rotation of the earth is aligned with the reference north pole, although this is not exactly the case. Any of the geostationary satellite coordinate systems in Section 2 can be obtained from the ECEF coordinate system by a rotation that maps the point on the equator at 0° longitude to the projection of the satellite onto the surface of the earth. A major goal of this section is to define a geosynchronous satellite coordinate system that is obtained from the ECEF coordinate system by a rotation that maps the north pole of the earth onto a normal vector to the orbital plane of the satellite (a slight tilt), and maps the point on the equator at 0° longitude to the projection of the satellite onto the surface of the earth (see Equation (4.13) below). Since the satellite moves with respect to a point on the earth, the geosynchronous satellite coordinate system changes with time.

Since we will make extensive use of vector algebra and since we need to convert between several different earth-centered rectangular coordinate systems we make use of the notion of the **frame** (i.e., the *ordered orthonormal basis*) that is canonically associated with a given positively oriented rectangular coordinate system. We begin by recalling the following results from Linear Algebra.

LEMMA 4.1. *Let $\mathcal{B} = \{\mathbf{v}_1, \mathbf{v}_2, \mathbf{v}_3\}$ be an ordered basis for $\mathbf{R}^3$ and let $\mathbf{u} \in \mathbf{R}^3$. Then*

$$\mathbf{u} = \sum_{j=1}^{3} \alpha_j \ \mathbf{v}_j \iff \mathbf{u} = \begin{bmatrix} \mathbf{v}_1 & \mathbf{v}_2 & \mathbf{v}_3 \end{bmatrix} \begin{bmatrix} \alpha_1 \\ \alpha_2 \\ \alpha_3 \end{bmatrix}. \tag{4.1}$$

Furthermore, if $\mathbf{B}$ is an orthonormal basis then $\alpha_j = \mathbf{u} \cdot \mathbf{v}_j$.

PROPOSITION 4.2. *Let $\mathcal{B} = \{\mathbf{v}_1, \mathbf{v}_2, \mathbf{v}_3\}$ and $\mathcal{C} = \{\mathbf{w}_1, \mathbf{w}_2, \mathbf{w}_3\}$ be two frames for $\mathbf{R}^3$. Then there is an orthogonal matrix, $\mathbf{R}$, so that*

$$\begin{bmatrix} \mathbf{w}_1 & \mathbf{w}_2 & \mathbf{w}_3 \end{bmatrix} = \begin{bmatrix} \mathbf{v}_1 & \mathbf{v}_2 & \mathbf{v}_3 \end{bmatrix} \mathbf{R}. \tag{4.2}$$

Geometrically, the matrix $\mathbf{R}$ rotates the frame $\mathcal{B}$ onto the frame $\mathcal{C}$.

In particular, we will use the orthogonal matrix

$$\mathbf{R}(\theta, \phi) = \begin{bmatrix} \cos\theta\cos\phi & -\sin\theta & \cos\theta\sin\phi \\ \sin\theta\cos\phi & \cos\theta & \sin\theta\sin\phi \\ -\sin\phi & 0 & \cos\phi \end{bmatrix}, \tag{4.3}$$

which has the properties that $\mathbf{R}(\theta) := \mathbf{R}(\theta, 0)$ is rotation through an angle θ about the z-axis, and

$$\mathbf{R}(\theta_1)\,\mathbf{R}(\theta_2, \phi) = \mathbf{R}(\theta_1 + \theta_2, \phi). \tag{4.4}$$

Let $\mathcal{E} = \{\mathbf{i}_E, \mathbf{j}_E, \mathbf{k}_E\}$ be the frame associated with the ECEF coordinate system and let $\mathcal{F} = \{\mathbf{i}_F, \mathbf{j}_F, \mathbf{k}_F\}$ be the frame associated with the non-rotating ECI coordinate system. The rotation of the earth about its axis is then modeled by applying

Proposition 4.2 to express the ECEF frame in terms of the ECI frame. Since our goal is to obtain a formula for the motion of the satellite with respect to the earth, we instead express the ECI frame in terms of the ECEF frame via the matrix equation

$$\begin{bmatrix}\mathbf{i}_F & \mathbf{j}_F & \mathbf{k}_F\end{bmatrix} = \begin{bmatrix}\mathbf{i}_E & \mathbf{j}_E & \mathbf{k}_E\end{bmatrix}\mathbf{R}(-\alpha t). \tag{4.5}$$

Here t denotes time and $\alpha = 2\pi/T$, where $T = 23.934$ hrs is the period of rotation of the earth about its axis [11].

An analysis of the satellite position and velocity data shows that the orbital plane of the satellite is a slight tilt (a rotation) of the equatorial plane of the earth, and that in this plane the satellite orbit is a small perturbation of a constant-speed circle. Specifically, we can choose a frame $\mathcal{P} = \{\mathbf{i}_P, \mathbf{j}_P, \mathbf{k}_P\}$ for which the vector, $\mathbf{k}_P$, is the normal vector to the orbital plane of the satellite, and which is a rotation of the ECI frame, $\mathcal{F}$, of the form

$$\begin{bmatrix}\mathbf{i}_P & \mathbf{j}_P & \mathbf{k}_P\end{bmatrix} = \begin{bmatrix}\mathbf{i}_F & \mathbf{j}_F & \mathbf{k}_F\end{bmatrix}\mathbf{R}(\theta_P, \phi_P) = \begin{bmatrix}\mathbf{i}_E & \mathbf{j}_E & \mathbf{k}_E\end{bmatrix}\mathbf{R}(\theta_P - \alpha t, \phi_P), \tag{4.6}$$

where the second equality follows from Equations (4.5) and (4.4). Since we will perform all numerical computations in the ECEF frame, we may assume that $\begin{bmatrix}\mathbf{i}_E & \mathbf{j}_E & \mathbf{k}_E\end{bmatrix}$ is the identity matrix.

Furthermore, using the satellite data we found that the distance, $R_S(t)$, of the satellite from the center of mass of the earth and the speed, $v_S(t)$, of the satellite are well approximated by functions of the form

$$R_S(t) = \overline{R}_S[1 + \epsilon_S \sin(\alpha(t - t_0))], \tag{4.7}$$
$$v_S(t) = \overline{v}_S[1 - \epsilon_S \sin(\alpha(t - t_0))], \tag{4.8}$$

where the mean radius is $\overline{R}_S = 4.216 \times 10^4$ km, the mean speed is $\overline{v}_S = \alpha\overline{R}_S = 1.107 \times 10^4$ km/hr, the offset time is $t_0 = 13.608$ hrs (UTC), and the perturbation parameter is $\epsilon_S = 5.298 \times 10^{-4}$. In addition, the satellite crosses the equatorial plane of the earth at the times $t \in \{t_0, t_0 + T/2\}$ for which $R_S(t) = \overline{R}_S$. Consequently, the satellite trajectory is well approximated by the parametrized curve

$$\mathbf{r}_S(t) = R_S(t)\left[\cos\theta_S(t)\,\mathbf{i}_P + \sin\theta_S(t)\,\mathbf{j}_P\right], \tag{4.9}$$

where

$$\theta_S(t) = \frac{\pi}{2} + \int_{t_0}^{t} \frac{v_S(s)}{R_S(s)}\,ds \approx \theta_0 + \alpha t + 2\epsilon_S C(t) + \mathcal{O}(\epsilon_S^2), \tag{4.10}$$

where $\theta_0 = \frac{\pi}{2} - \alpha t_0$ and $C(t) = \cos[\alpha(t - t_0)] - 1$. By construction, this curve has radial and speed functions given by $\|\mathbf{r}_S(t)\| = R_S(t)$ and $\|\mathbf{r}_S'(t)\| = v_S(t) + \mathcal{O}(\epsilon_S^2)$, respectively. Moreover, the curve lies in the plane through the origin with normal $\mathbf{k}_P$, and crosses the equator at time t_0 with $\mathbf{r}_S(t_0) = \overline{R}_S\mathbf{j}_P = \overline{R}_S[-\sin\theta_P\mathbf{i}_F + \cos\theta_P\mathbf{j}_F]$. Using the satellite position data, we estimated the vectors $\mathbf{j}_P$ and $\mathbf{k}_P$ and hence deduced that $(\theta_P, \phi_P) = (179.25°, 1.64°)$.

By Lemma 4.1 and Equations (4.9), (4.3) and (4.6),

$$\mathbf{r}_S(t) = R_S(t)\begin{bmatrix}\mathbf{i}_P & \mathbf{j}_P & \mathbf{k}_P\end{bmatrix}[\mathbf{R}(\theta_S(t))]_{*1} = R_S(t)\,\mathbf{R}(\theta_P - \alpha t, \phi_P)\,[\mathbf{R}(\theta_S(t))]_{*1}, \tag{4.11}$$

where $\mathbf{A}_{*j}$ denotes the j-th column of the matrix $\mathbf{A}$. A calculation then shows that

$$\mathbf{r}_S(t) = R_S(t)\begin{bmatrix} -\delta_C\cos[\theta_S(t) + \alpha t - \theta_P] + (1 - \delta_C)\cos[\theta_S(t) - \alpha t + \theta_P] \\ \delta_C\sin[\theta_S(t) + \alpha t - \theta_P] + (1 - \delta_C)\sin[\theta_S(t) - \alpha t + \theta_P] \\ -\delta_S\cos\theta_S(t)\end{bmatrix}, \tag{4.12}$$

where $\delta_C = \frac{1}{2}(1 - \cos\phi_P)$ and $\delta_S = \sin\phi_P$ are both close to zero. In Figure 1.2 (B), we show the projection of the satellite orbit onto the surface of the earth. Notice that the longitudinal scale is much smaller than the latitude scale. The position error between the data (blue) and model (red) is less than 6 km and the velocity error is less than 0.5 km/hr (as measured in the ECI coordinate system).

In analogy with the geostationary satellite coordinate system in Section 2, we introduce a time-dependent geosynchronous satellite coordinate system via the **moving satellite frame**, $\mathcal{S}(t)$, defined in terms of the ECEF frame, $\mathcal{E}$, by

$$\begin{bmatrix}\mathbf{i}_S(t) & \mathbf{j}_S(t) & \mathbf{k}_S(t)\end{bmatrix} = \begin{bmatrix}\mathbf{i}_E & \mathbf{j}_E & \mathbf{k}_E\end{bmatrix} \mathbf{R}(\theta_P - \alpha t, \phi_P)\, \mathbf{R}(\theta_S(t)). \tag{4.13}$$

Comparing the first column of Equation (4.13) to Equation (4.11), we have that

$$\mathbf{r}_S(t) = R_s(t)\, \mathbf{i}_S(t). \tag{4.14}$$

Explicit formula for $\mathbf{j}_S$ and $\mathbf{k}_S$ can be obtained from Equation (4.12) by observing that $\mathbf{j}_S = \frac{d}{d\theta_S}\mathbf{i}_S$ and $\mathbf{k}_S = \mathbf{i}_s \times \mathbf{j}_S$.

4.1. Problems.

1. Show that when $\epsilon_S = 0$ in Equation (4.10), $\mathbf{r}_S$ is a figure-eight curve that lies on the intersection of a sphere and a cylinder. Also, find an analytical relationship between the tilt angle, ϕ_P, and the amplitude of the oscillations in the latitude and longitude of $\mathbf{r}_S$.
2. Devise a method to estimate $\mathbf{k}_P$ from the satellite position data.
3. Prove the approximate formula for θ_S in Equation (4.10) and show that the curve, $\mathbf{r}_S$, defined by Equation (4.9) has the properties given below (4.10).$^{(*)}$
4. Verify Equation (4.12) and derive an explicit formula for $\mathbf{j}_S$.$^{(*)}$
5. The concept of a moving frame, due to E. Cartan, plays an important role in differential geometry. Cartan's basic idea is to assign a frame to each point of an object being studied (e.g., a curve or surface), and then use the orthonormal expansion in Lemma 4.1 to express the rate of change of the frame in terms of the frame itself [6]. Use this idea to find an explicit formula for the satellite velocity in terms of the moving satellite frame.
6. Write a computer program to reproduce Figure 1.2 (B).
7. Make animations of the satellite orbit viewed in both the ECI and ECEF coordinate systems.

5. Model II: The Unknown-Speed, Concatenation-of-Geodesics Model.

In this section, we describe a model in which the flight path of the aircraft is approximated by a concatenation of segments of constant-speed great circles (geodesics) on the sphere, but for which the different segments can have different *a priori* unknown speeds. We employ the geosynchronous satellite motion model developed in Section 4 and make use of Doppler shift data at the ping times. As in Model I, the initial position of the aircraft is an input parameter to the model. The equations in the model are generalizations to the case of a geosynchronous satellite of the ping arc equation (2.5) and the Doppler shift equation (3.3). Given knowledge of the aircraft position, $\mathbf{r}_n$, on the current ping arc, our goal is to derive a system of three equations in which the unknowns are the two components, $v_{\Theta,n}$ and $v_{\Phi,n}$, of the aircraft velocity at the current ping time and the position, Θ_{n+1}, of the aircraft on the next ping arc. These three equations are a vector ping arc equation (two scalar equations), which enforces the condition that the aircraft reaches the next ping arc at the next ping time, and a Doppler shift equation which enforces the condition that the aircraft

departs from the current ping arc with the correct Doppler shift. However, when we used this approach to reconstruct simulated flight paths we observed that in some cases the direction changes at the ping times were too small to track the simulated flight path. Instead, we found that a more accurate approach was to solve the overdetermined system consisting of the three equations described above together with a second Doppler shift equation, which enforces the condition that the aircraft arrives at the next ping arc with the correct Doppler shift.

To perform the calculations, we make use of two moving frames. These are the **moving satellite frame**, $\{\mathbf{i}_{\mathrm{S},n}, \mathbf{j}_{\mathrm{S},n}, \mathbf{k}_{\mathrm{S},n}\}$, given by evaluating Equation (4.13) at the n-th ping time, t_n, and the **moving aircraft frame**, $\{\mathbf{y}_n, \mathbf{y}_{\Phi,n}, \mathbf{y}_{\Theta,n}\}$, which is chosen so that at time t_n the aircraft position and velocity are of the form $\mathbf{r}_n = R_A\mathbf{y}(\Phi_n, \Theta_n) =: R_A\mathbf{y}_n$ and $\mathbf{v}_n = v_{\Theta,n}\mathbf{y}_{\Theta,n} + v_{\Phi,n}\mathbf{y}_{\Phi,n}$, as in Equations (2.2) and (3.2). If we let $\mathbf{F}_n$ be the 3×3 orthogonal matrix

$$\mathbf{F}_n = \begin{bmatrix} \mathbf{i}_{\mathrm{S},n} & \mathbf{j}_{\mathrm{S},n} & \mathbf{k}_{\mathrm{S},n} \end{bmatrix}, \tag{5.1}$$

then, by Lemma 4.1,

$$\begin{bmatrix} \mathbf{y}_n & \mathbf{y}_{\Phi,n} & \mathbf{y}_{\Theta,n} \end{bmatrix} = \mathbf{F}_n \begin{bmatrix} \cos\Phi_n & -\sin\Phi_n & 0 \\ \cos\Theta_n \sin\Phi_n & \cos\Theta_n \cos\Phi_n & -\sin\Theta_n \\ \sin\Theta_n \sin\Phi_n & \sin\Theta_n \cos\Phi_n & \cos\Theta_n \end{bmatrix} =: \mathbf{F}_n\mathbf{Y}_n, \tag{5.2}$$

where the ping arc angles, Φ_n, can be obtained from the BTO data.

Using Equations (4.14), (5.2), and (3.2), we can express the vectors $\widehat{\mathbf{u}}$ and $\mathbf{v}$ in the Doppler shift formula (3.1) in terms of the moving satellite frame, to obtain the **first Doppler shift equation**, which expresses the difference between measured Doppler shift data, Δf_n, at the n-th ping time and an analytical formula for the Doppler shift in terms of parameters describing the motion of the aircraft and satellite, as

$$\begin{aligned} f_{\mathrm{Doppler},1}(v_{\Phi,n}) := \Delta f_n - \frac{f}{cD_{\mathrm{SA},n}} [&-v_{\Phi,n}R_{S,n}\sin\Phi_n - (R_{S,n} - R_A\cos\Phi_n)(\mathbf{v}_{S,n})_1 \\ &+ R_A\cos\Theta_n\sin\Phi_n(\mathbf{v}_{S,n})_2 + R_A\sin\Theta_n\sin\Phi_n(\mathbf{v}_{S,n})_3] = 0. \end{aligned} \tag{5.3}$$

Here $R_{S,n} = \|\mathbf{r}_S(t_n)\|$ is the distance of the satellite from the center of the earth, and by Lemma (4.1), $\mathbf{v}_{S,n} = \mathbf{F}_n^T\mathbf{r}'_S(t_n)$ is the coordinate vector of the satellite velocity in the moving satellite frame. Note that we can analytically solve Equation (5.3) for $v_{\Phi,n}$ in terms of known quantities. More importantly, due to the motion of the geosynchronous satellite in the ECEF frame (*i.e.*, as $\mathbf{v}_{S,n} \neq 0$), we see that Δf_n depends on Θ_n. Therefore, the symmetry we observed between the positive and negative flight paths with the geostationary satellite in Model I is broken.

Next, we derive the ping arc equations. By Equation (5.2), we have that at time t_n the position and velocity of the aircraft are given by $\mathbf{r}_n = R_A\mathbf{F}_n(\mathbf{Y}_n)_{*1}$ and

$$\mathbf{v}_n = \mathbf{F}_n \begin{bmatrix} (\mathbf{Y}_n)_{*2} & (\mathbf{Y}_n)_{*3} \end{bmatrix} \begin{bmatrix} v_{\Phi,n} \\ v_{\Theta,n} \end{bmatrix}. \tag{5.4}$$

Substituting these expressions into the Equation (2.3) for the great circle path we find that the position of the aircraft at time t_{n+1} is given by

$$\mathbf{r}_{n+1} = R_A\mathbf{F}_n\mathbf{Y}_n\mathbf{x}_n, \tag{5.5}$$

where $\mathbf{x}_n = \mathbf{x}_n(v_{\Phi,n}, v_{\Theta,n})$ is the unit column vector defined by

$$\mathbf{x}_n \;=\; \frac{1}{v_n}\left[v_n\cos(v_n\Delta t_n/R_A) \quad v_{\Phi,n}\sin(v_n\Delta t_n/R_A) \quad v_{\Theta,n}\sin(v_n\Delta t_n/R_A)\right]^T. \quad (5.6)$$

Here $v_n = \sqrt{v_{\Phi,n}^2 + v_{\Theta,n}^2}$ is the aircraft speed at time t_n and $\Delta t_n = t_{n+1} - t_n$. On the other hand, the condition that the aircraft cross the $(n+1)$-st ping arc at time t_{n+1} can be expressed as $\mathbf{r}_{n+1} = R_A\mathbf{F}_{n+1}\mathbf{y}_{n+1}$, which together with Equation (5.5) yields the **vector ping arc equation**

$$\mathbf{x}_n(v_{\Phi,n}, v_{\Theta,n}) \;=\; \mathbf{A}_n y_{n+1}(\Phi_{n+1}, \Theta_{n+1}) \qquad \text{where } \mathbf{A}_n = \mathbf{Y}_n^T\mathbf{F}_n^T\mathbf{F}_{n+1} \text{ is orthogonal.} \quad (5.7)$$

Equation (5.7) is two independent equations in the three unknowns, $v_{\Phi,n}$, $v_{\Theta,n}$, and Θ_{n+1}. Just as in the derivation of Equation (2.6) for the aircraft heading, we can eliminate Θ_{n+1} to obtain the **scalar ping arc equation**

$$f_{\text{Ping}}(v_{\Phi,n}, v_{\Theta,n}) \;:=\; R_A\{(\mathbf{x}_n)_1 - a - \mathbf{b}^T\mathbf{x}_n\} \;=\; 0, \quad (5.8)$$

where $a = (\mathbf{A}_n)_{11}\cos\Phi_{n+1}$ and $\mathbf{b}^T = (\mathbf{A}_n)_{12}(\mathbf{A}_n^T)_{2*} + (\mathbf{A}_n)_{13}(\mathbf{A}_n^T)_{3*}$ are known.

Finally, we leave it as an exercise to the reader to formulate the **second Doppler shift equation** which is of the form[6]

$$f_{\text{Doppler},2}(v_{\Phi,n}, v_{\Theta,n}) \;=\; \Delta f_{n+1} \;-\; g(v_{\Phi,n}, v_{\Theta,n}) \;=\; 0. \quad (5.9)$$

The simplest method to solve for Θ_{n+1} is to use the first Doppler shift equation (5.3) to solve for $v_{\Phi,n}$, whereupon the scalar ping arc equation (5.8) can be used to solve for $v_{\Theta,n}$. Then Equation (5.7) can be inverted to obtain Θ_{n+1} from $\mathbf{y}_{n+1}$. While this method works well when the flight path is a great circle and the data is exact, it can fail for more general flight paths or for uncertain data. In that case, a more robust method is to minimize the function

$$F(v_{\Phi,n}, v_{\Theta,n}) = f_{\text{Doppler},1}^2(v_{\Phi,n}) + f_{\text{Ping}}^2(v_{\Phi,n}, v_{\Theta,n}) + f_{\text{Doppler},2}^2(v_{\Phi,n}, v_{\Theta,n}), \quad (5.10)$$

using unconstrained, gradient-based optimization (specifically, MATLAB's fminunc), and then solve for Θ_{n+1} using Equation (5.7). With a geostationary satellite, the analysis in Section 2 suggests that F has two local minima, corresponding to the positive and negative flight paths that go from the current ping arc to the next. With a geosynchronous satellite, numerical results strongly suggest that there is only a single local minimum, *i.e.*, that the symmetry between the positive and negative flight paths is indeed broken.

5.1. Problems.

1. Derive Equations (5.5) and (5.8).$^{(*)}$
2. Formulate Equation (5.9).$^{(*)}$
3. Given a value for $v_{\Phi,n}$ from Equation (5.3), use a Taylor series approximation and numerical simulations to show that Equation (5.8) is well approximated by a quadratic equation. Discuss the geometric significance of the roots of this quadratic.
4. Write a computer program that implements Model II and validate it by comparison with ping arc data obtained from simulated flight paths.
5. Using simulated flight paths, numerically investigate the uncertainty in the reconstructed flight path due to uncertainties in the Doppler shift data, Δf_n.

[6] A formula for g is given in the Appendix in the supplementary material.

6. Model III: The Concatenation of Small Circles, BFO Model. In this section, we develop a fully numerical model in which the flight path of the aircraft is approximated by a concatenation of segments of small circles, and we use the BFO data that was recorded by the satellite ground station rather than the aircraft-satellite Doppler shift we used in Section 5.

A **small circle** on a sphere is the curve of intersection of the sphere with a plane. Great circles and circles of latitude are examples of small circles. The red curves in Figure 2.1 are small circles. Given an initial position on a sphere of radius, R_A, an initial velocity vector that is tangent to the sphere at the initial position, and a radius, R_C, that is less than the radius of the sphere, there are two small circle paths with the given initial position, initial velocity, and radius. From the point of view of an aircraft pilot, one small circle flight path turns to the right and the other to the left. Rather than parametrizing small circles in terms of their radius, R_C, it is more convenient to parametrize them in terms of their geodesic curvature, κ_g. The geodesic curvature of a constant-speed smooth curve on a surface quantifies how much the curve is turning in the surface [6]. Since it does not turn in the surface, the geodesic curvature of a geodesic curve is zero. The geodesic curvature of a small circle path with constant speed, v, and radius, R_C, on a sphere of radius, R_A, is given by

$$\kappa_g = \pm v\sqrt{\frac{1}{R_C^2} - \frac{1}{R_A^2}}, \tag{6.1}$$

where the choice of sign depends on whether the small circle path is turning right or left. The geodesic curvature of a great circle is zero and, for small circles, $|\kappa_g| \to \infty$ as $R_C \to 0$.

A basic assumption in the models developed by the Satellite Working Group is that—after a certain time (19:41 UTC)—MH370 was operating without human control [1]. One possible scenario is that the aircraft was flying at constant speed and at a constant heading relative to the air. However, because of the effects of wind, the path of the aircraft over the earth may not have exactly been a great circle. Therefore a model based on small circles may produce a better approximation to the flight path than one based on great circles.

We now derive a parametrization of the small circle with geodesic curvature, κ_g, that lies on the sphere of radius, R_A, and which at time, t_n has position, $\mathbf{r}_n$, and velocity, $\mathbf{v}_n$. If we let $\mathbf{c}$ be the center and R_C be the radius of this small circle, then

$$\mathbf{r}(t) \;=\; \mathbf{c} \;+\; \cos\left[\frac{v(t-t_n)}{R_C}\right]\mathbf{r}_n^{\perp} \;+\; \frac{R_C}{v}\sin\left[\frac{v(t-t_n)}{R_C}\right]\mathbf{v}_n, \tag{6.2}$$

where $\mathbf{r}_n^{\perp} = \mathbf{r}_n - \mathbf{c}$ and $v = |\mathbf{v}_n|$. Let $\mathbf{w}_n = \frac{\mathbf{r}_n}{R_A} \times \frac{\mathbf{v}_n}{v}$, so that $\{\frac{\mathbf{r}_n}{R_A}, \frac{\mathbf{v}_n}{v}, \mathbf{w}_n\}$ is frame adapted to the small circle. Then a calculation shows that

$$\frac{\mathbf{r}(t)}{R_A} \;=\; \left[1 + \frac{\cos\alpha_n(t) - 1}{1+K^2}\right]\frac{\mathbf{r}_n}{R_A} \;+\; \frac{K(\cos\alpha_n(t)-1)}{1+K^2}\,\mathbf{w}_n \;+\; \frac{\sin\alpha_n(t)}{\sqrt{1+K^2}}\,\frac{\mathbf{v}_n}{v}, \tag{6.3}$$

where $K = R_A\kappa_g/v$ and $\alpha_n(t) = v(t-t_n)/R_C$.

One motivation for using small circles is that the ping arc equation and the two Doppler shift equations in the great circle model in Section 5 form an overdetermined system of three equations in two unknowns, $(v_{\Phi,n}, v_{\Theta,n})$. By adding the geodesic curvature, $\kappa_{g,n}$, as a third unknown, we can use the ping arc and BFO data to obtain

a system of three equations in three unknowns of the form

$$f_{\text{BFO},1}(v_{\Phi,n}, v_{\Theta,n}) = 0, \tag{6.4}$$
$$f_{\text{Ping}}(v_{\Phi,n}, v_{\Theta,n}, \kappa_{g,n}) = 0, \tag{6.5}$$
$$f_{\text{BFO},2}(v_{\Phi,n}, v_{\Theta,n}, \kappa_{g,n}) = 0. \tag{6.6}$$

Although we can derive BFO equations for small circle flight paths that are similar to the first and second Doppler shift equations (5.3) and (5.9), because of the need to transform between the geostationary and geosynchronous satellite coordinate systems, there is no longer any advantage to using an analytical approach such as that described in Section 5.

Instead, given a position, $\mathbf{r}_n$, on the n-th ping arc and a triple $(v_{\Phi,n}, v_{\Theta.n}, \kappa_{g,n})$, we define $f_{\text{Ping}}(v_{\Phi,n}, v_{\Theta.n}, \kappa_{g,n})$ to be the geodesic distance on the sphere of radius, R_A, between $\mathbf{r}(t_{n+1})$ and the $(n+1)$-st ping arc, where $\mathbf{r}(t_{n+1})$ is computed using the small circle parametrization (6.3). Similarly, we can use the definition (3.5) of the BFO to evaluate $f_{\text{BFO},1}$ at $(v_{\Phi,n}, v_{\Theta,n})$ by computing the Doppler shifts, $\Delta f_{\text{AS},n}$ and $\Delta f_{\text{AS-Comp},n}$ directly using the definition (3.1). Finally, we can evaluate $f_{\text{BFO},2}$ at $(v_{\Phi,n}, v_{\Theta.n}, \kappa_{g,n})$ using Equation (3.1), provided we first use the small circle parametrization (6.3) to calculate the position and velocity vectors of the aircraft at the next ping arc.

Since it is unlikely that the flight path of MH370 was really a concatenation of segments of small circles and since there is measurement error in the BTO and BFO data and additional uncertainty in some of the model parameters, we do not expect Equations (6.4), (6.5), and (6.6) to have an exact solution. For these reasons, we formulated the problem of solving the equations as a nonlinear least squares problem of the form: Find the set of parameters $(v_{\Phi,n}, v_{\Theta,n}, \kappa_{g,n})$ that minimizes the objective function

$$F = f_{\text{Ping}}^2 + f_{\text{BFO},1}^2 + f_{\text{BFO},2}^2 + f_{\text{Penalty}}^2, \tag{6.7}$$

where the function $f_{\text{Penalty}}(\kappa_g) = (\kappa_g/\kappa_{g,\text{Threshold}})^4$ is defined so as to penalize small circles that have a small radius and large speed. Without this penalty term the numerical solver can get stuck in physically unrealistic local minima. A numerical simulation study suggests that for the simulated flight paths we considered and for the recorded MH370 data, the function F has a unique global minimum, *i.e.*, its graph is bowl-shaped. If true, this observation is due to the fact that the satellite orbit is geosynchronous, and to the inclusion of the penalty term in Equation (6.7).

6.1. Problems.

1. Fill in the details of the derivation of Equation (6.3).$^{(*)}$
2. Provide a reasonable formula for the parameter $\kappa_{g,\text{Threshold}}$ in the penalty function, f_{Penalty}.
3. Discuss the relative merits of analytical versus fully numerical methods, both in the context of this article and more generally in engineering applications.
4. How are the methods developed in this article analogous to numerical methods for solving systems of ordinary differential equations?
5. Implement a fully numerical small circle model that uses Doppler shift rather than BFO data and study its performance.
6. Using a geosynchronous satellite model, try to construct two flight paths that have the same ping arc and Doppler shift data, but which are very far apart when they cross the final ping arc.

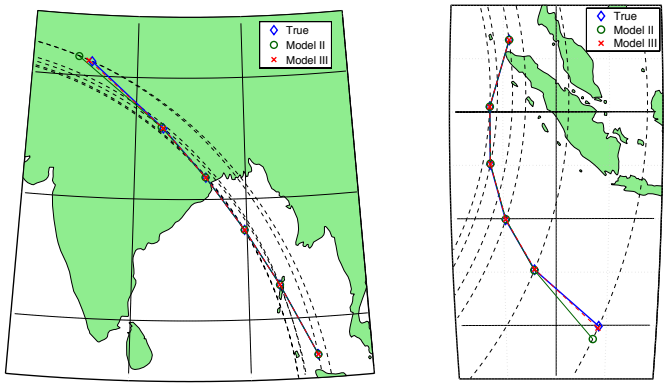

(A) (B)

FIG. 7.1 *Flight paths computed using Model II (green circles) and Model III (red crosses) for two simulated constant-speed, small circle flight paths (blue diamonds). (A) The aircraft starts in the southeast corner of the map and travels northwest. (B) The aircraft starts in the northwest corner of the map and travels south and east.*

7. Results. We verified Models II and III using several simulated flights, two of which are shown in Figure 7.1. Both of these flight paths are small circles that start at 95.6°E, 6.8°N (near the point of last radar contact of MH370) and have a constant speed of 600 km/h (325 knots). The radius of the small circle path is 80% of the radius of the earth in Figure 7.1 (A) and 35% of the radius of the earth in Figure 7.1 (B). The ping times were chosen to be the same as for MH370. The ping arcs for the two flights are shown with black dashed curves. In Figure 7.1 (A) the aircraft travels northwest almost tangent to the ping arcs. In Figure 7.1 (B) the aircraft travels south and then southeast along a path that is similar to the 325 knot flight path for MH370 shown in Figure 2.2. The positions at which the simulated flight path crosses the ping arcs are shown with blue diamonds. The green circles and red crosses show the corresponding aircraft positions computed using Models II and III, respectively. The agreement obtained between the results using the models and the simulated flight paths is excellent, although with Model II (based on great circles) the agreement is not quite as good as with Model III (based on small circles).

Next, we apply Model III to reconstruct the flight path of MH370, which requires addressing two major sources of uncertainty in the satellite data. First, because of large fluctuations in the BFO data recorded between 18:25 and 18:28, the flight path from 18:28 to 19:41 may not be well approximated by a segment of a small circle.[7] Following an approach taken in the ATSB report [2], we start the computation on the 19:41 ping arc using a range of initial positions, $\Theta_{19:41}$, that could reasonably be reached from the point of last radar contact at 18:15. In Figure 7.2 (A), we show this set of initial positions with a thin blue solid curve. The second source of uncertainty is the value of δf_{Bias} in Equation (3.5), which we varied from 145 Hz to 155 Hz to match the reported uncertainty [2]. For each pair $(\Theta_{19:41}, \delta f_{\text{Bias}})$, we used Model III to find the flight path that minimizes the objective function in Equation (6.7). To match the reported uncertainty in the BTO [2], we discarded flight paths for which

[7] This BFO data is not included in Table 1.1.

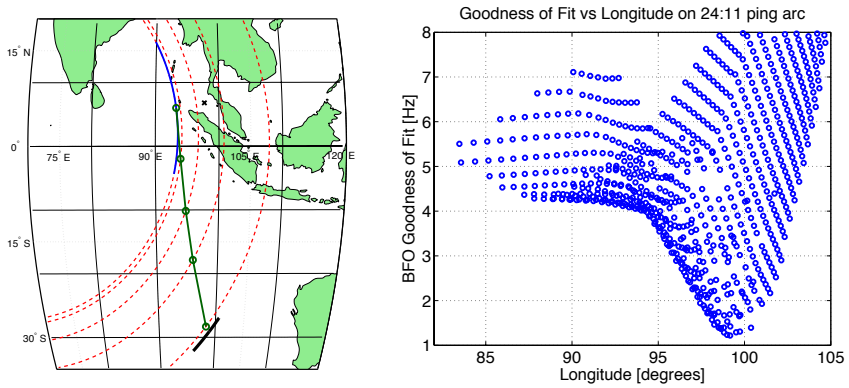

(A) (B)

FIG. 7.2 *(A) The flight path for MH370 computed using Model III with the values of* $(\Theta_{19:41}, \delta f_{Bias})$ *that minimize the BFO goodness of fit. The black cross shows the location of MH370 at last radar contact and the red dashed curves are the ping arcs from 19:41 to 24:11. The thin blue solid curve shows the set of initial positions,* $\Theta_{19:41}$*, on the 19:41 ping arc. The thick black curve shows the priority search area determined by the ATSB [2]. (B) Each blue circle shows the BFO goodness of fit of a flight path as a function of the longitude of the aircraft when it crosses the 24:11 ping arc. The different blue circles correspond to different values for* $(\Theta_{19:41}, \delta f_{Bias})$*. The minimum BFO goodness of fit,* GF_{BFO}*, occurs at longitude* $98.35°\,E$*. The figure shows only those points for which* $GF_{BFO} < 8$ *Hz. As the longitude increases from* $105°\,E$ *to* $107°\,E$*,* GF_{BFO} *increases from 8 to 40 Hz.*

there were ping times at which the distance of the aircraft from the ping arc exceeded 5 km. To quantify how well the computed flight paths fit the BFO data we calculated the **BFO goodness of fit**,

$$\mathrm{GF_{BFO}} = \left[\sum_{k=1}^{K-1} |f^{(k)}_{\mathrm{BFO},1}|^2\right]^{1/2} + \left[\sum_{k=2}^{K} |f^{(k)}_{\mathrm{BFO},2}|\right]^{1/2}, \tag{7.1}$$

where k indexes the ping times from 19:41 to 24:11.

In Figure 7.2 (B), we show the BFO goodness of fit as a function of the longitude of the position of the aircraft on the 24:11 ping arc. Each blue circle corresponds to a different choice of the parameters $(\Theta_{19:41}, \delta f_{\mathrm{Bias}})$. The minimum value of $\mathrm{GF_{BFO}}$ is 2.46 Hz at $(\Theta_{19:41}, \delta f_{\mathrm{Bias}}) = (9.5°, 155)$. In Figure 7.2 (A), we show the corresponding flight path with the green circles. This flight path crosses the 24:11 ping arc at longitude 98.35°E. The ground speed of the aircraft varies from 917 km/hr to 800 km/hr which compares well with the typical air speed of 905 km/hr for a Boeing 777 at an altitude of 35,000 ft [9]. The radii of the small circles for this flight path range from 50% to 57% of the radius of the earth.

8. Discussion. The mathematical models developed by the Satellite Working Group (SWG) were based on the assumption that the flight path of MH370 was smooth after 19:41 UTC and that it conformed to the performance limitations for a Boeing 777 (*e.g.*, minimum and maximum speeds at a given altitude) [2]. With the SWG model, between ping times the aircraft was assumed to be traveling along a great circle at constant speed relative to the air. To determine the flight path from one ping arc to the next, the initial velocity of the aircraft was varied to minimize the error between the calculated and recorded BFO values [3]. This approach is similar

to that taken in Model II. However, the SWG model also used meteorological data to incorporate the effect that winds had on the passage of the aircraft over the surface of the earth. The SWG verified their method by comparison with other flights in the same region on the same day, as well as with other flights of the same aircraft on the days immediately prior to the disappearance of MH370. The priority search area for MH370 that was announced by the ATSB on June 26th was based on the results obtained by the SWG. In Figure 7.2 (A), we show this search area with a thick black curve just below the 24:11 ping arc that extends from longitude 96°E to 101.5°E [2].

For the results presented in this paper, we used numerical optimization to determine the flight path that best fit the BTO and BFO data. To enrich the set of possible flight paths over which the optimization was performed, our model was based on segments of small circles rather than great circles. The results we obtained in Figure 7.2 (B) predict a very similar search area to that obtained by the ATSB [2]. This agreement between the two models—one based on wind-drifted great circles and the other on small circles—is encouraging.

One of the main reasons for developing a mathematical model of a phenomenon is to use the model for prediction. To be useful, a model needs to capture the most salient aspects of the phenomenon and the equations in the model need to be solved with robust and accurate algorithms. Moreover, accurate input data is needed to make accurate predictions. In the case of the search for MH370 this data includes the initial position of the aircraft on one of the ping arcs and the frequency shifts δf_{AI} and δf_{Bias} in the BFO Equation (3.5). A recent refinement of this data by the Satellite Working Group [3] prompted the ATSB to shift the priority search area to a region on the final ping arc immediately southwest of the priority search area shown with the thick black curve in Figure 7.2.

9. Acknowledgements. I thank the official Search Strategy Group coordinated by the Australian Transport Safety Bureau for releasing many details of their methods. Although the crash site of MH370 has not yet been found, the search would be hopeless without their efforts. I also learned much from the blog posts of Duncan Steel and his collaborators in the Independent Group. The manuscript was much improved thanks to the diligent work of two anonymous reviewers. Thanks also go to my Spring 2014 Multivariable Calculus class, to Yanping Chen and Brian Marks for their help with the figures, and to Alan Boyle, Matthew Goeckner, Justin Jacobs, Burkard Polster, Marty Ross, Yannan Shen, and my very supportive spouse and fellow mathematician Sue Minkoff.

REFERENCES

[1] C. Ashton, A. Shuster Bruce, G. Colledge, and M. Dickinson, The search for MH370, The Journal of Navigation, 68 (2015), pp. 1–22.

[2] Australian Transport Safety Bureau, MH 370 - Definition of Underwater Search Areas, 26 June, 2014. http://www.atsb.gov.au/mh370-pages/updates/reports.aspx [Online; accessed 9-September-2014].

[3] ———, MH 370 - Flight Path Analysis Update, 8 Oct, 2014. http://www.atsb.gov.au/mh370-pages/updates/reports.aspx [Online; accessed 16-October-2014].

[4] G. Chen, C. Gu, P. J. Morris, E. G. Paterson, A. Sergeev, Y. C. Wang, and T. Wierzbicki, Malaysian airlines flight MH370: Water entry of an airliner, Notices of the American Mathematical Society, 62 (2015), pp. 330–344.

[5] Inmarsat, MH370 Data Communications Logs, 2014. http://www.mh370.gov.my/index.php/en/95-data-communication-logs-for-mh370 [Online; accessed 27-March-2015].

[6] B. O'Neill, Elementary Differential Geometry, Academic Press, Waltham, Massachusetts, Second ed., 2006.

[7] Wikipedia, Aircraft Communications Addressing and Reporting System, 2014. https://en.wikipedia.org/w/index.php?title=Aircraft_Communications_Addressing_and_Reporting_System&oldid=672562871 [Online; accessed 17-September-2015].
[8] ———, Analemma, 2015. https://en.wikipedia.org/w/index.php?title=Analemma&oldid=680448005 [Online; accessed 17-September-2015].
[9] ———, Boeing 777, 2015. https://en.wikipedia.org/w/index.php?title=Boeing_777&oldid=681520569 [Online; accessed 17-September-2015].
[10] ———, Earth-centered inertial, 2015. https://en.wikipedia.org/w/index.php?title=Earth-centered_inertial&oldid=666290517 [Online; accessed 17-September-2015].
[11] ———, Earth's rotation, 2015. https://en.wikipedia.org/w/index.php?title=Earth%27s_rotation&oldid=679938189 [Online; accessed 17-September-2015].
[12] ———, ECEF, 2015. https://en.wikipedia.org/w/index.php?title=ECEF&oldid=673101265 [Online; accessed 17-September-2015].
[13] ———, Geostationary orbit, 2015. https://en.wikipedia.org/w/index.php?title=Geostationary_orbit&oldid=680719011 [Online; accessed 17-September-2015].
[14] ———, Malaysia Airlines Flight 370, 2015. https://en.wikipedia.org/w/index.php?title=Malaysia_Airlines_Flight_370&oldid=680952015 [Online; accessed 17-September-2015].
[15] J. Zweck, How did Inmarsat deduce possible flight paths for MH370?, SIAM News, 47 (2014), pp. 1,8. Also available online from http://www.siam.org/news/.

10. Appendix. In this Appendix, we outline solutions to some of the problems posed in the body of the paper.

Problem 2.1.1. We show that the constant speed great circle flight path, which at time, t_n, has position, $\mathbf{r}_n$, and velocity, $\mathbf{v}_n$, is parametrized by

$$\mathbf{r}_A(t) \;=\; \cos\left[\frac{v(t-t_n)}{R_A}\right]\mathbf{r}_n \;+\; \frac{R_A}{v}\sin\left[\frac{v(t-t_n)}{R_A}\right]\mathbf{v}_n, \tag{10.1}$$

where R_A is the radius of the sphere on which the great circle lies, and $v = |\mathbf{v}_n|$ is the speed of the aircraft.

Proof. Since the position vector, $\mathbf{r}_n$, is normal to the sphere and the velocity vector, $\mathbf{v}_n$, is tangent to the sphere, we have that $\mathbf{r}_n \perp \mathbf{v}_n$. Let $\mathbf{u}_n = \frac{R_A}{v}\mathbf{v}_n$. Then $\|\mathbf{r}_n\| = \|\mathbf{u}_n\| = R_A$. Let P be the plane centered at the origin with orthogonal basis $\{\mathbf{r}_n, \mathbf{u}_n\}$. The great circle lies in this plane. Then by vector algebra and trigonometry (draw a picture of the great circle in the plane P),

$$\mathbf{r}_A(t) \;=\; \cos[C(t-t_n)]\mathbf{r}_n + \sin[C(t-t_n)]\mathbf{u}_n, \tag{10.2}$$

for some constant C. To find C we calculate that $v = \|\mathbf{r}'_A(t)\| = R_A C$. □

Problem 2.1.3. Let $\mathbf{y}_\Theta$ and $\mathbf{y}_\Phi$ be unit vectors tangent to the coordinate curves, $\Phi = \Phi_n$ and $\Theta = \Theta_n$, respectively. Recall that the aircraft velocity at time t_n is

$$\mathbf{v}_n \;=\; v\cos\beta_n\,\mathbf{y}_\Theta \;+\; v\sin\beta_n\,\mathbf{y}_\Phi, \tag{10.3}$$

where the angle, β_n, is the heading direction of the aircraft. We will show that the ping arc equation,

$$\mathbf{r}_A(t_{n+1}) \;=\; R_A\mathbf{y}(\Phi_{n+1}, \Theta_{n+1}), \tag{10.4}$$

can be solved to obtain the formula for the heading direction given by

$$\sin\beta_n \;=\; \frac{\cos\left(\frac{v\Delta t_n}{R_A}\right)\cos\Phi_n \;-\; \cos\Phi_{n+1}}{\sin\left(\frac{v\Delta t_n}{R_A}\right)\sin\Phi_n}. \tag{10.5}$$

Proof. By Equation (10.1), the left hand side of the ping arc equation (10.4) is given by

$$\mathbf{r}_A(t_{n+1}) \;=\; \cos\left[\frac{v\Delta t_n}{R_A}\right]\mathbf{r}_n \;+\; \frac{R_A}{v}\sin\left[\frac{v\Delta t_n}{R_A}\right]\mathbf{v}_n, \tag{10.6}$$

where $\Delta t_n = t_{n+1} - t_n$. Recall that a satellite coordinate system is one for which the satellite is on the positive x-axis and the origin is at the center of the earth. Given any choice of satellite coordinate system, we can rotate it about the x-axis to obtain another satellite coordinate system which has the property that at time t_n the aircraft lies in the xy-plane, *i.e.*, $\Theta_n = 0$ (see Figure 2.1 (B)). With this choice of coordinates, by Equation (2.1), we have that

$$\mathbf{r}_n \;=\; R_A\mathbf{y}(\Phi_n, 0) \;=\; R_A\left[\cos\Phi_n\mathbf{i}_S \;+\; \sin\Phi_n\mathbf{j}_S\right]. \tag{10.7}$$

Next we calculate $\mathbf{v}_n$ in terms of Φ_n and β_n. First, the vector $\mathbf{y}_\Theta$ is the unit vector in the direction of $\frac{\partial \mathbf{y}}{\partial \Theta}$ and $\mathbf{y}_\Phi$ is the unit vector in the direction of $\frac{\partial \mathbf{y}}{\partial \Phi}$. Therefore,

$$\mathbf{y}_\Phi = -\sin\Phi\,\mathbf{i}_S + \cos\Theta\cos\Phi\,\mathbf{j}_S + \sin\Theta\cos\Phi\,\mathbf{k}_S, \tag{10.8}$$

$$\mathbf{y}_\Theta = -\sin\Theta\,\mathbf{j}_S + \cos\Theta\,\mathbf{k}_S. \tag{10.9}$$

Substituting these expressions into Equation (10.3) and using $\Theta_n = 0$, we obtain

$$\mathbf{v}_n = -v\sin\beta_n\sin\Phi_n\,\mathbf{i}_S + v\sin\beta_n\cos\Phi_n\,\mathbf{j}_S + v\cos\beta_n\,\mathbf{k}_S. \tag{10.10}$$

Substituting Equations (10.7) and (10.10) into Equation (10.6) we obtain an expression for the left-hand side, $\mathbf{r}_A(t_{n+1})$, of the ping arc equation (10.4) in terms of Φ_n and β_n. Next, we observe that by Equation (2.1), the $\mathbf{i}_S$-component of the right-hand side of the ping arc equation is the only component that is independent of the unknown angle, Θ_{n+1}. Therefore, to solve for β_n, we take the inner product of Equation (10.4) with $\mathbf{i}_S$. After an algebraic manipulation, we obtain the required Equation (10.5). □

Problem 3.1.1. We show that for a geostationary satellite, the aircraft-satellite Doppler shift, Δf_n, at the n-th ping arc is related to the component, $v_{\Phi,n}$, of the aircraft velocity that is perpendicular to the ping arc by

$$\Delta f_n = -\frac{f}{c}\frac{R_S}{D_{\mathrm{SA},n}}\,v_{\Phi,n}\sin\Phi_n, \tag{10.11}$$

where Φ_n is the ping arc angle and the distance, $D_{\mathrm{SA},n}$, between the satellite and aircraft is

$$D_{\mathrm{SA},n} = \sqrt{R_S^2 - 2R_SR_A\cos\Phi_n + R_A^2}. \tag{10.12}$$

Proof. Since $\{\mathbf{y}_n, \mathbf{y}_{\Phi,n}, \mathbf{y}_{\Theta,n}\}$ is an orthonormal basis,

$$\widehat{\mathbf{u}}(t_n)\cdot\mathbf{y}_{\Theta,n} = \frac{[\mathbf{r}_A(t_n)-\mathbf{r}_S]\cdot\mathbf{y}_{\Theta,n}}{\|\mathbf{r}_A(t_n)-\mathbf{r}_S\|} = \frac{[R_A\mathbf{y}_n - R_S\mathbf{i}_S]\cdot\mathbf{y}_{\Theta,n}}{D_{\mathrm{SA},n}} = 0, \tag{10.13}$$

since, by Equation (10.9), the $\mathbf{i}_S$-component of $\mathbf{y}_{\Theta,n}$ is zero. Therefore, by Equations (3.1), (3.2) and (10.8),

$$\Delta f_n = -\frac{f}{c}\frac{1}{D_{\mathrm{SA},n}}\,[R_A\mathbf{y}_n - R_S\mathbf{i}_S]\cdot[v_{\Theta,n}\mathbf{y}_{\Theta,n} + v_{\Phi,n}\mathbf{y}_{\Phi,n}] = -\frac{f}{c}\frac{R_S}{D_{\mathrm{SA},n}}\,v_{\Phi,n}\sin\Phi_n, \tag{10.14}$$

as required. □

Problem 4.1.3. Let

$$R_S(t) = \overline{R}_S[1+\epsilon_S\sin(\alpha(t-t_0))], \tag{10.15}$$

$$v_S(t) = \overline{v}_S[1-\epsilon_S\sin(\alpha(t-t_0))]. \tag{10.16}$$

We show that if

$$\mathbf{r}_S(t) = R_S(t)\left[\cos\theta_S(t)\,\mathbf{i}_P + \sin\theta_S(t)\,\mathbf{j}_P\right], \tag{10.17}$$

where

$$\theta_S(t) = \frac{\pi}{2} + \int_{t_0}^{t}\frac{v_S(s)}{R_S(s)}\,ds, \tag{10.18}$$

then

$$\theta_S(t) \approx \frac{\pi}{2} + \alpha(t-t_0) + 2\epsilon_S\left\{\cos[\alpha(t-t_0)] - 1\right\} + \mathcal{O}(\epsilon_S^2), \tag{10.19}$$

and

$$\|\mathbf{r}'_S(t)\| = v_S(t) + \mathcal{O}(\epsilon_S^2). \tag{10.20}$$

Proof. Substituting Equations (10.15) and (10.16) into Equation (10.18) and using the fact that $\overline{v}_S = \alpha\overline{R}_S$, we find that

$$\theta_S(t) = \frac{\pi}{2} + \alpha\int_0^{t-t_0} 1 - \frac{2\epsilon_S\sin\alpha s}{1+\epsilon_S\sin\alpha s}\,ds \tag{10.21}$$

$$= \frac{\pi}{2} + \alpha(t-t_0) - 2\epsilon_S\alpha\int_0^{t-t_0}\sin\alpha s\,ds + \mathcal{O}(\epsilon_S^2) \tag{10.22}$$

$$= \frac{\pi}{2} + \alpha(t-t_0) + 2\left\{\cos[\alpha(t-t_0)] - 1\right\} + \mathcal{O}(\epsilon_S^2), \tag{10.23}$$

as required.

Next, to prove Equation (10.20), we use (10.15) and (10.16) to show that

$$\mathbf{r}'_S(t) = [R'_S(t)\cos\theta_S(t) - v_S(t)\sin\theta_S(t)]\,\mathbf{i}_P + [R'_S(t)\sin\theta_S(t) + v_S(t)\cos\theta_S(t)]\,\mathbf{j}_P. \tag{10.24}$$

Therefore,

$$\|\mathbf{r}'_S(t)\|^2 = [R'_S(t)]^2 + [v_S(t)]^2 = \overline{v}_S^2\left\{1 - 2\epsilon_S\sin[\alpha(t-t_0)] + \epsilon_S^2\right\}, \tag{10.25}$$

and so

$$\|\mathbf{r}'_S(t)\| = \overline{v}_S\left\{1 - 2\epsilon_S\sin[\alpha(t-t_0)] + \epsilon_S^2\right\}^{1/2} \tag{10.26}$$

$$= \overline{v}_S\left\{1 + \tfrac{1}{2}(-2\epsilon_S\sin[\alpha(t-t_0)] + \epsilon_S^2)\right\} + \mathcal{O}(\epsilon_S^2) \tag{10.27}$$

$$= v_S(t) + \mathcal{O}(\epsilon_S^2), \tag{10.28}$$

as required. □

Problem 4.1.4. We show that if

$$\mathbf{r}_S(t) = R_S(t)\,\mathbf{R}(\theta_P - \alpha t, \phi_P)\,[\mathbf{R}(\theta_S(t))]_{*1}, \tag{10.29}$$

then

$$\mathbf{i}_S(t) := \frac{\mathbf{r}_S(t)}{R_S(t)} = \begin{bmatrix} -\delta_C\cos[\theta_S(t)+\alpha t-\theta_P] + (1-\delta_C)\cos[\theta_S(t)-\alpha t+\theta_P] \\ \delta_C\sin[\theta_S(t)+\alpha t-\theta_P] + (1-\delta_C)\sin[\theta_S(t)-\alpha t+\theta_P] \\ -\delta_S\cos\theta_S(t) \end{bmatrix}, \tag{10.30}$$

where $\delta_C = \frac{1}{2}(1-\cos\phi_P)$ and $\delta_S = \sin\phi_P$, and that

$$\mathbf{j}_S(t) = \frac{d}{d\theta_S}\mathbf{i}_S(t) = \begin{bmatrix} \delta_C\sin[\theta_S(t)+\alpha t-\theta_P] - (1-\delta_C)\sin[\theta_S(t)-\alpha t+\theta_P] \\ \delta_C\cos[\theta_S(t)+\alpha t-\theta_P] + (1-\delta_C)\cos[\theta_S(t)-\alpha t+\theta_P] \\ \delta_S\sin\theta_S(t) \end{bmatrix}. \tag{10.31}$$

Proof. Let $\theta_1 = \theta_P - \alpha t$ and $\theta_2 = \theta_S(t)$. Then by (10.29),

$$\begin{aligned}
\mathbf{i}_S(t) &= \mathbf{R}(\theta_P - \alpha t, \phi_P)\,[\mathbf{R}(\theta_S(t))]_{*1} \\
&= \begin{bmatrix} \cos\theta_1\cos\theta_2\cos\phi_P - \sin\theta_1\sin\theta_2 \\ \sin\theta_1\cos\theta_2\cos\phi_P + \cos\theta_1\sin\theta_2 \\ -\sin\phi_P\cos\theta_2 \end{bmatrix} \\
&= \begin{bmatrix} \frac{1}{2}\{[\cos(\theta_1+\theta_2)+\cos(\theta_1-\theta_2)]\cos\phi_P + [\cos(\theta_1+\theta_2)-\cos(\theta_1-\theta_2)]\} \\ \frac{1}{2}\{[\sin(\theta_1+\theta_2)+\sin(\theta_1-\theta_2)]\cos\phi_P + [\sin(\theta_1+\theta_2)-\sin(\theta_1-\theta_2)]\} \\ -\sin\phi_P\cos\theta_2 \end{bmatrix} \\
&= \begin{bmatrix} -\delta_C\cos[\theta_S(t)+\alpha t-\theta_P] + (1-\delta_C)\cos[\theta_S(t)-\alpha t+\theta_P] \\ \delta_C\sin[\theta_S(t)+\alpha t-\theta_P] + (1-\delta_C)\sin[\theta_S(t)-\alpha t+\theta_P] \\ -\delta_S\cos\theta_S(t) \end{bmatrix},
\end{aligned}$$

as required. To show that $\mathbf{j}_S(t) = \frac{d}{d\theta_S}\mathbf{i}_S(t)$ we recall from Equation (4.13) that

$$\begin{bmatrix}\mathbf{i}_S(t) & \mathbf{j}_S(t) & \mathbf{k}_S(t)\end{bmatrix} = \mathbf{R}(\theta_P - \alpha t, \phi_P)\,\mathbf{R}(\theta_S(t)). \tag{10.32}$$

So by linearity of the derivative and of matrix multiplication,

$$\frac{d}{d\theta_S}\begin{bmatrix}\mathbf{i}_S & \mathbf{j}_S & \mathbf{k}_S\end{bmatrix} \tag{10.33}$$

$$= \mathbf{R}(\theta_P - \alpha t, \phi_P)\,\frac{d}{d\theta_S}\mathbf{R}(\theta_S) \tag{10.34}$$

$$= \mathbf{R}(\theta_P - \alpha t, \phi_P)\,\frac{d}{d\theta_S}\begin{bmatrix}\cos\theta_S & -\sin\theta_S & 0 \\ \sin\theta_S & \cos\theta_S & 0 \\ 0 & 0 & 1\end{bmatrix}. \tag{10.35}$$

The required result now follows from the fact that the θ-derivative of the first column of the rotation matrix $\mathbf{R}(\theta)$ equals the second column of $\mathbf{R}(\theta)$. □

Problem 5.1.1. We show that the position of the aircraft at time t_{n+1} is given by

$$\mathbf{r}_{n+1} = R_A\mathbf{F}_n\mathbf{Y}_n\mathbf{x}_n, \tag{10.36}$$

where $\mathbf{x}_n = \mathbf{x}_n(v_{\Phi,n}, v_{\Theta,n})$ is the unit column vector defined by

$$\mathbf{x}_n = \frac{1}{v_n}\begin{bmatrix}v_n\cos(v_n\Delta t_n/R_A) & v_{\Phi,n}\sin(v_n\Delta t_n/R_A) & v_{\Theta,n}\sin(v_n\Delta t_n/R_A)\end{bmatrix}^T. \tag{10.37}$$

Here $v_n = \sqrt{v_{\Phi,n}^2 + v_{\Theta,n}^2}$ and $\Delta t_n = t_{n+1} - t_n$. We show that the **vector ping arc equation** which enforces the condition that the aircraft cross the $(n+1)$-st ping arc at time t_{n+1}, is given by

$$\mathbf{x}_n = \mathbf{A}_n\mathbf{y}_{n+1}, \qquad \text{where } \mathbf{A}_n = \mathbf{Y}_n^T\mathbf{F}_n^T\mathbf{F}_{n+1} \text{ is orthogonal,} \tag{10.38}$$

and that we can eliminate Θ_{n+1} from Equation (10.38) to obtain the **scalar ping arc equation**

$$f_{\text{Ping}}(v_{\Phi,n}, v_{\Theta,n}) := R_A\{(\mathbf{x}_n)_1 - a - \mathbf{b}^T\mathbf{x}_n\} = 0, \tag{10.39}$$

where $a = (\mathbf{A}_n)_{11}\cos\Phi_{n+1}$ and $\mathbf{b}^T = (\mathbf{A}_n)_{12}(\mathbf{A}_n^T)_{2*} + (\mathbf{A}_n)_{13}(\mathbf{A}_n^T)_{3*}$.

Proof. By Equation (2.3), the expressions for $\mathbf{r}_n$ and $\mathbf{v}_n$ given in and above Equation (5.4), and by Lemma 4.1,

$$\begin{aligned}\mathbf{r}_{n+1} &= \cos(v_n\Delta t_n/R_A)\,\mathbf{r}_n + \frac{R_A}{v_n}\sin(v_n\Delta t_n/R_A)\,\mathbf{v}_n,\\ &= R_A\mathbf{F}_n\left\{\cos(v_n\Delta t_n/R_A)(\mathbf{Y}_n)_{*1} + \frac{1}{v_n}\sin(v_n\Delta t_n/R_A)\begin{bmatrix}(\mathbf{Y}_n)_{*2} & (\mathbf{Y}_n)_{*3}\end{bmatrix}\begin{bmatrix}v_{\Phi,n}\\ v_{\Theta,n}\end{bmatrix}\right\}\\ &= R_A\mathbf{F}_n\mathbf{Y}_n\mathbf{x}_n,\end{aligned}$$

as required. Since the condition that the aircraft cross the $(n+1)$-st ping arc at time t_{n+1} can be expressed as $\mathbf{r}_{n+1} = R_A\mathbf{F}_{n+1}\mathbf{y}_{n+1}$, we have that $\mathbf{F}_n\mathbf{Y}_n\mathbf{x}_n = \mathbf{F}_{n+1}\mathbf{y}_{n+1}$. Since all matrices in this equation are orthogonal, multiplying on the left by $(\mathbf{F}_n\mathbf{Y}_n)^T$ yields (10.38) as required.

To derive Equation (10.39), we observe that by Equations (5.2) and (10.38)

$$\begin{bmatrix}\cos\Phi_{n+1}\\ \cos\Theta_{n+1}\sin\Phi_{n+1}\\ \sin\Theta_{n+1}\sin\Phi_{n+1}\end{bmatrix} = (\mathbf{Y}_{n+1})_{*1} = \mathbf{y}_{n+1} = \begin{bmatrix}(\mathbf{A}_n^T)_{1*}\mathbf{x}_n\\ (\mathbf{A}_n^T)_{2*}\mathbf{x}_n\\ (\mathbf{A}_n^T)_{3*}\mathbf{x}_n\end{bmatrix}. \tag{10.40}$$

On the other hand, also by (10.38), $(\mathbf{x}_n)_1 = (\mathbf{A}_n)_{1*}\mathbf{y}_{n+1}$. To eliminate Θ_{n+1} from this equation, we use the right hand side of (10.40) to obtain

$$\begin{aligned}(\mathbf{x}_n)_1 &= (\mathbf{A}_n)_{11}(\mathbf{y}_{n+1})_1 + (\mathbf{A}_n)_{12}(\mathbf{y}_{n+1})_2 + (\mathbf{A}_n)_{13}(\mathbf{y}_{n+1})_3\\ &= (\mathbf{A}_n)_{11}\cos\Phi_{n+1} + [(\mathbf{A}_n)_{12}(\mathbf{A}_n^T)_{2*} + (\mathbf{A}_n)_{13}(\mathbf{A}_n^T)_{3*}]\mathbf{x}_n,\end{aligned}$$

as required. □

Problem 5.1.2. The **second Doppler shift equation** is given by

$$f_{\text{Doppler},2}(v_{\Phi,n}, v_{\Theta,n}) = \Delta f_{n+1} - g(v_{\Phi,n}, v_{\Theta,n}) = 0, \tag{10.41}$$

where, arguing as in the first Doppler shift equation (5.3),

$$\begin{aligned}g(v_{\Phi,n}, v_{\Theta,n}) =\\ &\frac{f}{cD_{\text{SA},n+1}}\left[-v_{\Phi,n+1}R_{S,n+1}\sin\Phi_{n+1} - (R_{S,n+1} - R_A\cos\Phi_{n+1})(\mathbf{v}_{S,n+1})_1\right.\\ &\left. + R_A\cos\Theta_{n+1}\sin\Phi_{n+1}(\mathbf{v}_{S,n+1})_2 + R_A\sin\Theta_{n+1}\sin\Phi_{n+1}(\mathbf{v}_{S,n+1})_3\right].\end{aligned} \tag{10.42}$$

However because we do not know $v_{\Phi,n+1}$ and Θ_{n+1}, we need to express them in terms of $(v_{\Phi,n}, v_{\Theta,n})$. First, by Equation (10.40), Θ_{n+1} is given in terms of $(v_{\Phi,n}, v_{\Theta,n})$ by

$$\begin{bmatrix}\cos\Theta_{n+1} & \sin\Theta_{n+1}\end{bmatrix} = \begin{bmatrix}(\mathbf{A}_n^T)_{2*}\mathbf{x}_n & (\mathbf{A}_n^T)_{3*}\mathbf{x}_n\end{bmatrix}, \tag{10.43}$$

where $\mathbf{x}_n(v_{\Phi,n}, v_{\Theta,n})$ is given by Equation (10.37). Finally, using Equations (2.3) and (5.4), the definition of $\mathbf{A}$ given in Equation (5.7), and Lemma 4.1 it follows that $v_{\Phi,n+1}$ is given in terms of $(v_{\Phi,n}, v_{\Theta,n})$ by

$$v_{\Phi,n+1} = v_n(\mathbf{Y}_{n+1}^T\mathbf{A}_n^T)_{2*}\mathbf{u}_n, \tag{10.44}$$

where $\mathbf{Y}_{n+1} = \mathbf{Y}_{n+1}(\Phi_{n+1}, \Theta_{n+1})$ is given as in Equation (5.2) and

$$\mathbf{u}_n = \frac{1}{v_n}\begin{bmatrix}-v_n\sin(v_n\Delta t_n/R_A) & v_{\Phi,n}\cos(v_n\Delta t_n/R_A) & v_{\Theta,n}\cos(v_n\Delta t_n/R_A)\end{bmatrix}^T. \tag{10.45}$$

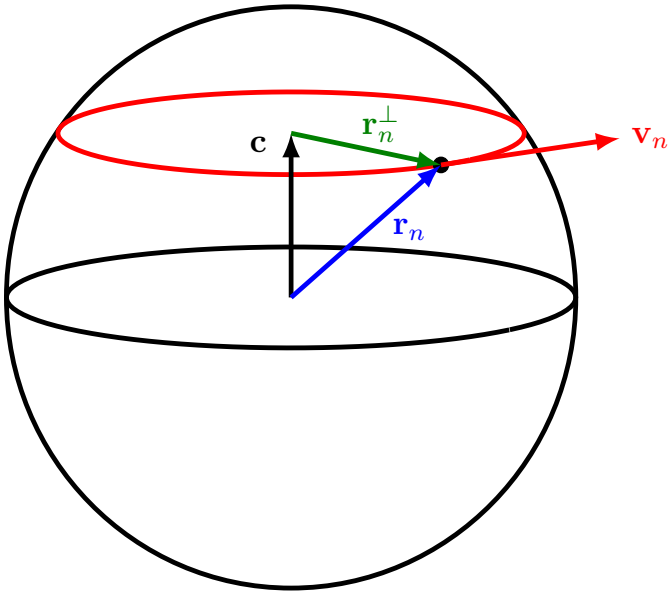

FIG. 10.1 *Sketch showing the vectors in the small circle parametrization* (10.46).

Problem 6.1.1. We show that the parametrization of the small circle of geodesic curvature, κ_g, that lies on the sphere of radius, R_A, and which at time, t_n, has position, $\mathbf{r}_n$, and velocity, $\mathbf{v}_n$, is given by

$$\mathbf{r}(t) \;=\; \mathbf{c} \;+\; \cos\left[\frac{v(t-t_n)}{R_C}\right]\mathbf{r}_n^\perp \;+\; \frac{R_C}{v}\sin\left[\frac{v(t-t_n)}{R_C}\right]\mathbf{v}_n, \tag{10.46}$$

where $\mathbf{c}$ is the center and R_C is the radius of the small circle, $\mathbf{r}_n^\perp = \mathbf{r}_n - \mathbf{c}$ and $v = |\mathbf{v}_n|$. Furthermore, if we let $\mathbf{w}_n = \frac{\mathbf{r}_n}{R_A} \times \frac{\mathbf{v}_n}{v}$, then $\mathcal{C} = \{\frac{\mathbf{r}_n}{R_A}, \frac{\mathbf{v}_n}{v}, \mathbf{w}_n\}$ is a frame at $\mathbf{r}_n$ adapted to the small circle, and

$$\frac{\mathbf{r}(t)}{R_A} \;=\; \left[1 + \frac{\cos\alpha_n(t) - 1}{1+K^2}\right]\frac{\mathbf{r}_n}{R_A} \;+\; \frac{K(\cos\alpha_n(t)-1)}{1+K^2}\,\mathbf{w}_n \;+\; \frac{\sin\alpha_n(t)}{\sqrt{1+K^2}}\,\frac{\mathbf{v}_n}{v}, \tag{10.47}$$

where $K = R_A\kappa_g/v$ and $\alpha_n(t) = v(t-t_n)/R_C$.

Proof. By Figure 10.1, we see that $\mathbf{r}_n^\perp$ is a radial vector to the small circle, C, with $\|\mathbf{r}_n^\perp\| = R_C$, and that $\mathbf{v}_n$ is a tangent vector to C at $\mathbf{r}_n$. Furthermore, $\mathbf{r}_n^\perp \perp \mathbf{v}_n$ as $\mathbf{v}_n \cdot \mathbf{r}_n^\perp = \mathbf{v}_n \cdot \mathbf{r}_n - \mathbf{v}_n \cdot \mathbf{c} = 0$, since on the one hand $\mathbf{r}_n$ is normal and $\mathbf{v}_n$ is tangent to the sphere, and on the other hand $\mathbf{c}$ is normal and $\mathbf{v}_n$ is tangent to the plane in which C lies. Equation (10.46) now follows by arguing as we did in the proof of Equation 10.1 above.

To prove Equation (10.47), we first express $\mathbf{r}_n^\perp$ in the frame $\mathcal{C}$ as

$$\mathbf{r}_n^\perp \;=\; R_C\left[\cos\gamma\,\frac{\mathbf{r}_n}{R_A} \;+\; \sin\gamma\,\mathbf{w}_n\right], \tag{10.48}$$

for some angle, γ. Here we have used the facts that $\mathbf{r}_n^\perp \perp \mathbf{v}_n$ and $\|\mathbf{r}_n^\perp\| = R_C$. To determine the angle γ, we observe that the vector $\mathbf{r}_n - 2\mathbf{r}_n^\perp$ lies on the sphere (see Figure 10.1), so that

$$R_A^2 \;=\; \|\mathbf{r}_n - 2\mathbf{r}_n^\perp\|^2 \;=\; R_A^2\left(1 - \frac{2R_C}{R_A}\cos\gamma\right)^2 + (2R_C\sin\gamma)^2. \tag{10.49}$$

Consequently

$$\cos\gamma \;=\; \frac{R_C}{R_A} \;=\; \frac{1}{\sqrt{1+K^2}} \qquad \text{and} \qquad \sin\gamma \;=\; \frac{K}{\sqrt{1+K^2}}, \tag{10.50}$$

by Equation (6.1). An algebraic calculation then yields Equation (10.47). □

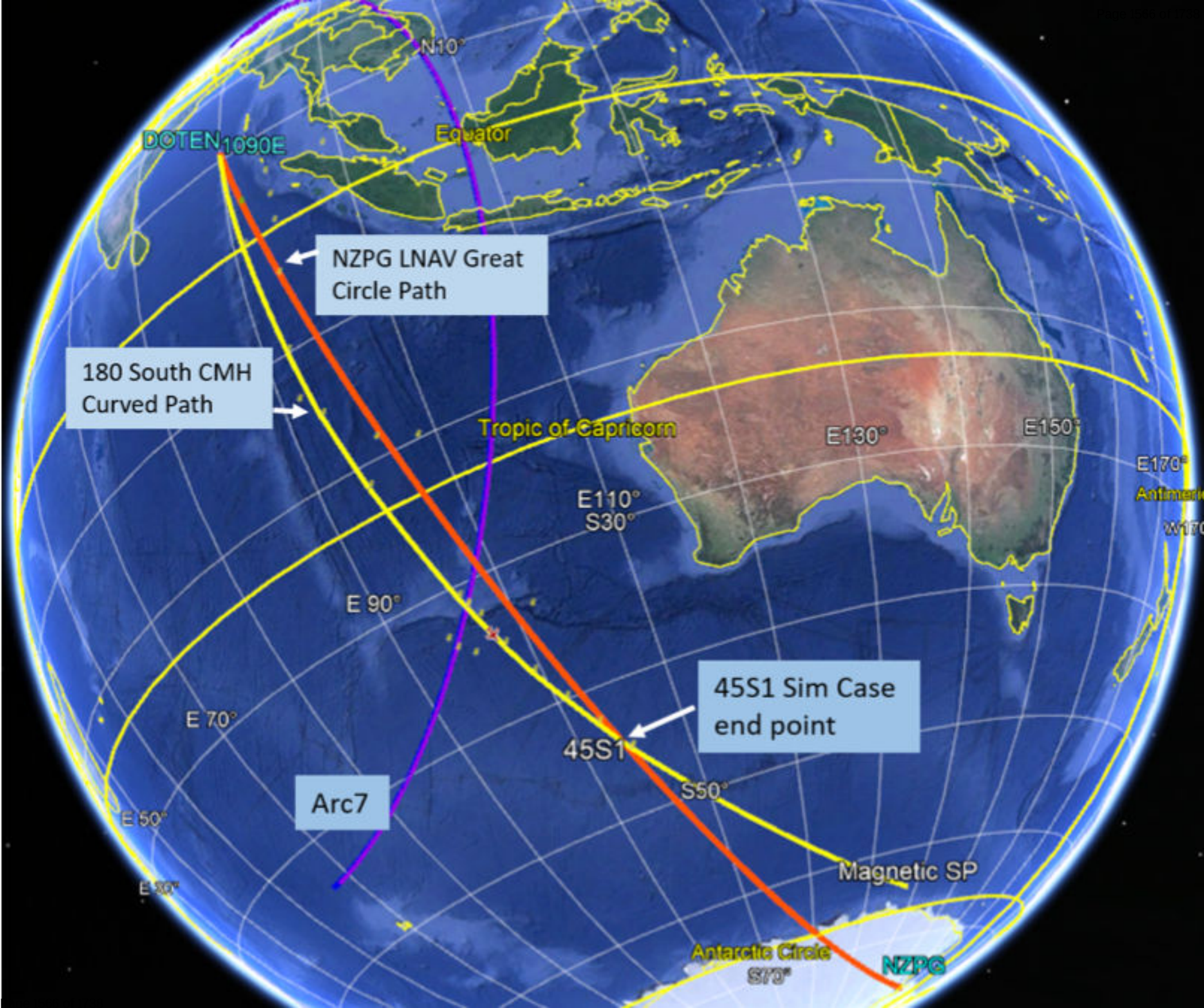
N10°
Equator
DOTEN
090E
NZPG LNAV Great Circle Path
180 South CMH Curved Path
Tropic of Capricorn
E130°
E150°
E170°
E110°
S30°
E 90°
E 70°
45S1
45S1 Sim Case end point
Arc7
S50°
E 50°
Magnetic SP
Antarctic Circle
S70°
NZPG

A Case Study In Public Data Release: Flight Path of Malaysia Airlines MH370

On Public Data Release

May 27, 2014, Malaysia DCA and Inmarsat released satellite communication logs for flight MH370.

"The goal of publication is transparency, not verification"

Mark Dickinson, Inmarsat

"The data itself is barely understandable, very opaque and you cannot draw too much from it."

"It is definitely not something someone can pick up and run with it and generate the same numbers."

The purpose of this talk is to demonstrate otherwise.

I. Timeline

II. Satellite Communication System

III. Public data products and analysis

IV. Breaking News

V. Lessons learned

A seemingly ordinary air disaster –

March 8, 2014 (MT) Malaysia Airlines Flight MH370, a Boeing 777 jet on a flight from Kuala Lumpur to Beijing, has lost contact. All indications are that it has crashed in the South China Sea between Malaysia and Vietnam.

[BOAC 781 (1954); Flying Tiger 739 (1961); Varig PP-VLU (1979); Air France 447 (2009)]

07:24 (MT) – MAS issues media statement

MEDIA STATEMENT released at 7.24am/8 Mar 2014 MH370 Incident

Sepang, 8 March 2014: Malaysia Airlines **confirms that flight MH370 has lost contact with Subang Air Traffic Control at 2.40am, today (8 March 2014).**

Flight MH370, operated on the B777-200 aircraft, departed Kuala Lumpur at 12.41am on 8 March 2014. MH370 ***was*** expected to land in Beijing at 6.30am the same day. The flight ***was*** carrying a total number of 227 passengers (including 2 infants), 12 crew members.

Malaysia Airlines is currently working with the authorities who have **activated their Search and Rescue team to locate the aircraft.**

However, there is one small detail ...

Unbeknownst to anyone, the plane is

STILL IN THE AIR!

I. Timeline of MH370

Planned Flight

- 16:00 to 24:19 UT, March 7, 2014
- Note: Malaysia and China timezone are 8 hours ahead of UT – hence March 8 MST.

16:00 UT – Passengers boarding MH370 at Kuala Lumpur airport satellite terminal, gate C1. SATCOM activated. ACARS message.

What are ACARS messages?

29 minutes later

16:29 UT - Plane pushes back from gate. ACARS message.

13 minutes later

16:42 UT - Takeoff for Beijing, runway 32R
6 hour flight. ACARS messages.

25 minutes later

17:07 UT - MH370 cruising at 35,000 feet 469 knots GS, heading for waypoint IGARI. Last ACARS message.

12 minutes later

17:19:29 UT – KL Radar signs off; transfer to HCM FIR. Last voice communication.

17:19:24 (ATC) “Malaysian three seven zero contact Ho Chi Minh 120 decimal nine. Good night.”

17:19:29 (MAS 370) “Good night, Malaysian three seven zero.”

62 seconds later

17:20:31 UT – Arrival at waypoint IGARI ("Transfer of Control Point" - TCP)

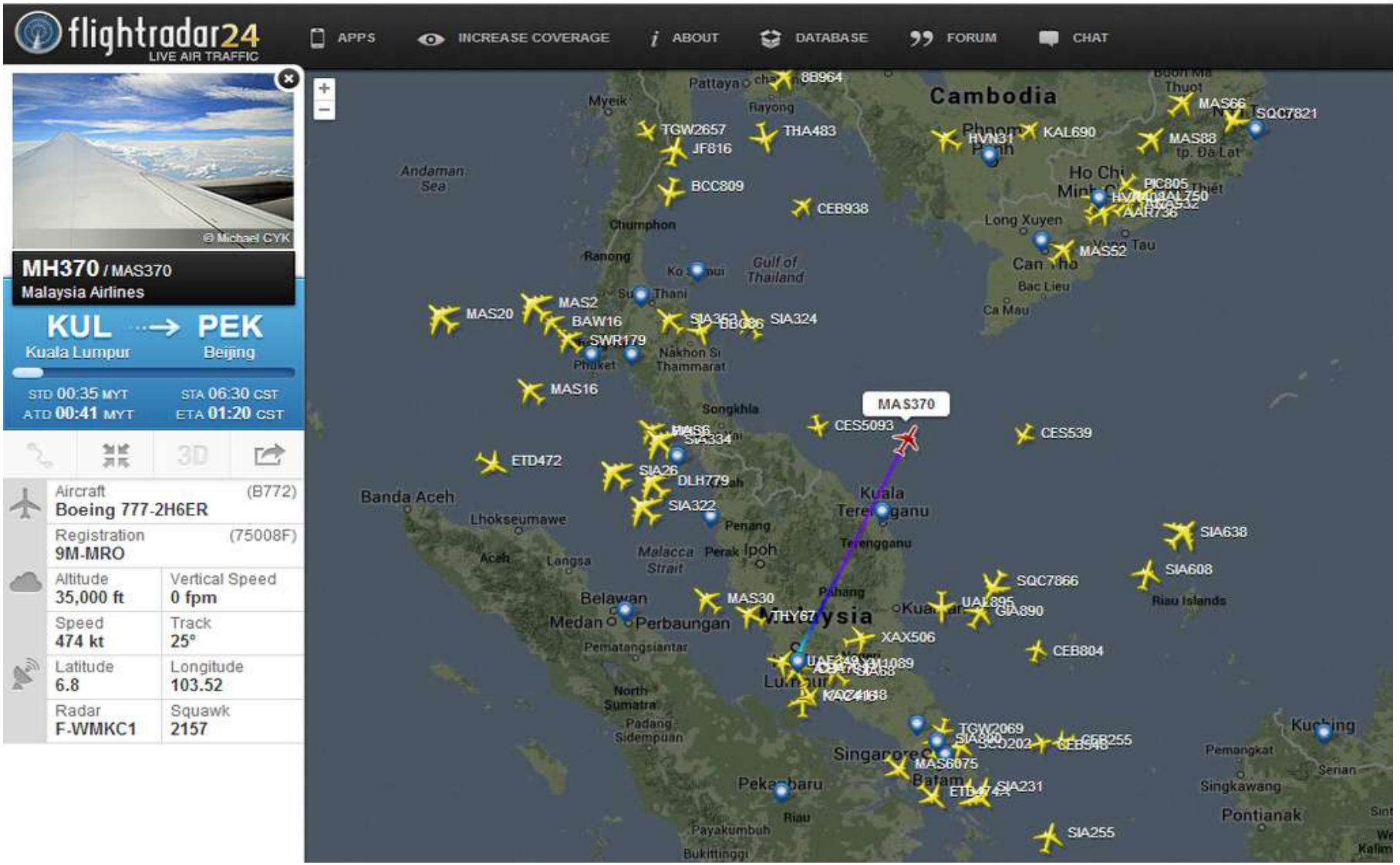

2-42 seconds later

17:20:33 UT – Aircraft symbols start dropping off Secondary Radar at HCM, KL, and Bangkok ATCC. Plane becomes invisible to ATC.

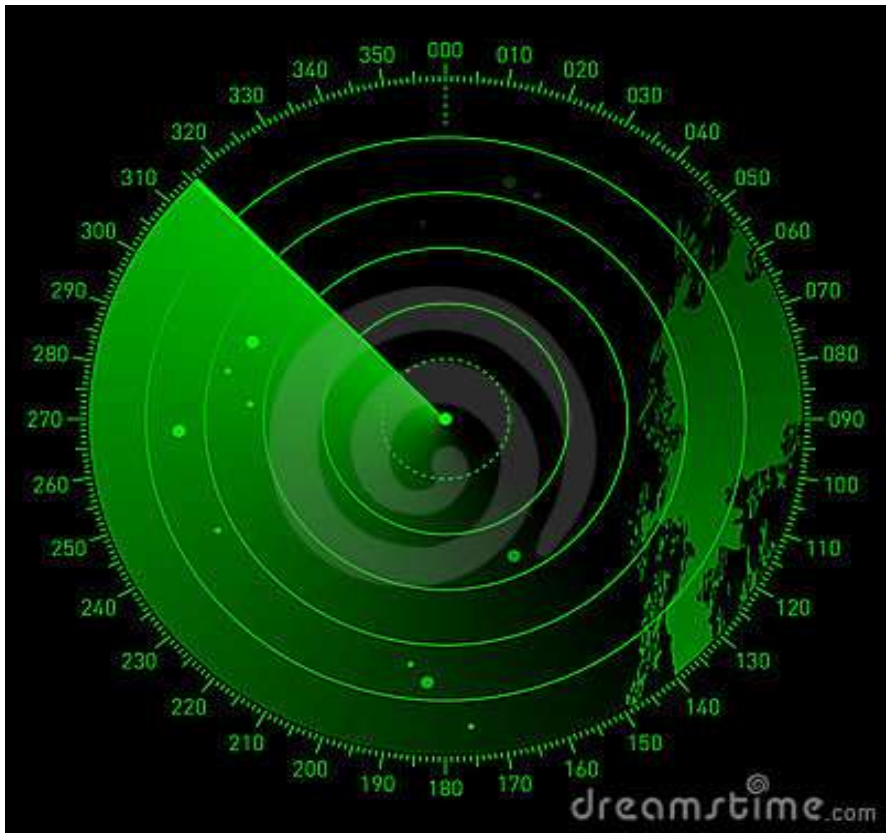

Primary Radar

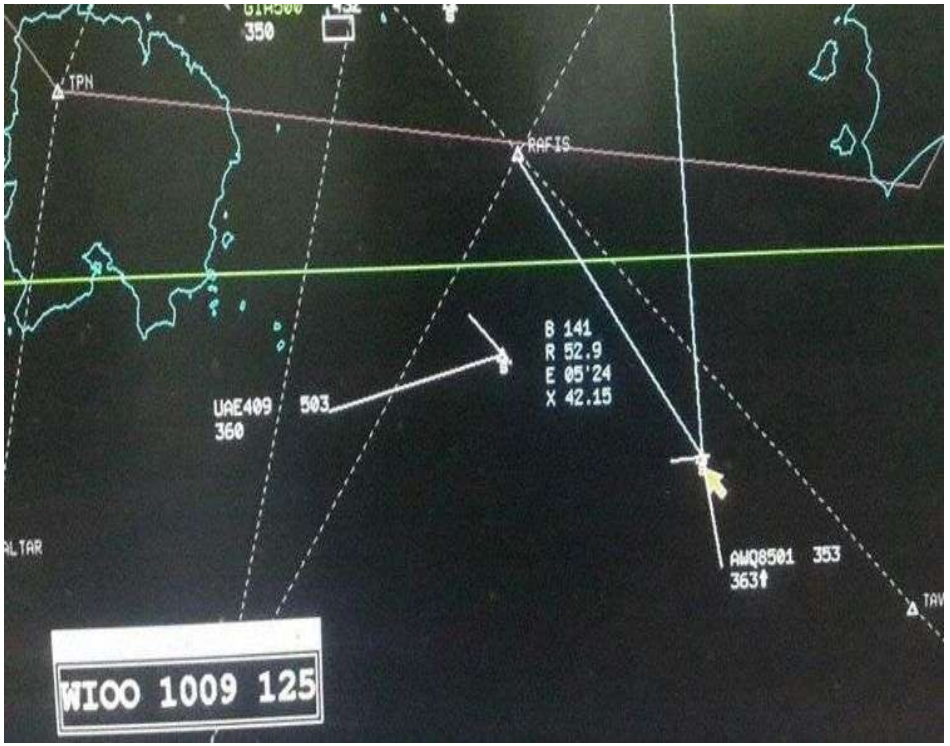

Secondary Radar

2 minutes later

17:23 UT – Plane is still tracked by military primary radar. Plane banks left; heads along Malaysia-Thailand border.

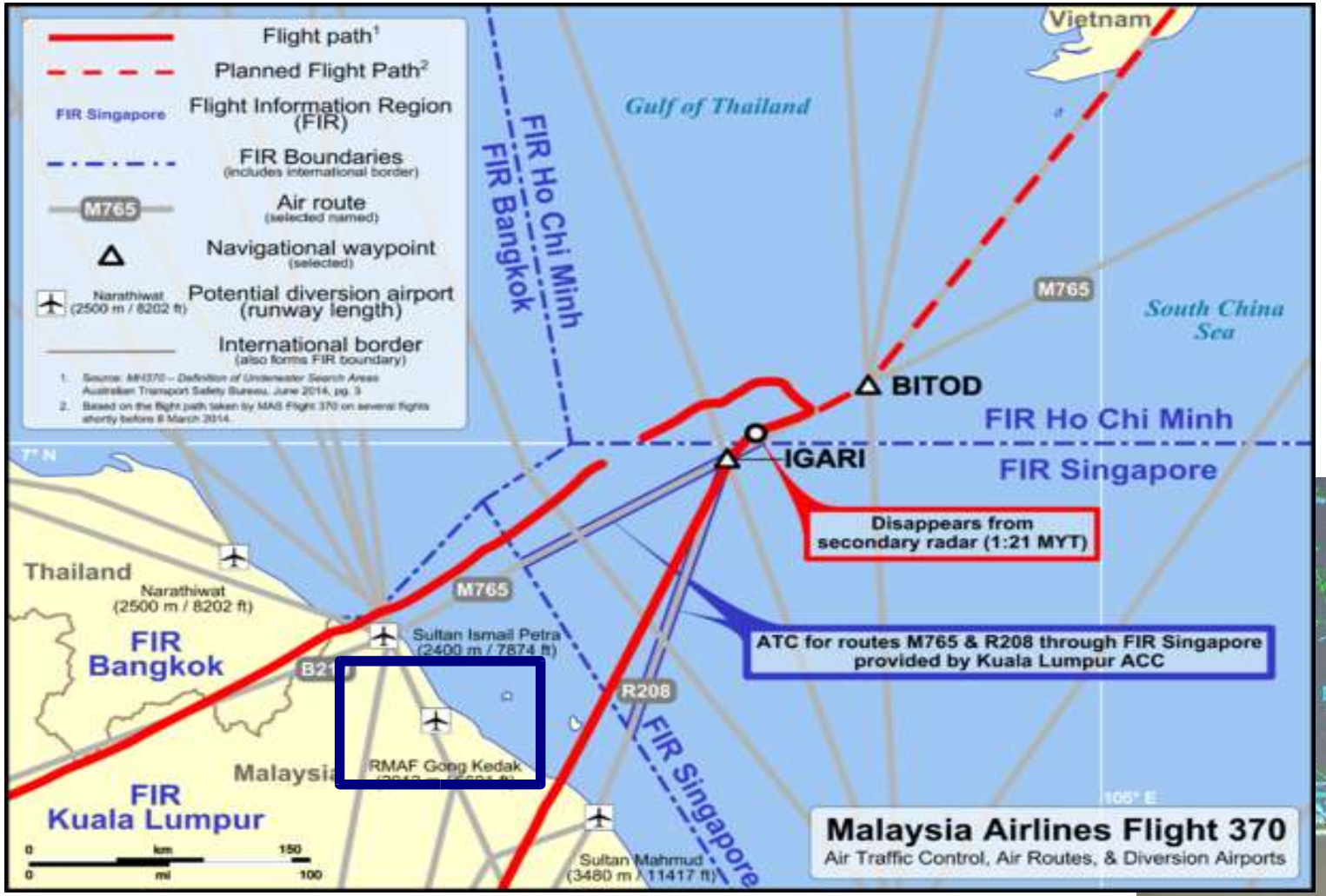

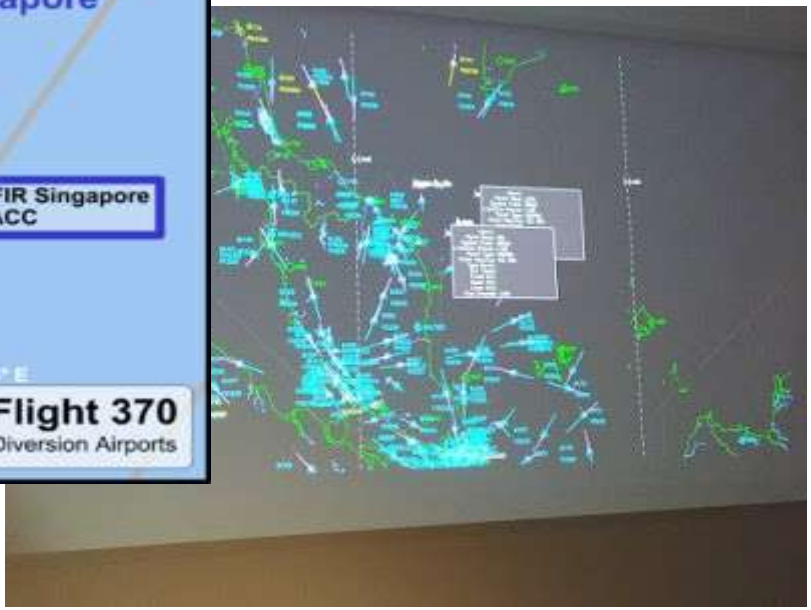

14 minutes later

17:37 UT – Next ACARS message due from aircraft - never sent

1 minute later

17:38 UT – HCM and KL ATC begin communicating r.e. location of MH370. Four hours pass before it is fully established that the plane is missing.

Event

17:38:19 Ho Chi Minh first enquired about MH370, informed KL-ATCC that verbal contact was not established with MH370 and radar target was last seen at BITOD.

13 minutes later

17:51 UT – Plane passes S of Penang Island and turns WNW along Strait of Malacca. Now being tracked by military radar on Penang Island

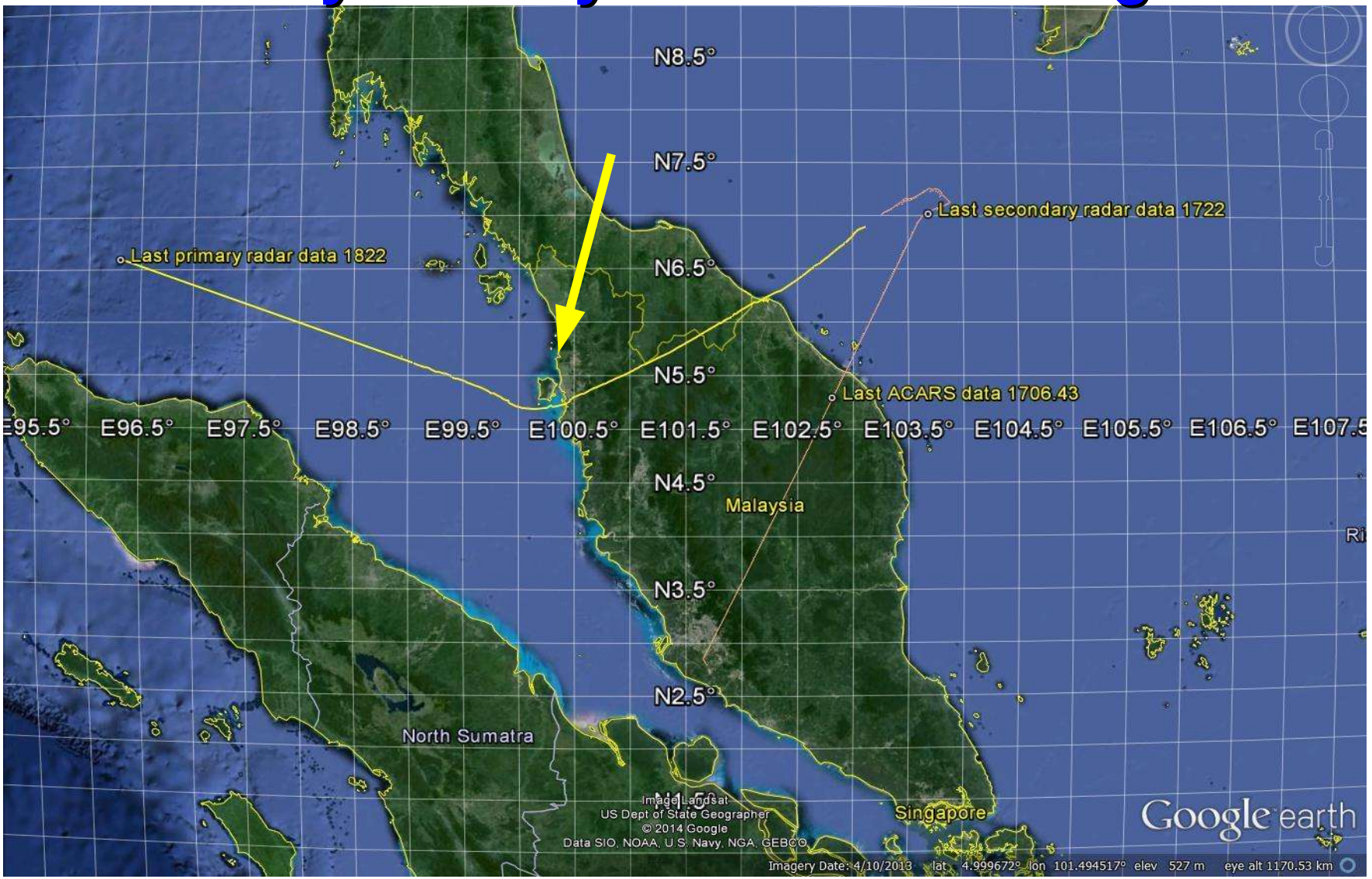

13 minutes later

18:04 UT – ACARS message sent from ground to aircraft via satellite; no response. SATCOM inoperative.

18:03 - No Response to Ground to Air DATA-2 ACARS Data. Link lost at sometime between 17:07:48 and here.

7/03/2014 18:03:41.405	IOR-P10500-0-3859	IOR	305	10	P-Channel TX	0x71 - User Data (ISU) - RLS
7/03/2014 18:03:41.405	IOR-P10500-0-3859	IOR	305	10	P-Channel TX	Subsequent Signalling Unit

"PLS CONTACT HO CHI MING ATC ASAP THEY COMPLAIN CANNOT TRACK YOU ON THEIR RADAR"

8 minutes later

18:12 UT – Plane reaches waypoint VAMPI; begins following airway N571

10 minutes later

18:22 UT – Plane passes out of range of military primary radar. Plane invisible to all.

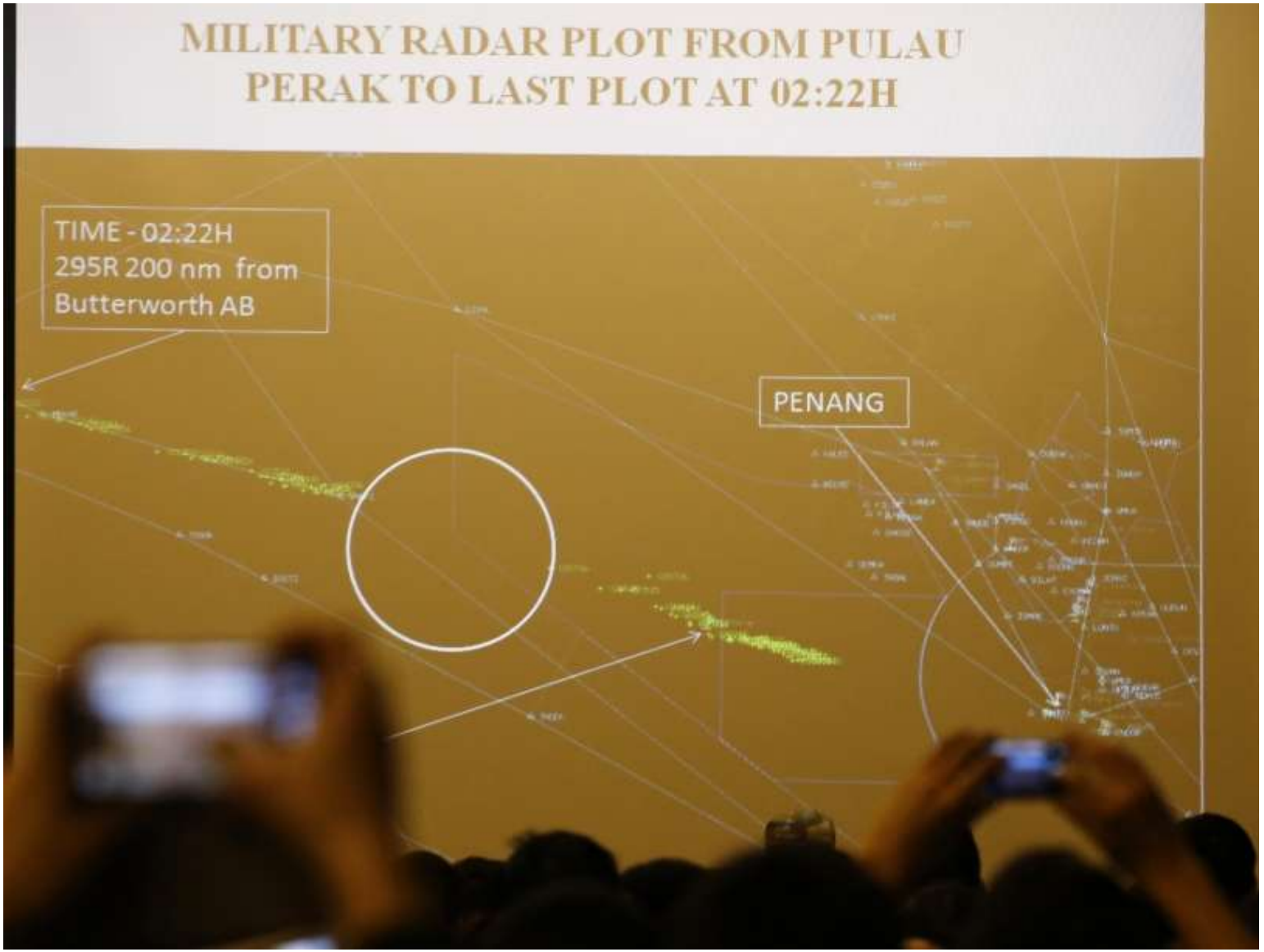

3 minutes later

18:25 UT – SATCOM reactivated; logs on to satellite network. Plane appears to be continuing WNW track

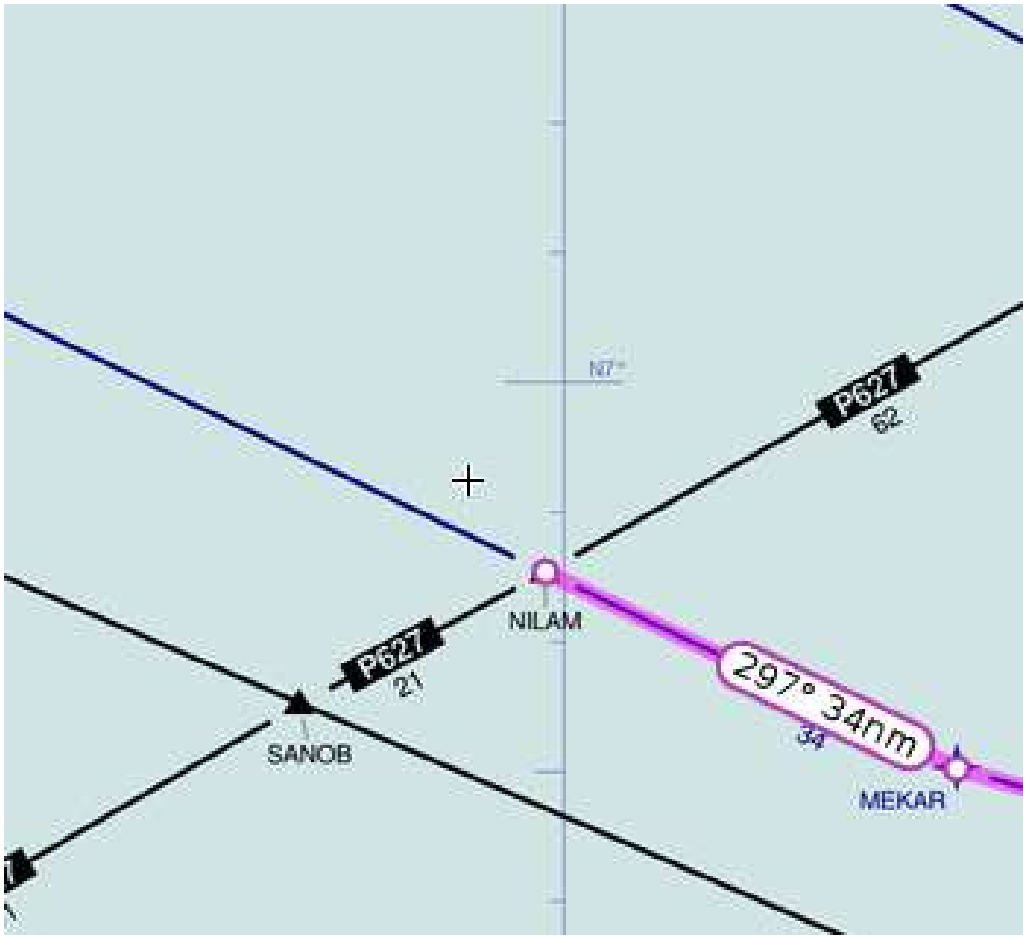

3-14 minutes later

18:28 – 18:39 UT – Sometime in here plane makes sharp turn South

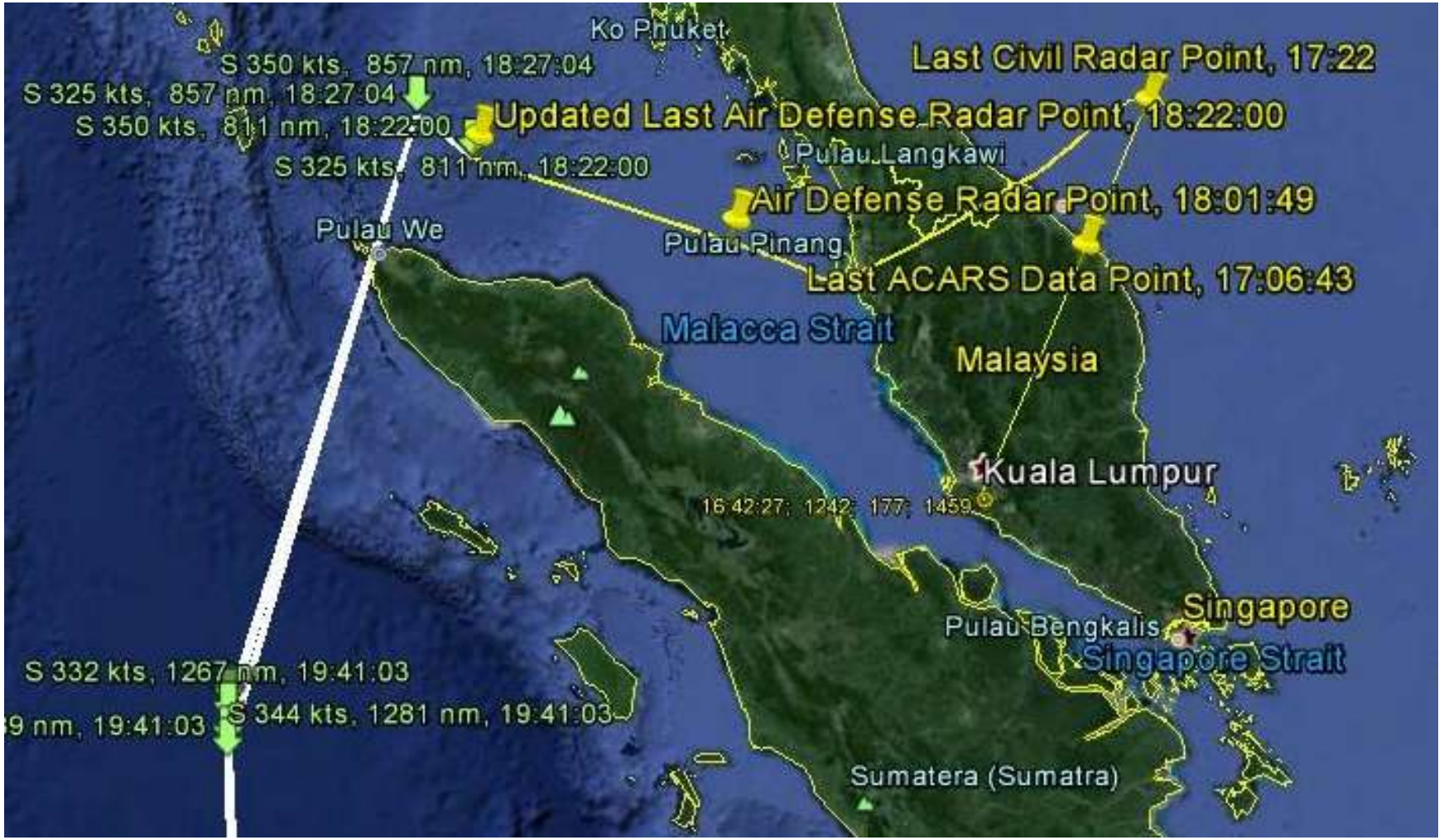

1 minute later

18:40 UT – Satellite call from Malaysian Airlines to MH370 attempted. SATCOM acknowledges, but call not answered.

61 minutes later

19:41 UT and hourly thereafter – ground station send “keep-alive pings” to aircraft SATCOM; acknowledgement returned.

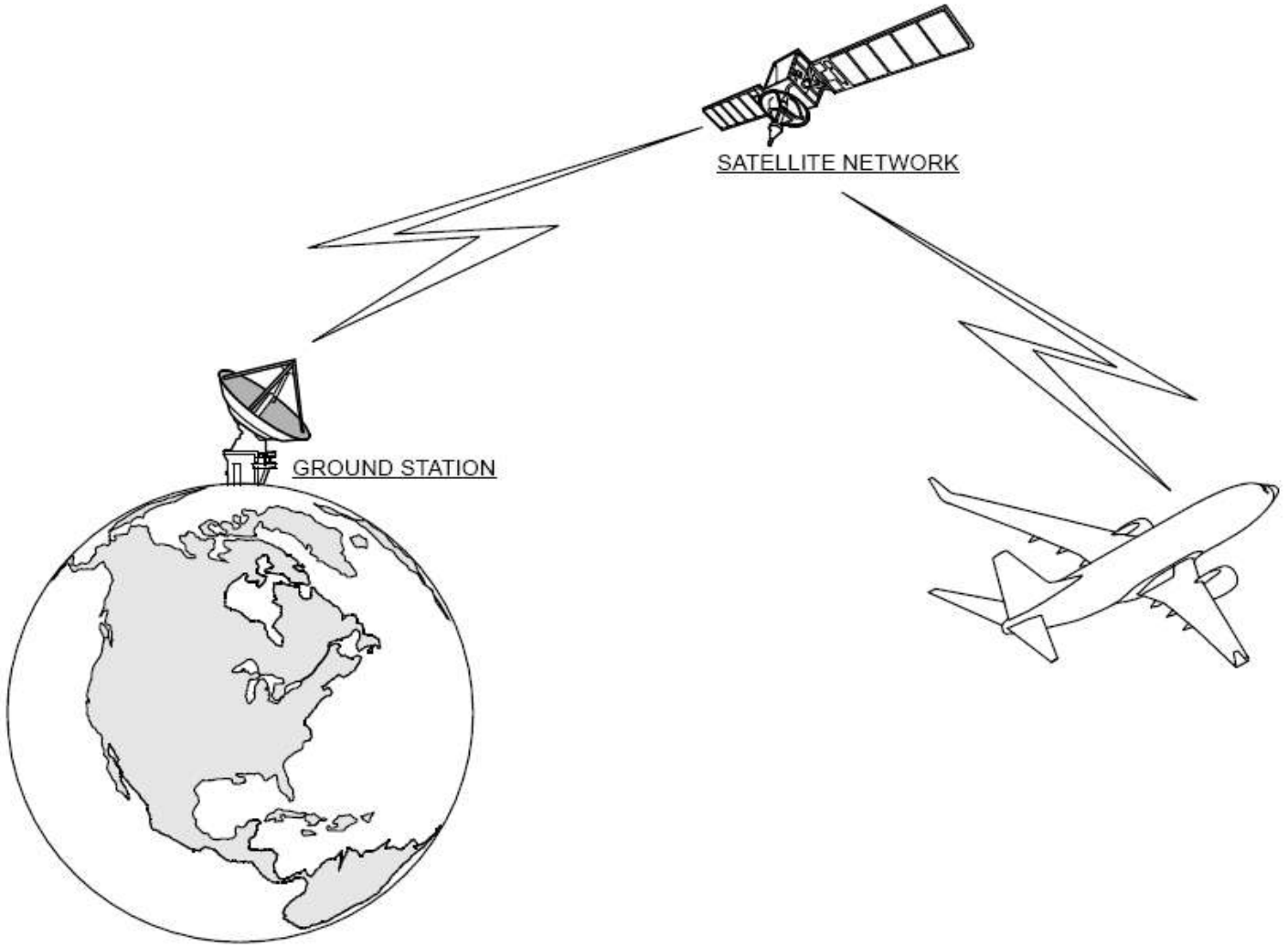

109 minutes later

21:30 UT – KL Rescue Coordination Center activated

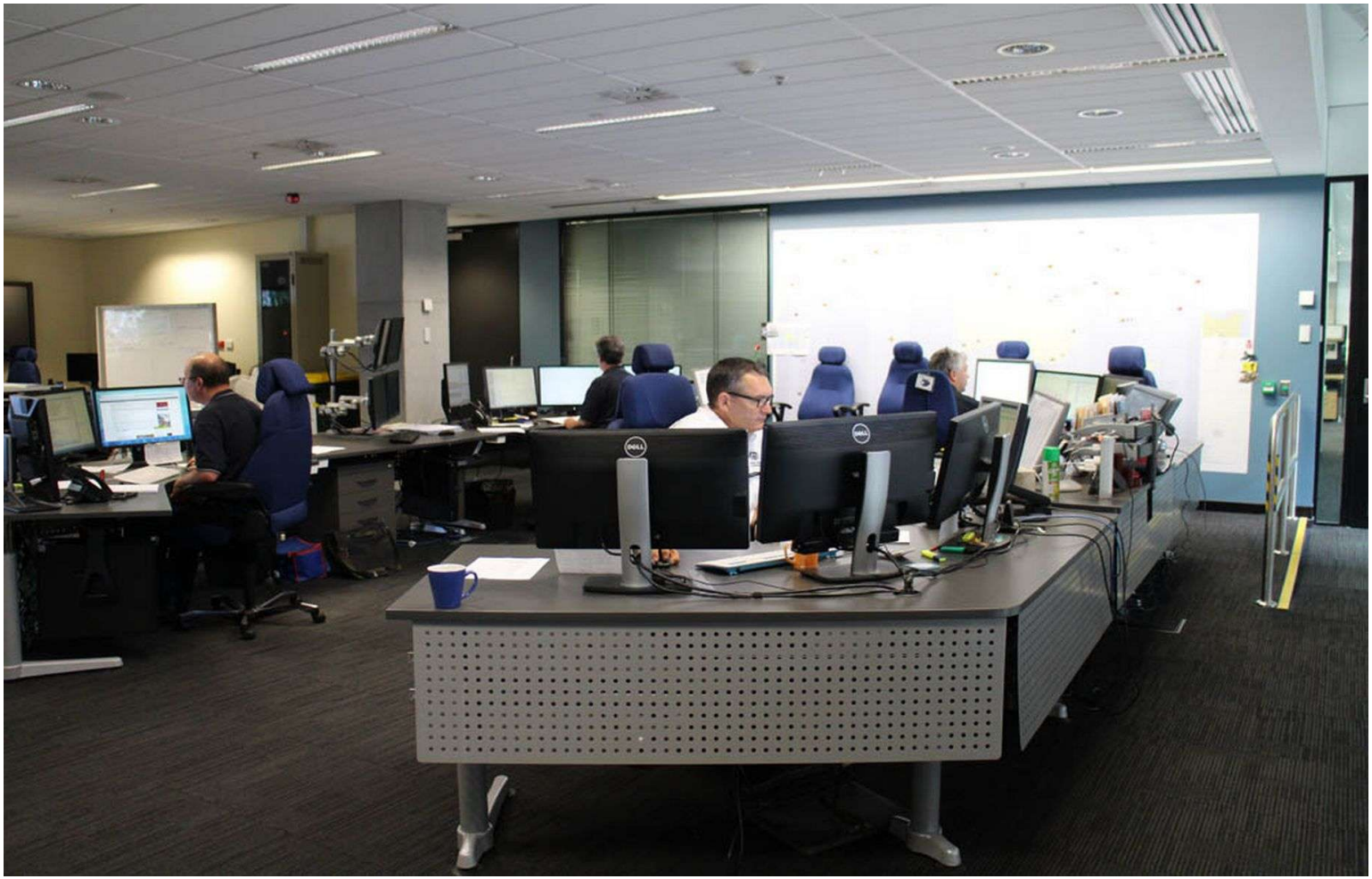

60 minutes later

22:30 UT – Plane is overdue in Beijing

40 minutes later

23:10 UT – Malaysia Airlines makes second attempted phone call; same result

14 minutes later

23:24 UT – MAS issues media statement

MEDIA STATEMENT released at 7.24am/8 Mar 2014 MH370 Incident

Sepang, 8 March 2014: Malaysia Airlines **confirms that flight MH370 has lost contact with Subang Air Traffic Control at 2.40am, today (8 March 2014).**

Flight MH370, operated on the B777-200 aircraft, departed Kuala Lumpur at 12.41am on 8 March 2014. MH370 ***was*** expected to land in Beijing at 6.30am the same day. The flight ***was*** carrying a total number of 227 passengers (including 2 infants), 12 crew members.

Malaysia Airlines is currently working with the authorities who have **activated their Search and Rescue team to locate the aircraft.**

47 minutes later

24:11 UT – Last ground-initiated "ping" exchange with aircraft (6th handshake)

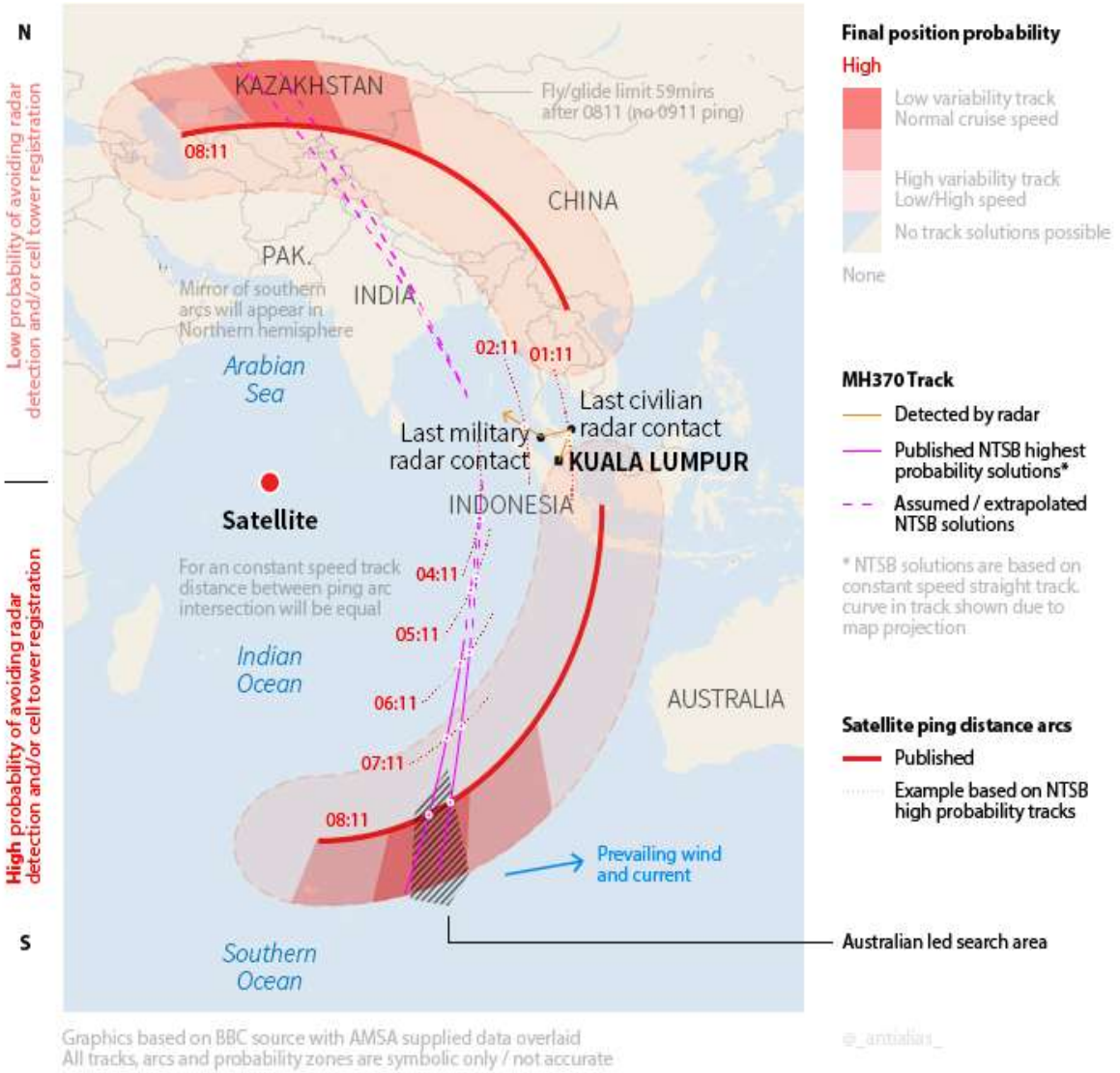

8 minutes later

24:19 UT – SATCOM sends another "Logon Request" message, but fails to complete the sequence. Possible engine flameout from fuel exhaustion; power loss; APU powerup.

00:19:29 - Log-On Request (reported as a Partial Handshake), initiated from the aircraft terminal

8/03/2014 00:19:29.416	IOR-R600-0-36F8	IOR	305	10	R-Channel RX	0x10 - Log-on Request (ISU)/Log-on Flight Information (SSU)	182
8/03/2014 00:19:31.572	IOR-P600-0-36FC	IOR	305	10	P-Channel TX	0x11 - Log-on Confirm	
8/03/2014 00:19:32.212	IOR-P600-0-36FC	IOR	305	10	P-Channel TX	0x40 - P-/R-Channel Control (ISU)	
8/03/2014 00:19:32.212	IOR-P600-0-36FC	IOR	305	10	P-Channel TX	Subsequent Signalling Unit	
8/03/2014 00:19:32.852	IOR-P600-0-36FC	IOR	305	10	P-Channel TX	0x41 - T-Channel Control (ISU)	
8/03/2014 00:19:32.852	IOR-P600-0-36FC	IOR	305	10	P-Channel TX	Subsequent Signalling Unit	

00:19:37 - Note that the following R-Channel burst at 00:19:37.443 is the last transmission received from the aircraft terminal

8/03/2014 00:19:37.443	IOR-R1200-0-36F6	IOR	305	10	R-Channel RX	0x15 - Log-on/Log-off Acknowledge	-2

Signal suggests plane is in a steep descent. Aircraft is presumed to have crashed near the location of the final transmission.

CNN Developing Story ...

II. Aircraft Communications Systems

- Primary systems:
  - HF Radio
  - VHF radio
  - Mode S / ADS-B (“extended squitter”) transponder
  - **Satellite Communications System (SATCOM)**
    - **Inmarsat**
    - Iridium

Inmarsat

- "International Marine Satellite" company
- Started 1979 to provide communications to ships out of reach of land stations

- Extended to cover land and air operations
- Operates fleet of geostationary satellites. Covers world up to 81 degrees latitude.
  - 3 generations (I3 to I5) in operation

Inmarsat Services

- Low bandwidth data
  - acars
  - SMS
- Voice (phone) / Fax
- ISDN
- Swift Broadband (internet; mobile circuit switched)
- **Service Providers**
  - **SITA** (no VHF in China)
  - ARINC

Classic Aero-H
(Used by MH370)

Service Allocation

1525 - 1660.5 MHz **L-Band**

MARITIME | ***AERONAUTICAL*** | LAND-MOBILE

Aero-H/H+ | Aero-I | Swift 64 | Aero-M | SBB

Bandwidth about the same as a dual frequency home wireless router

System is constrained

- Bandwidth is limited
  - Channel width 2.5 khz
  - Requires tight frequency control. For aircraft, Doppler effect is important. AES are required to adjust transmit frequency to compensate.
- Timing is important
  - AES to GES R-channels are shared
  - “Slotted Aloha” - requires synchronization with GES to AES signal
- Pilot signals used extensively to monitor system

System Monitoring

- “Burst Frequency Offset” (BFO) – measures error in frequency from AES to GES
  - 1 hz resolution

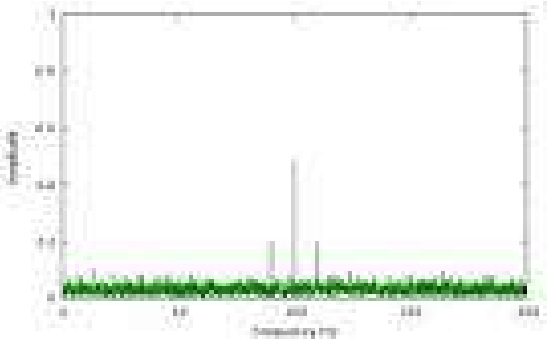

- “Burst Timing Offset” (BTO) – measures error in signal timing from AES to GES.
  - 20 microsecond resolution

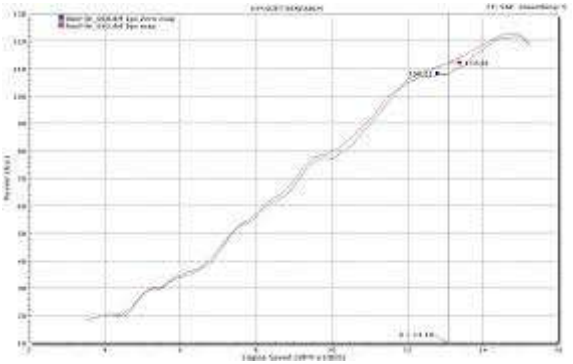

- Both recorded along with data packets at ground station in Perth, Australia

Inmarsat 3-F1

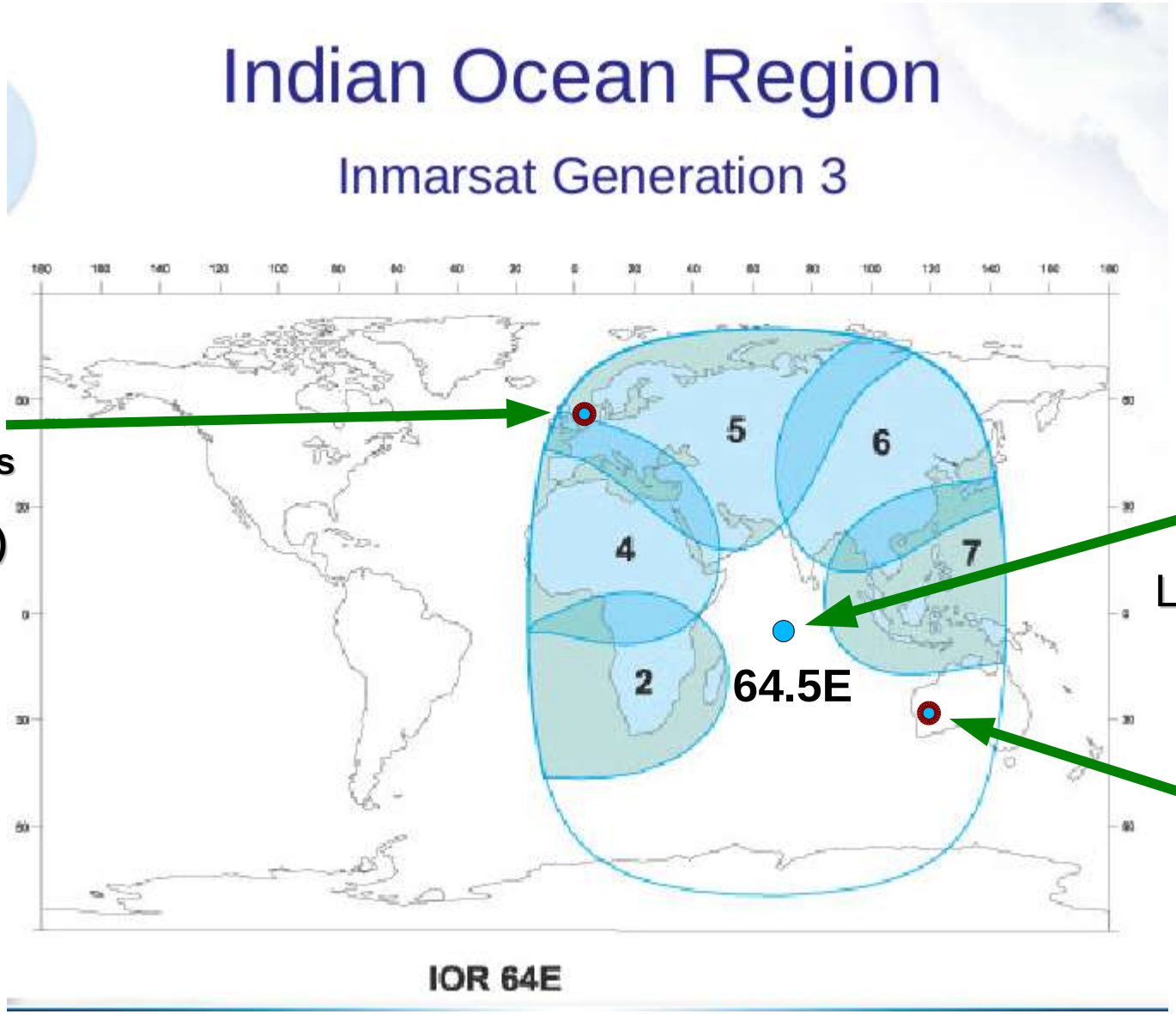

Burum, Netherlands (pilot transmitter)

Inmarsat-3

Launched 1996

Perth (ground station)

What we learn from BTOs

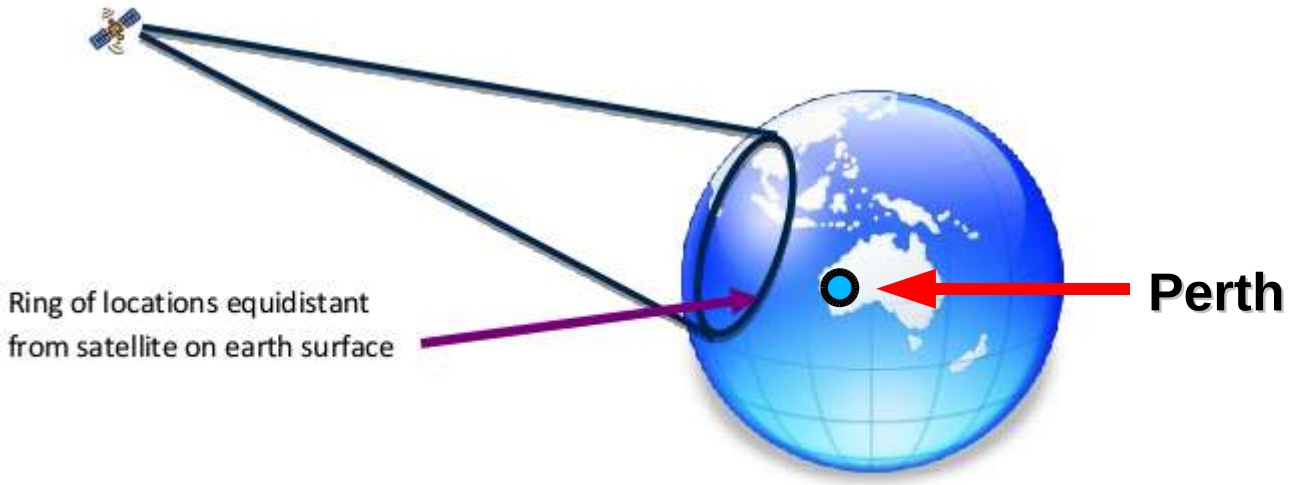

Light travel time (round trip) is ~ 0.5 seconds.
BTO depends on aircraft location on Earth.
Even sensitive to altitude.

Initial Analysis

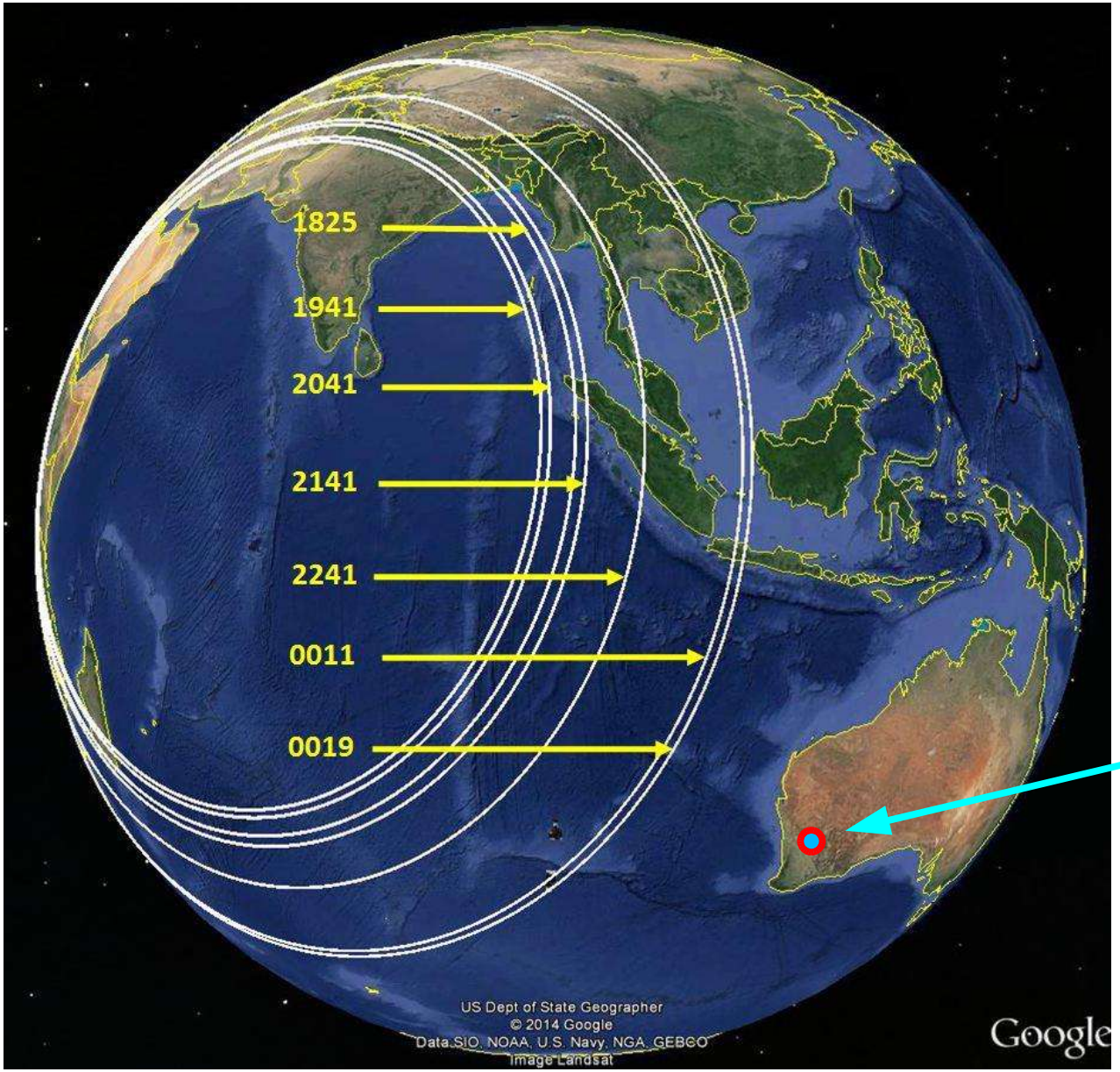

Seven sets of BTOs define 7 “ping rings” from 18:25 to 00:19 (24:19)

Perth

However, both North and South Corridors are possible

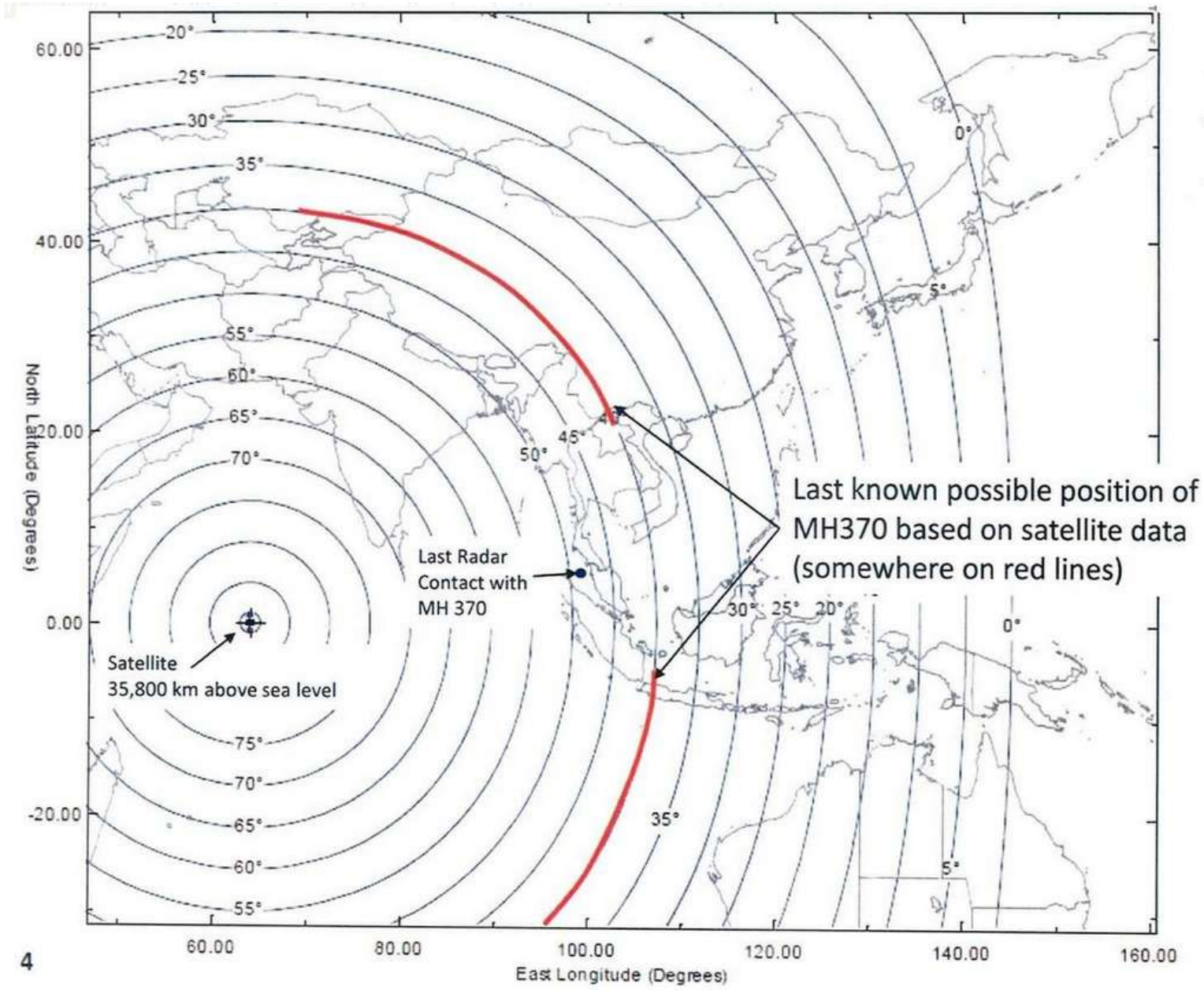

Inmarsat-3

A Note on Geostationary Satellites

- Main perturbation on geostationary satellite orbit due to Moon - causes inclination to increase.

- Satellites carry hydrazine for station-keeping; ~equal in mass to satellite at launch to control orbit.

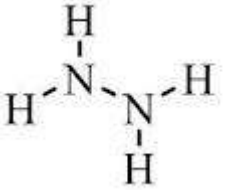

- 3-F1 is an old satellite – inclination no longer controlled.
  - **Inclination of 1.6 degrees on Mar 7, 2014 => Satellite oscillates above, below equator**

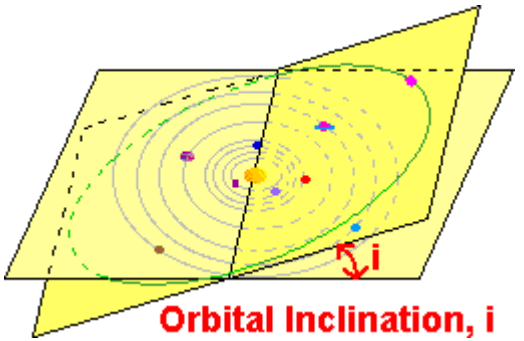

AES Doppler compensation mechanisms for aircraft

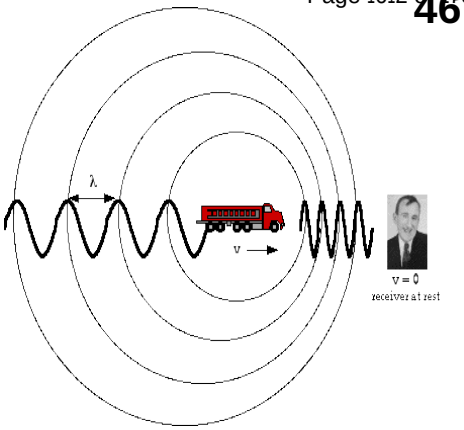

Inmarsat-3

- Doppler can be greater than 1 khz – exceeds tolerance of system.
- Compensation mechanism in MH370 SATCOM [Honeywell MCS-6000]
  - Use knowledge of plane's position, heading, and speed *along with knowledge of satellite position;* compute Doppler correction: $\vec{V} \cdot \vec{R}$
  - **Assumes satellite is exactly over equator**

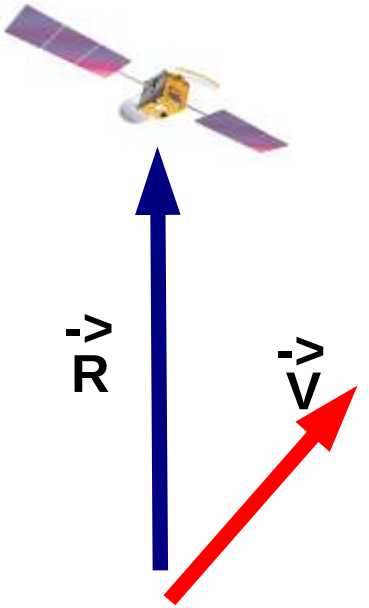

A fortuitous combination of circumstances

- **Because satellite orbit is inclined and AES assumes it is on the equator, the Doppler compensation is not perfect.** ***Error includes contributions from satellite motion and from aircraft motion – sensitive to location and to speed & direction of travel of aircraft!***
- Full BFO analysis is complex (contributions from GES AFC; satellite oscillator drift; satellite-GES Doppler)

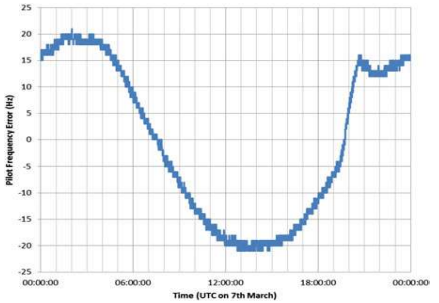

Original BFO Analysis (cleaned up a bit)

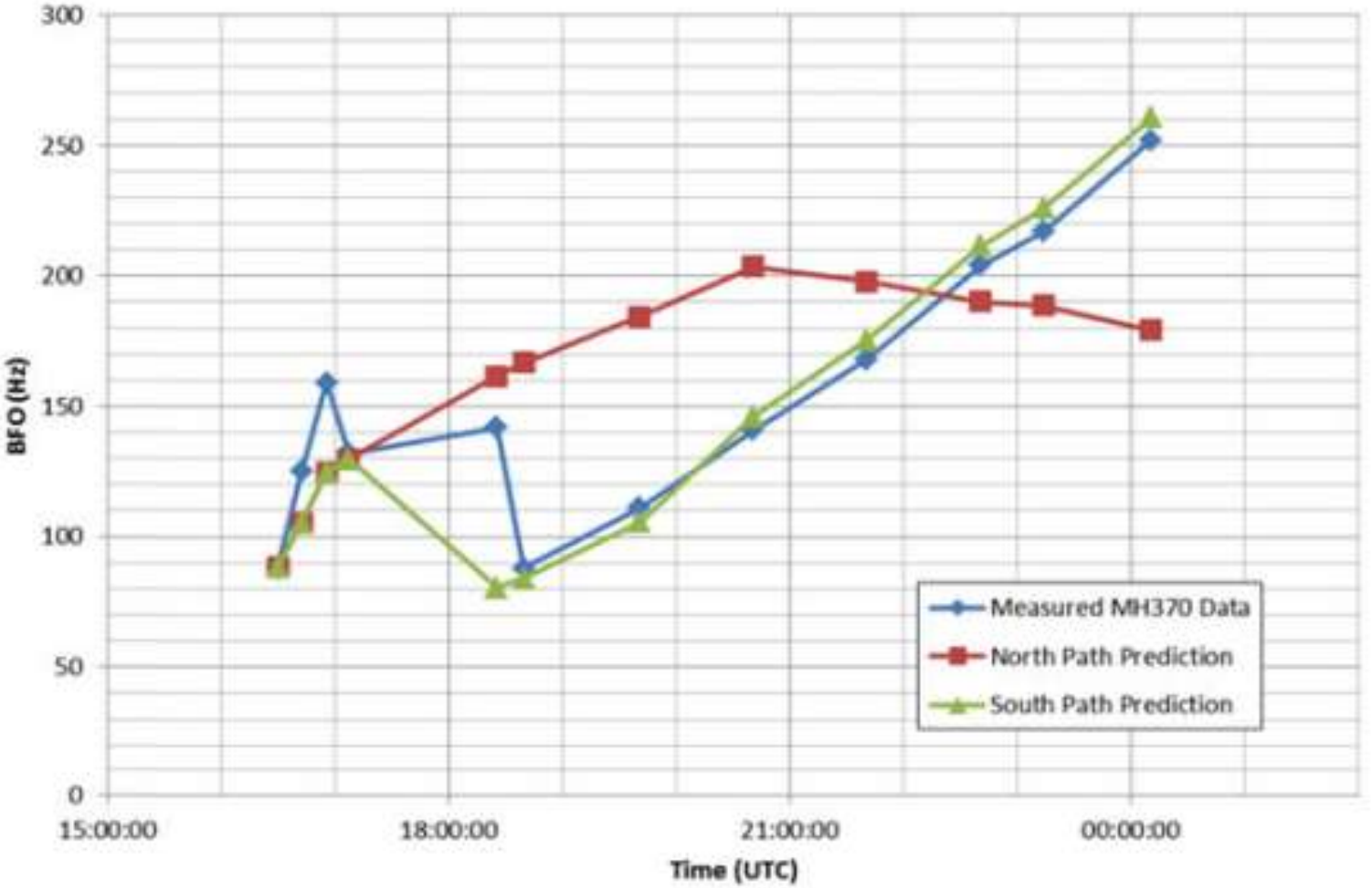

III. Investigation By the Public

Can We Reproduce Inmarsat's Result?

- Initially only figures available
- Many forums for discussion
  - tmfassociates.com
  - pprune.org
  - duncansteel.com
  - jeffwise.net
  - reddit.com
  - twitter.com
  - airliners.net

- Many people attempted to understand the ping ring; BFO plots poorly explained
  - Some features (e.g., AES Doppler) were decoded
  - Inaccuracies in published figures were detected

Public Data Release

- Authorities (Malaysian MOT and Australian ATSB) have been exceedingly reticent in sharing information. However, we now have
  - Inmarsat signal communication logs from 15:59 to end of flight
  - Documentation and calibration tables for BTO, BFO sufficient to understand and compute flight paths.
- Missing
  - Complete military radar data
  - Calibration data from similar and historical flights

Selex
ES RAT-31DL
3-D Phased array
Western Hill,
Penang Island

Example page - communications log

Time	Channel Name	Ocean Region	GES ID (octal)	Channel Unit ID	Channel Type	SU Type	Burst Frequency Offset (Hz) BFO	Burst Timing Offset (microseconds) BTO
7/03/2014 18:28:14.904	IOR-R1200-0-36ED	IOR	305	4	R-Channel RX	0x62 - Acknowledge User Data (R-channel)	143	12480
18:39 - Ground Initiated to Air Telephony Call - Zero Duration (Not Answered)								
7/03/2014 18:39:52.907	IOR-P10500-0-386B	IOR	301	10	P-Channel TX	0x20 - Access Request/Call Announcement Telephone/Circuit-Mode Data		
7/03/2014 18:39:52.907	IOR-P10500-0-386B	IOR	301	10	P-Channel TX	0x33 - C-Channel Assignment (Regularity)		
7/03/2014 18:39:52.907	IOR-P10500-0-386B	IOR	301	10	P-Channel TX	0x20 - Access Request/Call Announcement Telephone/Circuit-Mode Data		
7/03/2014 18:39:52.907	IOR-P10500-0-386B	IOR	301	10	P-Channel TX	0x33 - C-Channel Assignment (Regularity)		
7/03/2014 18:39:55.354	IOR-3730-21000	IOR	305	6	C-Channel RX	0x30 - Call Progress - Test	88	
.....								
84 C-Channel and 2 P-Channel messages moved into separate below table (see appendix 1) to ease the reading of key events. C-Channel messages have no BTO values								
.....								
7/03/2014 18:40:56.354	IOR-3730-21000	IOR	305	6	C-Channel RX	0x30 - Call Progress - Channel Release	90	
19:41 - Handshake Request, with response								
7/03/2014 19:41:00.910	IOR-P10500-0-386B	IOR	305	10	P-Channel TX	0x14 - Log Control - Log-on Interrogation		
7/03/2014 19:41:02.906	IOR-R1200-0-36ED	IOR	305	4	R-Channel RX	0x15 - Log-on/Log-off Acknowledge	111	11500
20:41 - Handshake Request, with response								
7/03/2014 20:41:02.907	IOR-P10500-0-386B	IOR	305	10	P-Channel TX	0x14 - Log Control - Log-on Interrogation		
7/03/2014 20:41:04.904	IOR-R1200-0-36ED	IOR	305	4	R-Channel RX	0x15 - Log-on/Log-off Acknowledge	141	11740
21.41 - Handshake Request, with response								
7/03/2014 21:41:24.907	IOR-P10500-0-386B	IOR	305	10	P-Channel TX	0x14 - Log Control - Log-on Interrogation		
7/03/2014 21:41:26.905	IOR-R1200-0-36ED	IOR	305	4	R-Channel RX	0x15 - Log-on/Log-off Acknowledge	168	12780
22:41 - Handshake Request, with response								
7/03/2014 22:41:19.907	IOR-P10500-0-386B	IOR	305	10	P-Channel TX	0x14 - Log Control - Log-on Interrogation		
7/03/2014 22:41:21.906	IOR-R1200-0-36ED	IOR	305	4	R-Channel RX	0x15 - Log-on/Log-off Acknowledge	204	14540
23:13 - Ground Initiated to Air Telephony Call - Zero Duration (Not Answered)								
7/03/2014 23:13:58.407	IOR-P10500-0-386B	IOR	305	10	P-Channel TX	0x20 - Access Request/Call Announcement Telephone/Circuit-Mode Data		
7/03/2014 23:13:58.407	IOR-P10500-0-386B	IOR	305	10	P-Channel TX	0x33 - C-Channel Assignment (Regularity)		
7/03/2014 23:14:00.904	IOR-3737-21000	IOR	305	6	C-Channel RX	0x30 - Call Progress - Test	216	

Publications

- www.malaysiaairlines.com/mh370 - Media releases
- Malaysia Ministry of Transport on Facebook
- Mar 22, 2014 - Cargo Manifest
  - https://s3.amazonaws.com/s3.documentcloud.org/documents/1151153/mh370-cargo-manifest-and-airway-bill.pdf
- Mar 25, 2014 - Original BFO figures and explanation
  - http://www.mot.gov.my/en/Newsroom/Press Release/Year 2014/Information Provided To MH370 Investigation by UK Air Accidents Investigation Branch (AAIB).pdf
  - http://www.inmarsat.com/wp-content/uploads/2014/03/Inmarsat-Differential-Doppler-Study.pdf

Publications (cont.)

- Apr 1, 2014 - Transcript of cockpit / ATC communications
  - http://www.bbc.co.uk/news/special/2014/newsspec_7440/transcript.pdf
- Apr 27, 2014 - MH 370 Preliminary Report to ICAO
  - http://www.dca.gov.my/MH370/Preliminary%20Report.pdf
- May 1. 2014 - HISHAMMUDDIN HUSSEIN - Actions taken on March 8.
  - http://www.abc.net.au/4corners/documents/2014/MH370/MH370Report_Actions_Taken.pdf
- Maps
  - https://www.facebook.com/HishammuddinH2O/

Publications (cont.)

Australian Government
Australian Transport Safety Bureau

- May 20, 2014 - Data Communication logs
  - http://www.dca.gov.my/mainpage/MH370%20Data%20Communication%20Logs.pdf
- ATSB (Australia)
  - http://www.atsb.gov.au/mh370.aspx
  - Includes links to June 26, 2014 report “MH370 Definition of Underwater Search Areas” (with updates Aug 18, 2014, Oct 8, 2014, and Dec 3, 2015)
- Oct 23, 2014 - "The Search for MH370" (Ashton et al.)
  - *Journal of Navigation* (2015), 68, 1

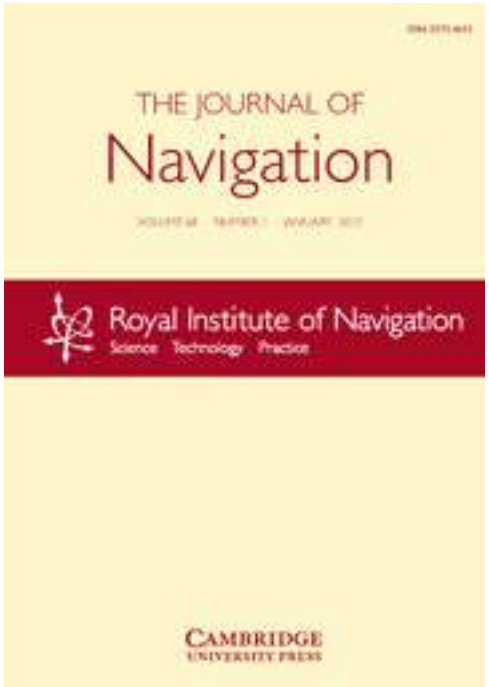

Publications (cont.)

INTERNATIONAL CIVIL AVIATION ORGANIZATION
A United Nations Specialized Agency

- Jan 29, 2015 - “SAR Response to MH370”
  - http://www.icao.int/APAC/Meetings/2015APSARTF3/WP05 ICAO Brief on the SAR Response to MH370.pdf
- Mar 8, 2015 - “Factual Information”
  - http://mh370.mot.gov.my/
- Nov 30, 2015 - “Bayesian Methods in the Search for MH370”
  - http://www.atsb.gov.au/media/5733804/Bayesian_Methods_MH370_Search_3Dec2015.pdf

MOT

The Malaysian ICAO Annex 13
Safety Investigation Team for MH370

FACTUAL INFORMATION

SAFETY INVESTIGATION FOR MH370

-

Malaysia Airlines MH370 Boeing B777-200ER (9M-MRO)
08 March 2014

By

The Malaysian ICAO Annex 13 Safety Investigation Team for MH370

Additional Documentation (partial)

- Wind, temp models (Air Resources Laboratory):
  - http://ready.arl.noaa.gov/gdas1.php
  - http://www.ecmwf.int/
- Magnetic declination maps (National Geophysical Data Center):
  - http://www.ngdc.noaa.gov/geomag/models.shtml
- Satellite orbital parameters
  - http://www.celestrak.com/
- Manual for Aeronautical Mobile Satellite (Route) Service (Inmarsat)
- Boeing 777 Flight Crew Operations Manual

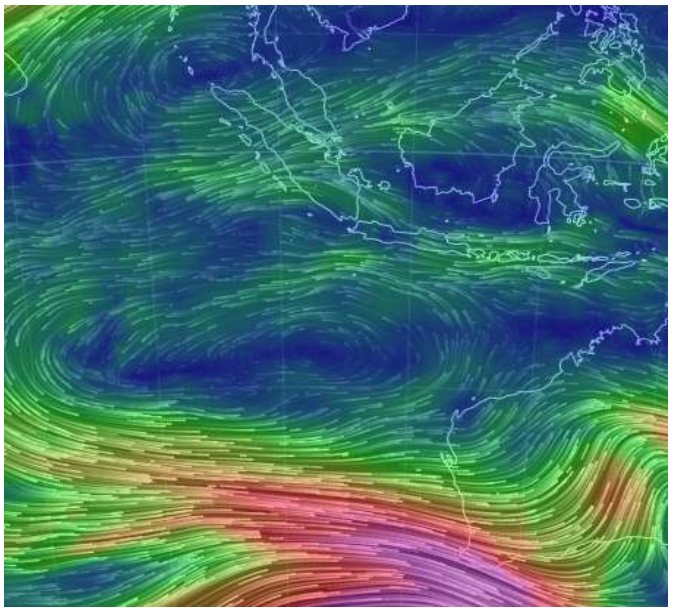

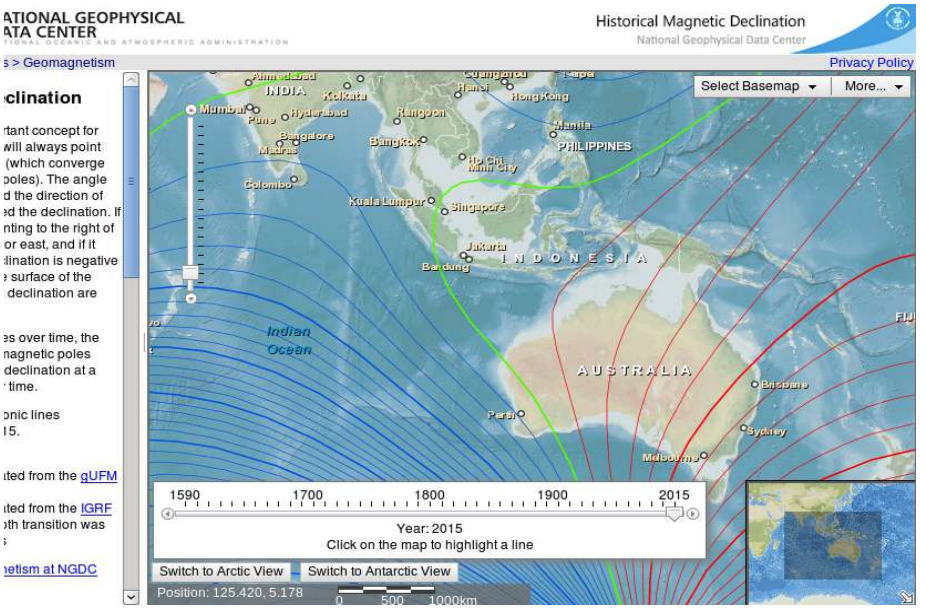

Additional details and information needed for models

- Spheroidal Earth
- Geodetic v. Geocentric latitude
- B-777 autopilot modes
- B-777 ranges v. fuel load
  - Amazing how much information is available on internet!

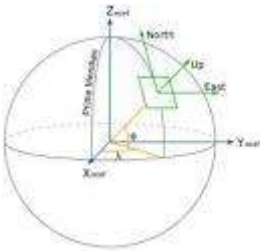

Public Data Analyses

- Once full logs and documentation were released, many people began computing potential flight paths (in parallel to official investigation)
- Key information not reverse-engineerable -
  - Perth GES AFC does not support negative latitudes!
  - Satellite frequency unstable – monitor by Burum pilot signal. Tables were released.
  - Some BTO and BFO values invalid

Table 4: Satellite and AFC values

Time UTC	(δf sat + δf AFC) Hz
16:30:00	29.1
16:42:00	27.6
16:55:00	25.8
17:07:00	24.1
18:25:00	10.7
19:41:00	-0.5
20:41:00	-1.5
21:41:00	-18.0
22:41:00	-28.5
00:11:00	-37.7
00:19:00	-37.8

Analysis Software

- **Excel**
- STK (free, commercial satellite tracking program)
- python
- octave

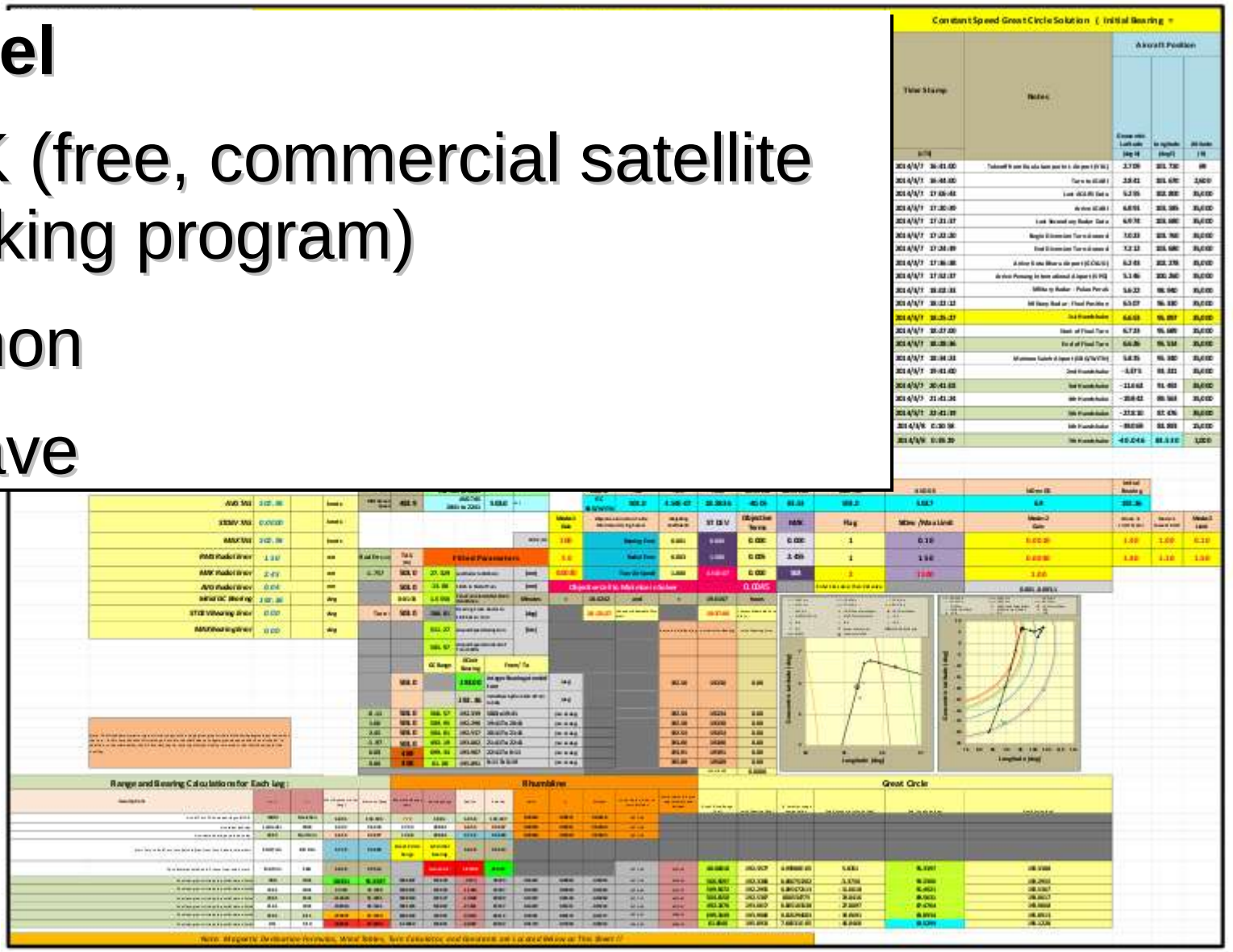

Where do people “publish”?

- dropbox
- google docs
- imgur
- twitter
- photobucket
- bitmath.org
- github
- Personal websites

Example: Magnetic track mode

Final latitude -34 deg.

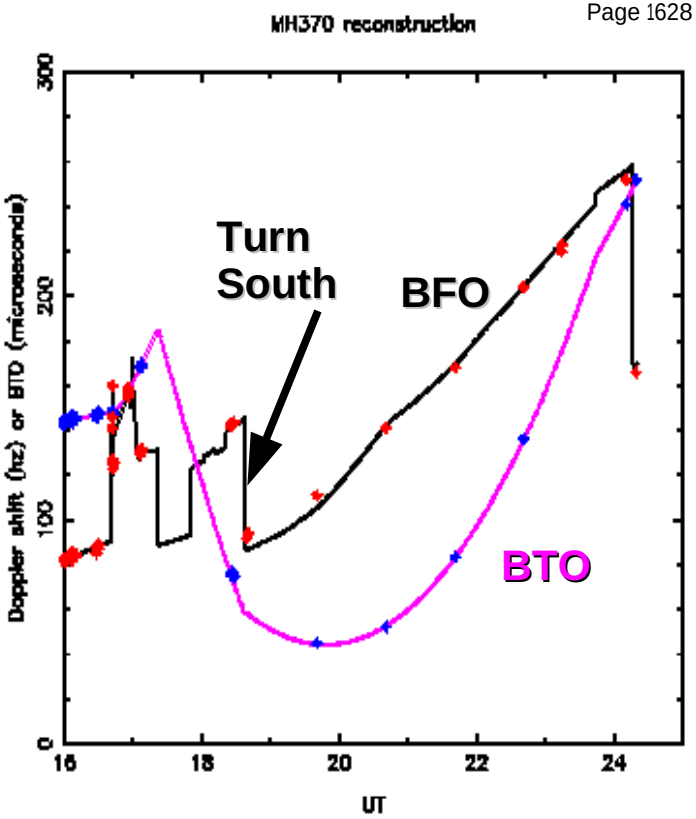

Initial ACARS data calibrate BTO, BFO and validate modeling

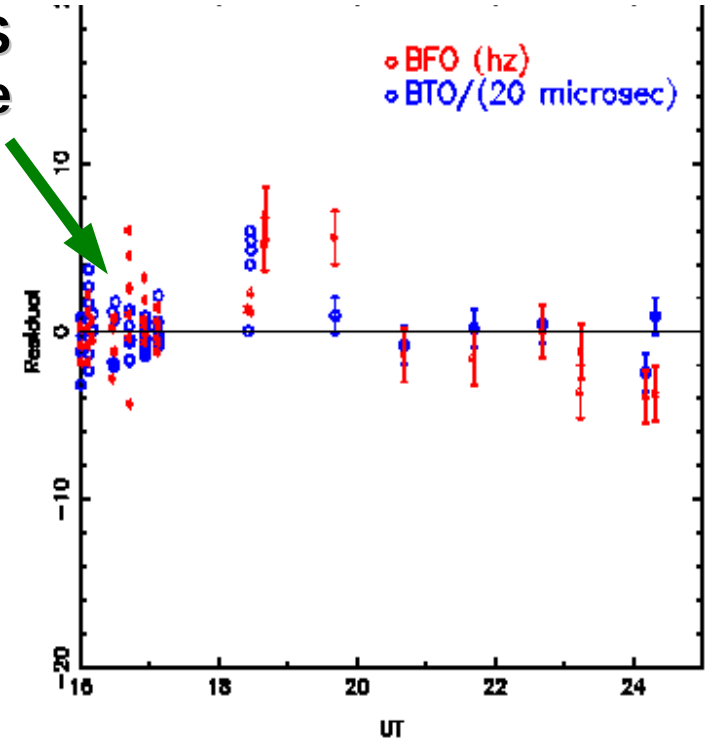

Example: Uncommanded Autopilot v. Active Pilot Flight Paths

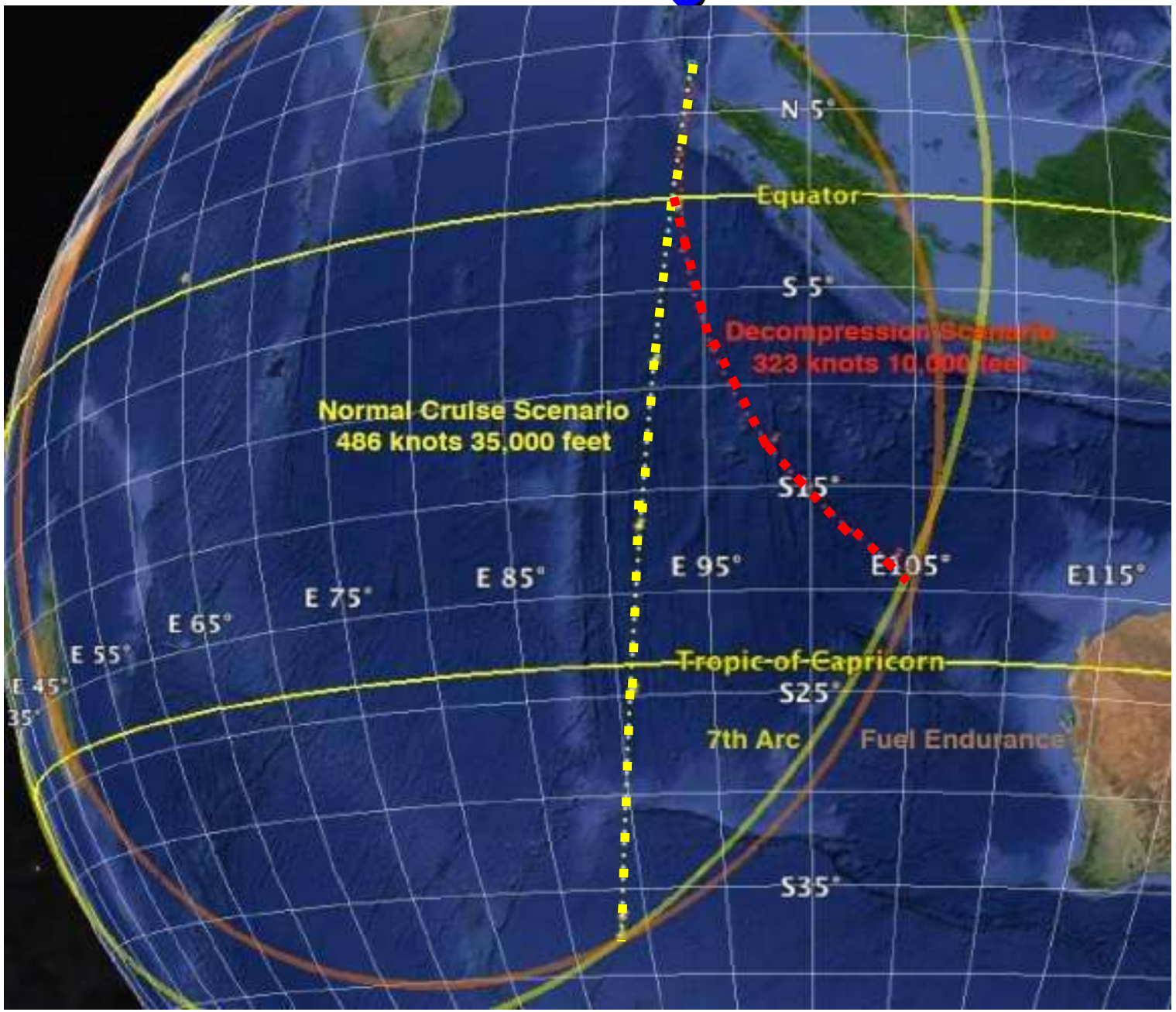

A Sample of Reports

"An Analysis of the Inmarsat Data from MH370" - R. Cole, June 20, 2014.

"MH370 Search Area Recommendation" - The Independent Group, Sept 9, 2014. ("We suggest you look *here.*")

"The Location of MH370" - Bobby Ulich, Sept 25, 2014. ("I suggest you look *there.*")

"Analytic Fuel Flow Model" - B. Martin, Mar 3, 2015.

"Some Observations on the Radar Data for MH370" - V. Iannello, Aug 18, 2015.

"MH370: On the possible interpretation of the abnormal BFO values" - Oleksandr N, Oct 1, 2015.

"The Routes Taken by Floating Debris from MH370" - R. Godfrey, Apr 2, 2016.

Predictions - JIT/JACC/ATSB v. Public

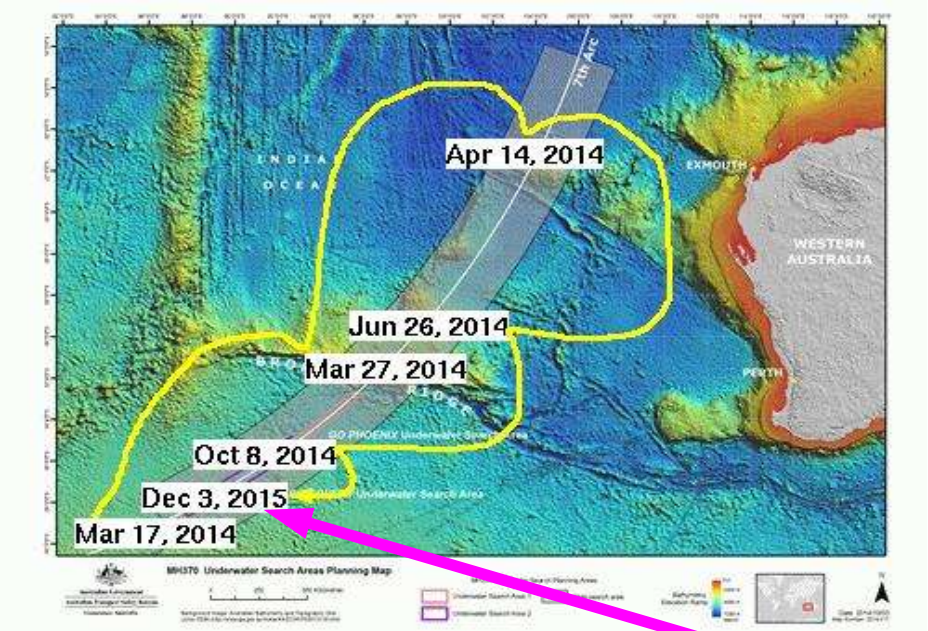

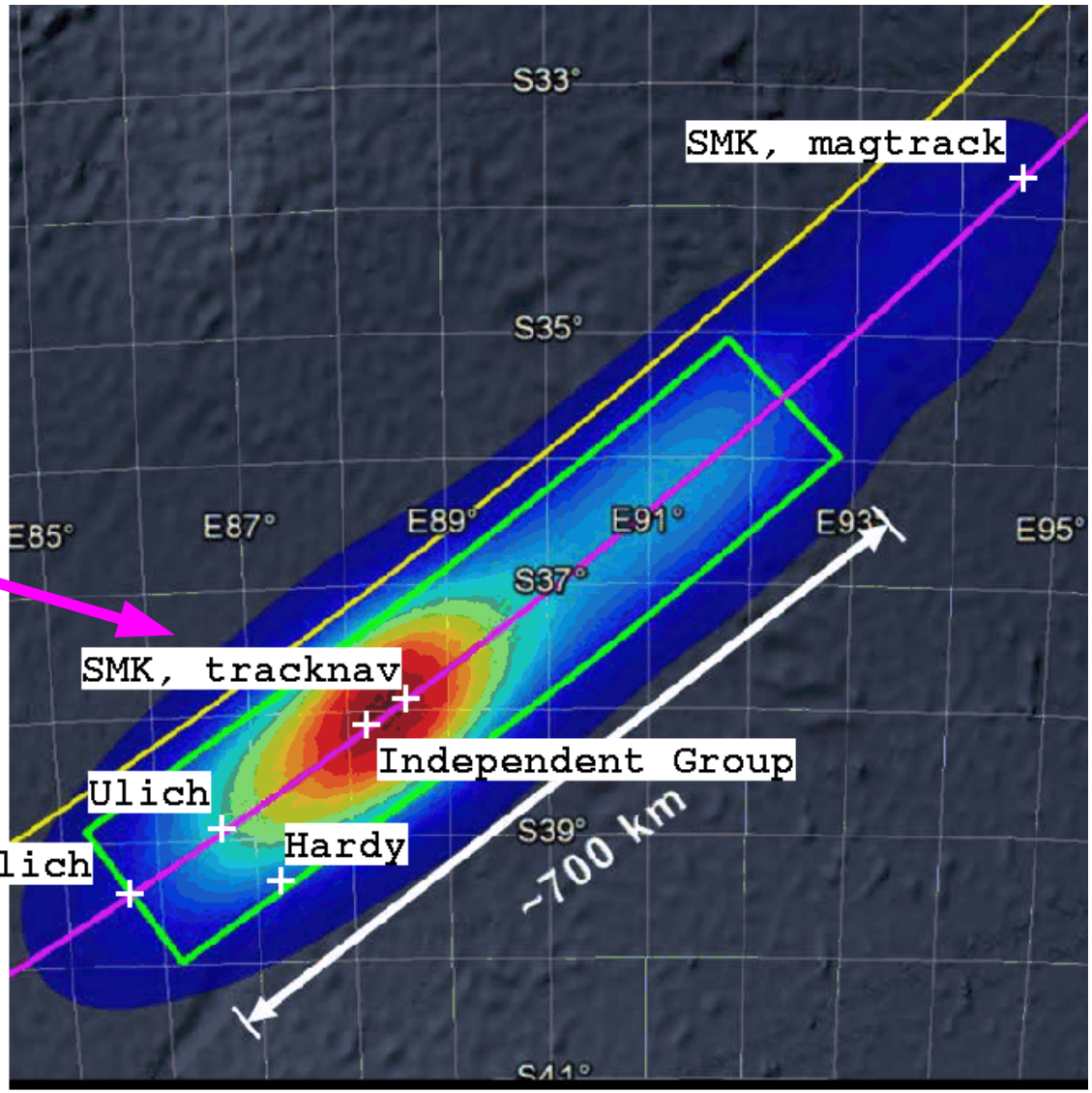

Early "official" search zones bounced up and down the 7th arc. Eventually settled on -35 to -39.

Nov 30, 2015: "Bayesian Methods in the Search for MH370" by DSTG. Highest probability region at -38° latitude.

Underwater Search (Australian ATSB lead) Currently 3 ships

Underwater search with towed side-scan sonar underway since Oct 2014.

High priority search area 120,000 sq. km. Cost US $100 million

Nothing found other than two unidentified shipwrecks.

Search will end ~July unless new evidence comes to light

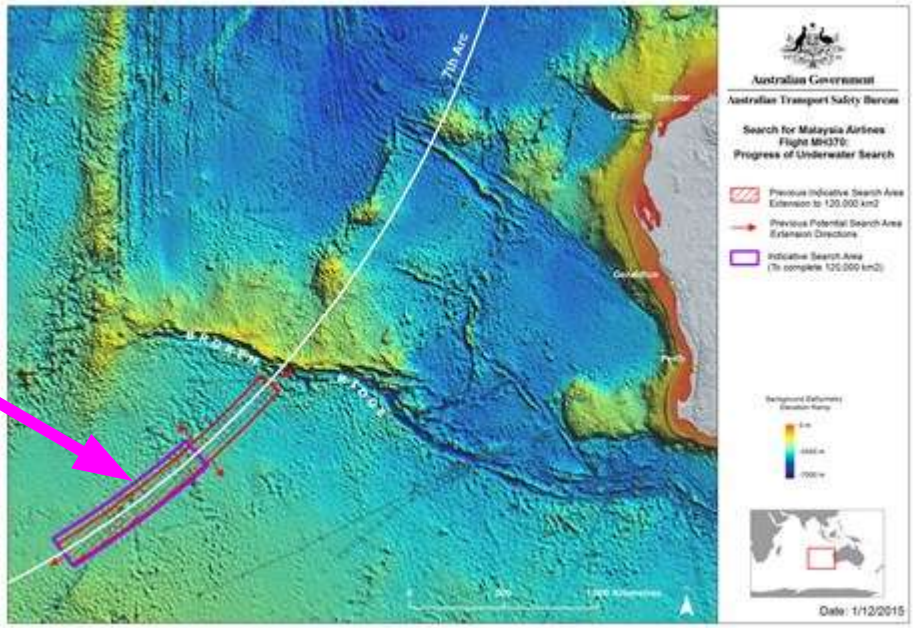

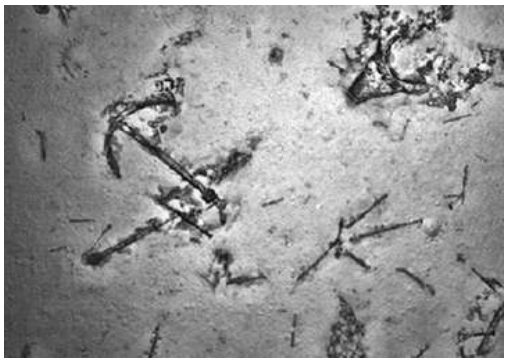

Where are we now?
Where do we go next?

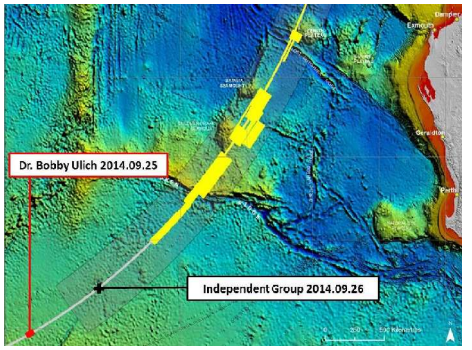

- Over a dozen people have modeled data.
- Large parameter space (speed, heading, timing, altitude, fuel model, etc.)
- Data-driven v. uncommanded autopilot-driven models
- End-of-flight scenarios studied - one person used a genuine B-777 simulator.

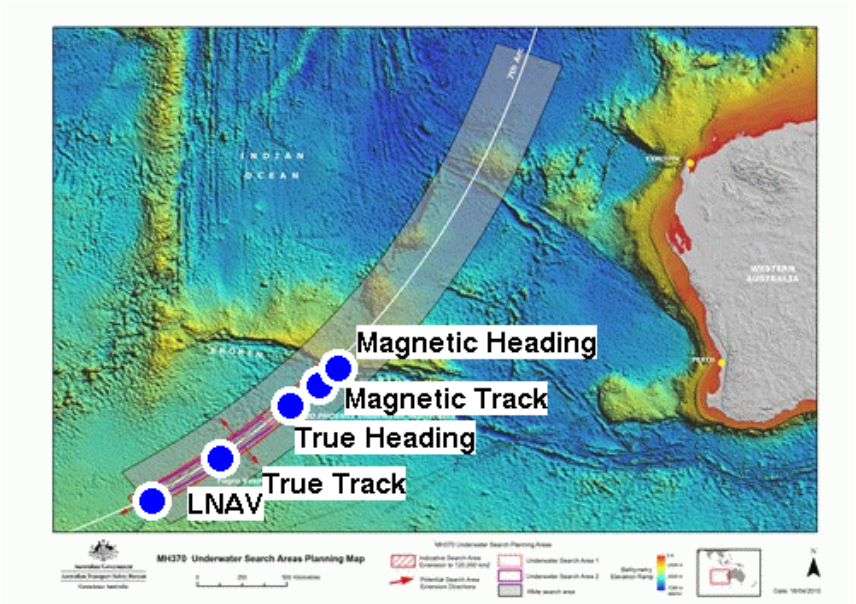

What if plane is not found?

- **Just missed in terrain?**
- **Revisit assumptions?**
- **Actively piloted?**
- **Conspiracy theory time!**

IV. Breaking News ...

July 29, 2015 Piece of right wing ("flaperon") discovered on Reunion Island, East of Madagascar.

(flaperon = flap + aileron)

Confirming evidence that MH370 went down in South Indian Ocean

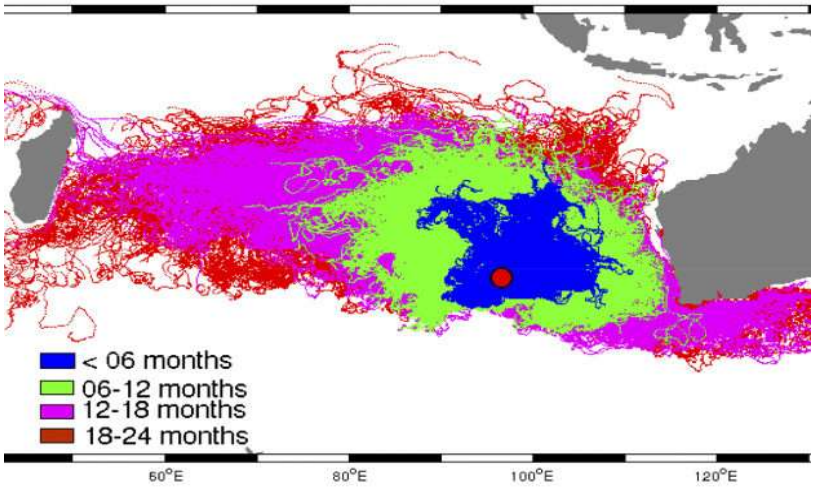

Drift modeling not accurate but favors more Northerly impact point

Goose barnacles - which species?

More Breaking News ...

Feb 27, 2016 Piece of right horizontal stabilizer discovered on sand bank off coast of Mozambique

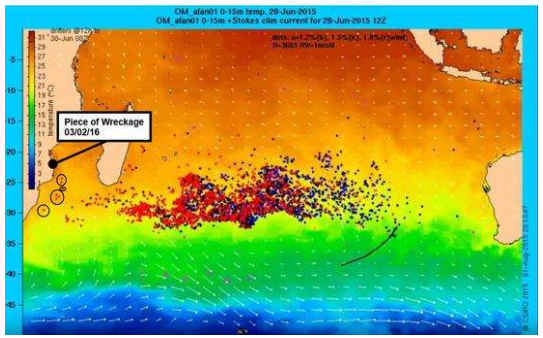

Glaser stencil font

No Goose barnacles - why?

Even More Breaking News ...

	Panel
676CR	Flap Support Fairing No. 7 Panel
676DB	Flap Support Fairing No. 7
676EB	Flap Support Fairing No. 7 - Aft
676FR	Flap Support Fairing No. 7 Panel
676GR	Flap Support Fairing No. 7 Panel
677AB	Flap Support Fairing No. 8 -

@航空事
weibo.com/606787403

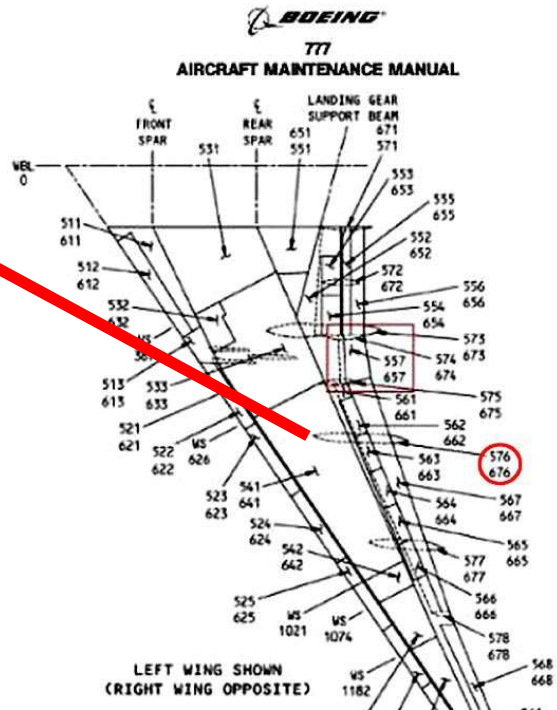

Mozambique, Dec 27, 2015.
676EB (Glaser Stencil Font) is B-777 outboard right wing flap track fairing.

Yet More Breaking News ...

Brenna Flaugher snapshot from plane window.

South Africa, Mossel Bay
Mar 22, 2016: Rolls Royce Engine logo from engine cowling. Same size and color scheme (grey letters on black background) as 9M-MRO (MH370).

And Yet Still More Breaking News ...

Piece of debris from Rodrigues Island, Mauritius, March 30, 2016.

Intricate metallic design matches interior bulkhead of Malaysia Airlines fleet.

Proposed location: Door 2R in business class.

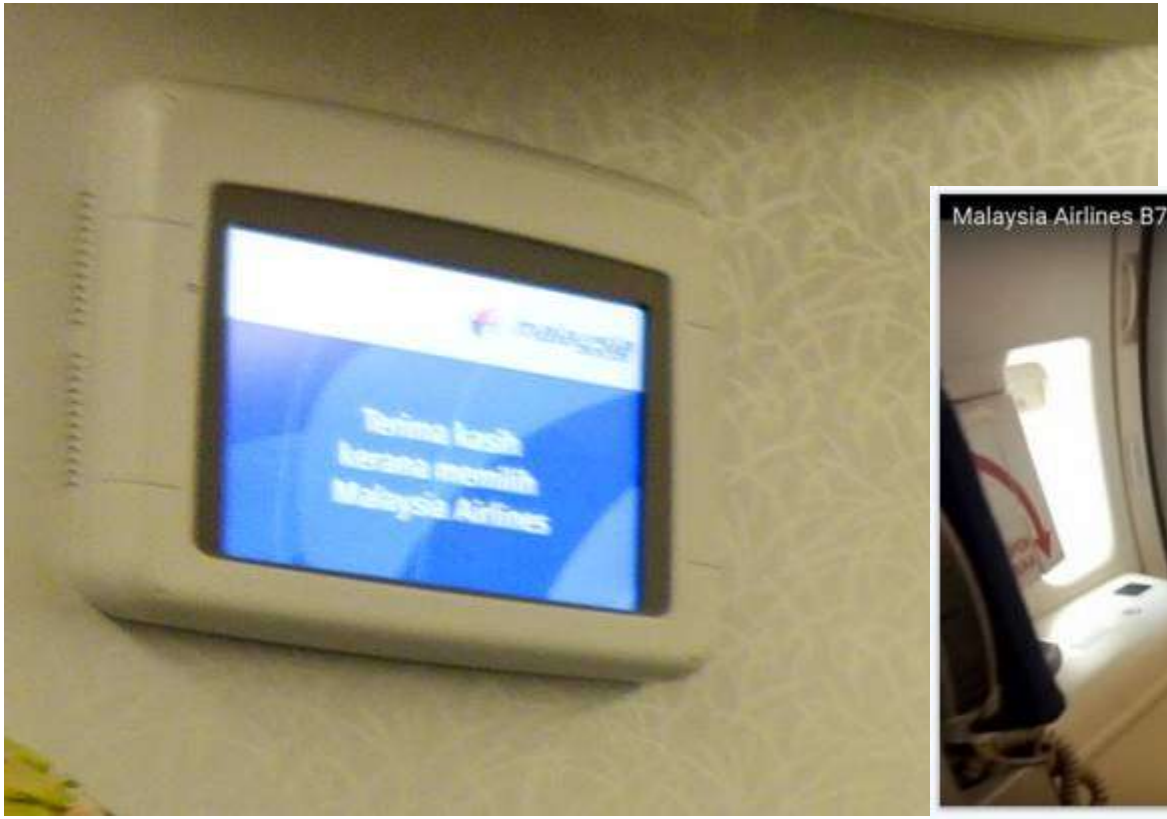

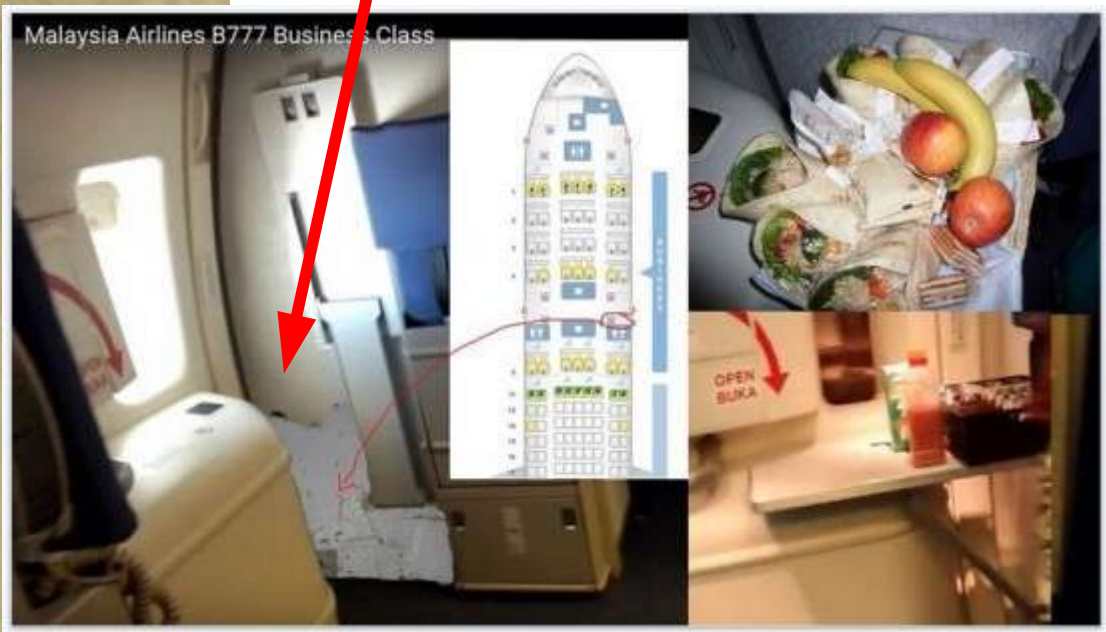

What Happened on Board?

- We know more about Amelia Earhart than MH370
- Much speculation about accident (fire) v. deliberate hijacking. Beyond scope of this talk.
  - Disabling Transponder
  - Disabling ACARS
  - Disabling SATCOM
    - Instrument bay
    - Power buses

V. Summary – Lessons Learned

- Public can make serious use of data from complex systems. Do not underestimate!
- In many ways, analysis of MH370 is similar to analyzing data from any experimental system:
  - Must understand how each part of system works (requires documentation)
  - Calibration data are crucial
- Do not hold back data that people might need - they will complain!

Backup Slides

MH21 - Kuala Lumpur to Amsterdam

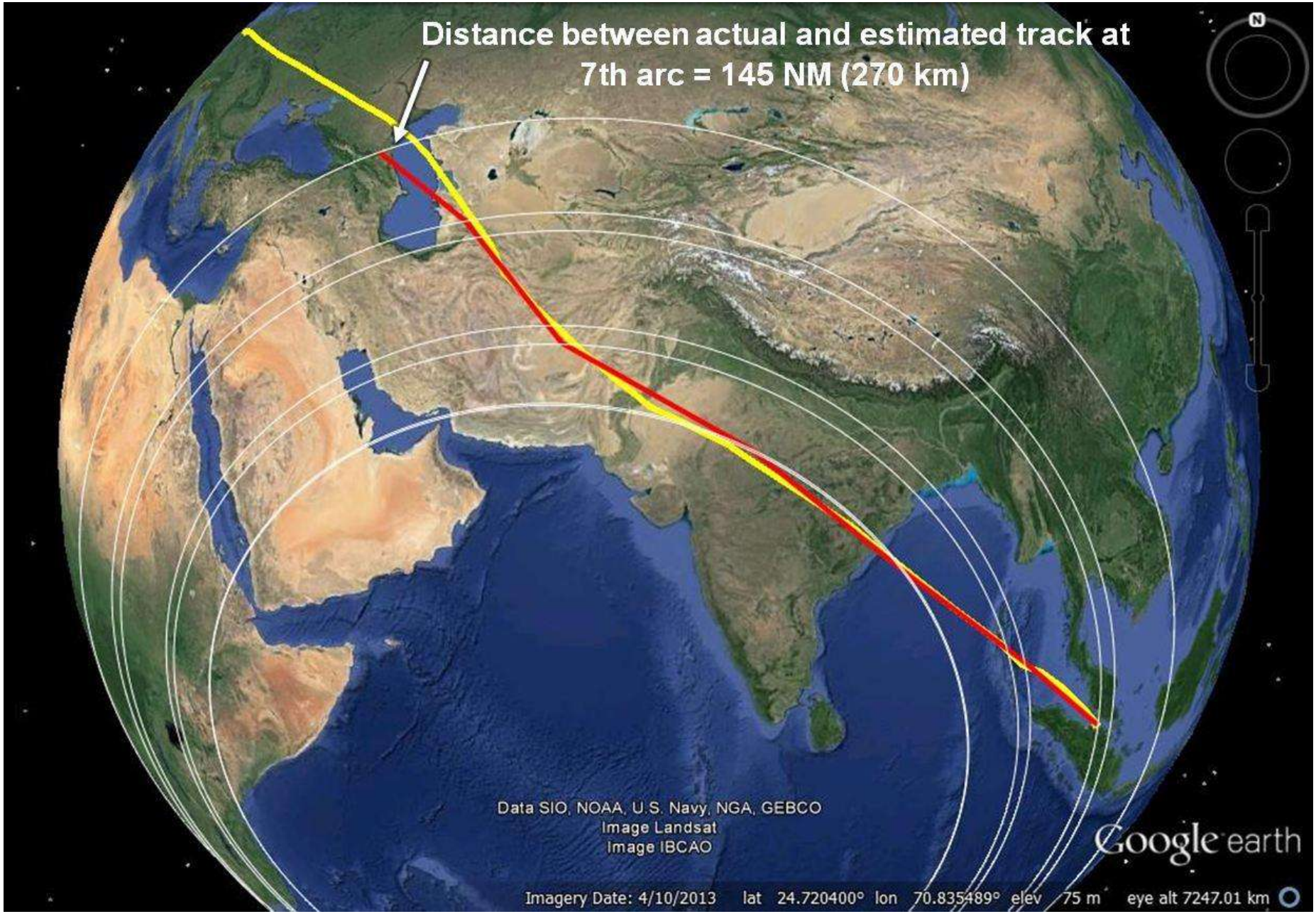

MH21 - BFO

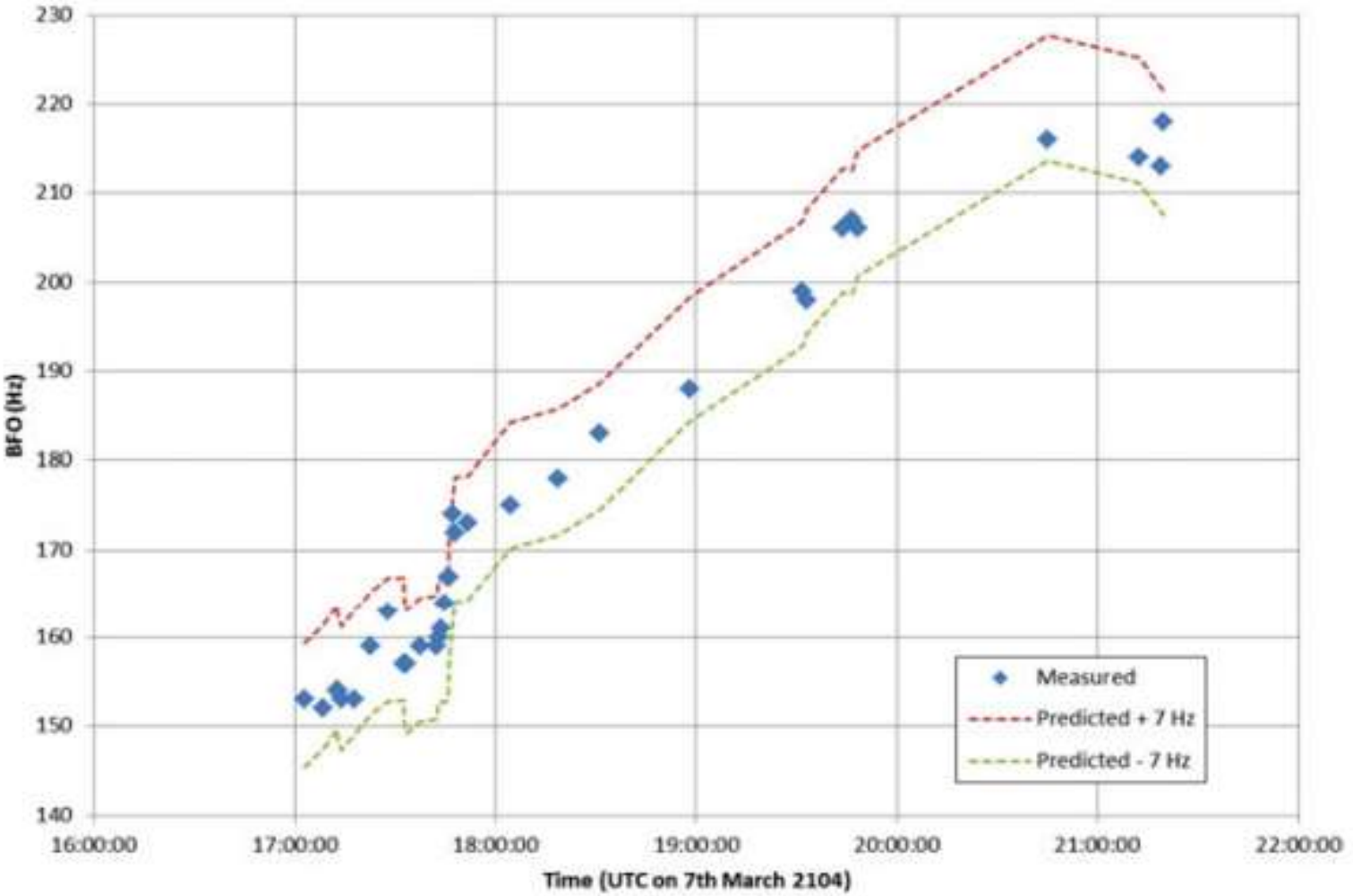

Figure 15. Burst Frequency Offset Validation (Amsterdam Flight).

Recent Analysis - Did Anyone Hear It Crash?

- Hydrophones
  - IMOS station Rottnest Island (W of Perth)
  - CTBTO station HA01 (Cape Leeuwin, Australia)
    - LANL claims detection at 00:52, bearing 246.9 deg

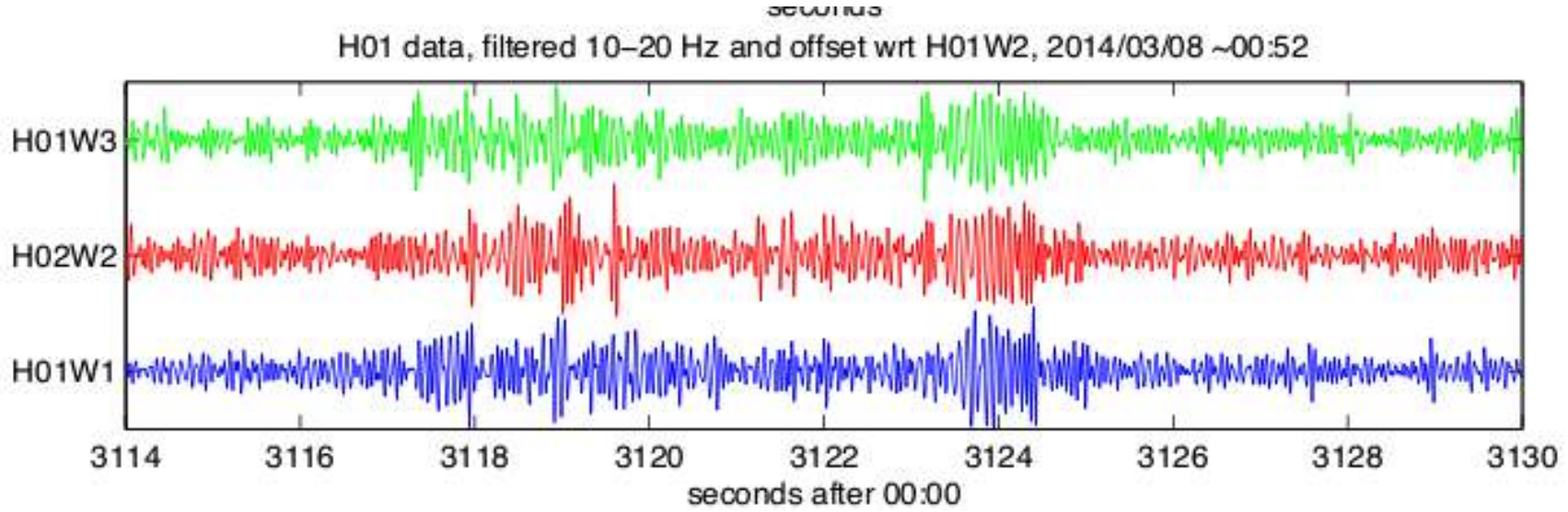

Recent Analysis - Did Anyone Feel It Crash?

- Seismic stations
  - Geoscope (French) and others - 11 stations around Indian Ocean
  - Data from IRIS-DMC

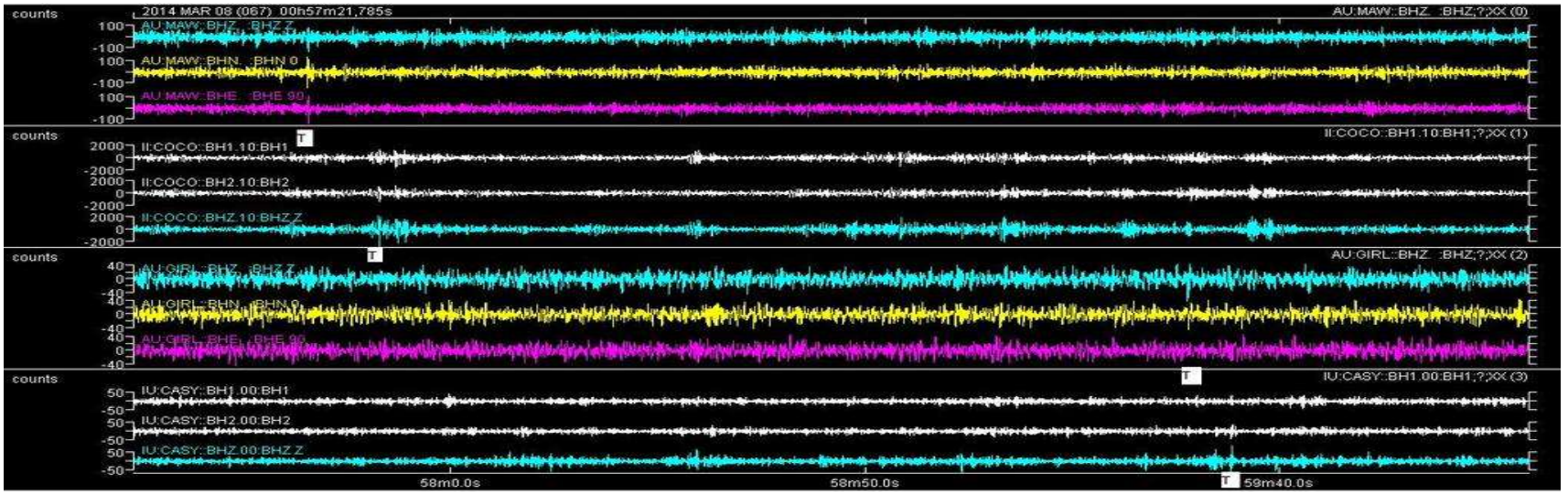

MH 370
08 March 2014
KUL - BJS

NAME	NATIONALITY	Age	Gender	Class	Seat No
TAN/CHONGLING	MYS	48	M	GCCL	1C
GAN/FUXIANG	CHN	49	M	GCCL	2A
CHNG/MEI LING	MYS	33	F	GCCL	2D
WEEKS/PAULMR	NZL	39	M	GCCL	2K
YUE/GUIJUMS	CHN	51	F	GCCL	3A
BRODSKII/NIKOLAI	RU	43	M	GCCL	3K
BAI/XIAOMO	CAN	37	F	GCCL	4A
MUKHERJEE/MUKTESH	CAN	42	M	GCCL	4C
MOHAMADSOFUAN/IBRAHIMMR	MYS	33	M	GCCL	4J
XING/QIAO	CHN	27	F	GCCL	4K
TIAN/QINGJUN	CHN	51	M	EYCL	11A
WOOD/PHILIP	USA	51	M	EYCL	11C
LIN/ANNANMR	CHN	27	M	EYCL	11D
XIE/LIPING	CHN	51	F	EYCL	11E
ZHANG/XUEWENMR	CHN	61	M	EYCL	11H
HUE/PUIHENGMR	MYS	66	M	EYCL	11J
LI/LE	CHN	36	M	EYCL	11K
BIBYNAZLI/MOHDHASSIM	MYS	62	F	EYCL	12A
DINA/MOHAMEDYUNUSRAMLI	MYS	30	F	EYCL	12C
MARIA/MOHAMEDYUNUSRAMLI	MYS	52	F	EYCL	12D
HASHIM/NOORIDA	MYS	57	F	EYCL	12E
WANG/SHOUXIAN	CHN	69	M	EYCL	12G
KOH/TIONGMENG	MYS	40	M	EYCL	12H
MUHAMMADRAZAHAN/ZAMANIMR	MYS	24	M	EYCL	12J
NORLIAKMAR/HAMIDMDM	MYS	33	M	EYCL	12K
ZHANG/SHAOHUA	CHN	32	F	EYCL	14A
ZHANG/HUALIAN	CHN	42	F	EYCL	14C
LI/YUCHEN	CHN	27	M	EYCL	14D
LI/YUAN	AUS	33	M	EYCL	14E
LI/JIE	CHN	27	F	EYCL	14F
KANG/XU	CHN	34	M	EYCL	14G

MH 370
08 March 2014
KUL - BJS

NAME	NATIONALITY	Age	Gender	Class	Seat No
GU/NAIJUN	AUS	31	F	EYCL	14H
SHARMA/CHANDRIKAMS	IND	51	F	EYCL	14J
CHAN/HUANPEENMR	MYS	46	M	EYCL	14K
LEE/SEWCHUMDM	MYS	55	F	EYCL	15A
NG/MAYLIMS	MYS	37	F	EYCL	15C
YANG/LI	CHN	35	F	EYCL	15D
LU/JIANHUA	CHN	57	M	EYCL	15E
MA/WENZHI	CHN	57	F	EYCL	15F
SIM/KENGWEI	MYS	53	M	EYCL	15G
ZHANG/CHI	CHN	58	F	EYCL	15H
WAN/HOCKKHOONMR	MYS	42	M	EYCL	15J
TEE/LINKEONGMR	MYS	50	M	EYCL	15K
LI/ZHIJIN	CHN	30	M	EYCL	16A
YAP/CHEEMENGMR	MYS	39	M	EYCL	16C
SUGIANTO/LOMR	IDN	47	M	EYCL	16D
VINNY/CHYNTHYATIOMRS	IDN	47	F	EYCL	16E
ZHANG/QIMS	CHN	31	F	EYCL	16G
BIAN/LIANGJING	CHN	27	M	EYCL	16H
MATRAHIM/NORFADZILLAHMISS	MYS	39	F	EYCL	16J
TONG/SOONLEEMR	MYS	31	M	EYCL	16K
WENG/MEI	CHN	39	F	EYCL	17A
ZHANG/NAMS	CHN	34	F	EYCL	17D
HU/XIAONINGMR	CHN	34	M	EYCL	17E
HU/SIWANCHD	CHN	3	F	EYCL	17F
SIREGAR/FIRMAN CHANDRA	IDN	25	M	EYCL	17G
SHIRSATH/KRANTI	IND	44	F	EYCL	17H
MUSTAFA/SUHAILIMISS	MYS	31	F	EYCL	17J
LEE/KAHKINMR	MYS	32	M	EYCL	17K
GAN/TAO	CHN	44	M	EYCL	18A
LU/XIANCHU	CHN	33	M	EYCL	18C
ZHAO/QIWEIMR	CHN	37	M	EYCL	18D

MH 370
08 March 2014
KUL - BJS

NAME	NATIONALITY	Age	Gender	Class	Seat No
ZHANG/XIAOLEIMS	CHN	32	F	EYCL	18E
ZHAO/YINGXINCHD	CHN	3	F	EYCL	18F
LIU/QIANG	CHN	40	M	EYCL	18H
RAMLAN/SAFUANMR	MYS	32	M	EYCL	18J
YUSOP/MUZIMR	MYS	50	M	EYCL	18K
JU/KUN	CHN	32	M	EYCL	19A
WANG/XIMIN	NZL	50	M	EYCL	19C
SUADAYA/FERRYINDRAMR	IDN	42	M	EYCL	19D
SUADAYA/HERRYINDRAMR	IDN	35	M	EYCL	19E
TANURISAM/INDRASURIAMR	IDN	57	M	EYCL	19F
WANG/WILLYSURIJANTOMR	IDN	53	M	EYCL	19G
YANG/AILINGMS	CHN	60	F	EYCL	19H
GUAN/HUAJINMS	MYS	34	F	EYCL	19J
JIA/PING	CHN	32	F	EYCL	19K
BURROWS/RODNEYMR	AUS	59	M	EYCL	20A
BURROWS/MARYMRS	AUS	54	F	EYCL	20C
CHEN/JIAN	CHN	58	M	EYCL	20D
FENG/JIXIN	CHN	70	M	EYCL	20F
WANG/YONGGANGMR	CHN	27	M	EYCL	20G
ZHANG/JIANWU	CHN	31	M	EYCL	20H
MENG/GAOSHENG	CHN	64	M	EYCL	20J
DING/LIJUN	CHN	43	M	EYCL	20K
LAWTON/CATHERINEMRS	AUS	54	F	EYCL	21A
LAWTON/ROBERTMR	AUS	58	M	EYCL	21C
XING/FENGTAO	CHN	36	M	EYCL	21D
CHEW/KARMOOIMS	MYS	31	F	EYCL	21E
WONG/SAISANGMR	MYS	53	M	EYCL	21F
LIM/POWCHUAMS	MYS	43	M	EYCL	21G
TAN/AHMENGMR	MYS	46	M	EYCL	21H
TAN/WEICHEWMR	MYS	19	M	EYCL	21J
CHUANG/HSIULINGMS	TWN	45	F	EYCL	21K

MH 370
08 March 2014
KUL - BJS

NAME	NATIONALITY	Age	Gender	Class	Seat No
GUAN/WENJIEMR	CHN	35	M	EYCL	22A
LIU/JINPENGMR	CHN	33	M	EYCL	22C
WANG/CHUNHUAMR	CHN	34	M	EYCL	22D
ZHANG/SIMING	CHN	71	F	EYCL	22H
DOU/YUNSHANMR	CHN	61	M	EYCL	22J
ZHANG/LIJUANMS	CHN	61	F	EYCL	22K
XIN/XIXIMS	CHN	32	F	EYCL	23A
HUANG/YIMS	CHN	30	F	EYCL	23C
LIU/ZHONGFU	CHN	72	M	EYCL	23D
MAIMAITIJIANG/A	CHN	35	M	EYCL	23E
MAO/TUGUI	CHN	72	M	EYCL	23F
ZHAO/GANGMR	CHN	46	M	EYCL	23H
WEN/HAO DONG	CHN	32	M	EYCL	23J
YAN/XIAO DAN	CHN	27	F	EYCL	23K
OUYANG/XIN	CHN	38	F	EYCL	24A
YIN/BOYAN	CHN	33	M	EYCL	24C
ZHANG/YANHUI	CHN	44	F	EYCL	24D
YANG/JIABAO	CHN	26	F	EYCL	24E
WANG/DAN	CHN	54	F	EYCL	24F
LI/HONGJING	CHN	20	F	EYCL	24G
LI/GUOHUI	CHN	56	M	EYCL	24H
HUANG/TIANHUI	CHN	43	M	EYCL	24J
JIANG/CUIYUN	CHN	62	F	EYCL	24K
LIU/SHUNCHAO	CHN	46	M	EYCL	25A
DI/JIABIN	CHN	36	M	EYCL	25C
WATTRELOS/AMBRE	FRA	14	F	EYCL	25D
WATTRELOS/HADRIEN	FRA	17	M	EYCL	25E
WATTRELOS/LAURENCE	FRA	52	F	EYCL	25F
ZHAO/YAN	FRA	18	F	EYCL	25G
TANG/XUDONG	CHN	31	M	EYCL	25H
YAN/LINGMR	CHN	29	M	EYCL	25J

MH 370
08 March 2014
KUL - BJS

NAME	NATIONALITY	Age	Gender	Class	Seat No
CHEN/CHANGJUNMR	CHN	35	M	EYCL	25K
ZHAO/PENG	CHN	25	M	EYCL	26A
TIAN/JUNWEI	CHN	29	M	EYCL	26C
LUI/CHING	CHN	45	F	EYCL	26D
WANG/SHU MIN	CHN	61	F	EYCL	26E
WANG/XIANJUN	CHN	61	M	EYCL	26F
LI/ZHIXIN	CHN	35	M	EYCL	26H
TAN/SIOH PENG	MYS	42	F	EYCL	26J
CHEN/WEI HOING	MYS	43	M	EYCL	26K
DEINEKA/SERGII	UKR	45	M	EYCL	27D
CHUSTRAK/OLEG	UKR	45	M	EYCL	27E
ZANG/LINGDI	CHN	58	F	EYCL	27G
LIANG/LUYANGMR	CHN	60	M	EYCL	27H
MOHDKHAIRULAMRI/SELAMATMR	MYS	29	M	EYCL	29A
PUSPANATHAN/SUBRAMANIAN	MYS	34	M	EYCL	29C
JIANG/XUEREN	CHN	62	M	EYCL	29J
LI/YANLIN	CHN	29	M	EYCL	29K
JIANG/YINGMS	CHN	27	F	EYCL	30A
KOZEL/CHRISTIAN	AUT	30	M	EYCL	30C
XU/CHUANE	CHN	57	M	EYCL	30D
ZHANG/YAN	CHN	36	F	EYCL	30E
MENG/BING	CHN	40	M	EYCL	30F
MENG/FANQUAN	CHN	70	M	EYCL	30G
MENG/NICOLECHD	USA	4	F	EYCL	30H
ZHANG/MENG	CHN	29	F	EYCL	30J
YAN/PENG	CHN	29	M	EYCL	30K
ZHOU/JINLING	CHN	61	M	EYCL	31A
ZHOU/FENG	CHN	56	F	EYCL	31C
ZHAO/ZHAOFANG	CHN	73	F	EYCL	31D
XIONG/DEMING	CHN	63	F	EYCL	31E
WANG/LINSHI	CHN	59	M	EYCL	31F

MH 370
08 March 2014
KUL - BJS

NAME	NATIONALITY	Age	Gender	Class	Seat No
LOU/BAOTANG	CHN	79	M	EYCL	31G
LIU/RUSHENG	CHN	76	M	EYCL	31H
DONG/GUOWEI	CHN	48	M	EYCL	31J
BAO/YUANHUA	CHN	63	F	EYCL	31K
CHEN/YUNMS	CHN	57	F	EYCL	32A
DING/YINGMS	CHN	62	F	EYCL	32C
HOU/AIQINMS	CHN	45	F	EYCL	32D
SONG/CHUNLINGMS	CHN	60	F	EYCL	32E
TANG/XUEZHUMS	CHN	57	F	EYCL	32F
YANG/QINGYUANMR	CHN	57	M	EYCL	32G
YANG/XIAOMINGMS	CHN	59	F	EYCL	32H
SURTIDAHLIA/MRS	NLD	50	F	EYCL	32J
FENG/DONG	CHN	21	M	EYCL	32K
CAO/RUI	CHN	32	F	EYCL	33A
MA/JUNMR	CHN	33	M	EYCL	33C
SONG/FEIFEIMR	CHN	32	M	EYCL	33D
ZHANG/HUAMR	CHN	43	M	EYCL	33E
TEOH/KIMLUNMR	MYS	36	M	EYCL	33G
YAO/LIFEI	CHN	31	M	EYCL	33H
YA/NA	CHN	26	F	EYCL	33J
HAN/JING	CHN	53	F	EYCL	33K
FU/BAOFENG	CHN	28	M	EYCL	34A
MARALDI/LUIGI	ITA	37	M	EYCL	34C
YUE/WENCHAO	CHN	26	M	EYCL	34D
ZHANG/YAN	CHN	45	F	EYCL	34G
WANG/YONGQIANG	CHN	30	M	EYCL	34H
SU/QIANGGUO	CHN	71	M	EYCL	34J
SONG/KUN	CHN	25	M	EYCL	34K
KOLEKAR/VINOD	IND	59	M	EYCL	35A
KOLEKAR/CHETANA	IND	55	F	EYCL	35C
KOLEKAR/SWANAND	IND	23	M	EYCL	35D

MH 370
08 March 2014
KUL - BJS

NAME	NATIONALITY	Age	Gender	Class	Seat No
WANG/HAITAO	CHN	26	M	EYCL	35G
LUO/WEI	CHN	29	M	EYCL	35H
LI/YAN	CHN	31	F	EYCL	35J
GAO/GE	CHN	27	F	EYCL	35K
HOU/BO	CHN	35	M	EYCL	36A
WEN/YONGSHENG	CHN	34	M	EYCL	36B
WANG/CHUNYONG	CHN	43	M	EYCL	36C
LI/ZHI	CHN	41	M	EYCL	36G
TAN/TEIKHINMR	MYS	32	M	EYCL	36H
DU/WENZHONG	CHN	50	M	EYCL	36J
LIN/MINGFENG	CHN	34	M	EYCL	36K
SHI/XIANWEN	CHN	26	M	EYCL	37A
WANG/LIJUN	CHN	49	M	EYCL	37C
WANG/RUI	CHN	35	M	EYCL	37D
JIAO/WEIWEI	CHN	32	F	EYCL	37H
ZHOU/SHIJIE	CHN	64	M	EYCL	37J
YIN/YUEWANG	CHN	21	M	EYCL	37K
LI/WENBO	CHN	29	F	EYCL	38A
ZHENG/RUIXIAN	CHN	42	F	EYCL	38C
JIAO/WENXUE	CHN	58	M	EYCL	38D
JINGHANG/JEE	MYS	41	M	EYCL	38G
DAI/SHULING	CHN	58	F	EYCL	38H
BIAN/MAOQIN	CHN	67	F	EYCL	38J
WANG/YONGHUI	CHN	33	M	EYCL	38K
LI/MINGZHONG	CHN	69	M	EYCL	39A
LIU/FENGYING	CHN	65	F	EYCL	39D
YUAN/JIN	CHN	63	F	EYCL	39G
ZHANG/LIQIN	CHN	43	F	EYCL	39J
WANG/HOUBIN	CHN	28	M	EYCL	39K
ZHU/JUNYAN	CHN	41	F	EYCL	40A
ZHANG/ZHONGHAI	CHN	43	M	EYCL	40C

MH 370
08 March 2014
KUL - BJS

NAME	NATIONALITY	Age	Gender	Class	Seat No
ZHANG/JINQUAN	CHN	72	M	EYCL	40D
YAO/JIANFENG	CHN	70	M	EYCL	40E
YANG/MEIHUA	CHN	65	F	EYCL	40F
DAISY/ANNE	MYS	56	F	EYCL	40G
AN/WENLAN	CHN	65	F	EYCL	40K
LIANG/XUYANG	CHN	30	M	EYCL	41D
DING/YING	CHN	28	F	EYCL	41G
CHE/JUNZHANG	CHN	68	F	EYCL	4J
WANG/MOHENG	CHN	2	M	EYCL	
ZHANG/YAN	USA	2	M	EYCL	

MAS 370 (Kuala Lumpur to Beijing)

PILOT-ATC RADIOTELEPHONY TRANSCRIPT

Departure from KLIA: 8 March 2014

ATC DELIVERY		
12:25:53	MAS 370	Delivery MAS 370 Good Morning
12:26:02	ATC	MAS 370 Standby and Malaysia Six is cleared to Frankfurt via AGOSA Alpha Departure six thousand feet squawk two one zero six
12:26:19	ATC	… MAS 370 request level
12:26:21	MAS 370	MAS 370 we are ready requesting flight level three five zero to Beijing
12:26:39	ATC	MAS 370 is cleared to Beijing via PIBOS A Departure Six Thousand Feet squawk two one five seven
12:26:45	MAS 370	Beijing PIBOS A Six Thousand Squawk two one five seven, MAS 370 Thank You
12:26:53	ATC	MAS 370 Welcome over to ground
12:26:55	MAS 370	Good Day
LUMPUR GROUND		
12:27:27	MAS 370	Ground MAS370 Good morning Charlie One Requesting push and start
12:27:34	ATC	MAS370 Lumpur Ground Morning Push back and start approved Runway 32 Right Exit via Sierra 4.
12:27:40	MAS 370	Push back and start approved 32 Right Exit via Sierra 4 POB 239 Mike Romeo Oscar
12:27:45	ATC	Copied
12:32:13	MAS 370	MAS377 request taxi.
12:32:26	ATC	MAS37..... (garbled) ... standard route. Hold short Bravo
12:32:30	MAS 370	Ground, MAS370. You are unreadable. Say again.
12:32:38	ATC	MAS370 taxi to holding point Alfa 11 Runway 32 Right via standard route. Hold short of Bravo.
12:32:42	MAS 370	Alfa 11 Standard route Hold short Bravo MAS370.
12:35:53	ATC	MAS 370 Tower
12:36:19	ATC	(garbled) ... Tower ... (garbled)
	MAS 370	1188 MAS370 Thank you

LUMPUR TOWER		
12:36:30	MAS 370	Tower MAS370 Morning
12:36:38	ATC	MAS370 good morning. Lumpur Tower. Holding point.. [garbled]..10 32 Right
12:36:50	MAS 370	Alfa 10 MAS370
12:38:43	ATC	370 line up 32 Right Alfa 10.
	MAS 370	Line up 32 Right Alfa 10 MAS370.
12:40:38	ATC	370 32 Right Cleared for take-off. Good night.
	MAS 370	32 Right Cleared for take-off MAS370. Thank you Bye.
LUMPUR APPROACH		
12:42:05	MAS 370	Departure Malaysian Three Seven Zero
12:42:10	ATC	Malaysian Three Seven Zero selamat pagi identified. Climb flight level one eight zero cancel SID turn right direct to IGARI
12:42:48	MAS 370	Okay level one eight zero direct IGARI Malaysian one err Three Seven Zero
12:42:52	ATC	Malaysian Three Seven Zero contact Lumpur Radar One Three Two Six good night
	MAS 370	Night One Three Two Six Malaysian Three Seven Zero
LUMPUR RADAR (AREA)		
12:46:51	MAS 370	Lumpur Control Malaysian Three Seven Zero
12:46:51	ATC	Malaysian Three Seven Zero Lumpur radar Good Morning climb flight level two five zero
12:46:54	MAS370	Morning level two five zero Malaysian Three Seven Zero
12:50:06	ATC	Malaysian Three Seven Zero climb flight level three five zero
12:50:09	MAS370	Flight level three five zero Malaysian Three Seven Zero
01:01:14	MAS370	Malaysian Three Seven Zero maintaining level three five zero
01:01:19	ATC	Malaysian Three Seven Zero
01:07:55	MAS370	Malaysian...Three Seven Zero maintaining level three five zero
01:08:00	ATC	Malaysian Three Seven Zero
01:19:24	ATC	Malaysian Three Seven Zero contact Ho Chi Minh 120 decimal 9 Good Night
01:19:29	MAS370	Good Night Malaysian Three Seven Zero

 # end of file/BIT 30 March #

Check for updates

Article

the International Communication Gazette

Framing the flight MH370 mystery: A content analysis of Malaysian, Chinese, and U.S. media

the International Communication Gazette
2018, Vol. 80(2) 158–184
© The Author(s) 2017
Reprints and permissions:
sagepub.co.uk/journalsPermissions.nav
DOI: 10.1177/1748048517707440
journals.sagepub.com/home/gaz
SAGE

Lindsey M Bier
University of Southern California, USA

Sejin Park
Republic of South Korea Army, Republic of Korea

Michael J Palenchar
University of Tennessee, USA

Abstract

This study analyzes frames related to the flight MH370 disappearance in Malaysian (N = 93), Chinese (N = 155), and U.S. (N = 150) newspapers. The results provide insight about media orientations in an international crisis, particularly regarding national interests and international citizenship. Attribution of responsibility is the dominant frame; secondary frames vary among conflict and human-interest frames, demonstrating that attribution of responsibility is the most important frame even with unknown controllability and ambiguous intentionality. Results also demonstrate significant differences in national interest frames and in the roles in the societal evaluation of risk. This study contextualizes the results in media systems, diplomatic relations, and cultures.

Keywords

Crisis communication, framing, international citizenship, international crisis, national interests

On 8 March 2014, about an hour after takeoff, Malaysia Airlines flight MH370 mysteriously disappeared from radar. In a news release to media after the disappearance, Malaysia Airlines confirmed the flight was carrying 239 passengers and crew from 14 different nationalities. The passengers included 154 Chinese, 50 Malaysian, seven Indonesian, six Australian, five Indian, four American,

Corresponding author:
Sejin Park, Public Affairs Officer, Republic of South Korea, PO Box 501, Key-Ryong Si, Choong-Nam, Republic of Korea 32801.
Email: sj4297@gmail.com

three French, two New Zealander, two Ukrainian, two Canadian, one Russian, one Italian, one Dutch, and one Austrian (Malaysia Airlines, 2014).

In the days and weeks after the mysterious event, international media reported extensively on the missing airplane. Such coverage doubled television audiences, increased primetime ratings, and generated immense internet traffic (news.com.acu, 2014). While many speculated the plane accidentally crashed with the fuselage now resting at the bottom of the Indian Ocean, others contended hijackers hid the plane to accomplish malicious purposes at a later time or supernatural forces snatched MH370 from the sky. Whether a rogue pilot, terrorists, or mechanical failure was attributed to blame, each story was nothing more than a conjecture because technological evidence about the actual fate of the flight remains sparse.

The MH370 investigation continues as the most expensive in aviation history (Australian Transport Safety Bureau, 2016; Wardell, 2014). Inhabitants of La Reunion, a remote Indian island, discovered debris on 29 July 2015, more than a year after the plane's disappearance. French and Malaysian authorities confirmed the debris was from MH370 (Jamieson and Ciganinero, 2015). In October 2016, authorities confirmed wing fragments, discovered in May 2016 in Mauritius and in June 2016 in Tanzania, came from MH370 (Westcott, 2016). However, the location of the fuselage and the conditions under which the plane disappeared remain a mystery that, more than three years after the event, continues to receive international media attention. For example, a British journalist released a book about MH370 in March 2016 (Quest, 2016) and an episode of the Australian edition of '60 Minutes' broadcast in July 2016 with accusations that the Malaysian government concealed its knowledge of the true fate of MH370 (Vankin, 2016). Further, the mystery of the missing plane still causes emotional suffering and anxiety for the 239 passengers' loved ones and has resulted in dozens of lawsuits (Glum, 2016).

The MH370 mystery permits a unique inquiry into media coverage of a crisis because multiple nations are involved and there is no clarity about what happened to the flight: This is a crisis without a known cause and, thus, without an individual, organization, or nation to attribute blame. Further, aviation crises are of interest because aviation is one of the technologies credited for creating a global community. According to the International Air Transport Association (2014), airlines safely transported more than 3.3 billion passengers, and, while doing so, sustained 58 million jobs and stimulated $2.4 trillion of economic output. Critical actions of large organizations, particularly aviation corporations such as Malaysia Airlines, attract global media attention and influence how the home country is perceived in other countries (Gotsi et al., 2011).

Media are a primary source of information about international events and issues, and coverage helps construct perceptions about and evaluations of unfamiliar nations, cultures, and ideologies for global audiences (Kucherenko and Christen, 2014; Orgeret, 2010). Media shape public opinions, particularly in crisis situations (Coombs, 2007; Knight, 1999). Considerable scholarly attention has been devoted to the manner in which media frame crises and to the relationship between national interests and media coverage of political events and wars

(Downing, 1988; Paletz and Vinson, 1994; Zaremba, 1988), but little empirical research has been conducted to elucidate the relationships among national interests, international citizenship, and communication about international crises. Therefore, the purpose of this study is to investigate the framing of the disappearance of flight MH370 in English-language newspapers from Malaysia, China, and the United States to provide insight about media orientation in an international crisis, particularly in relation to national interests and international citizenship.

Literature review

Theoretical framework

Media frames are 'schemata of interpretation' (Goffman, 1974: 21). Framing analysis investigates which attributes of an event or issue are presented as important by media (McCombs et al., 1997; Scheufele and Tewksbury, 2007). Thus, framing analysis is the interpretation of a reality in a message (McCombs, 2005). Through exposure to media with manifest and latent frames, audiences construct shared expectations and values, which affect behavior (Scheufele and Tewksbury, 2007). Therefore, in a strategic attempt not unlike persuasion, the media presentation of an event or issue influences public opinion and collective behavior (Ghanem, 1997).

National interests and media frames

National interests relate to the political, economic, militarist, sociocultural, and security objectives of a country and comprise value choices by policymakers to minimize costs and to maximize benefits for the good of the country (Li, 2003). Journalists employ national interest frames by explicitly highlighting or making implicit assumptions about these objectives and value choices to explain an event or issue and to resonate with domestic audiences (Brewer, 2006; Novais, 2007). In this manner, media reduce the complexity of foreign cultures (Said, 1993) and impose elite-defined national interests and agendas onto international matters (Akhavan-Majid and Ramaprasad, 1989; Dorogi, 2001). Although media often claim to offer a plurality of viewpoints, they are typically limited to those reflecting viewpoints from official sources (Ruigrok and Van Atteveldt, 2007) and there is a close relationship between media organizations and government agendas (Entman, 1991; Hook and Pu, 2006; Paterson, 1999). For example, national interests are prominent in U.S. media coverage of China, which commonly utilizes an anticommunist frame (Dorogi, 2001; Lee et al., 2011; Mao, 2014), whereas media about U.S.–Japan relations and U.S.–South Korea relations often employ a cooperative frame (Park, 2013).

National interests are reflected in culture and operate with the legitimacy of a country's citizenship, government, and/or economic activities. Such legitimacy may be justified with the fabrication of political authority and the coercive control of

cultural values. Culture is the expression of the character of a group of social actors and is molded by their backgrounds, languages, and beliefs (Bereciartu, 1994). In this sense, the framing of national interests can be further examined and understood from culture, for culture provides the foundation for social actors to generate knowledge and to assign meaning to external phenomena (Hall, 1997). Media content is a direct reflection of culture (Hall, 1980) and media frames are a part of culture (Entman, 1993; Goffman, 1974), for they link cognition and culture (Gamson et al., 1992; Lee and Basnyat, 2013). Media producers use cultural values in content and present them to audiences (Shoemaker and Reese, 1996), and culture functions to provide understanding between media producers and media consumers (Van Gorp, 2007).

Amid increased global interconnectedness from technological advancements in media and travel capabilities, national interests are often in tension with a country's desire to be perceived as a respectable international citizen. International citizenship, also called global citizenship, lacks a singular definition but is often related to neoliberal economic policy or a sense of cosmopolitanism based on moral responsibility to the global population. Journalists can function as agents to promote various facets of international citizenship (Schattle, 2015). According to Pert (2014), international citizenship is described according to the following frames: a legal frame featuring compliance with international law, a cooperation frame featuring support for bilateral or multilateral agreements, a willingness frame featuring completion of international tasks, an ethics frame featuring good deeds outside its national boundaries, a leadership frame featuring works to raise international standards, and a global peace frame as a primary actor in global peace and stability (Pert, 2014).

Generic roles in the societal evaluation of risk

Palmlund (1992, 2009) identified six generic roles in societal evaluation of risk, which can be used to examine media crisis frames, especially in relation to attribution of risk concerning individuals or organizations responsible for the crisis event or responsible for managing the crisis event. According to Palmlund's research, risk bearers are the victims of the negative consequences of the risk or perceive themselves as such. Risk bearers' advocates speak on behalf of the risk bearers. Risk generators create and/or fabricate the risks or are at least thought to do so by others involved. Risk researchers work through various methods to determine what occurred, why and how it can be abated or mitigated. Risk arbiters work to protect risk bearers from present or future risks, while risk informers are not directly affected or involved yet provide information and commentary.

Framing an international aviation crisis

While framing is a factor in media coverage, it becomes even more important in crisis communication because media frames affect audience perceptions of

organizations and behavior in emergency situations (Coombs, 2007). Entman (1993) identified four basic explicit and implicit media frames in crisis situations: definition of problem, specification of causes, conveyance of moral assessments, and endorsement of remedies. Such frames manifest in media through word choice, metaphors, exemplars, descriptions, arguments, and visual images (Pan and Kosicki, 1993). More recent studies, including those conducted by crisis communication scholars with a nuanced understanding of crisis frameworks, identified five media frames commonly utilized in crises, which will be the focal point of this present analysis: attribution of responsibility, conflict, economic consequences, human interest, and morality (An and Gower, 2009; Cho and Gower, 2006; Coombs and Holladay, 1996; Liu and Pennington-Gray, 2015; Neuman et al., 1992; Semetko and Valkenburg, 2000). In crisis situations, the morality frame situates the event within the context of moral or religious values (An and Gower, 2009; Neuman et al., 1992). The human-interest frame presents an emotional angle (An and Gower, 2009; Cho and Gower, 2006; Semetko and Valkenburg, 2000). The economic consequences frame reports the financial implications, either positive or negative, for individuals, groups, organizations, or countries (An and Gower, 2009; Neuman et al., 1992). The conflict frame highlights disagreements among individuals, groups, organizations, or countries (An and Gower, 2009; Neuman et al., 1992; Semetko and Valkenburg, 2000). Finally, the attribution of responsibility frame offers causes of or potential solutions (An and Gower, 2009; Semetko and Valkenburg, 2000).

Sociopolitical factors in Chinese, Malaysian, and U.S. crisis frames

The mysterious disappearance of the MH370 flight is a crisis involving several countries and, thus, diverse national interests and ideologies: Malaysia Airlines, a corporation in which the Malaysian government holds majority ownership, operated the flight; most of the 239 passengers onboard the flight were Chinese; and Boeing, a U.S. corporation with $81 trillion annual revenue, manufactured the aircraft (Defense News, 2013). While scholars and practitioners have acknowledged media play an important role in disseminating information about crises (Coombs, 2007), Schultz et al. (2012) contend U.S. media and foreign media present unlike solutions to crises. Molleda's research (2011) shows how media frame conflicts differently according to their geographic location in relation to the crisis location.

Moreover, countries have dissimilar journalistic standards and norms that affect how media frame crises. While objectivity is considered a universal journalistic norm, power relations within Malaysia, China, and the United States, respectively, influence media production, distribution, and consumption. Such power relations as well as Western and Asian cultural values, respectively, alter conceptualizations of objectivity and press freedom (Ramanathan, 2016). China is an especially interesting case because it is one of the few remaining communist states, and different political systems result in different media expectations (Mehra, 1993). The Chinese

media model is based on government censorship as Chinese media are state-owned extensions of the government that receive daily directives from the Publicity Department of the Communist Party of China (World Press Freedom Index, 2014). Economic reform has brought the expansion and diversification of Chinese media, but China still uses media to promote the government image (Zhao, 2000). Both mainstream print and broadcast as well as online media are controlled by legal restrictions, although online media expand the boundaries of permissible reporting (Hassid and Repnikova, 2016).

Media expectations are different in democratic countries than in communist countries (Mehra, 1993). Malaysia is a parliamentary democracy, and the United States is a democratic republic. While various political systems have long employed media to propagandize, spread ideology, and defend regimes, controlled communication has been an outcome of governments deemed communistic more so than of governments deemed democratic. In the case of Malaysia, however, media are censored more than media in most democracies (Freitag and Stokes, 2009). Ownership patterns and legal restrictions impact the content of mainstream media in Malaysia, whereas online media are fairly unrestricted (Brown, 2005; Jalarajan Raj and Sreekumar, 2012; Steele, 2011; Willnat and Wong, 2013). The Malaysian government uses media as instruments for national development, and, thus, Malaysian journalists generally report positively about their government (Jalarajan Raj and Sreekumar, 2012; Ramanathan, 2016). This 'development journalism' model (Taylor and Kent, 1999: 138) as well as Islamic cultural principles discourage journalists from divulging negative information (Steele, 2011, 2013). Unlike American journalists, Malaysian journalists often carefully ponder the consequences of their writings in accordance with Islamic social values (Steele, 2011, 2013). Malaysian journalists must practice 'responsible journalism,' particularly when reporting on race, religion, and politics—and some fear arrest for reporting in a manner deemed inappropriate by the government (Jalarajan Raj and Sreekumar, 2012: 25).

Free and open media have long been considered crucial to a healthy democracy. The U.S. media model, in theory, is based on diversity of viewpoints, programming, outlets, and ownership (Scherer, 2016). The concentration of U.S. media ownership, however, allows for information control. Moreover, journalistic norms change as U.S. society changes. For example, U.S. media historically reflected moderate viewpoints, but as viewpoints in society become more polarizing, so do media representations (McLuskey and Kim, 2012). While journalists in Southeast Asia exhibit values toward promoting national loyalty and building a sense of community, especially in print media (Massey, 2000; Menon, 1998), journalists in the United States and other Western countries are more likely to engage in 'aggressive journalism,' including the criticism of national leaders (Ramanathan, 2016: 23). According to the 2014 World Press Freedom Index, the United States ranks 46, Malaysia ranks 147, and China ranks 175 out of 180 countries in terms of a free and open media without government censorship.

Study rationale and research questions

Although framing theories have long been tested quantitatively through content analysis, Carragee and Roefs (2004) posit that a problem with framing research is it often fails to examine the framing process within the broader political and social context, and Park (2013) calls for additional framing research to provide a more comprehensive understanding of international media coverage. Van Gorp (2007) avows research does not adequately consider the influence of culture on archetypal media frames, and Hume (2010) indicates mediated communication as it pertains to culture is ripe for investigation. Lee (2004) suggests Western crisis frameworks are generalizable, but more research is necessary to understand differences in cross-cultural crisis communication. Pinsdorf (1991) argues an organization, particularly an airline operating transnationally, must reflect varying cultural values for survival after a crisis. Since the disappearance of flight MH370, Malaysia Airlines has incurred financial loss, and the future of the organization is bleak (Centre for Aviation, 2014; Skynews.com.au, 2016). Understanding how international media frame an aviation crisis without an obvious cause provides insight toward organizational survival by responding to publics with different political, social, and cultural backgrounds. As such, this present study addresses several of the shortcomings of the content analyses identified herein and extends the discussion beyond descriptive findings while maintaining the strengths of quantitative content analysis.

Furthermore, scholars suggest future framing research should pursue 'issue-specific frames related exclusively to a particular topic' (Santos et al., 2013: 67). Although the only crisis plagued by ongoing mystery, the MH370 flight was one of several aviation crises that made 2014 one of the deadliest years for flying in almost a decade (Grant, 2014). Thus, this study has implications for future research about response strategies for international aviation crises. Based on a synthesis of previous research, an analysis of English-language newspapers in Malaysia, China, and the United States elucidates variations in framing the flight MH370 crisis by answering the following research questions:

RQ1: How is the MH370 crisis framed in English-language Malaysian, Chinese, and U.S. newspapers in terms of attribution of responsibility, conflict, economic consequences, human interest, and morality?

RQ2: How does MH370 coverage in English-language Malaysian, Chinese, and U.S. newspapers reflect national interests in terms of the political, economic, militarist, sociocultural, and security objectives within each respective country?

RQ3: How does MH370 coverage in English-language Malaysian, Chinese, and U.S. newspapers reflect international citizenship in terms of each respective country's compliance with international law, cooperation with or toward formal agreements, willingness to work with other countries, ethical behavior, global leadership, and promotion of world peace and stability?

Method

Research design

Framing is one of the most commonly applied research approaches in the communication field (Bryant and Miron, 2004). This study employs a quantitative content analysis design to analyze statistically the differences among international media frames and to make inferences about communication about a crisis without an obvious cause. Content analyses are essential for understanding communication messages, and 'communication content merits systematic examination because of its assumed role as cause or antecedent of a variety of individual processes, effects, or uses people make of it' (Riffe et al., 2005: 11). The researchers conducted an analysis to reflect the overall trends of MH370-related coverage in English-language Malaysian, Chinese, and U.S. newspapers and counted frequencies and made comparisons to elucidate the significance of the frames.

Data collection and sample

Data were collected from Malaysian, Chinese, and U.S. sources based on (1) media primacy in each country, (2) the availability of newspapers in English, and (3) the availability of newspapers in the LexisNexis Academic database to ensure systematic sample collection. Malaysia was selected because it is the country of origin for Malaysia Airlines, China was selected because the majority of the MH370 passengers were Chinese citizens, and the United States was selected because it is the country of origin for the Boeing aircraft. English-language newspapers were used in part because of the researchers' language abilities but also because English-language media present global issues to an international readership and, thus, provide insight into the relationship between national interests and international citizenship. The oldest remaining newspaper and one of the top English newspapers by circulation in Malaysia is *New Straits Times*, a source used in comparative communication research among international sources (Massey, 2000; Park et al., 2016; Ramanathan, 2016); further, the *New Straits Times* is a part of the largest mass communication organization in Malaysia (Ramanathan, 2016). The top English newspaper in China is *China Daily*, which is state-owned and has been used in Chinese media content analyses (Luther and Zhou, 2005; Tai and Sun, 2007; Zhang et al., 2014). *The New York Times* is regarded as a model newspaper, is a top newspaper in the United States by circulation, and is frequently used in comparative research among international sources (Nossek, 2004; Tunstall, 1977).

All full-text articles related to flight MH370 from 8 March 2014 to 28 January 2015, inclusive, were obtained from *New Straits Times*, *China Daily*, and *The New York Times* through LexisNexis by key words. The time parameters were determined by the day flight MH370 disappeared to the day the Malaysian government declared MH370 likely crashed without survivors to allow insurers to pay the next of kin. The key words applied in headlines and full articles were 'MH370' and

'Malaysia Airlines' and '370.' Duplicates of articles were deleted. *Associated Press* articles published in *The New York Times* were included in the sample because it is a U.S. news agency and *The New York Times* in this study represents the U.S. perspective. Some articles related to flight MH370 also covered other aviation crises in 2014, particularly Malaysia Airlines Flight 17 and Air Asia Flight Q78501; these articles were included in the sample. The search yielded 93 articles from *New Straits Times*, 155 articles from *China Daily*, and 150 articles from *The New York Times* for a total of 398 articles.

Coding scheme and intercoder reliability

The unit of analysis for this study was the article. The coding scheme was based on the premise that media frames 'can be detected by probing for particular words. . .that consistently appear in a narrative and convey thematically consistent meanings' (Entman, 1991: 7). However, because multidimensional and abstract concepts are complex to study from a social scientific perspective (Riffe et al., 2005), the researchers developed precise conceptual and operational definitions of variables in a codebook.

The coding instrument was initially designed based on previous literature and prior to observation of the sample. The codebook explained the measures to the extent that each coding category allowed for replicability. First, the codebook consisted of basic information about the article such as publisher, publication date, and author of the article to ensure one particular journalist was not framing the crisis entirely differently than other journalists. The rest of the codebook focused on the appearance of the five media frames used in crisis communication and identified in previous literature (attribution of responsibility, conflict, economic consequences, human interest, and morality), the presence of national interests (operationalized as economy, military, sociocultural values, political system, and security), and the mention of international citizenship (operationalized as legal issues, cooperation in formal agreements, willingness to work together, ethical behavior, and global leadership).

To measure nuance within the crisis media frames, the researchers adapted the 20-question coding scheme used by Semetko and Valkenburg (2000) about attribution of responsibility, conflict, economic consequences, human interest, and morality. A total of 18 questions were added to account for the distinct attributes of the MH370 disappearance as an international crisis with an unknown cause. For example, the codebook included codes that distinguished between foreign and domestic governments both as a cause of the crisis and as a postcrisis alleviator, codes for the role of a corporation as a cause and as an alleviator, and codes for the presentation of multiple credible causes for the crisis. In total, there were 13 items about attribution of responsibility, eight items about conflict, nine items about economic consequences, five items about human interest, and three items about morality.

Because this study aims to investigate research questions rather than to support hypotheses, two authors served as the coders (Park and Reber, 2010). The coders

Table 1. Coding schemes.

Coding scheme		Explanation
Five crisis frames	Attribution of responsibility	Offers causes of or potential solutions for the crisis and a way of attributing responsibility
	Conflict	Highlights disagreements among individuals, groups, organizations, or countries
	Economic consequences	Reports the financial significance of the crisis for individuals, groups, organizations, or countries
	Human interest	Presents a human face or an emotional angle to the crisis
	Morality	Situates the event within the context of moral or religious values or social prescriptions
National interests	Economy	Discusses the country's activities related to the production, exchange, or consumption of goods
	Military	Includes information about the country's military, soldiers, or military affairs
	Culture and/or society	Gives information about the beliefs, myths, values, norms, special artifacts, and/or social practices of the country
	National security	Offers information about how the country is protecting citizens
	Political system	Contains messages about the country's political system
International citizenship	Legal issues	Presents the country's compliance with international law
	Cooperation	Expresses the country's support for bilateral or multilateral agreements
	Willingness	Reports the country's willingness to complete international tasks
	Ethics	Offers to do good deeds outside national boundaries because it is moral or right
	Leadership	Highlights the ways that the country is raising international standards
	Global peace	Situates global harmony as a priority for the country or the country as a primary actor in global peace

Table 2. Number of articles published by publisher.

Week postcrisis	1 n(%)	2 n(%)	3 n(%)	4 n(%)	5–8 n(%)	9–12 n(%)	12+ n(%)
NST	13(8.4)[a]	36(23.2)[a]	33(21.3)[b]	16(10.3)[b]	24(15.5)[b]	16(10.3)[a]	17(11.0)[b]
China Daily	16(17.2)[b]	10(10.8)[a]	11(11.8)[a]	8(8.6)[a]	16(17.2)[b]	9(9.7)[b]	23(24.7)[b]
NYT	43(30.3)[b]	20(14.1)[b]	19(13.4)[a]	7(4.9)[b]	23(16.2)[b]	8(5.6)[a]	22(15.5)[b]

NST: *New Straits Times*; *NYT*: *The New York Times*.
*$\chi^2(12) = 34.06$, $p < .01$.
[a]Higher than expected value.
[b]Lower than expected value.

completed three independent practice sessions, based on eight, 12, and 48 articles, respectively, prior to the actual coding. Between practice sessions, they discussed and agreed upon the classification of frames according to operational definitions and the codebook was modified as necessary. Intercoder reliability was assessed according to Cohen's Kappa. The scores ranged from .76 to .95, which are acceptable coefficients for a content analysis (Neuendorf, 2002).

The coders then independently read each article of the sample one at a time and coded frames in the article according to the codebook while disregarding outside knowledge about flight MH370 and other issues discussed in the article. After coding, the relationships among media frames and variables associated with national interests and international citizenship were examined statistically to answer the research questions about communication about an international crisis without an obvious cause.

Results

Before analyzing the five crisis media frames, though, the number of newspaper articles published was analyzed. As Table 2 shows, the majority of *New Straits Times* and *The New York Times* articles were published in the first month ($n = 98$, 66.6% and $n = 89$, 62.7%, respectively). In contrast, more than half of *China Daily* articles ($n = 48$, 51.2%) were published more than a month after the crisis happened. The difference among the three publishers was statistically significant, $\chi^2(12) = 34.06$, $p < .01$.

Research question 1

The first research question explores crisis media frames in *New Straits Times*, *China Daily*, and *The New York Times*. For all three publishers, attribution of responsibility was the dominant frame used (*New Straits Times*: $n = 97$, 62.6%; *China Daily*: $n = 67$, 72.0%; and *The New York Times*: $n = 100$, 70.4%). However, as shown in Table 3, the second most frequently used frames were different among the

Table 3. Crisis frames by publisher.

	Attribution of responsibility n(%)	Conflict n(%)	Economic consequence n(%)	Human interest n(%)	Morality n(%)
NST	97(62.6)[a]	21(13.5)[a]	3(1.9)[a]	18(11.6)[a]	16(10.3)[b]
China Daily	67(72.0)[b]	5(5.4)[b]	6(6.5)[b]	14(15.1)[a]	1(1.1)[b]
NYT	100(70.4)[b]	11(7.7)[b]	6(4.2)[b]	22(15.5)[b]	3(2.1)[a]

NST: *New Straits Times*; *NYT*: *The New York Times*.
*$\chi^2(8) = 23.57$, $p < .01$.
[a]Lower than expected value.
[b]Higher than expected value.

newspapers. For example, the conflict frame ($n = 21$, 13.5%) was the second for *New Straits Times*, while the human-interest frame was the second for *China Daily* and *The New York Times* ($n = 14$, 15.1% and $n = 22$, 15.5%, respectively). Overall, the proportions of frames in each newspaper were significantly different, $\chi^2(8) = 23.57$, $p < .01$.

To explore the details of the five crisis media frames employed by *New Straits Times*, *China Daily*, and *The New York Times*, Semetko and Valkenburg's (2000) coding scheme was adapted to suit an international crisis with an unknown cause. Some interesting results were found in the data. First, one of the coding items asked whether the publisher 'suggests that some level of domestic government has the ability to alleviate the crisis.' Among the 97 articles in *New Straits Times* that used the attribution of responsibility frame, 82.5% ($n = 80$) of the articles suggested the domestic government, in this case the Malaysian government, was an alleviator. The percentages for *China Daily* and for *The New York Times*, however, were relatively low ($n = 38$, 56.7% and $n = 39$, 39.0%, respectively).

Second, a coding item asked whether the publisher 'suggests that some level of foreign government has the ability to alleviate the crisis.' Among the 100 articles in *The New York Times* that used the attribution of responsibility frame, 86.0% ($n = 86$) suggested a foreign government was an alleviator. This compares with *New Straits Times* and *China Daily* in which 76.3% ($n = 74$) and 71.6% ($n = 48$) of articles, respectively, suggested a foreign government was a postcrisis alleviator.

Lastly, a coding item asked whether the article 'makes reference to God or a higher being or other religious tenets.' In *New Straits Times*, 50% ($n = 8$) of articles with a morality frame referred to a higher being or religious tenets. In *The New York Times*, 66.7% ($n = 2$) of articles with a morality frame referred to a higher being or religious tenets. No *China Daily* articles mentioned God or a higher being or any religious tenets.

A crosstab test yielded that the generic roles in the societal evaluation of risk were different among the newspapers, $\chi^2(10) = 47.72$, $p < .01$. As Table 4 indicates, the top three roles of each publisher were different. For example, risk arbiters, risk advocates, and risk informers were used most frequently by *New Straits Times* and

Table 4. Generic roles in the societal evaluation of risk by publisher.

	Risk bearers n(%)	Risk advocates n(%)	Risk generators n(%)	Risk researchers n(%)	Risk arbiters n(%)	Risk informers n(%)
NST	5(3.2)[a]	37(23.9)[b]	6(3.9)[a]	10(6.5)[a]	63(40.6)[b]	34(21.9)[b]
China Daily	8(8.6)[b]	9(9.7)[a]	4(4.3)[b]	8(8.6)[b]	40(43.0)[b]	24(25.8)[b]
NYT	16(11.3)[b]	6(4.2)[a]	11(7.7)[a]	12(8.5)[b]	40(43.0)[b]	24(25.8)[b]

NST: *New Straits Times*; *NYT*: *The New York Times*.
*$\chi^2(10) = 47.72$, $p < .01$.
[a]Lower than expected value.
[b]Higher than expected value.

Table 5. National interest by publisher.

	Economy n(%)	Military n(%)	Cultural/ society n(%)	National security n(%)	Political system n(%)	Nothing n(%)
NST	2(1.3)[a]	15(9.7)[b]	30(19.4)[a]	5(3.2)[a]	1(0.6)[a]	102(65.8)[b]
China Daily	1(1.1)[a]	15(16.1)[a]	7(7.5)[b]	0(0)[b]	0(0)[b]	70(75.3)[a]
NYT	0(0)[b]	32(22.5)[a]	1(0.7)[b]	1(0.7)[b]	0(0)[b]	108(76.1)[a]

NST: *New Straits Times*; *NYT*: *The New York Times*.
*$\chi^2(10) = 44.28$, $p < .01$.
[a]Higher than expected value.
[b]Lower than expected value.

China Daily. However, in articles in *The New York Times*, the dominant roles were risk informers followed by risk arbiters and risk bearers.

Research question 2

The second research question examines whether national interests were framed differently among the three newspapers. Table 5 shows the majority of *New Straits Times* articles did not contain any national interest frames ($n = 102$, 65.8%). Sociocultural ($n = 30$, 19.4%) frames followed by military ($n = 15$, 9.7%) frames appeared in *New Straits Times* articles. Likewise, the majority of *China Daily* and *The New York Times* articles did not have national interest frames ($n = 70$, 75.3% and $n = 108$, 76.1%, respectively). Both *China Daily* and *The New York Times* articles included military (16.1 and 22.5%, respectively) frames followed by sociocultural ($n = 7$, 7.5% and $n = 1$, 0.7%, respectively) frames.

Table 6. International citizenship by publisher.

	Legal issues n(%)	Cooperation n(%)	Willingness n(%)	Ethics n(%)	Leadership n(%)	Global peace n(%)	Nothing n(%)
NST	0(0)	7(4.5)[a]	62(40.0)[a]	6(3.9)[a]	2(1.3)[a]	0(0)	78(50.3)[a]
China Daily	0(0)	1(1.1)[b]	29(31.2)[b]	0(0)[b]	0(0)[b]	0(0)	63(67.7)[a]
NYT	0(0)	0(0)[b]	24(16.9)[b]	0(0)[b]	1(0.7)[b]	0(0)	117(82.4)[a]

NST: *New Straits Times*; *NYT*: *The New York Times*.
*$\chi^2(8) = 43.40$, $p < .01$.
[a]Higher than expected value.
[b]Lower than expected value.

The difference among the three publishers in terms of overall national interest frames was significant, $\chi^2(10) = 44.28$, $p < .01$.

Research question 3

Finally, the third research question investigates international citizenship frames within the three newspapers. In each of the three newspapers, the majority of articles did not include any frames about international citizenship and, thus, were coded as 'nothing.' The second most dominant frame for each of the three publishers was the willingness to work together to complete international tasks. Nevertheless, the proportions of the categories were significantly different, $\chi^2(8) = 43.40$, $p < .01$. For example, the majority of articles in *The New York Times* ($n = 117$, 82.4%) did not include any information about international citizenship, and only 16.9% of articles in *The New York Times* discussed the willingness of the United States to complete international tasks. However, for *New Straits Times* and *China Daily*, the proportion of the 'nothing' category decreased ($n = 78$, 50.3% and $n = 63$, 67.7%, respectively) and the proportion of the 'willingness' category increased ($n = 62$, 40.0% and $n = 29$, 31.2%, respectively). Interestingly, *New Straits Times* published articles about cooperation in formal agreements ($n = 7$, 4.5%), ethical behavior ($n = 6$, 3.9%), and global leadership ($n = 2$, 1.3%). For all three newspapers, there were no articles about legal issues and global peace.

Discussion

This study investigates media frames associated with an international crisis without a known cause and reveals that crisis frames, national interest frames, and international citizenship frames differ according to the country of origin of the publisher. Malaysia, China, and the United States have different media systems, and media 'reflect the values of the political and economic systems of the nations within which they operate' (Hachten, 1987: 16). Because the Chinese government

established *China Daily* to present information about China to an international English readership (Luther and Zhou, 2005), its articles are considered to characterize China as the Chinese government wishes China to be characterized within the global community (Ostini and Fung, 2002). In the MH370 disappearance, *China Daily* predictably focused on the activities of the Chinese government in relation to the crisis. For example, *China Daily* depicts Chinese officials as advocates for Chinese citizens, which supports previous comparative media framing research suggesting that during crises Chinese media frame the Chinese government positively whereas U.S. media frame the Chinese government negatively (Feng et al., 2012).

Diplomatic relations between and among countries also affect media coverage of an international aviation crisis (Yan and Kim, 2015). Malaysia–U.S. relations, although strained at times because of U.S. involvement in Islamic countries, are improving. China–U.S. relations are complicated as the two countries vie for global economic and militaristic power. The most salient diplomatic relationship in media coverage of the MH370 crisis, however, is Malaysia–China relations with Malaysians as the risk generators and Chinese as the risk bearers. Prior to the MH370 disappearance, Malaysia and China were organizing various activities throughout 2014 to celebrate diplomatic friendship between the two countries. China is well known for its panda diplomacy, or the gifting of Chinese pandas to a country as a sign of friendship and cooperation, but the scheduled delivery of pandas to Malaysia in honor of the 40th anniversary of China–Malaysia relations was initially postponed after the MH370 crisis. *New Straits Times* covered the panda delay and other aspects of China–Malaysia relations such as the Chinese boycott of Malaysia tourism more prominently than did *China Daily* and *The New York Times*. Though not state owned, *New Straits Times* is pro-government and nationalistic (Sani, 2005).

However, in an attempt to maintain good standing with the regional superpower, *New Straits Times* accepted China as a hegemon and emphasized Malaysia did not want the MH370 crisis to damage its cordial exchanges with China. With this background in mind, the three research questions are discussed in relation to the findings and literature review.

Crisis media frames

The first primary objective of this study was to assess how English-language newspapers in Malaysia, China, and the United States framed the MH370 crisis in terms of attribution of responsibility, conflict, economic consequences, human interest, and morality. Overall, the most common frame was attribution of responsibility, which involved responsibility for causing the disappearance of flight MH370 as well as responsibility for alleviating the harms resulting from the crisis. Among the three publishers, *The New York Times* most frequently employed information about causality within articles with the attribution frame and most frequently suggested multiple causes as credible, including accidental pressure loss or engine

failure, terrorism plots, and a pilot suicide mission. *The New York Times* also reported a CNN poll that indicated 9% of Americans believed space aliens hijacked the plane. In contrast, *China Daily* assigned causality the least frequently. Two reasons likely explain this result. First, from a cultural perspective, Chinese are more comfortable with uncertainty and ambiguity than are Malaysians and even more so than are Americans (The Hofstede Center, n.d.). Second, similar to the response of Chinese media during a 2013 aviation crisis, *China Daily* might be reluctant to ascribe causality in order to bolster a reputation as a good international citizen, as opposed to one as a menace, in the global community (Yan and Kim, 2015).

Entman (2005) contends a central function of media frames is to propose solutions to problems. In organizational crises, however, U.S. media and foreign media offer different solutions to problems associated with an international crisis (Schultz et al., 2012). Among the three publishers, *New Straits Times* most often attributed responsibility to the domestic government, provided solutions to the crisis, and specified the crisis required immediate action. For example, a 26 March 2014 article in *New Straits Times* reported 'the Malaysian investigation team has set up an international working group, comprising agencies with expertise in satellite communications and aircraft performance, to take this work forward' (Abas et al., 2014: 7), and a 27 March 2014 article reported Malaysia Airlines personnel were 'taking care of the next of kin and crafting ways and means to nurse the struggling airline back in shape' (Hamid, 2014: 6). Such responses are expected considering that in March 2014 the Malaysian government owned almost 70% of the Malaysia Airlines stock and a prompt, appropriate resolution to the crisis would increase the likelihood of organizational survival.

New Straits Times, *China Daily*, and *The New York Times* each suggested foreign governments are necessary to help alleviate the crisis and recognized the need for multiple actors in the global community to collaborate in the search for the missing aircraft. For example, in a 10 March 2014 article, *China Daily* praised China's 'all-out efforts to locate the missing passengers' and asserted 'experts have weighed in on the importance of China's role in the salvage mission' (China Daily, 2014a: A1). Li Jinming of Xiamen University said China's 'marine forces are better equipped compared with many neighboring countries' (China Daily, 2014a: A1). By highlighting China's advanced military technology and patrol vessels, the article reminded the world that China is indeed a regional, if not global, power. However, *China Daily* also emphasized international collaboration. For example, a 7 April 2014 article urged Chinese to voice frustrations 'in a proper and reasonable manner' because 'all the nations involved in the search need the cooperation and support of the [Chinese] people' (Zhao, 2014: A12). In an article published on 18 June 2014, *The New York Times* accentuated the coordinated military efforts among Australia, China, Japan, Malaysia, New Zealand, South Korea, and the United States—even 'countries that have had considerable frictions lately'—in the MH370 search (Bradsher, 2014: A4).

The conflict frame was second most common in *New Straits Times* articles, while the human-interest frame was second most common in both *China Daily* and *The New York Times* articles. For example, amid international criticism of the Malaysia Airlines' handling of the MH370 crisis, a 27 March 2014 article in *New Straits Times* used the conflict frame by reporting many Malaysians support Malaysia Airlines CEO Ahmad Jauhari Yahya because he 'handled the MH370 crisis in a composed and calm manner, and that there was no ground to call for his resignation' (Lingan, 2014: 12). Furthermore, *New Straits Times* articles addressed the domestic political conflict concurrent with the MH370 crisis in which government critics and civil society disparaged the hegemony of Malaysia's ruling elite. For example, a 9 April 2014 article accused the opposition party of posting MH370-related information online 'to provoke and incite hatred towards Malaysia' (News Straits Times, 2014: 8).

The human-interest frame most often employed personal vignettes to emphasize how the MH370 disappearance affected the next of kin. For example, *The New York Times* (2014) articles emphasized the anger, pain, and tears of Chinese whose children were on board MH370. *China Daily* articles accentuated the pain of Chinese, for example, by naming those who lost their lives and by quoting a woman who lost her mother on MH370: 'An airliner not only carries passengers but also the destinies of hundreds of families' (Hou and Zhu, 2014). An and Gower (2009) show the human-interest frame is commonly applied in coverage about crisis victims. Although it is logical for *China Daily* to provide a 'human face' on the crisis because most of the victims were Chinese, the congruence between *China Daily* and *The New York Times* partially deviates from previous framing studies. Molleda (2011) claims media frame differently according to their geographic location in relation to the crisis location. According to this argument, *New Straits Times* and *China Daily* would frame the crisis more similarly since they are geographically much closer to the organization responsible for the crisis and to the victims of the crisis than is *The New York Times*. In the context of an Asian health crisis, frames in *China Daily* were unlike frames in U.S. media (Luther and Zhou, 2005). However, like this present study, previous aviation crisis research indicates Chinese and U.S. media frames tend to mirror each other (Yan and Kim, 2015).

In coverage of the Asiana Airlines flight 214 crash in 2013, attribution of responsibility was the dominant frame and morality was second most common frame employed in Chinese media (Yan and Kim, 2015). The frequent use of the morality frame is presumably because all passengers except for three Chinese teenagers survived the crash and some of the survivors credited a higher being for their survival (Yan and Kim, 2015). This present study, however, is consistent with other crisis research in which morality was one of the least used frames (Semetko and Valkenburg, 2000). While the morality frame was not a dominant frame for any of the three publishers, the morality frame was lowest for *China Daily*. Fearing that religion will influence politics and detract from devotion to the government, the Communist Party of China discourages religious practice. According to the Global Index of Religiosity and Atheism, China is the most

atheistic among all countries, while Malaysia ranks very high for religiosity (Gallup, 2012). The dominant Islamic religious ideology in Malaysian culture impacted media frames as *New Straits Times* used the morality frame the most among the three publishers to relay moral messages and to offer social prescriptions for behavior. For example, Nazrin Shah, the Sultan of Perak in Malaysia, addressed the opening of the state legislative assembly by stating, 'Humans can only plan for the best, but Allah decides everything' (Hussain et al., 2014b: 7). Additional articles in *New Straits Times* made references to prayer and trusting in Allah, although the Malaysian government distanced itself from reports that a shaman with magic bamboo binoculars assisted with the search efforts.

National interest frames

The second primary objective of this study was to assess how English-language newspapers in Malaysia, China, and the United States used national interest frames. While Yan and Kim (2015) show that political context and national interests affect media coverage of an aviation crisis as far as the types of sources that journalists utilize, this present study analyzed the nuance of national interest frames in international media. *New Straits Times* used the sociocultural frame most frequently, which is consistent with previous research indicating that journalistic norms in Southeast Asia promote national loyalty and a sense of community (Massey, 2000; Menon, 1998). The sociocultural frame included information about the beliefs, myths, values, norms, special artifacts, and/or social practices of the country. For example, *New Straits Times* referred to Malaysian songs and poetry recitations to pacify mourners and to the educational and scientific endeavors of Malaysians, e.g., Dr Mohd Rizal Arshad of the University of Science in Malaysia, an expert on acoustic imaging devices, and Datuk Azharuddin Abdul Rahman, the director-general of Malaysia's Department of Civil Aviation, an expert in search-and-recovery missions (Arumugam, 2014; Hussain et al., 2014c). Chinese and U.S. media were again congruent and employed the military frame most frequently. For example, *China Daily* articles emphasized the use of Chinese satellites and naval vessels, including amphibious landing vessels, missile destroyers, and supply ships, to solve the MH370 mystery (China Daily, 2014b).

Another interesting point related to national interest frames is *New Straits Times* employed all five of the national interest frames (economy, military, sociocultural values, political system, and security) among the articles in the dataset, while *China Daily* and *The New York Times* articles applied only three national interest frames each. This is concurrent with research proposing journalists express more national loyalty when the news is perceived as 'ours' rather than 'theirs' (Nossek, 2004). *New Straits Times* was arguably closest to the crisis among the three publishers; thus, it was 'our' crisis and necessitated national interest frames within the dominant ideological culture. For example, in a 14 March 2014 statement, Defense and acting Transport Minister Datuk Seri Hishammuddin Hussein said Malaysia has a

'duty to follow every lead. We owe it to the families. And we will not give up' (Hussain et al., 2014a: 3). *China Daily* and *The New York Times* reported on 'their' crisis, which did not require as many national interest frames. For example, *The New York Times* reported on a meeting between Chinese officials and the families of MH370 passengers at which Liu Zhi, deputy secretary general of the Beijing government, indicated China was doing everything it could but the crisis was clearly Malaysia's responsibility; however, Liu contended 'the quality of the Malaysians' response would certainly be lower if the Chinese government were not involved' (Feng and Wong, 2014: A6). These findings support Dai and Hyun's (2010) summary of their research that 'lends support to the transformational view of globalization, which suggests that the nation state still matters in a globalized world, but is being recontextualized in a more complex world of politics and culture' (p. 299).

International citizenship frames

The third objective of this study was to assess how English-language newspapers in Malaysia, China, and the United States employed frames about international citizenship. While Yan and Kim (2015) focus on national interests within an aviation crisis, this present study expands a theoretical understanding of international citizenship frames within the context of a crisis with an unknown cause. The dominant frame for *New Straits Times*, *China Daily*, and *The New York Times* was the willingness to work together to complete international tasks, probably because of the enormity of the effort required to search for MH370 in the expansive Indian Ocean. *New Straits Times* used four of the frames (cooperation in formal agreements, willingness to work together, ethical behavior, and global leadership), while *China Daily* and *The New York Times* only used two distinct international citizenship frames each. For example, a 16 March 2014 article in *New Straits Times* used the ethical behavior frame by defending Malaysia's withholding of information, which was 'the responsible thing to do to avoid causing more anguish to family members' (Andres, 2014: 23). Further, a 15 May 2014 *New Straits Times* article used the cooperation frame as Prime Minister Datuk Seri Najib Razak 'urged the International Civil Aviation Organisation to increase regulations for real-time tracking of airliners' and the leadership frame as Najib commended Malaysia for overcoming diplomatic and military sensitivities and uniting 26 countries for the search (Latif, 2014: 2).

Another observation associated with international citizenship is the timing of articles among the three publishers. *The New York Times* published the highest number of articles about MH370 in the first week after the aircraft's disappearance. This is consisted with research that shows U.S. media typically report on aviation crises the most during the first week (Vincent et al., 1989; Yan and Kim, 2015). This study offers evidence that *New Straits Times* disseminated information about the MH370 crisis quickly to support the Malaysian global image and reputation as competent. *New Straits Times* published the highest number of articles in the

second week after the MH370 disappearance. *China Daily*, however, published the highest number of articles 12 weeks after the aircraft disappeared. Perhaps as time continued without much evidence to indicate what actually happened to MH370, it became more important for the Chinese government to establish an identity as a caregiver who helps citizens. For example, a 25 August 2014 article in *China Daily* quoted a Chinese graduate student: 'Malaysia Airlines and others are not doing their jobs, so we have to organize' (China Daily, 2014c: A2). *China Daily* focused on the Chinese perspective and rarely expressed an international perspective. In this manner, *China Daily* seemingly functioned as an official voice for the Chinese government in the MH370 crisis, while *New Straits Times* was more internationally focused during the crisis. Because Malaysia Airlines is an extension of the Malaysian government, Malaysia had to present itself as a good international citizen to preserve its global reputation.

Conclusion

An and Gower (2009) argued that attribution of responsibility is especially dominant in crises with controllability and intentionality. The results of this present study confirm previous research that indicates attribution of responsibility is the most commonly applied frame in crisis communication (Semetko and Valkenburg, 2000). In addition, this present study adds another dimension to theoretical knowledge in that attribution of responsibility is yet the most important frame even when the controllability of the crisis is unknown and the intentionality is ambiguous.

This present study further expands previous knowledge about the second common frame in an aviation crisis with an unknown cause. In business crises the economic consequences frame is the second most used (An and Gower, 2009), and in political crises the conflict frame is the second most used (Semetko and Valkenburg, 2000). The conflict frame in *New Straits Times* and the human-interest frame in *China Daily* and *The New York Times* were the second most used.

This present study's unique combination of media frames with national interests and international citizenship in the crisis context is a response to previous quantitative content analysis research. The results extend beyond descriptive analysis to provide insight about media orientations during an international crisis. Although each newspaper employed a different focus of responsibility, attribution of responsibility was the dominant frame, which demonstrates it is the most important frame even with unknown controllability and ambiguous intentionality. Results also demonstrate significant differences in national interest frames perhaps partially influenced by different national media systems and by diplomatic relations between and among countries, which reinforces the findings of Yan and Kim (2015). This present study differentiates international citizenship frames and considers the timing of information dissemination to give a more nuanced understanding of crisis media frames.

Since this present study is one of the first to frame a crisis with ambiguous causality, additional research to consider national interests and culture, international citizenship, and media related to a crisis without direct causality is warranted. Specifically, additional research is necessary to understand the interactions among national interest, international citizenship, and media frames. Furthermore, replication of this study is important to substantiate its findings. The results of additional studies combined with the present results have the potential to influence crisis typology research, attribution theory research, and even paracrisis-focused research.

Research with a greater sample size beyond English-language newspapers would be helpful to understand more acutely the frames employed in such crises to reach domestic and international audiences. Coauthoring with international scholars who study the culture and understand the nuances of other languages involved in international crises would strengthen this line of research.

Overall, this study advances theoretical knowledge about media frames within the context of an aviation crisis with an unknown cause. This study was a unique exploration of the role of national interest frames and international citizenship frames in media coverage of the flight MH370 disappearance, a mysterious international crisis without precedent.

Declaration of Conflicting Interests

The author(s) declared no potential conflicts of interest with respect to the research, authorship, and/or publication of this article.

Funding

The author(s) received no financial support for the research, authorship, and/or publication of this article.

References

Abas A, Jamaludin MH, Abdullah NI, et al. (2014) Doppler effect used to track jet. *New Straits Times*, 26 March, 7.

Akhavan-Majid R and Ramaprasad J (1989) Framing and ideology: A comparative analysis of U.S. and Chinese newspaper coverage of the Fourth United Nations Conference on Women and the NGO Forum. *Mass Communication and Society* 1(3/4): 131–152.

An SK and Gower KK (2009) How do the news media frame crises? A content analysis of crisis news coverage. *Public Relations Review* 35(2): 107–112.

Andres L (2014) Eyes of the world are on us. *New Straits Times*, 16 March, 23.

Arumugam T (2014) Tripartite meeting positive and productive. *New Straits Times*, 8 May, 8.

Australian Transport Safety Bureau (2016) Joint agency coordination center: MH370 operational search update. Available at: https://www.atsb.gov.au/mh370-pages/updates/operational-update/.

Bereciartu GJ (1994) *Decline of the Nation-State* (Trans. Douglass WA). Las Vegas: University of Nevada Press.

Bradsher K (2014). Australia to revisit area of Indian Ocean in search for missing jet. *The New York Times*, 18 June, A4.
Brewer P (2006) National interest frames and public opinion about world affairs. *The Harvard International Journal of Press/Politics* 11(4): 89–99.
Brown G (2005) The rough and rosy road: Sites of contestation in Malaysia's shackled media industry. *Pacific Affairs* 78: 39–56.
Bryant J and Miron D (2004) Theory and research in mass communication. *Journal of Communication* 54(4): 662–704.
Carragee M and Roefs W (2004) The neglect of power in recent framing research. *Journal of Communication* 54(2): 214–233.
Centre for Aviation (2014) Malaysia airlines 1H2015 outlook: More losses as capacity levels are maintained prior to transition. Available at: http://centreforaviation.com/analysis/malaysia-airlines-1h2015-outlook-more-losses-as-capacity-levels-are-maintained-prior-to-transition-201123.
China Daily (2014a) Experts emphasize China's role in rescue mission, 10 March.
China Daily (2014b) Chinese naval vessels move southward in MH370 search, 16 April.
China Daily (2014c) MH370 families unite so seek answers, 25 August.
Cho SH and Gower KK (2006) Framing effect on the public's response to crisis: Human interest frame and crisis type influences responsibility and blame. *Public Relations Review* 32(4): 420–422.
Coombs WT (2007) Protecting organization reputations during a crisis: The development and application of situational crisis communication theory. *Corporate Reputation Review* 10(3): 163–176.
Coombs WT and Holladay SJ (1996) Communication and attribution in a crisis: An experiment study in crisis communication. *Journal of Public Relations* 8(4): 279–295.
Dai J and Hyun K (2010) Global risk, domestic framing: Coverage of the North Korean nuclear test by US, Chinese, and South Korean news agencies. *Asian Communication Journal* 20(3): 299–317.
Defense News (2013) Defense news top 100 for 2013. Available at: http://special.defensenews.com/top-100/charts/rank_2013.php?c=FEAands=T1C.
Dorogi TL (2001) *Tainted Perceptions*. Lanham, MD: University Press of American.
Downing JDH (1988) Trouble in the backyard: Soviet media reporting on the Afghanistan conflict. *Journal of Communication* 38(2): 5–32.
Entman RM (1991) Framing U.S. coverage of international news: Contrasts in narratives of the KAL and Iran air incidents. *Journal of Communication* 41(4): 6–27.
Entman RM (1993) Framing: Toward clarification of a fractured paradigm. *Journal of Communication* 43(4): 51–58.
Entman RM (2005) *Projections of Power: Framing News, Public Opinion, and U.S. Foreign Policy*. Chicago, IL: University of Chicago Press.
Feng B and Wong E (2014) Anger over plane turns to frustration. *The New York Times*, 11 March, A6.
Feng M, Brewer PR and Ley BL (2012) Framing the Chinese baby formula scandal: A comparative analysis of US and Chinese news coverage. *Asian Journal of Communication* 22(3): 253–269.
Freitag AR and Stokes AQ (2009) *Global Public Relations: Spanning Borders, Spanning Cultures*. New York: Routledge.

Gallup (2012) Global index of religiosity and atheism. Available at: http://www.wingia.com/web/files/news/14/file/14.pdf.

Gamson WA, Croteau D, Hoynes W, et al. (1992) Media images and the social construction of reality. *Annual Review of Sociology* 18: 373–393.

Ghanem S (1997) Filling in the tapestry: The second level of agenda setting. In: McCombs ME, Shaw DL and Weaver DH (eds) *Communication and Democracy: Exploring the Intellectual Frontiers in Agenda-Setting Theory*. Mahwah, NJ: Lawrence Erlbaum, pp. 3–14.

Glum J (2016) Flight MH370 update: Search for missing plane prompts victims' families to seek legal help from American lawyers. Available at: http://www.ibtimes.com/flight-mh370-update-search-missing-plane-prompts-victims-families-seek-legal-help-2431672 .

Goffman E (1974) *Frame Analysis: An Essay on the Organization of Experience*. Boston, MA: Northeastern University Press.

Gotsi M, Lopez C and Andriopoulos C (2011) Building country image through corporate image: Exploring the factors that influence the image transfer. *Journal of Strategic Marketing* 19(3): 255–272.

Grant KB (2014) 2014: Deadly year for flying – But safer than ever. *CNBC*, 30 December. Available at: http://www.cnbc.com.

Hachten WA (1987) *The World News Prism: Changing Media of International Communication*. Ames: Iowa State University Press.

Hall S (1980) Encoding/decoding. In: Hall S, Hobson D, Lowe A, et al. (eds) *Culture, Media, Language: Working Papers in Cultural Studies, 1972–79*. London: Routledge, pp. 128–138.

Hall S (1997) The work of representation. In: Hall S (ed.) *Representation: Cultural Representations and Signifying Practices*. London: SAGE, pp. 13–64.

Hamid AJ (2014) Hard decisions lie ahead for MAS. *New Straits Times*, 27 March, 6.

Hassid J and Repnikova M (2016) Why Chinese print journalists embrace the Internet. *Journalism* 17(7): 882–898.

The Hofstede Center (n.d.) Available at: http://geert-hofstede.com.

Hook SW and Pu X (2006) Framing Sino-American relations under stress: A reexamination of news coverage of the 2001 spy plane crisis. *Asian Affairs: An American Review* 33(3): 167–183.

Hou L and Zhu X (2014) 'I know what they are feeling.' *China Daily*, 19 July.

Hume J (2010) Memory matters: The evolution of scholarship in collective memory and mass communication. *The Review of Communication* 10: 181–196.

Hussain H, Abas A, David A, et al. (2014a) 'We will spare nothing in our search efforts'. *New Straits Times*, 14 March, 3.

Hussain H, Abas A, Dermawan A, et al. (2014b) Regent: It's heart-wrenching. *New Straits Times*, 1 April, 7.

Hussain H, Karim, FN, Abas A, et al. (2014c) Netizens show they care. *New Straits Times*, 17 March, 5.

International Air Transport Association (2014) Annual review. Available at: http://www.iata.org/publications/Documents/iata-annual-review-2014-en.pdf.

Jalarajan Raj A and Sreekumar R (2012) Covenant cog or functional fourth estate: A survey of Malaysian journalists' attitude towards their profession. *Jurnalism si Comunicare* 7(1): 16–32.

Jamieson A and Ciganinero J (2015) MH370 flaperon is confirmed as first debris from missing Malaysian flight. Available at: http://www.nbcnews.com/storyline/missing-jet/mh370-flaperon-confirmed-first-debris-missing-malaysia-flight-n421061.

Knight MG (1999) Getting past the impasse: Framing as a tool for public relations. *Public Relations Review* 25(3): 381–398.

Kucherenko VV and Christen CT (2014) Ability to spot and resist manipulated news media about international affairs: Does political knowledge provide it? *Central European Journal of Communication* 12: 51–66.

Latif R (2014) Najib: Real-time tracking of aircraft long overdue. *New Straits Times*, 15 May, 2.

Lee BK (2004) Audience-oriented approach to crisis communication: A study of Hong Kong consumers' evaluation of an organizational crisis. *Communication Research* 31(5): 600–618.

Lee CC, Li H and Lee FLF (2011) Symbolic use of decisive events: Tiananmen as a news icon in the editorials of the elite U.S. press. *The International Journal of Press/Politics* 16(3): 335–356.

Lee ST and Basnyat I (2013) From press release to news: Mapping the framing of the 2009 H1N1 A influenza pandemic. *Health Communication* 28(2): 119–132.

Li X (2003) National interest and coverage of U.S.-China relations: A content analysis of *The New York Times* and *People's Daily* (1987–1996). *International Communication Bulletin* 38: 29–41.

Lingan L (2014) Union's quit demand to CEO draws flak. *New Straits Times*, 27 March, 12.

Liu B and Pennington-Gray L (2015) Bed bugs bite the hospitality industry? A framing analysis of bed bug news coverage. *Tourism Management* 48: 33–42.

Luther CA and Zhou X (2005) Within the boundaries of politics: News framing of SARS in China and the United States. *Journalism and Mass Communication Quarterly* 82(4): 857–872.

McCombs ME (2005) A look at agenda-setting: Past, present and future. *Journalism Studies* 6(4): 543–557.

McCombs ME, Llamas JP, Lopez-Escobar E, et al. (1997) Candidate images in Spanish elections: Second-Level agenda-setting effects. *Journalism and Mass Communication Quarterly* 74(4): 703–717.

McLuskey M and Kim YM (2012) Moderatism or polarization: Representations of advocacy groups' ideology in newspapers. *Journalism and Mass Communication Quarterly* 89(4): 565–584.

Malaysia Airlines (2014) *Malaysia Airlines flight incident* (news release). Available at: http://www.malaysiaairlines.com/my/en/site/mh370.html.

Malaysia Airlines' future still uncertain (2016) Available at: http://www.skynews.com.au/news/world/asiapacific/2016/03/08/malaysia-airlines–future-still-uncertain.html.

Mao Z (2014) Cosmopolitanism and global risk: News framing of the Asian financial crisis and the European debt crisis. *International Journal of Communication* 8: 1029–1048.

Massey BL (2000) How three Southeast-Asian newspapers framed "The Haze" of 1997–98. *Asian Journal of Communication* 10(1): 72–94.

Mehra A (1993) Introduction. In: Mehra A (ed.) *Press Systems in ASEAN States*. Singapore: Asian Media Information and Communication, pp. 1–11.

Menon V (1998) Forward. In: Latif A (ed.) *Walking the Tightrope: Press Freedom and Professional Standards in Asia*. Singapore: Asian Media Information and Communication, pp. iv–iiiv.

Missing Malaysia Airlines MH370 (2014) Available at: http://www.news.com.au/world/missing-malaysia-airlines-mh370-a-media-challenge/story-fndir2ev-1226859718262.

Molleda JC (2011) Advancing the theory of cross-national conflict shifting: A case discussion and quantitative content analysis of a transnational crisis' newswire coverage. *International Journal of Strategic Communication* 5(1): 49–70.

Neuendorf KA (2002) *The Content Analysis Guidebook*. Thousand Oaks, CA: SAGE.

Neuman WR, Just MR and Crigler AN (1992) *Common Knowledge*. Chicago, IL: University of Chicago Press.

New Straits Times (2014) Cyber troopers 'out to tarnish image', 8 April.

New York Times (2014) Frustration turns to anger over missing flight, 10 March.

Nossek H (2004) Our new and their news: The role of national identity in the coverage of foreign news. *Journalism* 5(3): 343–368.

Novais RA (2007) National influence in foreign news. *The International Communication Gazette* 69(6): 553–573.

Orgeret KS (2010) Mediated culture and the well-informed global citizen: Images of Africa in the global north. *Nordicom Review* 31(2): 47–61.

Ostini J and Fung AYF (2002) Beyond the four theories of the press: A new model of national media systems. *Mass Communication and Society* 5(1): 41–56.

Paletz DL and Vinson CD (1994) Constructing content and delimiting choice: International coverage of KAL Flight 007. *Argumentation* 8: 357–370.

Palmlund I (1992) Social drama and risk evaluation. In: Krimsky S and Golding D (eds) *Social Theories of Risk*. Westport, CT: Praeger, pp. 197–212.

Palmlund I (2009) Risk and social dramaturgy. In: Heath RL and O'Hair HD (eds) *Handbook of Risk and Crisis Communication*. New York: Routledge, pp. 192–204.

Pan ZP and Kosicki GM (1993) Framing analysis: An approach to news discourse. *Political Communication* 10(1): 55–75.

Park H and Reber BH (2010) Using public relations to promote health: A framing analysis of public relations strategies among health associations. *Journal of Health Communication* 15(1): 39–54.

Park J (2013) Contrasts in the coverage of Korea and Japan by US television networks: A frame analysis. *International Communication Gazette* 65(2): 145–164.

Park S, Bier LM and Palenchar MJ (2016) Framing a mystery: Information subsidies and media coverage of Malaysia Airlines flight 370. *Public Relations Review* 42(4): 654–664.

Paterson CA (1999) Agency source influence on television foreign reporting: Case of Mururoa and Tahiti. *Asia Pacific Media Educator* 7(2): 16–36.

Pert A (2014) *Australia as a Good International Citizen*. Annandale: The Federation Press.

Pinsdorf MK (1991) Flying different skies: How cultures respond to airline disasters. *Public Relations Review* 17(1): 37–56.

Quest R (2016) *The Vanishing of Flight MH370: The True Story of the Hunt for the Missing Malaysian Plane*. New York: Berkley.

Ramanathan S (2016) Cross-cultural perspectives and influences in reporting airline disasters: The MH370 episode. *Media Asia* 43(1): 23–34.

Riffe D, Lacy S and Fico FG (2005) *Analyzing Media Messages: Using Quantitative Content Analysis in Research*. New York: Routledge.

Ruigrok PC and van Atteveldt W (2007) Global angling with a local angle: How U.S., British, and Dutch newspapers frame global and local terrorist attacks. *The Harvard International Journal of Press and Politics* 12(1): 68–90.

Said EW (1993) *Culture and Imperialism*. New York: Knopf.

Sani MAM (2005) Media freedom in Malaysia. *Journal of Contemporary Asia* 35(3): 341–367.

Santos CA, Tainsky S, Schmidt KA, et al. (2013) Framing the octagon: An analysis of news-media coverage of mixed martial arts. *International Journal of Sport Communication* 6(1): 66–86 .

Schattle H (2015) Global citizenship as a national project: The evolution of *segye shimin* in South Korean public discourse. *Citizenship Studies* 19(1): 53–68.

Scherer DA (2016) The FCC's rules and policies regarding media ownership, attribution, and ownership diversity. *Journal of Current Issues in Media and Telecommunications* 8(1): 45–66.

Scheufele DA and Tewksbury D (2007) Framing, agenda setting, and priming: The evolution of three media effects models. *Journal of Communication* 57(1): 9–20.

Schultz F, Kleinnijenhuis J, Oegema D, et al. (2012) Strategic framing in the BP crisis: A semantic network analysis of associative frames. *Public Relations Review* 38(1): 97–107.

Semetko HA and Valkenburg PM (2000) Framing European politics: A content analysis of press and television news. *Journal of Communication* 50(2): 93–109.

Shoemaker PJ and Reese SD (1996) *Mediating the Message: Theories of Influences on Mass Media Content*. London: Longman.

Steele J (2011) Justice and journalism: Islam and journalistic values in Indonesia and Malaysia. *Journalism* 12(5): 533–549.

Steele J (2013) 'Trial by the press': An examination of journalism, ethics, and Islam in Indonesia and Malaysia. *The International Journal of Press/Politics* 18(3): 342–359.

Tai Z and Sun T (2007) Media dependencies in a changing media environment: The case of the 2003 SARS epidemic in China. *New Media and Society* 9(6): 987–1009.

Taylor M and Kent ML (1999) Challenging assumptions of international public relations: When government is the most important public. *Public Relations Review* 25(2): 131–144.

Tunstall J (1977) *The Media are American. Anglo-American Media in the World*. London: Constable.

Van Gorp B (2007) The constructionist approach to framing: Bringing culture back in. *Journal of Communication* 57(1): 60–78.

Vankin J (2016) Watch '60 Minutes' Malaysia Airlines flight MH370 story stream online: Cover-up of "rogue pilot" taking plane, program charges. Available at: http://www.inquisitr.com/3367944/malaysia-airlines-flight-mh370-60-minutes/.

Vincent RC, Crow BK and Davis DK (1989) When technology fails: The drama of airline crashes in network television news. *Journalism Monographs* 117: 46–54.

Wardell J (2014) Search for MH370 to be most expensive in aviation history. *Reuters*. Available at: http://www.reuters.com.

Westcott B (2016) Third piece of plane wreckage confirmed as MH370 debris. CNN, 7 October. Available at: http://www.cnn.com/2016/10/07/asia/mh370-mauritius-debris-confirmed/.

Willnat L and Wong WJ (2013) Online media and political participation: The case of Malaysia. *Mass Communication and Society* 16: 557–585.

World Press Freedom Index (2014) Available at: https://rsf.org/index2014.

Yan Y and Kim Y (2015) Framing the crisis by one's seat: A comparative study of newspaper frames of the Asiana crash in the U.S.A., Korea, and China. *Asian Journal of Communication* 25(5): 486–506.

Zaremba AJ (1988) *Mass Communication and International Politics: A Case Study of Press Reactions to the 1973 Arab-Israeli War*. Salem, WI: Sheffield.

Zhang Y, Jin Y and Tang Y (2015) Framing depression: Cultural and organizational influences on coverage of a public health threat and attribution of responsibilities in Chinese news media, 2000–2012. *Journalism and Mass Communication Quarterly* 92(1): 99–120.

Zhao L (2014) Calls for patience despite progress. *China Daily*, 7 April.

Zhao Y (2000) From commercialization to conglomeration: The transformation of the Chinese press within the orbit of the party state. *Journal of Communication* 50(2): 3–26.

Conspiracy Theories: Psychology Behind Flight MH370

Sara Moundi

Abstract

Recent research into the psychology of conspiracy theories has emphasized the importance of belief systems in the acceptance or rejection of conspiracy theories. As for the acceptance of conspiracy theories, a plethora of research has made the argument that the public buys into the idea of conspiracy theories because we as human beings need to be able to make sense of the world around us. We are curious of the unknown and cannot leave any questions unanswered. Many researchers have confirmed that this is the reason behind why people believe in conspiracy theories so this has become the 'accepted universal' as to why conspiracy theories are developed. However, there is scarce information available as to why people believe the particular conspiracy theory (or explanation(s)) that they do. This paper will use experimental data to analyze the top twelve conspiracy theories associated behind what happened to the Malaysia airlines flight number MH370 and the different personality types that would lead one to come to each conclusion.

Introduction

The significance of this study is to understand why people think what they do. Conspiracy theories have been around since the beginning of time. The explanation that many credible researchers, such as Marina Abalakina-Paap, have reached regarding why humans come up with conspiracy theories is that we constantly need to be able to make sense of the world around us, but there is little research behind why each person believes what he or she does. This paper looks at the twelve most popular theories that people have come up with for the explanation of the disappearance of the MH370 flight. The MH370 flight was a Malaysia airlines flight that disappeared on March 8, 2014 as it was flying from Kuala Lumpur, Malaysia to Beijing, China. There were 227 passengers and 12 crewmembers on board this flight. Through the extensive efforts of experts and search teams there still has been no confirmed debris or crash site of the plane, but there have been many conspiracy theories that have surfaced addressing what many think happened to the plane. This paper will address how the twelve most popular conspiracy theories associated with the MH370 disappearance correlate with the big five personality traits. The hypothesis is that each personality trait with correlate with specific conspiracy theories leading to the conclusion that personality factors into one's belief system.

Past Research

Other research that has been done which compares to this study was on conspiracy theories behind the 9/11 terrorist attacks by Michael J. Woods and Viram Swami. Woods' research he came to the conclusion that people come to believe in conspiracy theories because of the power of suggestion. He used different conspiracy theories behind the 9/11 attacks and simply just presented them in different ways. Woods found that the way the media or other external sources present ideas to people has a major role on persuading them to believe it. Woods use the same surveying tactics that this study suggests but his main focus does not examine the psychology behind conspiracy theories and why people believe the things that they do. Woods addresses this and measures conspiracy theories using personality factors but that was not the emphasis of his study. Another study that was done by Viram Swami focused looking at the actual psychology behind conspiracy theories. Swami uses the big five personality factor along with many other

demographics and descriptive statistics (such as age, ethnicity religion, etc.) to find a correlation between that and conspiracy beliefs. Swami's research tends to focus more on other descriptive statistics and not solely on personality. The focus of this research is exclusively on conspiracy theories and the big five personality factors. Because he was measuring more than just personality, Swami used a 17 item big five personality questionnaire and this research will use a 46 item questionnaire. This research will conduct a more comprehensive investigation to understand the personality types of individuals and then aim to find a more accurate correlation between personality types and different conspiracy theories.

Materials and Methods

In order to test the notion of this experiment, a survey will be conducted that measures the participant's personality type, and then list the top twelve conspiracy theories associated with the MH370 disappearance where the individual will state how much they believe in each theory. The conspiracies that are used in the survey were found on the comment sections of various online news articles. Samples were taken from news articles posted between March 8th and October 15, 2014 on four mainstream news websites: ABC (American Broadcasting Company) News, CNN, the *Independent*, and the *Daily Mail*. The four news sites were selected on the reasoning that an ideal sample would not be restricted to a single country, journalistic style, or ideological position, as well as for more practical reasons, such as search capabilities, comment archiving and unpaid access.

The following twelve conspiracy theories will be used:

Alien Abduction: This theory suggests that space aliens are behind the disappearance of the flight. It has been claimed that some passengers' cellular phones were ringing when they were called and satellites shoed no mid-air explosion.

MH370 and MH17 were the same plane: This theory suggests that the plane that crashed in a field in Ukraine was the lost MH370 flight and not flight MH17, which was scheduled to depart from Amsterdam and arrive in Kuala Lumpur, Malaysia.

The plane was shot down: This theory suggests that the plane was accidently shot down by US-Thai joint strike fighters in a military exercise in the South China Sea. This theory also claims that search and rescue efforts were deliberately sent in the wrong direction as part of a cover up.

Asian Bermuda Triangle: This theory suggests that the area where MH370 vanished is on the exact opposite side of the globe to the Bermuda Triangle and the plane disappeared there.

The CIA is behind it: This theory was suggests that in this day and age there is no way that a plane can just disappear and the American CIA is covering something up that it does not want the public to know.

9/11 style hijacking mission: This theory suggests that Israeli agents planned to crash the Malaysia Airlines plane into a building and then blame it on Iranian forces.

High-tech hijacking: This theory suggests that MH370 was the product of the world's first cyber hijacking, accomplished by accessing the airplane's flight computer and reprogramming the speed, altitude and direction of the plane.

Cracks in the plane: This theory suggests that slow decompression of the cabin left pilots and passengers unconscious. Pilots would not have been

able to put their oxygen masks on in time and passengers would not have been able to detect any oxygen deprivation.

Microchip 'Kinesis KL-02' motive: Kinesis KL-02 is the world's smallest microcontroller. Twenty tech employees working for Freescale Semiconductor, the company that invented the microcontroller and is currently testing it, were on board the flight. Drone technology using the microcontroller changed the course of the flight and left it undetectable. The flight landed in Diego Garcia in the Indian Ocean. The motive was to prevent the technology from falling in the hands of Iran because it would have become a nightmare for Israeli defense forces.

US Military Base: This theory suggests that MH370 landed at a US military base in Diego Garcia, which is located in the Indian Ocean.

Life Insurance Scam: This theory suggests that someone on board the flight bought a huge sum of life insurance and wants family to gain from it.

Pilot Suicide: This theory claims that the captain of the plane hijacked the plane on a suicide mission after his wife left him.

Based on a cognitive psychological standpoint, the big five personality factors will be used to establish a correlation between the participant's belief or denial in the top twelve conspiracy theories. The big five personality traits are the five basic dimensions of personality as proposed by personality psychologists:

Extraversion: This trait includes characteristics such as excitability, sociability, talkativeness, assertiveness and high amounts of emotional expressiveness.

Agreeableness: This personality dimension includes attributes such as trust, altruism, kindness, affection, and other pro social behaviors.

Conscientiousness: Common features of this dimension include high levels of thoughtfulness, with good impulse control and goal-directed behaviors. Those high in conscientiousness tend to be organized and mindful of details.

Neuroticism: Individuals high in this trait tend to experience emotional instability, anxiety, moodiness, irritability, and sadness.

Openness: This trait features characteristics such as imagination and insight, and those high in this trait also tend to have a broad range.

The survey will be assessed using two scales: The first will be a 46 item big five questionnaire, which was created by University of California Berkeley professor Oliver John; this questionnaire assesses the big five personality factors on a 5-point scale (1= strongly agree, 5= strongly disagree). The second will be a MH370 conspiracy belief scale that will be a 12-item scale based on a review of most popular MH370 conspiracy beliefs. Participants will state whether they believe each statement is true or false based on a 9-point scale (1=completely false, 9= completely true).

This experiment will aim to survey 500 participants and the participants will be recruited at random via email. Because this is a lengthy survey, it will take place online. Participants will be required to sign an informed consent form and then continue onto the survey itself.

Expected Results

The analysis of the survey results will be done using a multivariate multiple linear regression on the SPSS program. The results of this

examination of MH370 conspiracist theories can be predicted by a number of personality and individual difference variables. From research that was done conducting a similar experiments involving conspiracy theories behind what happened with the 9/11 terrorist attacks, it is expected that the belief in more radical conspiracy theories will be negatively associated with personality factors of agreeableness and neuroticism, while openness to experience, extraversion and conscientiousness will have a positive association. This experiments is expected to yield the same or very similar results.

Discussion

This research on conspiracy theories could be considered a great stepping-stone for the field of psychology. Other research that has been done aiming to explain the psychological reasoning behind conspiracy theories is that of the 9/11 terrorist attacks. The 9/11 research was not done as extensively as this experiment is because the goal of these other studies was not to solely find a correlation between conspiracy theories and the big five personality factors; there were many other factors involved. The reason why much research has not been done behind the psychology of conspiracy theories is because this is a grey area in psychology. It is ambiguous because it is not something that can be measured using numbers and it can be difficult to interpret; this does not mean that we should not try to understand the psychology behind conspiracy theories. This research can maybe further verify what was found in the study of the 9/11 terrorist attacks and future research can also be conducted with a different set on conspiracy theories so we can have a definite reasoning for why people believe what they do. There is not enough research available to fully verify the findings of this experiment or others like it. More research needs to be done so that the findings of these studies can be looked at as cold hard facts and not just a couple of congruencies among a couple of studies. This study is just one more step towards the goal of proving that there is a scientific reasoning behind why we believe what we do.

References

Abalakina-Paap, M., Stephan, W. G., Craig, T., and Gregory, W. L. (1999). Beliefs in conspiracies. *Pol. Psychol*. 20, 637–647.

John, Oliver P., The Big 5 Personality Test. Web. 2009.

Swami, V., (2010). Unanswered questions; a preliminary investigation of the personality and individual difference predictors of 9/11 conspiracy beliefs. Appl. Cogn. Psychol. 24, 749-761.

Wood, M. J., & Douglas, K. M. (2013). What about building 7? A social psychological study of online discussion of 9/11 conspiracy theories. *Frontiers in Psychology*, 4, 409.

Malaysia Airlines Flight 370

From Wikipedia, the free encyclopedia

Malaysia Airlines Flight 370 (MH370/MAS370)[b] was a scheduled international passenger flight that disappeared on 8 March 2014, while flying from Kuala Lumpur International Airport near Kuala Lumpur, Malaysia, to Beijing Capital International Airport in Beijing, China. The flight last made voice contact with air traffic control at 01:19 MYT (17:19 UTC, 7 March) when it was over the South China Sea, less than an hour after takeoff. The aircraft disappeared from air traffic controllers' radar screens at 01:22.[3][4] Malaysian military radar continued to track the aircraft as it deviated from its planned flight path and crossed the Malay Peninsula. It left the range of Malaysian military radar at 02:22 while over the Andaman Sea, 200 nautical miles (370 km; 230 mi) northwest of Penang in northwestern Malaysia.[5]:3[6] The aircraft, a Boeing 777-200ER, was carrying 12 Malaysian crew members and 227 passengers from 15 nations.[7]

Malaysia Airlines Flight 370

9M-MRO, the aircraft involved in the incident, photographed in 2011

Incident summary	
Date	8 March 2014
Summary	Missing, search ongoing; one flaperon found
Site	Southern Indian Ocean (presumed)
Passengers	227
Crew	12
Fatalities	239 (all, presumed)[a]
Survivors	0 (presumed)[a]
Aircraft type	Boeing 777-200ER
Operator	Malaysia Airlines
Registration	9M-MRO
Flight origin	Kuala Lumpur International Airport
Destination	Beijing Capital International Airport

A multinational search effort began in the Gulf of Thailand and the South China Sea, where the flight's signal was lost on secondary surveillance radar, and was soon[8][9] extended to the Strait of Malacca and Andaman Sea.[10][11][12] Analysis of satellite communications between the aircraft and Inmarsat's satellite communications network concluded that the flight continued until at least 08:19 MYT and flew south into the southern Indian Ocean, although the precise location cannot be determined;[13][14][15] Australia took charge of the search effort on 17 March, when the search shifted to the southern Indian Ocean.[16] On 24 March 2014, the Malaysian government, noting that the final location determined by the satellite communication is far from any possible landing sites, concluded that "flight MH370 ended in the southern Indian Ocean."[13][14][15][17] The current phase of the search is a comprehensive search of the seafloor about 1,800 kilometres (1,100 mi) southwest of Perth, Western Australia, which began in October 2014.[18][19][20] Despite the largest and most expensive search in aviation history,[21][22][23][24] no piece of the aircraft was found for more than a year, and the bulk of the aircraft has not been found, prompting many theories about its disappearance. On 29 July 2015, marine debris was found on Réunion Island which was later confirmed to be a flaperon from Flight 370.[25][26][27]

Malaysia established the Joint Investigation Team (JIT) to investigate the incident, working with foreign aviation authorities and experts.[5]:1 Neither the crew nor the aircraft's communication systems relayed a distress signal, indications of bad weather, or technical problems before the aircraft vanished.[28] Two passengers travelling on stolen passports were initially suspect in the disappearance, but they were later determined to be asylum seekers and terrorism has been ruled out.[29][30][31] Malaysian police have identified the Captain as the prime suspect if human intervention was the cause of the disappearance, after clearing all other passengers of any suspicious motives.[32] Power was lost to the aircraft's satellite data unit (SDU) at some point between 01:07 and 02:03; the SDU logged onto Inmarsat's satellite communication network at 02:25—three minutes after the aircraft left the range of radar.[5]:22 Based on analysis of the satellite communications, the aircraft turned south after passing north of Sumatra and flew for five hours with little deviation in its track, ending when fuel was exhausted.[5]:34[33][34][35]

At the time of its disappearance, and if the presumed loss of all on board is confirmed, Flight 370 would have been the deadliest aviation incident in Malaysia Airlines' history and the deadliest involving a Boeing 777.[36][37] It was surpassed in both regards 131 days later by the crash of another Malaysia Airlines Boeing 777 – Flight 17 – that was shot down over Ukraine.[38] Malaysia Airlines was struggling financially, a problem which was exacerbated by a decline in ticket sales after Flight 370 disappeared and before the crash of Flight 17; the airline was renationalised by the end of 2014. The Malaysian government received significant criticism, especially from China, for failing to disclose information in a timely manner during the early weeks of the search. Flight 370's disappearance brought to the public's attention the limits of aircraft tracking and flight recorders, including several issues raised four years earlier—but never mandated—following the loss of Air France Flight 447. A task force set up by the International Air Transport Association, with the support of the International Civil Aviation Organization, proposed a new standard that, by December 2015, commercial aircraft must report their position every 15 minutes.[39][40] The Malaysian Ministry of Transport issued an interim report on 8 March 2015.[41][42]

Contents

- 1 Disappearance
  - 1.1 Departure
  - 1.2 Communication lost
  - 1.3 Radar
  - 1.4 Satellite communication resumes
  - 1.5 Response by air traffic control
  - 1.6 Announcement of disappearance
  - 1.7 Timeline of disappearance
  - 1.8 Presumed loss
  - 1.9 Reported sightings
  - 1.10 Debris discovered
- 2 Search
  - 2.1 Southeast Asia
  - 2.2 Southern Indian Ocean
    - 2.2.1 Initial search
    - 2.2.2 Underwater search
    - 2.2.3 Marine debris

- 3 Aircraft
- 4 Passengers and crew
  - 4.1 Crew
  - 4.2 Passengers
- 5 Investigation
  - 5.1 International participation
  - 5.2 Analysis of satellite communication
    - 5.2.1 Background
    - 5.2.2 Communications from 02:25 to 08:19 MYT
    - 5.2.3 Deductions
    - 5.2.4 Analysis
  - 5.3 Possible in-flight events
    - 5.3.1 Power interruption
    - 5.3.2 Unresponsive crew or hypoxia
  - 5.4 Possible causes of disappearance
    - 5.4.1 Passenger involvement
    - 5.4.2 Crew involvement
    - 5.4.3 Cargo
- 6 Aftermath
  - 6.1 Information sharing
  - 6.2 Malaysia Airlines
    - 6.2.1 Financial troubles
    - 6.2.2 Compensation for passengers' kin
  - 6.3 Malaysia
  - 6.4 China
    - 6.4.1 Relatives of passengers
    - 6.4.2 Boycotts
  - 6.5 Air transport industry
    - 6.5.1 Aircraft tracking
    - 6.5.2 Transponders
    - 6.5.3 Flight recorders
    - 6.5.4 Safety recommendations
- 7 Timeline of events
- 8 In popular culture
- 9 See also
- 10 Notes
- 11 References
- 12 External links
  - 12.1 Reports
  - 12.2 Press releases / Media

Disappearance

Flight 370 was a scheduled red-eye flight in the early morning hours of 8 March 2014 from Kuala Lumpur, Malaysia to Beijing, China. It was one of two daily flights operated by Malaysia Airlines from its hub at Kuala Lumpur International Airport (KLIA) to Beijing Capital International Airport—scheduled to depart

at 00:35 local time (MYT; UTC+08:00) and arrive at 06:30 local time (CST; UTC+08:00).[43][44] On board Flight 370 were 227 passengers, 10 cabin crew, two pilots (a captain and first officer), and 14,296 kg (31,517 lb) of cargo.[41]:1, 12, 30

The planned flight duration was 5 hours, 34 minutes, which would consume an estimated 37,200 kg (82,000 lb) of jet A-1 fuel.[41]:1, 30 The aircraft carried 49,100 kilograms (108,200 lb) of jet fuel, including reserves, which allowed an endurance of 7 hours, 31 minutes.[41]:1, 30 The extra fuel was enough to divert to alternate airports—Jinan Yaoqiang International Airport and Hangzhou Xiaoshan International Airport—which would require 4,800 kg (10,600 lb) or 10,700 kg (23,600 lb), respectively, to reach from Beijing.[41]:30

Known flight path taken by Flight 370 (red), derived from primary (military) and secondary (ATC) radar data.

Departure

At 00:42, Flight 370 took off from runway 32R,[41]:1 and was cleared by air traffic control (ATC) to climb to flight level 180[c]—approximately 18,000 feet (5,500 m)—on a direct path to navigational waypoint IGARI (located at 6° 56' 12N 103° 35' 6E). Voice analysis has determined that the First Officer communicated with ATC while the flight was on the ground and that the Captain communicated with ATC after departure.[41]:21 Shortly after departure, the flight was transferred from the airport's air traffic control to "Lumpur Radar" air traffic control on frequency 132.6 MHz. Air traffic control over peninsular Malaysia and adjacent waters is provided by the Kuala Lumpur Area Control Centre (ACC); Lumpur Radar is the name of the frequency used for en route air traffic.[45] Lumpur Radar cleared Flight 370 to flight level 350[c]—approximately 35,000 ft (10,700 m). At 01:01, Flight 370's crew reported to Lumpur Radar that they had reached flight level 350, which they confirmed again at 01:08.[41]:1–2[46]

Communication lost

The aircraft's final automated position report and last transmission using the Aircraft Communications Addressing and Reporting System (ACARS) protocol was sent at 01:07;[5]:2[47][48]:36 among the data provided in the message was total fuel remaining—43,800 kg (96,600 lb).[49]:9 The final verbal contact with air traffic

External video

ATC conversations with Flight 370 (http://www.youtube.com/watch?v=q13aTqdMAFw) Audio recordings of conversations between ATC and Flight 370 from pre-departure to final contact (00:25 – 01:19).

control occurred at 01:19:30, when Captain Shah[41]:21 acknowledged a send-off by Lumpur Radar to Ho Chi Minh ACC:[d][41]:2[46][50]

> Lumpur Radar: "Malaysian three seven zero, contact Ho Chi Minh one two zero decimal nine. Good night."
>
> Flight 370: "Good night. Malaysian three seven zero."

The crew was expected to contact air traffic control in Ho Chi Minh City as the aircraft passed into Vietnamese airspace, just north of the point where contact was lost.[51][52] The captain of another aircraft attempted to reach the crew of Flight 370 "just after [01:30]"[53] using the international distress frequency to relay Vietnamese air traffic control's request for the crew to contact them; the captain said he was able to establish contact, but only heard "mumbling" and static.[53] Calls made to Flight 370's cockpit at 02:39 and 07:13 were unanswered but acknowledged by the aircraft's satellite data unit.[5]:18[48]:40

Radar

At 01:20:31, Flight 370 was observed on radar at the Kuala Lumpur ACC as it passed the navigational waypoint IGARI (6°56′12″N 103°35′6″E) in the Gulf of Thailand; five seconds later, the Mode-S symbol disappeared from radar screens.[41]:2 At 01:21:13, Flight 370 disappeared from the radar screen at Kuala Lumpur ACC and was lost about the same time on radar at Ho Chi Minh ACC, which claims the aircraft was at the nearby waypoint BITOD.[41]:2[46] Air traffic control uses secondary radar, which relies on a signal emitted by a transponder on aircraft; therefore, after 01:21 the transponder on Flight 370 was no longer functioning. The final data from the transponder indicated the aircraft was flying at its assigned cruise altitude of flight level 350[c] and was travelling at 471 knots (872 km/h; 542 mph) true airspeed.[54] There were few clouds around this point and no rain or lightning nearby.[41]:33–36 Later analysis estimated that Flight 370 had 41,500 kg (91,500 lb) of fuel when it disappeared from secondary radar.[41]:30

Data from Malaysian military radar showing Flight 370 (green) crossing the Strait of Malacca and Andaman Sea to where it was last seen by radar. The left of the two segments of the flight track follows air route N571 between waypoints VAMPI and MEKAR; the white circle appears to highlight a section where the aircraft was not tracked by radar.

At the time the transponder stopped functioning—01:21:13—military radar showed Flight 370 turning right, but "almost immediately"[41]:3 the aircraft began a left turn to a south-westerly direction.[41]:3 From 01:30:35–01:35, military radar showed Flight 370 at 35,700 ft (10,900 m)[e] on a 231° magnetic heading, with a ground speed of 496 knots (919 km/h; 571 mph).[41]:3 Flight 370 continued across the Malay Peninsula, fluctuating between 31,000–33,000 ft (9,400–10,100 m) in altitude.[41]:3 A civilian primary radar at Sultan Ismail Petra Airport with a 60 nmi (110 km; 69 mi) range made four detections of an unidentified aircraft between 01:30:37 and 01:52:35; the tracks of the unidentified aircraft are "consistent with those of the military data."[f][41]:3–4 At 01:52, Flight 370 was detected passing just south of Penang Island. From there, the aircraft flew

across the Strait of Malacca to or close to the waypoint VAMPI, passing over Pulau Perak at 02:03, after which it flew along air route N571 to waypoints MEKAR, NILAM, and possibly IGOGU.[5]:3, 38 The last known location, from and near the limits of Malaysian military radar, was at 02:22, 10 nautical miles (19 km; 12 mi) after passing waypoint MEKAR[41]:3, 7 and 200 nmi (370 km; 230 mi) northwest of Penang at an altitude of 29,500 ft (9,000 m).[55][56]

Because of sensitivity about revealing military radar capabilities, countries in the region where Flight 370 disappeared were reluctant to release information they may have collected from military radar. Despite the aircraft possibly having flown near or over the northern tip of Sumatra,[46] Indonesia—which has an early warning radar system—has publicly denied sighting Flight 370 on radar after contact was lost, although the Indonesian military did track Flight 370 earlier when en route to waypoint IGARI.[41]:4[57] Thailand and Vietnam also detected Flight 370 on radar before the transponder stopped working, but not afterwards.[41]:4–5 No radar contact was detected by Australia, including the JORN over-the-horizon radar system, which was believed to be looking north to detect illegal migrants and not west over the Indian Ocean where Flight 370 is presumed to have flown based on satellite communications.[58]

Satellite communication resumes

At 02:25, the aircraft's satellite communication system sent a "log-on request" message—the first message on the system since the ACARS transmission at 01:07—which was relayed by satellite to a ground station, both operated by satellite telecommunications company Inmarsat. After logging on to the network, the satellite data unit aboard the aircraft responded to hourly status requests from Inmarsat and two ground-to-aircraft phone calls, at 02:39 and 07:13, which went unanswered by the cockpit.[5]:18[48] The final status request and aircraft acknowledgement occurred at 08:10. The aircraft sent a log-on request at 08:19:29 which was followed, after a response from the ground station, by a "log-on acknowledgement" message at 08:19:37. The log-on acknowledgement is the last piece of data available from Flight 370. The aircraft did not respond to a status request from Inmarsat at 09:15.[5][48][59][60]

Response by air traffic control

At 01:38, Ho Chi Minh Area Control Centre (ACC) contacted Kuala Lumpur Area Control Centre to query the whereabouts of Flight 370 and informed them that they had not established verbal contact with Flight 370, which was last detected by radar at waypoint BITOD. The two centres exchanged four more calls over the next 20 minutes with no new information.[46][61]

At 02:03, Kuala Lumpur ACC relayed to Ho Chi Minh ACC information received from Malaysia Airlines' operations centre that Flight 370 was in Cambodian airspace. Ho Chi Minh ACC contacted Kuala Lumpur ACC twice in the following eight minutes asking for confirmation that Flight 370 was in Cambodian airspace.[46] At 02:15, the watch supervisor at Kuala Lumpur ACC queried Malaysia Airlines' operations centre, which said that it could exchange signals with Flight 370 and that Flight 370 was in Cambodian airspace.[61] Kuala Lumpur ACC contacted Ho Chi Minh ACC to ask whether the planned flight path for Flight 370 passed through Cambodian airspace. Ho Chi Minh ACC responded that Flight 370 was not supposed to enter Cambodian airspace and that they had already contacted Phnom Penh ACC (which controls Cambodian airspace), which had no contact with Flight 370.[46] Kuala Lumpur ACC contacted Malaysia Airlines' operations centre at 02:34, inquiring about the communication status with Flight 370,

and were informed that Flight 370 was in a normal condition based on a signal download and that it was located at 14°54′00″N 109°15′00″E.[46][61] Later, another Malaysia Airlines aircraft, Flight 386 bound for Shanghai, at the request of Ho Chi Minh ACC, attempted to contact Flight 370 on the Lumpur Radar frequency—the frequency on which Flight 370 last made contact with Malaysian air traffic control—and on emergency frequencies. The attempt was unsuccessful.[46][62]

At 03:30, Malaysia Airlines' operations centre informed Kuala Lumpur ACC that the locations it had provided earlier were "based on flight projection and not reliable for aircraft positioning."[46] Over the next hour, Kuala Lumpur ACC contacted Ho Chi Minh ACC asking whether they had contacted Chinese air traffic control. At 05:09, Singapore ACC was queried for information about Flight 370. At 05:20, an undisclosed official—identified in the preliminary report released by Malaysia as "Capt [name redacted]"—contacted Kuala Lumpur ACC requesting information about Flight 370; he opined that, based on known information, "MH370 never left Malaysian airspace."[46]

The watch supervisor at Kuala Lumpur ACC activated the Kuala Lumpur Aeronautical Rescue Coordination Centre (ARCC) at 05:30, over four hours after communication was lost with Flight 370.[61] The ARCC is a command post at an Area Control Centre that coordinates search-and-rescue activities when an aircraft is lost.

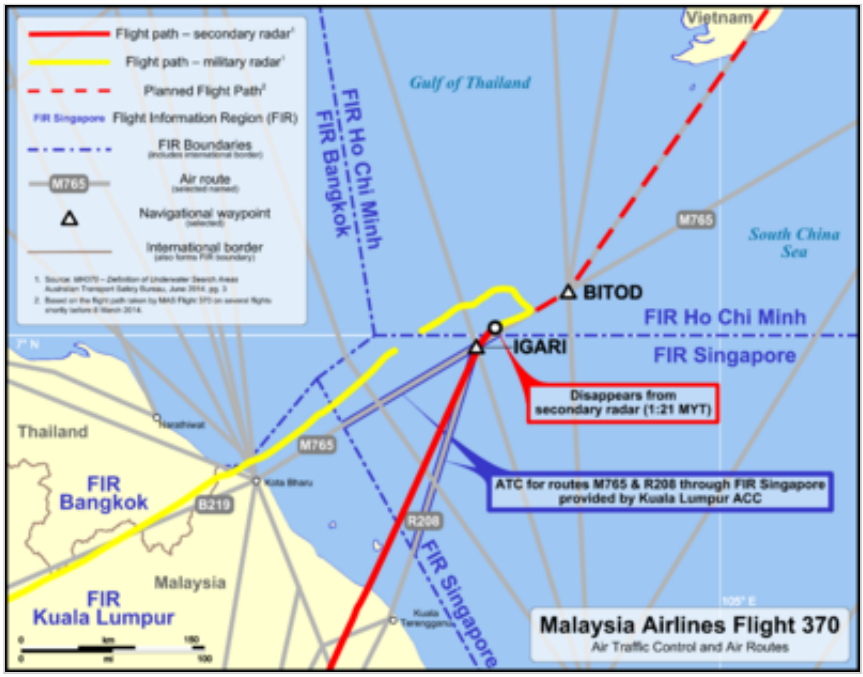

Flight Information Regions in the vicinity of where Flight 370 disappeared from secondary radar. Kuala Lumpur ACC provides ATC services on two routes, located within FIR Singapore, between Malaysia and Vietnam. (Air routes are depicted as roughly 5 nmi / 8–10 km wide, but vary in width, with some as wide as 20 nmi / 30–35 km.)

Announcement of disappearance

Malaysia Airlines issued a media statement at 07:24, one hour after the scheduled arrival time of the flight at Beijing, stating that contact with the flight had been lost by Malaysian ATC at 02:40 and that the government had initiated search and rescue operations;[63] the time when contact was lost was later corrected to 01:21.[64] Neither the crew nor the aircraft's communication systems relayed a distress signal, indications of bad weather, or technical problems before the aircraft vanished from radar screens.[28]

Timeline of disappearance

Elapsed (HH:MM)	Time		Event
	MYT	UTC	
00:00	8 March 00:41	7 March 16:41	Take-off from Kuala Lumpur International Airport

00:20	01:01	17:01	Crew confirms altitude of Flight Level 350 (approximately 35,000 ft / 10700 m)[50]
00:26	01:07	17:07	Last ACARS data transmission received;[47][48]:36 crew confirms altitude of Flight Level 350, a second time[50]
00:26–01:22	01:07–02:03	17:07–18:03	Satellite communication link lost sometime during this period.[48]:36
00:38	01:19	17:19	Last Malaysian ATC voice contact
00:40	01:21	17:21	Last secondary radar (transponder) contact at 6°55′15″N 103°34′43″E[3][4]
00:41	01:22	17:22	Transponder and ADS-B no longer operating.
00:44	01:25	17:25	Aircraft deviated from planned route[5]:2
00:49	01:30	17:30	Voice contact attempt by another aircraft, at request of Ho Chi Minh Area Control Centre (HCM ACC); mumbling and radio static heard in reply[53]
00:56	01:37	17:37	Missed expected half-hourly ACARS data transmission[47]
00:57	01:39	17:38	HCM ACC contacts Kuala Lumpur ACC (KL ACC) to inquire about Flight 370. HCM ACC tells them that verbal contact was not established and Flight 370 disappeared from its radar screens near BITOD waypoint. KL ACC responded that Flight 370 did not return to its frequency after passing waypoint IGARI.[41]:2[46]
01:05	01:46	17:46	HCM ACC contacts KL ACC again, inform them radar contact was established near IGARI, but lost near BITOD and that verbal contact was not established.[46]
01:16	01:57	17:57	HCM ACC informs KL ACC that there was no contact with Flight 370, despite attempts on many frequencies and aircraft in the vicinity.[46]
01:22	02:03	18:03	Malaysia Airlines dispatch centre sent a message to the cockpit instructing pilots to contact Vietnam ATC, which was not responded to.[65] A ground-to-aircraft ACARS data request, transmitted from the ground station multiple times between 02:03–02:05, was not acknowledged by the aircraft's satellite data unit.[48]:36–39
01:22	02:03	18:03	KL ACC contacts HCM ACC and relays information from Malaysia Airlines' operations centre that Flight 370 is in Cambodian airspace.[46]
01:34	02:15	18:15	KL ACC queries Malaysia Airlines' operations centre, which replies that it is able to exchange signals with flight which is in Cambodian airspace.[46]
01:37	02:18	18:18	KL ACC contacts HCM ACC asking them if Flight 370 was supposed to enter Cambodian airspace. HCM ACC replies that Flight 370's planned route did not take it into Cambodian airspace and that they had checked and Cambodia had no information or contact with Flight 370.[46]
01:41	02:22	18:22	Last primary radar contact by Malaysian military, 200 nautical miles (370 km; 230 mi) NW of Penang, 6°49′38″N 97°43′15″E[5]:3
01:44	02:25	18:25	"Log-on request" sent by aircraft to satellite. Satellite communication link is reestablished after being lost for between 22–68 min.[5]:18[48]:39 Sometimes referred to as the first hourly "handshake" after disappearing from radar.[59][66]
01:53	02:34	18:34	KL ACC queries Malaysia Airlines' operations centre about communication status with Flight 370, but it was not sure if a message sent to Flight 370 was successful or not.[46]
01:54	02:35	18:35	Malaysia Airlines' operations centre informs KL ACC that Flight 370 is in a normal condition based on signals from the aircraft and located at 14°54′00″N 109°15′00″E (Northern Vietnam) at 18:33 UTC. KL ACC relays this information to HCM ACC.[46]
			Ground-to-aircraft telephone call, via the aircraft's satellite link, went unanswered.

01:58	02:39	18:39	[5]:18[48]:40
02:49	03:30	19:30	Malaysia Airlines' operations centre informs KL ACC that position information was based on flight projection and not reliable for aircraft tracking. Between 03:30 and 04:25, KL and HCM ACCs query Chinese air traffic control.[46]
04:28	05:09	21:09	Singapore ACC queried for information about Flight 370.[46]
05:49	06:30	22:30	Missed scheduled arrival at Beijing Capital International Airport
05:51	06:32	22:32	Kuala Lumpur Aeronautical Rescue Coordination Centre (ARCC) is activated.[41]:2
06:32	07:13	23:13	Ground-to-aircraft telephone call placed by Malaysia Airlines,[65] via the aircraft's satellite link, went unanswered.[5]:18[48]:40
06:43	07:24	23:24	Malaysia Airlines issues a press statement announcing that Flight 370 is missing[64]
07:30	08:11	**8 March** 00:11	Sixth and last successful automated hourly handshake with Inmarsat-3 F1[59][67]
07:38	08:19:29	00:19:29	"Log-on request" sent by aircraft to satellite (sometimes referred to as a "partial handshake")[68][69] believed to have occurred when emergency power restarted the SDU shortly after fuel exhaustion and loss of power.[5]:18, 33[48]:41
07:38	08:19:37	00:19:37	After the ground station responded to the log-on request, the aircraft replied with a "log-on acknowledgement" transmission at 08:19:37.443. This is the last transmission received from Flight 370.[5]:18[48]:41
08:34	09:15	01:15	Aircraft did not respond to a scheduled, hourly handshake attempt by Inmarsat.[48]:41[59]

Presumed loss

On 24 March, Malaysian Prime Minister Najib Razak appeared before media at 22:00 local time to give a short statement regarding Flight 370, during which he announced:

> This evening I was briefed by representatives from the UK Air Accidents Investigation Branch. They informed me that Inmarsat, the UK company that provided the satellite data which indicated the northern and southern corridors, has been performing further calculations on the data. Using a type of analysis never before used in an investigation of this sort...Inmarsat and the AAIB have concluded that MH370 flew along the southern corridor, and that its last position was in the middle of the Indian Ocean, west of Perth. This is a remote location, far from any possible landing sites. It is therefore with deep sadness and regret that I must inform you that, according to this new data, flight MH370 ended in the southern Indian Ocean.[17]

Just before Najib spoke at 22:00 MYT, an emergency meeting was called in Beijing for relatives of Flight 370 passengers.[17] Malaysia Airlines announced that Flight 370 was assumed lost with no survivors. It notified most of the families in person or via telephone, and some received the following SMS (in English and Chinese):[17]

> Malaysia Airlines deeply regrets that we have to assume beyond any reasonable doubt that MH370 has been lost and that none of those on board survived. As you will hear in the next hour from Malaysia's Prime Minister, we must now accept all evidence suggests the plane went down in the Southern Indian Ocean.[13][14][15]

On 29 January 2015, the Director General of the Department of Civil Aviation Malaysia, Azharuddin Abdul Rahman, announced that the status of Flight 370 would be changed to an "accident", in accordance with the Chicago Convention on International Civil Aviation:[1]

> We have concluded that the aircraft exhausted its fuel over a defined area of the southern Indian Ocean, and that the aircraft is located on the sea floor close to that defined area. This is a remote location, far from any possible landing sites. It is also an area with adverse sea conditions with known depths of more than 6,000 metres. After 327 days...and based on all available data as well as circumstances mentioned earlier, survivability in the defined area is highly unlikely....On behalf of the Government of Malaysia, we officially declare Malaysia Airlines flight MH370 an accident in accordance with the Standards of Annexes 12 and 13 to the Chicago Convention and that all 239 of the passengers and crew onboard MH370 are presumed to have lost their lives.[1]

If the official assumption is confirmed, at the time of its disappearance Flight 370 was the deadliest aviation incident in the history of Malaysia Airlines (surpassing the 1977 hijacking and crash of Malaysian Airline System Flight 653 that killed all 100 passengers and crew on board) and the deadliest involving a Boeing 777, surpassing Asiana Airlines Flight 214 (3 fatalities).[36][37] In both of those categories, Flight 370 was surpassed 131 days later by Malaysia Airlines Flight 17, another Boeing 777-200ER, which was shot down on 17 July 2014, killing all 298 persons aboard.[38]

Reported sightings

The news media reported several sightings of an aircraft that fit the description of the missing aircraft. For example, on 19 March 2014, CNN reported that "several people on the ground or at sea claimed they saw Malaysia Airlines Flight 370 before it went missing after its post-midnight takeoff from Kuala Lumpur on March 8. The purported eyewitnesses include fishermen, an oil rig worker and islanders in an atoll. Some even alleged they saw it crash. While none of their claims have been substantiated, their assertions add to the ongoing mystery of the missing Boeing 777 and the 239 people aboard."[70]

Two days later, the London-based *Daily Mail* reported that "a Malaysian woman on a flight across the Indian Ocean claimed to have seen an aircraft in the water near the Andaman Islands on the day the jet disappeared."[71] Three months later, the London *Telegraph* reported that "a British woman sailing with her husband across the Indian Ocean from India to Thailand has claimed she may have seen the missing Malaysia Airlines plane on fire. Katherine Tee, 41, was on night watch on March 7–8 but said she did not report the sighting until Sunday because she was having marital problems and thought she was losing her mind."[72]

Debris discovered

On 29 July 2015, airliner marine debris was found on a beach in Saint-André, on Réunion, an island in the western Indian Ocean, about 4,000 km (2,500 mi) west of the underwater search area.[73] The object had a stenciled internal marking "657 BB" consistent with the code for a portion of a right wing flaperon (a trailing edge control surface) from a Boeing 777.[25][74] The following day, a damaged suitcase, which may be associated with Flight 370, was found.[75] The location is consistent with models of debris dispersal 16 months after an origin in the current search area, off the west coast of Australia.[76][77][73][78] On 31 July, a Chinese water bottle and an Indonesian cleaning product were found in the same area.[79][80]

The first object to be found was transported from Réunion—an overseas department of France—to Toulouse, for examination by France's civil aviation accident investigation agency, the Bureau d'Enquêtes et d'Analyses pour la Sécurité de l'Aviation Civile (BEA), and a French defence ministry laboratory.[73] Malaysia is sending investigators to both Réunion and Toulouse.[73][81] French police are conducting a search of the waters around Réunion for additional debris.[73] On 2 August, Malaysian officials confirmed that the object was a flaperon from a Boeing 777 aircraft and that the verification was made with investigators from France, Malaysia, Boeing, and the US NTSB.[82]

On 5 August, the Prime Minister of Malaysia announced that the found flaperon was confirmed to be from flight MH370's aircraft; French officials have only stated that there is a "very high probability"[83] the object is from Flight 370.[84][85][83] There have been many claims that additional debris had been found on Réunion which may have come from Flight 370, but none appears to have come from an aircraft as of 5 August.[77][86]

Boeing 777 flaperon

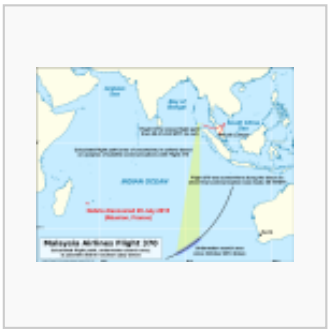

Location of found debris relative to Flight 370's flight path and the current search area

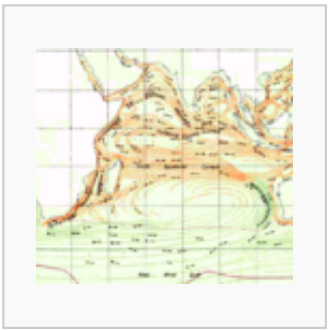

Currents within the Indian Ocean

Search

A search and rescue effort was launched soon after the aircraft's disappearance in Southeast Asia, but the following week, analysis of satellite communications between the aircraft and a communications satellite determined that the aircraft had continued flying for several hours and the final transmission from the aircraft was made over the Southern Indian Ocean, west of Australia. The surface search in the southern

Indian Ocean between 18 March and 28 April searched over 4,600,000 square kilometres (1,800,000 sq mi) and involved 19 vessels and 345 search sorties by military aircraft.[87] The current phase of the search is a bathymetric survey and sonar search of the seafloor, about 1,800 kilometres (1,100 mi) southwest of Perth, Australia.[18]

The search for Flight 370 is the most expensive search operation in aviation history.[21][22][88][89] In June 2014, *Time* estimated that the total search effort to that point had cost approximately US$70 million.[90] The tender for the underwater search is AU$52 million (US$43 million or €35 million)—shared by Australia and Malaysia—for 12 months, but would differ if found in more or less time.[19]

ADV *Ocean Shield* deploys the Bluefin-21 autonomous underwater vehicle, which conducted the seafloor sonar survey from 14 April to 28 May.

Since 30 March 2014, the search has been coordinated by the Joint Agency Coordination Centre (JACC), an Australian government agency established specifically to co-ordinate the search effort to locate and recover Flight 370, which primarily involves the Malaysian, Chinese, and Australian governments.[91]

Southeast Asia

The initial search area in Southeast Asia

The Kuala Lumpur Aeronautical Rescue Coordination Centre (ARCC) was activated at 05:30—four hours after communication was lost with Flight 370—to co-ordinate search and rescue efforts.[61] Search efforts began in the Gulf of Thailand and South China Sea. On the second day of the search, Malaysian officials revealed that radar recordings indicated Flight 370 may have turned around; the search zone was expanded to include part of the Strait of Malacca.[92] On 12 March, the chief of the Royal Malaysian Air Force announced that an unidentified aircraft—believed to be Flight 370—had travelled across the Malay peninsula and was last sighted on military radar 370 km (200 nmi; 230 mi) northwest of Penang Island; search efforts were subsequently increased in the Andaman Sea and Bay of Bengal.[56]

Records of signals sent between the aircraft and a communications satellite over the Indian Ocean revealed that the aircraft had continued flying for almost six hours after its final sighting on Malaysian military radar. Initial analysis of these communications determined that Flight 370 was along one of two arcs—equidistant from the satellite—when its last signal was sent; the same day this analysis was publicly

disclosed, 15 March, authorities announced they would abandon search efforts in the South China Sea, Gulf of Thailand, and Strait of Malacca to focus their efforts on the two corridors. The northern arc—from northern Thailand to Kazakhstan—was soon discounted as the aircraft would have to pass through heavily militarised airspace and those countries claimed their military radar would have detected an unidentified aircraft entering their airspace.[93][94][95]

Southern Indian Ocean

The focus of the search shifted to the Southern Indian Ocean west of Australia and within Australia's concurrent aeronautical and maritime Search and Rescue regions that extend to 75°E longitude.[96][97] Accordingly, on 17 March, Australia agreed to lead the search in the southern locus from Sumatra to the southern Indian Ocean.[16][98]

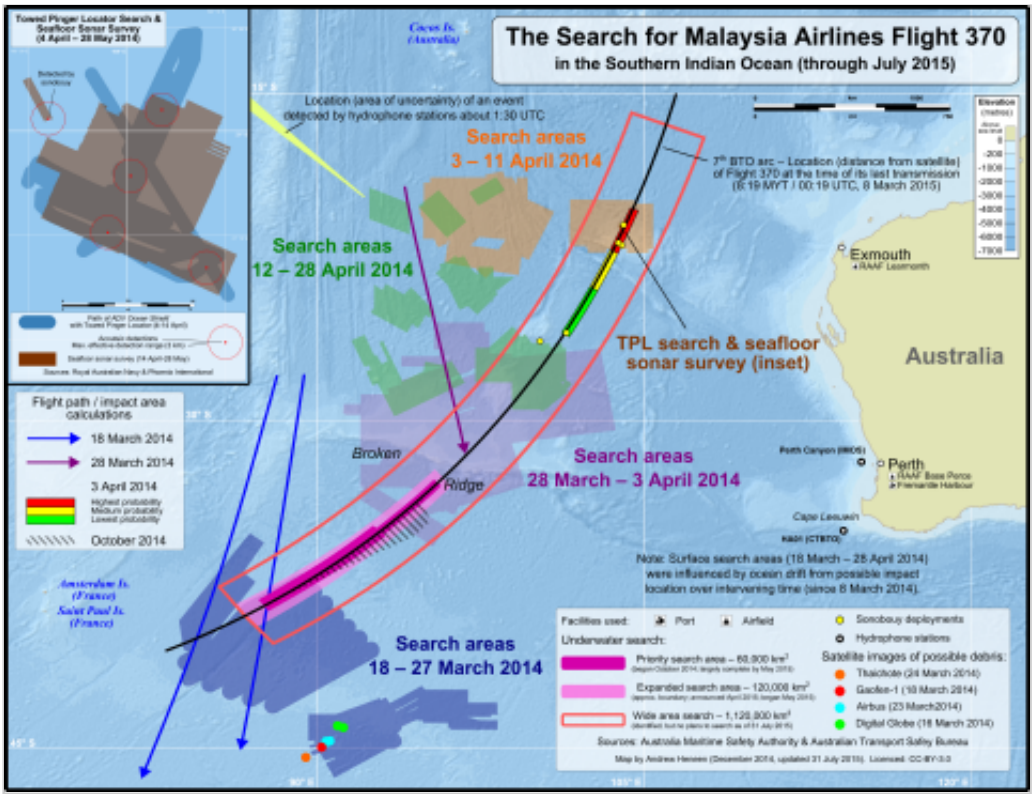

The shifting search zones for Flight 370 in the Southern Indian Ocean. The inset shows the path of taken by the vessel ADV *Ocean Shield* operating a towed pinger locator, acoustic detections, and the sonar search. The current underwater phase (both the wide area search and priority area) is shown in pink.

Initial search

From 18–27 March, the search effort focused on a 305,000 km^2 (118,000 sq mi) area about 2,600 km (1,600 mi) south-west of Perth[99] that Australian Prime Minister Tony Abbott said is "as close to nowhere as it's possible to be" and which is renowned for its strong winds, inhospitable climate, hostile seas, and deep ocean floors.[100][101] Satellite imagery of the region was analysed; several objects of interest and two possible debris fields were identified on images captured between 16–26 March. None of these possible objects were found by aircraft or ships.[102]

Revised estimates of the radar track and the aircraft's remaining fuel led to a move of the search 1,100 km (680 mi) north-east of the previous area on 28 March[103][104][105] which was followed by another shift on 4 April.[106][107] An intense effort began to locate the underwater locator beacons (ULBs; informally known as "pingers") attached to the aircraft's flight recorders, whose batteries were expected to expire around 7 April.[108][109] Two ships equipped with towed pinger locators (TPLs) and a submarine equipped with a hull-mounted acoustic system,[5]:11–12 began searching for pings along a 240-kilometre (150 mi) seabed line believed to be the Flight 370 impact area.[108][110][111] Operators considered it a shot in the dark,[112] when

comparing the vast search area with the fact that a TPL could only search up to 130 km^2 (50 sq mi) per day.[112] Between 4–8 April several acoustic detections were made that were close to the frequency and rhythm of the sound emitted by the flight recorders' ULBs; analysis of the acoustic detections determined that, although unlikely, the detections could have come from a damaged ULB.[5]:13 A sonar search of the seafloor near the detections was carried out between 14 April and 28 May without any sign of Flight 370.[5]:14 It was later revealed that the battery for the ULB attached to Flight 370's flight data recorder had expired in December 2012 and may not have been as capable.[113][114]

Underwater search

Wikimedia Commons has media related to: ***Search for Malaysia Airlines Flight 370*** (category)

In late June, details of the next phase of the search were announced;[115] officials have called this phase the "underwater search", despite the previous seafloor sonar survey.[20] Continued refinement of analysis of Flight 370's satellite communications identified a "wide area search" along the arc where Flight 370 was located when it last communicated with the satellite. The priority search area within the wide area search is in its southern extent.[116] Some of the equipment to be used for the underwater search operates best when towed 200 m (650 ft) above the seafloor at the end of a 10 km (6 mi) cable.[117] Available bathymetric data for this region was of poor resolution, thus necessitating a bathymetric survey of the search area before the underwater phase began.[118] Commencing in May, the bathymetric survey charted around 208,000 square kilometres (80,000 sq mi) of seafloor through 17 December 2014, when it was suspended for the ship conducting the survey to be mobilised in the underwater search.[119]

The underwater phase of the search, which began on 6 October 2014,[116] uses three vessels equipped with towed deep water vehicles, which use side-scan sonar, multi-beam echo sounders, and video cameras to locate and identify aircraft debris.[120] A fourth vessel participated in the search between January–May 2015; it had an autonomous underwater vehicle (AUV) to search areas which cannot be effectively searched by equipment on the other vessels.[121][122][123] As of 5 August 2015, nearly 60,000 km^2 (23,000 sq mi) of seafloor has been searched during the underwater phase of the search.[77]

Following the discovery of the flaperon on Réunion, the ATSB reviewed their drift calculations for debris from the aircraft and, according to the JACC, they are "satisfied that the discovery of the flaperon at La Réunion...is consistent with the current underwater search area in the southern Indian Ocean."[77] Reverse drift modelling of the debris, to determine its origin after 16 months, also supports the current underwater search area, although reverse drift modelling is very imprecise over long periods of time.[77]

Marine debris

A week after the discovery of a flaperon from Flight 370 on a beach on Réunion (an overseas department of France), France announced plans for an aerial search for possible marine debris around the island. On 7 August 2015, France began searching an area 120 km (75 mi) by 40 km (25 mi) along the east coast of Réunion.[83] Foot patrols for debris along beaches are also planned.[86] Malaysia has asked authorities in neighboring states to be on alert for marine debris which could be from an aircraft.[124]

Aircraft

Flight 370 was operated with a Boeing 777-2H6ER,[g] serial number 28420, registration 9M-MRO. The 404th Boeing 777 produced,[126] it first flew on 14 May 2002 and was delivered new to Malaysia Airlines on 31 May 2002. The aircraft was powered by two Rolls-Royce Trent 892 engines[126] and configured to carry 282 passengers.[127] It had accumulated 53,471.6 hours and 7,526 cycles in service[41]:22 and had not previously been involved in any major incidents,[128] though a minor incident while taxiing at Shanghai Pudong International Airport in August 2012 resulted in a broken wingtip.[129][130] Its last maintenance "A check" was carried out on 23 February 2014.[131] The aircraft was in compliance with all applicable Airworthiness Directives for the airframe and engines.[41]:27 A replenishment of the crew oxygen system—a routine maintenance task—was performed on 7 March 2014; an examination of this procedure found nothing unusual.[41]:27

Flightdeck of 9M-MRO in 2004.

Wikimedia Commons has media related to ***aircraft 9M-MRO***.

The Boeing 777, introduced in 1994, is generally regarded by aviation experts as having a safety record that is one of the best of any commercial aircraft.[36][37] Since its first commercial flight in June 1995, there have been only four other serious accidents involving hull-loss: British Airways Flight 38 in 2008; a cockpit fire in a parked EgyptAir 777-200 at Cairo International Airport in 2011;[132][133] the crash of Asiana Airlines Flight 214 in 2013, in which three people died; and Malaysia Airlines Flight 17, which was shot down over Ukraine with 298 people aboard in July 2014.[38][134]

Passengers and crew

People on board by nationality

Nationality	No.
Australia	6
Canada	2
China	152
France	4
Hong Kong[h]	1
India[136]	5
Indonesia	7
Iran[i]	2
Malaysia[j]	50
Netherlands	1
New Zealand	2
Russia	1
Taiwan	1
Ukraine	2
United States	3
Total	**239**

Malaysia Airlines released the names and nationalities of the 227 passengers and 12 crew members, based on the flight manifest, later modified to include two Iranian passengers travelling on stolen passports.[137]

Crew

All 12 crew members were Malaysian citizens. Two pilots were among the crew:[138]

- The pilot in command was 53-year-old Captain Zaharie Ahmad Shah from Penang. He joined Malaysia Airlines as a cadet pilot in 1981 and, after training and receiving his commercial pilot's licence, became a Second Officer with the airline in 1983. Shah was promoted to captain of the Boeing 737-400 in 1991, captain of Airbus A330-300 in 1996, and to captain of Boeing 777–200 in 1998. He had been a Type Rating Instructor and Type Rating Examiner since 2007 and had 18,365 hours of flying experience.[41]:13[138][139]
- The co-pilot was 27-year-old First Officer Fariq Abdul Hamid. He joined Malaysia Airlines as a cadet pilot in 2007 and became a Second Officer on Boeing 737–400 aircraft. He was promoted to first officer of Boeing 737–400 aircraft in 2010 and later transitioned to Airbus A330-300 aircraft in 2012. In November 2013, he began training as first officer on Boeing 777–200 aircraft. Flight 370 was his final training flight and he was scheduled to be examined on his next flight. Hamid had 2,763 hours of flying experience.[41]:14[140][141]

Passengers

Of the 227 passengers, 152 were Chinese citizens, including a group of 19 artists with 6 family members and 4 staff returning from a calligraphy exhibition of their work in Kuala Lumpur; 38 passengers were Malaysian. The remaining passengers were from 13 different countries.[142] Twenty passengers—12 of

whom were from Malaysia and 8 from China—were employees of Freescale Semiconductor.[143][144]

Under a 2007 agreement with Malaysia Airlines, Tzu Chi—an international Buddhist organisation—immediately sent specially trained teams to Beijing and Malaysia to give emotional support to passengers' families.[145][146] The airline also sent its own team of caregivers and volunteers[147] and agreed to bear the expenses of bringing family members of the passengers to Kuala Lumpur and providing them with accommodation, medical care, and counselling.[148] Altogether, 115 family members of the Chinese passengers flew to Kuala Lumpur.[149] Some other family members chose to remain in China, fearing they would feel too isolated in Malaysia.[150]

Investigation

International participation

Malaysia set up a Joint Investigation Team (JIT), composed of specialists from Malaysia, Australia, China, the UK, the US, and France,[5]:1[151] being led according to the ICAO standards by "an independent investigator in charge".[152][153][154] The team consists of an airworthiness group, an operations group, and a medical and human factors group. The airworthiness group will examine issues related to maintenance records, structures, and systems of the aircraft. The operations group will review flight recorders, operations, and meteorology. The medical and human factors group will investigate psychological, pathological, and survival factors.[155] Malaysia also announced, on 6 April, that it had set up three ministerial committees—a Next of Kin Committee, a committee to organise the formation of the Joint Investigation Team, and a committee responsible for Malaysian assets deployed in the search effort.[155] The criminal investigation is being led by the Royal Malaysia Police,[1]:9 assisted by Interpol and other relevant international law enforcement authorities.[156][157]

On 17 March, Australia took control for co-ordinating search, rescue, and recovery operations. For the following six weeks, the Australian Maritime Safety Authority (AMSA) and Australian Transport Safety Board (ATSB) worked to determine the search area, correlating information with the JIT and other government and academic sources, while the Joint Agency Coordination Centre (JACC) coordinated the search efforts. Following the fourth phase of the search, the ATSB took responsibility for defining the search area. In May, the *search strategy working group* was established by the ATSB to determine the most likely position on the aircraft at the 00:19 UTC satellite transmission. The group included aircraft and satellite experts from: Air Accidents Investigation Branch (UK), Boeing (US), Defence Science and Technology Organisation (Australia), Department of Civil Aviation (Malaysia), Inmarsat (UK), National Transportation Safety Board (US), and Thales (UK).[5]:1[158][159]

The Malaysian Ministry of Transport issued an interim report entitled "Factual Information: Safety Information for MH370" on 8 March 2015. As suggested by the report's title, it focused on providing factual information and not analysis of possible causes of the disappearance.[160]

Analysis of satellite communication

The communications between Flight 370 and the satellite communication network operated by Inmarsat, which were relayed by the Inmarsat-3 F1 satellite, provide the only significant clues to the location of Flight 370 after disappearing from Malaysian military radar at 02:22. These communications have also been used to deduce possible in-flight events (see next section). The investigative team was challenged with reconstructing the flight path of Flight 370 from a limited set of transmissions with no explicit information about the aircraft's location, heading, or speed.[5]:16–17[66]

Background

A depiction of an Inmarsat-3 series satellite. Flight 370 was in contact with Inmarsat-3 F1 (also known as "IOR" for Indian Ocean Region).

Aeronautical satellite communication (SATCOM) systems are used to transmit messages from the aircraft cockpit as well as automated messages from on-board systems using the ACARS communications protocol, but may also be used to transmit FANS and ATN messages and provide voice, fax and data links[161] using other protocols.[66][162][163] The aircraft's satellite data unit (SDU) is used to send and receive signals with the satellite communications network; it operates independently of other aircraft equipment which communicate through the SATCOM system, many using the ACARS protocol. Signals from the SDU are relayed by a satellite, which simply changes the signal's frequency, and then received by a ground station which processes the signal and, if applicable, routes it to its destination (e.g.. Malaysia Airlines' operations centre); signals to the aircraft are sent in reverse order. When the SDU is powered on and attempts to connect with the Inmarsat network, it will transmit a log-on request, which the ground station acknowledges.[5]:17[163] This is, in part, to determine that the SDU belongs to an active service subscriber and also used to determine which satellite should be used to transmit messages to the SDU.[163] After connecting, if a ground station has not received any contact from a terminal for one hour,[k] the ground station will transmit a "log-on interrogation" message—informally referred to as a "ping";[5]:18 an active terminal automatically responds. The entire process of interrogating the terminal is referred to as a 'handshake'.[59][164]

Communications from 02:25 to 08:19 MYT

Although the ACARS data link on Flight 370 stopped functioning between 01:07 and 02:03 MYT,[48]:36 the SDU remained operable.[5] After last contact by primary radar west of Malaysia, the following records were recorded in the log of Inmarsat's ground station at Perth, Western Australia (all times MYT/UTC+8):[5]:18 [48][l]

- 02:25:27 – First handshake – a log-on request initiated by aircraft
- 02:39:52 – Ground to aircraft telephone call, acknowledged by SDU, unanswered
- 03:41:00 – Second handshake (initiated by ground station)
- 04:41:02 – Third handshake (initiated by ground station)
- 05:41:24 – Fourth handshake (initiated by ground station)
- 06:41:19 – Fifth handshake (initiated by ground station)
- 07:13:58 – Ground to aircraft telephone call, acknowledged by SDU, unanswered
- 08:10:58 – Sixth handshake (initiated by ground station)

- 08:19:29 – Seventh handshake (initiated by aircraft); widely reported as a "partial handshake'", consisting of two transmissions:[48]
    - 08:19:29.416 – "log-on request" message transmitted by aircraft (seventh "partial" handshake)
    - 08:19:37.443 – "log-on acknowledge" message transmitted by aircraft, last transmission received from Flight 370

The aircraft did not respond to a ping at 09:15.[48]

Deductions

A few deductions can be made from the satellite communications. The first is that the aircraft remained operational until at least 08:19—seven hours after final contact was made with air traffic control over the South China Sea. The varying burst frequency offset (BFO) values indicate the aircraft was moving at speed. The aircraft's SDU needs location and track information to keep its antenna pointed towards the satellite, so it can also be deduced that the aircraft's navigation system was operational.[165]:4

Since the aircraft did not respond to a ping at 09:15, it can be concluded that at some point between 08:19 and 09:15, the aircraft lost the ability to communicate with the ground station.[59][60][164] The log-on message sent from the aircraft at 08:19:29 was "log-on request".[5]:22 There are only a few reasons the SDU would transmit a log-on request, such as a power interruption, software failure, loss of critical systems providing input to the SDU, or a loss of the link due to the aircraft's attitude.[5]:22 Investigators consider the most likely reason to be that they were sent during power-up after an electrical outage.[5]:33 At 08:19, the aircraft had been airborne for 7 h 38 min; the typical Kuala Lumpur-Beijing flight is $5\frac{1}{2}$ hours and fuel exhaustion was likely.[5]:33[5]:33[166] In the event of fuel exhaustion and engine flame-out—which would eliminate power to the SDU—the aircraft's ram air turbine would deploy, providing power to some instruments and flight controls, including the SDU.[5]:33 Approximately 90 seconds after the 02:25 handshake—also a log-on request—communications from the aircraft's inflight entertainment system were recorded in the ground station log. Similar messages would be expected following the 08:19 handshake but none were received, supporting the fuel starvation scenario.[5]:22

Analysis

Two parameters associated with these transmissions that were recorded in a log at the ground station were key to the investigation:

- Burst time offset (BTO) – the time difference between when a signal is sent from the ground station and when the response is received. This measure is twice the distance from the ground station to satellite to the aircraft and includes the time that the SDU takes between receiving and responding to the message and time between reception and processing at the ground station. This measure can be analysed to determine the distance between the satellite and the aircraft and results in a ring on the Earth's surface that is equidistant from the satellite at the calculated distance, which can be reduced to arcs by eliminating parts of the rings outside the aircraft's range.[5]:18[165]:4–6
- Burst frequency offset (BFO) – the difference between the expected and received frequency of transmissions. The difference is caused by Doppler shift as the signals travelled from the aircraft to the satellite to the ground station; the frequency translations made in the satellite and at the ground

station; a small, constant error (bias) in the SDU that results from drift and ageing; and compensation applied by the SDU to counter the Doppler shift on the uplink. This measure can be analysed to determine the aircraft's speed and heading, but multiple combinations of speed and heading can be valid solutions.[5]:18[165]:9–11

By combining the distance between the aircraft and satellite, speed, and heading with aircraft performance constraints (e.g. fuel consumption, possible speeds and altitudes), investigators generated candidate paths that were analysed separately by two methods. The first assumes the aircraft was flying on one of the three autopilot modes (two are further affected by whether the navigation system used magnetic north or true north as a reference) and calculates the BTO and BFO values along these routes and compares them with the values recorded from Flight 370. The second method generated paths which had the aircraft's speed and heading adjusted at the time of each handshake to minimise the difference between the calculated BFO of the path and the values recorded from Flight 370.[5]:18, 25–28[167]:10–11 A probability distribution for each method at the BTO arc of the sixth handshake of the two methods was created and then compared; 80 percent of the highest probability paths for both analyses combined intersect the BTO arc of the sixth handshake between 32.5°S and 38.1°S, which can be extrapolated to 33.5°S and 38.3°S along the BTO arc of the seventh handshake.[167]:12

Possible in-flight events

Power interruption

The SATCOM link functioned normally from pre-flight (beginning at 00:00 MYT) until it responded to a ground-to-air ACARS message with an acknowledge message at 01:07. Ground-to-air ACARS messages continued to be transmitted to Flight 370 until Inmarsat's network sent multiple "Request for Acknowledge" messages at 02:03, without a response from the aircraft. At some time between 01:07 and 02:03, power was lost to the SDU. At 02:25, the aircraft's SDU sent a "log-on request".[5]:22[48]:36–39 It is not common for a log-on request to be made in-flight, but it could occur for multiple reasons. An analysis of the characteristics and timing of these requests suggest a power interruption in-flight is the most likely culprit.[5]:33[168] As the power interruption was not due to engine flame-out, per ATSB, it may have been the result of manually switching off the aircraft's electrical system.[5]:33

Unresponsive crew or hypoxia

An analysis by the ATSB comparing the evidence available for Flight 370 with three categories of accidents—an in-flight upset (e.g., stall), a glide event (e.g., engine failure, fuel starvation), and an unresponsive crew or hypoxia event—concluded that an unresponsive crew or hypoxia event "best fit the available evidence"[5]:34 for the five-hour period of the flight as it travelled south over the Indian Ocean without communication or significant deviations in its track,[5]:34 likely on autopilot.[33][34][35] There is no consensus among investigators on the unresponsive crew or hypoxia theory.[33] If no control inputs were made following flameout and the disengagement of autopilot, the aircraft would likely have entered a spiral dive[5]:33 and enter the ocean within 20 nmi (37 km; 23 mi) of the flameout and disengagement of autopilot.[5]:35

Possible causes of disappearance

Passenger involvement

Two men boarded Flight 370 with stolen passports, which raised suspicion in the immediate aftermath of its disappearance.[169][170] The passports, one Austrian and one Italian, were reported stolen in Thailand in the preceding two years.[169] Interpol stated that both passports were listed on its database of lost and stolen passports, and that no check had been made against its database.[171][172] Malaysia's Home Minister, Ahmad Zahid Hamidi, criticised his country's immigration officials for failing to stop the passengers travelling on the stolen European passports.[172] The two one-way tickets purchased for the holders of the stolen passports were booked through China Southern Airlines.[169] It was reported that an Iranian had ordered the cheapest tickets to Europe via telephone in Bangkok, Thailand and paid in cash.[173][174] The two passengers were later identified as Iranian men, one aged 19 and the other 29, who had entered Malaysia on 28 February using valid Iranian passports. The head of Interpol said the organization was "inclined to conclude that it was not a terrorist incident".[29] The two men were believed to be asylum seekers.[30][31]

United States and Malaysian officials were reviewing the backgrounds of every passenger named on the manifest.[142] On 18 March, the Chinese government announced that it had checked all of the Chinese citizens on the aircraft and ruled out the possibility that any were potential hijackers.[175] One passenger who worked as a flight engineer for a Swiss jet charter company was briefly suspected as a potential hijacker because he was thought to have the relevant skill set.[176]

Crew involvement

Investigators believe someone in the cockpit of Flight 370 re-programmed the aircraft's autopilot before it travelled south across the Indian Ocean.[177][178] Police searched the homes of the pilots and seized financial records for all 12 crew members, including bank statements, credit card bills and mortgage documents.[179][180] On 2 April 2014, Malaysia's Police Inspector-General said that more than 170 interviews had been conducted as part of Malaysia's criminal investigation, including interviews with family members of the pilots and crew.[181][182]

Media reports have claimed that Malaysian police have identified Captain Shah as the prime suspect if human intervention is proven to be the cause of Flight 370's disappearance.[32][183][184][185] The United States' Federal Bureau of Investigation reconstructed the deleted data from Captain Shah's home flight simulator; a Malaysian government spokesman indicated that "nothing sinister"[186] had been found on it.[186][187] The preliminary report issued by Malaysia in March 2015 states that there was "no evidence of recent or imminent significant financial transactions carried out"[41]:20 by any of the pilots or crew and that analysis of the behaviour of the pilots on CCTV showed "no significant behavioural changes".[41]:21

Cargo

Flight 370 was carrying 10,806 kg (23,823 lb) of cargo, of which four ULDs of mangosteens and two pallets containing lithium-ion batteries are of interest, according to Malaysian investigators.[41]:103, 108–109 The four ULDs of mangosteens were loaded into the aft cargo bay of the aircraft. The lithium-ion batteries

were divided among two pallets in the forward cargo bay and one pallet placed in the rear of the aft cargo bay.[41]:106

There were 221 kg (487 lb) of lithium-ion batteries contained within a 2,453 kg (5,408 lb) consignment being transported between Motorola Solutions facilities in Bayan Lepas, Malaysia and Tianjin, China; the rest of the consignment consisted of walkie-talkie chargers and accessories.[41]:103 The lithium-ion batteries were assembled on 7 March and transported to the Penang Cargo Complex to be transported by MASkargo —Malaysia Airlines' cargo subsidiary—to be loaded onto a truck to transport it to Kuala Lumpur International Airport and onwards by air to Beijing.[41]:104 At the Penang Cargo Complex, the consignment was inspected by MASkargo employees and Malaysian customs officials, but did not go through a security screening, before the truck was sealed for transfer to the airport.[41]:104 The consignment did not go through any additional inspections at Kuala Lumpur International Airport before it was loaded onto Flight 370.[41]:104 Because the lithium-ion batteries were packaged in accordance with IATA guidelines,[m] they were not regulated as dangerous goods.[41]:106 Lithium-ion batteries can cause intense fires if they overheat and ignite, which has led to strict regulations on their transport aboard aircraft.[188][189] A fire fueled by lithium-ion batteries caused the crash of UPS Airlines Flight 6 and lithium-ion batteries are suspected to have caused a fire which resulted in the crash of Asiana Airlines Flight 991; both were cargo aircraft.[190][189][191] Some airlines have stopped carrying bulk shipments of lithium-ion batteries on passenger aircraft, citing safety concerns.[190][189]

A 4,566 kg (10,066 lb) consignment of mangosteens was aboard Flight 370, over half of which was harvested in Muar, Malaysia and the remainder from Sumatra, Indonesia.[41]:107 The mangosteens were packaged in plastic baskets containing 8–9 kg (18–20 lb) of mangosteens and covered with a water-soaked sponge to preserve their freshness.[41]:108 The mangosteens were loaded into four ULDs at Kuala Lumpur International Airport and inspected by officials from Malaysia's Federal Agriculture Marketing Authority before being loaded onto Flight 370.[41]:108 According to the head of Malaysian police, Inspector-General Tan Sir Khalid Abu Bakar, the people who handled the mangosteens as well as the Chinese importers were questioned to rule out sabotage.[192][193]

Aftermath

Information sharing

Public communication from Malaysian officials regarding the loss of the flight was initially beset with confusion.[n] The Malaysian government and the airline released imprecise, incomplete, and sometimes inaccurate information, with civilian officials sometimes contradicting military leaders.[207] Malaysian officials were criticised for such persistent release of contradictory information, most notably regarding the last point and time of contact with the aircraft.[208]

Although Malaysia's acting Transport Minister Hishammuddin Hussein, who is also the country's Defence Minister, denied the existence of problems between the participating countries, academics said that because of regional conflicts, there were genuine trust issues involved in co-operation and sharing intelligence, and that these were hampering the search.[209][210] International relations experts said entrenched rivalries over sovereignty, security, intelligence, and national interests made meaningful multilateral co-operation very

difficult.[209][210] A Chinese academic made the observation that the parties were searching independently, thus it was not a multilateral search effort.[210] *The Guardian* noted the Vietnamese permission given for Chinese aircraft to overfly its airspace as a positive sign of co-operation.[210] Vietnam temporarily scaled back its search operations after the country's Deputy Transport Minister cited a lack of communication from Malaysian officials despite requests for more information.[211] China, through the official Xinhua News Agency, said that the Malaysian government ought to take charge and conduct the operation with greater transparency, a point echoed by the Chinese Foreign Ministry days later.[209][212]

Malaysia had initially declined to release raw data from its military radar, deeming the information "too sensitive,"[209] but later acceded.[209][210] Defence experts suggested that giving others access to radar information could be sensitive on a military level. As an example: "The rate at which they can take the picture can also reveal how good the radar system is."[209] One suggested that some countries could already have had radar data on the aircraft but were reluctant to share any information that could potentially reveal their defence capabilities and compromise their own security.[209] Similarly, submarines patrolling the South China Sea might have information in the event of a water impact, and sharing such information could reveal their locations and listening capabilities.[213]

Criticism was also levelled at the delay of the search efforts. On 11 March, three days after the aircraft disappeared, British satellite company Inmarsat had provided officials (or its partner, SITA) with data suggesting the aircraft was nowhere near the areas in the Gulf of Thailand and the South China Sea being searched at that time; and may have diverted its course through a southern or northern corridor. This information was only publicly acknowledged and released by Najib on 15 March in a press conference.[66][214] Explaining why information about satellite signals had not been made available earlier, Malaysia Airlines said that the raw satellite signals needed to be verified and analysed "so that their significance could be properly understood" before it could publicly confirm their existence.[215] Hishammuddin said Malaysian and US investigators had immediately discussed the Inmarsat data upon receiving them on 12 March, and on two occasions, both groups agreed that it needed further processing and sent the data to the US twice for this purpose. Data analysis was completed on 14 March: by then, the AAIB had independently arrived at the same conclusion.[216]

In June 2014, relatives of passengers on Flight 370 began a crowdfunding campaign on Indiegogo to raise US$100,000—with an ultimate goal of raising US$5 million—as a reward to encourage anyone who knows the location of Flight 370 or the cause of its disappearance to reveal what they know.[217][218] The campaign, which ended 8 August 2014, raised US$100,516 from 1007 contributors.[217]

Malaysia Airlines

A month after the disappearance, Malaysia Airlines' chief executive Ahmad Jauhari Yahya acknowledged that ticket sales had declined but failed to provide specific details. This may partially result from the suspension of the airline's advertisement campaigns following the disappearance. Ahmad stated in an interview with the *Wall Street Journal* that the airline's "primary focus...is that we do take care of the families in terms of their emotional needs and also their financial needs. It is important that we provide answers for them. It is important that the world has answers, as well."[219] In further remarks, Ahmad said

he was not sure when the airline could start repairing its image, but that the airline was adequately insured to cover the financial loss stemming from Flight 370's disappearance.[219][220] In China, where the majority of passengers were from, bookings on Malaysia Airlines were down 60 percent in March.[221]

Malaysia Airlines retired the Flight 370 (MH370) flight number and replaced it with Flight 318 (MH318) beginning 14 March. This follows a common practice among airlines to rename flights following notorious accidents.[222][223] The flight—Malaysia Airline's second daily flight to Beijing—was later suspended beginning 2 May; according to insiders, this was due to lack of demand.[44][224]

Malaysia Airlines was given US$110 million from insurers in March 2014 to cover initial payments to passengers' families and the search effort.[225] In May, remarks from lead reinsurer of the flight, Allianz, indicated the insured market loss on Flight 370, including the search, was about US$350 million.[226][227]

Financial troubles

At the time of Flight 370's disappearance, Malaysia Airlines was struggling to cut costs to compete with a wave of new, low-cost carriers in the region. In the previous three years, Malaysia Airlines had booked losses of: RM1.17 billion (US$356 million) in 2013, RM433 million in 2012, and RM2.5 billion in 2011.[219] Malaysia Airlines lost RM443.4 million (US$137.4 million) in the first quarter of 2014 (January–March).[220] The second quarter—the first full quarter in the aftermath of Flight 370's disappearance—saw a loss of RM307.04 million (US$97.6 million), which represented a 75 percent increase over losses from the second-quarter of 2013.[228] Industry analysts expect Malaysia Airlines to lose further market share and face a challenging environment to stand out from competitors while addressing their financial plight.[219] The company's stock, down as much as 20 percent following the disappearance of Flight 370, had fallen 80 percent over the previous five years, which contrasts with a rise in the Malaysian stock market of about 80 percent over the same period.[221]

Many analysts and the media suggested that Malaysia Airlines would need to rebrand and repair its image and/or require government assistance to return to profitability.[229][230][231][232][233] The loss of Flight 17 in July greatly exacerbated Malaysia Airline's woes. The combined effect on consumer confidence of the loss of Flights 370 and 17 and the airline's poor financial performance led Khazanah Nasional—the majority shareholder (69.37 percent)[234] and a Malaysian state-run investment arm—to announce on 8 August its plan to purchase the remainder of the airline, thereby renationalising it.[235][236][237]

Compensation for passengers' kin

Lack of evidence in determining the cause of Flight 370's disappearance, indeed even physical evidence that the aircraft crashed, raises many issues regarding responsibility for the accident and payments made by insurance agencies.[238] Under the Montreal Convention, it is the carrier's responsibility to prove lack of fault in an accident and each passenger's next-of-kin are automatically entitled, regardless of fault, to a payment of approximately US$175,000[o] from the airline's insurance company—a total of nearly US$40 million for the 227 passengers on board.[238]

Malaysia Airlines would still be vulnerable to civil lawsuits from passengers' families.[238] Compensation awarded during or settled out-of-court during civil trials will likely vary widely among passengers based on country of the court. An American court could likely award upwards of US$8–10 million, while Chinese courts would likely award a small fraction of that.[239][240][241] Despite the announcement that Flight 370 ended in the southern Indian Ocean, it was not until 29 January 2015 that the Malaysian government officially declared Flight 370 an accident with no survivors, a move that would allow compensation claims to be made.[242] The first lawsuit related to the disappearance was filed in October 2014–before Flight 370 was declared an accident–on behalf of two Malaysian boys whose father was a passenger,[p] for negligence in failing to contact the aircraft soon after it was lost and for breach of contract for failing to bring the passenger to his destination.[245]

Malaysia Airlines offered *ex gratia* condolence payments soon after the disappearance. In China, families of passengers were offered ¥31,000 (about US$5,000) "comfort money";[246] but some families rejected the offer.[247] It was also reported that Malaysian relatives received only $2,000.[247] In June, Malaysia's deputy Foreign Minister Hamzah Zainuddin said that families of seven passengers received $50,000 advance compensation from Malaysia Airlines,[248] but that full payout would come after the aircraft is found or officially declared lost[249] (which later occurred in January 2015).[242]

Malaysia

Questions and criticisms were raised by air force experts and the Malaysian opposition about the current state of Malaysia's air force and radar capabilities. The failure of the Royal Malaysian Air Force to identify and respond to an unidentified aircraft (later determined to be Flight 370) flying through Malaysian airspace has been criticised by many.[250][251][252][253] The Malaysian military became aware of the unidentified flight only after reviewing radar recordings several hours after Flight 370's disappearance.[252] Not only was the failure to recognise and react to the unidentified aircraft a security blunder, it was also a missed opportunity to intercept Flight 370 and prevent the time-consuming and expensive search operation.[252][253]

Messages for MH370 at a bookstore in Malaysia

Malaysian Prime Minister Najib Razak responded to criticism of his government in an opinion piece published in the *The Wall Street Journal*:

> Without physical evidence, or a clear explanation for why this happened, peoples' attention has naturally focused on the authorities—and Malaysia has borne the brunt of the criticism. In the passage of time, I believe Malaysia will be credited for doing its best under near-impossible circumstances. It is no small feat for a country the size of ours to overcome diplomatic and military sensitivities and bring 26 different countries together to conduct one of the world's largest peacetime search operations. But we didn't get everything right...the response time should and will be investigated...I pledge that Malaysia will keep searching for the plane for as long as it takes.

> —Malaysian Prime Minister Najib Razak, *Malaysia's Lessons From the Vanished Airplane (The Wall Street Journal, 13 May 2014)*[254]

In the opinion piece, Najib goes on to emphasise the need for the aviation industry to "not only learn the lessons of MH370 but implement them," saying in closing that "the world learned from [Air France Flight 447] but didn't act. The same mistake must not be made again."[254]

Opposition leader Anwar Ibrahim strongly criticised the Malaysian government regarding its response to Flight 370's disappearance and the military's response when Flight 370 turned back over the Malay Peninsula; he has called for an international committee to take charge of the investigation "to save the image of the country and to save the country."[255] Malaysian authorities have accused Anwar—who was jailed on contentious charges the day before Flight 370 disappeared—of politicising the crisis. Flight 370's captain was a supporter of Anwar and the two knew each other.[255]

Malaysia's Defence and Transport Minister Hishammuddin Hussein—a central figure in the search and investigation of Flight 370 and active on Twitter—was criticised for responding/retweeting a tweet by a Malaysian journalist: "Right u are:) @IsmailAmsyar: #MH370 is a blessing in disguise 4 all of us. I understand now d beauty of unity & sweetness of having each other."[256] The remarks were viewed as insensitive to the victims' families. Both tweets were removed.[256][257] Questioned why Malaysia did not scramble fighter jets to intercept the aircraft as it tracked back across the Malay Peninsula, he noted that it was deemed a commercial aircraft and was not hostile, remarking: "If you're not going to shoot it down, what's the point of sending [a fighter jet] up?"[258]

The poor response to the crisis and lack of transparency in the response has brought attention to the state of media in Malaysia. After decades of having tight control of media, during which government officials were accustomed to passing over issues without scrutiny or accountability, Malaysia was suddenly thrust to the forefront of global media and unable to adjust to demands for transparency. Confronted by a foreign journalist about the slow response and conflicting information, Defence and Transport Minister Hishammuddin Hussein responded that he had received "a lot of feedback saying we've been very responsible in our actions...it's very irresponsible of you to say that."[259]

China

Chinese Deputy Foreign Minister Xie Hangsheng reacted sceptically to the conclusion by the Malaysian government that the aircraft had gone down with no survivors, demanding "all the relevant information and evidence about the satellite data analysis" and said that the Malaysian government must "finish all the work including search and rescue."[69][260] The following day, 25 March, Chinese president Xi Jinping sent a special envoy to Kuala Lumpur to consult with the Malaysian government over the missing aircraft.[261]

Relatives of passengers

On 25 March, around two hundred family members of the Chinese passengers protested outside the Malaysian embassy in Beijing.[262][263] Relatives who had arrived in Kuala Lumpur after the announcement continued with their protest, accusing Malaysia of hiding the truth and harbouring the murderer. They also wanted an apology for the Malaysian government's poor initial handling of the disaster and its "premature"

conclusion of loss, drawn without physical evidence.[264] An op-ed for *China Daily* said that Malaysia was not wholly to be blamed for its poor handling of such a "bizarre"[265] and "unprecedented crisis,"[265] and appealed to Chinese people not to allow emotions to prevail over evidence and rationality.[265] The Chinese ambassador to Malaysia defended the Malaysian government's response, stating that the relatives' "radical and irresponsible opinions do not represent the views of Chinese people and the Chinese government".[266] The ambassador also strongly criticised Western media for having "published false news, stoked conflict and even spread rumours"[267] to the detriment of relatives and of Sino–Malaysian relations.[267] On the other hand, a US Department of Defense official criticised China for what he perceived as providing apparently false leads that detracted from the search effort and wasted time and resources.[268][269]

Boycotts

Some Chinese have boycotted all things Malaysian, including vacations and singers, in protest of Malaysia's handling of the Flight 370 investigation.[270][271] Bookings on Malaysia Airlines from China, where the majority of passengers were from, were down 60 percent in March.[221] In late March, several major Chinese ticketing agencies—ELong, LY.com, Qunar and Mango—discontinued sale of airline tickets to Malaysia[270][272] and several large Chinese travel agencies reported a 50 percent drop in tourists compared to the same period the year before.[224] China is the third largest source of visitors for Malaysia, accounting for 1.79 million tourists.[224] One market analyst predicted a 20–40 percent drop in Chinese tourists to Malaysia, resulting in a loss of 4–8 billion yuan (RM2.1–4.2 billion; US$650 million-1.3 billion).[224][273]

The boycotts have largely been led or supported by celebrities.[224][274] Film star Chen Kun posted a message to Weibo—where he has 70 million followers—stating: "I...will start a boycott from my inner heart on any commercials and travel relating to Malaysia. This will last...until the Malaysian government takes down their clown-like mask and tells the truth."[224] The post was shared over 70,000 times and drew over 30,000 comments.[224] Over 337,000 people retweeted a tweet from TV host Meng Fei, which said "I've never been to Malaysia and I do not plan to go there in the future. If you feel the same, please retweet this message."[224]

China and Malaysia had dubbed 2014 to be the "Malaysia–China Friendship Year" to celebrate 40 years of diplomatic relations between the two countries.[272]

Air transport industry

The fact that, in a digitally-connected world, a modern aircraft could disappear has been met with surprise and disbelief by the public; and while changes in the aviation industry often take years to be implemented, airlines and air transport authorities have responded swiftly to take action on several measures to prevent a similar incident from occurring.[275][276][277][278]

Aircraft tracking

The International Air Transport Association—an industry trade organisation representing over 240 airlines (representing 84 percent of global air traffic)—and the United Nations' civil aviation body—the International Civil Aviation Organization (ICAO)—are working on implementing new measures to track aircraft in flight in real time.[279] The IATA created a task force (which includes several outside stakeholders)[279] to define a minimum set of requirements that any tracking system must meet, allowing airlines to decide the best solution to track their aircraft. The IATA's task force plans to come up with several short-, medium-, and long-term solutions to ensure that information is provided in a timely manner to support search, rescue, and recovery activities in the wake of an aircraft accident.[280] The task force was expected to provide a report to the ICAO on 30 September 2014, but on that day said that the report would be delayed, citing the need for further clarification on some issues.[281][282] In December 2014, the IATA task force recommended that, within 12 months, airlines track commercial aircraft in no longer than 15-minute intervals, although it still has not released its report and full details of proposed changes. The IATA itself did not support the deadline, which it believes cannot be met by all airlines, but the proposed standard has the support of the ICAO. Although the ICAO can set standards, it has no legal authority and such standards must be adopted by member states.[39][40]

In May 2014, Inmarsat said it would offer its tracking service for free to all aircraft equipped with an Inmarsat satellite connection (which amounts to nearly all commercial airliners).[283] Inmarsat has also changed the time period for handshakes with their terminals from one hour to 15 minutes.[165]:2

Transponders

There was a call for automated transponders after the 11 September 2001 terrorist attacks; no changes were made as aviation experts preferred flexible control, in case of malfunctions or electrical emergencies.[284] In the wake of Flight 370, the air transport industry is still resistant to the installation of automated transponders, which would likely entail significant costs. Pilots have also criticised changes of this kind, insisting on the need to cut power to equipment in the event of a fire. Nonetheless, new types of tamper-proof circuit breakers are being considered.[277]

Flight recorders

The frenzied search for the flight recorders in early April, due to the 30-day battery life of the underwater locator beacons (ULBs) attached to them, brought attention to the limitations of the ULBs.[q][285] Not only is the battery life of the ULBs limited, but the nominal distance at which the signal from the ULBs can be detected is 2,000–3,000 m (1.2–1.9 mi), up to 4,500 m (2.8 mi) under favourable conditions.[5]:11 Even if the flight recorders are located, the cockpit voice recorder memory has capacity to store only two hours of data, continuously recording over the oldest data. This length complies with regulations and it is usually only data from the last section of a flight that is needed to determine the cause of an accident. The events which caused Flight 370 to divert from its course and disappear happened more than two hours before the flight ended.[286] Given these limitations and the importance of the data stored on flight recorders, Flight 370 has brought attention to new technologies that enable data streaming to the ground.[287][288]

A call to increase the battery life of ULBs was made after the unsuccessful initial search in 2009 for the flight recorders on Air France Flight 447, which were not located until 2011. The ICAO did not make such a recommendation until 2014, with implementation by 2018.[287] The European Aviation Safety Agency has

stated its new regulations require that the transmitting time of ULBs fitted to aircraft flight recorders must range from 30 to 90 days. The agency proposed a new underwater locator beacon with a larger transmitting range to be fitted to aircraft flying over oceans.[280]

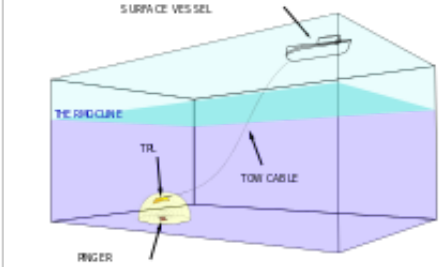

Detection of the acoustic signal from the ULBs must be made below the thermocline and within a maximum range, under nominal conditions, of 2,000–3,000 m (1.2–1.9 mi). With a ULB battery life of 30–40 days, searching for the important flight recorders is very difficult without precise coordinates of the location the aircraft entered the water.

Safety recommendations

In January 2015, the US NTSB cited Flight 370 and Air France Flight 447 when it issued eight safety recommendations[r] related to locating aircraft wreckage in remote or underwater locations and repeated recommendations for a crash-protected cockpit image recorder and tamper-resistant flight recorders and transponders.[289][290]

Timeline of events

8 March 2014
: Flight 370 disappears after departing Kuala Lumpur at 00:41 MYT (16:41 UTC, 7 March). A search and rescue effort is launched in the South China Sea and Gulf of Thailand.[291]

10 March
: Malaysia's military announces that Flight 370 may have turned back and flew west towards Malaysia. The search is expanded to include the Strait of Malacca.[92]

12 March
: Malaysia announces that Flight 370 crossed the Malay Peninsula and was last spotted on military radar 200 nmi (370 km; 230 mi) northwest of Penang on Malaysia's west coast. The focus of the search is shifted to the Andaman Sea and Strait of Malacca.[56][292]

15 March
: Officials announce that communications between Flight 370 and a communications satellite operated by Inmarsat indicate it continued to fly for several more hours and was along one of two corridors at the time of its last communication.[93]

18 March – 28 April
: Aerial search of the southern Indian Ocean, west of Australia, is conducted.[5][293]

24 March
: Prime Minister of Malaysia announces that Flight 370 is presumed to have gone down in the southern Indian Ocean; Malaysia Airlines states to families that it assumes "beyond reasonable doubt" there are no survivors.[294] The northern search corridor (northwest of Malaysia) and the northern half of the southern search corridor (the waters between Indonesia and Australia) are definitively ruled out.[295]

30 March
: The Joint Agency Coordination Centre is created to co-ordinate the multinational search effort.[296]

2–14 April
: An intense effort by several vessels and aircraft-deployed sonobuoys is made to detect underwater acoustic signals made by underwater locator beacons attached to the aircraft's data recorders. Several acoustic detections are made between 4–8 April.[5]

14 April – 28 May

A sonar survey of 860 km^2 (330 sq mi) of seafloor near the 4–8 April acoustic detections is conducted, yielding nil debris.[5]

1 May

A preliminary report from Malaysia to the ICAO (dated 9 April 2014) is publicly released along with: copies of cargo manifest documents; audio recordings (and transcript) of communications between air traffic control and Flight 370; a log of actions taken by air traffic control (Kuala Lumpur ACC) in the hours after Flight 370 disappeared from their radar (01:38–06:14 MYT).[46]

27 May

The data logs of satellite communications between Flight 370 and Inmarsat are released, following criticism over the way this data had been analysed and scepticism of whether Flight 370 really ended in the southern Indian Ocean.[297]

May–December

A bathymetric survey is conducted in the region to be searched.

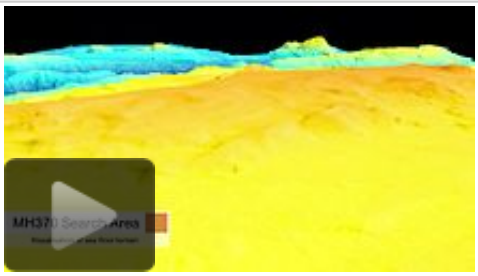

Video tour of bathymetry data collected during the bathymetric survey.

26 June

Plans for the next phase of the search (the "underwater search") are announced to the public in-depth for the first time and the Australian Transport Safety Bureau releases a report[5] detailing the previous search efforts, analysis of satellite communications, methodology used to determine the new search area.[298]

October 2014–ongoing

The underwater search began on 6 October and was expected to last up to 12 months. The search is conducted in areas where the bathymetric survey has been completed.[299][300]

8 October

Officials announce that the priority area to be searched is further south of the area identified in the June ATSB report.[116] The ATSB releases a report (a supplement to the June report) that details the methodology behind refinements to the analysis of satellite communications.[49]

29 January 2015

The Malaysian government officially declares Flight 370 an accident, in accordance with Annexes 12 and 13 to the Chicago Convention, with no survivors.[1]

8 March

The Malaysian Ministry of Transport publishes an interim report.[41]

29 July

A right wing flaperon from Flight 370 was found on the beach of Réunion Island in the Indian Ocean, 16 months after Flight 370 disappeared.[73]

In popular culture

The disappearance of Malaysia Airlines Flight 370 has been dubbed as one of the greatest aviation mysteries of all time.[301]

Several documentaries have been produced about the flight. The Smithsonian Channel aired a one-hour documentary about the flight on 6 April 2014, titled *Malaysia 370: The Plane That Vanished*.[302][303] The Discovery Channel broadcast a one-hour documentary about Flight 370 on 16 April 2014 titled *Flight 370: The Missing Links*.[304][305]

An episode of the television documentary series *Horizon* titled "Where is Flight MH370?" was broadcast on 17 June 2014 on BBC Two. The programme, narrated by Amanda Drew, documents how the aircraft disappeared, what experts believe happened to it, and how the search has unfolded. The programme also examines such new technologies as flight recorder streaming and Automatic dependent surveillance-broadcast (ADSB), which may help prevent similar disappearances in the future. It concludes by noting that *Ocean Shield* had spent two months searching 850 square kilometres (330 sq mi) of ocean, but that it had searched far to the north of the Inmarsat "hotspot" on the final arc, at approximately 28 degrees south, where the aircraft was most likely to have crashed.[306] On 8 October 2014, a modified version of the *Horizon* programme was broadcast in the US by PBS as an episode of *Nova*, titled "Why Planes Vanish", with a different narrator.[307][308][309]

The first fictional account of the mystery was Scott Maka's *MH370: A Novella*, published three months after the aircraft's disappearance.[310]

The aviation disaster documentary television series *Mayday* (also known as *Air Crash Investigation* or *Air Emergency*) produced an episode on the disaster, titled "Malaysia 370: What Happened?" In the UK, it aired on the first anniversary of Flight 370's disappearance, 8 March 2015.[311]

See also

- Accidents and incidents involving the Boeing 777 family
- Air safety
- List of accidents and incidents involving commercial aircraft
- List of aerial disappearances
- List of airline flights that required gliding
- List of unrecovered flight recorders
- Search for Malaysia Airlines Flight 370

Notes

a. No human remains of Flight 370 passengers or crew have been located; survival in the area where Flight 370 is believed to have entered the ocean is unlikely and the Malaysian government believes all passengers and crew are dead.[1] Additional details in the "presumed loss" section.
b. MH is the IATA designator and MAS is the ICAO airline designator.[2] The flight was also marketed as China Southern Airlines Flight 748 (CZ748/CSN748) through a codeshare.[2] It has been commonly referred to as "MH370", "Flight 370" or "Flight MH370".
c. Aircraft altitude is given in feet above sea level and measured, at higher altitudes, by air pressure, which declines linearly as altitude above sea level increases. Using a standard sea level pressure and formula, the nominal altitude of a given air pressure can be determined—referred to as the "pressure altitude". A flight level is the pressure altitude in 100s of feet. For example, flight level 350 corresponds to an altitude where air pressure is 179 mmHg (23.9 kPa), which is nominally 35,000 ft (10,700 m) but does not indicate the true altitude.
d. Responsibility for air traffic control is geographically partitioned, through international agreements, into flight information regions (FIRs). Although the airspace at the point where Flight 370 was lost is part of the Singapore FIR, the Kuala Lumpur ACC had been delegated responsibility to provide air traffic control services to aircraft in that part of its FIR.[45]:13
e. Heights given by primary radar are actual altitudes, unlike the pressure altitudes provided by secondary radar.
f. The interim report released by Malaysia in March 2015 says: "All the primary aircraft targets that were recorded by the DCA radar are consistent with those of the military data that were made available to the Investigation Team." The report does not *explicitly* state that the unidentified aircraft was Flight 370.[41]:3–4

Team." The report does not *explicitly* state that the unidentified aircraft was Flight 370.[illegible]

g. The aircraft is a Boeing 777-200ER (for Extended Range) model; Boeing assigns a unique customer code for each company that buys one of its aircraft, which is applied as an infix in the model number at the time the aircraft is built. The code for Malaysia Airlines is "H6", hence "777-2H6ER".[125]
h. One passenger boarded with a Hong Kong passport.[135]
i. The manifest initially released by Malaysia Airlines listed an Austrian and an Italian. These were subsequently identified as two Iranian nationals who boarded Flight 370 using stolen passports.[29]
j. 38 passengers and 12 crew.
k. The timing of the log-on interrogation message is determined by an inactivity timer, which was set to one hour at the time Flight 370 disappeared (it was later reduced to 15 minutes).[5]:18
l. Information released and reported publicly about SATCOM transmissions from Flight 370 have been inconsistent, especially the use of the terms "ping" and "handshake". It was initially reported as six "handshakes" or "pings" with one "partial handshake or ping" sent at 00:19 UTC by Flight 370, unprovoked by the ground station. The events listed may consist of several "transmissions" between the aircraft and ground station over the course of a few seconds. A readable copy of the ground station log of transmissions to and from Flight 370 is available here [1] (http://www.dca.gov.my/mainpage/MH370%20Data%20Communication%20Logs.pdf).
m. The 2014 IATA *Lithium Battery Guidance Document* (5 November 2013), which is based on the provisions of the ICAO's *Technical Instruction for the Safe Transport of Dangerous Goods by Air* (2013–2014 edition) and the 55th edition of the IATA's *Dangerous Goods Regulations*.[41]:106, Appendix 1.18I
n. Examples:
   * Malaysia Airlines' chief executive, Ahmad Jauhari Yahya, initially said air traffic control was in contact with the aircraft two hours into the flight when in fact the last contact with air traffic control was less than an hour after takeoff.[194]
   * Malaysian authorities initially reported that four passengers used stolen passports to board the aircraft before settling on two: one Italian and one Austrian.[195]
   * Malaysia abruptly widened the search area to the west on 9 March, and only later explained that military radar had detected the aircraft turning back.[195] This was later formally denied by Rodzali Daud.[196]
   * Malaysian authorities visited the homes of pilot Zaharie and co-pilot Fariq on 15 March, during which they took away a flight simulator belonging to Zaharie. Malaysian police chief Khalid Abu Bakar said this was the first police visit to those homes. On 17 March, the government contradicted this by saying police first visited the pilots' homes on the day following the flight's disappearance,[197] although this had been previously denied.[198]
   * On 16 March, Malaysia's acting transport minister contradicted the prime minister's account on the timing of the final data and communications received. Najib Razak had said that the ACARS system was switched off at 01:07. On 17 March, Malaysian officials said that the system was switched off sometime between 01:07, time of the last ACARS transmission, and 01:37, time of the next expected transmission.[199][200]
   * Three days after saying that the aircraft was not transporting anything hazardous, Malaysia Airlines' chief executive Ahmad said that potentially dangerous lithium batteries were on board.[201]
   * MAS chief executive initially claimed that the last voice communication from the aircraft was, "all right, good night", with the lack of a call sign fuelling speculation that the flight may have been hijacked.[202][203] Three weeks later Malaysian authorities published the transcript that indicated the last words were "Good night Malaysian three seven zero".[50][204][205][206]
o. The exact amount of this compensation is 113,100 special drawing rights. Using the official exchange rates (http://www.imf.org/external/np/fin/rates/rms_five.cfm) on 16 July 2014, this is worth approximately: RM557,000; ¥1,073,000; US$174,000; €129,000; or £102,000.
p. In March 2014, a petition for discovery was filed in a US court by a law firm, not representing relatives of families, against Boeing and Malaysia Airlines. It sought to obtain the names of manufacturers of aircraft parts along with maintenance records. It was reported in the media as a lawsuit or that Malaysia Airlines was being sued.[243][244]
q. Regulations require ULBs to transmit a minimum of 30 days. The ULBs on the flight recorders on Flight 370 had a minimum 30-day battery life after immersion. The ULB manufacturer predicted the maximum battery life was 40 days after immersion.[5]:11
r. A-15-1 through A-15-8

References

1. Rahma, Azharuddin Abdul (29 January 2015). "Announcement on MH370 by Director General – Department of Civil Aviation Malaysia" (http://www.mh370.gov.my/images/phocadownload/doa_announcement.pdf) (PDF). *Official Site for MH370*. Department of Civil Aviation Malaysia. Retrieved 31 January 2015.
2. MacLeod, Calum; Winter, Michael; Gray, Allison (8 March 2014). "Beijing-bound flight from Malaysia missing" (http://www.usatoday.com/story/news/world/2014/03/07/malaysia-airlines-beijing-flight-missiing/6187779/). *USA Today*. Retrieved 3 May 2014.
3. "Saturday, March 08, 04:20 PM MYT +0800 Media Statement – MH370 Incident released at 4.20pm" (http://www.malaysiaairlines.com/ksd-maintenance/DarkSites.html). Malaysia Airlines. scroll down to find "March 08, 04:20 PM MYT". Retrieved 8 March 2014.
4. "Saturday, March 08, 09:05 AM MYT +0800 Malaysia Airlines MH370 Flight Incident – 2nd Media Statement" (http://www.malaysiaairlines.com/ksd-maintenance/DarkSites.html). Malaysia Airlines. scroll down to find "2nd Media Statement". Archived (https://web.archive.org/web/20140308024002/http://www.malaysiaairlines.com/my/en/site/dark-site.html) from the original on 8 March 2014.
5. "MH 370 – Definition of Underwater Search Areas" (http://www.atsb.gov.au/media/5243942/ae-2014-054_mh370_-_definition_of_underwater_search_areas_18aug2014.pdf) (PDF). Australian Transport Safety Bureau. 26 June 2014. Archived (http://web.archive.org/web/20140827002931/http://www.atsb.gov.au/media/5243942/ae-2014-054_mh370_-_definition_of_underwater_search_areas_18aug2014.pdf) (PDF) from the original on 27 August 2014. Retrieved 12 April 2015. Lay summary (http://www.atsb.gov.au/mh370-pages/updates/reports.aspx).
6. "Radar data shows MH370 flew erratically, NYT reports" (http://www.themalaymailonline.com/malaysia/article/radar-data-shows-mh370-flew-erratically-nyt-reports). *Malay Mail Online*. 15 March 2014. Retrieved 18 December 2014.
7. "Saturday, March 08, 10:30 AM MYT +0800 Malaysia Airlines MH370 Flight Incident – 3rd Media Statement" (http://www.malaysiaairlines.com/ksd-maintenance/DarkSites.html). Malaysia Airlines. scroll down to find "3rd Media Statement". Retrieved 2 April 2014.
8. "Malaysia Airlines MH370: Last communication revealed" (http://www.bbc.com/news/world-asia-26541057). BBC News. 12 March 2014. Retrieved 8 May 2014.
9. Hildebrandt, Amber (10 March 2014). "Malaysia Airlines Flight MH370: 'Mystery compounded by mystery' " (http://www.cbc.ca/news/world/malaysia-airlines-flight-mh370-mystery-compounded-by-mystery-1.2566983). *CBC News* (Dominion of Canada: Canadian Broadcasting Corporation). Retrieved 14 February 2015.
10. Buncombe, Andrew; Withnall, Adam (10 March 2014). "Malaysia Airlines Flight MH370: Oil slicks in South China Sea 'not from missing jet', officials say" (http://www.independent.co.uk/news/world/asia/malaysia-airlines-flight-mh370-search-teams-scramble-helicopters-and-ships-to-investigate-sighting-of-possible-life-raft-9180759.html). *The Independent*. Retrieved 14 February 2015.
11. Grudgings, Stuart. "Malaysia Airlines plane crashes in South China Sea with 239 people aboard: report" (http://www.reuters.com/article/2014/03/08/us-malaysiaairlines-flight-idUSBREA2701720140308). Retrieved 8 March 2014.
12. Lokman, Tasnim (9 March 2014). "Missing MH370: Indonesia helps in search for airliner" (http://www2.nst.com.my/latest/font-color-red-missing-mh370-font-indonesia-helps-in-search-for-airliner-1.504168). *New Straits Times*. Retrieved 17 January 2015.
13. "Malaysia Airlines flight MH370: Distraught families told by text message to assume 'beyond doubt no one survived' " (http://www.independent.co.uk/news/world/asia/missing-malaysia-airlines-flight-mh370-distraught-families-told-by-text-message-to-assume-beyond-doubt-no-one-survived-9212722.html). *The Independent*. 24 March 2014. Retrieved 25 March 2014.
14. Thomas Fuller; Chris Buckley (24 March 2014). "Malaysian Leader Says Flight 370 Ended in Indian Ocean" (http://www.nytimes.com/2014/03/25/world/asia/malaysia-airlines-flight-370.html). *The New York Times*. Retrieved 12 April 2015.
15. "Flight MH370 'crashed in south Indian Ocean' – Malaysia PM" (http://www.bbc.co.uk/news/world-asia-26716572). BBC News. 24 March 2014. Retrieved 8 May 2014.
16. "Australia agrees to lead search in Indian Ocean for missing Malaysia Airlines flight MH370"

(https://web.archive.org/web/20140517130658/http://www.canberratimes.com.au/federal-politics/political-news/australia-agrees-to-lead-search-in-indian-ocean-for-missing-malaysia-airlines-flight-mh370-20140317-34xay.html). *The Canberra Times*. 17 March 2014. Archived from the original (http://www.canberratimes.com.au/federal-politics/political-news/australia-agrees-to-lead-search-in-indian-ocean-for-missing-malaysia-airlines-flight-mh370-20140317-34xay.html) on 17 May 2014. Retrieved 12 April 2015.
17. Weaver, Matthew (24 March 2014). "Blog: Malaysia Airlines flight MH370 (March 24) – MH370 families attack Malaysian government over loss of plane" (http://www.theguardian.com/world/2014/mar/24/mh370-chinese-plane-spots-white-objects-live-updates). *The Guardian*. Retrieved 11 May 2014.
18. "MH370 missing Malaysia Airlines plane: Search might be in wrong spot, investigators say" (http://www.news.com.au/travel/travel-updates/mh370-missing-malaysia-airlines-plane-search-might-be-in-wrong-spot-investigators-say/story-fnizu68q-1227084277721). *News.com.au*. 9 October 2014. Retrieved 19 October 2014.
19. "Transcript of Press Conference, 28 August 2014" (http://www.jacc.gov.au/media/interviews/2014/august/tr016.aspx). *jacc.gov.au*. JACC. Retrieved 14 December 2014.
20. "Search for MH370" (http://www.jacc.gov.au/search/index.aspx). *jacc.gov.au*. JACC. Retrieved 14 December 2014.
21. "New missing Malaysian plane MH370 search area announced" (http://www.bbc.com/news/world-asia-28031741). *BBC News*. 26 June 2014. Retrieved 15 November 2014. "The search for the missing airliner is already among most expensive in aviation history."
22. "Search for MH370 to be most expensive in aviation history" (http://www.reuters.com/article/2014/04/08/us-malaysia-airlines-costs-idUSBREA3709520140408). *Reuters*. Reuters. 8 April 2014. Retrieved 15 November 2014.
23. Neuman, Scott (17 March 2014). "Search For Flight MH370 Reportedly Largest in History" (http://www.npr.org/blogs/thetwo-way/2014/03/17/290890377/search-for-flight-mh370-reportedly-largest-in-history). *The Two-way*. NPR. Retrieved 11 May 2014.
24. Pearlman, Jonathan (29 May 2014). "MH370 search becomes most expensive aviation hunt in history, yet still no clues" (http://www.telegraph.co.uk/news/worldnews/asia/malaysia/10863605/MH370-search-becomes-most-expensive-aviation-hunt-in-history-yet-still-no-clues.html). *The Telegraph*. Telegraph Media Group. Retrieved 1 June 2014.
25. Safi, Michael and Holmes, Oliver "MH370 search: what is the 'flaperon' debris found in Réunion?" (http://www.theguardian.com/world/2015/jul/30/mh370-search-what-is-the-debris-found-in-la-reunion?CMP=soc_568) The *Guardian*, 30 July 2015
26. CBC News (29 July 2015). "MH370 Search: Too Early to Tell Whether Debris on Réunion Island is Part of Missing Jet" (http://www.cbc.ca/news/world/mh370-search-too-early-to-tell-whether-debris-on-r%C3%A9union-island-is-part-of-missing-jet-1.3172431). *CBC News*. Canada: Canadian Broadcasting Corporation. Retrieved 29 July 2015.
27. "MH370: Debris found on Réunion Island belongs to missing airliner" (http://www.cbc.ca/news/world/mh370-debris-found-on-r%C3%A9union-island-belongs-to-missing-airliner-1.3180272). *CBC News*. 5 August 2015. Retrieved 5 August 2015.
28. "No MH370 Distress Call, Search Area Widened" (http://www.aviationweek.com/Article.aspx?id=/article-xml/awx_03_11_2014_p0-671110.xml). *Aviation Week & Space Technology*. 12 March 2014. Retrieved 12 April 2015.
29. Budisatrijo, Alice; Westcott, Richard (11 March 2014). "Malaysia Airlines MH370: Stolen passports 'no terror link' " (http://www.bbc.com/news/world-asia-26525281). BBC News. Retrieved 9 May 2014.
30. "MISSING MH370: Man with stolen passport on jet is asylum seeker – Latest" (https://web.archive.org/web/20140313065137/http://www.nst.com.my/latest/font-color-red-missing-mh370-font-man-with-stolen-passport-on-jet-is-asylum-seeker-1.507657). *New Straits Times*. Archived from the original (http://www.nst.com.my/latest/font-color-red-missing-mh370-font-man-with-stolen-passport-on-jet-is-asylum-seeker-1.507657) on 13 March 2014. Retrieved 30 March 2014.
31. Dehghan, Saeed Kamali. "Iranians travelling on flight MH370 on forged passports 'not linked to terror' " (http://www.theguardian.com/world/2014/mar/11/passengers-malaysian-plane-mh370-iranian-forged-passports). *The Guardian*. Retrieved 30 March 2014.
32. "Malaysian police investigation names MH370 pilot prime suspect" (http://www.news.com.au/travel/travel-

updates/malaysian-police-investigation-names-mh370-pilot-prime-suspect/story-fnizu68q-1226962811653). *NewsComAu*. Retrieved 28 September 2014.
33. Bradsher, Keith (27 June 2014). "Pressure Loss Is Explored in Vanishing of Jetliner" (http://www.nytimes.com/2014/06/27/world/asia/malaysia-airlines-flight-370.html?_r=0). *New York Times*. Retrieved 29 June 2014.
34. Feast, Lincoln (26 June 2014). "Malaysia jet passengers likely suffocated, Australia says" (http://www.reuters.com/article/2014/06/27/us-malaysia-airlines-australia-idUSKBN0F10FE20140627). Reuters. Retrieved 29 June 2014.
35. Stacey, Daniel; Pasztor, Andy; Winning, David (26 June 2014). "Australian Report Postulates Malaysia Airlines Flight 370 Lost Oxygen" (http://online.wsj.com/articles/malaysia-airlines-flight-370-search-shifts-to-new-area-1403762350). *Wall Street Journal*. Retrieved 29 June 2014.
36. "Malaysia Airlines: experts surprised at disappearance of 'very safe' Boeing 777" (http://www.theguardian.com/world/2014/mar/08/malaysia-airlines-experts-surprised-at-disappearance-of-very-safe-boeing-777). *The Guardian*. 8 March 2014. Retrieved 11 May 2014.
37. "Malaysia Airlines has one of Asia's best safety records" (http://www.reuters.com/article/2014/03/08/us-malaysia-airlines-profile-idUSBREA2707Y20140308). Reuters. 8 March 2014. Retrieved 9 March 2014.
38. Patterson, Thom (17 July 2014). "A second lost Boeing 777 for Malaysia Airlines" (http://www.cnn.com/2014/07/17/world/europe/malaysia-airlines-sidebar/index.html?iid=article_sidebar). *CNN*. Retrieved 18 July 2014.
39. "UN Aviation Body to Propose 15-minute Flight Tracking Standard" (http://www.voanews.com/content/reu-un-aviation-body-to-propose-15-minute-flight-tracking-standard/2588127.html). *Voice of America*. Reuters. 6 January 2015. Retrieved 24 January 2015.
40. Peterson, Barbara (12 December 2014). "Here's Why Airliners Still Don't Have Real-Time Tracking Tech" (http://www.popularmechanics.com/technology/aviation/safety/mh370-missing-jets-tracking-technology-17521859). *Popular Mechanics*. Retrieved 24 January 2015.
41. Malaysia Ministry of Transport (8 March 2014). "Factual Information, Safety Investigation: Malaysia Airlines MH370 Boeing 777-200ER (9M-MRO)" (http://mh370.mot.gov.my/download/FactualInformation.pdf) (PDF). *Malaysia Ministry of Transport*. Malaysia: Malaysia Ministry of Transport. Archived (https://web.archive.org/web/20150309093347/http://mh370.mot.gov.my/download/FactualInformation.pdf) (PDF) from the original on 2015-03-09. Retrieved 9 March 2015.
42. Wise, Jeff (12 March 2015). "The Malaysian government just released a huge amount of new data on the MH370 crash. Here's what it reveals" (https://web.archive.org/web/20150314215013/http://www.nymag.com/daily/intelligencer/2015/03/with-new-batch-of-mh370-info-mystery-deepens.html). *New York Magazine*. New York Media. Archived from the original (http://www.nymag.com/daily/intelligencer/2015/03/with-new-batch-of-mh370-info-mystery-deepens.html) on 2015-03-14. Retrieved 14 March 2015.
43. "Tweet" (https://twitter.com/flightradar24/status/442118255511998464). *Twitter*. Flightradar24. 7 March 2014. Retrieved 24 October 2014.
44. "Malaysia Airlines 2Q loss widens. Restructuring is imminent but outlook remains bleak" (http://centreforaviation.com/analysis/malaysia-airlines-2q-loss-widens-restructuring-is-imminent-but-outlook-remains-bleak-184380). *CAPA Centre For Aviation*. 28 August 2014. Retrieved 24 October 2014. "The only significant cut MAS implemented in 2Q2014 was on the Beijing route, which is now served with one daily flight. (MH370 was one of two daily flights MAS had operated to Beijing.)"
45. "Airspace Delegated to Malaysia" (http://aip.dca.gov.my/aip%20pdf/ENR/ENR%202/ENR%202.1/Air%20Traffic%20Services%20Airspace.pdf) (PDF). *Department of Civil Aviation Malaysia*. Department of Civil Aviation Malaysia. 25 August 2011. Retrieved 24 October 2014.
46. "Documents: Preliminary report on missing Malaysia Airlines Flight 370" (http://www.cnn.com/interactive/2014/04/world/malaysia-flight-documents/). *CNN* (Malaysia Department of Civil Aviation). Retrieved 22 October 2014.
47. "MH370 PC live updates / 530 17th March" (https://web.archive.org/web/20140317135858/http://outofcontrolvideos.com/mh370-pc-live-updates-530-17th-march/). Out of Control Videos. Archived from the original (http://outofcontrolvideos.com/mh370-pc-live-updates-530-17th-march/) on 17 March 2014. Retrieved 16 July 2014. "Timing of ACARS deactivation unclear.

Last ACARS message at 01:07 was not necessarily point at which system was turned off"
48. "Signalling Unit Log for (9M-MRO) Flight MH370" (http://www.dca.gov.my/mainpage/MH370%20Data%20Communication%20Logs.pdf) (PDF). Inmarsat/Malaysia Department of Civil Aviation. Retrieved 29 June 2014.
49. "MH370 – Flight Path Analysis Update" (http://www.atsb.gov.au/media/5163181/AE-2014-054_MH370%20-FlightPathAnalysisUpdate.pdf) (PDF). *Australian Transport Safety Bureau*. 8 October 2014. Retrieved 15 November 2014.
50. "MH370: cockpit transcript in full" (http://www.theguardian.com/world/interactive/2014/apr/01/mh370-cockpit-transcript-full). *The Guardian*. 1 April 2014. Retrieved 11 May 2014.
51. "FlightRadar24.com MH370 7 March 2014" (http://www.flightradar24.com/data/flights/mh370#2d81a27). Retrieved 12 April 2015.
52. "Malaysian Airlines System (MH) No. 370 ✈ 08-Mar-2014 ✈ WMKK / KUL – ZBAA / PEK ✈" (http://uk.flightaware.com/live/flight/MAS370/history/20140307/1635Z/WMKK/ZBAA). flightaware. Retrieved 8 March 2014.
53. "Pilot: I established contact with plane" (http://www.nst.com.my/nation/general/font-color-red-missing-mh370-font-pilot-i-established-contact-with-plane-1.503464). *New Straits Times*. 9 March 2014. Retrieved 17 March 2014.
54. Cenciotti, David (11 March 2014). "What we know and what we don't about the mysterious Malaysia Airlines MH370 disappearance" (http://theaviationist.com/2014/03/11/mh370-known-unknown-facts/). *The Aviationist*. Retrieved 3 April 2014.
55. Forsythe, Michael; Schmidt, Michael (14 March 2014). "Radar Suggests Jet Shifted Path More Than Once" (http://www.nytimes.com/2014/03/15/world/asia/malaysia-military-radar.html?hp&_r=0). *The New York Times*. Retrieved 14 February 2015.
56. "Exclusive: Radar data suggests missing Malaysia plane deliberately flown way off course – sources" (http://www.reuters.com/article/2014/03/14/us-malaysia-airlines-radar-exclusive-idUSBREA2D0DG20140314). *Reuters*. Retrieved 28 September 2014.
57. Stacey, Daniel (1 May 2014). "Investigators to Re-Examine Clues in Missing Malaysia Airlines Flight 370" (http://online.wsj.com/news/articles/SB10001424052702303678404579535364189029806). Wall Street Journal. Retrieved 13 July 2014.
58. Stewart, Cameron (18 March 2014). "Malaysia Airlines flight MH370 'flew low to evade radars' " (http://www.theaustralian.com.au/business/aviation/malaysia-airlines-flight-mh370-flew-low-to-evade-radars/story-e6frg95x-1226857491352). *The Australian*. Retrieved 13 July 2014.
59. "Malaysian government publishes MH370 details from UK AAIB" (http://www.inmarsat.com/news/malaysian-government-publishes-mh370-details-uk-aaib/). Inmarsat. Retrieved 26 March 2014.
60. "Inmarsat breaks silence on probe into missing jet" (http://video.foxnews.com/v/3369208664001/inmarsat-breaks-silence-on-probe-into-missing-jet-/#sp=show-clips). Fox News Channel. Retrieved 26 March 2014.
61. Broderick, Sean (1 May 2014). "First MH370 Report Details Confusion In Hours After Flight Was Lost" (http://aviationweek.com/commercial-aviation/first-mh370-report-details-confusion-hours-after-flight-was-lost). *Aviation Week*. Retrieved 22 October 2014.
62. "Inquiry details controllers' hunt as MH370 vanished" (http://www.flightglobal.com/news/articles/inquiry-details-controllers39-hunt-as-mh370-vanished-398793/). *Flight Global*. 1 May 2014. Retrieved 12 April 2015.
63. "Sunday, March 09, 02:00 AM MYT +0800 Malaysia Airlines MH370 Flight Incident – 6th Media Statement" (http://www.malaysiaairlines.com/ksd-maintenance/DarkSites.html). Malaysia Airlines. scroll down to find "6th Media Statement". Retrieved 5 April 2014.
64. "Saturday, March 08, 07:30 AM MYT +0800 Media Statement – MH370 Incident released at 7.24am" (http://www.malaysiaairlines.com/ksd-maintenance/DarkSites.html). Malaysia Airlines. scroll to bottom of page. Retrieved 2 April 2014.
65. Watson, Ivan (29 April 2014). "MH370: Plane audio recording played in public for first time to Chinese families" (http://www.cnn.com/2014/04/29/world/asia/missing-plane-recordings/). *CNN*. Retrieved 14 July 2014. ""At 2:03 a.m. local time on March 8, the operational dispatch centre of Malaysia Airlines sent a message to the cockpit instructing the pilot to contact ground control in Vietnam, said Sayid Ruzaimi Syed Aris, an official with Malaysia's aviation authority...MH370 did not respond to the message...'At 7:13,' Sayid said, Malaysia Airlines tried to 'make a voice call to the aircraft, but no pickup.'"
66. Rayner, Gordon (24 March 2014). "MH370: Britain finds itself at centre of blame game over crucial delays"

(http://www.telegraph.co.uk/news/worldnews/asia/malaysia/10720009/MH370-Britain-finds-itself-at-centre-of-blame-game-over-crucial-delays.html). *The Telegraph*. Retrieved 26 March 2014.
67. Pearlman, Jonathan; Wu, Adam (21 March 2014). "Revealed: the final 54 minutes of communication from MH370" (http://www.telegraph.co.uk/news/worldnews/asia/malaysia/10714907/Revealed-the-final-54-minutes-of-communication-from-MH370.html). *The Daily Telegraph*.
68. "Missing Malaysia plane: What we know" (http://www.bbc.co.uk/news/world-asia-26503141). BBC News. 1 May 2014. Retrieved 8 May 2014.
69. Keith Bradsher, Edward Wong, Thomas Fuller. "Malaysia Releases Details of Last Contact With Missing Plane" (http://www.nytimes.com/2014/03/26/world/asia/malaysia-flight-370.html). *The New York Times*. Retrieved 25 March 2014.
70. Martinez, Michael (March 19, 2014). "Flying low? Burning object? Ground witnesses claim they saw Flight 370" (http://www.cnn.com/2014/03/19/world/asia/malaysia-airlines-plane-ground-witnesses/). CNN. Retrieved 19 May 2015.
71. Shears, Richard (March 21, 2014). "Malaysian woman claims to have seen missing MH370 in the water near Andaman Islands on day it disappeared" (http://www.dailymail.co.uk/news/article-2586013/Malaysian-woman-claims-seen-missing-MH370-water-near-Andaman-Islands-day-disappeared.html). London Daily Mail. Retrieved 19 May 2015.
72. Pearlman, Jonathan (June 3, 2014). "Malaysia Airlines plane search: British yachtswoman 'saw MH370 on fire'" (http://www.telegraph.co.uk/news/worldnews/asia/malaysia/10872261/Malaysia-Airlines-plane-search-British-yachtswoman-saw-MH370-on-fire.html). The Telegraph. Retrieved 19 May 2015.
73. "MH370 search: Réunion debris to be tested in France" (http://www.bbc.com/news/world-asia-33714780). *BBC News*. 30 July 2015. Retrieved 30 July 2015.
74. Boeing "777 Aircraft Maintenance Manual" [D633W101-RBA], Chapter 6 DIMENSIONS AND AREAS, Section 06-44 WINGS (Major zones 500 and 600), Page 221, May 3, 2008
75. Aubusson, Kate (31 July 2015). "MH370: Suitcase reportedly found on Reunion Island, close to where plane debris recovered" (http://www.smh.com.au/world/mh370-suitcase-reportedly-found-on-reunion-island-close-to-where-plane-debris-recovered-20150730-gio73i.html). *Sydney Morning Herald*. Retrieved 31 July 2015.
76. "MH370: Aircraft Debris and Drift Modelling" (http://www.atsb.gov.au/publications/2015/mh370-drift-analysis.aspx). Australian Transport Safety Bureau/The Commonwealth Scientific and Industrial Research Organisation. 4 August 2015. Retrieved 8 August 2015.
77. "MH370 Operational Search Update— 05 August 2015" (http://jacc.gov.au/families/operational_reports/opsearch-update-20150805.aspx). Joint Agency Coordination Centre. 5 August 2015. Retrieved 8 August 2015.
78. "Malaysia Airlines Flight 370 Searchers Treating Debris as Major Lead" (http://abcnews.go.com/International/malaysia-airlines-370-searchers-treating-debris-major-lead/story?id=32775033). Retrieved 30 July 2015.
79. "'Chinese water bottle, Indonesian canister' wash up on Reunion Island after possible MH370 wing flap find" (http://www.scmp.com/news/asia/southeast-asia/article/1845475/chinese-water-bottle-indonesian-canister-wash-reunion). *AFP, Reuters* (South China Morning Post). 31 July 2015. Retrieved 31 July 2015.
80. "MH370 Search: New Items Wash Ashore On Reunion" (http://news.sky.com/story/1528192/mh370-search-new-items-wash-ashore-on-reunion). *Sky News*. 31 July 2015. Retrieved 31 July 2015.
81. "MH370 search: Plane debris arrives in France" (http://www.bbc.com/news/world-europe-33739851). *BBC News*. 1 August 2015. Retrieved 2 August 2015.
82. Adamson, Thomas; Ng, Eileen (2 August 2015). "Malaysia Seeks Help in Finding More Possible MH370 Debris" (http://abcnews.go.com/International/wireStory/malaysia-seeks-expand-search-mh370-debris-32832669). *ABC News*. AP. Retrieved 8 August 2015. "Malaysia's transport ministry confirmed Sunday that the flaperon that was found has been identified as being from a 777, saying it had been verified by French authorities together with Boeing, the U.S. National Transportation Safety Board and a Malaysian team."
83. "France launches search for more MH370 debris on Réunion" (http://www.france24.com/en/20150807-france-steps-reunion-island-search-flight-mh370-wreckage). *France24*. 7 August 2015. Retrieved 8 August 2015. "The prefect of the French overseas department, Dominique Sorain, said Friday that a helicopter and water vehicles would scour an area 120 kilometres (75 miles) by 40 kilometres (25 miles) around the east coast of the island, where the wing part, known as a flaperon, was found. Bad weather forced the suspension of operations on Friday evening with the search set to begin again on Sunday morning."
84. "Plane debris is from missing MH370" (http://www.bbc.co.uk/news/world-asia-33794012). BBC News Online.

Retrieved 5 August 2015.
85. Shahrestani, Vin "MH370: Malaysian government confirms debris is from a Boeing 777" (http://www.telegraph.co.uk/news/worldnews/mh370/11779673/MH370-Malaysian-government-confirms-debris-is-from-a-Boeing-777.html) The *Telegraph* (UK), August 5, 2015
86. Mullen, Jethro; Shoichet, Catherine; Fantz, Ashley (6 August 2015). "MH370: More plane debris has washed up on Reunion, Malaysia says" (http://www.cnn.com/2015/08/06/world/mh370-investigation/). *CNN*. Retrieved 8 August 2015.
87. "Search for MH370 Facts and statistics Surface search of the southern Indian Ocean 17 March – 28 April 2014" (http://www.jacc.gov.au/search/files/MH370_Facts_and_statistics-Surface_search_of_the_southern_Indian_Ocean.pdf) (PDF). *jacc.gov.au*. Joint Agency Coordination Centre. Retrieved 5 December 2014.
88. Brown, Sophie (16 June 2014). "MH370: How long will the search continue?" (http://www.cnn.com/2014/06/16/world/asia/malaysia-airlines-how-long-will-search-continue/). *CNN.com*. Retrieved 15 November 2014.
89. "The Hunt for Malaysia Airlines Flight MH370 Continues" (http://www.newsweek.com/hunt-malaysia-airlines-flight-mh370-continues-263291). *Newsweek*. Reuters. 6 August 2014. Retrieved 15 November 2014.
90. "This Is the Country That's Spent the Most Searching for MH370" (http://time.com/2854385/mh370-search-spending/). *Time*. 11 June 2014. Retrieved 15 November 2014.
91. "About Us" (http://www.jacc.gov.au/about.aspx). *jacc.gov.au*. Joint Agency Coordination Centre. Retrieved 5 December 2014.
92. "RMAF chief: Recordings captured from radar indicate flight deviated from original route" (http://www.thestar.com.my/News/Nation/2014/03/10/Indications-of-turnback-by-MH370-RMAF-chief-Recordings-captured-from-radar-indicate-flight-deviated/). Retrieved 28 September 2014.
93. "MH370 possibly in one of two 'corridors', says PM" (http://www.themalaymailonline.com/malaysia/article/mh370-may-be-between-kazakhstan-and-south-indian-ocean-says-pm). Retrieved 28 September 2014.
94. Hodal, Kate (16 March 2014). "Flight MH370: Malaysia asks for help in continued search for missing plane" (http://www.theguardian.com/world/2014/mar/16/flight-mh370-malaysia-asks-help-missing-plane). *The Guardian*. Retrieved 4 November 2014.
95. "India Continues Search for MH370 as Malaysia Ends Hunt in South China Sea" (http://blogs.wsj.com/indiarealtime/2014/03/15/india-continues-search-for-mh370-as-malaysia-ends-hunt-in-south-china-sea/). *The Wall Street Journal*. 15 March 2014. Retrieved 12 April 2015.
96. "Arrangements in Australia" (https://www.amsa.gov.au/search-and-rescue/sar-in-australia/arrangements-in-australia/). *Australian Maritime Safety Authority*. Retrieved 12 November 2014.
97. "National Search and Rescue Manual – June 2014 edition" (http://natsar.amsa.gov.au/documents/NATSAR-Manual/Australian%20National%20SAR%20Manual%20June%202014%20FINAL.pdf) (PDF). *Australia Maritime Safety Authority*. p. 231. Retrieved 12 November 2014.
98. "Missing MH370: Australia to lead southern search for MH370" (http://www.thestar.com.my/News/Nation/2014/03/17/Missing-MH370-Australia/). *The Star*. 17 March 2014.
99. "Incident 2014/1475 search for Malaysian airlines flight MH370 planned search area 19 March 2014" (https://www.amsa.gov.au/media/incidents/mh370/day2-2014-03-19/190314_Day_Two_Search_Area_wide_handout_1.pdf) (PDF). Australian Maritime Safety Authority. 19 March 2014. Retrieved 12 April 2015.
100. Jacobs, Frank (27 March 2014). "MH370 and the Secrets of the Deep, Dark Southern Indian Ocean" (http://www.foreignpolicy.com/articles/2014/03/26/mh370_and_the_secrets_of_the_deep_dark_indian_ocean). *Foreign Policy*. Archived (http://web.archive.org/web/20150127175159/http://foreignpolicy.com/2014/03/27/mh370-and-the-secrets-of-the-deep-dark-southern-indian-ocean/) from the original on 27 January 2015. Retrieved 14 February 2015.
101. "AMSA_MH370_MediaKit " 18/03/2014 – AMSA Search Area Charts" (https://drive.google.com/folderview?id=0B4w6RpGjTiQpTUxRZzVULTRNaWc&usp=sharing&tid=0B4w6RpGjTiQpM1dxMzdSTHRMeW8). Australian Maritime Safety Authority. 18 March 2014. Retrieved 12 April 2015.
102. "Flight MH370: Images of ocean debris" (http://www.bbc.com/news/world-asia-26662641). *BBC News*. 28 March 2014. Retrieved 10 November 2014.
103. "Flight MH370: 'Objects spotted' in new search area" (http://www.bbc.com/news/world-asia-26786549). BBC

"Flight MH370: Objects spotted in new search area" (http://www.bbc.com/news/world-asia-26703549). BBC News. 28 March 2014. Retrieved 8 May 2014.
104. "MH370 Lost in Indian Ocean: "Credible lead" moves search to new area" (http://www2.nst.com.my/latest/font-color-red-mh370-lost-in-indian-ocean-font-credible-lead-moves-search-to-new-area-1.536483). *New Straits Times*. 28 March 2014. Retrieved 17 January 2015.
105. Shoichet, Catherine E.; Pearson, Michael; Mullen, Jethro. "Flight 370 search area shifts after credible lead" (http://edition.cnn.com/2014/03/27/world/asia/malaysia-airlines-plane/index.html). CNN. Retrieved 28 March 2014.
106. "Search and recovery continues for Malaysian flight MH370 (4 April 2014 am)" (http://www.jacc.gov.au/media/releases/2014/april/mr006.aspx). Joint Agency Coordination Centre. 4 April 2014. Retrieved 6 May 2014.
107. "Incident 2014/1475 – search for Malaysia Airlines flight MH370 – area searched (4 April)" (https://s3-ap-southeast-2.amazonaws.com/asset.amsa.gov.au/MH370+Day+18/Charts/2014_04_04_cumulative_search_handout.pdf) (PDF). Australian Maritime Safety Authority. 4 April 2014. Retrieved 12 April 2015.
108. Donnison, Jon (31 March 2014). "Malaysia flight MH370: No time limit on search, says Tony Abbott" (http://www.bbc.co.uk/news/world-asia-26814929). BBC News. Retrieved 8 May 2014.
109. "Royal Navy Submarine Joins MH370 Search" (http://news.sky.com/story/1235477/royal-navy-submarine-joins-mh370-search). Sky News. 2 April 2014. Retrieved 12 April 2015.
110. "Pinger Locators Deployed To Find MH370 Black Box Before Batteries Die" (http://www.investing.com/news/economy-news/pinger-locators-deployed-to-find-mh370-black-box-before-batteries-die-275800). Investing.com. 4 April 2014.
111. "Pinger locator equipment commences operation (4 April 2014)" (http://www.jacc.gov.au/media/releases/2014/april/mr007.aspx). Joint Agency Coordination Centre. 4 April 2014. Retrieved 6 May 2014.
112. "Only days left before Malaysia airlines flight 370's black box dies" (https://web.archive.org/web/20140407072117/http://www.wday.com/event/article/id/95224/group/News/). WDAY. 30 March 2014. Archived from the original (http://www.wday.com/event/article/id/95224/group/News/) on 7 April 2014. Retrieved 13 July 2014.
113. "MH370 Report: Underwater Locator Beacon Battery Had Expired" (http://www.nytimes.com/aponline/2015/03/08/world/asia/ap-as-malaysia-missing-plane.html?_r=0). *The New York Times*. Associated Press. 8 March 2015. Retrieved 8 March 2015.
114. Hawley, Samantha (8 March 2015). "Malaysia Airlines MH370: Report finds battery powering locator beacon on black box expired in 2012, no red flags raised over crew or aircraft" (http://www.abc.net.au/news/2015-03-08/mh370-report-says-black-box-locator-beacon-expired/6289462). *Australian Broadcasting Corp*. Retrieved 8 March 2015.
115. Smyth, Jamie (26 June 2014). "Search for Malaysia Airlines flight MH370 to resume in new area" (http://www.ft.com/cms/s/0/912130e8-fd06-11e3-8ca9-00144feab7de.html#axzz3JS0bpHI4). *Financial Times*. Retrieved 18 November 2014.
116. "MH370 Operational Search Update — 08 October 2014" (http://www.jacc.gov.au/families/operational_reports/opsearch-update-20141008.aspx). *Joint Agency Coordination Centre*. 8 October 2014. Retrieved 12 November 2014.
117. Innis, Michelle (6 October 2014). "Rugged Seabed Seen in New Maps Further Complicates Search for Malaysia Airlines Jet" (http://www.nytimes.com/2014/10/07/world/asia/search-resumes-for-missing-malaysian-airliner.html?_r=0). *The New York Times*. Retrieved 18 November 2014.
118. "MH370 Operational Search Update — 05 November 2014" (http://www.jacc.gov.au/families/operational_reports/opsearch-update-20141105.aspx). *Joint Agency Coordination Centre*. 5 November 2014. Retrieved 5 December 2014.
119. "MH370 Operational Search Update— 07 January 2015" (http://www.jacc.gov.au/families/operational_reports/opsearch-update-20150107.aspx). *Joint Agency Coordination Centre*. Retrieved 8 January 2015.
120. Stewart, Robb M (6 October 2014). "Malaysia Airlines Flight 370 Search Reboots" (http://online.wsj.com/articles/malaysia-airlines-flight-370-search-reboots-1412578236). *Wall Street Journal*. Retrieved 8 October 2014.
121. "MH370 Operational Search Update— 14 January 2015"

121. "MH370 Operational Search Update — 14 January 2015" (http://www.jacc.gov.au/families/operational_reports/opsearch-update-20150114.aspx). *JACC*. 14 January 2015. Retrieved 2 February 2015. "Fugro Supporter is expected to arrive in the search area and commence search activities in late January. Fugro Supporter has been equipped with a Kongsberg HUGIN 4500 autonomous underwater vehicle (AUV). The AUV will be used to scan those portions of the search area that cannot be searched effectively by the equipment on the other search vessels."
122. "MH370 Operational Search Update— 28 January 2015" (http://www.jacc.gov.au/families/operational_reports/opsearch-update-20150128.aspx). *JACC*. Retrieved 1 February 2015.
123. "MH370 Operational Search Update—13 May 2015" (http://www.jacc.gov.au/families/operational_reports/opsearch-update-20150513.aspx). *JACC*. 13 May 2015. Retrieved 2 June 2015.
124. Ng, Eileen; Adamson, Thomas (2 August 2015). "Malaysia Seeks Help in Finding More Possible MH370 Debris" (http://abcnews.go.com/International/wireStory/malaysia-seeks-expand-search-mh370-debris-32832669). *ABC News (US)*. AP. Retrieved 8 August 2015.
125. Pither, Tony (1998). *The Boeing 707 720 and C-135*. England: Air-Britain (Historians) Ltd. ISBN 0-85130-236-X.
126. "Malaysia Airlines 9M-MRO (Boeing 777 – MSN 28420)" (http://www.airfleets.net/ficheapp/plane-b777-28420.htm). *Airfleets*. Retrieved 7 March 2014.
127. "Boeing 777–200 – Fleet" (http://www.malaysiaairlines.com/hq/en/mh-experience/our-fleet/boeing-777-200.html). Malaysia Airlines. Retrieved 12 March 2014.
128. "Missing MAS 777-200 had no major prior incidents" (http://www.flightglobal.com/news/articles/missing-mas-777-200-had-no-major-prior-incidents-396793/). Flightglobal. 8 March 2014. Retrieved 9 March 2014.
129. 浦东机场滑行跑道内东航马航两飞机剐蹭 [Pudong airport taxiways Eastern Malaysia Airlines aircraft rub two] (http://news.xinhuanet.com/fortune/2012-08/10/c_123564158.htm) (in Chinese). Xinhua News Agency. 10 August 2012. Retrieved 6 May 2014.Translated article (http://translate.google.com/translate?hl=en&sl=zh-CN&tl=en&u=http%3A%2F%2Fnews.xinhuanet.com%2Ffortune%2F2012-08%2F10%2Fc_123564158.htm&sandbox=1) Note: this translation was made automatically and has low technical quality, lends itself only to specific queries.
130. "ASN Wikibase Occurrence # 147571" (http://aviation-safety.net/wikibase/wiki.php?id=147571). 9 August 2012. Retrieved 24 March 2014.
131. Toh, Mavis (9 March 2014). "MAS 777 underwent maintenance in Feb" (http://web.archive.org/web/20140309212334/http://www.flightglobal.com/news/articles/mas-777-underwent-maintenance-in-feb-396801/). Singapore: Flightglobal. Archived from the original (http://www.flightglobal.com/news/articles/mas-777-underwent-maintenance-in-feb-396801/) on 9 March 2014. Retrieved 12 April 2015.
132. "EgyptAir 777 fire probe inconclusive but short-circuit suspected" (http://www.flightglobal.com/news/articles/egyptair-777-fire-probe-inconclusive-but-short-circuit-379655/). Flightglobal. 30 November 2012. Retrieved 30 March 2014.
133. "Accident: Egyptair B772 at Cairo on Jul 29th 2011, cockpit fire" (http://www.avherald.com/h?article=44078aa7&opt=0). Avherald.com. 29 July 2011. Retrieved 30 March 2014.
134. CBC News (17 July 2014). "Malaysia Airlines Flight MH17 reportedly shot down near Ukraine-Russia border" (http://www.cbc.ca/news/world/malaysia-airlines-flight-mh17-reportedly-shot-down-near-ukraine-russia-border-1.2709881). *CBC News* (Dominion of Canada: Canadian Broadcasting Corporation). Retrieved 19 July 2014.
135. "HK resident was aboard missing plane" (http://rthk.hk/rthk/news/englishnews/20140309/news_20140309_56_990682.htm). *RTHK*. 10 March 2014. Retrieved 11 March 2014.
136. Ranjit Singh (12 March 2014). "MH370: Five Indian nationals identified" (http://english.astroawani.com/news/show/mh370-five-indian-nationals-identified-31687). astro AWANI. Retrieved 29 May 2014.
137. "MH370 Passenger Manifest" (http://www.malaysiaairlines.com/content/dam/malaysia-airlines/mas/PDF/MH370/8th%20Mar-Malaysia%20Airlines%20Flight%20MH%20370%20Passenger%20Manifest_Nationality.pdf) (PDF) (Press release). Malaysia Airlines. 8 March 2014. Archived (http://www.webcitation.org/6Nv7NSlhu) from the original on 8 March 2014.

on 8 March 2014.
138. "Missing MAS flight: Captain piloting MH370 a Penang boy" (http://www.straitstimes.com/the-big-story/missing-mas-plane/story/missing-mas-flight-captain-piloting-mh370-penang-boy-20140308). *The Straits Times*. 8 March 2014. Retrieved 9 March 2014.
139. Koswanage, Niluksi (9 March 2014). "Pilot of missing Malaysian flight an aviation tech geek" (http://in.reuters.com/article/2014/03/09/malaysia-crash-pilot-idINDEEA2804J20140309). Reuters. Retrieved 10 March 2014.
140. "MISSING MH370: Co-pilot family awaits for latest updates – Latest" (https://web.archive.org/web/20140604195716/http://www.nst.com.my/latest/font-color-red-missing-mh370-font-co-pilot-family-awaits-for-latest-updates-1.503079). *New Straits Times*. 8 March 2014. Archived from the original (http://www.nst.com.my/latest/font-color-red-missing-mh370-font-co-pilot-family-awaits-for-latest-updates-1.503079) on 4 June 2014.
141. Watkins, Tom (10 March 2014). "First officer on missing jet was transitioning to 777-200s" (http://edition.cnn.com/2014/03/08/world/asia/malaysia-airlines-first-officer/). CNN. Retrieved 10 March 2014.
142. McGuirk, Rod; Wright, Stephen (9 March 2014). "Behind jet's passenger list is rich human tapestry" (http://news.yahoo.com/behind-jets-passenger-list-rich-human-tapestry-134354700.html;_ylt=A0LEVzNMwLpUWvYAx0pXNyoA;_ylu=X3oDMTEzdWg4MWU4BHNlYwNzcgRwb3MDMQRjb2xvA2JmMQR2dGlkA1ZJUDI4NF8x). Associated Press. Retrieved 17 January 2015.
143. "No sign of Malaysia Airline wreckage; questions over stolen passports" (http://edition.cnn.com/2014/03/08/world/asia/malaysia-airlines-plane-missing/). CNN. 8 March 2014. Retrieved 10 March 2014.
144. "Loss of employees on Malaysia flight a blow, U.S. chipmaker says" (http://www.reuters.com/article/2014/03/09/us-malaysia-airlines-freescale-idUSBREA280T020140309). Reuters. 9 March 2014. Retrieved 15 March 2014.
145. "Caregiver sacrifices time for family of passengers" (http://www.nst.com.my/latest/font-color-red-missing-mh370-font-caregiver-sacrifices-time-for-family-of-passengers-1.521261). *New Straits Times*. Retrieved 2014.
146. Kuhn, Anthony (20 March 2014). "For Flight 370 Families, Every Day Is 'Torment' : Parallels" (http://www.npr.org/blogs/parallels/2014/03/20/291973274/for-flight-370-families-every-day-is-torment). NPR. Retrieved 11 May 2014.
147. "Missing MAS flight: Malaysia grateful for assistance in search and rescue operations, says Anifah" (http://www.thestar.com.my/News/Nation/2014/03/09/Missing-MAS-flight-Malaysia-grateful-for-assistance/). *The Star*. 9 March 2014. Retrieved 9 March 2014.
148. Melissa Chi (9 March 2014). "DCA: Search for MH370 intensifies with 74 vessels, 50 nautical miles near last-known site" (http://www.themalaymailonline.com/malaysia/article/dca-search-for-mh370-intensifies-with-74-vessels-50-nautical-miles-near-las). *The Malay Mail*. Retrieved 19 March 2014.
149. "Missing Malaysia jet may have veered off course" (http://www.cnbc.com/id/101485921). CNBC. Retrieved 12 March 2014.
150. "MISSING MH370: Families cling to faint hopes: psychologist" (http://www.nst.com.my/latest/font-color-red-missing-mh370-font-families-cling-to-faint-hopes-psychologist-1.506061). *New Straits Times*. 10 March 2014. Retrieved 12 March 2014.
151. Childs, Nick; Westcott, Richard (6 April 2014). "Malaysia flight MH370: Search ships to verify signals" (http://www.bbc.co.uk/news/world-asia-26912064). BBC News. Retrieved 9 May 2014.
152. "MH370 Tragedy: DCA has authority to analyse black box of missing plane Read more: MH370 Tragedy: DCA has authority to analyse black box of missing plane" (http://www2.nst.com.my/latest/font-color-red-mh370-tragedy-font-dca-has-authority-to-analyse-black-box-of-missing-plane-1.555040). *New Straits Times*. 7 April 2014. Retrieved 3 July 2014.
153. "International Panel To Look Into MH370 Incident – Hishammuddin" (http://www.bernama.com/bernama/v7/sp/newssports.php?id=1026000). Retrieved 28 September 2014.
154. "Malaysia Airlines flight MH370 puts UN search agency's protocol to the test" (http://www.scmp.com/news/asia/article/1458779/mh370-puts-un-search-agencys-protocol-test). *South China Morning Post*. Retrieved 28 September 2014.
155. "Malaysia Reorganizes Flight 370 Investigation, Appoints Independent Investigator" (http://www.frequentbusinesstraveler.com/2014/04/malaysia-reorganizes-flight-370-investigation-appoints-independent-investigator/#sthash.U2VCAmnR.dpuf). Frequent Business Traveler. 6 April 2014. Retrieved 6 April 2014.

6 April 2014.
156. "New phase of search starts on both corridors" (http://www.freemalaysiatoday.com/category/nation/2014/03/17/new-phase-of-search-starts-on-both-corridors/). Free Malaysia Today. Retrieved 30 March 2014.
157. Weaver, Matthew; McCarthy, Tom. "MH370: Australia takes lead in Indian Ocean as search area expands – live" (http://www.theguardian.com/world/blog/2014/mar/17/mh370-crew-of-missing-plane-investigated-for-more-than-a-week-live-updates). *The Guardian*. Retrieved 30 March 2014.
158. "Air Chief Marshal Angus Houston to lead Joint Agency Coordination Centre" (http://www.pm.gov.au/media/2014-03-30/air-chief-marshal-angus-houston-lead-joint-agency-coordination-centre). Retrieved 28 September 2014.
159. Milman, Oliver (30 March 2014). "Flight MH370: former Australian defence chief to co-ordinate search" (http://www.theguardian.com/world/2014/mar/30/flight-mh370-angus-houston-international-search-efforts). *The Guardian*. Retrieved 11 May 2014.
160. Mullen, Jethro (8 March 2015). "Investigators find no unusual signs among MH370 pilots and cabin crew" (http://www.cnn.com/2015/03/08/asia/malaysia-missing-plane-mh370/). *CNN*. Retrieved 9 March 2015. "The report, which contained factual information about the missing plane rather than analysis, offered relatives of the 239 people on board no apparent answers about why the aircraft dropped off radar."
161. "Classic Aero services and SwiftBroadband" (http://www.inmarsat.com/service/aviation-safety/). Inmarsat. Retrieved 28 March 2014.
162. Kirby, Mary. "SITA aids MH370 investigation; expert explains" (http://www.runwaygirlnetwork.com/2014/03/14/sita-aids-mh370-investigation-expert-explains/). *Runway Girl Network*. Retrieved 26 March 2014.
163. Turner, Aimee. "Malaysian MH370: SATCOMS 101 (Part One)" (http://www.airtrafficmanagement.net/2014/03/mh370-satcoms-101/). airtrafficmanagement.net. Retrieved 26 March 2014.
164. "Information provided to MH370 by AAIB: Information provided to MH370 investigation by UK Air Accidents Investigation Branch (AAIB)" (http://mh370.dca.gov.my/information-provided-to-mh370-by-aaib/). Department of Civil Aviation Malaysia. Retrieved 6 May 2014.
165. Ashton, Chris; Bruce, Alan Shuster; Colledge, Gary; Dickinson, Mark (14 September 2014). "The Search for MH370" (http://journals.cambridge.org/nav/mh370). *The Journal of Navigation* (The Royal Institute of Navigation). doi:10.1017/S037346331400068X (https://dx.doi.org/10.1017%2FS037346331400068X). Retrieved 19 October 2014.
166. "Considerations on defining the search area – MH370" (http://www.atsb.gov.au/publications/2014/considerations-on-defining-the-search-area-mh370.aspx). ATSB – Australian Transport Safety Bureau. Retrieved 28 May 2014.
167. "MH370 – Flight Path Analysis Update" (http://www.atsb.gov.au/media/5163181/AE-2014-054_MH370%20-FlightPathAnalysisUpdate.pdf) (PDF). Australian Transport Safety Bureau. 8 October 2014. Retrieved 19 October 2014.
168. Han, Esther. "MH370 power outage linked to possible hijacking attempt" (http://www.smh.com.au/world/mh370-power-outage-linked-to-possible-hijacking-attempt-20140630-zsqp2.html). *Sydney Morning Herald*. Retrieved 1 July 2014.
169. Keith Bradsher; Eric Schmitt (9 March 2014). "Passport Theft Adds to Mystery of Missing Malaysia Airlines Jet" (http://www.nytimes.com/2014/03/09/world/asia/malaysia-airlines-flight.html). *The New York Times*. Retrieved 12 April 2015.
170. Catherine E. Shoichet and Ray Sanchez (9 March 2014). "Plane bore painters, pilgrims, others from around the world" (http://edition.cnn.com/2014/03/08/world/asia/malaysia-airlines-plane-passengers/index.html). CNN. Retrieved 8 March 2014.
171. "INTERPOL confirms at least two stolen passports used by passengers on missing Malaysian Airlines flight 370 were registered in its databases" (http://www.interpol.int/News-and-media/News/2014/N2014-038). Interpol. Retrieved 9 March 2010.
172. Murdoch, Lindsay (10 March 2014). "Fake passports on Malaysia Airlines flight reveal flaw in airline safety" (http://www.smh.com.au/world/fake-passports-on-malaysia-airlines-flight-reveal-flaw-in-airline-safety-20140310-hvgv0.html). The Sydney Morning Herald. Retrieved 7 May 2014.
173. Mezzofiore, Gianluca (10 March 2014). "Missing Malaysia Airlines Flight MH370: Iranian Middleman Asked Thai Agent to Book Tickets on Stolen Passports" (http://www.ibtimes.co.uk/missing-malaysia-airlines-flight-

mh370-iranian-middleman-asked-thai-agent-book-two-stolen-1439631). *International Business Times* (UK). Retrieved 11 March 2014.
174. Ahmed, Saeed; Shoichet, Catherine E. (11 March 2014). "'There are no answers': Days later, no sign of Malaysia Airlines Flight 370" (http://edition.cnn.com/2014/03/10/world/asia/malaysia-airlines-plane/index.html). CNN. Retrieved 11 March 2014.
175. Chris Buckley and Keith Bradsher. "China Rules Out Terror Ties Among Citizens on Jet" (http://www.nytimes.com/2014/03/19/world/asia/beijing-says-no-chinese-passengers-were-involved-in-jets-disappearance.html?_r=0). *The New York Times*. Retrieved 19 March 2014.
176. "Malaysia police probe flight engineer on missing MH370" (http://www.straitstimes.com/asia/se-asia/malaysia-police-probe-flight-engineer-on-missing-mh370). *The Straits Times*. 17 March 2014. Retrieved 2015-08-02.
177. Barbara Starr, Chelsea J. Carter and Jim Clancy. "U.S. officials lean toward 'those in the cockpit' behind missing flight" (http://edition.cnn.com/2014/03/16/world/asia/malaysia-airlines-plane/index.html?hpt=hp_inthenews). CNN. Retrieved 16 March 2014.
178. "Deputy PM Warren Truss announces underwater search for missing plane will begin in August" (http://www.news.com.au/travel/travel-updates/mh370-deputy-pm-warren-truss-announces-underwater-search-for-missing-malaysia-airlines-plane-will-begin-in-august/story-fnizu68q-1226967783002). *NewsComAu*. Retrieved 28 September 2014.
179. "FBI to Quiz Wife of MH370 Pilot Amid Talk of Cockpit Hijack" (http://www.malaysia-chronicle.com/index.php?option=com_k2&view=item&id=249772:fbi-to-quiz-wife-of-mh370-pilot-amid-talk-of-cockpit-hijack&Itemid=2&tmpl=component&print=1#.U7V4WLHSSWa). *Malaysia Chronicle*. 24 March 2014. Retrieved 3 July 2014. "Police are also examining reports that he received a two-minute phone call shortly before take-off from a mystery woman using a mobile number obtained using a false identity."
180. Gardner, Frank; Fisher, Jonah (15 March 2014). "Missing Malaysia Airlines plane 'deliberately diverted'" (http://www.bbc.com/news/world-asia-26591056). BBC News. Retrieved 9 May 2014.
181. "MH370 passengers "cleared" in four probe areas: Malaysian police" (http://www.channelnewsasia.com/news/specialreports/mh370/news/mh370-passengers-cleared/1056364.html). Channel NewsAsia. 11 March 2014. Retrieved 12 April 2015.
182. "Missing plane MH370: Malaysia mystery 'may not be solved'" (http://www.bbc.com/news/world-asia-26847402). BBC News. 2 April 2014. Retrieved 9 May 2014.
183. Sheridan, Michael (22 June 2014). "Suspicion falls again on Malaysia Airlines flight 370's captain Zaharie Shah" (http://www.theaustralian.com.au/business/aviation/suspicion-falls-again-on-malaysia-airlines-flight-370s-captain-zaharie-shah/story-e6frg95x-1226962734150). *The Australian*. Retrieved 3 July 2014.
184. Sheridan, Michael (22 June 2014). "MH370 pilot 'chief suspect'" (http://www.thesundaytimes.co.uk/sto/news/world_news/Asia/article1425492.ece). *The Sunday Times*. Retrieved 3 July 2014.
185. "Malaysian police investigation names MH370 pilot 'prime suspect'" (http://www.news.com.au/travel/travel-updates/malaysian-police-investigation-names-mh370-pilot-prime-suspect/story-fnizu68q-1226962811653). *news.com.au*. 23 June 2014. Retrieved 3 July 2014.
186. Thomas, Pierre; Margolin, Josh (2 April 2014). "FBI Finishes Probe into Malaysia Airlines Captain's Flight Simulator" (http://abcnews.com/blogs/headlines/2014/04/no-clues-to-missing-malaysia-airlines-plane-in-captains-flight-simulator/). ABC News. Retrieved 7 May 2014.
187. Moore, Andy; Donnison, Jon (29 March 2014). "Flight MH370: Chinese and Australian ships draw blank" (http://www.bbc.com/news/world-asia-26797866). BBC News. Retrieved 9 May 2014.
188. Levin, Alan (11 August 2014). "Exploding Lithium Batteries Riskier to Planes: Research" (http://www.bloomberg.com/news/articles/2014-08-11/exploding-lithium-batteries-riskier-to-planes-research). *Bloomberg Business*. Retrieved 1 August 2015.
189. Knowler, Greg (15 April 2015). "Cathay slaps blanket ban on bulk lithium battery shipments" (http://www.joc.com/air-cargo/cathay-slaps-blanket-ban-bulk-lithium-battery-shipments_20150415.html). *The Journal of Commerce*. Retrieved 1 August 2015.
190. "Safety worries lead US airline to ban battery shipments" (http://www.bbc.com/news/technology-31709198). *BBC News*. 3 March 2015. Retrieved 1 August 2015.
191. Jansen, Bart (25 July 2013). "Crash investigators trace UPS plane fire to batteries" (http://www.usatoday.com/story/news/nation/2013/07/24/ups-crash-dubai-lithium/2582213/). *USA Today*. Retrieved 1 August 2015.

192. Shears, Richard (2 April 2014). "Malaysian police confirm they have interviewed farm workers who handled fruit cargo aboard missing MH370 in case they were used to smuggle a bomb onto the jet" (http://www.dailymail.co.uk/news/article-2595096/Malaysian-police-confirm-interviewed-farm-workers-handled-fruit-cargo-aboard-missing-MH370-case-used-smuggle-bomb-jet.html). *Daily Mail*. Retrieved 1 August 2015.
193. Pearlman, Jonathan (3 April 2014). "MH370: Malaysian police probe fruit farmers as investigation widens" (http://www.telegraph.co.uk/news/worldnews/asia/malaysia/10742287/MH370-Malaysian-police-probe-fruit-farmers-as-investigation-widens.html). *The Telegraph*. Retrieved 1 August 2015.
194. Hodal, Kate (14 March 2014). "Flight MH370: a week of false leads and confusion in hunt for missing plane" (http://www.theguardian.com/world/2014/mar/14/flight-mh370-false-leads-confusion-hunt-missing-plane). *The Guardian*. Retrieved 25 March 2014.
195. "Missing Malaysia Airlines flight MH370 – a week of confusion" (http://www.smh.com.au/world/missing-malaysia-airlines-flight-mh370--a-week-of-confusion-20140314-hviqs.html). The Sydney Morning Herald. 14 March 2014. Retrieved 7 May 2014.
196. "Missing Malaysia Airlines plane: Air force chief denies tracking jet to Strait of Malacca" (http://www.straitstimes.com/the-big-story/missing-mas-plane/story/missing-malaysia-airlines-plane-air-force-chief-denies-trackin). Retrieved 28 September 2014.
197. "MH370: Further confusion over timing of last words" (http://www.3news.co.nz/MH370-Further-confusion-over-timing-of-last-words/tabid/417/articleID/336342/Default.aspx). Retrieved 28 September 2014.
198. Jamieson, Alastair (13 March 2014). "Officials Deny Engine Data Report From Missing MH370" (http://www.nbcnews.com/storyline/missing-jet/officials-deny-engine-data-report-missing-mh370-n51576). NBC News. Retrieved 12 April 2015.
199. Calder, Simon; Withnall, Adam (17 March 2014). "Missing Malaysia Airlines Flight MH370: Confusion deepens over 'missing 30 minutes' at heart of mystery engulfing stricken jet" (http://www.independent.co.uk/news/world/asia/missing-malaysia-airlines-flight-mh370-confusion-deepens-over-missing-30-minutes-at-heart-of-mystery-engulfing-stricken-jet-9197375.html). *The Independent*. Retrieved 2014.
200. Woodrow Bellamy III (19 March 2014). "Avionics Magazine :: Malaysian PM Clarifies MH370 Avionics Disablement" (http://www.aviationtoday.com/av/commercial/Malaysian-PM-Clarifies-MH370-Avionics-Disablement_81658.html). Aviationtoday.com. Retrieved 12 April 2015.
201. "Not just mangosteens on board, MH370 also carried lithium-ion batteries, says daily" (http://www.themalaysianinsider.com/malaysia/article/not-just-mangosteens-on-board-mh370-also-carried-lithium-ion-batteries-says). *The Malaysian Insider*. 22 March 2014. Retrieved 12 April 2015.
202. "MH370: "All right, good night" came after system shut down" (http://www.themalaysiantimes.com.my/mh370-all-right-good-night-came-after-system-shut-down/). *The Malaysian Times*. 17 March 2014. Retrieved 31 March 2014.
203. "Malaysia Airlines flight MH370 co-pilot's last message was 'all right, good night' – video" (http://www.theguardian.com/world/video/2014/mar/17/malaysia-airlines-flight-mh370-co-pilot-all-right-good-night-video). *The Guardian*. 17 March 2014. Retrieved 31 March 2014.
204. "Last words transmitted from missing Malaysia Airlines plane were actually 'Good night, Malaysian three seven zero' " (http://www.news.com.au/travel/travel-updates/last-words-transmitted-from-missing-malaysia-airlines-plane-were-actually-good-night-malaysian-three-seven-zero/story-fnizu68q-1226869250467). News.com.au. 1 April 2014. Retrieved 1 April 2014.
205. "New account of MH370 pilot's final words" (http://www.aljazeera.com/news/asia-pacific/2014/03/malaysia-changes-final-words-mh370-pilot-201433117524180624 2.html). Al Jazeera. Retrieved 31 March 2014.
206. Donnison, Jon; Westcott, Richard (31 March 2014). "MH370: New account of cockpit last words" (http://www.bbc.co.uk/news/world-asia-26825184). BBC News. Retrieved 8 May 2014.
207. "Stolen Passports on Plane Not Seen as Terror Link" (http://www.nytimes.com/2014/03/12/world/asia/malaysia-flight.html). *The New York Times*. 11 March 2014. Retrieved 15 March 2014.
208. Denyer, Simon (12 March 2014). "Contradictory statements from Malaysia over missing airliner perplex, infuriate" (http://www.washingtonpost.com/blogs/worldviews/wp/2014/03/12/contradictory-statements-from-malaysia-over-missing-airliner-perplex-infuriate/). *The Washington Post*. Retrieved 14 March 2014.
209. Malakunas, Karl (14 March 2014). "Distrust adding to Malaysian jet confusion: analysts" (http://sg.news.yahoo.com/distrust-adding-malaysian-jet-confusion-analysts-181507988.html). Agence France-Presse. Retrieved 17 January 2015.
210. Branigan, Tania (14 March 2014). "Malaysia flight MH370 hunt sees suspicion and cooperation"

(http://www.theguardian.com/world/2014/mar/14/malaysia-flight-mh370-hunt-sees-suspicion-and-cooperation-china-us). *The Guardian* (Beijing). Retrieved 11 May 2014.
211. Harlan, Chico (11 March 2014). "Malaysia Airlines plane may have veered wildly off course during flight, military says" (http://www.washingtonpost.com/world/search-expands-for-missing-malaysia-airlines-flight/2014/03/11/fea6df4a-a8e8-11e3-8599-ce7295b6851c_story.html). *The Washington Post*. Retrieved 14 March 2014.
212. "China appeals to Malaysia for search information" (http://bigstory.ap.org/article/china-appeals-malaysia-search-information). *Associated Press*. 14 March 2014. Retrieved 14 March 2014.
213. Spoonts, Sean (22 March 2014). "'"Alright, Goodnight" – Does Malaysia Want To Know What Happened To Flight MH-370?" (http://sofrep.com/34084/alright-goodnight-malaysia-want-know-happened-flight-mh-370/). *SOFREP.COM (Special Operations Forces Report-Special Ops News & Intel)*. Sean Spoonts. Retrieved 10 May 2014.
214. Pasztor, Andy; Ostrower, Jon; Hookway, James (19 March 2013). "Critical Data Was Delayed in Search for Missing Malaysia Airlines Flight MH 370" (http://online.wsj.com/news/article_email/SB10001424052702304026304579449680167673144-lMyQjAxMTA0MDEwOTExNDkyWj). *The Wall Street Journal*. Retrieved 12 April 2015.
215. "Saturday, March 15, 05:45 PM MYT +0800 Malaysia Airlines MH370 Flight Incident – 19th Media Statement" (http://www.malaysiaairlines.com/ksd-maintenance/DarkSites.html). Malaysia Airlines. scroll down to find "19th Media Statement". Retrieved 15 March 2014.
216. Hishammuddin Hussein (21 March 2014). "MH370 Press Briefing by Hishammuddin Hussein on 21st March 2014" (http://mh370.dca.gov.my/mh370-press-briefing-by-hishammuddin-hussein-on-21st-march-2014/). Malaysia: Department of Civil Aviation Malaysia. Retrieved 6 May 2014.
217. "MH370 Is Missing With 239 People On Board, Help The Families Find The Truth" (https://www.indiegogo.com/projects/mh370-is-missing-with-239-people-on-board-help-the-families-find-the-truth). *Indiegogo*. Archived (http://web.archive.org/web/20150410023633/https://www.indiegogo.com/projects/mh370-is-missing-with-239-people-on-board-help-the-families-find-the-truth) from the original on 10 April 2015. Retrieved 10 April 2015.
218. Molko, David; Yan, Holly (9 June 2014). "MH370 families seek $5 million for investigation, reward" (http://www.cnn.com/2014/06/08/world/asia/malaysia-airlines-families-fund/index.html). *CNN*. Retrieved 10 April 2015.
219. Raghuvanshi, Gaurav; Ng, Jason (6 April 2014). "Malaysia Airlines Says Priority Is Families of the Missing, Though Ticket Sales Fall" (http://online.wsj.com/news/articles/SB10001424052702303532704579483060366249526). *Wall Street Journal*. Retrieved 3 July 2014.
220. "Malaysia Airlines Records RM443 million Loss for Q1 2014" (http://www.malaysiaairlines.com/my/en/corporate-info/press-room/latest/malaysia-airlines-records-rm443-million-loss-for-q12014.html). *Malaysia Airlines*. 15 May 2014. Retrieved 3 July 2014. "Much of the costs associated by MH370 will be covered by insurance."
221. "Flight's Disappearance Knocks Malaysia Airlines" (http://www.nytimes.com/2014/05/16/business/international/flights-disappearance-knocks-malaysia-airlines.html?_r=1). *New York Times*. 15 May 2014. Retrieved 3 July 2014.
222. "Malaysia Airlines to Retire Call Sign 370" (http://blogs.wsj.com/searealtime/2014/03/13/airline-to-retire-call-sign-370/). *The Wall Street Journal*. 13 March 2014. Retrieved 30 August 2014.
223. Neuman, Scott (13 March 2014). "When Bad Things Happen To Planes, Flight Codes Get 'Retired'" (http://www.npr.org/blogs/thetwo-way/2014/03/13/289800435/when-bad-things-happen-to-planes-flight-codes-get-retired). Retrieved 30 August 2014.
224. Hong, Zhang; Zhou, Laura (26 March 2014). "Chinese tourists boycott Malaysia in wake of MH370 disappearance" (http://www.scmp.com/article/1457902/malaysia-tourism-hit-sharp-drop-chinese-visitors-wake-mh370-incident?page=all). *South China Morning Post*. Retrieved 30 August 2014.
225. Wilson, Harry (23 March 2014). "Flight MH370: insurers make first pay out on missing Malaysia Airlines plane" (http://www.telegraph.co.uk/news/worldnews/asia/malaysia/10717604/Flight-MH370-insurers-make-first-pay-out-on-missing-Malaysia-Airlines-plane.html). *The Telegraph*. Retrieved 17 July 2014. "Malaysia Airlines has already been handed $110 million (£67 million) by insurers over the loss of its missing Boeing 777 on flight MH370"

226. Boyle, Charles (27 March 2014). "Complex Situation Occludes Details on Loss of Malaysian Airlines Flight MH370" (http://www.insurancejournal.com/news/international/2014/03/27/324543.htm). *Insurance Journal*. Retrieved 17 July 2014. "Allianz Global Corporate & Specialty has been identified as both the lead insurer and the lead reinsurer. An Allianz spokesperson in London confirmed that it is officially the latter."
227. Mathew, Jerin (15 May 2014). "Missing Malaysian Airlines Flight MH370 Hits Allianz with $30m Bill" (http://www.ibtimes.co.uk/missing-malaysian-airlines-flight-mh370-hits-allianz-30m-bill-1448613). *International Business Times*. Retrieved 17 July 2014. "The insured market loss on the aeroplane is about $350m, which include the costs for searching."
228. "Malaysia Airlines Financial Losses Grow" (http://www.nytimes.com/2014/08/29/business/malaysia-airlines-financial-losses-grow.html?_r=1). *New York Times*. Reuters. 29 August 2014. Retrieved 30 August 2014.
229. Venkat, P.R.; Raghuvanshi, Gaurav (2 July 2014). "Malaysia Airlines Could Go Private" (http://online.wsj.com/articles/malaysia-airlines-could-go-private-1404301103). Wall Street Journal. Retrieved 9 August 2014.
230. Patterson, Thom (18 July 2014). "Malaysia Air faces new, serious threat as company" (http://www.cnn.com/2014/07/17/world/europe/malaysia-airlines-sidebar/index.html?iid=article_sidebar). CNN. Retrieved 9 August 2014. "Analysts said it may take a government rescue to save the company from financial disaster."
231. "Malaysia Airlines considers tie-up with Etihad Airways as restructuring process slowly begins" (http://centreforaviation.com/analysis/malaysia-airlines-considers-tie-up-with-etihad-as-restructuring-process-slowly-begins-172934). *centreforaviation.com*. Centre for Aviation. 17 June 2014. Retrieved 9 August 2014.
232. Ngui, Yantoultra (2 July 2014). "Exclusive: State fund plans to take Malaysia Airlines private for restructuring: sources" (http://www.reuters.com/article/2014/07/02/us-malaysia-airlines-idUSKBN0F70UR20140702). Reuters. Retrieved 9 August 2014.
233. Zhang, Benjamin. "How Malaysia Airlines Can Be Saved From Financial And Reputational Ruin" (http://www.businessinsider.com/malaysia-airlines-uncertain-future-2014-7). *Business Insider*. Retrieved 23 July 2014.
234. Hamzah, Al-Zaquan Amer; Leong, Trinna; Ngui, Yantoultra (8 August 2014). "Malaysia Airlines To Go Private With A $435 Million Government Investment" (http://www.businessinsider.com/malaysia-airlines-overhaul-2014-8). *Business Insider*. Retrieved 9 August 2014.
235. MOUAWAD, JAD (8 August 2014). "Malaysia Steps In to Save Its Reeling National Airline" (http://www.nytimes.com/2014/08/09/business/international/malaysia-airlines-to-be-taken-over-by-government.html). *New York Times*. Retrieved 9 August 2014.
236. Creedy, Steve (9 August 2014). "Malaysia Airlines in $460m bid to clear air" (http://www.theaustralian.com.au/business/aviation/malaysia-airlines-in-460m-bid-to-clear-air/story-e6frg95x-1227018472442?nk=70b32bc1815c4b34c2328e2c878caf76). *The Australian*. Retrieved 9 August 2014.
237. Hamzah, Al-Zaquan Amer; Ngui, Yantoultra (8 August 2014). "State fund to take over Malaysia Airlines, plans 'complete overhaul' " (http://www.reuters.com/article/2014/08/08/us-malaysia-airline-idUSKBN0G807E20140808). *Reuters.com*. Reuters. Retrieved 9 August 2014.
238. "Missing Malaysia Airlines flight MH370 puzzle raises legal problems" (http://www.smh.com.au/world/missing-malaysia-airlines-flight-mh370-puzzle-raises-legal-problems-20140511-zr9fz.html). *Sydney Morning Herald*. 11 May 2014. Retrieved 17 July 2014.
239. Bishop, Katrina (25 March 2014). "MH370 families face huge compensation disparity" (http://www.cnbc.com/id/101522502#.). *CNBC*. Retrieved 17 July 2014.
240. Wallace, Gregory (26 March 2014). "Malaysia Airlines Flight 370: How much will families be paid?" (http://money.cnn.com/2014/03/25/news/companies/malaysia-airlines-compensation/). *CNN Money*. Retrieved 17 July 2014.
241. Bishop, Katrina. "MH370 families face huge compensation disparity" (http://www.cnbc.com/id/101522502#.). *CNBC*. Retrieved 31 January 2015.
242. "BBC News – MH370: Malaysia declares flight disappearance an accident" (http://www.bbc.co.uk/news/world-asia-31039460). *BBC News*. Retrieved 29 January 2015.
243. "American law firm plans to bring suit against Boeing and Malaysia Airlines" (http://www.scmp.com/news/asia/article/1457610/american-law-firm-plans-bring-suit-against-boeing-and-malaysia-airlines). *South China Morning Post*. Reuters. Retrieved 31 January 2015.
244. Liljas, Per (26 March 2014). "Family Member Files Lawsuit Over Missing Jet as Frustrating Search Continues"

(http://time.com/38260/malaysia-airlines-sued-over-mh370-disappearance/). *Time*. Retrieved 31 January 2015.
245. Philipp, Abby (31 October 2014). "Two Malaysian boys sue airline, government in first case after MH370s mysterious disappearance" (http://www.washingtonpost.com/news/morning-mix/wp/2014/10/31/two-malaysian-boys-sue-airline-government-in-first-case-after-mh-370s-mysterious-disappearance/). *Washington Post*. Retrieved 31 January 2015.
246. Ip, Kelly (13 March 2014). "Families of missing accept 'comfort money' " (http://www.thestandard.com.hk/news_detail.asp?we_cat=11&art_id=143440&sid=41796153&con_type=1&d_str=20140313&fc=8). *The Standard*. Retrieved 2014.
247. "MAS cash aid snubbed by kin of Chinese aboard MH370" (http://www.themalaymailonline.com/malaysia/article/mas-cash-aid-snubbed-by-kin-of-chinese-aboard-mh370). *The Malay Mail*. 11 March 2014. Retrieved 12 March 2014.
248. "7 MH370 passenger's families receive $50000 from Malaysia airlines" (http://news.biharprabha.com/2014/06/7-mh370-passengers-families-receive-50000-from-malaysia-airlines/). *IANS*. news.biharprabha.com. Retrieved 12 June 2014.
249. "Flight 370: Malaysia Airlines begins insurance payments" (http://timesofindia.indiatimes.com/world/rest-of-world/Flight-370-Malaysia-Airlines-begins-insurance-payments/articleshow/36488455.cms). *The Times of India*. 13 June 2014. Retrieved 17 July 2014. "[Hamzah Zainuddin] said full payout would come after the plane is found or officially declared lost."
250. Malaysia Insider (8 July 2011). "MH370 throws spotlight on Malaysia's air force and radar capabilities" (http://www.themalaysianinsider.com/malaysia/article/mh370-throws-spotlight-on-malaysias-air-force-and-radar-capabilities). The Malaysian Insider. Retrieved 12 April 2015.
251. Childs, Nick (16 March 2014). "Missing Malaysia plane: MH370 and the military gaps" (http://www.bbc.com/news/world-asia-26603830). BBC News. Retrieved 9 May 2014.
252. "Malaysia lets slip chance to intercept MH370" (http://www.malaysiakini.com/news/257320). *malaysiakini*. Malaysiakini. 17 March 2014. Retrieved 6 April 2014.
253. Campbell, Charlie (17 March 2014). "Another Lesson from MH370: Nobody is Watching Malaysian Airspace" (http://time.com/26883/malaysian-air-force-slammed-for-failing-to-intercepted-mh370/). *Time*. Retrieved 20 November 2014.
254. Razak, Najib (13 May 2014). "Malaysia's Lessons From the Vanished Airplane" (http://online.wsj.com/articles/SB10001424052702303627504579559170123401220). *The Wall Street Journal*. Retrieved 22 November 2014.
255. Henderson, Barney (3 April 2014). "MH370 Malaysia Airlines: Anwar Ibrahim says government purposefully concealing information" (http://www.telegraph.co.uk/news/worldnews/asia/malaysia/10743378/MH370-Malaysia-Airlines-Anwar-Ibrahim-says-government-purposefully-concealing-information.html). *The Daily Telegraph*. Retrieved 6 April 2014.
256. "Hishammuddin caught in social media storm over 'insensitive' MH370 tweet" (http://www.themalaysianinsider.com/malaysia/article/hishammuddin-caught-in-social-media-storm-over-insensitive-mh370-tweet). *The Malaysian Insider*. 3 April 2014. Retrieved 20 November 2014.
257. Rajca, Jennifer; Shorten, Kristin; Toohey, Paul; Swallow, Julian (3 April 2014). "Angus Houston pledges to help 'our mate' Malaysia in search for missing Malaysia Airlines flight MH370" (http://www.news.com.au/travel/travel-updates/angus-houston-pledges-to-help-our-mate-malaysia-in-search-for-missing-malaysia-airlines-flight-mh370/story-fnizu68q-1226872887918). *news.com.au*. News Corp Australia. Retrieved 20 November 2014.
258. "Multiple authorities let Malaysia Airlines flight MH370 disappear: ABC" (https://au.news.yahoo.com/world/a/23664489/multiple-authorities-let-malaysia-airlines-flight-mh370-disappear-abc/). *Yahoo News 7*. 20 March 2014. Retrieved 22 November 2014.
259. Kingsbury, Damien (20 March 2014). "A sclerotic Malaysian government stumbles in MH370 crisis" (http://www.crikey.com.au/2014/03/20/a-sclerotic-malaysian-government-stumbles-in-mh370-crisis/). *Crikey*. Retrieved 22 November 2014.
260. Hatton, Celia (25 March 2014). "Malaysia Airlines MH370: Relatives in Beijing scuffles" (http://www.bbc.com/news/world-asia-26728045). BBC News. Retrieved 9 May 2014.
261. "China's Xi to send special envoy to Malaysia over missing plane" (http://news.yahoo.com/chinas-xi-send-special-envoy-malaysia-over-missing-092920386--business.html). Yahoo! News. 25 March 2014. Retrieved

1 April 2014.
262. "MH370 passengers' relatives protest in China" (http://www.aljazeera.com/news/asia-pacific/2014/03/mh370-passengers-relatives-protest-china-20143254173613347.html). Al Jazeera. 25 March 2014. Retrieved 25 March 2014.
263. "(Flight MH370) Message from Beijing: "Liars" " (http://www.thestandard.com.hk/breaking_news_detail.asp?id=47913). *The Standard*. 25 March 2014. Retrieved 6 April 2014.
264. Branigan, Tania (30 March 2014). "Flight MH370: Chinese relatives demand apology from Malaysia" (http://www.theguardian.com/world/2014/mar/30/flight-mh370-chinese-relatives-apology-malaysia-missing-plane). *The Guardian*. Retrieved 6 April 2014.
265. Mei, Xinyu (31 March 2014). "Treat MH370 tragedy rationally" (http://www.chinadaily.com.cn/opinion/2014-03/31/content_17390638.htm). *China Daily*. Retrieved 2014.
266. Jha, Supriya (3 April 2014). "Developments over Malaysian jet search: As it happened" (http://zeenews.india.com/news/world/live-malaysia-australia-vow-to-solve-the-great-mh370-mystery_922001.html). *Z News*. Retrieved 6 April 2014.
267. Murdoch, Lindsay (3 April 2014). "Flight MH370: Police investigate whether food on missing plane was poisoned" (http://www.smh.com.au/world/flight-mh370-police-investigate-whether-food-on-missing-plane-was-poisoned-20140403-zqq33.html). The Sydney Morning Herald. Retrieved 3 April 2014.
268. Schmitt, Eric; Semple, Kirk (15 April 2014). "Flight MH370: Missteps by China slowed search for missing jet" (http://economictimes.indiatimes.com/news/international/world-news/flight-mh370-missteps-by-china-slowed-search-for-missing-jet/articleshow/33772008.cms). *The Economic Times*. Retrieved 17 January 2015.
269. "China gets taste of world criticism in MH370 hunt" (http://www.themalaymailonline.com/malaysia/article/china-gets-taste-of-world-criticism-in-mh370-hunt). *The Malay Mail*. Retrieved 23 April 2014.
270. Demick, Barbara (28 March 2014). "Chinese boycott Malaysia over missing jetliner" (http://articles.latimes.com/2014/mar/28/world/la-fg-wn-chinese-boycott-malaysia-over-missing-jetliner-20140328). *Los Angeles Times*. Retrieved 30 August 2014.
271. Millward, Steven (28 March 2014). "As outrage grows over missing flight, Chinese websites ban Malaysia Airlines ticket sales" (http://www.techinasia.com/china-flight-ticket-sites-boycott-malaysia-airlines-over-mh370/). *TechInAsia*. Retrieved 30 August 2014.
272. Gat, Aviva. "Several Chinese travel booking sites boycott Malaysia Airlines" (http://www.geektime.com/2014/03/31/several-chinese-travel-booking-sites-boycott-malaysia-airlines/). *Geektime*. Retrieved 30 August 2014.
273. "Malaysia to face losses of up to RM4 billion in tourism revenue due to MH370, say analysts" (http://www.themalaysianinsider.com/malaysia/article/malaysia-to-face-losses-of-up-to-rm4-billion-in-tourism-revenue-due-to-mh37). *The Malaysian Insider*. 27 March 2014. Retrieved 30 August 2014.
274. "Chinese celebs lash out at M'sia over MH370" (https://web.archive.org/web/20140904090815/https://my.news.yahoo.com/chinese-celebs-lash-out-at-m-sia-over-mh370-112920894.html). *Yahoo! Malaysia*. Malaysiakini. 27 March 2014. Archived from the original (https://my.news.yahoo.com/chinese-celebs-lash-out-at-m-sia-over-mh370-112920894.html) on 4 September 2014. Retrieved 30 August 2014.
275. "How do you track a plane?" (http://www.bbc.com/news/world-asia-pacific-26544554). *BBC News*. 17 March 2014. Retrieved 25 November 2014.
276. Rolphe, Martin (17 September 2014). "The future of aircraft surveillance and tracking" (http://nats.aero/blog/2014/09/future-aircraft-surveillance-tracking/). *nats.aero*. Retrieved 12 April 2015.
277. Pasztor, Andy (13 July 2014). "How to Avoid Another Malaysia Flight 370" (http://online.wsj.com/articles/how-to-avoid-another-malaysia-flight-370-1405100436). *The Wall Street Journal*. Retrieved 3 December 2014.
278. Pasztor, Andy (14 May 2014). "After MH370, Air-Tracking Plan Unveiled" (http://online.wsj.com/articles/SB10001424052702303851804579560962991371096). *The Wall Street Journal*. Retrieved 3 December 2014.
279. "Industry Addressing Aircraft Tracking Options" (http://www.iata.org/pressroom/pr/pages/2014-06-03-1.aspx). *IATA*. 3 June 2014. Retrieved 25 November 2014.
280. Domínguez, Gabriel (22 August 2014). "What has the aviation industry learned from Flight MH370?" (http://www.dw.de/what-has-the-aviation-industry-learned-from-flight-mh370/a-17871162). *Deutsche Welle*. Retrieved 19 October 2014.
281. "IATA wants new airline tracking equipment"

(http://www.malaysiasun.com/index.php/sid/222727817/scat/5e8a9e9456185a7e/ht/IATA-wants-new-airline-tracking-equipment). *Malaysia Sun*. Retrieved 10 June 2014.
282. Martell, Allison (30 September 2014). "Task force delays aircraft tracking plans promised after MH370 mystery" (http://uk.reuters.com/article/2014/09/30/uk-airlines-safety-tracking-idUKKCN0HP2C420140930). *Reuters*. Reuters. Retrieved 8 October 2014.
283. "Inmarsat offers to track aircraft for free after Malaysia Airlines disaster – Telegraph" (http://www.telegraph.co.uk/technology/news/10824544/Inmarsat-offers-to-track-aircraft-for-free-after-Malaysia-Airlines-disaster.html). *The Daily Telegraph*. 12 May 2014. Retrieved 4 April 2015.
284. "Why can plane transponders be turned off from the cockpit?" (http://www.cbsnews.com/news/malaysia-airlines-flight-370-mystery-raises-new-transponder-questions/). CBS News. 19 March 2014. Retrieved 19 March 2014.
285. Stupples, David (9 April 2014). "MH370 should make us rethink how we monitor planes" (http://phys.org/news/2014-04-mh370-rethink-planes.html). *Phys.org*. Retrieved 20 January 2015.
286. de Castella, Tom (25 March 2014). "Malaysia plane: Why black boxes can't always provide the answers" (http://www.bbc.com/news/magazine-26721975). *BBC News*. Retrieved 22 January 2015.
287. Allard, Tom (28 April 2014). "MH370: Expert demands better black box technology" (http://www.smh.com.au/world/mh370-expert-demands-better-black-box-technology-20140428-zr0vn.html). *Sydney Morning Herald*. Retrieved 21 January 2015.
288. Yu, Yijun (19 March 2014). "If we'd used the cloud, we might know where MH370 is now" (http://phys.org/news/2014-03-cloud-mh370.html#nRlv). *Phys.org*. Retrieved 21 January 2015.
289. Huerta, Michael P. (22 January 2015). "Safety Recommendation: A – 15 – 1 through – 8" (http://www.ntsb.gov/safety/safety-recs/recletters/A-15-001-008.pdf) (PDF). *NTSB*. Retrieved 13 February 2015.
290. "NTSB Calls for Better Ways to Find Aircraft Accident Sites and Retrieve Critical Flight Data" (http://www.ntsb.gov/news/press-releases/Pages/PR20150122.aspx). *NTSB*. 22 January 2015. Retrieved 13 February 2015.
291. Rivera, Gloria (7 March 2014). "Malaysia Airlines Flight Vanishes, Three Americans on Board" (http://abcnews.com/International/malaysia-airlines-flight-missing-en-route-china/story?id=22827892). ABC News. Retrieved 7 May 2014.
292. "MH370 Malaysia Airlines: Anwar Ibrahim says government purposefully concealing information" (http://www.telegraph.co.uk/news/worldnews/asia/malaysia/10743378/MH370-Malaysia-Airlines-Anwar-Ibrahim-says-government-purposefully-concealing-information.html). *Telegraph.co.uk*. 3 April 2014. Retrieved 28 September 2014.
293. "Search operation for Malaysian airlines aircraft: Update 2" (https://www.amsa.gov.au/media/documents/18032014MH370Update2.pdf) (PDF). Australian Maritime Safety Authority. 18 March 2014. Retrieved 12 April 2015.
294. "Malaysia plane: Bad weather halts search for flight MH370" (http://www.bbc.com/news/world-asia-26726427). BBC News. 25 March 2014. Retrieved 9 May 2014.
295. Austin, Henry (24 March 2014). "Missing Jet: 'Orange Rectangular Object' Spotted in Sea" (http://www.nbcnews.com/storyline/missing-jet/missing-jet-orange-rectangular-object-spotted-sea-n60261). NBC News. Retrieved 24 March 2014.
296. "About the Joint Agency Coordination Centre" (http://www.jacc.gov.au/). Joint Agency Coordination Centre. Retrieved 6 May 2014.
297. "MH370: Inmarsat satellite data revealed to the public — CNN.com" (http://edition.cnn.com/2014/05/27/world/asia/malaysia-missing-plane/index.html). CNN. 27 May 2014. Retrieved 29 May 2014.
298. "Media Release by The Hon Warren Truss MP, Deputy Prime Minister 26 June 2014" (http://www.jacc.gov.au/media/releases/2014/june/mr052.aspx). *JACC*. Australia Department of Infrastructure and Regional Development. Retrieved 27 June 2014.
299. "MH370 search resumes in Indian Ocean" (http://www.bbc.com/news/world-asia-29502013). *BBC News*. 6 October 2014. Retrieved 8 October 2014.
300. "MH370 seabed search begins in deep Indian Ocean waters" (http://www.smh.com.au/national/mh370-seabed-search-begins-in-deep-indian-ocean-waters-20141005-10qli2.html). *Sydney Morning Herald*. 5 October 2014. Retrieved 8 October 2014.
301. The disappearance of flight MH370:
    - "Malaysia Airlines MH370: One year on, still no trace of plane that disappeared with 239 people onboard"

(http://web.archive.org/save/http://australiaplus.com/international/2015-03-08/malaysia-airlines-mh370-one-year-on-still-no-trace-of-plane-that-disappeared-with-239-people-onboard/1422759). *Australia Plus* (Australian Broadcasting Corporation). 8 March 2015. Archived from the original (http://australiaplus.com/international/2015-03-08/malaysia-airlines-mh370-one-year-on-still-no-trace-of-plane-that-disappeared-with-239-people-onboard/1422759) on 18 March 2015. Retrieved 18 March 2015. "Addressing Parliament on Thursday, [Australian Prime Minister Tony Abbott] said the disappearance of the passenger jet was 'one of the great mysteries of our time.'"
    - "Can Malaysia Airlines Survive Another Tragedy?" (http://www.huffingtonpost.co.uk/2014/07/18/mh17-mh370-plane-disaster-malaysia-airlines_n_5598334.html). *Huffington Post*. Retrieved 4 January 2015.
    - "Reporter Velez-Mitchell: Saturation News Coverage 'Twists Reality' " (http://www.newsmax.com/Newsmax-Tv/Jane-Velez-Mitchell-media-coverage-obsessive/2014/12/30/id/615713/). *Newsmax*. Retrieved 4 January 2015.
    - "Transcripts" (http://edition.cnn.com/TRANSCRIPTS/1410/07/ath.02.html). *CNN*. Retrieved 12 April 2015.
    - "Malaysia Airlines disappearance joins greatest mysteries of all time" (http://pix11.com/2014/03/17/malaysia-airlines-disappearance-joins-greatest-mysteries-of-all-time/). *PIX 11*. Retrieved 4 January 2015.
    - "The most read stories of 2014 on KOMONews.com" (http://www.komonews.com/news/local/The-most-popular-stories-of-2014-287041471.html). *KOMO News*. Retrieved 4 January 2015.
    - "World Headlines" (https://www.osv.com/OSVNewsweekly/RSS/RSSWorld/TabId/970/ArtMID/14185/ArticleID/14292/The-ongoing-mystery-of-Malaysia-Airlines-Flight-370.aspx). *OSV Newsweekly*. Retrieved 4 January 2015.
302. "Malaysia 370: The Plane That Vanished" (http://www.smithsonianchannel.com/sc/web/show/3406766/malaysia-370-the-plane-that-vanished). *Smithsonian Channel*. Retrieved 18 June 2014.
303. Morabito, Andrea (3 April 2014). "Smithsonian Channel will air documentary on missing jet" (http://nypost.com/2014/04/03/smithsonian-channel-will-air-documentary-on-missing-jet/). *New York Post*. Retrieved 18 June 2014.
304. "Flight 370: The Missing Links" (http://www.discoverychannelasia.com/shows/flight-370-the-missing-links/). *Discovery Channel (Asia)*. Discovery Networks International. Retrieved 18 June 2014.
305. Kemp, Stuart (2 April 2014). "Discovery Networks International Orders Special on Malaysia Flight 370" (http://www.hollywoodreporter.com/news/discovery-networks-international-orders-special-692946). *The Hollywood Reporter*. Retrieved 18 June 2014.
306. "Where is Flight MH370?" (http://www.bbc.co.uk/programmes/b047czkj). *BBC Two*. BBC. Retrieved 12 June 2014.
307. "Why Planes Vanish" (http://www.pbs.org/wgbh/nova/space/why-planes-vanish.html). *NOVA*. WGBH. Retrieved 10 October 2014. "FOR BBC Where is Flight MH370?"
308. "NOVA — Why Planes Vanish" (http://video.pbs.org/video/2365334815/). *pbs.org*. PBS. Retrieved 10 October 2014.
309. John Goglia (8 October 2014). "Why Planes Vanish: NOVA Documentary Explores What Happened to Missing Malaysia Boeing-777" (http://www.forbes.com/sites/johngoglia/2014/10/08/why-planes-vanish-nova-documentary-explores-what-happened-to-missing-malaysia-boeing-777/). *Forbes*. Retrieved 11 October 2014.
310. "The Surprisingly Good Flight 370 Novel: Author Scott Maka Defends His Controversial Book" (http://www.thedailybeast.com/articles/2014/06/14/the-surprisingly-good-flight-370-novel-author-scott-maka-defends-his-controversial-book.html). The Daily Beast. Retrieved 3 July 2014.
311. "Air Crash Investigation" (http://web.archive.org/web/20150213212719/http://natgeotv.com/uk/air-crash-investigation/about). *National Geographic*. Archived from the original (http://natgeotv.com/uk/air-crash-investigation/about) on 13 February 2015. Retrieved 13 February 2015.

External links

- Official website (http://www.mh370.gov.my/index.php/en/) – maintained by the Malaysian government

- Joint Agency Coordination Centre (JACC) (http://www.jacc.gov.au/)
- Accident description (http://aviation-safety.net/database/record.php?id=20140308-0) at the Aviation Safety Network
- ATSB investigation of Flight 370 (http://www.atsb.gov.au/publications/investigation_reports/2014/aair/ae-2014-054.aspx) – webpage of Australian Transport Safety Bureau's investigation (Investigation number: AE-2014-054; Investigation title: *"Assistance to Malaysian Ministry of Transport in support of missing Malaysia Airlines flight MH370 on 7 March 2014 UTC"*)
- ICAO statement on the first anniversary of the Flight 370 disappearance (http://www.icao.int/Newsroom/NewsDoc2015/COM%20Statement_MH370-Anniversary.EN.pdf)

Reports

- MH 370 Preliminary Report (http://www.cnn.com/interactive/2014/04/world/malaysia-flight-documents/) – Preliminary report issued by the Malaysia Ministry of Transport. Dated 9 April 2014 and released publicly on 1 May 2014.
- MH370 – Definition of Underwater Search Areas (http://atsb.gov.au/media/5243942/ae-2014-054_mh370_-_definition_of_underwater_search_areas_18aug2014.pdf) – Report by the Australian Transport Safety Bureau, released 26 June 2014, and the most comprehensive report on Flight 370 publicly released at that time. The report focuses on defining the search area for the fifth phase, but in doing so provides a comprehensive overview/examination of satellite data, the failed searches, and possible "end-of-flight scenarios".
- Factual Information: Safety Investigation for MH370 (http://mh370.mot.gov.my/download/FactualInformation.pdf) – Interim report released 8 March 2015 (584 pages).

Press releases / Media

- Australian Maritime Safety Authority (http://amsa.gov.au/media/incidents/mh370-search.asp)
- Australian Transport Safety Bureau (http://www.atsb.gov.au/mh370)
- Malaysia Airlines (http://www.malaysiaairlines.com/my/en/site/mh370.html)
- Malaysian Ministry of Transport (http://www.mot.gov.my/my/Kenyataan%20Media%20MH%20370/MH370%20Press%20Statement%20by%20Hishammuddin%20Hussein%20on%202%20April%202014.pdf)
- US Department of Defense (http://www.defense.gov/home/features/2014/0314_flight370/)

Retrieved from "https://en.wikipedia.org/w/index.php?title=Malaysia_Airlines_Flight_370&oldid=675380482"

Categories: Malaysia Airlines Flight 370 | 2014 in Australia | 2014 in China | 2014 in international relations | 2014 in Malaysia | Accidents and incidents involving the Boeing 777 | Airliner accidents and incidents with an unknown cause | Australia–China relations | Australia–Malaysia relations | Aviation accidents and incidents in 2014 | Aviation accidents and incidents in international airspace | Aviation accidents and incidents in Malaysia | China–Malaysia relations | History of the Indian Ocean | Malaysia Airlines accidents and incidents | Missing aircraft

- This page was last modified on 10 August 2015, at 06:48.
- Text is available under the Creative Commons Attribution-ShareAlike License; additional terms may apply. By using this site, you agree to the Terms of Use and Privacy Policy. Wikipedia® is a registered trademark of the Wikimedia Foundation, Inc., a non-profit organization.